N73-73940

Vol. I

ORBITAL FLIGHT HANDBOOK

for the

NATIONAL AERONAUTICS AND SPACE ADMINISTRATION

George C. Marshall Space Flight Center
Huntsville, Alabama

MARTIN MARIETTA
SPACE SYSTEMS DIVISION Baltimore 3, Maryland

REPRODUCED BY
NATIONAL TECHNICAL
INFORMATION SERVICE
U.S. DEPARTMENT OF COMMERCE
SPRINGFIELD, VA. 22161

1119

© Copyright by Martin Company

FOREWORD

This handbook has been produced by the Space Systems Division of the Martin Company under Contract NAS 8-5031 with the George C. Marshall Space Flight Center of the National Aeronautics and Space Administration. The handbook expands and updates work previously done by the Martin Company and also incorporates, as indicated in the text, some of the work done by Space Technology Laboratories, Inc. and Norair Division of Northrop Corporation under previous contracts with the George C. Marshall Space Flight Center. The Orbital Flight Handbook is considered the first in a series of volumes by various contractors, sponsored by MSFC, treating the dynamics of space flight in a variety of aspects of interest to the mission designer and evaluator. The primary purpose of these books is to serve as a basic tool in preliminary mission planning. In condensed form they provide background data and material collected through several years of intensive studies in each space mission area, such as earth orbital flight, lunar flight and interplanetary flight. Volume I, the present volume, is concerned with earth orbital missions.

The Martin Company Program Manager for this project has been Jorgen Jensen; George Townsend has been Technical Director. George Townsend has also had the direct responsibility for the coordination and preparation of this volume. Donald Kraft is one of the principal contributors to this volume; information has also been supplied by Jyri Kork and Sidney Russak. Barclay E. Tucker and John Magnus have assisted in preparing the handbook for publication.

The assistance given by the Future Project Office at MSFC and by the MSFC Contract Management Panel, directed by Conrad D. Swanson, is gratefully acknowledged.

CONTENTS

		Page
I	Introduction	I-1
II	Physical Data	II-1
III	Orbital Mechanics	III-1
IV	Perturbations	IV-1
V	Satellite Lifetimes	V-1
VI	Maneuvers	VI-1
VII	Rendezvous	VII-1
VIII	Orbital Departure	VIII-1
IX	Satellite Re-Entry	IX-1
X	Waiting Orbit Criteria	X-1
XI	Orbit Computations	XI-1
XII	Guidance and Control Requirements	XII-1
XIII	Mission Requirements	XIII-1
	Appendix A	A-1
	Appendix B	B-1

NOTICE

THIS DOCUMENT HAS BEEN REPRODUCED FROM THE BEST COPY FURNISHED US BY THE SPONSORING AGENCY. ALTHOUGH IT IS RECOGNIZED THAT CERTAIN PORTIONS ARE ILLEGIBLE, IT IS BEING RELEASED IN THE INTEREST OF MAKING AVAILABLE AS MUCH INFORMATION AS POSSIBLE.

I. INTRODUCTION

The material within the manual is arranged in three major areas and these areas are further divided into related discussions. The classification of material is as follows:

Basic Techniques and Data--Chapters II through V.

Mission Sequencing Problems--Chapters VI through IX.

Requirements--Chapters X through XIII.

These areas encompass most of the material in the field of earth orbital mechanics. The intent in all of these discussions is to provide analytic relationships which define the problem, and to augment these discussions with an error analysis and graphical or tabular data. In some of the material, however, the number of variables is so large that it is not practical to present graphical data; in others, the problem is so involved that it is not possible to obtain analytic solutions (such investigations were conducted numerically). In all cases, however, the prescribed purpose has been achieved without sacrificing the scope of the investigation.

A brief resume of some of the more important features of these chapters is presented in the following paragraphs.

II. PHYSICAL DATA

The material in this chapter reviews some of the work published by R. M. L. and by W. M. Kaula for the purpose of presenting a set of constants necessary in the computation of trajectories. Appendix B extending this data is an internally consistent set of constants developed by Dr. H. G. L. Krause.

The chapter then discusses other geophysical factors which can affect the selection of an orbit. Included in these discussions is material on the radiation environment, the meteoroid environment and the upper atmosphere and its variability.

The chapter concludes with a discussion of the measurement of time, distance, mass, etc. This portion of the chapter contains tables constructed for the purposes of making the transformation of units as simple and accurate as possible.

III. ORBITAL MECHANICS

The discussions of this chapter present the basic central motion trajectory equations to be used in the balance of the text. Relations defining the 3-D motion are developed and a large number of identities and equations are presented for elliptic motion. These equations (numbering in excess of 400) are followed by approximately 75 series expansions of the time variant orbital parameters with arguments of the mean anomaly, the true anomaly, and the eccentric anomaly. The chapter concludes with a discussion of the n-body problems.

IV. PERTURBATIONS

Special and general perturbation techniques are discussed, and the results of several general perturbation theories are catalogued and compared. This presentation provides the reader with the information necessary to evaluate the theories for each individual application and with an awareness of the subtle differences in the approaches and results.

V. SATELLITE LIFETIMES

The material of this chapter presents in succession discussions pertaining to the aerodynamic forces in free molecular flow, to analytic approximations for use in determining the lifetime of satellites in circular orbits in a nonrotating atmosphere, and, finally, to decay rates in a rotating oblate atmosphere. Where possible, analytic expressions have been obtained, but accuracy has not been sacrificed for form, and extensive use has been made of numerical computation facilities. Here again, however, attention to detail revealed several nondimensional decay parameters and made it possible to make these computations more efficiently.

VI. MANEUVERS

The general problem of orbital maneuvering is approached from several directions. First, the case of independent adjustment of each of the six constants of integration is presented both for the case of circular motion and elliptic motion. Then the general problem of transferring between two specified terminals in space is developed. These discussions, like those of the other chapters, are fully documented.

The chapter concludes with a discussion of the effects of finite burning time, of the requirements for the propulsion system to accomplish the previously described maneuvers, a discussion of the error sensitivities, and a discussion of the statistical distribution of errors in the resultant orbital elements.

VII. RENDEZVOUS

Rendezvous is broken into two basic phases for the purpose of the discussion in this handbook. The first of these phases contains the launch and ascent timing problems, the problems of maneuvers and of the relative merits of direct ascent versus the use of intermittent orbits or rendezvous compatible orbits. The second phase is the discussion of the terminal maneuvers. Included in this final section are the equations of relative motion, a discussion of possible types of guidance laws, and information necessary to evaluate the energy and timing of the terminal maneuver whether it be of a short or long term nature.

VIII. ORBITAL DEPARTURE

The problem of recovering a satellite from orbit at a specific point on earth at a specific time is essentially the reverse of the rendezvous problem, and the approach taken here is the same. First, an intermediate orbit is established which satisfies the timing constraints, then the maneuver is completed by deorbiting without requiring a lateral maneuver. For cases where this approach should prove impractical, data for a maneuverable re-entry is also presented.

The presentation progresses from the timing problem to the analyses of the intervals between acceptable departures, the finite burning simulation of the deorbit maneuver, and the error sensitivities for deorbiting.

IX. SATELLITE RE-ENTRY

Once the satellite leaves orbit it must penetrate the more dense regions of the atmosphere prior to being landed. This chapter treats analytically and parametrically (i.e., as function of the re-entry velocity vector) the various factors which are characteristic of this trajectory: Included are the time histories of altitude, velocity and flight path angle; also included are the range attained in descent, the maximum deceleration, the maximum dynamic pressure, and equilibrium radiative skin temperatures, as well as a discussion of aerodynamic maneuverability. Thus, this chapter makes it possible to analyze the trajectory all the way from launch to impact in a reasonably accurate manner before progressing to a detailed numerical study of a particular vehicle flying a particular trajectory.

X. WAITING ORBIT CRITERIA

The balance of the book treats problems associated with the flight mechanics aspects of specific missions. However, these are some problems which are not of this nature but which can influence the selection of orbits. (The radiation environment etc., of Chapter II is an example of this type material.) Accordingly, Chapter X presents some information pertaining to the solar radiation heat level, and to the storage of cryogenic fluids. This information is treated only qualitatively because it is outside the general field of orbital mechanics and is itself the subject for an extensive study. The material is included however, because of the requirement for fuel in many of the discussions of maneuver outlined in the rest of the text.

XI. ORBIT COMPUTATION

The discussions of this chapter tie many of the previous chapters together since all trajectories to be of value must be known. The discussions progress from the basic definitions of the basic coordinate systems and transformations between them, to the determination of initial values of the six constants of integration, to the theory of observational errors, and finally to the subject of orbit improvement. In this process, data is presented for most of the current tracking facilities and for many basic techniques applicable to the various problem areas (e.g., orbit improvement via least squares, weighted least squares, minimum variance, etc.). The chapter concludes with a presentation of data useful in the preliminary analysis of orbits.

XII. GUIDANCE AND CONTROL REQUIREMENTS

The discussions of this chapter relate the errors in the six constants of integration to errors in a set of six defining parameters. This 6 x 6 matrix of error partials has been inverted to rotate the parameter errors to errors in the elements. The result is that it is possible to progress from a set of parameter errors at some time directly to the errors in the same parameters at any other time. This formulation has proved itself useful not only in the study of error propagation but in the analysis of differential corrections and the long time rendezvous maneuver.

Also included in the chapter is information related to problems of guidance system design, the attitude disturbing torques and the attitude control system.

XIII. MISSION REQUIREMENTS

The purpose of this chapter is to present many problems which directly affect the selection of orbits for various missions and experiments. The data include satellite coverage (both area and point), satellite illumination and solar eclipses, solar elevation above the horizon, surface orientation relative to the sun, sensor limitations (e.g., photographic resolution considerations, radar limitations), and ground tracks. Thus, given a particular mission, one can translate the accompanying requirements to limitations on the orbital elements and, in turn, pick a compromise set which best satisfies these requirements (when the radiation environment, meteoroid hazard and radiation heat loads have been factored into the selection).

CHAPTER II

PHYSICAL DATA

Prepared by:

G. E. Townsend, Jr.
S. L. Russak
Martin Company (Baltimore)
Aerospace Mechanics Department
March 1963

		Page
	Symbols	II-1
	Introduction	II-2
A.	Astronautical Constants	II-2
B.	Astrophysical Constants	II-15
C.	Conversion Data	II-50
D.	References	II-56
E.	Bibliographies	II-59
	Illustrations	II-63

LIST OF ILLUSTRATIONS

Figure	Title	Page
1	Confidence Level for the Value of μ' as a Function of the Number of Data Points and Size of Interval. . .	II-65
2	Present Standard and Model Atmospheres, and Proposed Revision of U.S. Standard Atmosphere. . .	II-66
3	Temperature Versus Altitude, Defining Molecular Scale Temperature and Kinetic Temperature of the Proposed Revision to the United States Standard Atmosphere.	II-67
4	Molecular-Scale Temperature Versus Geometric Altitude Proposed United States Standard Atmosphere Compared with United States Detailed Data, Russian Average Data, and ARDC Model Atmosphere 1959 for Altitudes Above 80 km Only	II-68
5	Density Versus Geometric Altitude for Proposed United States Standard Atmosphere Compared with United States Detailed Data, Russian Average Data, and ARDC Model Atmosphere 1959	II-69
6	Pressure Versus Geometric Altitude for Proposed United States Standard Atmosphere Compared with United States Detailed Data, Russian Average Data, and ARDC Model Atmosphere 1959	II-70
7	Molecular Weight Versus Altitude.	II-71
8	Average Daytime Atmospheric Densities at the Extremes of the Sunspot Cycle	II-72
9	Density of the Upper Atmosphere Obtained from the Orbits of 21 Satellites.	II-73
10	Dependence of Atmospheric Density on $\Delta\alpha = \alpha_\pi - \alpha_\odot$ in the Equatorial Zone (diurnal effect)	II-73
11a	Diurnal and Seasonal Variations in Atmospheric Density at 210 km Dervied from Observations of the Satellite 1958 δ 2. (The lower x-scale gives true local time, the upper $\Delta\alpha = \alpha_\pi - \alpha_\odot$. The parameter of the curves is $\Delta\delta = \delta_\pi - \delta_\odot$ where α is right ascension, δ is declination, π is perigee, $\odot$ is sun.)	II-74

LIST OF ILLUSTRATIONS (continued)

Figure	Title	Page
11b	Variations in Atmospheric Density at 562 km Above the Earth Ellipsoid Derived from the Observations of Satellite 1959 α 1	II-74
11c	Variations in Atmospheric Density at 660 km Derived from the Observations of Satellite 1958 β 2	II-74
12	Diurnal Variations of Atmospheric Density at Altitudes from 150 to 700 km Above the Earth Ellipsoid for $\lvert\Delta\,\delta\rvert < 20°$	II-75
13	Model of the Seasonal Variation of Mean Density to 200 km	II-75
14	Radiation Dose from Solar Flares Versus Skin Thickness	II-76
15	Solar Proton Dose, May 10, 1959 Flare, 30-Hour Duration	II-77
16	Solar Proton Dosages from February 23, 1956 Flare	II-78
17	Solid Angle Subtended by Earth as a Function of Altitude	II-79
18	Magnetic Dip Equator (1) from USN Hydrographic Office, 1955 and Geocentric Magnetic Equator (2) Inclined 13° to the Equator at Longitude 290°	II-79
19	Inner Van Allen Belt	II-80
20	Flux of Protons at One Longitude in the Van Allen Belt	II-81
21	Proton Differential Kinetic Energy Spectrum for the Inner Van Allen Belt	II-82
22	Flux of Electrons in the Van Allen Belts	II-83
23	Differential Kinetic Energy Spectrum Van Allen Belt Electrons	II-84

LIST OF ILLUSTRATIONS (continued)

Figure	Title	Page
24	Electron Dose Rates	II-85
25	X-Ray Dose Rates	II-85
26	Cosmic Radiation Intensity as a Function of Geomagnetic Latitude for High Altitudes During a Period of Low Solar Activity	II-86
27	Relative Biological Effectiveness for Cosmic Rays as a Function of Altitude and Geomagnetic Latitude During a Time of Low Solar Activity	II-86
28	Cosmic-Radiation Dosage as a Function of Shield Mass	II-87
29	Differential Energy Spectrum Measured During Rocket Flight NN 8.75 CF	II-87
30	Meteoric Mass Versus Apparent Visual Magnitude	II-88
31	Meteoroid Frequency Versus Mass	II-88
32	Average Meteoroid Distribution Curve from Microphone System Measurements	II-89
33	Meteoroid Penetration Relations	II-89

II. PHYSICAL DATA

SYMBOLS

a	Semimajor axis of the instantaneous elliptical orbit
e	Eccentricity of the instantaneous elliptical orbit
f	Flattening = $(R_{equatorial} - R_{polar}) \div R_{equatorial}$
G	Universal gravitational constant
i	Inclination of the instantaneous elliptical orbit
J_n	Coefficients of the potential function
K_s	Solar gravitational constant = $Gm_\odot$
L	Latitude
L'	Coefficient of the lunar equation
m	Mass
M_o	Mean anomaly of epoch
n	Number
P	Probability
$P_n()$	Legendre polynomial of order n
r	Radius
r^*	Radius of action (Tisserand's criteria)
t_b	Coefficient obtained from t distribution
U	Potential function
$\bar{x}$	Mean of a sample of size n
μ	Gravitational constant for a planet = Gm_p
μ'	Mean of population from which sample is taken
π	Parallax = ratio of two distances
σ	Variance of population from which sample is taken
$\sigma_{\bar{x}}$	Estimate of the variance assuming the parent population is normal $\left(\sigma^2_{\bar{x}} = \frac{1}{n} \sum (x_i - \bar{x})^2\right)$
τ	Orbital period
Ω	Longitude of the ascending node of the instantaneous elliptical orbit
ω	Argument of perigee of the instantaneous elliptical orbit

Subscripts

$\mathbb{C}$	Lunar
$\odot$	Solar
$\oplus$	Earth
p	Planet

INTRODUCTION

In the study of trajectories about the earth, factors defining the trajectory must be accurately known. Since these factors fall into two areas:

Astronautical constants

Geophysical constants

each of these general areas will be investigated. In addition, information which is not of a flight mechanics nature but which can effect the selection of orbits will also be presented. This type of information includes:

Radiation hazard data (all types)

Micrometeoroid data

Shielding data.

Finally, information necessary to convert this data from one set of units to another will be presented. This discussion goes beyond unit conversion, however, to include a review of time standards and measurement. This review is applicable to the material presented in all of the chapters which follow.

A. ASTRONAUTICAL CONSTANTS

Three noteworthy articles dealing with the constants which define the trajectory of a missile or space vehicle have been published within the past two years. These articles are:

"Analysis and Standardization of Astro-Dynamic Constants" by M. W. Makemson, R. M. L. Baker, Jr., and G. B. Westrom, Journal of the Astronautical Sciences, Vol. 8, No. 1, Spring 1961, pages 1 through 13.

"A Geoid and World Geodetic System Based on a Combination of Gravimetric, Astrogeodetic and Satellite Data" by W. M. Kaula, Journal of Geophysical Research, Vol. 66, No. 6, June 1961, pages 1799 through 1811.

"On a Consistent System of Astrodynamic Constants" by H. G. L. Krause, NASA Report MTP-P&VE-F-62-12, Marshall Space Flight Center, 12 December 1962.

The first paper reviews measurements of heliocentric, planetocentric and selenocentric constants; the second treats the determination of the geocentric constants by statistical methods using the gravimetric, astrogeodetic and satellite data. The work reported in these papers is excellent and will not be reproduced since it is readily available. Rather the published data will be summarized and the best values selected for use in trajectory analysis. It is felt that this step is necessary because (1) there are small inconsistencies in the data, and (2) there is no mention in the first article of a method of analysis or an approximate confidence interval. "Confidence interval" will be used here to indicate that the sample interval brackets the true mean some prescribed percentage of the time.

The discussion of these constants will be followed by a presentation of desirable data which is obtained from the constants and tables of conversions relating these quantities to the corresponding quantities in other sets of units. This latter set of tables is particularly important since there is much confusion as to the meaning of generally used units and the accuracy of the conversion factors.

Dr. Krause's paper, which is presented as Appendix B to this volume by consent of the author, presents a slightly different set of constants. This results from the fact that the approach taken was to produce an internally consistent set of constants based on the author's adopted values of the independent quantities rather than to accept the slight inconsistencies resulting from the development of "best values" for each of the quantities. It is noted, however, that in nearly every instance Dr. Krause's values differ from those quoted in this section by a quantity less than the uncertainties quoted in this chapter. Thus, the two approaches seem to complement each other.

1. Analysis of Constants

Although Baker's exact analytical procedure is not known, his results indicate a process similar to the following:

(1) Collect all available data pertinent to a particular quantity.

(2) Obtain the mean and standard deviation of this sample

$$\bar{x} = \frac{1}{n} \sum_{i=1}^{n} x_i$$

$$\sigma_{\bar{x}}^2 = \frac{1}{n} \sum_{i=1}^{n} (x_i - \bar{x})^2$$

$$\sigma^2 = \frac{n-1}{n} \sigma_{\bar{x}}^2$$

(3) Throw out all points deviating from the mean by more than one standard deviation.

(4) Recompute the mean and standard deviation.

Assuming that the various pieces of data are of roughly the same accuracy (this assumption is necessary since the uncertainties quoted for the number are inconsistent) and that there is no uniform bias to the determinations, this procedure will result in a reasonable estimate for the quantity and its uncertainty, provided that the sample size is sufficiently large. However, there is no guarantee that the estimate will be reasonable for small samples. A general feel for the maximum number of random, unbiased determinations required for a specified accuracy of the resultant analysis can be obtained from Tchebycheff's inequality.

$$P\left[-b < (\bar{x} - \mu') < b\right] \geq 1 - \frac{\sigma^2}{nb^2}$$

$$n^* = \frac{\sigma^2}{b^2 (1 - p)}$$

= an estimate of the minimum sample size.

Since the general accuracy of the determinations is quoted to about 1 to 5 parts in 10^4 and since the standard deviations are of the same order,

$$n^* \approx \frac{K}{(1 - P)} \quad ; \quad K \approx 1$$

or

$$n^* \approx 10K \qquad P = 90\%$$
$$\approx 100K \qquad P = 99\%$$

where K is a constant of proportionality. Because the sample sizes are generally smaller than 10, it may appear that the confidence level for the quoted constants will be less than 90% but probably greater than 80% for most but not all of the constants. This, however, is not true as will be shown in the following paragraphs.

Tchebycheff's inequality provides a general feel for the concept of assigning a probability of correctness to the quoted value of any of the discussed constants. However, the question arises as to the definition of the number K; moreover, even if K is defined, the estimates are in general too conservative. For this reason, the method described below will be utilized.

Assuming once again, that the samples come from a normal distribution, the probability P that a given value will fall in a quoted region about the mean is

$$P\left[\bar{x} - a\frac{\sigma}{\sqrt{n}} < \mu' < \bar{x} + a\frac{\sigma}{\sqrt{n}}\right] = P.$$

However, care must be taken because the quantities μ' and σ used in this expression are the mean and variance of the true population, not the estimates of μ', $\bar{x} = \frac{1}{n}\sum x_i$, and σ, $\hat{\sigma} = \sqrt{\frac{\sum (x_i - \bar{x})^2}{n}}$. While these estimates may be utilized there is no assurance for the correctness for any but the large sample. The solution to this problem is found in the "t" distribution

$$t = \frac{\bar{x} - \mu'}{\sqrt{\frac{\sum (x_i - \bar{x})^2}{n(n-1)}}} = \frac{\bar{x} - \mu'}{\hat{\sigma}} (n - 1)^{1/2}$$

This distribution involves only μ' and the data x_i and is of n - 1 degree of freedom. Since this distribution is also tabulated it is possible to write

$$P(-t_b < t < t_b) = \int_{-t_b}^{t_b} f(t; n - 1)\, dt = P = 1 - b$$

and convert the inequalities to obtain

$$P\left[\bar{x} - t_b\sqrt{\frac{\sum (x_i - \bar{x})^2}{n(n-1)}} < \mu' < \bar{x} + t_b\sqrt{\frac{\sum (x_i - \bar{x})^2}{n(n-1)}}\right] = 1 - b$$

The coefficient t_b is called the b percent level of t and locates points which cut off b/2 percent of the area under f(t) on each tail (f(t) is symmetric about t = 0).

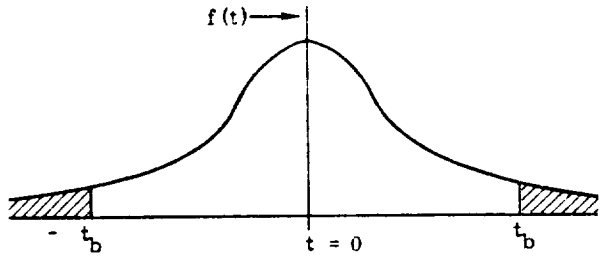

Thus, the problem of defining the probability of correctness which can be assigned to a quoted constant is one of defining t_b. Since in all the work to be discussed 1σ variation will be quoted, t_b times the radical can be defined as σ. This assumption results in an estimate of the probable correctness of the quoted constant which is a function only of the number of data points.

$$t_b = \sqrt{n - 1}$$

At this point it is possible to refer to a table of a cumulative t distribution and obtain the estimate of the confidence level for a given value of t_b (i.e., a specified sample size). However, since this solution requires nonlinear interpolation, the confidence levels have been plotted as a function of the sample size in Fig. 1. These data will be utilized for all estimates to be made in this section.

In view of the facts that the original measurements do not agree to within the probable errors quoted for the experiments and that the confidence levels for the results are reasonable, this procedure appears to be the most attractive means of resolving the confusion associated with these

constants until more and better data can be obtained. This is not meant to imply that Baker's data should be used as presented because in several cases his constants deserve special attention. In any event, when superior data become available they should either be weighted heavily $\left[\bar{x} \text{ obtained from } 0 = \sum_{i=1}^{n} \frac{(x_i - \bar{x})}{\sigma_i^2} \right]$ or utilized in preference to any other value.

Kaula's data will not be reviewed specifically because it is included in the analysis which follows. However, in the discussion of the geocentric constants, special note will be made of the agreement of Kaula's data with Baker's and that obtained by the criteria outlined above.

2. Heliocentric Constants

a. Solar parallax

Planetary observations and theories of planetary motion permit precise computation of the angular position of the planets. Although angular measurements are quite accurate, no distance scale is readily available. Attempts to resolve this problem have led to the comparison of large, unknown interplanetary distances to the largest of the known distances available to man, the equatorial radius of the earth. In the process, solar parallax was defined as the ratio of the earth's equatorial radius to the mean distance to the sun from a fictitious unperturbed planet whose mass and sidereal period are those utilized by Gauss in his computation of the solar gravitation constant (i.e., one astronomical unit). This definition renders unnecessary the revisions in planetary tables as more accurate fundamental constants are made available, since the length of the astronomical unit can be modified.

In the broadest sense, the solar parallax is the ratio between two sets of units: (1) the astronomical set utilizing the solar mass, the astronomical unit and the mean solar day, and (2) the laboratory set (cgs, etc.).

Before reviewing solar parallax data obtained from the literature, it is worthwhile to consider the means of computing the values and their uncertainties.

The first method, purely geometric, is triangulation based on the distance between two planets, between a planet and the sun, etc. One such computation was made by Rabe following a close approach of the minor planet Eros. The second method is an indirect approach based on Kepler's third law (referred to in the literature as the dynamical method). The third method employs the spectral shift of radiation from stars produced by the motion of the earth. Perturbations on the moon produced by the sun constitute a fourth means of computing solar parallax to good precision provided that the ratio of the masses of the earth and moon is well known. A fifth approach utilizes direct measurements of distance between bodies in space obtained from radar equipment.

Other approaches have also been advanced, but the five listed constitute the most frequently employed.

Table 1 presents the adopted value of solar parallax (from Baker) along with the unweighted mean of the data and the mean of the adjusted sample. (Special note is made that the value adopted by Baker corresponds most closely to that of Rabe which has been widely utilized during recent years.) The corresponding value of the astronomical unit is also presented.

TABLE 1

Solar Parallax

	Adopted by Baker	Uncorrected Mean and Standard Deviation	Adjusted Mean and Standard Deviation
Solar parallax (sec)	8.798± 0.002	8.7995± 0.0049	8.8002± 0.0024
Astronomical unit (10^6 km)	149.53± 0.03	149.507± 0.083	149.495± 0.041
Confidence level	?	99%	92%

The data in Table 1 show reasonably good agreement between the various estimates. However, it is interesting to note that the adjusted mean moved away from the value adopted by Baker. This behavior is undesirable but was not unforeseen because of the limitations of the method and the fact that more of the measurements were situated in this direction. However, most of the reported measurements were made before 1945 and the general trend during subsequent years has been toward slightly lower values of the solar parallax. If it is assumed that this trend reflects increased accuracy in the measurements (resulting in part from the availability of radar data), and if the more recent measurements are weighted by the time of determination (since the uncertainty in the various measurements is much larger than the quoted error in the experiment), a value of solar parallax of 8.7975 sec ± 0.0005 is obtained. This value is almost identical to Baker's which, as was noted, agrees with that of Rabe (generally accepted by those performing astronomical computations). For this reason, and for consistency in calculations by various groups within industry and the government, Baker's value of the solar parallax should be used. However, his assignment of probable error in this constant apparently is too large in view of the agreement of these data. A maximum uncertainty of ± 0.001 is more realistic.

b. Solar gravitational constant

In 1938 it was internationally agreed (IAU 1938) that to maintain the Gaussian value of the solar gravitational constant ($K_s^2 = Gm_\odot$ where G = Universal gravitational constant) in spite of changes in the definition of the sidereal year and the mass of the earth, the astronomical unit (AU) would be modified when necessary. Thus the solar gravitational constant has remained.

$$K_s = \frac{2\pi}{\tau} \sqrt{\frac{a_\oplus^3}{m_\odot + \frac{m_\oplus}{m_\odot}}}$$

$$= 0.017,\ 202,\ 098,\ 95 \ \frac{AU^{3/2}}{\text{solar day}}$$

where

$a_\oplus$ = 1 AU

τ = 365.256,383,5 mean solar days

$m_\odot$ = solar mass = 1

$\frac{m_\oplus}{m_\odot}$ = ratio of earth mass to solar mass = 0.000,002,819

This value of K_s is accurate to its ninth significant figure by definition. The precision in this determination is contrasted to the accuracy of a determination in laboratory units from the following equation

$$K_s^2 = Gm_\odot$$

where

G = the universal gravitational constant in the cgs or English system of units (mass in same system).

Utilizing even the most accurately known values of G and m (obtained from Westrom) the result is accurate only to its third place.

$$K_s^2 = \left\{\left[6.670\ (1 \pm 0.0007)\ 10^{-8}\right] \cdot \left[1.9866\ (1 \pm 0.007)\ 10^{33}\right]\right\}$$

$$K_s = 1.511\ (1 \pm 0.0005)\ 10^{13}\ cm^{3/2}/sec$$

The evaluation of K_s in laboratory units using the solar parallax proves equally as inadequate since the uncertainty is large. When the adopted value indicated in Table 1 is used, K_s is found to be

$$K_s = 1.1509\ (1 \pm 0.00015)\ 10^{13}\ cm^{3/2}/sec$$

It is thus advantageous to compute in the astronomical system of units, converting only when necessary. This procedure assures that the results will become more accurate as better values for the astronomical unit are obtained and produces a much lower end figure error due to round-off.

3. Planetocentric Constants

a. Planetary masses

Planetary masses are significant in computing transfer trajectories to the planets and trajectories about these bodies. The two most common methods of determining planetary mass are by the perturbation actions on other bodies or by observations of the moons of the planet. While the accuracies of the two approaches differ, each involves such complex functions as nearness of approach, mass of the planets, size and number of moons, etc., that no general conclusion can be made as to the superiority of one to the other.

Table 2 presents data reduced from determinations of the mass of each of the planets in terms of the solar mass, the related mass in kilograms, and the probable uncertainty in the measurement. In addition, since the number of points in the sample varies from planet to planet, this quantity is noted along with an estimate of the confidence level for the result.

In each case shown in Table 2 the results obtained with the adjusted sample approach those of Baker to within the uncertainties quoted for the masses and are practically identical. However, it should be noted that the uncertainties quoted for these masses are different at times. This discrepancy is believed to result from the somewhat arbitrary handling of the limits in the reviewed reference. On the basis of the data available, it seems more proper to use the standard deviation, as obtained from the adjusted sample, rather than Baker's value.

b. Planetary dimensions

While the physical dimensions of the planets have no effect on the trajectories of interplanetary vehicles and the dimensions are generally smaller than the uncertainty in the astronomical unit, the constants must be known for self-contained guidance techniques and for impact and launch studies. For these reasons the best shape of the various planets will be discussed.

Table 3 presents equatorial and polar radii and a quantity referred to in the literature as the flattening which is defined to be

$$f = \frac{R_{equatorial} - R_{polar}}{R_{equatorial}}$$

The table also presents comparisons of various data, the number of points in the sample and an estimate of the confidence level.

The sample size for the planet Uranus is questioned because Baker references only one source for this planet and that is a weighted average of several determinations. In the tabulation on Mars, note should be made of the excellent agreement on the best value of the radius given by the statistical approach and by Baker, and of the slight discrepancies in the uncertainties of the radius and in the best value of the flattening. Therefore, it is once again proposed that Baker's value of the radii and flattening (with one exception) be utilized but that the uncertainty obtained via statistics be associated with this number. The exception exists in the case of Mars for which it is proposed that 1/f be 75 ± 12, rather than Baker's value (150 ± 50) since this estimate is consistent with the data.

TABLE 2

Planetary Masses

Planet	Quantity of Interest	Adopted by Baker	Uncorrected Sample	Adjusted Sample
Mercury	Solar mass/mass of Mercury	6,100,000 ± 50,000	6.400.000 ± 630,000	6,030,000 ± 65,000
	Mass of Mercury in kg	$0.32\underline{567} \times 10^{24}$	$0.3\underline{1041} \times 10^{24}$	$0.3\underline{2945} \times 10^{24}$
	Sample size	4	4	3
	Confidence level	-	81%	70%
Venus	Solar mass/mass of Venus	407,000 ± 1,000	406,200 ± 1,000	407,000 ± 1,300
	Mass of Venus in kg	$4.8\underline{811} \times 10^{24}$	$4.8\underline{907} \times 10^{24}$	$4.8\underline{811} \times 10^{24}$
	Sample size	8	8	6
	Confidence level	-	97%	92%
Earth-Moon	Solar mass/earth-moon mass	328,450 ± 50	328,500 ± 100	328,430 ± 25
	Mass of earth-moon in kg	$6.0484\underline{1} \times 10^{24}$	$6.0474\underline{9} \times 10^{24}$	$6.0487\underline{8} \times 10^{24}$
	Sample size	6	6	4
	Confidence level	-	92%	81%
Mars	Solar mass/mass of Mars	3,090,000 ± 10,000	3,271,000 ± 795,000	3,092,000 ± 12,000
	Mass of Mars in kg	$6.0429\underline{1} \times 10^{24}$	$0.6073\underline{3} \times 10^{24}$	$0.6425\underline{0} \times 10^{24}$
	Sample size	6	6	4
	Confidence level	-	92%	81%
Jupiter	Solar mass/mass of Jupiter	1047.4 ± 0.1	1047.89 ± 1.87	1047.41 ± 0.08
	Mass of Jupiter in kg	$1.8967\underline{0} \times 10^{27}$	$1.8958\underline{1} \times 10^{27}$	$1.8967\underline{0} \times 10^{27}$
	Sample size	8	8	4
	Confidence level	-	97%	81%
Saturn	Solar mass/mass of Saturn	3500.0 ± 3	3497.3 ± 4.5	3499.8 ± 1.7
	Mass of Saturn in kg	$0.5676\underline{0} \times 10^{27}$	$0.5680\underline{4} \times 10^{27}$	$0.5676\underline{3} \times 10^{27}$
	Sample size	4	4	3
	Confidence level	-	81%	70%
Uranus	Solar mass/mass of Uranus	32,800 ± 100	22,810 ± 60	---
	Mass of Uranus in kg	$87.\underline{132} \times 10^{24}$	$87.\underline{093} \times 10^{24}$	---
	Sample size	2	2	---
	Confidence level	-	50%	---
Neptune	Solar mass/mass of Neptune	19,500 ± 200	19,500 ± 200	---
	Mass of Neptune in kg	$101.\underline{88} \times 10^{24}$	$101.\underline{88} \times 10^{24}$	---
	Sample size	3	3	---
	Confidence level	-	70%	---
Pluto	Solar mass/mass of Pluto	350,000 ± 50,000	333,000 ± 27,000	---
	Mass of Pluto in kg	$5.6\underline{760} \times 10^{24}$	$5.9\underline{658} \times 10^{24}$	---
	Sample size	3	3	---
	Confidence level	-	70%	---

____ Underlined digits are questionable

TABLE 3

Planetary Dimensions

Planet	Quantity of Interest	Adopted by Baker	Uncorrected Sample	Adjusted Sample
Mercury	Equatorial radius (km)	2,330 ± 15	2,355 ± 39	2,333 ± 11
	1/f	?	?	?
	Polar radius (km)	?	?	?
	Sample size	4	4	3
	Confidence level	?	81%	70%
Venus	Equatorial radius* (km)	6,100 ± 10	6,154 ± 100	6,106 ± 12
	1/f	?	?	?
	Polar radius (km)	?	?	?
	Sample size	6	6	3
	Confidence level	?	92%	70%
Mars	Equatorial radius (km)	3,415 ± 5	3,377 ± 47	3,414 ± 12
	1/f	150 ± 50	108.4 ± 54	75 ± 12
	Polar radius (km)	3,392 ± 12	3,346 ± 55	3,403 ± 12
	Sample size	9	9	5
	Confidence level	?	98%	88%
Jupiter	Equatorial radius (km)	71,375 ± 50	71,375 ± 30	---
	1/f	15.2 ± 0.1	15.2 ± 0.1	---
	Polar radius (km)	66,679 ± 50	66,679 ± 50	---
	Sample size	2	2	---
	Confidence level	?	50%	---
Saturn	Equatorial radius (km)	60,500 ± 50	60,160 ± 480	---
	1/f	10.2 ± ?	10.2 ± ?	---
	Polar radius (km)	54,569 ± 45	54,262 ± 450	---
	Sample size	2	2	---
	Confidence level	?	50%	---
Uranus	Equatorial radius (km)	24,850 ± 50	24,847 ± 50	---
	1/f	?	14 ± ?**	---
	Polar radius (km)	?	23,072 ± 50	---
	Sample size	?	?	---
Neptune	Equatorial radius (km)	25,000 ± 250	24,400 ± 2100	---
	1/f	58.5 ± ?	58.5 ± ?	---
	Polar radius (km)	24,573 ± 250	23,983 ± 2000	---
	Sample size	2	2	---
	Confidence level	?	50%	---
Pluto	Equatorial radius (km)	3,000 ± 500	2,934 ± 500	---
	1/f	?	?	---
	Polar radius (km)	?	?	---
	Sample size	1	1	---
	Confidence level	?	20%	---

*Equatorial radius for Venus includes the distance from the surface to the outer boundary of the dense atmosphere.

**From K. A. Ehricke's book "Space Flight Trajectories."

As was the case with some of the planetary masses, there was insufficient data available to allow for refining dimensional computations for all planets. Even where such computations were possible the confidence level of the resultant quantity was low.

c. Planetary orbits

Because the motion of a planet about the sun approximates an ellipse for relatively long periods of time, it has become standard practice to express the paths in terms of an ellipse with time-varying or osculating elements. To assure that the terminology is familiar, the six elements (or constants of integration) necessary to determine planetary motion are defined below.

(1) Planar elements

(1) Semimajor axis (a)--This element is a constant, being one-half the sum of the minimum and maximum radii. Element (a) is also a function of radius and velocity at any point.

(2) Eccentricity (e)--This element is related to the difference in maximum and minimum radii and is used to express a deviation in the path from circularity.

(3) Mean anomaly of epoch (M_0)--This element (referenced to any fixed known time) defines the position of the orbiting body in the plane of motion at any time.

(2) Orientation elements

(1) Argument of perigee (ω)--This is the angle measured in the orbital plane from the radius vector defining the ascending node to the minimum radius.

(2) Orbital inclination (i)--This angle expresses rotation of the orbital plane about a line in the ecliptic (or fundamental) plane.

(3) Longitude of the ascending node (Ω)--This is the angle measured in the fundamental plane from a fixed reference direction to the radius at which the satellite crosses the fundamental plane from the south to the north.

These osculating elements obviously are of primary importance in the computation of interplanetary transfer trajectories. Thus, the procedure for obtaining these elements will be reviewed; then the values of the elements will be presented. It is assumed only that a table of the time variation of acceleration is available. One such table is presented in Planetary Coordinates 1960 to 1980 available through Her Majesty's Stationery Office.

This reference quotes position and acceleration components in ecliptic rectangular coordinates. The most direct transformation is thus via the vectorial elements P, Q and R (where P points toward perihelion, Q in the direction of the true anomaly equals 90° and R completes the right handed set). The computation proceeds as follows: First the velocity components at the instant are computed. This is accomplished by numerical integration of the acceleration components rather than by differentiation of the position data in order to obtain better accuracy.

Argument	Sums		Function (Acceleration)	Differences			
	2nd	1st		1st	2nd	3rd	4th
t_{-2}		$\delta^{-1}\ddot{x}_{-3/2}$	$\ddot{x}_{-2}$	$\delta\ddot{x}_{-3/2}$			
t_{-1}	$\delta^{-2}\ddot{x}_{-1}$	$\delta^{-1}\ddot{x}_{-1/2}$	$\ddot{x}_{-1}$	$\delta\ddot{x}_{-1/2}$	$\delta^{2}\ddot{x}_{-1}$	$\delta^{3}\ddot{x}_{-1/2}$	
t_0	$\delta^{-2}\ddot{x}_{0}$	$\delta^{-1}\ddot{x}_{1/2}$	$\ddot{x}_{0}$	$\delta\ddot{x}_{1/2}$	$\delta^{2}\ddot{x}_{0}$	$\delta^{3}\ddot{x}_{1/2}$	$\delta^{4}\ddot{x}_{0}$
t_1	$\delta^{-2}\ddot{x}_{1}$	$\delta^{-1}\ddot{x}_{3/2}$	$\ddot{x}_{2}$	$\delta\ddot{x}_{3/2}$	$\delta^{2}\ddot{x}_{1}$		
t_2			$\ddot{x}_{2}$				

Thus, at the argument t_0

$$\dot{x} = \frac{1}{wK_s}\left[\mu\delta^{-1}\ddot{x} - \frac{1}{12}\mu\delta\ddot{x} + \frac{11}{720}\mu\delta^{3}\ddot{x} - \ldots\right]$$

where

w = the interval between points in mean solar days

K_s = Gaussian constant

$$= 0.017,202,098,95 \ \frac{AU^{3/2}}{\text{solar day}}$$

$$\mu\delta^{-1}\ddot{x} = 1/2\left(\delta^{-1}\ddot{x}_{-1/2} + \delta^{-1}\ddot{x}_{1/2}\right)$$

$$\mu\delta\ddot{x} = 1/2\left(\delta\ddot{x}_{-1/2} + \delta\ddot{x}_{1/2}\right)$$

$$\mu\delta^{3}\ddot{x} = 1/2\left(\delta^{3}\ddot{x}_{-1/2} + \delta^{3}\ddot{x}_{1/2}\right)$$

and similarly for $\dot{y}$ and $\dot{z}$.

Now

$$r^2 = x^2 + y^2 + z^2 \text{ (evaluated at } t_0)$$

$$v^2 = \dot{x}^2 + \dot{y}^2 + \dot{z}^2$$

$$H = x\dot{x} + y\dot{y} + z\dot{z}$$

$$a = \frac{1}{2/r - G^2} \qquad (1)$$

$$e \sin E = H/\sqrt{a} \qquad (2)$$

$$e \cos E = rG^2 - 1 \qquad (3)$$

$$\sqrt{p}\,\vec{R} = (y\dot{z} - z\dot{y})\,\hat{x} + (z\dot{x} - x\dot{z})\,\hat{y} + (x\dot{y} - y\dot{x})\,\hat{z}$$

$$\sqrt{1 - e^2}\,\vec{Q} = \vec{r}\,\frac{1}{r}\sin E + \vec{v}\,a^{1/2} \cdot (\cos E - e)$$

$$\vec{P} = \vec{r}\,\frac{1}{r}\cos E + \vec{v}\,a^{1/2}\sin E$$

And finally

$$\sin i \sin \Omega = R_x \tag{4}$$

$$\sin i \cos \Omega = -R_y \cos \epsilon - R_z \sin \epsilon \tag{5}$$

$$\cos i = R_z \cos \epsilon - R_y \sin \epsilon \tag{6}$$

And

$$(1 \pm \cos i) \sin (\omega \pm \Omega) = \pm P_y \cos \epsilon \pm P_z \sin \epsilon - Q_x \tag{7}$$

$$(1 \pm \cos i) \cos (\omega \pm \Omega) = \pm Q_y \cos \epsilon \pm Q_z \sin \epsilon + P_x \tag{8}$$

where: ϵ = obliquity of the ecliptic of date given below:

t = 1960	ϵ = 23°26'40.15"	sin ϵ = 0.39786035	cos ϵ = 0.91744599
1962	23°26'39.21"	0.39785618	0.91744780
1964	23°26'38.28"	0.39785201	0.91744960
1966	23°26'37.34"	0.39784784	0.91745141
1968	23°26'36.40"	0.39784368	0.91745322
1970	23°26'35.93"	0.39783951	0.91745503

Equations (1), (2) and (3) define a, e and E (analogous to M) at the selected epoch. Then Eqs (4) through (8) define the orbital planes and the quadrants of the three orientation elements.

Data for these six elements is presented in Tables 4 and 5. These tables present each of the six elements for a two-year period and the regression and precession rates of the nodal angle and the argument of perigee, respectively. These data are accurate to the last quoted digit for the quoted epochs and provide reasonably good accuracy when linearly interpolated. In order to maintain precision in such computations it is necessary to have the elements evaluated at much smaller time intervals.

4. Geocentric Constants

a. Potential function

The potential function of the earth (i.e., the relationship between potential energy and position relative to the earth) is not simply $-\frac{Gm}{r}_{\oplus}$ as is assumed in most Keplerian orbit studies because this approximation assumes that the mass is spherically symmetric. This assumption is sufficiently accurate for many preliminary studies but is not valid for precise orbital studies. For this reason it is general practice to expand the potential function in a series of Legendre polynomials. The coefficients of this series may then be evaluated from satellite observation.

Since the perturbations in the motion (i.e., deviations due to the presence of the terms involving mass asymmetry of the earth) are very sensitive to the uncertainties in the coefficients of the resulting potential function, one form of this function will be presented and discussed. The form selected, because of its simplicity and the fact that it was recently adopted by the IAU (1961), is that of J. Vinti of the National Bureau of Standards. The coefficients of other generally used expansions will be related to this set in later paragraphs.

$$U = -\frac{\mu}{r}\left[1 - \sum_{n=2}^{\infty} J_n \left(\frac{R}{r}\right)^n P_n (\sin L)\right]$$

where

μ = gravitational constant = $Gm_{\oplus}$

J_n = coefficients

R = equatorial radius of the earth

r = satellite radius

P_n (sin L) = Legendre polynomials

L = instantaneous latitude

The first few terms of this series are:

$$U = -\frac{\mu}{r}\left[1 - \frac{J_2}{2}\left(\frac{R}{r}\right)^2 (3\sin^2 L - 1) - \frac{J_3}{2}\left(\frac{R}{r}\right)^3 (5\sin^3 L - 3\sin L) - \frac{J_4}{8}\left(\frac{R}{r}\right)^4 (35\sin^4 L - 30\sin^2 L + 3) - \frac{J_5}{8}\left(\frac{R}{r}\right)^5 (63\sin^5 L - 70\sin^3 L + 15\sin L) - \frac{J_6}{16}\left(\frac{R}{r}\right)^6 (231\sin^6 L - 315\sin^4 L + 105\sin^2 L - 5)\right]$$

As is immediately obvious, this function contains the potential function for a mass spherically symmetric earth and a series of correction terms referred to as zonal harmonics. The odd ordered harmonics are antisymmetric about the equatorial plane (L = 0) and the even ordered harmonics, symmetric. This function was introduced merely to aid in the discussion of the factors affecting motion in geocentric orbits; therefore, the function as a whole will not be discussed further but its coefficients will be treated.

TABLE 4

Mean Elements of Inner Planets (from American Ephemeris, 1960, 1961, 1962; referred to mean equinox and ecliptic of date.)

Epochs: 1960 September 23.0 = J.D. 243 7200.5
1961 October 28.0 = J.D. 243 7600.5
1962 December 2.0 = J.D. 243 8000.5

Planet	Year	i* (deg)	Ω* (deg)	$\tilde{\omega}$* (deg)	a (AU)	e	M_0** (deg)
Mercury	1960	7.00400 + 1	47.86575 + 325	76.84441 + 426	0.387099	0.205627	152.303
	1961	7.00402 + 1	47.87873 + 325	76.86145 + 426	0.387099	0.205627	349.237
	1962	7.00404 + 1	47.89171 + 325	76.87849 + 426	0.387099	0.205627	186.171
Venus	1960	3.39424 + 0	76.32625 + 247	131.01853 + 385	0.723332	0.006792	108.652
	1961	3.39425 + 0	76.33611 + 247	131.03394 + 385	0.723332	0.006791	29.504
	1962	3.39426 + 0	76.34597 + 247	131.04934 + 385	0.723332	0.006791	310.356
Mars	1960	1.84993 + 0	49.25464 + 211	335.33609 + 504	1.523691	0.093369	62.572
	1961	1.84992 + 0	49.26308 + 211	335.35625 + 504	1.523691	0.093370	272.180
	1962	1.84991 + 0	49.27153 + 211	335.37641 + 504	1.523691	0.093371	121.789

*Plus variation per 100 days.

**The large differences between the mean anomalies at epoch are due primarily to the shift in the epoch and not to perturbations.

$\tilde{\omega} = \omega + \Omega$

TABLE 5

Osculating Elements of Outer Planets (from American Ephemeris, 1960, 1961, 1962; referred to mean equinox and ecliptic of date.)

Planet*	Date	i (deg)	Ω (deg)	$\tilde{\omega}$ (deg)	a (AU)	e	M_0 (deg)
Jupiter	1960 Jan. 27	1.30641	100.0560	12.3279	5.208041	0.048,335,1	249.7967
	1961 Jan. 21	1.30626	100.0651	13.2393	5.203825	0.048,589,9	278.7932
	1962 Jan. 16	1.30616	100.0725	13.2614	5.203520	0.048,459,7	308.6768
Saturn	1960 Jan. 27	2.48722	113.3161	92.1031	9.582589	0.050,548,4	188.9699
	1961 Jan. 21	2.48718	113.3273	90.7422	9.580399	0.051,145,6	202.4677
	1962 Jan. 16	2.48714	113.3385	89.3436	9.581007	0.051,778,3	216.0551
Uranus	1960 Jan. 27	0.77236	73.7218	172.5311	19.16306	0.046,906,5	329.2259
	1961 Jan. 21	0.77222	73.6971	172.8809	19.13202	0.045,282,3	333.0587
	1962 Jan. 16	0.77221	73.6942	172.3515	19.11431	0.044,112,4	337.7453
Neptune	1960 Jan. 27	1.77329	131.3233	25.9372	30.23803	0.003,139,4	191.3613
	1961 Jan. 21	1.77325	131.3709	22.4739	30.17541	0.005,351,5	197.0665
	1962 Jan. 16	1.77318	131.4144	26.5510	30.09783	0.007,911,7	195.1770
Pluto	1960 Jan. 27	17.16644	109.8642	223.8342	39.52392	0.251,35532	316.9810
	1961 Mar. 2	17.17057	109.8943	224.3400	39.38437	0.249,400,9	317.9194
	1962 Jan. 16	17.16791	109.8958	224.5629	39.29379	0.247,695,2	318.8914

*Osculating elements are given for every 40 days for Jupiter, Saturn, Uranus and Neptune, and for every 80 days for Pluto.

$\tilde{\omega} = \omega + \Omega$

Since the earth is almost spherically symmetric, the J_n are all small compared to one (as will be shown later); thus, the prime factor affecting motion is the gravitational constant, μ, which is defined directly from Newtonian Mechanics as $Gm_{\oplus}$. Data for this constant were not presented in the referenced paper (Baker) though a value was adopted. For this reason a review of some of the more recent determinations was made and a comparison constructed (Table 6).

Baker's value corresponds to that of Herrick (1958) and no data were found which ascribe an uncertainty or confidence level to this value. The value corresponds very closely to mean of the adjusted sample; for this reason an estimated uncertainty would be ±0.00004.

While Herrick's value appears valid, a better estimate in view of the work done by Kaula would seem to be Kaula's value (or the mean of the adjusted sample which is the same). It is proposed, therefore, that the value of μ be $1.407648 \cdot 10^{16} \pm 0.000035 \cdot 10^{16}$ ft^3/sec^2 or $398,601.5 \pm 9.9$ km^3/sec^2. The selection of this constant, which is obviously related to the mass of the earth-moon system (previously adopted), does not produce large inconsistencies due to the fact that the conversion between solar mass and earth mass is accurate to only four places, and to this order the two answers agree.

The remaining coefficients, J_n, are related to the earth's equatorial radius, the average rotational rate of the earth, the gravitational constant, and the flattening of the earth. For this reason, it is clear that the arbitrary selection of a set of constants will result in slight numerical inconsistencies. However, these uncertainties are small and of the same order as the uncertainty in the numerical values of the J_n. Data for the J_n are presented in Table 7.

Baker's values of the J_n correspond almost identically to those of the adjusted sample while Kaula's do not for J_4, J_5 and J_6. No satisfactory

TABLE 6

Gravitational Constant for the Earth

Date	ft^3/sec^2	Author
1957	1.407754×10^{16}	Elfers (Project Vanguard)
1958	1.407639	Herrick
1959	1.40760	Jeffreys
1959	1.40771	O'Keefe
1960	1.407645	Department of Defense (see Baker)
1961	1.40765	Kaula

	Adopted by Baker	Unadjusted Sample	Adjusted Sample
Gravitational constant (ft^3/sec^2)	1.407639×10^{16}	1.407666×10^{16}	1.407648×10^{16}
(km^3/sec^2)	398,599.9	398,606.6	398,601.5
Uncertainty (1)	± ?	$\pm 0.000050 \times 10^{16}$	$\pm 0.000035 \times 10^{16}$
(2)	± ?	±14.2	±9.9
Sample size	?	6	5
Confidence level	?	92%	88%

TABLE 7

Coefficients of the Potential Function

	Baker	Kaula	Uncorrected Sample	Adjusted Sample
J_2	1082.28×10^{-6}	1082.61×10^{-6}	1082.396×10^{-6}	1082.303×10^{-6}
$\sigma(J_2)$	$\pm 0.2 \times 10^{-6}$	$\pm 0.06 \times 10^{-6}$	$\pm 0.241 \times 10^{-6}$	$\pm 0.185 \times 10^{-6}$
Confidence level	?	?	98%	95%
J_3	-2.30×10^{-6}	-2.05×10^{-6}	-2.39×10^{-6}	-2.39×10^{-6}
$\sigma(J_3)$	$\pm 0.20 \times 10^{-6}$	$\pm 0.10 \times 10^{-6}$	$\pm 0.23 \times 10^{-6}$	$\pm 0.23 \times 10^{-6}$
Confidence level	?	?	98%	90%
J_4	-2.12×10^{-6}	-1.43×10^{-6}	-1.82×10^{-6}	-2.03×10^{-6}
$\sigma(J_4)$	$\pm 0.50 \times 10^{-6}$	$\pm 0.06 \times 10^{-6}$	$\pm 0.35 \times 10^{-6}$	$\pm 0.24 \times 10^{-6}$
Confidence level	?	?	98%	92%
J_5	-0.20×10^{-6}	-0.08×10^{-6}	-0.25×10^{-6}	-0.19×10^{-6}
$\sigma(J_5)$	$\pm 0.1 \times 10^{-6}$	$\pm 0.11 \times 10^{-6}$	$\pm 0.16 \times 10^{-6}$	$\pm 0.08 \times 10^{-6}$
Confidence level	?	?	92%	88%
J_6	1.0×10^{-6}	0.20×10^{-6}	0.68×10^{-6}	0.83×10^{-6}
$\sigma(J_6)$	$\pm 0.8 \times 10^{-6}$	$\pm 0.05 \times 10^{-6}$	$\pm 0.29 \times 10^{-6}$	$\pm 0.10 \times 10^{-6}$
Confidence level	?	?	81%	70%

reason was obtained for this difference, though it is believed that the data utilized by Kaula in the determination of J_4, J_5 and J_6 may have been biased. This conclusion is strengthened slightly by the fact that the results of Kaula for these three constants are somewhat below the majority of the other independent determinations. Even if the uncertainty in these three values is increased an amount sufficient to include all values, no appreciable change will be noted in the computation of trajectories, since the numbers are very small compared to unity and are even small compared to J_2.

It is proposed that the values adopted by Baker be accepted without change. This procedure seems justifiable on the basis of the data and has the advantage that the set is presumably consistent. This advantage is not clear cut since, even though the J_n's are interrelated, the uncertainties in the values are relatively large.

At this point Vinti's set of coefficients will be related to those utilized by other authors. Rather than discuss each potential, however, the potentials will be tabulated for comparison. Then, the coefficients of the various terms will be equated. This data is presented in Tables 8a and 8b.

b. Equatorial radius and flattening

The average figure of the earth is best represented as an ellipsoid of revolution (about the polar axis) with the major axis the equatorial diameter. Obviously this model is not exact; however, the accuracy afforded is generally adequate when computing the ground track of a satellite, determining tracking azimuths, etc. For this reason the best values for the parameters of the ellipsoid are desired. These data are presented in Table 9 in the form of values of the equatorial radius and flattening (previously defined) along with polar radii, also for each pair of values.

Although the discrepancies in the sets of data shown in Table 9 are minor, they are sufficient to justify the selection of one particular set. Based on the data reviewed, it is felt that the data of Kaula is probably slightly superior to the remaining values. This conclusion is strengthened by the good agreement between Kaula and some of the more recent standards. While this is by no means conclusive proof, the fact indicates a wide degree of acceptance. For this reason, an estimate of the confidence level would be greater than 90%.

TABLE 8a

Potential Functions Found in the Literature
(Kork, J "First Order Satellite Moitons in Near Circular Orbits About an Oblate Earth" Martin Company (Baltimore) ER 12202, January 1962)

Author	Potential function
Vinti	$U = -\frac{\mu}{r}\left[1 - J_2\left(\frac{R}{r}\right)^2\left(\frac{3}{2}\sin^2 L - \frac{1}{2}\right) - J_3\left(\frac{R}{r}\right)^3\left(\frac{5}{2}\sin^3 L - \frac{3}{2}\sin L\right) - J_4\left(\frac{R}{r}\right)^4\left(\frac{35}{8}\sin^4 L - \frac{30}{8}\sin^2 L + \frac{3}{8}\right) - \ldots\right] = -\frac{\mu}{r}\left[1 - \sum_{k=2}^{\infty} J_k\left(\frac{R}{r}\right)^k P_k(\sin L)\right]$
Jeffreys	$U = -\frac{\mu}{r}\left[1 + J\left(\frac{R}{r}\right)^2\left(\frac{1}{3} - \cos^2\alpha\right) + \frac{D}{35}\left(\frac{R}{r}\right)^4(35\cos^4\alpha - 30\cos^2 + 3)\right]$ where $\alpha = 90° - L$
Kozai	$U = -\frac{GM_E}{r}\left[1 + \frac{A_2}{r^2}\left(\frac{1}{3} - \sin^2 L\right) + \frac{A_3}{r^3}\left(\frac{5}{2}\sin^2 L - \frac{3}{2}\right)\sin L + \frac{A_4}{r^4}\left(\frac{3}{35} + \frac{1}{7}\sin^2 L - \frac{1}{4}\sin^2 2L\right) + \ldots\right]$
Brouwer	$U = -\frac{\mu}{r}\left[1 + \frac{k_2}{r^2}\left(1 - 3\sin^2 L\right) + \frac{A_{3,0}}{r^3}\left(-\frac{3}{2}\sin L + \frac{5}{2}\sin^3 L\right) + \frac{k_4}{r^4}\left(1 - 10\sin^2 L + \frac{35}{3}\sin^4 L\right) + \frac{A_{5,0}}{r^5}\left(\frac{15}{8}\sin L - \frac{35}{4}\sin^3 L + \frac{63}{8}\sin^5 L\right) + \ldots\right]$
O'Keefe, Eckels, Squires	$U = -\frac{A_{0,0}}{r} + \frac{A_{2,0}}{r^3}P_2^0 + \frac{A_{3,0}}{r^4}P_3^0 + \frac{A_{4,0}}{r^5}P_4^0 + \ldots$ where $A_{0,0} = \mu$; $P_k^0 = P_k(\sin L)$
Roberson	$U = -\frac{GM_E}{r}\left[1 + \mu\left(\frac{R}{r}\right)^2(1 - 3\sin^2 L) + \mu_2\left(\frac{R}{r}\right)^4(3 - 30\sin^2 L + 35\sin^4 L) + \ldots\right]$
Garfinkel	$U = -\frac{1}{r}\left[1 - \frac{2k}{r^2}P_2(\sin L) - \frac{k'}{r^4}P_4(\sin L)\right]$
Krause	$U = -\frac{fE}{r}\left[1 + \frac{k_2}{r^2}\left(1 - 3\sin^2 L\right) + \frac{k_4}{r^4}\left(1 - 10\sin^2 L + \frac{35}{3}\sin^4 L\right) + \ldots\right]$
Sterne	$U = -\frac{\mu}{r}\left[1 + \frac{B}{r^2}\left(1 - \frac{3}{2}\sin^2 L\right)\right]$
Herget and Musen	$U = -\frac{\mu}{r}\left[1 + \frac{k_2}{r^2}\left(1 - 3\psi^2\right) + \frac{k_4}{r^4}(3 - 30\psi^2 + 35\psi^4)\right]$ where $\psi = \sin^2 L$
Struble	$U = -\frac{gR^2}{r}\left[1 + J\left(\frac{R}{r}\right)^2\left(\frac{1}{3} - \cos^2\theta\right) + D\left(\frac{R}{4}\right)^4\left(\cos^4\theta - \frac{6}{7}\cos^2\theta + \frac{3}{35}\right)\right]$ where $\theta = 90 - L$
Laplace	$U = -\frac{fM_E}{r}\left[1 + \frac{B_2}{r^2}\left(\frac{3}{2}\sin^2 L - \frac{1}{2}\right) + \frac{B_4}{r^4}\left(\frac{35}{8}\sin^4 L - \frac{15}{4}\sin^2 L + \frac{3}{8}\right) + \ldots\right]$
Proskurin and Batrakov	$U = -\frac{fm}{r}\left[1 - \frac{J}{3}\left(\frac{R}{r}\right)^2(3\sin^2 L - 1) + \frac{D}{35}\left(\frac{R}{r}\right)^4(35\sin^4 L - 30\sin^2 L + 3)\right]$
Baker	$U = -\frac{k_e m_1}{r}\left[1 + \frac{1}{3}\frac{J}{r^2}(1 - 3\sin^2 L) + \frac{1}{5}\frac{H}{r^3}(3 - 5\sin^2 L)\sin L + \frac{1}{30}\frac{K}{r^4}(3 - 30\sin^2 L + 35\sin^4 L) + \ldots\right]$

TABLE 8b

Comparisons of Constants Used in Potential Functions

Vinti	J_2	J_3	J_4	Recommended
Laplace	$-B_2/R^2$	$-B_3/R^3$	$-B_4/R^4$	
Jeffreys	$\frac{2}{3} J$	H	$-\frac{8}{35} D$	
Kozai	$\frac{2}{3}\frac{A_2}{R^2}$	$-A_3/R^3$	$-\frac{8}{35}\frac{A_4}{R^4}$	
Brouwer	$\frac{2k_2}{R^2}$	$-A_3/R^3$	$-\frac{8}{3}\frac{k_4}{R^4}$	
O'Keefe, Eckels, Squires	$-A_{2,0}/\mu R^2$	$-A_{3,0}/\mu R^3$	$-A_{4,0}/\mu R^4$	
R. E. Roberson	2μ	None	$-8\mu_2$	
Garfinkel	$2k/R^2$	None	k'/R^4	
Struble	$\frac{2}{3} J$	None	$-\frac{8}{35} D$	
Krause	$2k_2/R^2$	None	$-\frac{8}{3}\frac{k_4}{R^4}$	
Sterne	$\frac{2B}{R^2}$	None	None	
Herget and Musen	$2k_2/R^2$	None	$-8k_4/R^4$	
Proskurin and Batrakov	$-\frac{2}{3} J$	None	$-\frac{3}{35} D$	
W. deSitter	$\frac{2}{3} J$	None	$-\frac{4}{15} K$	

TABLE 9

Equatorial Radius and Flattening

	Baker	Kaula	Uncorrected Sample	Adjusted Sample
Equatorial radius (km)	6378.150 ±0.050	6378.163 ±0.021	6378.215 ±0.105	6378.210 ±0.045
1/f	298.30 ±0.05	298.24 ±0.01	298.27 ±0.05	298.27 ±0.03
Polar radius (km) = Req $(1 - \frac{1}{1/f})$	6356.768 ±0.050	6356.777 ±0.021	6356.831 ±0.105	6356.826 ±0.045
Sample size	9	?	10	7
Confidence level	?	?	98%	95%

5. Selenocentric Constants

The determination of the lunar mass has been made from the lunar equation (involved in the reduction of geocentric coordinates to those of the barycenter, i.e., the center of mass of the earth-moon system), through the evaluation of the coefficient, L, defined to be

$$L' = \frac{\frac{m_\ell}{m_\oplus}}{1 + \frac{m_\ell}{m_\oplus}} \quad \frac{\pi_\odot}{\sin \pi_\ell}$$

where

π_ℓ is the lunar parallax (i.e., $\frac{R_{\oplus \text{ equatorial}}}{\text{average lunar distance}}$)

Since there are no lunar satellites whose orbits can be used in determining lunar mass, the calculations for the most part have been based on observations of Eros at the time of closest approach.

The method consists of finding the solar and lunar parallaxes, comparing the observed positions of Eros when nearest the earth with an accurate ephemeris, fitting the residuals to a smooth curve that has the periodicity and zero points of the lunar equation, and using the curve to improve the adopted value of L'. Once this is accomplished $\frac{m_\ell}{m_\oplus}$ is evaluated from the previous equation. Thus, the first step in the evaluation of the lunar mass is the evaluation of the lunar parallax or equivalently the lunar distance.

Baker presents data for the lunar distance evaluated by several different methods. These data have been used to produce Table 10.

TABLE 10

Lunar Distance

	Adopted by Baker	Uncorrected Sample	Adjusted Sample
Lunar distance (km)	384,402	384,402.6	384,401.6
Uncertainty (km)	±1	±2.6	±1.1
Lunar parallax (rad)	0.016,592,4	0.016,592,4	0.016,592,4
(sec)	3422.428	3422.428	3422.428
Uncertainty (rad)	±0.000,000,1	±0.000,000,1	±0.000,000,1
(sec)	±.021	±.021	±.021
Sample size	6	6	5
Confidence level	?	92%	88%

The data of Table 10 all agree very well and exhibit no inconsistencies of the type shown in other data. For this reason it is believed that Baker's value should be utilized as it is quoted in Table 10. It is interesting to note that the value of the lunar parallax and its uncertainty were the same for all of the evaluations.

The next step in the evaluation of the lunar mass is the determination of the best value of the coefficient of the lunar equation. Once again several values are available, each determined by different individuals at different times. The results of the analysis of these data are presented in Table 11.

TABLE 11

Coefficient of Lunar Equation

	Adopted by Baker	Uncorrected Sample	Adjusted Sample
Coefficient L'(sec)	6.4385	6.430	6.4381
Uncertainty (sec)	±0.0015	±0.005	±0.0016
Sample size	?	8	6
Confidence level	?	97%	92%

Once again good general agreement is noted. It is proposed, therefore, that the value of L' be 6.4385 ± 0.0015 with a confidence level of about 90%. With this value of L' and that of lunar parallax adopted in Table 10, the best value of the quantity $\frac{m_\oplus}{m_\ell}$ is found as

$$\frac{m_\oplus}{m_\ell} = \frac{\pi_\odot}{\sin \pi_\ell} \frac{1}{L'} - 1$$

$$= \frac{8.798}{0.016592} \quad \frac{8.7981}{6.4385} - 1 = 81.357$$

The estimate of the uncertainty is obtained by differentiating this equation with respect to π and L'. It is not necessary to differentiate with respect to $\pi_{\mathbb{C}}$ since this constant is known to a much higher precision.

$$\left|\Delta \frac{m_\oplus}{m_{\mathbb{C}}}\right| = \left(\frac{m_\oplus}{m_{\mathbb{C}}} + 1\right)\left(\frac{dL}{L'} - \frac{d\pi_\odot}{\pi_\odot}\right)$$

$$= 82.357\left(\frac{0.0015}{6.4385} - \frac{0.001}{8.798}\right)$$

$$= 0.0098$$

Thus the best value of the quantity $\frac{m_\oplus}{m_{\mathbb{C}}}$ is 81.357 ± 0.010 with a confidence level of approximately 90%. This value was obtained using Baker's data and is contrasted to his adopted value of 81.35 ± 0.05. Since the uncertainty of Baker's value seems inconsistent, it is proposed that the value and uncertainty developed here be utilized.

The remaining information required pertains to the figure of the moon. The figure of the moon is best represented by a triaxial ellipsoid with the radii of lengths a, b and c where a is directed toward the earth, c is along the axis of rotation and b forms an orthogonal set. Very little data are available for these lengths. Some information, however, is presented in:

> Alexandrov, I, "The Lunar Gravitational Potential" in Advances in the Astronautical Sciences, Vol. 5, Plenum Press (N. Y.), 1960, pages 320 through 324.

This reference gives data for determinations of the dynamic dimensions and the methods of computation as:

	Forced Libration	Free Libration	Adopted by Baker
Semiaxis a(km)	1738.67 ± 0.07	1738.57 ± 0.07	1738.57 ± 0.07
Semiaxis b(km)	1738.21 ± 0.07	1738.31 ± 0.07	1738.31 ± 0.07
Semiaxis c(km)	1737.58 ± 0.07	1737.58 ± 0.07	1737.58 ± 0.07

There is no reason to assume a value other than that of Baker due to the general lack of data.

6. Summary of Constants and Derivable Data

Because several values have been discussed for each constant, there is need to combine in one table the best value, its uncertainty and approximate confidence level. This is done in Table 12. Note is made of the source of each number given.

In addition to a tabulation of constants, there generally exists a requirement for data which are easily derivable from this more basic data. Table 13 presents the mass, the gravitational constant ($\mu = Gm$) and the radius of action* in metric, English and astronomical units. Table 14 presents the geometry of the planets in metric and English units, and Table 15 presents surface values for the circular and escape velocities and for gravity.

*Tisserand's criteria, $r^* = d\left(\frac{m}{M}\right)^{2/5}$ where d is the average distance between the two bodies, m is the mass of the smaller body and M is the mass of the larger body.

B. ASTROPHYSICAL CONSTANTS

In the previous section certain of the astronautical constants were reviewed. The purpose of this section is to include other factors affecting the trajectory. Accordingly, atmospheric models and density variability will first be discussed. The discussions will then be oriented toward the definition of other factors which must be considered in satellite orbit selection such as the radiation and meteorid environments.

1. Development of Model Atmospheres for Extreme Altitudes

In November 1953 an unofficial group of scientific and engineering organizations, each holding national responsibilities related to the requirement for accurate tables of the atmosphere to high altitudes formed the "Committee on the Extension of the Standard Atmosphere" (COESA). A Working Group, appointed at the first meeting, met frequently between 1953 and the end of 1956. This committee developed a model atmosphere to 300 km based on the data available at that time. This model was published in 1958 as the "U. S. Extension to the ICAO Standard Atmosphere," (Ref. 1).

At the time of the development of this standard only two methods of direct measurement of upper atmosphere densities were available:

(1) High altitude sounding rockets.

(2) Observations of meteor trails.

Both methods have severe limitations in the interpretation of the measured data. First, the rocket made only short flights into the upper atmosphere and the density measurements were made mostly inside the rocket's flow field, not in the undistrubed free stream. Second, meteors were visible only in a small range of altitude (85 to 130 km) and their aerodynamic characteristics contained too many unknowns (unsymmetrical shapes, loss of momentum by evaporation of melting surface layers, etc.).

The extent of the limitations of the rocket and meteor trail data became evident with the launching of the first satellites. The orbital periods of the first Sputnik indicated that the densities of the upper atmosphere were off by approximately an order of magnitude.

The Smithsonian 1957-2 atmosphere (Ref. 2) was developed based on the density estimates from the decay histories of the Sputnik satellites. This standard was soon superseded by the ARDC 1959 Model Atmosphere (Ref. 3). Up to about 50 km this atmosphere was the same as the U.S. extension to the ICAO Standard Atmosphere. Above that altitude some IGY rocket and early satellite data were used. Since all these data were obtained during the period of maximum

TABLE 12

Adopted Constants

	Best Value	Uncertainty	Approximate Confidence Level[b] (%)
Heliocentric Constants			
Solar parallax	[a] 8.798 sec	[b] ±0.001	90
Astronomical unit	[a] 149.53×10^6 km	[a] ±0.03	90
K_s^2	[c] 0.2959122083 AU^3/solar day^2	[a] $\pm 0.010^{-10}$	99+
Planetocentric Constants			
Mercury			
Solar mass/mass Mercury	[a] 6,100,000	[b] ±65,000	70
Equatorial radius	[a] 2330 km	[b] ±11	70
1/f	?	?	?
Venus			
Solar mass/mass Venus	[a] 407,000	[b] ±1300	90
Equatorial radius	[a] 6100 km (incl atmos)	[b] ±12	70
1/f	?	?	?
Earth-Moon			
Solar mass/earth-moon mass	[a] 328,450	[b] ±25	81
Equatorial radius	--	--	--
1/f	--	--	--
Mars			
Solar mass/mass Mars	[a] 3,090,000	[b] ±12,000	81
Equatorial radius	[a] 3415 km	[b] ±12	88
1/f	[b] 75	[b] ±12	80
Jupiter			
Solar mass/mass Jupiter	[a] 1047.4	[b] ±0.1	81
Equatorial radius	[a] 71,875 km	[b] ±20	50
1/f	[a] 15.2	[b] ±0.1	50
Saturn			
Solar mass/mass Saturn	[a] 3500	[b] ±2.0	70
Equatorial radius	[a] 60,500 km	[b] ±480	50
1/f	[a] 10.2	± ?	?

(continued)

NOTE:

[a] Baker's value.

[b] Value obtained in this report.

[c] Gaussian value.

[d] Ehricke's value.

[e] Kaula's value.

TABLE 12 (continued)

	Best Value	Uncertainty	Approximate Confidence Level[b] (%)
Uranus			
Solar mass/mass Uranus	[a]22,800	[b]±60	50
Equatorial radius	[a]24,850 km	[b]±50	?
1/f	[a]14.0	± ?	?
Neptune			
Solar mass/mass Neptune	[a]19,500	[b]±200	70
Equatorial radius	[a]25,000 km	[b]±2100	50
1/f	[a]58.5	± ?	?
Pluto			
*Solar mass/mass Pluto	[a]350,000	[b]±27,000	70
Equatorial radius	[a]3000 km	[b]±500	20
1/f	?	?	?
Geocentric Constants			
μ (km^3/sec^2)	[e]398,601.5	[e]±9.9	88
J_2	[a]1082.28×10^{-6}	[a]$\pm 0.2 \times 10^{-6}$	95
J_3	[a]-2.30×10^{-6}	[a]$\pm 0.2 \times 10^{-6}$	90
J_4	[a]-2.12×10^{-6}	[a]$\pm 0.5 \times 10^{-6}$	92
J_5	[a]-0.20×10^{-6}	[a]$\pm 0.1 \times 10^{-6}$	88
J_6	[a]-1.0×10^{-6}	[a]$\pm 0.8 \times 10^{-6}$	70
Equatorial radius (km)	[e]6378.163	[e]±0.021	95
1/f	[e]298.24	[e]±0.01	95
Selenocentric Constants			
Lunar distance (km)	[a]384,402 km	[a]±1 km	88
L'	[a]6.4385	[a]±0.0015	92
$m_\oplus / m_\leftmoon$	[b]81.357	[b]±0.01	90
Semiaxis a (km)	[a]1738.57 km	[a]±0.17 km	50
b (km)	[a]1738.31 km	[a]±0.07 km	50
c (km)	[a]1737.58 km	[a]±0.07 km	50

NOTE:

[a]Baker's value.

[b]Value obtained in this report.

[c]Gaussian value.

[d]Ehricke's value.

[e]Kaula's value.

TABLE 13

Gravitational Properties of the Planets

Planet	Mass (10^{24} kg)	Mass (10^{24} slugs)	Mass $m_\odot / m_p$	μ (km^3/sec^2 x 10^6)	μ (ft^3/sec^2 x 10^{16})	μ (AU^3 (solar day^2 x 10^{-9}))	r^* (10^6 km)	r^* (10^9 ft)	r^* AU	1960 Epoch
Mercury	0.3257	0.02232	6,100,000 ±65,000	0.021,725	0.076,721	0.048,509	0.11178	0.36674	0.000,747,6	No change
Venus	4.8811	0.3345	407,000 ±1300	0.325,581	1.149.78	0.726,987	0.61696	2.0241	0.004,126	No change
*Earth	5.9758	0.40947	332,440 ±50	0.398,601,5	1.407,648	0.890,033	0.92482	3.03429	0.006,185,0	No change
Earth-Moon	6.0484	0.41444	328,400 ±25	0.403,444	1.424,75	0.900,847	0.92933	3.04898	0.006,215,1	No change
Moon	0.073451	0.0050330	$\frac{m_\oplus}{m_\zeta}$ = 81.357 ±0.010	0.004,899,4	0.017302,1	0.010,939,8	0.066282	0.217460	0.000,443,3	No change
Mars	0.6429	0.04405	3,090,000 ±12,000	0.042,883,0	0.151,440	0.095,753,1	0.57763	1.8951	0.003,863	No change
Jupiter	1896.7	129.97	1,047.4 ±0.1	126.515	446.783	282.493	48.141	157.943	0.321,96	January 27, 1962
Saturn	567.60	38.89	3500 ±1.7	37.860,4	133.703	84.538,3	54.774	179.70	0.366,31	January 27, 1962
Uranus	87.132	5.970	22,800 ±100	5.811,91	20.524,6	12.977,4	51.755	169.80	0.346,13	January 27, 1962
Neptune	101.88	6.981	19,500 ±200	6.795,75	23.999,0	15.174,2	86.952	285.28	0.581,51	January 27, 1962
Pluto	5.676	0.3889	350,000 ±27,000	0.378,596	1.337,0	0.845,364	35,812	117.49	0.239,5	January 27, 1962
Sun	1.9866×10^6	0.13613×10^6	1.00000	132,511	467,960	295,912,208,3*	--	--	--	--

—— Underlined digits are questionable.

*Solar gravitational constant is Gaussian value.

TABLE 14

Geometry of the Planets

Planet	Equatorial Radius (km)	Equatorial Radius (stat mi)	Equatorial Radius (naut mi)	Equatorial Radius (ft x 10^7)	1/f	Polar Radius (km)	Polar Radius (stat mi)	Polar Radius (naut mi)	Polar Radius (ft x 10^7)	Radius of Sphere of Equivalent Volume ($R^3 = R_e^2 R_p$) (km)	Radius of Sphere of Equivalent Volume ($R^3 = R_e^2 R_p$) (stat mi)	Radius of Sphere of Equivalent Volume ($R^3 = R_e^2 R_p$) (naut mi)	Radius of Sphere of Equivalent Volume ($R^3 = R_e^2 R_p$) (ft x 10^7)
Mercury	2330 ±10	1448 ±6	1258 ±5	0.7644 ±0.0032	∞*	2330 ±10	1448 ±6	1258 ±5	0.7644 ±0.0032	2330 ±10	1488 ±6	1258 ±5	0.7644 ±0.0032
Venus	6100 ±50	3790 ±30	3290 ±25	2.001 ±0.016	∞*	6100 ±50	3790 ±30	3290 ±25	2.001 ±0.016	6100 ±50	3790 ±30	3290 ±25	2.001 ±0.016
Earth	6378.16 ±0.02	3963.20 ±0.03	3443.93 ±0.02	2.09257 $\pm 164 \times 10^{-7}$	298.24 ±0.01	6356.77 ±0.05	3949.77 ±0.03	3432.38 ±0.02	2.08555 $\pm 164 \times 10^{-7}$	6371.02 ±0.05	3958.77 ±0.03	3440.08 ±0.02	2.09023 $\pm 164 \times 10^{-7}$
Earth-Moon	--	--	--	--	--	--	--	--	--	--	--	--	--
Moon** a	1738.57 ±0.07	1080.30 ±0.04	938.75 ±0.03	0.57040 ±0.00002	--	--	--	--	--	--	--	--	--
b	1738.31 ±0.07	1080.14 ±0.04	938.61 ±0.03	0.57031 ±0.00002	--	1737.58 ±0.07	1079.68 ±0.07	938.22 ±0.03	0.57007 ±0.00002	1738.16 ±0.07	1080.04 ±0.04	938.53 ±0.03	0.57026 ±0.00002
c	1737.58 ±0.07	1079.68 ±0.04	938.22 ±0.03	0.57007 ±0.00002	--	--	--	--	--	--	--	--	--
Mars	3415 ±5	2122 ±3	1844 ±2	1.1204 ±0.0016	75 ±12	3369 ±5	2094 ±3	1819 ±2	1.1055 ±0.0016	3400 ±5	2113 ±3	1836 ±2	1.1155 ±0.0016
Jupiter	71,375 ±50	44,350 ±30	38,539 ±25	23.417 ±0.016	15.2 ±0.1	66,679 ±50	41,432 ±30	36,004 ±25	21.876 ±0.016	69,774 ±50	43,356 ±30	37,675 ±25	22.892 ±0.016
Saturn	60,500 ±50	37,590 ±30	32,670 ±25	19.849 ±0.016	10.2 ± ?	54,560 ±50	33,900 ±30	29,470 ±25	17.990 ±0.016	58,450 ±50	36,320 ±30	31,560 ±25	19.176 ±0.016
Uranus	24,850 ±50	15,440 ±30	13,420 ±25	8.153 ±0.016	14* ± ?	23,070 ±50	14,340 ±30	12,460 ±25	7.571 ±0.016	24,240 ±50	15,060 ±30	13,090 ±25	7.953 ±0.016
Neptune	25,000 ±250	15,530 ±150	13,500 ±130	8.202 ±0.080	58.5 ± ?	24,600 ±250	15,260 ±150	13,270 ±130	8.062 ±0.080	24,870 ±250	15,450 ±150	13,430 ±130	8.159 ±0.080
Pluto	3000 ±500	1860 ±300	1620 ±250	0.984 ±0.16	--	--	--	--	--	3000 ±500	1860 ±300	1620 ±250	0.984 ±0.16
Sun	696,500 ±500	432,800 ±300	376,100 ±250	228.51 ±0.16	--	--	--	--	--	696,500 ±500	432,800 ±300	376,100 ±250	228.51 ±0.16

*Taken from K. A. Ehricke. "Space Flight," D. Van Nostrand, 1960.

**Moon is best presented by triaxial ellipsoid--a: toward earth
b: orthogonal to "a" and "c"
c: along axis of rotation.

TABLE 15

Planetary Circular and Escape Velocities and Planetary Gravity

	Circular Velocity at Sea Level				Escape Velocity at Sea Level				Gravity at Sea Level			
Planet	(km/sec)	(ft/sec)	(stat mi/hr)	(AU/solar day)	(km/sec)	(ft/sec)	(stat mi/hr)	(AU/solar day)	(cm/sec^2)	(ft/sec^2)	($stat\ mi/hr^2$)	($AU/solar\ day^2$)
Mercury	3.05361	10,018.4	6,830.73	0.00176444	4.31846	14,168.2	9,660.13	0.00249530	400.212	13.1303	32,228.9	0.199801
Venus	7.30630	23,970.8	16,343.7	0.00422174	10.33266	33,899.8	23,113.5	0.00597043	875.261	28.7159	70,484.5	0.436964
Earth	7.909773	25,950.7	17,693.7	0.00457044	11.18610	36,699.8	25,022.6	0.00646357	982.0214	32.21855	79,081.88	0.4902632
Earth-Moon	--	--	--	--	--	--	--	--	--	--	--	--
Moon	1.678900	5,508.2	3,755.59	0.00097010	2.374831	7,789.8	5,311.23	0.00137194	162.169	5.32049	13,059.38	0.0809608
Mars	3.55141	11,651.6	7,944.27	0.00205208	5.02243	16,477.8	11,234.9	0.00290207	370.951	12.1703	29,872.5	0.185193
Jupiter	42.5818	139,704	95,252.7	0.0246047	60.2196	197,571	134,707	0.0347962	2598.63	85.2569	209,267	1.29734
Saturn	25.4511	83,500.9	56,932.4	0.0147062	35.9932	118,088	80,514.5	0.0207977	1108.26	36.3601	89,247.5	0.553284
Uranus	15.4841	50,800.9	34,637.0	0.00894705	21.8978	71,843.3	48,984.1	0.0126530	989.073	32.4499	79,649.7	0.493784
Neptune	16.5308	54,234.8	36,978.3	0.00955183	23.3780	76,699.6	52,295.2	0.0135083	1098.84	36.0512	88,489.3	0.548584
Pluto	11.23(?)	36,860(?)	25,130(?)	0.00649(?)	15.89(?)	52,130(?)	35,540(?)	0.00918(?)	4209(?)	138.1(?)	338,900(?)	2.101(?)
Sun	436.181	1,431,040	975,709	0.252035	616.853	2,023,795	1,379,860	0.356431	27,315.7	896.186	2,199,730	13.6371

____ Underlined digits are questionable.

solar activity, the resulting model was more representative of these conditions than average atmospheric properties. An example of the effect of solar conditions on upper atmosphere density is shown in the following sketches taken from Ref. 4. These sketches show the data calculated from the orbits of Explorer IX compared to earlier satellite data and the 1959 ARDC Model Atmosphere. Also shown are the portions of the solar sunspot cycle represented by the data.

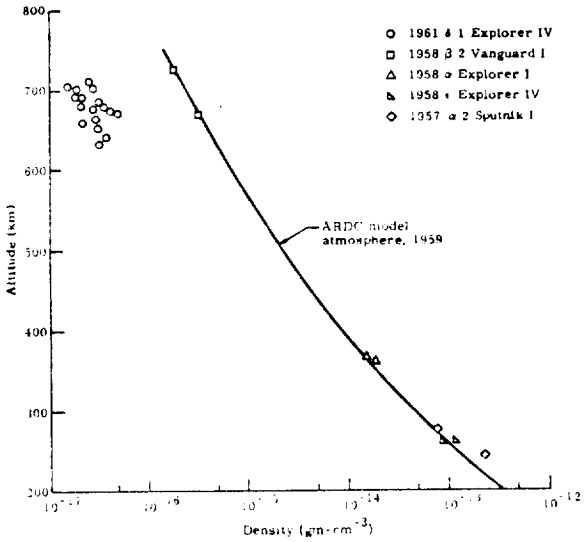

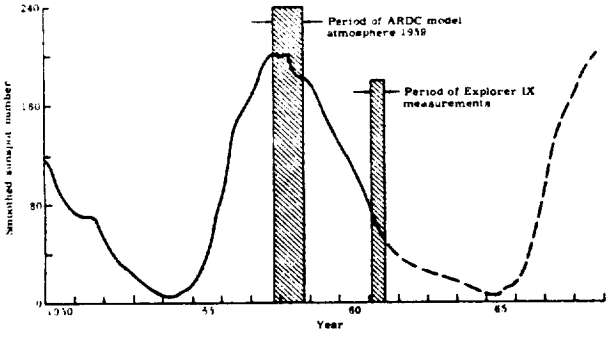

A new COESA Working Group was convened in January 1960. Using data and theories from more recent satellite and rocket flights, the Working Groups prepared a new standard atmosphere that was accepted by the entire committee on March 15, 1962 (Ref. 5). This new U. S. Standard Atmosphere depicts a typical mid-latitude year-round condition averaged for daylight hours and for the range of solar activity that occurs between sunspot minimum and maximum. Supplemental presentations are being developed to represent variability of density above 200 km with solar position and a set of supplemental atmospheres that will represent mean summer and winter conditions by 15° latitude intervals to an altitude of 90 km.

a. U.S. Standard Atmosphere--1962

The U.S. Standard Atmosphere--1962 was developed by four Task Groups of the Working Group of COESA. (Although U. S. Standard Atmosphere--1962 is the general terminology, the Working Group considers the region above 32 km as "tentative" and above 90 km as "speculative.") The recommendations of Task Group I for the region from 20 to 90 km were adopted. However, Task Group IV was appointed to resolve the discontinuity and inconsistency of the models prepared by Task Groups II (70 to 200 km) and III (200 to 700 km). The reports of Task Groups I and IV (Refs. 6 and 7) have been used extensively in describing the new atmosphere.

Suggestions agreed upon by the Working Group were that up to 79.006 geopotential km (80.000 geometric km using the ICAO gravity relations) geopotential altitude would be the basic height measure. Geometric heights would be basic above this level. Above 20 km (the top of the ICAO Standard), temperature lapse rate is positive at 1 deg/km to 32 km. This gives a value of 228.66 which is in good agreement with measurements. From 32 to 90 km, the temperature lapse would be linear in geopotential height with changes (of whole or half degrees Celsius) to occur at whole kilometer levels. A 5-km isothermal layer (268.66 °K) at 50 km was suggested, and densities close to 1 g/m^3 and 0.02 g/m^3 at 50 and 80 km (geometric), respectively were recommended.

Re-examination of constants from those used previously resulted in new proposed values as follows:

	ICAO	U.S. Ext	Proposed	Units
Universal gas constant	8.31436	8.31439	8.31470	joules/g-deg
Speed of sound	331.43	331.316	331.317	m/sec at 0° C
Sutherland's constant	120.0	110.4	110.4	°K

The new value of the gas constant decreases temperature values by 0.01° (0° C = 273.15° K) and density and pressure values. The differences are summarized in Table 16 (from Ref. 6). The column labeled "N" is the adopted revision, while "H" and "D" refer to earlier revisions. The speed of sound at 0° C also changes slightly and the new relationship is

$$C_S = 20.046707\ T^{1/2}\ \text{m/sec, T in °K}$$

The dynamic viscosity, μ, is slightly changed by the new value for Sutherland's constant, S, so that

$$\mu = 1.458 \times 10^{-6}\ T^{3/2} / (T + S)$$

In analyzing the temperature and density observations an average temperature of 270.65° K was indicated at 50 km, meeting the requirements of linear temperature lapse (above 32 km) that fit the observed data then placed the isothermal region at 47 km. The value of density at 50 km fell within the suggested value of the Working Group. From 30 to 50 km the new temperature profile is between the mean annual measured temperature for high and low latitudes as indicated in Fig. 2 (from Ref. 6). Above the isothermal layer, two temperature lapse regions define temperature to the next isothermal layer

TABLE 16

Comparison of Properties of ICAO, U. S. Extension, ARDC 1959 Model and U. S. Standard Atmospheres--1962

Height	Temperature				Pressure (mb's x 10^n)					Density (g/m^3 x 10^n)				
Geopot (km)	U.S. Ext 56-58	ARDC 59	"H"	"N"	U.S. Ext 56-58	ARDC 59	"H"	"N"	n	U.S. Ext 56-58	ARDC 59	"H"	"N"	n
88.743	196.86 0.0	165.66 0.0	190.65 0.0	180.65 0.0	2.258	1.353	1.8980	1.6437	-3	3.995	2.846	3.4682	3.1698	-3
79.006	196.86 0.0	165.66 0.0	190.65 0.0	180.65 0.0	1.224	1.008	1.0868	1.0364	-2	2.165	2.120	1.9859	1.9986	-2
79.000	196.86 0.0	165.66* -4.5	190.65* -3.2	180.65* -4.0	1.225	1.009	1.0879	1.0376	-2	2.167	2.122	1.9879	2.0009	-2
75.000	196.86* -3.9	183.66 -4.5	203.45 -3.2	196.65 -4.0	2.452	2.1707	2.1771	2.1420	-2	4.3394	4.1176	3.7279	3.7946	-2
61.000	251.46 -3.9	246.66 -4.5	248.25 -3.2	252.65 -2.0	2.0934	2.0372	1.8224	1.8209	-1	2.9002	2.8774	2.5574	2.5108	-1
54.000	278.76 -3.9	278.16 -4.5	270.65* 0.0	266.65 -2.0	5.1637	5.1630	4.5834	4.5748	-1	6.4534	6.4664	5.8996	5.9769	-1
53.000	282.66* =	282.66* 0.0	270.65 0.0	268.65 -2.0	5.8320 =	5.8320	5.2001	5.1977	-1	7.1881 =	7.1881	6.6934	6.7401	-1
52.000		282.66 0.0	270.65 "D"	= 270.65* 0.0		6.5813	5.8997 "D"	= 5.8997	-1		8.1113	7.5939 "D"	= 7.5939	-1
49.610		282.66 0.0	268.66 0.0	270.65 0.0		8.7858	7.9969	7.9772	-1		1.0829	1.0370	1.0268	+0
48.000		282.66 0.0	268.66* +2.5	270.65 0.0		1.0673	9.5880	9.7748	-1		1.3155	1.2433	1.2582	+0
47.000		282.66* +3.0	266.16 +2.5	270.65* +2.8		1.2044	1.0895	1.1090	+0		1.4845	1.4261	1.4275	+0
32.000		237.66 +3.0	228.66* +1.0	228.65* +1.0		8.6776	8.6800	8.6798	+0		1.2721	1.3225	1.3225	+1
25.000	ICAO	216.66* 0.0	221.66 +1.0	221.65 +1.0	ICAO	2.4886		2.5110	+1	ICAO	4.0016		3.9466	+1
20.000	216.66 = 0.0	216.66 = 0.0	216.66*	216.65* 0.0	5.4749	5.4748 =	5.4748	5.4747	+1	8.8035	8.8034 =	8.8034	8.8033	+1
11.000	216.66* -6.5	216.66* -6.5		216.65* -6.5	2.2632 =	2.2632		2.2632	+2	3.6392	3.6391		3.6392	+2
0.000	288.16	288.16		288.15	1.01325			1.01325	+3	1.2250 =	1.2250		1.2250	+3

*Breakpoint in temperature gradient, given in deg/km.

79 km (geopotential). The upper segment 61 to 79 (km) is based upon observed densities which have been considered more reliable than measured temperatures. Adopted temperatures are seen to be at least 20° colder than reported temperatures near 80 km. The isothermal layer of 180.65° K above 79 km provides continuity for density in the region above the isothermal layer. The new density value at 80 km (geometric) agrees very closely with the target value. The properties of this portion of the new standard atmosphere are shown on Table 17 (from Ref. 6).

The basic obstacle to a consistent, continuous standard atmosphere above 90 km was the development of a mean molecular weight (M) profile for the atmospheric gases together with a molecular scale temperature T_M profile with linear lapse rates which would give the secondary atmospheric parameters in agreement with theoretical and empirical data.

The boundary conditions applied to the model were:

(1) The density, pressure and temperature at 90 km must coincide with those of Task Group I, namely: density 3.1698 x 10^{-6} kgm/m^3, pressure 1.6437 x 10^{-3} millibars, molecular scale temperature 180.65° K.

(2) The density at 200 km should lie within the range 3.3 ± 0.3 x 10^{-10} kgm/m^3 for mean solar conditions.

(3) The model should agree as closely as possible with the densities in the altitude range 90 to 200 km recommended by Task Group II and based on rocket and satellite data.

TABLE 17

Properties, to 90 km,
of the U. S. Standard Atmosphere--1962

Kilometers Geomet	Kilometers Geopot	Temperature Grad	Temperature °K	Pressure (mb x 10^n)	n	Density ($\frac{gm}{m^3} \cdot 10^n$)	n	Sound Speed ($\frac{m}{sec} \cdot 10^2$)	Dyn Visc ($\frac{gm}{m\text{-}sec} \cdot 10^2$)
90.000	88.743	0.0	180.65	1.6437	-3	3.1698	-3	2.6944	1.2163
89.235	88.000	↓	180.65	1.8917	↓	3.6480	↓	2.6944	1.2163
87.179	86.000	↓	180.65	2.7613	↓	5.3250	↓	2.6944	1.2163
85.125	84.000	↓	180.65	4.0307	↓	7.7729	↓	2.6944	1.2163
83.072	82.000	↓	180.65	5.8836	↓	1.1346	-2	2.6944	1.2163
81.020	80.000	↓	180.65	8.5883	↓	1.6562	↓	2.6944	1.2163
79.994	79.000	***	180.65	1.0376	-2	2.0009	↓	2.6944	1.2163
78.969	78.000	-4.0	184.65	1.2512	↓	2.3606	↓	2.7241	1.2399
76.920	76.000	↓	192.65	1.7975	↓	3.2504	↓	2.7825	1.2865
74.872	74.000	↓	200.65	2.5444	↓	4.4176	↓	2.8396	1.3323
72.825	72.000	↓	208.65	3.5530	↓	5.9322	↓	2.8957	1.3773
70.779	70.000	↓	216.65	4.8994	↓	7.8782	↓	2.9507	1.4216
68.735	68.000	↓	224.65	6.6776	↓	1.0355	-1	3.0047	1.4652
66.692	66.000	↓	232.65	9.0034	↓	1.3482	↓	3.0577	1.5082
64.651	64.000	↓	240.65	1.2017	-1	1.7396	↓	3.1098	1.5505
62.611	62.000	↓	248.65	1.5889	↓	2.2261	↓	3.1611	1.5922
61.591	61.000	***	252.65	1.8209	↓	2.5108	↓	3.1864	1.6128
60.572	60.000	-2.0	254.65	2.0835	↓	2.8503	↓	3.1990	1.6230
58.534	58.000	↓	258.65	2.7190	↓	3.6622	↓	3.2240	1.6434
56.498	56.000	↓	262.65	3.5339	↓	4.6873	↓	3.2489	1.6636
54.463	54.000	↓	266.65	4.5749	↓	5.9769	↓	3.2735	1.6837
52.429	52.000	***	270.65	5.8997	↓	7.5939	↓	3.2980	1.7037
50.396	50.000	0.0	270.65	7.5940	↓	9.7747	-1	3.2980	1.7037
48.365	48.000	0.0	270.65	9.7748	↓	1.2582	+0	3.2980	1.7037
47.350	47.000	***	270.65	1.1090	+0	1.4275	↓	3.2980	1.7037
46.335	46.000	+2.8	267.85	1.2591	↓	1.6376	↓	3.2809	1.6897
44.307	44.000	↓	262.25	1.6294	↓	2.1645	↓	3.2464	1.6616
42.279	42.000	↓	256.65	2.1203	↓	2.8780	↓	3.2115	1.6332
40.253	40.000	↓	251.05	2.7752	↓	3.8510	↓	3.1763	1.6045
38.229	38.000	↓	245.45	3.6544	↓	5.1867	↓	3.1407	1.5756
36.205	36.000	↓	239.85	4.8430	↓	7.0342	↓	3.1047	1.5463
34.183	34.000	↓	234.25	6.4610	↓	9.6086	↓	3.0682	1.5167
32.162	32.000	***	228.65	8.6798	↓	1.3225	+1	3.0313	1.4868
30.142	30.000	+1.0	226.65	1.1718	+1	1.8011	↓	3.0180	1.4760
28.124	28.000	↓	224.65	1.5862	↓	2.4598	↓	3.0047	1.4652
26.107	26.000	↓	222.65	2.1530	↓	3.3687	↓	2.9913	1.4544
24.091	24.000	↓	220.65	2.9304	↓	4.6266	↓	2.9778	1.4435
22.076	22.000	↓	218.65	3.9997	↓	6.3726	↓	2.9643	1.4326
20.063	20.000	***	216.65	5.4747	↓	8.8033	+1	2.9507	1.4216
18.051	18.000	0.0	216.65	7.5045	↓	1.2067	+2	2.9507	1.4216
16.040	16.000	↓	216.65	1.0287	+2	1.6541	↓	2.9507	1.4216
14.031	14.000	↓	216.65	1.4101	↓	2.2674	↓	2.9507	1.4216
12.023	12.000	↓	216.65	1.9330	↓	3.1082	↓	2.9507	1.4216
11.019	11.000	***	216.65	2.2632	↓	3.6392	↓	2.9507	1.4216
10.016	10.000	-6.5	223.15	2.6443	↓	4.1282	↓	2.9946	1.4571
8.010	8.000	↓	236.15	3.5601	↓	5.2519	↓	3.0806	1.5268
6.006	6.000	↓	249.15	4.7183	↓	6.5973	↓	3.1643	1.5947
4.003	4.000	↓	262.15	6.1642	↓	8.1916	+2	3.2458	1.6611
2.001	2.000	↓	275.15	7.9496	↓	1.0065	+3	3.3253	1.7260
0.000	0.000	↓	288.15	10.1325	↓	1.2250	+3	3.4029	1.7894

***Altitude at which temperature gradient experiences discontinuity.

(4) At higher altitudes the density should match satellite density data under mean solar conditions and agree as closely as possible with the density values recommended by Task Group III.

(5) The molecular scale temperature gradients dT_M/dz should be linear and kept to a maximum of two significant figures and, where possible, to one significant figure.

(6) The number of breakpoints or segments in the $T_M(z)$ function should be kept to a minimum, consistent with accurate representation of the properties of a mean atmosphere.

(7) The value of T at 150 km should be as low as possible, consistent with the observed density values, to give some weight to Blamont's measurement of T at this altitude. (These temperature measurements are not consistent with temperatures deduced from density measurements.)

(8) The value of dT/dz should approach zero above 350 km.

(9) The value of T above 350 km should lie in the range 1500 ± 200° K.

b. Properties

The model defined in terms of molecular-scale temperature as a function of geometric altitude is shown in Fig. 3 (from Ref. 7) together with the corresponding defining functions for the ARDC 1959 model and the current U.S. standard atmosphere (ARDC 1956). In Fig. 4 (from Ref. 1) the adopted profile (up to 300 km) is compared with profiles deduced from several types of observations.

The gradients dT_M/dz increase steadily from 0° K/km at 90 km to a maximum value of 20° K/km between 120 and 150 km, then steadily decrease to 5° K/km at 200 km and finally to 1.1° K/km at 600 km. Because of the requirement that dT/dz tend to zero above 350 km, dT_M/dz must be maintained at a small positive value determined by the rate of decrease of M in the same region. When dT/dz = 0

$$dT_M/dz = - T/M^2 \, (dM/dz)$$

where dM/dz is negative

Figure 5 (from Ref. 1) presents density versus geometric altitude for the new standard compared with some U.S. and Russian data and the 1959 ARDC Model Atmosphere. A comparison of the pressure versus altitude curves for the new U.S. standard atmosphere with other standards is presented in Fig. 6 (from Ref. 1). Figure 7 (from Ref. 7) is a comparison of the molecular weight versus altitude for the different standards. A table of the defining properties of the 90- to 700- km portion of the U.S. Standard Atmosphere 1962 is presented in Table 18 (from Ref. 1). Table 19 (from Ref. 1) shows the detailed properties of this upper part of the new atmosphere. A brief outline of the new standard from 0 to 700 km in skeleton form is presented in Table 20 (from Ref. 1). This table is included along with the data of Table 19 because of its compact form and because of the fact that other data is also presented.

TABLE 18

Defining Properties of the Proposed Standard Atmosphere

z (km)	T_M (°K)	L (°K/km)	M	T
90	180.65		28.966	180.65
		+3		
100	210.65		28.88	210.02
		+5		
110	260.65		28.56	257.00
		+10		
120	360.65		28.07	349.49
		+20		
150	960.65		26.92	892.79
		+15		
160	1110.65		26.66	1022.2
		+10		
170	1210.65		26.40	1103.4
		+7		
190	1350.65		25.85	1205.4
		+5		
230	1550.65		24.70	1322.3
		+4		
300	1830.65		22.66	1432.1
		+3.3		
400	2160.65		19.94	1487.4
		+2.6		
500	2420.65		17.94	1499.2
		+1.7		
600	2590.65		16.84	1506.1
		+1.1		
700	2700.65		16.17	1507.6

z = geometric altitude

T_M = molecular scale temperature = TM_0/M

T = kinetic temperature

M = mean molecular weight

M_0 = sea-level value of M

L = dT_M/dz, gradient of molecular scale temperature

2. Density Variability

a. Measurements

Variations in density of the upper atmosphere affect the orbital lifetime and re-entry of satellites. For these reasons considerable attention has been given recently to evaluation of these variations.

Tidal variations in the atmosphere are attributed to gravitational variations caused by the sum and moon. This tidal energy is supplied

TABLE 19

Defining Molecular Scale Temperature and Related Properties for the U. S. Standard Atmosphere--1962

z (km)	T_M (°K)	L (°K/km)	H_p (km)	p (mb x 10^n) n	p (mm Hg x 10^n) n	ρ $\text{Log}_{10} p/p_o$	ρ $\left(\frac{kg}{m^3} \cdot 10^n\right)$ n	$\text{Log}_{10}\rho/\rho_o$
90	180.65	↑	5.438	1.6437 -3	1.2329 -3	-5.7899	3.1698 -6	-5.5871
92	186.65	↑	5.623	1.1448 ↓	8.5869 -4	-5.9496	2.1368 ↓	-5.7584
94	192.65	3.0	5.807	8.0674 -4	6.0511 ↓	-6.0990	1.4589 ↓	-5.9241
96	198.65	↓	5.991	5.7476 ↓	4.3110 ↓	-6.2462	1.0080 ↓	-6.0847
98	204.65	↓	6.176	4.1372 ↓	3.1031 ↓	-6.3890	7.0428 -7	-6.2404
100	210.65	↑	6.361	3.0070 ↓	2.2554 ↓	-6.5276	4.9731 ↓	-6.3915
102	220.65	↑	6.667	2.2119 ↓	1.6591 ↓	-6.6610	3.4924 ↓	-6.5450
104	230.65	5.0	6.974	1.6497 ↓	1.2374 ↓	-6.7883	2.4918 ↓	-6.6916
106	240.65	↓	7.280	1.2460 ↓	9.3456 ↓	-6.9102	1.8038 ↓	-6.8320
108	250.65	↓	7.588	9.5205 -5 ↓	7.1410 ↓	-7.0271	1.3233 ↓	-6.9665
110	260.65	↓	7.895	7.3527 -5	5.5150 -5	-7.1393	9.8277 -8	-7.0957
112	280.65	↑	8.507	5.7609 ↓	4.3210 ↓	-7.2452	7.1512 ↓	-7.2338
114	300.65	10.	9.117	4.5908 ↓	3.4434 ↓	-7.3438	5.3196 ↓	-7.3623
116	320.65	↓	9.731	3.7127 ↓	2.7848 ↓	-7.4360	4.0338 ↓	-7.4824
118	340.65	↓	10.34	3.0418 ↓	2.2816 ↓	-7.5226	3.1109 ↓	-7.5953
120	360.65	↓	10.96	2.5209 ↓	1.8909 ↓	-7.6042	2.4352 ↓	-7.7016
122	400.65	↑	12.18	2.1204 ↓	1.5904 ↓	-7.6793	1.8435 ↓	-7.8224
124	440.65	↑	13.41	1.8133 ↓	1.3601 ↓	-7.7472	1.4336 ↓	-7.9317
126	480.65	↑	14.63	1.5721 ↓	1.1792 ↓	-7.8092	1.1395 ↓	-8.0314
128	520.65	↑	15.86	1.3787 ↓	1.0341 ↓	-7.8663	9.2254 -9	-8.1232
130	560.65	↑	17.09	1.2210 -5	9.1584 -6	-7.9190	7.5873 -9	-8.2080
132	600.65	↑	18.32	1.0905 ↓	8.1797 ↓	-7.9681	6.3252 ↓	-8.2871
134	640.65	↓	19.55	9.8118 -6 ↓	7.3595 ↓	-8.0140	5.3357 ↓	-8.3610
136	680.65	20.	20.78	8.8852 ↓	6.6645 ↓	-8.0571	4.5478 ↓	-8.4303
138	720.65	↓	22.02	8.0923 ↓	6.0697 ↓	-8.0977	3.9121 ↓	-8.4957
140	760.65	↓	23.25	7.4079 ↓	5.5563 ↓	-8.1360	3.3929 ↓	-8.5576
142	800.65	↓	24.49	6.8124 ↓	5.1098 ↓	-8.1724	2.9643 ↓	-8.6162
144	840.65	↓	25.73	6.2908 ↓	4.7185 ↓	-8.2070	2.6071 ↓	-8.6720
146	880.65	↓	26.98	5.8310 ↓	4.3736 ↓	-8.2400	2.3067 ↓	-8.7251
148	920.65	↓	28.22	5.4233 ↓	4.0678 ↓	-8.2715	2.0522 ↓	-8.7759
150	960.65	↓	29.46	5.0599 -6 ↓	3.7952 -6 ↓	-8.3016	1.8350 -9	-8.8245
152	990.65	↑	30.39	4.7328 ↓	3.5499 ↓	-8.3306	1.6644 ↓	-8.8669
154	1020.65	15.	31.34	4.4359 ↓	3.3272 ↓	-8.3587	1.5141 ↓	-8.9080
156	1050.65	↓	32.28	4.1655 ↓	3.1244 ↓	-8.3861	1.3812 ↓	-8.9479
158	1080.65	↓	33.22	3.9187 ↓	2.9393 ↓	-8.4126	1.2633 ↓	-8.9866
160	1110.65	↓	34.17	3.6929 ↓	2.7699 ↓	-8.4384	1.1584 ↓	-9.0243
162	1130.65	↑	34.80	3.4848 ↓	2.6138 ↓	-8.4635	1.0738 ↓	-9.0572
164	1150.65	↓	35.44	3.2919 ↓	2.4691 ↓	-8.4883	9.9669 -10	-9.0896

Z = geometric altitude

H = geopotential altitude

$= \frac{RZ}{R+Z}$

R = radius of earth at 45° 32' 40" = 6356.766 km

TABLE 19 (continued)

z (km)	T_M (°K)	L (°K/km)	H_p (km)	p (mb x 10^n) n	p (mm Hg x 10^n) n	ρ $Log_{10}p/p_0$	ρ $\left(\frac{kg}{m^3} \cdot 10^n\right)_n$	$Log_{10}\rho/\rho_0$
166	1170.65		36.08	3.1128 -6	2.3348 -6	-8.5126	9.2637 -10	-9.1214
168	1190.65	10.0	36.72	2.9464	2.2100	-8.5364	8.6211 -10	-9.1526
170	1210.65		37.36	2.7915 -6	2.0938 -6	-8.5599	8.0330 -10	-9.1833
172	1224.65		37.81	2.6468	1.9853	-8.5830	7.5296	-9.2114
174	1236.65		38.27	2.5113	1.8836	-8.6058	7.0632	-9.2391
176	1252.65		38.73	2.3841	1.7882	-8.6284	6.6307	-9.2666
178	1266.65		39.18	2.2648	1.6987	-8.6507	6.2292	-9.2937
180	1280.65	7.0	39.64	2.1527	1.6147	-8.6727	5.8562	-9.3205
182	1294.65		40.10	2.0474	1.5357	-8.6945	5.5094	-9.3470
184	1308.65		40.55	1.9483	1.4614	-8.7161	5.1868	-9.3732
186	1322.65		41.01	1.8551	1.3914	-8.7374	4.8863	-9.3992
188	1336.65		41.47	1.7673	1.3256	-8.7584	4.6062	-9.4248
190	1350.65		41.93	1.6845 -6	1.2635 -6	-8.7793	4.3450 -10	-9.4502
192	1360.65		42.27	1.6064	1.2049	-8.7999	4.1130	-9.4740
194	1370.65		42.61	1.5324	1.1494	-8.8204	3.8950	-9.4976
196	1380.65		42.94	1.4624	1.0969	-8.8407	3.6901	-9.5211
198	1390.65		43.28	1.3961	1.0472	-8.8608	3.4975	-9.5444
200	1400.65		43.62	1.3333	1.0001	-8.8808	3.3163	-9.5675
202	1410.65		43.96	1.2738	9.5541	-8.9006	3.1458	-9.5904
204	1420.65		44.30	1.2173	9.1307	-8.9203	2.9852	-9.6132
206	1430.65		44.63	1.1638	8.7291	-8.9399	2.8340	-9.6358
208	1440.65		44.97	1.1130	8.3480	-8.9592	2.6915	-9.6582
210	1450.65	5.0	45.31	1.0647 -6	7.9862 -7	-8.9785	2.5571 -10	-9.6804
212	1460.65		45.65	1.0189	7.6427	-8.9976	2.4303	-9.7025
214	1470.65		45.99	9.7542 -7	7.3163	-9.0165	2.3107	-9.7244
216	1480.65		46.33	9.3407	7.0061	-9.0353	2.1978	-9.7462
218	1490.65		46.68	8.9475	6.7112	-9.0540	2.0911	-9.7678
220	1500.65		47.02	8.5735	6.4307	-9.0726	1.9904	-9.7892
222	1510.65		47.36	8.2177	6.1638	-9.0910	1.8952	-9.8105
224	1520.65		47.70	7.8721	5.9046	-9.1092	1.8051	-9.8316
226	1530.65		48.04	7.5567	5.6680	-9.1274	1.7200	-9.8526
228	1540.65		48.39	7.2497	5.4377	-9.1454	1.6394	-9.8735
230	1550.65		48.73	6.9572 -7	5.2183 -7	-9.1633	1.5631 -10	-9.8942
232	1558.65		49.01	6.6782	5.0091	-9.1811	1.4927	-9.9142
234	1566.65		49.29	6.4119	4.8093	-9.1987	1.4259	-9.9341
236	1574.65	4.0	49.58	6.1577	4.6187	-9.2163	1.3624	-9.9538
238	1582.65		49.86	5.9149	4.4366	-9.2338	1.3020	-9.9735
240	1590.65		50.14	5.6830	4.2626	-9.2511	1.2447	-9.9931
242	1598.65		50.43	5.4614	4.0964	-9.2684	1.1902	-10.0125

TABLE 19 (continued)

z (km)	T_M (°K)	L (°K/km)	H_p (km)	p (mb x 10^n) n	p (mm Hg x 10^n) n	ρ $Log_{10} p/p_0$	ρ $\left(\frac{kg}{m^3} \cdot 10^n\right)_n$	$Log_{10} \rho/\rho_0$
244	1606.65	4.0	50.71	5.2496 -7	3.9375 -7	-9.2856	1.1383 -10	-10.0319
246	1614.65		50.99	5.0471	3.7856	-9.3027	1.0890	-10.0511
248	1622.65		51.27	4.8535	3.6404	-9.3197	1.0421	-10.0703
250	1630.65		51.56	4.6683 -7	3.5015 -7	-9.3366	9.9738 -11	-10.0893
252	1638.65		51.84	4.4912	3.3687	-9.3534	9.5485	-10.1082
254	1646.65		52.13	4.3217	3.2415	-9.3701	9.1434	-10.1270
256	1654.65		52.41	4.1594	3.1198	-9.3867	8.7576	-10.1458
258	1662.65		52.70	4.0041	3.0033	-9.4032	8.3901	-10.1644
260	1670.65		52.98	3.8554	2.8918	-9.4197	8.0397	-10.1829
262	1678.65		53.27	3.7130	2.7849	-9.4360	7.7058	-10.2013
264	1686.65		53.55	3.5765	2.6826	-9.4523	7.3874	-10.2197
266	1694.65		53.84	3.4457	2.5845	-9.4684	7.0837	-10.2379
268	1702.65		54.13	3.3204	2.4905	-9.4845	6.7940	-10.2560
270	1710.65		54.41	3.2003 -7	2.4004 -7	-9.5005	6.5176 -11	-10.2741
272	1718.65		54.70	3.0851	2.3140	-9.5165	6.2537	-10.2920
274	1726.65		54.99	2.9746	2.2311	-9.5323	6.0018	-10.3099
276	1734.65	4.0	55.28	2.8686	2.1517	-9.5480	5.7613	-10.3276
278	1742.65		55.57	2.7670	2.0754	-9.5637	5.5316	-10.3453
280	1750.65		55.86	2.6694	2.0022	-9.5793	5.3122	-10.3629
282	1758.65		56.15	2.5758	1.9320	-9.5948	5.1025	-10.3804
284	1766.65		56.43	2.4858	1.8645	-9.6103	4.9021	-10.3978
286	1774.65		56.73	2.3995	1.7998	-9.6256	4.7105	-10.4151
288	1782.65		57.01	2.3166	1.7376	-9.6409	4.5273	-10.4323
290	1790.65		57.31	2.2369 -7	1.6778 -7	-9.6561	4.3521 -11	-10.4494
292	1798.65		57.60	2.1604	1.6204	-9.6712	4.1845	-10.4665
294	1806.65		57.88	2.0868	1.5653	-9.6862	4.0241	-10.4835
296	1814.65		58.18	2.0162	1.5122	-9.7012	3.8707	-10.5004
298	1822.65		58.47	1.9482	1.4613	-9.7161	3.7238	-10.5172
300	1830.65		58.76	1.8828	1.4122	-9.7309	3.5831	-10.5339
305	1847.15		59.38	1.7300	1.2976	-9.7677	3.2629	-10.5745
310	1863.65		60.00	1.5910	1.1934	-9.8041	2.9742	-10.6148
315	1880.15		60.62	1.4644	1.0984	-9.8401	2.7135	-10.6546
320	1896.65		61.25	1.3491	1.0119	-9.8757	2.4780	-10.6940
325	1913.15	3.3	61.88	1.2438 -7	9.3293 -8	-9.9110	2.2650 -11	-10.7331
330	1929.65		62.50	1.1477	8.6086	-9.9459	2.0721	-10.7717
335	1946.15		63.13	1.0599	7.9499	-9.9805	1.8973	-10.8100
340	1962.65		63.76	9.7957 -8	7.3474	-10.0147	1.7388	-10.8479
345	1979.15		64.40	9.0604	6.7958	-10.0486	1.5949	-10.8854

TABLE 19 (continued)

z (km)	T_M (°K)	L (°K/km)	H_p (km)	p (mb x 10^n) n	p (mm Hg x 10^n) n	ρ $Log_{10} p/p_0$	ρ $\left(\frac{kg}{m^3} \cdot 10^n\right)$ n	$Log_{10} \rho/\rho_0$
350	1995.65		65.02	8.3866 -8	6.2905 -8	-10.0821	1.4641 -11	-10.9226
355	2012.15		65.66	7.7688	5.8271	-10.1154	1.3451	-10.9594
360	2028.65		66.30	7.2018	5.4018	-10.1483	1.2368	-10.9958
365	2045.15		66.94	6.6810	5.0112	-10.1809	1.1381	-11.0320
370	2061.65		67.58	6.2024	4.6522	-10.2132	1.0481	-11.0677
375	2078.15	3.3	68.22	5.7620	4.3219	-10.2400	9.6595 -12	-11.1032
380	2094.65		68.86	5.3567	4.0178	-10.2768	8.9092	-11.1383
385	2111.15		69.51	4.9832	3.7377	-10.3082	8.2233	-11.1731
390	2127.65		70.16	4.6389	3.4794	-10.3393	7.5957	-11.2076
395	2144.15		70.81	4.3212	3.2411	-10.3701	7.0211	-11.2417
400	2160.65		71.45	4.0278 -8	3.0211 -8	-10.4007	6.4945 -12	-11.2756
410	2186.65		72.53	3.5055	2.6293	-10.4610	5.5850	-11.3411
420	2212.65		73.61	3.0571	2.2930	-10.5214	4.8134	-11.4057
430	2238.65		74.69	2.6714	2.0037	-10.5790	4.1573	-11.4693
440	2264.65		75.78	2.2339	1.7543	-10.6367	3.5981	-11.5321
450	2290.65	2.6	76.88	2.0517	1.5389	-10.6936	3.1204	-11.5939
460	2316.65		77.98	1.8031	1.3525	-10.7497	2.7116	-11.6549
470	2342.65		79.09	1.5875	1.1908	-10.8050	2.3609	-11.7151
480	2368.65		80.20	1.4002	1.0502	-10.8595	2.0595	-11.7744
490	2394.65		81.32	1.2371	9.2792 -9	-10.9133	1.7998	-11.8329
500	2420.65		82.44	1.0949 -8	8.2124 -9	-10.9664	1.5758 -12	-11.8906
510	2437.65		83.27	9.7042 -9	7.2787	-11.0188	1.3869	-11.9461
520	2454.65		84.09	8.6110	6.4588	-11.0707	1.2222	-12.0010
530	2471.65		84.91	7.6500	5.7380	-11.1221	1.0783	-12.0554
540	2488.65		85.75	6.8041	5.1035	-11.1730	9.5250 -13	-12.1093
550	2505.65	1.7	86.59	6.0585	4.5443	-11.2234	8.4238	-12.1626
560	2522.65		87.43	5.4007	4.0509	-11.2733	7.4585	-12.2155
570	2539.65		88.28	4.8197	3.6150	-11.3227	6.6115	-12.2678
580	2556.65		89.12	4.3058	3.2296	-11.3717	5.8673	-12.3197
590	2573.65		89.97	3.8508	2.8883	-11.4202	5.2127	-12.3711
600	2590.65		90.83	3.4475 -9	2.5859 -9	-11.4682	4.6362 -13	-12.4220
610	2601.65		91.47	3.0893	2.3172	-11.5159	4.1369	-12.4715
620	2612.65		92.13	2.7705	2.0780	-11.5632	3.6943	-12.5206
630	2623.65		92.78	2.4865	1.8650	-11.6101	3.3017	-12.5694
640	2634.65		93.43	2.2333	1.6751	-11.6568	2.9531	-12.6179
650	2645.65	1.1	94.09	2.0074	1.5056	-11.7031	2.6433	-12.6660
660	2656.65		94.75	1.8057	1.3544	-11.7491	2.3679	-12.7138
670	2667.65		95.42	1.6254	1.2192	-11.7948	2.1227	-12.7613
680	2678.65		96.09	1.4642	1.0983	-11.8401	1.9044	-12.8084
690	2689.65		96.76	1.3200	9.9007 -10	-11.8852	1.7097	-12.8552
700	2700.65		97.42	1.1908 -9	8.9317 -10	-11.9299	1.5361 -13	-12.9017

TABLE 20

Skeleton of the U. S. Standard Atmosphere--1962

Defining temperature and molecular weights of the proposed U. S. Standard Atmosphere and computed pressures and densities, where z = geometric altitude, h = geopotential altitude, T = kinetic temperature, M = mean molecular weight, L = gradient of molecular scale temperature = dT_M/dh (below 79 geopotential km) = dT_M/dz (above 79 geopotential km), T_M = molecular scale temperature = $(T/M)\,M_0$; and M_0 = sea level value of M.

z (km)	h (km)	T_M (°K)	L (°K/km)	M	T (°K)	P (mb x 10^n) n	ρ ($\frac{gm}{m^3} \cdot 10^n$)$_n$
0.000	0.000	288.15	-6.5	28.966	288.15	10.1325 2*	1.2250 3
11.019	11.000	216.65	0.0	28.966	216.65	2.2632 2	3.6392 2
20.063	20.000	216.65	1.0	28.966	216.65	5.4747 1	8.8033 1
32.162	32.000	228.65	2.8	28.966	228.65	8.6798 0	1.3225 1
47.350	47.000	270.65	0.0	28.966	270.65	1.1090 0	1.4275 0
52.429	52.000	270.65	-2.0	28.966	270.65	5.8997 - 1	7.5939 - 1
61.591	61.000	252.65	-4.0	28.966	252.65	1.8209 - 1	2.5108 - 1
79.994	79.000	180.65	0.0	28.966	180.65	1.0376 - 2	2.0009 - 2
90.000	88.743	180.65	3.0	28.966	180.65	1.6437 - 3	3.1698 - 3
100.000	98.451	210.65	5.0	28.88	210.02	3.0070 - 4	4.9731 - 4
110.000	108.129	260.65	10.0	28.56	257.00	7.3527 - 5	9.8277 - 5
120.000	117.777	360.65	20.0	28.07	349.49	2.5209 - 5	2.4352 - 5
150.000	146.542	960.65	15.0	26.92	892.79	5.0599 - 6	1.8350 - 6
160.000	156.071	1,110.65	10.0	26.66	1,022.20	3.6929 - 6	1.1584 - 6
170.000	165.572	1,210.65	7.0	26.40	1,103.40	2.7915 - 6	8.0330 - 7
190.000	184.485	1,350.65	5.0	25.85	1,205.40	1.6845 - 6	4.3450 - 7
230.000	221.968	1,550.65	4.0	24.70	1,322.30	6.9572 - 7	1.5631 - 7
300.000	286.478	1,830.65	3.3	22.66	1,432.10	1.8828 - 7	3.5831 - 8
400.000	376.315	2,160.65	2.6	19.94	1,487.40	4.0278 - 8	6.4945 - 9
500.000	463.530	2,420.65	1.7	17.94	1,499.20	1.0949 - 8	1.5758 - 9
600.000	548.235	2,590.65	1.1	16.84	1,506.10	3.4475 - 9	4.6362 - 10
700.000	630.536	2,700.65		16.17	1,507.60	1.1908 - 9	1.5361 - 10

to the atmosphere in the high density region and the diurnal tidal component propagates upward to about 105 to 305 km where it is damped. The semidiurnal components of the lunar and solar tidal variation, because of their shorter period, are usually detected between 50 and 80 km. The maximum density variation resulting from these tidal effects is of the order of 25%. At 96 km, Greenhow and Hall (Ref. 8) have found a diurnal density variation of about 13% and a semidiurnal variation of about 7%. Other causes of density variability are solar heating which may be expected to vary with local time, latitude, season and altitude (as selective portions of the solar radiation are absorbed). In addition to gravitational and thermal causes of fairly regular density variability there may be an irregular component analagous to storm systems in the lower atmosphere.

Nicolet (Ref. 9) indicates that atmospheric density variations may also be produced by solar flares and sunspot activity. Sunspot variation effects on density would be expected to vary from one year to the next with solar flare activity being associated with the sunspot activity. It is presumed that these effects would cause density variations of the order of 30 to 40% at altitudes of 200 km. The effect of the 11-year sunspot cycle on density has been estimated by Johnson (Ref. 10) as shown in Fig. 8. The maximum decrease occurs at about 1000 km where density is lower by a factor of 100. The effect reverses at 1700 km. If these estimates are correct, then the solar cycle variation may be the largest change in density.

One of the most useful techniques in determining densities has been from changes measured in the orbits of satellites having fairly precisely defined

elements. King-Hele and Walker (Ref. 11) have determined density from 21 satellites. Figure 9 shows the density ratio (to sea level density) from these determinations. These data confirm that at altitudes between 180 and 300 km "the density did not depart from the long term average of 1957 - 1959 by a factor of more than 1.5" as a result of latitudinal, seasonal or day-night effects, although it is possible that larger variations might have occurred over intervals of less than 1 day and not have been detected by this technique (which requires about 10 orbits for a determination).

A grouping of the data from 180 to 250 km in Fig. 9 into those points up to January 1959 and after August 1959 would indicate density curves, respectively, 10% higher and 10% lower than the average shown on Fig. 9. This small decrease in density with time is attributed to the decrease in solar activity.

At altitudes between 300 and 700 km, Fig. 9 shows an increasingly pronounced day-night variation. The authors note that this is a solar zenith angle effect and should not be attributed to latitude or season beyond the fact that solar zenith angle is related to latitude and season.

In evaluating the large apparent day-night effect shown, it should be noted that some of the variation is due to solar activity as the midday data all refer to early 1959 and the midnight values to late 1959 and early 1960.

Jacchia (Ref. 12) has found from observations of satellite motion that a large diurnal variation in atmospheric density primarily due to solar heating effects occurs at altitudes greater than 325 km and decreases at the 200-km level. This bulge occurs in the general direction of the sun with a 25° to 30° lag produced by the earth's rotation. This atmospheric bulge represents the bulk of the density variations at altitudes above 200 km with variations ranging from about 5% of the mean density at 200 km to about 25% at 800 km.

A separation of the day-night, seasonal, terrestrial (latitude) and solar activity effects has been indicated by Martin and Priester (Ref. 13) using observations of Vanguard I. At 660 km, a factor of 10 day-to-night variation in density was determined. This is considerably larger than Jacchia's value at 800 km. The value of density shown in Fig. 10 is a function of the difference in right ascension $\Delta\alpha$ of the sun and satellite perigee (and therefore a function of true local time). The shift of maximum density at 660 km by 25° from local noon is well defined and in agreement with Jacchia.

The seasonal and latitude effects are superimposed and at 660 km and over latitudes and declinations 0° to 30° they are each about 1/10 of the day-night effect. The analysis of Discoverer satellite orbits (Ref. 14) has indicated that the latitude-seasonal effect was only about 20%. Kallmann-Bijl (Ref. 15) in a recent survey has indicated that the separation of yearly, latitudinal, seasonal and solar cycle effects still remains a problem and her belief is borne out by the lack of agreement among different estimates of these effects.

Data from Vanguard 2 and Sputnik in addition to Vanguard I data were further investigated (Ref. 16) and yielded the diurnal (plus seasonal) density variations shown in Fig. 11. At 210 km the diurnal variation of density is about a factor of 2, at 562 km it is between 5 and 6 and at 660 km it is almost 10 as mentioned earlier. The difference in density between the solid and dashed lines is a measure of the seasonal effect at each altitude since

$$\Delta\delta = \delta_{\pi} - \delta_{\odot}$$

is the difference in declination between the satellite perigee π and the sun $\odot$. The seasonal density decrease at an average $\Delta\delta$ of about 40° is about 5% at each altitude. (Parkyn (Ref. 17) has determined the ratio of polar to equatorial density of 0.65 at about 250 km.) Figure 12 (taken from Ref. 17) is a model of the diurnal variations of atmospheric density. The "wiggle" at 200 km was first suggested by Kallmann (Ref. 18) and derived more exactly and with better definition by Priester and Martin (Ref. 19) using more data. The wiggle occurs in the F1 region of the ionosphere and is considered as the beginning of the density "solar effect." It is caused by absorption of the relatively intense solar helium line at 304Å. The diurnal variation of density at 200 km is small because of the poor heat conduction. The increasing diurnal effect "fan shape" with altitude results from the combination of absorbed solar electromagnetic radiation and increasing heat conductivity of the atmosphere. Another density "wiggle" at 300 to 500 km expected from the absorption of the 584Å solar helium line is apparently smoothed out by the large heat conductivity.

The flux of solar radiations (short ultraviolet as well as perhaps X-rays and particles) which cause the diurnal density variation are themselves variables. Therefore a "solar activity effect" upon density (above 200 km) also occurs. The best index of this effect is the intensity of radiation (in the 3- to 30-cm wavelength) from the sun which is emitted from the same solar regions (coronal condensations and flares) as the much more highly ionizing radiations which modulate atmosphere density.

The relation between density and 20-cm solar radio waves has been found to be approximately linear over the range of values of solar flux between 100 and 240 x 10^{-22} w/m^2-cps. If 170 x 10^{-22} is used as a standard flux, the density variation due to solar activity is about ±41%. This is over and above the diurnal variation. It is known that some of the ionizing solar radiations have their largest variations in intensity over relatively short intervals of minutes during solar flares. Short transients in density that result from the absorption of these radiations are not distinguishable using the relatively long technique of variations in satellite acceleration. On the other hand, some of the sources of increased ionizing radiation are relatively long-lived, as a 27-day periodicity of density has been detected. This corresponds to the rotational period of the sun.

An estimate of density at 1518 km has been made from the orbit of the Echo satellite (Ref. 20).

The variation in orbital period corresponded to a mean density of 1.1×10^{-18} gm/cm^3. However, at this altitude, density variations of 2 orders of magnitude are indicated, so the value of the mean is very limited.

At lower altitudes, Quiroz (Ref. 21) has constructed a model of the seasonal variation of mean density as shown in Fig. 13. This author notes that the variations indicated on this figure join quite well with the factor of 1.5 at 220 km from Ref. 11. At altitudes up to 30 km there is considerably more data available. In Refs. 22 and 23, summaries have been prepared and are available for a number of specific stations and by latitude and season.

b. Variable models from satellite orbits (Ref. 24)

Jacchia (Ref. 12) and Priester (Ref. 25) both devised variable models of the upper atmosphere based on the observed correlation with the decimeter solar flux and the angle between perigee and the sun. An annual variation in atmospheric density was then discovered by Paetzold (Ref. 26) who constructed a variable atmospheric model based on all three effects. A C_D of 2 should be used with these variable atmospheric models. (Paetzold has recently reported that he now uses $C_D = 2.2$.) In all the models mentioned above the density is calculated as if all the drag were caused by neutral particles. At the higher altitudes charge drag may be important, but the gross effects of the interaction would be the same in any case for satellites with conducting skins.

The model atmospheres based on satellite observations are constructed mostly from acceleration data smoothed over 2-day intervals. Therefore, these models can give no information about shorter term fluctuations. Little is known about short term fluctuations in the upper atmosphere.

Jacchia's Variable Model. According to Jacchia, the density of the upper atmosphere is given by the following formula.

$$\rho = \rho_0(h)\, F_{20} \left\{ 1 + 0.19 \left[\exp(0.01887h) - 1.9 \right] \cos^6 \psi/2 \quad \ldots \right\}$$

$\rho_0(h)$, which is the density when $\psi = 180°$ and $F_{20} = 1$, is given by

$$\log \rho_0(h) = -15.733 - 0.006,808,3h + 6.363 \exp(-0.008,917h).$$

The quantities appearing in these formulas are

h = height in km $(185 < h < 750)$

F_{20} = 20-cm solar flux in units of 100×10^{-22} w/m^2 - cps

ψ = the angle between the satellite and the peak of the diurnal bulge of the atmosphere. (The bulge is assumed to lag behind the sun by approximately 25° in Jacchia's atmosphere.)

ρ = atmospheric density in slugs/ft^3 (1 slug/ft^3 = 515.2 kg/m^3)

Priester's Variable Model. Priester's model is similar to Jacchia's, since both are based on the correlation with the 20-cm solar flux and the angle between perigee and the sun. In Priester's model, the atmospheric density is directly proportional to F_{20}, the 20-cm solar flux, and the peak of the diurnal bulge lags 1 hr (15°) behind the sun.

Paetzold's Variable Model. Paetzold's atmosphere is one of the more recent modes (July 1961). It also covers the greatest range of altitudes (150 to 1600 km), and uses the most dependable and readily available solar flux data (the 10-cm measurements made by Arthur Covington at the National Research Council, Ottawa, Canada). Since Paetzold's atmosphere includes more effects, it is more complicated than Jacchia's or Priester's.

In Paetzold's model, the density of the upper atmosphere, $\rho(h)$ is described by

$$\log \rho(h) = \log \rho_s(h) - i_{220}(h) \frac{220 - F_{10}}{120} - a(h)\, g(a) - \theta(h)\, f(\theta) \ldots .$$

where $\rho_s(h)$ is the standard density function given in Table 21. It represents the density in slugs/ft^3 (1 slug/ft^3 = 515.2 kg/m^3) at the maximum of the diurnal bulge (local time, θ = 14.00 hr), when the 10-cm solar flux, F_{10} is 220 (in units of 10^{-22} w/m^2-cps), and when the annual variation is at its peak. The function $i_{220}(h)$ represents the effect of solar ultraviolet emission, which is correlated with the 10-cm solar flux and with sunspots. The effect of the diurnal bulge is represented by $\theta(h)$, where

$$\theta(h) = \theta_s(h) - \Delta_1 \theta(h) \cdot \frac{i_{220}(h) \frac{220 - F_{10}}{120} + a(h)\, g(a)}{i_{220}(h) + a(h)} - \Delta_2 \theta(h) \cdot \left(\frac{220 - F_{10}}{120} \right)$$

All three functions, $\theta_s(h)$, $\Delta_1\theta(h)$ and $\Delta_2\theta(h)$ are given in Table 21. Below 650 km, the corrections $\Delta_1\theta(h)$ and $\Delta_2\theta(h)$ are small. The function $f(\theta)$ appears in Table 22. The annual variation in density is represented by the product $g(a)\, a(h)$, in which $g(a)$ is a function of the month of the year, and $a(h)$ is a function of the height.

TABLE 21

The Standard Functions for the Air Density and Its Variations

$\left(1 \text{ naut mi} = 1.852 \text{ km};\ 1 \text{ slug/ft}^3 = 515.2 \ \frac{\text{kg}}{\text{m}^3}\right)$

h (naut mi)	$\rho_s(h)$ (slugs/ft^3)	$\log \rho_s(h)$	$\theta_s(h)$	$a_{220}(h)$	$i_{220}(h)$	$\Delta_1\theta(h)$	$\Delta_2\theta(h)$
80	7.220×10^{-12}	-11.122	-0.009	0.031	0.041	0.000	0.000
85	3.845	0.443	-0.014	0.036	0.064	0	0
90	2.098	0.694	-0.018	0.041	0.091	0	0
95	1.347	0.879	-0.023	0.047	0.121	0	0
100	9.787×10^{-13}	-12.0133	-0.017	0.053	0.156	0	0
110	7.206	0.1438	+0.032	0.066	0.246	0	0
120	5.135	0.2913	0.070	0.079	0.325	0	0
130	3.296	0.4832	0.049	0.093	0.356	0	0
140	2.060	0.6868	0.054	0.108	0.373	0	0
150	1.423	0.8477	0.094	0.122	0.387	0	0
160	1.060	0.9756	0.133	0.137	0.398	0	0
170	8.046×10^{-14}	-13.0957	0.170	0.152	0.409	0	0
180	6.087	0.2167	0.207	0.168	0.420	0	0
190	4.612	0.3369	0.242	0.185	0.431	0.001	0
200	3.507	0.4553	0.276	0.203	0.442	0.001	0
210	2.712	0.5671	0.314	0.221	0.454	0.002	0
220	2.151	0.6705	0.344	0.240	0.465	0.002	0
230	1.714	0.7684	0.375	0.259	0.476	0.003	0
240	1.385	0.8604	0.425	0.278	0.487	0.004	0
250	1.130	0.9479	0.462	0.295	0.498	0.005	0
260	9.326×10^{-15}	-14.0316	0.499	0.312	0.509	0.007	0
270	7.901	0.1107	0.536	0.327	0.520	0.009	0
280	6.474	0.1898	0.573	0.342	0.531	0.010	0
290	5.443	0.2650	0.605	0.356	0.542	0.012	0
300	4.608	0.3376	0.642	0.370	0.554	0.014	0
310	3.921	0.4080	0.679	0.384	0.565	0.016	0
320	3.352	0.4762	0.716	0.397	0.576	0.020	0
330	2.873	0.5430	0.753	0.410	0.587	0.023	0
340	2.473	0.6082	0.790	0.422	0.598	0.028	0
350	2.196	0.6717	0.827	0.433	0.609	0.033	0
360	1.938	0.7340	0.863	0.444	0.620	0.038	0
370	1.606	0.7953	0.895	0.455	0.631	0.044	0
380	1.397	0.8557	0.927	0.467	0.643	0.049	0
390	1.217	0.9153	0.960	0.478	0.654	0.055	0
400	1.063	0.9739	0.992	0.991	0.665	0.061	0
410	9.300×10^{-16}	-15.0316	1.025	0.498	0.676	0.068	0
420	8.161	0.0886	1.053	0.508	0.687	0.074	0
430	7.174	0.1448	1.080	0.518	0.698	0.081	0
440	6.316	0.2003	1.108	0.528	0.709	0.087	0
450	5.564	0.2555	1.135	0.537	0.720	0.094	0
460	4.905	0.3103	1.162	0.546	0.732	0.101	0
470	4.333	0.3642	1.188	0.556	0.743	0.108	0
480	3.834	0.4174	1.213	0.565	0.754	0.116	0

TABLE 21 (continued)

$\left(1 \text{ naut mi} = 1.852 \text{ km};\ 1 \text{ slug/ft}^3 = 515.2 \ \frac{\text{kg}}{\text{m}^3}\right)$

h (naut mi)	$\rho_s(h)$ (slugs/ft^3)	log $\rho_s(h)$	$\theta_s(h)$	$a_{220}(h)$	$i_{220}(h)$	$\Delta_1\theta(h)$	$\Delta_2\theta(h)$
490	3.395	0.4701	1.239	0.574	0.765	0.123	0
500	3.009	0.5223	1.264	0.583	0.776	0.131	0
520	2.371	0.6256	1.310	0.602	0.798	0.145	-0.002
540	1.875	0.7274	1.353	0.620	0.819	0.160	-0.007
560	1.500	0.8278	1.396	0.637	0.836	0.175	-0.016
580	1.195	0.9276	1.435	0.654	0.852	0.190	-0.024
600	9.477×10^{-17}	-16.0268	1.471	0.671	0.868	0.206	-0.032
620	7.499	0.1254	1.504	0.689	0.885	0.223	-0.038
640	6.049	0.2225	1.536	0.706	0.901	0.239	-0.038
660	4.854	0.3186	1.565	0.726	0.917	0.255	-0.033
680	3.882	0.4137	1.590	0.745	0.932	0.271	-0.024
700	3.116	0.5075	1.611	0.754	0.947	0.287	-0.011
720	2.538	0.5995	1.630	0.768	0.961	0.302	+0.006
740	2.059	0.6905	1.647	0.781	0.975	0.316	0.029
760	1.666	0.7805	1.663	0.793	0.988	0.328	0.053
780	1.356	0.8691	1.676	0.804	1.000	0.339	0.077
800	1.115	0.9566	1.692	0.815	1.012	0.346	0.096
825	8.692×10^{-18}	-17.0649	1.708	0.829	1.028	0.354	0.114
350	6.786	0.1721	1.720	0.843	1.043	0.360	0.126

TABLE 22

The Phase-Functions, $f(\theta)$ and $g(a)$

$f(\theta)$		$g(a)$	
$0^h.0$	0.870	12.0 Mon.	0.120
1.0	0.945	1.0	0.320
2.0	0.980	2.0	0.265
3.0	0.995	3.0	0.180
4.0	1.000	4.0	0.170
5.0	0.975	5.0	0.300
6.0	0.850	6.0	0.640
7.0	0.655	7.0	0.980
8.0	0.490	8.0	0.900
9.0	0.295	9.0	0.475
10.0	0.130	10.0	0.485
11.0	0.055	11.0	0.025
12.0	0.030		
13.0	0.010	1.0 ... means the beginning of the first month, etc.	
14.0	0.000		
15.0	0.010		
16.0	0.045		
17.0	0.120		
18.0	0.210		
19.0	0.300		
20.0	0.400		
21.0	0.505		
22.0	0.615		
23.0	0.740		

The relative amplitude of the annual variation decreases toward a sunspot minimum. The product $[g(a)\ a(h)]$ is represented by the equation

$$g(a)\ a(h) = a_{220}(h)\{\ g(a) + (220 - F)\ [0.0043 - g(a)\ 0.0028]\} + \ldots$$

The quantity $g(a)$ appears in Table 22, while $a_{220}(h)$ is given in Table 21.

Five special examples have been calculated in Tables 23 through 27 in order to demonstrate the effect of the different influences. The scale height H, mean molecular weight $\overline{M}$, and temperature T, are given, in addition to the density ρ.

TABLE 23

Standard Model

$$\log \rho\,(h) = \log \rho_s\,(h)$$

This example contains the greatest values of density and temperature which will occur in an average sunspot cycle.

h (naut mi) (1 naut mi = 1.852 km)	$\rho(h)$ (slugs/ft^3) $\left(1 \frac{\text{slug}}{\text{ft}^3} = 515.2 \frac{\text{kg}}{\text{m}^3}\right)$	H (h) (naut mi) (1 naut mi = 1.852 km)	M(h)	T (h) (°K)
80	7.220×10^{-12}	10.1	28.0	589
85	3.845	15.6	27.8	899
90	2.098	21.0	27.7	1192
95	1.347	25.7	27.5	1455
100	9.787×10^{-13}	28.5	27.3	1603
110	7.206	27.9	26.9	1541
120	5.135	27.3	26.4	1469
130	3.296	29.3	25.9	1544
140	2.060	34.2	25.3	1734
150	1.423	36.7	24.8	1821
160	1.060	39.4	24.1	1888
180	6.087×10^{-14}	43.7	23.0	1987
200	3.507	49.2	21.7	2067
220	2.151	54.2	20.4	2118
240	1.385	57.8	19.2	2111
260	9.326×10^{-15}	61.4	18.2	2110
280	6.474	65.1	17.5	2118
300	4.608	68.9	16.8	2130
350	2.196	73.4	16.1	2125
400	1.063	76.1	15.8	2116
450	5.564×10^{-16}	78.6	15.7	2107
500	3.009	81.3	15.6	2105
550	1.650	84.3	15.5	2118
600	9.477×10^{-17}	88.0	15.3	2112
650	5.450	93.1	14.9	2130
700	3.116	99.6	14.2	2130
750	1.863	108.5	13.4	2112
800	1.115	119.3	12.5	2118
850	6.786×10^{-18}	133.6	11.5	2128

TABLE 24

Solar Flux Effect

$$\log \rho(h) = \log \rho_s(h) - i_{220}(h)$$

This example represents the mean amplitude at a sunspot minimum, while the diurnal bulge and annual variation have their maximum values.

h (naut mi) (1 naut mi = 1.852 km)	$\rho(h)$ (slugs/ft^3) $\left(1 \frac{\text{slug}}{\text{ft}^3} = 515.2 \frac{\text{kg}}{\text{m}^3}\right)$	H (h) (naut mi) (1 naut mi = 1.852 km)	$\overline{M}(h)$	T(h) (°K)
80	6.525×10^{-12}	9.7	28.0	569
85	3.353	14.1	27.8	784
90	1.720	18.9	27.7	1066
95	1.028	23.3	27.5	1344
100	6.878×10^{-13}	24.5	27.3	1468
110	4.179	25.0	26.9	1383
120	2.449	23.8	26.4	1280
130	1.459	25.8	25.9	1357
140	8.752×10^{-14}	29.0	25.4	1496
150	5.905	31.5	24.8	1554
160	4.276	33.4	24.0	1593
180	2.498	36.4	22.8	1634
200	1.372	40.2	21.5	1667
220	7.542×10^{-15}	44.4	20.1	1693
240	4.620	47.6	18.9	1708
260	3.019	50.4	17.9	1704
280	1.972	53.2	17.1	1700
300	1.297	55.9	16.4	1701
350	5.685×10^{-16}	59.6	16.0	1710
400	2.513	61.9	15.8	1710
450	1.135	64.0	15.6	1707
500	5.847×10^{-17}	66.8	15.3	1700
550	4.185	70.6	14.9	1702
600	1.303	75.8	14.4	1709
650	6.764×10^{-18}	82.5	13.4	1700
700	3.544	92.0	12.2	1700
750	1.963	107.3	10.8	1691
800	1.110	131.3	9.1	1698
850	6.343×10^{-19}	169.7	7.3	1708

TABLE 25

Day-Night Effect ("Diurnal Bulge")

$$\log \rho(h) = \log \rho_s(h) - \theta_s(h)$$

From this function the day-night variation can be seen. It represents the minimum of the diurnal variation, while the other influences retain their maximum values.

h (naut mi) (1 naut mi = 1.852 km)	$\rho(h)$ (slugs/ft^3) $\left(1 \frac{\text{slug}}{\text{ft}^3} = 515.2 \frac{\text{kg}}{\text{m}^3}\right)$	H (h) (naut mi) (1 naut mi = 1.852 km)	$\overline{M}(h)$	T(h) (°K)
80	7.373×10^{-12}	9.7	28.0	562
85	3.962	14.4	27.8	838
90	2.186	18.4	27.7	1054
95	1.419	21.2	27.5	1199
100	1.021	23.1	27.3	1298
110	6.788×10^{-13}	23.4	26.9	1280
120	4.399	22.9	26.4	1241
130	2.945	24.0	25.9	1250
140	1.822	25.1	25.4	1260
150	1.163	26.3	24.7	1278
160	7.908×10^{-14}	27.6	23.9	1288
180	4.485	29.6	22.7	1303
200	2.279	31.9	21.3	1314
220	9.931×10^{-15}	34.5	19.9	1318
240	5.413	36.7	18.7	1311
260	3.174	38.9	17.5	1316
280	1.835	41.1	16.8	1316
300	1.070	43.1	16.4	1312
350	3.854×10^{-16}	45.5	15.9	1330
400	1.254	47.8	15.6	1322
450	4.524×10^{-17}	50.0	15.3	1310
500	1.773	52.9	14.9	1310
550	7.429×10^{-18}	58.1	14.0	1312
600	3.274	68.3	12.3	1321
650	1.523	83.5	10.5	1332
700	7.681×10^{-19}	101.9	9.0	1369
750	4.166	131.7	7.2	1370
800	2.318	179.5	5.3	1353
850	1.333	277.8	3.6	1327

TABLE 26

Annual Effect

$$\log \rho(h) = \log \rho_s(h) - a(h)$$

This example gives the density at the annual minimum, while the remaining influences are at their maximum

h (naut mi) (1 naut mi = 1.852 km)	$\rho(h)$ (slugs/ft^3) $\left(1 \frac{\text{slug}}{\text{ft}^3} = 515.2 \frac{\text{kg}}{\text{m}^3}\right)$	H (h) (naut mi) (1 naut mi = 1.852 km)	$\overline{M}(h)$	T(h) (°K)
80	6.702×10^{-12}	7.9	28.0	469
85	3.548	11.6	27.8	668
90	1.912	15.0	27.7	850
100	1.211	18.1	27.5	1002
100	8.678×10^{-13}	20.4	27.3	1119
110	6.224	22.0	26.9	1208
120	4.328	22.7	26.4	1212
130	2.671	25.0	25.9	1312
140	1.614	29.4	25.4	1553
150	1.085	31.8	24.8	1623
160	7.797×10^{-14}	34.8	24.0	1663
180	4.482	37.9	22.8	1697
200	2.397	41.3	21.5	1727
220	1.270	45.3	20.1	1752
240	7.523×10^{-15}	48.9	18.9	1759
260	4.791	51.9	17.9	1754
280	3.059	55.0	17.1	1754
300	1.988	58.0	16.4	1759
350	8.818×10^{-16}	60.7	16.0	1755
400	3.777	62.6	15.8	1760
450	1.725	65.3	15.6	1757
500	8.257×10^{-17}	68.4	15.4	1750
550	4.064	72.0	15.0	1748
600	2.049	76.3	14.5	1741
650	1.045	82.4	13.8	1750
700	5.524×10^{-18}	91.4	12.6	1740
750	3.073	106.3	11.2	1740
800	1.747	128.4	9.5	1748
850	1.004	162.8	7.6	1750

TABLE 27

Total Variation

$$\log \rho(h) = \log \rho_s(h) - i_{220}(h) - \theta(h) - a(h)$$

This is the lower limit which will be possible in an average sunspot cycle.

h (naut mi) (1 naut mi = 1.852 km)	$\rho(h)$ (slugs/ft^3) $\left(1 \frac{\text{slug}}{\text{ft}^3} = 515.2 \frac{\text{kg}}{\text{m}^3}\right)$	H(h) (naut mi) (1 naut mi = 1.852 km)	$\bar{M}(h)$	T(h) (°K)	$\frac{\rho_s(h)}{\rho(h)}$
80	6.213×10^{-12}	7.5	28.0	429	1.155
85	3.146	10.3	27.8	605	1.219
90	1.616	12.9	27.7	739	1.30
95	9.738×10^{-13}	14.8	27.5	841	1.40
100	6.365	16.5	27.3	928	1.56
110	3.396	18.5	26.9	1026	2.20
120	1.748	18.8	26.4	1017	2.96
130	1.050	20.5	25.9	1071	3.15
140	6.026×10^{-14}	21.6	25.4	1099	3.43
150	3.618	22.0	24.7	1091	4.01
160	2.318	23.3	23.8	1098	4.66
180	1.141	24.5	22.4	1087	6.32
200	4.851×10^{-15}	26.6	20.9	1088	8.53
220	2.000	29.4	19.3	1098	11.42
240	9.621×10^{-16}	31.5	17.8	1091	15.38
260	5.048	33.0	17.1	1084	20.86
280	2.575	34.0	16.6	1080	27.60
300	1.329	34.7	16.2	1080	35.86
350	4.036×10^{-17}	37.3	16.0	1085	54.4
400	1.066	39.1	15.8	1094	99.9
450	3.213×10^{-18}	41.7	15.3	1107	173
500	1.035	46.3	14.4	1117	291
550	3.768×10^{-19}	54.5	12.7	1108	489
600	1.417	72.8	9.8	1102	668
650	7.403×10^{-20}	111.0	6.6	1118	736
700	2.908	160.4	4.5	1071	1071
750	1.698	254.1	3.96	1079	1096
800	9.625×10^{-21}	429.4	1.85	1080	1162
850	5.405	659.1	1.24	1115	1252

4. Radiation

a. Solar flare radiations

One of the most extensive manifestations of solar activity is the chromospheric flare. Flares are ranked according to their area on the solar disk and their brightness (in the red line of Hα, 6563 Å) as indicated in Table 28 (from Ref. 27). The frequency of flares of different importance (or class) is shown in Table 29.

TABLE 28

Flare Characteristics

Class	Duration (min) Average	Duration (min) Range	Area Limits 10^{-6} Visible Disk	Hα Line Width at Maximum (Å)
1-	--	--	100	1.5
1	20	4 to 43	100 to 250	3.0
2	30	10 to 90	250 to 600	4.5
3	60	20 to 155	600 to 1200	8
3+	180	50 to 430	1200	18

TABLE 29

Flare Frequency

Class	Relative Frequency	Absolute Frequency (R)
1	0.72	0.044
2	0.25	0.015
3	0.03	0.002

The number of flares per year varies with the cycle of sunspots and is defined by the Wolfe sunspot number R, which is

$$R = k(10g + f)$$

where f is the number of individual spots, g is the number of spot groups and k is an instrument and observer's correction factor. The mean sunspot period is 11.07 yr with mean maximum and minimum Wolfe numbers of 103 and 5.2, respectively (Ref. 28). The average time from sunspot maximum to minimum is 6.5 yr and the time from minimum to maximum is 4.5 yr. The last sunspot maximum occurred in 1958 with a record number of 185. Thus, the next maximum will occur probably in 1969. However, since there is a periodicity to sunspot cycle maximum which is not very well defined, it may be that the next maximum will be the end of the present period (with the 1969 peak exceeding the 1958 peak) or the beginning of the next period (with a sunspot number possibly as low as 50 during 1969). During 1958 more than 3100 flares of Class 1 or greater occurred, while the number of flares during the last sunspot minimum in 1954 was only 16; none larger than Class 1 were reported (Ref. 29). Solar flares may have electron temperatures as high as 2×10^8 °K (Ref. 30) as compared to effective temperatures in the umbra and perumbra of sunspots of 4300°K and 5500°K, respectively. Prior to the IGY, high energy particles from solar flares had been detected by ground-based measurements. Four such events were noted in the 15 yr preceding 1953. Three more of these events have occurred since that time, namely 23 February 1956, 4 May and 11 November 1960. During the IGY and IGC-59 (July 1957 to December 1959) 25 additional solar flare particle events were detected. These particles were detected by balloons and satellites but were not energetic enough to produce secondaries detectable at ground level. During this period 707 Class 2 or larger solar flares occurred (of which 71 were Class 3 or 3+). Therefore, although solar flares of Class 2 or greater have occurred on the average of once a day during solar maximum, only 25 times in 2.5 yr did these flares result in the arrival of flare particles in the vicinity of the earth. It should be noted here that during the last sunspot minimum (1954) no flares of Class 2 or larger occurred.

The flare particles are mostly protons (alphas and some heavier nuclei have also been detected) with kinetic energies extending from a few million electron volts (Mev) to a few tens of billion electron volts. These energies are considerably below the energies of cosmic ray particles although the particle flux is greater than the galactic cosmic ray flux. The first high energy solar particles were detected at ground-based cosmic ray (secondary) monitors and one of the first names given them was solar cosmic rays. Other names are "solar proton event," "solar flare radiation event," and "solar bursts." But solar high energy particles (SHEP) has been offered by a group of researchers in this field as a standard nomenclature. More confusing is the terminology "Giant" and "Large," sometimes used to describe the type of proton flux. Proton fluxes from the "Giant" flares of 23 February 1956, 4 May 1960 and 11 May 1960 were not as large as from the "Large" flares of 10 May, 10, 14 and 16 July 1959. Furthermore, the radiation doses from the "Giant" events were not as great as from the "Large" events. The only explanation for this ranking is that protons from the "Giant" events produced secondaries in the atmosphere that were energetic enough to penetrate and be detected at the ground. A better way to describe these events is by their differential or integral kinetic energy fluxes. Shown below are the differential spectra for two solar events, 23 February 1956 as derived from Foelsche's plot (Ref. 31) and 10 May 1959 as derived from Winckler's observations (Ref. 32).

Flare Model No. 1

$$dN_1 = 2.563 \times 10^{-1}\ KE^{-1.2985}\ dE;\quad 0.60 < E < 130\ \text{Mev}$$
$$dN_2 = 7.859 \times 10^{-1}\ KE^{-1.4460}\ dE;\quad 130 < E < 550$$
$$dN_3 = 2.957 \times 10^{3}\ KE^{-2.5520}\ dE;\quad 550 < E < 1600$$
$$dN_4 = 6.961 \times 10^{11}\ KE^{-5.040}\ dE;\quad 1600 < E < 5000$$
$$dN_5 = 2.802 \times 10^{22}\ KE^{-7.850}\ dE;\quad 5000 < E < 10,000$$
$$K = \sum_i \int dN_i = 5.0 \times 10^4\ \text{protons/cm}^2\text{-sec-ster}$$

Flare Model No. 2

$$dN = 9.39 \times 10^{9}\ E^{-4.8}\ dE;\quad 20 < E < 10,000\ \text{Mev}$$

A reasonably simple yet unambigious ranking of the severity of these events can be seen directly from these equations to be the coefficient indicating the total flux of particles and the exponent indicating how these are distributed with energy. Figure 14 shows the radiation dose inside different thicknesses of absorber for these events and clearly shows that the relative hazard from these events varies with the amount of shielding provided.

Figure 14 also shows that the radiation doses to an unshielded astronaut exceed the lethal doses but are shielded rather efficiently by even small amounts of absorbers. The shielding afforded by the materials and equipment of two spacecraft is shown on Table 30.

TABLE 30

Solar Flare Event Radiation Dose Inside Mercury Capsule and Apollo Command Module (Including Secondaries)

Vehicle	10 May 1959	23 February 1956
Mercury Capsule	3.8×10^3 rem	48.33 rem
Apollo Command Module	60.5 rem	42.5 rem
Ambient	$\sim 5 \times 10^6$ rem (1.8×10^4 assuming no protons below 20 Mev)	5.4×10^2 rem

The greater shielding inherent in the Apollo vehicle is apparent. However, it should be noted that the orbit of Mercury is such that the Earth's magnetic field would shield a large fraction of these solar particles. In Ref. 32 Obayashi and Hakura have developed a model of proton cutoff energies versus geomagnetic latitude during a solar plasma induced geomagnetic disturbance. At these times, the normal cutoff energies are reduced and the solar flare particles are "allowed" at normally "forbidden" regions near the earth. Using this model of cutoff energies to modify the incident solar flare proton spectra results in decreasing values of dose from polar to equatorial latitudes. Satellites which spend little or no time at magnetic latitudes less than 50° will not encounter solar flare protons. Correspondingly, polar orbital satellites will receive the highest dose. Figures 15 and 16 show dose versus orbital inclination for the two solar flare events at different values of shielding. The dose versus latitude cutoff for the May flare is seen to be much sharper than for the February flare. This is, of course, due to its relatively larger number of low energy particles which are excluded before the higher energy particles.

Also shown in these figures are the free space proton doses given in Fig. 14 from Ref. 33. It is seen that even at a 90° orbit the satellite dose under 1 gm/cm^2 is reduced to about 40% of the free space dose. Actually, the doses within orbital vehicles will be even lower due to shadow shielding by the earth. This is a function of altitude as shown in Fig. 17.

One further qualification in the use of Figs. 15 and 16 is necessary because they are plotted in terms of magnetic inclination. Figure 18 shows the magnetic dip equator and a great circle approximation. This latter curve may be used together with Fig. 17 to estimate the orbital dose.

The following example is given for illustration. We will assume an orbital inclination of 60°, 500-km circular orbit extending to 60°N over 280° longitude. The assumed duration of the February flare event is about 1 hr as compared to about 1 day for the May event. In 1 hr the magnetic inclination of the orbit has changed little, so that the February flare dose may be read from Fig. 16 at 60° + 13° (or 73°). This is about 35 rad under 1 gm/cm^2. However, during the day's duration of the May event, the magnetic inclination has gone to 47° and back again to 73°. Averaging the dose at these two latitudes gives 1200 rad under 1 gm/cm^2. At 500 km the earth intercepts 0.314 of the incident protons giving 35 (1-0.314) or about 24 rad from the February flare and 823 rad for the May flare as the final answers. In calculating dosages from the May 1959 event, the flux of protons was assumed constant for 30 hr. This gives a total flux of 3×10^9/cm^2-ster above 20 Mev. In calculating dosages from the February event, the flux was assumed to decay immediately from the given value as t^{-2}. This gives a total flux of 1.8×10^8/cm^2-ster above 0.60 Mev or 6.33×10^7/cm^2-ster above 20 Mev. During maximum periods of solar activity, it is believed that the total yearly flux of protons with energies greater than 20 Mev is 10^9-10^{10}/cm^2-ster. Therefore, the maximum yearly dose would be equivalent to approximately

$$\frac{10^{10}}{3 \times 10^9} \approx 3.3 \text{ times the May 1959 dose or}$$

$$\frac{10^{10}}{6.33 \times 10^7} \approx 158 \text{ times the February flare dose.}$$

However, it is fairly certain that an event such as that of February 1956 occurs no more frequently than once every 4 to 5 years, so that the maximum total yearly dose (during the peak years of the sunspot cycle) should be about 3.3 times the May 10, 1959 doses. This may be used to estimate the hazard relative to mission duration.

b. Van Allen belts (geomagnetically trapped particles)

In the vicinity of the earth, there are intense regions of charged particles trapped in the earth's magnetic field. In the four years since Dr. Van Allen confirmed the existence of these regions from measurements made on the early Explorer satellites, a considerable body of data has been gathered to "map" these regions.

The trapped particles form a generally toroidal region beginning at approximately 500-km altitude. The earth's field is not geocentric and has a number of signficant anomalies from a dipole resulting in the radiation belt shape like that shown in Fig. 19 (for part of the "inner" belt). Yoshida, Ludwig and Van Allen (Ref. 34) have shown that the location of the trapped particles is related to the dip latitude and scalar intensity of the real magnetic field. In effect, the belt varies over about 800 km in altitude and about 13° in latitude around the earth.

The belt position shown in Fig. 19 was determined from the relationships found in the last reference and with the use of a spherical harmonic fit to the magnetic field obtained from D. Jensen of the Air Force Special Weapons Center. The adiabatic invariant integral has also been noted by a number of workers in this field as having a better physical basis for determining the structure of the belts.

Most recently McIlwain (Ref. 35) has shown that the magnetic intensity scalar B and the parameter L define a practical and accurate coordinate system for the trapped particles. The parameter L is related to the adiabatic invariant integral and would be the equatorial radius of a magnetic shell in a dipole field. In the real field the physical interpretation of L is more complex.

The energy spectrum and particle flux for inner belt protons were calculated using the experimental data of Freden and White (Ref. 36), Van Allen (Ref. 37), and Van Allen, McIlwain and Ludwig (Ref. 38). Figure 20 shows the proton flux contours at one location over the earth, and Fig. 21 the differential kinetic energy spectrum of protons. The peak flux shown agrees with Van Allen's recent estimates.

The model of electrons, by far the most abundant constituents of the trapped radiation belts, was determined using flux and spectral measurements of Holley (Ref. 39), and Walt, Chase, Cladis, Imhof and Knecht (Ref. 40), together with the Anton 302 geiger counter data from a number of satellites and space probes (Refs. 41 and 42). Figure 22 shows the electron flux contours at one location over the earth and Fig. 23 shows the differential kinetic energy spectrum.

This spectrum agrees well in shape with the recent determination by Pizzella, Laughlin and O'Brien (Ref. 43) for the inner radiation belt at an altitude of 1000 km. The highest flux at this altitude is 5×10^6 electrons/cm^2-sec-steradian as given by Frank, Dennison and Van Allen (Ref. 44). This agrees well with the flux at this altitude shown in Figs. 22 and 23.

For the outer radiation belt, Van Allen has given the following peak electron distribution

10^8 cm^{-2} sec^{-1} above 40 Kev

10^5 cm^{-2} sec^{-1} above 2 Mev

10^2 cm^{-2} sec^{-1} above 5 Mev

This is two orders of magnitude less in flux than Van Allen's earlier estimates of the outer zone electrons. Extending the new spectrum to 20 Kev gives 2×10^9 electrons/cm^2-sec or 1.6×10^8 electron/cm^2-sec-steradian, which agrees closely with the peak outer belt flux shown in Fig. 22. Figures 24 and 25 show the electron and bremsstrahlung dose rates versus aluminum absorber from electrons at the peak of the inner and outer regions (Ref. 45). These may be compared with the Van Allen belt proton doses also shown in Fig. 14 as a function of absorber thickness for protons at the center of the inner belt. Proton doses for orbiting satellites may be obtained from Tables 31 and 32 as a function of orbital altitude, inclination and aluminum absorber thickness. Due to the belt asymmetry, the dose on each successive orbit differs. For example, at an orbital inclination of 40° (geographic) and an altitude of 740 km under 6 gm/cm^2 of aluminum, the accumulated dose is 0.0214 rem after the first orbit and 0.0249 rem after two orbits. For integer orbits, the dose accumulation cycle should repeat itself every 24 hr. The doses in Tables 31 and 32 are 12-hr totals, so that the orbital lifetime dose may be closely approximated by 2 (number of days in orbit) (12-hr cumulative dose). Table 33 from Ref. 45 gives dose versus orbital inclination, altitude and absorber thickness for a satellite exposed to the electrons of the inner Van Allen belt.

c. Primary cosmic radiation

Steady-state cosmic radiation values (Ref. 46) that have been generally accepted for a number of years (Ref. 47) were based on the belief that the primary spectrum contained few particles in the energy region below a fraction of a Bev. This meant the ionization at geomagnetic latitudes greater than 60° was taken to be the same as that at 60° and this indeed appeared to be true during 1950 to 1952. However, in 1954, a time of minimum solar activity, low energy protons caused an increase in the ionization levels at latitudes above 60° (Ref. 48). It should be remembered, though, that the most favorable periods for extended space flight are these same times of low solar (but higher cosmic ray) activity, because of the great reduction in flare occurrences. For this reason, values of the ionization rate that include the effect of the increase above 60° as would be expected during a typical time of solar quiescence are plotted in Fig. 26 as functions of altitude and geomagnetic latitude, both for near-earth and high altitude positions of measurement (Ref. 49). Not shown at the scale of Fig. 26 is that as the surface of the earth is approached, there is an ionization increase, followed by a decrease. The increase begins at 130,000 ft, continues down to heights of 80,000 ft (at 90° latitude) or 50,000 ft (at 0° latitude), and has its source in the shower, or cascade formation of mesons, nucleons, electrons and high energy photons, all of which are created by interaction of high energy cosmic particles with atmospheric constituents. The decrease in ionization with decreasing altitude below 80,000 to 50,000 ft comes about through atmospheric radiation absorption, while the decrease with decreasing magnetic latitude results from the increased shielding offered by the earth's magnetic field against the lowered energy cosmic particles. Figure 26 shows that the increase in cosmic detector ionization at increasingly great distances from the earth arises from a combination of the decrease in the solid angle subtended by the earth and the decrease in geomagnetic field strength, with a corresponding decrease in the cosmic particle deflection.

An estimate of the biological whole-body radiation intensity as a function of altitude and geomagnetic latitude can be obtained from Fig. 26 only if the conversion can be made from the ionization itself, in units of roentgen, to rem, the unit which gives an idea of the biological effectiveness of the

TABLE 31

Inner Van Allen Belt Proton Radiation Dose (rems)
Orbiting Aluminum Sphere

Orbital Inclination (deg)	Orbital Altitude	Aluminum Shield Thickness (gm/cm^2) No. Orbits	Rems 1.0	2.0	6.0	10.0	20.0	60.0	100.0
0	555 km 300 n mi	1	+0.00372	+0.00272	+0.00145	+0.00104	+0.00062	+0.00024	+0.00014
		2	+0.01852	+0.01354	+0.00720	+0.00517	+0.00312	+0.00120	+0.00070
		3	+0.02203	+0.01611	+0.00857	+0.00615	+0.00371	+0.00143	+0.00083
		4	+0.02744	+0.02006	+0.01067	+0.00766	+0.00462	+0.00178	+0.00103
		5	+0.03642	+0.02664	+0.01417	+0.01017	+0.00613	+0.00237	+0.00137
		6	+0.06091	+0.04455	+0.02370	+0.01701	+0.01026	+0.00396	+0.00230
		7	+0.07287	+0.05329	+0.02835	+0.02035	+0.01228	+0.00474	+0.00275
	740 km 400 n mi	1	+0.02093	+0.01530	+0.00814	+0.00584	+0.00352	+0.00136	+0.00079
		2	+0.08120	+0.05938	+0.03159	+0.02268	+0.01368	+0.00528	+0.00307
		3	+0.09957	+0.07282	+0.03874	+0.02781	+0.01678	+0.00647	+0.00376
		4	+0.15308	+0.11195	+0.05956	+0.04276	+0.02579	+0.00996	+0.00579
		5	+0.19437	+0.14215	+0.07563	+0.05429	+0.03275	+0.01264	+0.00735
		6	+0.24586	+0.17981	+0.09566	+0.06868	+0.04143	+0.01599	+0.00930
		7	+0.27285	+0.19955	+0.10616	+0.07622	+0.04598	+0.01775	+0.01032
	1110 km 600 n mi	1	+0.63995	+0.46803	+0.24900	+0.17876	+0.10784	+0.04163	+0.02420
		2	+1.13415	+0.82947	+0.44130	+0.31682	+0.19113	+0.07379	+0.04290
		3	+1.62798	+1.19063	+0.63345	+0.45477	+0.27435	+0.10592	+0.06158
		4	+2.40827	+1.76130	+0.93707	+0.67274	+0.40584	+0.15669	+0.09110
		5	+3.02077	+2.20925	+1.17540	+0.84385	+0.50906	+0.19655	+0.11427
		6	+4.13293	+3.02264	+1.60814	+1.15453	+0.69649	+0.26891	+0.15634
	1852 km 1000 n mi	1	+8.14456	+5.95656	+3.16909	+2.27517	+1.37253	+0.52993	+0.30810
		2	+16.08871	+11.76655	+6.26020	+4.49436	+2.71130	+1.04682	+0.60862
		3	+24.51561	+17.92961	+9.53915	+6.84841	+4.13142	+1.59513	+0.92741
		4	+33.35166	+24.39190	+12.97731	+9.31674	+5.62049	+2.17006	+1.26167
		5	+41.75440	+30.53728	+16.24686	+11.66404	+7.03653	+2.71679	+1.57954
20	555 km 300 n mi	1	+0.07177	+0.05249	+0.02792	+0.02005	+0.01209	+0.00467	+0.00271
		2	+0.07767	+0.05680	+0.03022	+0.02169	+0.01309	+0.00505	+0.00293
		3	+0.07838	+0.05732	+0.03050	+0.02189	+0.01321	+0.00510	+0.00296
		4	+0.07838	+0.05732	+0.03050	+0.02189	+0.01321	+0.00510	+0.00296
		5	+0.07890	+0.05770	+0.03070	+0.02204	+0.01329	+0.00513	+0.00298
		6	+0.08052	+0.05889	+0.03133	+0.02249	+0.01356	+0.00523	+0.00304
		7	+0.08355	+0.06110	+0.03251	+0.02334	+0.01408	+0.00543	+0.00316
	740 km 400 n mi	1	+0.05174	+0.03784	+0.02013	+0.01445	+0.00871	+0.00336	+0.00195
		2	+0.07776	+0.05687	+0.03025	+0.02172	+0.01310	+0.00505	+0.00294
		3	+0.08903	+0.06511	+0.03464	+0.02487	+0.01500	+0.00579	+0.00336
		4	+0.08907	+0.06514	+0.03465	+0.02488	+0.01501	+0.00579	+0.00336
		5	+0.09400	+0.06875	+0.03657	+0.02626	+0.01584	+0.00611	+0.00355
		6	+0.12011	+0.08784	+0.04673	+0.03355	+0.02024	+0.00781	+0.00454
		7	+0.14274	+0.10439	+0.05554	+0.03987	+0.02405	+0.00928	+0.00539
	1110 km 600 n mi	1	+0.60988	+0.44604	+0.23730	+0.17037	+0.10277	+0.03968	+0.02307
		2	+1.11837	+0.81792	+0.43516	+0.31241	+0.18847	+0.07276	+0.04230
		3	+1.36262	+0.99656	+0.53020	+0.38064	+0.22963	+0.08866	+0.05154
		4	+1.62606	+1.18922	+0.63270	+0.45423	+0.27402	+0.10580	+0.06151
		5	+1.86481	+1.36384	+0.72560	+0.52093	+0.31426	+0.12133	+0.07054
		6	+2.46111	+1.79994	+0.95763	+0.68750	+0.41475	+0.16013	+0.09310
	1852 km 1000 n mi	1	+7.25229	+5.30399	+2.82190	+2.02591	+1.22217	+0.47187	+0.27434
		2	+14.12855	+10.33298	+5.49749	+3.94679	+2.38097	+0.91928	+0.53447
		3	+19.89605	+14.55107	+7.74166	+5.55794	+3.35292	+1.29455	+0.75265
		4	+25.14740	+18.39168	+9.78499	+7.02490	+4.23789	+1.63624	+0.95131
		5	+30.67196	+22.43209	+11.93462	+8.56817	+5.16890	+1.99570	+1.16030
40	555 km 300 n mi	1	+0.03171	+0.02319	+0.01234	+0.00886	+0.00534	+0.00206	+0.00119
		2	+0.03866	+0.02828	+0.01504	+0.01080	+0.00651	+0.00251	+0.00146
		3	+0.03866	+0.02828	+0.01504	+0.01080	+0.00651	+0.00251	+0.00146
		4	+0.03866	+0.02828	+0.01504	+0.01080	+0.00651	+0.00251	+0.00146
		5	+0.03866	+0.02828	+0.01504	+0.01080	+0.00651	+0.00251	+0.00146
		6	+0.03866	+0.02828	+0.01504	+0.01080	+0.00651	+0.00251	+0.00146
		7	+0.03866	+0.02828	+0.01504	+0.01080	+0.00651	+0.00251	+0.00146
	740 km 400 n mi	1	+0.05504	+0.04025	+0.02141	+0.01537	+0.00927	+0.00358	+0.00208
		2	+0.06403	+0.04683	+0.02491	+0.01788	+0.01079	+0.00416	+0.00242
		3	+0.06958	+0.05088	+0.02707	+0.01943	+0.01172	+0.00452	+0.00263
		4	+0.07104	+0.05195	+0.02764	+0.01984	+0.01197	+0.00462	+0.00268
		5	+0.07155	+0.05233	+0.02784	+0.01998	+0.01205	+0.00465	+0.00270
		6	+0.07749	+0.05667	+0.03015	+0.02164	+0.01305	+0.00504	+0.00293
		7	+0.08057	+0.05892	+0.03135	+0.02250	+0.01357	+0.00524	+0.00304
	1110 km 600 n mi	1	+0.43148	+0.31556	+0.16789	+0.12053	+0.07271	+0.02807	+0.01632
		2	+0.81762	+0.59797	+0.31814	+0.22840	+0.13778	+0.05319	+0.03093
		3	+0.93977	+0.68731	+0.36567	+0.26252	+0.15837	+0.06114	+0.03555
		4	+1.02163	+0.74717	+0.39752	+0.28539	+0.17216	+0.06647	+0.03864
		5	+1.14910	+0.84040	+0.44712	+0.32100	+0.19364	+0.07476	+0.04346
		6	+1.52201	+1.11313	+0.59222	+0.42517	+0.25649	+0.09903	+0.05757
	1852 km 1000 n mi	1	+4.77857	+3.49483	+1.85936	+1.33488	+0.80529	+0.31092	+0.18077
		2	+8.78610	+6.42576	+3.41872	+2.45438	+1.48065	+0.57167	+0.33237
		3	+11.22799	+8.21165	+4.36887	+3.13652	+1.89216	+0.73056	+0.42474
		4	+13.73962	+10.04854	+5.34616	+3.83814	+2.31543	+0.89398	+0.51976
		5	+17.46029	+12.76966	+6.79389	+4.87751	+2.94244	+1.13607	+0.66051

TABLE 32

Van Allen Proton Radiation Dose (rems)
Orbiting Aluminum Sphere
Launched From Vandenburg

Altitude	No. Orbits	Orbit Inclination 60° gm/cm² 0	2.5	5	10	15	Orbit Inclination 60° gm/cm² 0	2.5	5	10	15	Orbit Inclination 90° gm/cm² 0	2.5	5	10	15
740 km	1	0.0292	0.00134	0.00103	0.000592	0.000453	0.0471	0.00219	0.001689	0.000968	0.000743	0.0980	0.00451	0.003466	0.001986	0.001525
400 n mi	2	0.0594	0.00262	0.002108	0.001208	0.000827	0.0629	0.00290	0.002230	0.001278	0.000981	0.1200	0.00555	0.004262	0.002442	0.001875
	3	0.0662	0.00306	0.002356	0.001350	0.001036	0.0643	0.00296	0.002280	0.001306	0.001003	0.1228	0.00561	0.004351	0.002493	0.001914
	4	0.0667	0.00307	0.002365	0.001355	0.001041	0.0643	0.00296	0.002280	0.001306	0.001003	0.1228	0.00561	0.004351	0.002493	0.001914
	5	0.0667	0.00307	0.002365	0.001355	0.001041	0.0645	0.00298	0.002287	0.001310	0.001006	0.1230	0.00566	0.004368	0.002503	0.001922
	6	0.0667	0.00308	0.002367	0.001356	0.001041	0.0680	0.00300	0.002408	0.001380	0.001059	0.1305	0.00601	0.004637	0.002657	0.002040
	7	0.0705	0.00326	0.002506	0.001436	0.001103	0.0681	0.00314	0.002419	0.001386	0.001064	0.1320	0.00608	0.004687	0.002686	0.002062
	8															
1480 km	1	3.025	0.1398	0.10762	0.0600	0.0473	4.320	0.1996	0.15357	0.0880	0.0676	4.950	0.2286	0.17588	0.1008	0.0774
800 n mi	2	5.545	0.2560	0.19689	0.1128	0.0865	6.850	0.3164	0.24335	0.1394	0.1071	7.349	0.3390	0.26078	0.1494	0.1147
	3	6.795	0.3138	0.24168	0.1381	0.1060	7.850	0.3628	0.27909	0.1599	0.1228	8.360	0.3864	0.29726	0.1703	0.1308
	4	7.400	0.3416	0.26274	0.1505	0.1158	8.185	0.3782	0.29091	0.1667	0.1280	9.160	0.4233	0.32565	0.1866	0.1433
	5	7.875	0.3625	0.27955	0.1600	0.1229	9.390	0.4335	0.33345	0.1911	0.1467	9.760	0.4512	0.34710	0.1989	0.1527
	6	8.915	0.4110	0.31645	0.1812	0.1393	11.210	0.5176	0.39837	0.2283	0.1753	12.110	0.5584	0.42955	0.2461	0.1890
	7															
	8															
2222 km	1	24.600	1.1324	0.87110	0.4991	0.3833	20.400	0.9422	0.72477	0.4153	0.3189	26.580	1.2258	0.94296	0.5403	0.4149
1200 n mi	2	45.550	2.1013	1.6164	0.9262	0.7112	40.100	1.8519	1.42450	0.8162	0.6268	51.300	2.3674	1.81645	1.0408	0.7992
	3	64.700	2.9865	2.2973	1.3164	1.0108	55.150	2.5444	1.95722	1.1215	0.8612	66.700	3.0759	2.36609	1.3578	1.0411
	4	88.550	4.0905	3.1465	1.8029	1.3845	71.500	3.2976	2.53684	1.4535	1.1161	83.500	3.8527	2.96365	1.6982	1.3040
	5	99.900	4.6047	3.5421	2.2096	1.5585	82.500	3.8144	2.93418	1.6813	1.2910	100.000	4.6139	3.54915	2.0337	1.5616
	6															
	7															
	8															
2960 km	1	59.300	2.7331	2.1024	1.2047	0.9251	63.550	2.9373	2.2595	1.2947	0.9942	64.150	2.9587	2.2759	1.3040	1.0014
1600 n mi	2	121.900	5.6169	4.3207	2.4758	1.9011	126.200	5.8287	4.4835	2.5691	1.9729	127.200	5.8720	4.5169	2.5862	1.9874
	3	179.200	8.2674	6.3595	3.6440	2.7982	174.800	8.0668	6.1975	3.5512	2.7269	176.000	8.1143	6.2418	3.5766	2.7464
	4	244.000	10.8105	8.3158	4.7650	3.6590	233.800	10.7673	8.2825	4.7458	3.6443	226.150	10.4359	8.0276	4.5998	3.5321
	5	286.500	13.2344	10.1803	5.8333	4.4793	265.300	12.2364	9.4126	5.3934	4.1415	275.800	12.6998	9.7691	5.5977	4.2984
	6															
	7															
	8															
3700 km	1	111.800	5.1518	3.9629	2.2707	1.7437	99.50	4.5972	3.5363	2.0263	1.5559	101.000	4.6618	3.5860	2.0547	1.5778
2000 n mi	2	214.400	9.9144	7.6265	4.3700	3.3557	176.00	8.0995	6.2304	3.5700	2.7413	212.000	9.7774	7.5211	4.3096	3.3093
	3	308.200	14.2183	10.9372	6.2670	4.8123	272.000	12.5644	9.6649	5.5380	4.2526	296.00	13.6474	10.4980	6.0153	4.6191
	4	404.400	18.5992	14.3071	8.1980	6.2951	365.00	16.8568	12.9668	7.4300	5.7054	380.00	17.5463	13.4972	7.7338	5.9388
4075 km	1	120.00	5.5367	4.2590	2.4404	1.8739	98.100	4.5348	3.4883	1.9988	1.5348	107.15	4.9528	3.8099	2.1831	1.6764
2200 n mi	2	247.60	11.3916	8.7628	5.0211	3.8556	195.80	9.0345	6.9496	3.9821	3.0578	208.15	9.6143	7.3956	4.2377	3.2540
	3	362.10	16.7222	12.8633	7.3707	5.6598	298.00	13.7327	10.5636	6.0529	4.6479	346.00	15.9763	12.2915	7.0428	5.4081
	4	493.00	22.7372	17.4902	10.0219	7.6957	370.00	17.1083	13.1663	7.5408	5.7906	451.00	20.8289	16.0222	9.1807	7.0498

TABLE 33

Twelve-Hour Orbital Dose (rad) Within Van Allen Belt

Altitude	Orbital Inclination (deg)	Aluminum Sphere Thickness (gm/cm^2)					
		0.1		1.0		2.0	
		Electrons	X-rays	Electrons	X-rays	Electrons	X-rays
555 km	0	4.598×10^{3}	0.7569	1.137×10^{-3}	0.2301		0.1575
(200 naut mi)	40	1.444×10^{3}	0.2377	3.574×10^{-4}	0.0723	$<10^{-5}$	0.0494
	90	6.811×10^{2}	0.1121	1.686×10^{-4}	0.0341		0.0233
740 km	0	1.1690×10^{4}	1.9241	2.892×10^{-3}	0.5849		0.4003
(400 naut mi)	40	5.046×10^{3}	0.8306	1.248×10^{-3}	0.2525	$<10^{-5}$	0.1728
	90	3.693×10^{3}	0.6078	9.136×10^{-4}	0.1848		0.1264
1110 km	0	6.634×10^{4}	10.9197	1.641×10^{-2}	3.3196		2.2716
(600 naut mi)	40	4.129×10^{4}	6.7964	1.021×10^{-2}	2.0661	$<10^{-4}$	1.4138
	90	2.359×10^{4}	3.8825	5.835×10^{-3}	1.1803		0.8077
1852 km	0	2.625×10^{5}	43.2147	6.495×10^{-2}	13.1373	1.803×10^{-4}	8.9898
(1000 naut mi)	40	2.088×10^{5}	34.3755	5.166×10^{-2}	10.4502	1.434×10^{-4}	7.1510
	90	1.097×10^{5}	18.0597	2.714×10^{-2}	5.4901	7.534×10^{-5}	3.7569

ionization. The factor of conversion, Relative Biological Effectiveness (RBE), yields a measure of the degree of localization, or nonuniformity, of tissue ionization. Ionization localization along the path of penetration is singularly noticeable for heavy (atomic number 6 or greater) particles. Although all atomic species through iron have regularly been observed, the biologically noteworthy heavy constituents of the primary radiation are carbon, nitrogen, oxygen, the magnesium and calcium groups, and iron. When these medium and high energy particles enter tissue, they first produce an ionization trail of great density. The high energy particles, in general, undergo nuclear disintegration during the penetration process, with a resulting large reduction in specific ionization, since afterward the ionization is caused by several particles of reduced charge travelling in different directions. These primaries which have a reduced impinging energy have a significant probability of being completely stopped through ionization only. This leads to extremely large specific ionizations near the ends of the paths, since the rates of energy loss increase as the particle energies decrease, down to very low energies. These thindown hits are capable of causing cell destruction. Their effects in nonreparable regions of the body, such as certain brain areas, have not yet been demonstrated. The RBE conversion from roentgen to rem obtained from a weighted analysis of particle type and tissue ionization characteristics between 30° and 55° latitude at the top of the atmosphere and extrapolation elsewhere, increases with increasing altitude and geomagnetic latitude, as seen in Fig. 27. This is explained by noting that at a position requiring decreased particle penetration of the magnetic field, there is a slight increase in the relative number of heavy constituents, compared with hydrogen and helium. At the same time, the heavy component energy range extends to lower values. It must be emphasized, however, that little actual biological experimentation has been performed to test the validity of the relation between ionization track density and the RBE for particles of large atomic number, which produce the greater fraction of the unshielded biological intensity.

Shielding against cosmic radiation is not ordinarily advisable, since it requires thicknesses of aluminum greater than 25 gm/cm^2 for heavy particles, and at least 200 gm/cm^2 (400 lb/ft^2 of shielded area) for hydrogen and helium, which have far higher penetrating power and constitute about 15 percent of the unshielded biological dose and 99 percent of the incident particle number. In fact, the biological dose increases for shielding thicknesses up to 15 gm/cm^2 for the carbon, nitrogen, and oxygen group, up to 10 gm/cm^2 for magnesium, up to 6 gm/cm^2 for calcium, and up to 5 gm/cm^2 for iron.

An estimate of the effectiveness of shielding against cosmic radiation is shown in Fig. 28 taken from Wallner and Kaufman (Ref. 50). A comparison with the curves shown in Fig. 14 shows the relatively slow decrease of dose with absorber thickness for cosmic rays as compared to other space radiations. The dose peak at about 10 gm/cm^2 is due to the increase of ionization

rate before significant numbers of particles are stopped in the absorbing material.

d. Penetrating electromagnetic radiation

Previous estimates of the high energy end of the solar system indicated intensities of the order of 10^{-4} erg/cm^2-sec below 8Å. Recent measurements indicated that during a solar flare (class 2+) this intensity increased to about 10^{-2} erg/cm^2-sec with 2 Å as the lower limit of the radiation detected (Ref. 51). More recently, measurements have indicated that X-ray flashes during solar flares had energies as high as 80 kev (0.15 Å (Ref. 52).

During a class 2 solar flare on 20 March 1958 an intense burst of electromagnetic energy was recorded which lasted 18 seconds (or less) (Ref. 53). This was determined to have an intensity of 2×10^{-4} erg/cm^2-sec above 20 kev and peaking in the region of 200 to 500 kev (0.06 to 0.025 Å). Measurements during a class 2+ flare on 31 August 1959 indicated a peak intensity of 4.5×10^{-6} erg/cm^2-sec ($\sim$ 20 kev) arriving at the top of the earth's atmosphere (Ref. 54). The spectrum decreases in photon count by a factor of 10 for an energy increase of about 20 kev. Although these photons are quite penetrating (the half-thickness value of aluminum for 500 kev photon is 3.0 cm) their intensity is so low as to produce an insignificant dose (of the order of 10^{-5} roentgen from the March 1958 event). Intensity enhancements in the region of 8-20 Å were also observed during the August 1959 event. In this region about 1 erg/cm^2-sec was measured. This would result in a much greater dose than the less intense higher energy photons; their penetration is very much less. The half-thickness values are less than 10^{-1} cm of aluminum.

A solar X-ray spectrum from a class 2+ flare is shown in Fig. 29 taken from Ref. 30. X-rays with energies in excess of 20 kev appear to be emitted only for short periods (a few minutes) during large flares. The X-ray dose rate to an unprotected man from a flux as shown in Fig. 29 would be about 3 rem/hr. However, since the emission lasts for much less than 1 hr we may conclude that high energy solar electromagnetic radiation will not be of concern to space flight. Saylor, et al. (Ref. 55) point out that ultraviolet light on bare skin can cause severe burns and even skin cancer. It will therefore be advisable to use windows or shutter arrangements to filter the otherwise unattenuated solar ultraviolet rays. In space there will be no warning glare of scattered light to alert the observer that his line of sight is approaching the sun. An inadvertent glance at the sun could cause temporary vision failure and ten seconds of exposure would cause permanent retinal burn. These authors conclude that protection of the eyes against sunlight is a necessity.

e. Radiation damage thresholds

Of all the components of a space vehicle, man has the lowest threshold to damage by ionizing radiation as shown in Table 34.

TABLE 34

Radiation Damage Dose Limitations

	Roentgen Equivalent	
People	10^2 (sickness)	10^3 (lethal)
Semiconductor	10^6 (damage)	10^7 (failure)
Electronics	10^8	10^{10}
Elastomers	10^7	10^8
Plastics	10^8	10^9
Metals	10^{15}	
Ceramics	10^{17}	

Ref. Nucleonics Sept 1956

More detailed treatment of radiation damage mechanism are shown in Refs. 56 and 57 and in the very comprehensive Radiation Effects Information Center Series of Battelle Memorial Institute.

Semiconductors are seen to be the second easiest damaged component. This is caused by the fact that their properties arise from their form of very nearly perfect single crystals. Most metals and ceramics used for structural, electrical or magnetic applications are already in a disordered polycrystalline form and their properties are only moderately changed by further disorder (ionization).

It should be noted that certain types of sensing elements may give erroneous readings due to spurious signals from the Van Allen or other radiation environments. While this does not represent damage by radiation, it is nevertheless undesirable and can be easily avoided by proper selection, design and calibration of these devices.

As contrasted to actually "reading" unwanted signals from ionizing radiations in sensitive "front end" components it is known that electronic components and circuits may operate improperly while in the presence of large fluxes of ionizing radiation. Measurements made under conditions simulating a nuclear explosion in space have indicated that the threshold of susceptibility to these effects is at peak dose rates of 10^6 to 10^7 roentgen per second. This again is greatly in excess of what will be encountered from the natural radiation environments.

The radiation problem therefore reduces to protection of the crew.

Maximum allowable radiation doses for manned space flight have been revised upward from 25 rem considerably in the past year. Presently the Apollo maximum allowable emergency dosages are as shown in Column 4 of Table 35 from Ref. 58. The normal mission dosages are as shown in Column 3. These values are more meaningful than the single so-called "whole body" value used previously.

TABLE 35

Radiation Dosage

	5 Year Dose (rem)	RBE	Average Year Dose (rad)	Maximum Single Acute Exposure (rad)	Design Dose (rad)
Skin body dose 0.07 mm depth	1630	1.3	235	500	125
Skin body dose extremities, hands, etc.	3910	1.4	559	700	175
Blood forming organism	271	1.0	54	200	50
Eyes	271	2.0	27	100	25

4. Meteoroids

Empirical data on meteoroids has come either from optical and radar meteor observations or from impact detectors on board rockets and satellites. In the first type of observation, velocity and luminous intensity history are directly measurable. The mass and density of the meteoroid is then determined using the drag equation, the shape of the light curve and the vaporization equation. Due to the variety of assumptions and dependencies in this analysis, there is a large uncertainty in flux estimates from the same type of data. The relation between meteoroid mass and visual magnitude is shown in Fig. 30 from an early survey (Ref. 59). The relation between mass and flux is shown in Fig. 31 from a later survey article (Ref. 60). The flux uncertainty is dealt with in a number of other survey articles (Refs. 61, 62 and 63), and an examination of the assumptions employed in the analysis procedure will show why it is as large as 10^3. The best known model of the meteoroid environment was developed by Whipple in 1957 and summarized in Table 36. The following equation fits the distribution presented by Whipple in 1957.

$$\phi = 1.3 \times 10^{-12}\ m^{-1}$$

where ϕ is the flux/m^2-sec of particles with mass m grams and greater. This was revised by Whipple (Ref. 64) in 1960 to

$\phi = 10^{-12.6}\ m^{-1.186}$ to include empirical data from rockets and satellites. A recent evaluation of rocket and satellite data (Ref. 65) (obtained from acoustic detectors) obtained

$\phi = 10^{-17.0}\ m^{-1.70}$ applicable between masses of 10^{-10} to 10^{-6} gm. These distributions are shown in Fig. 32 taken from the last cited reference. It should be noted that meteoroid masses of greatest interest to space vehicle designers lie between the mass regions measured by the meteor or satellite-borne microphone techniques. Observations of meteors simulated by shaped charge firings from an Aerobee Rocket (Ref. 66) have indicated that Whipple may have underestimated meteor luminous efficiencies. This may be accounted for by a downward revision by an order of magnitude in mass (Ref. 67) of the 1957 flux estimate of Whipple so that

$$\phi = 1.3 \times 10^{-13}\ m^{-1}.$$

Various investigators have put forth penetration models--some based on empirical equations derived from test data and some based on theoretical considerations and most all giving the penetration in a thick target. Since structural skins are usually made of aluminum alloy materials, a good basis of comparison is the penetration of meteorites into aluminum. Four penetration equations were investigated to obtain a comparison of the meteorite penetrations given by the different equations. These equations were:

a. Whipple's equation

This equation is given in (Ref. 63) as

$$P = K_1 \left(\frac{1}{\pi\rho\epsilon}\right)^{1/3} E^{1/3}$$

where

P = penetration in a thick target

K_1 = constant of proportionality

E = meteorite energy

ρ = target density

ϵ = heat to fusion of target material

For a meteorite of diameter (d) moving at a velocity (V) cm/sec and with a meteoroid density $\rho_M = 0.05$ gm/cm^3 and $\epsilon = 248$ cal/gm Whipple's equation is

TABLE 36

Data Concerning Meteoroids and Their Penetrating Probabilities

F. L. Whipple, Ref. 5

Meteor Visual Magnitude	Mass (g)	Radius (u)	Assumed Vel (km/sec)	KE (ergs)	Pen. in Al † (cm)	No. Striking Earth (per day)**	No. Striking 3m (Radius) Sphere (per day)***
0	25.0	49,200	28	1.0×10^{14}	21.3	--	--
1	9.95	36,200	28	3.98×10^{13}	15.7	--	--
2	3.96	26,600	28	1.58×10^{13}	11.5	--	--
3	1.58	19,600	28	6.31×10^{12}	8.48	--	--
4	0.628	14,400	28	2.51×10^{12}	6.24	--	--
5	0.250	10,600	28	1.00×10^{12}	4.59	2×10^{8}	2.22×10^{-5}
6	9.95×10^{-2}	7,800	28	3.98×10^{11}	3.38	5.84×10^{8}	6.48×10^{-5}
7	3.96×10^{-2}	5,740	28	1.58×10^{11}	2.48	1.47×10^{9}	1.63×10^{-4}
8	1.58×10^{-2}	4,220	27	5.87×10^{10}	1.79	3.69×10^{9}	4.09×10^{-4}
9	6.28×10^{-3}	3,110	26	2.17×10^{10}	1.28	9.26×10^{9}	1.03×10^{-3}
10	2.50×10^{-3}	2,290	25	7.97×10^{9}	0.917	2.33×10^{10}	2.58×10^{-3}
11	9.95×10^{-4}	1,680	24	2.93×10^{9}	0.656	5.84×10^{10}	6.48×10^{-3}
12	3.96×10^{-4}	1,240	23	1.07×10^{9}	0.469	1.47×10^{11}	1.63×10^{-2}
13	1.58×10^{-4}	910	22	3.89×10^{8}	0.335	3.69×10^{11}	4.09×10^{-2}
14	6.28×10^{-5}	669	21	1.41×10^{8}	0.238	9.26×10^{11}	1.03×10^{-1}
15	2.50×10^{-5}	492	20	5.10×10^{7}	0.170	2.33×10^{12}	2.58×10^{-1}
16	9.95×10^{-6}	362	19	1.83×10^{7}	0.121	5.84×10^{12}	6.48×10^{-1}
17	3.96×10^{-6}	266	18	6.55×10^{6}	0.0859	1.47×10^{13}	1.63
18	1.58×10^{-6}	196	17	2.33×10^{6}	0.0608	3.69×10^{13}	4.09
19	6.28×10^{-7}	144	16	8.20×10^{5}	0.0430	9.26×10^{13}	1.03 x 10
20	2.50×10^{-7}	106	15	2.87×10^{5}	0.0303	2.33×10^{14}	2.58 x 10
21	9.95×10^{-8}	78.0	15	1.14×10^{5}	0.0223	5.84×10^{14}	6.48 x 10
22	3.96×10^{-8}	57.4	15	4.55×10^{4}	0.0164	1.47×10^{15}	1.63×10^{2}
23	1.58×10^{-8}	39.8*	15	1.81×10^{4}	0.0121	3.69×10^{15}	4.09×10^{2}
24	6.28×10^{-9}	25.1*	15	7.21×10^{3}	0.00884	9.26×10^{15}	1.03×10^{3}
25	2.50×10^{-9}	15.8*	15	2.87×10^{3}	0.00653	2.33×10^{16}	2.58×10^{3}
26	9.95×10^{-10}	10.0*	15	1.14×10^{3}	0.00480	5.84×10^{16}	6.48×10^{3}
27	3.96×10^{-10}	6.30*	15	4.55×10^{2}	0.00353	1.47×10^{17}	1.63×10^{4}
28	1.58×10^{-10}	3.98*	15	1.81×10^{2}	0.00260	3.69×10^{17}	4.09×10^{4}
29	6.28×10^{-11}	2.51*	15	7.21 x 10	0.00191	9.26×10^{17}	1.03×10^{5}
30	2.50×10^{-11}	1.58*	15	2.87 x 10	0.00141	2.33×10^{18}	2.58×10^{5}
31	9.95×10^{-12}	1.00	15	1.14 x 10	0.00103	5.84×10^{18}	6.48×10^{5}

* Maximum radius permitted by solar light pressure.

** These No. based on entrance to atmosphere at 100 km approx

*** Includes earth's shading effect of 1/2

† $P = \left(\frac{9E}{\pi \rho^2 \epsilon}\right)^{1/3}$; ϵ = 447 x 778.3 ft lb/lb for Al

$$\frac{P}{d} = 1.08 \times 10^{-4} V^{2/3}$$

where

P = penetration in thick target

d = meteorite diameter

V = meteorite velocity in cm/sec.

Whipple's equation is theoretical and is believed to give penetration depths for hypervelocity impacts that are too high.

b. Kornhauser's equation

This equation is given in (Ref. 68) as

$$h = K_2 \left(\frac{T}{E}\right)^{1/3} \left(\frac{E}{E_o}\right)^{0.09}$$

where

h = penetration (depth of crater)

K_2 = constant of proportionality

T = kinetic energy of projectile

E = modulus of elasticity of target material

E_0 = reference modulus

This equation yields

$$\frac{h}{d} = 0.282 \times 10^{-4} V^{2/3}$$

which is identical to Whipple's except that the value of the constant is lower.

c. Summer's equation

This equation is an empirical equation based on experimental test data using many different projectile and target material combinations. As given in Ref. 69, the equation has the form of:

$$\frac{P}{d} = 2.28 \left(\frac{\rho_p}{\rho_t}\right)^{2/3} \left(\frac{V}{C}\right)^{2/3}$$

where

P = penetration in a thick target

d = diameter of projectile

ρ_p = density of projectile

ρ_t = density of target

V = projectile velocity

C = speed of sound in target material

For Whipple's meteorite density of $\rho_p = 0.05$ gm/cm^3, an aluminum target density of $\rho_t = 2.8$ gm/cm^3 and $C = 5.1 \times 10^5$ cm/sec, the equation reduces to

$$\frac{P}{d} = 0.243 \times 10^{-4} V^{2/3}$$

The agreement between this constant and that of Kornhauser is noted.

d. Bjork's equation

This is a theoretical equation developed by Bjork (Ref. 70) using a hydrodynamic model to explain hypervelocity impact. He derived equations for the impact of aluminum projectiles on aluminum targets and also iron projectiles on iron targets. In Ref. 71, Bjork gives the penetration of an aluminum projectile into an aluminum target as:

$$P = 1.09 (m v)^{1/3}$$

where

P = penetration in cm

m = projectile mass in gm

v = impact velocity in km/sec

Bjork in Ref. 72 states that the use of a correction factor of the form $\left(\frac{\rho_P}{\rho_t}\right)^{\phi}$ is subject to a great deal of conjecture as it rests on no theoretical basis. He also stated that he would favor the value of $\phi = 1/3$ and $\theta = 1/3$ in a general penetration equation such as:

$$P = K_3 m^{1/3} \rho_t^{-\phi} \rho_P^{(\phi - 1/3)} \left(\frac{V}{C}\right)^{\theta}$$

equating the general and empirical relations.

$$1.09 (mv)^{1/3} = K_3 m^{1/3} \rho_t^{-1/3} \left(\frac{V}{C}\right)^{1/3}$$

$$1.09 = K_3 \rho_t^{-1/3} \left(\frac{1}{C}\right)^{1/3}$$

For aluminum targets, $\rho_t = 2.8$ gm/cm^3 and $C = 5.1$ km/sec, $K_3 = 2.63$.

Thus we may write

$$P = 2.63 m^{1/3} \rho_t^{-1/3} \left(\frac{V}{C}\right)^{1/3}$$

Then, letting "d" equal the meteorite diameter in cm and its density $\rho_P = 0.05$ gm/cm^3 yields

$$P = 2.63 \left(\frac{\pi}{6} d^3 \rho_p\right)^{1/3} \rho_t^{-1/3} \left(\frac{V}{C}\right)^{1/3}$$

$$\frac{P}{d} = 0.322 V^{1/3}$$

where

P = penetration = cm

d = meteorite dia = cm

V = meteorite velocity = $\frac{km}{sec}$

This probably stretches Bjork's work more than he would care to see done but it is necessary to obtain a comparison with the other formulas.

e. Engineering model

For purposes of evaluating meteoroid effects upon propellant storage vessel design, the following model has been recommended (Ref. 73).

(1) The integral mass flux of particles is given by

$\Phi = 10^{-13}\ m^{-10/9}$ hits/m^2/sec, by particles of mass m gm and greater. Approximately 90% of the meteoroid flux is assumed to have a density of 0.05 gm/cm^3. The effective flux used in computing probability of hits is therefore reduced by an order of magnitude to compensate for the very low density meteoroids which will not follow the given penetration law.

(2) The particle velocity (v) is 30 km/sec.

(3) Penetration of impacting particles into a single thickness of steel is given by

$P = 1.5\ (mv)^{1/3}$, cm

(4) Aluminum is half as effective as steel in withstanding penetration.

(5) The use of spaced sheets (Whipple bumpers) allows a reduction factor, $B_f = 5$, in the total thickness required to withstand penetration.

(6) Particle density, (ρ) is 3 gm/cu cm.

(7) The area exposed to meteoroids is the total unshadowed surface area of the object. The shadowing can be expressed in terms of an effective area by computing a factor to be multiplied by the actual area. This reduction factor will be in the ratio of a sphere with a conical segment removed to a sphere. The center of this sphere is the spacecraft and the conical segment is that volume intersected, as an example, by the Earth. Consider the following sketch

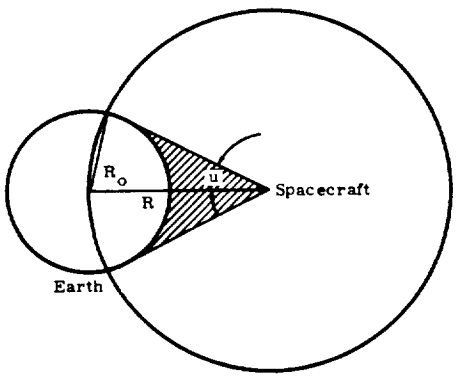

where

$$u = \sin^{-1} R_o/R.$$

Then

$$S_f = 1 - 1/2\ (1 - \cos u)$$

$$= 1 - \frac{1 + \cos (\sin^{-1} R_o/R)}{2}$$

The integral mass flux thus becomes

$$\Phi = 10^{-14}\ m^{-10/9}\ \text{hits/m}^2\ \text{sec}$$

$$N\ (\geq m) = 8.64 \times 10^{-10} m^{-10/9}\ \text{hits/m}^2\text{-day}$$

Eliminating the constant meteoroid velocity (30 km/sec), and expressing the penetration law in terms of mass gives

$$m = \frac{P^3}{101.25}$$

as the mass in grams required to penetrate X cm of steel. With the flux and penetration expressed only by mass, it is convenient to combine the two relationships, obtaining

$$N\ (\geq m) = 8.64 \times 10^{-10}\ (P^3/101.25)^{-10/9}$$

$$= \frac{1.46 \times 10^{-7}}{P^{10/3}}$$

hits per square meter per day capable of penetrating P cm of steel. The reciprocal of this relation is the average number of days between penetrations. To determine the thickness required so that an area of A meters is not penetrated on the average for at least T days,

$$P = (AT \cdot 1.46 \times 10^{-7})^{3/10}$$

$$P = \frac{8.901}{10^3}\ (AT)^{3/10},\ \text{cm of steel}$$

This relationship is convenient to use for purposes of design after the effects of the time distribution of meteoroid encounters have been included. The Poisson distribution model has been used to elaborate on meteorite encounter probabilities. This distribution which is valid for uniform masses of low density is

$$P_{kt} = \frac{\left(\frac{t}{T}\right)^K e^{-\frac{t}{T}}}{K!}$$

where t is any selected interval, and $\frac{1}{T}$ is the average number of penetrations per day. Thus the probability of any number, K, penetrations during time, t can be estimated. To determine the probability of no penetrations during T days (T = t) the relation reduces to

$$P_{kt} = e^{-1} = 0.368$$

so that the probability is 0.368 that there will be no penetrations within the average number of days between penetrations. To find the time at the end of which the probability of no penetrations is 0.99.

$$0.99 = e^{-t/T}$$

$$t = -T \ln 0.99$$

$$t = 0.0101T$$

For 0.95 and 0.90 probabilities, the correction factors are, respectively, 0.05 and 0.10. For example, the average time between penetrations for a 93 m^2 steel surface 2.5 cm thick is about 1.6×10^6 days. There is a 0.368 probability that there will be no penetrations by the end of this time. For this structure, the limiting time for 0.99 probability of no penetrations is 1.6×10^4 days; for 0.95 probability, 8×10^4 days; and for 0.90 probability, 1.6×10^5 days.

Correspondingly, if the probability for no penetration of X thickness within T is 0.368, then the thickness required for a 0.99 probability of no penetrations in T days is

$$(P_{kt} \text{ at } 0.99)^{10/3} = \frac{P^{10/3}}{0.0101}$$

$$P_{kt} \text{ at } 0.99 = 3.97P$$

for 0.90 probability.

$$P_{kt} \text{ at } 0.90 = 1.96X$$

More generally

$$\ln (\text{prob}) = \frac{-t\,(1.46 \times 10^{-7})\,A}{P^{10/3}}$$

The relationships between exposed area and time, aluminum thickness and penetration probability are illustrated in Fig. 33.

C. CONVERSION DATA

1. Definition of Time Standards and Conversions (Ref. 74)

Time measurement may be based upon the period of motion of a stable oscillator, the decay of a radioactive isotope, or the period of any celestial body relative to the observer. The latter is the body chosen sometimes referred to as the time reckoner and a clock in most astronomical research. The particular day is defined to be the time span between two successive upper or lower transits of the given time reckoner across the celestial meridian of the observer. Noon is the time of upper transit (the transit in the northern celestial hemisphere). Angles measured in the equatorial plane of the celestial sphere from the observer's meridian, O, westward are called local hour angles (see following sketch). Thus O_γ is the local hour angle of vernal equinox. Then local time of day is the hour angle of the time reckoner for days beginning at noon. Since an international agreement in 1925, astronomical time is reckoned from midnight, so that the local time of day based on this origin is

$$T = \tau + 12^h$$

where τ is the hour angle of the time reckoner. Because astronomers refer to two time reckoners, the sun and vernal equinox, there are two kinds of days; the solar day and the sidereal day.

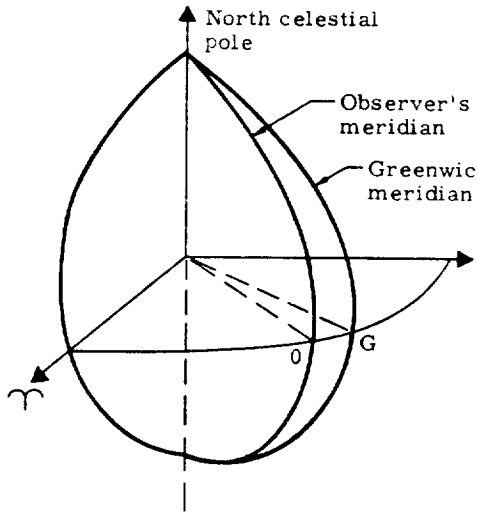

The sidereal day is the interval between two successive upper transits of vernal equinox. Because this time reckoner is a point on the celestial sphere, an infinite distance from the earth, the sidereal day is the period of earth rotation relative to inertial space. Because sidereal time is the hour angle of vernal equinox, it is given at any instant by the right ascension of a star that is crossing the observer's meridian at that instant. The best value for the sidereal day is 86164.091 mean solar sec.

The solar day, the interval between two successive upper transits of the sun, is $3^m\ 56^s$ longer than the sidereal day because the earth moves almost one degree each day in its orbit around the sun. Thus, the solar day is not exactly equal to the period of earth rotation. Also, the apparent sun (the sun we see) is not a precisely uniform time reckoner because the orbit of the earth is slightly eccentric and the eliptic is inclined about 23° to the equatorial plane. Because the apparent sun is a nonuniform time reckoner, the mean sun is used to measure civil time. The time unit is the average of the apparent solar days, the mean solar day and its length is defined to be 86400 mean solar sec. The difference between apparent and mean solar time is called the "equation of time," ET:

$$ET = AT - MT = \tau_A - \tau_M = A_M - A_A$$

where

AT = apparent time

MT = mean solar time

τ_A = hour angle of apparent sun

τ_M = hour angle of mean sun

A_M = right ascension of mean sun

A_A = right ascension of apparent sun

Civil time, CT, is mean solar time measured from midnight,

$$CT = \tau_M + 12^h$$

The local civil time at the Greenwich meridian is known as universal time, UT, or Greenwich mean time, GMT.

The difference in local time at two places for the same physical instant is the difference in longitude, λ:

$$T_1 - T_2 = \lambda_2 - \lambda_1$$

where λ, in the astronomer's convention, is measured positive westward from the Greenwich meridian. This equation applies for T measured in any system of local time, i.e., civil, apparent solar or sidereal times. For example,

$$LMT = LCT = UT - \lambda$$

Fifteen degrees of longitude corresponds to an hour of time difference, so that for local midnight at Greenwich, the corresponding local times at λ = 15° W and 30° W are 11:00 p.m. and 10:00 p.m., respectively. The local time increases for eastward longitude changes.

Since local civil times are the same only along a given meridian, some confusion is avoided by the use of time zones. The earth is divided into 24 zones, each fifteen degrees of longitude wide. In the middle of each zone, at the "standard meridian," local time differs from Greenwich time by an integral number of hours. The time read on a clock at any place, i.e., standard time, is the local civil time of the standard meridian nearest the clock. Standard time differs in some places from zonal time where boundaries are twisted to suit geographical and political boundaries.

Greenwich civil time is generally the system employed in astronomical almanacs. Therefore, conversions required most often are standard to GMT and GMT to standard. The conversion from a zone time to GMT is effected by dividing the longitude (in degrees) of the observation site by 15 and obtaining the nearest whole number. This value is added to the zone time for sites west of Greenwich and subtracted for sites east of Greenwich.

$$GMT = ZT \pm \frac{\lambda^o}{15}$$

The same rule applies for conversion of standard times, except that the irregular boundaries for the time zones must be utilized.

The preceding discussions provide the basis for an appreciation of the measurement of time intervals; however, in order to relate any two events in time it is necessary to refer them to the same time reference. For earth satellite problems this requires only that an epoch be selected and that the universal time be recorded at the instant. A record of time by days and/or seconds from this epoch thus relates all of the events. In other problems where two or more bodies are involved such an arbitrary solution of the time origin for one body may lead to unnecessary complexity due to the fact that all of the various time scales must be correlated each time a computation is performed. To avoid such a situation the Julian day calendar was established by the astronomers. This calendar takes the origin to be mean moon 4713 years before Christ and is a chronological and continuous time scale, i.e., days have been counted consecutively from this date to present. This practice avoids problems resulting from the nonintegral period of the earth (365.2563835 mean solar days) and the difficulties of months of different length. On this calendar January 0 (i.e., mean noon January 1) 1900 is 2415020 mean solar days. The conversion of other dates in the later half of the 20th century is facilitated by Table 37 obtained from The American Ephemeris and Nautical Almanac.

2. Review of Standards of Length and Mass

For many engineering purposes the conversions between units of measure need be known only to two or three significant figures. For this reason a general unawareness of the definition and use of these units has resulted and is evidenced by inconsistencies in the literature. The purpose of this section is to redefine a set of units and specify accepted conversions from this set to other commonly used systems.

a. Standard units

The United States' system of mass and measures has been defined in terms of the metric system since approximately 1900; it was refined in metric terms in 1959. Therefore, care must be exercised to assure that proper standards are used for all precise computations. Before going further it is necessary to obtain an appreciation for the bases for measurement.

The meter was originally defined to be $1/10^7$ part of 1/4 of a meridian of the earth. A bar of this length was constructed and kept under standard conditions in the Archives. Since subsequent measurements of the earth proved this definition to be incorrect, a new international standard, the Prototype Meter, was defined to be the distance between two marks on a platinum-iridium bar at standard conditions. This bar was selected by precise measurement to have the same length as the bar in the Archives. National standards were also produced and compared to the Prototype Meter. In October 1960, at the Eleventh General Conference on weights and measures, the meter was redefined to be 1,650,763.73 wavelengths of the orange-red radiation of Krypton 86. However, the bar standards are also maintained because of the ease of measurement.

The kilogram was originally defined to be the mass of 1000 cubic centimeters of water at its maximum density (i.e., 4° C). However, at the time the Prototype Meter was defined, the kilo-

TABLE 37

Julian Day Numbers for the Years 1950-2000
(based on Greenwich Noon)

Year	Jan. 0.5	Feb. 0.5	Mar. 0.5	Apr. 0.5	May 0.5	June 0.5	July 0.5	Aug. 0.5	Sept. 0.5	Oct. 0.5	Nov. 0.5	Dec. 0.5
1950	243 3282	3313	3341	3372	3402	3433	3463	3494	3525	3555	3586	3616
1951	3647	3678	3706	3737	3767	3798	3828	3859	3890	3920	3951	3981
1952	4012	4043	4072	4103	4133	4164	4194	4225	4256	4286	4317	4347
1953	4378	4409	4437	4468	4498	4529	4559	4590	4621	4651	4682	4712
1954	4743	4774	4802	4833	4863	4894	4924	4955	4986	5016	5047	5077
1955	243 5108	5139	5167	5198	5228	5259	5289	5320	5351	5381	5412	5442
1956	5473	5504	5533	5564	5594	5625	5655	5686	5717	5747	5778	5808
1957	5839	5870	5898	5929	5959	5990	6020	6051	6082	6112	6143	6173
1958	6204	6235	6263	6294	6324	6355	6385	6416	6447	6477	6508	6538
1959	6569	6600	6628	6659	6689	6720	6750	6781	6812	6842	6873	6903
1960	243 6934	6965	6994	7025	7055	7086	7116	7147	7178	7208	7239	7269
1961	7300	7331	7359	7390	7420	7451	7481	7512	7543	7573	7604	7634
1962	7665	7696	7724	7750	7785	7816	7846	7877	7908	7938	7969	7999
1963	8030	8061	8089	8120	8150	8181	8211	8242	8273	8303	8334	8364
1964	8395	8426	8455	8486	8516	8547	8577	8608	8639	8669	8700	8730
1965	243 8761	8792	8820	8851	8881	8912	8942	8973	9004	9034	9065	9095
1966	9126	9157	9185	9216	9246	9277	9307	9338	9369	9399	9430	9460
1967	9491	9522	9550	9581	9611	9642	9672	9703	9734	9764	9795	9825
1968	9856	9887	9916	9947	9977	*0008	*0038	*0069	*0100	*0130	*0161	*0191
1969	244 0222	0253	0281	0312	0342	0373	0403	0434	0465	0495	0526	0556
1970	244 0587	0618	0646	0677	0707	0738	0768	0799	0830	0860	0891	0921
1971	0952	0983	1011	1042	1072	1103	1133	1164	1195	1225	1256	1286
1972	1317	1348	1377	1408	1438	1469	1499	1530	1561	1591	1622	1652
1973	1683	1714	1742	1773	1803	1834	1864	1895	1926	1956	1987	2017
1974	2048	2079	2107	2138	2168	2199	2229	2260	2291	2321	2352	2382
1975	244 2413	2444	2472	2503	2533	2564	2594	2625	2656	2686	2717	2747
1976	2778	2809	2838	2869	2899	2930	2960	2991	3022	3052	3083	3113
1977	3144	3175	3203	3234	3264	3295	3325	3356	3387	3417	3448	3478
1978	3509	3540	3568	3599	3629	3660	3690	3721	3752	3782	3813	3843
1979	3874	3905	3933	3964	3994	4025	4055	4086	4117	4147	4178	4208
1980	244 4239	4270	4299	4330	4360	4391	4421	4452	4483	4513	4544	4574
1981	4605	4636	4664	4695	4725	4756	4786	4817	4848	4878	4909	4939
1982	4970	5001	5029	5060	5090	5121	5151	5182	5213	5243	5274	5304
1983	5335	5366	5394	5425	5455	5486	5516	5547	5578	5608	5639	5669
1984	5700	5731	5760	5791	5821	5852	5882	5913	5944	5974	6005	6035
1985	244 6066	6097	6125	6156	6186	6217	6247	6278	6309	6339	6370	6400
1986	6431	6462	6490	6521	6551	6582	6612	6643	6674	6704	6735	6765
1987	6796	6827	6855	6886	6916	6947	6977	7008	7039	7069	7100	7130
1988	7161	7192	7221	7252	7282	7313	7343	7374	7405	7435	7466	7496
1989	7527	7558	7586	7617	7647	7678	7708	7739	7770	7800	7831	7861
1990	244 7892	7923	7951	7982	8012	8043	8073	8104	8135	8165	8196	8226
1991	8257	8288	8316	8347	8377	8408	8438	8469	8500	8530	8561	8591
1992	8622	8653	8682	8713	8743	8774	8804	8835	8866	8896	8927	8957
1993	8988	9019	9047	9078	9108	9139	9169	9200	9231	9261	9292	9322
1994	9353	9384	9412	9443	9473	9504	9534	9565	9596	9626	9657	9687
1995	244 9718	9749	9777	9808	9838	9869	9899	9930	9961	9991	*0022	*0052
1996	245 0083	0114	0143	0174	0204	0235	0265	0296	0327	0357	0388	0418
1997	0449	0480	0508	0539	0569	0600	0630	0661	0692	0722	0753	0783
1998	0814	0845	0873	0904	0934	0965	0995	1026	1057	1087	1118	1148
1999	245 1179	1210	1238	1269	1299	1330	1360	1391	1422	1452	1483	1513
2000	245 1544	1575	1604	1635	1665	1696	1726	1757	1788	1818	1849	1879

1900 Jan 0.5 ET = Julian Day 2,415,020.0 = Greenwich Noon, January 1, 1900, a common epoch
1950 Jan 0.5 ET = Julian Day 2,433,282.0 = Greenwich Noon, January 1, 1950, another common epoch and first entry in this table

gram was redefined to be the mass of the Prototype Kilogram and, as was the case with the Prototype Meter, national standards were obtained by comparison to the Prototype Kilogram. This unit has not been changed to date though proposals have been made to base the measurement on some atomic standard. The conversion from mass to force is accomplished by the standardized constant $g_0 = 9.80665\ m/sec^2$.

Effective July 1, 1959, the English speaking people defined their standards of length and mass in terms of the metric system of units. This was accomplished through the definition of an international yard and an international pound.

1 yard ≡ 0.9144 meter

1 pound (avdp) ≡ 0.453,592,37 kilogram

These two units constitute the basis for all measure with the exception of those accomplished by the U.S. Coast and Geodetic Survey which continues to use a foot defined by the old standard:

$$1 \text{ foot} = \frac{1200}{3937} \text{ meter}$$

or

$$1 \text{ yard} = \frac{3600}{3937} \text{ meter}$$

$$= 0.91440182 \text{ meter}$$

Of course, other units of length, area, volume, etc., can be related by their definition to these more basic units. These second generation units (for example: statute mile, nautical mile, etc.) are in general peculiar to particular regions and thus only a few will be discussed in the following paragraphs.

The astronomical unit (AU) is defined as the mean distance from the sun to a fictitious planet whose mass and sidereal period are the same as those used by Gauss for the earth in his determination of the solar gravitation constant. This definition enables the astronomer to improve his knowledge of the scale of the solar system as more accurate data become available but does not require recomputation of planetary tables since angular data can be computed with an accuracy of eight or nine significant figures. The best value of this unit is presently 149.53×10^6 km and the mean distance from the earth to the sun is presently considered to be 1.000,000,03 AU.

The nautical mile was originally defined to be one minute of arc on the earth's equator. On this basis the best value of this unit appears to be approximately 6087 feet. Various attempts have been made to adopt a standard length, e.g., the British nautical mile was defined to be 6080 feet and the U.S. nautical mile was defined to be 6080.20 feet. In 1954, it was agreed to standardize the nautical mile by defining it in terms of the meter. As a result, the international nautical mile was defined to be 1852 meters, or, based on the conversion between feet and meters at the time, 6076.10333 feet. But with the redefinition of the foot (1 foot ≡ 0.3048 meter) as of July 1959, the nautical mile changed once again to 6076.11549 international feet, approximately. This value has been accepted by the National Bureau of Standards and all responsible agencies.

The statute mile ≡ 5280 international feet.

The meter was previously defined; however, many units of length have been defined based on the prime unit and related by powers of 10. Accordingly the following prefixes have been introduced and are generally recognized:

tera, meaning 10^{12}

giga, meaning 10^9

mega, meaning 10^6

kilo, meaning 10^3

hecto, meaning 10^2

deka, meaning 10^1

deci, meaning 10^{-1}

centi, meaning 10^{-2}

milli, meaning 10^{-3}

micro, meaning 10^{-6}

nano, meaning 10^{-9}

pico, meaning 10^{-12}

The yard ≡ 0.9144 meter

≡ 3 international feet

The foot ≡ 0.3048 meter

≡ 12 international inches

The inch ≡ 0.0254 meter

≡ 10^3 mils

The micron ≡ 10^{-6} meter

The angstrom ≡ 10^{-10} meter

3. Mathematical Constants

π	= 3.141,592,653,6
2π	= 6.283,185,307,2
3π	= 9.424,777,960,8
$\log_{10}\pi$	= 0.497,149,872,7
$\log_e\pi$	= 1.144,729,885,8
e	= 2.718,281,828,5
$\log_{10}e$	= 0.434,294,481,9
e^2	= 7,389,056,102
$\log_e 10$	= 2.302,585,091
$1/\pi$	= 0.318,309,886,0
$1/2\pi$	= 0.159,154,943,0
$1/3\pi$	= 0.106,103,295,3
$360/2\pi$	= 57,295,779,51

$1/e = 0.367,879,441,0$

$1/e^2 = 0.135,335,283,1$

4. Time Standards

$$1 \text{ second} = \frac{10^{-7}}{3.155,692,597,47}$$

times the Besselian (tropical, solar) year at 1900.0 and 12 hr ephemeris time

1 mean solar sec $\approx (1 + 10^{-9})$ ephemeris seconds in 1960

sidereal day = 86,164.091 mean solar seconds

sidereal year = 365.256,383,5 mean solar days

sidereal year = $3.155,814,9 \times 10^7$ mean solar seconds

5. Conversion Tables

Ready conversions for the more generally used units of astronomical measurements will be found in the following tables:

Table 38--Length Conversions

Table 39--Velocity Conversions

Table 40--Acceleration Conversions

Table 41--Mass Conversions

Table 42--Angular Conversions

Table 43--Time Conversions

Table 44--Force Conversions

TABLE 38

Length Conversions

	Astronomical Units	International Nautical Miles	Statute Miles	Meters	International Yards	International Feet	International Inches
1 Astronomical Unit =	1	$80.737,90 \times 10^6$	$92.911,52 \times 10^6$	149.5266×10^9	$163.524,3 \times 10^9$	490.5728×10^9	$588.687,4 \times 10^{10}$
1 International Nautical Mile =	$1.238,575 \times 10^{-8}$	1	1.150,779,447	1852*	2025.371,828	6076.115,485	72,913.385,826
1 Statute Mile =	$1.076,292 \times 10^{-8}$	0.868,976,242	1	1609.344*	1760*	5280*	63,360*
1 Meter =	$0.668,777,3 \times 10^{-11}$	$0.539,956,803 \times 10^{-3}$	$0.621,371,192 \times 10^{-3}$	1	1.093,613,298	3.280,839,895	39.370,078,740
1 International Yard =	$0.611,529,9 \times 10^{-11}$	$0.493,736,501 \times 10^{-3}$	$0.568,181,818 \times 10^{-3}$	0.9144*	1	3*	36*
1 International Foot =	$0.203,843,3 \times 10^{-11}$	$0.164,578,833 \times 10^{-3}$	$0.189,393,939 \times 10^{-3}$	0.3048*	0.333,333,333	1	12*
1 International Inch =	$0.169,869,4 \times 10^{-12}$	$0.137,149,028 \times 10^{-4}$	$0.157,828,282 \times 10^{-4}$	0.0254*	0.027,777,777	0.083,333,333	1

TABLE 39

Velocity Conversions

	Astronomical Units per Mean Solar Day	Astronomical Units per Sidereal Day	International Nautical Miles per Hour	Statute Miles per Hour	Kilometers per Hour	Meters per Second	Feet per Second
1 Astronomical Unit per Mean Solar Day =	1	1.002,737,90	$3.364,079 \times 10^5$	$3.871,313 \times 10^5$	$6.230,273 \times 10^5$	$1.730,632 \times 10^5$	$5.677,928 \times 10^5$
1 Astronomical Unit per Sidereal Day =	0.997,269,57	1	$3.354,892 \times 10^5$	$3.860,743 \times 10^5$	$6.213,260 \times 10^5$	$1.725,907 \times 10^5$	$5.662,424 \times 10^5$
1 International Nautical Mile per Hour =	$0.297,258,2 \times 10^{-6}$	$0.298,073,1 \times 10^{-6}$	1	1.150,779,447	1.852*	0.514,444,444	1.687,809,856
1 Statute Mile per Hour =	$0.258,310,3 \times 10^{-6}$	$0.259,017,5 \times 10^{-6}$	0.868,976,242,6	1	1.609,344*	0.447,040*	1.466,666,666
1 Kilometer per Hour =	$0.160,506,6 \times 10^{-6}$	$0.160,946,1 \times 10^{-6}$	0.539,956,803,4	0.621,371,192	1	0.277,777,777	0.911,344,415
1 Meter per Second =	$0.577,823,6 \times 10^{-6}$	$0.579,405,6 \times 10^{-6}$	1.943,844,491	2.236,936,288	3.600*	1	3.280,839,895
1 Foot per Second =	$0.176,210,6 \times 10^{-6}$	$0.176,602,8 \times 10^{-6}$	0.592,483,800	0.681,818,181	1.097,280*	0.3048*	1

—Underlined digits are questionable.

*Denotes exact conversion factor.

TABLE 40
Acceleration Conversions

	Astronomical Units per Mean Solar Day^2	Astronomical Units per Sidereal Day^2	International Nautical Miles per Hour^2	Statute Miles per Hour^2	Kilometers per Hour^2	Meters per Second^2	International Feet per Second^2
1 Astronomical Unit per Solar Day^2 =	1	1.005,483,30	$1.401,700 \times 10^3$	$1.613,047 \times 10^5$	$2.595,989 \times 10^5$	20.030,46	65.718,76
1 Astronomical Unit per Sidereal Day^2 =	0.994,546,60	1	$1.394,056 \times 10^3$	$1.604,250 \times 10^3$	$2.581,832 \times 10^5$	19.921,23	65.358,38
1 International Nautical Mile per Hour^2 =	$0.713,418,4 \times 10^{-5}$	$0.717,331,1 \times 10^{-5}$	1	1.150,779,447	1.852*	$1.429,012,345 \times 10^{-4}$	$4.688,360,711 \times 10^{-4}$
1 Statute Mile per Hour^2 =	$0.619,944,7 \times 10^{-5}$	$0.623,344,2 \times 10^{-5}$	0.868,976,242,8	1	1.609,344*	$1.241,777,778 \times 10^{-4}$	$4.074,074,074 \times 10^{-4}$
1 Kilometer per Hour^2 =	0.385,200,8 $\times 10^{-5}$	0.387,321,9 $\times 10^{-5}$	0.539,956,803,4	0.621,371,192	1	0.771,604,938,2 $\times 10^{-4}$	2.531,512,264 $\times 10^{-4}$
1 Meter per Second^2 =	0.048,923,97	0.050,197,70	0.699,784,017,6 $\times 10^4$	0.805,297,064,9 $\times 10^4$	12,960*	1	3.280,839,895
1 International Foot per Second^2 =	0.015,218,82	0.015,300,26	0.213,294,168,6 $\times 10^4$	0.245,245,245,2 $\times 10^4$	0.395,020,800	0.3048*	1

TABLE 41
Mass Conversions

	Solar Mass	Earth Mass	Moon Mass	Slugs	Kilograms	Pounds (avdp)	Ounces (avdp)
1 Solar Mass =	1	332,440	27,046,500	$1.361,25 \times 10^{29}$	$1.986,6 \times 10^{30}$	$4.379,70 \times 10^{30}$	$70.075,2 \times 10^{30}$
1 Earth Mass =	$3.088,062 \times 10^{-6}$	1	81,358	$4.094,2 \times 10^{23}$	$5.977,3 \times 10^{24}$	$13.172,8 \times 10^{24}$	$210,76 \times 10^{24}$
1 Moon Mass =	$3.697,320 \times 10^{-8}$	$1.229,14 \times 10^{-2}$	1	$5.032,3 \times 10^{21}$	$7.344,0 \times 10^{22}$	$16.191,0 \times 10^{22}$	$259,06 \times 10^{22}$
1 Slug =	$7.346,18 \times 10^{-29}$	$0.244,25 \times 10^{-23}$	$0.198,72 \times 10^{-21}$	1	14.593,902,976	32.174,048,556	514,784,777.0
1 Kilogram =	$5.033,73 \times 10^{-31}$	$0.167,36 \times 10^{-24}$	$0.136,16 \times 10^{-22}$	$6.852,176,612 \times 10^{-2}$	1	2.204,622,621	35.273,961,94
1 Pound (avdp) =	$2.283,26 \times 10^{-31}$	$0.759,15 \times 10^{-25}$	$0.617,63 \times 10^{-23}$	$3.108,095,016 \times 10^{-2}$	0.453,592,37*	1	16.0*
1 Ounce (avdp) =	$1.427,04 \times 10^{-32}$	$0.474,47 \times 10^{-26}$	$0.386,01 \times 10^{-24}$	$1.942,559,385 \times 10^{-3}$	$0.283,495,231 \times 10^{-2}$	0.062,5*	1

—Underlined digits are questionable.

*Denotes exact conversion factor.

$g_0 = 9.80665^* \frac{\text{meters}}{\text{sec}} = 32.174,048,556 \text{ ft/sec}^2$

TABLE 42
Angular Conversions

	Revolutions	Radians	Degrees	Minutes of Arc	Seconds of Arc	Angular Mills
1 Revolution =	1	6.283,185,307	360.*	21,600.0*	1,296,000.0*	6400.*
1 Radian =	0.159,154,943	1	57.295,779,511	3,437,746,771	206,264,806,236	1018.591,636
1 Degree =	$2.777,777,777 \times 10^{-3}$	$1.745,329,252 \times 10^{-2}$	1	60.0*	3,600.0*	17.7,777,777
1 Minute of Arc =	$4.629,629,629 \times 10^{-5}$	$2.908,882,086 \times 10^{-4}$	$1.666,666,666 \times 10^{-2}$	1	60.0*	0.296,296,296
1 Second of Arc =	$7.716,049,382 \times 10^{-7}$	$4.848,136,812 \times 10^{-6}$	$2.777,777,777 \times 10^{-4}$	0.016,666,666	1	$4.938,271,605 \times 10^{-3}$
1 Angular Mil =	1.5625×10^{-4}*	$9.817,477,040 \times 10^{-4}$	5.6250×10^{-2}*	3.375*	202.5*	1

*Denotes exact conversion

TABLE 43

Time Conversions

		Solar Year	Julian Year	Mean Solar Day	Sidereal Day	Mean Solar Sec	Sidereal Sec
1 Solar or Besselian Year	=	1	0.999,978,641	365.242,198	366.242,198	$3.155,692,59 \times 10^{7}$	$3.164,332,57 \times 10^{7}$
1 Julian Year	=	1.000,021,358	1	365.25*	366.250,00*	$3.155,760^{*} \times 10^{7}$	$3.164,400,16 \times 10^{7}$
1 Mean Solar Day	=	$2.737,909,26 \times 10^{-3}$	$2.737,850,787 \times 10^{-3}$	1	1.002,737,90	86400*	86636.555
1 Sidereal Day	=	$2.730,433,61 \times 10^{-3}$	$2.730,375,42 \times 10^{-3}$	0.997,269,57	1	86164.091	86400*
1 Mean Solar Sec	=	$3.168,876,46 \times 10^{-8}$	$3.168,808,78 \times 10^{-8}$	$1.157,407,40 \times 10^{-5}$	$1.160,576,27 \times 10^{-5}$	1	1.002,737,90
1 Sidereal Sec	=	$3.160,224,08 \times 10^{-8}$	$3.160,156,38 \times 10^{-8}$	$1.154,247,18 \times 10^{-5}$	$1.157,407,40 \times 10^{-5}$	0.997,269,57	1

*Exact conversion

TABLE 44

Force Conversions

	Kg (force)	Pound (force)	Newton	Poundal	Dyne
1 Kg Force	1	2.204,622,621	9.806,65*	70.931,635,35	$9.806,65 \times 10^{5}$*
1 Pound	0.453,592,370,1	1	4.448,221,62	32.174,048,6	$4.448,221,62 \times 10^{5}$
1 Newton	0.101,971,621,2	0.224,808,943	1	7.233,013,85	10^{5}
1 Poundal	$1.409,808,183 \times 10^{-2}$	$3.108,095,501 \times 10^{-2}$	0.138,254,954	1	$0.138,254,954 \times 10^{5}$
1 Dyne	$1.019,716,212 \times 10^{-6}$	$0.224,808,943 \times 10^{-5}$	10^{-5}	$7.233,013,85 \times 10^{-5}$	1

*Exact conversion

D. REFERENCES

1. Minzner, R. A., Ripley, W. S. and Condron, T. P, "U. S. Extension to the ICAO Standard Atmosphere--Tables and Data to 300 Standard Geopotential Kilometers," U. S. Government Printing Office, Washington, D. C., 1958.
2. Sterne, T. E., Folkart, B. M. and Schilling, G. F., "An Interim Model Atmosphere Fitted to Preliminary Densities Inferred from USSR Satellites," Special Report No. 7, Smithsonian Institute, Astrophysical Observatory.
3. Minzner, R. A., Champion, K. S. W. and Pond, H. L., "ARDC Model Atmosphere 1959," Air Force Survey in Geophysics No. 115, AFCRC TR-59-267, 1959.
4. O'Sullivan, W. J., Jr., Coffee, C. W. and Keating, G. M., "Upper-Atmosphere Density Measurements Results from Analysis of Orbital Perturbations of Explorer IX," IG Bulletin No. 63, September 1962 (from paper presented at the Third International Space Science Symposium, 30 April to 9 May 1962, Washington, D. C.).
5. Sissenwine, H., "Announcing the U. S. Standard Atmosphere--1962," Astronautics, Vol. 7, No. 8, August 1962.
6. Cole, A. E., Court, A. and Kantor, A. J., "Standard Atmosphere Revision to 90 Km," Report of Task Group I to COESA Working Group, AFCRL INAP-7 (Rev. 2), March 1961.
7. Champion, K. S. W. and Minzner, R. A., "Proposed Revision of U. S. Standard Atmosphere 90 to 700 Km," Research Report, AFCRL-62-802, 1962.
8. Greenhow, J. S. and Hall, J. E., "Diurnal Variations of Density and Scale Height in the Upper Atmosphere," Journal Atmos. and Terres. Physics, Vol. 18, No. 2/3 pp 203 to 214, June 1960.
9. Nicolet, M., "The Constitution and Composition of the Upper Atmosphere," IRE Proceedings, Vol. 47, No. 2, February 1959.
10. Johnson, F. S., "Structure of the Upper Atmosphere," Satellite Environment Handbook, Stanford University Press, Stanford, 1961.
11. King-Hele, D. G. and Walker, D. M. C., "Density of the Upper Atmosphere and Its Dependence on the Sun as Revealed by Satellite Orbits, Nature," Vol. 186, No. 4729, pp 928 to 931, 18 June 1960.

12. Jacchia, L. G., "A Variable Atmospheric-Density Model from Satellite Observations," Journ. Geophys. Res., Vol. 65, No. 9, September 1960.

13. Martin, H. A. and Priester, W., "Measurement of Solar and Diurnal Effects in the High Atmosphere by Artificial Satellites," Nature, Vol. 185, No. 4713, pp 600 to 601, 27 February 1960.

14. Groves, G. V., "Latitude and Diurnal Variations of Air Densities from 190 to 280 km from Discoverer Satellites," Proc. Royal Soc. A, Vol. 263, No. 1313, pp 212 to 216, 5 September 1961.

15. Kallman-Bijl, H. K., "Daytime and Nighttime Atmospheric Properties," Journ. Geophys. Res., Vol. 66, No. 3, pp 787 to 795, March 1961.

16. Priester, W., Martin, H. A. and Kramp, K., "Diurnal and Seasonal Density Variations in the Upper Atmosphere," Nature, Vol. 188, No. 4746, pp 202 to 204, 15 October 1960.

17. Parkyn, D. G., "Satellite Orbits in an Oblate Atmosphere," Journ. Geophys. Res., Vol. 65, No. 1, pp 9 to 17, January 1960.

18. Kallman, H. K., "A Preliminary Model Atmosphere Based on Rocket and Satellite Data," Journ. Geophys. Res., Vol. 64, No. 6, pp 615 to 623, June 1959.

19. Priester, W. and Martin, H. A., "Earth Satellite Observations and the Upper Atmosphere," Nature, Vol. 188, No. 4746, pp 200 to 202, 15 October 1960.

20. Jastrow, R. and Bryant, R., "Variations in the Orbit of the Echo Satellite," Journ. Geophys. Res., Vol. 65, No. 10, pp 3512 to 3513, October 1960.

21. Quiroz, R. S., "Air Density in the Mesosphere," Journ. Geophys. Res., Vol. 66, No. 7, pp 2129 to 2139, July 1961.

22. Sissenwine, N., Ripley, W. S. and Cole, A. E., "Behavior of Atmospheric Density Profiles," AFCRC-TN-58-627, Air Force Surveys in Geophysics, No. 109, December 1958.

23. Alfuth, W. H., Dickey, L. R. and Alsobrook, A. P., "An Attempt to Establish a Standard Atmospheric Density Profile Under Consideration of Its Time and Space Variation," RR-TR-3-60, Marshall Space Flight Center, 30 December 1960.

24. Anonymous, "Variable Atmospheric Models," Flight Performance Handbook, Wolverton, R. W. ed., STL, pp 2 to 336, September 1961.

25. Priester, W. and Martin, H. A., "Solar and Diurnal Effects in the Upper Atmosphere," Royal Aircraft Establishment Library Translation 901, Ministry of Aviation, London W. C. 2, England.

26. Paetzold, H. K., "A Proposal for a Self-Consistent Model of the Upper Atmosphere and Its Variations," Technische Hochschule, Munich, West Germany, 1961.

27. Friedman, H., Physics of the Upper Atmosphere, Edited by J. A. Ratcliffe, Academic Press, New York, 1960.

28. Allen, C. W., Astrophysical Quantities, The Athlone Press, University of London, London, 1955.

29. Dugas, D. J., "Solar Flare Radiation and Manned Space Flight," RM-2825-PR, The Rand Corp., November 1961.

30. Russak, S. and Kaplan, I., "Rocket Measurements of Energetic X-Rays During Solar Flares," ER 12440, The Martin Company, June 1962.

31. Foelsche, T., "Protection Against Solar Flare Protons," presented at 7th Annual Meeting of American Astronautical Society, Dallas, 16 to 18 January 1961.

32. Winckler, J. R. and Bhavsar, P. D., "Low Energy Solar Cosmic Rays and the Geomagnetic Storm of May 12, 1959," Journ. Geophys. Res., Vol. 65, No. 9, p 2637, 1960.

33. Beck, A. J. and Divita, E. L., "Evaluation of Space Radiation Doses Received Within a Typical Spacecraft," ARS Journal, Vol. 32, No. 11, pp 1668 to 1676, November 1962.

34. Yoshida, S., Ludwig, G. H. and Van Allen, J. A., "Distribution of Trapped Radiation in the Geomagnetic Field," Journ. Geophys. Res., Vol. 65, No. 3, p 807, 1960.

35. McIlwain, C. E., "Coordinates for Mapping the Distribution of Magnetically Trapped Particles, Journ. Geophys. Res., Vol. 66, No. 11, p 3681, November 1961.

36. Freden, S. C. and White, R. S., "Particle Fluxes in the Inner Radiation Belt," Journ. Geophys. Res., Vol. 65, No. 5, p 1377, 1960.

37. Van Allen, J. A., "The Geomagnetically Trapped Corpuscular Radiation," Journ. Geophys. Res., Vol. 64, No. 11, p 1683, 1959.

38. Van Allen, J. A., McIlwain, C. E. and Ludwig, G. H., "Radiation Observations with Satellite 1958E," Journ. Geophys. Res., Vol. 64, No. 3, p 271, 1959.

39. Holley, F. E., "Radiation Measurements to 1500 Kilometers with Atlas Pods," Air Force Special Weapons Center, TR 60-9, May 1960.

40. Walt, M., Chase, L. F., Cladis, J. B., Imhof, W. L. and Knecht, D. J., "Energy Spectra and Altitude Dependence of Electrons Trapped in the Earth's Magnetic Field," Proceedings of First International Space Science Symposium, Nice, 1960.

41. Van Allen, J. A. and Frank, L. A., "Radiation Around the Earth to a Radial Distance of 107,400 km, "Nature, Vol. 183, p 430, 1959.

42. Van Allen, J. A. and Frank, L. A., "Radiation Measurements to 658,300 km with Pioneer IV," Nature, Vol. 184, p 219, 1959.

43. Pizzella, G., Laughlin, C. D. and O'Brien, B. J., "Note on the Electron Energy Spectrum in the Inner Van Allen Belt," Journ. Geophys. Res., Vol. 67, No. 9, p 3281, 1962.

44. Frank, L. A., Dennison, D. C. and Van Allen, J. A., "Electrons in the Earth's Inner Radiation Zone, Abstract," Journ. Geophys. Res., Vol. 67, No. 9, p 3558, 1962.

45. Russak, S., "Radiation Doses from Electrons and Bremsstrahlung in the Van Allen Belts," presented at Symposium on the Protection of Man Against the Radiation Hazards of Space, Gatlinburg, 7 November 1962.

46. Van Allen, J. A., "The Nature and Intensity of Cosmic Radiation," Physics and Medicine of the Upper Atmosphere, University of New Mexico Press, 1952.

47. Haber, H., "Physical Factors of the Space Environment," Space Technology, John Wiley and Sons, 1959.

48. Singer, S. F., "The Primary Cosmic Radiation and Its Time Variations," Progress in Elementary Particle and Cosmic Ray Physics, Vol. IV, North Holland Publishing Co., Amsterdam, 1958.

49. Reitz, D., "Cosmic Rays, Nuclear Reactors, and Manned Space Systems," Aerospace Engineering, Vol. 20, No. 4, p 28, April 1961.

50. Wallner, L. E. and Kaufman, H. R., "Radiation Shielding for Manned Space Flight," NASA TN D-681, July 1961.

51. Friedman, H., "Solar Flare Patrol and Ionizing Radiation in the Night Sky," Paper presented to the American Rocket Society, June 1958.

52. Peterson, L. E. and Winckler, J. R., "Gamma Ray Burst from a Solar Flare," Journ. Geophys, Res., Vol. 64, No. 7, July 1959.

53. Chubb, T. A., Friedman, H. and Kreplin, R. W., "Measurements Made of High Energy X-Rays Accompanying Three Class 2+ Solar Flares," Journ. Geophys. Res., Vol. 65, No. 6, June 1960.

54. Ibid.

55. Saylor, W. P, et al., "Space Radiation Guide," AMRL-TDR-62-86, Biomedical Laboratory, AFSC, WPAFB, Ohio, August 1962.

56. Gardner, R. E., "Effects of Ionizing Radiation on Solid Rocket Motor Components," Jet Propulsion Laboratory Tech Rep No. 32-234, December 1961.

57. Jaffe, L. D. and Rittenhouse, J. B., "Behavior of Materials in Space Environments," Jet Propulsion Laboratory, Tech Rep No. 32-150, November 1961.

58. "Physical Protection of Man Against Ionizing Radiation of Extra-Terrestrial Origin," The Martin Company (Baltimore), ER 12354P, March 1962.

59. Naumann, R. J., "Meteoric Effects on Long Range and Orbital Vehicles," Army Ballistic Missile Agency Report No. DS-TN-94, 27 September 1957.

60. Rodriguez, D., "A Technical Note Concerning Meteoric Problems Related to Space Vehicles," ASI No. 11407 Aeronutronic Systems, Inc., 6 April 1959.

61. Rodriguez, D., "Meteoric Shielding for Space Vehicles," Aerospace Engineering, December 1960.

62. Davison, E. H. and Winslow, P. C., Jr., "Space Debris Hazard Evaluation," NASA TN D-1105, December 1961.

63. Whipple, F. L., "The Meteoric Risk to Space Vehicles," Proceedings of the 8th Congress of the International Astronautical Federation, Springer Verlag, Vienna, 1958.

64. Whipple, F. L., "Particulate Contents of Space," Presented at Symposium on the Medical and Biological Aspects of the Energies of Space, U. S. School of Aviation Medicine, San Antonio, 1960.

65. McCracken, C. W. and Alexander, W. M., "The Distribution of Small Interplanetary Dust Particles in the Vicinity of Earth," Presented at International Symposium on the Astronomy and Physics of Meteors held at Cambridge, Mass., 28 August to 1 September 1961.

66. McCrosky, R. E., "Observations of Simulated Meteors," Smithsonian Contributions to Astrophysics, Vol. 5, No. 4, 1961.

67. Davidson, J. R., Sandorff, P. E., et al., "Environmental Problems of Space Flight Structures, II Meteoroid Hazard," NASA TN D-1493 Langley Research Center, Va. (preliminary).

68. Kornhauser, M., "Satellite Pressure Losses Caused by Meteoroid Impacts," ARS Journal, May 1960.

69. Summers, J. L., "Investigation of High-Speed Impact: Regions of Impact and Impact at Oblique Angles," NASA TN D-94, October 1959.

70. Bjork, R. L., "Effects of a Meteoroid Impact on Steel and Aluminum in Space," Proceedings 10th International Astronautical Congress, London, 1959.

71. Bjork, R. L., "A Conservative Estimate of the Meteoroid Penetrating Flux," Rand Corporation Report P-1913, 11 February 1960.

72. Bjork, R. L., Comments on "The Effect of Micrometeoritic on Reflecting Surfaces," Rand Corporation Report P-1936, 29 February 1960.

73. "Earth Lunar Transportation System," Martin ER 12387-1, Martin Company, Space Systems Division, Baltimore, 1962.

74. Kraft, J. D., "Position of the Sun with Respect to an Earth Satellite," Martin Company, Baltimore, ER 12507, April 1962.

E. BIBLIOGRAPHIES

Alexandrov, I., "The Lunar Gravitational Potential," Advances in the Astronautical Sciences, Plenum Press, New York, Vol. 5, pp 320 to 324, 1960.

American Ephemeris and Nautical Almanac, Washington, D.C., U.S. Government Printing Office (Annual).

Baker, R. M. L., Jr. and Makemson, M. W., "Introduction to Astrodynamics," Academic Press, New York, 1960.

Belkovich, I. V., "The Physical Libration of the Moon," Pub Engelhardt Obs, 1949, No. 24 (also, Transactions of the IAU, Vol. 8, p 220, 1952.

Brouwer, D., "A New Determination of the Solar Parallax from the Parallactic Inequality in the Moon's Longitude; Comments on the Masses of the Inner Planets; Notes on Investigations in Progress," BANS, Vol. 15, p 165, 1950.

Brouwer, D. and Ashbrook, J., "The Minor Planet (619) Tribergs and the Mass of the Moon," Astronomical Journal, Vol. 56, p 57, 1951.

Brown, E. W., "Tables of the Motion of the Moon," Yale University Press, New Haven, Connecticut, 1919.

Chovitz, B. and Fischer, I., "Hough Ellipsoid," Transactions of the American Geophysical Union, Vol. 37, pp 339, 534, 1956.

Christie, Sir W. H. M. and Gill, Sir D., "Determination of the Moon's Parallax from Meridian Observations of the Crater Mösting A at the Royal Observatories of Greenwich and the Cape of Good Hope in the Years 1906-1910," MNRAS, Vol. 71, p 426, 1911.

Clemence, G. M.,
"Coordinates of the Center of Mass of the Sun and the Five Outer Planets," Astronomical Papers, American Ephemeris, Vol. 13, Part 4, p 323, 1953.
"Motion of Jupiter and Mass of Saturn," Astronomical Journal, Vol. 65, p 21, 1960.
"The Motion of Mercury, 1765-1937," Astronomical Journal, American Ephemeris, Vol. 11, Part 1, 1943.
"On the System of Astronomical Constants," Astronomical Journal, Vol. 53, p 169, 1948.

Clemence, G. M. and Scott, F. F., "Note on the Mass of Venus Derived from the Observations of Mars," Astronomical Journal, Vol. 49, p 188, 1942.

Cohen, C. J. and Anderle, R. J., "Verification of the Earth's 'Pear Shape' Gravitational Harmonic," Science, Vol. 131, pp 807 to 808, 1960.

Cook, A. H., "Reports on the Progress of Geophysics Developments in Dynamical Geodesy," Geophysical Journal Royal Astronomical Society, Vol. 2, p 222, 1959.

Delano, E., "The Lunar Equation from Observations of Eros 1930-31," Astronomical Journal, Vol. 55, p 192, 1950.

DeMarcus, W. C., "Planetary Interiors," Encyclopedia of Physics, Springer Verlag, Berlin, pp 419 to 448, 1959.

DeSitter, W.,
"On the Flattening and the Constitution of the Earth," Bulletin of the Astronomical Institute of the Netherlands, Vol. 2, p 97, 1924.
"On the Most Probable Values of Some Astronomical Constants, First Paper, Constants Connected with the Earth," Bulletin of the Astronomical Institute of the Netherlands, Vol. 4, p 57, 1927.

DeSitter, W. and Brouwer, D., "On the System of Astronomical Constants," Bulletin of the Astronomical Institute of the Netherlands, Vol. 8, p 213, 1938.

DeVaucouleurs, G.,
"Remarks on Mars and Venus," The Exploration of Space, The Macmillan Company, New York, pp 94 to 99, 1960.
"The Planet Mars," Astron. Soc. Pac. Leaflet, No. 276, 1952.
"The Astronomical Unit of Distance," Geophysics Corporation of America Report, Boston, January 1961.

Duncombe, R. L., "The Motion of Venus, 1750-1949," Astronomical Journal, Vol. 61, pp 266 to 268, 1956.

Dunham, T., "Spectroscopic Observations of the Planets at Mt. Wilson," The Atmospheres of the Earth and Planets, University of Chicago Press, Chicago, Illinois, pp 286 to 303, 1949.

Elfers, W. A., Satellite Data Handbook, Project Vanguard, Martin Company, Baltimore, Maryland, Engineering Report No. MR 6193-W, January 1957.

Encke, J. F., "Elements and Ephemerides of Vesta," Berliner Jahrbuch, 1838.

Fischer, I., "Parallax of the Moon in Terms of a World Geodetic System," Astronomical Journal, Vol. 67, No. 6, p 363, August 1962.

Fotheringham, J. K., "Note on the Mass of Venus," MNRAS, Vol. 86, p 296, 1926

Gill, Sir D., "Determination of the Solar Parallax and the Mass of the Moon from Heliometer Observations of Iris, Victoria and Sappho Made in the Years 1888 and 1889," Ann. Cape Observatory, Vols. 6 and 7, 1896 and 1897.

Hansen, P. A., "Auseinandersetzung einer Zweckmässigen Methode zur Berechnung Absoluten Störungen der Kleinen Planeten," Abhand, de K. S. Gesell. de Wiss., Vols. 5, 6 and 7, p 189, 1861.

Hayn, F., "Selenographische Koordinaten III," Leipzig Abhand., Vol. 30, pp 1 to 103, 1907.

Herrick, S., "Icarus and the Variation of Parameters," Astronomical Journal, Vol. 58, p 156, 1953

Herrick, S., Baker, R. M. L., Jr. and Hilton, C. G., "Gravitational and Related Constants for Accurate Space Navigation," UCLA Astronomical Papers, Vol. 1, No. 14, p 297, 1958.

Herrick, S., Westrom, G. B. and Makemson, M. W., "The Astronomical Unit and the Solar Parallax," UCLA Astrodynamical Report, No. 5, September 1959.

Hertz, H. G., "The Mass of Saturn and the Motion of Jupiter," Astronomical Papers, American Ephemeris, Vol. 15, Part 2, 1953.

Hess, S. L., "Atmospheres of Other Planets," Science, Vol. 128, pp 809 to 814, 1958.

Hinks, A. R., "Solar Parallax," MNRAS, Vol. 70, No. 9, p 588, 1909.

Hirose, H. and Manabe, R., "Motion and Figure of the Moon," Transactions of the IAU, Vol. 9, p 265, 1955.

Jacchia, L. G.,
"Slow Fluctuations Connected with Variable Solar Radiation," Smith. Astrophys. Obs. Special Report, No. 29, 1959.
"The Earth's Gravitational Potential as Derived from Satellites 1957 β_1 and 1958 β_2," Smith. Astrophys. Obs. Special Report, No. 19, pp 1 to 5, 1958.

Jastrow, R., et al., "Geophysical and Astrophysical Fundamentals," Handbook of Astronautical Engineering, McGraw-Hill Book Company, Inc., New York (Koelle, ed.) 1961.

Jeffreys, H.,
"The Moon's Libration in Longitude," MNRAS, Vol. 117, No. 5, p 475, 1957.
"On the Figures of the Earth and Moon," MNRAS, Vol. 97, p 3, 1936.
"The Figures of the Earth and Moon," Geophys. Supp. of MNRAS, Vol. 5, No. 7, p 219, 1948
"On the Figures of the Earth and Moon, Second Paper," MNRAS, Vol. 101, p 34, 1941.

Kaula, W. M., "A Geoid and World Geodetic System Based on a Combination of Gravimetric, Astro-Geodetic, and Satellite Data," Journ. Geophys. Res., Vol. 66, No. 6, June 1961.
"Estimation of Longitudinal Variations in the Earth's Gravitational Field from Satellite Observations," American Astronautical Society Preprint 61-26, 1961.
"Tesseral Harmonics of the Gravitational Field and Geodetic Datum Shifts Derived from Camera Observations of Satellites," Journal of Geophysical Research, Vol. 68, No. 2, 15 January 1963, pp 473 to 484.

Kiess, C. C., Karrer, S. and Kiess, H. K., "A New Interpretation of Martian Phenomena," Publ. Astron. Soc. Pac., Vol. 72, pp 256 to 267, 1960.

King-Hele, D. G., "Evaluation of the Second, Fourth and Sixth Harmonics in the Earth's Gravitational Potential," Nature, Vol. 187, pp 490 to 491, 1960.

King-Hele, D. G. and Merson R. K., "A New Value for the Earth's Flattening Derived from Measurements of Satellite Orbits," Nature, Vol. 183, pp 881 to 882, 1959.

Kozai, Y.,
"Note on the Secular Motions of the Node and Perigee of an Artificial Satellite," Smith. Astrophys. Obs. Special Report, No. 30, p 14, 1959.
"The Earth's Gravitational Potential Derived from the Motion of Satellite 1958 β_2," Smith. Astrophys. Obs. Special Report, No. 22, 1959.

Krüger, A., "Orbit of 24 Themis," Astron. Nach., Vol. 81, pp 331 to 334.

Kuiper, G. P., ed.,
The Atmospheres of the Earth and Planets, University of Chicago Press, Chicago, p 374, 1949.
"The Diameter of Neptune," Astrophysical Journal, Vol. 110, p 93, 1949.
"The Diameter of Pluto," Pub. ASP, Vol. 62, p 133, 1950.

Lambert, W. D., "The Figure of the Earth and the Parallax of the Moon," Astronomical Journal, Vol. 38, p 181, 1928.

Lecar, M., Sorenson, J. and Eckels, A., "A Determination of the Coefficient J of the Second Harmonic in the Earth's Gravitational Potential from the Orbit of Satellite 1958 β_2," Journ. Geophys. Res., Vol. 64, pp 209 to 216, 1959.

Ledersteger, K., "Die Näherungsmethoden des Astronomischen Nivellements und da im Nordteil des Meridianbogens Grossenhai Osterr. Z. Vermessungswesen, Vol. 39, Sonderheft 12, pp 37 to 45, 1951.

Leveau, G.,
"Determination des Elements Solaires et des Masses de Mars et Jupiter par les Observations Meridiennes de Vesta," Comptes Rendus, Vol. 145, p 903, 1907.
"Tables of Vesta," Paris Annales, Vol. 22, 1890.

Makemson, M., Baker, R. M. L., Jr. and Westrom, G. B., Analysis and Standardization of Astrodynamic Constants, 7th Annual Meeting of the American Astronautical Society, Dallas, Texas, January 1961. (Also, Journal of Astronautical Sciences, Vol. 8, No. 1, 1961.)

Martin, H. A. and Priester, W., "Measurement of Solar and Diurnal Effects in the High Atmosphere by Artificial Satellites," Nature, Vol. 185, pp 600 and 601, 1960.

McGuire, J. P., et al.,
"The Size of the Solar System," Scientific American, April 1961.
"A Dynamical Determination of the Astronomical Unit by a Least Squares Fit to the Orbit of Pioneer V," 106th Meeting of the American Astronautical Society, Mexico City, Paper No. 74, 1960.

Michielsen, H. F.,
"Fifth Harmonic of Earth's Gravitational Field," ARS Journal, Vol. 30, pp 976 to 978, 1960.
"The Odd Harmonics of the Earth's Gravitational Field," American Astronautical Society Preprint 61-25," 1961.

Mingner, R. A., Champion, K. S. W. and Pond, H. L., "ARDC Model Atmosphere, 1959," AFCRC-TR-59-267, Air Force Surveys in Geophysics No. 115, 1959.

Morgan, H. R. and Scott, F. F., "Observations of the Sun 1900-1937 Compared with Newcomb's Tables," Astronomical Journal, Vol. 47, p 193, 1939.

Müller, P., "Sur la Mesure des Diamètres Planétaires," Comité National Francaise d'Astronomia, 1948

Nefediev, A. A.,
Pub Engelhardt Obs., No. 26, 1951.
"Motion and Figure of the Moon," Transactions of the IAU, Vol. 8, p 218, 1952.
"Motion and Figure of the Moon," Transactions of the IAU, Vol. 9, p 264, 1955.

Newcomb, S.,
Elements of the Four Inner Planets and Astronomical Constants, Washington, 1895.
"On the Mass of Jupiter and the Orbit of Polyhymnia," Astronomical Papers, American Ephemeris, Vol. 5, Part 5, p 379, 1895.

Nicholson, S. B. and Mayall, N. U., "The Probable Value of the Mass of Pluto," Pub. ASP, Vol. 43, p 74, 1931.

O'Keefe, J. A.,
"IGY Results on the Shape of the Earth," ARS Journal, Vol. 29, No. 12, December 1959.
"Oblateness of the Earth by Artificial Satellites," Harvard College Obs. Announcement Card, 1408, June 1958.

O'Keefe, J. A. and Anderson, J. P., "The Earth's Equatorial Radius and the Distance of the Moon," Astronomical Journal, Vol. 57, p 108, 1952.

O'Keefe, J. A., Eckels, A. and Squires, R. K., "The Gravitational Field of the Earth," Astronomical Journal, Vol. 64, p 245, 1959.

O'Keefe, J. A. and Eckels, A., "Satellite 1958 β_2," Harvard College Obs. Announcement Card, 1420, December 1958.

Pettit, E. and Nicholson, S. B., "Temperatures on the Bright and Dark Sides of Venus," Pub. ASP, Vol. 67, p 293, 1955.

Price, R., Green. P. E., et al., "Radar Echoes from Venus," Science, Vol. 129, p 751, 1959.

Rabe, E.,
"Derivation of Fundamental Astronomical Constants from Observations of Eros During 1926-1945," Astronomical Journal, Vol. 55, p 112, 1949.
"Orbital Motion of Minor Planet (1362) Grique and the Mass of Jupiter," Astronomical Journal, Vol. 64, p 53, 1959.
"Additional Note on the Solar Parallax from Eros," Astronomical Journal, Vol. 59, pp 409 to 411, 1954.

Rabe, W., "Uber die Durchmesser der Grossen Planeten," Astron. Nach., Vol. 234, p 200, 1928.

Ratcliffe, J. A., ed.,
"Physics of the Upper Atmosphere," Academic Press, New York, p 586, 1960.
"The Thermosphere--the Earth's Outermost Atmosphere," Chapman, S., pp 1 to 16.
"The Properties and Consititution of the Upper Atmosphere," Nicolet, M., pp 17 to 72.
"The Upper Atmosphere Studied by Rockets and Satellites," Newell, H. E., Jr., pp 73 to 132.
"The Sun's Ionizing Radiations," Friedman, H., pp 133 to 218.
"The Airglow," Bates, D. R., pp 219 to 267.
"General Character of Auroras," Bates, D. R., pp 269 to 298.
"The Auroral Spectrum and Its Interpretation," Bates, D. R,, pp 299 to 353.
"Radar Studies of the Aurora," Booker, H. G., pp 355 to 375.
"The Ionosphere," Ratcliffe, J. A. and Weeks, K., pp 377 to 470.
"The Upper Atmosphere and Meteors," Greenhow, J. S. and Lovell, A. C. B., pp. 513 to 549.
"Advances During the IGY 1957/58," Greenhow, J. S. and Lovell, A. C. B., pp 551 to 563.

Reuyl, D., "Photographic Determination of the Diameter of Mars," Astronomical Journal, Vol. 49, p 125, 1941.

Ross, F. E.,
"New Elements of Mars," Astronomical Papers, American Ephemeris, Vol. 9, Part 2, p 251, 1916.
"Photographs of Venus," Astrophysical Journal, Vol. 68, p 57, 1928.

Sampson, R. A., "Theory of the Four Great Satellites of Jupiter," Memoirs of RAS, Vol. 63, pp 1 to 270, 1921.

Schmid, E., "Preliminary Values of the Ellipsoid Obtained by Using Deflections of the Vertical. . . in Hayford's Computations," Bull. Geodesique, Vol. 30, p 412, 1953.

See, T. J. J., "Preliminary Investigation of the Diameter of Mars," Astron. Nach., Vol. 157, p 98, 1901.

Smith, D. E., "Determination of the Earth's Gravitational Potential from Satellite Orbits," Planetary and Space Sci., Vol. 8, pp 43 to 49, October 1961.

Spencer-Jones, H.,
"Determination of the Solar Parallax from Eros Observations," Mem. RAS, Vol. 46, 1941.
"Discussion of the Greenwich Observations of the Sun, 1836-1923," MNRAS, Vol. 86, p 426, 1926.
"Solar Parallax from Radial Velocities of Stars," Ann. Cape Obs., Vol. 10, Part 8, 1928.
"The Solar Parallax and the Mass of the Moon from Observations of Eros at the Observations of 1931," Mem. RAS, Vol. 66, Part 2, p 56, 1941.

Struve, H., "Bestimmung der Abplattung und des Aequators von Mars," Astron. Nach., Vol. 138, p 217, 1895.

Townsend, G. and Musser, T., "Design Guide to Orbital Flight," McGraw-Hill Book Company, Inc., New York, Chapter 3, 1962.

Tross, C. "Astronomical Constants and Their Importance in Lunar Trajectory Determination," ARS Journal, Vol. 30, No. 10, pp 938 to 941, 1960.

Trumpler, R. J., "Observations of Mars at Opposition of 1924," Lick Obs. Bull., Vol. 13, p 19, 1927.

Urey, H.,
"The Atmospheres of the Planets," Handbuch der Physic, Vol. 52, pp 363 to 414, 1959.
The Planets, Yale University Press, New Haven, Connecticut, 1952.

Van De Kamp, P., "A Determination of the Diameter of Mars," Astronomical Journal, Vol. 38, p 61, 1928.

Watts, C. B., "A New Method of Measuring the Inclination of the Moon's Equator," Astronomical Journal, Vol. 60, p 443, 1955.

Westrom, G. B., "Trajectory Constants," Space Trajectories, Academic Press, New York, 1960.

Witt, G.,
"Baryzentrische Ephemeride des Planeten 433 Eros für 1930-31," Astron. Abhand to Astron. Nach., Vol. 9, 1933.
"Solar Parallax and Mass of Earth from the Orbit of Eros Between 1893 and 1931," Astron. Abhand to Astron. Nach., Vol. 9, 1935.

Woolard, E. W., "The Secular Perturbations of the Satellites of Mars," Astronomical Journal. Vol. 51, p 33, 1944.

Yakovkin, A. A.,
"General Characteristics of the Contour of the Moon," Transactions IAU, Vol. 8, p 229, 1952; Vol. 9, p 264, 1955.
"The Free Libration of the Moon," Transactions IAU, Vol. 8, p 231, 1952.

Yaplee, B. S., Bruton, R. H., Craig, K. J. and Roman, N. G., "Radar Echoes from the Moon at Wavelength 10 cm," Proceedings IRE, Vol. 46, p 293, 1958.

Yaplee, B. S., Bruton, R. H. and Miller, A. C., "Results of 10-cm Lunar Radar Range Study," paper presented to 8th General Assembly, URSI, London, 5 to 15 September 1960.

Yanow, G., "A Study of the Martian Upper Atmosphere and Ionosphere," Douglas Aircraft Company, Santa Monica, California, Engineering Paper No. 974, January 1961.

ILLUSTRATIONS

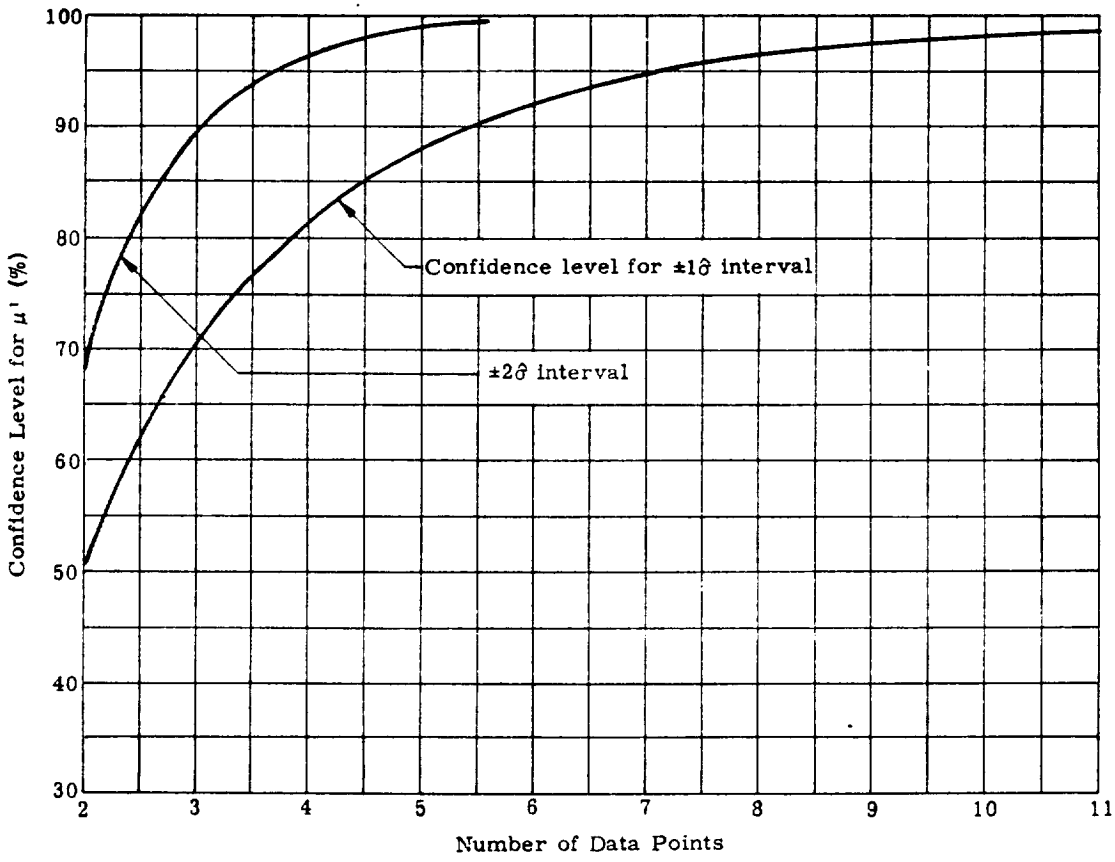

Fig. 1. Confidence Level for the Value of μ' as a Function of the Number of Data Points and Size of Interval

Preceding page blank

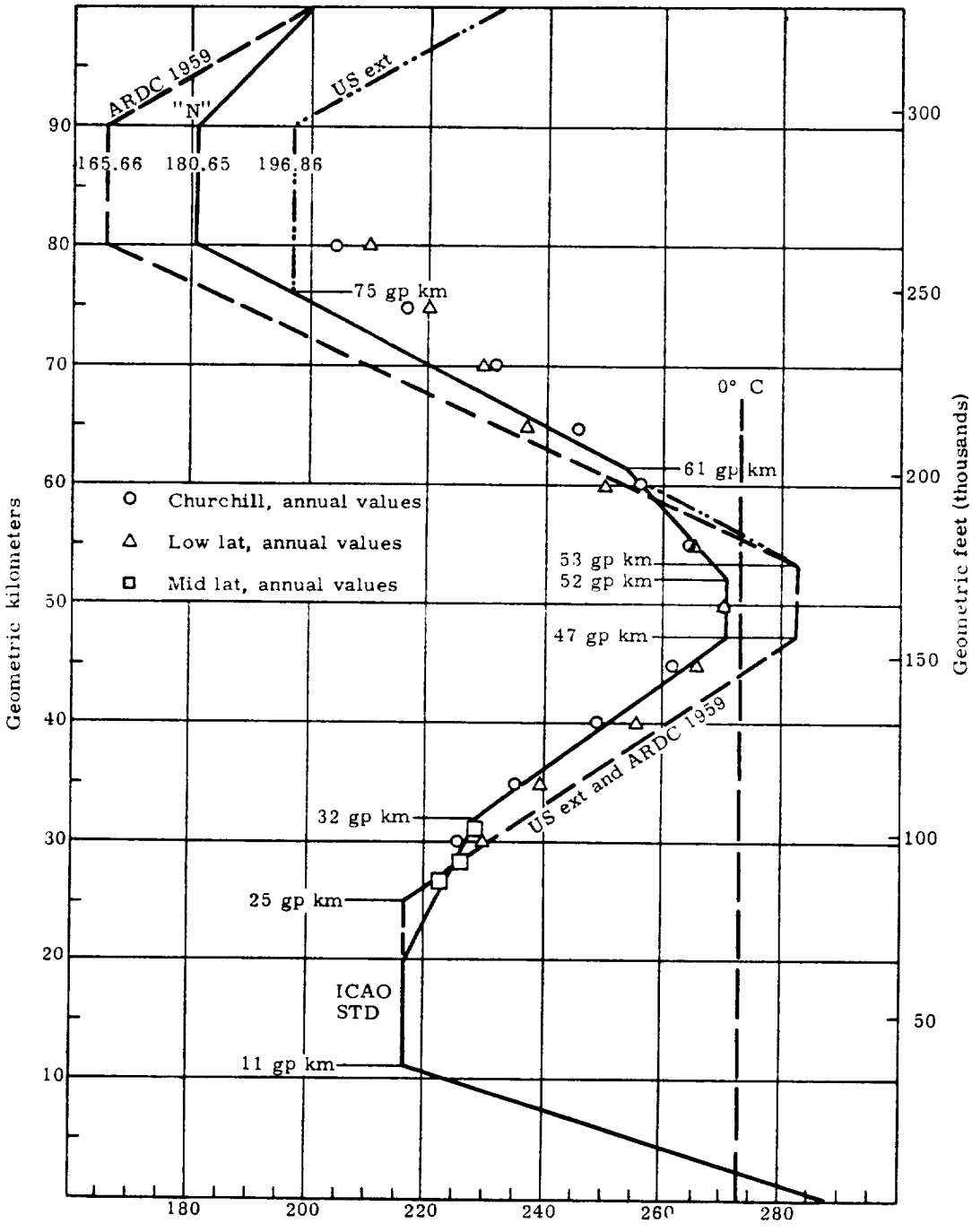

Fig. 2. Present Standard and Model Atmospheres, and Proposed Revision of U.S. Standard Atmosphere

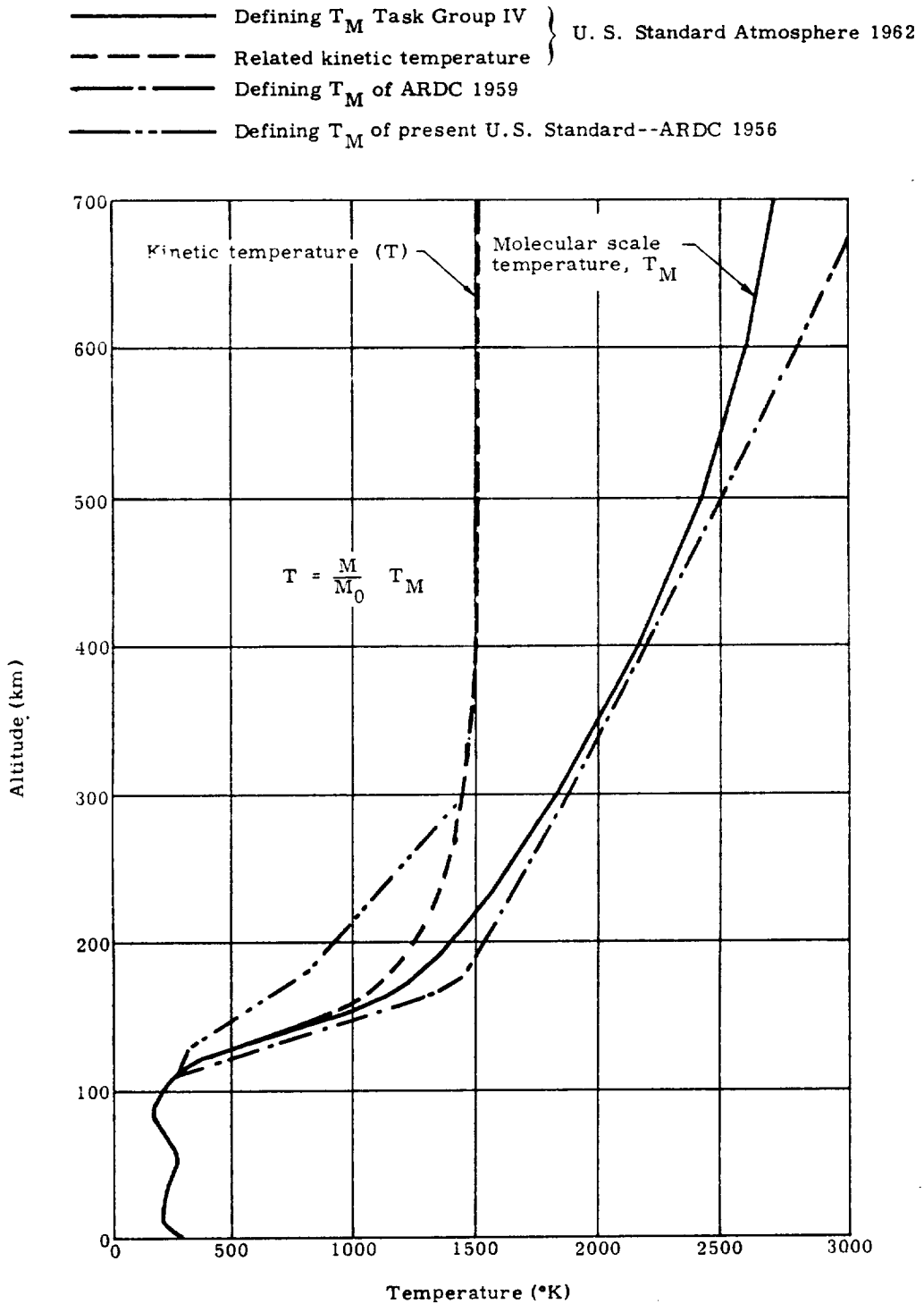

Fig. 3. Temperature Versus Altitude, Defining Molecular Scale Temperature and Kinetic Temperature of the Proposed Revision to the United States Standard Atmosphere

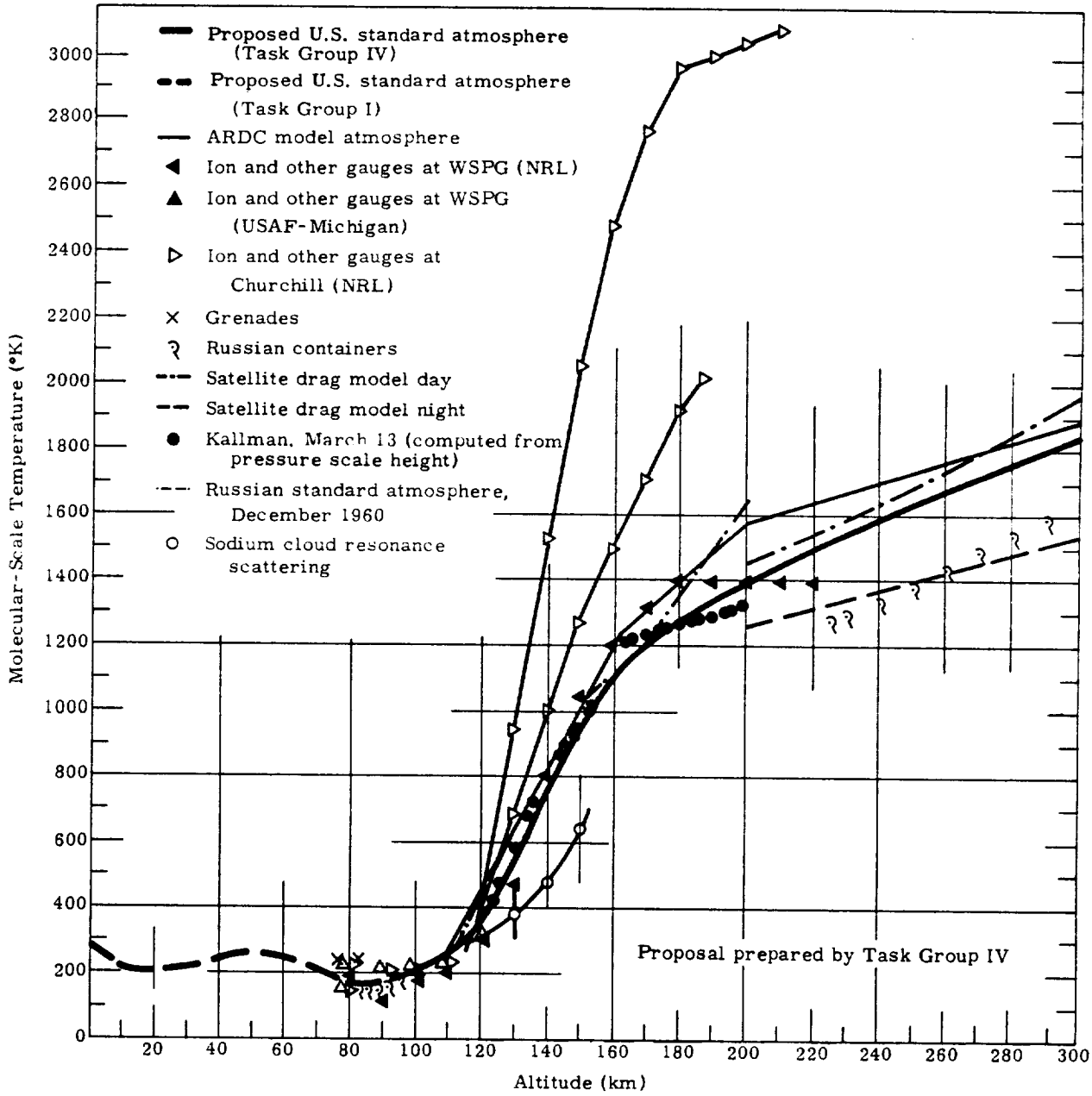

Fig. 4. Molecular-Scale Temperature Versus Geometric Altitude Proposed United States Standard Atmosphere Compared with United States Detailed Data, Russian Average Data, and ARDC Model Atmosphere 1959 for Altitudes Above 80 km Only

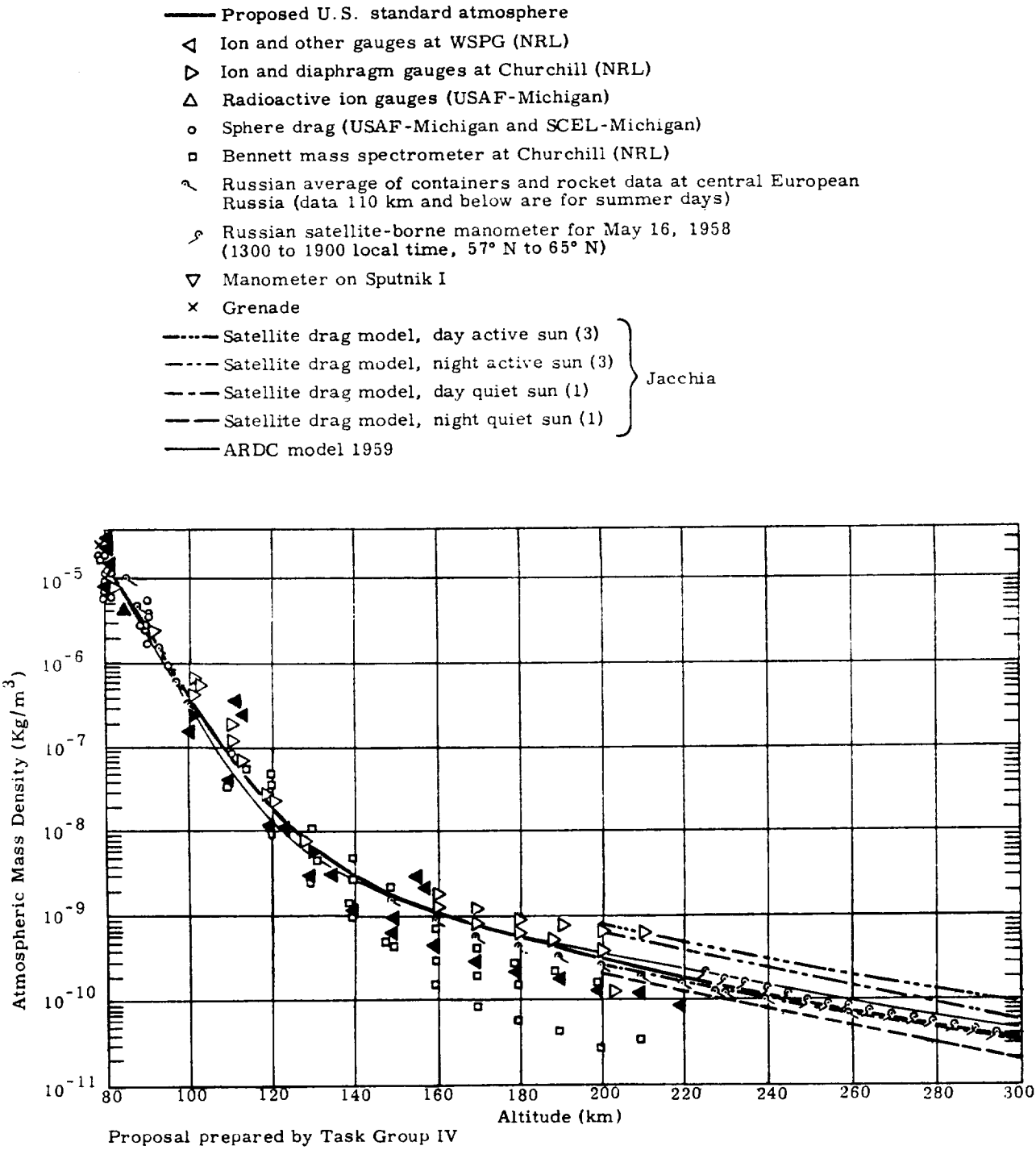

Fig. 5. Density Versus Geometric Altitude for Proposed United States Standard Atmosphere Compared with United States Detailed Data, Russian Average Data, and ARDC Model Atmosphere 1959

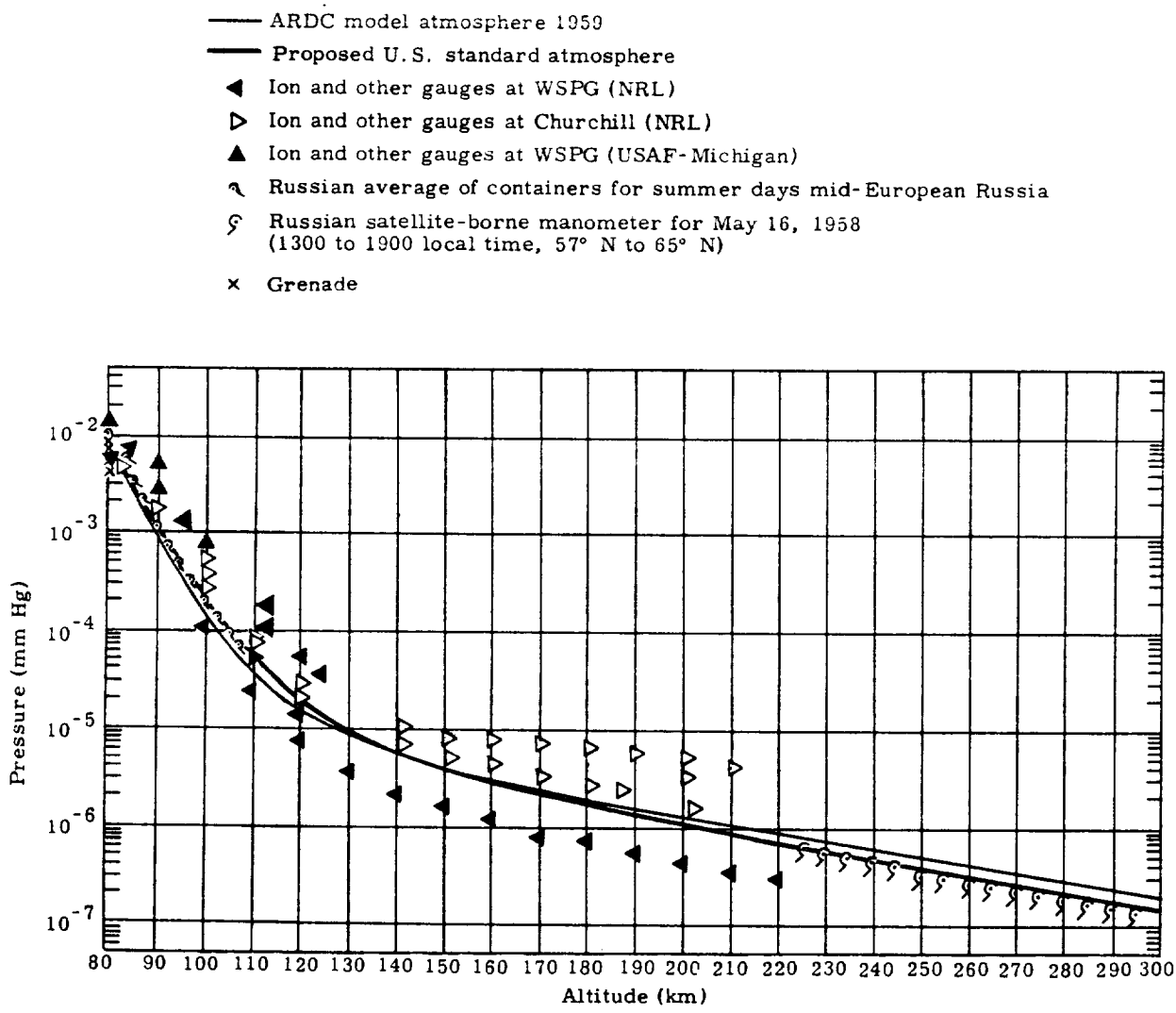

Proposal prepared by Task Group IV

October 15, 1961

Fig. 6. Pressure Versus Geometric Altitude for Proposed United States Standard Atmosphere Compared with United States Detailed Data, Russian Average Data and ARDC Model Atmosphere 1959

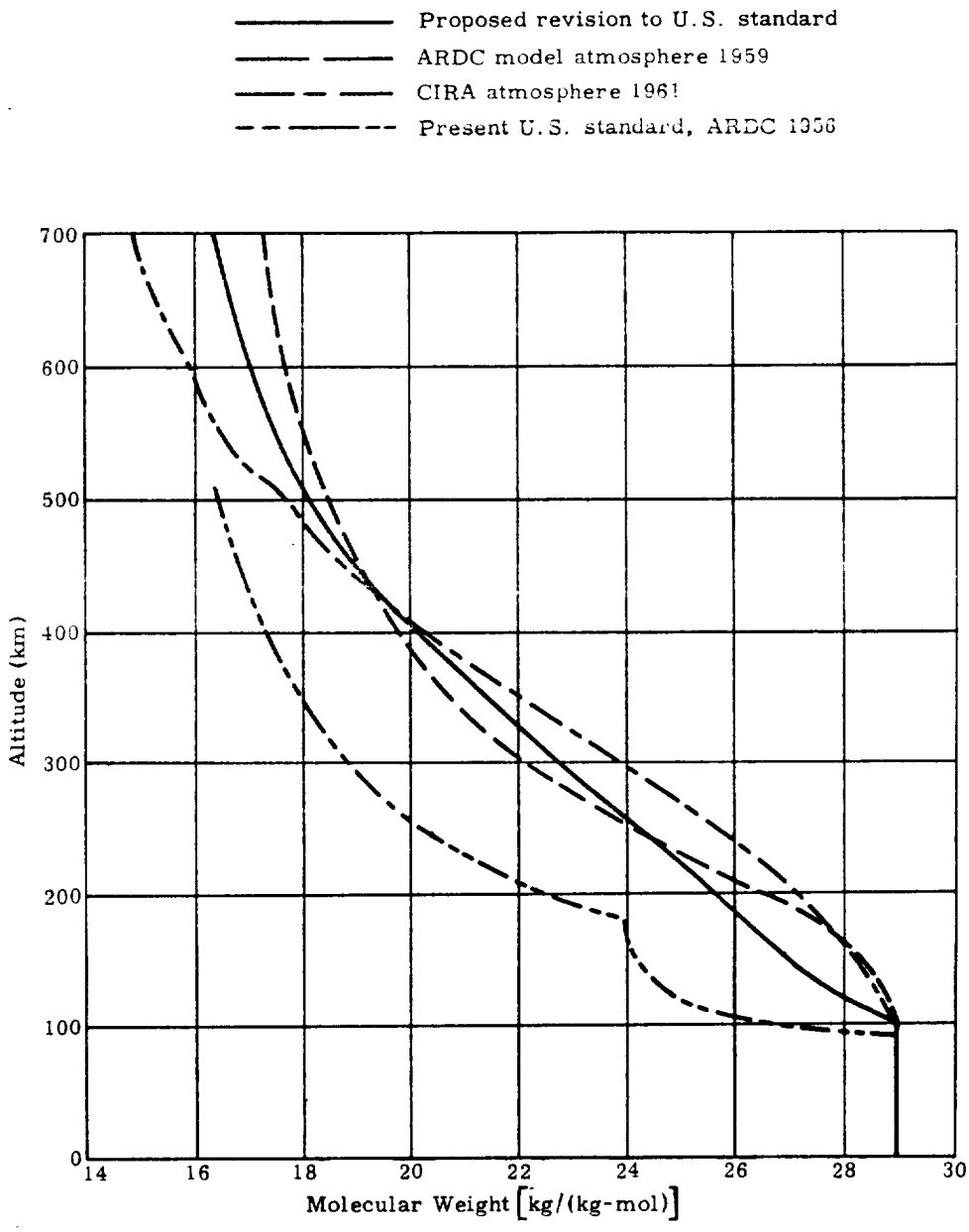

Fig. 7. Molecular Weight Versus Altitude

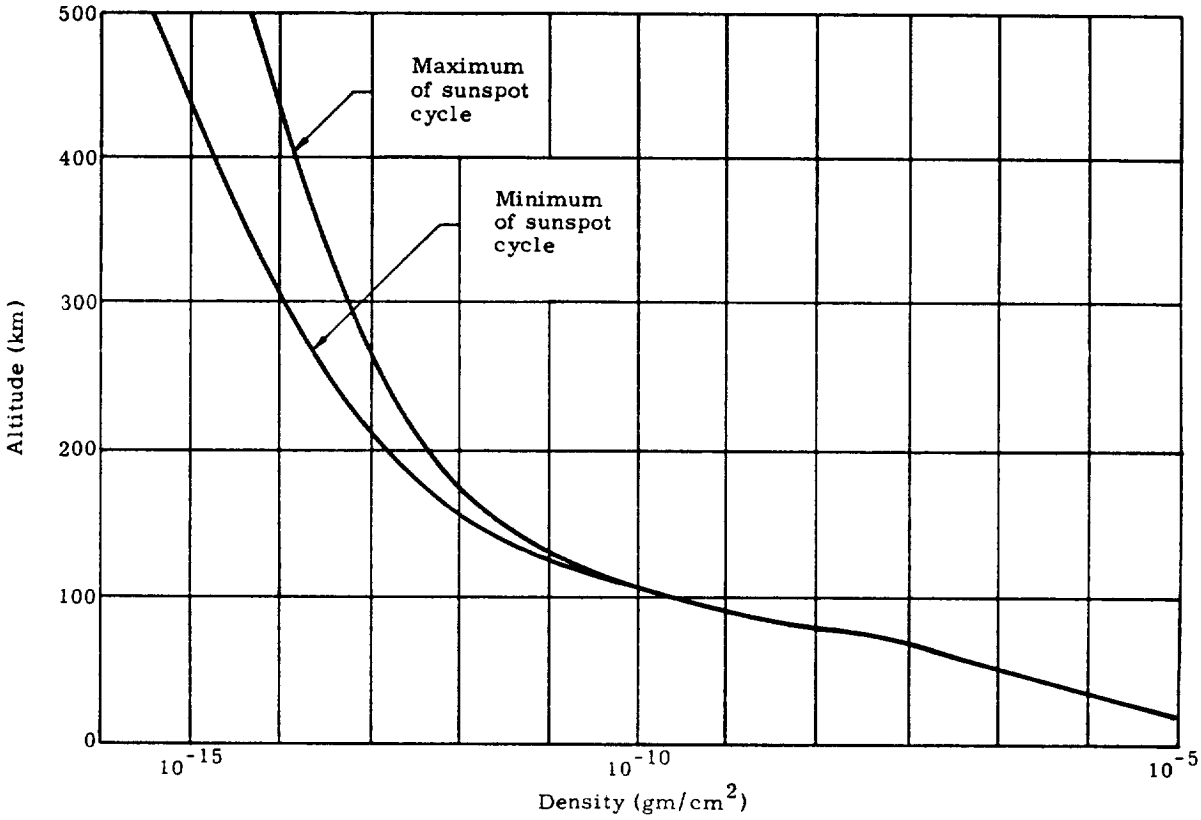

a. 0 to 500 km

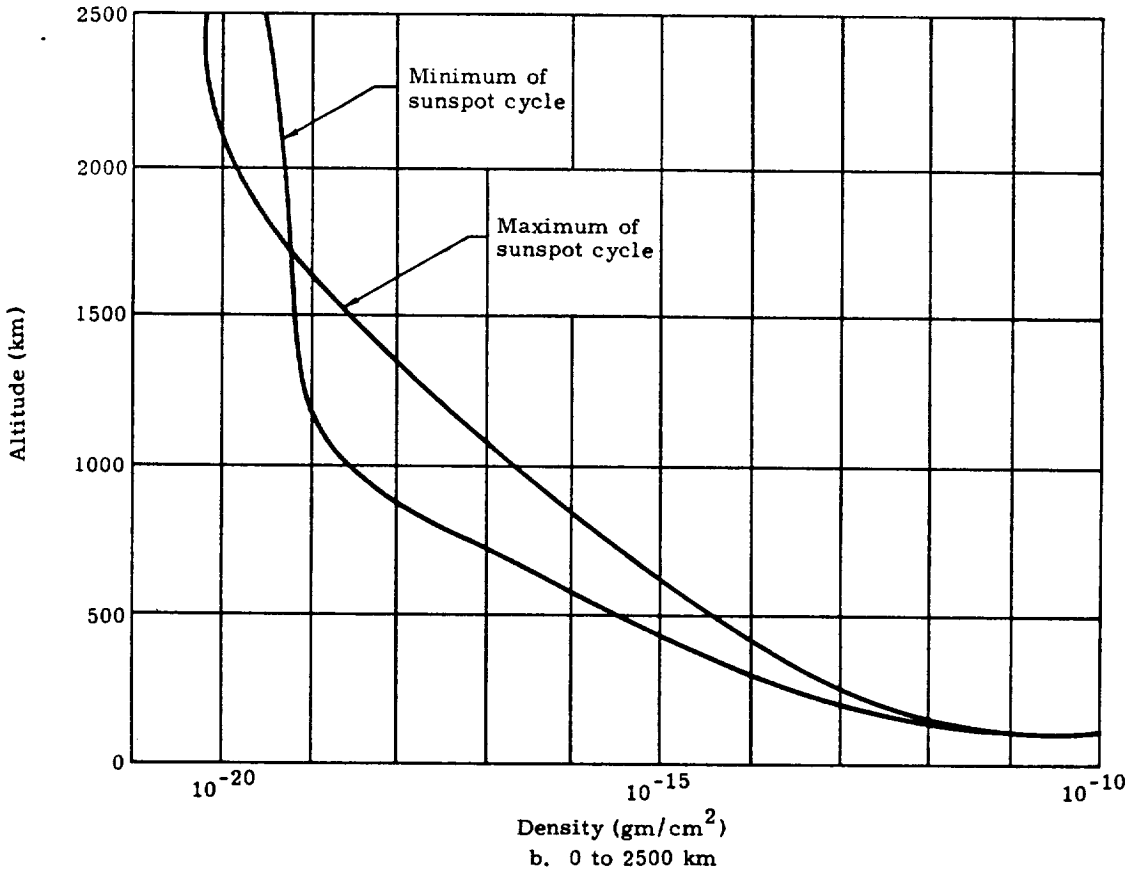

b. 0 to 2500 km

Fig. 8. Average Daytime Atmospheric Densities at the Extremes of the Sunspot Cycle

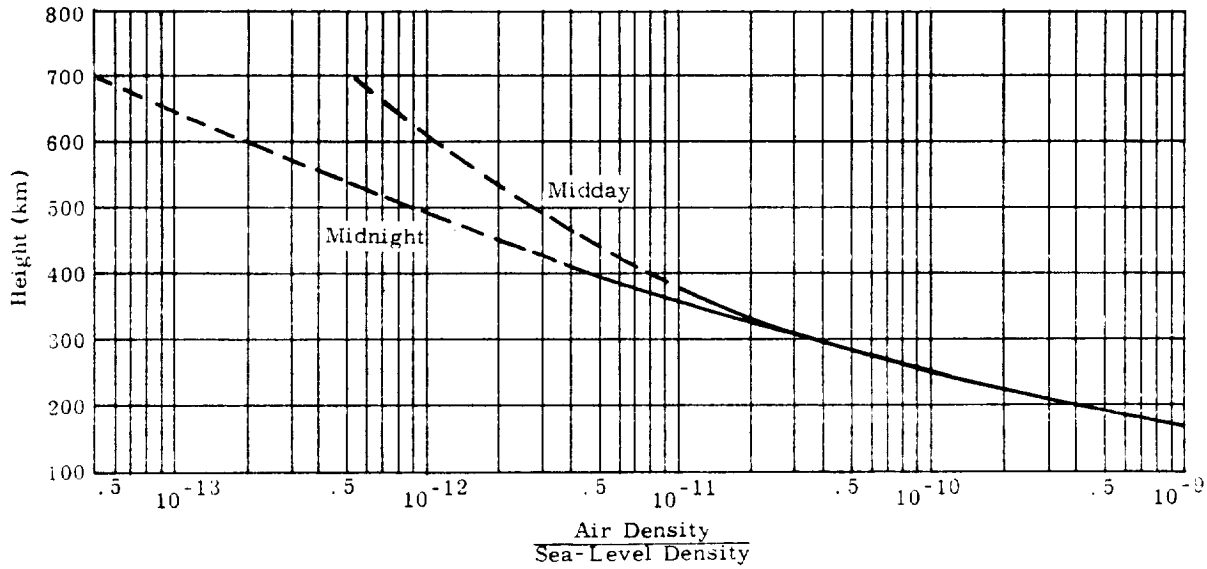

Fig. 9. Density of the Upper Atmosphere Obtained from the Orbits of 21 Satellites

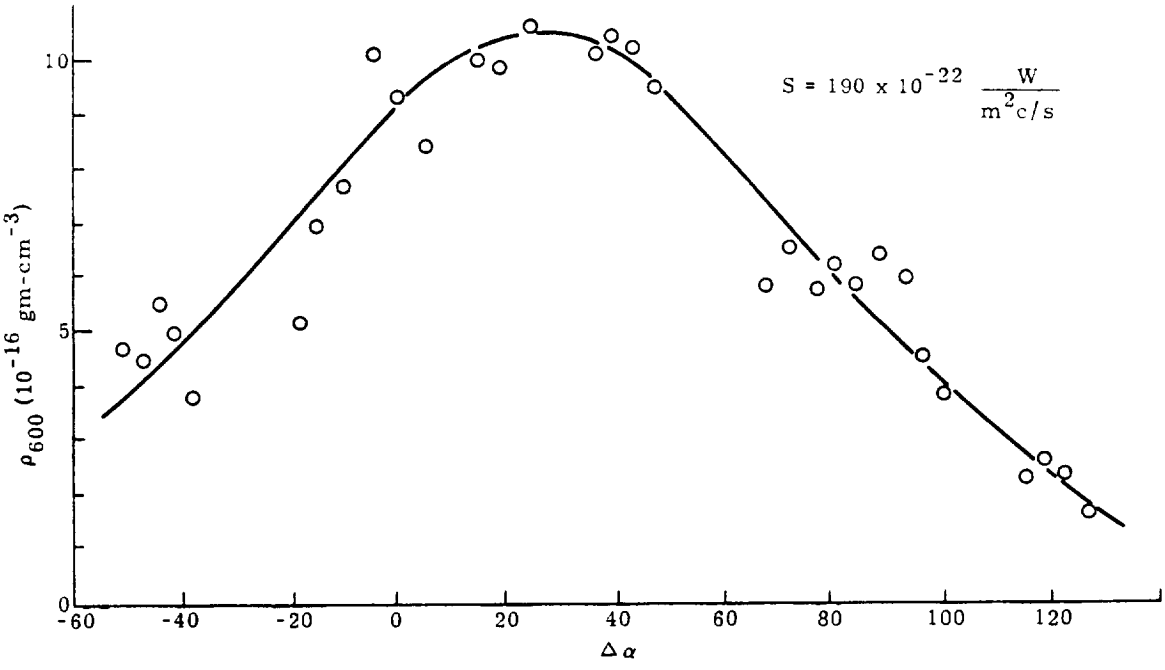

Fig. 10. Dependence of Atmospheric Density on $\Delta\alpha = \alpha_{\pi} - \alpha_{\odot}$ in the Equatorial Zone (diurnal effect)

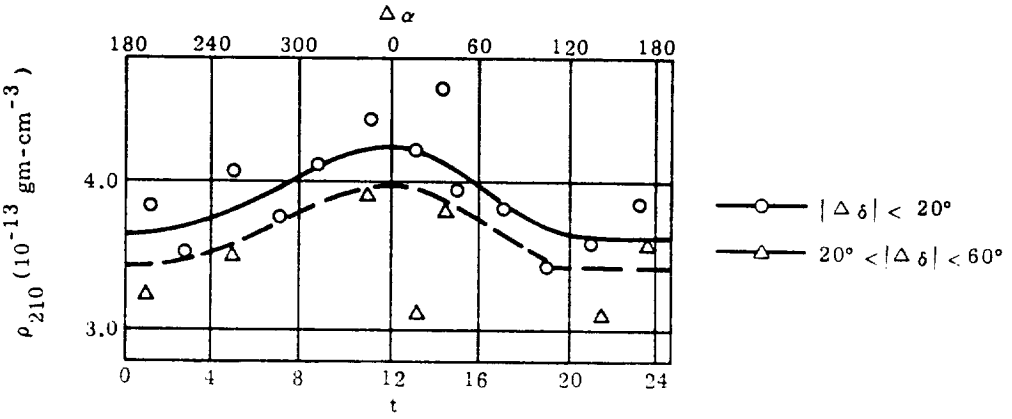

Fig. 11a. Diurnal and Seasonal Variations in Atmospheric Density at 210 km Derived from Observations of the Satellite 1958 δ 2. (The lower x-scale gives true local time, the upper $\Delta\alpha = \alpha_\pi - \alpha_\odot$. The parameter of the curves is $\Delta\delta = \delta_\pi - \delta_\odot$ where α is right ascension, δ is declination, π is perigee, ⊙ is sun.)

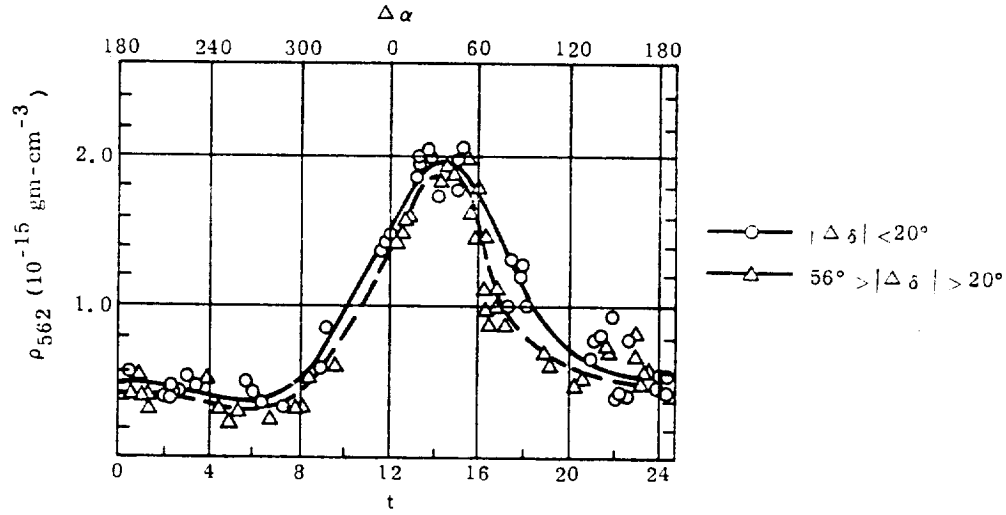

Fig. 11b. Variations in Atmospheric Density at 562 km Above the Earth Ellipsoid Derived from the Observations of Satellite 1959 α 1

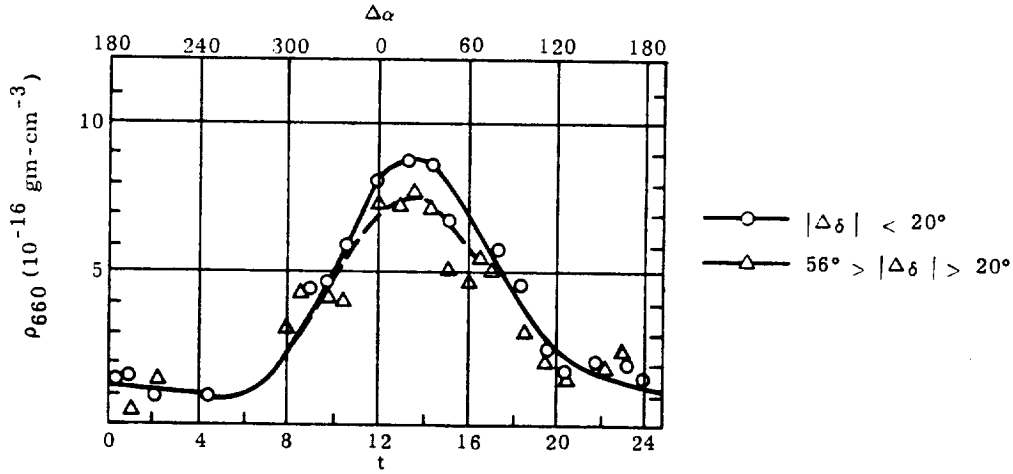

Fig. 11c. Variations in Atmospheric Density at 660 km Derived from the Observations of Satellite 1958 β 2

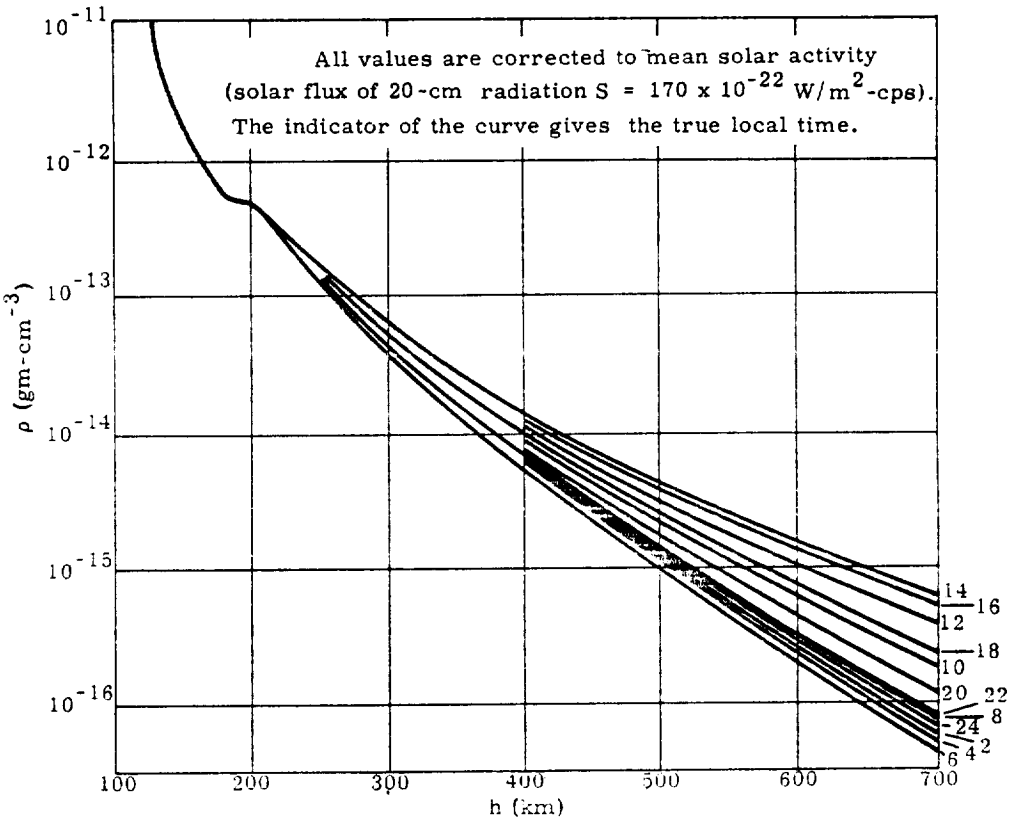

Fig. 12. Diurnal Variations of Atmospheric Density at Altitudes from 150 to 700 km above the Earth Ellipsoid for $|\Delta\delta| < 20°$

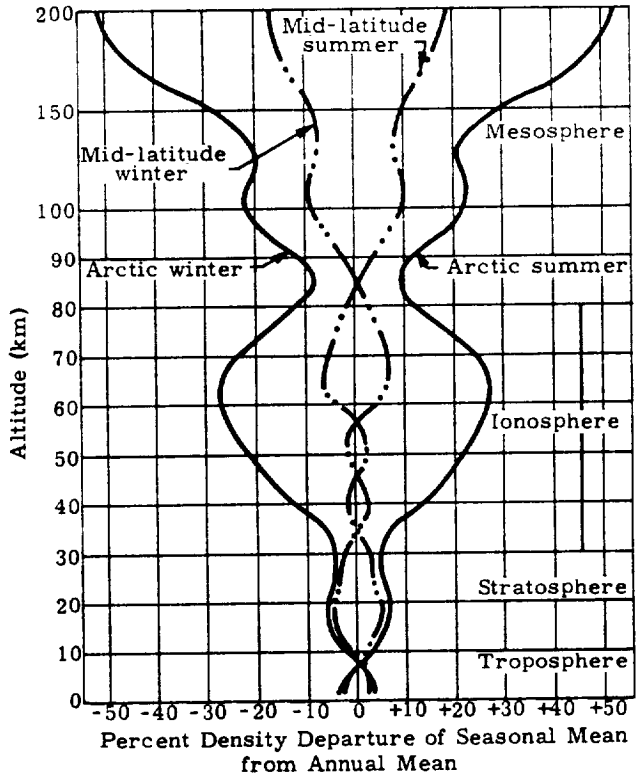

Fig. 13. Model of the Seasonal Variation of Mean Density to 200 km

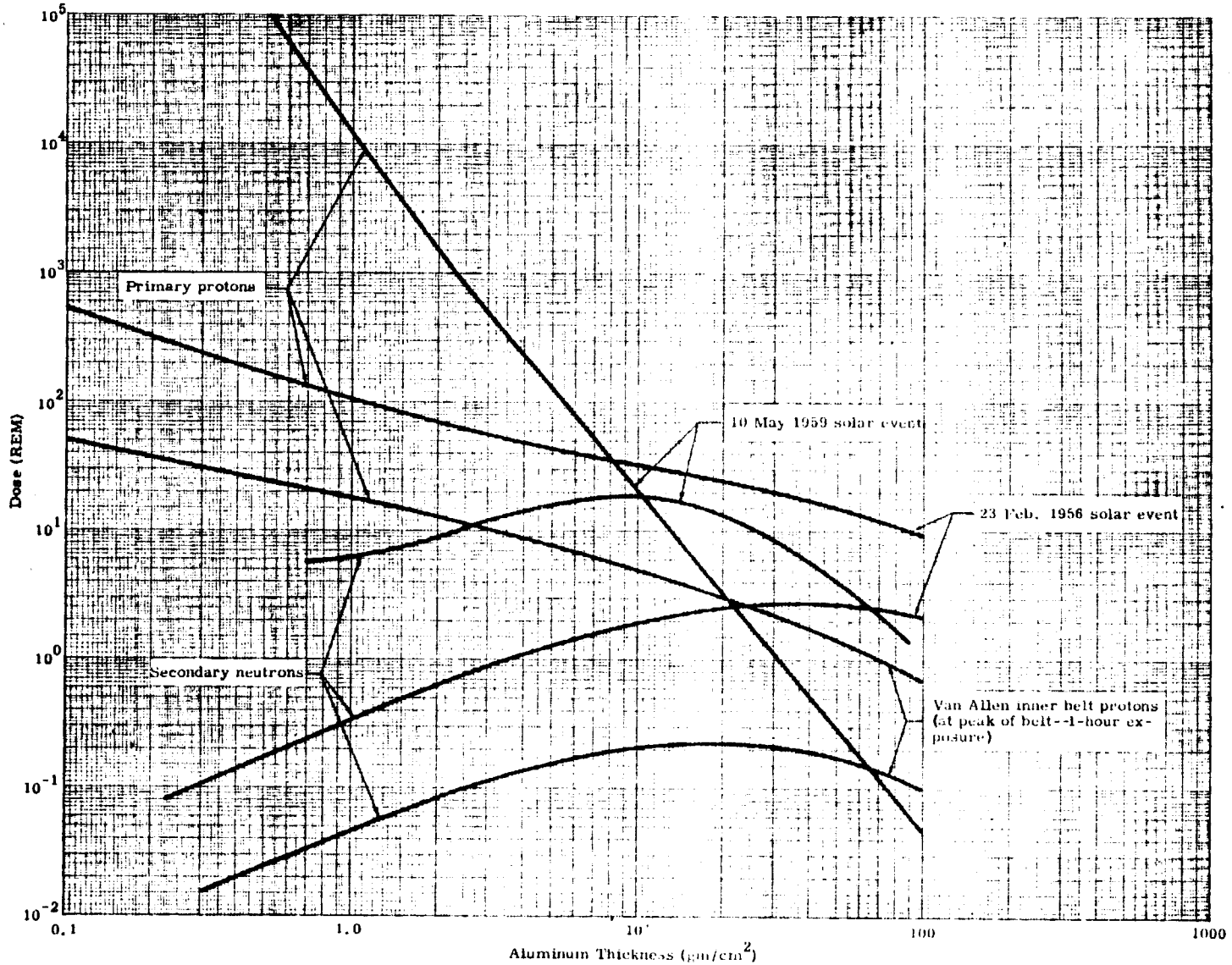

Fig. 14. Radiation Dose from Solar Flares Versus Skin Thickness

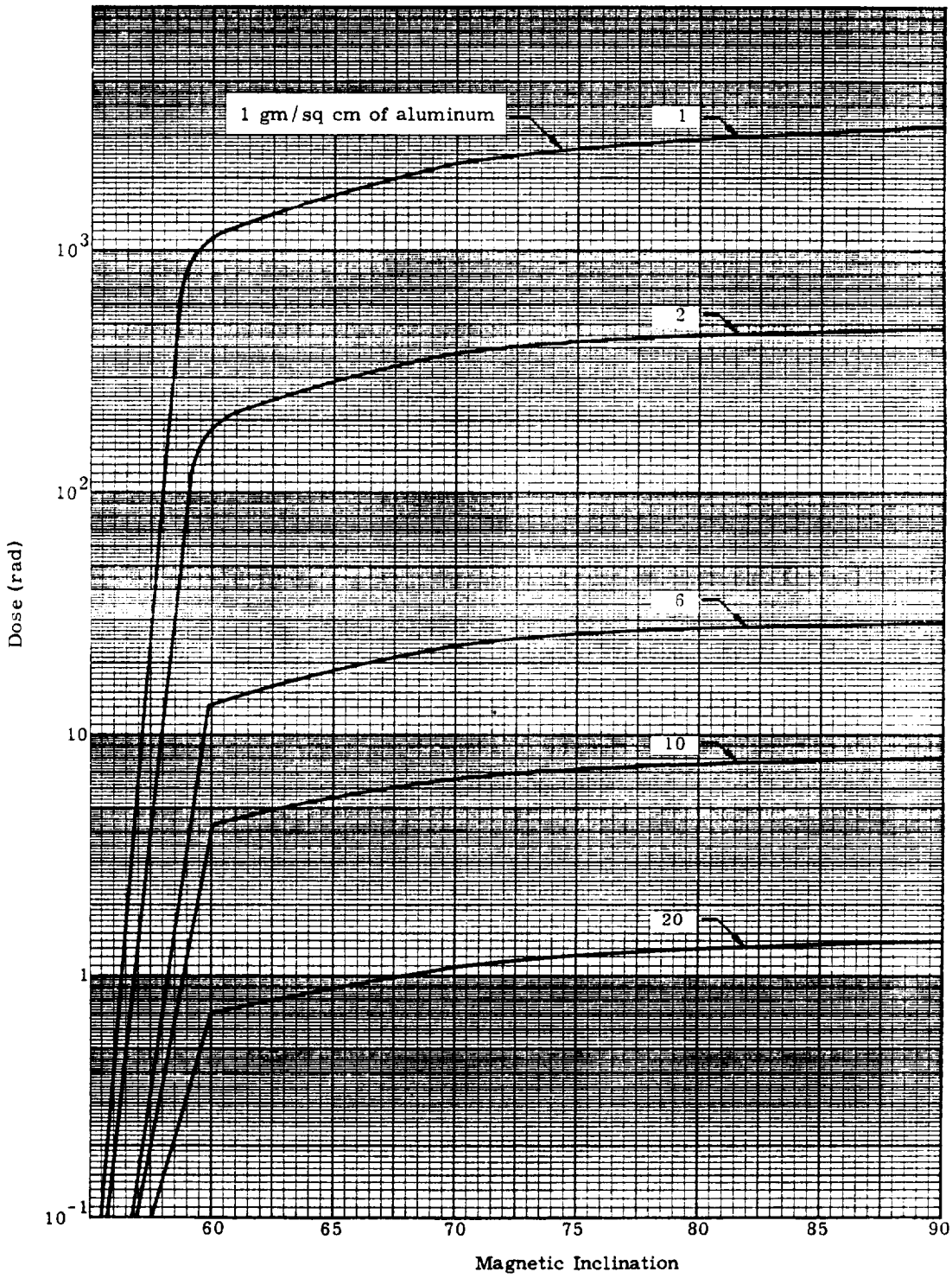

Fig. 15. Solar Proton Dose, May 10, 1959 Flare, 30-Hour Duration

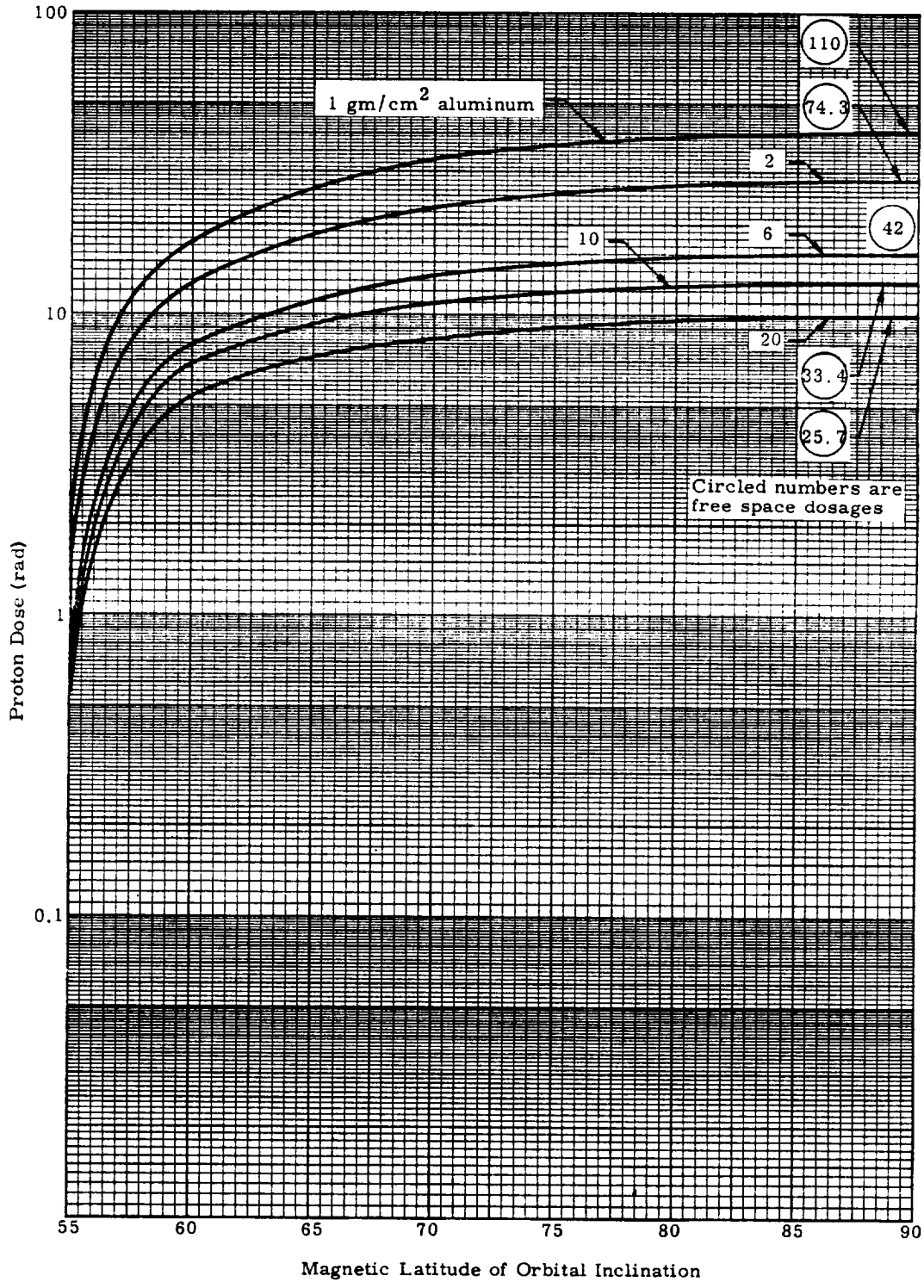

Fig. 16. Solar Proton Dosages from February 23, 1956 Flare.

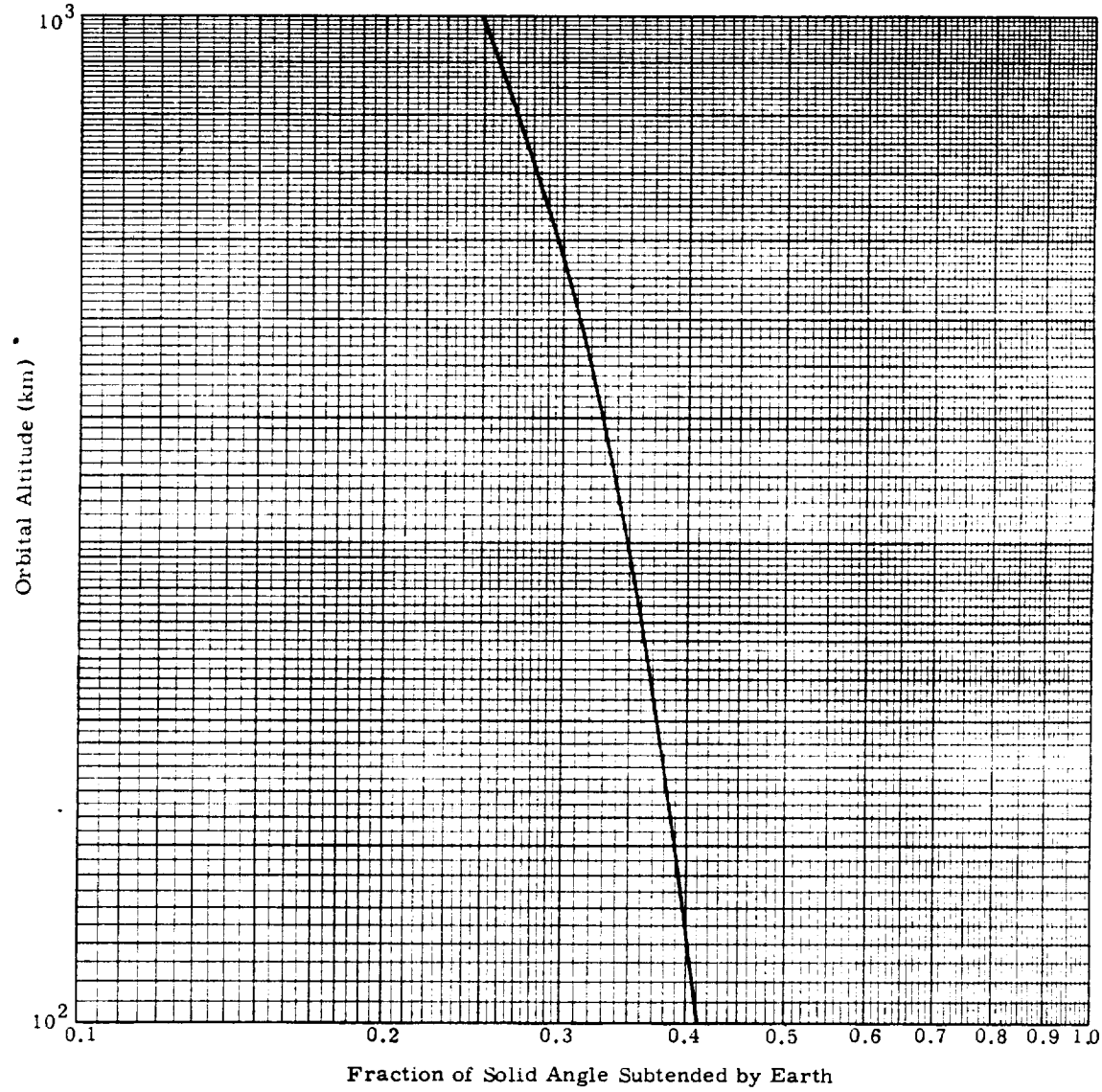

Fig. 17. Solid Angle Subtended by Earth as a Function of Altitude

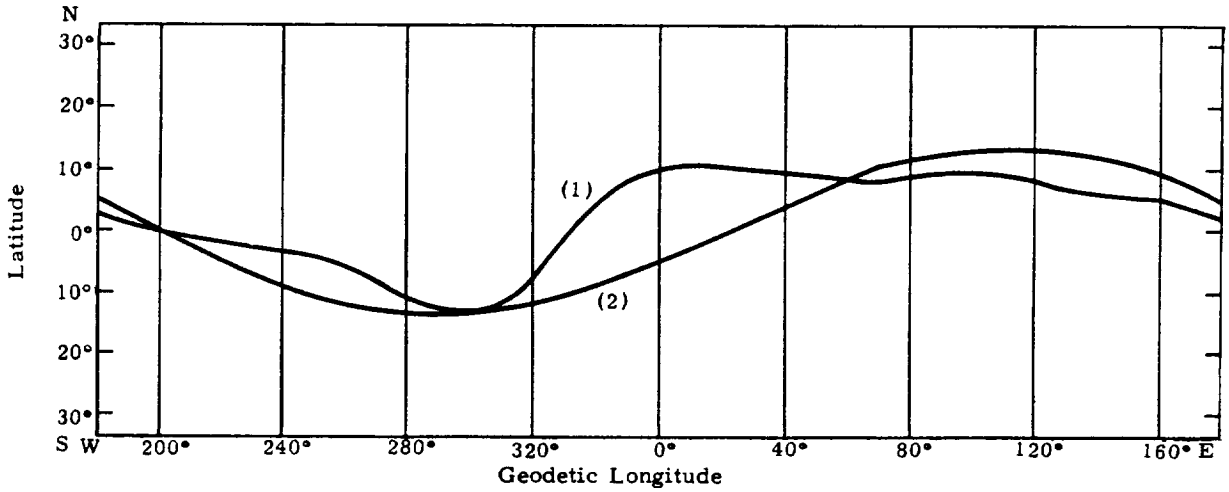

Fig. 18. Magnetic Dip Equator (1) from USN Hydrographic Office, 1955 and Geocentric Magnetic Equator (2) Inclined 13° to the Equator at Longitude 290°

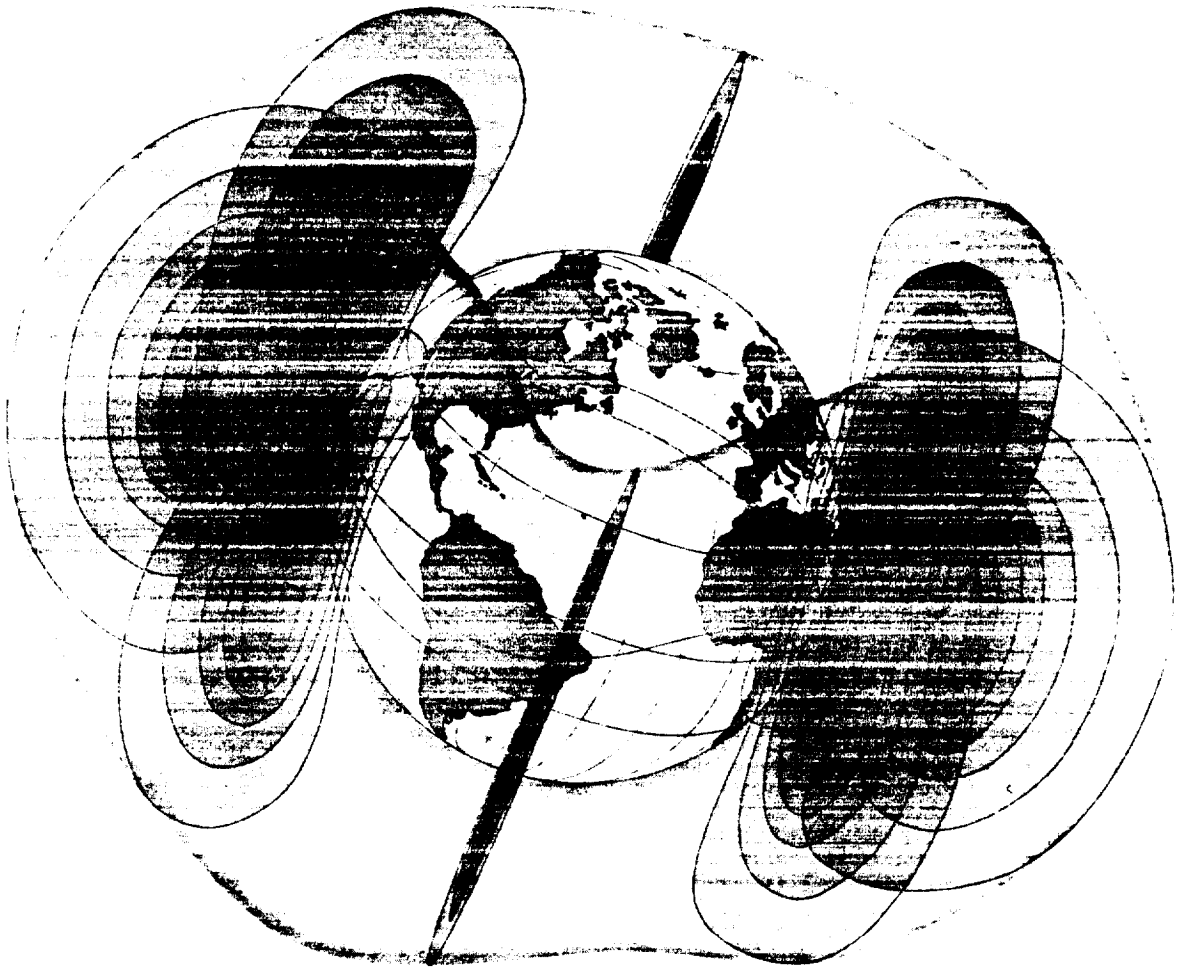

Fig. 19. Inner Van Allen Belt

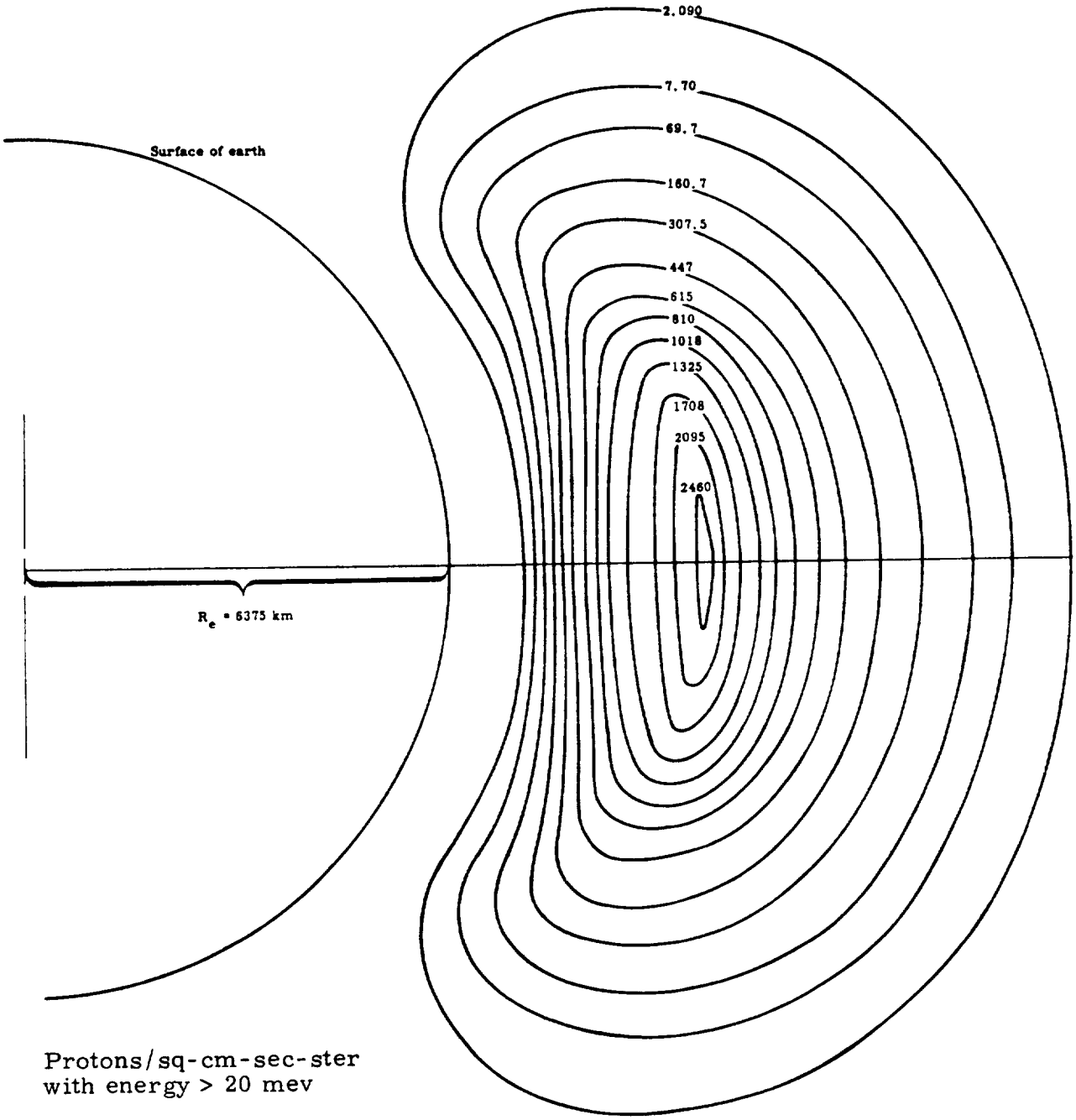

Fig. 20. Flux of Protons at One Longitude in the Van Allen Belt

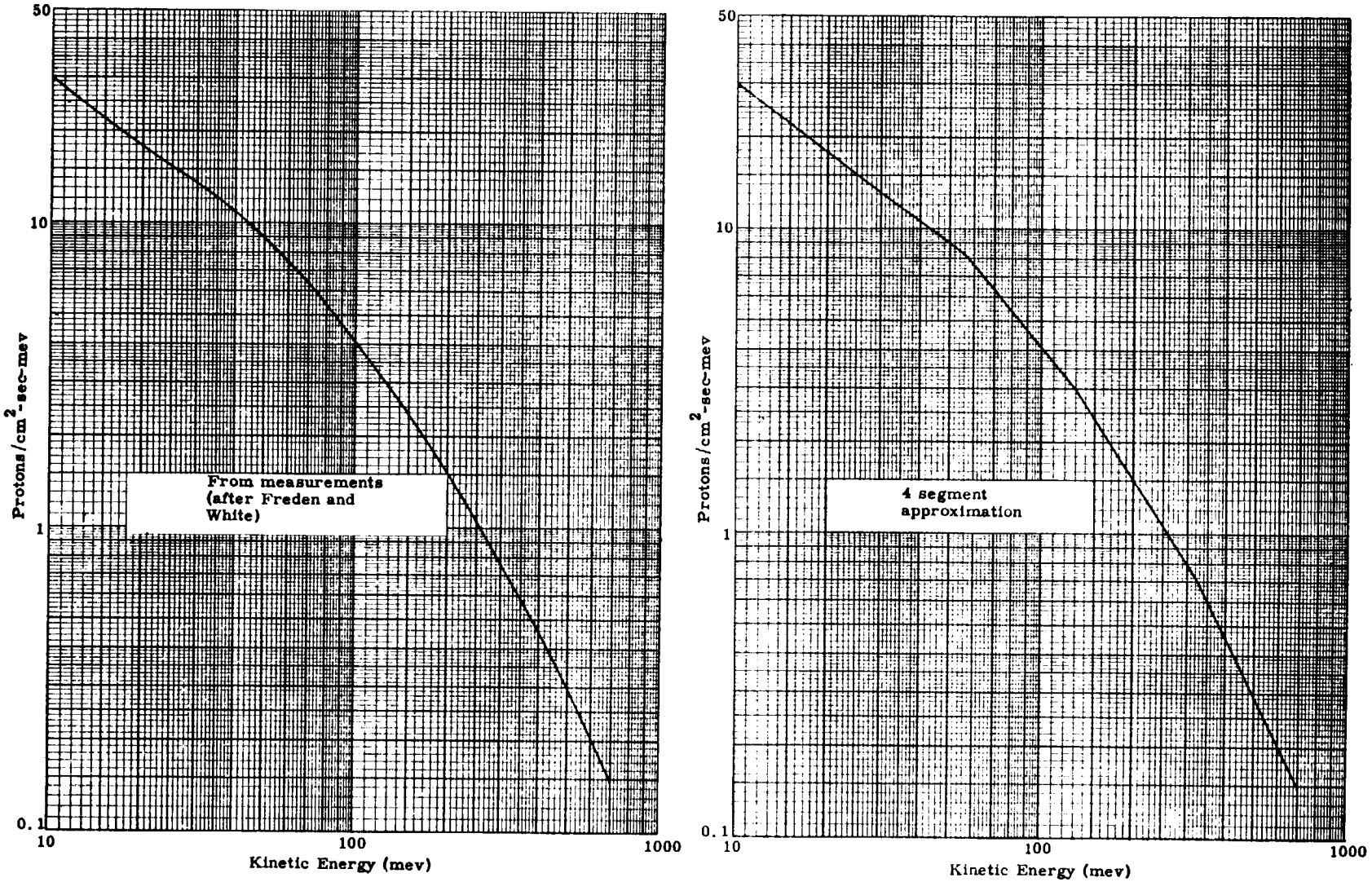

Fig. 21. Proton Differential Kinetic Energy Spectrum for the Inner Van Allen Belt

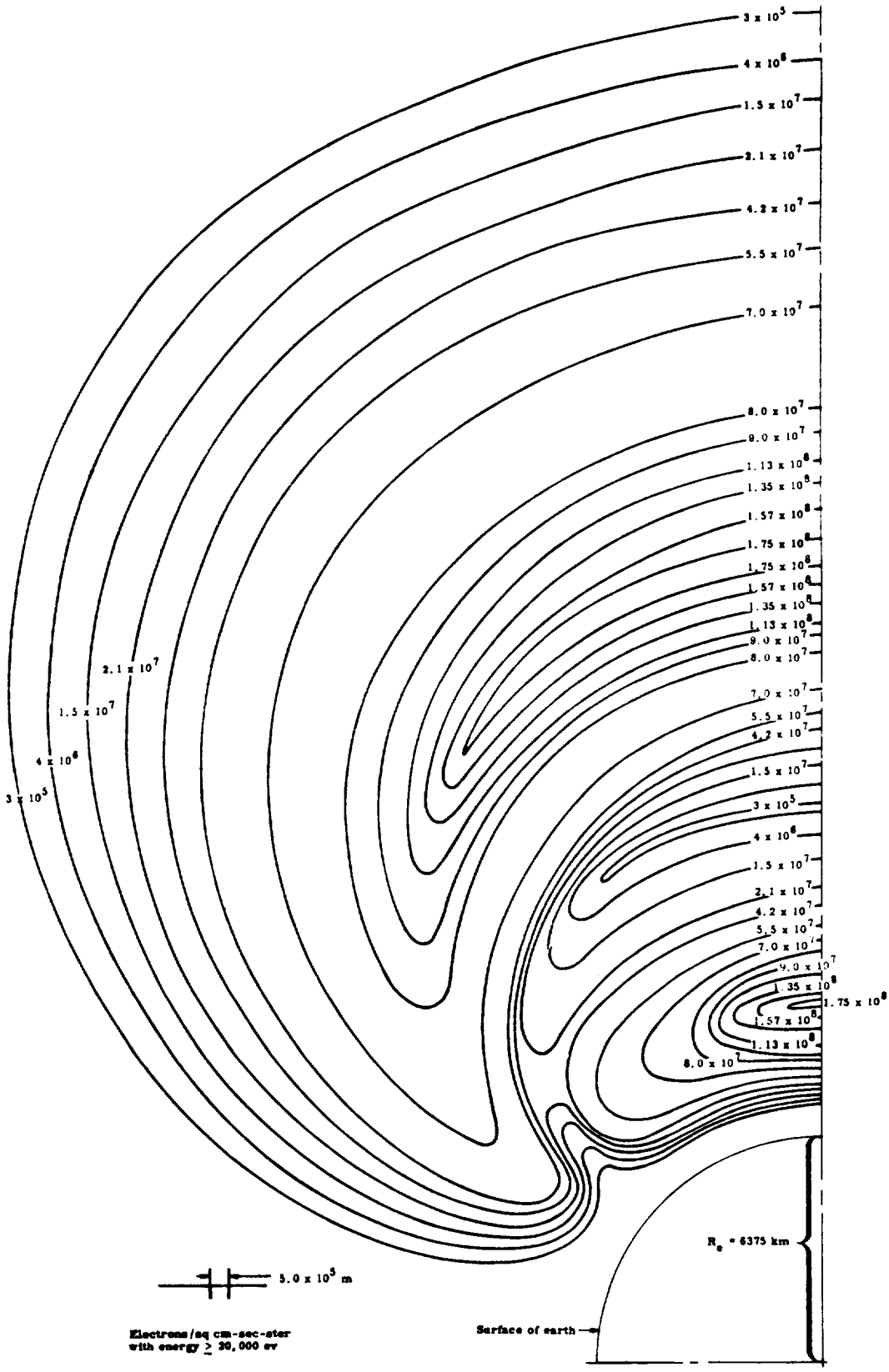

Fig. 22. Flux of Electrons in the Van Allen Belts

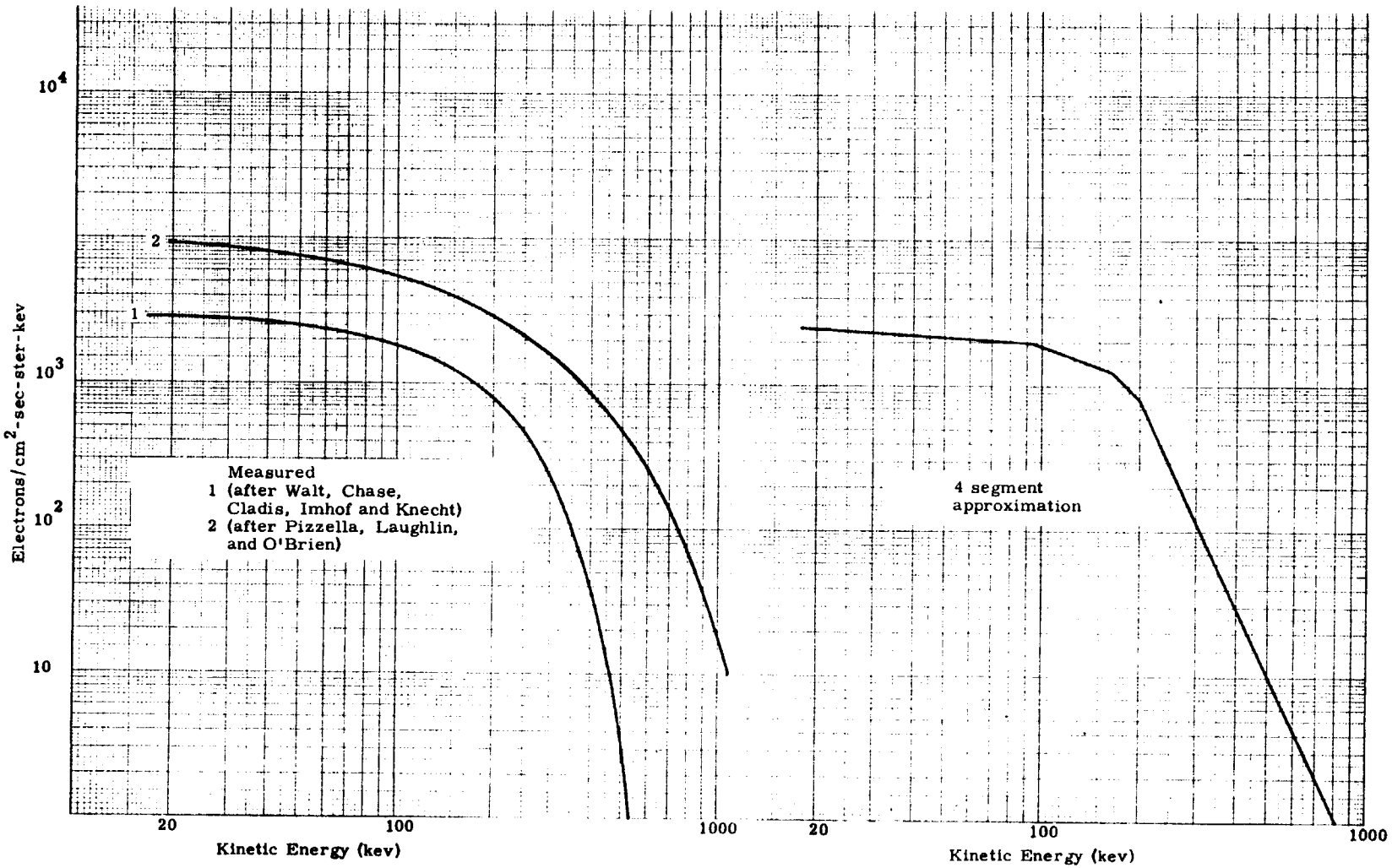

Fig. 23. Differential Kinetic Energy Spectrum Van Allen Belt Electrons

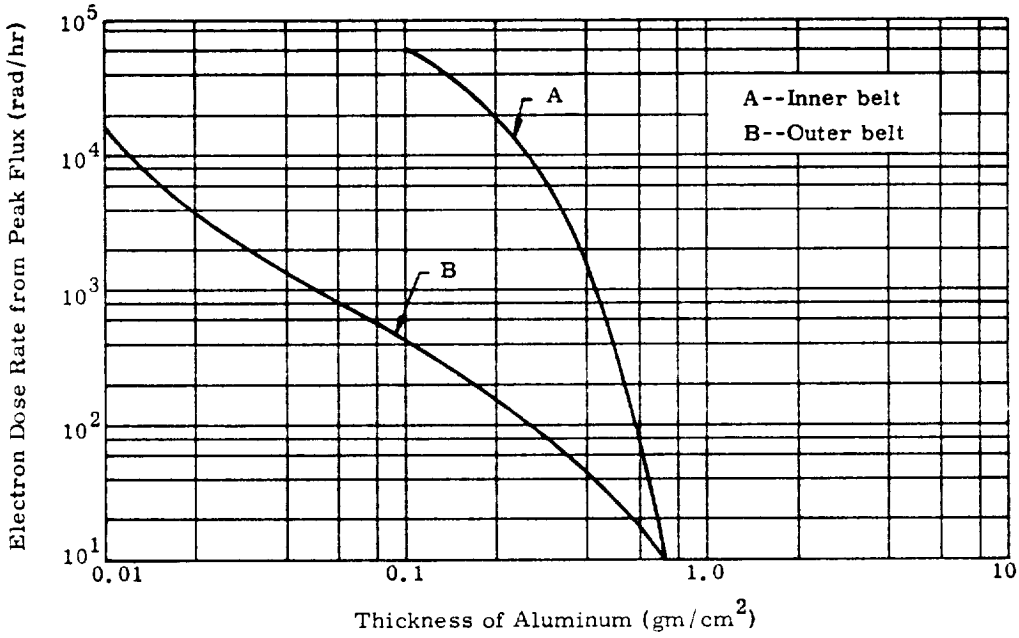

Fig. 24. Electron Dose Rates

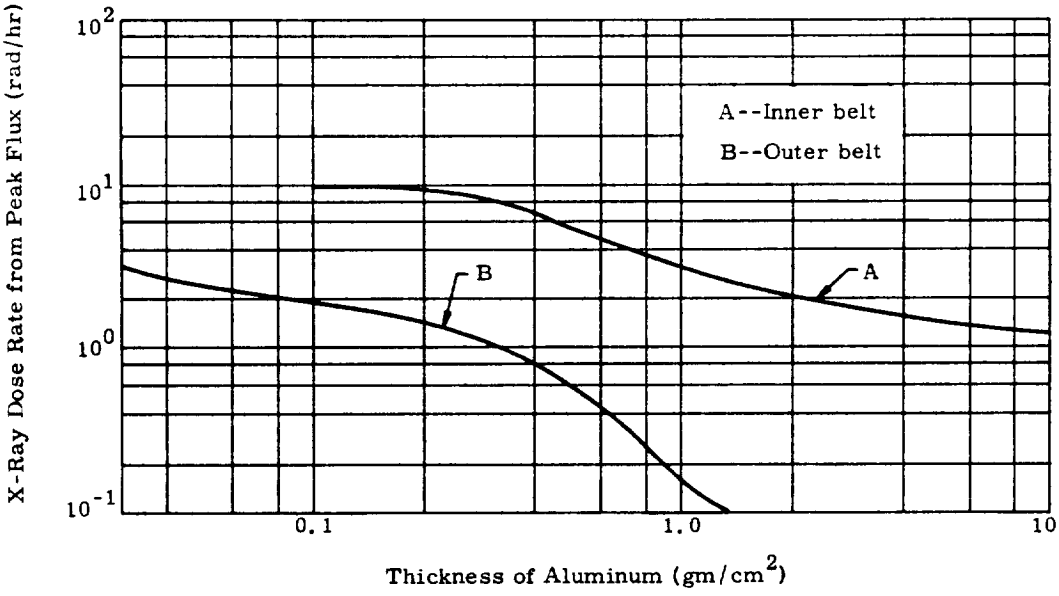

Fig. 25. X-Ray Dose Rates

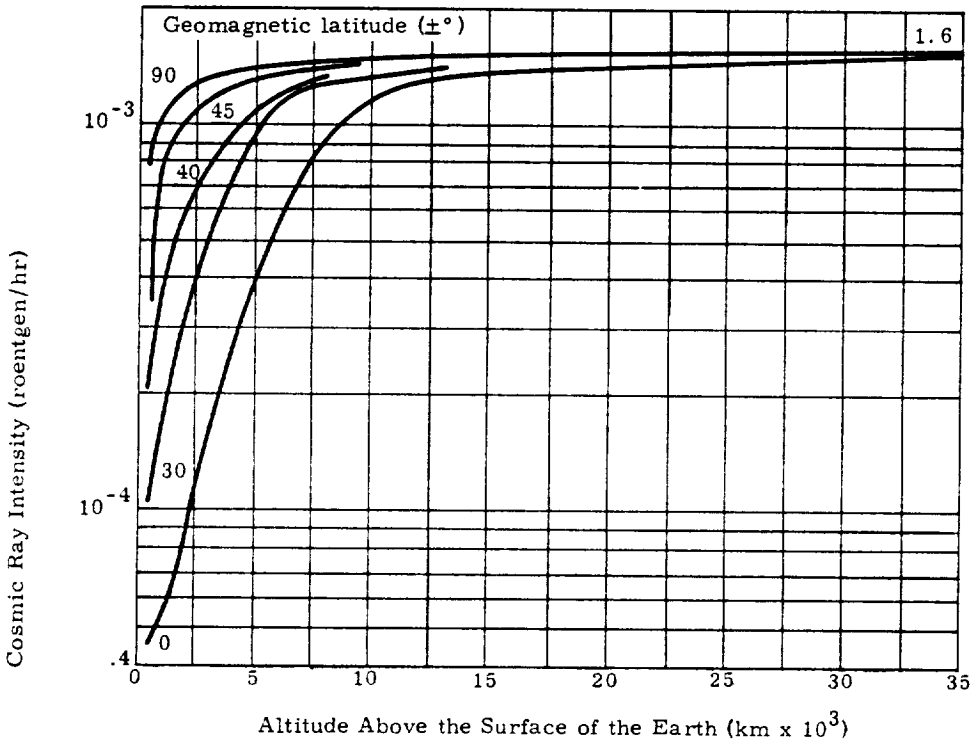

Fig. 26. Cosmic Radiation Intensity as a Function of Geomagnetic Latitude for High Altitudes During a Period of Low Solar Activity

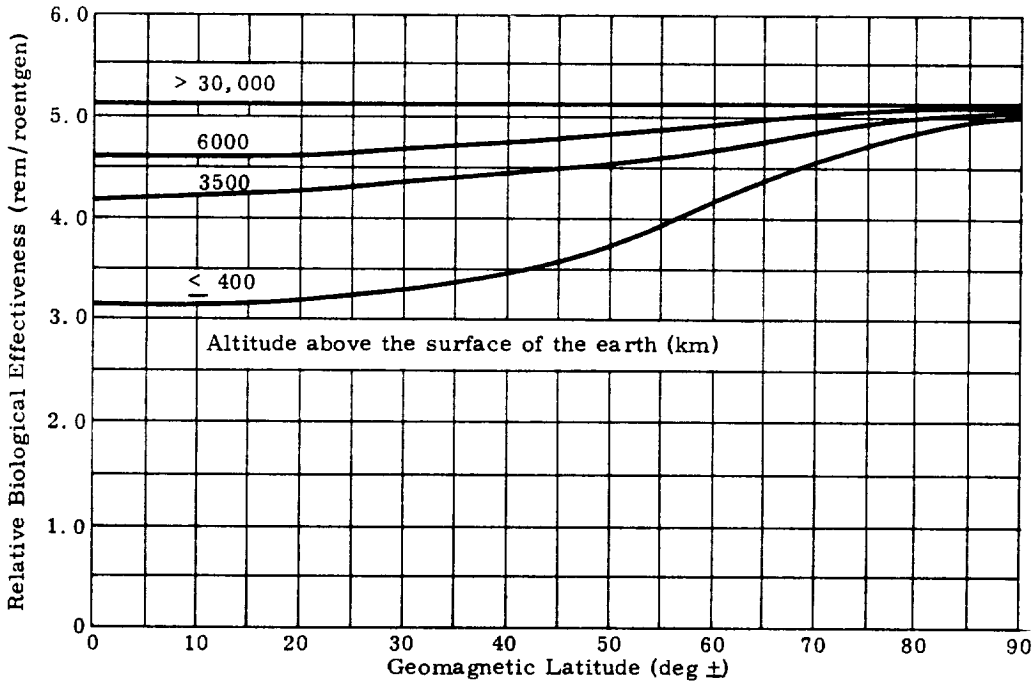

Fig. 27. Relative Biological Effectiveness for Cosmic Rays as a Function of Altitude and Geomagnetic Latitude During a Time of Low Solar Activity

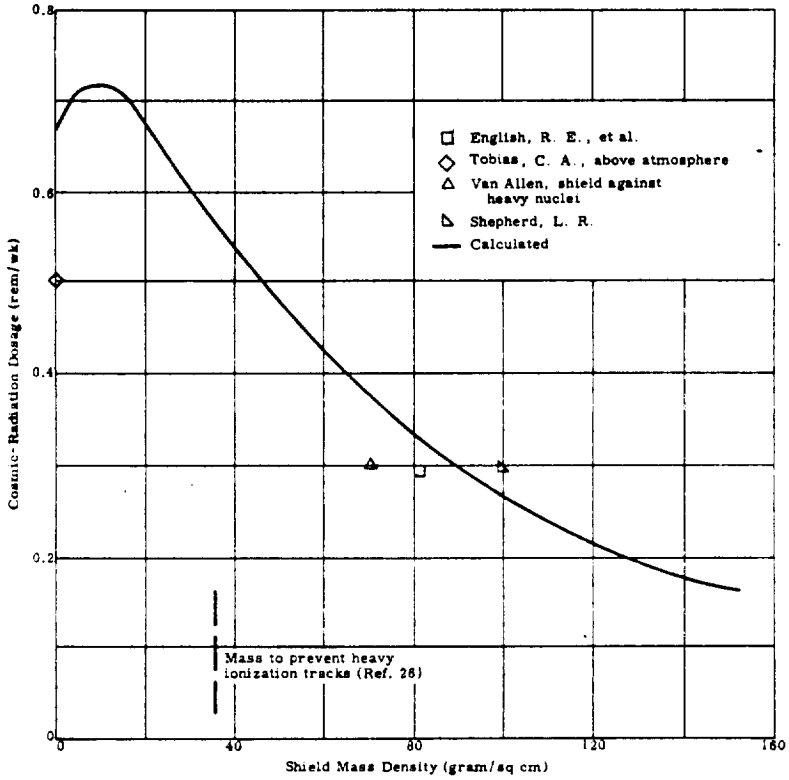

Fig. 28. Cosmic-Radiation Dosage as a Function of Shield Mass

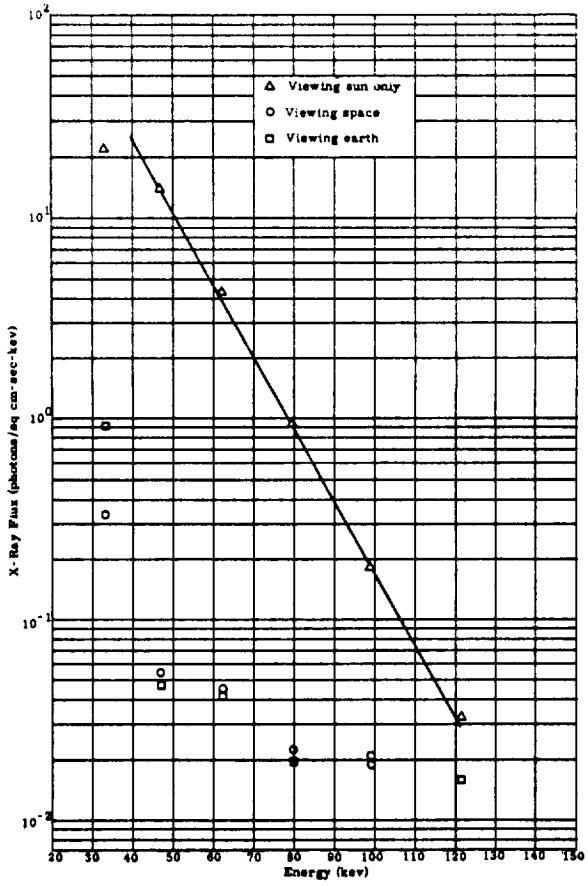

Fig. 29. Differential Energy Spectrum Measured During Rocket Flight NN 8.75 CF

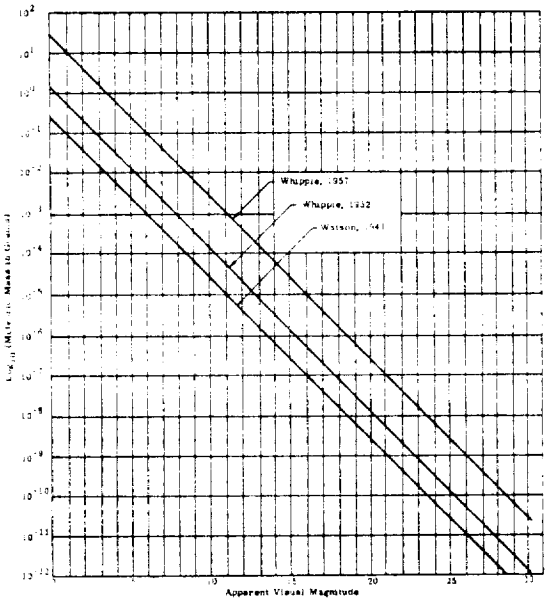

Fig. 30. Meteoric Mass Versus Apparent Visual Magnitude

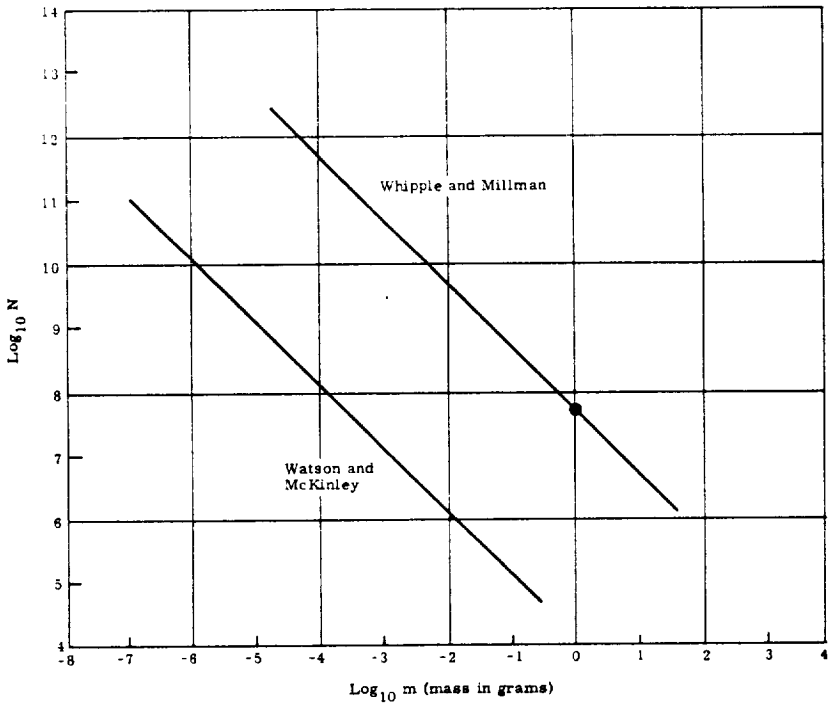

Fig. 31. Meteoroid Frequency Versus Mass

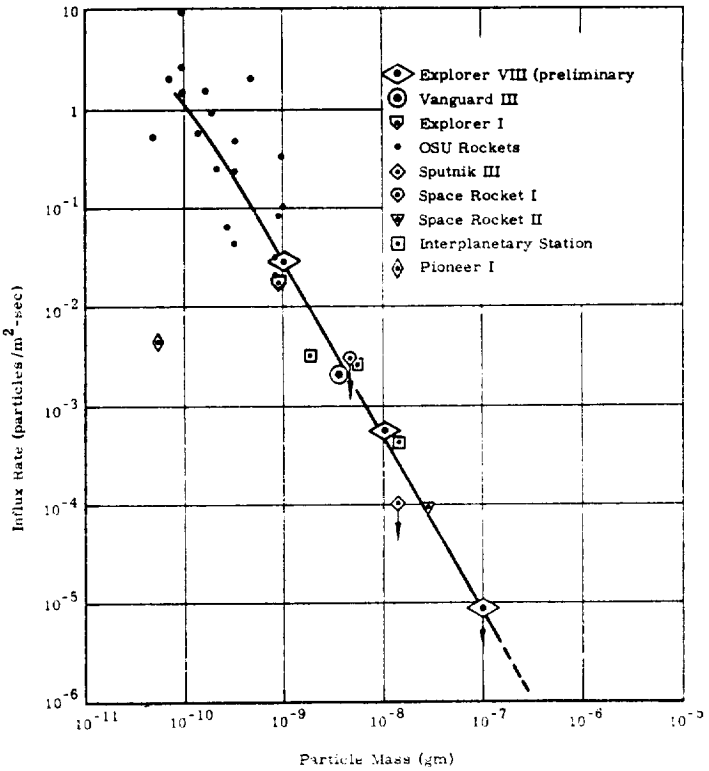

Fig. 32. Average Meteoroid Distribution Curve from Microphone System Measurements

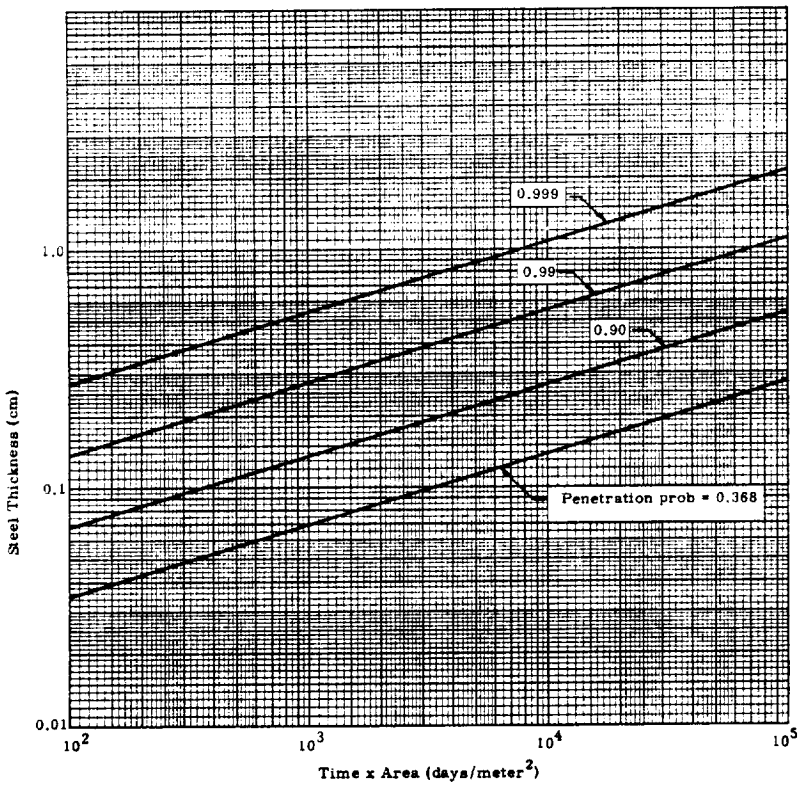

Fig. 33. Meteoroid Penetration Relations

CHAPTER III

ORBITAL MECHANICS

Prepared by:

J. Jensen, J. D. Kraft and G. E. Townsend, Jr.
Martin Company (Baltimore)
Aerospace Mechanics Department
March 1963

		Page
	Symbols	III-1
A.	Introduction	III-2
B.	Motion in a Central Field	III-2
C.	Lagrangian Equation	III-3
D.	Orbital Elements	III-3
E.	Motion in Three Dimensions	III-4
F.	Properties of Elliptic Motion	III-4
G.	Lambert's Theorem	III-7
H.	The N Body Problem	III-9
I.	Series Expansions for Elliptic Orbits	III-12
J.	Nomograms	III-14
K.	Tables of Equations of Elliptic Motion	III-15
L.	Presentation of Graphical Data	III-39
M.	References	III-39
N.	Bibliography	III-39
	Illustrations	III-41

LIST OF ILLUSTRATIONS

Figure		Page
1a	Semimajor Axis as a Function of the Radius and Velocity at Any Point	III-43
1b	Velocity--Escape Speed Ratio	III-44
2	The Relationship Between Orbital Position and Eccentricity and Time from Perigee (Kepler's Equation)	III-45
3	Three-Dimensional Geometry of the Orbit	III-46
4	Geometry of the Ellipse	III-46
5	Geometry of the Parabola	III-47
6	Geometry of the Hyperbola	III-47
7	The Parameter $\frac{1}{n} = \frac{\tau}{2\pi}$, as a Function of Semimajor Axis	III-48
8	Velocity of a Satellite in a Circular Orbit as a Function of Altitude	III-57
9	Parameters of Lambert's Theorem	III-60
10a	Lambert's Theorem (case 1)	III-61
10b	Lambert's Theorem (case 2)	III-62
11a	Solution for Eccentricity	III-63
11b	Solution for Eccentricity	III-64
12	Solution for Apogee and Perigee Radii	III-65
13a	True Anomaly as a Function of r_a/r_p and r_a/r_r	III-66
13b	True Anomaly as a Function of r/a, e, and γ	III-67
13c	True Anomaly as a Function of r/a, e, and γ	III-68
14	Solution for the Eccentric Anomaly as a Function of θ, and e or r_a/r_p	III-69
15	Q-Parameter as a Function of Orbital Semimajor Axis and Radius	III-70
16	Relationship Between Radius, Eccentricity, and Central Angle from Perigee--in Elliptic Orbit	III-71
17	Local Flight Path Angle	III-72

LIST OF ILLUSTRATIONS (continued)

Figure		Page
18	Solution for the Semiparameter as a Function of r, V and γ	III-73
19	Q-Parameter as a Function of Local Flight Path Angle and Eccentricity	III-74
20	The Solution for Local Flight Path Angle	III-75
21	Index for Figs 22a through 22i'	III-76
22a	Mean Anomaly as a Function of Eccentricity and Central Angle from Perigee	III-77
22a'	Mean Anomaly as a Function of Eccentricity and Central Angle from Perigee	III-78
22b	Mean Anomaly as a Function of Eccentricity and Central Angle from Perigee	III-79
22c	Mean Anomaly as a Function of Eccentricity and Central Angle from Perigee	III-80
22d	Mean Anomaly as a Function of Eccentricity and Central Angle from Perigee	III-81
22e	Mean Anomaly as a Function of Eccentricity and Central Angle from Perigee	III-82
22f	Mean Anomaly as a Function of Eccentricity and Central Angle from Perigee	III-83
22g	Mean Anomaly as a Function of Eccentricity and Central Angle from Perigee	III-84
22h	Mean Anomaly as a Function of Eccentricity and Central Angle from Perigee	III-85
22i	Mean Anomaly as a Function of Eccentricity and Central Angle from Perigee	III-86
22i'	Mean Anomaly as a Function of Eccentricity and Central Angle from Perigee	III-87

III. ORBITAL MECHANICS

SYMBOLS

a	Semimajor axis
A	Right ascension
b	Semiminor axis
e	Eccentricity
E	Eccentric anomaly
f	Force per unit mass
F	Force or hyperbolic anomaly
g	Acceleration due to gravity
h	Angular momentum
i	Inclination angle of the orbit to the equatorial plane
I	Moment of inertia; integral
K	Kinetic energy per unit mass
L	Latitude
m	Mass
M	Mean anomaly
n	Mean motion (mean angular velocity)
p	Semiparameter or semilatus rectum
P	Potential energy per unit mass
r	Orbital radius
r_a	Apogee radius
r_m	Radius to semiminor axis
r_p	Perigee radius
$\dot{r}$	Radial velocity
$\ddot{r}$	Radial acceleration
t	Time
t_p	Time of perigee passage
T	Kinetic energy per unit mass
U	Potential energy per unit mass
v	Velocity
v_a	Orbital velocity at apogee
v_p	Orbital velocity at perigee
x, y, z	Components of position
α	Angle of elevation above the horizontal plane
β	Azimuth angle measured from North in the horizontal plane
γ	Flight path angle relative to local horizontal
ϵ	Total energy per unit mass
θ	Orbital central angle between perigee and satellite position
$\dot{\theta}$	Angular velocity
$\ddot{\theta}$	Angular acceleration
Λ	Longitude (positive for East longitude)
μ	Earth's gravitational constant 1.4077×10^{16} ft^3/sec^2 (398,601.5 km^3/sec^2)
ν	Angle between the ascending node and the projection of the satellite position on the equatorial plane
τ	Orbital period over a spherical earth
ϕ	Orbital central angle between the ascending node and the satellite ($\theta + \omega$)
ω	Argument of perigee
Ω	Longitude of ascending node
Ω_e	Rotation rate of the earth (2π rad each 86164.091 mean solar sec

A. INTRODUCTION

The purpose of this chapter is to present data pertaining to the more elementary laws and concepts of orbit mechanics. The bulk of the material consists of graphs and tabulations of formulas for motion in elliptical orbits. In addition, a brief introductory treatment is given of the theoretical background. Many excellent books are available in the areas of analytical dynamics and celestial mechanics (see the bibliography at the end of the chapter). Therefore this chapter will only treat the material in outline form with no particular attempt to present a generalized and rigorous treatise on classical mechanics.

B. MOTION IN A CENTRAL FIELD

To a first approximation the earth can, dynamically, be considered as a point mass located at the geometrical center of the earth. This implies that the mass distribution of the earth exhibits spherical symmetry, an assumption that does not strictly hold true and will be discussed further in the next chapter. Additionally, the earth's mass will be considered infinite with respect to that of a satellite moving in its gravitational field. Finally, no additional forces will be assumed to act on the satellite. Under these assumptions the gravitational force $F = \frac{m\mu}{r^2}$ (μ = the earth's gravitational constant) acting on the satellite will be directed toward the stationary center of the earth. The ensuing motion will be planar.

In a rectangular coordinate system (in the plane of motion) as shown in the sketch below (assuming m to be constant), we get

$$f_x = \frac{F_x}{m} = -\frac{\mu}{r^2}\cos\theta = -f\cos\theta = -f\frac{x}{r} = \ddot{x} \tag{1}$$

$$f_y = \frac{F_y}{m} = -\frac{\mu}{r^2}\sin\theta = -f\sin\theta = -f\frac{y}{r} = \ddot{y} \tag{2}$$

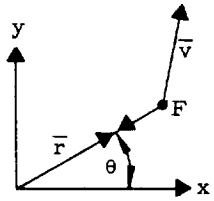

The motion is, however, more easily found in a polar coordinate system (r, θ) as shown in the sketch below.

In this system:

$$\frac{F_r}{m} = -f = -\frac{\mu}{r^2} = \ddot{r} - r\dot{\theta}^2 \tag{3}$$

$$\frac{F_\theta}{m} = 0 = r\ddot{\theta} + 2\dot{r}\dot{\theta} = \frac{1}{r}\frac{d}{dt}\left(r^2\dot{\theta}\right) \tag{4}$$

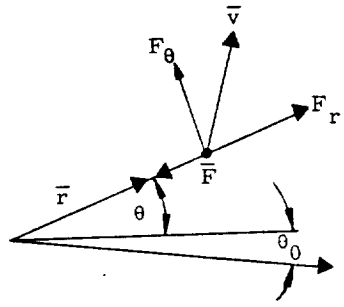

From Eq (4) it follows that:

$$r^2\dot{\theta} = \text{constant} = h \tag{5}$$

This constant is the angular momentum defined from vector mechanics. Substituting Eq (5) in Eq (3) results in

$$\ddot{r} = \frac{h^2}{r^3} - f.$$

Now letting $r = \frac{1}{u}$ it follows that

$$f = h^2 u^2\left(u + \frac{d^2u}{d\theta^2}\right) = \mu u^2 \tag{6}$$

where time has been eliminated by:

$$\dot{r} = -\frac{1}{u^2}\dot{u} = -\frac{1}{u^2}\frac{du}{d\theta}\dot{\theta} = -h\frac{du}{d\theta}$$

and

$$\ddot{r} = -h\frac{d}{dt}\left(\frac{du}{d\theta}\right) = -h^2u^2\frac{d^2u}{d\theta^2}$$

Equation (6) can be written

$$\frac{d^2u}{d\theta^2} + u = \frac{\mu}{h^2}$$

the solution to which can be recognized as:

$$u = \frac{\mu}{h^2} + C\cos(\theta - \theta_0)$$

or in terms of r the solution is

$$r = \frac{\frac{h^2}{\mu}}{1 + \frac{h^2}{\mu}C\cos(\theta - \theta_0)} = \frac{p}{1 + e\cos(\theta - \theta_0)} \tag{7}$$

The last form of Eq (7) is the standard form of a conic with the origin at one of the foci. From Eq (7) it can be seen that the semiparameter p (semilatus rectum) is $p = \frac{h^2}{\mu}$ and the eccentricity e is $\frac{h^2}{\mu}C = pC$. If $e < 1$ the conic is an

ellipse; if e = 0 it is a circle; if e = 1 it is a parabola, and if e > 1 it is an hyperbola.

C. LAGRANGIAN EQUATION

The preceding integration of the equations of motion is based on an elementary approach. At this point a brief digression will be made into the more general Lagrangian technique often used in orbit mechanics, and encountered in Chapter IV.

The Lagrangian equation for a conservative system is:

$$\frac{d}{dt}\left(\frac{\partial L}{\partial \dot{q}_i}\right) - \frac{\partial L}{\partial q_i} = 0 \qquad (8)$$

where the Lagrangian is L = T - U, T is the kinetic energy of the system and U the potential energy. The q's are generalized coordinates.

For a two-body central force case the Lagrangian is (in polar coordinates) $L = T - U = \frac{1}{2} m (\dot{r}^2 + r^2\dot{\theta}^2) - U(r)$. With $q_1 = \theta$ and $q_2 = r$ we get:

$$\frac{d}{dt}\left(\frac{\partial L}{\partial \dot{\theta}}\right) - \frac{\partial L}{\partial \theta} = \frac{d}{dt}\left[m r^2 \dot{\theta}\right] = 0 = \dot{p}_\theta \qquad (9)$$

where $p_\theta = m r^2 \dot{\theta}$ is the angular momentum of the system

and

$$\frac{d}{dt}\left(\frac{\partial L}{\partial \dot{r}}\right) - \frac{\partial L}{\partial r} = \frac{d}{dt}\left[m\dot{r}\right] - m r\dot{\theta}^2 - \frac{\partial U(r)}{\partial r} = 0$$

or, since

$$\frac{\partial U}{\partial r} = - F(r)$$

$$\frac{d}{dt}(m\dot{r}) - m r\dot{\theta}^2 = - F(r) \qquad (10)$$

From Eq (9) it follows that $r^2 \dot{\theta}$ = constant. (This is commonly referred to as the law of areas.)

The orbit can be found by eliminating t from Eq (10). From Eq (9)

$$m r^2 \frac{d\theta}{dt} = p_\theta$$

we can conclude that

$$\frac{d}{dt} = \frac{p_\theta}{m r^2}\frac{d}{d\theta}$$

and

$$\frac{d^2}{dt^2} = \frac{p_\theta}{m r^2}\frac{d}{d\theta}\left(\frac{p_\theta}{m r^2}\frac{d}{d\theta}\right)$$

Substituting this in Eq (10) we get:

$$\frac{p_\theta}{r^2}\frac{d}{d\theta}\left(\frac{p_\theta}{m r^2}\frac{dr}{d\theta}\right) - \frac{p_\theta^2}{m r^3} = - F(r) \qquad (11)$$

or using $u = \frac{1}{r}$

$$\frac{p_\theta^2 u^2}{m}\left(\frac{d^2u}{d\theta^2} + u\right) = + F\left(\frac{1}{u}\right) = m\mu u^2$$

which, since $p_\theta = hm$, is identical to Eq (6).

D. ORBITAL ELEMENTS

Equation (7) for the conic which embodies Kepler's first law defines the planar orbit of the satellite when the constants p, e and θ_0 are properly evaluated from a set of initial conditions, such as V, r and γ, where γ is the flight path angle as shown in the sketch below. Note that $\dot{\theta} r = V \cos\gamma$ and hence $\dot{\theta} r^2 = r V \cos\gamma = h$ = constant = $\sqrt{\mu p}$.

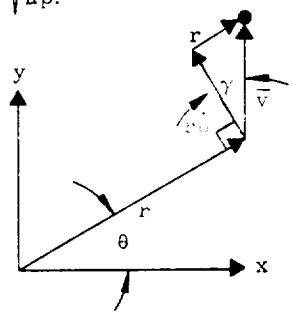

The three constants p, e and θ_0, or any of a number of equivalent sets of constants, describe completely the geometrical properties of the ellipse in the plane of motion. From a kinematic standpoint one more quantity is needed to specify the position of the satellite in its orbit. Frequently this specification is given in the form of the time of perigee passage, although a knowledge of the position at any time is sufficient.

Finally the plane of the satellite orbit must be described with respect to some reference plane. This description requires that two additional quantities be specified, for example, the inclination of the orbital plane with respect to the reference plane and the orientation in the reference plane of the line of intersection between the two planes. The complete specification of the orbit therefore requires knowledge of six quantities, commonly called six elements of the orbit. Under the simplifying assumptions made in this chapter with respect to the dynamics of the orbital motion, these elements will be constants, whereas in the actual physical situation they will generally be varying as functions of time.

A set of orbital elements in common usage is:

Semilatus rectum = p

Eccentricity = e

Time of perigee passage = t_p

Inclination of orbit plane (with respect to earth equatorial plane) = i

Argument of perigee (with respect to ascending node) = ω

Longitude of ascending node (with respect to vernal equinox) = Ω.

E. MOTION IN THREE DIMENSIONS

From the solution of the orbit as expressed in the orbital plane, i.e., $r = \frac{p}{1 + e \cos\theta}$, an expression can readily be obtained for the three-dimensional description of the motion in any coordinate system. For this purpose define a coordinate system (x, y, z) in the orbital plane with the x-axis pointing toward perigee, the y-axis pointing in the direction of r at $\theta = 90°$, and with the z-axis completing a right-handed Cartesian coordinate system. In this system the defining equations for the motion are $x = r \cos\theta$, $y = r \sin\theta$ and $z = 0$. To transform these equations into the (x', y', z') system shown in the sketch, the following transformation applies:

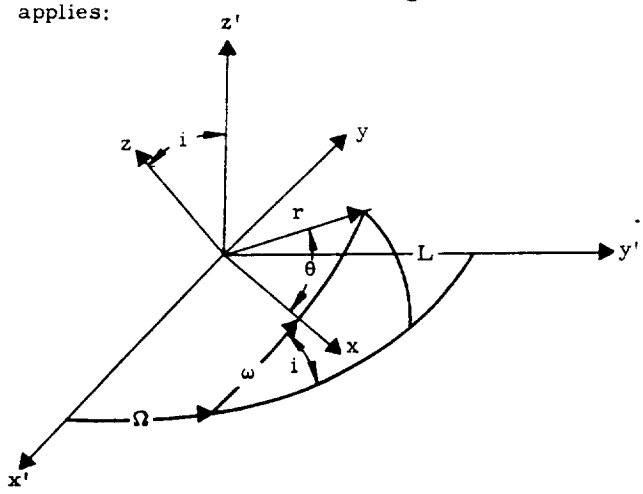

$$\begin{bmatrix} x' \\ y' \\ z' \end{bmatrix} = \begin{bmatrix} \cos\Omega\cos\omega - \sin\Omega\cos i\sin\omega & -\cos\Omega\sin\omega - \sin\Omega\cos i\cos\omega & \sin\Omega\sin i \\ \sin\Omega\cos\omega + \cos\Omega\cos i\sin\omega & -\sin\Omega\sin\omega + \cos\Omega\cos i\cos\omega & -\cos\Omega\sin i \\ \sin i\sin\omega & \sin i\cos\omega & \cos i \end{bmatrix} \begin{bmatrix} x \\ y \\ z \end{bmatrix}$$

Hence, since $x = r\cos\theta$, $y = r\sin\theta$, $z = 0$, $x' = A' r\cos\theta + B' r\sin\theta$, etc., etc.

where

$$A' = \cos\Omega\cos\omega - \sin\Omega\cos i\sin\omega$$

and

$$B' = -\cos\Omega\sin\omega - \sin\Omega\cos i\cos\omega$$

Now, since the orbital elements Ω, ω and i are constant for this discussion the velocity components are:

$$\dot{x}' = A'(\dot{r}\cos\theta - r\sin\theta\,\dot{\theta}) + B'(\dot{r}\sin\theta + r\cos\theta\,\dot{\theta})$$

where

$$r\dot{\theta} = \sqrt{\frac{\mu}{p}}\,(1 + e\cos\theta)$$

and

$$\dot{r} = e\sqrt{\frac{\mu}{p}}\sin\theta$$

Similar expressions are found for the other coordinates. To reduce this description in inertial space to one of position relative to the rotating earth the following transformation is required

$$\begin{bmatrix} x_r \\ y_r \\ z_r \end{bmatrix} = \begin{bmatrix} \cos\Omega_e t & \sin\Omega_e t & 0 \\ -\sin\Omega_e t & \cos\Omega_e t & 0 \\ 0 & 0 & 1 \end{bmatrix} \begin{bmatrix} x \\ y \\ z \end{bmatrix}$$

where Ω_e is the rotational rate of the earth and t is the time since the x_r-axis, being in the prime meridian, passed the x'-axis, the x' axis is oriented toward the vernal equinox.

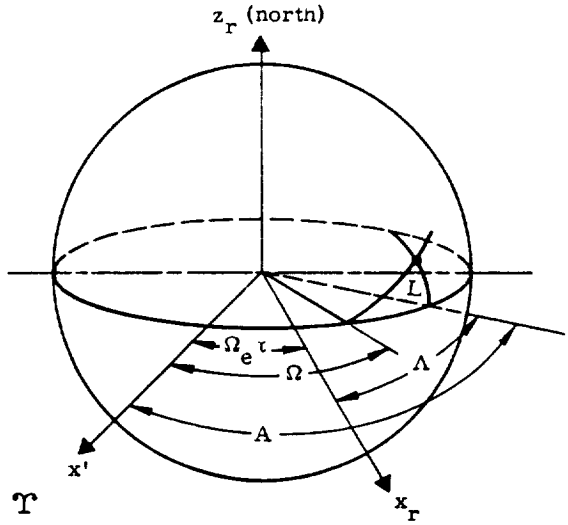

The sketch also shows the right ascension A and the geocentric latitude L.

$$A = \arccos\frac{x'}{\sqrt{r^2 - z'^2}}$$

and

$$L = \arcsin\frac{z'}{r} = \arcsin\frac{z}{r}$$

The longitude relative to the prime meridian measured positive in the direction of rotation is thus $\Lambda = A - \Omega_e t$.

F. PROPERTIES OF ELLIPTIC MOTION

Before progressing to a detailed discussion of the motion, two general properties should be considered.

Equation (5): $r^2 \dot{\theta} = r(r\dot{\theta}) = 2dA = h = \text{constant}$ expresses the conservation of angular momentum and is a consequence of the fact that the moment of force about the center of motion is 0. It is also the equivalent of the "Law of Equal Areas" known as Kepler's second law. It is a general law of central motion (i.e., for any force directed toward a fixed center of attraction and hence having zero moment about this point) since it was obtained without recourse to any specific force law. Since $\frac{1}{2} r(r\dot{\theta})$ is the differential area dA swept by the radius vector, one obtains $A = \frac{1}{2} ht + \text{constant}$, and hence, Kepler's second law: the radius vector of any given planet sweeps through equal areas in equal time.

The time τ to complete a revolution can easily be found since the area of the ellipse is πab and since $b = \sqrt{ap}$, one obtains

$$\tau = \frac{2\pi}{\sqrt{\mu}} a^{3/2}$$

Hence, Kepler's third law: the squares of the periods of the planets are to each other as the cubes of their semimajor orbital axes, or

$$\frac{\tau_1^2}{\tau_2^2} = \frac{a_1^3}{a_2^3} .$$

It also follows from Eq (5) that $\dot{\theta} = \frac{h}{r^2}$ or the angular velocity is inversely proportional to the square of the radius vector.

An important integral of the equations can be obtained by multiplying Eq (1) by $2\dot{x}$ and Eq (2) by $2\dot{y}$, and adding them.

$$2\ddot{x}\dot{x} + 2\ddot{y}\dot{y} = -\frac{2f}{r}(x\dot{x} + y\dot{y})$$

or

$$\frac{d}{dt}\left(\dot{x}^2 + \dot{y}^2\right) = -\frac{f}{r}\frac{d}{dt}\left(x^2 + y^2\right)$$

$$= -\frac{f}{r}\frac{d}{dt}(r^2) = -2f\dot{r}$$

If now f is a function of r only, the entire equation can be integrated to yield:

$$\dot{x}^2 + \dot{y}^2 = v^2 = -2\int f(r)\,dr + \text{constant} =$$

$$2V(r) + c,$$

where V(r) in a physical problem is a single valued function of r. This equation is known as the "vis viva" integral. The velocity is, in other words, only a function of the distance from the center of attraction. V(r) is the potential of the force f(r) (in our case, $f(r) = -\frac{\mu}{r^2}$). Thus, $V(r) = \frac{\mu}{r}$ and $v^2 = \frac{2\mu}{r} + \text{constant}$, where the constant is found to be equal to $-\mu/a$ for elliptical motion, zero for parabolic motion, and $+\mu/a$ for hyperbolic motion. In terms of the initial conditions v and r, the motion is elliptical, parabolic or hyperbolic depending on whether $v^2 - \frac{2\mu}{r}$ is negative, zero or positive, respectively. This equation is independent of the initial flight path angle γ. For elliptical orbits the resulting semimajor axis is given by

$$a = \frac{r\mu}{2\mu - rv^2} \quad \text{(Fig. 1)}$$

or

$$V = \sqrt{\frac{\mu}{a}\left(\frac{2a}{r} - 1\right)} .$$

For a circular orbit $r = a$ and the circular orbit velocity is given by

$$V_C = \sqrt{\frac{\mu}{a}} .$$

For a parabolic orbit a is infinite and the so-called escape speed or parabolic orbital velocity becomes

$$V_{esc} = \sqrt{\frac{2\mu}{r}} .$$

So far only the geometry of the orbit has been determined, and it has been obtained through the elimination of time from the equations. To complete the solution for elliptic motion, time is reintroduced by substituting the area integral

$$r^2\dot{\theta} = h = \sqrt{\mu a(1 - e^2)}$$

[Eq (5)], into the "vis viva" integral which in polar coordinates for elliptic motion takes the form:

$$v^2 = \dot{r}^2 + r^2\dot{\theta}^2 = \mu\left(\frac{2}{r} - \frac{1}{a}\right).$$

Thus

$$\dot{r} = \frac{dr}{dt} = \sqrt{\frac{\mu}{a r^2}\left[a^2 e^2 - (a - r)^2\right]}$$

or

$$dt = \frac{r\sqrt{a/\mu}\,dr}{\sqrt{a^2 e^2 - (a - r)^2}}$$

Now, introducing the mean angular motion

$$n = \frac{2\pi}{\tau} = \frac{1}{a}\sqrt{\frac{\mu}{a}}$$

results in the equation

$$n\,dt = \frac{r}{a}\,\frac{dr}{\sqrt{a^2 e^2 - (a - r)^2}}$$

To clean up this equation a new variable E is introduced defined by $a - r = a e \cos E$ from which $r = a(1 - e \cos E)$ and

$$n\,dt = (1 - e \cos E)\,dE.$$

This equation is integrable and yields upon integration

$$n(t - t_o) = E - \sin E$$

This equation is commonly referred to as Kepler's equation.

Because of the importance of and general interest in circular velocity, period and the mean angular velocity (mean motion), these quantities have been computed and presented in various forms in Figs. 7 and 8 and in Table 9 in both English and metric units.

The quantity E is called the eccentric anomaly (anomaly = angle or deviation). Its geometrical significance is shown in Fig. 4. The angle θ is referred to as the true anomaly. The quantity $n(t - t_o)$ is the angle which would be described by the radius vector had it moved uniformly at the average angular motion. It is called the mean anomaly and designated by $M = n(t - t_o)$.

Hence, $M = E - e \sin E$. This transcendental equation in E is known as Kepler's equation. Time from perigee passage for elliptical orbits is now obtained from:

$$t - t_p = \sqrt{\frac{a^3}{\mu}}\,M = \sqrt{\frac{a^3}{\mu}}\,(E - e \sin E).$$

The solution of Kepler's equation for time as a function of position is direct since there exists a unique value of E for each value of r or θ. However, the reverse determination (for position as a function of time) involves the solution of Kepler's equation for E. This solution is transcendental and thus requires iteration for convergence to the proper value of E. The best form of this iteration (assuming that a reasonable estimate of E is available) is Newton's method which is obtained directly from the Taylor series expansion of M as a function of the estimate of E and the mean anomaly. All higher order terms are neglected.

$$M = M_o + \frac{d}{dE}(M)\,\Delta E + \ldots$$

or

$$\Delta E = \frac{M - M_0}{\frac{d}{dE}(M)}$$

$$= \frac{M - M_0}{1 - e \cos E} = \frac{(E_0 - e \sin E_0) + M}{1 - e \cos E_0}$$

This form can be further modified to yield the new estimate of E directly by substituting

$$E_{n+1} = E_n + \Delta E$$

$$= \frac{e(\sin E_n - E_n \cos E_n) + M}{1 - e \cos E_n}$$

This series solution converges very rapidly and generally requires only two iterations for six or seven significant figures (given a two-place estimate). Since one means of obtaining such an initial estimate is a graph or nomogram, a numerical solution of Kepler's equation may be found in Fig. 2.

A peculiar property of elliptic orbits is that the velocity vector at any point can be broken into components, V_b and V_d ($\vec{V} = \vec{V}_b + \vec{V}_d$), such that V_b is constant in magnitude and perpendicular to the radius from the point of attraction to the instantaneous point in the orbit and V_d is constant in magnitude and continuously directed normal to the major axis of the ellipse. This behavior is illustrated in the following sketch.

Since $\overline{V}_d$ is constant, only $\overline{V}_b$ contributes to the acceleration, and solely by a change of direction, i.e., the acceleration must be radial and such that

$$a = a_r = - V_b \dot{\theta}$$

where $\dot{\theta}$ is the angular rate of the radius vector. But, the acceleration at any point can also be obtained from the gradient of the potential function (which, in the case of a spherical homogeneous earth, or one constructed in spherically concentric homogeneous layers is $\frac{\mu}{r}$).

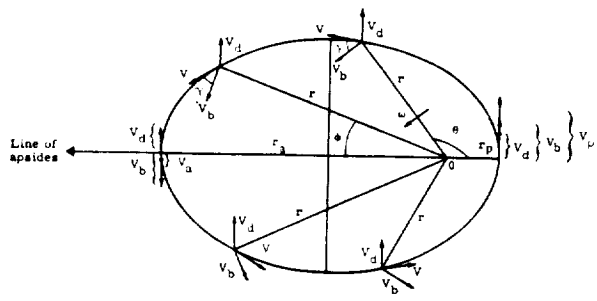

Therefore

$$-a_r = V_b \dot{\theta} = \frac{\mu}{r^2} \quad \text{or} \quad V_b = \frac{\mu}{\dot{\theta} r^2}$$

Now since the acceleration is directed toward the center of mass, the moment with respect to this center must be zero, or

$$r^2 \dot{\theta} = \text{constant} = h = r V \cos \gamma$$

This equation is recognized as the equation for conservation of angular momentum, or the area law.

Thus

$$V_b = \frac{\mu}{\dot{\theta} r^2} = \frac{\mu}{h} = \frac{\mu}{r V \cos \gamma} = \sqrt{\frac{\mu}{p}}$$

The second component of the velocity, V_d, can be evaluated from the law of cosines.

$$V_d^2 = V_b^2 + V^2 - 2V_b V \cos \gamma$$

This equation reduces to the following upon substitution

$$V_d = \sqrt{V^2 + \mu \left(\frac{1}{p} - \frac{2}{r}\right)} = eV_b$$

The quantities V_b and V_d can also be evaluated from the sketch when it is noted that

$$V_p = V_b + V_d$$

$$V_a = V_b - V_d$$

Now assuming that the apogee and perigee radii are known

$$V_b = \sqrt{\frac{\mu}{2r_p}\left(1 + \frac{r_p}{r_a}\right)}$$

$$V_d = \frac{\mu}{2V_b r_p}\left(1 - \frac{r_p}{r_a}\right) = eV_b$$

The total energy in the orbit can also be related to these fundamental quantities. This is accomplished as follows:

$$\frac{\text{Potential energy}}{\text{unit mass}} = -\frac{\mu}{r}$$

$$= -\frac{V^2}{2} - \frac{\mu}{2a} = -KE - \frac{\mu}{2a}$$

$$\frac{\text{Total energy}}{\text{unit mass}} = \frac{\text{Kinetic energy}}{\text{unit mass}} + \frac{\text{Potential energy}}{\text{unit mass}}$$

$$= -\frac{\mu}{2a} = -\frac{V_b^2 - V_d^2}{2}$$

This representation of the orbit also offers a simple means of determining the direction of the line of apsides of the orbit . The line of apsides is determined from the preceding sketch by

$$\tan \phi = \frac{\sin \gamma}{\frac{V_b}{V} - \cos \gamma} = \frac{\tan \gamma}{\frac{r}{p} - 1}$$

G. LAMBERT'S THEOREM

In Chapter VI, the problem arises of determining an ellipse from a given time interval between two points on an arc of the ellipse as described by the two radius vectors terminating on the arc. From Kepler's equation and the definition of the true anomaly, one obtains

$$n \Delta t = E_2 - E_1 - e(\sin E_2 - \sin E_1)$$

$$\Delta\theta = \cos^{-1}\left(\frac{p - r_2}{e r_2}\right) - \cos^{-1}\left(\frac{p - r_1}{e r_1}\right)$$

From these equations the ellipse can be determined. The simultaneous solution of these equations for a and e is, however, very difficult since the numerical iterative solution is quite sensitive to the accuracy of the first estimates of a and e. This problem is circumvented by the use of Lambert's theorem which can be developed as follows: Let

$$2G = E_2 + E_1 \text{ and } 2g = E_2 - E_1$$

$$r_1 = a(1 - e \cos E_1)$$

$$r_2 = a(1 - e \cos E_2)$$

Thus

$$r_1 + r_2 = 2a(1 - e \cos G \cos g)$$

Let C be the chord joining the extremes of r_1 and r_2 as shown in the following sketch.

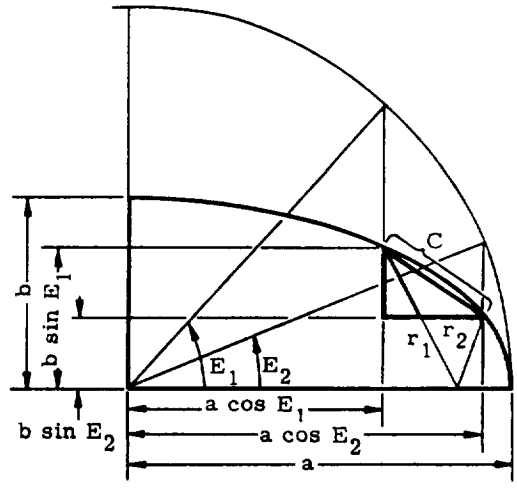

$$C^2 = (a \cos E_2 - a \cos E_1)^2 + (b \sin E_2 - b \sin E_1)^2$$

But the quadratic forms in $\cos E_1$, $\cos E_2$ and $\sin E_1$, $\sin E_2$ can be reduced to functions of G and g to yield

$$C^2 = 4a^2 \sin^2 G \sin^2 g + 4a^2 (1 - e^2) \cos^2 G \sin^2 g$$

Now introducing a new variable h defined as follows:

$$\cos h = e \cos G$$

leads to

$$C^2 = 4a^2 \sin^2 g (1 - \cos^2 h)$$

$$C = 2a \sin g \sin h$$

and

$$r_1 + r_2 = 2a (1 - \cos g \cos h)$$

Now introducing two new variables

$$\epsilon = h + g$$

$$\delta = h - g$$

enables the following equations to be written

$$\cos \frac{1}{2}(\epsilon + \delta) = e \cos \frac{1}{2}(E_2 + E_1)$$

$$r_1 + r_2 + C = 2a \left\{1 - \cos (h + g)\right\} = 4a \sin^2 \frac{\epsilon}{2}$$

$$r_1 + r_2 - C = 2a \left\{1 - \cos (h - g)\right\} = 4a \sin^2 \frac{\delta}{2}$$

These equations serve as the definition of the quantities $\epsilon + \delta$. But

$$n (\Delta t) = E_2 - E_1 - e (\sin E_2 - \sin E_1)$$

$$= (\epsilon - \delta) - 2 \sin \frac{1}{2}(\epsilon - \delta) \cos \frac{1}{2}(\epsilon + \delta)$$

$$= \epsilon - \delta - (\sin \epsilon - \sin \delta)$$

which is known as Lambert's theorem.

This form of the time equation may seem to have no major advantages. Closer examination, however, shows that for the case where the Δt is specified for transfer from r_1 to r_2 through a given $\Delta\theta$, and it is desired to find the unique ellipse whose parameters are a + e, this form may prove preferable. This conclusion is based on the fact that for this case only one variable of interest a appears explicitly though it is necessary in the process to solve for the auxiliary parameters $\epsilon + \delta$. One source of possible error is the selection of the proper quadrants for the angles ϵ and δ. This selection may be accomplished by referring to the following statements.

(1) $\sin \frac{\delta}{2}$ is +
- (a) the arc includes perigee and the chord intersects the perigee radius
- (b) the arc excludes perigee and the chord does not intersect the perigee radius

(That is, $\sin \delta/2$ is positive when the segment of the ellipse formed by the arc and chord does not contain the center of mass.)

(2) $\cos \frac{\epsilon}{2}$ is +
- (a) the arc contains perigee and the chord intersects the apogee radius
- (b) the arc does not contain perigee and does not intersect the apogee radius

(That is, $\sin \epsilon/2$ is positive when the segment of the ellipse formed by the arc and chord does not intersect the apogee radius.)

(3) $0 < \frac{1}{2}\epsilon < \pi$

(4) $-\frac{\pi}{2} < \frac{1}{2}\delta < \frac{\pi}{2}$

More detailed discussions of the reasoning for selecting these quadrants are presented in Ref. 1.

Graphical solutions to this form of the time equation are also possible. One such solution was prepared by Gedeon (Ref. 2). Let

$$2s = r_1 + r_0 + C$$

and

$$C^2 = r_1^2 + r_2^2 - 2 r_1 r_2 \cos \Delta\theta$$

Now define a function w

$$w = \pm \sqrt{1 - C/S}$$

where the + sign is utilized if $\Delta\theta < \pi$ and the - sign is for $\Delta\theta > \pi$.

Expanding the previous solution $n\Delta t$ in a power series for the case that the empty focus falls outside of the area enclosed by the arc and the chord yields

$$n\Delta t = \sqrt{2} \sum_{n=0}^{\infty} A_n \frac{1 - (W)^{2n+3}}{2n+3} \left(\frac{S}{2a}\right)^n$$

$$A_0 = 1$$

$$A_n = \frac{1.3.5 \ldots (2n-1)}{2.4.6.8 \ldots 2n} = \frac{(2n-1)!}{2n!}$$

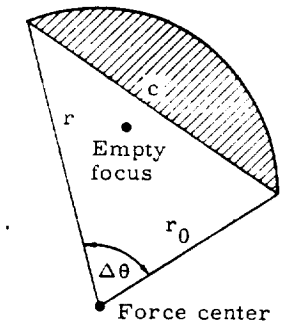

In a similar manner, a power series representation can be obtained for the case in which the arc and chord enclose the empty focus

$$n\Delta t = \sqrt{2}\left[\frac{\pi/2}{(S/2a)^{3/2}} - \sum_{n=0}^{\infty} A_n \frac{1 + (W)^{2n+3}}{2n+3} \left(\frac{S}{2a}\right)^n\right]$$

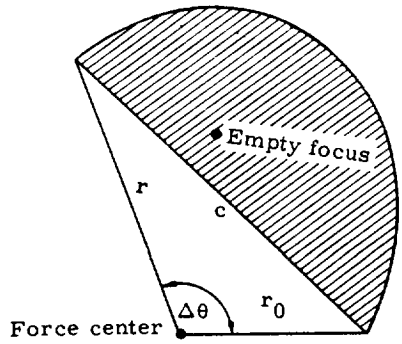

where the A_n are the same as those defined above.

Graphical presentation of this material is found in Figs. 9 and 10.

H. THE N-BODY PROBLEM

The previous discussions have been directed toward the description of the motion of a particle in the gravitational field of a mass sufficiently large that the perturbation due to the particle is completely negligible. Indeed the attractions of all other masses on both the particle and the central mass were neglected. The discussions of this section are intended to provide the generalizations which are possible in order that the discussions of perturbation methods of Chapter IV will be appreciated.

Consider the differential equations

$$m_i \ddot{\vec{r}}_i = -G m_i \sum_{\substack{j=1 \\ j \neq i}}^{n} m_j \frac{(\vec{r}_i - \vec{r}_j)}{r_{ij}^3}$$

This set is of the order 6 n due to the fact that there are 3 n coordinates $(x_i y_i z_i)$ expressed as second order differential equations. A rigorous solution thus involves the simultaneous solution of the n second order vector equations.

Since these forces are all conservative, it is also possible to express the total force acting on the vehicle as the gradient of a work function. Let

$$\vec{F}_i = -\vec{\nabla}_i U$$

Then

$$F_{xi} = m_i \ddot{x}_i = -\frac{\partial U}{\partial x_i}$$

$$F_{yi} = m_i \ddot{y}_i = -\frac{\partial U}{\partial y_i}$$

$$F_{zi} = m_i \ddot{z}_i = -\frac{\partial U}{\partial z_i} \qquad i = 1, \ldots, h$$

multiply F_{xi} by $\dot{x}$, F_{yi} by $\dot{y}$, F_{zi} by $\dot{z}$ and add

$$\sum_{i=1}^{n} m_i (\ddot{x}_i \dot{x}_i + \ddot{y}_i \dot{y}_i + \ddot{z}_i \dot{z}_i) =$$

$$-\sum_{i=1}^{n} \left(\frac{\partial U}{\partial x_i} \dot{x}_i + \frac{\partial U}{\partial y_i} \dot{y}_i + \frac{\partial U}{\partial z_i} \dot{z}_i\right)$$

But if a potential exists, U is a function of the 3n variables x_i, y_i, z_i alone. Thus, the right-hand side is the total derivative of U with respect to t. Thus, upon integration

$$\frac{1}{2} \sum m_i (\dot{x}_i^2 + \dot{y}_i^2 + \dot{z}_i^2) = -U + \text{constant}$$

or

$$T + U = \text{constant (energy equation)}$$

Now, potential energy is the amount of work required to change one configuration to another. Thus, since the bodies attract each other according to the law of inverse squares, the force between bodies is

$$\vec{F} = - \frac{G_i m_i m_j}{r_{ij}^2} \hat{r}_{ij}$$

Thus, the work is moving along the radius r_{ij} is

$$w_{ij} = - G m_i m_j \int_{r(0)_{ij}}^{r_{ij}} \frac{dr_{ij}}{r_{ij}^2}$$

$$= - G m_i m_j \left[\frac{1}{r_0} - \frac{1}{r}\right]_{ij}$$

Now if r (0) is ∞, all possible system configurations are included. Thus

$$w_{ij} = \frac{G m_i m_j}{r_{ij}}$$

Now the total work is the double summation of the individual works

$$w_T = U = \frac{1}{2} \sum_{j=1}^{n} \sum_{\substack{i=1 \\ \neq j}}^{n} \frac{G m_i m_j}{r_{ij}}$$

The one-half arises from the fact that if i and j are both allowed to assume all values, each term in the series will appear twice in the equation. Now following an argument of Moulton (Ref. 3), it can be stated that since the potential function depends solely on the relative positions of the n particles and not on the choice of origin, the origin can be considered to be displaced to any new point, yielding:

$$\vec{r}_i' = \vec{r}_i + \vec{r}_0$$

$$\vec{r}_0 = \alpha \hat{x} + \beta \hat{y} + \alpha \hat{z}$$

Thus

$$\frac{\partial U}{\partial \alpha} = \sum_{i=1}^{n} \frac{\partial U}{\partial x_i'} \frac{\partial x_i'}{\partial \alpha}$$

where

$$x_i' = x_i + \alpha; \quad \frac{\partial x_i}{\partial \alpha} = 1$$

But U does not involve α explicitly, since it is a function of relative position thus upon dropping the prime which is now of no value

$$\sum_{i=1}^{n} \frac{\partial U}{\partial x_i} = 0$$

Similarly for $\sum_{i=1}^{n} \frac{\partial U}{\partial y_i}$ and $\sum_{i=1}^{n} \frac{\partial U}{\partial z_i}$.

Thus

$$\sum_{i=1}^{n} m_i \ddot{\vec{r}}_i = 0$$

$$\sum_{i=1}^{n} m_i \dot{\vec{r}}_i = \vec{C}$$

and

$$\sum_{i=1}^{n} m_i \vec{r}_i = \vec{C} t + \vec{B}$$

But $\sum m_i \vec{r}_i$ is by definition $M \vec{R}$ which is the product of the total mass of the system and the position vector for the center of mass. Thus

$$M \vec{R} = \vec{C} t + \vec{B}$$

This equation states that the center of mass obeys Newton's law $\vec{F} = m \vec{a}$ (where F = 0 = the resultant force) and moves with a constant velocity in a straight line under the assumption that there are no net forces acting on the center of mass. This integral introduces six constants of integration to the system requiring 6 n such constants. Now consider:

$$m_i \ddot{\vec{r}}_i = \vec{\nabla}_i U$$

$$\vec{r}_i \times m_i \ddot{\vec{r}}_i = \vec{r}_i \times \vec{\nabla}_i U$$

$$\sum_{i=1}^{n} \vec{r}_i \times m_i \ddot{\vec{r}}_i = \sum_{i=1}^{n} \vec{r}_i \times \vec{\nabla}_i U$$

But the forces occur in equal magnitude and opposite directions for any given pair of masses. Thus, the right-hand side of the equation is zero when summed over all the masses and

$$\sum_{i=1}^{n} \vec{r}_i \times m_i \ddot{\vec{r}}_i = 0$$

$$= \sum_{i=1}^{n} \frac{d}{dt} (\vec{r}_i \times m_i \dot{\vec{r}}_i)$$

$$= \frac{d}{dt} \sum_{i=1}^{n} (\vec{r}_i \times m_i \dot{\vec{r}}_i)$$

Thus by direct integration once again it is seen that the total angular momentum is conserved

$$\sum_{i=1}^{n} (\vec{r}_i \times m_i \dot{\vec{r}}_i) = h$$

Since this is a vector equation, three additional constants have been introduced.

One more relationship between the coordinates and velocities can be obtained from the energy integral, the general form of which was presented earlier. Thus, ten integrals exist. These ten are the only integrals known and are the only integrals available from existing algebraic functions. Thus, the general solution of the n body problem requiring 6 n integrals is at this time impossible even though several operations can be performed to eliminate two variables, the line of node and the time. (The latter simplification is obtained by expressing each of the coordinates as a function of a given coordinate.) The sole exception to this rule is the 2-body problem.

Consider the equations of motion

$$m_1 \ddot{\vec{r}}_1 = -G m_1 m_2 \frac{(\vec{r}_1 - \vec{r}_2)}{r_{12}^3}$$

$$m_2 \ddot{\vec{r}}_2 = -G m_1 m_2 \frac{(\vec{r}_2 - \vec{r}_1)}{r_{12}^3}$$

Changing origin to the center of mass by substituting

$$\vec{R}_1 = \vec{r}_1 - \vec{R}_0$$

$$\vec{R}_2 = \vec{r}_2 - \vec{R}_0$$

yields

$$m_1 \ddot{\vec{R}}_1 = -G m_1 m_2 \frac{\vec{R}_1 - \vec{R}_2}{R_{12}^3}$$

$$m_2 \ddot{\vec{R}}_2 = -G m_1 m_2 \frac{\vec{R}_2 - \vec{R}_1}{R_{12}^3}$$

But the center of mass satisfies the equation

$$m_1 \vec{R}_1 + m_2 \vec{R}_2 = 0$$

or

$$\vec{R}_2 = -\frac{m_1}{m_2} \vec{R}_1$$

Substitution of this equality eliminates $\vec{R}_2$ from the equations

$$\ddot{\vec{R}}_1 = -G m_2 (1 + \frac{m_1}{m_2}) \frac{\vec{R}_1}{R_{12}^3}$$

$$= -G(m_1 + m_2) \frac{\vec{R}_1}{R_{12}^3}$$

$$\ddot{\vec{R}}_2 = -G(m_1 + m_2) \frac{\vec{R}_2}{R_{12}^3}$$

where

$$\vec{R}_{12} = \vec{R}_1 - \vec{R}_2$$

$$= (1 + \frac{m_1}{m_2}) \vec{R}_1 = \frac{M}{m_2} \vec{R}_1$$

$$= \frac{-M}{m_1} \vec{R}_2$$

Thus

$$\ddot{\vec{R}}_1 = -\frac{G m_2^3}{M^2} \frac{\vec{R}_1}{R_1^3}$$

$$\ddot{\vec{R}}_2 = -\frac{G m_1^3}{M^2} \frac{\vec{R}_2}{R_2^3}$$

With this substitution, the differential equations become uncoupled in the coordinates. But these equations are immediately recognizable as the differential equation for a conic section with the center of mass at the focus. Thus, as before, the solution will be of the form

$$R_1 = \frac{P_1}{1 + e_1 \cos \theta_1}$$

$$R_2 = \frac{P_2}{1 + e_2 \cos \theta_2}$$

But it is important to note that the elements of these conics are not the same though they must be related. Indeed, the effective masses as seen by the two bodies will be different. This latter requirement is the result of requiring that the line between the two bodies contains the fixed center of mass at any time. However, it is possible to obtain a set of six constants of integration a_1, e_1, i_1, ω_1, Ω_1, t_{01} and a dependent set a_2, e_2, i_2, ω_2, Ω_2 and t_{02} which will produce

the desired motion. This is accomplished by considering various elliptic relations and the geometry of the plane of motion. To illustrate the relationships, consider the requirement that the mean motions be the same.

$$n_1 = n_2$$

$$\frac{\mu_1}{a_1^3} = \frac{\mu_2}{a_2^3}$$

$$a_1 = \left(\frac{\mu_1}{\mu_2}\right)^{\frac{1}{3}} \cdot a_2 = \frac{m_2}{m_1}\ a_2$$

The other elements are determined in an analogous fashion.

I. SERIES EXPANSIONS FOR ELLIPTIC ORBITS

Many of the solutions to trajectory problems can be greatly simplified by utilizing approximate forms for the parameters involved. The general forms of several useful series are developed in this section, and a list of expansions is given in Table 6 (see Section K).

Kepler's equation can be rewritten as

$$E = M + e \sin E \qquad (12)$$

By Lagrange's expansion theorem, this expression can be developed (see Goursat and Hedrick, "Mathematical Analysis," Vol. I, p 404) in powers of eccentricity, e.

$$E = M + \sum_{n=1}^{\infty} \frac{e^n}{n!} \frac{d^{n-1}}{dM^{n-1}} (\sin^n M) \qquad (13)$$

From Eq (12) it follows immediately that

$$\sin E = \frac{E - M}{e}$$

Therefore,

$$\sin E = \sum_{n=1}^{\infty} \frac{e^{n-1}}{n!} \frac{d^{n-1}}{dM^{n-1}} (\sin^n M) \qquad (14)$$

To obtain the expansion for cos E, the auxiliary integral function I is needed.

$$I = -\int (E - M)\, dM$$

$$= -\int \sum_{n=1}^{\infty} \frac{e^n}{n!} \frac{d^{n-1}}{dM^{n-1}} (\sin^n M)\, dM$$

$$= -\sum_{n=1}^{\infty} \frac{e^n}{n!} \int d \frac{d^{n-2}}{dM^{n-2}} (\sin^n M)$$

$$= -\sum_{n=1}^{\infty} \frac{e^n}{n!} \frac{d^{n-2}}{dM^{n-2}} (\sin^n M) \qquad (15)$$

From Eq (12) by integration,

$$I = -\int (E - M)\, dM = -\int e \sin E\, dM$$

$$= -e \int \sin E (1 - e \cos E)\, dE$$

$$= -e \int \left(\sin E - \frac{e}{2} \sin 2E\right) dE$$

and using an arbitrary integration constant c,

$$I = c + e \cos E - \frac{e^2}{4} \cos 2E \qquad (16)$$

but integrating Eq (15) with respect to dM,

$$\int_0^{2\pi} I\, dM = \int_0^{2\pi} \left(-\frac{e^2}{4}\right) dM + \int_0^{2\pi} \left[\text{cosine terms}\right] dM$$

$$= \int_0^{2\pi} \left(-\frac{e^2}{4}\right) dM \qquad (17)$$

Similarly, from Eq (16),

$$\int_0^{2\pi} I\, dM = \int_0^{2\pi} \left(c + e \cos E - \frac{e^2}{4} \cos 2E\right)(1 - e \cos E)\, dE \qquad (18)$$

Equating Eqs (17) and (18),

$$\int_0^{2\pi} \left(-\frac{e^2}{4}\right) dM = \int_0^{2\pi} \left(-\frac{e^2}{4} + \frac{e^3}{4} \cos E\right) dE$$

$$= \int_0^{2\pi} \left[c - \frac{e^2}{2} + \left(e - ec + \frac{e^3}{8}\right) \cos E - \frac{3e^2}{4} \cos 2E + \frac{e^3}{8} \cos 3E\right] dE$$

As for the complete integral, all the cosine terms are zero; it follows that,

$$c = \frac{e^2}{4}$$

Finally, the auxiliary integral function becomes

$$I = e \cos E + \frac{e^2}{4} (1 - \cos 2E) \qquad (19)$$

Next, Kepler's equation is expressed in a functional form:

$$F(E, e, M) = E - e \sin E - M = 0 \quad (20)$$

The derivative of E with respect to e is found by the use of Jacobians as follows:

$$\frac{dE}{de} = -\frac{F_e}{F_E} = \frac{\sin E}{1 - e \cos E} \quad (21)$$

Differentiating, Eq (19) yields

$$\frac{dI}{de} = \cos E + \frac{e}{2} - \frac{e}{2} \cos 2E$$

$$+ e \sin E \frac{dE}{de} + \frac{e^2}{2} \sin 2E \frac{dE}{de} \quad (22)$$

Substituting Eq (21) into Eq (22) and collecting terms yields

$$\frac{dI}{de} = \cos E \quad (23)$$

Finally, the expansion for cos E is found from Eqs (23) and (15) as

$$\cos E = -\sum_{n=1}^{\infty} \frac{e^{n-1}}{(n-1)!} \frac{d^{n-2}}{dM^{n-2}} (\sin^n M) \quad (24)$$

Note: $\frac{d^{-1}}{dM^{-1}} (F) = \int F dM$ and $\frac{d^0}{dM^0} (F) = F$

From the basic equations of orbital mechanics,

$$\frac{r}{a} = 1 - e \cos E \quad (25a)$$

From Eq (24), it follows that

$$\frac{r}{a} = 1 + \sum_{n=1}^{\infty} \frac{e^n}{(n-1)!} \frac{d^{n-2}}{dM^{n-2}} (\sin^n M) \quad (25b)$$

Squaring Eq (25a),

$$\left(\frac{r}{a}\right)^2 = 1 + \frac{1}{2} e^2 - 2e \cos E + \frac{1}{2} e^2 \cos 2E \quad (26a)$$

Comparing Eq (26a) with Eq (19),

$$\left(\frac{r}{a}\right)^2 = 1 + e^2 - 2I \quad (26b)$$

and immediately from Eq (15),

$$\left(\frac{r}{a}\right)^2 = 1 + e^2 + 2 \sum_{n=1}^{\infty} \frac{e^n}{n!} \frac{d^{n-2}}{dM^{n-2}} (\sin^n M) \quad (27)$$

From Eq (20),

$$\frac{dE}{dM} = -\frac{F_M}{F_E} = \frac{1}{1 - e \cos E} = \frac{a}{r} \quad (28)$$

From Eqs (13) and (28),

$$\frac{a}{r} = 1 + \sum_{n=1}^{\infty} \frac{e^n}{n!} \frac{d^n}{dM^n} (\sin^n M) \quad (29)$$

It is known that

$$\left.\begin{aligned} \frac{x}{a} &= \cos E - e \\ \frac{y}{a} &= \sqrt{1-e^2} \sin E \end{aligned}\right\} \quad (30)$$

Combining Eqs (30), (24) and (14),

$$\frac{x}{a} = -e - \sum_{n=1}^{\infty} \frac{e^{n-1}}{(n-1)!} \frac{d^{n-2}}{dM^{n-2}} (\sin^n M) \quad (31)$$

$$\frac{y}{a} = \sqrt{1-e^2} \sum_{n=1}^{\infty} \frac{e^{n-1}}{n!} \frac{d^{n-1}}{dM^{n-1}} (\sin^n M) \quad (32)$$

The relationships between the true anomaly and eccentric anomaly are expressed as follows:

$$\left.\begin{aligned} \sin \theta &= \frac{\sqrt{1-e^2} \sin E}{1 - e \cos E} = \sqrt{1 - e^2} \frac{dE}{de} \\ \cos \theta &= \frac{\cos E - e}{1 - e \cos E} = -\frac{d}{de} \left(\frac{r}{a}\right) \end{aligned}\right\} \quad (33)$$

The first equation follows from Eq (21) and the second by Eq (25a)

$$\frac{d}{de} \left(\frac{r}{a}\right) = -\cos E + e \sin E \frac{dE}{de} = \frac{-\cos E + e}{1 - e \cos E}$$

Substituting Eqs (13) and (25b) into (33),

$$\sin \theta = \sqrt{1 - e^2} \sum_{n=1}^{\infty} \frac{e^{n-1}}{(n-1)!} \frac{d^{n-1}}{dM^{n-1}} (\sin^n M) \quad (34)$$

$$\cos \theta = -\sum_{n=1}^{\infty} \frac{n e^{n-1}}{(n-1)!} \frac{d^{n-2}}{dM^{n-2}} (\sin^n M) \quad (35)$$

The general form derivation of the time anomaly is somewhat more complicated and will not be attempted here. If a finite number of terms is carried, it follows from Eq (33) that

$$\frac{d\theta}{dM} = \frac{\sqrt{1 - e^2}}{(1 - e \cos E)^2} = \sqrt{1 - e^2} \left(\frac{a}{r}\right)^2$$

and after multiplying out $\left(\frac{a}{r}\right)^2$, the true anomaly follows by integration

$$\theta = \int \sqrt{1 - e^2} \left(\frac{a}{r}\right)^2 dM$$

Such an expression up to the sixth power of eccentricity has been derived by Moulton.

This concludes the derivation of the series expansions in powers of increasing eccentricity. In general form these series are presented in Table 6-1a. The results are given in Section K in Table 6-1b for eccentricities up to sixth and seventh powers.

Table 6-2a gives the n-th power of sin M in order to simplify the use of the general equations for expansions up to e^{13}. Table 6-2b indicates the determination of numerical constants for the expansions.

The general forms of the Fourier-Bessel expansions are given in Table 6-3a with the corresponding expansions of Bessel functions in Table 6-3b. Table 6-4 gives the Fourier-Bessel series expanded up to the seventh powers of eccentricity.

It has been shown by Laplace that for some values at M, the series expansions may diverge if the eccentricity e exceeds 0.662743 . . . For small eccentricities, the convergence is rather rapid. Table 6-5 presents the series for small values of e ($e^2 << 1$) as a function of mean anomaly. Finally, Table 6-6 presents the variables as a function of the true anomaly rather than the mean anomaly.

J. NOMOGRAMS

Many of the formulas of the previous sections are of sufficiently general interest to warrant numerical data being prepared for use in preliminary orbit computation. Accordingly, a set of figures will be presented relating the parameters which have been discussed. Use will be made in this presentation of the techniques of nomography (Refs. 3 and 4) and of more conventional forms of presentation.

Before presenting the data however, it is desirable to discuss the basis for construction of a nomogram. If the equation can be expressed as a determinant with the three variables separated into different rows of the determinant and if by manipulation, the equation can be put in the following form

$$\begin{vmatrix} f_1(\alpha) & f_2(\alpha) & 1 \\ f_1(\beta) & f_2(\beta) & 1 \\ f_1(\gamma) & f_2(\gamma) & 1 \end{vmatrix} = 0$$

Then a nomographic presentation is obtained by plotting the values of $f_1(\alpha)$ versus $f_2(\alpha)$, $f_1(\beta)$ versus $f_2(\beta)$ and $f_1(\gamma)$ versus $f_2(\gamma)$ on linear graph paper. It is important to note that the same scale must be utilized for each of the three curves. It is also important to note that the shape of the scales thus generated is defined entirely by the functional forms within the determinant.

By utilizing this technique, the equations defining the two body problem have been analyzed. The type of presentation is considered to be, in many ways, superior to any other available because of the fact that interpolation anywhere other than on a graduated scale is eliminated, and by the fact that more than a nominal number of variables may be handled without losing simplicity or accuracy of presentation. The nomograph obtained for equations of three variables, generally results in three arbitrarily curved scales, U, V, and W, as shown in this sketch.

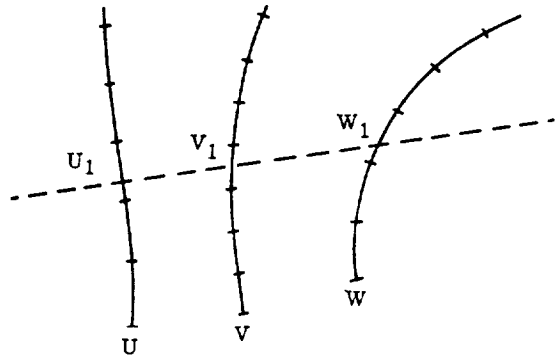

For the simpler cases, the scales may be simply three parallel straight lines, or two straight scales plus one curved scale. In all cases, however, the solution procedures remain the same.

Given any two values of the two independent variables, say $U = U_1$, and $V = V_1$, a straight line drawn between the two given points intersects the third scale at the desired value of the unknown function ($W = W_1$). The straight line (U_1, V_1, W_1) is called the index line or isopleth. It is immaterial which two variables are given and which is considered to be the unknown function.

Four or more variables will generally result in a sequence of 3-variable nomographs as shown in the following sketch.

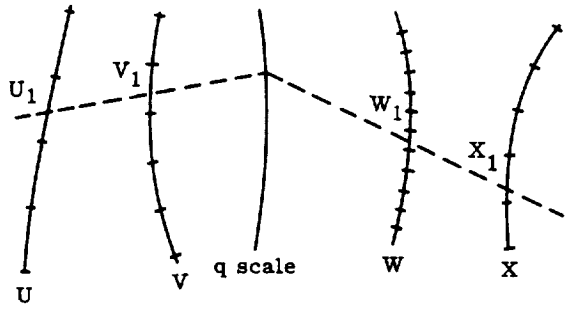

Ungraduated auxiliary scales (e. g., scale q in the given example) are employed, and the number of auxiliary scales is N-3, where N = number of all the variables (e. g., N = 4 in the present example).

A special case of the four-variable solution exists for equations of the form

$$\frac{f_1(U)}{f_2(V)} = \frac{f_3(W)}{f_4(X)}$$

These equations may be expressed in the form of a proportional chart illustrated below.

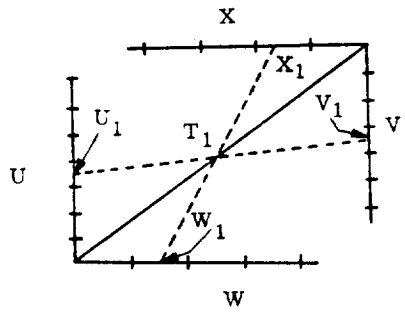

Given any three values of three independent variables $U = U_1$, $V = V_1$, $W = W_1$, the unknown $X = X_1$ is found as follows:

(1) Connect U_1 and V_1 with a straight line.

(2) Draw a straight line through W_1 and the intersection point T_1, reading X_1 on the X scale.

K. TABLES OF EQUATIONS OF ELLIPTIC MOTION

Because of their applicability, the equations of elliptic motion have been collected and are presented in the form of tables. The tabular content is as follows:

Table 1 Elliptical Orbit Element Relations.

This table presents a large number of formulas relating the various fixed parameters defining the ellipse. The index to Table 1 (next page) is a key for locating equations of a given parameter in terms of other parameters. For example, parameter b is expressed in terms of parameters a and e in Eq (20) of Table 1.

Table 2 Time Dependent Variables of Elliptic Orbits.

This table gives the relationship between the time varying parameters of the ellipse. The index (next page) is a key to Table 2.

Table 3 Elliptic Orbital Elements in Terms of Rectangular Position and Velocity Coordinates.

This table is so brief that no special index is required.

Table 4 Elliptic Orbital Elements in Terms of r, v, γ.

This brief table enables one to determine the orbital elements from given kinematic initial conditions.

Table 5 Miscellaneous Relations for Elliptic Orbits.

This table contains some of the special expressions not readily classified under the other tables such as energy relationship, time relationship and certain angular relationships.

Table 6 General Forms of Series Expansions in Powers of Eccentricity.

This table presents a variety of series expansions as follows:

(1a) General Terms of Series Expansions in Powers of Eccentricity

(1b) Power Series Expansions up to e^7 (Eq 6-1 to 6-11)

(2a) Expansion of Powers of Sin M (Eq 6-12 to 6-24)

(2b) Pascal's Triangle and Its Modification

(3a) General Forms of Fourier-Bessel Expansion (Eq 6-25 to 6-36)

(3b) Expansions of J_n (ne) (Eq 6-37)

(4) Fourier-Bessel Expansion up to e^7 (Eq 6-38 to 6-49)

(5) Expansions for Near-Circular Orbits (Eq 6-50 to 6-61)

(6) Expansions in True Anomaly and Eccentricity (Eq 6-62 to 6-76)

Table 7 Hyperbolic Orbit Element Relations.

This table gives the basic parameters for the hyperbola as follows:

(1) Hyperbolic Orbit Element Relations Basic Constant Parameters (Eq 7-1 to 7-56)

(2) Time Variant Hyperbolic Relations (Eq 7-57 to 7-68)

Table 8 Spherical Trigonometric Relations.

This auxiliary table expresses the relationship between the various geometric elements of the three-dimensional orbit. An index to this table is found (next page).

Indexes to some of the tables follow.

Index to Table 1 $X_1 = f(X_2, X_3)$

Parameter	a	b	e	p	r_a	r_p	v_a	v_p
a, b			41	60	79	98	117	137
a, e		20		† 61	† 80	† 99	118	138
a, p					81	100	119	139
		21	† 42		81a	100a		
a, r_a				62		101	120	140
		22	† 43	62a		100a	120a	
a, r_p				63	82		121	141
		23	† 44	63a	81a		120a	
a, v_a		24	45	64	83	102		142
a, v_p		25	46	65	84	103	122	
b, e	1			66	85	104	123	143
b, p	2		47		86	105	124	144
b, r_a	3		48	67		106	125	145
b, r_p	4		49	68	87		126	146
b, v_a								
b, v_p								
e, p	† 5	26			88	107	127	147
e, r_a	† 6	27		69		108	† 128	148
e, r_p	† 7	28		70	89		129	† 149
e, v_a	8	29		71	† 90	109		150
e, v_p	9	30		72	91	† 110	130	
p, r_a	10					111		
	11a	31	50			100a	131	
p, r_p	11	32	51		92		132	151
	11a				81a			
p, v_a	12	33	52		93	112		152
p, v_p	13	34	53		94	113	133	
r_a, r_p	14	35	54	73			134	153
	11a			63a			120a	153a
r_a, v_a	15	36	† 55	74		114		{ 154
r_a, v_p	16	37	56	75		115	135	153a
r_p, v_a	17	38	57	76	95			155
					95a			153a
r_p, v_p	18	39	† 58	77	96		136	
					95a			
v_a, v_p	19	40	54	78	97	116		
					95a			

† figure available

NOTE:
This index to Table 1 is a key for locating equations of a given parameter in terms of other parameters. For example, parameter b is expressed in terms of parameters a and e in equation 20 of Table 1.

Index to Table 2 $X_1 = f(a, e, X_2)$

Parameters	f(E)	f(r)	$f(\dot{r})$	f(v)	$f(\gamma)$	$f(\theta)$	$f(\dot{\theta})$
E		1 2*	3	4	5	† 6 7 8 2*	9
r	10 11*		12	† 13	† 14 15*	† 16 17 11* 15*	18
$\dot{r}$	19	20 21* 22* 23*		24 21* 25*	26 22* 25*	27 23*	28
$\ddot{r}$	29	30 31*	32	33	34	35 31*	36
v	37	† 38 39 40* 41*	42		43 40*	44 41*	45
γ	46	† 47 48 49* 50*	51	52 49*		† 53 54 55 50*	56
θ	†57 58 59 60* 61*	† 62 63 60* 61* 64* 65*	66	67	† 68 64* 65*		69
$\dot{\theta}$	70	71 72*	73	74	75	76 72*	
$\ddot{\theta}$	77	78	79	80	81	82	83

*Function of more than one time-dependent variable

†Figure available

See Note with Table 1

Index to Table 8

Parameters	i	L	β	ν	ϕ
f(i, L)			21	31	41
(i, β)		11		34	44
(i, ν)		14	24		46
(i, ϕ)		16	26	36	
(L, β)	1			37	47
(L, ν)	4		27		49
(L, ϕ)	6		29	39	
(β, ν)	7	17			50
(β, ϕ)	9	19		40	
(ν, ϕ)	10	20	30		
(i, L, β)				32	42
(i, L, ν)			22		43
(i, L, ϕ)			23	33	
(i, β, ν)		12			45
f(i, β, ϕ)		13		35	
(i, ν, ϕ)		15	25		
(L, β, ν)	2				48
(L, β, ϕ)	3			38	
(L, ν, ϕ)	5		28		
(β, ν, ϕ)	8	18			

See Note with Table 1

TABLE 1

Elliptic Orbit Element Relations
(see Fig. 4)

$$a = \frac{b}{\sqrt{1 - e^2}} \qquad (1\text{-}1)$$

$$= \frac{b^2}{p} = \frac{h^2}{\mu(1 - e^2)} \qquad (1\text{-}2)$$

$$= \frac{r_a^2 + b^2}{2r_a} \qquad (1\text{-}3)$$

$$= \frac{r_p^2 + b^2}{2r_p} \qquad (1\text{-}4)$$

$$= \frac{p}{1 - e^2} \quad \text{(Fig. 11)} \qquad (1\text{-}5)$$

$$= \frac{r_a}{1 + e} \quad \text{(Fig. 12)} \qquad (1\text{-}6)$$

$$= \frac{r_p}{1 - e} \quad \text{(Fig. 12)} \qquad (1\text{-}7)$$

TABLE 1 (continued)

$$a = \frac{\mu}{v_a^2}\left(\frac{1-e}{1+e}\right) \quad (1\text{-}8)$$

$$= \frac{\mu}{v_p^2}\left(\frac{1+e}{1-e}\right) \quad (1\text{-}9)$$

$$= \frac{r_a^2}{2r_a - p} \quad (1\text{-}10)$$

$$= \frac{r_p^2}{2r_p - p} \quad (1\text{-}11)$$

$$= \frac{r_a r_p}{p} \quad (1\text{-}11a)$$

$$= \frac{\mu}{v_a\left(2\sqrt{\frac{\mu}{p}} - v_a\right)} \quad (1\text{-}12)$$

$$= \frac{\mu}{v_p\left(2\sqrt{\frac{\mu}{p}} - v_p\right)} \quad (1\text{-}13)$$

$$= \frac{r_a + r_p}{2} \quad (1\text{-}14)$$

$$= \frac{\mu r_a}{2\mu - r_a v_a^2} \quad (1\text{-}15)$$

$$= \frac{1}{4v_p}\left(r_a v_p + \sqrt{r_a^2 v_p^2 + 8\mu r_a}\right) \quad (1\text{-}16)$$

$$= \frac{1}{4v_a}\left(r_p v_a + \sqrt{r_p^2 v_a^2 + 8\mu r_p}\right) \quad (1\text{-}17)$$

$$= \frac{\mu r_p}{2\mu - r_p v_p^2} \quad (1\text{-}18)$$

$$= \frac{\mu}{v_a v_p} = \left(\frac{\tau\sqrt{\mu}}{2\pi}\right)^{2/3} \text{ (Fig. 1)} \quad (1\text{-}19)$$

$$b = a\sqrt{1 - e^2} \quad (1\text{-}20)$$

$$= \sqrt{ap} \quad (1\text{-}21)$$

$$= \sqrt{r_a(2a - r_a)} \quad (1\text{-}22)$$

$$= \sqrt{r_p(2a - r_p)} \quad (1\text{-}23)$$

$$= \frac{2\sqrt{\mu}\, a^{3/2} v_a}{\mu + a v_a^2} \quad (1\text{-}24)$$

$$= \frac{2\sqrt{\mu}\, a^{3/2} v_p}{\mu + a v_p^2} \quad (1\text{-}25)$$

$$b = \frac{p}{\sqrt{1 - e^2}} \quad (1\text{-}26)$$

$$= r_a\sqrt{\frac{1-e}{1+e}} \quad (1\text{-}27)$$

$$= r_p\sqrt{\frac{1+e}{1-e}} \quad (1\text{-}28)$$

$$= \frac{\mu(1-e)^{3/2}}{v_a^2(1+e)^{1/2}} \quad (1\text{-}29)$$

$$= \frac{\mu(1+e)^{3/2}}{v_p^2(1-e)^{1/2}} \quad (1\text{-}30)$$

$$= r_a\sqrt{\frac{p}{2r_a - p}} \quad (1\text{-}31)$$

$$= r_p\sqrt{\frac{p}{2r_p - p}} \quad (1\text{-}32)$$

$$= \sqrt{\frac{(p\mu)^{3/2}}{v_a(2\mu - v_a\sqrt{p\mu})}} \quad (1\text{-}33)$$

$$= \sqrt{\frac{(p\mu)^{3/2}}{v_p(2\mu - v_a\sqrt{p\mu})}} \quad (1\text{-}34)$$

$$= \sqrt{r_a r_p} \quad (1\text{-}35)$$

$$= \sqrt{\frac{r_a^3 v_a^2}{2\mu - r_a v_a^2}} \quad (1\text{-}36)$$

$$= \sqrt{\frac{r_a}{2v_p}\left[\sqrt{r_a^2 v_p^2 + 8\mu r_a} - r_a v_p\right]} \quad (1\text{-}37)$$

$$= \sqrt{\frac{r_p}{2v_a}\left[\sqrt{r_p^2 v_a^2 + 8\mu r_p} - r_p v_a\right]} \quad (1\text{-}38)$$

$$= \sqrt{\frac{r_p^3 v_p^2}{2\mu - r_p v_p^2}} \quad (1\text{-}39)$$

$$= \frac{2\mu}{(v_a + v_p)\sqrt{v_a v_p}} \quad (1\text{-}40)$$

$$e = \sqrt{1 - \left(\frac{b}{a}\right)^2} = \sqrt{1 - \frac{h^2}{\mu a}} \quad (1\text{-}41)$$

$$= \sqrt{1 - \frac{p}{a}} \quad \text{(Fig. 11)} \quad (1\text{-}42)$$

$$= \frac{r_a}{a} - 1 \quad \text{(Fig. 12)} \quad (1\text{-}43)$$

$$= 1 - \frac{r_p}{a} \quad \text{(Fig. 12)} \quad (1\text{-}44)$$

TABLE 1 (continued)

$$e = \frac{\mu - a v_a^2}{\mu + a v_a^2} \quad (1\text{-}45)$$

$$= \frac{a v_p^2 - \mu}{a v_p^2 + \mu} \quad (1\text{-}46)$$

$$= \sqrt{1 - \left(\frac{p}{b}\right)^2} \quad (1\text{-}47)$$

$$= \frac{r_a^2 - b^2}{r_a^2 + b^2} \quad (1\text{-}48)$$

$$= \frac{b^2 - r_p^2}{b^2 + r_p^2} \quad (1\text{-}49)$$

$$= 1 - \frac{p}{r_a} \quad (1\text{-}50)$$

$$= \frac{p}{r_p} - 1 \quad (1\text{-}51)$$

$$= 1 - v_a \sqrt{\frac{p}{\mu}} \quad (1\text{-}52)$$

$$= v_p \sqrt{\frac{p}{\mu}} - 1 \quad (1\text{-}53)$$

$$= \frac{r_a - r_p}{r_a + r_p} = \frac{v_p - v_a}{v_p + v_a} \quad (1\text{-}54)$$

$$= 1 - \frac{r_a v_a^2}{\mu} \quad (1\text{-}55)$$

$$= \frac{1}{2\mu}\left(v_p \sqrt{r_a^2 v_p^2 + 8\mu r_a} - 2\mu - r_a v_p^2\right) \quad (1\text{-}56)$$

$$= \frac{1}{2\mu}\left(2\mu + r_p v_a^2 - v_a \sqrt{r_p^2 v_a^2 + 8\mu r_p}\right) \quad (1\text{-}57)$$

$$= \frac{r_p v_p^2}{\mu} - 1 \quad (1\text{-}58)$$

$$h = \sqrt{\mu p} = r^2 \dot{\theta} \quad (1\text{-}59)$$

$$p = \frac{b^2}{a} \quad (1\text{-}60)$$

$$= a(1 - e^2) \qquad \text{(Fig. 11)} \quad (1\text{-}61)$$

$$= \frac{r_a}{a}(2a - r_a) \quad (1\text{-}62)$$

$$= \frac{r_p}{a}(2a - r_p) \quad (1\text{-}63)$$

$$p = \frac{r_a r_p}{a} \quad (1\text{-}63a)$$

$$= \frac{4\mu}{\left(v_a + \frac{\mu}{a v_a}\right)^2} \quad (1\text{-}64)$$

$$= \frac{4\mu}{\left(v_p + \frac{\mu}{a v_p}\right)^2} \quad (1\text{-}65)$$

$$= b\sqrt{1 - e^2} \quad (1\text{-}66)$$

$$= \frac{2b^2 r_a}{b^2 + r_a^2} \quad (1\text{-}67)$$

$$= \frac{2b^2 r_p}{b^2 + r_p^2} \quad (1\text{-}68)$$

$$= r_a(1 - e) \quad (1\text{-}69)$$

$$= r_p(1 + e) \quad (1\text{-}70)$$

$$= \mu\left(\frac{1 - e}{v_a}\right)^2 \quad (1\text{-}71)$$

$$= \mu\left(\frac{1 + e}{v_p}\right)^2 \quad (1\text{-}72)$$

$$= \frac{2 r_a r_p}{r_a + r_p} \quad (1\text{-}73)$$

$$= \frac{r_a^2 v_a^2}{\mu} \quad (1\text{-}74)$$

$$= \frac{r_a}{2\mu}\left[4\mu - v_p \sqrt{r_a^2 v_p^2 + 8\mu r_a} + r_a v_p^2\right] \quad (1\text{-}75)$$

$$= \frac{r_p}{2\mu}\left[4\mu + r_p v_a^2 - v_a \sqrt{r_p^2 v_a^2 + 8\mu r_p}\right] \quad (1\text{-}76)$$

$$= \frac{r_p^2 v_p^2}{\mu} \quad (1\text{-}77)$$

$$= \frac{4\mu}{\left(v_a + v_p\right)^2} \quad (1\text{-}78)$$

$$r_a = a + \sqrt{a^2 - b^2} \quad (1\text{-}79)$$

$$= a(1 + e) \qquad \text{(Fig. 12)} \quad (1\text{-}80)$$

$$= a\left(1 + \sqrt{1 - \frac{p}{a}}\right) \quad (1\text{-}81)$$

$$= \frac{ap}{r_p} \quad (1\text{-}81a)$$

TABLE 1 (continued)

$$r_a = 2a - r_p \tag{1-82}$$

$$= \frac{2\mu a}{\mu + a v_a^2} \tag{1-83}$$

$$= \frac{2a^2 v_p^2}{\mu + a v_p^2} \tag{1-84}$$

$$= b\sqrt{\frac{1+e}{1-e}} \tag{1-85}$$

$$= \frac{p}{1 - \sqrt{1 - \left(\frac{p}{b}\right)^2}} \tag{1-86}$$

$$= \frac{b^2}{r_p} \tag{1-87}$$

$$= \frac{p}{1-e} \tag{1-88}$$

$$= r_p \left(\frac{1+e}{1-e}\right) \tag{1-89}$$

$$= \frac{\mu (1-e)}{v_a^2} \tag{1-90}$$

$$= \frac{\mu (1+e)^2}{v_p^2 (1-e)} \tag{1-91}$$

$$= \frac{r_p p}{2r_p - p} \tag{1-92}$$

$$= \frac{\mu}{v_a}\sqrt{\frac{p}{\mu}} \tag{1-93}$$

$$= \frac{\sqrt{p\mu}}{2\sqrt{\frac{\mu}{p}} - v_p} \tag{1-94}$$

$$= \sqrt{\frac{r_p^2}{4} + \frac{2\mu r_p}{v_a^2}} - \frac{r_p}{2} \tag{1-95}$$

$$= \frac{r_p v_p}{v_a} \tag{1-95a}$$

$$= \frac{r_p}{\frac{2\mu}{r_p v_p^2} - 1} \tag{1-96}$$

$$= \frac{2\mu}{v_a (v_a + v_p)} \tag{1-97}$$

$$r_p = a - \sqrt{a^2 - b^2} \tag{1-98}$$

$$= a(1-e) \qquad \text{(Fig. 12)} \tag{1-99}$$

$$= \frac{p}{1 + \sqrt{1 - \frac{p}{a}}} \tag{1-100}$$

$$= \frac{ap}{r_a} \tag{1-100a}$$

$$= 2a - r_a \tag{1-101}$$

$$= \frac{2a}{1 + \frac{\mu}{a v_a^2}} \tag{1-102}$$

$$= \frac{2a}{1 + \frac{a v_p^2}{\mu}} \tag{1-103}$$

$$= b\sqrt{\frac{1-e}{1+e}} \tag{1-104}$$

$$= \frac{p}{1 + \sqrt{1 - \left(\frac{p}{b}\right)^2}} \tag{1-105}$$

$$= \frac{b^2}{r_a} \tag{1-106}$$

$$= \frac{p}{1+e} \tag{1-107}$$

$$= r_a \frac{1-e}{1+e} \tag{1-108}$$

$$= \frac{\mu (1-e)^2}{v_a^2 (1+e)} \tag{1-109}$$

$$= \frac{\mu (1+e)}{v_p^2} \tag{1-110}$$

$$= \frac{p r_a}{2r_a - p} \tag{1-111}$$

$$= \frac{\sqrt{p\mu}}{2\sqrt{\frac{\mu}{p}} - v_a} \tag{1-112}$$

$$= \frac{\sqrt{p\mu}}{v_p} \tag{1-113}$$

$$= \frac{r_a^2 v_a^2}{2\mu - r_a v_a^2} \tag{1-114}$$

$$= \sqrt{\frac{r_a^2}{4} + \frac{2\mu r_a}{v_p^2}} - \frac{r_a}{2} \tag{1-115}$$

$$= \frac{2\mu}{v_p (v_a + v_p)} \tag{1-116}$$

TABLE 1 (continued)

$$v_a = \sqrt{\frac{\mu}{a}\left[\frac{1-\sqrt{1-\left(\frac{b}{a}\right)^2}}{1+\sqrt{1-\left(\frac{b}{a}\right)^2}}\right]} \quad (1\text{-}117)$$

$$= \sqrt{\frac{\mu}{a}\left(\frac{1-e}{1+e}\right)} \quad (1\text{-}118)$$

$$= \sqrt{\mu}\left(\sqrt{\frac{1}{p}} - \sqrt{\frac{1}{p}-\frac{1}{a}}\right) \quad (1\text{-}119)$$

$$= \sqrt{\frac{\mu}{a}\left(\frac{2a-r_a}{r_a}\right)} \quad (1\text{-}120)$$

$$= \sqrt{\frac{\mu r_p}{a r_a}} \quad (1\text{-}120a)$$

$$= \sqrt{\frac{\mu}{a}\left(\frac{r_p}{2a-r_p}\right)} \quad (1\text{-}121)$$

$$= \frac{\mu}{a v_p} \quad (1\text{-}122)$$

$$= \sqrt{\frac{\mu\sqrt{1-e^2}}{b}\left(\frac{1-e}{1+e}\right)} \quad (1\text{-}123)$$

$$= \sqrt{\frac{\mu}{p}\left[1-\sqrt{1-\left(\frac{p}{b}\right)^2}\right]} \quad (1\text{-}124)$$

$$= \sqrt{\frac{2\mu b^2}{r_a\left(b^2+r_a^2\right)}} \quad (1\text{-}125)$$

$$= \sqrt{\frac{2\mu r_p^3}{b^2\left(b^2+r_p^2\right)}} \quad (1\text{-}126)$$

$$= \sqrt{\frac{\mu}{p}}\,(1-e) \quad (1\text{-}127)$$

$$= \sqrt{\frac{\mu(1-e)}{r_a}} \quad (1\text{-}128)$$

$$= \sqrt{\frac{\mu(1-e)^2}{r_p(1+e)}} \quad (1\text{-}129)$$

$$= v_p\left(\frac{1-e}{1+e}\right) \quad (1\text{-}130)$$

$$= \frac{\sqrt{\mu p}}{r_a} \quad (1\text{-}131)$$

$$= \sqrt{\frac{\mu}{p}}\left(2-\frac{p}{r_p}\right) \quad (1\text{-}132)$$

$$v_a = 2\sqrt{\frac{\mu}{p}} - v_p \quad (1\text{-}133)$$

$$= \sqrt{\frac{2\mu r_p}{r_a\left(r_a+r_p\right)}} \quad (1\text{-}134)$$

$$= \sqrt{\frac{v_p^2}{4} + \frac{2\mu}{r_a}} - \frac{v_p}{2} \quad (1\text{-}135)$$

$$= \frac{2\mu - r_p v_p^2}{r_p v_p} \quad (1\text{-}136)$$

$$v_p = \sqrt{\frac{\mu}{a}\left[\frac{1+\sqrt{1-\left(\frac{b}{a}\right)^2}}{1-\sqrt{1-\left(\frac{b}{a}\right)^2}}\right]} \quad (1\text{-}137)$$

$$= \sqrt{\frac{\mu}{a}\left(\frac{1+e}{1-e}\right)} \quad (1\text{-}138)$$

$$= \sqrt{\mu}\left(\frac{1}{r_p} + \sqrt{\frac{1}{p}-\frac{1}{a}}\right) \quad (1\text{-}139)$$

$$= \sqrt{\frac{\mu}{a}\left(\frac{r_a}{2a-r_a}\right)} \quad (1\text{-}140)$$

$$= \sqrt{\frac{\mu r_a}{a r_p}} \quad (1\text{-}140a)$$

$$= \sqrt{\frac{\mu}{a}\left(\frac{2a-r_p}{r_p}\right)} \quad (1\text{-}141)$$

$$= \frac{\mu}{a v_a} \quad (1\text{-}142)$$

$$= \sqrt{\frac{\mu\sqrt{1-e^2}}{b}\left(\frac{1+e}{1-e}\right)} \quad (1\text{-}143)$$

$$= \sqrt{\frac{\mu}{p}\left[1+\sqrt{1-\left(\frac{p}{b}\right)^2}\right]} \quad (1\text{-}144)$$

$$= \sqrt{\frac{2\mu r_a^3}{b^2\left(r_a^2+b^2\right)}} \quad (1\text{-}145)$$

$$= \sqrt{\frac{2\mu b^2}{r_p\left(r_p^2+b^2\right)}} \quad (1\text{-}146)$$

$$= \sqrt{\frac{\mu}{p}}\,(1+e) \quad (1\text{-}147)$$

$$= \sqrt{\frac{\mu(1+e)^2}{r_a(1-e)}} \quad (1\text{-}148)$$

TABLE 1 (continued)

$$v_p = \sqrt{\frac{\mu}{r_p}(1+e)} \quad (1\text{-}149)$$

$$= v_a\left(\frac{1+e}{1-e}\right) \quad (1\text{-}150)$$

$$= \sqrt{\frac{\mu p}{r_p}} \quad (1\text{-}151)$$

$$= 2\sqrt{\frac{\mu}{p}} - v_a \quad (1\text{-}152)$$

$$= \sqrt{\frac{2\mu r_a}{r_p(r_a+r_p)}} \quad (1\text{-}153)$$

$$= \frac{r_a v_a}{r_p} \quad (1\text{-}153a)$$

$$= \frac{2\mu - r_a v_a^2}{r_a v_a} \quad (1\text{-}154)$$

$$= \sqrt{\frac{v_a^2}{4} + \frac{2\mu}{r_p}} - \frac{v_a}{2} \quad (1\text{-}155)$$

TABLE 2

Time Dependent Variables of Elliptic Orbits
(see Fig. 4)

$$E = \cos^{-1}\left(\frac{a-r}{ae}\right) \quad (2\text{-}1)$$

$$= \sin^{-1}\left(\frac{r\sin\theta}{a\sqrt{1-e^2}}\right) \quad \text{(Fig. 13)} \quad (2\text{-}2)$$

$$= \cos^{-1}\left[\frac{\mu e^2 \pm \left[\mu^2 e^2 - \mu a(1-e^2)\dot{r}^2\right]^{1/2}}{\mu e \pm e\left[\mu^2 e^2 - \mu a(1-e^2)\dot{r}^2\right]^{1/2}}\right] \quad (2\text{-}3)$$

$$= \cos^{-1}\left[\frac{1}{e}\left(\frac{av^2-\mu}{av^2+\mu}\right)\right] \quad (2\text{-}4)$$

$$= \cos^{-1}\left[\frac{1}{e}\left(\pm\sqrt{1-(1-e^2)\sec^2\gamma}\right)\right] \quad (2\text{-}5)$$

$$= \sin^{-1}\left(\frac{\sqrt{1-e^2}\sin\theta}{1+e\cos\theta}\right) \quad \text{(Fig. 14)} \quad (2\text{-}6)$$

$$= \cos^{-1}\left[\frac{e+\cos\theta}{1+e\cos\theta}\right] \quad \text{(Fig. 14)} \quad (2\text{-}7)$$

$$E = 2\tan^{-1}\left[\left(\frac{1-e}{1+e}\right)^{1/2}\tan\frac{\theta}{2}\right] \quad \text{(Fig. 14)} \quad (2\text{-}8)$$

$$= \cos^{-1}\left[\frac{1}{e}\left(1 - \frac{\left[\mu a(1-e^2)\right]^{1/4}}{a\dot{\theta}^{1/2}}\right)\right] \quad (2\text{-}9)$$

$$r = a(1-e\cos E) \quad (2\text{-}10)$$

$$= a\sqrt{1-e^2}\,\frac{\sin E}{\sin\theta} \quad (2\text{-}11)$$

$$= \frac{\mu a(1-e^2)}{\mu \pm \left[\mu^2 e^2 - \mu a(1-e^2)\dot{r}^2\right]^{1/2}} \quad (2\text{-}12)$$

$$= \frac{2\mu a}{av^2+\mu} \quad \text{(Fig. 15)} \quad (2\text{-}13)$$

$$= a\left[1 \pm \sqrt{1-(1-e^2)\sec^2\gamma}\right] \quad \text{(Fig. 17)} \quad (2\text{-}14)$$

$$= \frac{a(1-e^2)\tan\gamma}{e\sin\theta} \quad (2\text{-}15)$$

$$= \frac{a(1-e^2)}{1+e\cos\theta} \quad \text{(Fig. 16)} \quad (2\text{-}16)$$

$$= \frac{2r_a r_p}{(r_a+r_p)+(r_a-r_p)\cos\theta} \quad \text{(Fig. 13)} \quad (2\text{-}17)$$

$$= \left[\frac{\sqrt{\mu a(1-e^2)}}{\dot{\theta}}\right]^{1/2} \quad (2\text{-}18)$$

$$\dot{r} = \sqrt{\frac{\mu}{a}}\,\frac{e\sin E}{1-e\cos E} \quad (2\text{-}19)$$

$$= \pm\sqrt{\frac{\mu\left[2ar - r^2 - a^2(1-e^2)\right]}{ar^2}} \quad (2\text{-}20)$$

$$= \sqrt{v^2 - \frac{\mu a(1-e^2)}{r^2}} \quad (2\text{-}21)$$

$$= \frac{\sqrt{\mu a(1-e^2)}\tan\gamma}{r} \quad (2\text{-}22)$$

$$= \sqrt{\frac{\mu a(1-e^2)}{r}}\left(1 - \frac{r}{a(1-e^2)}\right)\tan\theta \quad (2\text{-}23)$$

$$= \pm\sqrt{\frac{4\mu a v^2 - (av^2+\mu)^2(1-e^2)}{4\mu a}} \quad (2\text{-}24)$$

$$= v\sin\gamma \quad (2\text{-}25)$$

TABLE 2 (continued)

$$\dot{r} = \pm\left[\frac{\mu\,(1-e^2)\tan^2\gamma}{a\left[1\pm\sqrt{1-(1-e^2)\sec^2\gamma}\right]^2}\right]^{1/2} \quad (2\text{-}26)$$

$$= e\left[\frac{\mu}{a\,(1-e^2)}\right]^{1/2}\sin\theta \quad (2\text{-}27)$$

$$= \pm\left\{\frac{2\mu\,\dot{\theta}^{1/2}}{\left[\mu a\,(1-e^2)\right]^{1/4}} - \frac{\mu}{a} - \left[\mu a\,(1-e^2)\right]^{1/2}\dot{\theta}\right\}^{1/2} \quad (2\text{-}28)$$

$$\ddot{r} = \frac{\mu}{a^2}\,\frac{e\,(\cos E - e)}{(1-e\cos E)^3} \quad (2\text{-}29)$$

$$= \frac{\mu\left[a\,(1-e^2)-r\right]}{r^3} \quad (2\text{-}30)$$

$$= \frac{\mu e}{r^2}\cos\theta \quad (2\text{-}31)$$

$$= \left\{\pm\,\mu\left[\mu e^2 - a\,(1-e^2)\,\dot{r}^2\right]^{1/2} + 2\mu^{1/2}\left[\mu e^2 - a\,(1-e^2)\,\dot{r}^2\right] \pm\left[\mu e^2 - a\,(1-e^2)\,\dot{r}^2\right]^{3/2}\right\} \Big/ \left[\mu^{1/2}\,a^2\,(1-e^2)^2\right] \quad (2\text{-}32)$$

$$= \frac{(av^2+\mu)^2}{8\mu a^2}\left[(av^2+\mu)\,(1-e^2) - 2\mu\right] \quad (2\text{-}33)$$

$$= \frac{\mu\left[(1-e^2) - (1\pm\sqrt{1-(1-e^2)\sec^2\gamma})\right]}{a^2\left[1\pm\sqrt{1-(1-e^2)\sec^2\gamma}\right]^3} \quad (2\text{-}34)$$

$$= \frac{\mu e}{a^2\,(1-e^2)^2}\,(1+e\cos\theta)^2\cos\theta \quad (2\text{-}35)$$

$$= \mu\left[\frac{a\,(1-e^2)\,\dot{\theta}^{3/2} - \left[\mu a\,(1-e^2)\right]^{1/4}\dot{\theta}}{\left[\mu a\,(1-e^2)\right]^{3/4}}\right] \quad (2\text{-}36)$$

$$v = \sqrt{\frac{\mu\,(1+e\cos E)}{a\,(1-e\cos E)}} \quad (2\text{-}37)$$

$$= \sqrt{\mu\left(\frac{2}{r} - \frac{1}{a}\right)} \quad \text{(Figs. 1 and 15)} \quad (2\text{-}38)$$

$$= \sqrt{v_0^2 + 2\mu\left(\frac{1}{r} - \frac{1}{r_0}\right)} \quad (2\text{-}39)$$

$$= \sqrt{\frac{\mu a\,(1-e^2)}{r\cos\gamma}} \quad \text{(Fig. 18)} \quad (2\text{-}40)$$

$$= \sqrt{\frac{\mu\,(1+2e\cos\theta+e^2)}{r\,(1+e\cos\theta)}} \quad (2\text{-}41)$$

$$= \left\{\frac{\mu\,(1+e^2) \pm 2\left\{\mu\left[\mu e^2 - a\,(1-e^2)\,\dot{r}^2\right]\right\}^{1/2}}{a\,(1-e^2)}\right\}^{1/2} \quad (2\text{-}42)$$

$$= \left[\frac{\mu}{a}\left(\frac{1\mp\sqrt{1-(1-e^2)\sec^2\gamma}}{1\pm\sqrt{1-(1-e^2)\sec^2\gamma}}\right)\right]^{1/2} \quad (2\text{-}43)$$

$$= \left[\frac{\mu\,(1+e^2+2e\cos\theta)}{a\,(1-e^2)}\right]^{1/2} \quad (2\text{-}44)$$

$$= \mu^{1/2}\left\{\frac{2a\dot{\theta}^{1/2} - \left[\mu a\,(1-e^2)\right]^{1/4}}{a\left[\mu a\,(1-e^2)\right]^{1/4}}\right\}^{1/2} \quad (2\text{-}45)$$

$$\gamma = \tan^{-1}\left[\frac{e}{\sqrt{1-e^2}}\sin E\right] \quad (2\text{-}46)$$

$$= \cos^{-1}\sqrt{\frac{a^2\,(1-e^2)}{r\,(2a-r)}} \quad \text{(Fig. 17)} \quad (2\text{-}47)$$

$$= \cos^{-1}\sqrt{\frac{r_a r_p}{r\,(r_a+r_p-r)}} \quad \text{(Fig. 17)} \quad (2\text{-}48)$$

$$= \cos^{-1}\left(\frac{\sqrt{\mu a\,(1-e^2)}}{r\,v}\right) \quad \text{(Fig. 18)} \quad (2\text{-}49)$$

$$= \tan^{-1}\left[\left(1 - \frac{r}{a(1-e^2)}\right)\tan\theta\right] \quad (2\text{-}50)$$

$$= \pm\tan^{-1}\left[\frac{\dot{r}\left[a\,(1-e^2)\right]^{1/2}}{\left\{\mu^{1/2} \pm \left[\mu e^2 - a\,(1-e^2)\dot{r}^2\right]^{1/2}\right\}}\right] \quad (2\text{-}51)$$

$$= \pm\tan^{-1}\left(\frac{\sqrt{(1-e^2)\left[4\mu a v^2 - (av^2+\mu)^2\,(1-e^2)\right]}}{(av^2+\mu)\,(1-e^2)}\right) \quad (2\text{-}52)$$

(Fig. 19)

TABLE 2 (continued)

$$\gamma = \tan^{-1}\left(\frac{e \sin\theta}{1+e\cos\theta}\right) \quad \text{(Fig. 20)} \quad (2\text{-}53)$$

$$= \sin^{-1}\left(\frac{e\sin\theta}{\sqrt{1+2e\cos\theta+e^2}}\right) \quad \text{(Fig. 20)} \quad (2\text{-}54)$$

$$= \cos^{-1}\left(\frac{1+e\cos\theta}{\sqrt{1+2e\cos\theta+e^2}}\right) \quad \text{(Fig. 20)} \quad (2\text{-}55)$$

$$= \pm\tan^{-1}\left\{\frac{2a\dot{\theta}^{1/2}\left[\mu a(1-e^2)\right]^{1/4} - \left[\mu a(1-e^2)\right]^{1/2}}{a^2(1-e^2)\ \dot{\theta}} - 1\right\}^{1/2} \quad (2\text{-}56)$$

$$\theta = \cos^{-1}\left(\frac{\cos E - e}{1-e\cos E}\right) \quad \text{(Fig. 14)} \quad (2\text{-}57)$$

$$= 2\tan^{-1}\left[\left(\frac{1+e}{1-e}\right)^{1/2}\tan\frac{E}{2}\right] \text{(Fig. 14)} \quad (2\text{-}58)$$

$$= \sin^{-1}\left(\frac{\sin E\sqrt{1-e^2}}{1-e\cos E}\right) \quad \text{(Fig. 14)} \quad (2\text{-}59)$$

$$= \cos^{-1}\left(\frac{a}{r}\left[\cos E - e\right]\right) \quad (2\text{-}60)$$

$$= \sin^{-1}\left(\frac{a\sqrt{1-e^2}\ \sin E}{r}\right) \quad (2\text{-}61)$$

$$= \cos^{-1}\left[\frac{a(1-e^2)-r}{er}\right] \quad \text{(Figs. 12 \& 13)} \quad (2\text{-}62)$$

$$= \cos^{-1}\left[\frac{2r_a r_p - r(r_a+r_p)}{r(r_a-r_p)}\right] \quad \text{(Figs. 12 \& 13)} \quad (2\text{-}63)$$

$$= \sin^{-1}\left[\frac{a(1-e^2)\tan\gamma}{er}\right] \quad (2\text{-}64)$$

$$= \tan^{-1}\left[\frac{a(1-e^2)\tan\gamma}{a(1-e^2)-r}\right] \quad (2\text{-}65)$$

$$= \sin^{-1}\left\{\frac{\dot{r}}{e}\left[\frac{a(1-e^2)}{\mu}\right]^{1/2}\right\} \quad (2\text{-}66)$$

$$= \cos^{-1}\left[\frac{(av^2+\mu)(1-e^2)-2\mu}{2\mu e}\right] \quad (2\text{-}67)$$

$$= \cos^{-1}\left[\frac{1}{e}\left\{\cos^2\gamma - 1 \pm \cos\gamma\sqrt{\cos^2\gamma-(1-e^2)}\right\}\right] \quad \text{(Fig. 20)} \quad (2\text{-}68)$$

$$= \cos^{-1}\left[\frac{1}{e}\left\{\left[\frac{a^3(1-e^2)^3}{\mu}\right]^{1/4}\dot{\theta}^{1/2} - 1\right\}\right] \quad (2\text{-}69)$$

$$\dot{\theta} = \left(\frac{\mu}{a^3}\right)^{1/2}\frac{(1-e^2)^{1/2}}{(1-e\cos E)^2} \quad (2\text{-}70)$$

$$= \frac{\left[\mu a(1-e^2)\right]^{1/2}}{r^2} \quad (2\text{-}71)$$

$$= \sqrt{\frac{\mu(1+e\cos\theta)}{r^3}} \quad (2\text{-}72)$$

$$= \frac{\left\{\mu^{1/2} \pm \left[\mu e^2 - a(1-e^2)\dot{r}^2\right]^{1/2}\right\}^{1/2}}{\left[\mu a^3(1-e^2)^3\right]^{1/2}} \quad (2\text{-}73)$$

$$= \frac{(av^2+\mu)^2\left[\mu a(1-e^2)\right]^{1/2}}{4\mu^2 a^2} \quad (2\text{-}74)$$

$$= \frac{\left[\mu a(1-e^2)\right]^{1/2}}{a^2\left[1 \pm \sqrt{1-(1-e^2)\sec^2\gamma}\right]^2} \quad (2\text{-}75)$$

$$= \left[\frac{\mu}{a^3(1-e^2)^3}\right]^{1/2}(1+e\cos\theta)^2 \quad (2\text{-}76)$$

$$\ddot{\theta} = -\frac{\mu}{a^3}\frac{2e(1-e^2)^{1/2}\sin E}{(1-e\cos E)^4} \quad (2\text{-}77)$$

$$= \pm\frac{2\mu}{r^4}\left[(2ar-r^2)(1-e^2) - a^2(1-e^2)^2\right]^{1/2} \quad (2\text{-}78)$$

$$= -2\dot{r}\left[a(1-e^2)\right]^{-5/2}\left\{\mu^{1/2} \pm \left[\mu e^2 - a(1-e^2)\dot{r}^2\right]^{1/2}\right\}^3 \quad (2\text{-}79)$$

$$= \pm\left[\frac{av^2+\mu}{2\mu a}\right]^3\left\{(1-e^2)\left[2\mu a v^2(1+e^2) - (a^2v^4+\mu^2)(1-e^2)\right]\right\}^{1/2} \quad (2\text{-}80)$$

$$= \pm\frac{2\mu(1-e^2)\tan\gamma}{a^3\left[1 \pm \sqrt{1-(1-e^2)\sec^2\gamma}\right]^4} \quad (2\text{-}81)$$

$$= -\frac{2\mu e}{a^3(1-e^2)^3}(1+e\cos\theta)^3\sin\theta \quad (2\text{-}82)$$

$$= \pm\frac{2\dot{\theta}^{2/3}}{a(1-e^2)}\left\{2a(1-e^2)\dot{\theta}^{1/2}\left[\mu a(1-e^2)\right]^{1/4} - (1-e^2)\left[\mu a(1-e^2)\right]^{1/2} - a^2(1-e^2)^2\dot{\theta}\right\}^{1/2} \quad (2\text{-}83)$$

TABLE 3

Elliptic Orbital Elements in Terms of Rectangular Position and Velocity Coordinates

$$a = \left[2\left(x^2+y^2+z^2\right)^{-1/2} - \frac{1}{\mu}\left(\dot{x}^2+\dot{y}^2+\dot{z}^2\right)\right]^{-1}$$

$$A = \tan^{-1}\left(\frac{y}{x}\right) \qquad (3\text{-}1)$$

$$e = \left\{1 - \frac{1}{\mu}\left[(x\dot{y}-y\dot{x})^2 + (x\dot{z}-z\dot{x})^2 + (y\dot{z}-z\dot{y})^2\right]\left[2\left(x^2+y^2+z^2\right)^{-1/2} - \frac{1}{\mu}\left(\dot{x}^2+\dot{y}^2+\dot{z}^2\right)\right]\right\}^{1/2} \qquad (3\text{-}2)$$

$$i = \cos^{-1}\left\{(x\dot{y}-y\dot{x})\left[(x\dot{y}-y\dot{x})^2 + (x\dot{z}-z\dot{x})^2 + (y\dot{z}-z\dot{y})^2\right]^{1/2}\right\} \qquad (3\text{-}3)$$

$$= \tan^{-1}\left(\frac{zr_n}{yx_n - xy_n}\right) \qquad (3\text{-}4)$$

$$= \cot^{-1}\left[\frac{y}{z}\cos\Omega - \frac{x}{z}\sin\Omega\right] \qquad (3\text{-}5)$$

$$L = \sin^{-1}\left[z\left(x^2+y^2+z^2\right)^{-1/2}\right] \qquad (3\text{-}6)$$

$$P = \frac{1}{\mu}\left[(x\dot{y}-y\dot{x})^2 + (x\dot{z}-z\dot{x})^2 + (y\dot{z}-z\dot{y})^2\right] \qquad (3\text{-}7)$$

$$r = \sqrt{x^2+y^2+z^2} \qquad (3\text{-}8)$$

$$v = \sqrt{\dot{x}^2+\dot{y}^2+\dot{z}^2} \qquad (3\text{-}9)$$

$$x = r\left[\cos(\omega+\theta)\cos\Omega - \cos i\sin(\omega+\theta)\sin\Omega\right] \qquad (3\text{-}10)$$

$$y = r\left[\cos(\omega+\theta)\sin\Omega + \cos i\sin(\omega+\theta)\cos\Omega\right] \qquad (3\text{-}11)$$

$$z = r\sin(\omega+\theta)\sin i \qquad (3\text{-}12)$$

$$x = \left[\cos\theta(\cos\omega\cos\Omega - \cos i\sin\Omega\sin\omega) + \sin\theta(-\sin\omega\cos\Omega - \cos i\sin\Omega\cos\omega)\right]\frac{p}{1+e\cos\theta} \qquad (3\text{-}13)$$

$$y = \left[\cos\theta(\cos\omega\sin\Omega + \cos i\cos\Omega\sin\omega) + \sin\theta(-\sin\omega\sin\Omega + \cos i\cos\Omega\cos\omega)\right]\frac{p}{1+e\cos\theta} \qquad (3\text{-}14)$$

$$z = \left[\cos\theta\sin i\sin\omega + \sin\theta\sin i\cos\omega\right]\frac{p}{1+e\cos\theta} \qquad (3\text{-}15)$$

$$\dot{x} = \sqrt{\frac{\mu}{p}}\left[(\cos\theta+e)(-\sin\omega\cos\Omega - \cos i\sin\Omega\cos\omega) - \sin\theta(\cos\omega\cos\Omega - \cos i\sin\Omega\sin\omega)\right] \qquad (3\text{-}16)$$

$$\dot{y} = \sqrt{\frac{\mu}{p}}\left[(\cos\theta+e)(-\sin\omega\sin\Omega + \cos i\cos\Omega\cos\omega) - \sin\theta(\cos\omega\sin\Omega + \cos i\cos\Omega\sin\omega)\right] \qquad (3\text{-}17)$$

$$\dot{z} = \sqrt{\frac{\mu}{p}}\left[(\cos\theta+e)\sin i\cos\omega - \sin\theta\sin i\sin\omega\right] \qquad (3\text{-}18)$$

$$\gamma = \sin^{-1}\left[(x\dot{x}+y\dot{y}+z\dot{z})\left(x^2+y^2+z^2\right)^{-1/2}\left(\dot{x}^2+\dot{y}^2+\dot{z}^2\right)^{-1/2}\right] \qquad (3\text{-}19)$$

$$\theta = \cos^{-1}\left[(xx_p+yy_p+zz_p)\left(x^2+y^2+z^2\right)^{-1/2}\left(x_p^2+y_p^2+z_p^2\right)^{-1/2}\right] \qquad (3\text{-}20)$$

$$\phi = \cos^{-1}\left[(xx_n+yy_n+zz_n)\left(x^2+y^2+z^2\right)^{-1/2}\left(x_n^2+y_n^2+z_n^2\right)^{-1/2}\right] \qquad (3\text{-}21)$$

$$\omega = \cos^{-1}\left[(x_nx_p+y_ny_p+z_nz_p)\left(x_n^2+y_n^2+z_n^2\right)^{-1/2}\left(x_p^2+y_p^2+z_p^2\right)^{-1/2}\right] \qquad (3\text{-}22)$$

where:

n = node

p = perigee

$$\Omega = \tan^{-1}\left(\frac{\dot{y}z - y\dot{z}}{\dot{x}z - x\dot{z}}\right) \qquad (3\text{-}23)$$

TABLE 4

Elliptic Orbital Elements in Terms of r, v, γ

$$a = \frac{r}{2 - \frac{rv^2}{\mu}} \quad \text{(Fig. 15)} \qquad (4\text{-}1)$$

$$= \frac{r}{2-Q} \quad \text{(Fig. 15)} \qquad (4\text{-}2)$$

$$b = \frac{r^2\cos^2\gamma}{\frac{2\mu}{rv^2} - 1} \qquad (4\text{-}3)$$

$$= \frac{(r\cos\gamma)^2}{\frac{2}{Q} - 1} \qquad (4\text{-}4)$$

$$e = \sqrt{1 - \left(\frac{2}{r} - \frac{v^2}{\mu}\right)\left(\frac{r^2 v^2 \cos^2\gamma}{\mu}\right)} \quad (4\text{-}5)$$

$$= \sqrt{1 - Q(2 - Q)\cos^2\gamma} \quad \text{(Fig. 19)} \quad (4\text{-}6)$$

$$p = \frac{1}{\mu}(r\, v \cos\gamma)^2 \quad \text{(Fig. 18)} \quad (4\text{-}7)$$

$$= \frac{Q}{r}\cos^2\gamma \quad (4\text{-}8)$$

$$Q = \left(\frac{v}{v_c}\right)^2 = \frac{rv^2}{\mu} \quad \text{(Figs. 15 and 19)} \quad (4\text{-}9)$$

$$r_a = \frac{r}{2 - \frac{rv^2}{\mu}}\left[1 + \sqrt{1 - \frac{1}{\mu}(rv\cos\gamma)^2\left(\frac{2}{r} - \frac{v^2}{\mu}\right)}\right] \quad (4\text{-}10)$$

$$= \frac{r}{2 - Q}\left[1 + \sqrt{1 - Q(2 - Q)\cos^2\gamma}\right] \quad (4\text{-}11)$$

$$r_p = \frac{r}{2 - \frac{rv^2}{\mu}}\left[1 - \sqrt{1 - \frac{1}{\mu}(rv\cos\gamma)^2\left(\frac{2}{r} - \frac{v^2}{\mu}\right)}\right] \quad (4\text{-}12)$$

$$= \frac{r}{2 - Q}\left[1 - \sqrt{1 - Q(2 - Q)\cos^2\gamma}\right] \quad (4\text{-}13)$$

$$v_a = \frac{\mu}{rv\cos\gamma}\left[1 - \sqrt{1 - \frac{1}{\mu}(rv\cos\gamma)^2\left(\frac{2}{r} - \frac{v^2}{\mu}\right)}\right] \quad (4\text{-}14)$$

$$= \frac{v}{Q\cos\gamma}\left[1 - \sqrt{1 - Q(2 - Q)\cos^2\gamma}\right] \quad (4\text{-}15)$$

$$v_p = \frac{\mu}{rv\cos\gamma}\left[1 + \sqrt{1 - \frac{1}{\mu}(rv\cos\gamma)^2\left(\frac{2}{r} - \frac{v^2}{\mu}\right)}\right] \quad (4\text{-}16)$$

$$= \frac{v}{Q\cos\gamma}\left[1 + \sqrt{1 - Q(2 - Q)\cos^2\gamma}\right] \quad (4\text{-}17)$$

TABLE 5

Miscellaneous Relations for Elliptic Orbits

$$\mathcal{E} = -\frac{\mu}{2a} \quad (5\text{-}1)$$

(see Eqs 1-1 through 1-19 for parametric variations of a)

$$= K + P \quad (5\text{-}2)$$

$$= \frac{v^2}{2} - \frac{\mu}{r} \quad (5\text{-}3)$$

$$K = \frac{v^2}{2} \quad (5\text{-}4)$$

$$M = E - e\sin E \quad \text{(Figs. 2 and 22a to i)} \quad (5\text{-}5)$$

(see Eqs 2-1 through 2-9 for parametric variations of E)

$$n = \frac{2\pi}{\tau} \quad \text{(Fig. 7)} \quad (5\text{-}6)$$

$$= \sqrt{\mu}\, a^{-3/2} \quad (5\text{-}7)$$

(see Eqs 1-1 through 1-19 for parametric variations of a)

$$= \frac{M}{t - t_p} \quad (5\text{-}8)$$

$$P = -\frac{\mu}{r} \quad (5\text{-}9)$$

r_m = a (see Eqs 1-1 through 1-19 for parametric variations of a) (5-10)

$$t = \frac{M}{n} + t_p \quad (5\text{-}11)$$

$$= \frac{a^{3/2}}{\sqrt{\mu}}(E - e\sin E) + t_p \quad (5\text{-}12)$$

(see Eqs 2-1 through 2-9 for parametric variations of E)

$$v_c = \sqrt{\frac{\mu}{r}} \quad \text{(Fig. 8)} \quad (5\text{-}13)$$

(see Eqs 2-10 through 2-18 for parametric variations of r)

$$v_e = \sqrt{2}\, v_c \quad (5\text{-}14)$$

$$= \sqrt{\frac{2\mu}{r}} \quad (5\text{-}15)$$

(see Eqs 2-10 through 2-18 for parametric variations of r)

$$\gamma_m = \sin^{-1}(\pm e) \quad (5\text{-}16)$$

(see Eqs 1-41 through 1-59 for parametric variations of e)

$$= \tan^{-1}\left(\frac{ea}{b}\right) \quad (5\text{-}17)$$

$$= \tan^{-1}\left(\frac{r_a - r_p}{2\sqrt{r_a r_p}}\right) \quad (5\text{-}18)$$

$$\theta_m = \cos^{-1}(-e) \quad (5\text{-}19)$$

$$= \sin^{-1}\left(\frac{b}{a}\right) \quad (5\text{-}20)$$

$$\tau = 2\pi a\sqrt{\frac{a}{\mu}} \quad \text{(Table 9 and Fig. 1)} \quad (5\text{-}21)$$

(see Eqs 1-1 through 1-19 for parametric variations of a)

TABLE 6-1a

General Forms of Series Expansions in Powers of Eccentricity (see Fig. 4)

$$E = M + \sum_{n=1}^{\infty} \frac{e^n}{n!} \frac{d^{n-1}}{dM^{n-1}} (\sin^n M) \qquad (6\text{-}1)$$

$$\sin E = \sum_{n=1}^{\infty} \frac{e^{n-1}}{n!} \frac{d^{n-1}}{dM^{n-1}} (\sin^n M) \qquad (6\text{-}2)$$

$$\cos E = -\sum_{n=1}^{\infty} \frac{e^{n-1}}{(n-1)!} \frac{d^{n-2}}{dM^{n-2}} (\sin^n M) \qquad (6\text{-}3)$$

$$\left(\frac{r}{a}\right) = 1 + \sum_{n=1}^{\infty} \frac{e^n}{(n-1)!} \frac{d^{n-2}}{dM^{n-2}} (\sin^n M) \qquad (6\text{-}4)$$

$$\left(\frac{r}{a}\right)^2 = 1 + e^2 + 2 \sum_{n=1}^{\infty} \frac{e^n}{n!} \frac{d^{n-2}}{dM^{n-2}} (\sin^n M) \qquad (6\text{-}5)$$

$$\left(\frac{a}{r}\right) = 1 + \sum_{n=1}^{\infty} \frac{e^n}{n!} \frac{d^n}{dM^n} (\sin^n M) \qquad (6\text{-}6)$$

$$\frac{x}{a} = -e - \sum_{n=1}^{\infty} \frac{e^{n-1}}{(n-1)!} \frac{d^{n-2}}{dM^{n-2}} (\sin^n M) \qquad (6\text{-}7)$$

$$\frac{y}{a} = \sqrt{1-e^2} \sum_{n=1}^{\infty} \frac{e^{n-1}}{n!} \frac{d^{n-1}}{dM^{n-1}} (\sin^n M) \qquad (6\text{-}8)$$

$$\sin\theta = \sqrt{1-e^2} \sum_{n=1}^{\infty} \frac{e^{n-1}}{(n-1)!} \frac{d^{n-1}}{dM^{n-1}} (\sin^n M) \qquad (6\text{-}9)$$

$$\cos\theta = -\sum_{n=1}^{\infty} \frac{ne^{n-1}}{(n-1)!} \frac{d^{n-2}}{dM^{n-2}} (\sin^n M) \qquad (6\text{-}10)$$

$$\theta = \int \sqrt{1-e^2} \left(\frac{a}{r}\right)^2 dM \qquad (6\text{-}11)$$

NOTE: Divergence for $e > 0.662743\ldots$

TABLE 6-1b

Power Series Expansions up to e^7

$$E = M + e \sin M + \frac{e^2}{2!} \sin 2M$$

$$+ \frac{e^3}{3!2^2} (3^2 \sin 3M - 3 \sin M)$$

$$+ \frac{e^4}{4!2^3} (4^3 \sin 4M - 4 \cdot 2^3 \sin 2M) +$$

(continued)

TABLE 6-1b (continued)

$$+ \frac{e^5}{5!2^4} (5^4 \sin 5M - 5 \cdot 3^4 \sin 3M + 5 \cdot 2 \sin M)$$

$$+ \frac{e^6}{6!2^5} (6^5 \sin 6M - 6 \cdot 4^5 \sin 4M + 5 \cdot 3 \cdot 2^5 \sin 2M)$$

$$+ \frac{e^7}{7!2^6} (7^6 \sin 7M - 7 \cdot 5^6 \sin 5M$$

$$+ 7 \cdot 3 \cdot 3^6 \sin 3M - 7 \cdot 5 \sin M)$$

$$+ \ldots\ldots \qquad \text{(Fig. 2)} \qquad (6\text{-}12)$$

$$\sin E = \sin M + \frac{e}{2} \sin 2M$$

$$+ \frac{e^2}{3!2^2} (3^2 \sin 3M - 3 \sin M)$$

$$+ \frac{e^3}{4!2^3} (4^3 \sin 4M - 4 \cdot 2^3 \sin 2M)$$

$$+ \frac{e^4}{5!2^4} (5^4 \sin 5M - 5 \cdot 3^4 \sin 3M + 5 \cdot 2 \sin M)$$

$$+ \frac{e^5}{6!2^5} (6^5 \sin 6M - 6 \cdot 4^5 \sin 4M + 5 \cdot 3 \cdot 2^5 \sin 2M)$$

$$+ \frac{e^6}{7!2^6} (7^6 \sin 7M - 7 \cdot 5^6 \sin 5M$$

$$+ 7 \cdot 3 \cdot 3^6 \sin 3M - 7 \cdot 5 \sin M)$$

$$+ \frac{e^7}{8!2^7} (8^7 \sin 8M - 8 \cdot 6^7 \sin 6M$$

$$+ 7 \cdot 4 \cdot 4^7 \sin 4M - 8 \cdot 7 \cdot 2^7 \sin 2M)$$

$$+ \ldots\ldots \qquad (6\text{-}13)$$

$$\cos E = \cos M + \frac{e}{2} (\cos 2M - 1)$$

$$+ \frac{e^2}{2!\,2^2} (3 \cos 3M - 3 \cos M)$$

$$+ \frac{e^3}{3!\,2^3} (4^2 \cos 4M - 4 \cdot 2^2 \cos 2M)$$

$$+ \frac{e^4}{4!\,2^4} (5^3 \cos 5M - 5 \cdot 3^3 \cos 3M + 5 \cdot 2 \cos M)$$

$$+ \frac{e^5}{5!\,2^5} (6^4 \cos 6M - 6 \cdot 4^4 \cos 4M + 5 \cdot 3 \cdot 2^4 \cos 2M)$$

$$+$$

(continued)

TABLE 6-1b (continued)

$$+\frac{e^6}{6!\,2^6}\,(7^5\cos 7M - 7\cdot 5^5\cos 5M + 7\cdot 3\cdot 3^5\cos 3M - 7\cdot 5\cos M)$$

$$+\frac{e^7}{7!\,2^7}\,(8^6\cos 8M - 8\cdot 6^6\cos 6M + 7\cdot 4\cdot 4^6\cos 4M - 8\cdot 7\cdot 2^6\cos 2M)$$

$$+ \ldots\ldots \qquad (6\text{-}14)$$

$$\theta = M + 2e\sin M + \frac{5e^2}{4}\sin 2M + \frac{e^3}{12}\,(13\sin 3M - 3\sin M) + \frac{e^4}{96}\,(103\sin 4M - 44\sin 2M) + \frac{e^5}{960}\,(1097\sin 5M - 645\sin 3M + 50\sin M) + \frac{e^6}{960}\,(1223\sin 6M - 902\sin 4M + 85\sin 2M) + \frac{e^7}{32,256}\,(47,273\sin 7M - 41,699\sin 5M + 5985\sin 3M + 749\cos M) + \ldots\ldots \qquad (6\text{-}15)$$

$$\sin\theta = \sqrt{1-e^2}\left\{\sin M + e\sin 2M + \frac{e^2}{2!\,2^2}\,(3^2\sin 3M - 3\sin M) + \frac{e^3}{3!\,2^3}\,(4^3\sin 4M - 4\cdot 2^3\sin 2M) + \frac{e^4}{4!\,2^4}\,(5^4\sin 5M - 5\cdot 3^4\sin 3M + 5\cdot 2\sin M) + \frac{e^5}{5!\,2^5}\,(6^5\sin 6M - 6\cdot 4^5\sin 4M + 5\cdot 3\cdot 2^5\sin 2M) + \frac{e^6}{6!\,2^6}\,(7^6\sin 7M - 7\cdot 5^6\sin 5M + 7\cdot 3\cdot 3^6\sin 3M - 7\cdot 5\sin M) + \frac{e^7}{7!\,2^7}\,(8^7\sin 3M - 8\cdot 6^7\sin 6M + 7\cdot 4\cdot 4^7\sin 4M - 8\cdot 7^2\sin M) + \ldots\ldots\right\} \qquad (6\text{-}16)$$

TABLE 6-1b (continued)

$$\cos\theta = \cos M + e(\cos 2M - 1) + \frac{3e^2}{2!\,2^2}\,(3\cos 3M - 3\cos M) + \frac{4e^3}{3!\,2^3}\,(4^2\cos 4M - 4\cdot 2^2\cos 2M) + \frac{5e^4}{4!\,2^4}\,(5^3\cos 5M - 5\cdot 3^3\cos 3M + 5\cdot 2\cos M) + \frac{6e^5}{5!\,2^5}\,(6^4\cos 6M - 6\cdot 4^4\cos 4M + 5\cdot 3\cdot 2^4\cos 2M) + \frac{7e^6}{6!\,2^6}\,(7^5\cos 7M - 7\cdot 5^5\cos 5M + 7\cdot 3\cdot 3^5\cos 3M - 7\cdot 5\cos M) + \frac{8e^7}{7!\,2^7}\,(8^6\cos 8M - 8\cdot 6^6\cos 6M + 7\cdot 4\cdot 4^6\cos 4M - 8\cdot 7\cdot 2^6\cos 2M) + \ldots\ldots \qquad (6\text{-}17)$$

$$\frac{r}{a} = 1 - e\cos M - \frac{e^2}{2}(\cos 2M - 1) - \frac{e^3}{2!\,2^2}\,(3\cos 3M - 3\cos M) - \frac{e^4}{3!\,2^3}\,(4^2\cos 4M - 4\cdot 2^2\cos 2M) - \frac{e^5}{4!\,2^4}\,(5^3\cos 5M - 5\cdot 3^3\cos 3M + 5\cdot 2\cos M) - \frac{e^6}{5!\,2^5}\,(6^4\cos 6M - 6\cdot 4^4\cos 4M + 5\cdot 3\cdot 2^4\cos 2M) - \frac{e^7}{6!\,2^6}\,(7^5\cos 7M - 7\cdot 5^5\cos 5M + 7\cdot 3\cdot 3^5\cos 3M - 7\cdot 5\cos M) - \ldots\ldots \qquad (6\text{-}18)$$

TABLE 6-1b (continued)

$$\left(\frac{r}{a}\right)^2 = 1 - 2e\cos M - \frac{e^2}{2!}(\cos 2M - 3)$$
$$- \frac{e^3}{3!\,2}(3\cos 3M - 3\cos M)$$
$$- \frac{e^4}{4!\,2^2}(4^2\cos 4M - 4\cdot 2^2\cos 2M)$$
$$- \frac{e^5}{5!\,2^3}(5^3\cos 5M - 5\cdot 3^3\cos 3M + 5\cdot 2\cos M)$$
$$- \frac{e^6}{6!\,2^4}(6^4\cos 6M - 6\cdot 4^4\cos 4M + 5\cdot 3\cdot 2^4\cos 2M)$$
$$- \frac{e^7}{7!\,2^5}(7^5\cos 7M - 7\cdot 5^5\cos 5M + 7\cdot 3\cdot 3^5\cos 3M - 7\cdot 5\cos M)$$
$$- \ldots\ldots \qquad (6\text{-}19)$$

$$\frac{a}{r} = 1 + e\cos M + e^2\cos 2M$$
$$+ \frac{e^3}{3!\,2^2}(3^3\cos 3M - 3\cos M)$$
$$+ \frac{e^4}{4!\,2^3}(4^4\cos 4M - 4\cdot 2^4\cos 2M)$$
$$+ \frac{e^5}{5!\,2^4}(5^5\cos 5M - 5\cdot 3^5\cos 3M + 5\cdot 2\cos M)$$
$$+ \frac{e^6}{6!\,2^5}(6^6\cos 6M - 6\cdot 4^6\cos 4M + 5\cdot 3\cdot 2^6\cos 2M)$$
$$+ \frac{e^7}{7!\,2^6}(7^7\cos 7M - 7\cdot 5^7\cos 5M + 7\cdot 3\cdot 3^7\cos 3M - 7\cdot 5\cos M)$$
$$+ \ldots\ldots \qquad (6\text{-}20)$$

$$\left(\frac{a}{r}\right)^2 = 1 + 2e\cos M + \frac{e^2}{2}(5\cos 2M + 1)$$
$$+ \frac{e^3}{4}(13\cos 3M + 3\cos M)$$

TABLE 6-1b (continued)

$$+ \frac{e^4}{24}(103\cos 4M + 8\cos 2M + 9)$$
$$+ \frac{e^5}{192}(1097\cos 5M - 75\cos 3M + 130\cos M)$$
$$+ \frac{e^6}{160}(1223\cos 6M - 258\cos 4M + 105\cos 2M + 50)$$
$$+ \frac{e^7}{23,040}(236,365\cos 7M - 83,105\cos 5M + 17,685\cos 3M + 13,375\cos M)$$
$$+ \ldots\ldots \qquad (6\text{-}21)$$

$$\frac{x}{a} = -e + \cos M + \frac{e}{2}(\cos 2M - 1)$$
$$+ \frac{e^2}{2!\,2^2}(3\cos 3M - 3\cos M)$$
$$+ \frac{e^3}{3!\,2^3}(4^2\cos 4M - 4\cdot 2^2\cos 2M)$$
$$+ \frac{e^4}{4!\,2^4}(5^3\cos 5M - 5\cdot 3^3\cos 3M + 5\cdot 2\cos M)$$
$$+ \frac{e^5}{5!\,2^5}(6^4\cos 6M - 6\cdot 4^4\cos 4M + 5\cdot 3\cdot 2^4\cos 2M)$$
$$+ \frac{e^6}{6!\,2^6}(7^5\cos 7M - 7\cdot 5^5\cos 5M + 7\cdot 3\cdot 3^5\cos 3M - 7\cdot 5\cos M)$$
$$+ \frac{e^7}{7!\,2^7}(8^6\cos 8M - 8\cdot 6^6\cos 6M + 7\cdot 4\cdot 4^6\cos 4M - 8\cdot 7\cdot 2^6\cos 2M)$$
$$+ \ldots\ldots \qquad (6\text{-}22)$$

$$\frac{y}{a} = \sqrt{1-e^2}\left\{\sin M + \frac{e}{2}\sin 2M\right.$$
$$+ \frac{e^2}{3!\,2^2}(3^2\sin 3M - 3\sin M) +$$

(continued)

TABLE 6-1b (continued)

$$+ \frac{e^3}{4!\,2^3}(4^3 \sin 4M - 4\cdot 2^3 \sin 2M)$$

$$+ \frac{e^4}{5!\,2^4}(5^4 \sin 5M - 5\cdot 3^4 \sin 3M + 5\cdot 2 \sin M)$$

$$+ \frac{e^5}{6!\,2^5}(6^5 \sin 6M - 6\cdot 4^5 \sin 4M + 5\cdot 3\cdot 2^5 \sin 2M)$$

$$+ \frac{e^6}{7!\,2^6}(7^6 \sin 7M - 7\cdot 5^6 \sin 5M + 7\cdot 3\cdot 3^6 \sin 3M - 7\cdot 5 \sin M)$$

$$+ \frac{e^7}{8!\,2^7}(8^7 \sin 8M - 8\cdot 6^7 \sin 6M + 7\cdot 4\cdot 4^7 \sin 4M - 3\cdot 7\cdot 2^7 \sin 2M)$$

$$+ \ldots\ldots\Big\} \qquad (6\text{-}23)$$

TABLE 6-1b (continued)

$$\sqrt{1-e^2} = 1 - \frac{e^2}{2} - \frac{e^4}{2\cdot 4} - \frac{1\cdot 3\, e^6}{2\cdot 4\cdot 6} - \frac{1\cdot 3\cdot 5\, e^8}{2\cdot 4\cdot 6\cdot 8} - \ldots$$

$$= 1 - \frac{e^2}{2} - \frac{e^4}{8} - \frac{e^6}{16} - \frac{5\, e^8}{128} - \frac{7\, e^{10}}{256} - \frac{21\, e^{12}}{1024} - \ldots \qquad (6\text{-}24)$$

TABLE 6-2a

Expansions of Powers of Sin M

$$\sin^2 M = \frac{1}{2}(1 - \cos 2M)$$

$$\sin^3 M = \frac{1}{4}(3 \sin M - \sin 3M)$$

$$\sin^4 M = \frac{1}{8}(3 - 4 \cos 2M + \cos 4M)$$

$$\sin^5 M = \frac{1}{16}(10 \sin M - 5 \sin 3M + \sin 5M)$$

$$\sin^6 M = \frac{1}{32}(10 - 15 \cos 2M + 6 \cos 4M - \cos 6M)$$

$$\sin^7 M = \frac{1}{64}(35 \sin M - 21 \sin 3M + 7 \sin 5M - \sin 7M)$$

$$\sin^8 M = \frac{1}{128}(35 - 56 \cos 2M + 28 \cos 4M - 8 \cos 6M + \cos 8M)$$

$$\sin^9 M = \frac{1}{256}(126 \sin M - 84 \sin 3M + 36 \sin 5M - 9 \sin 7M + \sin 9M)$$

$$\sin^{10} M = \frac{1}{512}(126 - 210 \cos 2M + 120 \cos 4M - 45 \cos 6M + 10 \cos 8M - \cos 10M)$$

$$\sin^{11} M = \frac{1}{1024}(462 \sin M - 330 \sin 3M + 165 \sin 5M - 55 \sin 7M + 11 \sin 9M - \sin 11M)$$

$$\sin^{12} M = \frac{1}{2048}(462 - 792 \cos 2M + 495 \cos 4M - 220 \cos 6M + 66 \cos 8M - 12 \cos 10M + \cos 12M)$$

$$\sin^{13} M = \frac{1}{4096}(1716 \sin M - 1287 \sin 3M + 715 \sin 5M - 286 \sin 7M + 78 \sin 9M - 13 \sin 11M + \sin 13M)$$

NOTE:

The numerical coefficients are easily obtained from the Pascal's triangle (cut in half), as shown in Table 6-2b.

TABLE 6-2b

Pascal's Triangle and its Modification

```
                    1
                  1   1
                1   2   1
              1   3   3   1
            1   4   6   4   1
          1   5  10  10   5   1
        1   6  15  20  15   6   1
      1   7  21  35 (35)(21)  7   1
    1   8  28  56  70 (56) 28  8   1
  . . . . . . . . . . . . . . . . .
```

Note: In the Pascal's triangle, each term is the sum of the two terms immediately above it (e.g., 35 + 21 = 56). The coefficients for the expansions of $\sin^n M$ in Table 6-2a result if the Pascal's triangle is cut in half as shown below.

n	The Coefficients of Expansion of $\sin^n M$
0	$\frac{1}{2}$
1	1
2	1 1
3	3 1
4	3 4 1
5	10 5 1
6	10 15 6 1
7	35 21 7 1
8	35 56 28 8 1
...	... ...
...	... ...

TABLE 6-3a

General Forms of Fourier-Bessel Expansion (see any reference on celestial mechanics, e.g., Smart)

$$E = M + 2\sum_{n=1}^{\infty} \frac{1}{n} J_n(ne) \sin n M \qquad (6\text{-}25)$$

$$\sin E = \frac{2}{e}\sum_{n=1}^{\infty} \frac{1}{n} J_n(ne) \sin n M \qquad (6\text{-}26)$$

$$\cos E = -\frac{1}{2} e + \sum_{n=1}^{\infty} \frac{2}{n^2} \frac{d}{de}\left\{J_n(ne)\right\} \cos n M \qquad (6\text{-}27)$$

$$\theta = M + \sum_{n=1}^{\infty} \frac{2}{n} \sin n M \sum_{k=-\infty}^{+\infty} f^{|n|} J_{n+k}(ne) \qquad (6\text{-}28)$$

where

$$f = \frac{1-\sqrt{1-e^2}}{e} = \frac{e}{2} + \frac{e^3}{8} + \frac{e^5}{16} + \frac{5e^7}{128} + \ldots \qquad (6\text{-}29)$$

$$\sin\theta = 2\sqrt{1-e^2}\sum_{n=1}^{\infty} \frac{1}{n}\frac{d}{de}\left\{J_n(ne)\right\} \sin n M \qquad (6\text{-}30)$$

$$\cos\theta = -e + \frac{2(1-e^2)}{e}\sum_{n=1}^{\infty} J_n(ne) \cos n M \qquad (6\text{-}31)$$

$$\frac{r}{a} = 1 + \frac{e^2}{2} - 2e\sum_{n=1}^{\infty} \frac{1}{n^2} \frac{d}{de}\left\{J_n(ne)\right\} \cos n M \qquad (6\text{-}32)$$

$$\left(\frac{r}{a}\right)^2 = 1 + \frac{3e^2}{2} - 4\sum_{n=1}^{\infty} \frac{1}{n^2} J_n(ne) \cos n M \qquad (6\text{-}33)$$

$$\frac{a}{r} = 1 + 2\sum_{n=1}^{\infty} J_n(ne) \cos n M \qquad (6\text{-}34)$$

$$\frac{x}{a} = -\frac{3e}{2} + 2\sum_{n=1}^{\infty} \frac{1}{n^2} \frac{d}{de}\left\{J_n(ne)\right\} \cos n M \qquad (6\text{-}35)$$

$$\frac{y}{a} = \frac{2}{e}\sqrt{1-e^2}\sum_{n=1}^{\infty} \frac{1}{n} J_n(ne) \sin n M \qquad (6\text{-}36)$$

Note: Divergence for $e > 0.662743\ldots$

TABLE 6-3b

Expansions of $J_n(ne)$

and $\frac{d}{de}\left\{J_n(ne)\right\} = J_n'(ne)$

$$J_n(x) = \sum_{k=0}^{\infty} (-1)^k \frac{x^{n+2k}}{2^{n+2k}\, k!\,(n+k)!}$$

$$J_1(e) = \frac{e}{2} - \frac{e^3}{16} + \frac{e^5}{384} - \frac{e^7}{18,432} + \ldots$$

$$J_2(2e) = \frac{e^2}{2} - \frac{e^4}{6} + \frac{e^6}{48} - \frac{e^8}{720} + \ldots$$

$$J_3(3e) = \frac{9e^3}{16} - \frac{81e^5}{256} + \frac{729e^7}{10,240} - \ldots$$

$$J_4(4e) = \frac{2e^4}{3} - \frac{8e^6}{15} + \frac{8e^8}{45} - \ldots$$

$$J_5(5e) = \frac{625e^5}{768} - \frac{15,625e^7}{18,432} + \ldots$$

$$J_6(6e) = \frac{81e^6}{80} - \frac{729e^8}{560} + \ldots$$

$$J_7(7e) = \frac{117,649e^7}{92,160} - \ldots$$

$$J_8(8e) = \frac{512e^8}{315} - \ldots$$

$$J_1'(e) = \frac{1}{2} - \frac{3e^2}{16} + \frac{5e^4}{384} - \frac{7e^6}{18,432} + \ldots$$

$$J_2'(2e) = e - \frac{2e^3}{3} + \frac{e^5}{8} - \frac{e^7}{90} + \ldots$$

$$J_3'(3e) = \frac{27e^2}{16} - \frac{405e^4}{256} + \frac{5103e^6}{10,240} - \ldots$$

$$J_4'(4e) = \frac{8e^3}{3} - \frac{16e^5}{5} + \frac{64e^7}{45} - \ldots$$

$$J_5'(5e) = \frac{3125e^4}{768} - \frac{109,375e^6}{18,432} + \ldots$$

$$J_6'(6e) = \frac{243e^5}{40} - \frac{729e^7}{70} + \ldots$$

$$J_7'(7e) = \frac{823,543e^6}{92,160} - \ldots$$

$$J_8'(8e) = \frac{4096e^7}{315} - \ldots$$

(6-37)

TABLE 6-4

Fourier-Bessel Expansions up to e^7

$$E = M + \left(e - \frac{e^3}{8} + \frac{e^5}{192} - \frac{e^7}{9216} + \ldots\right)\sin M$$
$$+ \left(\frac{e^2}{2} - \frac{e^4}{6} + \frac{e^6}{48} - \ldots\right)\sin 2M$$
$$+ \left(\frac{3e^3}{8} - \frac{27e^5}{128} + \frac{243e^7}{5120} - \ldots\right)\sin 3M$$
$$+ \left(\frac{e^4}{3} - \frac{4e^6}{15} + \ldots\right)\sin 4M$$
$$+ \left(\frac{125e^5}{384} - \frac{3125e^7}{9216} + \ldots\right)\sin 5M$$
$$+ \left(\frac{27e^6}{80} - \ldots\right)\sin 6M$$
$$+ \left(\frac{16,807e^7}{46,080} - \ldots\right)\sin 7M + \ldots \quad (6\text{-}38)$$

$$\sin E = \left(1 - \frac{e^2}{8} + \frac{e^4}{192} - \frac{e^6}{9216} + \ldots\right)\sin M$$
$$+ \left(\frac{e}{2} - \frac{e^3}{6} + \frac{e^5}{48} - \frac{e^7}{720} + \ldots\right)\sin 2M$$
$$+ \left(\frac{3e^2}{8} - \frac{27e^4}{128} + \frac{243e^6}{5120} - \ldots\right)\sin 3M$$
$$+ \left(\frac{e^3}{3} - \frac{4e^5}{15} + \frac{4e^7}{45} - \ldots\right)\sin 4M$$
$$+ \left(\frac{125e^4}{384} - \frac{3125e^6}{9216} + \ldots\right)\sin 5M$$
$$+ \left(\frac{27e^5}{80} - \frac{243e^7}{560} + \ldots\right)\sin 6M$$
$$+ \left(\frac{16,807e^6}{46,080} - \ldots\right)\sin 7M$$
$$+ \left(\frac{128e^7}{315} - \ldots\right)\sin 8M + \ldots\ldots \quad (6\text{-}39)$$

$$\cos E = -\frac{e}{2}$$
$$+ \left(1 - \frac{3e^2}{8} + \frac{5e^4}{192} - \frac{7e^6}{9216} + \ldots\right)\cos M$$
$$+ \left(\frac{e}{2} - \frac{e^3}{3} + \frac{e^5}{16} - \frac{e^7}{180} + \ldots\right)\cos 2M$$
$$+$$

(continued)

TABLE 6-4 (continued)

$$+\left(\frac{3\,e^2}{8} - \frac{45\,e^4}{128} + \frac{567\,e^6}{5120} - \ldots\right) \cos 3M$$

$$+\left(\frac{e^3}{3} - \frac{2\,e^5}{5} + \frac{8\,e^7}{45} - \ldots\right) \cos 4M$$

$$+\left(\frac{125\,e^4}{384} - \frac{4375\,e^6}{9216} + \ldots\right) \cos 5M$$

$$+\left(\frac{81\,e^5}{240} - \frac{81\,e^7}{140} + \ldots\right) \cos 6M$$

$$+\left(\frac{16,807\,e^6}{46,080} - \ldots\right) \cos 7M$$

$$+\left(\frac{128\,e^7}{315} - \ldots\right) \cos 8M + \ldots\ldots \quad (6\text{-}40)$$

$$\theta = M + \left(2\,e - \frac{e^3}{4} + \frac{5\,e^5}{96} + \frac{107\,e^7}{4608} + \ldots\right) \sin M$$

$$+\left(\frac{5\,e^2}{4} - \frac{11\,e^4}{24} + \frac{17\,e^6}{192} - \ldots\right) \sin 2M$$

$$+\left(\frac{13\,e^2}{12} - \frac{43\,e^5}{192} + \frac{95\,e^7}{512} - \ldots\right) \sin 3M$$

$$+\left(\frac{103\,e^4}{96} - \frac{451\,e^6}{480} + \ldots\right) \sin 4M$$

$$+\left(\frac{1097\,e^5}{960} - \frac{5957\,e^7}{4608} + \ldots\right) \sin 5M$$

$$+\left(\frac{1223\,e^6}{960} - \ldots\right) \sin 6M$$

$$+\left(\frac{47,273\,e^7}{32,256} - \ldots\right) \sin 7M + \ldots\ldots \quad (6\text{-}41)$$

$$\sin\theta = \left(1 - \frac{7\,e^2}{8} + \frac{17\,e^4}{192} - \frac{317\,e^6}{9216} + \ldots\right) \sin M$$

$$+\left(e - \frac{7\,e^3}{6} + \frac{e^5}{3} - \frac{19\,e^7}{360} + \ldots\right) \sin 2M$$

$$+\left(\frac{9\,e^2}{8} - \frac{207\,e^4}{128} + \frac{3681\,e^6}{5120} - \ldots\right) \sin 3M$$

$$+\left(\frac{4\,e^3}{3} - \frac{34\,e^5}{15} + \frac{121\,e^7}{90} - \ldots\right) \sin 4M$$

$$+\left(\frac{625\,e^4}{384} - \frac{29,363\,e^6}{9216} + \ldots\right) \sin 5M$$

$$+\left(\frac{81\,e^5}{40} - \frac{313\,e^7}{70} + \ldots\right) \sin 6M$$

$$+\left(\frac{117,649\,e^6}{46,080} - \ldots\right) \sin 7M$$

$$+\left(\frac{1024\,e^7}{315} - \ldots\right) \sin 8M + \ldots\ldots \quad (6\text{-}42)$$

TABLE 6-4 (continued)

$$\cos\theta = -e + \left(1 - \frac{9\,e^2}{8} + \frac{25\,e^4}{192} - \frac{49\,e^6}{9216} + \ldots\right) \cos M$$

$$+\left(e - \frac{4\,e^3}{3} + \frac{3\,e^5}{8} - \frac{2\,e^7}{45} + \ldots\right) \cos 2M$$

$$+\left(\frac{9\,e^2}{8} - \frac{225\,e^4}{128} + \frac{3969\,e^6}{5120} - \ldots\right) \cos 3M$$

$$+\left(\frac{4\,e^3}{3} - \frac{12\,e^5}{5} + \frac{64\,e^7}{45} - \ldots\right) \cos 4M$$

$$+\left(\frac{625\,e^4}{384} - \frac{30,625\,e^6}{9216} + \ldots\right) \cos 5M$$

$$+\left(\frac{81\,e^5}{40} - \frac{486\,e^7}{105} + \ldots\right) \cos 6M$$

$$+\left(\frac{117,649\,e^6}{46,080} - \ldots\right) \cos 7M$$

$$+\left(\frac{1024\,e^7}{315} - \ldots\right) \cos 8M + \ldots\ldots \quad (6\text{-}43)$$

$$\frac{r}{a} = 1 + \frac{e^2}{2} - \left(e - \frac{3e^3}{8} + \frac{5e^5}{192} - \frac{7e^7}{9216} + \ldots\right) \cos M$$

$$-\left(\frac{e^2}{2} - \frac{e^4}{3} + \frac{e^6}{16} - \ldots\right) \cos 2M$$

$$-\left(\frac{3e^3}{8} - \frac{45e^5}{128} + \frac{567e^7}{5120} - \ldots\right) \cos 3M$$

$$-\left(\frac{e^4}{3} - \frac{2e^6}{5} + \ldots\right) \cos 4M$$

$$-\left(\frac{125}{384} - \frac{4375e^7}{9216} + \ldots\right) \cos 5M$$

$$-\left(\frac{81e^6}{240} - \ldots\right) \cos 6M$$

$$-\left(\frac{16,807e^7}{46,080} - \ldots\right) \cos 7M - \ldots\ldots \quad (6\text{-}44)$$

$$\left(\frac{r}{a}\right)^2 = 1 + \frac{3e^2}{2} - \left(2e - \frac{e^3}{4} + \frac{e^5}{96} - \frac{e^7}{4608} + \ldots\right) \cos M$$

$$-\left(\frac{e^2}{2} - \frac{e^4}{6} + \frac{e^6}{48} - \ldots\right) \cos 2M +$$

(continued)

TABLE 6-4 (continued)

$$+\left(\frac{e^3}{4}-\frac{9e^5}{64}+\frac{81e^7}{2560}-\ldots\right)\cos 3M$$

$$+\left(\frac{e^4}{6}-\frac{2e^6}{15}+\ldots\right)\cos 4M$$

$$+\left(\frac{25e^5}{192}-\frac{625e^7}{4608}+\ldots\right)\cos 5M$$

$$+\left(\frac{9e^6}{80}-\frac{81e^8}{560}+\ldots\right)\cos 6M$$

$$+\left(\frac{2401e^7}{23,040}-\ldots\right)\cos 7M+\ldots\ldots \quad (6\text{-}45)$$

$$\frac{a}{r}=1+\left(e-\frac{e^3}{8}+\frac{e^5}{192}\right.$$

$$\left.-\frac{e^7}{9216}+\ldots\right)\cos M+\left(e^2-\frac{e^4}{3}+\frac{e^6}{24}\right.$$

$$\left.-\ldots\right)\cos 2M$$

$$+\left(\frac{9e^3}{8}-\frac{81e^5}{128}+\frac{729e^7}{5120}-\ldots\right)\cos 3M$$

$$+\left(\frac{4e^4}{3}-\frac{16e^6}{15}+\ldots\right)\cos 4M$$

$$+\left(\frac{625e^5}{384}-\frac{15,625e^7}{9216}+\ldots\right)\cos 5M$$

$$+\left(\frac{81e^6}{40}-\ldots\right)\cos 6M$$

$$+\left(\frac{117,649e^7}{46,080}-\ldots\right)\cos 7M+\ldots\ldots \quad (6\text{-}46)$$

$$\left(\frac{a}{r}\right)^2=\left(1+\frac{e^2}{2}+\frac{3e^4}{8}+\frac{15e^6}{16}+\ldots\right)$$

$$+\left(2e+\frac{3e^3}{4}+\frac{65e^5}{96}+\frac{2675e^7}{4608}\right.$$

$$\left.+\ldots\right)\cos M$$

$$+\left(\frac{5e^2}{2}+\frac{e^4}{3}+\frac{21e^6}{32}+\ldots\right)\cos 2M$$

$$+\left(\frac{13e^3}{4}-\frac{25e^5}{64}+\frac{393e^7}{512}-\ldots\right)\cos 3M$$

$$+$$

(continued)

TABLE 6-4 (continued)

$$+\left(\frac{103e^4}{24}-\frac{129e^6}{80}+\ldots\right)\cos 4M$$

$$+\left(\frac{1097e^5}{192}-\frac{16,621e^7}{4608}\right.$$

$$\left.+\ldots\right)\cos 5M+\left(\frac{1223e^6}{160}-\ldots\right)\cos 6M$$

$$+\left(\frac{47,273e^7}{4608}-\ldots\right)\cos 7M+\ldots\ldots (6\text{-}47)$$

$$\frac{x}{a}=-\frac{3e}{2}+\left(1-\frac{3e^2}{8}+\frac{5e^4}{192}-\frac{7e^6}{9216}\right.$$

$$\left.+\ldots\right)\cos M+\left(\frac{e}{2}-\frac{e^3}{3}\right.$$

$$\left.+\frac{e^5}{16}-\frac{e^7}{180}+\ldots\right)\cos 2M$$

$$+\left(\frac{3e^2}{8}-\frac{45e^4}{128}+\frac{567e^6}{5120}-\ldots\right)\cos 3M$$

$$+\left(\frac{e^3}{3}-\frac{2e^5}{5}+\frac{8e^7}{45}-\ldots\right)\cos 4M$$

$$+\left(\frac{125e^4}{384}-\frac{4375e^6}{9216}+\ldots\right)\cos 5M$$

$$+\left(\frac{81e^5}{240}-\frac{81e^7}{140}+\ldots\right)\cos 6M$$

$$+\left(\frac{16,807e^6}{46,080}-\ldots\right)\cos 7M$$

$$+\left(\frac{128e^7}{315}-\ldots\right)\cos 8M+\ldots\ldots \quad (6\text{-}48)$$

$$\frac{y}{a}=\left(1-\frac{5e^2}{8}-\frac{11e^4}{192}-\frac{457e^6}{9216}-\ldots\right)\sin M$$

$$+\left(\frac{e}{2}-\frac{5e^3}{12}+\frac{e^5}{24}-\frac{e^7}{45}+\ldots\right)\sin 2M$$

$$+\left(\frac{3e^2}{8}-\frac{51e^4}{128}+\frac{543e^6}{5120}-\ldots\right)\sin 3M$$

$$+\left(\frac{e^3}{3}-\frac{13e^5}{30}+\frac{13e^7}{72}-\ldots\right)\sin 4M$$

$$+\left(\frac{125e^4}{384}-\frac{4625e^6}{9216}+\ldots\right)\sin 5M$$

$$+\left(\frac{27e^5}{80}-\frac{135e^7}{224}+\ldots\right)\sin 6M+$$

(continued)

TABLE 6-4 (continued)

$$+\left(\frac{16,807e^6}{46,080}-\ldots\right)\sin 7M$$

$$+\left(\frac{128e^7}{315}-\ldots\right)\sin 8M+\ldots\ldots \quad (6\text{-}49)$$

TABLE 6-5

Expansions for Near-Circular Orbit ($e^2 << 1$)

$$E = M + e\sin M + \ldots \quad (6\text{-}50)$$

$$\sin E = \sin M + \frac{e}{2}\sin 2M + \ldots \quad (6\text{-}51)$$

$$\cos E = -\frac{e}{2} + \cos M + \frac{e}{2}\cos 2M + \ldots \quad (6\text{-}52)$$

$$\theta = M + 2e\sin M + \ldots \quad (6\text{-}53)$$

$$\sin\theta = \sin M + e\sin 2M + \ldots \quad (6\text{-}54)$$

$$\cos\theta = -e + \cos M + e\cos 2M + \ldots \quad (6\text{-}55)$$

$$\left(\frac{r}{a}\right) = 1 - e\cos M - \ldots \quad (6\text{-}56)$$

$$\left(\frac{r}{a}\right)^2 = 1 - 2e\cos M - \ldots \quad (6\text{-}57)$$

$$\left(\frac{a}{r}\right) = 1 + e\cos M + \ldots \quad (6\text{-}58)$$

$$\left(\frac{a}{r}\right)^2 = 1 + 2e\cos M + \ldots \quad (6\text{-}59)$$

$$\frac{x}{a} = -\frac{3e}{2} + \cos M + \frac{e}{2}\cos 2M + \ldots \quad (6\text{-}60)$$

$$\frac{y}{a} = \sin M + \frac{e}{2}\sin 2M + \ldots \quad (6\text{-}61)$$

TABLE 6-6

Expansions in True Anomaly and Eccentricity

$$E = \theta - e\sin\theta + \frac{e^2}{4}\sin 2\theta - \frac{e^3}{4}\left(\sin\theta + \frac{1}{3}\sin 3\theta\right) + \ldots \quad (6\text{-}62)$$

$$\sin E = \sin\theta - \frac{e}{2}\sin 2\theta - \frac{e^2}{4}(\sin\theta - \sin 3\theta) - \frac{e^3}{8}\sin 4\theta - \ldots \quad (6\text{-}63)$$

$$\cos E = \cos\theta + \frac{e}{2}(1 - \cos 2\theta) - \frac{e^2}{4}(\cos\theta - \cos 3\theta) + \frac{e^3}{8} \quad (6\text{-}64)$$

$$\cos^2 E = \cos^2\theta + \frac{e}{2}(\cos\theta - \cos 3\theta) + \frac{e^2}{4}\left(-2\cos 2\theta + \frac{3}{2}\cos 4\theta + \frac{1}{2}\right) + \frac{e^3}{8}(3\cos 3\theta - \cos 5\theta) \quad (6\text{-}65)$$

$$M = \theta - 2e\sin\theta + \frac{3}{4}e^2\sin 2\theta - \frac{1}{3}e^3\sin 3\theta + \ldots \quad (6\text{-}66)$$

$$\frac{r}{a} = 1 - e\cos\theta - \frac{e^2}{2}(1 - \cos 2\theta) - \frac{e^3}{4}(\cos 3\theta - \cos\theta) - \ldots \quad (6\text{-}67)$$

$$\frac{a}{r} = 1 + e\cos\theta + e^2 + e^3\cos\theta \quad (6\text{-}68)$$

$$\dot{r} = \sqrt{\frac{\mu}{a}}\, e\left(1 + \frac{e^2}{2} + \ldots\right)\sin\theta \quad (6\text{-}69)$$

$$\ddot{r} = \frac{\mu}{a^2}e\cos\theta\left[1 + 2e\cos\theta + \frac{e^2}{2}(\cos 2\theta + 5) + 4e^3\cos\theta + \ldots\right] \quad (7\text{-}70)$$

$$v = \sqrt{\frac{\mu}{a}}\left[1 + e\cos\theta + \frac{e^2}{4}(3 - \cos 2\theta) + \frac{e^3}{8}(4\cos\theta - \cos 3\theta - 7) + \ldots\right] \quad (6\text{-}71)$$

$$\gamma = e\sin\theta - \frac{e^2}{2}\sin 2\theta + \frac{e^3}{3}\sin 3\theta - \frac{e^4}{4}\sin 4\theta + \ldots \quad (6\text{-}72)$$

$$\sin\gamma = e\sin\theta - \frac{e^2}{2}\sin 2\theta + \frac{1}{24}e^3(\sin 3\theta - 3\sin\theta) - \frac{1}{16}e^4(\sin 4\theta - 2\sin 2\theta) + \ldots \quad (6\text{-}73)$$

$$\cos\gamma = 1 + \frac{e^2}{4}(\cos 2\theta - 1) + \frac{e^3}{8}(\cos 3\theta + 7) + \ldots \quad (6\text{-}74)$$

$$\dot{\theta} = \sqrt{\frac{\mu}{a^3}}\left[1 + 2e\cos\theta + \frac{e^2}{2}(4 + \cos 2\theta) + 3e^3\cos\theta + \ldots\right] \quad (6\text{-}75)$$

TABLE 6-6 (continued)

$$\ddot{\theta} = -\frac{2\mu}{a^3} e \sin\theta \left[1 + 3e\cos\theta + \frac{3e^2}{2}(3 + \cos 2\theta) + \ldots\right] \quad (6\text{-}76)$$

TABLE 7-1

Hyperbolic Orbit Element Relations
(see Fig. 6)

$$a = \frac{b}{\sqrt{e^2 - 1}} \quad (7\text{-}1)$$

$$= \frac{b^2}{p} \quad (7\text{-}2)$$

$$= \frac{b^2 - r_p^2}{2r_p} \quad (7\text{-}3)$$

$$= \frac{p}{e^2 - 1} \quad (7\text{-}4)$$

$$= \frac{r_p}{e - 1} \quad (7\text{-}5)$$

$$= \frac{\mu(1 + e)}{v_p^2 (e - 1)} \quad (7\text{-}6)$$

$$= \frac{r_p^2}{p - 2r_p} \quad (7\text{-}7)$$

$$= \frac{\mu}{v_p\left(v_p - 2\sqrt{\frac{\mu}{p}}\right)} \quad (7\text{-}8)$$

$$= \frac{\mu r_p}{r_p v_p^2 - 2\mu} \quad (7\text{-}9)$$

$$b = a\sqrt{e^2 - 1} \quad (7\text{-}10)$$

$$= \sqrt{ap} \quad (7\text{-}11)$$

$$= \sqrt{r_p(r_p + 2a)} \quad (7\text{-}12)$$

$$= \frac{2\sqrt{\mu}\, a^{3/2} v_p}{a v_p^2 - \mu} \quad (7\text{-}13)$$

$$= \frac{p}{\sqrt{e^2 - 1}} \quad (7\text{-}14)$$

TABLE 7-1 (continued)

$$b = r_p\sqrt{\frac{e + 1}{e - 1}} \quad (7\text{-}15)$$

$$= \frac{\mu(e + 1)^{3/2}}{v_p^2 (e - 1)^{1/2}} \quad (7\text{-}16)$$

$$= r_p\sqrt{\frac{p}{p - 2r_p}} \quad (7\text{-}17)$$

$$= \frac{1}{v_p}\sqrt{\frac{\mu p^2}{p - 2\sqrt{\frac{\mu p}{v_p}}}} \quad (7\text{-}18)$$

$$= r_p v_p\sqrt{\frac{r_p}{r_p v_p^2 - 2\mu}} \quad (7\text{-}19)$$

$$e = \sqrt{\left(\frac{b}{a}\right)^2 + 1} \quad (7\text{-}20)$$

$$= \sqrt{\frac{p}{a} + 1} \quad (7\text{-}21)$$

$$= \frac{r_p}{a} + 1 \quad (7\text{-}22)$$

$$= \frac{a v_p^2 + \mu}{a v_p^2 - \mu} \quad (7\text{-}23)$$

$$= \sqrt{\left(\frac{p}{b}\right)^2 + 1} \quad (7\text{-}24)$$

$$= \frac{b^2 + r_p^2}{b^2 - r_p^2} \quad (7\text{-}25)$$

$$= \frac{p}{r_p} - 1 \quad (7\text{-}26)$$

$$= \sqrt{\frac{p}{\mu}}\, v_p - 1 \quad (7\text{-}27)$$

$$= \frac{r_p v_p^2}{\mu} - 1 \quad (7\text{-}28)$$

$$p = \frac{b^2}{a} \quad (7\text{-}29)$$

$$= a(e^2 - 1) \quad (7\text{-}30)$$

$$= \frac{r_p}{a}(r_p + 2a) \quad (7\text{-}31)$$

$$= \mu\left(\frac{2a\, v_p}{a v_p^2 - \mu}\right)^2 \quad (7\text{-}32)$$

TABLE 7-1 (continued)

$$p = b\sqrt{e^2 - 1} \tag{7-33}$$

$$= \frac{2r_p b^2}{b^2 - r_p^2} \tag{7-34}$$

$$= r_p (e + 1) \tag{7-35}$$

$$= \mu \left(\frac{e + 1}{v_p}\right)^2 \tag{7-36}$$

$$= \frac{r_p^2 v_p^2}{\mu} \tag{7-37}$$

$$r_p = \sqrt{a^2 + b^2} - a \tag{7-38}$$

$$= a (e - 1) \tag{7-39}$$

$$= a \left(\sqrt{1 + \frac{p}{a}} - 1\right) \tag{7-40}$$

$$= \frac{2\mu a}{a v_p^2 - \mu} \tag{7-41}$$

$$= b\sqrt{\frac{e - 1}{e + 1}} \tag{7-42}$$

$$= \frac{p}{1 + \sqrt{1 + \left(\frac{p}{b}\right)^2}} \tag{7-43}$$

$$= \frac{p}{1 + e} \tag{7-44}$$

$$= \frac{\mu (1 + e)}{v_p^2} \tag{7-45}$$

$$= \frac{\sqrt{\mu p}}{v_p} \tag{7-46}$$

$$v_p = \frac{b\sqrt{\frac{\mu}{a}}}{\sqrt{a^2 + b^2} - a} \tag{7-47}$$

$$= \sqrt{\frac{\mu (e + 1)}{a (e - 1)}} \tag{7-48}$$

$$= \frac{\sqrt{\mu p}}{a \left(\sqrt{1 + \frac{p}{a}} - 1\right)} \tag{7-49}$$

$$= \sqrt{\frac{\mu}{r_p} \left(2 + \frac{r_p}{a}\right)} \tag{7-50}$$

$$= \sqrt{\frac{\mu (e + 1)^{3/2}}{b (e - 1)^{1/2}}} \tag{7-51}$$

TABLE 7-1 (continued)

$$v_p = \frac{p\sqrt{\mu p}}{b\left(\sqrt{b^2 + p^2} - b\right)} \tag{7-52}$$

$$= \sqrt{\frac{2\mu b^2}{r_p (b^2 - r_p^2)}} \tag{7-53}$$

$$= \sqrt{\frac{\mu}{p}} (1 + e) \tag{7-54}$$

$$= \sqrt{\frac{\mu}{r_p} (1 + e)} \tag{7-55}$$

$$= \sqrt{\frac{\mu p}{r_p}} \tag{7-56}$$

TABLE 7-2

Time Variant Hyperbolic Relations
(see Fig. 6)

Elements

$$a = \frac{\mu r}{r v^2 - 2\mu} \tag{7-57}$$

$$b = \sqrt{\frac{r^3 v^2 \cos^2 \gamma}{r v^2 - 2\mu}} \tag{7-58}$$

$$e = \sqrt{1 + \frac{1}{\mu^2} r v^2 \cos^2 \gamma (r v^2 - 2\mu)} \tag{7-59}$$

$$p = \frac{r^2 v^2 \cos^2 \gamma}{\mu} \tag{7-60}$$

$$r_p = \frac{\mu r}{r v^2 - 2\mu} \left(\sqrt{1 + \frac{1}{\mu^2} r v^2 \cos^2 \gamma (r v^2 - 2\mu)} - 1\right) \tag{7-61}$$

$$v_p = \frac{\mu}{r v \cos \gamma} \left(1 + \sqrt{1 + \frac{1}{\mu^2} r v^2 \cos^2 \gamma (r v^2 - 2\mu)}\right) \tag{7-62}$$

Time variants

$$F = iE$$

$$= \cosh^{-1} \left[\frac{1}{e} \left(1 + \frac{r}{a}\right)\right] \tag{7-63}$$

$$= \cosh^{-1} \left[\frac{e + \cos \theta}{1 + e \cos \theta}\right] \tag{7-63a}$$

$$= 2 \tanh^{-1} \left[\sqrt{\frac{e - 1}{e + 1}} \tan \frac{\theta}{2}\right] \tag{7-63b}$$

$$r = \frac{p}{1 + e \cos \theta} \tag{7-64}$$

$$t = \sqrt{\frac{p^3}{\mu}} \frac{1}{e^2 - 1} \left[\pm \frac{r}{p} \sqrt{e^2 r^2 - (p - r)^2} + \right.$$

(continued)

TABLE 7-2 (continued)

$$- \frac{1}{\sqrt{e^2 - 1}} \ln\left\{\frac{r}{p}\left(e + \frac{p - r}{er} \pm \sqrt{e^2 - 1}\sqrt{r^2 - \left(\frac{p - r}{e}\right)^2}\right)\right\}\Bigg] + t_p \quad (7\text{-}65a)$$

$$= \sqrt{\frac{a^3}{\mu}}\left[- F + e \sinh F\right]$$

$$= \sqrt{\frac{p^3}{\mu}} \frac{1}{e^2 - 1}\left[\frac{e \sin\theta}{1 + e\cos\theta} - \frac{1}{\sqrt{e^2 - 1}} \ln\left(\frac{e + \cos\theta + \sqrt{e^2 - 1}\sin\theta}{1 + e\cos\theta}\right)\right]$$

$$+ t_p \quad (7\text{-}65b)$$

$$v = \sqrt{\mu\left(\frac{2}{r} + \frac{1}{a}\right)} = \sqrt{\mu\left(\frac{2}{r} + \frac{e^2 - 1}{p}\right)} \quad (7\text{-}66a)$$

$$= \sqrt{\frac{\mu}{p}\left[1 + 2e\cos\theta + e^2\right]} \quad (7\text{-}66b)$$

$$\gamma = \sqrt{\frac{p^2}{r\left[2p + r(e^2 - 1)\right]}} \quad (7\text{-}67)$$

$$= \frac{1 + e\cos\theta}{\sqrt{1 + 2e\cos\theta + e^2}} \quad (7\text{-}68)$$

$$\theta = \cos^{-1}\left(\frac{p - r}{er}\right) \quad (7\text{-}69)$$

TABLE 8

Spherical Trigonometric Relations

$$i = \cos^{-1}(\cos L \sin\beta) \quad (8\text{-}1)$$

$$= \sin^{-1}\left(\frac{\sin L \sin\beta}{\sin\nu}\right) \quad (8\text{-}2)$$

$$= \tan^{-1}\left(\frac{\tan L}{\sin\phi \sin\beta}\right) \quad (8\text{-}3)$$

$$= \tan^{-1}\left(\frac{\tan L}{\sin\nu}\right) \quad (8\text{-}4)$$

$$= \cos^{-1}\left(\frac{\cos L \sin\nu}{\sin\phi}\right) \quad (8\text{-}5)$$

$$= \sin^{-1}\left(\frac{\sin L}{\sin\phi}\right) \quad (8\text{-}6)$$

$$= \sin^{-1}\left(\frac{\cos\beta}{\cos\nu}\right) \quad (8\text{-}7)$$

$$= \tan^{-1}\left(\frac{\cos\beta \tan\phi}{\sin\nu}\right) \quad (8\text{-}8)$$

TABLE 8 (continued)

$$i = \tan^{-1}\left(\frac{\cot\beta}{\cos\phi}\right) \quad (8\text{-}9)$$

$$= \cos^{-1}\left(\frac{\tan\nu}{\tan\phi}\right) \quad (8\text{-}10)$$

$$L = \cos^{-1}\left(\frac{\cos i}{\sin\beta}\right) \quad (8\text{-}11)$$

$$= \sin^{-1}\left(\frac{\sin i \sin\nu}{\sin\beta}\right) \quad (8\text{-}12)$$

$$= \tan^{-1}(\tan i \sin\beta \sin\phi) \quad (8\text{-}13)$$

$$= \tan^{-1}(\tan i \sin\nu) \quad (8\text{-}14)$$

$$= \tan^{-1}(\sin i \cos\nu \tan\phi) \quad (8\text{-}15)$$

$$= \sin^{-1}(\sin i \sin\phi) \quad (8\text{-}16)$$

$$= \sin^{-1}\left(\frac{\tan\nu}{\tan\beta}\right) \quad (8\text{-}17)$$

$$= \sin^{-1}\left(\frac{\cos\beta \sin\phi}{\cos\nu}\right) \quad (8\text{-}18)$$

$$= \tan^{-1}(\cos\beta \tan\phi) \quad (8\text{-}19)$$

$$= \cos^{-1}\left(\frac{\cos\phi}{\cos\nu}\right) \quad (8\text{-}20)$$

$$\beta = \sin^{-1}\left(\frac{\cos i}{\cos L}\right) \quad (8\text{-}21)$$

$$= \sin^{-1}\left(\frac{\sin i \sin\nu}{\sin L}\right) \quad (8\text{-}22)$$

$$= \cos^{-1}\left(\frac{\sin i \cos\phi}{\cos L}\right) \quad (8\text{-}23)$$

$$= \cos^{-1}(\sin i \cos\nu) \quad (8\text{-}24)$$

$$= \cos^{-1}\left(\frac{\tan i \sin\nu}{\tan\phi}\right) \quad (8\text{-}25)$$

$$= \tan^{-1}\left(\frac{\cot i}{\cos\phi}\right) \quad (8\text{-}26)$$

$$= \tan^{-1}\left(\frac{\tan\nu}{\sin L}\right) \quad (8\text{-}27)$$

$$= \sin^{-1}\left(\frac{\tan\nu}{\cos L \tan\phi}\right) \quad (8\text{-}28)$$

$$= \cos^{-1}\left(\frac{\tan L}{\tan\phi}\right) \quad (8\text{-}29)$$

$$= \sin^{-1}\left(\frac{\sin\nu}{\sin\phi}\right) \quad (8\text{-}30)$$

$$\nu = \sin^{-1}\left(\frac{\tan L}{\tan i}\right) \quad (8\text{-}31)$$

$$= \sin^{-1}\left(\frac{\sin L \sin\beta}{\sin i}\right) \quad (8\text{-}32)$$

$$= \tan^{-1}\left(\frac{\sin L}{\tan i \cos\phi}\right) \quad (8\text{-}33)$$

TABLE 8 (continued)

$$\nu = \cos^{-1}\left(\frac{\cos\beta}{\sin i}\right) \tag{8-34}$$

$$= \cos^{-1}\left(\frac{\sin\beta\cos\phi}{\cos i}\right) \tag{8-35}$$

$$= \tan^{-1}\left(\cos i \tan\phi\right) \tag{8-36}$$

$$= \tan^{-1}\left(\sin L \tan\beta\right) \tag{8-37}$$

$$= \cos^{-1}\left(\frac{\cos\beta\sin\phi}{\sin L}\right) \tag{8-38}$$

$$= \cos^{-1}\left(\frac{\cos\phi}{\cos L}\right) \tag{8-39}$$

$$= \sin^{-1}\left(\sin\beta\sin\phi\right) \tag{8-40}$$

$$\phi = \sin^{-1}\left(\frac{\sin L}{\sin i}\right) \tag{8-41}$$

$$= \cos^{-1}\left(\frac{\cos L\cos\beta}{\sin i}\right) \tag{8-42}$$

$$= \tan^{-1}\left(\frac{\tan L}{\sin i\cos\nu}\right) \tag{8-43}$$

$$= \cos^{-1}\left(\cot i\cot\beta\right) \tag{8-44}$$

$$= \sin^{-1}\left(\frac{\tan\nu}{\sin i\tan\beta}\right) \tag{8-45}$$

$$= \tan^{-1}\left(\frac{\tan\nu}{\cos i}\right) \tag{8-46}$$

$$= \tan^{-1}\left(\frac{\tan L}{\cos\beta}\right) \tag{8-47}$$

$$= \sin^{-1}\left(\frac{\sin L\cos\nu}{\cos\beta}\right) \tag{8-48}$$

$$= \cos^{-1}\left(\cos L\cos\nu\right) \tag{8-49}$$

$$= \sin^{-1}\left(\frac{\sin\nu}{\sin\beta}\right) \tag{8-50}$$

L. PRESENTATION OF GRAPHICAL DATA

The figures presented at the end of this chapter will not be discussed here. A list of figures is given at the beginning of this chapter.

M. REFERENCES

1. Plummer, H. C., "Introductory Treatise on Dynamical Astronomy," Dover Press, New York, 1960.

2. Gedeon, "Orbital Segment Mechanics," Norair Division of Northrop Corporation, Los Angeles, Report ASG-TM-61-43, 1961.

3. Moulton, F. R., "Introduction to Celestial Mechanics," Second Revised Edition, MacMillan Company, New York, 1958.

4. Epstein, L. I., "Nomography Interscience Publishers Incorporated, New York, 1958.

5. Levens, A. S., "Nomography," John Wiley and Sons Incorporated, New York, 1948.

N. BIBLIOGRAPHY

Baker, R. M. L., Jr. and Makemson, M. W. "An Introduction to Astro-dynamics," New York, Academic Press, 1960.

Beard, R. B. and Rotherham, A. C., "Space Flight and Satellite Vehicles," New York, Putnam, 1957.

Bellman, R.
"Stability Theory of Differential Equations," New York, McGraw-Hill Book Company, Inc., 1953.
"Dynamic Programming," Princeton University Press, Princeton, New Jersey, 1957.

Benedikt, E. T., "Collision Trajectories in the Three-Body Problem," Journal of the Astronautical Sciences, Summer 1959, Vol. 6, No. 2.

Berman, A. I., "The Physical Principles of Astronautics; Fundamentals of Dynamical Astronomy and Space Flight," New York, John Wiley & Sons, Inc., 1961.

Bizony, M. T., ed., "The Space Encyclopedia," New York, E. P. Dutton and Company, Inc., 1958.

Bowden, G. E., and Flis, J., "Notes of the Summer Institute in Dynamical Astronomy at Yale University, Yale University Press, New Haven, Connecticut, 1959.

Brillouin, L., "Poincare and the Shortcomings of the Hamilton-Jacobi Method for Classical or Quantized Mechanics," Archive for Rational Mechanics and Analysis, Vol. 5, No. 1, pp 76 to 94, 1960.

Brouwer, D., and Clemence, G. M., "Methods of Celestial Mechanics," New York, Academic Press, 1960.

Corben, H. C., and Stehle, P., "Classical Mechanics," New York, John Wiley & Sons, Inc., 1950.

Danby, J. M. A., "Fundamentals of Celestial Mechanics," MacMillan, New York, 1962.

Darwin, G. H., "Periodic Orbits," Acta Mathematica, Vol. 21, 1899.

Dubyago, A. D., "Determination of Orbits," MacMillan, New York, 1961.

Eckert, W. J., Brouwer, D., and Clemence, G. M., "Coordinates of the Five Outer Planets," The American Ephemeris and Nautical Almanac, U. S. Government Printing Office, Washington, D. C., Vol. 12, pp 1653 to 2060, 1951.

Ehricke, K. A.
"Space Flight," New York, D. Van Nostrand Company, Inc., 1960.
"Cislunar Orbits," Convair Astronautics, AZP-004, March 1957.
"Restricted 3 Body System Flight Mechanics in Cislunar Space and the Effect of Solar Perturbations," AZM-013, March 1957.
"The Solar System," AZM-008, June 1957.
"Space Flight Mechanics of Nonpowered Motion," AZM-010, November 1957.
"Space Craft," AZM-020, February 1958.
"Powered Space Flight Mechanics," AZM-011
"Celestial Mechanics," AZM-009, August 1957.

Felling, W., "Summer Institute in Dynamical Astronomy at Yale University July 1960," McDonnell Aircraft, St. Louis, 1961.

Finlay-Freundlich, E., "Celestial Mechanics," New York, Pergamon Press, Inc., 1958.

Goldstein, H., "Classical Mechanics," Reading, Massachusetts, Addison-Wesley Publishing Company, 1950.

Herget, P., "The Computation of Orbits," University of Cincinnati, 1948 (published privately by author).

Herrick, S.
"Astrodynamics and Rocket Navigation," New York, D. Van Nostrand Company (to be published).
"Tables for Rocket and Comet Orbits," U. S. Government Printing Office, Washington, D. C., 100 pp, 1953.

Herrick, S., Baker, R., and Hilton, C., "Gravitational and Related Constants for Accurate Space Navigation," American Rocket Society Preprint 497-57, 1957.

Hohmann, W., "The Attainability of Celestial Bodies," Munich, R. Oldenburg, 1926.

Jastrow, R., "Exploration of Space," MacMillan, New York, 1960.

Jensen, J., Townsend, G., Kork, J., and Kraft, D., "Design Guide to Orbital Flight," New York, McGraw-Hill Book Company, Inc., 1962.

Kellogg, O. D., "Foundations of Potential Theory," New York, Dover Publications, Inc., 1953.

Koelle, H. H., ed., "Handbook of Astronautical Engineering," New York, McGraw-Hill Book Company, Inc., 1961.

Kraft, J. D., Kork, J., and Townsend, G. E., "Mean Anomaly for Elliptic, Parabolic and Hyperbolic Orbits as Functions of the Central Angle from Perigee," The Martin Company (Baltimore), Engineering Report No. ER 12083, November 1961.

Krogdahl, W. S., "The Astronomical Universe," MacMillan, New York, 1962 (2nd ed.).

Legalley, D. P., ed., "Guidance Navigation, Tracking and Space Physics, Symposium on Ballistic Missile and Space Technology, Los Angeles, August 1960," Ballistic Missile and Space Technology, New York, Academic Press, Vol. 3, 450 pp, 1960.

MacMillian, W. D.
"Dynamics of Rigid Bodies," New York, McGraw-Hill Book Company, Inc., 1936.
"Statics and the Dynamics of a Particle," Theoretical Mechanics, New York, McGraw-Hill Book Company, Inc., Vol. I, 1927.

Mehlin, T. G., 1906, "Astronomy," New York, Wiley, 1959.

Moulton, F. R.
"An Introduction to Celestial Mechanics," New York, The MacMillan Company, 1914.
"Periodic Orbits," The Carnegie Institute, Washington, Publication No. 161, 1920.

Oertel, G. K., and Singer, S. F., "Some Aspects of the Three Body Problem," University of Maryland, Physics Department Report No. AFOSR TN 59-405, March 1959.

Payne-Gaposchkin, C., "Introduction to Astronomy," New York, Prentice-Hall, Inc., 1954.

Plummer, H. C., "Introductory Treatise on Dynamical Astronomy," New York, Dover Publications, Inc., 1960.

Proell, W., and Bowman, N. J., "A Handbook of Space Flight," 2nd edition, Chicago, Parastadion Press, 1958.

Russel, H. N., Dugan, R. S., and Stewart, J. Q., "Astronomy," 2nd edition, Boston, Ginn & Company, Vol. 1, 1945.

Scarborough, J. B., "Numerical Mathematical Analysis," Baltimore, The John Hopkins University Press, 1955.

Siefert, H. S., "Space Technology," New York, John Wiley & Sons, Inc., 1959.

Siegle, C. L., "Topics in Celestial Mechanics," Baltimore, The Johns Hopkins University Press, 1954.

Soule, P. W., et al., "Performance Manual for Orbital Operations," Northrop Corporation, Report No. NOR 61-208, September 1961.

Smart, W., "Celestial Mechanics," New York, Longmans, Green and Company, 1953.

Sternberg, W. J., and Smith, T. L., "Theory of Potential and Spherical Harmonics," Toronto, Canada, University of Toronto Press, 1944.

Synge, J. L., and Griffith, B. A., "Principles of Mechanics," New York, McGraw-Hill Book Company, Inc., 1959.

Timoshenko, S. P., "Advanced Dynamics," New York, McGraw-Hill Book Company, Inc., 1948.

Vertregt, M., "Principles of Astronautics," New York, Elsevier Publishing Company, 1960.

Watson, C., "Theoretical Astronomy," 2nd edition, Philadelphia, J. B. Lippincott Company, 1892.

Whittaker, E. T., "Analytical Dynamics," New York, Dover Publications, Inc., 1944.

Wintner, A., "The Analytical Foundations of Celestial Mechanics," Princeton University Press, Princeton, New Jersey, 1947.

Introduction to Ballistic Missiles. Prepared by STL for the Air Force Ballistic Missile Division, March 1960.
Vol. I--Mathematical and Physical Foundations, ASTIA No. 240177.
Vol. II--Trajectory and Performance Analysis, ASTIA No. 240178.
Vol. III--Design and Engineering Subsystems, ASTIA No. 240179.
Vol. IV--Guidance Techniques, ASTIA No. 240180.

Notes on Space Technology. Langley Field, Virginia, Langley Aeronautical Laboratory, Flight Research Division, May 1958.

ILLUSTRATIONS

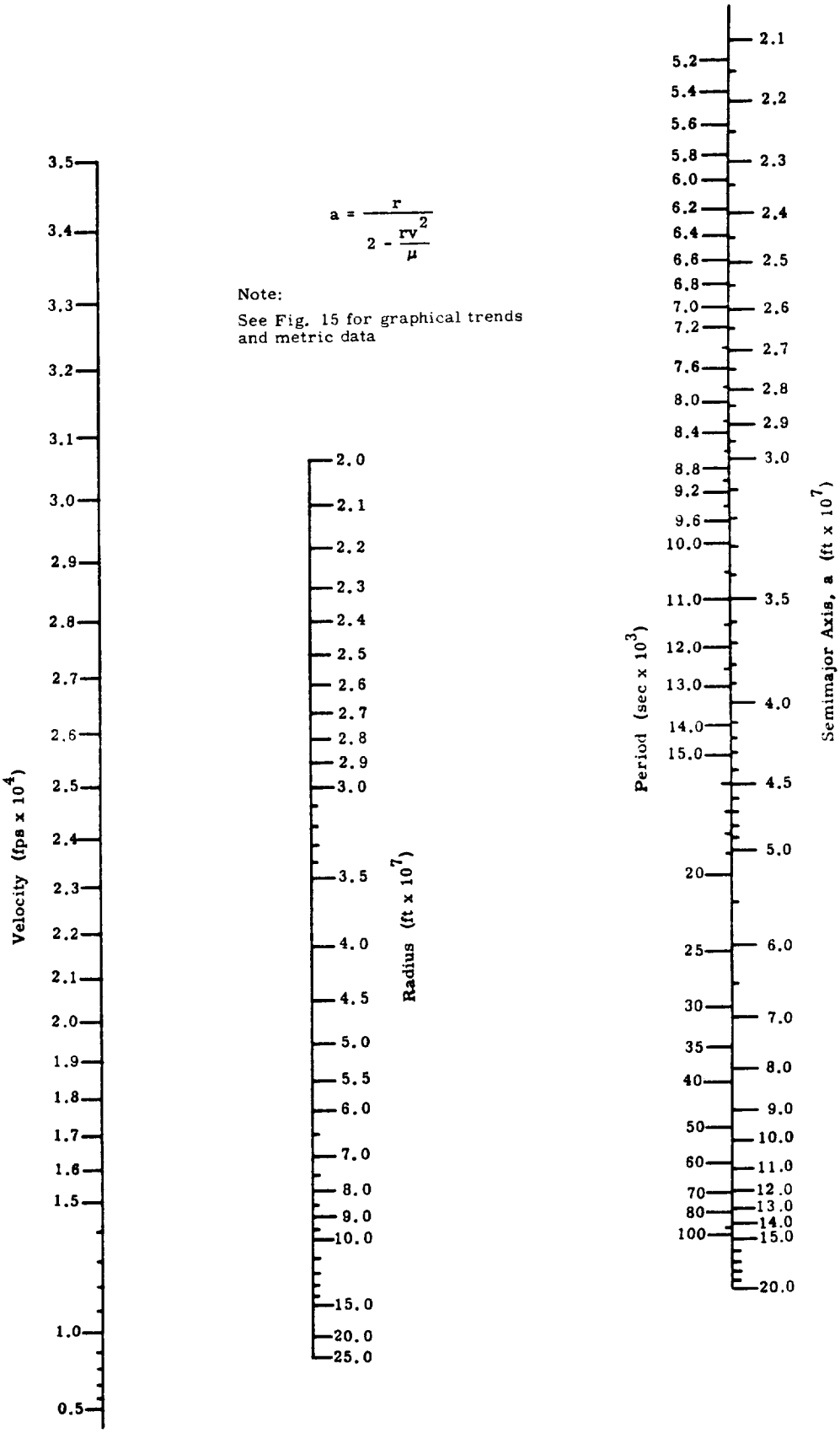

Fig. 1a. Semimajor Axis as a Function of the Radius and Velocity at any Point (English Units - see Figs. 1b and 15 for Other Units)

Preceding page blank

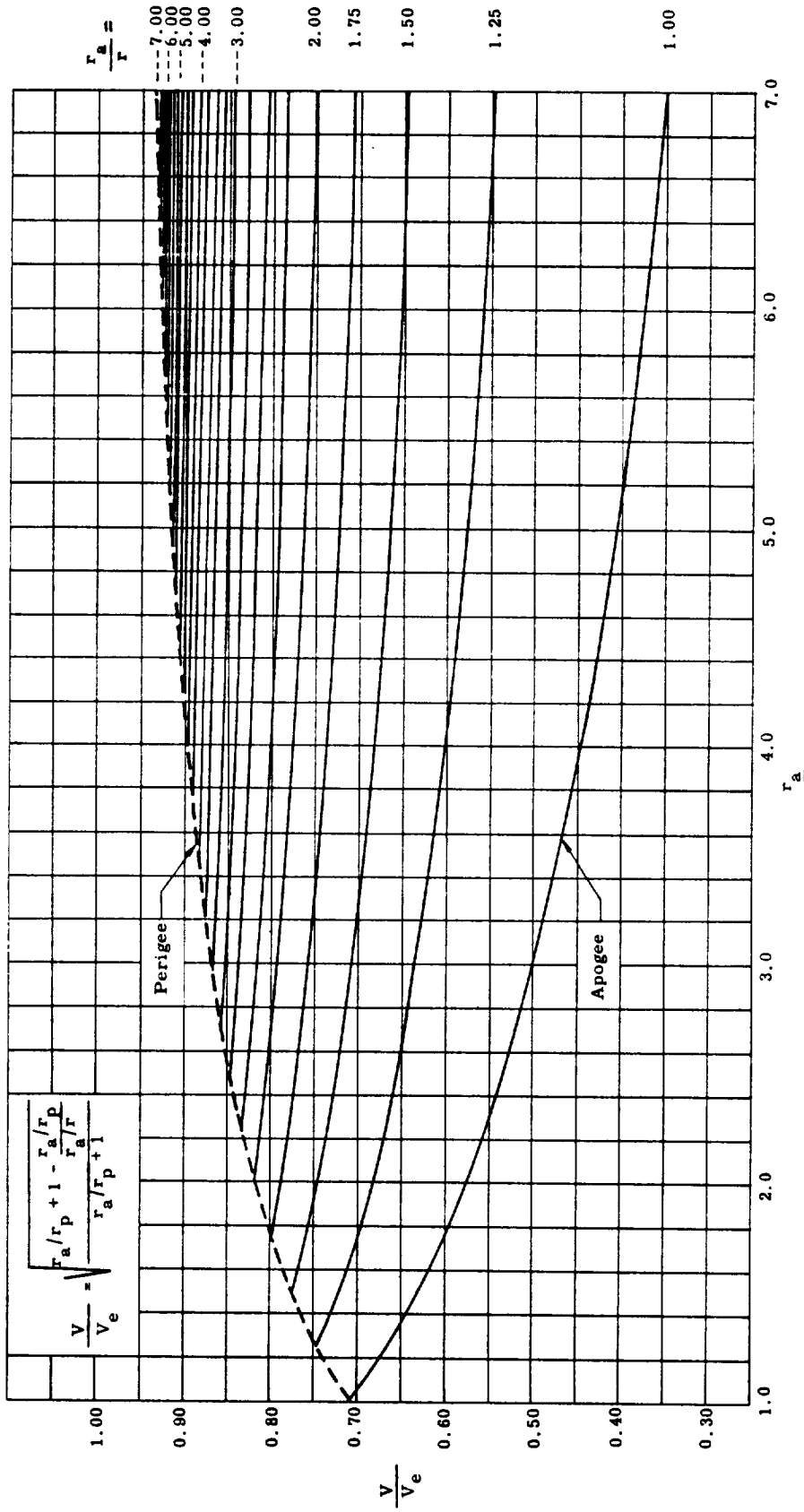

Fig. 1b. Velocity--Escape Speed Ratio

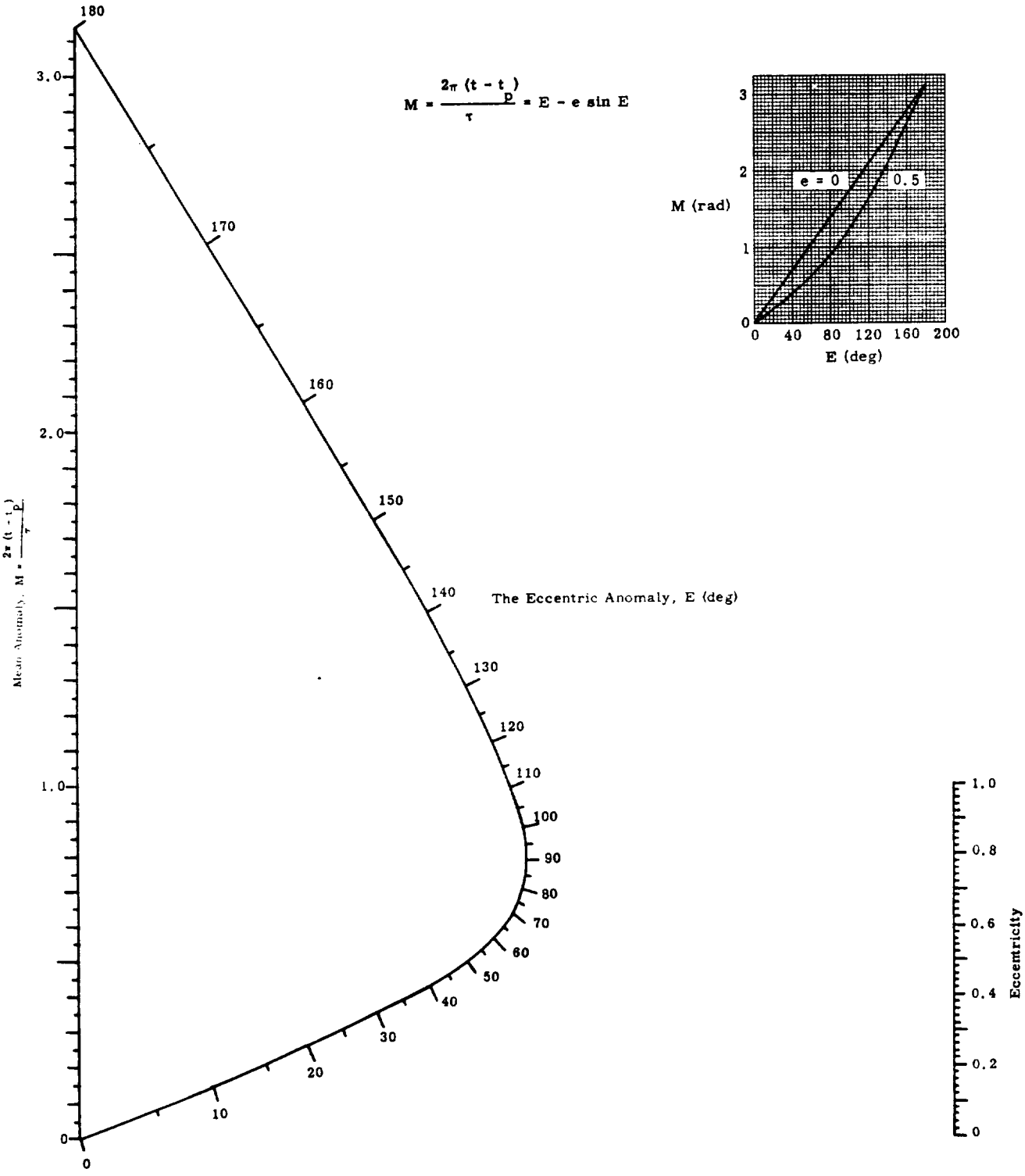

Fig. 2. The Relationship Between Orbital Position and Eccentricity and Time from Perigee (Kepler's Equation) (also see Fig. 22)

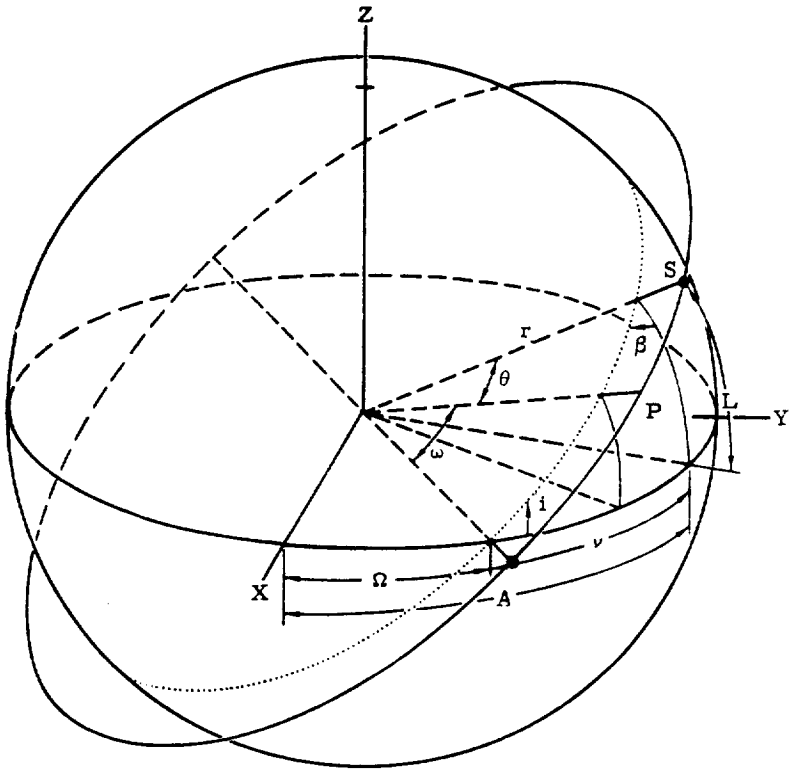

Fig. 3. Three-Dimensional Geometry of the Orbit

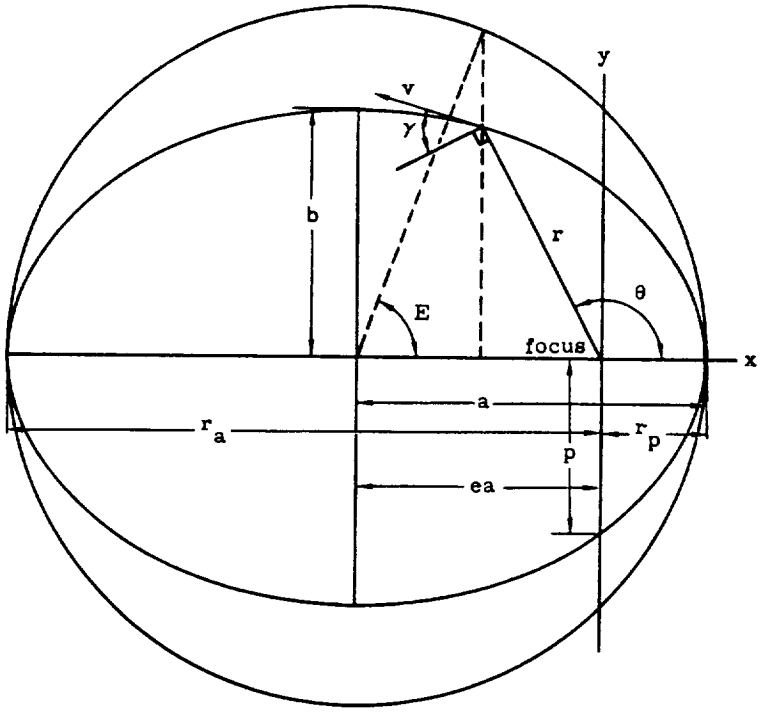

Fig. 4. Geometry of the Ellipse

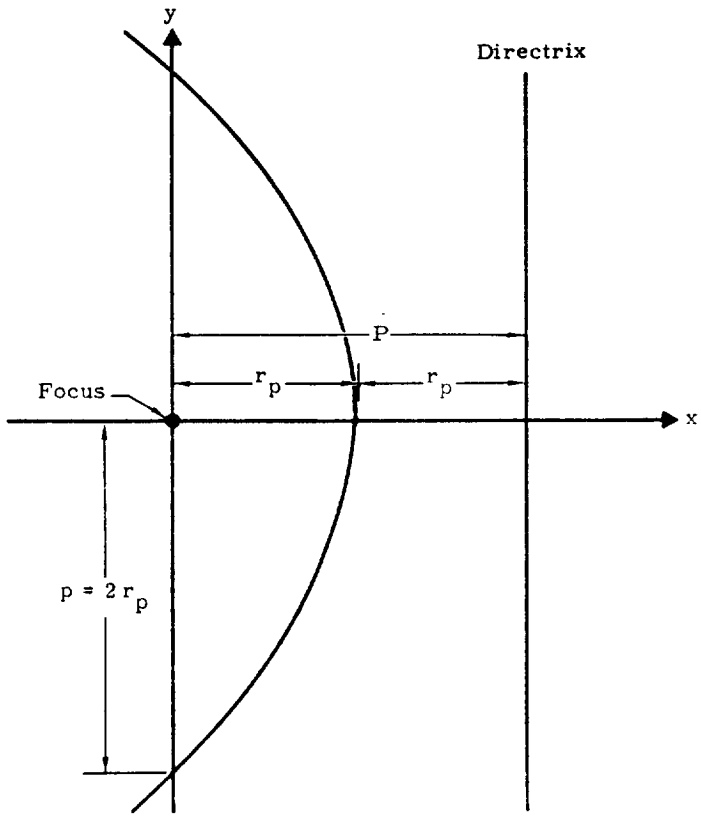

Fig. 5. Geometry of the Parabola

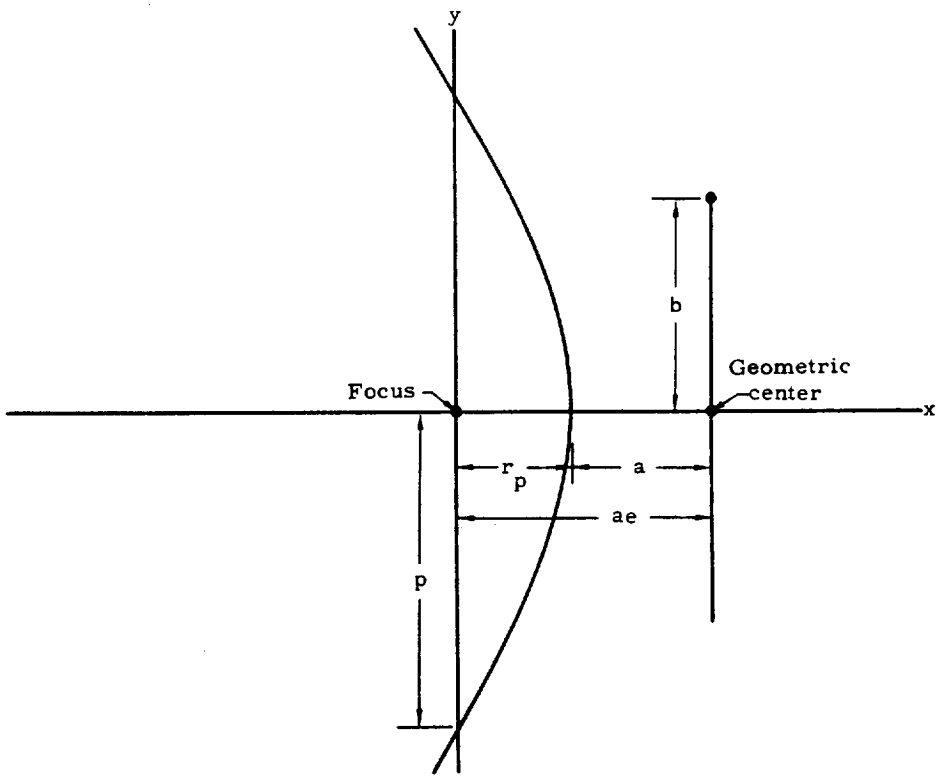

Fig. 6. Geometry of the Hyperbola

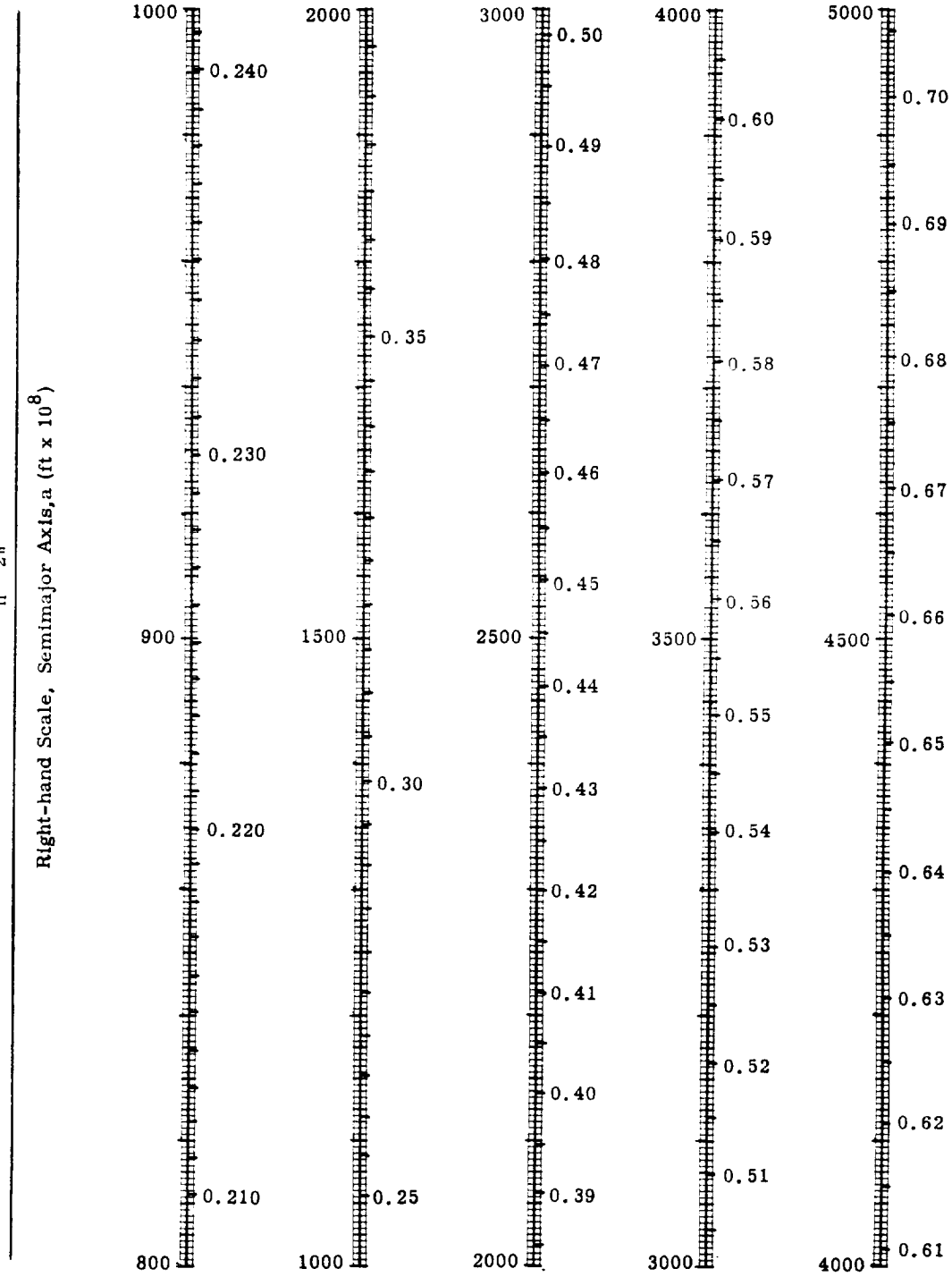

Fig. 7. The Parameter $\frac{1}{n} = \frac{\tau}{2\pi}$ as a Function of Semimajor Axis (English Units - see Table 9 for Metric Data)

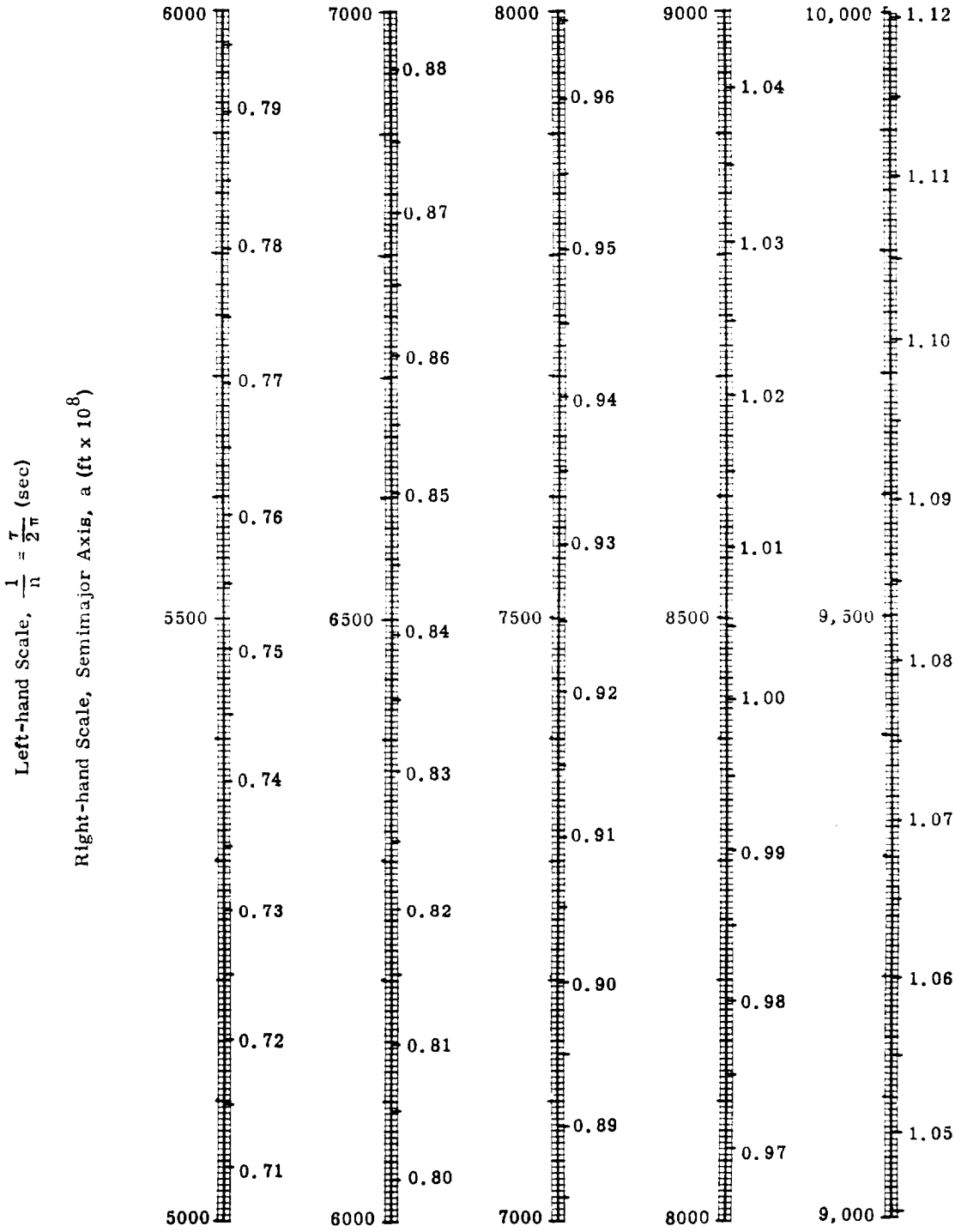

Fig. 7. (continued)

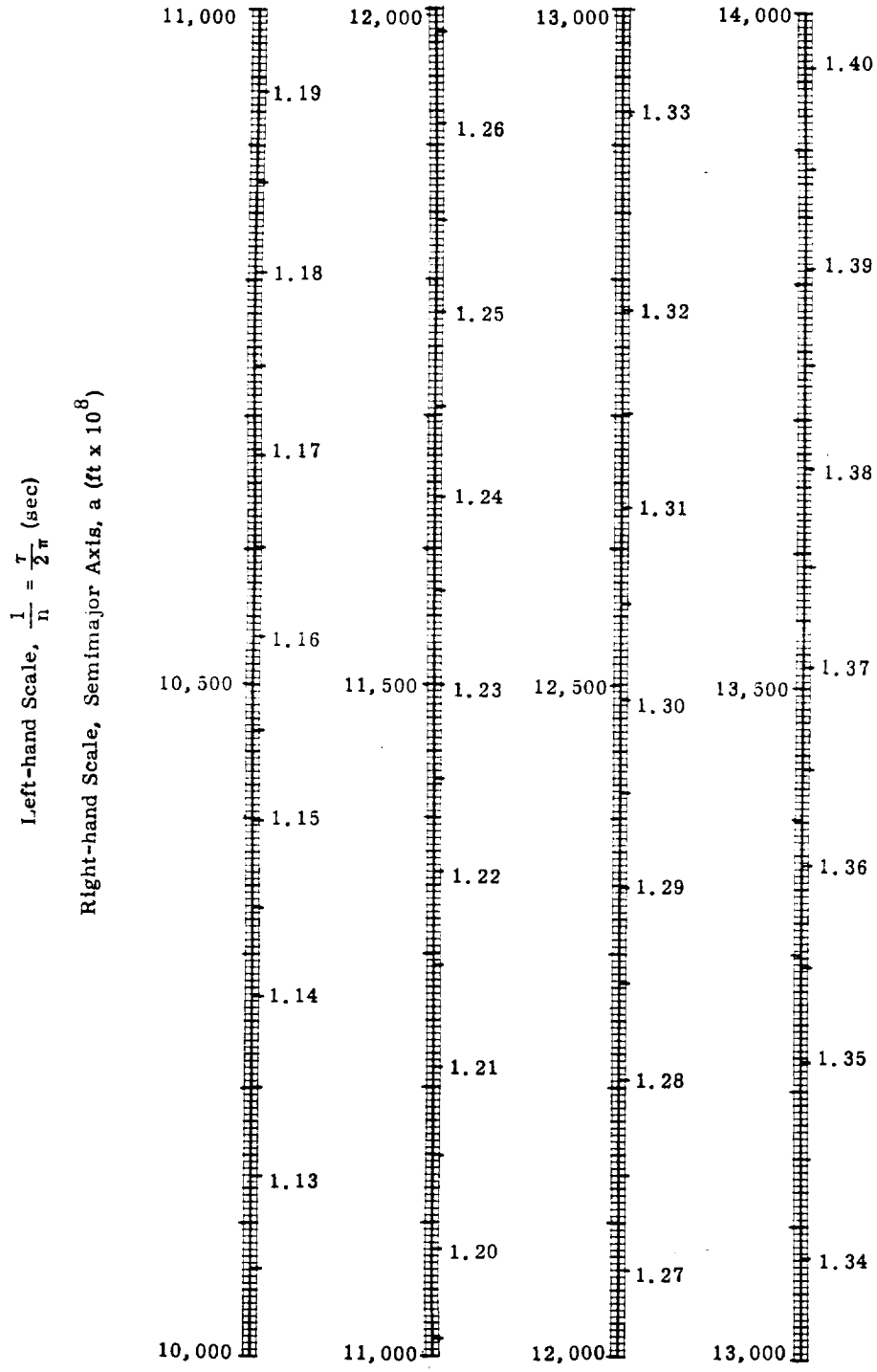

Fig. 7. (continued)

TABLE 9

Circular Velocity, Period and Angular Rate
(metric data; see Figs. 7 and 8 for English data)

RADIUS KILOMETERS

		0.	5.	10.	15.	20.	25.	30.	35.	40.	45.	50.	55.	60.	65.	70.	75.	80.	85.	90.	95.
6000	Velocity	8.191	8.167	8.144	8.121	8.127	8.134	8.130	8.127	8.124	8.120	8.117	8.114	8.110	8.107	8.104	8.100	8.097	8.094	8.090	8.087
	Period	1.285	1.286	1.288	1.290	1.291	1.293	1.294	1.296	1.298	1.299	1.301	1.303	1.304	1.306	1.307	1.309	1.311	1.312	1.314	1.315
	Ang. Vel.	4.890	4.884	4.878	4.872	4.866	4.860	4.854	4.848	4.842	4.836	4.830	4.824	4.818	4.812	4.806	4.800	4.794	4.788	4.782	4.777
6100	Velocity	8.084	8.080	8.077	8.074	8.070	8.067	8.064	8.061	8.057	8.054	8.051	8.047	8.044	8.041	8.038	8.034	8.031	8.028	8.025	8.021
	Period	1.317	1.319	1.320	1.322	1.324	1.325	1.327	1.328	1.330	1.332	1.333	1.335	1.337	1.338	1.340	1.341	1.343	1.345	1.346	1.348
	Ang. Vel.	4.771	4.765	4.759	4.753	4.747	4.741	4.736	4.730	4.724	4.718	4.713	4.707	4.701	4.695	4.690	4.684	4.678	4.673	4.667	4.661
6200	Velocity	8.018	8.015	8.012	8.008	8.005	8.002	7.999	7.996	7.992	7.989	7.986	7.983	7.980	7.976	7.973	7.970	7.967	7.964	7.961	7.957
	Period	1.350	1.351	1.353	1.354	1.356	1.358	1.359	1.361	1.363	1.364	1.366	1.368	1.369	1.371	1.372	1.374	1.376	1.377	1.379	1.381
	Ang. Vel.	4.656	4.650	4.644	4.639	4.633	4.628	4.622	4.617	4.611	4.605	4.600	4.594	4.589	4.583	4.578	4.572	4.567	4.562	4.556	4.551
6300	Velocity	7.954	7.951	7.948	7.945	7.942	7.939	7.936	7.932	7.929	7.926	7.923	7.920	7.917	7.914	7.910	7.907	7.904	7.901	7.898	7.895
	Period	1.382	1.384	1.386	1.387	1.389	1.391	1.392	1.394	1.396	1.397	1.399	1.400	1.402	1.404	1.405	1.407	1.409	1.410	1.412	1.414
	Ang. Vel.	4.545	4.540	4.534	4.529	4.524	4.518	4.513	4.508	4.502	4.497	4.492	4.486	4.481	4.476	4.471	4.465	4.460	4.455	4.450	4.444
6400	Velocity	7.892	7.889	7.886	7.883	7.880	7.876	7.873	7.870	7.867	7.864	7.861	7.858	7.855	7.852	7.849	7.846	7.843	7.840	7.837	7.834
	Period	1.415	1.417	1.419	1.420	1.422	1.424	1.425	1.427	1.429	1.430	1.432	1.434	1.435	1.437	1.439	1.440	1.442	1.444	1.445	1.447
	Ang. Vel.	4.439	4.434	4.429	4.424	4.418	4.413	4.408	4.403	4.398	4.393	4.388	4.383	4.377	4.372	4.367	4.362	4.357	4.352	4.347	4.342
6500	Velocity	7.831	7.828	7.825	7.822	7.819	7.816	7.813	7.810	7.807	7.804	7.801	7.798	7.795	7.792	7.789	7.786	7.783	7.780	7.777	7.774
	Period	1.449	1.450	1.452	1.454	1.455	1.457	1.459	1.460	1.462	1.464	1.465	1.467	1.469	1.470	1.472	1.474	1.476	1.477	1.479	1.481
	Ang. Vel.	4.337	4.332	4.327	4.322	4.317	4.312	4.307	4.302	4.297	4.292	4.288	4.283	4.278	4.273	4.268	4.263	4.258	4.253	4.249	4.244
6600	Velocity	7.771	7.768	7.765	7.763	7.760	7.757	7.754	7.751	7.748	7.745	7.742	7.739	7.736	7.733	7.730	7.728	7.725	7.722	7.719	7.716
	Period	1.482	1.484	1.486	1.487	1.489	1.491	1.492	1.494	1.496	1.497	1.499	1.501	1.503	1.504	1.506	1.508	1.509	1.511	1.513	1.514
	Ang. Vel.	4.239	4.234	4.229	4.225	4.220	4.215	4.210	4.205	4.201	4.196	4.191	4.186	4.182	4.177	4.172	4.168	4.163	4.158	4.154	4.149
6700	Velocity	7.713	7.710	7.707	7.705	7.702	7.699	7.696	7.693	7.690	7.687	7.685	7.682	7.679	7.676	7.673	7.670	7.668	7.665	7.662	7.659
	Period	1.516	1.518	1.519	1.521	1.523	1.525	1.526	1.528	1.530	1.531	1.533	1.535	1.536	1.538	1.540	1.542	1.543	1.545	1.547	1.548
	Ang. Vel.	4.144	4.140	4.135	4.131	4.126	4.121	4.117	4.112	4.108	4.103	4.099	4.094	4.089	4.085	4.080	4.076	4.071	4.067	4.062	4.058
6800	Velocity	7.656	7.653	7.651	7.648	7.645	7.642	7.639	7.637	7.634	7.631	7.628	7.625	7.623	7.620	7.617	7.614	7.612	7.609	7.606	7.604
	Period	1.550	1.552	1.554	1.555	1.557	1.559	1.560	1.562	1.564	1.566	1.567	1.569	1.571	1.572	1.574	1.576	1.578	1.579	1.581	1.583
	Ang. Vel.	4.053	4.049	4.044	4.040	4.035	4.031	4.027	4.022	4.018	4.013	4.009	4.005	4.000	3.996	3.992	3.987	3.983	3.978	3.974	3.970
6900	Velocity	7.601	7.598	7.595	7.592	7.590	7.587	7.584	7.581	7.579	7.576	7.573	7.570	7.568	7.565	7.562	7.560	7.557	7.554	7.551	7.549
	Period	1.584	1.586	1.588	1.590	1.591	1.593	1.595	1.597	1.598	1.600	1.602	1.603	1.605	1.607	1.609	1.610	1.612	1.614	1.616	1.617
	Ang. Vel.	3.966	3.961	3.957	3.953	3.948	3.944	3.940	3.936	3.931	3.927	3.923	3.919	3.914	3.910	3.906	3.902	3.898	3.893	3.889	3.885
7000	Velocity	7.546	7.543	7.541	7.538	7.535	7.533	7.530	7.527	7.525	7.522	7.519	7.517	7.514	7.511	7.509	7.506	7.503	7.501	7.498	7.495
	Period	1.619	1.621	1.622	1.624	1.626	1.628	1.629	1.631	1.633	1.635	1.636	1.638	1.640	1.642	1.643	1.645	1.647	1.649	1.650	1.652
	Ang. Vel.	3.881	3.877	3.873	3.868	3.864	3.860	3.856	3.852	3.848	3.844	3.840	3.836	3.831	3.827	3.823	3.819	3.815	3.811	3.807	3.803
7100	Velocity	7.493	7.490	7.487	7.485	7.482	7.480	7.477	7.474	7.472	7.469	7.466	7.464	7.461	7.459	7.456	7.453	7.451	7.448	7.446	7.443
	Period	1.654	1.656	1.657	1.659	1.661	1.663	1.664	1.666	1.668	1.670	1.671	1.673	1.675	1.677	1.678	1.680	1.682	1.684	1.685	1.687
	Ang. Vel.	3.799	3.795	3.791	3.787	3.783	3.779	3.775	3.771	3.767	3.763	3.759	3.755	3.751	3.748	3.744	3.740	3.736	3.732	3.728	3.724
7200	Velocity	7.441	7.438	7.435	7.433	7.430	7.428	7.425	7.423	7.420	7.417	7.415	7.412	7.410	7.407	7.405	7.402	7.400	7.397	7.394	7.392
	Period	1.689	1.691	1.692	1.694	1.696	1.698	1.699	1.701	1.703	1.705	1.707	1.708	1.710	1.712	1.714	1.715	1.717	1.719	1.721	1.722
	Ang. Vel.	3.720	3.716	3.713	3.709	3.705	3.701	3.697	3.693	3.689	3.686	3.682	3.678	3.674	3.670	3.667	3.663	3.659	3.655	3.652	3.648
7300	Velocity	7.389	7.387	7.384	7.382	7.379	7.377	7.374	7.372	7.369	7.367	7.364	7.362	7.359	7.357	7.354	7.352	7.349	7.347	7.344	7.342
	Period	1.724	1.726	1.728	1.730	1.731	1.733	1.735	1.737	1.738	1.740	1.742	1.744	1.746	1.747	1.749	1.751	1.753	1.754	1.756	1.758
	Ang. Vel.	3.644	3.640	3.637	3.633	3.629	3.625	3.622	3.618	3.614	3.611	3.607	3.603	3.600	3.596	3.592	3.589	3.585	3.581	3.578	3.574
7400	Velocity	7.339	7.337	7.334	7.332	7.329	7.327	7.324	7.322	7.320	7.317	7.315	7.312	7.310	7.307	7.305	7.302	7.300	7.297	7.295	7.293
	Period	1.760	1.762	1.763	1.765	1.767	1.769	1.770	1.772	1.774	1.776	1.778	1.779	1.781	1.783	1.785	1.787	1.788	1.790	1.792	1.794
	Ang. Vel.	3.570	3.567	3.563	3.560	3.556	3.552	3.549	3.545	3.542	3.538	3.535	3.531	3.527	3.524	3.520	3.517	3.513	3.510	3.506	3.503

RADIUS KILOMETERS

		0.	5.	10.	15.	20.	25.	30.	35.	40.	45.	50.	55.	60.	65.	70.	75.	80.	85.	90.	95.
7500	Velocity	7.290	7.288	7.285	7.283	7.280	7.278	7.276	7.273	7.271	7.268	7.266	7.264	7.261	7.259	7.256	7.254	7.252	7.249	7.247	7.244
	Period	1.796	1.797	1.799	1.801	1.803	1.805	1.806	1.808	1.810	1.812	1.814	1.815	1.817	1.819	1.821	1.823	1.824	1.826	1.828	1.830
	Ang. Vel.	3.499	3.496	3.492	3.489	3.485	3.482	3.478	3.475	3.471	3.468	3.465	3.461	3.458	3.454	3.451	3.447	3.444	3.441	3.437	3.434
7600	Velocity	7.242	7.240	7.237	7.235	7.233	7.230	7.228	7.225	7.223	7.221	7.219	7.216	7.214	7.211	7.209	7.207	7.204	7.202	7.200	7.197
	Period	1.832	1.833	1.835	1.837	1.839	1.841	1.842	1.844	1.846	1.848	1.850	1.852	1.853	1.855	1.857	1.859	1.861	1.862	1.864	1.866
	Ang. Vel.	3.430	3.427	3.424	3.420	3.417	3.414	3.410	3.407	3.404	3.400	3.397	3.394	3.390	3.387	3.384	3.380	3.377	3.374	3.370	3.367
7700	Velocity	7.195	7.193	7.190	7.188	7.186	7.183	7.181	7.179	7.176	7.174	7.172	7.169	7.167	7.165	7.162	7.160	7.158	7.156	7.153	7.151
	Period	1.868	1.870	1.871	1.873	1.875	1.877	1.879	1.881	1.882	1.884	1.886	1.888	1.890	1.892	1.893	1.895	1.897	1.899	1.901	1.903
	Ang. Vel.	3.364	3.361	3.357	3.354	3.351	3.348	3.344	3.341	3.338	3.335	3.331	3.328	3.325	3.322	3.318	3.315	3.312	3.309	3.306	3.303
7800	Velocity	7.149	7.146	7.144	7.142	7.139	7.137	7.135	7.133	7.130	7.128	7.126	7.124	7.121	7.119	7.117	7.115	7.112	7.110	7.108	7.105
	Period	1.904	1.906	1.908	1.910	1.912	1.914	1.915	1.917	1.919	1.921	1.923	1.925	1.926	1.928	1.930	1.932	1.934	1.936	1.937	1.939
	Ang. Vel.	3.299	3.296	3.293	3.290	3.287	3.284	3.280	3.277	3.274	3.271	3.268	3.265	3.262	3.259	3.255	3.252	3.249	3.246	3.243	3.240
7900	Velocity	7.103	7.101	7.099	7.097	7.094	7.092	7.090	7.088	7.085	7.083	7.081	7.079	7.076	7.074	7.072	7.070	7.068	7.065	7.063	7.061
	Period	1.941	1.943	1.945	1.947	1.948	1.950	1.952	1.954	1.956	1.958	1.960	1.961	1.963	1.965	1.967	1.969	1.971	1.973	1.974	1.976
	Ang. Vel.	3.237	3.234	3.231	3.228	3.225	3.222	3.219	3.216	3.212	3.209	3.206	3.203	3.200	3.197	3.194	3.191	3.188	3.185	3.182	3.179
8000	Velocity	7.059	7.056	7.054	7.052	7.050	7.048	7.046	7.043	7.041	7.039	7.037	7.035	7.032	7.030	7.028	7.026	7.024	7.021	7.019	7.017
	Period	1.978	1.980	1.982	1.984	1.985	1.987	1.989	1.991	1.993	1.995	1.997	1.999	2.000	2.002	2.004	2.006	2.008	2.010	2.012	2.013
	Ang. Vel.	3.176	3.173	3.170	3.168	3.165	3.162	3.159	3.156	3.153	3.150	3.147	3.144	3.141	3.138	3.135	3.132	3.129	3.126	3.124	3.121
8100	Velocity	7.015	7.013	7.011	7.009	7.006	7.004	7.002	7.000	6.998	6.996	6.993	6.991	6.989	6.987	6.985	6.983	6.981	6.978	6.976	6.974
	Period	2.015	2.017	2.019	2.021	2.023	2.025	2.026	2.028	2.030	2.032	2.034	2.036	2.038	2.040	2.041	2.043	2.045	2.047	2.049	2.051
	Ang. Vel.	3.118	3.115	3.112	3.109	3.106	3.103	3.101	3.098	3.095	3.092	3.089	3.086	3.083	3.081	3.078	3.075	3.072	3.069	3.067	3.064
8200	Velocity	6.972	6.970	6.968	6.966	6.964	6.961	6.959	6.957	6.955	6.953	6.951	6.949	6.947	6.945	6.943	6.940	6.938	6.936	6.934	6.932
	Period	2.053	2.055	2.056	2.058	2.060	2.062	2.064	2.066	2.068	2.070	2.072	2.073	2.075	2.077	2.079	2.081	2.083	2.085	2.087	2.088
	Ang. Vel.	3.061	3.058	3.055	3.053	3.050	3.047	3.044	3.041	3.039	3.036	3.033	3.030	3.028	3.025	3.022	3.019	3.017	3.014	3.011	3.008
8300	Velocity	6.930	6.928	6.926	6.924	6.922	6.920	6.917	6.915	6.913	6.911	6.909	6.907	6.905	6.903	6.901	6.899	6.897	6.895	6.893	6.891
	Period	2.090	2.092	2.094	2.096	2.098	2.100	2.102	2.104	2.106	2.107	2.109	2.111	2.113	2.115	2.117	2.119	2.121	2.123	2.124	2.126
	Ang. Vel.	3.004	3.003	3.000	2.998	2.995	2.992	2.990	2.987	2.984	2.981	2.979	2.976	2.973	2.971	2.968	2.965	2.963	2.960	2.958	2.955
8400	Velocity	6.889	6.887	6.884	6.882	6.880	6.878	6.876	6.874	6.872	6.870	6.868	6.866	6.864	6.862	6.860	6.858	6.856	6.854	6.852	6.850
	Period	2.128	2.130	2.132	2.134	2.136	2.138	2.140	2.142	2.143	2.145	2.147	2.149	2.151	2.153	2.155	2.157	2.159	2.161	2.163	2.164
	Ang. Vel.	2.952	2.950	2.947	2.944	2.942	2.939	2.937	2.934	2.931	2.929	2.926	2.923	2.921	2.918	2.916	2.913	2.911	2.908	2.905	2.903
8500	Velocity	6.848	6.846	6.844	6.842	6.840	6.838	6.836	6.834	6.832	6.830	6.828	6.826	6.824	6.822	6.820	6.818	6.816	6.814	6.812	6.810
	Period	2.166	2.168	2.170	2.172	2.174	2.176	2.178	2.180	2.182	2.184	2.186	2.187	2.189	2.191	2.193	2.195	2.197	2.199	2.201	2.203
	Ang. Vel.	2.900	2.898	2.895	2.893	2.890	2.888	2.885	2.882	2.880	2.877	2.875	2.872	2.870	2.867	2.865	2.862	2.860	2.857	2.855	2.852
8600	Velocity	6.808	6.806	6.804	6.802	6.800	6.798	6.796	6.794	6.792	6.790	6.788	6.786	6.784	6.782	6.780	6.779	6.777	6.775	6.773	6.771
	Period	2.205	2.207	2.209	2.211	2.212	2.214	2.216	2.218	2.220	2.222	2.224	2.226	2.228	2.230	2.232	2.234	2.236	2.237	2.239	2.241
	Ang. Vel.	2.850	2.847	2.845	2.842	2.840	2.837	2.835	2.833	2.830	2.828	2.825	2.823	2.820	2.818	2.815	2.813	2.811	2.808	2.806	2.803
8700	Velocity	6.769	6.767	6.765	6.763	6.761	6.759	6.757	6.755	6.753	6.751	6.749	6.747	6.746	6.744	6.742	6.740	6.738	6.736	6.734	6.732
	Period	2.243	2.245	2.247	2.249	2.251	2.253	2.255	2.257	2.259	2.261	2.263	2.265	2.267	2.268	2.270	2.272	2.274	2.276	2.278	2.280
	Ang. Vel.	2.801	2.798	2.796	2.794	2.791	2.789	2.786	2.784	2.782	2.779	2.777	2.775	2.772	2.770	2.767	2.765	2.763	2.760	2.758	2.756
8800	Velocity	6.730	6.728	6.726	6.724	6.723	6.721	6.719	6.717	6.715	6.713	6.711	6.709	6.707	6.705	6.704	6.702	6.700	6.698	6.696	6.694
	Period	2.282	2.284	2.286	2.288	2.290	2.292	2.294	2.296	2.298	2.300	2.302	2.304	2.305	2.307	2.309	2.311	2.313	2.315	2.317	2.319
	Ang. Vel.	2.753	2.751	2.749	2.746	2.744	2.742	2.739	2.737	2.735	2.732	2.730	2.728	2.725	2.723	2.721	2.718	2.716	2.714	2.712	2.709
8900	Velocity	6.692	6.690	6.689	6.687	6.685	6.683	6.681	6.679	6.677	6.675	6.674	6.672	6.670	6.668	6.666	6.664	6.662	6.661	6.659	6.657
	Period	2.321	2.323	2.325	2.327	2.329	2.331	2.333	2.335	2.337	2.339	2.341	2.343	2.345	2.347	2.349	2.350	2.352	2.354	2.356	2.358
	Ang. Vel.	2.707	2.705	2.702	2.700	2.698	2.696	2.693	2.691	2.689	2.687	2.684	2.682	2.680	2.678	2.675	2.673	2.671	2.669	2.666	2.664

Velocity --- Velocity in Kilometers per Second
Period --- Period in Hours
Ang. Vel. --- Angular Velocity in Radians per Hour

TABLE 9 (continued)

RADIUS KILOMETERS

		0.	1.	10.	12.	20.	25.	30.	35.	40.	45.	50.	55.	60.	65.	70.	75.	80.	85.	90.
9000	Velocity	6.655	6.653	6.651	6.649	6.648	6.646	6.644	6.642	6.640	6.638	6.637	6.635	6.633	6.631	6.629	6.627	6.626	6.624	6.622	6.620
	Period	2.360	2.362	2.364	2.366	2.368	2.370	2.372	2.374	2.376	2.378	2.380	2.382	2.384	2.386	2.388	2.390	2.392	2.394	2.396	2.398
	Ang. Vel.	2.662	2.660	2.658	2.655	2.653	2.651	2.649	2.647	2.644	2.642	2.640	2.638	2.636	2.633	2.631	2.629	2.627	2.625	2.623	2.620
9100	Velocity	6.618	6.617	6.615	6.613	6.611	6.609	6.607	6.606	6.604	6.602	6.600	6.598	6.597	6.595	6.593	6.591	6.589	6.588	6.586	6.584
	Period	2.400	2.402	2.404	2.406	2.408	2.410	2.412	2.414	2.416	2.418	2.420	2.422	2.424	2.426	2.428	2.429	2.431	2.433	2.435	2.437
	Ang. Vel.	2.618	2.616	2.614	2.612	2.610	2.607	2.605	2.603	2.601	2.599	2.597	2.595	2.593	2.590	2.588	2.586	2.584	2.582	2.580	2.578
9200	Velocity	6.582	6.580	6.579	6.577	6.575	6.573	6.572	6.570	6.568	6.566	6.564	6.563	6.561	6.559	6.557	6.556	6.554	6.552	6.550	6.549
	Period	2.439	2.441	2.443	2.445	2.447	2.449	2.451	2.453	2.455	2.457	2.459	2.461	2.463	2.465	2.467	2.469	2.471	2.473	2.475	2.477
	Ang. Vel.	2.576	2.574	2.571	2.569	2.567	2.565	2.563	2.561	2.559	2.557	2.555	2.553	2.551	2.549	2.547	2.544	2.542	2.540	2.538	2.536
9300	Velocity	6.547	6.545	6.543	6.542	6.540	6.538	6.536	6.535	6.533	6.531	6.529	6.529	6.526	6.524	6.522	6.521	6.519	6.517	6.515	6.514
	Period	2.479	2.481	2.483	2.485	2.487	2.489	2.491	2.493	2.495	2.497	2.499	2.501	2.503	2.505	2.507	2.509	2.511	2.513	2.515	2.517
	Ang. Vel.	2.534	2.532	2.530	2.528	2.526	2.524	2.522	2.520	2.518	2.516	2.514	2.512	2.510	2.508	2.506	2.504	2.502	2.500	2.498	2.496
9400	Velocity	6.512	6.510	6.508	6.507	6.505	6.503	6.502	6.500	6.498	6.496	6.495	6.493	6.491	6.489	6.488	6.486	6.484	6.483	6.481	6.479
	Period	2.519	2.521	2.523	2.525	2.527	2.529	2.531	2.533	2.536	2.538	2.540	2.542	2.544	2.546	2.548	2.550	2.552	2.554	2.556	2.558
	Ang. Vel.	2.494	2.492	2.490	2.488	2.486	2.484	2.482	2.480	2.478	2.476	2.474	2.472	2.470	2.468	2.466	2.464	2.462	2.460	2.459	2.457
9500	Velocity	6.478	6.476	6.474	6.472	6.471	6.469	6.467	6.466	6.464	6.462	6.461	6.459	6.457	6.455	6.454	6.452	6.450	6.449	6.447	6.445
	Period	2.560	2.562	2.564	2.566	2.568	2.570	2.572	2.574	2.576	2.578	2.580	2.582	2.584	2.586	2.588	2.590	2.592	2.594	2.596	2.598
	Ang. Vel.	2.455	2.453	2.451	2.449	2.447	2.445	2.443	2.441	2.439	2.437	2.435	2.433	2.432	2.430	2.428	2.426	2.424	2.422	2.420	2.418
9600	Velocity	6.444	6.442	6.440	6.439	6.437	6.435	6.434	6.432	6.430	6.429	6.427	6.425	6.424	6.422	6.420	6.419	6.417	6.415	6.414	6.412
	Period	2.600	2.602	2.604	2.606	2.608	2.610	2.612	2.614	2.617	2.619	2.621	2.623	2.625	2.627	2.629	2.631	2.633	2.635	2.637	2.639
	Ang. Vel.	2.416	2.414	2.413	2.411	2.409	2.407	2.405	2.403	2.401	2.399	2.398	2.396	2.394	2.392	2.390	2.388	2.386	2.385	2.383	2.381
9700	Velocity	6.410	6.409	6.407	6.405	6.404	6.402	6.400	6.399	6.397	6.396	6.394	6.392	6.391	6.389	6.387	6.386	6.384	6.382	6.381	6.379
	Period	2.641	2.643	2.645	2.647	2.649	2.651	2.653	2.655	2.657	2.659	2.661	2.663	2.666	2.668	2.670	2.672	2.674	2.676	2.678	2.680
	Ang. Vel.	2.379	2.377	2.375	2.374	2.372	2.370	2.368	2.366	2.364	2.363	2.361	2.359	2.357	2.355	2.354	2.352	2.350	2.348	2.346	2.345
9800	Velocity	6.378	6.376	6.374	6.373	6.371	6.369	6.368	6.366	6.365	6.363	6.361	6.360	6.358	6.357	6.355	6.353	6.352	6.350	6.349	6.347
	Period	2.682	2.684	2.686	2.688	2.690	2.692	2.694	2.696	2.698	2.700	2.702	2.705	2.707	2.709	2.711	2.713	2.715	2.717	2.719	2.721
	Ang. Vel.	2.343	2.341	2.339	2.337	2.336	2.334	2.332	2.330	2.329	2.327	2.325	2.323	2.321	2.320	2.318	2.316	2.314	2.313	2.311	2.309
9900	Velocity	6.345	6.344	6.342	6.340	6.339	6.337	6.336	6.334	6.333	6.331	6.329	6.328	6.326	6.325	6.323	6.321	6.320	6.318	6.317	6.315
	Period	2.723	2.725	2.727	2.729	2.731	2.733	2.735	2.738	2.740	2.742	2.744	2.746	2.748	2.750	2.752	2.754	2.756	2.758	2.760	2.762
	Ang. Vel.	2.307	2.306	2.304	2.302	2.300	2.299	2.297	2.295	2.293	2.292	2.290	2.288	2.287	2.285	2.283	2.281	2.280	2.278	2.276	2.275
10000	Velocity	6.313	6.312	6.310	6.309	6.307	6.306	6.304	6.302	6.301	6.299	6.298	6.296	6.295	6.293	6.292	6.290	6.288	6.287	6.285	6.284
	Period	2.764	2.767	2.769	2.771	2.773	2.775	2.777	2.779	2.781	2.783	2.785	2.787	2.789	2.791	2.794	2.796	2.798	2.800	2.802	2.804
	Ang. Vel.	2.273	2.271	2.269	2.268	2.266	2.264	2.263	2.261	2.259	2.258	2.256	2.254	2.253	2.251	2.249	2.248	2.246	2.244	2.243	2.241
10100	Velocity	6.282	6.281	6.279	6.278	6.276	6.274	6.273	6.271	6.270	6.268	6.267	6.265	6.264	6.262	6.261	6.259	6.257	6.256	6.254	6.253
	Period	2.806	2.808	2.810	2.812	2.814	2.816	2.819	2.821	2.823	2.825	2.827	2.829	2.831	2.833	2.835	2.837	2.839	2.842	2.844	2.846
	Ang. Vel.	2.239	2.238	2.236	2.234	2.233	2.231	2.229	2.228	2.226	2.224	2.223	2.221	2.219	2.218	2.216	2.214	2.213	2.211	2.210	2.208
10200	Velocity	6.251	6.250	6.248	6.247	6.245	6.244	6.242	6.241	6.239	6.238	6.236	6.235	6.233	6.231	6.230	6.228	6.227	6.225	6.224	6.222
	Period	2.848	2.850	2.852	2.854	2.856	2.858	2.860	2.862	2.865	2.867	2.869	2.871	2.873	2.875	2.877	2.879	2.881	2.883	2.886	2.888
	Ang. Vel.	2.206	2.205	2.203	2.201	2.200	2.198	2.197	2.195	2.193	2.192	2.190	2.189	2.187	2.185	2.184	2.182	2.181	2.179	2.177	2.176
10300	Velocity	6.221	6.219	6.218	6.216	6.215	6.213	6.212	6.210	6.209	6.207	6.206	6.204	6.203	6.201	6.200	6.198	6.197	6.195	6.194	6.192
	Period	2.890	2.892	2.894	2.896	2.898	2.900	2.902	2.905	2.907	2.909	2.911	2.913	2.915	2.917	2.919	2.921	2.924	2.926	2.928	2.930
	Ang. Vel.	2.174	2.173	2.171	2.170	2.168	2.166	2.165	2.163	2.162	2.160	2.159	2.157	2.155	2.154	2.152	2.151	2.149	2.148	2.146	2.145
10400	Velocity	6.191	6.189	6.188	6.186	6.185	6.183	6.182	6.180	6.179	6.178	6.176	6.175	6.173	6.172	6.170	6.169	6.167	6.166	6.164	6.163
	Period	2.932	2.934	2.936	2.938	2.940	2.943	2.945	2.947	2.949	2.951	2.953	2.955	2.957	2.959	2.962	2.964	2.966	2.968	2.970	2.972
	Ang. Vel.	2.143	2.141	2.140	2.138	2.137	2.135	2.134	2.132	2.131	2.129	2.128	2.126	2.125	2.123	2.122	2.120	2.119	2.117	2.115	2.114

		0.	1.	10.	12.	20.	25.	30.	35.	40.	45.	50.	55.	60.	65.	70.	75.	80.	85.	90.
10400	Velocity	6.161	6.160	6.158	6.157	6.155	6.154	6.153	6.151	6.150	6.148	6.147	6.145	6.144	6.142	6.141	6.139	6.138	6.137	6.135	6.134
	Period	2.974	2.976	2.979	2.981	2.983	2.985	2.987	2.989	2.991	2.993	2.996	2.998	3.000	3.002	3.004	3.006	3.008	3.011	3.013	3.015
	Ang. Vel.	2.112	2.111	2.109	2.108	2.106	2.105	2.103	2.102	2.100	2.099	2.097	2.096	2.094	2.093	2.092	2.090	2.089	2.087	2.086	2.084
10500	Velocity	6.132	6.131	6.129	6.128	6.126	6.125	6.124	6.122	6.121	6.119	6.118	6.116	6.115	6.113	6.112	6.111	6.109	6.108	6.106	6.105
	Period	3.017	3.019	3.021	3.023	3.025	3.028	3.030	3.032	3.034	3.036	3.038	3.040	3.043	3.045	3.047	3.049	3.051	3.053	3.055	3.058
	Ang. Vel.	2.083	2.081	2.080	2.078	2.077	2.075	2.074	2.072	2.071	2.069	2.068	2.067	2.065	2.064	2.062	2.061	2.059	2.058	2.056	2.055
10600	Velocity	6.103	6.102	6.101	6.099	6.098	6.096	6.095	6.094	6.092	6.091	6.089	6.088	6.086	6.085	6.084	6.082	6.081	6.079	6.078	6.077
	Period	3.060	3.062	3.064	3.066	3.068	3.070	3.073	3.075	3.077	3.079	3.081	3.083	3.086	3.088	3.090	3.092	3.094	3.096	3.098	3.101
	Ang. Vel.	2.054	2.052	2.051	2.049	2.048	2.046	2.045	2.043	2.042	2.041	2.039	2.038	2.036	2.035	2.034	2.032	2.031	2.029	2.028	2.026
10700	Velocity	6.075	6.074	6.072	6.071	6.070	6.068	6.067	6.065	6.064	6.063	6.061	6.060	6.058	6.057	6.056	6.054	6.053	6.051	6.050	6.049
	Period	3.103	3.105	3.107	3.109	3.111	3.114	3.116	3.118	3.120	3.122	3.124	3.126	3.129	3.131	3.133	3.135	3.139	3.139	3.142	3.144
	Ang. Vel.	2.025	2.024	2.022	2.021	2.019	2.018	2.017	2.015	2.014	2.012	2.011	2.010	2.008	2.007	2.006	2.004	2.003	2.001	2.000	1.999
10800	Velocity	6.047	6.046	6.044	6.043	6.042	6.040	6.039	6.038	6.036	6.035	6.033	6.032	6.031	6.029	6.028	6.027	6.025	6.024	6.022	6.021
	Period	3.146	3.148	3.150	3.152	3.155	3.157	3.159	3.161	3.163	3.165	3.168	3.170	3.172	3.174	3.176	3.178	3.181	3.183	3.185	3.187
	Ang. Vel.	1.997	1.996	1.995	1.993	1.992	1.990	1.989	1.988	1.986	1.985	1.984	1.982	1.981	1.980	1.978	1.977	1.975	1.974	1.973	1.971
10900	Velocity	6.020	6.018	6.017	6.016	6.014	6.013	6.011	6.010	6.009	6.007	6.006	6.005	6.003	6.002	6.001	5.999	5.998	5.997	5.995	5.994
	Period	3.189	3.191	3.194	3.196	3.198	3.200	3.202	3.205	3.207	3.209	3.211	3.213	3.215	3.218	3.220	3.222	3.224	3.226	3.229	3.231
	Ang. Vel.	1.970	1.969	1.967	1.966	1.965	1.963	1.962	1.961	1.959	1.958	1.957	1.955	1.954	1.953	1.951	1.950	1.949	1.947	1.946	1.945
11000	Velocity	5.993	5.991	5.990	5.988	5.987	5.986	5.984	5.983	5.982	5.980	5.979	5.978	5.976	5.975	5.974	5.972	5.971	5.970	5.968	5.967
	Period	3.233	3.235	3.237	3.239	3.242	3.244	3.246	3.248	3.250	3.253	3.255	3.257	3.259	3.261	3.264	3.266	3.268	3.270	3.272	3.274
	Ang. Vel.	1.944	1.942	1.941	1.940	1.938	1.937	1.936	1.934	1.933	1.932	1.930	1.929	1.928	1.927	1.925	1.924	1.923	1.921	1.920	1.919
11100	Velocity	5.966	5.964	5.963	5.962	5.960	5.959	5.958	5.956	5.955	5.954	5.952	5.951	5.950	5.948	5.947	5.946	5.944	5.943	5.942	5.941
	Period	3.277	3.279	3.281	3.283	3.285	3.288	3.290	3.292	3.294	3.296	3.299	3.301	3.303	3.305	3.307	3.310	3.312	3.314	3.316	3.318
	Ang. Vel.	1.918	1.916	1.915	1.914	1.912	1.911	1.910	1.909	1.907	1.906	1.905	1.904	1.902	1.901	1.900	1.898	1.897	1.896	1.895	1.893
11200	Velocity	5.939	5.938	5.937	5.935	5.934	5.933	5.931	5.930	5.929	5.927	5.926	5.925	5.924	5.922	5.921	5.920	5.918	5.917	5.916	5.914
	Period	3.321	3.323	3.325	3.327	3.329	3.332	3.334	3.336	3.338	3.341	3.343	3.345	3.347	3.349	3.352	3.354	3.356	3.358	3.360	3.362
	Ang. Vel.	1.892	1.891	1.890	1.888	1.887	1.886	1.885	1.883	1.882	1.881	1.880	1.878	1.877	1.876	1.875	1.873	1.872	1.871	1.870	1.869
11300	Velocity	5.913	5.912	5.911	5.909	5.908	5.907	5.905	5.904	5.903	5.901	5.900	5.899	5.898	5.896	5.895	5.894	5.892	5.891	5.890	5.889
	Period	3.365	3.367	3.369	3.371	3.374	3.376	3.378	3.380	3.383	3.385	3.387	3.389	3.391	3.394	3.396	3.398	3.400	3.403	3.405	3.407
	Ang. Vel.	1.867	1.866	1.865	1.864	1.862	1.861	1.860	1.859	1.858	1.856	1.855	1.854	1.853	1.851	1.850	1.849	1.848	1.847	1.845	1.844
11400	Velocity	5.887	5.886	5.885	5.884	5.882	5.881	5.880	5.878	5.877	5.876	5.875	5.873	5.872	5.871	5.870	5.868	5.867	5.866	5.864	5.863
	Period	3.409	3.411	3.414	3.416	3.418	3.420	3.423	3.425	3.427	3.429	3.431	3.434	3.436	3.438	3.440	3.443	3.445	3.447	3.449	3.452
	Ang. Vel.	1.843	1.842	1.841	1.839	1.838	1.837	1.836	1.835	1.833	1.832	1.831	1.830	1.829	1.827	1.826	1.825	1.824	1.823	1.822	1.820
11500	Velocity	5.862	5.861	5.859	5.858	5.857	5.856	5.854	5.853	5.852	5.851	5.849	5.848	5.847	5.846	5.844	5.843	5.842	5.841	5.839	5.838
	Period	3.454	3.456	3.458	3.460	3.463	3.465	3.467	3.469	3.472	3.474	3.476	3.478	3.481	3.483	3.485	3.487	3.490	3.492	3.494	3.496
	Ang. Vel.	1.819	1.818	1.817	1.816	1.815	1.813	1.812	1.811	1.810	1.809	1.808	1.806	1.805	1.804	1.803	1.802	1.801	1.799	1.798	1.797
11600	Velocity	5.837	5.836	5.834	5.833	5.832	5.831	5.829	5.828	5.827	5.826	5.824	5.823	5.822	5.821	5.819	5.818	5.817	5.816	5.815	5.813
	Period	3.499	3.501	3.503	3.505	3.508	3.510	3.512	3.514	3.516	3.519	3.521	3.523	3.525	3.528	3.530	3.532	3.534	3.537	3.539	3.541
	Ang. Vel.	1.796	1.795	1.794	1.792	1.791	1.790	1.789	1.788	1.787	1.786	1.784	1.783	1.782	1.781	1.780	1.779	1.778	1.777	1.775	1.774
11700	Velocity	5.812	5.811	5.810	5.808	5.807	5.806	5.805	5.803	5.802	5.801	5.800	5.799	5.797	5.796	5.795	5.794	5.792	5.791	5.790	5.789
	Period	3.543	3.546	3.548	3.550	3.552	3.555	3.557	3.559	3.562	3.564	3.566	3.568	3.571	3.573	3.575	3.577	3.580	3.582	3.584	3.586
	Ang. Vel.	1.773	1.772	1.771	1.770	1.769	1.768	1.766	1.765	1.764	1.763	1.762	1.761	1.760	1.759	1.758	1.756	1.755	1.754	1.753	1.752
11800	Velocity	5.788	5.786	5.785	5.784	5.783	5.781	5.780	5.779	5.778	5.777	5.775	5.774	5.773	5.772	5.771	5.769	5.768	5.767	5.766	5.765
	Period	3.589	3.591	3.593	3.595	3.598	3.600	3.602	3.604	3.607	3.609	3.611	3.614	3.616	3.618	3.620	3.623	3.625	3.627	3.629	3.632
	Ang. Vel.	1.751	1.750	1.749	1.748	1.746	1.745	1.744	1.743	1.742	1.741	1.740	1.739	1.738	1.737	1.736	1.734	1.733	1.732	1.731	1.730

Velocity --- Velocity in Kilometers per Second
Period --- Period in Hours
Ang. Vel. --- Angular Velocity in Radians per Hour

TABLE 9 (continued)

RADIUS KILOMETERS		0.	10.	20.	30.	40.	50.	60.	70.	80.	90.	100.	110.	120.	130.	140.	150.	160.	170.	180.	190.
12000	Velocity	5.763	5.761	5.759	5.756	5.754	5.751	5.749	5.747	5.744	5.742	5.740	5.737	5.735	5.732	5.730	5.728	5.725	5.723	5.721	5.718
	Period	3.634	3.638	3.643	3.648	3.652	3.657	3.661	3.666	3.670	3.675	3.679	3.684	3.689	3.693	3.698	3.702	3.707	3.711	3.716	3.721
	Ang. Vel.	41.497	41.465	41.393	41.361	41.290	41.258	41.187	41.156	41.085	41.054	40.983	40.932	40.882	40.831	40.781	40.730	40.680	40.630	40.580	40.530
12200	Velocity	5.716	5.714	5.711	5.709	5.707	5.704	5.702	5.700	5.697	5.695	5.693	5.690	5.688	5.686	5.683	5.681	5.679	5.677	5.674	5.672
	Period	3.725	3.730	3.734	3.739	3.744	3.748	3.753	3.757	3.762	3.766	3.771	3.776	3.780	3.785	3.789	3.794	3.799	3.803	3.808	3.813
	Ang. Vel.	40.480	40.431	40.381	40.331	40.282	40.233	40.183	40.134	40.085	40.036	39.988	39.939	39.890	39.842	39.793	39.745	39.697	39.649	39.601	39.553
12400	Velocity	5.670	5.667	5.665	5.663	5.661	5.658	5.656	5.654	5.651	5.649	5.647	5.645	5.642	5.640	5.638	5.636	5.633	5.631	5.629	5.627
	Period	3.817	3.822	3.826	3.831	3.836	3.840	3.845	3.850	3.854	3.859	3.863	3.868	3.873	3.877	3.882	3.887	3.891	3.896	3.901	3.905
	Ang. Vel.	39.505	39.457	39.410	39.362	39.315	39.267	39.220	39.173	39.126	39.079	39.032	38.985	38.938	38.892	38.845	38.799	38.752	38.706	38.660	38.614
12600	Velocity	5.625	5.622	5.620	5.618	5.616	5.613	5.611	5.609	5.607	5.605	5.602	5.600	5.598	5.596	5.594	5.591	5.589	5.587	5.585	5.583
	Period	3.910	3.915	3.919	3.924	3.929	3.933	3.938	3.943	3.947	3.952	3.957	3.961	3.966	3.971	3.975	3.980	3.985	3.989	3.994	3.999
	Ang. Vel.	38.568	38.522	38.476	38.431	38.385	38.340	38.294	38.249	38.204	38.158	38.113	38.068	38.024	37.979	37.934	37.889	37.845	37.800	37.756	37.712
12800	Velocity	5.580	5.578	5.576	5.574	5.572	5.570	5.567	5.565	5.563	5.561	5.559	5.557	5.554	5.552	5.550	5.548	5.546	5.544	5.542	5.539
	Period	4.003	4.008	4.013	4.017	4.022	4.027	4.032	4.036	4.041	4.046	4.050	4.055	4.060	4.064	4.069	4.074	4.079	4.083	4.088	4.093
	Ang. Vel.	37.568	37.524	37.480	37.436	37.392	37.348	37.304	37.261	37.217	37.174	37.130	37.087	37.044	37.001	36.958	36.915	36.872	36.830	36.787	36.744
13000	Velocity	5.537	5.535	5.533	5.531	5.529	5.527	5.525	5.522	5.520	5.518	5.516	5.514	5.512	5.510	5.508	5.506	5.504	5.501	5.499	5.497
	Period	4.098	4.102	4.107	4.112	4.116	4.121	4.126	4.131	4.135	4.140	4.145	4.150	4.154	4.159	4.164	4.169	4.173	4.178	4.183	4.188
	Ang. Vel.	36.802	36.759	36.717	36.675	36.633	36.590	36.548	36.506	36.465	36.423	36.381	36.340	36.299	36.257	36.215	36.174	36.133	36.091	36.050	36.009
13200	Velocity	5.495	5.493	5.491	5.489	5.487	5.485	5.483	5.481	5.479	5.477	5.474	5.472	5.470	5.468	5.466	5.464	5.462	5.460	5.458	5.456
	Period	4.192	4.197	4.202	4.207	4.212	4.216	4.221	4.226	4.231	4.235	4.240	4.245	4.250	4.255	4.259	4.264	4.269	4.274	4.279	4.284
	Ang. Vel.	35.969	35.928	35.887	35.846	35.806	35.765	35.725	35.684	35.644	35.604	35.564	35.524	35.484	35.444	35.404	35.364	35.324	35.285	35.245	35.206
13400	Velocity	5.454	5.452	5.450	5.448	5.446	5.444	5.442	5.440	5.438	5.436	5.434	5.432	5.430	5.428	5.426	5.424	5.422	5.420	5.418	5.416
	Period	4.288	4.293	4.298	4.303	4.307	4.312	4.317	4.322	4.327	4.331	4.336	4.341	4.346	4.351	4.355	4.360	4.365	4.370	4.375	4.380
	Ang. Vel.	35.166	35.127	35.088	35.048	35.009	34.970	34.931	34.892	34.854	34.815	34.776	34.738	34.699	34.661	34.622	34.584	34.546	34.508	34.469	34.431
13600	Velocity	5.414	5.412	5.410	5.408	5.406	5.404	5.402	5.400	5.398	5.396	5.394	5.392	5.390	5.388	5.386	5.384	5.382	5.380	5.378	5.376
	Period	4.384	4.389	4.394	4.399	4.404	4.409	4.414	4.418	4.423	4.428	4.433	4.438	4.443	4.447	4.452	4.457	4.462	4.467	4.472	4.477
	Ang. Vel.	34.393	34.355	34.318	34.280	34.242	34.205	34.167	34.130	34.092	34.055	34.018	33.980	33.943	33.906	33.869	33.832	33.795	33.758	33.722	33.685
13800	Velocity	5.374	5.372	5.371	5.369	5.367	5.365	5.363	5.361	5.359	5.357	5.355	5.353	5.351	5.349	5.347	5.345	5.344	5.342	5.340	5.338
	Period	4.482	4.486	4.491	4.496	4.501	4.506	4.511	4.516	4.521	4.525	4.530	4.535	4.540	4.545	4.550	4.555	4.560	4.565	4.569	4.574
	Ang. Vel.	33.648	33.612	33.575	33.539	33.503	33.466	33.430	33.394	33.358	33.322	33.286	33.250	33.214	33.178	33.143	33.107	33.072	33.036	33.001	32.965
14000	Velocity	5.336	5.334	5.332	5.330	5.328	5.326	5.324	5.323	5.321	5.319	5.317	5.315	5.313	5.311	5.309	5.308	5.306	5.304	5.302	5.300
	Period	4.579	4.584	4.589	4.594	4.599	4.604	4.609	4.614	4.619	4.624	4.628	4.633	4.638	4.643	4.648	4.653	4.658	4.663	4.668	4.673
	Ang. Vel.	32.930	32.895	32.860	32.824	32.789	32.754	32.719	32.683	32.650	32.615	32.580	32.546	32.511	32.477	32.442	32.408	32.373	32.339	32.305	32.271
14200	Velocity	5.298	5.296	5.294	5.293	5.291	5.289	5.287	5.285	5.283	5.281	5.280	5.278	5.276	5.274	5.272	5.270	5.269	5.267	5.265	5.263
	Period	4.678	4.683	4.688	4.693	4.698	4.703	4.707	4.712	4.717	4.722	4.727	4.732	4.737	4.742	4.747	4.752	4.757	4.762	4.767	4.772
	Ang. Vel.	32.237	32.203	32.169	32.135	32.101	32.067	32.033	32.000	31.966	31.933	31.899	31.866	31.832	31.799	31.766	31.733	31.699	31.666	31.633	31.600
14400	Velocity	5.261	5.259	5.258	5.256	5.254	5.252	5.250	5.249	5.247	5.245	5.243	5.241	5.239	5.238	5.236	5.234	5.232	5.230	5.229	5.227
	Period	4.777	4.782	4.787	4.792	4.797	4.802	4.807	4.812	4.817	4.822	4.827	4.832	4.837	4.842	4.847	4.852	4.857	4.862	4.867	4.872
	Ang. Vel.	31.567	31.535	31.502	31.469	31.436	31.404	31.371	31.339	31.306	31.274	31.241	31.209	31.177	31.145	31.113	31.081	31.049	31.017	30.985	30.953
14600	Velocity	5.225	5.223	5.221	5.220	5.218	5.216	5.214	5.213	5.211	5.209	5.207	5.206	5.204	5.202	5.200	5.198	5.197	5.195	5.193	5.191
	Period	4.877	4.882	4.887	4.892	4.897	4.902	4.907	4.912	4.917	4.922	4.927	4.932	4.937	4.942	4.947	4.952	4.957	4.962	4.967	4.972
	Ang. Vel.	30.921	30.889	30.858	30.826	30.794	30.763	30.731	30.700	30.669	30.637	30.606	30.575	30.544	30.513	30.482	30.451	30.420	30.389	30.358	30.327
14800	Velocity	5.190	5.188	5.186	5.184	5.183	5.181	5.179	5.177	5.176	5.174	5.172	5.170	5.169	5.167	5.165	5.164	5.162	5.160	5.158	5.157
	Period	4.977	4.981	4.987	4.993	4.998	5.003	5.008	5.013	5.018	5.023	5.028	5.033	5.038	5.043	5.048	5.053	5.058	5.063	5.068	5.074
	Ang. Vel.	30.296	30.266	30.235	30.205	30.174	30.144	30.113	30.083	30.052	30.022	29.992	29.962	29.932	29.902	29.872	29.842	29.812	29.782	29.752	29.722

RADIUS KILOMETERS		0	10.	20.	30.	40.	50.	60.	70.	80.	90.	100.	110.	120.	130.	140.	150.	160.	170.	180.	190.
15000	Velocity	5.155	5.153	5.152	5.150	5.148	5.146	5.145	5.143	5.141	5.140	5.138	5.136	5.134	5.133	5.131	5.130	5.128	5.126	5.124	5.123
	Period	5.079	5.084	5.089	5.094	5.099	5.104	5.109	5.114	5.119	5.124	5.129	5.135	5.140	5.145	5.150	5.155	5.160	5.165	5.170	5.175
	Ang. Vel.	29.692	29.663	29.633	29.604	29.574	29.545	29.515	29.486	29.457	29.427	29.398	29.369	29.340	29.311	29.282	29.253	29.224	29.195	29.166	29.137
15200	Velocity	5.121	5.119	5.118	5.116	5.114	5.113	5.111	5.109	5.107	5.106	5.104	5.102	5.101	5.099	5.097	5.096	5.094	5.093	5.091	5.089
	Period	5.181	5.186	5.191	5.196	5.201	5.206	5.211	5.216	5.221	5.227	5.232	5.237	5.242	5.247	5.252	5.257	5.263	5.268	5.273	5.278
	Ang. Vel.	29.108	29.080	29.051	29.022	28.994	28.965	28.937	28.908	28.880	28.852	28.823	28.795	28.767	28.739	28.711	28.683	28.655	28.627	28.599	28.571
15400	Velocity	5.088	5.086	5.084	5.083	5.081	5.079	5.078	5.076	5.074	5.073	5.071	5.069	5.068	5.066	5.065	5.063	5.061	5.060	5.058	5.056
	Period	5.283	5.288	5.293	5.298	5.304	5.309	5.314	5.319	5.324	5.329	5.335	5.340	5.345	5.350	5.355	5.360	5.366	5.371	5.376	5.381
	Ang. Vel.	28.543	28.515	28.488	28.460	28.432	28.405	28.377	28.350	28.322	28.295	28.267	28.240	28.213	28.186	28.159	28.131	28.104	28.077	28.050	28.023
15600	Velocity	5.055	5.053	5.052	5.050	5.048	5.047	5.045	5.044	5.042	5.040	5.039	5.037	5.036	5.034	5.032	5.031	5.029	5.028	5.026	5.024
	Period	5.386	5.392	5.397	5.402	5.407	5.412	5.417	5.423	5.428	5.433	5.438	5.443	5.449	5.454	5.459	5.464	5.469	5.475	5.480	5.485
	Ang. Vel.	27.996	27.969	27.942	27.915	27.889	27.862	27.835	27.809	27.782	27.755	27.729	27.703	27.676	27.650	27.623	27.597	27.571	27.545	27.518	27.492
15800	Velocity	5.023	5.021	5.020	5.018	5.016	5.015	5.013	5.012	5.010	5.009	5.007	5.005	5.004	5.002	5.001	4.999	4.998	4.996	4.994	4.993
	Period	5.490	5.495	5.501	5.506	5.511	5.516	5.522	5.527	5.532	5.537	5.542	5.548	5.553	5.558	5.563	5.569	5.574	5.579	5.584	5.590
	Ang. Vel.	27.466	27.440	27.414	27.388	27.362	27.336	27.310	27.285	27.259	27.233	27.207	27.182	27.156	27.131	27.105	27.080	27.054	27.029	27.003	26.978
16000	Velocity	4.991	4.990	4.988	4.987	4.985	4.983	4.982	4.980	4.979	4.977	4.976	4.974	4.973	4.971	4.970	4.968	4.966	4.965	4.963	4.962
	Period	5.595	5.600	5.605	5.611	5.616	5.621	5.626	5.632	5.637	5.642	5.647	5.653	5.658	5.663	5.668	5.674	5.679	5.684	5.690	5.695
	Ang. Vel.	26.953	26.928	26.902	26.877	26.852	26.827	26.802	26.777	26.752	26.727	26.702	26.677	26.652	26.628	26.603	26.578	26.553	26.529	26.504	26.480
16200	Velocity	4.960	4.959	4.957	4.956	4.954	4.953	4.951	4.950	4.948	4.947	4.945	4.944	4.942	4.941	4.939	4.938	4.936	4.935	4.933	4.932
	Period	5.700	5.705	5.711	5.716	5.721	5.726	5.732	5.737	5.742	5.748	5.753	5.758	5.764	5.769	5.774	5.779	5.785	5.790	5.795	5.801
	Ang. Vel.	26.455	26.431	26.406	26.382	26.358	26.333	26.309	26.285	26.260	26.236	26.212	26.188	26.164	26.140	26.116	26.092	26.068	26.044	26.020	25.997
16400	Velocity	4.930	4.929	4.927	4.926	4.924	4.923	4.921	4.920	4.918	4.917	4.915	4.914	4.912	4.911	4.909	4.908	4.906	4.905	4.903	4.902
	Period	5.806	5.811	5.817	5.822	5.827	5.833	5.838	5.843	5.848	5.854	5.859	5.864	5.870	5.875	5.880	5.886	5.891	5.896	5.902	5.907
	Ang. Vel.	25.973	25.949	25.925	25.902	25.878	25.854	25.831	25.807	25.784	25.760	25.737	25.714	25.690	25.667	25.644	25.620	25.597	25.574	25.551	25.528
16600	Velocity	4.900	4.899	4.897	4.896	4.894	4.893	4.891	4.890	4.888	4.887	4.886	4.884	4.883	4.881	4.880	4.878	4.877	4.875	4.874	4.872
	Period	5.912	5.918	5.923	5.929	5.934	5.939	5.945	5.950	5.955	5.961	5.966	5.971	5.977	5.982	5.987	5.993	5.998	6.004	6.009	6.014
	Ang. Vel.	25.505	25.482	25.459	25.436	25.413	25.390	25.367	25.344	25.321	25.299	25.276	25.253	25.231	25.208	25.185	25.163	25.140	25.118	25.095	25.073
16800	Velocity	4.871	4.870	4.868	4.867	4.865	4.864	4.862	4.861	4.859	4.858	4.857	4.855	4.854	4.852	4.851	4.849	4.848	4.847	4.845	4.844
	Period	6.020	6.025	6.030	6.036	6.041	6.047	6.052	6.057	6.063	6.068	6.073	6.079	6.084	6.090	6.095	6.100	6.106	6.111	6.117	6.122
	Ang. Vel.	25.051	25.028	25.004	24.984	24.961	24.939	24.917	24.895	24.873	24.851	24.829	24.807	24.785	24.763	24.741	24.719	24.697	24.675	24.653	24.632
17000	Velocity	4.842	4.841	4.839	4.838	4.837	4.835	4.834	4.832	4.831	4.829	4.828	4.827	4.825	4.824	4.822	4.821	4.820	4.818	4.817	4.815
	Period	6.127	6.133	6.138	6.144	6.149	6.155	6.160	6.165	6.171	6.176	6.182	6.187	6.192	6.198	6.203	6.209	6.214	6.220	6.225	6.230
	Ang. Vel.	24.610	24.588	24.567	24.545	24.523	24.502	24.480	24.459	24.437	24.416	24.394	24.373	24.352	24.330	24.309	24.288	24.267	24.245	24.224	24.203
17200	Velocity	4.814	4.813	4.811	4.810	4.808	4.807	4.806	4.804	4.803	4.801	4.800	4.799	4.797	4.796	4.795	4.793	4.792	4.790	4.789	4.788
	Period	6.236	6.241	6.247	6.252	6.258	6.263	6.269	6.274	6.279	6.285	6.290	6.296	6.301	6.307	6.312	6.318	6.323	6.329	6.334	6.340
	Ang. Vel.	24.182	24.161	24.140	24.119	24.098	24.077	24.056	24.035	24.014	23.993	23.973	23.952	23.931	23.910	23.890	23.869	23.848	23.828	23.807	23.787
17400	Velocity	4.786	4.785	4.783	4.782	4.781	4.779	4.778	4.777	4.775	4.774	4.773	4.771	4.770	4.768	4.767	4.766	4.764	4.763	4.762	4.760
	Period	6.345	6.350	6.356	6.361	6.367	6.372	6.378	6.383	6.389	6.394	6.400	6.405	6.411	6.416	6.422	6.427	6.433	6.438	6.444	6.449
	Ang. Vel.	23.766	23.746	23.725	23.705	23.684	23.664	23.644	23.623	23.603	23.583	23.563	23.543	23.522	23.502	23.482	23.462	23.442	23.422	23.402	23.382
17600	Velocity	4.759	4.758	4.756	4.755	4.754	4.752	4.751	4.750	4.748	4.747	4.746	4.744	4.743	4.741	4.740	4.739	4.737	4.736	4.735	4.733
	Period	6.455	6.460	6.466	6.471	6.477	6.482	6.488	6.493	6.499	6.504	6.510	6.515	6.521	6.526	6.532	6.537	6.543	6.548	6.554	6.560
	Ang. Vel.	23.362	23.342	23.322	23.303	23.283	23.263	23.243	23.224	23.204	23.184	23.165	23.145	23.125	23.106	23.086	23.067	23.047	23.028	23.008	22.989
17800	Velocity	4.732	4.731	4.730	4.728	4.727	4.726	4.724	4.723	4.722	4.720	4.719	4.718	4.716	4.715	4.714	4.712	4.711	4.710	4.708	4.707
	Period	6.565	6.571	6.576	6.582	6.587	6.593	6.598	6.604	6.609	6.615	6.620	6.626	6.632	6.637	6.643	6.648	6.654	6.659	6.665	6.670
	Ang. Vel.	22.970	22.950	22.931	22.912	22.892	22.873	22.854	22.835	22.816	22.796	22.777	22.758	22.739	22.720	22.701	22.682	22.663	22.644	22.626	22.607

Velocity --- Velocity in Kilometers per Second
Period --- Period in Hours
Ang. Vel. --- Angular Velocity in Radians per Day

TABLE 9 (continued)

RADIUS KILOMETERS

		0.	10.	20.	30.	40.	50.	60.	70.	80.	90.	100.	110.	120.	130.	140.	150.	160.	170.	180.	190.
18000	Velocity	4.706	4.704	4.703	4.702	4.701	4.699	4.698	4.697	4.695	4.694	4.693	4.691	4.690	4.689	4.688	4.686	4.685	4.684	4.682	4.681
	Period	6.676	6.680	6.687	6.693	6.698	6.704	6.709	6.715	6.721	6.726	6.732	6.737	6.743	6.748	6.754	6.760	6.765	6.771	6.776	6.782
	Ang. Vel.	22.588	22.569	22.550	22.531	22.513	22.494	22.475	22.457	22.438	22.419	22.401	22.382	22.364	22.345	22.327	22.308	22.290	22.272	22.253	22.235
18200	Velocity	4.680	4.679	4.677	4.676	4.675	4.673	4.672	4.671	4.670	4.668	4.667	4.666	4.665	4.663	4.662	4.661	4.659	4.658	4.657	4.656
	Period	6.708	6.793	6.799	6.804	6.810	6.816	6.821	6.827	6.832	6.838	6.844	6.849	6.855	6.860	6.866	6.872	6.877	6.883	6.889	6.894
	Ang. Vel.	22.217	22.198	22.180	22.162	22.143	22.125	22.107	22.089	22.071	22.053	22.035	22.017	21.999	21.981	21.963	21.945	21.927	21.909	21.891	21.873
18400	Velocity	4.654	4.653	4.652	4.651	4.649	4.648	4.647	4.646	4.644	4.643	4.642	4.641	4.639	4.638	4.637	4.636	4.634	4.633	4.632	4.631
	Period	6.900	6.905	6.911	6.917	6.922	6.928	6.934	6.939	6.945	6.950	6.956	6.962	6.967	6.973	6.979	6.984	6.990	6.996	7.001	7.007
	Ang. Vel.	21.855	21.837	21.820	21.802	21.784	21.767	21.749	21.731	21.714	21.696	21.678	21.661	21.643	21.626	21.608	21.591	21.573	21.556	21.538	21.521
18600	Velocity	4.629	4.628	4.627	4.626	4.624	4.623	4.622	4.621	4.619	4.618	4.617	4.616	4.614	4.613	4.612	4.611	4.609	4.608	4.607	4.606
	Period	7.013	7.018	7.024	7.030	7.035	7.041	7.047	7.052	7.058	7.064	7.069	7.075	7.081	7.086	7.092	7.098	7.103	7.109	7.115	7.120
	Ang. Vel.	21.504	21.486	21.469	21.452	21.435	21.417	21.400	21.383	21.366	21.349	21.331	21.314	21.297	21.280	21.263	21.246	21.229	21.212	21.195	21.178
18800	Velocity	4.605	4.603	4.602	4.601	4.600	4.598	4.597	4.596	4.595	4.594	4.592	4.591	4.590	4.589	4.588	4.586	4.585	4.584	4.583	4.581
	Period	7.126	7.132	7.137	7.143	7.149	7.154	7.160	7.166	7.172	7.177	7.183	7.189	7.194	7.200	7.206	7.211	7.217	7.223	7.229	7.234
	Ang. Vel.	21.162	21.145	21.128	21.111	21.094	21.077	21.061	21.044	21.027	21.010	20.994	20.977	20.961	20.944	20.927	20.911	20.894	20.878	20.861	20.845
19000	Velocity	4.580	4.579	4.578	4.577	4.575	4.574	4.573	4.572	4.571	4.569	4.568	4.567	4.566	4.565	4.564	4.562	4.561	4.560	4.559	4.558
	Period	7.240	7.246	7.251	7.257	7.263	7.269	7.274	7.280	7.286	7.291	7.297	7.303	7.309	7.314	7.320	7.326	7.332	7.337	7.343	7.349
	Ang. Vel.	20.628	20.612	20.795	20.779	20.763	20.746	20.730	20.714	20.697	20.681	20.665	20.649	20.632	20.616	20.600	20.584	20.568	20.552	20.536	20.520
19200	Velocity	4.556	4.555	4.554	4.553	4.552	4.550	4.549	4.548	4.547	4.546	4.545	4.543	4.542	4.541	4.540	4.539	4.538	4.536	4.535	4.534
	Period	7.355	7.360	7.366	7.372	7.378	7.383	7.389	7.395	7.401	7.406	7.412	7.418	7.424	7.429	7.435	7.441	7.447	7.453	7.458	7.464
	Ang. Vel.	20.504	20.488	20.472	20.456	20.440	20.424	20.408	20.392	20.376	20.360	20.345	20.329	20.313	20.297	20.281	20.266	20.250	20.234	20.219	20.203
19400	Velocity	4.533	4.532	4.530	4.529	4.528	4.527	4.526	4.525	4.524	4.522	4.521	4.520	4.519	4.518	4.517	4.515	4.514	4.513	4.512	4.511
	Period	7.470	7.476	7.481	7.487	7.493	7.499	7.505	7.510	7.516	7.522	7.528	7.533	7.539	7.545	7.551	7.557	7.562	7.568	7.574	7.580
	Ang. Vel.	20.187	20.172	20.156	20.141	20.125	20.110	20.094	20.079	20.063	20.049	20.032	20.017	20.002	19.986	19.971	19.956	19.940	19.925	19.910	19.894
19600	Velocity	4.510	4.508	4.507	4.506	4.505	4.504	4.503	4.502	4.500	4.499	4.498	4.497	4.496	4.495	4.494	4.492	4.491	4.490	4.489	4.488
	Period	7.586	7.591	7.597	7.603	7.609	7.615	7.620	7.626	7.632	7.638	7.644	7.650	7.656	7.661	7.667	7.673	7.679	7.685	7.690	7.696
	Ang. Vel.	19.879	19.864	19.849	19.834	19.819	19.803	19.788	19.773	19.758	19.743	19.728	19.713	19.698	19.683	19.668	19.653	19.638	19.623	19.608	19.594
19800	Velocity	4.487	4.486	4.485	4.483	4.482	4.481	4.480	4.479	4.478	4.477	4.476	4.474	4.473	4.472	4.471	4.470	4.469	4.468	4.467	4.465
	Period	7.702	7.708	7.714	7.720	7.725	7.731	7.737	7.743	7.749	7.755	7.760	7.766	7.772	7.778	7.784	7.790	7.796	7.801	7.807	7.813
	Ang. Vel.	19.579	19.564	19.549	19.534	19.520	19.505	19.490	19.475	19.461	19.446	19.431	19.417	19.402	19.388	19.373	19.358	19.344	19.329	19.315	19.300
20000	Velocity	4.464	4.463	4.462	4.461	4.460	4.459	4.458	4.457	4.455	4.454	4.453	4.452	4.451	4.450	4.449	4.448	4.447	4.445	4.444	4.443
	Period	7.819	7.825	7.831	7.837	7.842	7.848	7.854	7.860	7.866	7.872	7.878	7.884	7.890	7.895	7.901	7.907	7.913	7.919	7.925	7.931
	Ang. Vel.	19.286	19.271	19.257	19.243	19.228	19.214	19.199	19.185	19.171	19.156	19.142	19.128	19.114	19.099	19.085	19.071	19.057	19.043	19.028	19.014
20200	Velocity	4.442	4.441	4.440	4.439	4.438	4.437	4.436	4.434	4.433	4.432	4.431	4.430	4.429	4.428	4.427	4.426	4.425	4.424	4.422	4.421
	Period	7.937	7.942	7.948	7.954	7.960	7.966	7.972	7.978	7.984	7.990	7.996	8.002	8.007	8.013	8.019	8.025	8.031	8.037	8.043	8.049
	Ang. Vel.	19.000	18.986	18.972	18.958	18.944	18.930	18.916	18.902	18.888	18.874	18.860	18.846	18.832	18.818	18.804	18.790	18.777	18.763	18.749	18.735
20400	Velocity	4.420	4.419	4.418	4.417	4.416	4.415	4.414	4.413	4.412	4.411	4.410	4.408	4.407	4.406	4.405	4.404	4.403	4.402	4.401	4.400
	Period	8.055	8.061	8.067	8.073	8.078	8.084	8.090	8.096	8.102	8.108	8.114	8.120	8.126	8.132	8.138	8.144	8.150	8.156	8.162	8.168
	Ang. Vel.	18.721	18.708	18.694	18.680	18.666	18.653	18.639	18.625	18.612	18.598	18.585	18.571	18.557	18.544	18.530	18.517	18.503	18.490	18.476	18.463
20600	Velocity	4.399	4.398	4.397	4.396	4.395	4.393	4.392	4.391	4.390	4.389	4.388	4.387	4.386	4.385	4.384	4.383	4.382	4.381	4.380	4.379
	Period	8.174	8.179	8.185	8.191	8.197	8.203	8.209	8.215	8.221	8.227	8.233	8.239	8.245	8.251	8.257	8.263	8.269	8.275	8.281	8.287
	Ang. Vel.	18.449	18.436	18.423	18.409	18.396	18.382	18.369	18.356	18.342	18.329	18.316	18.303	18.289	18.276	18.263	18.250	18.237	18.223	18.210	18.197
20800	Velocity	4.378	4.377	4.376	4.374	4.373	4.372	4.371	4.370	4.369	4.368	4.367	4.366	4.365	4.364	4.363	4.362	4.361	4.360	4.359	4.358
	Period	8.293	8.299	8.305	8.311	8.317	8.323	8.329	8.335	8.341	8.347	8.353	8.359	8.365	8.371	8.377	8.383	8.389	8.395	8.401	8.407
	Ang. Vel.	18.184	18.171	18.158	18.145	18.132	18.119	18.106	18.093	18.080	18.067	18.054	18.041	18.028	18.015	18.002	17.989	17.976	17.963	17.950	17.938

RADIUS KILOMETERS

		0.	10.	20.	30.	40.	50.	60.	70.	80.	90.	100.	110.	120.	130.	140.	150.	160.	170.	180.	190.
21000	Velocity	4.357	4.356	4.355	4.354	4.353	4.352	4.351	4.349	4.348	4.347	4.346	4.345	4.344	4.343	4.342	4.341	4.340	4.339	4.338	4.337
	Period	8.413	8.419	8.425	8.431	8.437	8.443	8.449	8.455	8.461	8.467	8.473	8.479	8.485	8.491	8.497	8.503	8.509	8.515	8.521	8.527
	Ang. Vel.	17.925	17.912	17.899	17.886	17.874	17.861	17.848	17.836	17.823	17.810	17.798	17.785	17.772	17.760	17.747	17.734	17.722	17.709	17.697	17.684
21200	Velocity	4.336	4.335	4.334	4.333	4.332	4.331	4.330	4.329	4.328	4.327	4.326	4.325	4.324	4.323	4.322	4.321	4.320	4.319	4.318	4.317
	Period	8.533	8.539	8.545	8.551	8.557	8.563	8.569	8.575	8.581	8.588	8.594	8.600	8.606	8.612	8.618	8.624	8.630	8.636	8.642	8.648
	Ang. Vel.	17.672	17.659	17.647	17.634	17.622	17.609	17.597	17.585	17.572	17.560	17.547	17.535	17.523	17.510	17.498	17.486	17.474	17.461	17.449	17.437
21400	Velocity	4.316	4.315	4.314	4.313	4.312	4.311	4.310	4.309	4.308	4.307	4.306	4.305	4.304	4.303	4.302	4.301	4.300	4.299	4.298	4.297
	Period	8.654	8.660	8.666	8.672	8.679	8.685	8.691	8.697	8.703	8.709	8.715	8.721	8.727	8.733	8.739	8.745	8.751	8.758	8.764	8.770
	Ang. Vel.	17.425	17.412	17.400	17.388	17.376	17.364	17.352	17.339	17.327	17.315	17.303	17.291	17.279	17.267	17.255	17.243	17.231	17.219	17.207	17.195
21600	Velocity	4.296	4.295	4.294	4.293	4.292	4.291	4.290	4.289	4.288	4.287	4.286	4.285	4.284	4.283	4.282	4.281	4.280	4.279	4.278	4.277
	Period	8.776	8.782	8.788	8.794	8.800	8.806	8.812	8.819	8.825	8.831	8.837	8.843	8.849	8.855	8.861	8.867	8.874	8.880	8.886	8.892
	Ang. Vel.	17.183	17.171	17.159	17.147	17.136	17.124	17.112	17.100	17.088	17.076	17.065	17.053	17.041	17.029	17.017	17.006	16.994	16.982	16.971	16.959
21800	Velocity	4.276	4.275	4.274	4.273	4.272	4.271	4.270	4.269	4.268	4.267	4.266	4.265	4.264	4.263	4.262	4.261	4.260	4.259	4.258	4.258
	Period	8.898	8.904	8.910	8.916	8.923	8.929	8.935	8.941	8.947	8.953	8.959	8.965	8.971	8.978	8.984	8.990	8.996	9.002	9.008	9.015
	Ang. Vel.	16.947	16.936	16.924	16.912	16.901	16.889	16.878	16.866	16.854	16.843	16.831	16.820	16.808	16.797	16.785	16.774	16.762	16.751	16.739	16.728
22000	Velocity	4.257	4.256	4.255	4.254	4.253	4.252	4.251	4.250	4.249	4.248	4.247	4.246	4.245	4.244	4.243	4.242	4.241	4.240	4.239	4.238
	Period	9.021	9.027	9.033	9.039	9.045	9.052	9.058	9.064	9.070	9.076	9.082	9.088	9.095	9.101	9.107	9.113	9.119	9.125	9.132	9.138
	Ang. Vel.	16.717	16.705	16.694	16.683	16.671	16.660	16.649	16.637	16.626	16.615	16.603	16.592	16.581	16.570	16.558	16.547	16.536	16.525	16.514	16.502
22200	Velocity	4.237	4.236	4.235	4.234	4.234	4.233	4.232	4.231	4.230	4.229	4.228	4.227	4.226	4.225	4.224	4.223	4.222	4.221	4.220	4.219
	Period	9.144	9.150	9.156	9.163	9.169	9.175	9.181	9.187	9.193	9.200	9.206	9.212	9.218	9.224	9.231	9.237	9.243	9.249	9.255	9.262
	Ang. Vel.	16.491	16.480	16.469	16.458	16.447	16.436	16.425	16.414	16.403	16.391	16.380	16.369	16.358	16.347	16.336	16.326	16.315	16.304	16.293	16.282
22400	Velocity	4.218	4.217	4.216	4.216	4.215	4.214	4.213	4.212	4.211	4.210	4.209	4.208	4.207	4.206	4.205	4.204	4.203	4.202	4.202	4.201
	Period	9.268	9.274	9.280	9.286	9.293	9.299	9.305	9.311	9.318	9.324	9.330	9.336	9.342	9.349	9.355	9.361	9.367	9.374	9.380	9.386
	Ang. Vel.	16.271	16.260	16.249	16.238	16.227	16.217	16.206	16.195	16.184	16.173	16.163	16.152	16.141	16.130	16.120	16.109	16.098	16.087	16.077	16.066
22600	Velocity	4.200	4.199	4.198	4.197	4.196	4.195	4.194	4.193	4.192	4.191	4.190	4.189	4.189	4.188	4.187	4.186	4.185	4.184	4.183	4.182
	Period	9.392	9.398	9.405	9.411	9.417	9.423	9.430	9.436	9.442	9.448	9.455	9.461	9.467	9.473	9.480	9.486	9.492	9.498	9.505	9.511
	Ang. Vel.	16.055	16.045	16.034	16.023	16.013	16.002	15.992	15.981	15.971	15.960	15.949	15.939	15.928	15.918	15.907	15.897	15.886	15.876	15.865	15.855
22800	Velocity	4.181	4.180	4.179	4.178	4.178	4.177	4.176	4.175	4.174	4.173	4.172	4.171	4.170	4.169	4.168	4.168	4.167	4.166	4.165	4.164
	Period	9.517	9.523	9.530	9.536	9.542	9.549	9.555	9.561	9.567	9.574	9.580	9.586	9.592	9.599	9.605	9.611	9.618	9.624	9.630	9.636
	Ang. Vel.	15.845	15.834	15.824	15.813	15.803	15.793	15.782	15.772	15.762	15.751	15.741	15.731	15.720	15.710	15.700	15.690	15.679	15.669	15.659	15.649
23000	Velocity	4.163	4.162	4.161	4.160	4.159	4.158	4.158	4.157	4.156	4.155	4.154	4.153	4.152	4.151	4.150	4.149	4.149	4.148	4.147	4.146
	Period	9.643	9.649	9.655	9.662	9.668	9.674	9.680	9.687	9.693	9.699	9.706	9.712	9.718	9.725	9.731	9.737	9.744	9.750	9.756	9.762
	Ang. Vel.	15.638	15.628	15.618	15.608	15.598	15.588	15.577	15.567	15.557	15.547	15.537	15.527	15.517	15.507	15.497	15.487	15.477	15.467	15.457	15.447
23200	Velocity	4.145	4.144	4.143	4.142	4.141	4.141	4.140	4.139	4.138	4.137	4.136	4.135	4.134	4.133	4.133	4.132	4.131	4.130	4.129	4.128
	Period	9.769	9.775	9.781	9.788	9.794	9.800	9.807	9.813	9.819	9.826	9.832	9.838	9.845	9.851	9.857	9.864	9.870	9.876	9.883	9.889
	Ang. Vel.	15.437	15.427	15.417	15.407	15.397	15.387	15.377	15.367	15.357	15.347	15.337	15.327	15.318	15.308	15.298	15.288	15.278	15.268	15.259	15.249
23400	Velocity	4.127	4.126	4.125	4.125	4.124	4.123	4.122	4.121	4.120	4.119	4.118	4.118	4.117	4.116	4.115	4.114	4.113	4.112	4.111	4.111
	Period	9.895	9.902	9.908	9.914	9.921	9.927	9.933	9.940	9.946	9.953	9.959	9.965	9.972	9.978	9.984	9.991	9.997	10.003	10.010	10.016
	Ang. Vel.	15.239	15.229	15.220	15.210	15.200	15.190	15.181	15.171	15.161	15.152	15.142	15.132	15.123	15.113	15.103	15.094	15.084	15.075	15.065	15.055
23600	Velocity	4.110	4.109	4.108	4.107	4.106	4.105	4.105	4.104	4.103	4.102	4.101	4.100	4.099	4.098	4.098	4.097	4.096	4.095	4.094	4.093
	Period	10.022	10.029	10.035	10.042	10.048	10.054	10.061	10.067	10.073	10.080	10.086	10.093	10.099	10.105	10.112	10.118	10.125	10.131	10.137	10.144
	Ang. Vel.	15.046	15.036	15.027	15.017	15.008	14.998	14.988	14.979	14.970	14.960	14.951	14.941	14.932	14.922	14.913	14.903	14.894	14.885	14.875	14.866
23800	Velocity	4.092	4.092	4.091	4.090	4.089	4.088	4.087	4.086	4.086	4.085	4.084	4.083	4.082	4.081	4.080	4.080	4.079	4.078	4.077	4.076
	Period	10.150	10.157	10.163	10.169	10.176	10.182	10.189	10.195	10.201	10.208	10.214	10.221	10.227	10.233	10.240	10.246	10.253	10.259	10.266	10.272
	Ang. Vel.	14.857	14.847	14.838	14.829	14.819	14.810	14.801	14.791	14.782	14.773	14.763	14.754	14.745	14.736	14.726	14.717	14.708	14.699	14.690	14.680

Velocity --- Velocity in Kilometers per Second
Period --- Period in Hours
Ang. Vel. --- Angular Velocity in Radians per Day

TABLE 9 (continued)

RADIUS KILOMETERS

		0.	10.	20.	30.	40.	50.	60.	70.	80.	90.	100.	110.	120.	130.	140.	150.	160.	170.	180.	190.
24000	Velocity	4.075	4.074	4.074	4.073	4.072	4.071	4.070	4.069	4.069	4.068	4.067	4.066	4.065	4.064	4.064	4.063	4.062	4.061	4.060	4.059
	Period	10.278	10.285	10.291	10.298	10.304	10.311	10.317	10.323	10.330	10.336	10.343	10.349	10.356	10.362	10.368	10.375	10.381	10.388	10.394	10.401
	Ang. Vel.	14.671	14.662	14.653	14.644	14.635	14.626	14.616	14.607	14.598	14.589	14.580	14.571	14.562	14.553	14.544	14.535	14.526	14.517	14.508	14.499
24200	Velocity	4.058	4.058	4.057	4.056	4.055	4.054	4.053	4.053	4.052	4.051	4.050	4.049	4.048	4.048	4.047	4.046	4.045	4.044	4.043	4.043
	Period	10.407	10.414	10.420	10.426	10.433	10.439	10.446	10.452	10.459	10.465	10.472	10.478	10.485	10.491	10.498	10.504	10.511	10.517	10.523	10.530
	Ang. Vel.	14.490	14.481	14.472	14.463	14.454	14.445	14.436	14.427	14.418	14.409	14.400	14.391	14.383	14.374	14.365	14.356	14.347	14.338	14.330	14.321
24400	Velocity	4.042	4.041	4.040	4.039	4.038	4.038	4.037	4.036	4.035	4.034	4.034	4.033	4.032	4.031	4.030	4.029	4.029	4.028	4.027	4.026
	Period	10.536	10.543	10.549	10.556	10.562	10.569	10.575	10.582	10.588	10.595	10.601	10.608	10.614	10.621	10.627	10.634	10.640	10.647	10.653	10.660
	Ang. Vel.	14.312	14.303	14.294	14.286	14.277	14.268	14.259	14.251	14.242	14.233	14.224	14.216	14.207	14.198	14.190	14.181	14.172	14.164	14.155	14.146
24600	Velocity	4.025	4.025	4.024	4.023	4.022	4.021	4.020	4.020	4.019	4.018	4.017	4.016	4.016	4.015	4.014	4.013	4.012	4.011	4.011	4.010
	Period	10.666	10.673	10.679	10.686	10.692	10.699	10.705	10.712	10.718	10.725	10.731	10.738	10.744	10.751	10.757	10.764	10.770	10.777	10.783	10.790
	Ang. Vel.	14.138	14.129	14.121	14.112	14.103	14.095	14.086	14.078	14.069	14.061	14.052	14.043	14.035	14.026	14.018	14.009	14.001	13.992	13.984	13.975
24800	Velocity	4.009	4.008	4.007	4.007	4.006	4.005	4.004	4.003	4.003	4.002	4.001	4.000	3.999	3.999	3.998	3.997	3.996	3.995	3.995	3.994
	Period	10.797	10.803	10.810	10.816	10.823	10.829	10.836	10.842	10.849	10.855	10.862	10.868	10.875	10.882	10.888	10.895	10.901	10.908	10.914	10.921
	Ang. Vel.	13.967	13.959	13.950	13.942	13.933	13.925	13.917	13.908	13.900	13.891	13.883	13.875	13.866	13.858	13.850	13.841	13.833	13.825	13.816	13.808
25000	Velocity	3.993	3.992	3.991	3.991	3.990	3.989	3.988	3.987	3.987	3.986	3.985	3.984	3.983	3.983	3.982	3.981	3.980	3.979	3.979	3.978
	Period	10.927	10.934	10.941	10.947	10.954	10.960	10.967	10.973	10.980	10.986	10.993	11.000	11.006	11.013	11.019	11.026	11.032	11.039	11.046	11.052
	Ang. Vel.	13.800	13.792	13.783	13.775	13.767	13.759	13.750	13.742	13.734	13.726	13.717	13.709	13.701	13.693	13.685	13.677	13.668	13.660	13.652	13.644
25200	Velocity	3.977	3.976	3.976	3.975	3.974	3.973	3.972	3.972	3.971	3.970	3.969	3.968	3.968	3.967	3.966	3.965	3.965	3.964	3.963	3.962
	Period	11.059	11.065	11.072	11.079	11.085	11.092	11.098	11.105	11.112	11.118	11.125	11.131	11.138	11.144	11.151	11.158	11.164	11.171	11.178	11.184
	Ang. Vel.	13.636	13.628	13.620	13.612	13.603	13.595	13.587	13.579	13.571	13.563	13.555	13.547	13.539	13.531	13.523	13.515	13.507	13.499	13.491	13.483
25400	Velocity	3.961	3.961	3.960	3.959	3.958	3.958	3.957	3.956	3.955	3.954	3.954	3.953	3.952	3.951	3.951	3.950	3.949	3.948	3.947	3.947
	Period	11.191	11.197	11.204	11.211	11.217	11.224	11.230	11.237	11.244	11.250	11.257	11.264	11.270	11.277	11.283	11.290	11.297	11.303	11.310	11.317
	Ang. Vel.	13.475	13.467	13.459	13.451	13.443	13.435	13.428	13.420	13.412	13.404	13.396	13.388	13.380	13.372	13.364	13.357	13.349	13.341	13.333	13.325
25600	Velocity	3.946	3.945	3.944	3.944	3.943	3.942	3.941	3.941	3.940	3.939	3.938	3.937	3.937	3.936	3.935	3.934	3.933	3.933	3.932	3.931
	Period	11.323	11.330	11.336	11.343	11.350	11.356	11.363	11.370	11.376	11.383	11.390	11.396	11.403	11.410	11.416	11.423	11.429	11.436	11.443	11.449
	Ang. Vel.	13.318	13.310	13.302	13.294	13.286	13.279	13.271	13.263	13.255	13.248	13.240	13.232	13.224	13.217	13.209	13.201	13.194	13.186	13.178	13.171
25800	Velocity	3.931	3.930	3.929	3.928	3.928	3.927	3.926	3.925	3.925	3.924	3.923	3.922	3.921	3.921	3.920	3.919	3.918	3.918	3.917	3.916
	Period	11.496	11.503	11.509	11.516	11.523	11.529	11.536	11.543	11.549	11.556	11.562	11.569	11.576	11.582	11.589	11.595	11.602	11.609	11.615	11.622
	Ang. Vel.	13.163	13.155	13.148	13.140	13.132	13.125	13.117	13.110	13.102	13.094	13.087	13.079	13.072	13.064	13.057	13.049	13.041	13.034	13.026	13.019
26000	Velocity	3.915	3.915	3.914	3.913	3.912	3.912	3.911	3.910	3.909	3.909	3.908	3.907	3.906	3.906	3.905	3.904	3.903	3.903	3.902	3.901
	Period	11.590	11.596	11.603	11.610	11.616	11.623	11.630	11.636	11.643	11.650	11.657	11.663	11.670	11.677	11.683	11.690	11.697	11.703	11.710	11.717
	Ang. Vel.	13.011	13.004	12.996	12.989	12.981	12.974	12.966	12.959	12.952	12.944	12.937	12.929	12.922	12.914	12.907	12.900	12.892	12.885	12.877	12.870
26200	Velocity	3.900	3.900	3.899	3.898	3.898	3.897	3.896	3.895	3.895	3.894	3.893	3.892	3.892	3.891	3.890	3.889	3.889	3.888	3.887	3.886
	Period	11.724	11.730	11.737	11.744	11.750	11.757	11.764	11.771	11.777	11.784	11.791	11.797	11.804	11.811	11.818	11.824	11.831	11.838	11.845	11.851
	Ang. Vel.	12.863	12.855	12.848	12.841	12.833	12.826	12.819	12.811	12.804	12.797	12.789	12.782	12.775	12.768	12.760	12.753	12.746	12.738	12.731	12.724
26400	Velocity	3.886	3.885	3.884	3.883	3.883	3.882	3.881	3.881	3.880	3.879	3.878	3.878	3.877	3.876	3.875	3.875	3.874	3.873	3.873	3.872
	Period	11.858	11.865	11.872	11.878	11.885	11.892	11.899	11.905	11.912	11.919	11.925	11.932	11.939	11.946	11.953	11.959	11.966	11.973	11.980	11.986
	Ang. Vel.	12.717	12.710	12.702	12.695	12.688	12.681	12.674	12.666	12.659	12.652	12.645	12.638	12.631	12.623	12.616	12.609	12.602	12.595	12.588	12.581
26600	Velocity	3.871	3.870	3.870	3.869	3.868	3.867	3.867	3.866	3.865	3.865	3.864	3.863	3.862	3.862	3.861	3.860	3.859	3.859	3.858	3.857
	Period	11.993	12.000	12.007	12.013	12.020	12.027	12.034	12.040	12.047	12.054	12.061	12.068	12.074	12.081	12.088	12.095	12.101	12.108	12.115	12.122
	Ang. Vel.	12.574	12.567	12.559	12.552	12.545	12.538	12.531	12.524	12.517	12.510	12.503	12.496	12.489	12.482	12.475	12.468	12.461	12.454	12.447	12.440
26800	Velocity	3.857	3.856	3.855	3.854	3.854	3.853	3.852	3.852	3.851	3.850	3.849	3.848	3.848	3.847	3.847	3.846	3.845	3.844	3.844	3.843
	Period	12.129	12.135	12.142	12.149	12.155	12.162	12.169	12.176	12.183	12.190	12.197	12.203	12.210	12.217	12.224	12.231	12.237	12.244	12.251	12.258
	Ang. Vel.	12.432	12.426	12.419	12.412	12.405	12.398	12.392	12.385	12.378	12.371	12.364	12.357	12.350	12.343	12.336	12.329	12.323	12.316	12.309	12.302

RADIUS KILOMETERS

		0.	10.	20.	30.	40.	50.	60.	70.	80.	90.	100.	110.	120.	130.	140.	150.	160.	170.	180.	190.
27000	Velocity	3.842	3.842	3.841	3.840	3.839	3.838	3.837	3.837	3.836	3.835	3.834	3.834	3.833	3.832	3.832	3.831	3.830	3.830	3.829	
	Period	12.265	12.271	12.278	12.284	12.291	12.297	12.304	12.310	12.317	12.324	12.330	12.337	12.343	12.350	12.356	12.363	12.369	12.376	12.382	12.389
	Ang. Vel.	12.295	12.288	12.282	12.275	12.268	12.261	12.254	12.248	12.241	12.234	12.227	12.221	12.214	12.207	12.200	12.194	12.187	12.180	12.173	12.167
27200	Velocity	3.828	3.827	3.827	3.826	3.825	3.825	3.824	3.823	3.823	3.822	3.821	3.820	3.820	3.819	3.818	3.818	3.817	3.816	3.816	3.815
	Period	12.401	12.408	12.414	12.421	12.428	12.434	12.441	12.447	12.454	12.461	12.467	12.474	12.481	12.487	12.494	12.500	12.507	12.513	12.520	12.527
	Ang. Vel.	12.160	12.153	12.147	12.140	12.133	12.126	12.120	12.113	12.106	12.100	12.093	12.087	12.080	12.073	12.067	12.060	12.053	12.047	12.040	12.034
27400	Velocity	3.814	3.813	3.813	3.812	3.811	3.811	3.810	3.809	3.809	3.808	3.807	3.806	3.806	3.805	3.804	3.804	3.803	3.802	3.802	3.801
	Period	12.538	12.545	12.552	12.559	12.566	12.572	12.579	12.586	12.593	12.600	12.607	12.614	12.621	12.627	12.634	12.641	12.648	12.655	12.662	12.669
	Ang. Vel.	12.027	12.020	12.014	12.007	12.001	11.994	11.988	11.981	11.975	11.968	11.961	11.955	11.948	11.942	11.935	11.929	11.922	11.916	11.909	11.903
27600	Velocity	3.800	3.800	3.799	3.798	3.798	3.797	3.796	3.795	3.795	3.794	3.793	3.793	3.792	3.791	3.791	3.790	3.789	3.789	3.788	3.787
	Period	12.676	12.683	12.689	12.696	12.703	12.710	12.717	12.724	12.731	12.738	12.745	12.752	12.759	12.765	12.772	12.779	12.786	12.793	12.800	12.807
	Ang. Vel.	11.897	11.890	11.884	11.877	11.871	11.864	11.858	11.851	11.845	11.839	11.832	11.826	11.819	11.813	11.807	11.800	11.794	11.787	11.781	11.775
27800	Velocity	3.787	3.786	3.785	3.785	3.784	3.783	3.783	3.782	3.781	3.780	3.780	3.779	3.778	3.778	3.777	3.776	3.776	3.775	3.774	3.774
	Period	12.814	12.821	12.828	12.834	12.841	12.848	12.855	12.862	12.869	12.876	12.883	12.890	12.897	12.904	12.911	12.918	12.924	12.931	12.938	12.945
	Ang. Vel.	11.768	11.762	11.756	11.749	11.743	11.737	11.730	11.724	11.718	11.711	11.705	11.699	11.693	11.686	11.680	11.674	11.667	11.661	11.655	11.649
28000	Velocity	3.773	3.772	3.772	3.771	3.770	3.770	3.769	3.768	3.768	3.767	3.766	3.766	3.765	3.764	3.764	3.763	3.762	3.762	3.761	3.760
	Period	12.952	12.959	12.966	12.973	12.980	12.987	12.994	13.001	13.008	13.015	13.022	13.029	13.036	13.043	13.049	13.056	13.063	13.070	13.077	13.084
	Ang. Vel.	11.643	11.636	11.630	11.624	11.618	11.611	11.605	11.599	11.593	11.587	11.580	11.574	11.568	11.562	11.556	11.550	11.543	11.537	11.531	11.525
28200	Velocity	3.760	3.759	3.758	3.758	3.757	3.756	3.756	3.755	3.754	3.754	3.753	3.752	3.752	3.751	3.750	3.750	3.749	3.748	3.748	3.747
	Period	13.091	13.098	13.105	13.112	13.119	13.126	13.133	13.140	13.147	13.154	13.161	13.168	13.175	13.182	13.189	13.196	13.203	13.210	13.217	13.224
	Ang. Vel.	11.519	11.513	11.507	11.501	11.494	11.488	11.482	11.476	11.470	11.464	11.458	11.452	11.446	11.440	11.434	11.428	11.422	11.415	11.409	11.403
28400	Velocity	3.746	3.746	3.745	3.744	3.744	3.743	3.742	3.742	3.741	3.740	3.740	3.739	3.738	3.738	3.737	3.737	3.736	3.735	3.735	3.734
	Period	13.231	13.238	13.245	13.252	13.259	13.266	13.273	13.280	13.287	13.294	13.301	13.308	13.315	13.322	13.329	13.336	13.343	13.350	13.357	13.364
	Ang. Vel.	11.397	11.391	11.385	11.379	11.373	11.367	11.361	11.355	11.349	11.343	11.337	11.332	11.326	11.320	11.314	11.308	11.302	11.296	11.290	11.284
28600	Velocity	3.733	3.733	3.732	3.731	3.731	3.730	3.729	3.729	3.728	3.727	3.727	3.726	3.726	3.725	3.724	3.723	3.723	3.722	3.722	3.721
	Period	13.371	13.378	13.385	13.392	13.399	13.406	13.413	13.420	13.427	13.434	13.441	13.448	13.455	13.462	13.469	13.476	13.483	13.490	13.497	13.504
	Ang. Vel.	11.278	11.272	11.266	11.260	11.254	11.249	11.243	11.237	11.231	11.225	11.219	11.213	11.207	11.202	11.196	11.190	11.184	11.178	11.172	11.167
28800	Velocity	3.720	3.720	3.719	3.718	3.718	3.717	3.716	3.716	3.715	3.714	3.714	3.713	3.713	3.712	3.711	3.711	3.710	3.709	3.709	3.708
	Period	13.511	13.518	13.525	13.532	13.539	13.546	13.554	13.561	13.568	13.575	13.582	13.589	13.596	13.603	13.610	13.617	13.624	13.631	13.638	13.645
	Ang. Vel.	11.161	11.155	11.149	11.143	11.138	11.132	11.126	11.120	11.114	11.109	11.103	11.097	11.091	11.086	11.080	11.074	11.068	11.063	11.057	11.051
29000	Velocity	3.707	3.707	3.706	3.705	3.705	3.704	3.704	3.703	3.702	3.702	3.701	3.700	3.700	3.699	3.698	3.698	3.697	3.697	3.696	3.695
	Period	13.652	13.659	13.666	13.673	13.681	13.688	13.695	13.702	13.709	13.716	13.723	13.730	13.737	13.744	13.751	13.758	13.765	13.772	13.780	13.787
	Ang. Vel.	11.046	11.040	11.034	11.028	11.022	11.017	11.011	11.006	11.000	10.994	10.989	10.983	10.977	10.972	10.966	10.960	10.955	10.949	10.943	10.938
29200	Velocity	3.695	3.694	3.693	3.693	3.692	3.692	3.691	3.690	3.690	3.689	3.688	3.688	3.687	3.686	3.686	3.685	3.685	3.684	3.683	3.683
	Period	13.794	13.801	13.808	13.815	13.822	13.829	13.836	13.843	13.850	13.858	13.865	13.872	13.879	13.886	13.893	13.900	13.907	13.914	13.921	13.929
	Ang. Vel.	10.932	10.927	10.921	10.915	10.910	10.904	10.898	10.893	10.887	10.882	10.876	10.871	10.865	10.860	10.854	10.849	10.843	10.837	10.832	10.826
29400	Velocity	3.682	3.681	3.681	3.680	3.680	3.679	3.678	3.678	3.677	3.676	3.676	3.675	3.675	3.674	3.673	3.673	3.672	3.672	3.671	3.670
	Period	13.936	13.943	13.950	13.957	13.964	13.971	13.978	13.985	13.993	14.000	14.007	14.014	14.021	14.028	14.035	14.042	14.050	14.057	14.064	14.071
	Ang. Vel.	10.821	10.815	10.810	10.804	10.799	10.793	10.788	10.782	10.777	10.771	10.766	10.760	10.755	10.749	10.744	10.739	10.733	10.728	10.722	10.717
29600	Velocity	3.670	3.669	3.668	3.668	3.667	3.667	3.666	3.665	3.665	3.664	3.663	3.663	3.662	3.662	3.661	3.660	3.660	3.659	3.659	3.658
	Period	14.078	14.085	14.092	14.100	14.107	14.114	14.121	14.128	14.135	14.142	14.150	14.157	14.164	14.171	14.178	14.185	14.192	14.200	14.207	14.214
	Ang. Vel.	10.711	10.706	10.701	10.695	10.690	10.684	10.679	10.674	10.668	10.663	10.657	10.652	10.647	10.641	10.636	10.630	10.625	10.620	10.614	10.609
29800	Velocity	3.657	3.657	3.656	3.655	3.655	3.654	3.654	3.653	3.652	3.652	3.651	3.651	3.650	3.649	3.649	3.648	3.648	3.647	3.646	3.646
	Period	14.221	14.228	14.235	14.243	14.250	14.257	14.264	14.271	14.278	14.286	14.293	14.300	14.307	14.314	14.321	14.329	14.336	14.343	14.350	14.357
	Ang. Vel.	10.604	10.598	10.593	10.588	10.582	10.577	10.572	10.566	10.561	10.556	10.551	10.545	10.540	10.535	10.529	10.524	10.519	10.514	10.508	10.503

Velocity --- Velocity in Kilometers per Second
Period --- Period in Hours
Ang. Vel. --- Angular Velocity in Radians per Day

TABLE 9 (continued)

RADIUS KILOMETERS		0.	20.	40.	60.	80.	100.	120.	140.	160.	180.	200.	220.	240.	260.	280.	300.	320.	340.
50000	Velocity	3.648	3.642	3.639	3.636	3.633	3.630	3.627	3.624	3.621	3.618	3.615	3.612	3.609	3.606	3.603	3.600	3.597	3.595
	Period	14.364	14.400	14.436	14.472	14.508	14.544	14.580	14.617	14.653	14.689	14.725	14.761	14.798	14.834	14.870	14.906	14.943	14.979
	Ang. Vel.	10.498	10.472	10.446	10.420	10.394	10.368	10.342	10.317	10.291	10.266	10.241	10.216	10.191	10.166	10.141	10.116	10.092	10.067
49000	Velocity	3.586	3.583	3.580	3.577	3.574	3.571	3.569	3.566	3.563	3.560	3.557	3.554	3.552	3.549	3.546	3.543	3.540	3.538
	Period	15.089	15.125	15.162	15.198	15.235	15.272	15.308	15.345	15.382	15.418	15.455	15.492	15.529	15.566	15.603	15.640	15.676	15.713
	Ang. Vel.	9.994	9.970	9.946	9.922	9.898	9.874	9.851	9.827	9.804	9.780	9.757	9.734	9.711	9.688	9.665	9.642	9.619	9.597
48000	Velocity	3.529	3.527	3.524	3.521	3.518	3.516	3.513	3.510	3.507	3.505	3.502	3.499	3.497	3.494	3.491	3.489	3.486	3.483
	Period	15.825	15.862	15.899	15.936	15.973	16.010	16.048	16.085	16.122	16.160	16.197	16.234	16.272	16.309	16.347	16.384	16.422	16.459
	Ang. Vel.	9.529	9.507	9.485	9.463	9.441	9.419	9.397	9.375	9.353	9.332	9.310	9.289	9.267	9.246	9.225	9.204	9.183	9.162
47000	Velocity	3.475	3.473	3.470	3.468	3.465	3.462	3.460	3.457	3.455	3.452	3.449	3.447	3.444	3.442	3.439	3.437	3.434	3.432
	Period	16.572	16.610	16.648	16.685	16.723	16.761	16.799	16.836	16.874	16.912	16.950	16.988	17.026	17.064	17.102	17.140	17.178	17.217
	Ang. Vel.	9.099	9.079	9.058	9.038	9.017	8.997	8.977	8.957	8.936	8.916	8.896	8.877	8.857	8.837	8.817	8.798	8.778	8.759
46000	Velocity	3.424	3.421	3.419	3.416	3.414	3.411	3.409	3.406	3.404	3.402	3.399	3.397	3.394	3.392	3.389	3.387	3.384	3.382
	Period	17.331	17.369	17.408	17.446	17.484	17.522	17.561	17.599	17.638	17.676	17.715	17.753	17.792	17.830	17.869	17.908	17.946	17.985
	Ang. Vel.	8.701	8.682	8.663	8.644	8.625	8.606	8.587	8.568	8.550	8.531	8.512	8.494	8.476	8.457	8.439	8.421	8.403	8.385
45000	Velocity	3.375	3.372	3.370	3.367	3.365	3.363	3.360	3.358	3.356	3.353	3.351	3.348	3.346	3.344	3.341	3.339	3.337	3.334
	Period	18.101	18.140	18.179	18.218	18.257	18.296	18.335	18.373	18.412	18.452	18.491	18.530	18.569	18.608	18.647	18.686	18.725	18.765
	Ang. Vel.	8.331	8.313	8.295	8.277	8.260	8.242	8.225	8.207	8.190	8.173	8.155	8.138	8.121	8.104	8.087	8.070	8.053	8.036
44000	Velocity	3.328	3.325	3.323	3.321	3.318	3.316	3.314	3.311	3.309	3.307	3.305	3.302	3.300	3.298	3.296	3.293	3.291	3.289
	Period	18.883	18.922	18.961	19.001	19.040	19.080	19.119	19.159	19.198	19.238	19.277	19.317	19.357	19.396	19.436	19.476	19.515	19.555
	Ang. Vel.	7.986	7.969	7.953	7.936	7.920	7.904	7.887	7.871	7.855	7.839	7.822	7.806	7.790	7.774	7.759	7.743	7.727	7.711
43000	Velocity	3.282	3.280	3.278	3.276	3.273	3.271	3.269	3.267	3.265	3.262	3.260	3.258	3.256	3.254	3.252	3.249	3.247	3.245
	Period	19.675	19.715	19.755	19.795	19.835	19.875	19.915	19.955	19.995	20.035	20.075	20.115	20.155	20.196	20.236	20.276	20.316	20.357
	Ang. Vel.	7.644	7.629	7.613	7.598	7.583	7.567	7.552	7.537	7.522	7.507	7.492	7.477	7.462	7.447	7.432	7.417	7.402	7.388
42000	Velocity	3.239	3.237	3.235	3.232	3.230	3.228	3.226	3.224	3.222	3.220	3.218	3.216	3.213	3.211	3.209	3.207	3.205	3.203
	Period	20.478	20.518	20.559	20.599	20.640	20.680	20.721	20.761	20.802	20.843	20.883	20.924	20.965	21.005	21.046	21.087	21.128	21.169
	Ang. Vel.	7.364	7.349	7.335	7.321	7.306	7.292	7.278	7.263	7.249	7.235	7.221	7.207	7.193	7.179	7.165	7.151	7.137	7.124
41000	Velocity	3.197	3.195	3.193	3.191	3.189	3.187	3.185	3.183	3.181	3.179	3.177	3.175	3.173	3.171	3.169	3.167	3.165	3.163
	Period	21.291	21.332	21.373	21.414	21.455	21.496	21.538	21.579	21.620	21.661	21.702	21.743	21.785	21.826	21.867	21.909	21.950	21.991
	Ang. Vel.	7.082	7.069	7.055	7.042	7.028	7.015	7.002	6.988	6.975	6.962	6.948	6.935	6.922	6.909	6.896	6.883	6.870	6.857
40000	Velocity	3.157	3.155	3.153	3.151	3.149	3.147	3.145	3.143	3.141	3.139	3.137	3.135	3.133	3.131	3.129	3.128	3.126	3.124
	Period	22.116	22.157	22.199	22.240	22.282	22.323	22.365	22.406	22.448	22.490	22.532	22.573	22.615	22.657	22.699	22.740	22.782	22.824
	Ang. Vel.	6.819	6.806	6.793	6.780	6.768	6.755	6.743	6.730	6.718	6.705	6.693	6.680	6.668	6.656	6.643	6.631	6.619	6.607
39000	Velocity	3.118	3.116	3.114	3.112	3.110	3.108	3.107	3.105	3.103	3.101	3.099	3.097	3.095	3.094	3.092	3.090	3.088	3.086
	Period	22.950	22.992	23.034	23.076	23.118	23.160	23.202	23.245	23.287	23.329	23.371	23.413	23.456	23.498	23.540	23.583	23.625	23.667
	Ang. Vel.	6.571	6.559	6.547	6.535	6.523	6.511	6.499	6.487	6.476	6.464	6.452	6.441	6.429	6.417	6.406	6.394	6.383	6.371
38000	Velocity	3.081	3.079	3.077	3.075	3.073	3.072	3.070	3.068	3.066	3.064	3.062	3.061	3.059	3.057	3.055	3.054	3.052	3.050
	Period	23.795	23.837	23.880	23.922	23.965	24.008	24.050	24.093	24.136	24.178	24.221	24.264	24.306	24.349	24.392	24.435	24.478	24.521
	Ang. Vel.	6.327	6.316	6.305	6.294	6.282	6.271	6.260	6.249	6.238	6.227	6.216	6.205	6.194	6.183	6.172	6.161	6.150	6.139
37000	Velocity	3.045	3.043	3.041	3.039	3.038	3.036	3.034	3.032	3.031	3.029	3.027	3.025	3.024	3.022	3.020	3.018	3.017	3.015
	Period	24.650	24.693	24.736	24.779	24.822	24.865	24.908	24.951	24.994	25.038	25.081	25.124	25.167	25.211	25.254	25.297	25.341	25.384
	Ang. Vel.	6.118	6.107	6.096	6.086	6.075	6.065	6.054	6.044	6.033	6.023	6.012	6.002	5.992	5.981	5.971	5.961	5.951	5.941
36000	Velocity	3.010	3.008	3.006	3.005	3.003	3.001	3.000	2.998	2.996	2.995	2.993	2.991	2.990	2.988	2.986	2.985	2.983	2.981
	Period	25.514	25.558	25.602	25.645	25.689	25.732	25.776	25.820	25.863	25.907	25.951	25.994	26.038	26.082	26.126	26.170	26.213	26.257
	Ang. Vel.	5.910	5.900	5.890	5.880	5.870	5.860	5.850	5.840	5.831	5.821	5.811	5.801	5.791	5.782	5.772	5.762	5.753	5.743

RADIUS KILOMETERS		0.	20.	40.	60.	80.	100.	120.	140.	160.	180.	200.	220.	240.	260.	280.	300.	320.	340.
35000	Velocity	2.976	2.973	2.973	2.971	2.970	2.968	2.966	2.965	2.963	2.961	2.960	2.958	2.957	2.955	2.953	2.952	2.950	2.948
	Period	26.389	26.433	26.477	26.521	26.565	26.609	26.654	26.698	26.742	26.786	26.830	26.874	26.919	26.963	27.007	27.052	27.096	27.140
	Ang. Vel.	5.714	5.705	5.695	5.686	5.676	5.667	5.658	5.649	5.639	5.630	5.620	5.611	5.602	5.593	5.584	5.574	5.565	5.556
34000	Velocity	2.944	2.942	2.940	2.939	2.937	2.936	2.934	2.933	2.931	2.929	2.928	2.926	2.925	2.923	2.922	2.920	2.918	2.917
	Period	27.274	27.318	27.363	27.407	27.452	27.496	27.541	27.586	27.630	27.675	27.720	27.764	27.809	27.854	27.899	27.943	27.988	28.033
	Ang. Vel.	5.529	5.520	5.511	5.502	5.493	5.484	5.475	5.466	5.458	5.449	5.440	5.431	5.423	5.414	5.405	5.396	5.388	5.379
33000	Velocity	2.912	2.911	2.909	2.908	2.906	2.904	2.903	2.901	2.900	2.898	2.897	2.895	2.894	2.892	2.891	2.889	2.888	2.886
	Period	28.168	28.213	28.258	28.303	28.348	28.393	28.438	28.483	28.528	28.573	28.619	28.664	28.709	28.754	28.800	28.845	28.890	28.935
	Ang. Vel.	5.383	5.375	5.366	5.358	5.349	5.341	5.332	5.324	5.316	5.307	5.299	5.291	5.283	5.274	5.266	5.258	5.250	5.241
32000	Velocity	2.882	2.880	2.879	2.877	2.876	2.874	2.873	2.871	2.870	2.868	2.867	2.865	2.864	2.862	2.861	2.859	2.858	2.857
	Period	29.072	29.117	29.163	29.208	29.254	29.299	29.345	29.390	29.436	29.481	29.527	29.573	29.618	29.664	29.710	29.756	29.801	29.847
	Ang. Vel.	5.187	5.179	5.171	5.163	5.155	5.147	5.139	5.131	5.123	5.115	5.107	5.099	5.091	5.083	5.076	5.068	5.060	5.052
31000	Velocity	2.852	2.851	2.849	2.848	2.846	2.845	2.843	2.842	2.841	2.839	2.838	2.836	2.835	2.833	2.832	2.831	2.829	2.828
	Period	29.985	30.031	30.077	30.123	30.169	30.215	30.261	30.307	30.353	30.399	30.445	30.491	30.537	30.583	30.630	30.676	30.722	30.768
	Ang. Vel.	5.029	5.021	5.014	5.006	4.998	4.991	4.983	4.976	4.968	4.961	4.953	4.946	4.938	4.931	4.923	4.916	4.908	4.901
30000	Velocity	2.823	2.822	2.821	2.819	2.818	2.816	2.815	2.814	2.812	2.811	2.809	2.808	2.807	2.805	2.804	2.803	2.801	2.800
	Period	30.907	30.954	31.000	31.047	31.093	31.140	31.186	31.233	31.279	31.326	31.372	31.419	31.465	31.512	31.559	31.605	31.652	31.699
	Ang. Vel.	4.879	4.872	4.864	4.857	4.850	4.843	4.835	4.828	4.821	4.814	4.807	4.800	4.792	4.785	4.778	4.771	4.764	4.757
29000	Velocity	2.796	2.794	2.793	2.792	2.790	2.789	2.787	2.786	2.785	2.783	2.782	2.781	2.779	2.778	2.777	2.775	2.774	2.773
	Period	31.839	31.886	31.933	31.980	32.027	32.074	32.121	32.168	32.215	32.262	32.309	32.356	32.403	32.450	32.497	32.544	32.591	32.639
	Ang. Vel.	4.736	4.729	4.722	4.715	4.708	4.702	4.695	4.688	4.681	4.674	4.667	4.661	4.654	4.647	4.640	4.634	4.627	4.620
28000	Velocity	2.768	2.767	2.766	2.765	2.763	2.762	2.761	2.759	2.758	2.757	2.755	2.754	2.753	2.752	2.750	2.749	2.748	2.746
	Period	32.780	32.828	32.875	32.922	32.970	33.017	33.064	33.112	33.159	33.207	33.254	33.302	33.349	33.397	33.444	33.492	33.540	33.587
	Ang. Vel.	4.600	4.594	4.587	4.580	4.574	4.567	4.561	4.554	4.548	4.541	4.535	4.528	4.522	4.515	4.509	4.502	4.496	4.490
27000	Velocity	2.742	2.741	2.740	2.739	2.737	2.736	2.735	2.733	2.732	2.731	2.730	2.728	2.727	2.726	2.724	2.723	2.722	2.721
	Period	33.730	33.778	33.826	33.874	33.922	33.969	34.017	34.065	34.113	34.161	34.209	34.257	34.305	34.353	34.401	34.449	34.497	34.545
	Ang. Vel.	4.477	4.464	4.458	4.452	4.445	4.439	4.433	4.427	4.421	4.414	4.408	4.402	4.396	4.390	4.384	4.377	4.371	4.365
26000	Velocity	2.717	2.716	2.714	2.713	2.712	2.711	2.709	2.708	2.707	2.706	2.704	2.703	2.702	2.701	2.699	2.698	2.697	2.696
	Period	34.690	34.738	34.786	34.834	34.882	34.931	34.979	35.027	35.076	35.124	35.172	35.221	35.269	35.318	35.366	35.415	35.463	35.512
	Ang. Vel.	4.347	4.341	4.335	4.329	4.323	4.317	4.311	4.305	4.299	4.293	4.287	4.281	4.276	4.270	4.264	4.258	4.252	4.246
25000	Velocity	2.692	2.691	2.690	2.688	2.687	2.686	2.685	2.684	2.682	2.681	2.680	2.679	2.678	2.676	2.675	2.674	2.673	2.672
	Period	35.658	35.706	35.755	35.804	35.852	35.901	35.950	35.998	36.047	36.096	36.145	36.194	36.243	36.292	36.340	36.389	36.438	36.487
	Ang. Vel.	4.229	4.223	4.218	4.212	4.206	4.200	4.195	4.189	4.183	4.178	4.172	4.166	4.161	4.155	4.150	4.144	4.138	4.133
24000	Velocity	2.668	2.667	2.666	2.664	2.663	2.662	2.661	2.660	2.658	2.657	2.656	2.655	2.654	2.653	2.651	2.650	2.649	2.648
	Period	36.634	36.684	36.733	36.782	36.831	36.880	36.929	36.978	37.028	37.077	37.126	37.175	37.225	37.274	37.323	37.373	37.422	37.472
	Ang. Vel.	4.116	4.111	4.105	4.100	4.094	4.089	4.083	4.078	4.073	4.067	4.062	4.056	4.051	4.046	4.040	4.035	4.030	4.024
23000	Velocity	2.644	2.643	2.642	2.641	2.640	2.639	2.637	2.636	2.635	2.634	2.633	2.632	2.631	2.629	2.628	2.627	2.626	2.625
	Period	37.620	37.670	37.719	37.769	37.818	37.868	37.917	37.967	38.017	38.066	38.116	38.166	38.216	38.265	38.315	38.365	38.415	38.465
	Ang. Vel.	4.008	4.003	3.998	3.993	3.987	3.982	3.977	3.972	3.967	3.961	3.956	3.951	3.946	3.941	3.936	3.931	3.925	3.920
22000	Velocity	2.622	2.620	2.619	2.618	2.617	2.616	2.615	2.614	2.613	2.611	2.610	2.609	2.608	2.607	2.606	2.605	2.604	2.603
	Period	38.614	38.664	38.714	38.764	38.814	38.864	38.914	38.964	39.015	39.065	39.115	39.165	39.215	39.265	39.316	39.366	39.416	39.466
	Ang. Vel.	3.908	3.900	3.895	3.890	3.885	3.880	3.875	3.870	3.865	3.860	3.855	3.850	3.845	3.840	3.836	3.831	3.826	3.821
21000	Velocity	2.599	2.598	2.597	2.596	2.595	2.594	2.593	2.592	2.590	2.589	2.588	2.587	2.586	2.585	2.584	2.583	2.582	2.581
	Period	39.617	39.668	39.718	39.769	39.819	39.869	39.920	39.970	40.021	40.071	40.122	40.173	40.223	40.274	40.325	40.375	40.426	40.477
	Ang. Vel.	3.804	3.801	3.797	3.792	3.787	3.782	3.777	3.773	3.768	3.763	3.758	3.754	3.749	3.744	3.740	3.735	3.730	3.726

Velocity --- Velocity in Kilometers per Second
Period --- Period in Hours
Ang. Vel. --- Angular Velocity in Radians per Day

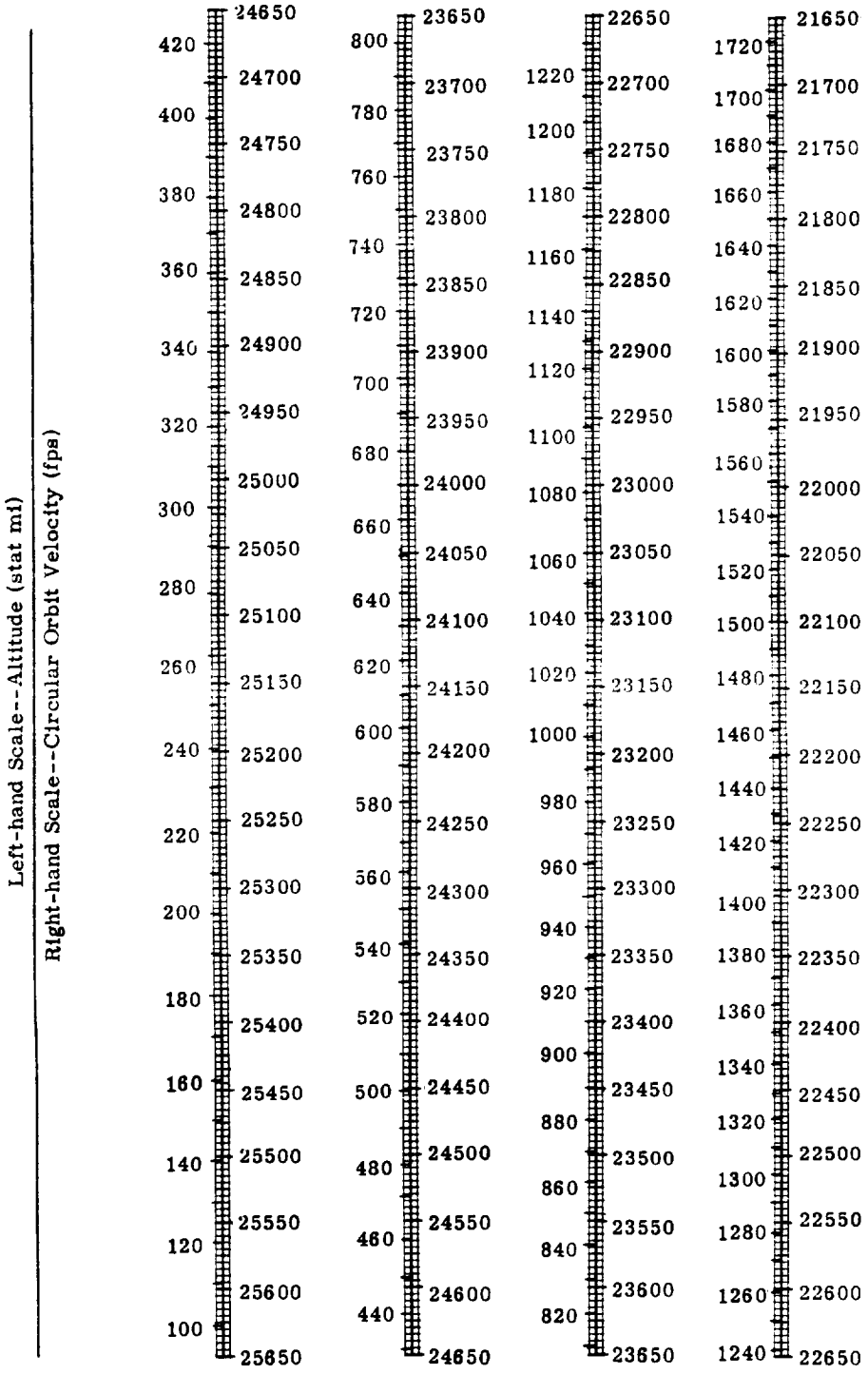

Fig. 8. Velocity of a Satellite in a Circular Orbit as a Function of Altitude (English Unit - see Table 9 for Metric Data)

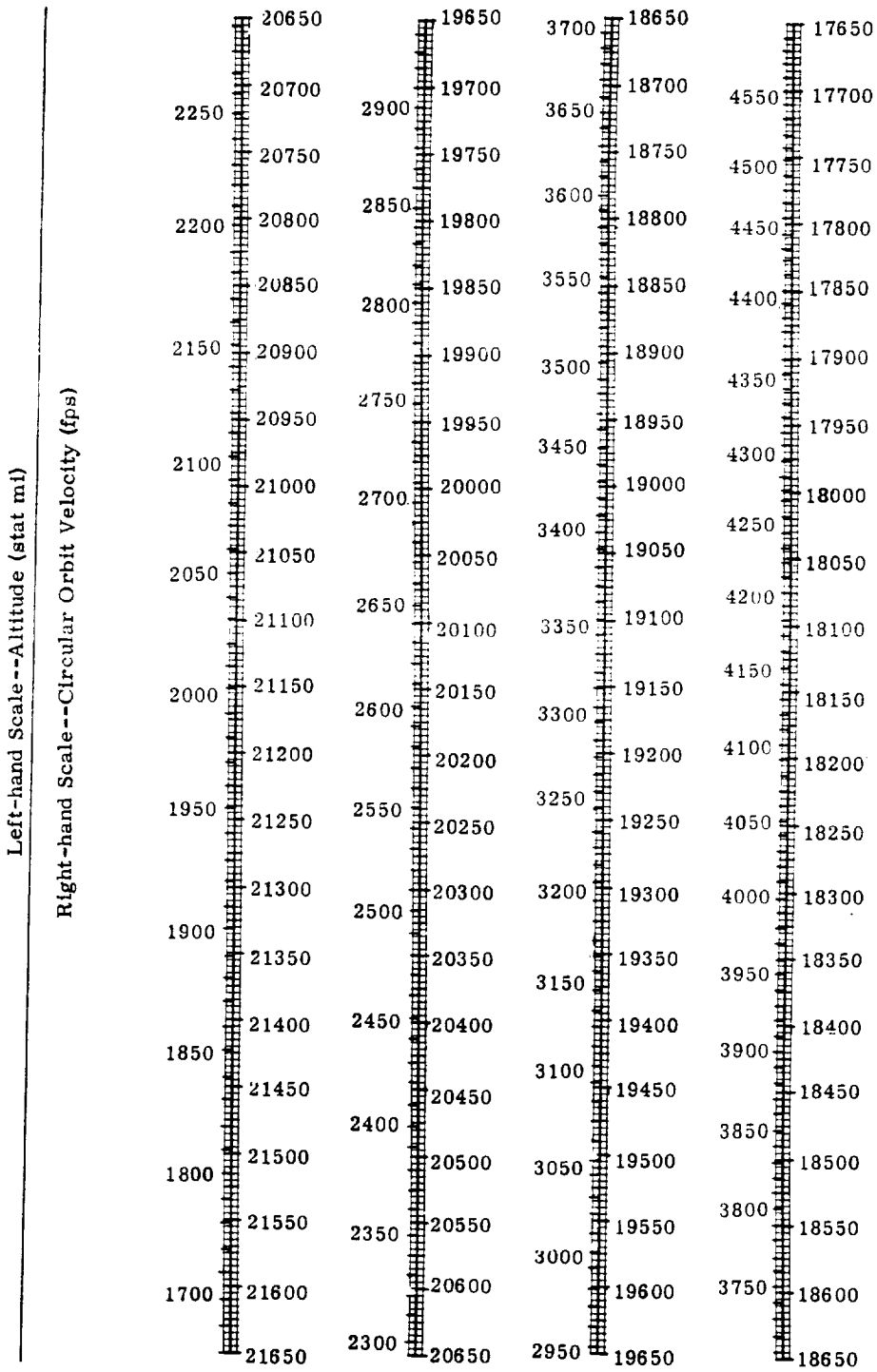

Fig. 8. (continued)

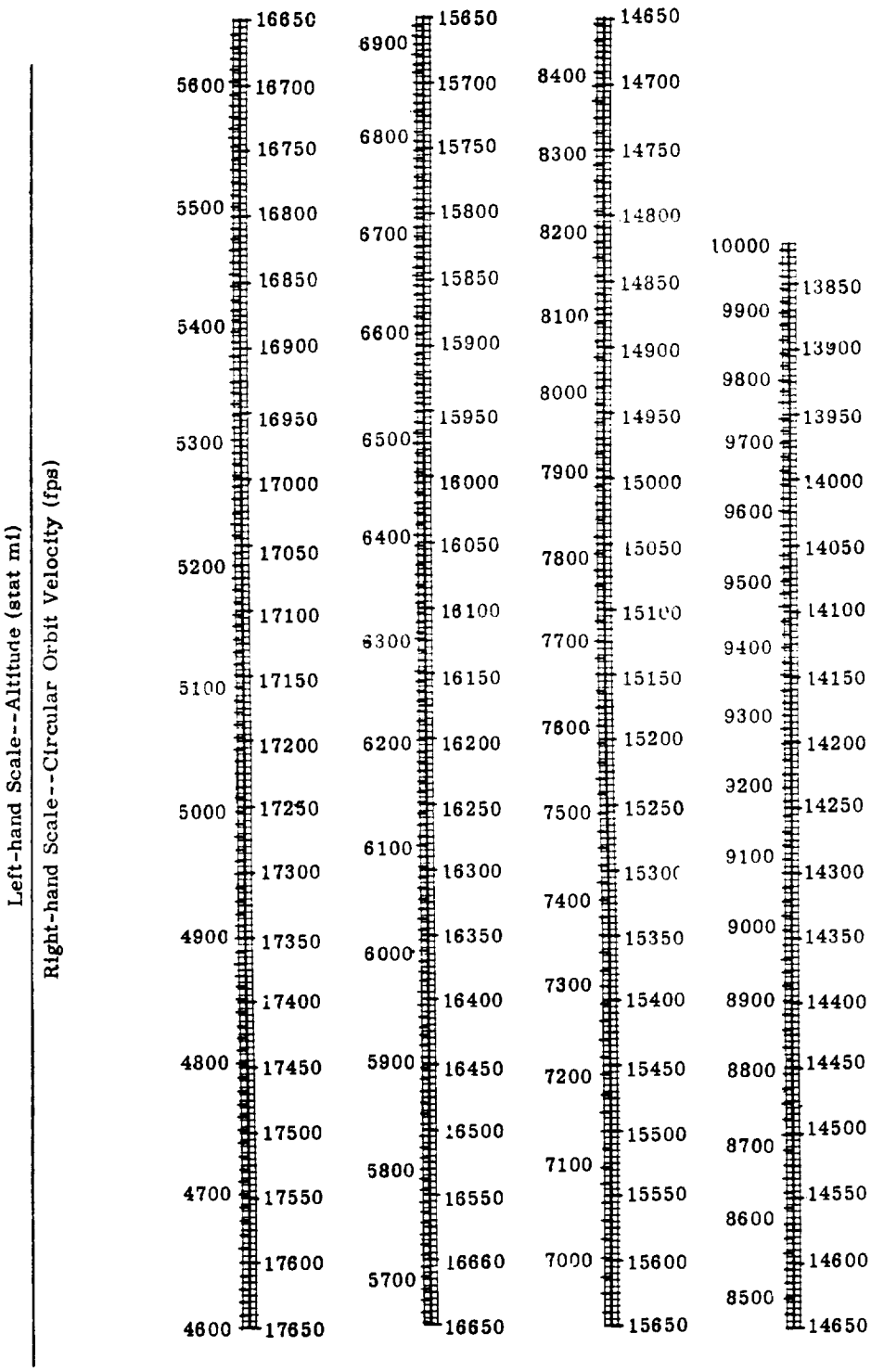

Fig. 8. (continued)

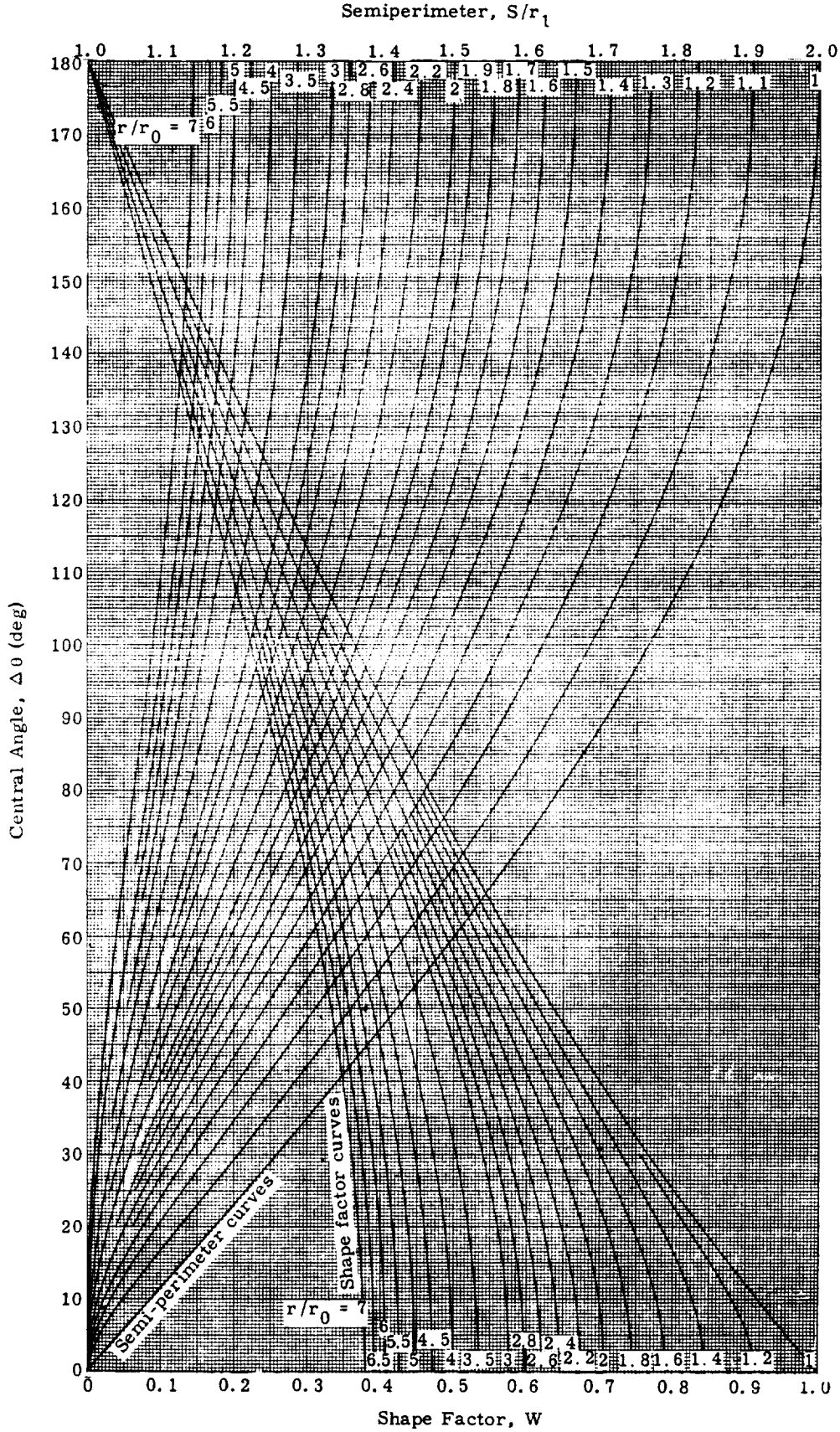

Fig. 9. Parameters of Lambert's Theorem

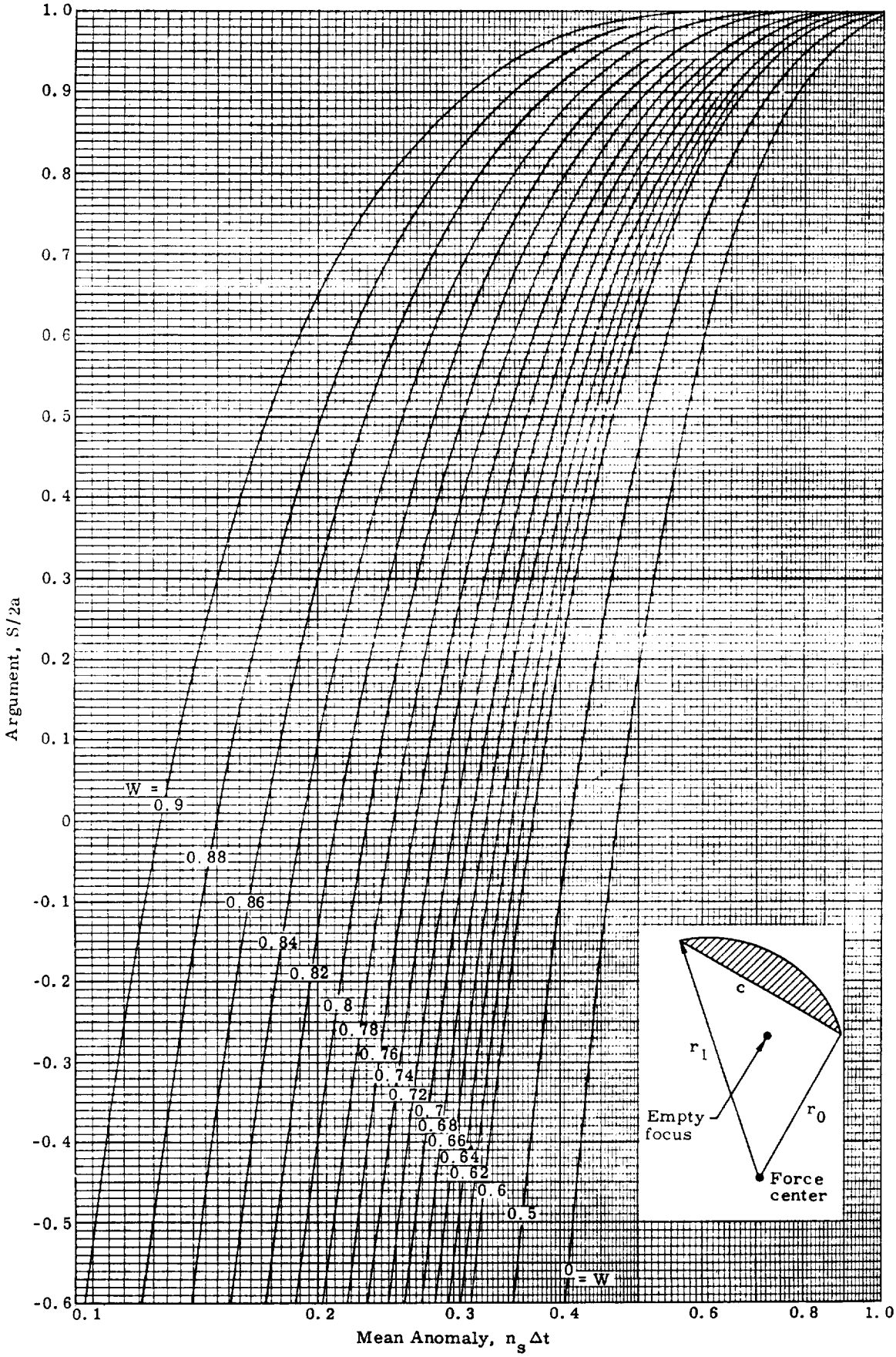

Fig. 10a. Lambert's Theorem (case 1)

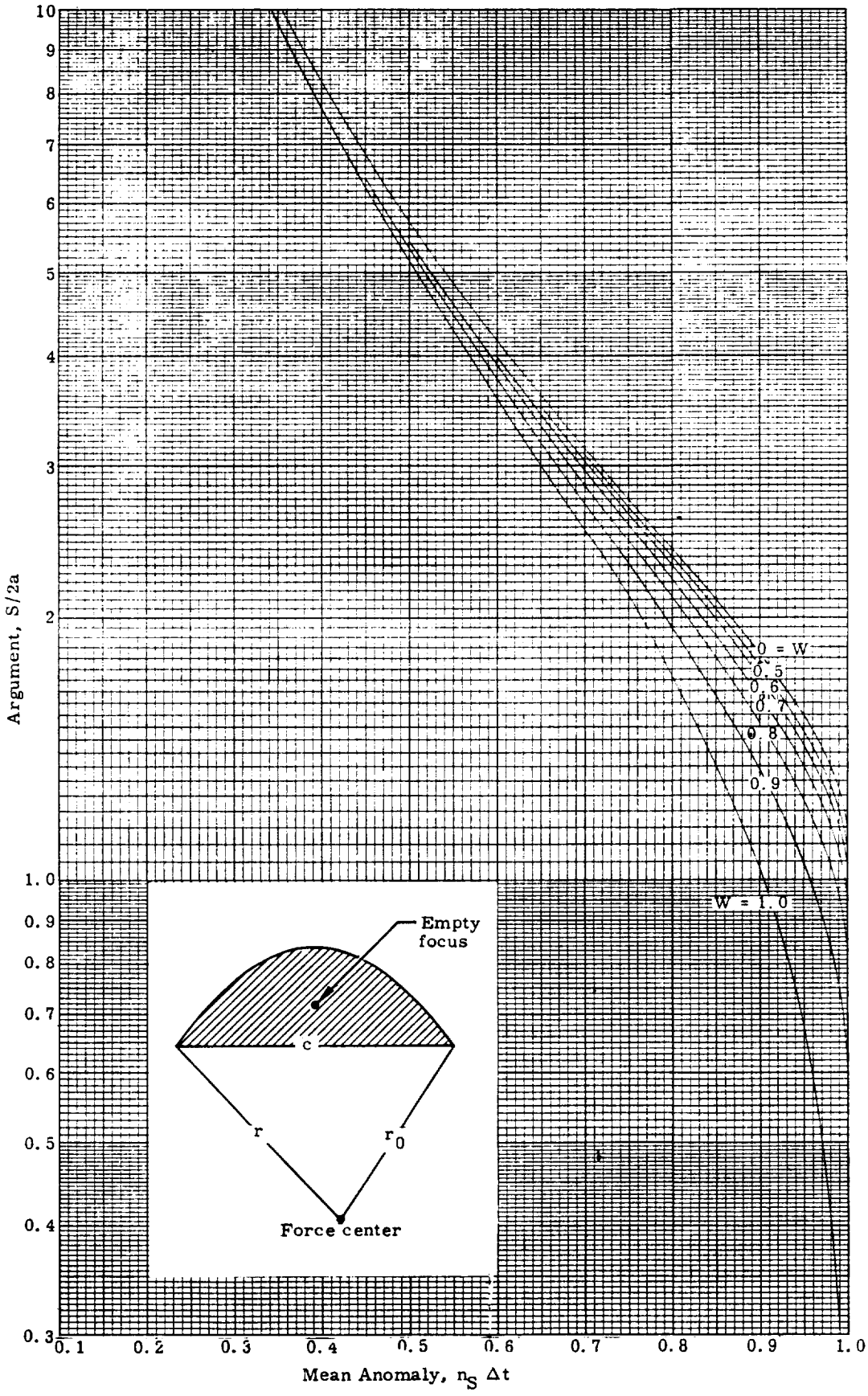

Fig. 10b. Lambert's Theorem (case 2)

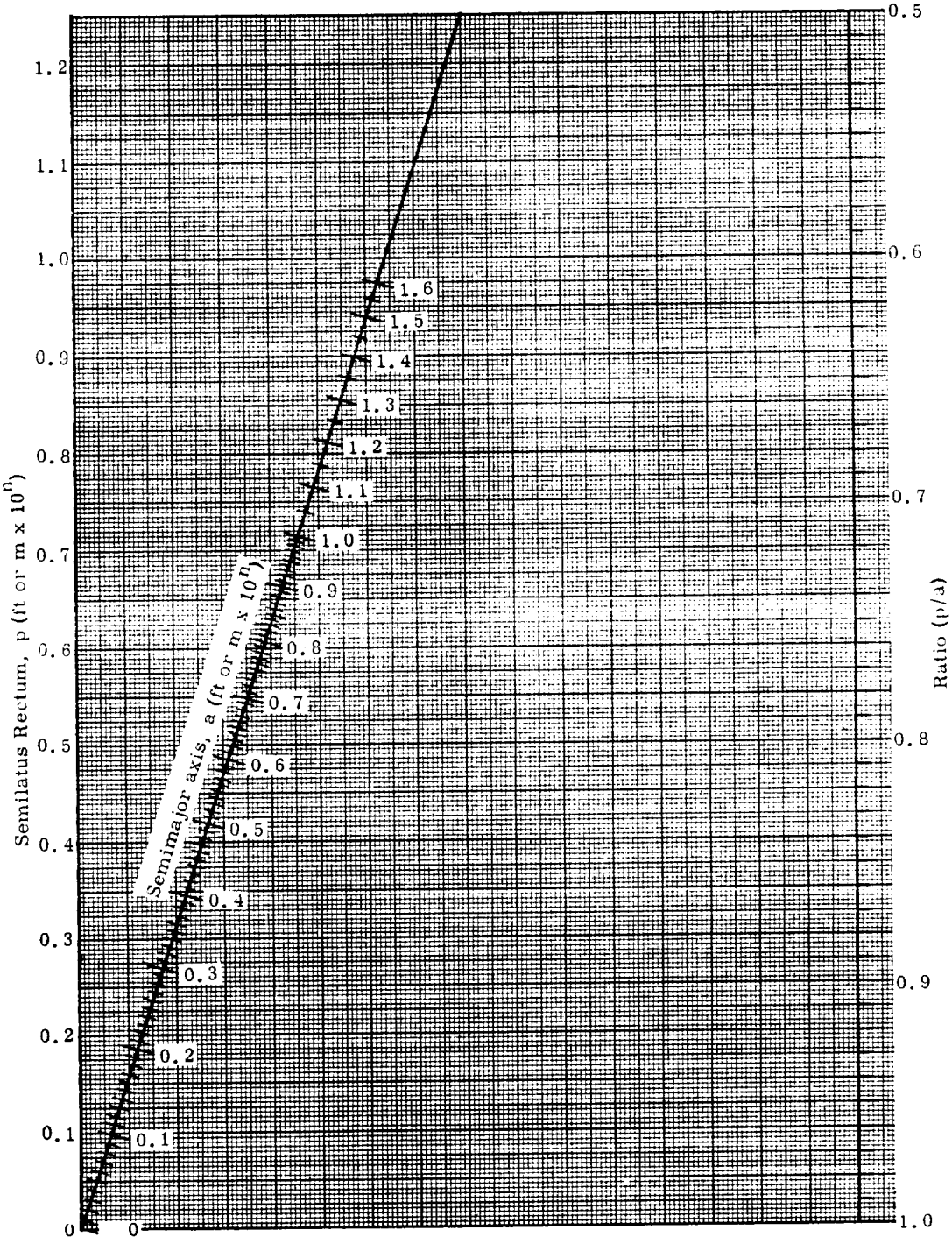

Fig. 11a. Solution for Eccentricity

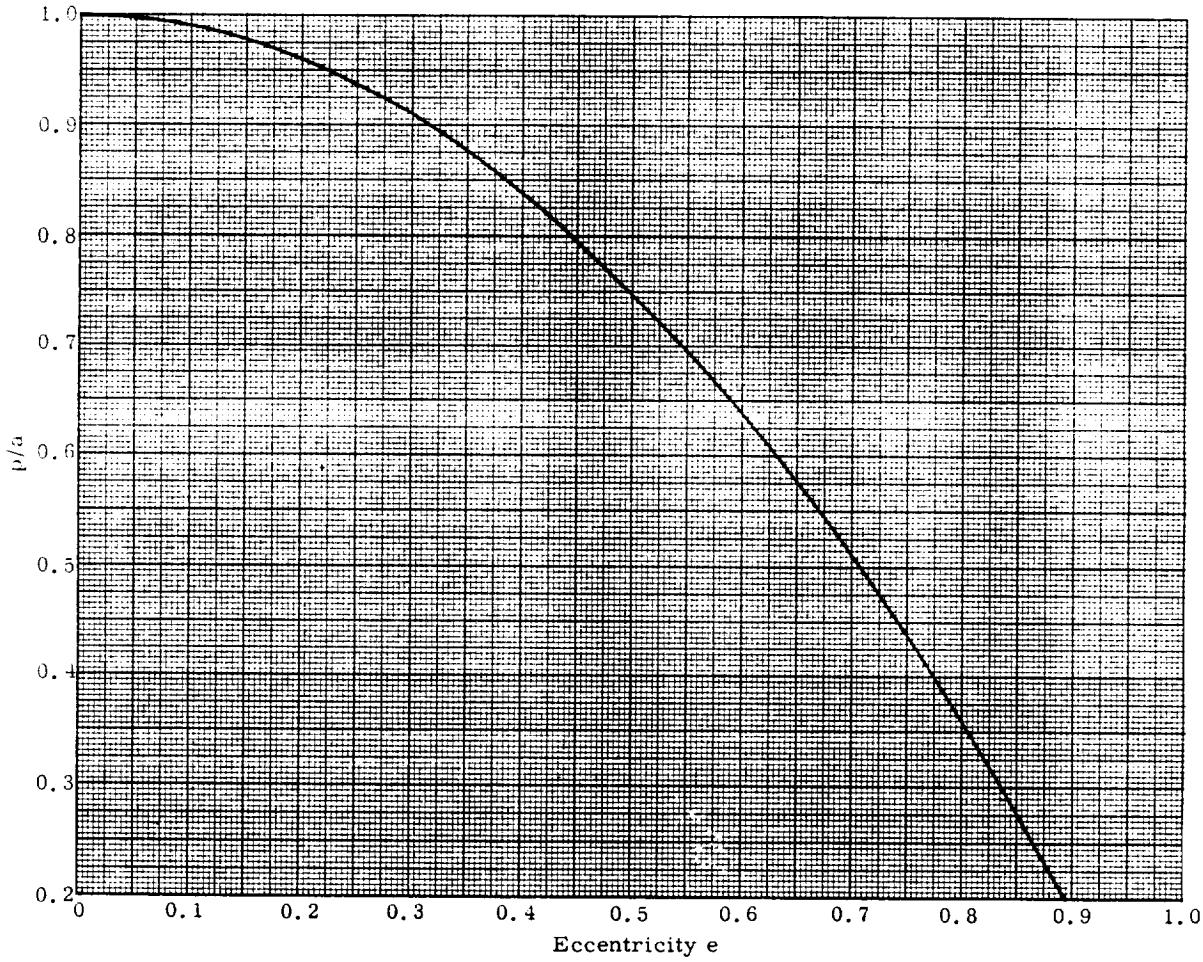

Fig. 11b. Solution for Eccentricity

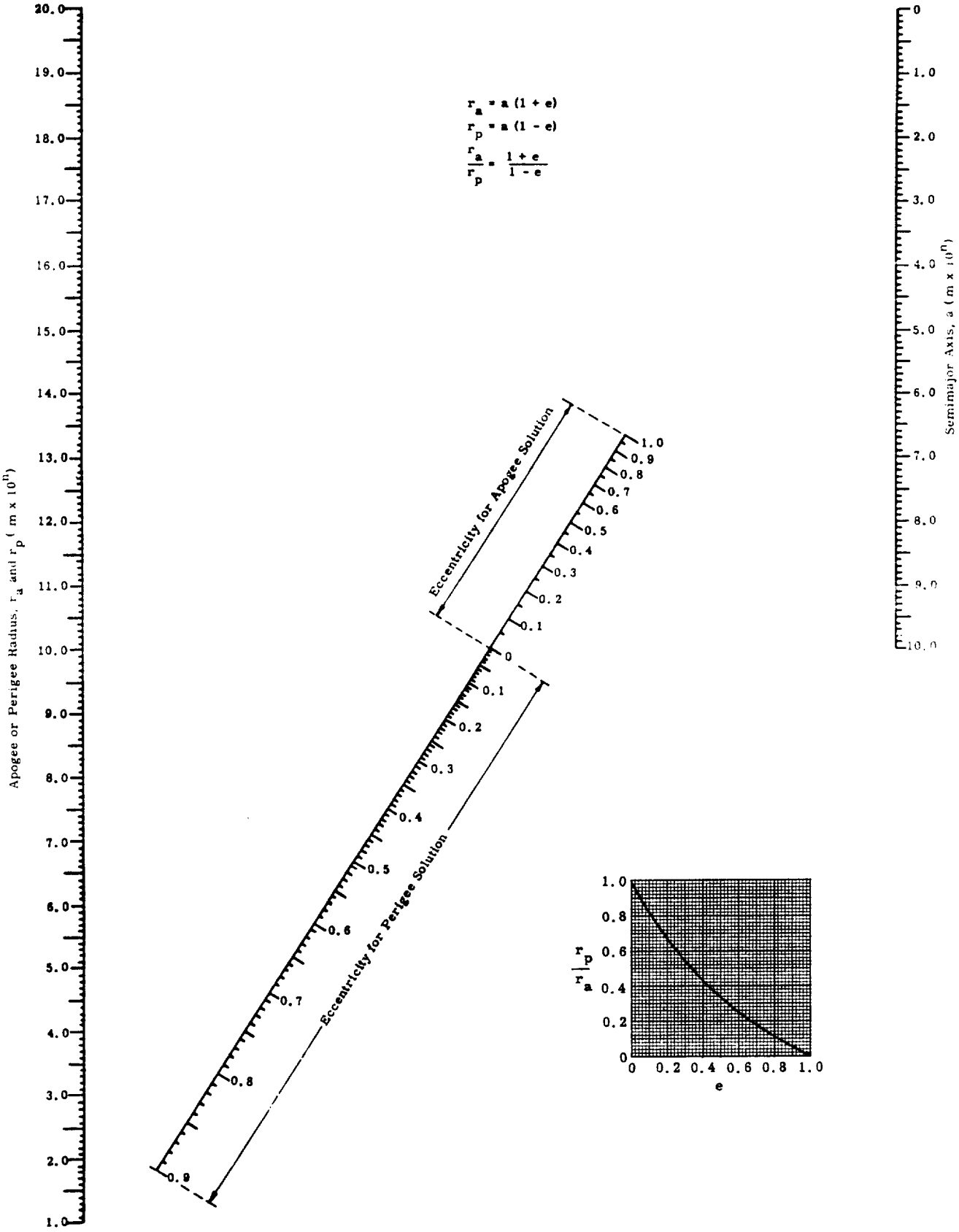

Fig. 12. Solution for Apogee and Perigee Radii

$$\theta = \cos^{-1} \frac{\frac{2r_a}{r} - \left(\frac{r_a}{r_p} + 1\right)}{\frac{r_a}{r_p} - 1}$$

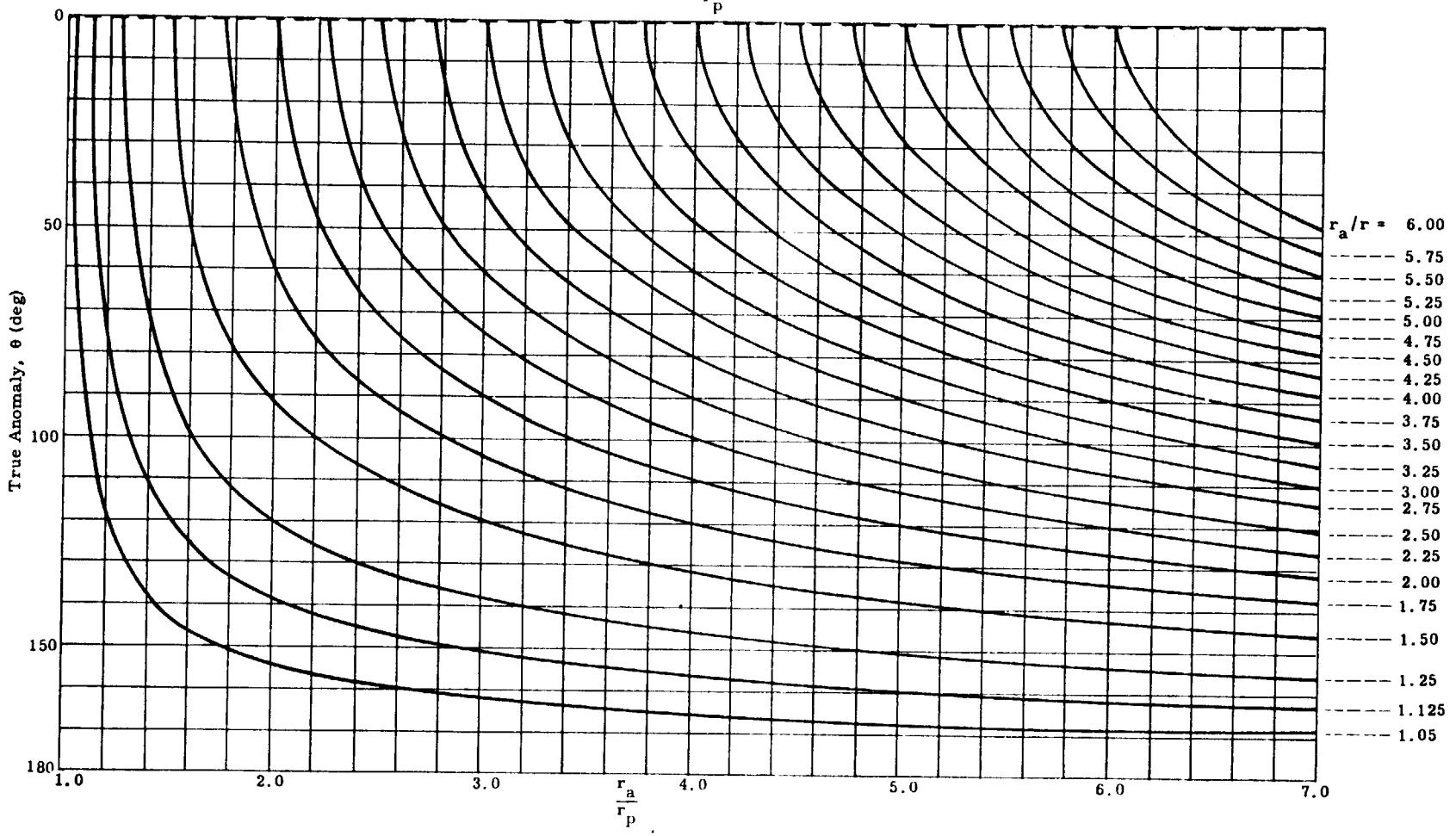

Fig. 13a. True Anomaly as a Function of r_a/r_p and r_a/r

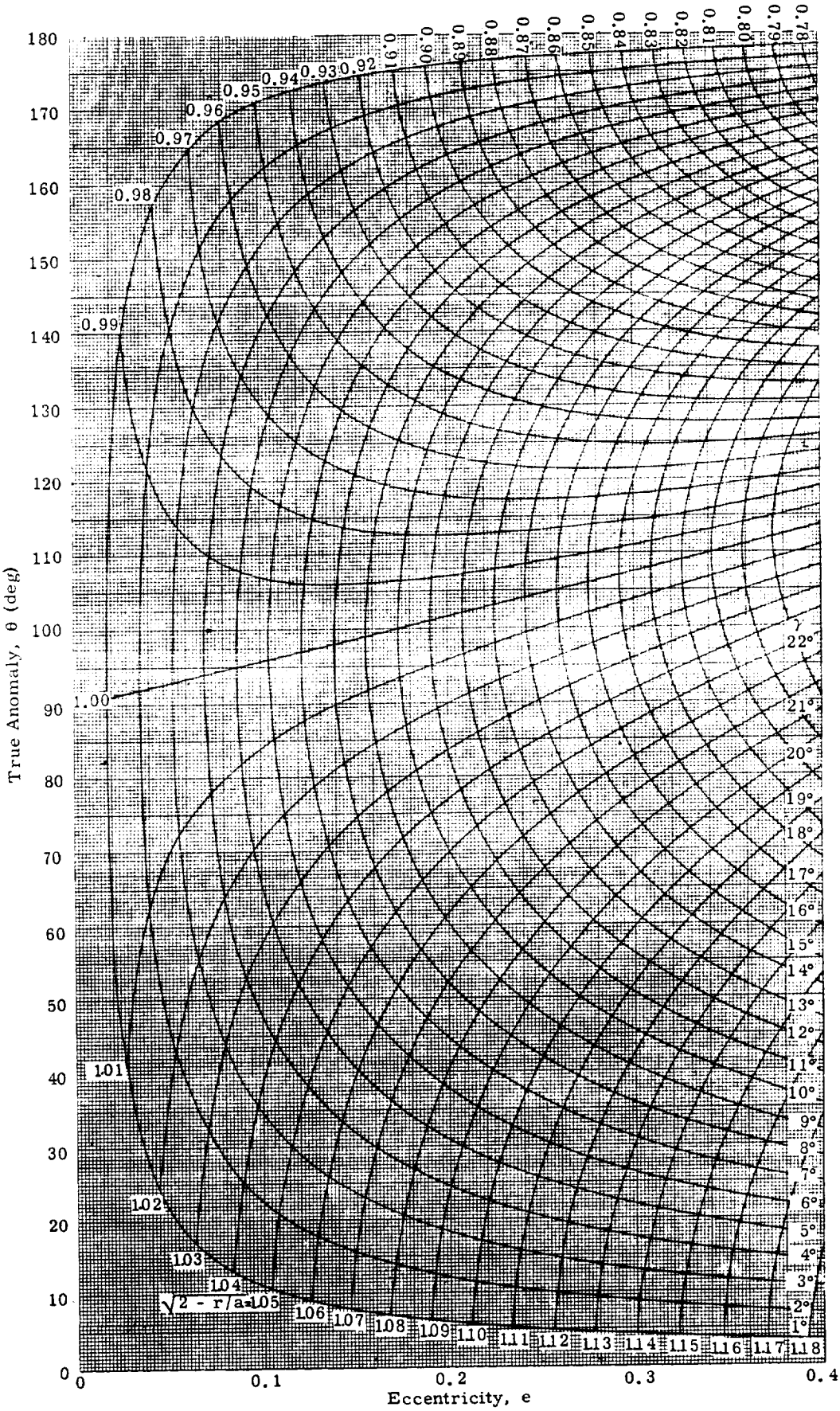

Fig. 13b. True Anomaly as a Function of r/a, e and γ

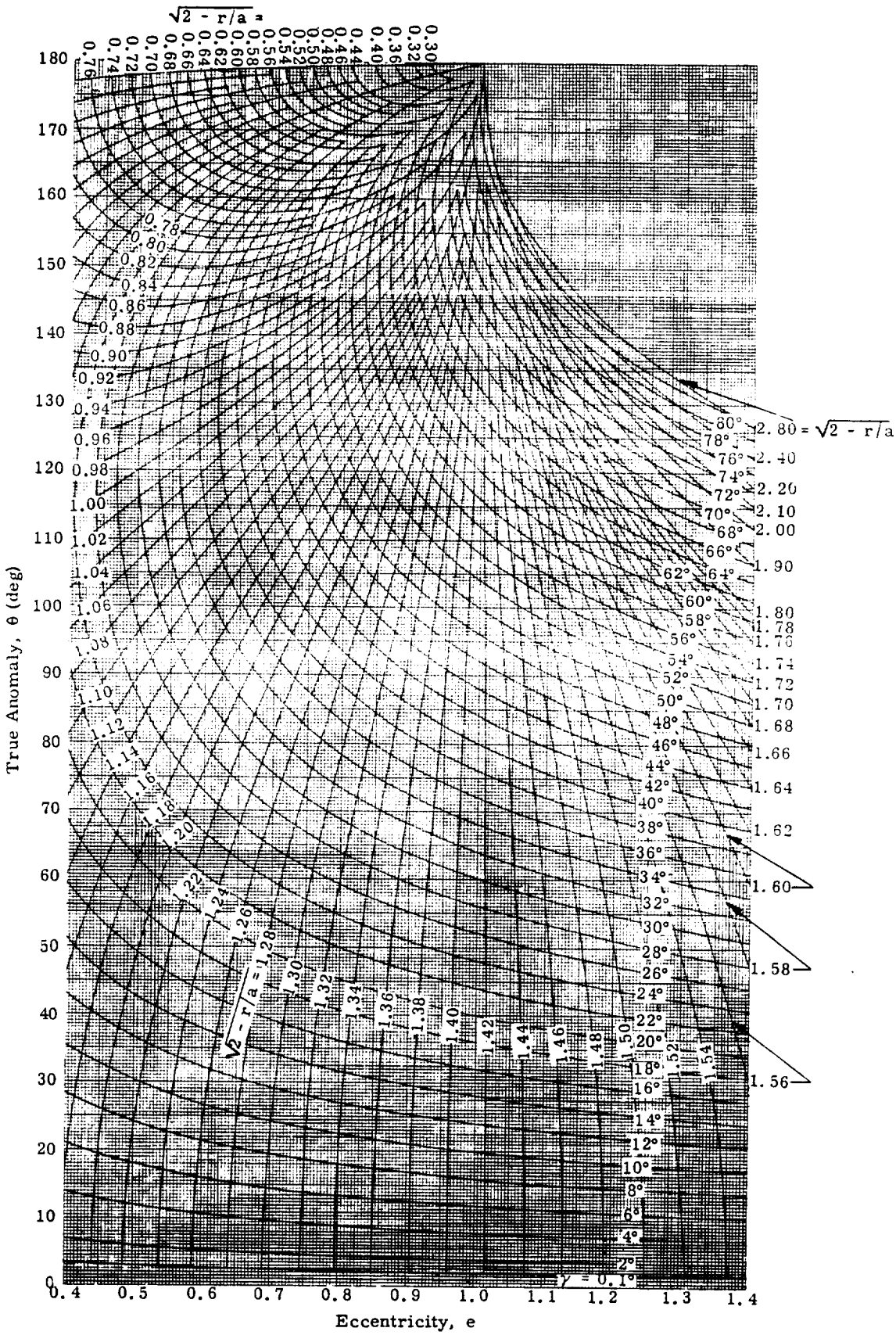

Fig. 13c. True Anomaly as a Function of r/a, e, and γ

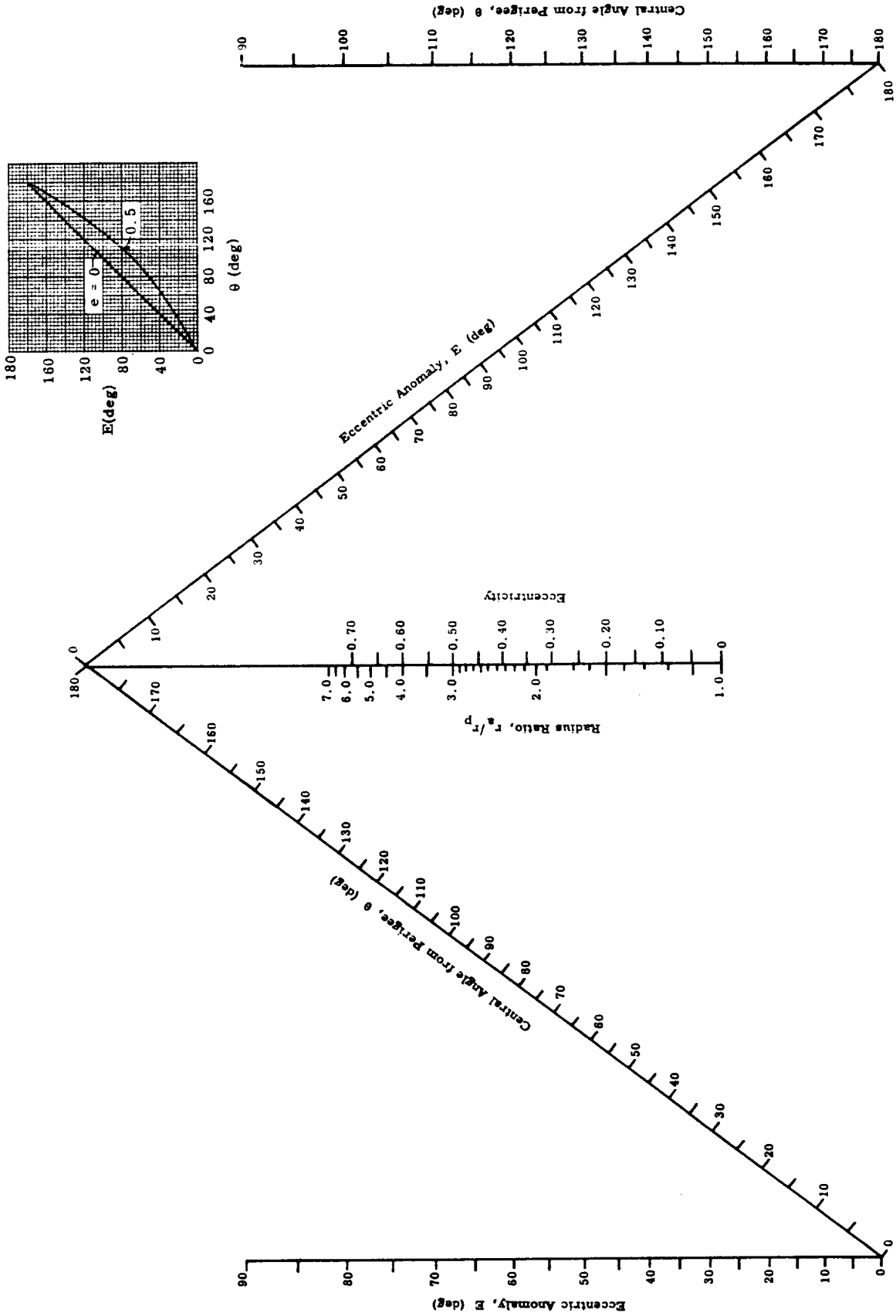

Fig. 14. Solution for the Eccentric Anomaly as a Function of θ, and e or r_a/r_p

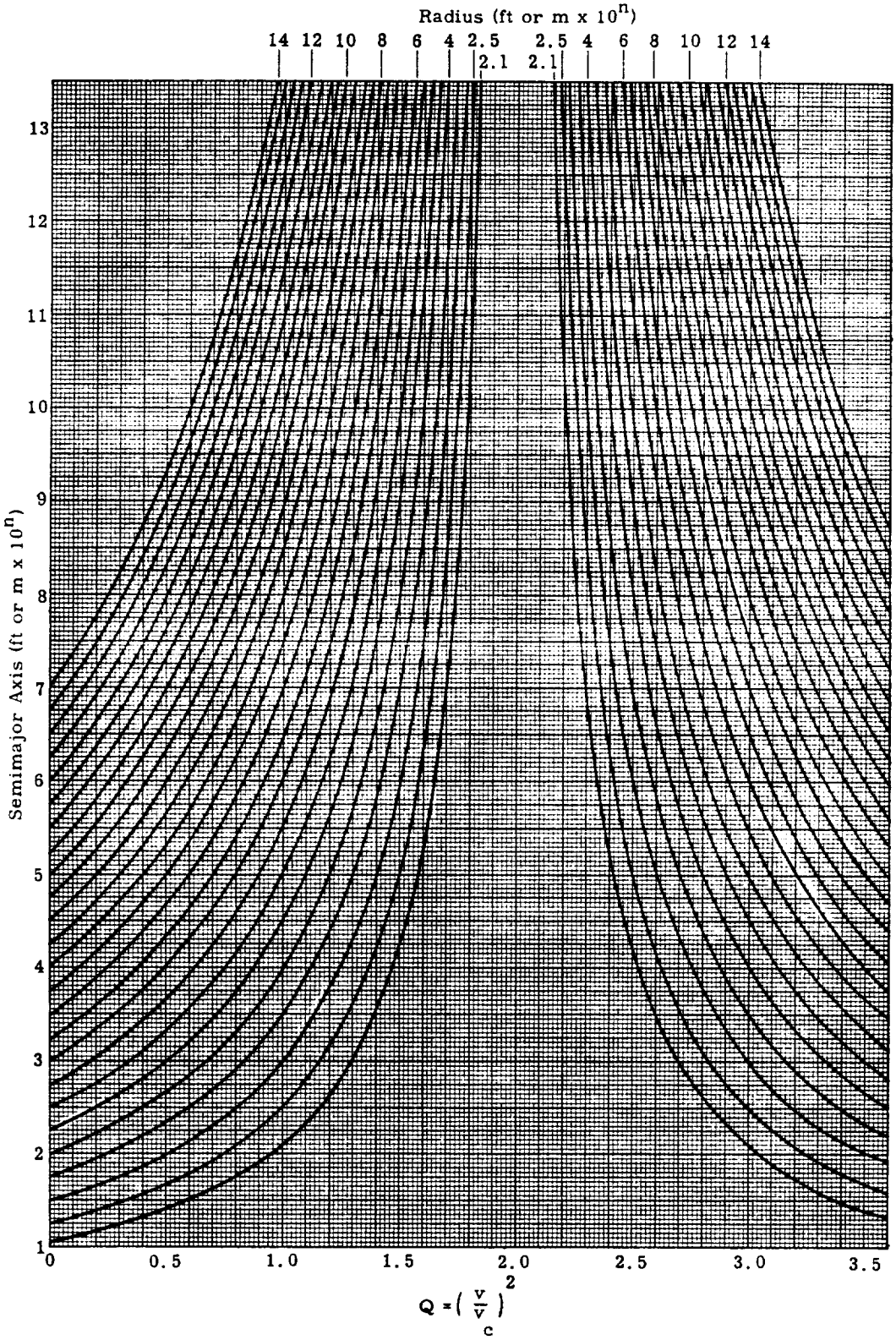

Fig. 15. Q-Parameter as a Function of Orbital Semimajor Axis and Radius

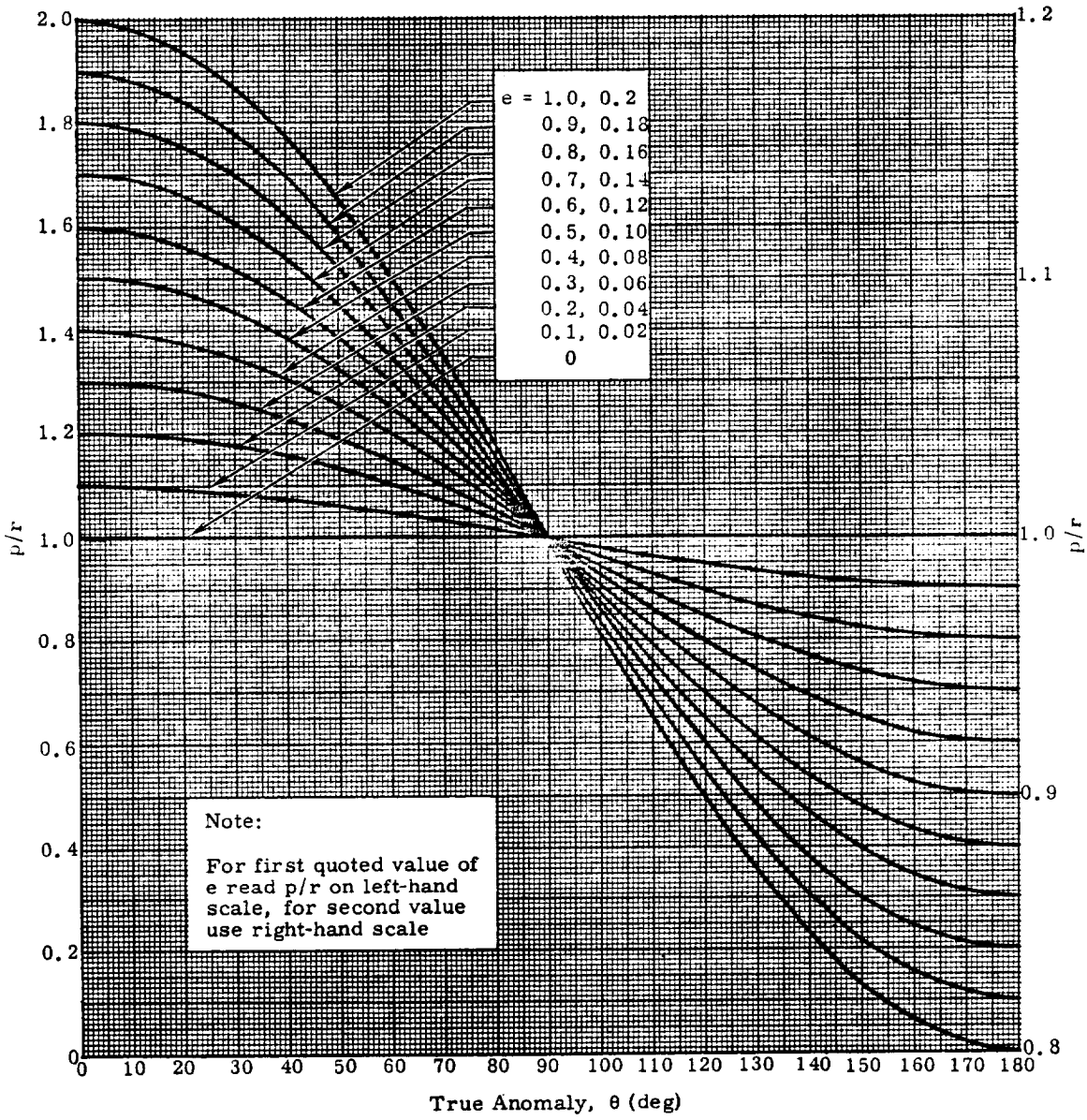

Fig. 16. Relationship Between Radius, Eccentricity and Central Angle from Perigee in an Elliptic Orbit

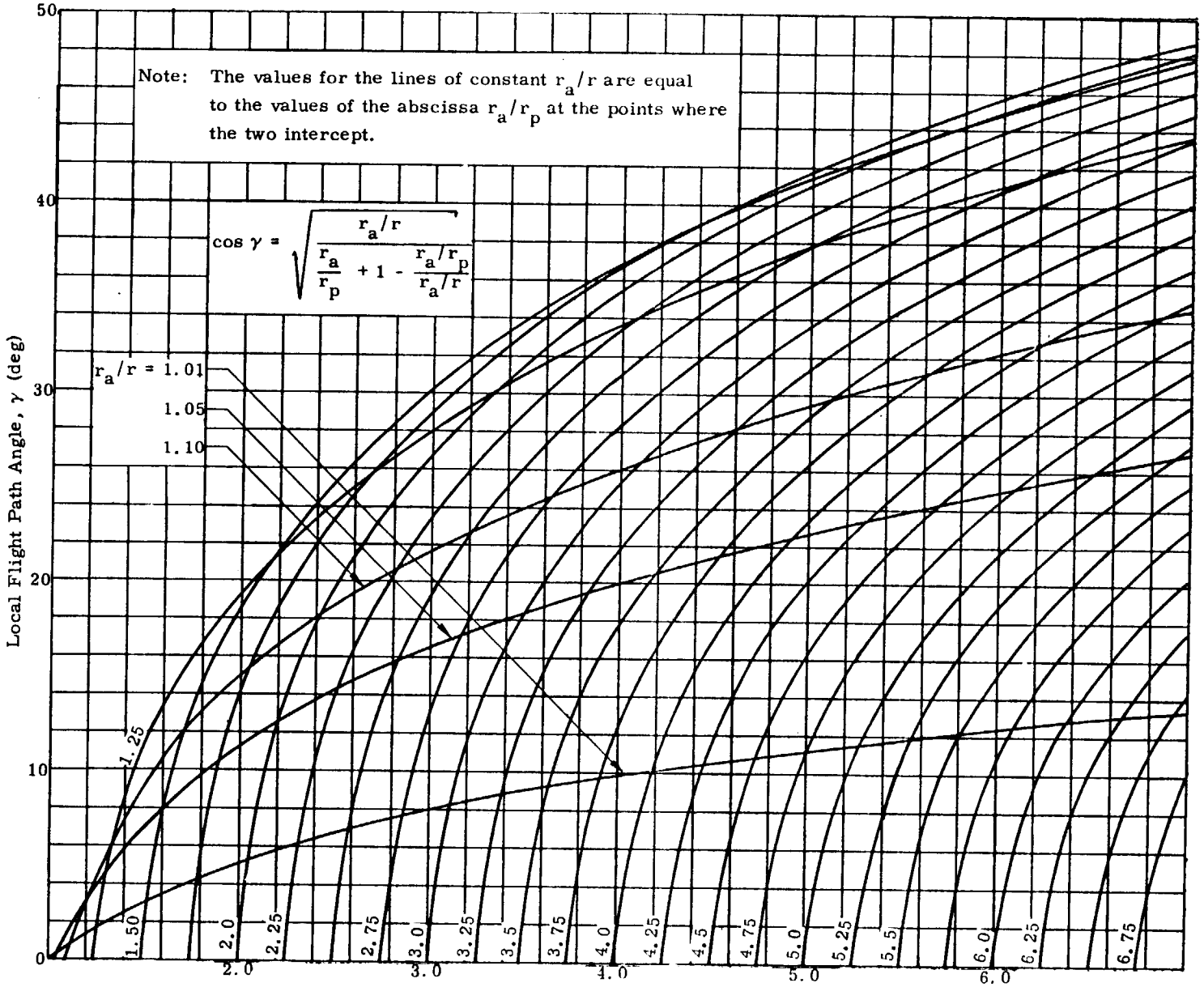

Fig. 17. Velocity-Escape Speed Ratio

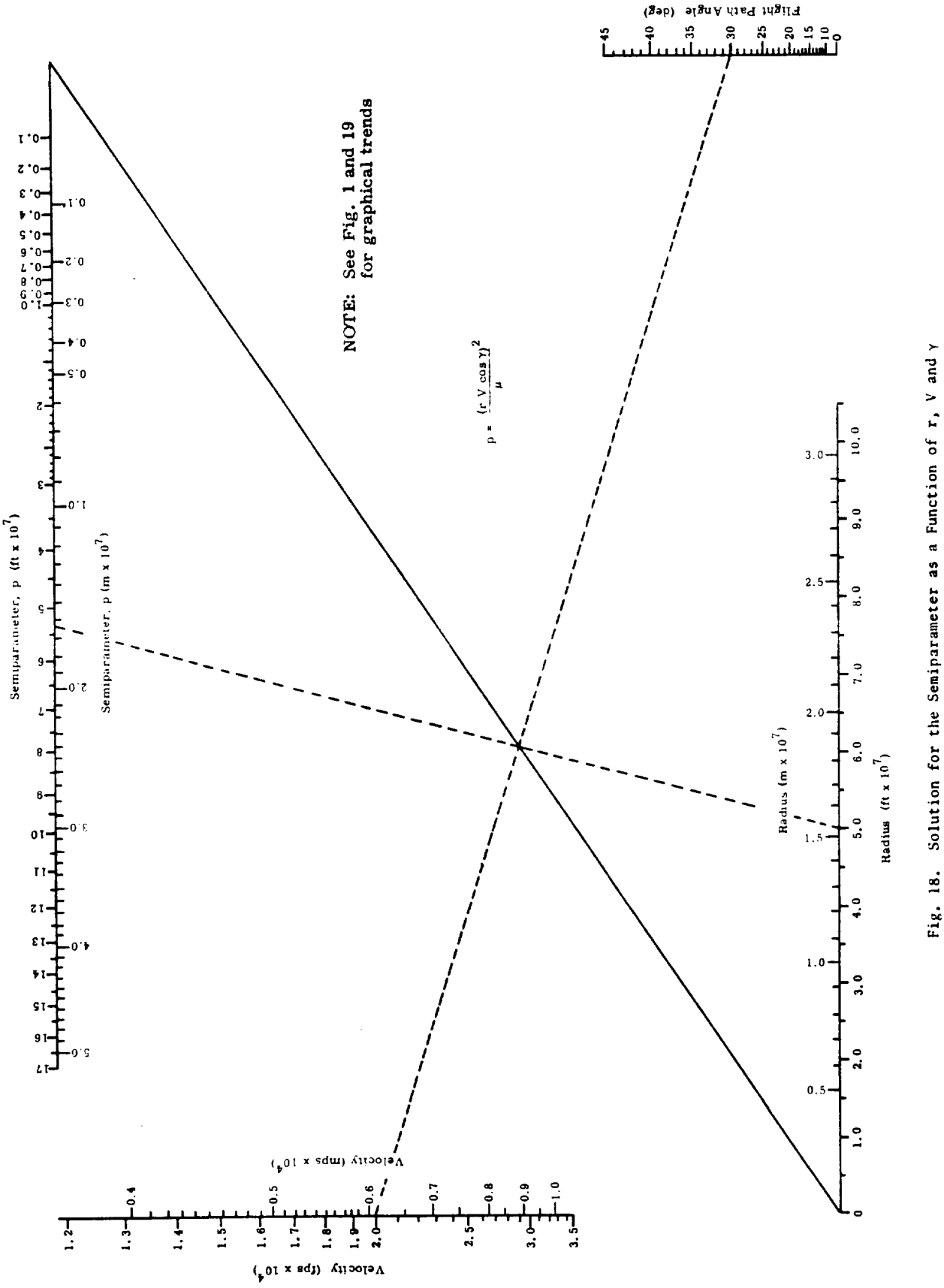

Fig. 18. Solution for the Semiparameter as a Function of r, V and γ

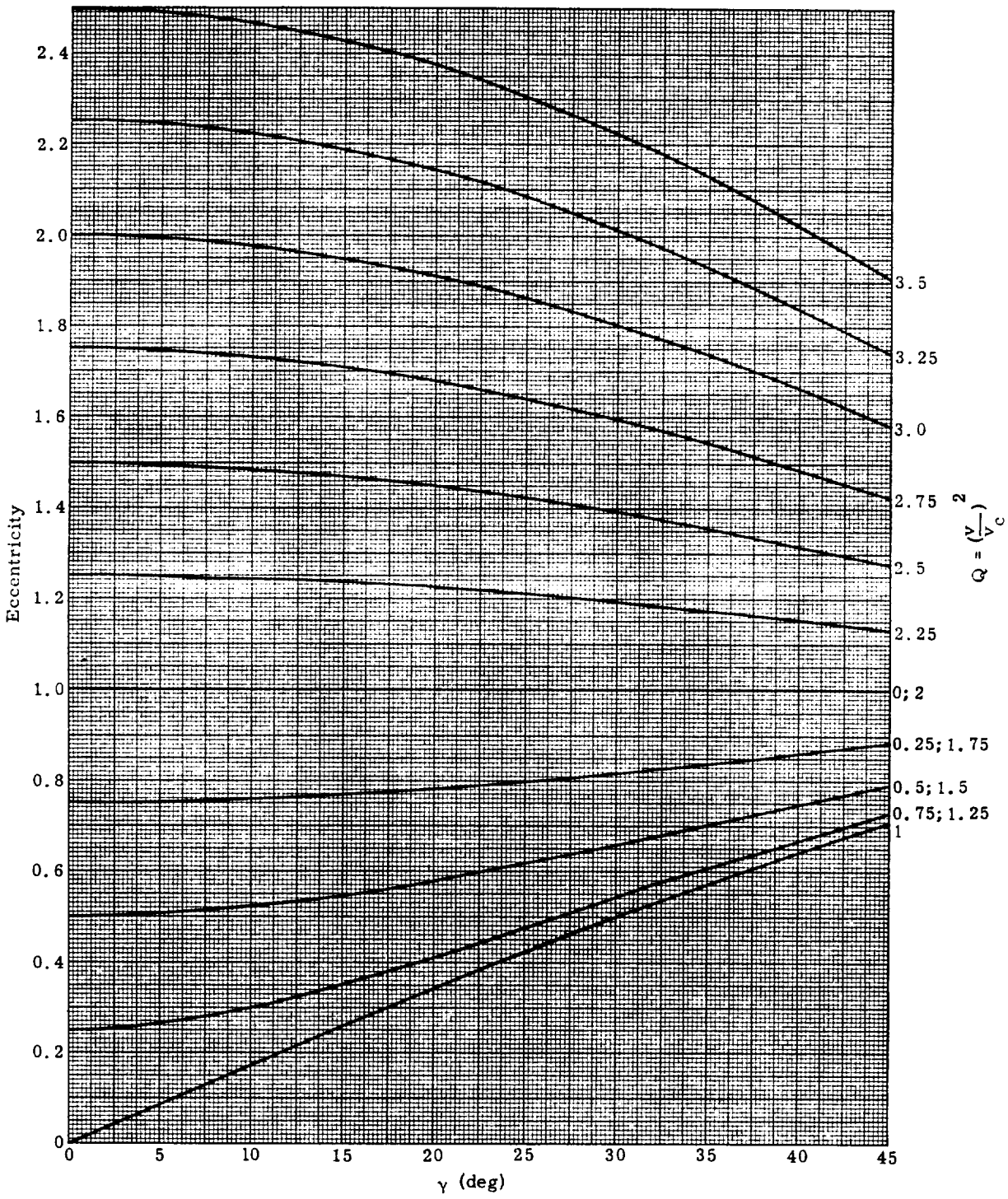

Fig. 19. Q-Parameter as a Function of Local Flight Path Angle and Eccentricity

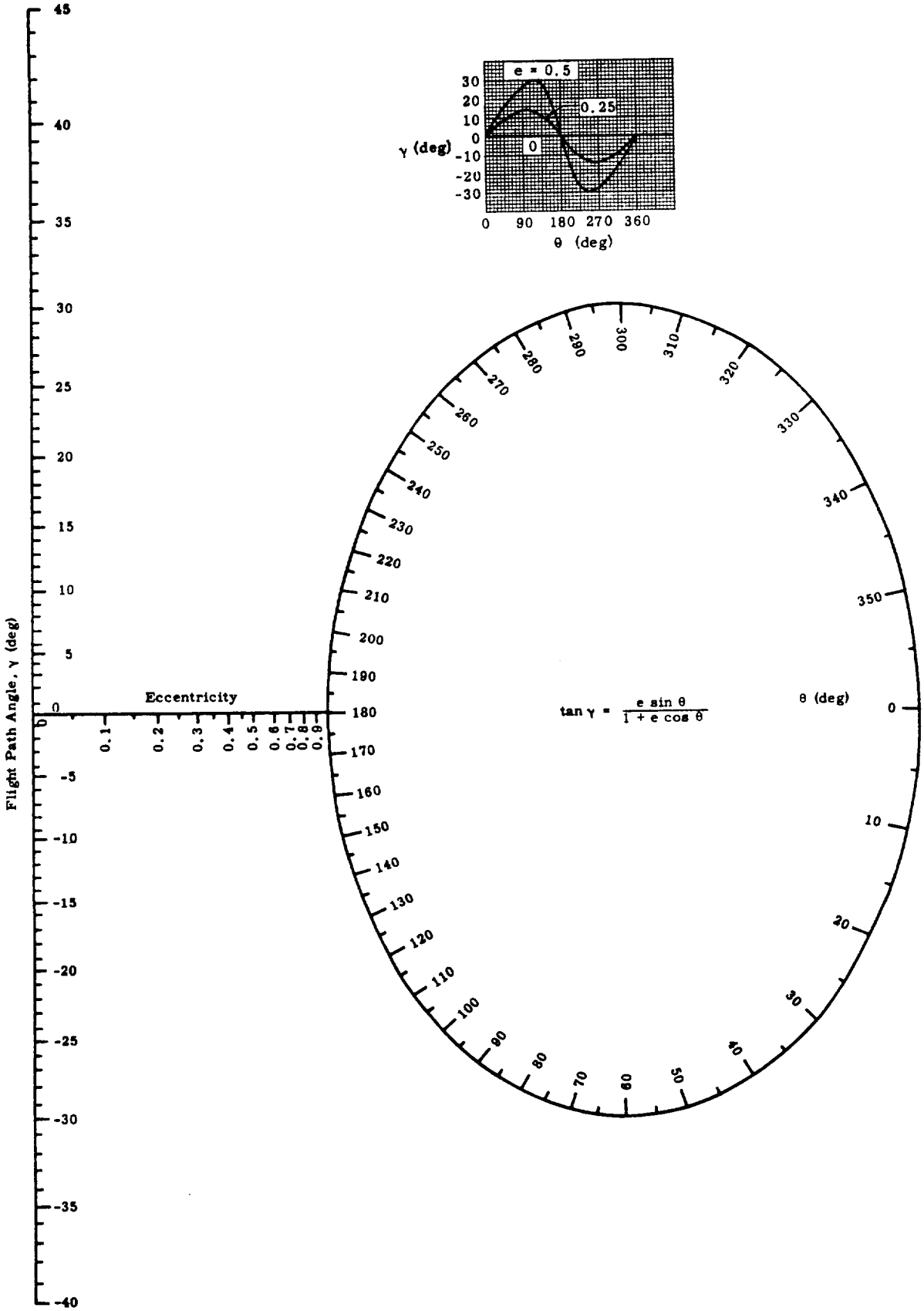

Fig. 20. The Solution for Local Flight Path Angle

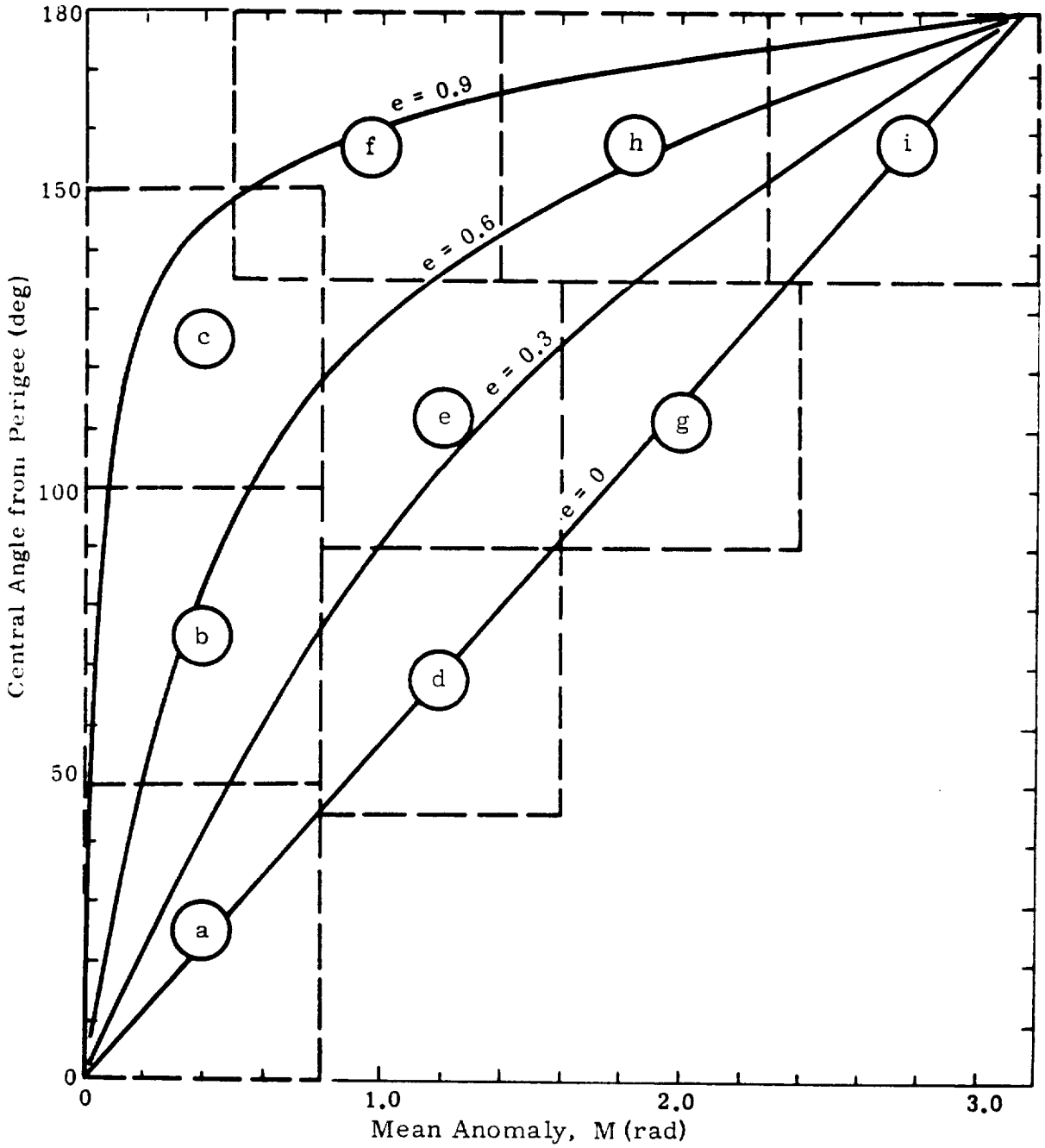

Time from perigee: $(t - t_p) = \frac{1}{n} M$

where $\frac{1}{n}$ is tabulated as a function of a in Fig. 7 and Table 9.

Fig. 21. Index for Figs. 22a Through 22i'
(circled numbers in field designate areas covered by corresponding figure numbers)

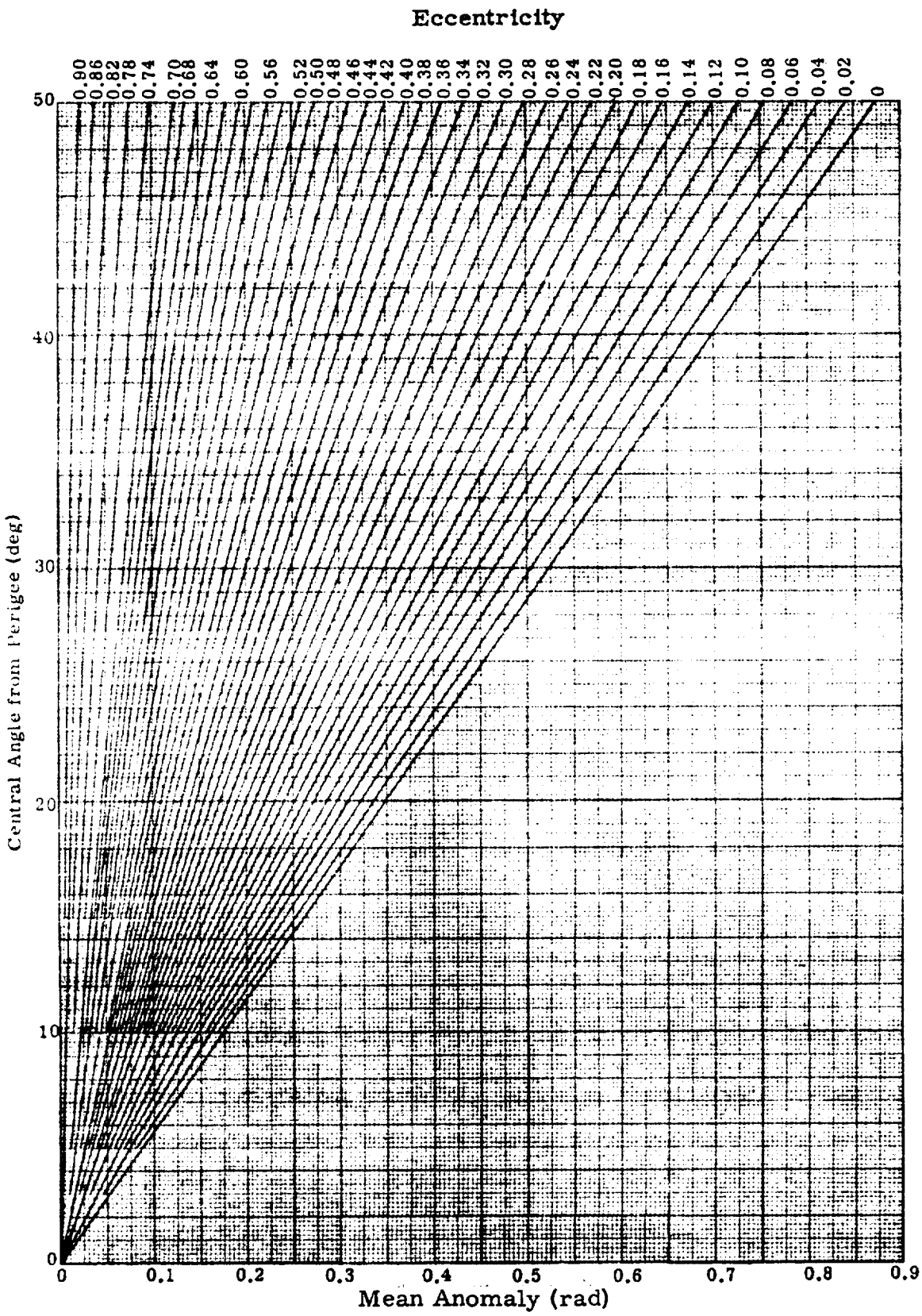

Fig. 22a. Mean Anomaly as a Function of Eccentricity and Central Angle from Perigee

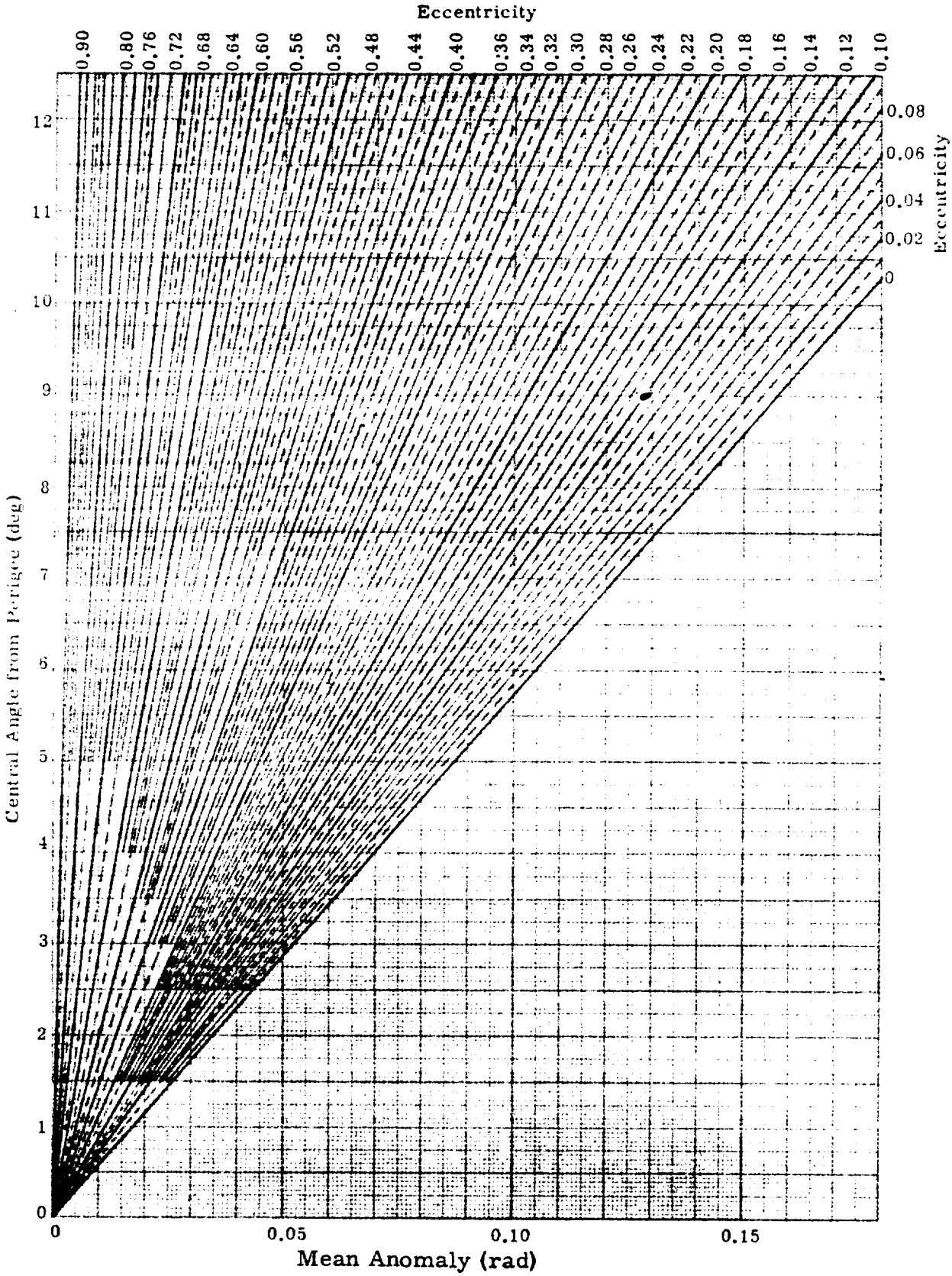

Fig. 22a' Mean Anomaly as a Function of Eccentricity and Central Angle from Perigee

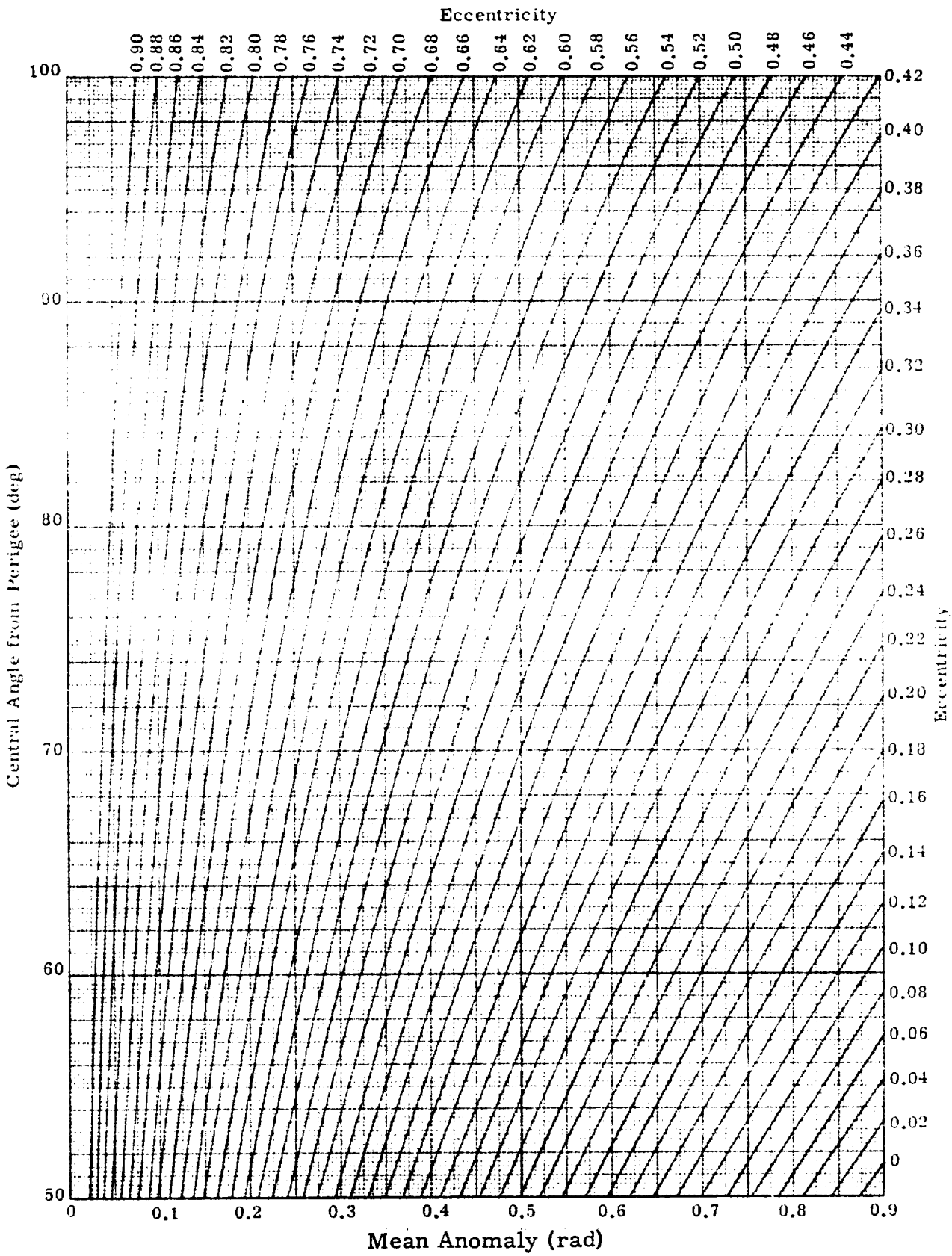

Fig. 22b. Mean Anomaly as a Function of Eccentricity and Central Angle from Perigee

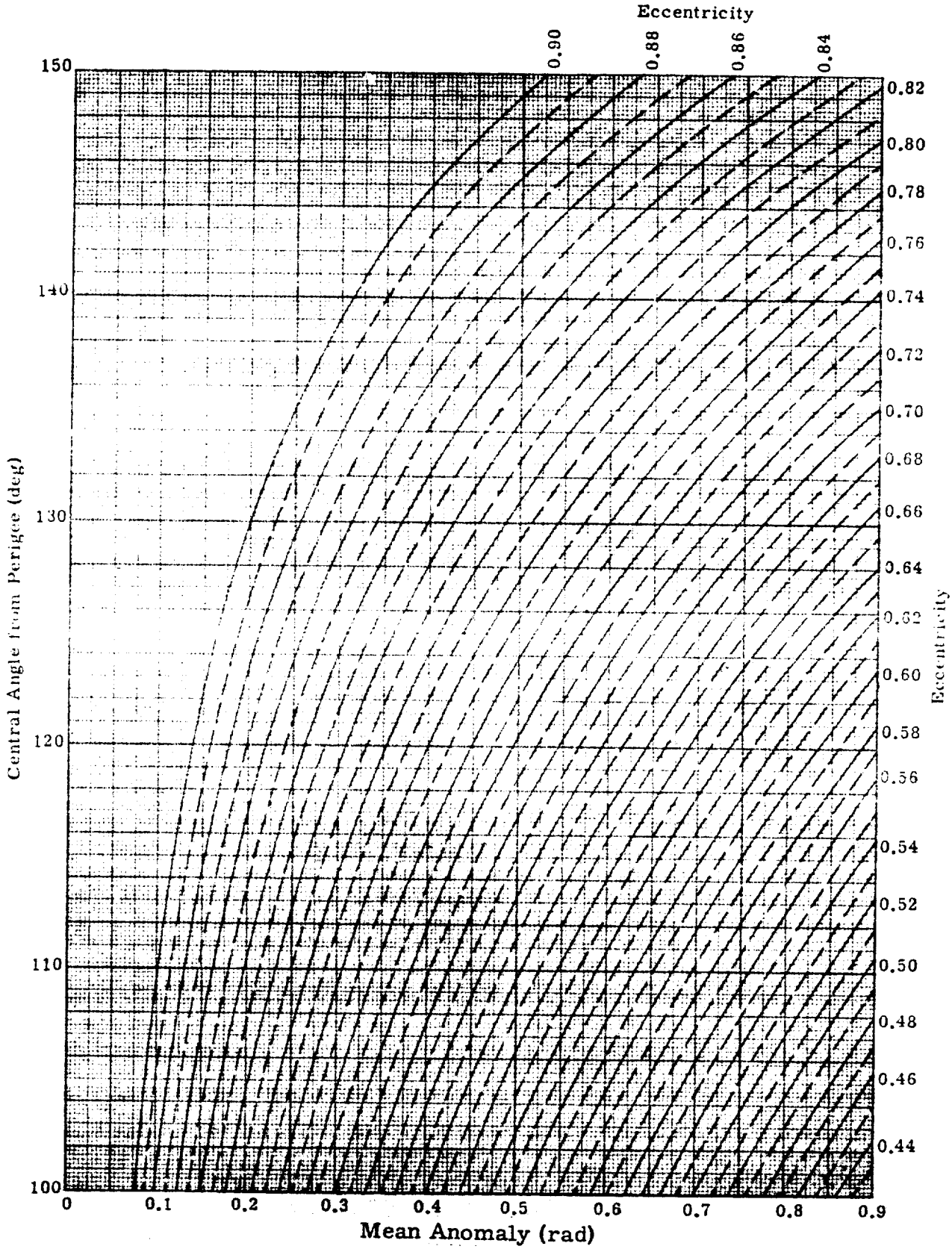

Fig. 22c. Mean Anomaly as a Function of Eccentricity and Central Angle from Perigee

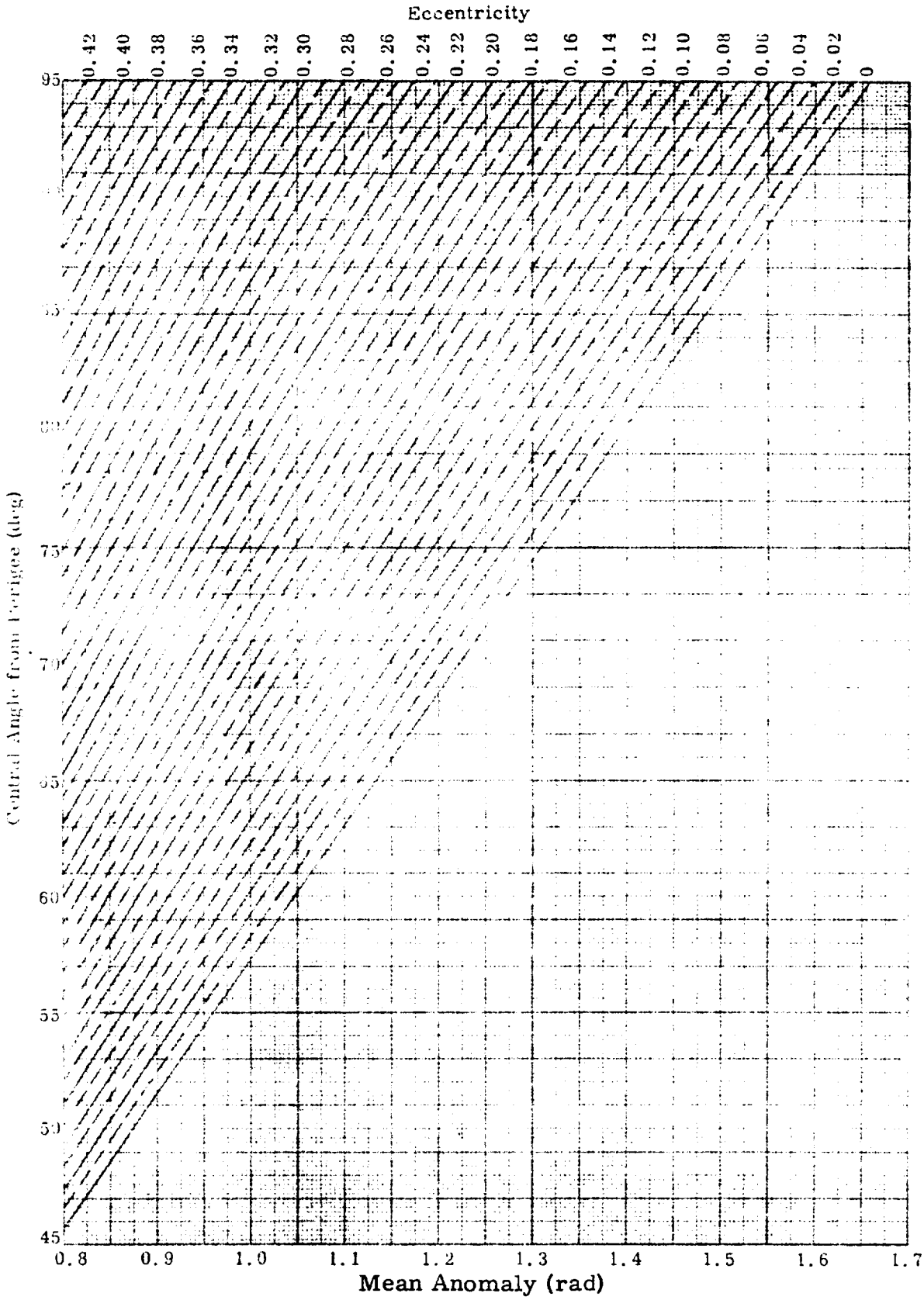

Fig. 22d. Mean Anomaly as a Function of Eccentricity and Central Angle from Perigee

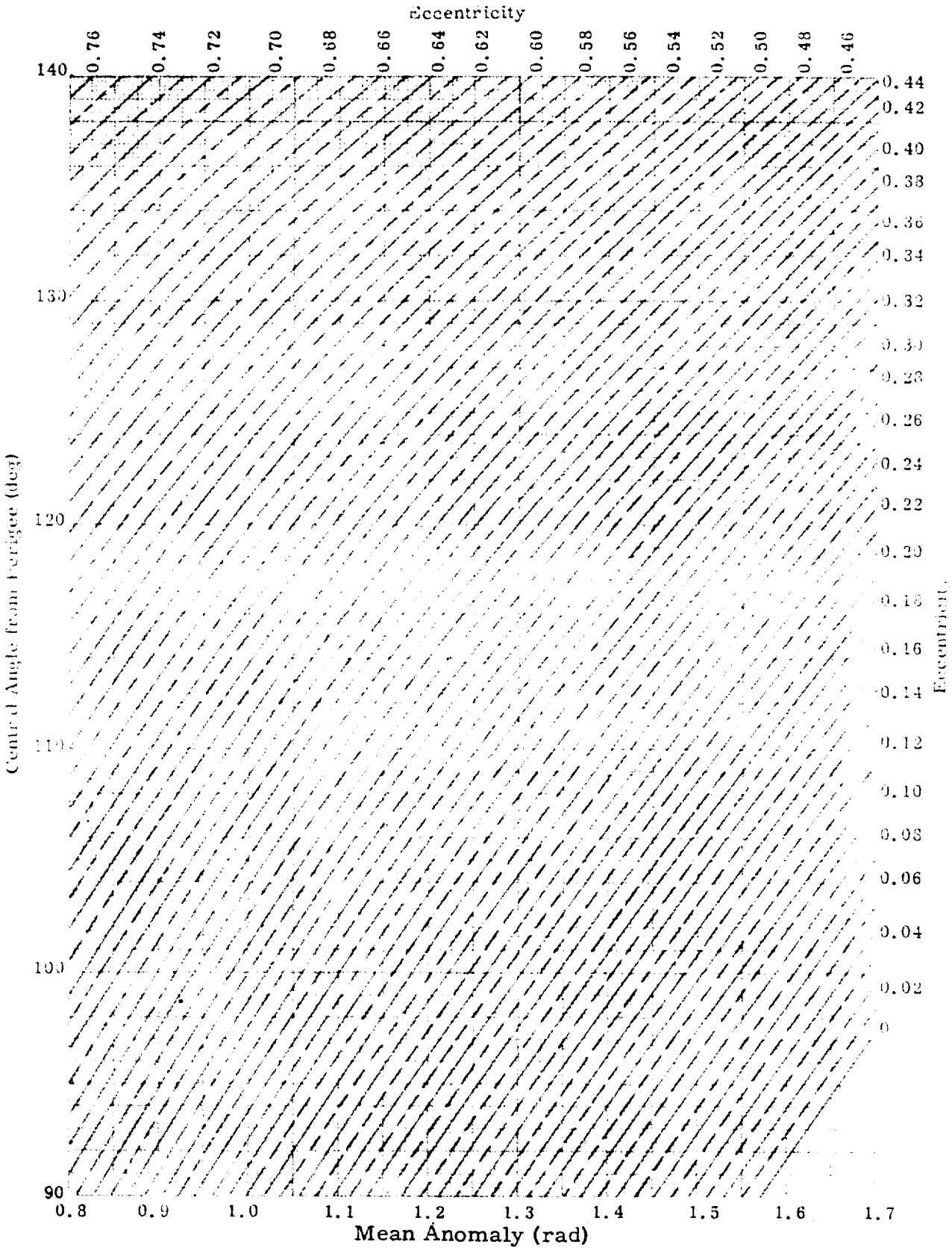

Fig. 22e. Mean Anomaly as a Function of Eccentricity and Central Angle from Perigee

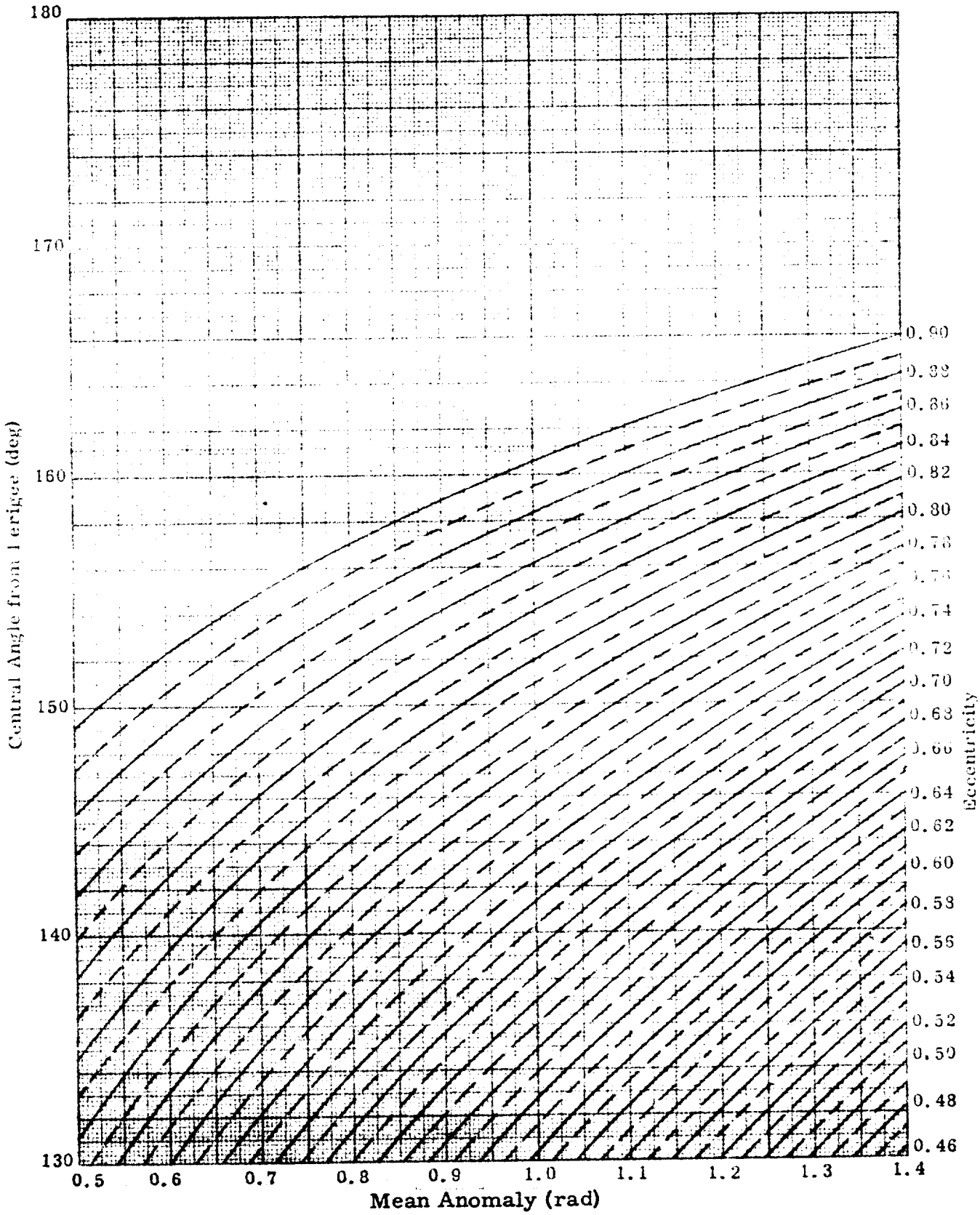

Fig. 22f. Mean Anomaly as a Function of Eccentricity and Central Angle from Perigee

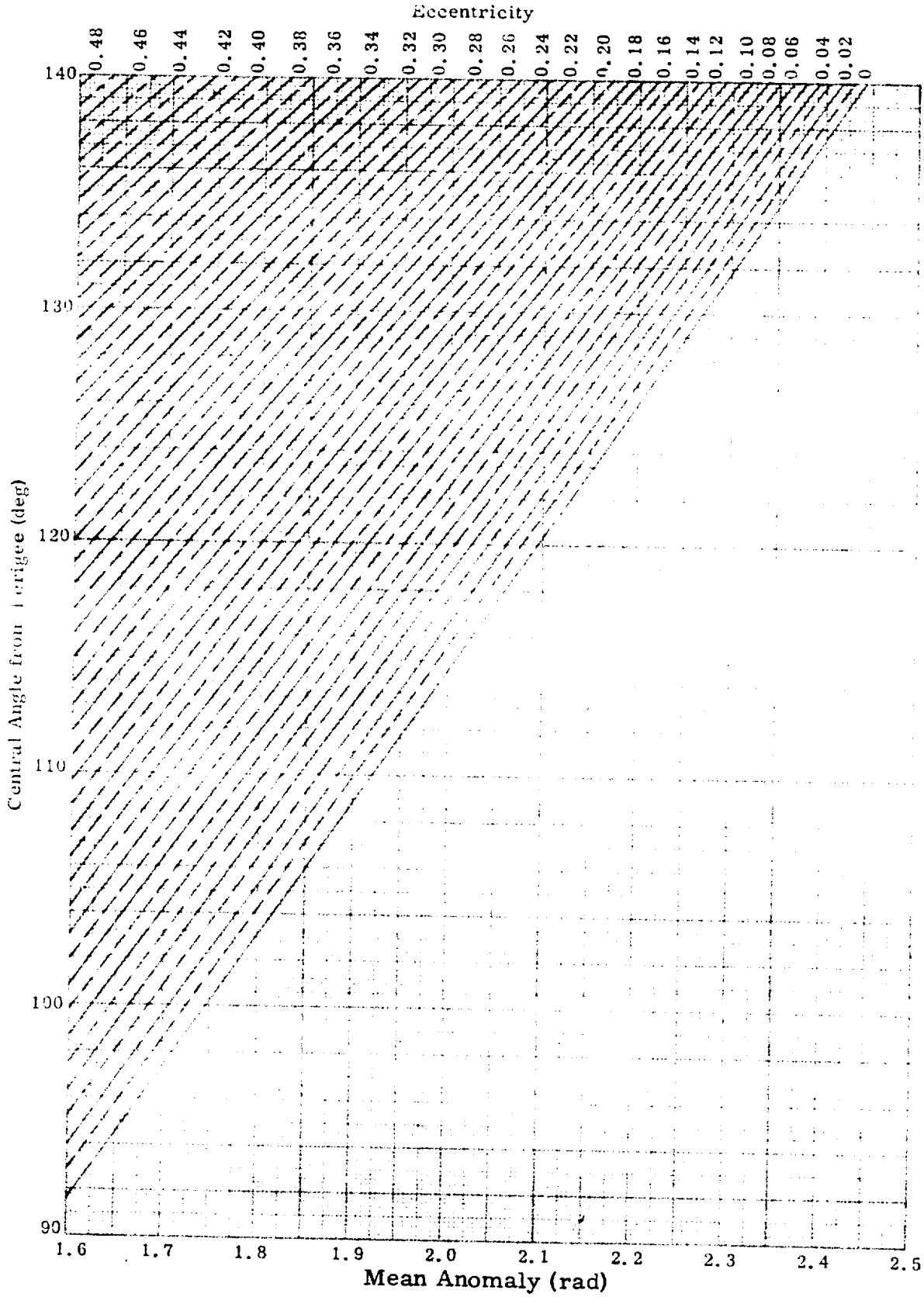

Fig. 22g. Mean Anomaly as a Function of Eccentricity and Central Angle from Perigee

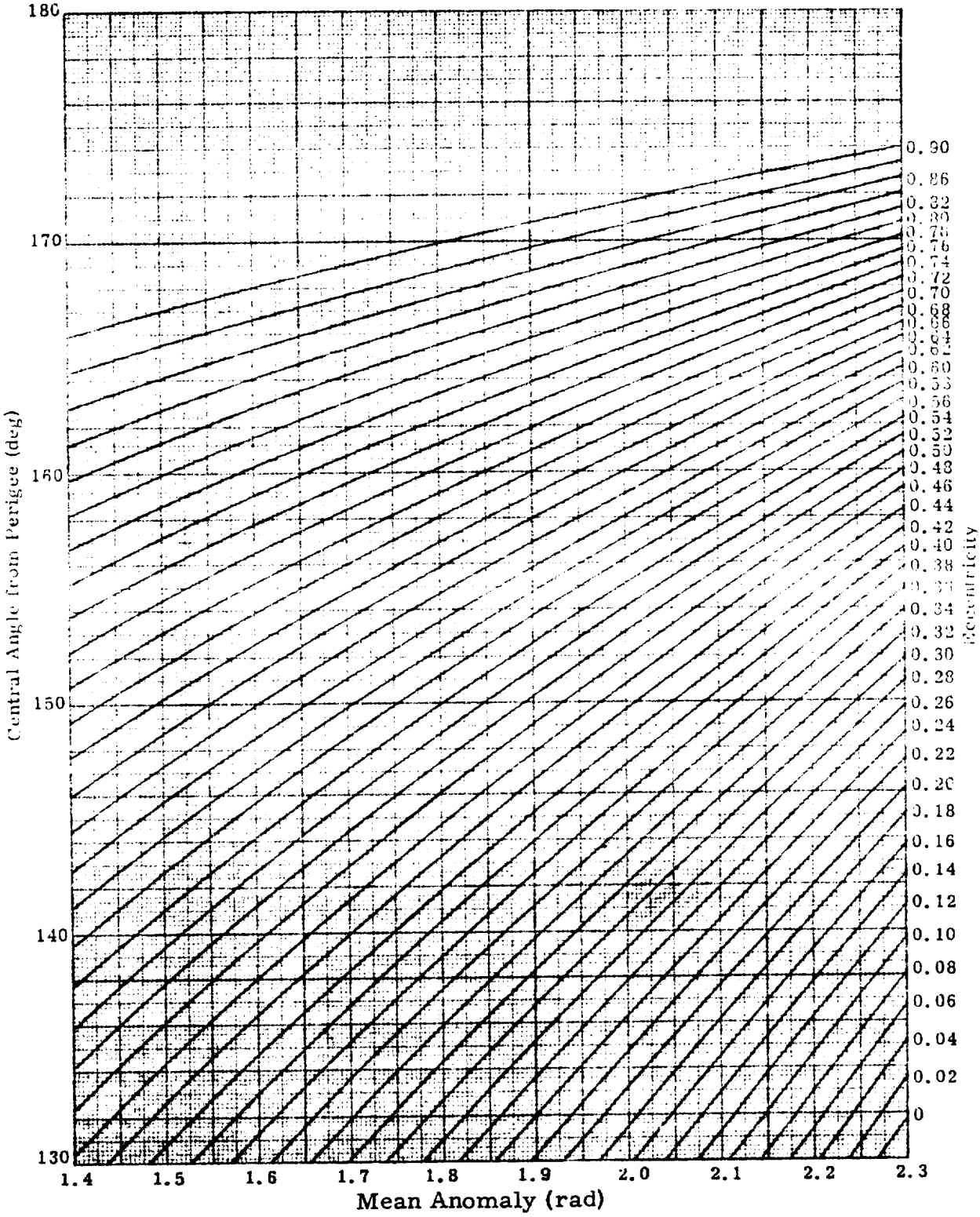

Fig. 22h. Mean Anomaly as a Function of Eccentricity and Central Angle from Perigee

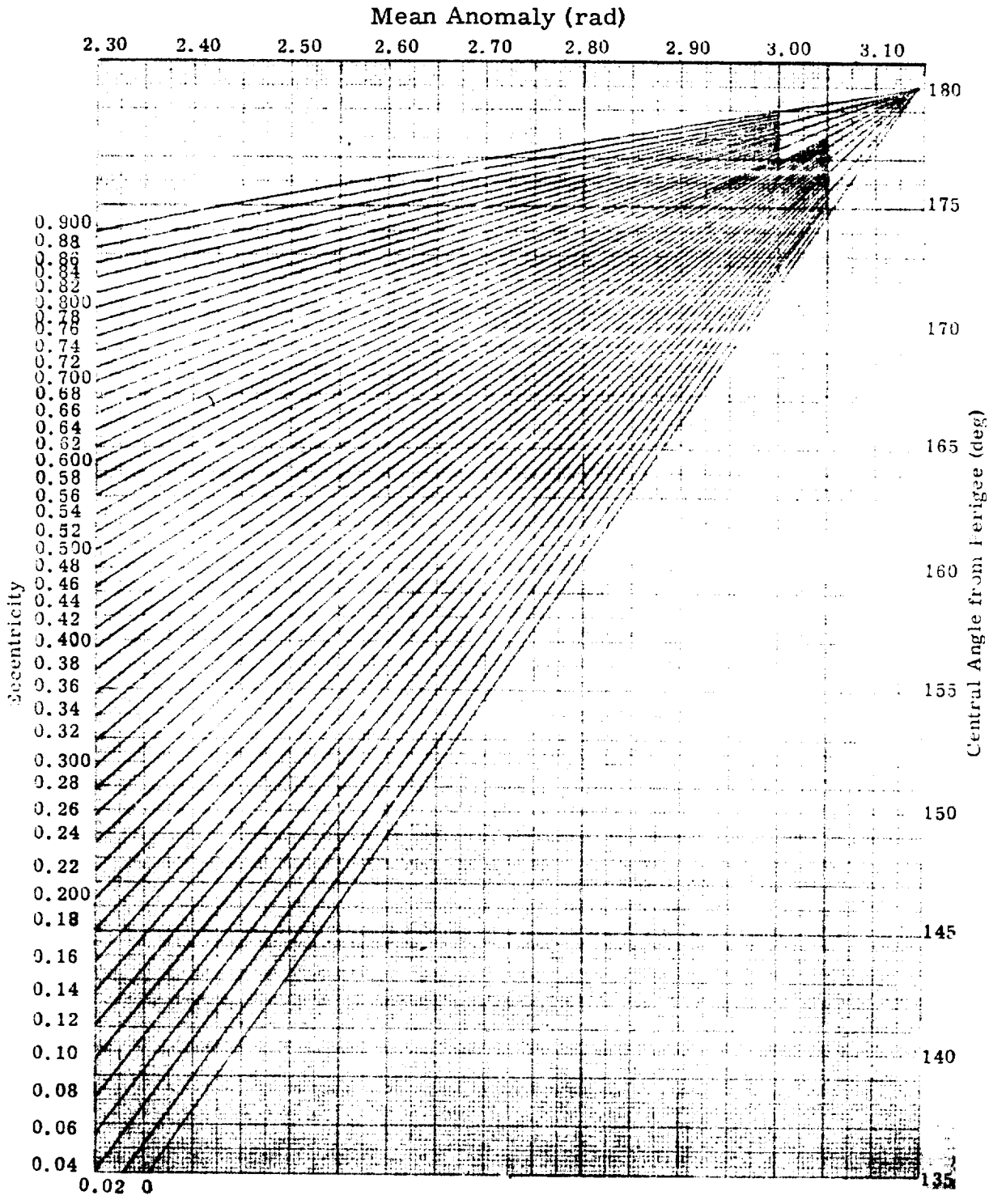

Fig. 22i. Mean Anomaly as a Function of Eccentricity and Central Angle from Perigee

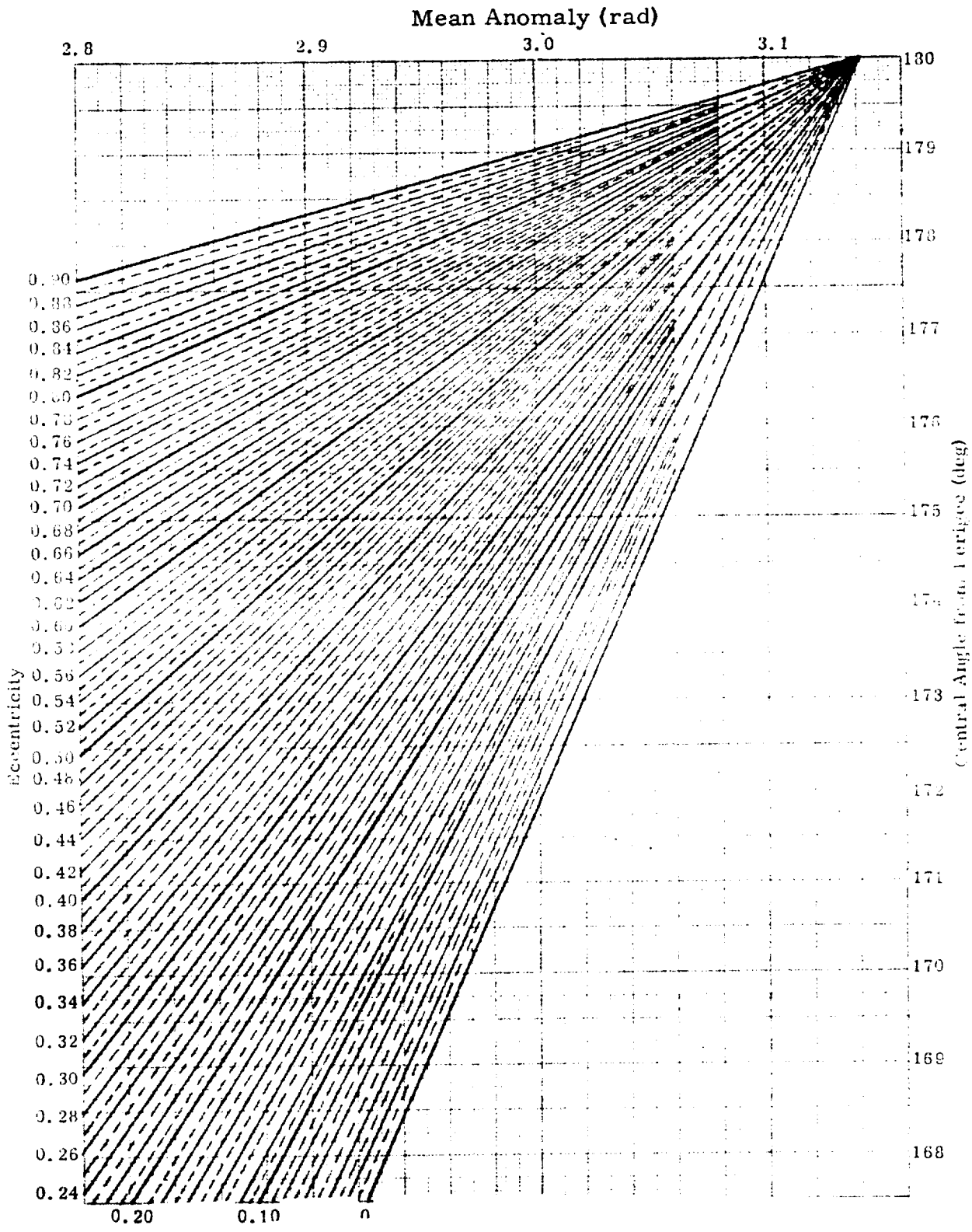

Fig. 22i'. Mean Anomaly as a Function of Eccentricity and Central Angle from Perigee

CHAPTER IV

PERTURBATIONS

Prepared by:

G. E. Townsend, Jr.
Martin Company (Baltimore)
Aerospace Mechanics Department
March 1963

		Page
	Symbols	IV-1
A.	Introduction	IV-2
B.	Special Perturbations	IV-2
C.	Methods for Numerical Integration	IV-7
D.	General Perturbations	IV-14
E.	References	IV-50
F.	Bibliography	IV-52
	Illustrations	IV-59

LIST OF ILLUSTRATIONS

Figure	Title	Page
1	Comparison of Perturbation Magnitudes (for equinoctial lunar conjunction)	IV-61
2	Solution for the Secular Precession Rate as a Function of Orbital Inclination and Semi-parameter	IV-62
3	Change in the Mean Anomaly Due to Earth's Oblateness	IV-63
4	Solution for the Secular Regression Rate as a Function of Orbital Inclination and the Semi-parameter	IV-64
5	Change in the Anomalistic Period Due to the Earth's Oblateness	IV-65
6	Change in the Nodal Period Due to the Earth's Oblateness (for small eccentricities)	IV-66
7	The Variations of the Radial Distance as Functions of the True Anomaly e and	IV-67
8	Maximum Radial Perturbation Due to Attraction of the Sun and Moon	IV-68
9	Satellite Orbit Geometry	IV-69
10	Effects of Solar Activity on Echo I	IV-70
11	Apogee and Perigee Heights on Echo I (40-day interval)	IV-70
12	Minimum Perigee Height as a Function of Days from Launch, Showing Effect of Oblateness, Drag, and Lunisolar Perturbations	IV-71
13	Minimum Perigee Height of Satellite as a Function of Days from Launch (8 to 14 hr, expanded scale)	IV-72

LIST OF ILLUSTRATIONS (continued)

Figure	Title	Page
14	Comparison of Approximate and Exact Solutions of Satellite Motions	IV-73
15	Minimum Perigee Height of Satellite as a Function of Days from Launch, Showing Effect of Neglecting Oblateness	IV-73
16	Minimum Perigee Height of Satellite as a Function of Days from Launch, Showing Effect of Neglecting Moon, Sun.	IV-74
17	Minimum Perigee Height of Satellite as a Function of Days from Launch, Showing Effect of Sun and Moon 90° Out of Phase	IV-74
18	Minimum Perigee Height of Satellite as a Function of Days from Launch, Showing Effect of Changing Orbit Size	IV-75
19	Minimum Perigee Height of Satellite as a Function of Days from Launch, Showing Effect of Change in Inclination	IV-75
20	Minimum Perigee Height of Satellite as a Function of Days from Launch, Showing Effect of Change in Argument of Perigee	IV-76
21	Minimum Perigee Height of Satellite as a Function of Days of Launch for About a 10-Year Period	IV-76

IV. PERTURBATIONS

SYMBOLS

A	Right ascension, area
a	Semimajor axis
B	Ballistic coefficient $C_D A/2m$
C_D	Drag coefficient
E	Eccentric anomaly
e	Eccentricity
G	Universal gravitation constant $[6.670 (1 \pm 0.0007) \times 10^{-8}$ cm^3/kg-sec$^2]$
h	Magnitude of the angular momentum per unit mass; step size in numerical integration
i	Orbital inclination
J_n	Coefficients of the zonal harmonics in the Vinti potential
L	Latitude
M	Mean anomaly $n(t - t_0) = E - e \sin E$
m	Mass
n	Mean motion $= 2\pi/\tau = \sqrt{\mu/a^3}$
p	Semilatus rectum $= a(1 - e^2)$
q	Perigee radius $= a(1 - e)$ also quantity in Encke's equation $= \frac{1}{2}\left[\left(\frac{r}{r_e}\right)^3 - 1\right]$
R, S, W	Vehicle coordinates R = $\hat{r}$, S normal to R in the plane of instantaneous motion ($\vec{S} \cdot \vec{V}$ = positive number), W completes the set
r	Radius
$\dot{r}$	$\frac{dr}{dt}$
$\ddot{r}$	d^2r/dt^2
t	Time
U	Potential function
$\vec{V}$	Velocity vector
x, y, z	Equatorial Cartesian coordinates
Γ, Γ_p	Angular coordinates of perturbing mass
γ	$\cos^{-1}(\vec{r} \cdot \vec{V}) - 90°$
ϵ	$-\mu/2a$ = energy per unit mass
η	Dimensionless parameter $\frac{V_0^2 r}{\mu} - 1$
θ	True anomaly
μ	= GM = masses' gravitational constant
Ξ	Disturbing potential
ξ	Perturbed ϕ in Anthony and Fosdick theory
ξ,η,ζ	$(x - x_e)$, $(y - y_e)$, $(z - z_e)$ in Encke's solution--also vehicle-centered coordinates
τ	Orbital period
τ_p	Time of perigee passage
ϕ	Central angle measured from the ascending node
Ω	Right ascension of the ascending node
Ω_e	Rotational rate of the earth, 1 revolution every 86,164.091 mean solar seconds
ω	Argument of perigee
$\tilde{\omega}$	$\Omega + \omega$

A. INTRODUCTION

The Keplerian relations, as discussed in Chapter III, give convenient approximations for use in preliminary orbit computations. However, in order to obtain precise earth satellite orbits, the various perturbing factors which give rise to accelerations (in addition to that of the central force field) and cause the motion to deviate from pure conic form must be considered. These perturbative accelerations may be due to the mass asymmetry of the earth, the gravitational attraction of other bodies, atmospheric drag, electromagnetic drag, radiation pressure, thrust, or may be required to account for relativity effects. These factors affect the motion of the satellite to a varying degree depending on the shape and mass of the satellite and the type of trajectory.

Special perturbation methods involve the formulation of the differential equations of motion in such a manner that the computation of an orbit is achieved by numerical integration. The perturbation method to be used is determined by the type of problem that is under consideration. Similarly, all combinations of integration techniques and perturbation methods are not equally suited to the solution of a particular problem, even though the use of such combinations is possible. Because numerical integration is subject to the inevitable accumulation of errors which eventually destroy the validity of the results, special perturbation methods are restricted to the prediction of earth satellite orbits for times dependent upon the desired accuracy, the formulation of the problem and the number of digits carried in the computations.

One source of error in the numerical integration process is roundoff error, resulting from the limited number of digits which can be carried in computation. The roundoff error is not reduced by double-precision computation where tabulated values to be interpolated at each integration step are known to less than single-precision accuracy. This error obviously increases with the number of computations, which in turn increases with decreased integration step size. Roundoff propagates through the numerical integration so that, assuming a normal error distribution, the absolute error incurred in double integration is

(the product of the number of steps and the original roundoff)$^{3/2}$

A second source of error is truncation. This error arises because of the finite polynomial approximations in the integration formulas. Since the terms in the polynomials involve powers or differences of the integration interval, the truncation error can be reduced by choosing a smaller integration step. Therefore, increasing the number of integration steps decreases the truncation error, but increases the roundoff error.

B. SPECIAL PERTURBATIONS

1. Perturbative Forces

The equation of motion of a perturbed orbit is of the form:

$$\ddot{\vec{r}} = -\mu \frac{\vec{r}}{r^3} + \vec{F} \tag{1}$$

where $\vec{F}$ is the sum of the accelerations due to the various perturbing forces. If $\vec{F} = 0$, there are no perturbations and the motion is Keplerian.

If the position coordinates of the vehicle and the perturbation accelerations are given in rectangular equatorial coordinates, Eq (1) can be written:

$$\ddot{x} = -\mu \frac{x}{r^3} + \sum_i \overset{oo}{x}_i, \quad x \rightarrow y, z \tag{2}$$

where $\sum_i \overset{oo}{x}_i$ is the sum of the perturbation accelerations. These terms are discussed in the following paragraphs.

a. Vinti potential

If the earth were homogeneous in concentric spherical shells, its potential would be that of a point mass. The effects of the flattening of the poles and lack of symmetry about the equator, however, manifest themselves as perturbative forces on satellites in the vicinity of the earth. The acceleration due to the oblateness of the earth can be written in a simple form attributable to J. Vinti of the National Bureau of Standards:

$$\begin{aligned}
\overset{oo}{x} = -\frac{\mu x}{r^3} \Bigg[& J_2 \left(\frac{R}{r}\right)^2 \frac{3}{2} \left(1 - 5\frac{z^2}{r^2}\right) \\
& J_3 \frac{z}{r} \left(\frac{R}{r}\right)^3 \frac{5}{2} \left(3 - 7\frac{z^2}{r^2}\right) \\
& + J_4 \left(\frac{R}{r}\right)^4 \frac{5}{8} \left(-3 + 42\frac{z^2}{r^2} - 63\frac{z^4}{r^4}\right) \\
& + J_5 \left(\frac{R}{r}\right)^5 \frac{z}{r} \frac{1}{8} \left(-693\frac{z^4}{r^4} + 630\frac{z^2}{r^2} - 105\right) + \ldots \Bigg]
\end{aligned} \tag{3}$$

$$\overset{oo}{y} = \overset{oo}{x} \frac{y}{x}$$

$$\begin{aligned}
\overset{oo}{z} = -\frac{\mu z}{r^3} \Bigg[& J_2 \left(\frac{R}{r}\right)^3 \frac{3}{2} \left(3 - 5\frac{z}{r}\right) \\
& + J_3 \left(\frac{R}{r}\right)^3 \frac{r}{z} \frac{3}{2} \left(-1 + 10\frac{z^2}{r^2} - \frac{35}{3}\frac{z^4}{r^4}\right) \\
& + J_4 \left(\frac{R}{r}\right)^4 \frac{5}{8} \left(-15 + 70\frac{z^2}{r^2} - 63\frac{z^4}{r^4}\right) \\
& + J_5 \left(\frac{R}{r}\right)^5 \frac{r}{z} \frac{1}{8} \left(15 - 315\frac{z^2}{r^2} + 945\frac{z^4}{r^4} \right. \\
& \left. - 693\frac{z^6}{r^6}\right) + \ldots \Bigg]
\end{aligned}$$

where J_i are the harmonic coefficients. Since the earth is almost spherically symmetric, the J_i are all small compared to 1 (see Chapter II).

b. Perturbative terms due to remote bodies

The perturbative terms due to remote bodies which can be considered as point masses can be written directly from the integrals for the n-body problem as developed in Moulton (Ref. 1) and in other texts on celestial mechanics.

$$\ddot{x} = \sum_{i=1}^{n} \mu_i \left(\frac{x_{\Delta i}}{r_{\Delta i}^3} - \frac{x_i}{r_i^3} \right)$$

$$\ddot{y} = \sum_{i=1}^{n} \mu_i \left(\frac{y_{\Delta i}}{r_{\Delta i}^3} - \frac{y_i}{r_i^3} \right) \qquad (4)$$

$$\ddot{z} = \sum_{i=1}^{n} \mu_i \left(\frac{z_{\Delta i}}{r_{\Delta i}^3} - \frac{z_i}{r_i^3} \right)$$

where $r_{\Delta i}$ is the distance from the satellite to the ith body and r_i is the radius from the center of the earth to the ith perturbing body. For the case of an earth satellite, lunar and solar attractions are the major sources of perturbations for short term orbits. The order of magnitude of these perturbing forces may be observed in Fig. 1. (Subsequent discussions appear in Section C of this Chapter.)

c. Thrust

If thrust is applied, it may also be handled as a perturbation. The general procedure, however, for large thrust-to-mass ratios is to treat the thrust periods in a different fashion by considering the vector sum of the thrust and central force terms as defining the reference trajectory rather than the central force term alone. Since the thrust vector is determined by the maneuver requirements and the guidance law to be utilized, no analytic solutions are available for this reference trajectory; thus, numerical integration is necessary. Indeed, no single form of the perturbing acceleration can be written other than its resolution in terms of generalized vectorial components; for example: $\frac{T_x}{m}$, $\frac{T_y}{m}$ and $\frac{T_z}{m}$.

d. Atmospheric lift and drag (Ref. 2)

$$\ddot{\vec{x}} = D_0^2 \dot{s}^2 \left\{ \left[\mu' \gamma(\nu)\, \sigma(H)\, \gamma(\sigma)\, \nu \frac{\nu_x}{\dot{s}^2} - \mu' \left(A + \frac{B}{\dot{s}} \right) \frac{f(r)}{D_0^2} Q_x \right] - \mu' \gamma(\nu)\, \sigma(H)\, \gamma(\sigma) \frac{\nu^2}{\dot{s}^2} \frac{C_L}{C_{D_0}} \left[\left(\hat{r} \times \frac{\vec{\nu}}{\nu} \right)_x \sin \xi + \left\{ \frac{\vec{\nu}}{\nu} \times \left(\hat{r} \times \frac{\vec{\nu}}{\nu} \right) \right\}_x \cos \xi \right] \right\} \quad \ddot{x} \rightarrow \ddot{y}, \ddot{z}$$

(5)

where the vehicle velocity relative to a rotating atmosphere with cross winds is given by

$$\nu_x = \dot{x} + y\Omega_e + q(\cos\alpha \sin\phi' \cos\beta + \sin\alpha \sin\beta)$$

$$\nu_y = \dot{y} - x\Omega_e + q(\sin\alpha \sin\phi' \cos\beta - \cos\alpha \sin\beta)$$

$$\nu_z = \dot{z} - q \cos\phi' \cos\beta$$

where

A = constant fitted to the Mach number variation of the drag coefficient with a mean sonic speed $\tilde{=} 1$

A_0 = Initial projected frontal area of the vehicle, m^2

B = constant fitted to Mach number variation of the drag coefficient with a mean sonic speed

$$\tilde{=} C_s \left(\frac{C_{D_T}}{C_{D_0}} - 1 \right)$$

C_{D_0} = reference (hypersonic continuum) value of the drag coefficient (0.92 for a sphere, 1.5 for a typical entry capsule)

C_L = lift coefficient

C_s = local sonic speed in terms of surface circular satellite speed

$D_0^2 = C_{D_0} A_0 \rho_0 V_{C0}^2 / 2 g_0 m_0$

$f(r) = \mu_0 D_0^2 \sigma \gamma(\sigma)$

g_0 = acceleration of gravity at unit distance (surface of earth)

H = altitude above an oblate earth = r - 1 $+ f \sin^2\phi' + \frac{f^2}{2}\left(\frac{1}{r} - \frac{1}{4}\right) \sin^2 2\phi' + \ldots$ where the flattening $f = \frac{1}{298.3}$ (units of earth radii)

m = mass of space vehicle (kg)

$\vec{Q}$ = unit vector in the orbit plane perpendicular to the line of apsides

q = speed of the cross wind measured in a system rotating with earth's angular rate (units of surface circular satellite speed V_{CO})

r = radius from the geocenter to the vehicle

$\dot{s}$ = speed of the vehicle with respect to an inertial frame, directed along $\vec{Q}$

V_{CO} = Surface speed for circular orbit--7905.258 m/sec

x, y, z = equatorial coordinates in units of equatorial earth radii

α = right ascension of the vehicle (radians)

β = azimuth of the direction from which the wind is coming

$\gamma(\nu)$ = $C_D(\nu/C_s)/C_{D_0}$, the drag coefficient variation with Mach number

$\gamma(\sigma)$ = $C_D(\sigma)/C_{D_0}$, the drag coefficient variation in the transitional regime

Ω_e = constant relating to the rotational rate of the earth, 0.058834470

μ' = m_0/m

ξ = bank angle

ρ = atmospheric density, kg/m^3

ρ_0 = "sea level" atmospheric density, 1.225 kg/m^3

σ = $\frac{\rho}{\rho_0}$

ϕ' = geocentric latitude, radians

e. Radiation pressure

A body in the region of the earth is subjected to solar radiation pressure amounting to about 4.5×10^{-5} dyne/cm^2, the order of the force being the same for complete absorption and specular reflection of the radiation. Radiation pressure is an important source of perturbations for satellites with area-to-mass ratios greater than about 25 cm^2/gm. The effects of radiation pressure on lifetime are discussed in Chapter V and also in Section C-7 of this chapter.

The rectangular coordinates (X-axis toward vernal equinox) of the accelerations are:

$$\left.\begin{aligned} \ddot{x} &= f \cos A_\odot \\ \ddot{y} &= f \cos i_\odot \sin A_\odot \\ \ddot{z} &= f \sin i_\odot \sin A_\odot \end{aligned}\right\} \qquad (6)$$

where:

$i_\odot$ = inclination of the ecliptic to the equator, 23.4349°

$A_\odot$ = mean right ascension of the sun during the computation

f = $4.5 \times 10^{-5} \left(\frac{A}{m}\right) \frac{cm}{sec^2}$.

f. Electromagnetic forces

As a satellite moves through a partly ionized medium, the incident flux of electrons on the satellite surface is larger than the ion flux, so that the satellite acquires a negative potential. On the day side of the earth, this effect is opposed by the photoejection of electrons. Jastrow (Ref. 3) estimates that the satellite potential may approach -60 volts on the day side and will not be greater than -10 volts on the night side.

In addition to the potential acquired by ionic collision, the motion of a conducting satellite through the magnetic field of the earth causes the satellite to acquire a potential gradient which is proportional to the strength of the magnetic field and the velocity of the satellite. The interaction of the electric currents thus induced in the satellite skin with the magnetic field causes a magnetic drag to act upon the satellite; this drag is proportional to the cube of the satellite dimensions.

If these forces are found not to be negligible, they can be included directly by the use of Maxwell's equations or indirectly by use of an atmospheric model which takes the effects into account.

g. The effects of relativity

Perturbations caused by relativity are of the order $\alpha = \frac{V_0^2}{c^2} = \frac{\mu}{rc^2}$, where c is the speed of light. Since α is a very small quantity and any measurable deviations occur only after a long period of time, relativistic effects can usually be ignored in the case of earth satellites. A modification of Newton's law as a consequence of the theory of relativity can be found in Danby (Ref. 4).

Substitution of these perturbative accelerations (a through g) in Eq (2) yields the complete equation of motion.

2. Special Perturbation Methods

Three special perturbation methods currently used for computing earth satellite orbits will now be discussed with an evaluation of the main advantages and disadvantages of each.

a. Cowell's method

In Cowell's method, the total acceleration, central as well as perturbative, acting on a satellite is integrated directly by one of the numerical integration techniques (Section B of this chapter). The equations of motion which must be integrated twice to obtain position coordinates are:

$$\ddot{x} = -\frac{\mu x}{r^3} + \sum_i \ddot{x}_i, \quad x \to y, z.$$

These equations are symmetrical in the rectangular coordinates and are simple in form; they apply to elliptic parabolic and hyperbolic orbits, and require no conversion from one coordinate system to another.

A disadvantage of the method is the large number of places which must be carried because of the large central force term to prevent loss of significance for the small perturbations. Also, since the total acceleration, which is subject to fairly rapid changes, is being integrated, it is necessary to use a smaller integration step to maintain a given accuracy. This requires an increase in the number of integration steps and the inherent roundoff error accumulation. Detection of small perturbation effects such as those caused by radiation pressure may be impossible due to roundoff and truncation errors. Cowell's method is especially useful when the perturbation forces, such as thrust, are of the same order as the central force.

b. Encke's method

In the Encke method, only the deviations of the actual motion from a reference orbit, which is assumed to be reasonably close to the actual orbit, are integrated. Usually a two-body reference orbit is used since the position at any time on this orbit can be determined analytically. However, more complicated reference orbits such as Garfinkel's solution (Ref. 5), which is known analytically and which incorporates some of the oblateness effects in the earth's gravitational potential, might be used on an earth satellite orbit.

Let x, y, z denote the actual position of the satellite and x_e, y_e, z_e the position on a Keplerian reference orbit.

The equations of motion in an inertial frame of reference are then:

$$\ddot{x} = -\frac{\mu x}{r^3} + \sum_i \overset{oo}{x}_i \qquad x \to y, z \tag{7}$$

$$\ddot{x}_e = -\mu \frac{x_e}{r_e^3} \qquad x_e \to y_e, z_e \tag{8}$$

Let the deviations from the reference orbit be ξ, η, ζ so that:

$$\left.\begin{aligned} \xi &= x - x_e \\ \eta &= y - y_e \\ \zeta &= z - z_e \end{aligned}\right\} \tag{9}$$

Differentiation of Eq (9) and substitution of Eqs (7) and (8) into the result yield:

$$\ddot{\xi} = \ddot{x} - \ddot{x}_e \qquad x \to y, z \text{ for } \xi \to \eta, \zeta$$

$$= \mu\left(\frac{x_e}{r_e^3} - \frac{x}{r^3}\right) + \sum_i \overset{oo}{x}_i \tag{10}$$

$$= \frac{\mu}{r_e^3}\left\{x\left[1 - \left(\frac{r_e}{r}\right)^3\right] - \xi\right\} + \sum_i \overset{oo}{x}_i$$

Because of the possible loss of significance in subtracting nearly equal quantities in Eq (10), it is necessary to rewrite Eq (10) in better computational form.

Substitute Eq (9) into the defining equation for r^2:

$$r^2 = x^2 + y^2 + z^2 \tag{11}$$

$$= (x_e + \xi)^2 + (y_e + \eta)^2 + (z_e + \zeta)^2 \tag{12}$$

$$= r_e^2 + 2\left[\xi\left(x_e + \tfrac{1}{2}\xi\right) + \eta\left(y_e + \tfrac{1}{2}\eta\right) + \zeta\left(z_e + \tfrac{1}{2}\zeta\right)\right] \tag{13}$$

Define q to be:

$$q = \frac{1}{r_e^2}\left[\xi\left(x_e + \tfrac{1}{2}\xi\right) + \eta\left(y_e + \tfrac{1}{2}\eta\right) + \zeta\left(z_e + \tfrac{1}{2}\zeta\right)\right] \tag{14}$$

So that Eq (13) becomes:

$$\left(\frac{r}{r_e}\right)^2 = 1 + 2q \text{ or } \left(\frac{r_e}{r}\right)^3 = (1 + 2q)^{-3/2} \tag{15}$$

Encke's series, using a binomial expansion, is defined by:

$$1 - \left(\frac{r_e}{r}\right)^2 = 1 - (1 + 2q)^{-3/2}$$

$$= \sum_{k=1}^{\infty} (-1)^{k-1} \frac{(2k+1)!}{2^k (k!)^2} q^k = fq$$

$$-1/2 < q < 1/2 \tag{16}$$

Substitution of Eq (16) into Eq (10) yields Encke's formula:

$$\ddot{\xi} = \frac{\mu}{r_e^3}(fqx - \xi) + \sum_i \overset{oo}{x}_i \tag{17}$$

This equation, which employs series expansion, yields more accurate deviations when the terms are small. When the terms exceed a certain limit, a process of rectification is initiated, that is, a new reference orbit is computed. The limits on q needed for rectification are established as:

$$|q| < \left[r_e^2\left(\frac{\Delta\ddot{\xi}}{a_{n+1}}\right)\right]^{\frac{n+1}{2}} \tag{18}$$

where $\Delta\ddot{\xi}$ is the allowable error in $\ddot{\xi}$ and a_{n+1} is the coefficient of the first neglected term of the Encke series.

In contrast to Cowell's method, only the differential accelerations due to perturbations are integrated to obtain deviations from a two-body orbit. These deviations are then added onto the coordinates of the satellite as found from the two-body orbit to obtain the actual position of the satellite. Since the deviations are much smaller and, therefore, need not be determined as accurately, it is possible to maintain a given accuracy with larger integrating steps. As a consequence of the larger integrating steps, there is less danger of serious roundoff accumulation. Moreover, the integration errors affect only the least significant figures in the deviations and, when added to the much larger positions determined from the reference orbit, should have a less serious effect on the overall accuracy. Although the roundoff error is less, Encke's method involves expressions that are much more complicated and often less symmetric than Cowell's simple formulas. In addition, both the necessity of solving the two-body formulas at every step and the possible need for rectification introduce additional sources of error. In the former case, the frequency of rectification affects the attainable accuracy and also introduces small errors in the determination of the mean anomaly M. For the case of nearly parabolic orbits, errors in the use of the two-body formulas in an unaltered form are especially critical. This is due to the fact that when the eccentricity $e \sim 1$, and the eccentric anomaly E is small, cancellation errors arise in forming the radial distance $r = a(1 - e \cos E)$ and the mean anomaly $M = E - e \sin E$. In addition, small division errors will be introduced in forming $p/a = (1 - e^2)$.

The Encke method is especially suited to problems in which the perturbative accelerations are not large and have their major effect over a limited portion of the orbit, e.g., lunar and interplanetary orbits except microthrust or long-thrust trajectories.

c. Variation-of-parameters method

The variation-of-parameters or variation-of-elements method differs from the Encke method in that there is a continuous set of elements for the reference orbit. The reference motion of the satellite can be represented by a set of parameters that, in the absence of perturbative forces, would remain constant with time. The perturbed motion of a satellite may thus be described by a conic section, the elements of which change continuously. The variable Keplerian orbit is tangent to the actual orbit at all times, and the velocity at any time is the same in both orbits. This reference orbit thus osculates with the actual orbit. The variations in the elements used to describe the osculating conic can be integrated numerically to solve for the motion.

Any set of six independent constants can be utilized for this purpose though it is conventional to use the geometrical set a, e, T_p, ω, Ω and i. Lagrange's planetary equations, which specify the variations for this set of parameters, are derived in Section C of this chapter.

It is also possible to choose a different form for the reference motion. As in Encke's method, Garfinkel's solution which includes part of the perturbative forces caused by the nonspherical shape of the earth might be employed. If the drag force predominates, as in the case of entry, a rectilinear gravity-free drag orbit as applied by Baker (Ref. 6) can be used instead.

Many variation-of-parameters methods have been proposed including those of Hansen, Strömgren, Oppolzer, Merton and Herrick. These methods differ in the choice of elements or parameters and of the independent variable. Of these, the parameters suggested by Herrick (Ref. 7) will be briefly described here.

Let x_ω, y_ω be rectangular coordinate axes in the instantaneous orbit plane with x_ω the axis along the perigee radius as shown. Let $\vec{P}$ be the unit vector in the orbit plane in the direction of perigee, $\vec{Q}$ be the unit vector perpendicular to $\vec{P}$ in the direction of motion along the y_ω-axis and $\vec{W}$ be the unit vector normal to the orbit plane in a right-hand system.

The parameters selected by Herrick for orbits of moderate eccentricity are vectors $\vec{A}(t)$ and $\vec{B}(t)$, the mean anomaly M and the mean motion n. The vectors $\vec{A}$ and $\vec{B}$ are defined by:

$$\vec{A} = e\vec{P}$$

$$\vec{B} = e\sqrt{p}\,\vec{Q}$$

$$M = n(t - t_0)$$

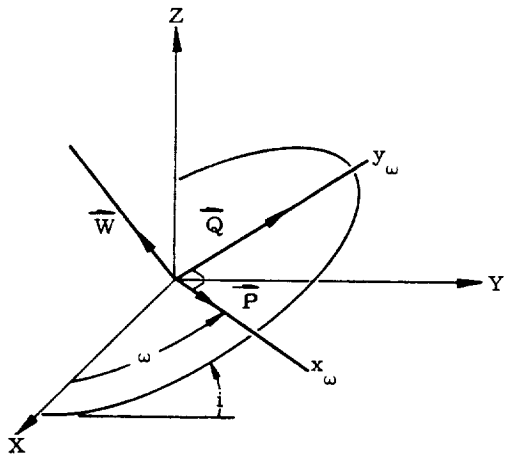

$$n = k_e\sqrt{\frac{1}{a^3}}$$

where

a = semimajor axis

e = eccentricity

p = semilatus rectum

$k_e = \sqrt{GM}$

The differential equations in the parameters have the form:

$$\vec{A} = \vec{A}_0 + k_e \int_{t_0}^{t} \vec{A}' \, dt$$

$$\vec{B} = \vec{B}_0 + k_e \int_{t_0}^{t} \vec{B}' \, dt$$

$$n(t) = n_0 + k_e \int_{t_0}^{t} n' \, dt$$

$$M(t) = M_0 + n_0 (t - t_0) + k_e \iint_{t_0}^{t} n' \, dt \, dt + k_e \int_{t_0}^{t} M' \, dt$$

and the perturbative variations $\vec{A}'$, $\vec{B}'$, n', M' are defined as:

$$D = e \sqrt{a} \sin E = \vec{r} \cdot \frac{\vec{B}}{p}$$

$$H = e x_\omega = -\vec{r} \cdot \vec{A}$$

$$\sqrt{\mu} D' = \vec{r} \cdot \vec{F} = xF_x + yF_y + zF_z$$

$$\mu \frac{dD'}{dt} = 2 \frac{d\vec{r}}{dt} \cdot \vec{F} = 2\left(\frac{dx}{dt} F_x + \frac{dy}{dt} F_y + \frac{dz}{dt} F_z\right)$$

$$H' = 2 DD' - \frac{r^2}{\sqrt{\mu}} \frac{dD'}{dt}$$

$$\frac{dH'}{dt} = \sqrt{\mu} \frac{D'}{r}$$

$$\sqrt{\mu} \vec{B}' = \vec{r} \frac{dH'}{dt} - \frac{d\vec{r}}{dt} H' - \vec{F} H$$

$$\sqrt{\mu} \vec{A}' = \vec{r} \frac{dD'}{dt} - \frac{d\vec{r}}{dt} D' - \vec{F} D$$

$$e^2 \sqrt{p} v' = \vec{A} \cdot \vec{B}' = A_x B_x' + A_y B_y' + A_z B_z'$$

$$\sqrt{a} M' = \sqrt{p} v' - 2 D'$$

$$n' = -\frac{3}{2} \frac{n a}{\sqrt{\mu}} \frac{dD'}{dt}$$

The Herrick elements must be related to the rectangular coordinates and to the usual elliptic elements because the perturbative forces $\vec{F}$ are given in rectangular coordinates. It is thus necessary to go through the two-body formulas at every step, as in the Encke method, and through some complicated conversions as well.

The essential characteristic of this method is that the integration is carried out on parameters which are much more slowly changing functions of time than rectangular coordinates. Since they vary slowly, the error accumulation from the calculation of the derivative is, for a long time, far beyond the eighth significant digit of the initial calculation. Thus, it is expected that truncation error would appear only for very large intervals and much larger integrating steps can be taken for a given accuracy. Since in this method a system of first order equations is being integrated, there is less danger of round-off error accumulation. A disadvantage is that the programming and numerical analysis involved in this method are the most complicated of the three methods discussed. Because of this, the computing time per integration step is at least twice as long as for a Cowell method. The Herrick formulas given here lead to special difficulties on low eccentricity orbits because of small division problems. Similar difficulties arise with other variation-of-parameter methods for low inclination orbits, as well as for hyperbolic and parabolic orbits. Such cases all require special consideration, thus detracting from the usefulness of parameter methods as basic integration tools. A new method due to Pines (Ref. 8) is apparently suitable for all earth satellite orbits. The variation of parameters method is primarily applicable to missions in which small perturbations act throughout the orbit, e.g., microthrust transfer.

C. METHODS FOR NUMERICAL INTEGRATION (REF. 9)

Of the factors affecting the choice of an integration method for space trajectory calculations, the two most important are speed and accuracy. Other factors, such as storage requirements, complexity, and flexibility, are of secondary importance with most modern computers such as the IBM 7090. A good integration subroutine should have the following features:

(1) It should permit as large a step-size as possible. Thus, higher order methods should generally be given preference over lower order methods.

(2) It should allow for the automatic selection of the largest possible integrating step for a required accuracy. The procedure for increasing or decreasing the step-size should be reasonably simple and reasonably fast.

(3) It should be reasonably economical in computing time.

(4) It should be stable; that is, errors introduced in the computation from any source should not grow exponentially.

(5) It should not be overly sensitive to the growth of roundoff errors, and every effort should be made to reduce roundoff error accumulation.

Some of the more commonly used integration methods are compared in detail on the basis of these criteria.

1. Single Step Methods

Of the various Runge-Kutta methods the Gill variation is most popular. It was devised to reduce the storage requirements and to inhibit roundoff error growth. There seems to be little reason to choose the Gill variation over the standard fourth order method when modern computers are available, because the storage savings are insignificant and the roundoff error control can be achieved more simply and more effectively by double precision accumulation of the dependent variables.

The process of double precision accumulation can be used with any integration method. It is extremely effective in inhibiting roundoff error growth and very inexpensive in machine time. The process consists simply of carrying all dependent variables in double precision, computing the derivatives and the increment in single precision, and adding this precision increment to the double precision dependent variables. For integrating a single equation of the form $Y' = dy/dt = f(t, y)$, the formulas for the standard Runge-Kutta fourth order method are

$$\left.\begin{aligned} k_1 &= hf(t_n, y_n) \\ k_2 &= hf\left(t_n + \frac{h}{2}, y_n + \frac{k_1}{2}\right) \\ k_3 &= hf\left(t_n + \frac{h}{2}, y_n + \frac{k_2}{2}\right) \\ k_4 &= hf\left(t_n + h, y_n + k_3\right) \end{aligned}\right\} \qquad (19)$$

(continued)

$$y_{n+1} = y_n + \frac{1}{6}\left(k_1 + 2k_2 + 2k_3 + k_4\right)$$

where h denotes the integration step-size and n denotes the integration step.

Runge-Kutta methods are stable, follow the solution curves well, have a relatively small truncation error among fourth order methods, and do not require any special starting procedure. However,

(1) They tend to require more computing time, since four derivative evaluations per step must be made compared to one or two for other multistep methods.

(2) The usual fourth order methods restrict the step-size for a required accuracy.

(3) There is no simple way to determine the local truncation error and, as a consequence, it is difficult to decide on the optimum step-size for a required accuracy.

Various suggestions have been made for overcoming this deficiency. The same trajectory could be integrated twice: first with step-size h and then with step-size h/2. The difference between the two values at a time t can then be used to decide whether the step-size should be increased or decreased. This process involves three times as much computing and, therefore, cannot be seriously considered. The simplest method, proposed by Aeronutronic, is to integrate over two intervals of length h and then to recompute the dependent variable using Simpson's rule,

$$y^{(s)}_{n+1} = y_{n-1} + \frac{h}{3}\left(y'_{n+1} + 4y'_n + y'_{n-1}\right)$$

The difference between this value and that obtained by the Runge-Kutta method at time t_{n+1} is then used as a criterion. This procedure is relatively simple and inexpensive, but there is no mathematical justification for it. Any decision to change the step-size based on it might be erroneous.

Other single step methods include several attributable to Heun, the improved polygon or Euler-Cauchy method, and a method employed by C. Bowie and incorporated in many Martin programs. Bowie's method is outlined below.

$$\ddot{x}_0 = f_0$$

$$\ddot{y}_0 = g_0$$

$$\dot{x}_{h/2} = \dot{x}_0 + \ddot{x}_0 \frac{h}{2}$$

$$\dot{y}_{h/2} = \dot{y}_0 + \ddot{y}_0 \frac{h}{2}$$

$$x_{h/2} = x_0 + \dot{x}_0 \frac{h}{2} + \ddot{x}_0 \frac{h^2}{8}$$

$$y_{h/2} = y_0 + \dot{y}_0 \frac{h}{2} + \ddot{y}_0 \frac{h^2}{8}$$

$$\dot{x}_h = \dot{x}_0 + \ddot{x}_0 h$$

$$\dot{y}_h = \dot{y}_0 + \ddot{y}_0 h$$

$$x_h = x_0 + \dot{x}_0 h + \ddot{x}_0 \frac{h^2}{2}$$

$$y_h = y_0 + \dot{y}_0 h + \ddot{y}_0 \frac{h^2}{2}$$

Step A

$$\ddot{x}_{h/2} = f_{h/2},\ \ddot{y}_{h/2} = g_{h/2},\ \ddot{x}_h = f_h,\ \ddot{y}_h = g_h$$

$$\dot{x}_{h/2} = \dot{x}_0 + \frac{h}{24}\left\{5\ddot{x}_0 + 8\ddot{x}_{h/2} - \ddot{x}_h\right\}$$

$$\dot{y}_{h/2} = \dot{y}_0 + \frac{h}{24}\left\{5\ddot{y}_0 + 8\ddot{y}_{h/2} - \ddot{y}_h\right\}$$

$$x_{h/2} = x_0 + \dot{x}_0 \frac{h}{2} + \frac{h^2}{96}\left(7\ddot{x}_0 + 6\ddot{x}_{h/2} - \ddot{x}_h\right)$$

$$y_{h/2} = y_0 + \dot{y}_0 \frac{h}{2} + \frac{h^2}{96}\left(7\ddot{y}_0 + 6\ddot{y}_{h/2} - \ddot{y}_h\right)$$

$$\dot{x}_h = \dot{x}_0 + \frac{h}{6}\left\{\ddot{x}_0 + 4\ddot{x}_{h/2} + \ddot{x}_h\right\}$$

$$\dot{y}_h = \dot{y}_0 + \frac{h}{6}\left\{\ddot{y}_0 + 4\,\ddot{y}_{h/2} + \ddot{y}_h\right\}$$

$$x_h = x_0 + \dot{x}_0\,h + \frac{h^2}{6}\left\{\ddot{x}_0 + 2\,\ddot{x}_{h/2}\right\}$$

$$y_h = y_0 + \dot{y}_0\,h + \frac{h^2}{6}\left\{\ddot{y}_0 + 2\,\ddot{y}_{h/2}\right\}$$

Step B

$$\ddot{x}_{h/2} = f_{h/2},\ \ddot{y}_{h/2} = g_{h/2},\ \ddot{x}_h = f_h,\ \ddot{y}_h = g_h$$

$$\dot{x}_h = \dot{x}_0 + \frac{h}{6}\left\{\ddot{x}_0 + 4\,\ddot{x}_{h/2} + \ddot{x}_h\right\}$$

$$\dot{y}_h = \dot{y}_0 + \frac{h}{6}\left\{\ddot{y}_0 + 4\,\ddot{y}_{h/2} + \ddot{y}_h\right\}$$

$$x_h = x_0 + \dot{x}_0\,h + \frac{h^2}{6}\left\{\ddot{x}_0 + 2\,\ddot{x}_{h/2}\right\}$$

$$y_h = y_0 + \dot{y}_0\,h + \frac{h^2}{6}\left\{\ddot{y}_0 + 2\,\ddot{y}_{h/2}\right\}$$

If the functions f, g do not actually involve $\dot{x}$, $\dot{y}$ it is clear that $\dot{x}_{h/2}$, $\dot{y}_{h/2}$ need never be computed and that $\dot{x}_h$, $\dot{y}_h$ need only be computed at the point they occur for the last time in the above list.

It will be noted that the process as described above involves two iterations and requires that the functions f, g be evaluated five times. If further iterations are desired, one simply goes back to the point marked "A" when he completes all the steps of the preceding page. Note that Steps "A" and "B" are identical, though the formulas immediately following them are not.

If the number of iterations are continued until there is no (sensible) change, the solution is exact on the assumption that $\ddot{x}$ and $\ddot{y}$ vary quadratically over each interval. Since this assumption is exactly realized only in trivial cases (for which it would be unreasonable to use any stepwise method), the optimum procedure seems to be to do only the two iterations as the list of steps implies. Put another way: when the overall accuracy is not sufficient, it is better to shorten the time interval than to increase the number of iterations beyond two per interval.

2. Fourth Order Multistep Prediction-Correct Method

Of this type, for a first order system $y' = f(t, y)$ are the Milne and Adams-Moulton methods. The Milne formulas are:

$$\left.\begin{aligned} y^{(p)}_{n+1} &= y_{n-3} + \frac{4h}{3}\left(2y'_n - y'_{n-1} + 2y'_{n-2}\right) + \frac{14}{45}\,h^5 y^{v}(\xi) \\ y^{(c)}_{n+1} &= y_{n-1} + \frac{h}{3}\left(y'_{n+1} + 4y'_n + y'_{n-1}\right) - \frac{h^5}{90}\,y^{v}(\xi) \end{aligned}\right\} \quad (20)$$

and the Adams-Moulton formulas are

$$\left.\begin{aligned} y^{(p)}_{n+1} &= y_n + \frac{h}{24}\left(55y'_n - 59y'_{n-1} + 37y'_{n-2} - 9y'_{n-3}\right) + \frac{251}{720}\,h^5 y^{v}(\eta) \\ y^{(c)}_{n+1} &= y_n + \frac{h}{24}\left(9y'_{n+1} + 19y'_n - 5y'_{n-1} + y'_{n-2}\right) - \frac{19}{720}\,h^5 y^{v}(\eta) \end{aligned}\right\} \quad (21)$$

For these methods, as well as for all multistep methods, special formulas must be used to obtain starting values at the beginning of the integration and wherever it is desired to double or halve. A Runge-Kutta method is the most convenient for obtaining these starting values. The difference between the predicted and corrected values provides a good estimate of the local truncation error and this estimate can then be used to decide on whether to increase or reduce the step-size.

The Milne method has a somewhat smaller local truncation error, but for some equations it may be unstable (i.e., errors introduced into the computation will grow exponentially) and, while some techniques have been suggested to eliminate this instability, it is probably advisable to avoid the use of the Milne method.

The Adams-Moulton formulas are unconditionally stable and lead to a fast and reasonably accurate method. Its principal disadvantage is its low order of accuracy which restricts the integration step-size.

3. Higher Order Multistep Methods

Variation-of-parameter methods lead to systems of equations which are essentially first-order in form as contrasted to Cowell and Encke methods which lead to systems of second order equations. For second order systems, special integration methods are available.

Before considering these, the Adams backward difference method applicable to first order systems must be mentioned. If the system has the form $y' = f(t, y)$, the Adams formulas are

$$y_{n+1} = y_n + h\sum_{k=0}^{N} \alpha_k \nabla^k f_n \quad (22)$$

where ∇^k is the backward difference operator defined by

$$\nabla^k f_n = \nabla^{k-1} f_n - \nabla^{k-1} f_{n-1};\ \nabla^0 f_n = f_n$$

The first few values of α_k are (1, 1/2, 5/12, 3/8, 251/720, 95/288) for k = 0, 1, 2, 3, 4, 5. If Nth differences are retained, the principal part of the local truncation error is $0(h^{N+2})$. If Nth differences are retained, then N + 1 consecutive values of y_i must be available, and

these must be supplied by some independent method. This Adams formula is of the open type and, therefore, not as accurate as a closed type formula of the same order would be. However, it involves only one derivative evaluation per step and this, combined with the smaller truncation error, leads to a very fast, stable integration method for first order systems.

The Adams method can be modified for second order systems. Thus, if the system to be solved has the form $y'' = \frac{d^2y}{dt^2} = f(t, y, y')$, the method consists of applying the formulas

$$\left.\begin{aligned} y'_{n+1} &= \dot{y}'_n + h \sum_{k=0}^{N} \alpha_k \nabla^k f_n \\ y_{n+1} &= y_n + h\, y'_n + h^2 \sum_{k=0}^{N} \beta_k \nabla^k f_n \end{aligned}\right\} \quad (23)$$

The first six values of α_k are the same as those given above, while the first six values of β_k are (1/2, 1/6, 1/8, 19/180, 3/32, 863/10080).

In contrast to the straight use of differences as exemplified by the Adams method the Gauss-Jackson method makes use of a summation process. The formulas may be expressed in terms of differences or in terms of ordinates. In ordinate form, predicted values for y at time $t = t_n$ are given by the equations

$$\left.\begin{aligned} y_n^p &= h^2 \left({}''f_n + \sum_{k=0}^{n-1} c_k f_k \right) \\ \left(\frac{dy}{dt}\right)_n^p &= h \left({}'f_{n-1/2} + \sum_{k=1}^{n-1} d_k f_k \right) \end{aligned}\right\} \quad (24)$$

where the first sums ${}'f_{n-1/2}$ and the second sums ${}''f_n$ are defined by the recurrence relations

$$\left.\begin{aligned} {}'f_{n-1/2} &= f_{n-1} + {}'f_{n-3/2} \\ {}''f_n &= {}'f_{n-1/2} + {}''f_{n-1}. \end{aligned}\right\} \quad (25)$$

Using these predicted values, y_n, $d/dt(y_n)$, and the attractions f_n may be computed from the equations. The following corrector formulas can then be used to obtain improved values for y_n, $d/dt(y_n)$

$$\left.\begin{aligned} y_n^c &= h^2 \left({}''f_n + \sum_{k=1}^{n} c_k^1 f_k \right) \\ \left(\frac{dy^c}{dt_n}\right) &= h \left({}'f_{n-1/2} + \sum_{k=1}^{n} d_k^1 f_k \right) \end{aligned}\right\} \quad (26)$$

The coefficients c_k, d_k, c_k^1, d^1, depend upon the number of differences retained. For n = 11, the coefficients are given in Ref. 10. With a single precision machine, it is recommended that eight differences be retained in these formulas. The starting values as well as the first and second sums must be supplied by an independent method. The difference between the predicted and corrected values can be used to decide whether to double or halve the step-size. A convenient method for starting or changing the step-size is the Runge-Kutta method, but, since this is a lower order method, several Runge-Kutta steps will have to be taken for each Gauss-Jackson step.

The Gauss-Jackson second-sum method is strongly recommended for use in either Encke or Cowell programs. For comparable accuracy, it will allow step-sizes larger by factors of four or more than any of the fourth order methods. The overall savings in computing time will not be nearly so large, however, because per step computing time is somewhat greater and because the procedure for starting and changing the interval is quite expensive. As compared with unsummed methods of comparable accuracy, the Gauss-Jackson method has the very important advantage that roundoff error growth is inhibited. It can be shown that, in unsummed methods roundoff error growth is proportional to $N^{3/2}$, where N is the number of integration steps compared with $N^{1/2}$ for summed methods. The Gauss-Jackson method is particularly suitable on orbits where infrequent changes in the step-size are necessary. Frequent changes in the step-size will result not only in increased computing time but in decreased accuracy as well.

Finally mentioned is a higher order method, associated with the name of Obrechkoff, which makes use of higher derivatives. A two-point predictor-corrector version as applied to a first order system y' = f(t, y) makes use of the formulas

$$\left.\begin{aligned} y_{n+1}^{(p)} &= y_{n-1} + 2h \left(4y'_n - 3y'_{n-1}\right) - \frac{2h^2}{5} \left(8y''_n + 7y''_{n-1}\right) + \frac{2h^2}{15} \left(7y'''_n - 3y'''_{n-1}\right) + \frac{13h^7}{6300} y^{vii}(\xi) \\ y_{n+1}^{(c)} &= y_n + \frac{h}{2} \left(y'_{n+1} + y'_n\right) - \frac{h^2}{10} \left(y''_{n+1} - y''_n\right) + \frac{h^4}{120} \left(y'''_{n+1} + y'''_n\right) - \frac{h^7}{100,800} y^{vii}(\xi) \end{aligned}\right\} \quad (27)$$

where the higher order primes mean the higher order derivative of y with respect to t. The disadvantage of this method is that the higher derivatives of the dependent variable must be available. Thus, to use these formulas, the first order system would have to be differentiated two times.

Moreover, as the force terms in the equations of motion change, these higher derivatives will also have to be changed. Thus, in spite of the favorable truncation error, this method cannot be recommended as a general purpose subroutine for space trajectory computations. However, the method appears clearly tailored to the lunar trajectory problem (Ref. 11).

4. Special Second Order Equations of the Form $y'' = f(t, y)$

The free-flight equations in the absence of thrust or drag forces can be written in the form $y'' = f(t, y)$ with missing first derivative terms. Some formulas which take advantage of this form have been proposed. The following special Runge-Kutta method, for example, requires only three derivative evaluations per step and, thus, results in a saving of about 25 percent over the standard Runge-Kutta formulas:

$$\left.\begin{aligned} k_1 &= hf(t_n,\ y_n) \\ k_2 &= hf\left(t_n + \frac{h}{2},\ y_n + \frac{h}{2}y_n' + \frac{h}{8}k_1\right) \\ k_3 &= hf\left(t_n + h,\ y_n + hy_n' + \frac{h}{2}k_2\right) \\ y_{n+1} &= y_n + h\left[y_n' + 1/6\ (k_1 + 2k_2)\right] \\ y_{n+1}' &= y_n' + 1/6\ (k_1 + 4k_2 + k_3). \end{aligned}\right\} \quad (28)$$

A predictor-corrector method (due to Milne and Stormer) adapted to this form makes use of the formulas

$$\left.\begin{aligned} y_{n+1}^p &= y_n + y_{n-2} - y_{n-3} + \frac{h^2}{4}(5f_n + 2f_{n-1} + 5f_{n-2}) + \frac{17h^6}{240}\,y^{vi}(\xi) \\ y_{n+1}^c &= 2y_n - y_{n-1} + \frac{h^2}{12}(f_{n+1} + 10f_n + f_{n-1}) - \frac{h^6}{240}\,y^{vi}(\eta). \end{aligned}\right\} \quad (29)$$

These formulas appear to achieve a local truncation error of $0(h^6)$ while retaining only four ordinates, compared with an $0(h^5)$ error for other fourth order methods. However, this advantage is illusory since the overall error is still $0(h^4)$ as in fourth order methods. In addition these formulas are somewhat unstable relative to roundoff error propagation. In practice there appears to be little to recommend the Milne-Stormer method.

The characteristics of these various integration routines are summarized in Table 1.

5. Evaluation of Integration Methods

The more important integration methods in general usage will be evaluated below as they are utilized with the various special perturbation formulations.

a. Cowell method

For the Cowell method, the choice of an integrating routine is very important because of the greater danger of loss of significance due to roundoff error accumulation. The Gauss-

TABLE 1

Comparison Criteria

Method of Numerical Integration	Truncation Error	Ease of Changing Step-Size	Speed	Stability	Roundoff Error Accumulation
Single Step Methods					
Runge-Kutta	h^5	*	Slow	Stable	Satisfactory
Runge-Kutta Gill	h^5	*	Slow	Stable	Satisfactory
Bowie	h^3	Trivial (step-size varied by error control)	Fast	Stable	Satisfactory
Fourth Order Multistep Predictor-corrector					
Milne	h^5	Excellent	Very fast	Unstable	Poor
Adams-Moulton	h^5	Excellent	Very fast	Unconditionally stable	Satisfactory
Higher Order Multistep					
Adams Backward Difference	Arbitrary	Good	Very fast	Moderately stable	Satisfactory
Gauss-Jackson**	Arbitrary	Awkward and expensive	Fast	Stable	Excellent
Obrechkoff	h^7	Excellent	***	Stable	Satisfactory
Special Second Order Equations [$y'' = f(t, y)$]					
Special Runge-Kutta	h^5	*	Slow	Stable	Satisfactory
Milne-Stormer	h^6	Excellent	Very fast	Moderately stable	Poor

*R-K (single step) trivial to change steps, very difficult to determine proper size.
**Gauss-Jackson is for second order equations.
***Speed of Obrechkoff depends on complexity of the higher order derivatives required; it could be very fast.

Jackson method of integration is recommended for Cowell programs because it allows larger step-sizes and because it inhibits roundoff error growth.

b. Encke method

For the Encke method, the choice of an integration method is less important relative to accuracy. There is some advantage in computing time, however, in choosing a single step method which will allow frequent changes in step-size without the necessity of going through an expensive restart procedure. For lunar flights, it has been found that the Obrechkoff method is especially useful in reducing computing time, but this method does not appear to be easily adaptable to other types of orbits or to other formulations. Although the Gauss-Jackson method is recommended in Encke programs, its advantages over other methods are not as great as in Cowell programs.

c. Variation-of-parameters method

For variation-of-parameters methods, the Adams backward difference formulas are recommended among higher order methods and the Adams-Moulton formulas among lower order methods.

In general, multistep integration methods which allow for automatic adjustment of the size based on an error criterion are preferred.

With any integration method, the process of double precision accumulation of the dependent variables should be used to prevent excessive roundoff error growth.

6. Summary of Studies on Special Perturbation Methods

In order to provide the mission analyst with a set of guide lines in determining the best integration methods for various special perturbation methods used in computing precise satellite trajectories, it is useful to examine the results obtained by others in the industry. This section is intended to show the interrelation of the mission, formulation of the problem, and method of integration so that the most efficient, accurate, and economical balance is achieved. Several serious questions, which must be carefully considered by the mission analyst, are raised in connection with the balance between the type of orbit and the scheme of integration.

a. Aeronutronic report (Refs. 12 and 13)

The Cowell, Encke and Herrick methods are compared for the following problems: a selenoidal satellite which is physically unstable, but for which an analytic solution is known; a low thrust trajectory; a high thrust trajectory and a ballistic lunar trajectory. In all cases the integration is carried out with a Runge-Kutta method with variable step-size adjustment. Their conclusions are:

(1) For the Cowell method, the effect of roundoff error is felt very quickly--within a few hundred steps.

(2) Overall, the Encke and Herrick methods are computationally more efficient than the Cowell method.

(3) On ballistic lunar trajectories, the Encke method is best. The Cowell method requires almost ten times as many integrating steps as the Encke method and three times as many as the Herrick method.

(4) On continuous low thrust trajectories, the Herrick method is superior.

(5) On trajectories where high thrust corrective maneuvers are introduced, the Cowell method is superior.

Although the trend of the conclusions in this study is probably correct, there are serious questions as to the validity of the conclusions on the degree of superiority of the perturbation methods. For one thing the method of integration (Runge-Kutta) favors the perturbation method. For the Cowell method, the choice of integration method is much more important, as indicated earlier. Experience has shown that roundoff error effects are not nearly so critical as concluded here. Both the use of the Gauss-Jackson integration method and double precision accumulation make roundoff error much less serious for the Cowell method than indicated here. The evidence presented, moreover, is not conclusive relative to accuracy. The numerical results, for example, are not given at corresponding times, and no accurate standard for comparison is available except for the unstable selenoidal satellite. The selenoidal satellite is by no means typical of the earth satellite problems and any generalizations of results based on a study of this orbit must certainly be viewed with skepticism.

b. Republic Aviation report (Ref. 14)

The orbit selected is that of a vehicle moving in the gravitational field of two fixed centers. An analytic solution in terms of elliptic functions is available for this orbit so that an accurate standard is thus available. This study compares the Encke, Cowell and Herrick methods with two different integration routines: a fourth order Runge-Kutta method and a sixth order Adams method. The conclusions of this study are:

(1) The Encke method was superior to the others in both accuracy and machine time. For an integration over a 100-hr period the Encke method required 0.5 min, the Herrick method 2.5 min and the Cowell method 3.5 min. All of those programs used the same integration method and the results were comparable as to accuracy.

(2) The Herrick method is superior to the Cowell method relative to attainable

accuracy and slightly better relative to computing time.

(3) An integral of the motion, such as the energy integral or a component of the angular momentum, is a poor positive test of accuracy.

(4) The Adams method is considerably faster than the Runge-Kutta method by a factor of almost three.

(5) Double precision accumulation is very effective in reducing errors due to roundoff.

(6) The largest error in the Encke and Herrick methods arises from errors in solving the two-body formulas, particularly as such errors affect the mean anomaly calculation.

The conclusions of this study appear to be well grounded. The only serious consideration is that the orbit selected is quite specialized and that no strong perturbations such as those due to oblateness or thrust are considered. Thus the extent to which these results can be assumed typical for satellite orbits is in some doubt.

c. Experiments at STL

The relative efficiency of the special perturbation methods is a function of (1) the type of orbit and (2) the method of integration. A given integration subroutine may favor one of the methods over another, so that the use of the same subroutine for all methods does not constitute a fair test.

In general there appears to be no doubt that the Encke method is computationally the most efficient on ballistic lunar trajectories. For comparable accuracy, however, the advantage in computing time is probably on the order of two or three, rather than ten as is sometimes quoted, when any of the standard integration subroutines are used.

There is no doubt that the Cowell method requires much greater care to ensure that roundoff errors do not become a serious factor in the accuracy. However, effective methods are available to curb roundoff error growth. When these are used, the Cowell method is still a very useful tool for many space computations.

None of the orbits considered in the reports by Aeronutronic and Republic Aviation appear to be applicable to the earth satellite problem in which a small but significant force, such as that of oblateness, is continuously applied.

To obtain information about the comparative performance of these special perturbation methods on earth satellite orbits, a numerical study was recently completed at STL. An idealized orbit was selected for the study with initial elements:

$a = 1.5$ earth radii

$e = 0.2$

$i = 45°$

$\Omega = \omega = M_0 = 0$

period of the unperturbed orbit = 155 min

perigee distance = 800 mi

apogee distance = 3200 mi

The only perturbation force considered was that due to the second harmonic in the earth's gravitational potential (J_2). An accurate standard against which to check the programs was provided by a double precision Cowell program. The double precision program yielded results on the unperturbed orbit ($J_2 = 0$) which agreed with the known analytic solution to a few digits in the eighth significant figure. For the perturbed orbit, the results provided by the standard are correct to at least seven significant figures.

Single precision floating point programs for the Cowell, Encke and Herrick methods were run on an IBM 7090 and compared with the double precision standard. Great care was used to ensure that all physical constants and initial conditions were identical in all programs. The integration was performed over 64 revolutions with output at 20-min intervals. Table 2 gives the method of integration used, the local truncation error criterion, the number of integration steps required, the computing time for 64 revolutions, and the maximum error in the distance Δr over the 64 revolutions. For each method several runs were made with successively tighter error criteria, and the most accurate of these was selected for the comparison. While the Cowell method required almost twice as many integrating steps, overall computing time was only slightly greater than the Encke method and, moreover, the accuracy was somewhat better. The Herrick method gave the best accuracy. The relatively large computing time required by the Herrick method is partially accounted for by the fact that the Adams-Moulton formulas (fourth order) are of lower order than the Gauss-Jackson formulas (sixth order). Since the latter will allow integrating steps perhaps twice as large for the same accuracy, the adjusted computed time would be comparable to that for the Cowell method.

A more detailed comparison of achievable accuracy is contained in Table 3 where the maximum errors in the distance r, the mean anomaly M, the semimajor axis a, and energy integral E are given on the 20th, 40th and 64th revolutions. It is clear that the Herrick method consistently yields the most accurate results and the Encke method yields the worst results. For all methods, there is a strong correlation between mean anomaly errors and position errors, indicating that the error is largely along the path of the motion. This conclusion also follows from the energy integral errors which are seen to be relatively constant and much smaller than the position errors. It may also be concluded that the constancy of the energy integral is a poor positive test of accuracy in the position coordinates. The

TABLE 2

Numerical Results--Special Perturbation Methods

Formulation	Method of Integration	Error Criterion	Number of Steps	Computing Time (min)	Maximum Δr (ft)
Cowell	Gauss-Jackson	1×10^{-10}	10,200	5.75	800
Encke	Gauss-Jackson	7×10^{-10}	6395	5.31	1700
Herrick	Adams-Moulton	5×10^{-10}	7000	11.45	400

TABLE 3

Maximum Error--Special Perturbation Methods

Method	Cowell			Encke			Herrick		
Revolution	20	40	64	20	40	64	20	40	64
$\Delta r \times 10^{6}$ (er)	1.2	2.2	4.0	2.2	6	8.4	0.2	0.8	2
$\Delta M \times 10^{3}$ (deg)	0.3	0.6	1	1	2	2.7	0.1	0.2	0.6
$\Delta a \times 10^{7}$ (er)	1.6	1.4	1	3	3.5	3	2.2	2.2	2.2
$\Delta E \times 10^{9}$ $\left(\frac{er}{min}\right)^2$	1	1	1	4	6	9	2	2	2

error in the semimajor axis is also seen to be smaller than the position errors, indicating that the geometry of the orbit is much more accurately determined than position in the orbit.

Although these results show that the Herrick method yields the most accurate results and the Encke method takes the least computing time, the order of magnitude of the difference is not sufficient to lead to a clear preference for any one method. Some improvement in the Encke and Herrick results could probably be obtained by even more careful analysis of the two-body formula computations. The Encke method, for example, is quite sensitive to the frequency of rectification and some improvement might be obtained by experimenting with rectification. There appears to be little reason to prefer either the Encke or the Herrick methods on earth satellite orbits of moderate eccentricity particularly, since they are considerably more complicated and require much more careful numerical analysis. In addition, special difficulties will arise in limiting type orbits (low eccentricity, high eccentricity, critical inclination) which do not arise when the Cowell method is used.

D. GENERAL PERTURBATIONS

Chapter III presented the discussion of motion about point mass (or a spherically symmetric mass). Although that discussion is revealing, it does not in general constitute a solution to the problem because the assumptions utilized prevent the solution from behaving as it should for the true gravitational field. In the preceding sections of this chapter, discussions have been presented which circumvent these limitations; however, in the process much generality has been lost since nothing can be said for trajectories beyond the neighborhood of the numerically obtained trajectory and nothing can be said about the long-term behavior of the orbit. (Before proceeding, it must be added in defense of numerical integration that the solutions thus obtained are valid to a very high order of approximation.) For these reasons it is desired that analytic expressions be presented which can be utilized to describe the motion of a satellite to varying orders of approximation. The approach taken here will be first to discuss the variation of the orbital elements and secondly, the first order secular or cumulative perturbations which can be added as linear functions of time or as discrete corrections to the two-body solution to improve the fit of the resulting motion. Then as a third step, the various general perturbation theories (i.e., approximate analytic

solutions for the perturbed motion obtained by series expansion) which present second order secular and periodic effects will be discussed. The advantages and disadvantages of this approach are summarized at this point.

Advantages of general perturbation methods are:

(1) They are very fast both because no step-by-step integration is necessary to obtain the elements at a given time and because the computing time per point is very small (on the order of 1 sec per point on an IBM 704).

(2) The accuracy of the computation is limited only by the order to which the expansion is carried out, and not by the accumulation of roundoff and truncation errors.

(3) They can maintain reasonable accuracy over many hundreds of revolutions.

(4) They allow for a clearer interpretation of the sources of the perturbation forces and the qualitative nature of an orbit.

Disadvantages of general perturbation methods are:

(1) Nonconservative forces, such as drag, are not easily included in the theory. No simple and adequate theory has yet been prepared which includes such forces in a form suitable for numerical computation.

(2) The effect of other forces, such as luni-solar perturbations and radiation pressure, are difficult to incorporate since they involve substantial amounts of new analysis and checkout.

(3) The series expansions are very complicated, and programs based upon them are complicated to write and difficult to check out even for a first order theory.

(4) There is a serious degradation in accuracy for special types of orbits including the important case of nearly circular orbits (e ~ 0), highly elliptical orbits (e ~ 1) and orbits near the critical inclination (i ~ 63.4°).

(5) Although agreement with observations does confirm practical convergence, no mathematical proof of convergence has yet been given for any of the general perturbation methods, nor are any estimates of the error in the truncated series available.

Finally, these discussions will be followed by those of atmospheric effects and extra-terrestrial effects.

1. Rates of Change of Satellite Orbital Elements Caused by a Perturbing Force (Ref. 15)

The instantaneous rates of change of satellite orbital elements caused by a perturbing force, as given, for example, by Moulton (Ref. 1, pp 404 and 405) are derived from astronomical perturbation theory involving tedious mathematical transformations. The purpose of this development is to give a simplified derivation of the same equations by using only elementary principles of mechanics. It is hoped that this approach will make the equations more meaningful and the discussions which follow later in the chapter more readily appreciated.

Consider a satellite of mass m moving in the inverse square force field of the earth. Its orbit is a Kepler ellipse (Ref. 1, Chapter V) specified by the following orbital elements a, e, h, ω, i and M_0 (see following sketch). The location of the satellite in its orbit is given by the angular position ϕ which is measured in the orbital plane from the node. The angular distance of the satellite from perigee is called the true anomaly, θ. Therefore,

$$\phi = \omega + \theta \tag{30}$$

The radial distance, r, from the center of the earth to the satellite is given by

$$r = \frac{p}{1 + e \cos \theta} . \tag{31}$$

The satellite's energy per unit mass, ϵ, and its angular momentum per unit mass, h, are related to the orbital elements by the equations

$$\epsilon = - \frac{\mu}{2a} \tag{32}$$

and

$$h = r^2 \dot{\theta} = \sqrt{\mu p} = na^2 \sqrt{1 - e^2} \tag{33}$$

where: μ = GM (the product of the gravitational constant and the earth's mass) and a dot over a quantity indicates a time rate and

$$n = \sqrt{\frac{\mu}{a^3}} . \tag{34}$$

Now suppose that a perturbing force $\vec{F}$ acts on the satellite. The orbit will no longer be a Kepler ellipse, but at every instant we can associate an "instantaneous osculating ellipse" with the new orbit by choosing the Kepler orbit corresponding to the instantaneous radius and velocity vectors of the satellite and to the potential energy, $-\frac{\mu}{r}$, of the satellite in the gravitational field of the spherical earth. This is the orbit the satellite would follow if the perturbing force were removed at that instant. The true orbit can thus be specified completely by a series of elements of the instantaneous osculating ellipse. Therefore, the set of differential equations which shows how these elements change with time is equivalent

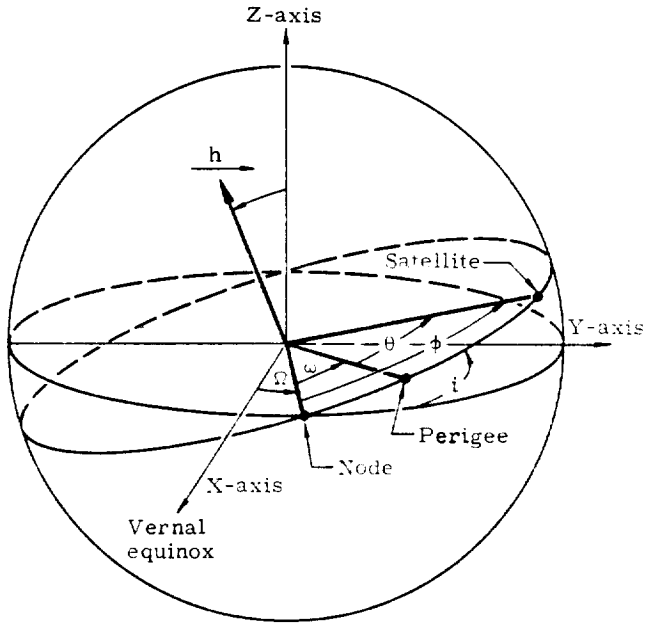

to the Newton or LaGrange set involving the coordinates and their rate of change with time. With this discussion as background, the rates of change of the orbital elements a, e, Ω, ω and i will now be derived.

Following Moulton (Ref. 1, p 402), the perturbing acceleration, $\vec{F}/m$, may be resolved into a component R along the radius vector (measured positive away from the center of the earth), a transverse component S in the instantaneous plane of the orbit (measured positive when making an angle less than 90 deg with the velocity vector $\vec{V}$), and a component W normal to the instantaneous plane (measured positive when making an angle less than 90 deg with the north pole or z-axis).

Let the unit vectors along the three directions be denoted by $\vec{n}_r$, $\vec{n}_s$ and $\vec{n}_w$. That is,

$$\vec{F} = m(R\vec{n}_r + S\vec{n}_s + W\vec{n}_w). \tag{35}$$

To find the rate of change of the semimajor axis, a, refer to Eq (32) for the relationship to the energy

$$\frac{da}{dt} = \frac{2a^2}{\mu}\frac{d\epsilon}{dt}. \tag{36}$$

The energy change (per unit mass) may be found from the definition of the work done on the satellite by the perturbing force.

$$\frac{d\epsilon}{dt} = \frac{\vec{F}}{m} \cdot \vec{V} \tag{37}$$

where $\vec{V}$ is the instantaneous velocity vector,

$$\vec{V} = \dot{r}\vec{n}_r + r\dot{\theta}\vec{n}_v = \dot{\theta}\left(\frac{dr}{d\theta}\vec{n}_r + r\vec{n}_s\right). \tag{38}$$

Now from the definition of the instantaneous osculating ellipse, it is clear that its velocity vector is the same as the instantaneous velocity vector of the actual orbit. Therefore $\dot{\theta}$ and $\frac{dr}{d\theta}$ in Eq (38) may be evaluated from Eqs (31) and (33) to obtain

$$\vec{V} = \frac{na^2\sqrt{1-e^2}}{r^2}\left(\frac{re\sin\theta}{1+e\cos\theta}\vec{n}_r + r\vec{n}_s\right). \tag{39}$$

Forming the dot product with $\vec{F}/m$ and substituting the resulting expression for $\frac{d\epsilon}{dt}$ in Eq (36) yields

$$\frac{da}{dt} = \frac{2e\sin\theta}{n\sqrt{1-e^2}}R + \frac{2a\sqrt{1-e^2}}{nr}S \tag{40}$$

which is the expression given for $\frac{da}{dt}$ by Moulton (Ref. 16).

To derive the changes in the other orbital elements, it is necessary to know the rate at which the angular momentum vector $\vec{h}$ (per unit mass) changes. This rate of change of $\vec{h}$ is then known to be equal to the summation of the external moments acting on the satellite.

$$\frac{d\vec{h}}{dt} = \frac{1}{m}(\vec{r} \times \vec{F})$$

$$= r\vec{n}_r \times (R\vec{n}_r + S\vec{n}_s + W\vec{n}_w) \qquad (41)$$

$$= rS\vec{n}_w - rW\vec{n}_s$$

The rate of change of $\vec{h}$ can also be written as

$$\frac{d\vec{h}}{dt} = \frac{dh}{dt}\vec{n}_w + h\frac{d\alpha}{dt}\vec{n}_s \qquad (42)$$

where $d\alpha$ is the angle through which the angular momentum vector is rotated in time dt. Therefore,

$$\frac{dh}{dt} = rS \qquad (43)$$

and

$$\frac{d\alpha}{dt} = -\frac{rW}{h}. \qquad (44)$$

Now, the eccentricity of the orbit may be expressed in terms of a and h through Eqs (33) and (34) which yield

$$e = \left(1 - \frac{h^2}{\mu a}\right)^{1/2} = (1 - p/a)^{1/2}$$

By differentiating, the following is obtained

$$\frac{de}{dt} = -\frac{h}{2\mu ae}\left(2\frac{dh}{dt} - \frac{h}{a}\frac{da}{dt}\right)$$

$$= -\frac{\sqrt{1-e^2}}{2na^2 e}\left(2\frac{dh}{dt} - na\sqrt{1-e^2}\frac{da}{dt}\right). \qquad (45)$$

Upon substituting Eqs (40) and (43) for $\frac{dh}{dt}$ and $\frac{da}{dt}$, Eq (45) takes the final form,

$$\frac{de}{dt} = \frac{\sqrt{1-e^2}\sin\theta}{na}R + \frac{\sqrt{1-e^2}}{na^2 e}\left[\frac{a^2(1-e^2)}{r} - r\right]S. \qquad (46)$$

The motion of the node is the same as the motion of the projection of $\vec{h}$ on the equatorial plane (see the following sketch). Let the subscript p denote the projection of any vector on the equatorial plane. Then it can be seen that

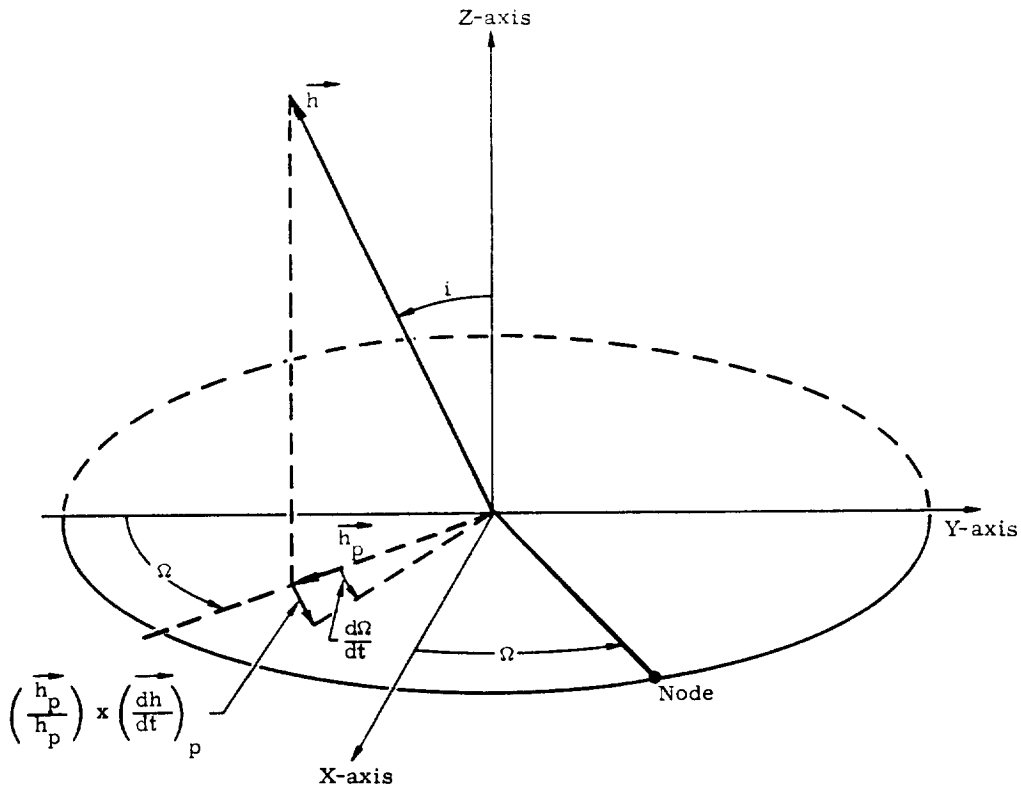

$\vec{h}_p$ = projection of $\vec{h}$ on the equatorial plane.

$\left(\frac{\vec{dh}}{dt}\right)_p$ = projection of $\frac{\vec{dh}}{dt}$ on the equatorial plane.

$\left(\frac{\vec{h}_p}{h_p}\right) \times \left(\frac{\vec{dh}}{dt}\right)_p$ = the component of $\left(\frac{\vec{dh}}{dt}\right)_p$ which is normal to $\vec{h}_p$.

$$\frac{d\Omega}{dt} = \frac{\left|\frac{\vec{h}_p}{h_p} \times \left(\frac{\vec{dh}}{dt}\right)_p\right|}{h_p} \qquad (47)$$

$$= \frac{\left|\vec{h}_p \times \left(h \frac{d\alpha}{dt} \vec{n}_s\right)_p\right|}{h_p^2}$$

But

$$\vec{h}_p = h \sin i \, (\hat{i} \sin \Omega - \hat{j} \cos \Omega)$$

where $\hat{i}$ and $\hat{j}$ are unit vectors along the X- and Y-axes, respectively, and

$$\left(h \frac{d\theta}{dt} \vec{n}_s\right)_p = -rW \left[\hat{i}(-\cos\phi \cos i \sin\Omega - \sin\phi \cos\Omega) + \hat{j}(-\sin\phi \sin\Omega + \cos\phi \cos i \cos\Omega)\right].$$

Thus, upon performing the cross product, Eq (47) becomes

$$\frac{d\Omega}{dt} = \frac{rW \sin\phi}{na^2 \sqrt{1 - e^2} \sin i} \qquad (48)$$

The change in the orbital inclination is related to the change in the node. This can be seen by referring to the following sketch in which two positions of the node, Ω_0 and Ω_1, are shown with

$$\Delta\Omega = \Omega_1 - \Omega_0$$

and

$$\Delta i = i_1 - i_0.$$

By spherical trigonometry, it can be shown that

$$\sin \Delta i = \sin i_1 \cos i_0 - \sin i_0 \cos i_1$$

$$= \frac{\sin i_0}{\sin \phi_1} \left[\cos i_0 \sin \phi_0 (1 - \cos \Delta\Omega) + \cos \phi_0 \sin \Delta\Omega\right].$$

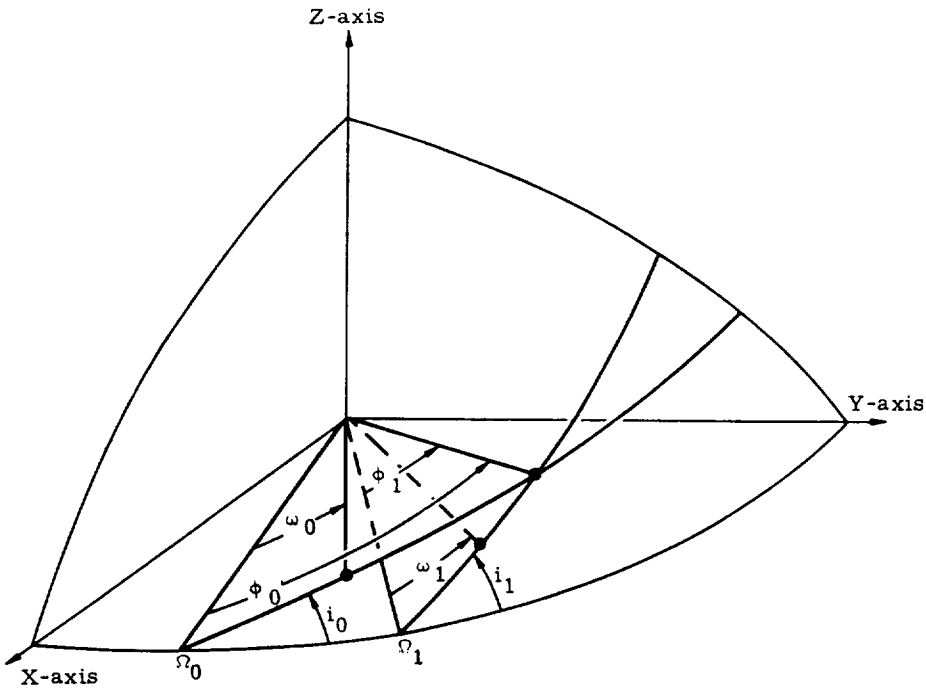

Differentiating and taking the limit as $\Delta\Omega \rightarrow 0$, the following is obtained

$$\frac{di}{dt} = \frac{\sin i}{\sin \phi} \cos \phi \frac{d\Omega}{dt}. \tag{49}$$

Therefore,

$$\frac{di}{dt} = \frac{rW \cos \phi}{na^2 \sqrt{1 - e^2}} \tag{50}$$

The change in the argument of perigee, ω, arises from two sources. One is the motion of perigee caused by the forces in the orbital plane tending to rotate the ellipse in its plane. The other change occurs because ω is measured from the moving node (see preceding sketch). To evaluate the latter changes, assume that the in-plane perturbing forces are zero. Then the change in ω equals the change in ϕ. According to the relations in a spherical triangle,

$$\cos \phi_1 = \cos \Delta\Omega \cos \phi_0 + \sin \Delta\Omega \sin \phi_0 \cos i_0.$$

Differentiating and taking the limit as $\Delta\Omega \rightarrow 0$, yields

$$\frac{d\phi}{dt} = \left(\frac{d\omega}{dt}\right)_W = -\cos i \frac{d\Omega}{dt} = \frac{-r \sin \phi \cot i}{na^2 \sqrt{1 - e^2}} W, \tag{51}$$

where the subscript W means that this is the change in ω contributed by the nodal motion which is caused by the component of the perturbing acceleration, W, normal to the orbital plane. The change caused by the in-plane components, R and S, is denoted by $\left(\frac{d\omega}{dt}\right)_{R,S}$. The effect of these in-plane forces is to change the instantaneous velocity vector which must, at every instant, remain tangent to the instantaneous osculating ellipse. This ellipse will therefore have a changing perigee position. The resulting rate of change of the argument of perigee will clearly be

$$\left(\frac{d\omega}{dt}\right)_{R,S} = -\frac{d\theta}{dt}. \tag{52}$$

Here $\frac{d\theta}{dt}$, the rate of change of the true anomaly caused by the perturbing force, must not be confused with $\dot{\theta}$ which is the rate of change of θ in an unperturbed Kepler orbit. To evaluate $\frac{d\theta}{dt}$, refer to the following sketch.

After the force m $(R\vec{n}_r + S\vec{n}_s)$ has been applied for the time dt, the velocity vector is changed from $\vec{V}$ to $\vec{V} + d\vec{V}$, the true anomaly from θ to $\theta + d\theta$ and the angle γ, between $\vec{n}_s$ and $\vec{V}$, is changed from γ to $\gamma + d\gamma$. The expression for γ is obtained from the angular momentum,

$$h = rV \cos \gamma.$$

Since $h = r^2\dot{\theta}$ and $V = (\dot{r}^2 + r^2\dot{\theta}^2)^{1/2}$, it follows that

$$\cos \gamma = \left[1 + \frac{1}{r^2}\left(\frac{dr}{d\theta}\right)^2\right]^{-1/2}.$$

Computing $\frac{dr}{d\theta}$ from Eq (31) yields

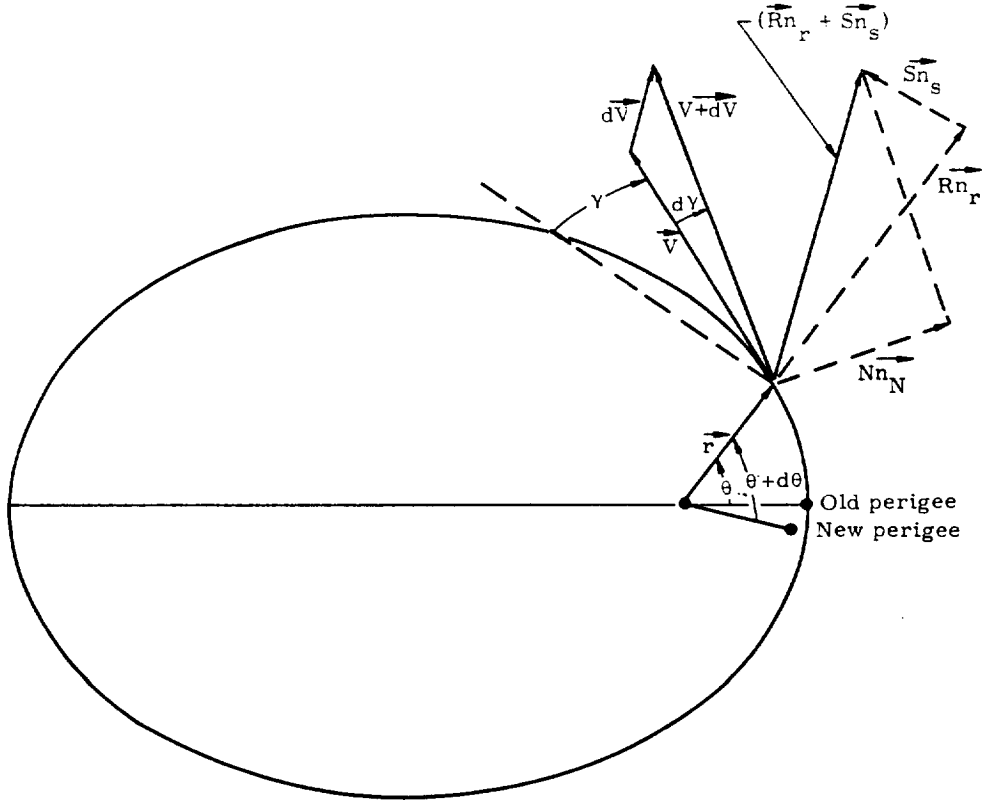

$$\cos\gamma = \frac{1 + e\cos\theta}{\sqrt{1 + e^2 + 2e\cos\theta}} \qquad (53)$$

and

$$\sin\gamma = \frac{e\sin\theta}{\sqrt{1 + e^2 + 2e\cos\theta}} \qquad (54)$$

Differentiating Eq (54) with respect to time and using Eq (52), it is found that

$$\left(\frac{d\omega}{dt}\right)_{R,S} = \left[\frac{1+e^2+2e\cos\theta}{e(e+\cos\theta)} \cdot \left(\frac{\sin\theta}{1+e^2+2e\cos\theta}\ \frac{de}{dt} - \frac{d\gamma}{dt}\right)\right] \qquad (55)$$

If N is the component of the force normal to $\vec{V}$,

$$d\gamma = \frac{N\,dt}{V}.$$

But

$$N = R\cos\gamma - S\sin\gamma,$$

and

$$V = \frac{h}{r}\sqrt{\frac{1 + e^2 + 2e\cos\theta}{1 + e\cos\theta}}$$

Therefore,

$$\frac{d\gamma}{dt} = \left\{\frac{r(1 + e\cos\theta)}{h(1 + e^2 + 2e\cos\theta)} \cdot [R(1 + e\cos\theta) - (e\sin\theta)S]\right\} \qquad (56)$$

Equation (56), along with Eq (46) for $\frac{de}{dt}$, yields

$$\left(\frac{d\omega}{dt}\right)_{R,S} = \frac{\sqrt{1 - e^2}}{nae}\left[-(\cos\theta)\,R + \sin\theta\left(1 + \frac{1}{1 + e\cos\theta}\right)S\right] \qquad (57)$$

The total rate of change of the argument of perigee is

$$\frac{d\omega}{dt} = \left(\frac{d\omega}{dt}\right)_W + \left(\frac{d\omega}{dt}\right)_{R,S} \qquad (58)$$

The final element, mean anomaly at epoch, which provides the position of the satellite at any time also has a time rate. This relationship is obtained directly from Kepler's equation

$$\sigma = M_0 = E - e\sin E - nt$$

and can be found by using the equations already obtained for $\frac{de}{dt}$ and $\frac{d\theta}{dt}$, with the relationship between E and θ given by

$$\cos\theta = \frac{\cos E - e}{1 - e\cos E}$$

$$\sin\theta = \frac{\sqrt{1 - e^2}\sin E}{1 - e\cos E}$$

The result is

$$\frac{d\sigma}{dt} = -\frac{1}{na}\left(\frac{2r}{a} - \frac{1 - e^2}{e}\cos\theta\right)R - \frac{(1 - e^2)}{nae}\left[1 + \frac{r}{a(1 - e^2)}\right](\sin\theta)\,S - t\frac{dn}{dt} \qquad (59)$$

Note is made at this point that the last term has been omitted in Moulton, Ref. 1, p 405.

This completes the set of equations for the orbital elements. The remaining 5 are summarized below for reference:

$$\left.\begin{aligned}
\frac{da}{dt} &= \frac{2e\sin\theta}{n\sqrt{1 - e^2}}R + \frac{2a\sqrt{1 - e^2}}{nr}S \\
\frac{de}{dt} &= \frac{\sqrt{1 - e^2}\sin\theta}{na}R + \frac{\sqrt{1 - e^2}}{na^2e}\left[\frac{a^2(1 - e^2)}{r} - r\right]S \\
\frac{d\Omega}{dt} &= \frac{r\sin\phi}{na^2\sqrt{1 - e^2}\sin i}W \\
\frac{di}{dt} &= \frac{r\cos\phi}{na^2\sqrt{1 - e^2}}W \\
\frac{d\omega}{dt} &= \frac{r\sin\phi\cot i}{na^2\sqrt{1 - e^2}}W - \frac{\sqrt{1 - e^2}\cos\theta}{nae}R + \frac{\sqrt{1 - e^2}}{nae}\left(1 + \frac{1}{1 + e\cos\theta}\right)\sin\theta\,S
\end{aligned}\right\} \qquad (60)$$

If at this point we introduce a disturbing function rather than the four components, we can put these equations in the Lagrangian form

$$\left.\begin{aligned}
R &\equiv \frac{\partial\Xi}{\partial r} \\
S &\equiv \frac{1}{r}\frac{\partial\Xi}{\partial\phi} \\
W &\equiv \frac{1}{r\sin\phi}\frac{\partial\Xi}{\partial i}
\end{aligned}\right\} \qquad (61)$$

$$
\left.
\begin{aligned}
\frac{da}{dt} &= \frac{2}{na}\ \frac{\partial \Xi}{\partial \sigma} \\
\frac{de}{dt} &= \frac{\sqrt{1-e^2}}{na^2 e}\left[\sqrt{1-e^2}\ \frac{\partial \Xi}{\partial \sigma} - \frac{\partial \Xi}{\partial \omega}\right] \\
\frac{d\omega}{dt} &= \frac{\sqrt{1-e^2}}{na^2 e}\ \frac{\partial \Xi}{\partial e} - \frac{\cot i}{na^2\sqrt{1-e^2}}\ \frac{\partial \Xi}{\partial i} \\
\frac{dM}{dt} &= -\frac{2}{na}\ \frac{\partial \Xi}{\partial a} - \frac{1-e^2}{na^2 e}\ \frac{\partial \Xi}{\partial e} + n \\
\frac{di}{dt} &= \frac{\cos i}{na^2\sqrt{1-e^2}\sin i}\ \frac{\partial \Xi}{\partial \omega} \\
\frac{d\Omega}{dt} &= \frac{1}{na^2\sqrt{1-e^2}\sin i}\ \frac{\partial \Xi}{\partial i}
\end{aligned}
\right\} \quad (62)
$$

2. First Order Secular Perturbations

For an oblate body having axial symmetry, the gravitational potential at any extension point may be represented by Vinti's potential (Chapter II). If for the present analysis we neglect terms with coefficients the order of J_2^2 (i.e., J_3, J_4...) we can write the work function (minus the potential) as:

$$
\begin{aligned}
U &= \frac{\mu}{r}\left[1 + \frac{J_2}{2}\left(\frac{R}{r}\right)^2 (3\sin^2 L - 1)\right] \qquad (63) \\
&= \frac{\mu}{r}\left[1 + \frac{J_2}{2}\left(\frac{R}{r}\right)^2 (3\sin^2 i \sin^2\phi - 1)\right]
\end{aligned}
$$

but since $\phi = \theta + \omega$ is a periodic quantity, $\sin^2\phi = \frac{1}{2} - \frac{1}{2}\cos 2\phi$ has a nonperiodic part $\frac{1}{2}$. Thus, the potential J will produce secular changes in the orbital elements as well as periodic changes. Before the magnitude of this change can be evaluated, however, the constant part of the function $(a/r)^3$ must be evaluated. Following the method of Dr. Krause (Ref. 16) we have:

$$
\left(\frac{a}{r}\right)^m = \frac{c_0}{2} + C_1\cos M + C_2\cos 2M + \ldots + c_n\cos n M
$$

where

$$
c_n = \frac{1}{\pi}\int_0^{2\pi}\left(\frac{a}{r}\right)^n \cos n M\, d M
$$

The C_n are simple functions of the eccentricity as may be seen in the expansions of Chapter III.

Thus,

$$
\begin{aligned}
\frac{C_0}{2} &= \frac{1}{2\pi}\int_0^{2\pi}\left(\frac{a}{r}\right)^3 dM \\
&= \frac{1}{2\pi}(1-e^2)^{-3/2}\int_0^{2\pi}(1 + e\cos\theta)\, d\theta \\
&= (1-e^2)^{3/2}
\end{aligned}
$$

and

$$
U = \frac{\mu}{r} + \Xi_{\text{secular}} \qquad (64)
$$

$$
\Xi_{\text{secular}} = \mu\left[J_2\frac{R^2}{a^3}(1-e^2)^{-3/2}(1 - 3/2\sin^2 i)\right] \qquad (65)
$$

At this point we refer to the Lagrangian equations of Section D-1 of this chapter and conclude that the secular variations in the elements are expressible to the first order in J_2 as:

$$
\Delta a = 0 \qquad (66)
$$

$$
\Delta e = 0 \qquad (67)
$$

$$
\Delta\omega = 3\pi J_2\left(\frac{R}{p}\right)^2(2 - 5/2\sin^2 i)\ (\text{rad/rev}) \qquad (68)
$$

$$
\frac{\Delta M}{nt} = \frac{3}{2}J_2\left(\frac{R}{p}\right)^2\sqrt{1-e^2}\ (1 - 3/2\sin^2 i)\ (\text{rad/rev}) \qquad (69)
$$

$$
\Delta i = 0 \qquad (70)
$$

$$
\Delta\Omega = -3\pi J_2\left(\frac{R}{p}\right)^2\cos i\ (\text{rad/rev}) \qquad (71)
$$

The physical significance for the fact that the secular variations in a, e and i are zero may be seen by looking at the potential function itself. The fact that J_2, J_3 and J_4 are small implies that to a first approximation the orbit will be nearly elliptical. Although one cannot assign an unambiguous major axis or eccentricity to the perturbed satellite orbit, the experience of astronomers has shown that it is convenient to refer the motion to an osculating ellipse. This is the orbit in which the satellite would move if at some instant the perturbing terms were to vanish ($J_2 = J_3 = J_4 = 0$) leaving the satellite under the attraction of the "spherical" earth. Hence the

actual position and velocity vector at each point define the osculating ellipse in terms of a set of elements a, e, and i, where a and e are the semimajor axis and eccentricity and i is the inclination of the plane of the ellipse to the equator.

The major axis a may be specified in terms of the energy E, associated with the osculating ellipse. When J_2, J_3 and J_4 are set equal to zero to calculate E, only the potential energy is altered, and it can be seen that unless r exhibits a secular (nonperiodic) variation, which is not possible here since we are dealing with bound orbits, only periodic variations in E can occur. Hence there can be only periodic variations in a.

Although p, i.e., a $(1 - c^2)$, is a constant of the motion, the total angular momentum $\vec{h}$ is not constant, because the equatorial bulge produces a nonradial component of force. But by the same arguments as above, the torque, and hence $\bar{h}$, can exhibit only periodic variations. Further, since at each equatorial crossing the momenta are related by

$$p = (h \cos i)_N = \text{constant.}$$

where N means node, it follows that the orbit inclination i behaves similarly. The same may be said for the orbit eccentricity, since the equation for eccentricity depends explicitly only on $|\vec{h}|$ and a.

It is noted at this point that since 3 of the 6 elements vary, the satellite periods will vary. The plural of period was intentionally utilized at this point because of the manner in which three distinct periods are defined (Ref. 17).

Anomalistic period is defined as the time from one perigee to the next. In that time the elliptic angles (true, mean, and eccentric anomaly) increase by 360°, while the central angle β increases by more or less than 360°, depending on whether the apsidal notation is against or in the direction of satellite motion.

Nodal period, also called synodic or draconic period, is defined as the time from one ascending node to the next. In that time the central angle β increases by 360°, since β is measured from the instantaneous position of the ascending node. The satellite does not, except at an orbit inclination of 90°, return to the same relative position in inertial space after one nodal period due to the regression of the nodes.

Sidereal period is defined as the time for the satellite to return to the same relative position in inertial space. In that time the satellite central angle as measured from a fixed reference, which is not to be confused with the central angle as measured from the ascending node, increases by 360°. In artificial satellite theory, the sidereal period is less important than the other two periods, it is rarely used, and it will not be discussed any further.

The perturbed anomalistic period can be evaluated from the average angular rate using the method of Kozai (Ref. 18) and a relation analogous to $n^2a^3 = \mu$.

$$\bar{n}^2\bar{a}^3 = \bar{\mu} = \mu \left\{1 - \frac{3}{2} J_2\left(\frac{R}{p}\right)^2 (1 - \frac{3}{2} \sin^2 i) \sqrt{1 - e^2}\right\}$$

where

$\bar{n}$ = perturbed mean angular rate

$\bar{a}$ = mean value of the semimajor axis

$$= a_0 \left\{1 - 3/2\, J_2\left(\frac{R}{p}\right)^2 (1 - 3/2 \sin^2 i) \cdot \sqrt{i - e^2}\right\}$$

$\bar{\mu}$ = effective gravitational constant as sensed by the satellite in its orbit.

This process yields

$$\tau_a = \frac{2\pi}{n_r} = \frac{2\pi}{\sqrt{\mu}} (\bar{a})^{3/2} \left\{1 + \frac{3 J_2 R_e^2}{\bar{a}^2 (1 - e^2)^{3/2}} \left(\frac{3\cos^2 i_0 - 1}{8}\right)\right\} \quad (72)$$

For a near-polar orbit the anomalistic period is longer than the unperturbed period, while for a near-equatorial orbit the anomalistic period is shorter. At inclination angles of $i_0 \simeq 54.7°$ and $i_0 \simeq 125.3°$, $3\cos^2 i_0 = 1$, and hence the anomalistic period equals the unperturbed period. Physically this is due to a combination of the mass distribution of the earth and the apsidal rotation at these inclination angles.

The perturbed nodal period, however, has been subject to much more confusion since the results of many of the authors are in conflict. Upon review of this work, however, it is felt that to the order J_2 the results of King Hele (Ref. 19) and Struble (Ref. 20) are the most preferable for small eccentricities. (Additional discussions and proofs appear in Ref. 17.) This result is:

$$\tau_n = 2\pi \sqrt{\frac{\bar{a}^3}{\mu}} \left\{1 - 3 J_2\left(\frac{R}{\bar{a}}\right)^2 \cdot \left(\frac{7\cos^2 i - 1}{8}\right)\right\} \quad (73)$$

These two period expressions (Eqs 72 and 73) may be seen to differ in both magnitude and in the algebraic sign of the corrective term. This

apparent discrepancy is due to the fact that the perigee is moving. Thus at the time the perigee has rotated through 360° the number of nodal and anomalistic periods should differ by 1.

Equations (68), (69), (71), (72) and (73) are presented in graphical form as Figs. 2, 3, 4, 5 and 6, respectively.

3. Higher Order Oblateness Perturbation

The errors inherent in numerical integration are not conducive to accurate computation of orbits over long time intervals. For this reason, general perturbations (analytic approximate solutions for the perturbed motion obtained by series expansions) are more useful in missions of long duration.

a. Oblateness of the earth

The potential function of the earth can be accurately expressed as an infinite series of zonal harmonics,

$$U = \frac{\mu}{r}\left[1 - \sum_{k=2}^{\infty} J_k \left(\frac{R}{r}\right)^k P_k (\sin L)\right]$$

where P_k (sin L) is the Legendre polynomial of order k, given by

$$P_k (x) = \frac{1}{2^k k!} \frac{d^k}{dx^k} (x^2 - 1)^k$$

This is the form of the potential function given by Vinti. The recommended values of the coefficients J_k and several expansions are given in Chapter II. The potential function determines the motion of a small body in the earth's field by

$$\ddot{x} = \frac{\partial U}{\partial x} \qquad x \rightarrow y, z.$$

The classic approach of the general perturbations method is the analytic integration of one of the sets of equations for variation of parameters, i.e., a set similar to that of Section C-1 (this chapter) with the perturbing function Ξ defined by

$$\Xi = U - \frac{\mu}{r}$$

This approach has been taken by several authors [Brouwer (Ref. 21), Kozai (Ref. 18), Garfinkel (Ref. 22), Izsak (Ref. 23) and Krause (Ref. 16) to name a few]. The method results in easily visualized perturbations since the variables are geometric quantities. However, because of a failing peculiar to the method of analysis, the equations exhibit singularities in certain elements in the vicinity of the "critical inclination," i.e., i = 63.4° and for i = 0 or e = 0. In the first case a physical explanation exists in that since the momenta of the canonical equations are bounded, the system is conditionally periodic. This situation admits 2 possibilities:

(1) Libration, min. $q_i \leq q_i \leq$ max q_i (i = 1, 2, 3).

(2) Circulation, $-\infty < q_i < \infty$.

These two possible regions are shown in the following sketch.

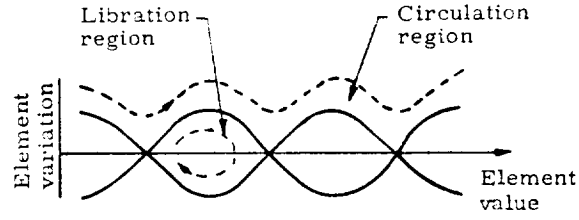

In the neighborhood of the so-called critical inclination, the elements which become indeterminant merely leave the circulation region and enter the libration region. Since the theory isn't prepared to handle points of this type along with the more regular points, it ceases to apply in this region. This behavior is no reflection on the theory in general, since other approaches can be utilized in these neighborhoods.

In the latter cases (i.e., e = 0 or i = 0) the problem is one of indeterminacy in one or more of the elements being utilized to describe the motion. More specifically, the angle ω cannot be utilized for e = 0 because of the fact that the line of apsides cannot be located. Similarly, the nodal angle Ω becomes meaningless if the plane of motion is the primary plane of reference. Special sets of elements have been developed however, which may be utilized effectively for very low eccentricity orbit. These sets will not be discussed.

One set of solutions obtained using this method including J_2 and J_4 terms in secular perturbations, J_2 to J_5 terms in long period perturbations and J_2 terms in short period perturbations, is presented below. This form is exactly analogous to those referenced previously; however, there are differences in the notation and in the coefficients

a. Secular terms

$$M_s = \frac{1}{a_0}\sqrt{\frac{\mu}{a_0}}\, t \left\{1 + \frac{3}{4} J_2 \left(\frac{R}{p_0}\right)^2 \sqrt{1 - e_0^2} \cdot (-1 + 3\cos^2 i_0) + \frac{3}{128} J_2^2 \left(\frac{R}{p_0}\right)^4 \sqrt{1 - e_0^2} \cdot \left[10 + 16\sqrt{1 - e_0^2} - 25 e_0^2 + (-60 - 96\sqrt{1 - e_0^2} + 90 e_0^2)\cos^2 i_0 + (130 + 144\sqrt{1 - e_0^2} +\right.\right.$$

continued

$$- 25\, e_0^2) \cos^4 i_0\Big] - \frac{45}{128} J_4 \left(\frac{R}{p_0}\right)^4 \sqrt{1 - e_0^2}\,(3$$

$$- 30 \cos^2 i_0 + 35 \cos^4 i_0)\Big\} + M_0 \qquad (74)$$

$$\omega_s = \frac{1}{a_0}\sqrt{\frac{\mu}{a_0}}\, t \left\{\frac{3}{4} J_2 \left(\frac{R}{p_0}\right)^2 (-1 + 5 \cos^2 i_0)\right.$$

$$+ \frac{3}{128} J_2^2 \left(\frac{R}{p_0}\right)^4 \left[-10 + 24\sqrt{1 - e_0^2} - 25\, e_0^2\right.$$

$$+ (-36 - 192\sqrt{1 - e_0^2} + 126\, e_0^2) \cos^2 i_0$$

$$\left. + (430 + 360\sqrt{1 - e_0^2} - 45\, e_0^2) \cos^4 i_0\right]$$

$$- \frac{45}{128} J_4 \left(\frac{R}{p_0}\right)^4 \left[12 + 9\, e_0^2 + (-144\right.$$

$$\left.\left. - 126\, e_0^2) \cos^2 i_0 + (196 + 189\, e_0^2) \cos^4 i_0\right]\right\}$$

$$+ \omega_0 \qquad (75)$$

$$\Omega_s = \frac{1}{a_0}\sqrt{\frac{\mu}{a_0}}\, t \left\{-\frac{3}{2} J_2 \left(\frac{R}{p_0}\right)^2 \cos i_0\right.$$

$$+ \frac{3}{32} J_2^2 \left(\frac{R}{p_0}\right)^4 \left[(4 + 12\sqrt{1 - e_0^2}\right.$$

$$- 9\, e_0^2) \cos i_0 + (-40 - 36\sqrt{1 - e_0^2}$$

$$\left. + 5\, e_0^2) \cos^3 i_0\right] - \frac{15}{32} J_4 \left(\frac{R}{p_0}\right)^4 (2 + 3\, e_0^2)\,(3$$

$$\left. - 7 \cos^2 i_0) \cos i_0\right\} + \Omega_0 \qquad (76)$$

b. Long period terms

$$e_\ell = \left\{\frac{1}{16} J_2 \left(\frac{R}{p_0}\right)^2 e_0 (1 - e_0^2) \left[1 - 11 \cos^2 i_0\right.\right.$$

$$\left. - \frac{40 \cos^4 i_0}{1 - 5 \cos^2 i_0}\right] + \frac{5}{16} \frac{J_4}{J_2} \left(\frac{R}{p_0}\right)^2 e_0\,(1$$

$$\left.\left. - e_0^2) \left[1 - 3 \cos^2 i_0 - \frac{8 \cos^4 i_0}{1 - 5 \cos^2 i_0}\right]\right\} \cos 2\omega_s$$

$$- \frac{1}{2} \frac{J_3}{J_2} \frac{R}{p_0} (1 - e_0^2) \sin i_0 \sin \omega_s \qquad (77)$$

$$i_\ell = - \frac{e_0\, e_\ell}{(1 - e_0^2) \tan i_0} \qquad (78)$$

$$M_\ell = \left[\frac{1}{16} J_2 \left(\frac{R}{p_0}\right)^2 (1 - e_0^2)^{3/2} \left(1 - 11 \cos^2 i_0\right.\right.$$

$$\left. - \frac{40 \cos^4 i_0}{1 - 5 \cos^2 i_0}\right) + \frac{5}{16} \frac{J_4}{J_2} \left(\frac{R}{p_0}\right)^2 (1 - e_0^2)^{3/2}$$

$$\left.\left(1 - 3 \cos^2 i_0 - \frac{8 \cos^4 i_0}{1 - 5 \cos^2 i_0}\right)\right] \sin 2\omega_s$$

$$+ \frac{1}{2} \frac{J_3}{J_2} \frac{R}{p_0} \frac{(1 - e_0)^{3/2}}{e_0} \sin i_0 \cos \omega_s \qquad (79)$$

$$\omega_\ell = \left\{-\frac{1}{32} J_2 \left(\frac{R}{p_0}\right)^2 \left[2 + e_0^2 - 11\,(2 + 3\, e_0^2) \cos^2 i_0\right.\right.$$

$$- 40\,(2 + 5\, e_0^2) \frac{\cos^4 i_0}{1 - 5 \cos^2 i_0} - \frac{400\, e_0^2 \cos^6 i_0}{\left(1 - 5 \cos^2 i_0\right)^2}\Big]$$

$$- \frac{5}{32} \frac{J_4}{J_2} \left(\frac{R}{p_0}\right)^2 \left[2 + e_0^2 - 3\,(2 + 3\, e_0^2) \cos^2 i_0\right.$$

$$- 8\,(2 + 5\, e_0^2) \frac{\cos^4 i_0}{1 - 5 \cos^2 i_0}$$

$$\left.\left. - \frac{80\, e_0^2 \cos^6 i_0}{(1 - 5 \cos^2 i_0)^2}\right]\right\} \sin 2\omega_s$$

$$- \frac{1}{2} \frac{J_3}{J_2} \frac{R}{p_0} \left(\frac{\sin i_0}{e_0} - \frac{e_0 \cos^2 i_0}{\sin i_0}\right) \cos \omega_s \qquad (80)$$

$$\Omega_\ell = \left\{-\frac{1}{16} J_2 \left(\frac{R}{p_0}\right)^2 e_0^2 \cos i_0 \left[11 + \frac{80 \cos^2 i_0}{1 - 5 \cos^2 i_0}\right.\right.$$

$$\left. + \frac{200 \cos^4 i_0}{\left(1 - 5 \cos^2 i_0\right)^2}\right] - \frac{5}{16} \frac{J_4}{J_2} \left(\frac{R}{p_0}\right)^2 e_0^2 \cos i_0 \left[3\right.$$

$$\left.\left. + \frac{16 \cos^2 i_0}{1 - 5 \cos^2 i_0} + \frac{40 \cos^4 i_0}{(1 - 5 \cos^2 i_0)^2}\right]\right\} \sin 2\omega_s$$

$$- \frac{1}{2} \frac{J_3}{J_2} \frac{R}{p_0} \frac{e_0 \cos i_0}{\sin i_0} \cos \omega_s \qquad (81)$$

b. Short period terms

$$a_p = \frac{3}{2} J_2 \frac{R^2}{a_0} \left\{\left(\frac{2}{3} - \sin^2 i_0\right) \left[\left(\frac{a_0}{r}\right)^3 - (1 - e_0^2)^{-3/2}\right]\right.$$

$$\left. + \left(\frac{a_0}{r}\right)^3 \sin^2 i_0 \cos 2\,(\theta + \omega_s + \omega_e)\right\} \qquad (82)$$

$$e_p = \frac{(1 - e_0^2)}{2 e_0} \left\{ \frac{1}{2} J_2 \left(\frac{R}{a_0}\right)^2 \left[(-1 + 3 \cos^2 i_0) \left\{ \left(\frac{a_0}{r}\right)^3 - (1 - e_0^2)^{-3/2} \right\} + 3 \sin^2 i_0 \left\{ \left(\frac{a_0}{r}\right)^3 - (1 - e_0^2)^{-2} \right\} \cos 2 (\theta + \omega_s + \omega_\ell) \right] - \frac{1}{2} J_2 \left(\frac{R}{p_0}\right)^2 \sin^2 i_0 \left[3 e_0 \cos (\theta + 2\omega_s + 2\omega_\ell) + e_0 \cos (3\theta + 2\omega_s + 2\omega_\ell) \right] \right\} \quad (83)$$

$$i_p = \frac{1}{4} J_2 \left(\frac{R}{r_0}\right)^2 \cos i_0 \sin i_0 \left[3 \cos 2 (\theta + \omega_s + \omega_\ell) + 3 e_0 \cos (\theta + 2\omega_s + 2\omega_\ell) + e_0 \cos (3\theta + 2\omega_s + 2\omega_\ell) \right] \quad (84)$$

$$\Omega_p = - \frac{1}{4} J_2 \left(\frac{R}{p_0}\right)^2 \cos i_0 \left[6 (\theta - M_s - M_\ell + e_0 \sin \theta) - 3 \sin 2 (\theta + \omega_s + \omega_\ell) - 3 e_0 \sin (\theta + 2\omega_s + 2\omega_\ell) - e_0 \sin (3\theta + 2\omega_s + 2\omega_\ell) \right] \quad (85)$$

$$M_p = - \frac{(1 - e_0^2)^{3/2}}{8 e_0} J_2 \left(\frac{R}{p_0}\right)^2 \left\{ 2 (-1 + 3 \cos^2 i_0) \left[\left(\frac{a_0}{r}\right)^2 (1 - e_0^2) + \left(\frac{a_0}{r}\right) + 1 \right] \sin \theta + 3 \sin^2 i_0 \left[\sin (\theta + 2\omega_s + 2\omega_\ell) \left\{ - \left(\frac{a_0}{r}\right)^2 (1 - e_0^2) - \frac{a_0}{r} + 1 \right\} + \sin (3\theta + 2\omega_s + 2\omega_\ell) \left\{ \left(\frac{a_0}{r}\right)^2 (1 - e_0^2) + \frac{a_0}{r} + \frac{1}{3} \right\} \right] \right\} \quad (86)$$

$$\omega_p = \frac{(1 - e_0^2)}{8 e_0} J_2 \left(\frac{R}{p_0}\right)^2 \left\{ 2 (-1 + 3 \cos^2 i_0) \left[\left(\frac{a_0}{r}\right)^2 (1 - e_0^2) + \frac{a_0}{r} + 1 \right] \sin \theta + 3 \sin^2 i_0 \left[\sin (\theta + 2\omega_s + 2\omega_\ell) \left\{ - \left(\frac{a_0}{r}\right)^2 (1 - e_0^2) - \frac{a_0}{r} + 1 \right\} + \sin (3\theta + 2\omega_s + 2\omega_\ell) \left\{ \left(\frac{a_0}{r}\right)^2 (1 - e_0^2) + \frac{a_0}{r} + \frac{1}{3} \right\} \right] \right\}$$

$$+ \frac{1}{8} J_2 \left(\frac{R}{p_0}\right)^2 \left\{ 6 (-1 + 5 \cos^2 i_0) (\theta - M_s - M_\ell + e_0 \sin \theta) + (3 - 5 \cos^2 i_0) \left[3 \sin 2 (\theta + \omega_s + \omega_\ell) + 3 e_0 \sin (\theta + 2\omega_s + 2\omega_\ell) + e_0 \sin (3\theta + 2\omega_s + 2\omega_\ell) \right] \right\} \quad (87)$$

where

$$E - e_0 \sin E = M_s + M_\ell ,$$

$$\tan \frac{\theta}{2} = \sqrt{\frac{1 + e_0}{1 - e_0}} \tan \frac{E}{2}$$

The solutions for the perturbed elements are then

$$x = x_s + x_\ell + x_p$$

where

$$x = a, e, i, \omega, \Omega, M.$$

These expressions provide all of the information necessary to describe the motion of a satellite to the order J_2^2. However, there exist requirements in many studies for the perturbed expressions for r and ϕ, ($\phi = \theta + \omega$). This information can be obtained from the equations presented above; however, the procedure is lengthy and unnecessary in view of some of the work quoted in (Ref. 18) by Kozai. This reference gives r and ϕ to the order J_2.

$$r = r_0 + \frac{1}{2} J_2 R^2 \frac{1}{p} \left(1 - \frac{3}{2} \sin^2 i\right) \left[-1 - \frac{1}{e} \left(1 - \sqrt{1 - e^2}\right) \cos \theta + \frac{r}{a} \frac{1}{\sqrt{1 - e^2}} \right] + \frac{1}{4} J_2 R^2 \frac{1}{p} \sin^2 i \cos 2 (\theta + \omega) \quad (88)$$

$$\phi = \phi_0 + \frac{3}{2} J_2 \left(\frac{R}{p}\right)^2 \left\{ \left(2 - \frac{5}{2} \sin^2 i\right) (\theta - M + e \sin \theta) + \left(1 - \frac{3}{2} \sin^2 i\right) \left[\frac{2}{3e} \left(1 - \frac{e^2}{2} - \sqrt{1 - e^2}\right) \sin \theta + \frac{1}{6} \left(1 - \sqrt{1 - e^2}\right) \sin 2\theta \right] - \left(\frac{1}{2} - \frac{5}{6} \sin^2 i\right) e \sin (\theta + 2\omega) - \left(\frac{1}{2} - \frac{7}{12} \sin^2 i\right) \sin 2 (\theta + \omega) - \frac{e}{6} \cos^2 i \sin (3\theta + 2\omega) \right\} \quad (89)$$

where r_0 and ϕ_0 are values computed from mean orbital elements.

Oblateness of the central body tends to make a twisted space curve out of the satellite orbit. It is customary to map this orbit as a plane curve on the orbital plane which contains at any instant the satellite radius and velocity vectors. In this plane one may either approximate the trajectory by an osculating ellipse (the astronomical approach) or try to assume the actual equation of the plane curve to the desired accuracy. This latter approach is the one taken by R. Struble (Refs. 20 and 24). Another significant difference is that in this work some of the conventional orbital elements become variables to the order J_2. Struble in this reference derives perturbations based on the following model

$$\frac{1}{r} \equiv u = \frac{1}{r_0}\left[1 + e\cos(\bar{\Phi} - \omega) - J_2\, c + J_2^2\, d\right]$$

$$\left[r_0,\ e,\ \omega,\ c,\ d \text{ variable}\right] . \qquad (90)$$

In the solution obtained, the short period perturbations are isolated in the c and d variables, while r_0, e and ω have only long period oscillations (with a secular variation in ω). The independent variable $\bar{\Phi}$ is related to the central angle from the node, ϕ, but provides simpler solutions than ϕ. In particular, $\bar{\Phi} = \phi$ when $J_2 = 0$. The solutions for some of the elements, accurate to the second order, are included below. Note is made of a shorthand notation employing a set of intermediate variables $\eta_2 \ldots \eta_6$ and ν_1 and ν_2. These terms are presented following the equations for the terms c and d defined in Eq (90).

$$u = \frac{1}{r_0}\left[1 + e\cos(\bar{\Phi} - \omega) - J_2\, c - J_2^2\, d\right]$$

$$\frac{1}{r_0} = \frac{\mu}{p^2}\cos^2 i_0 + \frac{3}{4}\frac{J_2}{r_0}\left(\frac{R}{r_0}\right)^2\left(1 + \frac{e^2}{2}\right)(2 - 3\sin^2 i_0) + \frac{9}{4}\frac{J_2^2}{r_0}\left(\frac{R}{r_0}\right)^4 \eta_2 \qquad (91)$$

$$p = r^2 \sin^2\theta^* \frac{dA}{dt}$$

where A is the right ascension and $\theta^* = 90 - L$.

$$e = e_0 - \frac{3}{2} J_2\, e\left(\frac{R}{r_0}\right)^2 (5\cos^2 i_0 - 1)^{-1}\left(\frac{1}{2}\eta_3 \cos 2\omega + \frac{1}{4}\eta_4 \sin 4\omega\right) \qquad (92)$$

$$\omega = \omega_0 + \left[\frac{3}{4} J_2\left(\frac{R}{r_0}\right)^2 (5\cos^2 i_0 - 1) + \eta_5 \frac{9}{4} J_2^2\left(\frac{R}{r_0}\right)^4\right]\bar{\Phi} +$$

$$+ \frac{3}{2} J_2\left(\frac{R}{r_0}\right)^2 (5\cos^2 i_0 - 1)^{-1}\left(\eta_6 \sin 2\omega - \frac{1}{2}\eta_4 \sin 4\omega\right) \qquad (93)$$

$$i = i_0 + \frac{3}{8} J_2\left(\frac{R}{r_0}\right)^2 \sin 2 i_0 \left[e\cos(\bar{\Phi} + \omega) + \cos 2\bar{\Phi} + \frac{e}{3}\cos(3\bar{\Phi} - \omega)\right] + \frac{9}{16} J_2^2\, \nu_1 \left(\frac{R}{r_0}\right)^4 \sin 2 i_0 \qquad (94)$$

$$i_0 = i_{00} + \frac{e^2}{32} J_2\left(\frac{R}{r_0}\right)^2 \sin 2 i_0 \left(5\cos^2 i_0 - 1\right)\left[-14 + 15\sin^2 i_0 - 5\frac{J_4}{J_2^2}(6 - 7\sin^2 i_0)\right]\cos 2\omega \qquad (95)$$

$$\phi = \bar{\Phi} + \frac{3}{8} J_2\left(\frac{R}{r_0}\right)^2 \left[4e\cos^2 i_0 \sin(\bar{\Phi} - \omega) + 2e(1 - 2\cos^2 i_0)\sin(\bar{\Phi} + \omega) + (1 - 3\cos^2 i_0)\sin 2\bar{\Phi} + \frac{2}{9} e(1 - 4\cos^2 i_0)\sin(3\bar{\Phi} - \omega)\right] + \frac{9}{4} J_2^2\, \nu_2 \qquad (96)$$

Now adopting the shorthand notation

$$D_1 = -\frac{35}{18}\frac{J_4}{J_2^2}$$

The short period terms c, d can be written

$$c = \frac{1}{8}\left(\frac{R}{r_0}\right)^2 \sin^2 i_0 \left[\left(2 + \frac{e^2}{3}\right)\cos 2\bar{\Phi} + e\cos(3\bar{\Phi} - \omega) + \frac{e^2}{6}\cos(4\bar{\Phi} - 2\omega) + \frac{3e^2}{2}\cos 2\omega\right] + \frac{1}{8}\left(\frac{R}{r_0}\right)^2 e^2 (2 - 3\sin^2 i_0)\cos(2\bar{\Phi} - 2\omega) \qquad (97)$$

$$\frac{d}{\frac{9}{4}\left(\frac{R}{r_0}\right)^4} = \left\{-\frac{e^4}{3}\left[\frac{27}{112} D_1 \sin^2 i_0 - \left(\frac{9}{8} + \frac{9}{32} D_1\right)\sin^4 i_0\right]\cos(2\bar{\Phi} - 4\omega) - \frac{1}{3}\left[e^2\left\{\left(\frac{1}{2} + \frac{9}{7} D_1\right) - \left(\frac{45}{7} D_1 + \frac{17}{6}\right)\sin^2 i_0\right.\right.\right.$$

continued

$$+\left(\frac{45}{8}D_1+\frac{281}{96}\right)\sin^4 i_0\Big\}+e^4\Big\{\left(\frac{3}{7}D_1-\frac{1}{4}\right)$$
$$-\left(\frac{3}{4}+\frac{15}{14}D_1\right)\sin^2 i_0$$
$$+\left(\frac{27}{16}+\frac{15}{16}D_1\right)\sin^4 i_0\Big\}\Big]\cos(2\bar{\phi}-2\omega)$$
$$-\frac{1}{3}\Big[\Big\{\left(\frac{9}{7}D_1-\frac{8}{3}\right)\sin^2 i_0+\left(\frac{37}{12}-\frac{3}{2}D_1\right)\sin^4 i_0$$
$$+e^2\Big\{\left(\frac{7}{8}+\frac{9}{2}D_1\right)\sin^2 i_0-\left(\frac{217}{72}+\frac{11}{2}D_1\right)\sin^4 i_0\Big\}$$
$$+e^4\Big\{\left(\frac{9}{14}D_1-\frac{1}{24}\right)\sin^2 i_0$$
$$-\left(\frac{13}{16}D_1+\frac{11}{8}\right)\sin^4 i_0\Big\}\Big]\cos 2\bar{\phi}$$
$$-\frac{1}{3}\Big[e^2\Big\{\frac{3}{4}\sin^2 i_0+\left(\frac{23}{48}D_1-\frac{41}{24}\right)\sin^4 i_0\Big\}$$
$$+e^4\Big\{D_1\frac{7}{96}\sin^4 i_0\Big\}\Big]\cos(2\bar{\phi}+2\omega)$$
$$-\frac{1}{8}\Big[e^3\Big\{\left(\frac{3}{7}D_1-\frac{1}{6}\right)-\left(\frac{7}{6}+\frac{15}{7}D_1\right)\sin^2 i_0$$
$$+\left(\frac{191}{96}+\frac{15}{8}D_1\right)\sin^4 i_0\Big\}\Big]\cos(3\bar{\phi}-3\omega)$$
$$-\frac{1}{8}\Big[e\Big\{(3D_1-\frac{5}{9})\sin^2 i_0$$
$$-\left(\frac{23}{36}+\frac{7}{2}D_1\right)\sin^4 i_0\Big\}+e^3\Big\{\left(\frac{123}{56}D_1-\frac{1}{48}\right)\sin^2 i_0$$
$$-\left(\frac{33}{32}+\frac{41}{16}D_1\right)\sin^4 i_0\Big\}\Big]\cos(3\bar{\phi}-\omega)$$
$$-\frac{1}{8}\Big[e\Big\{\left(\frac{29}{24}D_1-\frac{1}{16}\right)\sin^4 i_0\Big\}+e^3\Big\{\frac{1}{2}\sin^2 i_0$$
$$-\left(\frac{111}{144}+\frac{5}{48}D_1\right)\sin^4 i_0\Big\}\Big]\cos(3\bar{\phi}+\omega)$$
$$+\frac{1}{8}\Big[e^3\Big\{\frac{3}{4}\sin^2 i_0\cos^2 i_0\Big\}\Big]\cos(3\bar{\phi}+3\omega)$$
$$-\frac{1}{15}\Big[e^4\Big\{\frac{3}{5}D_1-\left(\frac{3}{4}+\frac{15}{56}D_1\right)\sin^2 i_0$$
$$+\left(\frac{9}{8}+\frac{15}{64}D_1\right)\sin^4 i_0\Big\}\Big]\cos(4\bar{\phi}-4\omega)$$
$$-\frac{1}{15}\Big[e^2\Big\{\left(\frac{69}{28}D_1-1\right)\sin^2 i_0$$
$$-\left(\frac{25}{72}+\frac{23}{8}D_1\right)\sin^4 i_0\Big\}$$
$$+e^4\Big\{\left(\frac{57}{140}D_1-\frac{5}{48}\right)\sin^2 i_0$$
$$-\left(\frac{3}{32}+\frac{19}{40}D_1\right)\sin^4 i_0\Big\}\Big]\cos(4\bar{\phi}-2\omega)$$
$$-\frac{1}{15}\Big[-\frac{3}{2}\sin^2 i_0+\left(\frac{3}{8}D_1+\frac{3}{2}\right)\sin^4 i_0$$
$$+e^2\Big\{-\frac{17}{24}\sin^2 i_0+\left(\frac{19}{15}D_1+\frac{41}{144}\right)\sin^4 i_0\Big\}$$
$$+e^4\Big\{\frac{169}{960}D_1\sin^4 i_0\Big\}\Big]\cos 4\bar{\phi}$$
$$+\frac{1}{15}\Big[e^2\Big\{\frac{8}{8}\sin^2 i_0\cos^2 i_0\Big\}\Big]\cos(4\bar{\phi}+2\omega)$$
$$-\frac{1}{24}\Big[e^3\Big\{\left(\frac{243}{280}D_1-\frac{31}{144}\right)\sin^2 i_0$$
$$-\left(\frac{35}{96}+\frac{81}{80}D_1\right)\sin^4 i_0\Big\}\Big]\cos(5\bar{\phi}-3\omega)$$
$$-\frac{1}{24}\Big[e\Big\{\frac{1}{12}\sin^2 i_0+\left(\frac{33}{40}D_1-\frac{35}{144}\right)\sin^4 i_0\Big\}$$
$$+e^3\Big\{-\left(\frac{1}{80}D_1+\frac{73}{864}\right)\sin^4 i_0\Big\}\Big]\cos(5\bar{\phi}-\omega)$$
$$-\frac{1}{24}\Big[\frac{1}{4}e^3\sin^2 i_0\cos^2 i_0\Big]\cos(5\bar{\phi}+\omega)$$
$$-\frac{1}{24}\Big[e^3\Big\{\frac{3}{16}\sin^4 i_0\Big\}\Big]\cos(5\bar{\phi}+3\omega)$$
$$-\frac{1}{35}\Big[e^4\Big\{\frac{63}{360}D_1\sin^2 i_0$$
$$-\left(\frac{21}{160}D_1+\frac{1}{16}\right)\sin^4 i_0\Big\}\Big]\cos(6\bar{\phi}-4\omega)$$
$$-\frac{1}{35}\Big[e^2\Big\{\frac{1}{24}\sin^2 i_0+\left(\frac{53}{80}D_1-\frac{23}{144}\right)\sin^4 i_0\Big\}$$
$$+e^4\Big\{D_1\frac{123}{1120}\sin^4 i_0\Big\}\Big]\cos(6\bar{\phi}-2\omega)$$
$$+\frac{1}{35}\Big[e^2\Big\{\frac{3}{32}(4\sin^2 i_0-5\sin^4 i_0)\Big\}\Big]\cos(6\bar{\phi}+2\omega)$$
$$-\frac{1}{48}\Big[e^3\Big\{\frac{287}{144}\sin^2 i_0$$
$$+\left(\frac{13}{56}D_1+\frac{845}{864}\right)\sin^4 i_0\Big\}\Big]\cos(7\bar{\phi}-3\omega)$$
$$-\frac{1}{48}\Big[e^3\Big\{\frac{3}{144}\sin^4 i_0\Big\}\Big]\cos(7\bar{\phi}-\omega)$$
$$-\frac{1}{63}\Big[e^4\Big\{D_1\frac{27}{896}\sin^4 i_0\Big\}\Big]\cos(8\bar{\phi}-4\omega)$$
$$+\Big[e^2\Big\{(3D_1+\frac{11}{6})\sin^2 i_0-\left(\frac{43}{16}+\frac{15}{4}D_1\right)\sin^4 i_0\Big\}$$
$$+e^4\Big\{\left(\frac{1}{16}+\frac{33}{56}D_1\right)\sin^2 i_0$$
$$-\left(\frac{79}{32}+\frac{3}{4}D_1\right)\sin^4 i_0\Big\}\Big]\cos 2\omega$$
$$-\Big[e^4\Big\{D_1\frac{3}{128}\sin^4 i_0\Big\}\Big]\cos 4\omega\Big\} \qquad (98)$$

Finally the pseudo variables $\eta_2 \cdots \eta_6$ and ν_1 and ν_2 can be defined in terms of the true variables.

$$\eta_2 = \left\{\left(\frac{3}{7}D_1 - 1\right) + \left(\frac{35}{8} - \frac{15}{7}D_1\right)\sin^2 i_0 + \left(\frac{15}{8}D_1 - \frac{109}{24}\right)\sin^4 i_0 + e^2\left[\left(\frac{9}{7}D_1 - 1\right) + \left(\frac{53}{18} - \frac{45}{7}D_1\right)\sin^2 i_0 + \left(\frac{45}{8}D_1 - \frac{95}{36}\right)\sin^4 i_0\right] + e^4\left[\left(\frac{9}{56}D_1 - \frac{1}{4}\right) - \left(\frac{45}{56}D_1\right)\sin^2 i_0 + \left(\frac{9}{16} + \frac{45}{64}D_1\right)\sin^4 i_0\right]\right\} \quad (99)$$

$$\eta_3 = \left\{\left(\frac{7}{3} + \frac{24}{7}D_1\right)\sin^2 i_0 - \left(\frac{17}{4} + \frac{9}{2}D_1\right)\sin^4 i_0 - e^2\left(\frac{8}{7}D_1 + \frac{13}{24}\right)\sin^2 i_0 + \left(\frac{3}{16} - \frac{7}{8}D_1\right)\sin^4 i_0\right]\right\} \quad (100)$$

$$\eta_4 = \left\{e^2\left[\frac{1}{2}\sin^2 i_0 - \frac{95}{96}\sin^4 i_0\right]\right\} \quad (101)$$

$$\eta_5 = \left\{\left(\frac{24}{7}D_1 - 4\right) + \left(\frac{151}{12} - \frac{93}{7}D_1\right)\sin^2 i_0 + \left(\frac{21}{2}D_1 - \frac{229}{24}\right)\sin^4 i_0 + e^2\left[\left(\frac{11}{12} - \frac{9}{14}D_1\right) - \left(\frac{9}{2}D_1 + \frac{23}{32}\right)\sin^2 i_0 + \left(\frac{45}{8}D_1 - \frac{77}{72}\right)\sin^4 i_0\right]\right\} \quad (102)$$

$$\eta_6 = \left\{\left(\frac{7}{3} + \frac{24}{7}D_1\right)\sin^2 i_0 - \left(\frac{17}{4} + \frac{9}{2}D_1\right)\sin^4 i_0 + e^2\left[\left(14 - \frac{9}{7}D_1\right) + \left(\frac{819}{28}D_1 - \frac{158}{3}\right)\sin^2 i_0 + \left(\frac{289}{8} - \frac{29}{4}D_1\right)\sin^4 i_0\right]\right\} \quad (103)$$

$$\nu_1 = \left\{-\frac{e^3}{28}D_1\left(6 - 7\sin^2 i_0\right)\cos\left(\bar{\phi} - 3\omega\right) + \frac{e}{36}\left(36 - 89\sin^2 i_0\right)\cos\left(\bar{\phi} - \omega\right) + \frac{e}{28}\left[3D_1\left(4 + e^2\right) - 28\left(6 - 7\sin^2 i_0\right) - 7e^2\left(2 - 3\sin^2 i_0\right)\right]\cos\left(\bar{\phi} + \omega\right) + \frac{e^3}{8}\sin^2 i_0\, D_1\cos\left(\bar{\phi} + 3\omega\right) + \frac{e^2}{36}\left(9 - 25\sin^2 i_0\right)\cos\left(2\bar{\phi} - 2\omega\right) + \frac{1}{14}\left[2D_1\left(6 - 7\sin^2 i_0\right) - 7\left(4 - 5\sin^2 i_0\right) + e^2\left\{3D_1\left(6 - 7\sin^2 i_0\right) - \frac{7}{2}\left(2 - 3\sin^2 i_0\right)\right\}\right]\cos 2\bar{\phi} + \frac{e^2}{16}\left[6D_1\sin^2 i_0 - \left(2 - \sin^2 i_0\right)\right]\cos\left(2\bar{\phi} + 2\omega\right) + \frac{e}{252}\left[28\left(2 - \sin^2 i_0\right) + 9D_1\left(4 + e^2\right)\left(6 - 7\sin^2 i_0\right) - 21e^2\left(2 - 3\sin^2 i_0\right)\right]\cos\left(3\bar{\phi} - \omega\right) + \frac{e}{24}\left[D_1\left(4 + e^2\right)\sin^2 i_0 - 2\left(3 - 2\sin^2 i_0\right)\right]\cos\left(3\bar{\phi} + \omega\right) + \frac{e^2}{336}\left[7\left(10 - 9\sin^2 i_0\right) + 18D_1\left(6 - 7\sin^2 i_0\right)\right]\cos\left(4\bar{\phi} - 2\omega\right) + \frac{1}{144}\left[18D_1\left(2 + 3e^2\right)\sin^2 i_0 - 6\left(3 + \sin^2 i_0\right) - e^2\left(12 - 7\sin^2 i_0\right)\right]\cos 4\bar{\phi} + \frac{e^3}{140}D_1\left(6 - 7\sin^2 i_0\right)\cos\left(5\bar{\phi} - 3\omega\right) + \frac{e}{360}\left[27D_1\left(4 + e^2\right)\sin^2 i_0 - 20\left(3 + \sin^2 i_0\right)\right]\cos\left(5\bar{\phi} - \omega\right) + \frac{e^2}{144}\left[18D_1\sin^2 i_0 - \left(2 + \sin^2 i_0\right)\right]\cos\left(6\bar{\phi} - 2\omega\right) + \frac{e^3}{56}D_1\sin^2 i_0\cos\left(7\bar{\phi} - 3\omega\right)\right\} \quad (104)$$

and

$$\nu_2 = \left\{\left[-D_1 e^3\frac{1}{56}\left(6 - 14\sin^2 i_0 + 7\sin^4 i_0\right)\right]\sin\left(\bar{\phi} - 3\omega\right) + \left[\frac{e}{2}\left\{\left(\frac{36}{7}D_1 - \frac{7}{3}\right) + \left(\frac{403}{36} - \frac{99}{7}D_1\right)\sin^2 i_0 + \left(9D_1 - \frac{29}{3}\right)\sin^4 i_0\right\} + e^3\cos^2 i_0\left\{\left(\frac{9}{14}D_1 - \frac{1}{2}\right) + \left(\frac{3}{4} - \frac{9}{8}D_1\right)\sin^2 i_0\right\}\right]\sin\left(\bar{\phi} - \omega\right) + \left[e\left\{\left(3 - \frac{9}{7}D_1\right) + \left(\frac{9}{2}D_1 - \frac{53}{4}\right)\sin^2 i_0 + \left(11 - 3D_1\right)\sin^4 i_0\right\} + e^3\left\{\left(\frac{1}{4} - \frac{9}{28}D_1\right) + \left(\frac{9}{8}D_1 - \frac{7}{8}\right)\sin^2 i_0 + \left(\frac{3}{4} - \frac{3}{4}D_1\right)\sin^4 i_0\right\}\right]\sin\left(\bar{\phi} + \omega\right) - \left[e^3\left\{D_1\frac{1}{16}\sin^2 i_0\left(1 - 2\sin^2 i_0\right)\right\}\right]\sin\left(\bar{\phi} + 3\omega\right) + \frac{1}{2}\left[e^2\left\{\left(\frac{9}{7}D_1 - \frac{1}{8}\right) + \left(\frac{91}{144} - \frac{99}{28}D_1\right)\sin^2 i_0 + \left(\frac{9}{4}D_1 - \frac{31}{48}\right)\sin^4 i_0\right\}\right]\sin\left(2\bar{\phi} - 2\omega\right)$$

$$+\frac{1}{2}\left[(3-\frac{6}{7}D_1)+(\frac{23}{7}D_1-\frac{61}{6})\sin^2 i_0\right.$$

$$+(\frac{89}{12}-\frac{5}{2}D_1)\sin^4 i_0+e^2\left\{(\frac{1}{2}-\frac{9}{7}D_1)\right.$$

$$+(\frac{69}{14}D_1-\frac{91}{36}\sin^2 i_0$$

$$\left.\left.+(\frac{155}{72}-\frac{15}{4}D_1)\sin^4 i_0\right\}\right]\sin 2\bar{\phi}+\frac{1}{2}\left[e^2\left\{-\frac{1}{12}\right.\right.$$

$$+(\frac{163}{144}-\frac{3}{8}D_1)\sin^2 i_0$$

$$\left.\left.+(\frac{9}{16}D_1-\frac{275}{288})\sin^4 i_0\right\}\right]\sin(2\bar{\phi}+2\omega)$$

$$+\frac{1}{3}\left[e^2\left\{D_1\frac{3}{56}(4-11\sin^2 i_0\right.\right.$$

$$\left.\left.+7\sin^4 i_0)\right\}\right]\sin(3\bar{\phi}-3\omega)$$

$$+\frac{1}{3}\left[e\left\{(\frac{5}{36}-\frac{9}{7}D_1)+(\frac{5}{216}+\frac{33}{7}D_1)\sin^2 i_0\right.\right.$$

$$\left.\left.-(\frac{25}{216}+\frac{7}{2}D_1)\sin^4 i_0\right\}\right]+e^3\left\{(\frac{1}{4}-\frac{9}{28}D_1)\right.$$

$$+(\frac{33}{28}D_1-\frac{17}{24})\sin^2 i_0$$

$$\left.\left.+(\frac{1}{2}-\frac{7}{8}D_1)\sin^4 i_0\right\}\right]\sin(3\bar{\phi}-\omega)+\frac{1}{3}\left[e\left\{\frac{3}{4}\right.\right.$$

$$\left.-(1+\frac{3}{4}D_1)\sin^2 i_0+(\frac{5}{8}D_1+\frac{11}{24})\sin^4 i_0\right\}$$

$$\left.-e^3\left\{D_1\sin^2 i_0(\frac{3}{16}-\frac{5}{24}\sin^2 i_0)\right\}\right]\sin(3\bar{\phi}+\omega)$$

$$+\frac{1}{4}\left[e^2\left\{-(\frac{5}{12}+\frac{9}{14}D_1)+(\frac{129}{56}D_1+\frac{91}{144})\sin^2 i_0\right.\right.$$

$$\left.\left.-(\frac{27}{16}D_1+\frac{59}{288})\sin^4 i_0\right\}\right]\sin(4\bar{\phi}-2\omega)$$

$$+\frac{1}{4}\left[\frac{1}{2}-(\frac{1}{2}D_1+\frac{5}{12})\sin^2 i_0+(\frac{5}{8}D_1-\frac{1}{24})\sin^4 i_0\right.$$

$$+e^2\left\{\frac{1}{3}-(\frac{65}{144}+\frac{3}{4}D_1)\sin^2 i_0\right.$$

$$\left.\left.+(\frac{15}{16}D_1+\frac{41}{288})\sin^4 i_0\right\}\right]\sin 4\bar{\phi}$$

$$+\frac{1}{5}\left[e^3\left\{D_1(-\frac{3}{28}+\frac{53}{140}\sin^2 i_0\right.\right.$$

$$\left.\left.-\frac{11}{40}\sin^4 i_0)\right\}\right]\sin(5\bar{\phi}-3\omega)+\frac{1}{5}\left[e\left\{\frac{5}{12}\right.\right.$$

$$\left.-(\frac{3}{4}D_1+\frac{7}{18})\sin^2 i_0+(\frac{9}{10}D_1-\frac{1}{18})\sin^4 i_0\right\}$$

$$\left.-e^3\left\{D_1\sin^2 i_0(\frac{3}{16}-\frac{9}{40}\sin^2 i_0)\right\}\right]\sin(5\bar{\phi}-\omega)$$

$$+\frac{1}{6}\left[e^2\left\{\frac{1}{12}-(\frac{1}{16}+\frac{3}{8}D_1)\sin^2 i_0\right.\right.$$

$$\left.\left.+(\frac{7}{16}D_1-\frac{5}{288})\sin^4 i_0\right\}\right]\sin(6\bar{\phi}-2\omega)$$

$$-\frac{1}{7}\left[e^3\left\{D_1\sin^2 i_0\frac{1}{112}(7-8\sin^2 i_0)\right\}\right]\sin(7\bar{\phi}-3\omega)\Big\} \quad (105)$$

In these equations ω_0, i_{00} and e_0 are integration constants and as before the singularity at $i = 63.4°$ occurs. However, Struble notes that for this inclination the motion is given by the simple pendulum equation and concludes, as was done earlier, that an oscillation occurs in the element ω.

Still a third approach, though somewhat more similar to the second than the first, to predicting the motions of a satellite has been developed by Anthony and Fosdick (Ref. 25). This work, based upon the method of Lindstedt, is the result of series expansions for all variables in power series of the small parameter J_2. Since the higher order coefficients (J_3, etc.) are neglected, these series are truncated following terms of the order J_2. This being the case, each of the variables may be represented as

$$\left.\begin{aligned} u &= \frac{1}{r} = u_0(\xi) + 3/2\, J_2\, u_1(\xi) \\ P &= r^2\dot{\phi} = P_0(\xi) + 3/2\, J_2\, P_i(\xi) \\ \theta' &= (90 - L) = \pi/2 + 3/2\, J_2\, \theta_1'(\xi) \end{aligned}\right\} \quad (106)$$

where the new variable ξ is defined by

$$\phi = \xi(1 + 3/2\, J_2\, \phi_1)$$

ϕ_1 = constant to eliminate secular variations in u

and $u_0 = 1/r$ (for Keplerian orbit)

Now starting the solution for the motion at an apse (i.e., at a point where $\dot{r} = 0$), the equations of motion were found to be as follows:

General First-Order Results (Arbitrary ξ_0)

$$\phi = \xi \left[1 + \frac{3J_2}{4c^4}\left(\frac{R}{r_0}\right)^2 (2 - 3\sin^2 i)\right] \text{ (given } \phi_0\text{, use this equation to find } \xi_0 \qquad (107)$$

$$\theta' = \frac{\pi}{2} + \frac{J_2 \sin 2i}{4c^4}\left(\frac{R}{r_0}\right)^2 \{3\eta \sin \xi_0 - 2\eta \sin \xi_0 \cos(\xi - \xi_0) + (3 + 2\eta)\cos \xi_0 \sin(\xi - \xi_0) - \eta \sin \xi_0 \cos 2(\xi - \xi_0) - \eta \cos \xi_0 \sin 2(\xi - \xi_0) - 3(\xi - \xi_0)[\cos \xi_0 (\xi - \xi_0) - \sin \xi_0 \sin(\xi - \xi_0)]\} \qquad (108)$$

$$P = r^2\dot{\phi} = r_0 V_0 \left\{1 - \frac{J_2}{4c^4}\left(\frac{R}{r_0}\right)^2 \sin^2 i \left[(3 + 4\eta)\cos 2\xi_0 - 3\eta \cos 2\xi_0 \cos(\xi - \xi_0) + 3\eta \sin 2\xi_0 \sin(\xi - \xi_0) - 3\cos 2\xi_0 \cos 2(\xi - \xi_0) + 3\sin 2\xi_0 \sin 2(\xi - \xi_0) - \eta \cos 2\xi_0 \cos 3(\xi - \xi_0) + \eta \sin 2\xi_0 \sin 3(\xi - \xi_0)\right]\right\} \qquad (109)$$

$$u = \frac{1}{r} = \frac{1}{r_0 c^2}\left\{1 + \eta \cos(\xi - \xi_0) + \frac{J_2}{16c^4}\left(\frac{R}{r_0}\right)^2 L_1\right\} \qquad (110)$$

$$r = r_0 \left\{\frac{1 + \eta}{1 + \eta \cos(\xi - \xi_0)} - \frac{J_2}{16}\left(\frac{R}{r_0}\right)^2 \frac{L_1}{(1 + \eta)\left[1 + \eta \cos(\xi - \xi_0)\right]^2}\right\} \qquad (111)$$

$$V^2 = \frac{V_0^2}{c^4}\left\{1 + \eta^2 + 2\eta \cos(\xi - \xi_0) + \frac{J_2}{16}\left(\frac{R}{r_0}\right)^2 \frac{M_1}{c^4}\right\} \qquad (112)$$

$$V = \frac{V_0\sqrt{1 + \eta^2 + 2\eta \cos(\xi - \xi_0)}}{1 + \eta}\left\{1 + \frac{J_2}{32}\left(\frac{R}{r_0}\right)^2 M_1 \left\{(1 + \eta)^2\left[1 + \eta^2 + 2\eta \cos(\xi - \xi_0)\right]\right\}^{-1}\right\} \qquad (113)$$

where

$$L_1 = \{24 + 12\eta^2 + (\sin^2 i)\left[-36 - 18\eta^2 + (24 + 32\eta + 3\eta^2)\cos 2\xi_0\right]\} + \{-24 - 8\eta^2 + (\sin^2 i)\left[(-20 - 27\eta + 4\eta^2)\cos 2\xi_0 + 36 + 12\eta^2\right]\}\cos(\xi - \xi_0) + \{-\left[8 + 15\eta + 16\eta^2\right](\sin^2 i)\sin 2\xi_0\}\sin(\xi - \xi_0) + \{-4\eta^2 + \left[6\eta^2 + (-4 - 6\eta^2)\cos 2\xi_0\right]\sin^2 i\}\cos 2(\xi - \xi_0) + \{(4 + 6\eta^2)(\sin^2 i)\sin 2\xi_0\}\sin 2(\xi - \xi_0) - \{5\eta(\sin^2 i)\cos 2\xi_0\}\cos 3(\xi - \xi_0) + \{5\eta(\sin^2 i)\sin 2\xi_0\}\sin 3(\xi - \xi_0) - \{\eta^2(\sin^2 i)\cos 2\xi_0\}\cos 4(\xi - \xi_0) + \{\eta^2(\sin^2 i)\sin 2\xi_0\}\sin 4(\xi - \xi_0) \qquad (114)$$

$$M_1 = \{16(3 - 3\eta - \eta^3) + (\sin^2 i)\left[24(-3 + 3\eta + \eta^3) + 8(3 - \eta - 6\eta^2 - 3\eta^3)\cos 2\xi_0\right]\} + \{4(-12 + 12\eta - 4\eta^2 + 3\eta^3) + (\sin^2 i)\left[6(12 - 12\eta + 4\eta^2 - 3\eta^3) + (-40 - 18\eta + 8\eta^2 + 12\eta^3)\cos 2\xi_0\right]\}\cos(\xi - \xi_0) + \{-(16 + 66\eta + 32\eta^2 + 6\eta^3)(\sin^2 i)\sin 2\xi_0\}\sin(\xi - \xi_0) + \{16\eta^2 + (\sin^2 i)\left[-24\eta^2 + (16 + 24\eta^2)\cos 2\xi_0\right]\}\cos 2(\xi - \xi_0) - \{(16 + 24\eta^2)(\sin^2 i)\sin 2\xi_0\}\sin 2(\xi - \xi_0) + \{4\eta^3 + (\sin^2 i)\left[-6\eta^3 + (26\eta + 9\eta^3)\cos 2\xi_0\right]\}\cos 3(\xi - \xi_0) - \{(26\eta + 9\eta^3)(\sin^2 i)\sin 2\xi_0\}\sin 3(\xi - \xi_0) + \{16\eta^2(\sin^2 i)\cos 2\xi_0\}\cos 4(\xi - \xi_0)$$

continued

$$- \left\{16\eta^2 (\sin^2 i) \sin 2\xi_0\right\} \sin 4(\xi - \xi_0)$$
$$+ \left\{3\eta^3 (\sin^2 i) \cos 2\xi_0\right\} \cos 5(\xi - \xi_0)$$
$$- \left\{3\eta^3 (\sin^2 i) \sin 2\xi_0\right\} \sin 5(\xi - \xi_0). \quad (115)$$

$$c^2 = \eta + 1 \quad (116)$$

$$\eta = \frac{V_0^2 r_0}{u} - 1 \quad (117)$$

Under the assumption that the trajectory is nearly circular these equations can be simplified to yield

Nearly Circular Orbits (Arbitrary ξ_0)

$$\phi = \left[1 + \frac{3J_2}{4}\left(\frac{R}{r_0}\right)^2 (2 - 3\sin^2 i)\right]\xi \text{ (given } \phi_0\text{, use this equation to find } \xi_0) \quad (118)$$

$$\theta' = \frac{\pi}{2} + \frac{3J_2}{4}\left(\frac{R}{r_0}\right)^2 \sin^2 i \left\{\cos \xi_0 \sin(\xi - \xi_0) - (\xi - \xi_0)\left[\cos \xi_0 \cos(\xi - \xi_0) - \sin \xi_0 \sin(\xi - \xi_0)\right]\right\} \quad (119)$$

$$P = r_0 V_0 \left\{1 - \frac{3J_2}{4}\left(\frac{R}{r_0}\right)^2 \sin^2 i \left[\cos 2\xi_0 - \cos 2\xi_0 \cos 2(\xi - \xi_0) + \sin 2\xi_0 \sin 2(\xi - \xi_0)\right]\right\} \quad (120)$$

$$u = \frac{1}{r_0}\left[1 - \eta \left\{1 - \cos(\xi - \xi_0)\right\} + \frac{J_2}{4}\left(\frac{R}{r_0}\right)^2 \left\{6\left[1 - \cos(\xi - \xi_0)\right] + (\sin^2 i)\left[-(9 - 6\cos 2\xi_0) + (9 - 5\cos 2\xi_0)\cos(\xi - \xi_0) - 2(\sin 2\xi_0)\sin(\xi - \xi_0) - (\cos 2\xi_0)\cos 2(\xi - \xi_0) + (\sin 2\xi_0)\sin 2(\xi - \xi_0)\right]\right\}\right] \quad (121)$$

$$r = r_0\left[1 + \eta \left\{1 - \cos(\xi - \xi_0)\right\} - \frac{J_2}{4}\left(\frac{R}{r_0}\right)^2 \left\{6\left[1 - \cos(\xi - \xi_0)\right] + (\sin^2 i)\left[-(9 - 6\cos 2\xi_0) + (9 - 5\cos 2\xi_0)\cos(\xi - \xi_0) - 2(\sin 2\xi_0)\sin(\xi - \xi_0) + \right.\right.$$

continued

$$\left.\left. - (\cos 2\xi_0)\cos 2(\xi - \xi_0) + (\sin 2\xi_0)\sin 2(\xi - \xi_0)\right]\right\}\right] \quad (122)$$

$$V^2 = V_0^2\left[1 - 2\eta \left\{1 - \cos(\xi - \xi_0)\right\} + J_2\left(\frac{R}{r_0}\right)^2 \left\{3\left[1 - \cos(\xi - \xi_0)\right] + (\sin^2 i)\left[\left(-\frac{9}{2} + \frac{3}{2}\cos 2\xi_0\right) + \left(\frac{9}{2} - \frac{5}{2}\cos 2\xi_0\right)\cos(\xi - \xi_0) - (\sin 2\xi_0)\sin(\xi - \xi_0) + (\cos 2\xi_0)\cos 2(\xi - \xi_0) - (\sin 2\xi_0)\sin 2(\xi - \xi_0)\right]\right\}\right] \quad (123)$$

$$V = V_0\left[1 - \eta \left\{1 - \cos(\xi - \xi_0)\right\} + \frac{J_2}{2}\left(\frac{R}{r_0}\right)^2 \left\{3\left[1 - \cos(\xi - \xi_0)\right] + (\sin^2 i)\left[\left(-\frac{9}{2} + \frac{3}{2}\cos 2\xi_0\right) + \left(\frac{9}{2} - \frac{5}{2}\cos 2\xi_0\right)\cos(\xi - \xi_0) - (\sin 2\xi_0)\sin(\xi - \xi_0) + (\cos 2\xi_0)\cos 2(\xi - \xi_0) - (\sin 2\xi_0)\sin 2(\xi - \xi_0)\right]\right\}\right] \quad (124)$$

The solution obtained using these equations exhibits no singularity at the "critical inclination" and indeed is well behaved at every point. For this reason this set of equations, though not precise, seems well suited to analytic studies involving computer programs.

4. Analytic Comparison of General Perturbations Formulations

Recently several analytical methods of determining the oblateness perturbations have been published (Refs. 18 and 23 to 28) in which basically different mathematical approaches are employed. These approaches include:

(1) The classical approach of general perturbation theory in celestial mechanics, using the concept of an osculating ellipse and solving for the variations in orbital elements.

(2) Integrating the equations of satellite motion by seeking a solution in the form

$$\frac{1}{r} = \frac{1}{r_0}\left[1 + e\cos(\bar{\phi} - \omega) - J_2 c + J_2^2 d\right]$$

where c and d are unknown functions in terms of short-period perturbations (to be determined by the integration process), while r_0, e and ω exhibit only long-period perturbations.

(3) Direct approximate integration of the equations of motion with oblateness perturbations, solving directly for the instantaneous coordinates of the body in orbital motion.

Depending on the variables and mathematical tools used, the final solutions of various authors are seemingly different and physical interpretations of certain important variables are sometimes hard to visualize. The transformations between the different sets of variables employed in the literature have not been obtained previously.

Due to these facts a somewhat bitter controversy has arisen about the merits of classical celestial mechanics (Refs. 20, 23 and 29) for the solutions of near-circular orbits. The present analysis, which was made by J. Kork (Ref. 30) compares the solutions obtained by all the above mentioned authors for nearly circular orbits within the first order accuracy in the oblateness parameter J_2 (i.e., neglecting J_3, J_4, J_2^2 terms).

a. Kozai's formulation (Refs. 18 and 26)

Upon a change in the notation utilized by Kozai to that utilized by Vinti and upon changing the symbols to be consistent with those presented in Chapter III, the first order perturbation in position may be written

$$\delta r = a \left\{ \frac{1}{2} J_2 \left(\frac{R^2}{ap}\right) \left(1 - \frac{3}{2}\sin^2 i\right) \left[-1 - \frac{1}{e}\left(1 - \sqrt{1-e^2}\right)\cos\theta + \frac{r}{a}\frac{1}{\sqrt{1-e^2}} \right] + \frac{1}{4} J_2 \left(\frac{R^2}{ap}\right) \sin^2 i \cos 2(\theta+\omega) \right\} \quad (125a)$$

$$\delta\phi = \frac{3}{2} J_2 \left(\frac{R}{p}\right)^2 \left\{ \left(2 - \frac{5}{2}\sin^2 i\right)(\theta - M + e\sin\theta) + \left(1 - \frac{3}{2}\sin^2 i\right)\left[\frac{2}{3e}\left(1-e^2\right) - \sqrt{1-e^2}\right)\sin\theta + \frac{1}{6}\left(1 - \sqrt{1-e^2}\right)\sin 2\theta \right] - \left(\frac{1}{2} - \frac{5}{6}\sin^2 i\right) e\sin(\theta+2\omega) - \left(\frac{1}{2} - \frac{7}{12}\sin^2 i\right)\sin 2(\theta+\omega) - \frac{e}{6}\cos^2 i \sin(3\theta+2\omega) \right\} \quad (125b)$$

and the secular perturbations in the orbital elements are

$$\bar{\omega} = \omega_0 + \frac{3}{2} J_2 \left(\frac{R}{p}\right)^2 \bar{n}\left(2 - \frac{5}{2}\sin^2 i\right) t \quad (126a)$$

$$\bar{\Omega} = \Omega_0 - \frac{3}{2} J_2 \left(\frac{R}{p}\right)^2 \bar{n} t \cos i \quad (126b)$$

$$\bar{M} = M_0 + \bar{n} t \quad (126c)$$

$$\bar{n} = n_0 + \frac{3}{2} J_2 \left(\frac{R}{p}\right)^2 n_0 \left(1 - \frac{3}{2}\sin^2 i\right)\sqrt{1-e^2} \quad (126d)$$

where ω_0, Ω_0 and M_0 are the mean values at the epoch, i.e., the initial values of the osculating elements from which the periodic perturbations have been subtracted.

There are no first order secular perturbations of the semimajor axis, a, of the eccentricity, e, and of the inclination, i.

The mean value of a (i.e., $\bar{a}$) is given by Kozai in terms of the unperturbed semimajor axis a_0, as

$$\bar{a} = a_0 \left\{ 1 - \frac{3}{2} J_2 \left(\frac{R}{p}\right)^2 \left(1 - \frac{3}{2}\sin^2 i\right)\sqrt{1-e^2} \right\} \quad (127)$$

Notice that the classical relationship $n_0^2 a_0^3 = \mu$, becomes in these variables

$$\bar{n}^2\bar{a}^3 = \mu \left\{ 1 - \frac{3}{2} J_2 \left(\frac{R}{p}\right)^2 \left(1 - \frac{3}{2}\sin^2 i\right)\sqrt{1-e^2} \right\} \quad (128)$$

The value of the mean semimajor axis, $\bar{a}$, has been already used in the derivations of Eq (5).

If the eccentricity, e, of the orbit is a small quantity of the first order or less, Eqs (125) can be reduced to the simple form given below (Ref. 26).

$$\delta r = \frac{1}{4}\bar{a} J_2 \left(\frac{R}{\bar{a}}\right)^2 \sin^2 i \cos 2\lambda = \frac{1}{8}\bar{a}\,\epsilon \sin^2 i \cos 2\lambda \quad (129a)$$

$$\delta\phi = -\frac{3}{2} J_2 \left(\frac{R}{\bar{a}}\right)^2 \left(\frac{1}{2} - \frac{7}{12}\sin^2 i\right)\sin 2\lambda = -\epsilon\left(\frac{1}{2} - \frac{7}{12}\sin^2 i\right)\sin 2\lambda \quad (129b)$$

where (within a first order accuracy)

$$\lambda = M + \omega$$

$$\epsilon = \frac{3}{2} J_2 \left(\frac{R}{r}\right)^2 \approx \frac{3}{2} J_2 \left(\frac{R}{\bar{a}}\right)^2$$

Since ϵ is a small quantity, and since the relationship between M and θ is (Ref. 31)

$$M = \theta - 2e\sin\theta + \ldots$$

it can be shown that for small eccentricities, i.e., $e = O(\epsilon)$

$$1 + \epsilon \cos 2\lambda \approx 1 + \epsilon \cos 2(\theta + \omega) + 4\epsilon \sin\theta \sin 2(\theta + \omega) \approx 1 + \epsilon \cos 2\phi \tag{130a}$$

and similarily

$$1 + \epsilon \sin 2\lambda \approx 1 + \epsilon \sin 2\phi \tag{130b}$$

Thus Eqs 129a and b can be written also as

$$\delta r \approx \frac{1}{6}\bar{a}\,\epsilon \sin^2 i \cos 2\phi$$

$$\delta\phi \approx -\epsilon \left(\frac{1}{2} - \frac{7}{12}\sin^2 i\right) \sin 2\phi \tag{131}$$

Finally, the expression for the instantaneous radius vector in near-circular orbits can be written as

$$r = \bar{a}\left[1 - e_0 \cos(\phi - \bar{\omega}) + \frac{1}{4} J_2 \left(\frac{R}{\bar{a}}\right)^2 \sin^2 i \cos 2\phi\right] \tag{132}$$

From Eqs (126) and (130a) it can be seen that for small eccentricities the average angle from node to perigee $\bar{\omega}$ can be approximated for one revolution by its initial value, ω_0.

Kozai's solution for near-circular orbits consists basically of two independent components varying about a mean radius, $\bar{a}$. These components are:

(1) An oblateness term, $\frac{1}{4}\epsilon \sin^2 i \cos 2\phi$ which has a period of π (double periodic within one full revolution) and depends mainly on the shape of earth seen by the satellite vehicle (i.e. oblateness parameter J_2 and inclination of the orbit, i) but is independent of the orbital eccentricity, e, and nodal angle to perigee, ω. The oblateness term depends also on the semimajor axis through the term $\epsilon = \frac{3}{2} J_2 \left(\frac{R}{\bar{a}}\right)^2$.

(2) An elliptical term, $e_0 \cos(\phi - \omega_0)$ depending only on the geometrical properties of the orbit, e_0 and ω_0 but being completely independent of the oblateness of the planet or the orbital inclination.

It is obvious from the mathematical form of Eq (132) that depending on the relative size of the oblateness and ellipticity terms, in connection with proper phase shifts between the two, two, three or four "apses" can be obtained during a single revolution (i.e. points where $\dot{r} = 0$).

This fact will be graphically illustrated in the discussion of Izsak's work.

b. Struble's formulation

If only terms to the first order in J are retained, Struble's main results, periodic in radius, can be presented in the following form (Ref. 24, p 93).

$$\frac{1}{r} = \frac{1}{r_0}\left[1 + e\cos(\bar{\phi} - \omega) - J_2 c\right] \tag{133a}$$

$$\frac{1}{r_0} = \frac{\mu}{p_m^2}\cos^2 i_0 + \frac{3}{4}\frac{J_2}{r_0}\left(\frac{R}{r_0}\right)^2 \left(1 + \frac{e^2}{2}\right)\left(2 - 3\sin^2 i_0\right) \tag{133b}$$

$$\phi = \bar{\phi} + \frac{3}{8} J_2 \left(\frac{R}{r_0}\right)^2 \left[4e\cos^2 i \sin(\bar{\phi} - \omega) + 2e(1 - 2\cos^2 i_0)\sin(\bar{\phi} + \omega) + (1 - 3\cos^2 i_0)\sin 2\bar{\phi} + \frac{2}{9} e (1 - 4\cos^2 i_0)\sin(3\bar{\phi} - \omega)\right] \tag{133c}$$

where

$$c = \frac{1}{8}\left(\frac{R}{r_0}\right)^2 \sin^2 i \left[\left(2 + \frac{e^2}{3}\right)\cos 2\bar{\phi} + e\cos(3\bar{\phi} - \omega) + \frac{e^2}{6}\cos(4\bar{\phi} - 2\omega) + \frac{3e^2}{2}\cos 2\omega\right] + \frac{1}{8}\left(\frac{R}{r_0}\right)^2 e^2 (2 - 3\sin^2 i_0)\cos(2\bar{\phi} - 2\omega) \tag{133d}$$

$$p_m = r^2 \sin\theta' \frac{dA_s}{dt} = \text{angular momentum about the polar axis}$$

$$\theta' = 90° - L \tag{133e}$$

In Ref. 32 it is shown that the angular momentum orbital plane is given by

$$h = r^2(\dot{\theta} + \dot{\omega} + \cos i\,\dot{\Omega}) = \sqrt{\mu p} \tag{134}$$

From Eqs (133) and (134) it can be shown that

$$p_m = \sqrt{\mu p}\cos i \text{ or } \frac{1}{p} = \frac{\mu \cos^2 i}{p_m^2} \tag{135}$$

For small eccentricities of the order J_2

$$1 + e\cos(\bar{\phi} - \omega) \approx 1 + e\cos(\phi - \omega) \tag{136}$$

at least for one revolution. Similarly all terms containing e^2, $J_2 e$, etc. can be neglected. Using Eqs (135) and (136) the results given in Eqs. (133) can be simplified to read

$$r = r_0\left[1 - e\cos(\phi - \omega) + \frac{1}{4} J_2 \left(\frac{R}{r_0}\right)^2 \sin^2 i \cos 2\phi\right] \tag{137a}$$

$$r_0 = p\left[1 - \frac{3}{4} J_2 \left(\frac{p}{r_0}\right)\left(\frac{R}{r_0}\right)^2 (2 - 3\sin^2 i)\right] \quad (137b)$$

Furthermore it should be noted that for small eccentricities

$$J_2 \left(\frac{p}{r_0}\right) \approx J_2$$

$$p = a(1 - e^2) \approx a \quad (138)$$

Remembering this approximation and comparing Eq (137b) with Eq (127) similarily Eq (137a) with Eq (132) it becomes obvious that for $e = O(J_2)$ the first order results of Struble are identical with Kozai's formulation and the constant r_0 is given simply by the mean semimajor axis:

$$r_0 = \bar{a} \quad (139)$$

c. Izsak's formulation (Ref. 23)

The instantaneous radius is given by Izsak as follows

$$r = a^*\left[1 - e\cos(\phi - \omega) + \frac{1}{2}e^2\cos 2(\phi - \omega) + \frac{1}{4}J_2\left(\frac{R}{\bar{a}}\right)^2 \sin^2 i \cos 2w + \ldots\right]$$

where

$$a^* = a\left[1 - \frac{1}{2}e^2 + \frac{1}{2}J_2\left(\frac{R}{\bar{a}}\right)^2 (1 - \frac{1}{2}\sin^2 i)\right]$$

$$w = (1 + \epsilon')\theta + \omega \quad (140)$$

ϵ' = a constant for the motion of the perigee of the order J_2

For $e = O(J_2)$ the solution for one revolution is simply

$$r = a^*\left[1 - e\cos(\phi - \omega) + \frac{1}{4}J_2\left(\frac{R}{\bar{a}}\right)^2 \sin^2 i \cos 2\phi\right] \quad (141)$$

Comparing Eq (141) with Eq (132) it is seen that Izsak's solution can be also reduced to the form given by Kozai and the parameter a^* is simply $a^* = \bar{a}$.

An interesting feature of Ref. 23 is a set which represents parametric families of curves obtained by solving Eq (141) of this study numerically for various values of e_0 (0.0, 0.00012, 0.00030, 0.00049) and for three particular cases of ω_0 (0°, 45°, 90°). The curves show clearly the possibilities of 2, 3 and 4 "apses" (i.e. points where $\dot{r} = 0$) during one revolution, depending on the relative sizes of ellipticity terms with respect to the oblateness terms and also on certain phase shifts between them. These figures have been reproduced and are presented for convenience as Fig. 7.

d. Equations derived by Anthony and Fosdick

The form of the resulting equations in Ref. 25 is completely different from the results obtained by the authors considered previously. In Ref. 28 the equations of motion in spherical coordinates are integrated directly and certain new variables are introduced, which do not have a simple physically intuitive connection with the variables used previously. There may exist some doubt, how the initial value, ξ_0, of the "independent variable for which the first-order analytical results for r and V are periodic" compares with the classical ω_0, and how the analog of eccentricity $\eta \equiv \frac{V_0^2}{V_c^2} - 1$ may depend on the classical eccentricity, e. These transformations are far from obvious, thus, they are derived in this section by reducing Anthony's solution to an analytical form similar to Kozai's results and then comparing the coefficients term-by-term.

The equations for arbitrary near-circular orbits are given as Eqs (118) through (124) assuming $\eta = \theta(J_2)$. Certain terms in these equations can be simplified by using the equality

$$\cos 2\xi_0 \cos 2(\xi - \xi_0) - \sin 2\xi_0 \sin 2(\xi - \xi_0) = \cos 2\xi \quad (143)$$

Next, using the previous notation $\epsilon = J_2\left(\frac{R}{r_0}\right)^2 = \frac{3}{2}J_2\left(\frac{R}{r_0}\right)^2$ the expressions for r and V can be written as follows

$$r = r_0\left\{1 + \eta\left[1 - \cos(\xi - \xi_0)\right] - \epsilon + \epsilon\cos(\xi - \xi_0) - \frac{1}{6}\epsilon\sin^2 i\left[(-9 + 6\cos 2\xi_0) + (9 - 5\cos 2\xi_0)\cos(\xi - \xi_0) - 2\sin 2\xi_0 \sin(\xi - \xi_0) - \cos 2\xi\right]\right\} \quad (144a)$$

$$V = V_0\left\{1 - \eta + \eta\cos(\xi - \xi_0) + \epsilon - \epsilon\cos(\xi - \xi_0) + \frac{1}{3}\epsilon\sin^2 i \cdot \left[\left(-\frac{9}{2} + \frac{3}{2}\cos 2\xi_0\right) + \left(\frac{9}{2} - \frac{5}{2}\cos 2\xi_0\right)\cos(\xi - \xi_0) - \sin 2\xi_0 \sin(\xi - \xi_0) + \cos 2\xi\right]\right\} \quad (144b)$$

where

$$\xi = \left[1 - \frac{1}{2}\epsilon(2 - 3\sin^2 i)\right]\phi \quad (144c)$$

Notice, that in Eqs (144a) and (144b) the sine and cosine terms appear combined with a small con-

stant of the form $\alpha_1 \cos \xi$, where $\xi = (1 - \alpha_2)\phi$. Since for the nearly circular orbit considered here both α_1 and α_2 are of the order ϵ, it follows by a reasoning similar to Eqs (130a) and (130b) that

$$1 + \alpha_1 \cos \xi \approx 1 + \alpha_1 \cos \phi, \text{ etc.} \qquad (145)$$

Equation (145) indicates that for the purposes of this analysis it does not make a noticeable difference, if during any single revolution ξ is simply visualized as the central angle from the ascending node, ϕ.

Next, collecting the cosine and sine terms in Eq (144a)

$$r = r_0 (1 + A_0) \left[1 - A_1 \cos (\xi - \xi_0) + A_2 \sin (\xi - \xi_0) + \frac{1}{6} \epsilon \sin^2 i \cos 2\xi\right] \qquad (146)$$

where

$$A_0 = \eta - \epsilon + \frac{3}{2} \epsilon \sin^2 i - \epsilon \sin^2 i \cos 2\xi_0$$

$$A_1 = \eta - \epsilon + \frac{3}{2} \epsilon \sin^2 i - \frac{5}{6} \epsilon \sin^2 i \cos 2\xi_0$$

$$A_2 = \frac{1}{3} \epsilon \sin^2 i \sin 2\xi_0$$

By trigonometry

$$- A_1 \cos x + A_2 \sin x = \sqrt{A_1^2 + A_2^2} \cos \left(x + \tan^{-1} \frac{A_2}{A_1}\right)$$

Thus Eq (146) becomes

$$r = r_0 (1 + A_0) \left[1 - \sqrt{A_1^2 + A_2^2} \cos (\xi - \xi_0 + \alpha_0) + \frac{1}{6} \epsilon \sin^2 i \cos 2\xi\right] \qquad (147)$$

where

$$\alpha_0 = \tan^{-1} \left(\frac{A_2}{A_1}\right)$$

Kozai's form of radius, given by Eq (132) can be written as follows

$$r = \bar{a} \left[1 - e \cos (\phi - \omega_0) + \frac{1}{6} \epsilon \sin^2 i \cos 2\phi\right] \qquad (148)$$

By comparing Eq (147) with Eq (148), while remembering that within the first order accuracy $\xi \approx \phi$, the following important transformation equations can be derived by equating the corresponding coefficients of two Fourier series expansions of the same function ϕ. Thus, Anthony's variables are related to Kozai's formulation by the following equations:

$$\bar{a} = r_0 \left[1 + \eta - \epsilon + \frac{3}{2} \epsilon \sin^2 i + \right.$$

continued

$$\left. - \epsilon \sin^2 i \cos 2\xi_0\right] \qquad (149a)$$

$$e = \left[\left(\eta - \epsilon + \frac{3}{2} \epsilon \sin^2 i - \frac{5}{6} \epsilon \sin^2 i \cos 2\xi_0\right)^2 + \left(\frac{1}{3} \epsilon \sin^2 i \sin 2\xi_0\right)^2\right]^{1/2} \qquad (149b)$$

$$\omega_0 = \xi_0 - \tan^{-1} \left[\left(\frac{1}{3} \epsilon \sin^2 i \sin 2\xi_0\right) \cdot \left(\eta - \epsilon + \frac{3}{2} \epsilon \sin^2 i - \frac{5}{6} \epsilon \sin^2 i \cos 2\xi_0\right)^{-1}\right] \qquad (149c)$$

The inverse transformation equations for η and r_0 can also be obtained from Eqs (149a) and (149b) to be:

$$\eta = \left[e^2 - \left(\frac{1}{3} \epsilon \sin^2 i \sin 2\xi_0\right)^2\right]^{1/2} + \epsilon - \frac{3}{2} \epsilon \sin^2 i + \frac{5}{6} \epsilon \sin^2 i \cos 2\xi_0 \qquad (150a)$$

$$r_0 = \bar{a} \left[1 - \eta + \epsilon - \frac{3}{2} \epsilon \sin^2 i + \epsilon \sin^2 i \cos 2\xi_0\right] \qquad (150b)$$

$$= \bar{a} \left[1 - \left(e^2 - \left(\frac{1}{3} \epsilon \sin^2 i \sin 2\xi_0\right)^2\right)^{1/2} + \frac{1}{6} \epsilon \sin^2 i \cos 2\xi_0\right]$$

$$\xi_0 = \xi_0 (\omega_0, i, e, \epsilon) \qquad (150c)$$

Unfortunately, Eq (149c) is transcendental and the third transformation must be found by numerical successive approximations. Characteristic solution curves for Eq (150c) can be obtained by the following procedure:

(1) For a given e, i, ϵ solve for various values of ω_0 by assuming values for ξ_0 in steps of 10°, for example.

(2) Plot the data and obtain a value of ξ_0 corresponding to the given ω_0.

For step (1) it is advantageous to write Eq (149c) in the following form

$$\omega_0 = \xi_0 - \tan^{-1} \left[\frac{\frac{1}{3} \epsilon \sin^2 i \sin 2\xi_0}{\left[e^2 - \left(\frac{1}{3} \epsilon \sin^2 i \sin 2\xi_0\right)^2\right]^{1/2}}\right] \qquad (151)$$

Note:

If in Eq (151) the eccentricity becomes smaller than a critical value $e^* = \frac{\epsilon}{3} \sin^2 i$, the values of ξ_0

can no longer be picked arbitrarily. This fact is illustrated by assuming e = 0 in Eq (149b) and observing that the required value of ξ_0 = 0°, 90°, 180°, 270°. Physically this means that for e = 0 the "apoapsis" always occurs at the equatorial crossings (ξ_0 = 0°, 180°) and "periapsis" always occurs at the maximum latitude (ξ_0 = 90°, 270°), there being four "apsidal" points during one revolution.

It is noted once again that ω_0 gives the location of the minimum point of the eccentrical components of orbital radius, while ξ_0, gives the extreme of the radius.

Finally, it should be remarked that the statement made in Ref. 28

"e = $|\eta|$ for an elliptical orbit"

is misleading since it is true only for the non-oblate case, while in general e = e (η, ϵ, i, ξ_0) and must be computed by Eq (149b). Only for large eccentricities is the approximation e ≈ $|\eta|$ valid for rough engineering estimates.

e. General comparisons

It was shown above that to the order J_2 in oblateness all the methods considered are identical at least in the case of nearly circular orbits. Mathematically, Kozai's formulations for the instantaneous radius, Eq (132), and secular perturbations, Eqs (126) are generally the simplest to use. However, if for any fixed orbit the orbital injection conditions are desired, the results of Anthony and Fosdick merit investigation. It was thus shown that the classical method of osculating ellipses is still valid for nearly circular orbits and that it provides a somewhat clearer geometrical interpretation of end results.

5. Solar and Lunar Perturbations

The problems of defining the changes in the motion of an earth satellite due to the presence of distant gravitating masses and the discussion of the stability of an orbit are of necessity closely related. This relationship exists because the two analyses differ only in the time intervals considered and the fact that forces other than those produced by external masses (for example atmospheric drag) must be included in the discussion of stability. For this reason much of the material presented in the following paragraphs is applicable to subsequent discussions.

Analytic expressions for the perturbations due to the gravitational attraction of a third body may be derived by techniques similar to those used in the oblateness derivations. This approach has been taken by Penzo (Ref. 33) with the result that one set of equations for the variations in the orbital elements may be obtained. This solution is outlined below:

Choose geocentric coordinates with the X-Y plane being the orbit plane of the disturbing body. Let Γ be the central angle between the ascending node and the disturbing body, and Γ_p be the central angle between perigee and the disturbing body. Also, let i_p be the angle between the vehicle orbit plane and the plane containing the origin, perigee and the disturbing body.

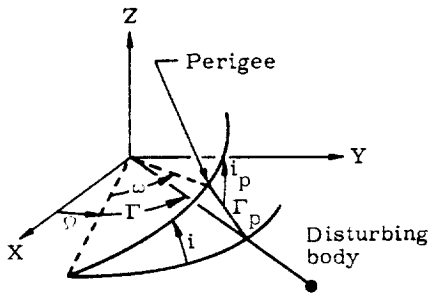

The deviations in the elements are derived in a system based on this latter plane. In this system, Ω_p = 0, ω_p = 0 and i_p is the inclination. The solutions obtained for the perigee system are then transformed into the solutions in the original X, Y, Z system. The solutions are:

$$\Delta i_p = \frac{\mu_d}{\mu} \frac{r_p^3 \sin \Gamma_p \cos \Gamma_p \sin i_p \sin \theta}{r_d (1-e)^3 (1+ e \cos \theta)^3} \left[(13 + 2e^2) e - 3 (1-9e^2 - 2e^4) \cos \theta - e(1-6e^4) \cos^2 \theta \right]$$

$$- \frac{\mu_d}{\mu} \frac{r_p^3 (1+e)^3 \sin^2 \Gamma_p \sin i_p \cos i_p}{r_d e^2 (1+ e \cos \theta)^3} (1 + 3e \cos \theta)$$

$$- \frac{\mu_d}{\mu} \frac{3 r_p^3 (1+4e^2) \sin \Gamma_p \cos \Gamma_p \sin i_p}{r_d (1-e)^3 \sqrt{1-e^2}} E + C_i \qquad (152)$$

$$\Delta \Omega_p = \frac{\mu_d}{\mu} \frac{r_p^3 (1+e) \sin^2 \Gamma_p \cos i_p \sin \theta}{r_d (1-e)^2 (1+e \cos \theta)} \left[3e + 3(1+e^2) \cos \theta + e (1+2e^2) \cos^2 \theta \right]$$

$$- \frac{\mu_d}{\mu} \frac{r_p^3 (1+e)^3 \sin \Gamma_p \cos \Gamma_p (1+3e \cos \theta)}{r_d e^2 (1+ e \cos \theta)^3}$$

$$- \frac{\mu_d}{\mu} \frac{3 r_p^3 (1+e) \sin^2 \Gamma_p \cos i_p}{r_d (1-e)^2 \sqrt{1-e^2}} E + C_\Omega \qquad (153)$$

$$\Delta\omega_p = -\cos i_p \Delta\Omega_p + \frac{\mu_d}{\mu} \frac{r_p^3 (1+e)^3 \sin 2\Gamma_p \cos i_p}{r_d 2e^4 (1+e\cos\theta)^3} \left[4 - 5e^2 + 3e(4-e^2)\cos\theta + 12e^2\cos^2\theta\right] - \frac{\mu_d}{\mu} \frac{r_p^3 (1+e)\sin\theta}{r_d e^3 (1-e)^2 (1+e\cos\theta)^3} \left\{\left[(6 - 44e^2 + 13e^4 - 2e^6) + 3e(4 - 25e^2 + 3e^4)\cos\theta + e^2(8 - 37e^2 + 2e^4)\cos^2\theta\right](\cos^2\Gamma_p - \sin^2\Gamma_p \cos^2 i_p) + e^2\left[(2+e^2) + 3e(1+e^2)\cos\theta + e^2(1+2e^2)\cos^2\theta\right](1 - 3\sin^2\Gamma_p\cos^2 i_p)\right\} + \frac{\mu_d}{\mu} \frac{3r_p^3 (1+e)(4\cos^2\Gamma_p - \sin^2\Gamma_p\cos^2 i_p - 1)}{r_d (1-e)^2 \sqrt{1-e^2}} E + C_\omega \quad (154)$$

$$\Delta a = \frac{\mu_d}{\mu} \frac{2a^2 p^2}{r_d e^2 (1+e\cos\theta)^2} \left[3e^2 \sin 2\Gamma_p \cos i_p \sin\theta\cos\theta - 6e(\cos^2\Gamma_p - \sin^2\Gamma_p\cos^2 i_p)\cos\theta - 3\cos^2\Gamma_p + 3(1+e^2)\sin^2\Gamma_p\cos^2 i_p - e^2\right] + C_a \quad (155)$$

$$\Delta e = \frac{p}{2ea^2}\Delta a - \frac{1}{ea}\sqrt{\frac{p}{\mu}} \left\{\frac{\mu_d}{\mu} \frac{\sqrt{\mu p}\, r_p^3 \sin 2\Gamma_p \cos i_p \sin\theta}{2r_d (1-e)^3 (1+e\cos\theta)^3} \left[e(2e^4 - 9e^2 - 8) + 3(2 - 9e^2 - 3e^4)\cos\theta + e(2 - 9e^2 - 8e^4)\cos^2\theta\right] + \frac{\mu_d}{\mu} \frac{\sqrt{\mu p}\, r_p^3 (1+e)^3}{r_d e^2 (1+e\cos\theta)^3} (\cos^2\Gamma_p - \sin^2\Gamma_p\cos^2 i_p)(1 + 3e\cos\theta) + \frac{\mu_d}{\mu} \frac{15\sqrt{\mu p}\, r_p^3 e^2 \sin 2\Gamma_p \cos i_p}{2r_d (1-e)^3 \sqrt{1-e^2}} E + C_e \quad (156)$$

where μ_d and r_d are the gravitational constant and orbital radius (assumed constant) of the disturbing body, respectively, and the C_i, C_Ω, etc., are constants of integration, i.e., they are functions of the initial conditions.

The transformations to the elements in the X, Y, Z system are

$$\Delta i = \frac{1}{\sin i}\left[(\cos\alpha \sin i_p - \sin\alpha \cos i_p \cos\Gamma_p)\Delta i_p - \sin\alpha \sin i_p \sin\Gamma_p \Delta\Omega_p\right] \quad (157)$$

$$\Delta\Omega = \frac{1}{\cos\nu \sin^3 i} \left\{\left[\sin i_p \sin\Gamma_p \cos i(\cos\alpha \sin i_p - \sin\alpha\cos i_p \cos\Gamma_p) - \sin^2 i \cos i_p \sin\Gamma_p\right]\Delta i_p + (\sin^2 i \sin i_p \cos\Gamma_p - \sin^2 i_p \sin^2\Gamma_p \cos i \sin\alpha)\Delta\Omega_p\right\} \quad (158)$$

$$\Delta\omega = \frac{\sin\alpha}{\cos\omega \sin^3 i}\left[(\sin\alpha \sin^2\Gamma_p \cos i \sin i_p - \sin^2 i \cos\Gamma_p)\Delta\Omega_p + \sin\Gamma_p \cos i(\cos\alpha \sin i_p - \sin\alpha\cos i_p\cos\Gamma_p)\Delta i_p\right] + \Delta\omega_p$$

where

$$\sin\alpha = \frac{\sin\omega \sin i}{\sin\Gamma_p}$$

The assumptions in the derivation of these solutions are that $r_d >> r$ and that the disturbing body does not move during the interval of variation.

Thus, in order to solve for the perturbed motion of a satellite it would be necessary to compute the perturbations (for some small time, say 1 period) due to each body being considered, resolve these perturbations into a common coordinate system, add the resultant motions, adjust the orbital elements and then continue the computation. This is obviously a lengthy procedure and is not intended to be performed by hand.

Another approach to perturbations has been reported by Geyling (Ref. 34), who presents the effects of these remote bodies in terms of variations in the position of the satellite in cartesian coordinates. Only circular satellite orbits, however, are considered.

Choose X, Y, Z axes such that the orbit plane of the disturbing body is the X-Y plane, the X axis being in the direction of the satellite's ascending node. The deviations from the nominal trajectory will be given in the ξ, η, ζ system, which moves with the position in the nominal orbit. ξ is radial, and η is in the direction of motion.

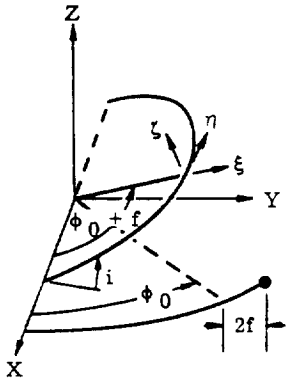

The position of the disturbing body in the X-Y plane is given by the central angle $\bar{\phi} = \bar{\phi}_0 + \lambda f$ where $\bar{\phi}_0$ is an initial value at $t = f = 0$ and λ is the ratio of the angular velocity of the disturbing body to that of the vehicle. Geyling's solutions are

$$\xi = -\frac{3}{8}\frac{\mu_d}{\mu}\frac{r_c^4}{r_d^3}\left[-\frac{2}{3}(2\cos^2 i - \sin^2 i) + \frac{4}{3}\sin^2 i\cos 2\phi + \frac{2}{4\lambda^2-1}\sin^2 i\cos 2\bar{\phi} + \frac{(\lambda+2)(1-\cos i)^2}{(\lambda+1)(2\lambda+1)(2\lambda+3)}\cos 2(\bar{\phi}+\phi) + \frac{(\lambda-2)(1+\cos i)^2}{(\lambda-1)(2\lambda-1)(2\lambda-3)}\cos 2(\bar{\phi}-\phi)\right] + k_1 + k_2\sin\phi + k_3\cos\phi \quad (160)$$

$$\eta = -\frac{3}{8}\frac{\mu_d}{\mu}\frac{r_c^4}{r_d^3}\left[\frac{4}{3}(2\cos^2 i - \sin^2 i)f - \frac{11}{6}\sin^2 i\sin 2\phi - \frac{2\sin^2 i}{\lambda(4\lambda^2-1)}\sin 2\bar{\phi} - \frac{(4\lambda^2+12\lambda+11)(1-\cos i)^2}{4(\lambda+1)^2(2\lambda+1)(2\lambda+3)}\sin 2(\bar{\phi}+\phi) + \frac{(4\lambda^2-12\lambda+11)(1+\cos i)^2}{4(\lambda-1)^2(2\lambda-1)(2\lambda-3)}\sin 2(\bar{\phi}-\phi)\right] + k_4 + k_5\phi + k_6\sin\phi + k_7\cos\phi \quad (161)$$

$$\zeta = -\frac{3}{8}\frac{\mu_d}{\mu}\frac{r_c^4}{r_d^3}\left[\frac{1}{2}\sin 2i\sin\phi - f\sin 2i\cos\phi - \frac{(1-\cos i)\sin i}{2\lambda(\lambda+1)}\sin(2\bar{\phi}+\phi) - \frac{(1+\cos i)\sin i}{2\lambda(\lambda-1)}\sin(2\bar{\phi}-\phi)\right] + k_8\cos\phi + k_9\sin\phi \quad (162)$$

where r_c = radius of the circular nominal orbit, and the k's are constants to be evaluated from initial conditions. These solutions are indeterminate for $\lambda = 0, \pm 1/2, \pm 3/2, \pm 1$. However, for $\lambda = 0$, i.e., for a stationary disturbing body, the particular solutions are

$$\xi = -\frac{3}{8}\frac{\mu_d}{\mu}\frac{r_c^4}{r_d^3}\left[-\frac{2}{3}(2\cos^2 i - \sin^2 i) + \frac{4}{3}\sin^2 i\cos 2\phi - 2\sin^2 i\cos 2\bar{\phi}_0 + \frac{2}{3}(1-\cos i)^2\cos 2(\phi+\bar{\phi}_0) + \frac{2}{3}(1+\cos i)^2\cos 2(\phi-\bar{\phi}_0)\right] \quad (163)$$

$$\eta = -\frac{3}{8}\frac{\mu_d}{\mu}\frac{r_c^4}{r_d^3}\left[\frac{4}{3}(2\cos^2 i - \sin^2 i + 3\sin^2 i\cos 2\bar{\phi}_0)f - \frac{11}{6}\sin^2 i\sin 2\phi - \frac{11}{12}(1-\cos i)^2\sin 2(\phi+\bar{\phi}_0) - \frac{11}{12}(1+\cos i)^2\sin 2(\phi-\bar{\phi}_0)\right] \quad (164)$$

$$\zeta = -\frac{3}{8}\frac{\mu_d}{\mu}\frac{r_c^4}{r_d^3}\left\{\left[(1+\cos i)\sin i\cos(\phi-2\bar{\phi}_0) - (1-\cos i)\sin i\cos(\phi+2\bar{\phi}_0) - \sin 2i\cos\phi\right]f + \frac{1}{2}\sin 2i\sin\phi + \frac{1}{2}(1-\cos i)\sin i\sin(\phi+2\bar{\phi}_0) - \frac{1}{2}(1+\cos i)\sin i\sin(\phi-2\bar{\phi}_0)\right\} \quad (165)$$

Again, if more than one disturbing body is considered, it is necessary to consider them independently, compute the resultant displacements η, ξ, ζ in the respective coordinate systems, resolve the displacement vectors and add. Despite the limitation imposed by the assumption of circular orbits, this approach affords a simple means of computing realistic coordinate variations for many satellite orbits.

The magnitude of these radial perturbations for near earth circular orbits can be seen in Fig. 8. This data is based on the work of Blitzer (Ref. 35).

Another approximate method for computing the effects of external masses on the orbit of an earth satellite has been reported by M. Moe (Ref. 36). This work is outlined below:

First consider the perturbations of a satellite orbit due to a disturbing body assumed to be in the X-Y plane. The geometry is shown in Fig. 9. The orbit will be described in terms of the osculating ellipse whose elements are a, e, M_0, Ω, ω, and i, and expressions will be derived to compute the approximate changes in the elements during one revolution of the satellite. The parameters i, ω, Ω, and Γ are taken relative to the disturbing body plane. For an earth satellite, this is either the ecliptic or the earth-moon plane.

Now, if the equations for the variation of elements of Section C-1 of this chapter are utilized together with the components of R, S and W, the approximate changes in the elements can be evaluated. Moulton (Ref. 1, p 340) gives the form of these forces. Under the assumption that the ratio of orbital radius to the distance to the disturbing body is small these components may be expanded in powers of r/a_d and all but first order terms can be neglected. This procedure yields:

$$R = K_d r (1 + 3 \cos 2\Gamma_p)$$

$$S = 6 K_d r \left[\cos\Gamma \sin(\omega + \theta) - \sin\Gamma \cos(\omega + \theta) \cos i\right] \cos\Gamma_p$$

$$W = -6 K_d r \cos\Gamma_p \sin i \sin\Gamma$$

where

$$K_d = \mu_d / 2a_d^3 \equiv \mu H$$

a_d = assumed constant.

Letting ϵ stand for any orbital element and $\Delta\epsilon$ for the change in that element after one revolution of the satellite (from perigee to perigee), we have

$$\Delta\epsilon = \int_{t=0}^{t=2\pi/n} \frac{d\epsilon}{dt}\, dt = \int_{\theta=0}^{2\pi} \frac{d\epsilon}{dt}\frac{dt}{d\theta}\, d\theta \qquad (166)$$

where t is time measured from perigee passage of the satellite. Since $\Delta\epsilon$ is supposed to be small compared to ϵ, it is permissible to approximate all variables in the equations for element variations for $d\epsilon/dt$ by the values they would have in the unperturbed orbit, and to approximate $dt/d\theta$ by its relationship to the conservation of angular momentum, h

$$\frac{dt}{d\theta} = \frac{r^2}{h}$$

where $h = na^2\sqrt{1 - e^2}$ is assumed constant. Since the angular velocity of the satellite is usually large compared to the angular velocity of the disturbing body, we may further assume that Γ is constant during the time the satellite takes to complete one revolution. Then integrals of the type in Eq. (166) can be evaluated easily. The results are

$$\Delta a = 0 \qquad (167)$$

$$\Delta q = 15\, H\pi a^4 e \sqrt{1 - e^2} \left\{\sin 2\Gamma \cos 2\omega \cos i - \sin 2\omega (\cos^2\Gamma - \sin^2\Gamma \cos^2 i)\right\} \qquad (168)$$

where $q = r_p = a(1 - e)$

$$\Delta e = -\frac{1}{a}\Delta q \qquad (169)$$

$$\Delta i = \frac{-3 H\pi a^3}{2\sqrt{1 - e^2}} \left\{2 \sin 2\Gamma \sin i \left[1 - e^2 (1 - 5\cos^2\omega)\right] + 5 e^2 \sin^2\Gamma \sin 2\omega \sin 2i\right\} \qquad (170)$$

$$\Delta\Omega = \frac{-3 H\pi a^3}{2\sqrt{1 - e^2}} \left\{5 e^2 \sin 2\Gamma \sin 2\omega + 4 \sin^2\Gamma \cos i \left[(1 - e^2)\cos^2\omega + 4(1 + 4e^2)\sin^2\omega\right]\right\} \qquad (171)$$

$$\Delta\omega = -\cos i\, \Delta\Omega + 6 H\pi a^2 \sqrt{1 - e^2} \left\{5 \sin 2\Gamma \sin\omega \cos\omega \cos i - 1 + 3 \sin^2\Gamma \cos^2 i - (5\sin^2\omega - 4)(\cos^2\Gamma - \sin^2\Gamma \cos^2 i)\right\} \qquad (172)$$

where

$$H = \frac{M_D}{2 a_D^3 M_E} = \frac{GM_D}{2\eta^2 a_D^3 a^3}$$

Here, M_E and M_D are the masses of the earth and the disturbing body, a_D is the average distance to the disturbing body.

G is the universal gravitational constant and n is the satellite's mean angular motion.

For the moon as the disturbing body

$$H = H_m = 0.68736 \times 10^{-18} \text{ (naut mi)}^{-3}$$

$$= 10.8207 \times 10^{-20} \text{ km}^{-3}$$

$$= 2.80763 \times 10^{-8} \text{ (earth radii)}^{-3}$$

If the disturbing body is the sun, then

$$H = H_s = 0.31584 \times 10^{-18} \text{ (naut mi)}^{-3}$$

$$= 4.97207 \times 10^{-20} \text{ km}^{-3}$$

$$= 1.29010 \times 10^{-8} \text{ (earth radii)}^{-3}$$

Note that $H_m = 2.17631\ H_s$, but remember that the fundamental planes are different for the two perturbations. Assuming that the other variables (a, e, i, and ω) remain constant during one period, Δq can be integrated from 0 to π (the period of Γ) to give the approximate total change. Dividing by π gives the average change in q for one revolution of the satellite. Similarly, formulas for the average change in the other parameters can be determined to be:

$$\Delta q_{sec} = -7.5\, H\pi a^4 e \sqrt{1 - e^2} \sin 2\omega \sin^2 i \qquad (173)$$

$$\Delta e_{sec} = -\frac{1}{a} \Delta q_{sec} \qquad (174)$$

$$\Delta \omega_{sec} = 6\, H\pi a^3 \sqrt{1 - e^2} \left[1 + \frac{5 \sin^2 \omega}{2(1 - e^2)} (e^2 - \sin^2 i)\right] \qquad (175)$$

$$\Delta i_{sec} = \frac{-3.75\, H\pi a^3}{\sqrt{1 - e^2}} (e^2 \sin 2\omega \sin 2i) \qquad (176)$$

$$\Delta \Omega_{sec} = \frac{-3\, H\pi a^3 \cos i}{\sqrt{1 - e^2}} \left[(1 - e^2)\cos^2 \omega + (1 + 4e^2)\sin^2 \omega\right] \qquad (177)$$

where the subscript sec means secular. To compute the changes per unit time, divide by the period of the satellite in the specified time units. Note also that H and a must be in units consistent with those used for q.

The above expressions indicate the secular trend in the various parameters due to a disturbing body, for example, the moon. To illustrate the meaning and importance of these formulas, it is helpful to return to the complete formula for the perturbation of perigee distance q.

Recall from Eq. (157) that

$$\Delta q = A \left\{\sin 2\Gamma \cos 2\omega \cos i - \sin 2\omega \left(\cos^2 \Gamma - \sin^2 \Gamma \cos^2 i\right)\right\}$$

where

$$A = 15\, H\pi a^4 e \sqrt{1 - e^2}.$$

Using trigonometric identities, the expression for Δq can be written in the following form:

$$\Delta q = \Delta q_{per} + \Delta q_{sec}.$$

where subscript per means periodic

$$\Delta q_{per} = A \left[\sin 2\Gamma \cos 2\omega \cos i - \frac{1}{2} \cos 2\Gamma \sin 2\omega (1 + \cos^2 i)\right]$$

and

$$\Delta q_{sec} = -\frac{1}{2} A \sin 2\omega \sin^2 i.$$

Thus Δq can be expressed as the sum of two terms; the first of which is a periodic function of Γ, and the second is independent of Γ. This nonperiodic or secular term is precisely Δq_{sec} which was previously derived.

The effect indicated by the periodic term (Δq_{per}) can be better understood if its form is changed as follows

$$\Delta q_{per} = AB (\sin 2\Gamma \cos \alpha - \cos 2\Gamma \sin \alpha)$$

$$= AB \sin (2\Gamma - \alpha)$$

where

$$B = \sqrt{\cos^2 i + \frac{1}{4} \sin^2 2\omega \sin^4 i}$$

and $\alpha = \pm \cos^{-1} \frac{\cos 2\omega \cos i}{B}$ with the minus sign holding if $\sin 2\omega$ is negative.

The formulas for $\Delta \omega$, Δi, and $\Delta \Omega$ can each be expressed in a similar form, and in each case the secular terms have already been derived. Since the forms of the periodic terms are not important for most purposes, they will not be given.

From this point the method of computation parallels Penzo's.

6. Drag Perturbation of a Satellite Orbit

The effect of air drag on the osculating orbital elements of a satellite can be determined using the approach outlined by Moe and discussed under solar lunar perturbation. The effect on each element is expressed as the change in that element in one orbital revolution. That is, if the elements at a certain perigee are a, e, i, ω, and Ω, then

the elements at the following perigee will be changed by the amounts Δa, Δe, Δi, $\Delta \omega$, and $\Delta \Omega$ (Refs. 37 and 38).

a. Perturbation equations and the drag force

To obtain expressions for these changes, start with Eqs. (178) through (181), relating the time derivatives of the orbital elements to the components of a general perturbing force. A particular form of these equations, given by Moulton (Ref. 1, pp. 404 to 405) and Moe (Ref. 39), is

$$\frac{da}{dt} = \frac{2e \sin\theta}{n\sqrt{1-e^2}} R + \frac{2a\sqrt{1-e^2}}{nr} S \qquad (178a)$$

$$\frac{de}{dt} = \frac{\sqrt{1-e^2}\sin\theta}{na} R + \frac{\sqrt{1-e^2}}{na^2 e}\left[\frac{a^2(1-e^2)}{r} - r\right] S \qquad (178b)$$

$$\frac{d\Omega}{dt} = \frac{r\sin(\theta+\omega)}{na^2\sqrt{1-e^2}\sin i} W \qquad (178c)$$

$$\frac{di}{dt} = \frac{r\cos(\theta+\omega)}{na^2\sqrt{1-e^2}} W \qquad (178d)$$

$$\frac{d\omega}{dt} = \frac{r\sin(\theta+\omega)\cot i}{na^2\sqrt{1-e^2}} W - \frac{\sqrt{1-e^2}\cos\theta}{nae} R + \frac{\sqrt{1-e^2}}{nae}\left(1 + \frac{1}{1+e\cos\theta}\right)\sin\theta\, S \qquad (178e)$$

R is the component along the radius vector (measured positive away from the center of the earth), S is the transverse component in the instantaneous plane of the orbit (measured positive when making an angle less than 90° with the satellite's velocity vector), and W is the component normal to the instantaneous plane (measured positive when making an angle less than 90° with the north pole).

When the disturbing force is caused by air drag, the perturbing acceleration is

$$\frac{1}{2}\rho(\underline{r})\, V^2 \frac{C_D A}{m} = B\,\rho(\underline{r})\, V^2$$

which has the components,

$$R = -B\,\rho(\underline{r})\, V\, V_0 \frac{e\sin\theta}{\sqrt{1+e^2+2e\cos\theta}} \qquad (179a)$$

$$S = -B\,\rho(\underline{r})\, V\left[\frac{V_0(1+e\cos\theta)}{\sqrt{1+e^2+2e\cos\theta}} - V_a\cos\beta\right] \qquad (179b)$$

and

$$W = -B\,\rho(\underline{r})\, V\, V_a \sin\beta \qquad (179c)$$

where

$B = \frac{C_D A}{2m}$

m = mass of the satellite

C_D = drag coefficient

A = effective area of the satellite

$\underline{r}$ = radius vector from the center of the earth to the satellite

$\rho(\underline{r})$ = density of the atmosphere at $\underline{r}$

V = velocity of satellite relative to the atmosphere

V_0 = velocity of satellite relative to inertial space

V_a = velocity of the atmosphere relative to inertial space

β = the angle between V_a and the plane of the orbit

b. Assumptions and approximations

Equations (168a), (168b) and (168c) can also be expressed in terms of the eccentric anomaly E, instead of the true anomaly θ. This step is desirable since the integration of Eqs. (167a) through (167e) over an orbital revolution can be most easily carried out by using E as the variable of integration (limits 0 to 2π). To facilitate the integration, the following assumptions and approximations are made:

(1) The density, $\rho(\underline{r})$, is spherically symmetric. It is assumed to change exponentially above perigee height, i.e.,

$$\rho(\underline{r}) = \rho_p\, e^{-(h-h_p)/H} \qquad (180)$$

where ρ_p is the density at perigee. It is a function of the height, h_p, of perigee above the surface of the earth. H is the scale height at perigee altitude and h is the height of the satellite above the surface of the earth.

(2) In integrating the effect of the perturbing force over one revolution, the satellite is assumed to move along the unperturbed Kepler orbit. This is a good approximation because the perturbation has little effect on the orbit over one revolution. This is not true during the last few revolutions of the lifetime. Other methods must be used to determine the effect of air drag during that short time.

(3) The integrand is expanded in the quantity e (1 - cos E) (which is always small

wherever the perturbing force is important). Only the most important terms of the series are integrated.

(4) The entire atmosphere rotates at a uniform angular rate equal to the rate of rotation of the earth about its axis.

Several investigators (Refs. 40 and 41) have carried out integrations using variants of the above approximations. Sterne (Ref. 41), for example, in addition to treating the problem with a spherically symmetric atmosphere, also made a more refined analysis taking account of the atmosphere's flattening. However, for altitudes above 200 naut mi or 370 km, the neglect of the diurnal bulge causes errors, which overshadow the improvement obtained by considering atmospheric flattening. This was shown by Wyatt (Ref. 42). Moreover, fluctuation in the density of the atmosphere causes uncertainties large enough that highly refined expressions for the changes in orbital elements are not warranted for most purposes.

c. Approximate changes in osculating orbital elements

Given below are methods useful in simplified programs, based on approximations (1), (2), (3) and (4). Most of the results were obtained in series form, but only the dominant terms are given here. For higher order terms see Sterne's paper (Ref. 41).

The case of $ae/H > 2$. When the parameter $ae/H > 2$, the changes in the orbital elements per revolution are

$$\Delta a = -Q\left[1 + \frac{1 - 8e + 3e^2}{8c\,(1 - e^2)}\right] \tag{181a}$$

$$\Delta e = -Q\left(\frac{1 - e}{a}\right)\left[1 - \frac{(3 + 4e - 3e^2)}{8c\,(1 - e^2)}\right] \tag{181b}$$

$$\Delta i = -D(1 - e)^2\left\{\cos^2\omega + \frac{1}{8c}\left[8\left(\frac{1 + e}{1 - e}\right) + \left(4f^* + \frac{9e^2 + 6e - 15}{(1 - e)^2}\right)\cos^2\omega\right]\right\}\sin i \tag{181c}$$

$$\Delta\Omega = -D\,(1 - e)^2\left\{1 + \frac{1}{8c}\left[4f^* + \frac{9e^2 + 6e - 15}{(1 - e)^2}\right]\right\}\sin\omega\cos\omega \tag{181d}$$

$$\Delta\omega = -\Delta\Omega\cos i \tag{181e}$$

where

$$Q = 2B\,\rho_p\,a^2\,f\,\frac{(1 + e)^2}{(1 - e^2)^{1/2}}\left(\frac{2\pi}{c}\right)^{1/2}$$

$$c = ae/H$$

$$f = 1 - \frac{2\Omega_e}{n}\,(1 - e)\left(\frac{1 - e}{1 + e}\right)^{1/2}\cos i$$

$$f^* = \frac{e}{1 - e^2}\left(e + \frac{f - 1}{f^{1/2}}\right)$$

$$D = 2\pi B\,\frac{\Omega_e}{n}\,a\,\rho_p f^{1/2}\,(2\pi c)^{-1/2}$$

Ω_e = angular rate of rotation of the earth's atmosphere in inertial space (2π in approximately 24 hr)

It might also be useful to know how the radius of perigee, q, changes in a revolution; q is simply related to a and e through the equation

$$q = a\,(1 - e)$$

Thus, the change in q, when $ae/H > 2$, is

$$\Delta q = -Q\left(\frac{1 - e}{1 + e}\right)\frac{1}{2c} \tag{181f}$$

and the change in the period can be found from the change in a through the relation

$$\Delta\tau/\tau = \left(\frac{3}{2}\right)\Delta a/a$$

The case of $ae/H \leq 2$. When the parameter $ae/H \leq 2$, the appropriate changes are

$$\Delta a = -G\,\frac{(1 + e)^{3/2}}{(1 - e)^{1/2}}\left[(1 - 2e)\,I_o(c) + 2e\,I_1(c)\right] \tag{182a}$$

$$\Delta e = -\frac{G}{a}\sqrt{\frac{1 + e}{1 - e}}\left\{(1 - e)\,I_1(c) + \frac{e}{2}\left[I_o(c) + I_2(c)\right]\right\} \tag{182b}$$

$$\Delta i = -K\left\{\frac{1}{2}\left[I_o(c) - I_2(c)\right] + (\cos^2\omega)\left[I_2(c) - 2e\,I_1(c)\right]\right\}\sin i \tag{182c}$$

$$\Delta\Omega = -K\left[I_2(c) - 2e\,I_1(c)\right]\sin\omega\cos\omega \tag{182d}$$

$$\Delta\omega = -\Delta\Omega\cos i \tag{182e}$$

and

$$\Delta q = -G\sqrt{\frac{1 + e}{1 - e}}\left[\left(1 - \frac{5}{2}\,e\right)I_o(c) - (1 - 3e)\,I_1(c) - \frac{e}{2}\,I_2(c)\right] \tag{182f}$$

where

$$G = 2\pi\,\frac{C_D A}{m}\,a^2\,\rho_p f\,e^{-c}$$

$$K = \pi \frac{C_D A}{m} \frac{\Omega_e}{n} a \rho_p \sqrt{f}\, e^{-c}$$

and I_n is the Bessel function of imaginary argument and nth order. The secular time rate of change of the elements may be obtained by dividing Eqs. (181a) through (181f) and Eqs. (182a) through (182f) by the Kepler period, $\tau = 2\pi a^{3/2} / \sqrt{\mu}$.

From Eqs. (181) and (182) it can be seen that the rotation of the earth's atmosphere relative to the satellite affects the inclination, node, and argument of perigee of the orbit. If there were no atmospheric rotation ($\omega_e = 0$), only the semimajor axis and eccentricity (hence the height of perigee) would be affected.

The orbital parameters most sensitive to drag are the heights of apogee and perigee, the period, and the eccentricity. The reason for this sensitivity is primarily the fact that V relative to the atmosphere is not vastly different than V relative to space. Thus, the perturbing force is nearly planar and therefore affects semimajor axes and eccentricity.

The procedure for evaluating the effects due to drag is now clear: First the element variations are computed, then the elements are adjusted and the process continued. If a sufficiently small interval of time is utilized for the stepping procedure, say 1 revolution for satellites above approximately 180 km, then the element changes will be sufficiently small so that they may be added to those produced by the sun, moon, ablateness, etc., to produce a first order approximation to the total solution. Numerical data and discussions of the planar effects are presented in Chapter V (Satellite Lifetime). Thus, graphical data will not be included at this point. Data for the nonplanar parameters will not be prepared because of the fact that too many parameters are involved to make such a presentation meaningful. Rather it is suggested that these effects be evaluated for each orbit.

d. Contribution of random drag fluctuations to error in predicted time of nodal crossing of a satellite, assuming perfect initial elements*

If the period is known to be exactly P(0) during the zeroth revolution, then the period will be predicted to be P'(n) during the nth revolution. This prediction will be based on the average rate of change of period during the preceding revolutions. But suppose there are random fluctuations about the average change in period. Let these random fluctuations be $\rho_1, \rho_2, \ldots, \rho_j, \ldots, \rho_N$. Then after N revolutions the period will actually be

$$P(N) = P'(N) + \sum_{j=1}^{N} \rho_j$$

*This subsection was included as "Appendix E, Special Derivations" in Flight Performance Handbook for Orbital Operation, STL report prepared under Contract NAS 8-863.

The time of nodal crossing will be predicted to be

$$t'(N) = t(0) + \sum_{n=1}^{N} P'(n)$$

while the actual time of nodal crossing will be

$$t(N) = t(0) + \sum_{n=1}^{N} P'(n) + \sum_{n=1}^{N} r(n)$$

where

$$r(n) \equiv \sum_{j=1}^{n} \rho_j .$$

The error, E(N), in the prediction is

$$E(N) = -\sum_{n=1}^{N} r(n) = -\sum_{n=1}^{N} \sum_{j=1}^{n} \rho_j .$$

This double sum can be written out explicitly as

$$E(N) = -\left[(\rho_1) + (\rho_1 + \rho_2) + \ldots + (\rho_1 + \rho_2 + \ldots + \rho_N)\right].$$

Rearranging terms, we obtain

$$E(N) = -\left[N\rho_1 + (N-1)\rho_2 + \ldots + \rho_N\right]. \quad (183)$$

Case a: Fluctuations Independent from Revolution to Revolution. If each ρ_j is independent and has the standard deviation F, then the standard deviation of E(N) is

$$G_{rms}(N) \equiv E(N)_{rms} = \left(F \sum_{n=1}^{N} n^2\right)^{1/2}$$

$$= F\left[N(N+1)(2N+1)/6\right]^{1/2}. \quad (184)$$

Case b: Fluctuations Correlated over 25 Revolutions. On the other hand, suppose that the random drag fluctuations are perfectly correlated over intervals of 25 revolutions, but independent from one interval to the next. A 25-revolution interval is chosen because it is the usual smoothing interval in published orbits. We begin with Eq (183).

Since the accelerations are assumed to be correlated over intervals of 25 revolutions,

$$\rho_1 = \rho_2 = \ldots = \rho_q = \rho_A$$

$$\rho_{q+1} = \rho_{q+2} = \ldots = \rho_{q+25} = \rho_B$$

$$\rho_{q+26} = \rho_{q+27} = \ldots = \rho_{q+50} = \rho_C$$

The fluctuations in acceleration about the smoothed value are illustrated in the following sketch.

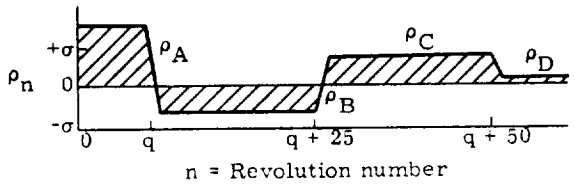

The possible values of q range from 1 to 25. In the absence of particular information, all values of q will be assigned equal weights. When n = 1, $\rho = \rho_A$. When n = 2, ρ will equal ρ_A if $2 \leq q \leq 25$, and $\rho = \rho_B$ if q = 1. When n = 3, $\rho = \rho_A$ if $3 \leq q \leq 25$, and $\rho = \rho_B$ if q = 1 or 2, etc. The equal weighting of the 25 values of q can be expressed by averaging over the ensemble of possible values, that is

$$\rho_1 = \rho_A$$

$$\rho_2 = (1/25)\,(24\,\rho_A + \rho_B)$$

$$\rho_3 = (1/25)\,(23\,\rho_A + 2\,\rho_B)$$

$$\cdots\cdots\cdots\cdots\cdots\cdots$$

$$\rho_{25} = (1/25)\,(\rho_A + 24\,\rho_B)$$

$$\rho_{26} = \rho_B$$

$$\rho_{27} = (1/25)\,(24\,\rho_B + \rho_C)$$

$$\cdots\cdots\cdots\cdots\cdots\cdots$$

$$\rho_{50} = (1/25)\,(\rho_B + 24\,\rho_C), \text{ etc.}$$

The timing error, averaged over the ensemble of possible values of q, is found by substituting these ρ_j's into Eq (184).

$$\overline{E(N)} = -\Big[N\rho_A + (N-1)\,(24\,\rho_A + \rho_B)/25 + (N-2)\,(23\,\rho_A + 2\,\rho_B)/25 + \ldots + (N-24)\,(\rho_A + 24\,\rho_B)/25 + (N-25)\,\rho_B + (N-26)\,(24\,\rho_B + \rho_C)/25 + \ldots + (N-49)\,(\rho_B + 24\,\rho_C)/25 + (N-50)\,\rho_C + (N-51)\,(24\,\rho_C + \rho_D)/25 + \ldots\Big], \quad \text{for all } (N-k) > 0 \ldots \tag{185}$$

Collecting coefficients of ρ_A, ρ_B, and ρ_C

$$\overline{E(N)} = -(\rho_A/25)\,\big[25\,N + 24\,(N-1) + \ldots + (N-24)\big] - (\rho_B/25)\,\big[(N-1) + 2(N-2) + \ldots + 24(N-24) + 25(N-25) + 24(N-26) + \ldots + (N-49)\big] - (\rho_C/25)\,\big[(N-26) + 2(N-27) + \ldots + 24(N-49) + \ldots\big] - \ldots,$$

$$\text{for all } (N-k) > 0 \ldots$$

Let

$$a(N) \equiv \big[25\,N + 24(N-1) + \ldots + (N-24)\big].$$

$$b(N) \equiv \big[(N-1) + 2(N-2) + \ldots + 24(N-24) + 25(N-25) + 24(N-26) + \ldots + (N-49)\big]$$

$$c(N) \equiv \big[(N-26) + 2(N-27) + \ldots 24(N-49) + 25\,(N-50) + 24(N-51) + \ldots + (N-74)\big]$$

$$d(N) \equiv \big[(N-51) + 2(N-52) + \ldots + 25(N-75) + \ldots\big]$$

$$e(N) \equiv \ldots \text{ etc.,}$$

$$\text{for all } (N-k) > 0.$$

If the standard deviation of ρ_j is σ, and each ρ_j is independent, then the standard deviation of $\overline{E(N)}$ is

$$K_{rms}(N) \equiv \Big[\overline{E(N)}\Big]_{rms} = (\sigma/25)\,\Big[a^2(N) + b^2(N) + c^2(N) + \ldots\Big]^{1/2}. \tag{186}$$

In case $N \leq 25$, a(n), b(n), and c(N) are calculated as

$$b(N) = (N-1) + 2(N-2) + \ldots + 24(N-24), \quad \text{for all } (N-k) > 0 \text{ and for } N \leq 25$$

$$= \sum_{q=1}^{N-1} q(N-q) = N\sum_{1}^{N-1} q - \sum_{1}^{N-1} q^2$$

$$= N^2(N-1)/2 - N(N-1)\,(2N-1)/6$$

$$b(N) = \big[N(N-1)/2\big]\,\big[N - (2N-1)/3\big].$$

$$\text{for } N \leq 25$$

$$a(N) = 25(N + N - 1 + \ldots + 1) - b(N)$$

$$a(N) = 25\,N\,(N+1)/2 - b(N).$$

for $N \leq 25$

$$c(N) = 0. \qquad \text{for} \quad N \leq 25.$$

In case N is greater than 25, the contribution of the first 25 terms in Eq (185) to b(N) is

$$b_1(N) = \sum_{q=1}^{24} q(N-q) = N\sum_{1}^{24} q - \sum_{1}^{24} q^2$$

$$o_1(N) = 100\,(3\,N - 49),$$

for $N \geq 25$.

a(N) is then given by

$$a(N) = 25(N + N - 1 + \ldots + N - 24) - b_1(N)$$

$$a(N) = 625\,(N - 12) - b_1(N),$$

for $N \geq 25$.

We define $b_2(N)$ to be the contribution to b(N) of all those terms of the second 25 terms in Eq (185) for which the quantity N - k is positive. For $N \leq 25$, $b_2(N) = 0$, and for $N \geq 26$, $b_2(N)$ is given by

$$b_2(N) = a(N - 25),$$

for $N \geq 26$.

b(N) is given by

$$b(N) = b_1(N) + b_2(N).$$

The quantities c(N), d(N), etc., are given by

$$c(N) = 0, \qquad \text{for} \quad N \leq 26$$

$$c(N) = b(N - 25),$$

for $N \geq 27$

$$d(N) = 0, \qquad \text{for} \quad N \leq 51$$

$$d(N) = b(N - 50),$$

for $N \geq 52$

etc.

Comparison of Case a and Case b. The limits of the equations for correlated and uncorrelated errors will now be calculated, to show how the two cases are related. For uncorrelated errors (Case a), take the limit of Eq (184).

$$\lim_{N\to\infty} F\left[N(N+1)\,(2\,N+1)/6\right]^{1/2} = F(N^3/3)^{1/2}. \tag{187}$$

For correlated errors (Case b), take the limit of Eq (186)

$$\lim_{N\to\infty} (\sigma/25)\left\{\left[625\,(N-12) - 100\,(3\,N-49)\right]^2\right.$$

$$+\left[100\,(3\,N-49) + 625(N-37)\right.$$

$$\left.\left. - 100\,(3\,N-124)\right]^2 + \right.$$ continued

$$+\left[100\,(3\,N-124) + 625\,(N-62)\right.$$

$$\left.\left. - 100\,(3\,N-199)\right]^2 + \ldots\right\}^{1/2}$$

$$= \lim_{N\to\infty} \sigma\left\{\left[13\,(N-8)\right]^2 + \left[25\,(N-25)\right]^2\right.$$

$$\left. + \left[25\,(N-50)\right]^2 + \ldots\right\}^{1/2}.$$

Let N = 25 M, where M is an integer. Then the above limit becomes

$$\lim_{M\to\infty} (25)^2\,\sigma\left\{M^2 + (M-1)^2 + (M-2)^2 \ldots\right.$$

$$\left. + 1^2 - M^2 + \left[(13/25)\,(M - 8/25)\right]^2\right\}^{1/2}$$

$$= \lim_{M\to\infty} (25)^2\,\sigma\left\{M\,(M+1)\,(2\,M+1)/6\right.$$

$$\left. - M^2 + \left[(13/25)\,(M-8/25)\right]^2\right\}^{1/2}$$

$$= \lim_{M\to\infty} (25)^2\,\sigma\left\{M\,(M+1)\,(2\,M+1)/6\right\}^{1/2}$$

$$= (25)^2\,\sigma\,(M^3/3)^{1/2} = 5\sigma\,(N^3/3)^{1/2}. \tag{188}$$

Thus, the limits (5) and (6) for correlated and uncorrelated errors approach the same asymptotic form for large N. This makes it possible to evaluate the constant F, which must equal 5σ. The relationship $F = 5\sigma$ corresponds exactly to the situation in the theory of errors, in which the standard deviation of the mean of k independent observations equals the standard deviation of one observation divided by the square root of k. The asymptotic form Eq (188) is a convenient approximation to represent the error contributed by random fluctuations, when the initial elements are perfect. The satellite accelerations, i.e., the rate of change of the period published to July 1961, furnish no evidence for choosing between Case a and Case b, because they are smoothed over intervals of 25 revolutions.

7. Radiation Pressure

Above a height of 500 naut mi or 926 km, radiation pressure usually has a greater effect on the orbit of an artificial satellite than air drag (though for ordinary satellites, the effects of radiation and drag both are very small). However, both effects are significant for balloon satellites since the area-to-mass ratio is large. (The area-to-mass ratio of the Echo I balloon satellite was 600 times that of Vanguard I.) At first glance it may appear that it is possible to handle this force as was done in the previous sections. However, this is not the case because of the fact that the earth affords a shield from the sun's rays during a portion of the orbit. This shadow effect is investigated in detail in Chapter XIII.

Kozai (Ref. 43) has integrated the perturbations of first order over one revolution, in terms of the eccentric anomaly, E. The satellite leaves the shadow when E equals E_1, and enters the shadow when E equals E_2. (Reradiation from the earth is ignored.)

The perturbations over one revolution are given by

$$\delta a = 2a^3F \left(S \cos E + T \sqrt{1 - e^2} \sin E\right)\Big|_{E_1}^{E_2} \tag{189}$$

$$\delta e = a^2F \sqrt{1 - e^2} \left[\frac{1}{4} S \sqrt{1 - e^2} \cos 2E + T \left(-2e \sin E + \frac{1}{4} \sin 2E\right)\Big|_{E_1}^{E_2} + \frac{3}{2} \int TdE \right] \tag{190}$$

$$\delta i = a^2F \frac{W}{\sqrt{1 - e^2}} \left[\left\{(1 + e^2) \sin E - \frac{e}{4} \sin 2E\right\} \cos \omega + \sqrt{1 - e^2} (\cos E - \frac{e}{4} \cos 2E) \sin \omega \Big|_{E_1}^{E_2} - \frac{3}{2} e \int W \cos \omega \, dE \right] \tag{191}$$

$$\sin i \, \delta\Omega = a^2F \frac{W}{\sqrt{1 - e^2}} \left[\left\{(1 + e^2) \sin E - \frac{e}{4} \sin 2E\right\} \sin \omega - \sqrt{1 - e^2} (\cos E - \frac{e}{4} \cos 2E) \cos \omega \Big|_{E_1}^{E_2} - \frac{3}{2} e \int W \sin \omega \, dE \right] \tag{192}$$

$$\delta\omega = - \cos i \, \delta\Omega + a^2F \frac{\sqrt{1 - e^2}}{e} \left[S(e \sin E + \frac{1}{4} \sin 2E) + T \sqrt{1 - e^2} (e \cos E - \frac{1}{4} \cos 2E \Big|_{E_1}^{E_2} - \frac{3}{2} \int SdE \right] \tag{193}$$

$$\delta M = - \frac{3}{2} \int_0^{2\pi} \frac{\delta a}{a} \, dM - \sqrt{1 - e^2} \, \delta\omega - \sqrt{1 - e^2} \cos i \, \delta\Omega - 2a^2F \left[\left\{S \, (1 + e^2) \sin E - \frac{e}{4} \sin 2E\right\} - T \sqrt{1 - e^2} \, (\cos E - \frac{e}{4} \cos 2E)\Big|_{E_1}^{E_2} - \frac{3}{2} e \int SdE \right] \tag{194}$$

where the limits of integration are E_1 and E_2 unless other values are written; S and T are the expressions of $S(\theta)$ and $T(\theta)$, in which ϕ is replaced by ω; that is,

$$\left.\begin{aligned} S &= S(0), \\ T &= T(0). \end{aligned}\right\} \tag{195}$$

If the satellite does not enter the shadow during one revolution, the terms depending explicitly on E vanish, and, in particular, δa vanishes.

In the expressions of $\delta\omega$ and $\delta\Omega$, indirect effects of the solar radiation pressure through $\dot{\omega}$ and $\dot{\Omega}$ must be considered as

$$\left.\begin{aligned} \frac{d\delta\omega}{dt} &= \frac{d\dot{\omega}}{de} \delta e + \frac{d\dot{\omega}}{di} \delta i + \frac{d\dot{\omega}}{da} \delta a, \\ \frac{d\delta\Omega}{dt} &= \frac{d\dot{\Omega}}{de} \delta e + \frac{d\dot{\Omega}}{di} \delta i + \frac{d\dot{\Omega}}{da} \delta a. \end{aligned}\right\} \tag{196}$$

The disturbing functions $S(\theta)$, $T(\theta)$, and W are

$$\begin{aligned} S(\theta) = &- \cos^2 \frac{i}{2} \cos^2 \frac{\epsilon}{2} \cos (\lambda_0 - \phi - \Omega) \\ &- \sin^2 \frac{i}{2} \sin^2 \frac{\epsilon}{2} \cos (\lambda_0 + \Omega - \phi) \\ &- \frac{1}{2} \sin i \sin \epsilon \left\{\cos (\lambda_0 - \phi) - \cos (-\lambda_0 - \phi)\right\} \\ &- \sin^2 \frac{i}{2} \cos^2 \frac{\epsilon}{2} \cos (\Omega - \lambda_0 - \phi) \\ &- \cos^2 \frac{i}{2} \sin^2 \frac{\epsilon}{2} \cos (-\lambda_0 - \phi - \Omega), \end{aligned} \tag{197}$$

$$\begin{aligned} W = &\sin i \cos^2 \frac{\epsilon}{2} \sin (\lambda_0 - \Omega) \\ &- \sin i \sin^2 \frac{\epsilon}{2} \sin (\lambda_0 + \Omega) \\ &- \cos i \sin \epsilon \sin \lambda_0 \end{aligned} \tag{198}$$

where λ_0 is the longitude of the sun, and ϵ is the obliquity. The expression of $T(\theta)$ is obtained if cos in $S(\theta)$ is replaced by sin except for the trigonometrical terms with an argument i, ϵ, $i/2$, or $\epsilon/2$.

The conventional symbols are used for the orbital elements: a is the major axis, e the eccentricity, i the inclination, Ω the node, ω the argument of perigee, M the mean anomaly, and θ the true anomaly. In addition,

$$\phi = \theta + \omega$$

and

$$p = a (1 - e^2);$$

$n^2a^3F \, S(\theta)$, $n^2a^3F \, T(\theta)$, and $n^2a^3F \, W$ are three components of the disturbing force due to the solar radiation pressure in the direction of the

radius vector of the satellite, in the direction perpendicular to it in the orbital plane, and in the normal to the orbital plane; and F is a product of the mass area ratio, solar radiation pressure, and a reciprocal of GM.

The smallness of the effect of radiation pressure on an ordinary satellite is illustrated by the orbit of Vanguard I (Refs. 44, 45 and 46). Radiation pressure periodically changes its height of perigee by about one mile. The effect of radiation pressure on the period is obscured by the fluctuations in air drag. Both radiation pressure and air drag would have had very small effects on a conventional satellite at the original perigee height of Echo I, but both effects were magnified by the area-to-mass ratio, which was 600 times that of Vanguard I. The consequent large effects on the rate of change of period are shown in Fig. 10, which originally appeared in Ref. 45. The correlation of air drag with the decimeter solar flux is also shown to persist to this great height (see Chapter II). Note also in Fig. 10 that radiation pressure sometimes has no effect on the period. This occurs when the whole orbit is in sunlight. [$E_2 = E_1 + 2\pi$ in the expression for δa of Eq (194).]

The radiation pressure sometimes acts to increase the period. Echo I was the first satellite for which this was observed (Ref. 45). It was also the first satellite for which the eccentricity was observed to increase. This can be clearly seen from the increasing distance between perigee and apogee in Fig. 11, which is modified from the NASA Satellite Situation Report of July 18, 1961, though for most satellites the eccentricity has decreased during the lifetime. Detailed behavior of a satellite due to this perturbation cannot be tabulated in a parametric form due to the large number of factors affecting the solution. These factors include longitude of the nodes, orbital inclination, position of the earth in its orbit and semimajor axis and eccentricity of the orbit. Thus, it is necessary to obtain a particular solution for the perturbed rates of the elements given a set of desired elements, then incorporate them in a numerical manner with the rates produced by other forces.

The analyst is urged to consult a growing body of literature for this perturbative influence. Some of these references have been collected and presented as Refs. 1, 34, and 43 through 57.

8. Satellite Stability

The study of satellite stability concerns the long term orbital behavior of artificial satellites. It attempts to provide the mission analyst with answers to such questions as: How will the various orbital elements change? What will be the magnitude of these changes? Will their pattern be highly erratic or regular? Will there be a change in the pattern from erratic to regular or vice versa? In order to answer these and other questions it is necessary to combine the perturbing forces acting upon the satellite orbit and their effect upon the various orbital elements of interest for a particular mission.

This section discusses some approximate methods for dealing with satellite stability problems. The formulas and methods given here can be used to: (1) construct approximate computer programs, which are much faster and cheaper than "exact" programs; (2) solve some satellite stability problems without the need for a high speed computer; (3) help in gaining more insight into the behavior of satellites.

Section C2 of this chapter discussed the approximate method of M. Moe and presented most of the formulas which will be used in this section. The following discussions present some of the results obtained using this method. Although only earth satellite results are given here, these methods have also been used extensively for lunar satellites and can be applied to orbits about other planets. Part 2 illustrates a method for computing satellite trajectories by hand.

Care must be taken not to use the methods of this section on orbits which are physically too large, in which case the approximations for luni-solar perturbations break down. While definite rules cannot be laid down, Table 4 should prove helpful. The table lists the various bodies and the approximate upper limits where "very good," "good," and "fair" results can be obtained. The parameter used is the period of the satellite in days.

TABLE 4

Validity of the "Approximate" Method as a Function of Orbital Period (days)

	Very Good	Good	Fair
Earth	2.	4.	[illegible]
Moon	0.5	1.	1.5
Mars	45.	60.	90.
Venus	15.	25.	35.
Mercury	5.	8.	10.

A special case arises for very remote earth satellites which do not pass near the moon. These may also be treated by approximate methods and in these cases some orbits with periods as long as 45 days can be studied. For this class of orbits the effects of the moon are ignored and the sun is treated as the only disturbing body. Another class of orbits for which the methods of this section are not very helpful is the very near earth orbit where drag and oblateness perturbations are predominant.

Accurately predicting the future history of an artificial satellite is difficult and expensive. Fortunately approximate methods often give good results. This section discusses approximate methods which have been extensively used for terrestrial and lunar satellite orbits.

It is convenient to consider the stability of the orbit of an earth satellite as a two-body problem with perturbations introduced by the sun, moon,

earth shape, drag and radiation pressure. These effects must be analyzed separately and then combined. This procedure is accomplished only after allowing for the fact that the various equations refer to different planes; the results can then be summed to yield the new orbit. The process can then be repeated.

Performing this operation by slide rule or desk calculator is very slow and requires about 8 hr to compute the change for one revolution, or 1 man-year for 1 month of the satellite's orbit. However, the combined equations can be evaluated on a high speed computer such as the IBM 7090 at the rate of about 5 rev/sec. Subsequent paragraphs of this section discuss results obtained in the latter manner.

When high speed computers are not available, good results can be obtained by using the secular terms to estimate the results over many revolutions. This method is illustrated in Part 2.

Part 1: Sample Results by "Approximate" Method. Early in 1961, a study (Ref. 58) was made at STL to determine the lifetimes of earth satellites in highly eccentric orbits. The project was the Eccentric Geophysical Observatory (EGO). Some of the results of this study will be used to illustrate the approximate method and the general problem of orbital stability.

The experimental objectives of Project EGO made it desirable to keep perigee height as low as possible consistent with lifetime requirements. A graph of the suggested nominal answering these requirements is shown in Fig. 12. This graph will be discussed in detail since it illustrates most of the important features of this type of orbit. The initial conditions in terms of equatorial spherical coordinates are given in the figure. These were the suggested burnout conditions of the missile which were to inject the satellite into orbit. The resulting orbital parameters in terms of equatorial coordinates are as follows:

a = 32,879 naut mi = 60,892 km	ω_α = 135.617
e = 0.891057	Launch time = 3 hr 30 min GMT
i_α = 31.289°	
Ω_α = 41.796°	Launch date = 1 April 1963

The most important parameter in the EGO study is perigee height or equivalently perigee distance q and to the first order, the only perturbations affecting q are caused by the sun and the moon. The periodic term for the lunar perturbations of q may be written as

$$\Delta q_{per} = A_m B_m \sin (2\Gamma_m + \alpha_m)$$

where A_m, B_m, and α_m are as given in Section C5 of this chapter. Therefore the moon causes the satellite's perigee to alternately rise and fall. The period is one-half the moon's sidereal period or a little less than fourteen days. The amplitude for EGO-type satellites is about 40 naut mi or 74 km. The sun has a similar effect but the period is one-half year and the amplitude is about 200 naut mi or 370 km. Figure 12 is a graph of perigee height versus time. Note that the moon waves are shown only for the first 100 days. The rest of the curve shows the envelope of minimum perigee height. This simplification is adopted for all similar graphs in this section. Note also that the moon waves should be just a sequence of separate points plotted at 1.73-day intervals since perigee is reached only once each revolution of the satellite whose period was 1.73 days.

Now consider the combined secular effect caused by the sun and moon. This is given by the following formula which is derived in Section C5 of this chapter.

$$\Delta q_{sec} = -\frac{1}{2}\left(A_m \sin 2\omega_m \sin^2 i_m + A_\epsilon \sin 2\omega_\epsilon \sin^2 i_\epsilon\right) \qquad (199)$$

where

$$A_m = 15\, H_m\, \pi\, a^4\, e \sqrt{1 - e^2}$$

and

$$A_\epsilon = 15\, H_s\, \pi\, a^4\, e \sqrt{1 - e^2}.$$

Recall that H_m and H_s are positive constants. Note that the subscripts m and ϵ indicate moon plane and ecliptic plane parameters. Equatorial parameters will be indicated by the subscript α in the following discussions.

Initially, the nominal orbit had equatorial parameters i_α = 31.29°, Ω_α = 41.80° and ω_α = 135.62°, and ω_m = 94.68°, i_ϵ = 20.30°, Ω_ϵ = 87.47°, and ω_ϵ = 85.69°, respectively. At the end of 402 days, the orbit parameters take on the values: a = 32,793 naut mi or 60,733 km, e = 0.8893, i_α = 37.58°, Ω_α = 8.55°, ω_α = 181.38°, i_m = 16.11°, ω_m = 187.07°, i_ϵ = 14.75°, and ω_ϵ = 167.96°. Note that the secular trend is now nearly 0, which is again shown in Fig. 12. At the end of 554 days, the orbit parameters are: a = 32,779 naut mi or 60,707 km, e = 0.8902, i_α = 36.87°, Ω_α = -1.65°, ω_α = 195.61°, i_m = 16.77°, ω_m = 214.50°, i_ϵ = 13.45°, and ω = 198.43°. The secular trend is now negative.

Now a brief discussion will be given of the other figures in this section. In the initial EGO study (Ref. 58), the burnout conditions of the missile were given. The only variation permitted was in time of launch. A series of satellite lifetime runs (Ref. 59) were made on the IBM 7090 with 1 April 1963 as launch day. The first run was at 0 hr GMT, the next at 2 hr and so forth to 24 hr. The results are illustrated in Fig. 13.

At first glance, it is surprising that merely changing the launch time would have such a large effect on the satellite's future history. This

behavior results since changing the launch time of day changes the satellite's nodal longitude (Ω_α). At 0 h, Ω_α = -10.849. From then on Ω_α increases by 30.083° for each 2 hr added to the launch time. This, of course, is due to the earth rotating 360.996° in 24 mean solar hours.

Changing Ω_α does two important things. First, it changes the phase of the sun and moon designated by Γ_m and Γ_ϵ. For EGO-type satellites, the moon's periodic effect is only about 40 naut mi or 74 km in amplitude and hence is not too critical. The sun's periodic effect, however, is very important. Secondly, changing Ω_α changes the ecliptic and moon plane parameters of the orbit and hence changes the secular trend of the satellite. The secular trend is large and positive for the 8-, 10-, 12-, and 14-hr orbits.

In Fig. 14 comparison is made between approximate results as obtained from the Satellite Lifetime Program (Ref. 59) and results obtained by integrating the equations of motion in a way that is essentially exact. Note that the agreement is good.

Figure 15 illustrates how oblateness indirectly affects perigee height even though its direct effect is zero to first order. It does this by changing the equatorial inclination i_α and the nodal longitude Ω_α. This in turn changes the ecliptic and moon-plane parameters i_ϵ, ω_ϵ, i_m, and ω_m. This then changes the secular effect as is shown.

In Fig. 16 the effect of leaving out the effects of sun or moon is demonstrated. Here the nominal graph is shown in comparison with the same orbit computed with the sun only and with the moon only. Note especially the difference in secular trend.

The effect of making various changes in the initial parameters of the nominal orbit is shown in Figs. 17, 18, 19 and 20.

The graph of the 6-hr orbit for a period of 10 yr is shown in Fig. 21. This orbit illustrates an important phenomenon. From the secular trend in perigee distance given by Eq (185) it follows that Δq_{sec} depends mainly on the inclination and argument of perigee. The inclination does not change very rapidly; however, the argument of perigee is perturbed very much by oblateness and to a lesser extent by luni-solar effects. As i_α increases, oblateness perturbations get smaller ($0 \leq i \leq 63.7°$) and as a result ω_m and ω_ϵ change slowly. Thus the secular term can be nearly constant over a long period of time. If this happened when the secular trend was down, the satellite would probably expire. This effect also explains the short life of most lunar satellites (Ref. 58).

Part 2: Hand Calculation of an Earth Satellite Orbit. The detailed revolution by revolution approximate calculation of a satellite orbit is too slow and tedious to be practical by hand. However, the process can be accelerated by treating the periodic and secular terms separately.

To illustrate this method, part of the trajectory of the EGO Nominal will be calculated (see Fig. 12).

Consider first the periodic term for the lunar perturbations (given in Section C2 of this chapter).

$$\Delta q_{per(mt)} = A_m B_m \sin (2\Gamma_{mt} - \alpha_m)$$

where

$H_m = 0.68736 \times 10^{-18}$ (naut mi)$^{-3}$ was evaluated in Part 2.

A_m = 15.3 naut mi = 28.3 km

B_m = 0.961

α_m = -170.64°

(Note that the minus sign is taken when $\sin 2\omega_m$ is negative.)

The parameter Γ_{mt} denotes the angular position of the moon measured from the satellite's ascending node at time t (see Fig. 9). This parameter is given by the following formula.

$$\Gamma_{mt} = (t - t_m) n_m - \Omega_{mt}$$

where

t_m = time the moon was at its ascending equatorial node

n_m = moon's angular rate = $\frac{2\pi}{\tau_m}$

Ω_{mt} = satellite's moon-plane ascending node measured from the moon's equatorial node

t = time.

If time is measured in days, and angles in degrees and if the initial time $t_0 = 0$

then

t_m = -6.9658 days (ephemeris)

n_m = 13.176°/day

Ω_m = 67.58°

t = 0 (initially)

Γ_{mo} = 24.14°

Γ_{mt} = 24.14 + 13.176°

where t is measured in days.

Substituting the computed values of A_m, B_m, and α_m gives

$$\Delta q_{per(mt)} = 14.7 \sin (2\Gamma_{mt} + 170.60)$$
$$= 14.7 \sin (218.92 + 26.352\ t).$$

The period of the satellite once again is 1.73 days. Hence the periodic term alone indicates that the moon's gravitational field will push the satellite down for four revolutions. The satellite will then be at a minimum height as far as the periodic effect of the moon is concerned. From then on this periodic motion can be ignored (see Fig. 12).

Evaluating $\Delta q_{per(mt)}$ for time t = 0, t = 1.73, t = 3.46, and t = 5.19 days, and then summing gives the initial downward push by the moon to be 36.2 naut mi or 67.0 km.

Consider now the periodic term of the sun's perturbation in perigee distance as measured from the center of the earth (q)

$$\Delta q_{per(\epsilon t)} = A_\epsilon \, B_\epsilon \, \sin (2\Gamma_{\epsilon t} - \alpha_\epsilon)$$

where

$$A_\epsilon = 7.03 \text{ naut mi} \approx 13 \text{ km}$$

$$B_\epsilon = 0.961$$

$$\alpha_\epsilon = 171.38°.$$

The parameter $\Gamma_{\epsilon t}$ is given by

$$\Gamma_{\epsilon t} = (t - t_\epsilon) N_\epsilon - \Omega_{\epsilon t}°$$

$$t_\epsilon = - 11.4258 \text{ days}$$

$$n_\epsilon = 0.9856°/\text{day}$$

$$\Omega_{\epsilon t} = 87.47° \text{ when } t = 0$$

$$\Gamma_{\epsilon 0} = - 76.21°.$$

Thus

$$\Gamma_{\epsilon t} = - 76.21 + 0.9856\, t°$$

where t is measured in days.

Combining the above equations gives

$$\Delta q_{per(\epsilon t)} = 6.59 \sin (2\,\Gamma_{\epsilon t} - 171.38)$$

$$= 6.59 \sin (36.20 + 1.9712\, t).$$

Note that the sun's periodic effect is initially upward. But after about 146 days, this upward move is cancelled. The satellite than has about 18.4 days or eleven revolutions to reach a minimum. Evaluation $\Delta q_{per(\epsilon t)}$ at time t = 147.05, t = 148.78, t = 150.051, $\cdots$, t = 164.35--that is, once each revolution from time t = 147.05 to t = 164.35--and summing yields the net downward push of the sun as 21 naut mi or 39 km. The satellite will then be at a minimum height as far as the periodic effect of the sun is concerned. From then on this periodic motion can be ignored (see Fig. 12).

Now consider the combined secular effects of the sun and moon on perigee distance q:

$$\Delta q_{sec} = - \frac{1}{2} \left(A_m \sin 2\omega_m \sin^2 i_m + \right.$$

$$\left. + A_\epsilon \sin 2\omega_\epsilon \sin^2 i_\epsilon \right)$$

$$\Delta q_{sec} = +0.0319 \text{ naut mi/rev.} = +0.0591 \text{ km/rev}$$

Assuming the various parameters are relatively invariant during the first 164.35 days, the secular rise in perigee height for this period can be computed as

$$\Sigma \Delta q_{sec} = \frac{164.35}{1.73} (0.0319) = 3.0 \text{ naut mi or}$$

$$5.6 \text{ km}.$$

The combined periodic and secular results indicate that perigee height should have decreased by

$$36.2 + 21.0 - 3.0 = 54.2 \text{ naut mi or } 100.4 \text{ km}.$$

This checks reasonably well with the results shown in Fig. 12.

Better results could be obtained by summing the secular perturbations over perhaps 20- or 50-day intervals and taking into account changes in the parameters e, i_m, ω_m, i_ϵ and ω_ϵ (in such computations the periodic terms in these parameters are not important). The main difficulty here would be in converting solar and lunar perturbations into changes in the equatorial parameters.

Using this method with, say, 50-day steps should yield results of fair accuracy for many satellite orbits. For example, the 0 hr, 2 hr, 8 hr, 10 hr, 12 hr and 14 hr would be quite easy to compute by hand (see Fig. 13). Hand computation of the orbit of a lunar satellite is also easy because the moon's equator is very close to the ecliptic, and because the sun's effect is very small compared with the effect of earth.

E. REFERENCES

1. Moulton, F. R., "An Introduction to Celestial Mechanics," Second Revised Edition, Macmillan Co.

2. Baker, R., "Three Dimensional Drag Perturbation Technique," ARS Journal, Vol. 30, No. 8, August 1960.

3. Jastrow, R., "Atmospheric Drag on Satellites," J Geophysical Res., Vol. 62, 1957, pp 413 to 423.

4. Danby, J., "Fundamentals of Celestial Mechanics," Macmillan Co. + 1962.

5. Garfinkel, B., "On the Motion of a Satellite of an Oblate Earth," Astronomical Journal, Vol. 63, 1958.

6. Baker, R., "Encke's and the Variation of Parameters Methods as Applied to Re-Entry Trajectories," J. Amer. Astron. Soc., Vol. 6, No. 1, Spring 1959.

7. Herrick, S., "Astrodynamics," Von Nostrand (to be published).

8. Pines, S., "Variation of Parameters for Elliptic and Near Circular Orbits," Astronomical Journal, Vol. 66, No. 5, June 1961.

9. Conte, S. D., "An Evaluation of Special Perturbation Methods and Integration Routines for Space Trajectory Computations," Space Technology Laboratories Report 9850-66, 17 April 1961.

10. Garrett, J., et al., "Satellite Orbit Determination and Error Analysis of Procedures," Prepared for Holloman Air Force Base, Project No. A-398, September 1959.

11. Herrick, C. and Leger, R., "Trajectory Computation in Systems Design," Space Trajectories, Academic Press, Ch 6, 1960.

12. Baker, R., Westrom, G., et al., "Efficient Precision Orbit Computation Techniques," Aeronutronics Report, 1959.

13. Baker, R., Westrom, G., et al., "Efficient Precision Orbit Computation Techniques," Astrodynamical Report No. 3, University of California (Los Angeles), June 1959.

14. Pines, S., Payne, M. and Wolf, H., "Comparison of Special Perturbation Methods in Celestial Mechanics," Aero Research Laboratory Report No. 60-281, Wright-Patterson Air Force Base, August 1960.

15. Moe, M. M., "Rates of Change of Satellite Orbital Elements Caused by a Perturbing Force," Space Technology Laboratories Report STL-TR-59-0000-09893, 22 October 1959.

16. Krause, H. G. L., "The Secular and Periodic Perturbations of the Orbit of an Artificial Earth Satellite," Presented at the 7th International Astronautic Congress, Rome, September 1956.

17. Kalil, F. and Martikan, F., "Minimum Altitude Variation Orbits About an Oblate Earth," the Martin Company (Baltimore), Report ER 12380, February 1962.

18. Kozai, Y., "The Motion of a Close Earth Satellite," Astronomical Journal, Vol. 64, No. 9, 1959, pp 367 to 377.

19. King Hele, "The Effect of the Earth's Oblateness on the Orbit of a Near Satellite," Proceedings of the Royal Soc., Vol. 247A, No. 4, August 1958, p 49.

20. Struble, R. A. and Campbell, W. F., "Theory of Motion of a Near Earth Satellite," ARS Journal, Vol. 31, No. 1, January 1961, pp 154 and 155.

21. Brouwer, D., "Solution of the Problem of Artificial Satellite Theory Without Drag," Astron.J., Vol. 64, No. 9, 1959, pp 378 to 396.

22. Garfinkel, B., "On the Motion of a Satellite in the Vicinity of the Critical Inclination," Astron.J., Vol. 65, No. 10, 1960, pp 624 to 627.

23. Izsak, I. G., "On Satellite Orbits with Very Small Eccentricities," The Astronomical Journal, Vol. 66, No. 3, April 1961, p 129.

24. Struble, R. A., "The Geometry of the Orbits of Artificial Satellites," Archives for National Mechanical and Analysis, Vol. 7, No. 2, 1961, pp 87 to 104.

25. Anthony, M. L. and Fosdick, G. E., "Satellite Motions About an Oblate Planet," Jour. of Aerospace Sciences, Vol. 28, No. 10, October 1961, p 789.

26. Kozai, Y., "Note on the Motion of a Close Earth Satellite with a Small Eccentricity," The Astronomical Journal, Vol. 66, No. 3, April 1961, p 132.

27. Struble, R. A., "An Application of the Method of Averaging in the Theory of Satellite Motion," Journal of Math and Mech, Vol. 10, No. 5, 1961, p 691.

28. Izsak, I. G., "A Theory of Satellite Motion About an Oblate Planet," SAO Special Report No. 52, Cambridge, Mass., 21 November 1960.

29. Kozai, Y., "Comments on Use of Osculating Ellipse in Analysis of Near Circular Orbits," ARS Jour, Vol. 31, No. 5, May 1961, p 676.

30. Kork, J., "First Order Satellite Motion in Near-Circular Orbits About an Oblate Earth," the Martin Company (Baltimore), Report ER 12202, January 1962.

31. Jensen, J., Townsend, G. E., Kork, J., and Kraft, J. D., "Design Guide for Orbital Flight," McGraw-Hill, January 1962.

32. Taratynova, G. H., "The Motion of an Artificial Earth Satellite in the Non-Central Gravitational Field of the Earth When Atmospheric Resistance Is Present," in The Russian Literature of Satellites, Part I, International Physical Index, Inc., New York, 1958, p 74.

33. Penzo, P., "Analytical Perturbation Expressions for the Restricted Three-Body Problem," Space Trajectories Session, AFBMD-STL-Aerospace 5th Symposium on Ballistic Missiles and Space Technology, 1960.

34. Geyling, F. T., "Satellite Perturbation from Extra Terrestrial Gravitation and Radiation Pressure," J. Franklin Inst., Vol. 269, No. 5, 1960, pp 375 to 407.

35. Blitzer, L., "Lunar-Solar Perturbations of an Earth Satellite," Amer. J. Physics, Vol. 27, No. 9, 1959, pp 634 to 645.

36. Moe, M. M., "Solar-Lunar Perturbations of the Orbit of an Earth Satellite," Space Technology Laboratories, STL-TR-60-0000-00871, 29 September 1959, and reprinted in ARS Journal, May 1960.

37. Plummer, H. C., "Dynamical Astronomy," University Press, Cambridge, 1918.

38. Smart, W. M., "Celestial Mechanics," Longmans, Green and Co., New York and London, 1953.

39. Moe, M. M., "The Rates of Change of Satellite Orbital Elements Caused by a Perturbing Force," Space Technology Laboratories, STL-TR-59-0000-09893, 22 October 1959.

40. Leeper, E., "Atmospheric Perturbations of Artificial Satellites," The RAND Corporation, 24 September 1958, p 1496.

41. Sterne, T. E., "Effect of the Rotation of a Planetary Atmosphere upon the Orbit of a Close Satellite," ARS Journal, Vol. 29, 1959, p 777.

42. Wyatt, S. P., "Rate of Change of Period Caused by a Diurnal Bulge," Smithsonian Astrophysical Observatory, Special Report No. 63.

43. Kozai, Y., "Effects of Solar Radiation Pressure on the Motion of an Artificial Satellite," Smithsonian Astroph Obs, Special Report No. 56, 1961, pp 25 to 33.

44. Musen, P., Bryant, R., and Bailie, A., "Perturbations in Perigee Height of Vanguard I," Science, Vol. 131, 1960, pp 935 and 936.

45. Zadunaisky, Shapiro, and Jones, "Experimental and Theoretical Results on the Orbit of Echo I," Smithsonian Astrophysical Observatory, Special Report No. 61, 1961.

46. Musen, P., "The Influence of the Solar Radiation Pressure on the Motion of an Artificial Satellite," Jour. Geophys. Res., Vol. 65, pp 1391 to 1396.

47. Parkinson, R. W., Jones, H. M., and Shapiro, I. I., "Effects of Solar Radiation Pressure on Earth Satellite Orbits," Science, Vol. 131, 1960, pp 920 and 921.

48. Shapiro, I. I., and Jones, H. M., "Perturbations of the Orbit of the Echo Balloon," Science, Vol. 132, 1960, pp 1484 to 1486.

49. Wyatt, S. P., "The Effect of Radiation Pressure on the Secular Acceleration of Satellites," Smithsonian Astroph. Obs., Special Report No. 60, 1961.

50. Bryant, R., "Report on the Orbit of Echo I," NASA (Goddard), 1961.

51. McElvain, R. J., "Effects of Solar Radiation Pressure on Satellite Attitude Control," Space Technology Laboratories Report 2313-0003-NU-000, July 1961.

52. Poynting, J. H., "Collected Scientific Papers," Cambridge University Press, 1920.

53. Robertson, H. P., "Dynamical Effects of Radiation in the Solar System," Monthly Notices Royal Astron.Soc., Vol. 97, 1937, pp 423 to 438.

54. Wyatt, S. P., and Whipple, F. L., "The Poynting-Robertson Effect on Meteor Orbits," Astrophys. Jour., Vol. 111, 1950, pp 134 to 141.

55. Garwin, L. I., "Solar Sailing--a Practical Method of Propulsion Within the Solar System," Jet Propulsion, Vol. 28, 1958, pp 188 to 190.

56. Tsu, T. C., "Interplanetary Travel by Solar Sail," ARS Journal, Vol. 29, 1959, p 422.

57. Lindon, H. S., "Some Exact Solutions of the Equations of Motion of a Solar Sail with Constant Sail Setting," ARS Journal, Vol. 30, No. 2, 1960, pp 198 to 200.

58. Dunn, R. L., "Satellite Stability Study for Project EGO," Space Technology Laboratories, STL-TR-2311-0007-RU-000, August 1961.

59. Buckingham, J. R., "Computer Program Guide for Satellite Lifetime (AT4.Z)," Space Technology Laboratories, STL/CDRC Report No. 9830.30-022, 30 January 1960.

F. BIBLIOGRAPHY

Allen, W., "Effect on a Rocket of the Oblateness of a Planet," ARS Journal, Vol. 30, No. 7, July 1960.

Anthony, M. L., and Fosdick, G. E.,
"Planar Motions About an Oblate Planet," American Rocket Society, Preprint No. 1231-60, 1960.
"An Analytical Study of the Effects of Oblateness on Satellite Orbits (U)." Denver, Colorado, the Martin Company, Report No. R-60-2, April 1960, 155 pp.
"Satellite Motions About an Oblate Planet." Denver, Colorado, the Martin Company, 1960. (Presented at the Summer Meeting of IAS (Los Angeles).) (Also, Journal of Aerospace Sciences, October 1961, pp 789 to 802.)

Anthony, M. L., and Perko, L. M., "Vehicle Motion of the Equatorial Plane of a Planet," (A Second Order Analysis in Ellipticity). Martin Company, Denver, 8 December 1960. (Also, ARS Journal, Vol. 31, No. 10, October 1961, pp 1413 to 1421.)

Bailie, A., and Bryant, R., "Osculating Elements Derived from the Modified Hansen Theory for the Motion of an Artificial Satellite," Astronomical Journal, Vol. 65, No. 8, October 1960, pp 451 to 453. (Also, NASA TN D-568.)

Baker, R. M. L., Jr.,
"Librations on a Slightly Eccentric Orbit," ARS Journal, Vol. 30, No. 1, January 1960, pp 124 to 126.
"Plane Librations of a Prolate Ellipsoidal Shell," ARS Journal, Vol. 30, No. 1, January 1960, pp 126 to 128.
"Three Dimensional Drag Perturbation Technique," ARS Journal, Vol. 30, No. 8, August 1960, pp 748 to 753.

Baker, R. M. L., Jr., and Makemson, M. W., "Fundamentals of Astrodynamics," University of California, Los Angeles, Astrodynamical Report No. 6, 20 September 1959.

Baker, R. M. L., Jr., et al., "Efficient Precision Orbit Computational Techniques." Los Angeles, California, University of California, Astrodynamical Report No. 3, 11 June 1959.

Bandeen, W. R., "Earth Oblateness and Relative Sun Motion Considerations in the Determination of an Ideal Orbit for the Nimbus Meteorological Satellite." NASA TN D-1045, July 1961, 10 pp.

Barrar, R. B., "Some Remarks on the Motion of a Satellite of an Oblate Planet," Astronomical Journal, Vol. 66, No. 1, February 1961, pp 11 to 15.

Batrakov, Yu. V. and Proskurin, V. F., "Perturbations of Orbits of Artificial Satellites due to Air Resistance," ARS Journal, Russian Supplement, Vol. 30, No. 7, July 1960, pp 700 to 704. (Also, NASA Technical Translation F-46, November 1960, 13 pp.)

Batrakov, Yu. V., et al., "Perturbations in the Motion of Artificial Satellites Due to the Oblateness of the Earth," ARS Journal, Vol. 31, No. 1, January 1961.

"National Aeronautics and Space Administration. PAPERS ON ANALYSIS OF ORBITS," March 1962, p 29. $0.75. (NASA Technical Translation F-74. Translation of Bulletin of the Stations for Optical Observation of Artificial Earth Satellites, No. 7 (17), 1960.)

Beard, D. and Johnson, F., "Charge and Magnetic Field Interaction with Satellites," Journal of Geophysical Research, Vol. 65, No. 1, 1960, pp 1 to 7.

Beletskiy, V. V., "The Libration of a Satellite," Artificial Satellites of the Earth. USSR, Academy of Sciences, No. 3, 1959.

Berman, L. J., "The Correction of Epoch Error in Circular Orbits," American Rocket Society, 30 April 1959, Reprint No. 792-59.

Blitzer, L.,
"Effect of Earth's Oblateness on Satellite Period," Jet Propulsion, Vol. 27, 1957, p 406.
"Apsidal Motion of an IGY Satellite Orbit," Journal of Applied Physics, Vol. 28, 1957, p 1362.
"Lunar-Solar Perturbations of an Earth Satellite," American Journal of Physics, Vol. 27, No. 9, 1959, pp 634 to 645.

Blitzer, L., and Wheelon, A. D., "Oblateness Perturbations of Elliptical Satellite Orbits," Journal of Applied Physics, Vol. 28, 1957, p 279.

Blitzer, L., Weisfield, M., and Wheelon, A. D., "Perturbations of a Satellite's Orbit Due to the Earth's Oblateness," Journal of Applied Physics, Vol. 27, 1956, p 1141.

Bowden, G., and Flis, I. (Editors), "Notes of the Summer Institute in Dynamical Astronomy at Yale University, July 1959," New Haven, Connecticut, Yale University Observatory, 1960.

Brouwer, D.,
"Motion of a Particle of Negligible Mass Under the Gravitational Attraction of a Spheroid," Astronomical Journal, Vol. 51, No. 1156, 1946.
"A Study of the Changes in the Rate of Rotation of the Earth," Astronomical Journal, Vol. 57, 1952, pp 125 to 147.
"Solution of the Problem of Artificial Satellite Theory Without Drag," Astronomical Journal, Vol. 64, No. 9, November 1959, pp 378 to 396.
"Outlines of General Theories of the Hill-Brown and Delauney Types, for Orbits of Artificial Satellites," Astronomical Journal, Vol. 63, November 1958, pp 433 to 438.

Brouwer, D. and Hori, G.,
"Theoretical Evaluation of Atmospheric Drag Effects in the Motion of an Artificial Satellite," Astronomical Journal, Vol. 66, No. 5, June 1961, pp 193 to 225.
"Appendix to Theoretical Evaluation of Atmospheric Drag Effects on the Motion of an Artificial Satellite," Astronomical Journal, Vol. 66, No. 6, August 1961, pp 264 and 265.

Caldwell, G. C., Struble, R. A. and Yionoulis, S. M., "The Secular Characteristics of the Motion of an Earth Satellite," North Carolina State College, Department of Mathematics and Engineering Research (Raleigh), 1960, File No. ERD 106/5.

Callender, E. D., "On the Almost Periodicity of Satellite Motion," Astronomical Journal, Vol. 66, No. 3, April 1961, pp 134 to 137.

Castruccio, P. A., Bass, R. W. and Slotnick, D. L., "New Methods in Celestial Mechanics," Aeronca Astromechanics Institute, 1960, Technical Report 60-25.

Chopra, K. and Singer, F., "Drag of a Sphere Moving in a Conducting Fluid," University of Maryland, Physics Department (College Park), Technical Report No. 97, January 1958.

Cohen, S., "Multi-Body Effects on Orbit Transfer," American Rocket Society, December 1960, Preprint No. 1478-60.

Crane, J. A., "On the Motion of a Particle About an Oblate Spheroid III. Parabolic and Highly Elliptic Orbits," Journal of the British Interplanetary Society, Vol. 17, No. 12, November and December 1960, pp 437 to 440.

Diliberto, S. P., Kyner, W. T. and Freund, R. B., "The Application of Periodic Surface Theory to the Study of Satellite Orbits," Astronomical Journal, Vol. 66, No. 3, April 1961, pp 118 to 128.

Dobson, W. F., Huff, V. N., and Zimmerman, A. V., "Elements and Parameters of the Osculating Orbit and Their Derivatives," NASA TN D-1106, January 1962, 49 pp.

Dunn, J. C., "Green's Functions for Space Trajectory Perturbation Analysis," J. Astronaut. Sci., Vol. 8, No. 4, Winter 1961, pp 95 to 102.

El'Yasberg, P. E., "Dependence of Secular Variations of Orbit Elements on Air Resistance," ARS Journal, Russian Supplement, Vol. 30, No. 7, July 1960, pp 672 to 675. (Also, NASA Technical Translation F-47, November 1960, 10 pp.)

Ewart, D., "On the Motion of a Particle About an Oblate Spheroid," Journal of the British Interplanetary Society, Vol. 17, No. 6, 1959, pp 162 to 168.

Garfinkel, B.,
"On the Motion of a Satellite of an Oblate Planet." Aberdeen Proving Ground, Maryland, 1957, Ballistic Research Laboratory Report No. 1018. (Also, Astronomical Journal, Vol. 63, No. 1257, March 1958, pp 88 to 96.)
"On the Motion of a Satellite in the Vicinity of the Critical Inclination," Astronomical Journal, Vol. 65, No. 10, December 1960, pp 624 to 627.
"The Orbit of a Satellite of an Oblate Planet," Astronomical Journal, Vol. 64, No. 9, November 1959, pp 353 to 367.

Garofalo, A. M., "New Set of Variables for Astronomical Problems," Astronomical Journal, Vol. 65, No. 3, 1960, pp 117 to 121.

Geyling, F. T.,
"Fundamental Satellite Perturbations," ARS Journal, Vol. 30, No. 11, 1960.
"Drag Displacements and Decay of Near-Circular Satellite Orbits," Stockholm, XIth International Astronautical Congress, 1960.
"Satellite Perturbation from Extra Terrestrial Gravitation and Radiation Pressure," Journal of the Franklin Institute, Vol. 269, No. 5, 1960, pp 375 to 407.

Grebenikov, E. A.,
"Secular Perturbations in the Theory of Motion of an Artificial Earth Satellites," Russian Astronomical Journal, Vol. 36, No. 6, 1959, pp 1111 to 1121.
"Secular Perturbations in the Theory of Motion of an Artificial Satellite," Soviet Astronomical Journal, Vol. 3, No. 6, 1960, pp 1023 to 1032.

Groves, G. W., "On Tidal Torque and Eccentricity of a Satellite's Orbit," Royal Astronomical Society, Monthly Notices, Vol. 212, No. 5, 1960, pp 497 to 502.

Hall, N. S., Galowicz, H. G., and Wallman, E. J., Jr., The Choice of Unperturbed Orbit in the Use of Encke's Method for the Effects of Oblateness and Drag," Los Angeles, California, American Rocket Society Semiannual Meeting, ARS Paper 1232-60, May 1960.

Hall, N. S., et al., "Oblatory Perturbations of Satellite Orbits," Advances in the Astronautical Sciences, Macmillan Company, Vol. 6, 1960.

Heinrich, W., "On New Short Periodic and Secular Solutions of the Problem of the Moon and Satellites," Bull. Astron. Inst. Czechoslovakia, Vol. 11, No. 4, 1960, pp 121 to 129.

Herget, P. and Musen, P., "A Modified Hansen Lunar Theory for Artificial Satellites," Astronomical Journal, Vol. 63, November 1958, pp 430 to 433.

Herrick, S.,
"Variation of Parameters," Los Angeles, California, University of California, July 1960, Astrodynamical Report No. 9 (AFOSR TN 60-812.)
"A Modification of the Variation of Constants Method for Special Perturbations," Publs. Astron. Soc Pacific, Vol. 60. No. 356, 1948, pp 321 to 323.

Herrick, S., and Walters, L. G., "Contribution to Astrodynamics: Space Vehicle Ephemeris and Differential Correction Program, Unified Theory," Newport Beach, California, Aeronutronic Systems, Inc., Publication No. U-908, 1960.

Hori, G.,
"The Motion of an Artificial Satellite in the Vicinity of the Critical Inclination," Astronomical Journal, Vol. 65, No. 5, June 1960, pp 291 to 300.
"The Motion of a Hyperbolic Artificial Satellite Around the Oblate Earth," Astronomical Journal, Vol. 66, No. 6, August 1961, pp 258 to 263.

Izsak, I.,
"On Satellite Orbits with Very Small Eccentricities," Astronomical Journal, Vol. 66, No. 3, April 1961, pp 129 to 131.
"Periodic Drag Perturbations of Artificial Satellites," Astronomical Journal, Vol. 65, No. 6, August 1960, pp 355 to 357.

Jastrow, R., "Atmospheric Drag on Satellites," Journal of Geophysical Research, Vol. 62, September 1957, pp 413 to 423.

Kalensher, B. E., "Equations of Motion of a Missile and a Satellite for an Oblate Spheroidal Rotating Earth," California Institute of Technology, Pasadena, JPL Report No. 20-142, April 1957.

Karrenberg, H. K., Levin, E. and Lewis, D. H., "Variation of Satellite Position with Uncertainties in the Mean Atmosphere Density," Aerospace Corporation, ElSegundo, California, June 1961, IAS Preprint No. 61-138-1832.

Kaula, W. M., "A Development of the Lunar and Solar Disturbing Functions for a Close Satellite, NASA TN D-1126, January 1962, 11 pp.

King, J. P., "Motion of an Orbiting Vehicle About Its Center of Mass Due to the Gravity Gradient," American Rocket Society, May 1960, Preprint 122-60.

King-Hele, D.,
"The Effect of the Earth's Oblateness on the Orbit of a Near Satellite," Proc. Roy. Soc. (London), Vol. A247, No. 1248, 1958.
"Determination of Air Density and the Earth's Gravitational Field from the Orbits of Artificial Satellites," Proceedings of the Xth International Astronautical Congress, London, 1959. Vienna, Austria, Wien-Springer-Verlag, Vol. I, 1960, pp 1 to 20.

King-Hele, D., and Walker, D. M. C.,
"Variation of Upper Atmosphere Density with Latitude and Season: Further Evidence from Satellite Orbits," Nature, Vol. 185, No. 4715, 1960, pp 727 to 729.
"Methods for Predicting the Orbits of Near Earth-Satellites," Journal of the British Interplanetary Society, Vol. 17, No. 1, 1959, pp 2 to 14.

Kochi, K. C., and Staley, R. M., "Methods for Analysis of Satellite Trajectories," Autonetics, A Division of North American Aviation, Inc., Downey, California, September 1960, 330 pp incl illus (Project 1772; Task 17722) (Report No. EM-2075; WADD TR 60-214).

Kooy, J. M. J., "On the Application of the Method of Variation of Elliptic Orbit Elements in the Case of a Satellite Vehicle," Astronautica Acta, Vol. 3, No. 3, 1956.

Kovalevsky, J., "Numerical Method for the Calculation of General Perturbations: Application to the VIIIth Satellite of Jupiter," Paris, France, University of Paris, 1959, Thesis.

Kozai, Y.,
"Tesseral Harmonics of the Gravitational Potential of the Earth as Derived from Satellite Motions," Astronomical Journal, Vol. 66, No. 7, September 1961, pp 355 to 358.
"On the Effect of the Sun and the Moon upon the Motion of a Close Earth Satellite," Smithsonian Astrophysical Observatory, (Cambridge), Special Report No. 22, pp 7 to 10.
"Semi-Analytical Calculations of Orbital Perturbations of Earth Satellites," Smithsonian Astrophysical Observatory, (Cambridge), ARS Preprint No. 871-59.
"The Motion of a Close Earth Satellite," Astronomical Journal, Vol. 64, No. 9, November 1959, pp 367 to 377.
"Effects of Solar Radiation Pressure on the Motion of an Artificial Satellite," Smithsonian Astrophysical Observatory, (Cambridge), Special Report No. 56, January 1960.
"Osculating Elements," Smithsonian Astrophysical Observatory, (Cambridge), Special Report No. 31, January 1960, pp 8 and 9.
"Effect of Precession and Nutation on the Orbital Elements of a Close Earth Satellite," Astronomical Journal, Vol. 65, No. 10, December 1960, pp 621 to 623.
"On the Motion of a Close Earth Satellite with a Small Eccentricity," Astronomical Journal, Vol. 66, No. 3, April 1961, pp 132 to 134.
"The Gravitational Field of the Earth Derived from Motions of Three Satellites," Astronomical Journal, Vol. 66, No. 1, February 1961, pp 8 to 10.

Kozai, Y., and Whitney, C. A., "Anticipated Orbital Perturbations of Satellite 1959 Delta Two," Smithsonian Astrophysical Observatory, (Cambridge), Special Report No. 30, November 1959, pp 1 to 8.

Knoll, F. W. A., "Rapid and Precise Method of Numerical Integration of the Motion of Planetary Bodies and Space Vehicles in the Solar System," American Astronautical Society, 1960, Preprint 60-32.

Krauss, L., and Yoshihara, H., "Electrogas-Dynamic Motion of a Charged Body in a Plasma," Journal of Aerospace Sciences, Vol. 27, No. 3, 1960, pp 229 to 233.

Krause, H. G. L., "The Secular and Periodic Perturbations of the Orbit of an Artificial Earth Satellite," Proceedings of the 8th International Astronautical Federation Congress, Rome. Vienna, Austria, Springer-Verlag, 1956.

Lanzano, P.,
"Application of Lunar Theory to the Motion of Satellites," Advances in the Astronautical Sciences. Macmillan Company, Vol. 6, 1960.
"Application of the Jacobi Integral of Celestial Mechanics to the Terminal Guidance of Space Probes," Stockholm, XIth International Astronautical Congress, Astrodynamics Colloquium, 1960.

Lass, H., and Solloway, C. B., "Motion of a Satellite Under the Influence of a Constant Normal Thrust," ARS J. 32, 1962, pp 97 to 100.

Lecar, M., "A Method of Estimating Residuals in Orbital Theory," NASA TN D-493, January 1961.

Levin, E., "Satellite Perturbations Resulting from Lunar and Solar Gravitation," Santa Monica, California, The Rand Corporation, Report No. P-1561, 1 December 1958.

Ljah, R. A., "On the Influence of Atmospheric Resistance upon the Motion of the Artificial Satellite," Bull. Inst. Theoretical Astron., USSR, Academy of Science, Vol. 7, No. 5, 1959, pp 321 to 326.

London, H., "Some Exact Solutions of the Equations of Motion of a Solar Sail with Constant Sail Setting," ARS Journal, Vol. 30, No. 2, 1960, pp 198 to 200.

Lur'e, A. I., "The Equations of the Perturbative Motion in the Problem of Kepler," Russian Math and Applied Mechanics, Vol. 23, No. 2, 1959, pp 412 and 413.

Mace, D., and Thomas, L., "An Extrapolation Formula for Stepping the Calculation of the Orbit of an Artificial Satellite Several Revolutions Ahead at a Time," Astronomical Journal, Vol. 65, No. 5, 1960, pp 300 to 303.

Makarov, E. N., "On the Simultaneous Determination of Systematic Errors of Stellar Catalogues and of the Masses of Planets from

Observations of Asteroids," Bull. Inst. Theoretical Astron. USSR, Academy of Science, Vol. 7, 1958, pp 1 to 18.

Mersman, W. A., "Theory of the Secular Variations in the Orbit of a Satellite of an Oblate Planet," NASA TR R-99, 1961.

Message, P. F., "On Mr. King-Hele's Theory of the Effect of the Earth's Oblateness on the Orbit of a Close Satellite," Monthly Notices of the Royal Astronomical Society, Vol. 121, No. 1, 1960.

Miachin, V. F., "Estimation of Errors in the Numerical Integration of the Equations of Celestial Mechanics," Silver Springs, Maryland, The Johns Hopkins University, Applied Physics Laboratory, TG 230-T230, April 1961, 36 pp. (Translated from Bull. Instituta Theoreticheskoi Astronomii, Vol. 7, No. 4 (87), 1959, pp 257 to 280.)

Michaels, J. E., and Strawbridge, E. A., "Planetary Perturbations of Interplanetary Orbits," American Rocket Society, 1959, Preprint No. 957-59.

Miller, G. K., Jr., "Determination of Ballistic Missile Dispersion by Use of First-Order Perturbation Theory," (NASA Technical Memorandum X-667) May 1962, 32 pp.

Moe, M. M., and Karp, E. E., "Effect of Earth's Oblateness on the Anomalistic Period of a Satellite," ARS Journal, Vol. 31, No. 10, October 1961, pp 1462 to 1464.

Moran, J. P., "The Effects of Plane Librations on the Orbital Motion of a Dumbbell Satellite (U)," American Rocket Society, 8 December 1960, Preprint No. 1446-60.

Mullikin, T. W., "Oblateness Perturbations of Near-Earth Satellites," The Rand Corporation, Santa Monica, California, Report No. RM-2643, 25 October 1960.

Musen, P.,
"Application of Hansen's Theory to the Motion of an Artificial Satellite in the Gravitational Field of the Earth," Journal of Geophysical Research, Vol. 64, No. 12, 1959, pp 2271 to 2279.
"The Influence of the Solar Radiation Pressure on the Motion of an Artificial Satellite," Journal of Geophysical Research, Vol. 65, No. 5, May 1960, pp 1391 to 1396.
"Motion of a Satellite in an Asymmetrical Gravitational Field," Journal of Geophysical Research, Vol. 65, No. 9, September 1960, pp 2783 to 2792. (Also, NASA TN D-569, January 1961.)
"A Modified Hansen's Theory as Applied to the Motion of Artificial Satellites," NASA TN D-492, November 1960.
"The Theory of Artificial Satellites in Terms of the Orbital True Longitude," Journal of Geophysical Research, Vol. 66, No. 2, February 1961, pp 403 to 409.
"On the Long Period Luni-Solar Effect in the Motion of an Artificial Satellite," NASA TN D-1041, July 1961, 17 pp.

Musen, P., Bailie, A., and Upton, E., "Development of the Lunar and Solar Perturbations in the Motion of an Artificial Satellite," Committee on Space Research, First International Space Symposium, Nice, France, January 1960. (Also, NASA TN D-494.)

Nielson, J., et al., "Three-Dimensional Orbits of Earth Satellites, Including Effects of Earth's Oblateness and Atmospheric Rotation," NASA Memo 12-4-58A, December 1958.

Nonweiler, T. R. F., "Perturbations of Elliptic Orbits by Atmospheric Contact," Journal of the British Interplanetary Society, Vol. 16, April 1958, pp 368 to 379. (Also Journal of the British Interplanetary Society, Vol. 17, No. 1, January-February 1959, pp 14 to 20.)

O'Keefe, J. A.,
"An Application of Jacobi's Integral to the Motion of an Earth Satellite," Astronomical Journal, Vol. 62, October 1957, pp 265 and 266.
"Determination of the Earth's Gravitational Field," Science, Vol. 131, 1960, pp 607 and 608.
"Zonal Harmonics of the Earth's Gravitational Field and the Basic Hypothesis of Geodesy," Journal of Geophysical Research, Vol. 64, No. 12, December 1959, p 2389.

O'Keefe, J. A., and Batchlor, C. D., "Perturbations of a Close Satellite by the Equatorial Ellipticity of the Earth," Astronomical Journal, Vol. 62, 1957, p 183.

O'Keefe, J. A., Eckels, A., and Squires, R., "Vanguard Measurements Give Pear-Shaped Component of Earth's Figure," Science, Vol. 129, No. 3348, 1959, pp 565 and 566.

O'Keefe, J. A., et al., "The Gravitational Field of the Earth," Astronomical Journal, Vol. 64, No. 7, September 1959, pp 245 to 253. (Also, American Rocket Society, Preprint No. 873-59.)

Okhotsimskij, D. E., Eneyev, T. M., and Taratynova, G. P., "Determination of the Life of an Artificial Earth Satellite and an Investigation of the Secular Perturbations," Uspekhi Fiz. Nauk, Vol. 63, No. 1a, 1957.

Orlov, A. A., "Formulas for Computing Perturbations in Elliptical and Hyperbolic Motion," USSR, Vestnik Moskovskogo Gosudarstvenngo Universiteta, Seria Fizikii Astronomicheskii, No. 2, March-April 1960, pp 51 to 60. (Abstracted in Physics Express, Vol. 3, No. 3, November 1960, pp 28 and 29.)

Parkinson, R., Jones, H., and Shapiro, I., "The Effects of Solar Radiation Pressure on Earth Satellite Orbits," Science, Vol. 131, 1960, pp 920 and 921.

Parkyn, D. G., "Satellite Orbits in an Oblate Atmosphere," Journal of Geophysical Research, Vol. 65, No. 1, January 1960, pp 9 to 17.

Penzo, P., "Analytical Perturbation Expressions for the Restricted Three-Body Problem," AFBMD-STL-Aerospace 5th Symposium on

Ballistic Missiles and Space Technology, Space Trajectories Session, 1960.

Petty, C. M., and Breakwell, J. V., "Satellite Orbits About a Planet with Rotational Symmetry," Journal of the Franklin Institute, Vol. 270, No. 4, October 1960, pp 259 to 282.

Pines, S., "Variation of Parameters for Elliptic and Near Circular Orbits," Astronomical Journal, Vol. 66, No. 3, February 1961.

Pines, S., Payne, M., and Wolfe, H., "Comparison of Special Perturbations Methods in Celestial Mechanics," Silver Springs, Maryland, The Johns Hopkins University, Applied Research Laboratory, Report No. 60-281, 1960.

Porter, J. G., "Comparative Study of Perturbation Methods," Astronomical Journal, Vol. 63, No. 10, 1958, pp 405 and 406.

Proskurin, V. F., and Batrakov, V. V., "Perturbations in the Motion of Artificial Satellites Due to the Oblateness of the Earth," ARS Journal, Russian Supplement, Vol. 31, No. 1, January 1961, pp 117 to 125.

Reitz, D., "Solar Influences on Space Flight," Martin Company (Denver), September 1961, 213 pp.

Reynolds, G. E., and Kerr, O. E., "Approximating the Immediate Path of a Satellite," Air Force Cambridge Research Center, Electromagnetic Radiation Laboratory, AFCRL 377, June 1961.

Roberson, R. E., "Orbital Behavior of Earth Satellites," Journal of the Franklin Institute, Vol. 264, September and October 1957, pp 181 to 202, 269 to 285.

Roberson, R. E., and Tatistcheff, D., "The Potential Energy of a Small Rigid Body in the Gravitational Field of an Oblate Spheroid," Journal of the Franklin Institute, September 1956.

Sarychev, V. A., "Influence of the Earth's Oblateness on the Rotational Motion of an Artificial Satellite," Planetary and Space Science, Vol. 8, December 1961, pp 171 to 178.

Savet, P. H., "Satellite Orbits Derived from a Gravitational Model of the Earth," Planetary and Space Science, Vol. 7, July 1961. (Also, Proceedings of the 4th AFBMD/STL Symposium on Space Technology.)

Schliesinger, S., "Intergration Methods for Differential Equations," Journal of Astronautical Science, Vol. 6, No. 4, 1960, pp 53 to 57.

Schilt, J., "The Correction to the Motion of the Equinox," Astronomical Journal, Vol. 65, No. 4, 1960, pp 218 to 221.

Sedwick, J. L., Jr., "Interpretations of Observed Perturbations on a Minimal Earth Satellite," Scientific Uses of Earth Satellites, University of Michigan Press, (Ann Arbor), 1956, p 44. (Van Allen, J. A., ed.)

Singer, F., "The Effect of Meteoric Particles on a Satellite," Jet Propulsion, Vol. 26, No. 12, December 1956.

Smith, O. K.,
"Oblateness Terms for Variational Equations," Space Technology Laboratories, Los Angeles, Report No. PA-1951-16/1, 14 July 1959.
"Computation of Coordinates from Brouwer's Solution of the Artificial Satellite Problem," Astronomical Journal, Vol. 66, No. 7, September 1961, pp 359 and 360.

Socilina, A. S., "On Accumulation of Errors in Numerical Integration in Some Problems of Celestial Mechanics," Bull. Inst. Theoretical Astron. USSR, Academy of Science, Vol. 7, 1959, pp 281 to 286.

Spencer-Jones, H., "The Rotation of the Earth and the Secular Acceleration of the Sun, Moon and Planets," Monthly Notices, Royal Astronomical Society, Vol. 99, 1939, pp 541 to 558.

Spitzer, L., "Perturbations of a Satellite," Journal of the British Interplanetary Society, Vol. 9, 1950, p 131.

Sterne, T. E.,
"Effect of the Rotation of a Planetary Atmosphere upon the Orbit of a Close Satellite," ARS Journal, Vol. 29, 1959, pp 777 to 782.
"The Gravitational Orbit of a Satellite of an Oblate Planet," Astronomical Journal, Vol. 63, No. 1, 1958.

Struble, R. A.,
"Some New Satellite Equations," ARS Journal, Vol. 30, No. 7, July 1960.
"A Geometrical Derivation of the Satellite Equations," Journal of Mathematical Analysis and Applications, Vol. 1, No. 3, December 1960, pp 300 to 307.
"The Geometry of the Orbits of Artificial Satellites," Archive for Rational Mechanics and Analysis, Vol. 7, No. 2, 1961, pp 87 to 104. (Also, North Carolina State College, Department of Mathematics and Engineering Research, (Raleigh), July 1960, File No. ERD 106/4.)
"A Rigorous Theory of Satellite Motion," Stresa, Italy, Tenth International Congress of Applied Mechanics, 1960.
"An Application of the Method of Averaging in the Theory of Satellite Motion," Journal of Mathematics and Mechanics, Vol. 10, No. 5, September 1961, pp 691 to 704.

Struble, R. A., and Campbell, W. F., "Theory of Motion of a Near Earth Satellite," ARS Journal, Vol. 31, No. 1, January 1961, pp 154 and 155.

Taratynova, G. P.,
"Numerical Solution of Equations of Finite Differences and Their Application to the Calculation of Orbits of Artificial Earth Satellites," ARS Journal, Russian Supplement, Vol. 31, No. 7, July 1961, pp 976 to 988.
"Method for Orbit Calculations with Perturbations and Derivations of Equation of Motion of a Satellite in the Eccentric Gravity Field," Uspekhi Fiz. Nauk, Vol. 51, No. 1a, 1957.

"Motion of an Artificial Earth Satellite in the Non-Central Gravitational Field of the Earth When Atmospheric Resistance Is Present," The Russian Literature of Satellites, New York, International Physics Index, Inc., Part 1, 1958.

Upton, E., Bailie, A., and Musen, P., "Lunar and Solar Perturbations on Satellite Orbits," American Rocket Society, Preprint No. 920-59, 1959.

Vinti, J. P.,
"Theory of the Effect of Drag on the Orbital Inclination of an Earth Satellite," Journal of Research, National Bureau of Standards, Vol. 62, No. 2, February 1959, pp 79 to 88.
"New Method of Solution for Unretarded Satellite Orbits," Journal of Research, National Bureau of Standards, Vol. 62B, No. 2, October to December 1959, pp 105 to 116.
"Theory of an Accurate Intermediate Orbit for Satellite Astronomy," Journal of Research, National Bureau of Standards, Vol. 65B, No. 3, September 1961.
"Intermediary Equatorial Orbits of an Artificial Satellite," National Bureau of Standards, Report No. 7345, October 1961.
"Formulae for an Accurate Intermediary Orbit of an Artificial Satellite," Astron. J. 66, No. 9, November 1961, pp 514 to 516.

Ward, G. N., "On the Secular Variations of the Elements of Satellite Orbits," Proc. Roy. Soc. (London) 266A, 27 February 1962, pp 130 to 137.

Westerman, H. R., "Perturbation Approach to the Effect of the Geomagnetic Field on a Charged Satellite," ARS Journal, Vol. 30, No. 2, February 1960, pp 204 and 205.

Whittaker, E., and Robinson, G., "The Calculus of Observations," Blackie and Son, London, 1924.

Wong, P., "Nonsingular Variation of Parameter Equations for Computation of Space Trajectories," ARS Journal, Vol. 32, 1962, pp 264 and 265.

Yatsienskii, I. M., "Effect of Geophysical Factors upon the Motion of an Artificial Satellite," Uspekhi Fiz. Nauk, No. 1a, 1957, p 59.

ILLUSTRATIONS

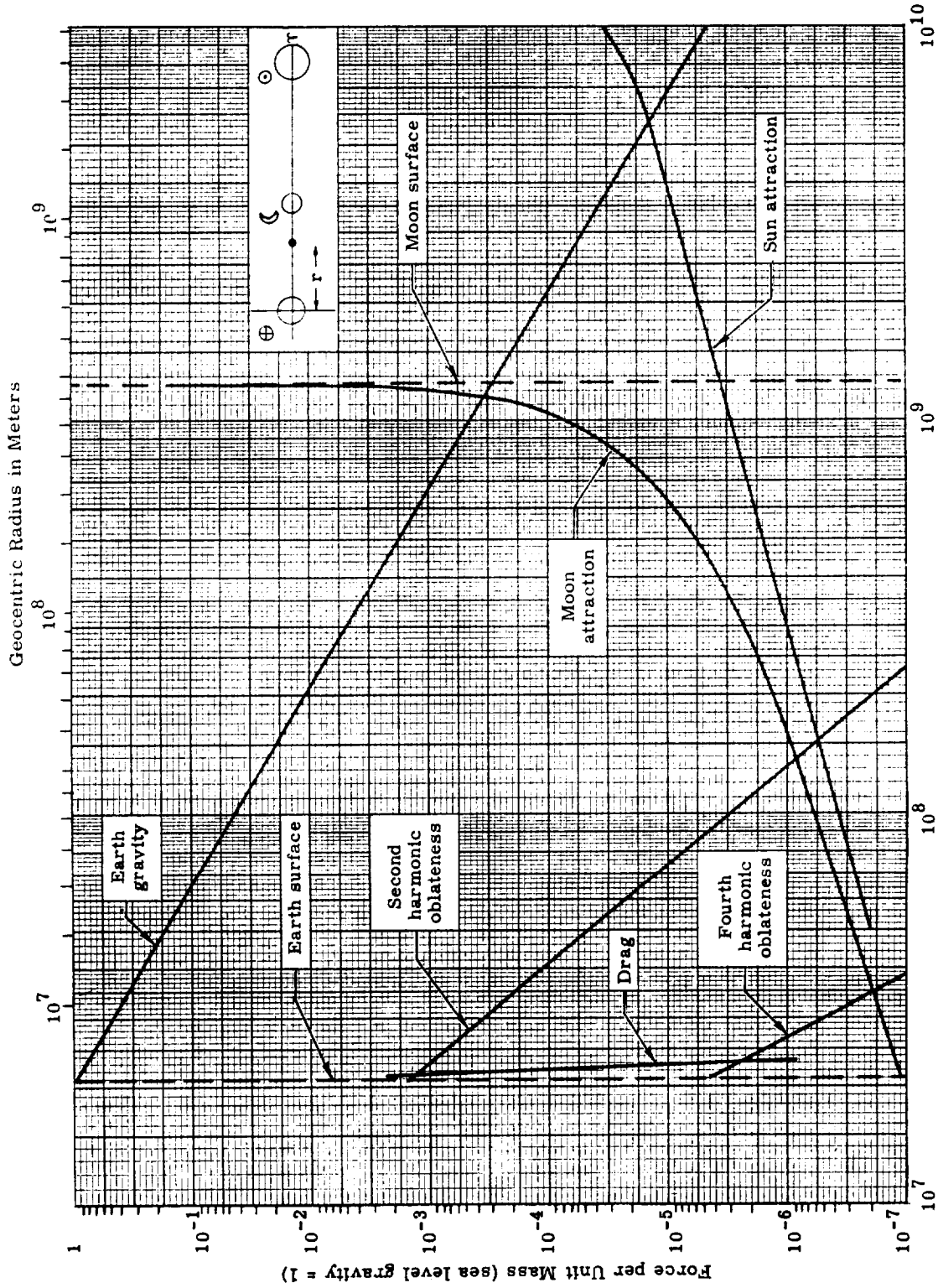

Fig. 1. Comparison of Perturbation Magnitudes (for equinoctial lunar conjunction)

Preceding page blank

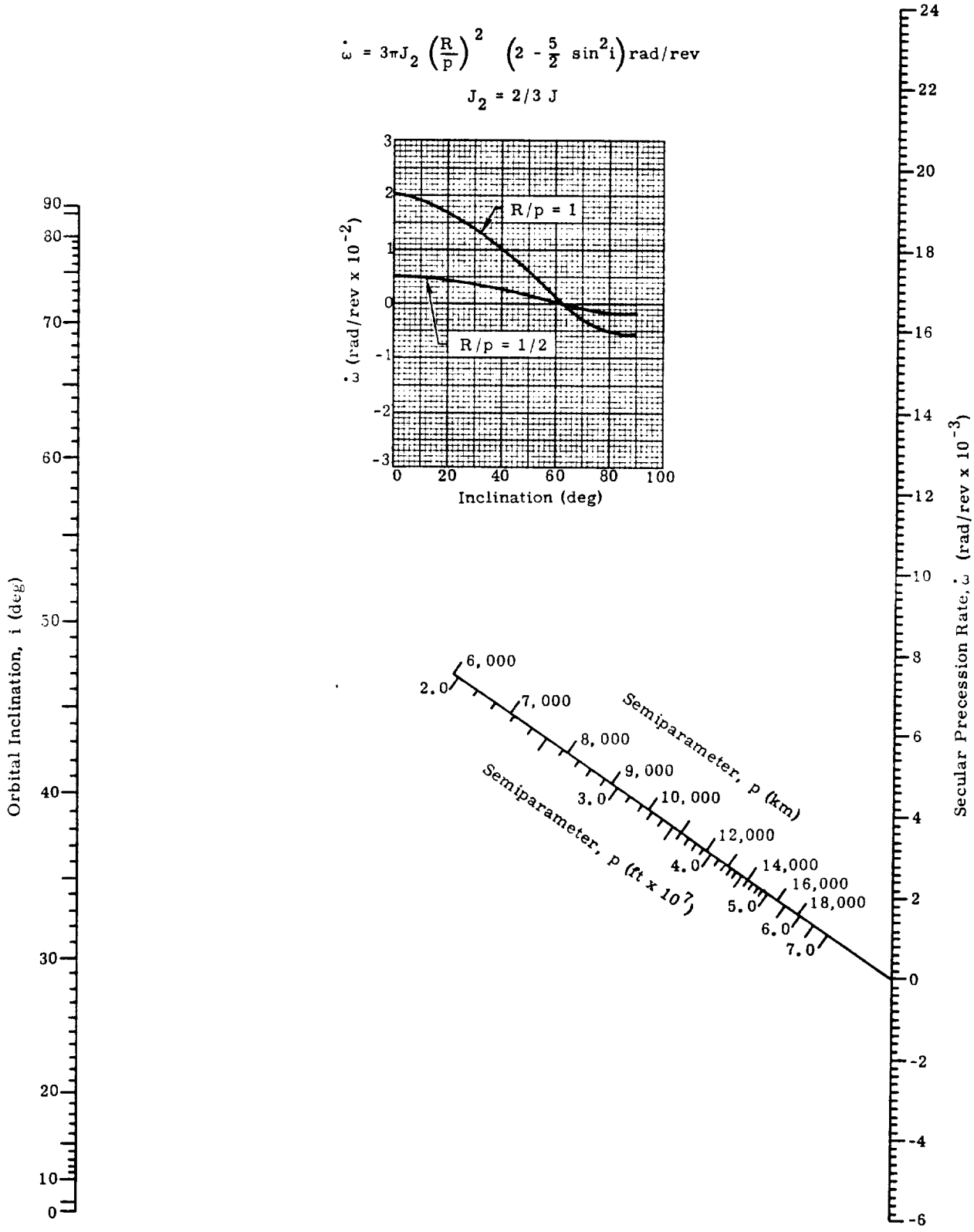

Fig. 2. Solution for the Secular Precession Rate as a Function of Orbital Inclination and Semiparameter

$$\frac{\Delta M}{M} = \frac{3}{2} J_2 \left(\frac{R}{p}\right)^2 \sqrt{1 - e^2} \quad (1 - 3/2 \sin^2 i)$$

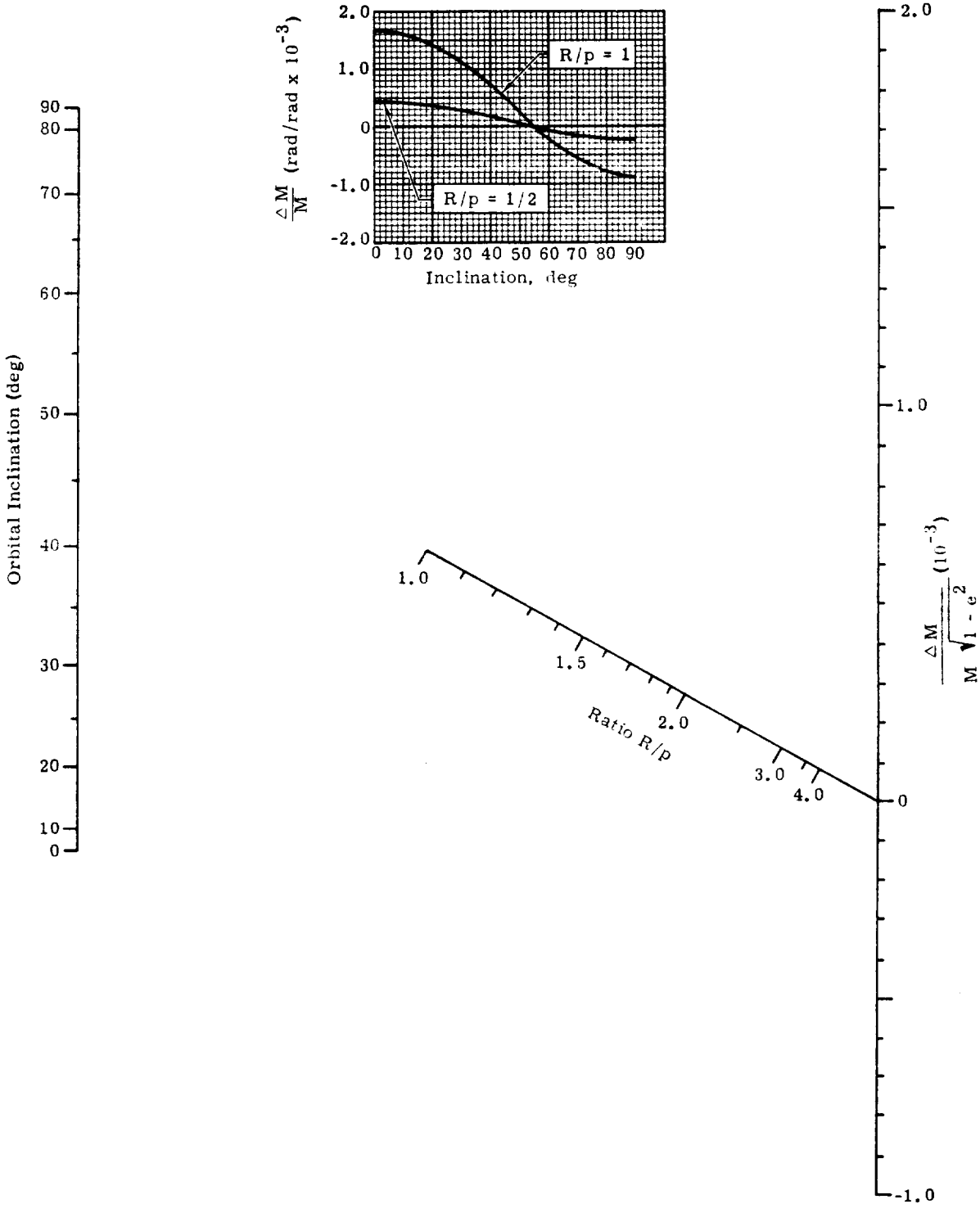

Fig. 3. Change in the Mean Anomaly Due to the Earth's Oblateness

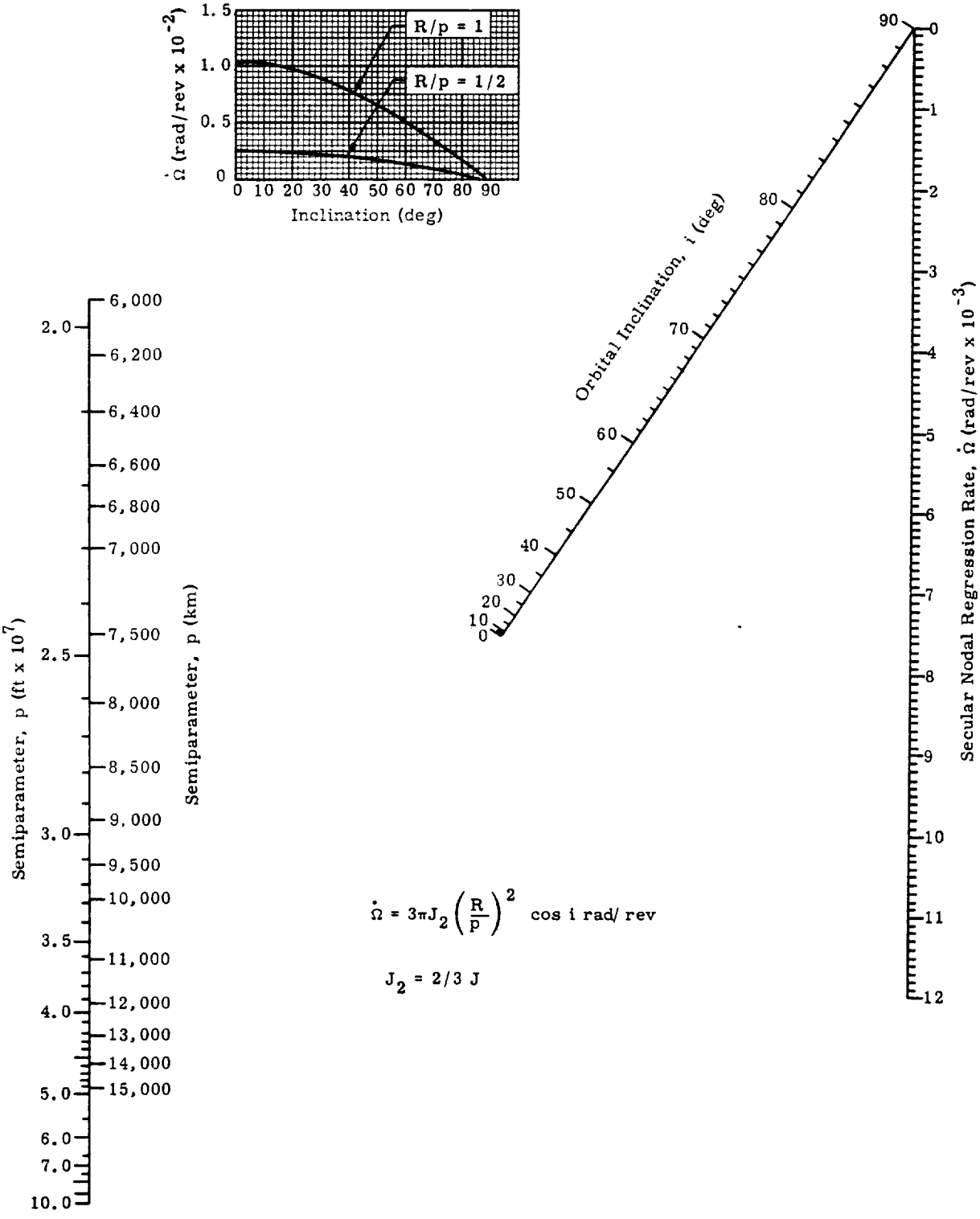

Fig. 4. Solution for the Secular Regression Rate as a Function of Orbital Inclination and the Semiparameter

$$\frac{\Delta \tau_a}{\bar{\tau}\sqrt{1 - e^2}} = \left(\frac{\tau_a}{\bar{\tau}} - 1\right)\frac{1}{\sqrt{1 - e^2}} = 3J_2\left(\frac{R}{p}\right)^2\left(\frac{3\cos^2 i - 1}{8}\right)$$

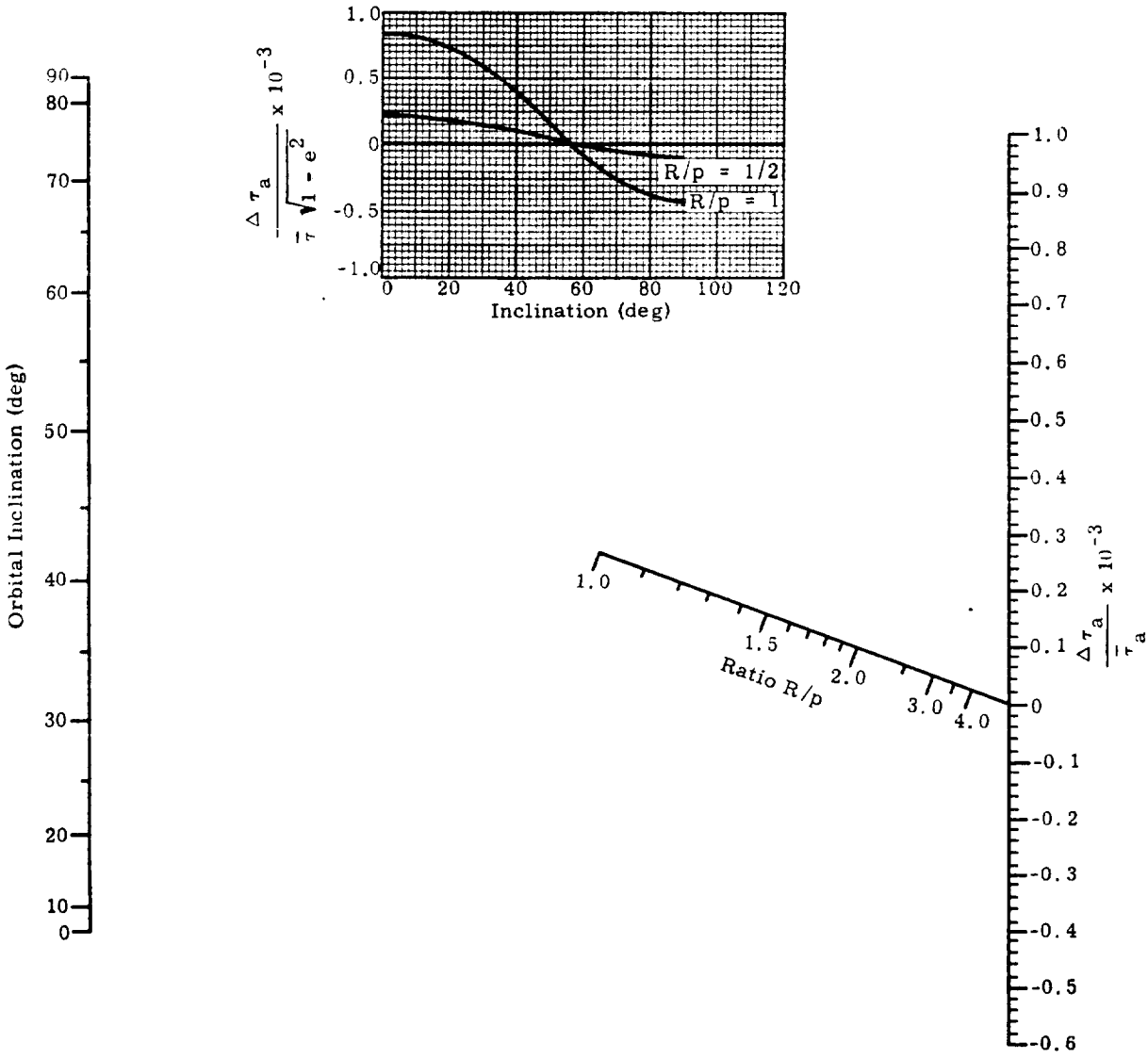

Fig. 5. Change in the Anomalistic Period Due to the Earth's Oblateness

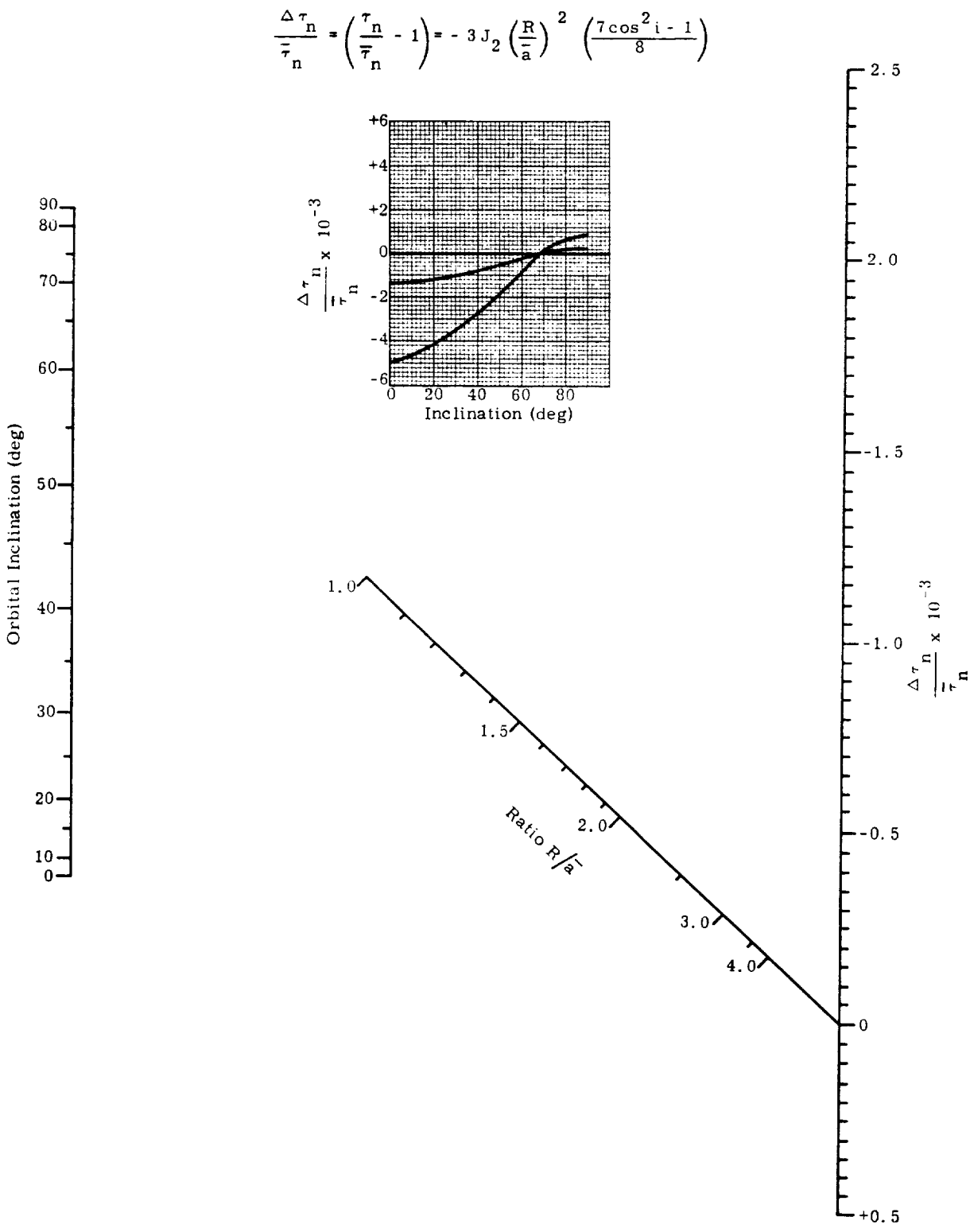

Fig. 6. Change in the Nodal Period Due to the Earth's Oblateness (for small eccentricities)

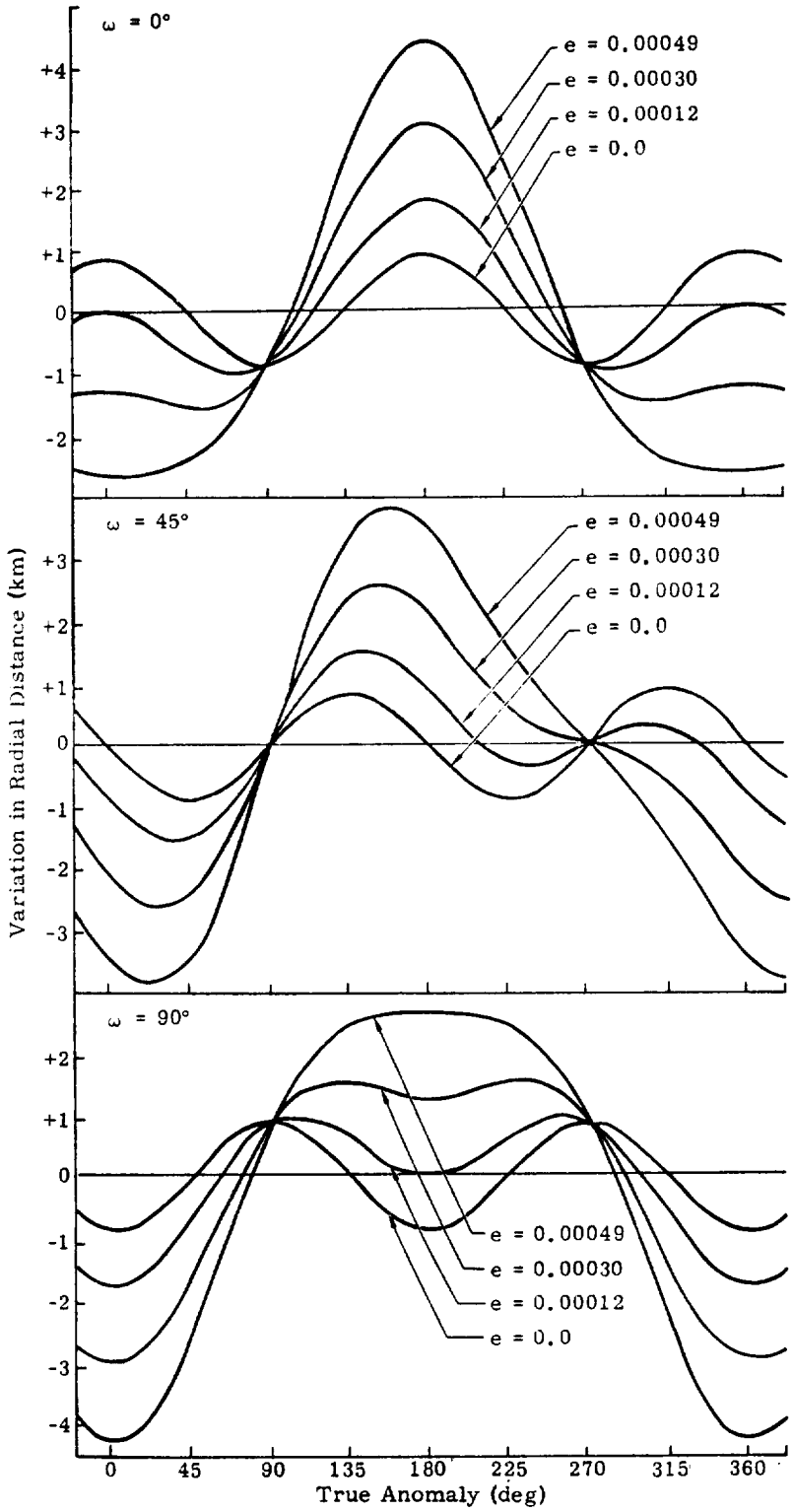

Fig. 7. The Variations of the Radial Distance as Functions of the True Anomaly, e and ω

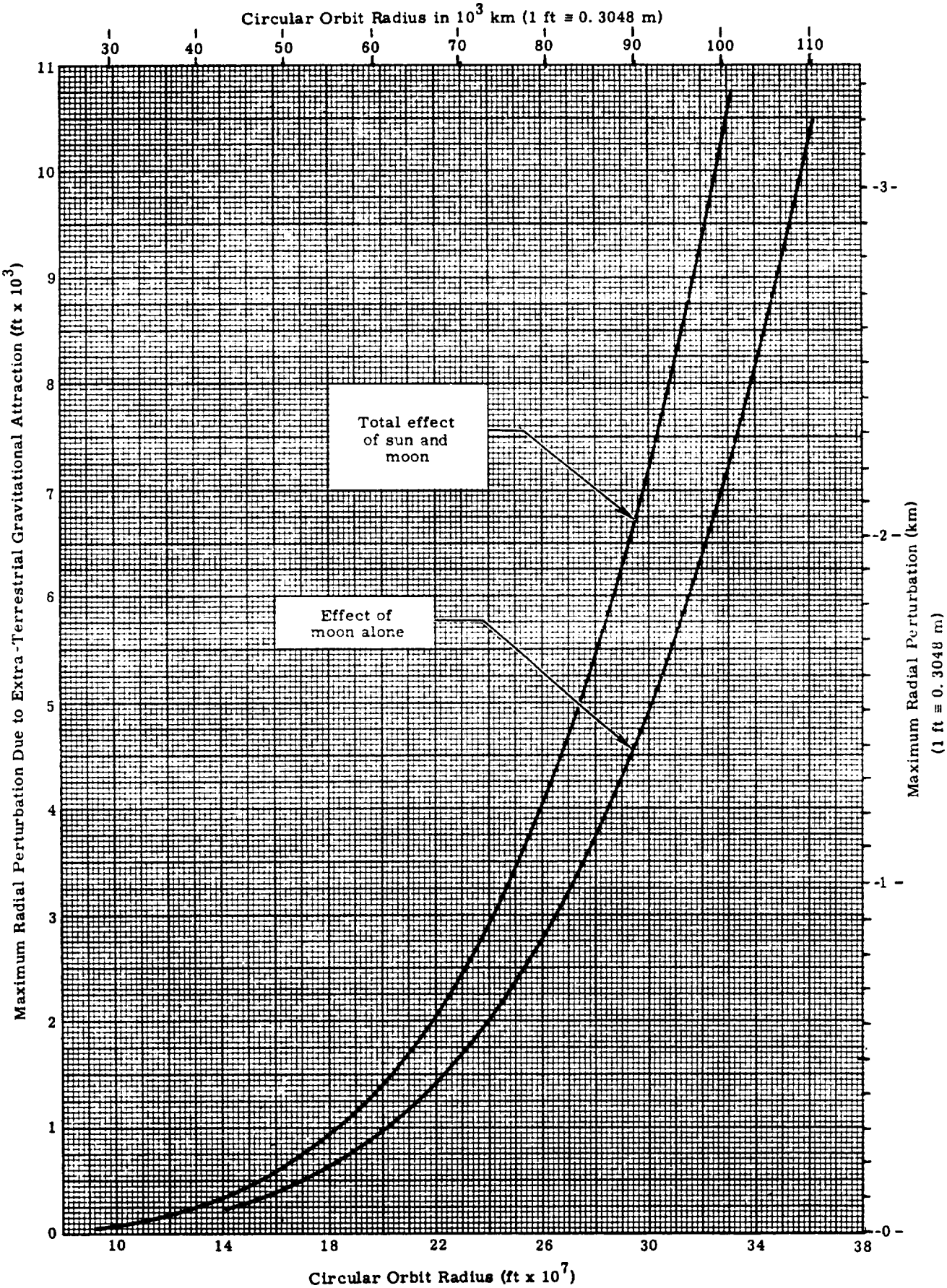

Fig. 8. Maximum Radial Perturbation Due to Attraction of the Sun and Moon

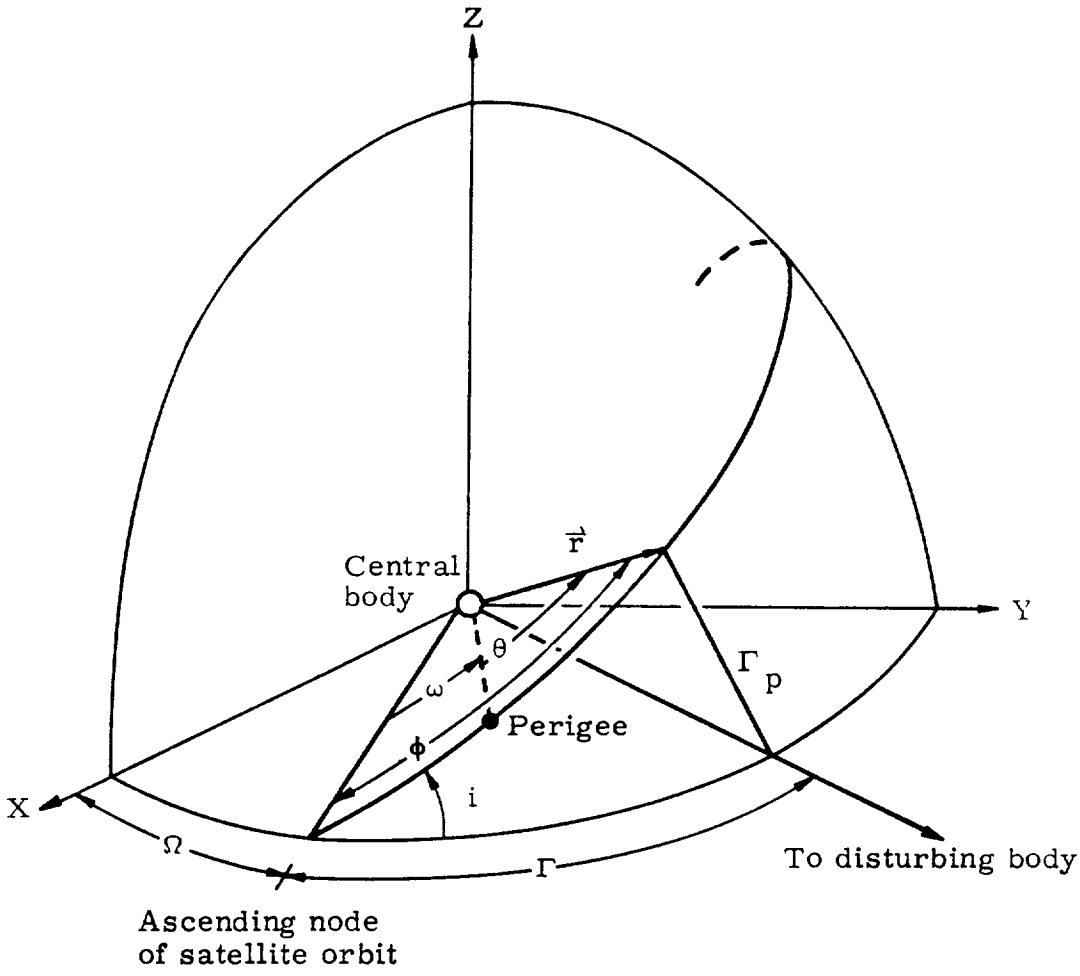

Fig. 9. Satellite Orbit Geometry

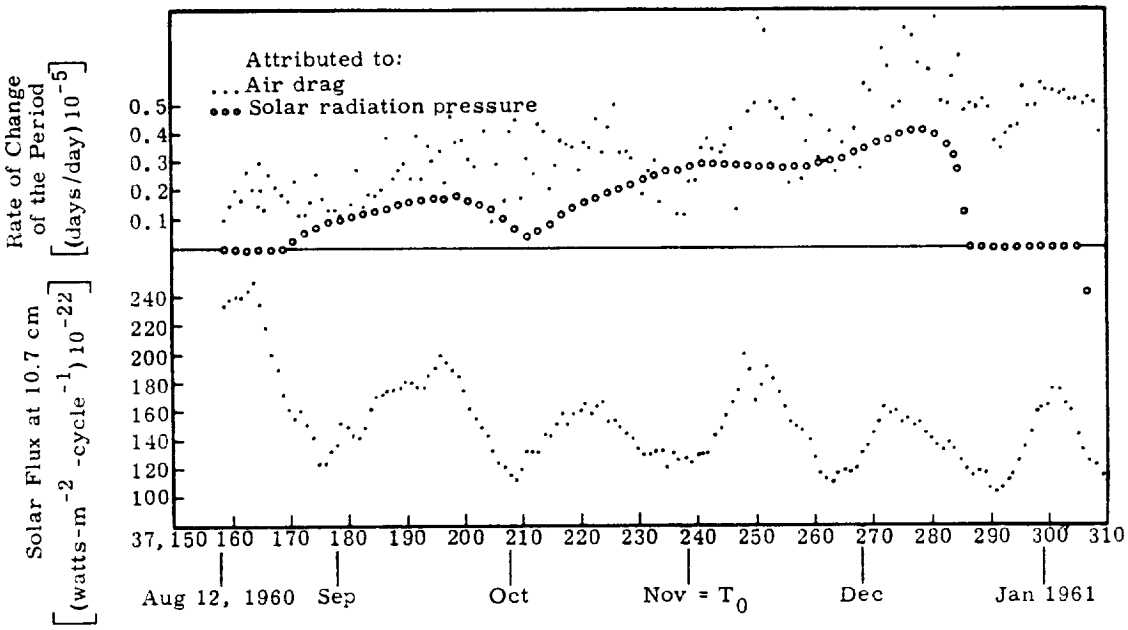

Fig. 10. Effects of Solar Activity on Echo I

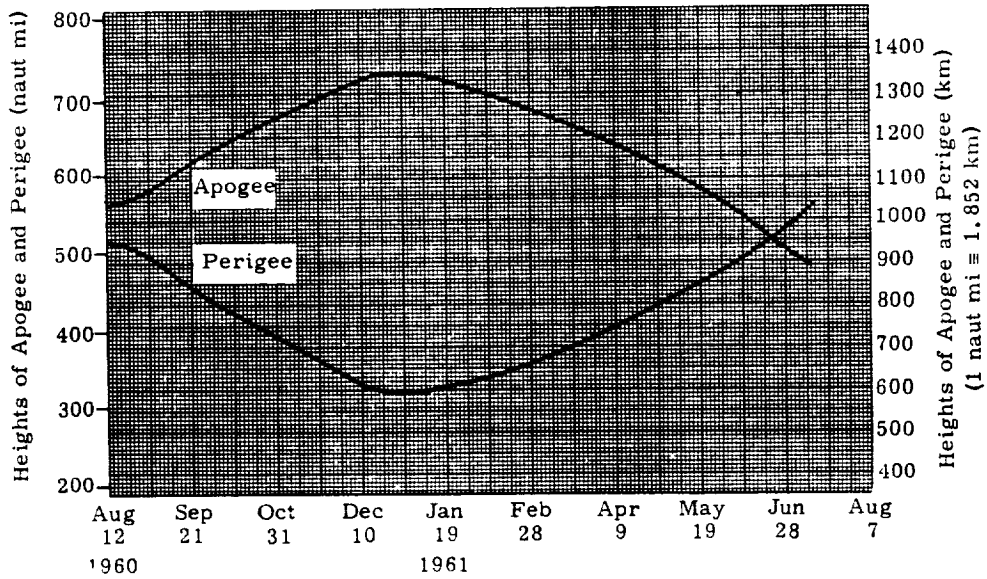

Fig. 11. Apogee and Perigee Heights on Echo I
(40-day interval)

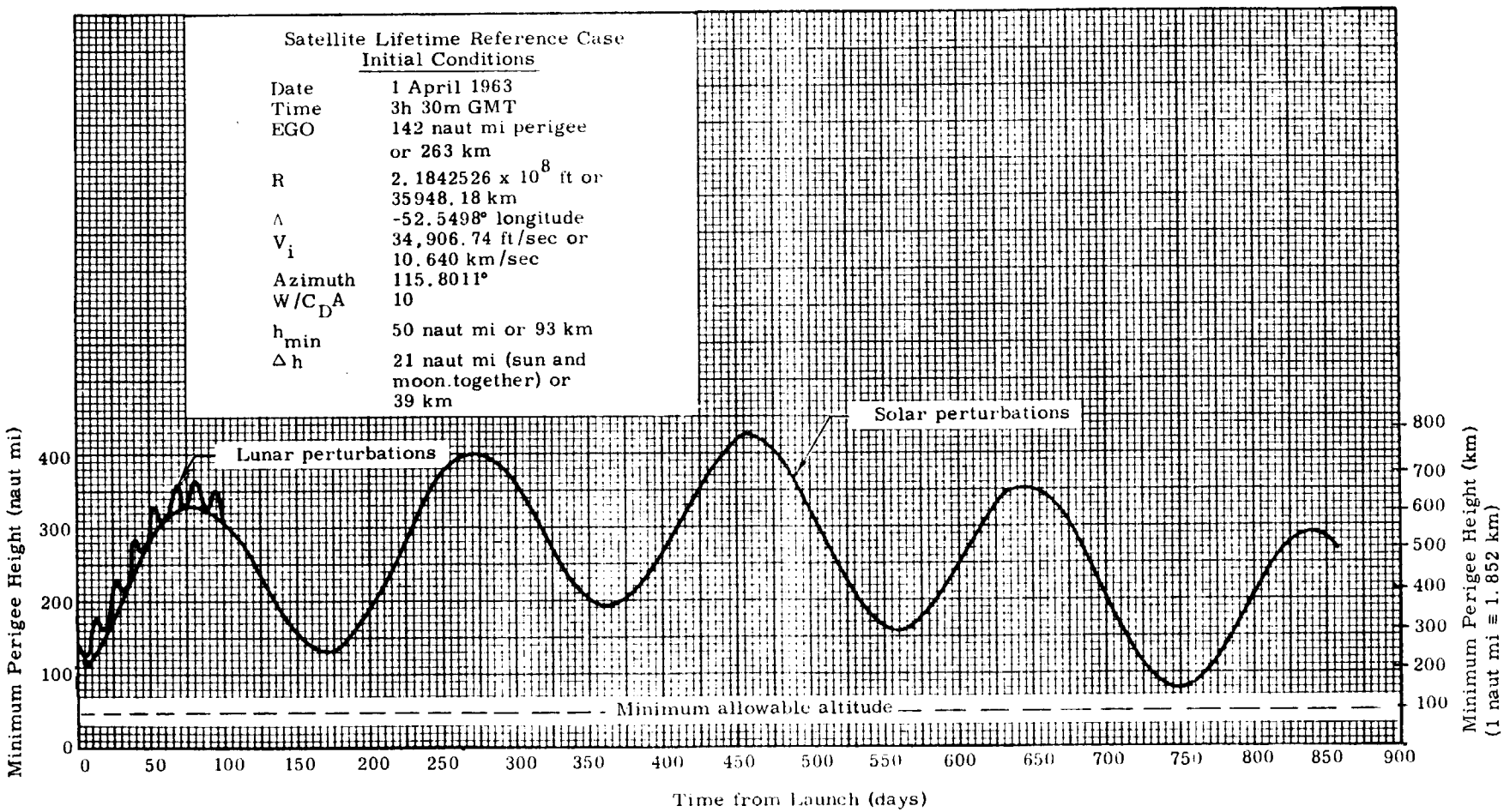

Fig. 12. Minimum Perigee Height as a Function of Days from Launch, Showing Effect of Oblateness, Drag, and Lunisolar Perturbations

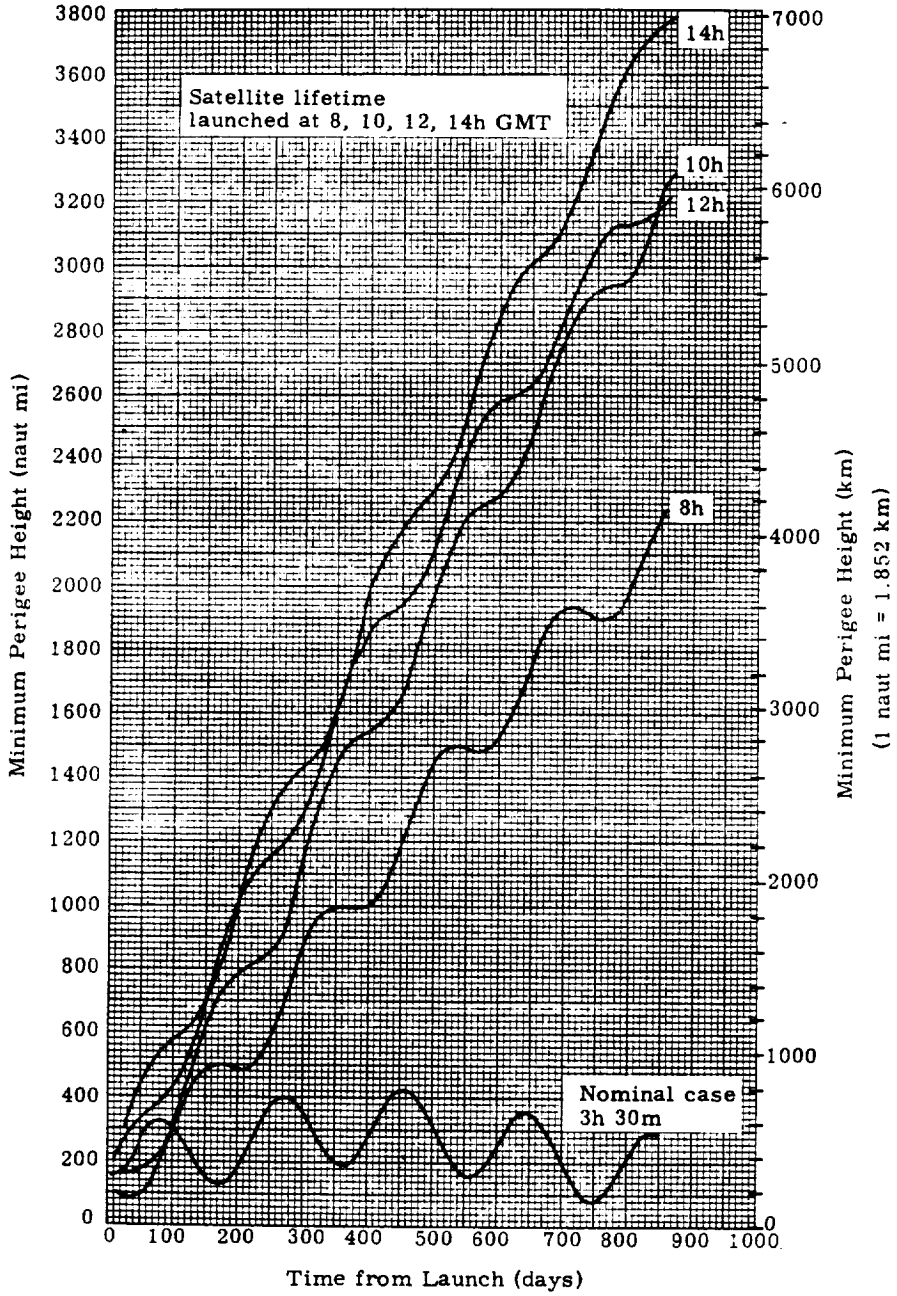

Fig. 13. Minimum Perigee Height of Satellite as a Function of Days from Launch (8 to 14 hr, expanded scale)

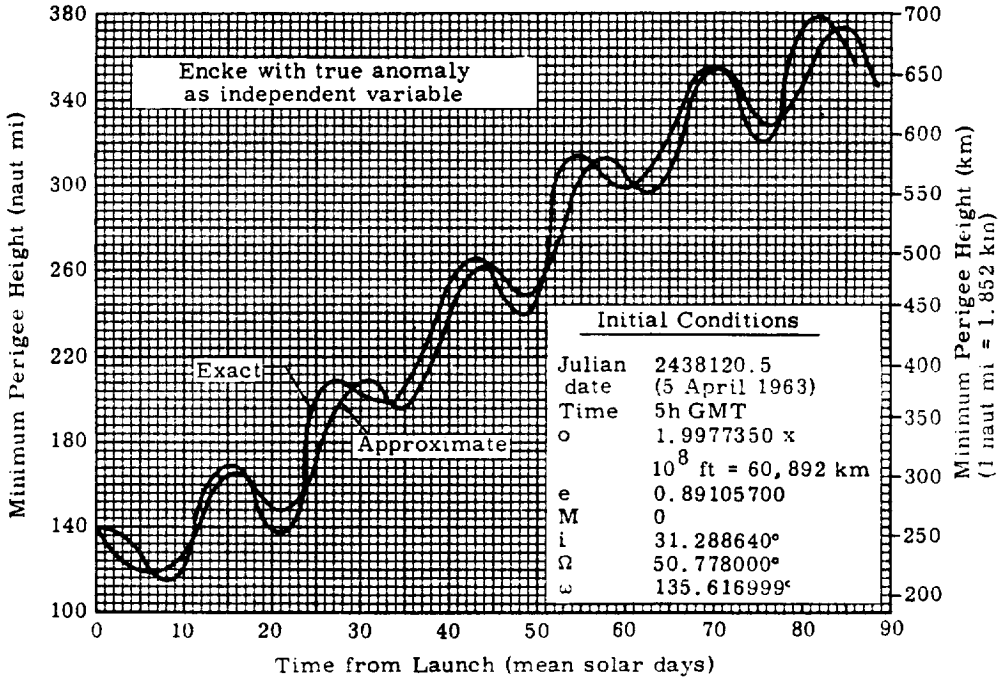

Fig. 14. Comparison of Approximate and Exact Solutions of Satellite Motions

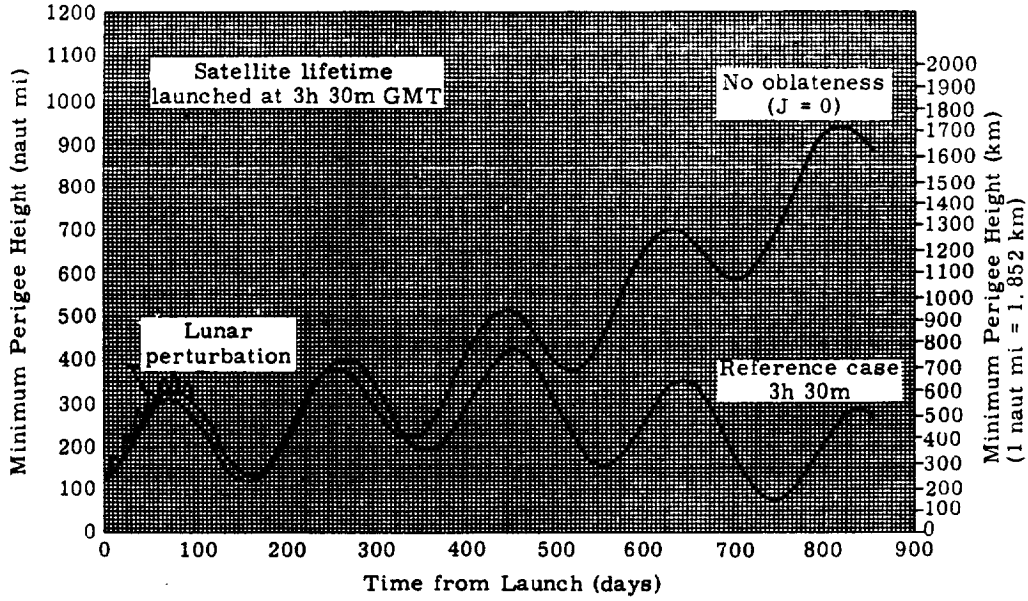

Fig. 15. Minimum Perigee Height of Satellite as a Function of Days from Launch, Showing Effect of Neglecting Oblateness

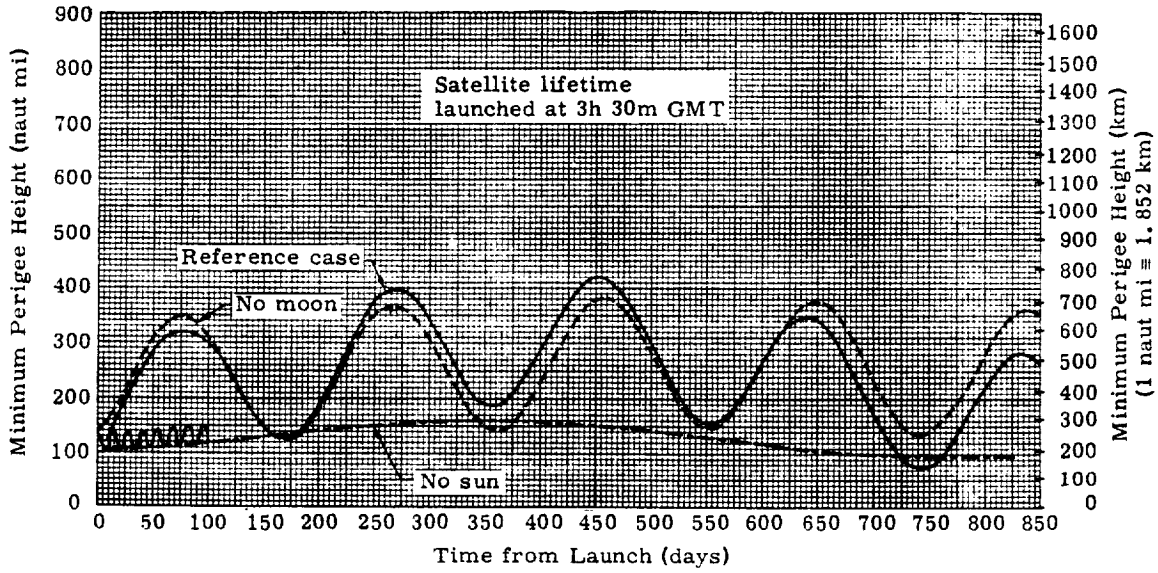

Fig. 16. Minimum Perigee Height of Satellite as a Function of Days from Launch, Showing Effect of Neglecting Moon, Sun

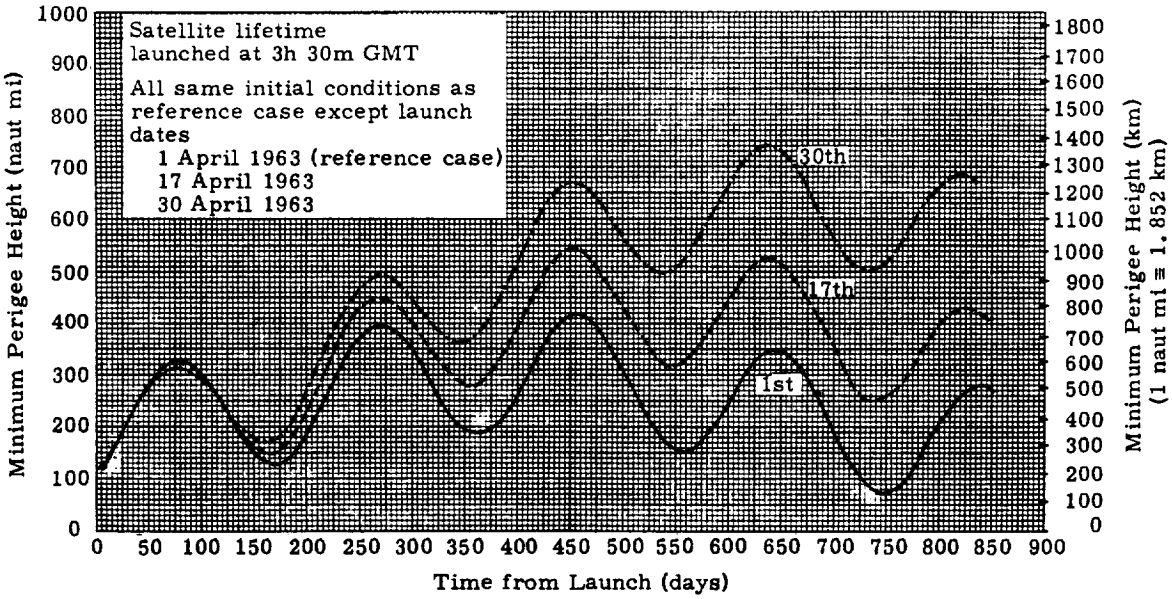

Fig. 17. Minimum Perigee Height of Satellite as a Function of Days from Launch, Showing Effect of Sun and Moon 90° Out of Phase

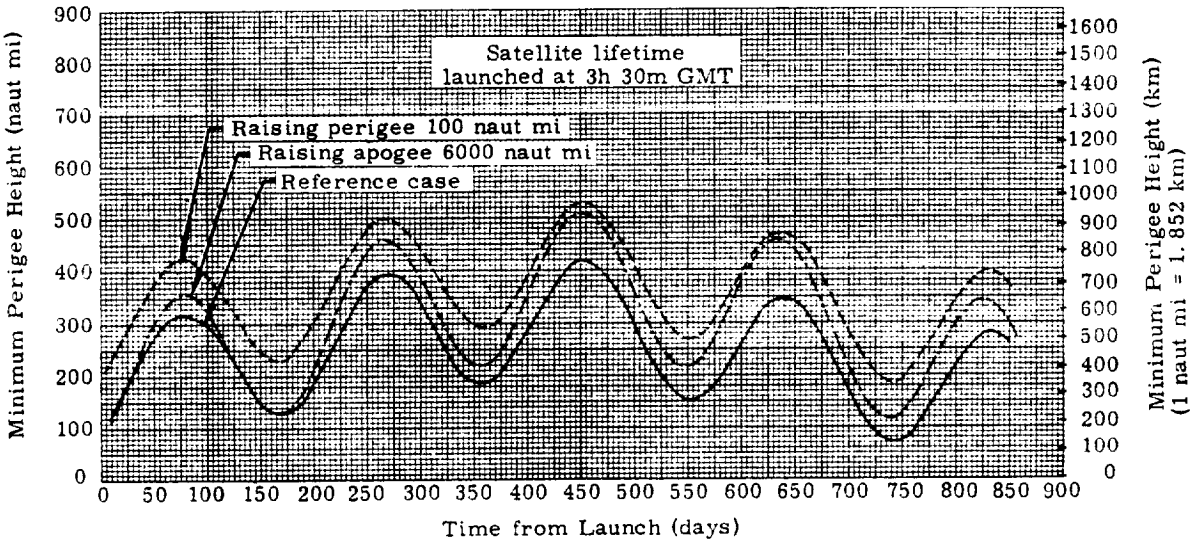

Fig. 18. Minimum Perigee Height of Satellite as a Function of Days from Launch, Showing Effect of Changing Orbit Size (Δr_{min} = 100, Δr_{max} = 6000 naut mi)

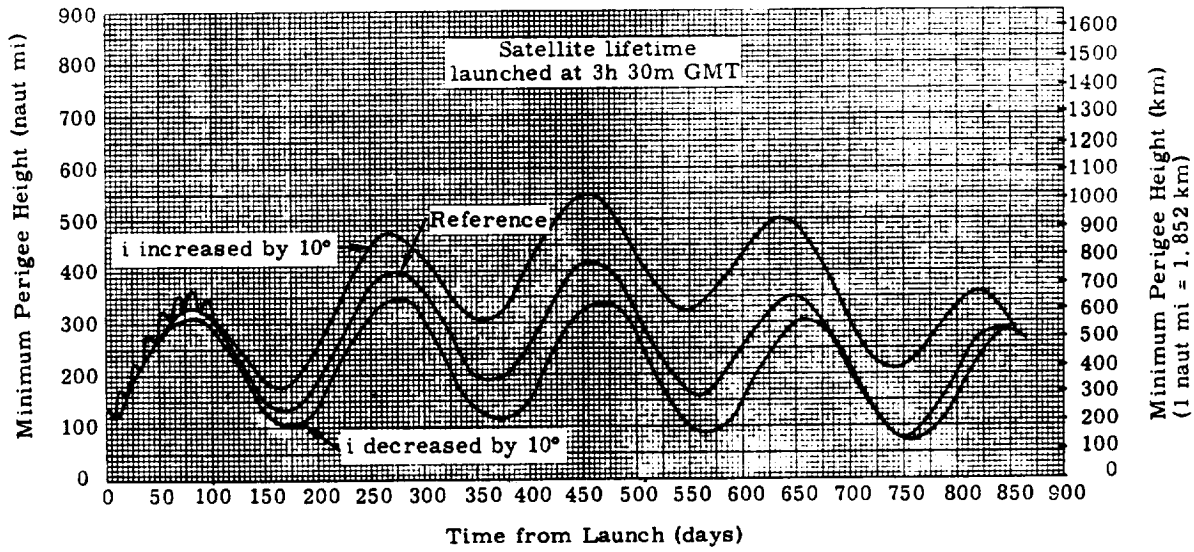

Fig. 19. Minimum Perigee Height of Satellite as a Function of Days from Launch, Showing Effect of Change in Inclination

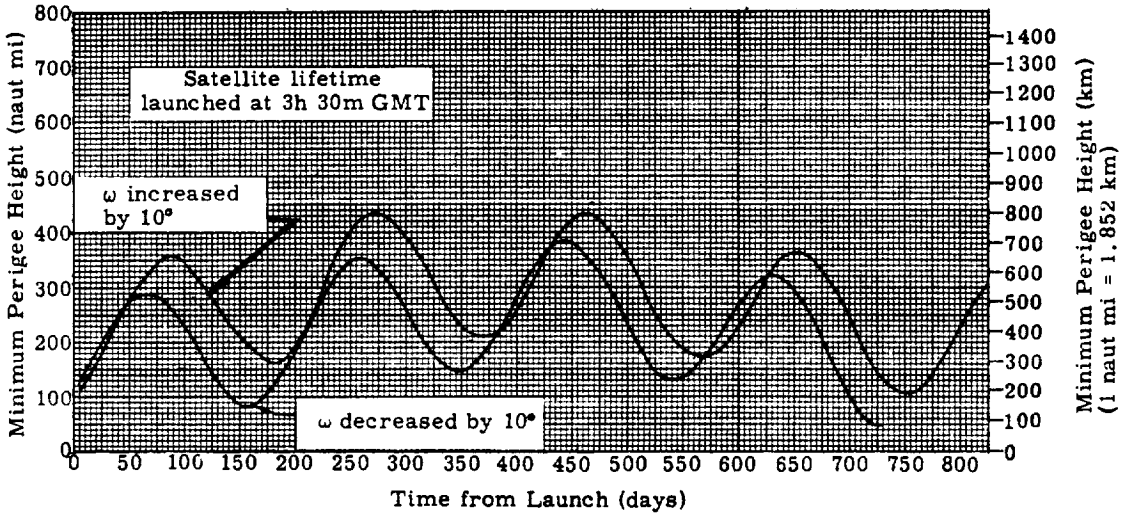

Fig. 20. Minimum Perigee Height of Satellite as a Function of Days from Launch, Showing Effect of Change in Argument of Perigee

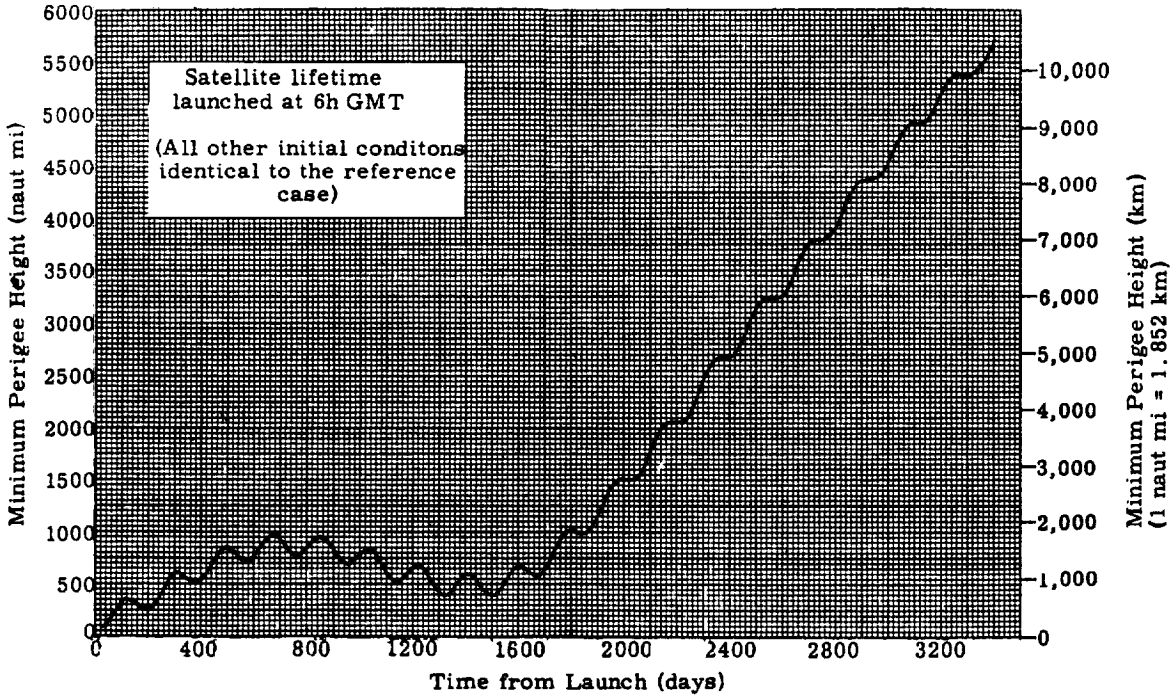

Fig. 21. Minimum Perigee Height of Satellite as a Function of Days from Launch for About a 10-Year Period

CHAPTER V

SATELLITE LIFETIMES

Prepared by:

G. E. Townsend, Jr.
Martin Company (Baltimore)
Aerospace Mechanics Department
March 1963

		Page
	Symbols	V-1
A.	Introduction	V-2
B.	The Drag Force	V-2
C.	Two-Dimensional Atmospheric Perturbations . . .	V-8
D.	Three-Dimensional Atmospheric Perturbations . .	V-21
E.	The Effects of Density Variability	V-25
F.	References	V-30
G.	Bibliography	V-30
	Illustrations	V-35

LIST OF ILLUSTRATIONS

Figure	Title	Page
1.	Drag Coefficient for a Sphere at 120 km Versus M_∞	V-37
2.	Cone Drag Coefficient, Diffuse Reflection	V-37
3.	Drag Coefficient for a Rich Circular Cylinder with Axis Normal to the Stream at 120 km Versus M_∞	V-37
4.	Comparison of Drag Coefficient of a Transverse Cylinder for Specular and Diffuse Reflection	V-38
5.	Cone Drag Coefficient, Comparison of Free Molecular and Continuum Flow Theory; $\alpha = 0$	V-38
6a.	ARDC 1959 Model Atmosphere	V-39
6b.	ARDC 1959 Model Atmosphere	V-40
7a.	Logarithmic Slope of Air Density Curve	V-41
7b.	Logarithmic Slope of 1959 ARDC Atmosphere	V-41
8.	Values of True Anomaly as a Function of Eccentricity for Which $\rho/\rho\,(h_p)$ = Constant (exponential fit to ARDC 1959 atmosphere)	V-42
9.	Nondimensional Drag Decay Parameters for Elliptic Satellite Orbits	V-43
10.	Decay Parameters P^+ and P^- for Elliptic Orbits	V-44
11a.	Apogee Decay Rate Versus Perigee Altitude	V-45
11b.	Perigee Decay Rate Versus Perigee Altitude (Part I)	V-46
11c.	Perigee Decay Rate Versus Perigee Altitude (Part II)	V-47

LIST OF ILLUSTRATIONS (continued)

Figure	Title	Page
12a.	Apogee Decay Rate Versus Perigee Altitude	V-48
12b.	Perigee Decay Rate Versus Perigee Altitude (Part I)	V-49
12c.	Perigee Decay Rate Versus Perigee Altitude (Part II)	V-50
13.	Satellite Lifetimes in Elliptic Orbits	V-51
14.	Generalized Orbital Decay Curves for Air Drag	V-52
15.	Comparison of Errors in Orbital Prediction for Correlated and Uncorrelated Atmospheric Density Fluctuation	V-53
16a.	The Ratio of the rms Error in Orbital Prediction Caused by Sinusoidal Drag Variations to the Amplitude of the Sinusoidal Variation	V-54
16b.	The Ratio of the rms Error in Orbital Prediction Caused by Sinusoidal Drag Variations to the Amplitude of the Sinusoidal Variation	V-54
16c.	The Ratio of the rms Error in Orbital Prediction Caused by Sinusoidal Drag Variations to the Amplitude of the Sinusoidal Variation	V-54
16d.	The Ratio of the rms Error in Orbital Prediction Caused by Sinusoidal Drag Variations to the Amplitude of the Sinusoidal Variation	V-54
17.	The Ratio of the rms Error in Orbital Prediction Caused by Random Drag Fluctuation from Period to Period	V-55
18.	The Ratio of the Error in Orbital Prediction Caused by Smoothed Observational Errors to the rms Error of a Single Observation	V-55

CHAPTER V. SATELLITE LIFETIMES

SYMBOLS

A	Area
a	Semimajor axis
B	Ballistic coefficient $C_D A/2m$
C_D	Drag coefficient
C_L	Lift coefficient
c_p/c_v	Ratio of specific heats
D	Drag force
E	Eccentric anomaly
E_T	Total energy
erf (x)	Error function of argument x
$F_1(z, \epsilon)$, $F_2(z, \epsilon)$	Nondimensional decay parameters
$G_1(z, \epsilon)$, $G_2(z, \epsilon)$	Nondimensional decay parameters
H	Angular momentum per unit mass
h	Altitude
$I_n(z)$	Modified Bessel function of n^{th} order
i	Orbital inclination; smoothing interval
K	Inverse of square of most probable velocity, negative log slope of atmospheric density
K_N	Knudsen number
ℓ, m, n	Direction cosines
M	Mach number
M_∞	Molecular speed ratio
m	Mass
N	Disturbing force normal to velocity in the plane of motion; number of revolutions since epoch; number of molecules hitting satellite surface.
P^+, P^-	Drag parameters for low eccentricity
p	Semilatus rectum
R	Universal gas constant; radius of the earth; radial component of disturbing force
R_N	Reynolds number
r	Radius
S	Circumferential component of disturbing force
T	Tangential component of disturbing force; temperature
T_L	Lifetime
t	Time
V	Velocity
W	Component of the disturbing force normal to plane of motion
x, y, z	Position coordinates in Cartesian coordinates
Z	Lifetime parameter $Ka\epsilon$
α	Angle of attack
β	Emissivity of surface
$\Gamma(n)$	Gamma function
γ	Flight path angle
ϵ	Eccentricity (to differentiate from base of natural logs)
θ	True anomaly; 1/2 angle of a cone
λ	Mean free path
μ	Gravitational constant for the earth = GM
Ξ	Yaw angle
ρ	Atmospheric density
σ	Stefan-Boltzmann constant; statistical variance; ratio ρ/ρ_0
τ	Orbital period
Ω	Right ascension of the ascending node
Ω_e	Rotational rate of the earth's atmosphere
ω	Argument of perigee

Subscripts

c	Circular
i	Initial incident
o	Original
p	Perigee
r	Relative
w	Wall; surface

A. INTRODUCTION

For most of the low altitude orbits for satellite payloads it is either interesting or necessary to study the effects of the atmospheric perturbations on the orbital elements of the satellite and on the lifetime. (Some material of this sort is in Chapter IV; however, the scope of the previous discussion of this subject is not adequate for the present task.) Many analytic approximations to these effects are presented in the literature; however, in obtaining these solutions approximations have been made which at times drastically restrict the validity of the results. For this reason, it is the purpose of this chapter to present not only the information but also higher order solutions to the nonlinear equations of motion for the effects of atmospheric drag. The combination of these effects with those due to gravitational accelerations, etc., will not be discussed beyond the statement that such a process requires the simultaneous utilization of special perturbations and general perturbation techniques as discussed in Chapter IV. (The present analysis, of course, falls into the latter category.) As a matter of fact, special perturbations will be utilized even in this study in the integration of the analytically determined decay rates.

It is believed that this approach is inherently more accurate than those utilizing either general or special perturbation techniques alone. It should be noted in support of this statement, that even though numerical integration of the equations of motion has become increasingly popular with the advent of faster digital computers, special perturbations have three definite limitations:

(1) Loss of numerical accuracy, if long integration times are involved (hundreds or thousands of revolutions).

(2) Long running times even with IBM 7090. or 7094.

(3) Lack of general trends, since only isolated particular cases are solved.

As an additional step to enhance the value of the results, the analysis will be conducted, where possible, carrying the density as a parameter. Thus, the final result of the study will be of value for all atmospheres. This advantage is quite significant due to the fact that the atmospheric models are constantly changing and the fact that there are seasonal and other variations (discussed in Chapter II).

In order to develop an appreciation of the material and methods of analysis, this chapter will be presented in three basic parts:

(1) The drag force.

(2) Two-dimensional atmospheric perturbations.

(3) Three-dimensional atmospheric perturbations.

B. THE DRAG FORCE

As a preface to the discussion of atmospheric perturbations, certain phenomena and techniques must be presented. These discussions will be divided into three general areas:

(1) Gaseous flow regimes.

(2) The force exerted by the atmosphere on the vehicle.

(3) Tumbling satellites.

Each of these areas will be divided in turn into discussions of the factors necessary in subsequent discussions. In particular they are slanted toward the evaluation of the quantity $\frac{C_D A}{2m}$, which will be designated the ballistic coefficient.

1. Gaseous Flow Regimes

The work in the field of aerodynamics has been divided into investigations in four general regions or flight regimes:

(1) Continuum flow.

(2) Slip flow.

(3) Transition flow.

(4) Free molecule flow.

These regimes are defined in terms of the Knudsen number:

$$K_N = \frac{\lambda}{\ell} = \frac{\text{mean free path}}{\text{characteristic length of body}}$$

$$= \sqrt{\frac{\pi}{2}\frac{c_p}{c_v}}\,\frac{M}{R_N} \quad \text{for small } R_N \text{ (Ref. 1)}$$

$$\approx \frac{M}{R_N} \quad \text{for large } R_N$$

where

c_p/c_v = ratio of specific heats

M = Mach number

$$= \frac{V}{\sqrt{\frac{c_p}{c_v} g RT}}$$

R_N = Reynolds number

Though there is overlap of the regions, and though no truly definitive numerical values of K_N for these regions exist, generally accepted values for the four flight regimes are:

Continuum flow--$K_N < 0.01$.

Slip flow--$0.01 < K_N < 0.1$.

Transition flow--$0.1 < K_N < 10$.

Free molecule flow--$10 < K_N$.

These flow regimes are illustrated in the following sketch (Ref. 1):

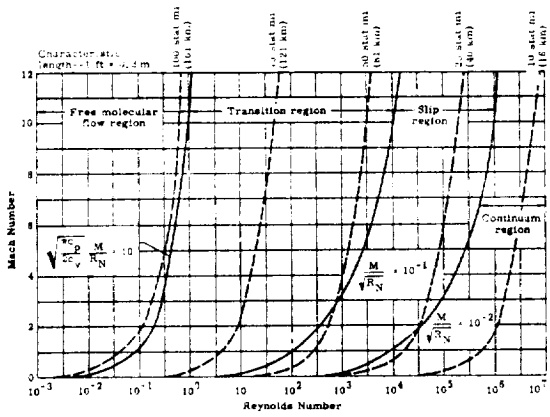

It is noted that in addition to the defining lines mentioned above, a second set of lines denoting altitude is also included on this figure. It is also noted that for any satellite above the altitude of 100 stat mi (161 km), the flow is always free molecule and that free molecule flow could be considered to extend down to as low as 75 stat mi (121 km) without introducing significant errors in the analysis. Since this region (121 to 161 km) is the lowest possible altitude for even moderate durations in orbit, the entire lifetime analysis can be conducted, based on the assumption of free molecule flow. This assumption, however, makes it necessary in subsequent calculations to stop the decay analysis or integration at the aforementioned altitude of 120 km (≈400,000 ft). At this altitude the mean free path is 20.49 ft (6.25 meters); thus the Knudsen number for all but extremely large vehicles is such that the analyses will be valid.

2. The Force Exerted by the Atmosphere on the Vehicle

In order to determine the drag coefficients analytically it is necessary to study the mechanism by which the force is exerted on the satellite. This step will be accomplished in the following analyses utilizing the work reported in Ref. 2 as the basis for the discussions.

Let $\dot{x}'$, $\dot{y}'$ and $\dot{z}'$ be the velocity components of a molecule of gas relative to the mean velocity of the gas. In addition, assume that the distribution of these velocities is normal--i.e., that the number of molecules with velocities in the region $\dot{x}$ to $\dot{x} + d\dot{x}$, etc., is

$$dN = N_0 \left(\frac{K}{\pi}\right)^{3/2} \exp\left[-K\left(\dot{x}'^2 + \dot{y}'^2 + \dot{z}'^2\right)\right] d\dot{x}'\, d\dot{y}'\, d\dot{z}'$$

where

N_0 = the number of molecules per unit volume

K = the reciprocal of the square of the most probable velocity = $\frac{1}{2RT}$

R = universal gas constant

T = absolute temperature

These molecules impact on a surface whose velocity components in the same coordinate system are ℓV, mV, nV (ℓ, m and n being the direction cosines for V). Thus, the velocity relative to the surface is

$$\dot{x} = \dot{x}' - \ell V$$
$$\dot{y} = \dot{y}' - mV$$
$$\dot{z} = \dot{z}' - nV$$

and the distribution of the impacting molecules with velocities $\dot{x} + \ell V$ to $\dot{x} + \ell V + d\dot{x}$, etc., is:

$$dN = N_0 \left(\frac{K}{\pi}\right)^{3/2} \exp\left\{-K\left[(\dot{x} + \ell V)^2 + (\dot{y} + mV)^2 + (\dot{z} + nV)^2\right]\right\} d\dot{x}\, d\dot{y}\, d\dot{z}$$

It is noted at this point that while either positive or negative values of $\dot{y}$ and $\dot{z}$ are permissible, only negative values of $\dot{x}$ will yield impacts; thus the total number of particles of all velocities hitting the surface is

$$N = -N_0 \left(\frac{K}{\pi}\right)^{3/2} \int_{-\infty}^{0} d\dot{x} \int_{-\infty}^{\infty} d\dot{y} \int_{-\infty}^{\infty} \exp\{-K\left[(\dot{x} + \ell V)^2 + (\dot{y} + mV)^2 + (\dot{z} + nV)^2\right]\} \dot{x}\, dz$$
$$= \frac{N_0}{2\sqrt{\pi K}} e^{-\ell^2 V^2 K} + \frac{N_0 \ell V}{2}\left[1 + \operatorname{erf}(\ell V \sqrt{K})\right]$$

where

$$\operatorname{erf}(\ell V \sqrt{K}) = \frac{2}{\sqrt{\pi}} \int_0^{\ell V \sqrt{K}} e^{-s^2} ds$$

At this point it is possible to relate the number of particles hitting the plate to the mass and hence to the momentum transferred. The force acting on the surface is the integral of the momenta

imparted by the molecules for all possible velocities. Assuming for the moment that complete energy transfer is made and that the direction cosines of the stream are ℓ', m' and n', this pressure on the surface is:

$$p = -\rho\left(\frac{K}{\pi}\right)^{3/2}\int_{-\infty}^{0} d\dot{x}\int_{-\infty}^{\infty} d\dot{y}\int_{-\infty}^{\infty}\dot{x}(\ell'\,\dot{x} + m'\,\dot{y} + n'\,\dot{z})\exp\left\{-K\left[(\dot{x}+\ell V)^2 + (\dot{y}+mV)^2 + (\dot{z}+nV)^2\right]\right\} d\dot{z}$$

$$= -\rho\frac{V^2}{2}\left\{\frac{1}{V\sqrt{\pi K}}(\ell\ell' + mm' + nn')\,e^{-\ell^2 V^2 K} + \left[\frac{\ell'}{2K V^2} + \ell(\ell\ell' + mm' + nn')\right]\cdot\left[1 + \text{erf}(\ell\, V\sqrt{K})\right]\right\}$$

This estimate is not correct, however, because of the molecules impacting the surface. Some are reflected specularly (i.e., according to Snell's law), while the others are temporarily absorbed and reflected diffusely (i.e., in random directions) at a later time. For specular reflection, the effective pressure is thus,

$$p_{eff} = 2\,p$$

while for diffuse reflection, the equation remains unaltered. Thus, the two types of reflection bracket the actual process and the true force can be written

$$p = (2 - f)\,p_{incident} + f\,p_{reflected}$$

where

f is the fraction of the total molecules which is diffusely reflected. (Experiment indicates the value lies in the range $0.9 < f < 1.0$.)

At this point attention is turned to the computation of the drag and lift coefficients, defined as follows:

$$C_D A = \frac{D}{\frac{1}{2}\rho V^2} = \frac{\int p_D\, dA}{\frac{1}{2}\rho V^2}$$

$$C_L A = \frac{L}{\frac{1}{2}\rho V^2} = \frac{\int p_L\, dA}{\frac{1}{2}\rho V^2}$$

Since dA is a function of geometry and orientation, these coefficients can be defined for various shapes. The succeeding paragraphs present data for C_D both for specular and diffuse reflection (see Ref. 2). Note is made that the surface temperature, which is calculable as a function of the same set of variables, has been included in the diffuse results. The derivations are in themselves not unique or necessary for this discussion; thus, only the final forms will be presented. Additional material may be found in the reference and in the literature.

Sphere ($A = \pi r^2$)

$$\text{Specular } C_D = \text{erf}(M_\infty)\left[2 + \frac{2}{M_\infty^2} - \frac{1}{2M_\infty^4}\right] + \frac{e^{-M_\infty^2}}{\sqrt{\pi}}\left[\frac{1}{M_\infty^3} + \frac{2}{M_\infty}\right] \quad (1a)$$

$$\text{Diffuse } C_D = C_{D_{specular}} + \left(\frac{2\sqrt{\pi}}{3M_\infty}\right)\sqrt{\frac{T_w}{T_i}} \quad (1b)$$

where T_w is the surface temperature obtained by iterating the following equation:

$$T_w\left(\frac{8\sqrt{K}\,\beta\,\sigma\,T_w^3}{3\rho R\,\phi} + 1\right) = T_i\left(\frac{5}{3} + \frac{2}{3}M_\infty^2\right)$$

M_∞ = speed ratio $= \dfrac{V}{\sqrt{2RT}}$

T_i = temperature of incident stream

β = surface emissivity

σ = Stefan-Boltzmann constant

$\phi = \int_{\text{surface}} \rho N$

$= \dfrac{e^{-M_\infty^2}}{\sqrt{\pi}} + \text{erf}(M_\infty)\left(M_\infty + \dfrac{1}{2M_\infty}\right)$ for a monatomic atmosphere of oxygen and nitrogen in the shadow.

Since the properties of the atmosphere are integrally associated with this evaluation of these coefficients only specific data can be generated for C_D. An example of the application is presented in Fig. 1. This figure, obtained from Ref. 2, presents C_D as a function of M_∞ and for an altitude of 120 km. Though computations for this figure were made with atmospheric data available in 1949, the variations which are shown are representative and the limiting values, which are rapidly approached, valid for this reference altitude. Data for other altitudes must be generated as needed.

Flat plate at angle of attack α to the flow ($A = ab$)

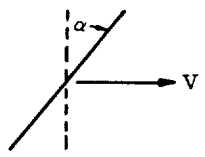

For this body configuration the drag coefficients vary according to the following equations:

$$\text{Specular } C_D = \frac{4 \sin^2 \alpha}{M_\infty \sqrt{\pi}} e^{-M_\infty^2 \sin^2 \alpha} + \left(\frac{2 \sin \alpha}{M_\infty^2} + 4 \sin^3 \alpha \right) \text{erf} (M_\infty \sin \alpha) \quad (2a)$$

$$\text{Diffuse } C_D = \frac{2}{M_\infty \sqrt{\pi}} e^{-M_\infty^2 \sin^2 \alpha} + 2 \sin \alpha \left(1 + \frac{1}{2 M_\infty^2} \right) \text{erf} (M_\infty \sin \alpha) + \frac{\sqrt{\pi} \sin^2 \alpha}{M_\infty} \sqrt{\frac{T_w}{T_i}} \quad (2b)$$

where T_w is obtained from

$$\beta \sigma T_w^4 \approx \rho \frac{N}{N_0} \left[\frac{1}{2} V^2 + \frac{5}{2} R T_i - \frac{3}{2} R T_w \right] \sin \alpha$$

Cone with axis parallel to flow ($A = \pi r^2$)

$$\text{Specular } C_D = \frac{2 \sin \theta}{M_\infty \sqrt{\pi}} e^{-M_\infty^2 \sin^2 \theta} + \left(\frac{1}{M_\infty} + 2 \sin^2 \theta \right) [1 + \text{erf} (M_\infty \sin \theta)] \quad (3a)$$

$$\text{Diffuse } C_D = \left[\frac{1}{M_\infty \sin \theta \sqrt{\pi}} + \frac{1}{2 M_\infty^2} \sqrt{\frac{T_w}{T_i}} \right] e^{-M_\infty^2 \sin^2 \theta} + \left[1 + \frac{1}{2 M_\infty^2} + \frac{\sin \theta \sqrt{\pi}}{2 M_\infty} \sqrt{\frac{T_w}{T_i}} \right] \left[1 + \text{erf} (M_\infty \sin \theta) \right] \quad (3b)$$

where T_w is obtained from

$$T_w \left(\frac{4 \sqrt{\pi K} \beta \sigma T_w^3}{3 \rho R \phi} + 1 \right) = T_i \left(1 + \frac{2}{3} M_\infty^2 \right)$$

and where θ is the half angle of the cone. These results can be extended to nonzero incidence angles by utilizing the flat-plate results mentioned earlier. Such calculations are presented graphically in Fig. 2 (Ref. 3).

Right circular cylinder with axis perpendicular to flow ($A = 2 r L$)

$$\text{Specular } C_D = \frac{2}{M_\infty} \sum_{M=\infty}^{\infty} (-1)^n \frac{M_\infty^{2n} \Gamma\left(\frac{2n+3}{2}\right)}{n! \, \Gamma(n+2)} + \frac{1}{M_\infty} \sum_{n=0}^{\infty} (-1)^n \frac{M_\infty^{2n} \Gamma\left(\frac{2n+1}{2}\right)}{n! \, \Gamma(n+2)} + \sqrt{\frac{\pi}{3}} \sum_{n=0}^{\infty} (-1)^n \frac{M_\infty^{2n}}{n!} \left\{ \frac{\Gamma\left(\frac{2n+3}{2}\right)}{\Gamma(n+3)} + \frac{2 \Gamma\left(\frac{2n+1}{2}\right)}{\Gamma(n+2)} \right\} \quad (4a)$$

$$\text{Diffuse } C_D = \frac{1}{M_\infty} \sum_{n=0}^{\infty} (-1)^n \frac{M_\infty^{2n} \Gamma\left(\frac{2n+1}{2}\right)}{n! \, \Gamma(n+1)} + \frac{\pi^{3/2}}{4 M_\infty} \sqrt{\frac{T_w}{T_i}} + \left(M_\infty + \frac{1}{M_\infty} \right) \sum_{n=0}^{\infty} (-1)^n \frac{M_\infty^{2n}}{n!} \frac{\Gamma\left(\frac{2n+1}{2}\right)}{\Gamma(n+2)} \quad (4b)$$

where T_w is computed from

$$\frac{\pi \beta \sigma \sqrt{K} T_w^4}{\rho R} = \frac{T_i}{2} \left[M_\infty^2 + \frac{3}{2} \left(\frac{5}{3} - \frac{T_w}{T_i} \right) \right] \left\{ \sum_{n=0}^{\infty} (-1)^n \frac{M_\infty^{2n}}{n!} \frac{\Gamma\left(\frac{2n+1}{2}\right)}{\Gamma(n+1)} + M_\infty^2 \sum (-1)^n \frac{M_\infty^{2n}}{n!} \frac{\Gamma\left(\frac{2n+1}{2}\right)}{\Gamma(n+2)} \right\}$$

Figure 3 presents data comparable to that discussed in conjunction with the sphere. Of particular interest is the fact that this coefficient approaches a limit which is not unlike that of the sphere.

Circular-arc ogive ($A = \pi r^2$)

This figure is constructed by rotating an arc of a circle about its chord then cutting the body of revolution perpendicular to the axis at its midpoint. The angle of the nose (2θ) analogous to the half angle of the cone is utilized to describe the shape.

$$\text{Specular } C_D = \frac{1}{1 - \cos \theta} \left\{ \left[\frac{4}{3} + \frac{1}{M_\infty^2} \right] (1 - \cos \theta) - \frac{2 \theta^2}{3} \cos \theta + \frac{e^{-M_\infty^2 \theta^2}}{\sqrt{\pi}} \left[\frac{\theta}{4 M_\infty^3} + \frac{\theta^3}{2 M_\infty} \right] + \text{erf} (M_\infty \theta) \left[\frac{\theta^4}{2} + \frac{\theta^2}{2 M_\infty^2} - \frac{1}{8 M_\infty^4} \right] \right\} \quad (5a)$$

$$\text{Diffuse } C_D = \frac{1}{1-\cos\theta}\left\{\left(1+\frac{1}{2M_\infty^2}\right)(1-\cos\theta)\right.$$

$$+\operatorname{erf}(M_\infty\theta)\left[\frac{\theta^2}{2}+\frac{\theta^2+1}{4M_\infty^2}-\frac{1}{8M_\infty^4}\right]$$

$$+\frac{e^{-M_\infty^2\theta^2}}{\sqrt{\pi}}\left[\frac{\theta}{2M_\infty}+\frac{\theta^3\sqrt{\pi}}{4M_\infty^3}\right]$$

$$+\sqrt{\frac{T_w}{T_i}}\left[\frac{1}{12M_\infty^4}+\frac{\theta^3\sqrt{\pi}}{6M_\infty}\left(1+\operatorname{erf}(M_\infty\theta)\right)\right.$$

$$\left.\left.+e^{-M_\infty^2\theta^2}\left(\frac{\theta^2}{6M_\infty^2}-\frac{1}{12M_\infty^4}\right)\right]\right\} \quad (5b)$$

where T_w is obtained from

$$\beta\sigma T_w^4 \approx \frac{\rho N}{N_0}\left[\frac{1}{2}V^2+\frac{5}{2}RT_i-\frac{3}{2}RT_w\right]\sin\frac{\theta}{2}$$

To provide a feel for the validity of these results, tests have been performed (Refs. 3 and 4) and data prepared for the transverse right circular cylinder. The results of these tests are shown in Figs. 4 and 5. These figures depict the variation in the critical region for molecular speed ratios in the vicinity of 0.7 to 2.5. The agreement between these data and the theoretical values is observed to be very good. Also noted is the tendency for the results to agree better at higher values of the speed ratio with the specular reflection theory than with the diffuse theory and vice-versa at the lower speeds.

3. Tumbling Satellites

The preceding discussions have presented data for bodies fixed relative to the flow field. However, in most satellite applications this is not the case. The first class of such exceptions consists of those satellites which by design orient themselves relative to the earth or space in order to perform some mission. The time history of attitude for this vehicle is thus known, and a time history of the drag coefficient can be constructed. The second class of vehicles consists of those which tumble in both time and space, thus complicating their aerodynamic description. One path around this impasse is to describe the parameters statistically and assume that they are independently distributed. This approach, while not rigorous for either class of exception, provides a convenient means of computation for the latter case and an approximate method for long time intervals in the former case. Consider the following sketches.

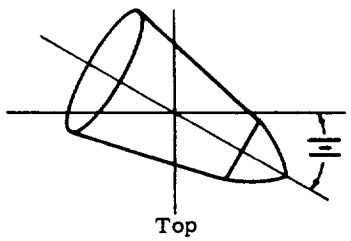

Top

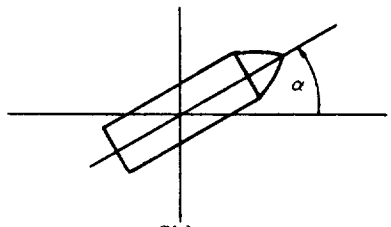

Side

Now approximating the effective drag coefficient based on one of the surfaces (say A_1)

$$C_D^* = C_{D_1}\cos\alpha\cos\Xi + C_{D_2}\frac{A_2}{A_1}\cos\Xi\sin\alpha$$

$$+C_{D_3}\frac{A_3}{A_1}\cos\alpha\sin\Xi + C_{D_4}\frac{A_4}{A_1}\sin\alpha\sin\Xi$$

where α and Ξ are uniformly randomly selected variates always lying in the range 0 to $\pi/2$

C_D^* is the affective drag coefficient for the body

A_n is the reference area for the nth geometrical shape

Since the distributions of α and Ξ are known (the joint density function is $\left(\frac{2}{\pi}\right)^2$), it is desired to determine the distribution of the function C_D^*. This is accomplished as follows:

$$g(C_D^*, \alpha) = f\left[\alpha, \Xi(C_D^*, \alpha)\right]\left|\frac{\partial\Xi}{\partial C_D^*}\right|$$

but $\Xi(C_D^*, \alpha)$ must be obtained from

$$C_D^* = a_1\cos\Xi + a_2\sin\Xi$$

$$= a_3\cos(\Xi - w)$$

where

$$a_1 = C_{D_1}\cos\alpha + C_{D_2}\frac{A_2}{A_1}\sin\alpha$$

$$a_2 = C_{D_3}\frac{A_3}{A_1}\cos\alpha + C_{D_4}\frac{A_4}{A_1}\sin\alpha$$

$$\left.\begin{aligned} a_3\cos w &= a_1 \\ a_3\sin w &= a_2 \end{aligned}\right\} \quad \text{or} \quad \begin{aligned} w &= \tan^{-1}(a_2/a_1) \\ a_3 &= \sqrt{a_1^2+a_2^2} \end{aligned}$$

thus

$$\Xi = \cos^{-1}\left(\frac{C_D^*}{a_3}\right) + w$$

also

$$\frac{\partial\Xi}{\partial C_D^*} = \left[-a_1\sin\Xi + a_2\cos\Xi\right]^{-1}$$

or,

$$\frac{\partial \Xi}{\partial C_D^*} = \left\{ -a_1 \sin\left[\cos^{-1}\left(\frac{C_D^*}{a_3}\right) + w\right] + a_2 \cos\left[\cos^{-1}\left(\frac{C_D^*}{a_3}\right) + w\right]\right\}^{-1}$$

$$= \left[\left[-a_1 \left\{ \sin\left[\cos^{-1}\left(\frac{C_D^*}{a_3}\right)\right] \cos w + \frac{C_D^*}{a_3} \sin w \right\} + a_2 \left\{ \frac{C_D^*}{a_3} \cos w - \sin\left[\cos^{-1}\left(\frac{C_D^*}{a_3}\right)\right] \sin w \right\}\right]\right]^{-1}$$

$$= \left\{ -a_1 \left[\frac{\sqrt{a_3^2 - C_D^{*}}}{a_3} \left(\frac{a_1}{a_3}\right) + \frac{C_D^*}{a_3} \left(\frac{a_2}{a_3}\right)\right] + a_2 \left[\frac{C_D^*}{a_3} \left(\frac{a_1}{a_3}\right) + \frac{\sqrt{a_3^2 - C_D^{*}}}{a_3} \left(\frac{a_2}{a_3}\right)\right]\right\}^{-1}$$

$$= \frac{a_3^2}{\sqrt{a_3^2 - C_D^{*2}} \left(a_2^2 - a_1^2\right)}$$

thus

$$g\left(C_D^*, \alpha\right) = \left(\frac{2}{\pi}\right)^2 \left| \frac{a_3^2}{\sqrt{a_3^2 - C_D^{*2}} \left(a_2^2 - a_1^2\right)} \right|$$

The distribution of C_D^* is obtained at this point by integrating $g\left(C_D^*, \alpha\right)$ with respect to α over the range 0 to $\pi/2$. First, however, it is necessary to replace α in the joint density function.

$$g\left(C_D^*, \alpha\right) = \left(\frac{2}{\pi}\right)^2 \left| \frac{a_1^2 + a_2^2}{\sqrt{a_1^2 + a_2^2 - C_D^{*2}} \left(a_2^2 - a_1^2\right)} \right|$$

$$a_1^2 = \left(C_{D1} \cos\alpha + C_{D2} \frac{A_2}{A_1} \sin\alpha\right)^2$$

$$= \left(C_1 \cos\alpha + C_2 \sin\alpha\right)^2$$

$$= C_1^2 \cos^2\alpha + 2 C_1 C_2 \cos\alpha \sin\alpha + C_2^2 \sin^2\alpha$$

$$a_2^2 = \left(C_{D3} \frac{A_3}{A_1} \cos\alpha + C_{D4} \frac{A_4}{A_1} \sin\alpha\right)^2$$

$$= \left(C_3 \cos\alpha + C_4 \sin\alpha\right)^2$$

$$= C_3^2 \cos^2\alpha + 2 C_3 C_4 \cos\alpha \sin\alpha + C_4^2 \sin^2\alpha$$

$$a_1^2 + a_2^2 = C_5 \cos^2\alpha + C_6 \cos\alpha \sin\alpha + C_7 \sin^2\alpha$$

$$a_2^2 - a_1^2 = C_8 \cos^2\alpha + C_9 \cos\alpha \sin\alpha + C_{10} \sin^2\alpha$$

At this point it is noted that the area A_1 can be selected so that $a_2^2 > a_1^2$; thus, since α and Ξ are always between 0 and $\pi/2$ the function defined is everywhere positive in every term. Thus, the absolute value signs can be dropped

and

$$g(C_D^*) = \left(\frac{2}{\pi}\right)^2 \int_0^{\frac{\pi}{2}} \frac{\sum_{i=0}^{2} d_i \cos^{2-i}\alpha \sin^i\alpha}{\sqrt{\sum_{i=0}^{6} D_i \cos^{6-i}\alpha \sin^i\alpha}} d\alpha \qquad (6)$$

This function may be approximated analytically upon studying the behavior or integrated numerically. Analytic integration, however, does not appear attractive. It is noted that for the special case of 2-D analysis this problem is circumvented, since integration is not required. For this case $g\left(C_D^*\right)$ is obtained directly to be:

$$g\left(C_D\right) = \left(\frac{2}{\pi}\right) \frac{a_1^2 + a_2^2}{\sqrt{a_1^2 + a_2^2 - C_D^{*2}} \left(a_2^2 - a_1^2\right)}$$

where

$$a_1^2 = C_{D1}^2$$

$$a_2^2 = C_{D3}^2 \left(\frac{A_3}{A_1}\right)^2$$

A_2, A_4, C_{D2} and C_{D4} do not appear in this form for the reason that only a 2-D analysis is made. Thus, if the vehicle is tumbling in a known plane this much simpler solution can be utilized.

The density function is known or at least definable for the 3-D case and known analytically for the 2-D case, the problem turns to one of evaluating the moments of the distribution. These moments may be obtained directly from the moment generating function in the following manner:

$$m(t) = \int\int \cdots \int \left(e^{tu(x_1 \cdots x_n)} f(x_1 \cdots x_n) \prod_{i=1}^{n} dx_i \right)$$

$$\frac{d^r}{dt^r} m(t) \Big|_{t=0} = \mu'_r$$

where

μ'_1 = the mean

$\sigma^2 = \mu'_2 - \mu'^2_1$ = the variance

Substitution for this problem into the previous formula yields:

$$m(t) = \left(\frac{2}{\pi}\right)^2 \int_0^{\frac{\pi}{2}} \int_0^{\frac{\pi}{2}} \exp\Big\{ t \Big[h_1 \cos\alpha \cos\Xi + h_2 \cos\alpha \sin\Xi + h_3 \sin\alpha \cos\Xi + h_4 \sin\alpha \sin\Xi \Big] \Big\} d\alpha\, d\Xi$$

where

$$h_i = C_{D_i} \frac{A_i}{A_1} \quad i = 1, 2, 3, 4$$

But this problem, like the first, is not easily integrable. Thus, a numerical evaluation is suggested for each case of interest. In fact, even for the 2-D case, in which

$$m(t) = \int_{-\infty}^{\infty} e^{C_D^* t} \left(\frac{2}{\pi}\right) \frac{C_1}{\sqrt{C_2 - C_D^{*2}}}\, dC_D^*$$

where

$$C_1 = \frac{C_{D1}^2 + C_{D3}^2 \left(\frac{A_3}{A_1}\right)^2}{C_{D1}^2 - C_{D3}^2 \left(\frac{A_3}{A_1}\right)^2}$$

$$C_2 = C_{D1}^2 + C_{D3}^2 \left(\frac{A_3}{A_1}\right)^2$$

an analytic form is not readily available.

Since the mean is not available in analytic form, little can be said relative to the best value of $C_D^* A_1$ in the general problem. Many investigators avoid this problem by using the approximation derived from consideration of a spherical satellite.

$$C_D^* A = C_{D_{sphere}} (A_{surface}) \cdot \left[\frac{A_{surface\ of\ sphere}}{A_{projected\ area\ of\ sphere}} \right]^{-1} = C_{D_{sphere}} \left(\frac{A_{surface}}{4} \right)$$

Though this may seem to be a crude approximation, there are many cases in which it is reasonable. In fact, Ref. 5 reports an investigation in which a body randomly tumbling (about three principal axes) is analyzed and in which the author concludes that for convex surfaces the average drag on a surface element in random orientation is the same as that on a sphere of equal area. This work thus lends credibility to the previous assumption and provides a numerical value which can be utilized as an initial estimate in the numerical calculations outlined previously.

C. TWO-DIMENSIONAL ATMOSPHERIC PERTURBATIONS (REF. 6)

The motion of a point mass in a nonrotating atmosphere surrounding a central force is given by the following set of simultaneous differential equations

$$\left.\begin{aligned} \ddot{r} &= r\dot{\theta}^2 - \frac{\mu}{r^2} - B\rho\dot{r}V \\ \frac{d}{dt}(r^2\dot{\theta}) &= -B\rho V r\dot{\theta} \end{aligned}\right\} \qquad (7)$$

where

$V = \sqrt{(r\dot{\theta})^2 + \dot{r}^2}$

μ = earth's gravitational constant

$\dot{\theta} = \frac{d\theta}{dt}$ = angular velocity (rad/sec)

$B = \frac{C_D A}{2m}$ = ballistic coefficient

(8)

It is noted that this set of equations is nonlinear and that a solution can be obtained only by numerical integration. This fact is somewhat disconcerting, since these equations neglect atmospheric rotation, which introduces considerations of a third dimension and complicates the analysis further by entering the equations explicitly in the drag term. This latter factor results in the replacement of V as defined previously with

V_r = velocity relative to the atmosphere

$= \left| \vec{V} + \vec{V}_{atm} \right|$

Thus, if analytic approximations are desired, it becomes necessary to divide the problem into two phases--a perturbed orbit phase and an aerodynamic entry phase. In the first phase, a region is considered where the orbit is determined by the inverse square gravity field and only small perturbations are caused by the relatively small drag forces. In the entry phase, the aerodynamic forces (lift, drag, etc.) become the important factors influencing the trajectory of the satellite and gravity forces become less important. This last phase is by far the more complicated, and fortunately for a lifetime study it can be neglected, since relatively short periods of time are spent at the altitudes where drag forces become dominant. Thus, the present problem is the analysis of only the first phase. References 7 through 20 present a portion of the pertinent literature and will be discussed as the presentation progresses.

1. Near-Circular Orbits (approximate solution)

To initiate these discussions, consider the decay of a circular orbit. The energy loss due to drag during one revolution, ΔE_D, is given by the loss in total energy

$$\Delta E_D = E_{T1} - E_{T2}$$

$$= \left(\frac{V_{c1}^2}{2} - \frac{\mu}{r_1} \right) - \left(\frac{V_{c2}^2}{2} - \frac{\mu}{r_2} \right) \qquad (9)$$

Using the equation for circular velocity and letting

$$\Delta r = r_2 - r_1 ,$$

$$\Delta E_D = - \frac{\mu \Delta r}{2 r_1 r_2} \qquad (10)$$

The energy loss per unit mass due to drag is also equal to the drag force per unit mass integrated over a full revolution

$$\Delta E_D = \oint \frac{D}{m} \cdot ds \qquad (11)$$

Assuming small altitude losses during each single revolution

$$\Delta E_D \approx \frac{D}{M} \oint ds = \left(\frac{D}{m} \right) 2\pi \left(\frac{r_1 + r_2}{2} \right) \qquad (12)$$

where $\frac{r_1 + r_2}{2}$ = an average radius for the revolution.

Now using the approximation that the circular velocity is averaged approximately as

$$V_c^2 = \frac{2\mu}{r_1 + r_2} , \qquad (13)$$

Eqs (12) and (13) and the relation $\frac{D}{m} = \beta \rho V^2$ yield

$$\Delta E_D = 2\pi \mu B \rho_{av} \qquad (14)$$

If $\frac{\Delta r}{r_1} << 1$, then $r_1 r_2 \approx r_{av}^2$ and Eq (10) with Eq (14) results in the decay rate of the orbital altitude per revolution

$$\frac{\Delta r}{rev} = - 4\pi B \rho_{av} r_{av}^2 \qquad (15)$$

This decay rate can be converted to $\frac{\Delta r}{sec}$ by considering that the orbital period for this perturbed circle is

$$\tau = 2\pi \sqrt{\frac{r_{av}^3}{\mu}}$$

Thus

$$\frac{\Delta r}{\Delta t} = - 2 B \rho_{av} \sqrt{\mu r_{av}} \qquad (16)$$

Equation (16) shows that the decay rate for this special case is a linear function of the ballistic coefficient. This fact will be utilized in much of the future work in order to restrict the number of variables in the analysis. Equation (16) is not directly integrable because of the odd fashion in which the true density varies. However, if the density is assumed to vary exponentially with altitude, approximate lifetimes for circular orbits can be obtained:

$$\int_0^{t_L} dt = \int_{r_0}^{r_f} \frac{- dr}{2 B \rho_0 e^{K(r - r_a)} \sqrt{\mu r}} \qquad (17)$$

where

r_f = the final radius = R + 120 km

ρ_0 = the density at the $\frac{r_o + r_f}{2}$ (see Figs. 6a and 6b)

K = the negative of the logarithmic density slope (see Figs. 7a and 7b).

(Note: This data is for the 1959 ARDC Atmosphere. Data for the U. S. Standard 1962 Atmosphere is presented in Chapter II. Either can be utilized if the lifetimes are adjusted, as will be discussed on p V-20.)

Thus

$$T_L = \frac{- 1}{2 \sqrt{\mu} B \rho_0 e^{-m r_a}} \int_{r_0}^{r_f} \frac{e^{-K r} dr}{\sqrt{r}}$$

let

$$x^2 = Kr$$

$$2x\,dx = K\,dr \text{ or } dr = \frac{2x}{K} dx = \frac{1}{\sqrt{K}} 2 \sqrt{r}\, dx$$

Thus

$$\int_{r_0}^{r_f} \frac{e^{-Kr} dr}{\sqrt{r}} = \frac{2}{\sqrt{K}} \int_{\sqrt{K r_0}}^{\sqrt{K r_f}} e^{-x^2} dx$$

$$= \sqrt{\frac{\pi}{K}} \left[\text{erf} \left(\sqrt{K r_f} \right) - \text{erf} \left(\sqrt{K r_o} \right) \right]$$

and

$$T_L = \frac{e^{-K r_a}}{2 \sqrt{\mu} B \rho_0} \sqrt{\frac{\pi}{K}} \left[\text{erf} \left(\sqrt{K r_0} \right) - \text{erf} \left(\sqrt{K r_f} \right) \right] \qquad (18)$$

The disadvantage of utilizing this form for the complete lifetime is that the density does not vary exponentially, and thus the approximation becomes poorer as the difference in r_0 and r_f becomes large. This deficiency can be circumvented through the simple expedient of breaking the true radial increment into several subdivisions and evaluating the times required to descend through each interval. These times can then be summed to yield the lifetime. Computations utilizing this philosophy will yield accurate estimates provided that the intervals are no larger than 50 stat mi or 80 km.

The case of even slightly elliptic orbits must be treated in a different fashion since the assumptions made in generating circular orbit lifetimes are not valid for other orbits. Thus, it is necessary to consider the equations of variation of elements derived in Chapter IV or to approximate the motion in some other fashion. If the latter approach is taken, one possible avenue of investigation is to linearize the equations of motion by expanding the variables in Taylor series and retaining only first-order terms. This approach is valid only for small variations in the parameters. One such investigation is reported in Ref. 12. The author utilizes a small parameter β' defined as

$$\beta' = B \rho_0 r_0 \tag{19}$$

All orbital parameters are expressed as power series of β, considering only the first order terms

$$\left.\begin{aligned} r &= r_0 + \beta' r_1 \\ \theta &= \theta_0 + \beta' \theta_1 \\ V &= V_0 + \beta' V_1 \\ H &= H_0 + \beta' H_1 \end{aligned}\right\} \tag{20}$$

where

$H = r^2 \dot{\theta}$ is the angular momentum per unit mass (to differentiate from h = altitude).

Substituting Eq (20) into the differential equations, Eq (7), the following relationships are obtained

$$\left.\begin{aligned} \theta &= \theta_0 \left[1 + \frac{B \rho_0 r_0}{\theta_0} \left(4 \cos \theta_0 + \frac{3}{2} \theta_0^2 - 4 \right) \right] \\ r &= r_0 \left[1 + 2 B \rho_0 r_0 (\sin \theta_0 - \theta_0) \right] \\ V &= V_c \left[1 + B \rho_0 r_0 (-2 \sin \theta_0 + \theta_0) \right] \\ H &= H_0 \left[1 - B \rho_0 r_0 \theta_0 \right] \end{aligned}\right\} \tag{21}$$

where

$$\theta_0 = \frac{V_c t}{r_0}$$

Expressions for these quantities on a per revolution basis are next obtained from the differences in Eq (21) evaluated at the limits $\theta_0 = 0$ and 2π:

$$\left.\begin{aligned} \frac{\Delta r}{rev} &= -4\pi B \rho_0 r_0^2 \\ \frac{\Delta V}{rev} &= 2\pi B \rho_0 r_0 V_c \\ \frac{\Delta H}{rev} &= -2 B \rho_0 r_0 \end{aligned}\right\} \tag{22}$$

But, for circular orbits $V_c = \sqrt{\frac{\mu}{r}}$ and $\frac{dV_c}{dr} = -\frac{1}{2r}\sqrt{\frac{\mu}{r}}$, giving the following condition:

$$\frac{\Delta V_c}{rev} = -\frac{1}{2} \frac{V_c}{r} \frac{\Delta r}{rev} \tag{23}$$

Now, from the first two relationships in Eq (22), exactly the same relationship follows:

$$\frac{\Delta V}{rev} = -\frac{V_c}{2r} \frac{\Delta r}{rev}$$

This implies that for a first order approximation in $B \rho_0 r_0$ the speed at any given altitude remains exactly equal to the circular speed during the drag decay of a circular orbit.

And, from Eq (21) for $\theta_0 = 2\pi$ the corresponding angle θ is obtained as

$$\theta = 2\pi + 6\pi^2 B \rho_0 r_0 \tag{24}$$

Equation (24) indicates that the line of apsides is advancing by the amount

$$\Delta \omega = 6\pi^2 B \rho_0 r_0 \text{ (rad)} \tag{25}$$

Since the equation for the change in the radius per revolution is the same as that for the circular orbit. The lifetime of this slightly elliptic orbit will be the same as that presented earlier. Actually, as will be shown later, the lifetime is slightly longer, but a quantitative analysis is left until subsequent paragraphs. These subsequent discussions will concern the behavior of these and other more elliptic orbits.

2. Elliptic Orbits (approximate solution)

The type of expansion outlined for near-circular orbits can also be utilized for elliptic orbits as was shown in Ref. 12. This reference presented power series expansions for decay rates in elliptic orbits utilizing the small parameter

$$\beta = B \rho(h_{p0}) r_{p0} \tag{26}$$

where

$\rho(h_p)$ = air density at perigee radius

r_{p0} = initial perigee radius.

Next, a density ratio is defined

$$\sigma_0 = \rho / \rho(h_{p0}).$$

For these orbits Eq (7) becomes

$$\left.\begin{aligned} \ddot{r} - r\dot{\theta} &= -\frac{\mu}{r^2} - \beta \sigma_0 \frac{\dot{r} V}{r_{p0}} \\ \frac{1}{r} \frac{d}{dt}(r^2 \dot{\theta}) &= -\beta \sigma_0 \frac{r \dot{\theta} V}{r_{p0}} \end{aligned}\right\} \tag{27}$$

Using a change of variables $u = \frac{1}{r}$, and neglecting higher order terms in β, the power series expansions assume the following form:

$$\left.\begin{aligned} u &= u_0 + \beta u_1 \\ V &= V_0 + \beta V_1 \\ H &= H_0 + \beta H_1 \end{aligned}\right\} \tag{28}$$

Now the ratio of the initial speed at the perigee radius to the circular speed at r_{p0} is defined as

$$C = \frac{V_{p0}}{V_c} \tag{29}$$

and the corresponding eccentricity is expressed as

$$\epsilon = C^2 - 1 = \left(\frac{V_{p0}}{V_c}\right)^2 - 1 \tag{30}$$

An exponential atmosphere is assumed in the form

$$\sigma_0 = \frac{\rho}{\rho(h_{p_1})} = e^{-K(r - r_{p0})} \tag{31}$$

The differential equations given by Eq (27) are then solved for the two cases below:

Case I: near-circular orbits

Case II: eccentric orbits

Case I--near-circular orbits. The solutions derived by Ref. 12 are summarized below. First, the orbit parameters:

$$H = r_{p0} V_{p0} \left\{\left[1 - B\rho(h_p) r_{p0}\right]\theta \left[1 - Kr_{p0}\epsilon + \frac{3}{4}(Kr_{p0}\epsilon)^2 - \frac{5}{12}(Kr_{p0}\epsilon)^3\right] + \sin\theta\left[Kr_{p0}\epsilon\left(1 - Kr_{p0}\epsilon + \frac{5}{8}(Kr_{p0}\epsilon)^2\right)\right] + \sin 2\theta\left[\frac{(Kr_{p0}\epsilon)^2}{2}\left(\frac{1}{4} - \frac{1}{8}Kr_{p0}\epsilon\right)\right] + \sin 3\theta\,\frac{(Kr_{p0}\epsilon)^3}{72}\right]\right\} \tag{32a}$$

$$\frac{r}{r_{p0}} = \frac{1+\epsilon}{1+\epsilon\cos\theta}\left\{1 - 2B\rho(h_p)\frac{r_{p0}(1+\epsilon)}{1+\epsilon\cos\theta}\left\{\left[1 - Kr_{p0}\epsilon + \frac{3}{4}(Kr_{p0}\epsilon)^2 - \frac{5}{12}(Kr_{p0}\epsilon)^3\right]\theta - \frac{5}{144}(Kr_{p0}\epsilon)^3\,\theta\cos\theta - \left[1 - \frac{3}{2}Kr_{p0}\epsilon + \frac{3}{4}(Kr_{p0}\epsilon)^2 + \frac{125}{192}(Kr_{p0}\epsilon)^3\right]\sin\theta - \frac{(Kr_{p0}\epsilon)^2}{24}(1 - Kr_{p0}\epsilon)\sin 2\theta - \frac{(Kr_{p0}\epsilon)^3}{576}\sin 3\theta\right\}\right\} \tag{32b}$$

Second, the decay rates obtained from the above equations:

$$\frac{\Delta H}{rev} = -2\pi B\rho(h_{p0}) V_{p0} r_{p0}^2 \left[1 - Kr_{p0}\epsilon + \frac{3}{4}(Kr_{p0}\epsilon)^2 - \frac{5}{12}(Kr_{p0}\epsilon)^3\right] \tag{33a}$$

$$\frac{\Delta r_p}{rev} = r_{(\theta = 2\pi)} - r_{(\theta = 0)} = -4\pi B\rho(h_{p0}) r_{p0}^2 \left[1 - Kr_{p0}\epsilon + \frac{3}{4}(Kr_{p0}\epsilon)^2 - \frac{65}{144}(Kr_{p0}\epsilon)^3\right] \tag{33b}$$

$$\frac{\Delta r_a}{rev} = r_{(\theta = 3\pi)} - r_{(\theta = \pi)} = -4\pi B\rho(h_{p0}) r_{p0}^2 \left(\frac{1+\epsilon}{1-\epsilon}\right)^2 \left[1 - Kr_{p0}\epsilon + \frac{3}{4}(Kr_{p0}\epsilon)^2 - \frac{55}{144}(Kr_{p0}\epsilon)^3\right] \tag{33c}$$

Note that for $\epsilon = 0$ both Eqs (33b) and (33c) reduce to the circular decay rate given previously by Eq (22).

The given series expansions are adequate only for small values of $Kr_{p0}\epsilon$, the upper limit being suggested as $Kr_{p0}\epsilon < 0.5$. Reference 12 gives the following table, indicating the upper limits of eccentricity for various altitudes from sea level satisfying this condition:

h_{p0} (km)	h_{p0} (stat mi)	K (ft^{-1})	K (m^{-1})	ϵ
161	100	9.3×10^{-6}	30.5×10^{-6}	0.0025
322	200	5.1×10^{-6}	16.7×10^{-6}	0.0045
483	300	3.65×10^{-6}	12.0×10^{-6}	0.0061

(1 stat mi = 1.609 km; 1 ft = 0.3048 meter)

Case II--elliptic orbits. For values of $Kr_{p0}\epsilon > 1$, terms up to the seventh power were carried. The resulting series expansions are shown below.

$$H = r_{p0} V_{p0}\left[1 - e^{-Kr_{p0}\epsilon}\left(C_1\theta + \sum_{n=1}^{7} C_{n+1}\sin n\theta\right)\right] \tag{34a}$$

$$\frac{r}{r_{p0}} = \frac{1+\epsilon}{1+\epsilon\cos\theta}\left\{1 - \frac{B\rho(h_{p0}) r_{p0}\, e^{-Kr_{p0}\epsilon}}{1+\epsilon\cos\theta}\cdot\left[2C_1\theta - C_2\theta\cos\theta + C^*\sin\theta - \frac{2}{3}C_3\sin 2\theta - \frac{1}{4}C_4\sin 3\theta - \frac{2}{15}C_5\sin 4\theta - \frac{1}{12}C_6\sin 5\theta + \frac{3}{35}C_7\sin 6\theta + \frac{C_8}{12}\sin 7\theta\right]\right\} \tag{34b}$$

where

$$C_1 = 1 + \frac{1}{4}(Kr_{p0}\epsilon)^2 + \frac{1}{64}(Kr_{p0}\epsilon)^4 + \frac{1}{2304}(Kr_{p0}\epsilon)^6 + \ldots$$

$$C_2 = Kr_{p0}\epsilon + \frac{1}{8}(Kr_{p0}\epsilon)^3 + \frac{1}{192}(Kr_{p0}\epsilon)^5 + \frac{1}{2632}(Kr_{p0}\epsilon)^7 + \ldots$$

$$C_3 = \frac{1}{8}(Kr_{p0}\epsilon)^2 + \frac{1}{96}(Kr_{p0}\epsilon)^4 + \frac{1}{3072}(Kr_{p0}\epsilon)^6 + \ldots$$

$$C_4 = \frac{1}{72}(Kr_{p0}\epsilon)^3 + \frac{1}{1152}(Kr_{p0}\epsilon)^5 + \frac{1}{3412}(Kr_{p0}\epsilon)^7 + \ldots$$

$$C_5 = \frac{1}{768}(Kr_{p0}\epsilon)^4 + \frac{1}{1536}(Kr_{p0}\epsilon)^6 + \ldots$$

$$C_6 = \frac{1}{9600}(Kr_{p0}\epsilon)^5 + \frac{1}{230,400}(Kr_{p0}\epsilon)^7 + \ldots$$

$$C_7 = \frac{1}{138,240}(Kr_{p0}\epsilon)^6 + \ldots$$

$$C_8 = \frac{1}{2,358,720}(Kr_{p0}\epsilon)^7 + \ldots$$

$$C^* = -2C_1 + C_2 + \frac{4}{3}C_3 + \frac{3}{4}C_4 + \frac{8}{15}C_5 + \frac{5}{12}C_6 - \frac{18}{35}C_7 - \frac{7}{12}C_8 + \ldots$$

The accuracy of the series solution is limited to a region near the perigee, due to expansion of σ_0 aroung the perigee point. Therefore a limiting central angle, θ_{lim}, was designated, such that $\frac{\rho}{\rho(h_p)} \leq 0.01$ for $\theta \leq \theta_{lim}$. The limiting angle is given as

$$\cos\theta_{lim} = \left(\frac{1+\epsilon}{\epsilon}\right)\frac{1}{\frac{4.605}{Kr_p} + 1} - \frac{1}{\epsilon}. \qquad (34c)$$

For $\frac{\rho}{\rho(h_p)} \leq 0.1$ the constant 4.60 is replaced by 2.30. Figure 8 presents θ_{lim} plotted versus the orbital eccentricity for two values of density ratios and two initial perigee altitudes. Since the air density has decreased to 1% of the perigee value at a central angle of θ_{lim}, the following assumptions can be made:

(1) The drag effects are negligible for the arc BCD.

(2) All the drag takes place in the region DAB.

(3) A symmetry exists about the line AOC (i.e., $Drag_{DA} = Drag_{AB}$).

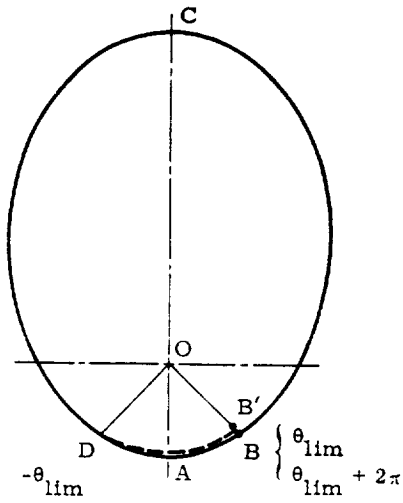

Therefore, the change of orbital radius at a central angle θ_{lim} is expressed as

$$\frac{\Delta r}{rev} = r_{B'} - r_B = r(\theta_{lim} + 2\pi) - r(\theta_{lim}) \approx r(\theta_{lim}) - r(-\theta_{lim}). \qquad (35a)$$

From Eq (34b)

$$\frac{\Delta r}{rev} = \left\{ -\frac{B\rho(h_{p0})r_{p0}^2 e^{-Kr_{p0}\epsilon}}{1+\epsilon\cos\theta}\left[2C_1\theta - C_2\theta\cos\theta + \ldots\right]\right\}_{-\theta_{lim}}^{\theta_{lim}} \qquad (35b)$$

But

$$\Delta\epsilon = \left(\frac{1-\epsilon}{a}\right)\Delta a \qquad (36a)$$

From the chain rule

$$\Delta r = \left(\frac{\partial r}{\partial a}\right)\Delta a + \left(\frac{\partial r}{\partial e}\right)\Delta\epsilon \qquad (36b)$$

and from Eqs (36a) and (36b) it can be shown that the following orbital parameters can be obtained from Eq (35b):

$$\Delta a \approx \frac{(1+\epsilon\cos\theta)^2}{(1-\epsilon)^2(1-\cos\theta)}\Delta r \qquad (37a)$$

$$\Delta h_a \approx \frac{2(1+\epsilon\cos\theta)^2}{(1-\epsilon)^2(1-\cos\theta)}\Delta r \qquad (37b)$$

Equations (37a) and (37b) are based on the assumption that $\Delta h_a >> \Delta h_p$. Thus the apogee decay rates can be obtained by the expansion of a small parameter method by Eqs (35b) and (37b). For perigee decay rates no information is given by this solution.

3. Variation of Elements

As was noted in the previous paragraphs, a second method of solution for the effects of drag is available in the form of the equations for variation of elements. These equations will be utilized in the investigations of elliptic orbits which follow.

Since the interest in this discussion is in the solution for the lifetime of a satellite in a nonrotating atmosphere, the disturbing acceleration will be due to drag and will act along the velocity vector that is tangent to the path. Thus, since

$$S = \frac{(1 + \epsilon \cos\theta)\, T}{\sqrt{1 + \epsilon^2 + 2\epsilon \cos\theta}} + \frac{(\epsilon \sin\theta)\, N}{\sqrt{1 + \epsilon^2 + 2\epsilon \cos\theta}}$$

$$R = -\frac{(\epsilon \sin\theta)\, T}{\sqrt{1 + \epsilon^2 + 2\epsilon \cos\theta}} + \frac{(1 + \epsilon \cos\theta)\, N}{\sqrt{1 + \epsilon^2 + 2\epsilon \cos\theta}}$$

where

S = circumferential disturbance

R = radial disturbances

T = the tangential acceleration

N = the normal acceleration $\equiv 0$

ϵ = the eccentricity to differentiate from the base of natural logarithms

The equations of variations of constants can be written as

$$\frac{da}{dt} = \frac{2\sqrt{1 + \epsilon^2 + 2\epsilon \cos\theta}}{n\sqrt{1 - \epsilon^2}}\, T$$

$$\frac{de}{dt} = \frac{2\sqrt{1 - \epsilon^2}\,(\cos\theta + \epsilon)}{na\sqrt{1 + \epsilon^2 + 2\epsilon \cos\theta}}\, T$$

$$\frac{d\omega}{dt} = \frac{2\sqrt{1 - \epsilon^2}}{na\epsilon}\, \frac{\sin\theta}{\sqrt{1 + \epsilon^2 + 2\epsilon \cos\theta}}\, T$$

$$\frac{d\sigma}{dt} = -\left[2(1 - \epsilon^2)(1 + \epsilon^2 + \epsilon \cos\theta)\sin\theta\right]\left[na\epsilon(1 + \epsilon \cos\theta)(1 + \epsilon^2 + 2\epsilon \cos\theta)^{1/2}\right]^{-1} T$$

$$\frac{d\Omega}{dt} = 0\,, \quad \frac{di}{dt} = 0 \qquad (38)$$

where

$n = \frac{2\pi}{\tau}\sqrt{\frac{\mu}{a^3}}$ mean angular velocity

$T = -\frac{D}{m}$ drag deceleration.

From Eq (38) it follows that for a nonrotating atmosphere, drag does not cause any variations in the inclination or the nodal position of the orbit. Aerodynamic drag will, however, cause a forward rotation of the perigee in the orbital plane, as was shown quantitatively in Eq (25). An appreciation of the reason for this advance can be obtained from the following qualitative analysis.

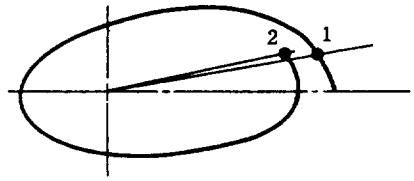

Consider a slowly decaying elliptical orbit as shown on the sketch. Take points 1 and 2 as shown in the sketch in such a manner that the angle from perigee is constant.

Then $\theta_1 = \theta_2$, $r_1 > r_2$ and $\rho_1 < \rho_2$. From the basic equations of elliptic orbits

$$V^2 = \frac{\mu}{a}\left[\frac{1 + 2\epsilon \cos\theta + \epsilon^2}{1 - \epsilon^2}\right] \qquad (39)$$

From Eq (38)

$$\dot{\omega} = 2B\rho \sin\theta \sqrt{\frac{\mu}{a}\left(\frac{1 + \epsilon^2 + 2\epsilon \cos\theta}{1 - \epsilon^2}\right)} \qquad (40)$$

The ratio $\dot{\omega}/\dot{\omega}_2$ becomes

$$\frac{\dot{\omega}_1}{\dot{\omega}_2} = \frac{\rho_1}{\rho_2}\,\frac{\epsilon_2}{\epsilon_1}\left(\frac{a_2}{a_1}\right)^{1/2}\left(\frac{1 + \epsilon_1^2 + 2\epsilon_1 \cos\theta_1}{1 + \epsilon_2^2 + 2\epsilon_2 \cos\theta_2}\right)^{1/2} \cdot \left(\frac{1 - \epsilon_2^2}{1 - \epsilon_1^2}\right)^{1/2}\,\frac{\sin\theta_1}{\sin\theta_2}$$

Then for the first order of eccentricity

$$\frac{\dot{\omega}_1}{\dot{\omega}_2} \approx \frac{\rho_1}{\rho_2}\,\frac{\epsilon_2}{\epsilon_1}\left(\frac{a_2}{a_1}\right)^{1/2}\left(\frac{1 + \epsilon_1 \cos\theta_1}{1 + \epsilon_2 \cos\theta_1}\right) \qquad (41)$$

But, $\frac{1 + \epsilon_1 \cos\theta_1}{1 + \epsilon_2 \cos\theta_2} \approx 1$

$$\frac{a_2}{a_1} < 1,\ \frac{\epsilon_2}{\epsilon_1} < 1 \text{ and } \frac{\rho_1}{\rho_2} < 1$$

Therefore $\frac{\dot{\omega}_1}{\dot{\omega}_2} < 1$ and the perigee advances due to air drag as was stated. This advance does not affect the lifetime of the satellite to the order of approximation of this analysis; however, since the atmosphere is not considered to rotate, density need not be considered to vary with position around the earth. Thus, the orientation of the orbit while it changes does not change the decay history (again, to this order of approximation). For this reason, attention can be focused on the change of the three elements in the plane of the

orbit (a, ϵ and σ). Further, since σ relates position in the orbit as a function of time and not a change in the size or shape of the orbit, the elements of primary concern are a and ϵ. Variations in both of these elements are discussed in the following paragraphs. However, before these discussions it is desirable to relate the change in altitude of apogee and perigee to the changes in the elements a and ϵ.

The altitude variations during one revolution are quite large for elliptic orbits with high eccentricity, and therefore it is necessary to pick certain reference points during one revolution, for which the altitude, air density and decay rate can be found more easily. Since this geometry of a two-dimensional ellipse is completely determined by the perigee and apogee altitudes, and since air drag occurs primarily in the vicinity of perigee, apogee and perigee radii will be utilized as the reference points. These radii are expressed in terms of the semimajor axis and eccentricity as

$$\left.\begin{aligned} r_a &= a(1+\epsilon) \\ r_p &= a(1-\epsilon) \end{aligned}\right\} \qquad (42)$$

Now, orbital altitude is given by $h_i = r_i - R_e$, where R_e is the radius of the equivalent spherical earth. Therefore the partial derivatives become, since $\frac{\partial h_i}{\partial x} = \frac{\partial r_i}{\partial x}$

$$\left.\begin{aligned} \frac{\partial h_a}{\partial a} &= 1+\epsilon & \frac{\partial h_p}{\partial a} &= 1-\epsilon \\ \frac{\partial h_a}{\partial \epsilon} &= a & \frac{\partial h_p}{\partial \epsilon} &= -a \end{aligned}\right\} \qquad (43)$$

And from the chain rule for derivatives

$$\left.\begin{aligned} \frac{dh_a}{dt} &= \frac{\partial h_a}{\partial a}\frac{da}{dt} + \frac{\partial h_a}{\partial \epsilon}\frac{d\epsilon}{dt} \\ \frac{dh_p}{dt} &= \frac{\partial h_p}{\partial a}\frac{da}{dt} + \frac{\partial h_p}{\partial \epsilon}\frac{d\epsilon}{dt} \end{aligned}\right\} \qquad (44)$$

Substituting Eqs (43) into Eqs (44) yields

$$\left.\begin{aligned} \frac{dh_a}{dt} &= (1+\epsilon)\frac{da}{dt} + a\frac{d\epsilon}{dt} \\ \frac{dh_p}{dt} &= (1-\epsilon)\frac{da}{dt} - a\frac{d\epsilon}{dt} \end{aligned}\right\} \qquad (45)$$

Thus, after the time derivatives of semimajor axis and eccentricity are determined from the Lagrange planetary equations, the time rates of the perigee and apogee altitudes can be found by substitution. The instantaneous orbital altitudes can be determined by integrations of Eq (45) either by numerical or analytical expressions.

Assuming an orbit with a very high eccentricity, the significant part of air drag takes place near the perigee and the maximum variations of orbital parameters can be found approximately by setting $\cos\theta \approx 1.0$. Equations (38) become

$$\left.\begin{aligned} \frac{da}{dt} &= \frac{2(1+\epsilon)}{n\sqrt{1-\epsilon^2}}\,T \\ \frac{de}{dt} &= \frac{2\sqrt{1-\epsilon^2}}{na}\,T \end{aligned}\right\} \qquad (46)$$

and the ratio of $\dot{a}$ to $\dot{\epsilon}$ is found as

$$\frac{\dot{a}}{\dot{\epsilon}} = \frac{a}{1-\epsilon} \quad \text{or} \quad \frac{da}{dt} = \left(\frac{a}{1-\epsilon}\right)\frac{d\epsilon}{dt} \qquad (47)$$

Substituting Eq (47) into Eq (45) yields

$$\left.\begin{aligned} \frac{dh_a}{dt} &= \left(\frac{2a}{1-\epsilon}\right)\frac{d\epsilon}{dt} = 2\frac{da}{dt} \\ \frac{dh_p}{dt} &= a\frac{d\epsilon}{dt} - a\frac{d\epsilon}{dt} = 0 \end{aligned}\right\} \qquad (47a)$$

Equations (47a) indicate that orbits with large eccentricities tend to become more circular during the drag decay process. For highly elliptic orbits the perigee decay rate is zero for a first approximation and in all cases it is considerably smaller than the apogee decay rate, as proven by numerical integrations (Ref. 10).

Now continuing, using the expression for drag deceleration

$$T = -\frac{D}{m} = -B\rho V^2 \qquad (48)$$

Equations (38) become

$$\left.\begin{aligned} \frac{da}{dt} &= -\frac{2a^2}{\mu}B\rho V^3 \\ \frac{de}{dt} &= -2\rho V(\cos\theta + \epsilon) \end{aligned}\right\} \qquad (49)$$

Substituting for V and $\dot{\theta}$ from

$$V^2 = \frac{\mu}{a}\left(\frac{1+2\epsilon\cos\theta+\epsilon^2}{1-\epsilon^2}\right) \qquad (50a)$$

$$\frac{dt}{d\theta} = \frac{r^2}{na^2\sqrt{1-\epsilon^2}} \qquad (50b)$$

the equations for the variation of elements can be expressed as derivatives with respect to the central angle θ. At this point it should be noted that Eq (50b) applies rigorously only if angular momentum is conserved, i.e., $r^2\dot{\theta} = \sqrt{\mu p} = na^2\sqrt{1-\epsilon^2}$. In Ref. 17 the correct expression is given in terms of the osculating elements as

$$r^2\left[\dot{\theta} + \dot{\omega} + \cos i\,\frac{d\Omega}{dt}\right] = \sqrt{\mu p} \qquad (51)$$

However, as seen from Eq (25)

$$\frac{\Delta\omega}{\Delta\theta} \approx 3\pi B \rho_0 r_0 \text{ (rad/rad)}.$$

But since $1 >> \frac{\dot{\omega}}{\dot{\theta}}$, Eq (50b) is justified for the present analysis. Thus, Eqs (49) become

$$\frac{da}{d\theta} = -2a^2 B\rho \frac{(1 + 2\epsilon\cos\theta + \epsilon^2)^{3/2}}{(1 + \epsilon\cos\theta)^2} \quad (52a)$$

$$\frac{de}{d\theta} = -2aB\rho(1-\epsilon^2)\left[\frac{(1 + 2\epsilon\cos\theta + \epsilon^2)^{1/2}}{(1 + \epsilon\cos\theta)^2} \cdot (\cos\theta + \epsilon)\right] \quad (52b)$$

Next, the functions of the central angle are expressed as functions of the eccentric anomaly by the following relationships:

$$\left.\begin{aligned} r &= a(1 - \epsilon\cos E) \\ \sin\theta &= \frac{\sqrt{1-\epsilon^2}\sin E}{1 - \epsilon\cos E} \\ \cos\theta &= \frac{\cos E - \epsilon}{1 - \epsilon\cos E} \\ d\theta &= \frac{\sqrt{1-\epsilon^2}}{1 - \epsilon\cos E} dE \end{aligned}\right\} \quad (53)$$

Substituting Eq (53) into Eq (52) and using the approximate symmetry relationship of drag decay functions

$$\int_0^{2\pi} f\, d\theta = 2\int_0^{\pi} f\, d\theta$$

The decays per revolution are found by the following integrals:

$$\frac{\Delta a}{rev} = -4a^2 B\rho_0 \int_0^{\pi} \frac{\rho}{\rho_0} \frac{(1 + \epsilon\cos E)^{3/2}}{(1 - \epsilon\cos E)^{1/2}} dE \quad (54a)$$

$$\frac{\Delta e}{rev} = -4aB\rho_0(1-\epsilon^2)\int_0^{\pi} \frac{\rho}{\rho_0} \frac{(1+\epsilon\cos E)^{1/2}}{(1-\epsilon\cos E)^{1/2}} \cos E\, dE \quad (54b)$$

Note that Eqs (54) basically involve the application of the Krylov and Bogoliuboff averaging method (Refs. 13 and 14), by which approximate differential equations are obtained for the variation of orbital elements by averaging the original equations over one full revolution (i.e., $E = 0$ to $E = 2\pi$). This removes all trigonometric terms from Eqs (54) and is actually equivalent to a conservation of energy approach (Ref. 14, p. 238).

The fraction in Eqs (54) can be expressed in a simplified form by employing power series expansions as:

$$\frac{\Delta a}{rev} = -4a^2 B\rho_0 \int_0^{\pi} \frac{\rho}{\rho_0}\left[1 + 2\epsilon\cos E + \frac{3}{2}\epsilon^2\cos^2 E + \epsilon^3\cos^3 E + \frac{7}{8}\epsilon^4\cos^4 E + \ldots\right] dE \quad (55a)$$

+ (continued)

$$\frac{\Delta e}{rev} = -4aB\rho_0(1-\epsilon^2)\int_0^{\pi} \frac{\rho}{\rho_0}\left[\cos E + \epsilon\cos^2 E + \frac{1}{2}\epsilon^2\cos^3 E + \frac{1}{2}\epsilon^3\cos^4 E + \frac{3}{8}\epsilon^4\cos^5 E + \ldots\right] dE \quad (55b)$$

In general, the density function $\frac{\rho}{\rho_0}$ is empirically found (see atmospheric models) and cannot be expressed in a simple exact analytical form. Thus, the analytic integration of Eqs (55) is not possible. Numerical integrations of Eqs (54) or (55) can be performed on a high speed digital computer, however. If this step is to be taken, the density is related to eccentric anomaly in two steps:

(1) Altitude: $h = r - R_e = a(1 - \epsilon\cos E) - R_e$

(2) Density: $\rho(h)$ from atmospheric density tables. (56)

Defining $S = 1 + 2\epsilon\cos E + \frac{3}{2}\epsilon^2\cos^2 E + \ldots$, and dropping terms higher than the second power of eccentricity (Ref. 12) has numerically computed the function of the integrand in Eq (55a) for Explorer IV, considering both Smithsonian 1957-2 and ARDC 1959 model atmospheres.

The most important conclusion from this study and related studies performed elsewhere is that even for orbits of relatively small eccentricities (Explorer IV had $\epsilon = 0.14$). The most significant portion of the drag perturbation takes place in the vicinity of perigee in a region where $|E| < 40°$. Utilizing this conclusion (not the limit on $|E|$) and approximating the density in this region by an exponential, Eqs (55) can be put in an integrable form. Let

$$\frac{\rho}{\rho_0} = e^{-K(h-h_p)} \quad (57a)$$

where K is the negative logarithmic slope given in Figs. 7a and 7b. Equation (57a) implies a straight line variation of ρ versus h on a semilog paper, which does not exist for any altitude range. Nevertheless, for a relatively small region, say 50,000 ft (15 km) around the perigee point, this approximation is valid to a very high order if an instantaneous value of K is selected.

Using relationships $r = a(1 - \epsilon\cos E)$ and $r_p = a(1 - \epsilon)$, Eq (57b) can be written as

$$\frac{\rho}{\rho_0} = e^{-Ka\epsilon} e^{Ka\epsilon\cos E} \quad (57b)$$

Now substituting Eq (57b) into (55a, b) yields

$$\frac{\Delta a}{rev} = -4a^2 B\rho_0 \, e^{-Ka\epsilon} \int_0^{\pi} e^{Ka\epsilon \cos E} (1 + 2\epsilon \cos E + \ldots) \, dE \tag{58a}$$

$$\frac{\Delta e}{rev} = -4aB\rho_0 (1-\epsilon^2) \, e^{-Ka\epsilon} \int_0^{\pi} e^{Ka\epsilon \cos E} (\cos E + \epsilon \cos^2 E + \ldots) \, dE \tag{58b}$$

The integrals above could be evaluated in the form of modified Bessel functions of imaginary argument, if the brackets contained a series of sine terms. Therefore, at this point a further crucial approximation is introduced. It is assumed that significant drag exists only near the perigee. This assumption breaks down for very small eccentricities (i.e., as $\epsilon \to 0$), but the validity of it is good for moderately elliptic orbits.

Assuming that $\sin^2 E << 1$ then $\cos^n E$ can be written as an infinite series of sines for odd n or as a finite polynomial in sines for n even. The first five sine expansions are as follows:

$$\left.\begin{aligned}
\cos E &= 1 - \tfrac{1}{2}\sin^2 E - \tfrac{1}{8}\sin^4 E - \tfrac{1}{16}\sin^6 E - \tfrac{5}{128}\sin^8 E - \ldots \\
\cos^2 E &= 1 - \sin^2 E \\
\cos^3 E &= 1 - \tfrac{3}{2}\sin^2 E + \tfrac{3}{8}\sin^4 E + \tfrac{1}{16}\sin^6 E + \tfrac{3}{128}\sin^8 E + \ldots \\
\cos^4 E &= 1 - 2\sin^2 E + \sin^4 E \\
\cos^5 E &= 1 - \tfrac{5}{2}\sin^2 E + \tfrac{15}{8}\sin^4 E - \tfrac{5}{16}\sin^6 E - \tfrac{5}{128}\sin^8 E + \ldots
\end{aligned}\right\} \tag{59}$$

Substituting Eq (59) into Eqs (58a, b) the following expressions are obtained:

$$\frac{\Delta a}{rev} = -4a^2 B\rho_0 e^{-z} \int_0^{\pi} e^{z\cos E} (\alpha_0 - \alpha_1 \sin^2 E - \alpha_2 \sin^4 E - \alpha_3 \sin^6 E - \alpha_4 \sin^8 E - \ldots) dE \tag{60a}$$

$$\frac{\Delta \epsilon}{rev} = -4aB\rho_0 e^{-z} \int_0^{\pi} e^{z\cos E} (\beta_0 - \beta_1 \sin^2 E - \beta_2 \sin^4 E - \beta_3 \sin^6 E - \beta_4 \sin^8 E - \ldots) dE \tag{60b}$$

where

$$z \equiv Ka\epsilon$$

and the constants α_i, β_i are power series in terms of eccentricity, up to ϵ^4, as follows:

$$\left.\begin{aligned}
\alpha_0 &= 1 + 2\epsilon + \tfrac{3}{2}\epsilon^2 + \epsilon^3 + \tfrac{7}{8}\epsilon^4 + \tfrac{3}{4}\epsilon^5 + \tfrac{11}{16}\epsilon^6 + \ldots \\
\alpha_1 &= \epsilon + \tfrac{3}{2}\epsilon^2 + \tfrac{3}{2}\epsilon^3 + \tfrac{7}{4}\epsilon^4 + \ldots \\
\alpha_2 &= \tfrac{1}{4}\epsilon - \tfrac{3}{8}\epsilon^3 - \tfrac{7}{8}\epsilon^4 - \ldots \\
\alpha_3 &= \tfrac{1}{8}\epsilon - \tfrac{1}{16}\epsilon^3 - \ldots \\
\alpha_4 &= \tfrac{56}{64}\epsilon - \tfrac{3}{128}\epsilon^3 - \ldots
\end{aligned}\right\} \tag{61a}$$

$$\left.\begin{aligned}
\beta_0 &= 1 + \epsilon - \tfrac{1}{2}\epsilon^2 - \tfrac{1}{2}\epsilon^3 - \tfrac{1}{8}\epsilon^4 - \tfrac{1}{8}\epsilon^5 - \tfrac{1}{16}\epsilon^6 - \ldots \\
\beta_1 &= \tfrac{1}{2} + \epsilon + \tfrac{1}{4}\epsilon^2 + \tfrac{3}{16}\epsilon^4 + \ldots \\
\beta_2 &= \tfrac{1}{8} - \tfrac{5}{16}\epsilon^2 - \tfrac{1}{2}\epsilon^3 - \tfrac{33}{64}\epsilon^4 - \ldots \\
\beta_3 &= \tfrac{1}{16} - \tfrac{3}{32}\epsilon^2 + \tfrac{19}{128}\epsilon^4 + \ldots \\
\beta_4 &= \tfrac{5}{128} - \tfrac{13}{256}\epsilon^2 + \tfrac{27}{1024}\epsilon^4 + \ldots
\end{aligned}\right\} \tag{61b}$$

It is noted that Eqs (60a, b) conform to the modified Bessel functions of imaginary argument, which can be written as

$$I_p(z) = \frac{\left(\frac{1}{2}z\right)^p}{\Gamma(p + \frac{1}{2})\,\Gamma(\frac{1}{2})} \int_0^{\pi} e^{z\cos E} \sin^{2p} E \, dE \tag{62}$$

where:

$$p = (1, 2, 3 \text{ ---})$$

$$\Gamma(n+1) = h\Gamma(n)$$

and

$$\Gamma(\tfrac{1}{2}) = \sqrt{\pi}$$

The integrals in Eqs (60a, b) can now be expressed in terms of Bessel functions as

$$\left.\begin{aligned}
\int_0^{\pi} e^{z\cos E} dE &= \pi I_0(z) \\
\int_0^{\pi} e^{z\cos E} \sin^2 E \, dE &= \frac{\pi I_1(z)}{z} \\
\int_0^{\pi} e^{z\cos E} \sin^4 E \, dE &= \frac{3\pi I_2(z)}{z^2} \\
\int_0^{\pi} e^{z\cos E} \sin^6 E \, dE &= \frac{3\cdot 5\,\pi I_3(z)}{z^3} \\
\int_0^{\pi} e^{z\cos E} \sin^8 E \, dE &= \frac{3\cdot 5\cdot 7\,\pi I_4(z)}{z^4}
\end{aligned}\right\} \tag{63a}$$

NOTE: For modified Bessel functions $I_0(0) = 1$ and $I_2(0) = I_3(0) = \ldots = I_p(0) = 0$, so that for $z = 0$, Eqs (63a) are seemingly indeterminate for $p \geq 2$. The limiting values, however, can actually be found to be finite:

$$\lim_{z \to 0} \frac{I_p(z)}{z^p} = \frac{1}{2^p (p!)} \tag{63b}$$

Now in terms of modified Bessel functions the integrals of the orbital decay rates can be expressed as:

$$\int_0^{\pi} [\,]\,dE = \alpha_0 \pi I_0(z) - \alpha_1 \frac{\pi I_1(z)}{z} - \alpha_2 \frac{3\pi I_2(z)}{z^2} - \alpha_3 \frac{3 \cdot 5\pi I_3(z)}{z^3} - \alpha_4 \frac{3 \cdot 5 \cdot 7\pi I_4(z)}{z^4} - \ldots \tag{64}$$

(and a similar equation involving β_1).

Thus, both Δa and $\Delta \epsilon$ can be expressed as series of the same form but differing coefficients. However, the computation of these changes is unnecessarily complex due to the fact that higher order modified Bessel functions can be reduced to a linear combination of orders zero and one ($I_0(z)$ and $I_1(z)$) by the use of the reduction formula

$$I_{p+1}(z) = I_{p-1}(z) - \frac{2p}{z} I_p(z) \tag{65}$$

The reduction formulas up to the order four are

$$\left.\begin{aligned} I_2(z) &= I_0(z) - \frac{2}{z} I_1(z) \\ I_3(z) &= \left(1 + \frac{2^2}{z^2}\right) I_1(z) - \frac{2^2}{z} I_0(z) \\ I_4(z) &= \left(1 + \frac{2^3 \cdot 3}{z^2}\right) I_0(z) - \frac{2^3}{z}\left(1 + \frac{2 \cdot 3}{z^3}\right) I_1(z) \end{aligned}\right\} \tag{66}$$

Now using Eqs (66) the decay rates of elements can be written in the final form for elliptic orbits

$$\frac{\Delta a}{rev} = -4\pi a^2 B \rho_0 F_1(z, \epsilon) \tag{67a}$$

$$\frac{\Delta e}{rev} = -4\pi a B \rho_0 F_2(z, \epsilon) \tag{67b}$$

where the following nondimensional functions are used:

$$F_1(z,\epsilon) \equiv e^{-z}\left\{\left[\alpha_0 - \frac{3\alpha_2}{z^2} + \frac{60\alpha_3}{z^4} - \frac{105\alpha_4 (z^2 + 24)}{z^6} + \ldots\right] I_0(z) - \left[\alpha_1 - \frac{6\alpha_2}{z^2} + \frac{15\alpha_3 (z^2 + 8)}{z^4} - \frac{840\alpha_4 (z^2 + 6)}{z^6} + \ldots\right] \frac{I_1(z)}{z}\right\} \tag{68a}$$

+ (continued)

$$F_2(z,\epsilon) = e^{-z}\left\{\left[\beta_0 - \frac{3\beta_2}{z^2} + \frac{60\beta_3}{z^4} - \frac{105\beta_4 (z^2 + 24)}{z^6} + \ldots\right] I_0(z) - \left[\beta_1 - \frac{6\beta_2}{z^2} + \frac{15\beta_3 (z^2 + 8)}{z^4} - \frac{840\beta_4 (z^2 + 6)}{z^6} + \ldots\right] \frac{I_1(z)}{z}\right\} \tag{68b}$$

Note is made that Ref. 16 tabulates $e^{-z} I_0(z)$, $e^{-z} I_1(z)$. Note also that the following asymptotic series are given in Ref. 16, p. 271 for large z:

$$e^{-z} I_0(z) \approx \frac{1}{(2\pi z)^{1/2}}\left\{1 + \frac{1^2}{1!\,8z} + \frac{1^2 \cdot 3^2}{2!\,(8z)^2} + \frac{1^2 \cdot 3^2 \cdot 5^2}{3!\,(8z)^3} + \frac{1^2 \cdot 3^2 \cdot 5^2 \cdot 7^2}{4!\,(8z)^4} + \ldots\right\} \tag{69a}$$

$$e^{-z} I_1(z) \approx \frac{1}{(2\pi z)^{1/2}}\left\{1 - \frac{1 \cdot 3}{1!\,8z} - \frac{1^2 \cdot 3 \cdot 5}{2!\,(8z)^2} - \frac{1^2 \cdot 3^2 \cdot 5 \cdot 7}{3!\,(8z)^3} - \frac{1^2 \cdot 3^2 \cdot 5^2 \cdot 7 \cdot 9}{4!\,(8z)^4} - \ldots\right\} \tag{69b}$$

Note is made at this point that decay rates as predicted by these formulas have been checked against the numerically determined rates and agreement shown to be good for the cases of moderate eccentricity. In no case, however, should the method be employed for eccentricities less than approximately 0.03 since the assumptions made previously restrict the range of applicability of the method. The value 0.03 was determined numerically.

Now, noting that $a = \frac{r_p}{1 - e}$, Eqs (67a, b) can be written in the following form:

$$\left.\begin{aligned} \frac{da}{dt} &= -2B\rho_0 \sqrt{\frac{\mu r_p}{1-\epsilon}}\, F_1 \\ \frac{de}{dt} &= -\frac{1}{a}\left(2B\rho_0 \sqrt{\frac{\mu r_p}{1-\epsilon}}\right) F_2 \end{aligned}\right\} \tag{70}$$

But, since $(-2B\rho_0 \sqrt{\mu r_p})$ is simply the decay rate for a circular orbit at initial perigee altitude, $\left(\frac{dr_p}{dt}\right)_{\epsilon = 0}$, the equations can be rewritten as

$$\frac{da}{dt} = \left(\frac{dr_p}{dt}\right)_{\epsilon = 0} (1 - \epsilon)^{-1/2} F_1 \tag{71a}$$

$$\frac{de}{dt} = \frac{1}{a}\left(\frac{dr_p}{dt}\right)_{\epsilon=0}(1-\epsilon)^{-1/2} F_2 \qquad (71b)$$

From Eqs (45) and (71) the final decay rates are obtained

$$\left.\begin{aligned}\frac{dh_a}{dt} &= \left(\frac{dr_p}{dt}\right)_{\epsilon=0}(1-\epsilon)^{-1/2} G_1 \\ \frac{dh_p}{dt} &= \left(\frac{dr_p}{dt}\right)_{\epsilon=0}(1-\epsilon)^{-1/2} G_2\end{aligned}\right\} \quad 0.03<\epsilon<0.4 \qquad (72)$$

where

$$\left(\frac{dr_p}{dt}\right)_{\epsilon=0} = -2B\rho_0\sqrt{\mu r_p}$$

$$G_1 = (1+\epsilon) F_1 + F_2 \qquad \text{(nondimensional)}$$

$$G_2 = (1-\epsilon) F_1 - F_2 \qquad \text{(nondimensional)}$$

At this point it should be noted that the functions G_1 and G_2, although they are relatively complicated, are nondimensional and need be computed only once. In the present study these nondimensional drag decay parameters for elliptic satellite orbits were hand computed, carrying terms up to ϵ^4. The resulting parametric curves are presented in Fig. 9. Thus, the upper limit on ϵ, $\epsilon_{max} < 0.4$.

This figure shows G_2, the perigee parameter, to be independent of ϵ to a high order of approximation though there is a variation of G_2 with the parameter Z. This behavior is not the case with G_1, the apogee parameter, the reason for this behavior being that apogee decays much more rapidly than perigee for an elliptic orbit. Special attention is also drawn to the curves denoting low eccentricities. These curves will be discussed in subsequent paragraphs.

4. The Case of Small Eccentricities

Since the Bessel function expansions of the previous section are not valid for eccentricities below 0.03, an alternate approach will be applied in this region. This approach was developed by Perkins (Ref. 8) and again assumes an exponential atmospheric model $\rho = \rho_0 e^{-k\Delta r}$. In this analysis a nondimensional parameter C and a drag constant K are defined to be

$$C \equiv kr_p\left[1-\left(\frac{V_c}{V}\right)_p^2\right] = \frac{kr_p\epsilon}{1+\epsilon} = \frac{Z}{(1+\epsilon)^2} \qquad (73)$$

$$K \equiv g_0\frac{C_D A}{W}\rho_0 r_0^2 = 2B\rho_0 r_{p_i}^2 \qquad (74)$$

Using Laplace transformations, the decay rates are found as

$$\left.\begin{aligned}\frac{dr_a}{dt} &= -K\left(\frac{V_{p_0}}{r_{p_0}}\right)e^{-C\left(a+\frac{b}{2}\right)} \\ \frac{dr_p}{dt} &= -K\left(\frac{V_{p_0}}{r_{p_0}}\right)e^{-C\left(a-\frac{b}{2}\right)}\end{aligned}\right\} \qquad (75)$$

But since $V_p r_p = \sqrt{\mu r_p}\,(1+\epsilon)$, Eq (92) can be written as

$$\frac{dr_a}{dt} = \left(\frac{dr_p}{dt}\right)_{\epsilon=0}\sqrt{1+\epsilon}\;\; P^+ \qquad (76a)$$

$$\frac{dr_p}{dt} = \left(\frac{dr_p}{dt}\right)_{\epsilon=0}\sqrt{1+\epsilon}\;\; P^- \qquad (76b)$$

where

$$\left.\begin{aligned}&\left(\frac{\partial r_p}{dt}\right)_{\epsilon=0} = -2B\rho_0\sqrt{\mu r_p} \\ &P^+ = e^{-C\left(a+\frac{b}{2}\right)} \\ &P^- = e^{-C\left(a-\frac{b}{2}\right)} \\ &a = \sum_{n=0}^{\infty}\frac{x^n}{(n!)^2} = 1 + \frac{x}{(1!)^2} + \frac{x^2}{(2!)^2} + \cdots \\ &b = C\sum_{n=0}^{\infty}\frac{x^n}{(n!)^2(n+1)} = C\left[1 + \frac{x}{2(1!)^2} + \frac{x^2}{3(2!)^2} + \cdots\right] \\ &x = (C/2)^2 = \left(\frac{kr_p\epsilon}{2(1+\epsilon)}\right)^2\end{aligned}\right\} \qquad (77)$$

and

The nondimensional parameters P^+ and P^- of Eq (76) are plotted in Fig. 10. The trends of the curves are noted to be the same as those obtained by numerical integrations.

Figure 10 is, of course, limited to small eccentricities, as can be seen from the following example:

Assume:

h_{pi} = 85 stat mi = 448,800 ft = 136,794 meters

r_{pi} = $2.135,170 \times 10^7$ ft = 6.507998×10^6 meters

ϵ = 0.02

Solution

From Fig. 7a:

$$k_0 = 1.98 \times 10^{-5}/\text{ft} = 6.50 \times 10^{-5}/\text{meter}$$

$$\rho_0 = 7.15 \times 10^{-12} \text{ slug/ft}^3$$

$$= 3.684 \times 10^{-9} \text{ kg/meter}^3 \text{ (from Chapter II)}$$

$$\left(\frac{dr_p}{dt}\right)_{\epsilon=0} = -2B\rho_0\sqrt{\mu r_p} = -7.84 \text{ fps} = -2.39 \text{ mps}$$

From Eq (73):

$$C = \frac{kr_p\epsilon}{1+\epsilon} = 8.24$$

From Fig. 10:

$$P^+ = 2.73, \quad P^- = 0.0088$$

From Eq (76a): $\dot{r}_a = \left(\frac{dr_p}{dt}\right)_{\epsilon=0}\sqrt{1+\epsilon}\ P^+$

$$= 2.16 \text{ fps} = 0.658 \text{ mps}$$

From Eq (76b): $\dot{r}_p = \left(\frac{dr_p}{dt}\right)_{\epsilon=0}\sqrt{1+\epsilon}\ P^-$

$$= 0.070 \text{ fps} = 0.021 \text{ mps}$$

Consider the same example for a slightly larger ϵ. If $\epsilon = 0.04$, then $C = 16.1$ and $x = 64$. Proper convergence of Eq (77) now requires an extremely large number of terms (at least 25) thus making the solution impractical.

Thus, since Perkins' methods and the Bessel method are applicable in different regions and since the solutions have the same form, i.e.,

$$\dot{r}_a = \left(\frac{dr_p}{dt}\right)_{\epsilon=0}\sqrt{1+e}\ P^+ \quad \epsilon < 0.03$$

$$\dot{r}_a = \left(\frac{dr_p}{dt}\right)_{\epsilon=0}\sqrt{1+e}\ G_1(z) \quad \epsilon > 0.03$$

and similarly for $\dot{r}_p$. Perkins' parameters P^+ and P^-, can thus be considered to be analytic extensions of the parameters G_1 and G_2. This fact was noted to be responsible for the low eccentricity curves of Fig. 9.

5. Apogee and Perigee Decay Rates and Satellite Lifetimes

The previous Subsections C-3 and -4 have presented in nondimensional form equations and graphical data for $\dot{r}_a$ and $\dot{r}_p$. However, before determining an estimate of the lifetime of a satellite it is necessary to dimensionalize the various parameters. This has been done in Figs. 11a, b, c and 12a, b, c, which present apogee and perigee decay rates both in English and metric units for altitudes in the range 75 to 400 stat mi (120 to 640 km) and eccentricities from 0 to 0.4. It is noted that there are bumps on these curves. These irregularities are the direct result of similar behavior for the density slope of the ARDC 1959 atmosphere. Correction of this data for atmospheric variation will be discussed in Subsection C-6. Changes resulting from changes in the model atmosphere (e.g., 59 ARDC to 62 U.S. Standard) require recomputation of Figs. 11, 12, 13 and 14.

These decay rates must be integrated to yield the lifetime. As was mentioned earlier, this portion of the analysis will be conducted numerically. The reason for this step is simple--it is not desired to introduce further approximation, which could materially affect the accuracy of study. To be sure, approximations have been made to this point; however, the validity of each has been well founded. If a further assumption were made to obtain an integrable form, the accuracy would suffer materially and the attention to detail exhibited earlier would be for naught. Some have argued that since the atmosphere is not known and since the other approximations have been made, such core is unnecessary. While this is true to a degree, a philosophy such as this will never yield good estimates even as the various density variability factors become known, while the philosophy of this section will reflect such improvements.

The integration procedure for this computation is

$$\Delta t_j = \frac{(\Delta h_a)_j}{\left(\frac{dh_a}{dt}\right)_j}$$

where

$(\Delta h_a)_j$ is the j-th apogee altitude increment

$\left(\frac{dh_a}{dt}\right)_j$ is the apogee decay rate at this altitude

thus

$$T_L = \sum_{j=0}^{\text{reentry}} \Delta t_j$$

This integration is very simple and can be rapidly performed even for small values of $(\Delta h_a)_j$. This type of integration also admits several refinements involving the use of iteration and average decay rates rather than instantaneous rates. However, if the step size is sufficiently small this is not necessary. The correct value of $(\Delta h_a)_j$ is determined by the repetition of the same integration until the values of T_L for successive values agree to within a prescribed error. This step size need not be the same for all orbits, but for orbits of similar a and e, the step sizes generally are the same (a value of 500 ft or 150 meters was utilized). The results of this integration are presented in Figs. 13 and 14 in both English and metric units

for a value of B = 1 $\frac{ft^2}{slug}$ or 0.6365×10^{-2} $\frac{meters^2}{kg}$

Decay histories for typical satellites were added in dotted lines in order to indicate the changes in eccentricity and perigee altitude as functions of time.

Lifetimes for all other values of B are obtained via the approximation

$$T_{L_1} B_1 = T_{L_2} B_2$$

or

$$T_{L_2} = \frac{T_{L_1} B_1}{B_2}$$

The basis for this approximation is that the decay rates were all noted to be linear functions of B. Thus, since B is a constant, it does not affect the integration, and as a result lifetime is inversely proportional to B. This behavior is true in free molecular flow; however, as B is made significantly larger or as the altitude is decreased, the vehicle leaves the free molecule region, and the assumptions of this chapter deteriorate. Thus, the simpler conversion must not be used indiscriminately. If there is a question as to the regime of flight, specific data should be prepared. Otherwise the conversion is justifiable.

Though much has been written on the variation of lifetime with eccentricity, it is noted that these figures show the extreme sensitivity of this parameter even for small eccentricities. This sensitivity explains why satellites with the same total energy per unit mass (i.e., same a) do not necessarily have the same lifetime.

6. Comparison with Satellite Data

In the final analysis, the value of a computational technique such as this must be assessed in terms of its ability to predict phenomena correctly. Thus, the actual lifetimes of several satellites will be checked in order to provide this information. First the value of B to be utilized must be computed for initial determinations of lifetime or for preliminary estimates. The value of B must be computed based on estimates made earlier in the discussion of free molecular flow. However, once the initial tracking data from the satellite is available, a more accurate method is available. This method is based on the formulas developed for the change in the element a.

$$a = \frac{r_a + r_p}{2}$$

$$\dot{a} = \frac{\dot{r}_a + \dot{r}_p}{2} = \frac{\dot{h}_a + \dot{h}_p}{2}$$

Thus, if a is known, an effective ballistic coefficient B_{eff} can be found by utilizing the computed $\dot{h}_a$ and $\dot{h}_p$ for B = 1 (rather than the observed values). Thus

$$B_{eff} = \frac{2\,\dot{a}_{observed}}{(\dot{h}_a + \dot{h}_p)_{theoretical}}$$

$$= \frac{\dot{a}_{observed}}{2\,\rho_p \sqrt{\mu a}\,(G_1 + G_2)}$$

This approach compensates for a variety of sins since the nature of the body in question, the mass, the nature of the tumble, and even variations in the density of the atmosphere are factors included in the correction.

TABLE 1

Comparison of Satellite Lifetime Estimates

Name	Effective B* (ft^2/slug)	Effective B* (m^2/kg)	Estimated Lifetimes (days)	Actual Lifetimes (Ref. 15) (days)
Sputnik I	0.69	0.44×10^{-2}	145	92
Sputnik II	1.00	0.64	155	162
Sputnik III	1.13	0.72	221	202
	--	--	--	593
Explorer III	3.69	2.35	84	93
Explorer IV	1.55	0.98	469	455
Score	2.98	1.91	32	34
Discoverer I	~1.5	0.95	12.6	5
Discoverer II	1.50	0.95	11.0	13
Discoverer V	1.46	0.93	45	46
Discoverer VI	1.13	0.72	62	62
Discoverer VII	1.53	0.97	14	19
Discoverer VIII	1.38	0.88	100	109
Discoverer XI	1.65	1.05	9	11
Discoverer XIII	1.04	0.66	87	97
Discoverer XIV	1.30	0.83	24	29
Discoverer XV	1.50	0.95	30	35
Discoverer XVII	0.95	0.61	51	47

*Computed from the satellite data of the initial decay rates of semimajor axis.

(1 ft^2/slug = 0.6365×10^{-2} m^2/kg)

Since effective ballistic coefficient is considered the more accurate, it was used in the construction of the following table.

Two things in Table 1 are important and should be noted. First, the values of B_{eff} as computed from the orbital decay during the first few orbital revolutions are not in all cases in good agreement with the values predicted theoretically. Consider the following examples:

Satellite	B_{eff} (ft^2/slug)	B_{theo} (ft^2/slug)	Agreement	Remarks
Sputnik I	0.69	0.603	Good	Neglecting antennas
Explorer III	3.69	3.71	Good	Random tumbling
Explorer IV	1.55	3.21	Poor	Random tumbling

This being the case, it is necessary to update the knowledge of B as data becomes available in order to obtain reasonable lifetime estimates. The second point is that the agreement between the computed data and the true data is good. To provide an appreciation of the level of improvement, several previous works in the field were reviewed (Refs. 7, 9, 10, 11, 12 and 15). Data for these references are not included here because of the

fact that different atmospheric models and different data for the satellites have been assumed and different corrective procedures (i.e., B_{eff}) utilized in the correction of the results. As a general rule the estimates obtained here are superior to these works, though there were cases for which other curves were more accurate. Since this was expected, the relative value of the approach was determined by a root mean square estimate of the errors in the predicted lifetimes. (The results included here produced approximately 13% error, while those of the literature varied from approximately 15% to 35%.)

This improvement in the agreement seems very significant. However, the magnitude of the final error is still large. The reason for this large error lies in the fact that the method does not provide for atmospheric rotation, for density variability for variations in B, or for the oblate nature of the atmosphere. This being the case, subsequent paragraphs will be devoted to refining the previous work.

D. THREE-DIMENSIONAL ATMOSPHERIC PERTURBATIONS

Due to the fact that the atmosphere rotates, the velocity of the vehicle relative to the atmosphere will not be the velocity of the vehicle relative to space. Thus, the drag force will not lie in the plane of unperturbed motion and each of the six elements or constants of integration will be affected rather than just the three considered previously. Since the equations for variation in the elliptic constants have previously been developed, it thus remains to describe the perturbing force and discuss the resulting motion.

1. The Perturbing Force

The drag acceleration which acts on the vehicle is

$$\frac{\vec{D}}{m} = -B \rho V_r^2 \hat{V}_r$$

where

$$\vec{V}_r = (\vec{V} - \vec{V}_{atm})$$

$$\vec{V}_{atm} = \vec{\Omega}_e \times \vec{r}$$

This acceleration must now be resolved into components in order to permit evaluation of the resultant motion. The specific set of components to be utilized is the set R, S, W discussed in Chapter IV.

$\hat{R}$ is measured along the radius

$\hat{S}$ is measured in the general direction of motion perpendicular to $\hat{R}$

$\hat{W}$ completes the right handed set.

First, the atmospheric velocity

$$\vec{V}_{atm} = \Omega_e \begin{vmatrix} \hat{R} & \hat{S} & \hat{W} \\ \sin i \sin(\theta+\omega) & \sin i \cos(\theta+\omega) & \cos i \\ r & 0 & 0 \end{vmatrix}$$

$$= r \Omega_e \left[\cos i \, \hat{S} - \sin i \cos(\theta + \omega) \, \hat{W} \right]$$

Secondly, the vehicle velocity

$$\vec{V} = \dot{r} \hat{R} + r \dot{\theta} \hat{S}$$

thus

$$\vec{V}_r = \dot{r} \hat{R} + (r\dot{\theta} - r \Omega_e \cos i) \hat{S} + r \Omega_e \sin i \cos(\theta + \omega) \hat{W}$$

and

$$|V_r|^2 = \dot{r}^2 + (r\dot{\theta})^2 - 2r^2 \dot{\theta} \Omega_e \cos i + (r \Omega_e \cos i)^2 + \left[r \Omega_e \sin i \cos(\theta + \omega) \right]^2$$

$$= V^2 - 2H\Omega_e \cos i + r^2 \Omega_e^2 \left[\cos^2 i + \sin^2 i \cos^2(\theta + \omega) \right]$$

$$= V^2 - 2H\Omega_e \cos i + r^2 \Omega_e^2 \left[1 - \sin^2 i \sin^2(\theta + \omega) \right]$$

where

H = the angular momentum per unit mass

$= \sqrt{\mu p}$

This result was also obtained by Sterne (Ref. 18) and Kalil (Refs. 19 and 20). Now at this point the function $|V_r|^2$ must be expressed in terms of the eccentric anomaly in order to facilitate integration with respect to time.

$$V^2 = \frac{\mu}{a} \frac{1 + \epsilon \cos E}{1 - \epsilon \cos E}$$

$$r^2 = a^2 (1 - 2\epsilon \cos E + \epsilon^2 \cos^2 E)$$

thus

$$V_r^2 = \frac{\mu}{a} \frac{1 + \epsilon \cos E}{1 - \epsilon \cos E} \left[1 - \frac{\Omega_e \sqrt{1 - \epsilon^2}}{n} \cos i \frac{1 - \epsilon \cos E}{1 + \epsilon \cos E} + \frac{\Omega_e^2}{n^2} \frac{(1 - \epsilon \cos E)^3}{(1 + \epsilon \cos E)} (1 - \sin^2 i \sin^2(\theta + \omega)) \right]$$

$$n^2 = \mu / a^3$$

But, as was noted by Sterne, Ω_e / n can be no larger than approximately 1/15 for earth satellites; thus V_r can be obtained in an approximate sense by the binomial expansion of the quantity within the braces by neglecting terms of the order

$(\Omega_e/n)^2$. This step appears justifiable in view of the fact that there is such a large uncertainty in the atmospheric density at any time and in the aerodynamic characteristics of the vehicle. Under this assumption, V_r can be expressed as

$$V_r \approx \sqrt{\frac{\mu}{a}\frac{1+\epsilon\cos E}{1-\epsilon\cos E}}\left[1 - \frac{\Omega_e\sqrt{1-\epsilon^2}}{n}\cos i\ \frac{1-\epsilon\cos E}{1+\epsilon\cos E}\right]$$

This equation shows that to the order of corrective terms smaller than approximately $\frac{1}{2}\left(\frac{1}{15}\right)^2$ or $\frac{1}{450}$ the effect of the earth's rotation is a simple function of the inclination and of time. The form of this corrective term being sufficiently simple, the subsequent integration of the equations of motion appears attractive. Now, the drag acceleration is:

$$\frac{\vec{D}}{m} = -B\rho\frac{\mu}{a}\sqrt{\frac{1+\epsilon\cos E}{(1-\epsilon\cos E)^3}}\left[1 - C\frac{1-\epsilon\cos E}{1+\epsilon\cos E}\right]\Big[e\sin E\,\hat{R}$$

$$+\left(\sqrt{1-\epsilon^2} - \Omega_e\cos i\sqrt{\frac{a^3}{\mu}}(1-\epsilon\cos E)^2\right)\hat{S}$$

$$+\Omega_e\sin i\cos(\theta+\omega)\sqrt{\frac{a^3}{\mu}}(1-\epsilon\cos E)^2\,\hat{W}\Big]$$

where

$$C = \frac{\Omega_e\sqrt{1-\epsilon^2}\cos i}{n}$$

But

$$\cos(\theta+\omega) = \cos\theta\cos\omega - \sin\theta\sin\omega$$

$$= \frac{\cos E - \epsilon}{1-\epsilon\cos E}\cos\omega - \frac{\sin E\sqrt{1-\epsilon^2}}{1-\epsilon\cos E}\sin\omega$$

Thus the final form of the drag acceleration is

$$\frac{\vec{D}}{m} = -B\rho\frac{\mu}{a}\sqrt{\frac{1+\epsilon\cos E}{(1-\epsilon\cos E)^3}}\left[1 - C\frac{1-\epsilon\cos E}{1+\epsilon\cos E}\right]\Big[\epsilon\sin E\,\hat{R}$$

$$+\left(\sqrt{1-\epsilon^2} - \frac{C}{\sqrt{1-\epsilon^2}}\sqrt{\frac{a^3}{\mu}}(1-\epsilon\cos E)^2\right)\hat{S}$$

$$+\left(\Omega_e\sin i\sqrt{\frac{a^3}{\mu}}(1-\epsilon\cos E)\right)\left((\cos E - \epsilon)\cos\omega\right.$$

$$\left.-(\sin E\sqrt{1-\epsilon^2})\sin\omega\right)\hat{W}\Big]$$

2. The Change in the Orbit

At this point it is necessary to refer to equations for the time variations of the orbital elements (Eqs (60), Chapter IV) or to the form utilized by Sterne and presented in Plummer (Ref. 21):

$$\frac{da}{dt} = \frac{2}{n}\left[R\tan\phi\sin\theta + S\sec\phi(1+\epsilon\cos\theta)\right]$$

$$\frac{d\epsilon}{dt} = \frac{a}{n}\cos\phi\left[R\sin\theta + S(\cos\theta+\cos E)\right]$$

$$\frac{di}{dt} = \frac{r\cos(\theta+\omega)}{n\,a^2\sin i\cos\phi}W$$

$$\frac{d\Omega}{dt} = \frac{r\sin(\theta+\omega)}{n\,a^2\sin i\cos\phi}W$$

$$\frac{d\omega}{dt} = -\frac{a\cos^2\phi\cos^2\theta\,R - r\sin\theta(2+\epsilon\cos\theta)}{n\,a^2\sin\phi\cos\phi}S$$

$$+\frac{r\sin(\theta+\omega)}{n\,a^2\cos\phi\tan i}W$$

$$\frac{d\epsilon'}{dt} = -\frac{2r\,R}{n\,a^2} + 2\sin^2\frac{\phi}{2}\frac{d(\omega+\Omega)}{dt}$$

$$+2\cos\phi\sin^2\frac{i}{2}\frac{d\Omega}{dt}$$

where

$\sin\phi = (1-\epsilon^2)^{1/2}$ as is customary in some of the astronomical texts

ϵ' = mean longitude at the epoch

R, S, W = the components of the disturbing acceleration

At this point it is noted that since

$$n(t-t_0) = E - \epsilon\sin E,$$

$$\dot{E} = \frac{n}{1-\epsilon\cos E}$$

Also from Chapter III,

$$\cos\theta = \frac{\cos E - \epsilon}{1-\epsilon\cos E}$$

$$\sin\theta = \frac{\sqrt{1-\epsilon^2}\sin E}{1-\epsilon\cos E}$$

Thus the expressions for the changes in the orbital elements obtained by substituting for R, S and W can be transformed into functions of the independent variable E and its time rate $\dot{E}$. Integration for the secular change in each element would then be possible (utilizing the limits for E of 0 to 2π) if the density could also be expressed as a function of the variable E.

As was noted in previous sections of this chapter, the density of the true atmosphere does not vary exponentially with altitude. However, as was also noted for small variations in the altitude the approximation is valid. Selecting once again the perigee altitude as the reference for the approximation (since the largest portion of the drag force occurs near perigee), the density can be written as

$$\rho = \rho_0\, e^{-K(h - hp)}$$

where

ρ_0 = density at perigee

$h = a(1 - \epsilon \cos E) - R_e \left[1 - f \sin^2 i \sin^2(\theta + \omega)\right]$

$h_p = a(1 - \epsilon) - R_e \left[1 - f \sin^2 i \sin^2 \omega\right]$

$h - h_p = a\epsilon(1 - \cos E) + R_e f \sin^2 i \left[\sin^2(\theta + \omega) - \sin^2 \omega\right]$

R_e = earth's equatorial radius

Thus the approximate density is

$$\rho = \rho_0 \exp\left[-Z(1 - \cos E) + q(\sin^2(\theta + \omega) - \sin^2 \omega)\right]$$

where Z was previously defined to be $Ka\epsilon$, and where

$$q \equiv K R_e f \sin^2 i$$

At this point Sterne presents a Taylor expansion of ρ in the form

$$\rho = \rho_0 e^{-Z} e^{Z \cos E} \sum_{\ell=0}^{\infty} \frac{(-q)^\ell}{\ell!} (\sin^2(\theta + \omega) - \sin^2 \omega)^\ell$$

$$= \rho_0 e^{-Z} e^{Z \cos E} \sum_{m=0}^{\infty} q'_{2m} \frac{\sin^{2m} E}{(1 - \epsilon \cos E)^{2m}}$$

In the series, the terms which are odd functions of θ are also odd functions of E and may be ignored since they will not contribute to the complete integral for the secular changes in the elements. Using the even part of the series through terms in q^4, which gives the series accurately to about 1 part in 1000 for the altitudes in which this study is concerned, Kalil obtained

$$q_0 = 1$$

$$q_1 = (1 - \epsilon^2)\left(-q \cos 2\omega + \frac{q^2}{2} \sin^2 2\omega\right)$$

$$q_2 = (1 - \epsilon^2)^2 \left[\frac{q^2}{2} \cos 4\omega - \frac{q^3}{2} \cos 2\omega \sin^2 2\omega + \frac{q^4}{24} \sin^4 2\omega\right]$$

$$q_3 = (1 - \epsilon^2)^3 \left[-\frac{q^3}{6} \cos^3 2\omega + \frac{q^3}{2} \cos 2\omega \sin^2 2\omega + \frac{q^4}{24} \cos^2 2\omega \sin^2 2\omega - \frac{q^4}{12} \sin^4 2\omega\right]$$

$$q_4 = (1 - \epsilon^2)^4 \left[\frac{q^4}{24} \cos^4 2\omega - \frac{q^4}{16} \sin^2 4\omega + \frac{q^4}{24} \sin^4 2\omega\right]$$

Since the angle ω is approximately constant during any single revolution, the q_i can be treated as approximate constants when integrating over one revolution, without the introduction of appreciable error.

It is noted that according to the remainder theorem for alternating series, a series whose terms are alternately positive and negative, and such that their absolute values form a monotone null sequence, is convergent (this is the case here for the series expansion of the atmospheric density). This being the case, the absolute value of the remainder after n terms of such a series does not exceed the absolute value of the (n + 1) st term. Hence, the relative error introduced in the series expansion of the atmospheric density by retaining only terms through q^n is

$$\Delta \rho < \frac{q^{n+1}}{(n+1)!} \exp(q)$$

Thus, by retaining terms through q^2, the relative error in ρ is 3.4% at altitudes of 100 naut mi (185 km) where $q \sim 0.5$, and only 0.16% at altitudes of 200 naut mi (370 km) where $q \sim 0.2$.

Upon substitution of this density model into the equations of variation of constants and performing the integration, Sterne reported the following secular changes in the elements:

$$(\Delta a)_{sec} = -2B \sqrt{\mu a} \frac{(1 + \epsilon)^{3/2}}{(1 - \epsilon)^{1/2}} \left[1 - C \frac{1 - \epsilon}{1 + \epsilon}\right]^2 \rho_0 \sqrt{\frac{1}{2\pi Z}} \cdot \left[1 + \frac{f_1}{8Z} + \frac{9 f_2}{128 Z^2} + \cdots\right]$$

$$(\Delta \epsilon)_{sec} = -2B(1 - \epsilon^2) \sqrt{\frac{1 + \epsilon}{1 - \epsilon}} \left[1 - C \frac{1 - \epsilon}{1 + \epsilon}\right]^2 \rho_0 \sqrt{\frac{\mu}{2\pi a}} \left[1 - \frac{1}{8Z}\left(3 + 4\epsilon N + \frac{4\epsilon^2}{1 - \epsilon^2} + \frac{4\epsilon C}{1 - C + \epsilon + \epsilon C}\right) + \cdots\right]$$

$$(\Delta i)_{sec} = -\frac{B}{2} \Omega_e \sin i (1 - \epsilon^2)\left(1 - C \frac{1 - \epsilon}{1 + \epsilon}\right) a \rho_0 \sqrt{\frac{1}{2\pi Z}} \cdot \left\{1 + \frac{1}{8Z}\left[1 - 4\epsilon N + 4\epsilon \frac{3 + 2\epsilon}{1 + \epsilon^2}\right] + \cdots + \cos 2\omega \left[1 - \frac{1}{8Z}\left(15 + 4\epsilon N + 4\epsilon \frac{5 + 6\epsilon}{1 - \epsilon^2}\right) + \cdots\right]\right\}$$

$$(\Delta \Omega)_{sec} = -\frac{B}{2} \Omega_e \sin 2\omega (1 - \epsilon^2)\left(1 - C \frac{1 - \epsilon}{1 + \epsilon}\right) a \rho_0 \sqrt{\frac{1}{2\pi Z}} \cdot \left\{1 - \frac{1}{8Z}\left(15 - 4\epsilon \frac{3 - 2\epsilon}{1 - \epsilon^2} + 4\epsilon N\right) + \cdots\right\}$$

$$(\Delta \omega)_{sec} = -\cos i \, (\Delta \Omega)_{sec}$$

$$(\Delta \epsilon')_{sec} = (1 - \cos i)(\Delta \Omega)_{sec}$$

or

$$(\Delta M)_{sec} = 0$$

where

$$f_1 = 1 - 8\epsilon N - \frac{4\epsilon^2}{1-\epsilon^2} + 8q_1 \frac{1}{(1-\epsilon)^2}$$

$$f_2 = 1 + \frac{8}{3}\frac{\epsilon^2(1+5\epsilon^2)}{(1-\epsilon^2)^2} + \frac{16}{3}\frac{\epsilon N(5\epsilon^2-1)}{1-\epsilon^2} + \frac{32}{3}\epsilon^2 N^2 - \frac{16}{3}q_1(1+10\epsilon+8\epsilon N) + \frac{128}{3}q_2(1+4\epsilon)$$

$$N = \frac{1+C}{1-C+\epsilon+\epsilon C}$$

These results are believed valid for all of the cases for which $Z > 2$ to the order of q_2 and represent the solution well for such cases. However, if $Z < 2$ a more general solution is necessary. This solution suggested in Sterne's paper (carried out for the element a) is reported for the elements a and e by Kalil. The results are shown below.

$$(\Delta\tau)_{sec} = -6\pi\tau B a (1-C)^2 \rho_0 e^{-Z} \sum_{n=0}^{5} A_n I_n(Z)$$

$$(\Delta a)_{sec} = -4\pi B a^2 (1-C)^2 \rho_0 e^{-Z} \sum_{n=0}^{5} A_n I_n(Z)$$

$$(\Delta e)_{sec} = -4\pi B a (1-\epsilon^2) \rho_0 e^{-Z} \sum_{n=0}^{5} B_n I_n(Z)$$

where the constants evaluated for small eccentricities (i.e., $e^3 << 1$) are presented below:

$$A_0 = 1 + \epsilon^2(j^2 + \tfrac{1}{2})$$

$$A_1 = 2j\epsilon - \frac{\epsilon^2}{Z}(j^2+\tfrac{1}{2}) + \frac{q}{Z}\left[1 + \epsilon^2(j^2+4j+\tfrac{7}{2})\right]$$

$$A_2 = 2q_1\frac{\epsilon}{Z}(j+1) - 3\frac{\epsilon^2}{Z^2}q_1(j^2+4j+\tfrac{7}{2}) + 3\frac{q_2}{Z^2}$$

$$A_3 = 6\frac{\epsilon}{Z}q_2(j+2) + 15\frac{q_3}{Z^3}$$

$$A_4 = \frac{15q_3}{Z^3}\left[2\epsilon(j+3) + \frac{\epsilon^2}{Z}(j^2+12j+\tfrac{43}{2})\right] + \frac{105q_4}{Z^4}$$

$$A_5 = 210\, q_4 \frac{\epsilon}{Z^4}(j+4)$$

$$B_0 = \epsilon(2C+1)$$

$$B_1 = (1-C)^2 - \frac{3C+2}{2Ka} + \frac{q_1}{Ka}(3-2C)$$

$$B_2 = \frac{q_1}{Z}\left[(1-C)^2 - \frac{3}{2Ka}(6-5C)\right]$$

$$B_3 = \frac{q_1}{Z^2}\frac{33}{2}\epsilon^2 + \frac{3q_2}{Z^2}\left[(1-C)^2 + \frac{1}{2Ka}(10+17C)\right] + \frac{q_3}{Z^2}\frac{15}{Ka}(7-10d+6C^2)$$

$$B_4 = \frac{3q_2}{Z^2}\left[\frac{97}{2Ka} + \epsilon(5-4C)\right] + \frac{15q_3}{Z^3}\left[(1-C)^2 - \frac{7}{Ka}(7 - \frac{21}{2}C + 6C^2) + \epsilon^2(\frac{55}{2} - 30C + 21C^2)\right] + \frac{q_4}{Z^3}\frac{105}{Ka}(9-14C+8C^2)$$

$$B_5 = -\frac{q_3}{Z^4}(105\epsilon^2)\left[\frac{55}{2} - 33C + 21C^2\right] + \frac{q_4}{Z^4}(105)\left[(1-C)^2 - \frac{9}{Ka}(9 - \frac{29}{2}C + 8C^2) + \epsilon^2(\frac{89}{2} - 56C)\right]$$

$$j = \frac{1+C}{1-C}$$

K = negative log density slope

The symbols C, Z, ϵ and q_i are the same in this set of equations as previously defined. The reduction formulas discussed earlier can also be utilized, to relate all of the higher order Bessel functions to the fundamental functions $I_0(Z)$ and $I_1(Z)$. This step simplifies the numerical evaluation of the time history of the decay; however, it only serves to make the functional form of the resultant equations more complex. For this reason the equations are left in their present form.

This set of equations is believed valid for satellite orbits extending down to approximately 180 km with errors less than several percent. Thus, if the inclination of the orbit were to be specified, the equations could be integrated numerically to yield realistic lifetime and decay histories for the vehicle as was done in the discussion of the nonrotating atmosphere. The possibility of being able to construct a family of lifetime figures for various inclinations is also noted, though to date this has not been accomplished. Indeed, this step does not appear attractive for general computations because the procedure would result in an error source when data is applied for values of B other than that utilized in the construction of the figures. Thus, the most attractive procedure involves the numerical integration of the decay rates for each satellite of interest. This approach, though more cumbersome, will be more numerically exact and should result in errors approaching an order of magnitude less than those obtained with the nonrotating atmospheric analysis.

Though numerical data is not presented, several general observations will be made. First, the equations show that the effect of the atmospheric rotation is to decrease inclination for all orbits (inclination defined $0° \leq i \leq 180°$). Secondly, the effect is to decrease the rate at which a and ϵ vary for $i < 90°$ and increase the rate $i > 90°$. Thirdly, rotation produces secular regression and precession of the osculating ellipse.

Numerical computations reported by Sterne substantiate not only these general trends but also to a good degree, the numerical values of the perturbed elements. This being the case, the theory as evinced by the equations of this section is believed to represent the best theoretical estimate of the behavior of the vehicle.

E. THE EFFECTS OF DENSITY VARIABILITY (Ref. 22)

To this point the approximations made in the discussion of atmospheric effects have been refined to include oblateness and rotation. Still no mention has been made of the effects of density variability. If the time intervals are large and the altitudes sufficiently high that the forces are not extremely large, the density variability effects will tend to null out due to the fact that the model atmosphere approximates average conditions. These cases are treated in previous discussions to varying degrees of approximation. However, if the time intervals are short or the densities more significant, the effect of variability will be more pronounced, and the equation should be integrated with the estimated density rather then with the model density. One approach to the problem of analysis of this latter case was shown in Chapter IV-C-6-d, which discusses random drag fluctuations. The following paragraphs (Ref. 22) extend this approach and provide some numerical data which is of general interest. The parameter of these discussions is the time of nodal crossing, a readily observable and easily computed quantity; the other parameters, be they orbital elements or position and velocity, should be checked as time permits. One such investigation is reported in Ref. 23.

1. Errors in the Time of Nodal Crossing due to Drag Fluctuations Alone

The contribution of random drag fluctuations to the rms error in predicted time of nodal crossing depends on the correlation function of the random fluctuations, which is unknown. Upper and lower bounds, however, can be constructed. These bounds on the random error are given in Fig. 15. In the upper bound, the random drag fluctuations are assumed independent from one revolution to the next. In the lower bound, the random fluctuations are assumed perfectly correlated over intervals of 25 revolutions, but uncorrelated from interval to interval. The curves actually show the ratio of the standard deviation of the prediction to the standard deviation of the random fluctuation, σ, which is calculated from observations smoothed over intervals of 25 revolutions.

The estimation of σ is thus necessary to translate the data of this figure to errors in the predicted time. No completely satisfactory method is available to perform this function; however, observations of satellites with perigees in the range 220 to 650 km indicate that σ (in minutes/revolution) is given by the empirical equation

$$\sigma = 2.2 \times 10^{-3} h_p \left|\dot{\tau}\right| . \qquad (78)$$

where h_p is the height of perigee in km, and $\dot{\tau}$ is the smoothed rate of change of period (unperturbed by sinusoidal and random fluctuations) in minutes per revolution.

For orbiting satellites the smoothed rate of change of period, $\dot{\tau}$, can be determined from observations. For satellites not yet launched, the values obtained from the previous discussions can be used as an estimate for the smoothed rate of change of period.

A simple approximation for the prediction error caused by both of the assumed random drag fluctuations is dashed in between the two bounds in Fig. 15. It is

$$G_{rms}(N)/\sigma = 5\,(N^3/3)^{1/2} \qquad (79)$$

where $G_{rms}(N)$ is the rms error in the predicted time of nodal crossing (in minutes), N revolutions after the orbit was perfectly known. Equation (79) is asymptotic to both bounds and all three curves derived in Chapter IV.

The contribution of a different assumption (i.e., of a sinusoidal drag variation) to the error in the time of nodal crossing is given by

$$H_{rms}(N) = (2)^{-1/2} A (k)^{-2} \left\{ \left[1 - \cos(kN) - (kN)^2/2 \right]^2 + \left[kN - \sin(kN) \right]^2 \right\}^{1/2} \qquad (80)$$

where:

H_{rms} = the rms sinusoidal prediction error (in minutes) for arbitrary initial phase of the sinusoidal drag

$A = 1.8\, h_p \left|D\right| \times 10^{-3}$ (empirically determined for same conditions as σ, Eq (78)). (81)

h_p = perigee altitude(km)

$k = (1.61\,\tau)\, 10^{-4}$

τ = the period in minutes

Thus the sinusoidal and random errors can be combined to give the rms error in timing of an orbital prediction when the initial elements are perfect:

$$\Delta \tau_n (N) = \left\{ G^2_{rms} (N) + H^2_{rms} (N) \right\}^{1/2} . \quad (82)$$

Now, if the local speed of nadir point is V_0, and changes only slightly during the N periods over which the prediction is made, then the corresponding positional error tangential to the projection of the orbit on the earth is

$$X (N) = V_0 \Delta \tau_n (N) \quad (83)$$

2. Errors in Orbital Predictions When the Elements and Rate of Change of Period are Obtained by Smoothing Observations

In the preceding simplified formulas, a perfect knowledge of the orbit at the initial time, or epoch, has been assumed. In actual orbital predictions, the elements at the epoch and the rate of change of period are usually found by some smoothing procedure, using data containing observational errors. (Discussions of the errors made by various satellite tracking devices appear in Chapter XI.) Thus, to be rigorous these error sources must also be included in the analysis.

Suppose that the rate of change of period is calculated from $M(\leq i)$ "measured" times of nodal crossing, which are uniformly distributed throughout an interval of i revolutions. Assume that there are three independent causes of fluctuations in the "measured" time of nodal crossing:

(1) A 27-day sinusoidal variation in the rate of change of period

(2) A random fluctuation in the rate of change of period, which is independent from revolution to revolution

(3) A measurement error introduced by the tracking device.

Of course, only (3) can be regarded as an error of measurement, but (1) and (2) will contribute an error to the smoothed values of the period and the rate of change of period. The errors will be given as a function of the number of revolutions N, after the epoch. The epoch is taken to be at the center of the smoothing intervals.

(1) The contribution of the smoothed sinusoidal drag variation to the rms error in an orbital prediction which runs for N revolutions from the epoch is

$$S(N) = \frac{A}{k^2 \sqrt{2}} \left(\alpha^2 + \beta^2 \right)^{1/2} \quad (84)$$

where

$$\alpha = \cos kN - \frac{2i}{k} \sin \left(\frac{ik}{2} \right) + \frac{64}{i^3 k} \sin \left(\frac{ki}{4} \right) \cdot \left[1 - \cos \left(\frac{ki}{4} \right) \right] \left[N^2 - \frac{(i+2)i}{12} \right]$$

$$\beta = \sin kN - kN + 8N \left[i (i+2) k \right]^{-1} \cdot \left[\cos \left(\frac{ki}{2} \right) - 1 + \frac{i^2 k^2}{8} \right]$$

and A is given by Eq (81), i is the smoothing interval in revolutions, and $k = 1.61 \times 10^{-4} \tau$, where τ is the period in minutes.

As the smoothing interval, i, approaches zero, Eq (84) approaches Eq (80), which represents the sinusoidal error when there is no smoothing. The quantity S(N)/A is graphed in Figs. 16a through 16d.

(2) The contribution of the smoothed random fluctuation to the rms error in orbital prediction is

$$R(N) = 5\sigma \left\{ \frac{N^3}{3} + 2 \left(\frac{i}{4} \right)^3 \left[\frac{64}{5} \left(\frac{N}{i} \right)^4 - 16 \left(\frac{N}{i} \right)^3 + \left(\frac{N}{i} \right)^2 - \frac{1}{20} \right] \right\}^{1/2} \quad \text{for } i >> 1 \quad (85)$$

where σ is given by Eq (78).

Equation (85) should be compared with its unsmoothed counterpart, Eq (79). The quantity $R(N)/(5\sigma)$ is graphed in Fig. 17.

The contribution of smoothed measurement errors to the rms error in the predicted time of the Nth nodal crossing is

$$O(N) = \sigma_0 (M)^{-1/2} (i)^{-2} \left\{ (i)^4 \cdot \left[M (M+2)^{-1} + (16/9) (M+2)^2 / M^2 \right] + 256 N^4 + 16 (Ni)^2 \left[M (M+2)^{-1} - (8/3) (M+2)/M - 2M (M+2)^{-2} \right] + 32 N i \cdot \left[(i)^2/(3M) - 4N^2 (M+2)^{-1} \right] \right\}^{1/2} \quad (86)$$

where all the observations are assumed to have the same standard deviation, σ_0, and M is the number of observations in a smoothing interval of i revolutions. The quantity $O(N)/\sigma_0$ is graphed in Fig. 18. The observational errors, σ_0, made by various tracking devices are given in Chapter XI. In order to have the error given by Eq (86) in minutes of time, it is necessary to use σ_0, the error of a single observation in minutes of time. Angular errors, $\Delta\theta$ (in radians), can be approximately converted to timing errors, σ_0 (in minutes)

by

$$\sigma_0 \approx \left(1 + \frac{h}{R_e}\right)^{-1} h \frac{\Delta\theta}{V_0} , \qquad (87)$$

where h is the height of the satellite, and R_e is the radius of the earth, and V_0 is the local speed of the nadir point in units of length per minute.

Doppler errors are more difficult to convert to errors in timing. They are subject to refraction and azimuth uncertainties, and it is difficult to tell how many independent observations are made in one pass. In addition, refraction and oscillator instability can create biases as large as the random errors of observations, and these biases cannot be reduced by smoothing observations from a pass over a single station. The observational error in minutes for one independent doppler observation is approximately

$$\sigma_0 \approx (t_f - t_i) \frac{\Delta\dot{r}}{(\dot{r}_i - \dot{r}_i)} , \qquad (88)$$

where the range rate changes from an initial value of $\dot{r}_i$ to a final value $\dot{r}_f$ during the time $(t_f - t_i)$, in minutes, that a doppler signal is being measured by the station. The range-rate error in a doppler observation is $\Delta\dot{r}$. For a typical case, $(t_f - t_i)$ is 10 minutes, and $(\dot{r}_i - \dot{r}_f)$ is 20,000 feet per second (or 6100 mps).

There is an important difference between Eq (87) on the one hand, and Eq (88) on the other. Equation (87) is applicable to each individual observation, hence to the average of a group of observations. Equation (88) only represent average conditions, so they only apply to the average of a group of observations, such as would be used with Eq (86).

The errors are given as a function of the number of revolutions after the epoch assumed to be at the center of the smoothing interval. Now assuming that the observational, sinusoidal, and random errors are independent, they can be combined to give

$$E_{rms}(N) = \left\{ [O(N)]^2 + [S(N)]^2 + [R(N)]^2 \right\}^{1/2} \qquad (89)$$

where $E_{rms}(N)$ is the standard deviation of the predicted time of the Nth nodal crossing after the epoch, when the elements and rate of change of period are obtained by smoothing observations. $E_{rms}(N)$ represents the error tangential to the orbit of the satellite projected on the celestial sphere. Errors at right angles to the orbit are usually an order of magnitude smaller.

Errors in actual predictions issued by the Vanguard Computing Center, NASA Computing Center, Smithsonian Astrophysical Observatory, and Naval Weapons Laboratory are compared with the theoretical model in Tables 2 and 3. Table 2 contains the errors in one to two-week predictions made near the peak of the sunspot cycle. Table 3 shows the errors in predictions half-way between sunspot maximum and sunspot minimum. In the tables, N is the number of revolutions predicted, beginning at the center of the smoothing interval. The smoothed rate of change of period is $\dot{\tau}$ (minutes per revolution). The root-mean-square prediction error, E_{rms} (N) (in minutes), includes the contributions of observational errors and drag fluctuations. theoretical prediction error caused by obse errors alone is designated by O(N).

TABLE 2

Prediction Errors Near Peak of Sunspot Cycle

Satellite	Dates	No. of Predictions	$-\dot{\tau}$ (Min/Rev)	N (Rev)	O(N) (Min)	E_{rms} (N) Actual (Min)	E_{rms} (N) Theoretical (Min)
Explorer IV	1958	8	2.15×10^{-3}	165	0.024	3.2	3.7
Sputnik III	1958	7	1.32×10^{-3}	220	0.01	3.3	1.9
Vanguard I	Fall, 1958	20	5.5×10^{-5}	154	0.056	0.25	0.22
Vanguard I	Summer, 1959	11	2.1×10^{-5}	154	0.056	0.13	0.097
Vanguard I	Winter, 1959 to 1960	7	6.5×10^{-6}	154	0.056	0.062	0.061
Atlas-Score	Dec. 1958 to Jan. 1959	1*	2.2×10^{-2}	271	0.3	67.0	74.0

*A single observation has no statistical significance. This case is included merely to show how large the error can be when the rate of change of period is large.

TABLE 3

Prediction Errors Half-Way Between Sunspot Maximum and Minimum

Satellite	Dates	No. of Predictions	$-\dot{\tau}$ (Min/Rev)	N (Rev)	O (N) (Min)	E_{rms} (N)	
						Actual (Min)	Theoretical (Min)
Tiros II	Dec. 1960 to May 1961	12	3.7×10^{-6}	250	0.08	0.12	0.08
Vanguard I	Oct. 1960 to May 1961	12	7.4×10^{-6}	150	0.06	0.12	0.06
Transit III-B	Feb. to Mar. 1961	10	1.05×10^{-2}	22	0.04	0.74	0.50
Echo I	Oct. to Dec. 1960	6	6.8×10^{-4}	145	0.04	4.4	3.3

TABLE 4

Errors in Individual Orbital Predictions for Vanguard I

Number of Pass	Errors (seconds of time)	Number of Pass	Errors (seconds of time)
2309	+37	2159	-12
2986	-25	1708	-12
2836	+21	2685	-11
2234	-21	2009	- 9
2459	+17	1633	- 7
2535	-16	2384	+ 6
3173	+14	2760	- 3
1934	-14	2084	+ 2
2911	+12	1858	+ 2
2610	-12	1783	+ 1

E_{rms} = 15 seconds = 0.25 minutes

It is interesting to note that observational errors were the principal cause of errors in orbital predictions for only one of the cases shown, that of Vanguard I with its perigee in darkness (Winter 1959-1960). In all the cases, the prediction errors attributable to observational errors were smaller than the total error for Vanguard I in darkness. If the errors in predictions had been caused mainly by observational errors, then the prediction errors would have been independent of the smoothed rate of change of period. A detailed discussion of the theory and the method of calculation is given in Ref. 21.

Theoretical calculations of the errors in orbital predictions by the methods described above are subject to uncertainties because of variations in methods of fitting, spin of nonspherical satellites, and sampling errors as well as uncertainties in the estimates of the smoothing intervals. The uncertainty in the theoretical rms error is approximately +100 to -50 percent. All of the examples in Tables 2 and 3 were within these bounds. Deviations from the theoretical model have tended to be on the high side so far (1958 to 1961). During the two years near sunspot minimum, the percentage variations of the decimeter solar flux (which is correlated with atmospheric density) are only one-third as large as during the rest of the sunspot cycle, so the deviations from the theoretical model can be expected to be on the low side during 1963 and 1964.

E_{rms} (N) in Tables 2 and 3 is, of course, a root-mean-square error. The error in an individual prediction can be larger or smaller than the root-mean-square value, and can be positive or negative. The distribution function appears to be normal. Table 4 shows the individual errors in twenty predictions made for Vanguard I when its perigee was in sunlight (Fall, 1958).

3. Errors in Orbital Predictions When the Rate of Change Period is Calculated from a Standard Atmosphere

The usual way of making satellite orbital predictions is to compute the elements and rate of change of period at the epoch by smoothing all the observations made during a certain time interval (usually a few days). This orbit is then projected forward in time. All of the predictions listed in Tables 2 and 3, with the possible exception of the predictions for Transit III-B, were made by this method. The theory appropriate to this method of making predictions has been described above. The theory for the case in which the rate of change of period is derived from a standard atmosphere will now be described. Such a method might be used when there are not enough observations to determine the rate of change of period. In this case, the error can be separated into three parts, described under the following headings:

(1) The error in the period and the time of nodal crossing.

(2) The error caused by computing the rate of change of period from a standard atmosphere.

(3) The error caused by the sinusoidal and random drag fluctuations.

(1) If the period and the time of nodal crossing at the epoch are obtained by a single orbital fit over N revolutions containing M independent observations, then the errors in the period, $\Delta\tau$ (in minutes), and time, Δt (in minutes), caused by observational errors, are

$$\Delta t \approx \sigma_0 M^{-1/2} \tag{90}$$

and

$$\Delta\tau \approx 4\sigma_0 i^{-1} M^{-1/2} \tag{91}$$

where σ_0 is the error of a single independent observation (in minutes of time) and may be obtained from the observational errors in angular and doppler units by Eqs (87) and (88), respectively.

In the case of precision doppler observations, an alternative method of calculating the period is feasible but is not recommended, because it produces large errors in the period. This method is to compute independent values of the elements from each pass of doppler data recorded by a station, and average all the sets of elements derived during i revolutions. The errors in period and timing (caused by observational errors) produced by this method are roughly

$$\Delta t \approx \sigma_0 (M)^{-1/2} \tag{90a}$$

and

$$\Delta\tau \approx \sigma_0 \left(\frac{2}{M}\right)^{1/2} \frac{\tau}{t_f - t_i} , \tag{91a}$$

where $(t_f - t_i)$ is the time interval during which a single station is recording doppler data during a pass.

(2) The rate of change of period $\dot{\tau}$ can be approximately calculated by using the theory of drag perturbations in Chapter IV and one of the standard atmospheres described in Chapter II. This method is not precise and a certain amount of error is thus inserted. However, the magnitude of this error can not be described analytically and must thus be accepted.

(3) The errors caused by sinusoidal and random drag fluctuations are given by Eqs (80) and (79), respectively. The reason for using models which do not include smoothing is that $\dot{\tau}$ is obtained from a standard atmosphere.

Now that the three factors have been discussed, the predicted time of nodal crossing can be written in the following form:

$$t_p(N) = t + N\tau + \left(\frac{N^2}{N}\right)\dot{\tau} \tag{92}$$

where the errors in predictions contributed by the time of nodal crossing, the period, and the rate of change of period are Δt, $N\Delta\tau$, and $(N^2/2)\,\tau$, respectively.

If the coupling among the period and the time of nodal crossing (which should not cause much error) is ignored, then the root mean square error in a prediction made with a standard atmosphere, N revolutions after the epoch, is approximately

$$E_{rms}^*(N) = \left\{ (\Delta t)^2 + (N\Delta\tau)^2 + \left(\frac{N^2}{N}\,fD\right)^2 + \left[G_{rms}(N)\right]^2 + \left[H_{rms}(N)\right]^2 \right\}^{1/2} , \tag{93}$$

where the epoch is taken to be the center of the smoothing interval employed in calculating the period and time of nodal crossing. Equation (93) applies in cases in which a standard atmosphere is used for calculating the rate of change of period. The error $E_{rms}^*(N)$ is tangential to the orbit of the satellite projected on the celestial sphere. The error at right angles to the orbit is usually smaller.

4. Example

Problem:

Calculate the root-mean-square error in an orbital prediction for Explorer IV, 165 revolutions from the center of the smoothing interval. The period at the time of interest was 109 minutes, and the heights of perigee and apogee were 142 and 1190 naut mi or 263 and 2200 km, respectively. The smoothing interval is estimated to be i = 100 revolutions, the number of observations, M = 25, and the prediction interval, N = 165. The smoothed rate of change of period, $\dot{\tau} = -2.15 \times 10^{-3}$ min/rev, and the observational error is estimated to have been 0.7 milliradian. The elements and rate of change of period were derived by smoothing observations.

Solution:

The errors given by Eqs (84) through (89) are appropriate. The average height of the satellite h, was 666 naut mi or 1232 km and the approximate speed of the nadir point was $V_0 \approx 2\pi R_e/P = 198$ naut mi per minute or 367 km/min, so Eq (87) gives for the average error of an observation, $\sigma_0 = 2 \times 10^{-3}$ minutes. From Fig. 18, $O(N)/\sigma_0 = 12$, so the contribution of observational errors to the error

in an orbital prediction is 2.4×10^{-2} minutes. The normalized random error, $R(N)/(5\sigma)$ is 1.6×10^{3}, from Fig. 17. According to Eq (78), σ is 3.7×10^{-4} minutes per revolution. Therefore, the prediction error caused by random fluctuations is 2.95 minutes. The normalized sinusoidal error is $S(N)/A = 7.5 \times 10^{3}$, interpolating between Figs. 16b and 16c. According to Eq (81), A is 3.06×10^{-4} minutes per revolution. Therefore, the prediction error caused by the sinusoidal variation is 2.3 minutes. Combining the three errors by Eq (89), the theoretical error of prediction is 3.7 minutes. For comparison, the root-mean-square error of eight predictions issued by the Vanguard Computing Center was 3.2 minutes.

F. REFERENCES

1. Eckert, E. and Drake, R., "Heat and Mass Transfer," McGraw-Hill Publishing Company (New York), 1959.
2. Ashley, H., "Applications of the Theory of Free Molecule Flow to Aeronautics," IAS Journal, Vol. 16, 1949, pp 95 to 105.
3. Stalder, J. R. and Zurick, V. J., "Theoretical Aerodynamic Characteristics of Bodies in a Free Molecule Flow Field," NASA TN2423, 1951.
4. Stalder, J. R., et al., "A Comparison of Theory and Experiment for High Speed Free Molecule Flow," NASA TN 2244, 1950.
5. Schramberg, R., "A New Analytical Representation of Surface Interaction for Hyperthermal Free Molecule Flow with Application to Satellite Drag," Heat Transfer and Fluid Mechanics Institute, June 1959.
6. Kork, J., "Satellite Lifetimes in Elliptic Orbits," Chapter V, "Design Guide to Orbital Flight," McGraw-Hill, 1962.
7. Roberson, R. E., "Effect of Air Drag on Elliptic Satellite Orbits," Jet Propulsion, Vol. 28, No. 2, February 1958, p 90.
8. Perkins, F. M., "An Analytical Solution for Flight Time of Satellites in Eccentric and Circular Orbits," Astronautica Acta, Vol. IV, Fasc. 2, 1958, p 113.
9. Breakwell, J. V. and Koehler, L. F. "Elliptical Orbit Lifetimes," American Astronomical Society, Preprint No. 58-34, August 1958.
10. "Dynamic Analysis and Design Performance Requirements for Satellite Vehicle Guidance Systems," Martin-Baltimore Engineering Report ER 10470-6, 31 January 1959.
11. Billik, B., "The Lifetime of an Earth Satellite," Aerospace Corporation, TN-594-1105-1, December 1960.
12. Fosdick, G. E., "Orbital Lifetime and Perturbations Due to Atmospheric Drag," Lecture No. 10, Space Flight Dynamics Course, Martin-Denver, Spring, 1960.
13. Krylov, N. M. and Bogoliuboff, N., "Introduction to Nonlinear Mechanics," Princeton University Press, 1943.
14. Minorsky, N., "Nonlinear Mechanics," J. W. Edwards, Ann Arbor, 1947.
15. Stafford, W. H. and Craft, R. M., "Artificial Earth Satellites and Successful Solar Probes," NASA TN D-601, 1957 to 1960.
16. "Bessel Function, Part I," British Association Mathematical Tables VI, University Press, Cambridge, 1958.
17. Taratynova, G. P., "The Motion of an Artificial Earth Satellite in the Eccentric Gravitational Field of the Earth when Atmospheric Resistance is Taken into Account," The Russian Literature of Satellites, International Physical Index, Incorporated, New York, 1958.
18. Sterne, T. E., "Effect of the Rotation of a Planetary Atmosphere upon the Orbit of a Close Earth Satellite," ARS Journal, Vol. 29, No. 10, October 1959, pp 777-782.
19. Kalil, F., "The Effect of an Oblate Rotating Atmosphere on the Eccentricity of a Close Earth Satellite," the Martin Co., ER No. 12552, 1962.
20. Kalil, F., "The Effect of an Oblate Rotating Atmosphere on the Semi Major Axis of a Close Earth Satellite," the Martin Co. (Baltimore), ER 12511, August 1962.
21. Plummer, H., "An Introductory Treatise on Dynamical Astronomy," Dover Publications, New York, 1960.
22. Moe, K., "A Model for the Errors in Orbital Predictions Caused by Fluctuations in Drag," STL/TR 60-0000-09145, 27 April 1960.
23. Karrenberg, H., Levin, E. and Lewis, D., "Variation of Satellite Position with Uncertainties in the Mean Atmospheric Density," Aerospace Corporation (El Segundo), Report TDR-594(1150)TN-7, June 1961.

G. BIBLIOGRAPHY

Baker, R. M. L., Jr., "Three Dimensional Drag Perturbation Technique," ARS Journal, Vol. 30, No. 8, Aug 1960.

Baker, R. M. L., Jr. and Charwat, A. F., "Transitional Correction to the Drag of a Sphere in Free Molecule Flow," Physics of Fluids, Vol. 1, 1958, pp 78-81.

Beard, D. B. and Johnson, F. S., "Charge and Magnetic Field Interaction with Satellites," Journal of Geophysical Research, Vol. 65, No. 1, Jan 1960, p 1.

Billik, B.,
"The Lifetime of an Earth Satellite," Report No. TN-594-1105-1, Aerospace Corporation, Los Angeles, Dec 1960.

"Survey of Current Literature on Satellite Lifetimes," (Report No. TDR-594(1560-01) TN-1, Aerospace Corporation (El Segundo, Calif), 11 April 1961. (Also ARS Journal, Vol. 32, No. 11, Nov 1962, pp 1641-1650.)

Breakwell, J. V. and Koehler, L. F., "Elliptical Orbit Lifetimes," Preprint No. 58-34, American Astronomical Society, Aug 1958.

Bullis, E. P. and Campbell, L., Jr.,
"Moonwatch Catalogue," Special Report No. 12, Smithsonian Astrophysical Laboratory (Cambridge, Mass.), April 1958.

"Moonwatch Catalogue, July and August 1958," Report No. 18, Smithsonian Astrophysical Laboratory (Cambridge, Mass), Oct 1958.

Citron, S. J., "Satellite Lifetimes in Circular and Elliptical Orbits Under the Influence of Continuous Thrust, Atmospheric Drag and Planet Oblateness," ARS Preprint 2371-62, March 1962.

Chang, H. H. C. and Smith, M. C., "On the Drag of a Spherical Satellite Moving in a Partially Ionized Atmosphere," Journal of the British Interplanetary Society, Vol. 17, No. 7, Jan-Feb 1960, p 199.

Chopra, K. P. and Singer, S. F., "Drag of a Sphere Moving in a Conducting Fluid," Technical Report No. 97, University of Maryland, Physics Department (College Park), 1958.

Clark, J. B., "Technical Parameters of Satellites 1958 Delta and 1958 Epsilon," Report No. 18, Smithsonian Astrophysical Laboratory (Cambridge, Mass), Oct 1958.

Davis, R. J., Whipple, F. L. and Zirker, J. B., "The Orbit of a Small Earth Satellite," Scientific Uses of Earth Satellites, University of Michigan Press (Ann Arbor), 1958, 2nd ed.

Fejer, J. A., "Lifetime of an Artificial Satellite," Nature, Vol. 180, 21 Dec 1957, p 1413.

Fosdick, G. E., "Orbital Lifetime and Perturbations due to Atmospheric Drag," Lecture No. 10 Space Flight Dynamics Course, Martin Company (Denver), Spring 1960.

Good, R. E., "A Method for Predicting the Lifetime of a Near Satellite," Technical Report No. 418, Massachusetts Institute of Technology, Naval Supersonic Laboratory (Cambridge, Mass.), 1960.

Groves, G. V.,
"Effect of the Earth's Equatorial Bulge on the Lifetime of Artificial Satellites and Its Use in Determining Atmospheric Scale Heights," Nature, Vol. 1, 12 April 1958, p 1055.

"Air Density in the Upper Atmosphere from Satellite Observation," Nature, Vol. 184, Supplement No. 4, 18 July 1959, pp 178-179.

Harris, I. and Jastrow, R.,
"Upper Atmospheric Densities from Minitrack Observations on Sputnik I," Science, Vol. 127, 28 Feb 1958, p 471.

"An Interim Atmosphere Derived from Rocket and Satellite Data," Planetary and Space Science, Vol. 1, 1959, pp 20-26.

Henry, I. G., "Lifetimes of Artificial Satellites of the Earth," American Rocket Society (New York), 26-29 Nov 1956. (Also, Jet Propulsion, Vol. 27, No. 1, Jan 1957).

Iatsienski, I. M., "Effect of the Geophysical Factors upon the Motion of an Artificial Satellite," The Russian Literature of Satellites, International Physical Index, Inc. (New York), 1958.

Jacchia, L. G.,
"An Empirical Formula for Satellite Ephemerides near the End of Their Lifetime," Special Report No. 20, Smithsonian Astrophysical Observatory (Cambridge, Mass.), 1958.

"The Descent of Satellite 1957 Beta One," Special Report No. 15, Smithsonian Astrophysical Observatory (Cambridge, Mass.), 20 July 1958. (Also, IGY Satellite Report Series, No. 6, National Academy of Science, 15 Aug 1958.)

Orbital Results for Satellite 1957 Beta One," Special Report No. 13, Smithsonian Astrophysical Observatory (Cambridge, Mass.), May 21, 1958.

"Two Atmospheric Effects on the Orbital Acceleration of Artificial Satellites," Nature, Vol. 183, Feb 21, 1959, p 526.

Jacchia, L. G. and Briggs, R. E., "Orbital Acceleration of Satellite 1958 Beta Two," Report No. 18, Smithsonian Astrophysical Laboratory (Cambridge, Mass.), Oct 1958.

Jastrow, R. and Pearse, C. A., "Atmospheric Drag on the Satellite," Journal of Geophysics Research, Vol. 62, No. 9, Sep 1957.

Jones, L. M., Fishchbach, F. F., and Peterson, J. W., "Seasonal and Latitude Variations in Upper-Air Density," 5th General Assembly of CSAGI (Moscow), July 30 to Aug 9, 1958.

Kalensher, B.E., "Equations of Motion of a Missile and a Satellite for an Oblate Spheroidal Rotating Earth," Memo 20-142, California Institute of Technology, Jet Propulsion Laboratory (Pasadena), April 12, 1957.

Karrenberg, H. K., Levin, E., and Lewis, D. H., "Variation of Satellite Position with Uncertainties in the Mean Atmospheric Density," (Report No. TDR-594(1150)TN-7), Aerospace Corporation, El Segundo, California, 12 June 1961.

Kaula, W. M., "Analysis of Gravitational and Geometric Aspects of Geodetic Utilization of Satellites," NASA TN D-572, March 1961.

Ketchum, H. B., "The Orbit Lifetimes of the U. S. Artificial Satellites," Advances in Astronautical Sciences, Plenum Press, Inc. (N. Y.), 1957, Vol. 1, pp 31 to 41.

King-Hele, D. G., and Leslie, D. C. N., "The Descent of an Earth-Satellite Through the Upper-Atmosphere," Journal of the British Interplanetary Society, Vol. 15, Nov to Dec 1956, pp 314 to 323.

"Effect of Air Drag on the Orbit of the Russian Earth Satellite," Nature, Vol. 181, June 28, 1958, p 1761.

King-Hele, D. G., and Walker, D. M. C., "Irregularities in the Density of the Upper Atmosphere: Results from Satellites," Nature, Vol. 183, Feb 21, 1959, p 527.

Kooy, J. M. J., "On the Application of the Method of Variation of Elliptic Orbit Elements in the Case of a Satellite Vehicle," Astronautica Acta, Vol. 3, 1957, pp 180 to 214.

Kork, J., "Satellite Lifetimes," Design Guide to Orbital Flight, Chapter 5, McGraw-Hill Book Company (N. Y.), 1962.

Lee, V. A., "Atmosphere-Oblateness Correction Factor for Circular Satellite Orbits," ARS Journal Vol. 32, pp 102 to 103, 1962.

Lundbak, A., "Some Simple Formulas for Latitude Effects and Lifetimes of Satellites," Planetary and Space Science, Vol. 2, No. 4, Aug 1960, pp 212 to 213.

Michielsen, H., "Orbit Decay and Prediction of the Motion of Artificial Satellites," Advances in Astronautical Sciences, Plenum Press, Inc., (N. Y.), Vol. 4, 1959, pp 255 to 310.

Niemerow, J., "Lifetime of a Satellite with a Large Initial Eccentricity," GM 59-8023 2-14, Space Technology Laboratories, March 27, 1959.

Minzner, R. A., and Ripley, W. S., "The ARDC Model Atmosphere, 1956," Air Force Surveys in Geophysics No. 86, Geophysics Research Directorate, AFCRC, ARDC, Dec 1956 (also, AFCRC TN 56-204, ASTIA 110233).

"Higher Atmospheric Densities and Temperatures Demanded by Satellite and Recent Rocket Measurements," American Rocket Society Controllable Satellites Conference (Cambridge, Mass.), April 30 to May 1, 1959.

Mitra, S. K., "The Upper Atmosphere," The Royal Asiatic Society of Bengal, 1952, p 582.

Newton, R., "Lifetimes of Artificial Satellites," Jet Propulsion, Vol. 28, 1958, pp 331 to 333.

Nonweiler, T., "Perturbations of Elliptic Orbits by Atmospheric Contact," Journal of the British Interplanetary Society, Vol. 16, March to April 1958, pp 368 to 379.

Okhotsimskii, D. E., Eneev, T. M., and Taratynova, G. P., "Determining the Lifetime of an Artificial Earth Satellite and Investigating Secular Perturbations of Its Orbit," The Russian Literature of Satellites, International Physical Index, Inc. (N. Y.), 1958.

Parkyn, D. G., "Satellite Orbits in an Oblate Atmosphere," Journal of Geophysical Research, Vol. 65, No. 1, Jan 1960, pp 9 to 17.

Patterson, G. N., "Transport Properties of Free Molecule (Knudsen) Flow," Utia Review No. 11, Institute of Aerophysics, University of Toronto, March 1958.

"Recent Trends in the Mechanics of Highly Rarefied Gases," Utia Review No. 16, Institute of Aerophysics, University of Toronto, Jan 1960.

"Aerodynamics of Highly Rarefied Gases," Utia Review No. 18, Institute of Aerophysics, University of Toronto, March 1961.

Perkins, F. M., "An Analytical Solution for Flight Time of Satellites in Eccentric and Circular Orbits," Astronautica Acta, Vol. IV, 1958, p 113.

Petersen, N. V., "Lifetimes of Satellites in Near Circular Oribts," Jet Propulsion, Vol. 26, No. 5, May 1956, pp 341 to 351.

Peterson, C. M., "Communications Center of the Optical Satellite Tracking Program," Report No. 18, Smithsonian Astrophysical Laboratory, Cambridge, Mass., Oct 1958.

Roberson, R. E., "Effect of Air Drag on Elliptic Satellite Orbits," Jet Propulsion, Vol. 28, No. 2, Feb 1958.

Schamberg, R., "A New Analytical Representation of Surface Interaction for Hyperthermal Free Molecule Flow with Application to Satellite Drag," Heat Transfer and Fluid Mechanics Institute, June 1959.

Schilling, G. F., "Technical Parameters of the Artificial Satellites," Special Report No. 12, Smithsonian Astrophysical Laboratory, Cambridge, Mass., April 1958.

Schilling, G. F., and Rinehart, J. S., "Note on the Mass-Area Ratios of the USSR Satellites," Special Report No. 12, Smithsonian Astrophysical Laboratory, Cambridge, Mass., April 1958.

Schilling, G. F., and Sterne, T. E., "Densities of the Upper Atmosphere Derived from Satellite Observations," Special Report No. 12, Smithsonian Astrophysical Laboratory, Cambridge, Mass., April 1958.

Schilling, G. F., and Whitney, C. A., "Atmospheric Densities from Explorer IV," Report No. 18, Smithsonian Astrophysical Laboratory, Cambridge, Mass., Oct 1958.

Schilling, G. F., Whitney, C. A., and Folkart, B. M., "Preliminary Note of the Mass-Area Ratio of Satellites 1958 Delta 1 and Delta 2," IGY Satellite Report Series No. 6, National Academy of Science, Aug 15, 1958.

Scott, J. M. C., "Estimating the Life of a Satellite," Nature, Vol. 180, Dec 28, 1957, pp 1467 to 1468.

Sentman, L. H., "Free Molecule Flow Theory and Its Application to the Determination of Aerodynamic Forces," LMSC-448514, Lockheed Aircraft Corporation, Missiles and Space Division, Oct 1961.

Singer, S. F., "Studies of a Minimum Orbital Unmanned Satellite of Earth (MOUSE). Part II--Orbits and Lifetimes of Minimum Satellites," Preprint 160-54 American Rocket Society, Nov 30 to Dec 3, 1954.

Siry, J., "Satellite Orbits and Atmospheric Densities at Altitudes up to 750 Km Obtained from the Vanguard Orbit Determination Program," International Astronomical Union, 10th General Assembly, Aug 1958.

Spitzer, L., "On the Determination of Air Density from a Satellite," Scientific Uses of Earth Satellites, University of Michigan Press (Ann Arbor), 1958, 2nd ed.

Stafford, W. H., and Craft, R. M., "Artificial Earth Satellites and Successful Solar Probes, 1957 to 1960," NASA TN D-601, 1961.

Stalder, J. R., and Zurick, V. J., "Theoretical Aerodynamic Characteristics of Bodies in a Free-Molecule Flow Field," NACA TN 2423, July 1951.

Stalder, J. R., Goodwin, G., and Creager, M.O., "A Comparison of Theory and Experiment for High-Speed Free-Molecule Flow," NACA TN 2244, Dec 1950.

Sterne, T. E.,
"An Atmospheric Model and Some Remarks on the Inference of Density from the Orbit of a Close Earth Satellite," Astronomical Journal, Vol. 63, No. 3, March 1958.

"The Densities of the Upper Atmosphere," Special Report No. 11, Smithsonian Astrophysical Observatory, Cambridge, Mass., March 31, 1958, pp 18 to 22.

"Formula for Inferring Atmospheric Density from the Motion of Artificial Earth Satellites," Science, Vol. 127, May 23, 1958, p 1245.

"Effect of the Rotation of a Planetary Atmosphere upon the Orbit of a Close Satellite," ARS Journal, Vol. 29, No. 10, Oct 1959, pp 777 to 782.

Street, R. E., "Problem of Slip Flow in Aerodynamics," NACA RM 57A30, March 1957.

Taratynova, G. P., "The Motion of an Artificial Earth Satellite in the Eccentric Gravitational Field of the Earth When Atmospheric Resistance Is Taken into Account," The Russian Literature of Satellites, International Physical Index, Inc., New York, 1958.

Van Allen, J., ed., "Scientific Uses of Earth Satellites," University of Michigan Press (Ann Arbor), 1958, 2nd ed.

Van Sant, C. T., and Westrom, G., "Differential Correction of Earth Satellite Orbits Including the Drag Perturbation," IAS Paper 61-140-1834, June 13 to 16, 1961.

Veis, G., "The Orbit of Satellite 1958 Zeta," Special Report No. 23, Smithsonian Astrophysical Laboratory, Cambridge, Mass., March 30, 1959.

Venti, J., "Theory of the Effect of Drag on the Orbital Inclination of an Earth Satellite," Journal of Research, National Bureau of Standards, Vol. 62, 1959, pp 79 to 88.

Waldinger, H. V.,
"The Slow Descent of a Satellite in a Circular Orbit," Technical Note No. 61, Republic Aviation Corporation, Farmingdale, New York, 1960.

"The Slow Descent of a Satellite Under Drag," Technical Note No. 62, Republic Aviation Corporation, Farmingdale, New York, 1960.

Warwick, J. W., "Decay of Spin in Sputnik I," Planetary and Space Science, Vol. I, pp 43 to 49.

Whitney, C. A.,
"The Acceleration of Satellites 1958 Alpha and Gamma," Special Report No. 12, Smithsonian Astrophysical Laboratory, Cambridge, Mass., April 1958.

"The Structure of the High Atmosphere--I. Linear Models," Special Report No. 21, Smithsonian Astrophysical Laboratory, Cambridge, Mass., Feb 27, 1959.

"The Structure of the High Atmosphere--II. A Conduction Model," Special Report, Smithsonian Astrophysical Laboratory, Cambridge, Mass., 1961 (in press).

"Atmospheric Conditions at High Altitudes from Satellite Observations," American Rocket Society Controllable Satellites Conference, Cambridge, Mass., April 30 to May 1, 1959.

Wyatt, P. J., "Induction Drag on a Large Negatively Charged Satellite Moving in a Magnetic-Field-Free Ionosphere," Journal of Geophysical Research, Vol. 65, No. 6, June 1960, p 1673.

Yengst, W. C., "Comments on a Variable Atmospheric-Density Model," Report No. A-61-1733.1-1, Aerospace Corporation, Los Angeles, Feb 9, 1961.

ILLUSTRATIONS

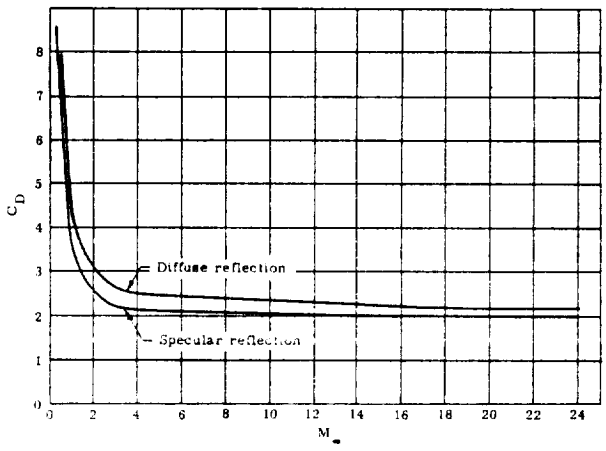

Fig. 1. Drag Coefficient for a Sphere at 120 km Versus M_∞

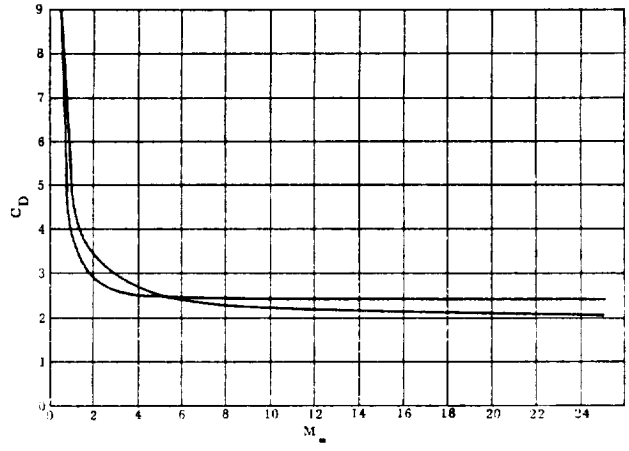

Fig. 3. Drag Coefficient for a Rich Circular Cylinder with Axis Normal to the Stream at 120 km Versus M_∞

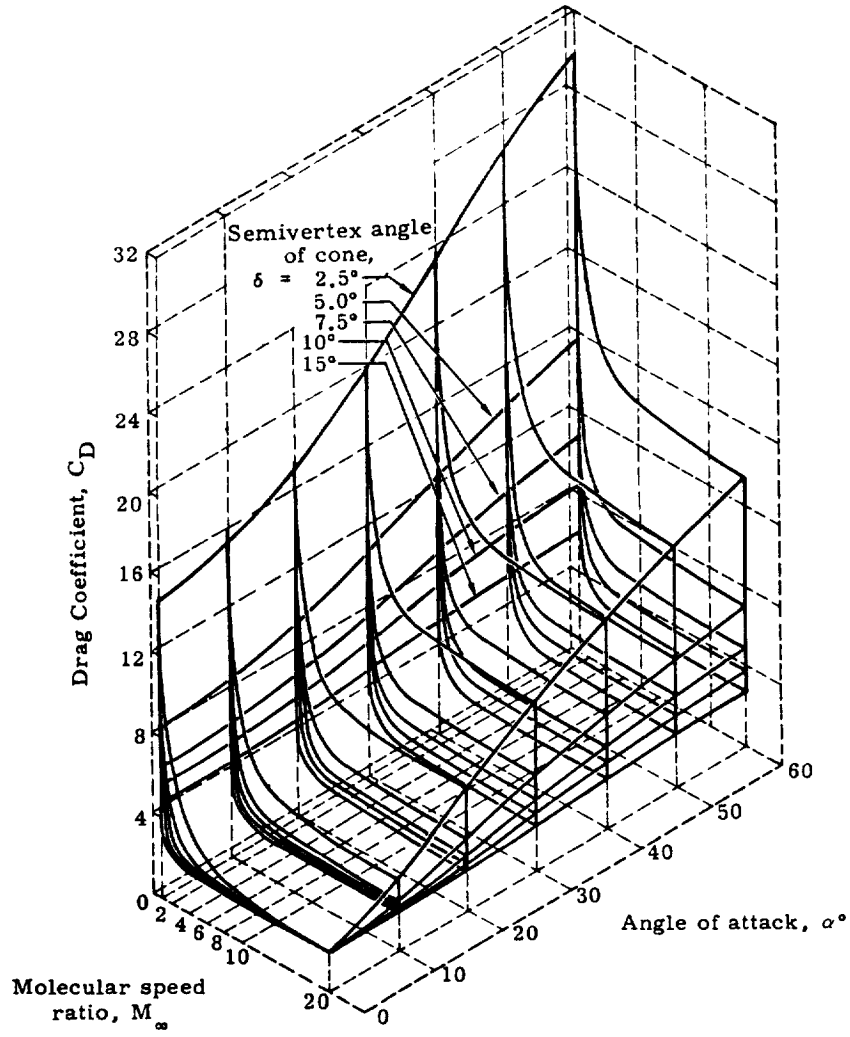

Fig. 2. Cone Drag Coefficient, Diffuse Reflection

Preceding page blank

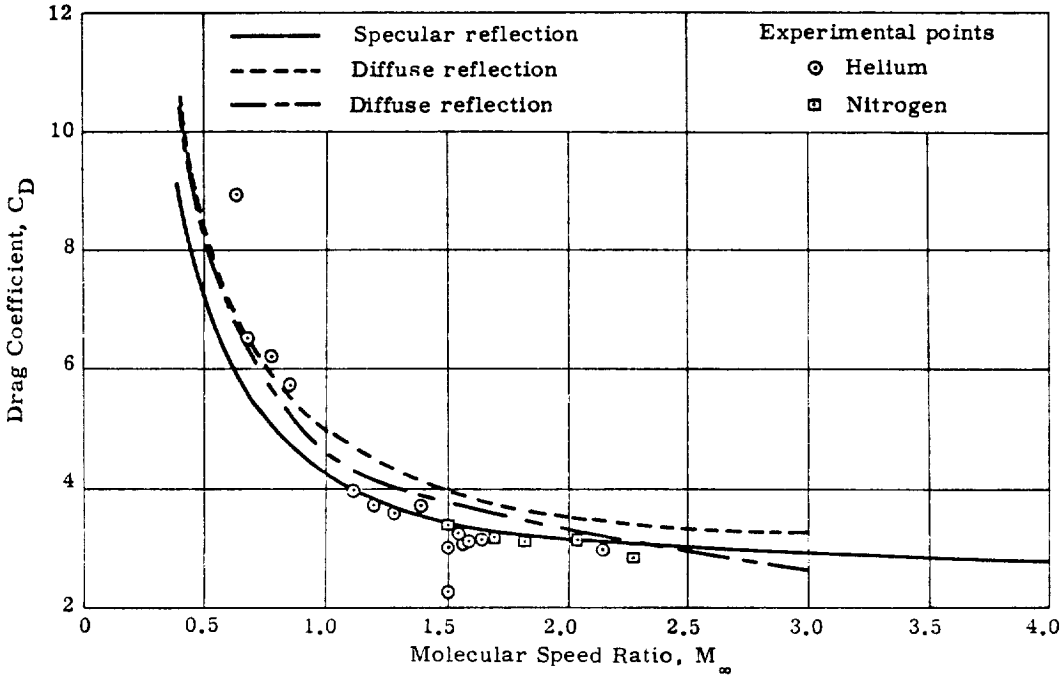

Fig. 4. Comparison of Drag Coefficient of a Transverse Cylinder for Specular and Diffuse Reflection

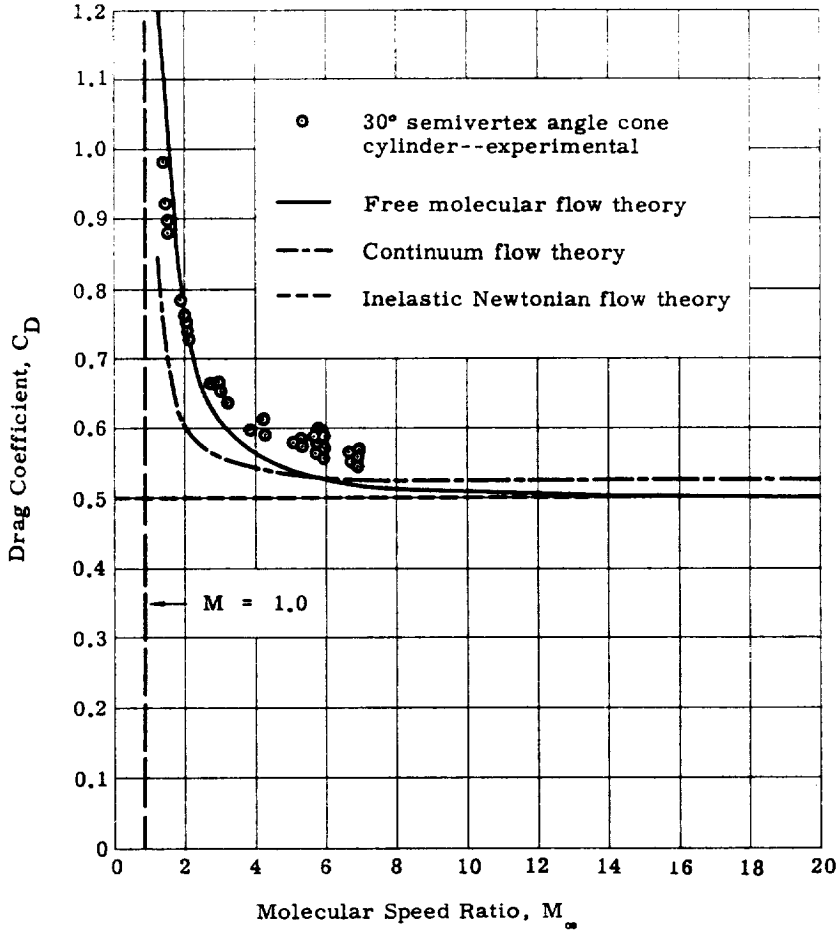

Fig. 5. Cone Drag Coefficient, Comparison of Free Molecular and Continuum Flow Theory; $\alpha = 0°$

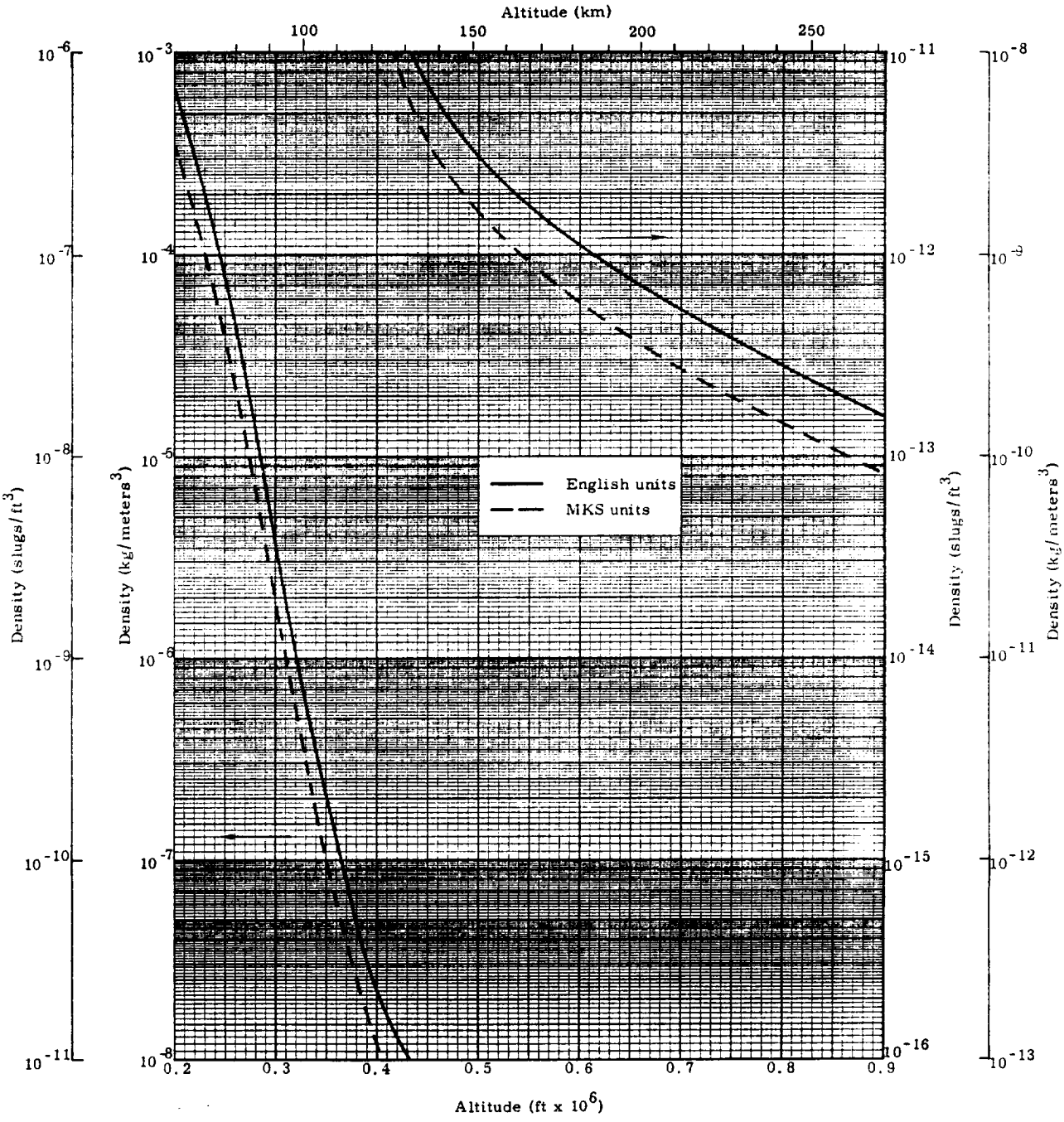

Fig. 6a. ARDC 1959 Model Atmosphere (1 slug/ft^3 = 512 kg/m^3)

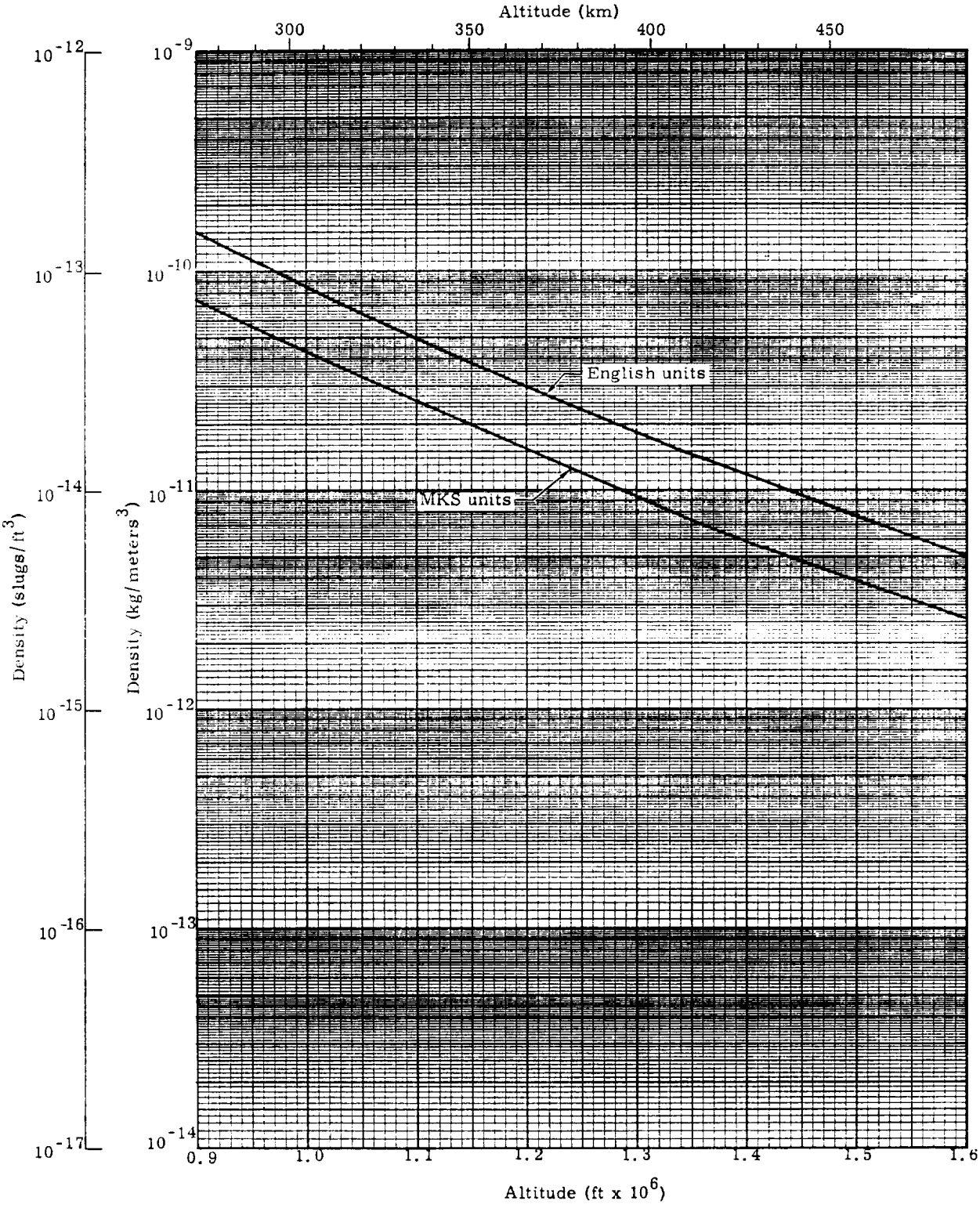

Fig. 6b. ARDC 1959 Model Atmosphere

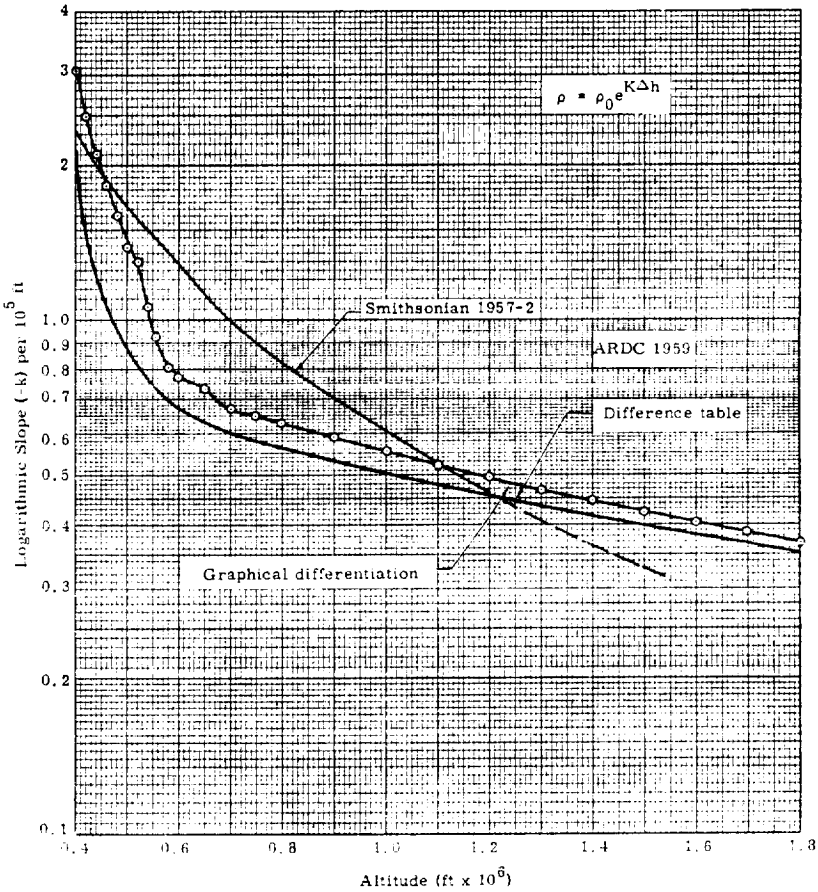

Fig. 7a. Logarithmic Slope of Air Density Curve

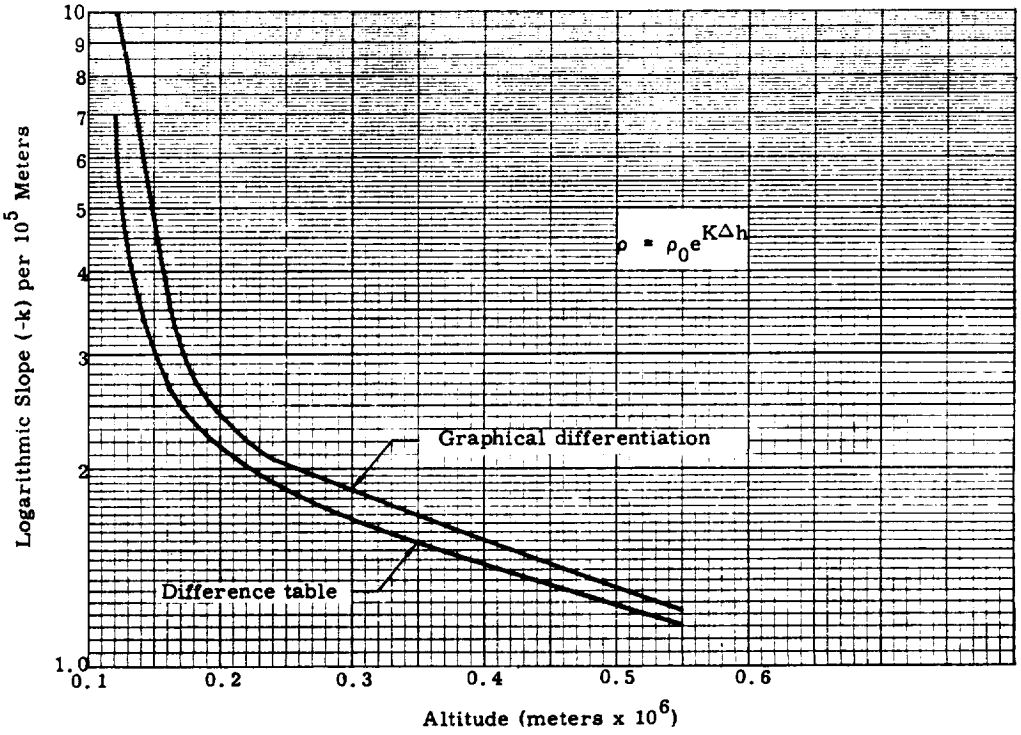

Fig. 7b. Logarithmic Slope of 1959 ARDC Atmosphere

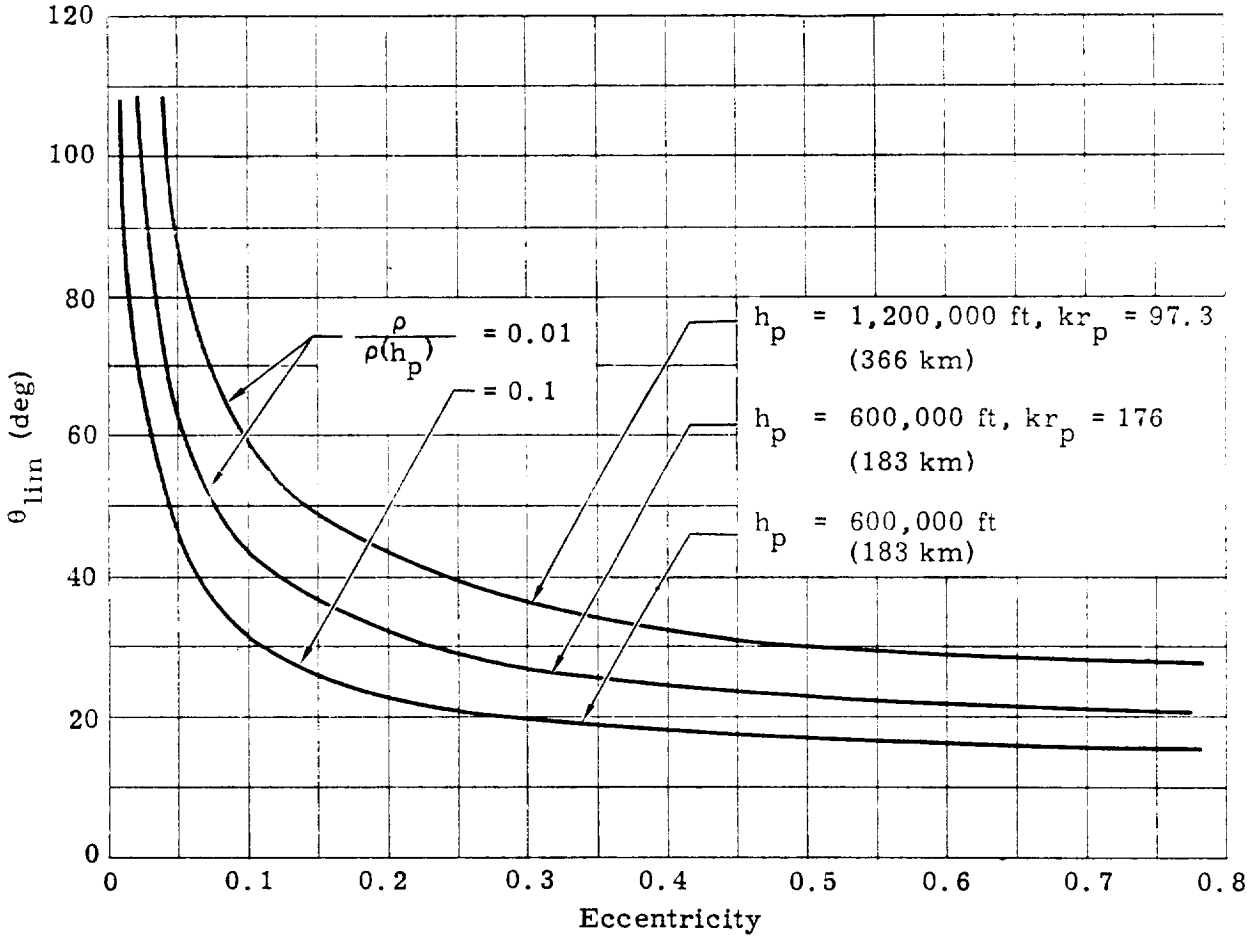

Fig. 8. Values of True Anomaly as a Function of Eccentricity for Which $\rho/\rho(h_p)$ = Constant (exponential fit to ARDC 1959 atmosphere)

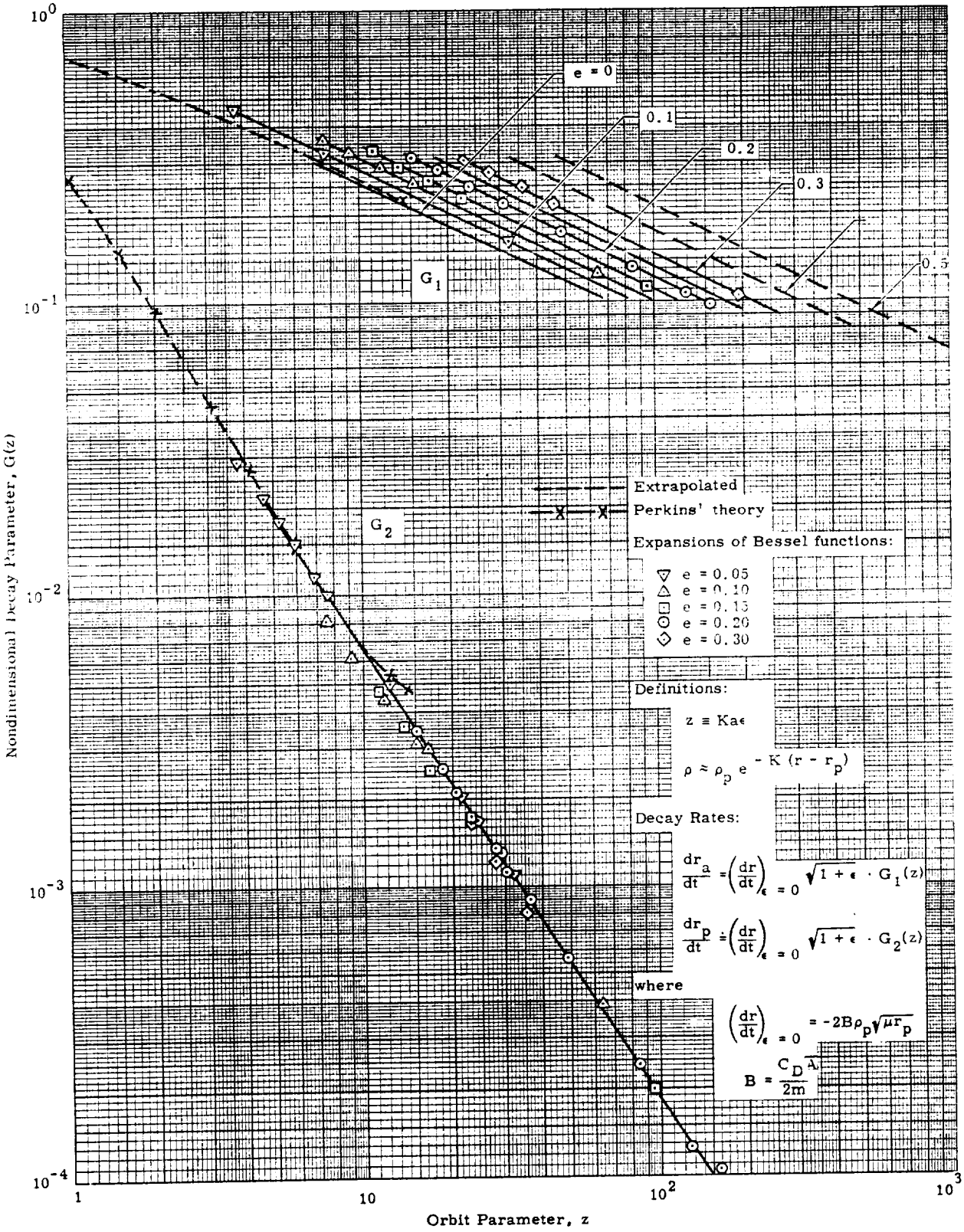

Fig. 9. Nondimensional Drag Decay Parameters for Elliptic Satellite Orbits

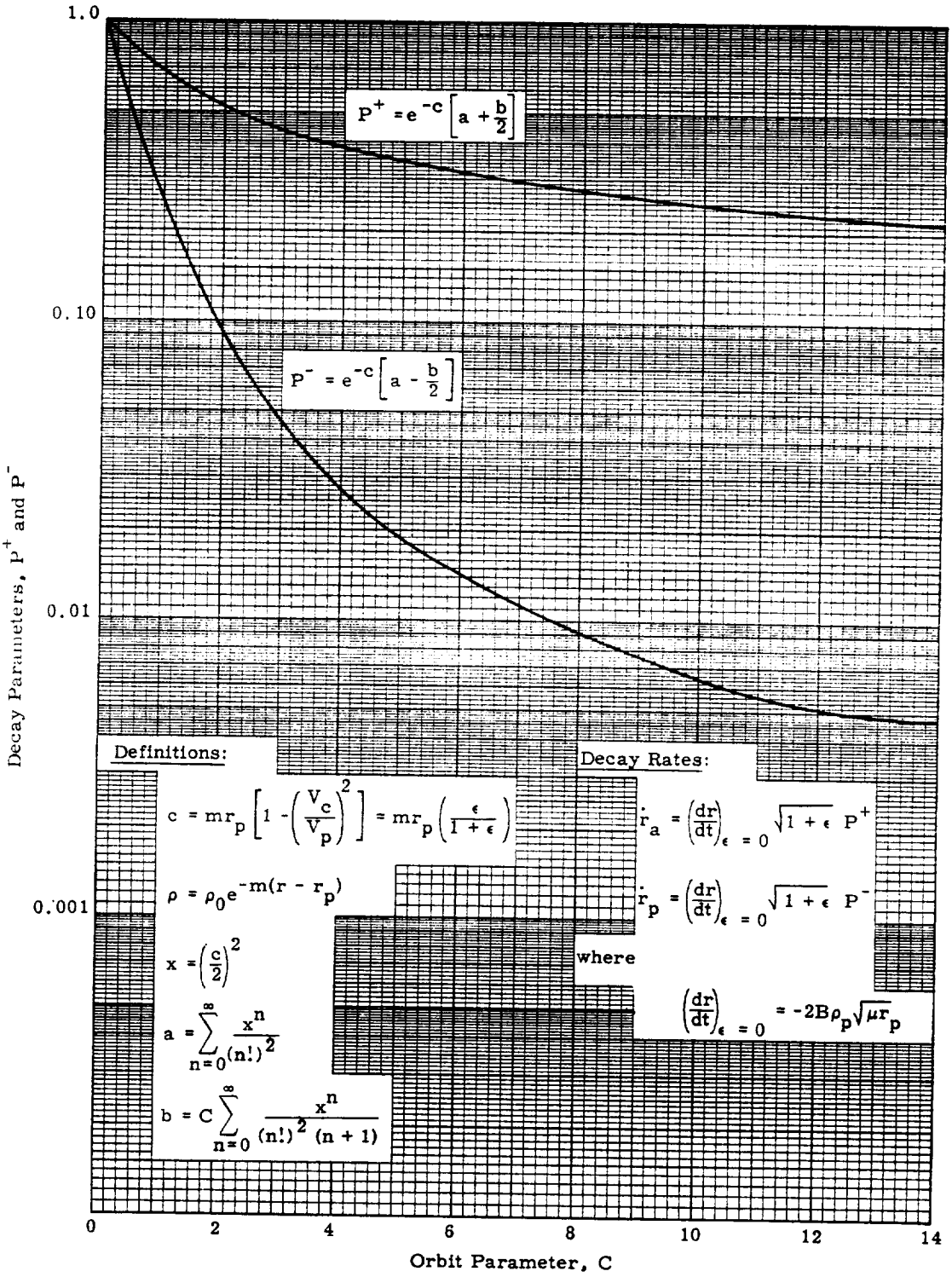

Fig. 10. Decay Parameters P^+ and P^- for Elliptic Orbits

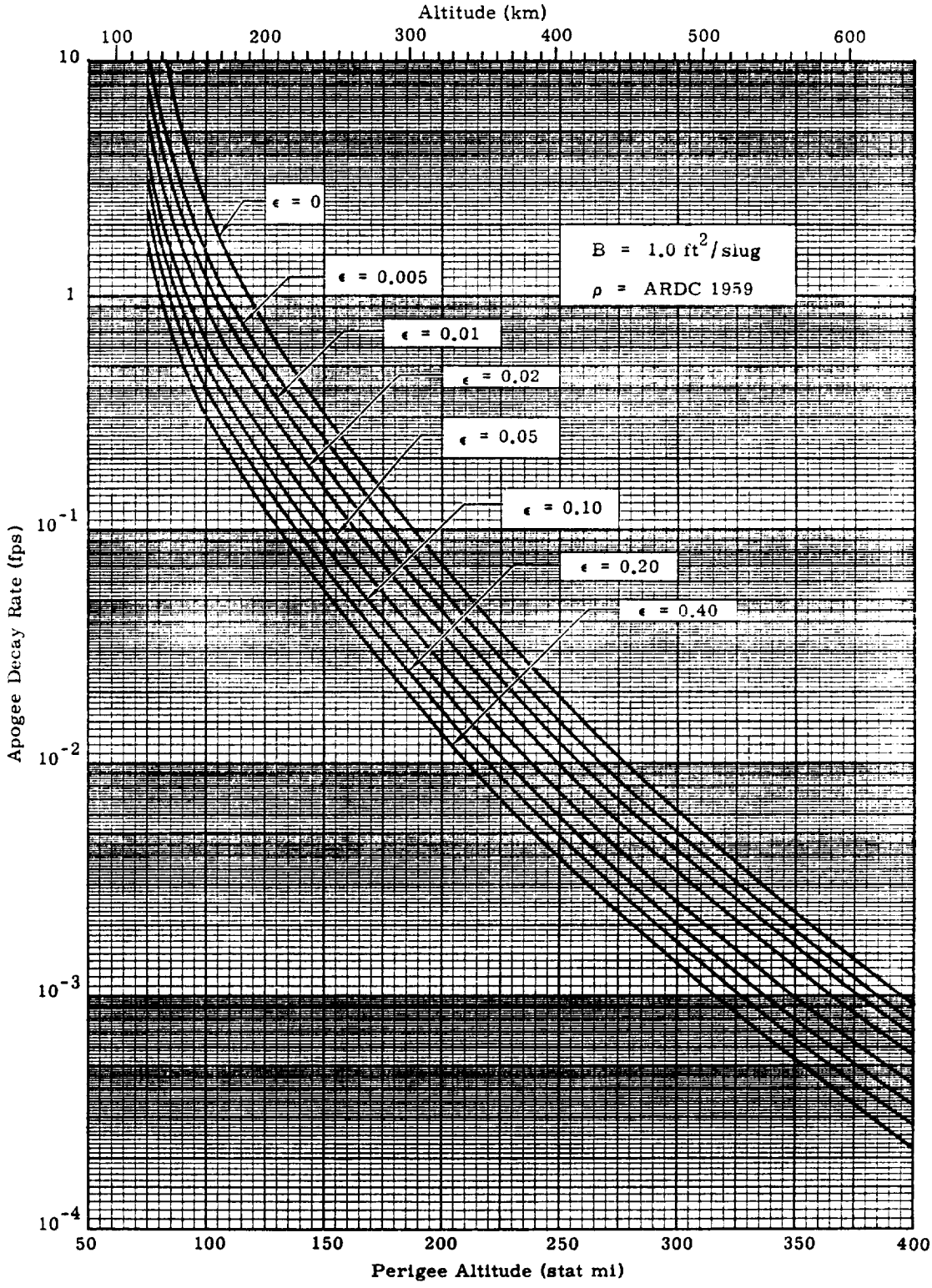

Fig. 11a. Apogee Decay Rate Versus Perigee Altitude (see Fig. 12a for metric data)

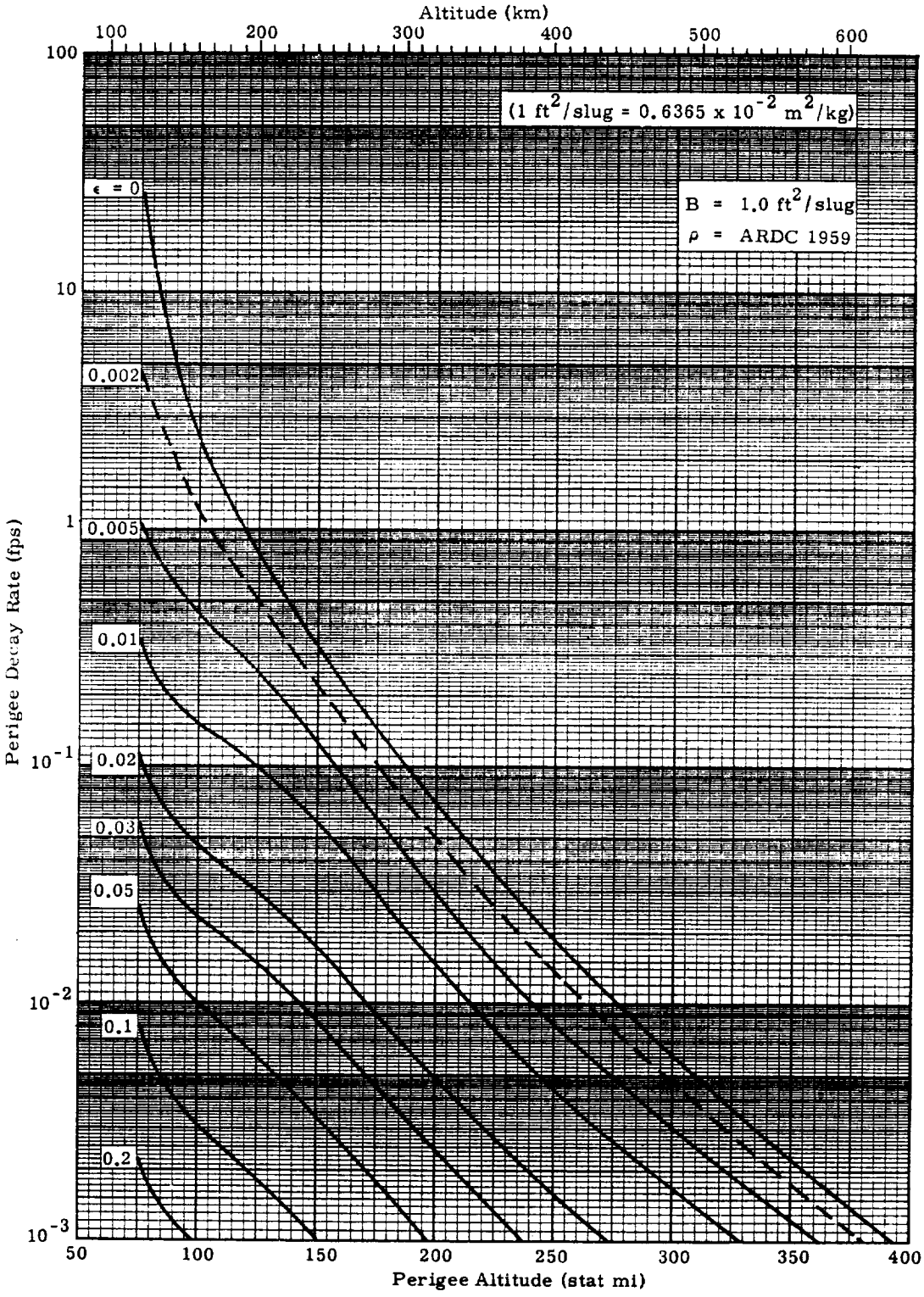

Fig. 11b. Perigee Decay Rate Versus Perigee Altitude (Part I)
(see Fig. 12b for metric data)

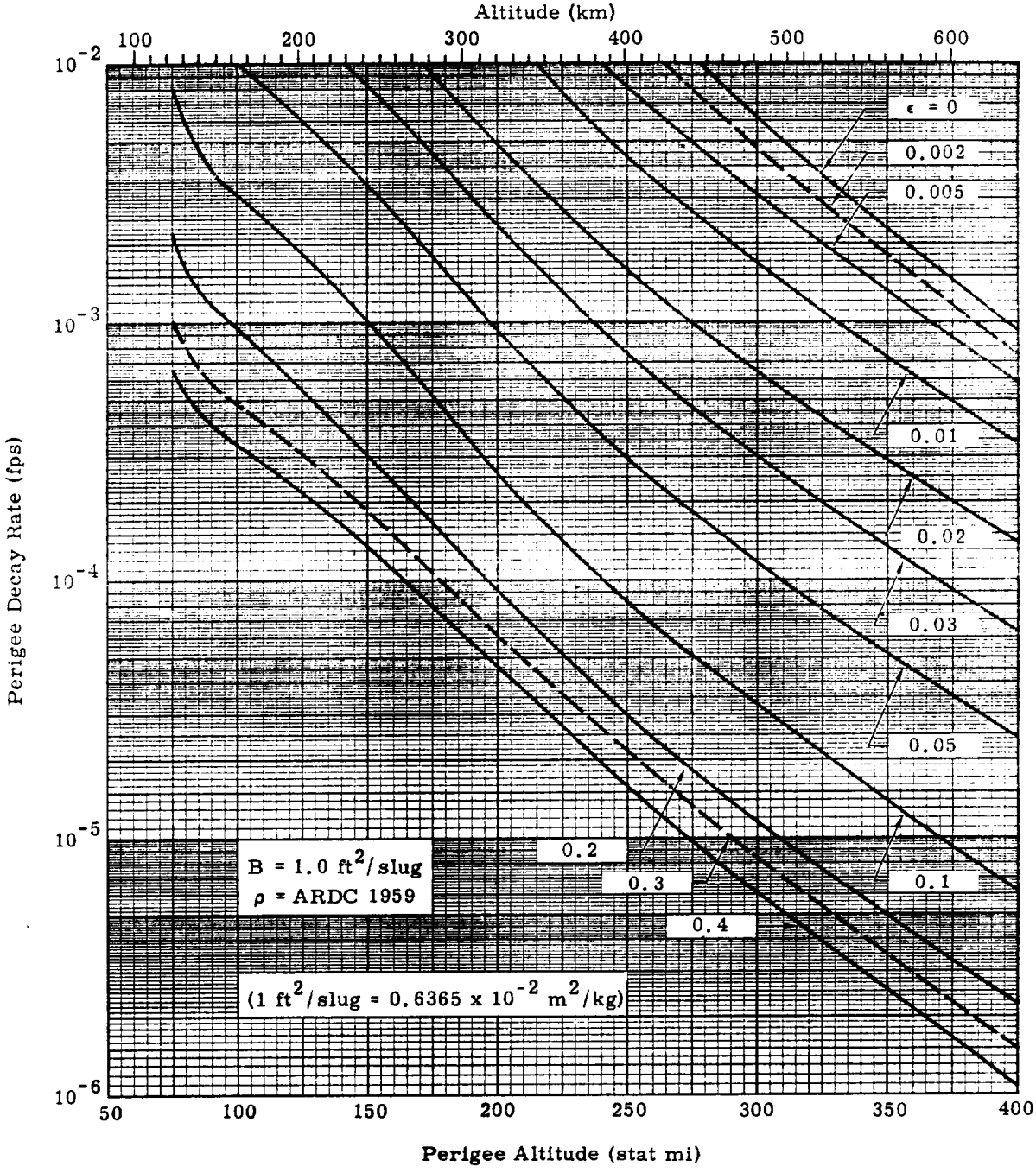

Fig. 11c. Perigee Decay Rate Versus Perigee Altitude (Part II)
(see Fig. 12c for metric data)

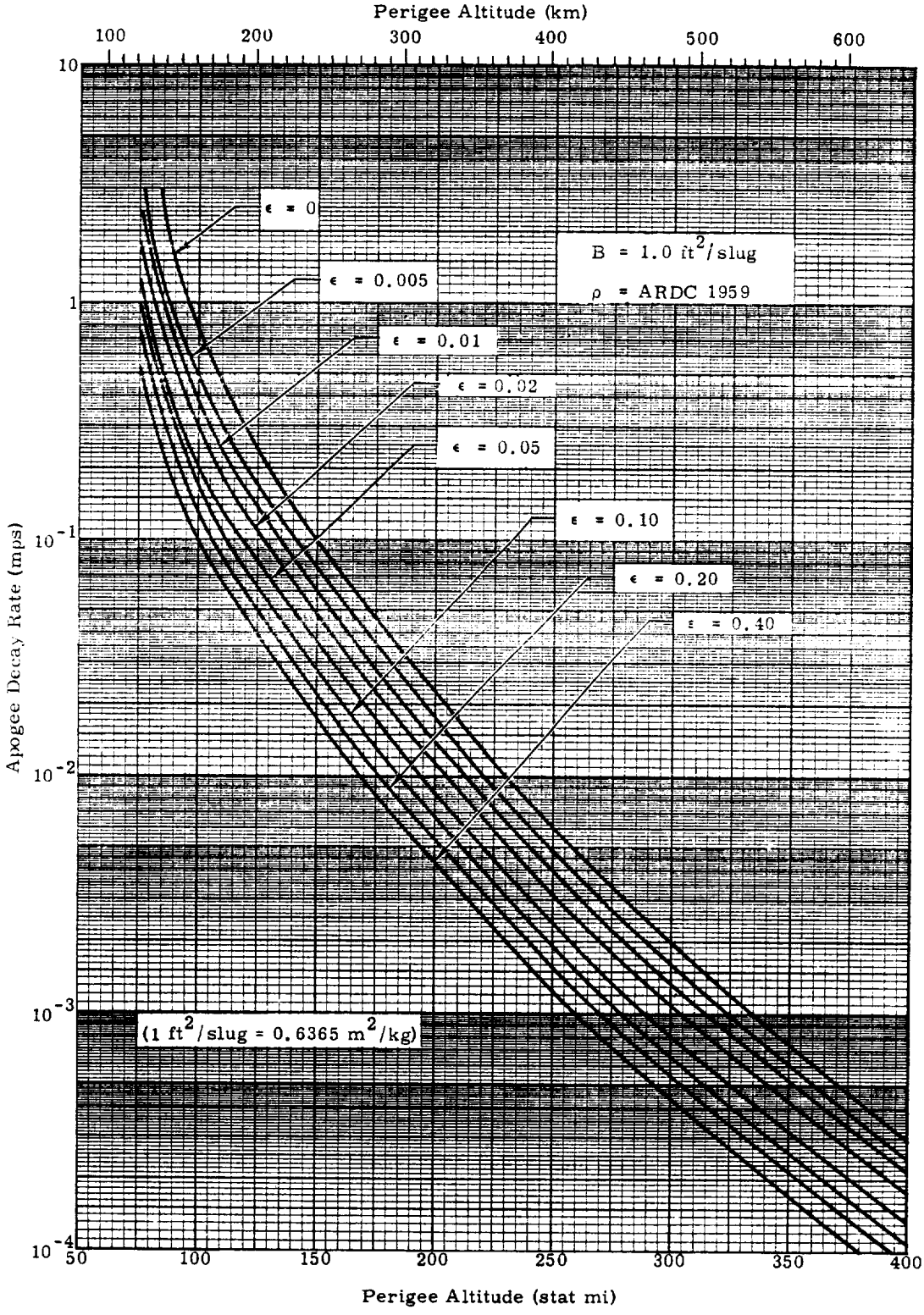

Fig. 12a. Apogee Decay Rate Versus Perigee Altitude

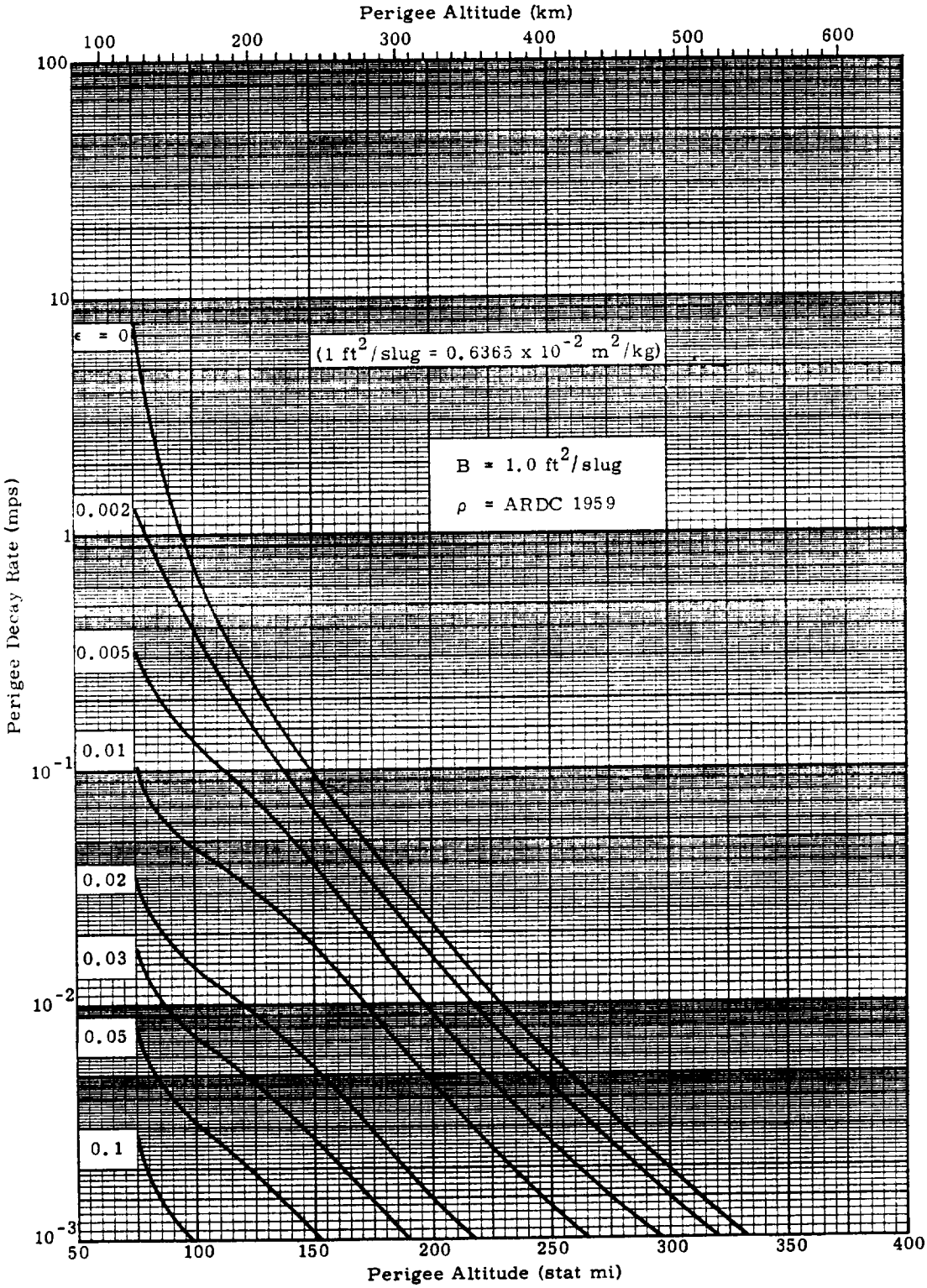

Fig. 12b. Perigee Decay Rate Versus Perigee Altitude (Part I)
(see Fig. 11b for English data)

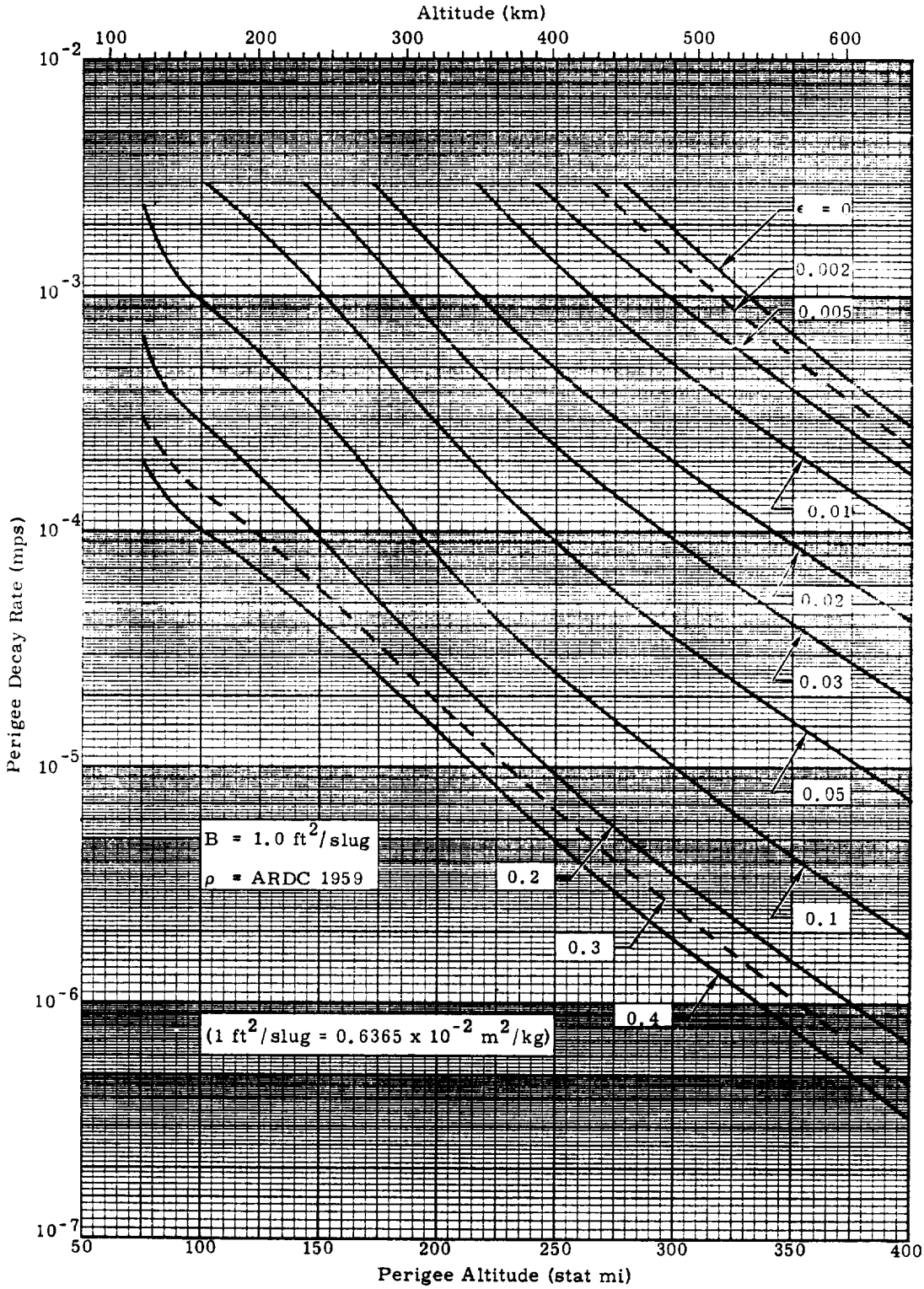

Fig. 12c. Perigee Decay Rate Versus Perigee Altitude (Part II)
(see Fig. 11c for English data)

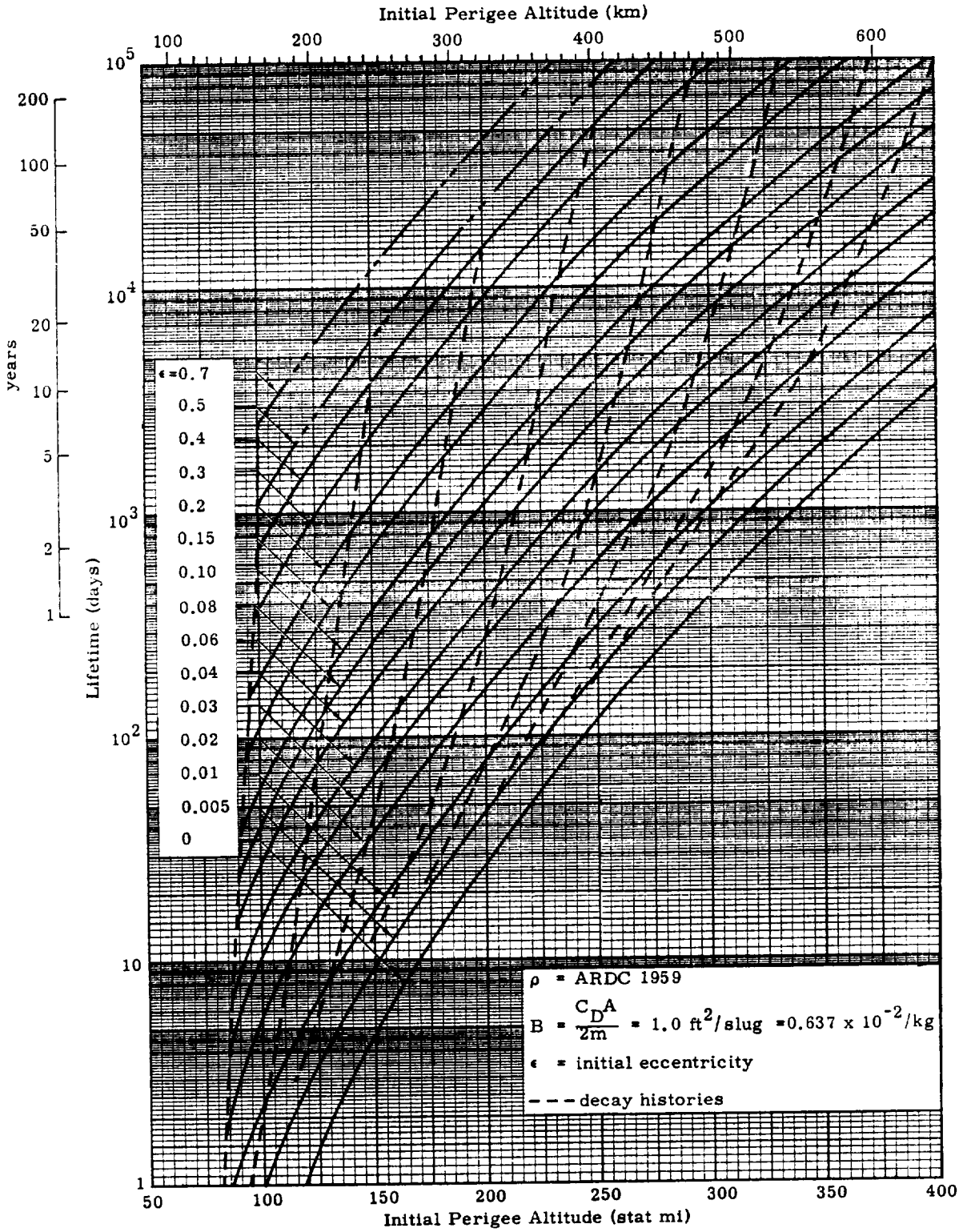

Fig. 13. Satellite Lifetimes in Elliptic Orbits

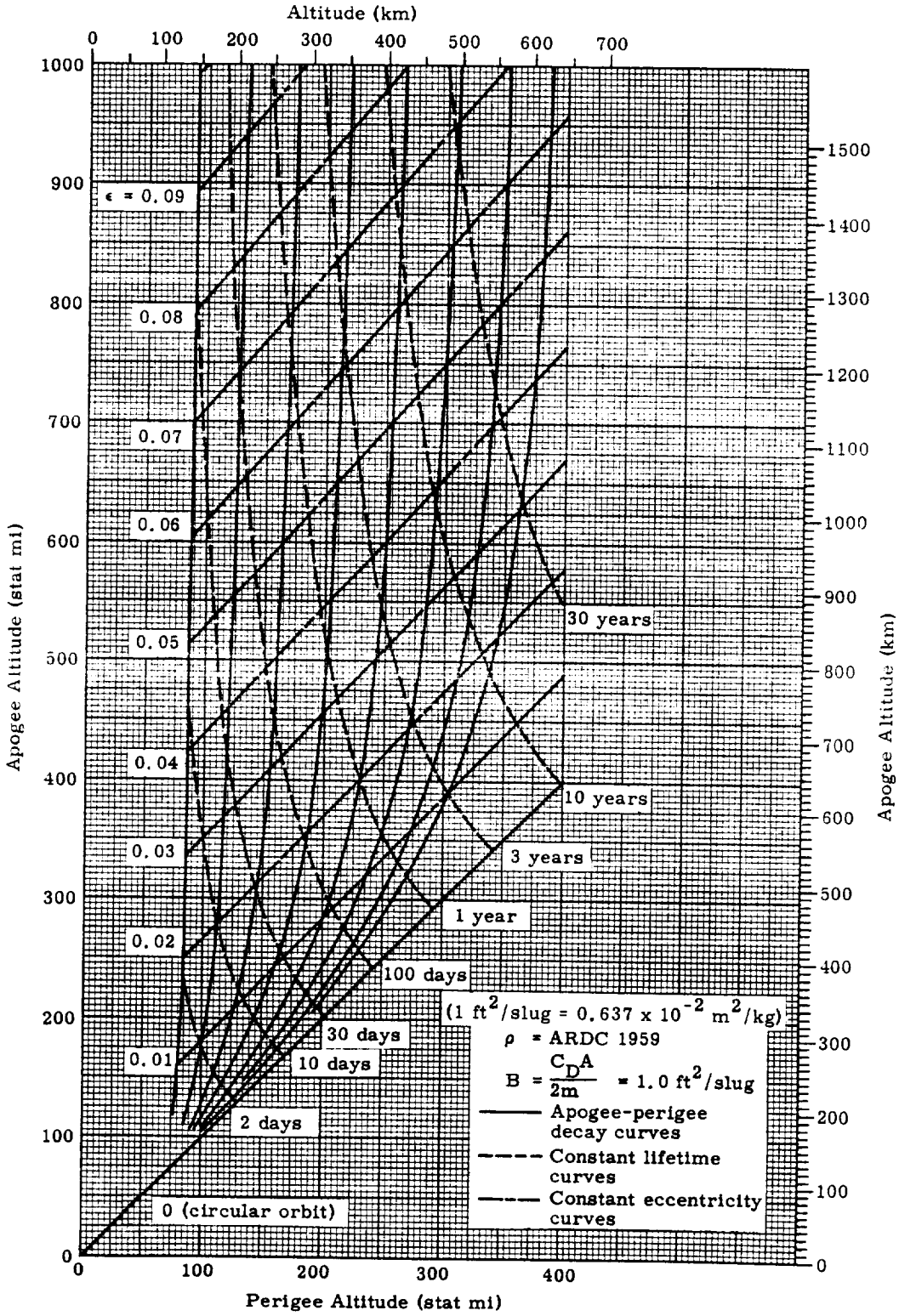

Fig. 14. Generalized Orbital Decay Curves for Air Drag

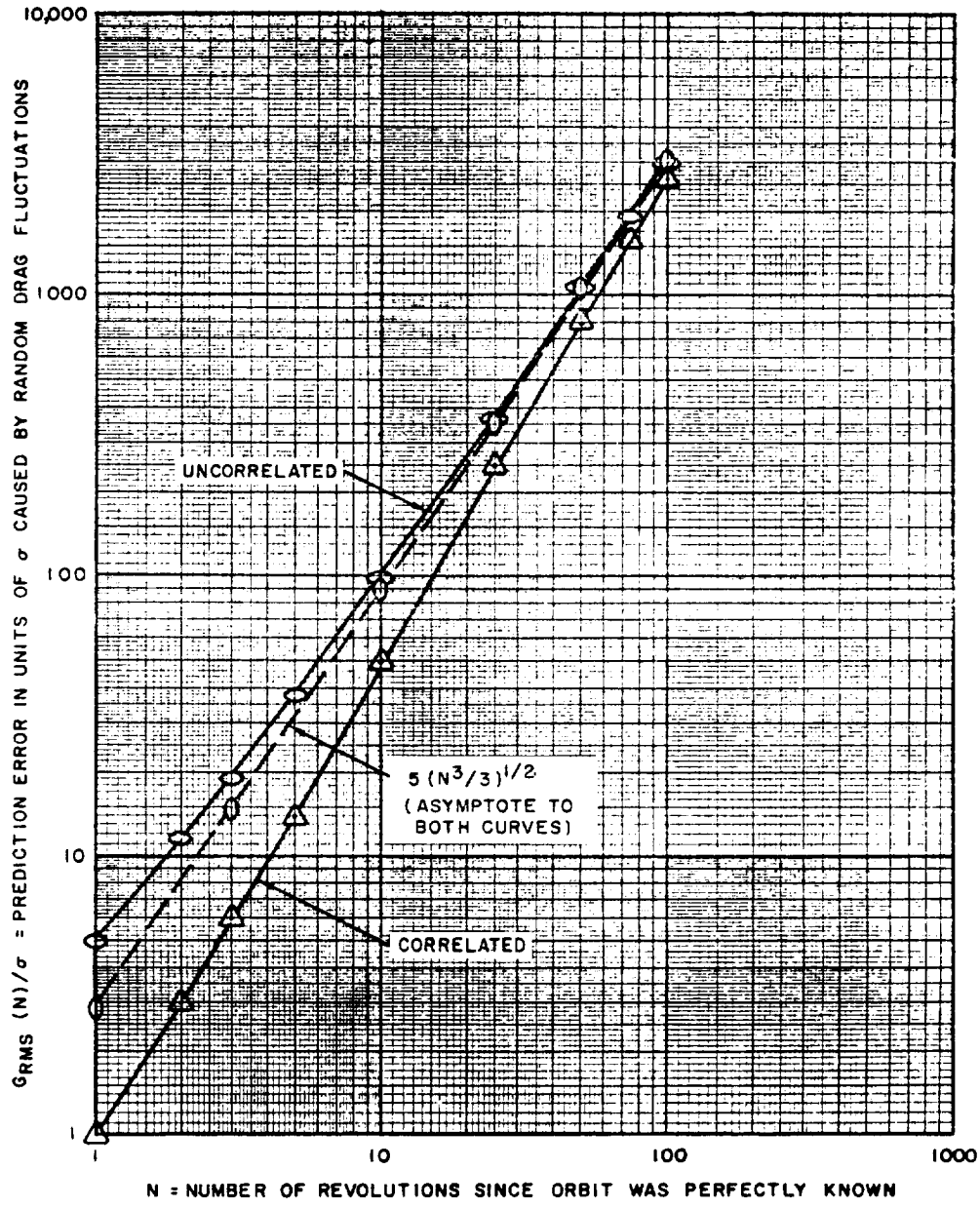

Fig. 15. Comparison of Errors in Orbital Prediction for Correlated and Uncorrelated Atmospheric Density Fluctuation

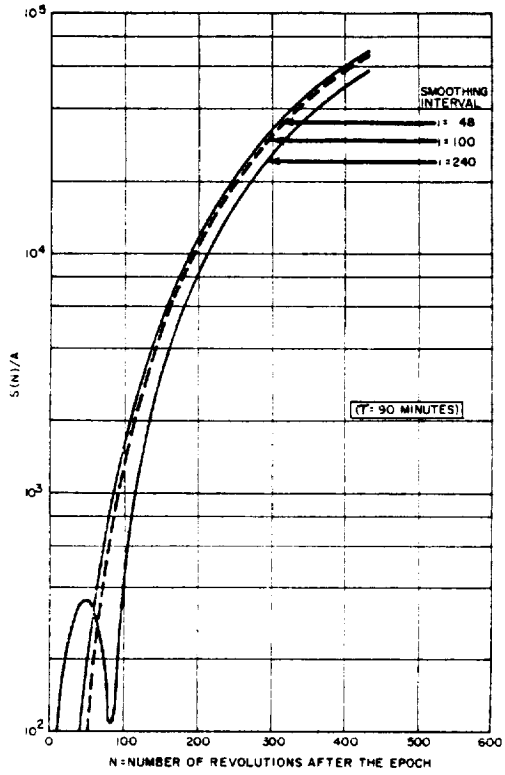

Fig. 16a. The Ratio of the rms Error in Orbital Prediction Caused by Sinusoidal Drag Variations to the Amplitude of the Sinusoidal Variation

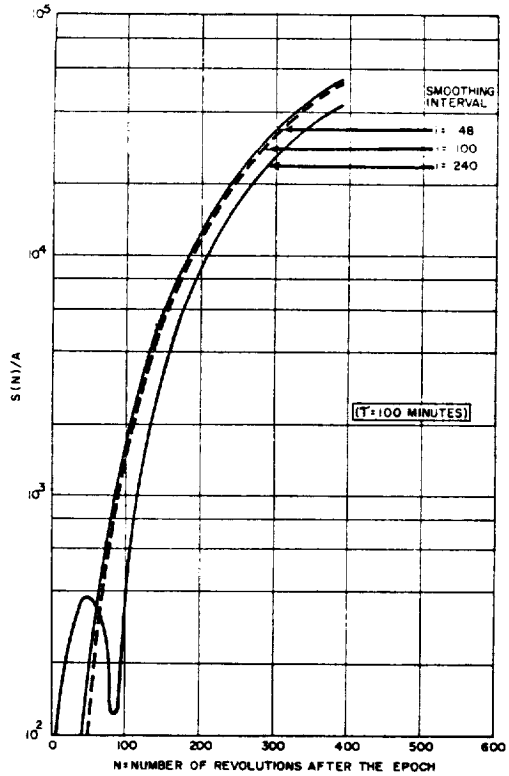

Fig. 16b. The Ratio of the rms Error in Orbital Prediction Caused by Sinusoidal Drag Variations to the Amplitude of the Sinusoidal Variation

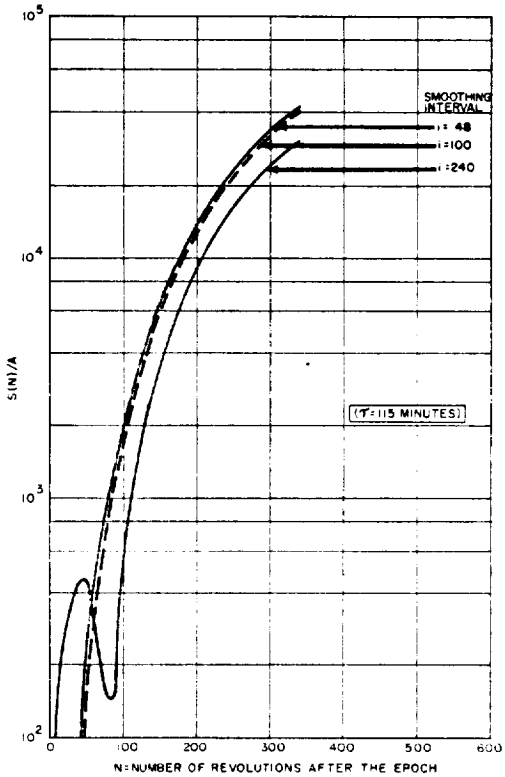

Fig. 16c. The Ratio of the rms Error in Orbital Prediction Caused by Sinusoidal Drag Variations to the Amplitude of the Sinusoidal Variation

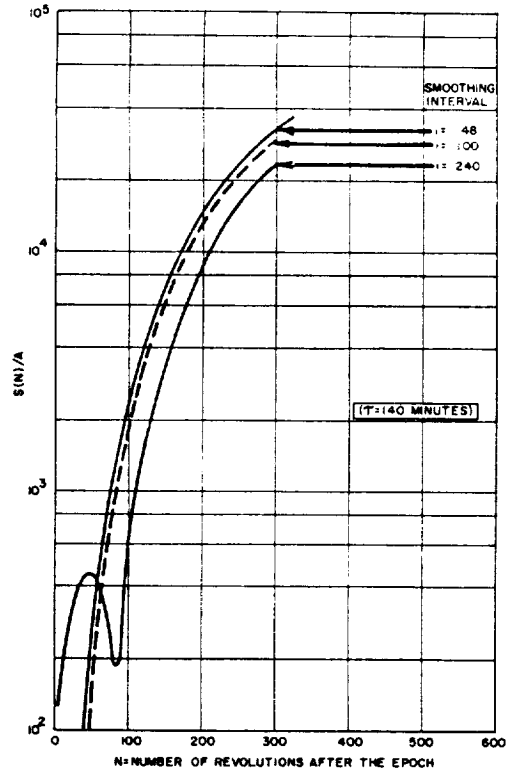

Fig. 16d. The Ratio of the rms Error in Orbital Prediction Caused by Sinusoidal Drag Variations to the Amplitude of the Sinusoidal Variation

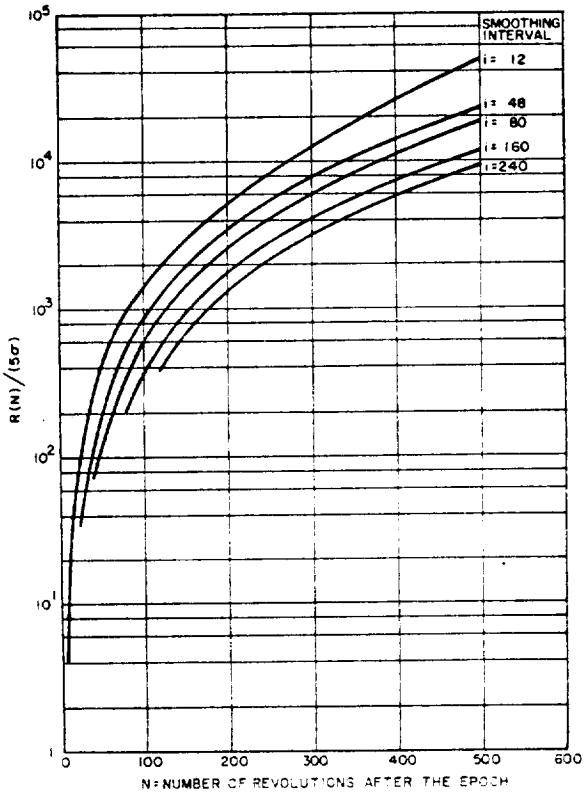

Fig. 17. The Ratio of the rms Error in Orbital Prediction Caused by Random Drag Fluctuation from Period to Period

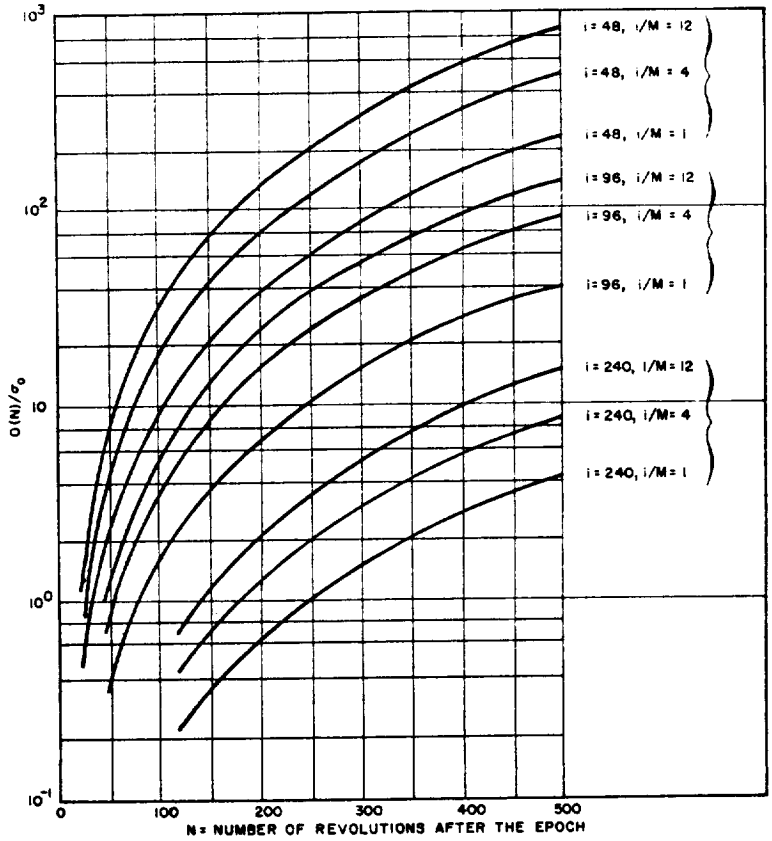

Fig. 18. The Ratio of the Error in Orbital Prediction Caused by Smoothed Observational Errors to the rms Error of a Single Observation

CHAPTER VI

MANEUVERS

Prepared by:

G. E. Townsend, Jr.
Martin Company (Baltimore)
Aerospace Mechanics Department
March 1963

		Page
	Symbols	VI-1
A.	Introduction	VI-2
B.	Impulsive Corrections	VI-2
C.	Independent Adjustment of Orbital Elements	VI-3
D.	Small Maneuvers in Nearly Circular Orbits	VI-15
E.	General Two-Impulse Maneuvers	VI-23
F.	Propulsion Requirements for Canceling the Effects of Drag and Oblateness	VI-26
G.	Differential Corrections in Orbit Transfer	VI-33
H.	The Statistical Distribution of the Elements of the Final Orbit	VI-39
I.	Transfer Trajectory Optimization	VI-43
J.	The Effects of Finite Burning Time	VI-50
K.	In-Orbit Propulsion System	VI-53
L.	Micro-Thrust Study	VI-56
M.	References	VI-64
N.	Bibliography	VI-65
	Illustrations	VI-75

LIST OF ILLUSTRATIONS

Figure		Page
1	Solution to the Law of Cosines	VI-77
2	Solution to the Law of Sines	VI-78
3	Total Velocity Increment Required for Two-Pulse Correction to a Circular Orbit	VI-79
4	Effects of Variations in Characteristic Velocity on the Velocity After the Maneuver	VI-80
5	Effects of Variations in the Pulse Attitude Angle on Vehicle Velocity After the Maneuver	VI-81
6	Effects of Variations in Characteristic Velocity on the Turn Angle.	VI-82
7	Effects of Variations in Thrust Pulse Angle on the Turn Angle	VI-83
8	Maneuvers in Circular Orbits to Change Orbital Inclination and/or the Node	VI-84
9	Nondimensionalized Impulsive Velocity Required to Transfer to a New Altitude, Rotate the Orbital Plane (at that altitude), and Recircularize Upon Arrival at the Initial Orbit	VI-85
10	Ratio of the Interceptor's Apogee Radius to the Radius of the Target's Circular Orbit as a Function of the Azimuth Change for Minimum Energy	VI-86
11	Nondimensionalized Orbital Period of the Interceptor in Its Maneuvering Orbit (elliptic orbit with apsidal radii equal to r_a and r_c)	VI-87
12	Fuel Required for Lateral Maneuvers in a Circular Orbit	VI-88
13	Nondimensionalized Impulsive Velocity Required to Rotate a Satellite's Orbital Plane	VI-89
14	Maneuver Angle as a Function of Thrust Attitude . . .	VI-90

LIST OF ILLUSTRATIONS (continued)

Figure		Page
15	Total Velocity Increment Required for Two-Pulse Correction to a Circular Orbit	VI-91
16	Velocity Increment for Maintenance of Circular Orbits by an Impulse at Orbit Intersection	VI-92
17	Error Analysis of Two-Pulse Correction of a Circular Orbit	VI-93
18	Absolute Magnitudes of the Nondimensionalized Components of the Thrust Vector as a Function of the True Anomaly for Orbit Inclinations from 0° to 90°	VI-94
19	Absolute Magnitude of the Nondimensionalized Thrust Vector as a Function of True Anomaly	VI-95
20	Magnitudes of the Nondimensionalized Corrective Force and Its Components, Averaged over the Orbit	VI-96
21	Discrete Velocity Sustaining System (h_0 = 300 naut mi = 555 km; I_{sp} = 300 sec)	VI-97
22	Discrete Velocity Sustaining System (h_0 = 200 naut mi = 370 km; I_{sp} = 300 sec)	VI-97
23	Discrete Velocity Sustaining System (h_0 = 100 naut mi = 185 km; I_{sp} = 300 sec)	VI-98
24	Discrete Velocity Sustaining System (h_0 = 50 naut mi = 93 km; I_{sp} = 300 sec)	VI-98
25	Velocity Required for Optimum 2-D Transfers Between Circular Orbits	VI-99
26	Independent Impulses for Optimum 2-D Transfers Between Circular Orbits	VI-100
27	Flight Path Angles for Optimum 2-D Transfer Between Circular Orbits	VI-101

LIST OF ILLUSTRATIONS (continued)

Figure		Page
28	Velocity Required for Optimum 3-D Transfers Between Circular Orbits	VI-102
29	Central Angles for Optimum 3-D Transfers Between Circular Orbits	VI-103
30	Flight Path Angles for Optimum 3-D Transfer Between Circular Orbits	VI-104
31	Total Energy Requirement for the Three-Pulse Transfer Between Circular Orbits as a Function of r_1, r_2 and r_3	VI-105
32	Energy Requirements for Transfer Between Coplanar Circular Orbits via the Hohmann Ellipse	VI-106
33	Lead Time Versus Acceleration Time	VI-107
34	Lead Time Versus Acceleration Time	VI-107
35	Velocity Difference Between Finite and Zero Time Acceleration Assumptions	VI-108
36	Difference in Velocity Increments Due to Zero and Finite Thrust Time Assumptions	VI-108
37	The Maximum Uncertainty in the Velocity Increment for Present Control Parameters as a Function of the Initial Thrust-to-Weight Ratio (specific impulse = 300 sec)	VI-109
38a	The Maximum Error in the Velocity Increment for a Velocity Monitored Propulsion System.	VI-110
38b	The Maximum Error in the Velocity Increment for a Velocity Monitored Propulsion System (error in the integrated velocity increment = $10^{-4} \Delta V$)	VI-111
39	Characteristic Chamber Length for a UDMH-IRFNA Motor	VI-112

LIST OF ILLUSTRATIONS (continued)

Figure		Page
40	Relative Total Pressure Loss (measured at the throat) as a Function of Chamber Cross Section for a UDMH-IRFNA Rocket Motor	VI-113
41	Sea Level Specific Impulse for a UDMH-IRFNA Motor as a Function of Chamber Pressure (mixture ratio = 2.60:1)	VI-113

VI. MANEUVERS

SYMBOLS

A	Right ascension
A_T	Throat area
a	Semimajor axis
C_F	Coefficient of Thrust
D	Drag force
ΔV	Velocity increment due to impulsive thrusts
E	Eccentric anomaly
e	Eccentricity
$\mathfrak{F}(\ )$	Hypergeometric series
F	Force; Function
g_0	Gravity acceleration
h	Altitude
$I_0(z)$	Modified Bessel function of the first kind
I_{sp}	Specific impulse
i	Inclination
J, J_2	First coefficients of the potential function
L	Latitude
m	Mean anomaly relative to the injection point
M	Mean anomaly relative to perigee; Mach number
$m, \dot{m}$	Mass and mass rate
$P_n^m(z)$	Generalized Legendre polynomial
p	Semiparameter of ellipse
R	Range, equatorial radius
r	radius
r_a, r_p	Apogee and perigee radii
T_s	Period of sustained lifetime
t	Time
t_b	Burning time
U	Potential function
V	Velocity
V_c	Circular speed $\sqrt{\mu/r}$
W_o	Initial weight
W_p	Propellant weight
X_K	Acceleration
x, y, z	Coordinate components
β	Azimuth relative to north point on horizon; Log-log slope of atmospheric density approximation
γ	Flight path angle relative to local horizontal; ratio of specific heats for a gas
ϵ	Base of natural logarithms utilized to prevent confusion with eccentricity
ζ	Mass ratio W_p/W_o
θ	Central angle measured from perigee, i.e., true anomaly
μ	Gravitational constant = GM ; statistical mean
ν	Angle in the equatorial plane measured from the ascending node to the intersection of the equatorial plane and the instantaneous meridian
ρ	Atmospheric mass density
σ	Variance of a statistical density function
τ	Orbital period
ϕ	Central angle measured from the ascending node $= \theta + \omega$
ϕ_T	Thrust orientation angle relative to velocity vector
Ω	Right ascension of the ascending node
Ω_e	Rotational rate of the earth
$\dot{\Omega}$	Secular regression rate of the line of nodes due to the earth's oblateness
ω	Argument of perigee
ω'	Secular precession rate of the argument of perigee due to the earth's oblateness

A. INTRODUCTION

Because of many reasons, including guidance inaccuracies in launch and ascent, change of mission for the satellite, and evasion or rendezvous maneuvers, a requirement exists to transfer from one position and velocity in space to another at some subsequent time. This chapter treats some of the problems associated with such maneuvers and presents computation routines and data useful in analyses of these maneuvers.

Due to the fact that two general trajectories do not intersect, it is necessary to perform at least two maneuvers in order to produce the desired trajectory. Thus, the first order of business is the analyses of impulses (the mechanism of investigation) and of the independent adjustment of the six constants of integration or elements. These discussions will be followed by the analysis of small maneuvers in nearly circular orbits, a general two-impulse transfer discussion, propulsion requirements for correcting the effect of atmospheric drag and the earth's oblateness. At this point, the emphasis changes slightly to the presentation of material pertinent to differential corrections, the errors in the final orbit and trajectory optimization. These discussions are followed in turn by the analysis of the effects of finite burning time and the in-orbit propulsion system. The chapter concludes with a discussion of the adaptability of microthrusts for orbital corrections.

B. IMPULSIVE CORRECTIONS

Because the impulse is the medium of analysis in these discussions, the accompanying assumptions and methods will first be reviewed. Because the burning time is infinitesimal, the effects of gravity, variations in position due to thrust, etc., can be neglected and the governing law considered to be the law of cosines.

By this law, the characteristic velocity of the maneuver (ΔV) may be expressed as a function of the velocity vector prior to maneuver (V_1), the velocity vector after the maneuver (V_2), the turning angle of the maneuver (ψ) and the angle of thrust application relative to the initial flight direction (ϕ_T).

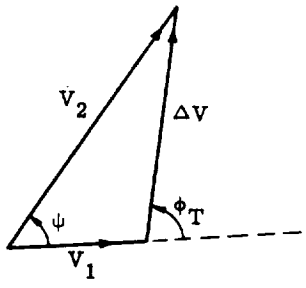

$$\Delta V^2 = V_1^2 + V_2^2 - 2 V_1 V_2 \cos \psi \qquad (1)$$

where

$$\Delta V = g_0 I_{sp} \ln \left(\frac{1}{1 - \frac{\dot{m} t_b}{m_0}} \right) \qquad (2)$$

= the ideal velocity increment obtainable.

A convenient graphical representation of this law can be found if it is first nondimensionalized.

$$\left(\frac{\Delta V}{V_1} \right)^2 = 1 + \left(\frac{V_2}{V_1} \right)^2 - 2 \left(\frac{V_2}{V_1} \right) \cos \psi \qquad (3)$$

Similarly the law of sines is:

$$\frac{\Delta V}{V_1} \sin \phi_T = \frac{V_2}{V_1} \sin \psi \qquad (4)$$

These equations are presented in Figs. 1 and 2. The velocity increment itself is related to the mass fraction $\left(\frac{\dot{m} t_b}{m_0} \right)$ in Fig. 3. The form of these figures is the nomogram; the philosophy of construction along with a general description of the utilization of such a figure is presented in Chapter III. The effects of errors in ΔV and ϕ_T on the final velocity V_2 can be seen immediately from the law of cosines to be

$$\left(\frac{\partial x}{\partial y} \right)_{\phi_T} = \frac{y + \cos \phi_T}{x} \qquad (5)$$

$$\left(\frac{\partial x}{\partial \phi_T} \right)_y = - \frac{y}{x} \sin \phi_T \qquad (6)$$

$$\left(\frac{\partial \psi}{\partial y} \right)_{\phi_T} = \frac{\sin \phi_T}{x^2} \qquad (7)$$

$$\left(\frac{\partial \psi}{\partial \phi_T} \right)_y = \frac{y}{x} \left(\frac{\partial x}{\partial y} \right)_{\phi_T} \qquad (8)$$

where

$$x = \frac{V_2}{V_1}$$

$$y = \frac{\Delta V}{V_1}$$

and the subscript on the partial derivative indicates the parameter held constant. Figures 4 through 7 show these error coefficients.

C. INDEPENDENT ADJUSTMENT OF ORBITAL ELEMENTS

The impulse having been considered, attention can be turned to the correction of the orbital elements. This series of corrections will be treated first for the case when the target orbit is circular then for the case of elliptic orbits. (The distinction is made because of minor differences in the maneuver formulation.)

1. Circular Orbits

In general, the ascent guidance system will not be capable of placing the vehicle in a specified precisely circular orbit (even for a spherical earth). Therefore, maneuvers to change each element must be defined.

a. Correction of eccentricity and semimajor axis

The first of these maneuvers is the placement of the satellite in the proper orbit. This problem is considered in three cases, in which the planar orbit will be described by apogee and perigee radii and the time of perigee crossing. The three cases are:

(1) $r_a > r_n > r_p$

(2) $r_a > r_p > r_n$

(3) $r_n > r_a > r_p$.

The r_n is that radius which is specified for the satellite.

Case 1--$r_a > r_n > r_p$. Consider first the pulse necessary to change an initially elliptical orbit to a circular orbit.

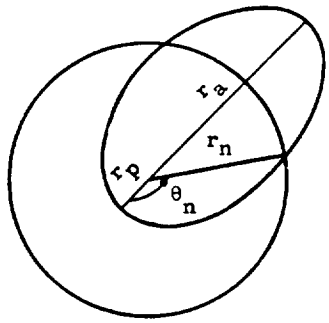

From the law of cosines

$$\Delta V_\epsilon^2 = V_c^2 + V_n^2 - 2 V_c V_n \cos \Delta\gamma$$

where

$V_c = \sqrt{\frac{\mu}{r_n}}$

V_n = velocity in the incorrect orbit at r_n

$\Delta\gamma$ = change in flight path angle

This expression may be written in terms of the knowns by considering

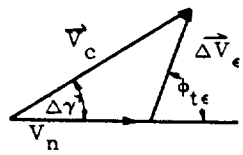

$$\Delta\gamma = \cos^{-1} \sqrt{\frac{r_a r_p}{r_n (r_a + r_p - r_n)}}$$

$$V_n^2 = \frac{\mu p}{r_n^2 \cos^2 \Delta\gamma} = 2 V_c^2 \left(1 - \frac{r_n}{r_a + r_p}\right)$$

$$2 V_c V_n \cos \Delta\gamma = 2 \sqrt{\frac{\mu}{r_n}} \frac{\sqrt{\mu p}}{r_n \cos \Delta\gamma} \cos \Delta\gamma$$

$$= 2 V_c^2 \sqrt{\frac{2 r_a r_p}{r_n (r_a + r_p)}}$$

Then, the nondimension solution for the corrective pulse may be written so as to involve only two ratios.

$$\left(\frac{\Delta V_\epsilon}{2 V_c}\right)^2 = \frac{3}{2} - \frac{\frac{r_n}{r_p}}{\frac{r_a}{r_p} + 1} - \sqrt{\frac{2 \frac{r_a}{r_p}}{\frac{r_n}{r_p}\left(\frac{r_a}{r_p} + 1\right)}} \qquad (9)$$

The direction of thrust application is determined by noting that

$$\Delta V_\epsilon \sin \phi_{t\epsilon} = V_c \sin \Delta\gamma$$

or

$$\phi_{t\epsilon} = \sin^{-1} \left(\frac{V_c}{\Delta V_\epsilon} \sin \Delta\gamma\right) \qquad (10)$$

If a timer signal is used to trigger the pulse, the time to make the correction must also be computed.

$$t = \frac{1}{\sqrt{\mu}} \left(\frac{r_a + r_p}{2}\right)^{3/2} \left[E - \frac{r_a - r_p}{r_a + r_p} \sin E\right] + t_p \qquad (11)$$

where

$$\sin E = \frac{r_n}{r_a - r_p} \left[\frac{r_a}{r_p}\left(1 + 2 \frac{r_p}{r_n}\right) + \frac{r_p}{r_a}\left(1 + 2 \frac{r_a}{r_n}\right) + \right.$$

(continued)

$$- 2 \left(1 + 2 \frac{r_a}{r_n} \frac{r_p}{r_n}\right)\Bigg]^{1/2}$$

and t is the time to initiate the correction.

The orbit resulting from the correction(s), the magnitude, direction and time of which are given by Eqs (9), (10) and (11) is a circular orbit of the desired period. However, this orbit may be slightly in error due to inherent inaccuracies. For this reason, the following error analysis for changing the size and shape of the orbit to a circular orbit was conducted.

$$\sin \Delta\gamma = \frac{\Delta V}{V_c} \sin \phi_t$$

$$\cos \Delta\gamma \, \partial(\Delta\gamma) = \frac{\partial(\Delta V)}{V_c} \sin \phi_t + \frac{\Delta V}{V_c} \cos \phi_t \, \partial \phi_t - \frac{\Delta V}{V_c^2} \sin \phi_t \, \Delta V_c$$

where

$$V_c = \sqrt{\frac{\mu}{r}} \text{ and}$$

$$\frac{\partial V_c}{\partial r} = - \frac{V_c}{2r}.$$

Thus,

$$\cos \Delta\gamma \, \delta(\Delta\gamma) = \frac{\delta(\Delta V)}{V_c} \sin \phi_t + \frac{\Delta V}{V_c} \cos \phi_t \, \Delta\phi_t + \frac{\Delta V \Delta r}{2 V_c r} \sin \phi_t$$

or

$$\frac{\cos \Delta\gamma \, \delta(\Delta\gamma)}{\sin \phi_t} = \frac{\delta(\Delta V)}{V_c} + \frac{\Delta V}{V_c} \left[\frac{\Delta r}{2r} + \cot \phi_t \, \Delta\phi_t\right].$$

It is noted that both sides of the last equation become infinite as ϕ_t goes to zero. This problem may be resolved by going back one step to the preceding equation and noting that for $\phi_t = 0$, $\Delta\gamma = 0$.

$$\delta(\Delta\gamma) = \frac{\Delta V \Delta\phi_t}{V_c}$$

b. Correction of the plane

The second maneuver to be considered is that necessary to change the orbital plane. Consider the case of maneuvers in circular orbits to change orbital inclination or the node (Fig. 8). A vehicle in a circular orbit with inclination angle (i) and nodal longitude (Ω) is given a horizontal thrust pulse (ΔV, the characteristic velocity of the maneuver) at latitude (L) so that the orbital velocity remains constant in magnitude, but changes in azimuth by an angle $\Delta\beta$. (Azimuth is determined by the intersection of the meridian at the point of the maneuver and the great circle projection of the orbital path.) Using primes to indicate quantities after the maneuver,

$$\beta' = \beta + \Delta\beta.$$

A new node (Ω') and new inclination (i') result from such a maneuver. If d is the longitude of the maneuver, measured from the reference axis, then

$$\nu = \Omega \pm d.$$

(Note: Use a plus sign if Ω and d are on opposite sides of the reference axis, and a minus sign if they are on the same side.)

Since d is fixed, the longitude of the new node is

$$\Omega' = \nu' - d.$$

From spherical trigonometry,

$$\cos i = \cos L \sin \beta$$

$$\sin \nu = \tan L \cot i$$

$$\cot \beta = \sin L \cot \nu$$

These expressions can be manipulated by maintaining L constant to yield

$$\nu' = \tan^{-1}(\sin L \tan \beta'), \qquad (12)$$

and

$$i' = \cos^{-1}(\cos L \sin \beta'). \qquad (13)$$

The energy requirement to accomplish this constant speed turn is then simply

$$\frac{\Delta V}{V_c} = 2 \sin \Delta\beta/2 \qquad (14)$$

and the impulse must be directed according to

$$\phi_t = \pm \left(\frac{\Delta\beta}{2} + 90°\right)$$

in the plane normal to the radius vector.

The error derivatives $\left(\frac{\partial i}{\partial \beta}\right)_{L = \text{constant}}$ and $\left(\frac{\partial \nu}{\partial \beta}\right)_{L = \text{constant}}$ may be readily determined as

$$\left(\frac{\partial i}{\partial \beta}\right)_L = - \frac{\cos L \cos \beta}{\sin i} = - \sin L \cot i \cot \nu \qquad (15)$$

and

$$\left(\frac{\partial \nu}{\partial \beta}\right)_L = \frac{\sin L \sec^2 \beta}{\sec^2 \nu} = \cos^2 \nu \sin L + \frac{\sin^2 \nu}{\sin L} . \tag{16}$$

At this point, it is of interest to note that if it is desired that the nodal position be maintained constant, the maneuver must occur at one of the equatorial crossings. If, however, the inclination is to be maintained constant, all maneuvers must be made at $\pm \frac{\Delta\Omega}{2}$ (sign depends on the direction of the $\Delta\Omega$) from the longitude corresponding to the maximum latitude.

Equation (14) shows the very large energy requirements for significant changes in azimuth at low altitudes where V_c is of the order of 8000 mps and suggests that a more efficient procedure might result if the maneuver could be made at a point where the velocity is low. Pursuing this thought further, consider the following sketch.

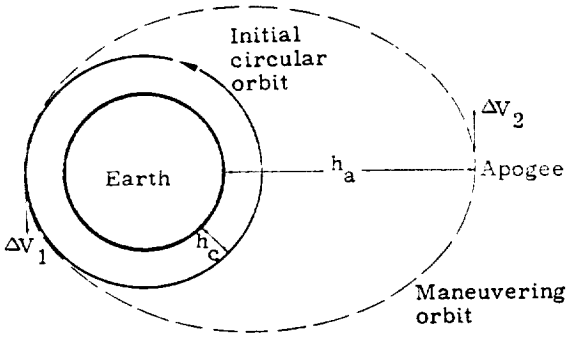

The philosophy is first to inject into an elliptic orbit the parameters of which will be investigated, secondly to change azimuth at the maximum radius (minimum velocity) and thirdly, reestablish the desired circular orbit but in a new plane. Now

$$V_p = V_c + \Delta V_1$$

$$V_p^2 - V_a^2 = 2\mu \left(\frac{1}{r_p} - \frac{1}{r_a}\right)$$

or

$$V_a = \frac{2V_c^2}{V_p} - V_p$$

Having reached apogee, the second increment of magnitude defined by

$$\frac{\Delta V_2}{V_a} = 2 \sin \frac{\Delta\beta_2}{2}$$

is applied.

Then at perigee, the initial velocity adjustment must be canceled; thus

$$\Delta V_{total} = 2\Delta V_1 + \Delta V_2 .$$

By combining the above equations, the following explicit expression for ΔV_T in terms of the radius of the circular orbit and the ratio of apogee to perigee radii can be obtained.

$$\Delta V_T = 2V_c \left\{ \left(\frac{r_a}{r_c}\right)^{1/2} \left[1 + \left(\frac{r_a}{r_c}\right)^{-1} \cdot \sin \frac{\Delta\beta}{2}\right] \left[\frac{1}{2}\left(1 + \frac{r_a}{r_c}\right)\right]^{-1/2} - 1 \right\}$$

$$(r_a \geq r_c) \tag{15}$$

This function has been plotted in Fig. 9 ($r_a \geq r_c$) in nondimensionalized form (by dividing through by V_c) for various values of $\Delta\beta$. For the smaller values of $\Delta\beta$, the impulsive incremental velocity required to perform the transfer maneuver is seen to be greater when the vehicle is injected into an elliptic orbit, that is, when the nodal point is stretched or lengthened. On the other hand, for the larger values of $\Delta\beta$, the three-impulse maneuver becomes more efficient, and, in fact, there is a definite ratio of r_a/r_c at which the total energy required for the maneuver is a minimum.

This condition is more clearly illustrated by analyzing the variation of ΔV_T with respect to r_a for a given value of r_c. Performing the indicated differentiation yields

$$\frac{\partial(\Delta V_T)}{\partial r_a} = \frac{V_c}{2r_c} \left\{ \left[\frac{1}{2}\frac{r_a}{r_c}\left(1 + \frac{r_a}{r_c}\right)\right]^{-3/2} \cdot \left[\frac{r_a}{r_c} - \left(1 + 2\frac{r_a}{r_c}\right) \sin \frac{\Delta\beta}{2}\right] \right\} \tag{16}$$

This function defines the minimum points when

$$\frac{\partial(\Delta V_T)}{\partial r_a} = 0 \tag{17}$$

that is, when

$$\frac{r_a}{r_c} = \left(1 + 2\frac{r_a}{r_c}\right) \sin \frac{\Delta\beta}{2} \tag{18}$$

or when

$$\frac{r_a}{r_c} = \frac{\sin \frac{\Delta\beta}{2}}{1 - 2 \sin \frac{\Delta\beta}{2}} \qquad (19)$$

The right-hand side of Eq (19) is plotted in Fig. 10 for the range $0^\circ \leq \Delta i \leq 90^\circ$ and also in Fig. 9 as a dotted line. The values given by the curve are the minima, while values selected within the shaded area represent choices which require more energy than the minimum, but less than that required to make the correction on the initial circular orbit itself. Another factor which in inferred from this curve is that since $r_a \geq r_c$, the value of $\Delta\beta$, at which the function is exactly unity (about 39°), defines the minimum azimuth change for which it becomes profitable to effect the transfer to an eccentric orbit.

The vertical boundary at $\Delta\beta = 60^\circ$ arises because of the fact that the formulation breaks down at this point because the vehicle is required to transfer to infinity (i.e., escape) maneuver, then return. In this region all maneuvers will require the same energy, since the velocities at these large radii are essentially zero. However, this solution is of academic interest because of the impracticality of such an approach.

Another factor of interest in this study is the period T of the elliptical orbits being considered, since one would normally want to keep the transfer time within reasonable limits. The equation for the period of a vehicle in an elliptic orbit about the spherical earth is

$$\tau = \frac{2\pi}{\mu^{1/2}} a^{3/2} \qquad (20)$$

which may be reduced in terms of the variables used in the previous equations to the form:

$$\tau = \frac{2\pi r_c^{3/2}}{\mu^{1/2}} \left[\frac{1}{2}\left(1 + \frac{r_a}{r_c}\right)\right]^{3/2}$$

$$= \tau_c \left[\frac{1}{2}\left(1 + \frac{r_a}{r_c}\right)\right]^{3/2} \qquad (21)$$

where τ_c is the period of the (target's) circular orbit. Figure 11 is a plot of the nondimensionalized orbital period of the interceptor

$$\frac{\tau}{\tau_c} = \left[\frac{1}{2}\left(1 + \frac{r_a}{r_c}\right)\right]^{3/2} \qquad (22)$$

as a function of the parameter r_a/r_c for the same range as was considered previously, with the same equation applying in this case, for the entire range of r_a/r_c.

The factor of interest here, however, is the additional amount of time required to perform the eccentric maneuver, as compared to the period of the circular orbit. This factor is given by

$$\tau - \tau_c = \left(\frac{\tau}{\tau_c} - 1\right) \tau_c \qquad (23)$$

The new circular orbit may also be described in terms of the lateral separation from the old orbit as a function of the central angle from the point at which the maneuver is made (ϕ_0) if the maneuver is small. Let the spherical separation of the new orbit from the original orbit be $\bar{z}$ expressed in radians.

Then

$$\frac{\sin \bar{z}}{\sin \Delta\beta} = \frac{\sin \phi_0}{\sin \phi_T}$$

but $\sin \Delta\beta = \Delta V / V_c \sin \phi_T$ from pulse geometry.

Therefore,

$$\sin \bar{z} = \frac{\Delta V}{V_c} \sin \phi_0.$$

For small angles ($\bar{z} < 0.1$ radian) $\sin \bar{z} \tilde{=} \bar{z}$ (radian) $\tilde{=} \frac{z}{r_0} \frac{(\text{km})}{(\text{km})}$, and with a maximum error of about 1% we have:

$$\frac{z}{r_0} \tilde{=} \frac{\Delta V}{V_0} \sin \phi_0 \qquad (24)$$

The separation z (km) versus mass ratio required is plotted in nomograph form in Fig. 12 for circular orbits at altitudes of 0, 200, 400, 600, 800 and 1000 km for various ϕ_0 and I_{sp} = 200, 250, 300, 350 and 400 sec. The maximum separation between the orbits is seen to occur at

$$\phi_0 = (2n - 1)\ 90^\circ,\ n = 1, 2, \ldots$$

This fact is true because both orbits must contain the original radius vector.

There is no time separation between satellites because the satellite is in a circular orbit at the same altitude with the same period both before and after the maneuver.

c. Correction of position

The equations to correct the position of the satellite in its corrected circular orbit are derived as follows. If it is assumed the satellite is displaced $\Delta\theta$ from some desired position, then the time in which the satellite passes through $\Delta\theta$ is

$$\Delta t = \frac{\tau}{2\pi} \Delta\theta \qquad (25)$$

This Δt must be lost or made up, depending upon whether the satellite is ahead of, or behind its desired zenith. The simplest solution, from the standpoint of computations involved, is to cause the satellite to enter an elliptical orbit possessing a period $\tau \pm \Delta t/n$ (with perigee or apogee, as the case may be, at the altitude of the desired orbit) by a pulse tangent to the original orbit, and to re-enter the original orbit by an equal and opposite pulse after n periods of the transfer orbit. Then, if τ_t and a are parameters of the transfer orbit,

$$\frac{\Delta t}{n} = \pm (\tau_t - \tau) = \pm \tau \left\{ \left(\frac{a}{r_n} \right)^{3/2} - 1 \right\} \quad (26)$$

Combining Eqs (25) and (26) and noting that

$$a = \frac{\mu r_n}{2\mu - r_n V_n^2},$$

V_n is determined as

$$\left(\frac{V_n}{V_c} \right)^2 = 2 - \frac{1}{\left(\frac{\Delta\theta}{2\pi} + 1 \right)^{2/3}}.$$

Then,

$$\frac{\Delta V_{\theta 1}}{n V_c} = \frac{V_n}{V_c} - 1 = \sqrt{2 - \frac{1}{\left(\frac{\Delta\theta}{2\pi} + 1 \right)^{2/3}}} - 1 \quad (27a)$$

and

$$\Delta V_{\theta 2} = - \Delta V_{\theta 1}$$

where:

$\Delta V_{\theta 1}$, $\Delta V_{\theta 2}$ are the first and second corrective pulses applied tangentially at an interval $n\tau \left(1 \pm \frac{\Delta\theta}{2\pi n} \right)$.

n = number of revolutions in transfer orbit

$\Delta\theta$ = + if vehicle is to move backward in orbit (i.e., ΔV along velocity vector)
= - if vehicle is to move ahead in orbit (i.e., ΔV opposes velocity vector)

Equation (27a) is presented in Fig. 13.

For large values of $\Delta\theta$, ΔV approaches

$$\Delta V = \sqrt{\frac{\mu}{r}} \, (\sqrt{2} - 1),$$

which is the difference between escape and circular orbit velocities. For small values of $\Delta\theta$,

$$\Delta V \approx \sqrt{\frac{\mu}{r}} \left(\frac{\Delta\theta}{6\pi} \right).$$

The time required for carrying out the maneuver is

$$t = \frac{2\pi n}{\sqrt{\mu}} \sqrt{\left(\frac{r\mu}{2\mu - r(V + \Delta V)^2} \right)^3}$$

where ΔV is negative if $\Delta\theta$ is + and positive if $\Delta\theta$ is -.

The more general case where thrust is not assumed to be along the velocity vector results in the following expression

$$\Delta\theta = (1 - K_2)\,\pi \left\{ 1 - \frac{1}{\left(2 - K_2^2 \right)^{3/2}} \right\} + 2 K_2 \left\{ \tan^{-1} \left[\frac{\tan\alpha}{\frac{K_2^2}{2} - 1} \right] + \alpha - \frac{E - e \sin E}{\left[2 - K_2^2 \right]^{3/2}} \right\} \quad (27b)$$

where

$$\alpha = \tan^{-1} \left\{ \frac{(K_2 - K_1) \, |\sin \phi_T|}{1 + (K_2 - K_1) \cos \phi_T} \right\}$$

$$K = \sqrt{2 - \frac{r}{a}}$$

and

$$E = \tan^{-1} \left\{ (K_2 - K_1) \sqrt{\frac{2 - K_2^2}{K_2^2 - 1}} \, |\sin \phi_T| \right\}$$

This relationship is presented in Fig. 14.

Equation (27) assumes that the maneuver may be initiated at any time and considers only the magnitude of the error in the central angle. If it is desired to produce a specific node (on a rotating earth) at a specified time, the basic approach must be altered. The new problem may be restated as follows: Assume that it is desired to move from a known position B (relative to the ascending node) to a nodal position Ω_2 on a rotating earth in the same time that it takes to move from a position α to the node Ω_1. This problem is illustrated in the following sketch.

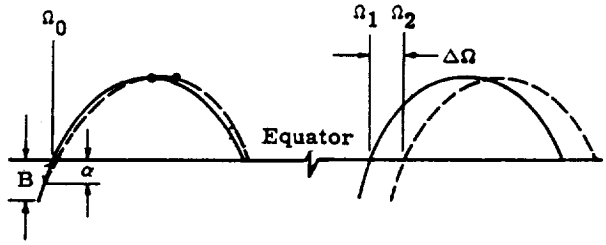

For the case of nearly circular orbits, this implies that ($t_1 = t_2$):

$$\frac{\tau}{2\pi}\left[2\pi n + \alpha - n\dot{\omega}\right] = \frac{\tau'}{2\pi}\left[2\pi n' + B - n'\dot{\omega}'\right] \tag{28}$$

If $n = n'$ and $\dot{\omega}' \approx \dot{\omega}$,

$$\frac{\tau}{\tau'} = \frac{n'(2\pi - \dot{\omega}') + B}{n(2\pi - \dot{\omega}) + \alpha}$$

$$\simeq 1 + \frac{B - \alpha}{n(2\pi - \dot{\omega}) + \alpha} .$$

Another relationship between τ and τ' can be obtained by observing the nodal motion as a function of period change:

$$n\Delta\tau\Omega_e = \Delta\Omega + \dot{\Omega}n$$

and

$$\frac{\tau}{\tau'} = 1 + \frac{\Delta\Omega + n\dot{\Omega}}{n\Omega_e\tau'}$$

Equating

$$\frac{B - \alpha}{n(2\pi - \dot{\omega}) + \alpha} = \frac{\Delta\Omega + n\dot{\Omega}}{n\Omega_e\tau'} \tag{29}$$

The angle α is included in the analysis for the sole purpose of providing a means for including errors in the time of passage through the node Ω_0. Therefore,

$$\alpha = f(t_{error}) = \frac{2\pi\Delta t_0}{\tau} .$$

Substituting this relationship into Eq (29) yields

$$\frac{B}{2\pi} = \left[1 - \frac{\dot{\omega}}{2\pi} + \frac{\Delta t_0}{n\tau}\right]\left[\frac{\Delta\Omega + n\dot{\Omega}}{\Omega_e\tau + \frac{\Delta\Omega}{n} + \dot{\Omega}}\right] + \frac{\Delta t_0}{\tau} \tag{30}$$

Thus, the position of the point at which the first corrective pulse is to be made is defined, but the magnitude of the correction itself has not yet been evaluated. This portion of the analysis can be accomplished when it is noted that the orbits of interest for this study are circular.

Thus,

$$\Delta\tau = 3\tau\left[\frac{\Delta r}{r} + \frac{\Delta V}{V_c}\right] \tag{31}$$

If the period change is to result solely from a velocity pulse (that is, no change in radius during the application of the pulse), the period change is:

$$\Delta\tau = \frac{3\tau\Delta V}{V_c} .$$

Again,

$$\Delta\tau = \frac{\Delta\Omega + n\dot{\Omega}}{n\Omega_e} .$$

Therefore,

$$\Delta V = \frac{\mu}{6\pi r^2}\left[\frac{\Delta\Omega + n\dot{\Omega}}{n\Omega_e}\right] \tag{32}$$

This equation defines the first pulse, which alters the period to produce the desired position change. However, a second pulse approximately equal to, but in the opposite direction from the first, is required at the desired node to produce the correct orbit. Both of these pulses should be directed along the velocity vector. The magnitude of this second pulse is:

$$\Delta V_2 = \Delta V_1 + (V_c - \delta V_1)$$

where the corrective term is included to compensate for the small radius and velocity errors which produced the initial displacement.

Case 2. $r_a > r_p > r_n$. For this case, the determination of ΔV_ϵ must be modified as follows:

$$\frac{\Delta V_\epsilon}{\sqrt{2}V_{ca}} = \frac{1}{\sqrt{\frac{r_a}{r_n} + 1}} - \frac{1}{\sqrt{\frac{r_a}{r_p} + 1}} \tag{33}$$

$$\frac{\Delta V_{\epsilon 2}}{V_c} = 1 - \sqrt{\frac{2}{1 + \frac{r_n}{r_a}}} \tag{34}$$

where $V_{ca} = \sqrt{\frac{\mu}{r_a}}$. Tangential pulses ($\Delta V_{\epsilon 1}$ and $\Delta V_{\epsilon 2}$) are applied at

$$t_p + \frac{\pi}{\sqrt{\mu}}\left(\frac{r_a + r_p}{2}\right)^{3/2}$$

and

$$t_p + \frac{2\pi}{\sqrt{\mu}}\left(\frac{r_a + r_p}{2}\right)^{3/2}, \text{ respectively.}$$

The subsequent corrections for i, Ω proceed exactly as in the first case.

Case 3. $r_n > r_a > r_p$. Proceeding in a manner similar to Case 2,

$$\frac{\Delta V_{\epsilon 1}}{\sqrt{2}V_{cp}} = \frac{1}{\sqrt{1 + \frac{r_p}{r_n}}} - \frac{1}{\sqrt{1 + \frac{r_p}{r_a}}} \tag{35}$$

$$\frac{\Delta V_{\epsilon 2}}{V_c} = 1 - \sqrt{\frac{2}{\frac{r_n}{r_p} + 1}} \tag{36}$$

where $V_{cp} = \sqrt{\frac{\mu}{r_p}}$ and $\Delta V_{\epsilon 1}$ and $\Delta V_{\epsilon 2}$ are applied tangentially at times

$$t_p + \frac{2\pi}{\sqrt{\mu}} \left(\frac{r_a + r_p}{2}\right)^{3/2}$$

and

$$t_p + \frac{3\pi}{\sqrt{\mu}} \left(\frac{r_a + r_p}{2}\right)^{3/2} .$$

The subsequent corrections for i, Ω proceed exactly as in the first case.

2. Elliptical Orbits

The presentation here considers the orbit to be defined in terms of the six usual elements a, e, t_p, i, ω, Ω and discusses the adjustment of each.

a. Transition from incorrect orbit

The first step in the final correction of an elliptical orbit is a transition from the incorrect orbit to an orbit of the desired size and shape in the plane of the incorrect orbit, but rotated in the plane through an angle ω - ω', where ω' is the angle from perigee to node for the incorrect orbit and ω the angle from perigee to node in the orbit ultimately desired.

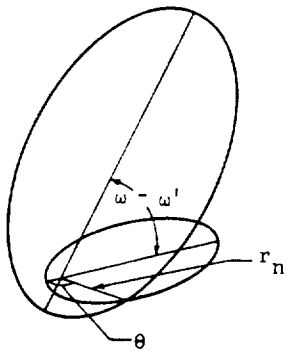

Known or calculable quantities are r'_a, r'_p, r_a, r_p, ω and ω', where primes denote quantities in the incorrect orbit. The angle from perigee to intersection in the original orbit (θ) may be determined as follows.

$$r_n = \frac{p'}{1 + e' \cos\theta} = \frac{p}{1 + e \cos(\theta - \omega + \omega')}$$

Writing this expression in terms of the known radii,

$$\left(\frac{r'_a}{r'_p} - 1\right)\cos\theta + \frac{r'_a}{r'_p} + 1 = \frac{r'_a}{r_a}\left[\frac{r_a}{r_p} + 1 + \left(\frac{r_a}{r_p} - 1\right)\cos(\theta - \psi)\right] \quad (37)$$

where

$$\psi = \omega - \omega' .$$

This expression can be easily solved for θ by an iteration technique. However, a direct solution is also available

$$\cos\theta = \frac{B(1 - A\cos\psi)}{1 + A^2 - 2A\cos\psi} \pm \left[B^2(1 - A\cos\psi)^2 - (1 + A^2 - 2A\cos\psi)(B^2 - A^2\sin^2\psi)\right]^{1/2} \cdot (1 + A^2 - 2A\cos\psi)^{-1}$$

where

$$A = \frac{1/r_p - 1/r_a}{1/r'_p - 1/r'_a} = \frac{e'}{e}\frac{p}{p'} ,$$

$$B = \frac{1/r_a + 1/r_p}{1/r'_p - 1/r'_a} \cdot \frac{\frac{r'_a}{r'_p} + 1}{\frac{r'_a}{r'_p} - 1} = \frac{e'}{p'}\frac{p}{} - \frac{1}{e'}$$

$$\psi = \omega - \omega' .$$

The change in flight path angle in the maneuver is

$$\Delta\gamma = \cos^{-1}\sqrt{\frac{r'_a/r_n}{r'_a/r'_p - (r_n/r'_p) + 1}} - \cos^{-1}\sqrt{\frac{r_a/r_n}{\frac{r_a}{r_p} - \frac{r_n}{r_p} + 1}} \quad (38)$$

The characteristic velocity necessary to effect the maneuver may be determined from the law of cosines.

$$\frac{\Delta V_\epsilon^2}{2 V_{cr}^2} = 2 - \frac{1}{\frac{r'_a}{r_n} + \frac{r'_p}{r_n}} - \frac{1}{\frac{r_a}{r_n} + \frac{r_p}{r_n}} - 2\sqrt{\left[1 - \frac{1}{\frac{r'_a}{r_n} + \frac{r'_p}{r_n}}\right]\left[1 - \frac{1}{\frac{r_a}{r_n} + \frac{r_p}{r_n}}\right]}\cos\Delta\gamma , \quad (39)$$

where ΔV_ϵ is the characteristic velocity of the correction and V_{cr} is the circular velocity at r.

Thus, if r_p, r_a, r'_a, r'_p, ω and ω' are known, θ (and hence r_n and the time for correction), ΔV and Δγ are determined.

b. Correction of inclination

After the size and shape correction is completed, it is possible to correct inclination to the desired value by a constant speed turn at the node (ω). The error in inclination (Δi) will be determined as data. The characteristic velocity of the inclination correction is then

$$\Delta V_i = 2V_n \sin \frac{\Delta i}{2} \qquad (40)$$

where the velocity at the node (V_n) is determined as

$$V_n = \sqrt{\mu\left(\frac{2}{r_n} - \frac{1}{a}\right)}$$

$$= V_{ca}\left[\frac{r_a}{r_p} + 1 + \left(\frac{r_a}{r_p} - 1\right)\cos\omega - \frac{2\frac{r_a}{r_p}}{\frac{r_a}{r_p} + 1}\right]^{1/2}$$

(V_{ca} is circular velocity at r_a.)

Then, the inclination correction may be expressed in nondimensional form as

$$\frac{\Delta V_i}{V_{ca}} = 2 \sin \frac{\Delta i}{2} \sqrt{\frac{r_a}{r_p} + 1 + \left(\frac{r_a}{r_p} - 1\right)\cos\omega - \frac{2\frac{r_a}{r_p}}{\frac{r_a}{r_p}+1}} \qquad (41)$$

and the direction of thrust application is

$$\phi_{ti} = \frac{\Delta i}{2} + 90° \qquad (42)$$

from the initial direction of motion because the thrust possesses no component along the principal normal to the orbit.

The thrust is applied at a time

$$t - t_p = \frac{\tau}{2\pi}(E_n - e \sin E_n)$$

where

$$E_n = 2 \tan^{-1}\left[\sqrt{\frac{r_p}{r_a}} \tan \frac{\omega}{2}\right]. \qquad (43)$$

c. Correction of nodal position

The next corrective maneuver is the correction of nodal position.

The inclination (i) is to be maintained and the latitude of the satellite at transition is L. Consider the spherical triangles formed by the projections of the original and corrected orbits on a spherical earth.

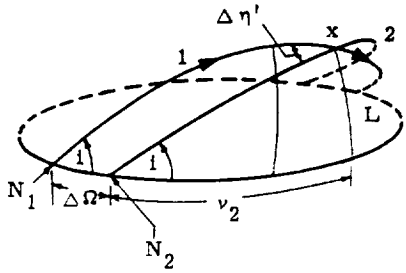

$$\tan i = \frac{\tan L}{\sin(\nu_2 + \Delta\Omega)} = \frac{\tan L}{\sin \nu_2}$$

$$\sin(\nu_2 + \Delta\Omega) = \sin \nu_2$$

Thus

$$\nu_2 = 90° - \frac{\Delta\Omega}{2}$$

Let the angle from node to transition (x) at the incorrect orbit be ϕ_x.

Then,

$$\phi_x = \tan^{-1}\left[\frac{\tan\left(90° + \frac{\Delta\Omega}{2}\right)}{\cos i}\right].$$

The velocity at x should be changed to the velocity possessed in the original orbit at $90° - \frac{\Delta\Omega}{2}$ longitude from N_1. To obtain this condition, a constant speed turn, the change in yaw angle at x in the actual orbits ($\Delta\eta$), and a consequent rotation of the orbit through an angle in its plane is necessary.

Again considering spherical trigonometry, the projected change in yaw angle is

$$\Delta\eta' = 180 - 2\cos^{-1}\left(\sin\frac{\Delta\Omega}{2}\sin i\right) \qquad (44)$$

The actual change in yaw angle is given by

$$\Delta\eta = 2\sin^{-1}\left(\cos\gamma_x \sin\frac{\Delta\eta'}{2}\right) \qquad (45)$$

where γ_x is the flight path angle in both orbits at the transition point.

The first pulse required in the nodal correction is then

$$\Delta V'_n = 2V_x \sin\frac{\Delta\eta}{2} = 2V_x \cos\gamma_x \sin\frac{\Delta\Omega}{2}\sin i.$$

However, $r_x V_x \cos\gamma_x = \sqrt{\mu p}$.

Then,

$$\Delta V'_n = 2\sqrt{\frac{\mu}{p}}\,(1 + e\cos\theta_x)\sin\frac{\Delta\Omega}{2}\sin i \qquad (46)$$

where $\theta_x = \phi_x - \omega_1$ and $\Delta\eta'$ is given by Eq (44). The time for the correction is determined by θ_t.

Since the orbit is elliptic and since this orbit rotates about the line through the point of thrust application and the center of the earth, the line of apsides is rotated in the orbit plane during this maneuver. For some satellite applications, this rotation is very objectionable and must be canceled. Therefore, a second pulse is required ($\Delta V''_n$) to rotate the orbit a specified angle (α) in its plane. If r' is the radius at transition, $\Delta V''_n = 2\,V'\sin\gamma'$.

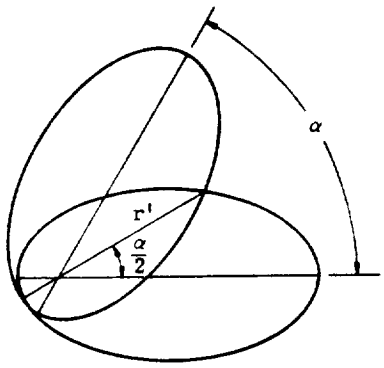

But, $V' = \dfrac{\sqrt{p\mu}}{r'\cos\gamma'} = \sqrt{\dfrac{\mu}{p}}\dfrac{1 - e\cos\frac{\alpha}{2}}{\cos\gamma'}$

and, therefore, since $\tan\gamma' = \dfrac{-e\sin\frac{\alpha}{2}}{1 - e\cos\frac{\alpha}{2}}$

$$V' = \sqrt{\frac{\mu}{p}}\left(\frac{-e\sin\frac{\alpha}{2}}{\sin\gamma'}\right)$$

Then

$$\Delta V''_n = 2V'\sin\gamma' = -2\sqrt{\frac{\mu}{p}}\,e\sin\frac{\alpha}{2} \qquad (47)$$

where p, e are parameters of the desired orbit, and α is determined as

$$\alpha = 180^\circ - 2\tan^{-1}\left[\frac{\tan\left(90 - \frac{\Delta\Omega}{2}\right)}{\cos i}\right] \qquad (48)$$

The corrective pulse is applied at

$$t = \frac{\tau}{2\pi}\,(E' - e\sin E')$$

seconds after the time of perigee passage, where

$$E' = 2\tan^{-1}\left(\sqrt{\frac{r_p}{r_a}}\cot\frac{\alpha}{4}\right) \qquad (49)$$

Note is made at this point that the analysis of the second nodal pulse is identically that which is required to change the argument of perigee an amount $\Delta\omega$ for the case where this element alone is to be changed.

d. Correction of position

The elliptical orbit is now correct with the exception of the position correction or analogously the correction to the time of perigee passage. Since the orientation of the orbit is correct, this final adjustment must be made either at apogee or perigee.

If the observed time of perigee passage is t'_p and the time at which the satellite should cross perigee is t_p, the period of the transfer orbit tangent at perigee is $\tau + \Delta t$, where $\Delta t = t'_p - t_p$.

And, the corrective pulse to be applied at perigee is

$$\frac{\Delta V_t}{n} = \sqrt{\frac{\mu}{r_p}}\left[\sqrt{2 - r_p\left(\frac{2\pi}{\sqrt{\mu}\,(\tau + \Delta t)}\right)^{2/3}} - \sqrt{\frac{2}{1 + \frac{r_p}{r_a}}}\right] \qquad (50)$$

An equal and opposite pulse applied at $t_p + n\,(\tau + \Delta t)$ completes the maneuver and prevents further drift.

Equations (10) to (50) comprise a method of correction calculation which is theoretically sufficient to achieve the desired properties in a given orbit.

Repetitions of the various maneuvers may be required to achieve desired accuracies. The number of repetitions will depend on sensor and control accuracies, and on the mission itself.

3. Sequence for Corrections for Maneuvers

Several requirements restrict the selection of a routine to correct the positions of a satellite. Since the mission of most satellites is intrinsically one of long duration, and corrections to an accurate orbit might be required daily, economy is an important factor. Secondly, the transfer orbits involved in the correction should closely approximate the nominal orbit, so that the mission (communication, surveillance, etc.) will not be interrupted. Also, the correction routine should be as simple as possible with the other imposed conditions. The following correction calculation routine has been selected on the basis of these requirements.

At any given reference time t_0, the data for the correction calculation are a_0, e_0, i_0, Ω_0, ω_0, θ_0. These quantities are in error compared to the corresponding parameters of the nominal orbit at the same time, a_n, e_n, i_n, Ω_{0n}, ω_{0n}, θ_{0n}.

Because of their frequent occurrence in the correction equations chosen, it is convenient to define six parameters, η, λ, ξ, σ, $\varkappa$, ψ. These parameters are defined (for the case of the incorrect orbit, denoted by subscript "0") as follows:

$$\begin{aligned}
\eta_0 &= \cos\omega_0 \sin\Omega_0 + \cos i_0 \cos\Omega_0 \sin\omega_0 \\
\lambda_0 &= -\sin\omega_0 \sin\Omega_0 + \cos i_0 \cos\Omega_0 \cos\omega_0 \\
\xi_0 &= \cos\omega_0 \cos\Omega_0 - \cos i_0 \sin\Omega_0 \sin\omega_0 \\
\sigma_0 &= -\sin\omega_0 \cos\Omega_0 - \cos i_0 \sin\Omega_0 \cos\omega_0 \\
\varkappa_0 &= \sin i_0 \sin\omega_0 \\
\psi_0 &= \sin i_0 \cos\omega_0
\end{aligned} \tag{51}$$

Then the incorrect orbit may be expressed in spherical coordinates (r, A, L) by the three equations:

$$\begin{aligned}
r &= \frac{a_0 (1 - e_0^2)}{1 + e_0 \cos\theta} \\
A &= \tan^{-1}\left(\frac{\eta_0 \cos\theta + \lambda_0 \sin\theta}{\xi_0 \cos\theta + \sigma_0 \sin\theta}\right) \\
L &= \sin^{-1}(\varkappa_0 \cos\theta + \psi_0 \sin\theta)
\end{aligned} \tag{52}$$

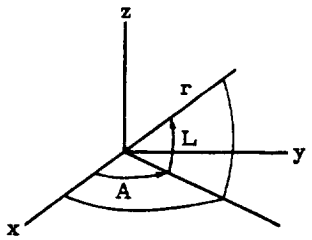

Although all six orbital elements may require correction, economy can be improved by correcting more than one element with a single thrust. The corrections of inclination and the node, which are both nonplanar corrections, can be simply combined, as can the planar corrections (size, shape and position of the satellite within the orbit). Although, for maximum economy, the order in which the planar and nonplanar corrections are made depends on the energies of the incorrect and required orbits, the increased economy derived from employing separate corrective routines for each case is not sufficient to justify the increased complexity of the routine (for small changes in the orbital elements). For example, in the case of circular orbits of radii $r_n = 5.488164 \times 10^7 \pm 6000$ ft ($1.672792 \times 10^7 \pm 1830$ m) the velocity increments required to rotate the orbit planes through 0.10° are 27.961 fps and 27.965 fps (8.5225 and 8.5237 mps), a difference in the fifth significant figure or third decimal place. Even though the error in radius should approach $r_n \pm 25,000$ ft (7620 m), the difference in the increments is in the fourth place. Thus, for orbital maintenance the order of correction for the nodal and inclination changes has very little effect on the resultant energy requirement. Even though the errors to be corrected during initial placement are much larger and the differences in the velocity increments more significant, the order still produces only minor differences. For this reason the position of the planar change in the routine will be considered inmaterial for simplicity.

The first thrust in the corrective sequence is chosen as a thrust to eliminate error in inclination and node by a constant speed turn at the intersection of the incorrect orbit and the nominal orbit plane. If quantities associated with this intersection point are denoted by the subscript 1, this point may be determined by setting $r = r_1$, $\theta = \theta_1$ in Eq (52) and simultaneously solving this equation and Eq (53) of the nominal orbit plane for θ_1 and r_1

$$\begin{aligned}
&\cos L \cos A \sin i_n \sin\Omega_{0n} \\
&- \cos L \sin A \sin i_n \cos\Omega_{0n} + \sin L \cos i_n = 0
\end{aligned}$$

which yields (53)

$$\begin{aligned}
&(\xi_0 \cos\theta_1 + \sigma_0 \sin\theta_1) \sin i_n \sin\Omega_n \\
&- (\eta_0 \cos\theta_1 + \lambda_0 \sin\theta_1) \sin i_n \cos\Omega_{0n} \\
&+ (\varkappa_0 \cos\theta_1 + \psi_0 \sin\theta_1) \cos i_n = 0
\end{aligned}$$

Solving this equation for θ_1 gives

$$\cos\theta_1 = \pm \frac{Q}{\sqrt{T^2 + Q^2}} \tag{54}$$

where

$$\begin{aligned}
Q &= \sigma_0 \sin i_n \sin\Omega_{0n} - \lambda_0 \sin i_n \cos\Omega_{0n} \\
&\quad + \psi_0 \cos i_n, \\
T &= \xi_0 \sin i_n \sin\Omega_{0n} - \eta_0 \sin i_n \cos\Omega_{0n} \\
&\quad + \varkappa_0 \cos i_n,
\end{aligned}$$

and the sign chosen in Eq (54) is that which satisfies

$$\cos\theta_1 = -\frac{Q}{T}\sin\theta_1.$$

In computing the velocity increment required at the intersection point, latitude, flight path angle, orbit velocity and change of flight path azimuth during the maneuver are necessary.

$$L_1 = \sin^{-1}\left[\sin i_n \sin(\theta_1 + \omega_1)\right] \tag{55}$$

where

$$\omega_1 = \sin^{-1}\left[\frac{\sin i_0 \sin(\theta_1 + \omega_0)}{\sin i_n}\right]$$

$$\gamma_1 = \tan^{-1}\left[\frac{e_0 \sin\theta_1}{1 + e_0 \cos\theta_1}\right] \quad (56)$$

$$V_1 = \sqrt{\mu\left(\frac{2}{r_1} - \frac{1}{a_0}\right)} \quad (57)$$

$$\Delta\beta_1 = \sin^{-1}\left(\frac{\cos i_n}{\cos L_1}\right) - \sin^{-1}\left(\frac{\cos i_0}{\cos L_1}\right) \quad (58)$$

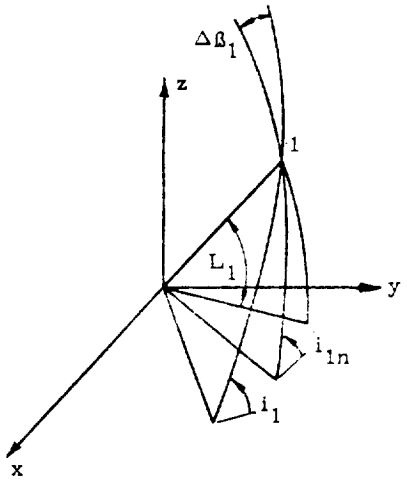

The magnitude of the velocity increment required to correct the orbit inclination and node is

$$\Delta V_1 = 2V_1 \sin\frac{\Delta\beta_1}{2} \cos\gamma_1 \quad (59)$$

The parameters in the corrected orbit corresponding to Eq 51 are:

$$\eta_1 = \cos\omega_1 \sin\Omega_{1n} + \cos i_n \cos\Omega_{1n} \sin\omega_1$$

$$\lambda_1 = -\sin\omega_1 \sin\Omega_{1n} + \cos i_n \cos\Omega_{1n} \cos\omega_1$$

$$\xi_1 = \cos\omega_1 \cos\Omega_{1n} - \cos i_n \sin\Omega_{1n} \sin\omega_1$$

$$\sigma_1 = -\sin\omega_1 \cos\Omega_{1n} - \cos i_n \sin\Omega_{1n} \cos\omega_1$$

$$\chi_1 = \sin i_n \sin\omega_1$$

$$\psi_1 = \sin i_n \cos\omega_1 \quad (60)$$

The orientation of the corrective thrust can then be obtained. Since the general elliptical orbit in three dimensions may be expressed as:

$$\vec{r} = \left[\xi p \frac{\cos\theta}{1 + e\cos\theta} + \sigma p \frac{\sin\theta}{1 + e\cos\theta}\right] \vec{i}$$

(continued)

$$+ \left[\eta p \frac{\cos\theta}{1 + e\cos\theta} + \lambda p \frac{\sin\theta}{1 + e\cos\theta}\right] \vec{j}$$

$$+ \left[\chi p \frac{\cos\theta}{1 + e\cos\theta} + \psi p \frac{\sin\theta}{1 + e\cos\theta}\right] \vec{k}, \quad (61)$$

the orbital velocity may be determined as $\frac{d\vec{r}}{dt}$.

$$\vec{V} = \sqrt{\frac{\mu}{p}}\left[\sigma(\cos\theta + e) - \xi\sin\theta\right]\vec{i}$$

$$+ \sqrt{\frac{\mu}{p}}\left[\lambda(\cos\theta + e) - \eta\sin\theta\right]\vec{j}$$

$$+ \sqrt{\frac{\mu}{p}}\left[\psi(\cos\theta + e) - \chi\sin\theta\right]\vec{k} \quad (62)$$

Orbital velocity in spherical coordinates may then be expressed as:

$$V = \sqrt{\mu\left(\frac{2}{r} - \frac{1}{a}\right)}$$

$$\nu^* = \tan^{-1}\left[\frac{\lambda(\cos\theta + e) - \eta\sin\theta}{\sigma(\cos\theta + e) - \xi\sin\theta}\right]$$

$$\phi^* = \sin^{-1}\left[\frac{1}{V}\sqrt{\frac{\mu}{p}}\left\{\psi(\cos\theta + e) - \chi\sin\theta\right\}\right]. \quad (63)$$

where

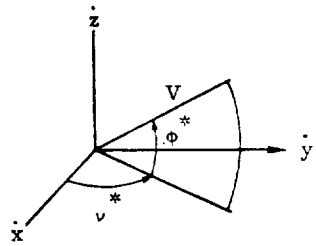

Corresponding to Eq (63), the orientation of the velocity increment ΔV_1 is given by:

$$\Delta\nu_1^* = \tan^{-1}\left\{\left[(\lambda_1 - \lambda_0)(\cos\theta_1 + e_0) - (\eta_1 - \eta_0)\sin\theta_1\right]\left[(\sigma_1 - \sigma_0)(\cos\theta_1 + e_0) - (\xi_1 - \xi_0)\sin\theta_1\right]^{-1}\right\}$$

$$\Delta\varphi_1^* = \sin^{-1}\left[\frac{1}{\Delta V_1}\sqrt{\frac{\mu}{p_0}}\left\{(\psi_1 - \psi_0)(\cos\theta_1 + e_0) - (\chi_1 - \chi_0)\sin\theta_1\right\}\right] \quad (64)$$

After addition of the velocity increment defined by Eqs (59) and (64), the vehicle occupies an orbit which lies in the correct plane, but which has the original incorrect size and shape. The next step in the selected correction routine is a transfer from apogee of the incorrect orbit to a point in the nominal orbit (for this case assumed

circular). This approach is not always the most efficient means of making a transfer, however, for the small period changes required (even for the initial placement problem), the energy differences are extremely small. The equations defining this correction are:

$$\Delta V_2 = \sqrt{\frac{\mu}{r_a}}\left(\sqrt{\frac{2r_n}{r_a + r_n}} - \sqrt{2 - \frac{r_a}{a_0}}\right)$$

$$\Delta\nu_2^* = \tan^{-1}\left(\frac{\lambda_1}{\sigma_1}\right)$$

$$\Delta\phi_2^* = \sin^{-1}(-\psi_1), \qquad (65)$$

where

$$r_a = a_0(1 + e_0)$$

When the vehicle completes the transfer to nominal orbit altitude, a tangential thrust could be applied to cause the vehicle to enter a circular orbit at this altitude. However, the vehicle would still not be synchronized because the orbital central angle would remain uncorrected. Correction of this quantity, which is discussed earlier, involves two thrusts applied tangentially at any point in the circular orbit. Selecting the terminus of the Hohmann transfer orbit, i.e. the point at which the vehicle first reaches nominal altitude, as the point for initiating the change of position improves the economy of the correction routine in certain cases. For example, if the vehicle reaches the nominal radius, r_n, with a velocity greater than circular velocity, and the vehicle is ahead of the nominal position desired in the orbit, part or all of the excess velocity can be used as part or all of the first velocity increment of the angular position correction.

The third corrective thrust, computed as the combination of the tangential thrust to achieve circularity and the first of two tangential thrusts to change the orbital central angle, is

$$\Delta V_3 = \sqrt{\frac{\mu}{r_n}}\left(\sqrt{2 - \left(1 - \frac{\Delta\theta}{2\pi}\right)^{-2/3}} - \sqrt{\frac{2r_a}{r_n + r_a}}\right)$$

$$\Delta\nu_3^* = \tan^{-1}\left(\frac{\lambda_1}{\sigma_1}\right) + 180^\circ$$

$$\Delta\phi_3^* = -\sin^{-1}(-\psi_1) \qquad (66)$$

The direction of $\Delta\vec{V}_3$ is opposite to that of $\Delta\vec{V}_2$. In Eq (66), the angle of required position change, $\Delta\theta$, is positive for the case in which the vehicle lags its nominal position in the pattern orbit. The first equation of (66) holds whether $r_a > r_n$ or $r_n > r_a$. The final corrective thrust is

$$\Delta V_4 = \sqrt{\frac{\mu}{r_n}}\left(\sqrt{2 - \left(1 - \frac{\Delta\theta}{2\pi}\right)^{-2/3}} - 1\right)$$

$$\Delta\nu_4^* = \tan^{-1}\left(\frac{\lambda_1}{\sigma_1}\right)$$

$$\Delta\phi_4^* = \sin^{-1}(-\psi_1). \qquad (67)$$

As noted, economy can be improved by substituting $\frac{\Delta\theta}{n}$ (n = an integer) for $\Delta\theta$ in the first equation of (67) and increasing the transfer time by a factor of n.

If the value of $\Delta\theta$ in Eqs (66) and (67) is to be computed from the initial data (e_0, e_n, a_0, a_n, etc.), the time interval from the time of data sensing to the time of initiating the correction of orbital central angle is

$$\Delta t = a_0\sqrt{\frac{a_0}{\mu}}\left[\pi - \sin^{-1}\left(\frac{\sqrt{1 - e_0^2}\sin\theta}{1 + e_0\cos\theta_0}\right) + \frac{e_0\sqrt{1 - e_0^2}\sin\theta_0}{1 + e_0\cos\theta_0}\right] + \frac{\pi}{2}\left(\frac{p_0}{1 - e_0} + r\right)\sqrt{\frac{1}{2\mu}\left(\frac{p_0}{1 - e_0} + r\right)} \qquad (68)$$

The location of the nominal position at the time of initiation of the angular position correction is:

$$r_{3n} = r_n$$

$$L_{3n} = \sin^{-1}\left[\sin L_{0n}\cos\frac{\Delta t}{\tau_n}\,2\pi + \sqrt{\sin^2 i_n - \sin^2 L_{0n}}\sin\frac{\Delta t}{\tau_n}\,2\pi\right]$$

$$A_{3n} = \tan^{-1}\left[\frac{\cos i_n}{\sqrt{\left(\frac{\sin i_n}{\sin L_{3_n}}\right)^2 - 1}}\right] + A_{0n} - \sin^{-1}\left(\frac{\tan L_{0n}}{\tan i_n}\right) \qquad (69)$$

and the position of the vehicle at this time is given by:

$$r_3 = r_n$$

$$L_3 = \sin^{-1}(x_1)$$

$$A_3 = \tan^{-1}\left(\frac{\eta_1}{\xi_1}\right). \qquad (70)$$

The required change in central angle is then

$$\Delta\theta = \cos^{-1}\left[\cos L_3 \cos L_{3n} \cos (A_3 - A_{3n}) + \sin L_3 \sin L_{3n}\right]$$

The four maneuvers given by Eqs (59), (65), (66) and (67) comprise the complete correction routine.

Although the proximity of the correction transfer orbits to the nominal orbit means that the difference in perturbation of the transfer and nominal (perturbed) orbits is negligible, the perturbations affect the times of correction initiation and must, therefore, be included in the routine. This may be done by considering the orbit parameters ω and Ω involved in the equations as functions of time and adding a perturbation correction to the computed times.

A sample problem has been calculated using this routine in order to provide an appreciation of the magnitude of the propulsion requirement for each correction. The data for the sample problem are:

$a_{0n} = 5.488164 \times 10^7$ ft (1.672792×10^7 m)	$a_0 = 5.4889664 \times 10^7$ ft (1.673037×10^7 m)
$e_{0n} = 0$	$e_0 = 0.0001$
$i_{0n} = 54.736°$	$i_0 = 54.741°$
$\Omega_{0n} = 0$	$\Omega_0 = 0.005°$
$\omega_{0n} = 0$	$\omega_0 = -60°$
$\theta_{0n} = 0$	$\theta_0 = 60.005°$

The radius at this time is $r_0 = 5.488692 \times 10^7$ ft (1.672953×10^7 m) which is r_n plus 1 stat mi or 1.609 km.

Proceeding through the correction routine yields the following correction magnitudes.

ΔV_1 = 1.804 fps (0.5499 m/s)

ΔV_2 = 0.185 fps (0.0564 m/s)

ΔV_3 = 1.899 fps (0.5788 m/s)

ΔV_4 = 0.914 fps (0.2786 m/s)

Total ΔV = 4.802 fps (1.463 m/s).

Thus if the satellite possesses propellants capable of supplying a total of 5000 fps (1524 m/s) and 5 fps (1.524 m/s) is assumed to be the average correction required twice per day, the system can function for about 500 days.

Thus, the routine seems adequate to satisfy the requirements of economy and proximity of the transfer and nominal orbits with a reasonably simple calculation routine.

D. SMALL MANEUVERS IN NEARLY CIRCULAR ORBITS (REF. 1)

1. Linearization of Maneuvers

The discussions of Section B have been general and are not restricted to small eccentricities. Generally, however, for the cases in which the target orbit is circular and no intermediate orbits are utilized, the actual orbit obtainable will deviate slightly from circularity. If this deviation is to be corrected, some of the maneuvers of the previous discussions can be simplified using first order differentials. This approach has two major advantages:

(1) The functional form of the solution can be simplified.

(2) The roundoff error arising from subtracting to nearly equal quantities can be reduced.

As before, the discussions will be divided into three cases for investigation:

(1) Correction by means of two velocity increments tangent to the flight path, the first impulse (ΔV_1) being applied at apogee in the incorrect orbit and the second at the altitude of the nominal circular orbit.

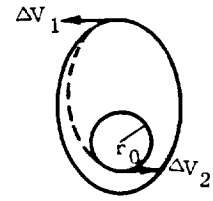

(2) Correction by means of two tangential impulses, the first (ΔV_1) being applied at perigee in the incorrect orbit.

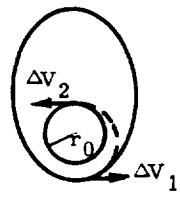

(3) Correction by means of one impulse (ΔV) applied at the intersection of the incorrect and correct orbits, if the orbits intersect.

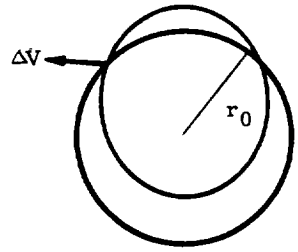

It is noted that while the circular orbit is shown within the ellipse for Cases (1) and (2), the cases for exterior circular orbits will also be discussed.

Consider

$$\Delta a = a - r_0$$

$$\Delta e = e \qquad e^2 << 1$$

for Case 1

$$r_1 = a(1+e) = r_0 + \Delta a + e(r_0 + \Delta a)$$
$$\approx r_0 + \Delta a + e r_0$$

$$\Delta V_1 \approx \sqrt{\frac{\mu}{r_0}} \left[\left(1 - \frac{\Delta a}{2 r_0} - \frac{e}{2}\right) \left(1 - \frac{\Delta a}{4 r_0} - \frac{e}{4}\right) - \left(1 - \frac{\Delta a}{2 r_0}\right)(1 - e) \right], \quad e^2 << 1, \quad \left(\frac{\Delta a}{r_0}\right)^2 << 1$$

The latter approximation utilizes the following expansions.

$$(1 \pm \epsilon)^{-1} = 1 \mp \epsilon + \epsilon^2 \mp \epsilon^3 + \ldots$$

$$(1 \pm \epsilon)^{1/2} = 1 \pm \frac{\epsilon}{2} - \frac{\epsilon^2}{8} \pm \frac{\epsilon^3}{16} - \ldots$$

Then

$$\Delta V_1 \approx \frac{1}{4} \left[\frac{\mu}{r_0}\right]^{1/2} \left[e - \frac{\Delta a}{r_0}\right]$$

$$\Delta V_2 = \left[\frac{\mu}{r_0}\right]^{1/2} - \left[\frac{2\mu\left(1 + \frac{\Delta a}{r_0}\right)(1+e)}{r_0\left[\left(1+\frac{\Delta a}{r_0}\right)(1+e)+1\right]}\right]^{1/2}$$

$$\approx \left[\frac{\mu}{r_0}\right]^{1/2} \left\{1 - \left[\left(1 + \frac{\Delta a}{2 r_0} + \frac{e}{2}\right) \cdot \left(1 - \frac{\Delta a}{4 r_0} - \frac{e}{4}\right)\right]\right\}$$

The procedure is similar in Case (2), the results being summarized below. For Case (3),

$$\Delta V^2 = \frac{\mu}{r_0} \left[3 - \frac{1}{1 + \frac{\Delta a}{r_0}} - 2 \sqrt{\left(1 + \frac{\Delta a}{r_0}\right)\left(1 - e^2\right)} \right]$$

$$\Delta V^2 \approx \frac{\mu}{r_0} \left[3 - \left\{ 1 - \frac{\Delta a}{r_0} + \left(\frac{\Delta a}{r_0}\right)^2 \right\} - 2 \left\{ 1 + \frac{\Delta a}{2 r_0} - \frac{1}{8} \left(\frac{\Delta a}{r_0}\right)^2 \right\} \left(1 - \frac{e^2}{2}\right) \right]$$

$$\Delta V^2 \approx \frac{\mu}{r_0} \left[e^2 - \frac{3}{4} \left(\frac{\Delta a}{r_0}\right)^2 \right]$$

The final results are as follows. For Case (1):

$$\Delta V_1 \approx \frac{1}{4} \sqrt{\frac{\mu}{r_0}} \left(e - \frac{\Delta a}{r_0}\right) \tag{71}$$

$$\Delta V_2 \approx \frac{1}{4} \sqrt{\frac{\mu}{r_0}} \left(-e - \frac{\Delta a}{r_0}\right) \tag{72}$$

$$\Delta V_T = |\Delta V_1| + |\Delta V_2|$$

$e^2 << 1$,
$\Delta a = a - r_0$

Case (2):

$$\Delta V_1 \approx \frac{1}{4} \sqrt{\frac{\mu}{r_0}} \left(-e - \frac{\Delta a}{r_0}\right) \tag{73}$$

$$\Delta V_2 \approx \frac{1}{4} \sqrt{\frac{\mu}{r_0}} \left(e - \frac{\Delta a}{r_0}\right) \tag{74}$$

$$\Delta V_{total} = |\Delta V_1| + |\Delta V_2|$$

$e^2 << 1$

Case (3):

$$\Delta V \approx \left[\frac{\mu}{r_0}\right]^{1/2} \left[e^2 - \frac{3}{4} \left(\frac{\Delta a}{r_0}\right)^2\right]^{1/2}, \quad e^2 << 1; \quad \frac{\Delta a}{r_0} < e \tag{75}$$

The symmetry is obvious in Cases (1) and (2), and the total velocity requirement is the same in these cases:

$$\frac{\Delta V_{total}}{V_0} \approx \frac{1}{2} e, \qquad -e < \frac{\Delta a}{r_0} < e$$

$$\approx \frac{1}{2} \frac{\Delta a}{r_0}, \quad \left|\frac{\Delta a}{r_0}\right| > e$$

Since for intersection of the correct and incorrect orbits

$$a(1-e) = r_p < r_0 < r_a = a(1+e)$$

then

$$r_0 + \Delta a - e r_0 < r_0 < r_0 + \Delta a + e r_0$$

or

$$\left|\frac{\Delta a}{r_0}\right| < e,$$

and, from Eq (75), the impulses required for Case (3) have the range

$$\frac{e}{2}\sqrt{\frac{\mu}{r_0}} < \Delta V < e\sqrt{\frac{\mu}{r_0}}$$

However, if the orbits intersect (i.e., $e > \left|\frac{\Delta a}{r_0}\right|$), the total velocity required for correction by two tangential impulses at extrema, Case (1) or Case (2), is

$$\Delta V_{total} \approx \frac{e}{2}\sqrt{\frac{\mu}{r_0}},$$

which indicates the anticipated superiority of efficiency in Cases (1) and (2). Equations (71) through (74) are plotted in Fig. 15 for the error ranges of interest. Equation (75) is plotted in Fig. 16. As an example, consider the following table.

Errors in Original Orbit		Velocity Increment Required for Correction ΔV_{total} (mps)
Δa (km)	e	
10	0.00167	6.72
9.3	0.001	5.44
0	0.001	3.91 2 pulse 7.77 1 pulse

2. Error Analysis

Orbit correction sensitivities will also be developed for the case of correction of a slightly eccentric orbit to a circular orbit by two impulses tangent to the flight path. The following nomenclature will be involved:

- V_1 = orbit speed at r_1 before the first correction
- V_1' = orbit speed at r_1 after the first correction
- ΔV_1 = characteristic velocity of the first corrective impulse
- r_2 = radius at extremum where second impulse is applied (nominally r_0)
- V_2 = orbit speed at r_2 before the second correction
- V_2' = orbit speed at r_2 after the second correction
- ΔV_2 = characteristic velocity of the second corrective impulse
- γ = flight path angle with respect to local horizontal
- ϕ_T = thrust attitude angle

Primes will denote corrected parameters.

The errors in the final orbit parameters, $\Delta a'$ and e', will be functions of errors in the injection parameters (Δr_2, $\Delta V_2'$ and γ_2), which, in turn, will be functions of errors in the magnitude and orientation of the second corrective thrust and errors in the conditions r_2, V_2 and γ_2 before thrust. The errors in r_2, V_2 and γ_2 are functions of errors in magnitude and orientation of the first corrective impulse and errors in the determined values of r_1, V_1 and γ_1. Therefore, the error equations are conveniently developed in several steps.

a. Errors contributed by corrective thrusts

The orbit errors contributed by errors in the corrective thrusts may be induced intuitively, but a rigorous general analysis is not difficult. The equations describing addition of a vector impulse ΔV are

$$f_1 = -\Delta V^2 + V^2 + V'^2 - 2VV'\cos(\gamma' - \gamma) = 0 \quad (76)$$

$$f_2 = -\Delta V \sin\phi_T + V' \sin(\gamma' - \gamma) = 0 \quad (77)$$

Symbols are consistent with previous notation and are further defined in the sketch.

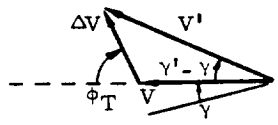

Errors in V' and γ' are to be determined as functions of errors in V, γ, ϕ_T and ΔV. From Eqs (76) and (77) the error relationships, to the order of linear differentials, can be expressed as follows.

$$-\Delta V\, d(\Delta V) + V'\, dV' + VV'\left[\sin(\gamma' - \gamma)\cdot(d\gamma' - d\gamma)\right] - \left[\cos(\gamma' - \gamma)\cdot(V\, dV' + V'\, dV)\right] + V\, dV = 0$$

and

$$-\sin\phi_T\, d(\Delta V) - \Delta V \cos\phi_T d\phi_T + \sin(\gamma' - \gamma)\, dV' + V'\left[\cos(\gamma' - \gamma)\cdot(d\gamma' - d\gamma)\right] = 0$$

Terms may be collected, and the resulting expressions solved by application of Cramer's rule for the errors dV' and $d\gamma'$: In this solution the Jacobian

$$\frac{\partial(f_1, f_2)}{\partial(V', \gamma')} = 2\begin{vmatrix} V' - V\cos(\gamma' - \gamma) & VV'\sin(\gamma' - \gamma) \\ \sin(\gamma' - \gamma) & V'\cos(\gamma' - \gamma) \end{vmatrix} = 2V'\left[V'\cos(\gamma' - \gamma) - V\right]$$

is useful. The results are

$$dV' = \left[\frac{\Delta V\cos(\gamma' - \gamma) - \frac{VV'}{\Delta V}\sin^2(\gamma' - \gamma)}{V'\cos(\gamma' - \gamma) - V}\right] d(\Delta V) + \cos(\gamma' - \gamma)\, dV - V\sin(\gamma' - \gamma)\, d\phi_T$$

$$d\gamma' = \frac{\sin(\gamma' - \gamma)\left[\left\{V' - V\cos(\gamma' - \gamma)\right\}\frac{V'}{\Delta V} - \Delta V\right]}{V'\left[V'\cos(\gamma' - \gamma) - V\right]} d(\Delta V) - \frac{\sin(\gamma' - \gamma)}{V'} dV + \left[1 - \frac{V}{V'}\cos(\gamma' - \gamma)\right] d\phi_T + d\gamma$$

In terms of $(\gamma' - \gamma)$ or, in terms of ϕ_T,

$$dV' = \left(\frac{\Delta V}{V'} + \frac{V}{V'}\cos\phi_T\right) d(\Delta V) + \left(\frac{\Delta V}{V'}\cos\phi_T + \frac{V}{V'}\right) dV - V\frac{\Delta V}{V'}\sin\phi_T d\phi_T \quad (78)$$

$$d\gamma' = \frac{V}{V'^2}\sin\phi_T\, d(\Delta V) - \frac{\Delta V}{V'^2}\sin\phi_T\, dV + \frac{\Delta V}{V'^2}(\Delta V + V\cos\phi)\, d\phi_T + d\gamma \quad (79)$$

For the case of interest, tangential corrective impulses applied at orbit extrema, the following nominal values are involved in evaluation of the sensitivities.

$$\phi_T = 0$$

$$V' = V + \Delta V$$

$$\gamma' - \gamma = 0$$

Then Eqs (78) and (79) become

$$dV' = d(\Delta V) + dV \quad (80)$$

$$d\gamma' = \frac{\Delta V}{V'} d\phi + d\gamma \quad (81)$$

(tangential impulses at extrema)

which agree with intuition for this simple case.

b. Errors prior to second impulse

Errors in the orbit conditions r_2, V_2, γ_2 prior to the second impulse will be developed from a general analysis giving errors at extrema in terms of errors in any injection condition r, V, γ. Specification of the conditions (r, V, γ) at any time completely determines the planar properties of the orbit. From the energy equation and the geometry of an ellipse, simple expressions can be developed relating r_a, r_p, v_a and v_p to a and e:

$$r_a = a(1 + e) \quad (82)$$

$$r_p = a(1 - e) \quad (83)$$

$$v_a = \sqrt{\frac{\mu}{a}\left(\frac{1 - e}{1 + e}\right)} \quad (84)$$

$$v_p = \sqrt{\frac{\mu}{a}\left(\frac{1 + e}{1 - e}\right)} \quad (85)$$

Then

$$dr_a = (1 + e)\, da + ade \quad (86)$$

$$dr_p = (1 - e)\, da - ade \quad (87)$$

$$dv_a = -\frac{V_a}{2a} da - \frac{V_p}{(1 + e)^2} de \quad (88)$$

$$dv_p = -\frac{V_p}{2a} da + \frac{V_a}{(1 - e)^2} de \quad (89)$$

In turn, from the energy equation,

$$a = \left[\frac{2}{r} - \frac{V^2}{\mu}\right]^{-1},$$

and Kepler's second law, which can be restated in the form

$$e = \sqrt{1 - \left(\frac{2}{r} - \frac{V^2}{\mu}\right)\left(\frac{r^2V^2\cos^2\gamma}{\mu}\right)}$$

the differentials of a and e are

$$da = \frac{2a^2}{r^2} dr + \frac{2a^2V}{\mu} dV$$

$$de = \frac{1}{2e}\left[-\frac{1}{a}\left(-2\frac{r^2V^2}{\mu}\cos\gamma\sin\gamma\, d\gamma +\right.\right.$$

(continued)

$$+\frac{\cos^2\gamma}{\mu}\left(2rV^2\,dr+2Vr^2\,dV\right)\Bigg)$$

$$-\frac{r^2V^2\cos^2\gamma}{\mu}\left(-\frac{2}{r^2}\,dr-\frac{2V}{\mu}\,dV\right)\Bigg]$$

which, after simplification and substitution of

$$r=\frac{a(1-e^2)}{1+e\cos\theta}$$

give

$$da=\frac{2(1+e\cos\theta)^2}{(1-e^2)^2}\,dr+2a\left[\sqrt{\frac{a}{\mu}}\sqrt{\frac{1+2e\cos\theta+e^2}{1-e^2}}\right]dV \tag{90}$$

$$de=\frac{(e+\cos\theta)(1+e\cos\theta)}{a(1-e^2)}\,dr+2(e+\cos\theta)\sqrt{\frac{a(1-e^2)}{\mu(1+2e\cos\theta+e^2)}}\,dV+(1-e^2)\frac{\sin\theta}{1+e\cos\theta}\,d\gamma \tag{91}$$

Substitution of Eqs (90) and (91) in Eqs (86) through (89) gives the required error relationships:

$$dr_a=\frac{1+e}{(1-e^2)^2}(1+e\cos\theta)(2+e-e^2+e\cos\theta+\cos\theta)\,dr+2a\sqrt{\frac{a}{\mu}}\frac{(1+e)^2}{\sqrt{1-e^2}}\frac{1+\cos\theta}{\sqrt{1+2e\cos\theta+e^2}}\,dV+a(1-e^2)\frac{\sin\theta}{1+e\cos\theta}\,d\gamma \tag{92}$$

$$dr_p=\frac{1-e}{(1-e^2)^2}(1+e\cos\theta)(2-e-e^2+e\cos\theta-\cos\theta)\,dr+2a\sqrt{\frac{a}{\mu}}\frac{(1-e)^2}{\sqrt{1-e^2}}\frac{1-\cos\theta}{\sqrt{1+2e\cos\theta+e^2}}\,dV-a(1-e^2)\frac{\sin\theta}{1+e\cos\theta}\,d\gamma \tag{93}$$

$$dV_a=-\frac{(1+e\cos\theta)}{1-e^2}\left[\frac{V_a}{a}\frac{(1+e\cos\theta)}{1-e^2}+\frac{V_p}{a}\frac{(e+\cos\theta)}{(1-e)^2}\right]dr+$$

(continued)

$$-\sqrt{\frac{a}{\mu}}\left[V_a\sqrt{\frac{1+2e\cos\theta+e^2}{1-e^2}}+2V_p\frac{\sqrt{1-e^2}}{(1+e)^2}\frac{(e+\cos\theta)}{\sqrt{1+2e\cos\theta+e^2}}\right]dV-V_p\frac{1-e^2}{(1+e)^2}\frac{\sin\theta}{1+e\cos\theta}\,d\gamma \tag{94}$$

$$dV_p=-\frac{(1+e\cos\theta)}{1-e^2}\left[\frac{V_p}{a}\frac{(1+e\cos\theta)}{1-e^2}-\frac{V_a}{a}\frac{(e+\cos\theta)}{(1-e)^2}\right]dr-\sqrt{\frac{a}{\mu}}\left[V_p\sqrt{\frac{1+2e\cos\theta+e^2}{1-e^2}}-2V_a\frac{\sqrt{1-e^2}}{(1-e)^2}\frac{(e+\cos\theta)}{\sqrt{1+2e\cos\theta+e^2}}\right]dV+V_a\frac{1+e}{1-e}\frac{\sin\theta}{1+e\cos\theta}\,d\gamma \tag{95}$$

These equations relate errors in conditions at orbit extrema to errors in injection conditions (r, V, γ).

For $e^2 \ll 1$ Eqs (92) through (95) reduce to

$$dr_a\approx\left[2+\cos\theta+2e(3+\cos\theta)\cos^2\frac{\theta}{2}\right]dr+2a\sqrt{\frac{a}{\mu}}\left[1+\cos\theta+2e(2-\cos\theta)\cos^2\frac{\theta}{2}\right]dV+\left[a\sin\theta-\frac{ea}{2}\sin 2\theta\right]d\gamma \tag{96}$$

$$dr_p\approx\left[2-\cos\theta-2e(3-\cos\theta)\sin^2\frac{\theta}{2}\right]dr+2a\sqrt{\frac{a}{\mu}}\left[1-\cos\theta-2e(2+\cos\theta)\sin^2\frac{\theta}{2}\right]dV+\left[-a\sin\theta+\frac{ea}{2}\sin 2\theta\right]d\gamma \tag{97}$$

$$dV_a\approx-\frac{1}{a}\sqrt{\frac{\mu}{a}}(1+\cos\theta)(1+e\cos\theta)\,dr-\left[(1-e\cos\theta)(1+2\cos\theta)+e\right]dV-\sqrt{\frac{\mu}{a}}\sin\theta(1-e\cos\theta-e)\,d\gamma \tag{98}$$

$$dV_p\approx-\frac{1}{a}\sqrt{\frac{\mu}{a}}(1-\cos\theta)(1+e\cos\theta)\,dr-\left[(1-e\cos\theta)(1-2\cos\theta)-e\right]dV+\sqrt{\frac{\mu}{a}}\sin\theta(1+e-\cos\theta)\,d\gamma \tag{99}$$

For $e^2 \ll 1$ and impulses applied near apogee or perigee ($\theta = 0°$ or $180°$), the case of interest for the two-impulse correction previously described, Eqs (96) through (99) reduce still further to the following results: perigee injection, $e^2 \ll 1$:

$$dr_a \approx (3 + 8e)\, dr_p + 4a \sqrt{\frac{a}{\mu}}\,(1 + e)\, dV_p \qquad (100)$$

$$dV_a \approx -\frac{2}{a}\sqrt{\frac{\mu}{a}}\,(1 + e)\, dr_p - (3 - 2e)\, dV_p \qquad (101)$$

apogee injection, $e^2 \ll 1$:

$$dr_p \approx (3 - 8e)\, dr_a + 4a \sqrt{\frac{a}{\mu}}\,(1 - e)\, dV_a \qquad (102)$$

$$dV_p \approx -\frac{2}{a}\sqrt{\frac{\mu}{a}}\,(1 - e)\, dr_a - (3 + 2e)\, dV_a \qquad (103)$$

For e, $\frac{\Delta a}{r_.} < 0.001$ the errors are given to three significant figures by the following very simple formulas.

$$\frac{dr_2}{r_0} \approx 3\frac{dr_1}{r_0} + 4\frac{dV_1}{V_0} \qquad (104)$$

$$\frac{dV_2}{V_1} \approx -2\frac{dr_1}{r_0} - 3\frac{dV_1}{V_0} \qquad (105)$$

The relation of errors in conditions before the second impulse to errors just after the first impulse must also consider errors in orbit central angle, θ, and local flight path angle, γ. Because the orbits of interest are nearly circular, a variational approach is necessary to define errors in these angular quantities. Therefore, a general analysis of errors in r, V, θ and γ anywhere in a near-circular orbit as functions of launch errors will be performed, and the results for r and V will be compared to Eqs (104) and (105).

Series expansions for the variables of interest are available in Chapter III.

$$\frac{r}{a} = 1 - e\cos M - \frac{e^2}{2}(\cos 2M - 1) - \frac{e^3}{2!\,2^2}(3\cos 3M - 3\cos M) - \ldots$$

$$\frac{V}{\sqrt{\frac{\mu}{a}}} = 1 + e\cos\theta + \frac{e^2}{4}(3 - \cos 2\theta) + \frac{e^3}{8}(4\cos\theta - \cos 3\theta - 7) + \ldots$$

$$\theta = M + 2e\sin M + \frac{5e^2}{4}\sin 2M + \frac{e^3}{12}(13\sin 3M - 3\sin M) + \ldots$$

$$\gamma = e\sin\theta - \frac{e^2}{2}\sin 2\theta + \frac{e^3}{3}\sin 3\theta - \ldots$$

$$M = \text{mean anomaly} = \sqrt{\frac{\mu}{a^3}}\,(t - t_p) \qquad (106)$$

For $e^2 \ll 1$, approximate relations can be written.

$$r \approx a(1 - e\cos M) \qquad (107)$$

$$V \approx \sqrt{\frac{\mu}{a}}\,(1 + e\cos M) \qquad (108)$$

$$\theta \approx M + 2e\sin M \qquad (109)$$

$$\gamma \approx e\sin M \qquad (110)$$

Deviations from the nominal circle r_0 and v_0 at launch are $\delta r_1 = r_1 - r_0$, $\delta V_1 = V_1 - V_o$, $\delta\gamma_1 = \gamma_1$ and $\delta\theta_1 = \theta_1 - \theta_0$. From Eq (47)

$$M = M_0 + \Delta M = \sqrt{\frac{\mu}{r_0^3\left(1 + \frac{\Delta a}{r_0}\right)^3}}\,(t - t_{po} - \Delta t_p)$$

or

$$\Delta M = -\frac{3}{2}\frac{\Delta a}{r_0}M_0 - \sqrt{\frac{\mu}{r_0^3}}\,\Delta t_p. \qquad (111)$$

The errors at any later time δr_2, δV_2, γ and $\delta\theta_2$ will be determined by varying one injection parameter at a time and assuming a linear combination of the individual errors.

Case (1) $[\delta r_1 = 0,\ \delta V_1 = 0,\ \delta\gamma_1 \neq 0]$. If γ_1 is the only launch parameter which is in error, $\delta r_1 = 0$, $\delta V_1 = 0$, $\gamma_1 = \delta\gamma_1$, and from Eq (133), $e \approx |\delta\gamma_1|$, where $\delta\gamma_1$ is an error due to a velocity component normal to the desired circular orbit velocity at launch. For the circular orbit, M and t_p are referenced to the perigee direction in the incorrect orbit. Since the semimajor axis a is a function of r and V but not γ, $\delta a = 0$ for this case. That is, if only the orientation of the injection velocity is varied, there will be generated a family of orbits in which the eccentricity varies, but the semimajor axis remains constant. Then, from Eqs (107) through (111),

$$\delta r_{(1)} \approx -er_0\cos M_0 \approx -r_0|\delta\gamma_1|\cos M_0$$

$$\frac{\delta V_{(1)}}{V_0} \approx |\delta\gamma_1|\cos M_0$$

$$\delta\theta_{(1)} \approx -\sqrt{\frac{\mu}{r_0^3}}\,\Delta t_p + 2|\delta\gamma_1|\sin M_0$$

$$\delta\gamma_{(1)} \approx |\delta\gamma_1|\sin M_0$$

From the δr_1 equation, $\delta r = 0$ when $\cos M_0 = 0$. Therefore, for Case (1), $M_0 = 90°$ (for γ_1 positive) or $M_0 = 270°$ (for γ_1 negative). The absolute magnitudes in these equations may be removed by

defining a mean anomaly $\mathcal{M}_0$, referenced to the launch point. Then $\mathcal{M}_0 = M_0 - 90°$ for positive $\delta\gamma_1$, and $\mathcal{M}_0 = M_0 + 90°$ for negative $\delta\gamma_1$. Substitution in the previous equations gives, for either positive or negative $\delta\gamma_1$.

$$\frac{\delta r_{(1)}}{r_0} \approx \Delta\gamma_1 \sin \mathcal{M}_0 \tag{112}$$

$$\frac{\delta V_{(1)}}{V_0} \approx -\Delta\gamma_1 \sin \mathcal{M}_0 \tag{113}$$

$$\delta\theta_{(1)} \approx 2\,\Delta\gamma_1 (\cos \mathcal{M}_0 - 1) \tag{114}$$

$$\delta\gamma_{(1)} \approx \Delta\gamma_1 \cos \mathcal{M}_0 \tag{115}$$

In derivation of Eq (114) use is made of the fact that $\delta\theta_{(1)} = 0$ at $\mathcal{M}_0 = 0$ since the correct and incorrect orbits intersect at launch.

Case (2) $[\delta\gamma_1 = 0,\ \delta V_1 = 0,\ \delta r_1 \neq 0]$. For $\delta\gamma_1 = 0,\ \delta V_1 = 0,\ \delta r_1 \neq 0$, Eqs (90) and (91) give $\frac{\delta a}{r_0}(2) \approx 2\frac{\delta r_1}{r_0}$

$$e_{(2)} \approx \frac{|\Delta r_1|}{r_0}.$$

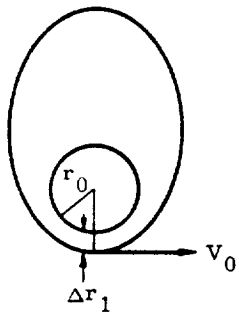

Then, from Eqs (48) through (52)

$$\frac{\delta r_{(3)}}{r_0} \approx 2\frac{\delta r_1}{r_0} - \frac{|\delta r_1|}{r_0}\cos M_0$$

$$\frac{\delta V_{(2)}}{V_0} \approx -\frac{\delta r_1}{r_0} + \frac{|\delta r_1|}{r_0}\cos M_0$$

$$\delta\theta_{(2)} \approx -3\frac{\delta r_1}{r_0} M_0 - \sqrt{\frac{\mu}{r_0^3}}\,\delta t_p + 2\frac{|\delta r_1|}{r_0}\sin M_0$$

$$\delta\gamma_{(2)} \approx \frac{|\delta r_1|}{r_0}\sin M_0$$

But $M_0 = 0°$ for Δr_1 positive, and $M = 180°$ for δr_1 negative. Then, for $\mathcal{M}_0 = 0°$ at launch,

$$\frac{\delta r_{(2)}}{r_0} \approx \frac{\delta r_1}{r_0}(2 - \cos \mathcal{M}_0) \tag{116}$$

$$\frac{\delta V_{(2)}}{V_0} \approx \frac{\delta r_1}{r_0}(\cos \mathcal{M}_0 - 1) \tag{117}$$

$$\delta\theta_{(2)} \approx \frac{\delta r_1}{r_0}(2 \sin \mathcal{M}_0 - 3\,\mathcal{M}_0) \tag{118}$$

$$\delta\gamma_{(2)} \approx \frac{\delta r_1}{r_0}\sin \mathcal{M}_0 \tag{119}$$

Case (3) $[\delta r_1 = 0,\ \delta\gamma_1 = 0,\ \delta V_1 \neq 0]$. For the remaining case, where $\delta r_1 = 0$, $\delta\gamma_1 = 0$ and $\delta V_1 \neq 0$, Eqs (90) and (91) give

$$\frac{\delta a_{(3)}}{r_0} \approx 2\frac{\delta V_1}{V_0}$$

$$e_{(3)} \approx 2\frac{|\delta V_1|}{V_0}.$$

A procedure similar to that used in Cases (1) and (2) gives

$$\frac{\delta r_{(3)}}{r_0} \approx 2\frac{\delta V_1}{V_0}(1 - \cos \mathcal{M}_0) \tag{120}$$

$$\frac{\delta V_{(3)}}{V_0} \approx \frac{\delta V_1}{V_0}(2 \cos \mathcal{M}_0 - 1) \tag{121}$$

$$\delta\theta_{(3)} \approx -3\,\mathcal{M}_0\frac{\delta V_1}{V_0} + 4\frac{\delta V_1}{V_0}\sin \mathcal{M}_0 \tag{122}$$

$$\delta\gamma_{(3)} \approx 2\frac{\delta V_1}{V_0}\sin \mathcal{M}_0. \tag{123}$$

The total error solutions are obtained by adding Eqs (112), (116) and (120); Eqs (113), (117) and (121); etc.

$$\frac{\delta r}{r_0} \approx \sin \mathcal{M}_0\,\delta\gamma_1 + (2 - \cos \mathcal{M}_0)\frac{\delta r_1}{r_0} + 2(1 - \cos \mathcal{M}_0)\frac{\delta V_1}{V_0} \tag{124}$$

$$\frac{\delta V}{V_0} \approx -\sin \mathcal{M}_0\,\delta\gamma_1 + (\cos \mathcal{M}_0 - 1)\frac{\delta r_1}{r_0} + (2 \cos \mathcal{M}_0 - 1)\frac{\delta V_1}{V_0} \tag{125}$$

$$\delta\theta \approx \delta\theta_1 + 2(\cos \mathcal{M}_0 - 1)\,\delta\gamma_1 + (2 \sin \mathcal{M}_0 - 3\,\mathcal{M}_0)\frac{\delta r_1}{r_0} + (4 \sin \mathcal{M}_0 - 3\,\mathcal{M}_0)\frac{\delta V_1}{V_0} \tag{126}$$

$$\delta\gamma \approx \cos \mathcal{M}_0\,\delta\gamma_1 + \sin \mathcal{M}_0\frac{\delta r_1}{r_0} + 2 \sin \mathcal{M}_0\frac{\delta V_1}{V_0} \tag{127}$$

for $e^2 \ll 1$

For the problem of relating errors at one orbit extremum to those at the previous extremum, $m_0 = 180°$ in Eqs (124) through (127).

$$\frac{\delta r_2}{r_0} \approx 3\frac{\delta r_1}{r_0} + 4\frac{\delta V_1}{V_0} \tag{128}$$

$$\frac{\delta V_2}{V_0} \approx -2\frac{\delta r_1}{r_0} - 3\frac{\delta V_1}{V_0} \tag{129}$$

$$\delta\theta_2 \approx \delta\theta_1 - 4\delta\gamma_1 - 3\pi\frac{\delta r_1}{r_0} - 3\pi\frac{\delta V_1}{V_0} \tag{130}$$

$$\delta\gamma_2 \approx -\delta\gamma_1 \tag{131}$$

$e^2 << 1$, points 1 and 2 extrema

Eqs (128) and (129) agree exactly with Eqs (104) and (105), in which the errors were derived as differentials.

c. Errors in final orbit elements

Errors in the final orbit elements $\delta a'$ and e' may be determined as functions of errors in the orbit conditions just after the second impulse, r_2, V'_2, γ'_2 by letting $r = r_0 + \delta r$, $V = V_0 + \delta V$ and $\cos^2\gamma = 1 - \gamma^2 + \ldots$ in

$$e^2 = 1 - \left(\frac{2}{r} - \frac{V^2}{\mu}\right)\left(\frac{r^2V^2\cos^2\gamma}{\mu}\right)$$

(neglecting terms of third and higher orders) and in

$$a = \left(\frac{2}{r} - \frac{V^2}{\mu}\right)^{-1}$$

(neglecting terms of second and higher orders). The results are

$$\Delta a \approx 2\delta r + 2\frac{r_0}{V_0}\delta V \tag{132}$$

$$e^2 \approx \left(2\frac{\delta V}{V_0} + \frac{\delta r}{r_0}\right)^2 + \gamma^2 \tag{133}$$

d. Combination of the errors

The errors in the final orbit parameters can now be written completely in terms of errors in tracking and prediction of the original orbit and errors in the corrective thrusts by adding the individual errors derived previously. Let the errors in tracking and prediction of the original orbit at the time of the first corrective impulse be δr_1, δV_1, and $\delta\gamma_1$, and let the errors in the first corrective impulse magnitude and orientation be $\delta(\Delta V_1)$ and $\delta\phi_1$. Then, from Eqs (80) and (81), the errors just after the corrective maneuvers are

$$\delta r_1' \approx \delta r_1$$

$$\delta V_1' \approx \delta(\Delta V_1) + \delta V_1$$

$$\delta\theta_1' \approx \delta\theta$$

$$\delta\gamma' \approx \frac{\Delta V_1}{V_0}\delta\phi_{T_1} + \delta\gamma_1.$$

These errors are transformed to errors at the next orbit extremum, where the second corrective impulse is to be applied by Eqs (104), (105) and (128) through (131).

$$\frac{\delta r_2}{r_0} \approx 3\frac{\delta r_1'}{r_0} + 4\frac{\delta V_1'}{V_0} \approx 3\frac{\delta r_1}{r_0} + 4\left[\frac{\delta(\Delta V_1)}{V_0} + \frac{\delta V_1}{V_0}\right]$$

$$\frac{\delta V_2}{V_0} \approx -2\frac{\delta r_1'}{r_0} - 3\frac{\delta V_1'}{V_0} \approx -2\frac{\delta r_1}{r_0} - 3\left[\frac{\delta(\Delta V_1)}{V_0} + \frac{\delta V_1}{V_0}\right]$$

$$\delta\theta_2 \approx \delta\theta_1' - 4\delta\gamma' - 3\pi\frac{\delta r_1'}{r_0} - 3\pi\frac{\delta V_1'}{V_0}$$

$$\approx \delta\theta_1 - 4\left(\frac{\Delta V_1}{V_0}\delta\phi_{T_1} + \delta\gamma_1\right) - 3\pi\left[\frac{\delta r_1}{r_0} + \frac{\delta(\Delta V_1)}{V_0} + \frac{\delta V_1}{V_0}\right]$$

$$\delta\gamma_2 \approx -\delta\gamma_1' \approx -\frac{\Delta V_1}{V_0}\delta\phi_{T_1} - \delta\gamma_1$$

Equations (80) and (81) are then applied to these equations to include the errors in the second impulse magnitude and orientation, $\delta(\Delta V_2)$ and $\delta\phi_{T_2}$

$$\frac{\delta r_2'}{r_0} = \frac{\delta r_2}{r_0} \approx 3\frac{\delta r_1}{r_0} + 4\left(\frac{\delta(\Delta V_1)}{V_0} + \frac{\delta V_1}{V_0}\right)$$

$$\frac{\delta V_2'}{V_0} \approx \frac{\delta(\Delta V_2)}{V_0} + \frac{\delta V_2}{V_0} \approx \frac{\delta(\Delta V_2)}{V_0} - 2\frac{\delta r_1}{r_0} - 3\left(\frac{\delta(\Delta V_1)}{V_0} + \frac{\delta V_1}{V_0}\right)$$

$$\delta\theta_2' = \delta\theta_2 \approx \delta\theta_1 - 4\left(\frac{\Delta V_1}{V_0}\delta\phi_{T_1} + \delta\gamma_1\right) - 3\pi\left(\frac{\delta r_1}{r_0} + \frac{\delta(\Delta V_1)}{V_0} + \frac{\delta V_1}{V_0}\right)$$

$$\delta\gamma_2' \approx \frac{\Delta V_2}{V_0}\,\Delta\phi_{T_2} + \delta\gamma_2 \approx \frac{\Delta V_2}{V_0}\,\delta\phi_{T_2} - \frac{\Delta V_1}{V_0}\,\delta\phi_{T_1} - \delta\gamma_1$$

Finally, these errors are transformed to the errors in final orbit elements by Eqs (132) and (133).

$$\frac{\delta a'}{r_0} \approx 2\left[\frac{\delta r_1}{r_0} + \frac{\delta V_1}{V_0} + \frac{\delta(\Delta V_1)}{V_0} + \frac{\delta(\Delta V_2)}{V_0}\right] \quad (134)$$

$$e'^2 \approx \left[-\frac{\delta r_1}{r_0} - 2\frac{\delta V_1}{V_0} - 2\frac{\delta(\Delta V_1)}{V_0} + 2\frac{\delta(\Delta V_2)}{V_0}\right]^2 + \left[\frac{\Delta V_2}{V_0}\,\delta\phi_{T_2} - \frac{\Delta V_1}{V_0}\,\delta\phi_{T_1} - \delta\gamma_1\right]^2 \quad (135)$$

Equation (134) is plotted in Fig. 17. For the assumption that $\delta(\Delta V_1) = \delta(\Delta V_2)$.

E. GENERAL TWO-IMPULSE MANEUVERS

For the case where it is desired to transfer between orbits and where the maximum change in the azimuth is not large, it is possible to accomplish the transfer efficiently with two impulses. This may be visualized from the following sketch.

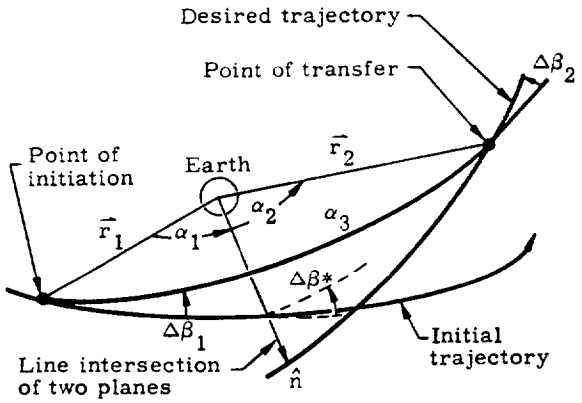

The plane of the transfer is thus defined by $\vec{r} \cdot \vec{r}_1 \times \vec{r}_2 = 0$ where $\vec{r}$ is a general radius vector for points on the transfer trajectory. However, this expression will not serve the purposes we desire. Thus, consider the unit vector $\hat{n}$ along the intersection of the planes.

$$\cos\alpha_1 = \frac{\vec{r}_1 \cdot \hat{n}}{r_1} = \hat{r}_1 \cdot \hat{n}$$

$$\cos\alpha_2 = \hat{r}_2 \cdot \hat{n}$$

$$\cos\alpha_3 = \hat{r}_1 \cdot \hat{r}_2$$

$$\sin\Delta\beta_1 = \sin\Delta\beta^* \frac{\sin\alpha_2}{\sin\alpha_3}$$

where $\Delta\beta^*$ is a known angle for the two orbits as a function of the latitude at which the planes intersect.

Now at this point, the plane of motion is defined. The initial and final radii and the angle between are known; however, the transfer has not been uniquely defined because many elliptical trajectories could be constructed to satisfy these conditions. To completely define the problem, one additional parameter must thus be selected. This parameter could be a geometrical element such as a, p, or e, a time variant parameter at r_1 or r_2 at the time of transfer. Since the latter piece of data is more general than the others, it is assumed to apply for this purpose.

Thus the problem evolves into the solution of a set of simultaneous equations for the planar elements of the orbit.

$$\Delta t = t_{arrival} - t_{injection} = \sqrt{\frac{\mu}{a^3}}\left[E_2 - E_1 - e(\sin E_2 - \sin E_1)\right]$$

$$\alpha_3 = \theta_2 - \theta_1 = \cos^{-1}\left[\frac{a(1-e^2) - r_2}{e r_2}\right] - \cos^{-1}\left[\frac{a(1-e^2) - r_1}{e r_1}\right]$$

where

$$\cos E_2 = \frac{a - r_2}{e a}$$

$$\cos E_1 = \frac{2 - r_1}{e a}$$

This solution is transcendental and thus requires the simultaneous iteration of 4 equations unless Lambert's theorem (discussed in Chapter III) is utilized in place of Kepler's equation. (If Lambert's theorem is utilized, the semimajor axis is evaluated by an iteration which does not involve eccentricity, and the equation for α_3 can then be utilized to define eccentricity.) Two iterative processes are valid for this solution and are sufficiently simple that their use is justified in automatic computation. The first such process is the Newton-Raphson iteration. This procedure is applicable for functions

$$y_1 = f_1(E_1, E_2, a, e) = f_1(x_i) \equiv 0 \qquad i = 1, 2, 3, 4$$

$$y_2 = f_2(E_1, E_2, a, e) = f_2(x_i) \equiv 0$$

$$y_3 = f_3(E_1, E_2, a, e) = f_3(x_i) \equiv 0$$

$$y_4 = f_4(E_1, E_2, a, e) = f_4(x_i) \equiv 0$$

Now assume

$$x_1 = x_{1,0} + h$$

$$x_2 = x_{2,0} + k$$

$$x_3 = x_{3,0} + m$$

$$x_4 = x_{4,0} + n$$

Thus

$$f_i (x_{1,0} + h, x_{2,0} + k, x_{3,0} + m, x_{4,0} + n) = 0$$

etc.

Expanding these f_i in Taylor series and neglecting higher order terms in h, k, m and n now yields

$$f_1(x_{1,0} + h, \cdots x_{4,0} + n) = f_1 (x_{1,0}, x_{2,0}, x_{3,0}, x_{4,0}) + h \left(\frac{\partial f_1}{\partial x_1}\right)_{x_i = x_{i,0}} + k \left(\frac{\partial f_1}{\partial x_2}\right)_{x_i = x_{i,0}} + m \left(\frac{\partial f_1}{\partial x_3}\right)_{x_i = x_{i,0}} + n \left(\frac{\partial f_1}{\partial x_4}\right)_{x_i = x_{i,0}}$$

and similarly for f_2, f_3 and f_4. Now treating the coefficients h, k, m and n as the unknowns, the solution is

$$h = \frac{\begin{vmatrix} f_1 & \partial f_1/\partial x_2 & \partial f_1/\partial x_3 & \partial f_1/\partial x_4 \\ f_2 & \cdot & \cdot & \cdot \\ f_3 & \cdot & \cdot & \cdot \\ f_4 & \partial f_4/\partial x_2 & \partial f_4/\partial x_3 & \partial f_4/\partial x_4 \end{vmatrix}}{\begin{vmatrix} \partial f_1/\partial x_1 & \cdot & \cdot & \partial f_1/\partial x_4 \\ \cdot & \cdot & \cdot & \cdot \\ \cdot & \cdot & \cdot & \cdot \\ \partial f_4/\partial x_1 & \cdot & \cdot & \partial f_4/\partial x_4 \end{vmatrix}}$$

and k, m and n are determined in a similar manner (i.e., by replacing in turn the second, third and fourth columns of the determinant by the column f_1, f_2, f_3, f_4 and dividing the resultant determinant by the same denominator as presented above). Once the process is completed numerically, it is repeated until the values of the increments h, k, m and n are smaller than some value which must be specified.

This solution has been tested and proven to converge; however, it must be noted that the functions which are being iterated are of a very complex nature and have many relative minima and maxima. Thus, unless the first guesses for a and e are reasonably valid, the method will not converge to the proper root. First estimates may be obtained from series expansions or approximate forms discussed in Chapter III.

The second iterative solution which has been checked is a purely numerical evaluation and proceeds as follows. First, the variable E is eliminated by direct substitution into the equations for Δt and $\Delta\theta$. Then functions f_1, f_2 and f_3 are defined as follows

$$f_1 = (\Delta t_{given} - \Delta t_{computed})\, 2\pi/\tau$$

$$f_2 = \Delta\theta_{given} - \Delta\theta_{computed}$$

$$f_3 = |f_1| + |f_2|$$

As before, a value for each of the variables a and e is guessed, but this time one value (say a) is incremented positively and negatively and the function f_3 evaluated for each set of variables $(a + \Delta a, e)$; (a, e); and $(a - \Delta a, e)$. The value of a which results in the smallest value of f_3 is then selected and the process is repeated after incrementing e. A fairly coarse grid (i.e., large Δa and Δe) can be utilized initially, and this grid is halved each time the previous root is selected as the minimizing value. Once the grid is sufficiently small or once the value of f_3 (which is the total error of the solution) is less than a specified number the solution can be halted. In all cases f_3 should be checked because unless it is nearly zero, the set of variables selected corresponds to a local minimum, not the true root. In such cases, both a and e can be incremented varying amounts to see if there is any set of roots in the vicinity yielding a smaller f_3. If so, the procedure continues. This solution is illustrated below for the case in which point A represents the first repeated root

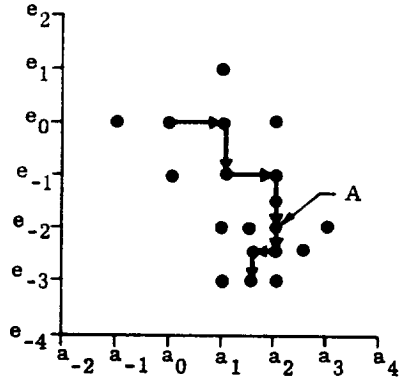

This solution was found ideally suited to automatic computation, since no functions other than those required in the definition of the problem

need be programmed and since the logic involved is very simple. In addition, it is possible to ascertain whether convergence to the proper roots has been obtained by checking the value of f_3.

This method also proved to require less accurate initial estimates of a and e and was never subject to the problem of division by zero as is possible in the definition of h, k, m and n of the Newton-Raphson method.

Once the elements a and e are known to the desired accuracy, the development of the maneuvers can continue. The term $\Delta\beta$, was defined previously; therefore, consider the azimuths in the two orbits at the point of the second maneuver

$$\sin\beta_1 = \frac{\cos i_1}{\cos L}$$

$$\sin\beta_2 = \frac{\cos i_2}{\cos L}$$

$$\sin\beta_1 = \frac{\cos i_1}{\cos i_2}\sin\beta_2$$

but

$$\Delta\beta_2 = \beta_2 - \beta_1$$

Thus

$$1 = \frac{\cos i_1}{\cos i_2}\left[\cos\Delta\beta_2 + \sin\Delta\beta_2 \cot\beta_1\right]$$

or

$$\frac{\cos i_2}{\cos i_1} = \cos\Delta\beta_2 + \sin\Delta\beta_2\cot\beta_1$$

$\Delta\beta_2$ can be evaluated directly from this equation; however, unless $\Delta\beta_2$ is small a simple solution would be to evaluate both β_1 and β_2 then subtract. For the case where $\Delta\beta_2$ is small (as is in general true)

$$\Delta\beta_2 \approx \left(\frac{\cos i_2}{\cos i_1} - 1\right)\left[\left(\frac{\cos L}{\cos i_1}\right)^2 - 1\right]^{-1/2}$$

But the velocity vector must be rotated through another angle ($\Delta\gamma$) in order to change the direction of the velocity in the plane to attain the correct ellipse. This angle is obtained from

$$\Delta\gamma_1 = \cos^{-1}\sqrt{\frac{a^2(1-e^2)}{r_1(2a - r_1)}} - \cos^{-1}\sqrt{\frac{a_0^2(1-e_0^2)}{r_1(2a_0 - r_1)}}$$

$$\Delta\gamma_2 = \cos^{-1}\sqrt{\frac{a_f^2(1-e_f^2)}{r_2(2a_f - r_2}} +$$

(continued)

$$- \cos^{-1}\sqrt{\frac{a(1-e^2)}{r_2(2a - r_2)}}$$

where: the absence of a subscript denotes the transfer orbit
subscript 0 denotes the initial orbit
subscript f denotes the final orbit

Now the total turn angle for the velocity vector is obtained from the following sketch to be

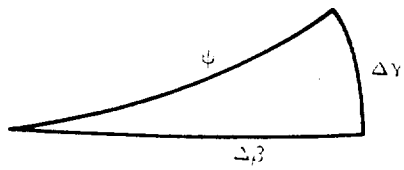

$$\psi_1 = \cos^{-1}(\cos\Delta\gamma_1\cos\Delta\beta_1)$$

$$\psi_2 = \cos^{-1}(\cos\Delta\gamma_2\cos\Delta\beta_2)$$

and the changes in the required velocities are:

$$\Delta V_1^2 = V_0^2 + V_1^2 - 2V_0V_1\cos\psi_1$$

$$= \mu\left[\frac{4}{r_1} - \frac{1}{a_0} - \frac{1}{a} - \sqrt{\left(\frac{2}{r_1} - \frac{1}{a_0}\right)\left(\frac{2}{r_1} - \frac{1}{a}\right)}\cdot\cos\Delta\gamma_1\cos\Delta\beta_1\right]$$

and

$$\Delta V_2^2 = \mu\left[\frac{4}{r_2} - \frac{1}{a} - \frac{1}{a_f} - \sqrt{\left(\frac{2}{r_2} - \frac{1}{a}\right)\left(\frac{2}{r_2} - \frac{1}{a_f}\right)}\cos\Delta\gamma_2\cos\Delta\beta_2\right]$$

No provision has been made at any point in this analysis for nonzero burning times. Actually, however, these equations have been utilized in a digital program to simulate powered maneuvers. The process was as follows.

(1) The impulsive analysis was made.

(2) A finite burning simulation was attempted.

(3) The error in the position and velocity at burnout was determined from the computed position and velocity and the values were predicted for the transfer orbit the same number of seconds after the impulse.

(4) The magnitude of the errors was utilized to adjust the time for initiating the thrust and the thrust program.

(5) The process was repeated until the desired transfer orbit was obtained to a specified accuracy. The allowable errors for the initial computations were $(\Delta x, \Delta y, \Delta z)_{B0} \leq 1000$ ft (or 300 m) and $(\Delta\dot{x}, \Delta\dot{y}, \Delta\dot{z})_{B0} \leq 0.1$ fps (or 0.03 mps).

The validity of the impulsive analysis was in this manner proven for moderate to large accelerations. The low acceleration runs, however, required more computations in order to converge to a proper thrust program. This fact should be expected, since the accuracy of the impulsive analysis deteriorates as the time of thrusting increases. The results of these runs indicated generally good agreement for the computation of the actual propellant mass required but indicated that the maneuver should be anticipated in order to find the proper thrust program in a limited number of trials. The physical significance of this statement is seen directly from the following sketch.

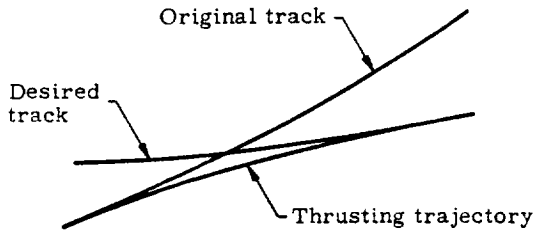

F. PROPULSION REQUIREMENTS FOR CANCELLING THE EFFECTS OF DRAG AND OBLATENESS

For most earth satellites only two relatively large perturbing accelerations act on the vehicle, the first due to earth's oblateness and the second due to atmospheric drag. Generally these effects are sufficiently large that it is necessary to accept them; however, for some orbits and for some specific satellite applications it may be desirable to cancel them. This section treats these two problems.

1. Counteracting the Effects of the Earth's Oblateness (Ref. 2)

The potential function of the earth in Jeffrey's notation is:

$$U(r, L) = -\frac{\mu}{R}\left[\frac{R}{r} + \frac{JR^3}{3r^3}(1 - 3\sin^2 L) + O(J^2)\right]$$

where

$J = 3/2\, J_2$

and where terms of the order J^2 have been neglected

while for a spherical earth it is

$$U_s = -\frac{\mu}{r}$$

The gravitational force acting on the satellite is given by the negative gradient of the potential function. In polar coordinates

$$\text{grad } U = \hat{r}\frac{\partial U}{\partial r} + \hat{L}\frac{1}{r}\frac{\partial U}{\partial L} + \hat{\phi}\frac{1}{r\cos L}\frac{\partial U}{\partial \phi}$$

therefore

$$F_{ob} = -\text{grad } U(r, L) = -\hat{r}\frac{\mu}{R^2\rho^2}\left[1 + \frac{J}{\rho^2}(1 - 3\sin^2 L)\right] + \frac{\hat{L}\mu}{R^2\rho^4} J \sin 2L \qquad (136)$$

and

$$F_s = -\text{grad } U_s = -\hat{r}\frac{\mu}{R^2\rho^2}$$

where

$$\rho = \frac{r}{R} \qquad (137)$$

The corrective force which must be exerted on the satellite to remain in an unperturbed orbit is the difference between these two forces represented by Eqs (136) and (137).

$$\vec{F}_{req} = -m(F_{ob} - F_s)$$

$$\vec{F}_{req} = m(\text{grad } U - \text{grad } U_s)$$

so that the general force equation giving the corrective force per unit mass is

$$\vec{F}_{req} = \hat{r}\frac{\mu}{R^2\rho^4}\left[J(1 - 3\sin^2 L)\right] - \hat{L}\frac{\mu}{R^2\rho^4} J \sin 2L \qquad (138)$$

Consider the following sketch which shows the projection of the actual orbit on a sphere of radius equal to that value of r occurring at the highest latitude of the orbit. The X-axis in this case is 90° out of phase with the ascending node.

By inspection, the relation between the latitude L and the angle from perigee θ is

$$\sin L = \sin i \cos \tau \qquad (139)$$

where

$$\tau = \theta - \alpha$$

$$\alpha = 90 - \omega$$

From the standard form of the conic for the orbit of a satellite about a spherical earth,

$$r = \frac{p}{1 + e\cos\theta} \qquad (140)$$

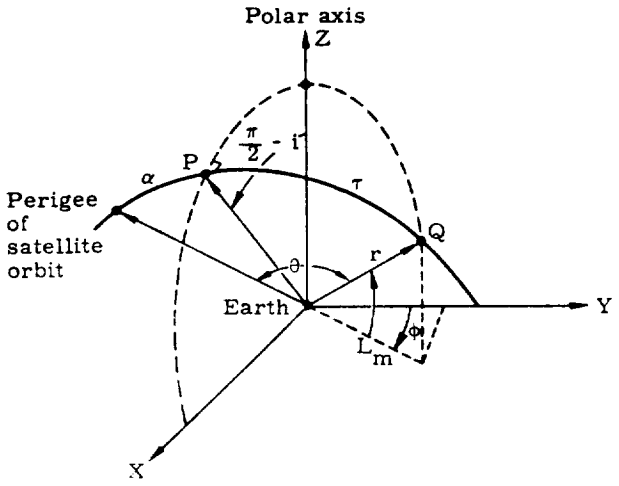

Substituting these expressions into the force equation per unit mass (Eq (138)) yields

$$\vec{F}_{req} = \hat{r}\,\frac{\mu R^2}{p^4}\,(1 + e\cos\theta)^4 \left[J\left(1 - 3\sin^2 i\cos^2(\theta - \alpha)\right)\right] - \frac{\hat{L}\,2J\mu R^2}{p^4}\,(1 + e\cos\theta)^4 \sin i\cos(\theta - \alpha)\sqrt{1 - \sin^2 i\cos^2(\theta - \alpha)} \tag{141}$$

Now to relate the force to time, rather than true anomaly, replace θ by E, using the geometric relationship

$$\cos\theta = \frac{\cos E - e}{1 - e\cos E} \tag{142}$$

and

$$\cos(\theta - \alpha) = \frac{H}{1 - e\cos E} \tag{143}$$

where

$$H = (\cos E - e)\cos\alpha + \sqrt{1 - e^2}\,\sin E\sin\alpha \tag{144}$$

Substitution of Eqs (142) and (143) into Eq (68) to get the corrective thrust requirements in terms of obital elements gives

$$\vec{F}_{req} = m\left(\hat{r}\,F_r + \hat{L}\,F_L\right) \tag{145}$$

where

$$F_r = \frac{J\mu R^2}{p^4}\left(\frac{1 - e^2}{1 - e\cos E}\right)^4 \left[1 - \frac{3H^2\sin^2 i}{(1 - e\cos E)^2}\right]$$

and

$$F_L = \frac{J\,2\mu R^2 H\sin i}{p^4(1 - e\cos E)}\left(\frac{1 - e^2}{1 - e\cos E}\right)^4 \left[1 - \frac{H^2\sin^2 i}{(1 - e\cos E)^2}\right]^{\frac{1}{2}}$$

Now the mass of the satellite must be considered a function of time. If the mass rate is small relative to the mass of the satellite, this time variation can be written as

$$m = m_o\left(1 - \frac{\dot{m}t}{m_0} + O(\dot{m}/m)^2\right)$$

or as a function of the eccentric anomaly

$$m = m_o - \frac{dm}{dE}\frac{dE}{dt}\,t = m_o - \frac{dm}{dE}\left(\frac{dt}{dE}\right)^{-1} t. \tag{146}$$

But for a spherical earth,

$$t = \frac{\tau}{2\pi}\,(E - e\sin E) \tag{147}$$

so that

$$\frac{dt}{dE} = \frac{\tau}{2\pi}\,(1 - e\cos E) \tag{147a}$$

and hence m (and therefore W in units of weight) can be expressed as a function only of the eccentric anomaly:

$$W = W_0 - \frac{E - e\sin E}{1 - e\cos E}\,\frac{dW}{dE}. \tag{148}$$

Substituting Eq (148) into the force equation (145) gives

$$F_{req} = \frac{1}{g_0}\left[W_0 - \frac{E - e\sin E}{1 - e\cos E}\,\frac{dW}{dE}\right]\left[\hat{r}\,F_r + \hat{L}\,F_L\right] \tag{149}$$

Now expressing the thrust as a function of the specific impulse

$$F_{req} = I_{sp}\,\dot{W}$$

or as a function of eccentric anomaly and weight

$$F_{req} = I_{sp} \frac{dW}{dE} \left(\frac{dt}{dE}\right)^{-1} \tag{150}$$

Therefore

$$I_{sp} \frac{dW}{dE} = \frac{\tau}{2\pi g_0} \left[W_0 (1 - e \cos E) - (E - e \sin E) \frac{dW}{dE} \right] \sqrt{F_r^2 + F_L^2} \tag{151}$$

thus,

$$\frac{dW}{dE} = \frac{W_0 (1 - e \cos E) \sqrt{F_r^2 + F_L^2}}{\frac{2\pi I_{sp} g_0}{\tau} + (E - e \sin E) \sqrt{F_r^2 + F_L^2}} \tag{151a}$$

Integration of Eq (151a) over limits of one revolution (0 to 2π) gives the amount of propellant used in that orbital pass

$$W_p = \int_0^{2\pi} \frac{dW}{dE} \, dE \tag{152}$$

Also, by a slight rearrangement of terms, using Eqs (147a) and (151), the integral equation for the corrective thrust is

$$\left|F_{req}\right| = W_0 \int_0^E \frac{\sqrt{F_r^2 + F_L^2}}{g_0 + \frac{T}{2\pi I_{sp}} (E - e \sin E) \sqrt{F_r^2 + F_L^2}} \, dE \tag{153}$$

Both of these equations are difficult if not impossible to integrate analytically. However, a simplification will result if the mass of the vehicle is assumed constant for a complete revolution. The magnitude of the error of this assumption is small as will be apparent in subsequent discussions.

Each component of the force can be related to the propellant flow by Eq (151)

$$I_{sp} \frac{dW_r}{dE} = \frac{W\tau}{2\pi g_0} (1 - e \cos E) F_r \tag{154}$$

$$I_{sp} \frac{dW_L}{dE} = \frac{W\tau}{2\pi g_0} (1 - e \cos E) F_L \tag{154a}$$

The actual propellant flow rate is

$$I_{sp} \frac{dW}{dE} = \frac{W\tau}{2\pi g_0} (1 - e \cos E) F_{req} \tag{155}$$

or upon substituting for F_{req} in terms of its components

$$I_{sp} \frac{dW}{dE} = \frac{W\tau}{2\pi g_0} (1 - e \cos E) \sqrt{F_r^2 + F_L^2} \tag{155a}$$

so that

$$\frac{dW}{dE} = \sqrt{\left(\frac{dW_r}{dE}\right)^2 + \left(\frac{dW_L}{dE}\right)^2} \tag{156}$$

and hence, the weight of propellant consumption per revolution is

$$W_p = \frac{W\tau \mu R^2 J}{2\pi g_0 a^4 I_{sp}} \int_0^{2\pi} \left\{ \left[\frac{1}{(1 - e \cos E)^5} \right] \cdot \left[5H^4 \sin^4 i - 2H^2 (1 - e \cos E)^2 \sin^2 i + (1 - e \cos E)^4 \right]^{1/2} \right\} dE \tag{157}$$

Probably the most common case for which the oblateness correction will be made will be for satellites in circular orbits. It would therefore be of interest at this time to determine the thrust and propellant equations for circular orbits.

The simplifying conditions for circular orbits are: (1) eccentricity is by definition zero, (2) perigee is undefined and may be selected to make the angle a zero, and (3) the eccentric anomaly E and the true anomaly θ are coincident. Then

$$F_r = \frac{\mu R^2}{a^4} J (1 - 3 \sin^2 L) \tag{158}$$

$$F_L = -\frac{\mu R^2}{a^4} J \sin^2 L \tag{158a}$$

$$F_{req} = m \sqrt{F_r^2 + F_L^2} \tag{158b}$$

$$W_p = \frac{W\tau \mu R^2 J}{2\pi g_0 a^4 I_{sp}} \int_0^{2\pi} \left[5 \cos^4 E \sin^4 i - 2 \cos^2 E \sin^2 i + 1 \right]^{1/2} dE \tag{159}$$

Also, for circular orbits, the true anomaly is related to the time since perigee passage by

$$\theta = \frac{2\pi t}{\tau} .$$

Thus, the corrective thrust F_{req} can be rewritten from Eqs (158) and (159) as

$$F_r = \frac{\mu R^2 J}{a^4} (1 - 3 \sin^2 \cos^2 \theta) \qquad (160)$$

$$F_L = \frac{-2\mu R^2 J}{a^4} \sin i \cos \theta \sqrt{1 - \sin^2 i \cos^2 \theta} \qquad (160a)$$

$$F_{req} = M \sqrt{F_r^2 + F_L^2} \qquad (160b)$$

The variation of the absolute values of these functions as functions of the true anomaly θ, and orbit inclination i are illustrated in Figs. 18 and 19. The parameter for these figures is a non-dimensional acceleration x defined as follows:

$$x_r = \frac{a^4}{\mu R^2 J} |F_r|$$

$$x_\theta = \frac{a^4}{\mu R^2 J} |F_\theta|$$

$$x_{req} = \frac{a^4}{\mu R^2 J} |F_{req}|$$

Estimated average values derived from these curves are illustrated in Fig. 20 as a function of the orbit inclination i. The curve for $\bar{x}_{req}$ represents the averages derived from the curves in Fig. 19, not from $\bar{x}_r$ and $\bar{x}_L$, since

$$\bar{x}_{req} \neq \sqrt{\bar{x}_r^2 + \bar{x}_L^2}$$

but rather

$$\bar{x}_{req} = \overline{\sqrt{x_r^2 + x_L^2}}$$

Evaluation of the propellant requirement is now a simple matter, since

$$I_{sp} \int_0^{W_p} dW_p = \int_0^{\tau} F_{req} \, dt$$

hence,

$$W_p = \frac{\tau}{I_{sp}} F_{req}$$

or

$$W_p = \frac{W \tau \mu R^2 J}{g_0 I_{sp} a^4} \bar{x}_{req}$$

where $\bar{x}_{req}$ is as illustrated in Fig. 20.

Example 1. Consider a 10,000-lb (44,500 newton) satellite on a 300-naut mi or 556-km equatorial circular orbit. The parameters for this case would be as follows:

$m = 311$ slugs $= 4530$ kg

$I_{sp} = 500$ sec (assumed)

$R = 20.9264 \times 10^6$ ft $= 6378.2$ km

$a = 22.72 \times 10^6$ ft $= 6930$ km

$\mu = 1.407645 \times 10^{16}$ ft^3/sec^2 $=$ 398601.5 km^3/sec^2

$i = 0$ deg

$\tau = 5740$ sec

$J = 1.637 \times 10^{-3}$

For this case

$\bar{x}_{req} = 1$

$F_{req} = 11.8$ lb (average value) $\doteq 52.5$ newton

and

$W_p = 136$ lb/orbit $= 605$ newtons/orbit

Example 2. Consider the same 10,000-lb (44,500 newton) vehicle on a 300-naut mi (556-km) polar circular orbit. The parameters are the same as before, except that now,

$i = 90°$.

For this case

$\bar{x}_{req} = 1.31$

Hence,

$F_{req} = 15.5$ lb (average value) $= 69$ newton

$W_p = 178$ lb/orbit $= 794$ newtons/orbit

Example 3. Consider the same 10,000-lb (44,500 newton) vehicle on a 300-naut mi (556-km) circular orbit inclined 28° to the equator (east-launching from the AMR). The parameters are the same as in Example 1, except that now,

$i = 28°$.

For this case

$$\bar{x}_{req} = 0.935$$

Hence,

$$F_{req} = 11.05 \text{ lb (average value)} = 49.2 \text{ newtons}$$

$$W_p = 127 \text{ lb/orbit} = 566 \text{ newtons/orbit}$$

Example 4. Consider the same 10,000-lb (44,500 newton) vehicle on a "24-hr" circular equatorial orbit. The parameters are the same as in Example 1, except that now,

$$a = 1.4 \times 10^8 \text{ ft} = 0.42 \times 10^8 \text{ m}$$

$$\tau = 86,164 \text{ sec}$$

For this case

$$\bar{x}_{req} = 1$$

Hence,

$$F_{req} = 0.00815 \text{ lb (average value)} = 0.0363 \text{ newton}$$

$$W_p = 1.4 \text{ lb/orbit} = 6.24 \text{ newtons/orbit}$$

Conclusions. Some general observations may be made from Figs. 18, 19 and 20.

(1) In an equatorial orbit, the corrective force required to maintain an unperturbed orbit is constant and directed away from the earth (Fig. 18). As the inclination of the orbit is increased to about 30° the radial component of the force decreases somewhat, indicating the diminishing effect of the equatorial bulge as the vehicle gets farther away from it. Beyond an inclination of 30°, the vehicle begins to feel the full effect of the oblate shape of the earth and results in the high values of F_{req} (Fig. 19) for low values of θ.

(2) The correction required on a polar orbit is greater than that required on an equatorial orbit. As an illustrative example, consider a satellite on a polar orbit. Beginning with its position at $\theta = 0$ (over the earth's North Pole), the field is symmetric, and only a negative component of radial force exists (i.e., thrust directed toward center of earth). As the vehicle's latitude decreases (increasing θ) the force decreases and rotates away from the center of the earth until at $\theta = 55°$, it is tangent to the orbit, and directed away from the equator. Finally, as the vehicle passes over the equator on its way toward the South Pole, the only force is the radial component acting away from the earth.

(3) Another result is that an orbit inclination of about 30° requires the least amount of energy expenditure to maintain the orbit (Fig. 20).

2. Propulsion Requirements for Counteracting Drag

Corrective propulsion needed for drag cancellation may be applied either by a continuous thrust device or in discrete impulses. In the first case, either thrust must be varied in such a manner that the drag is balanced at every instant or the time integral of the thrust dotted into the velocity around the orbit must be equal to the work done by the drag force. This drag force is

$$\frac{\vec{D}}{m} = -\frac{1}{2}\frac{C_D A}{m}\rho\,(\vec{V} + \vec{V}_{aT}) \cdot (\vec{V} + \vec{V}_{aT})\frac{\vec{V} + \vec{V}_{aT}}{\left|\vec{V} + \vec{V}_{aT}\right|}$$

where

$\vec{V}_{aT}$ = the velocity of the atmosphere

V = the velocity due to elliptic motion

ρ = mass density as function of position

Thus

$$\frac{\vec{T}}{m} = \frac{\vec{D}}{m}$$

Assuming that the orbit is specified (both planar and orientation elements) and that a model of atmospheric density is available which includes as many of the effects due to solar radiation, atmospheric oblateness, etc., as desirable, and that the product $C_D A$ can be defined with some accuracy, the time history of thrust can be computed. This procedure would best be handled numerically though the possibility exists that series expansions in the various terms might also prove useful. The major drawbacks, however, that the method is cumbersome and requires a variable thrust, are sufficient to eliminate this method from consideration in a parametric study of this nature.

The time integral approach to drag cancellation may be stated as

$$W_{thrust} = -W_{drag}$$

$$\int_0^\tau \vec{F} \cdot (\vec{V} + \vec{V}_{aT})\,dt = \int_0^\tau \vec{D} \cdot (\vec{V} + \vec{V}_{aT})\,dt$$

$$= \int_0^\tau \frac{1}{2} C_D A\,\rho \frac{\left[(\vec{V} + \vec{V}_{aT}) \cdot (\vec{V} + \vec{V}_{aT})\right]^2}{\left|\vec{V} + \vec{V}_{aT}\right|}\,dt$$

where τ is the orbital period

But if

$$F = F \frac{(\vec{V} + \vec{V}_{aT})}{\left|\vec{V} + \vec{V}_{aT}\right|}$$

where

F = scalar constant

The left-hand side of the previous integral reduces to:

$$F \int_0^T \frac{(\vec{V} + \vec{V}_{aT}) \cdot (\vec{V} + \vec{V}_{aT})}{\left|\vec{V} + \vec{V}_{aT}\right|} dt$$

which is by definition

$$F \int_0^T \left|\vec{V} + \vec{V}_{aT}\right| dt$$

Similarly the right-hand side of the equation is

$$\frac{1}{2} \int_0^T C_D A \rho \left|\vec{V} + \vec{V}_{aT}\right|^3 dt$$

This solution, like the first, is such that a numerical solution is quite attractive for the general case. For special cases when the term $\vec{V}_{aT}$ can be neglected or considered to be colinear with $\vec{V}$ (that is for very high satellites or nearly circular equatorial orbits). The general order of complexity can be reduced and analytic solutions become attractive. Material pertinent to these cases is covered in Chapter V. Because of the restrictive nature of this material it is not presented here. Rather, it is noted that the procedure is simply the matching of the work done by thrust and by drag. The matching procedure is at times very tedious but may nonetheless be accomplished. An approximation to this impulse could be obtained by integrating the drag force over a revolution and observing the change in the orbital elements; then via the methods described in previous sections the impulse required to correct elements could be computed and the average thrust obtained by dividing by the orbital period.

The final approach to this maintenance maneuver is one in which the orbit is allowed to decay until one of the elements has changed an amount equal to or greater than a prescribed tolerance for that element. At this time a two-impulse maneuver is initiated which transfers the vehicle back to the original orbit. Since atmospheric velocity is small compared to the vehicle velocity, the perturbing forces occur approximately in the plane of motion and thus the transfer will be approximately coplanar. Chapter V again presents all of the data pertinent to the decay of satellites and the first section of this chapter ties these changes into the propulsion requirements. Thus, the procedure to be followed for an analysis of this nature is:

(1) The specification of the geometrical elements.

(2) The establishment of tolerances for the elements.

(3) The evaluation of the rates of change of the elements.

(4) The assessment of the times at which corrective action is required, the same maneuver being required each time.

(5) The calculation of the maneuver requirements.

Since each of these discussions is presented in detail in the respective sections of pertinent chapters repetition of this material for the general solution is superfluous. However, because circular orbits pose a unique problem the solution of which can be obtained, the following paragraphs are presented for this restricted problem. The discussions follow those of Ref. (3).

The total required velocity, ΔV, is the sum of the separate velocity additions ΔV_1 and ΔV_2, where ΔV_1 refers to the velocity addition necessary to obtain a Hohmann transfer back to the desired altitude, and where ΔV_2 is the velocity addition necessary to circularize the orbit having once reached the desired altitude. The total required velocity for a single two-impulse correction maneuver is just ΔV. The following sketch describes the geometry of these maneuvers.

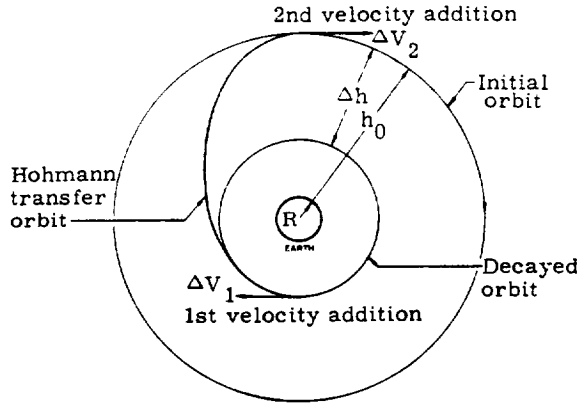

The separate velocity additions, ΔV_1 and ΔV_2, may be determined from the energy equation to be

$$\Delta V_1 = \sqrt{\mu \left(\frac{1}{R + h_0 - \Delta h} - \frac{1}{R + h_0 - \Delta h/2}\right)} - \sqrt{\mu \frac{1}{R + h_0 - \Delta h}} \qquad (161)$$

$$\Delta V_2 = \sqrt{\mu \frac{1}{R + h_0}} - \left[\mu \left(\frac{2}{R + h_0} - \frac{1}{R + h_0 - \Delta h/2}\right)\right]^{\frac{1}{2}} \quad (162)$$

The velocity addition available from a given engine is related to the propellant mass fraction, W_p/W_0, by the familiar rocket equation

$$\Delta V_i = I_{sp} g_0 \ln \frac{1}{1 - W_{pi}/W_{0i}} \quad (163)$$

or

$$\frac{W_{pi}}{W_{0i}} = 1 - e^{-\Delta V_i / I_{sp} g_0} \quad (164)$$

where ΔV_i is the ith total velocity addition and W_{pi} is the amount of propellant required for that particular velocity addition.

Since all the ΔV requirements are the same for each maneuver, it follows that

$$\frac{W_{p1}}{W_0} = \frac{W_{p2}}{W_0 - W_{p1}} = \frac{W_{p3}}{W_0 - W_{p1} - W_{p2}} = 1 - e^{-\Delta V / I_{sp} g_0} \quad (165)$$

where the subscripts 1, 2, 3, etc., denote successive corrective maneuvers. The total amount of propellant used after n maneuvers is then,

$$W_p = \sum_{i=1}^{n} W_{pi} \quad (166)$$

where,

$$W_{p1} = W_0 \left(1 - e^{-\Delta V / I_{sp} g_0}\right) \quad (167)$$

$$W_{p2} = (W_0 - W_{p1}) \left(1 - e^{-\Delta V / I_{sp} g_0}\right) \quad (168)$$

$$W_{pn} = \left\{\left(W_0 - W_{p1} - W_{p2} - \cdots - W_{pn-1}\right) \cdot \left[1 - \exp\left(\Delta V / I_{sp}\, g_0\right)\right]\right\} \quad (169)$$

The total time elapsed after n maneuvers is the summation of the increments of time between successive maneuvers, where it is recalled that the amount Δh has been lost in altitude from one maneuver to the next. This time may be found as follows:

$$dE_T = -\frac{\mu m}{2(R + h)^2}\, dh \quad (170)$$

(where E_T is the total energy of a satellite of mass m in a circular orbit at an altitude h.)

From the drag force D acting on the satellite.

$$dE_T = DV\, dt = \frac{1}{2} \rho V^3 C_D A\, dt \quad (171)$$

(if the atmospheric velocity is neglected).

Now combining Equations (170) and (171) with the expression for circular velocity, and approximating the atmospheric density, to make integration possible, by

$$\rho = \rho_0 e^{-\beta h} \quad (172)$$

yields

$$\frac{(W/C_D A)}{g_0 \rho_0 \sqrt{\mu R}} \int_{h_0}^{h_0 - \Delta h} e^{\beta h}\, dh = -\int_0^{\Delta T} dt \quad (L \ll R) \quad (173)$$

which after integrating and rearranging is the time interval between maneuvers

$$\Delta T = \frac{(W/C_D A)}{\beta g_0 \rho_0 \sqrt{\mu R}} e^{\beta h_0} \left(1 - e^{-\beta \Delta h}\right) + \pi \sqrt{\frac{\left[2(R + h) - \Delta h\right]^3}{\mu}} \quad (174)$$

where the corrective term is 1/2 of the period of the transfer orbit.

An appreciation of the validity of the density approximation may be seen in Chapter V. It is noted, however, that generally good agreement between the true density and that predicted can be obtained for an altitude range from 185 km to 370 km and from 370 km to 750 km using

$\rho_0 = 1.60 \times 10^{-10}$ slugs/ft^3 or 0.824×10^{-7} kg/m^3

$\beta = 7.21 \times 10^{-6}$ ft^{-1} or 23.7×10^{-6} m^{-1}

and

$\rho_0 = 1.92 \times 10^{-12}$ slugs/ft^3 or $.988 \times 10^{-9}$ kg/m^3

$\beta = 3.58 \times 10^{-6}$ ft^{-1} or 11.74×10^{-6} m^{-1}

respectively.

Now, denoting successive maneuvers by the subscripts 1, 2, 3, n, it follows that

$$\Delta T_n = \left\{\left(W_0 - W_{p1} - W_{p2} - \cdots - W_{pn-1}\right)\right.$$

(continued)

$$\cdot \left[\frac{e^{\beta h_0}(1 - e^{-\beta \Delta h})}{\beta C_D A g_0 \rho_0 \sqrt{\mu R}} \right] \Bigg\} + \pi \sqrt{\frac{[2(R + h) - \Delta h]^3}{\mu}} \qquad (175)$$

Thus the total time elapsed after n maneuvers is

$$T_s = \sum_{i=1}^{n} \Delta T_i \qquad (176)$$

Now if the corrective term for transfer time is neglected as being small compared to the total time, and the equation for T_s divided by the total amount of propellant used after n maneuvers, the series common to both equations (involving the weights) may be eliminated to arrive at the desired expression

$$T_s / \frac{W_0}{C_D A} = \frac{W_p}{W_0} \left[\frac{e^{\beta h_0}(1 - e^{-\beta \Delta h})}{\beta g_0 \rho_0 \sqrt{\mu R}\left(1 - e^{-\Delta V / I_{sp} g_0}\right)} \right] \qquad (177)$$

This relationship between the propellant mass fraction required to sustain a satellite a specified lifetime is explicitly independent of the number of impulse corrections, and like the continuous thrust method, shows a linear dependence of the propellant mass fraction, W_p/W_0, upon the sustained lifetime, T_s, for a given set of initial conditions. Figures 21 through 24 show the linear relationship as predicted by Eq (177) as a function of the ballistic coefficient for various $\Delta h/h_0$, and initial altitudes for a specific impulse of 300 sec.

One of the values on these curves is for the case where $\Delta h = 0$. This curve was obtained as follows.

$$F = \frac{1}{2} C_D A \rho V^2 = \dot{W} I_{sp}$$

$$W_p = \frac{1}{2} \frac{C_D A \rho V^2}{I_{sp}} T_s$$

$$\frac{T_s}{W_0 / C_D A} = \frac{2 W_p I_{sp}}{W_0 \rho V^2} = \frac{2 W_p}{W_0} \frac{I_{sp}(R + h)}{\rho \mu}$$

Although it will not be shown here, this is the same limit that would be obtained if Δh and the various maneuver increments (ΔV_i) were allowed to approach zero simultaneously in Eq 177 with the corrective term for time being neglected, (the corrective term must be neglected because the vehicle is never coasting back to the initial orbit; i.e., there is no Hohmann transfer). These figures show that the longest sustained lifetime per unit weight of propellant is obtained from the continuous thrust sustaining method. In the case of satellites utilizing the discrete velocity-addition sustaining method, longer lifetimes are realized (for a given propellant mass fraction) as the increment is decreased in altitude, Δh, the point below the desired altitude at which the first and successive corrective maneuvers are initiated.

Another interesting fact which may be observed by comparing the sustained and unsustained lifetimes is that the advantages of a sustained satellite over an unsustained satellite are greatest at the lower altitudes, where they are needed most.

G. DIFFERENTIAL CORRECTIONS IN ORBIT TRANSFER

The fundamental goal of space vehicle guidance is placing the vehicle at a certain point in space at a certain time, perhaps with a particular velocity. An approximate method of computing guidance commands to accomplish this objective is by differential corrections based on the ideal transfer profile. The sensed data, in the form of deviations from the ideal transfer orbit, are transformed into the desired vehicle velocity component corrections by a matrix of precomputed error sensitivities stored in the vehicle-borne computer.

The primary advantage of the differential correction technique is a simplification of guidance system input calculations performed aboard the vehicle. These calculations involve only matrix multiplication, which can be mechanized in a simple, lightweight vehicle-borne computer.

The technique is feasible wherever deviations from the desired transfer orbit and perturbations to Keplerian motion are reasonably small. Orbit deviations must be small to admit the use of a linear differential approximation. Also, if the deviations are small, the effect of small perturbations on both nominal and incorrect orbits is essentially the same, i.e., the deviation is independent of small perturbations. The orbit correction, being dependent only on the deviation, is thus independent of small perturbations.

The problem may be formulated in several ways (Refs. 4 and 5), depending on choice of coordinates and orbital elements. The formulation considered is that of Lawden (Ref. 4), the solution being obtained by a somewhat different mathematical approach. Let the center of coordinates be located at the center of the force field, the X-axis be the line of intersection of the ideal vehicle transfer orbit and the orbit plane of the target point, the Z-axis be normal to the target point orbit plane, and the Y-axis complete a right-hand system, as shown in the sketch.

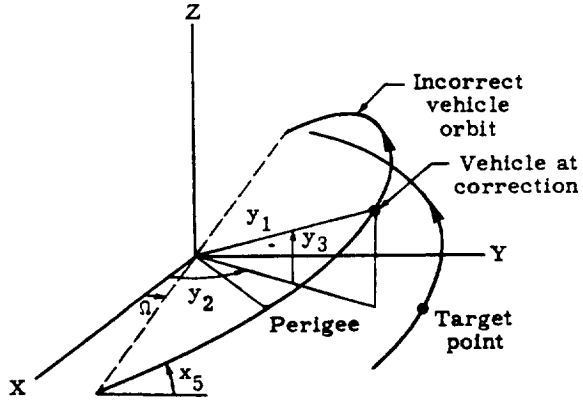

The following nomenclature will be used

x_0 Semimajor axis of the preselected transfer orbit

x_1 Eccentricity of the preselected transfer orbit

x_2 "Curly pi" or sum of the longitude of ascending node and argument of perigee of the transfer orbit

x_3 Eccentric anomaly of the vehicle position at the time of correction

x_4 Eccentric anomaly of the vehicle position in the transfer orbit at the time of rendezvous with the target point

x_5 Inclination of the preselected transfer orbit to the target point orbit plane

x_6 Sum of x_2 and the true anomaly of the vehicle at the time of correction

x_7 180° + longitude of the ascending node of the transfer orbit

x_8 Radius at the rendezvous point

x_9 Eccentric anomaly of the target point in its orbit at the time of rendezvous

y_1 Radius to the vehicle at the time of correction

y_2 Angle in the XY-plane from the X-axis to the projection on the XY-plane of the vehicle radius at the time of correction

y_3 Angle measured in a plane normal to the XY-plane from the XY-plane to the vehicle at the time of correction

y_4 Time between correction and rendezvous

u_1 Radial velocity component of the vehicle at the time of correction

u_2 Vehicle velocity component normal to u_1 and parallel to the XY-plane (at the time of correction)

u_3 Velocity component which completes a right-hand system with u_1 and u_2

v_i Velocity components of the vehicle in the transfer orbit at rendezvous (directions analogous to u_i)

w_i Target point velocity components at rendezvous

a_0 Semimajor axis of the target point orbit

e_0 Eccentricity of the target point orbit

E_0 Eccentric anomaly of the target point at the time of correction

$\tilde{\omega}_0$ Angle in the XY-plane from the X-axis to perigee of the target point orbit.

The problem may be stated as follows. At a certain preselected time, at which errors are to be determined and corrections executed, the vehicle position (y_1, y_2, y_3) is found to be in error relative to the preselected transfer by amounts dy_1, dy_2, dy_3. The velocity components at this point are in error by Δu_1, Δu_2, Δu_3. If the desired velocity at the incorrect point (the velocity to rendezvous $y_4 + dy_u$ later) is $u_i + du_i$, the correction to be applied is $du_i - \Delta u_i$, where the correction relative to the programmed velocity (du_1, du_2, du_3) is to be determined as a function of the dy's. If the velocity, as well as the position, the vehicle is to be matched to that of the target point, a second velocity correction, to be added to the programmed thrust at rendezvous, must be computed.

The required transformation matrix may be obtained by differentiation of the following functions, which describe the Keplerian motion of the vehicle and the target point.

$$
\begin{aligned}
\Phi_0 &= x_4 - x_3 - x_1 (\sin x_4 - \sin x_3) - \frac{y_4}{x_0}\sqrt{\frac{\mu}{x_0}} \\
\Phi_1 &= \tan\frac{x_6 - x_2}{2} - \sqrt{\frac{1+x_1}{1-x_1}}\tan\frac{x_3}{2} \\
\Phi_2 &= \tan\frac{x_7 - x_2}{2} - \sqrt{\frac{1+x_1}{1-x_1}}\tan\frac{x_4}{2} \\
\Phi_3 &= x_8 - x_0 (1 - x_1 \cos x_4) \\
\Phi_4 &= y_1 - x_0 (1 - x_1 \cos x_3) \\
\Phi_5 &= x_9 - E_0 - e_0 (\sin x_9 - \sin E_0) - \frac{y_4}{a_0}\sqrt{\frac{\mu}{a_0}} \\
\Phi_6 &= \tan\frac{x_7 - \tilde{\omega}_0}{2} - \sqrt{\frac{1+e_0}{1-e_0}}\tan\frac{x_9}{2} \\
\Phi_7 &= x_8 - a_0 (1 - e_0 \cos x_9) \\
\Phi_8 &= \tan (x_7 - y_2) - \tan (x_7 - x_6) \cos x_5 \\
\Phi_9 &= \sin y_3 - \sin (x_7 - x_6) \sin x_5 \\
U_1 &= u_1 - x_1 \sin (x_6 - x_2)\sqrt{\frac{\mu}{x_0 (1 - x_1^2)}} \\
U_2 &= u_2 - \frac{\cos x_5}{\cos y_3}\cdot\frac{\sqrt{\mu x_0 (1 - x_1^2)}}{y_1} \\
U_3 &= u_3 - \frac{\tan y_3}{\tan (x_6 - x_7)}\cdot\frac{\sqrt{\mu x_0 (1 - x_1^2)}}{y_1}
\end{aligned}
\qquad (178)
$$

The desired velocity components are $u_k + du_k$ where u_k are the programmed velocity components at correction and (in Einsteinian summation notation)

$$du_k = \frac{\partial u_k}{\partial y_m}\, dy_m, \quad k = 1, 2, 3; \; m = 1, 2, 3, 4. \tag{179}$$

The solution of the problem is then complete upon evaluation of the partial derivatives of this expression. These partials are obtained immediately from the Jacobian

$$\Delta = \begin{vmatrix} a_{ij} \\ u_{\ell j} \end{vmatrix} \begin{vmatrix} O \\ I \end{vmatrix}$$

where

$$a_{ij} = \frac{\partial \Phi_i}{\partial x_j} \qquad i, j = 0, 1, \ldots, 9$$

$$u_{\ell j} = \frac{\partial U_\ell}{\partial x_j} \qquad \ell = 1, 2, 3$$

$$O = [0]_3^{10}$$

$$I = [1]_3^3$$

The partial $\frac{\partial u_k}{\partial y_m}$ of Eq (179) is obtained by dividing the negative of the determinant Δ into the same determinant with the $(10 + k)^{th}$ column replaced by the column vector

$$\left\{ \frac{\partial \Phi_i}{\partial y_m}, \frac{\partial U_\ell}{\partial y_m} \right\}$$

For example,

$$\frac{\partial u_1}{\partial y_1} = -\frac{1}{\Delta} \begin{vmatrix} & \frac{\partial \Phi_0}{\partial y_1} & 0 & 0 \\ & \frac{\partial \Phi_1}{\partial y_1} & 0 & 0 \\ a_{ij} & \cdots & \cdots & \cdots \\ & \frac{\partial \Phi_9}{\partial y_1} & 0 & 0 \\ \hline & \frac{\partial U_1}{\partial y_1} & 0 & 0 \\ u_{\ell j} & \frac{\partial U_2}{\partial y_1} & 1 & 0 \\ & \frac{\partial U_3}{\partial y_1} & 0 & 1 \end{vmatrix}$$

This completes the solution for the components of the midcourse differential correction. The thirteenth order determinants (Δ and substituted Δ's) may be evaluated for a particular mission by a computer program and the resulting matrix

$$\left[\frac{\partial u_k}{\partial y_m} \right]$$

stored in the vehicle-borne computer memory.

However, for hand computations, the solution can be expressed in a more convenient form. This is possible because of the large number of zeros in the determinant Δ. Specifically,

$$|a_{ij}| = \begin{vmatrix} a_{00} & a_{01} & 0 & a_{03} & a_{04} & 0 & 0 & 0 & 0 & 0 \\ 0 & a_{11} & a_{12} & a_{13} & 0 & 0 & a_{16} & 0 & 0 & 0 \\ 0 & a_{21} & a_{22} & 0 & a_{24} & 0 & 0 & a_{27} & 0 & 0 \\ a_{30} & a_{31} & 0 & 0 & a_{34} & 0 & 0 & 0 & a_{38} & 0 \\ a_{40} & a_{41} & 0 & a_{43} & 0 & 0 & 0 & 0 & 0 & 0 \\ 0 & 0 & 0 & 0 & 0 & 0 & 0 & 0 & 0 & a_{59} \\ 0 & 0 & 0 & 0 & 0 & 0 & 0 & a_{67} & 0 & a_{69} \\ 0 & 0 & 0 & 0 & 0 & 0 & 0 & 0 & a_{78} & a_{79} \\ 0 & 0 & 0 & 0 & 0 & a_{85} & a_{86} & a_{87} & 0 & 0 \\ 0 & 0 & 0 & 0 & 0 & a_{95} & a_{96} & a_{97} & 0 & 0 \end{vmatrix} \tag{180}$$

which, by Laplace's development of the first five columns, reduces to

$$|a_{ij}| = a_{59}\, a_{67} (a_{85} a_{96} - a_{86} a_{95}) \begin{vmatrix} a_{00} & a_{01} & 0 & a_{03} & a_{04} \\ 0 & a_{11} & a_{12} & a_{13} & 0 \\ 0 & a_{21} & a_{22} & 0 & a_{24} \\ a_{30} & a_{31} & 0 & 0 & a_{34} \\ a_{40} & a_{41} & 0 & a_{43} & 0 \end{vmatrix}$$

where

$$a_{00} = \frac{3}{2}\sqrt{\mu}\, x_0^{-5/2}\, y_4$$

$$a_{01} = \sin x_3 - \sin x_4$$

$$a_{03} = -\frac{y_1}{x_0}$$

$$a_{04} = \frac{x_8}{x_0}$$

$$a_{11} = -\tan\frac{x_3}{2}\sqrt{\frac{1-x_1}{1+x_1}}\,\frac{1}{(1-x_1)^2}$$

$$a_{12} = -\frac{1}{2}\sec^2\frac{x_6 - x_2}{2}$$

$$a_{13} = -\frac{1}{2}\left[\sqrt{\frac{1-x_1}{1+x_1}}\sec^2\frac{x_6 - x_2}{2} + \sqrt{\frac{1+x_1}{1-x_1}}\right]$$

$$a_{21} = -\tan\frac{x_4}{2}\sqrt{\frac{1-x_1}{1+x_1}}\frac{1}{(1-x_1)^2}$$

$$a_{22} = -\frac{1}{2}\csc^2\frac{x_2}{2}$$

$$a_{24} = -\frac{1}{2}\sqrt{\frac{1+x_1}{1-x_1}}\sec^2\frac{x_4}{2}$$

$$a_{30} = -\frac{x_8}{x_0}$$

$$a_{31} = x_0 - x_8$$

$$a_{34} = -x_0 x_1 \sin x_4$$

$$a_{40} = -\frac{y_1}{x_0}$$

$$a_{41} = x_0 - y_1$$

$$a_{43} = -x_0 x_1 \sin x_3$$

$$a_{16} = \frac{1}{2}\sec^2\frac{x_6 - x_2}{2}$$

$$a_{27} = \frac{1}{2}\csc^2\frac{x_2}{2}$$

$$a_{38} = 1$$

$$a_{59} = \frac{x_8}{a_0}$$

$$a_{67} = \frac{1}{2}\csc^2\frac{\tilde{\omega}_0}{2}$$

$$a_{69} = -\frac{1}{2}\sqrt{\frac{1+e_0}{1-e_0}}\sec^2\frac{x_9}{2}$$

$$a_{78} = 1$$

$$a_{79} = -a_0 e_0 \sin x_9$$

$$a_{85} = -\tan x_6 \sin x_5$$

$$a_{86} = \sec^2 x_6 \cos x_5$$

$$a_{87} = \sec^2 y_2 - \sec^2 x_6 \cos x_5$$

$$a_{95} = -\sin x_6 \cos x_5$$

$$a_{96} = -\cos x_6 \sin x_5$$

$$a_{97} = -a_{96}$$

Also

$$\left[u_{\ell j}\right] = \begin{bmatrix} u_{10} & u_{11} & u_{12} & 0 & 0 & 0 & u_{16} & 0 & 0 & 0 \\ u_{20} & u_{21} & 0 & 0 & 0 & u_{25} & 0 & 0 & 0 & 0 \\ u_{30} & u_{31} & 0 & 0 & 0 & 0 & u_{36} & u_{37} & 0 & 0 \end{bmatrix}$$

where (181)

$$u_{10} = \frac{u_1}{2x_0}$$

$$u_{20} = -\frac{u_2}{2x_0}$$

$$u_{30} = -\frac{u_3}{2x_0}$$

$$u_{11} = -\frac{u_1}{x_1(1-x_1^2)}$$

$$u_{21} = \frac{u_2 x_1}{1 - x_1^2}$$

$$u_{31} = \frac{u_3 x_1}{1 - x_1^2}$$

$$u_{12} = -u_1 \cot(x_6 - x_2)$$

$$u_{25} = u_2 \tan x_5$$

$$u_{16} = u_{12}$$

$$u_{36} = u_3 \sec x_6 \csc x_6$$

$$u_{37} = -u_{36}$$

and

$$\left\{\frac{\partial\Phi_1}{\partial y_1}, \frac{\partial U_\ell}{\partial y_1}\right\} = \left\{0,0,0,0,1,0,0,0,0,0,0, \frac{u_2}{y_1}, \frac{u_3}{y_1}\right\}$$

$$\left\{\frac{\partial\Phi_1}{\partial y_2}, \frac{\partial U_\ell}{\partial y_2}\right\} = \{0,0,0,0,0,0,0,0, -\sec^2 y_2, 0,0,0,0\}$$

$$\left\{\frac{\partial\Phi_1}{\partial y_3}, \frac{\partial U_\ell}{\partial y_3}\right\} = \{0,0,0,0,0,0,0,0,0, \cos y_3, 0, -u_2 \tan y_3, -u_3 \sec y_3 \csc y_3\}$$

$$\left\{\frac{\partial \Phi_i}{\partial y_4} \quad \frac{\partial U_l}{\partial y_4}\right\} = \left\{-\frac{1}{x_0}\sqrt{\frac{\mu}{x_0}},\ 0,0,0,0,\right.$$

$$\left. -\frac{1}{a_0}\sqrt{\frac{\mu}{a_0}},\ 0,0,0,0,0,0,0\right\}$$

The determinant $|a_{ij}|$ is interesting in itself since the differentials in the transfer orbit geometry

$$dx_j = \frac{\partial x_j}{\partial y_i}\, dy_i \qquad (182)$$

are given by $|a_{ij}|$ in the same manner that the corrections in vehicle velocity are given directly by Δ. From $|a_{ij}|$, after simplification and factoring, the following error sensitivities are obtained.

$j = 0, \ldots, 4$	$J = 5, \ldots, 9$
$\frac{\partial x_j}{\partial y_1} = (-1)^{j+1}\ \frac{M_{4j}}{D}$	$\frac{\partial x_j}{\partial y_1} = 0\ ,\ j = 5, \ldots, 9$
$\frac{\partial x_j}{\partial y_2} = (-1)^{j+1}\ C_4\ \frac{M_{1j}}{D}$	$\frac{\partial x_5}{\partial y_2} = -k_1,\ \frac{\partial x_6}{\partial y_2} = k_2,\ \frac{\partial x_j}{\partial y_2} = 0,\ j = 7, 8, 9$
$\frac{\partial x_j}{\partial y_3} = (-1)^{j+1}\ C_5\ \frac{M_{1j}}{D}$	$\frac{\partial x_5}{\partial y_3} = \frac{k_2 k_3}{k_4}\ ,\ \frac{\partial x_6}{\partial y_3} = k_1 k_3 k_4,\ \frac{\partial x_j}{\partial x_3} = 0,\ j=7, 8, 9$
$\frac{\partial x_j}{\partial y_4} = (-1)^j \sum_{k=0}^{3} C_k\ \frac{M_{kj}}{D}$	$\frac{\partial x_5}{\partial y_4} = k_1 k_5,\ \frac{\partial x_6}{\partial y_4} = k_5 (1 - k_2),\ \frac{\partial x_7}{\partial y_4} = k_5,\ \frac{\partial x_8}{\partial y_4} = C_3,\ \frac{\partial x_9}{\partial y_4} = \frac{1}{x_8}\sqrt{\frac{\mu}{a_0}}$

(125)

where M_{ij} are the 4 x 4 minors of the determinant

$$D = \begin{vmatrix} d_{00} & d_{01} & 0 & d_{03} & d_{04} \\ 0 & d_{11} & -1 & d_{13} & 0 \\ 0 & d_{21} & -1 & 0 & d_{24} \\ d_{30} & d_{31} & 0 & 0 & d_{34} \\ d_{40} & d_{41} & 0 & d_{43} & 0 \end{vmatrix}$$

and

$$d_{00} = \frac{3y_4}{2x_0^2}\ \sqrt{\frac{\mu}{x_0}}$$

$$d_{01} = \frac{1}{x_1}\left(\frac{y_4}{x_0}\sqrt{\frac{\mu}{x_0}} + x_3 - x_4\right)$$

$$d_{03} = -\frac{y_1}{x_0}$$

$$d_{04} = \frac{x_8}{x_0}$$

$$d_{11} = \frac{1}{1 - x_1^2}\ \sin (x_6 - x_2)$$

$$d_{13} = -\left(\sqrt{\frac{1 - x_1}{1 + x_1}} + \frac{2x_1}{\sqrt{1 - x_1^2}}\ \cos^2 \frac{x_6 - x_2}{2}\right)$$

$$d_{21} = \frac{1}{1 - x_1^2}\ \sin x_2$$

$$d_{24} = -\left(\sqrt{\frac{1 - x_1}{1 + x_1}} + \frac{2x_1}{\sqrt{1 - x_1^2}}\ \sin^2 \frac{x_2}{2}\right)$$

$$d_{30} = -d_{04}$$

$$d_{31} = x_0 - x_8$$

$$d_{34} = -x_0 x_1 \sin x_4$$

$$d_{40} = d_{03}$$

$$d_{41} = x_0 - y_1$$

$$d_{43} = -x_0 x_1 \sin x_3$$

$$C_0 = \frac{1}{x_0}\sqrt{\frac{\mu}{x_0}}$$

$$C_1 = K_5 (1 - \cos x_5)$$

$$C_2 = -K_5$$

$$c_3 = \frac{1}{x_8}\sqrt{\mu\, a_0}\, e_0 \sin x_9$$

$$c_4 = \cos x_5$$

$$c_5 = k_1 k_3 k_4$$

$$k_1 = \frac{\sin x_5}{\tan x_6}$$

$$k_2 = \cos x_5$$

$$k_3 = \frac{\cos^2 y_2 \cos y_3}{\cos^2 x_6}$$

$$k_4 = \sin x_6$$

$$k_5 = \frac{1}{x_8}\sqrt{\frac{\mu}{a_0}}\left[\sqrt{\frac{1-e_0}{1+e_0}} + \frac{2\,e_0}{\sqrt{1-e_0^2}}\sin^2\frac{\tilde{\omega}_0}{2}\right]$$

The orbit to be achieved by the velocity correction is thus determined in terms of the data.

Special note is made at this point that further development of these determinants is possible resulting in a set of analytic expressions for the corrections. Some of these expressions, however, are very complex in form. For this reason, it is felt that the present form of the solution is most useful.

As an alternative to evaluation of the velocity corrections (du_k) from the 13 x 13 Δ determinants as previously outlined, the corrections may be determined as functions of the orbit element corrections since

$$du_k = \frac{\partial u_k}{\partial x_j}\,\frac{\partial x_j}{\partial y_i}\,dy_i \qquad (184)$$

where $\frac{\partial x_j}{\partial y_i}$ are given by Eq (183) and

$$\frac{\partial u_k}{\partial x_j} = -u_{kj}$$

from Eq (181).

If the velocity, as well as the position, of the vehicle is to be matched with that of the target point, the required correction to the programmed velocity increment at rendezvous may be determined as follows. The velocity components of the vehicle just before rendezvous are

$$v_1 = \sqrt{\frac{\mu}{x_0\,(1-x_1^2)}}\; x_1 \sin(x_7 - x_2)$$

$$v_2 = \frac{\sqrt{\mu\, x_0\,(1-x_1^2)}}{x_8}\cos x_5$$

$$v_3 = \frac{\sqrt{\mu\, x_0\,(1-x_1^2)}}{x_8}\sin x_5 \qquad (185)$$

The deviations of these components from those of the preselected transfer are given by

$$dv_i = \frac{\partial v_i}{\partial x_k}\,\frac{\partial x_k}{\partial y_j}\,dy_j \qquad (186)$$

where the $\frac{\partial x_k}{\partial y_j}$ are given by Eq (183) and the

$\frac{\partial v_i}{\partial x_k}$ are, from Eq (185)

$$\frac{\partial v_1}{\partial x_0} = -\frac{v_1}{2x_0}\;;\quad \frac{\partial v_1}{\partial x_1} = \frac{v_1}{x_1\,(1-x_1^2)}$$

$$\frac{\partial v_1}{\partial x_2} = v_1 \cot x_2\;;\quad \frac{\partial v_1}{\partial x_7} = -v_1 \cot x_2$$

$$\frac{\partial v_2}{\partial x_0} = \frac{v_2}{2x_0}\;;\quad \frac{\partial v_2}{\partial x_1} = -\frac{v_2\, x_1}{1-x_1^2}$$

$$\frac{\partial v_2}{\partial x_5} = -v_2 \tan x_5\;;\quad \frac{\partial v_2}{\partial x_8} = -\frac{v_2}{x_8}$$

$$\frac{\partial v_3}{\partial x_0} = \frac{v_3}{2x_0}\;;\quad \frac{\partial v_3}{\partial x_1} = -\frac{v_3\, x_1}{1-x_1^2}$$

$$\frac{\partial v_3}{\partial x_5} = v_3 \cot x_5\;;\quad \frac{\partial v_3}{\partial x_8} = -\frac{v_3}{x_8}$$

Similarly, from the velocity components of the target point at rendezvous,

$$w_1 = \sqrt{\frac{\mu}{a_0\,(1-e_0^2)}}\; e_0 \sin(x_7 - \tilde{\omega}_0)$$

$$w_2 = \frac{\sqrt{\mu\, a_0\,(1-e_0^2)}}{x_8}$$

$$w_3 = 0\,, \qquad (187)$$

the change in the desired rendezvous velocity from the programmed value is given by

$$dw_1 = w_1 \cot(x_7 - \tilde{\omega}_0)\, dx_7 = -w_1 \cot\tilde{\omega}_0 \frac{\partial x_7}{\partial y_4}\, dy_4$$

$$dw_2 = -\frac{w_2}{x_8}\, dx_8 = -\frac{w_2}{x_8}\,\frac{\partial x_8}{\partial y_4}\, dy_4 \qquad (188)$$

The partials are given by Eq (183). Then the required velocity correction to the stored velocity increment at rendezvous is

$$\Delta v_i = dv_i - dw_i$$

In the previous analyses dy_4 has been considered as an arbitrary increment in the time between correction and rendezvous. If the time of rendezvous is to be maintained at the programmed value, $dy_4 = 0$ and the computations and storage requirements are simplified. On the other hand, if some flexibility is acceptable, then the increment in time may be selected so as to minimize the energy requirement of the correction. Lawden (Ref. 4) gives the value of dy_4 which minimizes the propellant expenditure as

$$dy_4 = -\frac{\delta_3}{\delta_0}\sqrt{\frac{\delta_0\,\delta_2 - \delta_1^2}{\delta_0 - \delta_3^2}} - \frac{\delta_1}{\delta_0} \qquad (189)$$

where

$$\delta_0 = \left(\frac{\partial u_1}{\partial y_4}\right)^2 + \left(\frac{\partial u_2}{\partial y_4}\right)^2 + \left(\frac{\partial u_3}{\partial y_4}\right)^2$$

$$\delta_1 = \sum_{i=1}^{3} \frac{\partial u_i}{\partial y_4}\left(\frac{\partial u_i}{\partial y_1}\, dy_1 + \frac{\partial u_i}{\partial y_2}\, dy_2 + \frac{\partial u_i}{\partial y_3}\, dy_3 - \Delta u_i\right)$$

$$\delta_2 = \sum_{i=1}^{3}\left(\frac{\partial u_i}{\partial y_1}\, dy_1 + \frac{\partial u_i}{\partial y_2}\, dy_2 + \frac{\partial u_i}{\partial y_3}\, dy_3 - \Delta u_i\right)^2$$

$$\delta_3 = \frac{\partial v}{\partial y_4}$$

dy_1, dy_2, dy_3 = position component errors at correction

Δu_i = velocity component errors at correction

v = velocity increment at rendezvous

Many formulations of the differential correction technique are possible. Reference 5 presents rectangular coordinate routine. However, regardless of the form of the data, the approach presented is applicable. By modification of the Φ functions, transformation matrices for any adequate data system may be obtained.

This formulation has been checked for efficacy in several specific examples, one of which is transferred to a 24-hr orbit. The results of these checks indicated a very high degree of approximation in the commanded velocity corrections. In no case were the resultant position and velocity errors greater than 10% of the uncorrected value for errors in position less than 100,000 ft (or 30 km) or more than 3% for errors in initial velocity as large as 20 fps (or 6 mps). In fact the general order of the resultant errors was approximately 3% for errors in initial position in this range and 0.5 to 1% for errors in initial velocity less than 20 fps. The method is thus seen to be ideally suited to midcourse guidance problems and to the problem of small maneuvers.

H. THE STATISTICAL DISTRIBUTION OF THE ELEMENTS OF THE FINAL ORBIT (REF. 6)

Preceding discussions (for example Eqs 134 and 135) related the errors in the resultant orbit elements due to a combination of tracking and control errors. However, these relationships provide no insight as to the probability of occurrence of a given error. This additional information is obtained by relating the probability distributions of the total errors $\Delta a'$ and $\Delta e'$ to the distributions of the individual tracking and control errors. The development of these distributions will be based on the customary assumption that the individual errors (Δr_1, ΔV_1, etc.) are independently and normally distributed.

Since the forms of Eqs 134 and 135 are different, i.e., $\Delta a'$ is the sum of linear differentials and $\Delta e'$ is the square root of the sum of the squares of differential terms. The distribution of both forms will be derived. Consider

$$u = \sum_i a_i x_i, \qquad i = 1, 2, \ldots, k$$

where the a_i are constants and the x_i are independently and normally distributed with means μ_i and variance σ_i^2. Then the moment generating function m (t) for the distribution of the variate u is given as follows:

$$m(t) = \left(\frac{1}{2\pi}\right)^{\frac{k}{2}}\left(\prod_{i=1}^{K}\frac{1}{\sigma_i}\right)\int_{-\infty}^{\infty}\int_{-\infty}^{\infty}\cdots\int_{-\infty}^{\infty}\exp\left[t\sum_i a_i x_i - \frac{1}{2}\sum_i\left(\frac{x_i - \mu_i}{\sigma_i}\right)^2\right]\prod_{i=1}^{K} dx_i$$

where ϵ is the base of natural logarithms (utilized to differentiate from eccentricity).

Transformation to the standard form is convenient.

Now letting ϵ be the base of natural logarithms (to differentiate from eccentricity) and

$$y_i = \frac{x_i - \mu_i}{\sigma_i}$$

then

$$m(t) = \left(\frac{1}{2\pi}\right)^{\frac{k}{2}} \prod_{i=1}^{K} \int_{-\infty}^{\infty} \left(\epsilon^{t a_i \mu_i}\right)\left(\epsilon^{t a_i y_i \sigma_i}\right) \epsilon^{-\frac{1}{2} y_i^2} \, dy_i$$

$$= \left(\frac{1}{2\pi}\right)^{\frac{k}{2}} \prod_{i=1}^{K} \left[\epsilon^{t a_i \mu_i} \epsilon^{\frac{1}{2} t^2 a_i^2 \sigma_i^2}\right] \left[\int_{-\infty}^{\infty} \epsilon^{-\frac{1}{2}\left(y_i^2 - 2 t a_i y_i \sigma_i + t^2 a_i^2 \sigma_i^2\right)} dy_i\right]$$

$$= \epsilon^{\left[t \sum_i a_i \mu_i + \frac{t^2}{2} \sum_i a_i^2 \sigma_i^2\right]} \qquad (190)$$

However, the moment generating function for the normal distribution is

$$m_n(t) = \epsilon^{t\mu + \frac{1}{2} t^2 \sigma^2}$$

Therefore, Eq (190) is the moment generating function for a normal distribution with mean and variance given by

$$\mu = \sum_i a_i \mu_i \qquad (191)$$

$$\sigma^2 = \sum_i a_i^2 \sigma_i^2 \qquad (192)$$

In particular, application of this result to Eq (134) provides the distribution of the error $\Delta a'$. The error in semimajor axis of the corrected orbit is normally distributed with zero mean and variance

$$\sigma^2_{\Delta a'} = 4\sigma^2_{r_1} + 4\frac{r_0^2}{V_0^2}\left(\sigma^2_{\delta V_1} + \sigma^2_{\delta(\Delta V_1)} + \sigma^2_{\delta(\Delta V_2)}\right)$$

That is, the distribution of $\Delta a'$ is

$$f(\Delta a') = \left\{8\pi\left[\sigma^2_{r_1} + \frac{r_0^3}{\mu}\left(\sigma^2_{\delta V_1} + \sigma^2_{\delta(\Delta V_1)} + \sigma^2_{\delta(\Delta V_2)}\right)\right]\right\}^{-1} \epsilon^{-\frac{\Delta a^2 \sigma_{r_1}^2}{8}}$$

$$\epsilon^{-\frac{\Delta a^2 r_0^3}{8\mu}\left(\sigma^2_{\delta V_1} + \sigma^2_{\delta(\Delta V_1)} + \sigma^2_{\delta(\Delta V_2)}\right)}$$

The distribution of the eccentricity error is more difficult to obtain because Eq (135) is not linear. Equation (135) is of the form

$$u = \sqrt{x_1^2 + x_2^2}$$

where x_1 and x_2 are assumed normally and independently distributed, i.e.,

$$n(x_1, x_2) = \frac{1}{2\pi\sigma_{x_1}\sigma_{x_2}}\left[\epsilon^{-\frac{1}{2}\left(\frac{x_1}{\sigma_{x_1}}\right)^2} \epsilon^{-\frac{1}{2}\left(\frac{x_2}{\sigma_{x_2}}\right)^2}\right]$$

The distribution of u may be obtained by eliminating either x_1 or x_2 in terms of u to obtain a density

$$g(u, x_2) = \sum_i n\left[x_1(u, x_2), x_2\right]\left|\frac{\partial x_i}{\partial u}\right|_i$$

where each term in the summation represents one branch of a possibly nonmonotone function $u(x_1)$. The desired distribution, g(u), may then be obtained by integrating over the x_2 in g (u, x_2).

$$g(u) = \int_{-\infty}^{\infty} g(u, x_2)\, dx_2$$

In particular, for

$$u = \sqrt{x_1^2 + x_2^2}$$

$$x_1 = \pm\sqrt{u^2 - x_2^2}$$

$$\left|\frac{\partial x_1}{\partial u}\right| = \frac{u}{\sqrt{u^2 - x_2^2}}$$

Since the function g(u) is not single valued, it must be evaluated on each branch

$$g(u, x_2) = f(x_1^+)\left|\frac{\partial x_1^+}{\partial u}\right| + f(x_1^-)\left|\frac{\partial x_1^-}{\partial u}\right|$$

But

$$f(x_1^+) = f(x_1^-)$$

$$\left|\frac{\partial x_1^{+}}{\partial u}\right| = \left|\frac{\partial x_1^{-}}{\partial u}\right|$$

Thus

$$g(u, x_2) = 2 f(x_1) \left|\frac{\partial x_1}{\partial u}\right|$$

$$g(u, x_2) = 2\left[\frac{1}{2\pi \sigma_{x_1} \sigma_{x_2}} \epsilon^{-\frac{1}{2} \frac{u^2 - x_2^2}{\sigma_{x_1}^2}} \epsilon^{-\frac{1}{2}\frac{x_2^2}{\sigma_{x_2}^2}} \frac{u}{\sqrt{u^2 - x_2^2}}\right]$$

$$g(u) = \frac{u \epsilon^{-\frac{1}{2}\frac{u^2}{\sigma_{x_1}^2}}}{\pi \sigma_{x_1} \sigma_{x_2}} \int_{-\infty}^{\infty} \left\{ \frac{1}{\sqrt{u^2 - x_2^2}} \epsilon^{-\frac{1}{2}\left[x_2^2\left(\frac{1}{\sigma_{x_2}^2} - \frac{1}{\sigma_{x_1}^2}\right)\right]} dx_2 \right\}$$

After the transformation

$$t = x_2^2$$

this expression may be integrated to yield the required distribution

$$g(u) = \left\{\frac{u}{\sigma_{x_1} \sigma_{x_2}} \epsilon^{-\frac{u^2}{4}\left(\frac{1}{\sigma_{x_1}^2} + \frac{1}{\sigma_{x_2}^2}\right)} I_0\left[\frac{u^2}{4}\left(\frac{1}{\sigma_{x_2}^2} - \frac{1}{\sigma_{x_1}^2}\right)\right]\right\} \quad (193)$$

$$\left(0 < x_2^2 < u^2\right)$$

$$= 0, \; x_2^2 > u^2$$

This g(u) (and, in particular, the distribution of corrected orbit eccentricity error) is a skewed, single-sided distribution with positive mean and and a shape similar to that of the gamma distribution.

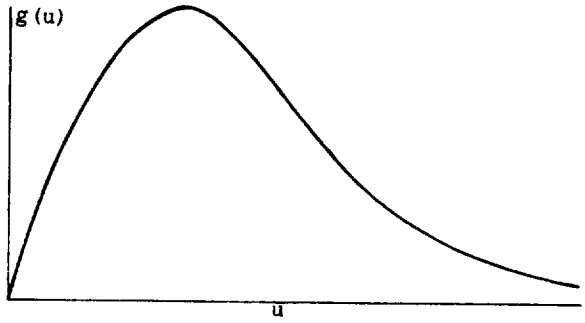

In manipulation of the distribution g(u) the following definitions are convenient.

$$K_1 \equiv \frac{1}{\sigma_{x_1} \sigma_{x_2}}$$

$$K_2 \equiv \frac{1}{4}\left(\frac{1}{\sigma_{x_1}^2} + \frac{1}{\sigma_{x_2}^2}\right)$$

$$K_3 \equiv \frac{1}{4}\left(\frac{1}{\sigma_{x_2}^2} - \frac{1}{\sigma_{x_1}^2}\right)$$

The distribution is then

$$g(u) \equiv K_1 u \epsilon^{-K_2 u^2} I_0(K_3 u^2)$$

This final form has been checked both analytically and numerically utilizing randomly selected variates from normal distributions. The results show excellent correlation.

Quantities of some significance in describing the properties of the distribution (e.g., central value, spread, skewness, etc.) are the moments of the distribution. The rth moment of g(u) is

$$\bar{\mu}_r = \int_0^{\infty} u^r g(u) \, du$$

$$= K_1 \int_0^{\infty} u^{r+1} \epsilon^{-K_2 u^2} I_0(K_3 u^2) \, du \quad (194)$$

After the transformation $t = u^2$, the integral can be evaluated in various forms.

$$\int_0^{\infty} t^n \epsilon^{-K_2 t} I_\nu(K_3 t) \, dt =$$

$$\left[\Gamma(n + \nu + 1)\left(K_2^2 - K_3^2\right)^{-\frac{1}{2}(n+1)} P_n^{-\nu}\left(\frac{K_2}{\sqrt{K_2^2 - K_3^2}}\right)\right] \quad K_2 > |K_3|$$

where the generalized Legendre function is given by

$$P_n^m(z) = \frac{1}{\Gamma(1-m)}\left(\frac{z+1}{z-1}\right)^{\frac{m}{2}} {}_2\mathcal{F}_1\left(-n,\ n+1;\ 1-m;\ \frac{1}{2}-\frac{1}{2}z\right)$$

and the hypergeometric series is given by

$${}_m\mathcal{F}_n\ (a_1, \ldots, a_m;\ \gamma_1, \ldots, \gamma_n;\ z) =$$

$$\sum_{i=0}^{\infty} \frac{(a_1)_i \ldots (a_m)_i}{(\gamma_1)_i \ldots (\gamma_n)_i} \frac{z^i}{i!}$$

Then

$$\bar{\mu}_r = \frac{K_1}{2} \frac{\Gamma\left(\frac{r}{2}+1\right)}{K_2^{\frac{r}{2}+1}} \mathcal{F}\left[\frac{r+2}{4}, \frac{r+4}{4}, 1; \left(\frac{K_3}{K_2}\right)^2\right]$$

$$= \frac{K_1}{2}\left\{\frac{\Gamma\left(\frac{r}{2}+1\right)}{K_2^{\frac{r}{2}+1}} \sum_{i=0}^{\infty} \frac{\left(\frac{r+2}{4};\ 1;\ i\right)\left(\frac{r+4}{4};\ 1;\ i\right)}{i!\ (1;\ 1;\ i)} \left(\frac{K_3}{K_2}\right)^{2i}\right\} \qquad (195)$$

In particular, the mean of the distribution g(u) is given by

$$\bar{\mu}_1 = \frac{K_1\,\Gamma(3/2)}{2\,K_3^{\frac{3}{2}}} \mathcal{F}\left[\frac{3}{4}, \frac{5}{4}, 1; \left(\frac{K_3}{K_2}\right)^2\right]$$

$$= \frac{K_1\sqrt{\pi}}{4\,K_2^{\frac{3}{2}}}\left[1 + \frac{\frac{3}{4}\cdot\frac{5}{4}}{1\cdot 1}\left(\frac{K_3}{K_2}\right)^2 + \frac{\frac{3}{4}\cdot\frac{7}{4}\cdot\frac{5}{4}\cdot\frac{9}{4}}{(2!)^2}\left(\frac{K_3}{K_2}\right)^4 + \frac{\frac{3}{4}\cdot\frac{7}{4}\cdot\frac{11}{4}\cdot\frac{5}{4}\cdot\frac{9}{4}\cdot\frac{13}{4}}{(3!)^2}\left(\frac{K_3}{K_2}\right)^6 + \ldots\right] \qquad (196)$$

The second moment is of interest in determination of the variance of g(u).

$$\bar{\mu}_2 = \frac{K_1}{2}\frac{\Gamma(2)}{K_2^2}\mathcal{F}\left[1, \frac{3}{2}, 1; \left(\frac{K_3}{K_2}\right)^2\right]$$

$$= \frac{K_1}{2\,K_2^2}\left[1 + \frac{3}{2}\left(\frac{K_3}{K_2}\right)^2 + \frac{1}{2!}\,\frac{3}{2}\cdot\frac{5}{2}\left(\frac{K_3}{K_2}\right)^4 + \frac{1}{3!}\cdot\frac{3}{2}\cdot\frac{5}{2}\cdot\frac{7}{2}\left(\frac{K_3}{K_2}\right)^6 + \ldots\right] \qquad (197)$$

Then the variance is

$$\sigma_u^2 = \bar{\mu}_2 - (\bar{\mu}_1)^2 \qquad (198)$$

Another factor of interest is the probability of occurrence of extreme values of u. Direct computation of areas under the distribution of Eq (193) is rather tedious. However, for large values of the variate u, the modified Bessel function of the first kind of order zero may be approximated by the following series.

$$I_0(x) \approx \frac{\epsilon^x}{\sqrt{2\pi x}}\left(1 + \frac{1^2}{1!\ 8x} + \frac{1^2\cdot 3^2}{2!\ (8x)^2} + \frac{1^2\cdot 3^2\cdot 5^2}{3!\ (8x)^3} + \ldots\right)$$

(x large)

If only the fundamental term of this series is retained, the distribution of Eq (193) becomes

$$g(u) \approx \sqrt{\frac{2}{\pi}}\ \frac{1}{\sqrt{\sigma_{x_1}^2 - \sigma_{x_2}^2}}\ \epsilon^{-\frac{u^2}{2}\frac{1}{\sigma_{x_1}^2}}$$

(u large) (199)

Thus, available tabulations of the normal density area

$$n(x) = \frac{1}{\sqrt{2\pi}}\int_x^{\infty} \epsilon^{-\frac{y^2}{2}}\,dy$$

can be used to evaluate probability of occurrence of extreme values of u with good accuracy.

I. TRANSFER TRAJECTORY OPTIMIZATION

1. Variational Approach

The problem of trajectory optimization has received attention in much of the literature referenced. However, the work of D. F. Lawden (Refs. 7, 8, 9) is felt to be particularly meritorious. For this reason, his work has been followed quite closely in this material which is included to provide insight into the general maneuver problem and the basis for the formulation of the differential correction routine discussed later.

The general problem of optimizing a maneuver trajectory with respect to the energy requirement may be expressed as: it is required that two points in space be connected by a curve along which the vehicle can be maneuvered with a minimum energy expenditure. Because aerodynamic, electromagnetic and other forces are extremely complex in nature, only thrust and gravity forces will be considered.

Consider the reference frame in the following sketch:

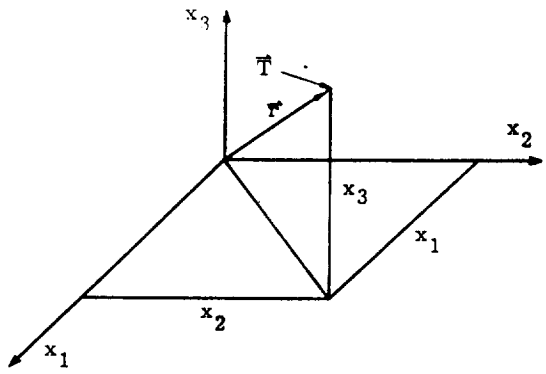

We have

$$m\,\ddot{\vec{r}} = \vec{T} + m\,\vec{g} = \vec{T} - \frac{m\mu}{r^2}\,\hat{r} \qquad (200)$$

where the symbol $\wedge$ denotes a unit vector.

If f_i (i = 1, 2, 3) denote the gravitation components along the three axes at the point (x_1, x_2, x_3) and the time is t we can assume the f_i are known functions of t, t_0, t_1, Λ_k, x_i (where t_0 is the time of departure, t_1 is the time of arrival and the Λ_k are parameters whose values change for different problems). Now we can form the following functions:

$$\phi_i = \dot{V}_i - \frac{T}{m}\,\ell_i - f_i = 0 \qquad (201)$$

$$\phi_{i+3} = \dot{x}_i - V_i = 0 \qquad (202)$$

where again

$$f_i = f_i\,(t, t_0, t_1, \Lambda_k, x_i) \qquad (203)$$

ℓ_i = the direction cosines of the thrust vector

i = 1, 2, 3.

Now noting that $T = c\beta$ (where β is the mass rate of change) and utilizing the cosine identity, we can form the following functions:

$$\phi_i = \dot{V}_i - \frac{c}{m}\,\beta\,\ell_i - f_i = 0 \qquad (204)$$

$$\phi_{i+3} = \dot{x}_i - V_i = 0 \qquad (205)$$

$$\phi_7 = \dot{m} + \beta = 0 \qquad (206)$$

$$\phi_8 = \sum_{i=1}^{3} \ell_i^{\,2} - 1 = 0 \qquad (207)$$

But β is positive and bounded ($\beta_1 \le \beta \le \beta_2$) to overcome problems arising from the fact that the ℓ_i are undefined when $\beta = 0$. However, we shall let $\beta_1 \to 0$ to allow for unpowered flight. β is assumed to be a monotonically increasing function of some parameter of no physical significance [$\alpha = \alpha\,(t)$] such that as α changes from $-\infty$ to ∞, β changes from β_1 to β_2. Thus, $\frac{d\beta}{d\alpha} = 0$ for some large value of $|\alpha|$. Conversely, the vanishing of $\frac{d\beta}{d\alpha}$ implies either maximum or minimum thrust (Ref. 10).

These eleven functions of t (x_i, V_i, ℓ_i, α and m) must be chosen in such a manner that the energy (or characteristic velocity of the maneuver) is minimized, subject to a particular set of boundary conditions.

Now the boundary conditions for the problem are x_{i0}, x_{if}, $\dot{x}_{i0}$ and $\dot{x}_{if}$. These conditions can be stated as

$$\xi_i = x_{i0} - d_i = 0 \qquad (208)$$

$$\xi_{i+3} = x_{if} - a_i = 0 \qquad (209)$$

$$\xi_{i+6} = V_{i0} - \dot{d}_i = 0 \qquad (210)$$

$$\xi_{i+9} = V_{if} - \dot{a}_i = 0 \qquad (211)$$

where the subscripts 0 and f indicate the initial and final values of x_i and $\dot{x}_i$, respectively, and the d and a denote the points of departure and arrival, respectively. If, in addition, the times of departure and the time of transfer are specified, two additional boundary conditions are

$$\xi_{13} = t_0 - T_0 = 0 \qquad (212)$$

$$\xi_{14} = t_f - T_f = 0 \tag{213}$$

Now we introduce 8 Lagrangian multipliers (λ_j) and form the fundamental function

$$F = \sum_{j=1}^{8} \lambda_j \phi_j \tag{214}$$

Using two sets of running indices (the summation convention) the Euler-Lagrange equations can now be written as:

$$\dot{\lambda}_i + \lambda_{i+3} = 0 \qquad (i, k = 1, 2, 3) \tag{215}$$

$$\dot{\lambda}_{i+3} + \lambda_k \frac{\partial f_k}{\partial x_i} = 0 \tag{216}$$

$$2\lambda_8 \ell_i - \frac{c\beta}{m} \lambda_i = 0 \tag{217}$$

$$\lambda_7 = 2 \frac{c\beta}{m} \lambda_i \ell_i \tag{218}$$

$$\frac{d\beta}{d\alpha} \left(\lambda_7 - \frac{c}{m} \lambda_i \ell_i\right) = 0 \tag{219}$$

It follows from these equations that the λ_i must satisfy

$$\ddot{\lambda}_i = \lambda_k \frac{\partial f_k}{\partial x_i} \tag{220}$$

and

$$\lambda_i = \frac{2m}{c\beta} \lambda_8 \ell_i \tag{221}$$

This latter equation states that the vector composed of the three components λ_i (mutually orthogonal and referred to by Lawden as the primer) is always parallel to the thrust direction except in those cases when $\beta = 0$ (i.e., no thrust).

It further follows from Eq (219) that

$$\frac{d\beta}{d\alpha} = 0 \tag{222}$$

or

$$\lambda_7 = \frac{c}{m} \lambda_i \ell_i \tag{223}$$

The first alternative implies that $\beta \to 0$ or $\beta = \beta_u$ or again that the thrust level is either zero or maximum. If $\beta = 0$ the vehicle coast in an orbit under the influence of gravity alone and λ_7 = constant, $\lambda_8 = 0$ and the ℓ_i are not defined. If $\beta = \beta_u$, the thrust is parallel to the primer as mentioned previously and

$$\lambda_8 = \frac{c\beta_\mu}{2m} \sqrt{\sum_{i=1}^{3} \lambda_i^2} \tag{224}$$

$$\dot{\lambda}_7 = \frac{c\beta_\mu}{m^2} \sqrt{\sum_{i=1}^{3} \lambda_i^2} \tag{225}$$

The second alternative in conjunction with Eq (218) yields

$$\dot{\lambda}_7 = \frac{\beta}{m} \lambda_7 \tag{226}$$

which upon integration gives

$$\lambda_7 = \frac{\text{constant}}{m} \tag{227}$$

However

$$\ell_i = \frac{\lambda_i}{\sqrt{\sum_{i=1}^{3} \lambda_i^2}} \tag{228}$$

therefore

$$\sum_{i=1}^{3} \lambda_i^2 = c \tag{229}$$

This equation states that the primer vector has a constant magnitude which is a contradiction to earlier proofs of Lawden (Ref 8). Therefore, this alternative is not possible, leaving the first alternative (Eq 222) as the only possibility.

Now since the $\dot{V}_i$, ℓ_i and β need only be piecewise continuous in the interval $t_0 \le t \le t_f$, the extremal arc may have corners. If such corners exist, the Weierstrass-Erdman corner conditions must be satisfied for the instants at which thrust is applied or terminated. This implies that the λ_j ($j = 1, 2, 3, 4, 5, 6, 7$) must be continuous at these times. But since $\dot{\lambda}_i = -\lambda_{i+3}$ ($i = 1, 2, 3$), the primer and its first derivative must be continuous. Now the corner condition must be satisfied:

$$\left(F - V_i \frac{\partial F}{\partial V_i}\right)_+ = \left(F - V_i \frac{\partial F}{\partial V_i}\right)_- \tag{230}$$

This equation requires that the following function be continuous

$$-\lambda_i \left(\frac{c\beta}{m} \ell_i + f_i\right) - \lambda_{i+3} V_i + \lambda_7 \beta$$

which in turn requires that

$$\frac{c\beta}{m} \lambda_i \ell_I - \lambda_7 \beta$$

be continuous since f_i and V_i are by definition continuous, and since the λ_i were shown to be continuous for this class of problems (Eq 91). This function is shown to be continuous in Ref 7. Further it is shown that

$$\lambda_i f_i - \dot{\lambda}_i V_i + \beta \left(\frac{c}{m} \lambda_i \ell_i - \lambda_7\right) = \text{constant}$$

where the constant takes on the same value for the entire minimum energy trajectory.

We now form another function, H, from the constraints (Eqs 208 through 213) and the expression for the characteristic velocity of the maneuver.

$$H = c \log \frac{M_0}{M_1} + \eta_i (x_{i0} - d_i) + \eta_{i+3} (x_{i1} - a_i)$$

$$+ \eta_{i+6} (V_{i0} - \dot{d}_i) + \eta_{i+9} (V_{i1} - \dot{a}_i)$$

$$+ \eta_{13} (t_0 - T_0) + \eta_{14} (t_1 - T_1) \qquad (231)$$

At this point it is noted that if the time of transfer and the time of initiation constraints are removed, η_{13} and η_{14} are zero.

Now, from the generalized problem of Mayer, the necessary conditions for the minimization of H can be evaluated

$$\eta_i - \lambda_{i+3,\,0} = 0 \qquad (232)$$

$$\eta_{i+6} - \lambda_{i,\,0} = 0 \qquad (233)$$

$$\eta_{i+3} + \lambda_{i+3,\,f} = 0 \qquad (234)$$

$$\eta_{i+9} + \lambda_{i,\,f} = 0 \qquad (235)$$

$$\frac{c}{M_0} - \lambda_{7,\,0} = 0 \qquad (236)$$

$$-\frac{c}{M_f} + \lambda_{7,\,f} = 0 \qquad (237)$$

$$\int_{t_0}^{t_f} \lambda_i \frac{\partial f_i}{\partial \Lambda_k} \, dt = 0 \qquad (238)$$

$$\eta_{13} + \eta_i \dot{x}_{i0} + \eta_{i+6} \dot{V}_{i0} + \frac{c}{M_0} \dot{M}_0 - \int_{t_0}^{t_f} \lambda_i \frac{\partial f_i}{\partial t_0} \, dt = 0 \qquad (239)$$

$$\eta_{14} + \eta_{i+3} \dot{x}_{if} + \eta_{i+9} \dot{V}_{if} + \frac{c}{M_f} \dot{M}_f - \int_{t_0}^{t_f} \lambda_i \frac{\partial f_i}{\partial t_f} \, dt = 0 \qquad (240)$$

where the subscripts 0 and f refer to the initial and final times for the orbital transfer. If the time restraints are removed (to find the minimum energy trajectory), η_{13} and η_{14} are zero and η_i and η_{i+6} can be eliminated from Eq (239) and η_{i+3} and η_{i+9} can be eliminated from Eq (111) yielding

$$\lambda_i \dot{V}_i - \dot{\lambda}_i V_i - \frac{c}{M_0} \dot{M}_0 = \int_{t_0}^{t_f} \lambda_i \frac{\partial f_i}{\partial t_0} \, dt \qquad (241)$$

$$\lambda_i \dot{V}_i - \dot{\lambda}_i V_i - \frac{c}{M_f} \dot{M}_f = \int_{t_0}^{t_f} \lambda_i \frac{\partial f_i}{\partial t_f} \, dt \qquad (242)$$

The conditions of Eq 232 to Eq 242 must necessarily be satisfied if the external arc is to be optimum with respect to the energy requirement. As is evident from the complexity of these expressions, exact solutions are not easily come by, and general solutions to the optimum transfer problem appear doomed. In fact, numerical evaluation is generally necessary. This conclusion is strengthened when it is noted that the absolute minimum energy maneuver is not the only solution satisfying these conditions. Thus, it is generally necessary to investigate each of the resulting "optimum" solutions. However, several conclusions can be drawn from this work and that reported in Ref. 11.

(1) The optimum trajectory is composed of maximum thrust arcs and coasting arcs.

(2) There are in general only 3 sub arcs in the trajectory, 2 of which are thrust arcs.

(3) The thrust arcs generally occur at the two terminals.

To aid in the visualization of the transfer problem and provide information which is of value in the analysis of trajectory problems, the general problem will be reduced to one of pulse transfer. This assumption is valid for most maneuvers since the magnitude of the correction (ΔV) and the time of burning (t_b) are generally small compared to V_0 or V_1 and the time of transfer, respectively. Under this assumption the optimum trajectory connects the two specified radii with impulses at either end.

Variations in all of the parameters during thrust periods are assumed small. This infers that since the primer vector and its derivatives are continuous during initiation and termination of a thrust phase, they are continuous across any null thrust arc. Thus, Eq 225 reduces to

$$\Delta \lambda_7 = \Delta \frac{c}{M} \sqrt{\sum_{i=1}^{3} \lambda_i^2} \qquad (243)$$

By considering the equations for λ_7 it can be shown that Eq 223 implies that

$$\sqrt{\sum_{i=1}^{3} \lambda_i^2} = 1 \qquad (244)$$

at the beginning of the maneuver.

Now, since the λ_i are the direction ratios for the thrust vector, this equation states that, for the pulse case, they are equal to the direction cosines of the impulse. The other constraints are

$$\lambda_i \dot{V}_i = \frac{c}{M} \beta + \lambda_i f_i \qquad (245)$$

$$\lambda_i f_i - \dot{\lambda}_i V_i = \int_{t_0}^{t_f} \lambda_i \frac{\partial f_i}{\partial t_0} \, dt \qquad (246)$$

$$\lambda_i f_i - \dot{\lambda}_i V_i = -\int_{t_0}^{t_f} \lambda_i \frac{\partial f_i}{\partial f_f} \, dt \qquad (247)$$

$$\lambda_i f_i - \dot{\lambda}_i V_i = \text{constant} \qquad (248)$$

where t_0 and t_f are not specified, and the constant of Eq 248 is zero if the f_i components are time invariant and independent of t_0 and t_1.

Investigations of these equations are reported in Ref. 7 for motion in Keplerian orbits. Therefore, it is not deemed necessary to repeat this material. Rather, conclusions pertaining to these investigations will be presented for the case of transfer between elliptic orbits.

(1) If the orbits intersect, a single impulse can be used to effect the maneuver, and the conditions for optimum transfer are satisfied. However, in some cases this type of transfer is not the absolute minimum energy maneuver (i.e., minimum of the minimum energy maneuvers). For this reason it is necessary to check the energy requirements of each solution satisfying the conditions for minimum energy maneuvers.

(2) If the orbits do not intersect, two impulses are generally required (one at each terminal) to effect the maneuver. This conclusion must be modified in certain classes of transfers as is indicated in the analysis of 3 impulse transfers.

(3) If the eccentricities of the two orbits go to zero, the optimum mode of transfer is via the well known Hohmann ellipse which is tangent at perigee to one circular orbit and tangent at apogee to the other. This conclusion is also modified for certain orbits for 3 impulse-transfers.

(4) If the eccentricities of the two orbits are small, the line of apsides of the minimum energy transfer ellipse aligns itself in the approximate direction of the line of apsides of the terminal ellipse (initial or final) having the greater eccentricity.

(5) If the two terminal ellipses are not coplanar, little in the way of a general conclusion can be made. If, however, the eccentricities of both the initial and final orbits are small, the optimum maneuver occurs when the transfer orbit is tangent to the respective orbits at the points of departure and arrival and when the line of apsides of the transfer orbit is the line of intersection of the two orbital planes.

Utilizing the second of these "general rules" numerical data may be generated relating the parameters of the "optimum" transfer orbit. However, because of the number of variables involved, parametric studies generally prove extremely lengthy in all but the most simple cases. Among these simple cases is the analysis of transfer between circular orbits. For this reason and for the reason that many satellite applications require circular orbits, certain of the parameters will be discussed in the following paragraphs.

Consider the following sketches depicting coplanar and noncoplanar transfer.

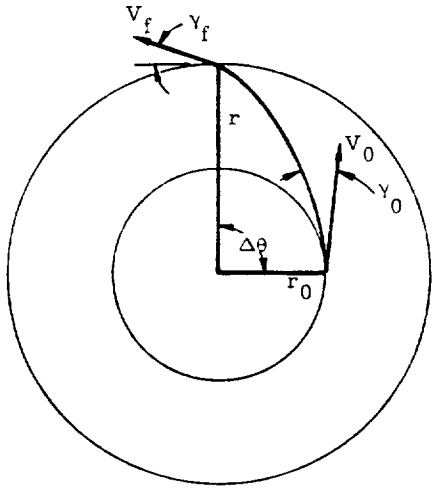

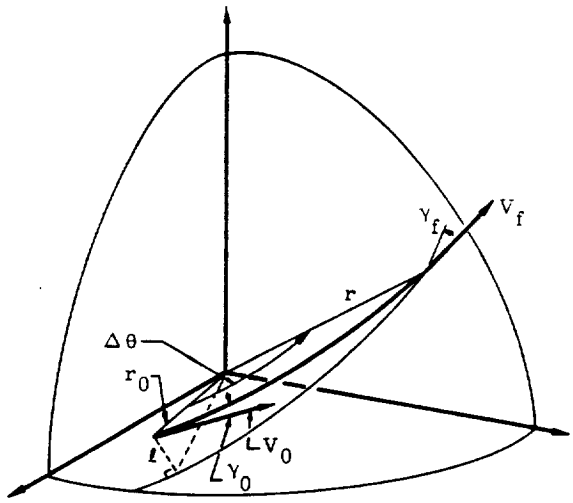

The first of these sketches (showing transfer between circular coplanar orbits) points up the fact that the maneuver required must change both the magnitude and the direction of the velocity in the plane of transfer (both of the effects have been discussed earlier). Thus, it is desired to show what types of orbits will be required to minimize ΔV_{total} for various types of transfer. The equation for this maneuver are:

$$\frac{\Delta V_T}{V_{c1}} = \sqrt{1 + \left(\frac{V_0}{V_{c1}}\right)^2 - 2\,\frac{V_0}{V_{c1}}\cos\gamma} + \sqrt{\frac{r_0}{r_f}}\sqrt{1 + \left(\frac{V_f}{V_{c2}}\right)^2 - 2\,\frac{V_f}{V_{c2}}\cos\gamma_2}$$

$$\tan \gamma_0 = \left[\frac{1 - \frac{r_0}{2a}}{\tan \frac{\Delta\theta}{2}} - \frac{\sqrt{\left(1 - \frac{r_0}{2a}\right) \frac{r_0}{r} - \frac{r_0}{2a}\left(1 - \frac{r_0}{2a}\cos^2 \frac{\Delta\theta}{2}\right)}}{\sin \frac{\Delta\theta}{2}} \right]$$

$$\tan \gamma_f = \left[- \frac{1 - \frac{r_f}{2a}}{\tan \frac{\Delta\theta}{2}} + \frac{\sqrt{\left(1 - \frac{r}{2a}\right) \frac{r}{r_0} - \frac{r}{2a}\left(1 - \frac{r}{2a}\cos^2 \frac{\Delta\theta}{2}\right)}}{\sin \frac{\Delta\theta}{2}} \right]$$

$$\frac{V}{V_c} = \frac{\sqrt{\left(\frac{2}{r} - \frac{1}{a}\right)}}{\sqrt{\frac{1}{r}}} = \sqrt{2 - \frac{r}{a}}$$

Thus, if r_f, r_0, r_f and $\Delta\theta$ are specified, the quantity a which will require the smallest value of ΔV_T can be determined. This was done numerically in Ref 12. The results of these computations are presented in Figs. 25, 26 and 27.

The second sketch shows the nonplanar transfer between circular orbits. The equations for this maneuver can be obtained in a simple form if the second impulse alone is responsible for altering the plane of motion. This assumption will not always yield a true minimum energy transfer; however, more rigorous attention to detail leads to a very complex form of solution, thus making such an approach less suited to parametric analyses of this nature.

$$\frac{V_0}{V_{c1}} = \sqrt{\frac{2}{\frac{r}{r_0} - \frac{\cos(\Delta\theta - \gamma_f)}{\cos \gamma_f}}} \cdot \frac{\sin \frac{\Delta\theta}{2}}{\cos \gamma_f}$$

$$\frac{\Delta V_1}{V_{c1}} = \sqrt{2 - \frac{2 - \left(\frac{V_0}{V_{c1}}\right)^2}{\frac{r}{r_0}}}$$

$$\frac{\Delta V_2}{V_{c1}} = \left\{ \left[\sin \Delta\theta - 2\left(\frac{V_0}{V_{c1}}\right) \cos \gamma_f \right. \right.$$

$$(\sin^2 \Delta\theta - \sin^2 \ell\ )^{1/2}$$

$$\left. + \left(\frac{V_0}{V_{c1}}\right)^2 \sin \Delta\theta \right] \left[\left(\frac{r}{r_0}\right) \right.$$

$$\left. \left. \cdot \sin \Delta\theta \right]^{-1} \right\}^{1/2}$$

$$\frac{\Delta V_T}{V_{c1}} = \frac{\Delta V_1 + \Delta V_2}{V_{c1}}$$

These equations have also been solved numerically to yield the smallest values of ΔV_T. The results of these studies are shown in Figs. 28, 29 and 30.

As was noted in the discussion of the optimum trajectories, and again in the previous paragraph, these solutions may not in general be the minimum energy transfers. However, in all cases, this solution will belong to the set of relative minima.

2. Minimum Energy Transfers

The preceding discussions present the variational formulation of the general maneuver optimization procedure along with several conclusions derivable therefrom. The solution, while rigorous, does not provide data which would be of general interest due to the fact that a lengthy numerical evaluation is necessary to evaluate each optimum solution. This being the case, numerical data for the special case of transfer between circular orbits was also presented. However, two questions arise in regard to the application of the "rules" for approximate maneuver optimization. These questions are:

(1) Under what condition is the two-pulse transfer between circular orbits minimum energy?

(2) What is the minimum energy two-impulse transfer between circular and elliptic orbits?

To answer the first of these questions consider the three-impulse maneuver.

a. Three-pulse transfers between circular orbits

Some of the orbits which have been proposed for various satellite missions require large amounts of energy for the ascent and injection maneuvers because of their extreme altitudes. Thus the three-impulse maneuver philosophy can be divided into three classes:

$$r_2 \geq r_3 > r_1$$

$$r_3 \geq r_2 \geq r_1$$

$$r_3 > r_1 \geq r_2$$

where

r_1 = radius of the initial circular orbit

r_2 = apogee radius of the first transfer orbit (the intermediate radius)

r_3 = radius of the final circular orbit.

The transfers have all been assumed to be of the 180° type since any other transfer would require more energy, and since the primary purpose of this material is to show the existence of three impulse optimum solutions.

Case No. 1 $(r_2 > r_3 > r_1)$

The velocity increment required for this case is defined by the difference in the circular velocity and the perigee velocity for the first transfer orbit, plus the difference in the apogee velocity in the first and second transfer orbits, plus the difference in the perigee velocity in the second transfer orbit and the circular velocity in the desired orbit; i.e.,

$$\Delta V_t = |\Delta V_1| + |\Delta V_2| + |\Delta V_3|$$

$$= (V_{p1} - V_{c1}) + (V_{a2} - V_{a1}) + (V_{p2} - V_{c3})$$

$$\frac{\Delta V_t}{V_{c1}} = \left[\sqrt{\frac{2r_2}{r_2 + r_1}} - 1\right] + \frac{V_{c2}}{V_{c1}}\left[\sqrt{\frac{2r_3}{r_2 + r_3}} - \sqrt{\frac{2r_1}{r_2 + r_1}}\right] + \frac{V_{c3}}{V_{c1}}\left[\sqrt{\frac{2r_2}{r_2 + r_3}} - 1\right]$$

This equation is presented graphically in Fig. 31. The dashed curve denotes the Hohmann transfer. Curves for all r_3/r_1 originate at this single curve since it is, in essence, the limit of the family (i.e., $r_1 = r_3$). The investigation must now be turned to the problem of determining whether or not any of the curves of this family eventually diminish by an amount sufficient to result in a value of $\frac{\Delta V_t}{V_{c1}}$ less than that of the Hohmann transfer; (data for this type of transfer are presented as Fig. 32).

This has been accomplished in Ref. 13, where the equation for $\frac{\Delta V_t}{V_{c1}}$ is differentiated with respect to r_2/r_1 and the resultant equated to zero. The complete solution thus found is:

$$\frac{r_2}{r_1} = \frac{3 + \frac{r_1}{r_3}}{3\left(1 + \frac{r_1}{r_3}\right) - 2\sqrt{3 - \frac{2r_1}{r_3}}}$$

Now by using the constraint $\frac{r_2}{r_1} \geq \frac{r_3}{r_1} > 1$, which is a restatement of the condition assumed in formulating this case, the value of, $\frac{r_3}{r_1}$, i.e., $\frac{r_3^*}{r_1}$ for which the three-pulse approach is more efficient is obtained as 15.582 approximately.

For all $\frac{r_3}{r_1} \geq \frac{r_3^*}{r_1}$, the curves possess no relative maxima or minima and the curves continually decrease. Therefore, the three-pulse method is always more efficient than the Hohmann transfer. If $11.939 < \frac{r_3}{r_1} < \frac{r_3^*}{r_1}$, the solution for those values of $\frac{r_3}{r_1}$ for which $\frac{\Delta V_t}{V_{c1}}$ is less than that for the Hohmann transfer can also be found. However, this value of $\frac{r_3}{r_1}$ is a function of the altitude of the intermediate point which must be placed above a critical altitude greater than the altitude of either of the circular orbits and approaching infinity as $\frac{r_3}{r_1}$ approaches 11.939. If $\frac{r_3}{r_1} < 11.939$, the Hohmann two-pulse transfer is always the more economical approach.

Case No. 2 $(r_3 \geq r_2 \geq r_1)$

The velocity increment required for this case is defined by the difference in circular velocity at the first altitude and the perigee velocity of the first transfer orbit, plus the difference in the apogee velocity of the first transfer orbit and the perigee velocity of the second, plus the difference in the apogee velocity of the second transfer orbit and the circular velocity of the second circular orbit.

$$\frac{\Delta V_t}{V_{c1}} = \left[\sqrt{\frac{2r_2}{r_1 + r_2}} - 1\right] + \frac{V_{c1}}{V_{c2}}\left[\sqrt{\frac{2r_3}{r_2 + r_3}} - \sqrt{\frac{2r_1}{r_1 + r_2}}\right] + \frac{V_{c3}}{V_{c1}}\left[1 - \sqrt{\frac{2r_2}{r_3 + r_2}}\right]$$

When this equation is differentiated with respect to the radius ratio $\frac{r_2}{r_1}$, it can once again be shown that the quantity $\frac{\Delta V_t}{V_{c1}}$ is a single zero derivative which for this case corresponds to a maximum. Further it can be shown that the end points of the curve correspond to the energy requirement for the Hohmann transfer; therefore, this mode of transfer is always less economical than the Hohmann transfer.

Case No. 3 $(r_3 > r_1 \geq r_2)$

The velocity increment required for this case is defined by the difference in the circular velocity of the first orbit and the apogee velocity of the first transfer orbit, plus the difference in the perigee velocity in the second and first transfer orbits, plus the difference in the circular velocity in the final orbit and the apogee velocity of the second transfer orbit; i.e.,

$$\frac{\Delta V_t}{V_{c1}} = \left[1 - \sqrt{\frac{2r_2}{r_1+r_2}}\right] + \frac{V_{c2}}{V_{c1}}\left[\sqrt{\frac{2r_3}{r_3+r_2}} - \sqrt{\frac{2r_1}{r_1+r_2}}\right] + \frac{V_{c3}}{V_{c1}}\left[1 - \sqrt{\frac{2r_2}{r_3+r_2}}\right]$$

The curves obtained from this equation increase for all $r_2 < r_1$ and have no maximum value. Thus, this approach can never be as efficient as the Hohmann transfer.

b. The two-pulse transfer between coplanar, circular and elliptic orbits

This problem has been formulated in Refs. 14, 15 and 16 and, therefore, will only be summarized in this presentation. Detailed proofs of each step in the formulation are left to the reader.

The problem is that of transferring from one terminal (defined by a scalar distance and a velocity vector) to another. If V_{n1} and V_{r1} are the normal and radial components of velocity at the first position and V_{n2} and V_{r2} the components at the second point, the total velocity pulse required for the transfer (assuming two pulses) is

$$\Delta V = \sqrt{(V_{no} - V_{n1})^2 + (V_{ro} - V_{r1})^2} + \sqrt{(V_{nx} - V_{n2})^2 + (V_{rx} - V_{r2})^2}$$

where

V_{ro}, V_{no} denote velocity components following first pulse (that is, at burnout)

V_{rx}, V_{nx} denote velocity components just prior to second pulse.

Now assuming a conservative field, this equation can be reduced to nondimensional form by using the conservation of angular momentum

$$\frac{\Delta V}{V_{c1}} = \sqrt{\left(\frac{V_{no}}{V_{c1}} - \frac{V_{n1}}{V_{c1}}\right)^2 + \left(\frac{V_{ro}}{V_{c1}} - \frac{V_{r1}}{V_{c1}}\right)^2} + \sqrt{\left(\frac{r_1}{r_2}\frac{V_{no}}{V_{c1}} - \frac{V_{n2}}{V_{c1}}\right)^2 + \left(\frac{V_{rx}}{V_{c1}} - \frac{V_{r2}}{V_{c1}}\right)^2}$$

where

V_{c1} = circular speed at the distance r_1

r_1, r_2 = radial distances for the two terminals.

The problem is now to minimize this quantity under the constraint that the radial velocities are always real, i.e.,

$$\left(1 - \frac{r_1^2}{r_2^2}\right)\left(\frac{V_{no}}{V_{c1}}\right)^2 + \left(\frac{V_{ro}}{V_{c1}}\right)^2 + \left(\frac{r_1}{r_2} - 1\right) \geq 0$$

(This is a restatement of the conservation of total energy)

where

$$0 < \frac{r_1}{r_2} < 1.$$

This minimization is accomplished as follows since in the region of interest the function is differentiable.

$$\frac{\partial\left(\frac{\Delta V}{V_{c1}}\right)}{\partial\left(\frac{V_{ro}}{V_{c1}}\right)} = \frac{\partial\left(\frac{\Delta V}{V_{c1}}\right)}{\partial\left(\frac{V_{no}}{V_{c1}}\right)} = 0$$

Justification for this step is shown in Ref. 15 when the function $\frac{\Delta V}{V_{c1}}$ is shown to have a relative minimum interior to the limits which $\frac{V_{rx}}{V_{c1}}$ can assume, $\left(\text{i.e., } 0 < \frac{V_{rx}}{V_{c1}} < \frac{V_{r2}}{V_{c1}}\right)$. Performing this differentiation and simplifying the resultant equations leads to the conclusion that $\left(\frac{\Delta V}{V_{c1}}\right)_{\min}$ must be compatible with one of the following equations

$$\frac{r_1}{r_2}\frac{V_{no}}{V_{c1}} = \frac{V_{n2}}{V_{c1}}\frac{V_{rx}}{V_{r2}} \pm \left(\frac{V_{rx}}{V_{r2}} - 1\right)\sqrt{\frac{2r_2}{r_2+r_1}}.$$

After combining terms and using the equations for the partial derivatives obtained previously, four pairs of expressions are obtained

$$\frac{V_{rx} - V_{r2}}{V_{nx} - V_{n2}} = \frac{V_{r2}}{V_{n2} \pm \sqrt{\left(\frac{\mu}{r_1}\right)\frac{2r_2}{r_1+r_2}}}$$

$$\frac{V_{ro} - V_{r1}}{V_{no} - V_{n1}} = \frac{V_{r1}}{V_{n1} \pm \frac{r_1}{r_2}\sqrt{\left(\frac{\mu}{r_1}\right)\frac{2r_2}{r_1+r_2}}}$$

When these four equations are divided into two sets both with positive (or negative) radicals and solved for the values of $\frac{V_{no}}{V_{c1}}$ and $\frac{V_{ro}}{V_{c1}}$, four independent solutions are obtained (two for each quadratic equation). The smallest of the four solutions is then the minimum energy (two-pulse) maneuver between the two terminals. This is the basic approach and the solution to the problem first formulated in Ref. 14. In general, it is not possible to select the correct solution analytically; however, in particular cases this selection is possible.

Investigation of these equations is now directed toward the definition of the type of transfer which is most efficient. First, it is obvious that unless the relative radial velocity approaches zero at a given terminal, the condition defined is not one of tangential transfer from the circular orbit or arrival at apogee or perigee in the elliptic orbit. Additional investigations reveal that for nonintersecting circular and elliptic orbits, the optimum path is tangent to the circular orbit but is not, in general, tangent to the elliptic orbit. This fact is illustrated in the following sketch. Numerical studies of the parameters of the optimum path must, of course, be deferred until such time as the orbits in question are completely specified.

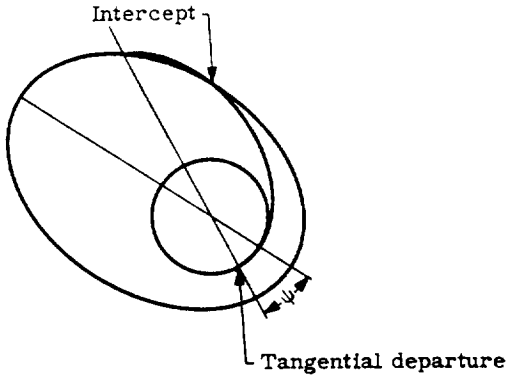

J. THE EFFECTS OF FINITE BURNING TIME

The simplest means of evaluating the effects of burning time on a maneuver in space is to study the numerical simulation of a maneuver, that is, to program a set of equations which describes a maneuver and compare the results to those predicted by an impulsive analysis. This approach, however, is somewhat restrictive because:

(1) The results of the analysis are valid only in the neighborhood of the maneuvers which were simulated.

(2) The results are strongly dependent upon the manner in which the thrust vector is controlled to yield the desired maneuver.

(3) Unless large numbers of simulations are made it is quite possible to overlook the effects of particular variables and trends in the results.

For these reasons, the approach taken here will be to present an analytic approximation to the equations of powered motion which will yield the desired information in a form which exhibits the necessary functional relationships. Consider the following sketch.

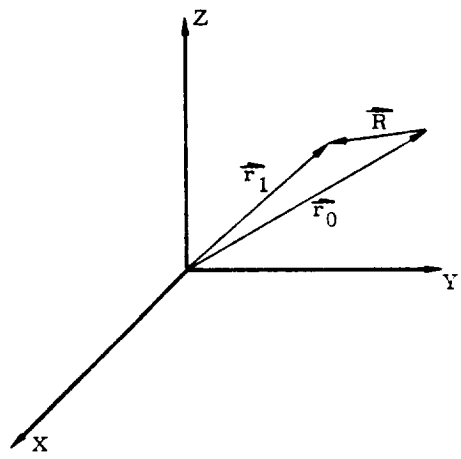

$$\vec{R} = \vec{r}_1 - \vec{r}_0$$

$$\ddot{\vec{R}} = \vec{a}_T + \ddot{\vec{r}}_1 - \ddot{\vec{r}}_0$$

where $\vec{a}_T$ = the thrust acceleration and where the acceleration due to the mutual attraction of the vehicles and the differences in the perturbation accelerations have been neglected. But the radial acceleration vector $\ddot{\vec{r}}_1$ can be developed in terms of r_0 to be

$$\ddot{\vec{r}}_1 = \ddot{\vec{r}}_0 + (\vec{R} \cdot \vec{\nabla})\, \ddot{\vec{r}}_0 + \ldots$$

where

$\ddot{\vec{r}}_0$ = acceleration due to the central force

$$\ddot{\vec{R}} = \vec{a}_T + (\vec{R} \cdot \vec{\nabla})\, \ddot{\vec{r}}_0$$

But

$$\ddot{\vec{r}}_0 = -\frac{\mu}{r_3}\, \vec{r}_0$$

Thus

$$\ddot{\vec{R}} = \vec{a}_T - \frac{\mu}{r_0^2}\left[\frac{\vec{R}}{r_0} - \frac{3\,\vec{r}_0\,(\vec{R} \cdot \vec{r}_0)}{r_0^3}\right]$$

Thus, for motion in a nearly circular orbit the small displacements from the unperturbed position are:

$$\ddot{x} = 3\omega^2 x + 2\omega \dot{y} + a_x \qquad \text{(along radius)}$$

$$\ddot{y} = -2\omega \dot{x} + a_y \qquad \text{(along velocity of origin)}$$

$$\ddot{z} = -\omega^2 z + a_z \qquad \text{(normal to plane)}$$

where ω is the angular rate of the origin about the earth $= \sqrt{\frac{\mu}{r_0^3}}$. Now, following the method of Darby (Ref 17), assume that the thrust is applied as a series of small impulses of magnitude

$$\Delta V = a \Delta T$$

Thus each of the equations listed above can be considered to be unperturbed for a time (i.e., the thrust acceleration is zero) then at a small time later the velocity is changed and the process repeated. Consider the equation for Z.

$$\ddot{z} + \omega^2 z = 0$$

$$z = A \sin \omega (t - T) \qquad t_1 < t < t_2$$

$$\dot{z} = \omega A \cos \omega (t - T)$$

$$= B \cos \omega (t - T)$$

$$\dot{z}_1 = (B + a_z T) \cos \omega (t - T) \qquad t_2 < t < t_3$$

$$d\dot{z} = \lim_{\Delta t_0 \to 0} (\dot{z}_1 - \dot{z}) = a_z \cos \omega (t - T)\, dT$$

Thus

$$\dot{z} = \int_0^t a_z \cos \omega (t - T)\, dT_0$$

$$z = \frac{1}{\omega} \int_0^t a_z \sin \omega (t - T)\, dT$$

and similarly

$$y = \int_0^t a_y \left[\frac{4}{\omega} \sin \omega (t - T) - 3(t - T)\right] dT$$

$$- \frac{2}{\omega} \int_0^t a_x \left[1 - \cos \omega (t - T)\right] dT$$

$$\dot{y} = \int_0^t a_y \left[4 \cos \omega (t - T) - 3\right] dT$$

$$- 2 \int_0^t a_x \left[\sin \omega (t - T)\right] dT$$

$$x = \frac{1}{\omega} \int_0^t a_x \sin \omega (t - T)\, dT$$

$$+ \frac{2}{\omega} \int_0^t a_y \left[1 - \cos \omega (t - T)\right] dT$$

$$\dot{x} = \int_0^t a_x \cos \omega (t - T)\, dT$$

$$+ 2 \int_0^t a_y \sin \omega (t - T)\, dT$$

At this point the solution is no further progressed than would have resulted if the functions x, y, z, $\dot{x}$ and $\dot{z}$ had been expressed as inverse Laplace transforms since the time history of a_x, a_y and a_z has not been specified. However, if it is assumed that once firing is initiated the direction of the thrust vector is unaltered, then, the acceleration will vary with time according to

$$a(t) = \frac{a(0)}{1 - \dot{m} T}$$

where: $\dot{m}$ is the % change in mass, i.e., $\frac{1}{m_0} \frac{dm}{dt}$

At this point the terms $\cos \omega (t - T)$ and $\sin \omega (t - T)$ can be expanded in a power series to yield

$$\cos \omega (t - T) = 1 - \frac{\omega^2 (t - T)^2}{2} + \omega^4 \frac{(t - T)^4}{24} - \cdots$$

$$\sin \omega (t - T) = \omega (t - T) - \omega^3 \frac{(t - T)^3}{6} + \cdots$$

Thus, since ω is a constant, the solution evolves into the evaluation of integrals of the form

$$\int_0^t \frac{(t - T)^n}{1 - \dot{m} T}\, dT \qquad n = 1, 2, 3, 4, \cdots$$

If only two terms of each expansion are retained (i.e., $n < 4$) the results of Darby can be obtained as:

$$\int_0^t \frac{(t - T)}{1 - \dot{m} T}\, dT = \frac{1}{\dot{m}^2} \left[\dot{m}t - (1 - \dot{m}t) \ln \frac{1}{1 - \dot{m}t}\right]$$

$$= \frac{A}{\dot{m}^2}$$

$$\int_0^t \frac{(t - T)^2}{1 - \dot{m} T}\, dT = \frac{1}{\dot{m}^3} \left[(1 - \dot{m}t)^2 \ln \frac{1}{1 - \dot{m}t} - \dot{m}t + \frac{3}{2} (\dot{m}t)^2\right] = \frac{B}{\dot{m}^3}$$

$$\int_0^t \frac{(t - T)^3}{1 - \dot{m} T}\, dT = \frac{1}{\dot{m}^4} \left[(1 - \dot{m}t)^3 \ln \frac{1}{1 - \dot{m}t} - \dot{m}t + \frac{5}{2} (\dot{m}t)^2 - \frac{11}{6} (\dot{m}t)^3\right] = \frac{C}{\dot{m}^4}$$

$$\int_0^t \frac{(t - T)^4}{1 - \dot{m} T}\, dT = \frac{1}{\dot{m}^5} \left[(1 - \dot{m}t)^4 \ln \frac{1}{1 - \dot{m}t} - \dot{m}t + \frac{7}{2} (\dot{m}t)^2 - \frac{13}{3} (\dot{m}t)^3 + \frac{25}{12} (\dot{m}t)^4\right] = \frac{D}{\dot{m}^5}$$

and

$$x = \frac{a_{x0}}{\dot{m}^2} \left(A - \frac{\omega^2}{6 \dot{m}^2} C\right) + \frac{a_{y0}\, \omega}{\dot{m}^3} \left(B - \frac{\omega^2}{12 \dot{m}^2} D\right)$$

$$y = \frac{a_{y0}}{\dot{m}^2}\left(A - \frac{2\omega^2}{3\dot{m}^2}C\right) - \frac{a_{x0}\,\omega}{\dot{m}^3}\left(B - \frac{\omega^2}{12\dot{m}^2}D\right)$$

$$z = \frac{a_{z0}}{\dot{m}^2}\left(A - \frac{\omega^2}{6\dot{m}^2}\right)$$

$$\dot{x} = \frac{a_{x0}}{\dot{m}}\left(\ln\frac{1}{1-\dot{m}t} - \frac{\omega^2}{2\dot{m}^2}B\right) + \frac{2\,a_{y0}\,\omega}{\dot{m}^2}\left(A - \frac{\omega^2}{6\dot{m}^2}C\right)$$

$$\dot{y} = \frac{a_{y0}}{\dot{m}}\left(\ln\frac{1}{1-\dot{m}t} - \frac{2\omega^2}{\dot{m}^2}B\right) - \frac{2\,a_{x0}\,\omega}{\dot{m}^2}\left(A - \frac{\omega^2}{6\dot{m}^2}C\right)$$

$$\dot{z} = \frac{a_{z0}}{\dot{m}}\left(\ln\frac{1}{1-\dot{m}t} - \frac{\omega^2}{2\dot{m}^2}B\right)$$

As is done in Chapter VII (Rendezvous), the set of definitions for A, B, C and D can be simplified for the case where $\dot{m}t_{max}$ (or $\dot{m}t_b$) is small compared to 1, for then

$$\ln\frac{1}{1-\dot{m}t} = -\ln(1-\dot{m}t)$$

$$= \dot{m}t + \frac{(\dot{m}t)^2}{2} + \frac{(\dot{m}t)^3}{3} + \cdots$$

Thus

$$A = \dot{m}t - (1-\dot{m}t)\left[\dot{m}t + \frac{(\dot{m}t)^2}{2} + \frac{(mt)^3}{3} + \cdots\right]$$

$$= \frac{(\dot{m}t)^2}{2}\left[1 + \frac{\dot{m}t}{3} + \frac{(\dot{m}t)^2}{6} + \frac{(\dot{m}t)^3}{10} + \cdots\right]$$

$$B = \frac{(\dot{m}t)^3}{3}\left[1 + \frac{\dot{m}t}{4} + \frac{(\dot{m}t)^2}{10} + \frac{(\dot{m}t)^3}{20} + \cdots\right]$$

$$C = \frac{(\dot{m}t)^4}{4}\left[1 + \frac{\dot{m}t}{5} + \frac{(\dot{m}t)^2}{15} + \frac{(\dot{m}t)^3}{35} + \cdots\right]$$

$$D = \frac{(\dot{m}t)^5}{5}\left[1 + \frac{\dot{m}t}{6} + \frac{(\dot{m}t)^2}{21} + \frac{(\dot{m}t)^3}{56} + \cdots\right]$$

Now since the motion of the origin of the relative coordinates is known to move in a circle, the position and velocity of the vehicle are known as a function of time. In particular, they are known at the end of burning. Thus, the effects of the burning can be computed by comparing the position and velocity vectors at this time with those that would have resulted at the same time if the maneuver had been impulsive. It is further possible to determine the effect on the six orbital elements since the position and velocity at the end of burning determine these constants uniquely via the equations of Chapter III.

The accuracy of this solution is limited or restricted by four assumptions.

(1) The locus of the origin of coordinates was assumed circular. This assumption can of course be violated if the interval of burning is known by using the average velocity corresponding to that interval and correcting for the radial motion of the origin. The resultant accuracy will of course deteriorate.

(2) The vehicle is assumed to be at the origin with zero velocity at time = 0. Should these conditions not be satisfied, however, suitable constants can be introduced via the medium of the Laplace transform. A similar solution employing nonzero initial boundary conditions is illustrated in Chapter VII (Rendezvous).

(3) Only first-order terms were carried in the expansion of $\vec{r}_1 - \vec{r}_0$. This assumption effectively limits the allowable deviation of the vehicle from the origin of coordinates. Although no analysis of this restriction will be made here, it is noted that for single thrust periods of no more than approximately 2 to 4% of the orbital period and accelerations no larger than 1 g, the total displacements will be no more than 10^6 ft or 0.3×10^6 m. For such displacements the accuracy of the method is still adequate for hand computations of first-order effects.

(4) Higher order terms in $\dot{m}t$ were neglected in the series for A, B, C and D. This assumption is generally not serious due to the rapid convergence of the series for most values of this parameter. However, should this convergence problem be such that additional terms would not resolve the difficulty, the original definition of these constants could be utilized at the expense of simplicity in the form.

Because of the manner in which the variables are related and the large number of ways which can be used to assess the effects of finite burning times, parametric data based on these solutions will not be provided. Rather it is suggested that the computations be made as outlined and that the results be compared to the unperturbed solution utilizing the equations of Chapter III or the differential expression relating elemental errors to position and velocity errors of Chapter VII.

Reference 17 does, however, present a set of figures which relate to the time interval necessary to "anticipate" a maneuver (or lead time) and the difference in the magnitude of the ideal and actual velocity increments as functions of specific impulse, acceleration level, azimuth and flight path angle. Because of the interest in these results they are included.

Figures 33 and 34 show the approximately linear manner in which the lead time varies with both acceleration level and specific impulse. In

both cases the curvature is the result of mass changes and is less noticeable for the small maneuvers.

Figures 35 and 36 show the effects of finite burning time on the magnitude of the velocity increment. These figures show the importance of consideration of these effects in any computations beyond those of a preliminary nature.

Though not shown in figures, several trends can also be noted.

(1) Finite burning times tend to result in a smaller value of eccentricity for a given mass fraction due largely to the fact that work is generally done against gravity forces.

(2) These times tend to produce perigee radii which are greater than their impulse counterparts.

(3) The change in inclination of the plane will tend to be larger for the finite burning time case than for the impulse case.

K. IN-ORBIT PROPULSION SYSTEM

1. Propulsion System Requirements

Each of the maneuvers to be performed in orbit (including injection into the various transfer orbits) requires the application of corrective impulses. The control of these impulses is the determining factor in the evaluation of the utility of the satellite in performing the particular function. In the navigation problem, the control tolerances are specified (based upon some maximum allowable drift rate for the satellites with respect to each other) and the subsystem requirements remain to be evaluated. In order to provide insight into these problems, the following analysis of two different types of propulsion control techniques has been made. These techniques are:

(1) Monitored propulsive inputs.

(2) Monitored velocity increment.

The first of these techniques attempts to control or at least compensate for variations in each of the parameters contributing to the velocity increment. Therefore, errors in each of the parameters will be reflected directly in an error in the velocity pulse. These effects may be evaluated from the following equation (where the loss due to finite burning time is neglected):

$$\Delta V = -g_0 I_{sp} \ell n (1 - \zeta) \qquad (249)$$

$$\delta(\Delta V) = \frac{\partial(\Delta V)}{\partial t_b} \Delta t_b + \frac{\partial(\Delta V)}{\partial \dot{w}_p} \Delta \dot{w}_p + \frac{\partial(\Delta V)}{\partial I_{sp}} \Delta I_{sp} + \frac{\partial(\Delta V)}{\partial W_0} \Delta W_0$$

$$= \frac{g_0 I_{sp} \zeta}{1 - \zeta} \left[\frac{\Delta t_b}{t_b} + \frac{\Delta \dot{w}_p}{\dot{w}_p} - \zeta (1 - \zeta) \ell n (1 - \zeta) - \frac{\Delta W_0}{W_0} \right] \qquad (250)$$

$$= \frac{(T/W_0) g_0 \Delta t_b}{1 - \zeta} + \frac{g_0 I_{sp} \zeta}{1 - \zeta} \frac{\Delta \dot{w}_p}{\dot{w}_p} + \zeta^2 \Delta V \frac{\Delta I_{sp}}{I_{sp}} - \frac{g_0 I_{sp} \zeta}{1 - \zeta} \frac{\Delta W_0}{W_0}$$

This equation may be reduced to a more simple form by employing data which is representative of current technology for each of the control parameters. These data are:

$$\Delta t_b \approx 0.030 \text{ sec}$$

$$\Delta \dot{w}_p \approx 0.005 \dot{w}_p$$

$$\frac{\Delta I_{sp}}{I_{sp}} \approx 1/260$$

Thus, for a specific impulse of 300 sec:

$$\delta(\Delta V) = \frac{0.066 T/W_0}{1 - \zeta} + \frac{0.161 I_{sp} \zeta}{1 - \zeta} + \frac{\zeta^2 \Delta V}{260} - \frac{g_0 I_{sp} \zeta}{1 - \zeta} \left(\sum_{i=1}^{n} \frac{t_{b_i} \Delta \dot{w}_{p_i} + \dot{w}_{p_i} \Delta t_{b_i}}{W_{0_i}} + \frac{\Delta W_0}{W_0} \right) \qquad (251)$$

where ΔW_0 is the initial error in the weight of the vehicle. The last group of terms in this equation (the summation) is small compared to the other three for small or even moderately large increments; therefore, it may be neglected. The maximum magnitude of the remaining terms is presented in Fig. 37 as a function of the initial thrust-to-weight ratio. As may be noted from this figure, a system of this type would have difficulty in satisfying extreme accuracy requirements since to limit a maximum error in the velocity increment to less than 0.5 fps appears difficult.

If the velocity increment itself is monitored by integrating the acceleration due to thrust, the maximum error in the increment is a function only of the error in the time of burning and that in the integration itself. Assuming that the integrated accelerometers are accurate to 1 part in 10^5 g (which is the expected accuracy of future integrating accelerometers), the error in the integrated acceleration should be accurate to approximately 1 part in 10^4. Thus, the maximum error is

$$\delta(\Delta V) = \frac{\Delta V}{10^4} + \frac{0.966 T/W_0}{1 - \zeta} \qquad (252)$$

This equation has also been plotted and appears as Fig. 38a. This figure shows that with control

parameters as quoted the error in the velocity pulse can be controlled to well within 0.5 fps for thrust-weight ratios as high as 0.4 ($\Delta V < 100$ fps). Thus, the precision required for small corrections can be obtained with this system. Since the error plotted in this figure is the maximum expected, this figure implies that the error will generally be negligible. Figure 38b shows the effect of reducing the error in the shutdown time on the resultant velocity error. The parameter in this figure ($\Delta t_b \frac{T}{W_0}$) is immediately recognizable as the error in the total impulse.

2. Selection of Thrust Level and Propellants

While the detailed design of a propulsion system is obviously beyond the scope of an effort of this type, the general sizing and capabilities of such a system can be established.

As shown in Eq (252), if the velocity increment is to be controlled within 0.1 fps for increments of less than 500 fps, the ratio of the error in the impulse to the initial weight must be

$$\frac{T\Delta t_b}{W_0} \leq \left[\delta(\Delta V) - \frac{\Delta V}{10^4}\right] \frac{1-\zeta}{g_0}$$

$$\leq \frac{0.05\,(1-\zeta)}{g} \approx \frac{0.05}{g_0} \cdot \left[1 - \frac{\Delta V}{g_0 I_{sp}}\right]$$

$$\leq 0.0015 \text{ (for } I_{sp} = 300 \text{ sec)} \quad .$$

From this it may be seen that (for reasonable errors in the shutdown time, say 0.05 sec) the thrust-to-initial-weight ratio should be ≤ 0.03. It should be noted, however, that the thrust levels should not be extremely low because of the assumption made in the formulation of the corrective maneuvers. For these reasons, an initial thrust-to-weight ratio of say 0.01 should be selected. If this ratio were maintained constant, the thrust for successive corrections would have to decrease according to the following equation.

$$T = 0.01 \left[W_0 - \sum_{i=1}^{m} \dot{w}_p t_{bi}\right]$$

However, since the vehicles in orbit will possess fuel fractions of less than 2/3 in order to assure reasonable payload capabilities, the thrust-to-initial-weight ratio for each correction will always be > 0.03 which is the allowable upper limit. Thus, no provision for thrust variation is necessary.

With thrust level thus established, the remaining propulsion parameters can be evaluated once the propellant characteristics are known. This requires the selection of a propellant or propellant combination capable of performing as required. These considerations are beyond the scope of the present effort and will not be discussed.

3. Nozzle Sizing

The second step in the analysis of the propulsion system is the sizing of the rocket motor and nozzle. This will be accomplished through the utilization of the theoretical relationships developed in gas dynamics and the experimental propulsion systems data available.

The first assumption concerning the motor which must be made pertains to the expansion ratio which is feasible for the nozzle of a motor operating in a vacuum. From this ratio and the average value of the ratio of specific heats for the products of combustion, it is possible to determine the pressure ratio across the nozzle.

$$\frac{p_e}{p_c}\sqrt{1 - \left(\frac{p_e}{p_c}\right)^{\frac{\gamma-1}{\gamma}}} = \frac{A_T}{A_e}\left(\frac{2}{\gamma+1}\right)^{1/\gamma-1}\sqrt{\frac{\gamma-1}{\gamma+1}} \qquad (253)$$

where γ is the average value of the ratio of specific heats of the products of combustion. This equation is of the form

$$\left(\frac{p_e}{p_c}\right)^2 - \left(\frac{p_e}{p_c}\right)^{\frac{3\gamma-1}{\gamma}} - C = 0$$

The simplest solution to this equation is by iteration. Newton's method will be utilized because of convergence

$$X_{n+1} = X_n - \frac{f(X_n)}{f'(X_n)}$$

where, for this solution, X_n is the nth estimate of p_e/p_c. This solution results in the following equation

$$X_{n+1} = X_n - \frac{X_n^2 - X_n^{\frac{3\gamma-1}{\gamma}} - C}{2X_n - \frac{3\gamma-1}{\gamma} X_n^{\frac{2\gamma-1}{\gamma}}}$$

If p_e/p_c is assumed to be $\ll 1$, the first trial of p_e/p_c should be approximately the square root of C.

From this point, it is possible to establish the theoretical thrust coefficient of a gas with the given value of the ratio of specific heats.

$$C_F = \sqrt{\gamma^2 \frac{2}{\gamma-1}}\sqrt{\left(\frac{2}{\gamma+1}\right)^{\frac{\gamma+1}{\gamma-1}}\left(1 - \frac{P_e}{P_c}\right)^{\frac{\gamma-1}{\gamma}}} + \frac{p_e}{p_c}\frac{A_e}{A_i} \qquad (254)$$

Now from the definition of the thrust coefficient

$$C_F = T/A_t P_c$$

it is possible to size the nozzle for any selected chamber pressure. First, however, it should be noted that the theoretical thrust coefficients are approximately 5% higher than indicated from experimental data, thus a better estimate of these areas should account for this discrepancy.

The length of the nozzle may be obtained once the equivalent value of the half angle of divergence has been selected. Care must be exercised in this selection to assure that the flow doesn't separate from the nozzle, and that the nozzle is not excessively long. The length is then obtained as follows:

$$A_e - A_t = \pi \left(r_e^2 - r_t^2 \right) = A_t \left[\left(\frac{r_e}{r_t} \right)^2 - 1 \right]$$

but

$$r_e = r_t + L \tan \alpha$$

thus

$$A_e - A_t = A_t \left[\left(1 + \frac{L}{r_t} \tan \alpha \right)^2 - 1 \right]$$

$$L = \frac{\left(\sqrt{\frac{A_e}{A_t}} - 1 \right) \sqrt{A_t}}{\sqrt{\pi} \tan \alpha} \qquad (255)$$

These data define the general size of the nozzle; however, due to the fact that the optimum nozzle is not conical but rather more nearly a segment of a paraboloid of revolution, they do not define the optimum geometry. This refinement, however, is not deemed necessary due to the fact that the thrust levels are small.

4. Combustion Chamber Sizing

The combustion chamber to be fitted to the nozzle, which has been described in terms of the design parameters utilized, must now be investigated. This may be done through the investigation of an additional parameter, the characteristic chamber length (L*). This parameter, which affects the cycle efficiency, is defined as the ratio of the chamber volume to the nozzle throat area and is a function of the oxidizer-to-fuel weight ratio of the propellants utilized. Experimental data must be utilized for this determination. One such curve is presented in Fig. 39. The curve presented here is an average value curve since the data available were for slightly different propellant combinations operating in different test facilities under different pressures. Nonetheless, these data are sufficient to indicate a characteristic chamber length of approximately 100 in. or greater is recommendable. Similar data for any other propellant combination thus yield the chamber volumes:

$$V_c \approx L^* A_t$$

Before the motor can be sized, however, the geometry of the combustion chamber must be specified as either cylindrical or spherical.

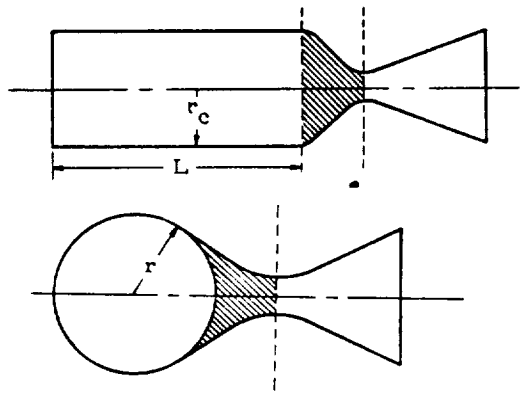

The former is particularly well suited for small motors since production is greatly simplified; the latter is a better design for larger motors due principally to the fact that the surface area exposed for heat transfer within the chamber is minimized for a given volume. Both of these chambers may be defined when a restriction is placed on the ratio of the chamber-to-throat area ratio of the cylindrical motor. This may in turn be accomplished by investigating the pressure drop through the chamber.

$$\frac{P_{inj}}{P_1} = \frac{1 + \gamma M_1^2}{1 + \gamma M_{inj}^2} \qquad (256)$$

where the point 1 is a section passing through the nozzle throat.

$$\frac{P_T}{P_S} = \left[1 + \frac{\gamma - 1}{2} M^2 \right]^{\frac{\gamma}{\gamma - 1}} \qquad (257)$$

Thus

$$\frac{P_{T\,inj}}{P_{T_1}} = \left[\frac{1 + \gamma M_1^2}{1 + \gamma M_{inj}^2} \right] \left[\frac{1 + \frac{\gamma - 1}{2} M_{inj}^2}{1 + \frac{\gamma - 1}{2} M_1^2} \right]^{\frac{\gamma}{\gamma - 1}}$$

If now M_{inj}^2 is small compared to M_1^2.

$$\frac{P_{T\,inj}}{P_{T_1}} = \frac{1 + \gamma M_1^2}{\left(1 + \frac{\gamma - 1}{2} M_1^2 \right)^{\frac{\gamma}{\gamma - 1}}}$$

This is also the ratio of the total pressure at the throat of an ideal motor to that of a tubular motor. This ratio may be related directly to the chamber-to-throat area ratio from the continuity equation as

$$\frac{A_1}{A_T} = \frac{1}{M_1}\left[\frac{2\left(1+\frac{\gamma-1}{2}M_1^2\right)}{\gamma+1}\right]^{\frac{\gamma+1}{2(\gamma-1)}} \quad (258)$$

The graphical relationship between the total pressures at the throat for tubular and ideal motors and the chamber-to-throat area ratio can thus be plotted in a figure similar to Fig. 40, and the minimum ratio $\frac{A_c}{A_t}$ assessed. Once this is done, the geometry of the chamber is:

$$V_c = L^* A_t = \frac{4}{3}\pi r^3 \text{ (spherical chamber)}$$

$$= \left(\frac{A_c}{A_t}\right) A_t L \text{ (cylindrical chamber)}$$

Thus

$$L = L^* \frac{A_t}{A_c}$$

Note is made that since, as is shown in Fig. 40, $\frac{A_c}{A_t}$ should be equal to or greater than 3.0 and since this ratio corresponds to an awkward length-to-diameter ratio for the chamber (approximately 30), the length may be selected based on other criteria.

5. Propellant Flow Rates

The propellant flow rates for the range of chamber pressures can be obtained once the variation in specific impulse for a given oxidizer-to-fuel weight ratio is established. A review of the abundance of data available will generally reveal no well defined curve for this variation due to differences in assumptions, fuel properties, etc.; therefore, an average curve such as Fig. 41 must be utilized.

Now

$$\dot{w}_p = T/I_{sp}$$

and

$$\dot{w}_f = \frac{1}{1+r}\dot{w}_p = \frac{1}{1+r}T/I_{sp}$$

$$\dot{w}_o = \frac{r}{1+r}\dot{w}_p = \frac{r}{1+r}T/I_{sp}$$

The propellants may be fed to the motor by any of a number of types of pumps. However, two schemes appear particularly attractive for small thrusts. The first utilizes positive displacement pump (which can be electrically driven), a hydraulic accumulator and a pressure regulator to supply the propellants to the nozzle under a constant pressure. This system can have one significant advantage due to the fact that the utilization of the accumulator makes it possible to employ a very small pump which operates between the corrections to keep the system charged. This possibility results in a reduced peak power requirement and a reduced pump-drive unit weight without increasing the size of the accumulator beyond allowable bounds. However, due to the fact that the unit will be constantly pressurized, the seal between the diaphragm and the propellant will require special attention. The second technique utilizes a small vane-type pump of such size as to make an accumulator unnecessary. The accumulator could be used in this application as it was in the other; however, the positive displacement pump is more efficient for this type of operation. Note should be made at this point that a positive propellant feed system is required to assure flow to the pump in either case.

Pumps of both these types exist in the sizes required though it is probable that special materials would be required because of the corrosive nature of the fluids.

The piston pumps are available in a variety of sizes capable of providing exit pressures up to approximately 3000 psia (20.7×10^6 newtons/m^2 at overall efficiencies varying from 85 to 92% (see sketch) for $500 \leq p \leq 3000$ (3.5 to 20.7×10^6 newtons/m^2).

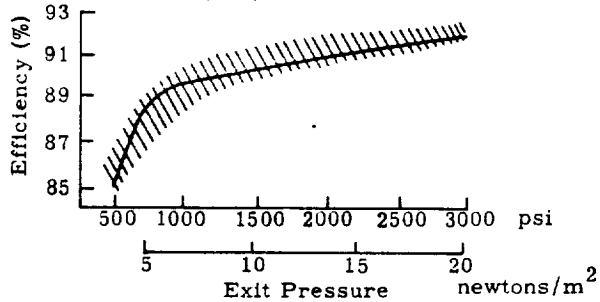

The required power input for these pumps is obtained from the following equations.

$$hp = 0.000583\,(psi)\,(gal/min) = \frac{0.00419\,(psi)\,(lb/sec)}{(density)(overall\ efficiency)}$$

$$Torque = \frac{(in.^3/rev)\,(psi)}{2}$$

$$rpm = (lb/min) \,/\, (in.^3/rev)\,(lb/in.^3)\,(volumetric\ efficiency)$$

L. MICRO-THRUST STUDY

The purpose of this study is to evaluate the performance and applicability of micro-thrust devices for small corrections in various orbital parameters. For each specific correction maneuver, a definite thrust orientation law (considering thrust magnitude, direction and duration) exists. The analytical expressions derived from the basic laws of celestial mechanics are obtained and their applicability in case of micro-thrust maneuvers investigated. Solutions in closed form are obtained in several cases. Low thrust systems

capable of producing these thrusts are discussed conceptually as well as in detail in the literature. For this reason, such data will not be presented here.

1. Planar Study of Radial Circumferential and Tangential Thrusts

Consider a set of equations of planar motion in polar coordinates. If R is used as the sum of radial accelerations and T as the sum of circumferential accelerations, then

$$\ddot{r} - r\dot{\theta}^2 + \frac{\mu}{r^2} = R$$

$$\frac{1}{r}\frac{d}{dt}\left(r^2\dot{\theta}\right) = T \qquad (259)$$

It is noticed from Eqs (259) that angular momentum is conserved only if there is no component of the tangential thrust applied to the satellite.

Several special cases for thrusting in the two-dimensional micro-thrust problem are discussed in the literature. The most important results of these solutions are summarized below and will serve as an introduction to further discussions.

a. Radial thrust

This problem is treated in Refs. 18 through 20. The outline presented here follows basically Ref. 20.

Equations (259) for the given case become

$$\ddot{r} - r\dot{\theta}^2 + \frac{\mu}{r^2} = R$$

$$r^2\dot{\theta} = \sqrt{\mu p} = \text{constant} \qquad (260)$$

where p is the semiparameter at the instant.

Now introducing nondimensional variables defined in terms of the instantaneous orbital elements.

$R^* = \frac{R}{g_a}$ (acceleration compared to gravity at a)

$r^* = \frac{r}{a}$ (distance in number of semimajor axes)

$t^* = t/\sqrt{a/g_a}$ (time compared to the orbital period)

By these substitutions, the Eqs (260) become (neglecting e^2 terms)

$$\ddot{r}^* - r^*\dot{\theta}^2 + \frac{1}{r^{*2}} = R^*$$

$$r^{*2}\dot{\theta} = 1 \qquad (261)$$

where differentiation is with respect to t*.

Now eliminating $\dot{\theta}$ in Eq (261) yields

$$\ddot{r}^* - \frac{1}{r^{*3}} + \frac{1}{r^{*2}} = R^* \qquad (262)$$

Eq (262) can now be integrated assuming an initially circular orbit at r* = 1 to yield

$$\dot{r}^{*2} = \frac{2}{r^*} - \frac{1}{r^{*2}} + 2R^*(r^* - 1) - 1 \qquad (263)$$

From Eq (263), it is apparent that the radial velocity is zero at the radial distances where

$$2R^* r^{*3} - (2R^* + 1) r^{*2} + 2r^* - 1 = 0 \qquad (264)$$

or

$$r^* = 1$$

and

$$r^* = \frac{1 \pm \sqrt{1 - 8R^*}}{4R^*} \qquad (265)$$

From Eq (265), the fact is seen that the orbit remains bounded for radial accelerations $R^* < \frac{1}{8}$. In the opposite case, $R^* > \frac{1}{8}$, no real roots exist in Eq (265), which indicates that large changes in the planar elements are possible or that escape from the earth's gravitational field may occur if a constant radial acceleration is applied for a sufficiently long time period.

The condition for critical acceleration $R^* = \frac{1}{8}$ implies

$$R = R^* g_a = \frac{1}{8} g_a = \frac{1}{8}\frac{\mu}{a^2} = \frac{1}{8}\left(\frac{r}{a}\right)^2 g$$

$$= \frac{1}{8}\left(\frac{R_0}{a}\right)^2 g_0$$

R_0 = radius of $\oplus$

g_0 = surface gravity.

Since the micro-thrust devices have, in general, a thrust level of 10^{-4} to 10^{-5} g_0, they are obviously not adequate for large orbital changes employing radial thrust applications. Nevertheless, as shown in Ref. 19, such radial micro-thrust can be used effectively to change the eccentricity of an orbit.

If $x_1 > x_2 > x_3$ are the roots of Eq (264), the solutions for a central angle and flight time as functions of the radial distance are:

(1) Radial inward thrust, $R^* < 0$

$$\theta(r^*) = \frac{2\delta}{\gamma\alpha}\left[\frac{\delta}{\beta}\pi\left(\phi, \frac{\alpha}{\beta}, k\right) + cF(\phi, k)\right] + \text{const.} \qquad (266)$$

$$t^*(r^*) = \frac{2\delta}{\gamma}\left[x_3 F(\phi, k) + (x_1 - x_3) E(\phi, k) + \frac{(x_1 - x_2)\sin 2\phi}{2\sqrt{1 - k^2 \sin^2\phi}}\right] + \text{const}$$

where

$$\alpha = -x_3 k^2$$

$$\beta = x_2$$

$$\delta = (x_2 - x_3) k^2$$

$$r^* = \frac{\alpha \sin^2\phi + \beta}{c \sin^2\phi + 1}$$

$$\gamma = (x_2 - x_3) k^2 \sqrt{-2R^* (x_1 - x_3)}$$

$$c = -k^2 = -\frac{x_1 - x_2}{x_1 - x_3}$$

$F(\phi, k)$, $E(\phi, k)$ and $\pi(\phi, \frac{\alpha}{\beta}, k)$ are elliptic integrals of the first, second and third kind.

(2) Radial outward thrust, $0 < R^* < \frac{1}{\delta}$

$$\theta(r^*) = \frac{2\delta^2}{\gamma\alpha\beta}\pi(\phi, \frac{\alpha}{\beta}, k) + \text{const.}$$

$$t^*(r^*) = \frac{2\delta}{\gamma}\left[x_1 F(\phi, k) - (x_1 - x_3) E(\phi, k)\right] + \text{const.} \quad (267)$$

where

$$\alpha = x_2 - x_3$$

$$\beta = x_3$$

$$r = \alpha \sin^2(\phi + \beta)$$

$$\delta = x_2 - x_3$$

$$\gamma = (x_2 - x_3)\sqrt{2R^*(x_1 - x_3)}$$

$$k^2 = \frac{x_2 - x_3}{x_1 - x_3}$$

$$r^* = \frac{\alpha \sin^2\phi + \beta}{c \sin^2\phi + 1}$$

b. Circumferential thrust

This problem is also solved in Ref. 18, using a series expansion method for large thrust ratios and a simple first order approximation for the very small thrust ratios. For circumferential thrust, the equations of motion corresponding to Eq (261) are

$$\ddot{r}^* - r^* \dot{\theta}^2 + \frac{1}{r^{*2}} = 0$$

$$\frac{d}{dt^*}(r^{*2}\dot{\theta}) = r^* T^* \quad (268)$$

where

$$T^* = T/g_a \quad (269)$$

Eliminating $\dot{\theta}$ from Eqs (268),

$$\frac{d}{dt^*}(r^{*3}\dot{r}^* + r^*)^{1/2} = r^* T^* \quad (270)$$

for very small accelerations, $r^{*3}\ddot{r}^* << r^*$ and the approximate differential equation is

$$\frac{d}{dt^*} r^{*1/2} = r^* T^* \quad (271)$$

and

$$r^* = \frac{1}{(1 - T^* t^*)^2} \quad (272)$$

which is a good approximation.

c. Tangential thrust

The problem of tangential micro-thrust application is treated in Refs. 21 through 23. It is shown that the mass ratio is slightly smaller for tangential than for circumferential micro-thrust for all but circular orbits. The approximate solution for radius is basically the same as Eq (270), if the first order approximation in T_t^* is considered (T_t = tangential acceleration):

$$r^* \approx \frac{1}{1 - 2 T_t^* (\frac{s}{a})} \quad (273)$$

where s = distance traversed by the rocket.

In Ref. 16 the altitude change per revolution is given for the tangential micro-thrust as:

$$\Delta r_{rev} = 4\pi T_t^* r_o \quad (274)$$

and the number of revolutions to reach a certain altitude is

$$n = \frac{1}{8\pi T_t^*} \left(\frac{r_o + r_1}{r_1^2} \right) \Delta r \qquad (275)$$

If r_1 tends to infinity, this last equation tends to

$$n_\infty = \frac{1}{8\pi T^*}$$

This equation states that the number of revolutions to escape is inversely proportional to T*. The following sketches obtained from numerical integration exhibit this behavior. Also shown is the fact that the orbit grows in such a manner that most of the revolutions approximate concentric circular orbits. Thus a tangential thrust is a very simple and accurate means of changing the radius of a circular orbit.

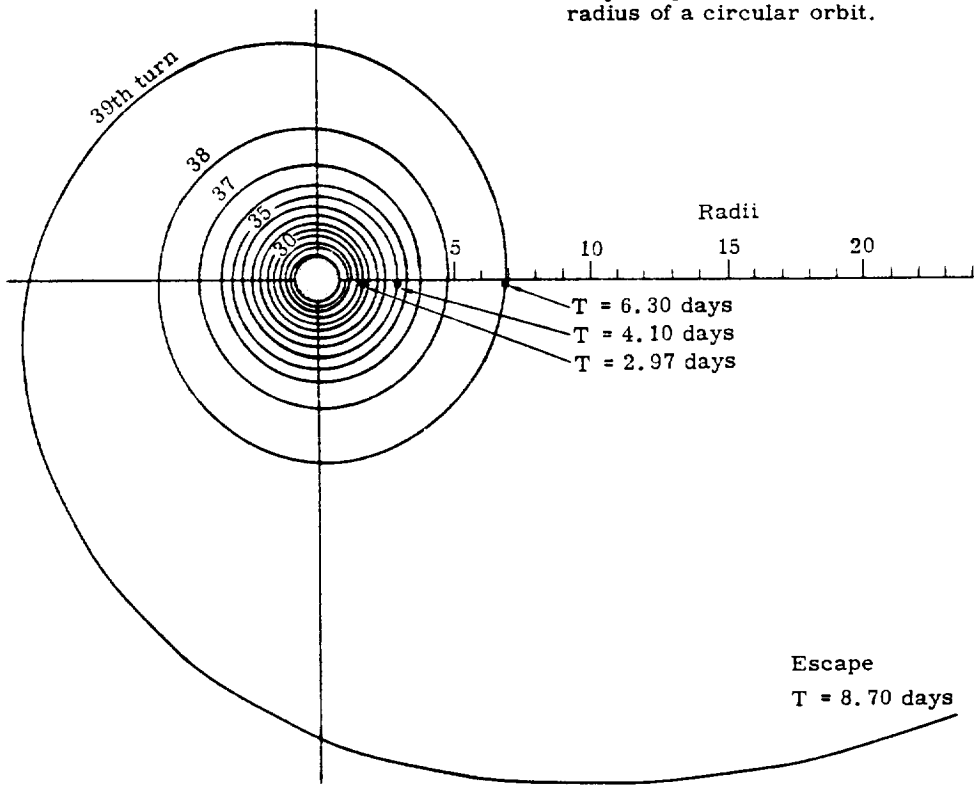

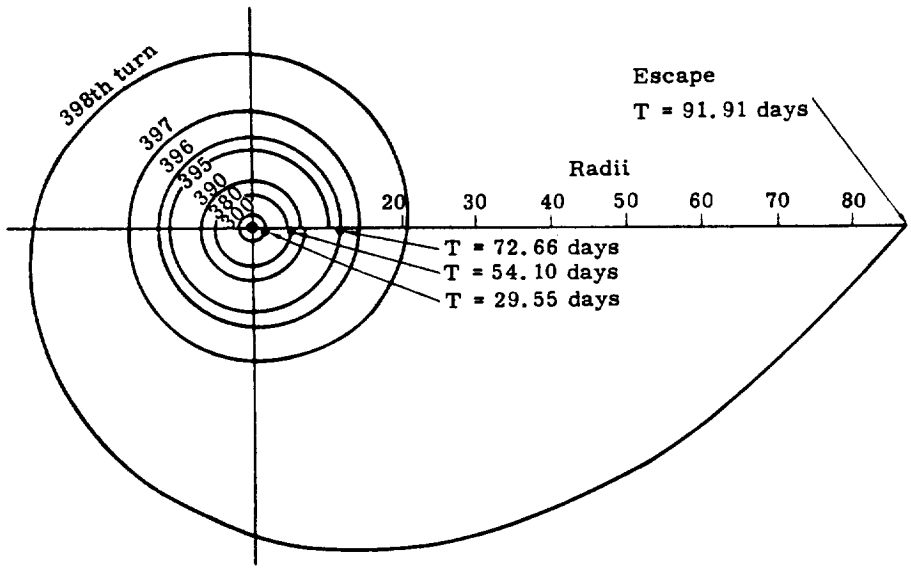

2. The Equations of Motion

The preceding discussion (Eqs (259) through (275)) showed the motion of the vehicle in polar coordinates under the influence of a micro-thrust. Unfortunately, this formulation is not always satisfactory for presenting the most readily comprehended information pertaining to the micro-thrust problem. For this reason, the equations have been written in terms of osculating orbital elements (i.e., the elements of the instantaneous elliptic orbit resulting from thrust termination at that time). This derivation is presented in Chapter IV.

$$
\left[\begin{aligned}
\frac{da}{dt} &= \frac{2}{n\sqrt{1-e^2}}\left(e\sin\theta \cdot R + \frac{p}{r}T\right)\\
\frac{de}{dt} &= \frac{\sqrt{1-e^2}}{na}\left[\sin\theta \cdot R + (\cos\theta + \cos E)\,T\right.\\
\frac{di}{dt} &= \frac{r\cos(\omega+\theta)}{na^2\left(1-e^2\right)}W\\
\sin i\,\frac{d\Omega}{dt} &= \frac{r\sin(\omega+\theta)}{na^2\sqrt{1-e^2}}W\\
\frac{d\tilde{\omega}}{dt} &= 2\sin^2\frac{i}{2}\frac{d\Omega}{dt}\\
&\quad + \frac{\sqrt{1-e^2}}{nae}\left[-\cos\theta \cdot R + \sin\theta\left(1+\frac{r}{p}\right)T\right]\\
\frac{d\epsilon}{dt} &= -\frac{2r}{na^2}\cdot R + \frac{e^2}{1+\sqrt{1-e^2}}\frac{d\tilde{\omega}}{dt}\\
&\quad + 2\sqrt{1-e^2}\sin^2\frac{i}{2}\frac{d\Omega}{dt}
\end{aligned}\right] \qquad (276)
$$

where: $\tilde{\omega} = \omega + \Omega$

and where R, T and ω are the components of acceleration along the radius, the normal to the radius in the plane in the general direction of motion, and normal to the plane in the general direction of north, respectively (see sketch).

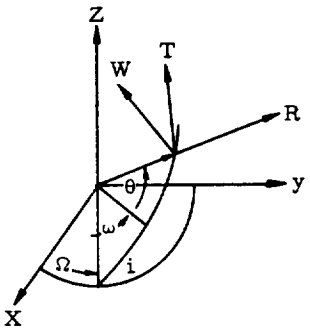

Equations (276) are the basic Lagrange planetary equations, from which special cases for a single component of disturbing acceleration can be derived. The resulting set of differential equations for the orbital parameters can be programmed for a digital computer, and the variations in the orbit computed as a function of time.

The equations can, however, be integrated under several conditions. The resulting equations are presented in following paragraphs. It should be noted, however, that, in certain cases, angular momentum is not conserved for long periods of time (tangential thrust) and that the integration formulas give a good approximation for only a few orbital revolutions.

a. Acceleration perpendicular to orbital plane

In this case both the radial and circumferential components of the acceleration are zero (i.e., R = 0 and T = 0), and the planetary equations for the disturbing acceleration follow from Eqs 276 simply as

$$
\left\{\begin{aligned}
\frac{da}{dt} &= \frac{de}{dt} = 0\\
\frac{di}{dt} &= \frac{r\cos(\omega+\theta)}{na^2\sqrt{1-e^2}}W\\
\frac{d\Omega}{dt} &= \frac{r\sin(\omega+\theta)}{na^2\sqrt{1-e^2}\sin i}W\\
\frac{d\tilde{\omega}}{dt} &= 2\sin^2\frac{i}{2}\frac{d\Omega}{dt}\\
\frac{d\epsilon}{dt} &= \frac{d\tilde{\omega}}{dt}
\end{aligned}\right\} \qquad (277)
$$

Define a nondimensional acceleration

$$W^* = \frac{W}{g_a} \qquad (278)$$

where g_a is the gravitational acceleration at a distance corresponding to the semimajor axis.

Since $\mu = n^2 a^3$, this acceleration is equal to

$$g_a = \frac{\mu}{a^2} = n^2 a$$

and

$$W = n^2 a W^* \qquad (279)$$

From the conservation of angular momentum,

$$\frac{d\theta}{dt} = \frac{\sqrt{\mu p}}{r^2}$$

it follows, by using $p = a(1-e^2)$, that

$$\frac{dt}{d\theta} = \frac{r^2}{na^2\sqrt{1-e^2}} \qquad (280)$$

Substituting Eqs (279) and (280) into Eqs (277):

$$\left\{\begin{aligned}
\frac{di}{d\theta} &= \frac{r^3 \cos(\omega+\theta)}{a^3 (1-e^2)} W^* = \\
&\quad \frac{(1-e^2)^2 \cos(\omega+\theta)}{(1+e\cos\theta)^3} W^* \\
\frac{d\Omega}{d\theta} &= \frac{(1-e^2)^2 \sin(\omega+\theta)}{\sin i\,(1+e\cos\theta)^3} W^* \\
\frac{d\tilde{\omega}}{d\theta} &= 2\sin^2\frac{i}{2}\,\frac{d\Omega}{d\theta} \\
\frac{d\epsilon}{d\theta} &= \frac{d\tilde{\omega}}{d\theta}
\end{aligned}\right\} \qquad (281)$$

Assuming the variation in i during a revolution to be extremely small, such that sin i can be considered essentially constant, these expressions can be integrated with respect to the central angle θ.

First, expand the sines and cosines:

$$\left.\begin{aligned}
\sin(\omega+\theta) &= \sin\omega\ \cos\theta + \cos\omega\ \sin\theta \\
\cos(\omega+\theta) &= \cos\omega\ \cos\theta - \sin\omega\ \sin\theta
\end{aligned}\right\} \qquad (282)$$

Substituting this into Eq (281),

$$\Delta i \equiv \int_{\theta_0}^{\theta} di = W^* (1-e^2)^2 \left[\cos\omega \int \frac{\cos\theta\, d\theta}{(1+e\cos\theta)^3} - \sin\omega \int \frac{\sin\theta\, d\theta}{(1+e\cos\theta)^3}\right]\Bigg|_{\theta_0}^{\theta} \qquad (283)$$

$$\Delta\Omega \equiv \int_{\theta_0}^{\theta} d\Omega = W^* \frac{(1-e^2)^2}{\sin i}\left[\sin\omega \int \frac{\cos\theta\, d\theta}{(1+e\cos\theta)^3} + \cos\omega \int \frac{\sin\theta\, d\theta}{(1+e\cos\theta)^3}\right]\Bigg|_{\theta_0}^{\theta} \qquad (284)$$

Both equations can be integrated by the use of the following integration formulas:

$$\int \frac{\sin\theta\, d\theta}{(1+e\cos\theta)^3} = \frac{1}{2e(1+e\cos\theta)^2}\Bigg|_{\theta_0}^{\theta}$$

$$\int \frac{d\theta}{(1+e\cos\theta)^2} = \frac{1}{(1-e^2)^{3/2}}\left[\frac{-e\sqrt{1-e^2}\sin\theta}{1+e\cos\theta} + 2\tan^{-1}\left(\sqrt{\frac{1-e}{1+e}}\tan\frac{\theta}{2}\right)\right]\Bigg|_{\theta_0}^{\theta}$$

$$\int \frac{\cos\theta\, d\theta}{(1+e\cos\theta)^2} = \frac{1}{(1-e^2)^{3/2}}\left[\frac{\sqrt{1-e^2}\sin\theta}{1+e\cos\theta} - 2e\tan^{-1}\left(\sqrt{\frac{1-e}{1+e}}\tan\frac{\theta}{2}\right)\right]\Bigg|_{\theta_0}^{\theta}$$

$$\int \frac{\cos\theta\, d\theta}{(1+e\cos\theta)^3} = \frac{1}{2(1-e^2)}\left[\frac{\sin\theta}{(1+e\cos\theta)^2} + \int \frac{-2e+\cos\theta}{(1+e\cos\theta)^2}\, d\theta\right] = \frac{1}{2(1-e^2)}\,\frac{\sin\theta}{(1+e\cos\theta)^2} + \frac{(1+2e^2)}{2(1-e^2)^2}\,\frac{\sin\theta}{(1+e\cos\theta)} - \frac{3e}{(1-e^2)^{5/2}}\tan^{-1}\left(\sqrt{\frac{1-e}{1+e}}\tan\frac{\theta}{2}\right)\Bigg|_{\theta_0}^{\theta} \qquad (285)$$

After some simplification, the change in orbital inclination caused by a constant micro-thrust perpendicularly oriented to the orbital plane is given by

$$\Delta i = W^* \left\{\frac{(1-e^2)}{2(1+e\cos\theta)^2}\left[\sin\theta\cos\omega - \left(\frac{1-e^2}{e}\right)\sin\omega\right] + \frac{(1+2e^2)\sin\theta\cos\omega}{2(1+e\cos\theta)} - \frac{3e\cos\omega}{(1-e^2)^{1/2}}\tan^{-1}\left(\sqrt{\frac{1-e}{1+e}}\tan\frac{\theta}{2}\right)\right\}\Bigg|_{\theta_0}^{\theta} \text{ (rad/rev)} \qquad (286)$$

and the change in the longitude of the ascending node is given in the form

$$\Delta\Omega = \frac{W^*}{\sin i}\left\{\frac{(1-e^2)}{2(1+e\cos\theta)^2}\left[\sin\theta\sin\omega + \left(\frac{1-e^2}{e}\right)\cos\omega\right] + \frac{(1+2e^2)\sin\theta\sin\omega}{2(1+e\cos\theta)} - \frac{3e\sin\omega}{(1-e^2)^{1/2}}\tan^{-1}\left(\sqrt{\frac{1-e}{1+e}}\tan\frac{\theta}{2}\right)\right\}\Bigg|_{\theta_0}^{\theta} \text{ (rad/rev)} \qquad (287)$$

The integrals for the longitude of perigee ($\tilde{\omega}$) and the mean longitude of epoch (ϵ) are both equal and are simply Eq (287) multiplied by $2 \sin^2 \frac{i}{2}$.

Of course, if i should be varying very rapidly, then sin i could not be taken outside the integral sign in Eq (172), and a closed form solution would be extremely difficult, if not impossible, to obtain.

b. Radial acceleration

Setting T = 0 and W = 0 in Lagrange's planetary equations, the following results are obtained:

$$\left\{ \begin{aligned} \frac{da}{dt} &= \frac{2 e \sin\theta}{n\sqrt{1-e^2}} R \\ \frac{de}{dt} &= \frac{\sqrt{1-e^2}\sin\theta}{na} R \\ \frac{di}{dt} &= \frac{d\Omega}{dt} = 0 \\ \frac{d\tilde{\omega}}{dt} &= -\frac{\sqrt{1-e^2}\cos\theta}{nae} R \\ \frac{d\epsilon}{dt} &= -\frac{1}{na}\left[2\frac{r}{a} + \frac{e\sqrt{1-e^2}}{1+\sqrt{1-e^2}}\cos\theta\right] R \end{aligned} \right\} \quad (288)$$

At this point it should be noted that for radial acceleration there is no change in the orbital inclination and in the longitude of the ascending node. The orbital plane remains essentially fixed in the inertial space, and only the shape and size of the ellipse are altered.

Now introduce a nondimensional acceleration, $R^* \equiv \frac{R}{g_a}$. Thus as before

$$R = n^2 a R^* \quad (289)$$

For the case of a radial acceleration, the angular momentum is conserved. Thus

$$\frac{dt}{d\theta} = \frac{r^2}{a^2 n\sqrt{1-e^2}}$$

and Eqs (288) become

$$\left\{ \begin{aligned} \frac{da}{d\theta} &= 2ae\frac{(1-e^2)\sin\theta}{(1+e\cos\theta)^2} R^* \\ \frac{de}{d\theta} &= \frac{(1-e^2)^2\sin\theta}{(1+e\cos\theta)^2} R^* \\ \frac{d\tilde{\omega}}{d\theta} &= -\frac{(1-e^2)^2\cos\theta}{e(1+e\cos\theta)^2} R^* \\ \frac{d\epsilon}{d\theta} &= -\left[\frac{2(1-e^2)^{5/2}}{(1+e\cos\theta)^3} + \frac{e(1-e^2)^2\cos\theta}{(1+\sqrt{1-e^2})(1+e\cos\theta)^2}\right] R^* \end{aligned} \right\} \quad (290)$$

As for micro-thrust applications, the changes in orbital parameters during one revolution are extremely small; thus it is possible to assume $e = e_0$, $a = a_0$, etc., and consider these variables as "almost constants" in integrating Eqs (290). This assumption can be proven analytically for certain cases, and it is a close first approximation for all cases.

The change in semimajor axis during one revolution in the orbit is found as

$$\Delta a = \int da = 2 ae R^* (1-e^2) \int \frac{\sin\theta\, d\theta}{(1+e\cos\theta)^2} = \frac{2a R^* (1-e^2)}{(1+e\cos\theta)}\Bigg|_{\theta_0}^{\theta} \quad (291)$$

Similarly, the change in eccentricity for intervals up to 1 rev is

$$\Delta e = \int de = R^* (1-e^2)^2 \int \frac{\sin\theta\, d\theta}{(1+e\cos\theta)^2} = \frac{R^* (1-e^2)^2}{e(1+e\cos\theta)}\Bigg|_{\theta_0}^{\theta} \quad (292)$$

If e = 0, the equation simplifies to

$$\Delta e = \int de = R^* \int \sin\theta\, d\theta = -R^* \cos\theta \Big|_{\theta_0}^{\theta}$$

The variation in the longitude of the perigee again for intervals up to 1 rev is

$$\Delta\tilde{\omega} = \int d\tilde{\omega} = -\frac{(1-e^2)}{e} R^* \int \frac{\cos\theta\, d\theta}{(1+e\cos\theta)^2}$$

or

$$\Delta\tilde{\omega} = -\frac{R^*}{e\sqrt{1-e^2}}\left[\frac{\sqrt{1-e^2}\sin\theta}{1+\cos\theta} - 2e\tan^{-1}\left(\sqrt{\frac{1-e}{1+e}}\tan\frac{\theta}{2}\right)\right]_{\theta_0}^{\theta} \quad (293)$$

Finally, the change in the mean longitude of epoch for this same interval is

$$\Delta\epsilon = \int d\epsilon = -\left[2(1-e^2)^{5/2}\int \frac{d\theta}{(1+e\cos\theta)^3}\right.$$

$$+ \frac{e(1-e^2)^2}{1+\sqrt{1-e^2}} \int \frac{\cos\theta \, d\theta}{(1+e\cos\theta)^2} \Bigg] R^*$$

Integrating and collecting terms,

$$\Delta\epsilon = -R^* \sqrt{1-e^2} \left\{ \frac{-e(1-e^2)\sin\theta}{(1+e\cos\theta)^2} \right.$$

$$- 2\tan^{-1}\left(\sqrt{\frac{1-e}{1+e}}\tan\frac{\theta}{2}\right) + \left(\frac{3}{\sqrt{1-e^2}} + \frac{e}{1+\sqrt{1-e}}\right)$$

$$\left. \cdot \left[\frac{-e\sqrt{1-e^2}\sin\theta}{1+e\cos\theta} + 2\tan^{-1}\left(\sqrt{\frac{1-e}{1+e}}\tan\frac{\theta}{2}\right)\right]\right\} \Bigg|_{\theta_0}^{\theta}$$

(294)

Equations (291), (292), (293) and (294) define all the changes in orbital parameters for a constant radial micro-thrust applied during a known change in the central angle during 1 orbit.

c. Circumferential acceleration

Last, the case is considered for radial and the normal components of the micro-thrust acceleration equal to zero; i.e., only the component in the orbital plane perpendicular to the radius vector exists. Then, Eqs (276) reduce to

$$\left\{ \begin{array}{l} \frac{da}{dt} = \frac{2}{n\sqrt{1-e^2}} \left(\frac{p}{r}\right) T \\ \\ \frac{de}{dt} = \frac{\sqrt{1-e^2}}{na} (\cos\theta + \cos E)\, T \\ \\ \frac{di}{dt} = \frac{d\Omega}{dt} = 0 \\ \\ \frac{d\tilde{\omega}}{dt} = \frac{\sqrt{1-e^2}}{nae} \sin\theta \left(1+\frac{r}{p}\right) T \\ \\ \frac{d\epsilon}{dt} = \frac{e\sqrt{1-e^2}}{na\left(1+\sqrt{1-e^2}\right)} \left(1+\frac{r}{p}\right) T \end{array} \right\} \quad (295)$$

Once more, using a nondimensional acceleration $T^* = \frac{T}{g_a}$, substituting $T = n^2 a\, T^*$ into Eq (295) and remembering from the definition of semiparameter that

$$\frac{p}{r} = (1-e^2)\frac{a}{r}$$

the following set of differential equations is obtained:

$$\left[\begin{array}{l} \frac{da}{d\theta} = 2r\,T^* = \frac{2p}{1+e\cos\theta} T^* \\ \\ \frac{de}{d\theta} = (1-e^2)^2 \frac{(\cos\theta + \cos E)}{(1+e\cos\theta)^2} T^* \\ \\ \frac{d\tilde{\omega}}{d\theta} = \frac{\sin\theta}{e}\left(1+\frac{r}{p}\right)\left(\frac{r}{a}\right)^2 T^* \\ \\ \frac{d\epsilon}{d\theta} = \frac{e}{1+\sqrt{1+e^2}}\left(1+\frac{r}{p}\right)\left(\frac{r}{a}\right)^2 T^* \end{array} \right] \quad (296)$$

Here, also, the assumption is made that the changes in orbital parameters during one revolution are extremely small. Thus, Eqs (296) can be integrated as follows, giving the change in semimajor axis

$$\Delta a \equiv \int da = 2pT^* \int \frac{d\theta}{1+e\cos\theta}$$

$$= \frac{2pT^*}{\sqrt{1-e^2}} \tan^{-1}\left(\frac{\sqrt{1-e^2}\sin\theta}{1+e\cos\theta}\right)\Bigg|_{\theta_0}^{\theta} \quad (297)$$

Now

$$\cos E = \frac{e+\cos\theta}{1+e\cos\theta}$$

Therefore, the change in eccentricity becomes

$$\Delta e \equiv \int de = (1-e^2)^2 T^* \left\{ \int \frac{\cos\theta\, d\theta}{(1+e\cos\theta)^2} \right.$$

$$\left. + e\int \frac{d\theta}{(1+e\cos\theta)^3} + \int \frac{\cos\theta\, d\theta}{(1+e\cos\theta)^3} \right\}$$

$$\Delta e = (1-e^2)^2 T^* \left\{ \frac{1}{(1-e^2)^{3/2}} \left[\frac{\sqrt{1-e^2}\sin\theta}{1+e\cos\theta} \right.\right.$$

$$\left.\left. - 2e\tan^{-1}\left(\sqrt{\frac{1-e}{1+e}}\tan\frac{\theta}{2}\right)\right] \right.$$

$$+ \frac{1}{2(1-e^2)^{3/2}} \left\{ \frac{-e\sqrt{1-e^2}\sin\theta}{(1+e\cos\theta)^2} + \right.$$

(continued)

$$+\frac{3}{1-e^2}\left[\frac{-e\sqrt{1-e^2}\sin\theta}{1+e\cos\theta}+2\tan^{-1}\left(\sqrt{\frac{1-e}{1+e}}\tan\frac{\theta}{2}\right)\right]$$

$$-2\tan^{-1}\left(\sqrt{\frac{1-e}{1+e}}\tan\frac{\theta}{2}\right)\Bigg\}+\frac{1}{2(1-e^2)^{5/2}}\left[\frac{(1-e^2)^{3/2}\sin\theta}{(1+e\cos\theta)^2}\right.$$

$$\left.+\frac{(1+2e^2)\sqrt{1-e^2}\sin\theta}{(1+e\cos\theta)}-6e\tan^{-1}\left(\sqrt{\frac{1-e}{1+e}}\tan\frac{\theta}{2}\right)\right]\Bigg\}\Bigg|_{\theta_0}^{\theta}$$

(298)

The change in the longitude of perigee is

$$\Delta\tilde{\omega}=\int d\tilde{\omega}=\frac{T^*(1-e^2)^2}{e}\left[\int\frac{\sin\theta\,d\theta}{(1+e\cos\theta)^2}+\int\frac{\sin\theta\,d\theta}{(1+e\cos\theta)^3}\right]$$

and, thus,

$$\Delta\tilde{\omega}=\frac{T^*(1-e^2)^2}{e^2}\left[\frac{1}{(1+e\cos\theta)}+\frac{1}{2(1+e\cos\theta)^2}\right]\Bigg|_{\theta_0}^{\theta}$$

(299)

The change in the mean longitude of epoch is

$$\Delta\epsilon\equiv\int d\epsilon=\frac{T^*e(1-e^2)^2}{1+\sqrt{1-e^2}}\left[\int\frac{d\theta}{(1+e\cos\theta)^2}+\int\frac{d\theta}{(1+e\cos\theta)^3}\right]$$

and, finally,

$$\Delta\epsilon=\frac{T^*e\sqrt{1-e^2}}{2\left(1+\sqrt{1-e^2}\right)}\Bigg\{2\left[\frac{-e\sqrt{1-e^2}\sin 0}{1+e\cos\theta}\right.$$

$$\left.+2\tan^{-1}\left(\sqrt{\frac{1-e}{1+e}}\tan\frac{\theta}{2}\right)\right]$$

$$-\frac{e\sqrt{1-e^2}\sin\theta}{(1+e\cos\theta)^2}+\frac{3}{1-e^2}\left[\frac{-e\sqrt{1-e^2}\sin\theta}{1+e\cos\theta}\right.$$

+ .

(continued)

$$+2\tan^{-1}\left(\sqrt{\frac{1-e}{1+e}}\tan\frac{\theta}{2}\right)$$

$$\left.-2\tan^{-1}\left(\sqrt{\frac{1-e}{1+e}}\tan\frac{\theta}{2}\right)\right]\Bigg\}\Bigg|_{\theta_0}^{\theta}$$

(300)

d. Conclusions

The equations of the preceding discussions are in the strictest sense only approximate, since the coupling of the equations has been neglected. However, if the interval of time is sufficiently small, the results will be quite accurate. The implication of this is that these expressions could be used to evaluate secular changes and a program written for an electronic computer to sum the various contributions. This is indeed true. The procedure has much to recommend it since the time of computation will be much reduced and the problems of numerical roundoff almost eliminated.

M. REFERENCES

1. Kraft, J. D., "Techniques and Requirements for Orbit Maintenance," ER 12493, Martin Company (Baltimore), 29 June 1962.

2. Levy, Ezra C., "Propulsion Requirement to Counteract One Effect of Earth's Oblateness," Space Technology Laboratories Memo 7720.2-130, 3 January 1961.

3. Bruce, R., "Satellite Orbit Sustaining Techniques," STL Report STL-TM-60-0000-94092, November 1961.

4. Lawden, D. F., and Long, R. S., "The Theory of Correctional Maneuvers in Interplanetary Space," RR-60-1186-11, Radiation Inc., 30 August 1960.

5. "Guidance Requirements for a 24-Hour Satellite," ER 10718-6, Martin Company, 15 October 1959.

6. Kraft, J. D., "Techniques and Requirements for Orbit Maintenance," ER 12493, Martin Company, June 1962.

7. Lawden, D. F., "Optimal Trajectories," Report RR-59-1186-7, Radiation Inc., (Melbourne), May 1959.

8. Lawden, D. F., "Minimal Rocket Trajectories," Journal of the American Rocket Society, Vol. 23, No. 6, 1953.

9. Lawden, D. F., "Fundamentals of Space Navigation," Journal of the British Interplanetary Society, Vol. 13, No. 2, 1954.

10. Miele, A., "General Variational Theory of the Flight Paths of Rocket-Powered Aircraft, Missiles and Satellite Carriers," Report No. A-58-2, Purdue Research Foundation, 1958.

11. Anthony, M., et al., "Variational Approach to Trajectory Optimization," University of Colorado Extension Lectures, Spring Semester 1960.

12. Gedeon, G. S., "Orbital Segment Mechanics," Norair Report ASG-TM-61-43.

13. Hoelker, R. F., and Silber, R., "Bi-Elliptical Transfer Between Circular Coplanar Orbits," ABMA Report DA-TM-2-59, January 1959.

14. Vargo, L. G., "Optimal Transfer Between Two Coplanar Terminals in a Gravitational Field," presented at the Western Regional Meeting, 13 to 19 August 1958 (AAS Preprint No. 58-20).

15. Munick, H., McGill, R., and Taylor, G. E., "Minimization of Characteristic Velocity for Transfer Between Arbitrary Terminals in an Inverse Square Field Using Two Impulses," presented at the ARS 14th Annual Meeting, Washington, D. C., 16 to 20 November 1959 (ARS Preprint No. 959-59). See also abridged version ARS Journal, July 1960.

16. Munick, H., McGill, R., and Taylor, G. E., "Analytic Solutions to Several Optimum Orbit Transfer Problems," Journal of the Astronautical Sciences, Vol. VII, No. 4, Winter 1960.

17. Darby, W. G., "Correction for the Effects of Finite Thrusting Times in Orbit Changing Maneuvers," IAS Preprint 61-154-1848, June 1961.

18. Tsien, H. S., "Takeoff from Satellite Orbit," ARS Journal, Vol. 23, No. 4, July 1953, p 233.

19. "Advances in Astronautical Sciences," Vol. 3 (Proceedings of the Western Regional Meeting of the AAS), Plenum Press, Inc. (New York), August 1958.

20. Copeland, J., "Interplanetary Trajectories Under Low Thrust Radial Acceleration," ARS Journal, Vol. 29, No. 4, April 1959, p 267.

21. Benney, D. J., "Escape from a Circular Orbit Using Tangential Thrust," Jet Propulsion, Vol. 28, No. 3, March 1958, p 167.

22. "Dynamic Analysis and Design Performance Requirements for Satellite Vehicle Guidance Systems," ER 10470-6, Martin Company, January 1959.

23. Bacon, R. H., "Logarithmic Spiral: An Ideal Trajectory for the Interplanetary Vehicle with Engines of Low Sustained Thrust," American Journal of Physics, Vol. 27, No. 3, March 1959, p 164.

N. BIBLIOGRAPHY

Altman, S. P, "Orbital Transfer for Satellites," Los Angeles, 4th Symposium on Ballistic Missiles and Space Technology, August 1959.

Anthony, M., et al., "Variational Approach to Trajectory Optimization," University of Colorado Extension Lectures (Boulder), Spring 1960.

Arthur, P., et al., "Simple Method for Approximating the Characteristics of Low Thrust Trajectories," ARS Journal, Vol. 30, No. 7, July 1960.

Augenstein, B. W., "Dynamic Problems Associated with Satellite Orbit Control," Lockheed Missile Systems Division (Palo Alto, California), 1959. (ASME Paper 59-AV-4).

Bakalyar, G., "Orbital Rendezvous and Point-to-Point Velocity Transfers," Report No. MI-59-61, Martin Company (Denver), November 1959.

Battin, R. H., and Laning, J. H., "A Navigation Theory for Round Trip Reconnaissance Missions to Venus and Mars," Massachusetts Institute of Technology, MIT Instrumentation Laboratory, Cambridge, August 1959.

Brown, H., and Nelson, J. R., "Thrust Orientation Patterns for Orbit Adjustment of Low Thrust Vehicles," ARS Journal, Vol. 30, No. 7, July 1960, pp 635 to 637.

Bruce, R. W., Satellite Orbit Sustaining Techniques (U)," Preprint No. 1448-60, American Rocket Society, 5 to 8 December 1960.

Buchheim, R. W., "Space Flight Trajectories, Navigation and Maneuvers (U)," Report No. P-1387, The Rand Corporation, Santa Monica, California, May 1958.

Burgess, E., "Satellite and Transfer Orbits," Pacific Rocket Society Bulletin, Vol. 4, No. 4, April 1951, pp 5 to 12.

Carstens, J., "Optimum Maneuvers for Launching Satellite into Circular Orbits of Arbitrary Radius and Inclination, Preprint No. 1450-60, American Rocket Society, December 1960.

Cohen, S. R., and Ruggiero, R. R., "Multi-Body Effects on Orbit Transfer (U)," Preprint No. 1478-60, American Rocket Society, 5 to 8 December 1960.

Darby, W. G., "Correction for the Effects of Finite Thrusting Time in Orbit Changing Maneuvers," Preprint No. 61-154-1848, Institute of Aerospace Sciences, June 1961.

De Bra, D., "Orbital Plane-Change Maneuver," Astronautical Sciences Review, Vol. 1, No. 4, October to December 1959.

Demetraides, S., "Orbital Propulsion System for Space Maneuvering," Astronautical Sciences Review, Vol. 1, No. 4, October to December 1959.

Edelbaum, T. N.,
"Propulsion Requirements for Controllable Satellites, Preprint No. 1228-60, American Rocket Society, 1960.

"Some Extensions of the Hohmann Transfer Maneuver," ARS Journal, Vol. 29, No. 11, 1959, pp 864 to 865.

Ehricke, K. A., "Error Analysis of Keplerian Flights Involving a Single Central Force Field and Transfer Between Two Central Force Fields," Navigation, Spring 1958, pp 5 to 23.

Fitzgibbon, M. C., "Satellite Orbit Control System," Preprint No. 59-7, American Astronautical Society, August 1959 (Also, Advances in the Astronautical Sciences, Vol. 5, New York, Plenum Press, 1960).

Fox, R., "Powered Trajectory Studies for Low Thrust Vehicles," ARS Journal, Vol. 31, No. 1, January 1961.

Gundel, B. H., and De Bra, D. B., "Circularization of Elliptic Orbits," Preprint No. 60-36, American Astronautical Society, 1960.

Hord, R. A., "Relative Motion in the Terminal Phase of Interception of a Satellite or Ballistic Missile," NASA TN 4399, September 1958.

Hoelker, R., and Silber, R., "Bi-Elliptic Transfer Between Co-Planar Circular Orbits," 4th Symposium on Ballistic Missile and Space Technology, Los Angeles, California, August 1959.

Johnson, P. G., et al., "Use of Perigee Propulsion for Orbital Launch of Nuclear Rockets," American Astronautical Society, 1960 (Presented at Seattle, Washington, Western National Meeting of the American Astronautical Society, 8 to 11 August 1960).

Kelber, C. C., "Maneuverable Satellite," Western Regional Meeting of the American Astronautical Society, August 1958.

Ketchum, H. B.,
"Navigational Calculations in Space Flight, Part I--Planetary Orbital Distances," Journal of Space Flight, Vol. 5, April 1953.

"Navigational Calculations in Space Flight; Part II--Planetary Orbital Velocities and Gravitational Fields," Journal of Space Flight, Vol. 5, September 1953.

"Navigational Calculations in Space Flight; Part III--Satellite Gravitational Field, Orbital Velocities and Elements of Orbits," Journal of Space Flight, Vol. 5, December 1953.

"Navigational Calculations in Space Flight; Part IV--The Effects of Atmospheric Friction," Journal of Space Flight, Vol. 6, June 1954.

Koskela, P. E., Nicola, L., and Walters, L. G., "The Station Keeping Implications of an Artificial Satellite," Preprint No. 1229-60, American Rocket Society, 1960.

Lass, H., "Low Thrust Takeoff from a Satellite Orbit," ARS Journal, Vol. 31, No. 1, January 1961.

Lawden, D. F.,
"Orbital Transfer Via Tangential Ellipses," Journal of the British Interplanetary Society, Vol. 11, No. 6, November 1952, pp 278 to 279.

"Inter-Orbital Transfer of a Rocket," Journal of the British Interplanetary Society, Vol. 11, No. 6, November 1952, pp 321 to 333.

"Minimal Rocket Trajectories," Jet Propulsion, Vol. 23, November to December 1953.

"Fundamentals of Space Navigation," Journal of the British Interplanetary Society, Vol. 13, No. 2, March 1954, pp 87 to 101.

"Perturbation Maneuvers," Journal of the British Interplanetary Society, Vol. 13, No. 6, November 1954.

"Transfer Between Circular Orbits," Jet Propulsion, Vol. 27, No. 7, July 1956, pp 555 to 558.

"Optimal Trajectories," Report No. RR-59-1186-7, Radiation, Inc. (Orlando), May 1959.

"Necessary Conditions for Optimal Rocket Trajectories," Quarterly Journal of Mechanics and Applied Mathematics, Vol. 12, November 1959.

"The Theory of Correctional Maneuvers in Interplanetary Space," Report No. RR-60-1186-11, Orlando, Florida, Radiation, Inc., August 1960.

"Optimal Program for Correctional Maneuvers," Report No. RR-1186-60-13, Radiation, Inc. (Orlando), 27 September 1960.

Leitmann, G., "On a Class of Variational Problems in Rocket Flight," Journal of the Aerospace Sciences, Vol. 26, September 1959.

Levin, E., "Low Thrust Transfer Between Circular Orbits (U)," Report No. P-1536, The Rand Corporation, Santa Monica, California, October 1958.

Loh, W. H. T., "Minor Circle Flight for Boost Glide on Orbital Re-entry Vehicles," Preprint No. 60-35, American Astronautical Society, 1960.

London, H. S., "Change of Satellite Orbit Plane by Aerodynamic Maneuvering, Report No. 61-5, Institute of Aerospace Sciences, January 1961.

Miele, A.,
"General Variational Theory of the Flight Paths of Rocket-Powered Aircraft, Missiles and Satellite Carriers," Report No. A-58-2, Purdue University, Purdue Research Foundation, Lafayette, 1958.

"Theorem of Image Trajectories," Report No. DI-82-0039, Boeing Airplane Company, Seattle, January 1960.

Morgenthaler, G. W.,
"On Midcourse Guidance in Satellite Interception," Astronautica Acta, Vol. 5, No. 6, 1959.

"On Midcourse Guidance in Satellite Interception, II," Caywood-Schiller Associates, 31 January 1959.

Munick, H., and McGill, R., "Analytical Estimates for Optimum Transfer Paths," ARS Journal, Vol. 30, January 1960.

Munick, H., McGill, R., and Taylor, G. E., "Analytic Solutions to Several Optimum Orbit Transfer Problems," Journal of the Astronautical Sciences, Vol. 7, No. 4, Winter 1960, pp 73 to 77.

Munick, H., et al., "Minimization of Characteristic Velocity for 2 Pulse Orbital Transfers," ARS Journal, Vol. 30, No. 7, July 1960.

Rider, L.,
"Ascent from Inner Circular to Outer Co-Planar Elliptic Orbits," ARS Journal, Vol. 30, No. 3, March 1960.

"Low Thrust Correction of Orbital Orientation," ARS Journal, Vol. 30, No. 7, July 1960, pp 647 to 648.

Schindler, G., "Minimum Time Flight Paths," ARS Journal, Vol. 30, No. 4, April 1960.

Silber, R., "Survey of Characteristic Velocity Requirements for Two-Impulse Transfers Between Circular and Coplanar Exterior Elliptical Orbit with Exposition of Local and Overall Optimum Solutions," NASA TN D-600, March 1961.

Skalafuris, A., et al., "Midcourse Guidance Problem in Satellite Interception," ARS Journal, Vol. 30, No. 1, January 1960.

Smith, F. T., "Optimization of Multistage Orbit Transfer Processes by Dynamic Programming," ARS Journal, Vol. 31, No. 11, November 1961, pp 1553 to 1560.

Szebehely, V. G., "Equations for Thrust Programs," Stockholm, XIth International Astronautical Congress, Trajectories Session, 1960.

Tanguay, A. R., and Hock, D. H., "Space Maneuvers," Space Trajectories, Academic Press (New York), 1960.

Ting, L.,
"Optimum Orbital Transfer by High Thrust Rockets," PIBAL Report No. 633, Polytechnic Institute of Brooklyn, New York, February 1961, 29 pp (Also, AFOSR 163).

"Optimum Orbital Transfer by Impulses," ARS Journal, Vol. 30, No. 11, November 1960.

Townsend, G., Kraft, D., and Kork, J., "Maneuvers," Design Guide to Orbital Flight, McGraw-Hill Book Company (New York), 1962.

Tsien, H. S., "Take-off from a Satellite Orbit (Radial Thrust)," Jet Propulsion, Vol. 23, No. 4, July to August 1953.

Vargo, L., "Generalization of Minimum Impulse Theorem to the Restricted Three Body Problem," Journal of the British Interplanetary Society, Vol. 17, September to October 1959.

Warzecha, L. W., "Performance and Design Considerations for Maneuvering Space Vehicles," Aero/Space Engineering, November 1960, pp 18 to 23.

Wolfe, J. F., and DeBra, D., "Two-Maneuver Ascents to Circular Orbits," J. Astron. Sci., Vol. 7, No. 2, 1960, pp 47 to 48.

Zilczer, P., "Space Navigation by Correlation," Preprint No. 60-18, American Astronautical Society, 1960.

Alderson, J. D., Jr., "Optimum Thrust Programs for High-Altitude Rockets," No GAE/AE-60-1, 88 pages, Wright-Patterson Air Force Base, Ohio, Air Force Institute of Technology, September 1960 (ASTIA No. AD-250795).

Baker, G. A., Jr., Ford, K. W., and Porter, C. E., "Optimal Accuracy Rocket Trajectories," Journal of Applied Physics, Vol. 30, No. 12, December 1959, pp 1925 to 1932.

Bellman, R.,
"An Introduction to the Theory of Dynamic Programming," Report No. R-245, The Rand Corporation (Santa Monica), 1953.

"The Theory of Dynamic Programming," Bulletin of the American Mathematical Society, Vol. 60, No. 6, p 503, November 1954.

Bellman, R., and Dreyfus, S. E.,
"Computational Solutions of Dynamic Programming; VI--on the Optimal Trajectory Problem," Report No. RM-1750, The Rand Corporation (Santa Monica), 16 April 1957 (ASTIA No. AD-123 553).

"An Application of Dynamic Programming to the Determination of Optimal Satellite Trajectories," Journal of the British Interplanetary Society, Vol. 17, Nos. 3-4, May-August 1959, pp 78 to 83.

Bender, D. F., "Optimum Co-Planar Two Impulse Transfers Between Elliptic Orbits," IAS Paper No. 62-4, IAS 30th Annual Meeting, January 1962.

Berman, L. J., "A Digital Computer Study of the Powered Flight Trajectories of Long Range Ballistic Missiles: Part III--Trajectory Optimization by Partial Variation," Report No. ARG-R-1, Massachusetts Institute of Technology (Cambridge), March 1958 (ASTIA No. AD-215 407).

Billik, B. H., "On the Maximum Burnout Velocity of a Vehicle Achieved Through a Throttling Process," Report No. STL 7720, Space Technology Laboratories (Los Angeles), 4 August 1960.

Breakwell, J. V.,
"The Optimization of Trajectories," Report No. AL-2706 NAA, North American Aviation (Los Angeles), August 1957 (Also, Journal of

the Society of Industrial and Applied Mathematics, Vol. 7, No. 2, June 1959, pp 215 to 247) (Also, Flight Dynamics and Space Mechanics, January 1960, LMSD-288139, Vol. III, Chapter 12) (Also, ASTIA No. AD-209 092).

"Optimal Ascent into a Circular Orbit," IAS Vehicle Systems Optimization Symposium (New York), 27-29 November 1961.

Bryson, A. E., and Ross, S. E., "Optimum Rocket Trajectories with Aerodynamic Drag," Jet Propulsion, Vol. 28, No. 7, July 1958, pp 465 to 469 (Also, Preprint 542-57, American Rocket Society, December 1957).

Carstens, J. P., and Edelbaum, T. N., "Optimum Two Impulse Ascents to Circular Orbits," Journal of the Astronautical Sciences, Vol. 7, No. 4, Winter 1960, pp 96 to 97.

"Optimum Maneuvers for Launching Satellites into Circular Orbits of Arbitrary Radius and Inclination," Preprint No. 1450-60, American Rocket Society, December 1960.

Cashmore, D. J., "Minimum Gravitational Losses for Rocket Motion near a Planetary Surface," Journal of the British Interplanetary Society, Vol. 17, No. 2, March-April 1959, pp 52 to 57.

Cicala, C., and Miele, A., "Brachistochronic Maneuvers of a Variable Mass Aircraft in a Vertical Plane," Journal of the Aeronautical Sciences, Vol. 22, No. 8, August 1955, pp 577 to 578.

"Generalized Theory of the Optimum Thrust Programming for the Level Flight of a Rocket-Powered Aircraft," Jet Propulsion, Vol. 26, No. 6, June 1956, pp 443 to 455.

Courant, R., "Calculus of Variations and Supplementary Notes," New York University, Institute of Mathematical Sciences (New York), 1949 to 1950.

Corben, H. C., "A Note on the Optimization of Powered Trajectories in an Arbitrary Gravitational Field," RW Report ERL-IM-150, Thompson Ramo-Wooldridge, 4 December 1957.

Deaton, A. W., and Brandon, P. D., "Saturn Missile SA-7: Optimum Trajectory Shape for Circular Orbit Mission (U)," MTP-AERO-60-8, Marshall Space Flight Center, 14 November 1960.

Desoer, C. A., "Pontriagin's Maximum Principle and the Principle of Optimality," Report 60-326 (U/Rpt.), University of California (Berkeley), 11 November 1960, 9 pages (Also, Journal of the Franklin Institute, Vol. 271, No. 5, May 1961, pp 361 to 367).

Edelbaum, T. N., and Carstens, J. P., "Optimum Maneuvers for Launching Satellites into Circular Orbits of Arbitrary Radius and Inclination," United Aircraft Corporation, Research Laboratories (East Hartford), 1960 (ARS Preprint No. 1450-60).

Eggers, A. J., Allen, H. J. and Neice, S. E., "Comparative Analysis of the Performance of Long-Range Hypervelocity Vehicles," NACA RM A 54 L10, March 1955 (Also, NACA TN-4046, October 1957).

Ehlers, E. E., "On the Trajectories of a Missile in a Constant Gravity Field with the Sine and the Tangent of the Thrust Angle Varying Linearly with Time," Document No. DI-82-0069, Math. Note No. 222, Washington, Boeing Scientific Research Laboratory (Seattle) October 1960 (ASTIA No. AD-245 134).

"Missile Trajectories with Linear Time Variation of the Sine or Tangent of the Thrust Angle," ARS Journal, Vol. 31, No. 5, May 1961, pp 631 to 636.

Egorov, V. A., "On the Solution of a Degenerate Variational Problem and the Optimum Climb of a Space Rocket," Journal of Applied Mathematics and Mechanics, Vol. 22, No. 1, 1959 (Translated).

Ewing, G. M., "A Fundamental Problem of Navigation in Free Space," Quarterly of Applied Mathematics, Vol. XVIII, No. 4, January 1961.

Faulkner, F. D., "The Problem of Goddard and Optimum Thrust Programming," Research Paper No. 11, Naval Postgraduate School (Monterey, California), March 1957 (Also, 3rd Annual Meeting of the American Astronautical Society (New York), 6-7 December 1956) (Also, Proceedings of the American Astronautical Society, 1956, pp 43 to 51).

"Some Results from Direct Methods Applied to Optimum Rocket Trajectories," Proceedings of the 10th International Astronautical Congress, Amsterdam, 1958, Springer-Verlag (Vienna), 1959, Vol. II, pp 694 to 701.

"Complete Elementary Solution to Some Optimum Trajectory Problems," ARS Journal, Vol. 31, No. 1, January 1961, pp 33 to 39.

Foote, J. R., Butler, T., Adney, J. E. and Thatcher, H. C., "Direct Variational Methods and Brachistochrone Problems," AFOSR-101, Holloman Air Force Base, New Mexico, Directorate of Research Analysis, January 1961 (Also, ASTIA No. AD-251 008).

Foulders, C. R., "Minimum-Time Steering Programs for Orbital Transfer with Low-Thrust Rockets," Astronautica Acta, Vol. 7, No. 1, 1961, pp 35 to 49.

Fox, R. H., "Optimum Exhaust Velocity Programming and Propulsion Efficiency," Report UCRL-5135, University of California, Lawrence Radiation Laboratory (Livermore), 26 May 1958 (Also, Journal of the Astronautical Society, Vol. VI, No. 1, Spring 1959, pp 13 to 16.

Fraeijs, De Veubeke, B., "Variational Methods in Optimizing Rocket Performance," Rocket Propulsion, Elsevier Publishing Company (New York), 1960, Chapter 12, pp 772 to 812.

Fried, B. D.,
"On the Powered Flight Trajectory of an Earth Satellite," Jet Propulsion, Vol. 27, No. 6, June 1957, pp 641 to 643.

"The Dynamics of Powered Flight with Application to Trajectory Optimization Problems," Report No. ARL-7-74, Thompson Ramo-Wooldridge Corporation, Physical Research Laboratory, 31 December 1957.

"Trajectory Optimization for Powered Flight in Two or Three Dimensions," Space Technology, John Wiley and Sons, Inc. (New York), 1959, Chapter 4 (Seifert, H. S., ed).

Graham, E. W., "A Class of Optimum Trajectory Problems in Gravitational Fields," Journal of the Aerospace Sciences, Vol. 27, No. 4, April 1960, pp 296 to 303.

Graham, E. W., and Beane, B. J., "Optimum Rocket Trajectories with Atmospheric Resistance," Report No. SM 23745, California, Douglas Aircraft Company (Santa Monica), November 1959 (Also, ASTIA No. AD-235 783).

Granton, J., Jr., et al., "The Trajectory of a Rocket with Thrust," Jet Propulsion, Vol. 28, No. 7, July 1958, pp 472 to 478.

Halkin, H., "Nondegenerate Variational Problems and the Principle of Optimal Evolution," IAS Vehicle Systems Optimization Symposium (New York), 27-29 November 1961.

Hestenes, M. R., "A General Problem in the Calculus of Variations with Applications to Paths of Least Time," Report No. RM-100, California, The Rand Corporation (Santa Monica), March 1950.

Horner, J., and Silber, R., "Impulse Minimization for Hohmann Transfer Between Inclined Circular Orbits of Different Radii," ABMA Report No. DA-TR-70-59, Army Ballistic Missile Agency (Huntsville), 1959.

Jurovics, S. A., and McIntyre, J. E.,
"The Adjoint Method and Its Application to Trajectory Optimization," MD 60-334, North American Aviation (Los Angeles), October 1960.

"Optimum Steering Program for the Entry of a Multistage Vehicle into a Circular Orbit," ARS Journal, Vol. 31, No. 4, April 1961, pp 518 to 523 (Also, MD 60-205, North American Aviation (Los Angeles), May 1960, Revised October 1960).

Kelley, H. J.,
"An Investigation by Variational Methods of Flight Paths for Optimum Performance," SCD Thesis, New York University, Guggenheim School of Aeronautics (New York), May 1958.

"Gradient Theory of Optimal Flight Paths," Preprint No. 1230-60, American Rocket Society, 1960 (Also, ARS Journal, Vol. 30, No. 10, October 1960).

"Successive Approximation Techniques for Trajectory Optimization," IAS Vehicle System Optimization Symposium (New York), 27-29 November 1961.

Krasovskii, N. N., "Sufficient Conditions for Optimization," (Prikl. Mat. Mekh.) Appl. Math. Mech., Vol. 23, No. 3, Pergamon Press (New York), 1959, pp 839 to 843.

Krotov, V, F., "Calculation of the Optimum Trajectory for the Entry of a Rocket into a Particular Circular Trajectory (Orbit) Around the Earth," Mekhanika, MVTU No. 50, Moscow, Oborongiz, 1956, pp 313 to 334.

Kulakowski, L. J., and Stancil, R. T., "Rocket Boost Trajectories for Maximum Burnout Velocity," ARS Journal, Vol. 30, No. 7, July 1960, pp 612 to 618.

Lawden, D. F.,
"Minimal Trajectories," Journal of the British Interplanetary Society, Vol. 9, No. 4, July 1950, pp 179 to 186.

"The Determination of Minimal Orbits," Journal of the British Interplanetary Society, Vol. 11, No. 5, September 1952, pp 216 to 224.

"Minimal Rocket Trajectories," Journal of the American Rocket Society, Vol. 23, No. 6, November 1953.

"Stationary Rocket Trajectories," Quarterly Journal of Mechanics and Applied Mathematics, Vol. 7, Part 4, December 1954, pp 488 to 504.

"Optimum Launching of a Rocket into an Orbit Around the Earth," Astronautica Acta, Vol. 1, Fasc. 4, 1955, pp 185 to 190 (Also, Copenhagen, 6th IAF Congress, 5 August 1955).

"Optimal Programming of Rocket Thrust Direction," Astronautica Acta, Vol. 1, Fasc. 1, January 1955, pp 41 to 46 (Also, Innsbruck, 5th IAF Congress, 6 August 1954).

"Maximum Ranges of Intercontinental Missiles," The Aeronautical Quarterly, Vol. VIII, Part 3, August 1957, pp 269 to 278.

"Mathematical Problems of Astronautics," Mathematical Gazette, October 1957, pp 168 to 179.

"Optimal Rocket Trajectories," Jet Propulsion, Vol. 27, No. 12, December 1957, p 1263.

"The Employment of Aerodynamic Forces to Obtain Maximum Range of a Rocket Missile," The Aeronautical Quarterly, Vol. 9, No. 2, May 1958, pp 97 to 109.

"Optimal Trajectories," Special Report 3, Report RR-59-1186-7, Radiation, Inc. (Melbourne, Fla.), May 1959 (Also, ASTIA No. AD-219 299).

"Necessary Conditions for Optimal Rockets Trajectories," Quarterly Journal of Mechanics and Applied Mathematics, Vol. 12, No. 4, November 1959, pp 476-487.

"Advances in Space Sciences," Interplanetary Rocket Trajectories, Vol. 1, Chapter 1, p 1053, Academic Press (New York), 1959 (Ordway, F. I., III, ed).

"Optimal Powered Arcs in an Inverse Square Law Field," ARS Journal, Vol. 31, No. 4, April 1961, pp 566 to 568.

Leitmann, G.,
"Optimum Thrust Programming for High Altitude Rockets--New Solutions," NOTS TN 5038-9 (China Lake, California), 18 July 1955.

"Integration of the Euler-Legrange Equation and Numerical Example for Optimum Thrust Programming," NOTS TN 5038-10 (China Lake, California), 25 July 1955, 8 pp.

"The Problem of Optimum Thrust Programming," NOTS TN 5038-11 (China Lake, California), 22 September 1955, 11 pp.

"A Calculus of Variations Solution of Goddard's Problem," Astronautica Acta, 1956, Vol. II, Fasc. 2, pp 55 to 62.

"Stationary Trajectory for a High-Altitude Rocket with Drop Away Booster," Astronautica Acta, Vol. II, Fasc. 3, 1956, pp 119 to 124. Correction: Vol. II, Fasc. 4, p 218 (Also, Aeronautical Engineering Review, Vol. 16, 1957, p 63).

"Optimum Thrust Programming for High-Altitude Rockets," Aeronautical Engineering Review, Vol. 16, No. 6, June 1957, pp 63 to 66 (Also, NOTS TN 5038-7, 1955) (Also, University of California, PhD Dissertation).

"A Note on Goddard's Problem," Astronautica Acta, Vol, 3, Fasc. 4, 1957, pp 237 to 240.

"Trajectory Programming for Maximum Range," Journal of the Franklin Institute, Vol. 264, No. 6, December 1957, pp 443 to 452.

"On a Class of Variational Problems in Rocket Flight, Report No. LMSD-5067, Lockheed Missile Systems Division (Sunnyvale), September 1958 (Also, Journal of the Aerospace Sciences, Vol. 26, No. 9, September 1959, pp 586 to 591) (Also, ASTIA No. AD-202-302).

"On a Minimum Fuel Satellite Transfer Trajectory," TM No. 491/2-01-60, The Martin Company (Baltimore), January 1960.

"Optimal Thrust Direction for Maximum Range," Journal of the British Interplanetary Society, Vol. 16, No. 9, September-October 1958, pp 503 to 507.

"Extremal Rocket Trajectories in Position and Time Dependent Force Fields," Preprint 61-30, American Astronautical Society, 7th Annual Meeting, 16 to 18 January 1961.

"The Optimization of Rocket Trajectories--A Survey," Progress in the Astronautical Sciences, North Holland Publishing Company, 1961 (Singer, S. F., ed).

"Minimum Transfer Time for a Power-Limited Rocket, Report No. LMSD-49769, Lockheed Aircraft Corporation (Sunnyvale), 14 August 1959 (Also, Stockholm, XIth International Astronautical Congress, Astrodynamics Colloquium, 1960) (Also, "General Research in Flight Sciences, January 1959-January 1960," Flight Dynamics and Space Mechanics, Report No. LMSD-288139, Vol. III, Chapter 2 Lockheed Aircraft Corporation (Sunnyvale), January 1960). (Also, Journal of Applied Mechanics, Paper No. 61-APM-6, pp 1 to 8) (Also, ASTIA No. AD-225 924).

"Propulsive Efficiency of Rockets," Third International Symposium on Rockets (Tokyo), 1961, Preliminary Preprint.

"Optimization Techniques," Variational Problems with Bounded Control Variables, Academic Press (New York), 1961, Chapter 5.

"On Some Optimum Rocket Trajectories," IAS Vehicle Systems Optimization Symposium (New York), November 27 to 29, 1961.

Leitmann, G. and Cowan, W. D., "A Preliminary Study of the Problem of Obtaining Maximum Range with a Large Surface-to-Surface Rocket (U)," NOTS TN 5038-17, 17 October 1955. Correction: 20 August 1956 (Also, ASTIA No. AD-143 266).

Levinsky, E. S.,
"Variational Procedure for Minimizing Heating Effects During the Re-entry of a Lifting Vehicle," Report No. ZA-309, Convair (San Diego), March 1960.

"Application of Inequality Constraints to Variational Problems of Lifting Re-entry," IAS 29th Annual Meeting, New York, IAS Paper No. 61-21, 23 to 25 January 1961.

Mackay, J. S., "Approximate Solution for Rocket Flight with Linear Tangent Thrust Attitude," ARS Journal, Vol. 30, No. 11, November 1960, pp 1091 to 1093.

McIntyre, J. E.,
"Optimum Trajectory Analysis," Report No. MD 60-309, North American Aviation (Los Angeles), 6 October 1960.

"Application of Optimum Trajectory Analysis to Boost Vehicle Design," IAS Vehicle Systems Optimization Symposium (New York), 27 to 29 November 1961.

Michaels, J. E. and Hartman, M. J.,
"The Determination of Optimum Initial Conditions for Interplanetary Travel from Any Launch Site on Earth," 7th AAS National Annual Meeting (Dallas), January 1961.

Michelson, I.,
"Ultimate Design of High Altitude Sounding Rockets," ARS Journal, Vol. 27, October 1957.

Miele, A.,
"General Variational Theory of the Flight Paths of Rocket-Powered Aircraft, Missiles, and Satellite Carriers," Purdue University, School of Aeronautical Engineering (Lafayette), January 1958, A-58-2 (Also, Astronautica Acta, Vol. 4, 1958, pp 264-288 (Condensed)) (Also, Amsterdam, Proceedings of the IXth International Astronautical Congress, 18 August 1958) (Also, Office of Scientific Research, Technical Note 58-246, Contract AF-18(603)-69) (Also, AFOSR TN 58-246) (Also, ASTIA No. AD-154 148).

"Minimal Maneuvers of High-Performance Aircraft in a Vertical Plane," Purdue University School of Aeronautical Engineering (Lafayette), May 1958, A-58-3 (Also, NASA TN D-155, September 1959) (Also, ASTIA No. AD-255 859).

"Lagrange Multipliers and Quasi-Steady Flight Mechanics," Purdue University, School of Aeronautical Engineering (Lafayette), May 1958, A-58-4. (Also, Journal of Aerospace Sciences, Vol. 26, No. 9, September 1959, pp 592-598).

"Minimality for Arbitrarily Inclined Rocket Trajectories," Jet Propulsion, Vol. 28, July 1958, pp 481-483.

"Stationary Conditions for Problems Involving Time Associated with Vertical Rocket Trajectories," Journal of the Aerospace Sciences, Vol. 25, No. 7, July 1958, pp 467-468.

"Trajectories of Minimum Aerodynamic Heating Including Drag Effects," Report No. SM-27789, Douglas Aircraft Company (Santa Monica), August 1958.

"On the Brachistochronic Thrust Program for a Rocket Powered Missile Traveling in an Isothermal Medium," Report No. SM-27790, Douglas Aircraft Company, Missiles Engineering Department (Santa Monica), August 1958.

"The Application of Green's Theorem to Variational Problems of Linear Type" Report No. SM-27791, Douglas Aircraft Company (Santa Monica), August 1958 (Also, Journal of the Aerospace Sciences, Vol. 25, No. 9, September 1958, pp 581-590).

"Some Recent Advances in the Mechanics of Terrestrial Flight," Jet Propulsion, Vol. 28, No. 9, September 1958, pp 581-587.

"Mathematical Theory of the Optimum Trajectories of a Rocket--Final Report," Purdue University, School of Aeronautical Engineering (Lafayette), November 1958, A-58-10 (Also, AFOSR TR 58-154) (Also, ASTIA No. AD-206 361).

"Interrelationship of Calculus of Variations and Ordinary Theory of Maxima and Minima for Flight Applications," ARS Journal, Vol. 29, No. 1, January 1959, pp 75-76.

"Variational Apporach to Problems of Hypervelocity Flight, Final Report," Purdue University, School of Aeronautical Engineering (Lafayette), June 1959, A-59-7.

"A General Survey of the Problem of Optimizing Flight Paths of Aircraft and Missiles," Preprint No. 1219-60, American Rocket Society, 9-16 May 1960 (Also, American Rocket Society Semi-Annual Meeting, 9-16 May 1960).

"A Survey of the Problem of Optimizing Flight Paths of Aircraft and Missiles," Document No. D1-82-0050, Boeing (Seattle), July 1960 (Also, ASTIA No. AD-244 056).

"Application of Green's Theorem to the Extremization of Linear Integrals," IAS Vehicle Systems Optimization Symposium (New York), 27-29 November 1961.

Miele, A., and Cappellari, J. O., Jr.,
"Approximate Solutions to Optimum Climbing Trajectory for a Rocket-Powered Aircraft," Purdue University, School of Aeronautical Engineering (Lafayette), July 1957, A-57-4 (Also, NASA TN D-150, September 1959) (Also, ASTIA No. AD-225 566).

"Approximate Solutions to Optimum Flight Trajectories for a Turbojet-Powered Aircraft," Purdue University, School of Aeronautical Engineering (Lafayette), December 1957, A-57-7 (Also, NASA TN D-152, September 1959, 33 pp) (Also, ASTIA No. AD-225 563).

"Topics in Dynamic Programming for Rockets," Purdue University, School of Aeronautical Engineering (Lafayette), July 1958, A-58-5 (Also, Zeitschrift für Flugwissenschaften, Vol. 7, No. 1, 1959) (Also, AFOSR TN 58-685) (Also, ASTIA No. AD-162 218).

"Some Variational Solutions to Rocket Trajectories Over a Spherical Earth," Purdue University, School of Aeronautical Engineering (Lafayette), November 1958, A-58-9 (Also, AFOSR TN 58-1012) (Also, ASTIA No. AD-206 155).

Miele, A., and Cavotti, C. R.,
"Generalized Variational Approach to the Optimum Thrust Programming for the Vertical Flight of a Rocket, Part II: Application of Green's Theorem to the Development of Sufficiency Proofs for Particular Classes of Solutions," Purdue University, School of Aeronautical Engineering (Lafayette), August 1957, A-57-2, v + 30 pp (Also, Zeitschrift für Flugwissenschaften, April 1958, Bd. 6, Heft 4, s. 102-109 (Condensed)) (Also, ASTIA No. AD-136 638).

Miner, W. E.,
"Studies Toward a Minimum Propellant Guidance System," ABMA Report No. DA-TR-15-60 (Huntsville), Army Ballistic Missile Agency, 5 April 1960.

Moskowitz, S., and Ting, Lu
"A Realistic Approach to Problems of Optimum Rocket Trajectories," PIBAL Report No. 625, Polytechnic Institute of Brooklyn (New York), October 1960, 18 pp (Also, ASTIA No. AD-247 226) (Also, ARS Journal, Vol. 31, No. 4, April 1961, pp 551-553).

Mueller, G.,
"Optimum Range of a Wingless Rocket About Rotating Earth," Report No. ATI 169 753, California Institute of Technology (Pasadena), 1952, (PhD Thesis).

Munick, H.,
"An Optimum Transfer Path from an Elliptical Orbit to a Higher Energy Circular Orbit," ARS Journal, Vol. 29, No. 6, June 1959, pp 449-453.

Munick, H., and McGill, R.,
"Minimization of Characteristic Velocity for Two-Impulse Orbital Transfer," ARS Journal, Vol. 30, No. 7, July 1960, pp 638-639.

"Analytical Estimates for Optimum Transfer Paths," ARS Journal, Vol. 30, January 1960, pp 120-121.

Munick, H., McGill, R., and Taylor, G. E.,
"Analytic Solutions to Several Optimum Orbit Transfer Problems," Journal of Astronautical Sciences, Vol. 7, No. 4, Winter 1960, pp 73-77.

Newton, R. R.,
"On the Optimum Trajectory of a Rocket," Journal of the Franklin Institute, No. 3, Vol. 266, September 1958, pp 155-187 (Also, New Orleans, Louisiana, Tulane University, 22 April 1957, Department of Physics Project TU 2-9F, R 5 16-7) (Also, Reprint Series, Report No. 475, Silver Spring, Maryland, The Johns Hopkins University, Applied Physics Laboratory, December 1958).

"On the Optimization of Physical Propulsion Systems," Jet Propulsion, Vol. 28, No. 11, November 1958, pp 752-753.

Olds, R. H.,
"Optimum Variation of Exhaust Velocity During Burning," NAVORD Report 6427, 28 October 1958, p 5 (Also, Jet Propulsion, Vol. 28, No. 6, June 1958, pp 405-406).

Okhotsimskii, D. E., and Eneev, T. M.,
"Some Variation Problems Connected with the Launching of Artificial Satellites of the Earth," Uspekhi Fiz. Nauk, Vol. 63, No. 1, September 1957 (In Russian) (Also, Journal of the British Interplanetary Society, Vol. 16, No. 5, January-February 1958, pp 263-294).

Pfeiffer, C.,
"Theory and Application of the Critical Direction Method of Trajectory Optimization," IAS Vehicle Systems Optimization Symposium (New York), 27-29 November 1961.

Rider, L.,
"A Functional Equation Approach to the Optimization of Plane Change Maneuvers in Space," 22 January 1962 (Report No. TDR-930(2560-30) TN-1, DCAS-TDR-62-6) (Contract No. AF04(647)-930).

Ross, S. E.,
"Variational Solutions to Optimum Rocket Trajectory Problems," Doctorate Thesis, Harvard University (Cambridge), January 1958.

"Minimality for Problems in Vertical and Horizontal Rocket Flight," Jet Propulsion, Vol. 28, No. 1, January 1958, pp 55-56.

"Composite Trajectories Yielding Maximum Coasting Apogee Velocity," ARS Journal, Vol. 29, No. 11, November 1959, pp 843-848.

"Optimum Rocket Trajectories with Aerodynamic Drag," Jet Propulsion, Vol. 28, No. 7, July 1958, pp 465-469.

"Low Acceleration Trajectory Optimization in a Strong Central Force Field," IAS Vehicle Systems Optimization Symposium (New York), 27-29 November 1961.

Rutowski, E. S.,
"Energy Approach to the General Aircraft Performance Problem," Journal of the Aeronautical Sciences, Vol. 21, No. 3, March 1954, pp 187-195 (Also, Annual Summer Meeting of the IAS Aerodynamics Session, 15-17 July 1953--Unrevised form).

Schindler, G. M.,
"Minimum Time Flight Paths," ARS Journal, Vol. 30, No. 4, April 1960, pp 352-355.

Shen, Y. C.,
"General Formulation of the Problem of Optimum Rocket Trajectories," TM-833, Aerojet-General (Azusa, California), November 1959.

"Multiplier Rule in the Calculus of Variations and Its Application to Optimum Performance of Rocket Vehicles," TM-832, Aerojet-General (Azusa, California), November 1959.

"Formulation of the Optimum Rocket Trajectory," ARS Journal, Vol. 31, No. 1, January 1961, pp 89-90.

Simon, W. E.,
"An Extension of the Method of Steepest Descent for Digital Computer Application," Research Report No. R-60-39, The Martin Company (Denver), January 1961.

"Philosophy and Technique for Application of the Modified Method of Steepest Descent

to a Wide Class of Problems," Report No. IOL 214-163-60, North American Aviation (Downey, California), September 1960.

"A Modified Method of Steepest Descent for the General Problem of Finding Extremal Solutions, with Particular Application to Non-linear Least Squares," Report No. IOL 214-139-60, North American Aviation (Downey, California), August 1960.

Smith, E. Q.,
"Optimum Intercept Trajectories for Supersonic Fighters (U)," Naval Air Missile Test Center Technical Memorandum Report 107, 30 August 1957.

Smith, E. Q., and Bok, J. R.,
"Optimum Thrust Programming for Air-to-Air Missiles," Naval Air Missile Test Center Informal Report No. CT-39-56, 20 February 1957 (Part I published in the Bulletin of the 12th Meeting of the Joint Army-Navy-Air Force Solid Propellant Group reporting the Symposium on Design and Performance Optimization, Naval Ordnance Laboratory (White Oak, Maryland), 7-9 May 1956).

Smith, G. C.,
"The Calculation of Minimal Orbits," Astronautica Acta, Vol. 5, No. 5, 1959, pp 253-254.

Stancil, R. T., and Kulakowski, L. J.,
"Rocket Boost Vehicle Mission Optimizations," Preprint No. 1449-60, American Rocket Society (New York), 1960 (Also, Report No. ERR-FW-024, Convair, 27 July 1960, 35 pp) (Also, ASTIA No. AD-255 027).

Stark, H. M.,
"Optimum Trajectories Between Two Terminals in Space," ARS Journal, Vol. 31, No. 2, February 1961, pp 261-262.

Szebehely, V. G.,
"Equations for Thrust Programs," XIth International Astronautical Congress (Stockholm), Trajectories Session, 1960.

Templeman, W. H.,
"Comparison of Minimum Energy Paths and Apogee Designation Paths," ARS Journal, Vol. 29, No. 2, November 1959.

Theodorsen, T.,
"Optimum Path of an Airplane-Minimum Time Climb," Journal of Aerospace Sciences, Vol. 26, No. 10, October 1959, pp 637-642.

Ting, L.
"Approximations in Variational Problems," PIBAL Report No. 610, AFOSR TN 60-789, Polytechnic Inistitute of Brooklyn (New York), July 1960 (Also, Aerospace Engineering, January 1961).

"Approximating Technique for Variational Problems," Aerospace Engineering, January 1961, pp 32-33 and 89-91.

Traenkle, C. A.,
"Design Parameters and Optimization of Missile Trajectories," Zeitschrift fur Flugwissenschaften, Vol. 7, No. 10, October 1959, pp 287-293 (Also, WADC TR 58-580, September 1958) (Also, ASTIA No. AD-204 805).

"Mechanics of the Power and Launching Phase for Missiles and Satellites," Ingenieur Archiv (Festschr), Vol. 28, 1959, pp 335-356) (Also, WADC TR 58-579, September 1958) (Also, ASTIA No. AD-204 804).

"Optimal Programming and Control of Satellite Orbits," ARDC Wright Air Development Center, Ohio, September 1958, WADC TR 58-581 (Also, Zeitschrift fur Flugwissenschaften, 1959) (Also, ASTIA No. AD-204 806).

"Outline of the Mechanics of the Power and Launching Phase for Missiles and Satellites," Technical Paper No. 958-59, 20 pp, American Rocket Society, 16-20 November 1959.

Valentine, F. A.,
"The Problem of Lagrange with Differential Inequalities as Added Side Conditions," Contributions to the Theory of Calculus of Variations, University of Chicago Press, 1933-1937, pp 405-447 (Also, University of Chicago Press, 1937, Dissertation).

Vargo, L. G.,
"A Generalization of the Minimum Impulse Theorem to the Restricted Three-Body Problem," Journal of the British Interplanetary Society, Vol. 17, September-October 1959, pp 124-126.

Wagnet, W. E.,
"Development and Formulation of an Optimum Trajectory Program for Missiles and Satellite Carriers," Report No. 60 H-515, North American Aviation (Los Angeles), September 1960.

Wang, C. J., Lawrence, H. R. and Anthony, G. W.,
"Optimum Thrust Programming of Nuclear Rockets," Preprint No. 691-58, 13 pp, American Rocket Society, 17-21 November 1958.

ILLUSTRATIONS

Preceding page blank

Preceding page blank

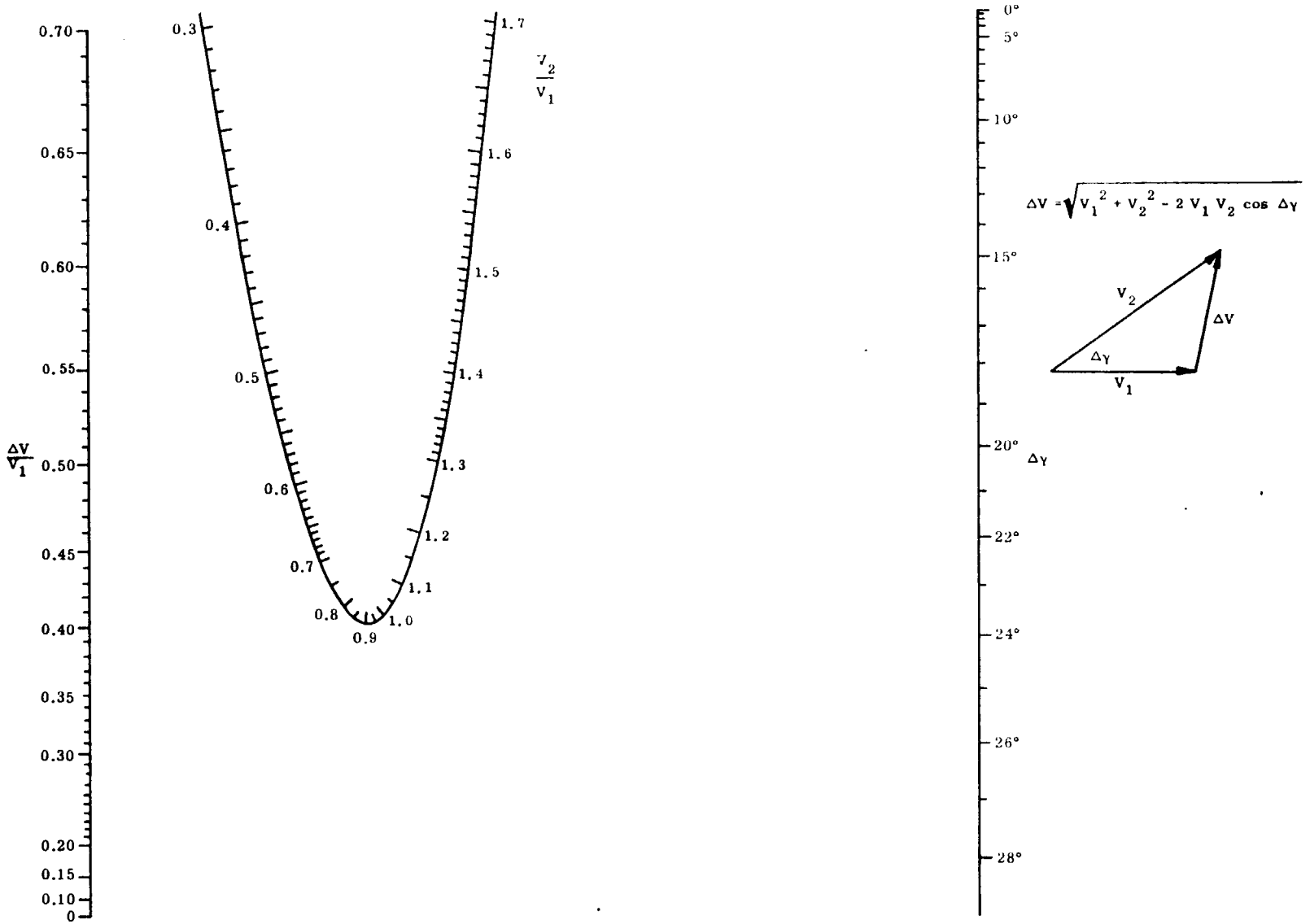

Fig. 1. Solution to the Law of Cosines

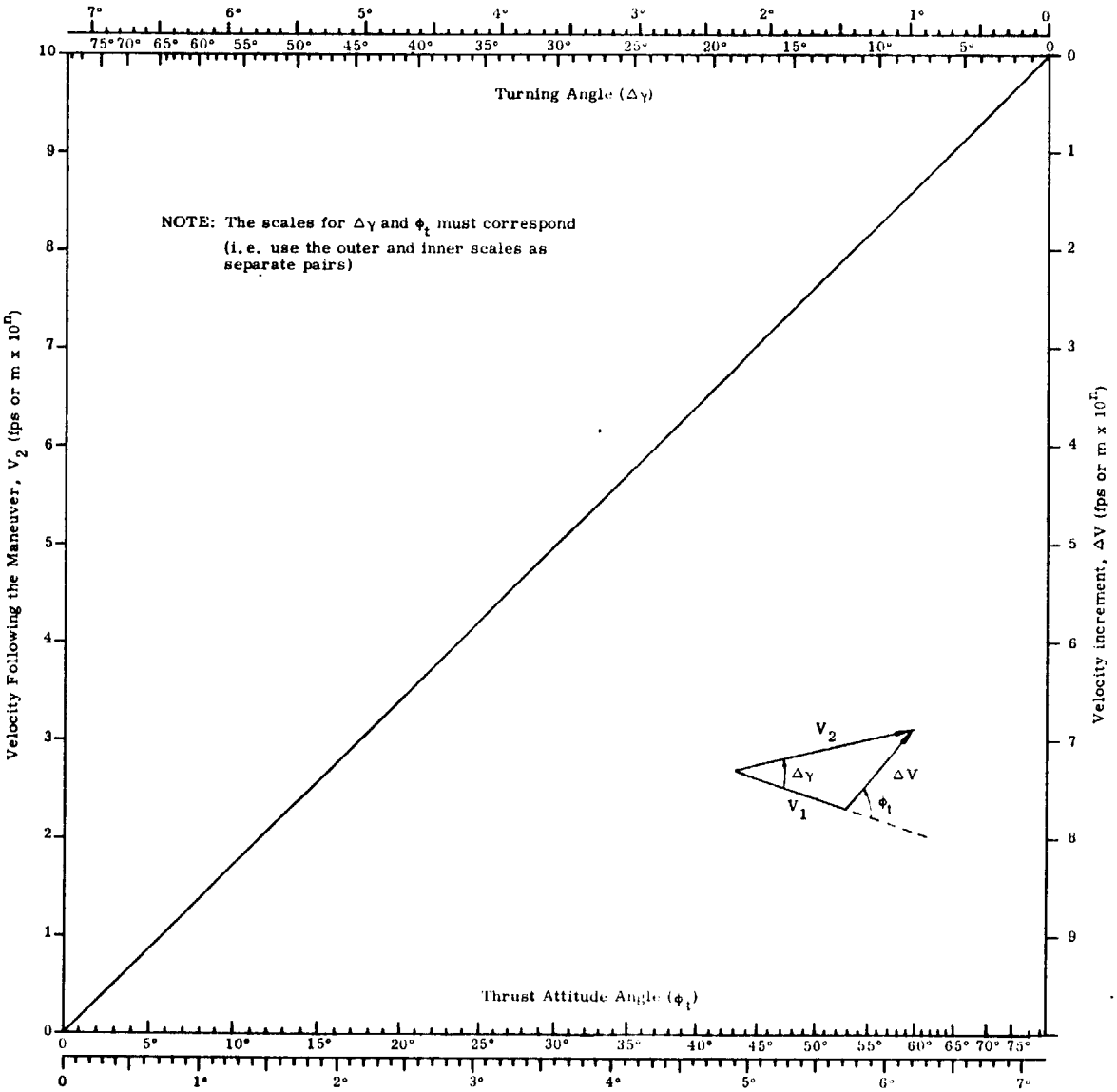

Fig. 2. Solution to the Law of Sines

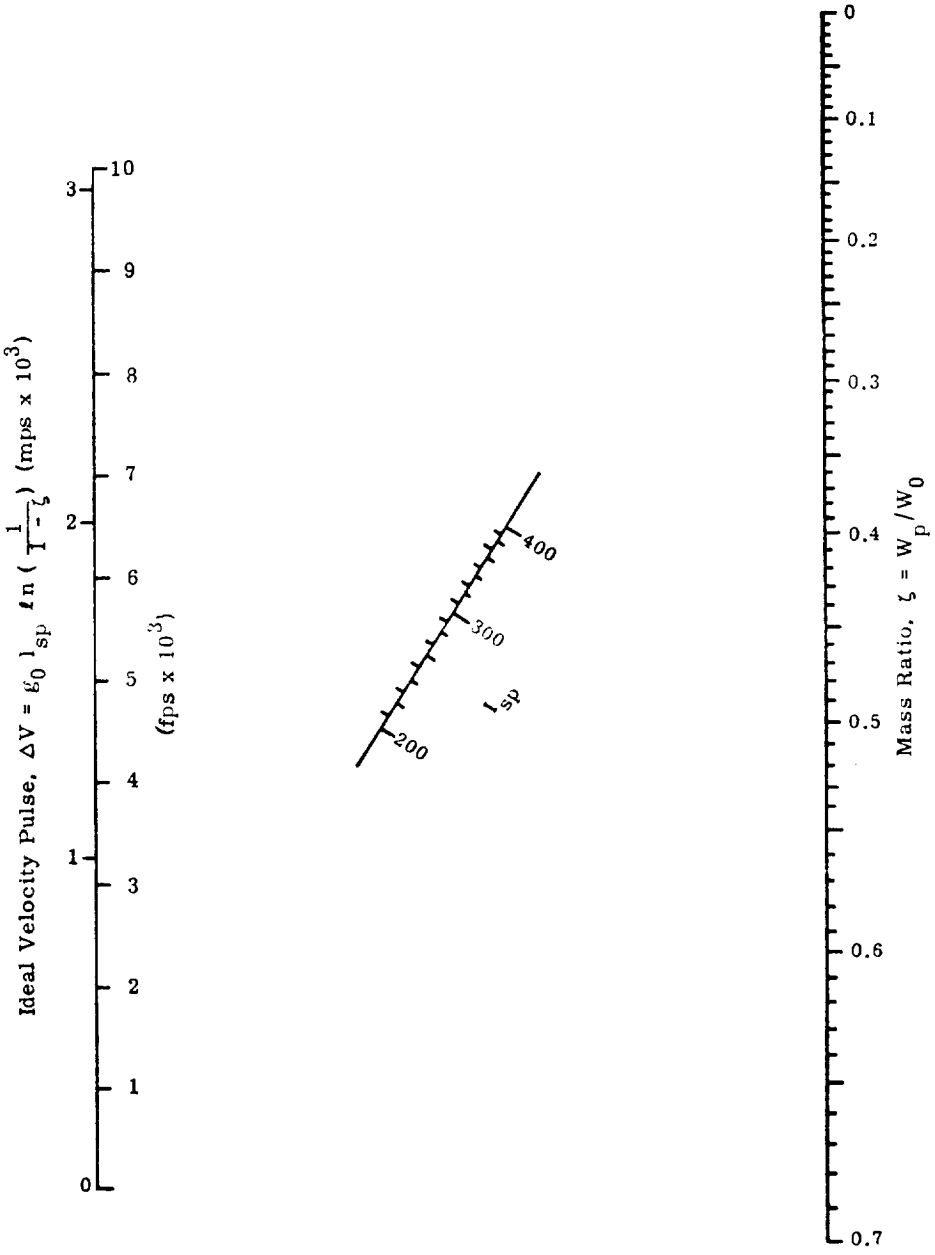

Fig. 3. Total Velocity Increment Required for Two-Pulse Correction to a Circular Orbit

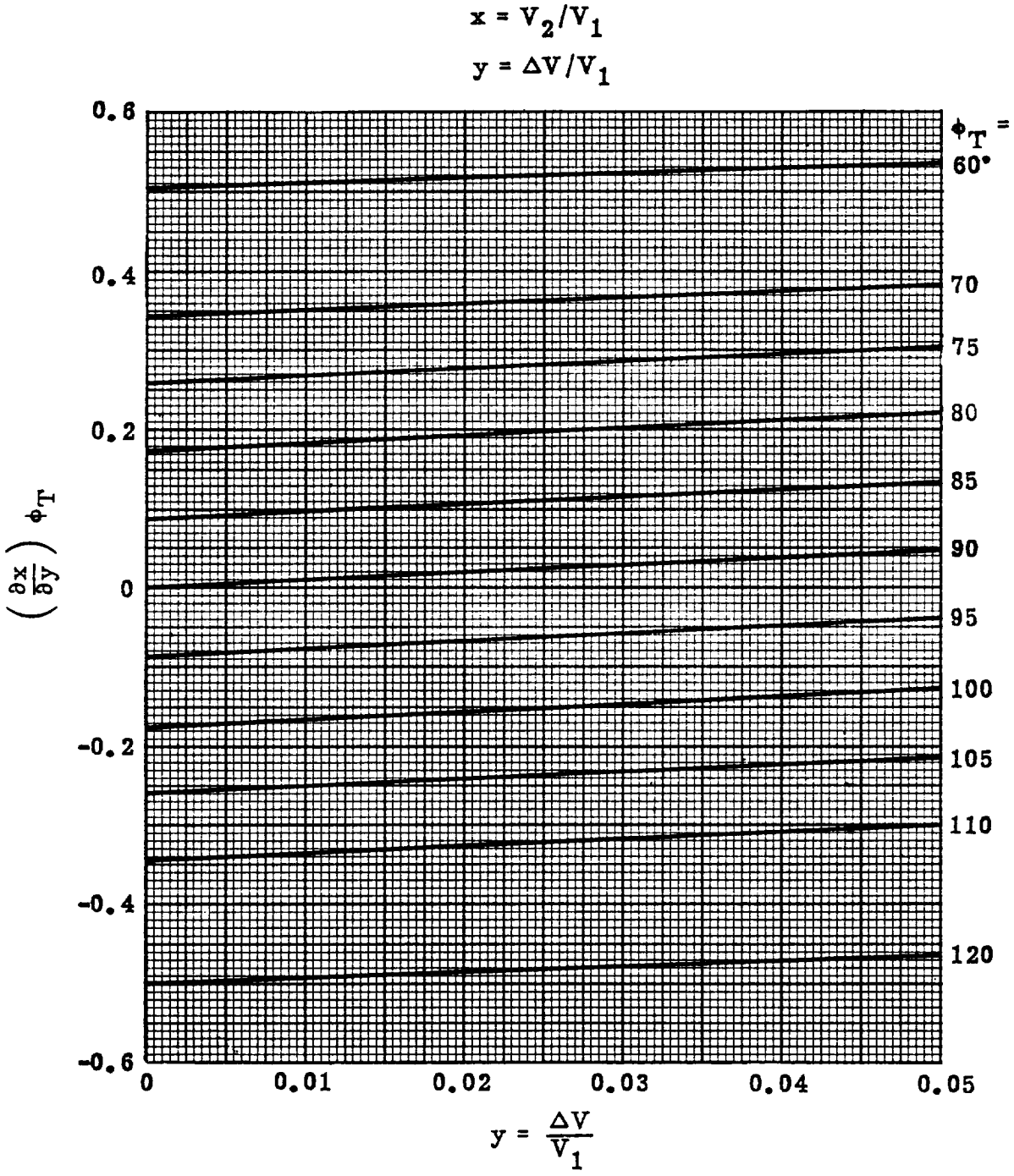

Fig. 4. Effects of Variations in Characteristic Velocity on the Velocity After the Maneuver

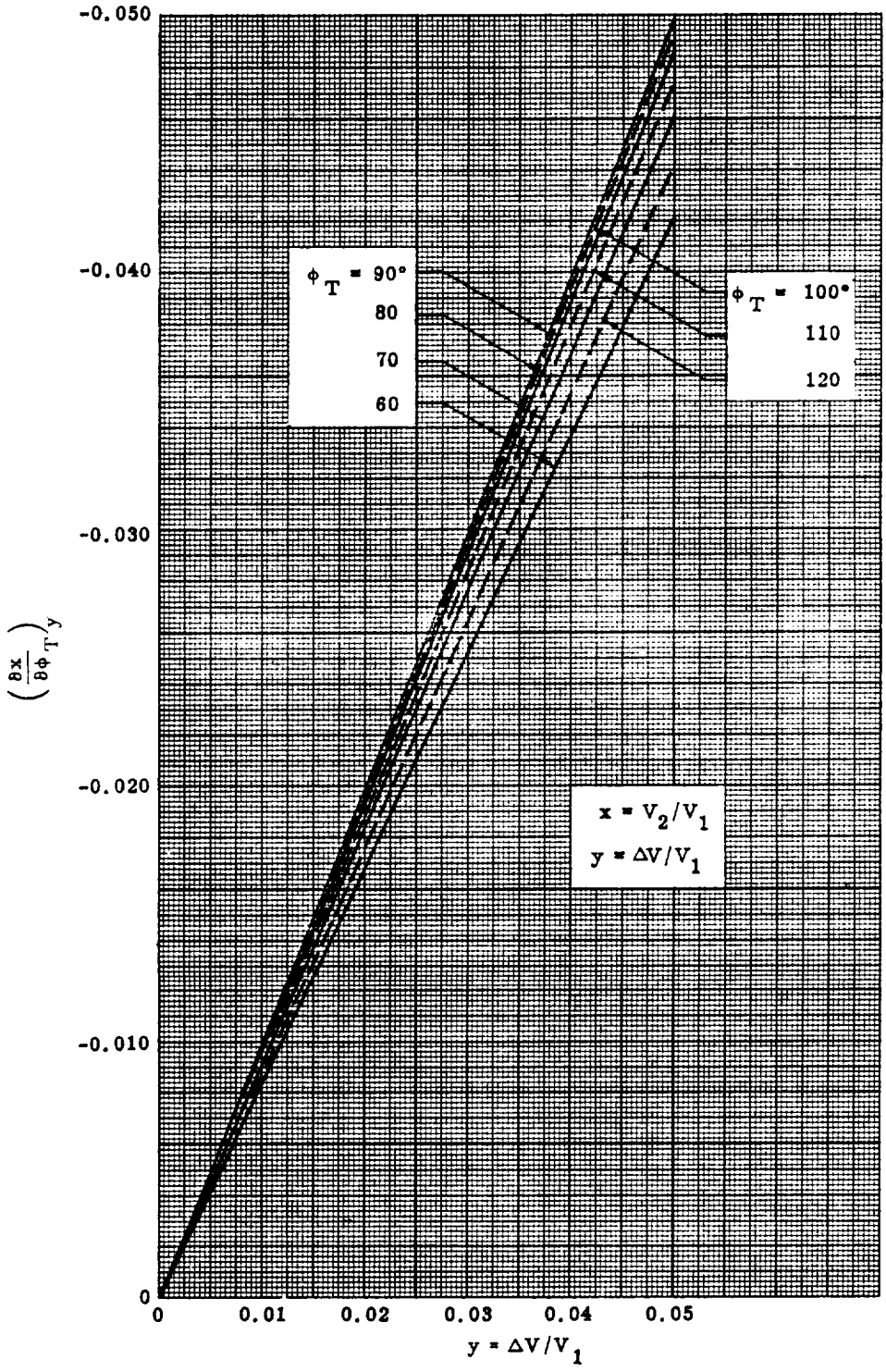

Fig. 5. Effects of Variations in the Pulse Attitude Angle on Vehicle Velocity After the Maneuver

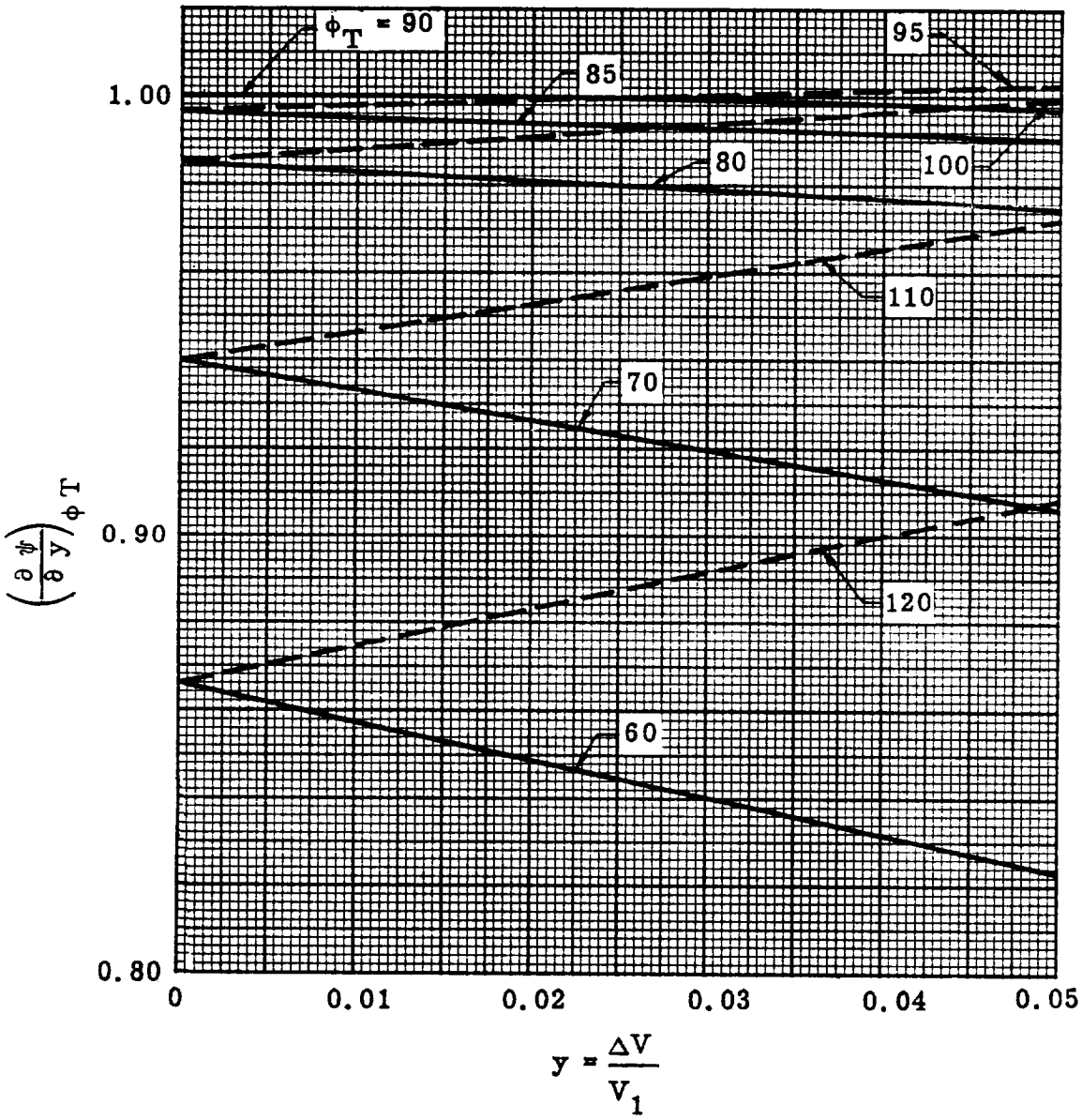

Fig. 6. Effects of Variations in Characteristic Velocity on the Turn Angle

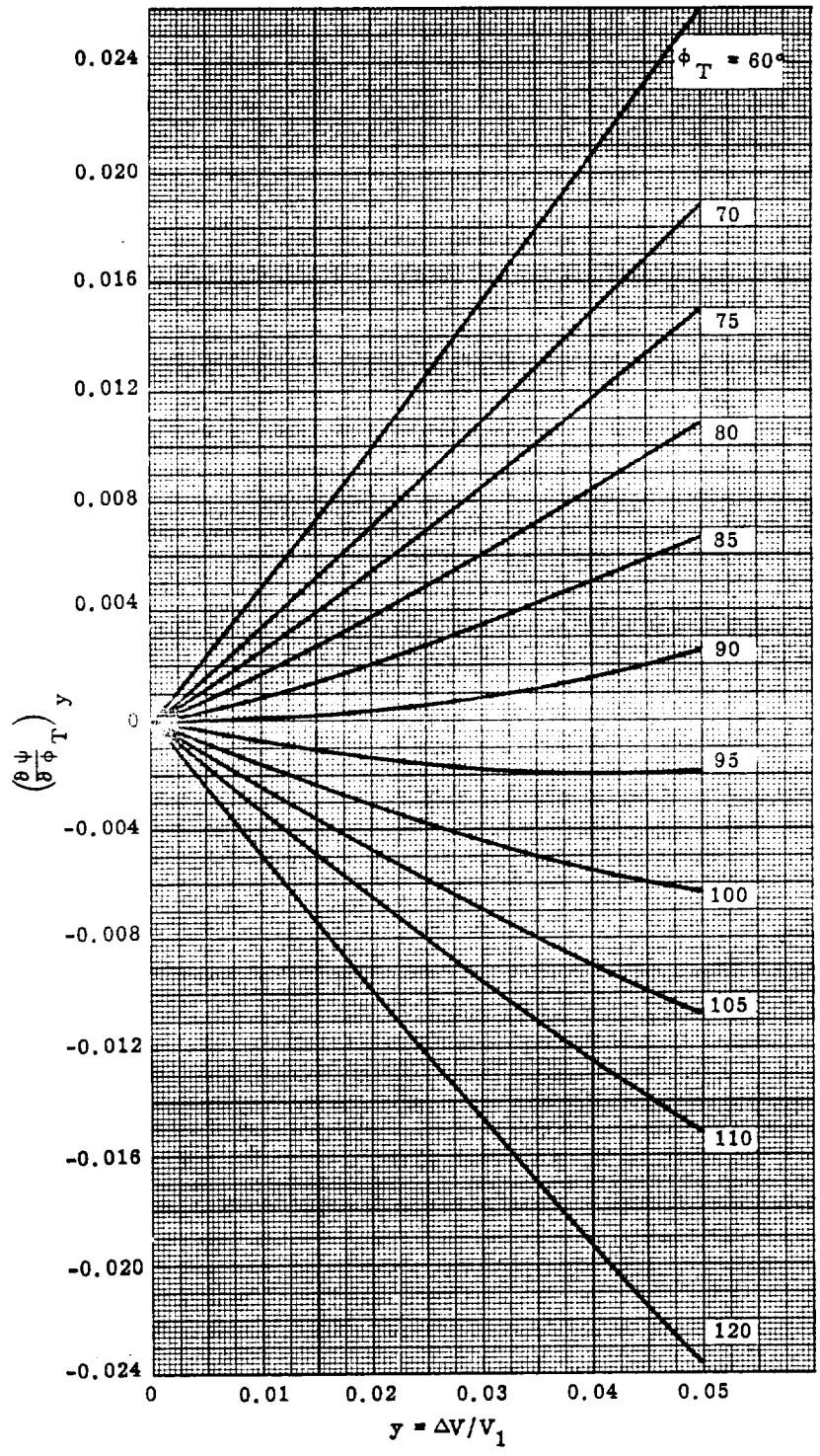

Fig 7. Effects of Variations in Thrust Pulse Angle on the Turn Angle

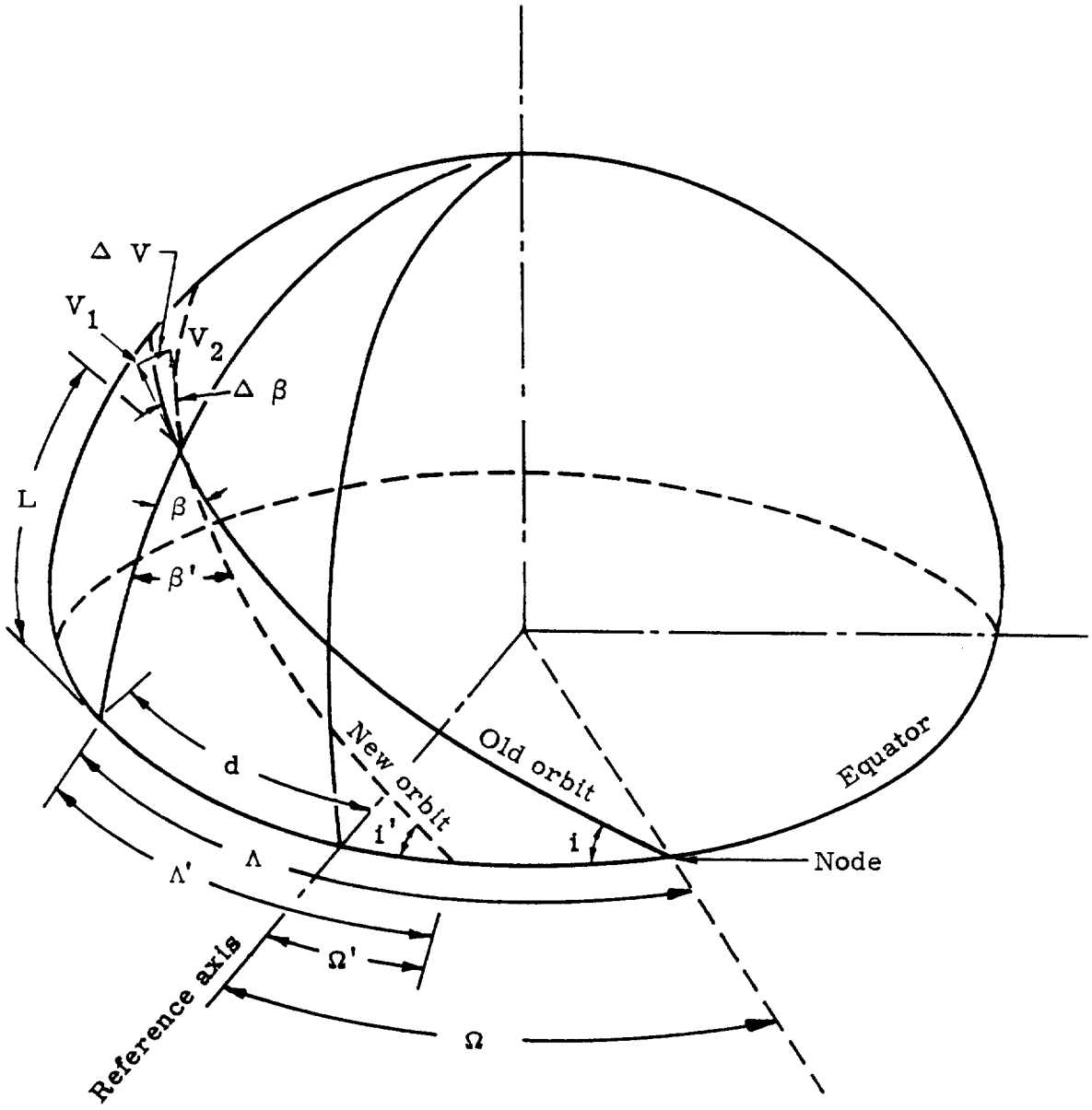

NOTE: No primes denote premaneuver

Primes denote post maneuver

Fig. 8. Maneuvers in Circular Orbits to Change Orbital Inclination and/or the Node

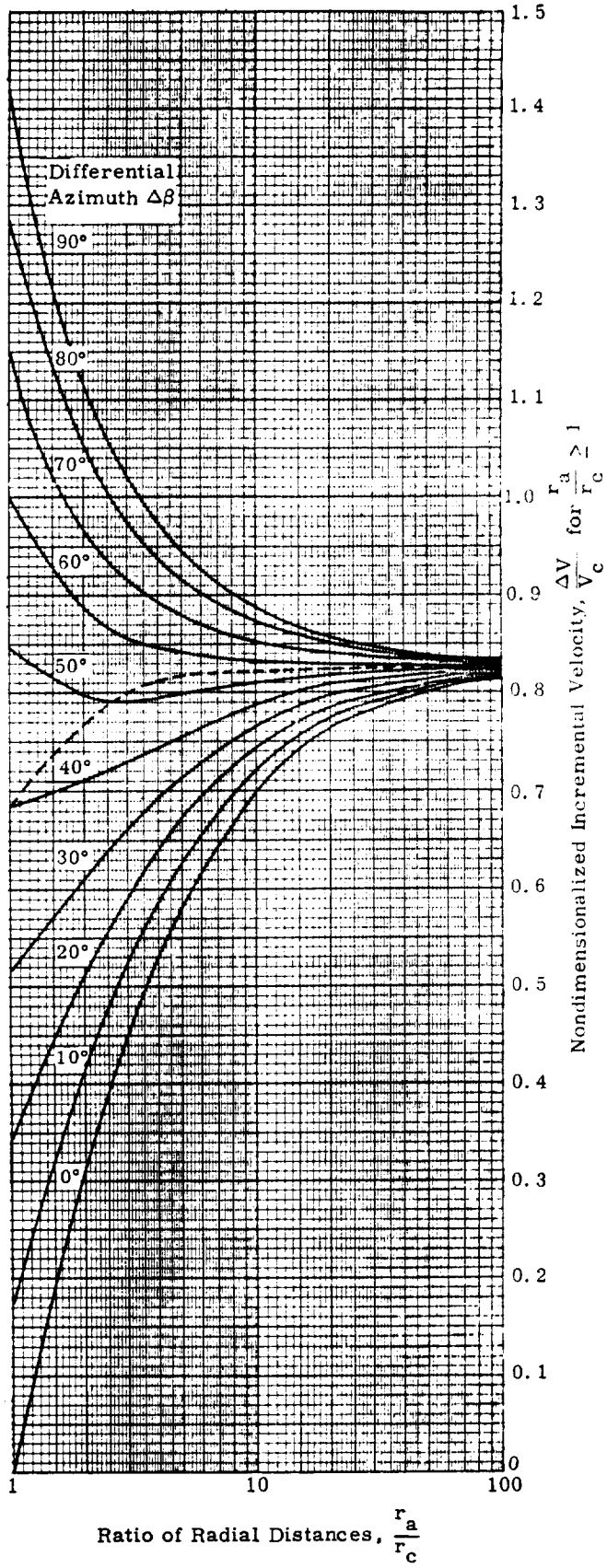

Fig. 9. Nondimensionalized Impulsive Velocity Required to Transfer to a New Altitude, Rotate the Orbital Plane (at that altitude), and Recircularize Upon Arrival at the Initial Orbit

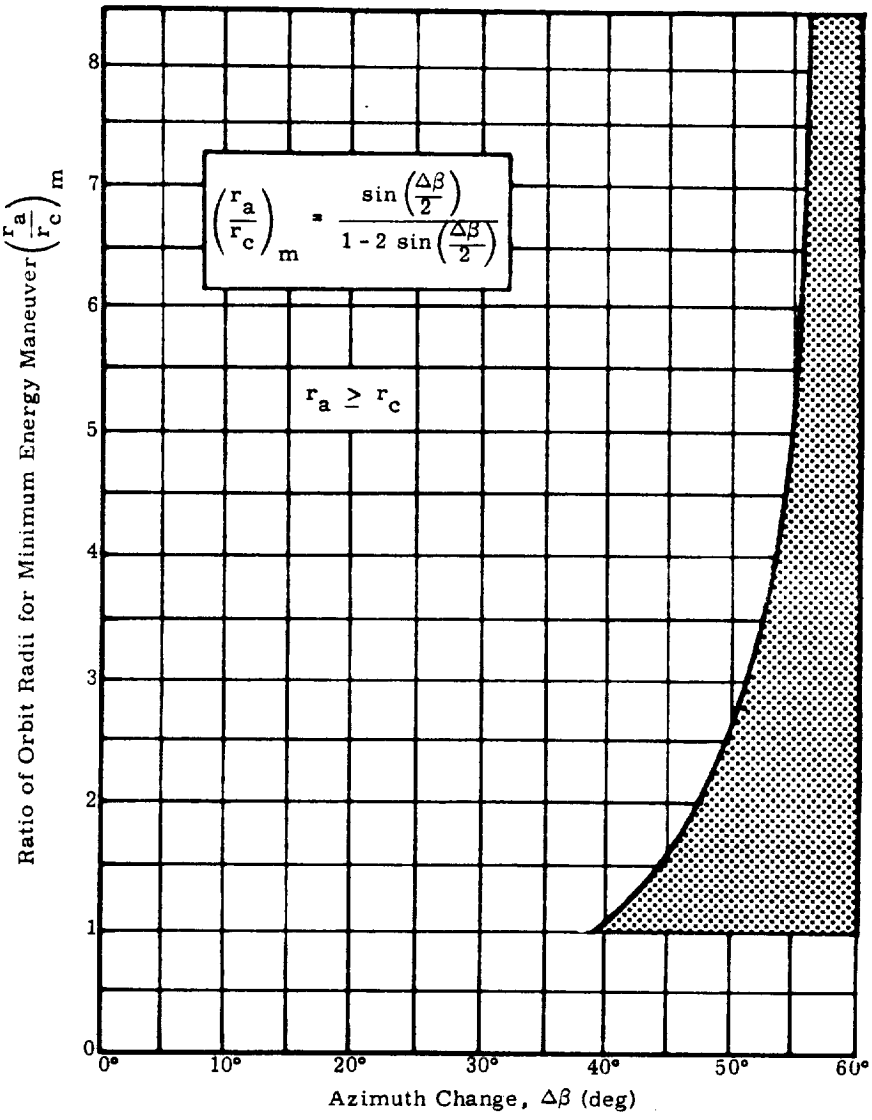

Fig. 10. Ratio of the Interceptor's Apogee Radius to the Radius of the Target's Circular Orbit as a Function of the Azimuth Change for Minimum Energy

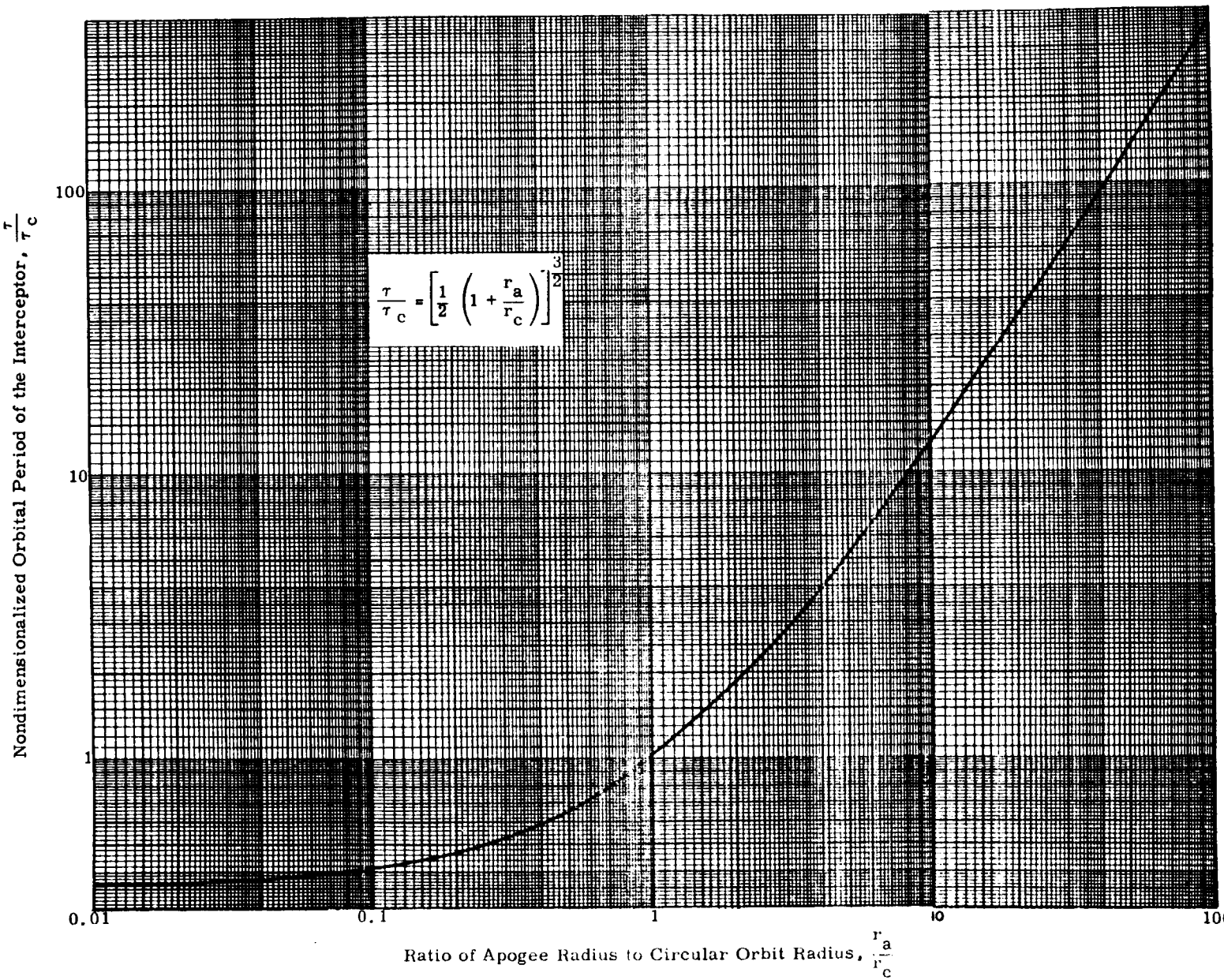

Fig. 11. Nondimensionalized Orbital Period of the Interceptor in Its Maneuvering Orbit (elliptic orbit with apsidal radii equal to r_a and r_c)

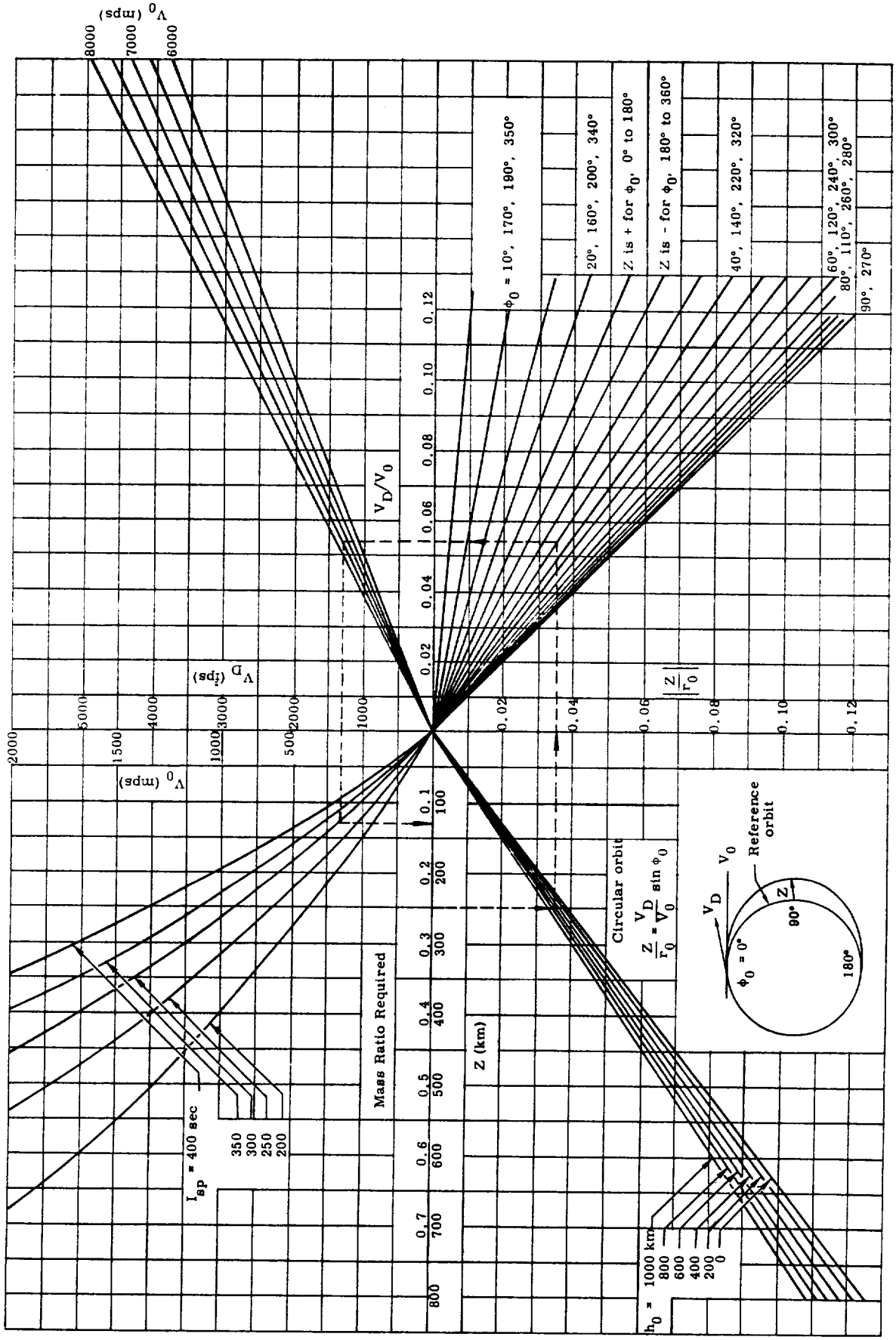

Fig. 12. Fuel Required for Lateral Maneuvers in a Circular Orbit

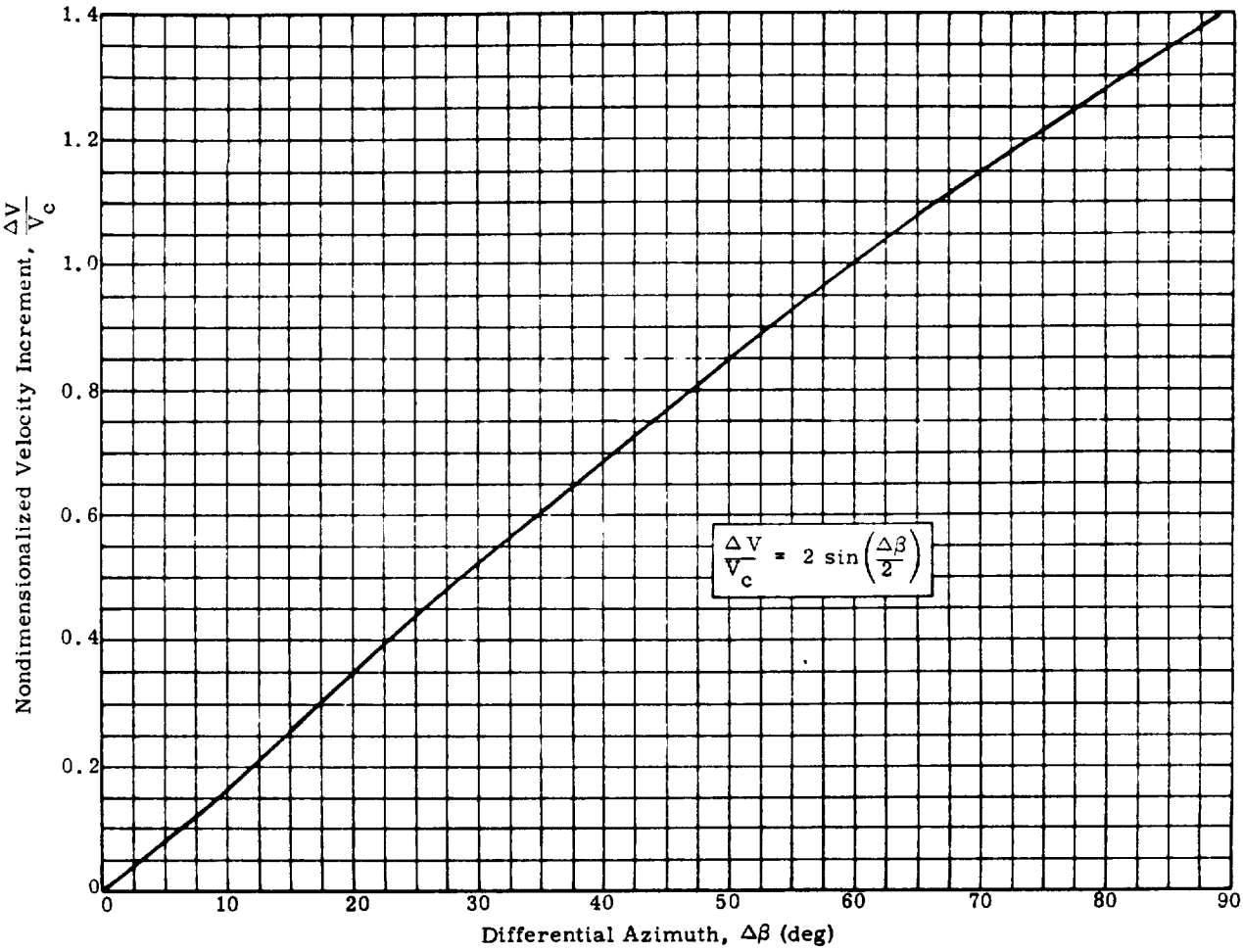

Fig. 13. Nondimensionalized Impulsive Velocity Required to Rotate a Satellite's Orbital Plane

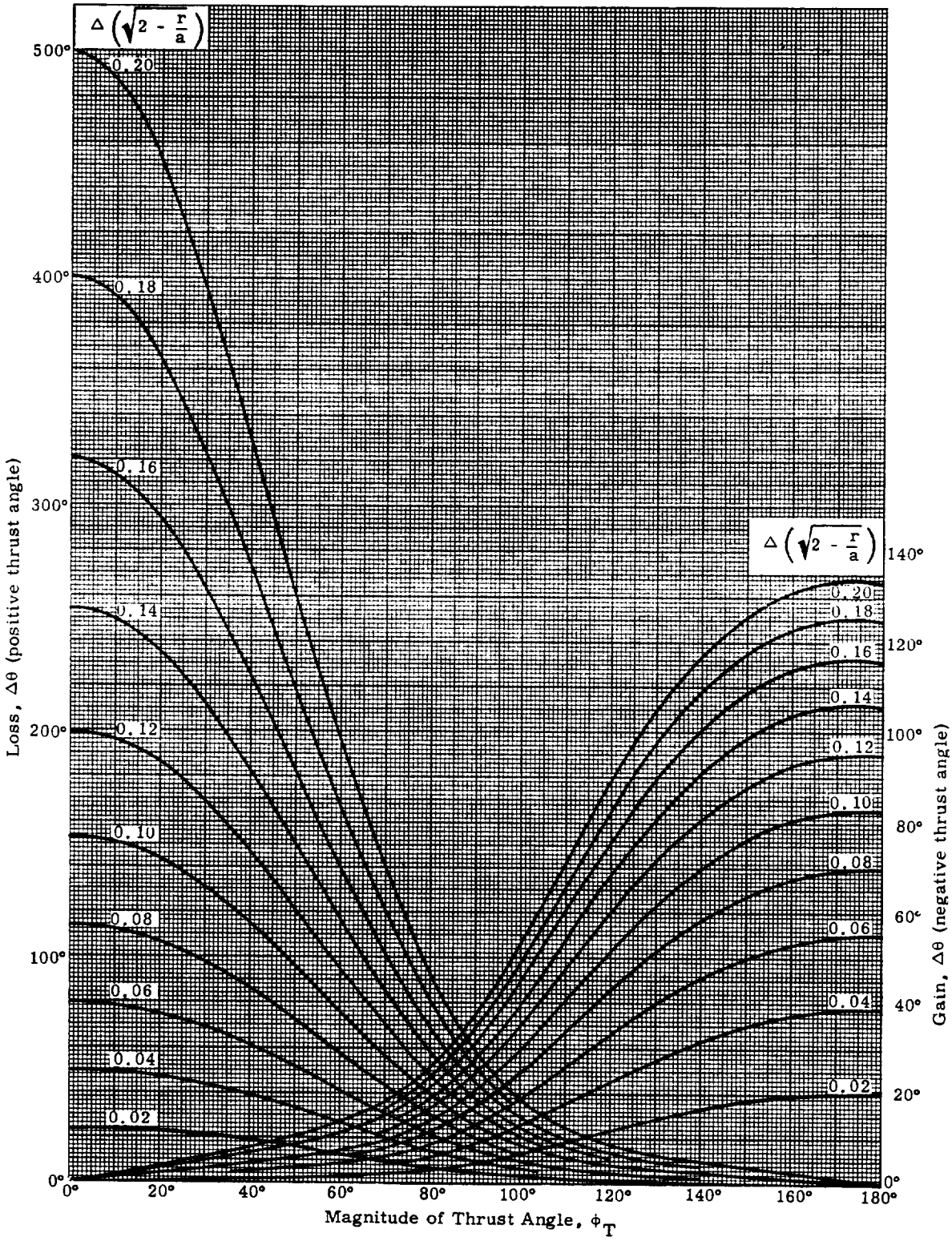

Fig. 14. Maneuver Angle as a Function of Thrust Attitude

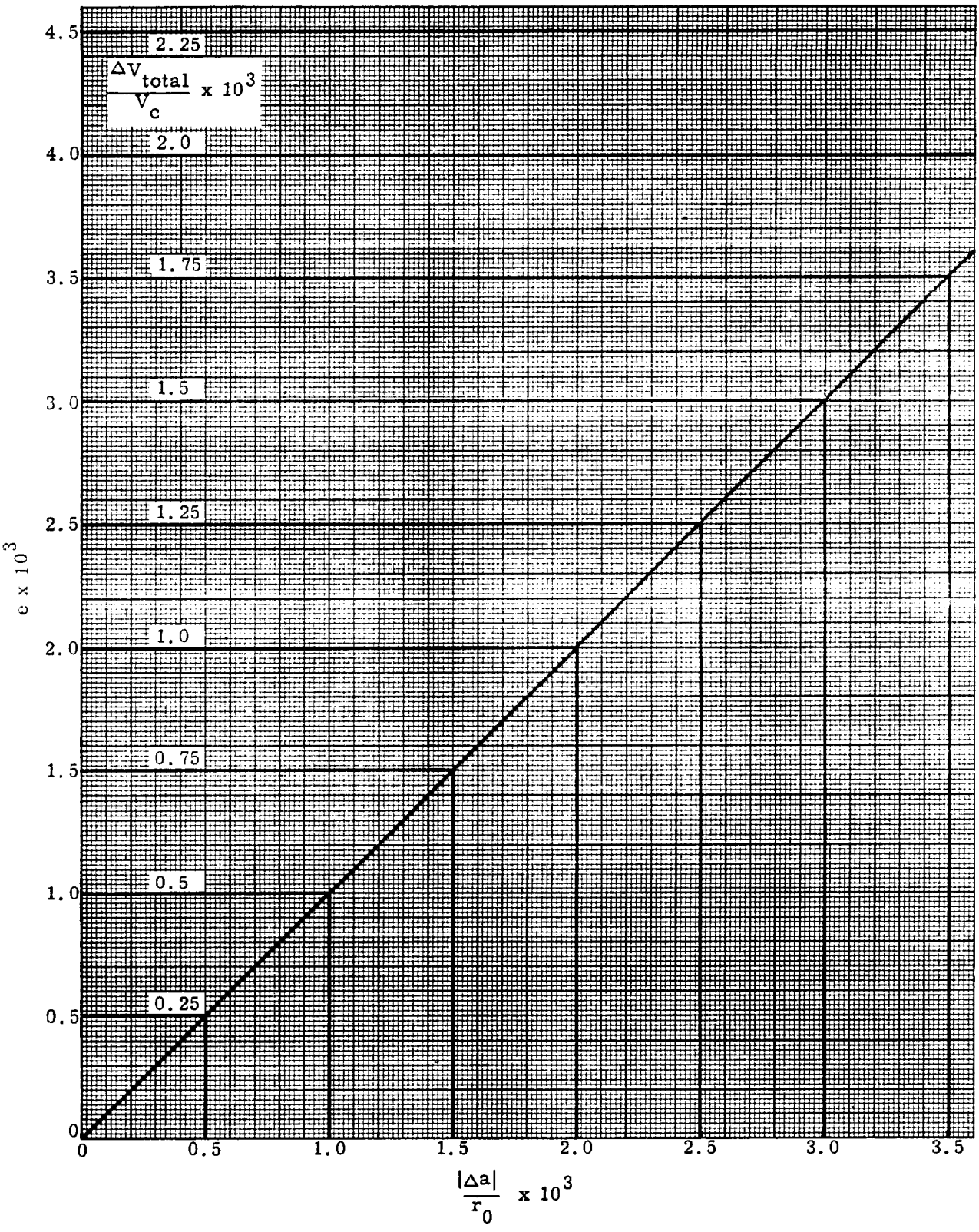

Fig. 15. Total Velocity Increment Required for Two-Pulse Correction to a Circular Orbit

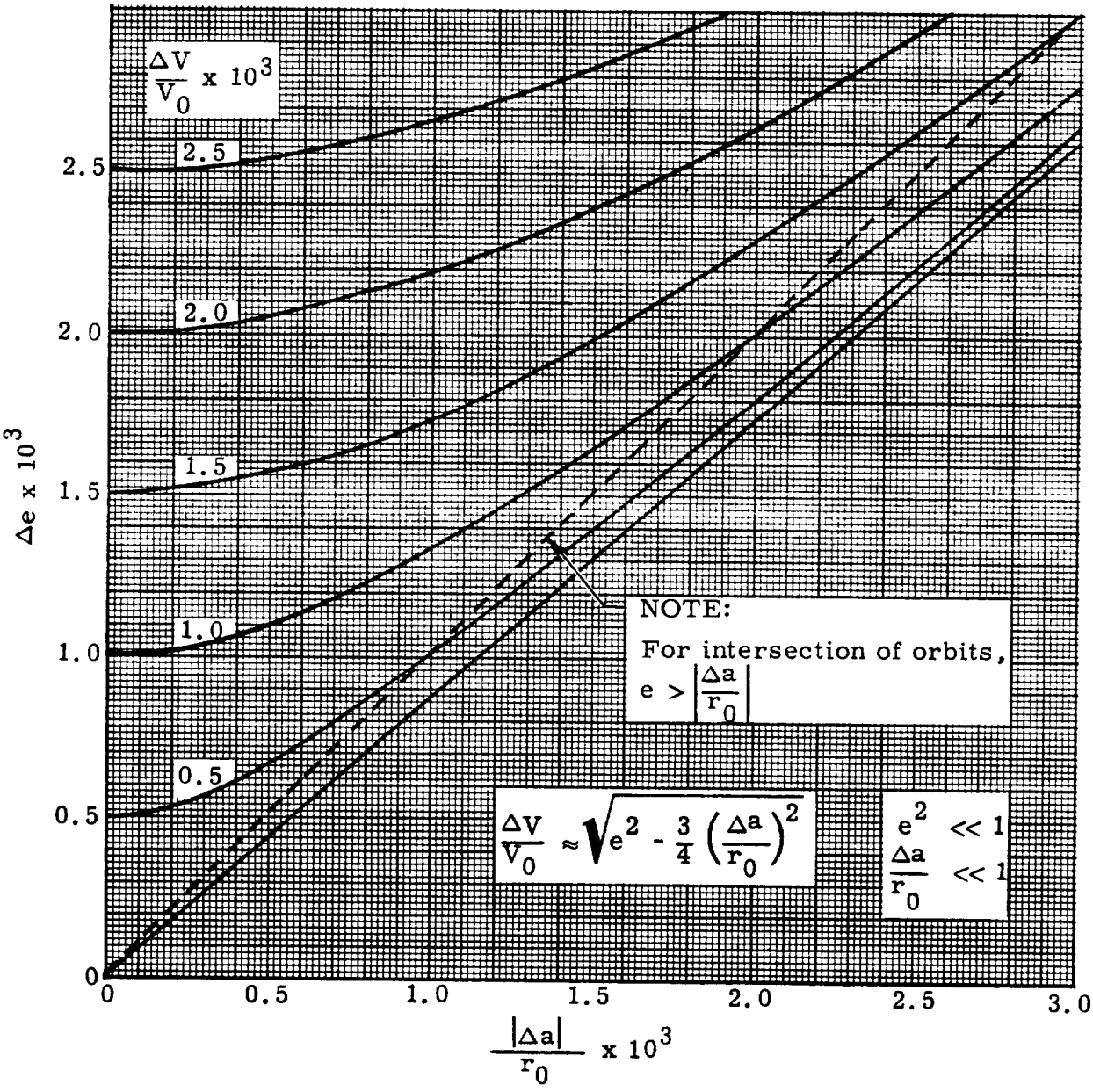

Fig. 16. Velocity Increment for Maintenance of Circular Orbits by an Impulse at Orbit Intersection

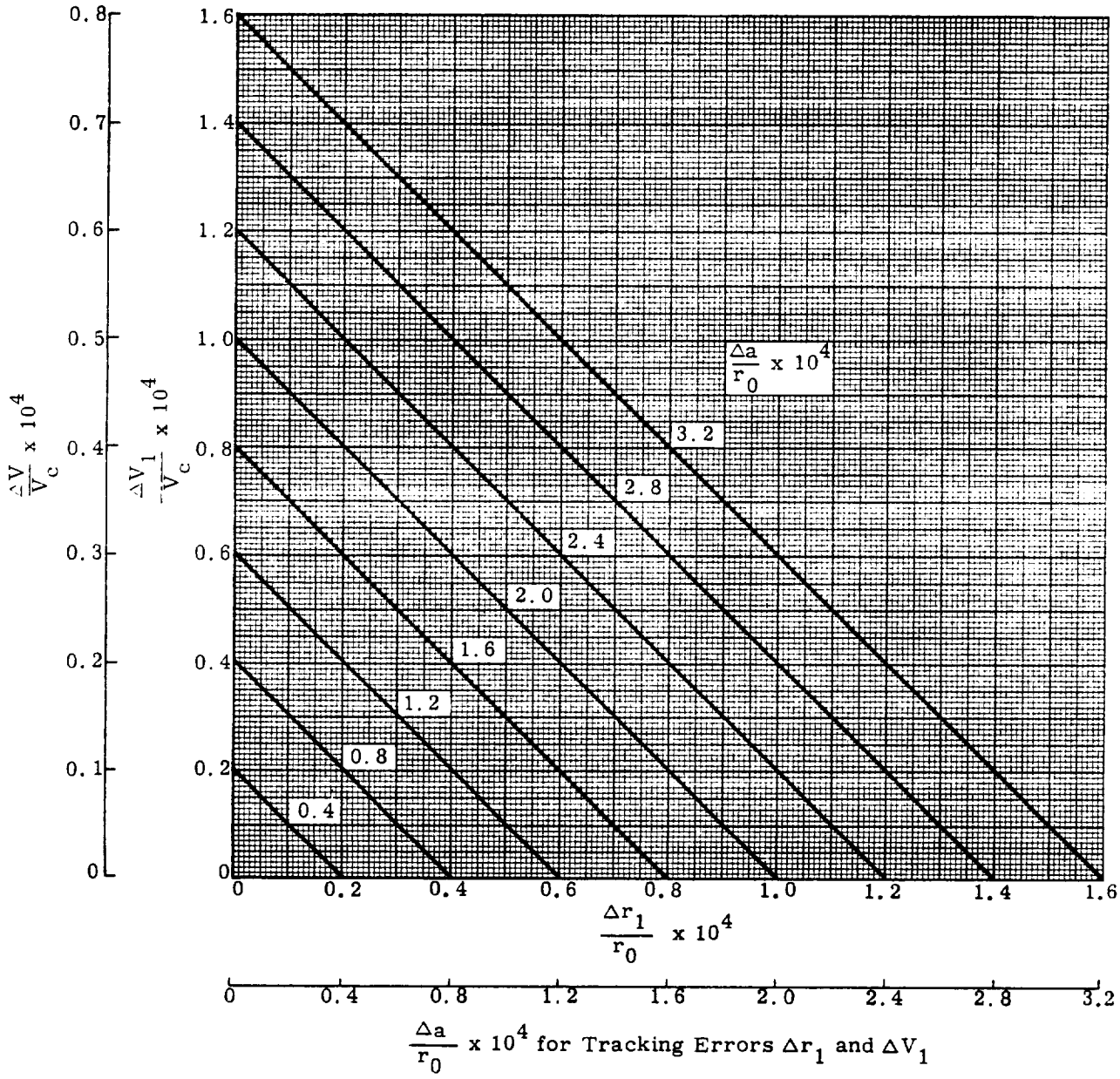

Fig. 17. Error Analysis of Two-Pulse Correction of a Circular Orbit

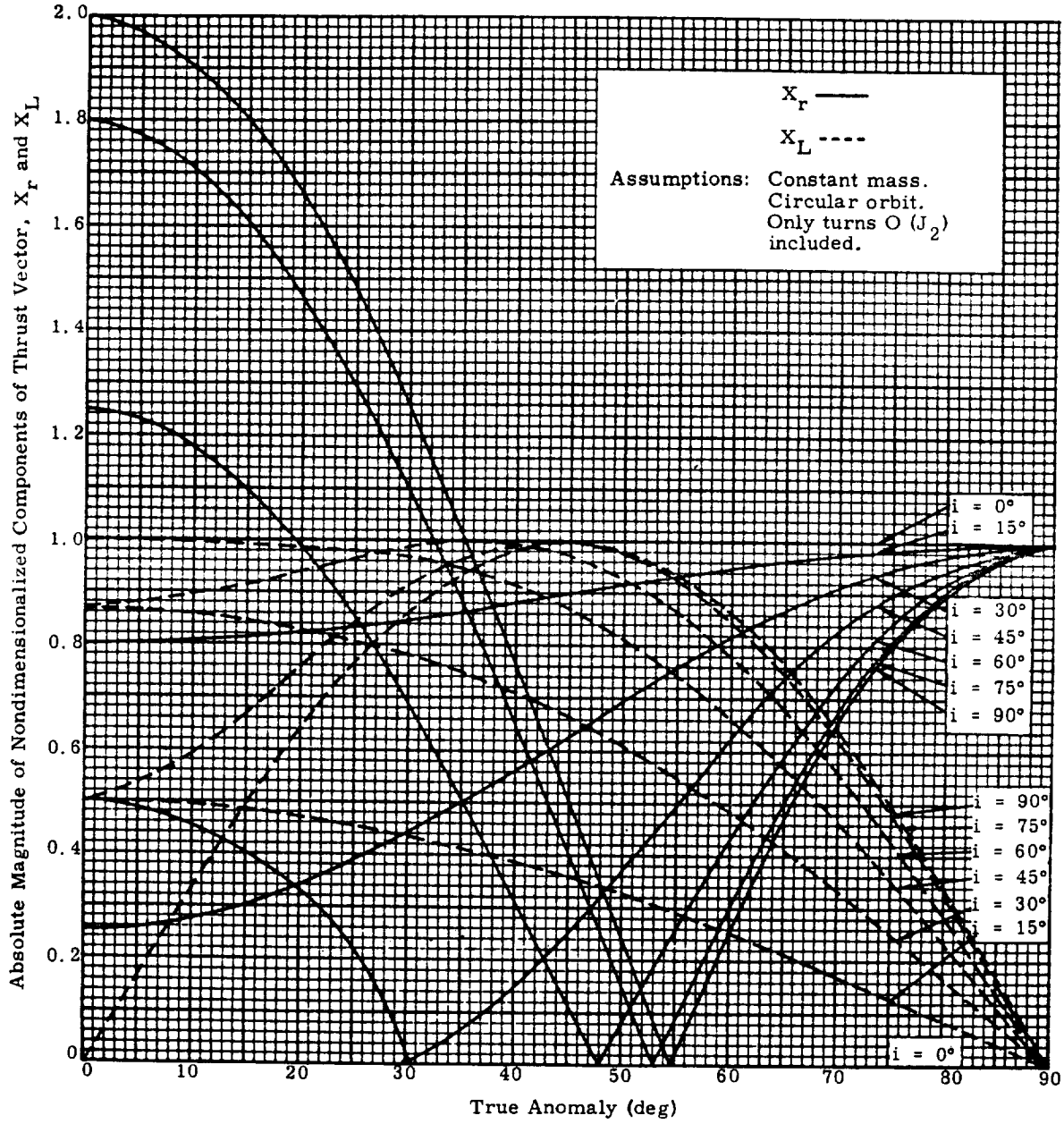

Fig. 18. Absolute Magnitudes of the Nondimensionalized Components of the Thrust Vector as a Function of the True Anomaly for Orbit Inclinations from 0° to 90°

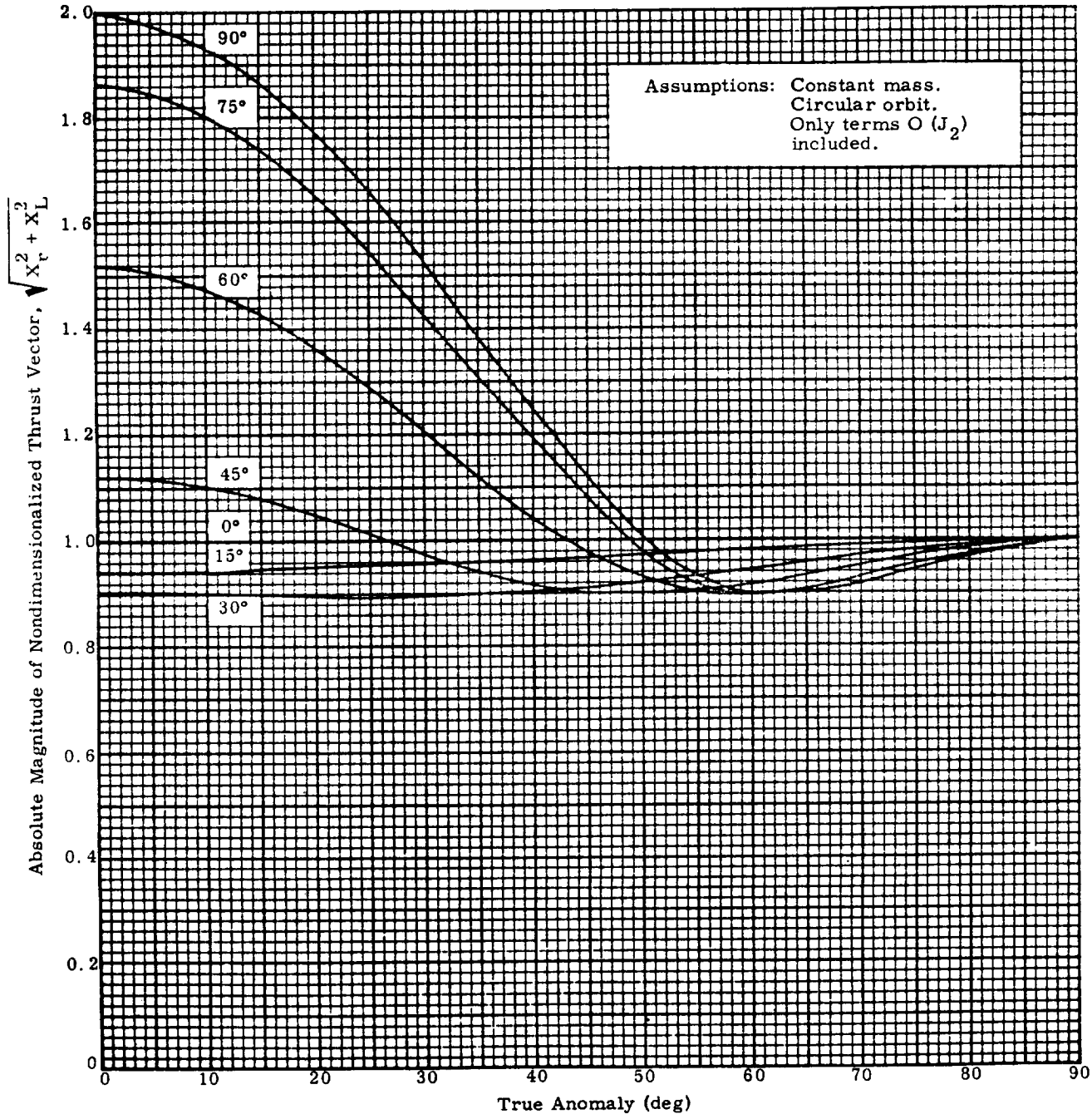

Fig. 19. Absolute Magnitude of the Nondimensionalized Thrust Vector as a Function of True Anomaly

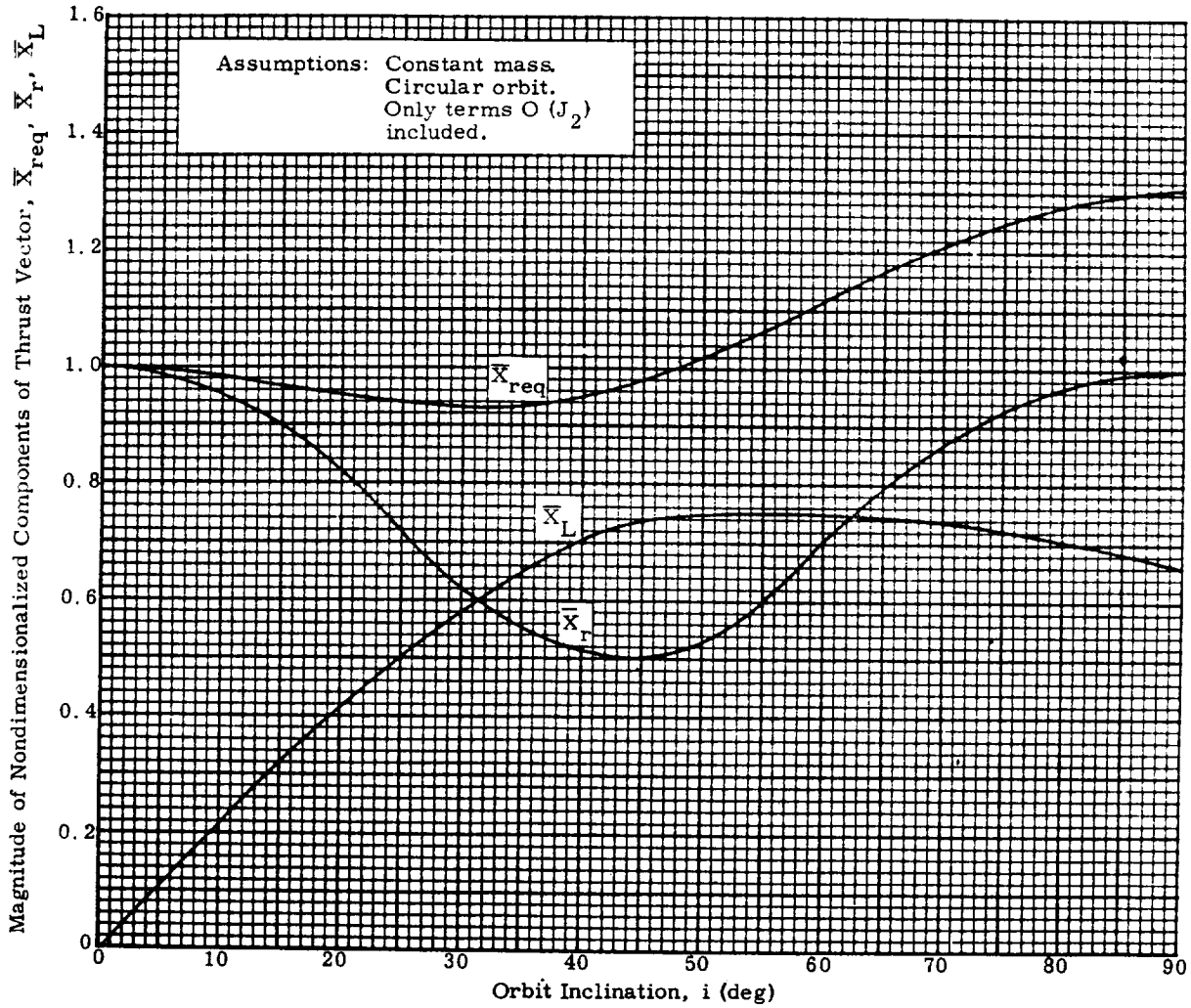

Fig. 20. Magnitudes of the Nondimensionalized Corrective Force and Its Components, Averaged over the Orbit

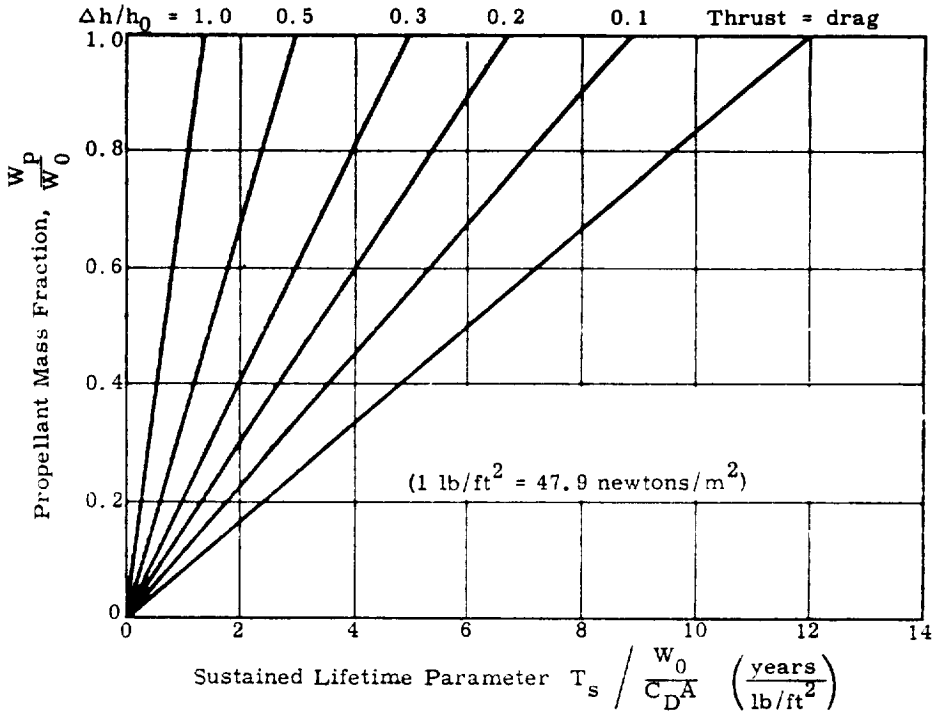

Fig. 21. Discrete Velocity Sustaining System
(h_0 = 300 naut mi = 555 km; I_{sp} = 300 sec)

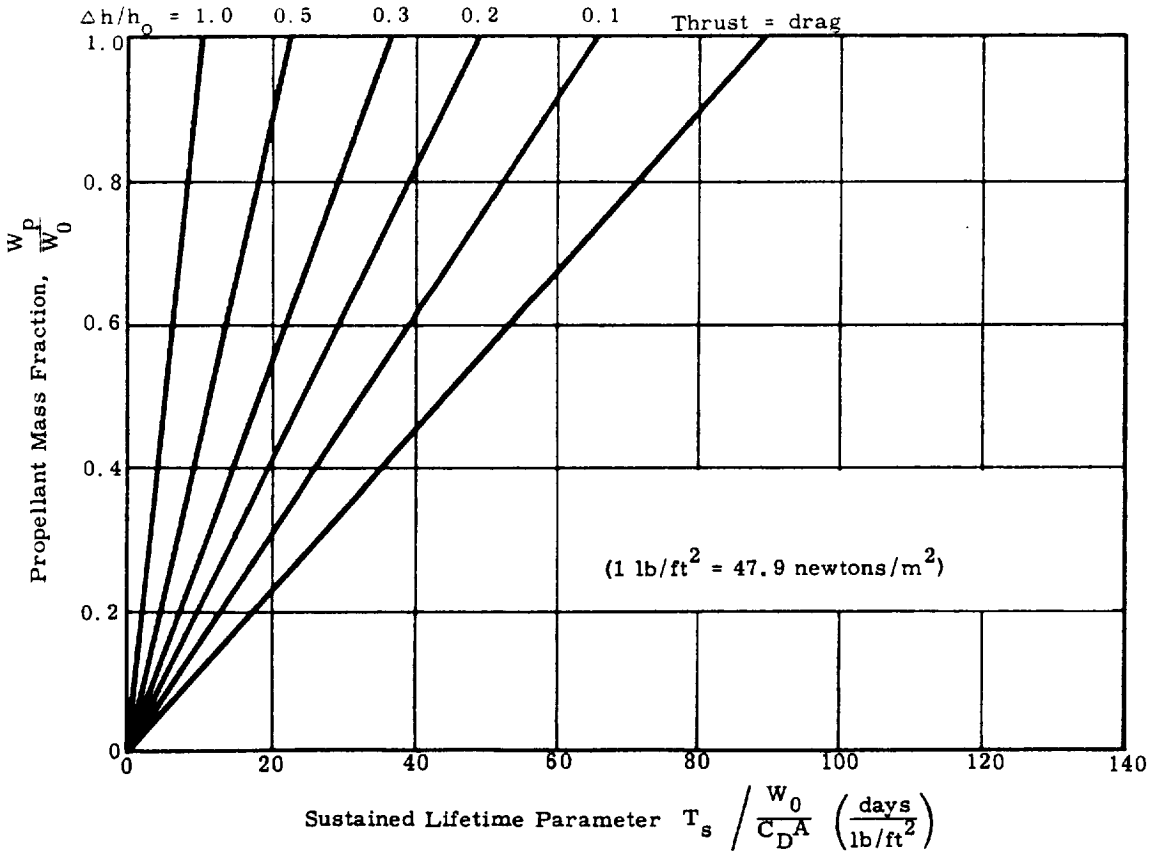

Fig. 22. Discrete Velocity Sustaining System
(h_0 = 200 naut mi = 370 km; I_{sp} = 300 sec)

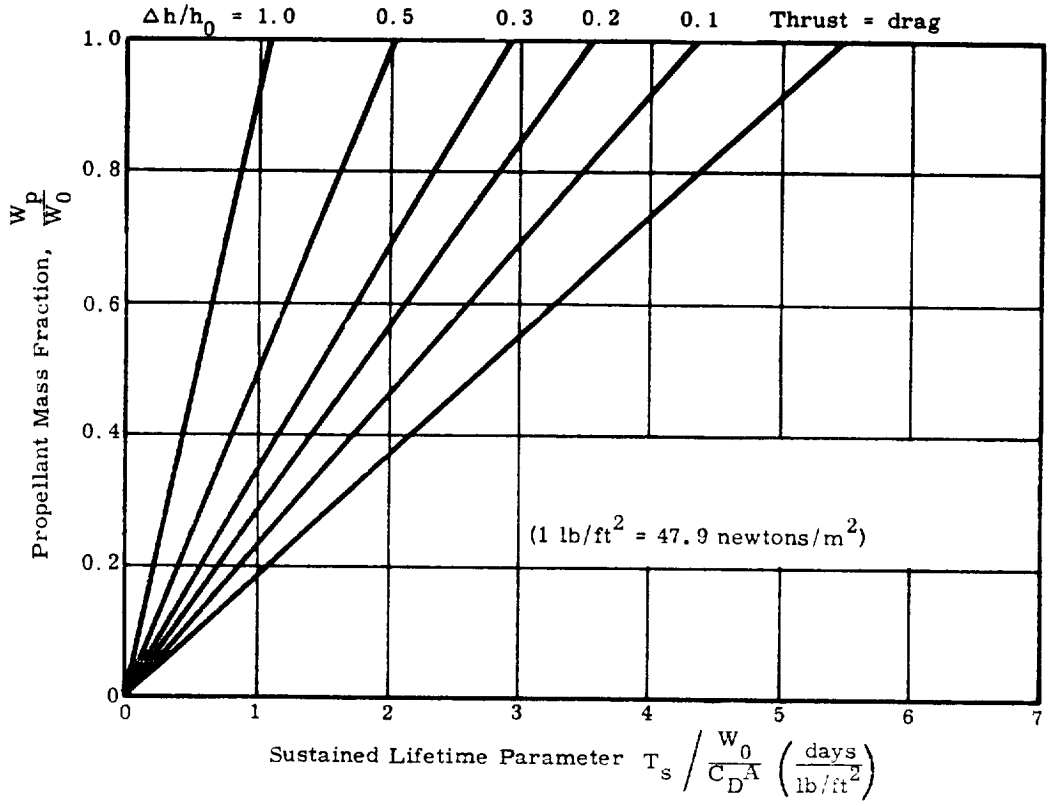

Fig. 23. Discrete Velocity Sustaining System
(h_0 = 100 naut mi = 185 km; I_{sp} = 300 sec)

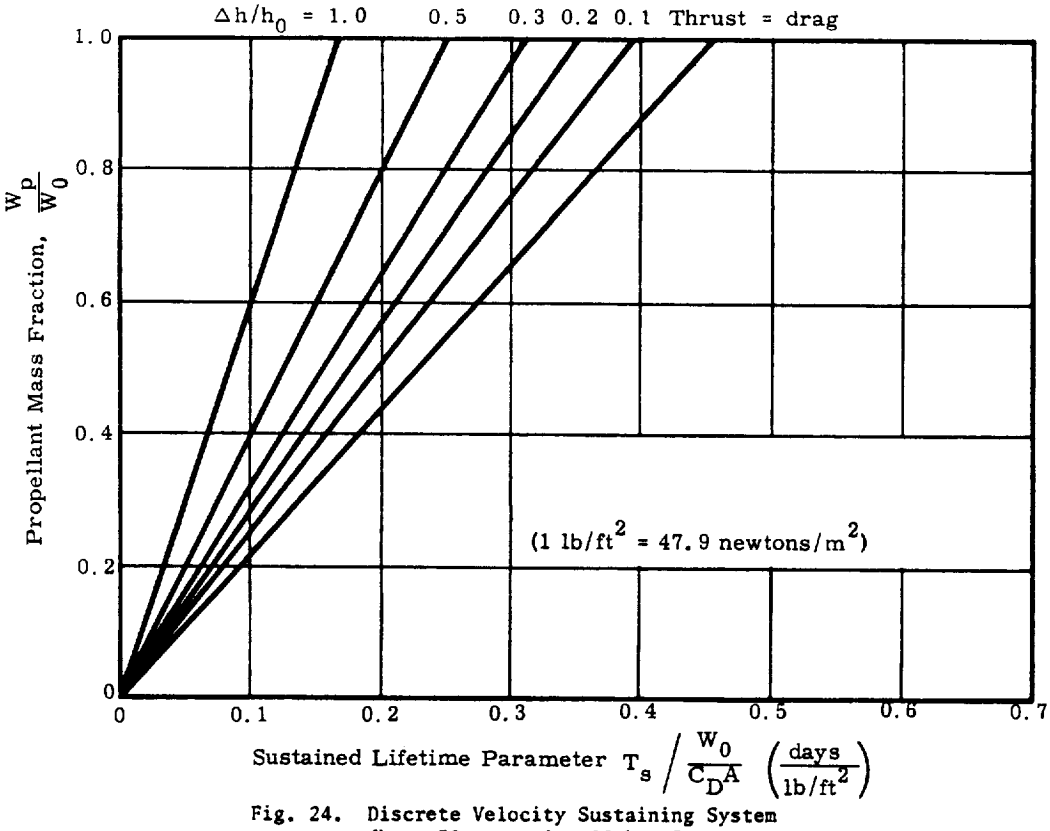

Fig. 24. Discrete Velocity Sustaining System
(h_0 = 50 naut mi = 93 km; I_{sp} = 300 sec)

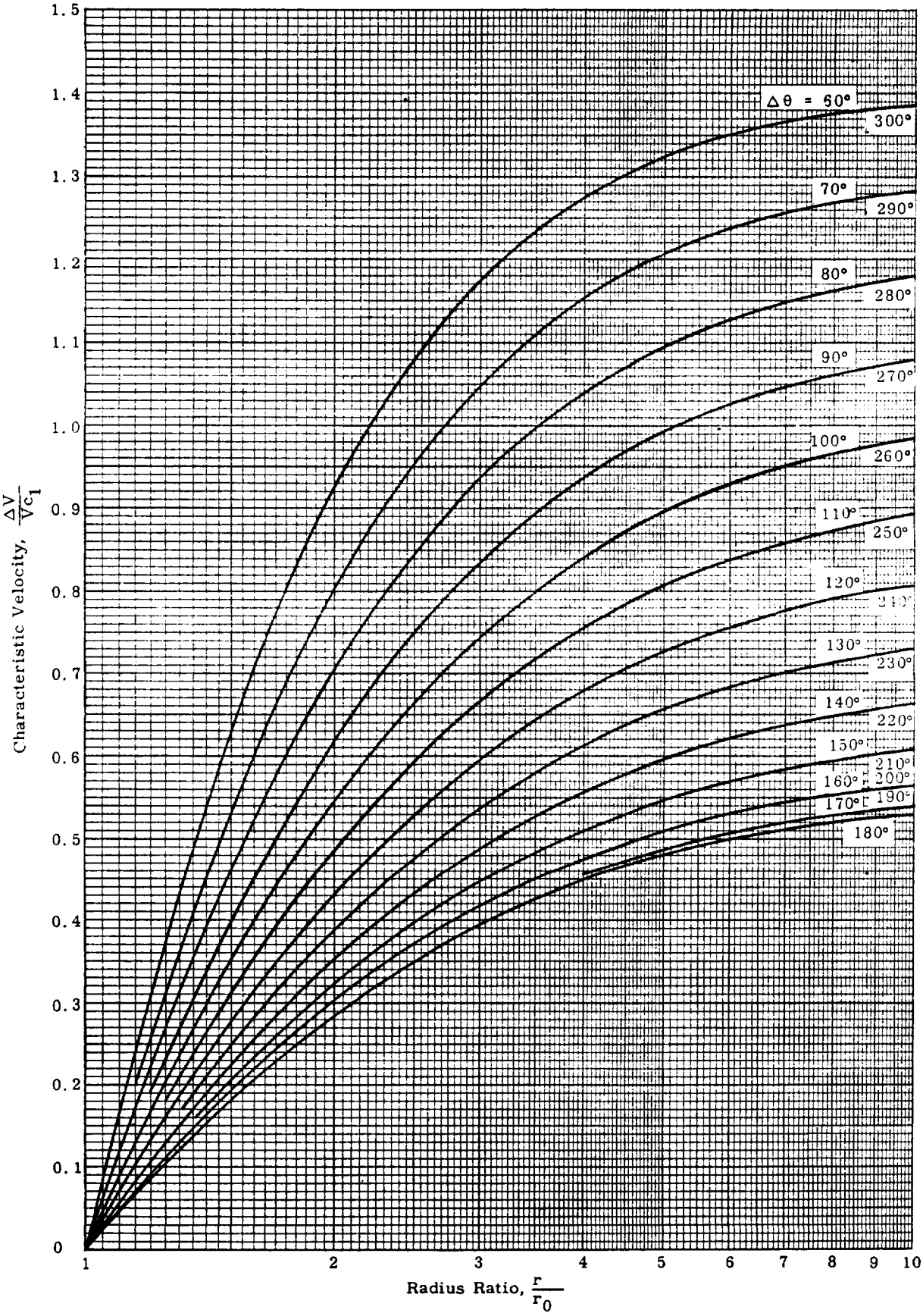

Fig. 25. Velocity Required for Optimum 2-D Transfers Between Circular Orbits

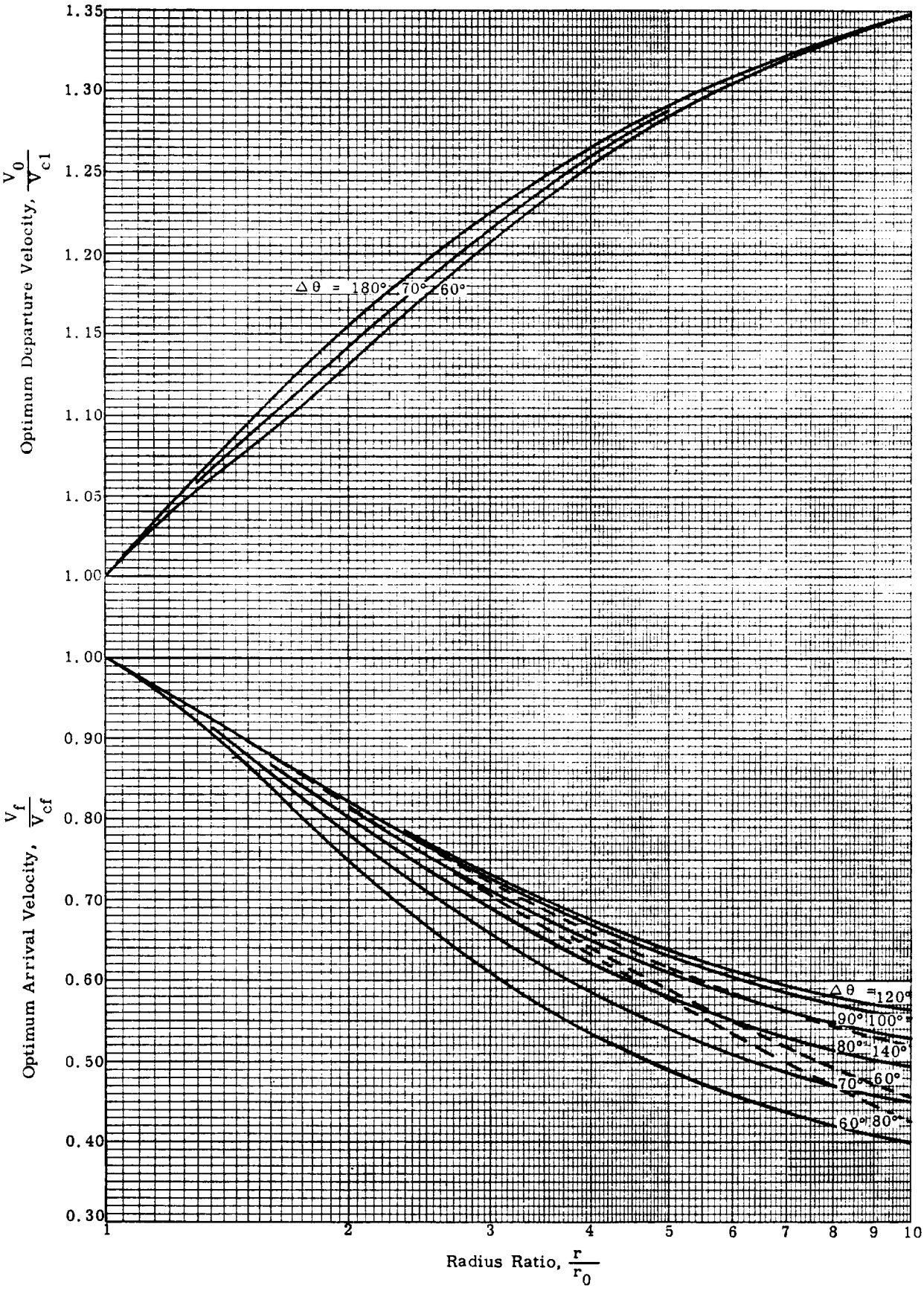

Fig. 26. Independent Impulses for Optimum 2-D Transfers Between Circular Orbits

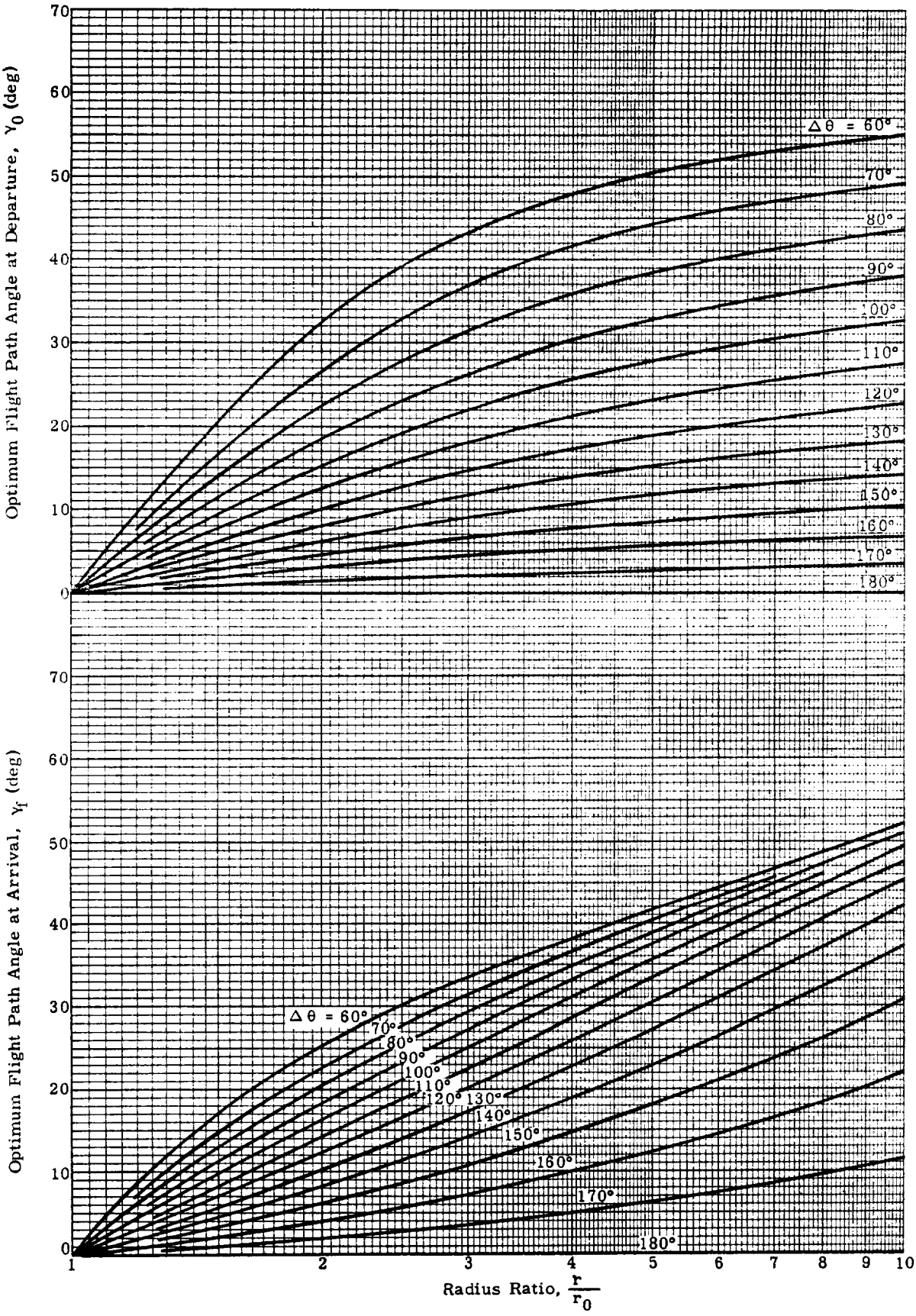

Fig. 27. Flight Path Angles for Optimum 2-D Transfer Between Circular Orbits

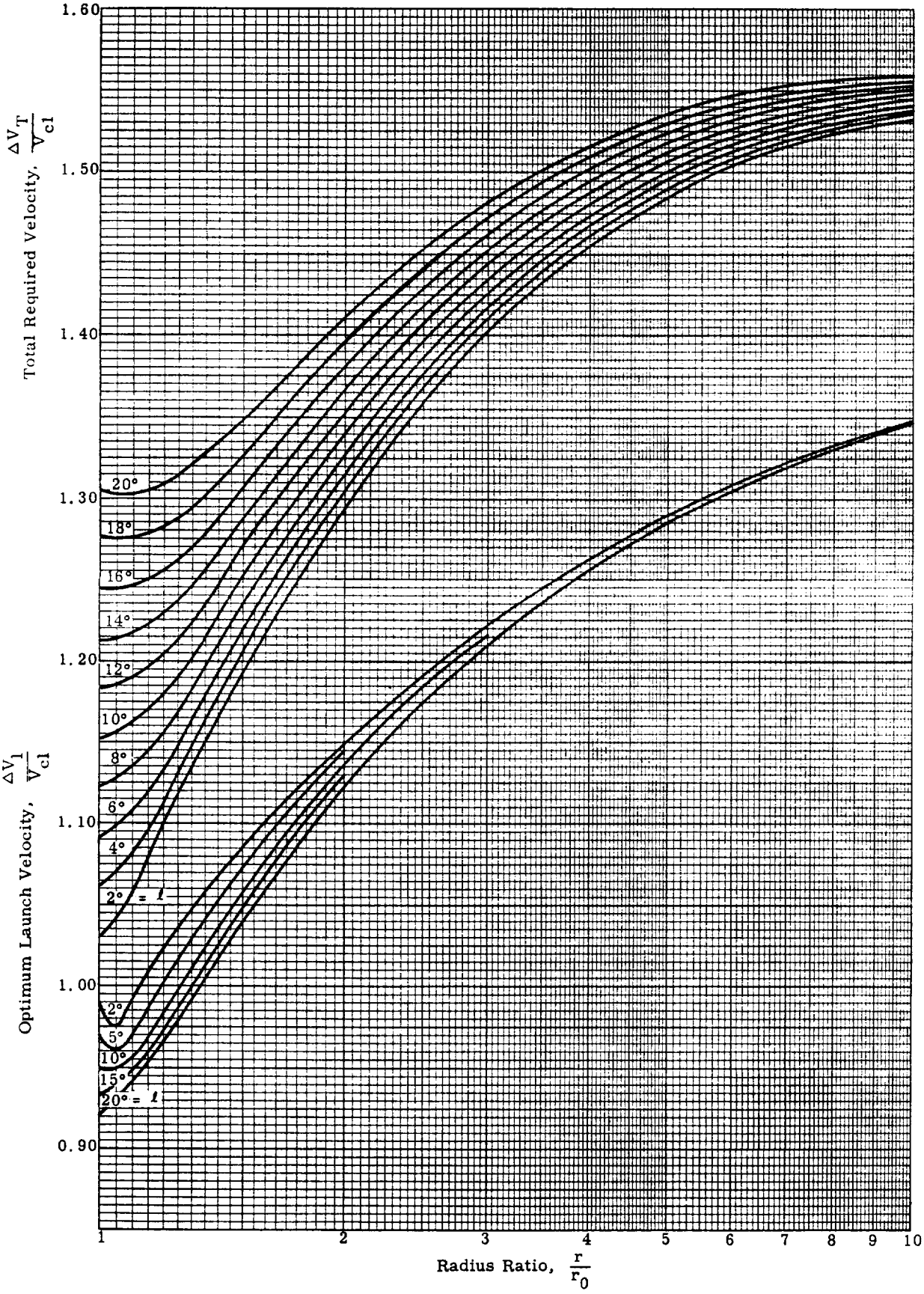

Fig. 28. Velocity Required for Optimum 3-D Transfers Between Circular Orbits

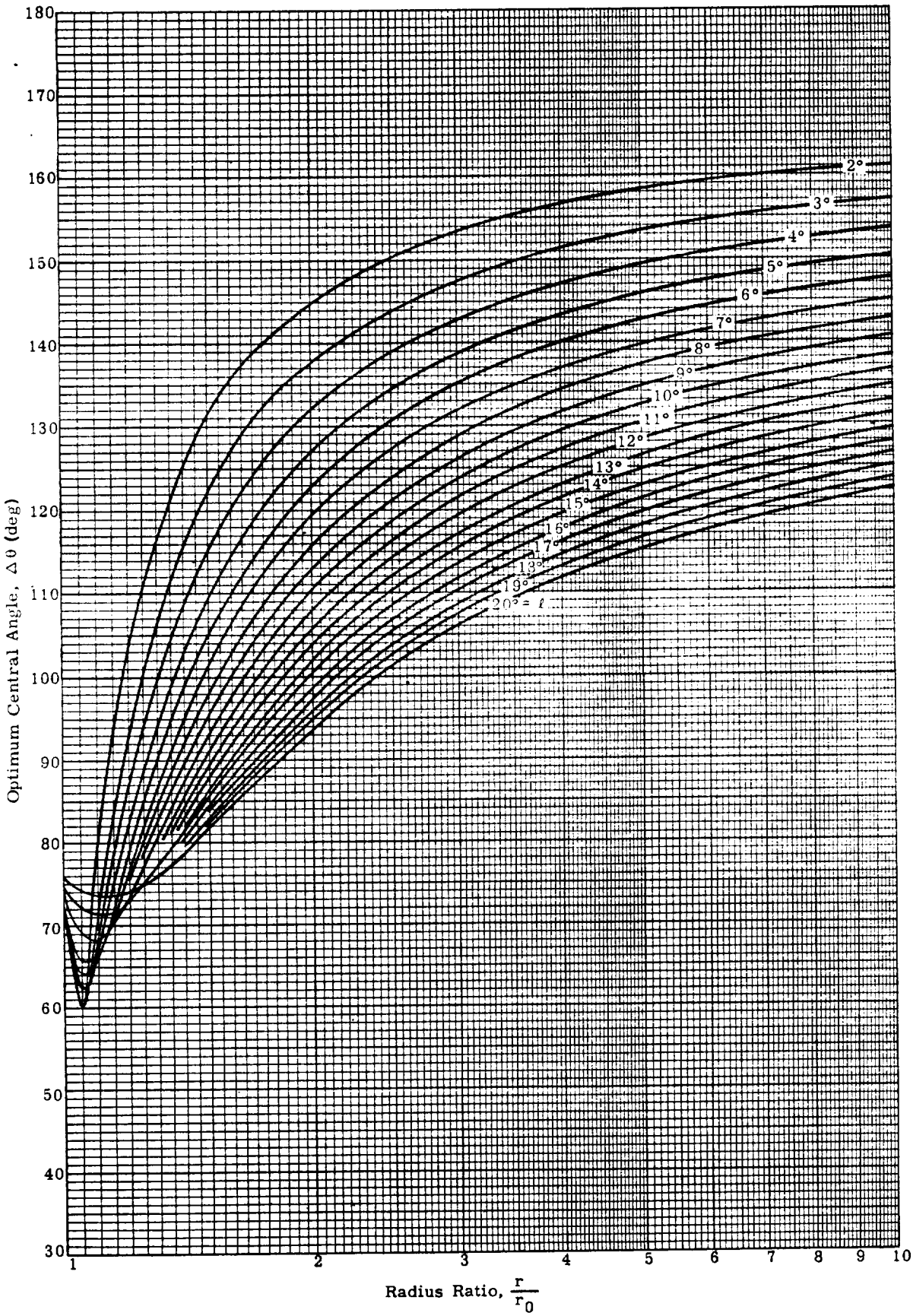

Fig. 29. Central Angles for Optimum 3-D Transfers Between Circular Orbits

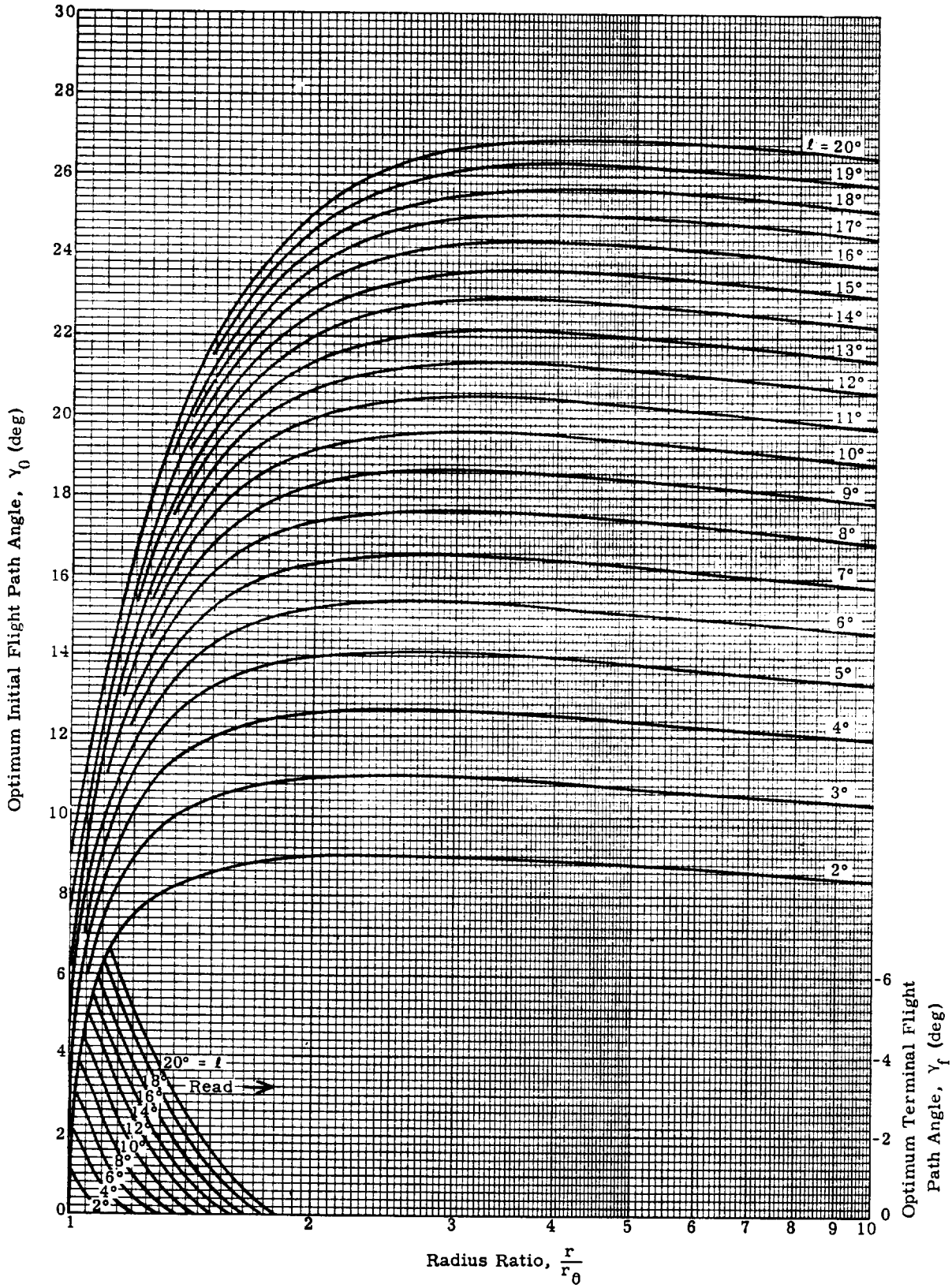

Fig. 30. Flight Path Angles for Optimum 3-D Transfer Between Circular Orbits

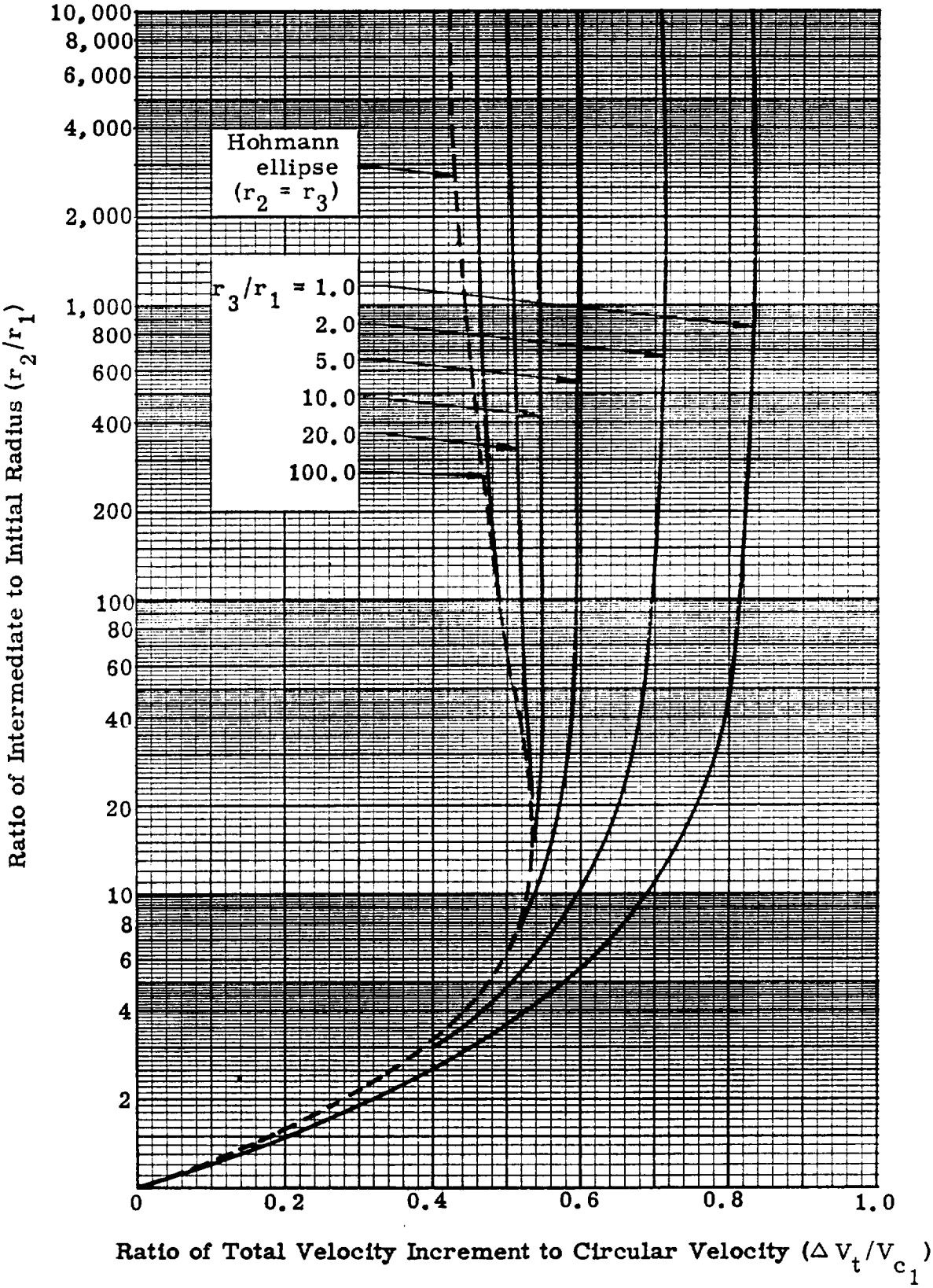

Fig. 31. Total Energy Requirement for the Three-Pulse Transfer Between Circular Orbits as a Function of r_1, r_2 and r_3

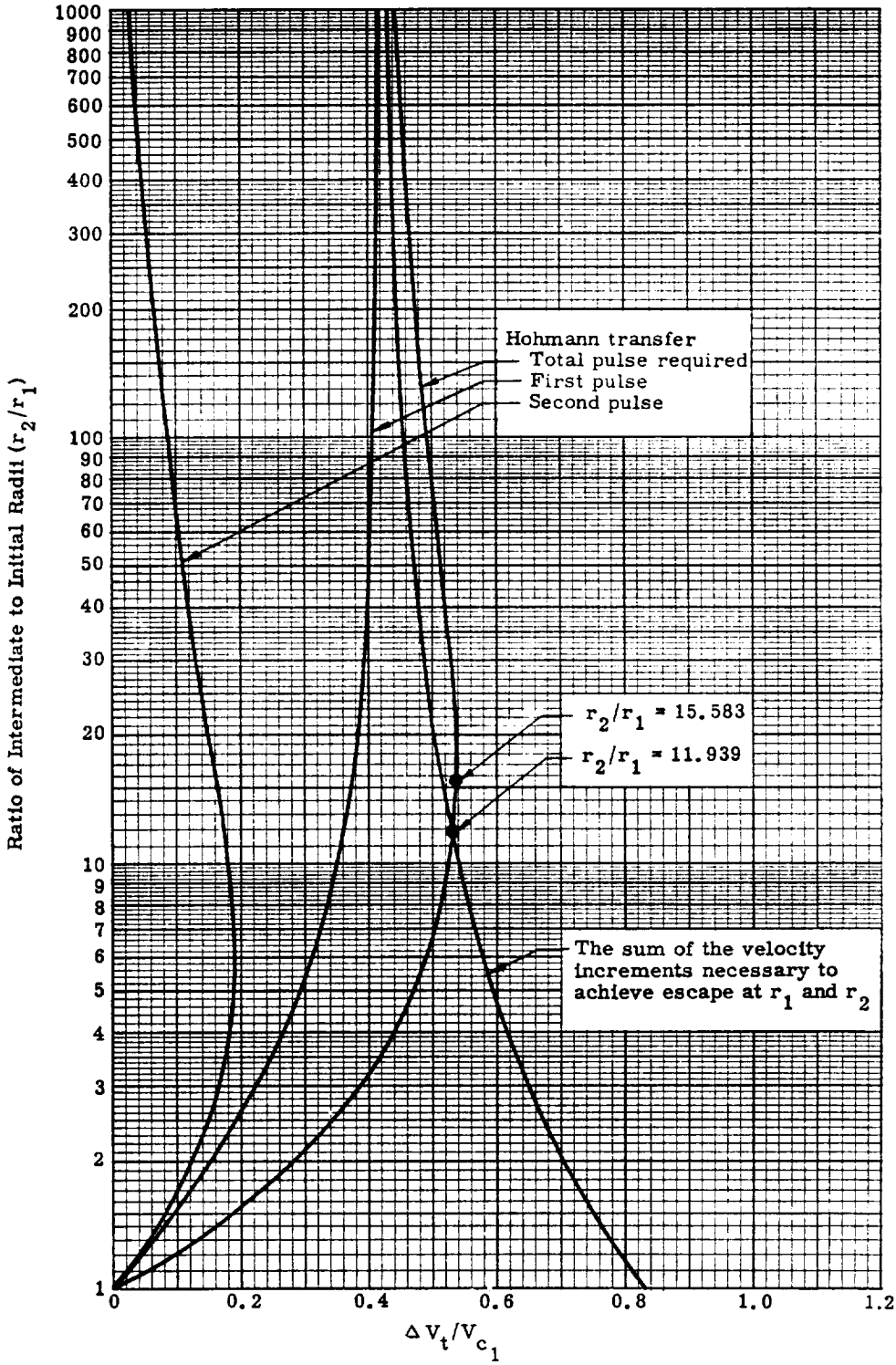

Fig. 32. Energy Requirements for Transfer Between Coplanar Circular Orbits via the Hohmann Ellipse

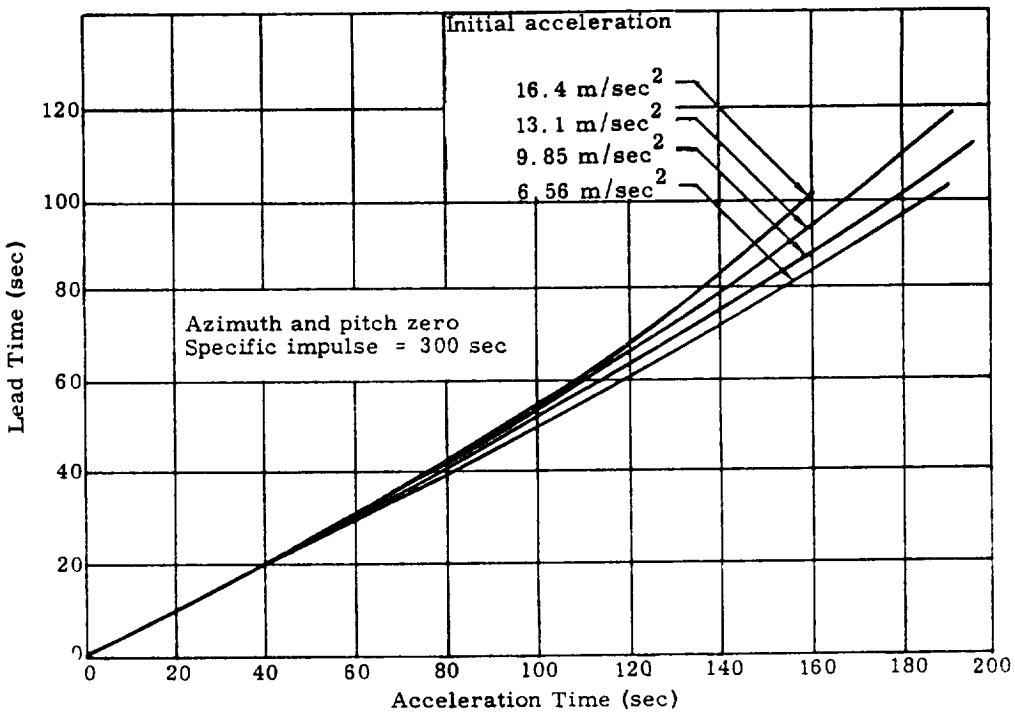

Fig. 33. Lead Time Versus Acceleration Time

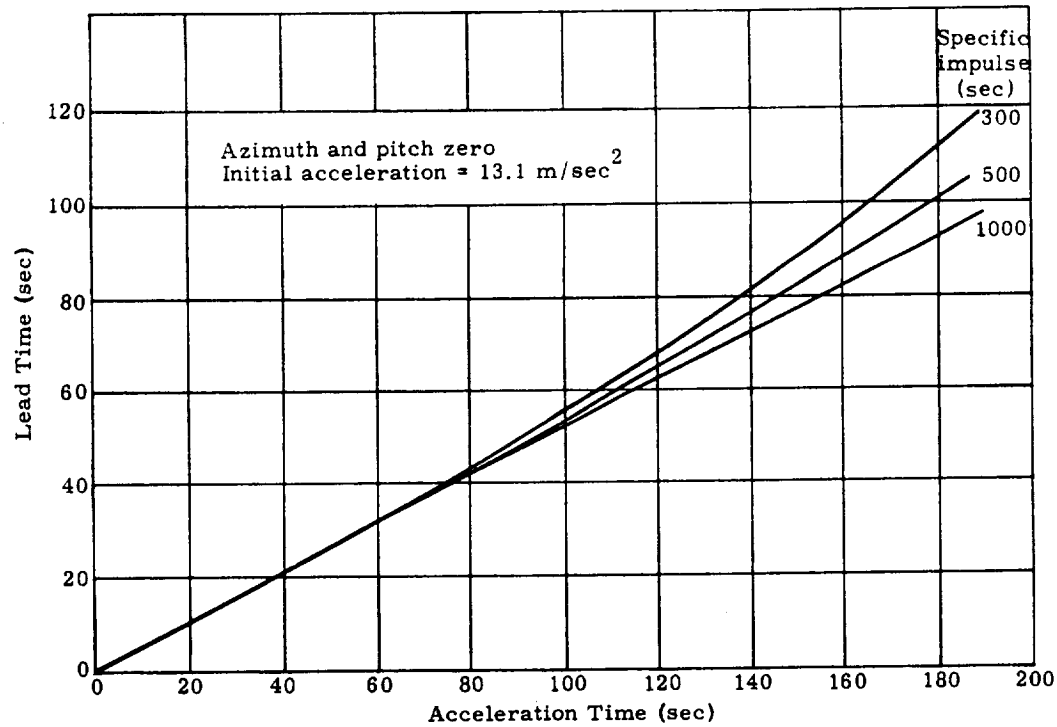

Fig. 34. Lead Time Versus Acceleration Time

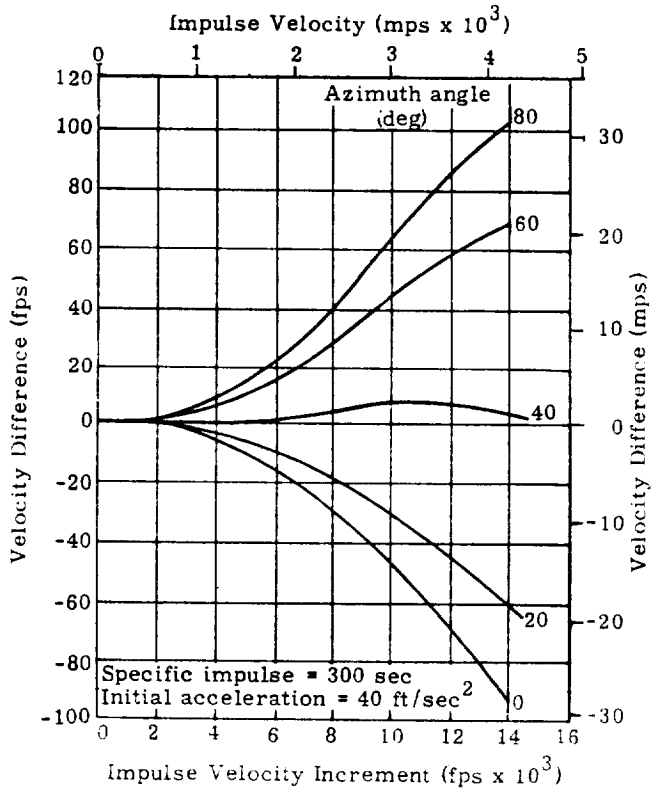

Fig. 35. Velocity Difference Between Finite and Zero Time Acceleration Assumptions

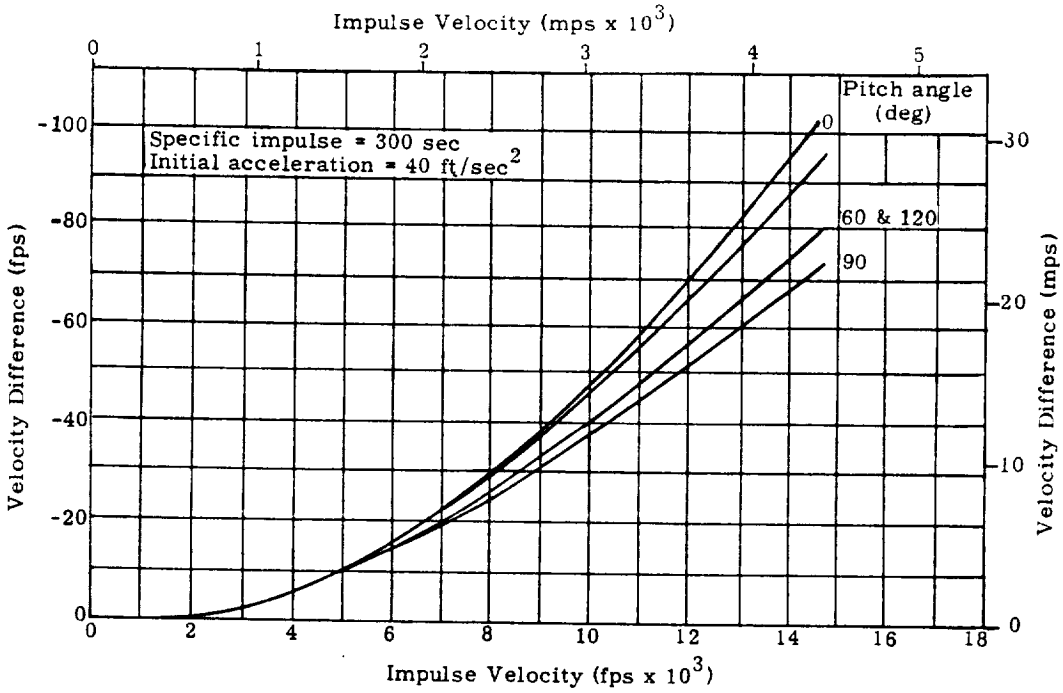

Fig. 36. Difference in Velocity Increments Due to Zero and Finite Thrust Time Assumptions

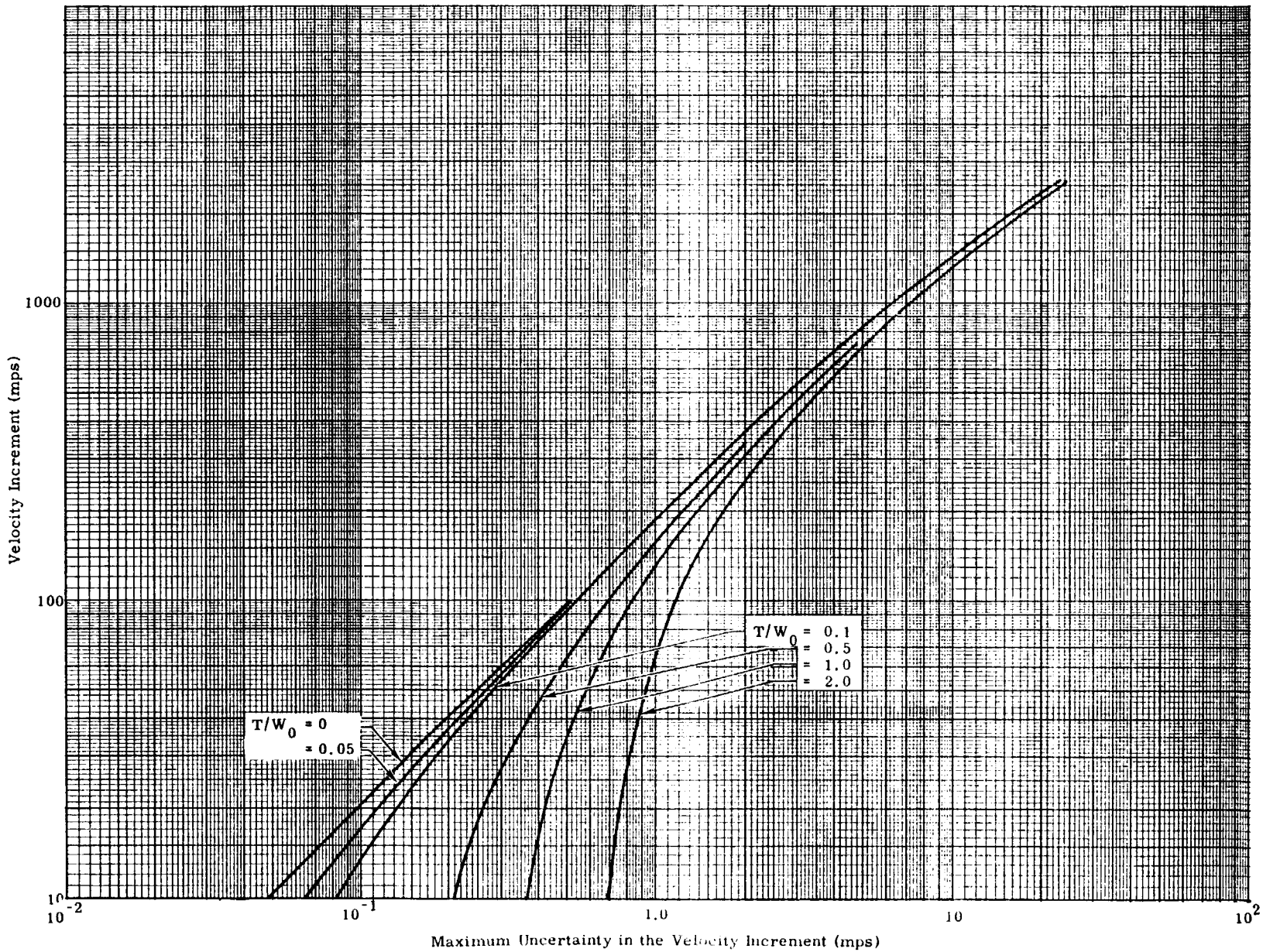

Fig. 37. The Maximum Uncertainty in the Velocity Increment for Present Control Parameters as a Function of the Initial Thrust-to-Weight Ratio (specific impulse = 300 sec)

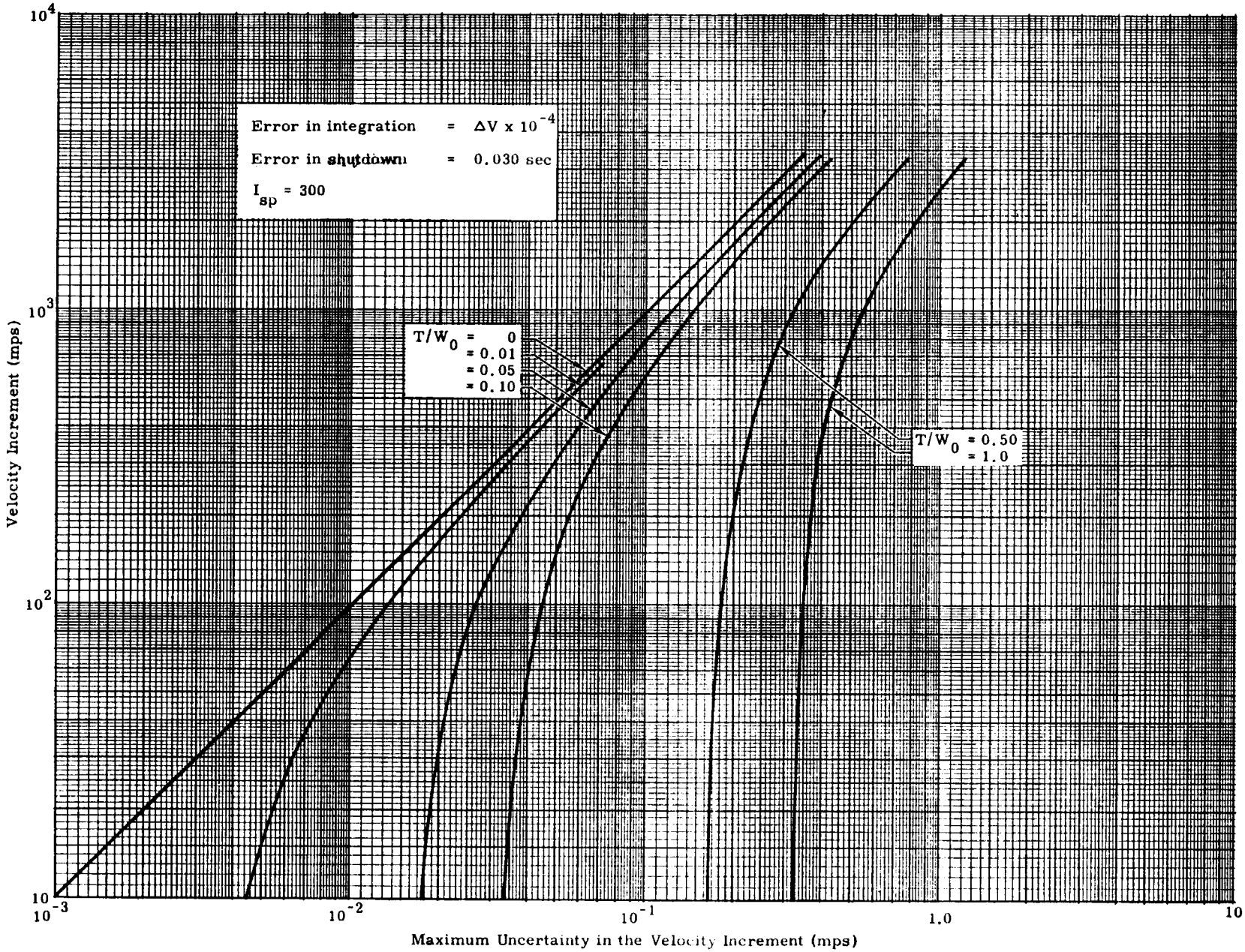

Fig. 38a. The Maximum Error in the Velocity Increment for a Velocity Monitored Propulsion System

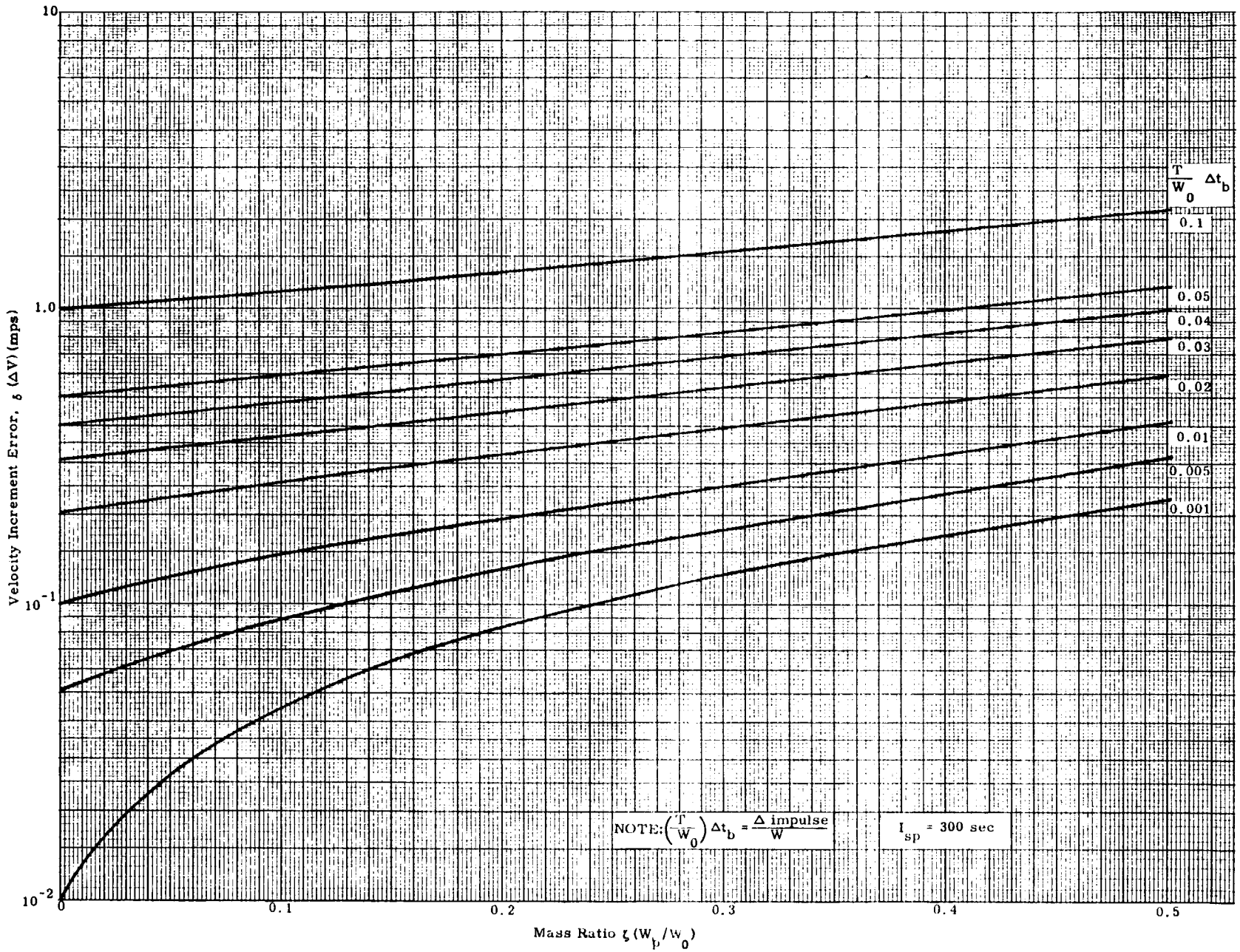

Fig. 38b. The Maximum Error in the Velocity Increment for a Velocity Monitored Propulsion System (error in the integrated velocity increment = 10^{-4} ΔV)

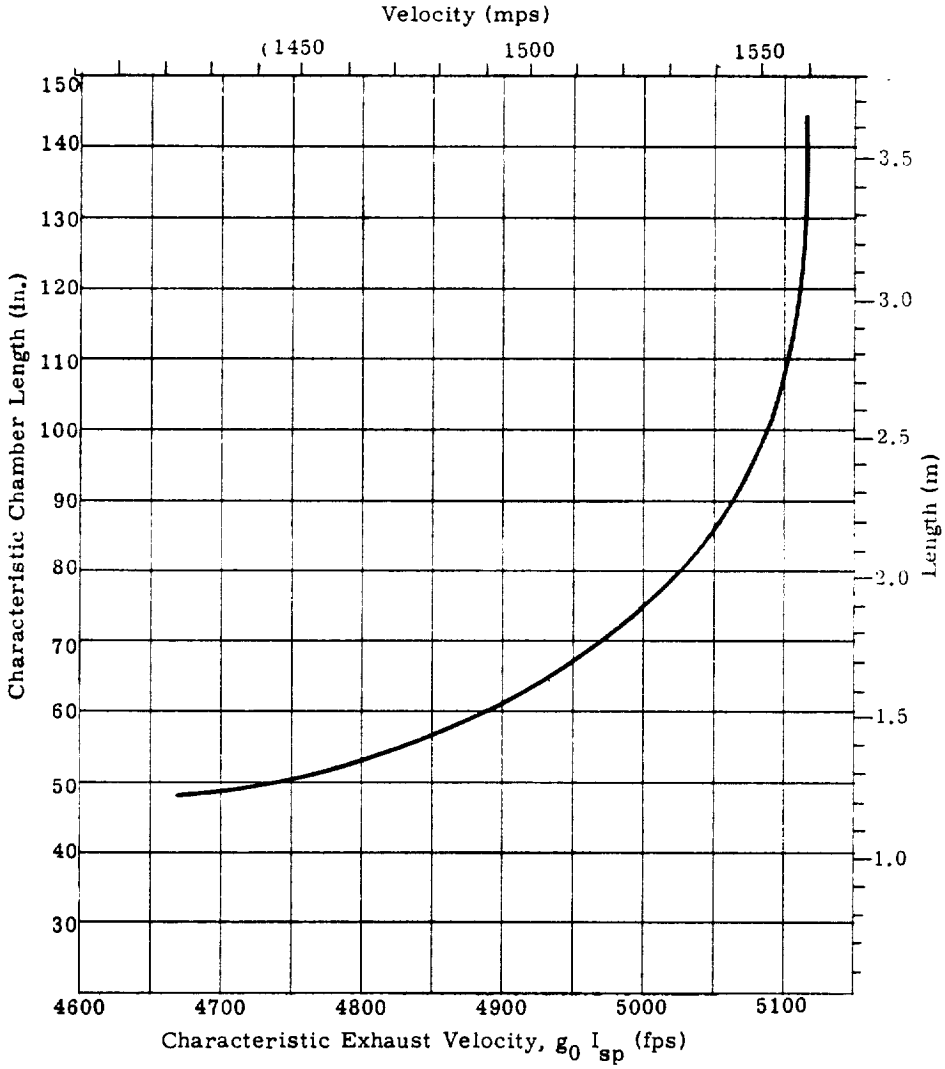

Fig. 39. Characteristic Chamber Length for a UDMH-IRFNA Motor (thrust = 20 to 1000 lb, chamber pressure = 300 to 800 psi, mixture ratio = 2.60:1)(1 psi = 6894 newtons/m^2)

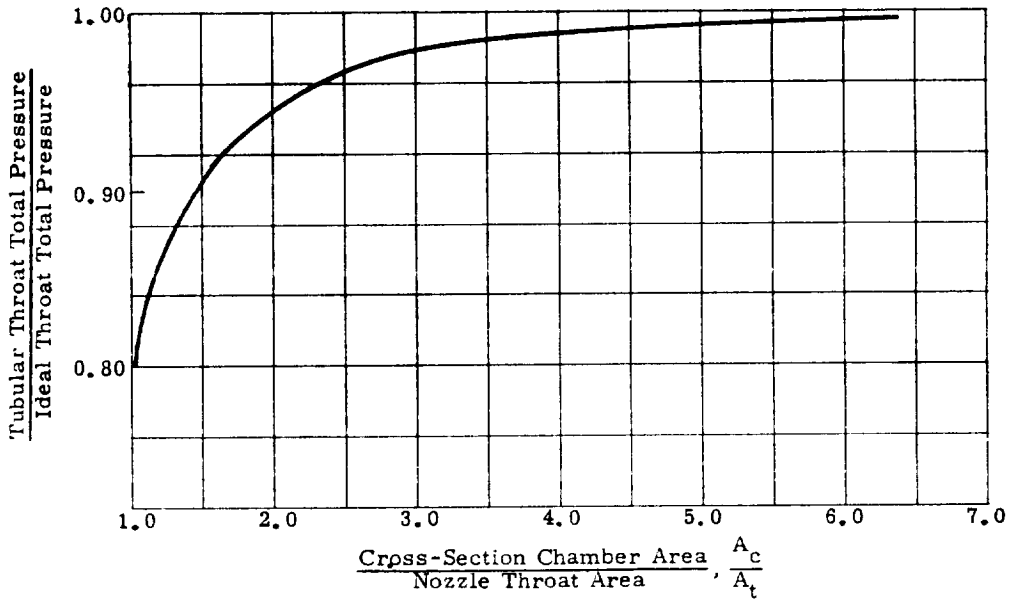

Fig. 40. Relative Total Pressure Loss (measured at the throat) as a Function of Chamber Cross Section for a UDMH-IRFNA Rocket Motor

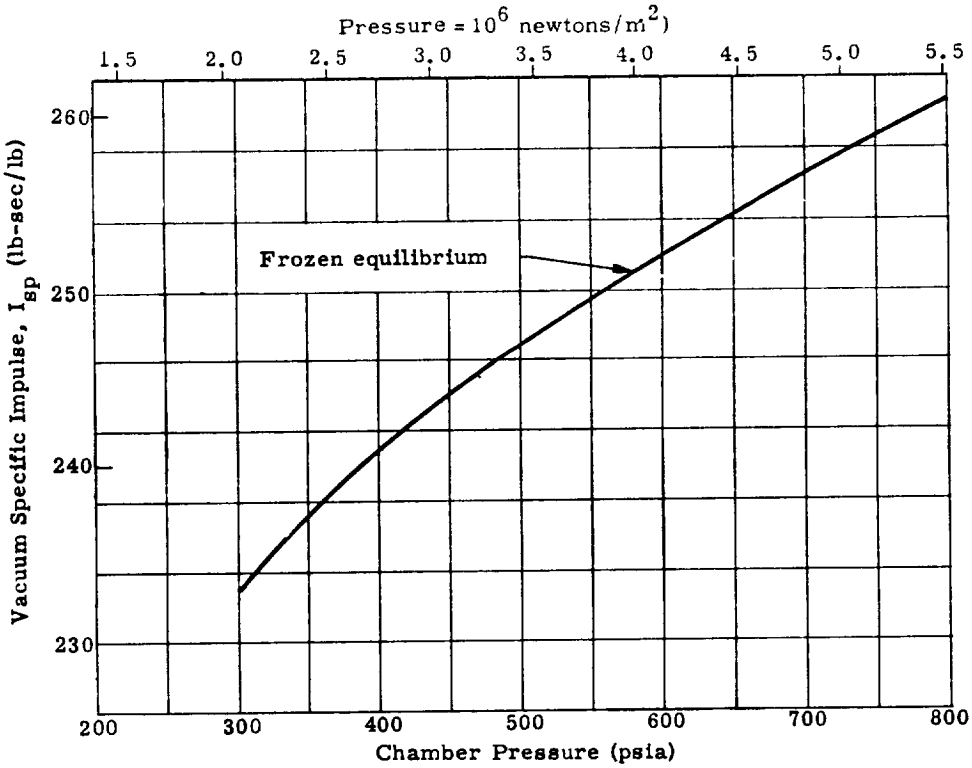

Fig. 41. Sea Level Specific Impulse for a UDMH-IRFNA Motor as a Function of Chamber Pressure (mixture ratio = 2.60:1)
(1 psia = (6894 newtons/m^2)

CHAPTER VII

RENDEZVOUS

Prepared by:

G. E. Townsend, Jr.
Martin Company (Baltimore)
Aerospace Mechanics Department
March 1963

		Page
	Symbols	VII-1
A.	Introduction	VII-3
B.	The Gross Maneuver	VII-3
C.	The Terminal Maneuver	VII-15
D.	References	VII-54
E.	Bibliography	VII-55

LIST OF ILLUSTRATIONS

Figure No.		Page
1	Graphical Solution to Kepler's Equation for E as a Function of M and e	VII-61
2	Launch Azimuth as a Function of Latitude and Inclination	VII-61
3	Launch Site Location for Rendezvous (sample problem)	VII-62
4	Variation of Semimajor Axis with n/m (n/m = 0 to 17)	VII-62
5	Variation of Semilatus Rectum with n/m (n/m = 11 to 17)	VII-62
6	Rendezvous Compatible Orbits (geometric effects)	
	N/m = 16/1	VII-63
	N/m = 31/2	VII-64
	N/m = 15/1	VII-65
	N/m = 29/2	VII-66
	N/m = 14/1	VII-67
7	Finite Burning Time Effects on Rendezvous Compatible Orbits	
	N/m = 15/1, L = 28.5°	VII-68
	N/m = 15/1, L = 34.5°	VII-69
8	Graphical Solution for $\frac{\Delta V}{V}$ in Eq 45a	VII-70
9	Circle Diagram Generatrix of In-Plane Motion	VII-71
10	In-Plane Circle Diagram at Injection	VII-71
11	Parametric Relation for Rendezvous ($\rho = 0$; $\alpha = 0$)	VII-72

LIST OF ILLUSTRATIONS (continued)

Figure No.		Page
12	Ratio of Rendezvous Time to Initial Time-to-Go Versus Initial Downrange Angle	VII-72
13	Rendezvous Geometry at Nodal Crossing	VII-73
14	Rendezvous Using Pure Loft (no period change) . . .	VII-73
15	Rendezvous Using Loft and Period Change	VII-74
16	Output of the Digital Filter (least squares estimate of the input with zero-lag)	VII-75
17	Output of the Digital Filter (least squares, zero-lag estimation of first derivative of the input)	VII-75
18	Output of the Digital Filter (least squares, zero-lag [a = 0] estimation of the second derivative of the input)	VII-75
19	RMS Residual Transverse Error Velocity	VII-76
20	Homing Profile for Extreme Errors	VII-76

VII. RENDEZVOUS

SYMBOLS

Symbols used frequently in this chapter are listed here.

a	semimajor axis (ft or m)
A	right ascension relative to vernal equinox; homing vehicle's yaw relative to target orbit
b	braking distance
e	eccentricity
E	eccentric anomaly (deg or rad)
F	thrust (lb or Newton's)
g	gravitational acceleration = $GM_{\oplus}/r^2$ (fps^2 or mps^2)
G	Newton's Universal Constant of Gravitation
h	angular momentum (ft^2/sec or m^2/sec)
i	inclination to the equatorial plane (deg or rad)
I_{sp}	specific impulse (lb-sec/lb)
J_2	coefficient of the potential function = 1.0823×10^{-3}
L	latitude (deg or rad)
m	mass (slugs or kg)
M	mean anomaly (deg or rad)
$M_{\oplus}$	mass of earth (slugs or kg)
n	number of revolutions; mean motion $\left(\frac{2\pi}{\tau}\right)$
p	semilatus rectum (ft or m)
$r, \dot{r}, \ddot{r}$	radial component of position, velocity and acceleration
r_a, r_p	apogee and perigee radii
R_e	equatorial radius of earth
R	radius of equivalent sphere for earth; relative range
$\dot{R}$	relative range rate $(R \cdot V)/R$
s	relative position vector
t	time
t_b	burning time; braking duration
t_G	rectilinear time to go $(R/\dot{R})$
T	normalized position variable for relative motion study = $\omega_0 t$
u_0	deviation in radial velocity for closure = $-V_R$
V	velocity
V_C, V_R, V_N	velocity components in the circumferential direction, radial direction, and normal to the plane, respectively
W_0	initial weight; deviation of velocity from circularity in discussion of relative motion = $-V_C$
x, y, z	Cartesian components of position
α	nondimensional position parameter for relative motion study (y/r)
β	azimuth relative to local north
γ	flight path angle relative to local horizontal
θ	central angle from perigee to instantaneous radius
λ	nondimensional position parameter for relative motion study (z/r)
Λ	longitude relative to prime meridian
μ	earth's gravitation constant = $GM_{\oplus}$
ν	longitude of the satellite relative to the ascending node
ρ	nondimensional position parameter for relative motion study (x/r)
ξ	ratio of propellant mass to initial vehicle mass
σ	standard deviation
τ	orbital period
ω	argument of perigee; angular rate
ω_0	angular rate in a circular orbit
$\dot{\omega}$	change in argument of perigee per revolution due to oblateness
Ω	right ascension of the ascending node
$\dot{\Omega}$	change in Ω per revolution due to oblateness
Ω_e	rotational rate of the earth 1 rev each 86164.091 mean solar sec

Subscripts

a	apogee

b	bias	R	along range vector
BO	burnout	S	smoothing
f	parameter in final orbit; final	t	value in transfer orbit; total; target
h	homing	T	transverse
L	launch	y	rotation about local vertical
ℓ	low altitude orbit	0	initial, at time = 0
n	node; nominal; running integer	$\oplus$	earth
p	perigee, proportional	$\leftmoon$	moon

A. INTRODUCTION

With the advent of large instrumented and manned satellites, a requirement has been generated for bringing two or more vehicles together in space. This maneuver is referred to as rendezvous and is differentiated from intercept by the fact that at the time of closure the velocity vectors of the two vehicles must match. The procedure for matching these position and velocity vectors is the subject of this chapter, and the various phases of the maneuver will be studied in detail.

Rendezvous can be broken into a series of problems for the purposes of discussion, these problems being:

(1) The gross maneuver.

(2) The terminal maneuver.

The gross maneuver refers to the powered and coasting periods necessary to place the shuttle or homing vehicle in the vicinity of the target satellite. This maneuver can be performed in a number of ways, among them being:

(1) Rendezvous utilizing an intermediate orbit.

(2) Direct ascent.

  (a) Rendezvous compatible orbits.

  (b) Direct ascent coupled with plane change maneuvers.

The first of these techniques concerns itself with the reduction of a three-dimensional problem to one of two dimensions by the simple expedient of launching into the plane of motion at the time the launch site is in the plane. Time then passes until the desired relative positions of the two vehicles are obtained; then a planar transfer is initiated.

A second approach (Rendezvous Compatible Orbits) is an attempt to once again reduce the problem to two dimensions but without utilizing the intermediate or parking orbit. This is possible if the orbital elements of the target satellite are judicially selected. Thus, the whole philosophy is predicated on the premise that rendezvous will be required at some future date and the orbit of the target selected accordingly. The third approach treats the problem as one of three dimensions and allows for the expenditure of propellant to turn the velocity vector at the time the vehicle enters the desired plane. Each of these approaches is investigated.

The terminal maneuver refers to the analysis of the procedures necessary to reduce the relative position and velocity of the shuttle vehicle with respect to the target to zero. Because the distances involved are small, this portion of the analysis is conducted utilizing the equations of relative motion which are derived and discussed in the text. The discussions pertain to the various guidance schemes which can be employed utilizing these equations and the behavior of the vehicle under the influence of such a law. Material is also presented which relates the energy and time of closure requirements for such motion, and schemes for data smoothing during closure. The chapter ends with a discussion of long time closure trajectories, and an analysis of homing phase errors.

B. THE GROSS MANEUVER

The analysis of closing with another vehicle requires that the velocity and radius vectors of the target vehicle be matched. In the process, however, it is generally required that as little propellant as possible be expended for maneuvering (i.e., changing the orbital inclination or nodal position). Thus, while not always practical, it is desirable that the analysis be reduced to the problem of nearly coplanar orbital transfer. Two schemes for defining the launch timing for nearly coplanar transfers and the general case of non-coplanar transfers are presented in the following paragraphs. These are:

(1) Launch utilizing parking orbits.

(2) Direct ascent to a rendezvous compatible orbit.

(3) Direct ascent to orbit considering planar adjustment.

The method of approach neglects the perturbative accelerations due to the sun and moon and assumes that the orbits are Keplerian ellipses (making adjustments for the secular perturbations due to the earth's oblateness). Similarly, the orbital decay rates in all orbits are assumed negligible (thus the analysis is restricted to orbits of greater than 200-mi (320-km) altitude or to short times at lower altitudes). And finally, the burning time of the rocket stages is assumed to be short (making it possible to treat the velocity increments obtainable from rocket stages as pulses). Justification for the final assumption is shown in Chapter VI.

1. Development of Equations To Be Utilized

The studies of orbital injection are directed toward the evaluation of the parameters affecting orbital injection and the establishment of the sensor accuracies and computer requirements necessary to produce a desired orbit. For this analysis the transfer orbit is assumed to be an ellipse, and the final orbit either circular or elliptical. To assure the maximum degree of flexibility, injection (i.e., the point at which the final trajectory is obtained) is assumed to occur at a point corresponding to the intersection of the transfer orbit and the desired orbit rather than at apogee of the transfer orbit or at the point of tangency of the two orbits. However, it must be pointed out that both of these methods of injection can also be obtained from the generalized approach as outlined. All of the equations derived are reduced to the fewest variables possible, thus maintaining simplicity both in the analysis and in the application of the equations to a vehicle-borne computer. While not absolutely necessary, the equations are reduced to a non-dimensional form, thus assuring that the analysis

is capable of handling transfer between any two elliptical orbits around any central body. The following sketch defines a typical transfer and points out the parameters which must be determined to define the maneuver.

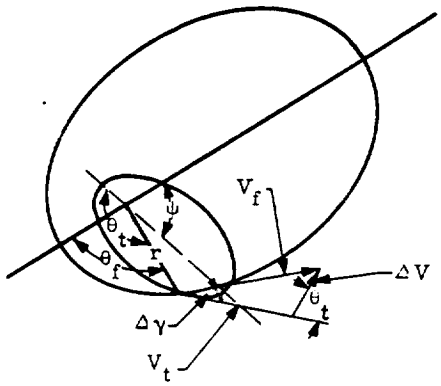

$$\psi = \theta_t - \theta_f \tag{1}$$

$$\Delta\gamma = \gamma_t - \gamma_f \tag{2}$$

$$\Delta V^2 = V_f^2 + V_t^2 - 2 V_f V_t \cos \Delta\gamma \tag{3}$$

$$\Delta V = g_0 I_{sp} \ell n \left(\frac{1}{1-\xi}\right) - \frac{g I_{sp} \xi \sin\gamma}{F/W_0} \tag{4}$$

$$\theta = \cos^{-1}\left[\frac{p-r}{re}\right] = \cos^{-1}\left[\frac{\frac{2r_a}{r} - \left(\frac{r_a}{r_p}+1\right)}{\frac{r_a}{r_p}-1}\right] \tag{5}$$

$$\gamma = \cos^{-1}\sqrt{\frac{r_a/r}{\left(\frac{r_a}{r_p}+1\right) - \frac{r_a/r_p}{r_a/r}}} \tag{6}$$

$$\sqrt{\frac{r}{u}}\, V = \sqrt{\frac{2\left[\left(\frac{r_a}{r_p}+1\right) - \frac{r_a/r_p}{r_a/r}\right]}{\left(\frac{r_a}{r_p}+1\right)}} \tag{7}$$

The determination of the radius of intercept is in reality a fairly complex solution since the exact size, shape and orientation of the transfer orbit are not known until the vehicle has been tracked for some interval of time. However, since the actual orbit differs but little from the predicted orbit and since there is an interval of time during coast when tracking data may be processed, it seems reasonable to assume that the actual transfer orbit is defined. Now, since the required information is available, the radius of interception may be evaluated as follows.

$$r = \frac{p_t}{1 + e_t \cos\theta_t} = \frac{p_f}{1 + e_f \cos\theta_f} = \frac{p_f}{1 + e_f \cos(\theta_t - \psi)} \tag{8}$$

Therefore:

$$\left(\frac{r_{af}}{r_{pf}}+1\right) + \left(\frac{r_{af}}{r_{pf}}-1\right)\cos(\theta_t - \psi) = \frac{r_{af}}{r_{at}}\left[\left(\frac{r_{at}}{r_{pt}}+1\right) + \left(\frac{r_{at}}{r_{pt}}-1\right)\cos\theta_t\right] \tag{9}$$

and:

$$\frac{2 r_{at}}{r} = \left(\frac{r_{at}}{r_{pt}}+1\right) + \left(\frac{r_{at}}{r_{pt}}-1\right)\cos\theta_t \tag{10}$$

The solution for θ_t from Eq (9) is somewhat involved, and the type of solution may well depend upon the material available for the solution and the number of times that the equation must be solved. If a small digital computer in the vehicle is programmed to handle the solution, an iterative solution would probably be the simplest. A direct solution may also be obtained for θ_t after manipulation of the terms in Eq (9); this direct solution is to be preferred for accuracy for manual evaluations of θ_t even though the form of the equation is complex.

$$\cos\theta_t = -A \pm \sqrt{B + A} \tag{11}$$

$$\left.\begin{aligned} A &= \frac{CD}{1+C^2} \\ B &= \frac{1-D^2}{1+C^2} \\ C &= \frac{x - yz\cos\psi}{yz\sin\psi} \\ D &= \frac{(x+2) - z(y+2)}{yz\sin\psi} \end{aligned}\right\} \tag{12}$$

$$\left.\begin{aligned} x &= \frac{r_{at}}{r_{pt}} - 1 \\ y &= \frac{r_{af}}{r_{pf}} - 1 \\ z &= \frac{r_{at}}{r_{af}} \end{aligned}\right\} \tag{13}$$

Timing for the injection pulse can be obtained by matching tracking data for the radius to the satellite with the value of the intercept radius as calculated, or the pulse may be initiated at some specified time corresponding to the time of flight from cutoff to the intercept radius. This time of flight may be computed by subtracting the time of flight from perigee to the cutoff radius from that corresponding to travel from perigee to the intercept radius. The time of flight from perigee may be determined as follows.

This approach is entirely general so that the case of tangency of the two orbits can also be evaluated. That case, however, provides another restraint (the flight path angle identity).

$$\cos \gamma = \sqrt{\frac{r_{af}/r}{\left(\frac{r_{af}}{r_{pf}} + 1\right) - \frac{r_{af}/r_{pf}}{r_{af}/r}}}$$

$$= \sqrt{\frac{r_{at}/r}{\left(\frac{r_{at}}{r_{pt}} + 1\right) - \frac{r_{at}/r_{pt}}{r_{at}/r}}}$$

$$r_{tan} = \frac{r_{af}\left(\frac{r_{at}}{r_{pt}} + 1\right) - r_{at}\left(\frac{r_{af}}{r_{pf}} + 1\right)}{\frac{r_{af}}{r_{pt}} - \frac{r_{at}}{r_{pf}}} \qquad (14)$$

The equations of this section have been plotted in nomographic form and are presented in Chapter III. The accuracy afforded by these figures is inadequate for most detailed analyses; however, preliminary calculations are greatly simplified by their use.

2. Launch Utilizing the Intermediate Orbit

a. Formulation

Since the majority of the missions envisioned for satellites suggest orbits inclined at greater than 30° to the equator and since in-orbit maneuvers are not necessary for these orbits, the first approach to be analyzed is that which requires accurate control of the time and azimuth of launch and which utilizes the intermediate orbit.

Kepler's equation defines the time the vehicle coasts in the transfer orbit. This time plus the total time in the intermediate orbit, the time of ascent to the intermediate orbit, and the time from perigee to the point of rendezvous in the target orbit, defines the time (in the target orbit) from perigee to the position of the target vehicle at the time of launch. This time in turn defines the position of the vehicle in its orbit. However, this reverse solution of Kepler's equation is transcendental and requires an independent investigation.

The time from perigee in the final orbit at the time of launch can be computed as

$$t_{1f} = t_{2f} - t_t - n\tau_1 - t_{ascent} \qquad (15)$$

where

$$t_{2f} = \frac{\tau_f}{2\pi}\left[E_{2f} - e_f \sin E_{2f}\right]$$

$$E_{2f} = 2\tan^{-1}\left[\sqrt{\frac{r_{pf}}{r_{af}}}\tan\frac{\theta_{2f}}{2}\right]$$

$$\theta_{2f} = \theta_t - \psi$$

Now

$$E_{1f} - e_f \sin E_1 = \frac{t_{1f}(2\pi)}{\tau_f} = M_{1f} \qquad (16)$$

This equation can be solved using any of a number of iterative processes; however, Newton's method appears to possess best convergence properties.

$$E_{k+1} = E_k - \frac{f(E_k)}{f'(E_k)}$$

$$f(E_k) = E_k - e \sin E_k - M_1$$

$$f'(E_k) = 1 - e\cos E_k$$

and

$$E_{k+1} = \frac{e\left[\sin E_k - E_k \cos E_k\right] + M}{1 - e\cos E_k} \qquad (17)$$

This series has been shown to converge for all E_k and to converge very rapidly if a reasonable estimate of E_k is utilized. Pursuing this thought further, it may be seen that Kepler's equation can be divided into two terms, each of which defines a line.

$$y = \sin E$$

$$y = \frac{1}{e}(E - M)$$

The intersection of these lines is the required solution. This graphical solution, presented in Fig. 1, would be employed as the first estimate of E. (The nomogram of Kepler's equation, Chapter III, may also be utilized.) Once this solution converges for E_1, the initial position of the target vehicle may be evaluated.

$$\theta_{1f} = 2\tan^{-1}\left[\sqrt{\frac{r_{af}}{r_{pf}}}\tan\frac{E_{1f}}{2}\right] \qquad (18)$$

To illustrate the power of this method, consider the following sample problem:

Sample problem

$M = 1.0$

$e = 0.3$

$E_k \approx 1.29$

$$E_{k+1} = \frac{0.3\ [0.960823 - 1.29\ (0.277174)] + 1.0}{1.0 - 0.3\ (0.277174)}$$

$$= 1.288087$$

$$E_{k+2} = \frac{0.3\ [0.960294 - 1.288087\ (0.278991)] + 1.0}{1.0 - 0.3\ (0.278991)}$$

$$= 1.288088$$

These equations only partially define the rendezvous problem since only the position of the target vehicle and the corresponding time of launch are evaluated. Consideration must now be given to the position of the launch site. This can be accomplished with spherical trigonometry; however, several quantities, shown in the following sketch must be defined before proceeding.

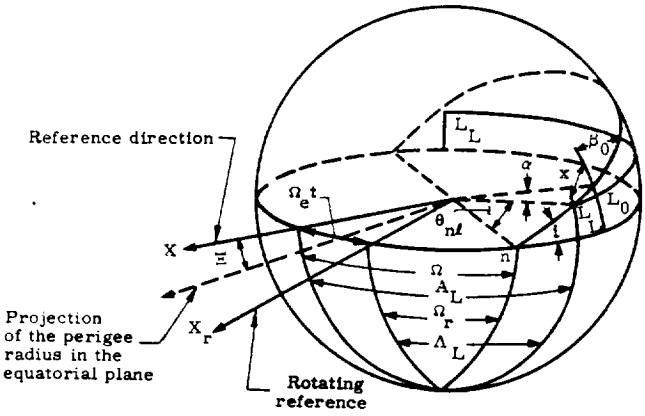

The angle from the ascending node to the radius at which transfer into the final orbit occurs (projected along the equator of a nonrotating earth) is

$$A_s - \Omega = \tan^{-1}\left[\cos i \tan(\omega_t + \theta_t)\right] \qquad (19)$$

where A_s is the right ascension of the satellite at the point of injection into the final orbit, and the latitude of the point of injection is

$$L_s = \sin^{-1}\left[\sin i_t \sin(\omega_t + \theta_t)\right] \qquad (20)$$

Similarly, the angle from the node to the perigee of the transfer orbit and the latitude of perigee may be computed as

$$A_p - \Omega = \tan^{-1}\left[\cos i_t \tan \omega_t\right] \qquad (21)$$

$$L_p = \sin^{-1}\left[\sin i_t \sin \omega_t\right] \qquad (22)$$

Continuing, the position of the required point for injection into the intermediate orbit is

$$A_{BO} - \Omega = \tan^{-1}\left[\cos i_t \tan(\omega_t - \phi)\right] \qquad (23)$$

$$L_{BO} = \sin^{-1}\left[\sin i_t \sin(\omega_t - \phi)\right] \qquad (24)$$

The last remaining step is to define the position of the launch site and the azimuth of burnout. This problem requires the value of the ground range attained in ascent to the low altitude orbit over a nonrotating earth (x).

$$A_L - \Omega = \tan^{-1}\left[\cos i_t \tan\left(\omega_t - \phi - \frac{x}{R_e}\right)\right] \qquad (25)$$

$$L_L = \sin^{-1}\left[\sin i_t \sin\left(\omega_t - \phi - \frac{x}{R_e}\right)\right] \qquad (26)$$

$$\beta_L = \sin^{-1}\left[\frac{\cos i_t}{\cos L_L}\right] \qquad (27)$$

If the assumption is made that the distance and time spent during ascent to the point of burnout are small, the azimuth in which the vehicle must be fired can be computed. This solution follows from the laws of sines and cosines and Eq (27).

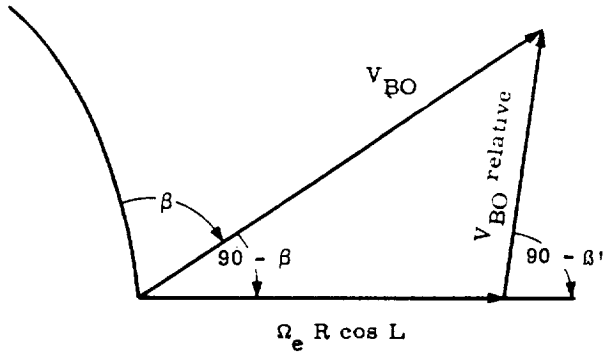

$$V_{BO}^2 = V_{BO}^2 + (\Omega_e R_e \cos L_L)^2 - 2 V_{BO} \Omega_e R \cos L \sin \beta$$

$$= V_{BO}^2 + (\Omega_e R_e \cos L_L)^2 - 2 V_{BO} \Omega_e R \cos i$$

$$\cos \beta' = V_{BO} \cos \beta \left[V_{BO}^2 + (\Omega_e R_e \cos L_L)^2 - 2 V_{BO} \Omega_e R_e \cos i\right]^{-1/2} \qquad (28)$$

The uncorrected launch azimuth (i.e., Eq (27) is presented in Fig. 2. The value of azimuth obtained in this manner is quite close to the corrected value since the velocity component produced by the earth's rotation is only 1524 cos L fps or 465 cos L mps. The magnitude of this vector is, thus, approximately one-tenth of the magnitude of the burnout velocity for most orbital shots with a resultant effect on the cosine of the azimuth between 0.5% and 10% depending on the orbital inclination.

Equations (25) through (28) define the position of the required launch site and the azimuth of launch both in space and relative to the launch site. However, if a particular launch site is to be utilized, consideration must be given to the problem of matching the desired time of launch with the time at which the launch site crosses the desired orbital plane.

$$t_L = t_1$$

where

t_L = the time of launch relative to the reference direction in the plane of the equator.

t_1 = the time from perigee in the final orbit to the vehicle at the launch of the shuttle.

Now

$$t_L = t_{2f} + t^* - t_t - t_{ascent} - n\tau_l \left[1 + \frac{\Delta\tau}{\tau}\right] \quad (20)$$

where

t^* = time required by the satellite to travel from the projection of the perigee radius in the equatorial plane to the reference direction (all times are thus related to a common base).

n = number of revolutions in intermediate orbit.

$\Delta\tau$ = oblateness correction to orbital period.

Numerical data can be generated for the time of ascent once it is known what the intermediate orbit will be and to what extent the trajectory from launch to burnout is shaped by the guidance law. It should be noted that since the selection of an intermediate orbit will depend on the duration of t_{ascent}, iteration for this quantity will be necessary.

This time must be matched with the following, if no error in the orbital plane is permissible.

$$t_L = \frac{(\Omega + n\dot{\Omega}_l) - \Lambda_L \pm \sin^{-1}\left(\frac{\tan L_L}{\tan i}\right) + \delta\pi}{\Omega_e} \quad (30)$$

where $\delta = 1$ for southerly launches, 0 otherwise.

$\dot{\Omega}_l$ = secular regression rate in the intermediate orbit $= \dfrac{-3\pi J_2 \cos i}{\left(\frac{a}{R}\right)^2 (1-e^2)^2}$ $\quad 0 < i < 180°$

and where the plus value of $\sin^{-1}\left(\frac{\tan L}{\tan i}\right)$ is used for northerly launches and the minus for southerly launches.

It should be noted at this point that range safety restrictions at both AMR and PMR currently restrict all launches to those in a southerly direction. For this reason only southerly launches are given attention, and therefore, only the negative sign is utilized. For convenience, the term π will also be combined with the angle Ω.

Since the solution of Eqs (29) and (30) may require that the satellite remain in the low altitude orbit for a long period, it may be possible (if small errors in the nodal position are acceptable) to launch at a time when the desired launch site is arbitrarily close to the desired plane. This is done in the following manner.

$$t_L - \frac{(\Omega + n\dot{\Omega}) - \Lambda_L - \sin^{-1}\left(\frac{\tan L_L}{\tan i}\right)}{\Omega_e} \leq \frac{\text{allowable nodal error}}{\Omega_e} \quad (31)$$

Since rendezvous cannot occur until this error has been removed, maneuvering is implied. Equation (31) thus introduces the concept of launch time tolerance (or launch windows as the subject is sometimes called) since

$$\Delta t_L = \frac{\Delta\Omega}{\Omega_e} .$$

It should be noted that the perturbing influence of the earth's oblateness has been included only in those terms involving the low altitude circular orbit. This assumption is reasonable, though not precise, if the final and initial orbits differ markedly in size. However, if more accuracy is desired, or if the various orbits are essentially the same size, the following equations should be employed.

$$t_L = t_{2f} + t^* + \Delta\tau_f\left(\frac{\theta_f}{2\pi}\right) - t_t + \Delta\tau_t\left(\frac{\theta_t}{2\pi}\right) - n\tau_L\left[1 + \frac{\Delta\tau}{\tau}\right] - t_{ascent} \quad (32)$$

$$t_L = \left\{\Omega + n\dot{\Omega}_l - \left(\frac{\theta_t}{2\pi}\right)\dot{\Omega}_t - \left(\frac{\theta_f}{2\pi}\right)\dot{\Omega}_f - \Lambda_L - \sin^{-1}\left[\frac{\tan L_L}{\tan i}\right]\right\}\frac{1}{\Omega_e} \quad (33)$$

Because of the large number of variables, it is impossible to obtain an intuitive feel for the manner in which the time in the intermediate orbit varies. However, if certain restrictions are made, a feel can be obtained for certain classes of orbits. If it is assumed that the orbits of interest are both circular and that the transfer is via the Hohmann ellipse, and if it is further assumed that perturbations are neglected because of plotting accuracy, then

$$n = \frac{t_{2f} + t^*}{\tau_L} - \frac{\tau_t}{2\tau_L} - \frac{t_{ascent}}{\tau_L} - \frac{(\Omega - \Lambda_L) - \sin^{-1}\left(\frac{\tan L_L}{\tan i}\right)}{\Omega_e \tau_L}$$

(continued)

$$= \frac{t_{2f} + t^* - t_{ascent}}{\tau_L} - \frac{1}{2}\sqrt{\frac{a_t^3}{a_L^3}} - \frac{(\Omega - \Lambda_L) - \sin^{-1}\left(\frac{\tan L_L}{\tan i}\right)}{\Omega_e \tau_L} \qquad (34)$$

Since the equation generally results in a negative value of t_L, the significance of such values must be discussed. Negative times simply imply that the shuttle vehicle is launched at a time prior to the beginning of the time record; negative times can be avoided by increasing t_{2f} by some integer of the orbital period (1, 2, 3, ---).

b. Sample problem

The rendezvous problem, exclusive of the final closure discussion, has been presented in the preceding sections. A numerical check of the flexibility, accuracy and utilization of the approach is in order. For the purposes of illustration, a target orbit of a 24-hr period is selected. In addition it is assumed that the latitude of the point of injection into the transfer orbit is the latitude of the launch site. The numerical analysis follows.

r_{af} = 42,400 stat mi ≈ 68,300 km

r_{pf} = 10,000 stat mi ≈ 27,900 km

e_f = 0.61832

L_1 = 28.5° N

L_2 = 28.5° N

$i_f = i_t$ = 70°

ω_f = -77.46°

r_{pt} = 4500 stat mi ≈ 7250 km

Elliptical orbits are tangent at point of rendezvous. In addition it is assumed that the type of transfer is specified and the time of ascent is known.

t_{ascent} = 1000 sec

$$\sin(\omega + \theta) = \frac{\sin L_2}{\sin i}$$

$(\omega + \theta_2)_{24}$ = 30.52°

$(\theta_2)_{24}$ = 107.98°

$$\frac{2 r_a}{r_{tan}} = \left(\frac{r_a}{r_p} + 1\right)_{24} + \left(\frac{r_a}{r_p} - 1\right)\cos(\theta_2)_{24}$$

r_{tan} = 20,000 stat mi ≈ 32,200 km

$$r_{at} = \frac{\frac{r_{tan}}{r_{pt}} - 1}{\frac{r_{tan}}{(r_a)_{24}(r_p)_{24}} - \frac{\frac{(r_a)_{24}}{(r_p)_{24}} + 1}{(r_a)_{24}} + \frac{1}{r_{pt}}}$$

= 23,623 stat mi ≈ 38,000 km

$$\frac{r_{at}}{r_{pt}} = 5.24956$$

$$e_t = \frac{\frac{r_{at}}{r_{pt}} - 1}{\frac{r_{at}}{r_{pt}} + 1} = 0.67998$$

$$\cos\theta_t = \frac{\frac{2 r_{at}}{r} - \left(\frac{r_{at}}{r_{pt}} + 1\right)}{\frac{r_{at}}{r_{pt}} - 1} = -0.91474$$

θ_t = 156.17°

$\psi = \theta_t - \theta_{24}$ = 48.19°

$\omega_t = \omega_{24} - \psi$ = - 125.65°

$$a_t = \frac{r_{at} + r_{pt}}{2} = 7.42447 \times 10^7 \text{ ft} \approx 22,600 \text{ km}$$

$$\left(\frac{\tau}{2\pi}\right)_t = \sqrt{\frac{a^3}{\mu}} = 5391.75 \text{ sec/rad}$$

$$E_t = 2\tan^{-1}\left[\sqrt{\frac{r_{pt}}{r_{at}}}\tan\frac{\theta_t}{2}\right] = 2.24059 \text{ rad}$$

$$t_t = \frac{\tau}{2\pi}\left[E_t + e_t \sin E_t\right] = 9206.6 \text{ sec}$$

$$E_{24} = 2\tan^{-1}\left[\sqrt{\frac{r_p}{r_a}}\tan\frac{\theta_{24}}{2}\right] = 67.60°$$

= 1.17978 rad

$$(t_2)_{24} = \frac{\tau_{24}}{2\pi}\left[E_{24} - e_{24}\sin E_{24}\right]$$

= 8339.5 sec

$$\tau_l = 2\pi\sqrt{\frac{a^3}{\mu}}$$

$$t_L = (t_2)_{24} - t_t - t_{ascent} - n\,\tau_l$$

Since $L_L = L_2$, t_L may be written as

t_L = - 1867.1 - 6133.2 n'

(neglecting perturbations)

This launch time must be made to correspond with that of the launch point as it crosses the orbital plane. This equation, which has all times referenced to the projection of the perigee radius on the equatorial plane, is as follows.

$$t_L = \frac{(\Omega - \Lambda_L) - \sin^{-1}\left[\frac{\tan L_L}{\tan i}\right]}{\Omega_e}$$

$$= \frac{(\Omega - \Lambda_L) - 0.19897}{0.729214 \times 10^{-4}}$$

$$\therefore (\Omega - \Lambda_L) = -n'(0.44724) + 0.06282$$

This equation is immediately recognizable as that of a straight line with a slope of -0.44724 and an ordinate intercept of 0.06282 radian. This equation can be solved for integral values of n' to determine if the desired trajectory can be obtained with the given bits of data. It is obvious that only a few launch sites provide the required timing considerations for this problem. However, if the time in the low altitude orbit is allowed to change by varying the period of this orbit, different results are obtained. This procedure was repeated and the altitude of the circular orbit allowed to vary. The results of these calculations are presented in Fig. 3. This figure shows the limitations on the altitude of the low-altitude orbit. It must be noted that these curves are not, in reality, continuous and that only the points of intersection of vertical lines for integral numbers of revolutions, and the horizontal lines for constant launch site latitude provide the required solution.

$i = 70°$

$L_L = 28.5°$

$L_2 = 28.5°$

$(r_a)_{24} = 42,400$ stat mi $\approx 68,300$ km

$(r_p)_{24} = 10,000$ stat mi $\approx 27,900$ km

$t_{ascent} = 1000$ sec

No perturbations

The effects of perturbation were not included in this analysis primarily because the magnitude is such that they are rounded off in plotting. However, for comparison purposes these calculations were made for the assumption that all of the influences are encountered in the low-altitude orbit. This assumption is believed to be reasonable because the time in the low-altitude orbit will probably be large compared to that in the transfer orbit, and the effects of the earth's oblateness fall off as the square of the semi-latus rectum. However, by using Chapter IV, it is possible to account for the cyclic perturbations occurring within fractions of revolutions, thus making it possible to account for the perturbing influence of the earth's oblateness for the entire time of flight.

The result of these computations is a slightly different slope for the lines of Fig. 3. The magnitude of this difference is approximately 0.0027 rad/rev and the maximum error produced is 0.046 rad (or 2.6 deg). Although this error is small it should not be neglected since it is capable of producing a linear displacement of approximately 900 stat mi or 1450 km at a radius of 20,000 stat mi or 32,200 km.

3. Compatible Orbits

If rendezvous is seen as a requirement prior to the time the target vehicle is launched, its orbit can be selected in such a manner that the correct relative position between the launch site and the satellite exists at a prescribed time. The selection of such an orbit enables the launch vehicle to utilize a direct ascent trajectory requiring a minimum amount of fuel and guidance. The orbits which satisfy these conditions are referred to as compatible orbits and the periods of such orbits are defined as follows.

$$\Delta t_L = \Delta t_{ascent} + n\tau\left[1 + \frac{\Delta\tau}{\tau}\right] \qquad (35)$$

$$\Delta t_L = \frac{(\Omega_0 + n\Omega) - \Lambda_{L1} \pm \sin^{-1}\left(\frac{\tan L_{L1}}{\tan i}\right) + 2m\pi}{\Omega_e}$$

$$- \frac{\Omega_0 - \Lambda_{L2} \pm \sin^{-1}\left(\frac{\tan L_{L2}}{\tan i}\right)}{\Omega_e} \qquad (36)$$

where

the subscripts 1 and 2 refer to the station from which the first and second satellites were launched in a southerly direction.

The term $\Delta\tau$ is an approximate correction to the orbital period over a spherical earth to account for the earth's equatorial bulge.

Equations (35) and (36) can be solved for the orbital period required to produce rendezvous from a given pair of launch sites after a given interval of time. The result is

$$\tau = \frac{2m\pi + (\Lambda_{L2} - \Lambda_{L1}) \pm \sin^{-1}\left(\frac{\tan L_{L1}}{\tan i}\right)}{n\Omega_e\left[1 + \frac{\Delta\tau}{\tau}\right]}$$

$$+ \frac{\mp\sin^{-1}\left(\frac{\tan L_{L2}}{\tan i}\right) - \Omega_e \Delta t_{asc} + n\dot{\Omega}}{n\Omega_e\left[1 + \frac{\Delta\tau}{\tau}\right]} \qquad (37)$$

To this point no constraints are placed on the values which n can assume. This is accomplished by referring to the spherical triangle shown below.

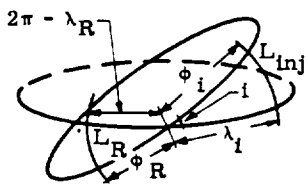

$$\phi = \sin^{-1}\left(\frac{\sin L}{\sin i}\right)$$

For northerly launches from the northern hemisphere, n must be of the form

$$n = p - (\phi_i - \phi_R)$$

and for southerly launches, n must be of the form

$$n = p + (\phi_i - \phi_R)$$

where p is an arbitrary integer and the subscripts i and R refer to the points of injection and rendezvous, respectively. As may be noted, the solution for ϕ is ambiguous unless an additional parameter is specified. The most readily available bit of information is the quadrant (relative to some point in the orbit) of ϕ or of the related angle λ. This information is known for any desired case.

Now, if one simplifying assumption is made, Eq (37) can be reduced to a form which is applicable for the case of a single launch site (i.e., $L_{L1} = L_{L2}$; $\Lambda_{L1} - \Lambda_{L2}$)

$$\tau = \frac{2m\pi - \Omega_e \Delta t_{asc} + n\dot{\Omega}}{n\Omega_e\left[1 + \frac{\Delta\tau}{\tau}\right]} \qquad (38)$$

Because of the interdependence of $\dot{\Omega}$ and τ, an iterative solution to this problem is generally required. However, because $\dot{\Omega}$ is very small, it is generally sufficient to use the value of τ, obtained, neglecting perturbations, to estimate the value of $\dot{\Omega}$ and then to correct the orbital period.

Figures 4 and 5 show the variation in the required semimajor axis for different values of n/m, neglecting perturbations and variations in the ascent trajectories. The auxiliary scale adjacent to the scale for semimajor axis presents the altitude of a circular orbit of the same period.

Table 1 (obtained from Ref. 1) presents the set of orbits obtainable from a launch site at 28.5° (AMR) which makes 15 revolutions per effective earth's rotation as a function of the time interval between easterly launches. The effective rotation of the earth is defined as the time or angular interval between successive passes of a point on earth through a given point in the regressing orbital plane (i.e., $t = \frac{2\pi + n\dot{\Omega}}{\Omega_e}$). Fifteen orbital periods per effective earth's rotation are selected for this presentation because for smaller integers (i.e., 14, 13, etc.), most of the orbits lie in the Van Allen radiation belts, thus making them unsuitable for many satellite missions, and because the only lower orbit suitable (i.e., 16 periods per effective rotation) presents problems due to the extremely short lifetime. Reference 1 also has this to say about the interval between the launches: "The selection of the value of N (the number of revolutions between launches) depends on the specific purpose of the space station. If the orbital inclination of the satellite must be large, a value of N approaching 7 is required. Orbits of this type have the additional advantage that the two possible launch times during each effective earth's revolution are more nearly equispaced; but as N approaches 1, the time spacing between the two possible launches becomes very unequal."

Swanson and Petersen have extended the work published in Ref. 1. This work is presented below as it appeared in Refs. 2 and 3.

For an orbital period corresponding to N revolutions every m earth revolutions to make a south-going pass over the launch base n revolutions after the north-going pass, the following relation must be satisfied.

$$n = \left(\frac{N/m - 1}{2}\right) + \left(\frac{N}{m}\right)M + \frac{1}{\pi}\left[\phi - \frac{N}{m}\nu\right] \qquad (39)$$

where M = integer number of earth revolutions completed between the north-going and south-going pass. For every value of n there is only one value of orbit inclination, i, that will satisfy the equation. No correction for finite burning time is included.

$\nu = \tan^{-1}[\tan\phi \cos i]$

$\varphi = \sin^{-1}[\sin L/\sin i]$

L = latitude of launch base

i = inclination of orbit plane

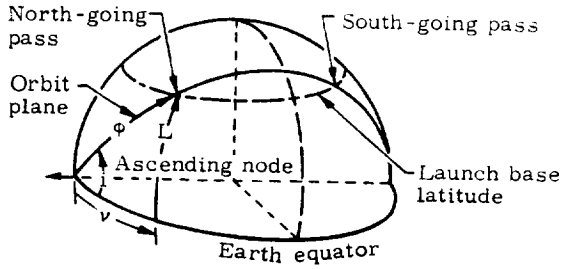

The relationship between n and N/m is presented in Figs. 6a, b, c, d and e.

The preceding figures neglect the effect of finite burning time on the problem. These effects can be observed from the following sketch and Figs. 7a and b.

These figures which present data for Canaveral launches show the effect of both burning time and the number n on the selection of orbital inclination.

TABLE 1

Rendezvous Compatible Orbits Making 15 Revolutions Per Effective Earth's Rotation (Launch from a Latitude of 28.5°)

Central Angle Between Launch and Injection		Revolutions Between Launches (N)												
		1	2	3	4	5	6	7	8	9	10	11	12	13
0	i°	29.13	31.03	34.66	40.72	50.56	65.82	86.60	65.82	50.56	40.72	34.66	31.03	29.13
arc = 0 naut mi	a	3701.7	3702.3	3703.6	3706.3	3711.4	3721.0	3738.0	3721.0	3711.4	3706.3	3703.6	3702.3	3701.7
	h(naut mi)	261.5	262.1	263.4	266.1	271.2	280.8	297.8	280.8	271.2	266.1	263.4	262.1	261.5
5	i°	29.14	31.05	34.71	40.80	50.69	66.05	86.68	66.05	50.69	40.80	34.71	31.05	29.14
arc = 300 naut mi	a	3701.7	3702.3	3703.6	3706.3	3711.5	3721.1	3738.0	3721.1	3711.5	3706.3	3703.6	3702.3	3701.7
	h(naut mi)	261.5	262.1	263.4	266.1	271.3	280.9	297.8	280.9	271.3	266.1	263.4	262.1	261.5
10	i°	29.15	31.11	34.81	41.06	51.04	66.46	86.76	66.46	51.04	41.06	34.81	31.11	29.15
arc = 600 naut mi	a	3701.7	3702.3	3703.7	3706.4	3711.7	3721.4	3738.1	3721.4	3711.7	3706.4	3703.7	3702.3	3701.7
	h(naut mi)	261.5	262.1	263.5	266.2	271.5	281.2	297.9	281.2	271.5	266.2	263.5	262.1	261.5
15	i°	29.17	31.18	35.00	41.46	51.80	67.26	86.90	67.26	51.80	41.46	35.00	31.18	29.17
arc = 900 naut mi	a	3701.7	3702.4	3703.8	3706.6	3712.1	3722.1	3738.2	3722.1	3712.1	3706.6	3703.8	3702.4	3701.7
	h(naut mi)	261.5	262.2	263.6	266.4	271.9	281.9	298.0	281.9	271.9	266.4	263.6	262.2	261.5
20	i°	29.18	31.28	35.28	42.09	53.02	68.52	87.10	68.52	53.02	42.09	35.28	31.28	29.18
arc = 1200 naut mi	a	3701.7	3702.4	3703.9	3707.0	3712.8	3723.0	3738.4	3723.0	3712.8	3707.0	3703.9	3702.4	3701.7
	h(naut mi)	261.5	262.2	263.7	266.8	272.6	282.8	298.2	282.8	272.6	266.8	263.7	262.2	261.5
25	i°	29.19	31.41	35.62	42.86	54.42	69.87	87.32	69.87	54.42	42.86	35.62	31.41	29.19
arc = 1500 naut mi	a	3701.7	3702.4	3704.0	3707.4	3713.6	3724.0	3738.6	3724.0	3713.6	3707.4	3704.0	3702.4	3701.7
	h(naut mi)	261.5	262.2	263.8	267.2	273.4	283.8	298.4	283.8	273.4	267.2	263.8	262.2	261.5
30	i°	29.22	31.55	36.01	43.84	55.86	71.23	87.56	71.23	55.86	43.84	36.01	31.55	29.22
arc = 1800 naut mi	a	3701.7	3702.5	3704.1	3707.8	3714.5	3725.2	3738.8	3725.2	3714.5	3707.8	3704.1	3702.5	3701.7
	h(naut mi)	261.5	262.3	263.9	267.6	274.3	285.0	298.6	285.0	274.3	267.6	263.9	262.3	261.5

(* 1 naut mi = 1.852 km)

L = latitude of launch base i = orbit inclination
ψ^* = burning time measured in degrees of travel of the target satellite. This angle is assumed to be a reasonably small quantity

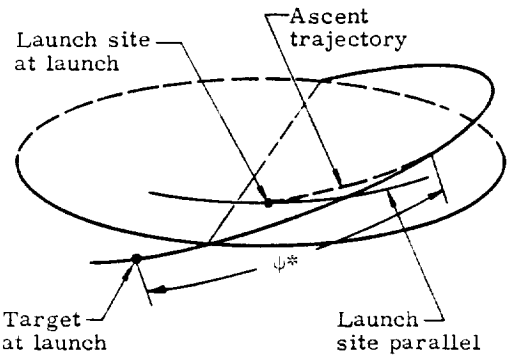

4. Direct Launch

This technique can be analyzed by referring to the development for the intermediate orbit case

$$t_L = t^* + \left(t_{2i}\right) - t_{BO} - t_{ascent} \tag{40}$$

$$t_L = \frac{\Omega - \Lambda_L \pm \sin^{-1}\left(\frac{\tan L}{\tan i}\right)}{\Omega_e} + \frac{\Delta\Omega}{\Omega_e} \tag{41}$$

The significance of all terms in these equations with the exception of the $\Delta\Omega$ term has been discussed in previous paragraphs. The significance of the final term and the energy requirements can be obtained from the following discussion.

$$(A_L - \Omega) = \nu$$

$$\Delta\eta' = \tan^{-1}\left(\frac{\tan L}{\sin \nu}\right) - \tan^{-1}\left(\frac{\tan L}{\sin (\nu + \Delta\Omega)}\right) \tag{42}$$

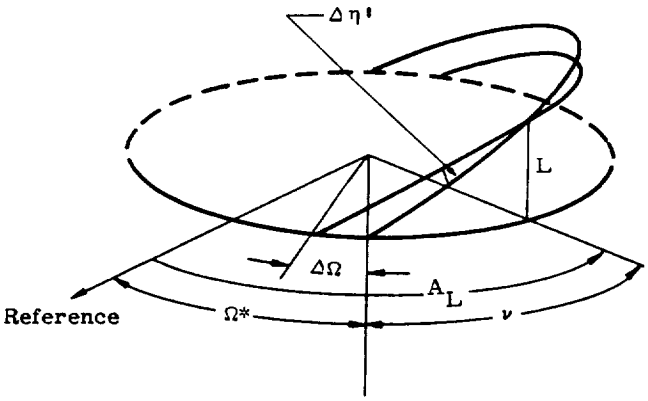

This angle ($\Delta\eta'$) is the projection of the actual change in yaw on the earth. The actual change may be seen from the following sketch to be

$$\Delta\eta = 2 \sin^{-1}\left(\cos \gamma_t \sin \frac{\Delta\eta'}{2}\right) \tag{43}$$

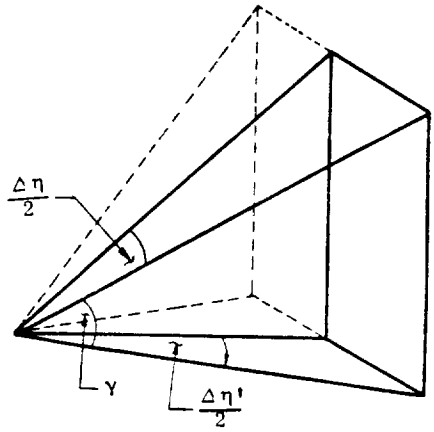

Now the velocity increment to produce this change is

$$\Delta V_n = 2 V_t \sin \frac{\Delta\eta}{2}$$

$$= 2 V_t \cos \gamma_t \sin \frac{\Delta\eta'}{2}$$

$$= 2 V_t \cos \gamma_t \sin \frac{1}{2}\left[\tan^{-1}\left(\frac{\tan L}{\sin \nu}\right) - \tan^{-1}\left(\frac{\tan L}{\sin (\nu + \Delta\Omega)}\right)\right] \tag{44}$$

If the change in yaw is small, and if the correction is made near apogee where the velocity V_t is minimum (just prior to injection into the final orbit), the relationship between the velocity increment and the change in node is

$$\frac{\Delta V_n}{V_a} = \tan^{-1}\left(\frac{\tan L}{\sin \nu}\right) - \tan^{-1}\left(\frac{\tan L}{\sin (\nu + \Delta\Omega)}\right) \tag{45}$$

The significance of negative values of $\frac{\Delta V_n}{V_a}$ is simply that the sign of $\Delta\Omega$ is negative or that the inclination of the transfer orbit is less than that of the desired orbit. A graphical solution to this equation is presented as Fig. 8.

This nodal and inclination correction results in a tolerance in the time of launch assuming that some specified amount of propellant is available for making such a correction.

$$\Delta t_L = \frac{\Delta\Omega}{\Omega_e} \tag{46}$$

$$\sin (\nu + \Delta\Omega) = \frac{\tan L}{\tan\left[\tan^{-1}\left(\frac{\tan L}{\sin \nu}\right) - \frac{\Delta V}{V_a}\right]} \tag{47}$$

$$\sin(\nu + \Delta\Omega) = \sin\nu\cos\Delta\Omega + \sin\Delta\Omega\cos\nu$$

$$\approx \sin\nu + \Delta\Omega\cos\nu$$

$$\therefore \Delta\Omega = \frac{\tan L}{\cos\nu \tan\left[\tan^{-1}\left(\frac{\tan L}{\sin\nu}\right) - \frac{\Delta V}{V_a}\right]} - \tan\nu; \quad (\nu \neq \pm\tfrac{\pi}{2}) \qquad (48)$$

and

$$\Delta t_L = \frac{\tan L - \sin\nu \tan\left[\tan^{-1}\left(\frac{\tan L}{\sin\nu}\right) - \frac{\Delta V}{V_a}\right]}{\Omega_e \cos\nu \tan\left[\tan^{-1}\left(\frac{\tan L}{\sin\nu}\right) - \frac{\Delta V}{V_a}\right]} \qquad (49)$$

As an example, consider the case

$L = 30°$

$\nu = (A_L - \Omega^*) = 30°$

$\Delta V_{max} = \pm 1000$ fps $= 305$ mps

$V_a = 10,000$ fps $= 3050$ mps

$\Delta t \approx \pm 1300$ sec

Should L have been negative in this example, ν would have remained unchanged because of the definition of Ω^* which is measured from the reference direction to the last nodal crossing, thus restricting the value of ν to less than 180°. Mathematically this says

$\Omega^* = \Omega \qquad 0 < L \leq 90$

$\Omega^* = \Omega - 180 \quad 0 > L \geq -90$

With these restrictions, the launch tolerance remains unchanged.

The resultant change in inclination can also be obtained, but it is of lesser significance since its effect on the energy requirements is already included.

From the sketch with Eq (42) and spherical trigonometry

$$\tan L = \tan i \sin\nu \qquad (50)$$

or

$$\tan i_f \sin\nu = \tan(i_f + \Delta i)\sin\left[\nu + \Delta\Omega\right]$$

but

$$\frac{\sin(\nu + \Delta\Omega)}{\sin\nu} = \cos\Delta\Omega + \cot\nu\sin\Delta\Omega$$

$$\frac{\tan(i + \Delta i)}{\tan i} = \frac{1 + \frac{\tan\Delta i}{\tan i}}{1 - \tan i\tan\Delta i} \approx \frac{1}{1 - \Delta i\tan i} \qquad (51)$$

This final approximation is valid under the assumption that the orbital inclination is greater than 30° and that the change in inclination is small.

Thus

$$1 - \Delta i\tan i \approx \cos\Delta\Omega + \cot\nu\sin\Delta\Omega$$

$$\Delta i \approx \frac{1 - \cos\Delta\Omega - \cot\nu\sin\Delta\Omega}{\tan i} \qquad (52)$$

If the nodal change is also small, this equation reduces to

$$\Delta i \approx \frac{-\Delta\Omega\cos\nu}{\tan i\sin\nu} \quad \begin{matrix} i \neq 0 \\ \nu \neq 0 \end{matrix} \qquad (53)$$

C. THE TERMINAL MANEUVER

The preceding discussions have been directed toward the placement of the shuttle or homing vehicle in the vicinity of the target. The following material is intended to provide an insight into the subsequent motion leading to docking or closure. The discussion proceeds as follows.

(1) Relative motion.

(2) Terminal guidance schemes.

(3) Closure times and energy requirements.

(4) Terminal guidance smoothing techniques.

(5) Long time closures.

(6) Homing phase errors

1. Relative Motion (Ref. 5)

In this section, the general relative equations of motion for the rendezvous maneuver are developed and explained. The purpose of this section is to show how the rendezvous dynamics are affected by orbital aspects as well as by vehicle-induced accelerations. The effects of initial conditions on the rendezvous problem will be discussed with respect to velocity and time requirements in sample problems.

a. Motion relative to target

Consider the earth-centered inertial frame shown in the following sketch. The target vehicle

is located by the position vector $\vec{r}_t$, and the homing vehicle by $\vec{r}_h$. The relative range vector $\vec{s}$ is defined from target vehicle to homing vehicle.

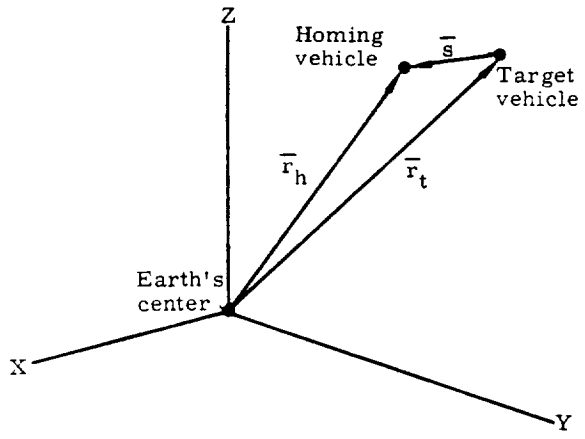

Let:

$\bar{g}(\bar{r})$ = gravitational acceleration for a spherical earth.

$\bar{a}_t$, $\bar{a}_h$ = thrust acceleration of target and homing vehicles.

$\bar{P}(\bar{r}, \dot{\bar{r}})$ = perturbative acceleration due to earth oblateness, moon, sun, atmosphere, and nearby planets combined.

Motion relative to the target, neglecting mutual attraction of the vehicles, is thus governed by

$$\frac{d^2\bar{s}}{dt^2} = \left[\bar{a}_h - \bar{a}_t + \bar{g}(\bar{r}_h) - \bar{g}(\bar{r}_t)\right] + \left[\bar{P}(\bar{r}_h, \dot{\bar{r}}_h) - \bar{P}(\bar{r}_t, \dot{\bar{r}}_t)\right] \quad (54)$$

Simplification of Eq (54) results if the following assumptions apply:

(1) $s << r_t$.

(2) r_t and r_h sufficiently large such that drag effects are small.

(3) Total rendezvous time sufficiently small so that the perturbative accelerations have only first order effects on the motion of each vehicle.

Then, the difference of perturbative accelerations appearing in Eq (54) may be neglected as second order in the perturbation. This follows since the proximity of the two vehicles in space and time yields

$$\bar{P}(\bar{r}_h, \dot{\bar{r}}_h) \sim \bar{P}(\bar{r}_t, \dot{\bar{r}}_t) + d\bar{P}(\bar{r}_t, \dot{\bar{r}}_t)$$

Inasmuch as $\bar{P}$ is itself of first order, $d\bar{P}$ is of second order.

Similarly, if $\bar{g}(\bar{r}_h)$ is developed in a Taylor series about $\bar{r}_t$,

$$\bar{g}(\bar{r}_h) = \bar{g}(\bar{r}_t) + (\bar{s} \cdot \nabla)\,\bar{g}(\bar{r}_t) + \tfrac{1}{2}(\bar{s} \cdot \nabla)^2\,\bar{g}(\bar{r}_t) + \ldots$$

where

∇ = gradient operator.

Neglecting second and higher order terms

$$\bar{g}(\bar{r}_h) - \bar{g}(\bar{r}_t) = (\bar{s} \cdot \nabla)\,\bar{g}(\bar{r}_t).$$

Substituting

$$\bar{g}(\bar{r}) = -\frac{GM}{r^3}\,\bar{r}$$

where

GM = Universal gravitational constant times mass of the earth.

$= \mu$.

$$\bar{g}(\bar{r}_h) - \bar{g}(\bar{r}_t) = -\frac{GM}{r_t^2}\left[\frac{\bar{s}}{r_t} - 3\bar{r}_t\,\frac{(\bar{s} \cdot \bar{r}_t)}{r_t^3}\right] \quad (55)$$

Thus Eq (54) becomes, valid to first order,

$$\frac{d^2\bar{s}}{dt^2} = \left[\bar{a}_h - \bar{a}_t\right] - \frac{GM}{r_t^2}\left[\frac{\bar{s}}{r_t} - 3\bar{r}_t\,\frac{(\bar{s} \cdot \bar{r}_t)}{r_t^3}\right] \quad (56)$$

This is the equation derived and discussed by Hord in Ref. 4.

The exact solution of Eq (56) for the general case is a difficult analytical task. Aside from the thrust accelerations which are general functionals of $\bar{s}$ and $d\bar{s}/dt$, the orbital nature of the problem, reflected through the gravity terms, complicates the analysis. This complexity, however, underscores the fact that the orbital aspects of the problem should never be overlooked in the general case. To cite an example, consider a coplanar rendezvous in which homing starts when the target is at the apogee of its assumed eccentric orbit. Assume the homing vehicle to be slightly behind the target, at the same altitude, and at sufficient overspeed to be closing on the target. On the

basis of rectilinear considerations one may compute a total closing time by dividing the initial relative range by the closing rate. This time, however, may be completely erroneous and moreover the vehicles may never close to a sufficiently small range for rendezvous purposes. The reason for this is seen by noting the orbital aspects of the situation. The target, initially at apogee, begins to speed up as it travels toward perigee; the homing vehicle, depending on the overspeed, may be at apogee of an elliptic orbit, in a circular orbit, or at perigee of an elliptic orbit. Clearly, the latter two conditions cause an expansion of the homing time, since the homing vehicle either remains at the same speed or slows down as it travels toward apogee. Hence, rendezvous may never occur, or, if it occurs, may undergo extreme time expansion.

Conditions permitting neglect of orbital aspects. If Eq (56) is integrated once with respect to time,

$$\frac{d\bar{s}}{dt} = \left(\frac{d\bar{s}}{dt}\right)_0 + \int_0^t \Delta\bar{a}\, dt - \int_0^t \Delta\bar{g}(\bar{s}, \bar{r}_t)\, dt \qquad (57)$$

where

$$\Delta\bar{a} = \bar{a}_h - \bar{a}_t$$

$$\Delta\bar{g}(\bar{s}, \bar{r}_t) = \frac{GM}{r_t^2}\left[\frac{\bar{s}}{r_t} - 3\,\bar{r}_t\,\frac{(\bar{s}\cdot\bar{r}_t)}{r_t^3}\right]$$

then the condition allowing neglect of the orbital aspects of the problem is obvious, since orbit parameters such as GM and r_t are vested solely in $\Delta\bar{g}(\bar{s}, \bar{r}_t)$. Hence, if

$$\left|\int_0^{T_0} \Delta\bar{g}\, dt\right| << \left|\frac{d\bar{s}}{dt}\right|_0 \text{ or } \left|\int_0^{T_0} \Delta\bar{a}\, dt\right| \qquad (58)$$

Eq (57) becomes

$$\frac{d\bar{s}}{dt} \approx \left(\frac{d\bar{s}}{dt}\right)_0 + \int_0^t \Delta\bar{a}\, dt \qquad (59)$$

and permits rectilinear analysis. Note that Eq (58) is a condition on the integrated effect of the gravity differential rather than on the magnitude of $\Delta\bar{g}$ itself.

b. Analysis of relative motion

Certain important special cases of Eq (56) can be analyzed by the method of Gilbert (Ref. 5). One such case is that of thrust-free motion. The method presented below is valid for thrust-free motion, but is easily extended to motion in the presence of impulsive thrusts.

The form of Eq (16) to be analyzed is

$$\frac{d^2\bar{s}}{dt^2} + \frac{GM}{r_t^2}\left[\frac{\bar{s}}{r_t} - 3\,\bar{r}_t\,\frac{(\bar{s}\cdot\bar{r}_t)}{r_t^3}\right] = 0 \qquad (60)$$

The analysis for a target in circular motion is studied first and later extended to targets in orbits of small eccentricities.

(1) Target in circular orbit. Let there be a rotating, relative coordinate frame centered at the target, whose axes as shown in the following sketch are defined by

$\bar{i}_x$ = unit vector along target's radius vector, $\bar{r}_t$

$\bar{i}_y$ completes the right-handed set

$\bar{i}_z$ = unit vector normal to target's orbit plane.

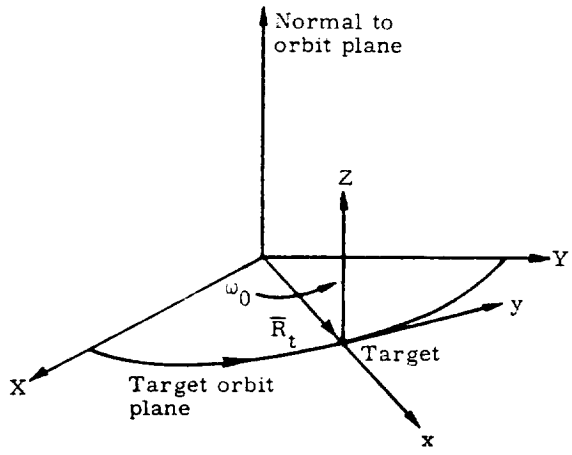

The vector $\bar{s}$ may be resolved into the three orthogonal directions and three coupled second order differential equations obtained.

Since

$$\frac{d^2\bar{s}}{dt^2} = \frac{\delta^2\bar{s}}{\delta t^2} + \left(2\bar{\omega}_0 \times \frac{\delta\bar{s}}{\delta t}\right) + \left(\bar{\omega}_0 \times \bar{\omega}_0 \times \bar{s}\right)$$

where

$\frac{\delta\bar{s}}{\delta t}$ = rate of change of $\bar{s}$ relative to observer in rotating frame

$\frac{\delta^2\bar{s}}{\delta t^2}$ = acceleration of $\bar{s}$ relative to observer in rotating frame

$\bar{\omega}_0$ = angular velocity vector of target in circular motion

Equation (60) becomes

$$\frac{\delta^2\bar{s}}{\delta t^2} + \left(2\bar{\omega}_0 \times \frac{\delta\bar{s}}{\delta t}\right) + \left(\bar{\omega}_0 \times \bar{\omega}_0 \times \bar{s}\right) + \frac{GM}{r_t^2}\left[\frac{\bar{s}}{r_t} - 3\bar{r}_t\,\frac{(\bar{s}\cdot\bar{r}_t)}{r_t^3}\right] = 0. \qquad (61)$$

Whence,

$$\left.\begin{aligned} \frac{d^2x}{dt^2} - 3\omega_0^2 x - 2\omega_0 \frac{dy}{dt} &= 0 \\ \frac{d^2y}{dt^2} + 2\omega_0 \frac{dx}{dt} &= 0 \\ \frac{d^2z}{dt^2} + \omega_0^2 z &= 0. \end{aligned}\right\} \qquad (62a, b, c)$$

These equations have the solution

$$\left.\begin{aligned} x &= \left(2\frac{\dot{x}_0}{\omega_0} - 3y_0\right)\cos\omega_0 t + \frac{\dot{y}_0}{\omega_0}\sin\omega_0 t \\ &\quad + \left(4y_0 - \frac{2\dot{x}_0}{\omega_0}\right) \\ y &= 2\left(\frac{2\dot{x}_0}{\omega_0} - 3y_0\right)\sin\omega_0 t - \frac{2\dot{y}_0}{\omega_0}\cos\omega_0 t \\ &\quad + (6\omega_0 y_0 - 3\dot{x}_0)t + \left(x_0 + \frac{2\dot{y}_0}{\omega_0}\right) \\ z &= z_0\cos\omega_0 t + \frac{\dot{z}_0}{\omega_0}\sin\omega_0 t \end{aligned}\right\} \qquad (62d, e, f)$$

These equations have been presented in numerous references, among them Refs. 6 and 7, and have been utilized in connection with various terminal guidance studies. However, the present goals are best served by altering the form of these equations by introducing a set of normalized variables.

$$\left.\begin{aligned} \rho &\equiv \frac{x}{r_t} \\ \alpha &\equiv \frac{y}{r_t} \\ \lambda &\equiv \frac{z}{r_t} \\ T &\equiv \omega_0 t \end{aligned}\right\} \qquad (63)$$

Note that α is the downrange angle of the homing vehicle relative to the target, while λ is the cross-range angle. The normalized time T is actually the angle of travel of the target from t = 0.

It is also beneficial to define the following normalized rates,

$$\left.\begin{aligned} A &\equiv \frac{\frac{dz}{dt}}{V_0} = \frac{d\lambda}{dT} \equiv \frac{V_N}{V_0} \\ B &\equiv \frac{\frac{dx}{dt} - \omega_0 y}{V_0} = \frac{d\rho}{dT} - \alpha \equiv \frac{V_R}{V_0} \\ C &\equiv \frac{\frac{dy}{dt} + \omega_0 x}{V_0} = \frac{d\alpha}{dT} + \rho \equiv \frac{V_C}{V_0} \end{aligned}\right\} \qquad (64)$$

where

$$\left.\begin{aligned} V_o &= \omega_0 r_t \\ V_C &= \left(\frac{d\bar{r}_h}{dt} - \frac{d\bar{r}_t}{dt}\right)\cdot \bar{\imath}_y \\ V_R &= \left(\frac{d\bar{r}_h}{dt} - \frac{d\bar{r}_t}{dt}\right)\cdot \bar{\imath}_x \\ V_N &= \left(\frac{d\bar{r}_h}{dt} - \frac{d\bar{r}_t}{dt}\right)\cdot \bar{\imath}_z \end{aligned}\right\} \qquad (65)$$

Note that V_C, V_R, V_N are the instantaneous differences of the inertial velocity vectors in the circumferential (y), radial (x), and normal (z) directions, respectively. Hence, C, B, and A are the normalized instantaneous differences of the inertial velocity components.

If the normalized position variables of Eq (63) are substituted in Eq (62), Eqs (66) result.

$$\left.\begin{aligned} \frac{d^2\rho}{dT^2} - 3\rho - 2\frac{d\alpha}{dT} &= 0 \\ \frac{d^2\alpha}{dT^2} + 2\frac{d\rho}{dT} &= 0 \\ \frac{d^2\lambda}{dT^2} + \lambda &= 0 \end{aligned}\right\} \qquad (66)$$

Solutions of Eqs (66), in terms of initial normalized positions and rates, are

$$\left.\begin{aligned} \rho &= 2(\rho_0 + C_0) + (B_0 + \alpha_0)\sin T \\ &\quad - (\rho_0 + 2C_0)\cos T \\ \alpha &= -(\alpha_0 + 2B_0) - 3(\rho_0 + C_0)T \\ &\quad + 2(B_0 + \alpha_0)\cos T \\ &\quad + 2(\rho_0 + 2C_0)\sin T \\ \lambda &= \lambda_0\cos T + A_0\sin T. \end{aligned}\right\} \qquad (67)$$

Also by straightforward differentiation,

$$\left.\begin{aligned} \frac{d\alpha}{dT} &= C - \rho = -3(\rho_0 + C_0) - 2(B_0 + \alpha_0)\sin T \\ &\quad + 2(\rho_0 + 2C_0)\cos T \end{aligned}\right.$$

$$\left.\begin{aligned} \frac{d\rho}{dT} &= B + \alpha = (B_0 + \alpha_0)\cos T \\ &\quad + (\rho_0 + 2C_0)\sin T \\ \frac{d\lambda}{dT} &= A = A_0 \cos T - \lambda_0 \sin T. \end{aligned}\right\} \qquad (68)$$

Inasmuch as Eqs (67) and (68) specify three independent position coordinates and their rates, the analytic solution of Eq (60) is complete. The value of the solution, however, is further enhanced if we utilize Gilbert's Method of Circle Diagrams, Ref. 7, to describe the motion.

(2) Gilbert's Method of Circle Diagrams. The information in Eqs (67) and (68) may be portrayed with two phase-plane plots. The out-of-plane variables, λ and A, may be plotted parametrically in a λ-A phase-plane. The remaining variables may be incorporated in a ρ versus $\alpha/2$ plot wherein the complete in-plane behavior is displayed. With such phase-plane plots, the orbital aspects of the problem will be made evident.

In order that we may assign special orbital significance to the normalized variables, the following assumptions are made:

(1) The inclination of the homing vehicle's orbit plane with respect to the target's is small.

(2) The eccentricity of the homing vehicle's orbit is small.

These assumptions are valid for a wide class of rendezvous missions and allow the following interpretation.

- A = homing vehicle's yaw or velocity azimuth angle with respect to the target's orbit
- λ = homing vehicle's cross-range angle with respect to the target's orbit plane
- α = homing vehicle's downrange angle with respect to the target
- ρ = normalized altitude of homing vehicle in excess of r_t.
- C = normalized speed of homing vehicle in excess of $V_0 = \omega_0 r_t$
- γ = $B + \alpha$ = homing vehicle's flight path angle (positive if measured upward from its local horizontal).

Out-of-plane motion. By elimination of T between λ and A, there results

$$A^2 + \lambda^2 = A_0^2 + \lambda_0^2 \qquad (69)$$

But for small inclinations i_0,

$$i_0^2 = A_0^2 + \lambda_0^2 \qquad (70)$$

Thus,

$$A^2 + \lambda^2 = i_0^2 \qquad (71)$$

The locus of Eq (71) is a circle of radius i_0 in the λ-A plane. The argument of the locus point is T. Hence, in one complete orbit revolution on the part of the target, T changes by 2π, returning the locus point to its initial location. The following sketch shows the circle diagram of out-of-plane motion.

The time history of the homing vehicle's cross-range and azimuth angles are portrayed conveniently in the sketch. The angle of travel of the radial segment i_0 is T and is related to time by Eq (63). The value $T = T_N$ corresponds to the crossing of the positive A-axis and defines the ascending (from -z to +z) node.

Important characteristics of the out-of-plane motion are easily obtained from the circle. For example, $z_{max} = R_t \lambda_{max} = R_t i_0$ and $(dz/dt)_{max} = V_0 A_{max} = V_0 i_0$.

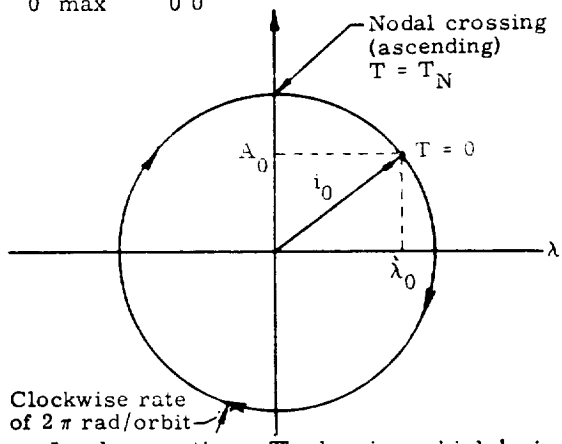

In-plane motion. The homing vehicle's in-plane orbit elements may be written directly in terms of the normalized variables in view of the interpretations allowed by the assumption of $e << 1$.

Hence,

$$\frac{\Delta E}{E_0} \equiv \frac{E - E_0}{E_0} = -2(C_0 + \rho_0) \qquad (72)$$

where E = energy of homing vehicle's orbit.

$E_0 = -1/2\, v_0^2$ = energy of target's orbit.

$$e^2 = (\rho_0 + 2C_0)^2 + \gamma_0^2 \qquad (73)$$

where e = eccentricity of homing vehicle's orbit.

$$T_p = -\tan^{-1} \frac{\gamma_0}{\rho_0 + 2C_0} \qquad (74)$$

where T_p = normalized time to perigee from T = 0

$$\alpha_P = \alpha_0 - 2\gamma_0 - 3(\rho_0 + C_0)\, T_p \qquad (75)$$

where α_P = downrange angle of homing vehicle at perigee passage ($T = T_p$).

Equations (72) through (75) permit the solutions of Eqs (67) and (68) to be written in terms of orbit elements of the homing vehicle.

$$\alpha = \alpha_P - 3(\rho_0 + C_0)(T - T_p) + 2e \sin (T - T_p)$$

$$\rho = 2(\rho_0 + C_0) - e \cos (T - T_p)$$

$$C = -(\rho_0 + C_0) + e \cos (T - T_p)$$

$$\gamma = e \cos (T - T_p). \qquad (76)$$

Portrayal of in-plane motion is obtained by a plot of ρ versus $\alpha/2$. The parametric relation is

$$\left[\rho - 2(\rho_o + C_0)\right]^2 + \left\{\frac{\alpha}{2} - \left[\frac{\alpha_p}{2} - \frac{3}{2}(\rho_0 + C_0)(T - T_p)\right]\right\}^2 = e^2 \qquad (77)$$

or,

$$\left[\rho - 2(\rho_0 + C_0)\right]^2 + \left\{\frac{\alpha}{2} - \left[\frac{\alpha_0}{2} - \gamma_0 - \frac{3}{2}(\rho_0 + C_0)\, T\right]\right\}^2 = e^2. \qquad (78)$$

Equation (77) or its equivalent, Eq (78), represents a circle of radius e in the $\rho - \alpha/2$ plane. The center of the circle is located at $2(\rho_0 + C_0)$ and

$$\left[\frac{\alpha_0}{2} - \gamma_0 - \frac{3}{2}(\rho_0 + C_0)\, T\right]$$

in the ρ and $\alpha/2$ directions, respectively. As the target moves in its orbit an angle T, the point on the circle representing the moving vehicle's relative coordinates travels an angle T counterclockwise. Simultaneously, the center of the circle drifts in the positive $\alpha/2$-direction at the rate of $-3/2(\rho_0 + C_0)$ radians per unit T. The idea of a point traversing a circle of radius e, which drifts at a uniform rate along the $\alpha/2$-direction, is the process by which the $\rho - \alpha/2$ trajectory is most easily visualized. This circle diagram generatrix is shown in Fig. 9.

The locus of relative motion in the $\rho - \alpha/2$ plane is, in general, a trochoid. For $3\left|\rho_0 + C_0\right| < 2e$, the generated curve has loops. For $3\left|\rho_0 + C_0\right| = 2e$, the curve reduces to a cycloid and has cusps. For $3\left|\rho_0 + C_0\right| > 2e$, the curve has neither loops nor cusps and tends toward a straight line for $3\left|\rho_0 + C_0\right| >> 2e$.

The values of the in-plane relative coordinates ρ, C, γ, and α are readily obtained by circle diagram sketches using the generatrix of Fig. 9. The value of α is slightly more difficult to obtain since the simultaneous motions of translation and rotation must be considered. On the other hand, the values of ρ, C, and γ are obtained by simply considering motion along the circle. The value of ρ at any time is equal to the ρ-coordinate of the locus point, and C is equal to $(\rho_0 + C_0) - \rho$. The value of γ is merely equal to horizontal displacement of the locus point from the vertical line joining apogee and perigee (line of apsides). Inasmuch as the argument of the locus point along the circle is T (the angular travel of the target), the values of ρ, C, and γ may be readily calculated.

(3) Sample analysis using circle diagrams. The convenience afforded by Gilbert's circle diagrams in establishing functional relations between various parameters and in generating trajectory requirements overshadows the desirability of graphical plots for the relative motion. In this section the application of Gilbert's method of circle diagrams as an analytical tool is illustrated. For purposes of illustration, the initial conditions will be

(1) Target in circular orbit with radius, r_t

(2) Homing vehicle injected ahead of target with

$$\left.\begin{aligned} x_0 &= 0 \\ y_0 &= s_0 > 0 \\ z_0 &= 0 \\ V_N &= 0 \\ V_C &= -W_0;\ W_0 > 0 \\ V_R &= -u_0;\ u_0 > 0 \end{aligned}\right\} \qquad (79)$$

The situation is shown in the following sketch.

Out-of-plane analysis. Since

$$z_0 = 0$$

$$V_N = \left(\frac{dz}{dt}\right)_0 = 0.$$

Equations (63) and (64) yield

$$\lambda_0 = A_0 = 0. \qquad (80)$$

Accordingly, Eqs (70) and (71) yield

$$i_0 = A\,(T > 0) = \lambda\,(T > 0) = 0. \qquad (81)$$

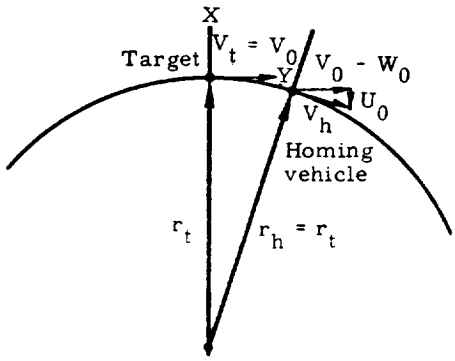

The out-of-plane circle diagram thus degenerates to a point at the origin of the λ-A phase plane, indicating coplanar motion.

In-plane analysis. From Eqs (63) and (64)

$$\left.\begin{aligned} \rho_0 &= 0 \\ \alpha_0 &= \frac{s_0}{r_t} \\ C_0 &= \frac{-W_0}{V_0} \\ \gamma_0 &= B_0 + \alpha_0 = \frac{s_0}{r_t} - \frac{u_0}{V_0} . \end{aligned}\right\} \qquad (82)$$

Equations (73), (74) and (75) then yield

$$e^2 = \left(\frac{2W_0}{V_0}\right)^2 + \left(\frac{s_0}{r_t} - \frac{u_0}{V_0}\right)^2 \qquad (83)$$

$$T_P = \pi + \tan^{-1}\left(\frac{s_0 V_0}{2W_0 r_t} - \frac{u_0}{2W_0}\right) \qquad (84)$$

$$\alpha_p = \left(2\frac{u_0}{V_0} - \frac{s_0}{r_t}\right) - \frac{3W_0}{V_0} T_p . \qquad (85)$$

The in-plane circle diagram is shown in Fig. 10 assuming

$$\frac{s_0}{2r_t} < \frac{u_0}{V_0} < \frac{s_0}{r_t} .$$

It is of interest to consider the following special cases

(1) $\gamma_0 = 0$ (homing vehicle's flight path angle is zero)

(2) $W_0 = 0$ (no speed deficit)

(3) Combination of s_0, W_0, γ_0 which causes locus point to pass through origin (coincidence of vehicles).

The circle diagram for $\gamma_0 = 0$ is shown in the following sketch. As can be seen, there exists the possibility of a being always positive, i.e., nonclosure, in spite of the speed deficit, W_0. The limiting condition for downrange angle closure ($\alpha = 0$) is obtained by locating the locus point having minimum $\frac{\alpha}{2}$ and requiring it to be zero. This point occurs when the circle's drift rate cancels out the "speed" of the tip of the radius vector in the negative $\alpha/2$-direction. Since the radius vector rotates at angular rate of 1 rad/unit τ and the radius is $e = 2W_0/V_0$, the speed of the tip of the radius vector is $2W_0/V_0$. Thus, its rate in the negative $\alpha/2$-direction is $2W_0/V_0$ cos T. Equating the rotational and translation rates in the $\alpha/2$-direction,

$$\frac{2W_0}{V_0} \cos T_{min} = \frac{3}{2} \frac{W_0}{V_0}$$

or

$$T_{min} = \cos^{-1} \frac{3}{4} . \qquad (86)$$

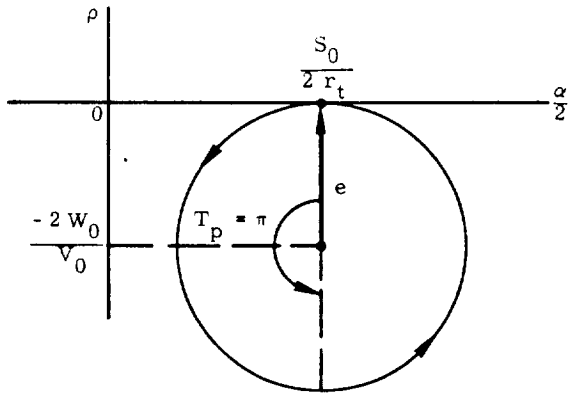

NOTE:
Center drifts to the right $\frac{3}{2} \frac{W_0}{V_0}$ units per unit T

The value of $\left(\frac{\alpha}{2}\right)$ at that point is

$$\left(\frac{\alpha}{2}\right)_{min} = \frac{s_0}{2r_t} - \frac{2W_0}{V_0} \sin T_{min} + \frac{3}{2} \frac{W_0}{V_0} T_{min}$$

$$= \frac{s_0}{2r_t} - 0.24 \frac{W_0}{V_0} . \qquad (87)$$

For the limiting case of downrange closure ($\alpha_{min} = 0$).

$$\left(\frac{W_0}{V_0}\right)_{min} = 2.26\ \frac{s_0}{r_t} \quad . \tag{88}$$

That is, if closure is to be obtained, the speed deficit W_0 must be greater than the minimum value specified in Eq (88). The limiting locus is shown in the following sketch along with the locus expected on the basis of rectilinear considerations.

The sketch shows that a rectilinear analysis for the specific injection conditions of $\gamma_0 = 0$ and $W_0 = W_{min}$ is far too optimistic. As indicated, the actual crossover time is given by $T_{min} = \omega_0 t_{min} = 0.724$ compared to $T_G = \omega_0 t_G = 0.442$, where $t_G = s_0/W_0$ is the rectilinear time-to-go. For the limiting case, the time expansion is

$$\frac{t_{min}}{t_G} = \frac{T_{min}}{T_G} = 1.64. \tag{89}$$

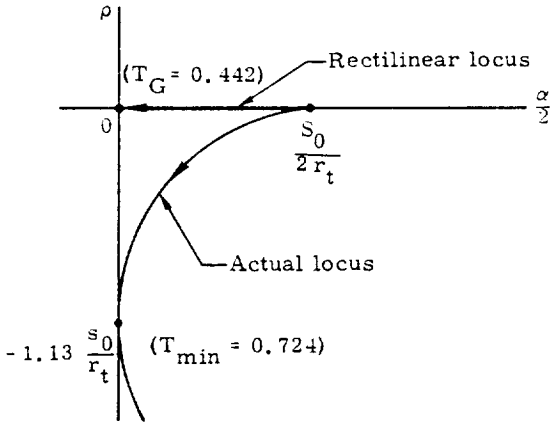

If $W_0 < (W_0)_{min}$ the expansion would be infinite since downrange closure cannot occur. Note also that the orbital nature of the problem causes the homing vehicle to be low in altitude by $1.13\ s_0$ at closure, while rectilinear analysis predicts no altitude deviation. This effect is due to the fact that the speed deficit causes the homing vehicle's injection point to be apogee. The homing vehicle's altitude thus decreases as it progresses toward perigee. This same effect accounts for the expansion in the time of downrange closure, since the homing vehicle's speed increases as it progresses toward perigee.

For the special case of $(W_0 = 0)$ the general circle diagram of Fig. 10 reduces to that of the following sketch.

It is evident that by proper choice of the flight path angle, γ_0, complete coincidence of the vehicles can be obtained. By inspection, the circle will pass through the origin at $T = \pi$ for

$$\gamma_0 = \frac{s_0}{4r_t} \quad . \tag{90}$$

Thus, coincidence occurs after the target moves through $T = \pi$ radians or 180 degrees, if the homing vehicle is lofted an angle

$$\frac{s_0}{4r_t} = \frac{\alpha_0}{4} \quad .$$

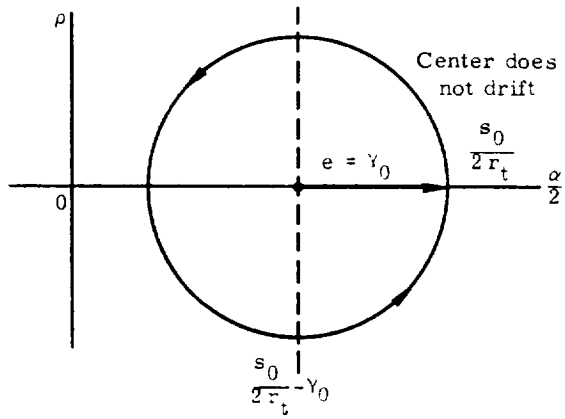

Rendezvous of the vehicles for the more general case of s_0, W_0, $\gamma_0 \neq 0$ may be obtained by considering the general circle diagram of Fig. 10. The first crossing of the $\alpha/2$-axis ($\rho = 0$) for $T > 0$ is at

$$T_1 = 2T_A \tag{91}$$

where

$$T_A = \text{normalized time to apogee} = T_P - \pi$$

$$= \tan^{-1}\ \frac{\gamma_0 V_0}{2W_0} \quad . \tag{92}$$

For complete coincidence we require

$$\alpha\,(T_1) = 0. \tag{93}$$

Hence, the drift of the circle must be such that at $T = T_1$, $\frac{\alpha}{2} = 0$. In Fig. 10, symmetry shows that the $\alpha/2$-component of the radius vector at $T = T_1$ is $-\gamma_0$. Considering the fact that the circle's center was initially at $(s_0/2r_t) - \gamma_0$ and drifted $(3/2)\,(W_0/V_0)\,T_1$ units in the plus $\alpha/2$-direction during the travel from $T = 0$ to $T = T_1$, the value of $\alpha\,(T_1)/2$ is

$$\frac{\alpha(T_1)}{2} = \left(\frac{s_0}{2r_t} - \gamma_0\right) + \frac{3}{2}\,\frac{W_0}{V_0}\,T_1 - \gamma_0 \quad . \tag{94}$$

Substituting Eqs (91) and (92) into (94) and invoking the requirement of (93), the following parametric relation is obtained.

$$\frac{s_0}{2r_t} = 2\gamma_0 - 3\,\frac{W_0}{V_0}\tan^{-1}\frac{\gamma_0}{2W_0/V_0} \quad (95)$$

This relation is analogous to the "Hit Equation" of ballistic missile theory (Ref. 8). Figure 11 shows a plot of γ_0 and s_0/r_t for various values of W_0/V_0. The required rendezvous time, t_R, is given by

$$T_R = \omega_0 t_R = T_1 = 2\tan^{-1}\frac{\gamma_0}{2W_0/V_0} \quad (96)$$

Thus, in terms of the target's orbital period, τ_0,

$$\left(\frac{t_R}{\tau_0}\right) = \frac{1}{\pi}\tan^{-1}\frac{\gamma_0}{2W_0/V_0} \quad (97)$$

On the basis of rectilinear analysis, the initial time-to-go is,

$$t_G \equiv \frac{s_0}{W_0} \quad (98)$$

Hence

$$\left(\frac{t_G}{\tau_0}\right) = \frac{1}{2\pi}\,\frac{(s_0/r_t)}{(W_0/V_0)} \quad (99)$$

The ratio of the actual rendezvous time to the initial time-to-go based on rectilinear analysis is thus

$$\frac{t_R}{t_G} = \left(\frac{2W_0/V_0}{s_0/r_t}\right)\tan^{-1}\frac{\gamma_0}{(2W_0/V_0)} \quad (100)$$

The ratio is plotted in Fig. 12 as a function of W_0/V_0 and $\alpha_0 = (s_0/r_t)$. The dependence on α_0 was introduced by utilizing Fig. 11 in a crossplot so that γ_0 could be expressed in terms of α_0 and W_0/V_0.

Note that in this example time compression occurs since $t_R/t_G \leq 1$. This is explained by the fact that for $W_0 > 0$ and $\gamma_0 > 0$, the homing vehicle is on its way toward apogee at the start of the problem. This is obvious in Fig. 10. Thus, the homing vehicle's speed over the lofted flight is less than its initial speed, causing more rapid closure than expected on the basis of rectilinear analysis.

Figure 12 may be used to compute the required rendezvous time. First compute $t_G \equiv s_0/W_0$; then locate the appropriate W_0/V_0 curve, interpolating if need be. The value of t_R/t_G then gives the attenuation factor for a particular $\alpha_0 = s_0/r_t$.

(4) Circle diagram extension to eccentric orbits. In the following paragraphs the basis upon which Gilbert's Method of Circle Diagrams can be extended to targets in eccentric orbits is presented. The eccentricity, however, must be small in order to retain a linear or first-order analysis. Only the in-plane motion is treated since out-of-plane motion is unaffected by target orbit eccentricities.

Circle Diagram of Target Motion. Previously the motion of the homing vehicle relative to a target moving in a circular orbit was analyzed. In this section all motion is referred to the target's mean motion. For small eccentricities the target's mean motion is circular with a radius equal to the semimajor axis. Thus, to obtain a circle diagram of eccentric target motion, it is merely necessary to replace the homing vehicle by the target vehicle and the target vehicle by the mean target in the previous results. The Circle Diagram of Target Motion referred to the mean target is shown in the following sketch. All the features of the in-plane circle diagram which were mentioned in previous sections still hold except that motion is strictly periodic. The center of the circle generatrix does not shift in time.

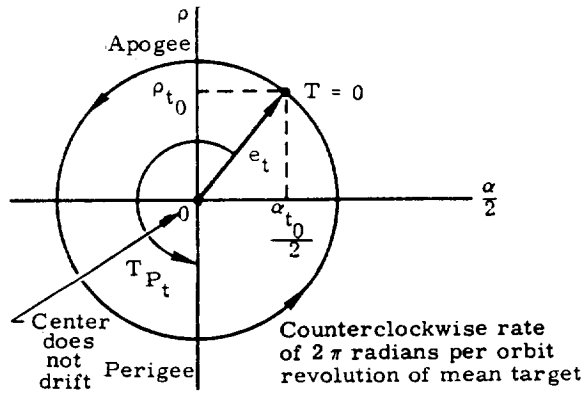

Composite Circle Diagram of Relative Motion. If the homing vehicle's circle diagram, referred to the mean target, is superimposed upon the target's, the composite circle diagram of the following sketch is obtained. Note that the circle diagram differs from that of Fig. 9 merely by the fact that the target locus is a circle of radius e_t (target orbit eccentricity) rather than the origin of the $\rho - \alpha/2$ plane. As e_t approaches zero the locus shrinks to a point at the origin, yielding the circle diagram of Fig. 9.

The relative motion is obtained by plotting both the target and homing vehicle loci and noting the differences in relative coordinates as a function of T (time).

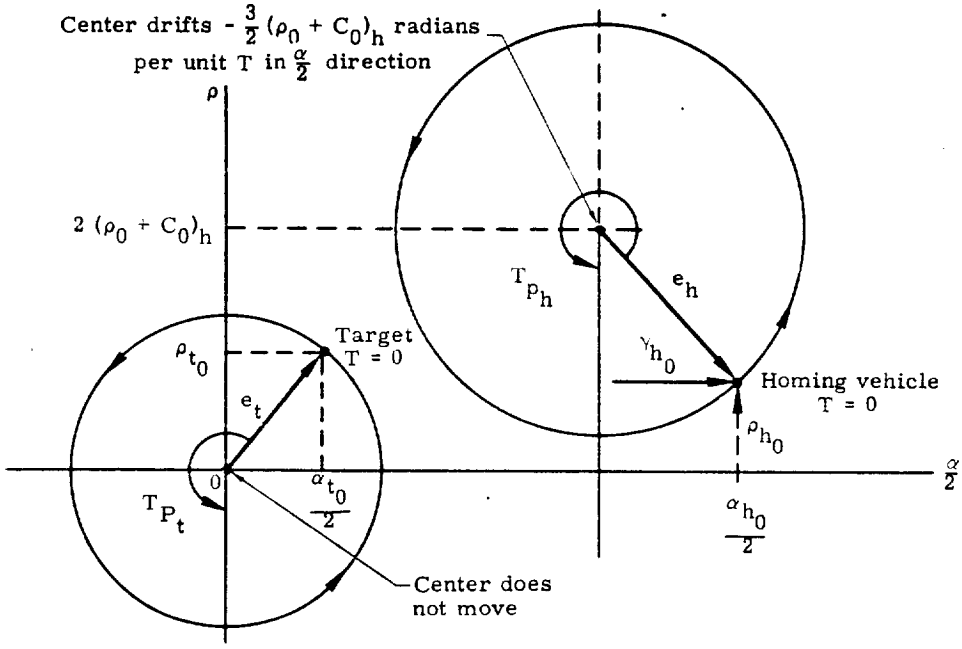

(5) Motion in presence of impulsive thrusts. In the presence of impulsive thrusts, there exists segments of thrust free motion which are separated by discrete changes in velocity. Hence complete motion is obtained by regarding it as a succession of thrust free segments under various initial conditions. Inasmuch as the position coordinates cannot change instantaneously, the final position coordinates before the impulse become the initial position coordinates after the impulse. The complete motion is readily obtained by sketches of circle diagrams. Each impulse changes the size and location of the circle generatrix. The effects of velocity increments in the normal, radial, and circumferential directions are demonstrated below.

Normal velocity increment. For small inclinations between the orbit planes of the target and homing vehicle, a velocity increment, ΔV_N, normal to the target's orbit plane produces an increment ΔA in the homing vehicle's velocity azimuth relative to the target's orbit plane. The relation is linear for small inclinations and velocity increments.

$$\Delta A = \frac{\Delta V_N}{V_0} \tag{101}$$

The relative out-of-plane motion is illustrated in the following sketch. This sketch shows the situations just prior to the impulse ($T = 0^-$) and just after the impulse ($T = 0^+$). Since position cannot change instantaneously, the crossrange angle, λ, remains unchanged. However, the azimuth angle changes by the amount given in Eq (101). The result is a change in inclination angle. Out-of-plane motion is thus typified by motion along the circle of radius, i_0, until the impulse is applied. After the impulse, the locus point moves along the circle of radius, i_1.

From this sketch it is apparent that inclination may be completely removed by applying a normal impulse at $\Delta A = \pm i_0$ and $\lambda = 0$. The velocity increment required would be

$$\Delta V_N = \mp V_0 i_0 \tag{102}$$

This corresponds to a velocity increment at the nodal crossings equal and opposite to the existing normal velocity.

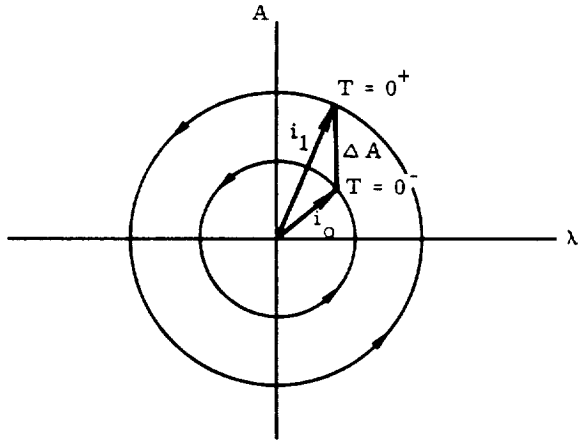

Radial velocity increment. A change in the homing vehicle's velocity vector by an increment, ΔV_R, parallel to the target vehicle's local vertical yields a change in the homing vehicle's flight path angle, B, measured with respect to the target's local horizontal.

$$\Delta B = \frac{\Delta V_R}{V_0} \tag{103}$$

Inasmuch as the homing vehicle's flight path angle measured with respect to its own local horizontal is given by

$$\gamma = B + \alpha$$

then, since α does not change instantaneously,

$$\Delta\gamma = \Delta B = \frac{\Delta V_R}{V_0} \tag{104}$$

The effect of a change in γ is shown in the following sketch. As shown in this sketch, a positive change in the flight path angle causes an increase in the horizontal displacement between the locus point and the center of the generatrix. Inasmuch as the position coordinates cannot change instantaneously, the center must move to the left by the amount, $\Delta\gamma$. This causes the radius to increase, indicating an increase in eccentricity. The center does not shift along the ρ-axis, since the location of the center in such a direction represents the orbit's energy level which is invariant for flight path angle changes.

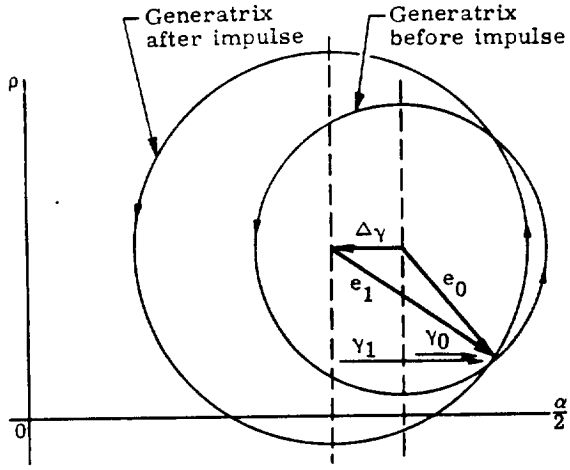

The complete relative motion is thus given by the locus of points generated by the circle of radius e_0 before the impulse and that generated by the circle of radius e_1 after the impulse. Since the energy level is unchanged by the radial impulse, both circles drift in the negative $\alpha/2$-direction at the same rate. It should be noted that if it is desired that the homing vehicle's orbit be circular using a single radial impulse, one should wait until

$$\gamma_0 = \pm e_0$$

and produce

$$\Delta\gamma = \mp e_0$$

by applying

$$\Delta V_R = \mp V_0 e_0 \tag{105}$$

These points correspond to points 90° away from the apsides where the flight path angle possesses extreme values.

Circumferential velocity or speed increments. A change in the homing vehicle's circumferential velocity, ΔV_C, is synonymous with a change in its orbital speed and, hence, a change in orbital energy or period. In terms of the normalized rate, C,

$$\Delta C = \frac{\Delta V_C}{V_0} \tag{106}$$

The effect on the relative motion is indicated in the following sketch. Since the position of the generatrix's center represents the homing vehicle's orbit energy, an increase in the homing vehicle's speed, ΔV_C, causes a vertical shift of the circle's center by the amount $2\Delta C = 2(\Delta V_C/V_0)$. This has two effects. First, the orbit eccentricity changes in general; secondly, the center drifts at a different rate in the $\alpha/2$-direction. As shown in the sketch, the energy level before the impulse is characterized by the ρ-position of the circle's center, $2(\rho_0 + C_0)$. This energy causes the circle to drift in the negative $\alpha/2$-direction at a rate of $3/2\ (\rho_0 + C_0)$. The increase in energy yields a new energy level, $2(\rho_0 + C_0) + 2\Delta C$, and causes the new circle to drift in the negative $\alpha/2$-direction at a rate of $3/2\ (\rho_0 + C_0) + 3/2\ \Delta C$. Thus, for a positive ΔC the new circle moves at a faster rate in the negative $\alpha/2$-direction.

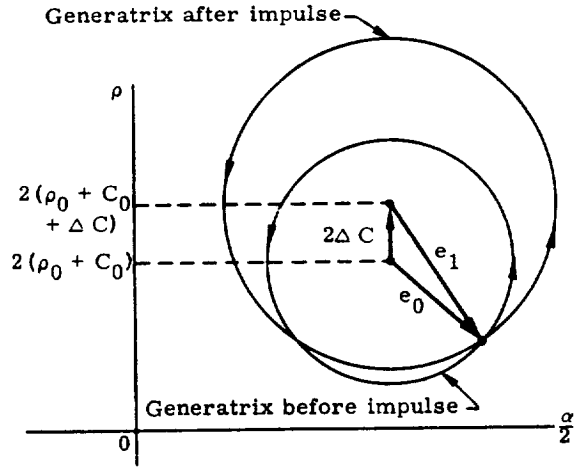

Note that, if desired, orbit eccentricity can be made zero by waiting until the locus point is either at the highest or lowest point of the circle of radius, e_0. If the locus point is at

$$\rho_{max} = 2(\rho_0 + C_0) + e_0$$

the resulting eccentricity, e_1, can be made zero by making $2\Delta C = e_0$ or

$$\Delta V_C = \frac{V_0 e_0}{2} \tag{107}$$

If the locus point is at ρ_{min}, e_1 can be made zero by $2\Delta C = -e_0$ or

$$\Delta V_C = -\frac{V_0 e_0}{2} \tag{108}$$

Comparison of either of these velocity increments with Eq (105) shows that for control of eccentricity circumferential increments can be twice as efficient as radial increments. Note, however, that circumferential increments also produce changes in the orbital energy or period, while radial increments affect only eccentricity.

(6) Sample problem. Assume the vehicles are in circular orbits of equal radii which are inclined at an angle i_0. Assume the phasing to be such that the homing vehicle crosses the target's orbit plane an angle α_0 ahead of the target. This is shown in Fig. 13.

Suppose it is desired that rendezvous be accomplished with only two thrust applications of an impulsive nature. One method by which this may be accomplished is to wait until the situation of Fig. 13 occurs and apply a velocity increment which rotates the homing vehicle's velocity vector into the target's plane while simultaneously changing the flight path angle so that a lofted flight is obtained. The loft should be chosen so that the two vehicles coincide when the homing vehicle returns to its original altitude. The trajectory is shown in Fig. 14. At coincidence, the second impulse is applied to restore the flight path angle to zero and, hence, restore circularity. Since no period changes are involved, the two vehicles will subsequently move in identical orbits and, hence, be in coincidence thereafter.

Another method also converts the situation depicted by this sketch into a coplanar situation but involves changing the flight path angle and period with the first impulse and restoring to the original values with the second impulse upon coincidence. The trajectory is shown in Fig. 15. It is similar to the method of Fig. 14 except that the required rendezvous time is reduced through the use of speed (period) changes as well. Recall that this situation was partially analyzed previously.

Both methods are analyzed below with respect to velocity and time requirements.

Method A: yaw and loft. To convert the situation of Fig. 13 into a coplanar situation a normal velocity component is required. According to Eq (102) we require

$$\Delta V_N = V_0 i_0 \tag{109}$$

Initially, the ρ - $\alpha/2$ phase diagram is as shown in the following sketch. To cause coincidence with a pure radial increment (flight path angle change) requires a flight path angle change of

$$\Delta\gamma_1 = \gamma_0 = \frac{\alpha_0}{4} \tag{110}$$

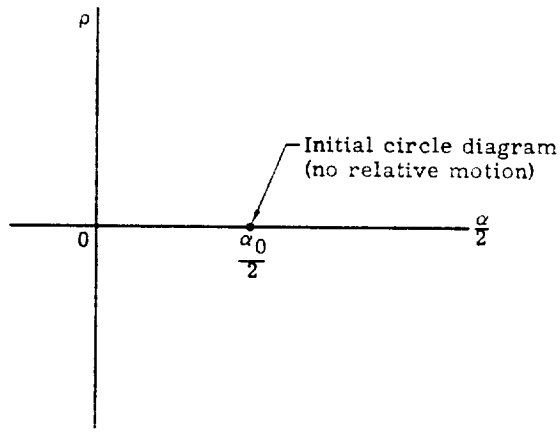

The resulting relative motion is shown in the following sketch. Note that rendezvous occurs at $T = \pi$ or one-half period later. At this time the second impulse must be directed radially outward to remove the existing flight path angle (reduce the ensuing circle diagram to a point at the origin). The second impulse must produce

$$\Delta\gamma_2 = \gamma_0 = \frac{\alpha_0}{4} \tag{111}$$

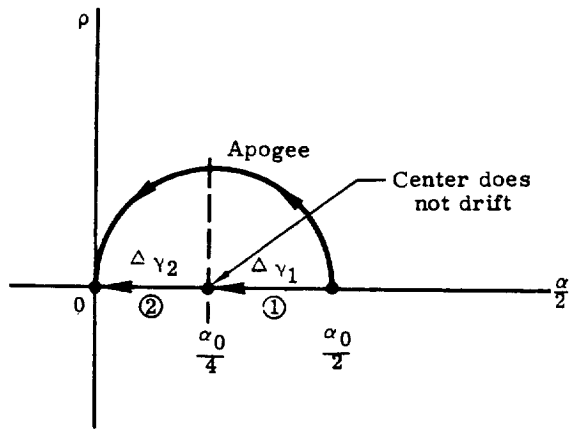

Thus, the actual radial components are

$$(\Delta V_R)_1 = V_0 \Delta\gamma_1 = V_0 \frac{\alpha_0}{4}$$

$$(\Delta V_R)_2 = V_0 \Delta\gamma_2 = V_0 \frac{\alpha_0}{4} \qquad (112)$$

Assuming an orientated thrust vector, the radial and normal velocity components of the first impulse require

$$\Delta V_1 = V_0 \sqrt{i^2_0 + \left(\frac{\alpha_0}{4}\right)^2} \qquad (113)$$

The second impulse requires

$$\Delta V_2 = (\Delta V_R)_2 = V_0 \frac{\alpha_0}{4} \qquad (114)$$

Thus,

$$(\Delta V)_{orien} = \Delta V_1 + \Delta V_2$$

$$= V_0 \left[\frac{\alpha_0}{4} + \sqrt{i^2_0 + \left(\frac{\alpha_0}{4}\right)^2} \right] \qquad (115)$$

If separate nozzles are used for increments in the various directions,

$$\Delta V_1 = V_0 \left(i_0 + \frac{\alpha_0}{4} \right) \qquad (116)$$

$$\Delta V_2 = V_0 \frac{\alpha_0}{4}$$

Hence,

$$(\Delta V)_{sep} = \Delta V_1 + \Delta V_2 = V_0 \left(i_0 + \frac{\alpha_0}{2} \right) \qquad (117)$$

in either case the total rendezvous time, as indicated in Fig. 14 and the preceding sketch ($T = \tau$), is

$$t_R = \frac{\tau_0}{2} \qquad (118)$$

where again

τ_0 = target's orbital period.

Method B: yaw, loft and period changes. In either method the yaw velocity required is the same,

$$\Delta V_N = \gamma_0 i_0 \qquad (119)$$

The radial and circumferential velocity increments depend on the desired time of rendezvous. Let us suppose that a rendezvous time of $\tau_0/4$ is desired. That is, rendezvous after the target moves through 90° rather than 180° as in Method A. Equation (97) shows that

$$\left(\frac{t_R}{\tau_0}\right) = \frac{1}{\pi} \tan^{-1} \frac{V_p}{2W_0} \qquad (120)$$

where $V_p = \gamma_0 V_0$

W_0 = speed (circumferential velocity) reduction.

Thus, for $t_R = \tau_0/4$

$$\frac{V_p}{W_0} = 2 \tan \frac{\pi}{4} = 2 \qquad (121)$$

The ratio of the radial velocity increment to the circumferential increment must, hence, be equal to 2 for rendezvous after the target moves through 90°.

Equation (95) shows that for this ratio

$$\frac{\alpha_0}{2} \equiv \frac{W_0}{V_0} \left(4 - \frac{3\pi}{4}\right) \qquad (122)$$

is the condition for rendezvous. Thus,

$$W_0 = \frac{V_0 \alpha_0}{8 - \frac{3\pi}{2}} = -\Delta V_{C_1} \qquad (123)$$

and

$$V_p = \frac{V_0 \alpha_0}{4 - \frac{3\pi}{4}} = \Delta V_{R_1} \qquad (124)$$

Equations (119), (123) and (124) are thus the yaw, speed reduction, and pitch components of the velocity increment applied at point ① in Fig. 15.

The pitch and speed components at point ② (Fig. 15) by symmetry are

$$W_0 = \frac{V_0 \alpha_0}{8 - \frac{3\pi}{2}} = \Delta V_{C_2} \qquad (125)$$

$$V_p = \frac{V_0 \alpha_0}{4 - \frac{3\pi}{4}} = \Delta V_{R_2} \qquad (126)$$

This may also be obtained from the circle diagram of the following which shows the flight path angle and energy changes required to reduce the circle generatrix to a point when the locus point is at the origin.

As shown in the following sketch, the generatrix is reduced to a point at the origin by shifting the center to the left by $\Delta_{\gamma_2} = \gamma_0$ and upward by $2\Delta C_2 = 2(W_0/V_0)$. These correspond to the velocity components of Eqs (125) and (126).

For an oriented engine nozzle, velocity requirements are as follows.

$$(\Delta V)_1 = \left[(\Delta V_N)^2 + \left(\Delta V_{C_1}\right)^2 + \left(\Delta V_{R_1}\right)^2 \right]^{1/2}$$

$$= V_0 \left[i^2_0 + 5 \left(\frac{\alpha_0}{8 - \frac{3\pi}{2}} \right)^2 \right]^{1/2} \qquad (127)$$

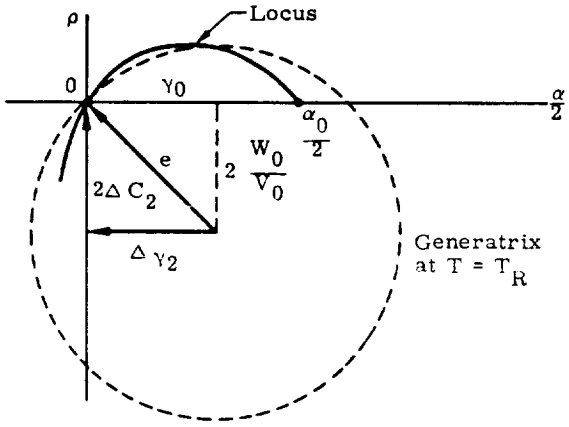

and

$$(\Delta V)_2 = \sqrt{5}\, V_0 \left(\frac{\alpha_0}{8 - \frac{3\pi}{2}} \right) \tag{128}$$

Thus,

$$(\Delta V)_{orien} = (\Delta V)_1 + (\Delta V)_2$$

$$= V_0 \left[i^2_0 + 5 \left(\frac{\alpha_0}{8 - \frac{3\pi}{2}} \right)^2 \right]^{1/2}$$

$$+ \sqrt{5}\, V_0 \left(\frac{\alpha_0}{8 - \frac{3\pi}{2}} \right) \tag{129}$$

For separate nozzles the absolute values of the components are added directly, yielding

$$(\Delta V)_{sep} = V_0 \left[i_0 + 6 \left(\frac{\alpha_0}{8 - \frac{3\pi}{2}} \right) \right] \tag{130}$$

By comparing Eqs (129) and (130) with (115) and (116) the reduction of rendezvous time from $\tau_0/2$ to $\tau_0/4$ can be seen to involve a considerable increase in velocity requirements. Assuming $i_0 = 0$

$$\frac{(\Delta V)_{\tau_0/4}}{(\Delta V)_{\tau_0/2}} = \begin{cases} \dfrac{4\sqrt{5}}{8 - \frac{3\pi}{2}} = 2.72 \text{ for oriented nozzle} \\ \dfrac{12}{8 - \frac{3\pi}{2}} = 3.64 \text{ for separate nozzles.} \end{cases}$$

2. Terminal Guidance Schemes (Ref. 10)

In the previous section the general linear differential equation of relative motion was derived as

$$\frac{d^2\bar{s}}{dt^2} = \bar{a}_h - \bar{a}_t - \frac{GM}{r_t^2} \left[\frac{\bar{s}}{r_t} - 3\bar{r}_t \frac{(\bar{s} \cdot \bar{r}_t)}{r_t^3} \right] \tag{131}$$

where

$\bar{s} \equiv \bar{r}_h - \bar{r}_t$ = relative position of homing vehicle with respect to target.

Equation (131) was derived in terms of motion relative to the target. In this section it is assumed that the homing phase is conducted by the homing vehicle utilizing an onboard guidance system and that the target does not execute thrust maneuvers of either an evasive or cooperative nature.

It is convenient to re-express the differential equation of relative motion so that the target's motion relative to the homing vehicle is obtained. This is readily obtained from Eq (131) by replacing $\bar{s}$ by $-\bar{R}$ where

$\bar{R} \equiv \bar{r}_t - \bar{r}_h$ = range vector of target with respect to homing vehicle (132)

Thus, since the thrust acceleration of the target is zero

$$\bar{a}_t = 0 \tag{133}$$

and the differential equation of motion relative to the homing vehicle is

$$\frac{d^2\bar{R}}{dt^2} = -\bar{a}_h - \frac{GM}{r_t^2} \left[\frac{\bar{R}}{r_t} - 3\bar{r}_t \frac{(\bar{R} \cdot \bar{r}_t)}{r_t^3} \right] \tag{134}$$

The effect of the gravity vector differential is obtained by inspection of Eq (134), that is, the apparent target acceleration is of magnitude

(1) $\frac{GM}{r_t^2} \left(\frac{R}{r_t} \right)$ directed inward along the line-of-sight.

(2) $\frac{GM}{r_t^2} \left(3 \frac{\bar{R} \cdot \bar{r}_t}{r_t^3} \right)$, directed upward along the target's local vertical.

Both effects decrease linearly with range. Note that they are not necessarily orthogonal unless the line of sight is normal to the local vertical. For such a situation, however, the vertical acceleration vanishes since it is proportional to $\bar{R} \cdot \bar{r}_t$.

A convenient description of the apparent target acceleration is obtained by resolving it into

components parallel and transverse to the line of sight. This is shown in the following sketch.

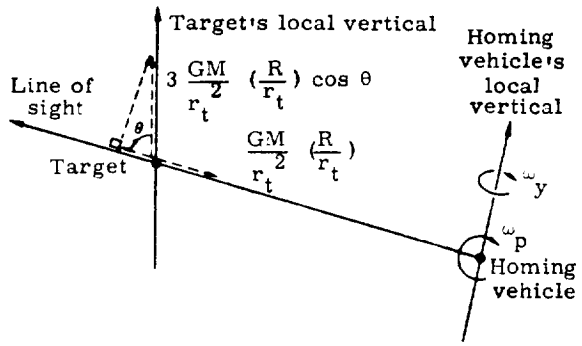

As may be seen in the sketch several new variables have been introduced. These are

θ = angle between target vertical and line-of-sight

ω_p = pitch (angular) rate of the line of sight

ω_y = yaw (angular) rate of the line of sight.

The apparent acceleration outward along the line of sight is

$$\Delta g_R = -\frac{GM}{r_t^2}\left(\frac{R}{r_t}\right)(1 - 3\cos^2\theta) \qquad (135)$$

The apparent acceleration normal to the line of sight tending to increase the pitch rate of the line of sight is

$$\Delta g_p = \frac{GM}{r_t^2}\left(\frac{R}{r_t}\right) \cdot 3\sin\theta\cos\theta \qquad (136)$$

Note that the apparent gravity effects act solely in the plane of the line of sight containing both the target and homing vehicle local verticals. Thus,

$$\Delta g_y = 0 \qquad (137)$$

a. Formulation with respect to line of sight

Since

$$\bar{R} = \bar{i}_R R \qquad (138)$$

where $\bar{i}_R \equiv$ unit vector along line of sight

$$\frac{d\bar{R}}{dt} = \bar{i}_R \frac{dR}{dt} + (\bar{\omega} \times \bar{R}) \qquad (139)$$

where $\bar{\omega} \equiv$ angular rate of line of sight in inertial space

and

$$\frac{d^2\bar{R}}{dt^2} = \bar{i}_R\left[\frac{d^2R}{dt^2} - R\omega^2\right] + \left[2\bar{\omega}\frac{dR}{dt} + \frac{d\bar{\omega}}{dt}R\right] x\,\bar{i}_R \qquad (140)$$

Equation (134) may be resolved into components along (parallel) and transverse to the line of sight.

The equation of motion along the line of sight is

$$\frac{d^2R}{dt^2} - R\omega^2 = -a_R + \Delta g_R \qquad (141)$$

where the subscript "R" denotes components along the line of sight and the superfluous subscript "h" on the thrust acceleration has been dropped.

The equation of motion transverse (normal) to the line-of-sight is

$$\frac{dh_{\omega_p}}{dt} = R(\Delta g_p - a_p) \qquad (142)$$

$$\frac{dh_{\omega_y}}{dt} = -Ra_y \qquad (143)$$

where

$h_{\omega_p} \equiv R^2\omega_p$ = angular momentum in pitch: (144)

$h_{\omega_y} \equiv R^2\omega_y$ = angular momentum in yaw: (145)

Note that in the absence of transverse thrusts $R^2\omega_y$ is conserved, while $R^2\omega_p$ is not generally conserved due to the torque, $R\Delta g_p$, exerted by the gravity differential.

b. Transverse corrections

The general transverse command logic takes the form

$$\Delta V_T^* = k_1\omega + k_2 V_T + k_3 \qquad (146)$$

where

ΔV_T^* = desired transverse velocity increment

k_1, k_2 = constants of proportionality

V_T = velocity of homing vehicle transverse (normal) to line of sight

k_3 = bias term.

Equation (146) may also be considered a vector statement wherein ΔV_T^*, ω, V_T and k_3 are two-element column vectors whose components are those of yaw and pitch. That is,

$$\Delta V_T^* = \begin{pmatrix} \Delta V_p^* \\ \Delta V_y^* \end{pmatrix} \qquad (147)$$

$$\omega = \begin{pmatrix} \omega_p \\ \omega_y \end{pmatrix} \tag{148}$$

$$V_T = \begin{pmatrix} V_p \\ V_y \end{pmatrix} \tag{149}$$

$$k_3 = \begin{pmatrix} k_{3p} \\ k_{3y} \end{pmatrix} \tag{150}$$

The "constants of proportionality" are then 2 x 2 matrices

$$k_1 = \begin{bmatrix} K^p_{1p} & K^y_{1p} \\ K^p_{1y} & K^y_{1y} \end{bmatrix} \tag{151}$$

$$k_2 = \begin{bmatrix} K^p_{2p} & K^y_{2p} \\ K^p_{2y} & K^y_{2y} \end{bmatrix} \tag{152}$$

where the subscripts indicate those elements belonging to the pitch or yaw velocity command, and the superscripts indicate the elements which scale the pitch and yaw components of ω and V_T. Except in cases where the homing vehicle is called upon to execute roll maneuvers, there will generally be no interchannel crossfeed terms in the command logic. Hence, in most situations the elements outside the principal diagonal are zero.

If k_2 and k_3 are zero while k_1 is equal to the instantaneous range to the target, a collision course results. A lead-collision or biased-collision course may be generated by defining k_3 appropriately so that the homing vehicle in effect steers on a collision course to a point offset from the actual target. If k_2 and k_3 are zero while k_1 is a constant other than the instantaneous range, a proportional navigation results if k_3 is other than zero. For k_1 and k_3 equal to zero while k_2 is -1, a pure pursuit course results since the homing vehicle is directed to fly along the instantaneous line-of-sight. Thus, by proper selection of the constants of proportionality all types of homing schemes are possible including hybrid schemes which do not completely fall into the above classes. It is also possible to fly a slightly different course in pitch than in yaw by choosing the constants of proportionality for the two channels differently. Moreover, the complete homing phase may be a blend of various types by varying the constants of proportionality as a function of range or some other appropriate variable.

Collision course. If range information is available a collision course may be flown. This will tend to minimize the homing time since in nonrotating relative coordinates the motion is completely along the line of sight, which maintains a fixed direction in inertial space. Thus, in nonrotating relative coordinates the motion of the target is radially inward toward the homing vehicle.

Integration of Eqs (144) and (145) with respect to time yields

$$R^2 \omega_p = R_0^2 \omega_{p_0} + \int_0^t R \Delta g_p \, dt - \int_0^t R a_p \, dt \tag{153}$$

$$R^2 \omega_y = R_0^2 \omega_{y_0} - \int_0^t R a_y \, dt \tag{154}$$

If proportional transverse jets are used (alternately, a gimbaled nozzle) the thrust accelerations are of the form

$$a_p = \frac{\Delta V_p^*}{\tau_p} = \frac{R \omega_p}{\tau_p} \tag{155}$$

$$a_y = \frac{\Delta V_y^*}{\tau_y} = \frac{R \omega_y}{\tau_y} \tag{156}$$

where τ_p and τ_y are the pitch and yaw channel time constants. Substituting Eqs (155) and (156) into (153) and (154) yields

$$\omega_y = \omega_{y_0} \left(\frac{R_0}{R}\right)^2 e^{-\frac{t}{\tau_y}} \tag{157}$$

$$\omega_p = \left(\omega_{p_0} R_0^2 + \int_0^t R \Delta g_p e^{\frac{\sigma}{\tau_p}} \, d\sigma\right) \frac{e^{-\frac{t}{\tau_p}}}{R^2} \tag{158}$$

Note that if the time constants are small enough that $\frac{R_0}{R}$ does not build up appreciably within, say three time constants, the initial rates ω_{p0} and ω_{y0} are steered out exponentially. In fact, if τ_p, τ_y, and the range rate are small enough such that values of range separated in time by time constants are nearly equal,

$$\omega_y \sim \omega_{y_0} e^{-t/\tau_y} \tag{159}$$

$$\omega_p \sim \omega_{p0} e^{-t/\tau_p} + \frac{\Delta g_p}{R} \tau_p \left(1 - e^{-t/\tau_p}\right) \tag{160}$$

Thus, in the steady state

$$\omega_y = 0 \tag{161}$$

$$\omega_p = \frac{\Delta g_p}{R} \tau_p \tag{162}$$

Note that a pitch rate exists due to the pitch component of the gravity differential. This emphasizes two significant points:

(1) A nonzero steady-state pitch acceleration of

$$a_p = \frac{R}{\tau_p}\ \omega_p = \Delta g_p \qquad (163)$$

will exist.

(2) A precise collision course cannot be realized in pitch if Eq (155) is used, since the gravity differential causes a small steady value of pitch rate to exist. For extensive homing time the pitch displacement of the line-of-sight may be appreciable.

The first point is, of course, clear upon inspection of Eq (142). The obvious remedy for the second point is to make τ_p sufficiently small so that the total displacement is negligible. This, however, is not always possible, since high control loop gains may result in control instability. In the next topic, "Biased-Collision Course," a solution to this problem is indicated.

If impulsive thrusts are used for transverse corrections, the accelerations assume the forms

$$a_p = \Delta V_p^* \delta(t) = r\omega_p\, \delta(t) \qquad (164)$$

$$a_y = \Delta V_y^* \delta(t) = r\omega_y\, \delta(t) \qquad (165)$$

where

$\delta(t) \equiv$ Dirac delta or impulse function.

Hence, Eqs (153) and (154) for $t > 0$ become

$$R^2 \omega_p = \int_0^t R\ \Delta g_p\ dt \qquad (166)$$

$$R^2 \omega_y = 0 \qquad (167)$$

Thus, ω_y does not require further corrections in the ideal case, but ω_p soon builds up such that if a set of transverse corrections are scheduled at $t = t_i$, the required velocity increment is

$$\Delta V_p(t_i) = \frac{1}{R_i} \int_0^{t_i} R\ \Delta g_p\ dt \qquad (168)$$

In many cases a control deadzone is used such that corrections are made whenever ω_p exceeds some threshold value. Equation (168) may be used to compute the range at which this occurs. Thus, if the previous correction occurred at $t = t_{i-1}$ when $R = R_{i-1}$, then the threshold value will be exceeded at the range $R = R_i$ given by

$$R^2 = \frac{1}{\Omega_p} \left| \int_{R_{i-1}}^{R_i} \Delta g_p\ \frac{R\,dR}{\dot{R}} \right| \qquad (169)$$

where

Ω_p = deadzone threshold value for ω_p

$\dot{R}$ = range rate = $\frac{dR}{dt}$ (assumed to be negative).

The magnitude of the correction at such a time is

$$\Delta V_i = R_i\, \Omega_p \qquad (170)$$

Hence, the total pitch velocity increment is

$$(\Delta V_p)_{\text{total}} = R_0\, \omega_{p_0} + \sum_{i=1}^{n} \Delta V_i$$

$$= R_0\, \omega_{p_0} + \Omega_p \sum_{i=1}^{n} R_i \qquad (171)$$

The total yaw velocity increment is

$$(\Delta V_y)_{\text{total}} = R_0\, \omega_{y_0} \qquad (172)$$

Thus, the total transverse velocity requirement is

$$(\Delta V_T)_{\text{total}} = R_0 \left(\omega_{p_0} + \omega_{y_0}\right) + \Omega_p \sum_{i=1}^{n} R_i \qquad (173)$$

where it is assumed that ω_{p_0} and ω_{y_0} are positive; if they are not positive, absolute values are to be used in Eqs (171), (172) and (173).

Biased-collision course. In this method the line-of-sight rates are controlled to appropriate bias values. If the biases are zero, a pure collision course results. One particular application of this technique is that which maintains the line of sight at constant angles with respect to the target's local vertical and orbit plane normal. Thus, if the target's body axes are maintained at fixed angles with respect to its local vertical and orbit plane normal, the homing vehicle approaches the target at a fixed aspect in target body coordinates. This is shown in the following sketch for a coplanar situation.

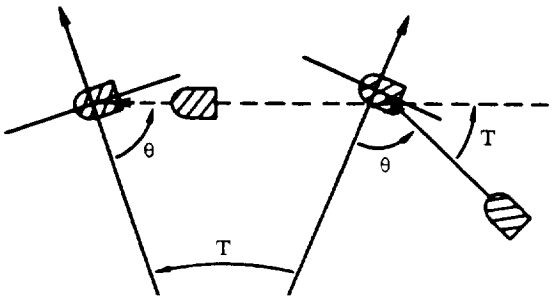

For a target in a circular orbit, the local vertical has an angular rate of

$$\omega_t = \sqrt{\frac{GM}{r_t^3}}$$

Thus, assuming coplanar rendezvous, the line-of-sight rate in pitch must have a magnitude ω_t. If the homing vehicle is behind the target the sign of ω_p must be negative (downward rotation); if ahead, positive. The yaw rotation must be zero in the case of coplanar rendezvous. Thus, there exists biased-collision steering in pitch and pure collision in yaw.

For continuous, proportional steering

$$a_p = \frac{\Delta V_p^*}{\tau_p} = \frac{R(\omega_p - \omega_b)}{\tau_p} \tag{174}$$

$$a_y = \frac{\Delta V_y^*}{\tau_y} = \frac{R\omega_y}{\tau_y} \tag{175}$$

where

$\omega_b \equiv$ desired bias rate

$= \pm\omega_t$.

Substituting the above into the general equations, Eqs (153) and (154) yields upon solution of the differential equations

$$\omega_y = \omega_{y_0}\left(\frac{R_0}{R}\right)^2 e^{-t/\tau_y} \tag{176}$$

$$\omega_p = \omega_{p_0}\left(\frac{R_0}{R}\right)^2 e^{-t/\tau_p} + \frac{1}{r^2}\int_0^t R\left(\Delta g_p + \frac{R\omega_b}{\tau_p}\right) e^{-\frac{(t-\sigma)}{\tau_p}}\, d\sigma \tag{177}$$

As before, if the ratio of range values separated in time by three time constants is approximately unity,

$$\omega_y \sim \omega_{y_0} e^{-t/\tau_y} \tag{178}$$

$$(\omega_p - \omega_b) \sim \left(\omega_{p_0} - \omega_b\right) e^{-t/\tau_p} + \frac{\Delta g_p}{R}\tau_p\left(1 - e^{-t/\tau_p}\right) \tag{179}$$

Thus, in the steady state

$$\omega_y = 0 \tag{180}$$

$$\omega_p = \omega_b + \frac{\Delta g_p}{R}\tau_p \tag{181}$$

This equation shows that the steady pitch rotation obtained using conventional collision steering can be removed by $\omega_b = -\Delta g_p/R\,\tau_p$ and implies use of angular acceleration measurements.

Using Eq (136) in Eq (181) yields

$$\omega_p = \omega_b + 3\frac{GM}{r_t^3}\tau_p \sin\theta_0 \cos\theta_0$$

$$= \omega_b + 3\omega_t^2 \tau_p \sin\theta_0 \cos\theta_0 \tag{182}$$

Then, for $\omega_b = \pm\omega_t$

$$\omega_p = \pm\omega_t(1 \mp 3\omega_t \tau_p \sin\theta_0 \cos\theta_0) \tag{183}$$

Since the maximum value of $\sin\theta_0 \cos\theta_0$ is 1/2 and τ_p is usually on the order of seconds, the bracketed term is approximately unity. Thus, in the steady state $\omega_p \cong \omega_b = \pm\omega_t$.

For impulsive thrusts,

$$a_p = \Delta V_p^* \delta(t) = R(\omega_p - \omega_b)\,\delta(t) \tag{184}$$

$$a_y = \Delta V_y^* \delta(t) = R\omega_y\,\delta(t) \tag{185}$$

Hence, after such a correction

$$R^2\omega_p = \int_0^t R\,\Delta g_p\, dt + R^2\omega_b \tag{186}$$

$$R^2\omega_y = 0 \tag{187}$$

As in the case of the collision course, the gravity differential requires subsequent corrections in pitch. Thus, if corrections are made whenever ω_p deviates from ω_b by Ω_p, the range at the time of each correction is given by Eq (169). For the present case since

$$\Delta g_p = 3R\omega_t^2 \sin\theta_0 \cos\theta_0 \tag{188}$$

Equation (169) becomes

$$R_i^2 = \frac{3\omega_t^2 \sin\theta_0 \cos\theta_0}{\Omega_p}\int_{R_{i-1}}^{R_i}\frac{R^2\, dr}{\dot{R}} \tag{189}$$

where the absolute value signs on the right member are implied. If the closing rate, $(-\dot{R})$, is constant between the ith and (i - 1)st corrections

$$R_i^2 = \frac{\omega_t^2 \sin\theta_0 \cos\theta_0}{\Omega_p (-\dot{R})_{i-1}} (R_{i-1}^3 - R_i^3) \quad (190)$$

The total pitch and yaw velocity increments are

$$(\Delta V_p)_{total} = R_0 \Delta\omega_{p_0} + \Omega_p \sum_{i=1}^{n} R_i \quad (191)$$

$$(\Delta V_y)_{total} = R_0 \omega_{y_0} \quad (192)$$

Hence,

$$(\Delta V_T)_{total} = R_0 \left(\Delta\omega_{p_0} + \omega_{y_0}\right) + \Omega_p \sum_{i=1}^{n} R_i \quad (193)$$

By comparison of Eq (193) with Eq (173) it might be inferred that "biased-collision" is most efficient for a coplanar rendezvous since $\Delta\omega_{p_0}$ is involved in biased-collision; whereas the full initial pitch rate, ω_{p_0}, is involved in "pure collision." This is deceiving unless it is realized that faster range closure occurs in pure collision and hence fewer number of pitch corrections are required, since the time-integrated effect of gravity is smaller. Thus, biased-collision does not necessarily require less velocity.

Proportional navigation. Proportional navigation involves transverse accelerations proportional to the line-of-sight rates. That is

$$a_p = K_{a_p} \omega_p \quad (194)$$

$$a_y = K_{a_y} \omega_y \quad (195)$$

If

$$K_{a_p} = \frac{R}{\tau_p} \quad (196)$$

$$K_{a_y} = \frac{R}{\tau_y} \quad (197)$$

then a collision course results. However, in the absence of range information a collision course may be approximated by Eqs (194) and (195) when K_{a_p} and K_{a_y} are constants. This is the prime purpose of proportional navigation.

Substituting Eqs (194) and (195) in Eqs (153) and (154) yields

$$\omega_y = \omega_{y_0} \left(\frac{R_0}{R}\right)^2 Q_y(t) \quad (198)$$

$$\omega_p = \left[R_0^2 \omega_{p_0} + \int_0^t \frac{R\Delta g_p}{Q_p(t)} dt\right] \frac{Q_p(t)}{R^2} \quad (199)$$

where

$$Q(t) \equiv \exp\left(-\int_0^t \frac{K_a}{R} dt\right) \quad (200)$$

Explicit solutions of Eqs (198) and (199) require knowledge of the time variation of range. If we assume that proportional transverse jets are used, then in the absence of accelerations along the line of sight,

$$R \sim R_0 + \dot{R}_0 t \quad (201)$$

It is also assumed that the initial closing rate $(-\dot{R}_0)$ is high enough so that Eq (201) is true in spite of gravity effects and line-of-sight rotations. With Eq (201), Eq (200) becomes

$$Q(t) = \left(\frac{R}{R_0}\right)^m \quad (202)$$

where

$$m \equiv \frac{K_a}{(-\dot{R}_0)} \quad (203)$$

yielding

$$\omega_y = \omega_{y_0} \left(\frac{R}{R_0}\right)^{m-2} \quad (204)$$

$$\omega_p = \left[\omega_{p_0} + \int_0^t \frac{\Delta g_p}{R} \left(\frac{R}{R_0}\right)^{2-m} dt\right] \left(\frac{R}{R_0}\right)^{m-2} \quad (205)$$

If the closing rate is sufficiently high so that $\frac{\Delta g_p}{R}$ can be taken outside of the integral

$$\omega_p \sim \omega_{p_0} \left(\frac{R}{R_0}\right)^{m-2} + \left(\frac{m}{m-3}\right) \frac{\Delta g_p}{K_{a_p}} \left[1 - \left(\frac{R}{R_0}\right)^{m-1}\right] \quad (206)$$

Note that in order to be effective

$$m = \frac{K_a}{(-\dot{R}_0)} > \begin{cases} 2 \text{ for yaw} \\ 3 \text{ for pitch} \end{cases} \qquad (207)$$

Thus, by choosing m sufficiently high (implying high K_{a_p}) in the steady state

$$\omega_y = 0$$

$$\omega_p = \frac{\Delta g_p}{K_{a_p}} \text{ (negligible for } K_{a_p} \text{ high enough).}$$

It is seen then that the proportional navigation course can adequately approximate the collision course for sufficiently high gains and closing rates.

Biased-proportional navigation. This technique is a generalization of proportional navigation, analogous to biased-collision in its generalization of collision steering. If this technique is applied to the coplanar situation analyzed for the case of biased-collision, one obtains

$$\omega_y = \omega_{y_0} \left(\frac{R}{R_0}\right)^{m-2} \qquad (208)$$

$$\omega_p = \left[\omega_{p_0} + \int_0^t \frac{\Delta g_p + K_{a_p} \omega_b}{R} \left(\frac{R}{R_0}\right)^{2-m} dt\right] \left(\frac{R}{R_0}\right)^{m-2} \qquad (209)$$

under the same restrictions imposed on the explicit analysis for proportional navigation. For this case

$$\frac{\Delta g_p}{R} = 3\omega_t^2 \sin\theta_0 \cos\theta_0.$$

Therefore,

$$\omega_p = \omega_{p_0} \left(\frac{R}{R_0}\right)^{m-2} + 3\left(\frac{m}{m-3}\right)\frac{\omega_t^2 \sin\theta_0 \cos\theta_0}{K_{a_p}} \left[1 - \left(\frac{R}{R_0}\right)^{m-1}\right] + \left(\frac{m}{m-2}\right)\omega_b \left[1 - \left(\frac{R}{R_0}\right)^{m-2}\right] \qquad (210)$$

Thus, in the steady state

$$\omega_p \sim 3\left(\frac{m}{m-3}\right)\frac{\omega_t^2 \sin\theta_0 \cos\theta_0}{K_{a_p}} + \left(\frac{m}{m-2}\right)\omega_b \qquad (211)$$

For $\omega_p \sim \pm\omega_t$, it is required that

$$\omega_b = \pm\omega_t \left[\frac{m-2}{m} \mp \left(\frac{m-2}{m-3}\right)\frac{\omega_t^2 \sin\theta_0 \cos\theta_0}{K_{a_p}}\right] \qquad (212)$$

where $m > 3$. For large m (large K_{a_p})

$$\omega_b = \pm\omega_t \qquad (213)$$

As in the case of proportional navigation, this technique can adequately approximate its collision counterpart for sufficiently high gains and closing rates.

c. Homing flight paths

The flight paths produced by the transverse steering techniques presented are simple to derive. For example, in the steady-state, collision and proportional navigation maintain the line of sight in a fixed inertial direction, assuming the flight times are small enough to warrant neglect of the gravity effect. Thus, in a nonrotating frame centered at the target, the homing vehicle closes radially on the target. On the other hand, for the coplanar biased-collision and biased-proportional navigation examples presented, the line of sight is maintained fixed in a rotating frame centered at the target. In this frame the biased-collision and biased-proportional schemes produce an apparent homing vehicle motion radially toward the target. The following two sketches show the flight paths in these frames. The mapping of a flight path from one frame to the other is relatively simple since the two frames differ by a rotational rate.

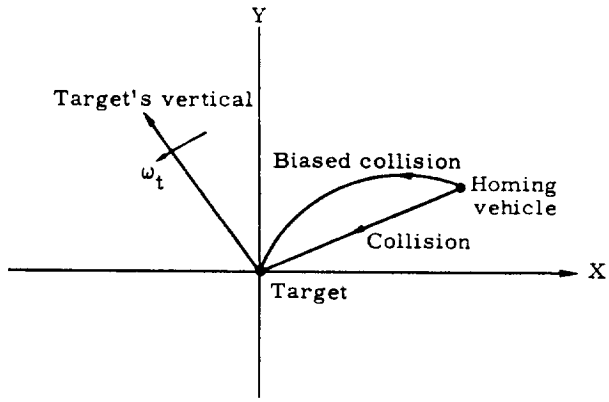

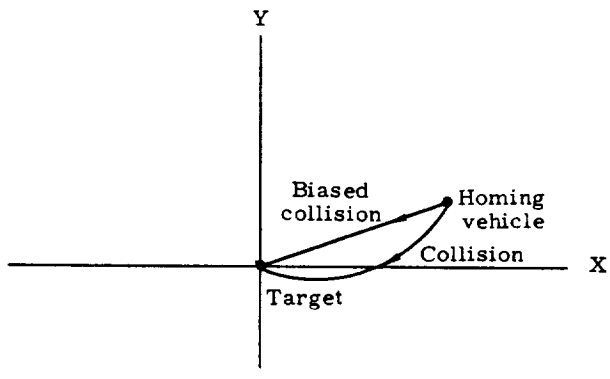

Note that if the target's body axes are continuously aligned with its local vertical, an observer on the target will see the homing vehicle approach along an apparent straight line if biased-collision is used. To this observer the collision course will appear curved. However, assuming no thrust accelerations along the line of sight and identical initial conditions, the homing vehicle reaches the target sooner along the collision course.

d. Motion along the line of sight (longitudinal)

The governing differential equation for this maneuver is Eq (141) which is repeated at this point.

$$\frac{d^2R}{dt^2} - R\omega^2 = -a_R + \Delta g_R \tag{214}$$

where

$$\Delta g_R = -\frac{GM}{r_t^2}\left(\frac{R}{r_t}\right)(1 - 3\cos^2\theta) \tag{215}$$

For a target in circular orbit, the differential equation can be written as

$$\frac{d^2R}{dt^2} + R\,\omega_t^2\left[(1 - 3\cos^2\theta) - \frac{\omega^2}{\omega_t^2}\right] = -a_R \tag{216}$$

where

ω_t = target's angular rate.

For the cases treated it was seen that biased-collision and biased-proportional navigation yield

$$\frac{d^2R}{dt^2} - R\,\omega_t^2\,(3\cos^2\theta_0) = -a_R \tag{217}$$

whereas collision and proportional navigation yield

$$\frac{d^2R}{dt^2} + R\,\omega_t^2\,(1 - 3\cos^2\theta) = -a_R \tag{218}$$

The above equations show that the gravity effects reduce the closing rate in the case of biased-collision and biased-proportional navigation. However, the gravity effects may actually increase the closing rate or at worse reduce it to a lesser extent in collision and proportional navigation. Hence, all else being equal, the latter produce shorter homing times. The differences are small when rapid rendezvous is involved. However, for extended or long-time rendezvous the differences may be significant.

Neglect of orbital aspects. The homogeneous solution of Eq (217) admits hyperbolic functions whose arguments are proportional to ω_t. For Eq (218) since $\theta = \theta_0 \pm \omega_t t$, Mathieu functions, whose arguments are likewise proportional to ω_t, are admitted. These homogeneous solutions represent the perturbative effect of the orbital aspects of the problem. If the homing phase is restricted to small homing times such that the arguments of the homogeneous functions differ negligibly from zero, the range variation will be approximately that which is obtained by letting $\omega_t = 0$ in Eqs (217) and (218). In such instances all techniques analyzed in subsection d have range variations governed by

$$\frac{d^2R}{dt^2} \simeq -a_R \tag{219}$$

In all ensuing work in this chapter it is assumed that Eq (219) is valid. The condition which must be satisfied for this to hold is

$$\omega_t\, t_R << 1 \tag{220}$$

or

$$t_R << \frac{\tau_0}{2\pi} \tag{221}$$

where

$t_R \equiv$ rendezvous (homing) time.

This implies, of course, that the initial closing rate must be sufficiently high so that the integrated effects of the gravity differential are negligible. If this is not the case, the problem becomes one of extended or long-time rendezvous, requiring the use of Eq (217) or (218).

e. Single longitudinal correction

Satellite rendezvous requires closing rate control and differs from interception because of this requirement. It is assumed that the homing vehicle possesses an initial closing rate $(-\dot{R}_0)$ such that longitudinal corrections may be devoted solely to closing rate reductions or braking. The initial closing rate is established either by the booster or homing vehicle upon injection.

The most obvious technique is one involving a single thrust application at the last possible moment, such that range and closing rate go to zero upon completion of the correction. This technique produces minimum flight times since the initial closing rate is not reduced until just prior to rendezvous.

Impulsive thrust. In the ideal case of an impulsive thrust, the initial closing rate is removed at R = 0. Thus, the rendezvous and interception problems are virtually identical in this ideal case. The rendezvous time is the same as that of interception. That is,

$$t_R = t_{G_0} = \frac{R_0}{(-\dot{R}_0)} \tag{222}$$

where

t_{G_0} ≡ initial time-to-go.

The longitudinal velocity requirement is just

$$\Delta V_L = (-\dot{R}_0) \tag{223}$$

Constant acceleration. Physically all thrusts are finite and, hence, regard must be given to the resultant nonzero braking distance. For constant thrust and negligible mass change, the braking acceleration is constant. The distance traveled over the time it takes to remove the closing rate is defined as the braking distance b and is given by

$$b = \frac{(-\dot{R}_0)^2}{2a_0} \tag{224}$$

where

$$a_0 = \frac{F_0}{m_0} = \text{initial thrust-to-mass ratio.}$$

Thus, the homing vehicle is allowed to close at the rate $(-\dot{R}_0)$ until R = b, whereupon the braking acceleration a_0 is applied so that R = 0 when $\dot{R}$ = 0. This results in a rendezvous time of

$$t_R = t_{G_0} + \frac{\Delta t_b}{2} \tag{225}$$

where

$$\Delta t_b \equiv \text{braking duration} = \frac{(-\dot{R}_0)}{a_0} \tag{226}$$

Constant thrust. For the general case of constant thrust wherein mass variation is non-negligible

$$a_R(t) = -\frac{F_0}{m_0 - \dot{m}_0 t} \tag{227}$$

where

$\dot{m}_0 \equiv$ mass flow rate > 0.

$$= \frac{F(t)}{g_0 I_{sp}}$$

For this case, the required braking distance is Refs. 10 and 11.

$$b = \left(e^{\dot{R}_0/c} - (1 + \dot{R}_0/c)\right)\left(-\frac{cm}{\dot{m}}\right) \tag{228}$$

where

$c \equiv$ effective mass exit velocity.

$$= g_0 I_{SP}$$

The rendezvous time is

$$t_R = t_{G_0} + \frac{c}{a_0}\left(\frac{c}{(-\dot{R}_0)} - \left(1 + \frac{c}{\dot{R}_0}\right)e^{\dot{R}_0/c}\right) \tag{229}$$

The following sketch shows a typical R versus $\dot{R}$ phase plane for this closure. Impulsive, constant acceleration and constant thrust braking are illustrated. It is noted, however, that the difference between the latter two is exaggerated.

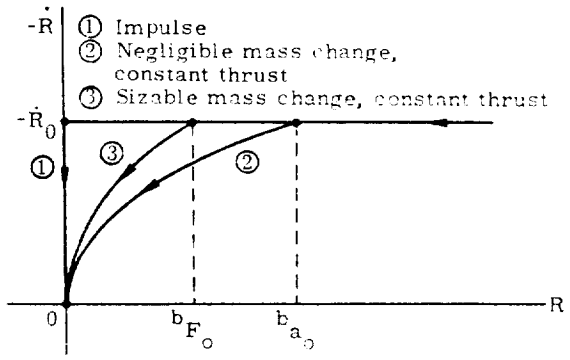

Multiple longitudinal corrections. There are many reasons for reducing the closing rate in multiple steps rather than in a single step. The most obvious reason is the presence of system errors which can cause significant range and range rate dispersions if large closing rates are removed in a single step. Therefore, there exists the possibility of biasing the nominal point of closing rate reduction so that the closing rate is nominally zero at some range R_b. Small vernier jets can then be used to adjust for position and residual range rate errors. However, for large initial closing rates, the residual errors may be quite high and may require considerable expenditure of gas since the thrust level and specific impulses of pneumatic jets are low. Compounding this is the weight penalty incurred by the tankage to contain such large pneumatic volumes. Thus, even if such fine jets are used, there still exists the desirability of multiple step reductions so that the single step braking thrust will not leave large residual errors for the vernier system.

The underlying idea of multiple step reduction of the closing rate is this: divide up the total closing rate to be reduced in smaller increments and allocate these increments at various ranges so that percent-type errors in the velocity increments are also allocated rather than occurring all at once near the target. Errors in each correction are than removed by each subsequent correction, assuming that sufficient time exists between corrections for closed-loop control.

If done properly, the closing rate control can be effected without need of a bilateral thrust capability during the multiple step reductions.

This is done by constraining each correction to yield a certain minimum closing rate even in the presence of system errors. Thus, each successive correction need only decrease the closing rate. This permits the use of a unilateral thrust, resulting in a weight saving since a comparable rear-mounted longitudinal engine is not required. In addition, since the closing rate decreases monotonically, the longitudinal velocity requirement is no more than the initial closing velocity $(-\dot{R}_0)$. There is the matter of the differential gravity effect and injection dispersions. However, these are also required of the single step technique.

It should be made clear that these refinements occur at the expense of a longer flight time. That is, under the constraint of minimum velocity requirement and unilateral thrust, final dispersions are traded off against time. However, except for emergency rendezvous, the longer homing time is usually more acceptable than the weight penalty which otherwise occurs.

A method for selecting the nominal closing rate profile which utilizes the minimum number of reductions is now described. To simplify the presentation, impulsive corrections are assumed. This is not a restriction, however, since, for nonimpulsive thrust, it is only necessary to start each correction at a range which is greater by the amount of distance traveled during each thrust period. Thus, if it is required that the closing rate be reduced from $(-\dot{R}_0)$ to $(-\dot{R}_1)$ at some range, the difference between the braking distances b_0 and b_1 yields the amount of lead distance. The corresponding difference between the stretch-out times yields the amount by which the total homing time is increased over the impulsive case.

Suppose the final braking correction is scheduled at a range R_B which provides a suitable bias such that errors in range measurement do not cause an overshoot in position and, possibly, premature impact. In addition, suppose the nominal closing rate at this point is made sufficiently high to ensure against negative closing rates in the presence of system dispersions. The following sketch shows this in the $(-\dot{R})$ versus R phase plane. The 3σ contour of dispersions is shown, assuming a bivariate gaussian distribution in closing rate and range.

It is implicitly assumed that the range dispersion is acceptable with regard to specifications or that use of small bilateral verniers for clocking maneuvers can comfortably accommodate the range errors. The primary concern then is to ensure that the closing rate dispersion is also within allowable limits. From this sketch it is apparent that the closing rate bias $(-\dot{R}_B)$ must be at least equal to the expected 3σ closing

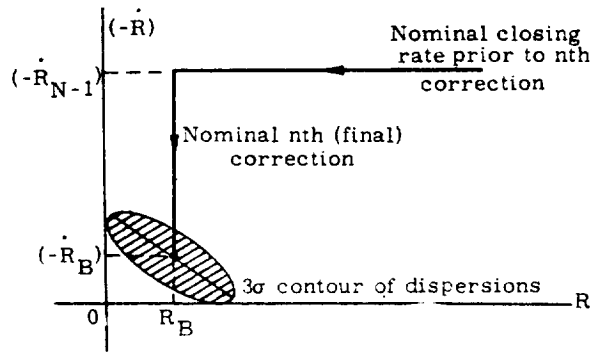

rate error if range is to decrease monotonically. Hence, for large dispersions in the final closing rate $(-\dot{R}_N)$ the bias becomes large and may be unacceptable in terms of vernier fuel and tank weight requirements. To avoid this the following process may be used to obtain the desired closing rate profile. Let

- N = total number of required corrections (to be determined)
- V_i = closing rate following ith correction
- ΔV_i = velocity increment of ith correction
- ΔV_i^* = commanded velocity increment of ith correction
- k_i, β_i = proportional (percent-type) and additive errors in execution of ΔV_i^*
- D_i = desired or nominal closing rate following ith correction
- ϵ_i = error in measurement of V_i.

The proportional error k_i is the per-unit error in execution of ΔV_i^* and may result from either accelerometer bias, scale factor errors, or from thrust and I_{sp} variations if corrections are metered on a time basis. The additive error β_i is the effect of residual impulse uncertainties.

Since

$$V_i = V_{i-1} - \Delta V_i \tag{230}$$

$$\Delta V_i^* = (V_{i-1} + \epsilon_{i-1}) - D_i \tag{231}$$

and

$$\Delta V_i = (1 + k_i)\,\Delta V_i^* + \beta_i \tag{232}$$

It is possible to write for the general correction

$$V_i = D_i - k_i (D_{i-1} - D_i) - (\epsilon_{i-1} + \beta_i) \quad (233)$$

if all cross-products of errors are assumed to be negligible. In particular for the Nth (final) correction,

$$D_N = (-\dot{R}_B)$$

yielding

$$\left[V_N - (-\dot{R}_B)\right] = -k_N \left[D_{N-1} - (-\dot{R}_B)\right] - \alpha_N \quad (234)$$

where

$\left[V_N - (-\dot{R}_B)\right]$ = closing rate error after Nth correction

$\alpha_N \equiv$ total additive error of Nth correction

$$\equiv \epsilon_N + \beta_N \quad (235)$$

Hence, if the 3σ dispersion in the final closing rate is allowed to be no greater than C [and by the preceding sketch $(-\dot{R}_B) \equiv C$], then it is required that

$$D_{N-1} \leq C + \left(\frac{C^2 - 9\sigma^2_{\alpha_N}}{9\sigma^2_{k_N}} \right)^{1/2} \quad (236)$$

Thus, if a single step correction (N = 1) is to be used, the following relation must hold.

$$D_0 = (-\dot{R}_0) \leq C + \left(\frac{C^2 - 9\sigma^2_{\alpha_1}}{9\sigma^2_{k_1}} \right)^{1/2} \quad (237)$$

If this is not the case, then a single step correction cannot be used and hence N must be greater than 1. This implies a prior correction at a range

$$R = R_{N-1} > R_N = R_B.$$

For this prior correction, the unilateral thrust constraint is invoked, requiring that $V_{N-1} > 0$. Using Eq (233) with i = N - 1, this is established with 3σ probability if

$$D^2_{N-1} > 9\sigma^2_{k_{N-1}} (D_{N-2} - D_{N-1})^2 + 9\sigma^2_{\alpha_{N-1}} \quad (238)$$

If D_{N-1} is assumed to be at the maximum value allowed by Eq (236) (to minimize the nominal closing time),

$$D_{N-2} < \underset{D_{N-1}}{\text{Max}} \left[D_{N-1} + \left(\frac{D^2_{N-1} - 9\sigma^2_{\alpha_{N-1}}}{9\sigma^2_{k_{N-1}}} \right)^{1/2} \right] \quad (239)$$

where the notation implies the maximum value with respect to D_{N-1}. Thus, in order for a two step reduction to be possible,

$$D_0 = (-\dot{R}_0) < \underset{D_1}{\text{Max}} \left[D_1 + \left(\frac{D^2_1 - 9\sigma^2_{\alpha_1}}{9\sigma^2_{k_1}} \right)^{1/2} \right] \quad (240)$$

where $(D_1)_{\text{max}}$ is given by Eq (236) for N = 2.

Usually, it is not necessary to proceed beyond the case of N = 2 since the presence of a small number $\sigma^2_{k_1}$ in the denominator of the square root expression in Eq (240) yields a very large number. In addition, the fact that the maximum value of D_1 is involved in Eq (240) further enhances the situation. However, should the initial closing rate be extremely high, so that Eq (240) does not hold, N must be made greater than 2. This implies a prior correction at

$$R = R_{N-2} > R_{N-1} > R_N = R_B$$

Again for this prior correction the unilateral thrust constraint is invoked, and an expression similar to Eq (238) results. If the maximum value of D_{N-2} is used, a constraint on D_{N-3}, similar to that of Eq (239), results.

$$D_{N-3} < \underset{D_{N-2}}{\text{Max}} \left[D_{N-2} + \left(\frac{D^2_{N-2} - 9\sigma^2_{\alpha_{N-2}}}{9\sigma^2_{k_{N-2}}} \right)^{1/2} \right] \quad (241)$$

where $(D_{N-2})_{\text{max}}$ is given by Eq (239). If three reductions are to suffice, then Eq (241) requires that

$$D_0 = (-\dot{R}_0) < \underset{D_1}{\text{Max}} \left[D_1 + \left(\frac{D^2_1 - 9\sigma^2_{\alpha_1}}{9\sigma^2_{k_1}} \right)^{1/2} \right]$$

which is identical to Eq (240), except that the unity subscripts apply to the first of three scheduled reductions, and, if written out cumulatively instead of recursively, implies

$$D_0 = (-\dot{R}_0) < \left\{ \begin{matrix} \text{Max} \\ D_1 \end{matrix} \quad \begin{matrix} \text{Max} \\ D_2 \end{matrix} \left[D_2 + \sum_{i=1}^{2} \left(\frac{D_{N-1}^2 - 9\sigma^2_{\alpha_{N-i}}}{9\sigma^2_{k_{N-i}}} \right)^{1/2} \right] \right\} \quad (242)$$

where $(D_1)_{\max}$ and $(D_2)_{\max}$ are given by Eqs (236) and (239) for N = 3.

What has taken place so far is an exercise in dynamic programming (Ref. 12) to determine the minimum number of reductions N necessary to satisfy the criterion C under the constraint of unilateral thrust. By inference, the general allocation policy for N reductions may be written as

$$D_{N-i} < \begin{matrix} \text{Max} \\ D_{N-i+1} \end{matrix} \left[D_{N-i+1} + \left(\frac{D_{N-i+1}^2 - 9\sigma^2_{\alpha_{N-i+1}}}{9\sigma^2_{k_{N-i+1}}} \right)^{1/2} \right] \quad (243)$$

for

$$i = 2, 3, \ldots, N$$

where

$$D_0 = (-\dot{R}_0) \quad (244)$$

$$\text{Max } D_{N-1} = C + \left(\frac{C^2 - 9\sigma^2_{\alpha_N}}{9\sigma^2_{k_N}} \right)^{1/2} \quad (245)$$

The process is continued until it is found that

$$D_0 = (-\dot{R}_0) < \text{Max } D_{N-i} \quad (246)$$

whereupon N is determined. The process also yields the desired closing rates at each step. Hence, upon satisfaction of Eq (246) all D_i's are determined.

There now remains the problem of allocating the desired set of closing rates at appropriate times or ranges. Generally, the choice should be made so that a sufficient amount of tracking and smoothing time exists between consecutive step reductions. Also, the reductions should be spaced so that the transverse channels have sufficient time to steer out errors. The nonimpulsive nature of each thrust application must also be taken into account. Thus, generally, the time between reductions is

$$\Delta t_i = \Delta t_{s_i} + \Delta t_{\ell_i} + \Delta t_{B_i} \quad (247)$$

where

Δt_i = time between ith and i - first reduction

Δt_{s_i} = ith smoothing time

Δt_{ℓ_i} = ith lag time (computing time, valve lag, etc.)

Δt_{B_i} = burning time of ith correction

The range difference between the ith and (i - 1)st correction is thus

$$\Delta R_i = \left(\Delta t_{s_i} + \Delta t_{\ell_i} \right) D_{i-1} + \Delta b_i \quad (248)$$

where

$\Delta b_i \equiv$ distance traveled in braking from D_{i-1} to D_i. (249)

Equations (248) and (249) then allow for the computation of the spacing of step reductions and, hence, the generation of the nominal closing rate profile. For any given set of spacings between corrections, the closing rate profile is the minimum time profile under unilateral constraints. This follows, since at each step the closing rate is assigned the highest possible value under unilateral thrust constraints.

g. Other rendezvous schemes

So far the work presented in this section has been based on the differential equations of relative motion. This approach is, however, not necessary as will be illustrated in the two remaining schemes to be discussed.

Combined injection and terminal guidance. By timing the initiation of thrust and providing thrust of a variable magnitude and direction, it is possible to perform the injection and any maneuvers necessary for closure simultaneously. The most notable studies conducted for this scheme have been conducted at the MIT Instrumentation Laboratory (see Refs. 13, 14, 15 and 16). These studies are concerned with a guidance equation of the form

$$\bar{f}_c = S_1 \bar{\ell}_r \left[\dot{R} + f(R) \right] + S_2 \left[R \bar{\omega}_{LS} \right] \quad (250)$$

where

$\bar{f}_c$ = commanded acceleration vector

S_1, S_2 = sensitivity coefficients

$\dot{R}$ = range rate

R = range

$\bar{\omega}_{LS}$ = angular velocity of the line of sight

$f(R)$ = desired range rate as a function of range

$\bar{\ell}_R$ = unit vector along the line of sight

For the studies conducted to this date, the $f(R)$ utilized has been $K\sqrt{R}$. This selection was made based on trials of several functions satisfying the boundary conditions for $f(R)$ (namely that $f(R)$ be defined for all R and go to zero at $R = 0$). A variety of values have been investigated for S_i and for K. With regard to K, the implications are that some linear function of the required velocity increment (i.e., $a + b\Delta v$) may be advantageous from the standpoint of propulsion system performance.

Because of the extreme initial closure velocities (as great as 4500 mps) and the limited range of the radar unit, it is, in general, necessary to begin the injection maneuver with a programmed thrust. Then at some time during the maneuver after the target is acquired, the guidance equation must be utilized. This sequencing is desirable in other respects as well, since it allows the planar change to be made while the velocity is near minimum, thus conserving the energy available.

A single variable thrust gimbaled motor (along with an adequate control system) comprises the propulsion system. The utilization of a single motor is made possible by restricting the initial conditions for closure to lie within a region ahead of and slightly below the target. Under these conditions the target overtakes the shuttle during the injection maneuver. The energy requirements for these maneuvers closely approximate the minimum (for small changes in the plane of motion).

The purpose of the variable thrust motor is to provide additional tolerance in the relative position of the two vehicles at the time the injection maneuver is initiated. In this manner it is possible to simultaneously compensate for errors in the ascent trajectory and launch timing.

The data obtained for the necessary computations are taken from a single radar unit mounted to the vehicle on a set of gimbals. The range and range rate are measured directly, whereas the angular velocity of the line of sight is computed from signals taken from the dish gimbals and the inertial platform.

An elementary functional block diagram of this system is shown in the following sketch.

Positive closure. Utilizing the analytic solutions for positive and velocity presented in the discussion of relative motion for nearly circular orbits, a purely numerical study of rendezvous has been conducted. The guidance scheme for this technique requires that the vehicle be accelerated toward the target with some given velocity. Then at a specified distance and range rate, thrust is again initiated to drive both the range and range rate to zero. This scheme has been investigated in studies conducted within the Martin Company.

In order to maintain the vehicle antennas in known orientations with respect to the earth, and to simplify the attitude control function to one of stabilization, the vehicle considered is assumed to be aligned with its fore and aft axis parallel to the orbital plane of the target satellite. Furthermore it is assumed that the fore-aft axis and the lateral axis lie in the plane normal to radius vector to the satellite. Thrust units are located so as to provide fore-aft, left-right and up-down accelerations. The attitude reference for this orientation is provided by an inertial platform.

Analog studies have been conducted to investigate vehicle to target closure employing on-off thrusts applied through the cg of the shuttle vehicle. The basic scheme utilized in these runs

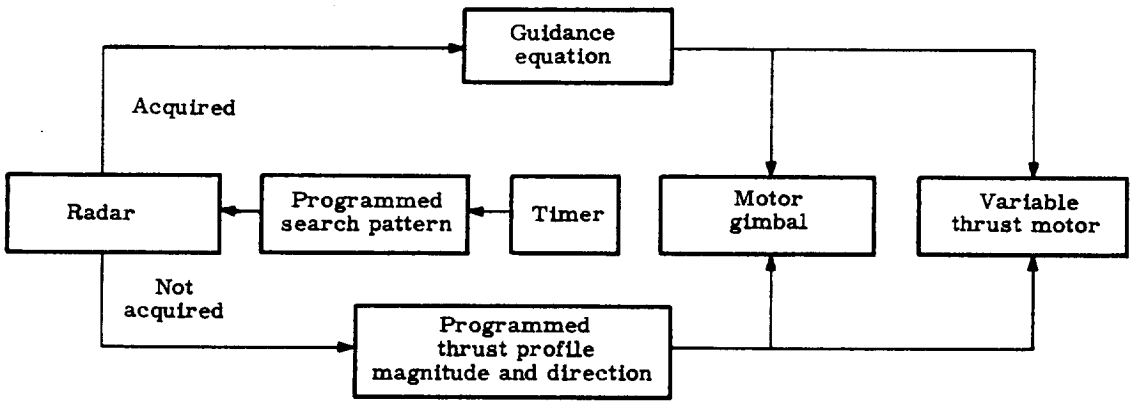

is illustrated in the following sketch. This sketch shows the relative range and range-rate phase plane (where Points A and B are two representative conditions existing at the time of radar lock-on).

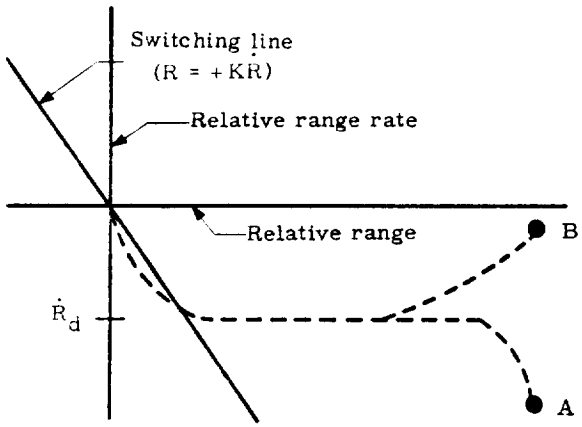

Thrust is applied in all cases to produce a given specified closure rate, $\dot{r}_d$. The vehicle is then allowed to coast until the switching line conditions are reached. At this point thrust is again initiated and the range and range rates are nulled to zero. The choice of K in the switching line equation is determined by knowledge of the acceleration available from the motors. Thrust must be initiated sufficiently early to avoid overrunning the target. Because of the on-off nature of the propulsion system, a dead spot must be provided to prevent chattering. In addition, it is necessary to bias the preselected closure velocity since the relative velocity components will change even in the absence of thrust due to slight differences in the orbits of the two vehicles and the differences in the perturbations effecting them.

The guidance law for each thrust component (neglecting the velocity bias previously discussed) is of the form

$$\left.\begin{aligned} T = +T_0 &\left\{\begin{aligned} &\left[(R-\epsilon)+K\dot{R}\right] > D\,;\ \dot{R} > -\dot{R}_d \\ &\text{or} \\ &\left[(R-\epsilon)+K\dot{R}\right] < -D\,;\ \dot{R} > \dot{R}_d \end{aligned}\right\} \\ T = -T_0 &\left\{\begin{aligned} &\left[(R-\epsilon)+K\dot{R}\right] > D\,;\ \dot{R} < -\dot{R}_d \\ &\left[(R-\epsilon)+K\dot{R}\right] < -D\,;\ \dot{R} < \dot{R}_d \end{aligned}\right\} \\ T = 0 \qquad & -D < \left[(R-\epsilon)+K\dot{R}\right] < D \end{aligned}\right\} \quad (251)$$

where

ϵ = stand off distance

D = dead spot (±) about ϵ

$\dot{R}_d$ = preselected closure rate.

It can be shown that closure from any point in a region about the target vehicle is possible. However, the most economic utilization of the propellant occurs when the shuttle is initially ahead of the target with a slightly lower velocity. If the vehicle is initially behind the target, two possibilities exist. First, thrust can be applied to produce closure without regard to propellant consumption. Or secondly, the orbital period of the shuttle vehicle can be adjusted so as to produce a gradual closure with respect to the target, and then at such time as the vehicles are appropriately located, the previous routine can be employed.

Studies conducted with initial separations of approximately 32 km and velocities of approximately 90 mps indicate that thrust-to-weight ratios of 0.1 to 0.2 g are quite adequate for control. Closure times for these runs were generally in the order of 400 to 800 sec with a fuel requirement of approximately $\frac{W_0}{8}$ which checks very closely to the estimate obtained from

$$\Delta V = g_0 I_{sp} \ell n \frac{1}{1-\xi}.$$

The motion of the shuttle vehicle under the influence of this set of control laws is illustrated in the following sketch which shows the projected motion in the vertical-longitudinal plane and the lateral longitudinal plane.

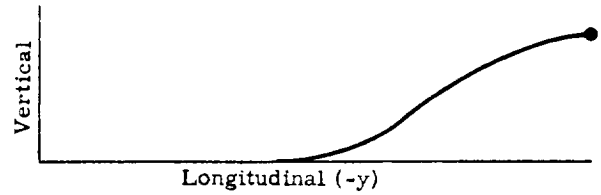

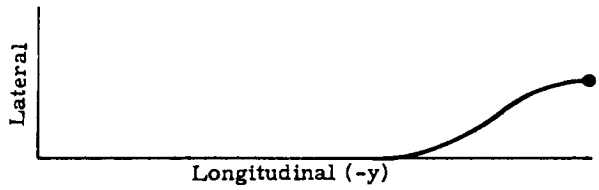

Signals for implementing this guidance law are derived from the radar data. Range (r) and range rate ($\dot{r}$) along the line of sight are measured by the tracking radar; the Euler angles defining relative position are provided by pickoffs on the radar dish gimbals, and the angular rate of the line of sight as computed from the signals from the rate gyros on the radar dish gimbals and the angular rate of the vehicle which is slaved to some reference (for example, local vertical).

h. Use of explicit control

The preselection of a nominal closing rate profile implies a fixed number of corrections at fixed ranges. In the early stages of mission planning, this is perhaps necessary for determination of sensor, propulsion, and time requirements in relation

to final accuracies and desired payload. However, whenever the question of optimization arises, the selection of a nominal profile can become an involved process, particularly when many corrections are necessary. Moreover, when the statistical interactions are considered, there may be some disadvantages in the idea of a fixed profile. Under such involved circumstances, it may be desirable to allow the vehicle to adjust the closing rate as a function of the conditions which exist at the time, rather than purely on the basis of range or time. Such a scheme would involve estimating the final range and closing rate dispersions which would result upon application of the final braking thrust, and an eventual adjustment of the closing rate if the estimated dispersions were unsatisfactory. Thus, the times and number of thrust applications would depend upon the particular circumstances encountered during homing, with due regard for system constraints.

3. Closure Times and Energy Requirements

The requirements for time and mass fraction to produce terminal closure under any one of the guidance laws discussed in the previous section can be obtained by programming the equations of motion for numerical solution and by substitution of given sets of initial conditions into the program. Although this technique has been employed frequently in the literature, it has the disadvantage that the solution is accurate only in the neighborhood of the initial set of conditions. Thus, for the present purposes a better approach is to present an analytic approximation which is reasonably valid than to discuss numerical solutions. This technique should have the advantage of pointing up the significant parameters.

Consider the two space curves representing the motion of the two vehicles in the following sketch.

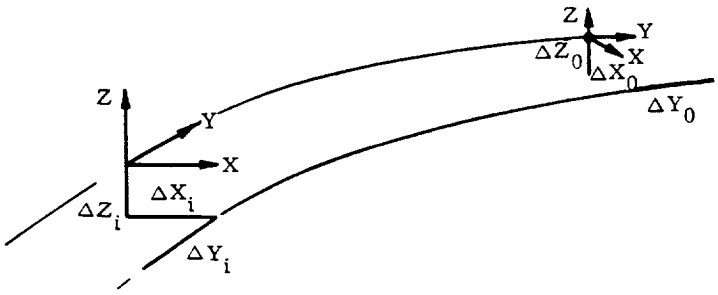

Given the position and velocity errors at a time corresponding to injection it is possible to compute the required change in position and velocity at a time in the future at which rendezvous is desired. This information is sufficient for a first order estimate of energy requirement if guidance schemes are not considered. (The energy requirement will be no more valid than this due to the fact that coupling of the differential equations will be neglected.)

The differential equations governing this maneuver are

$$\vec{F} = \dot{m}\vec{C} = (m_0 - \dot{m}t)\ddot{\vec{R}} \qquad (252)$$

or in terms of the various components of position

$$F_x = \dot{m}_x C = \left[m_0 - (\dot{m}_x + \dot{m}_y + \dot{m}_z)t\right] \ddot{x}(t)$$

$$= (m_0 - \dot{m}t)\ddot{x}$$

(where $\dot{m}$ represents the total mass flow rate assumed constant)

and the boundary conditions are $\vec{R} = \vec{R}_0$ and $\vec{V} = \vec{V}_0$ at $t = 0$ and $\vec{R} = \vec{V} = 0$ at $t = t_b$. The ground rule is that thrust be maintained constant. This, in turn, means that the induced velocity will be canceled at some point in the maneuver by reversing the thrust for the remaining burning time. It is noted that this is the general requirement. If the initial conditions are proper for a given thrust level and burning time, it will be possible to eliminate the necessity for thrust reversal. This will be seen in the discussions which follow.

Each of the components of position can be obtained as a function of burning time (prior to thrust reversal) by integrating

$$\ddot{x}(t) = \frac{\frac{F_x}{m_0}}{\left(1 - \frac{\dot{m}}{m_0}t\right)}$$

$$\dot{x}(t) = \frac{F_x}{m_0}\left[-\frac{m_0}{\dot{m}}\ell n\left(1 - \frac{\dot{m}}{m_0}t\right)\right] + C_1.$$

Now evaluating $\dot{x}$ at $t = 0$, yields $C_1 = \dot{x}_0$, thus

$$\dot{x}(t) = -\frac{F_x}{\dot{m}}\ell n\left(1 - \frac{\dot{m}}{m_0}t\right) + \dot{x}_0$$

$$x(t) = -\frac{F_x}{\dot{m}}\left(-\frac{m_0}{\dot{m}}\right)\left[\left(1 - \frac{\dot{m}}{m_0}t\right)\left\{\ell n\left(1 - \frac{\dot{m}}{m_0}t\right) - 1\right\}\right] + \dot{x}_0 t + C_2.$$

Again evaluating at $t = 0$ yields

$$x(t) = \frac{F_x m_0}{\dot{m}^2}\left[\left(1 - \frac{\dot{m}t}{m_0}\right)\left\{\ell n\left(1 - \frac{\dot{m}t}{m_0}\right) - 1\right\}\right]$$

(continued)

$$+ \dot{x}_0 t + x_0 + \frac{F_x m_0}{\dot{m}^2}$$

$$= \frac{F_x m_0}{\dot{m}^2}\left[\left(1 - \frac{\dot{m}t}{m_0}\right)\ell n\left(1 - \frac{\dot{m}t}{m_0}\right) + \frac{\dot{m}t}{m_0}\right] + \dot{x}_0 t + x_0 \quad (253)$$

and similarly for y and z. But this solution is valid only for $t < t_1$ where t_1 is the time at which this component of thrust is reversed. At times greater than t_1 the same procedure must be utilized but T_x must be of the opposite sense.

$$\dot{x}(t) = \frac{F_x}{\dot{m}}\left[\ell n\left(1 - \frac{\dot{m}t}{M_0}\right)\right] + C_3$$

where

$$M_0 = m_0 - \dot{m}t_1$$

But $\dot{x}$ must be $\dot{x}_1$ at $t = t_1$. Thus

$$C_3 = \dot{x}_1 - \frac{F_x}{\dot{m}}\left[\ell n\left(1 - \frac{\dot{m}t_1}{M_0}\right)\right]$$

and

$$\dot{x}(t) = \frac{F_x}{\dot{m}}\left[\ell n\left(1 - \frac{\dot{m}t}{M_0}\right) - \ell n\left(1 - \frac{\dot{m}t_1}{M_0}\right) - \ell n\left(1 - \frac{\dot{m}t_1}{M_0}\right)\right] + \dot{x}_0$$

$$= \frac{F_x}{\dot{m}}\left[\ell n\left(1 - \frac{\dot{m}t}{M_0}\right) - \ell n\left\{\left(1 - \frac{\dot{m}t_1}{M_0}\right)\cdot\left(1 - \frac{\dot{m}t_1}{m_0}\right)\right\}\right] + \dot{x}_0.$$

At this point the relationship between t_1 for this coordinate and t_b can be determined by requiring that $\dot{x} = 0$ at $t = t_b$. Thus

$$1 - \frac{\dot{m}t_b}{M_0} = \left(1 - \frac{\dot{m}t_1}{M_0}\right)\left(1 - \frac{\dot{m}t_1}{m_0}\right) e^{-\dot{x}_0 \frac{\dot{m}}{F_x}}$$

or

$$t_b = \frac{M_0}{\dot{m}}\left[1 - \left(1 - \frac{\dot{m}t_1}{M_0}\right)\left(1 - \frac{\dot{m}t_1}{m_0}\right) e^{-\dot{x}_0 \frac{\dot{m}}{F_x}}\right] \quad (254)$$

$$\approx 2t_1 - 2\frac{\dot{m}t_1^2}{m_0} \text{ for } \dot{x}_0 = 0$$

Now continuing to the definition of x(t) yields

$$x(t) = \frac{F_x}{\dot{m}}\left[-\frac{M_0}{\dot{m}}\left(1 - \frac{\dot{m}t}{M_0}\right)\left\{\ell n\left(1 - \frac{\dot{m}t}{M_0}\right) - 1\right\}\right.$$

(continued)

$$\left. - t\,\ell n\left\{\left(1 - \frac{\dot{m}t_1}{M_0}\right)\left(1 - \frac{\dot{m}t_1}{m_0}\right)\right\}\right] + \dot{x}_0 t + C_4$$

where

$$x(t) = x_1 \text{ at } t = t_1.$$

Thus

$$C_4 = x_1 + \frac{F_x}{\dot{m}}\left[\frac{M_0}{\dot{m}}\left(1 - \frac{\dot{m}t_1}{M_0}\right)\left\{\ell n\left(1 - \frac{\dot{m}t_1}{M_0}\right) - 1\right\} + t_1\,\ell n\left\{\left(1 - \frac{\dot{m}t_1}{M_0}\right)\left(1 - \frac{\dot{m}t_1}{m_0}\right)\right\}\right] - \dot{x}_0 t_1$$

$$= \frac{F_x}{\dot{m}^2}\left[m_0\left(1 - \frac{\dot{m}t_1}{m_0}\right)\ell n\left(1 - \frac{\dot{m}t_1}{m_0}\right) + \dot{m}t_1 + M_0\left(1 - \frac{\dot{m}t_1}{M_0}\right)\left\{\ell n\left(1 - \frac{\dot{m}t_1}{M_0}\right) - 1\right\} + t_1\,\ell n\left\{\left(1 - \frac{\dot{m}t_1}{M_0}\right)\left(1 - \frac{\dot{m}t_1}{m_0}\right)\right\}\right] + x_0$$

Now at $t = t_b$, $x = 0$, therefore

$$-x_0 = \frac{F_x}{\dot{m}^2}\left[-M_0\left(1 - \frac{\dot{m}t_b}{M_0}\right)\left\{\ell n\left(1 - \frac{\dot{m}t_b}{M_0}\right) - 1\right\} - \dot{m}(t_b - t_1)\,\ell n\left\{\left(1 - \frac{\dot{m}t_1}{M_0}\right)\left(1 - \frac{\dot{m}t_1}{m_0}\right)\right\} + m_0\left(1 - \frac{\dot{m}t_1}{m_0}\right)\ell n\left(1 - \frac{\dot{m}t_1}{m_0}\right) + \dot{m}t_1 + M_0\left(1 - \frac{\dot{m}t_1}{M_0}\right)\left\{\ell n\left(1 - \frac{\dot{m}t_1}{M_0}\right) - 1\right\}\right] \quad (255)$$

This expression can be simplified by eliminating t_b from the equation using

$$t_b = \frac{M_0}{\dot{m}}\left[1 - A\left(1 - \frac{\dot{m}t_1}{M_0}\right)\left(1 - \frac{\dot{m}t_1}{m_0}\right)\right]$$

$$A = e^{-\dot{x}_0 \dot{m}/F_x} \quad (256)$$

or

$$t_b = \frac{M_0}{\dot{m}}(1 - A) + A\,2t_1\left(1 - \frac{\dot{m}}{m_0}t_1\right)$$

$$= \frac{M_0}{\dot{m}}(1 - A) + 2At_1\frac{M_0}{m_0} \quad (257)$$

Now letting $\frac{\dot{m}t_1}{m_0} = \xi_1$.

$$t_b = \frac{m_0}{\dot m}(1-\xi_1)(1-A) + 2A(1-\xi_1)t_1$$

$$1 - \frac{\dot m t_b}{M_0} = 1 - \left[(1-A) + 2A\xi_1\right]$$

$$= A - 2A\xi_1 = A(1-2\xi_1).$$

Thus

$$-x_0 = \frac{F_x}{\dot m^2}\Big[-Am_0(1-\xi_1)(1$$
$$-2\xi_1)\left\{\ell n\, A(1-2\xi_1) - 1\right\}$$
$$-\left\{m_0(1-\xi_1)(1-A) + m_0\xi_1\right.$$
$$\left.\cdot(2A(1-\xi_1) - 1)\right\}\ell n(1-2\xi_1)$$
$$+\dot m_0(1-\xi_1)\ell n(1-\xi_1) + m_0\xi_1$$
$$+m_0(1-\xi_1)\left(1 - \frac{\xi_1}{1-\xi_1}\right)$$
$$\cdot\left\{\ell n\left(1 - \frac{\xi_1}{1-\xi_1}\right) - 1\right\}\Big]$$

$$-x_0 = \frac{F_x m_0}{\dot m^2}\Big[-A(1-3\xi_1+2\xi_1^2)\ell n(1-2\xi_1)$$
$$+(1-3\xi_1+2\xi_1^2)(1-\ell nA)$$
$$-\left\{(1-\xi_1)(1-A) + \xi_1\left[2A(1-\xi_1)\right.\right.$$
$$\left.\left.-1\right]\right\}\ell n(1-2\xi_1)$$
$$+(1-\xi_1)\ell n(1-\xi_1) + \xi_1 + (1-2\xi_1)$$
$$\left\{\ell n(1-2\xi_1) - \ell n(1-\xi_1) - 1\right\}\Big].$$

Now adding and subtracting $(1-3\xi_1+2\xi_1^2)\ell n(1-2\xi_1)$ within the bracket yields

$$-x_0 = m_0\frac{F_x}{\dot m^2}\left\{\left[\xi_1\ell n(1-\xi_1) + 2\xi_1^2\right]\right.$$
$$+(1-3\xi_1+2\xi_1^2)\left[(1-A)\ell n(1-2\xi_1)\right.$$
$$\left.\left.-\ell nA\right]\right\} \qquad (258)$$

This equation is solved for t_1; then the equation for t_b completes the solution. However, if ξ is of the order of 0.1 or less as it is for most maneuvers a further simplification can be achieved by expansion of $\ell n(1-\xi)$

$$\ell n(1-\xi) = -\xi - \xi_2^2.$$

Thus

$$-x = m_0\frac{F_x}{\dot m^2}\left\{\left[\xi_1^2 - \frac{\xi_1^3}{2}\right] + (1-3\xi_1+2\xi_1^2)\right.$$
$$\left.\left[(1-A)(-2\xi_1 - 2\xi_1^2) - \ell nA\right]\right\}$$

$$\frac{\dot m^2 x_0}{m_0 F_x} = \ell nA + 2\xi_1(1-A) + \xi_1^2(-1+8(1-A))$$
$$+\xi^3\left(-\frac{1}{2} - 2(1-A)\right) + \cdots \qquad (259)$$

This is a cubic equation which can be solved by successive approximations. Since there exist three such equations (one for each of the coordinates) parametric data seems extremely impractical. However, the form of the solution is sufficiently simple to facilitate hand computions for any given set of initial conditions.

Once t_1 and t_b are known, the total mass fraction is simply

$$\xi = \frac{\dot m t_b}{m_0} = \frac{T}{C}\frac{t_b}{m_0} \qquad (260)$$

and the corresponding impulsive velocity is

$$\Delta V = g_0 I_{sp}\,\ell n\frac{1}{(1-\xi)}$$
$$\approx g_0 I_{sp}\,\xi = g_0 I_{sp}\frac{\dot m t_b}{m_0}$$
$$= g_0 I_{sp}\frac{T}{C}\frac{t_b}{m_0} \qquad (261)$$

Thus, in this fashion it is possible to evaluate the energy requirements for a rendezvous maneuver which approximates the guided maneuver.

Example. Consider a maneuver in the x-direction for which the initial conditions are $x = R_0 = x_0$, $\dot x = 0$, $t = t_b$, and $\frac{F}{W_0} = B$ or $\frac{F}{m_0} = Bg_0$, where B is an unspecified constant. Since $\dot x = 0$, $A = 1$.
Thus

$$\frac{\dot m^2 x_0}{m_0 F_x} \approx -\xi_1^2 + O(\xi^3)$$

but

$$F_x = -\frac{F x_0}{R_0} = -F.$$

Thus

$$\frac{\dot m^2 x_0}{m_0 F} = \left(\frac{\dot m t_1}{m_0}\right)^2$$

$$t_1^2 = \frac{m_0 x_0}{F} = \frac{x_0}{Bg_0}$$

and

$$t_b = 2t_1\left(1 - \frac{\dot{m}t_1}{m_0}\right)$$

$$\frac{\dot{m}}{m_0} = \frac{\dot{W}}{W_0} = \frac{F}{W_0 I_{sp}} = \frac{B W_0}{W_0 I_{sp}} = \frac{B}{I_{sp}}$$

$$t_b = 2\left[\left(\frac{x_0}{B g_0}\right)^{1/2} - \frac{1}{I_{sp}}\left(\frac{x_0}{g_0}\right)\right]$$

or

$$B = \frac{x_0/g_0}{\left(\frac{t_b}{2} + \frac{x_0}{I_{sp} g_0}\right)^2}.$$

Also

$$\xi_b = \frac{\dot{m}}{m_0} t_b$$

$$= \frac{2B}{I_{sp}}\left[\left(\frac{x_0}{B g_0}\right)^{1/2} - \frac{1}{I_{sp}}\left(\frac{x_0}{g_0}\right)\right] \quad (262)$$

This expression shows the importance of several parameters. First, ξ_b will be larger for the higher acceleration levels (large B). This behavior results from the excessive propellant burned to cancel the velocity induced from t = 0 to t = t_1. The higher consumption, however, resulted in a lower value of closure time (t_b). The second parameter is the specific impulse (I_{sp}). This parameter enters into two stages: first, higher values of specific impulse reduce t_b, and second, the higher values of I_{sp} reduce $\dot{m}$. The contribution of both efforts is observed in the functional form of ξ_b, Eq (262).

To provide an idea of the magnitude of the required propellant fraction, consider

$x_0 = 10^5$ ft = 0.3048×10^5 m

B = 0.1

g_0 = 32.2 ft/sec^2 ≈ 980 cm/sec^2

I_{sp} = 300 sec

$$\xi_b = \frac{0.2}{0.300}\left[\frac{10^3}{5.68} - \frac{1}{300}\,\frac{10^5}{32.2}\right]$$

$$= 0.666\left[0.176 - 0.013\right] = 0.108$$

$$t_b = \xi_b \frac{m_0}{\dot{m}} = \xi_b\left(\frac{I_{sp}}{B}\right)$$

$$= 0.108\,\frac{(300)}{0.1} = 322 \text{ sec}$$

t_1 = 170 sec

$\Delta V \approx g_0 I_{sp} \xi_b$ = 32.2 (300) (0.108)

= 1030 fps or 315 mps

Now consider the some problem but with acceleration levels of 0.075, 0.05, 0.03 and 0.01.

	B = 0.1	B = 0.075	B = 0.05	B = 0.03	B = 0.01
ξ_b	0.108	0.0955	0.0783	0.0616	0.0364
t_b (sec)	322	382	469	616	1103
t_1 (sec)	170	203	244	318	562
ΔV fps	1030	922	756	594	352
ΔV mps	315	281	231	181	107

The first observation is that the energy requirements are large. This fact is due to the assumption that the closure velocity was zero initially (as may be seen in Eq (259), and the fact that the assumed range at t = 0 was large. To provide an appreciation of the validity of the solution, however, a numerical check was made of this set of initial conditions utilizing a line of sight guidance law. The results of this investigation proved the validity of this approximation since the agreement of the results for the same closure times was essentially the same as those predicted.

A more realistic approach utilizing the fact that the vehicle should be placed ahead of the target at a slightly lower velocity in order to produce an inverse tail chase would of necessity reduce these energy requirements to the numbers more conventionally quoted. In fact by selecting the proper value of F and t_b for a given $\dot{x}_0\,\dot{y}_0\,\dot{z}_0$ it would be possible to eliminate the first type of thrust (i.e., toward the target) and accelerate continuously to the desired rendezvous. To provide more specific information for a particular guidance system, it is necessary to produce a numerical simulation of the maneuver. This has been accomplished for two of the rendezvous schemes, the first being a constant line of sight in inertial space and the second being a combination of a differential correction procedure and Method I. Table 2 presents typical numerical results for these techniques for a circular target orbit of approximately 180 km. Burnout occurs at 37 km for all runs, and two ascent range angles (cut off to apocynthian 180° and 90°) are presented. The differences in the numerical results are due to the fact that more energy is required for injection for the 90° ascents and the fact that the relative velocities near apocynthian for the 180° ascents are sufficiently lower to require longer closure times. As may be seen from Eq (259), the maneuver requirements for a lunar rendezvous and for an earth rendezvous would be the same. The same cannot, however, be said for that portion of the velocity required to inject into the orbit. Thus, the total maneuver requirements should be increased by the amount of the difference in the injection velocities to provide a better estimate of the total requirements for earth rendezvous

$$\Delta V_{correction} = (V_c - V_a)_{\oplus} - (V_c - V_a)_{\text{☾}}$$

TABLE 2

Numerical Rendezvous Results

	Position			Velocity			Uncorrected Miss Distance	Method I		Method II	
ϕ Ascent	x_0(m)	y_0(m)	z_0(m)	$\dot{x}_0$(mps)	$\dot{y}_0$(mps)	$\dot{z}_0$(mps)	(km)	t	ΔV (mps)	t	ΔV (mps)
90	0	-33,109	-16,620	0	43.6	61.0	0	560	81.1	587	71.6
90	0	-35,693	-9,897	0	43.6	61.0	8.83	608	84.4	627	78.9
90	3,426	-35,528	-9,897	0	43.6	61.0	--	609	89.9	628	79.2
90	3,426	-28,554	-23,343	0	43.6	61.0	9.06	540	100.3	563	88.7
90	0	-28,760	-23,343	0	43.6	61.0	--	538	93.0	561	87.4
90	37,040	0	0	-64.6	0	0	0	557	71.9	580	71.9
90	33,617	0	6,723	-64.6	0	0	--	538	91.4	559	82.6
90	33,617	0	-6,723	-64.6	0	0	--	535	91.7	556	82.6
90	40,466	0	-6,723	-64.6	0	0	--	622	92.7	644	83.8
90	40,466	0	6,723	-64.6	0	0	8.98	616	92.7	644	83.8
180	0	-19,886	-31,299	0	-15.1	56.1	0	1081	66.1	1093	36.9
180	0	-27,729	-24,256	0	-15.1	56.1	14.48	1261	69.8	1269	45.1
180	23,706	-14,388	-24,256	0	-15.1	56.1	--	1162	101.5	470	57.0
180	23,706	-5,667	-27,891	0	-15.1	56.1	--	968	112.2	977	72.5
180	0	-5,667	-36,604	0	-15.1	56.1	--	843	66.8	853	64.6
180	37,040	0	0	-26.1	0	0	0	1061	40.8	1071	40.5
180	37,040	0	6,743	-26.1	0	0	--	1102	59.1	1112	51.8
180	45,003	0	6,743	-26.1	0	0	15.41	1207	64.6	1220	59.1
180	60,747	0	6,743	-26.1	0	0	--	1366	91.4	1383	68.3

Method 1 The inertial line of sight is maintained fixed.

Method 2 A computation is made using the equations of relative motion to yield a correction of position. Then as a final phase, the inertial line of sight is held constant as thrust nulls velocity and position errors.

NOTES:

x normal to track
y along track (i.e., along V)
z along radius

4. Terminal Guidance Smoothing Techniques

Tracking noise, in particular that which arises in radar skin tracking, has a profound effect on the probability of success in the rendezvous mission. Frequently, the basic accuracy of a homing tracker is not sufficient to allow guidance command computations without some smoothing. In this section two techniques for the smoothing of transverse angular rates of the line of sight are discussed. Emphasis is placed on the angular rates inasmuch as the effects of noise in these measurements are more severe than those in range. The two techniques are:

(1) Angular momentum smoothing.

(2) Sample data (digital) filtering.

The first technique takes advantage of the fact that the product of the square of range and the inertial angular rate of the line of sight is very nearly preserved during thrust-free flight. Thus, the average of this product over many points in time yields a near-optimal estimate of the "angular momentum" of the target-homing vehicle system. Division of this estimate by the square of the most recent value of range (suitably smoothed and updated) yields a near-optimal, updated estimate of the line-of-sight rate. Alternatively, division of the estimate of angular momentum by the most recent value of range yields a near-optimal, updated estimate of the transverse velocity.

The second technique is that of digital filtering of the line-of-sight rate, assumed to be of the form of a signal polynomial plus uncorrelated noise. This technique is the conventional sample data minimum mean square error scheme discussed by Blum (Ref. 17). While the angular momentum smoothing scheme is simple and effective, range measurements must be available. Sample data filtering on the angular rates does not depend on range information and is, hence, applicable to both collision and proportional navigation.

A third technique not discussed here is that of analog filtering of continuous data outputs from the tracker. The smoothing may involve either a straightforward low-pass filtering of the tracking outputs or the use of Wiener filters. The interested reader is directed to Refs. 18 through 26 on the topic of optimum mean square error filters for continuous processes.

The forms of the true rates ω_y and ω_p are suggested in the discussion of homing techniques formulated with respect to the line of sight. For thrust-free motion

$$\left.\begin{aligned} h_{\omega_p} &= R_0^2 \omega_{p_0} + \int_0^t R \Delta g_p \, dt \\ h_{\omega_y} &= R_0^2 \omega_{y_0} \end{aligned}\right\} \qquad (263)$$

where

$$\left.\begin{aligned} h_{\omega_p} &= R^2\omega_p \\ h_{\omega_y} &= R^2\omega_y \end{aligned}\right\} \quad (264)$$

Thus, for angular momentum smoothing, the yaw signal, h_{ω_y}, is a constant, while that of pitch is very nearly so if the gravity torque is small. For sample data filtering of the rates, ω_p and ω_y, substitution of Eq (264) into Eq (263) shows that

$$\left.\begin{aligned} \omega_p &= \frac{R_0^2\omega_{p_0}}{R^2} + \frac{1}{R^2}\int_0^t R\Delta g_p\, dt \\ \omega_y &= \frac{R_0^2\omega_{p_0}}{R^2} \end{aligned}\right\} \quad (265)$$

Over smoothing times much less than the total homing time, ω_p and ω_y, may be closely approximated by general polynomials in time. For example, if the closing rate is reasonably constant over the smoothing time,

$$R \cong R_0 - (-\dot{R}_0)\, t$$

$$\cong R_0\left(1 - \frac{t}{t_{G_0}}\right) \quad (266)$$

where

$$t_{G_0} = \text{initial time-to-go} = \frac{-\dot{R}_0}{R_0} \quad (267)$$

Thus,

$$\omega_y = \frac{\omega_{y_0}}{\left(1 - \frac{t}{t_{G_0}}\right)^2}$$

$$= \omega_{y_0}\left(1 + 2\frac{t}{t_{G_0}} - 5\frac{t^2}{t_{G_0}^2} + \cdots\right) \quad (268)$$

and similarly for ω_p except that an additional expansion is required due to the presence of the gravity torque.

Thus, in both schemes it can be said that the true signal is a polynomial in time. In the case of angular momentum smoothing the behavior is nearly a constant in pitch and truly a constant in yaw. The angular rates are polynomials of higher order depending on the smoothing time. For very short smoothing times a linear variation is valid. For moderate to reasonably long smoothing times a second or third order polynomial is valid.

a. Angular momentum smoothing

Let

$$h_{p,y} = \text{estimate of } h_{\omega_p},\ h_{\omega_y}$$

then assuming a large number of samples, N, over the smoothing interval,

$$h_{p,y} = \frac{1}{N}\sum_{i=1}^{N}\left(h_{\omega_{p,y}}\right)_i \quad (269)$$

may be used to smooth the angular momentum over thrust-free periods. In the following, the range measurements are considered to be noiseless since current trackers have range accuracies giving rise to negligible transverse guidance errors. The input to the smoothing process may be written as

$$\left.\begin{aligned} \left(h_{\omega_p}\right)_i &= R_0^2\omega_{p_0} + R_i^2\delta\omega_{p_i} \\ &\quad + \int_{t_0}^{t_0+t_i} R\Delta g_p\, dt \\ \left(h_{\omega_y}\right)_i &= R_0^2\omega_{y_0} + R_i^2\delta\omega_{y_i} \end{aligned}\right\} \quad (270)$$

where

$\delta\omega_p$ = pitch rate noise of line of sight

$\delta\omega_y$ = yaw rate noise of line of sight.

Thus,

$$\left.\begin{aligned} h_p &= R_0^2\omega_{p_0} + \frac{1}{N}\sum_{i=1}^{N} R_i^2\delta\omega_{p_i} \\ &\quad + \frac{1}{N}\sum_{i=1}^{N}\int_{t_0}^{t_0+t_i} R\Delta g_p\, dt \\ h_y &= R_0^2\omega_{y_0} + \frac{1}{N}\sum_{i=1}^{N} R_i^2\delta\omega_{y_i} \end{aligned}\right\} \quad (271)$$

At the end of the smoothing interval at which the estimates are to apply, the true values of the angular momenta are

$$h_p = R_0^2 \omega_{p_0} + \int_{t_0}^{t_0 + t_N} R\Delta g_p \, dt$$

$$h_y = R_0^2 \omega_{y_0} \qquad (272)$$

Hence, the errors in the estimates are

$$\delta h_p = \frac{1}{N} \sum_{i=1}^{N} R_i^2 \delta\omega_{p_i} - \frac{1}{N} \sum_{i=1}^{N} \int_{t_0+t_i}^{t_0+t_N} R\Delta g_p \, dt \qquad (273)$$

$$\delta h_y = \frac{1}{N} \sum_{i=1}^{N} R_i^2 \delta\omega_{y_i}$$

Utilizing the apparent gravity effects (discussed earlier) and the fact that range decreases monotonically, Eq (273) are seen to be bounded by

$$(\delta h_p)_{max} = \frac{R_0}{N} \sum_{i=1}^{N} \delta V_{p_i} + \frac{3}{4} \frac{GM}{r_t^3} R_0^2 t_N \qquad (274)$$

$$(\delta h_y)_{max} = \frac{R_0}{N} \sum_{i=1}^{N} \delta V_{y_i}$$

where

$$\delta V_{p_i} = R_i \delta\omega_{p_i} \qquad (275)$$

$$\delta V_{y_i} = R_i \delta\omega_{y_i}$$

Hence,

$$(\delta V_p)_{max} = \frac{(\delta h_p)_{max}}{R} = \left(\frac{R_0}{R}\right) \frac{1}{N} \sum_{i=1}^{N} \delta V_{p_i} + \frac{3}{4} \frac{GM}{r_t^3} \frac{R_0^2}{R} t_N \qquad (276)$$

$$(\delta V_y)_{max} = \frac{(\delta h_y)_{max}}{r} = \left(\frac{R_0}{R}\right) \frac{1}{N} \sum_{i=1}^{N} \delta V_{y_i}$$

Using Eq (266) with $t = t_N << t_{G_0}$

$$(\delta V_p)_{max} \cong \frac{1}{N} \sum_{i=1}^{N} \delta V_{p_i} + \frac{3\,GM}{4\,r_t^3} Rt_N \qquad (277)$$

$$(\delta V_y)_{max} \cong \frac{1}{N} \sum_{i=1}^{N} \delta V_{y_i}$$

Thus, since the samples are uncorrelated, the maximum values for the standard deviations are

$$\max \sigma_{V_p} = \frac{1}{\sqrt{N}} \left(\sigma_{V_{p_i}}\right)_{max} \qquad (278)$$

$$\max \sigma_{V_y} = \frac{1}{\sqrt{N}} \left(\sigma_{V_{y_i}}\right)_{max}$$

and the maximum mean pitch velocity error is

$$\max \mu_{V_p} = \frac{3}{4} \frac{GM}{r_t^3} Rt_N \qquad (279)$$

The fact that the velocity error due to the gravity torque is negligible is apparent upon substitution of some numbers. For a target in a circular orbit of 500 naut mi or 926 km altitude and a relative range of 25 naut mi or 46.3 km, a smoothing time of 10 sec yields

$$\max \mu_{V_p} \cong 1 \text{ fps or } 0.3 \text{ mps}$$

At a relative range of 5 mi or 8.7 km this maximum error becomes 0.2 fps or 0.036 mps; at 1 mi or 1.73 km; 0.04 fps or 0.012 mps. Thus, while the bias error is initially large, it quickly drops to a negligible level at small ranges where fine accuracy is required. This is to be expected since the differential gravity acceleration diminishes as range goes to zero. Thus, Eqs (278) and (279) remain as the principal errors, showing that the angular momentum smoothing scheme yields residual transverse velocity errors which decrease with the square root of the number of samples used in the process.

b. Sample data filtering

Blum (Ref. 17) presents an exact formula for the output noise power of an optimum digital filter designed to make a zero-lag estimate of the input or its derivatives. The input model consists of a polynomial signal plus stationary uncorrelated noise. Graphs and tables of the rms error for the zero-lag estimation of the 0th, 1st and 2nd derivatives are given as a function of the input polynomial up to degree 5 and memory spans up to 10 sample points.

The work of Blum in sampled data filters is discussed in this section, to the extent of introducing the variables and notation used in his graphs and tables, and the results that he derives.

Consider a set of equally spaced data points (u, y_u) $u = 1, 2, \ldots, M$. The problem is to fit a least squares polynomial of degree n to these points and to estimate the Kth derivative of the observed data from the curve fit at any point on the u scale.

For the purpose of the analysis it is convenient to utilize orthogonal polynomials in the curve fitting procedure. Thus let the true polynomial be given by

$$P(u) = \sum_{L=0}^{n} \alpha_L \xi_L(u), \quad u = 1, 2, \ldots, M \tag{280}$$

where the polynomials $\xi_L(u)$ are orthogonal, (Ref. 28) e. g., satisfy the following relationships

$$\sum_{u=1}^{M} \xi_h(u)\xi_L(u) = 0, \quad h \neq L, \tag{281}$$

$$\sum_{u=1}^{M} \xi_L{}^2(u) = S(L, M). \tag{282}$$

It is assumed that the observations y_u are given by

$$y_u = P(u) + N(u).$$

The N(u) are assumed to be random, stationary, and uncorrelated errors.

Then the least squares estimates $\hat{\alpha}_L$ of the coefficients α_L are obtained by minimizing

$$I = \sum_{u=1}^{M} \left[\sum_{L=0}^{n} \hat{\alpha}_L \xi_L(u) - y_u \right]^2 \tag{283}$$

with respect to each of the parameters $\hat{\alpha}_L$.

Thus one obtains

$$\frac{\partial I}{\partial \hat{\alpha}_L} = \sum_{u=1}^{M} 2 \left[\sum_{v=0}^{n} \hat{\alpha}_v \xi_v(u) - y_u \right] \xi_L(u) = 0, \quad L = 0, 1, \ldots, n. \tag{284}$$

Solving Eq (284) for α_L one obtains

$$\hat{\alpha}_L = \sum_{u=1}^{M} \frac{y_u \xi_L(u)}{S(L, M)}, \quad L = 0, 1, \ldots, n. \tag{285}$$

By substituting Eq (285) one obtains the curve fit relationship

$$Y(u) = \sum_{L=0}^{n} \hat{\alpha}_L \xi_L(u). \tag{286}$$

To evaluate the estimate of the Kth derivative at $u = M + \alpha$ one need only take the Kth derivative of both sides of Eq (286) (considering u as a continuous variable), and obtain

$$\left.\frac{d^K Y(u)}{du^K}\right|_{u=M+\alpha} \equiv Y^{(K)}_{(M+\alpha)} = \sum_{L=K}^{n} \hat{\alpha}_L \left.\frac{d^K}{du^K} \xi_L(u)\right|_{u=M+\alpha} \tag{287}$$

Let

$$\left.\frac{d^K}{du^K} \xi_L(u)\right|_{u=M+\alpha} \equiv \xi_L{}^{(K)}(M + \alpha) \tag{288}$$

Now, substituting Eqs (285) and (287) yields

$$Y^{(K)}(M + \alpha) = \sum_{L=K}^{n} \sum_{u=1}^{M} \frac{y_u \xi_L(u) \xi_L{}^{(K)}(M + \alpha)}{S(L, M)} \tag{289}$$

Let

$$W^*_{M-u} = \sum_{L=K}^{n} \frac{\xi_L(u)\xi_L{}^{(K)}(M + \alpha)}{S(L, M)}, \quad u = 1, 2, \ldots, M \tag{290}$$

then

$$Y^{(K)}_{M+j}(M + \alpha + j) = \sum_{u=1}^{M} W^*_{M-u} y_{u+j}, \quad j = 0 \pm 1 \pm 2 \ldots. \tag{291}$$

Equation (291) is directly interpreted as the input-output relationship of a digital filter with weighting sequence $W^*_0, W^*_1, \ldots, W^*_{M-1}$. The input is the sequence y_{u+j} and the output is $Y_{M+j}(M + j + \alpha)$. The output is available in real time after the last data point is sampled and estimates the Kth derivative of the input at $u = M + \alpha + j$. The filter has a finite memory over the interval $(M - 1)T$.

Since the estimators $\hat{\alpha}_L$ are unbiased, the error in estimate is given by (j = 0),

$$\Delta = \left[Y_M^{(K)}(M+\alpha) - \sum_{L=K}^{n} \alpha_L \xi_L^{(K)}(M+\alpha) \right]$$

$$\Delta = \sum_{u=1}^{M} W^*_{M-u} N(u). \tag{292}$$

The mean square error of estimate is given by

$$\sigma_\Delta^2 = \alpha_N^2 \sum_{u=1}^{M} \left[W^*_{M-u} \right]^2 \tag{293}$$

(σ_N^2 = noise mean square error).

Substituting Eqs (281) and (282) into Eq (293) yields,

$$\frac{\sigma_\Delta^2}{\sigma_N^2} \equiv \delta^2(M, \alpha, K, n) = \sum_{L=K}^{n} \frac{\left[\xi_L^{(K)}(M+\alpha) \right]^2}{S(L, M)} \tag{294}$$

which is the main result of this section.

Equation (294) has been derived for unit time between samples. If the interval between samples is given by T, then Eq (290) is modified as follows:

$$W^*_{M-u,\,T} = \frac{1}{(T)^K} W_{M-u}, \tag{295}$$

and Eq (294) becomes

$$\frac{\sigma_\Delta^2 (T)^{2K}}{\sigma_N^2} = \delta^2(M, \alpha, K, n). \tag{296}$$

Note that

$$\delta^2(M, \alpha, K, n) = \delta^2(M, \alpha, K, n-1) + \frac{\left[\xi_n^{(K)}(M+\alpha) \right]^2}{S(n, -M)}, \tag{297}$$

so that increasing the degree of curve fit is never associated with a decrease in σ_Δ^2 since the second term of Eq (297) is positive definite for fixed M, α, and K.

Special case. Special formulas for δ^2 are as follows. Let K = 0, α = 0, -1, -2, ..., (M - 1) then

$$\delta^2(M, \alpha, 0, n) = W^*_{-\alpha}.$$

As an example, when α = 0, K = 0, one obtains a zero-lag estimate of the input. The mean square error output is then proportional to W_0, the coefficient which multiplies the latest data point, e. g.,

$$\sigma_\Delta^2 = \sigma_N^2 \cdot W_0^*.$$

Other relationships on the δ which may be useful are as follows. Let the order of the derivative equal the order of degree of curve fit, e. g., K = n, then

$$\delta^2(M, \alpha, n, n) = \frac{(n!)^2}{S(n, M)} \tag{298}$$

and is independent of α.

Let the order of the derivative equal one less than the degree of the curve fitting polynomial, e. g., K = n - 1, then

$$\delta^2(M, \alpha, n-1, n) = \delta^2(M, \alpha, n-1, n-1) + \left[\frac{M + 2\alpha - 1}{2} \right]^2 \delta^2(M, \alpha, n, n) \tag{299}$$

$$= \frac{[(n-1)!]^2}{S(n-1, M)} + \left[\frac{M + 2\alpha - 1}{2} \right]^2 \frac{[n!]^2}{S(n, M)} \tag{300}$$

When α = - (M - 1)/2; e. g., the midpoint of the curve fitting interval,

$$\delta(M, \alpha = -\left[\frac{M-1}{2} \right], n-1, n) = \delta^2(M, \alpha, n-1, n-1). \tag{301}$$

This represents the minimum δ^2 obtainable with respect to α.

Tables 3, 4 and 5 present the exact values of δ using Eq (296). Figures 11, 12 and 13 present a plot of δ using Eq (294) for M = 10 to 100 for purposes of interpolation.

Equation (296) is identical with the results one would obtain from Blum (Ref. 30) as are the values of the weighting sequence.

The interpretation of the parameter α is as follows: when α = 0, one obtains a zero-lag estimate with respect to the latest data point, when - (M - u $\rightarrow$ 1) < α > 0, one obtains an extrapolation, and when (M - 1) < α < 0, one obtains interpolation of the input polynomial. A more

detailed discussion of σ_Δ^2 as a function of α is available (Ref. 28).

Table 6 contains a summary of a few useful properties of the orthogonal polynomials. A listing of the orthogonal polynomials in consistent notation is shown in Table 5 of Ref. 29.

The functions satisfy the following recursion relationship

$$\xi_{v+1}(u) \equiv \xi_1(u)\,\xi_v(u) - \frac{v^2(M^2 - v^2)}{4(4v^2 - 1)}\,\xi_{v-1}(u) \quad (302)$$

As indicated, the recursion is an identity so that by repeated differentiation one obtains

$$\xi_{v+1}^{(L)}(u) \equiv \xi_1(u)\,\xi_v^{(L)}(u) + L\,\xi_v^{(L-1)}(u) - \frac{v^2(M^2 - v^2)}{4(4v^2 - 1)}\,\xi_{v-1}^{(L)}(u), \quad (303)$$

where

$$\xi_x^{(L)}(u) = 0, \quad L < 0, \quad x < 0, \quad L > x, \text{ and}$$

where $\xi_L^{(L)} = L!$

so that

$$\xi_{v+1}^{(L)}(M+\alpha) \equiv \left[\frac{2\alpha + M - 1}{2}\right]\xi_v^{(L)}(M+\alpha) + L\,\xi_v^{(L-1)}(M+\alpha) - v^2\,\frac{[M - v^2]}{4(4v^2 - 1)}\,\xi_{v-1}^{(L)}(M+\alpha). \quad (304)$$

Finally, the sum of squares S(L, M) is given by Ref. 30.

$$S(L, M) = \frac{(L!)^4 \prod_{j=-L}^{+L}(M - j)}{(2L)!\,(2L+1)!} \quad (305)$$

Higher order polynomials to degree 10 are listed by Allen (Ref. 31). A very complete table of the values of $\xi_v(u)$ for v = 0, to 5, u from v + 2 to 104 is made available by Anderson and Houseman (Ref. 30).

c. Conclusion

An exact equation for the mean square error of the output of an optimum digital filter has been presented. The formula was derived using curve fitting concepts to demonstrate the relationship between the concepts of parameter estimation in curve fitting and weighting function optimization in linear filtering.

Equation (290) represents a convenient formula for computing the weighting sequence of the digital filter.

From Tables 3, 4 and 5, one may determine the exact value of δ for small M.

In Figures 16, 17 and 18, the values of δ can be determined for those values of M not tabulated. For M > 100, one can extrapolate linearly on log-log paper.

TABLE 3

Table of $\delta(M, \alpha, K, n)$, $\alpha = 0$, K = 0 for Evaluating the RMS Error for Zero-Lag ($\alpha = 0$) Estimation of the Input (K = 0) as a Function of the Degree of the Curve Fitting Polynomial (n) and the Number of Data Points (M)

M/n ⟶		0	1	2	3	4	5
2	δ	0.70711					
3	δ	0.57735	0.91287				
4	δ	0.50000	0.83666	0.97468			
5	δ	0.44721	0.77460	0.94112	0.99283		
6	δ	0.40825	0.72375	0.90633	0.97996	0.99801	
7	δ	0.37796	0.68139	0.87267	0.96362	0.99348	0.99946
8	δ	0.35355	0.64550	0.84162	0.94548	0.98655	0.99796
9	δ	0.33333	0.61464	0.81278	0.92660	0.97800	0.99533
10	δ	0.31623	0.58775	0.78625	0.90762	0.96802	0.99157
20	δ	0.22361	0.43095	0.60892	0.74985	0.85231	0.92022
50	δ	0.14142	0.27865	0.40784	0.52578	0.63011	0.71946
95	δ	0.10260	0.20359	0.30142	0.39471	0.48223	0.56299
1001	δ	0.031607	0.063167	0.094632	0.12596	0.15709	0.18800

TABLE 4

Table of $\delta(M, \alpha, K, n)$, $\alpha = 0$, K = 1 for Evaluating the RMS Error for Zero-Lag ($\alpha = 0$) Estimation of the First Derivative of the Input (K = 1) as a Function of the Degree of the Curve Fitting Polynomial (n) and the Number of Data Points (M)

M/n ⟶		1	2	3	4	5
2	δ	1.414				
3	δ	0.70711	2.5495			
4	δ	0.44721	1.5652	3.83895		
5	δ	0.31623	1.1148	2.52566	5.5839	
6	δ	0.23905	0.85252	1.90348	3.6802	8.2418
7	δ	0.18898	0.68138	1.52189	2.8226	5.2190
8	δ	0.15430	0.56167	1.26041	2.3028	3.9614
9	δ	0.12910	0.47377	1.06943	1.9445	3.2351
10	δ	0.11010	0.40685	0.92389	1.6794	2.7476
20	δ	0.038778	0.14855	0.35079	0.65608	1.0684
50	δ	0.0097999	0.038494	0.093871	0.18201	0.30714
95	δ	0.0037414	0.014821	0.036558	0.071883	0.12326
1001	δ	0.000109380	0.00043711	0.0010913	0.0021790	0.0038054

TABLE 5

Table of $\delta(M, a, K, n)$, a = 0, K = 2 for evaluating the RMS error for zero-lag (a = 0) estimation of the second derivative of the input (K = 2) as a function of the degree of the curve fitting polynomial (n) and the number of data points (M)

M/n ⟶		2	3	4	5
3	δ	2.4495			
4	δ	1.0	6.7823		
5	δ	0.53452	3.2071	14.017	
6	δ	0.32733	1.8919	7.0312	26.312
7	δ	0.21822	1.2440	4.3502	13.334
8	δ	0.15430	0.87535	2.9852	8.4113
9	δ	0.11396	0.64578	2.1729	5.8714
10	δ	0.087039	0.49355	1.6494	4.3527
20	δ	0.013094	0.087123	0.29179	0.74414
50	δ	0.0015194	0.0089549	0.030657	0.079685
75	δ	0.00050512	0.0018129	0.0062672	0.016468
1001	δ	0.84641×10^{-6}	0.50735×10^{-5}	0.17741×10^{-4}	0.47264×10^{-4}

TABLE 6

Orthogonal Polynomials

$$\xi_0(u) = 1$$

$$\xi_1(u) = (u - \bar{u}),\ \bar{u} = \frac{M+1}{2}$$

$$\xi_2(u) = (u - \bar{u})^2 - \frac{M^2 - 1}{12}$$

$$\xi_3(u) = (u - \bar{u})^3 - (u - \bar{u})\left[\frac{3M^2 - 7}{20}\right]$$

$$\xi_4(u) = (u - \bar{u})^4 - (u - \bar{u})^2\left[\frac{3M^2 - 13}{14}\right] + \frac{3(M^2 - 1)(M^2 - 9)}{560}$$

$$\xi_5(u) = (u - \bar{u})^5 - (u - \bar{u})^3\left[\frac{5(M^2 - 7)}{18}\right] + (u - \bar{u})\left[\frac{15M^4 - 230M^2 + 407}{1008}\right]$$

5. Long Time Closure

If relatively long times are acceptable for closure, several computational schemes may be employed. One such method has been developed by D. F. Lawden and is reported in Ref. 31. The solution outlined is directed primarily toward the correction of interplanetary orbits but is sufficiently general that it may be utilized for this problem as well. The major disadvantage of this solution for manual computation is the iteration procedure required to define the modified or closure orbit.

A general solution may be obtained by considering the requirements for closure (i.e., the radius identity at the point of rendezvous and specified time of closures). This analysis yields two equations with 3 unknowns (Δa, Δe and $\Delta\omega$); however, these new variables are in turn functions of Δr which is a known error and ΔV_1 and $\Delta\gamma_1$ which are the differences in velocity and flight path angle immediately after the corrective pulse relative to those of the target vehicle at the same time. This analysis yields the following equations when second order terms in Δa, Δe and $\Delta\omega$ are neglected.

$$\left[1 - \frac{2e_f \Delta e}{1 - e_f^2}\right]\left[1 + \frac{\Delta a}{a}\right] = \frac{1 + (e_f + \Delta e)\cos(\theta_{f2} + \Delta\omega)}{1 + e_f \cos\theta_{f2}}$$

$$\frac{\Delta t\, 2\pi}{\tau} = E_{t2} - E_{t1} - (e_f + \Delta e)(\sin E_{t2} - \sin E_{t1})$$

$$E_{t1} = 2\tan^{-1}\left[\sqrt{\frac{1-(e_f+\Delta e)}{1+(e_f+\Delta e)}}\ \tan\frac{(\theta_{f2} - \Delta\theta - \Delta\phi + \Delta\omega)}{2}\right]$$

$$E_{t2} = 2\tan^{-1}\left[\sqrt{\frac{1-(e_f+\Delta e)}{1+(e_f+\Delta e)}}\ \tan\frac{(\theta_{f2} + \Delta\omega)}{2}\right]$$

where

Δa, Δe and $\Delta\omega$ are the required changes in the orbital parameters as defined in the following discussion of the variation of parameters technique.

θ_{f2} is the angle from perigee to the point of rendezvous in the target orbit.

$\Delta\theta$ is the angle subtended by the target vehicle in moving from t_1 to t_2.

$\Delta\phi$ is the central angle between the two vehicles at t_1

The resultant equations for this solution are so complex in nature that the solution appears unattractive.

A third method may be obtained by adapting the "Variational Method for General Orbital Errors Analysis" reported in Chapter 12. The equations for this solution are summarized below.

$$\theta_{f2} = \theta_{f2}(\theta_{f1}, t_{closure}, e_f)$$

$$\Delta\phi_2 = \Delta\omega - \frac{(1+e\cos\theta_{f2})^2}{(1-e^2)^{3/2}}\left[\sqrt{\frac{\mu}{a^3}}\,\Delta t_p + \frac{3M\Delta a}{2a}\right] + \frac{\sin\theta_{f2}\,(2 + e\cos\theta_{f2})}{1 - e^2}\Delta e \qquad (306)$$

$$\Delta r_2 = \left[\frac{1 - e^2}{1 + e\cos\theta_{f2}} - \frac{3eM\sin\theta_{f2}}{2(1-e^2)^{1/2}}\right]\Delta a - a\cos\theta_{f2}\,\Delta e - \sqrt{\frac{\mu}{a}}\,\frac{e\sin\theta_{f2}\,\Delta t_p}{(1-e^2)^{1/2}} \qquad (307)$$

$$\Delta a = \frac{2(1 + e\cos\theta_{f1})^2 \Delta r_1}{(1 - e^2)^2} + \quad \text{(continued)}$$

$$+ 2\sqrt{\frac{a^3}{\mu}}\ \frac{(1+2e\cos\theta_{f1}+e^2)\Delta V_1}{1-e^2} \qquad (308)$$

$$\Delta e = \frac{(e+\cos\theta_{f1})(1+e\cos\theta_{f1})\Delta r_1}{a(1-e^2)^2}$$

$$+ 2(e+\cos\theta_{f1})\sqrt{\frac{a(1-e^2)}{\mu(1+2e\cos\theta_{f1}+e^2)}}\ \Delta V_1$$

$$+ \frac{(1-e^2)\sin\theta_{f1}}{1+e\cos\theta_{f1}}\ \Delta\gamma_1 \qquad (309)$$

$$\Delta\omega = \frac{\sin\theta_{f1}(1+e\cos\theta_{f1})\Delta r_1}{ae(1-e^2)}$$

$$+ 2\sin\theta_{f1}\sqrt{\frac{a(1-e^2)}{\mu(1+2e\cos\theta_{f1}+e^2)}}\ \Delta V_1$$

$$- \left[2 + \frac{(1-e^2)\cos\theta_{f1}}{e(1+e\cos\theta_{f1})}\right]\Delta\gamma_1 \qquad (310)$$

$$\Delta t_p = \sqrt{\frac{a^3}{\mu}}\left\{\frac{(1-e^2)^{3/2}}{(1+e\cos\theta_{f1})^2}\left[(\Delta\omega - \Delta\phi_1)\right.\right.$$

$$\left.\left. + \frac{\sin\theta_{f1}(2+e\cos\theta_{f1})}{1-e^2}\Delta e\right] - \frac{3M\Delta a}{2a}\right\} \qquad (311)$$

This analysis assumes that the orbits of the target and shuttle vehicle during closure are very similar and treats the displacement at the initially selected point of rendezvous, or any other point where the vehicles are sufficiently close, as an error in the position at that time of the target vehicle. The solution is made in the following sequence:

(1) The required changes in a, e, ω and t_p are computed in terms of known errors Δr_1 and $\Delta\phi_1$, and the desired parameters ΔV_1 and $\Delta\gamma_1$.

(2) These equations in terms of two unknowns are then substituted into the equations for Δr_2 and $\Delta\phi_2$.

(3) The equations for errors in position at point 2 are equated to 0 and the resultant equations solved simultaneously for ΔV_1 and $\Delta\gamma_1$.

(4) With knowledge of the velocity and flight path angle both before and after the application of the corrective pulse, the magnitude and direction of the pulse required may be computed from the law of cosines.

This analysis is general and could be employed for the case of short time closure as well (this implies large changes in a, e, ω, t_p) were it not for the fact that second order terms in ΔV_1, $\Delta\gamma_1$ and Δr_1 have been neglected in the derivation. This does not preclude the possibility of including these terms in the definition of Δa, Δe, $\Delta\omega$ and Δt_p; however, this incorporation is felt to be excessively laborious.

Sample problem. The utilization of this closure analysis is illustrated in the following sample problem.

$a_{24} = 1.38337 \times 10^8$ ft = 42165.1 km

$e_{24} = 0.61832$

$\theta_{f1} = 107.90°$

$t_{f1} = 8339.5$ sec

$V_{f1} = 12840$ fps = 3913.63 m/sec

$r_{f1} = 20{,}000$ stat mi = 32186.9 km

$\Delta r_1 = 16.6426$ stat mi = 26.7837 km

$\Delta\phi_1 = 0.019222$ rad

$V'_{t1} = 8776$ fps = 2675 m/sec

$t_{closure} = 20{,}000$ sec

$\gamma'_{t'} = 36.008°$

Note:

X'_{t1} parameter in transfer orbit before initiating closure

X_{t1} parameter in closure orbit at time of pulse

X_{f1} parameter in target orbit at time of pulse

X_{f2} parameter in target orbit at rendezvous

X_{24} target 24-hr orbit

$t_{f2} = 28340$ sec

$$M_{f2} = \frac{2\pi t_{f2}}{\tau} = 2.086592$$

From Fig. 1

$E_K \approx 2.46$ rad

$$E_{K+1} = \frac{e(\sin E_K - E_K\cos E_K) + M}{1 - e\cos E_K}$$

$= 2.457386$ rad $= 140.7984°$

$$\theta_{f2} = 2\tan^{-1}\left[\sqrt{\frac{1+e}{1-e}}\ \tan\frac{E_{f2}}{2}\right] = 160.3768°$$

$$\Delta a = \frac{2(1+e\cos\theta_{f1})\Delta r_1}{(1-e^2)^2} + 2\sqrt{\frac{a^3(1+2e\cos\theta_{f1}+e^2)}{\mu(1-e^2)}}\Delta V_1$$

$$= (30.1577 + 3.49074\,\Delta V_1) \times 10^4 \text{ (ft)}$$

where ΔV_1 is expressed in feet per second.

$$\Delta e = \frac{(e + \cos\theta_{f1})(1 + e\cos\theta_{f1})\,\Delta r_1}{a(1 - e^2)^2} + 2(e + \cos\theta_{f1})\sqrt{\frac{a(1-e^2)}{\mu(1 + 2e\cos\theta + e^2)}}\,\Delta V_1 + \frac{(1 - e^2)\sin\theta_{f1}\,\Delta\gamma}{1 + e\cos\theta_{f1}}$$

$$= \left[2.08560 + 0.482328\,\Delta V_1 + 7261.03\,\Delta\gamma\right] \times 10^{-4}$$

$$\Delta\omega = \frac{\sin\theta_{f1}(1 + e\cos\theta_{f1})\,\Delta r_1}{ae(1 - e^2)} + \frac{2\sin\theta}{e}\sqrt{\frac{a(1-e^2)}{\mu(1 + 2e\cos\theta_{f1} + e^2)}}\,\Delta V_1 - \left[2 + \frac{(1 - e^2)\cos\theta_{f1}}{e(1 + e\cos\theta_{f1})}\right]\Delta\gamma$$

$$= (12.80025 + 2.396265\,\Delta V_1 - 16188.96\,\Delta\gamma_1) \times 10^{-4}$$

$$\Delta t_p = \sqrt{\frac{a^3}{\mu}}\left\{\frac{(1-e^2)^{3/2}}{(1+e\cos\theta_{f1})^2}\left[\Delta\omega - \Delta\phi_1 + \frac{\sin\theta_{f1}(2+e\cos\theta_{f1})\,\Delta e}{1 - e^2}\right] - \frac{3M\Delta a}{2a}\right\}$$

$$\Delta t_p = \left[1.016824(\Delta\omega - \Delta\phi_1) + 2.832749\,\Delta e\right] - 0.452128 \times 10^{-8}\,\Delta a \times 10^4$$

$$= -190.165412 + 2.224632\,\Delta V_1 + 4107.37\,\Delta\gamma_1$$

Now since it is desired to rendezvous at θ_{f2}, it is known that $\Delta\phi_2 = \Delta r_2 = 0$. Re-evaluating the equations for $\Delta\phi$ and Δr at θ_{f2} and equating them to zero yields

$$\Delta\phi_2 = \Delta\omega - \frac{(1+e\cos\theta_{f2})^2}{(1-e^2)^{3/2}}\left[\sqrt{\frac{\mu}{a^3}}\,\Delta t_p + \frac{3M\Delta a}{2a}\right] + \frac{\sin\theta_{f2}(2 + e\cos\theta_{f2})\,\Delta e}{1 - e^2}$$

$$0 = \Delta\omega - 0.262335 \times 10^{-4}\,\Delta t_p - 0.806135 \times 10^{-8}\,\Delta a + 0.770742\,\Delta e$$

$$\Delta r_2 = \left[\frac{1 - e^2}{1 + e\cos\theta_{f2}} - \frac{3Me\sin\theta_{f2}}{2(1-e^2)^{1/2}}\right]\Delta a - a\cos\theta_{f2}\,\Delta e - \sqrt{\frac{\mu}{a}}\,\frac{e\sin\theta_{f2}\,\Delta t_p}{(1-e^2)^{1/2}}$$

$$0 = 0.660121\,\Delta a + 1.303016 \times 10^8\,\Delta e - 0.266530 \times 10^4\,\Delta t_p$$

Substituting for Δa, Δe, $\Delta\omega$ and Δt_p their equivalents in terms of ΔV_1 and $\Delta\gamma_1$ yields

$$0.629591\,\Delta V + 11670.08\,\Delta\gamma = 39.983576$$

$$2.33986\,\Delta V + 8366.51\,\Delta\gamma = -73.310088$$

Solving these equations simultaneously produces

$$\Delta V_1 = -53.998 \text{ fps} = -16.459 \text{ m/sec}$$

$$\Delta\gamma_1 = 0.00634 \text{ rad} = 0.3632°$$

These values of ΔV_1 and $\Delta\gamma_1$ are relative to those of the target vehicle at point one. The solution for the required maneuver follows:

$$V_{t1} = V_{f1} + \Delta V = 12786 \text{ fps} = 3897.2 \text{ m/sec}$$

$$V'_{t1} = 8775.5 \text{ fps} = 2674.8 \text{ m/sec}$$

$$\Delta\gamma = (\gamma_{f1} + \Delta\gamma_1) - \gamma'_{t1}$$

$$\gamma_{f1} = \tan^{-1}\left[\frac{e_f\sin\theta_{f1}}{1 + e_f\cos\theta_{f1}}\right] = 36.012°$$

$$\Delta\gamma = 0.3712°$$

The law of cosines yields the required pulse

$$\Delta V_1^2 = (V'_{t1})^2 + (V_{t1})^2 - 2V'_{t1}\,V_{t1}\cos\Delta\gamma$$

$$= 4011 \text{ fps} = 1223 \text{ m/sec}$$

This pulse represents half of the total maneuver. A second pulse is required at the point at which the two vehicles finally close. This second pulse must be sufficient to turn the shuttle vehicle and supplement its velocity vector. The laws of sines and cosines and the energy equation must be employed to define this second pulse.

$$r_{f2} = \frac{p}{1 + e\cos\theta_{f2}} = \frac{(r_{f1}\,V_{f1}\cos\gamma_{f1})^2}{\mu(1 + e_f\cos\theta_{f1})}$$

$$= 2.046322 \times 10^8 \text{ ft} = 62371.9 \text{ km}$$

$$V_{f2} = \sqrt{\mu\left(\frac{2}{r_2} - \frac{1}{a_f}\right)} = 5985.4 \text{ fps} = 1824.3 \text{ m/sec}$$

$$V_{t2} = \sqrt{\mu\left(\frac{2}{r_2} - \frac{1}{a_f + \Delta a}\right)} = 5886.3 \text{ fps} = 1794.1 \text{ m/sec}$$

$$\gamma_{f2} = \frac{e_f \sin \theta_{f2}}{1 + e_f \cos \theta_{f2}} = 26.4495°$$

$$\gamma_{t2} = \frac{(e_f + \Delta e) \sin (\theta_{f2} + \Delta\omega)}{1 + (e_f + \Delta e) \cos (\theta_{f2} + \Delta\omega)} = 27.7571°$$

$$\Delta\gamma_2 = 1.3076°$$

$$\Delta V_2^2 = (V_{f2})^2 + (V_{t2})^2 - 2\, V_{f2}\, V_{t2} \cos \Delta\gamma_2$$

$$= 168 \text{ fps} = 51.2 \text{ m/sec}$$

$$\Delta V_T = 4011 + 168 = 4279 \text{ fps.} = 1304 \text{ m/sec}$$

This value of ΔV_T represents the total impulse required for injection and correction of the orbits. It must not be compared to the impulse requirements for closure alone.

As was noted earlier in the discussion of this approach, the accuracy deteriorates as the deviation from the reference trajectory (in this case the target orbit from θ_{f1} to θ_{f2}) increases. The accuracy afforded by this technique as a function of the distances involved has not been determined.

In an analogous manner the differential corrections formulation presented in Chapter VI (Maneuvers) may be adapted for producing closure. The restrictions for usage are, however, roughly the same. Because this approach is discussed in detail in Chapter VI, no further discussion will be presented at this point.

6. Homing Phase Errors

Due to several error sources, errors will result in an inability to control both the transverse and the longitudinal motion of the shuttle vehicle. These sources and their effects are the subject of the following paragraphs. Particular sensors will not be discussed because of the rapid changes being made in the design and utilization of such equipments.

a. Transverse errors

Due to the effect of radar tracking noise, accelerometer error and engine shutoff uncertainty, a transverse velocity error remains at the end of the transverse correction pulses, including the final one.

Radar tracking noise arises from:

(1) Receiver thermal noise.

(2) Amplitude scintillation of the target.

(3) Angular scintillation of the target.

(4) Radar antenna servo jitter.

(5) Radar range measurement noise.

The first four sources result in a random error in the measured line-of-sight angle. This error has a nearly flat spectrum at frequencies below about 1 cps and is heavily attenuated at higher frequencies by action of the radar angle tracking loop. The standard deviations of the angular noise due to these sources are related to range as follows:

(1) Receiver noise varies with the square of range.

(2) Amplitude scintillation is invariant with range.

(3) Angular scintillation varies inversely with range.

(4) Servo jitter is invariant with range.

Since the computer accepts angular rate data, the angular noise is effectively differentiated before use. The computer then performs an arithmetic averaging of the angle rate noise over a smoothing period T. (Actually, the computer operates on H rather than ω but this is unimportant in the present discussion.) Since T is large compared to the reciprocal of angle noise bandwidth, the resulting angle rate noise after smoothing is given by

$$\omega_{RMS} = \frac{\psi_{RMS}}{T}$$

where ψ_{RMS} is the standard deviation of the total angle noise at the radar output due to all four noise sources. The error in measured transverse velocity due to radar tracking noise varies as the product of range and angle rate noise. Thus the velocity error due to radar tracking noise has the following relationship to range:

(1) Receiver noise varies with the cube of range.

(2) Amplitude scintillation varies directly with range.

(3) Angular scintillation is invariant with range.

(4) Servo jitter varies directly with range.

Figure 19 shows the transverse velocity error resulting from typical radar errors, plotted against range, with T = 10 sec.

The transverse velocity error due to radar range noise is a second order effect since the error is a product of range error and the small angular rate of the line of sight. The accelerometer error in terminating thrust has a negligible effect for a similar reason. The error due to transverse engine shutoff uncertainty is small and constant for any correction period, and is only important at the end of the last correction. Its value may be held less than 0.6 fps or 0.2 mps (3 σ) for a reasonable choice of engine thrust level.

Figure 19 shows a worst possible profile of transverse velocity during the homing phase. The correction threshold function shown has been chosen empirically and is not necessarily optimum. The 3σ noise envelope shown is just three times the value of the curve of Fig. 19. The pessimistic assumption has been made in Fig. 20 that the magnitude of the residual error at the end of each correction period is 3σ. This has been done for the purpose of sizing the propellant tanks of the homing vehicle for the worst case. The initial transverse error of 250 fps or 76 mps corresponds to a worst case for the launch guidance system.

In determining an acceptable correction threshold function it must be remembered that too high a threshold will generally result in a propellant penalty since corrections are unnecessarily delayed. Too low a threshold will result in frequent small corrections which are undesirable for several reasons, among them the fact that insufficient smoothing time is available between corrections.

Using typical numbers for a final transverse correction occurring at a range of 200 ft or 61 m a 3σ value of transverse velocity of less than 1.5 fps or 0.46 mps may be achieved, considering all sources of error.

b. Longitudinal errors

The longitudinal error analysis is quite straightforward for the system proposed. The errors in R and $\dot{R} = (-V_c)$ at the termination of any but the final longitudinal thrust period are quite unimportant, provided that the nominal closing profile (Fig. 10) has been chosen intelligently. Intelligent choice of this profile, that is, proper choice of the parameters of Eq (263) permits sufficiently long coast times, so that R and $\dot{R}$ may be adequately smoothed before the next correction begins. If this is done, errors in the radar measurement of r and $\dot{r}$ occurring at the beginning of a prior correction pulse, as well as accelerometer error, thrust acceleration uncertainty and thrust shutoff uncertainty occurring during the prior correction pulse, only serve to alter the range at which the subsequent correction begins (that is, lengthen or shorten the coast period before the next correction). No accumulation of error results.

The profile is also chosen so that the final correction in close velocity is small and begins at very close range. The terminal error in r and $\dot{r}$ results from the following sources:

(1) Radar measurement error of r at initiation of final longitudinal correction.

(2) Radar measurement error of $\dot{r}$ at initiation of final longitudinal correction.

(3) Accelerometer error.

(4) Thrust acceleration uncertainty (uncertainty in predicted a_i).

(5) Thrust shutoff uncertainty.

Items (1) and (4) produce only a terminal range error. Items (2), (3) and (5) are primarily responsible for a terminal closing velocity error. For a small final correction, the terminal range error is primarily due to item (1), and for a good radar is surely less than 50 ft or 15 m (3σ). The 3σ terminal closing velocity error due to item (2) is about 1 to 2 fps or 0.3 to 0.6 mps for a good radar. The 3σ error due to item (3) may be held to less than 0.4 fps or 0.12 mps with almost any decent accelerometer. The 3σ error due to item (5) may be held to less than 1 fps or 0.3 mps by proper choice of longitudinal engine size. Thus, the total 3σ error in terminal closing velocity is no more than 2.25 fps or 0.686 mps.

The total terminal velocity, including transverse velocity, is therefore no more than 2.7 fps or 0.82 mps (3σ). This velocity defines the quality of rendezvous obtainable with the vehicle described. If desired, a vernier system could be incorporated on the vehicle to effect either a soft contact with the target, or else a standoff position with respect to the target (Ref. 32).

D. REFERENCES

1. Petersen, N. V., Swanson, R. S., "Rendezvous in Space," Aerospace Engineering, Vol. 19, No. 5, May 1960.

2. Swanson, R. S. and Petersen, N. V., "Summary Report of Rendezvous Compatible Orbits," (ASG-TM-61-10), Northrop Corp., Norair Division, 1961.

3. Gedeon, G. S., et al., "Flight Performance Manual for Orbital Operations," Norair Division of Northrop Corp., Report NOR 61-208, September 1961.

4. Hord, R. A., "Relative Motion in the Terminal Phase of Interception of a Satellite or a Ballistic Missile," NACA TN 4399, September 1958.

5. Gilbert, E. O., "Orbit Control and Analysis Techniques for Equatorial 24-Hour Satellites," STL/TN-60-0000-27149, Space Technology Laboratories, August 1960.

6. Seifert, H. S., "Space Technology," John Wiley and Sons, 1959.

7. Clohessy, W. H., and Wiltshire, R. S., "Terminal Guidance System for Satellite Rendezvous," Journal of the Aerospace Sciences, Vol. 27, No. 9, September 1960.

8. Wheelon, A. D., "Free Flight of a Ballistic Missile," Space Technology Laboratories, Inc.

9. Anonymous, "The Rendezvous Maneuver," Chapter 4 of Flight Performance Handbook for Orbital Operations, STL (Redondo Beach), September 1961.

10. Passera, A. L., "Conditional-Switching Terminal Guidance (A Terminal Guidance Technique for Satellite Rendezvous)," IRE Transactions on Aeronautical and Navigational Electronics, Vol. ANE-7, No. 4, December 1960.

11. Nason, M. L., "Terminal Guidance Technique for Satellite Interception Utilizing a Constant Thrust Rocket Motor," ARS Journal, Vol. 30, No. 9, September 1960.

12. Bellman, Richard, "Dynamic Programming," Princeton University Press, Princeton, New Jersey, p 18, 1957.

13. Felleman, P., and Sears, N., "A Guidance Technique for Achieving Satellite Rendezvous," Aerospace Engineering, Vol. 19, May 1960.

14. Sears, N., and Felleman, P., "Continuously Powered Terminal Maneuver for Satellite Rendezvous," ARS Journal, Vol. 30, No. 8, August 1960.

15. Sears, N., and Felleman, P., "Terminal Guidance for a Satellite Rendezvous," ARS Preprint 778-59, 1959.

16. MIT Instrumentation Laboratory Reports, not reviewed here because of classification.

(a) "Satellite Rendezvous Guidance System," Report R-257, October 1959. SECRET

(b) "Satellite Rendezvous Guidance System," Study Report R-260, June 1960. SECRET

(c) "Satellite Rendezvous Guidance System," Study Report R-289, September 1960. SECRET

(d) "Space Mission Navigation and Guidance Techniques," Report R-234, March 1959. SECRET

17. Blum, M., "On the Mean Square Noise Power of a Linear Discrete Filter Operating on Polynomial Plus White Noise Input," IRE Transaction on Information Theory, December 1957.

18. Ling, Donald P., "Radio-Inertial Guidance," part of Space Technology edited by H. Seifert, John Wiley and Sons, New York, 1959, pp 25 to 108, 25-18.

19. Wiener, N., "The Extrapolation, Interpolation and Smoothing of Stationary Time Series," John Wiley and Sons, New York, 1949.

20. Bode, H. W., and Shannon, C. E., "A Simplified Derivation of Linear Least Square Smoothing and Prediction Theory," Proc IRE, 38, pp 417 to 425, 1950.

21. Darlington, S., "Linear Least Squares Smoothing and Prediction," BSTJ, 37, pp 1221 to 1294, 1958.

22. Bendat, J. S., "Optimum Filters for Independent Measurements of Two Related Perturbed Messages," IRE Trans Prof Group Circuit Theory, CT-4, pp 14 to 19, 1957.

23. Laning, J. H., and Battin, R. H., "Random Processes in Automatic Control," McGraw-Hill, New York, 1956.

24. Tukey, J. W., and Blackman, R. B., "The Measurement of Power Spectra from the Point of View of the Communications Engineer," Part I, BSTJ, 37, pp 185 to 282 (1958); Part 2, BSTJ, 37, pp 485 to 569 (1958).

25. Aseltine, J. A., "Transform Method in Linear System Analysis," McGraw-Hill Book Co., Inc., New York, 1958.

26. Van Valkenburg, M. E., "Introduction to Modern Network Synthesis," Wiley, New York, 1960.

27. Fischer, R. A., and Yates, F., "Statistical Tables for Biological, Agricultural and Medical Research," Oliver and Boyd, Edinburgh, Scotland, 1938.

28. Blum, M., "An Extension of the Minimum Mean Square Prediction Theory for Sampled Input Signals," IRE Transactions, Vol. IT-2, pp 176 to 184, September 1956.

29. Anderson, R. L., and Houseman, E. E., "Tables of Orthogonal Polynomial Values Extended to N = 104," Iowa State College of Agriculture and Mechanical Arts, Ames, Iowa, Res Bulletin 297; April 1942.

30. Allen, F. E., "The General Form of the Orthogonal Polynomials for Simple Series with Proofs of Their Simple Properties," Proc Roy Soc, Edinburgh, Vol. 50, pp 310 to 320, 1935.

31. Lawden, D. F., "Correction of Interplanetary Trajectories," Journal of the British Interplanetary Society, July 1954.

32. Schroeder, W., "A Terminal Guidance Scheme for Docking Satellites," Space Technology Laboratores, Inc., Summer 1961.

E. BIBLIOGRAPHY

Bakalyar, G.,
"Orbital Rendezvous and Point to Point Velocity Transfers," The Martin Company, Denver, Colorado, Report No. MI-59-61, November 1959.
"Continuous Thrust Rendezvous Transfers Approximately Mass Extremized (U)," The Martin Company, Denver, Colorado, Report No. R-61-22, August 1961.

Blizard, R. B., "Terminal Rendezvous Between a Ferry and a Satellite (U)," The Martin Company, Denver, Colorado, Report No. R-61-21, August 1961.

Brissenden, Roy F., and Lineberry, Edgar C., Jr., "Visual Control of Rendezvous," Aerospace Technologists, Guidance and Control Br., Aerospace Mechanics Div., Langley Research Center, NASA, IAS 30th Annual Meeting, IAS Paper No. 62-42.

Brissenden, R. F., Burton, B. B., Foudriat, E. D., and Whitten, J. B., "Analog Simulation of a Pilot-Controlled Rendezvous," NASA TN D-747, April 1961.

Brunk, W. E., and Flaherty, R. J., "Methods and Velocity Requirements for the Rendezvous of Satellites in Circumplanetary Orbits," NASA TN 81, October 1959.

Carney, T. M., "An Automatic Terminal Guidance System for Rendezvous with a Satellite," NASA TN D-923, August 1961.

Cicolani, L. S., "Trajectory Control in Rendezvous Problems Using Proportional Navigation," NASA TN D-772, April 1961.

Clohessy, W., and Wiltshire, R.,
"Problems Associated with Assembly of Multiunit Satellites in Orbit," The Martin Company, Denver, Colorado, ASME Paper No. 59-AV-25.

"Terminal Guidance System for Satellite Rendezvous," Los Angeles, California, IAS National Summer Meeting, June 1959, Paper No. 59-93. (Also, Journal of the Aerospace Sciences, Vol. 27, No. 9, September 1960.)

Duke, W. M., et al., "Error Analysis Considerations for Satellite Rendezvous," American Rocket Society, Preprint No. 1198-60, May 1960.

Eggleston, John M., "A Study of the Optimum Velocity Change to Intercept and Rendezvous," NASA TN D-1029, February 1962.

Eggleston, J. M., and Beck, H. D., "A Study of the Positions and Velocities of a Space Station and a Ferry Vehicle During Rendezvous and Return," NASA TR R-87, 1961.

Eggleston, J. M., and Dunning, R. S., "Analytical Evaluation of a Method of Midcourse Guidance for Rendezvous with Earth Satellites," NASA TN D-883, June 1961.

Faulkner, F. D.,
"Complete Solution to a Simple Rendezvous Problem," Monterey, California, Naval Postgraduate School, July 1960.
"Optimum Interception of a Ballistic Missile at Intermediate Range," Naval Postgraduate School, Res Paper 29, October 1961.

Feileman, P. G., and Sears, N. E., Jr., "A Guidance Technique for Achieving Rendezvous," Aerospace Engineering, Vol. 19, May 1960, pp 76 to 77.

Garber, T. B., "Ascent Guidance for Satellite Rendezvous," Aerospace Engineering, Vol. 19, No. 5, May 1960.

Grubin, C., "Docking Dynamics for Rigid-Body Spacecraft," Inst Aerospace Sci Paper 62-43, January 1962.

Heiss, W. H., Macek, W. M., Price, R. C., and Stark, E. W., "Space Rendezvous Terminal Sensors," National Aerospace Electronics Conference, Dayton, Ohio, Proceedings, 8 to 10 May 1961 (NAECON, Dayton, Ohio, 1961), pp 64 to 75.

Hord, R. A., "Relative Motion in the Terminal Phase of Interception of a Satellite or Ballistic Missile," NASA TN 4399, September 1958.

Hord, R. A., and Dürling, B. J., "Analysis of a Linear System for Variable-Thrust Control in the Terminal Phase of Rendezvous," NASA TN D-953, September 1961.

Hornby, H., "An Analytical Study of Orbital Rendezvous for Least Fuel and Least Energy," NASA TN D-1207, March 1962.

Jacobs, E., Morgenthaler, G., and Sevastian, R.,
"A Simplified Model for Computing Probability of Satellite Interception by a Preguided Missile," Chicago, Caywood-Schiller Associates, May 1959.
"Probability of Satellite Interception by an Air Launched Preguided Missile," ARS Journal, Vol. 31, No. 3, March 1961, pp 352 to 355.

Kamm, L. J., "SATRAC: Satellite Automatic Terminal Rendezvous and Coupling (U)," American Rocket Society, Preprint No. 1497-60, 5 to 8 December 1960.

Kaste, O., and Novak, D., "Study of Rendezvous Mission," Baltimore, Maryland, The Martin Company, Engineering Report No. ER 11522, October 1960. (Also, MLV Technical Note No. 13.)

Kidd, A. T., "Terminal Maneuvers for Satellite Ascent Rendezvous," Institute of Aerospace Sciences, Preprint No. 61-206-1900, June 1961.

Leitmann, G., "An Optimum Pursuit Problem," Journal of the Franklin Institute, Vol. 263, No. 6, June 1957, pp 499 to 503.

Levin, E., and Ward, J., "An Orbital Rendezvous Simulator," Astronautical Science Review, Vol. 1, No. 4, October to December 1959, pp 15 to 16, 21.

Levin, E., et al., "Manned Control of Orbital Rendezvous," Aerospace Engineering, Vol. 19, No. 5, May 1960.

Lindorfer, W., "Optimization of Missile Intercept Range," IAS Vehicle Systems Optimization Symposium, New York, 27 to 29 November 1961.

Lorell, J., "Velocity Increments Required to Reduce Target Miss on Coasting Trajectories," Institute of Aerospace Sciences, Preprint No. 60-30, January 1960.

Miller, D. M., "A Statistical-Mechanical Estimate of Orbital Collision Probabilities," Calif Inst Tech Jet Propulsion Lab. TR 32-211, March 1962.

Morgenthaler, G. W., "On Midcourse Guidance in Satellite Interception, II," Chicago, Caywood-Schiller Associates, January 1959. (Also Astronautica Acta, Vol. 5, No. 6, 1959, pp 328 to 346.

Munick, H., and McGill, R., "Analytical Estimates for Optimum Transfer Paths," ARS Journal, Vol. 30, No. 1, January 1960.

Nason, M. C.,
"Terminal Guidance Technique for Satellite Interception Utilizing a Constant Thrust Rocket Motor," ARS Journal, Vol. 30, No. 9, September 1960.
"Terminal Guidance and Rocket Fuel Requirements for Satellite Interception," American Rocket Society, Preprint No. 777-59, April 1959.

Niemi, N. J., "An Investigation of a Terminal Guidance System for a Satellite Rendezvous," American Rocket Society, Paper No. 1176-60, 1960.

Parker, G. H., and Daly, W. A., "Preliminary Design of a Satellite Rendezvous Vehicle," American Rocket Society, Preprint No. 1481-60, December 1960.

Petersen, N. V., "Rendezvous in Space--Effects of Launch Conditions," Aerospace Engineering, Vol. 19, May 1960.

Petersen, N. V., and Swanson, R. S., "Rendezvous Compatible Orbits," Astronautical Science Review, Vol. 1, October to December 1959, pp 13 to 14, 20.

Petersen, N. V., Swanson, R. S., and Hoover, L. R., "An Astrovehicle Rendezvous-Guidance Concept," Institute of Aerospace Sciences, Preprint No. 60-12, 1960.

Potter, N. S., "Controlled Rendezvous of Orbiting Space Stations," American Rocket Society, Preprint No. 1483-60, December 1960, also, ARS Journal, Vol. 31, No. 8, August 1961, pp 1096 to 1102.

Roberson, R. E., "Path Control for Satellite Rendezvous," American Astronautical Society, Preprint No. 60-15, January 1960. (Also, "Advances in Astronautical Sciences," Vol. 6, New York, The Macmillan Company, 1960.)

Schroeder, W., "A Terminal Guidance Scheme for Docking Satellites," ARS Preprint 1952-61, August 1961.

Sears, N. E., "Satellite-Rendezvous Guidance System (U)," Massachusetts Institute of Technology, Instrumentation Laboratory, Cambridge, Massachusetts, Report No. R-331, May 1961.

Sears, N. E., and Felleman, P. G.,
"Terminal Guidance for Satellite Rendezvous," American Rocket Society, Paper No. 778-59, April 1959.
"Continuously Powered Terminal Maneuver for Satellite Rendezvous," ARS Journal, Vol. 30, No. 8, August 1960, pp 734 to 739.

Shapiro, M.,
"Attenuated Intercept Satellite Rendezvous System," ARS Journal, Vol. 31, No. 12, December 1961, pp 1733 to 1744.
"An Attenuated Intercept Satellite Rendezvous System," Institute of Aerospace Sciences, Preprint No. 61-155-1849, June 1961.

Simon, E., Jr., "A Proposed Control System to Facilitate the Terminal Phase of Manned Rendezvous," American Rocket Society, Preprint No. 1480-60, 1960.

Skalafuris, A. J., and Schiller, D. H., "On Midcourse Guidance Problems in Satellite Interception," Chicago, Caywood-Schiller Associates, September 1958. (Also, ARS Journal, Vol. 30, pp 41 to 45, January 1960.)

Smith, R. A., "Establishing Contact Between Orbiting Vehicles," Journal of the British Interplanetary Society, Vol. 10, No. 6, November 1951, pp 295 to 299. (Also, London, 2nd International Congress on Astronautics, Symposium on Satellite Vehicles, 1951.)

Spradlin, L. W., "The Long-Time Satellite Rendezvous Trajectory," Aerospace Engineering, Vol. 19, June 1960.

Steffan, K. F., "A Satellite Rendezvous Terminal Guidance System," American Rocket Society, Preprint No. 1494-60, December 1960. (Also, ARS Journal, Vol. 31, No. 11, November 1961.)

Steinhoff, E., "Orbital Rendezvous and Guidance," Aerospace Engineering, Vol. 19, May 1960.

Straly, W. H.,
"Utilizing the Chasing Technique in Rendezvous," American Rocket Society, Preprint No. 2295-61, October 1961.
"The Phasing Technique in Rendezvous," ARS Journal, Vol. 32, No. 4, April 1962, p 620.

Swanson, R. S., and Petersen, N. V., "The Influence of Launch Conditions on the Friendly Rendezvous of Astrovehicles, American Astronautical Society, Preprint No. 59-16, August 1959. (Also, "Advances in Astronautical Sciences," New York, Plenum Press, 1960, Vol. 5.)

Swanson, R. S., Petersen, N. V., and Soule, P. W., "Station Keeping of Satellites in Rendezvous Compatible Orbits," ARS Preprint 1954-61, August 1961.

Swanson, R. S., et al., "An Astrovehicle Rendezvous Guidance Concept," Advances in Astronautical Sciences, The Macmillan Company, New York, Vol. 6, 1960.

Tempelman, W. H., "3-D Analysis of Minimum Energy Intercepts, Transfers and Rendezvous Using n Impulses," American Rocket Society, Preprint No. 1474-60, December 1960.

Townsend, G. E.,
"Satellite Rendezvous," Design Guide to Orbital Flight, McGraw-Hill Book Company, New York, 1962, Chapter 8.
"A Generalized Analytic Method of Satellite Rendezvous," The Martin Company, Baltimore, Maryland, Engineering Report No. ER 10882, October 1959.

Tsien, H. S., "Takeoff from a Satellite Orbit (radial thrust)," Jet Propulsion, Vol. 23, No. 4, July to August 1953.

Ward, J. W., and Williams, H. M., "Orbital Docking Dynamics," ARS Preprint 1953-61, August 1961.

Weber, R. J., and Pouson, N. M., "Achieving Satellite Rendezvous," ARS Journal, Vol. 29, No. 8, August 1959.

Wiltshire, R. S., and Clohessy, W. H., "Terminal Guidance for Rendezvous in Space," Astronautical Science Review, Vol. 1, No. 4, pp 9 to 10, October to December 1959.

ILLUSTRATIONS

Preceding page blank

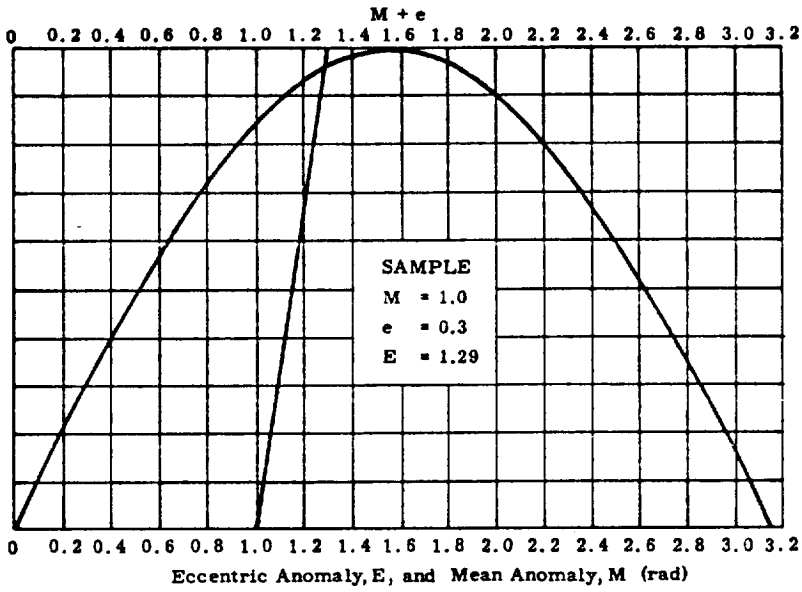

Fig. 1. Graphical Solution to Kepler's Equation for E as a Function of M and e

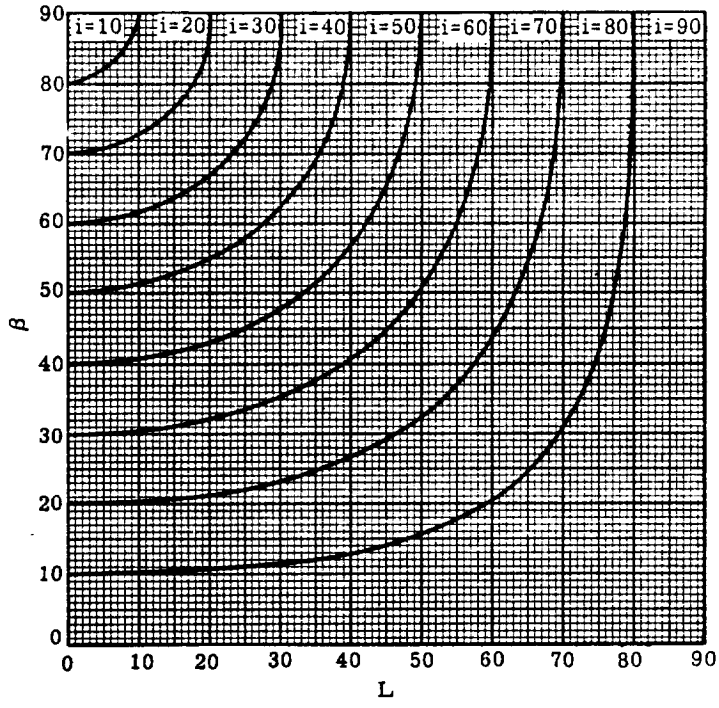

Fig. 2. Launch Azimuth as a Function of Latitude and Inclination

Preceding page blank

$i = 70°$
$L_L = 28.5°$
$L_2 = 28.5°$
$(r_a)_{24} = 42,400$ stat mi
$= 68,300$ km
$(r_p)_{24} = 10,000$ stat mi
$= 16,090$ km
$t_{ascent} = 1000$ sec

Fig. 3. Launch Site Location for Rendezvous (sample problem)

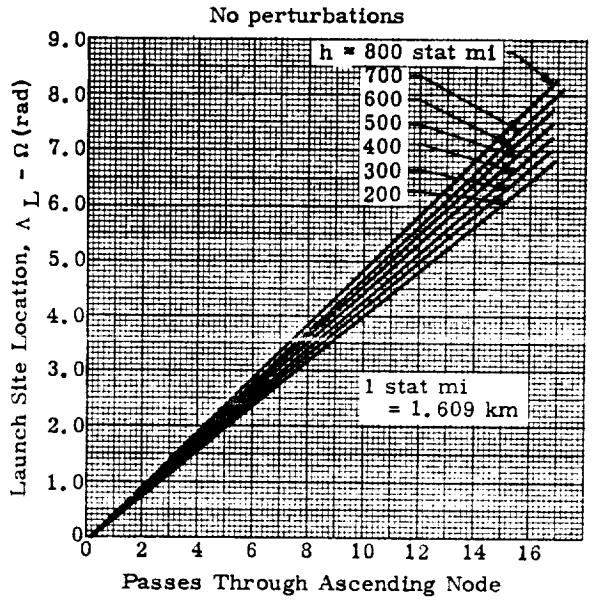

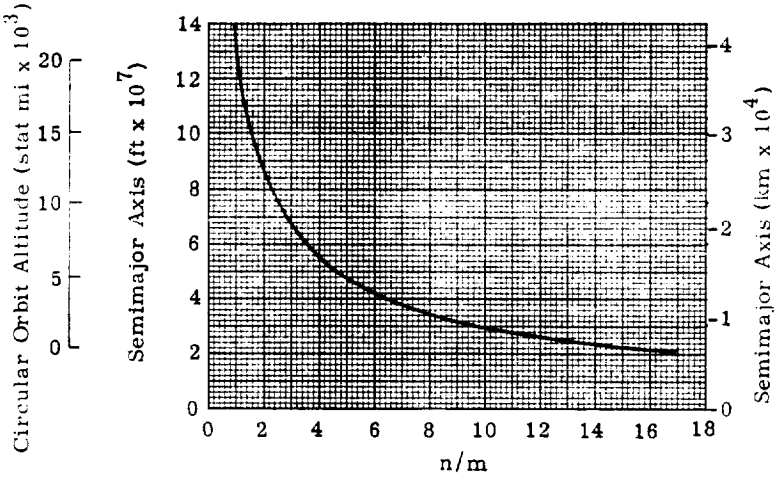

Fig. 4. Variation of Semimajor Axis with n/m (n/m = 0 to 17)

Fig. 5. Variation of Semilatus Rectum with n/m (n/m = 11 to 17)

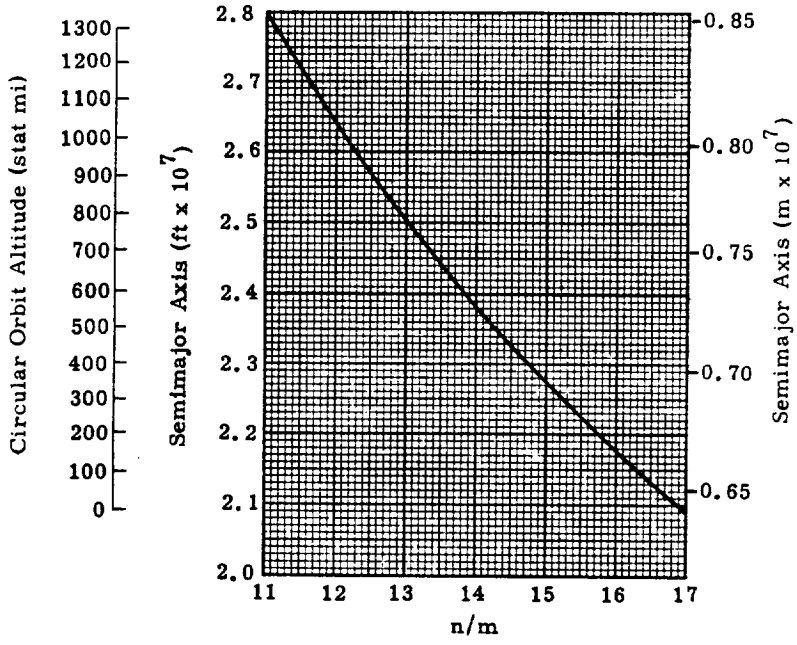

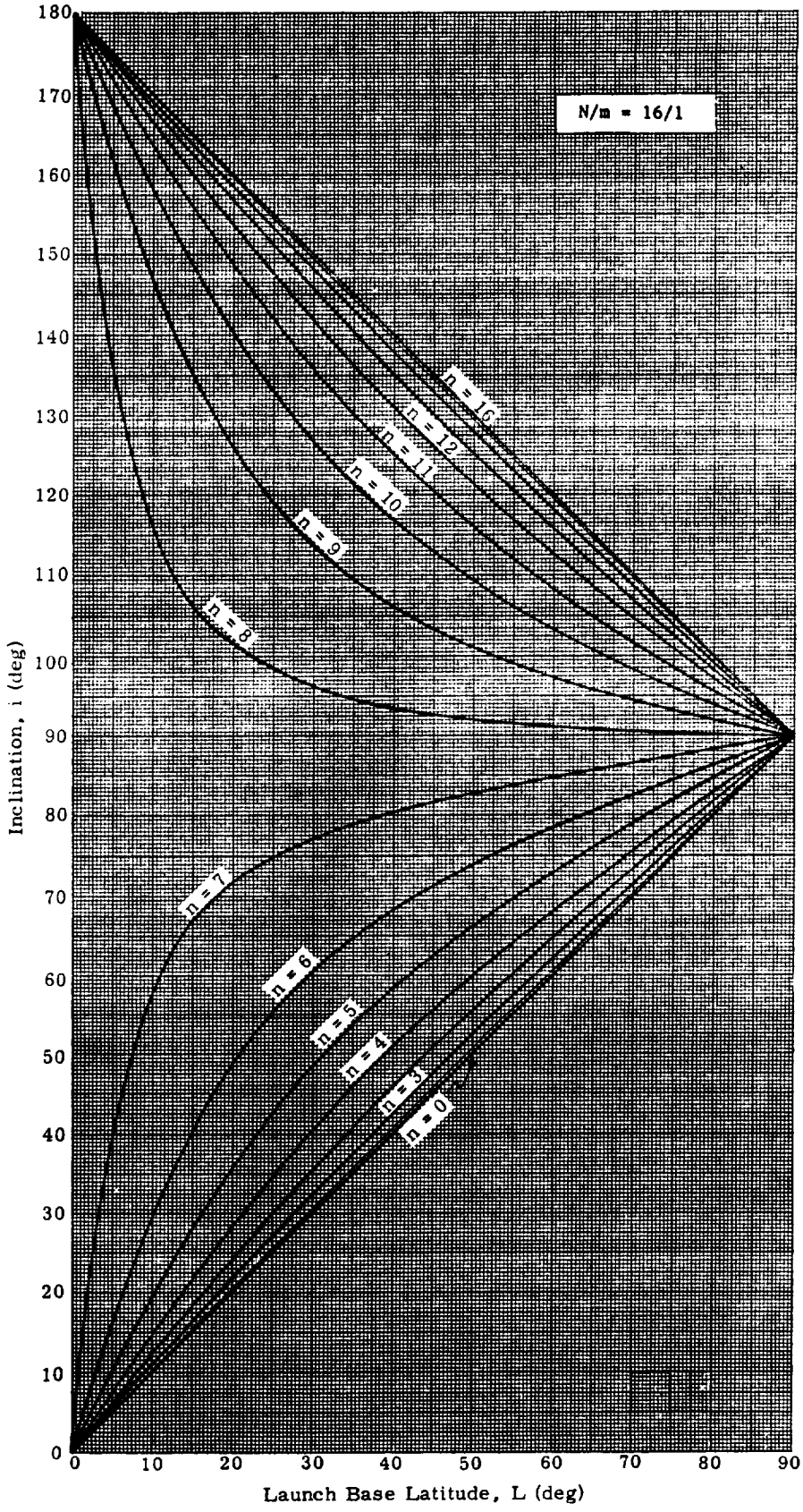

Fig. 6. Rendezvous Compatible Orbits (geometric effects)

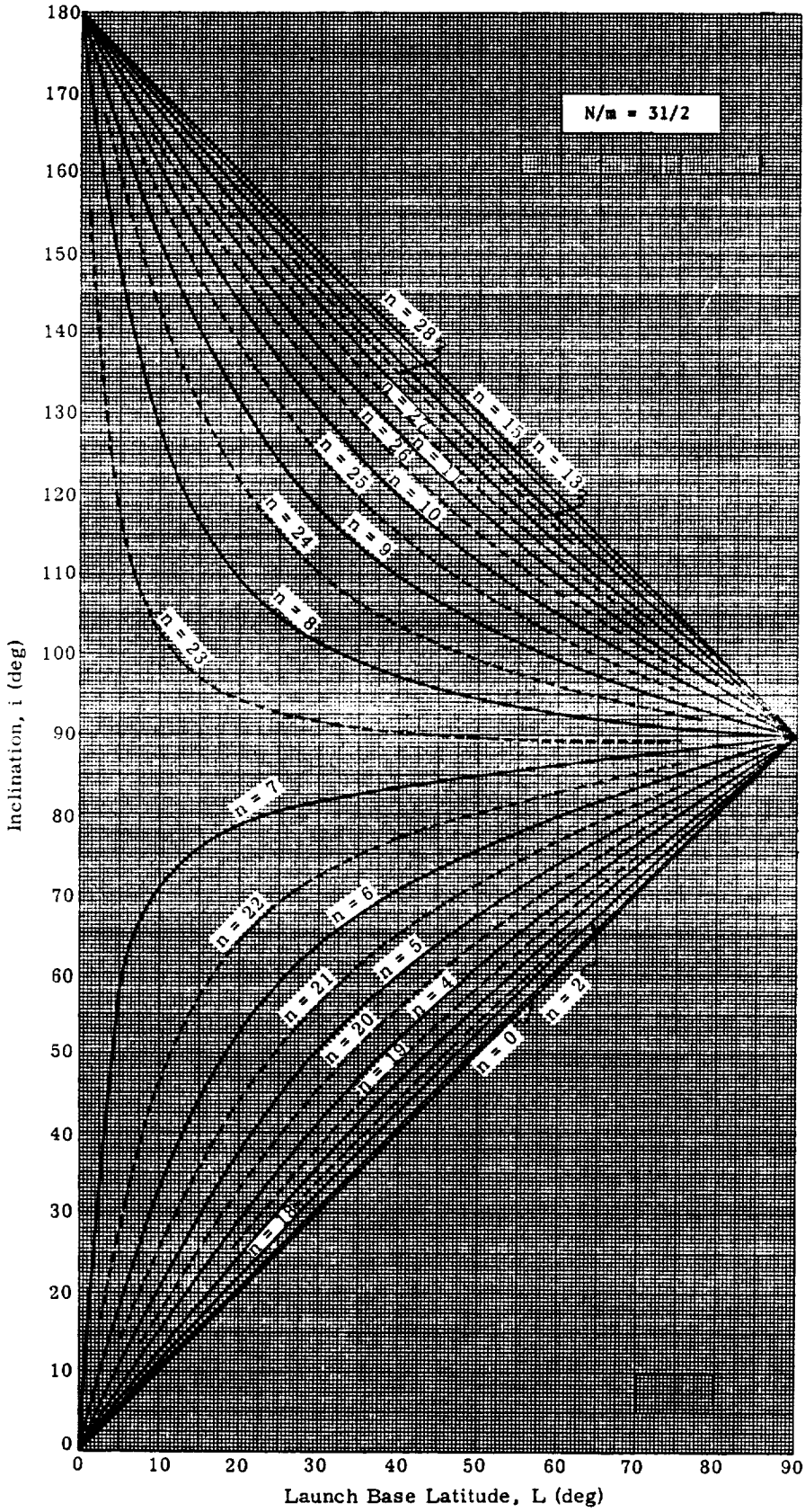

Fig. 6. Continued

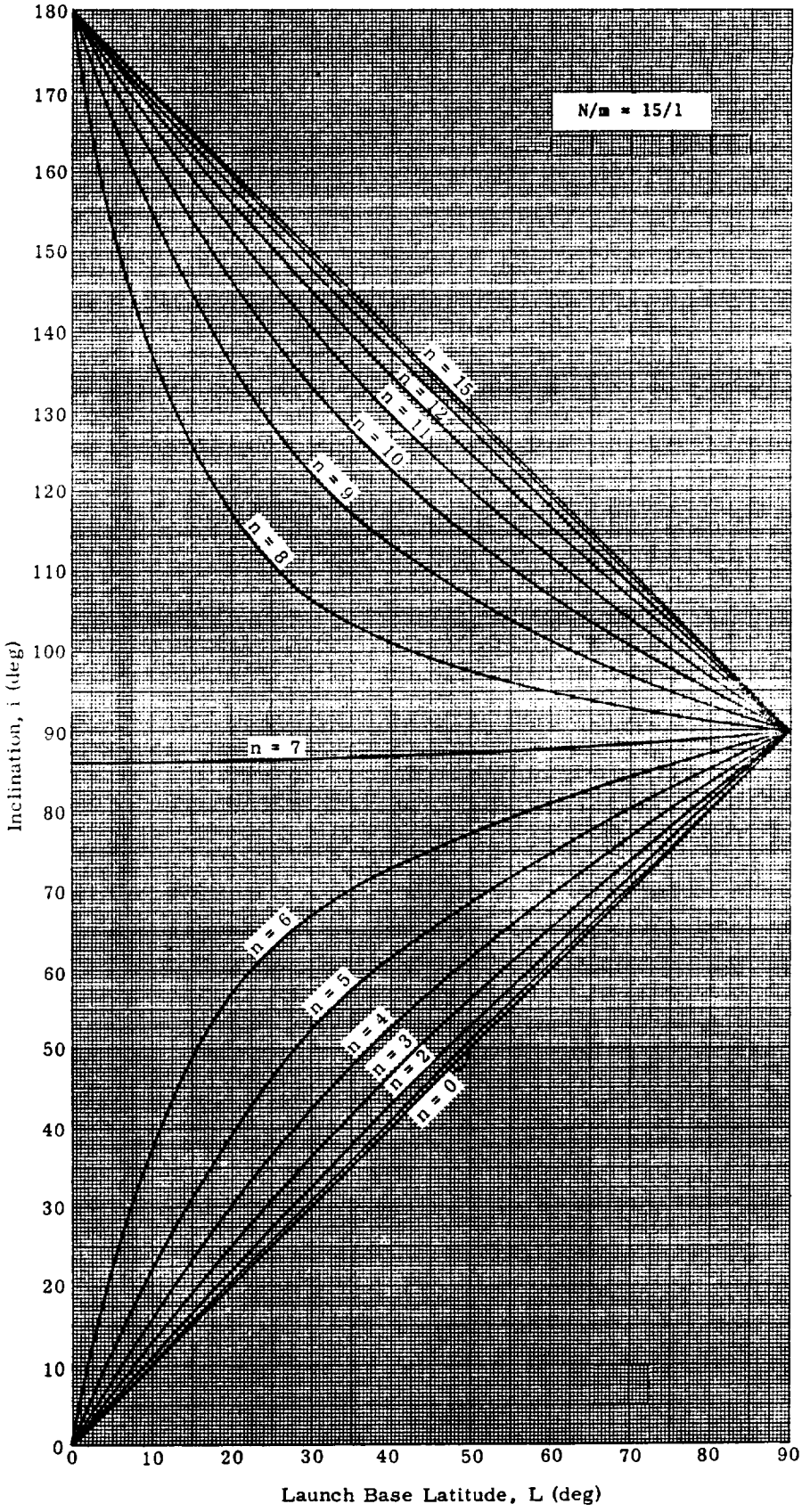

Fig. 6. Continued

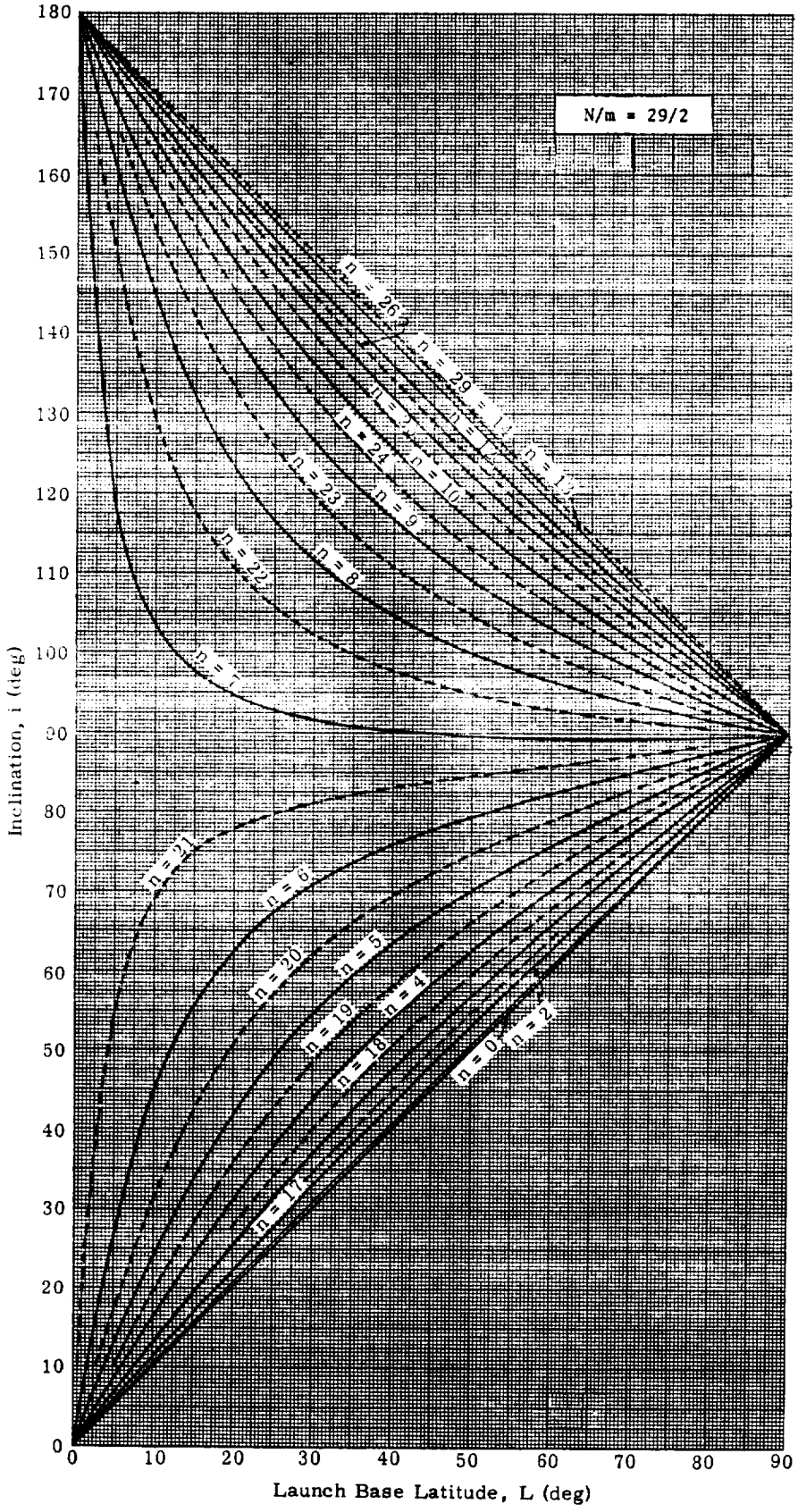

Fig. 6. Continued

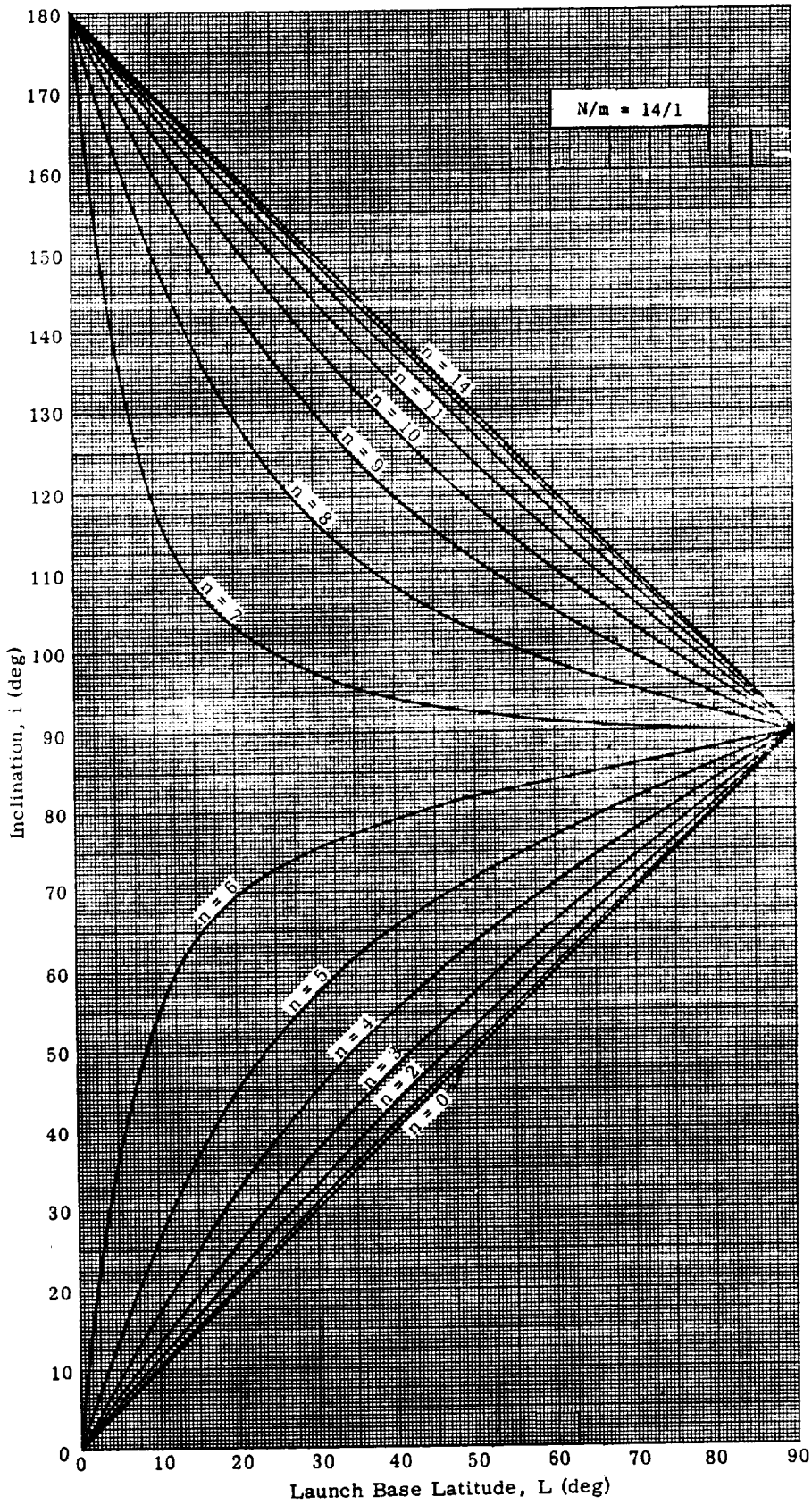

Fig. 6. Continued

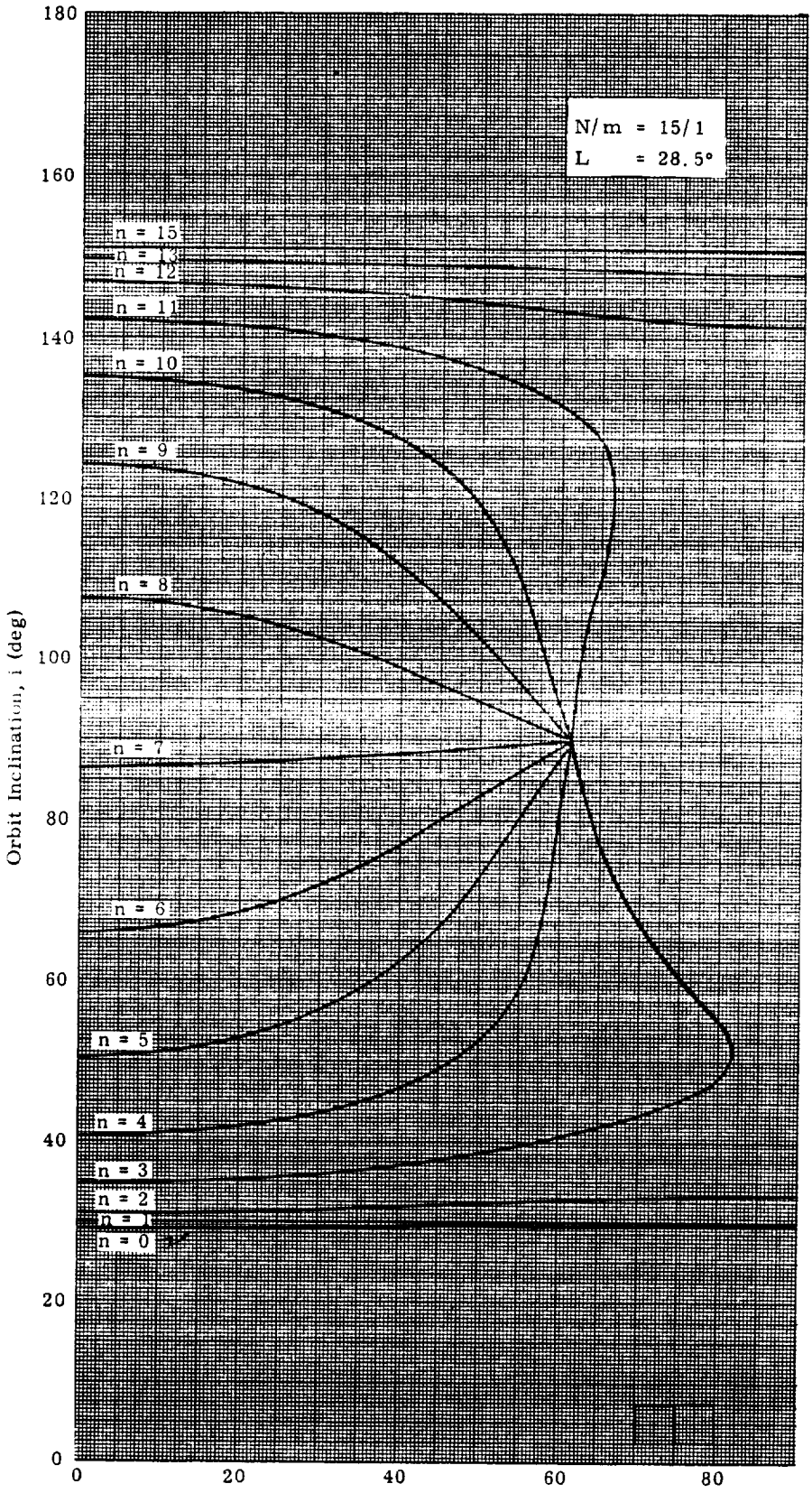

Fig. 7. Finite Burning Time Effects on Rendezvous Compatible Orbits

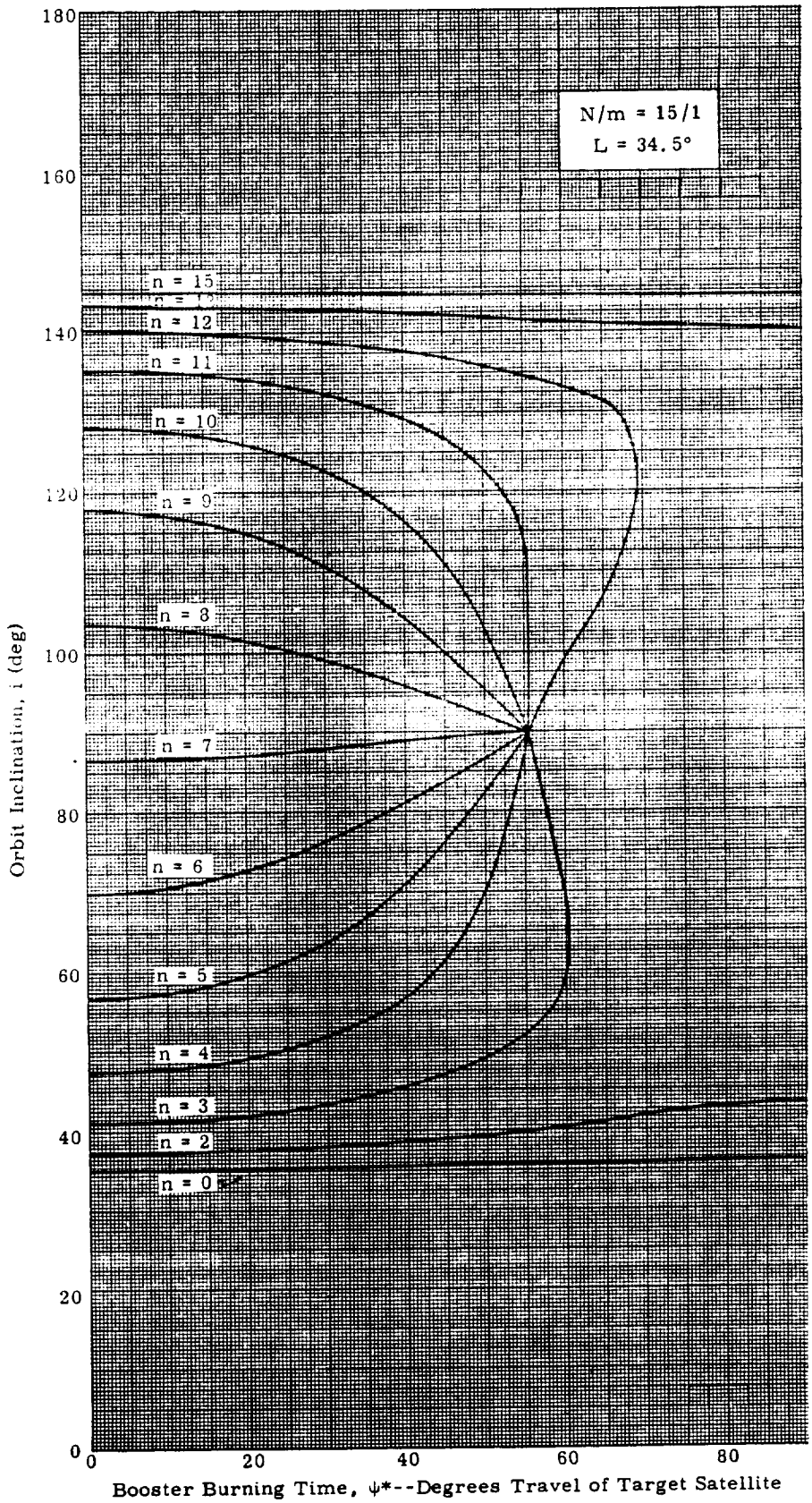

Fig. 7. Continued

The solution for the energy requirement utilized in adjusting the plane of the transfer orbit near its apogee for direct launches

$$\frac{\Delta V}{V} = \left|\beta_2 - \beta_1\right|$$

Example

$L = 40°$
$\nu = 70°$
$\nu + \Delta\Omega = 80°$

$$\frac{\Delta V}{V} = 0.73 - 0.71 = 0.02$$

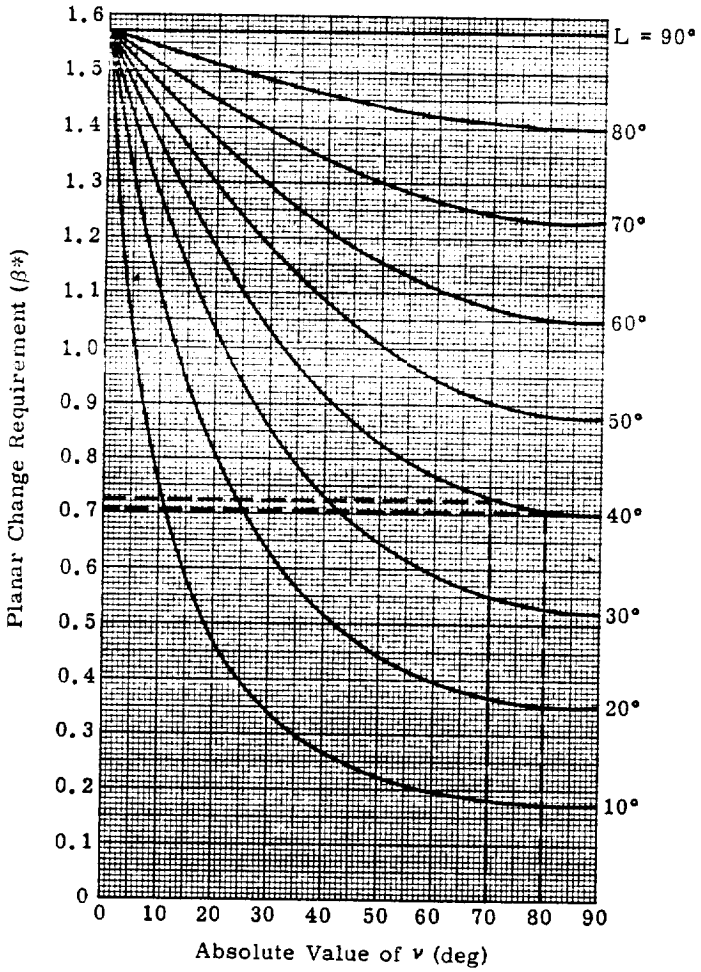

Fig. 8. Graphical Solution for $\frac{\Delta V}{V}$

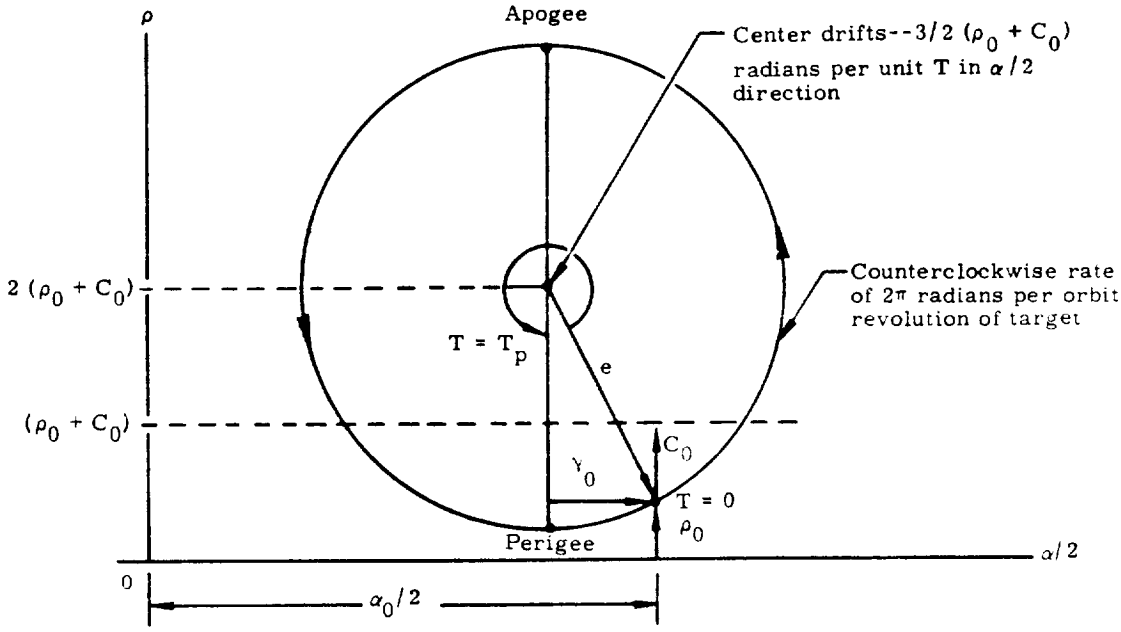

Fig. 9. Circle Diagram Generatrix of In-Plane Motion

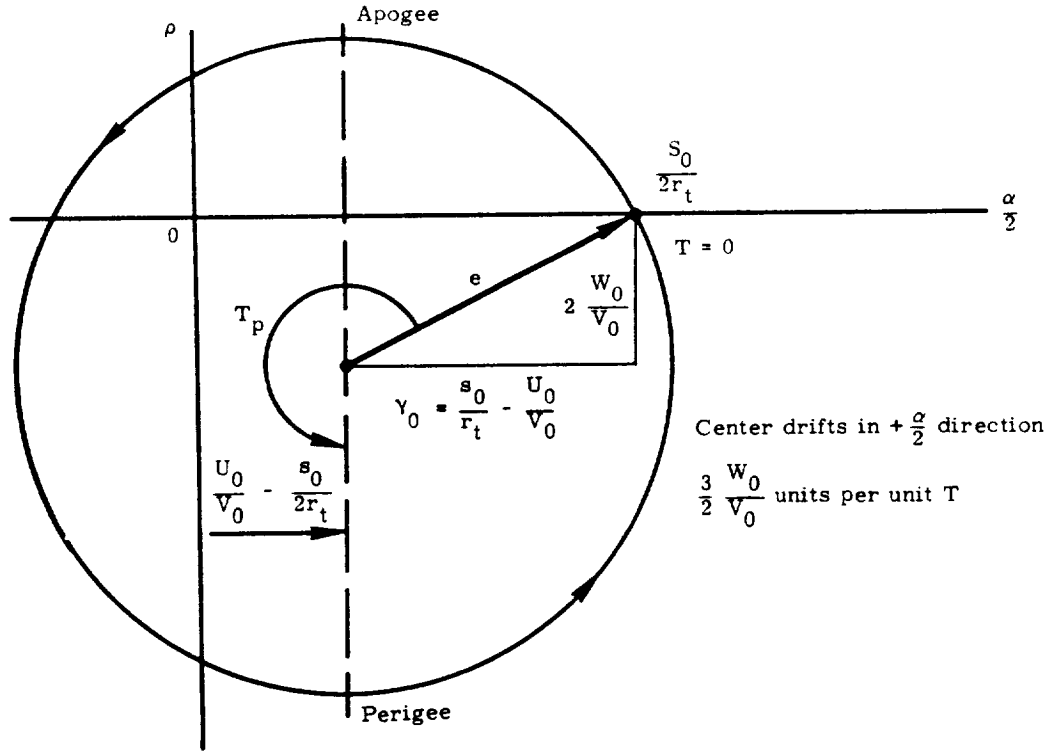

Fig. 10. In-Plane Circle Diagram at Injection

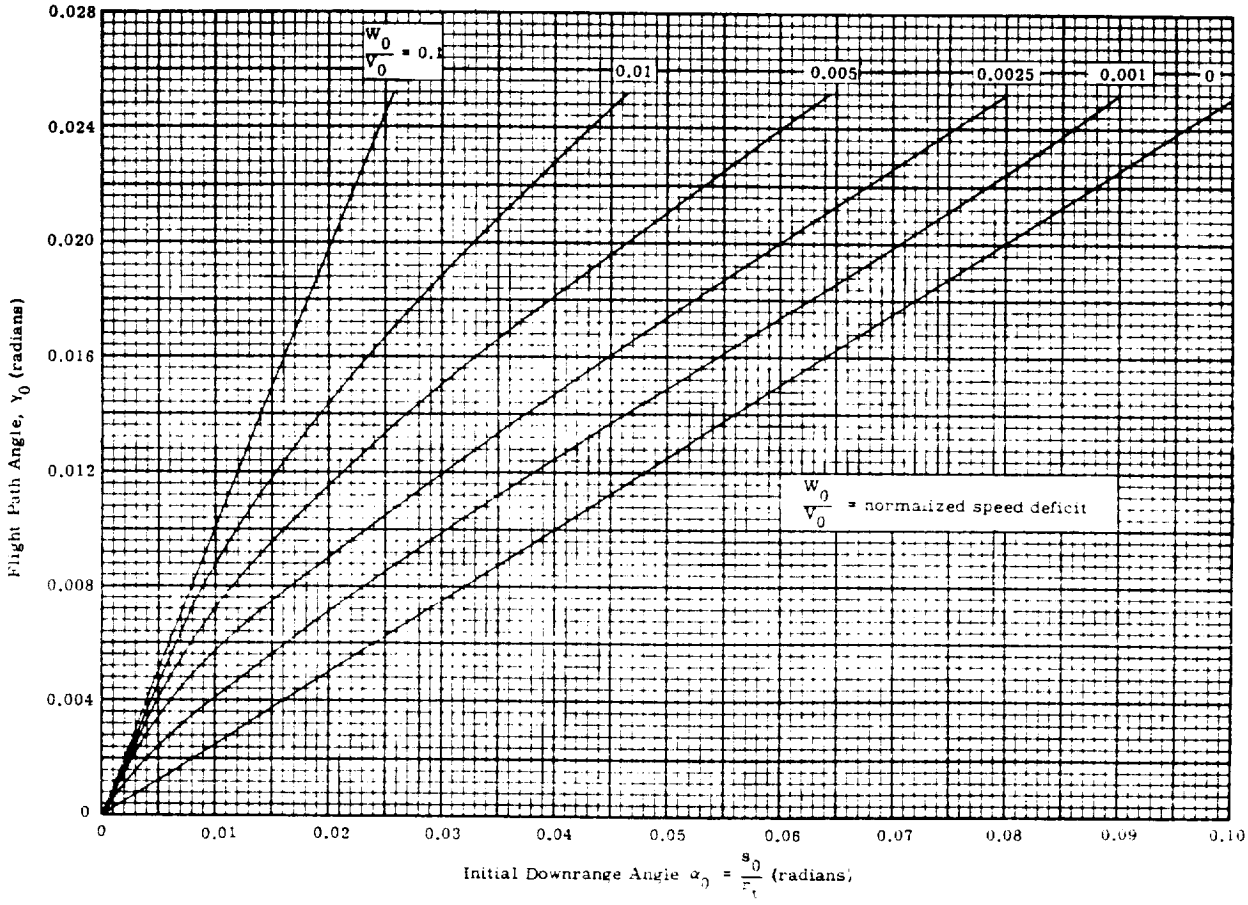

Fig. 11. Parametric Relation for Rendezvous (ρ = 0, α = 0)

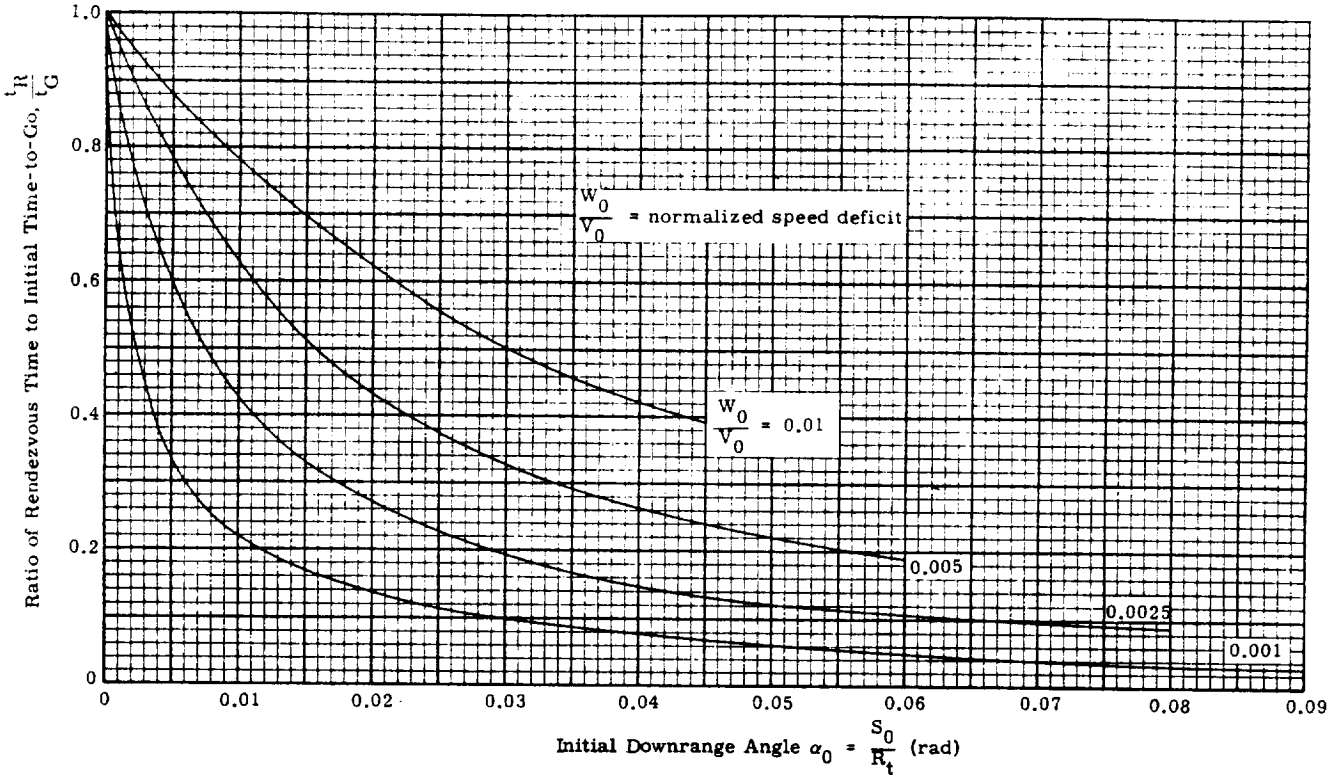

Fig. 12. Ratio of Rendezvous Time to Initial Time-to-Go Versus Initial Downrange Angle

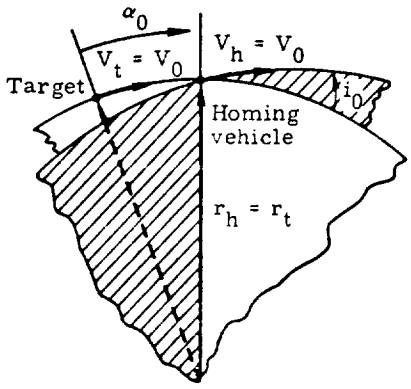

Fig. 13. Rendezvous Geometry at Nodal Crossing

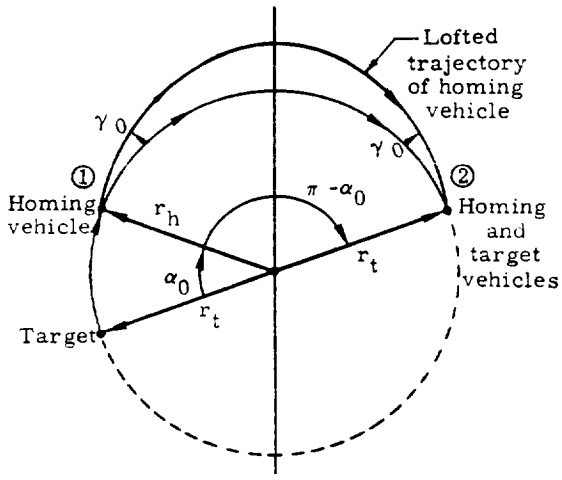

Fig. 14. Rendezvous Using Pure Loft (no period change)

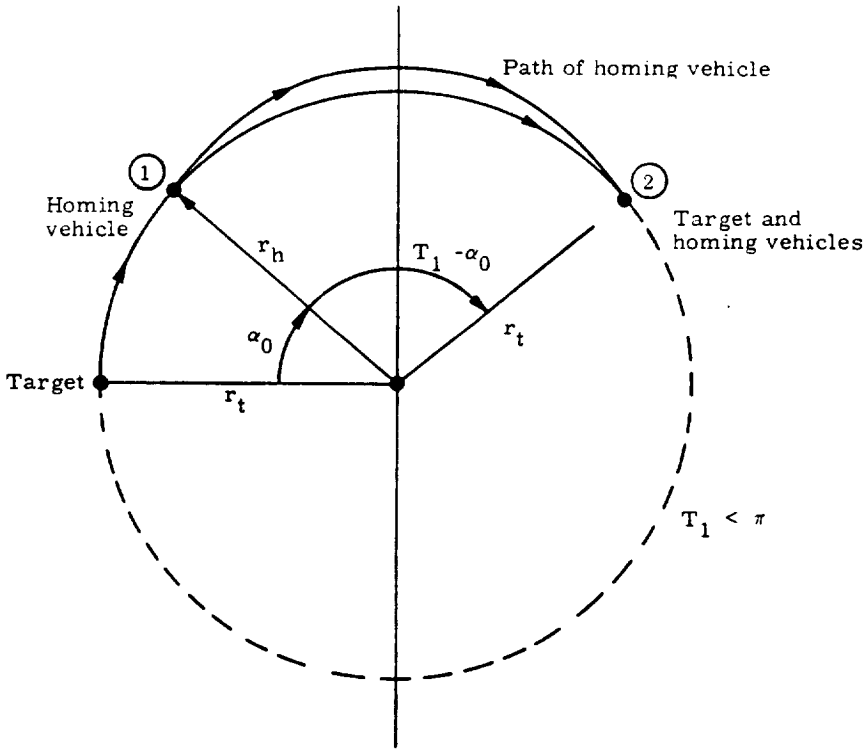

Fig. 15. Rendezvous Using Loft and Period Change

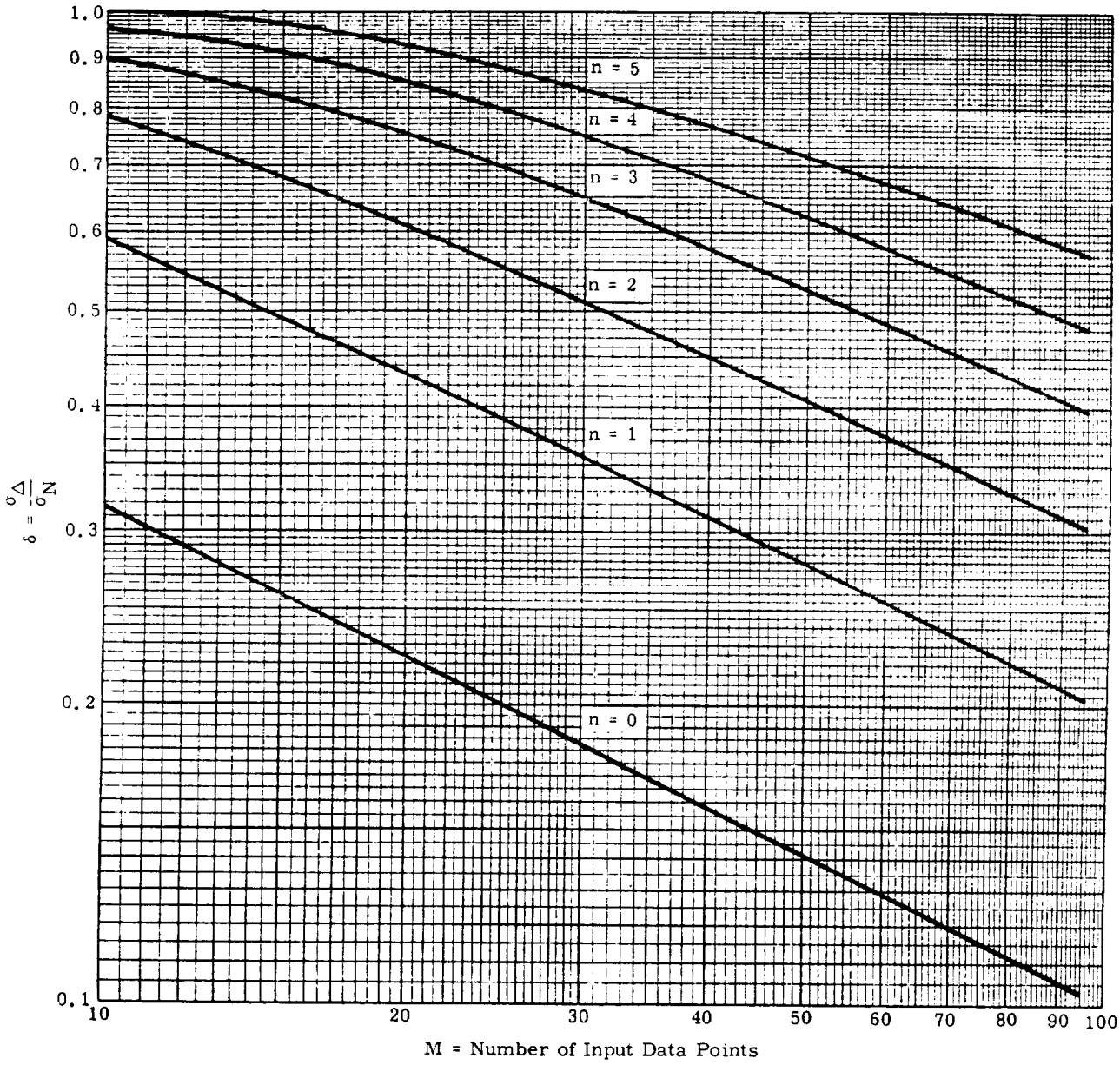

$\delta = \frac{\sigma_\Delta}{\sigma_N}$

σ_Δ = rms error output (zero-lag estimation)

σ_N = rms error of noise

n = degree of polynomial passed without error

(M - 1)T = memory span of filter

Fig. 16. Output of the Digital Filter (least squares estimate of the input with zero-lag)

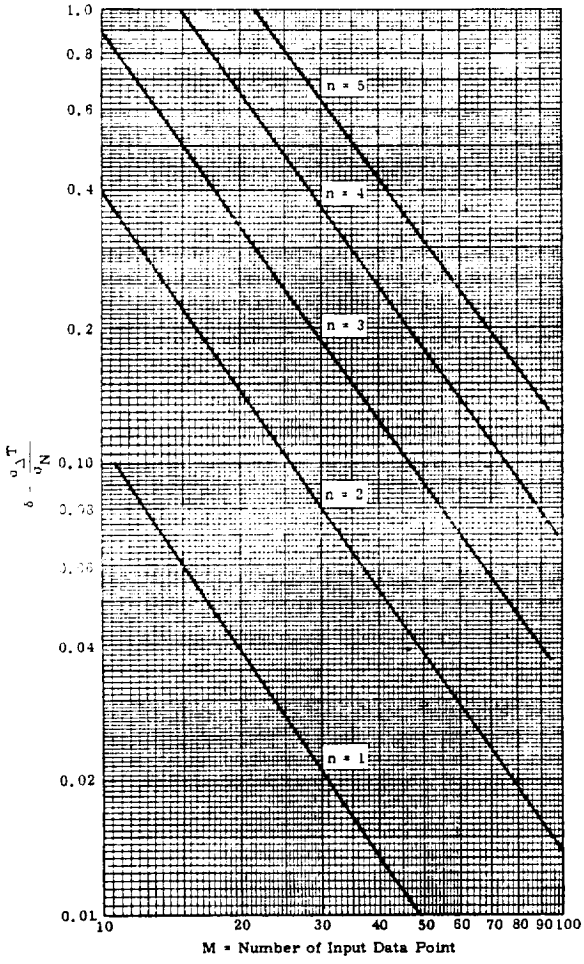

σ_Δ = rms of output

σ_N = rms of input

$\delta = \frac{\sigma_\Delta T}{\sigma_N}$

n = degree of polynomial passed by filter without error

T = interval between samples

(M - 1)T = finite memory of filter

Fig. 17. Output of the Digital Filter (least squares, zero-lag estimation of first derivative of the input)

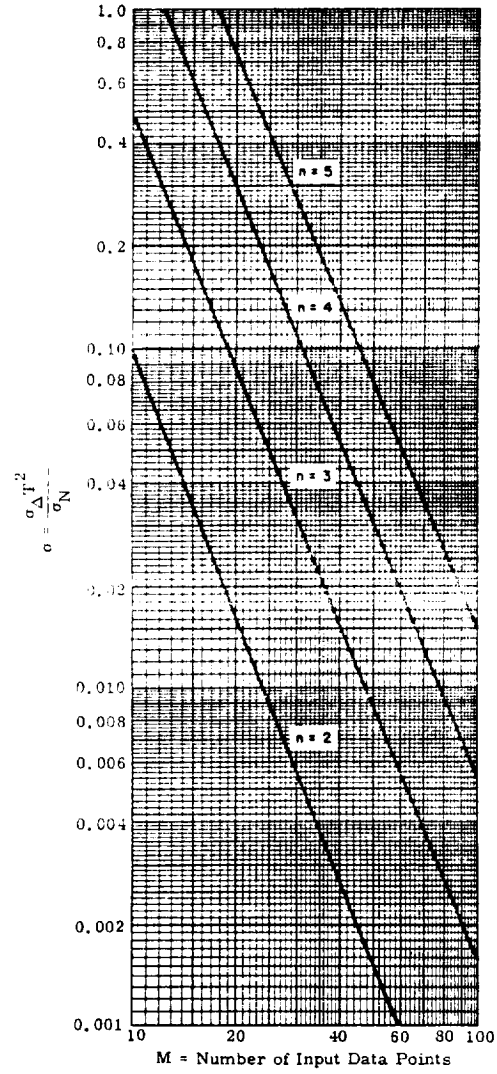

σ_Δ = rms of the output

σ_N = rms of the noise

$\delta = \frac{\sigma_\Delta T^2}{\sigma_N}$

n = degree of polynomial passed without error

T = interval between samples

(M - 1)T = finite memory of filter

Fig. 18. Output of the Digital Filter (least squares, zero-lag [a = 0] estimation of the second derivative of the input)

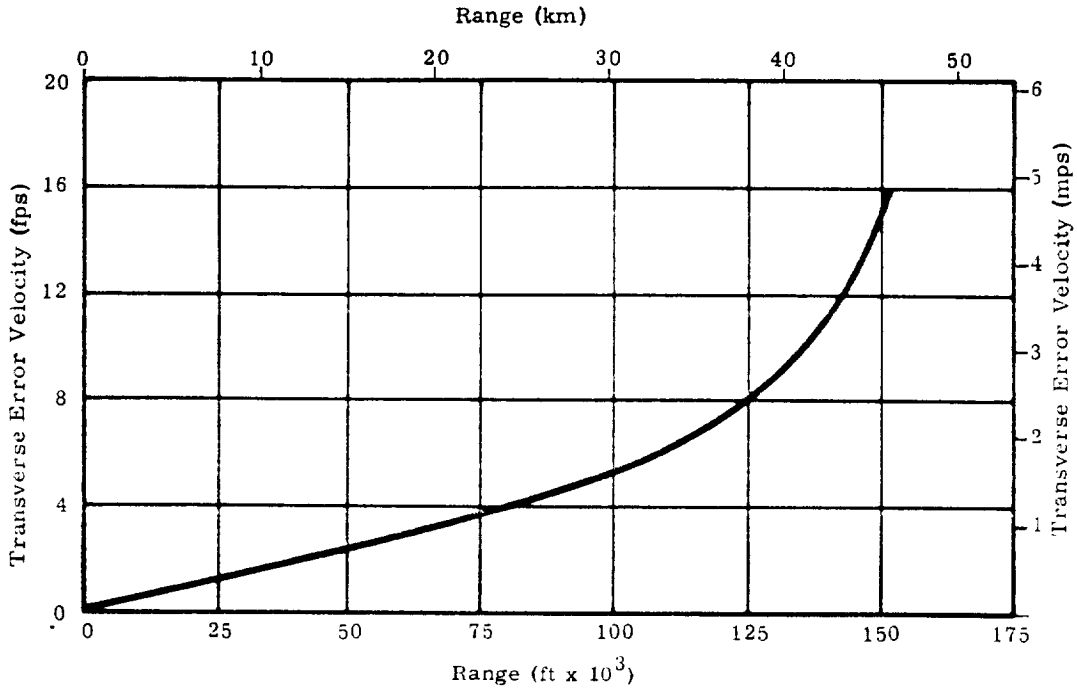

Fig. 19. RMS Residual Transverse Error Velocity

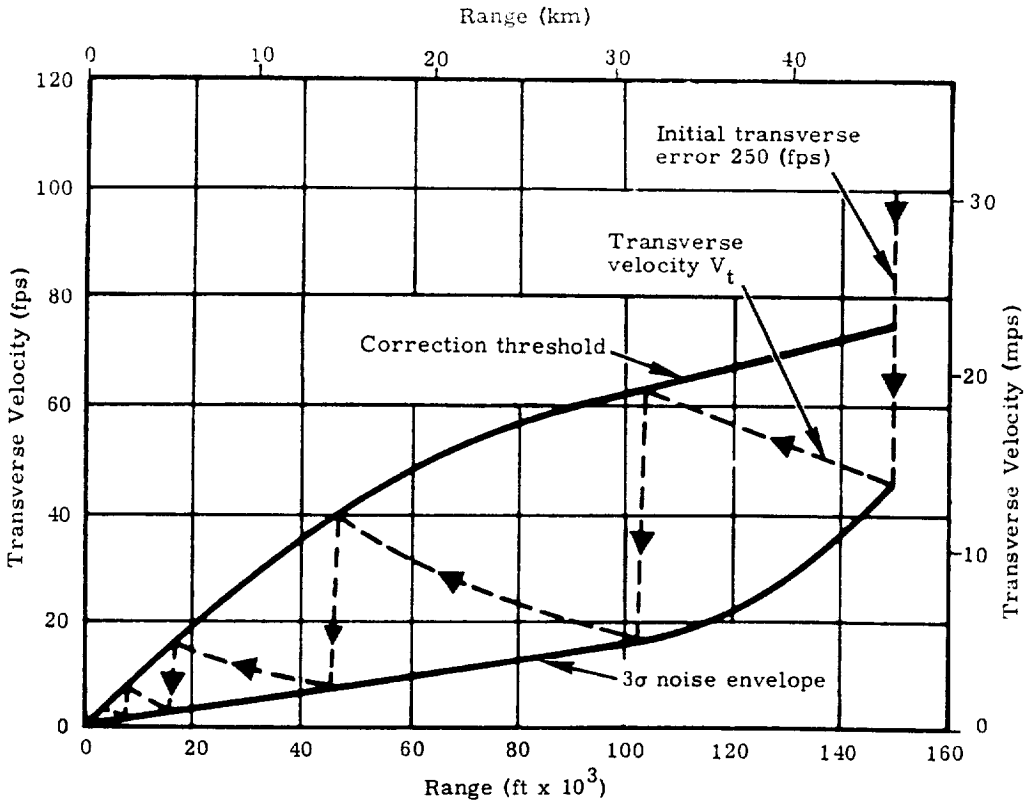

Fig. 20. Homing Profile for Extreme Errors
(1 ft = 0.3048 m)

CHAPTER VIII

ORBITAL DEPARTURE

Prepared by:

G. E. Townsend, Jr.
Martin Company (Baltimore)
Aerospace Mechanics Department
March 1963

		Page
	Symbols	VIII-1
A.	Introduction	VIII-3
B.	The Generalized Return Problem	VIII-3
C.	Planar Analysis of Departure from Low Altitude Orbits.	VIII-17
D.	Three-Dimensional Impulse Analysis for the Case of Circular Orbits	VIII-23
E.	Analysis of Orbital Departure Frequency	VIII-24
F.	Conclusions	VIII-30
G.	References	VIII-30
H.	Bibliography.	VIII-30
	Illustrations	VIII-31

LIST OF ILLUSTRATIONS

Figure	Title	Page
1	Geometry of the Return Problem.	VIII-33
2	Geometry of the Return Problem (expanded view). .	VIII-33
3a	3-D Geometry of the Return Shuttle Problem ($i \geq L_x$)	VIII-34
3b	Characteristic Angles of the Return Shuttle Trajectory	VIII-34
4a	Solution of Flight Time Equation	VIII-35
4b	Flight Time Versus Departure Angle	VIII-36
5	Critical Angle for the Return Flight-Time Solution.	VIII-37
6a	Location of the Return Shuttle in the Orbit Plane . .	VIII-37
6b	Altitude from Sea Level for the Return Shuttle . . .	VIII-38
7	Ground Track of the Return Shuttle	VIII-39
8	Flight Time Error Analysis	VIII-40
9	Error in Re-entry Parameters as Functions of Altitude and Retrorocket Mass Ratios	VIII-41
10	The Ratio of the Velocity Pulse Obtainable from a Rocket Stage to the Ideal Pulse Neglecting Finite Burning Times	VIII-42
11	Re-Entry Parameters as Functions of δ and T/W_0 .	VIII-43
12a	Re-Entry Parameters as Functions of Initial Thrust-to-Weight Ratio and Retrorocket Mass Ratio	VIII-44
12b	Re-Entry Parameters as Functions of Initial Thrust-to-Weight Ratio and Retrorocket Mass Ratio	VIII-45

LIST OF ILLUSTRATIONS (continued)

Figure	Title	Page
12c	Re-Entry Parameters as Functions of Initial Thrust-to-Weight Ratio and Retrorocket Mass Ratio	VIII-46
13	Range Attained in Descending from Re-Entry to Sea Level	VIII-47
14a	Mass Ratio Required to Exit from a 100-Stat Mi (161 km) Circular Orbit	VIII-48
14b	Mass Ratio Required to Exit from a 100-Stat Mi (161 km) Circular Orbit	VIII-48
14c	Mass Ratio Required to Exit from a 100-Stat Mi (161 km) Circular Orbit	VIII-49
15	Variations in the Re-Entry Conditions Due to Small Variations in Orbital Altitude and Velocity	VIII-50
16	Re-Entry Parameters as Functions of Initial Altitude and Retrorocket Mass Ratio	VIII-51
17	Re-Entry Parameters as Functions of Initial Orbital Altitude and Mass Ratio of the Retrorocket	VIII-52
18a	Re-Entry Parameters as Functions of Initial Orbital Velocity and Retrorocket Mass Ratio	VIII-53
18b	Re-Entry Parameters as Functions of Initial Velocity and Mass Ratio of the Retrorocket	VIII-54
18c	Re-Entry Parameters as Functions of Initial Velocity and Retrorocket Mass Ratio	VIII-55
18d	Re-Entry Parameters as Functions of Initial Velocity and Retrorocket Mass Ratio	VIII-56

LIST OF ILLUSTRATIONS (continued)

Figure	Title	Page
18e	Re-Entry Parameters as Functions of Initial Orbital Velocity and Retrorocket Mass Ratio.	VIII-57
19a	Re-Entry Parameters as Functions of ζ and γ_1 . .	VIII-58
19b	Re-Entry Parameters as Functions of ζ and γ_1 . .	VIII-59
19c	Re-Entry Parameters as Functions of ζ and γ_1 . .	VIII-60
19d	Re-Entry Parameters as Functions of ζ and γ_1 . .	VIII-61
19e	Re-Entry Parameters as Functions of ζ and γ_1 . .	VIII-62
20a	Variations in Re-Entry Position, Time and Flight Path Angle (per Second Error in t_B) with Initial Velocity and Retrorocket Mass Ratio	VIII-63
20b	Variations in Re-Entry Position, Time and Flight Path Angle (per Second Error in t_B) with Variations in Initial Velocity and Retrorocket Mass Ratio	VIII-64
20c	Variations in Re-Entry Position, Time and Flight Path Angle (per Second Error in t_B) with Variations in Initial Velocity and Retrorocket Mass Ratio	VIII-65
20d	Variations in Re-Entry Position, Time and Flight Path Angle (per Second Error in t_B) with Initial Velocity and Retrorocket Mass Ratio	VIII-66
20e	Variations in Re-Entry Position, Time and Flight Path Angle (per Second Error in t_B) with Initial Velocity and Retrorocket Mass Ratio	VIII-67

LIST OF ILLUSTRATIONS (continued)

Figure	Title	Page
21	Variations in Re-Entry Location, Time, Flight Path Angle, and Velocity with Initial Velocity as Functions of Retrorocket Mass Ratio and h_1	VIII-68
22a	Variations in Re-Entry Location, Time, Flight Path Angle and Velocity with Altitude as Functions of h_1 and Retrorocket Mass Ratio.	VIII-69
22b	Variations in Re-Entry Position, Time, Flight Path Angle and Velocity with Altitude as Functions of h_1 and Retrorocket Mass Ratio.	VIII-70
22c	Variations in Re-Entry Position, Time, Flight Path Angle and Velocity with Altitude as Functions of h_1 and Retrorocket Mass Ratio.	VIII-71
23a	Errors in the Re-Entry Parameters Due to a 1° Error in γ_1.	VIII-72
23b	Errors in the Re-Entry Parameters Due to a 1° Error in γ_1	VIII-73
23c	Errors in the Re-Entry Parameters Due to a 1° Error in γ_1	VIII-74
23d	Errors in the Re-Entry Parameters Due to a 1° Error in γ_1	VIII-75
23e	Errors in the Re-Entry Parameters Due to a 1° Error in γ_1	VIII-76
24	Optimum ΔK and γ for 3-D Departure	VIII-77
25	Optimum Central Angle and Arrival Path Angle for 3-D Departure	VIII-78
26	Optimum Central Angle and ΔK as a Function of d .	VIII-79
27	Plane Change Angle and Flight Path Angle as Functions of Mass Range Angle	VIII-80

VIII. ORBITAL DEPARTURE

Symbols

A	Reference area for C_D; right ascension (rad)
A_e	Exit area of rocket nozzle
a	Semimajor axis of the ellipse
B	Ballistic coefficient, $C_D A/2m$
D	Aerodynamic drag
D_m	Lateral maneuver distance
E	Eccentric anomaly
e	Eccentricity of the ellipse
g	Gravity at altitude
g_0	Gravity at sea level
h	Altitude above a spherical earth
I_{sp}	Specific impulse of the retrorocket
i	Orbital inclination
J_2	Coefficient of second harmonic of earths potential function 1.0823×10^{-3}
K	$\sqrt{2 - \frac{r}{a}}$
L	Aerodynamic lift; latitude
M	Mean anomaly
m	Mass of the vehicle
n	Number of revolutions; mean motion
P	Pressure
p	Semilatus rectum of ellipse
R	Radius of spherical earth
R_e	Equatorial radius of earth
r	Radius from the center of force
r_m	Mixture ratio (oxidizer/fuel)
T	Thrust
t	Time
t_B	Burning time
V_c	Circular orbital speed = $\sqrt{\mu/r}$
V	Velocity
W	Weight
W_p	Weight propellant
$\dot{W}_p$	Propellant flow rate
X	Range
$\bar{X}$ and $\bar{Y}$	Inertial components of the radius (2 dimensional)
$\dot{\bar{X}}$ and $\dot{\bar{Y}}$	Inertial components of velocity (2 dimensional)
$\ddot{\bar{X}}$ and $\ddot{\bar{Y}}$	Inertial components of acceleration (2 dimensional)
Z	Displacement perpendicular to the orbital plane
α	Angle of attack, cross range angle,
α	range angle
β	Azimuth from north
γ	Flight path angle referenced to local horizontal
$\bar{\gamma}$	Angle formed by $\dot{\bar{X}}$ and $\dot{\bar{Y}}$
Δ_i^j	Finite difference operator
δ	Thrust altitude with respect to the velocity vector
δ'	Supplement of the eccentric anomaly
ζ	Mass ratio (W_p/W_0)
θ	Central angle from perigee to the instantaneous radius
Λ	Longitude
μ	Gravitational constant (1.407645×10^{16} ft^3/sec^2 or 3.986005×10^{14} m^3/sec^2)
υ	Nondimensional velocity V/V_c
ρ	Density
ρ_B	bulk density $= \dfrac{r_m + 1}{\frac{r_m}{\rho_{ox}} + \frac{1}{\rho_{fuel}}}$
τ	Orbital period over a spherical earth (sec)
ϕ	Central angle between points in an orbit (deg); central angle $(\theta + \omega)$
ψ	Angle between major axes of 2 orbits
Ω	Longitude of the ascending node

Ω_e	Rotational rate of earth (7.292115 x 10^{-5} rad/sec)
$\dot{\Omega}$	Secular change in the right ascension of the ascending node due to the earth's oblateness (rad/rev)
ω	Argument of perigee

Subscripts

AD	Ascent and descent
a	Apogee or ambient
BO	Burnout
cl	Low altitude circular orbit
f	First or original orbit
i	Impact, intersection
L	Launch
o	Initial
p	Perigee
r	Rotating
SL	Sea level
t	Terminal
X	Impact

Superscript

*	Denotes point of injection from initial to transfer orbit

A. INTRODUCTION

Most satellite missions eventually require that the satellite or a portion thereof be recovered from orbit. This recovery process has been broken into two phases for presentation in the manual: departure and re-entry. The latter is discussed in Chapter IX and the former is presented here. The purpose of the departure discussions is to provide insight into: the timing limitations for return to a point on earth, the energy requirements, the error sensitivities for that portion of the trajectory occurring above the re-entry altitude (≈400,000 ft or 122 km).

In the analysis of the departure of a satellite from orbit, two general approaches present themselves for consideration:

(1) Departure at those times necessary to arrive at a position in the plane of motion at the same time that the impact site lies in the plane.

(2) Departure any time that the fuel required to maneuver onto a collision trajectory is equal to or less than some prescribed limit.

However, there are orbits which do not meet the requirements imposed by either of these approaches (e.g. some of the 24-hr orbits). Thus, it is necessary before investigating these approaches to first analyze the general problem of return from orbit utilizing an intermediate orbit (i.e. the reverse rendezvous technique of Chapter VII). Once this is done departure from the parking orbit (assumed to be nearly circular) can be discussed.

It should be noted at this point that the parking orbit approach is not a firm requirement since by properly restricting the times of departure and the descent trajectories, the position of the re-entry point can be matched to almost any specified point ($L \leq i$) without the use of the parking orbit. However, the only means for producing re-entry from an arbitrary orbit at a prescribed position and at a preselected time (assuming very limited or no maneuvering during descent) is the parking orbit. Other significant advantages will be discussed in turn during the presentation of the material.

B. THE GENERALIZED RETURN PROBLEM

1. Return Trajectories

Transfer from the elliptical orbit into a low altitude circular orbit is now considered. The time limitations (i.e., arrival at a given time over a fixed point) are not considered initially because time-imposed conditions can be obtained later by variations of the general return trajectory.

The transfer orbit is assumed to be an ellipse whose major axis is inclined at some unknown angle (ψ) to the major axis of the original orbit. Injection into the transfer orbit is accomplished tangentially at a departure point r^*, θ^* as shown in Fig. 1. A nonzero flight path angle at departure is specified because:

(1) Limitations may exist on the velocity pulses given by the rocket booster.

(2) Arrival time and location of the intersection with the low altitude orbit can be adjusted by changes in the departure angle.

(3) This approach results in a more generalized solution, where perigee departure is included as a particular case.

In order to ensure the certainty of intersection with the final low altitude circular orbit, a requirement exists that the perigee radius of the transfer orbit must be equal to or less than the radius of the final orbit. This can be given mathematically as

$$r_{pt} \leq r_{cl} \text{ or } r_{cl} = r_{pt} + \Delta r \qquad (1)$$

where Δr is determined by the probable errors caused by the guidance limitations at the departure point. In order to avoid the atmospheric effects distorting the transfer trajectory, the low altitude orbit should be at least 200 stat mi 322 km above sea level. In any case, the perigee radius of the transfer orbit has to be fixed before the maneuver. This considerably simplifies the solution for the remaining properties of the transfer orbit.

Knowing the parameters of the original orbit and having specified the departure time or the departure angle (θ^*), the departure radius is determined as

$$r^* = \frac{p_f}{1 + e_f \cos \theta^*} \quad . \qquad (2)$$

For greater generality, this can also be given in a nondimensional parameter form, using the perigee distance of the original orbit as a reference distance as

$$\frac{r^*}{r_{pf}} = \frac{1 + e_f}{1 + e_f \cos \theta^*} \quad . \qquad (2b)$$

At the departure point, the two ellipses are further assumed to be tangent, as shown in Fig. 1 for efficiency of propellant consumption. This means that the flight path angles are identical, i.e.,

$$\gamma_t = \gamma_f \equiv \gamma^* .$$

where: flight path angle is defined from the conservation of angular momentum by

$$V r \cos \gamma = \sqrt{p\mu},$$

Thus

$$\cos^2 \gamma = \frac{1}{\frac{r}{r_p}\left(1 + \frac{r_p}{r_a} - \frac{r}{r_a}\right)} \quad . \qquad (3)$$

where the sign of the flight angle is determined by the quadrant of the original ellipse.

Using $\gamma_t^* = \gamma^*$ and writing Eq (3) for the radii of the transfer ellipse and the initial orbit, it follows that the apogee radius of the transfer orbit is given by

$$\frac{r_{at}}{r^*} = \frac{\left(1 - \frac{r_{pt}}{r^*}\right)\cos^2\gamma^*}{\cos^2\gamma^* - \frac{r_{pt}}{r^*}} . \qquad (4)$$

From Eq (4), the semimajor axis of the transfer ellipse is obtained as

$$\frac{a_t}{r^*} = \frac{1}{2}\left[\frac{\cos^2\gamma^* - \left(\frac{r_{pt}}{r^*}\right)^2}{\cos^2\gamma^* - \frac{r_{pt}}{r^*}}\right] . \qquad (5)$$

Next, in order to determine the properties of the transfer orbit completely, the central angle from perigee (θ_t^*) is obtained. At the departure point, the following expression holds:

$$r^* = \frac{p_f}{1 + e_f \cos\theta^*} = \frac{p_t}{1 + e_t \cos\theta_t^*} .$$

Solving this for θ_t^*,

$$\cos\theta_t^* = \frac{\frac{r_{pt}}{r_{pf}}}{1 - \frac{r_{pt}}{r_{at}}}\left[\left(1 + \frac{r_{pf}}{r_{af}}\right) + \left(1 - \frac{r_{pf}}{r_{af}}\right)\cos\theta^* - \frac{r_{pf}}{r_{pt}}\left(1 + \frac{r_{pt}}{r_{at}}\right)\right] . \qquad (6a)$$

Using Eq (2b), this can be rewritten in a shorter form as

$$\cos\theta_t^* = \frac{2\frac{r_{pt}}{r^*} - \left(1 + \frac{r_{pt}}{r_{at}}\right)}{1 - \frac{r_{pt}}{r_{at}}} . \qquad (6b)$$

Assuming that transfer will be initiated near apogee of the transfer orbit, the quadrant of the initial central angle in the transfer orbit is determined by the rule:

if $0 \leq \theta^* \leq 180°$ then $90° < \theta_t^* \leq 180°$

if $180° \leq \theta^* \leq 360°$ then $180° \leq \theta_t^* < 270°$

Now from the geometry of the problem, the angle between the major axes of the transfer and target orbits is

$$\psi = 180° + \theta^* - \theta_t^* . \qquad (7)$$

Next, the magnitude of the velocity impulse applied at θ^* is determined (direction ΔV^* is opposite to the direction of motion for the assumed tangential transfer). Since the departure radius and semimajor axes for both ellipses are already computed, this velocity impulse is found by the numerical difference of the velocity required in the original orbit and the velocity corresponding to the transfer orbit at this particular point.

$$\Delta V^* = V_f^* - V_t^* . \qquad (8)$$

These velocities may be found from the energy equation.

$$V = \sqrt{\mu\left(\frac{2}{r} - \frac{1}{a}\right)} \qquad (9)$$

Equations (8) and (9) determine the required velocity impulse as

$$\Delta V^* = \sqrt{\frac{\mu}{r^*}}\left[\sqrt{2 - \frac{r^*}{a_f}} - \sqrt{2 - \frac{r^*}{a_t}}\right] \qquad (10)$$

Injection into the low altitude circular orbit is now accomplished at either the intersection point r_{1t} or point r_{2t}, as shown in Fig. 2.

In a manner similar to that of Eq (6b), the intersection central angle is given by

$$\cos\theta_{it} = \frac{2\frac{r_{pt}}{r_{it}} - \left(1 + \frac{r_{pt}}{r_{at}}\right)}{1 - \frac{r_{pt}}{r_{at}}} , \qquad (11)$$

where

$i = 1, 2$

$r_{it} = r_{cl}$

θ_{1t} is in the fourth quadrant and θ_{2t} is in the first quadrant for all reasonable return trajectories.

Now the maneuver angle at the circular orbit is defined by:

$$\cos^2\Delta\gamma_i = \frac{1}{\frac{r_{cl}}{r_{pt}}\left(1 + \frac{r_{pt}}{r_{at}} - \frac{r_{cl}}{r_{at}}\right)} \qquad (12)$$

where the following rules apply:

$$\Delta\gamma_1 \leq 0 \quad \text{(negative)}$$

$$\Delta\gamma_2 \geq 0 \quad \text{(positive)}$$

and the pulse required is

$$\Delta V_1^2 = V_{1t}^2 - 2V_{1t} V_{1\ell} \cos \Delta\gamma_1 + V_{1\ell}^2 \quad (13)$$

or

$$\left(\frac{\Delta V_1}{V_{1\ell}}\right)^2 = \left(\frac{V_{1t}}{V_{1\ell}}\right)^2 - 2\left(\frac{V_{1t}}{V_{1\ell}}\right)\cos \Delta\gamma_1 + 1. \quad (14)$$

where

$$V_{1t} = \sqrt{2 - \frac{r_{c\ell}}{a_t}}\ \sqrt{\frac{\mu}{r_{c\ell}}}$$

$$V_{1\ell} = \sqrt{\frac{\mu}{r_{c\ell}}}.$$

Thus, the following equation results:

$$\left(\frac{\Delta V_1}{V_{c\ell}}\right)^2 = \left(3 - \frac{r_{c\ell}}{a_t}\right) - 2\left(2 - \frac{r_{c\ell}}{a_t}\right)^{1/2} \cos \Delta\gamma_1 \quad (15)$$

Now the angle at which the thrust must be applied with respect to the velocity vector (δ) is found by the law of sines.

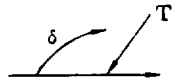

$$\sin \delta_1 = \left(\frac{V_{c\ell}}{\Delta V_1}\right) \sin \Delta\gamma_1 \quad (16)$$

To avoid the ambiguities in the sign of Eq (16), the law of cosines can also be applied to the angle δ, resulting in

$$\cos \delta_1 = \frac{+\sqrt{2 - \frac{r_{c\ell}}{a_t}} - \cos \Delta\gamma_1}{\left(\frac{\Delta V_1}{V_{c\ell}}\right)}. \quad (17)$$

At r_{2t}, a similar analysis can be applied since the drag loss is negligible for half a revolution and a symmetry about the major axis exists.

This analysis determines the trajectories and velocity pulses for a return into a circular orbit. The flight times and the positioning problems are considered in Subsection 3.

2. Departure Error Analysis

The problem arises concerning the effect of small errors of altitude, velocity or flight path angle on the perigee conditions. Partial derivatives of the perigee radius and velocity, with respect to initial conditions, are obtained in terms of eccentricity and central angle. In the conversion from the usual r, V and γ relationships, the following equations are found to be most useful:

$$\frac{r}{r_p} = \frac{1 + e}{1 + e \cos \theta} \quad (18)$$

$$\left(\frac{V}{V_c}\right)^2 = \frac{1 + 2 e \cos \theta + e^2}{1 + e \cos \theta} \quad (19)$$

$$\left(\frac{V_c}{V_{ca}}\right)^2 = \frac{1 + e \cos \theta}{1 - e} \quad (20)$$

$$\cos^2 \gamma = \frac{(1 + e \cos \theta)^2}{1 + 2 e \cos \theta + e^2} \quad (21)$$

The partials of r_p can be nondimensionalized as follows:

$$\frac{V}{r} \frac{\partial r_p}{\partial V} = \frac{2 (1 + e \cos \theta)(1 - \cos \theta)}{(1 + e)^2} \quad (22)$$

$$\frac{\partial r_p}{\partial r} = \frac{(1 - e)(1 + \cos \theta)}{(1 - e^2)^2} \quad (2 - e - e^2 - \cos \theta + e \cos \theta) \quad (23)$$

$$\frac{1}{r} \frac{\partial r_p}{\partial \gamma} = - \sin \theta. \quad (24)$$

The partials of V_p are derived from the conservation of angular momentum

$$V_p\ r_p = V\ r \cos \gamma.$$

Differentiating,

$$\frac{\partial (V_p\ r_p)}{\partial V} = V_p \frac{\partial r_p}{\partial V} + r_p \frac{\partial V_p}{\partial V} = r \cos \gamma. \quad (25)$$

Using Eqs (18) to (22), the final form of the partial is obtained.

$$\frac{\partial V_p}{\partial V} = \frac{e - 1 + 2 \cos \theta}{(1 + 2 e \cos \theta + e^2)^{1/2}}. \quad (26)$$

Using the method of Eq (25), the following equations are obtained:

$$\frac{r}{V}\frac{\partial V_p}{\partial r} = \frac{\cos\theta - 1}{(1 + 2e\cos + e^2)^{1/2}} \qquad (27)$$

$$\frac{1}{V}\frac{\partial V_p}{\partial \gamma} = \frac{(1+e)\sin\theta}{(1 + e\cos\theta)(1 + 2e\cos\theta + e^2)^{1/2}} \qquad (28)$$

As seen in Fig. 1, the departure usually occurs close to the apogee of the transfer ellipse, i.e., $\theta_t^* \approx 180°$. For this case

$$\cos\theta_t^* \approx -1$$

$$\cos\theta_t^* \approx 0.$$

Therefore, the partial derivatives for the case of departure point being near to the apogee of the transfer ellipse reduce to the following:

(1) Errors in perigee radius.

$$\frac{V_a}{r_a}\frac{\partial r_p}{\partial V_a} = \frac{4(1-e)}{(1+e)^2} = \left(2\frac{r_p}{r_a}\right)\left(1 + \frac{r_p}{r_a}\right) \qquad (29)$$

$$\frac{\partial r_p}{\partial r_a} = \frac{(1-e)(3+e)}{(1+e)^2} = \frac{r_p}{r_a}\left(2 + \frac{r_p}{r_a}\right) \qquad (30)$$

$$\frac{1}{r_a}\frac{\partial r_p}{\partial \gamma} = 0. \qquad (31)$$

(2) Errors in perigee velocity.

$$\frac{\partial V_p}{\partial V_a} = \frac{e-3}{1-e} = -\left(2 + \frac{r_a}{r_p}\right) \qquad (32)$$

$$\frac{r_a}{V_a}\frac{\partial V_p}{\partial r_a} = -\frac{2}{1-e} = -\left(1 + \frac{r_a}{r_p}\right) \qquad (33)$$

$$\frac{1}{V_a}\frac{\partial V_p}{\partial \gamma} = 0. \qquad (34)$$

In Eqs (22) to (34), it is implied that all the quantities pertain to the transfer ellipse.

The important point to notice is the insensitivity of the perigee radius and velocity to errors in flight path angle for near-apogee departures, as shown by Eqs (31) and (34).

For small deviations from the required departure conditions, the perigee errors can be approximated from the given partials by

$$\Delta r_p \approx \frac{\partial r_p}{\partial r_a}\Delta r_a + \frac{\partial r_p}{\partial V_a}\Delta V_a + \frac{\partial r_p}{\partial \gamma}\Delta\gamma \qquad (35)$$

and

$$\Delta V_p \approx \frac{\partial V_p}{\partial r_a}\Delta r_a + \frac{\partial V_p}{\partial V_a}\Delta V_a + \frac{\partial V_p}{\partial \gamma}\Delta\gamma \qquad (36)$$

By substituting Eqs (29) to (31) into (35), the radial errors for a near-apogee departure are obtained:

$$\frac{\Delta r_p}{r_a} \approx \frac{1-e}{(1+e)^2}\left[(3+e)\frac{\Delta r_a}{r_a} + 4\frac{\Delta V_a}{V_a}\right] \qquad (37)$$

or in terms of apogee and perigee radii:

$$\frac{\Delta r_p}{r_a} \approx \frac{r_p}{r_a}\left[\left(2 + \frac{r_p}{r_a}\right)\frac{\Delta r_a}{r_a} + 2\left(1 + \frac{r_p}{r_a}\right)\frac{\Delta V_a}{V_a}\right]. \qquad (38)$$

Similarly, the velocity error is found by substituting Eqs (32) to (34) into (36).

$$\frac{\Delta V_p}{V_a} \approx -\left(\frac{1}{1-e}\right)\left[2\frac{\Delta r_a}{r_a} + (3-e)\frac{\Delta V_a}{V_a}\right] \qquad (39)$$

or

$$\frac{\Delta V_p}{V_a} \approx -\left[\left(1 + \frac{r_a}{r_p}\right)\frac{\Delta r_a}{r_a} + \left(2 + \frac{r_a}{r_p}\right)\frac{\Delta V_a}{V_a}\right]. \qquad (40)$$

3. Timing Considerations

Assume that the trajectory problem of the return vehicle is defined as follows:

(1) **The vehicle must arrive in a low altitude orbit over a specified impact area at some predetermined time.**

(2) **There are possible limitations on the velocity pulses to be employed during the maneuver.**

Immediately, it becomes clear that unless the orbital plane for the return phase is different from that of the original orbit, only two times of

arrival in the low altitude orbit are acceptable during each day. These times correspond to the times at which the impact point crosses the orbital plane.

The following analysis of the return problem is quite general. However, because the number of variables involved is large, only those cases for which the orbital plane is unaltered are treated.

The initial location (at time t_0) of the final intersection point is determined by using spherical trigonometry and the symbols defined in Fig. 3a.

$$\sin L_0 = \sin i \sin \phi_0 . \tag{41}$$

Equation (41) applies only if $L_0 \leq i$. In case the inclination angle is less than the latitude of the impact area (note that $L_0 \equiv L_x$), a change in orbital inclination must be accomplished before or during the departure maneuver. The equations for such a maneuver are presented in Chapter VI.

From spherical trigonometry, the first intersection of the two planes is

$$\cos (\Lambda_0 - \Omega_0) = \frac{\cos \phi_0}{\cos L_x} . \tag{42}$$

The second intersection is

$$\Lambda_0' - \Omega_0 = \pi - \cos^{-1}\left(\frac{\cos \phi_0}{\cos L_x}\right). \tag{42a}$$

Next, the initial angular distance from the intersection point (P_i) to the impact point (P_x) is

$$\Delta\Lambda_0 = \Lambda_0 - \Lambda_x$$

$$= (\Omega_0 - \Lambda_x) + \cos^{-1}\left(\frac{\cos \phi_0}{\cos L_x}\right). \tag{43}$$

During each revolution of the earth there are two intersection points, P_i and P_i'

Time to intersection for the first day is

$$t_{j1} = \frac{\Delta\Lambda_0}{\Omega_e} = \frac{\Omega_0 - \Lambda_x}{\Omega_e} + \frac{1}{\Omega_e}\cos^{-1}\left(\frac{\cos \phi_0}{\cos L_0}\right). \tag{44}$$

Time to intersection for n days is

$$t_j = t_{j1} + (n - 1)\, d + \frac{n\Omega d}{\Omega_e \tau} \quad (j = n = 1, 2, 3 \ldots) \tag{45}$$

where d = sidereal day (86,164 sec)

Or using Eq (44),

$$t_j = \frac{\Omega_0 + n\dot{\Omega} d/\tau - \Lambda_x}{\Omega_e} + \frac{1}{\Omega_e}\cos^{-1}\left(\frac{\cos \phi_0}{\cos L_0}\right) + (n - 1)\, d \tag{46}$$

where $j = n = 1, 2, 3, \ldots$

Equation (46) gives the only possible flight times for target interception.

By changing the inclination at the original orbit in inertial space (i.e., changing i and/or Ω_0), a small range of possible intersection times can be achieved. Large changes in inclination become prohibitive due to exceedingly high mass ratios and should not be considered for most vehicles.

From the geometry of Fig. 3b,

$$\psi = 180° - (\theta_t^* - \theta^*) \tag{47}$$

and

$$\theta_l = 360° - \omega + \phi_0 + \theta_t^* - \theta^*. \tag{48}$$

Now, after the equation for the necessary intercept flight time has been derived and the angles for the transfer trajectory have been defined, a solution of the departure angle is required in mathematical form.

$$\theta^* = f(\theta_0, \Omega_0, i, \omega, p_f, e_f, r_l, \Lambda_x, L_x, t_t) . \tag{49}$$

To get the exact relationship indicated by Eq (49), an expression for the total flight time must be derived in terms of all other pertinent variables. In such an equation there is only one unknown (i.e., θ^*) and the proper value of the total flight time, corresponding to some fixed value determined by Eq (46), can be obtained by variations of θ^*.

In general, the total flight time is the sum of three separate components.

(1) Time in original orbit before departure (t_1).

(2) Time in transfer orbit (t_2).

(3) Time in the final low altitude orbit until the impact area is reached (t_3).

Consider the case where the departure angle from perigee (θ^*) is less than the initial central angle (θ_0), or $\theta^* < \theta_0$. Then, the components of flight time will be as follows.

(1) Original orbit

$$t_1 = \frac{\tau_f}{2\pi}\left[2\pi + (E^* - E_0) + e(\sin E_0 - \sin E^*)\right]$$

where

$$E = 2 \tan^{-1}\left[\sqrt{\frac{1-e}{1+e}}\ \tan\frac{\theta}{2}\right]$$

$$\sin E = \frac{\sqrt{1-e^2}\sin\theta}{1+e\cos\theta} \qquad (50)$$

(2) Transfer orbit

$$t_2 = \frac{\tau_t}{2\pi}\left\{2\pi - E_t^* + e_t \sin E_t^*\right\} \qquad (51)$$

(3) Low altitude circular orbit

$$t_3 = \frac{\tau_\ell}{2\pi}\theta_\ell = \sqrt{\frac{r_\ell^3}{\mu}}\,(2\pi - \omega + \phi_0 + \theta_t^* - \theta^*) \qquad (52)$$

The total flight time is given as

$$t_t = t_1(\theta^*) + t_2(\theta^*) + t_3(\theta^*) \qquad (53)$$

where it is desired that t_t be one of the characteristic time values given by Eq (46).

If the departure angle from perigee is greater than the initial central angle ($\theta^* > \theta_0$), then the transfer orbit is initiated before the next perigee passage and Eq (50) becomes

$$t_t = \frac{\tau_f}{2\pi}\left\{(E^* - E_0) + e(\sin E_0 - \sin E^*)\right. \qquad (54)$$

Equations (51), (52) and (53) remain identical even for the case of $\theta^* > \theta_0$.

The transformation of Eq (53) into (49) is obviously extremely complicated, if not impossible. Thus, it is necessary to revert to a trial-and-error method. One such method is described below.

4. Iteration Procedure for the Departure Angle

The approach presupposes that either the computer possesses plotting and curve-reading abilities, or that the first approximation of the departure angle is known.

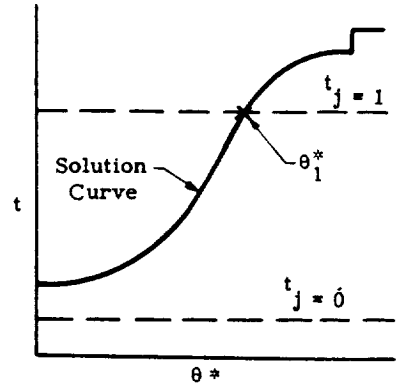

For a particular return mission, the most obvious method of solution is as follows.

(1) Determine the target point intercept times with the orbit plane (t_j).

(2) Establish the total flight time solution curve for a whole revolution in original orbit by the procedure shown in Table 1. Relatively large increments of central angle (e.g., $\Delta\theta^* = 30°$) can be used.

(3) Find the first intersection point (θ_1^*) of the solution curve and target intercept times.

(4) Determine the accurate departure angle by a linear iteration process.

(a) Use Eq (53) to compute t_{t1} for the first approximation of θ_1^*.

$$\text{If}\begin{cases} t_j > t_{t1}, \text{ assume } \theta_2^* = \theta_1^* + 1 \\ t_j < t_{t1}, \text{ assume } \theta_2^* = \theta_1^* - 1 \end{cases}.$$

(b) Compute t_{t2} for θ_2^*.

NOTE: t_{t1} and t_{t2} should be on the opposite sides of t_j. If both are on the same side, i.e.,

$$\begin{cases} t_{t1} > t_j \\ t_{t2} > t_j \end{cases} \text{ or } \begin{cases} t_{t1} < t_j \\ t_{t2} < t_j \end{cases},$$

use θ_2^* as θ_1^* and repeat step (4a).

(c) From θ_1^* and θ_2^*, compute the second approximation by the linear relationship

$$\theta_3^* = \frac{t_j - B}{A} \qquad (55)$$

where

$$A = \frac{t_{t1} - t_{t2}}{\theta_1^* - \theta_2^*} \qquad (56a)$$

$$B = \frac{t_{t2}\theta_1^* - t_{t1}\theta_2^*}{\theta_1^* - \theta_2^*}. \qquad (56b)$$

(d) Compute t_{t3} for θ_3^*. As for each linear approximation, the two points used must be on opposite sides of t_j line, the following rules apply.

$$\text{If}\begin{cases} t_{t3} > t_j, \text{ use min } \theta_k^* \\ t_{t3} < t_j, \text{ use max } \theta_k^* \end{cases} \text{where } \left\{ \theta_k : \theta_1^*,\ \theta_2^* \right\} .$$

(e) Compute the third approximation by using θ_3^* in connection with the correct θ_k^*.

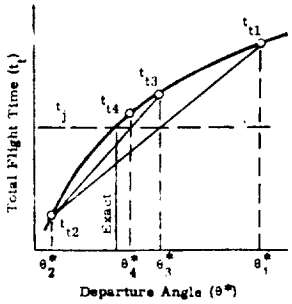

Thus,

$$\theta_4^* = \frac{t_j - B'}{A'} \qquad (57)$$

$$A' = \frac{t_{tk} - t_{t3}}{\theta_k^* - \theta_3^*} \qquad (58a)$$

$$B' = \frac{t_{t3}\theta_k^* - t_{tk}\theta_3^*}{\theta_k^* - \theta_3^*} \qquad (58b)$$

The iteration usually converges very rapidly because θ_1^* and θ_2^* are already within ± 1° of the exact answer desired. The geometrical interpretation of the convergence is shown in the preceding sketch. The reason for taking θ_k^* as one of the initial points is to avoid $(\theta_k^* - \theta_3^*) \to 0$ as the exact answer is approached. With this method, the values of $(\theta_k^* - \theta_3^*)$ remain finite for all approximations.

Table 1 presents the necessary variables arranged in the order of computation, and the equations used to aid in the visualization of the solution procedure.

TABLE 1
Return Shuttle Computations

	Variable	How Determined	Remarks
Desired Intercept Times	ϕ_o	Eq(41b)	
	t_j	Eq(46)	
Total Flight Curve	r^*	Eq(2a)	First assume θ^*
	$\cos^2 \gamma^*$	Eq(3)	
	r_{at}/r^*	Eq(4)	
	$\cos \theta_t^*$	Eq(6b)	
	a_t	$a_t = 1/2\ (r_{at} + r_{pt})$	
	e_t	$e_t = \frac{r_{at}}{a_t} - 1$	
	$\tau_t/2\pi$	$\frac{\tau_t}{2\pi} = \frac{a_t^3}{\mu}$	
	$\tau_\ell/2\pi$	$\frac{\tau_\ell}{2\pi} = \frac{r_\ell^3}{\mu}$	
	t_1	Eq(50) or (54)	
	t_2	Eq(51)	
	t_3	Eq(52)	
	t_t	$t_t = t_1 + t_2 + t_3$	Plot t_t vs θ^* (Fig. 4a)
Ground Track	M_i	$M_i = \frac{2\pi}{\tau} t_i$	For simplicity assume t_i in full hours
	θ_i	by iteration	
	L	Eq(59)	
	Λ	Eq(60)	

It should be noted that for a first approximation t_1, t_2, t_3 and θ_i can be found from Keplerian flight time curves (Chapter III). These curves are accurate to four significant figures and satisfactory for slide rule computations. After the flight time curve is plotted and the first estimate of departure angle is obtained, the exact equations should be used.

The desired intercept times and the ground track are computed only once (intercept times are independent of departure angle, and ground track is determined for only one final value of θ^*).

For the total flight time curve, values of θ^* are assumed at sufficient intervals (e.g., $\Delta\theta^* = 30°$) and t_t is found for each θ^*. From a plot of t_t versus θ^*, the intersections with the desired intercept times are determined.

5. Sample Problem

Assume that the following orbital and target parameters are specified (target refers to the specified low altitude orbit).

$\theta_0 = 0°$

$i = 70°$

$\omega = 270°$

$\Omega_0 = 135°\ E = +135°$

$\Lambda_x = 80°\ W = -80°$

$L_x = 28°\ N = +28°$

$\tau_f = 86,164.09$ sec (24-hour orbit)

$p_f = 1.037528 \times 10^8$ ft = 31623.9 km

$e_f = 0.500000$

$r_{af} = 2.075055 \times 10^8$ ft = 63247.7 km

$r_{pf} = 0.691685 \times 10^8$ ft = 21082.6 km

$r_t = r_{pt} = 0.224869 \times 10^8$ ft = 6854.0 km

The angle (ϕ_0) from the ascending node of the orbital plane to the intercept point of the target path and orbital plane is from Eq (41).

$$\phi_0 = \sin^{-1}\left(\frac{\sin 28°}{\sin 70°}\right) \approx \sin^{-1}(0.500)$$

$$\begin{cases} \phi_0 \approx 30° \\ \phi_0' \approx 150° \end{cases}$$

From Eq (43),

$$\Delta\Lambda_0 \approx 135° - (-80°) + \cos^{-1}\left(\frac{\cos 30°}{\cos 28°}\right)$$

$$\begin{cases} \Delta\Lambda_0 \approx 226.5° \\ \Delta\Lambda_0' \approx 383.5° \end{cases}$$

There is also the possibility of considering the angle $\Delta\Lambda_0' \approx 383.5° - 360° \approx 23.5°$, because $\Delta\Lambda_0'$ is actually ahead at the target point. Time to reach the first intersection points is as follows.

$$t_{j=1} \approx \frac{226.5}{4.18 \times 10^{-3}} = 54,200 \text{ sec} = 15.06 \text{ hr}$$

$$t'_{j=1} \approx \frac{383.5}{4.18 \times 10^{-3}} = 91,800 \text{ sec} = 25.5 \text{ hr}$$

$$t''_{j=1} \approx \frac{23.5}{4.18 \times 10^{-3}} = 5620 \text{ sec} = 1.56 \text{ hr}$$

The second set of possible flight times is derived from Eq (45).

$$t_{j=2} = 54,200 + (2-1)\,86,200 = 140,400 \text{ sec} = 39.0 \text{ hr}$$

$$t'_{j=2} = 91,800 + (2-1)\,86,200 = 178,000 \text{ sec} = 49.5 \text{ hr}$$

This means that during each day there are two possible arrival times over the target area.

Next, the total flight time is computed for $\theta^* = 0°, 30°, 60° \ldots 360°$, using Table 1 in connection with Chapter III. The sample calculations are given later for $\theta^* = 137°$.

The results for the departure angle within the first revolution of the 24-hr orbit are shown in Fig. 4a. The solid line gives the total flight times for the ascent crossing at the target latitude during the first revolution in the low altitude orbit. For the descent crossing during the first revolution, and for all crossings during succeeding revolutions in the low altitude orbit, the solid line retains its shape but will be displaced along the time axis by some constant flight time.

The first time the target crosses the orbital plane (1.56 hr) it falls short of the necessary transfer time. Therefore, this solution is imaginary.

For the given sample problem, the first possible departure angle is approximately $\theta^* \approx 137°$, corresponding to a flight time of 15 hr.

The important feature of Fig. 4a is the discontinuity in the total flight time solution. This irregularity is caused by the fact that overshooting the target interception by even a small angle results in the requirement for another revolution in the 24-hr orbit. For the given case, the third theoretically possible target intercept time is seen to fall into the region of discontinuity, indicating that this arrival time also represents an imaginary solution.

Of course, a possibility exists that the target intercept could be made during a succeeding revolution in the low altitude orbit. The optimum number of such revolutions will depend primarily upon the purpose of the return shuttle.

For example, the target intercept could be made at 25.5 hr by leaving at $\theta^* \approx 236°$ and staying for more than one full revolution in the low altitude orbit.

To explain the discontinuity at $\theta^*_{critical}$, flight times in the 24-hr orbit, the transfer orbit and the low altitude orbit are given separately in Fig. 4b. At $\theta^*_{critical} \approx 312°$, the overshooting of the target will require another revolution in the low orbit.

The determination of the critical departure angle is best accomplished by plotting θ_ℓ versus θ^*, as shown in Fig. 5. The flight time discontinuity exists at $\theta_\ell = 0°$.

Figure 4a indicates that $t_1 \approx 15$ hr is the most promising total maneuver time. Therefore, this solution is recomputed with more accuracy than that afforded by the preliminary slide rule results. From Eq (41),

$$\phi_0 = 29.9736°.$$

Time to reach the first intercept point is

$$t_{j=1} = \frac{\Omega_0 - \Lambda_x}{\Omega_e} + \frac{1}{\Omega_e} \cos^{-1}\left(\frac{\cos \phi_0}{\cos L_x}\right)$$

$$= 54,129.917 \text{ sec} = 15.036088 \text{ hr.}$$

The departure angle ($\theta^* = 137°$) is used to find t_{t1} by the procedure given in Table 1. All the steps are indicated for the sample problem in the following paragraphs.

(1) Departure radius

$$r^* = \frac{p_{24}}{1 + e_{24} \cos \theta^*} = 1.635645 \times 10^8 \text{ ft}$$
$$= 49,854.4 \text{ km}$$

(2) Cosine flight path angle

$$\cos^2 \gamma^* = \frac{1}{\frac{r^*}{r_{p24}}\left(1 + \frac{r_{p24}}{r_{a24}} - \frac{r^*}{r_{a24}}\right)} = 0.775799$$

(3) Apogee radius

$$\frac{r_{at}}{r^*} = \frac{\left(1 - \frac{r_{pt}}{r^*}\right)\cos^2 \gamma^*}{\cos^2 \gamma^* - \frac{r_{pt}}{r^*}} = 1.048287$$

(4) Central angle

$$\cos \theta_t^* = \frac{2\frac{r_{pt}}{r^*} - \left(1 + \frac{r_{pt}}{r_{at}}\right)}{1 - \frac{r_{pt}}{r_{at}}}; \quad \theta_t^* = 170.2047°$$

(5) Semimajor axis

$$a_t = \frac{1}{2}(r_{at} + r_{pt}) = 0.969747 \times 10^8 \text{ ft}$$
$$= 29557.8 \text{ km}$$

(6) Eccentricity

$$e_t = \frac{r_{at}}{a_t} - 1 = 0.768115$$

(7) Period of transfer orbit

$$\frac{\tau_t}{2\pi} = \sqrt{\frac{a_t^3}{\mu}} = 8048.71 \text{ sec}$$

(8) Period of low altitude orbit

$$\frac{\tau_\ell}{2\pi} = \sqrt{\frac{r_\ell^3}{\mu}} = 898.74 \text{ sec}$$

As $\theta^* > \theta_0$, from Eq (54),

$$t_1 = 20,276.50 \text{ sec} = 5.632361 \text{ hr}.$$

From Eq (51), the following is obtained.

$$t_2 = 31,796.37 \text{ sec} = 8.832325 \text{ hr}$$

(9) Angle in low orbit

$$\theta_\ell = 360° - \omega + \phi_0 + \theta_t^* - \theta^* = 153.1783°$$
$$= 2.673465 \text{ rad}$$

$$t_3 = \frac{\tau_\ell}{2\pi}\theta_\ell = 2402.75 \text{ sec} = 0.667430 \text{ hr}$$

(10) Total flight time

$$t_{t1} = t_1 + t_2 + t_3 = 15.132112 \text{ hr}$$

(11) Error in flight time

$$\Delta t_1 = t_t - t_j = 345.7 \text{ sec} = 5.76 \text{ min}$$

As $t_{t1} > t_j$, $\theta_2^* = \theta_1^* - 1 = 136°$ and, by the previous method, $t_{t2} = 14.960314$ hr.

Using the iteration process given in Eqs (55), (56a) and (56b), the next approximation is obtained.

$$A = \frac{t_{t1} - t_{t2}}{\theta_1^* - \theta_2^*} = 0.171802 \text{ hr/deg}$$

$$B = \frac{t_{t2}\theta_1^* - t_{t1}\theta_2^*}{\theta_1^* - \theta_2^*} = -8.404758 \text{ hr}$$

Finally,

$$\theta_3^* = \frac{t_j - B}{A} = 136.4411^\circ .$$

Using $\theta_3^* = 136.44^\circ$, $t_{t3} = 15.036515$ hr is obtained for the second approximation.

Since $t_{t3} > t_j$, by the rules given in subsection 5, min θ_k^* (i.e., θ_2^*) has to be used. Thus, Eqs (57), (58a) and (58b) become

$$A' = \frac{t_{t2} - t_{t3}}{\theta_2^* - \theta_3^*} = 0.173187 \text{ hr/deg}$$

$$B' = \frac{t_{t3}\,\theta_2^* - t_{t2}\,\theta_3^*}{\theta_2^* - \theta_3^*} = -8.592722 \text{ hr}$$

giving the third approximation as

$$\theta_4^* = \frac{t_j - B}{A} = 136.4376^\circ.$$

Thus, for the present example, the second and third approximations are almost identical and, for practical purposes, the convergence to the exact value is obtained. The following table presents the convergence of the solutions.

Approximation	θ^* (deg)	Error in Total Flight Time † (sec)
First	137	345.7
Second	136.44	1.535
† $t_{t = 54,129.917 \text{ sec}}$	136.4376	0.050

Since the shape and inclination of the transfer ellipse (θ_t^*, a_t, e_t, etc.,) were determined during the last iteration, it is relatively simple to obtain the location of the return shuttle in the orbit plane. The locations of the return shuttle treated here are given in Fig. 6a.

Altitude from sea level is given in Fig. 6b, as computed from the basic relationships.

$$r = \frac{p}{1 + e \cos \theta} \quad \text{and} \quad r = R + h$$

where R is the radius of earth at the given latitude. By neglecting the oblateness perturbation effects of the earth the ground track can be computed from the following equations.

(1) Latitude

$$L = \sin^{-1} [\sin i \sin (\omega + \theta)] \qquad (59)$$

(2) Longitude

$$\Lambda = \tan^{-1} [\cos i \tan (\omega + \theta)] + \Omega_0 - \Omega_e t \qquad (60)$$

where

$$\Omega_e = 0.004178074 \text{ deg/sec.}$$

The computed ground track for the sample problem is given in Fig. 7. Assuming the initial time to be zero hour, it gives the successive positions and a service time scale up to the desired landing point (Florida in the present case).

It should be noted that up to 12 hr, the transfer ground track deviates only slightly from the basic 24-hr ground track (given in dotted lines). The reason for this can be seen by comparing Figs. 6a and 7.

6. Flight Time Error Analysis

The total flight time error per unit departure angle can be approximated by taking the slopes of the total flight time curve (Fig. 4b). The solid line of Fig. 8 presents the slopes of the return flight time curve. Another approach utilizes the total flight time equation

$$t_t (\theta^*) = t_1 (\theta^*) + t_2 (\theta^*) + t_3 (\theta^*), \qquad (61)$$

Thus

$$\frac{dt_t}{d\theta^*} = \frac{dt_1}{d\theta^*} + \frac{dt_2}{d\theta^*} + \frac{dt_3}{d\theta^*} \qquad (62)$$

Since the period and eccentricity of the 24-hr orbit are dependent of θ^*, the first derivative in Eq 62 is found by using Kepler's equation

$$M = E - e \sin E \qquad (63)$$

where

$$M = nt = \frac{2\pi t}{\tau}.$$

Differentiating with respect to central angle

$$\frac{dM}{d\theta} = (1 - e \cos E) \frac{dE}{d\theta}, \qquad (64)$$

but

$$E = \sin^{-1} \left(\frac{\sqrt{1 - e^2} \sin \theta}{1 + e \cos \theta} \right), \qquad (65)$$

therefore

$$\frac{dE}{d\theta} = \frac{\sqrt{1 - e^2}}{1 + e \cos \theta}. \qquad (66)$$

From Eqs (64) and (66),

$$\frac{dM}{d\theta} = \frac{(1 - e^2)^{3/2}}{(1 + e \cos \theta)^2}. \qquad (67)$$

Using the definition of M, the error due to time spent in the 24-hr section of the return path is found from Eq (67).

$$\frac{dt_1}{d\theta^*} = \frac{\tau_f}{2\pi} \frac{(1 - e^2)^{3/2}}{(1 + e \cos \theta^*)^2} \tag{68}$$

Equation (68) is presented as the dotted line on Fig. 8. It is obviously symmetrical about 180°, as expected.

a. Approximate analysis

The low altitude orbit contribution to Eq (61) is approximately constant for the whole revolution of θ^* (Fig. 4b). Thus,

$$t_3 \approx \frac{\tau}{2\pi} (300° - \theta^*)$$

and

$$\frac{dt_3}{d\theta^*} \approx - \frac{\tau_f}{2\pi} = - 898.74 \text{ sec/rad} =$$

$$- 15.686 \text{ sec/deg.} \tag{69}$$

To obtain the contribution of the transfer orbit, the following approximation may be used first. Assuming that the transfer orbit is always entered at apogee (i.e., $r^* \approx r_{at}$), the time spent in transfer orbit is one-half of a period.

$$t_2 \approx \frac{\tau_t}{2} = \pi \sqrt{\frac{a_t^3}{\mu}} \tag{70}$$

Due to the previous assumptions,

$$a_t \approx \frac{1}{2} (r^* + r_{pt}) \tag{71}$$

and

$$a_t^3 \approx \frac{1}{8} \left(\frac{p_f}{1 + e_f \cos \theta^*} + r_{pt} \right)^3 . \tag{72}$$

Substituting Eq (72) into Eq (70) and differentiating with respect to θ^*,

$$\frac{dt_2}{d\theta^*} \approx \frac{3\pi e_f}{4\sqrt{\mu}} \left(\frac{r^{*2}}{p_f} \right) \left(\frac{r^* + r_{pt}}{2} \right)^2 \sin \theta^* . \tag{73}$$

The slope of the total flight time curve is the sum of these three components (i.e., the sum of Eqs (68), (69) and (73)).

b. Exact analysis

Actually, the transfer orbit is not usually entered at apogee, but rather at some small displacement from apogee. Since the vehicle moves very slowly in this region, the flight times may change considerably.

Thus, Eq (73) can be justified only for a preliminary estimate, and an exact analysis is needed. The exact derivative is obtained by differentiating the expression for t_2 assuming that γ^* is negative

$$t_2 = \frac{\tau_t}{2\pi} \left\{ 2\pi - M_t \right\} . \tag{74}$$

Differentiating Eq (74) with respect to θ^*,

$$\frac{dt_2}{d\theta^*} = \frac{1}{2\pi} \frac{d\tau_t}{d\theta^*} \left\{ 2\pi - M_t \right\} - \frac{\tau_t}{2\pi} \frac{dM_t}{d\theta^*} . \tag{75}$$

To evaluate these derivatives it is now necessary to define

$$A \equiv \frac{r_{pt}^2}{r_{af} r_{pf}} \tag{76a}$$

$$B \equiv \frac{r_{pt}}{r_{af}} + \frac{r_{pt}}{r_{pf}} , \tag{76b}$$

Thus

$$\cos \theta_t^* = \frac{B + 2 - \frac{r^*}{r_{pt}} (1 + A) - 2 \frac{r_{pt}}{r^*}}{\frac{r^*}{r_{pt}} (1 - A) + B - 2} \tag{77}$$

$$e_t = \frac{\frac{r^*}{r_{pt}} (1 - A) + B - 2}{\frac{r^*}{r_{pt}} (1 + A) - B} \tag{78}$$

$$a_t = \frac{1}{2} r^* \left[\frac{1 - \frac{r_{pt}}{r^*} B + A}{1 - B + \frac{r^*}{r_{pt}} A} \right] \tag{79}$$

Also, from Eqs (77) and (78), it follows that

$$1 + e_t \cos \theta_t^* = \frac{2 \left(1 - \frac{r_{pt}}{r^*} \right)}{\frac{r^*}{r_{pt}} (1 + A) - B} \tag{80}$$

Using the relationship

$$\frac{\tau_t}{2\pi} = \sqrt{\frac{a_t^3}{\mu}}$$

the first derivative is

$$\frac{d\tau_t}{d\theta^*} = \frac{3\pi}{\mu}\, a_t^{1/2}\left(\frac{da_t}{d\theta^*}\right)$$

$$= \frac{3\pi}{\mu}\, a_t^{1/2}\left(\frac{da_t}{dr^*}\right)\frac{dr^*}{d\theta^*} . \qquad (81)$$

From Eq (79) and also from

$$\frac{dr^*}{d\theta^*} = \frac{r^{*2}}{p_f}\, e_f \sin\theta^*, \qquad (82)$$

it follows that

$$\frac{da_t}{d\theta^*} = \frac{1}{2}\,\frac{1 - B + A}{\left(1 - B + \frac{r^*}{r_{pt}} A\right)^2}\,\frac{r^{*2}}{p_f}\, e_f \sin\theta^* . \qquad (83)$$

From Eqs (79), (81) and (83),

$$\frac{d\tau_t}{d\theta^*} = \left[\frac{3\sqrt{2}\pi}{4\sqrt{\mu}}\,\frac{r^{*5/2}}{p_f}\, e_f \left(\frac{1 - \frac{r_{pt}}{r^*} B + A}{1 - B + \frac{r^*}{r_{pt}} A}\right)\right]^{1/2} \cdot \left[\frac{1 - B + A}{\left(1 - B + \frac{r^*}{r_{pt}} A\right)^2}\right] \sin\theta^* . \qquad (84)$$

To obtain the second term in Eq (75), it should be noted that in this case τ_t = constant is implied, and

$$\frac{\tau_t}{2\pi}\,\frac{dM_t}{d\theta^*} = \frac{1}{n}\,\frac{dnt}{d\theta^*} = \frac{dt}{d\theta^*} = \frac{dt}{d\theta_t^*}\,\frac{d\theta_t^*}{d\theta^*} \qquad (85)$$

The first quantity in Eq (85) follows from Kepler's Law

$$\frac{dt}{d\theta_t^*} = \frac{r^{*2}}{\sqrt{\mu p_t}} . \qquad (86)$$

Substituting Eq (80) into Eq (86), (since $p = r(1 + e\cos\theta)$).

$$\frac{dt}{d\theta_t^*} = \frac{r^{*3/2}}{\sqrt{\mu}}\sqrt{\frac{\frac{r^*}{r_{pt}}(1 + A) - B}{2\left(1 - \frac{r_{pt}}{r^*}\right)}} \qquad (87)$$

To obtain the second quantity in Eq (85), the following shorthand notation of Eq (77) is used.

$$\cos\theta_t^* = f(r^*) \qquad (88)$$

Differentiating Eq (88) with respect to θ^*

$$-\sin\theta_t^*\,\frac{d\theta_t^*}{d\theta^*} = \frac{df}{d\theta^*}\,\frac{dr^*}{d\theta^*} . \qquad (89)$$

From Eq (77), it follows that

$$\frac{df}{dr^*} = -\frac{2}{r_{pt}}\left[\left(\frac{r_{pt}}{r^*}\right)^2 (2 - B) - 2\,\frac{r_{pt}}{r^*}(1 - A) + B - 2A\right]\left[\frac{r^*}{r_{pt}}(1 - A) + B - 2\right]^{-2} \qquad (90)$$

From Eqs (89), (90) and (82),

$$\frac{d\theta_t^*}{d\theta^*} = \frac{2r^{*2}}{r_{pt}\, p_f}\, e_f\left[\left(\frac{r_{pt}}{r^*}\right)^2 (2 - B) - 2\,\frac{r_{pt}}{r^*}(1 - A) + B - 2A\right]\left\{\left[\frac{r^*}{r_{pt}}(1 - A) + B - 2\right]^{-2} \cdot \frac{\sin\theta^*}{\sin\theta_t^*}\right\} . \qquad (91)$$

Substituting Eqs (87) and (91) into (85),

$$\frac{\tau_t}{2\pi}\,\frac{dM_t}{d\theta^*} = \frac{r^{*3/2}}{\mu}\sqrt{\frac{\frac{r^*}{r_{pt}}(1 + A) - B}{2\left(1 - \frac{r_{pt}}{r^*}\right)}}\,\frac{d\theta_t^*}{d\theta^*} . \qquad (92)$$

It should be noted that Eqs (91) and (92) are zero at the points where

$$\frac{r_{pt}}{r^*} = \frac{B - 2A}{2 - B} . \qquad (93)$$

The third error in time, i.e., the total flight time error contributed by the low altitude orbit is simply.

$$\frac{dt_3}{d\theta^*} = \frac{\tau_\ell}{2\pi}\,\frac{d\theta_\ell}{d\theta^*} \qquad (94)$$

since the period τ_ℓ is a constant.

As shown previously

$$\theta_\ell = 360^\circ - \omega + \phi_0 + \theta_t^* - \theta^*$$

therefore, Eq (94) becomes

$$\frac{dt_3}{d\theta^*} = \frac{\tau_\ell}{2\pi}\left(\frac{d\theta_t^*}{d\theta^*} - 1\right) . \qquad (95)$$

Finally, the equations for the flight time error are given as follows.

(1) Approximate equation

$$\frac{dt_t}{d\theta^*} \approx \frac{\tau_f}{2\pi} \frac{\left(1 - e_f^2\right)^{3/2}}{\left(1 + e_f \cos\theta^*\right)^2} + \frac{3\pi e_f}{4\sqrt{\mu}} \left(\frac{r^{*2}}{p_f}\right)\left(\frac{r^* + r_{pt}}{2}\right)^2 \sin\theta^* \quad (96)$$

-899

(2) Exact equation

$$\frac{dt_t}{d\theta^*} = \frac{\tau_f}{2\pi} \frac{\left(1 - e_f^2\right)^{3/2}}{\left(1 + e_f \cos\theta^*\right)^2} + \frac{1}{2\pi} \frac{d\tau_t}{d\theta^*} \left\{2\pi - M_t\right\} - \frac{\tau_t}{2\pi} \frac{dM_t}{d\theta^*} + \frac{\tau_f}{2\pi} \left(\frac{d\theta_t^*}{d\theta^*} - 1\right) \quad (97)$$

where

$\frac{d\tau_t}{d\theta^*}$ is given by Eq (84)

$\frac{\tau_t}{2\pi} \frac{dM_t}{d\theta^*}$ is given by Eq (92b)

$\frac{d\theta_t^*}{d\theta^*}$ is given by Eq (91).

In Fig. 8, the results of Eqs (96) and (97) are compared to the solid curve obtained from measuring the slopes of curves in Fig. 4b. It is seen that the approximate equation gives only the general trends and should not be used where exact numerical values are needed.

c. Limiting cases for the exact flight-time error analysis

In the previous material, the error analysis for the return shuttle flight times was derived. Due to the geometry of the problem, Eqs (91) and (92) become indeterminate for $\theta^* = 0°$ and 180°. This is caused by the fact that for the apogee and perigee departures from orbit, the corresponding transfer orbits are entered at apogee. Mathematically, as $\theta^* \to 0°$ and 180°, $\theta_t^* \to 180°$ and

$$\left(\frac{\sin\theta^*}{\sin\theta_t^*}\right) \longrightarrow \frac{0}{0} . \quad (98)$$

Equation (98) calls for a limiting procedure, since it is intuitively clear that the ratios must be finite.

Since

$$\cos\theta^* = \frac{1}{e_f}\left(\frac{p_f}{r^*} - 1\right) , \quad (99)$$

$$\sin^2\theta^* = 1 - \cos^2\theta^* = \frac{1}{e_f^2}\left[\left(\frac{p_f}{r^*}\right)\left(2 - \frac{p_f}{r^*}\right) - \left(1 - e_f^2\right)\right] . \quad (100)$$

Next, defining two new constants

$$u \equiv \frac{r_{pt}}{r_{af}} \quad (101a)$$

$$v \equiv \frac{r_{pt}}{r_{pf}} \quad (101b)$$

which correspond to the previous constants as follows.

$$A = u\,v \quad (102a)$$

$$B = u + v \quad (102b)$$

From the definition of eccentricity, it follows that

$$e_f = \frac{v - u}{v + u} \quad (103)$$

and

$$p_f = r_{pf}\,(1 + e_f) = \frac{2\,v\,r_{pf}}{u + v} . \quad (104)$$

Therefore, Eq (100) is shown to become, after substituting Eqs (101), (103) and (104),

$$\sin^2\theta^* = \frac{4\,(u + v)}{(v - u)^2}\left\{\frac{r_{pt}}{r^*}\left[1 - \left(\frac{r_{pt}}{r^*}\right)\cdot\left(\frac{1}{u + v}\right) - \frac{uv}{u + v}\right]\right\} . \quad (105)$$

From Eqs (77) and (102), it follows that

$$\sin^2\theta_t^* = 4\left[-\left(\frac{r_{pt}}{r^*}\right)^2 + \frac{r_{pt}}{r^*}(u + v + 2) - uv\left(\frac{r^*}{r_{pt}}\right)^2 + \frac{r^*}{r_{pt}}(u + v + 2uv) - 2\,(u + v) - (1 + uv)\right] \cdot \left[\frac{r^*}{r_{pt}}(1 - uv) + u + v - 2\right]^{-2} \quad (106)$$

Now, defining

$$x \equiv \frac{r_{pt}}{r^*} , \tag{107}$$

the following relationships exist.

$$\theta^* \to 0^\circ \quad \text{means } x \to v \tag{108}$$

$$\theta^* \to 180^\circ \text{ means } x \to u . \tag{109}$$

The problem of deriving the actual limits is somewhat simplified by the theorem that the square of the limit is equal to the limit of the square.

From Eqs (105), (106) and (107),

$$\frac{\sin^2 \theta^*}{\sin^2 \theta_t^*} = \frac{(u+v)\left[\frac{1}{x^2}(1 - uv) + u + v - 2\right]^2}{(v-u)^2} \frac{1}{I_x} \tag{110}$$

where

$$I_x = \frac{-x^2 + x(u+v+2) - \frac{uv}{x^2} + \frac{1}{x}(u+v+2uv)}{x - \frac{x^2}{u+v} - \frac{uv}{u+v}} + \frac{-2(u+v) - (1+uv)}{x - \frac{x^2}{u+v} - \frac{uv}{u+v}} . \tag{111}$$

Since the cases of interest in this investigation are elliptic orbits, $u \neq v$, the behavior of $\frac{1}{I_x}$ alone must be investigated.

Because Eq (111) still gives an indeterminate form $\frac{0}{0}$, L'Hospital's rule has to be used and

$$\lim_{x \to u \text{ or } v} (I_x) = \lim_{x \to u,\, v} \left\{ \left[-2x + u + v + 2 + \frac{2uv}{x^3} - \frac{1}{x^2}(u + v + 2uv) \right] \cdot \left[1 - \frac{2x}{u+v} \right]^{-1} \right\} \tag{112}$$

Finally, from Eqs (109), (110) and (112),

$$\lim_{\theta^* \to 0^\circ} \left(\frac{\sin \theta^*}{\sin \theta_t^*} \right) = \frac{1 - v}{v - u} . \tag{113}$$

Similarly,

$$\lim_{\theta^* \to 180^\circ} \left(\frac{\sin \theta^*}{\sin \theta_t^*} \right) = \frac{1 - u}{v - u} , \tag{114}$$

or simply

$$\lim_{\theta^* \to 180^\circ} \left(\frac{\sin \theta^*}{\sin \theta_t^*} \right) = \lim_{\theta^* \to 0^\circ} \left(\frac{\sin \theta^*}{\sin \theta_t^*} \right) + 1. \tag{115}$$

For the sample problem (24-hour orbit)

$$\left.\begin{aligned} r_{pt} &= 0.224869 \times 10^8 \text{ ft} \\ &= 6854.0 \text{ km} \\ r_{a24} &= 2.075055 \times 10^8 \text{ ft} \\ &= 63,247.7 \text{ km} \\ r_{p24} &= 0.691685 \times 10^8 \text{ ft} \\ &= 21,082.6 \text{ km} \end{aligned}\right\} \quad \begin{aligned} u &= \frac{r_{pt}}{r_{a24}} = 0.108368 \\ v &= \frac{r_{pt}}{r_{p24}} = 0.325103 \end{aligned}$$

and from Eqs (113) and (114),

$$\lim_{\theta^* \to 0^\circ} \left(\frac{\sin \theta^*}{\sin \theta_t^*} \right) = 3.113927$$

$$\lim_{\theta^* \to 180^\circ} \left(\frac{\sin \theta^*}{\sin \theta_t^*} \right) = 4.113927.$$

d. Error analysis by numerical differentiation

Since the total flight time curve (Fig. 4b) was computed in the sample problem, a numerical differentiation method can also be used.

First, assemble a central difference table in the following form.

θ_{-2}	$(t_t)_{-2}$			
		Δ^1_{-2}		
θ_{-1}	$(t_t)_{-1}$		Δ^2_{-2}	
		Δ^1_{-1}		Δ^3_{-2} .....
θ_0	$(t_t)_0$		Δ^2_{-1}	
		Δ^1_0		Δ^3_{-1} .....
θ_1	$(t_t)_1$		Δ^2_0	
		Δ^1_1		
θ_2	$(t_t)_2$			
.....				

where Δ^n is the n th difference of the value of t_t, when θ is increased to $\theta + \Delta\theta$.

It can be shown that for this central difference table, Stirling's interpolation formula is

$$t_t = (t_t)_0 + \frac{\delta\theta}{\Delta\theta}\left(\frac{\Delta^1_0 + \Delta^1_{-1}}{2}\right) + \frac{\delta\theta^2}{2!\,\Delta\theta^2}\Delta^2_{-1} + \frac{\delta\theta(\delta\theta^2 - \Delta\theta^2)}{3!\,\Delta\theta^3}\left(\frac{\Delta^3_{-1} + \Delta^3_{-2}}{2}\right) + \ldots \tag{116}$$

where

$\delta\theta$ is a small variation between θ_0 and θ_1

$\Delta\theta$ is the equal increment $\theta_1 - \theta_0$, $\theta_0 - \theta_{-1}$, ...

The slope of the total flight time curve is obtained by differentiating Eq (116) and setting $\delta\theta = 0$ in the result. Thus,

$$\frac{dt_t}{d\theta^*} = \frac{1}{\Delta\theta}\left(\frac{\Delta^1_0 + \Delta^1_{-1}}{2} - \frac{\Delta^3_{-1} + \Delta^3_{-2}}{12} + \frac{\Delta^5_{-2} + \Delta^5_{-3}}{60} - \ldots\right) . \qquad (117)$$

(Fig. 4b), the rough values for t_t were obtained from which the following table is constructed.

θ (deg)	t_t (sec)	Δ^1	Δ^2	Δ^3
0	12,910			
		3020		
30	15,930		2490	
		5510		+1470
$(60)_0$	$(21,440)_0$		3960	
		$(9470)_0$		-330
90	30,910		$(3630)_0$	
		13,100		
120	44,010			

From Eq (117),

$$\left(\frac{dt_t}{d\theta^*}\right)_{\theta^* = 60°} = \frac{1}{30°}\left(\frac{9470 + 5510}{2} - \frac{-330 + 1470}{12}\right)$$

$$= 246.5 \text{ sec/deg.}$$

The results of numerical differentiation are also given in Fig. 8, and they fit rather closely the slopes measured from Fig. 4b. Since numerical differentiation is extremely simple, as compared to the exact analysis, it should be used for all preliminary calculations.

NOTE: In the numerical differentiation method presented here, the difference columns should not be carried further than is consistent with the accuracy of the data. Otherwise, the higher order approximations could be less accurate than the lower ones. Thus, the differences should be carried only to the point where marked irregularities start to appear.

C. PLANAR ANALYSIS OF DEPARTURE FROM LOW ALTITUDE ORBITS

For high altitude orbits, where all estimates of atmospheric drag are negligible, orbital lifetime may be measured in terms of years. Thus, should impact with the earth be desired at a specific time and location, some device must be employed to alter the vehicle's velocity and/or flight path angle an amount sufficient to cause the vehicle to re-enter. Re-entry as used here is actually a misnomer due to the fact that there are finite values of atmospheric pressure for the entire range of altitudes to be investigated. The term, however, will be used throughout this section to refer to an altitude below which atmospheric drag is of such magnitude as to cause the vehicle's trajectory to degenerate and impact with the earth in one half of one revolution or less. Previous machine runs and calculations have revealed that for vehicles of ballistic or low lift design this re-entry altitude may be considered to be 300,000 ft (91.5 km). Therefore, for the purposes of this analysis, since drag is of negligible magnitude above the re-entry altitude, the atmosphere will be assumed to terminate at an altitude of 300,000 ft (91.5 km). The earth will be assumed to be both spherical and non-rotating. Thus the vehicle trajectories involved will be portions of Keplerian ellipses. Special note should be made at this point that even though the approaches made here are valid for vehicles of high lift design, the altitude at which drag must be considered may increase to 400,000 ft (122 km) or more. Motion within the earth's atmosphere will not be treated here; it is reported in Chapter IX. Since Section B resulted in a plane which continues the impact point at a given time the analysis of departure can be treated as 2 dimensional. The following paragraphs present this information both for the impulse and finite burning cases.

1. Analytic Approach to Orbital Departure

A method of analysis which neglects the effects of finite burning times will now be developed to provide a means of obtaining relatively accurate approximations of the re-entry parameters and retrorocket size requirements.

The velocity increment obtainable from a given rocket is:

$$\Delta V = g_0 I_{sp} \ln\left(\frac{1}{1-\zeta}\right) - g t_B \sin\gamma \qquad (118)$$

$$= g_0 I_{sp} \ln\left(\frac{1}{1-\zeta}\right) - g \frac{I_{sp}\zeta}{T/W_0} \sin\gamma .$$

If the assumption is made that the burning time is extremely short or that the flight path angle remains very close to 0° during burning, Eq (118) reduces to

$$\Delta V = g_0 I_{sp} \ln\left(\frac{1}{1-\zeta}\right) . \qquad (119)$$

This equation is plotted in Chapter VI.

For most cases in which departure is desired from low altitude orbits, the mass ratio required is quite small and one further simplification in this expression may be made by noting that:

$$\ln\left(\frac{1}{1-\zeta}\right) = \zeta + \frac{\zeta^2}{2} + \frac{\zeta^3}{3} + \ldots$$

$$\approx \zeta \text{ for small values of } \zeta .$$

Therefore:

$$\Delta V = g_0 I_{sp} \zeta . \qquad (120)$$

This equation may be rewritten to include propellant characteristics by substituting for ζ its equivalent

$$\zeta = \rho_0 g_0 V_P / W_0 .$$

Thus:

$$\Delta V = g_0^2 I_{sp} \rho_0 V_P / W_0 .$$

Where

V_P = total propellant volume

ρ_0 = bulk density of propellant combination

$$= \frac{r_m + 1}{\frac{r_m}{\rho_{oxidizer}} + \frac{1}{\rho_{fuel}}}$$

r_m = mixture ratio $\sim \frac{\text{weight of oxidizer}}{\text{weight of fuel}}$

$I_{sp} = \frac{\text{unit force thrust}}{\text{weight of propellant flow/sec}}$

Since the assumption has been made that the burning time is infinitesimal, the velocity increment obtained from a given retrorocket may be treated as a pulse and the laws of sines and cosines can be used to relate the velocity and the direction before and after the pulse. For the purposes of this analysis, the thrust vector will be in the plane of the orbit; therefore, both the change in flight path angle and the required thrust attitude angle may be computed.

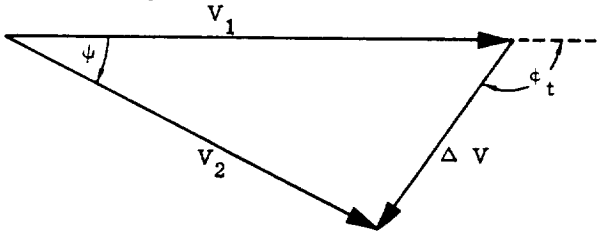

NOTE:
If the thrust vector lies in the orbital plane, $\psi = \Delta\gamma$ and $\phi_t = \delta$. (δ = the thrust attitude angle discussed in Section B.)

$$\Delta V^2 = V_1^2 + V_2^2 - 2V_1 V_2 \cos \Delta\gamma \qquad (121)$$

$$\left(\frac{\Delta V}{V_1}\right)^2 = \left(\frac{V_2}{V_1}\right)^2 - 2\frac{V_2}{V_1}\cos\Delta\gamma + 1$$

$$\frac{\sin\delta}{V_2} = \frac{\sin\Delta\gamma}{\Delta V}$$

$$\sin\delta = \frac{V_2/V_1}{\Delta V/V_1}\sin\Delta\gamma . \qquad (122)$$

Equation (121) is also presented in Chapter VI.

Now since the equation of any conic may be written as

$$\frac{V^2}{\mu} = \frac{2}{r} + \text{constant} \qquad (123)$$

$$\frac{V_1^2}{2} - \frac{\mu}{r_1} = \frac{V_2^2}{2} - \frac{\mu}{r_2} . \qquad (124)$$

a means of determining the vehicle velocity at any radius, if velocity and radius are known at some other point in the conic, is available. Point 2 is assumed to be that of re-entry at a radius of 2.12029×10^7 ft (6462.64 km). Thus, the velocity at re-entry may be determined once the velocity at burnout has been obtained. The energy equation is plotted in Chapter III.

The re-entry flight path angle can be obtained from the conservation of angular momentum and the radius, velocity and flight path angle at burnout of the retrorocket.

$$\cos\gamma_2 = \cos\gamma_1 \frac{r_1 V_1}{r_2 V_2} . \qquad (125)$$

Equation (125) can be used in conjunction with the energy equation to yield the relationship between the flight path angle at burnout of the retrorocket and that at re-entry.

If a tolerance is placed on the entry angle (e.g. 0 - 2°), the retropulse cannot be selected independently of other considerations. This fact may appear obvious, but is rigorously shown by combining the equations for the conservation of energy and angular momentum.

$$r_1 v_1 \cos\gamma_1 = r_2 v_2 \cos\gamma_2$$

$$r_1 \left|\vec{V}_0 + \vec{\Delta V}\right| \cos(\gamma_0 - \Delta\gamma)$$

$$= r_{entry}\sqrt{\left|\vec{V}_0 + \Delta\vec{V}\right|^2 - \frac{2\mu}{r} + \frac{2\mu}{r_{entry}}}\cos\gamma_{entry}$$

In order to determine the values of range and time of flight required for descent to re-entry, it is necessary to first consider the ellipse in question.

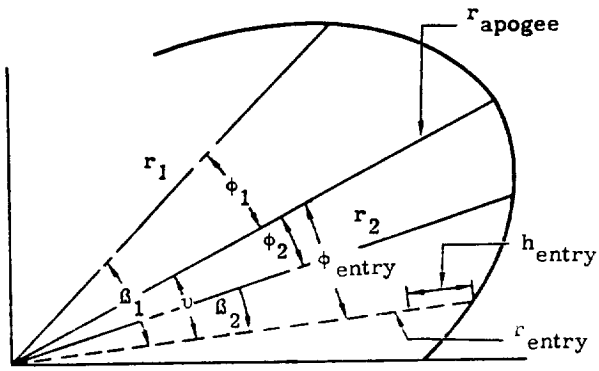

The range attained may be seen to be

$$X = R\beta \tag{126}$$

R = The radius of the earth

The problem then is to define the angle β in terms of the known quantities of the ellipse. This problem may be simplified by observing that

$$\beta = \upsilon - \phi. \tag{127}$$

Where

ϕ_1 is negative and ϕ_2 is positive and where the central angle from a given radius to apogee is

$$\phi = \cos^{-1}\left[\frac{r - p}{re}\right]. \tag{128}$$

Therefore:

$$\beta = \cos^{-1}\left[\frac{r_e - p}{r_e e}\right] \pm \cos^{-1}\left[\frac{r - p}{re}\right], \tag{129}$$

where:

$r_e = r_{entry}$

To define the time of flight a procedure similar to that employed to define the angle β is used. That is, the time of flight from one point to another is equal to the difference between the times from these points to apogee. The time of flight from a given point to apogee is defined by Eq (130)

$$t_a = \frac{\tau}{2\pi}\left[\delta' - e \sin \delta'\right]. \tag{130}$$

Where

δ' is measured in radians

$$\delta' = \cos^{-1}\left[\frac{\cos\phi - e}{1 - e\cos\phi}\right]. \tag{131}$$

The time of flight is thus

$$t_f = t_{entry} - t_a$$

where

δ'_{entry} is evaluated at $\phi = \phi_{entry}$

δ'_a is evaluated at $\phi = \phi_1$ or ϕ_2

t'_a is negative if vehicle passes through apogee before re-entry

Thus the complete maneuver can be described analytically under the assumption of impulsive burning.

This section has shown the results of flight path corrections and departures for the case in which instantaneous pulses were considered. Figure 9 shows the percentage deviation in the re-entry parameters obtained using this method as compared to that which includes the effects of finite burning time. The horizontal lines drawn at ± 4% error were arbitrarily selected to show the minimum mass ratios which could be considered as pulses in order to maintain this desired accuracy in all re-entry parameters as a function of initial altitude. A continuation of this analysis would be necessary to limit the maximum mass ratios which could be considered as pulses for the same accuracy limitation.

Figure 10 presents the error in the ideal velocity pulse due to finite burning times.

2. Orbital Departure from 100-stat mi (161-km) Orbits with Finite Burning Time

Finite burning time will now be included in the analysis as an additional variable: however, since no closed solution exists for this problem, the digital computer and a stepwise trajectory program were employed. This program considers the vehicle to be a point mass and the earth to be spherical. The trajectory during burning of a rocket or during travel within the sensible atmosphere is obtained by stepwise integration. The time interval for each integration is determined by the accuracy limitation placed on the extrapolated values of certain critical quantities. The equations for this program are presented in the simplified form required for this effort.

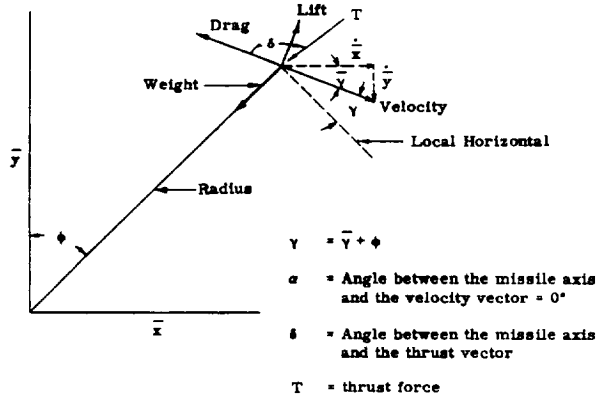

$$\dot{V} = \frac{T}{m}\cos(\alpha + \delta) - \frac{D}{m} - \frac{\mu}{r^2}\sin\gamma \tag{132}$$

$$= -\frac{T}{m} - \frac{\mu}{r^2}\sin\gamma = A$$

$$\dot{\bar{\gamma}} V = \frac{T}{m} \sin(\alpha + \delta) + \frac{L}{m} - \frac{\mu}{r^2} \cos \gamma \tag{133}$$

$$= -\frac{\mu}{r^2} \cos \gamma = B$$

$$\ddot{\bar{y}} = A \sin \bar{\gamma} + B \cos \bar{\gamma} \tag{134}$$

$$\ddot{\bar{x}} = A \cos \bar{\gamma} - B \sin \bar{\gamma} \tag{135}$$

$$\sin \gamma = \sin \bar{\gamma} \cos \phi + \cos \bar{\gamma} \sin \phi \tag{136}$$

$$\cos \gamma = \cos \bar{\gamma} \cos \phi - \sin \bar{\gamma} \sin \phi \tag{137}$$

where

$$\sin \bar{\gamma} = \frac{\dot{\bar{y}}}{V}$$

$$\cos \bar{\gamma} = \frac{\dot{\bar{x}}}{V}$$

$$\sin \phi = \frac{\bar{x}}{r}$$

$$\cos \phi = \frac{\bar{y}}{r}$$

$$T = T_{SL} + A_e (P_{SL} - P_a)$$

$$T_{SL} = T_{Vac} - A_e P_{SL} \tag{138}$$

$$m = \frac{W_0}{g_0} \left[1 - \frac{\dot{W}_p t}{W_0} \right] \tag{139}$$

$$\dot{W}_p = \text{constant}.$$

Once the retrorocket burns out, the trajectory is assumed to be unperturbed down to the altitude at which drag becomes appreciable. The equations for this portion of the trajectory are those of motion in a Keplerian ellipse.

For the purposes of this analysis two rocket parameters $\frac{W_p}{W_0}$ and $\frac{T}{W_0}$ (mass ratio and initial thrust-to-weight ratio) are investigated. In addition the thrust attitude angle (δ) was varied to show the effects of these quantities on the conditions at re-entry.

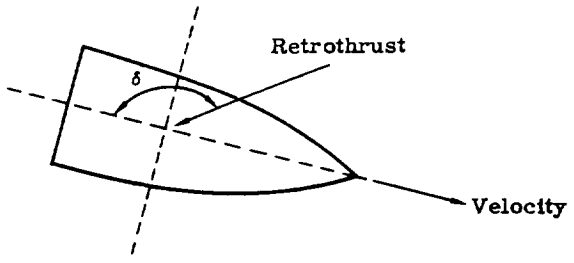

NOTE:
δ is measured in the plane of the trajectory.

The magnitude of the radial component of velocity is small, thus work done by the radial component of thrust will be small. It may, therefore, appear that a value of δ of 180° is optimum for all cases in which departure is desired; such is not the case. In the case of low altitude orbits small changes in the burnout altitude and flight path angle can affect the mass ratio required for orbital departure and on the re-entry parameters. This analysis, therefore, treats departure from a 100-stat mi (161 km) orbit separately from similar analysis for orbits of increased altitude.

There are many possible criteria which might be considered in the determination of an optimum retrorocket configuration. The selected configuration might be one for which the re-entry velocity is minimum, the re-entry flight path angle is minimum, the mass ratio required for departure is minimum or one which ensures a given value of range from the time of initiation to impact with the earth. The vehicle itself must also be considered in this process due to the sensitivity of some vehicles to small changes in the re-entry parameters.

Minimization of the re-entry flight path angle is not a realistic constraint for the vehicle configurations discussed due to the fact that the maximum values of both deceleration and aerodynamic heating can be held with allowable tolerances for manned re-entry for angles up to approximately -2°. Thus, this constraint need not be considered.

Since maneuver, either before initiating re-entry or sometime thereafter, is anticipated to assure impact in a given area, the criteria selected for the evaluation of retrorocket configurations should provide the maximum degree of flexibility in this respect. The analysis of maneuvering showed that the maximum displacement of the impact point in a plane normal to that of the unaltered trajectory, for a given amount of propellant, is obtained if the central angle measured from the radius at which the correction is made to that at which the trajectory impacts with the earth is 90° (10,000-km range). Thus, the selection of the retrorocket configuration which is near optimum for an orbit of this altitude is, determined by this value of total range and the minimum amount of propellant required for successful departure. This criteria must be modified, however, if the re-entry angle exceeds the allowable tolerances placed upon it.

Specific impulse will not be included in this analysis as a variable; however, because the mass ratios are small, the data presented here can be converted to obtain approximate answers corresponding to values of I_{sp} other than the assumed 300 sec. This can be accomplished by employing Eq (120).

$$\Delta V = g_0 I_{sp} \zeta = C$$

$$\zeta_1 I_{sp_1} = \zeta_2 I_{sp_2}$$

Figure 11 shows the variations in range, re-entry velocity and re-entry flight path angle as

functions of δ and $\frac{T}{W_0}$ for one value of mass ratio (0.1). This figure clearly shows that the range obtained in descent to 300,000 ft (91.5 km) can be minimized for a value of δ less than 180°. Also shown is the convergence of the curves of the higher values of $\frac{T}{W_0}$ implying that little is to be gained by increasing its magnitude above some value as yet undetermined (0.5, see Section 3. It is interesting to note that re-entry velocity which is a function of initial velocity, altitude, and velocity increment of the retrorocket is least sensitive to changes in thrust-to-weight ratio. This fact substantiates the assumption made in the impulse analyses that the velocity increment loss (a function of $\frac{T}{W_0}$) due to gravity is negligible for small values of mass ratio.

Figures 12a, b and c present time of flight required for descent from 100 stat mi (161 km) to 300,000 ft (91.5 km) and the re-entry parameters at 300,000 ft (91.5 km) as functions of thrust-to-weight ratio, mass ratio, and values of δ of 180, -135, and -90°, respectively. It is interesting to note that the hand computed instantaneous pulse points fared into the digital results for the δ = 180° case. The sensitivity of both range and time of flight to small changes in mass ratio may be observed to decrease as mass ratio increases; this portion of the analysis, however, will be discussed later.

If now a curve such as the one shown in Fig. 13 is employed to determine values of total range attained in descending to sea level Figs. 14a, b, and c may be obtained. These curves point up most effectively the proper combination of δ, $\frac{T}{W_0}$ and mass ratio required to accomplish a minimum energy orbital departure for a given range. Examination of these figures reveals that the minimum propellant requirement for a given value of total range is obtained for this special case for a value of δ of approximately -135°. Further examination indicates that both re-entry flight path angle and the required mass ratio are minimum for the higher thrust-to-weight ratio (0.5), again for a given value of total range.

Since the results obtained thus far pertain to only one set of initial conditions and since it is desired to show the effects of small variations in the conditions prior to initiation of the retrorocket on the re-entry parameters, another series of runs has been made. However, due to the scope of the program involved only one retrorocket configuration has been investigated. This particular configuration was selected to provide a minimum energy orbital departure for a total range of 5000 naut mi or 9270 km (δ = -135°, T/W = 0.5, ζ = 0.042, L/D = 0.5). The results of this series of runs are presented in Fig. 15.

3. Orbital Departure from Nearly Circular Orbits ($100 \leq h \leq 500$ stat mi i.e. 161 to 805 km) with Finite Burning Times

This section treats departure from orbits whose altitudes vary from 100 to 500 stat mi (161 to 805 km), whose velocities at the firing of the retrorocket vary between 100 ft/sec more than and 100 ft/sec less than the velocity of circularity ($v_c \pm 30.5$ m/sec) at the orbital altitude, and whose flight path angles will be between ±4°.

As was discussed in the previous paragraphs, the work done by the radial component of thrust is small; therefore, as the orbital altitude increases, the value of δ which provides for a minimum energy orbital departure rapidly changes from -90 to 180°. The value of δ to be used for the remainder of this study dealing with orbits of 100-stat mi (161-km) altitude and more will be 180°. The initial thrust-to-weight ratio will also be assigned a value to restrict the scope of the program which must be undertaken to provide the data for this report. Figure 16, a plot of the re-entry parameters as functions of orbital altitude and thrust-to-weight ratio, shows the reduced sensitivity of all of the re-entry quantities to thrust-to-weight ratio as $\frac{T}{W_0}$ increases. This figure indicates that no improvement in the re-entry parameters or reductions in the required mass ratio are to be realized by increasing $\frac{T}{W_0}$ to more than 1.5 and little above 0.5; therefore, a value of $\frac{T}{W_0}$ of 0.5 is used for the remainder of this analysis.

Figure 17 presents re-entry velocity, flight path angle, time of flight required for descent and the range attained in descent to 300,000 ft (91.5 km) as functions of the initial altitude and retrorocket mass ratio for several initially circular orbits. This figure clearly defines the minimum mass ratio required for departure from several initially circular orbits. Any mass ratio less than that which produces 0° as a re-entry angle would produce an elliptical orbit, the initial perigee of which would be above the nominally selected re-entry altitude, and the initial apogee of which would be approximately the altitude at burnout. This orbit would decay, possibly quite rapidly due to the existence of an atmosphere above the re-entry altitude, and the vehicle would eventually re-enter; these figures, however, are for those applications in which the vehicle would re-enter the sensible atmosphere, as defined, in one-half of one revolution or less. The time of flight for a vehicle traveling in a trajectory which did not initially pass within the atmosphere would be determined approximately by its closest approach to the earth and the quantity $\frac{C_D A}{2m}$.

Figures 18a, b, c, d, and e present the re-entry parameters as functions of orbital altitude, orbital velocity and retrorocket mass ratio (γ_1 = 0°). Conclusions pertaining to the minimum mass ratios acceptable for orbital departure for velocities other than that of circularity can be obtained from these figures in the manner discussed for Fig. 17.

Figures 19a, b, c, d, and e present the re-entry parameters as functions of retrorocket mass ratio, orbital altitude and flight path angle prior to firing the retrorocket. Several of these figures show discontinuities and bulges which at first glance may appear to be in error; however,

it must be noted that these irregularities occur for mass ratios which are marginal from the standpoint of energy required for successful orbital exit and only in the range of flight path angles from approximately -2° to +2°. This situation can best be explained by stating that a variation in the value of γ_1 (either positive or negative) produces an elliptical orbit one portion of which lies below the altitude at which the retrorocket is fired. The net result of this displacement of the perigee is to reduce the amount of propellant required for a successful departure from orbit or to make exit less marginal for a given amount of propellant.

Small thrust-to-initial-weight ratios $\left(\frac{T}{W_0} = 0.01\right)$ for orbital departure have also been considered. This device burned for the major portion of the time required for descent, thus, providing a force which could also be employed for minor maneuver or flight path corrections during descent. It was thought that significant reduction in the re-entry flight path angle could be realized with this approach; however, the results indicated little margin of superiority in this respect and showed an increase in the amount of propellant required.

4. Error Sensitivities for Departure from Nearly Circular Orbits Assuming Finite Burning Times

Generally, since the orbital velocity, altitude and flight path angle at any given time are not known exactly, it is desired to show the effects of errors in each of these orbital parameters prior to initiation of a retrorocket and in the retrorocket burning time on the re-entry parameters being evaluated. Due to the fact that no purely analytical expressions can be obtained which include the effects of retrorocket burning time on these errors, each error was evaluated manually by determining the slopes of the curves presented in the previous sections. An extension of this analysis to include such things as variations in the peak values of deceleration and vehicle skin temperatures due to the atmosphere, in the impact angle and velocity, and in impact dispersion, will not be made here due to the fact that each of these quantities is a complex function of the configuration of the re-entry vehicle.

The error in a given re-entry parameter resulting from any of the errors being investigated can be evaluated from the data presented here in the following manner.

$$\Delta X_1 = \Delta t_B \left(\frac{\Delta X}{\Delta t_B}\right) \quad (140)$$

$$\Delta X_2 = \Delta V_1 \left(\frac{\Delta X}{\Delta V_1}\right) \quad (141)$$

$$\Delta X_3 = \Delta h_1 \left(\frac{\Delta X}{\Delta h_1}\right) \quad (142)$$

$$\Delta X_4 = \Delta \gamma_1 \left(\frac{\Delta X}{\Delta \gamma_1}\right) \quad (143)$$

where

X can be any of the four re-entry quantities considered (range, flight time, velocity, and flight path angle).

The resultant error in any of the re-entry parameters due to an error in more than one of the quantities t_B, V_1, h_1 and γ_1 can now be evaluated through the utilization of the chain rule, i.e.,

$$\Delta X_{total} = \Delta X_1 + \Delta X_2 + \Delta X_3 + \Delta X_4. \quad (144)$$

This assumption is permissible only because the independent error terms are small for most cases; if a higher degree of accuracy is desired or if these independent errors are large, the method of successive approximations must be employed to improve the accuracy of the estimate. Once the resultant error has been determined, the actual value of the re-entry parameter may be obtained by adding the resultant error to the nominal value of quantity as defined in previous sections.

It is noted at this point that this procedure will not yield the most probable value of the error if the maximum errors in each parameter are substituted into the chain. To obtain this probable error, it is necessary to refer to statistical discussions similar to that presented in Chapter VI.

Due to the fact that it is at present impossible to place a vehicle in an exact predetermined orbit, it is necessary to provide the vehicle with a retrorocket large enough to remove the vehicle from the major portion of orbits into which injection is likely. This fact makes it necessary to physically control the burning time (and consequently the mass ratio) of the retrorocket in order to prevent the vehicle from assuming a trajectory which would produce maximum values of skin temperature and/or deceleration which exceed the limits placed on the trajectory by structural and personnel considerations.

Figures 20a, b, c, d and e present the errors in the re-entry parameters due to an error in t_B (assumed to be 1 sec) as functions of the orbital conditions prior to firing the retro-rocket and of the retrorocket mass ratio. The selection of this value of Δt_B is not intended to reflect the accuracy anticipated in controlling this quantity but rather is intended to make the data more readily applicable for all values of Δt_B. Actually, this error can be limited to approximately 0.05 sec barring malfunction for most motors of the size necessary for this maneuver.

Figure 21 presents the changes in the re-entry quantities due to an error of 1 ft/sec (0.3 mps) in V_1 as a function of the retrorocket mass ratio and the orbital conditions prior to firing the retrorocket. Very little data is available pertaining to the accuracies obtainable from the various velocity sensing schemes and mechanisms, but it is felt that vehicle velocity should be known within a

range of 1 to 10 parts in 100,000. These inaccuracies correspond to errors in V_1 from approximately 0.2 to 1.0 fps (±0.06 to ± 0.3 mps).

Figures 22a, b and c present the variations in the re-entry parameters due to a 1-stat mi (1.61 km) error in h_1. The accuracies obtainable even with present radar indicate that it would be unreasonable to assume an error in h_1 greater than approximately 300 ft $\left(\frac{1}{17.6}\right.$ stat mi or 91.5 m$\left.\right)$ will exist. Since all of the errors being evaluated are small even for an error in h_1 of 1.6 km, the effects of an error in h_1 of only 91 m are negligible. As may be observed from the energy equation, variations in altitude h_1 will have a definite effect on the re-entry velocity, an effect which is not reflected here. This apparent discrepancy is due to the fact that the assumed error in h_1 is so small that actual variations in the value of the re-entry velocity could not be obtained in this manner from the data.

Figures 23a, b, c, d and e present the errors in the re-entry parameters due to a 1° error in the flight path angle. This error can be the result of the fact that the flight path angle prior to the maneuver was not known correctly or to the fact that the impulse from the retrorocket was not applied in the proper direction. In either case very little data is available pertaining to the accuracy to which this quantity can be obtained; however, it is felt that if sufficiently accurate data is available this angle should be known to the order of 0.01 to 0.1 degree.

The data presented in this section indicates that the resultant errors in all of the re-entry parameters with the exception of range attained in descent will be quite small for the estimated errors in t_B, V_1, h_1 and γ_1. Range, however, is quite sensitive to errors in each of these quantities thus pointing up the probability of a marked impact dispersion pattern. The determination of this pattern, however, will not be attempted due to the necessity of including the vehicle ballistic coefficient and aerodynamic lift in such analysis. In any event, the presence of an atmosphere below the re-entry altitude will magnify the dispersion pattern existing at re-entry due to the aerodynamic uncertainties and the fact that γ and V were also affected by the previous errors.

D. THREE-DIMENSIONAL IMPULSE ANALYSIS FOR THE CASE OF CIRCULAR ORBITS

The approach in the previous sections has been to reduce the recovery problem to one of two dimensions by utilizing an intermediate orbit. The philosophy for this approach is governed by the consideration of the energy required for maneuvering. However, because timing errors can result, and because under some circumstances it may be desirable to recover promptly, it is also necessary to consider the three-dimensional nature of the problem (see following sketches).

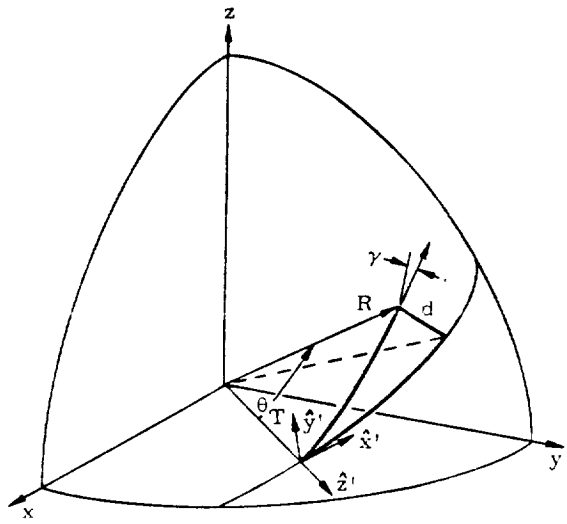

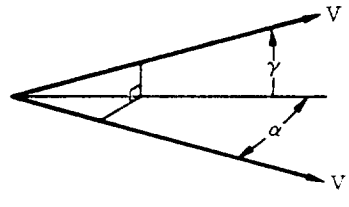

This particular problem has been analyzed by Fosdick and Anthony (Ref. 1). For this reason the complete solution will not be repeated here. However, it is noted that the problem is not unlike those discussed in Chapter VI (Maneuvers). The referenced paper gives the following:

(1) The direction cosines of the impulse in vehicle centered coordinates

$$\ell = \frac{\Delta\vec{V} \cdot \hat{X}'}{\Delta V} = (\nu \cos\alpha \cos\gamma - 1)/D^*$$

$$m = \frac{\Delta\vec{V} \cdot \hat{Y}'}{\Delta V} = (\alpha \cos\gamma \sin\alpha)/D^*$$

$$n = \frac{\Delta\vec{V} \cdot \hat{Z}'}{\Delta V} = (\nu \sin\gamma)/D^*$$

where

$$D^* = (1 - 2\nu \cos\alpha \cos\gamma + \nu^2)^{1/2}$$

α = The angle in the horizontal plane at the initial radius through which the velocity vector is rotated

γ = The flight path angle of the velocity vector following the impulse

$$\nu = \frac{V}{V_c}$$

$$\nu = \left\{ \left[1 - \cos\theta_T\right] \left[\cos^2\alpha \quad (1 - \cos\theta_T + \frac{r - R}{R} \cdot \right. \right.$$
$$\left. \left. + \tan\alpha \sin\theta_T \right]^{-1} \right\}^{1/2}$$

(2) Turn angle and impulse magnitude

$$\sin\alpha = \frac{\sin d}{\sin\theta_T}$$

$$\frac{\Delta V}{V_c} = \nu^2 + 1 - 2\nu\cos\gamma\cos\alpha$$

(3) Flight path angle.

To this point only the initial and final radii and the angle between have been fixed. Thus, the transfer ellipse is not unique and γ cannot be fixed. This condition is altered if the time of flight (or flight path angle or velocity at a point in the ellipse) is specified since then the ellipse is unique. The reason that this was not done was to leave an area for possible optimization of the impulsive correction.

Ref. 1 also reports some results obtained for the analytic optimization of the position of deorbit. The solution is, however, fairly lengthy. Gedeon (Ref. 2) took this work and developed some interesting results by numerical optimization of the following equation obtainable from Ref. 1.

$$\Delta K = \sqrt{1 - 2K\cos\gamma\sqrt{\sin^2\theta_T - \frac{\sin^2 d}{\sin\theta_T}} + K^2}$$

where: $K = \frac{\sin\theta_T/2}{\cos\gamma} \cdot \sqrt{\frac{2}{\frac{r_0}{r_1} - \frac{\cos(\theta_T - \gamma)}{\cos\gamma}}}$

r_0 = initial radius

r_1 = radius at which the displacement occurs

ΔK = The change in the quantity $\sqrt{2 - \frac{r}{a}}$

= a measure of ΔV since $a = \frac{r\mu}{2u - r\left|\vec{V} + \vec{\Delta V}\right|^2}$

$$= -2\frac{r}{K}\frac{\vec{V}\cdot\vec{\Delta V}}{\mu} \quad \frac{|\Delta V|^2}{|V|^2} \ll |$$

The results of these procedures are presented in Figures 24 through 27. One important factor should be noted. These figures have the parameter r_0/r_1; thus, they can be utilized for generating data down the re-entry altitude (or to impact if the effects of the atmosphere on the trajectory can be assumed negligible in the case of interest).

This being the case, the angle γ, takes on special value since it is the re-entry angle discussed previously and in Chapter IX.

This material completes this portion of the 3-D recovery discussion. As was noted previously, however, additional material on this problem and on maneuvers can be found in Chapter VI.

E. ANALYSIS OF ORBITAL DEPARTURE FREQUENCY

1. Defining Equations

For the purpose of defining the acceptable times of orbital departure from the low altitude orbit, a model of the earth and of the satellite orbit have been selected. The earth is assumed to be spherical and rotating at a uniform rate (see the following sketch). In order to partially compensate for errors involved in assuming a spherical earth, the orbital plane is assumed to be regressing about the equator at a uniform rate. The orbit of the satellite will be considered to be affected by drag forces; however, all other accelerations (such as second order oblateness effects, sun, moon, etc.) are neglected.

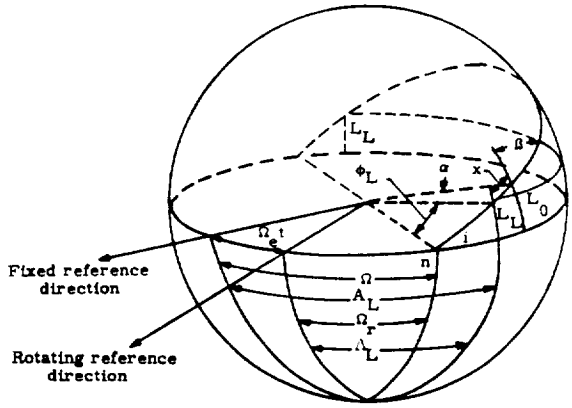

$$\alpha = \frac{X}{R_s} = \frac{\text{arc}}{\text{radius}}$$

Utilizing this sketch and the assumptions listed above, it is now possible to solve for the sidereal time at which the impact point lies in a prescribed plane.

$$t_{exit} = \frac{\Omega_0 + n\dot{\Omega} - (\Lambda + \Delta\Lambda \text{ maneuver})}{\Omega_e} + \frac{f_{impact}(L, i) + 2m\pi}{\Omega_e}$$

where: $\Delta\Lambda$ maneuver = angular displacement corresponding to thrust or aerodynamic maneuverability.

$$\dot{\Omega} = -3\pi J_2 \left(\frac{R}{p}\right)^2 \cos i \qquad 0° \leq i \leq 180°$$

m = positive integer for number of days; selected sufficiently large that $t \geq 0$

$$f(L, i) = \sin^{-1} \frac{\tan L_L}{\tan i}$$ northerly launches or southerly approach

$$= \pi - \sin^{-1} \frac{\tan L_L}{\tan i}$$ northerly approach southerly launches $0° < i < 90°$

$$= \pi + \sin^{-1} \frac{\tan L_L}{\tan i}$$ northerly approach southerly launch $90° < i < 180°$

n = number of revolutions in orbit (non-integer)

Similarly there is an expression for the time at which the launch point crosses the plane

$$t_{launch} = \Big(\Omega_0 - \Lambda_{launch} - \Delta\Lambda_{launch\ maneuver} + f_{launch}(L, i) \Big) \Omega_e^{-1}$$

Thus, the time duration for the satellite in orbit is $t_{exit} - t_{launch}$ or

$$t_{in\ orbit} = \Big[(\Lambda + \Delta\Lambda)_{impact} - (\Lambda + \Delta\Lambda)_{launch} + n\dot{\Omega} + 2m\pi + f_{impact}(L, i) - f_{launch}(L, i) \Big] \Omega_e^{-1}$$

It is noted at this point that though f_{impact} and f_{launch} have the same functional form, the numerical values of L_L, L_i, i and i_i need not be the same. Thus, this equation can reflect the effects of maneuvering in orbit in the interim between launch and recovery.

A second equation for the time in orbit may be written as

$$t_{in\ orbit} = n\tau_0 + \sum_{i=1}^{n} \Delta\tau_i + t_{AD}$$

where

n = the number of revolutions in the orbit (noninteger)

τ_0 = the period of the initial orbit over an oblate earth

$\Delta\tau_i$ = change in the i^{th} period due to drag shown in the next sketch

t_{AD} = the time required for ascent and descent.

Now, the two equations for $t_{in\ orbit}$ can be equated and solved for the unknown "n" which will be required to place the satellite and the impact point in the desired positions for recovery.

$$n = \Big[(\Lambda + \Delta\Lambda)_{impact} - (\Lambda + \Delta\Lambda)_{launch} + 2m\pi + f_{impact}(L, i) - f_{launch}(L, i) - \Big(\sum_{i=1}^{n} \Delta\tau_i + t_{AD} \Big) \Omega_e \Big] \Big[\tau_s \Omega_e \Big(1 + \frac{\Delta\tau}{\tau_s} - \frac{\dot{\Omega}}{\Omega_e}\Big)\Big]^{-1}$$

where

$\frac{\Delta\tau}{\tau_s}$ = oblateness correction for orbital period, see Chapter IV

τ_s = the orbital period over a spherical earth.

2. Drag Correction

Since the corrective term (i.e., the series) is a function of n (shown in the following sketch), the solution requires iteration.

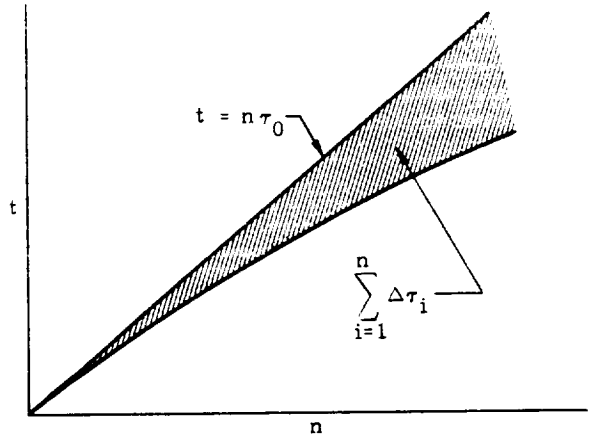

This process, however, is greatly simplified due to the fact that the size of the correction is small. Thus n can be estimated neglecting the correction and then refined. This refinement can be obtained in the following fashion.

$$a = \frac{r_a + r_p}{2}$$

$$\Delta a_{secular} = \frac{(\dot{h}_a + \dot{h}_p)}{2} \tau$$

$$\Delta\tau_{secular} = \frac{3}{2} \frac{\tau}{a} (\Delta a_D + \Delta a_0)$$

$$= -\frac{3}{4}\frac{\tau^2}{a}\left[G_1(z) + G_2(z)\right]\left[1 - e\right]^{1/2} 2B\rho_p\sqrt{\mu r_p}$$

where

Δa_D = the drag correction for secular changes in the semi-major axis

Δa_0 = the oblateness correction for secular changes in the semimajor axis = 0

$G_1(z)$, $G_2(z)$ = drag parameters for elliptic orbits, discussed in Chapter V

ρ_p = atmosphere density at perigee

$B = \frac{C_D A}{2m}$

Thus, as the elements are defined as a function of the revolution number, the correction corresponding to that revolution can be computed.

The approach above is vigorous but is somewhat more involved than desirable because it is necessary to compute a correction on each revolution. In view of the fact that the corrections are in general small and that the atmospheric uncertainties preclude high accuracies, an alternative solution is available for the case of circular and near circular orbits. This approach makes use of the fact that in a restricted range of altitudes the following approximations are valid.

$$\Delta\tau = (4\pi\rho B\sqrt{\mu r_p})\left(\frac{3}{2}\sqrt{\frac{a}{\mu}}\right)\Delta t = -6\pi B a\,\Delta t$$

But

$$t \approx n\tau_0$$

$$\Delta t \approx \tau_0\,\Delta n$$

Now replacing a by $(a_0 - 4\pi\rho a_0^2 Bn)$ yields:

$$\Delta\tau \approx -6\pi B\tau_0(a_0 - 4\pi\rho a_0^2 Bn)\rho\,\Delta n$$

and for nearly circular orbits

$$\rho \approx \rho_0 \exp K(a_0 - a) \approx \rho_0 \exp K(4\pi\rho_0 a_0^2 Bn)$$

$$\Delta\tau = \left\{-6\pi B\tau_0\left[(a_0 - 4\pi\rho_0 a_0^2 Bn \exp K(4\pi\rho_0 a_0^2 Bn)\right]\right.$$

$$\left.\cdot\,\rho_0 \exp K(4\pi\rho_0 a_0^2 Bn)\,\Delta n\right\}$$

Now adopting a shorthand notation to prevent bookkeeping problems with the constants, the equation for $\Delta\tau$ becomes

$$\Delta\tau = (A_1 + A_2 n e^{A_3 n})\, e^{A_3 n}\,\Delta n$$

$$A_1 = -6\pi B\tau_0 a_0\rho_0$$

$$A_2 = +24\pi^2 B^2\tau_0 a_0^2\rho_0$$

$$A_3 = 4\pi\rho_0 a_0^2 BK$$

If, at this point it is further assumed that the series $\sum_{i=1}^{n}\Delta i$ can be approximated by the integral, a simple expression can be obtained.

$$\sum_{i=1}^{n}\Delta\tau_i = \int_0^n (A_1 + A_2 n e^{A_3 n})\, e^{A_3 n}\, dn$$

$$= \frac{A_1}{A_3} e^{A_3 n} + \frac{A_2(2A_3 n - 1)}{(2A_3)^2} e^{2A_3 n}$$

This expression should be utilized for the evaluation of the series for most of the cases of interest. However, for special cases where $|2A_3 n| < 1$, it is of interest to look at the series expansion of the right-hand side of the previous equation.

$$\sum_{i=1}^{n}\Delta\tau_i = \frac{A_1}{A_3}\left(1 + A_3 n + \frac{(A_3 n)^2}{2} + \frac{(A_3 n)^2}{6} + \ldots\right)$$

$$+ \frac{A_2(2A_3 n - 1)}{(2A_3)^2}\left(1 + 2A_3 n + \frac{(2A_3 n)^2}{2} + \frac{(2A_3 n)^3}{6} + \ldots\right)$$

$$= \left(\frac{A_1}{A_3} - \frac{A_2}{4A_3^2}\right) + n\left(A_1 + \frac{A_2}{2A_3}\right) + n^2\left(\frac{A_1 A_3}{2} + \frac{A_2}{2}\right) + n^3\left(\frac{A_1 A_3^2}{6} + \frac{2A_2 A_3}{3}\right) + \text{other terms.}$$

This form of the series is preferable for the previously noted special cases because of the simple form.

It is noted at this point that either form for the correction will be more accurate if the altitude range is small. Thus, a logical extension could be obtained by breaking the decay range into regions which the assumptions were valid. This approach would entail the computation of several sets of constants A_i (i = 1, 2, 3).

3. Launch Maneuver Correction

To this point each factor in the definition of the quantity n has been discussed except the quantities $\Delta\Lambda_{launch}$ and $\Delta\Lambda_{impact}$. The first maneuver ($\Delta\Lambda_L$) is the direct result of launching into a plane other than the orbital plane and utilizing a portion of the propellant for the purpose of turning the vehicle into the desired plane. The magnitude of this maneuver thus depends on the amount of surplus propulsion available, the type of trajectory to be flown and the type of guidance law which is utilized. Although no detailed discussions of powered flight are presented in this volume, the related discussions for the case where the plane is altered impulsively can be presented. Consider the following sketch and the spherical relationships derivable therefrom:

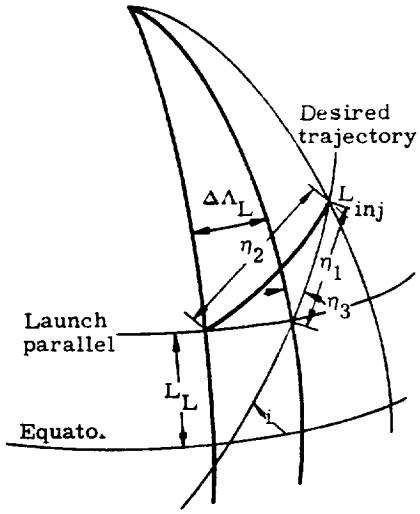

$$\sin \phi = \frac{\sin L}{\sin i}$$

$$\eta_1 = \phi_{inj} - \phi_L$$

$$= \sin^{-1}\left(\frac{\sin L_{inj}}{\sin i}\right) - \sin^{-1}\left(\frac{\sin L_L}{\sin i}\right)$$

$$\eta_2 = \frac{\text{ascent range}}{\text{Earth's radius}}$$

(i.e., the plane change is assumed to occur at point of injection into orbit but prior to injection for fuel economy)

$$\eta_3 = \beta_L$$

$$= \sin^{-1}\left(\frac{\cos i}{\cos L_L}\right)$$

Now the determination of $\Delta\Lambda$ can proceed based on Eqs (65) and (68) of Chapter XIII.

$$\sin(\Lambda - \Lambda_0) = \frac{\sin\alpha \sin\beta}{\cos L}$$

$$\sin L = \sin L_0 \cos\alpha + \cos L_0 \sin\alpha \cos\beta$$

or

$$\cos\beta = \frac{\sin L - \sin L_0 \cos\alpha}{\cos L_0 \sin\alpha}$$

These equations are the parametric equations for a polar cap with center at L_0, Λ_0 and of radius of α. The azimuth angle β is then the independent variable for generating the locus of points L, Λ. These two equations can be utilized as follows:

Let

$$\alpha = \eta_1$$

$$\beta = \eta_3$$

$$\Lambda_0 = 0$$

then

$$\sin\Lambda_1 = \frac{\sin\eta_1 \sin\eta_3}{\cos L_{inj}}$$

Now let

$$\alpha = \eta_2$$

$$L_0 = L_{inj} \text{ and } L = L_L$$

$$\cos\beta = \frac{\sin L_L - \sin L_{inj}\cos\eta_2}{\cos L_{inj}\sin\eta_2}$$

and

$$\sin(\Lambda_2 - \Lambda_1) = \frac{\sin\eta_2 \sin\beta}{\cos L_L}$$

At this point it is noted that the quantity of interest $\Delta\Lambda_L$ may be obtained to be:

$$\Delta\Lambda_L = \Lambda_2 - \Lambda_0 = \Lambda_2$$

This derivation tacitly assumed that the launch site would cross the orbital plane, thus as a consequence this value of $\Delta\Lambda_L$ is valid only for the cases for which

$$i > |L_L|$$

By varying the formulation above other cases can, however, be included.

4. Landing Maneuver Correction

The second maneuver to be discussed ($\Delta\Lambda_{impact}$) is, as was noted, the result of either

aerodynamic maneuverability or thrust. In either case, however, $\Delta\Lambda_{impact}$ is highly dependent on the guidance philosophy. This being the case, only the simplest of the possible maneuvers can be considered. The following sketch illustrates this problem for a lateral maneuver distance D_m and a descent range R.

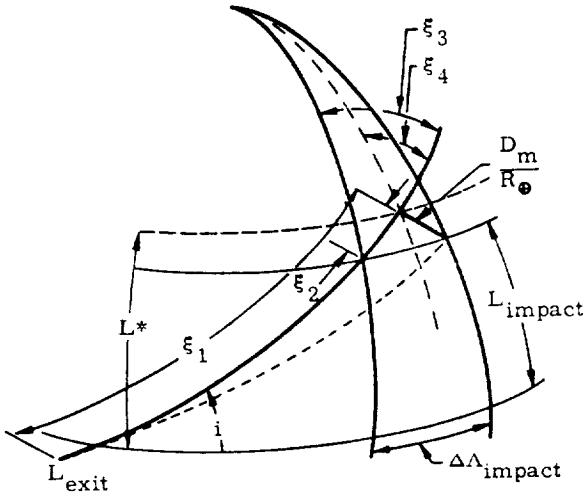

$$\xi_1 = \cos^{-1}\left[\frac{\cos\frac{R}{R_\oplus}}{\cos\frac{D_m}{R_\oplus}}\right]$$

$$\xi_2 = \xi_1 - \phi_2 + \phi_1$$

where

$$\phi_1 = \sin^{-1}\left(\frac{\sin L_{exit}}{\sin i}\right)$$

$$\phi_2 = \sin^{-1}\left(\frac{\sin L_{impact}}{\sin i}\right)$$

$$\xi_3 = \sin^{-1}\left(\frac{\cos i}{\cos L_{impact}}\right)$$

$$L^* = \sin^{-1}\left(\sin i \sin(\xi_2 + \phi_2)\right)$$

$$\xi_4 = \sin^{-1}\left(\frac{\cos i}{\cos L^*}\right)$$

Now, as before, the spherical segment equations can be utilized to yield $\Delta\Lambda_{impact}$.

let

$$\alpha = \xi_1$$

$$\beta = \xi_3$$

$$\Lambda_0 = 0$$

$$L_0 = L_{impact}$$

$$\sin\Lambda_1 = \frac{\sin\xi_1 \sin\xi_3}{\cos L^*}$$

Now let

$$\alpha = \frac{D_m}{R}$$

$$\beta = \xi_3$$

$$\Lambda_0 = \Lambda_1$$

$$L_0 = L^*$$

$$\sin(\Lambda_2 - \Lambda_1) = \frac{\sin\left(\frac{D_m}{R}\right)\sin\xi_4}{\cos L_{impact}}$$

and finally

$$\Delta\Lambda_{impact} = \Lambda_2 - \Lambda_0 = \Lambda_2$$

No stipulation has been made as to the restriction on the validity of this value of Λ_2; however, in the derivation an assumption has been made nonetheless. This assumption is that

$$i > |L_{impact}| + \frac{D_m}{R}$$

While this assumption is somewhat restrictive, it provides information for most of the orbits of practical value. Those orbits which are excluded will be discussed later.

Attention may now be turned to the description of the parameters assumed in this final discussion, R and D_m. The first quantity must be estimated from the combination of the free flight trajectory down to a re-entry altitude, the aerodynamic characteristics of the body and the re-entry conditions. This material is found in Chapters III and IX. The second quantity (D_m), however, must be handled in a slightly different fashion. If the maneuver is the result of a small impulsive correction, the lateral maneuverability is approximately

$$D_m = r_0 \frac{\Delta V}{V_0} \sin(\theta - \theta_0) \quad \text{(see Chapter VI)}$$

where

r_0 = initial radius

V_0 = initial velocity

$\theta - \theta_0$ = central angle from point of maneuver to impact

Whereas, if the maneuver results from aerodynamic forces

$$D_m \approx 623\left(\frac{L}{D^*}\right)^{1.875} \text{ naut mi}$$

$$\approx 1155\left(\frac{L}{D^*}\right)^{1.875} \text{ km} \qquad \frac{L}{D^*} < 1.0$$

$$D_m \approx 910\left(\frac{L}{D^*}\right) \text{ naut mi}$$

$$\approx 1688\left(\frac{L}{D^*}\right) \text{ km} \qquad 0.75 < \frac{L}{D^*} < 2.0$$

where

D_m = maximum distance normal to the orbital plane that is obtainable in descent from 300,000 ft (91.4 km).

L/D* = component of the L/D ratio normal to the plane of motion.

These latter relations were suggested by numerical integration of actual motions, although it is noted that the former relation $\left(\frac{L}{D^*} < 1\right)$ has some theoretical basis. (The theoretical constants are different.)

5. The Form of n

Now since each term in the definition of n is a known quantity, the number of revolutions having occurred at any time that the impact point is in or near the plane of motion can be evaluated. The attention must, therefore, be turned to those values of n which are acceptable for a particular problem. Consider the following sketch:

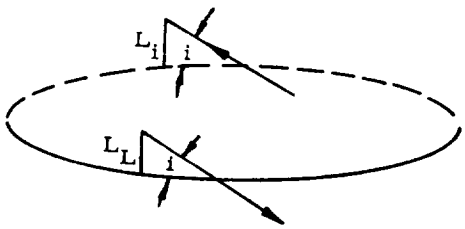

From this sketch, it is apparent that the number of revolutions must be of this form:

$$n' = p + \frac{1}{2\pi}\left[\pi + \sin^{-1}\left(\frac{\sin L_L}{\sin i}\right) + \sin^{-1}\left(\frac{\sin L_i}{\sin i}\right)\right]$$

southerly launches approach from the south

$$= p + \sin^{-1}\left(\frac{\sin L_L}{\sin i}\right) - \sin^{-1}\left(\frac{\sin L_i}{\sin i}\right)$$

southerly launches approach from north

$$n' = p - \sin^{-1}\left(\frac{\sin L_L}{\sin i}\right) + \sin^{-1}\left(\frac{\sin L_i}{\sin i}\right)$$

northerly launch approach from north

$$= p + \sin^{-1}\left(\frac{\sin L_L}{\sin i}\right) - \sin^{-1}\left(\frac{\sin L_i}{\sin i}\right)$$

northerly launch approach from south

where

p is a positive integer

n' is related to n in following paragraph

But portions of these distances will be required for ascent and descent. Since those distances are not explicitly in the equations for time in orbit (the times required are included), a correction to the value of n' must be made and the resultant form for n must be

$$n = n' - \frac{R_{ascent}}{R_\oplus} - \frac{R_{descent}}{R_\oplus}$$

The procedure is now to generate values of n for the various passes of the impact point through the plane of motion and compare these numbers to those required for successful return. In this comparison if $\pm D_m$ allows the computation of the required n, then a suitable maneuver can result in sucessful return. This process is sufficiently simple in that it can be performed manually if necessary; however, digital computers prove to be a definite asset. Once n is known, it can be determined whether the approach was from the north or south, what maneuverability is required, and even the time at which deorbit should occur.

6. Alternative Methods

As was noted in previous paragraphs, there have been assumptions made which restrict the applicability of the approach to orbits for which $i > |L_{impact}| + \frac{D_m}{R_\oplus}$. Though this assumption may not be too restrictive for some orbits, it proves troublesome for others. One approach around this impasse is to compute the ground swath defined by the maneuverability of the vehicle. (Ground swaths are discussed in Chapter XIII.) When the ground swath contains the impact site then recovery is possible. If several of these ground swaths are then computed in the vicinity of the positions which yielded satisfactory call-downs, the amount of maneuverability and the direction and the time for deorbit can be found. The approach is very simple and is not restricted as to applicability; however, the number of computations required even for relatively short durations in orbit is large and automatic computation is almost essential.

A third purely graphical approach involves the plotting of the ground track (see Chapter XVIII) for the orbit on vellum for a suitable map. (This track will be approximately constant for the entire duration in orbit under the assumption that large maneuvers or large changes resulting from drag do not occur.) Then the positions of the ascending nodes can be plotted on the map including the effects of drag, oblateness, etc. After this step, the maneuver envelope is superimposed on the ground track as the track is laid alternately on each of the ascending nodes and the possible call-downs are recorded. This final approach thus combines the advantages of both of the previous approachs in that it is not restricted to latitudes, can be performed manually and readily exhibits the information desired. Much work is still required, however, in order to develop the data.

Each of these three methods has its merits, and each has been utilized for analyses of this type. The selection of a method should be based on the method of computation, the information required in the analysis, and the availability of data in various forms.

F. CONCLUSIONS

In this chapter the geometry and the landing site intercept timing considerations for a generalized return trajectory from an elliptical orbit into a low altitude circular orbit are presented mathematically. An error analysis of the final low altitude orbit characteristics is derived for small errors in the departure velocity, altitude and flight path angle. The following conclusions are reached.

(1) The return trajectory is extremely sensitive to errors in departure velocity. A vernier correction of the velocity vector seems mandatory immediately after the initial departure injection for certain classes of orbits.

(2) Errors in departure radius cause an error of roughly the same order of magnitude at the perigee arrival.

(3) In case of departure close to the apogee of the transfer ellipse, the errors caused by deviations in flight path angle are extremely small and can be neglected for engineering purposes.

In the timing analysis of the return shuttle, it is shown that two possible target arrival times exist for each day. The solution for the exact departure angle required for a target intercept is best accomplished by an iterative method. For the sample problem the convergence of the iteration method is very rapid. The second approximation gives an answer within two decimal places and within 1.5 sec of total flight time (t_t = 54, 129.92 sec).

Three flight time error analyses are investigated. First, the approximate analytical method is seen to give only an order of magnitude result. Second, the exact analytical method is seen to be somewhat cumbersome algebraically, so far as manual computations are concerned (on the other hand, a digital computer can handle the exact equations easily). Third, the numerical differentiation method is found to be simple, fast and sufficiently accurate.

Call-down from an intermediate altitude circular orbit or from low altitude circular orbits in general is shown to be extremely sensitive to all error sources. Indeed, if a given landing point is selected with a very small allowable error, the only means of achieving a satisfactory landing at a prescribed time is with a maneuverable re-entry vehicle. Lateral maneuverability seems to afford the most rewarding avenue of investigation from this point of view.

The anlaysis of orbital departure with finite burning times shows the effect of thrust attitude and magnitude on the re-entry parameters. The analysis also shows that the optimum thrust vector is not always opposite in direction from that of the velocity vector and that thrust levels above approximately 1/2 mg alter the descent trajectory very little.

G. REFERENCES

1. Fosdick, G. and Anthony, M., "Three-Dimensional Pulse Optimization for Vehicles Disorbiting from Circular Orbits," ARS paper 61-156-1850, 13 June 1961.

2. Gedeon, G. S., "Flight Performance Manual for Orbital Operations," Norair Div Northrop Corp. (Hawthorne) Report NOR 61-208, September 1961.

H. BIBLIOGRAPHY

See Chapters III, V, VI, VII and IX for references pertinent to the problem of recovery. In addition, the following are offered.

Bull, G., Enkenhus, K. and Tiddy, G., "Exit and Re-entry Problems," Aerospace Engineering, Vol. 17, No. 6, June 1958.

Detra, R., Ryddell, F. and Rose, P., "Controlled Recovery of Nonlifting Satellites," ARS Journal, Vol. 30, No. 9, September 1960, p 892.

Fosdick, G. and Anthony, M., "3-D Pulse Optimization for Vehicles Disorbiting from Circular Orbits," ARS paper 61-156-1850, June 1961.

Hakes, R. C., "Some Fundamental Problems Associated with Injecting, Orbiting and Recovering Man from Orbit," presented at 27th Annual Meeting of IAS, New York, 26 to 29 January 1959.

Hoglund, R. and Thale, J., "Recovery from a Satellite Orbit," ARS Preprint 650-58, 1958.

Low, G. M., "Nearly Circular Transfer Trajectories for Descending Satellites," NASA report No. 3, Lewis Research Center.

Rosamond, D. L., "Satellite Recovery Techniques for Optimization of Touchdown Accuracy," Journal of Aerospace Sciences, Vol. 28, No. 3, March 1961.

Townsend, G. and Kork, J., "Satellite Recovery," Chapter 9 in Design Guide to Orbital Flight, McGraw-Hill Book Co., New York, 1962.

ILLUSTRATIONS

Preceding page blank

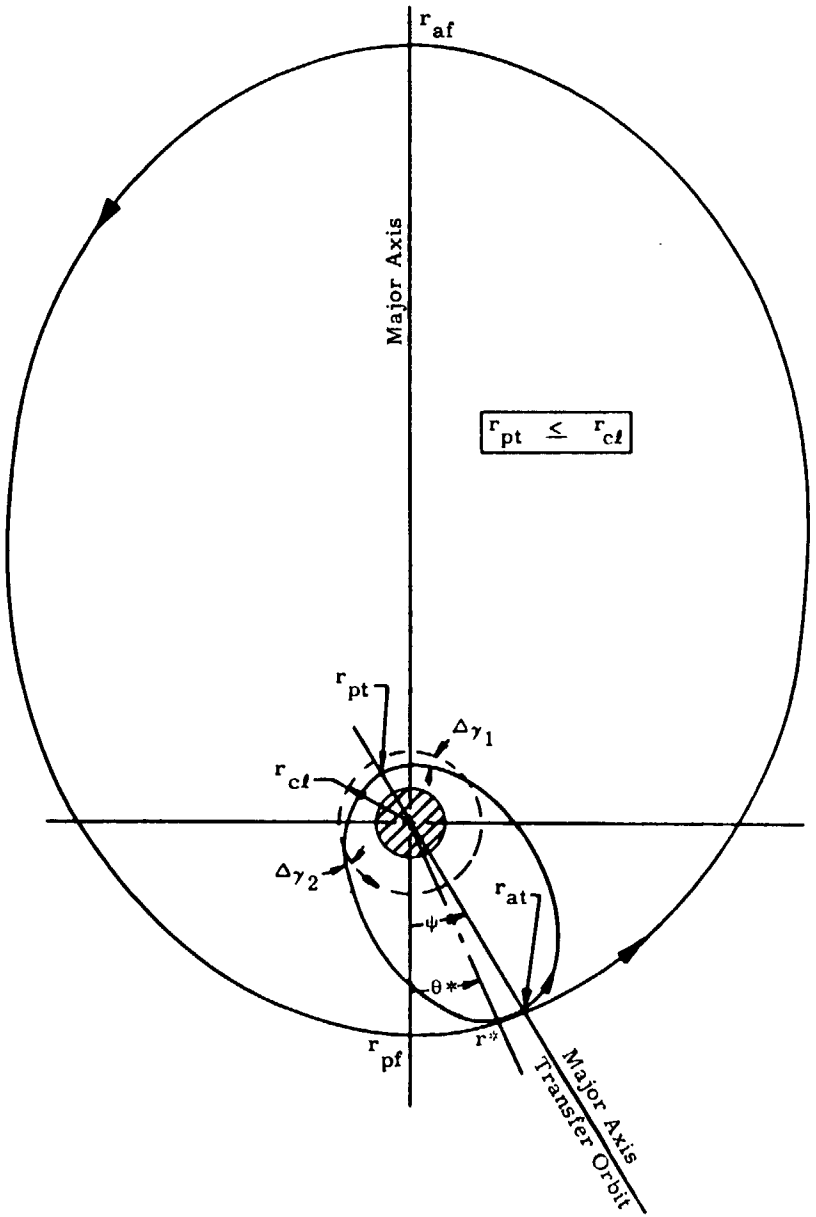

Fig. 1. Geometry of the Return Problem

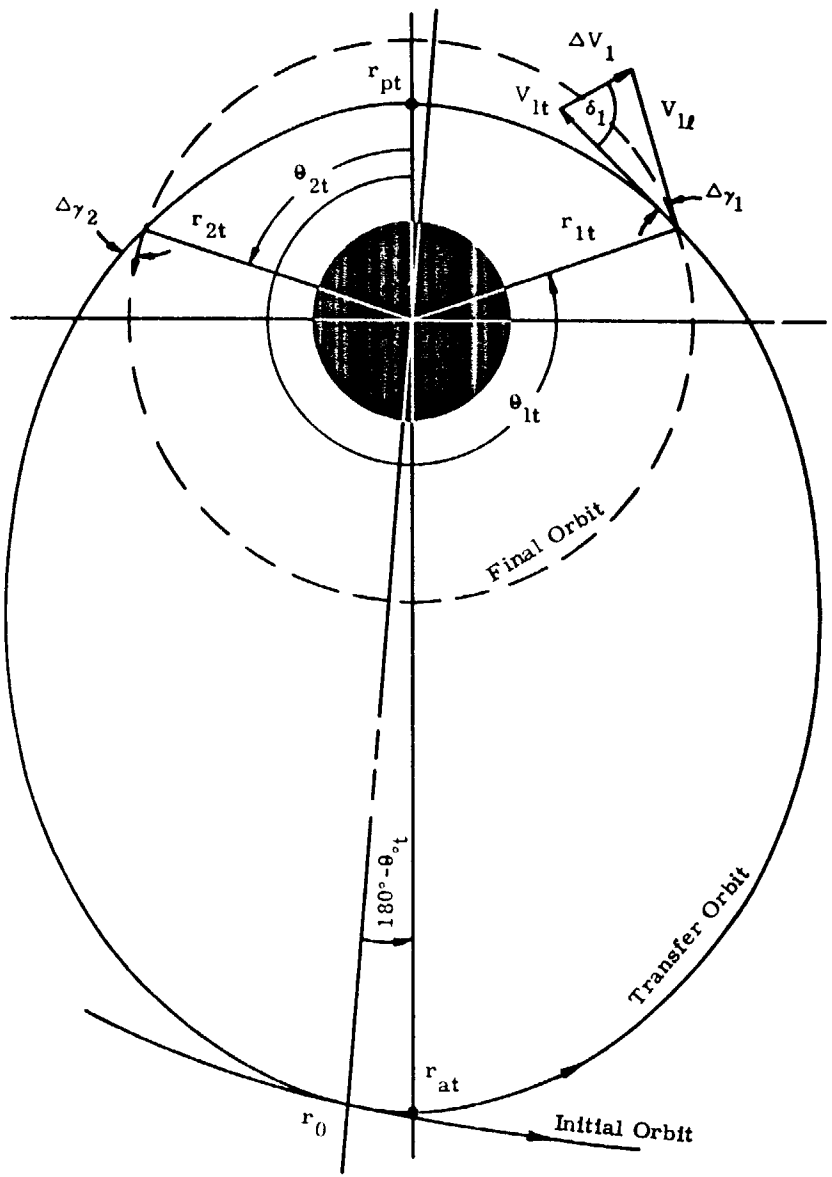

Fig. 2. Geometry of the Return Problem (expanded view)

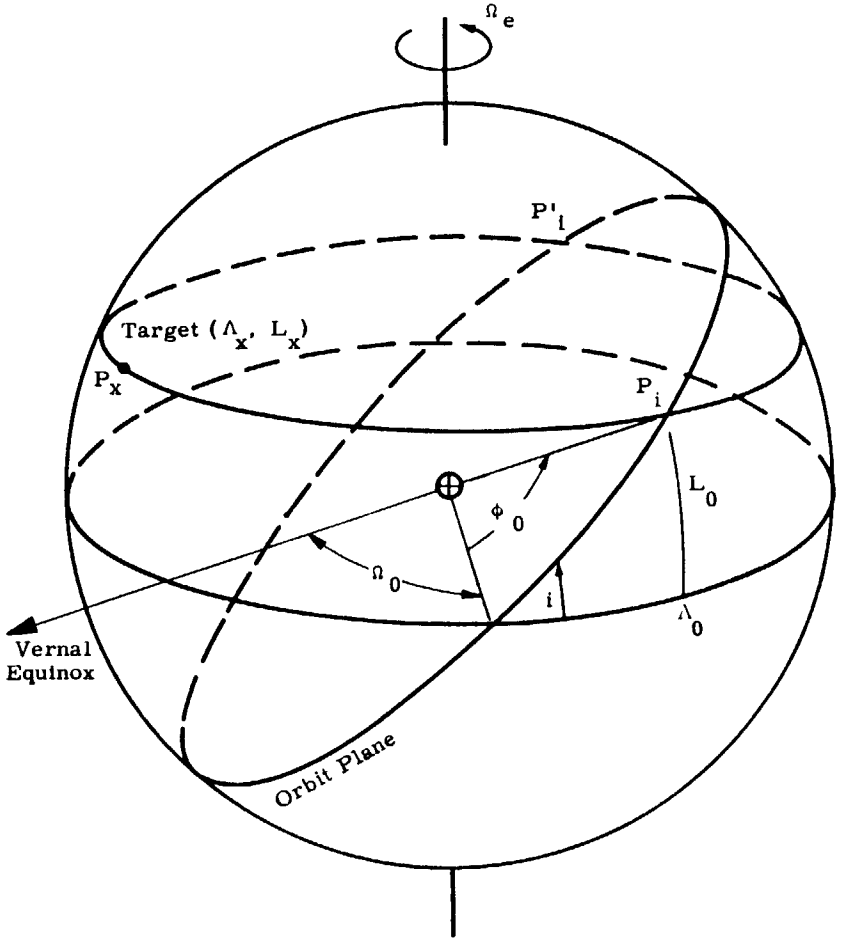

Fig. 3a. 3-D Geometry of the Return Shuttle Problem ($i \geq L_x$)

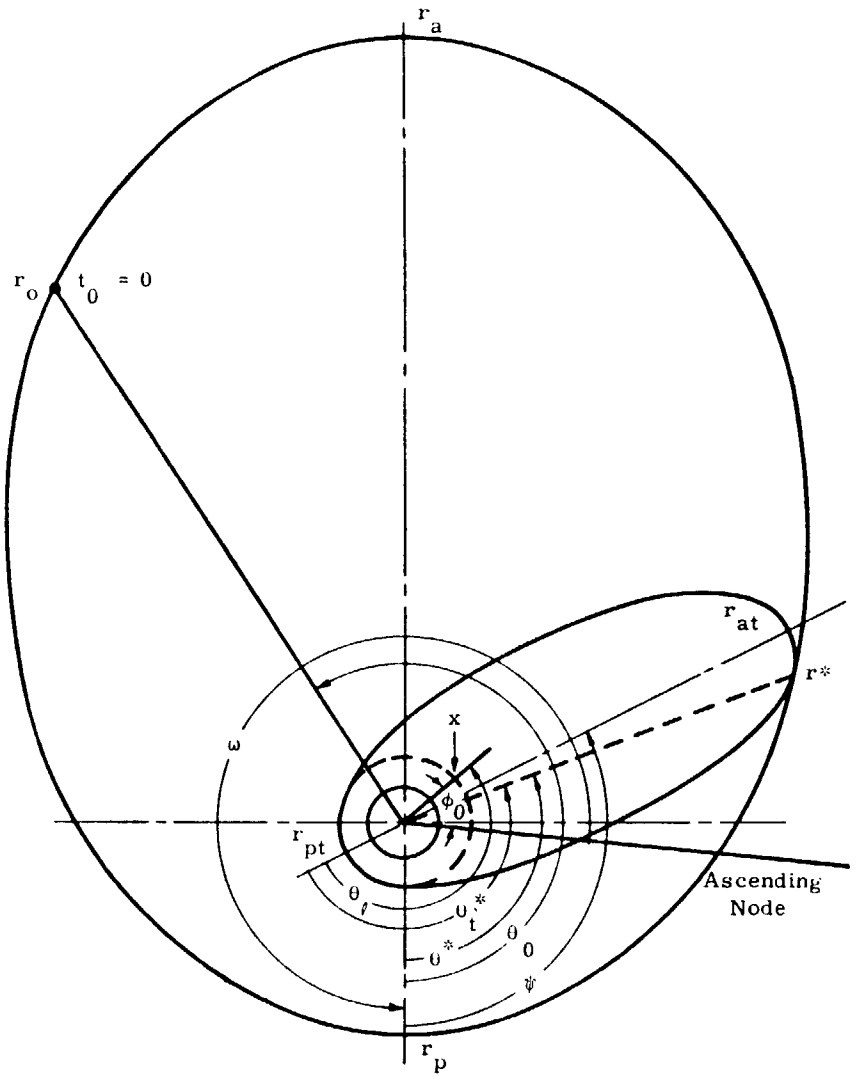

Fig. 3b. Characteristic Angles of the Return Shuttle Trajectory

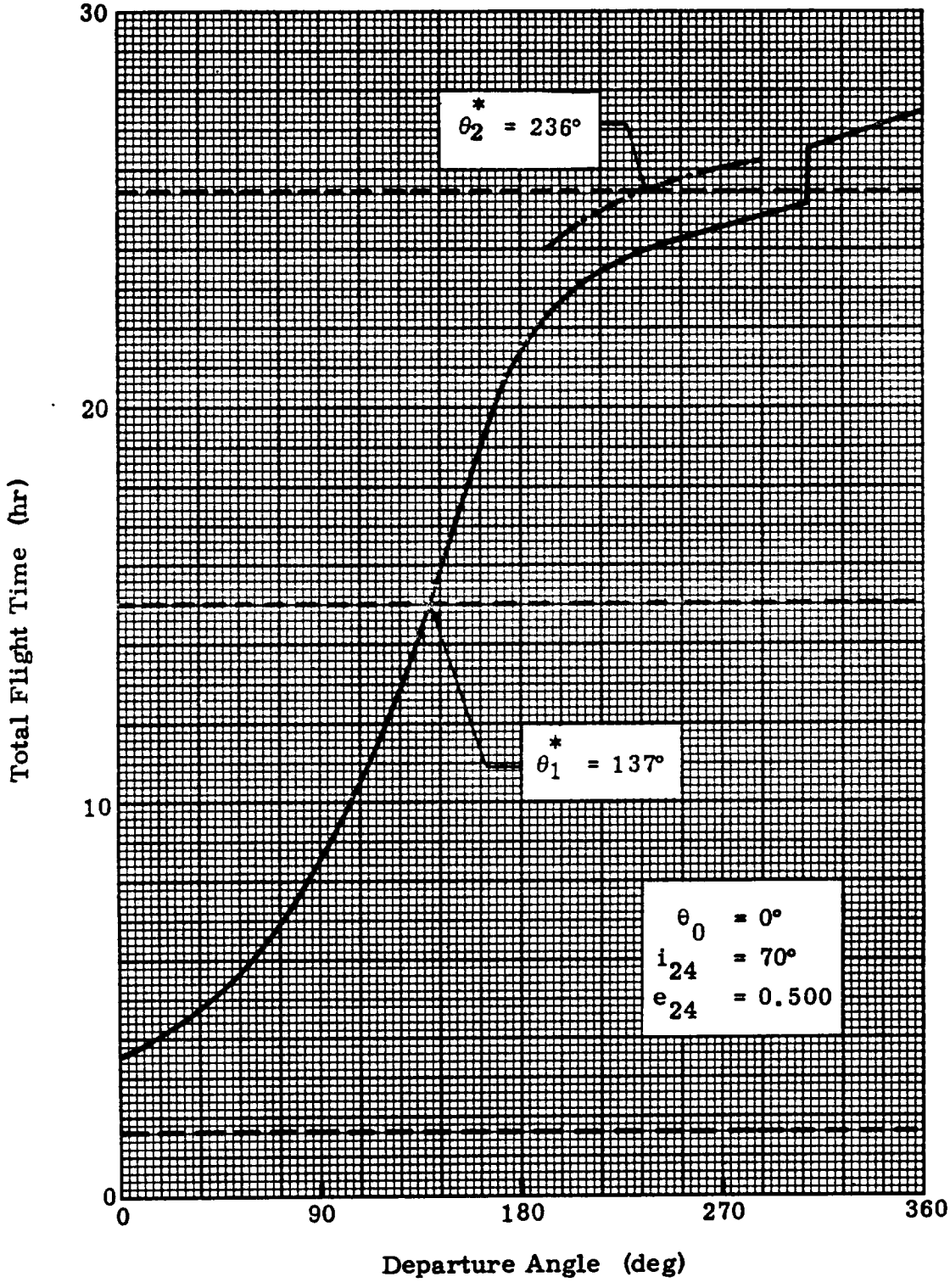

Fig. 4a. Solution of Flight Time Equation

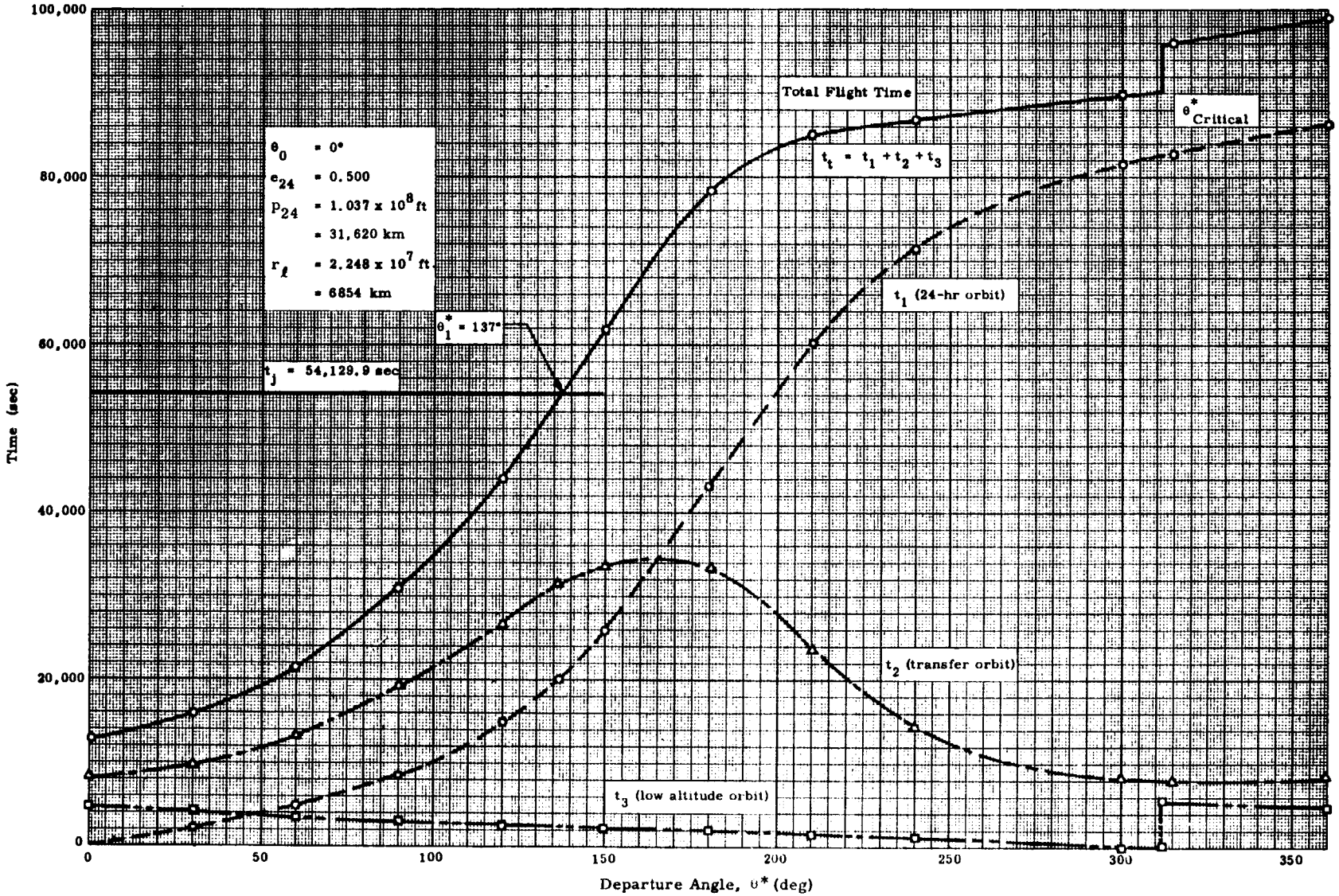

Fig. 4b. Flight Time Versus Departure Angle

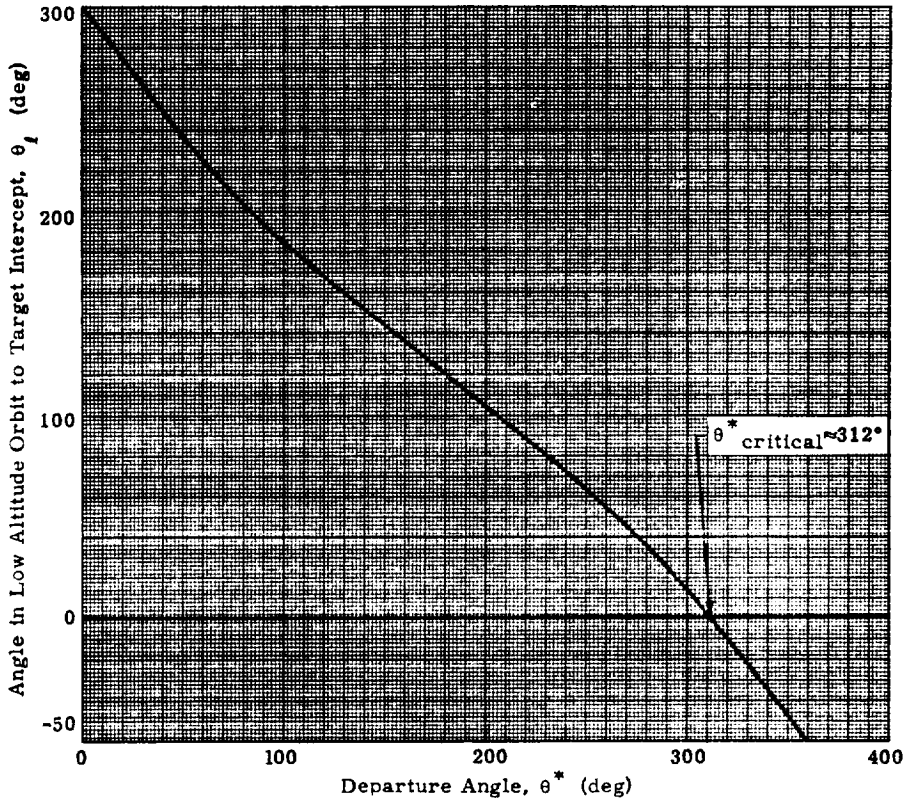

Fig. 5. Critical Angle for the Return Flight-Time Solution

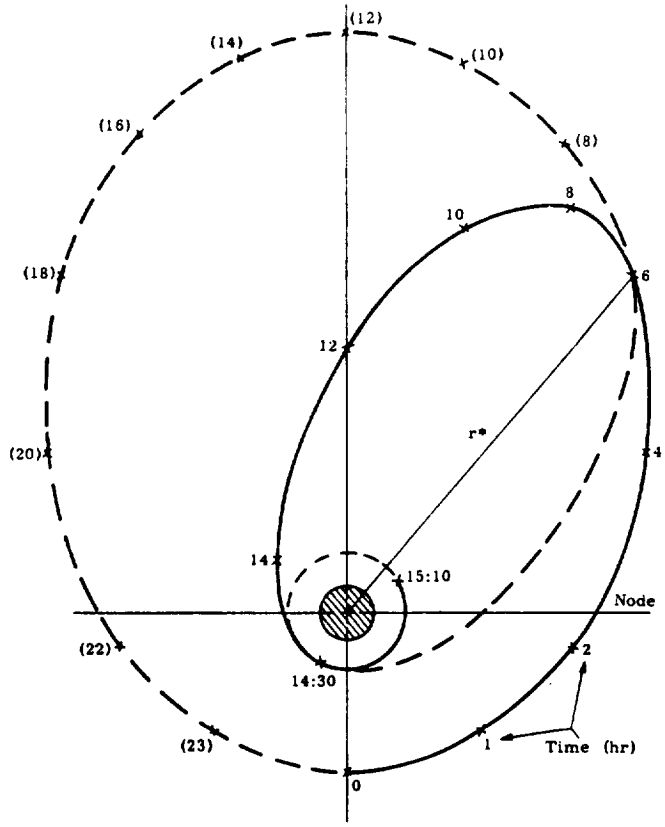

Fig. 6a. Location of the Return Shuttle in the Orbit Plane

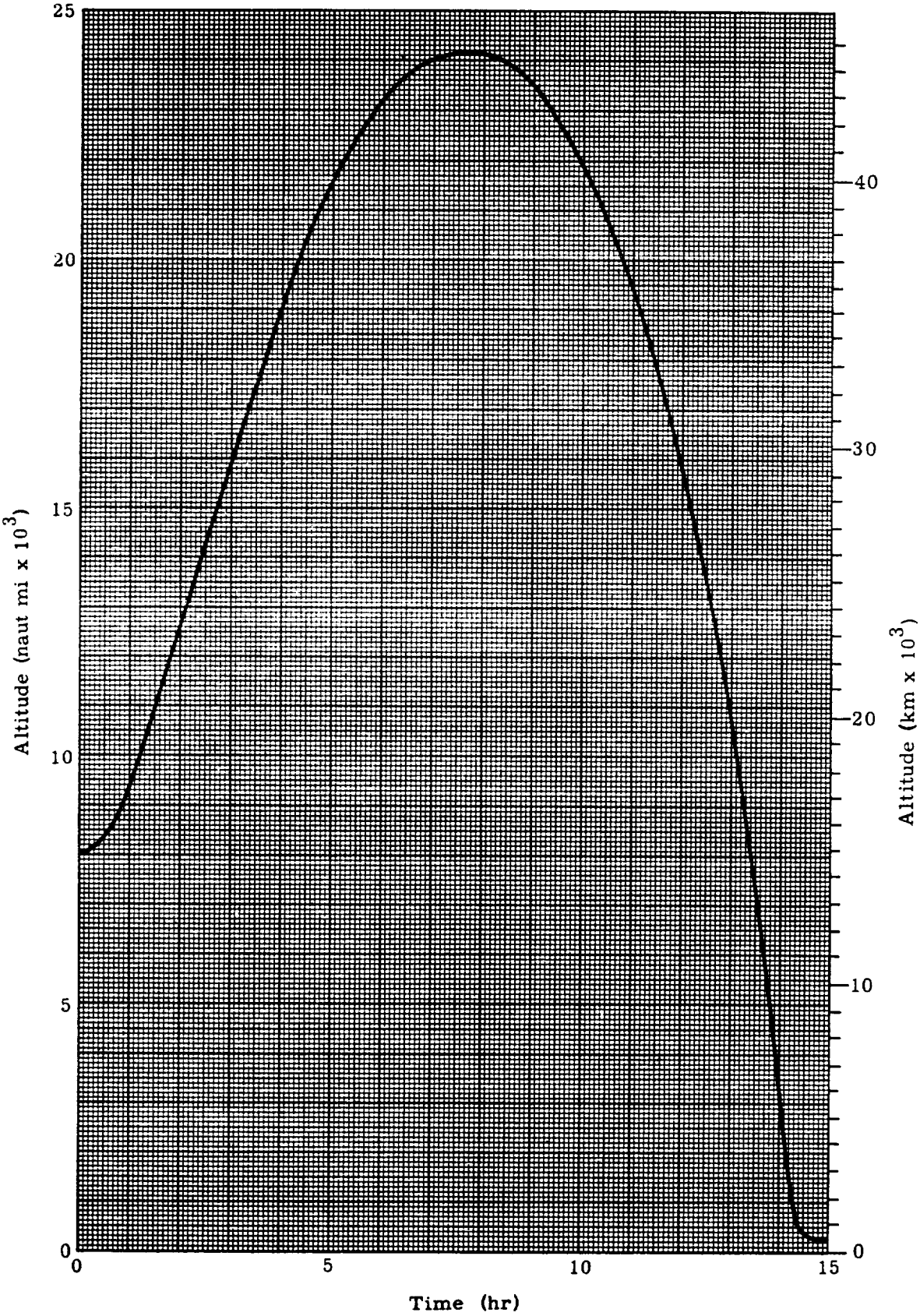

Fig. 6b. Altitude from Sea Level for the Return Shuttle

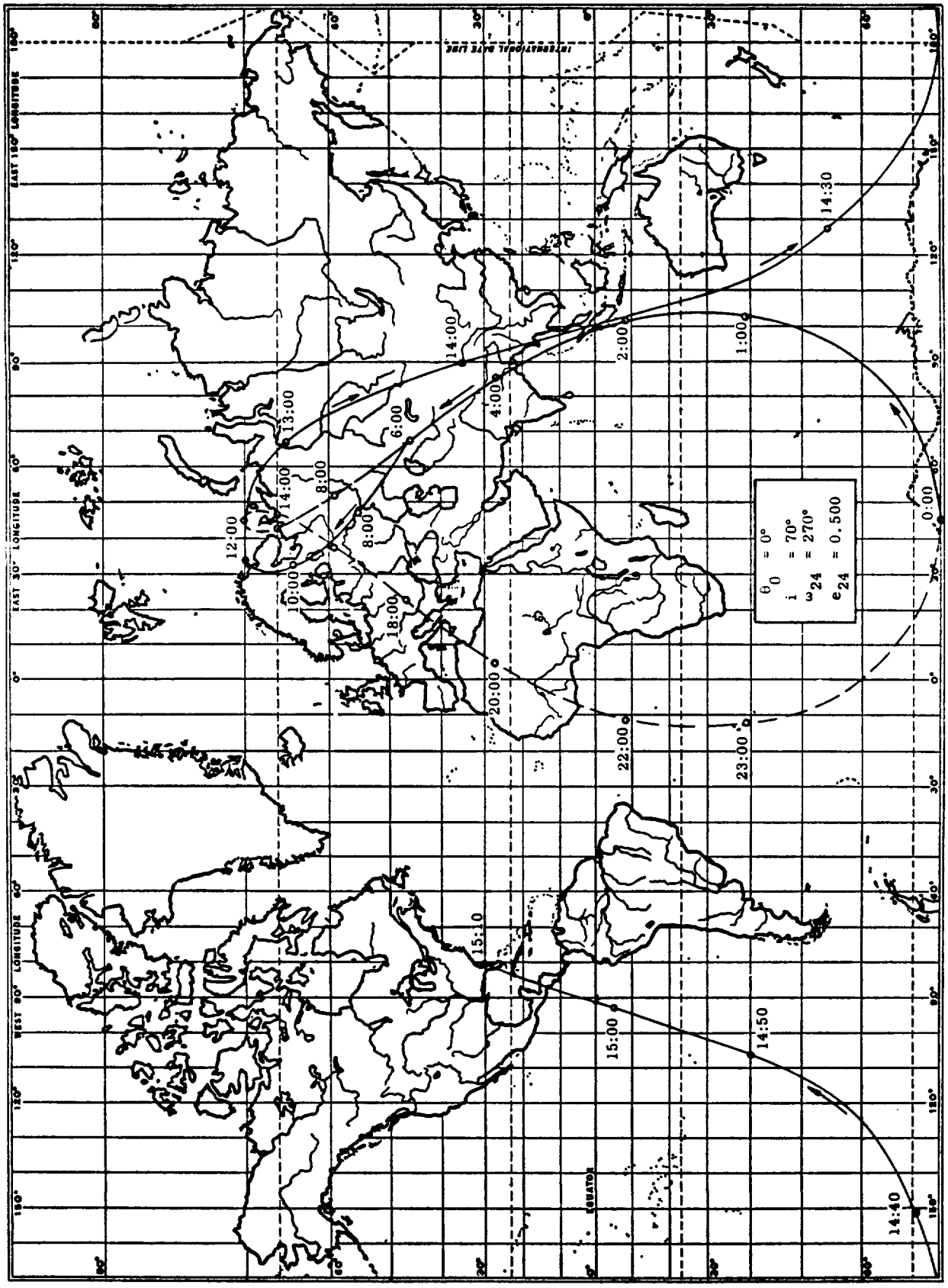

Fig. 7. Ground Track of the Return Shuttle

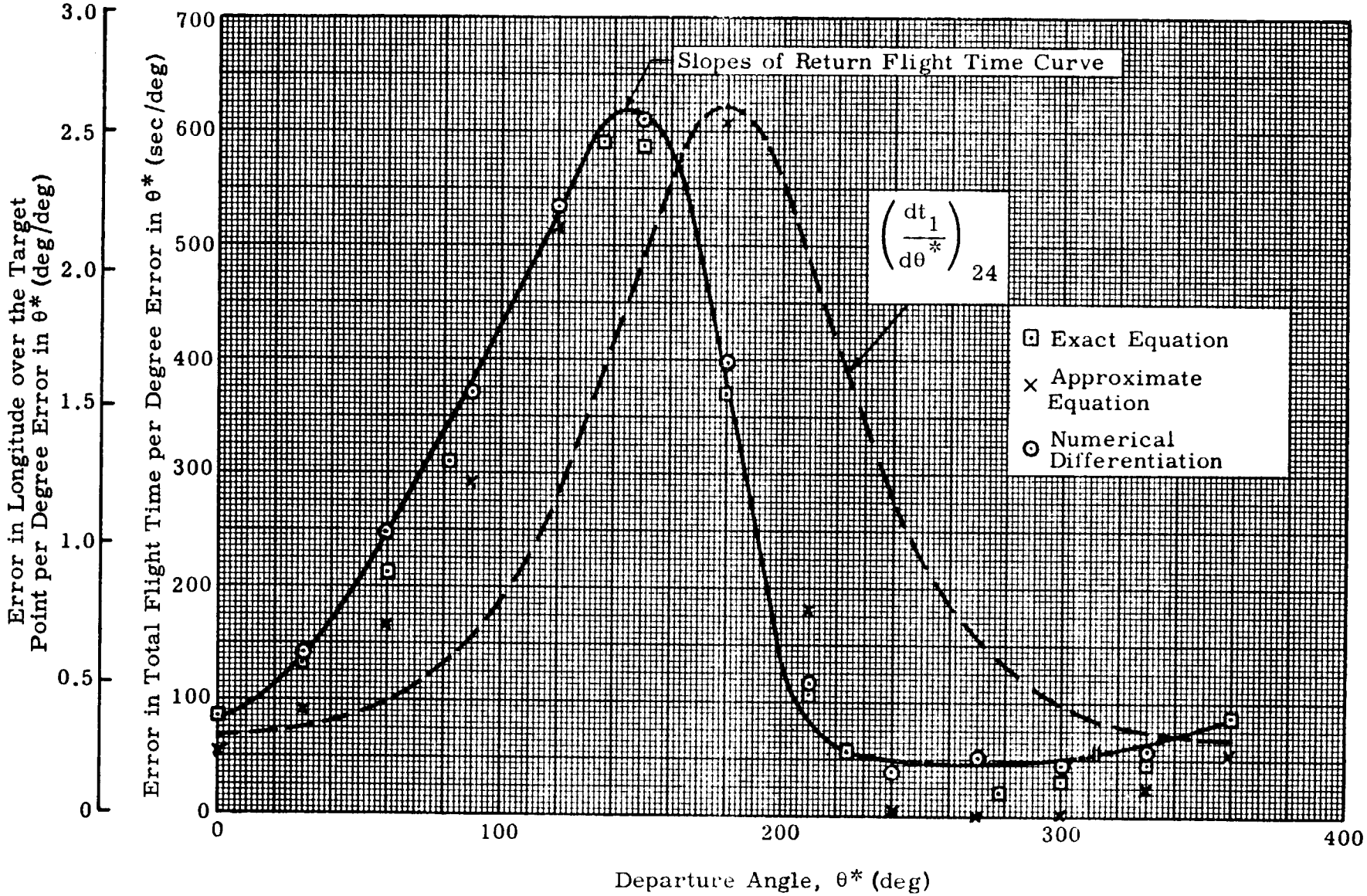

Fig. 8. Flight Time Error Analysis

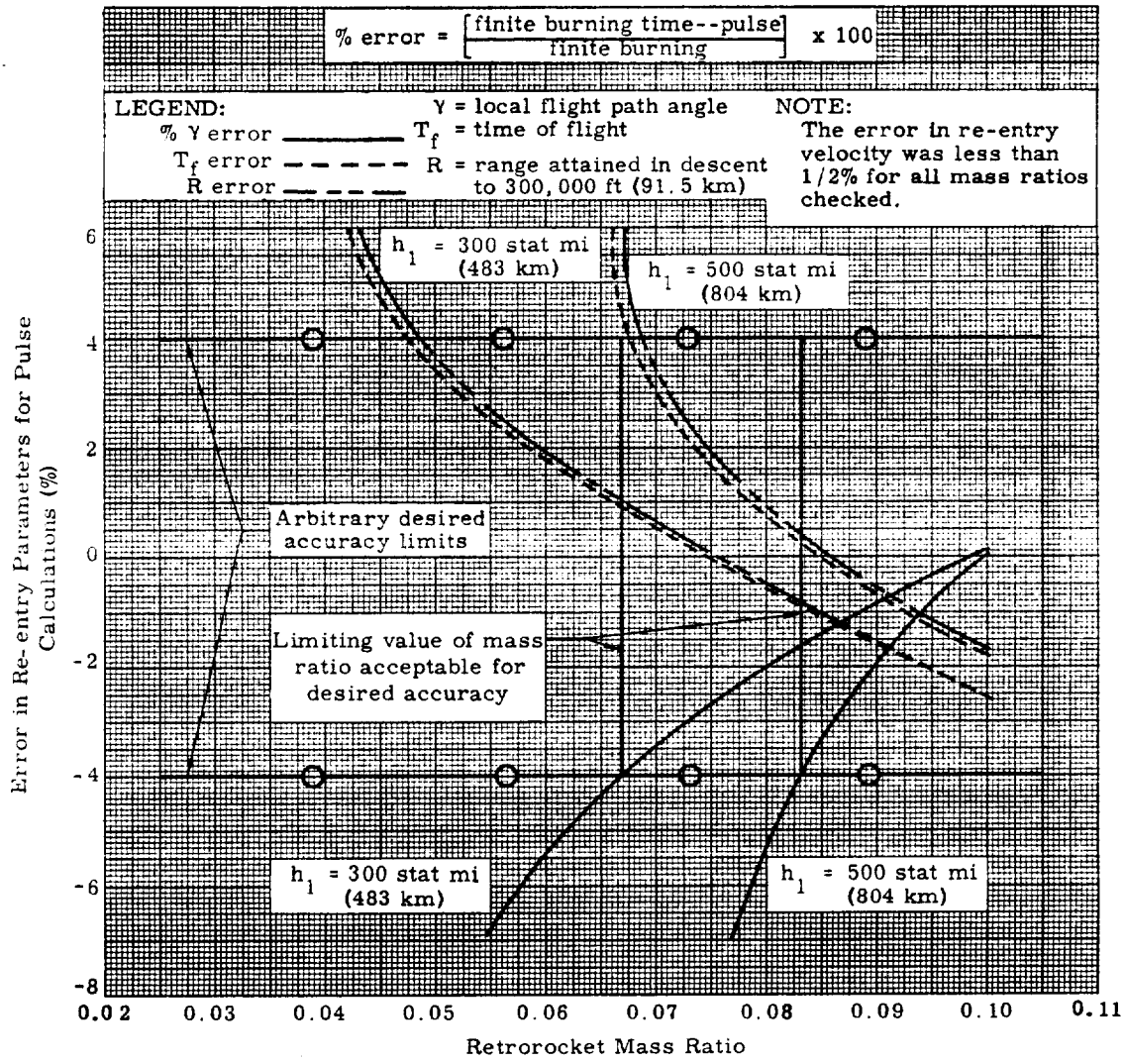

Fig. 9. Error in Re-entry Parameters as Functions of Altitude and Retrorocket Mass Ratios (1 stat mi ≈ 1.609 km)

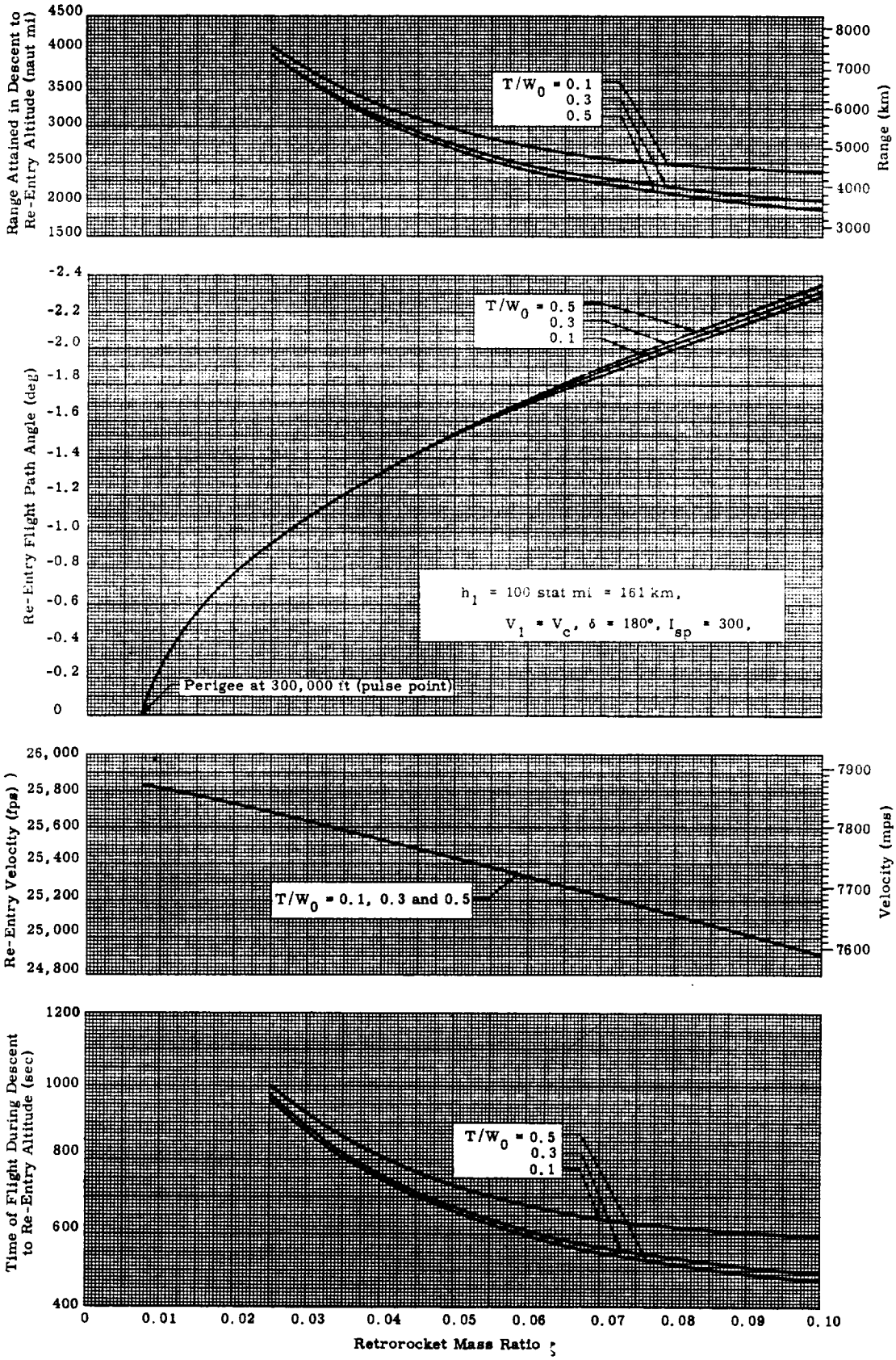

Fig. 10. The Ratio of the Velocity Pulse Obtainable from a Rocket Stage to the Ideal Pulse Neglecting Finite Burning Times

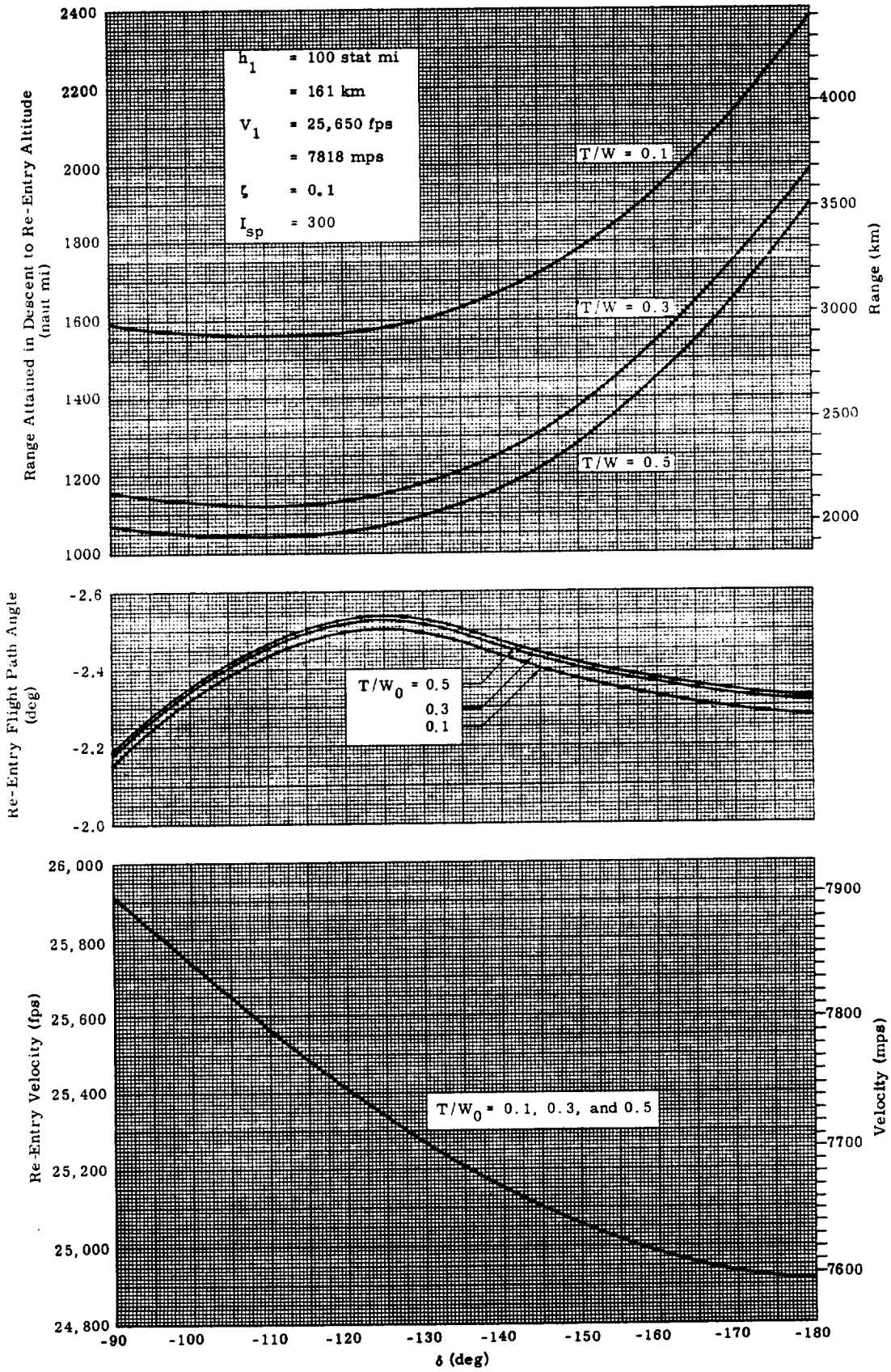

Fig. 11. Re-Entry Parameters as Functions of δ and T/W_0

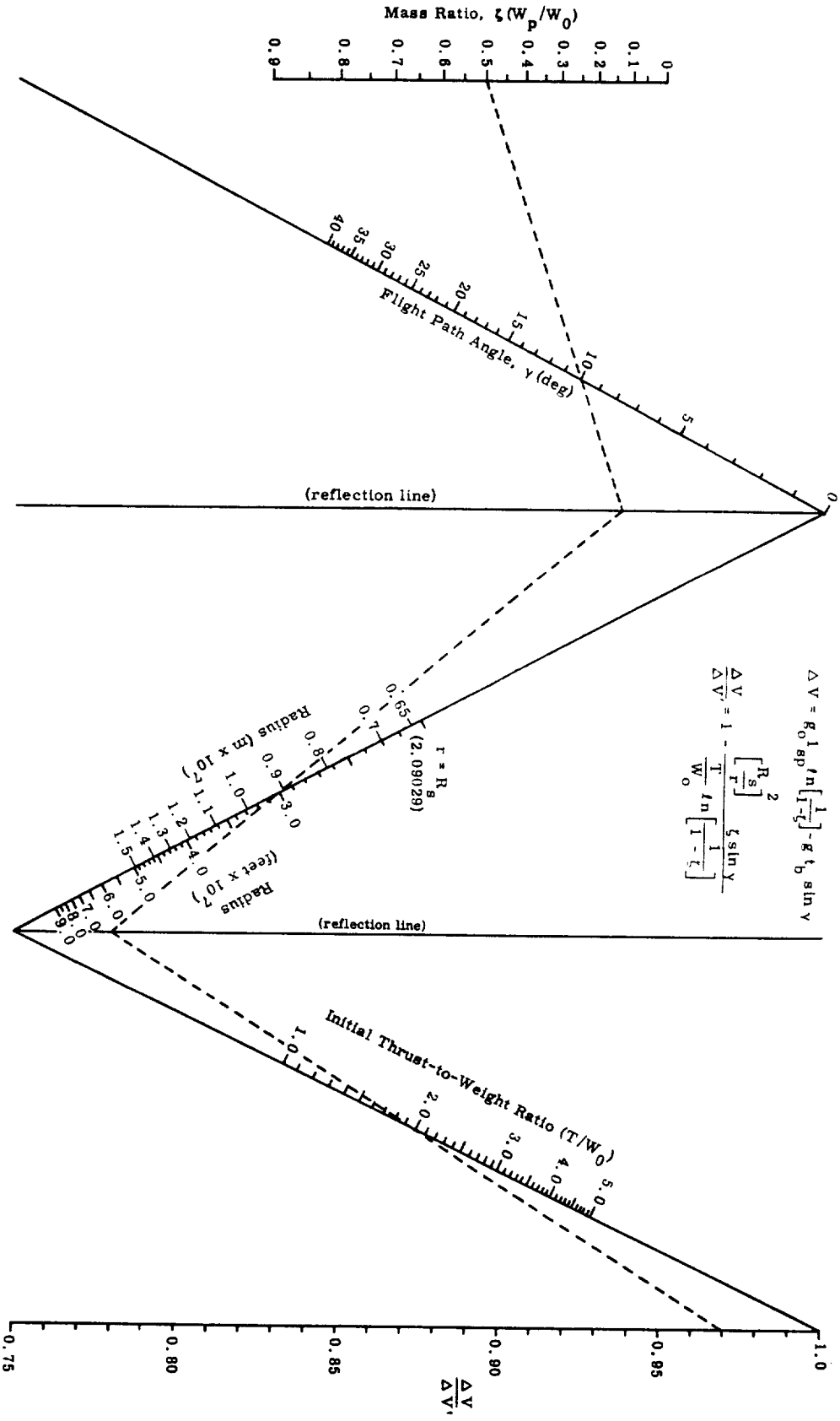

Fig. 12a. Re-Entry Parameters as Functions of Initial Thrust-to-Weight Ratio and Retrorocket Mass Ratio

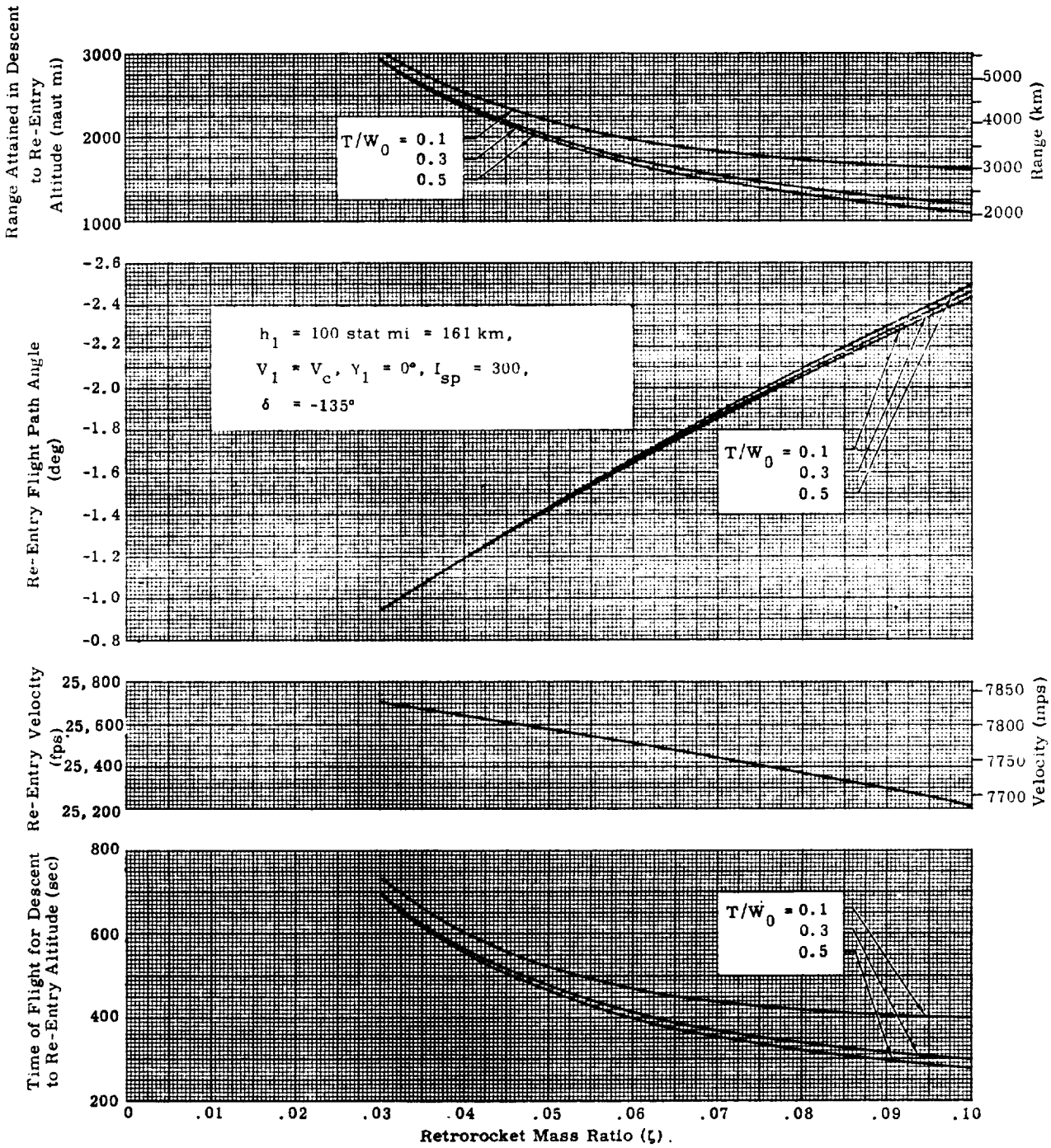

Fig. 12b. Re-Entry Parameters as Functions of Initial Thrust-to-Weight Ratio and Retrorocket Mass Ratio

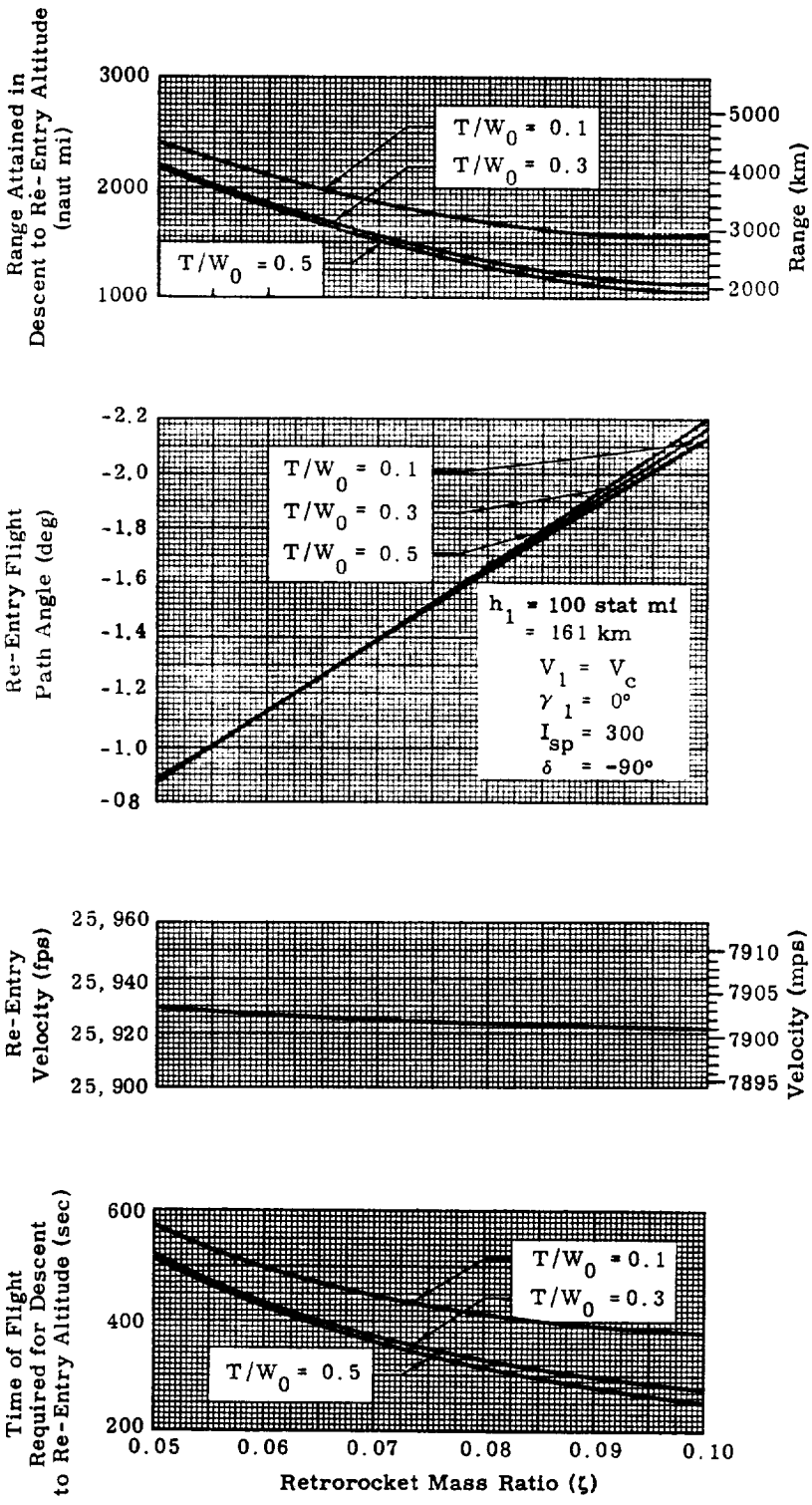

Fig. 12c. Re-Entry Parameters as Functions of Initial Thrust-to-Weight Ratio and Retrorocket Mass Ratio

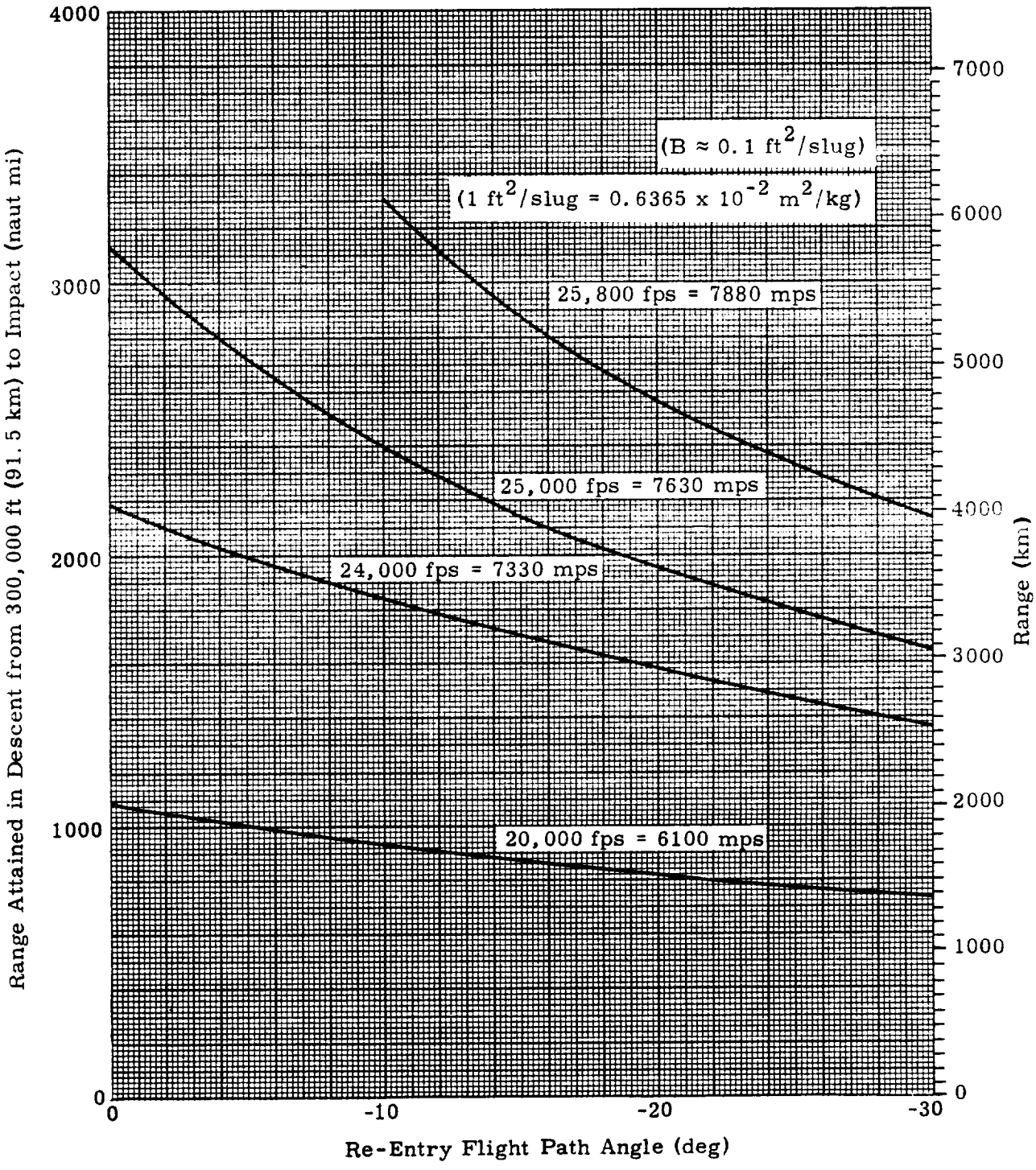

Fig. 13. Range Attained in Descending from 300,000 ft (91.5 km) to Sea Level

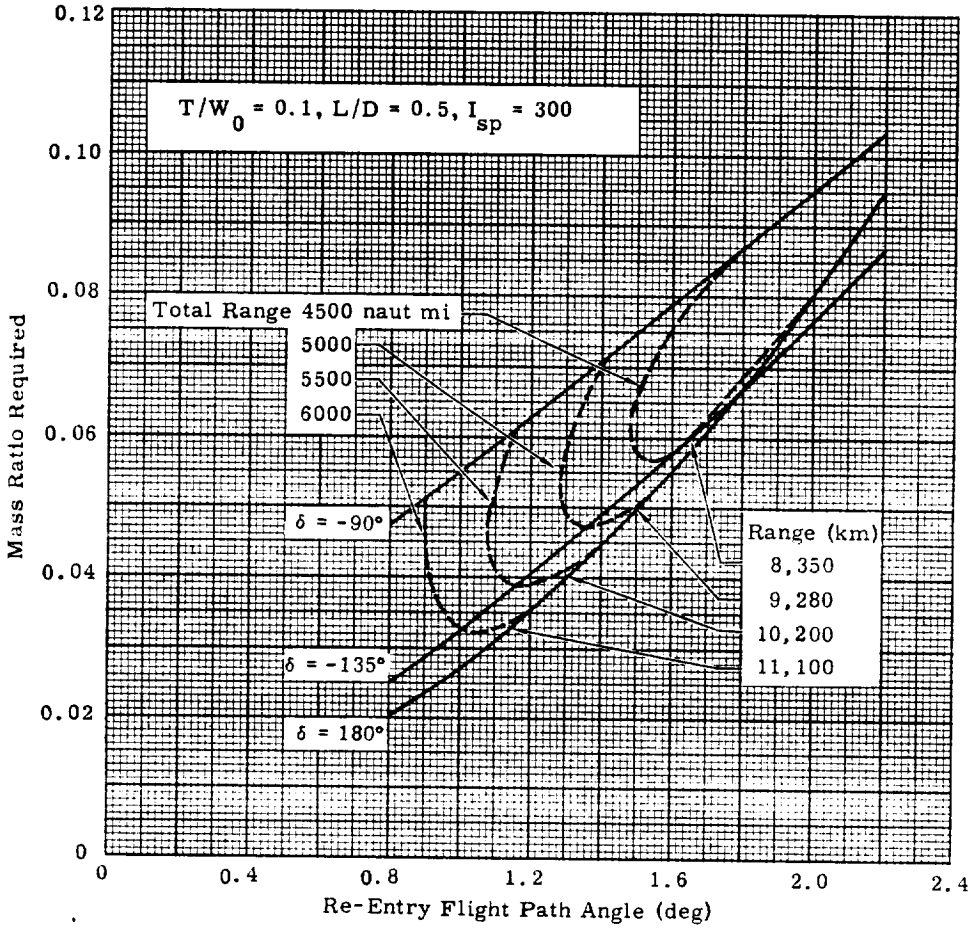

Fig. 14a. Mass Ratio Required to Exit from a 100-Stat Mi (161 km) Circular Orbit

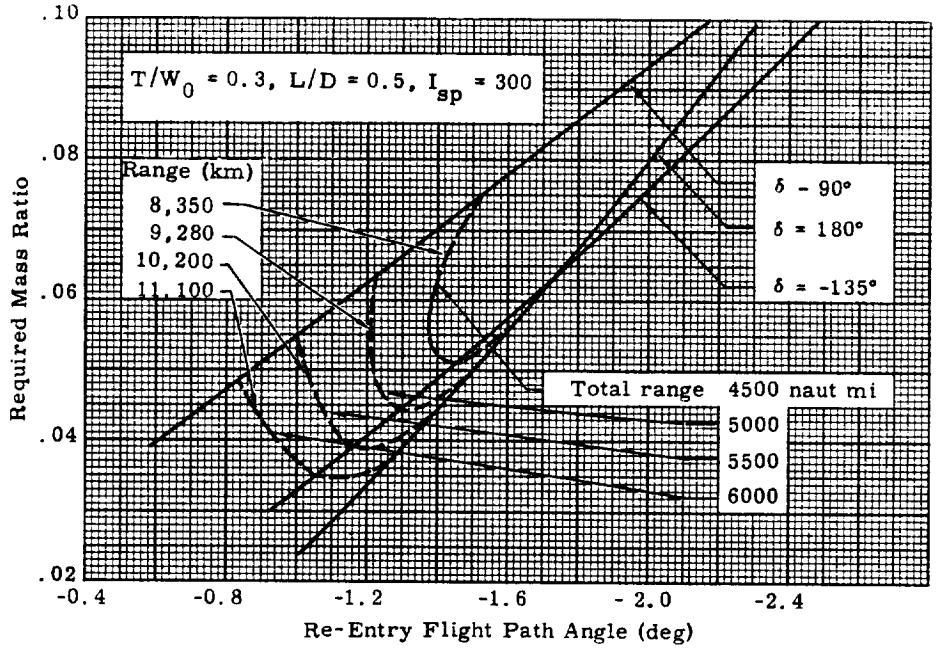

Fig. 14b. Mass Ratio Required to Exit from a 100-Stat Mi (161 km) Circular Orbit

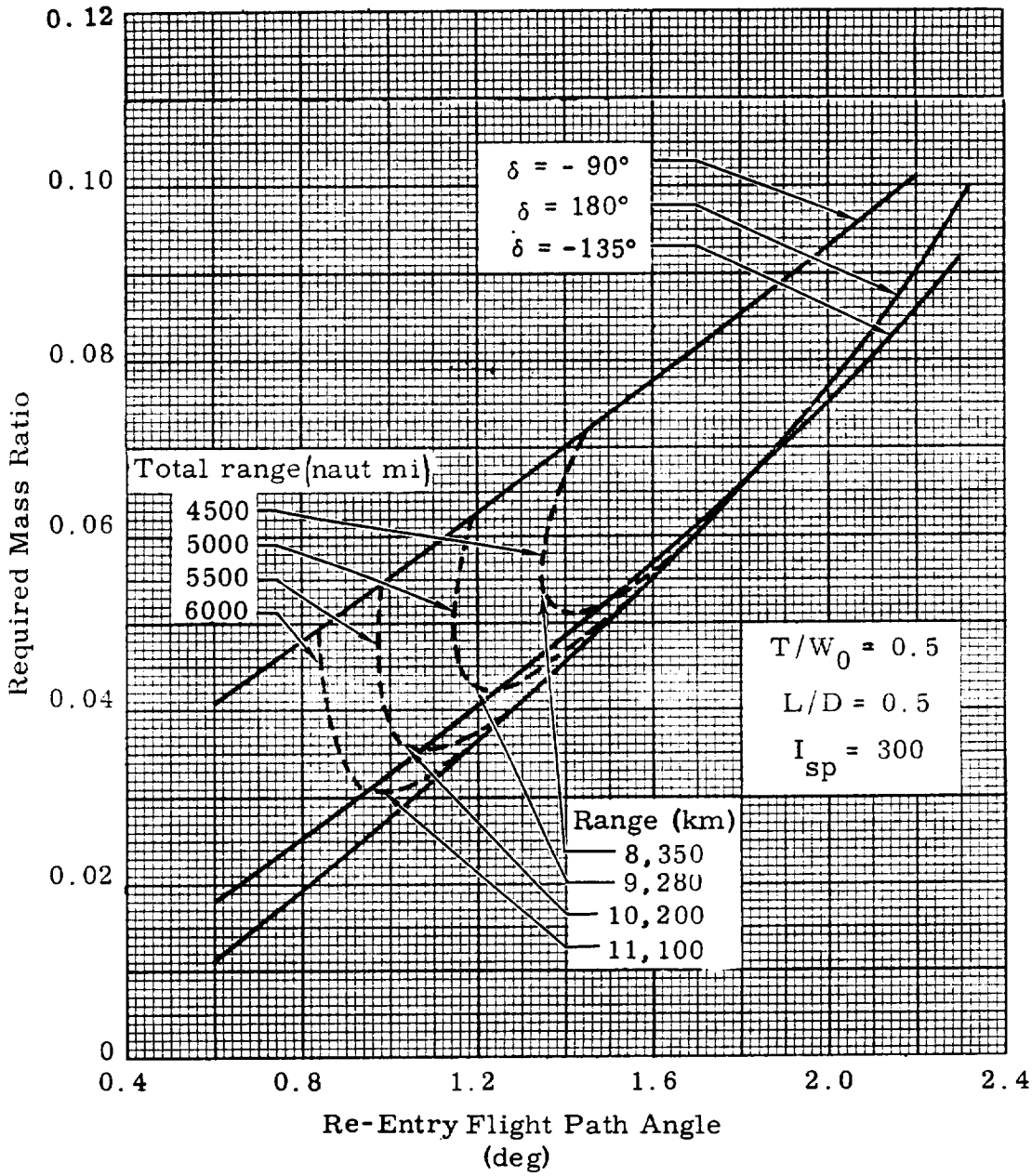

Fig. 14c. Mass Ratio Required to Exit from a 100-Stat Mi (161 km) Circular Orbit

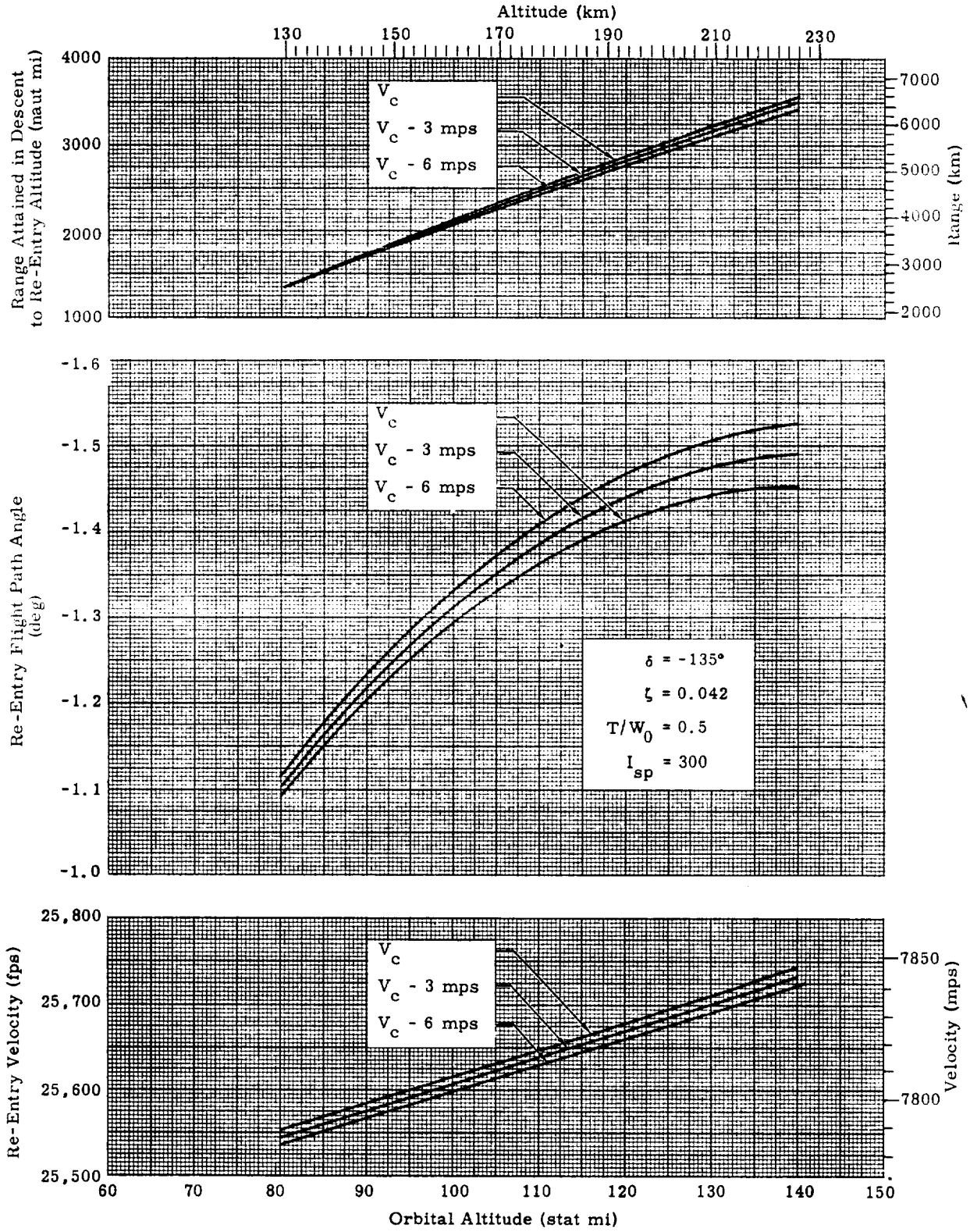

Fig. 15. Variations in the Re-Entry Conditions Due to Small Variations in Orbital Altitude and Velocity

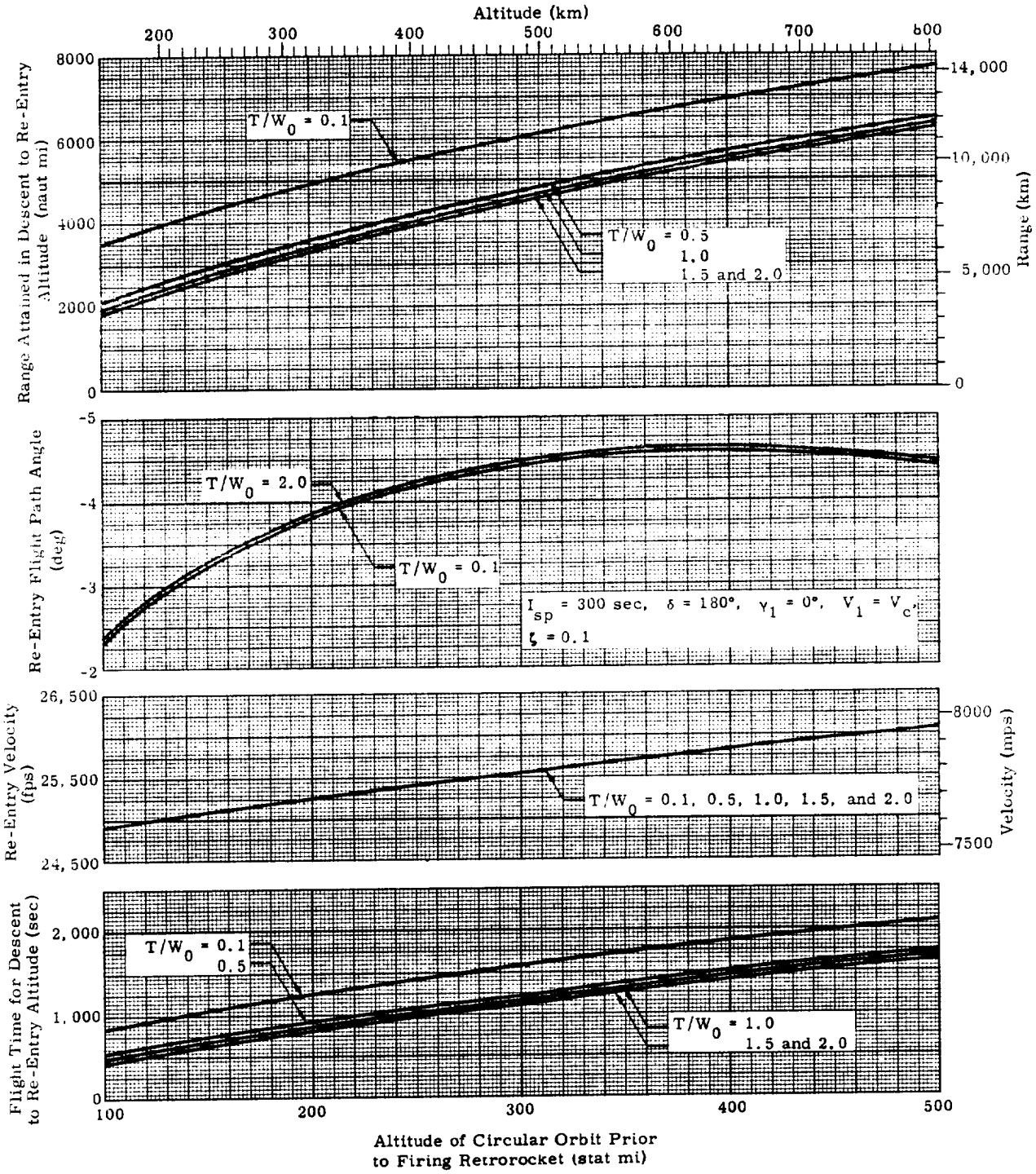

Fig. 16. Re-Entry Parameters as Functions of Initial Altitude and Retrorocket Mass Ratio

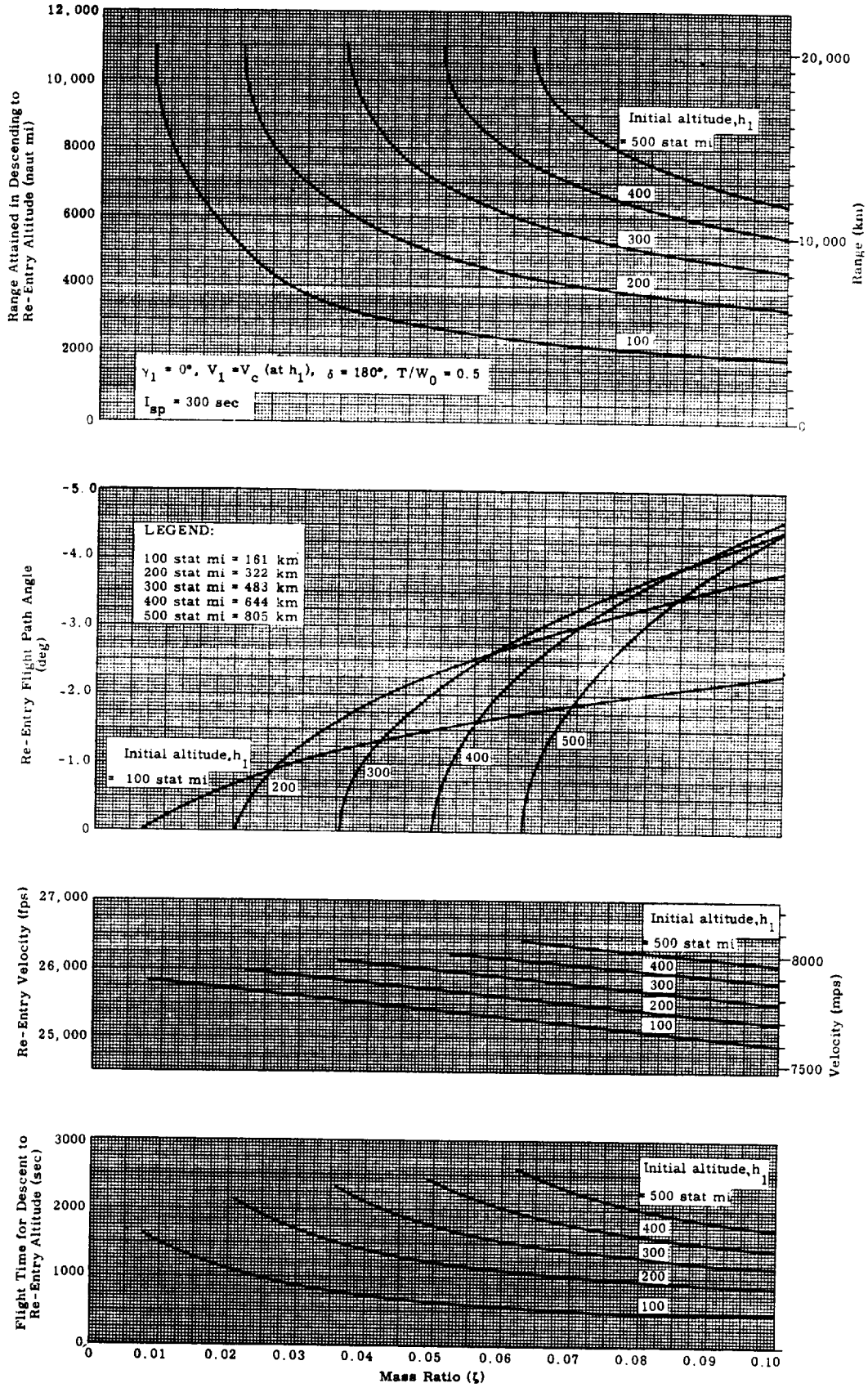

Fig. 17. Re-Entry Parameters as Functions of Initial Orbital Altitude and Mass Ratio of the Retrorocket

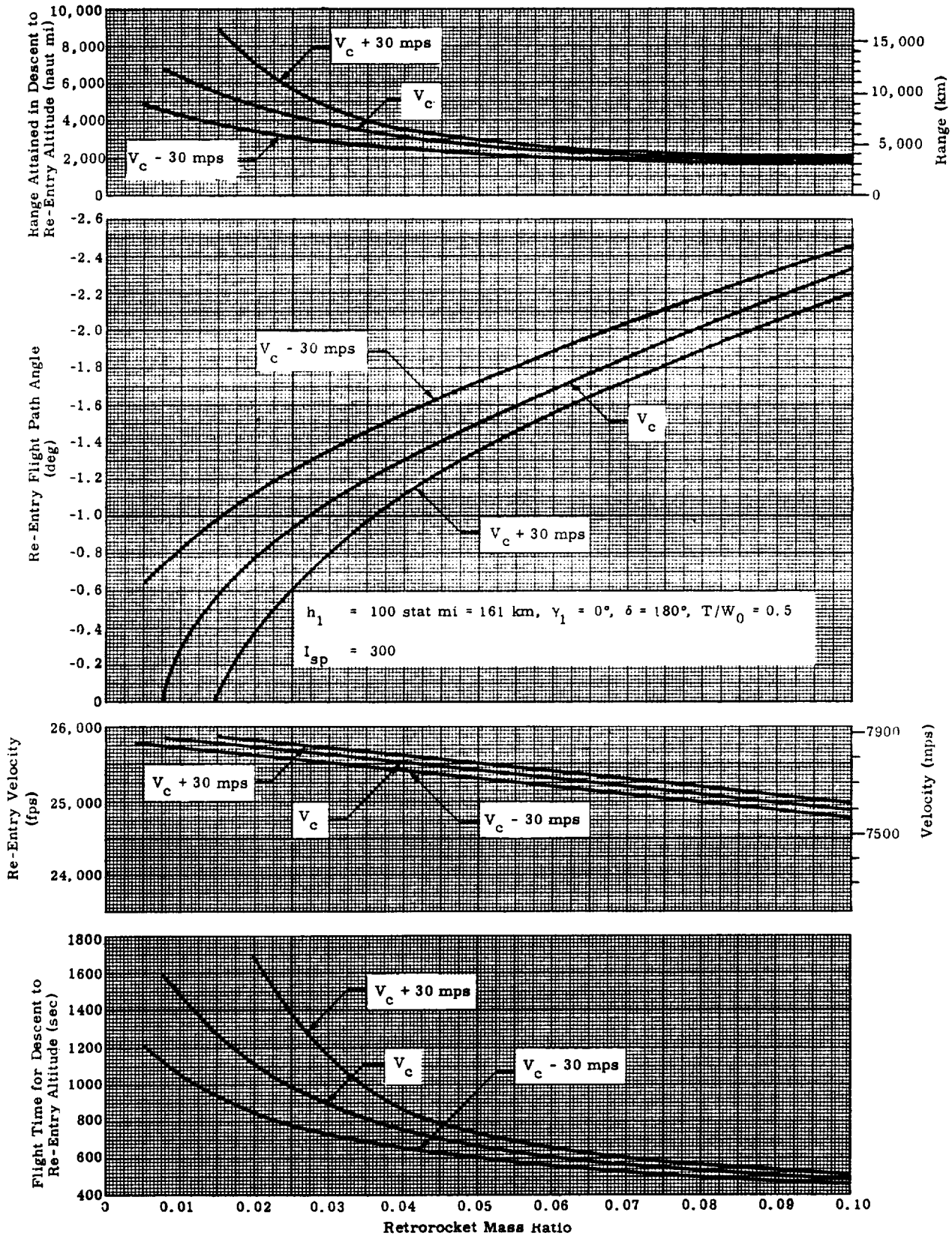

Fig. 18a. Re-Entry Parameters as Functions of Initial Orbital Velocity and Retrorocket Mass Ratio (30 mps = 100 fps)

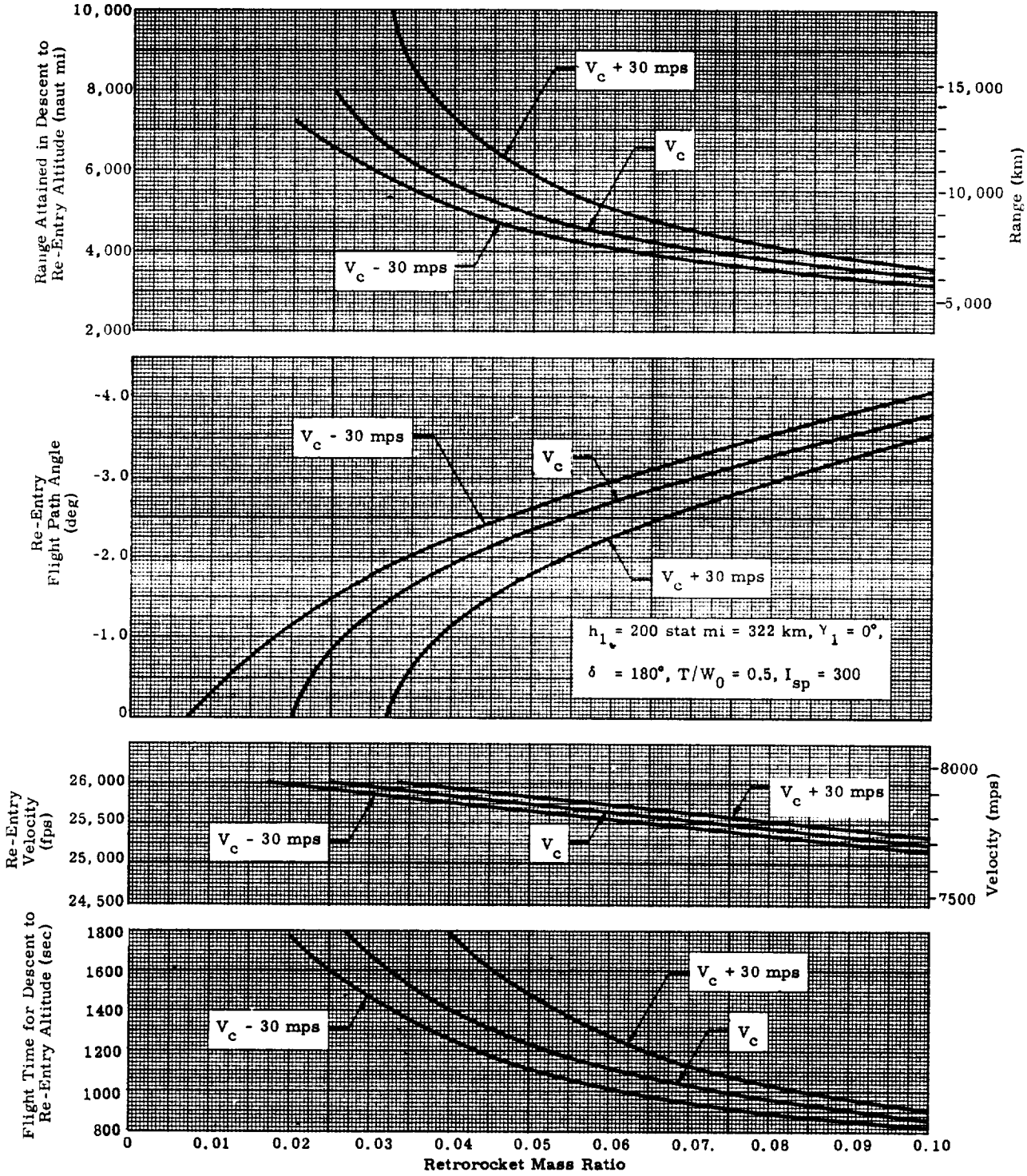

Fig. 18b. Re-Entry Parameters as Functions of Initial Velocity and Mass Ratio of the Retrorocket (100 fps ≈ 30 mps)

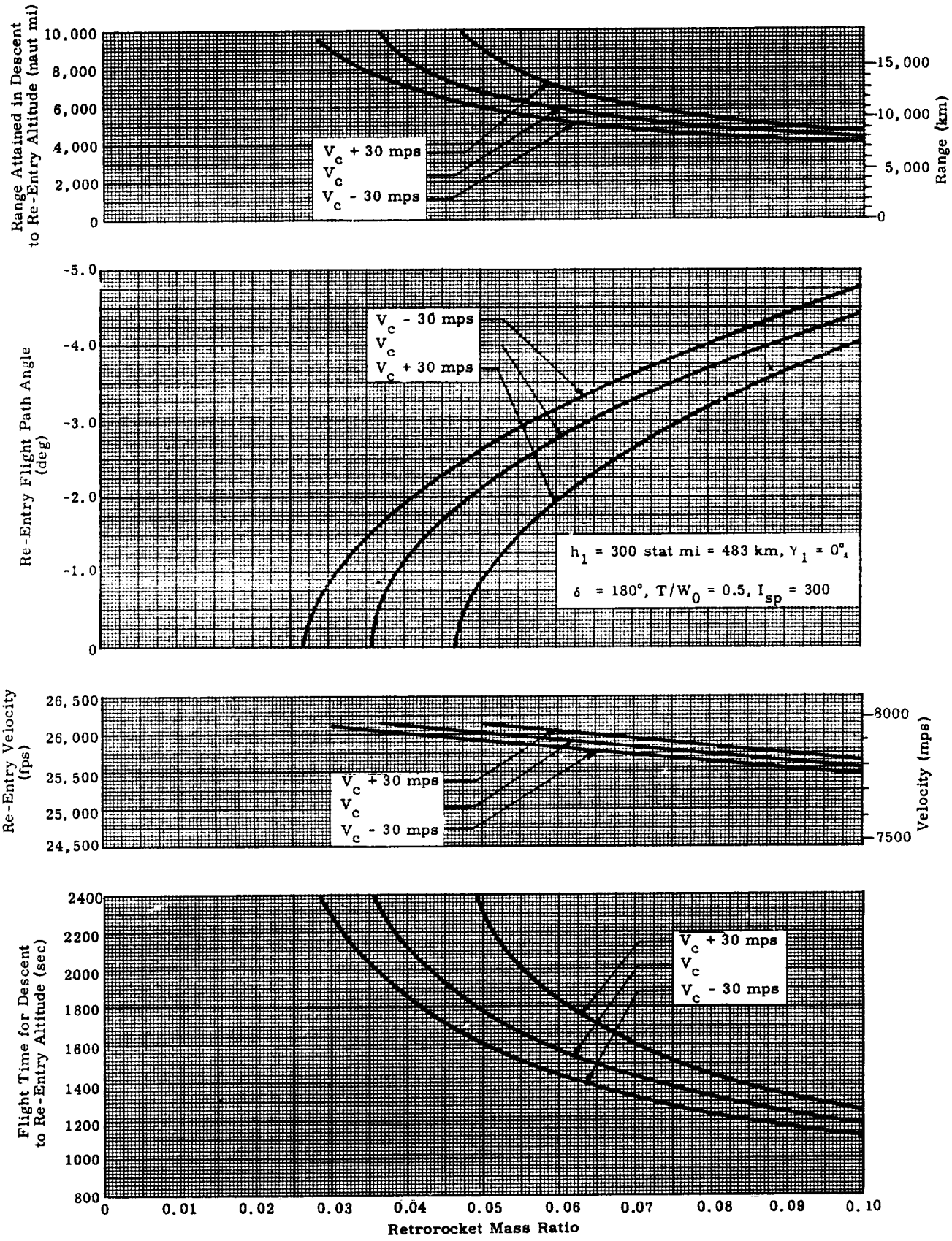

Fig. 18c. Re-Entry Parameters as Functions of Initial Velocity and Retrorocket Mass Ratio (100 fps $\approx$ 30 mps)

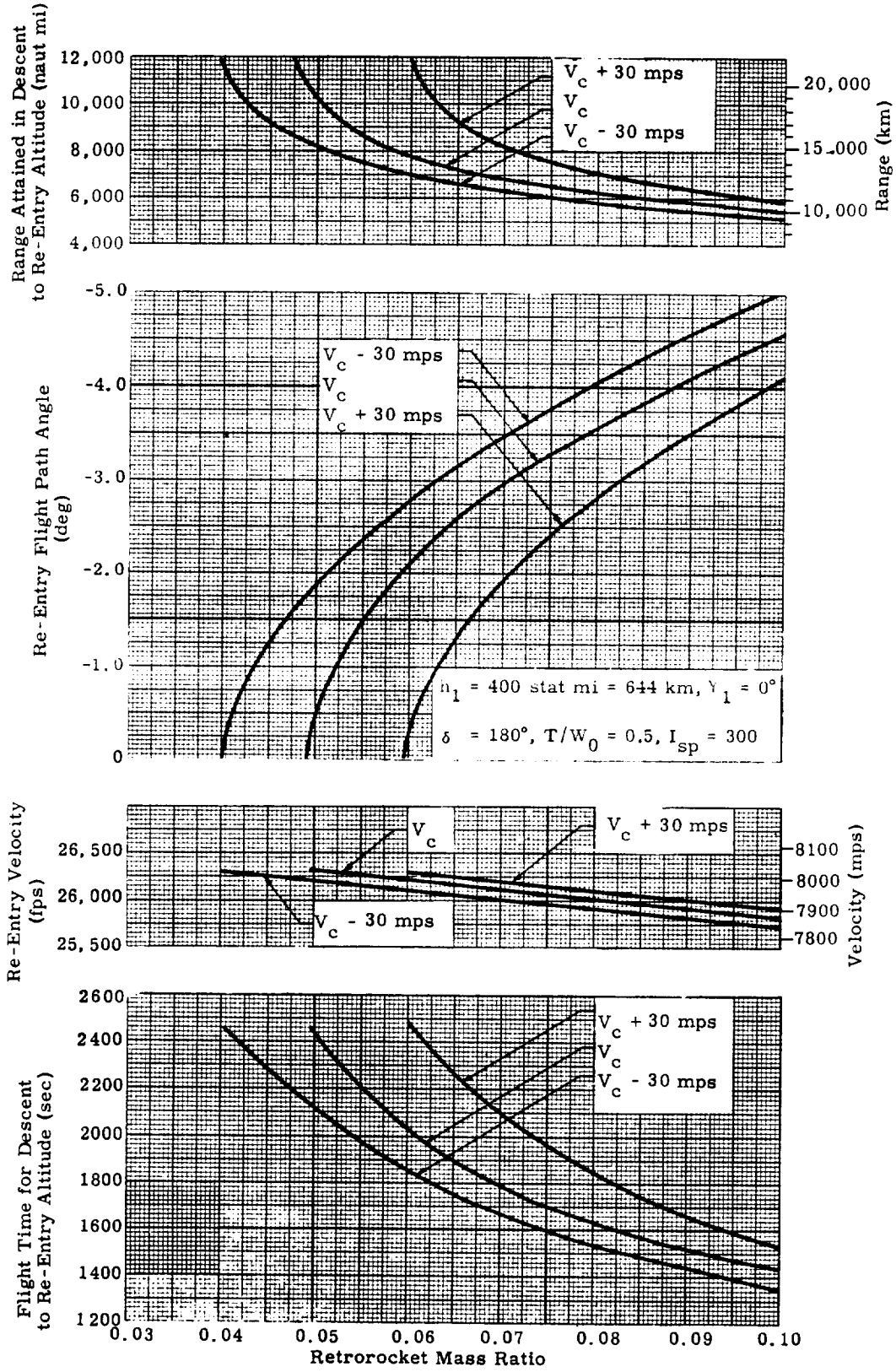

Fig. 18d. Re-Entry Parameters as Functions of Initial Velocity and Retrorocket Mass Ratio (100 fps ≈ 30 mps)

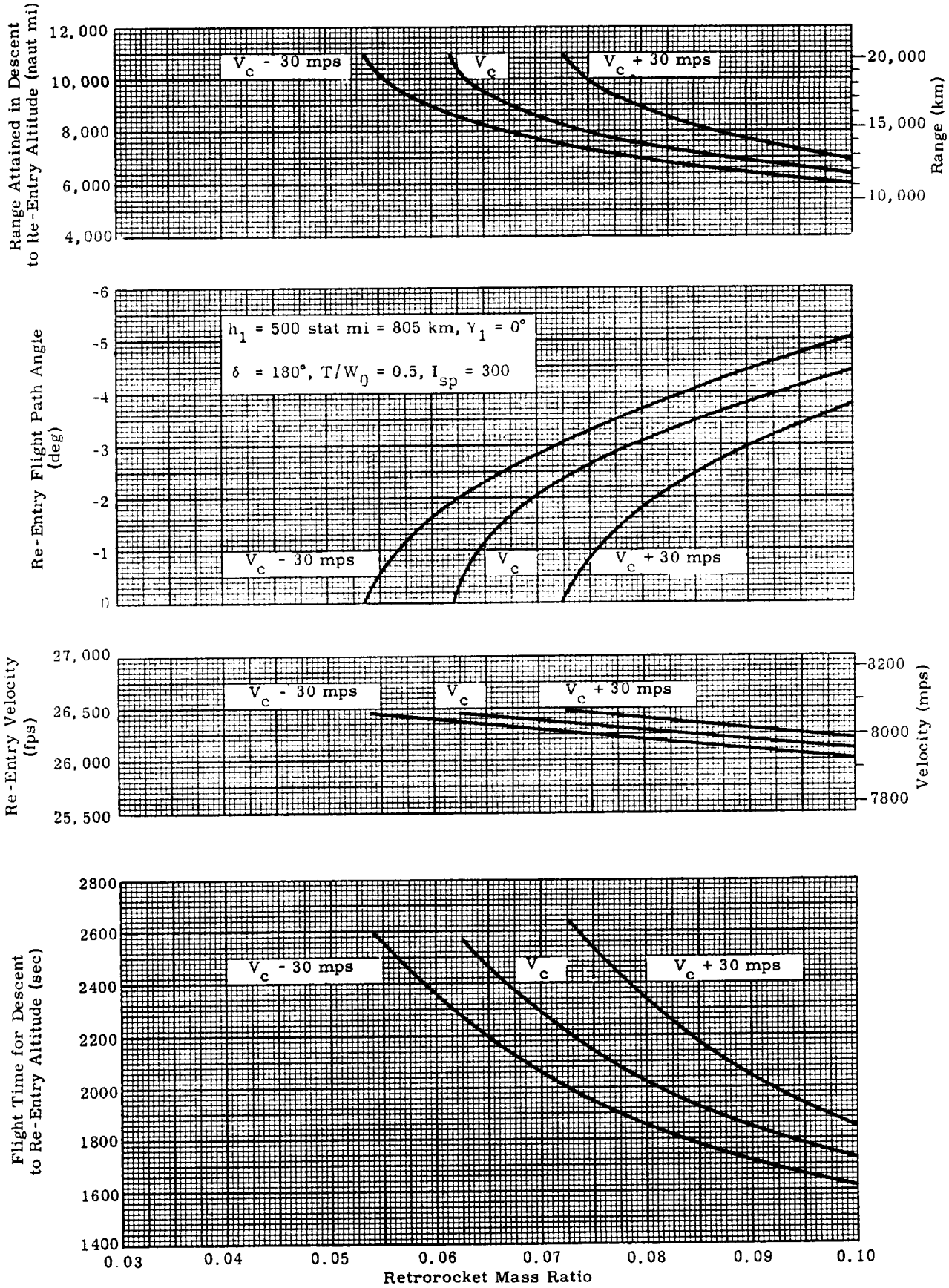

Fig. 18e. Re-Entry Parameters as Functions of Initial Orbital Velocity and Retrorocket Mass Ratio (100 fps ≈ 30 mps)

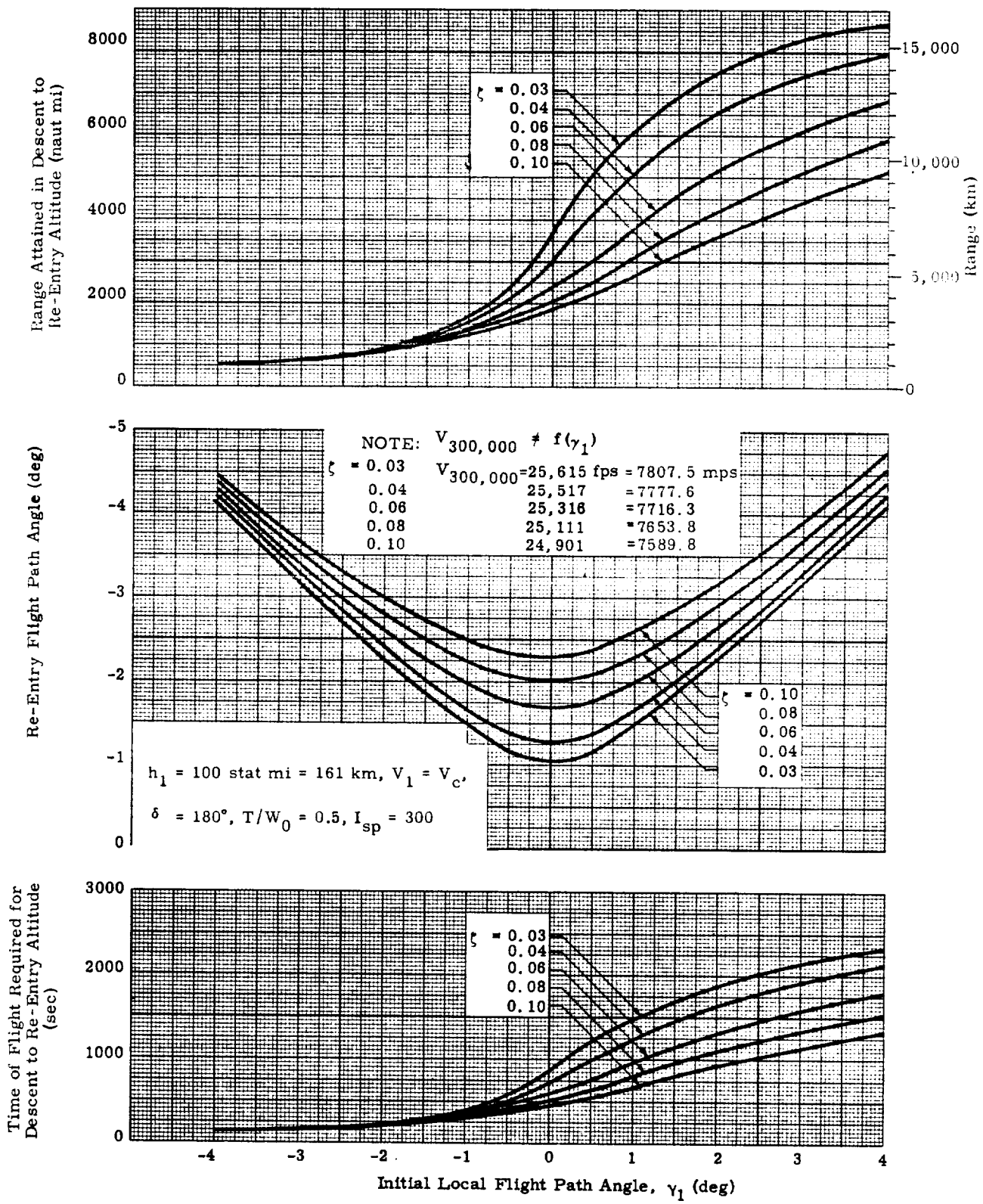

Fig. 19a. Re-Entry Parameters as Functions of ζ and γ_1

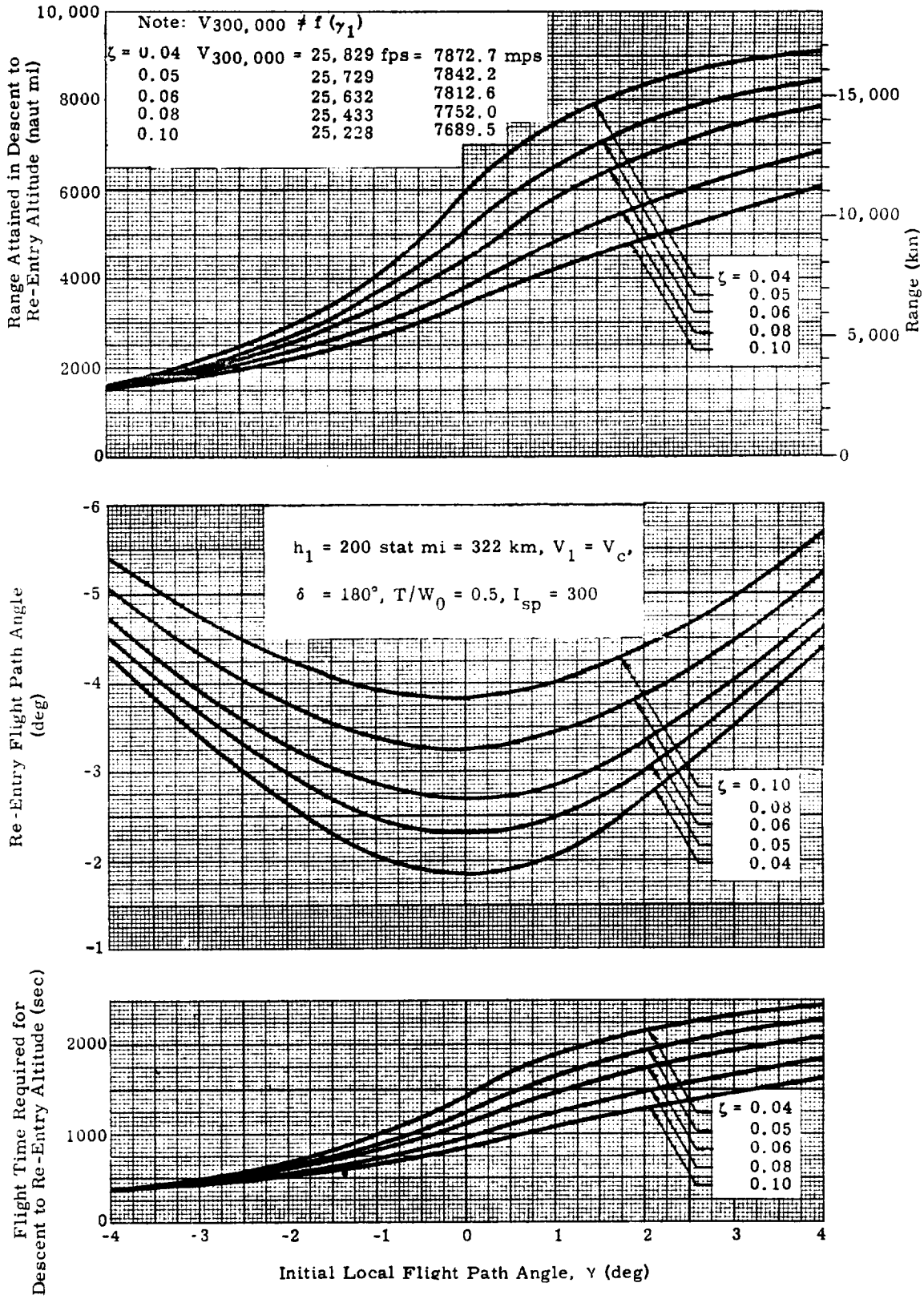

Fig. 19b. Re-Entry Parameters as Functions of ζ and γ_1

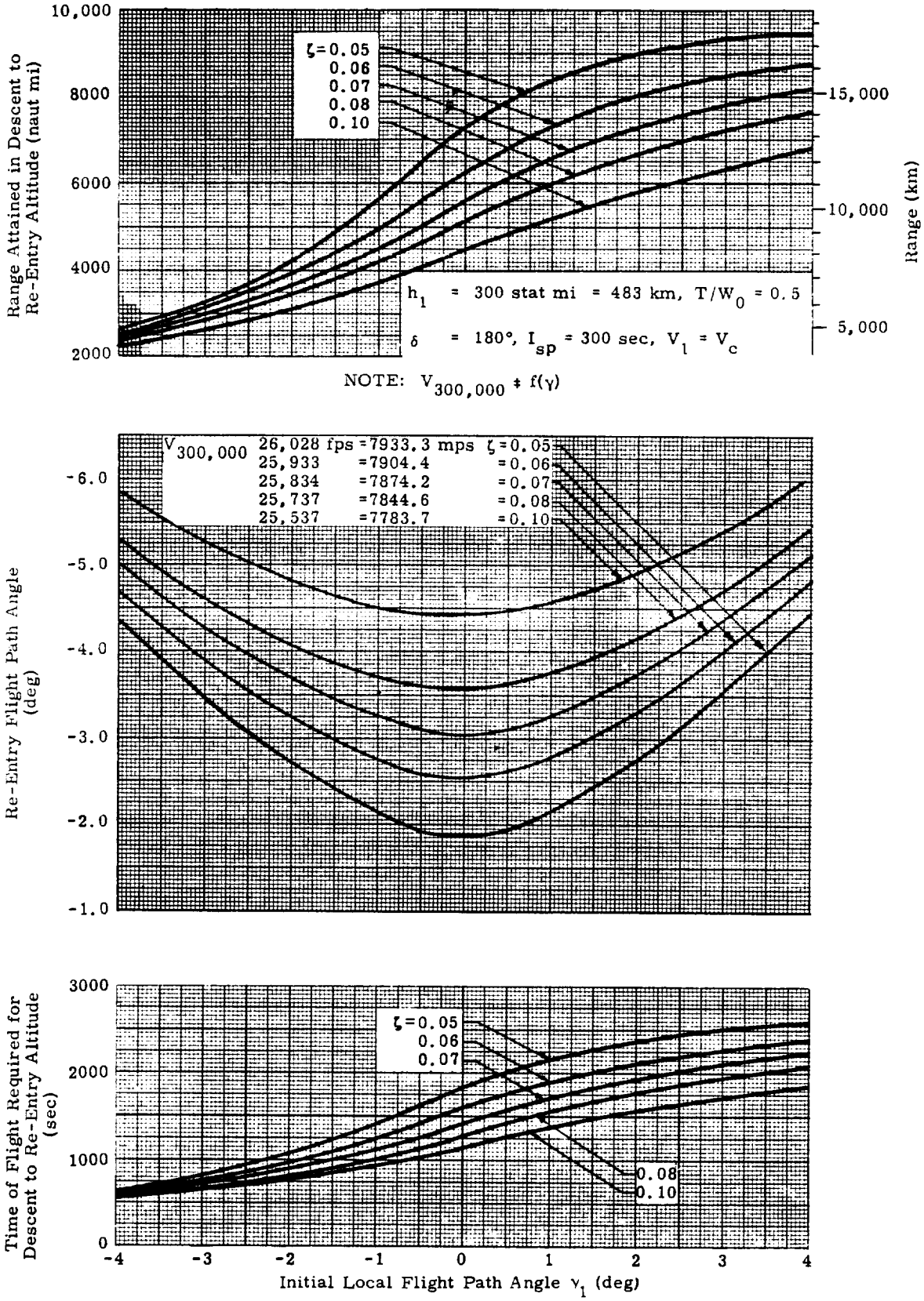

Fig. 19c. Re-Entry Parameters as Functions of ζ and γ_1

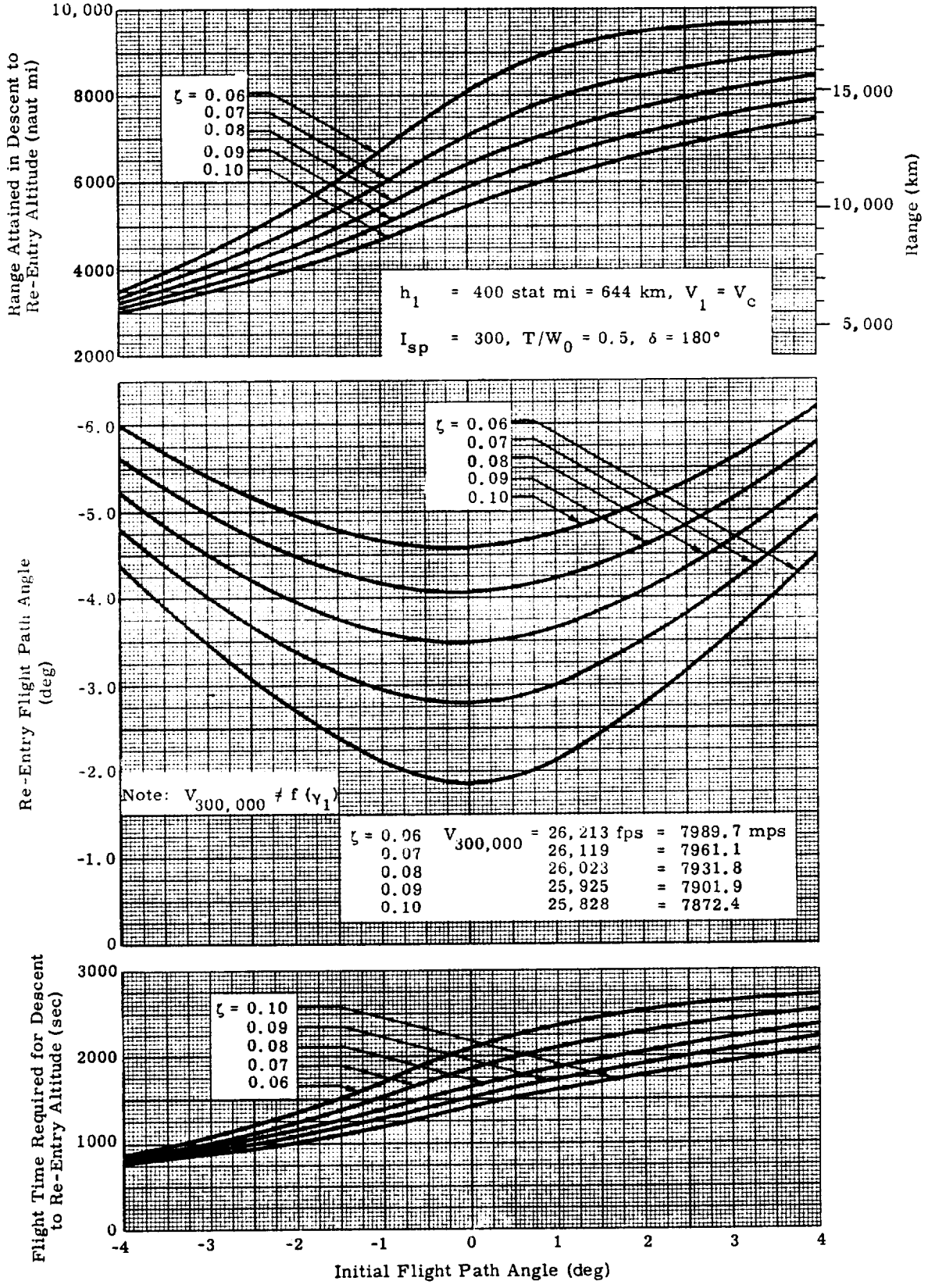

Fig. 19d. Re-Entry Parameters as Functions of ζ and γ_1

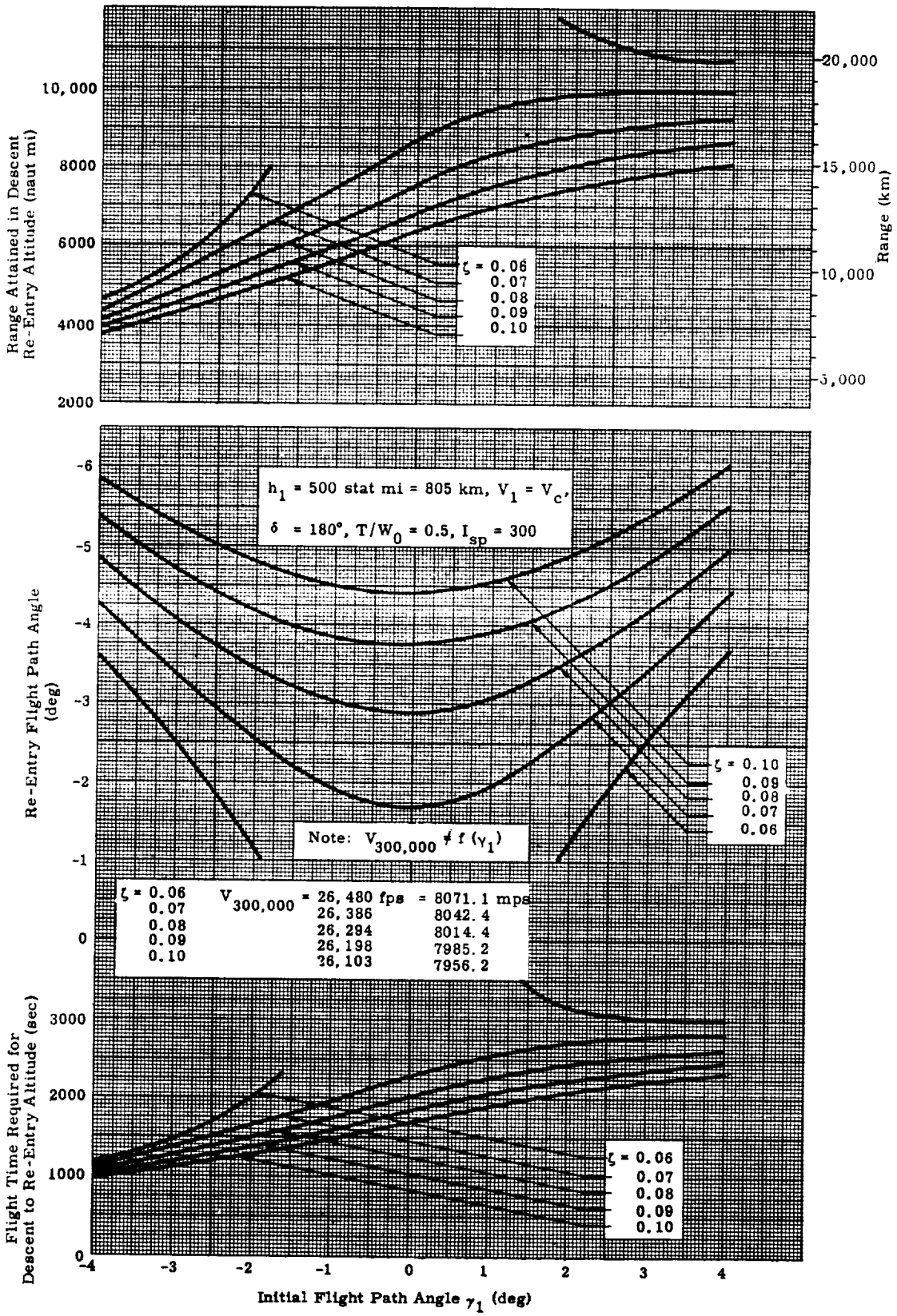

Fig. 19e. Re-Entry Parameters as Functions of ζ and γ_1

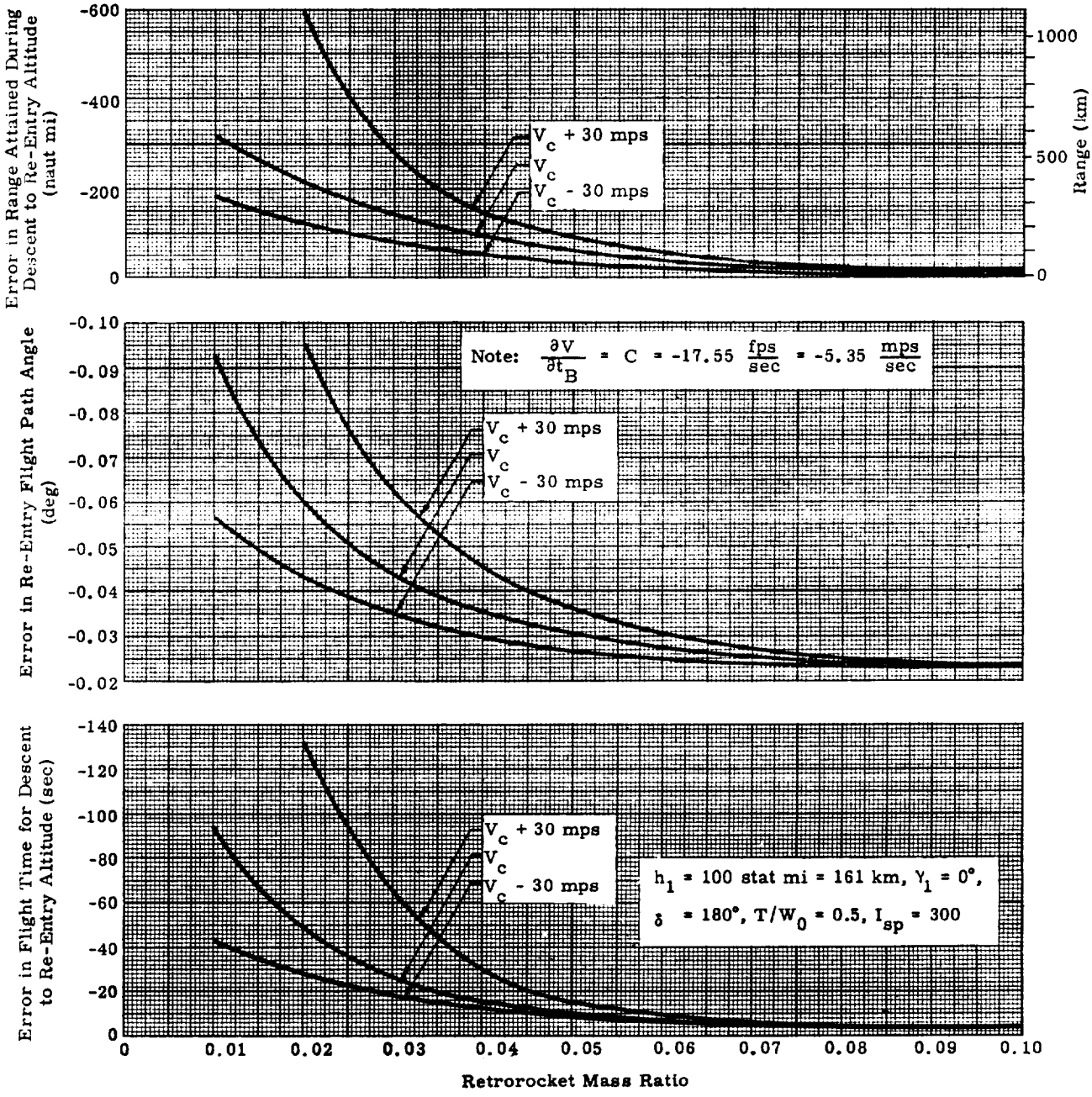

Fig. 20a. Variations in Re-Entry Position, Time and Flight Path Angle (per Second Error in t_B) with Initial Velocity and Retrorocket Mass Ratio (100 fps ≈ 30 mps)

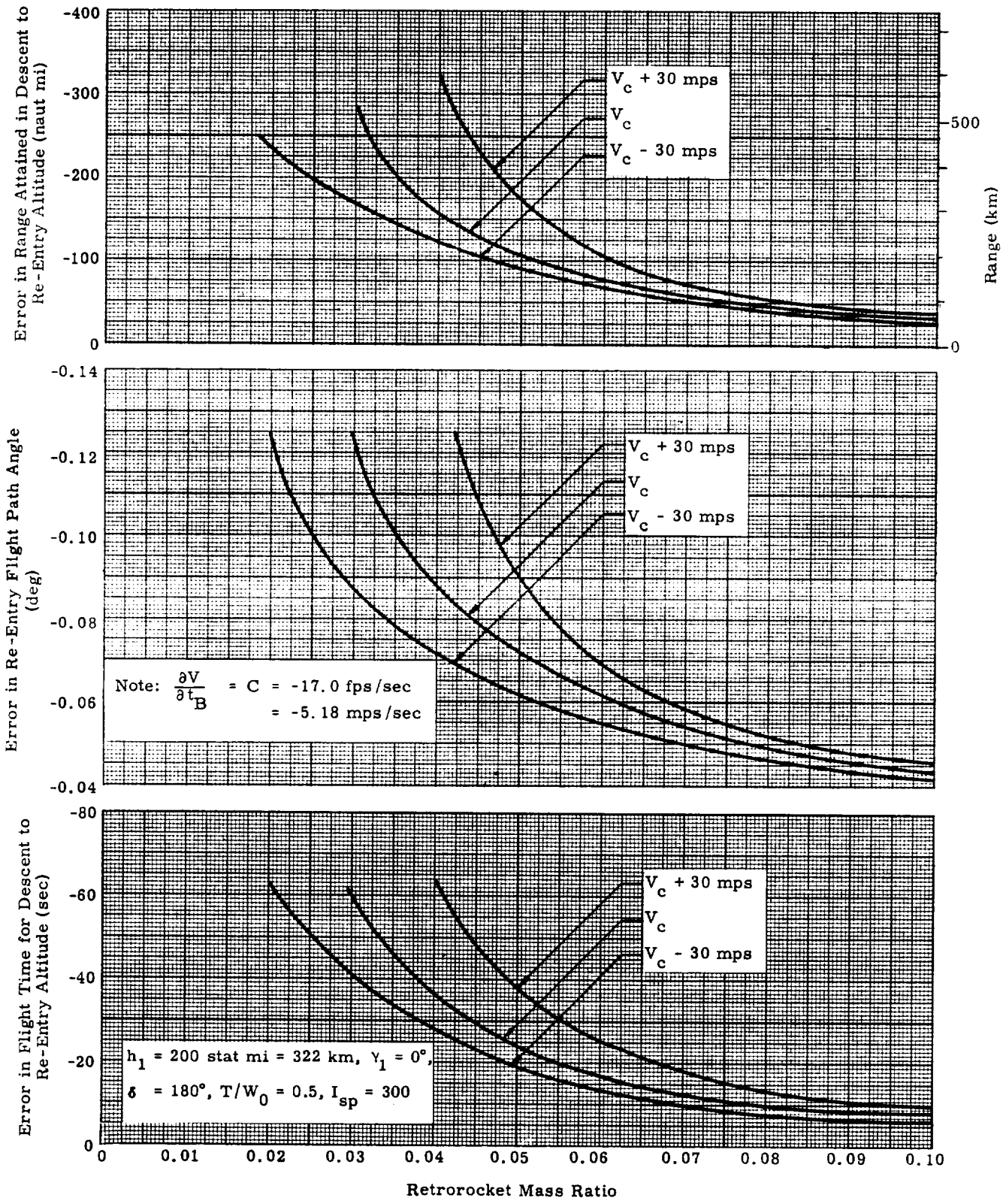

Fig. 20b. Variations in Re-Entry Position, Time, and Flight Path Angle (per Second Error in t_B) with Variations in Initial Velocity and Retrorocket Mass Ratio (100 fps ≈ 30 mps)

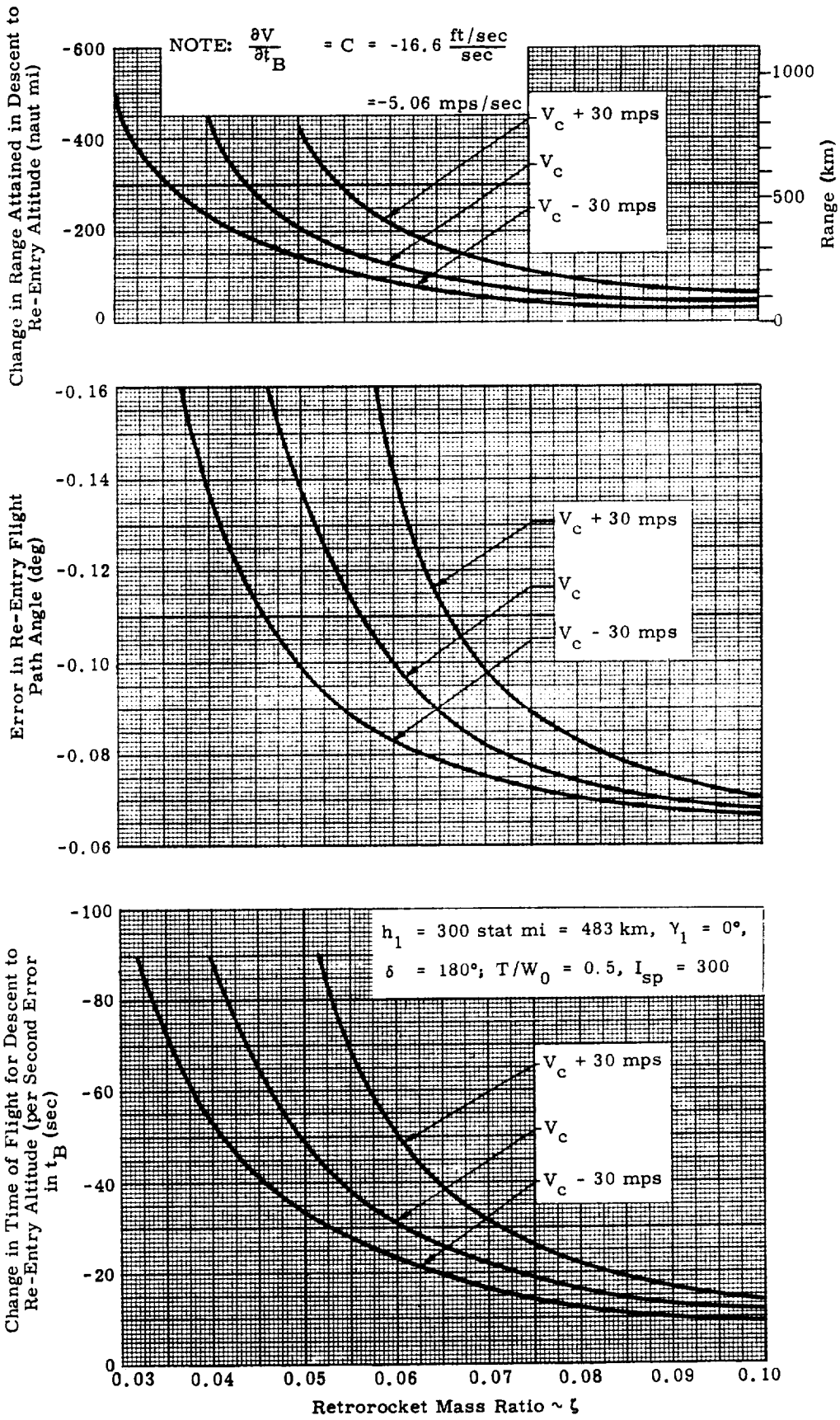

Fig. 20c. Variations in Re-entry Position, Time and Flight Path Angle (per Second Error in t_B) with Variations in Initial Velocity and Retrorocket Mass Ratio (100 fps = 30 mps)

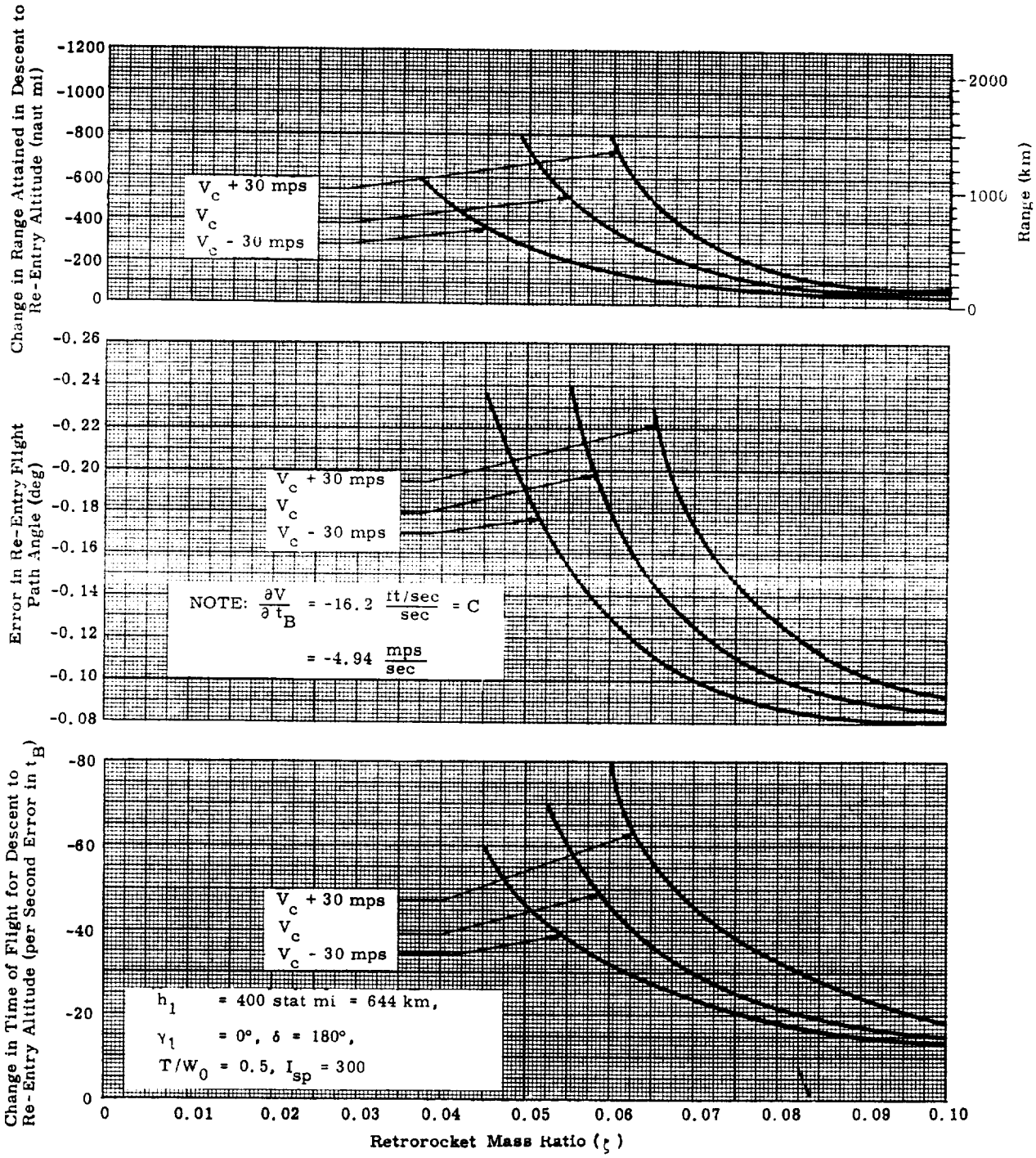

Fig. 20d. Variations in Re-Entry Position, Time and Flight Path Angle (per Second Error in t_B) with Initial Velocity and Retrorocket Mass Ratio (100 fps ≈ 30 mps)

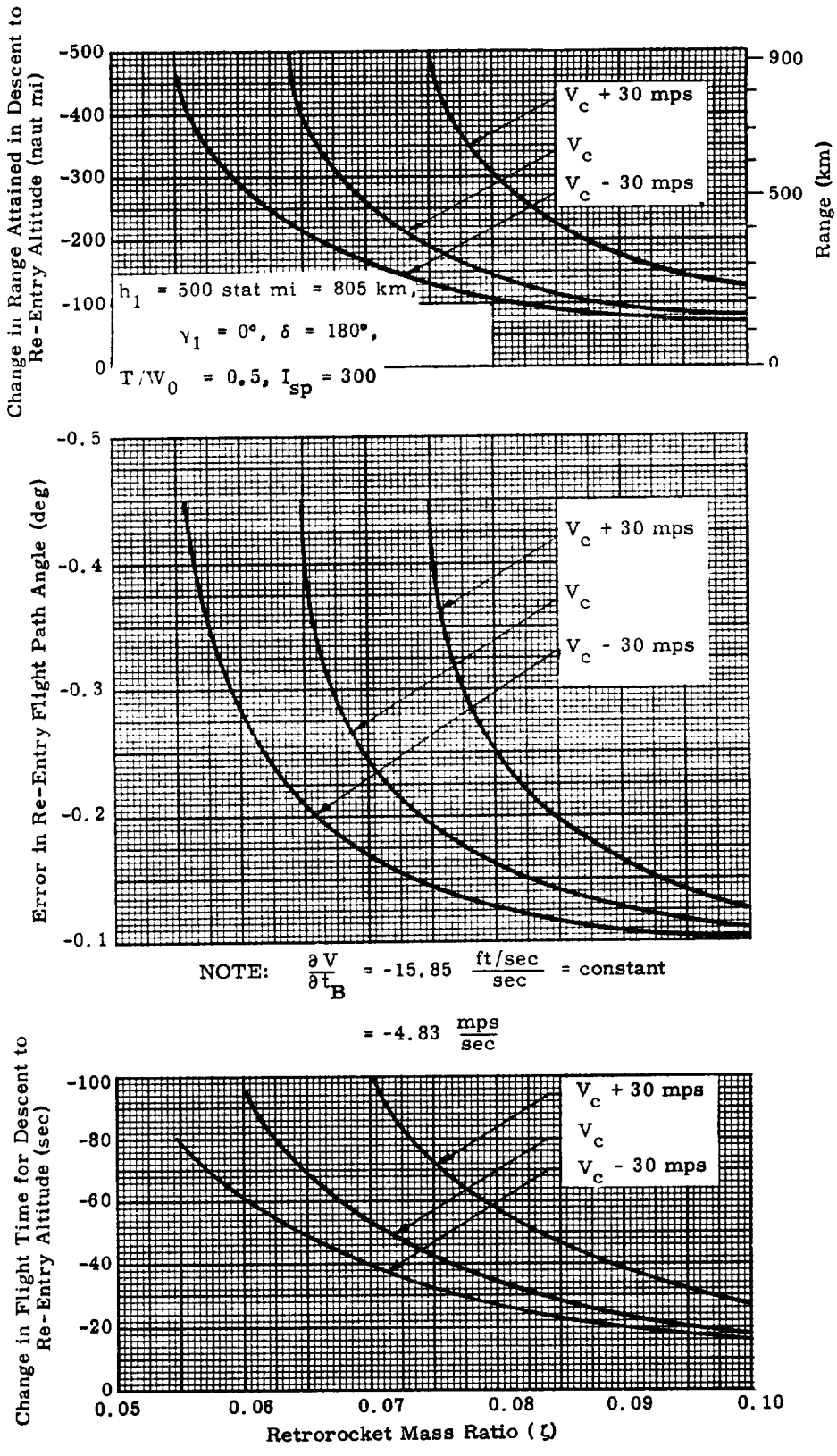

Fig. 20e. Variations in Re-Entry Position, Time and Flight Path Angle (per Second Error in t_B) with Initial Velocity and Retrorocket Mass Ratio (100 fps ≈ 30 mps)

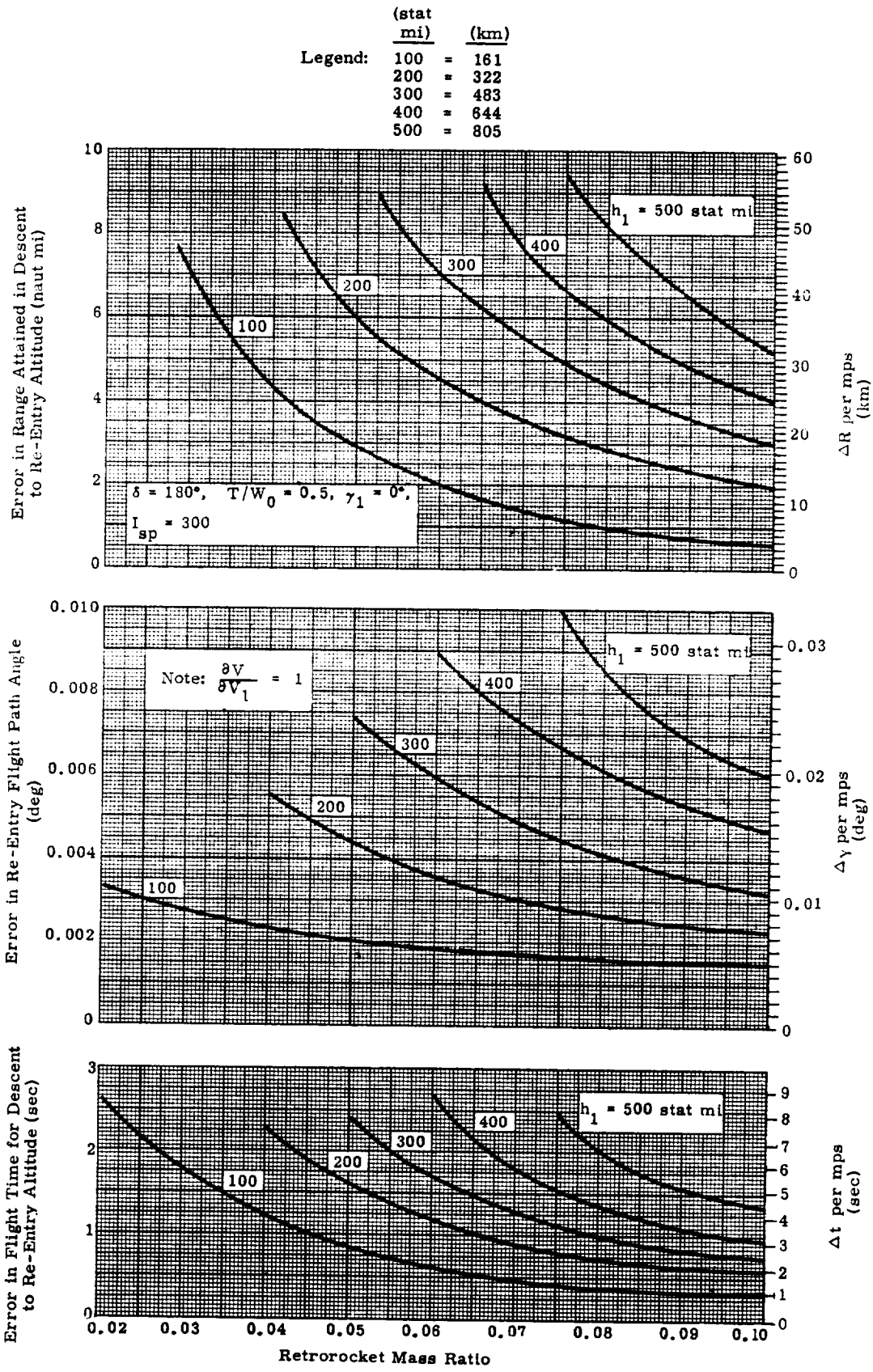

Fig. 21. Variations in Re-Entry Location, Time, Flight Path Angle, and Velocity with Initial Velocity as Functions of Retrorocket Mass Ratio and h_1

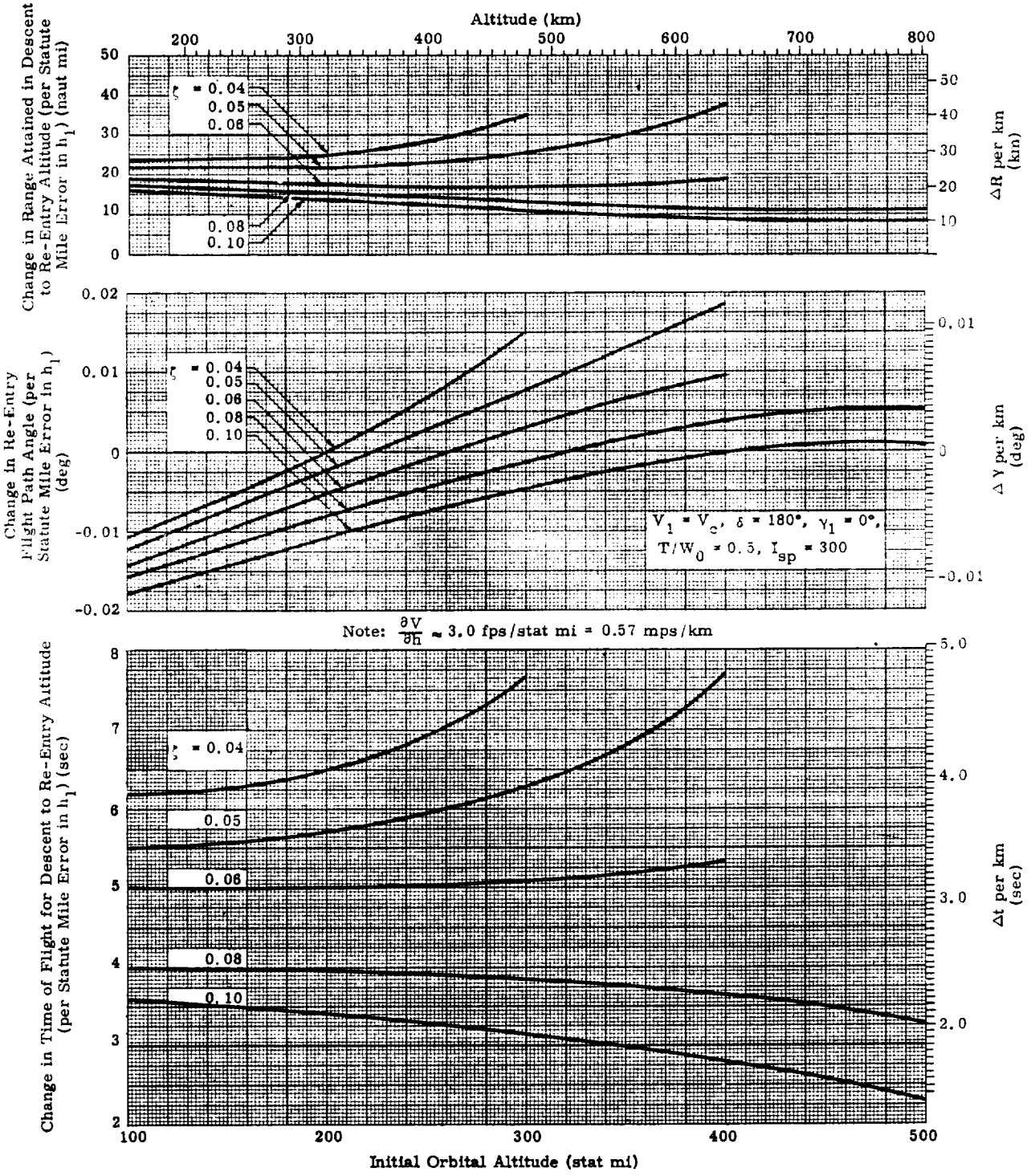

Fig. 22a. Variations in Re-Entry Location, Time, Flight Path Angle and Velocity with Altitude as Functions of h_1 and Retro-rocket Mass Ratio

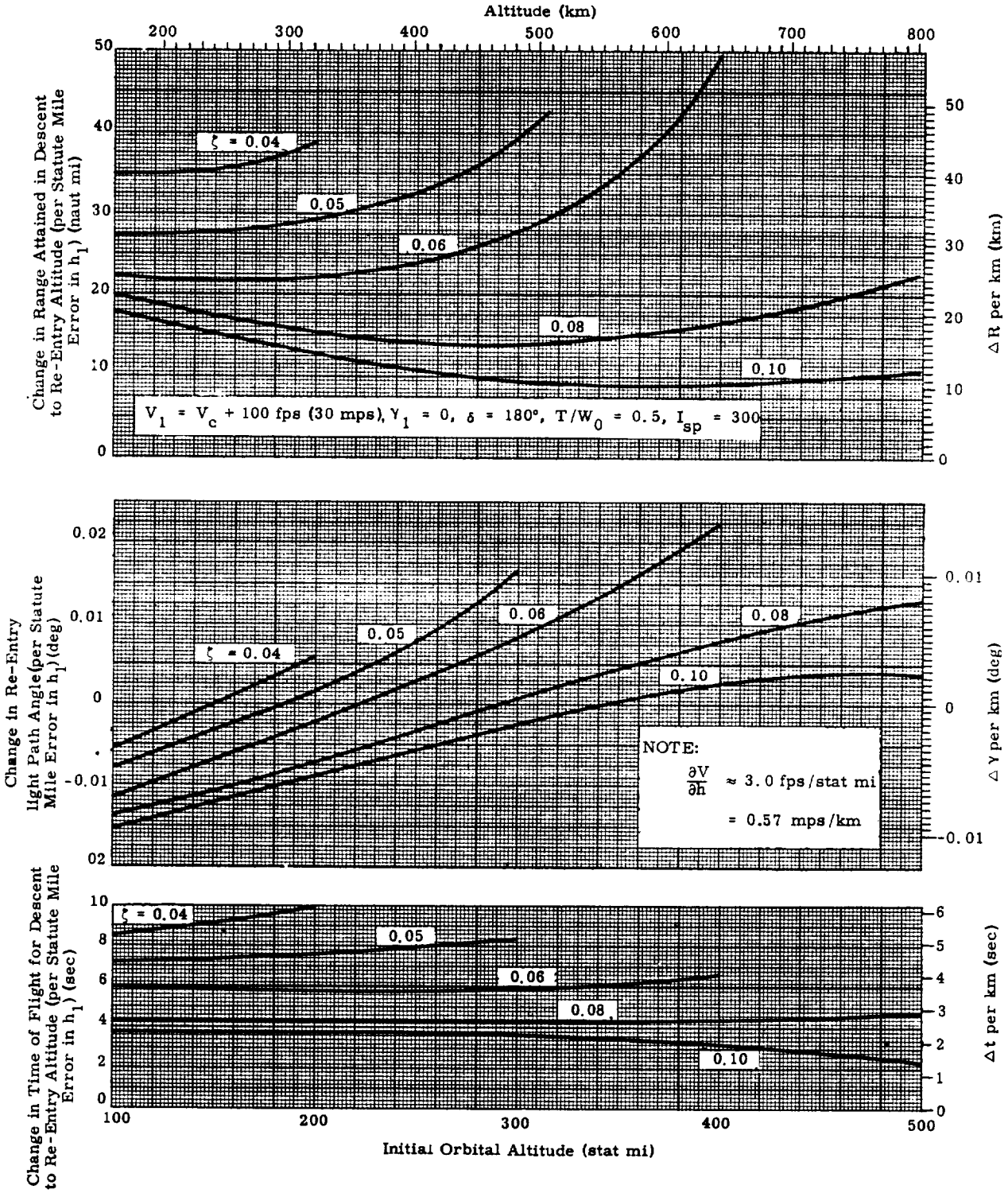

Fig. 22b. Variations in Re-Entry Position, Time, Flight Path Angle and Velocity with Altitude as Functions of h_1 and Retrorocket Mass Ratio

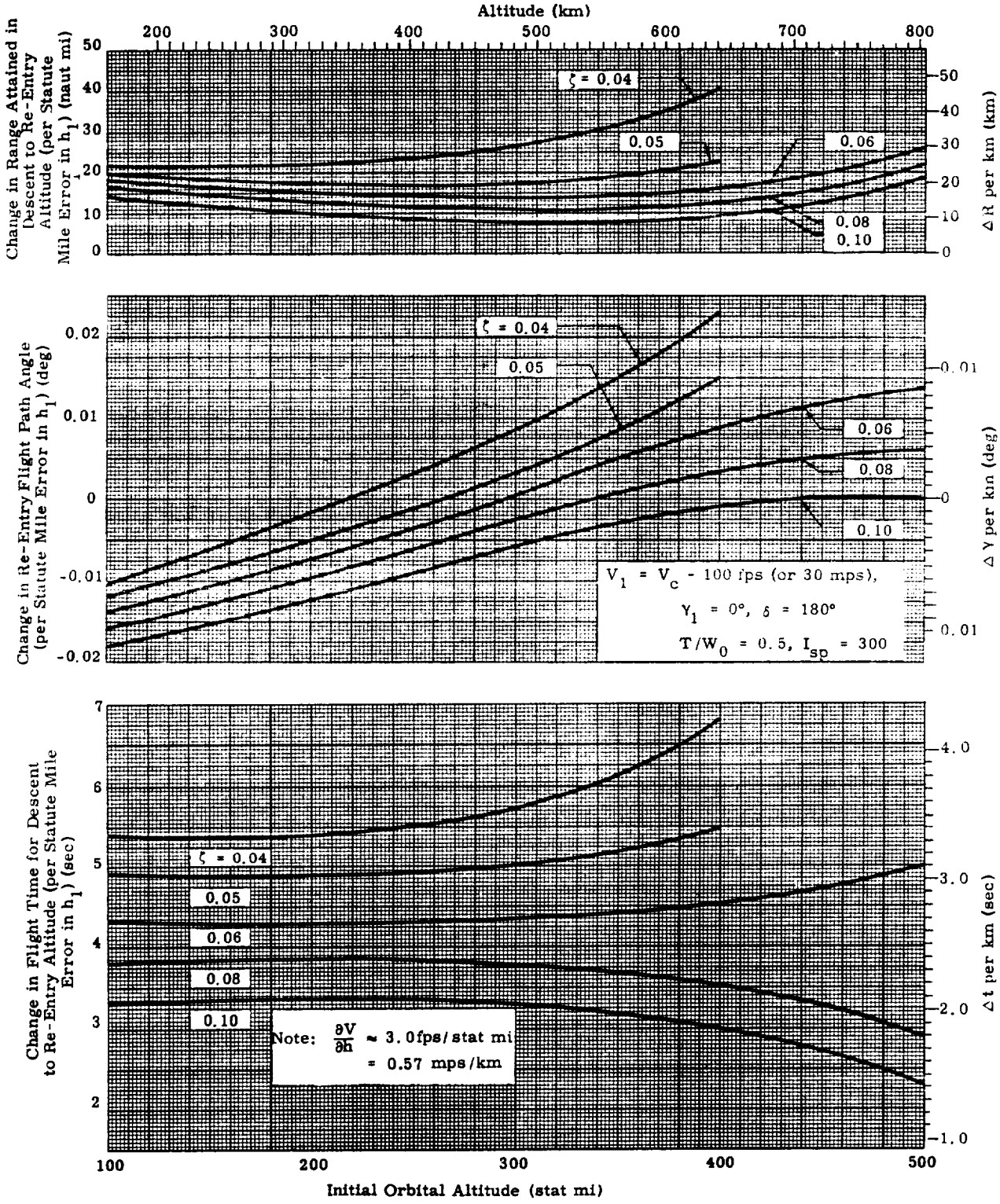

Fig. 22c. Variations in Re-Entry Position, Time, Flight Path Angle and Velocity with Altitude as Functions of h_1 and Retro-rocket Mass Ratio

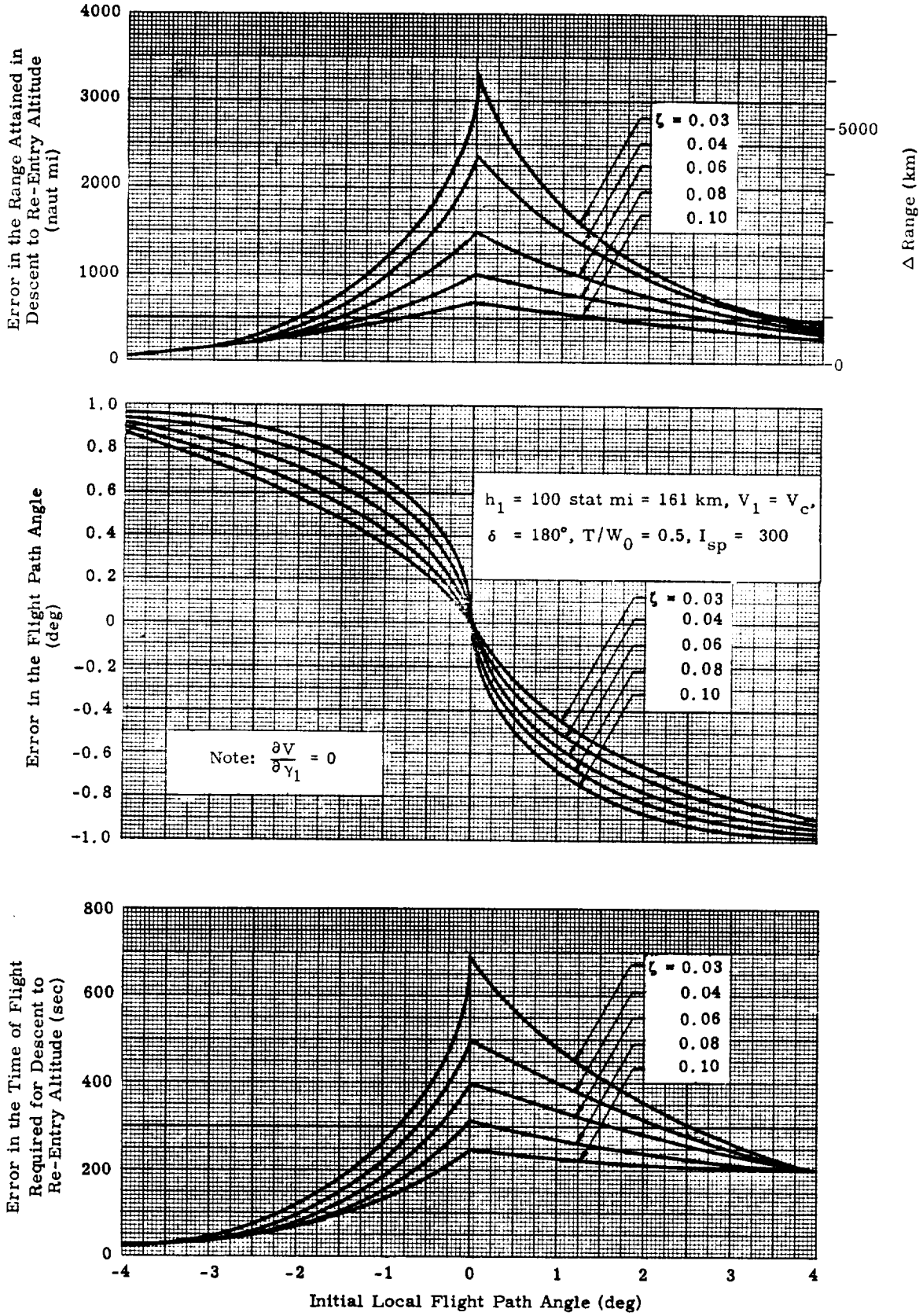

Fig. 23a. Errors in Re-Entry Parameters Due to a 1° Error in γ_1

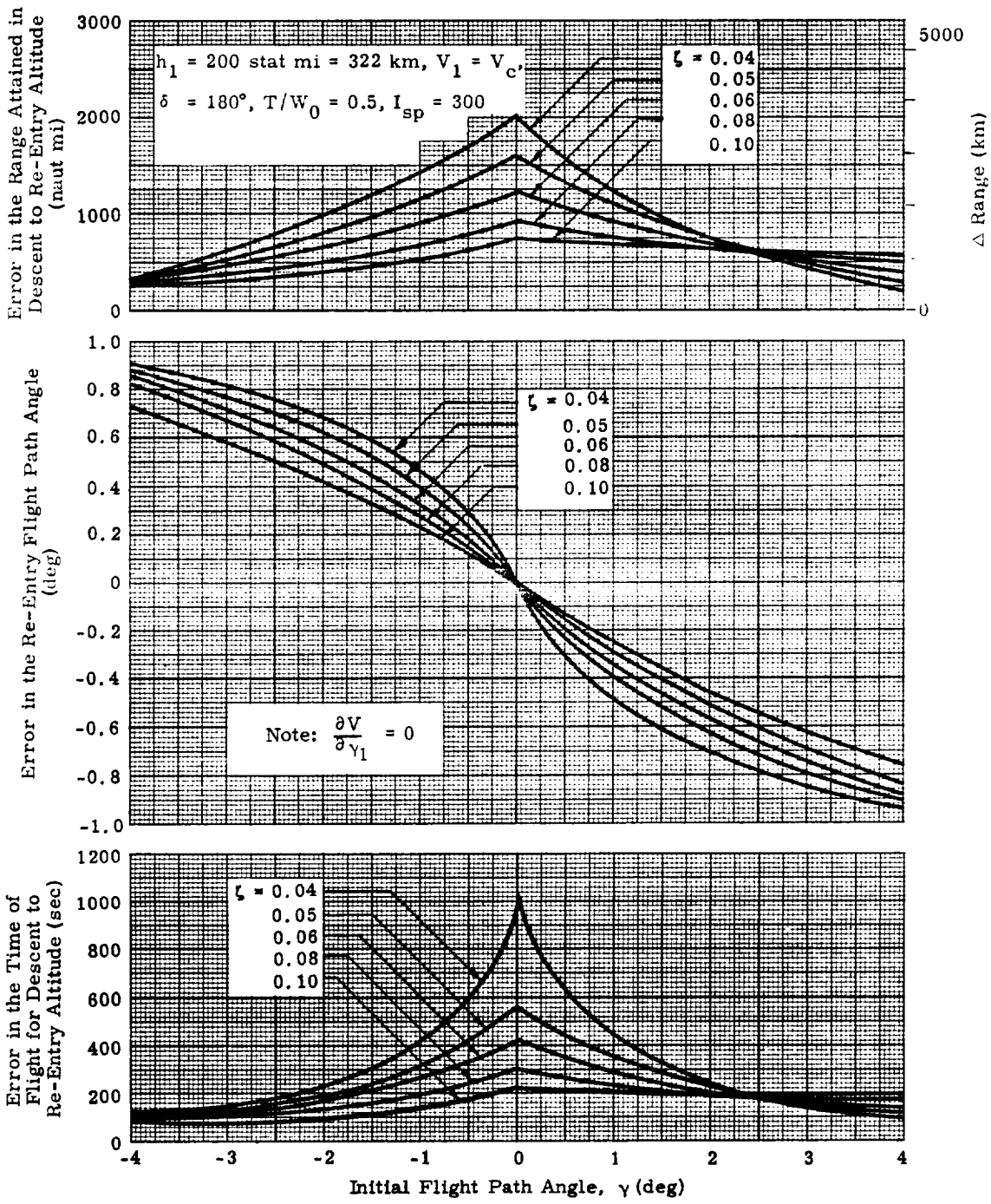

Fig. 23b. Errors in the Re-Entry Parameters Due to a 1° Error in γ_1

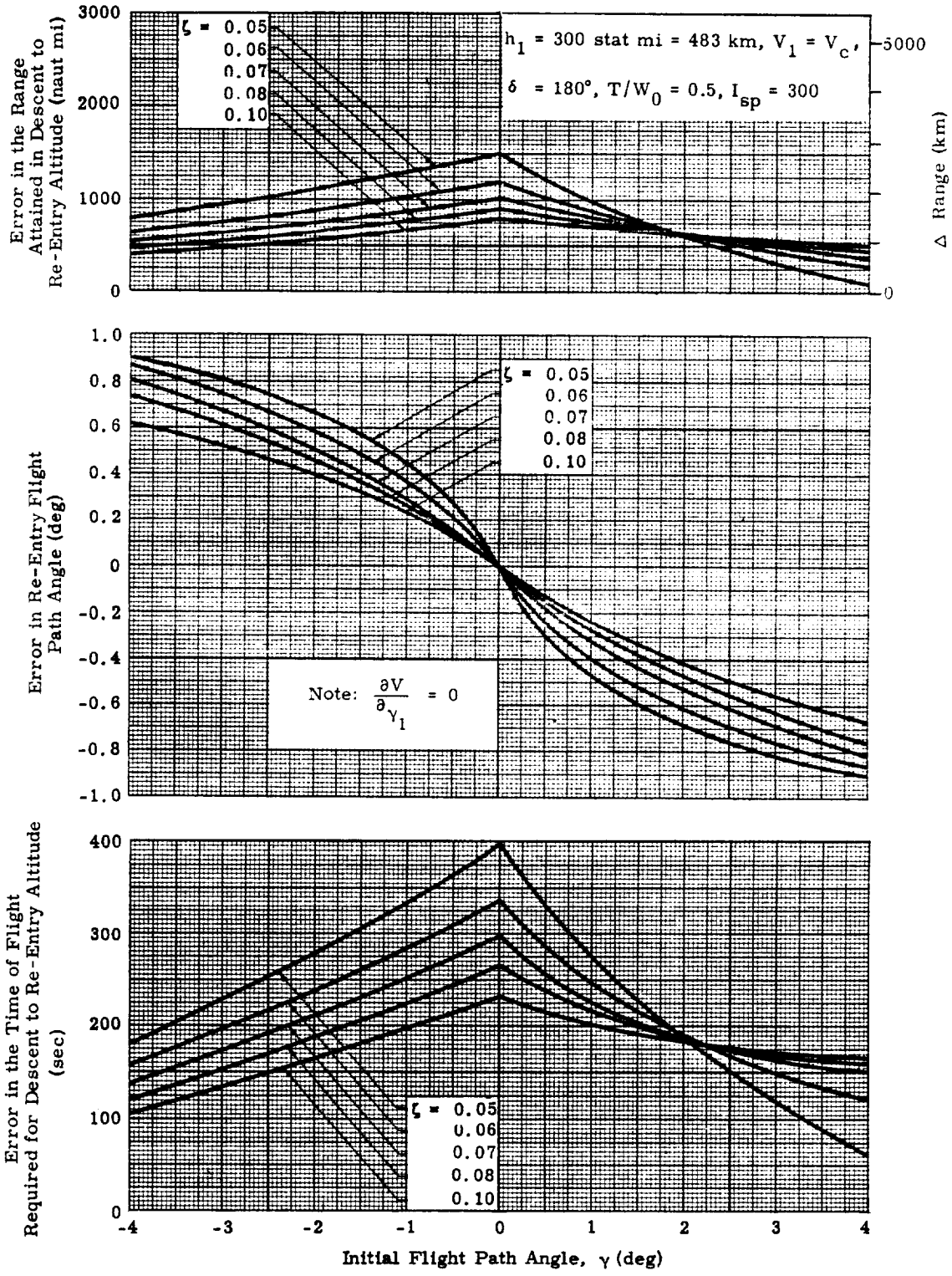

Fig. 23c. Errors in the Re-Entry Parameters Due to a 1° Error in γ_1

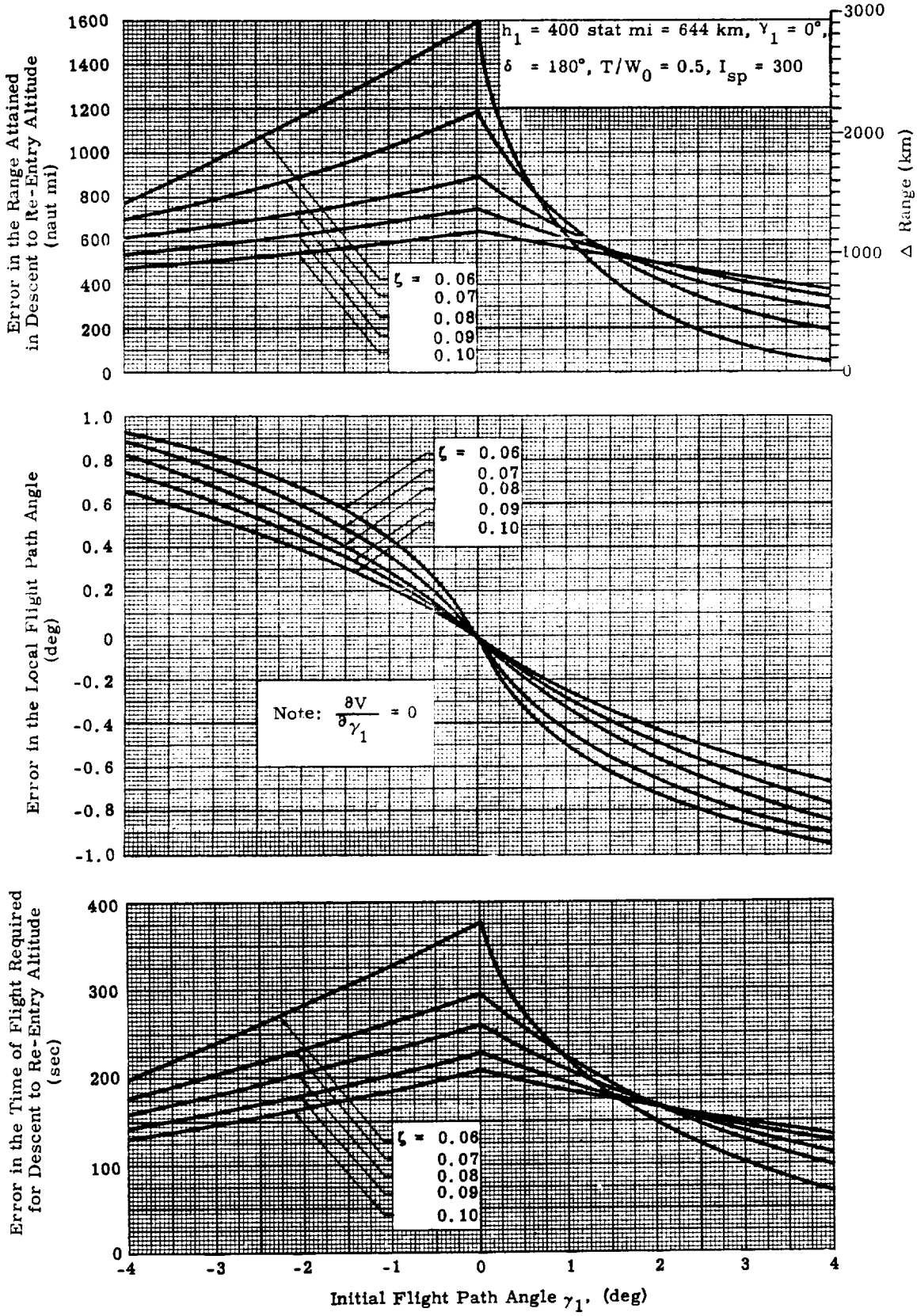

Fig. 23d. Errors in the Re-Entry Parameters Due to a 1° Error in γ_1

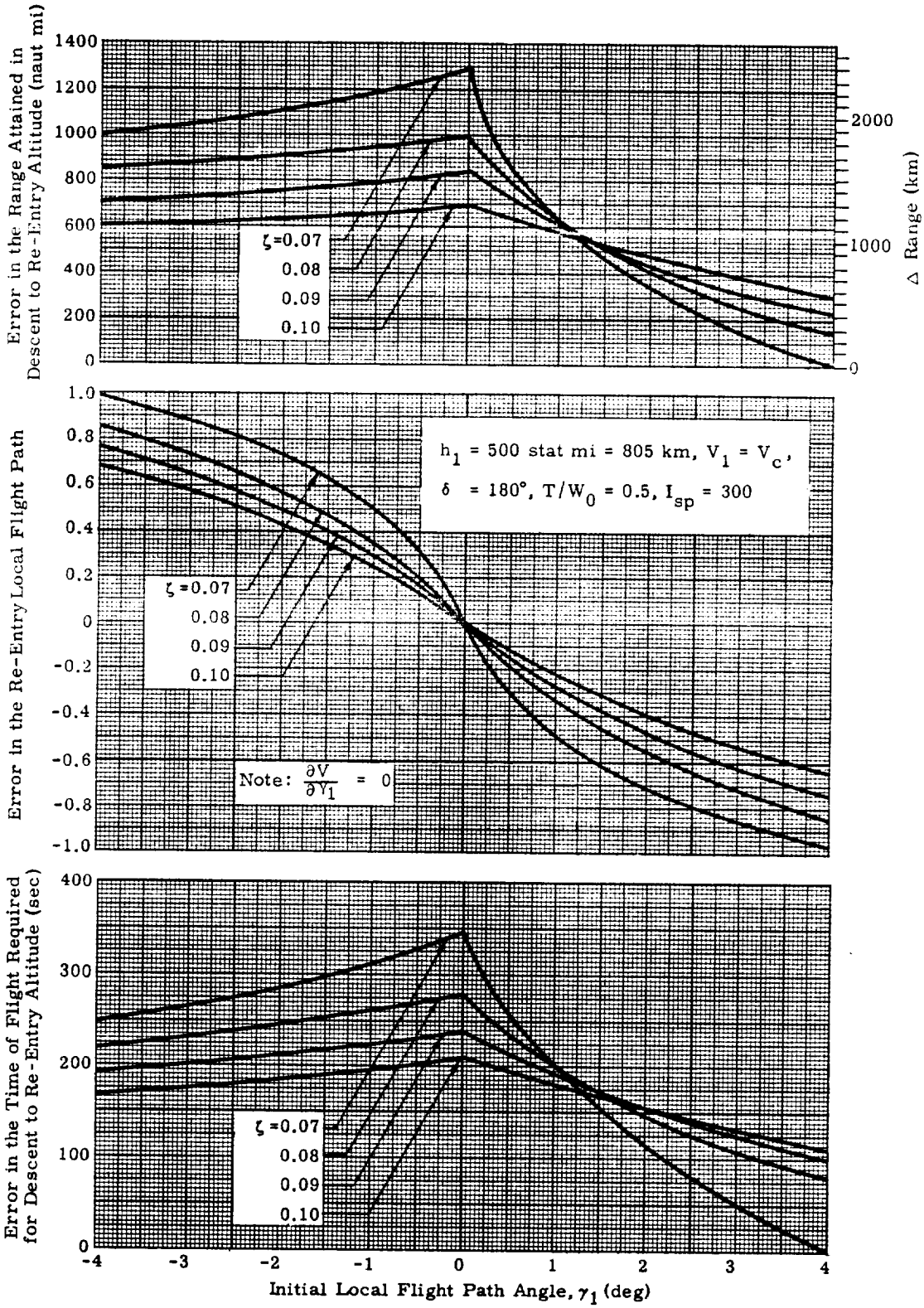

Fig. 23e. Errors in the Re-Entry Parameters Due to a 1° Error in γ_1

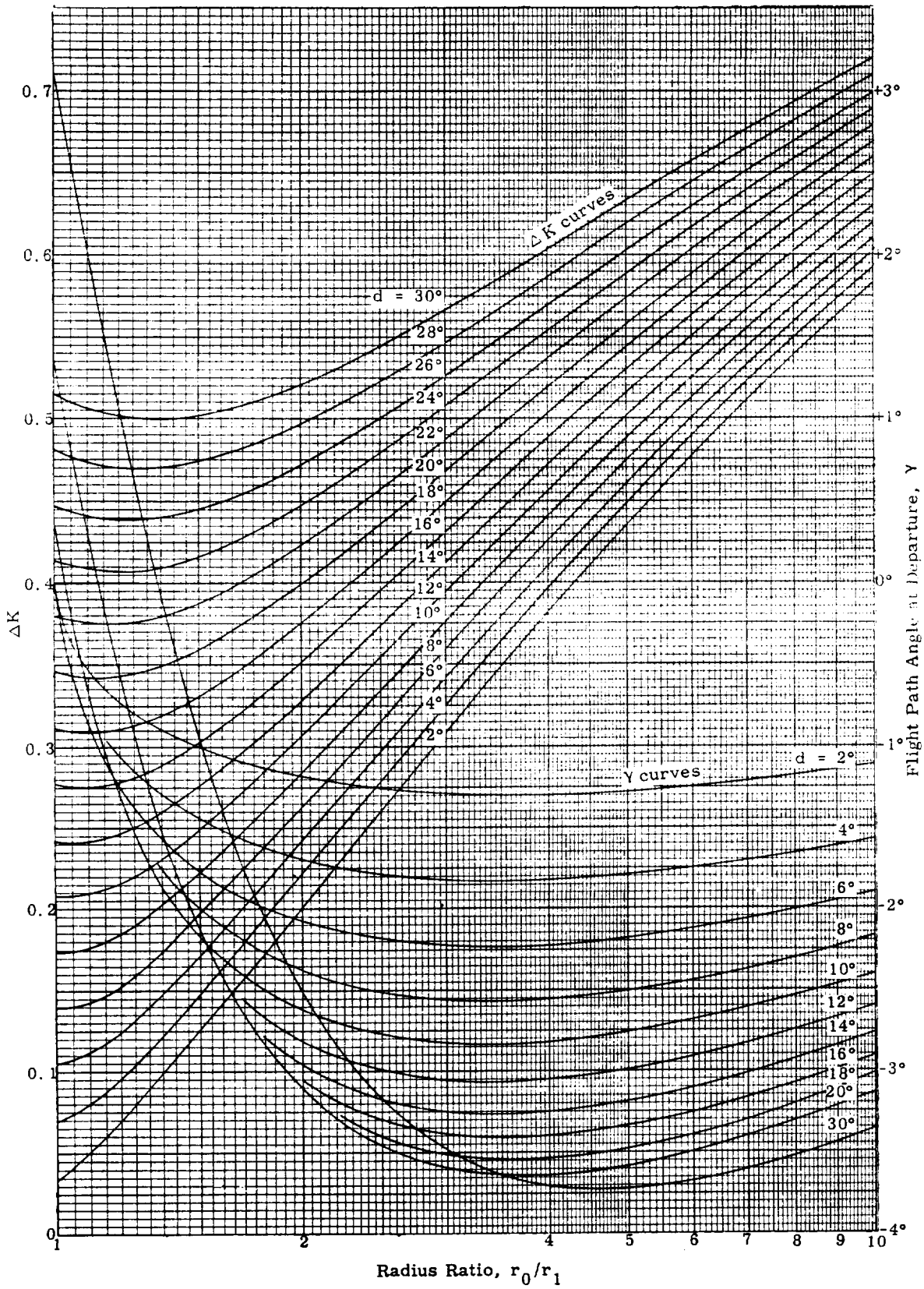

Fig. 24. Optimum ΔK and γ for 3-D-Departure

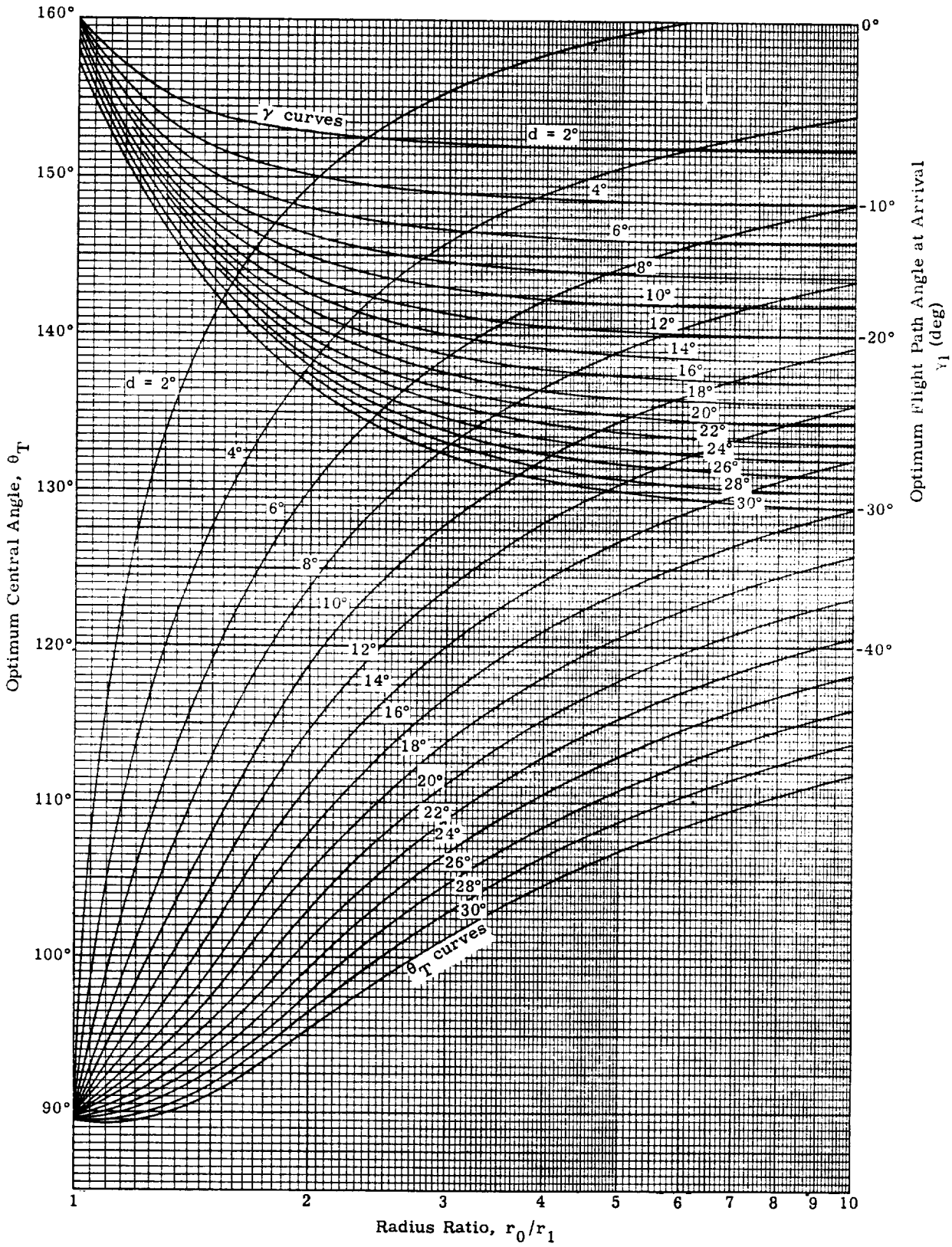

Fig. 25. Optimum Central Angle and Arrival Path Angle for 3-D Departure

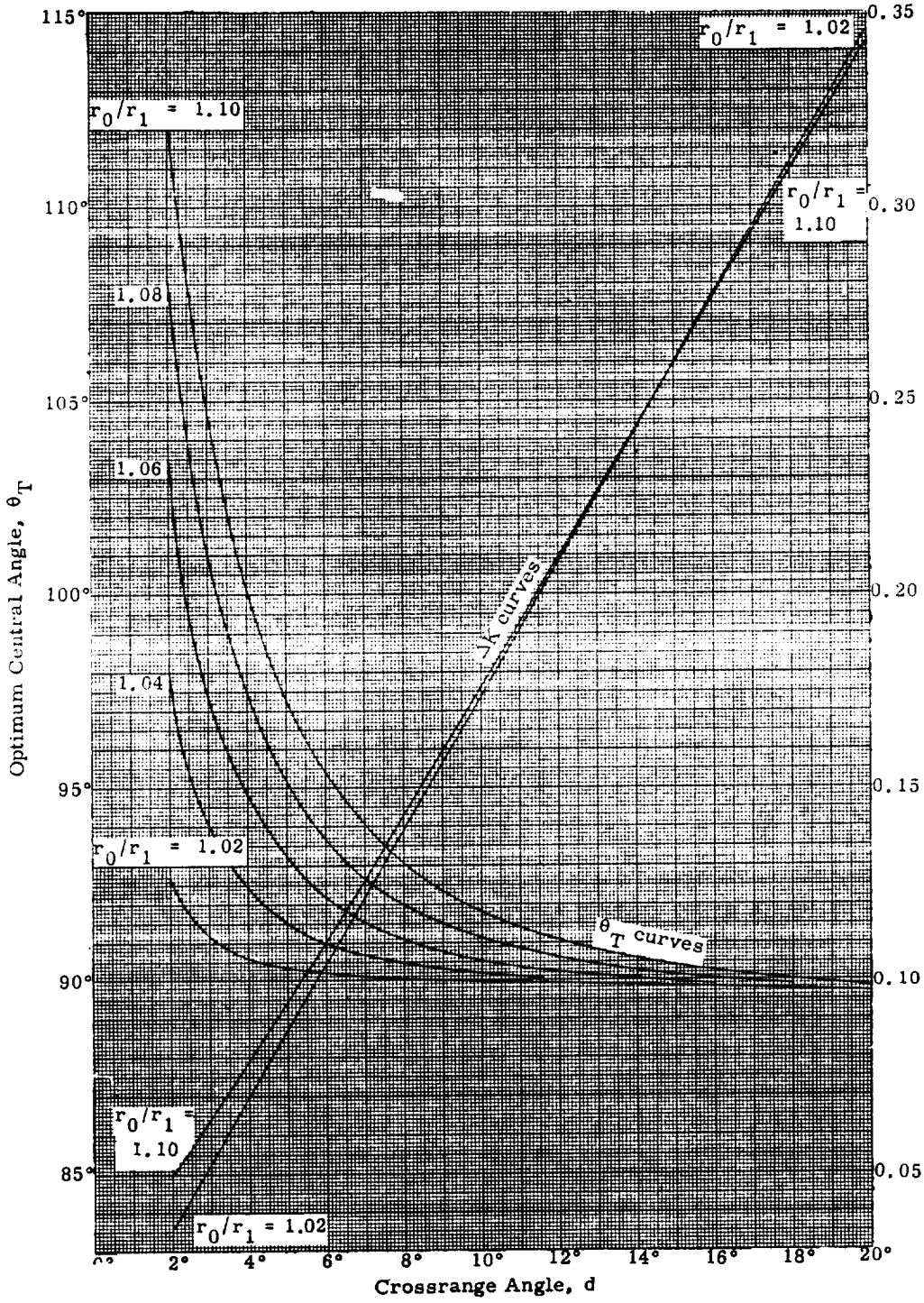

Fig. 26. Optimum Central Angle and ΔK as a Function of d

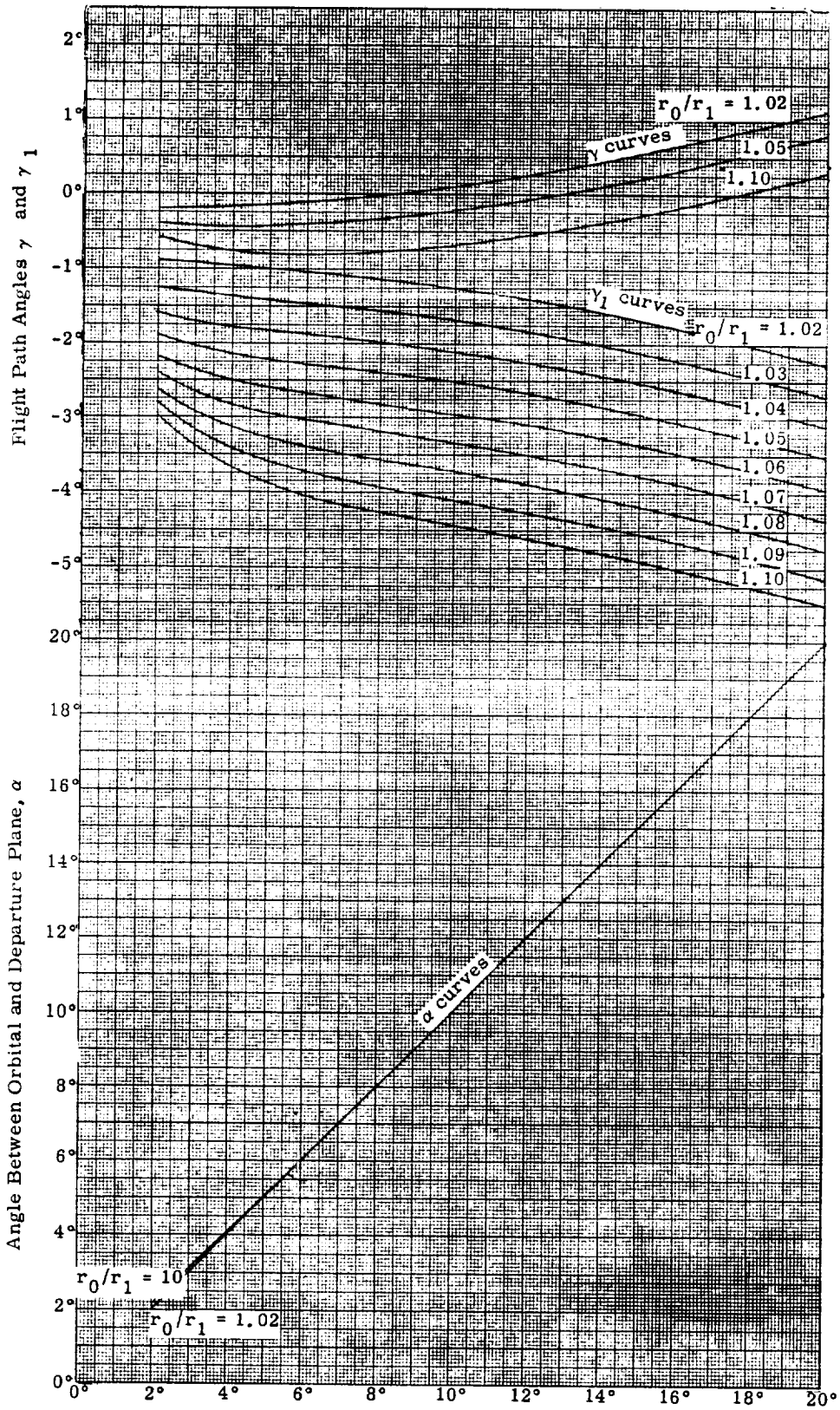

Fig. 27. Plane Change Angle and Flight Path Angle as Functions of Mass Range Angle

CHAPTER IX

SATELLITE RE-ENTRY

Prepared by

J. D. Kraft
Martin Company (Baltimore)
Aerospace Mechanics Department
March 1963

		Page
	Symbols	IX-1
A.	Introduction	IX-2
B.	Re-Entry Trajectories	IX-2
C.	Deceleration	IX-12
D.	Re-Entry Heating	IX-14
E.	Range and Time to Impact	IX-17
F.	Maneuverability	IX-18
G.	References	IX-21
H.	Bibliography	IX-22
	Illustrations	IX-29

LIST OF ILLUSTRATIONS

Figure	Title	Page
1	Values of z Functions for Entry from Decaying Orbits into Planetary Atmosphere	IX-31
2	Values of z Functions for Entry from Orbital Velocity at Initial Angles of Descent; $\bar{u}_0 = 1$	IX-32
3	Values of z Functions for Atmosphere Braking of Nonlifting Vehicles ($\bar{u}_0 = 1.4$, L/D = 0)	IX-34
4	Velocity Profile and Flight Path Angle Variation for Satellite Re-Entry	IX-35
5	Velocity Variation with Altitude (h_0 = 300,000 ft = 91,440 m, v_0 = 25,000 fps = 7,620 mps, L/D = 0) . .	IX-36
6	Flight Path Angle Variation with Altitude (h_0 = 300,000 ft = 91,440 m; v_0 = 25,000 fps = 7620 mps)	IX-41
7	Characteristic Re-Entry Altitude-Velocity Profiles for Lifting Vehicles	IX-44
8	Altitude Peak of First Skip (v_0 = 25,000 fps = 7,620 mps, h_0 = 400,000 ft = 122,000 m)	IX-45
9a	Entry Vehicle Comparison, Velocity-Altitude Profile	IX-47
9b	Effect of Entry Velocity on Altitude-Velocity Profile	IX-48
9c	Effect of Entry Angle on Velocity-Altitude Profiles .	IX-49
9d	Effect of Programmed C_L on Velocity-Altitude Profile	IX-50
9e	Program of C_L with Mach Number	IX-50
10a	Terminal Velocity	IX-51
10b	Terminal Flight Path Angle	IX-52

LIST OF ILLUSTRATIONS (continued)

Figure	Title	Page
11a	Entry Vehicle Comparison, Altitude-Time History . . .	IX-53
11b	Re-entry Vehicle Comparison--Time History	IX-54
11c	Re-Entry History with and Without Rotating Air . . . . . Mass	IX-55
12a	Effect of Lift-Drag Ratio on Deceleration for Entry into Earth Atmosphere From Decaying Orbits	IX-56
12b	Deceleration Profile and Load Factor for Satellite Re-Entry	IX-56
12c	Deceleration Variation with Altitude for Satellite Re-Entry	IX-57
13a	Maximum Decelerations for Ballistic Re-Entry	IX-58
13b	Optimum Ballistic Coefficients (to minimize re-entry decelerations)	IX-58
14a	Controlled Descent, General Ballistic Coefficient Variation	IX-59
14b	Controlled Descent, General Acceleration Profile . . .	IX-59
15	Length of Time Spent at Decelerations Equal to and Larger than the Shown Value	IX-60
16	Effect of Re-Entry Conditions on Maximum Total Decelerations (L/D = 0.5)	IX-62
17a	Maximum Load Factor Versus L/D (W/C_DA = 438 psf or B = 0.234×10^{-3} m^2/kg)	IX-62
17b	Maximum Load Factor Versus L/D (W/C_DA = 50 psf or B = 2.04×10^{-3} m^2/kg)	IX-63
17c	Maximum Total Acceleration Versus L/D Ratio (W/C_DA = 50 psf or B = 2.04×10^{-3} m^2/kg)	IX-63

LIST OF ILLUSTRATIONS (continued)

Figure	Title	Page
18	Maximum Re-Entry Load Factor Versus Ballistic Coefficient (h_0 = 400,000 ft = 121,920 m, v_0 = 25,000 fps = 7620 mps)	IX-64
19	Maximum Re-Entry Load Factor Versus Flight Path Angle (v_0 = 25,000 ft/sec = 7620 mps, h_0 = 400,000 ft = 121,920 m)	IX-65
20	Maximum Re-entry Load Factor Versus Velocity (h_0 = 400,000 ft, γ_0 = - 1°)	IX-66
21	Maximum Re-Entry Load Factor Versus L/D.	IX-68
22	Effect of Re-Entry Angle on Peak Deceleration, v_0 = v_c, $W/C_L A$ = 20 psf = 957 newton/m^2, L/D = 2 (Ref. 14)	IX-68
23	Maximum Re-Entry Dynamic Pressure (v_0 = 25,000 fps = 7620 mps; h_0 = 400,000 ft = 121,920 m)	IX-69
24	Maximum Re-Entry Dynamic Pressure Versus γ_0 (v_0 = 25,000 fps = 7620 mps, h_0 = 400,000 ft = 121,920 m)	IX-72
25	Maximum Re-entry Dynamic Pressure Versus Velocity (γ_0 = - 1°; h_0 = 400,000 ft = 121,920 m)	IX-73
26	Maximum Re-Entry Dynamic Pressure Versus L/D (v_0 = 25,000 fps = 7620 mps)	IX-75
27	Maximum Re-Entry Dynamic Pressure Versus L/D (γ_0 = -1°; h_0 = 400,000 ft = 121,920 m)	IX-76
28	Effects of Lift, Drag and Wing Loading on Maximum Dynamic Pressure	IX-78

LIST OF ILLUSTRATIONS (continued)

	Title	Page
29	Radius-Emissivity Parameter ($R^{1/8} \times \epsilon^{1/4}$) Versus Stagnation Nose Radius.	IX-78
30a	Heat Transfer Rate q_s at the Stagnation Point of a Blunt Body of 1-ft Nose Radius as a Function of Air Density Ratio, ρ/ρ_0	IX-79
30b	Ratio of the Heat Input Rate q_s to the Rate at Which Energy Is Dissipated by Drag $\frac{1}{2}\rho v^3$ as a Function of Air Density Ratio ρ/ρ_0	IX-79
31a	Effect of Re-Entry Angle on Maximum Heat Flux ($v_0 = v_c$, $W/C_L A$ = 20 psf, L/D = 2)	IX-80
31b	Equilibrium Radiation Temperature Versus Heat Transfer Rate	IX-80
32	Comparison of Radiation Equilibrium Method with an Exact Skin Temperature Computation (free fall from 1,000,000 ft = 304,800 m)	IX-81
33a	Nose Temperature Histories for Different Flight Conditions	IX-82
33b	Stagnation Point Temperature Profiles for Equilibrium Glides	IX-83
33c	Temperature Data for Inertial Velocity and Altitude . .	IX-84
34a	Maximum Equilibrium Nose Temperature Versus $W/C_L A$ for Equilibrium Glides	IX-85
34b	Altitude for Maximum Equilibrium Nose Temperature Versus $W/C_L A$ (equilibrium glides)	IX-85
34c	Altitude for Maximum Stagnation Nose Temperature (h_0 = 400,000 ft, v_0 = 25,000 fps)	IX-86
35	Maximum Re-Entry Stagnation Point Nose Temperature (h_0 = 400,000 (121,920 m), v_0 = 25,000 fps (7620 mps)	IX-87

LIST OF ILLUSTRATIONS (continued)

Figure	Title	Page
36	Maximum Re-Entry Stagnation Point Nose Temperature Versus γ_0 (h_0 = 400,000 ft = 121,920 m, v_0 = 25,000 fps = 7620 mps)	IX-88
37	Effect of Re-Entry Conditions on Maximum Stagnation Point Temperature (L/D = 0.5)	IX-90
38	Maximum Re-Entry Stagnation Point Temperature Parameter Versus Velocity (h_0 = 400,000 ft = 121,920 m; γ_0 = - 1°)	IX-91
39	Maximum $T_W R^{1/8} \epsilon^{1/4}$ Versus Re-Entry Velocity (h_0 = 400,000 ft = 121,920 m, $\frac{W}{C_D A}$ = 50 psf = 2390 Newtons/m^2	IX-93
40	Maximum Re-Entry Stagnation Point Nose Temperature Versus Velocity (h_0 = 400,000 ft = 121,920 m; $W/C_D A$ = 438 psf = 21,000 newtons/m^2	IX-95
41	$T_W R^{1/8} \epsilon^{1/4}$ Versus Lift-Drag Ratio (h_0 = 400,000 ft = 121,920 m)	IX-97
42	Equilibrium Temperature History, with and Without Rotating Air Mass	IX-98
43a	Maximum Stagnation Point Temperature Parameter Versus Ballistic Coefficient (ballistic re-entry--L/D = 0)	IX-98
43b	Maximum Radiation-Equilibrium Temperature at Laminar Stagnation Point for Entry from Decaying Orbits into Earth Atmosphere	IX-99
44	Effect of Lift-Drag Ratio on Maximum Laminar Heating Rate at Stagnation Point for Entry from Decaying Orbits	IX-99
45a	Surface Temperature Parameter $\epsilon^{1/4} R^{1/8} T_w$ as a Function of Air Density Ratio ρ/ρ_0. Simple drag bodies	IX-100

LIST OF ILLUSTRATIONS

Figure	Title	Page
45b	Lift Parameter $C_L A/W$ as a Function of Air Density Ratio ρ/ρ_0 for Several Values of the Drag Parameter $W/C_D A$. Constant Heat Transfer Trajectories.	IX-100
45c	Lift Parameter $C_L A/W$ as a Function of Air Density Ratio ρ/ρ_0 for Several Values of the Surface Temperature Parameter $\epsilon^{1/4} R^{1/8} T_w$ Constant Heat Transfer Trajectories	IX-101
46	Rate of Change of Stagnation Point Temperature Parameter as a Function of Re-Entry Angle (h_0 = 400,000 ft = 121,920 m, (v_0 = 25,000 fps = 7620 mps) .	IX-102
47	Maximum Surface Temperature for Entry into Various Planets from Decaying Orbits $v_0/v_c = 1$, $\gamma_0 = 0°$	IX 103
48	Range to Impact Versus Re-entry Angle	IX-104
49	Range Attained in Descent from 300,000 ft (91,440 m) ft to Sea Level (L/D = 0).	IX-105
50	Range to Impact from 400,000 ft = 121,920 m (v_0 = 25,000 fps = 7620 mps).	IX-107
51	Range to Impact from 400,000 ft = 121,920 m(γ_0 = -1°)	IX-109
52	Impact Range Versus Re-Entry Velocity ($\frac{W}{C_D A}$ = 50 psf = 2390 newtons/m^2, h_0 = 400,000 ft = 121,920 m) .	IX-111
53	Range to Impact from 400,000 ft (121,920 m) Versus L/D (v_0 = 25,000 fps = 7620 mps).	IX-115
54	Range Versus Lift-Drag, $\frac{W}{C_D A}$ = 50 psf (Applies for $5 < \frac{W}{C_D A} < 500$ psf; h_0 = 400,000 ft)	IX-116

LIST OF ILLUSTRATIONS (continued)

Figure	Title	Page
55	Equilibrium Glide Range (not dependent on $W/C_L A$) . .	IX-118
56a	Variation in Range as a Function of Angle of Attack and Entry Angle. (Nonrotating Earth; h_0 = 350,000 ft = 106,700 m; v_0 = 25,863 fps = 7870 mps; W/A = 20 lb/ft^2 = 956 newton/m^2)	IX-118
56b	Variation in Range as a Function of Initial Velocity and Entry Angle for Ballistic Vehicles (α = 90), (Nonrotating Earth; h_0 = 350,000 ft = 106,800 m; W/A = 20 lb/ft^2 = 955 newtons/m^2)	IX-119
56c	Variation in Range as a Function of Angle of Attack and Initial Velocity. (Nonrotating Earth; h_0 = 350,000 ft = 160,800 m; γ_0 = 1°)	IX-119
57	Time to Impact Versus Ballistic Coefficient (v_0 = 25,000 fps = 7620 mps)	IX-120
58	Time Versus Range to Impact from 400,000 ft = 121,920 m (v_0 = 25,000 fps = 7620 mps)	IX-120
59	Time to Impact Versus Re-Entry Velocity (h_0 = 400,000 ft = 121,920 m, $W/C_D A$ = 50 psf = 2390 newton/m^2)	IX-122
60	Re-Entry Time Versus L/D for Various Velocities ($\frac{W}{C_D A}$ = 50 psf = 2390 newtons/m^2; h_0 = 400,000 ft = 121,920 m)	IX-123
61	Velocity at Apogee Versus Range	IX-124
62	Range and Time to Impact for Ballistic Entry.	IX-125
63a	Conditions for Impact--Ballistic Case	IX-125
63b	Conditions for Impact, Lifting Case	IX-126
63c	Minimum Entry Angle for Capture (at escape velocity)	IX-126

LIST OF ILLUSTRATIONS (continued)

Figure	Title	Page
64	Range Corrections with Ballistic Coefficient Increments	IX-127
65a	Variation in Range as a Function of Angle of Attack and Entry Angle for Headings of 90° and 150° (Rotating Earth; h_0 = 350,000 ft = 106,680 m; v_0 = 25,743 fps = 7846 mps; W/A = 20 lb/ft^2 = 957 newtons/m^2)	IX-128
65b	Variation in Range and Maximum Deceleration as a Function of Heading and Initial Latitude (Rotating Earth; h_0 = 350,000 ft = 106,650 m; v_0 = 25,743 fps = 7846 mps; W/A = 20 lb/ft^2 = 957 newtons/m^2)	IX-128
66a	Effect of Roll Angle on Lateral Range	IX-129
66b	Lateral Range Capability ($v_0 = v_c$)	IX-129
66c	Effect of Entry Angle on Lateral Range	IX-130
66d	Effect of Velocity at Initiation of Maneuver on Lateral Range	IX-130
67a	Effect of Re-Entry Angle on the Azimuth Angle and Range to Maximum Lateral Deflection Point	IX-131
67b	Effect of Wing Loading on Azimuth Potential (γ_0 = 2°; constant altitude and equilibrium glide)	IX-132
67c	Effect of Wing Loading on Range to Maximum Azimuth Potential (γ_0 = -2°; constant altitude and equilibrium glide)	IX-132

LIST OF ILLUSTRATIONS (continued)

Figure	Title	Page
68	Total Maneuverability Envelope	IX-133
69	Range and Lateral Displacement for Lifting Body Re-Entry	IX-134

IX. SATELLITE RE-ENTRY

SYMBOLS

a	acceleration
A	reference area
B	ballistic coefficient, $\frac{C_D A}{2m}$
C_D	drag coefficient
C_L	lift coefficient
D	drag force $= \frac{1}{2} \rho v^2 C_D A$
g	gravitational acceleration
G	resultant acceleration magnitude experienced in addition to that due to gravity
h	altitude; also, enthalpy
k	conductivity
°K	degrees Kelvin
L	lift force $= \frac{1}{2} \rho v^2 C_L A$
Le	Lewis number
ℓ	characteristic length
m	vehicle mass
N	load factor, $\frac{G}{g}$
Nu	Nusselt number $= \frac{h\ell}{k}$
Pr	Prandtl number
q_s	Heating rate at the stagnation region
r	geocentric radius vector
R	earth radius
°R	degrees Rankine
Re	Reynolds number $= \frac{\rho v \ell}{\mu}$
R_s	body radius of curvature at the stagnation point
t	time
T_w	temperature at the vehicle wall
u	component of velocity normal to the radius vector in the trajectory plane
$\bar{u}$	normalized velocity component, $\frac{u}{v_c}$
v	velocity magnitude
v_c	circular orbit velocity magnitude
$\bar{v}$	normalized velocity, $\frac{v}{v_c}$
w	radial component of velocity
W	vehicle weight
x	longitudinal range
y	altitude
Y	side force
z	drag parameter $= \rho_0 B \sqrt{\frac{r}{\beta}}\ \bar{u}\, e^{-\beta y}$
β	logarithmic slope of the exponential atmospheric density function
γ	flight path angle with respect to the local horizontal
ϵ	emissivity
θ	flow inclination angle with respect to the free stream
λ	lateral range
μ	viscosity
ν	kinematic viscosity
ρ	density of the atmosphere
ρ_0	sea-level or reference density of the atmosphere
$\bar{\rho}$	normalized density $= \frac{\rho_\infty}{\rho_0}$
σ	radiation constant
ϕ	bank angle

Subscripts

e	entry condition
s	value at the stagnation point
0	initial value
∞	ambient value

A. INTRODUCTION

For missions involving manned satellites and recovery of scientific instrument payloads, re-entry of the vehicle into the atmosphere is an important problem area. The principal considerations involved are (1) protection of the vehicle structure and payload against the deceleration and loading encountered in entry, (2) protection of the vehicle structure and payload against the thermal environment, (3) assurance of dynamic stability of the entering vehicle, and (4) achieving sufficiently accurate trajectory control and landing point prediction. An investigation of any of these factors must rely on an analysis of the vehicle trajectory. This chapter, therefore, presents an entry trajectory analysis and subsequently considers the four previously noted mission considerations. Design information given is in the form of both analytic solutions and data generated by numerical methods.

B. RE-ENTRY TRAJECTORIES

During the re-entry phase of the satellite mission, aerodynamic forces become necessarily more important, and the relatively simple perturbed Keplerian orbit relationships can no longer be used. The equations of motion involve nonlinear drag terms, since air drag is a function of V^2 and atmospheric density, ρ, and ρ is a complicated function of altitude.

These nonlinear differential equations cannot be reduced to an exact closed form solution with present mathematical methods. Thus, two possible solution procedures must be investigated.

(1) Closed form solutions of approximate differential equations.

(2) Numerical parametric solutions of the exact differential equations using a high speed digital computer.

1. Approximate Analytic Solutions

A multitude of approximate analytic solutions to the equations of motion has appeared in the literature during the past few years. Many of these solutions differ somewhat in their simplifying assumptions as well as in mathematical approach. Therefore, in an attempt to consider the problem with both depth and scope, two somewhat different approximate analyses are presented in detail in Subsections a and b, following; and a rather comprehensive itemization of other solutions existing in the literature, together with pertinent assumptions and limitations, is given in Subsection c.

a. First approximate method (Ref. 1)

Chapman (Ref. 1) presents an interesting approximate solution as well as a convenient approach to numerical solution of the equations of motion. Assumptions include (1) spherically symmetric planet and atmosphere, (2) exponentially varying atmospheric density, (3) negligible peripheral velocity of the planet compared to the velocity of the entering vehicle, (4) small fractional change in radial distance compared to the fractional change in velocity in a given increment of time (i.e., $|\frac{dr}{r}| \ll |\frac{du}{u}|$), (5) small component of lift in the horizontal direction compared to the drag (i.e., $|\frac{L}{D}\tan\gamma| \ll 1$) and (6) a point mass vehicle. The derivation proceeds as follows: in the absence of forces normal to the trajectory plane, the motion may be described in two dimensions by the vector acceleration.

$$\vec{a} = \left(\frac{dw}{dt} - \frac{u^2}{r}\right)\vec{e}_r + \left(\frac{du}{dt} + \frac{uw}{r}\right)\vec{e}_\phi \qquad (1)$$

where $\vec{e}_r$ and $\vec{e}_\phi$ are unit vectors in the r and ϕ directions, r is the radius vector from the planet center to the entering body, and w and u are velocity components along and normal to the instantaneous radius vector, respectively. The

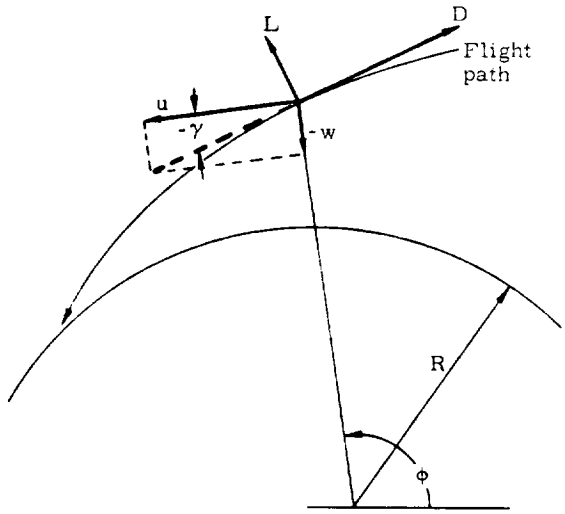

flight path angle with respect to local horizontal, γ (negative for descent) is

$$\gamma = \tan^{-1}\frac{w}{u} \qquad (2)$$

The vector force is

$$\vec{f} = (-mg + L\cos\gamma - D\sin\gamma)\,\vec{e}_r - (D\cos\gamma + L\sin\gamma)\,\vec{e}_\phi, \qquad (3)$$

so that two component equations of motion may be written from Eqs (1), (2) and (3):

$$-\frac{d^2y}{dt^2} = -\frac{dw}{dt} = g - \frac{u^2}{r} - \frac{L}{m}\cos\gamma + \frac{D}{m}\sin\gamma \qquad (4)$$

$$\frac{du}{dt} = -\frac{uw}{r} - \frac{D}{m}\left(\cos\gamma + \frac{L}{D}\sin\gamma\right) \qquad (5)$$

Ref. (1) neglects the term $\frac{uw}{r}$ in Eq (5), which is equivalent to assumption (4),

$$\frac{|\frac{uw}{r}|}{|\frac{du}{dt}|} = \frac{u}{r}\frac{|\frac{dr}{dt}|}{|\frac{du}{dt}|} = \frac{|\frac{dr}{r}|}{|\frac{du}{u}|} \ll 1.$$

This situation is realistic only when drag is large, so that the solutions will not apply to orbit motion above the sensible atmosphere. Then, using the exponential approximation to atmospheric density,

$$\rho = \rho_0 e^{-\beta y}, \tag{6}$$

and assumption (5),

$$\left|\frac{L}{D} \tan \gamma\right| \ll 1,$$

Eq (5) yields

$$\frac{du}{dt} = -\frac{\rho_0 e^{-\beta y}}{2 \frac{m}{C_D A}} \frac{u^2}{\cos \gamma} \tag{7}$$

since

$$D = \frac{1}{2} \rho V^2 C_D A \tag{8}$$

where

v = velocity magnitude = $\sqrt{u^2 + w^2}$

C_D = drag coefficient

A = reference cross-section area of entry vehicle

The variable u may be normalized by setting

$$\bar{u} = \frac{u}{v_c} = \frac{u}{\sqrt{gr}} . \tag{9}$$

Then

$$\frac{du}{dt} = \frac{d\left(\sqrt{gr}\, \bar{u}\right)}{dt} = \sqrt{gr} \frac{d\bar{u}}{dt} \tag{10}$$

since, from approximation (4) and the differential of Newton's law of gravitation, $g = \frac{\mu}{r^2}$,

$$\frac{dg}{g} = -2 \frac{dr}{r} ,$$

derivatives of g and r may be neglected relative to derivatives of u or $\bar{u}$. From Eq (10), Eq (7) for the normalized variable becomes

$$\frac{d\bar{u}}{dt} = -B \rho_0 e^{-\beta y} \frac{\bar{u}^2}{\cos \gamma} \sqrt{gr} \tag{11}$$

where B is the ballistic coefficient, $B = \frac{C_D A}{2m}$. Similarly, rewriting Eq (4) using Eqs (8) and (9) gives

$$-\frac{1}{g} \frac{dw}{dt} = -\frac{1}{g} \frac{d^2 y}{dt^2} = 1 - \bar{u}^2 + \rho_0 B \frac{r\bar{u}^2 e^{-\beta y}}{\cos^2 \gamma} (\sin \gamma - \frac{L}{D} \cos \gamma) \tag{12}$$

Reference (1) reduces the transformed pair of motion equations, Eqs (11) and (12), to a single equation by transforming to a dimensionless dependent variable z defined by

$$z \equiv \rho_0 B \sqrt{\frac{r}{\beta}}\, \bar{u}\, e^{-\beta y} \tag{13}$$

Then, with assumption (4),

$$\frac{1}{\bar{u}} \frac{dz}{d\bar{u}} - \frac{z}{\bar{u}^2} = -\rho_0 B \sqrt{r\beta}\, e^{-\beta y} \frac{dy}{d\bar{u}} = -\beta \frac{z}{\bar{u}} \frac{dy}{dt} \frac{dt}{d\bar{u}} . \tag{14}$$

But, from Eq (11),

$$\frac{d\bar{u}}{dt} = -\sqrt{g\beta}\, \frac{\bar{u} z}{\cos \gamma} \tag{15}$$

and

$$\frac{dy}{dt} = w = \bar{u} \sqrt{gr} \tan \gamma$$

so that Eq (14) becomes

$$\frac{dz}{d\bar{u}} - \frac{z}{\bar{u}} = \sqrt{\frac{\beta}{g}} \frac{\cos \gamma}{\bar{u}} \frac{dy}{dt} = \sqrt{\beta r} \sin \gamma. \tag{16}$$

Then

$$\frac{1}{g} \frac{dw}{dt} = \sqrt{\frac{r}{g}} \frac{d}{dt}\left(\frac{\bar{u} \sin \gamma}{\cos \gamma}\right) = \frac{1}{\sqrt{\beta g}} \frac{d\bar{u}}{dt}\left(\frac{\bar{u}}{\cos \gamma} \frac{d^2 z}{d\bar{u}^2} + \frac{\bar{u} \sqrt{\beta r} \sin^2 \gamma}{\cos^2 \gamma} \frac{d\gamma}{d\bar{u}}\right) \tag{17}$$

and

$$\bar{u} \frac{d}{d\bar{u}}\left(\frac{dz}{d\bar{u}} - \frac{z}{\bar{u}}\right) = \bar{u} \sqrt{\beta r} \frac{d}{d\bar{u}} (\sin \gamma)$$

$$= \bar{u} \frac{d^2 z}{d\bar{u}^2} - \frac{dz}{d\bar{u}} + \frac{z}{\bar{u}} \tag{18}$$

$$= \bar{u} \frac{d^2 z}{d\bar{u}^2} - \sqrt{\beta r} \sin \gamma.$$

From the first form of Eq (18), Eq (15) and Eq (17),

$$-\frac{1}{g} \frac{dw}{dt} = -\frac{1}{g} \frac{d^2 y}{dt^2} = \frac{\bar{u} z}{\cos^2 \gamma} \left[\left[\bar{u} \frac{d^2 z}{d\bar{u}^2} + \tan^2 \gamma \left[\bar{u} \frac{d}{d\bar{u}}\left(\frac{dz}{d\bar{u}} - \frac{z}{\bar{u}}\right)\right]\right]\right] \tag{19}$$

and from Eqs (12), (13) and (16),

$$-\frac{1}{g} \frac{dw}{dt} = -\frac{1}{g} \frac{d^2 y}{dt^2} = 1 - \bar{u}^2 + \frac{\bar{u} z}{\cos^2 \gamma}\left(\frac{dz}{dt} - \frac{z}{\bar{u}} - \sqrt{\beta r} \frac{L}{D} \cos \gamma\right) \tag{20}$$

A comparison of Eqs (19) and (20) gives the final equation to be solved.

$$u \frac{d}{d\bar{u}}\left(\frac{dz}{d\bar{u}} - \frac{z}{\bar{u}}\right) - \frac{1 - \bar{u}^2}{\bar{u}z} \cos^4 \gamma$$

$$\sqrt{\beta r}\, \frac{L}{D} \cos^3 \gamma = 0 \qquad (21)$$

where

$$\sqrt{\beta r} \sin \gamma = \frac{dz}{d\bar{u}} - \frac{z}{\bar{u}}$$

Consequently, the pair of component motion equations, Eqs (4) and (5), has been reduced to a single second order differential equation by transforming to the dependent variable z and the independent variable $\bar{u}$, subject to the assumptions noted.

The nonlinear differential Eq (21) may be solved by numerical integration; since Eq (21) depends only on the ratio of lift and drag coefficients, numerical solution of this equation has certain advantages over straightforward integration of the two component equations of motion, which depend on both coefficients. Alternatively, Eq (21) may be used to generate various approximate solutions.

(1) Approximation for straight line trajectories and ballistic vehicles

For the case of entry of a ballistic vehicle along a spiral path characterized by a constant flight path angle with respect to local horizontal $\bar{\gamma}$, Eq (18) gives

$$\frac{d}{d\bar{u}} (\sin \gamma) = 0 = \bar{u} z_1'' - \sqrt{\beta r} \sin \bar{\gamma} \qquad (22)$$

where z_1 is the z function defined by Eq (13) for this special case. Successive integration of Eq (22) yields, for initial conditions $\bar{u} = \bar{u}_0$, $z = 0$ (entry from high altitudes),

$$z_1' = \sqrt{\beta r} \sin \bar{\gamma} \ln \bar{u} + \text{costant}$$

and

$$\frac{z_1}{\bar{u} \sqrt{\beta r} \sin \bar{\gamma}} = \ln \frac{\bar{u}}{\bar{u}_0} = B \frac{\rho_0 e^{-\beta y}}{\beta \sin \bar{\gamma}} \qquad (23)$$

This solution is applicable in either of two circumstances: (1) the rather impractical case in which lift is programmed to maintain a constant flight path angle, or (2) the case of ballistic vehicles entering at such steep flight path angles that the difference of gravitational and centrifugal forces is small compared to the vertical component of drag force, so that the trajectory is essentially a straight line. This latter situation is that considered in Ref. 2, and Eq (23) is the solution obtained in that reference.

(2) Approximation for gliding vehicles

For the case of small entry angles ($|\sin \gamma| \approx |\gamma| << \frac{L}{D}$ and $\cos \gamma \approx 1$) with large $\frac{L}{D}$ and gliding hypersonic flight ($\bar{u} \approx 1$), the basic differential equation, Eq (21), gives the approximate solution

$$z_2 = \frac{1 - \bar{u}^2}{\bar{u} \sqrt{\beta r}\, \frac{L}{D}} \qquad (24)$$

which is the same as the gliding flight solution given by Ref. 3 and considered in Ref. 4.

(3) Approximation for a skipping vehicle

For the case in which the difference in gravitational and centrifugal forces, i.e., the term

$$\frac{1 - \bar{u}^2}{\bar{u} z} \cos^4 \gamma$$

of the basic equation, Eq (21), is relatively small, as for a skipping vehicle, Ref. 1 provides an approximate solution.

$$\frac{z_3}{\bar{u}} = \frac{z_0}{\bar{u}_0} + \sqrt{\beta r} \left[\sin \gamma_0 \ln \frac{\bar{u}}{\bar{u}_0} - \frac{\cos^3 \gamma_{av}}{2} \frac{L}{D} \ln^2 \frac{\bar{u}}{\bar{u}_0} \right] \qquad (25)$$

with

$$\sin \gamma = \sin \gamma_0 - \left(\cos^3 \gamma_{av}\right) \frac{L}{D} \ln \frac{\bar{u}}{\bar{u}_0} \qquad (26)$$

For $\frac{L}{D} = 0$ these equations reduce to Eq (23).

b. Second approximate method (Ref. 5)

Wang and Ting (Ref. 5) derive approximate solutions from the equations of motion expressed in the form of tangential and normal components.

$$\frac{dv}{dt} = -\frac{D}{m} - g \sin \gamma \qquad (27)$$

$$\frac{v d\gamma}{dt} = \frac{L}{m} - \left(g - \frac{v^2}{r}\right) \cos \gamma \qquad (28)$$

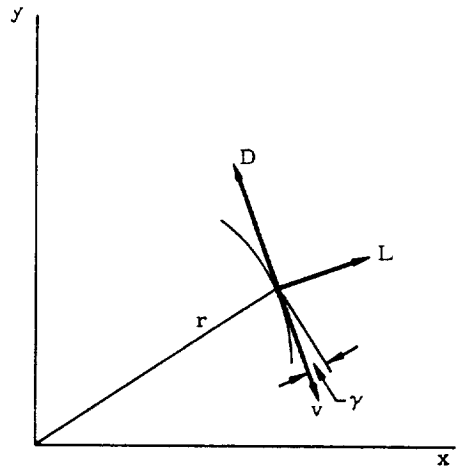

where

v = vehicle velocity magnitude

$D = \frac{1}{2}\rho v^2 C_D A$

= drag force

$L = \frac{1}{2}\rho v^2 C_L A$ (29)

= lift force

g = acceleration due to gravity

r = radial distance of vehicle from the center of the earth

m = mass of vehicle

γ = local flight path angle, positive for ascent

Since this formulation differs from that of Ref. 1 and provides somewhat more accurate approximate solutions, the derivation will be presented in some detail for reference. Assumptions, although noted in the derivation, are collected for convenience in the following list.

(1) The earth and its atmosphere are spherically symmetric.

(2) The atmospheric density varies exponentially.

(3) The atmosphere does not rotate.

(4) $\cos\gamma \approx \gamma_e$. For grazing entry, the local flight path angle is always small so that $\cos\gamma \approx 1$ and can be approximated by $\cos\gamma_e$. For steep entry, the flight path angle does not change greatly from the entry value, and the approximation is again valid.

(5) The aerodynamic coefficients C_L and C_D are assumed constant in the given solutions. (An extension does not require this assumption.)

(6) Although γ is not assumed to be very small, accuracy deteriorates because of series truncation assuming $1 \gg \gamma^3$. For reasonable accuracies, $\gamma < 60°$.

(7) The vehicle is considered as a point mass.

With the assumption of exponential atmospheric density, Eq (6) takes the form

$$\rho = \rho_0 \, e^{-\beta h}$$

$$\frac{d\rho}{dt} = -\beta\rho\frac{dh}{dt} = -\beta\rho v\sin\gamma$$

and from Eqs (8) and (29), Eqs (27) and (28) become

$$\frac{dv}{v} = \frac{C_D A}{2m\beta\sin\gamma}d\rho + \frac{g}{\beta\rho v^2}d\rho \qquad (30)$$

$$\sin\gamma\, d\gamma = -\frac{C_L A}{2m\beta}d\rho - \left(\frac{1}{r} - \frac{g}{v^2}\right)\frac{\cos\gamma_e}{\beta\rho}\,d\rho \qquad (31)$$

where the approximation $\cos\gamma \approx \cos\gamma_e$ has been made in Eq (31). The limitations imposed by this approximation are noted in the previous list of assumptions, Assumption (4). The quantities in parenthesis in Eq (31) represent the centrifugal and gravitational forces and are sometimes neglected in approximate solutions if entry velocities may be assumed close to circular orbit velocity. Reference 5 obtains a higher order solution by approximating the velocity in the centrifugal force term by the velocity-density relation given in Ref. 6,

$$\ln\frac{v}{v_e} = \frac{B}{\beta\sin\gamma_e}(\rho - \rho_e) \qquad (32)$$

where

$$B = \frac{C_D A}{2m}$$

Then, expanding the centrifugal force term in series,

$$\frac{g}{v^2} = \frac{g}{v_e^2}\left[1 + C_1\ln\frac{v}{v_e} + C_2\ln^2\frac{v}{v_e} + \ldots\right]$$

$$\approx \frac{g}{v_e^2}\left[1 + \frac{C_1 B}{\beta\sin\gamma_e}(\rho - \rho_e) + C_2\left(\frac{B}{\beta\sin\gamma_e}\right)^2(\rho - \rho_e)^2\right] \qquad (33)$$

where C_1 and C_2 are constant coefficients which can be determined by collocation. Substitution of Eq (33) in Eq (31) and integration gives, for constant C_L,

$$\cos\gamma = \cos\gamma_e + B_1(\rho - \rho_e) + B_2\ln\frac{\rho}{\rho_e} + B_3 f_1(\rho) \qquad (34)$$

where

$$B_1 = \frac{C_L A}{2m\beta},\quad B_2 = \frac{\cos\gamma_e}{\beta r},\quad B_3 = -\frac{g\cos\gamma_e}{\beta v_e^2}$$

$$f_1(\rho) = \left[(1 + B_4C_1 + B_4^2C_2)\ln\frac{\rho}{\rho_e} - (B_4C_1 + 2B_4^2C_2)\frac{\rho - \rho_e}{\rho_e} + \frac{1}{2}B_4^2C_2\left(\frac{\rho^2 - \rho_e^2}{\rho_e^2}\right)\right]$$

$$B_4 = -\frac{B\rho_e}{\beta\sin\gamma_e}$$

For constant C_D integration of Eq (30) proceeds as

$$\ln \frac{v_e}{v} = -\frac{B}{\beta}\int_{\rho_e}^{\rho} \frac{d\rho}{\sin\gamma} - \frac{g}{\beta}\int_{\rho_e}^{\rho} \frac{d\rho}{\rho v^2} \qquad (35)$$

Evaluation of the integrals is facilitated by the following expansions.

$$\frac{1}{\sin\gamma} \approx \frac{1}{\gamma - \frac{1}{6}\gamma^3} \approx \frac{1}{\gamma} + \frac{\gamma}{6}, \qquad 1 >> \gamma^4 \qquad (36)$$

or

$$\frac{1}{\sin\gamma} = \frac{1}{\sin[\gamma_e - (\gamma_e - \gamma)]} \approx \frac{1}{\sin\gamma_e - (\gamma_e - \gamma)\cos\gamma_e}$$

$$\approx \frac{1}{\sin\gamma_e} + \frac{\cos\gamma_e}{\sin^2\gamma_e}(\gamma_e - \gamma), \qquad (37)$$

$$\gamma > \frac{\pi}{4}, \quad 1 >> (\gamma - \gamma_e)$$

Also, $\cos\gamma \approx 1 - \frac{\gamma^2}{2}$ in Eq 34. Then integration of Eq (35) gives the following solutions:

Case I. K_2 positive, $\gamma_e < 45°$

$$\ln \frac{v_e}{v} = \frac{B_3}{\cos\gamma_e} f_1(\rho) + \frac{B_5}{\sqrt{K_2}} f_2(\rho) + f_3(\rho) \qquad (38)$$

where

$$B_5 = \frac{B}{\beta}\left[1 + \frac{4K_2\bar{\gamma}^2 - K_1^2}{48K_2}\right]$$

$$f_2(\rho) = \rho\ell n\left\{\left[K_1 + 2(1-\sigma)K_2 + 2\left[K_2\bar{\gamma}^2 + (K_1 + K_2 - \sigma K_2)(1-\sigma)K_2\right]^{1/2}\right\}\left\{\left[-2\sqrt{K_2}\,\bar{\gamma} + K_1\right]\right\}^{-1}$$

$$f_3(\rho) = \frac{B\rho}{24\beta K_2}\left\{\left[\left[2K_2(1-\sigma) + K_1\right]\left[\bar{\gamma}^2 + K_1(1-\sigma) + K_2(1-\sigma)^2\right]^{1/2} + K_1\bar{\gamma}\right]\right\}$$

$$\bar{\gamma}^2 = \gamma_e^2 - \left[2B_1 - \frac{2C_1B_3B_4}{\rho_e} + C_2B_3B_4^2\frac{(\rho - 3\rho_e)}{\rho_e^2}\right](\rho - \rho_e) - 2\left[B_3 + B_2 + C_1B_3B_4 + C_2B_3B_4^2\right]\ln\frac{\rho}{\rho_e}$$

$$K_1 = 2\left[B_1\rho + B_3 + B_2 - C_1B_3B_4\frac{(\rho - \rho_e)}{\rho_e} + C_2B_3B_4^2\frac{(\rho - \rho_e)^2}{\rho_e^2}\right]$$

$$\sigma = \frac{\rho_e}{\rho}$$

$$K_2 = B_3 + B_2 + C_1B_3B_4 - C_2B_3B_4^2\frac{(\rho^2 - \rho_e^2)}{\rho_e^2}$$

Case II. K_2 negative, $\gamma_e < 45°$

$$\ln \frac{v_e}{v} = \frac{B_3}{\cos\gamma_e} f_1(\rho) + \frac{B_5}{\sqrt{-K_2}} f_4(\rho) + f_3(\rho) \qquad (39)$$

where

$$f_4(\rho) = \rho\left[\sin^{-1}\frac{K_1}{\sqrt{K_1^2 - 4K_2\bar{\gamma}^2}} - \sin^{-1}\frac{K_1 + 2(1-\sigma)K_2}{\sqrt{K_1^2 - 4K_2\bar{\gamma}^2}}\right]$$

Case III. K_2 positive, $\gamma_e > 45°$

$$\ln \frac{v_e}{v} = \left(\frac{-1}{\sin\gamma_e} + \frac{\gamma_e\cos\gamma_e}{\sin^2\gamma_e}\right)\frac{B}{\beta}(\rho - \rho_e) - \frac{B_6}{\sqrt{K_2}} f_2(\rho) - 6f_3(\rho) \qquad (40)$$

where

$$B_6 = \frac{B\cos\gamma_e(4K_2\bar{\gamma}^2 - K_1^2)}{8\beta\sin^2\gamma_e K_2}$$

Case IV. K_2 negative, $\gamma_e > 45°$

$$\ln \frac{v_e}{v} = \left(\frac{-1}{\sin\gamma_e} + \frac{\gamma_e\cos\gamma_e}{\sin^2\gamma_e}\right)\frac{B}{\beta}(\rho - \rho_e) - \frac{B_6}{\sqrt{-K_2}} f_4(\rho) - 6f_3(\rho) \qquad (41)$$

These solutions can be used to determine the velocity at any point between entry and minimum γ.

c. Other approximate analytic solutions

The following list of approximate analytic solutions has been collected, along with pertinent assumptions and limitations for reference convenience.

(1) Reference (7)

Assumptions. (1) spherically symmetric earth and atmosphere, (2) exponential atmospheric density, (3) nonrotating atmosphere, (4) constant gravitational attraction, (5) ballistic entry

(6) the quantity $\frac{1}{\beta R}\frac{\cos\gamma}{\rho}\left(\frac{gR}{v^2}-1\right)$ is considered constant in integration over ρ or γ, and (7) point mass

Solution.

$$\cos\gamma = \frac{\cos\gamma_e}{1+\frac{1}{\beta R}\left(\frac{gR}{v^2}-1\right)\left(1-\frac{\rho_e}{\rho}\right)} \tag{42}$$

$$\left(\frac{v}{v_e}\right)^2 = \left(\frac{4}{\beta R}\right)\left(\frac{gR}{v_e^2}\right) F(\gamma) + \left[\left[\left(1-\frac{4}{\beta R}\right)\left(\frac{gR}{v_e^2}\right)F(\gamma_e)\exp\left[\frac{-R\,C_D A\,(\gamma_e-\gamma)\rho}{m\cos\gamma\left(\frac{gR}{v^2}-1\right)}\right]\right]\right] \tag{43}$$

where

$$F(\gamma) \equiv \left[\ln\left(\frac{-\gamma}{2}\right) - C_1\gamma + \frac{1}{4}(C_1\gamma)^2 - \frac{1}{18}(C_1\gamma)^3\right]e^{C_1\gamma} + \left[\frac{(C_1\gamma)^3}{720\,C_1^4} + \frac{(C_1\gamma)^2}{240\,C_1^4} + \left(\frac{1}{120\,C_1^4}+\frac{1}{12\,C_1^2}\right)C_1\gamma + \left(\frac{1}{120\,C_1^4}+\frac{1}{12\,C_1^2}\right)\right] \text{(for } \gamma \text{ small)}$$

or

$$F(\gamma) \equiv -C_2\left[C_1\sin\gamma+\cos\gamma\right] - C_3\left[\frac{1}{2}C_1\sin 2\gamma+\cos 2\gamma\right] + C_4\sin^2\gamma\,(C_1\sin\gamma+3\cos\gamma)$$

(for γ large)

$$C_1 = \left[\frac{\cos\gamma_m}{\rho_m R}\frac{m}{C_D A}\left(\frac{gR}{v_m^2}-1\right)\right]^{-1}$$

where m designates a reference point

$$C_2 = \frac{1}{2}\left[\frac{1}{\cos\gamma_e}+\frac{1}{\cos^2\gamma_e}(C_1^2+9) - 6\left(\frac{1}{\cos^3\gamma_e}\right)\right]\left[(C_1^2+1)(C_1^2+9)\right]^{-1}$$

$$C_3 = \frac{1}{2}\left[\cos^2\gamma_e\,(C_1^2+4)\right]^{-1}$$

$$C_4 = \frac{1}{2}\left[\cos^3\gamma_e\,(C_1^2+9)\right]^{-1}$$

Special Cases.

(i) For $\beta R > 200$ and $\gamma < 45°$ ($\beta R \approx 900$ for earth)

$$\left(\frac{v}{v_e}\right)^2 = \exp\left[\frac{C_D A}{m} R\left(\frac{\gamma-\gamma_e}{\cos\gamma}\right)\left(\frac{gR}{v^2}-1\right)\right]^{-1} \tag{44}$$

(ii) For constant γ (from Eq (42), this occurs for ρ small or close to ρ_e or for v large or close to gR). Then,

$$\cos\gamma = \cos\gamma_e \tag{45}$$

$$\left(\frac{v}{v_e}\right)^2 = \exp\left[\frac{C_D A}{m\beta}\frac{(\rho-\rho_e)}{\sin\gamma_e}\right] \tag{46}$$

(Compare with Eq (23).)

(2) Reference (8)

Assumptions. (1) spherically symmetric earth and atmosphere, (2) exponential atmospheric density, (3) nonrotating atmosphere, (4) small γ ($\sin\gamma \approx \gamma$ and $\cos\gamma \approx 1$) and the component of g along the flight path angle is small, (5) constant C_L and C_D, (6) constant gravity and constant $\frac{1}{r}$ over range of re-entry, (7) point mass.

Solution.

$$v^2 = \bar{v}^2 - 2\sqrt{\frac{g}{r}}(h-h_e) \tag{47}$$

where

$$\bar{v} = \frac{\bar{v}}{\bar{v}_1}\frac{\bar{v}_1}{v_e}v_e$$

$$\frac{v_1}{v_e} = \exp\left(-\frac{\gamma-\gamma_e}{\frac{L}{D}}\right)$$

$$\frac{\bar{v}}{\bar{v}_1} = \exp\left[\left[\frac{-4g\,e^{\phi_e}}{v_e^2\left(\frac{L}{D}\right)^2\beta}\left\{\left[\frac{v_e^2}{gr}e^{-\phi_e} - \left(1+\frac{k^2}{2}\right)\right]\frac{1}{2k}\left[\ell n\frac{k+\phi}{k+\phi_e} - \ell n\frac{k-\phi}{k-\phi_e}\right] - \frac{1}{2}\left(1+\frac{k^2}{6}\right)\left[\ell n\frac{k+\phi}{k+\phi_e}+\ell n\frac{k-\phi}{k-\phi_e}\right] - \frac{1}{2}(\phi_e-\phi)+\frac{1}{12}\left(\phi_e^2-\phi^2\right)\right\}\right]\right]$$

$$k^2 = \frac{8 K_D}{\beta r \frac{L}{D}} \left[e^{-\beta h_e} + \frac{\beta r \gamma_e^2}{2 \frac{L}{D} K_0} \right]$$

$$\phi = - \frac{2\gamma}{\frac{L}{D}}$$

$$K_D = \frac{C_D A \rho_0 r}{2m}$$

(3) Reference (9)

Assumptions. (1) spherically symmetric and atmosphere, (2) exponential atmospheric density, (3) nonrotating atmosphere, (4) γ is small, (5) constant aerodynamic coefficients C_L and C_D (6) $v \approx v_e$ in the gravitation term of the force equation $\frac{v^2}{r} \cos \gamma$, (7) constant r over the range of integration, (8) constant g, (9) point mass.

Solution.

$$\gamma^2 = \gamma_e^2 - \frac{C_L A}{m\beta} (\rho - \rho_e) - \left[\frac{2}{r\beta} - \frac{2}{\beta v_e^2} \right] \ell n \frac{\rho}{\rho_e} \qquad (48)$$

$$\ell n \frac{v_e}{v_m} = \frac{C_D A}{2m\beta\sqrt{C}} \ell n \left[\frac{\sqrt{a + b\rho_m + C\rho_m^2} + \sqrt{C}\rho_m + \frac{\beta}{2\sqrt{C}}}{\sqrt{a + b\rho_e + C\rho_e^2} + \sqrt{C}\rho_e + \frac{\beta}{2\sqrt{C}}} \right] \qquad (49)$$

where

$$a = \gamma_e^2 - \left[\frac{1}{r\beta} - \frac{g}{\beta v_e^2} \right] \left[2 \ell n \frac{\rho_m}{\rho_e} - 3 \right] + \frac{C_L A}{m\beta} \rho_e$$

$$b = - \left[\frac{C_L A}{m\beta} + \frac{4}{\rho_m} \left(\frac{1}{r\beta} - \frac{g}{\beta v_e^2} \right) \right]$$

$$C = \frac{1}{\rho_m^2} \left(\frac{1}{r\beta} - \frac{g}{\beta v_e^2} \right)$$

and the subscripts e and m signify values at entry and at peak acceleration or minimum flight path angle, respectively.

(4) Reference (2)

See Eq (23).

(5) Reference (10)

See Eq (46) or (23).

(6) Reference (11)

Assumptions. (1) spherically symmetric earth and atmosphere, (2) exponential atmospheric density, (3) point mass, (4) $1 - \frac{v^2}{gr} \approx 0$ in the equations of motion, (5) $\sin \gamma << \frac{\rho v^2 C_D A}{2 mg}$ (i.e., the component of gravity along the flight path is negligible compared to the aerodynamic drag load, (6) constant $\frac{C_L}{C_D}$.

Solution.

$$\frac{v}{v_e} = \exp \left[- \frac{C_D}{C_L} (\gamma - \gamma_e) \right] \qquad (50)$$

$$(\rho - \rho_e) = 2 \beta \frac{m}{C_D A} \frac{C_D}{C_L} (\cos \gamma - \cos \gamma_e) \left(\text{for constant } \frac{C_L A}{m} \right) \qquad (51)$$

or

$$\rho = \rho_e + \beta \frac{m}{C_D A} \frac{C_D}{C_L} (\gamma_e^2 - \gamma^2) \quad 1 >> \gamma^3$$

2. Numerical Solutions and Graphical Presentations

Since the equations of motion for entry (Eqs (4) and (5), or Eq (21), or Eqs (27) and (28)) cannot be solved analytically without use of simplifying assumptions, numerical integration offers the only means of highly accurate computation of general trajectories. Many techniques are possible in numerical solution, depending on the chosen formulation of the equations of motion and on the method of numerical integration used. Three formulations of the equations of motion are given in Eqs (4) and (5), Eq (21), and Eqs (27) and (28), and various numerical integration techniques are discussed in Chapter IV. In general, selection of a formulation and integration technique must be based upon the nature of the particular entry mission. However, it should be noted that Eq (21), although not completely exact, has an advantage in that only ratios of lift and drag coefficients are involved.

Consideration of numerical entry analyses will be limited to presentation of the solutions and will not consider the methods. The solutions are of interest for two reasons:

(1) Comparison of the numerical solutions with the results of approximate analytic analyses provides a check on the validity of these analytic solutions.

(2) The numerical solutions, presented in the form of parametric graphs, are useful in making preliminary design estimates.

Reference 1 provides various solutions determined numerically from the entry problem formulation of Section B.1.a. For entry of ballistic vehicle from a decaying orbit ($\gamma_e = 0°$, $\bar{u}_0 = 1$), Eq (2) reduces to

$$\bar{u}\frac{d}{d\bar{u}}\left[\frac{dz}{d\bar{u}} - \frac{z}{\bar{u}}\right] - \frac{1-\bar{u}^2}{\bar{u}z} + \sqrt{\beta r}\,\frac{L}{D} = 0 \qquad (52)$$

$$z_0 = 0,\ z_0' = 0$$

The solution of this equation, which has to be evaluated only once for each value of $\sqrt{\beta r}\,\frac{L}{D}$ is plotted in Fig. 1a for nonlifting vehicles and in Fig. 1b for lifting vehicles. It should be noted that in the case of circular decay, the lifting vehicle does not "skip," but follows a smooth equilibrium glide trajectory. For nonlifting vehicles entering from circular velocities and nonzero entry angles ($\bar{u}_0 = 1$, $\gamma_0 < 0$), Eq (21) reduces to

$$\bar{u}\frac{d}{d\bar{u}}\left[\frac{dz}{d\bar{u}} - \frac{z}{\bar{u}}\right] - \frac{1-\bar{u}^2}{\bar{u}z}\cos^4\gamma = 0 \qquad (53)$$

The z functions for this case are plotted in Fig. 2a. With lift and $\bar{u}_0 = 1$, $\gamma_0 < 0$, Eq (52) applies with $z_0 = 0$ and $Z_0' = \sqrt{\beta r}\gamma_0$. Solutions for this case are plotted in Figs. 2b through 2e. All exhibit severe skips except when $\gamma_0 = 0$.

In Fig. 3 the theoretical solutions for the atmospheric braking of ballistic vehicles entering at escape speeds are shown for different values of maximum deceleration during the first pass. The parameters used are $(30\bar{u}\,z)_{\text{first max.}}$ which correspond to the altitudes of deepest penetration during the first pass. Figure 3 shows, for example, that if $(30\bar{u}\,z)_{\text{first max.}} = 0.46$, then entry is completed on the seventh pass.

Figure 4 represents a numerical integration run on the IBM 704 digital computer, considering natural decay from a near-circular orbit. Velocity and flight path angle variations are given as functions of geometrical altitude above the sea level. Superimposed are the results obtained from the analytical solution given in Fig. 1a and the corresponding flight path angles given in Table 1. Correlation is seen to be good, justifying the approximations made in Ref. 1. [Table 1 also gives the ranges in terms of earth radii and the flight times from the initial re-entry altitude.]

Figures 5a to 5e show the velocity-altitude profiles for ballistic re-entry, as obtained by numerical integrations of the exact equations of motion. Using the ballistic coefficient (B) as a constant parameter, parametric trajectory curves are given for initial flight path angles of -1°, -2°, -3°, -5° and -10° for an initial velocity of 25,000 fps (7620 mps) and an initial altitude of 300,000 ft (91.4 km). It should be noted that these results also apply to any altitudes higher than 300,000 ft (91.4 km), since the drag effects above this altitude are extremely small for conventional ballistic coefficients. Interpolations between the curves can be accomplished.

In Fig. 5a the comparison with the analytical methods of Ref. 3 is presented, showing that for $B = 0.5$ to $5.0\ \text{ft}^2/\text{slug}$ (0.00318 to $0.0318\ \text{m}^2/\text{kg}$) relatively good agreement exists.

The corresponding local flight path angle versus altitude histories is shown in Figs. 6a to 6e. In Fig. 6a the comparison of analytical and numerical results is seen once more to be satisfactory for a first approximation.

Characteristic re-entry altitude-velocity profiles for lifting vehicles with $L/D = 1$ and $L/D = 3$ are indicated in Fig. 7 for an initial re-entry flight path angle of -10°.

Figures 8a, 8b and 8c present the peak altitudes of first skip for lifting re-entry vehicles in parametric form for $L/D = 0.5$ to 3.0.

Figure 9a compares the velocity-altitude profiles for various re-entry vehicles, both ballistic and lifting type. The severity of skips increases with increasing lift-to-drag ratios and atmospheric effects become significant at much higher altitudes in the case of lifting bodies, as compared to simple ballistic vehicles.

Figure 9b investigates the effects of variable entry velocities on the velocity-altitude profiles of a lifting body with $L/D = 0.5$. It should be noticed that a definite "skip envelope" exists for all entries regardless of the initial velocity and basically the same trajectories are reached at 100,000 ft (30.48 km) altitude.

The initial flight path angle produces somewhat larger deviations between the members of the same trajectory family as indicated in Fig. 9c.

The effects of programmed C_L on velocity-altitude profile are shown in Fig. 9d. The corresponding programs of C_L as functions of Mach number are given in Fig. 9e.

It should be noted that considerable variations in the lift coefficient are required for a relatively smooth trajectory and even small deviations from the desired lift coefficent program result in a pronounced phugoid motion of the vehicle.

Figure 10a presents the terminal velocities as a function of L/D for various parametric values $\frac{W}{C_D A}$, While Fig. 10b gives terminal flight path angles for lifting vchicles.

A comparison between the trajectories of ballistic, lifting and winged bodies is given in Fig. 11a. Further comparisons of velocities, flight path angles, dynamic pressures, accelerations and nose temperatures for the above three

TABLE 1

Values of z Functions and Related Quantities for $\frac{L}{D} = 0$ and $\bar{U}_0 = 1$ (Ref. 1)

$\bar{V}_1 = 1.0$ $\sqrt{(\delta r)_e} L/D = 0$

$\bar{U}$	z	G	γ DEG.	$\bar{Q}$	S	T
.00 DEG.						
.999	.00008	.00	-.15	.000	.000	.0
.995	.00058	.02	-.33	.275	.716	581.4
.990	.00163	.05	-.47	.431	.886	720.1
.985	.00299	.09	-.58	.535	.961	781.7
.980	.00461	.14	-.67	.614	1.006	818.6
.970	.00846	.25	-.82	.736	1.059	862.7
.960	.01301	.37	-.96	.828	1.091	889.3
.950	.01817	.52	-1.07	.903	1.112	907.6
.900	.05116	1.38	-1.56	1.154	1.166	954.5
.850	.09348	2.39	-1.98	1.309	1.190	976.6
.800	.14306	3.44	-2.36	1.419	1.205	990.7
.750	.19860	4.48	-2.73	1.503	1.214	1001.0
.700	.25915	5.46	-3.11	1.568	1.222	1009.2
.650	.32387	6.34	-3.50	1.619	1.228	1016.1
.600	.39203	7.09	-3.91	1.661	1.232	1022.1
.550	.46290	7.68	-4.36	1.694	1.236	1027.6
.500	.53570	8.09	-4.86	1.722	1.239	1032.7
.450	.60958	8.30	-5.43	1.743	1.242	1037.7
.400	.68355	8.30	-6.09	1.761	1.245	1042.6
.350	.75637	8.06	-6.89	1.775	1.247	1047.5
.300	.82646	7.58	-7.89	1.785	1.249	1052.8
.250	.89161	6.86	-9.21	1.793	1.251	1058.4
.200	.94852	5.91	-11.08	1.799	1.253	1064.9
.150	.99158	4.74	-14.03	1.803	1.255	1072.6
.100	1.00892	3.41	-19.50	1.805	1.256	1083.1
.050	.95725	2.05	-33.16	1.806	1.258	1100.0

$\bar{U}$	z	G	γ DEG.	$\bar{Q}$	S	T
-.50 DEG.						
.999	.00026	.01	-.50	.000	.000	.0
.995	.00137	.04	-.56	.151	.202	164.3
.990	.00291	.09	-.63	.260	.285	231.4
.985	.00462	.14	-.69	.341	.330	268.5
.980	.00648	.19	-.75	.406	.360	293.5
.970	.01065	.31	-.87	.512	.400	326.7
.960	.01536	.44	-.98	.595	.426	348.5
.950	.02058	.59	-1.08	.665	.445	364.4
.900	.05309	1.43	-1.54	.907	.495	407.8
.850	.09449	2.41	-1.94	1.060	.518	429.4
.800	.14308	3.44	-2.32	1.170	.532	443.4
.750	.19769	4.46	-2.69	1.254	.542	453.7
.700	.25741	5.42	-3.07	1.319	.550	461.9
.650	.32144	6.29	-3.47	1.371	.555	468.9
.600	.38905	7.04	-3.88	1.412	.560	475.0
.550	.45951	7.63	-4.34	1.446	.564	480.5
.500	.53205	8.04	-4.84	1.473	.567	485.7
.450	.60583	8.25	-5.41	1.495	.570	490.7
.400	.67984	8.25	-6.07	1.513	.573	495.6
.350	.75286	8.02	-6.88	1.526	.575	500.6
.300	.82328	7.55	-7.88	1.537	.577	505.8
.250	.88890	6.84	-9.21	1.545	.579	511.5
.200	.94640	5.90	-11.09	1.551	.581	517.9
.150	.99016	4.73	-14.04	1.555	.583	525.7
.100	1.00822	3.40	-19.52	1.557	.584	536.2
.050	.95713	2.05	-33.18	1.558	.586	553.2

$\bar{U}$	z	G	γ DEG.	$\bar{Q}$	S	T
-1.00 DEG.						
.999	.00052	.02	-1.00	.000	.000	.0
.995	.00264	.08	-1.03	.107	.102	83.1
.990	.00536	.16	-1.07	.187	.146	118.5
.985	.00817	.24	-1.10	.247	.171	139.1
.980	.01105	.32	-1.14	.297	.188	153.5
.970	.01704	.50	-1.21	.379	.212	173.5
.960	.02334	.67	-1.28	.446	.229	187.5
.950	.02993	.85	-1.35	.503	.242	198.2
.900	.06704	1.81	-1.69	.711	.278	230.2
.850	.11045	2.82	-2.02	.850	.298	248.0
.800	.15943	3.83	-2.35	.953	.310	260.2
.750	.21336	4.81	-2.69	1.033	.319	269.6
.700	.27166	5.72	-3.05	1.096	.326	277.4
.650	.33380	6.53	-3.42	1.146	.332	284.0
.600	.39921	7.22	-3.83	1.188	.336	289.9
.550	.46731	7.75	-4.27	1.221	.340	295.3
.500	.53744	8.12	-4.77	1.248	.343	300.4
.450	.60886	8.29	-5.33	1.270	.346	305.3
.400	.68066	8.26	-6.00	1.287	.349	310.3
.350	.75170	8.01	-6.80	1.301	.351	315.3
.300	.82048	7.52	-7.81	1.312	.353	320.5
.250	.88491	6.81	-9.14	1.320	.355	326.2
.200	.94177	5.87	-11.03	1.325	.357	332.7
.150	.98559	4.71	-14.00	1.329	.359	340.5
.100	1.00458	3.39	-19.50	1.332	.360	351.0
.050	.95536	2.05	-33.19	1.333	.362	368.0

$\bar{U}$	z	G	γ DEG.	$\bar{Q}$	S	T
-1.50 DEG.						
.999	.00078	.02	-1.50	.000	.000	.0
.995	.00394	.12	-1.52	.088	.068	55.5
.990	.00792	.24	-1.54	.153	.098	79.4
.985	.01195	.35	-1.57	.203	.115	93.3
.980	.01602	.47	-1.59	.244	.127	103.2
.970	.02428	.71	-1.64	.312	.143	117.2
.960	.03272	.94	-1.69	.369	.155	127.1
.950	.04132	1.18	-1.74	.417	.164	134.7
.900	.08677	2.35	-2.00	.597	.192	158.6
.850	.13605	3.47	-2.26	.721	.207	172.7
.800	.18889	4.54	-2.53	.815	.217	182.8
.750	.24501	5.53	-2.83	.888	.225	190.9
.700	.30408	6.40	-3.14	.948	.231	197.7
.650	.36579	7.16	-3.48	.996	.236	203.7
.600	.42976	7.77	-3.85	1.035	.240	209.1
.550	.49558	8.22	-4.27	1.068	.244	214.2
.500	.56274	8.50	-4.74	1.094	.247	219.0
.450	.63065	8.59	-5.28	1.115	.250	223.8
.400	.69854	8.47	-5.93	1.132	.252	228.5
.350	.76543	8.15	-6.71	1.146	.254	233.4
.300	.82999	7.61	-7.71	1.157	.257	238.6
.250	.89031	6.85	-9.03	1.165	.258	244.3
.200	.94346	5.87	-10.91	1.170	.260	250.7
.150	.98432	4.70	-13.89	1.174	.262	258.6
.100	1.00164	3.38	-19.41	1.177	.264	269.1
.050	.95288	2.04	-33.16	1.178	.265	286.2

TABLE 1 (continued)

$\bar{V}_1 = 1.0 \qquad \sqrt{(Br)_\oplus} L/D = 0$

γ = -2.00 DEG.

$\bar{U}$	Z	G	γ DEG.	$\bar{Q}$	S	T
.998	.00105	.03	-2.00	.000	.000	.0
.995	.00419	.13	-2.02	.062	.044	39.9
.990	.00946	.28	-2.04	.123	.070	56.9
.985	.01476	.44	-2.06	.168	.084	68.4
.980	.02009	.59	-2.08	.205	.094	76.3
.970	.03080	.90	-2.12	.266	.107	87.4
.960	.04161	1.20	-2.16	.316	.116	95.1
.950	.05250	1.50	-2.19	.359	.123	101.2
.900	.10818	2.93	-2.40	.519	.145	120.1
.850	.16579	4.24	-2.61	.631	.157	131.5
.800	.22515	5.42	-2.84	.716	.166	139.9
.750	.28608	6.46	-3.08	.784	.172	146.8
.700	.34838	7.34	-3.36	.839	.178	152.6
.650	.41183	8.06	-3.65	.884	.182	157.9
.600	.47615	8.61	-3.99	.921	.186	162.8
.550	.54101	8.98	-4.37	.952	.189	167.4
.500	.60602	9.15	-4.80	.978	.192	171.8
.450	.67066	9.13	-5.31	.998	.195	176.3
.400	.73430	8.91	-5.92	1.015	.197	180.8
.350	.79607	8.47	-6.67	1.028	.199	185.5
.300	.85481	7.83	-7.63	1.039	.201	190.5
.250	.90882	6.98	-8.92	1.046	.203	196.0
.200	.95545	5.94	-10.78	1.052	.205	202.3
.150	.99006	4.72	-13.73	1.056	.206	210.1
.100	1.00221	3.37	-19.25	1.058	.208	220.6
.050	.95100	2.03	-33.07	1.060	.210	237.7

γ = -2.50 DEG.

$\bar{U}$	Z	G	γ DEG.	$\bar{Q}$	S	T
.998	.00131	.04	-2.50	.000	.000	.0
.995	.00523	.16	-2.51	.055	.035	28.7
.990	.01179	.35	-2.53	.110	.056	45.6
.985	.01835	.54	-2.55	.150	.067	54.8
.980	.02493	.73	-2.56	.183	.075	61.2
.970	.03809	1.11	-2.59	.238	.086	70.1
.960	.05128	1.48	-2.62	.283	.093	76.4
.950	.06450	1.84	-2.66	.322	.099	81.3
.900	.13084	3.54	-2.82	.467	.117	96.8
.850	.19754	5.05	-3.00	.569	.127	106.3
.800	.26446	6.37	-3.19	.648	.134	113.4
.750	.33144	7.48	-3.40	.711	.140	119.2
.700	.39831	8.40	-3.64	.762	.144	124.3
.650	.46486	9.11	-3.90	.805	.148	129.0
.600	.53083	9.61	-4.20	.840	.152	133.3
.550	.59593	9.89	-4.54	.869	.155	137.5
.500	.65978	9.97	-4.94	.893	.157	141.6
.450	.72192	9.83	-5.41	.913	.160	145.7
.400	.78173	9.48	-5.97	.929	.162	149.9
.350	.83843	8.92	-6.68	.942	.164	154.3
.300	.89094	8.16	-7.60	.952	.166	159.1
.250	.93770	7.20	-8.85	.960	.168	164.4
.200	.97630	6.07	-10.66	.966	.169	170.6
.150	1.00252	4.77	-13.57	.969	.171	178.2
.100	1.00683	3.38	-19.06	.972	.173	188.7
.050	.95040	2.02	-32.92	.973	.174	205.8

γ = -3.00 DEG.

$\bar{U}$	Z	G	γ DEG.	$\bar{Q}$	S	T
.998	.00157	.05	-3.00	.000	.000	.0
.995	.00628	.19	-3.01	.050	.029	23.9
.990	.01413	.42	-3.03	.100	.047	38.0
.985	.02197	.65	-3.04	.137	.056	45.7
.980	.02981	.88	-3.05	.168	.063	51.0
.970	.04547	1.33	-3.08	.218	.071	58.4
.960	.06110	1.76	-3.11	.259	.078	63.7
.950	.07670	2.19	-3.13	.295	.083	67.8
.900	.15417	4.18	-3.27	.428	.098	80.9
.850	.23067	5.90	-3.42	.523	.106	89.0
.800	.30604	7.37	-3.59	.595	.113	95.1
.750	.38010	8.59	-3.77	.654	.117	100.2
.700	.45264	9.55	-3.98	.702	.121	104.7
.650	.52345	10.26	-4.21	.742	.125	108.8
.600	.59224	10.73	-4.47	.775	.128	112.6
.550	.65868	10.94	-4.78	.803	.131	116.4
.500	.72238	10.92	-5.14	.826	.133	120.1
.450	.78284	10.67	-5.57	.845	.135	123.9
.400	.83945	10.19	-6.10	.861	.137	127.8
.350	.89140	9.49	-6.76	.873	.139	131.9
.300	.93762	8.59	-7.63	.883	.141	136.4
.250	.97661	7.50	-8.82	.891	.143	141.5
.200	1.00608	6.25	-10.57	.896	.144	147.5
.150	1.02214	4.86	-13.41	.900	.146	155.0
.100	1.01610	3.40	-18.85	.902	.147	165.3
.050	.95150	2.02	-32.73	.904	.149	182.3

γ = -4.00 DEG.

$\bar{U}$	Z	G	γ DEG.	$\bar{Q}$	S	T
.997	.00209	.06	-4.00	.000	.000	.0
.995	.00628	.19	-4.01	.032	.017	14.2
.990	.01672	.50	-4.02	.080	.033	27.0
.985	.02714	.81	-4.03	.113	.041	33.3
.980	.03754	1.11	-4.04	.141	.046	37.6
.970	.05825	1.70	-4.06	.185	.053	43.4
.960	.07885	2.28	-4.08	.221	.058	47.5
.950	.09934	2.85	-4.10	.253	.062	50.7
.900	.19994	5.43	-4.21	.370	.073	60.8
.850	.29733	7.63	-4.33	.453	.080	67.0
.800	.39125	9.45	-4.46	.518	.085	71.8
.750	.48144	10.90	-4.60	.570	.089	75.8
.700	.56758	12.00	-4.76	.613	.092	79.3
.650	.64935	12.76	-4.95	.649	.095	82.6
.600	.72634	13.18	-5.16	.679	.097	85.7
.550	.79810	13.29	-5.41	.704	.099	88.8
.500	.86408	13.09	-5.71	.725	.101	91.9
.450	.92362	12.61	-6.07	.743	.103	95.0
.400	.97594	11.86	-6.52	.757	.105	98.4
.350	1.02004	10.88	-7.10	.769	.106	101.9
.300	1.05466	9.67	-7.86	.778	.108	105.9
.250	1.07811	8.29	-8.93	.785	.110	110.5
.200	1.08804	6.75	-10.53	.790	.111	116.0
.150	1.08071	5.13	-13.19	.794	.113	123.0
.100	1.04853	3.50	-18.43	.796	.114	132.8
.050	.95978	2.01	-32.24	.798	.116	149.7

types of re-entry bodies are given in Fig. 11b as functions of time. Finally, Fig.11c represents the effects of the rotating atmosphere on the entry of a lifting body with L/D = 0.5 and $\frac{W}{C_L A}$ = 155 lb/ft^2 $\left(7420 \frac{\text{newtons}}{\text{m}^2}\right)$. It can also be seen from the note that for entry from 300,000 ft (91.4 km) the range for a rotating air mass is 72.5 naut mi (135 km) longer than the value for a stationary air mass.

C. DECELERATION

Deceleration magnitude is one of the several factors to be considered in safeguarding the payload of an entering vehicle. External loading on the vehicle, due to air pressure created by motion of the vehicle through the atmosphere, varies directly with deceleration and ballistic coefficient. Another consideration involving deceleration is that of human tolerance to stress, which is a function not only of peak deceleration and rate of onset of deceleration, but of orientation of the body and duration of the stress.

1. Analytic Solutions

From the force equation for an entering body (for example Eq (3)) the total acceleration magnitude is

$$a = \left[\left(-g + \frac{L}{m} \cos\gamma - \frac{D}{m} \sin\gamma \right)^2 + \left(\frac{D}{m} \cos\gamma + \frac{L}{m} \sin\gamma \right)^2 \right]^{1/2} \quad (54)$$

and the resultant acceleration magnitude experienced in addition to that due to gravity can be written as

$$G = \left[\left(\frac{L}{m} \cos\gamma - \frac{D}{m} \sin\gamma \right)^2 + \left(\frac{D}{m} \right)^2 \left(\cos\gamma + \frac{L}{D} \sin\gamma \right)^2 \right]^{1/2} \quad (55)$$

or

$$G = \frac{C_D A}{2m} \rho V^2 \cos\gamma \left[\left(-\frac{L}{D} + \tan\gamma \right)^2 + \left(1 + \frac{L}{D} \tan\gamma \right)^2 \right]^{1/2} \quad (56)$$

This acceleration G is that actually experienced by a pilot or instrument package, i.e., the acceleration due to external forces (lift and drag) alone. Expressed in units of g, this quantity is sometimes referred to as the load factor, $N = \frac{G}{g}$. Two simple cases are of interest.

(1) Ballistic entry

For L = 0, Eq (55) reduces to

$$G = \frac{C_D A}{2m} \rho V^2 \quad (57)$$

L = 0

(2) lifting entry at small entry angles

From Eq (56)

$$G \approx \frac{C_D A}{2m} \rho V^2 \cos\gamma \left[1 + \left(\tan\gamma - \frac{C_L}{C_D} \right)^2 \right]^{1/2} \quad (58)$$

$$\left[1 >> \left| \frac{L}{D} \tan\gamma \right| \right]$$

For small entry angles

$$G \approx \frac{C_D A}{2m} \rho V^2 \left[1 + \left(\frac{C_L}{C_D} \right)^2 \right]^{1/2} \quad (59)$$

$$\left[\cos\gamma \approx 1, \frac{C_L}{C_D} >> \left| \tan\gamma \right| \right]$$

The maximum deceleration experienced can be determined from the previous equations by setting

$$\frac{dG}{dt} = 0$$

For the case of Eq (59), small entry angles, or Eq (57), ballistic entry, this condition gives

$$v^2 \frac{d\rho}{dt} + 2\rho v \frac{dv}{dt} = 0$$

From Eqs (29) and (27),

$$\left[1 + \frac{2g}{\beta v_m^2} \right] \sin\gamma_m = -\frac{C_D A}{m} \frac{\rho_m}{\beta} \quad (60)$$

or

$$\sin\gamma_m \approx -\frac{C_D A}{m} \frac{\rho_m}{\beta} \quad \left[1 >> \frac{2g}{\beta v_m^2} \right] \quad (61)$$

In the notation of Ref. 1, or Section B.1.a.,

$$N_{max} \approx \sqrt{\beta r}\, (\bar{u}z)_{max} \sqrt{1 + \left(\frac{L}{D} \right)^2} \quad \left[|\gamma| << \frac{L}{D}, \cos\gamma \approx 1 \right] \quad (62)$$

2. Numerical Solutions and Graphical Presentations

Fig. 12a from (Ref. 1) gives horizontal deceleration, $\frac{du}{dt}$, for entry into the earth's atmosphere from decaying orbits. From Eqs (10) and (15),

$$\frac{du}{dt} \approx -g \sqrt{\beta r} \frac{\bar{u}z}{\cos\gamma} \quad (63)$$

$$\approx 30\, \bar{u}z\ ,\ (g),\ 1 >> \gamma$$

Consequently, Fig. 2 is useful in generating Fig. 12a.

In Fig. 12b are shown the results of numerical integrations of the exact equations of motion by an IBM 704 digital computer for a zero lift decay trajectory from a near-circular orbit. From Fig. 12b it can be seen that below approximately 50,000 ft, the deceleration approaches zero because in this range terminal velocity is reached (drag = weight). On the same figure, the re-entry load factors

$$N = \frac{G}{g}$$

are also indicated. At least for small re-entry angles, both curves coincide (for practical purposes) in the region where really significant g loads are encountered. It should also be noted that the analytical values are considerably higher than the actual decelerations (theoretical max = 8.35 g and actual max = 6.9 g).

Furthermore, maximum deceleration is also a function of the ballistic coefficient, as indicated by Fig. 12c. For different entry angles the shapes of the curves presented in Fig. 12c are essentially maintained; only the region of maximum deceleration shifts out with decreasing γ_0.

The variations in maximum decelerations are given in Fig. 13a, which also gives the corresponding altitudes where they occur. Given a certain re-entry angle (e.g., γ_0 = 0 deg) and the ballistic coefficient of the satellite (e.g., B = 2 ft^2/slug), 0.0127 m^2/kg), the magnitude of the maximum acceleration and its point of occurrence (for the given example; $(\dot{v}/g_{max})$ = 6.65 and $h_{max\ acc}$ = 185, 000 ft) (56.4 km) can be determined. From Fig. 13a it can also be seen that for a fixed ballistic coefficient, optimum re-entry decelerations are always connected with a zero initial angle. However, for a fixed re-entry angle, there exists a variable optimum ballistic coefficient which minimizes the decelerations. These optimum ballistic coefficients are given as functions of γ_0 in Fig. 13b. The corresponding values of maximum deceleration are also given. It can be seen that the design values for ballistic coefficients in the range $1.0 < B < 1.5$ ft^2/slug (0.00637 to 0.00956 m^2/kg) are desirable.

Drag decelerations may be controlled by varying the configuration parameters. Figure 14a shows the effects of variations in the configuration parameters for normalized altitude variations (Ref. 12). The normalized altitude represents distances on either side of the original altitude for maximum deceleration. Figure 14b indicates the acceleration profiles for these programmed configuration changes. Taking the most drastic deceleration reduction (namely 60% of the maximum uncontrolled deceleration) only 4 g's are encountered if the configuration parameter is changed roughly by a factor of 8.

For manned satellite re-entry, the critical parameter is not the magnitude of maximum acceleration, but time spent at a given acceleration. Figure 15a compares the effects of re-entry angles on cumulative deceleration times (for B = 1.0 ft^2/slug 0.00637 m^2/kg) with human tolerance as given in Ref. 13. It should be noted that the tolerance curves seem to be the maximum permissible values and blackouts can possibly occur, even if the dotted lines are not reached. Although the interpretation of the curves for human tolerance is not clear, it appears that for a pilot in a sitting position (with a g suit), the re-entry angles must be less than 2°, preferably less than 1°. For a pilot in a prone position, re-entry must be less than 4°.

Figure 15b compares the effects of ballistic coefficients on deceleration times for $\gamma_0 = -1°$. It indicates that, for small re-entry angles, a relatively large range of ballistic coefficients permissible for manned re-entry exists. With the given data, the permissible range would be $0.5 < B < 5.0$ ft^2/slug (0.00318 to 0.0318 m^2/kg) for a pilot with a g suit in a sitting position. For a pilot in the prone position, $0.1 < B < 25.0$ ft^2/slug (0.000637 to 0.16 m^2/kg) seems to be safe.

The material presented for the ballistic entry was extended to show the effects of aerodynamic lift during re-entry. The data presented were obtained from an iterative solution by the 704 digital computer of a point mass moving in an inverse-square force field. Because the aerodynamic forces at 300,000 ft (91.4 km) are sufficiently high to cause an immediate skipping of the vehicle at the higher lift-to-drag ratio, the re-entry altitude was increased to 400,000 ft (122 km).

Figure 16 presents the effects of re-entry conditions on the maximum total deceleration for a lifting body. This is a specific example for a vehicle with $W/C_L A$ = 146.9 psf (7040 newton/m^2 and L/D = 0.5. It also indicates a trend that for small re-entry angles decelerations decrease as orbital velocity is approached.

Figure 17a shows the effects of increasing L/D ratios on the decrease of total deceleration for a fixed re-entry angle and velocity. For example, in case of $\gamma_0 = -1°$, maximum deceleration is decreased roughly by a factor of 1/5 as L/D increases from 0 to 0.5. Similar curves are presented in Figs. 17b and c.

Maximum load factors for a variation of ballistic coefficients with lift-to-drag ratios from zero to three are shown in Figs. 18a, b and c for initial re-entry flight path angles of -1°, -5° and -10°.

For the initial flight path angles considered, a re-entry vehicle with an L/D = 1 reduces intolerable or excessive accelerations experienced in a ballistic re-entry to within comfortable limits. It should be pointed out that the modest reductions achieved by increasing lift-to-drag ratios greater than 1 can lead to an excessive increase in the amplitude and number of cycles of a moderate skipping trajectory.

To facilitate interpolations between the curves, load factors are given as functions of the initial flight path angle γ_0, in Figs. 19a, b and c. Figures 20a, b and c show that for a ballistic re-entry the magnitude of the acceleration peaks between initial velocities of 10,000 and 25,000 fps (3048 and 7620 mps), but decreases throughout the complete velocity range for a lifting re-entry.

Figure 21 gives the maximum entry load factors as a function of L/D ratio for $\gamma_0 = -1°$ and $W/C_DA = 5$ psf considering initial velocities between 10,000 and 25,000 fps (3048 and 7620 mps).

Figure 22 indicates the peak decelerations for the constant altitude--equilibrium glide entry program (Ref. 14) as a function of initial entry flight path angle. For a suggested operational limit it is seen that $\gamma_0 \geq -7°$ is advisable for L/D = 2.

A parametric set of curves, similar to the deceleration presentation, is given for maximum re-entry dynamic pressures (dynamic pressure = $\frac{1}{2}\rho V^2$) in Figs. 23a to 27c. A comprehensive curve, expressing the effects of lift, drag and wing loading on the maximum re-entry dynamic pressure is presented in Fig. 28 for $\gamma_0 = -1°$, $v_0 = 25,000$ fps and $h_0 = 300,000$ ft (7620 mps and 91.4 km).

Figures 23a to c show that maximum entry dynamic pressures are essentially linear functions of ballistic coefficients throughout the initial flight path angles investigated.

In Figs. 25a to c the decrease of dynamic pressure with increase of initial entry velocity is an effect of the centrifugal force acting on the vehicle in earth's gravitational field during the hypersonic portion of the trajectory where the maximum values of the dynamic pressure are occurring.

D. RE-ENTRY HEATING

Two modes of heat transfer to an entry vehicle exist during the entry phase of flight. These are the laminar and turbulent aerodynamic boundary layer heat transfer and the radiant transfer of energy to the vehicle surface from the hot gas between the shock wave and the vehicle. The relative magnitude of these two modes of heat transfer are functions of vehicle shape and entry velocity. In general, the blunter the vehicle and the higher the entry velocity, the greater the radiation heat transfer rate relative to the aerodynamic rate. The radiation heat transfer rate is the earliest to reach its maximum during the entry trajectory; next is the laminar rate and finally the turbulent rate. As the entry angle is decreased, both the rate and total radiant heat transfer decrease; whereas, for aerodynamic heat transfer, only the rate decreases while the total increases.

Protection against this thermal environment may be accomplished in a number of ways, and the methods chosen are dependent primarily upon the magnitudes of both the total and the rate of heat transfer. If both rate and total are sufficiently low, a simple heat sink made of copper or beryllium may be adequate. The simple heat sink is heat rate limited only to prevent the outer surface from melting. If the total heat that must be absorbed is large, the weight of the heat sink becomes excessive. For rates that are relatively low, it is possible to absorb the heat in a thin skin and reradiate it to the external environment. For example, if a thin skin can withstand a temperature of 5000° R it can reradiate up to 300 Btu/ft^2-sec so that the heat protection system now becomes a matter of insulating the remainder of the vehicle from this high temperature skin. On the other hand, at low heat rates it is also possible to use low temperature ablating materials for heat absorption. This alleviates the insulation problem, but weight is now required as ablating material rather than insulation. At high heat transfer rates and for high total heating, the use of high surface temperature ablating materials is required.

Analysis of aerodynamic heating of re-entry vehicles becomes much more complicated than the trajectory analysis since heat transfer terms introduce new nonlinearities into the differential equations. The main difficulty with an exact skin temperature history calculation is the necessity of knowing all the characteristics of a particular re-entry body shape, its heat shield thickness, heat conductivities and related heat transfer parameters, surface interactions with the air-flow (ionization, melting, ablation, etc.) and certain further important heat transfer characteristics. The number of variables involved makes a parametric representation necessarily rather involved.

1. Analytic Solutions

During entry, intense heating occurs at the stagnation region of the entering body. It is customary to relate the heating rate at any point on the body, q, to the heating rate at the stagnation point, q_s. In hypersonic flow the heating rate at a stagnation point can be written (Ref. 1) as

$$q_s = \frac{C}{\sqrt{R_s}} \left[\frac{\rho_\infty}{\rho_0}\right]^n \left[\frac{v}{v_c}\right]^m \qquad (64)$$

where the constants C, n and m depend on the type of boundary layer flow, and

R_s = body radius of curvature at the stagnation point

ρ_∞ = density of the ambient atmosphere

ρ_0 = sea-level atmospheric density

v = vehicle velocity

$v_c = \sqrt{gr}$ = circular orbit velocity at altitude.

For laminar flow n = 0.5 and m ≈ 3.1. As in the case of analytic trajectory solutions (Section B.1.c), more than a few methods have been developed for computing the laminar heating rates at a stagnation region. A collection of these methods appears

in Ref. 15 and is presented in the following list.

Laminar Heating Rate at Stagnation Region

(1) Ref. 16

$$q_s = \frac{Nu}{D} k \left[T_w - T_\infty \right] \qquad (65)$$

where

Nu = Nusselt number

$$k_1 \left[\frac{v_\infty D}{2} \right]^{0.5} Pr^{0.4}$$

for a sphere ($k_1 = 1.696 \times 10^{-3}$ in English units, ft-lb-sec; $= 5.169 \times 10^{-4}$ in mks)

D = drag

k = conductivity

T_w = temperature at the wall

T_∞ = temperature of the free stream

v_∞ = free stream velocity

Pr = Prandtl number = 0.71

(2) Ref. 17

$$q_s = \frac{k_w (T_s - T_w)}{\sqrt{\nu_w}} \frac{Nu}{\sqrt{Re_w}} \left[\frac{dv_\delta}{dx} \right]_s^{0.5} \qquad (66)$$

where

$\frac{Nu}{Re_w}$ = ratio of Nusselt number to the square root of the Reynolds number (= 0.62 for Pr = 0.71, small $\frac{T_w}{T_s}$ and axially symmetric heating)

$\frac{dv_\delta}{dx}$ = stagnation point, velocity gradient

θ = flow inclination angle with respect to the free stream

s = subscript denoting value at stagnation point

w = subscript denoting value at the wall

ν = kinematic viscosity, $\frac{\mu}{\rho}$

(3) Ref. 18

(extreme cooling, small $\frac{T_w}{T_s}$)

$$q_s = \left\{ \frac{(0.5) 2^{0.5n}}{Pr^{2/3}} \left[\rho_s \mu_s v_\infty \right]^{1/2} \right.$$

(continued)

$$\left. \cdot \cdot h_s \left[\frac{dv_\delta}{v_\infty d\theta} \right]_s^{0.5} \sqrt{\frac{R_{sh}}{R_s^2}} \right\} \qquad (67)$$

when

n = 0 for a planar body (two-dimensional flow)

n = 1 for a body of revolution (axially symmetric flow)

R_{sh} = shock radius $\approx R_s + 0.1 R_s$

h = enthalpy

μ = viscosity

$\frac{dv_\delta}{v_\infty d\theta}$ = dimensionless stagnation point velocity gradiant (= 0.408 for spherical body, Newtonian flow and a 1.2 ratio of specific heats)

(4) Ref. 19

$$q_s = \left\{ \frac{26,300}{\sqrt{R_s}} \left[\frac{\rho_\infty}{\rho_0} \right]^{0.5} \left[\frac{v_\infty}{v_c} \right]^{3.15} \right.$$

$$\left. \cdot \left| \frac{h_s - h_w\, 6}{h_s - 3.2 \times 10^0} \right| \right\} \frac{kcal}{m^2 - sec} \qquad (68)$$

(5) Ref. 20

$$q_s = \left\{ \frac{0.54 \times 2^{n/2}}{Pr^{0.6} \sqrt{R_s}} \left[\frac{\rho_w \mu_w}{\rho_s \mu_s} \right]^{0.1} \right.$$

$$\cdot \cdot (\rho_s \mu_s v_\infty)^{0.5} (h_s - h_w) \left[\frac{dv_\delta}{v_\infty d\theta} \right]_s^{0.5}$$

$$\left. \cdot \left[1 + (Le^m - 1) \frac{h_D}{h_s} \right] \right\} \qquad (69)$$

where

Le = Lewis number $\neq$ 1 (Le $\approx$ 1.4)

m = 0.52 for equilibrium boundary layer flow

= 0.63 for frozen boundary layer flow

n = 0 or 1 as in case (3)

(6) Ref. 21

$$q_s = K' \frac{1 - \frac{h_w}{h_s}}{\sqrt{R_s}} 2^{0.5n} (\rho_\infty)^{0.5} (u_\infty)^3 \qquad (70)$$

where u_∞ is the component of ambient flow velocity parallel to the surface

and $K' = 15.5 \times 10^{-9}$ Btu/sec-(slug)$^{1/2}$-(ft)^3 = 36.1×10^{-9} kcal/sec-(kg)$^{1/2}$-(m)^3.

The previous solutions apply for the case of laminar stagnation point heating, which generally applies for the nose and leading edge of gliding vehicles. However, Ref. 15 provides the following solution for turbulent flow.

$$q = \left\{ 7.5 \left[\frac{\theta^{0.6} \cos^{1.6}\theta}{0.542\,(1-\beta^2\theta^2)^{0.7}} \right] \left[\frac{0.408}{\beta} \right]^{0.6} \frac{\bar{\rho}^{0.8}}{R_s^{0.2}} \cdot \left[\frac{v_\infty}{1000} \right]^3 \left[1 - \frac{h_w}{h_s} \right] \right\} \text{ kcal/m}^2\text{-sec} \quad (71)$$

where

$$\beta = \left[\frac{dv_\delta}{v_\infty\, d\theta} \right]_s$$

ρ = altitude density ratio, $\frac{\rho_\infty}{\rho_0}$

During entry the gas behind the shock wave in the stagnation region becomes very hot, and radiation from this hot gas is a source of heat transmission in addition to the convective heat input. Reference 21 provides the following empirical equation for the radiative heating rate:

$$q = 11.2\, R_s\, \bar{\rho}^{1.5} \left[\frac{v_\infty}{10{,}000} \right] \text{ kcal/m}^2\text{-sec} \quad (72)$$

2. Numerical Solutions and Graphical Presentations

The equations for heat transfer rates presented in the previous section obviously vary somewhat in complexity and in degree of approximation. For generation of graphical data to be used in preliminary design work, a very simple solution has the advantages of involving fewer parameters to be varied and necessitating fewer calculations. For this reason, the solution chosen for generation of graphical data is that of Eq (64)

$$q_s = \frac{17{,}000}{R_s^{1/2}} \left[\frac{\rho_\infty}{\rho_s} \right]^{1/2} \left[\frac{v}{v_c} \right]^3 \text{ Btu/ft}^2\text{-sec}$$

$$= \frac{25{,}400}{R_s^{1/2}} \left[\frac{\rho_\infty}{\rho_0} \right]^{1/2} \left[\frac{v}{v_c} \right]^3 \text{ kcal/m}^2\text{-sec (hypersonic flight)}$$

Furthermore, maximum stagnation point wall temperatures are presented in the parametric form

$$T_{ws} \cdot R_s^{1/8} \cdot \epsilon^{1/4}$$

to make the results independent of the nose radius at the stagnation point, R_s, and skin emissivity, ϵ. The values of the "radius-emissivity parameter" $R_s^{1/8} \cdot \epsilon^{1/4}$ are plotted in Fig. 29. The radiation heat loss is given by

$$q_{rad} = \epsilon\, \sigma\, T_{ws}^4 \quad (73)$$

where σ = radiation constant = 0.482×10^{-12} Btu/ft^2-sec-(°R)^4 = 1.372×10^{-11} kcal/m^2-sec-(°K)^4. At equilibrium, all of the heat flow from the boundary layer is radiated back into the atmosphere (i.e., the heat flux to the interior of the structure is negligible), and the maximum temperature attained by the stagnation region of the body is determined by equating the two heat flows:

$$T_{ws}\, R_s^{1/8}\, \epsilon^{1/4} = \left[\frac{17{,}000}{\sigma} \right]^{1/4} \left[\frac{\rho_\infty}{\rho_0} \right]^{1/8} \left[\frac{v}{v_c} \right]^{3/4} \quad (°\text{R-ft}^{1/8} \text{ or } 2.092°\text{ K-km}^{1/8}) \quad (74)$$

The maximum aerodynamic heating at the stagnation region of the nose can then be computed as:

$$q_s = \left[T_{w_s}\, R_s^{1/8}\, \epsilon^{1/4} \right]^4 \frac{\sigma}{\sqrt{R_s}} \quad (75)$$

The graphical information on re-entry heating presented in Figs. 30 through 47 is based primarily on Eqs (74) and (75), together with the related trajectory equations (Section B).

Figure 30a (Ref. 22) presents the approximate heat transfer rates for a blunt body of 1-ft (0.3 m) nose radius traveling at satellite velocities both for free molecule and for continuous flow. The definitions and ranges of flow regimes are given in Chapter 5. Figure 30b shows the ratios of heat input rates with respect to rate of energy dissipation by drag ($1/2\, \rho v^3$).

The effects of entry angles on maximum heat flux are given in Fig. 31a (Ref. 14). For example, as the re-entry angle is increased from -1° to -4°, the maximum heat flux is increased roughly by a factor of 4. Assuming radiation equilibrium temperatures of the satellite skin, Fig. 31b gives skin temperatures as a function of heat transfer rates for different values of the constant of emissivity, ϵ.

The assumption of radiation equilibrium becomes inadequate for steep ballistic entries or large heat shields. Figure 32 (Ref. 23) shows a sample history of aerodynamic heating, comparing the radiation equilibrium method with an exact skin temperature computation for a vertical entry. Temperature histories of the outer and inner surface of a 0.25-in. pyrex skin are shown for free fall from 1,000,000 ft (304.8 km).

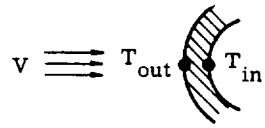

The estimated maximum temperatures are seen to be as follows:

T_{rad} = 2480° R = 1380° K

T_{out} = 1660° R = 920° K

T_{in} = 1080° R = 600° K

Thus, for the case considered, radiation equilibrium gives unrealistically high estimates, as the most important parameter for recovery programs is usually the temperature at the inner surface of the heat shield. In connection with Fig. 32, it should be further noted that below 100,000 ft (30.5 km) it would be advantageous to jettison the hot heat shield for the case investigated.

Figure 33a shows the trajectories for a family of re-entry vehicles, indicating the stagnation point radiation temperatures in dotted lines. Following a solid line of velocity-altitude variation, the corresponding skin temperature parameters can be read from the intersections with the dotted lines. Figure 33b presents the corresponding temperature profiles as a function of altitude. From theoretical considerations it can be shown that the maximum temperature occurs at $\frac{V}{V_c} = 0.81$, which agrees with the numerical results of the machine computations.

A family of curves similar to Fig. 33a is plotted for the initial altitude at 400,000 ft (122 km) in Fig. 33c.

Fig. 34a shows the maximum equilibrium nose temperatures as a function of the lift characteristics for equilibrium glides. It can be seen that the maximum equilibrium temperatures can be reduced by increasing the L/D ratios. The corresponding altitudes for maximum temperatures are expressed in Fig. 34b. The effects of the initial flight path angle on the altitude for maximum stagnation nose temperature are given in Fig. 34c.

In Figs. 35 through 41 the results of all the important Martin Company numerical integration results are collected. Maximum re-entry stagnation point nose temperatures are presented successively versus the ballistic coefficient, B, the initial entry angle, γ_0, the initial velocity, v_0, and lift-to-drag ratios, L/D.

Figures 35a through 36c show the maximum radiation-equilibrium temperature at the laminar stagnation point as a function of ballistic coefficient, lift-to-drag ratio and initial re-entry angles.

It can be seen that though aerodynamic lift reduces the higher temperatures experienced during a ballistic re-entry, the magnitude of the reduction is reduced as the initial flight path angle decreases. The effects of initial re-entry velocity are shown in Fig. 37 for L/D = 0.5 and in Figs. 38a through 40d for three ballistic coefficients and various values of L/D and entry angle.

The effect of considering a rotating air mass is presented in Fig. 42 for the equilibrium temperature history.

A comparison of the maximum temperature parameters for ballistic entry is shown in Fig. 43a for various initial flight path angles. Also shown is a comparison between the stagnation point and spherical nose solutions.

Figure 43b presents the maximum temperature parameters for various L/D ratios (Ref. 1). It can be used for various planetary atmosphere, if the proper logarithmic atmospheric densitys slope, b, is inserted in connection with the radial distance, r.

Obviously the preliminary design estimates based on the stagnation point solution may be considerably altered, if the particular shape of the vehicle nose is known. An indication of the dependency on body shape is given by Fig. 44 from Ref. 1.

Parametric temperature histories versus density ratios are given in Fig. 45a (Ref. 22) for simple drag bodies. Figures 45b and c present lift parameter requirements for constant heat transfer trajectories (Ref. 22).

The slopes of the stagnation point temperature parameter are given in Figs. 46a through 46c for three ballistic coefficients.

Finally the effects of lift-drag ratios on the maximum surface temperature parameter for entry into various planetary atmospheres is given in Fig. 47 (Ref. 1). It should be noted that optimum conditions are encountered at L/D from roughly 0.8 to 1.0 for most planets.

E. RANGE AND TIME TO IMPACT

Range to impact for ballistic vehicles is given as a function of the initial flight path angle in Fig. 48 for h_0 = 300,000 ft (91.4 km) and v_0 = 25,000 fps (7620 mps).

Figures 49a through e present the data obtained from a series of computer runs, giving the values of range attained in descent from 300,000 ft to sea level. Data are plotted as functions of re-entry velocity, re-entry flight path angle and ballistic coefficient for a zero-lift re-entry.

Figures 50a through c show range from 400,000 ft (122 km) for different ballistic coefficients, lift-to-drag ratios and re-entry angles. It is interesting to note that for a constant re-entry angle, range is rather insensitive to ballistic coefficient for the higher lift-to-drag ratios.

Figures 51a through 52g show the range to impact versus initial velocity for various parametric values of lift-drag ratios, L/D, and initial flight path angles, γ_0.

Further parametric studies of impact ranges are compiled in Figs. 53 through 54c, as functions of initial flight path angles and lift-drag ratios.

Equilibrium glide range variations as a function of initial velocities are indicated in Fig. 55.

The range characteristics of a high-drag, low variable lift vehicle (flat plate at almost 90° angles of attack) are treated in Figs. 56a to 56c (Ref. 25). Figure 56a expresses the variation in range as a

function of angle of attack and entry flight path angles. Figure 56b analyzes the range variations for ballistic vehicles as functions of initial velocities and entry angles, while Fig. 56c gives the range as a function of angle of attack and initial entry velocity.

Figure 57 shows times to impact for various ballistic coefficients, lift-drag ratios and re-entry angles. It should be observed that for high lift-drag ratios the flight time is rather sensitive to entry angles and ballistic coefficients.

Parametric curves of range versus flight time for lifting bodies are shown for three values of B in Figs. 58a to 58c, using $\gamma_0 = -1$, $-5°$ and $-10°$. The effects of initial entry velocity are expressed for $L/D = 0.5$, 1.25 and 2.0 in Figs. 59a to 59c. In Fig. 60 time to impact is expressed as a function of L/D, using as parameters the initial flight path angles and initial velocities.

Range is shown as a function of velocity at apogee for lifting vehicles traveling at sub-satellite speeds in Fig. 61, cross-plotting flight times as additional parameters.

For fast estimates of ballistic vehicle range and time to impact, a comprehensive parametric family of curves is presented in Fig. 62 for a large number of ballistic coefficients and initial flight path angles.

F. MANEUVERABILITY

Even if deceleration and heating are adequately controlled during entry, recovery of the vehicle is not assured unless it is capable of landing in a predesignated area. The size of the landing area could range from a very large region for parachute recovery by a large search group to an area comparable to that of an airport for glide-landing vehicles. It is apparent, in the latter case, that the vehicle must be capable of fairly extensive maneuvers during the entry phase if recovery is to be possible without long periods of waiting in orbit for a favorable landing site approach. Consequently, vehicle maneuverability is another problem in the area of entry requiring investigation.

As a first consideration in the problem of maneuvering a vehicle from certain initial conditions to a successful landing, the possibility that a landing, or even an impact, on the earth might not be possible for the given initial conditions, should be noted. Trajectories which are too high overshoot because they encounter too little atmospheric drag to slow the vehicle for entry; on the other hand, trajectories which are too low result in the vehicle experiencing too much deceleration for safe recovery.

Figures 63a and 63b show the range of values for both re-entry velocity and flight path angle necessary to ensure ballistic vehicle and lifting body impact with the earth in one revolution or less. Results apply for two initial altitudes, 300,000 and 400,000 ft (91.4 and 122 km). Several values of the ballistic coefficient from 0 to 1.07 are included.

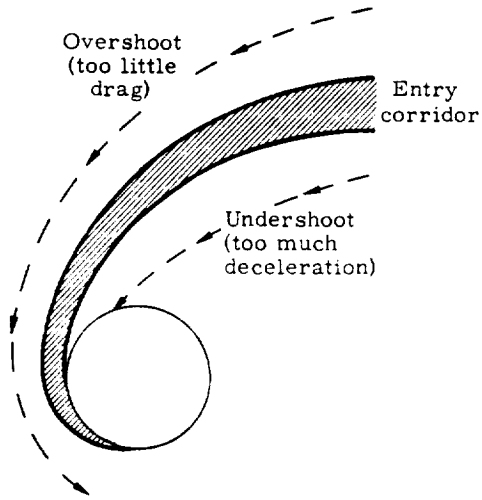

Figure 63c (Ref. 14) indicates the limitations on the minimum entry angles for capture of vehicles traveling at escape velocities.

Example:

$$W/C_L A = 50 \text{ lb/ft}^2 \ (2390 \text{ newtons/m}^2),$$

$$v_0 = v_e = \sqrt{2}\, v_c$$

For positive lift, vehicle is captured, if

$$\gamma_0 < -5.05°$$

For negative lift, vehicle is captured, if

$$\gamma_0 < -4.50°$$

Entry corridor conditions are considered in greater detail in Ref. 26.

Within certain bounds, the longitudinal and lateral range to the landing site may be varied by modifying the vehicle area or orientation (i.e., modifying the effective drag or lift). Figure 64 illustrates the correction of longitudinal range by varying the ballistic coefficient. This figure presents two graphs showing the ballistic coefficient increments needed to compensate for errors in entry angle if a fixed longitudinal range is to be attained.

Example:

$B_0 = 1.0 \text{ ft}^2/\text{slug} \ (0.00637 \text{ m}^2/\text{kg})$ } Range = 530 stat mi (Fig. 62) (853 km)

Programmed re-entry angle $\gamma_0 = -2$ deg }

Actual re-entry angle $\gamma_0' = -3$ deg

Thus, error = -1 deg (new range = 416 stat mi (670 km), Fig. 62).

From Fig. 64 $\dfrac{\Delta B_1}{B_0} = -0.8$

Therefore, approximately 80% of B ($\propto$ drag area) should be discarded in order to reach the predetermined range of 530 stat mi (853 km).

For the high-drag, low-lift vehicle already treated in Figs. 56a to 56c ($\alpha \approx 90°$, see Ref. 25). the variation of range as a function of angle of attack and initial flight path angle is shown for two azimuth angles in Fig. 65a. These changes in design range, created by the rotation of the earth, must be counteracted for a particular heading by proper changes in the angle of attack (i.e., changing the L/D ratio).

Figure 65b gives for the same type of entry vehicles the whole spectrum of variation of range as a function of heading for initial latitudes of 0° and 45°. Maneuver capabilities compensating these effects may be mandatory where exact impact at the point of destination is desired.

Reference 27 provides approximate analytic solutions for the lateral maneuverability available from banking the vehicle. These solutions, together with pertinent assumptions, are presented here for convenience in reference. They are based on equations of motion expressed in the following form (see Eqs (27) and (28)

$$m v \frac{dv}{ds} = - D - m g \sin \gamma \tag{76}$$

$$m v \frac{2 d\gamma}{ds} = L - m \cos \gamma \left(g - \frac{v^2}{r}\right) \tag{77}$$

$$m v^2 \frac{d\psi}{ds} = Y \tag{78}$$

where

Y = side force normal to L and D.

If the side force Y is produced by banking the vehicle, and if the vehicle exhibits a constant aerodynamic lift-drag ratio of $\left(\frac{L}{D}\right)_0$, then a bank angle ϕ results in

$$\frac{L}{D} = \left(\frac{L}{D}\right)_0 \cos \phi \tag{79}$$

$$\frac{Y}{D} = \left(\frac{L}{D}\right)_0 \sin \phi \tag{80}$$

1. Equilibrium-Glide Solution

Assumptions: vehicle weight is balanced by lift plus centrifugal force in the vertical direction (small γ).

$$\frac{\lambda}{R} \approx \frac{\pi^2}{24} \left(\frac{L}{D}\right)_0^2 \sin \phi \cos \phi \qquad \left[\psi << 1,\ v_0 = v_c,\ v_f = 0\right] \tag{81}$$

or, more generally

$$\frac{\lambda}{R} \approx \frac{L}{D}\left[\left(-\xi_0 + \frac{\xi_0^3}{3!} - \frac{\xi_0^5}{5!}\right)\Phi_0 + \left(1 - \frac{3}{3!}\xi_0^2 + \frac{5}{5!}\xi_0^4\right)\frac{Y}{D}\Phi_1 + \left(\frac{3}{3!}\xi_0 - \frac{10}{5!}\xi_0^3\right)\left(\frac{Y}{D}\right)^2 \Phi_2 + \left(-\frac{1}{3!} + \frac{10}{5!}\xi_0^2\right)\left(\frac{Y}{D}\right)^3 \Phi_3 + \frac{5}{5!}\xi_0\left(\frac{Y}{D}\right)^4 \Phi_4 + \frac{1}{5!}\left(\frac{Y}{D}\right)^5 \Phi_5\right] \tag{82}$$

$$\frac{x}{R} \approx \frac{L}{D}\left[\left(-1 + \frac{\xi_0^2}{2!} - \frac{\xi_0^4}{4!}\right)\Phi_0 + \left(-\frac{2}{2!}\xi_0 + \frac{4}{4!}\xi_0^3\right)\frac{Y}{D}\Phi_1 + \left(\frac{1}{2!} - \frac{6}{4!}\xi_0^2\right)\left(\frac{Y}{D}\right)^2 \Phi_2 + \frac{4}{4!}\xi_0\left(\frac{Y}{D}\right)^3 \Phi_3 - \frac{1}{4!}\left(\frac{Y}{D}\right)^4 \Phi_4\right] \tag{83}$$

$$\approx \frac{1}{2}\frac{L}{D} \ln \frac{1 - \bar{v}^2}{1 - \bar{v}_0^2} \quad \text{for} \quad \frac{Y}{D} = \xi_0 = 0 \tag{84}$$

where

λ = lateral range

x = longitudinal range

R = radius of earth

$\Phi_n = \int_{\bar{v}}^{\bar{v}} \frac{\bar{v}\,(\ln \bar{v})^n}{\bar{v}_0\,1 - \bar{v}^2}\, d\bar{v}$ in the difference between initial and final values tabulated as function of $\bar{v}$ in Table 2.

$\bar{v} = \frac{v}{v_c} = \bar{v}_0 \exp\left[-\frac{\psi}{(Y/D)}\right]$

$\bar{v}_0$ = normalized velocity at initiation of maneuver

$\xi = \frac{Y}{D} \ln \bar{v}$

2. Orbit Decay at Large Bank Angles ($\phi \approx 90°$)

Assumptions: zero lift in vertical plane $\frac{Y}{D} = \left(\frac{L}{D}\right)_0$, entry in decay from a satellite orbit.

$$\frac{\lambda}{R} = \sqrt{\frac{3}{2\beta R}\left[\frac{Y}{D}\right]}\,\psi \tag{85}$$

Figure 66a expresses the effects of roll angles on the lateral range for the study conducted in Ref. 27. It is seen roll angles equal to approximately 45° result in a maximum lateral range. Figure 66b represents the lateral range capabilities for increasing L/D ratios. The following empirical approximate equations can be fitted to these curves as follows, assuming the initial altitudes of 300,000 ft: (91.4 km)

TABLE 2

Values of the Function Φ_n

∇	Φ_0	Φ_1	Φ_2	Φ_3	Φ_4	Φ_5	∇	Φ_0	Φ_1	Φ_2	Φ_3	Φ_4	Φ_5
1.00	∞	0	0	0	0	0	0.49	0.1373	0.2492	-0.0773	0.0341	-0.0175	0.0097
.99	1.9585	.0050	.0000	.0000	.0000	.0000	.48	.1309	.2538	-.0806	.0366	-.0192	.0109
.98	1.6145	.0100	-.0001	.0000	.0000	.0000	.47	.1248	.2584	-.0840	.0391	-.0211	.0123
.97	1.4143	.0150	-.0002	.0000	.0000	.0000	.46	.1189	.2629	-.0875	.0417	-.0231	.0139
.96	1.2730	.0200	-.0004	.0000	.0000	.0000	.45	.1131	.2674	-.0910	.0445	-.0253	.0156
.95	1.1640	.0250	-.0006	.0000	.0000	.0000	.44	.1076	.2719	-.0947	.0475	-.0277	.0176
.94	1.0754	.0300	-.0009	.0000	.0000	.0000	.43	.1022	.2764	-.0984	.0506	-.0303	.0197
.93	1.0009	.0350	-.0012	.0001	.0000	.0000	.42	.0970	.2808	-.1022	.0538	-.0331	.0221
.92	.9367	.0400	-.0016	.0001	.0000	.0000	.41	.0920	.2852	-.1061	.0572	-.0361	.0247
.91	.8804	.0450	-.0021	.0001	.0000	.0000	.40	.0872	.2896	-.1100	.0608	-.0393	.0276
.90	.8304	.0500	-.0026	.0002	.0000	.0000	.39	.0825	.2940	-.1140	.0646	-.0428	.0309
.89	.7853	.0550	-.0031	.0002	.0000	.0000	.38	.0780	.2983	-.1182	.0685	-.0466	.0345
.88	.7445	.0600	-.0038	.0003	.0000	.0000	.37	.0736	.3026	-.1224	.0726	-.0506	.0384
.87	.7071	.0649	-.0044	.0004	.0000	.0000	.36	.0694	.3068	-.1266	.0769	-.0549	.0428
.86	.6728	.0699	-.0051	.0005	-.0001	.0000	.35	.0653	.3110	-.1310	.0814	-.0596	.0477
.85	.6410	.0749	-.0059	.0006	-.0001	.0000	.34	.0614	.3152	-.1354	.0862	-.0646	.0530
.84	.6114	.0799	-.0068	.0008	-.0001	.0000	.33	.0576	.3193	-.1400	.0911	-.0700	.0589
.83	.5838	.0848	-.0076	.0009	-.0001	.0000	.32	.0540	.3234	-.1445	.0963	-.0758	.0654
.82	.5580	.0898	-.0086	.0011	-.0002	.0000	.31	.0505	.3274	-.1492	.1016	-.0821	.0726
.81	.5337	.0948	-.0096	.0013	-.0002	.0000	.30	.0472	.3314	-.1540	.1073	-.0888	.0806
.80	.5108	.0997	-.0107	.0016	-.0003	.0000	.29	.0439	.3354	-.1588	.1132	-.0959	.0893
.79	.4892	.1047	-.0118	.0018	-.0003	.0001	.28	.0408	.3393	-.1636	.1193	-.1036	.0990
.78	.4688	.1096	-.0130	.0021	-.0004	.0001	.27	.0378	.3431	-.1686	.1257	-.1119	.1097
.77	.4493	.1146	-.0143	.0024	-.0005	.0001	.26	.0350	.3469	-.1736	.1324	-.1207	.1214
.76	.4309	.1195	-.0156	.0028	-.0006	.0001	.25	.0323	.3506	-.1787	.1393	-.1303	.1344
.75	.4133	.1245	-.0170	.0032	-.0007	.0002	.24	.0297	.3543	-.1839	.1466	-.1405	.1488
.74	.3966	.1294	-.0185	.0036	-.0008	.0002	.23	.0272	.3579	-.1891	.1541	-.1514	.1647
.73	.3806	.1343	-.0200	.0041	-.0009	.0002	.22	.0248	.3614	-.1944	.1620	-.1632	.1822
.72	.3653	.1392	-.0216	.0046	-.0011	.0003	.21	.0226	.3649	-.1997	.1702	-.1757	.2015
.71	.3507	.1441	-.0232	.0051	-.0013	.0004	.20	.0204	.3683	-.2051	.1787	-.1892	.2229
.70	.3367	.1490	-.0249	.0057	-.0015	.0004	.19	.0184	.3716	-.2105	.1876	-.2037	.2466
.69	.3232	.1539	-.0267	.0064	-.0017	.0005	.18	.0165	.3748	-.2160	.1968	-.2192	.2728
.68	.3103	.1588	-.0285	.0071	-.0020	.0006	.17	.0147	.3780	-.2214	.2063	-.2359	.3019
.67	.2979	.1637	-.0304	.0078	-.0023	.0007	.16	.0130	.3810	-.2269	.2162	-.2538	.3341
.66	.2860	.1686	-.0324	.0086	-.0026	.0009	.15	.0114	.3840	-.2325	.2265	-.2730	.3699
.65	.2745	.1734	-.0345	.0095	-.0030	.0010	.14	.0099	.3868	-.2380	.2372	-.2936	.4097
.64	.2635	.1782	-.0366	.0104	-.0034	.0012	.13	.0085	.3896	-.2435	.2482	-.3157	.4540
.63	.2528	.1831	-.0388	.0114	-.0039	.0014	.12	.0073	.3922	-.2490	.2597	-.3394	.5034
.62	.2426	.1879	-.0411	.0125	-.0044	.0016	.11	.0061	.3948	-.2544	.2715	-.3650	.5585
.61	.2327	.1927	-.0434	.0136	-.0049	.0019	.10	.0050	.3972	-.2598	.2836	-.3924	.6023
.60	.2231	.1975	-.0458	.0148	-.0055	.0022	.09	.0041	.3994	-.2651	.2961	-.4218	.6896
.59	.2139	.2023	-.0483	.0161	-.0062	.0026	.08	.0032	.4015	-.2703	.3089	-.4534	.7676
.58	.2050	.2071	-.0509	.0175	-.0069	.0030	.07	.0025	.4035	-.2754	.3220	-.4874	.8556
.57	.1964	.2118	-.0535	.0190	-.0077	.0034	.06	.0018	.4053	-.2803	.3354	-.5238	.9553
.56	.1881	.2166	-.0562	.0205	-.0086	.0039	.05	.0013	.4069	-.2849	.3488	-.5628	1.0686
.55	.1801	.2213	-.0590	.0222	-.0096	.0045	.04	.0008	.4083	-.2892	.3623	-.6046	1.1981
.54	.1724	.2260	-.0618	.0239	-.0106	.0051	.03	.0005	.4094	-.2932	.3754	-.6488	1.3466
.53	.1649	.2307	-.0648	.0257	-.0118	.0058	.02	.0002	.4104	-.2966	.3880	-.6950	1.5176
.52	.1576	.2353	-.0678	.0276	-.0130	.0066	.01	.0001	.4110	-.2992	.3990	-.7415	1.7134
.51	.1506	.2400	-.0709	.0297	-.0144	.0075	.00	.0000	.4112	-.3005	.4059	-.7777	1.9075
.50	.1438	.2446	-.0740	.0319	-.0159	.0085							

for $L/D \leq 1.0$ (due east): $\lambda \approx 623 \left(\frac{L}{D}\right)^{1.875}$ (naut mi) $= 1155 \left(\frac{L}{D}\right)^{1.875}$ (km)

for $0.75 \leq \frac{L}{D} \leq 2.0$ (due east): $\lambda \approx 910 \frac{L}{D} - 300$ (naut mi) $= 1688 \left(\frac{L}{D}\right) - 556$ (km)

The effects of the entry angle on the maximum lateral range are shown in Fig. 66c for roll angle of 45° and (L/D) = 1.0, while the effects of initial velocity are indicated in Fig. 66d.

In Ref. 14, the maneuvering performance of a re-entry vehicle is considered for a trajectory consisting of three parts:

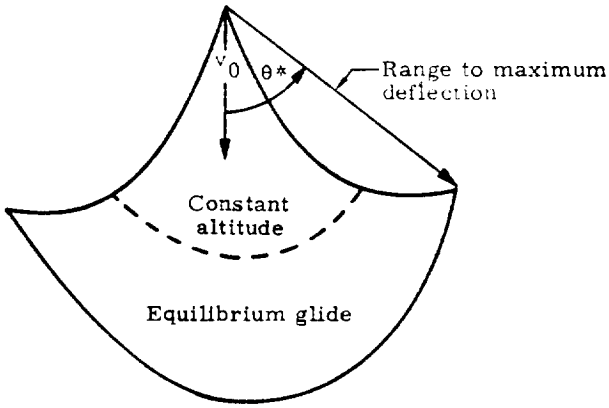

(1) Initial pull-out at $\left(\frac{L}{D}\right)_{max}$.

(2) Constant altitude glide at $\frac{L}{D} \leq \left(\frac{L}{D}\right)_{max}$.

(3) Equilibrium glide at $\left(\frac{L}{D}\right)_{max}$.

Range to maximum deflection point and the corresponding azimuth angle, θ*, are defined as shown in the above sketch.

The effects of re-entry angle on θ* and range are presented in Fig. 67a for $\frac{W}{C_L A} = 20$ psf (958 newtons/m^2 and $\frac{L}{D}$ ratios of 0.5, 1 and 2. It can be seen that the range capabilities are greatly reduced by large re-entry angles, the resulting ranges for $-10 \geq \gamma_0$ being almost independent of $\frac{L}{D}$. The reverse is true for azimuth angles.

Figures 67b and c give the effects of wing loading on the range to maximum deflection point and the maximum azimuth angle for $\gamma_0 = -2°$ and $\frac{L}{D}$ ratios 0.5, 1 and 2.

Figure 68a shows a typical maneuverability envelope for $\frac{W}{C_L A} = 20$ psf (958 newtons/m^2) and $v_0 = v_c$ (entry at circular orbit speeds). North pole is considered as the initial point of the trajectory calculations. For an initial flight path angle of -2°, the maneuver envelopes for the lift-drag ratios of 0.5, 1 and 2 are plotted. A comparison for $\gamma_0 = -4°$ and $\frac{L}{D} = 2$ is shown in dotted lines.

Similar maneuver envelopes are also shown in Fig. 68b for $\frac{W}{C_L A} = 100$ psf (4787 newtons/m^2) and $\gamma_0 = -6°$ for an entry at escape speeds.

Finally, Fig. 69 shows the maneuverability (that is the locus of impact points) of a lifting body as computed on the Martin Marietta powered trajectory program, using a maximum L/D = 0.5; the minimum which could be trimmed is 0.3. Bank angles varied from 0° for the fore and aft case to 60° for the maximum lateral deviation. Initial conditions were $h_0 = 300,000$ ft (91.4 km) $v_0 = 25,500$ fps (7770 mps) and $\gamma_0 = -1°$. An additional variable on the plot is the altitude at which initial deviation from the basic approach is effected (300,000, < 250,000, 225,000, 200,000 or 150,000 ft; (91.4 < 76.2, 68.6, 61.0, 45.7 km). Essentially, no maneuverability is afforded for initial altitude below 150,000 ft (45.7 km).

G. REFERENCES

1. Chapman, D. R., "An Approximate Analytical Method for Studying Entry into Planetary Atmospheres," NACA TN 4276, May 1958.

2. Allen, H. J., and Eggers, A. J., Jr., "A Study of the Motion and Aerodynamic Heating of Missiles Entering the Earth's Atmosphere at High Supersonic Speeds," NACA TN 4047, October 1957.

3. Sänger, E., "Raketen-Flugtechnik," R. Oldenbourg, Berlin, 1933.

4. Eggers, A. J., Jr., Allen, H. J., and Neice, S. E., "A Comparative Analysis of the Performance of Long-Range Hypervelocity Vehicles," NACA TN 4046, 1957.

5. Wang, K., and Ting, Lu, "Approximate Solutions for Reentry Trajectories with Aerodynamic Forces," Astronautics Acta, Fasc 8, pp 28 to 41, 1962.

6. Allen, H. J., and Eggers, A. J., Jr., "A Study of the Motion and Aerodynamic Heating of Ballistic Missiles Entering the Earth's Atmosphere at High Supersonic Speed," NACA Report 1381 1958.

7. Loh, W. H. T., "Ballistic Re-entry at Small Angles of Inclination," ARS Journal, Vol. 32, No. 5, May 1962, pp 718 to 721.

8. Bendor, E., Krenkel, A. R., and Kottler, C., "Trajectories of Lifting Bodies Entering Planetary Atmospheres at Shallow Angles," Fifth Symposium on Ballistic Missile and Space Technology, Academic Press, New York, 1960, pp 89 to 112.

9. Wang, K., and Ting, L., "An Approximate Analytic Solution of Re-entry Trajectory with

Aerodynamic Forces," ARS Journal, Vol. 30, No. 6, June 1960, pp 565 to 566.

10. Phillips, R. L., and Cohen, C. B., "Use of Drag Modulation to Reduce Deceleration Loads During Atmospheric Entry," ARS Journal, Vol. 29, No. 6, June 1959, pp 414 to 422.

11. Lees, L., Hartwig, F. W., and Cohen, C. B., "Use of Aerodynamic Lift During Entry into the Earth's Atmosphere," ARS Journal, Vol. 29, No. 9, September 1959, pp 633 to 641.

12. Robinson, A. C., Wolarer, L. E., and Besonis, A. J., "A Study of Nonlifting Satellites Re-entering the Earth's Atmosphere," WADC Aero Research Lab Working Paper, March 1958.

13 White, C., and Benson, O., "Physics and Medicine of the Upper Atmosphere," The University of New Mexico Press, Albuquerque, 1952.

14. Mandell, D. S., "Maneuvering Performance of Lifting Re-entry Vehicles," ARS Journal, Vol. 32, No. 3, March 1962, pp 346 to 354.

15. Hankey, W. L., Jr., Neumann, R. D., and Flinn, E. H., "Design Procedures for Computing Aerodynamic Heating at Hypersonic Speeds," WADC Technical Report 59-610, June 1960.

16. Sibulkin, M. J., "Heat Transfer Near the Forward Stagnation Point of a Body of Revolution," Journal of Aeronautical Sciences Vol. 19, No. 8, August 1952, pp 580 to 581.

17. Cohen, C. B., and Reshotko, E., "Heat Transfer at the Forward Stagnation of Blunt Bodies," NACA TN 3513, July 1955.

18. Lees, L., "Laminar Heat Transfer over Blunt Bodies at Hypersonic Flight Speeds," Jet Propulsion, Vol. 26, No. 4, April 1956, pp 259 to 269, 274.

19. Detra, R. W., Kemp, N. H., and Riddell, F. R., "Addendum to 'Heat Transfer to Satellite Vehicles Re-entering the Atmosphere,'" Jet Propulsion, Vol. 27, No. 4, December 1957, pp 1256 to 1257.

20. Fay, J. A., and Riddell, F. R., "Theory of Stagnation Point Heat Transfer in Dissociated Air," Journal of Aeronautical Sciences, Vol. 25, No. 2, February 1958, pp 73 to 86.

21. Lees, L., "Recovery Dynamics--Heat Transfer at Hypersonic Speed in a Planetary Atmosphere," Space Technology, John Wiley and Sons, Inc., 1958.

22. Kemp, N. H., and Riddell, F. R. "Heat Transfer to Satellite Vehicles Re-entering the Atmosphere," Jet Propulsion, Vol. 27, No. 2, February 1957, pp 132 to 137.

23. Kork, J., "A Practical Calculation Method of Aerodynamic Heating at the Stagnation Point," Master's Thesis, University of Maryland, May 1958.

24. Gazley, C., Jr., and Masson, D. J., "A Recoverable Scientific Satellite," Rand Report RM-1844, 1956.

25. Cheatham, D. C., Young, J. W., and Eggleston, John, "The Variation and Control of Range Traveled in the Atmosphere by a High-Drag Variable-Lift Entry Vehicle," NASA TN D-230, March 1960.

26. Chapman, D. R., "An Analysis of the Corridor and Guidance Requirements for Supercircular Entry into Planetary Atmospheres," NASA Technical Report R-55, 1960.

27. Slye, R. E., "An Analytical Method for Studying the Lateral Motion of Atmosphere Entry Vehicles," NASA TN D-325, September 1960.

H. BIBLIOGRAPHY

Adler, A. A., "Calculation of Re-entry Velocity Profile," Jet Propulsion, Vol. 28, No. 12, December 1958, pp 827 to 828.

Allen, H. J., "Motion of a Ballistic Missile Angularly Misaligned with the Flight Path upon Entering the Atmosphere and Its Effect upon Aerodynamic Heating, Aerodynamic Loads and Miss Distance," NACA TN 4048, October 1957.

Allen, H. J., and Eggers, A. J., Jr., "A Study of the Motion and Aerodynamic Heating of Missiles Entering the Earth's Atmosphere at Supersonic Speeds," NACA TN 4047, October 1957.

Ambrosio, A., "A General Atmospheric Entry Function and Its Characteristics," ARS Journal, Vol. 32, No. 6, June 1962, p 906.

Austin, R. W., "Trajectory Control of Lifting Re-entry Vehicles," IAS National Aerospace Support and Operations Meeting, Orlando, Florida, 4 December 1961.

Baker, R. M. L., Jr.,
"Encke's Method and Variation of Parameters as Applied to Re-entry Trajectories," Advances in Astronautical Sciences, New York, Plenum Press, Vol. 3, August 1958.
"Variation of Parameters as Applied to Re-entry Trajectories," American Astronautical Society Western Regional Meeting, 18 to 19 August 1958.
"Application of Astronomical Perturbation Techniques to the Return of Space Vehicles," ARS Journal, Vol. 29, No. 3, March 1959, pp 207 to 211.
"3-Dimensional Drag Perturbation Technique," ARS Journal, Vol. 30, No. 8, August 1960, pp 748 to 753.

Becker, J., "Re-entry from Space," Scientific American, Vol. 204, No. 1, January 1961, pp 49 to 57.

Berman, L. J., "Optimum Soft Landing Trajectories: Part I--Analysis" (U), Massachusetts Institute of Technology, Department of Aeronautics and Astronautics, Cambridge, Massachusetts, Report No. AFOSR 519, March 1961.

Bidwell, J. M., and Skulsky, R. S., "Maneuvering Re-entry for Maximum Lateral Range," The Martin Company, Denver, Colorado, Report No. Ml 60-36.

Blum, R., "Re-entry Trajectories--Flat Earth Approximation," ARS Journal, Vol. 32, No. 4, April 1962, p 616.

Boissevain, A. G., "The Effect of Lateral- and Longitudinal-Range Control on Allowable Entry Conditions for a Point Return from Space," NASA TN D-1067, July 1961.

Bowersox, R. B., et al., "Trajectory of a Vehicle Departing from a Circular Orbit, Lockheed Aircraft Corporation, Sunnyvale, California, Report No. LMSD-703049, July 1960.

Bressler, D. C., "Effects of Initial Re-entry Flight Conditions on a Recoverable Space Vehicle," The Martin Company, Baltimore, Maryland, Engineering Report No. ER 10625M, 1959.

Bull, G. V., Enkenhus, K. R., and Tiddy, G. H., "Exit and Re-entry Problems," Aero/Space Engineering, Vol. 17, No. 6, June 1958.

Bush, L. R., "A Study of the Accurate Re-entry and Precision Landing of an Orbital Earth Satellite, Part I," Cornell Aeronautical Laboratory, CAL Report No. VF-1351-H-1, 30 June 1959. (Also, ASTIA No. AD 245, 153.)

Brunner, M. J., "The Aerodynamic and Radiant Heat Input to Space Vehicles Which Re-enter at Satellite and Escape Velocity," American Rocket Society, Preprint No. 1558-60, December 1960.

Bryson, A. E., Denham, W. F., Carroll, F. J., and Mikand, K., "Determination of the Lift or Drag Program that Minimizes Re-entry Heating with Acceleration or Range Constraints Using a Steepest Descent Computation Procedure," Institute of the Aeronautical Sciences, Paper No. 61-6, 1961.

Cappellari, J. O., "The Effect of Drag Modulation on the Maximum Deceleration Encountered by a Re-entering Ballistic Missile," Purdue University, School of Aeronautical Engineering, Lafayette, Indiana, Report No. A-59-6, June 1959.

Chapman, D. R.,
"An Approximate Analytical Method for Studying Entry into Planetary Atmospheres," NASA TR R-11, 1959. (Also, NACA TN 4276, May 1958.)
"An Analysis of the Corridor and Guidance Requirements for Supercircular Entry into Planetary Atmospheres," NASA TR R-55.

Chapman, D. R., and Kapphahn, A. K., "Tables of Z Functions for Atmosphere Entry Analyses," NASA TR R-106, 1961.

Cheatham, D. C., Young, J. W., and Eggleston, J., "The Variation and Control of Range Traveled in the Atmosphere by a High-Drag Variable-Lift Entry Vehicle," NASA TN D-230, March 1960.

Cross, D. B.,
"A Study of Entry into the Earth's Atmosphere," American Astronautical Society, Preprint No. 58-48, December 1958.
"Re-entry Trajectory Analysis," The Martin Company, Denver, Colorado, Martin-Denver Course in Space Flight Dynamics, Lecture No. 13, 1960.
"Flight Dynamics and Heating Problems for Atmospheric Entry," The Martin Company, Denver, Colorado, Report No. R-60-12, May 1960.

Czarnecki, E. G., "Lifting Re-entry Vehicles," Astronautics, Vol. 6, No. 6, June 1961, pp 27 to 31, 50, 52.

Daskin, W., et al., "The Use of Lift for Re-entry from Satellite Trajectories," Jet Propulsion, Vol. 27, No. 11, November 1957, pp 1184 to 1189.

Detra, R. W., "Controlled Recovery of Nonlifting Satellites," ARS Journal, Vol. 30, No. 9, September 1960.

Detra, R. W., and Hidalgo, H., "Generalized Heat Transfer Formulas and Graphs for Nose Cone Re-entry into the Atmosphere," ARS Journal, Vol. 31, No. 3, March 1961, p 318.

Detra, R. W., Kemp, N. H., and Riddell, F. R., "Addendum to Heat Transfer to Satellite Vehicles Re-entering the Atmosphere," Jet Propulsion, Vol. 27, No. 12, December 1957.

Detra, R. W., and Riddell, F. R., "Controlled Recovery of Nonlifting Satellites," AVCO Research Laboratory and Advanced Development Division, Report No. RR 54, May 1959.

DiChristina, V., "Re-entry Performance of a High-Altitude Probe," Inst. Aerospace Sci., Paper 62-31, January 1962.

Dryer, M., "Propulsive Control of Atmospheric Entry Lifting Trajectories" (U), The Martin Company, Denver, Colorado, Report No. R-60-9, May 1960, 27 pp.

Edwards, R. H., and Campbell, G. S., "Prediction of Peak Temperature for Satellite Entries with Lift," ARS Journal, Vol. 30, No. 5, May 1960, p 496.

Eggers, A. J., Jr., Allen, H. J., and Neice, S. E., "A Comparative Analysis of the Performance of Long-Range Hypervelocity Vehicles," NASA TN 4046, October 1957.

Eggers, A. J., Jr., Hansen, C. F., and Cunningham, B. E., "Stagnation-Point Heat Transfer to Blunt Shapes in Hypersonic Flight, Including Effects of Yaw," NACA TN 4229, April 1958.

Eggleston, J. M., and Cheatham, D. C., "Piloted Entries into the Earth's Atmosphere," Institute of Aeronautical Sciences, Preprint No. 59-98, June 1959.

Ehricke, K. A.,
"On the Descent of Winged Orbital Vehicles," Astronautica Acta, Vol. 1, Fasc 3, 1955, pp 137 to 155.
"On Mechanics of Descent to Celestial Body," Journal of Astronautics, Vol. 2, No. 4, 1955, pp 137 to 144.
"Re-entry of Spherical Bodies into the Atmosphere at Very High Speeds," American Rocket Society, Spring Meeting, Washington, D. C., Reprint No. 428-57, April 1957.
"The Satelloid," Astronautica Acta, Vol. II, Fasc 2, 1956, pp 64 to 100.

Etkin, B., "The Entry of Manned Maneuverable Space Craft into Planetary Atmospheres," Toronto University, Inst. Aerophys., UTIA Rev. 20, October 1961.

Fay, J. A., and Riddell, F. R., "Theory of Stagnation-Point Heat Transfer in Dissociated Air," J. Aeronautical Science, Vol. 25, February 1958, pp 73 to 85.

Fay, J. A., "Hypersonic Heat Transfer in the Air Laminar Boundary Layer," AVCO Report AMP 71, March 1962.

Ferri, A., and Ting, L., "Practical Aspects of Re-entry Problems" (U), Polytechnic Institute of Brooklyn, Department of Aerospace Engineering, New York, Report No. PIBAL 705, July 1961.

Ferri, A., Feldman, L., and Daskin, W., "The Use of Lift for Re-entry from Satellite Trajectories," Jet Propulsion, Vol. 27, No. 11, November 1957.

Fine, J. H., "Stability of Flight Paths of Lifting Vehicles During Entry into Planetary Atmospheres," Toronto University, Inst. Aerophys., July 1961.

Fisher, L., "Landing Energy Dissipation for Manned Re-entry Vehicles," NASA TN D-453, 1960.

Gaines, L. M., and Surber, T. E., "Prediction of Optimum Approach and Landing Techniques for Manned Re-entry Gliders," North American Aviation, Inc., presented at the National IAS - ARS Joint Meeting, 13 to 16 June 1961, Ambassador Hotel, Los Angeles, California, IAS Paper 61-115-1809.

Galman, B. A.,
"Direct Re-entry at Escape Velocity," American Astronautical Society, Preprint No. 60-86, April 1960.
"Some Fundamental Considerations for Lifting Vehicles in Return from Satellite Orbit," General Electric Company, Philadelphia, Pennsylvania, Report No. GE-MSVD TIS R595D355, May 1959.

Garber, T. B.,
"Effects of Aerodynamic Forces upon the ICBM Re-entry Trajectory," The Rand Corporation, Santa Monica, California, Report No. RM 1782, August 1956.
"On the Rotational Motion of a Body Re-entering the Atmosphere," Journal of Aerospace Science, Vol. 26, No. 7, July 1959, p 443.

Gazley, C., Jr.,
"Recovery of a Circum-Lunar Instrument Carrier," The Rand Corporation, Santa Monica, California, Report No. P-119, 19 August 1957.
"The Penetration of Planetary Atmosphere," The Rand Corporation, Report No. P-1322, Santa Monica, California, February 1958.
"Deceleration and Heating of a Body Entering a Planetary Atmosphere from Space," Report No. P-955, The Rand Corporation, Santa Monica, California, 18 February 1957. (Also, Vistas in Astronautics, New York, Pergamon Press, Inc., 1958, Vol. 1, pp 8 to 32.)
"Atmospheric Entry of Manned Vehicles," The Rand Corporation, Research Memorandum RM-2579, Santa Monica, California, January 1960, p 42. (Also, Institute of Aerospace Sciences Space Stations Symposium, April 1960.)
"Atmospheric Entry," Handbook of Astronautical Engineering, McGraw-Hill Book Company, New York, 1961 (Koelle, ed.)

Gazley, C., Jr., and Masson, D. J., A Recoverable Scientific Satellite," Report No. RM-1844, The Rand Corporation, Santa Monica, California, 1956.

Grant, F. C.,
"Analysis of Low-Acceleration Lifting Entry from Escape Speed," NASA TN D-249, June 1960.
"Dynamic Analysis of a Simple Re-entry Maneuver for a Lifting Satellite," NASA TN D-47, September 1959.
"Importance of the Variation of Drag with Lift in Minimization of Satellite Entry Acceleration," NASA TN D-120, October 1959.
"Modulated Re-entry," Joint Conference on Lifting Manned Hypervelocity and Re-entry Vehicles, Langley Field, Virginia, April 1960.

Groves, G. V., "Velocity of a Body Falling Through the Atmosphere and the Propagation of Its Shock Wave to Earth," Journal of Atmospheric and Terrestrial Physics, Vol. 10, No. 2, February 1957, pp 73 to 83.

Guess, A. L., and Peline, V. P., "The Sensitivity of Ballistic Satellite Re-entry Trajectory Prediction to Differences in the Geophysical Properties," The Martin Company, Baltimore, Maryland, Report No. AP TN 60-3. (Also, Lockheed Aircraft Corporation, Sunnyvale, California, Report No. LMSD-447470.)

Hendrix, C. E., "Proposal for a Simple System for Achieving Soft Landing of a Rocket Vehicle," Naval Ordnance Test Station, China Lake, California, NOTS TP 2495, NavWEPS Report 7084.

Jackson, C. M., Jr., "Estimates of Minimum Energy Requirements for Range-Controlled Return of a Non-Lifting Satellite from a Circular Orbit," NASA Technical Note D-980, November 1961.

Hermann, R., "Ascent and Re-entry," Space Trajectories, Academic Press, New York, 1960.

Hilderbrand, R. B., "Aerodynamic Fundamentals," Handbook of Astronautical Engineering, McGraw-Hill Book Company, New York, 1961 (Koelle, ed.).

Hill, F. A. F., "Satellite Re-entry with Lightly Loaded Lifting Vehicles," Massachusetts Institute of Technology, Naval Supersonic Laboratory, Cambridge, Massachusetts, Technical Report No. 429, December 1959.

Hoglund, R., and Thale, J., "Recovery from a Satellitic Orbit," American Rocket Society, Preprint 650-58, 1958.

Hoshizaki, H., "Heat Transfer in Planetary Atmospheres at Super-Satellite Speeds, ARS Journal, Vol. 32, No. 10, p 1544.

Hunziker, R. R., "Re-entry Trajectories for Impact Prediction and Radar Acquisition," ARS Journal, Vol. 32, No. 8, August 1962, p 1261.

Kaeppeler, H. J., and Kubler, M. E., "Die Rückkehr von Geflugelten Geräten von Aussenstationsbahnen," Bericht uber den V. Internationalen Astronautischen Kongress. Vienna, Springer Publication, 1955 (F Hecht, ed.).

Katzen, E. D., "Terminal Phase of Satellite Entry into the Earth's Atmosphere," ARS Journal, Vol. 29, No. 2, February 1959, pp 147 to 148.

Katzen, E. D., and Levy, L. L., Jr., "Atmosphere Entries with Vehicle Lift-Drag Ratio Modulated to Limit Deceleration and Rate of Deceleration - Vehicles with Maximum Lift-Drag Ratio of 0.5," NASA Technical Note D-1145, December 1961.

Kemp, N. H., and Riddell, F. R., "Heat Transfer to Satellite Vehicles Re-entering the Atmosphere," Jet Propulsion, Vol. 27, No. 2, February 1957, pp 132 to 137.

Kemp, N. H., Rose, P. H., and Detra, R. W., "Laminar Heat Transfer Around Blunt Bodies in Dissociated Air," Journal of the Aerospace Sciences, Vol. 26, 1959, pp 424 to 450.

Kennet, H., and Strack, S. L., "Stagnation Point Radiative Transfer," ARS Journal, Vol. 31, No. 3, March 1961, p 370.

Kepler, D. I., "Concepts Influencing the Selection of a Configuration for Atmospheric Re-entry," American Rocket Society, Paper No. 786-59, April 1959.

King-Hele, D. G., "The Descent of an Earth-Satellite Through the Upper Atmosphere," Journal of the British Interplanetary Society, Vol. 15, December 1956, pp 314 to 323.

Kork, J., "Satellite Re-entry," Design Guide to Orbital Flight, McGraw-Hill Book Company, New York, Chapter X, 1962.

Lees, L.,
Ablation in Hypersonic Flow, New York, Seventh Anglo-American Aeronautical Conference, October 5 to 7, 1959.
"Laminar Heat Transfer Over Blunt-Nosed Bodies at Hypersonic Flight Speeds," Jet Propulsion, Vol. 26, No. 4, 1956, pp 259 to 269, 274.
"Recent Developments in Hypersonic Flow," Jet Propulsion, Vol. 27, No. 11, November 1957, pp 1162 to 1178.
"Recovery Dynamics--Heat Transfer at Hypersonic Speeds in a Planetary Atmosphere," Space Technology, New York, John Wiley and Sons, 1959.

Lees, L., Hartwig, F. W., and Cohen, C. B., "The Use of Lift During Entry into the Earth's Atmosphere," American Rocket Society, Preprint No. 785-59, April 1959. (Also, ARS Journal, Vol. 29, No. 9, September 1959).

Legalley, D. P., ed., "Re-entry and Vehicle Design," Ballistic Missile and Space Technology, Academic Press, New York, Vol. 4, 1960, p 422.

Levin, A. D., and Hopkins, E. J., "Re-entry Glide Maneuvers for Recovery of a Winged First-Stage Rocket Booster."

Levinsky, E. S., "Application of Inequality Constraints to Variational Problems of Lifting Re-entry," Institute of Aerospace Sciences, Report No. 61-21, January 1961.

Levy, L. L., Jr., "Atmosphere Entries with Spacecraft Lift-Drag Ratios Modulated to Limit Decelerations," NASA Technical Note D-1427, October 1962.

Lew, H. G., "Re-entry Physics," General Electric Company, Missile and Space Vehicle Department, Philadelphia, Pennsylvania, Contract No. DA 36-034-ORD-3187 (RD), December 1960. (Martin Library No. 6173-S-19.)

Linnell, R. D., "Vertical Re-entry into the Earth's Atmosphere for Both Light and Heavy Bodies," Jet Propulsion, Vol. 28, No. 5, pp 329-331, May 1958.

Loh, W. H. T.,
"Mechanics of Re-entry," 4th Symposium on Ballistic Missiles and Space Technology, Los Angeles, California, August 1959.
"Dynamics and Thermodynamics of Re-entry," Journal of the Aerospace Sciences, October 1960, pp 748 to 762.
"A Second Order Theory of Entry Mechanics into a Planetary Atmosphere," Institute of Aerospace Sciences, June 1961, Preprint No. 61-116-1810.
"Supercircular Gliding Entry," ARS Journal, Vol. 32, No. 9, September 1962, p 1398.
"Ballistic Re-entry at Small Angles of Inclination," ARS Journal, Vol. 32, No. 5, May 1962, p 718.

Luidens, R. W., "Approximate Analysis of G-Loads and Heating During Atmospheric Entries and Passes with Constant Aerodynamic Coefficients," NASA TN D1280, July 1962.

Mandell, D. S.
"A Study of the Maneuvering Performance of Lifting Re-entry Vehicles, Part I, Initial Atmospheric Re-entry," General Electric Company, Missile and Space Vehicle Department, Philadelphia, Pennsylvania, Flight Mechanics Data Memo No. 2:23, October 1960. (Also, American Rocket Society, Preprint No. 1555-60, December 1960.)
"Maneuvering Trajectory Program," General Electric Company, Missile and Space Vehicle Department, Philadelphia, Pennsylvania, Report No. TIS R50SD398, November 1960.
"Maneuvering Performance of Lifting Re-entry Vehicles," Vol. 32, No. 3, ARS Journal, March 1962, p 346.

Marshall, F. J., "Optimum Re-entry via a Variable Control Force," American Rocket Society, Preprint No. 956-59, 1959.

Miele, A., and Cavoti, C. R., "Variational Approach to the Re-entry of a Ballistic Missile, Parts I and II," Purdue University, School of Aeronautical Engineering, Lafayette, Indiana, Reports Nos. A-59-1 and A-59-3.

Miercort, F. A., "Re-entry into an Exponential Atmosphere, Ignoring Gravity," Martin-Denver, SR 1420-5, 30 November 1961, p 6.

Miller, B. P., "Approximate Velocity, Position and Time Relationship for Ballistic Re-entry," Vol. 31, No. 3, ARS Journal, March 1961, p 437.

Moe, M. M., "An Approximation to the Re-entry Trajectory," ARS Journal, Vol. 30, No. 1, ARS Journal, 1960, pp 50 to 53.

Morth, R. and Speyer, J. L., "Divergence from Equilibrium Glide Path at Supersatellite Velocities," ARS Journal, Vol. 31, No. 3, p 448.

Nielson, J. N., "Three-Dimensional Satellite Orbits with Emphasis on Re-entry Dynamics and Oblateness Effects," Aero/Space Engineering, Vol. 18, No. 4, April 1959, pp 60 to 66.

Nonweiler, T. R. F.,
"Problems of Interplanetary Navigation and Atmospheric Re-entry," Journal of the Royal Aeronautical Society, Vol. 64, 1960, pp 155 to 160.
"The Motion of an Earth Satellite on Re-entry to the Atmosphere," IXth International Astronautical Congress, Amsterdam, Vol. II, 1958, p 842. (Also, Astronautica Acta, Vol. 5, 1959.)

Norling, R. A., "Normal Dispersion of a Re-entry Body," ARS Journal, Vol. 30, No. 7, July 1960, p 652.

Offenhartz, E., Weisblatt, H., and Flagg, R. F., "Stagnation Point Heat Transfer Measurement at Super-Satellite Speeds," J. Royal Aeronautical Soc. Vol. 66, January 1962, p 53.

Olstad, W. B., "A Study of the Feasibility of Inflatable Re-entry Gliders," NASA TN D-538, 1960.

Phillips, R. L., and Cohen, C. B., "Use of Drag Modulation to Reduce Deceleration Loads During Atmospheric Entry," ARS Journal, Vol. 29, No. 6, June 1959.

Plascott, R. H., "The Re-entry of Manned Earth Satellites," Royal Aeroplane Establishment, Farnborough, England, Technical Note No. 2640, August 1959.

Probstein, R. F., "Methods of Calculating the Equilibrium Laminar Heat Transfer Rate at Hypersonic Flight Speeds," Jet Propulsion, Vol. 26, 1956, pp 497 to 499.

Quillinan, J. H., London, J. and Aston, B. A., "Configuration Selection of Re-entry Vehicles," Institute of Aeronautical Sciences, Preprint No. 59-97, June 1959.

Remmler, K. L., "Tumbling Bodies Entering the Atmosphere," ARS J. 32, 92-94, 1962.

Reshotko, E., "Simplified Method for Estimating Compressible Laminar Heat Transfer with Pressure Gradient," NACA TN 3888, December 1956.

Reshotko, E. and Cohen, C. B., "Heat Transfer at the Forward Stagnation Point of Blunt Bodies," NACA TN 3513, July 1955.

Rasamond, D. L., "Satellite Recovery Techniques for Optimization of Touchdown Accuracy," Institute of Aeronautical Sciences, Preprint No. 59-92, June 1959.

Riddell, F. R. and Detra, R. W., "Returning Alive from Space," American Astronautical Society, January 1958.

Riddell, F. R., and Winkler, H. B., "Meteorites and Re-entry of Space Vehicles at Meteor Velocities, ARS Journal, Vol. 32, No. 10, October 1962, p 1523.

Robinson, A. C., and Besonis, A. J., "On the Problems of Re-entry into the Earth's Atmosphere," USAF WADC TR 58-408, August 1958. (Also ASTIA No. AD 203790.) (Also, Journal of the Astronautical Sciences, No. 7, 1960, pp 7 to 21.)

Robinson, A. C., and Poli, C. R., "Development of Normalized Six-Degree-of-Freedom Equations for Analog Simulation of Atmospheric Re-entry," Synthesis and Analysis Division, Directorate of Systems Dynamic Analysis, Aeronautical Systems Division, Wright-Patterson Air Force Base, Ohio. (Task No. 70958) (ASD TR 61-448), November 1961.

Robinson, A. C., Wolaver, L. E. and Besonis, A. J., "A Study of Nonlifting Satellites Re-entering the Earth's Atmosphere," WADC Aero Research Laboratory Working Paper, March 1958.

Rogallo, F. M., and Lowry, J. G., "Flexible Re-entry Gliders," Society of Automotive Engineers, Inc., New York, Preprint No. 175C, 1960.

Rose, P. H., "Re-entry from Lunar Missions," AVCO Rpt AMP 69, December 1961.

Rute, L., "A Study of Aerodynamic Effects of Isothermal and Temperature Gradient Atmospheres on Re-entry Trajectories," Polytechnic Institute of Brooklyn, Department of Aerospace Eng and Applied Mechanics, AFOSR 2411, March 1962.

Scala, S., "Heating Problems of Entry into Planetary Atmospheres from Super Circular Orbiting Velocities," Proceedings of Symposium on Aerothermoelasticity, Aeronautical Systems Division, Wright-Patterson AFB, Ohio TR 61-645, October 1961.

Scherberg, M. G. and Rubin, T., "Decelerations of Ballistic Type Missile on Re-entry into Atmosphere," WADC TN WCRR53-2, February 1953.

Skulsky, R. S. and Summers, L. J., "Parametric Studies on Ballistic Re-entry Trajectories," The Martin Company, Denver, Colorado, Report MI-60-36, May 1960.

Slye, R. E., "An Analytical Method for Studying the Lateral Motion of Atmosphere Entry Vehicles," NASA TN D-325, September 1960.

Smith, R. H., "Supercircular Entry and Recovery with Maneuverable Manned Vehicles," Institute of Aerospace Sciences, Preprint No. 61-114-1808, June 1961.

Strack, S. L., "Radiant Heat Transfer Around Re-entry Bodies," ARS Journal, Vol. 32, No. 5, May 1962, p 744.

Surber, T. E. and Gaines, L. M., "Prediction of Optimum Approach and Landing Techniques for Manned Lifting Re-entry Gliders," Institute of Aerospace Sciences, Preprint No. 61-115-1809, June 1961.

Swanson, B. L.,
"A Study of Methods for Simulating the Atmosphere Entry of Vehicles with Small-Scale Models"
"Appendix A, B--Turbulent Heating Rates"
"Appendix C--Simulation of Highly Elliptic, Parabolic, and Hyperbolic Entries," NASA TN D-90, 1960, 51 pp.

Townsend, G. and Kork, J., "Satellite Recovery," Design Guide to Orbital Flight, McGraw-Hill Book Company, New York, Chapter 9, 1962.

Turnacliff, R. D. and Hartnett, J. P., "Generalized Trajectories for Free-Falling Bodies of High Drag," American Rocket Society, Preprint No. 543-57, December 1957.

Vargo, L. G., "Criteria for Orbital Re-entry," Jet Propulsion, Vol. 28, No. 1 January 1958, p 54.

Wang, K. and Ting, L., "An Approximate Analytic Solution of Re-entry Trajectory with Aerodynamic Forces," ARS Journal Vol. 30, No. 6, June 1960, p 565.
"Approximate Solutions for Re-entry Trajectories with Aerodynamic Forces," Astronaut Acta, 8, 28-41, 1962.

Warden, R. V., "Ballistic Re-entries with a Varying W/C_DA," ARS Journal, Vol. 31, No. 2, pp 208 to 213, February 1961.

Wick, B. H., "Radiative Heating of Vehicles Entering the Earth's Atmosphere," presented to the Fluid Mechanics Panel of Advisory Group for Aeronautical Research and Development, Brussels, Belgium, 3 to 6 April 1962.

Wong, T. J., et al., "Motion and Heating During Atmosphere Re-entry of Space Vehicles," NASA TN D-334, 1960.

"The Use of Aerodynamic Lift During Entry into The Earth's Atmosphere," Space Technology, Inc., Los Angeles, Cal., 20 November 1958.

"Trajectory Control for Vehicles Entering the Earth's Atmosphere at Small Flight-Path Angles," Langley Research Center, Langley Field, Va., February 1959.

"Variational Procedure for Minimizing Heating Effects During the Re-entry of a Lifting Vehicle: Heat Transfer to Slender Hypersonic Delta Wings Near 90° Incidence," Aeronautical Systems Division, Dir/Aeromechanics, Flight Dynamics Lab, Wright-Patterson AFB, Ohio, WADD TR 60-369, Vol. II, Final Report, April 1962.

"On the Mechanics of Descent to a Celestial Body," American Rocket Society, Report No. 146 A-54.

"Proceedings of the Recovery of Space Vehicles Symposium," Los Angeles, Cal., 31 August to 1 September 1960.

New York, Institute of the Aeronautical Sciences, 1960

"Recovery Technology and Space Operations," Evans, H. L.
"A Guided Parachute System," Kane, M. T.
"A Minimum Weight Landing System for Interplanetary Spacecraft," Ewing, E. G.
"Introduction to Dyna-Soar Recovery Session," Moore, W. L.
"The Effect of Search and Retrieval on Escape System Performance and Space Crew Safety," Edwards, H. H. and Garnett, R. J.

"Re-entry of Spherical Bodies into the Atmosphere at Very High Speed," American Rocket Society, Report No. 22128-57.

ILLUSTRATIONS

Preceding page blank

Preceding page blank

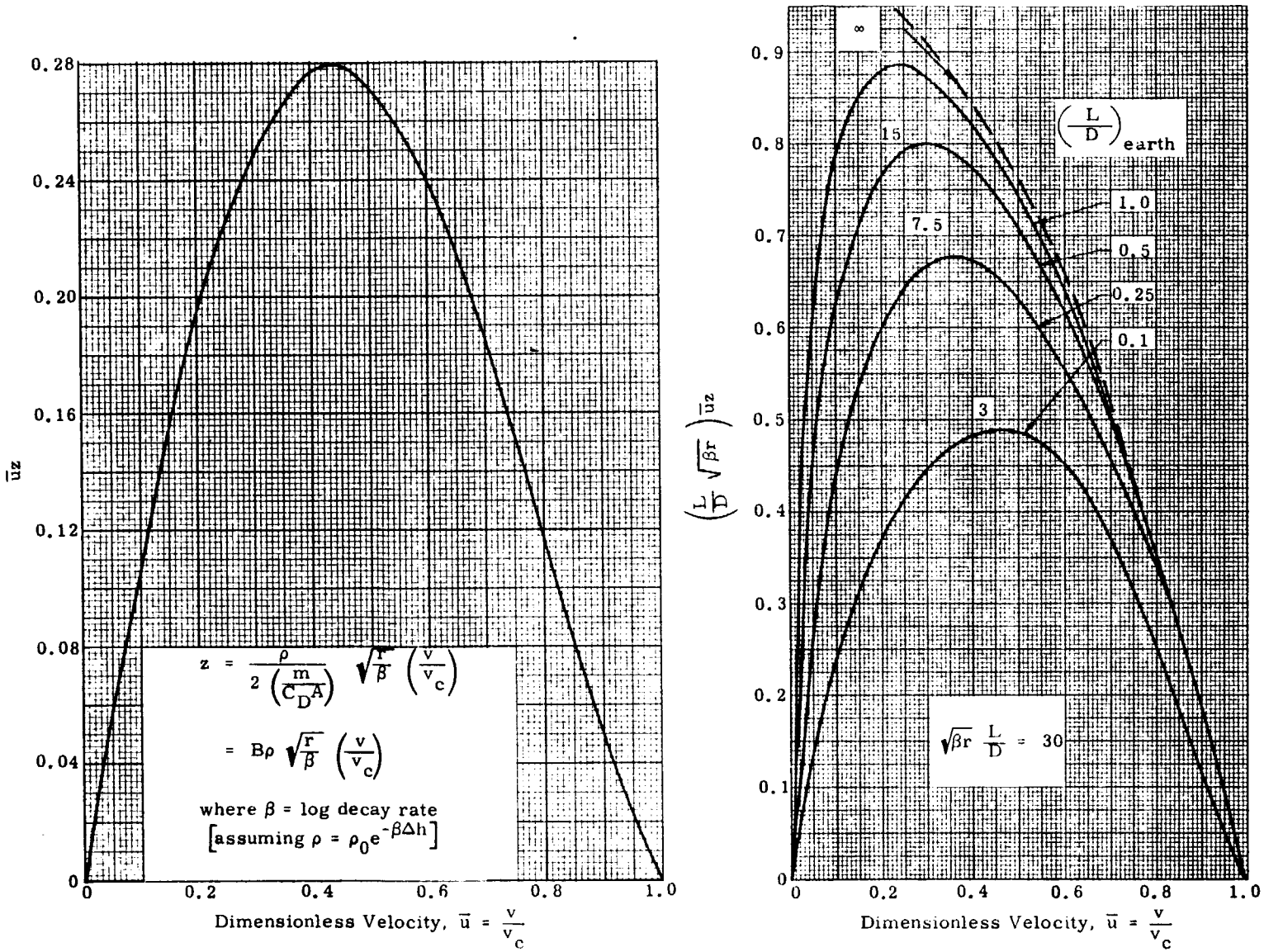

Fig. 1. Values of z Functions for Entry from Decaying Orbits into Planetary Atmosphere (Ref. 1)

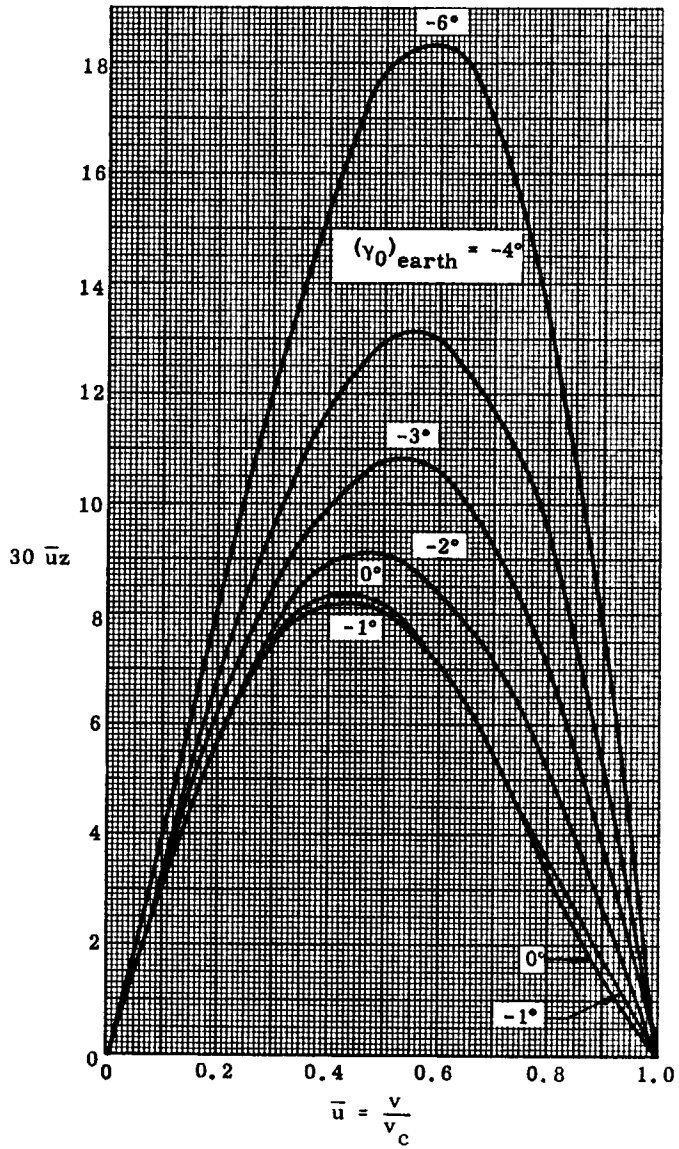

(a) Nonlifting Vehicles, L/D = 0

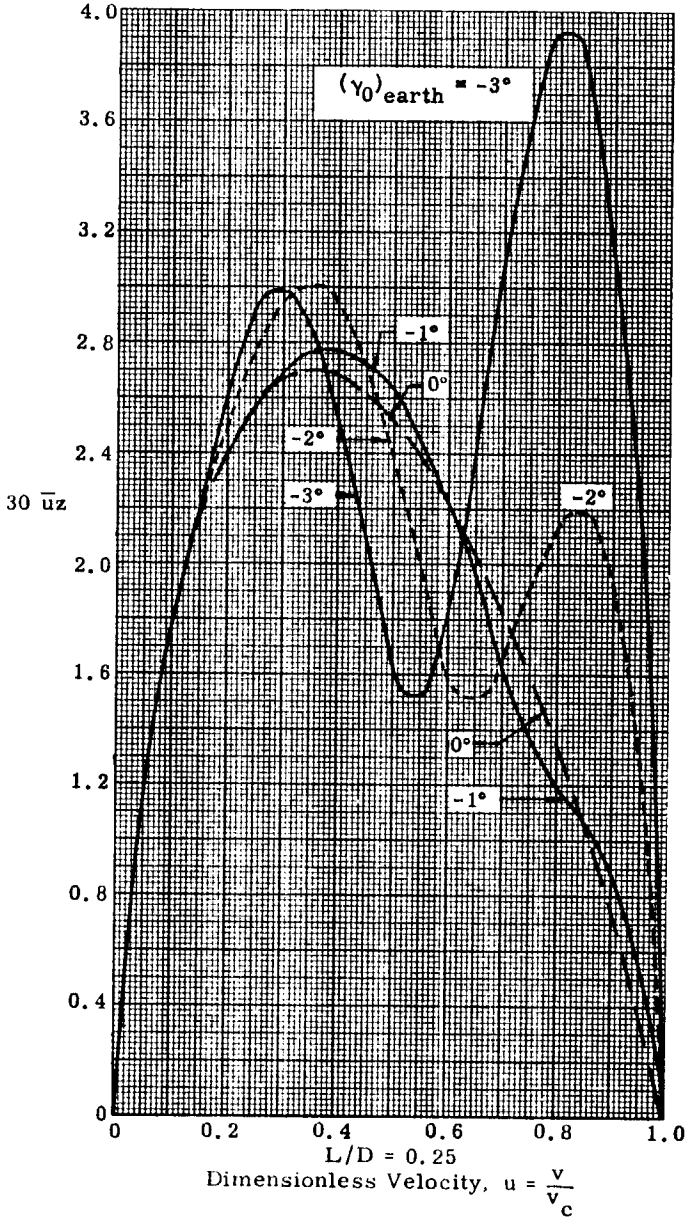

(b) Vehicles with L/D > 0 = 0.25

Fig. 2. Values of z Functions for Entry from Orbital Velocity at Initial Angles of Descent; $\bar{u}_0$ = 1 (Ref. 1)

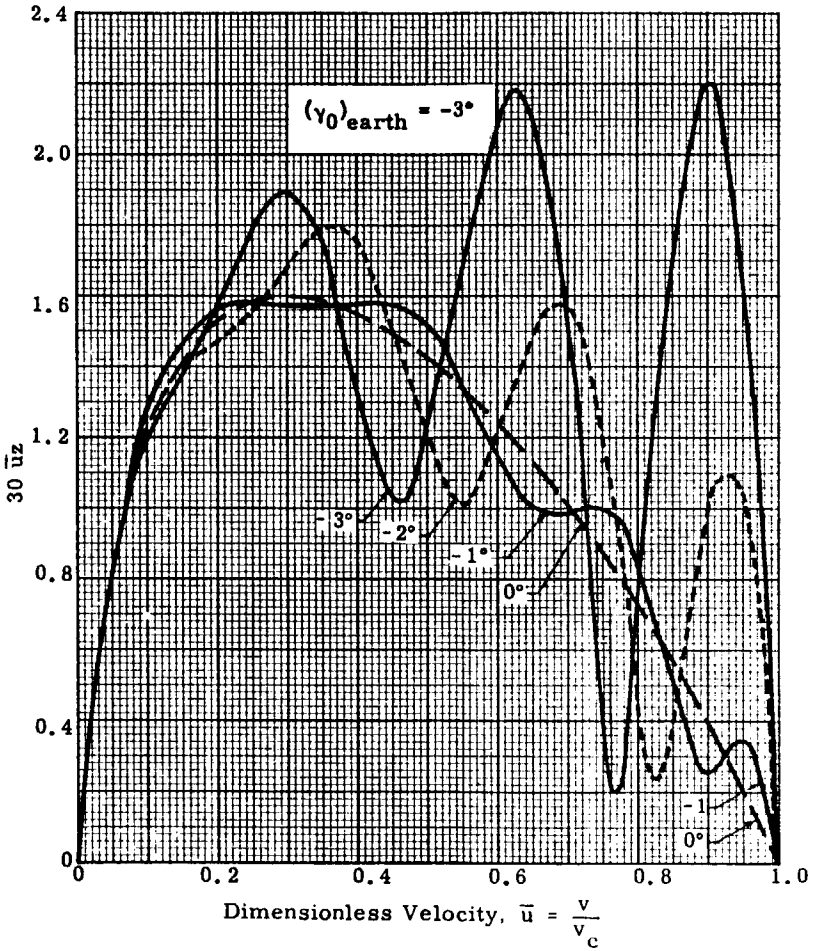

(c) Vehicles with L/D = 0.5

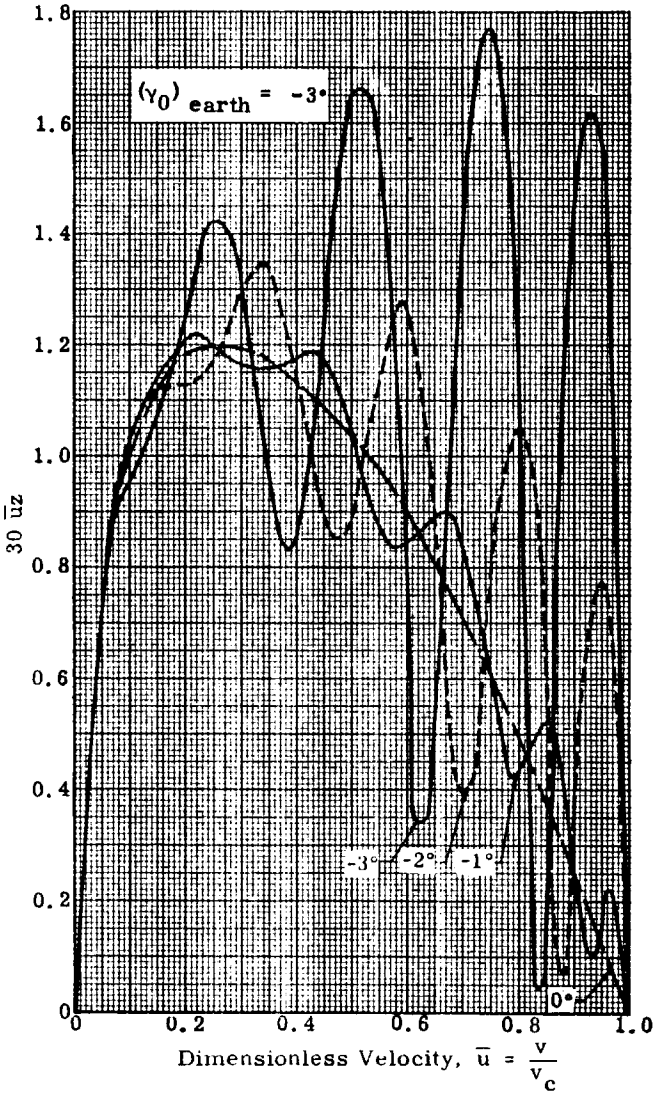

(d) Vehicles with L/D = 0.7

Fig. 2. (continued)

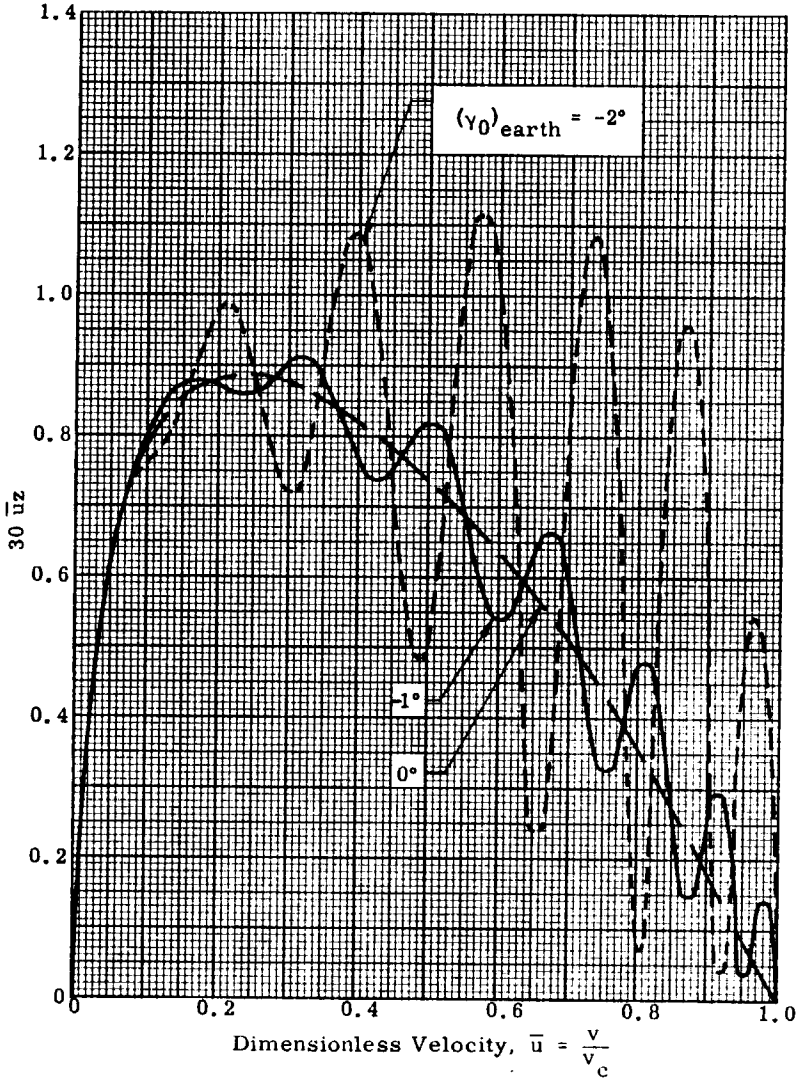

(e) Vehicles with L/D = 1

Fig. 2. (continued)

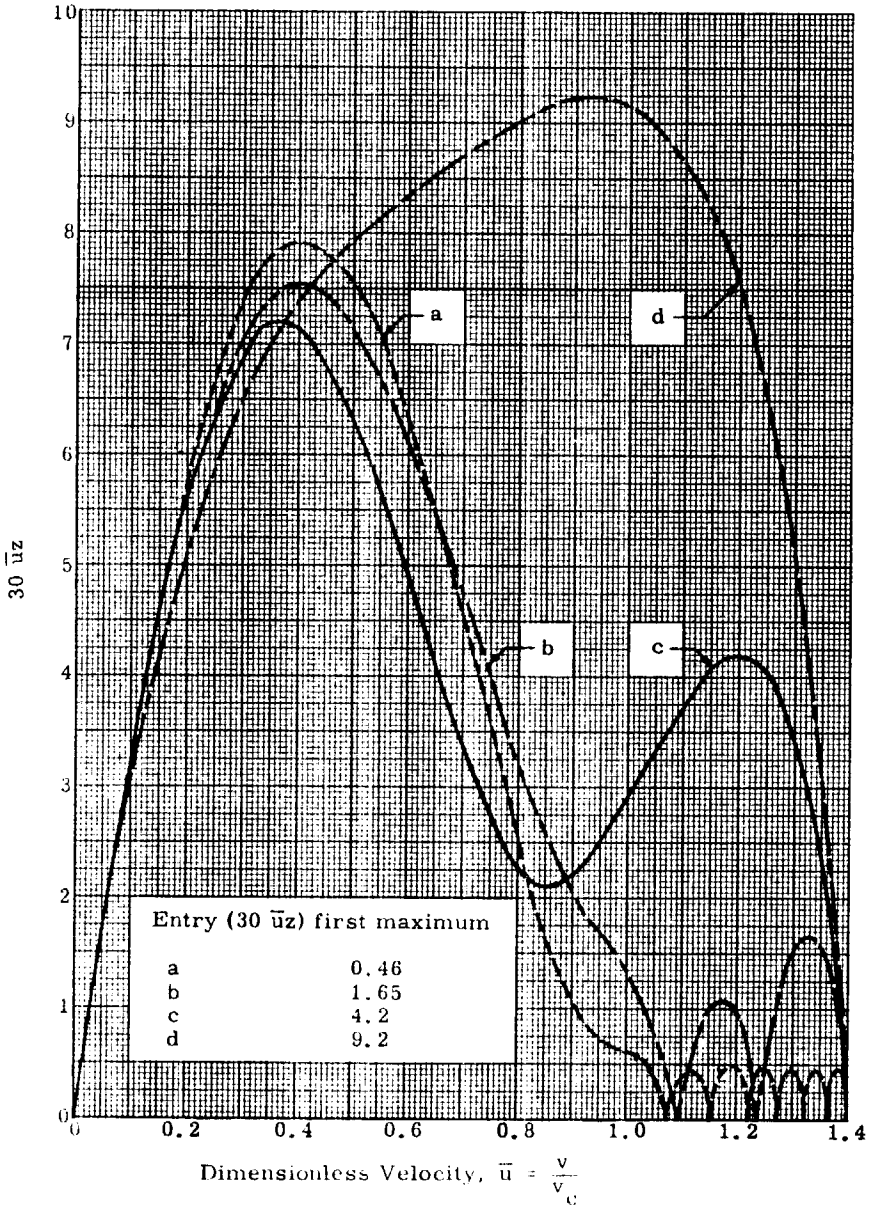

Fig. 3. Values of z Functions for Atmosphere Braking of Nonlifting Vehicles ($\bar{u}_0$ = 1.4, L/D = 0) (Ref. 1)

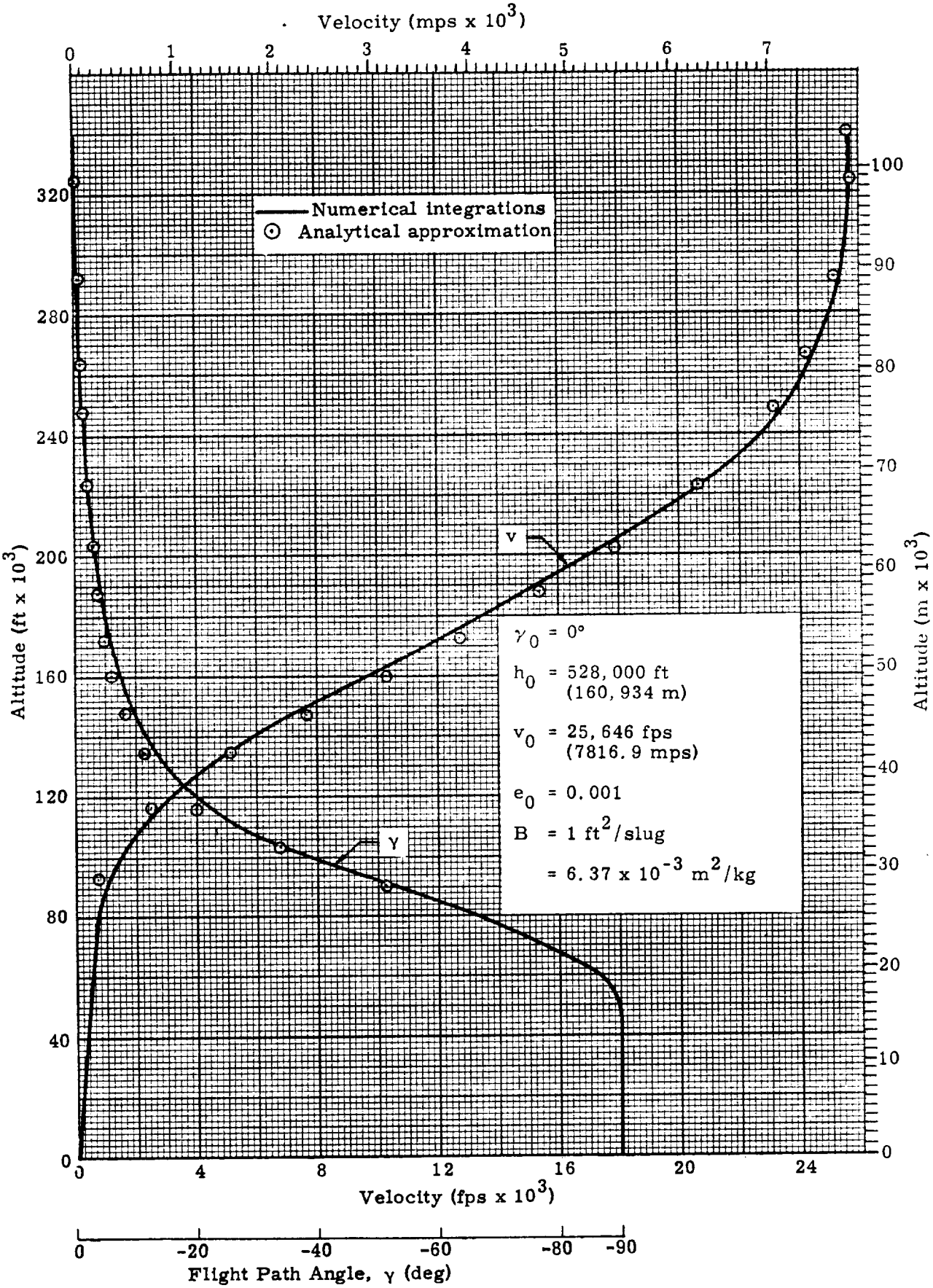

Fig. 4. Velocity Profile and Flight Path Angle Variation for Satellite Re-Entry

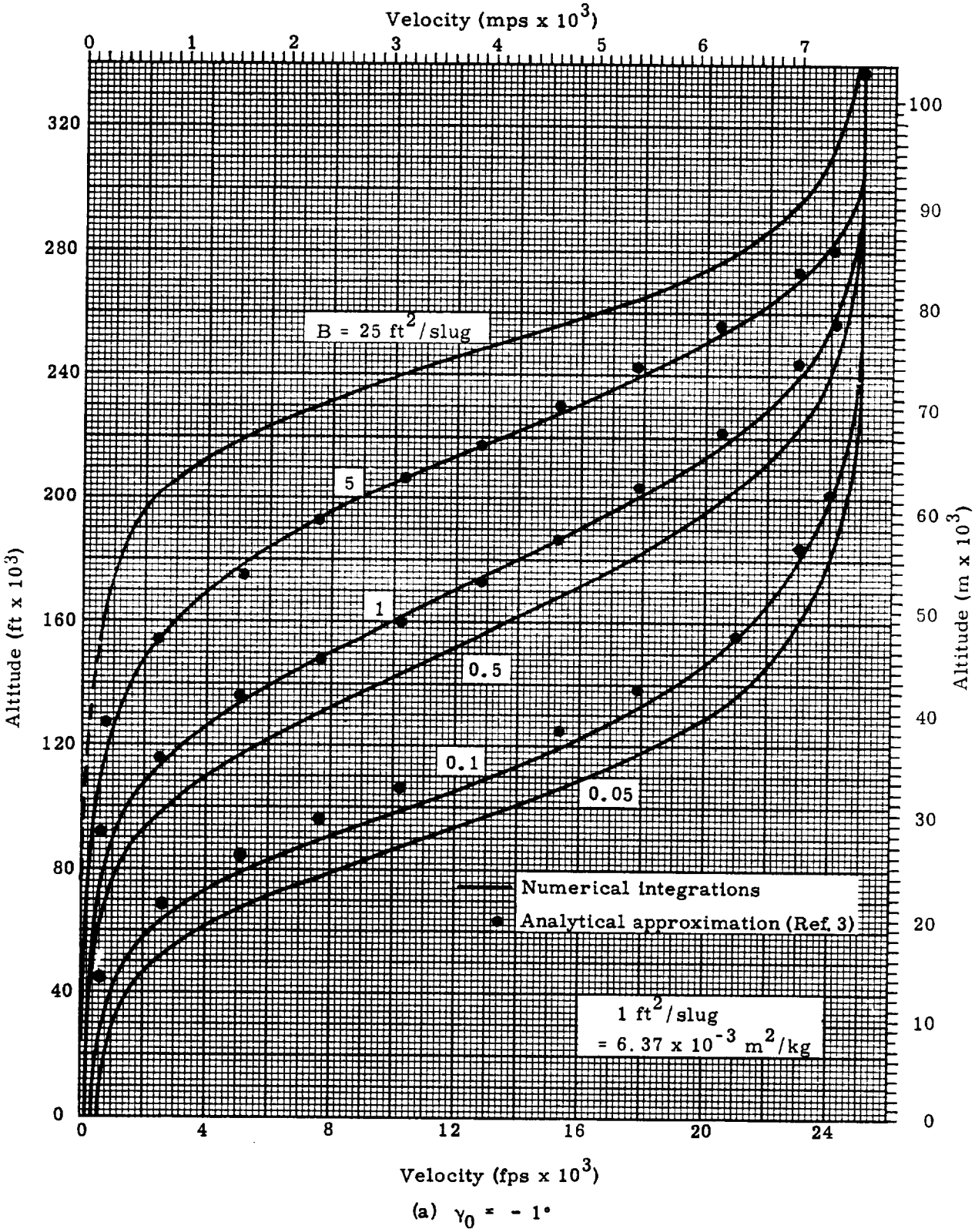

(a) $\gamma_0 = -1°$

Fig. 5. Velocity Variation with Altitude (h_0 = 300,000 ft = 91,440 m, v_0 = 25,000 fps = 7,620 mps, L/D = 0)

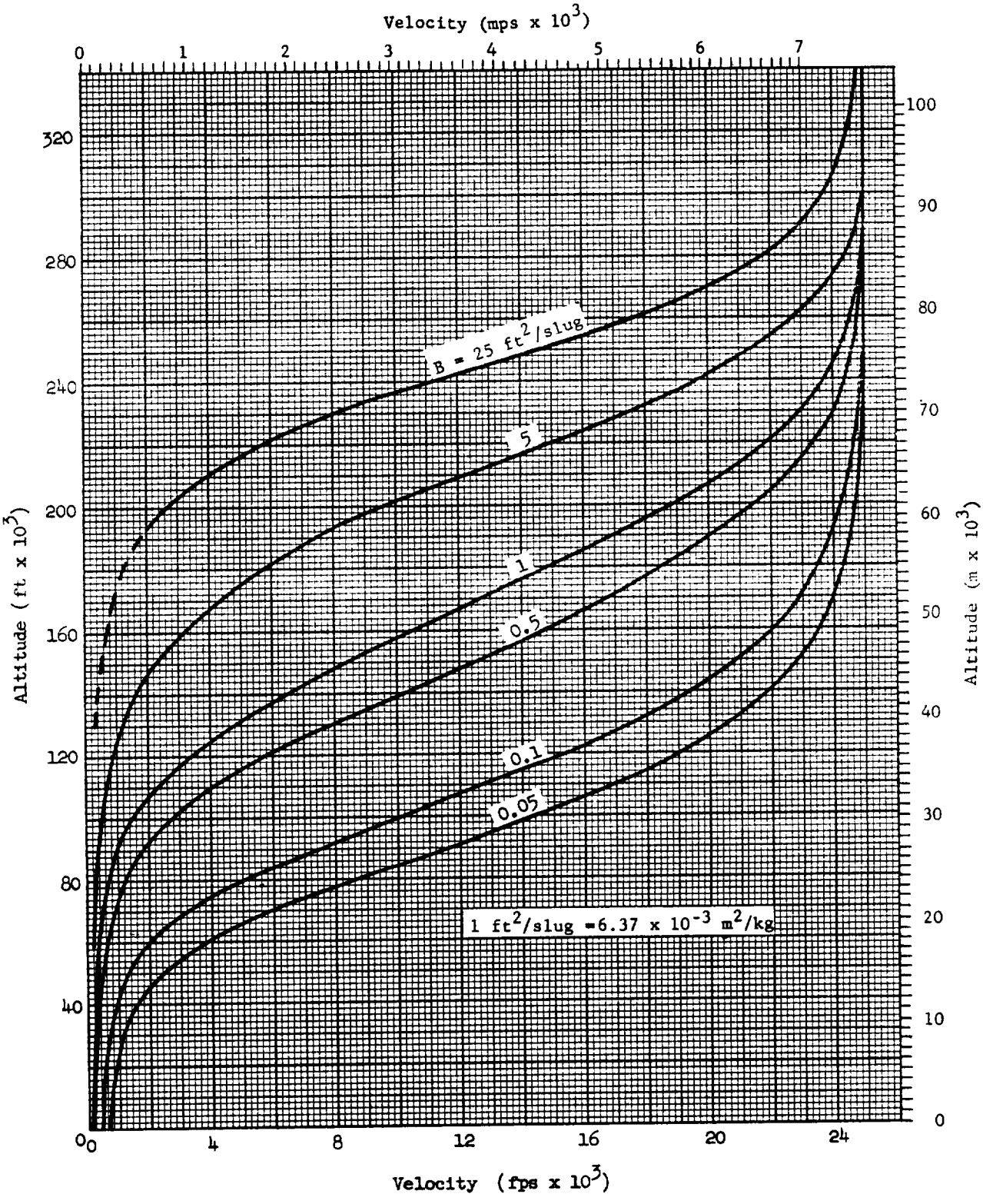

(b) $\gamma_0 = -2°$

Fig. 5. (continued)

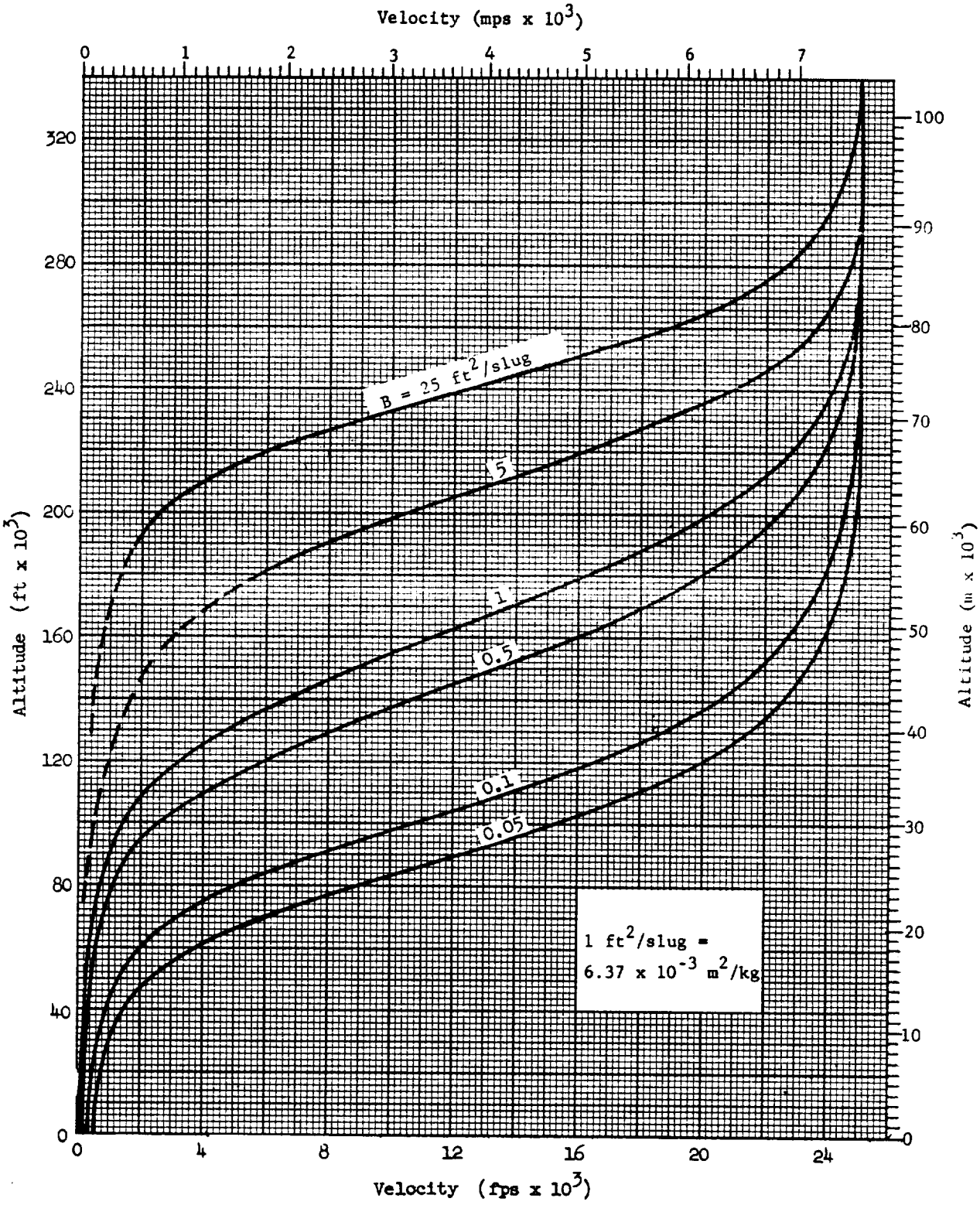

(c) $\gamma_0 = -3°$

Fig. 5. (continued)

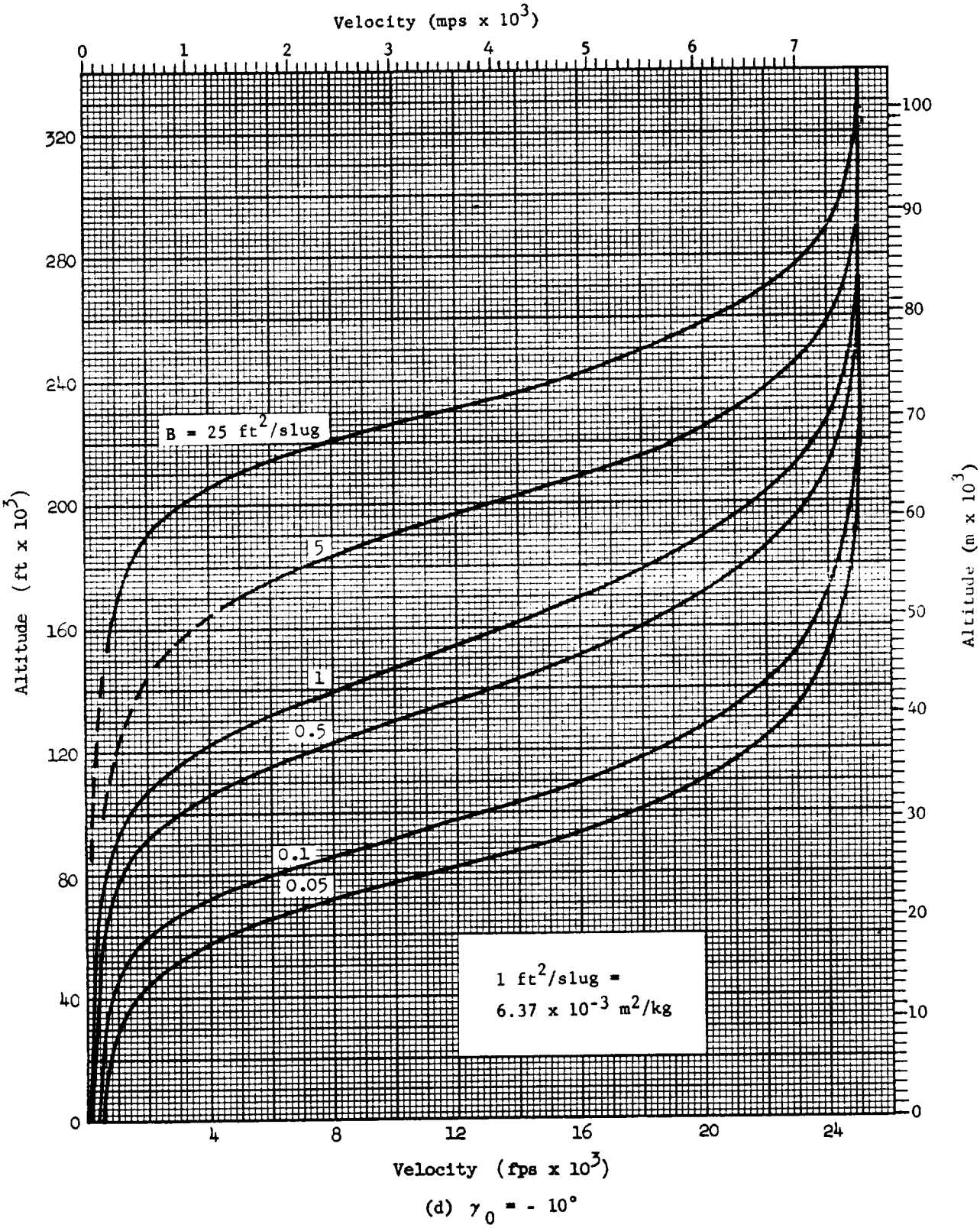

(d) γ_0 = - 10°

Fig. 5. (continued)

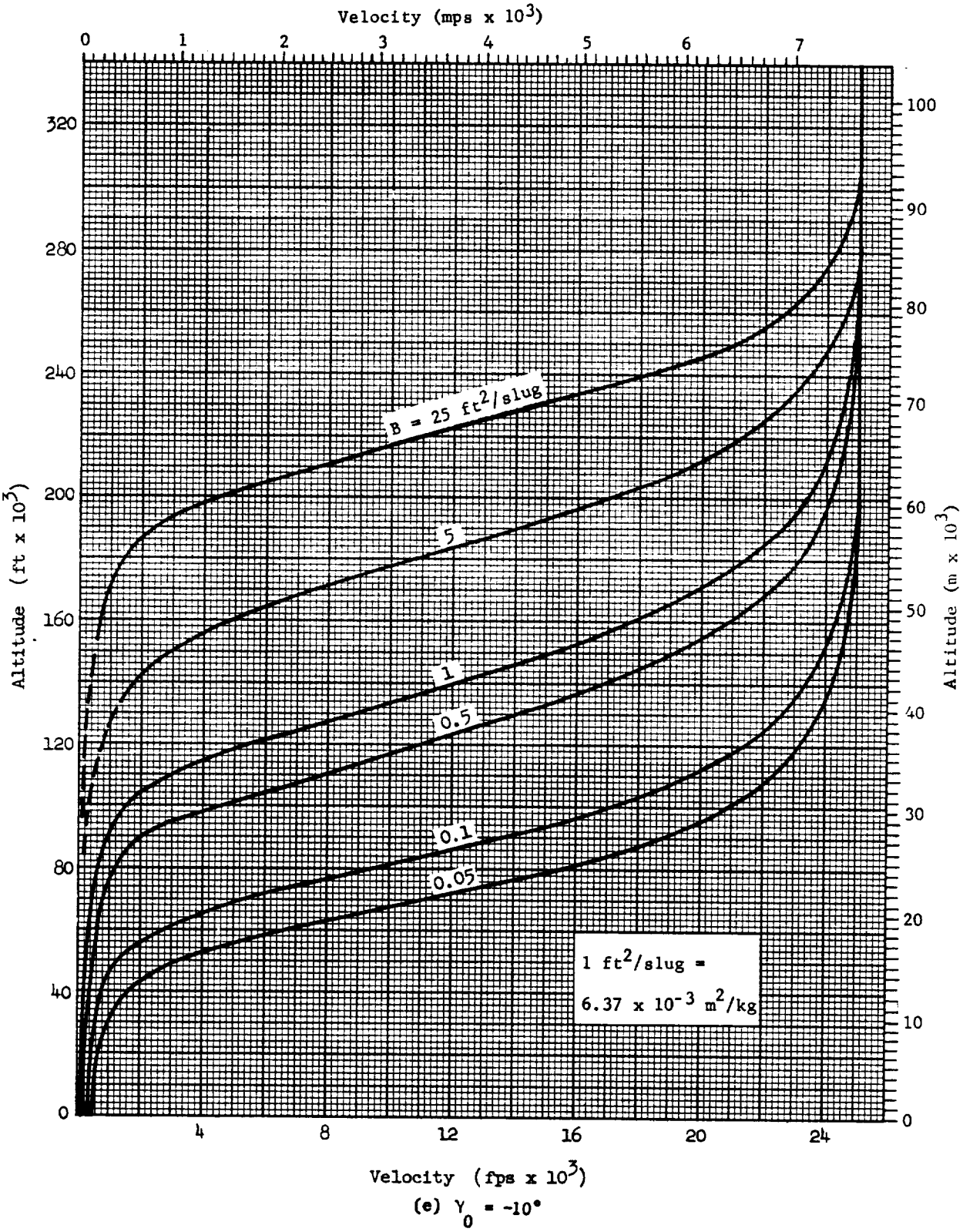

(e) $\gamma_0 = -10°$

Fig. 5. (continued)

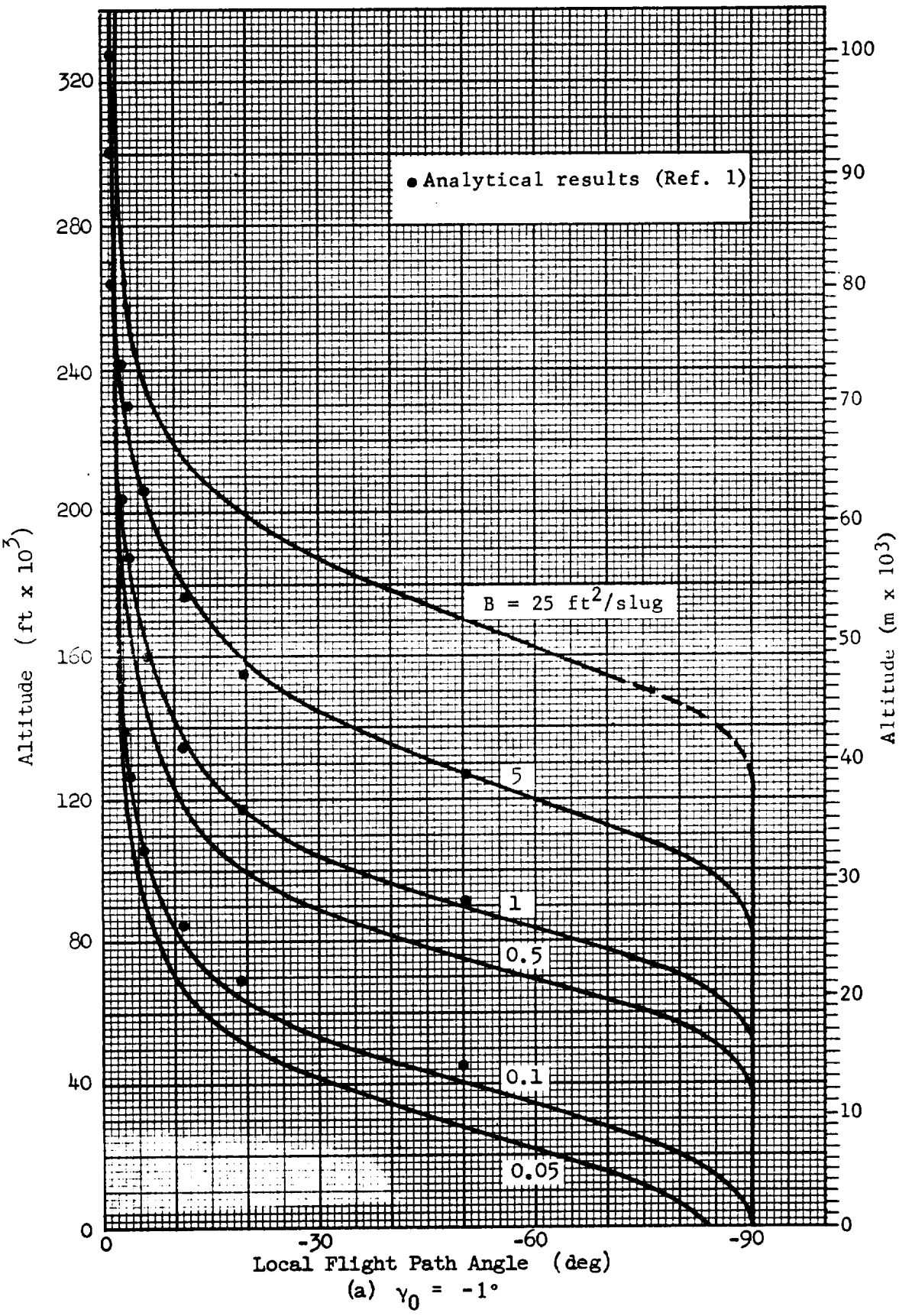

Fig. 6. Flight Path Angle Variation with Altitude (h_0 = 300,000 ft = 91,440 m; v_0 = 25,000 fps = 7620 mps)

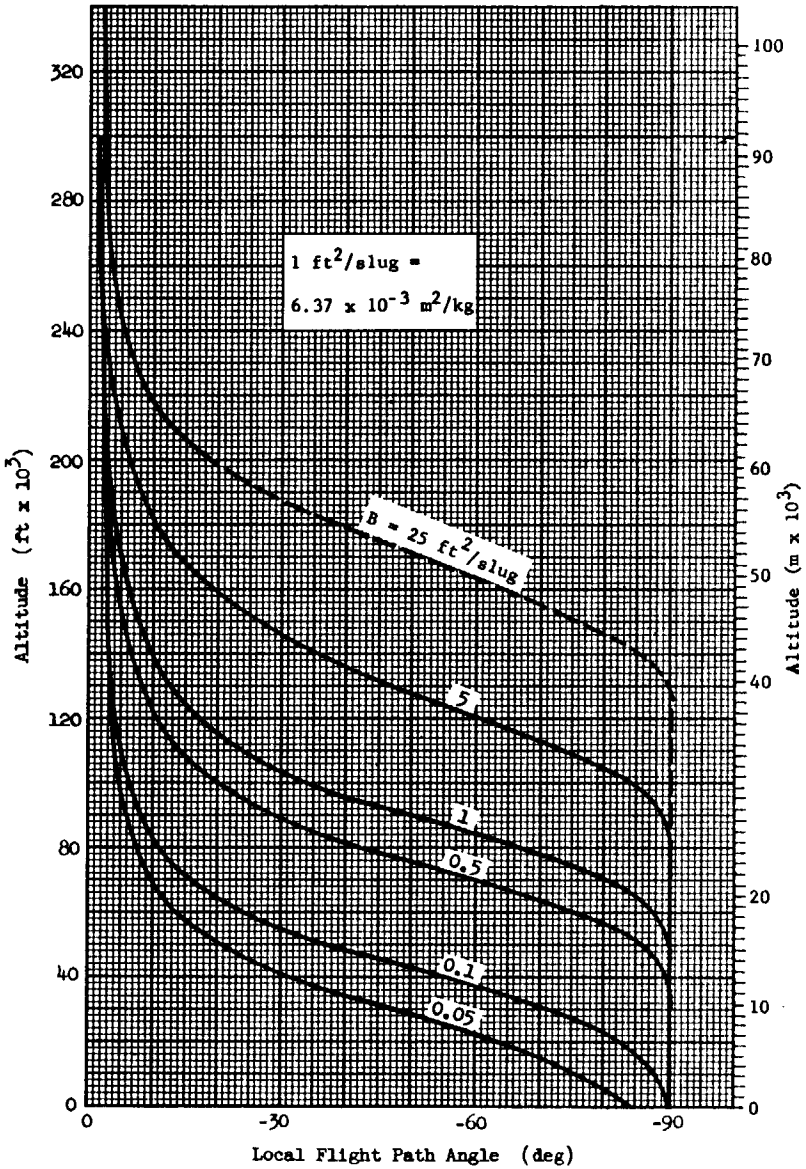

(b) $\gamma_0 = -2°$

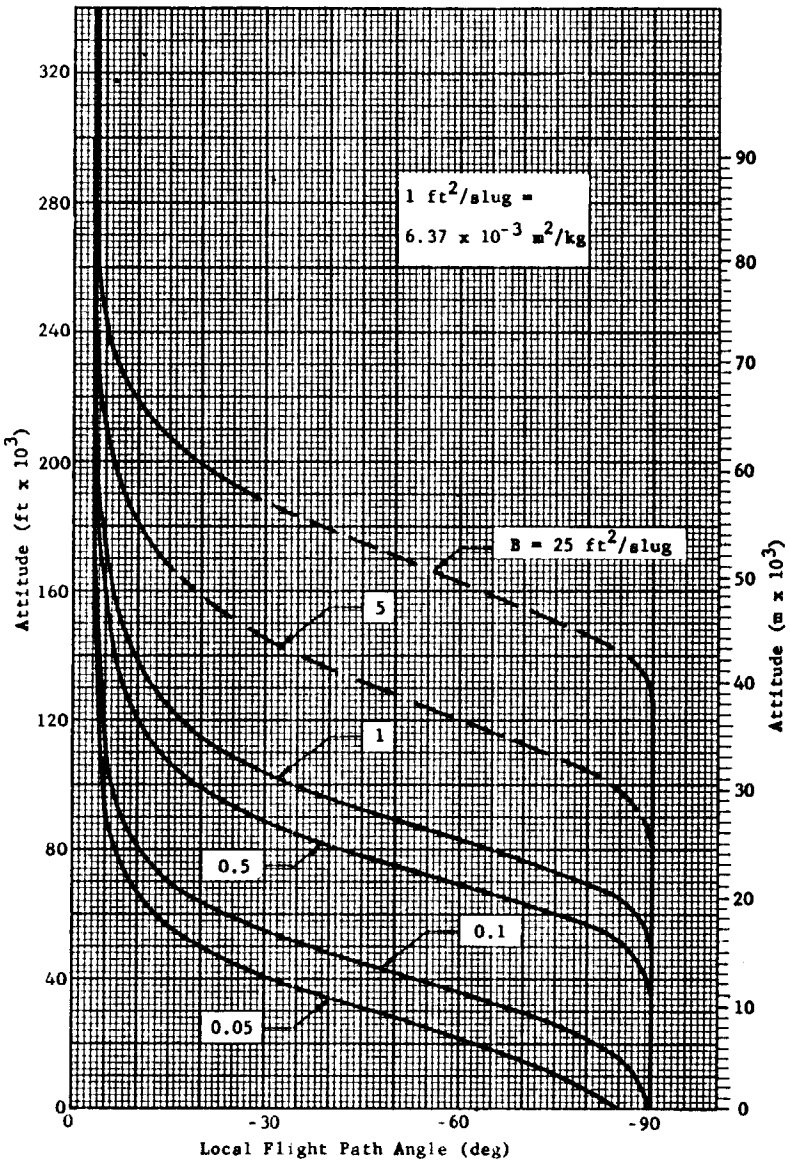

(c) $\gamma_0 = -3°$

Fig. 6. (continued)

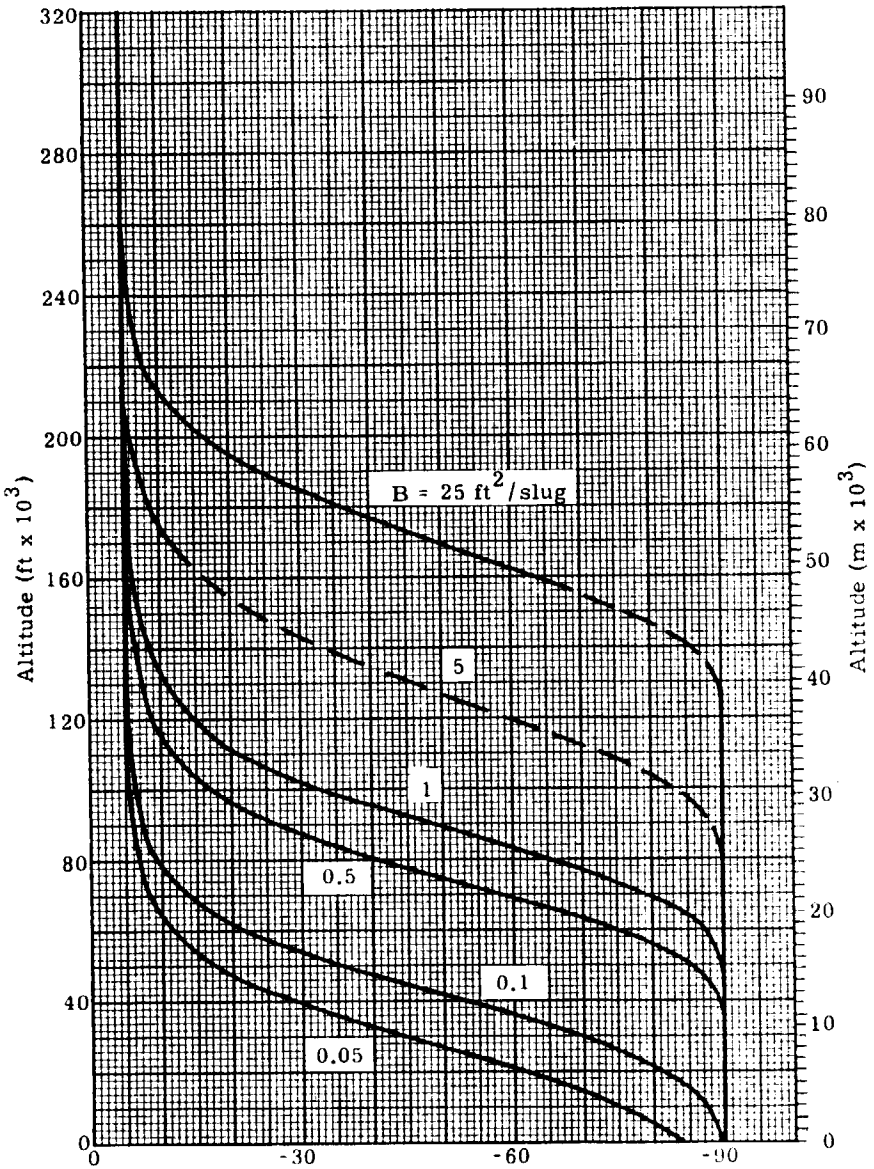

(d) $\gamma_0 = -5°$

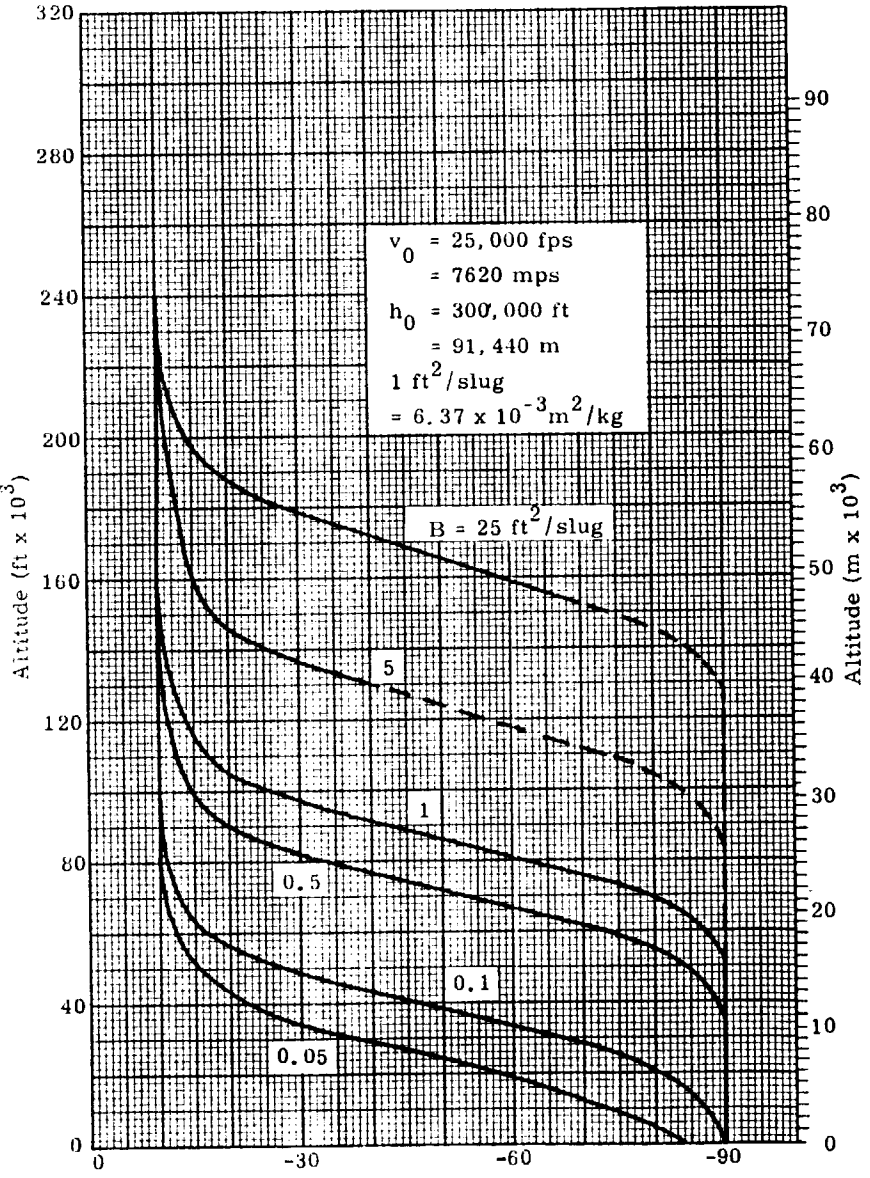

(e) $\gamma_0 = -10°$

Fig. 6. (continued)

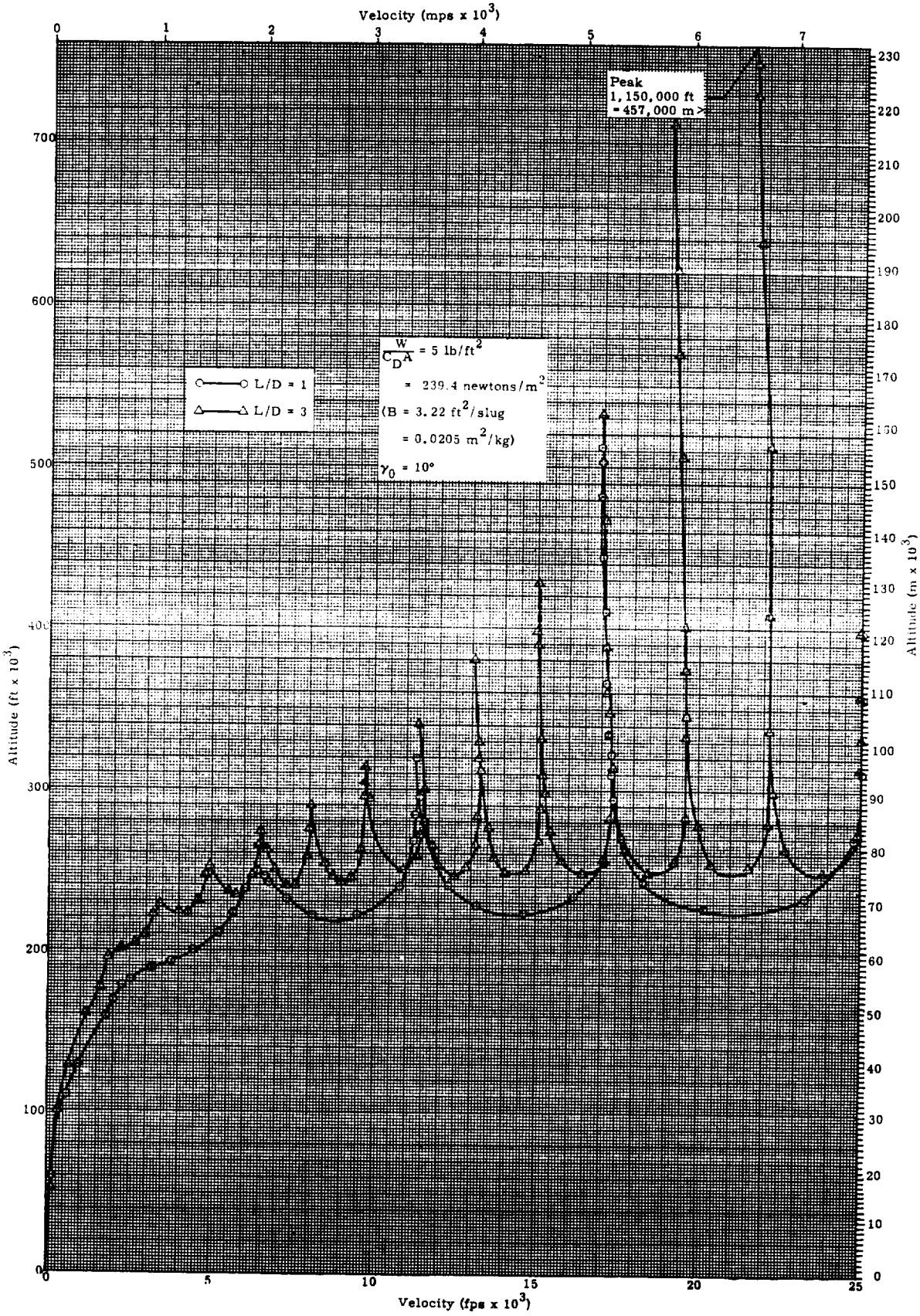

Fig. 7. Characteristic Re-Entry Altitude-Velocity Profiles for Lifting Vehicles

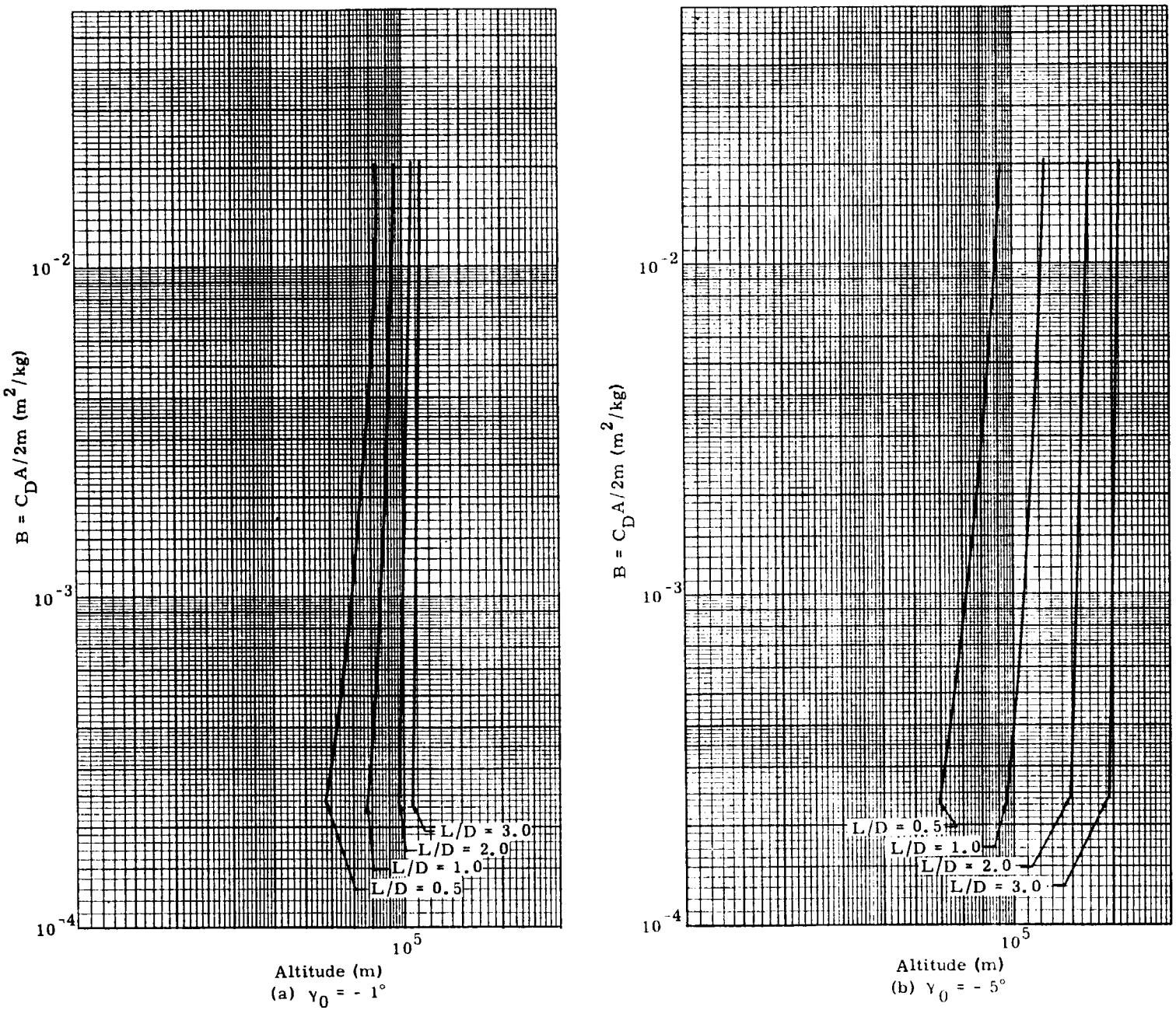

Fig. 8. Altitude Peak of First Skip (v_0 = 25000 fps = 7,620 mps, h_0 = 400,000 ft = 122,000 m)

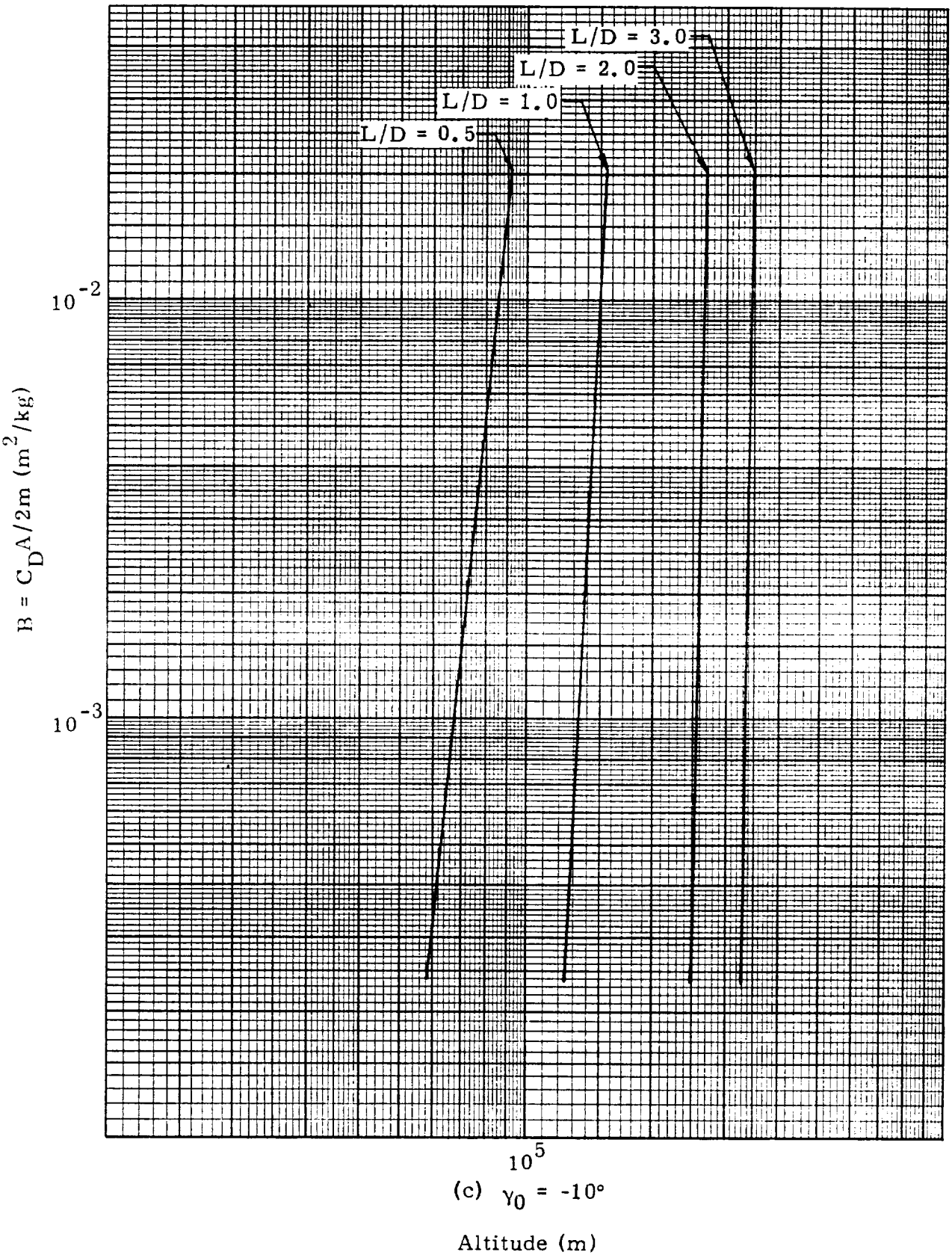

Fig. 8. (continued)

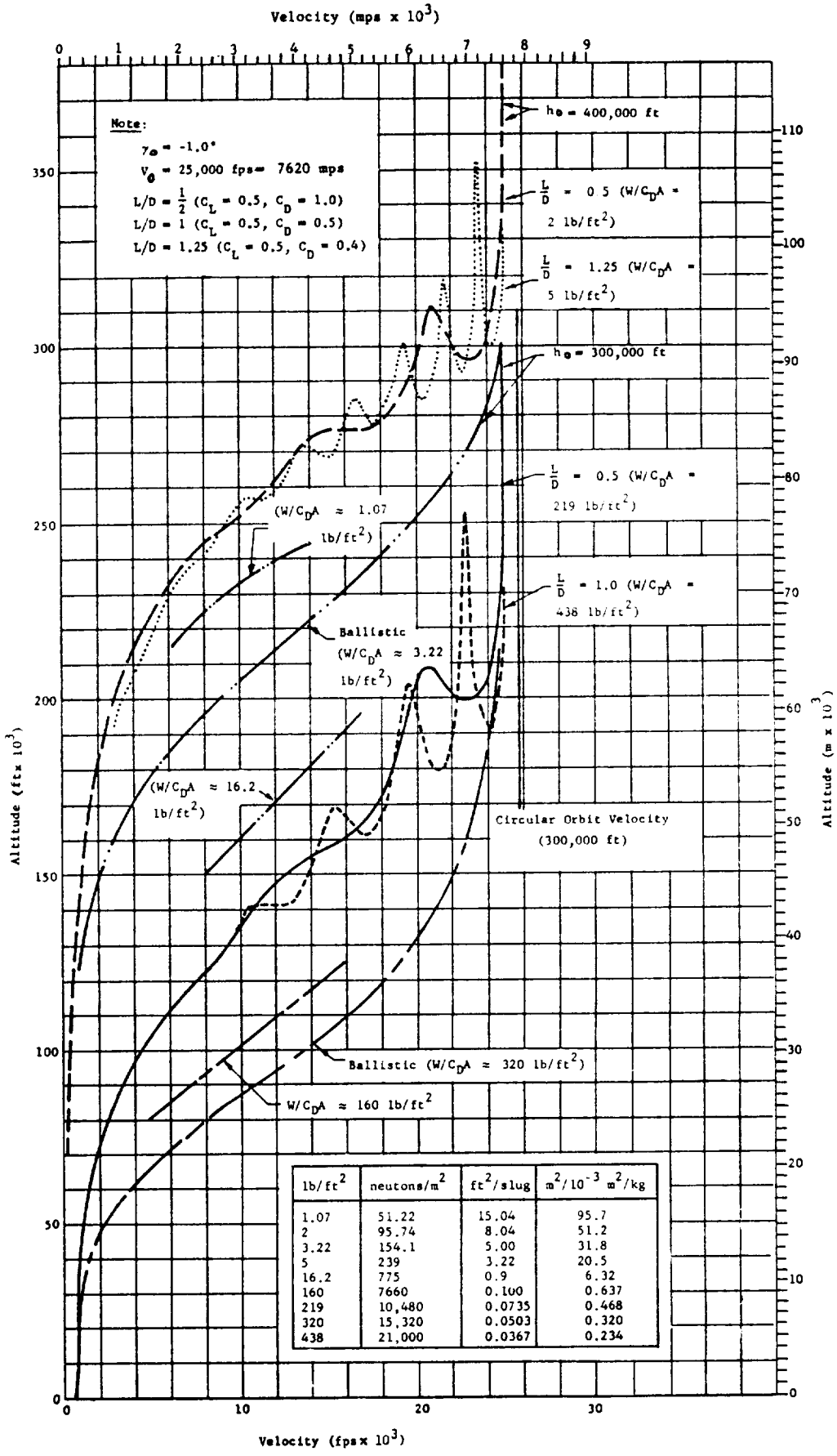

lb/ft^2	neutons/m^2	ft^2/slug	m^2/10^{-3} m^2/kg
1.07	51.22	15.04	95.7
2	95.74	8.04	51.2
3.22	154.1	5.00	31.8
5	239	3.22	20.5
16.2	775	0.9	6.32
160	7660	0.100	0.637
219	10,480	0.0735	0.468
320	15,320	0.0503	0.320
438	21,000	0.0367	0.234

Fig. 9a. Entry Vehicle Comparison, Velocity-Altitude Profile

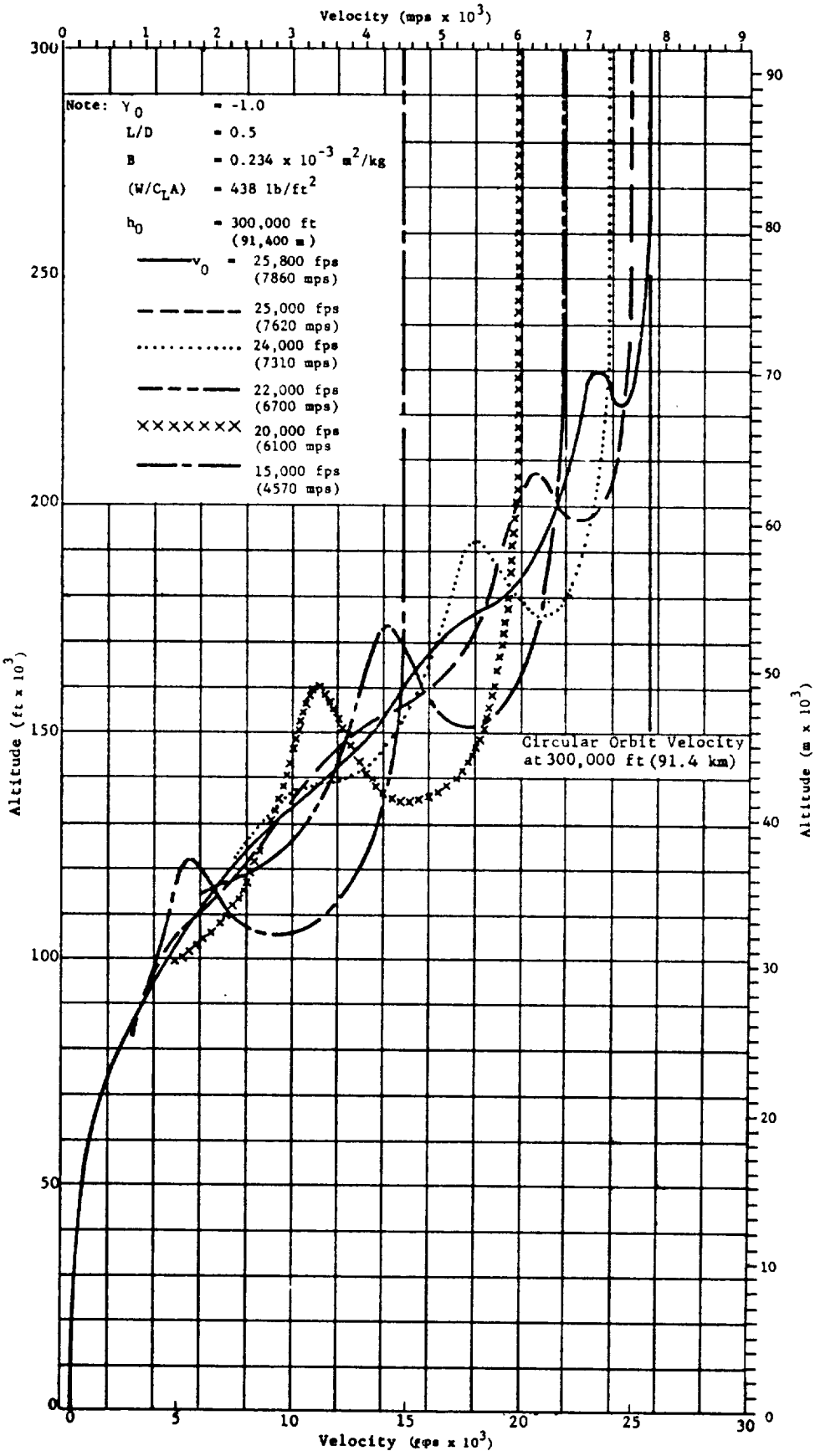

Fig. 9b. Effect of Entry Velocity on Altitude-Velocity Profile

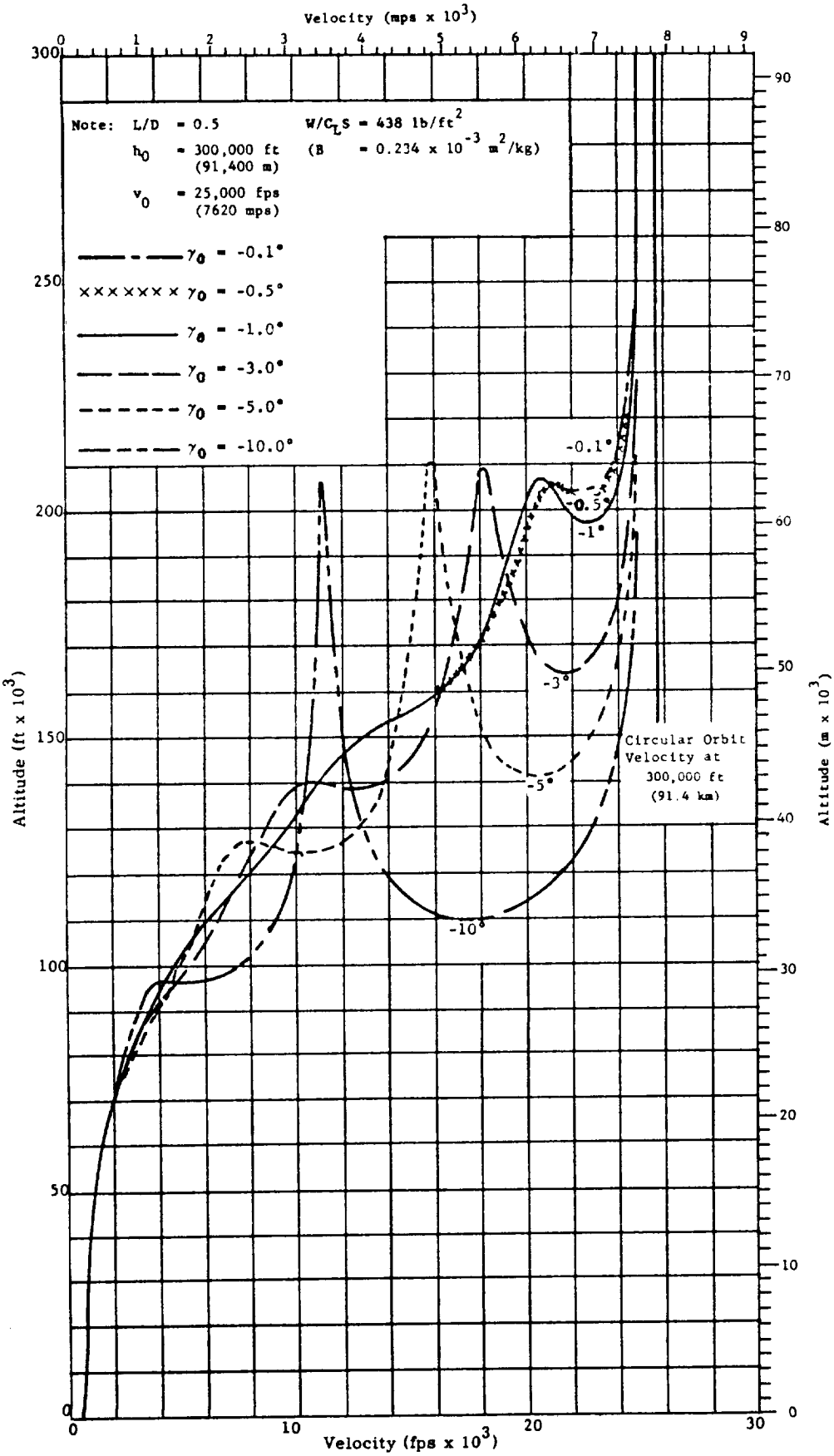

Fig. 9c. Effect of Entry Angle on Velocity-Altitude Profiles

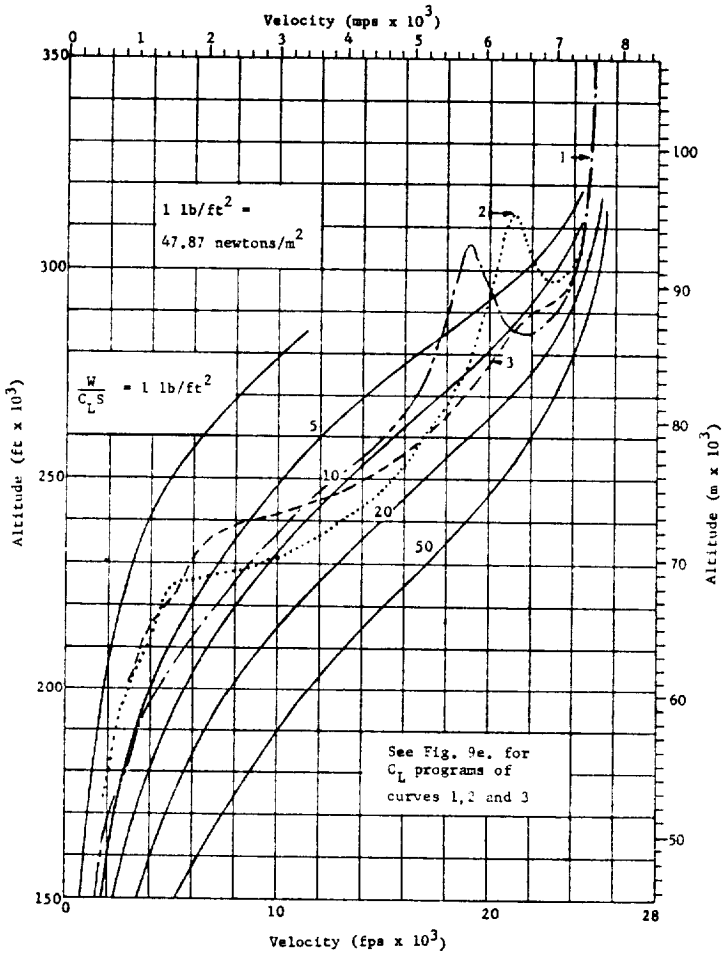

Fig. 9d. Effect of Programmed C_L on Velocity-Altitude Profile

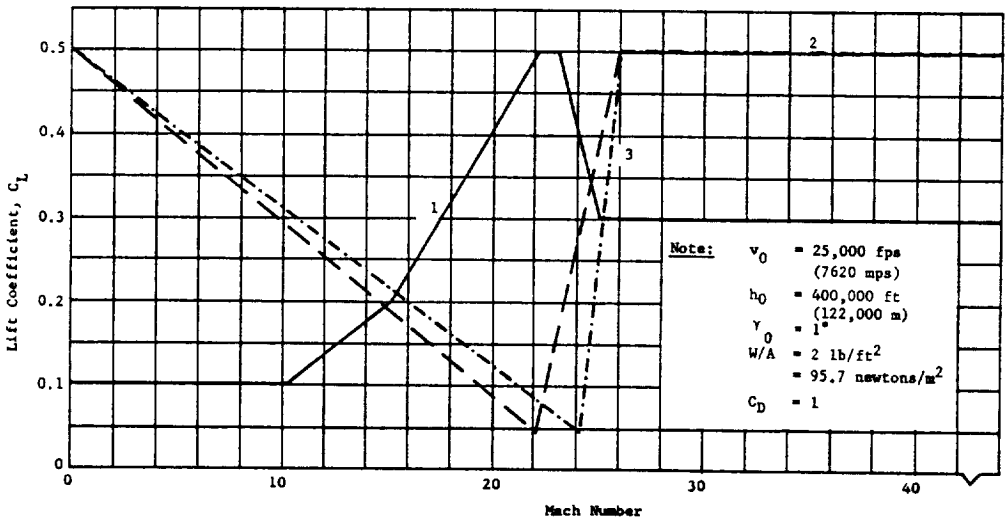

Fig. 9e. Program of C_L with Mach Number

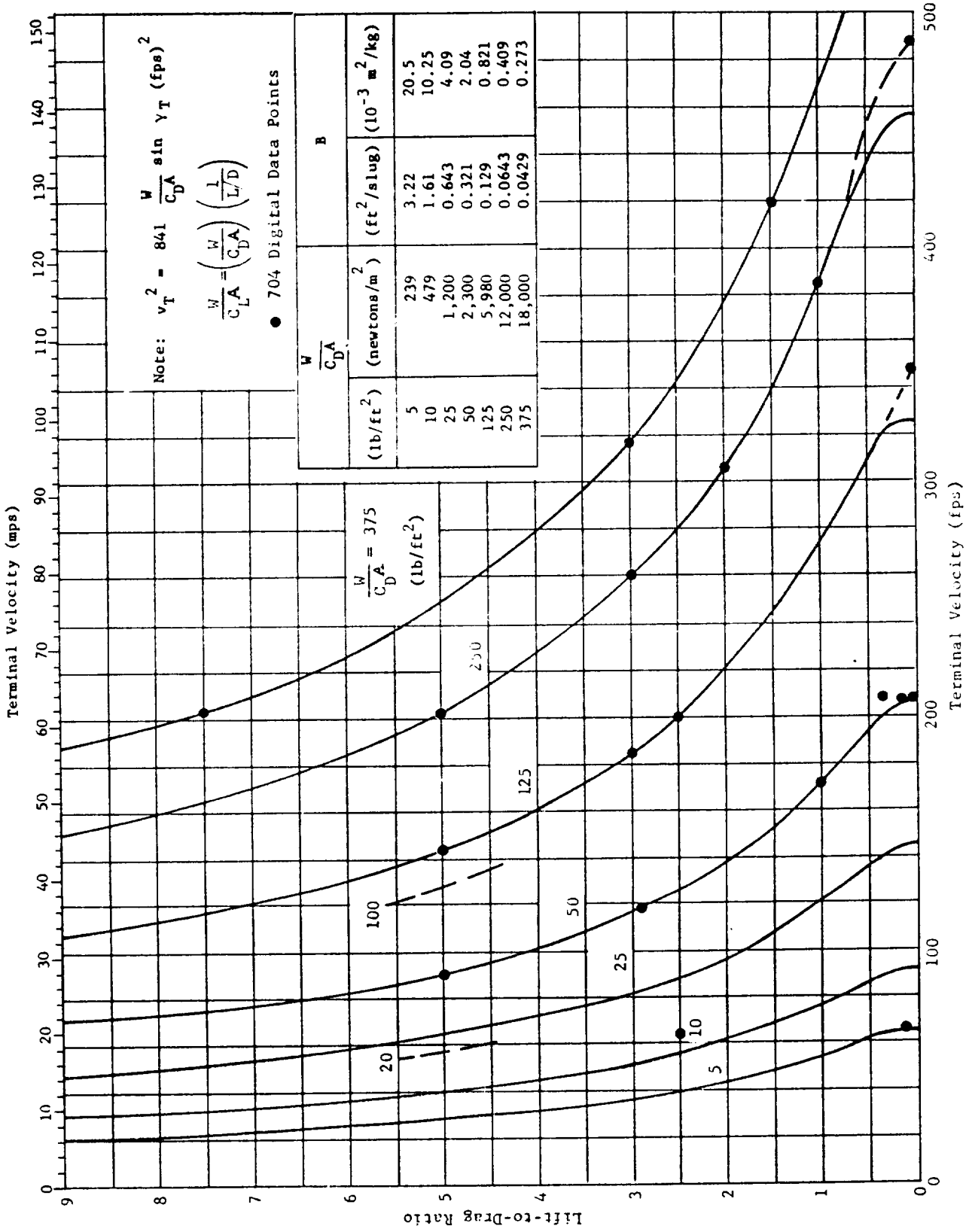

Fig. 10a. Terminal Velocity

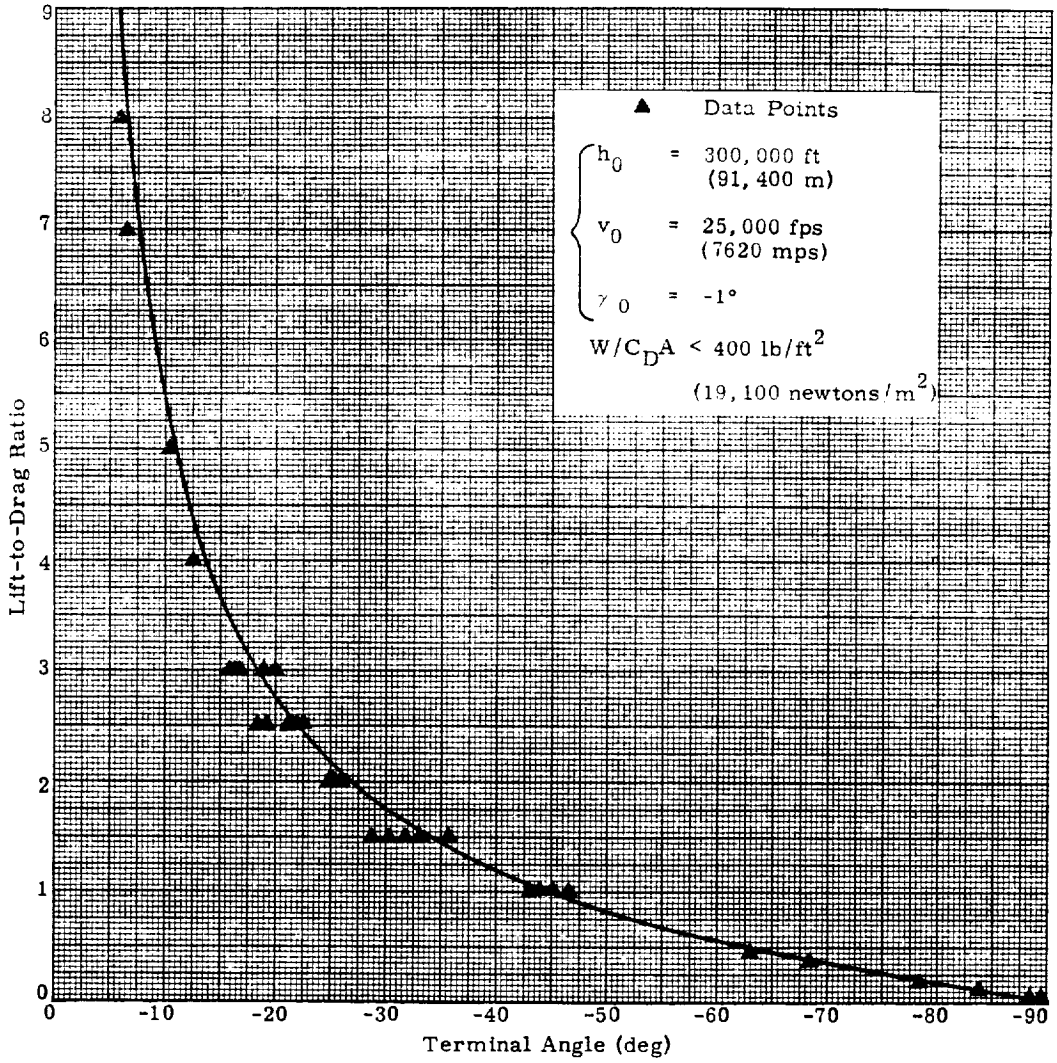

Fig. 10b. Terminal Flight Path Angle

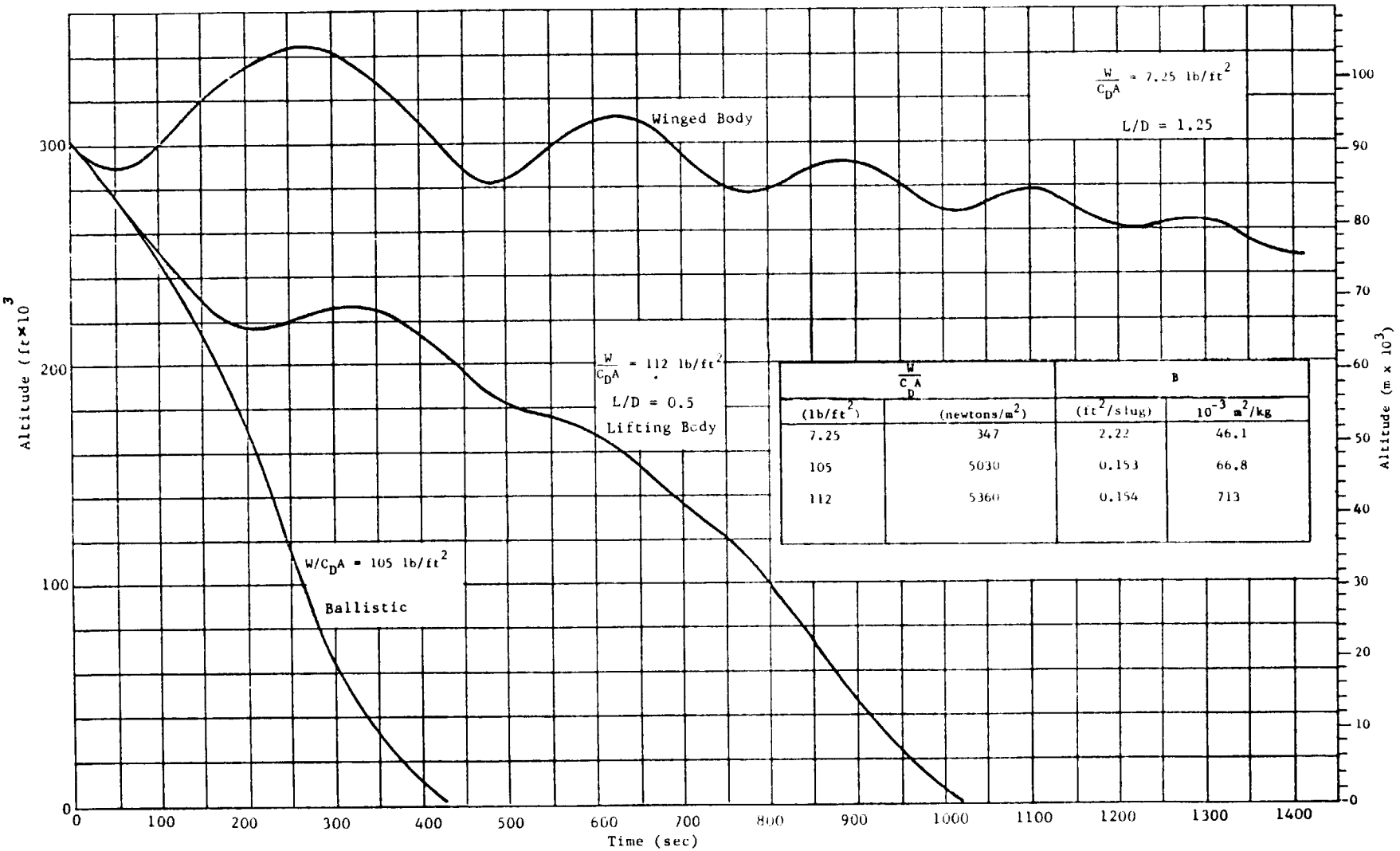

$\frac{W}{C_D A}$		B	
(lb/ft^2)	(newtons/m^2)	(ft^2/slug)	10^{-3} m^2/kg
7.25	347	2.22	46.1
105	5030	0.153	66.8
112	5360	0.154	713

Fig. 11a. Entry Vehicle Comparison, Altitude-Time History

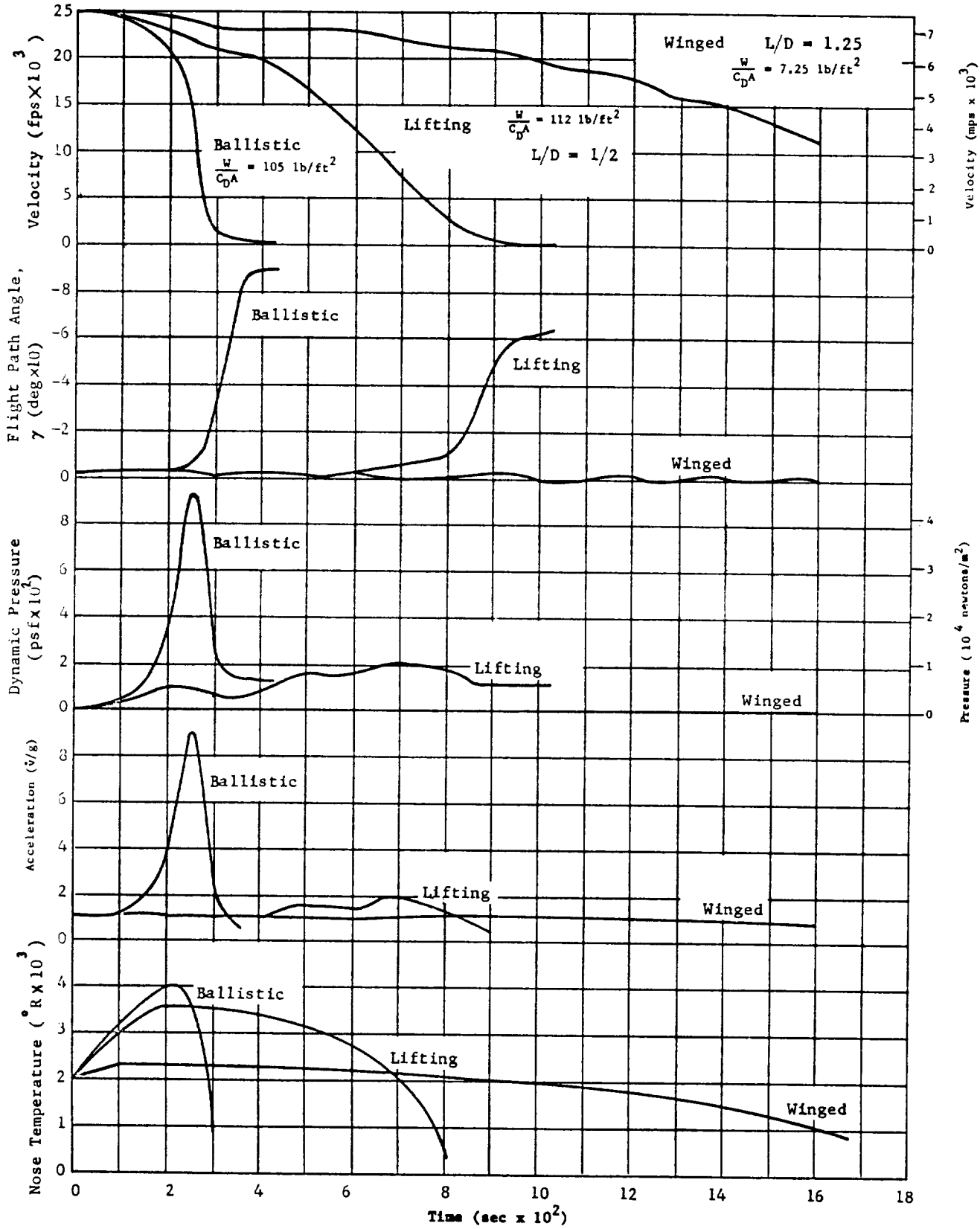

Fig. 11b. Re-entry Vehicle Comparison--Time History

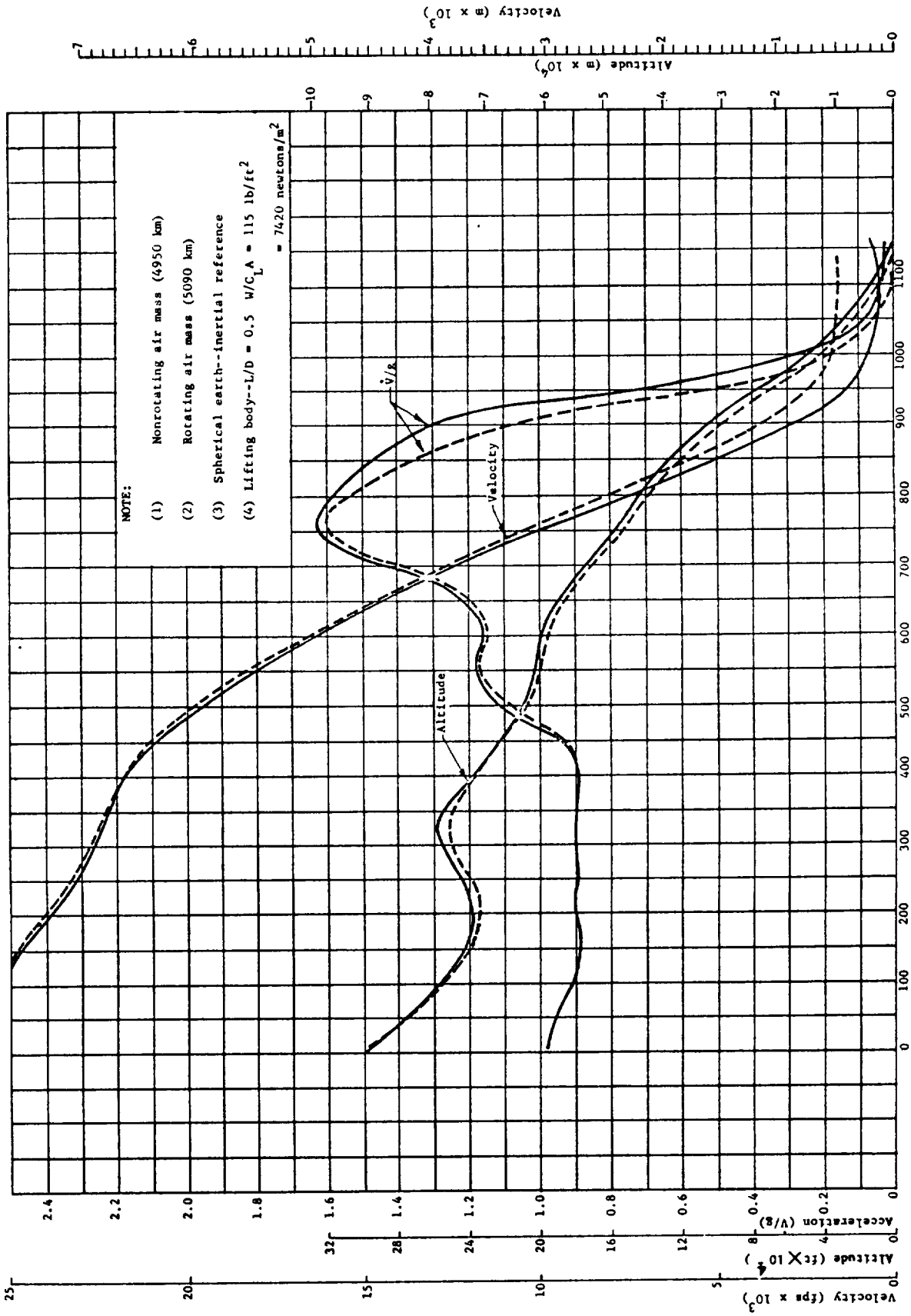

Fig. 11c. Re-Entry History with and Without Rotating Air Mass

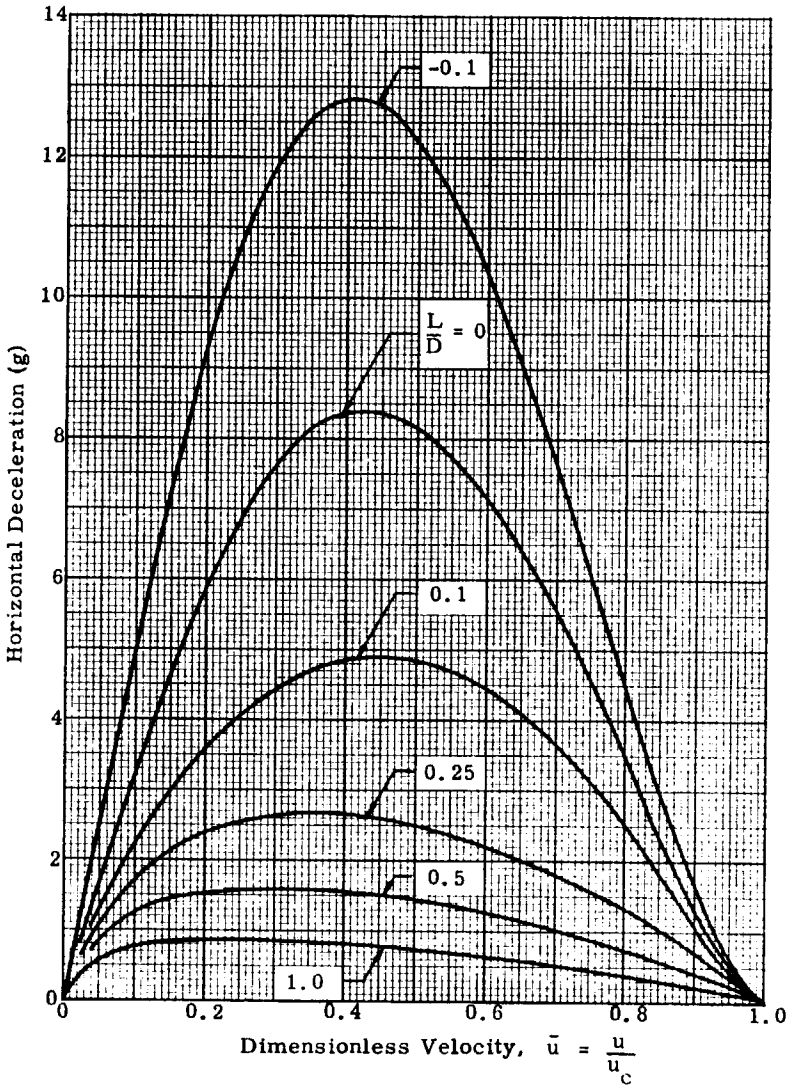

Fig. 12a. Effect of Lift-Drag Ratio on Deceleration for Entry into Earth Atmosphere From Decaying Orbits (Ref. 1)

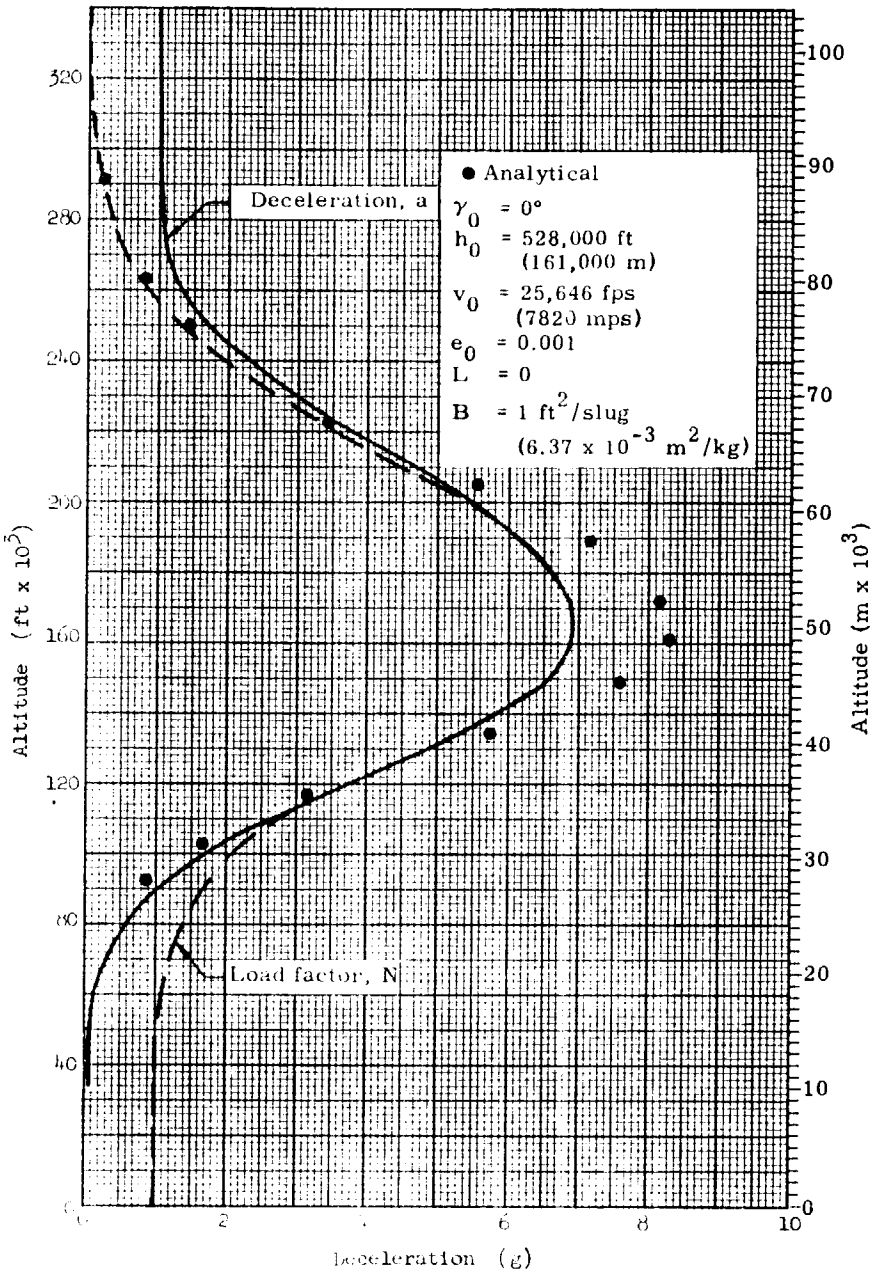

Fig. 12b. Decelleration Profile and Load Factor for Satellite Re-Entry

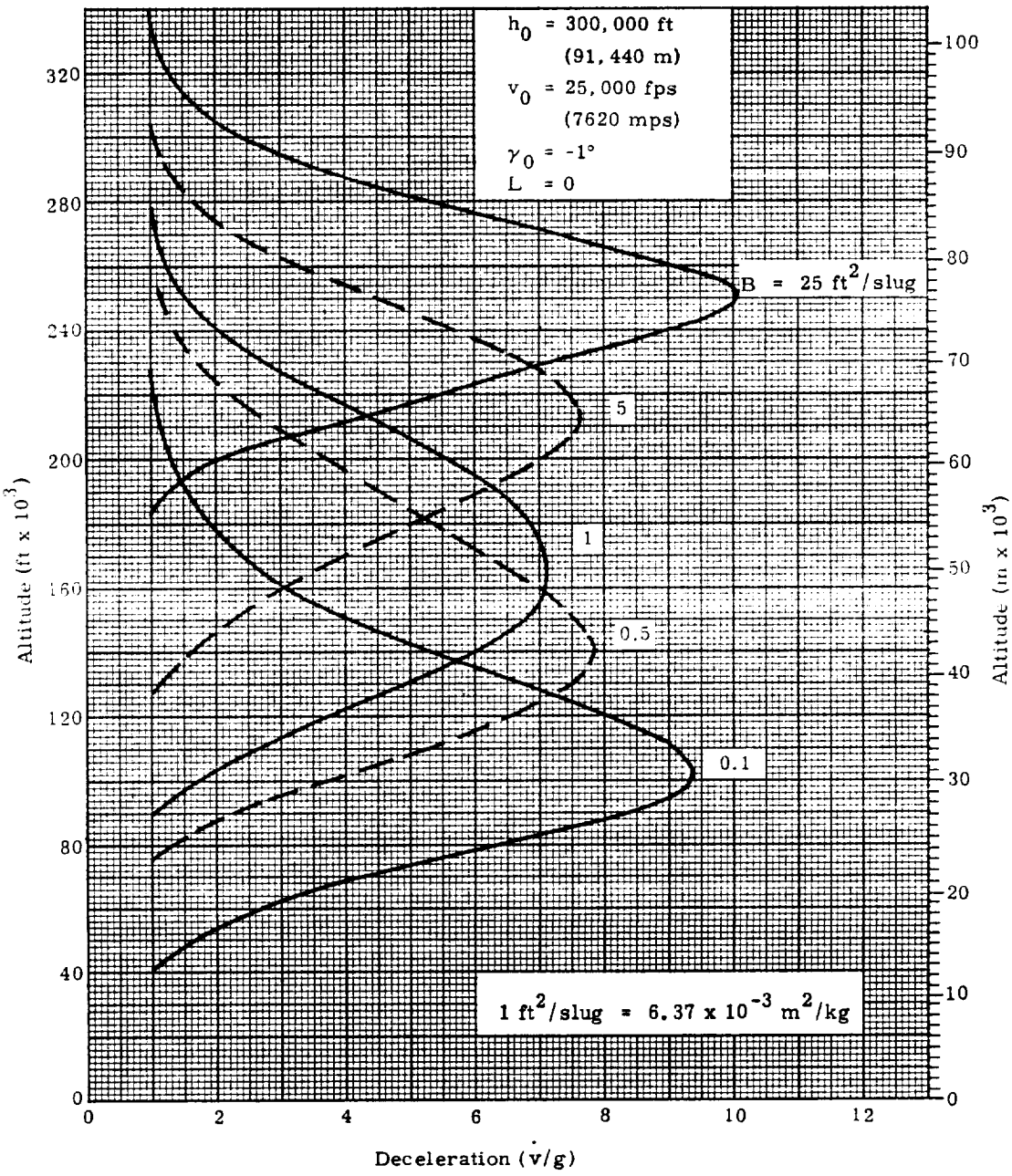

Fig. 12c. Deceleration Variation with Altitude for Satellite Re-Entry

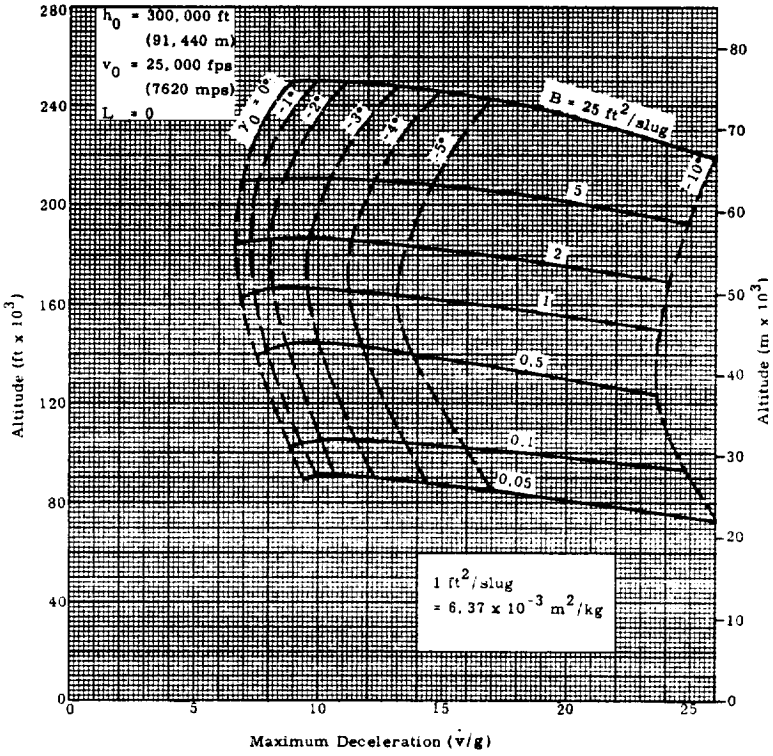

Fig. 13a. Maximum Decelerations for Ballistic Re-Entry

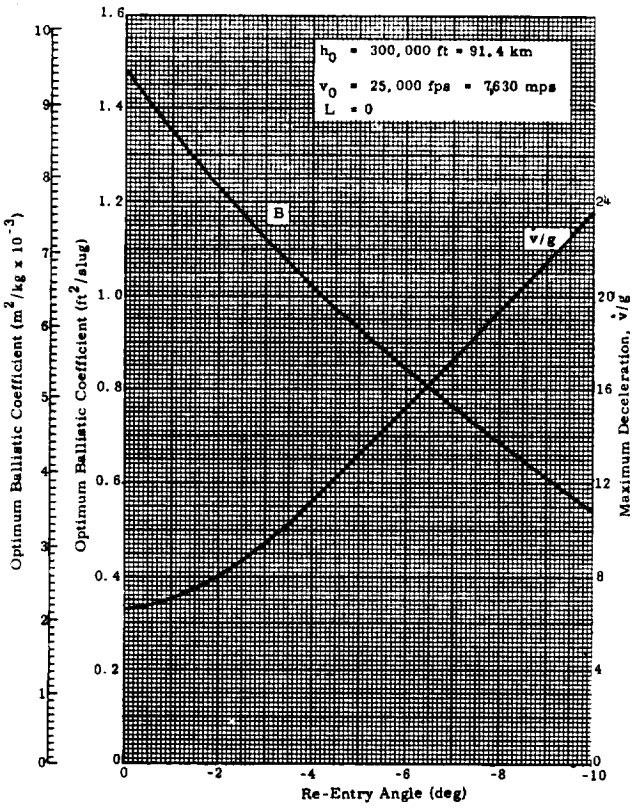

Fig. 13b. Optimum Ballistic Coefficients (to minimize re-entry decelerations)

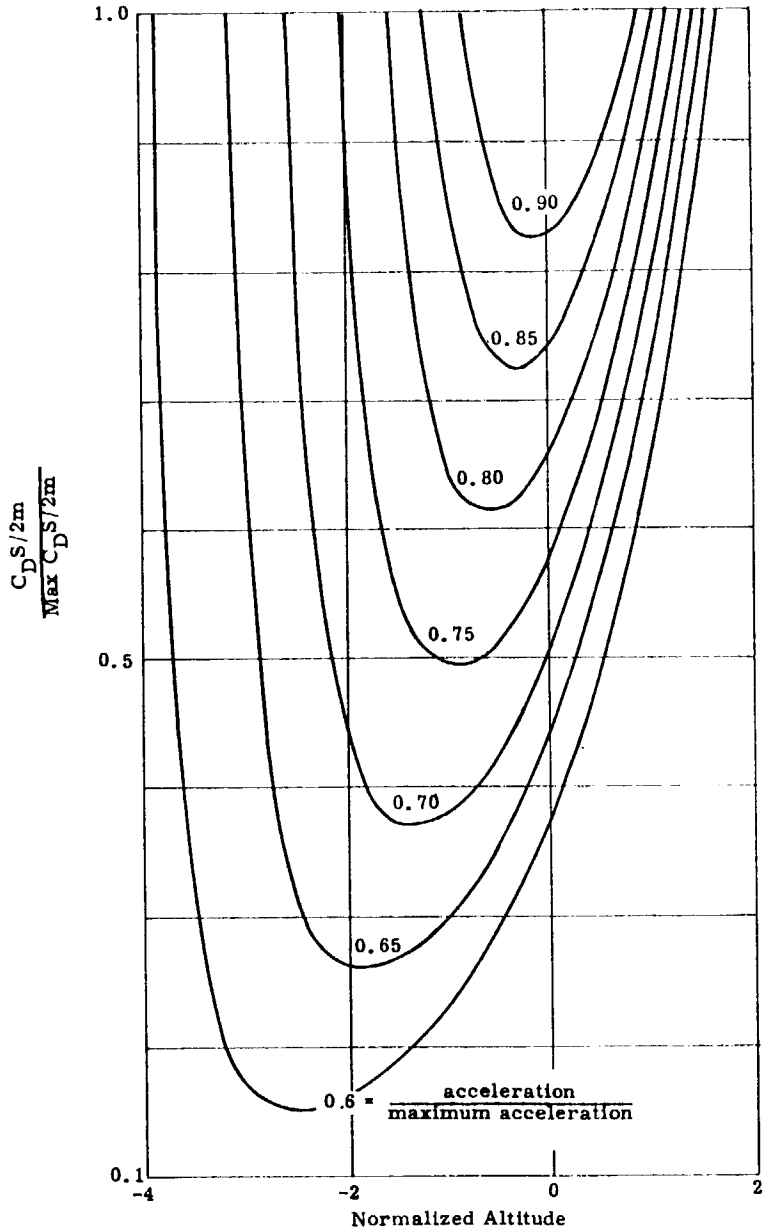

Fig. 14a. Controlled Descent, General Ballistic Coefficient Variation (Ref. 12)

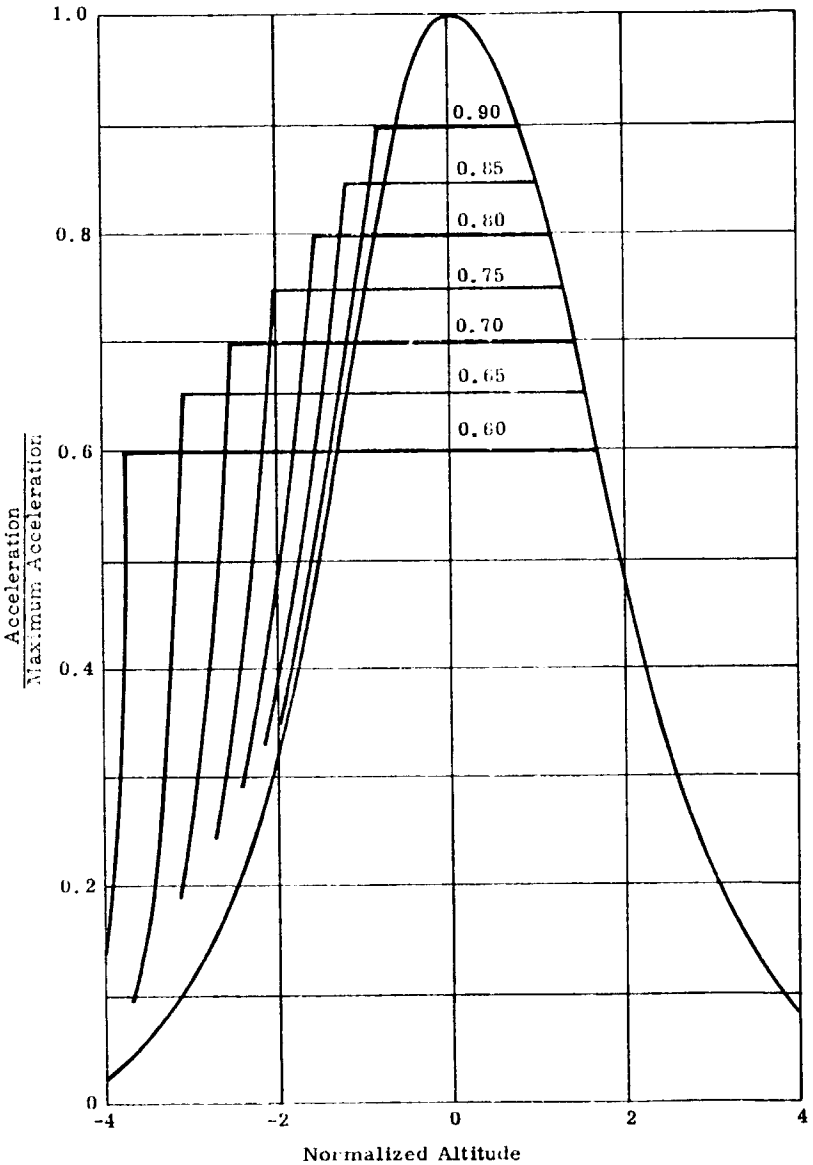

Fig. 14b. Controlled Descent, General Acceleration Profile

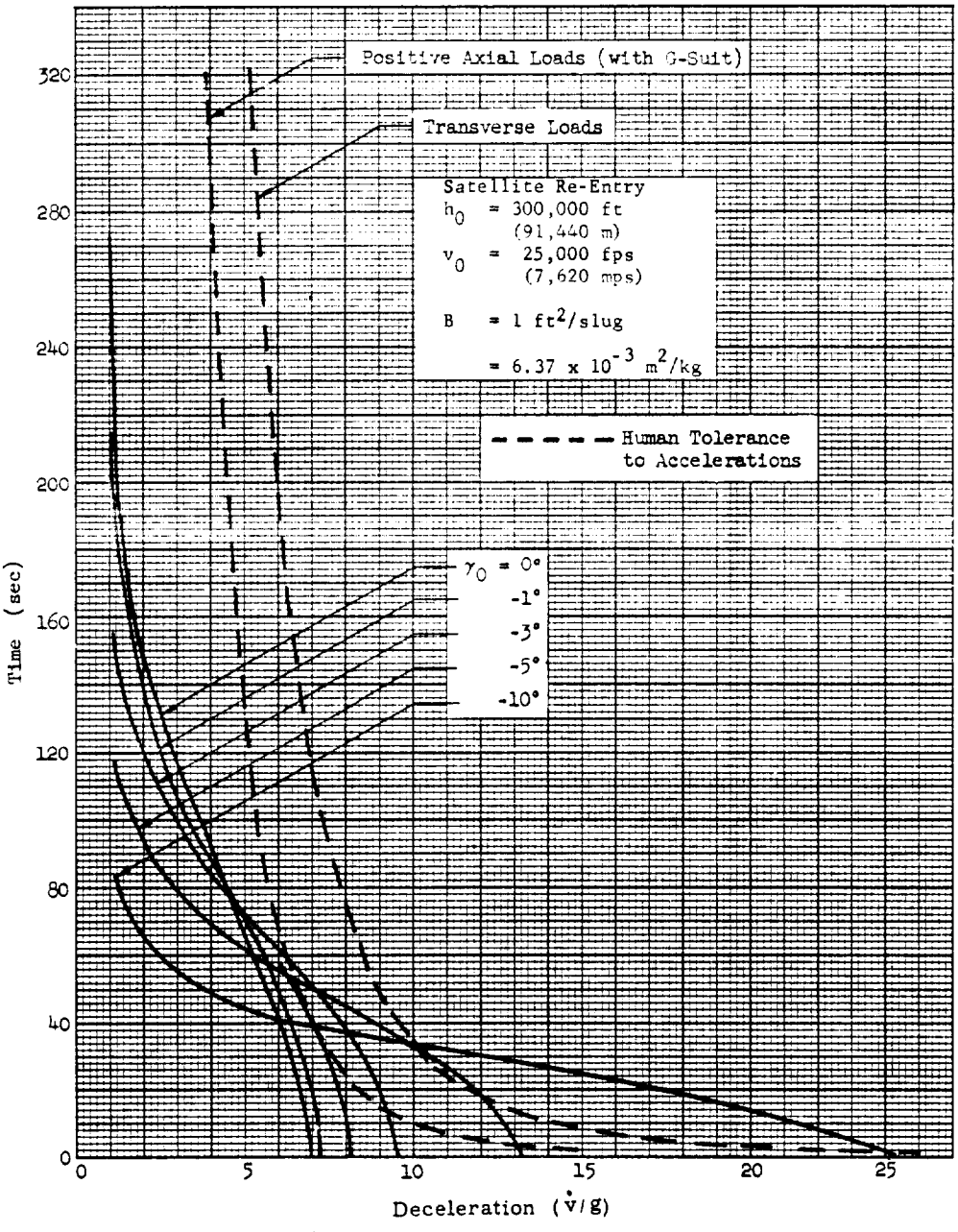

(a) Constant ballistic coefficient

Fig. 15. Length of Time Spent at Decelerations Equal to and Larger than the Shown Value

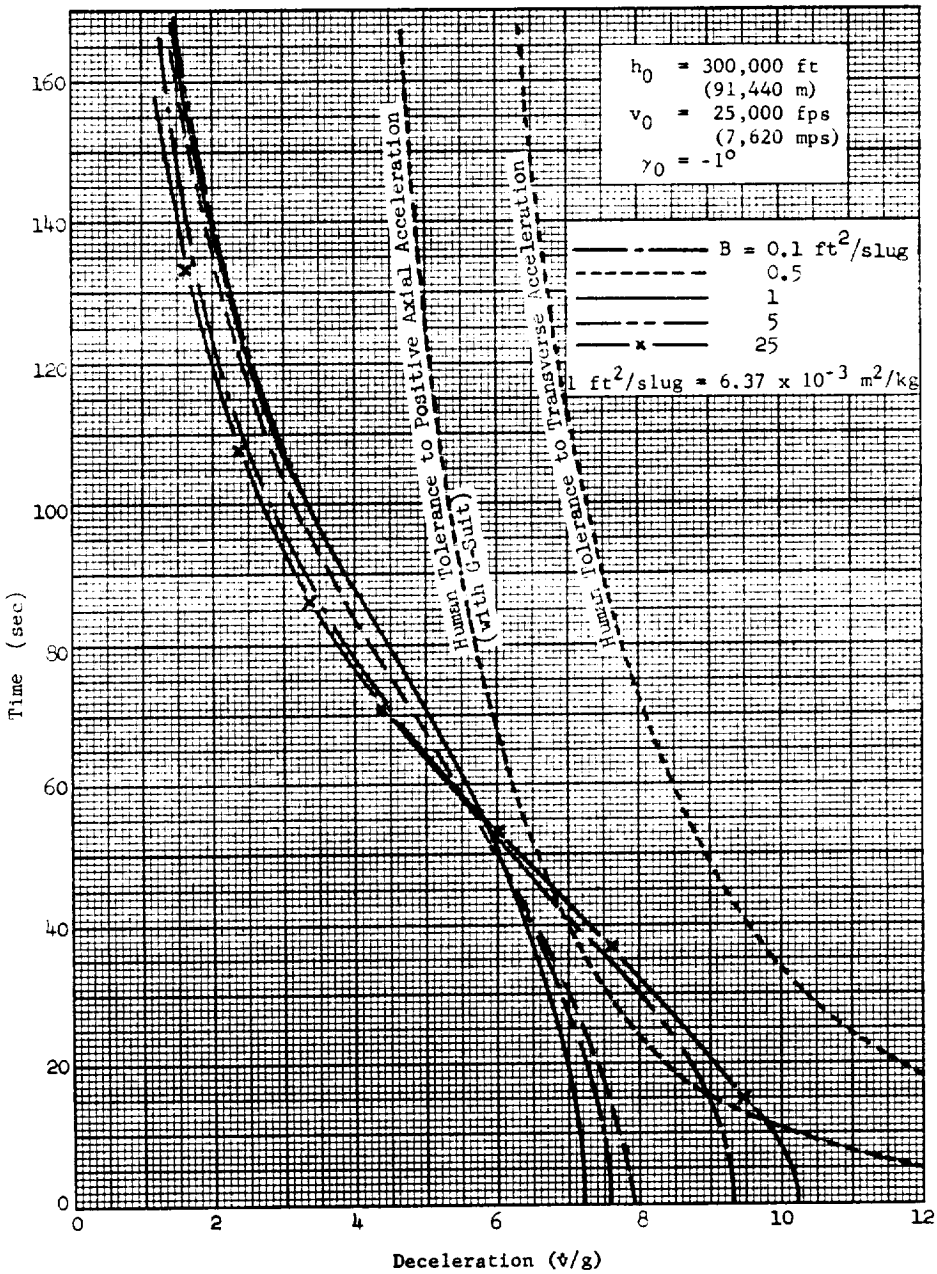

(b) Constant re-entry angle

Fig. 15. (continued)

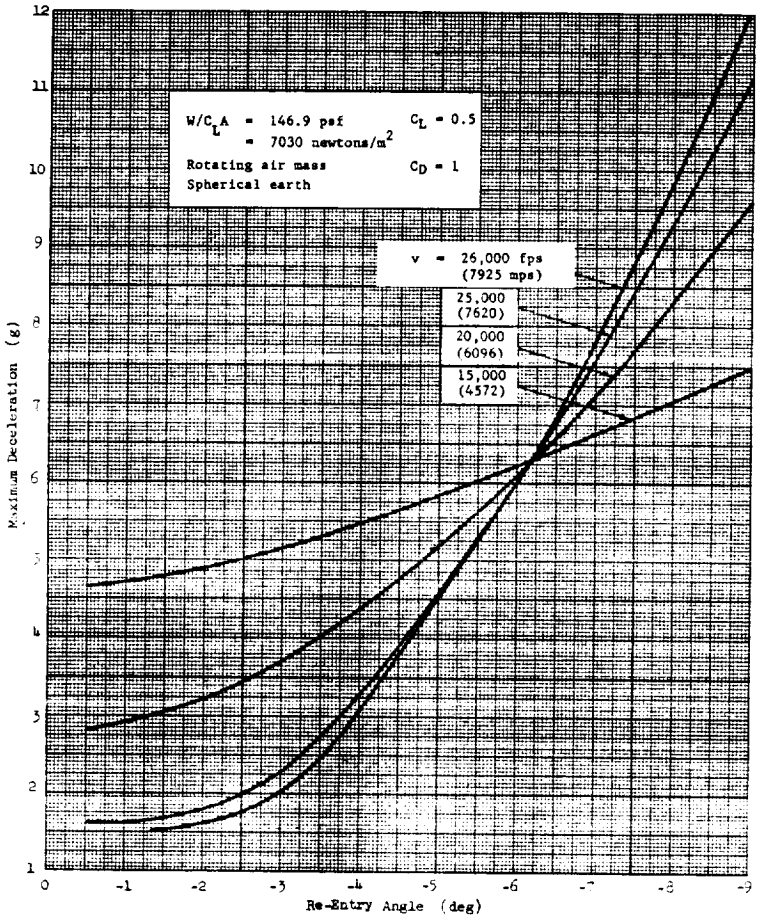

Fig. 16. Effect of Re-Entry Conditions on Maximum Total Decelerations (L/D = 0.5)

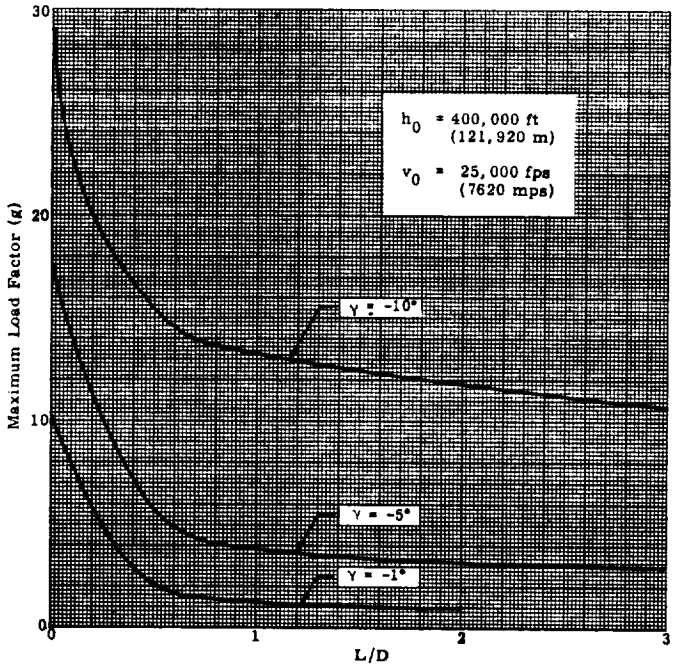

Fig. 17a. Maximum Load Factor Versus L/D (W/C_DA = 438 psf or B = 0.234 x 10^{-3} m^2/kg)

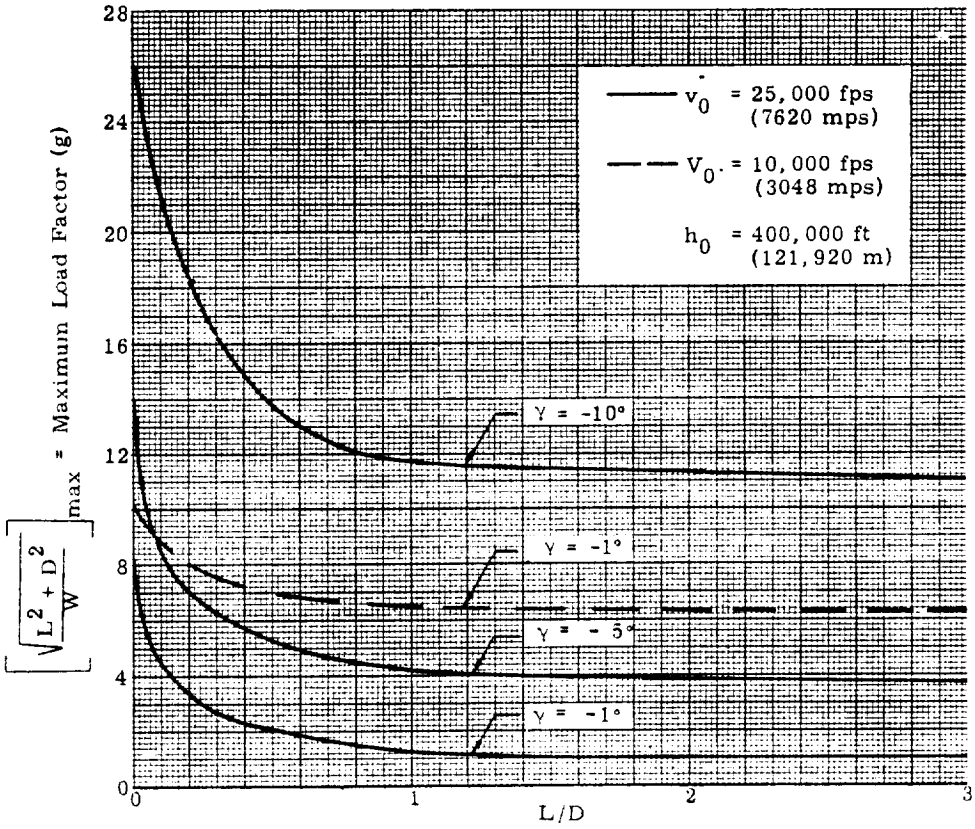

Fig. 17b. Maximum Load Factor Versus L/D (W/C_DA = 50 psf or B = 2.04 x 10^{-3} m^2/kg)

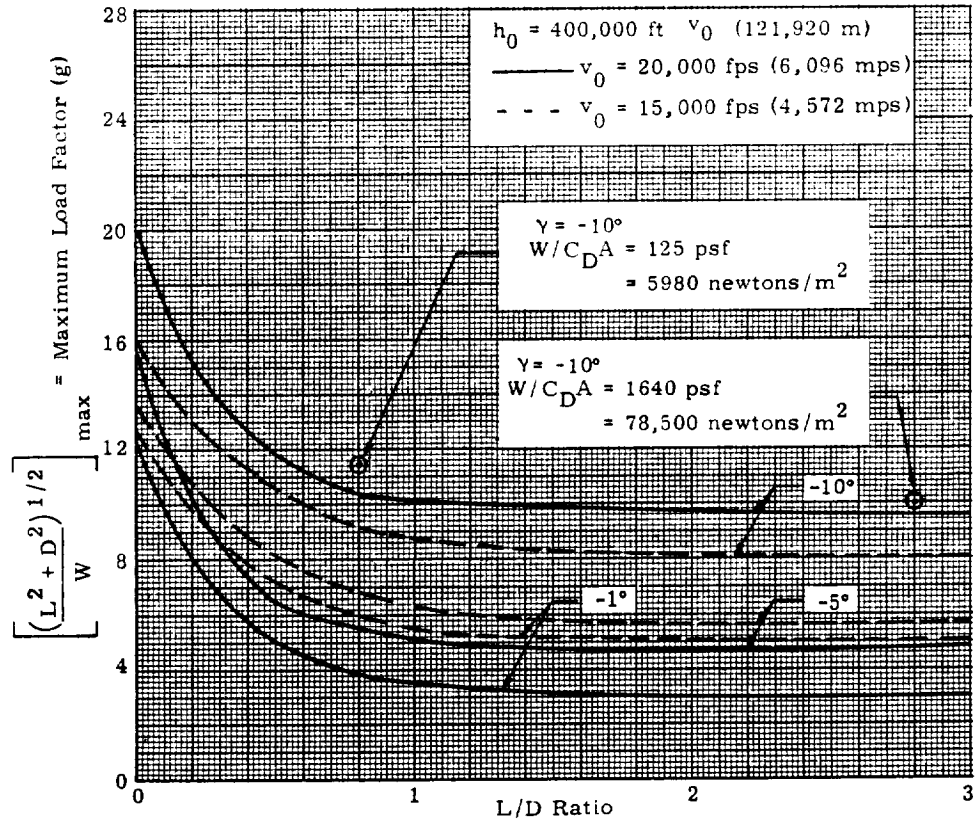

Fig. 17c. Maximum Total Acceleration Versus L/D Ratio (W/C_DA = 50 psf or B = 2.04 x 10^{-3} m^2/kg)

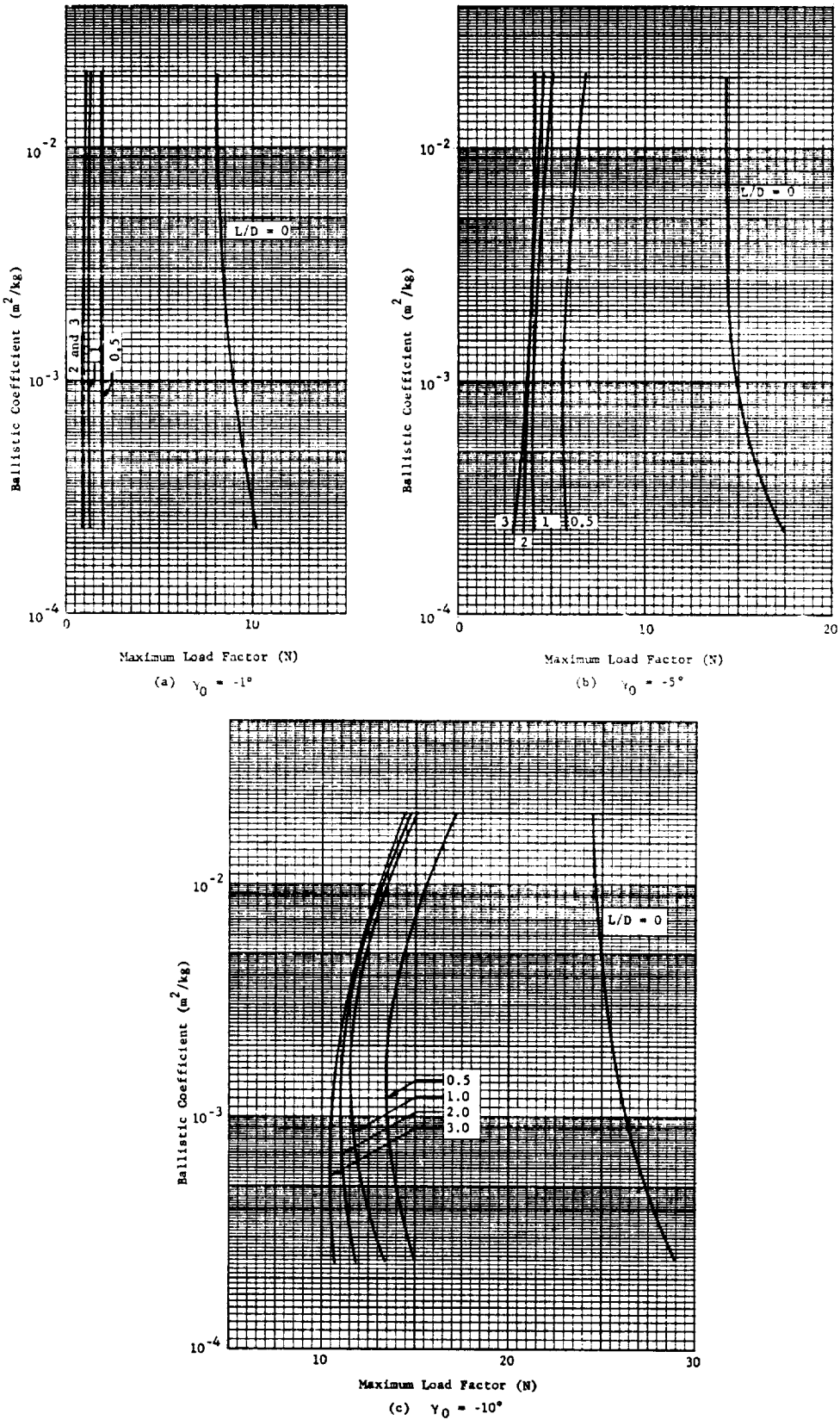

Fig. 18. Maximum Re-Entry Load Factor Versus Ballistic Coefficient (h_0 = 400,000 ft = 121,920 m; v_0 = 25,000 fps = 7620 mps)

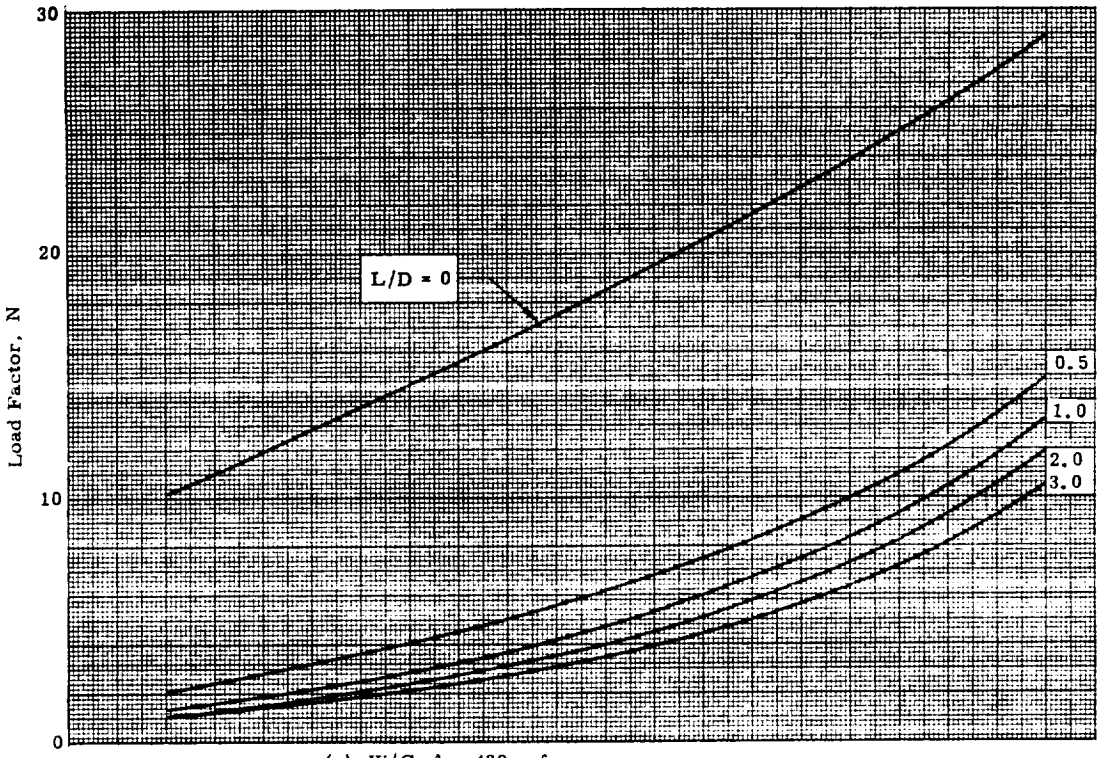

(a) W/C_DA = 438 psf

B = 0.037 $ft^2/slug$ = 0.234 x 10^{-3} m^2/kg

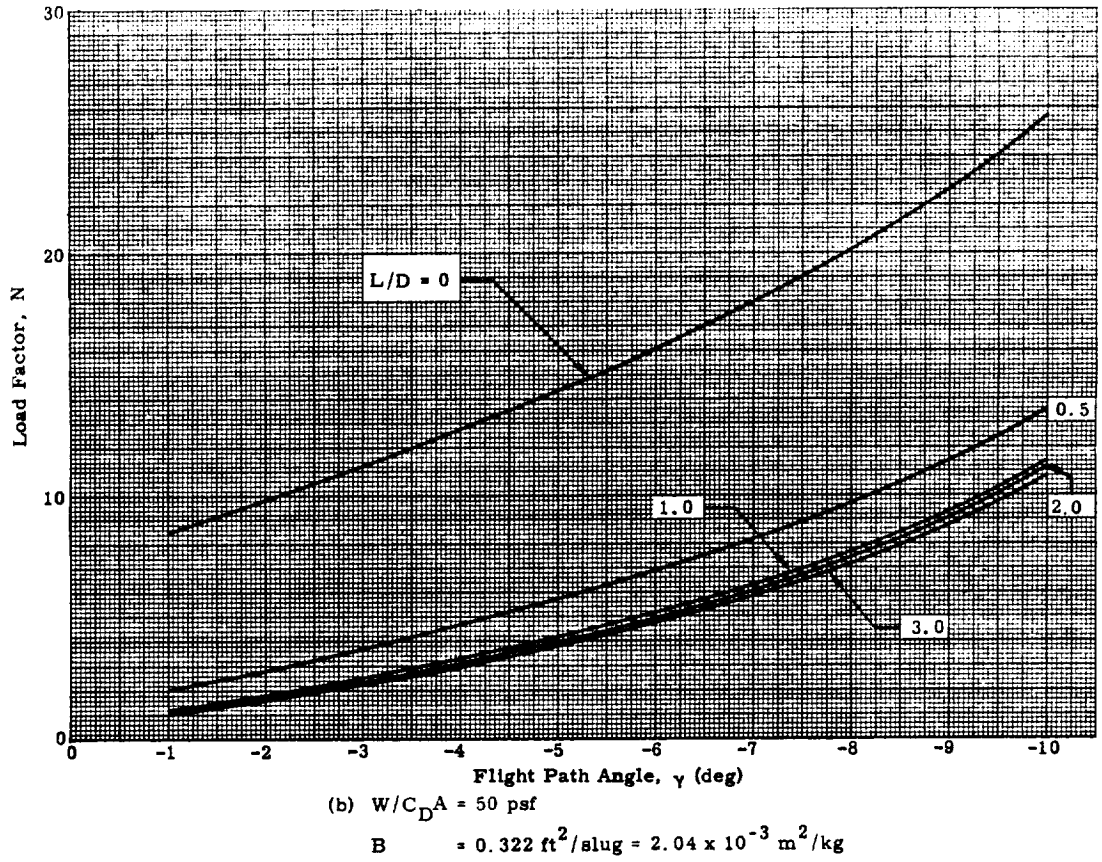

(b) W/C_DA = 50 psf

B = 0.322 $ft^2/slug$ = 2.04 x 10^{-3} m^2/kg

Fig. 19. Maximum Re-Entry Load Factor Versus Flight Path Angle (v_0 = 25,000 fps = 7620 mps; h_0 = 400,000 ft = 121,920m)

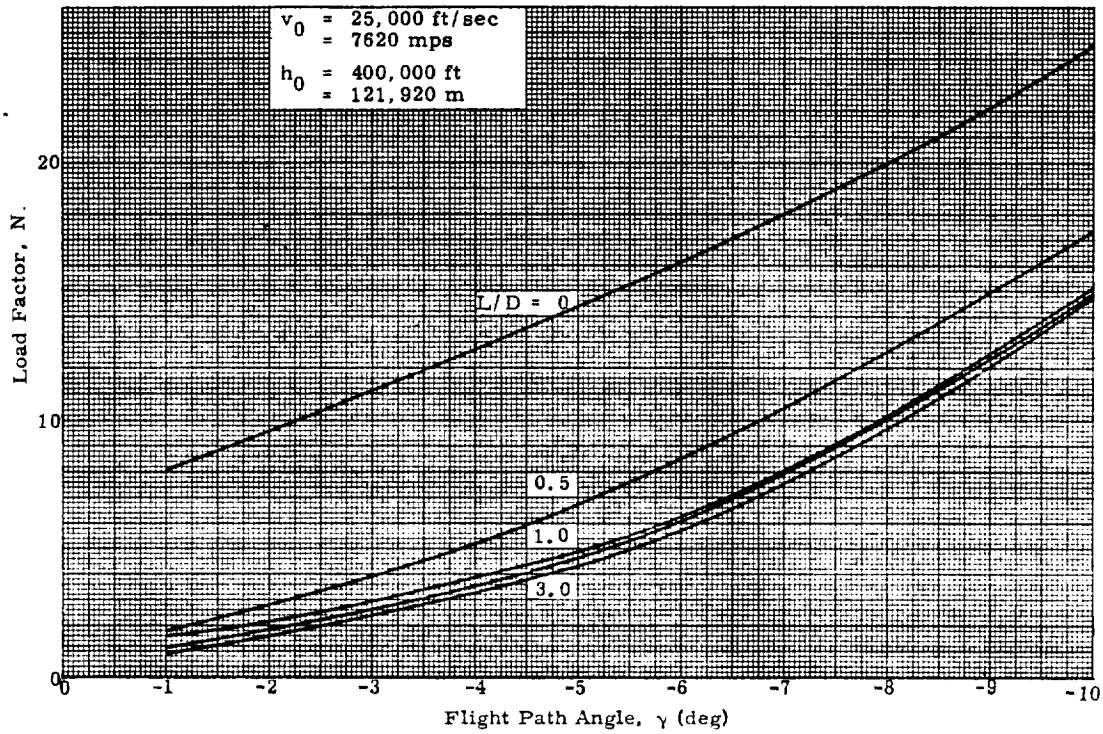

(c) W/C_DA = 5 psf, B = 3.22 ft^2/slug = 2.05 x 10^{-2} m^2/kg

Fig. 19. (continued)

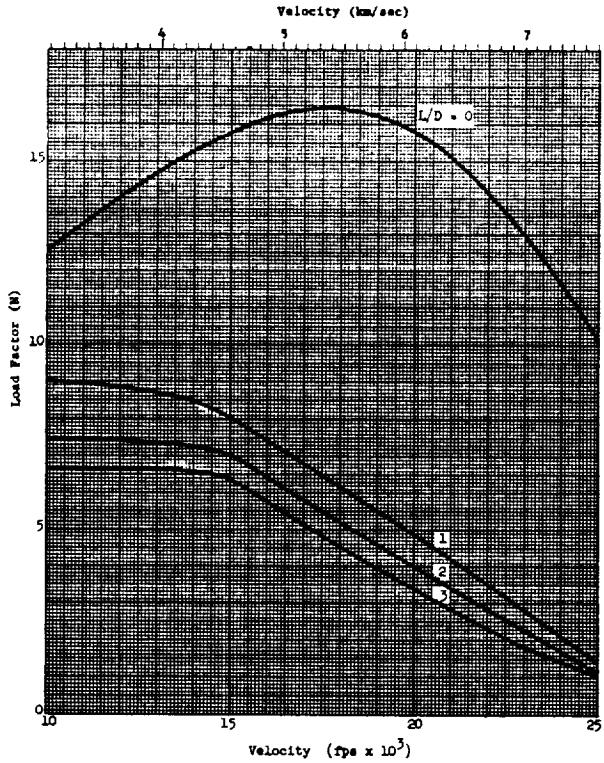

(a) B = 0.0367 ft^2/slug; W/C_DA = 438 psf
= 0.234 x 10^{-3} m^2/kg = 21,000 newton/m^2

Fig. 20. Maximum Re-entry Load Factor Versus Velocity (h_0 = 400,000 ft, γ_0 = -1°)

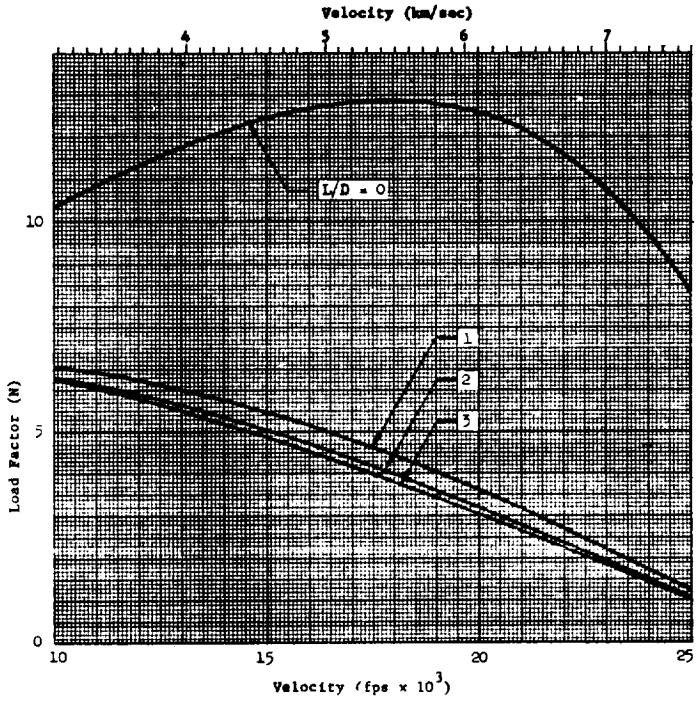

(b) B = 0.322 ft^2/slug; W/C_DA = 50 psf

= 2.04 x 10^{-3} m^2/kg = 2390 newtons/m^2

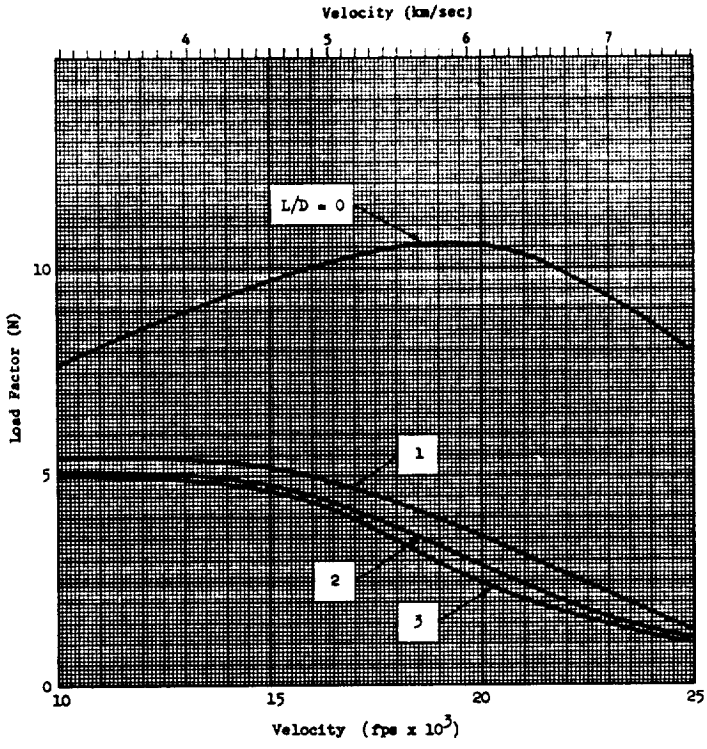

(c) W/C_DA = 5 psf = 239 newtons/m^2, B = 3.22 ft^2/slug = 2.05 x 10^{-2} m^2/kg

Fig. 20. Continued

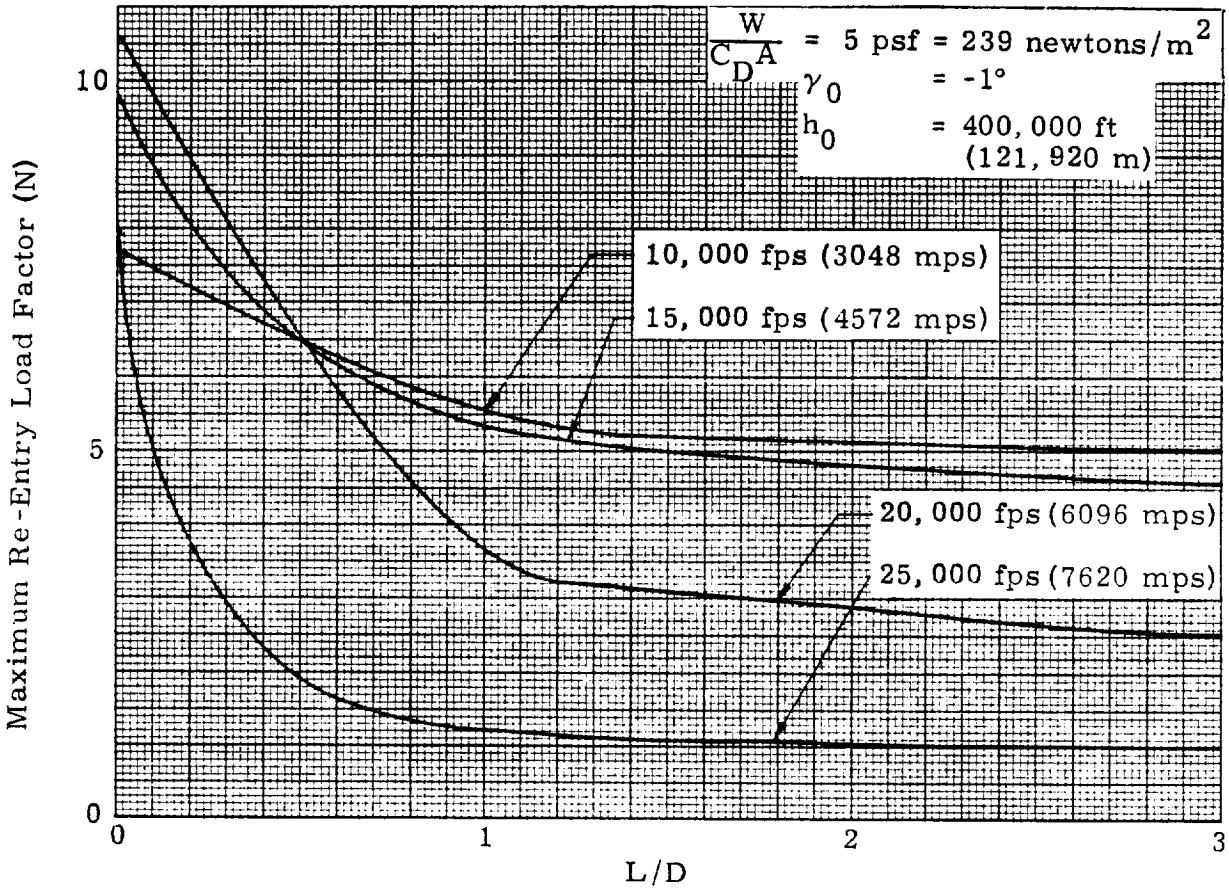

Fig. 21. Maximum Re-Entry Load Factor Versus L/D

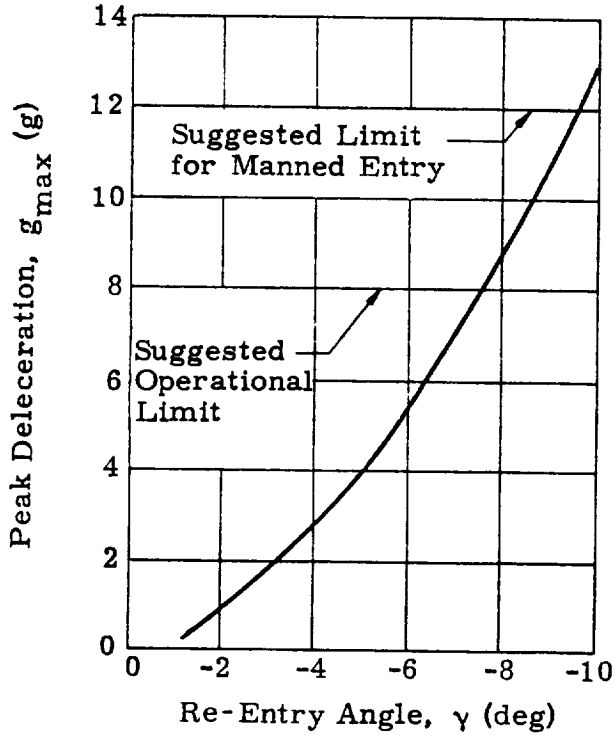

Fig. 22. Effect of Re-Entry Angle on Peak Deceleration, $v_0 = v_c$, $W/C_L A$ = 20 psf = 957 newton/m^2, L/D = 2 (Ref. 14)

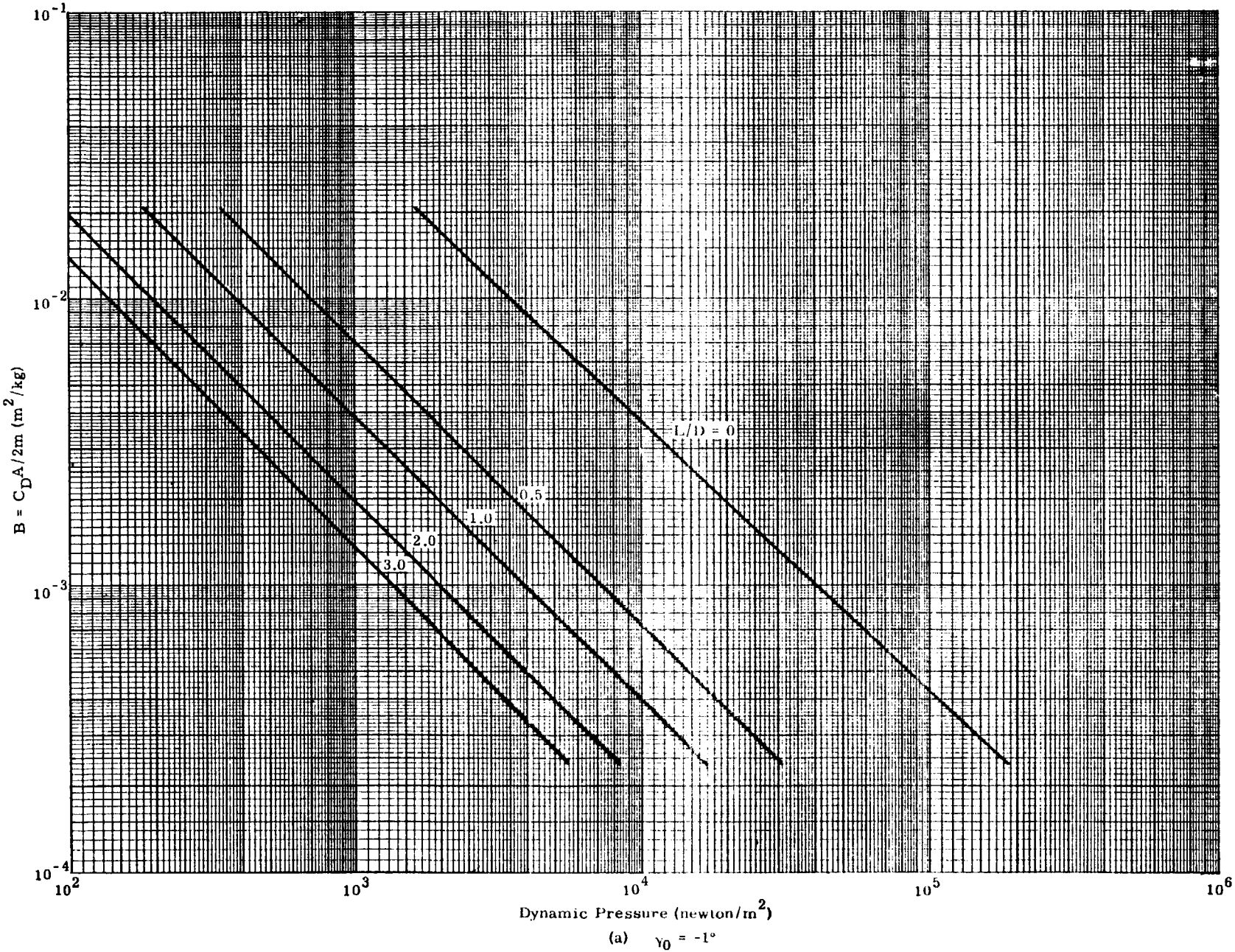

(a) $\gamma_0 = -1°$

Fig. 23. Maximum Re-Entry Dynamic Pressure (v_0 = 25,000 fps = 7620 mps; h_0 = 400,000 ft = 121,920 m)

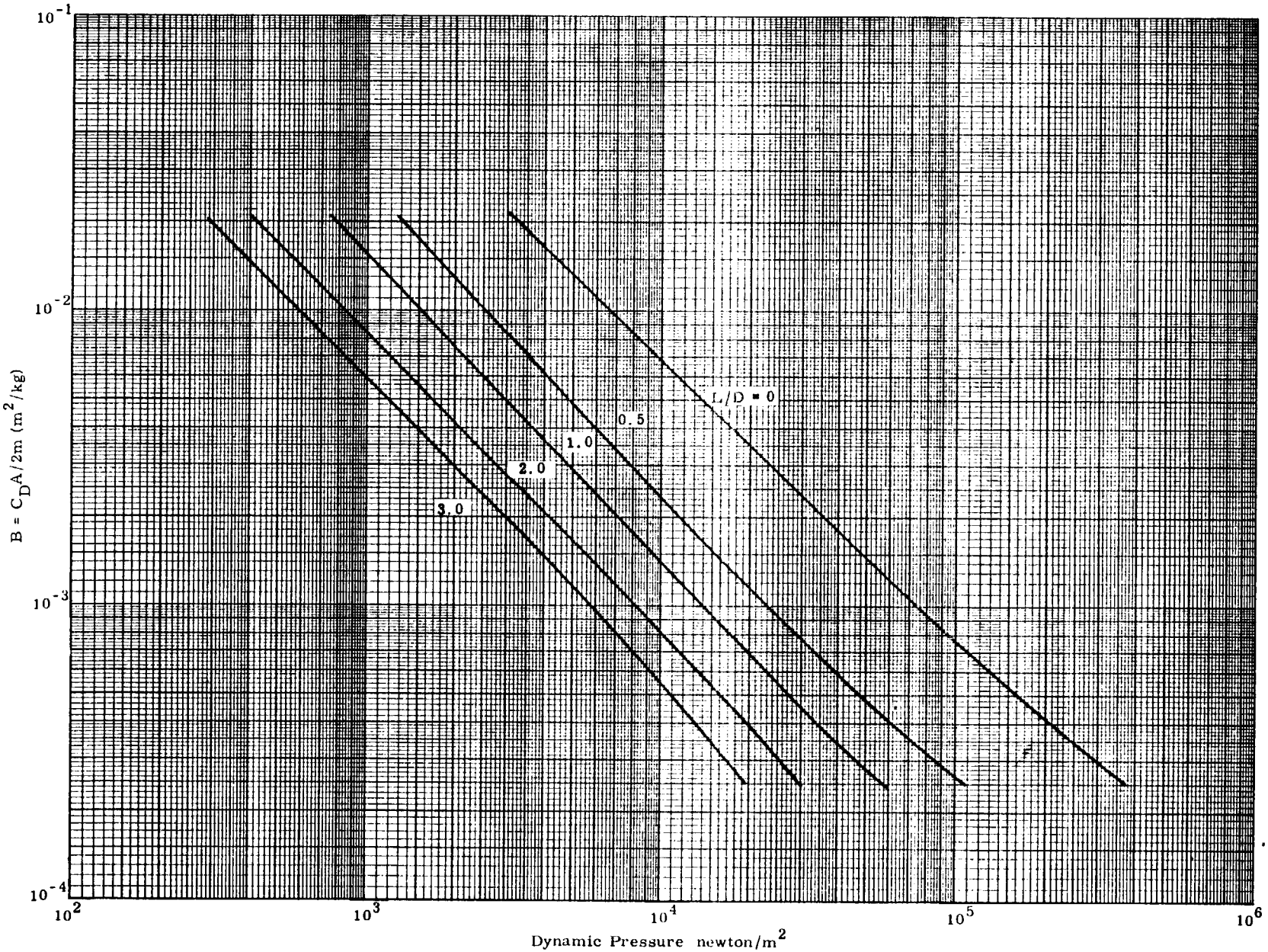

(b) $\gamma_0 = -5°$

Fig. 23. (continued)

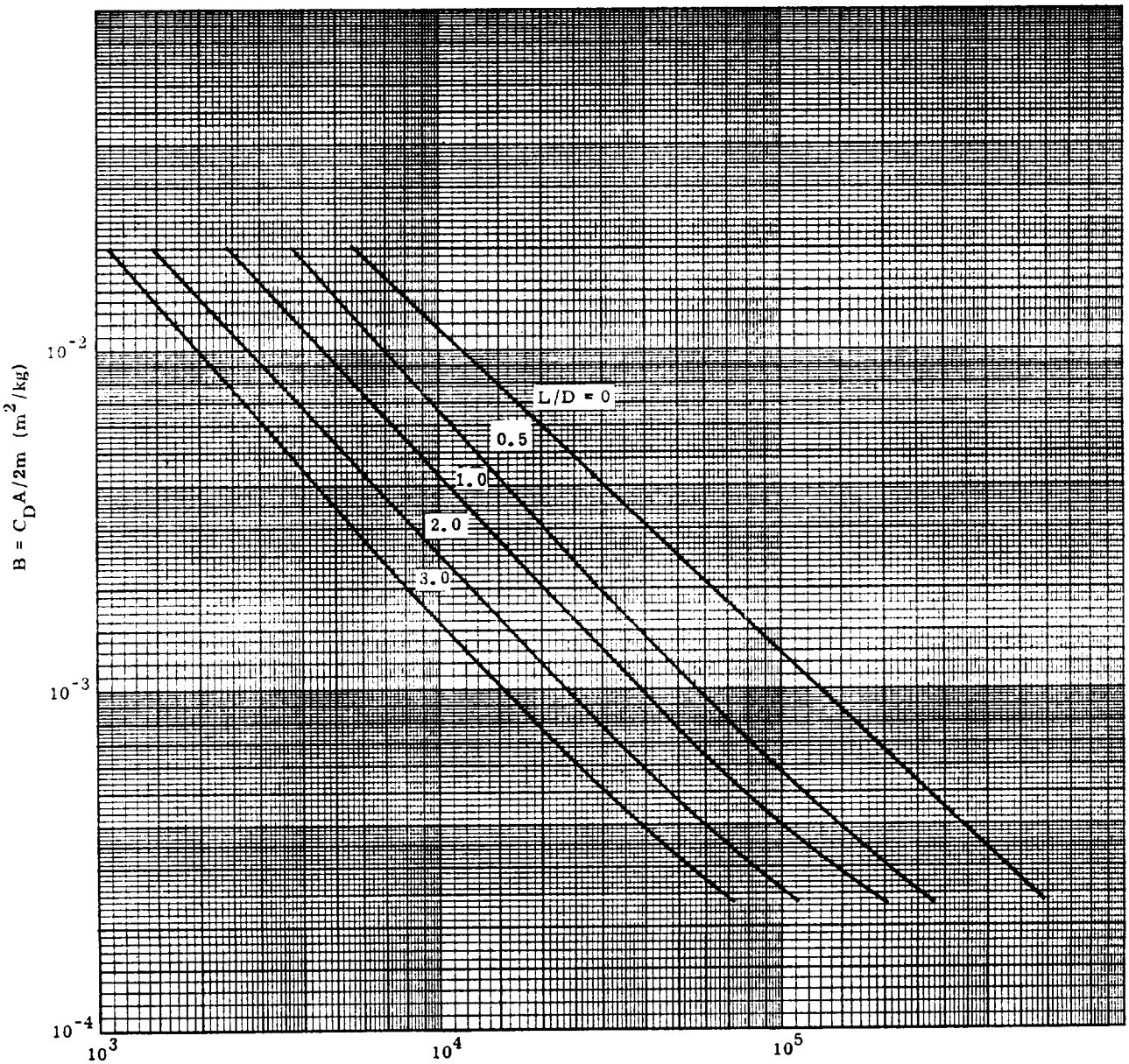

(c) $\gamma_0 = -10°$

Fig. 23. (continued)

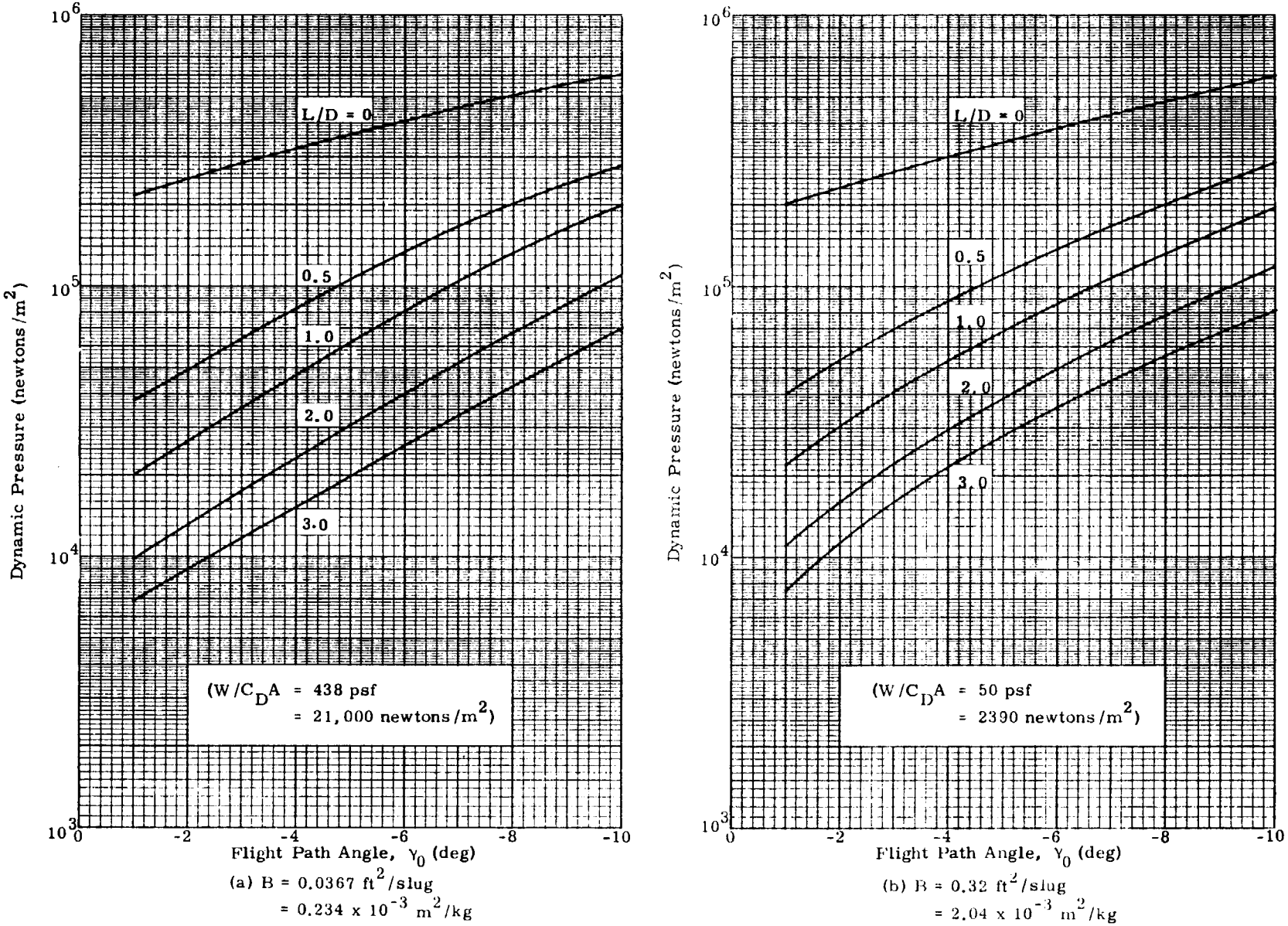

Fig. 24. Maximum Re-Entry Dynamic Pressure Versus γ_0 (v_0 = 25,000 fps = 7620 mps, h_0 = 400,000 ft = 121,920 m)

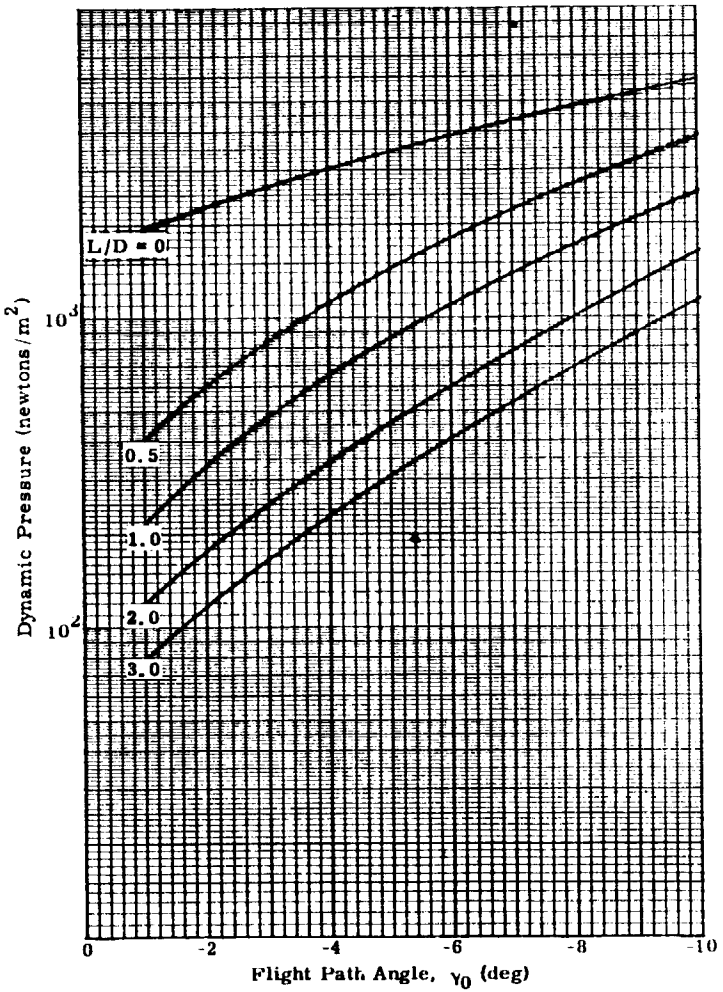

(c) W/C_DA = 5 psf = 239 newtons/m^2,
B = 3.2 ft^2/slug = 20.5 x 10^{-3} m^2/kg

Fig. 24. (continued)

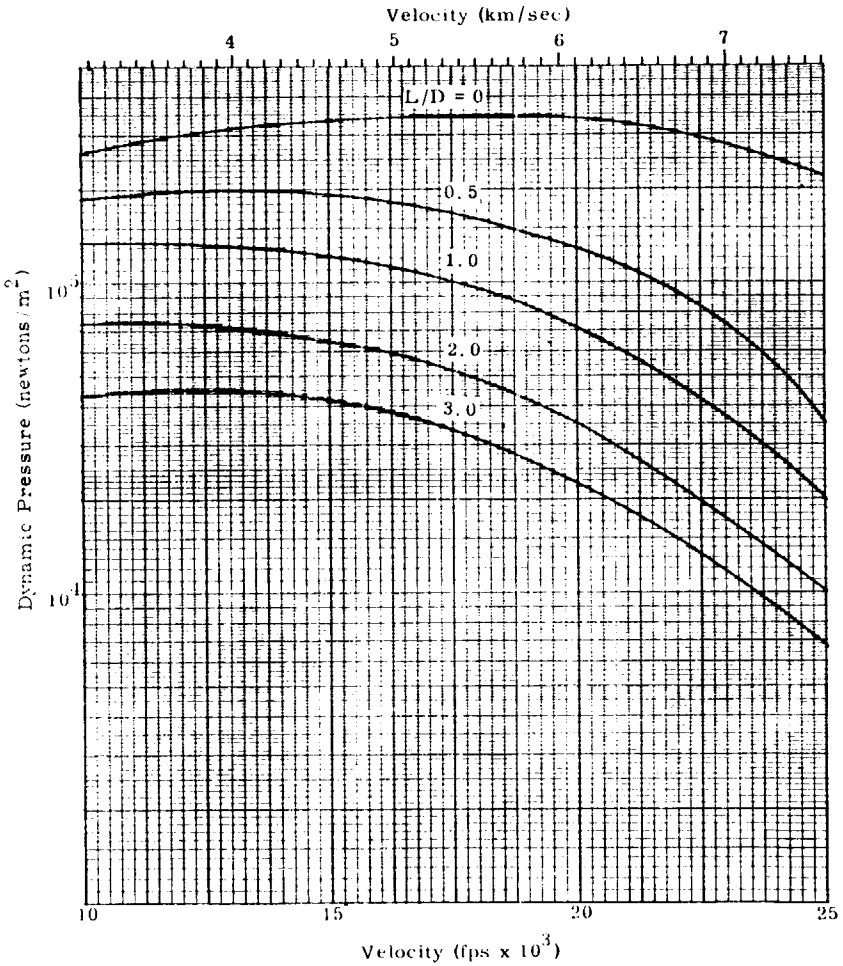

(a) W/C_DA = 438 psf
= 21,000 newtons/m^2

Fig. 25. Maximum Re-entry Dynamic Pressure Versus Velocity
(γ_0 = -1°; h_0 = 400,000 ft = 121,920 m)

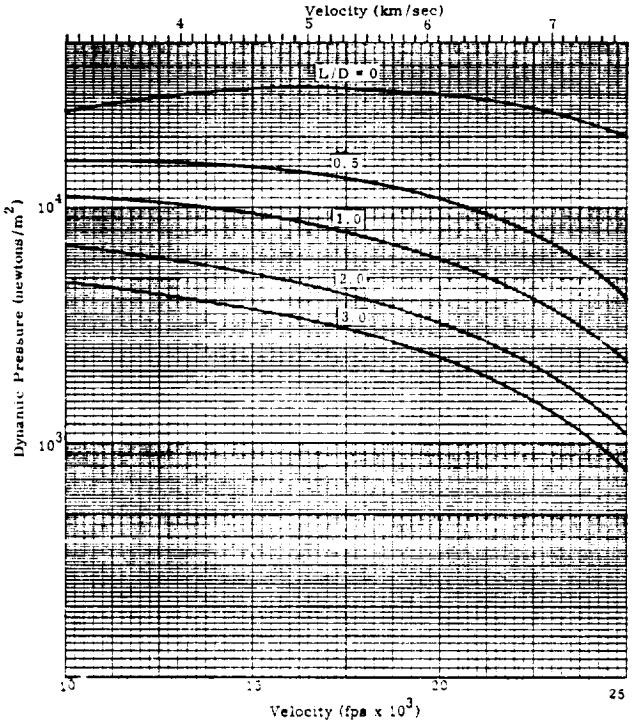

(b) W/C_DA = 50 psf
= 2390 newtons/m^2

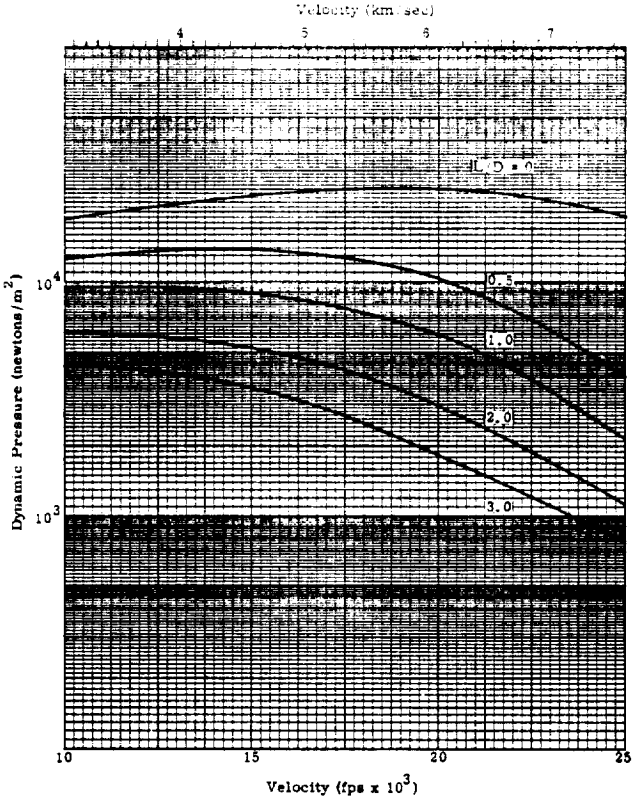

(c) W/C_DA = 5 psf
= 239 newtons/m^2

Fig. 25. (continued)

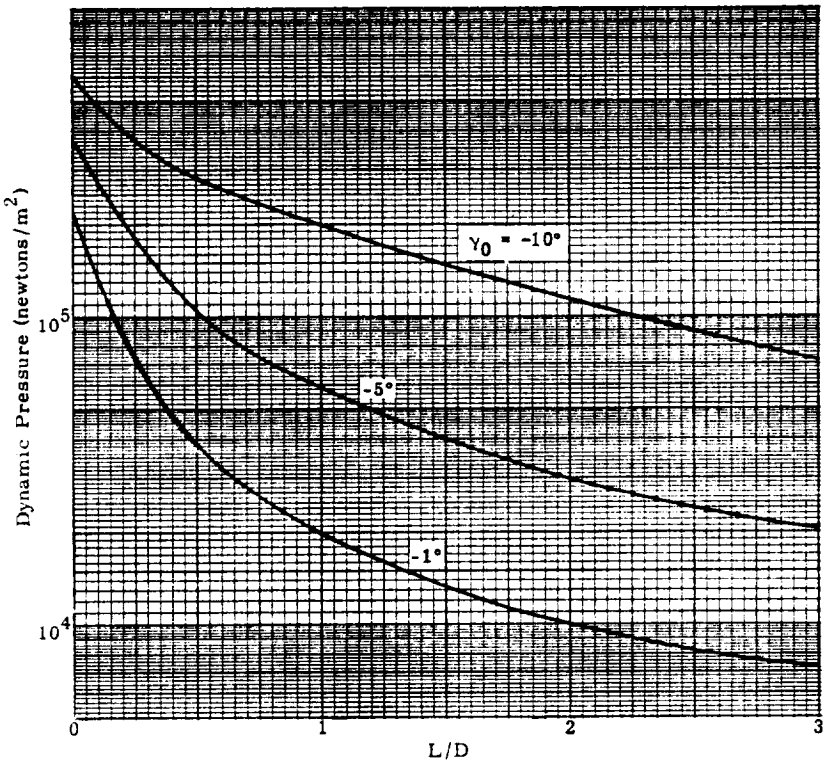

(a) W/C_DA = 438 psf = 21,000 newtons/m^2

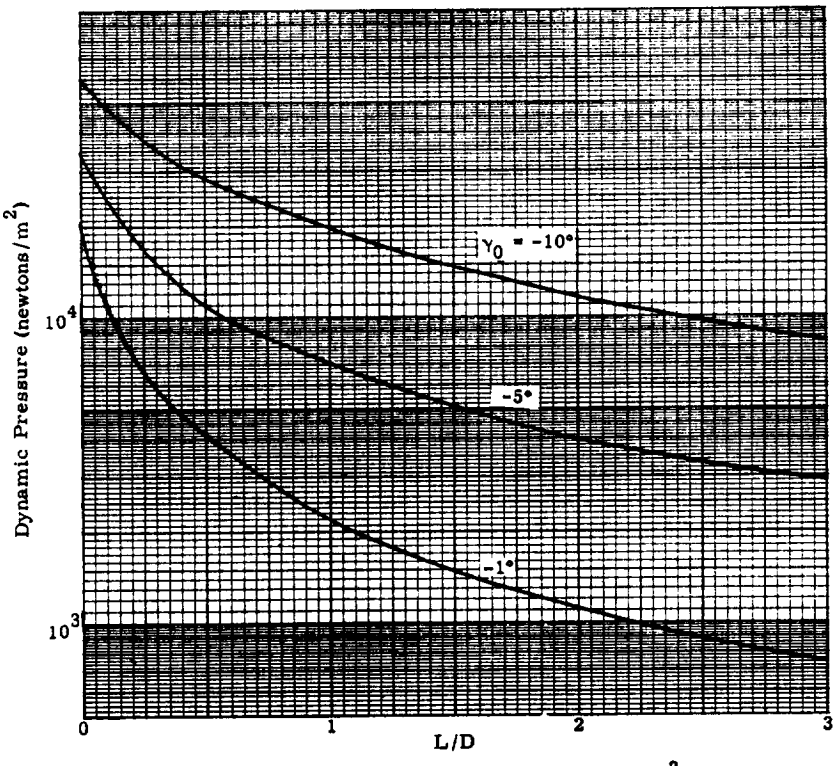

(b) W/C_DA = -50 psf = 2390 newtons/m^2

Fig. 26. Maximum Re-Entry Dynamic Pressure Versus L/D (v_0 = 25,000 fps = 7620 mps)

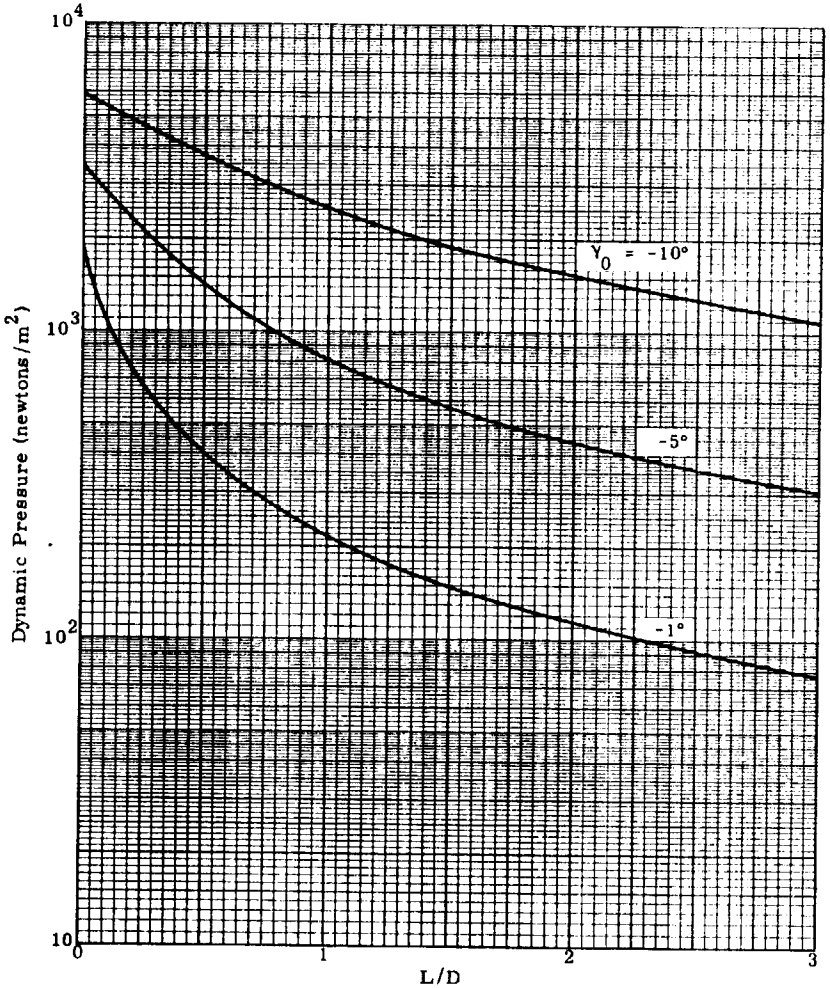

(c) W/C_DA = 5 psf = 239 newtons/m^2

Fig. 26. (continued)

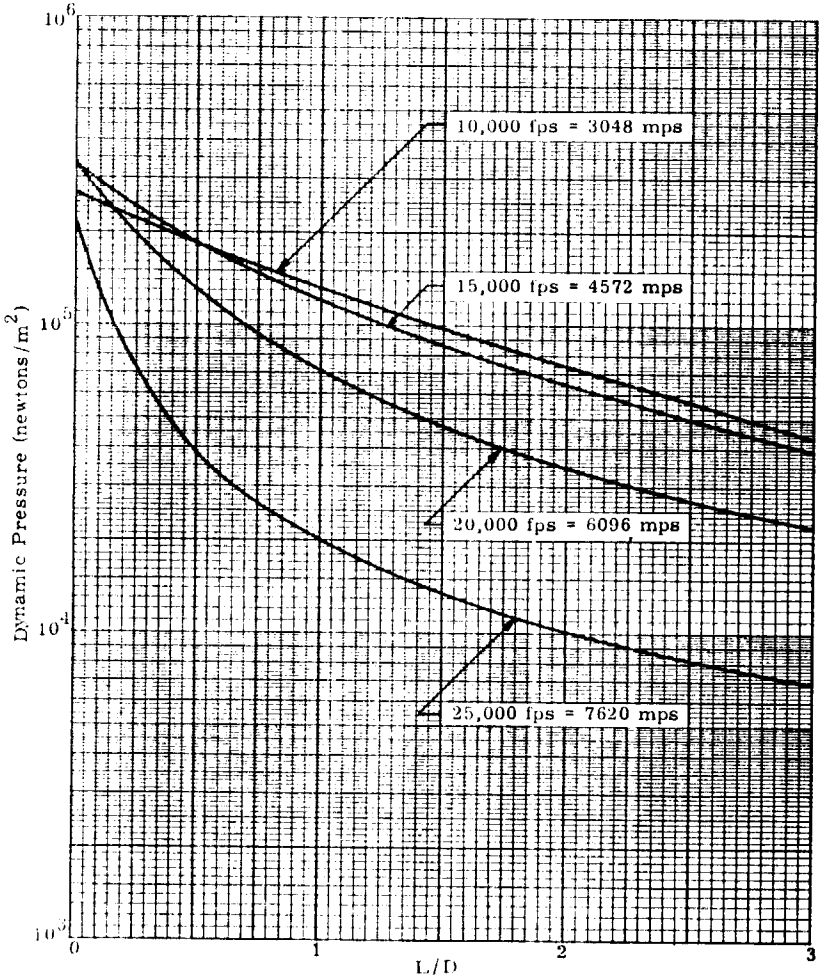

(a) W/C_DA = 458 psf = 21,000 newtons/m^2

Fig. 27. Maximum Re-Entry Dynamic Pressure Versus L/D
(γ_0 = -1°; h_0 = 400,000 ft = 121,920 m)

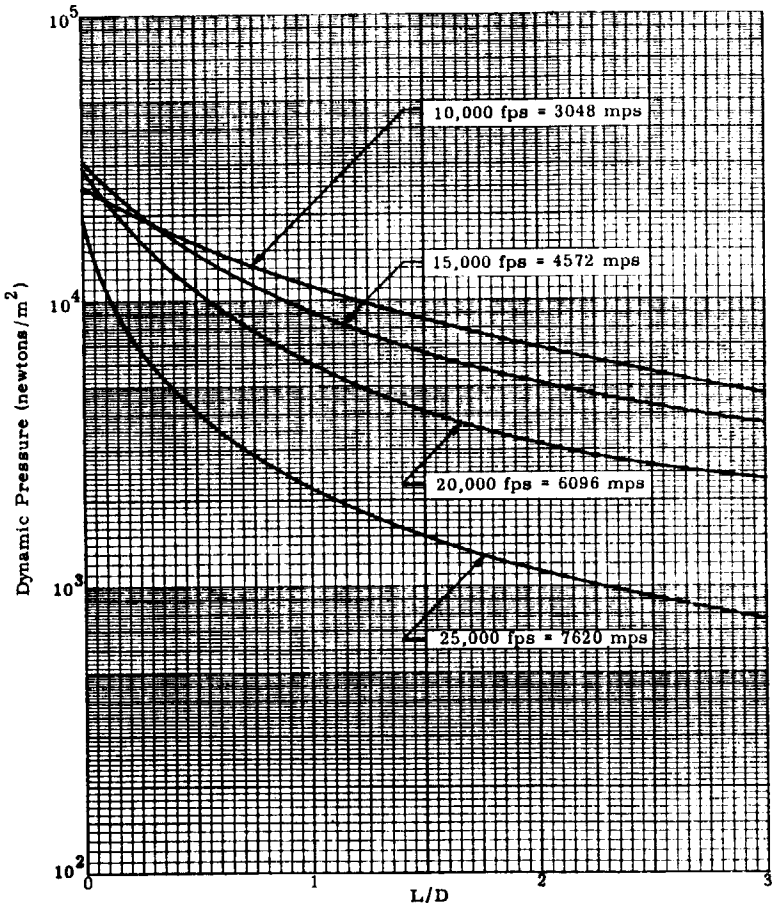

(b) W/C_DA = 50 psf = 2390 newtons/m^2

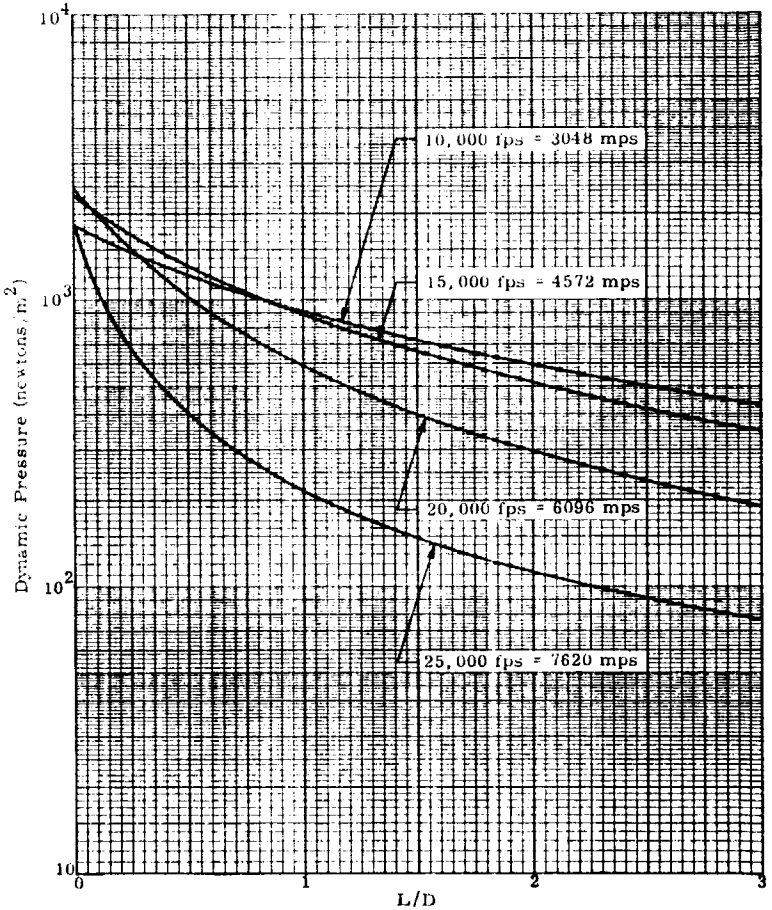

(c) W/C_DA = 5 psf = 239 newtons/m^2

Fig. 27. (continued)

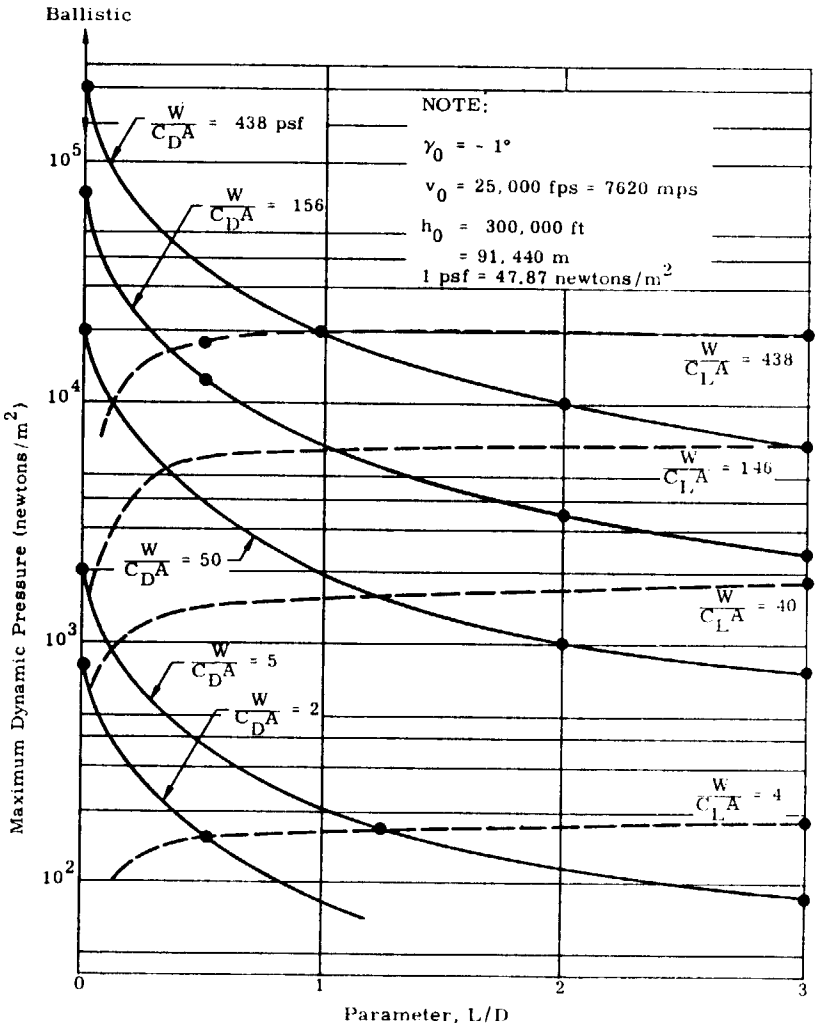

Fig. 28. Effects of Lift, Drag and Wing Loading on Maximum Dynamic Pressure

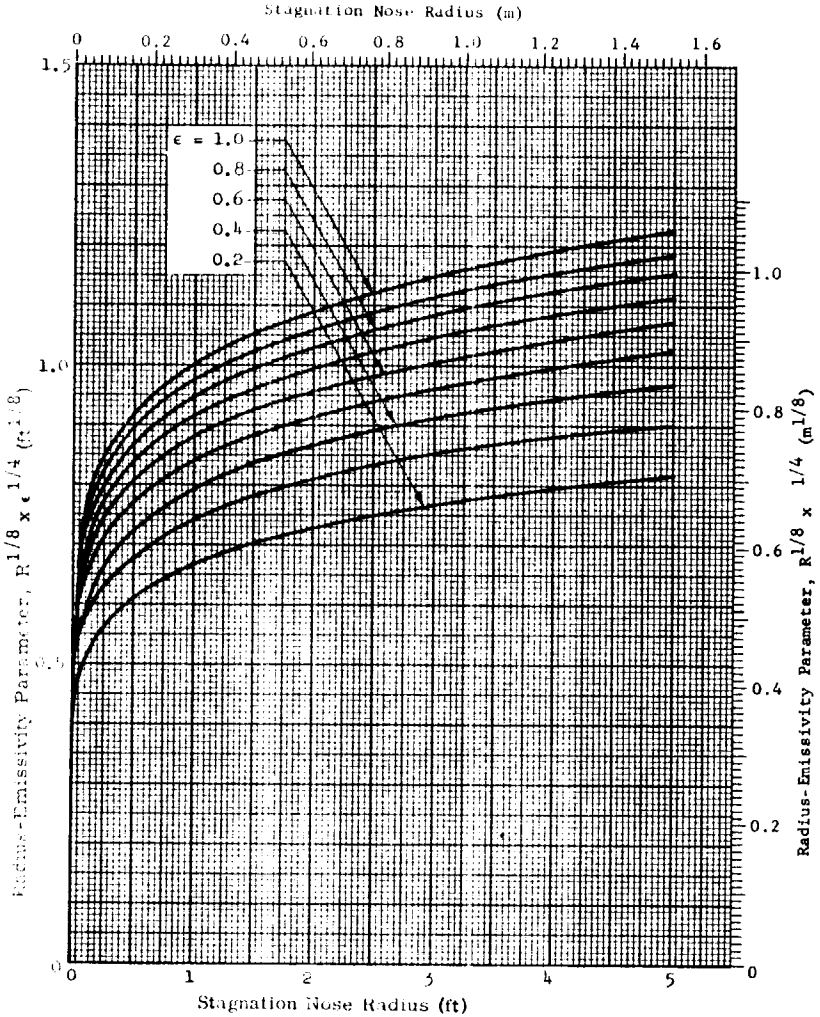

Fig. 29. Radius-Emissivity Parameter ($R^{1/8} \times \epsilon^{1/4}$) Versus Stagnation Nose Radius

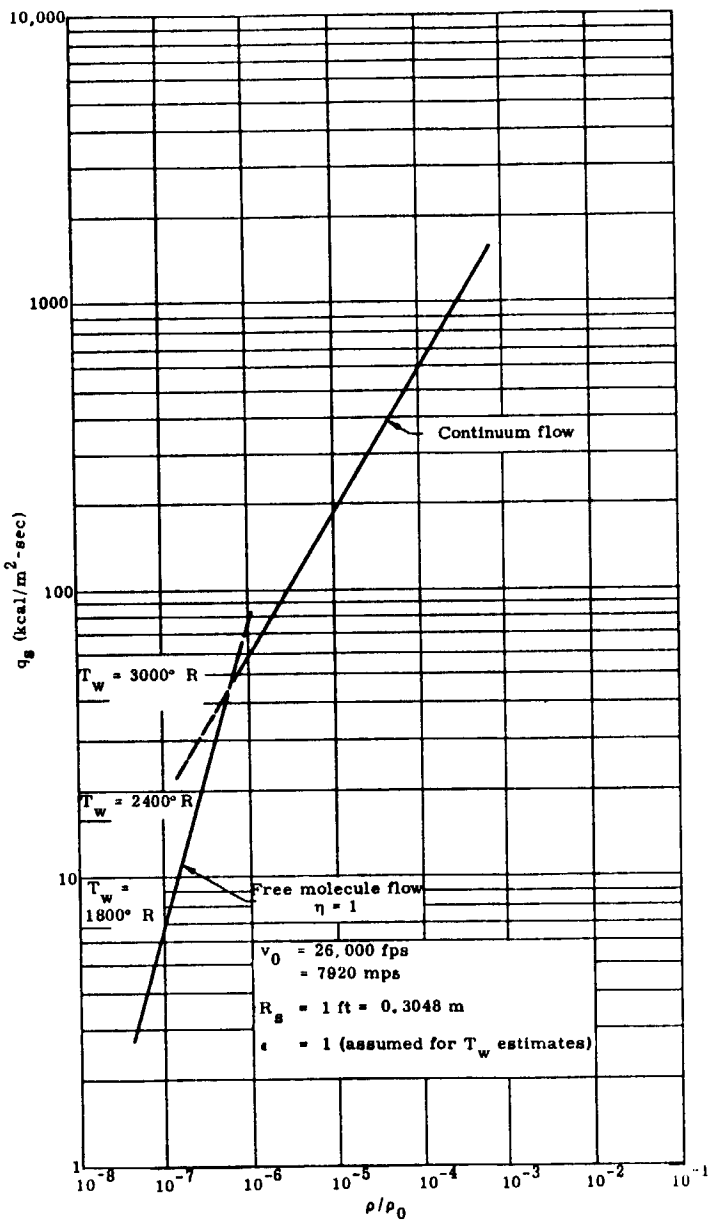

Fig. 30a. Heat Transfer Rate q_s at the Stagnation Point of a Blunt Body of 1-ft Nose Radius as a Function of Air Density Ratio, ρ/ρ_0 (Ref. 22)

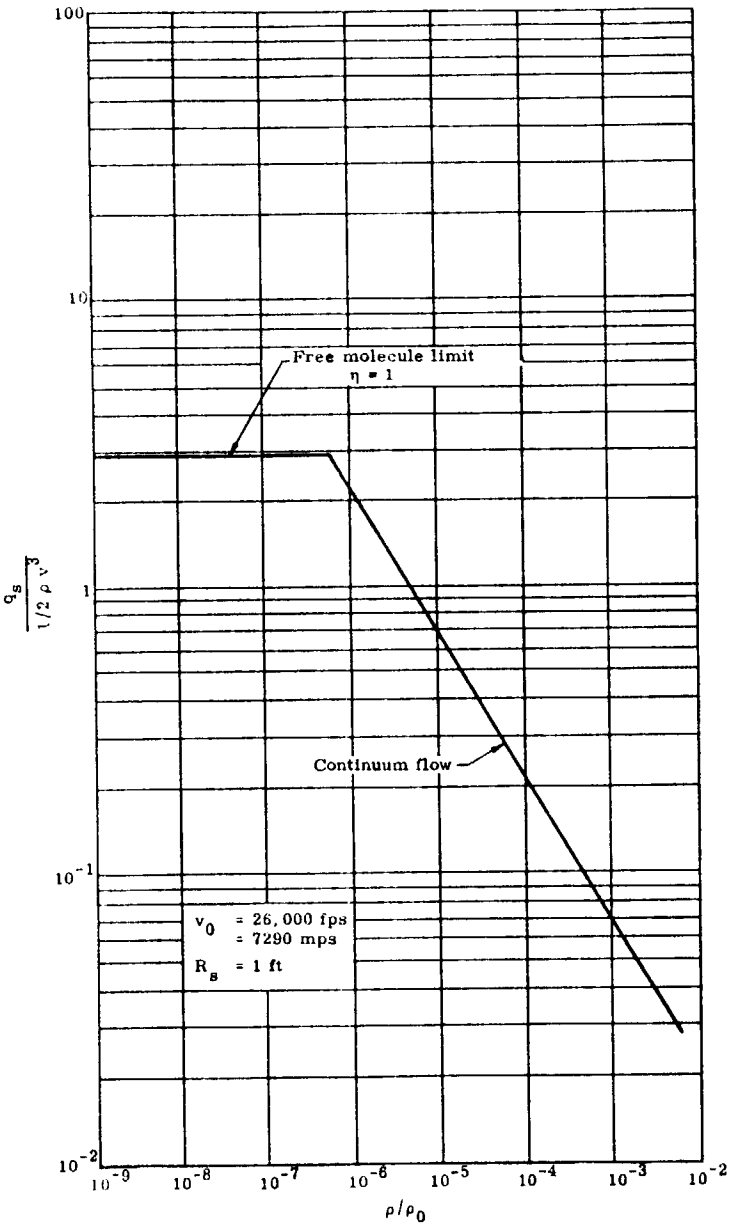

Fig. 30b. Ratio of the Heat Input Rate q_s to the Rate at Which Energy Is Dissipated by Drag $\frac{1}{2}\rho v^3$ as a Function of Air Density Ratio ρ/ρ_0 (Ref. 22)

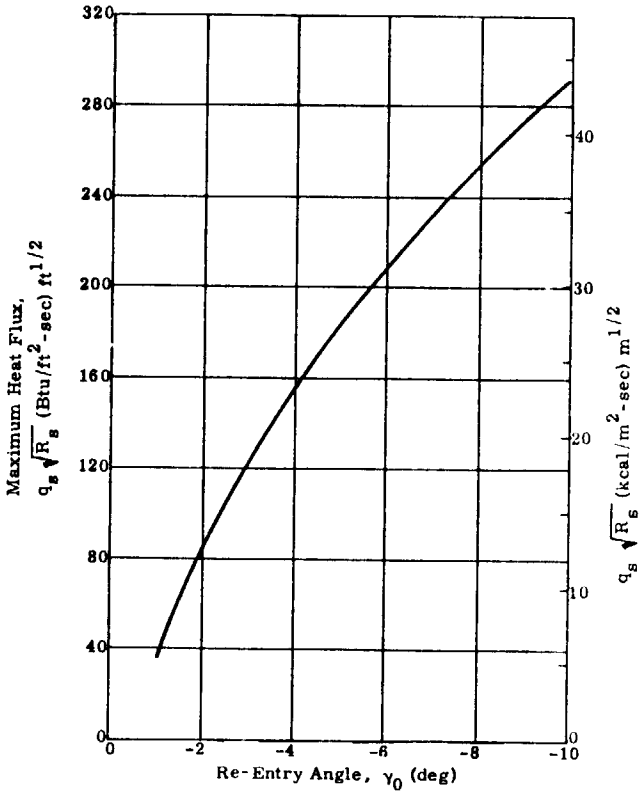

Fig. 31a. Effect of Re-Entry Angle on Maximum Heat Flux ($v_0 = v_c$, W/C_LA = 20 psf, L/D = 2) (Ref. 14)

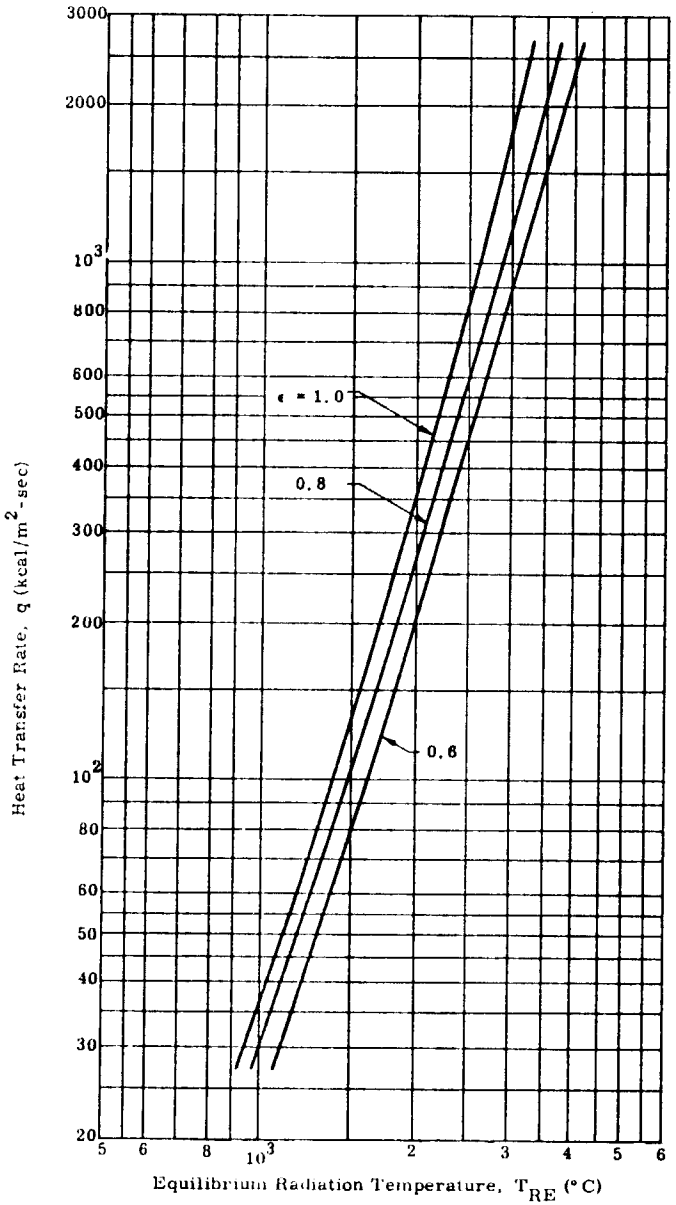

Fig. 31b. Equilibrium Radiation Temperature Versus Heat Transfer Rate (Ref. 14)

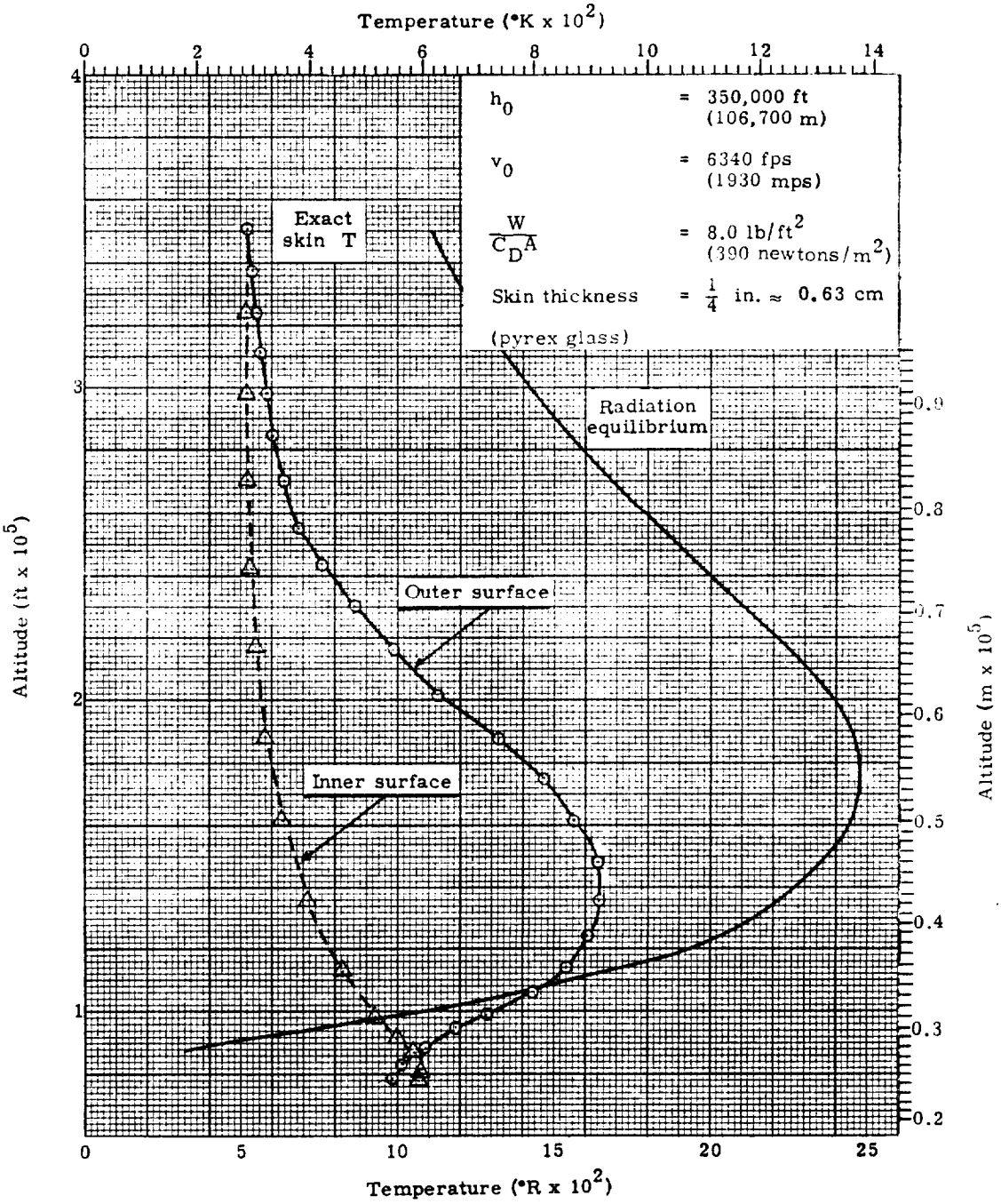

Fig. 32. Comparison of Radiation Equilibrium Method with an Exact Skin Temperature Computation (free fall from 1,000,000 ft = 304,800 m) (Ref 23)

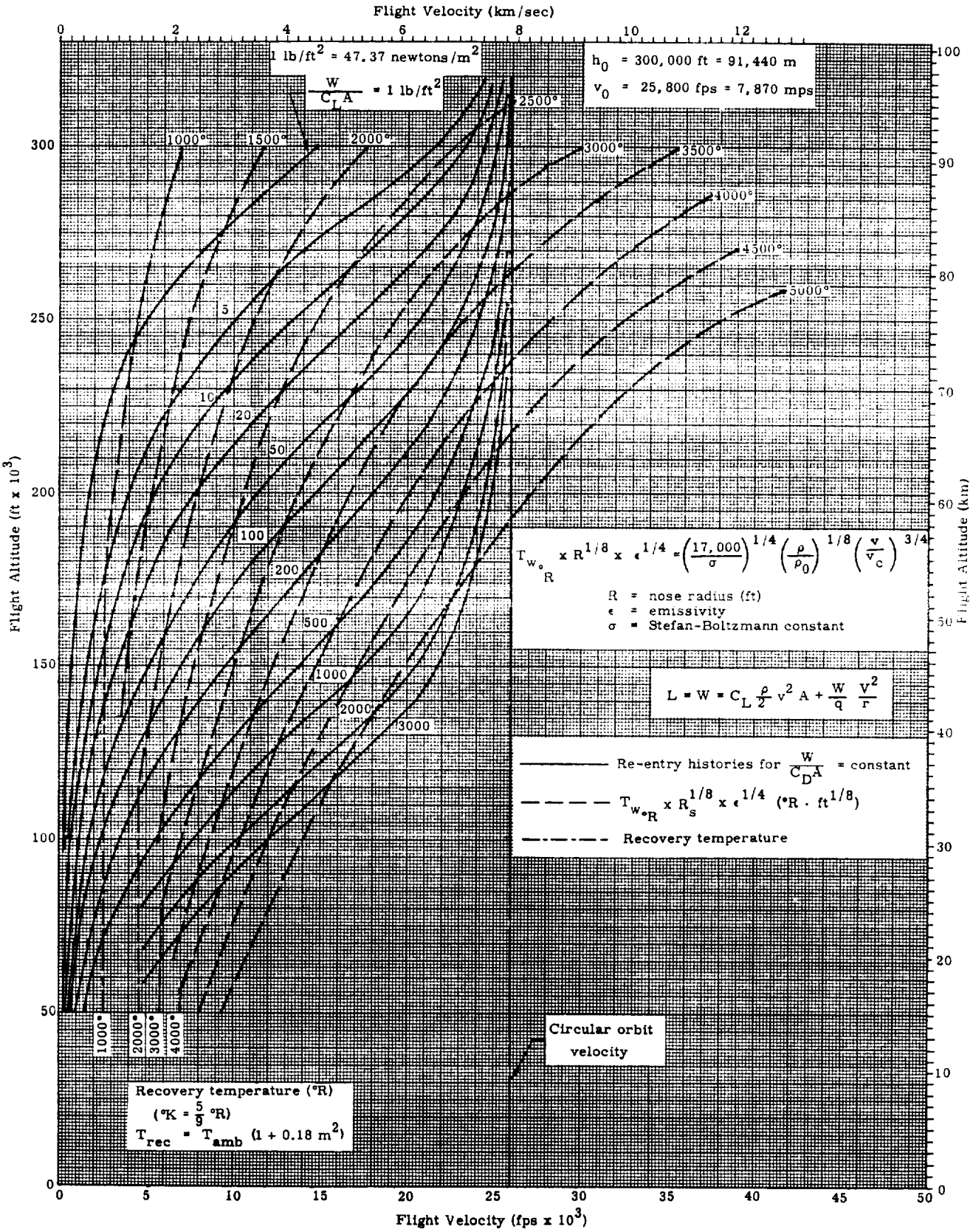

Fig. 33a. Nose Temperature Histories for Different Flight Conditions

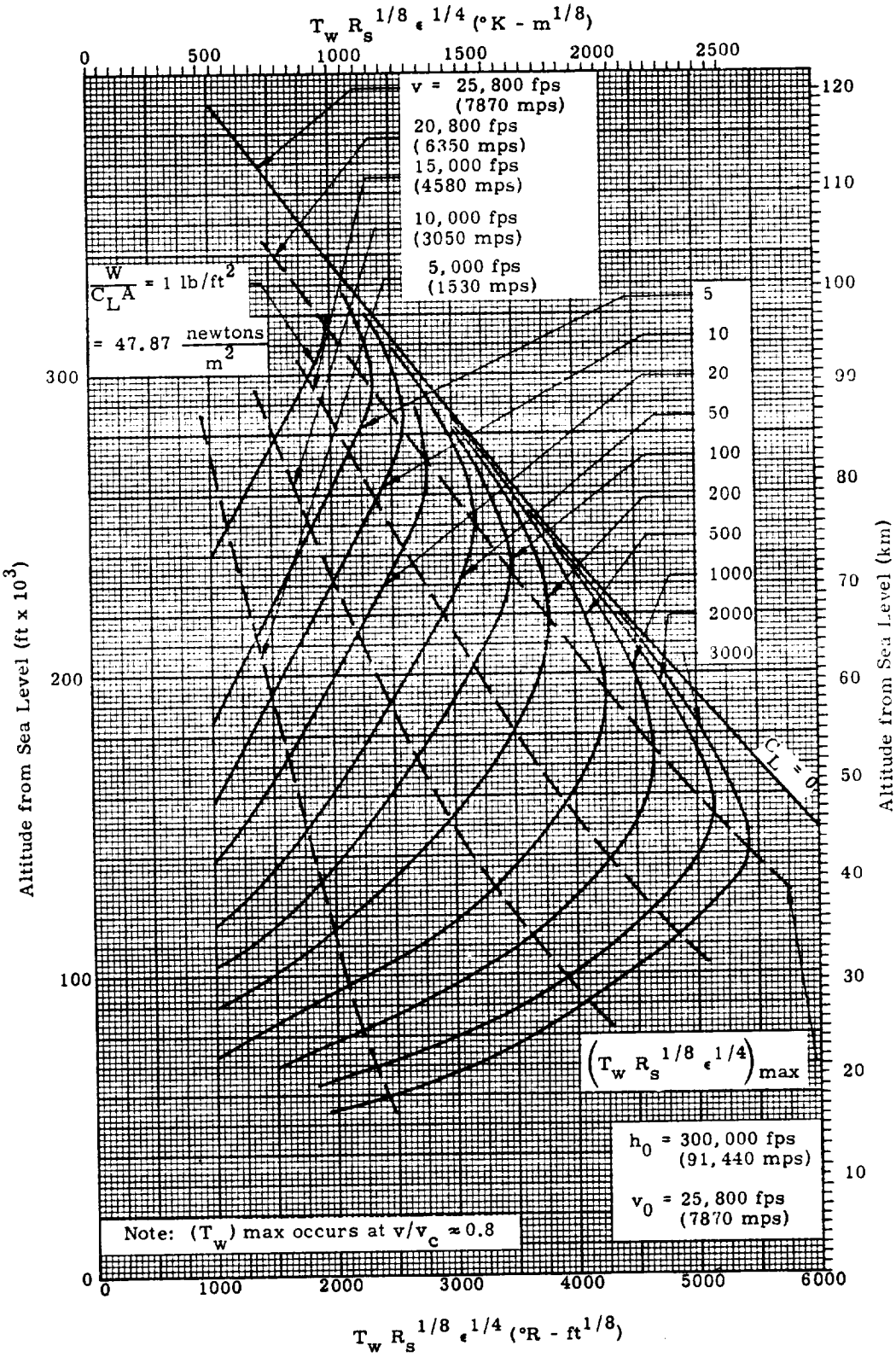

Fig. 33b. Stagnation Point Temperature Profiles for Equilibrium Glides

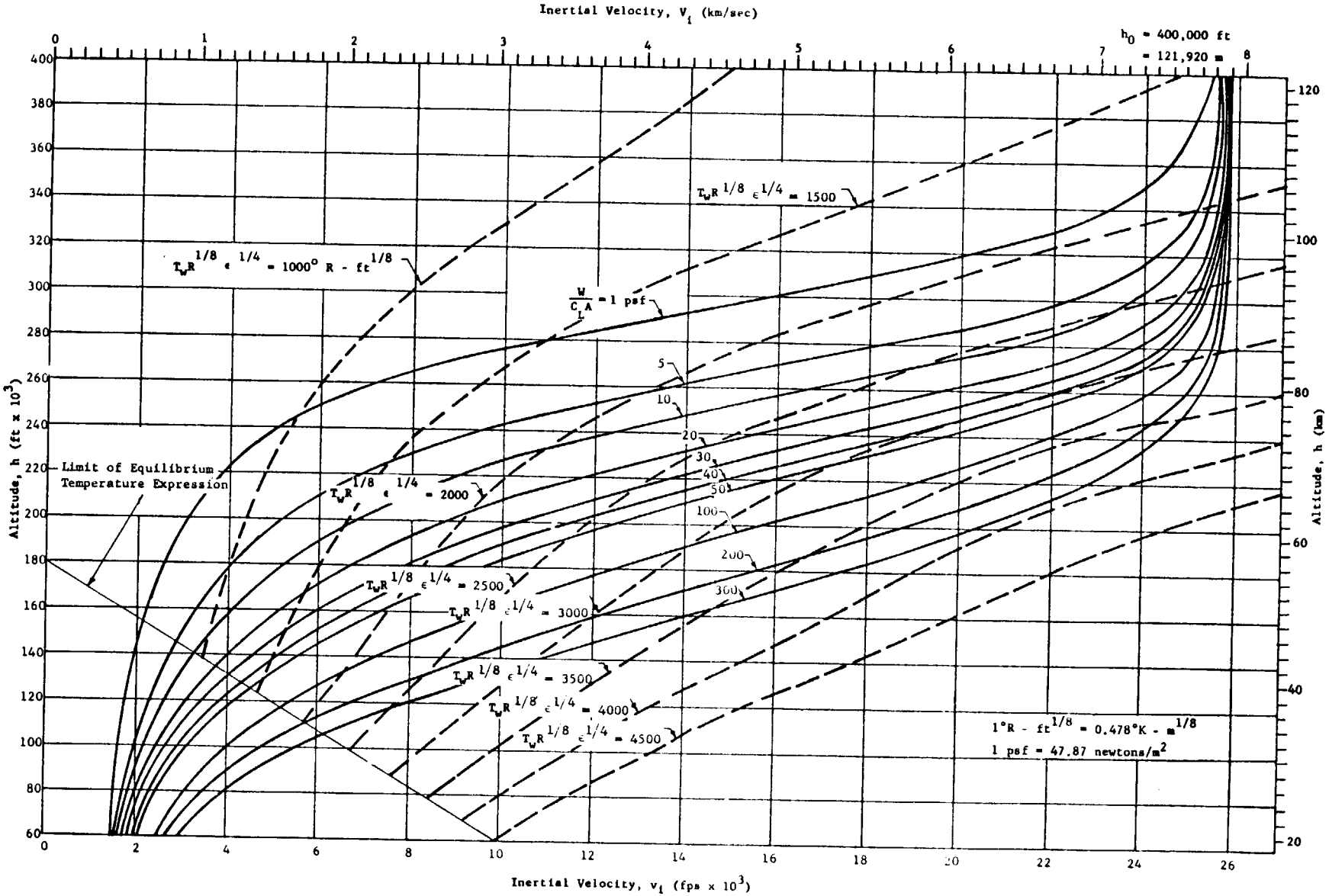

Fig. 33c. Temperature Data for Inertial Velocity and Altitude

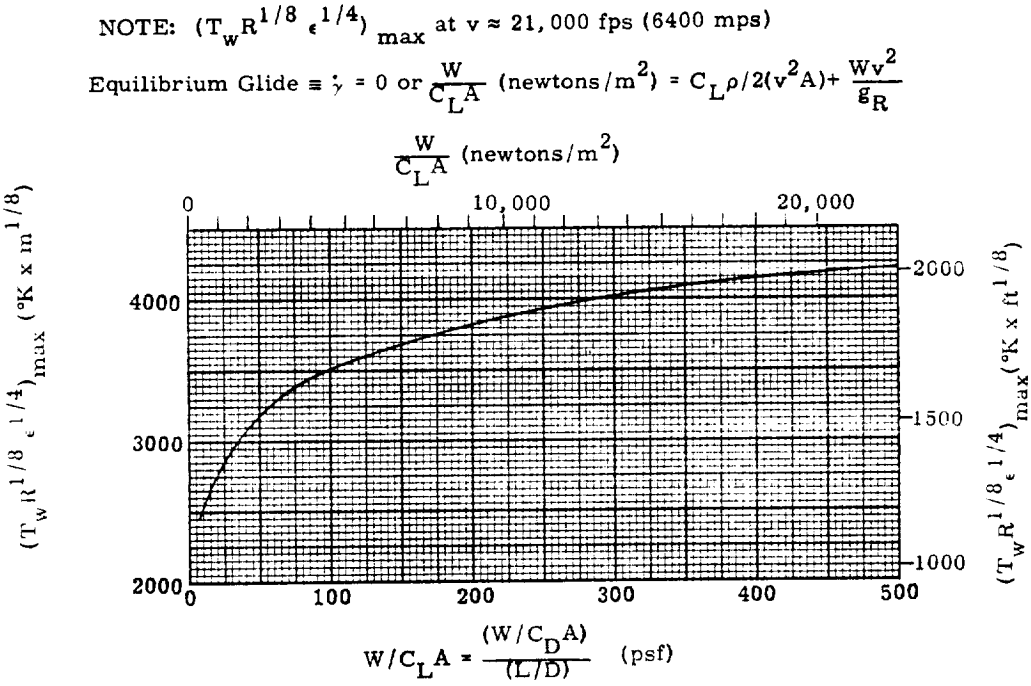

Fig. 34a. Maximum Equilibrium Nose Temperature Versus $W/C_L A$ for Equilibrium Glides

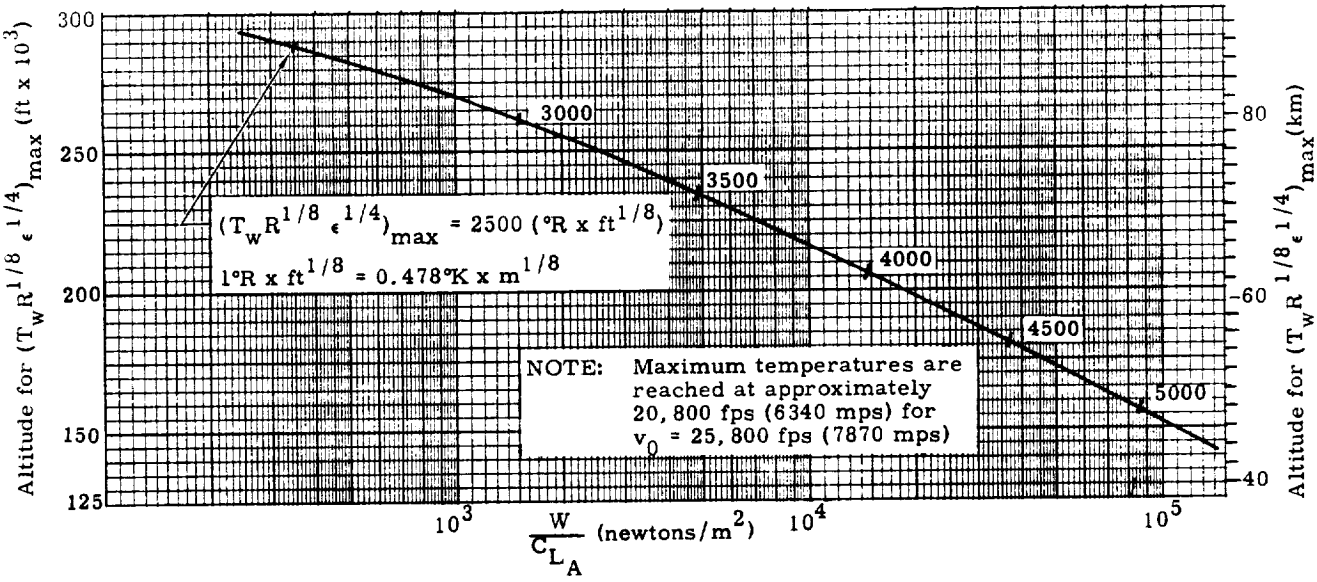

Fig. 34b. Altitude for Maximum Equilibrium Nose Temperature Versus $W/C_L A$ (equilibrium glides)

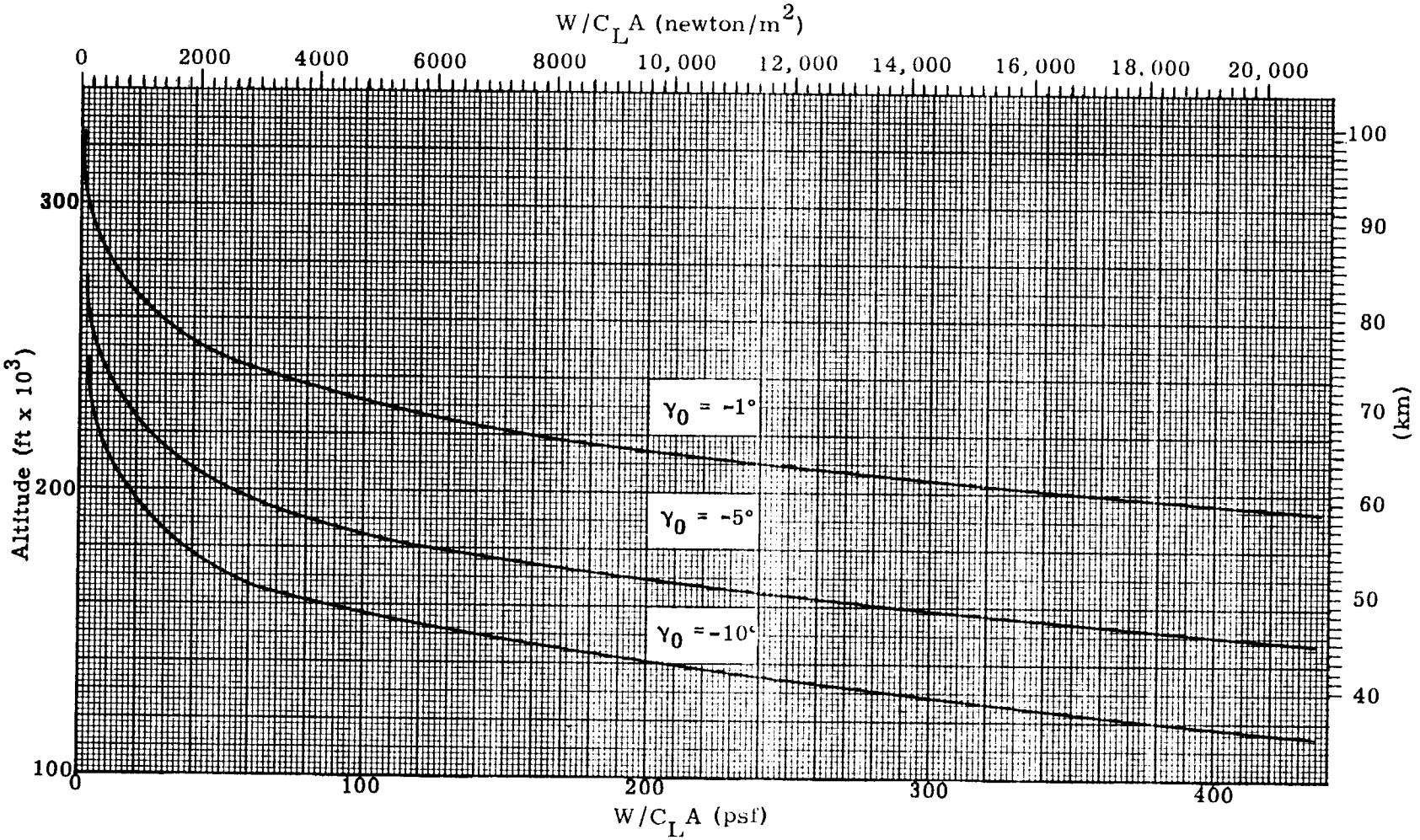

Fig. 34c. Altitude for Maximum Stagnation Nose Temperature (h_0 = 400,000 ft, v_0 = 25,000 fps)

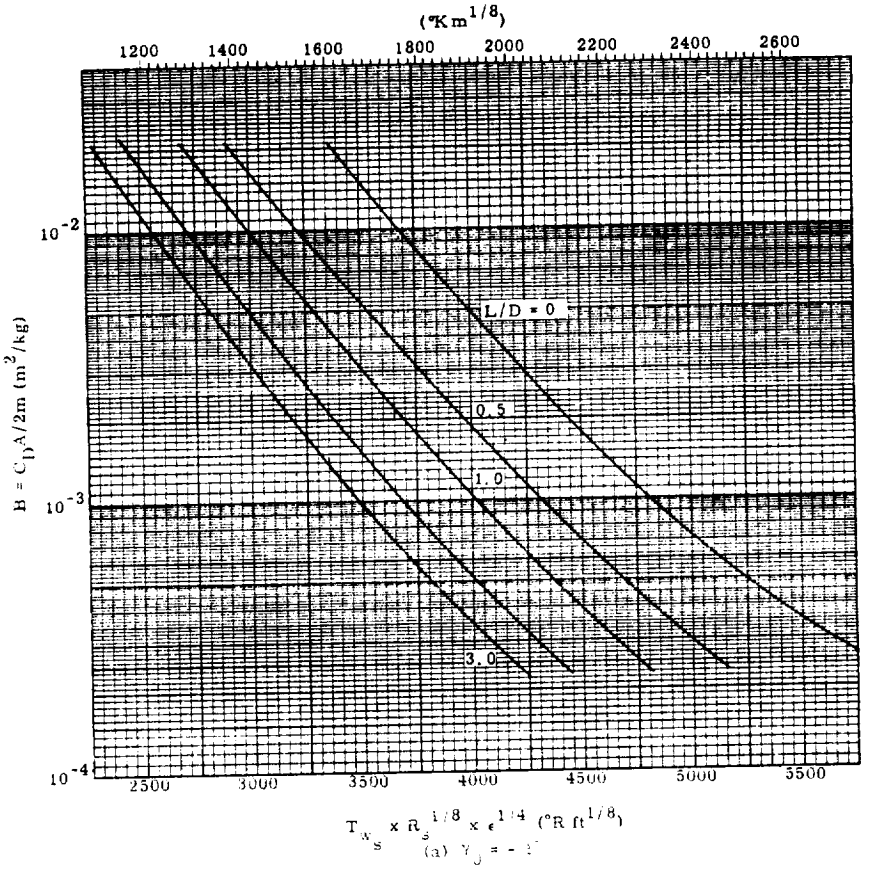

(a) $\gamma_0 = -1°$

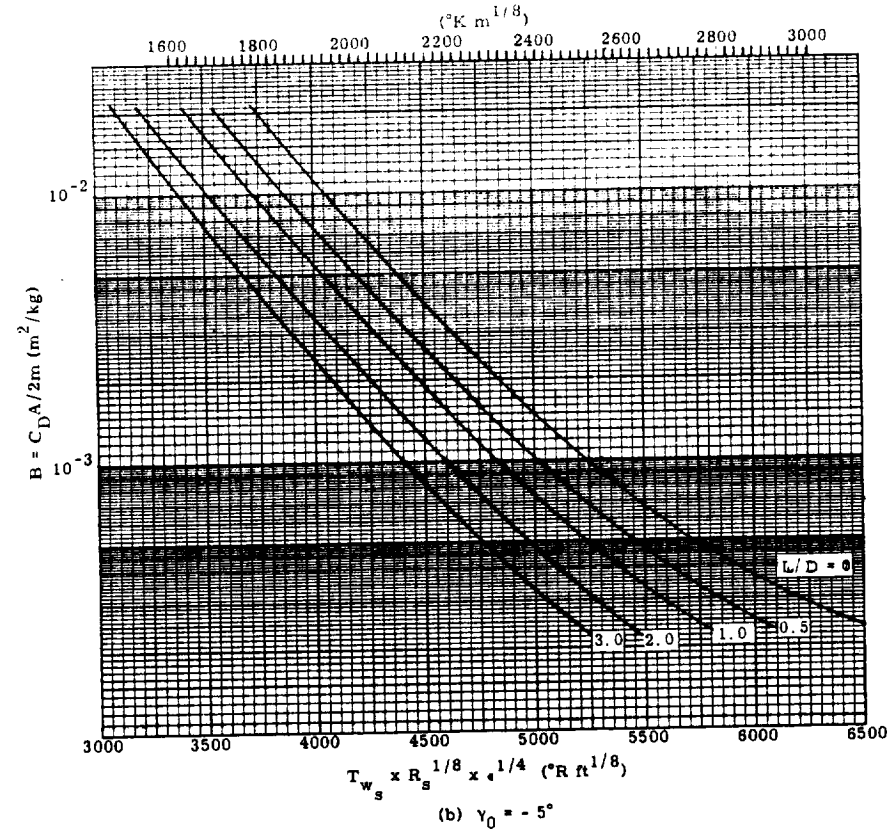

(b) $\gamma_0 = -5°$

Fig. 35. Maximum Re-Entry Stagnation Point Nose Temperature (h_0 = 400,000 (121,920 m), v_0 = 25,000 fps (7620 mps)

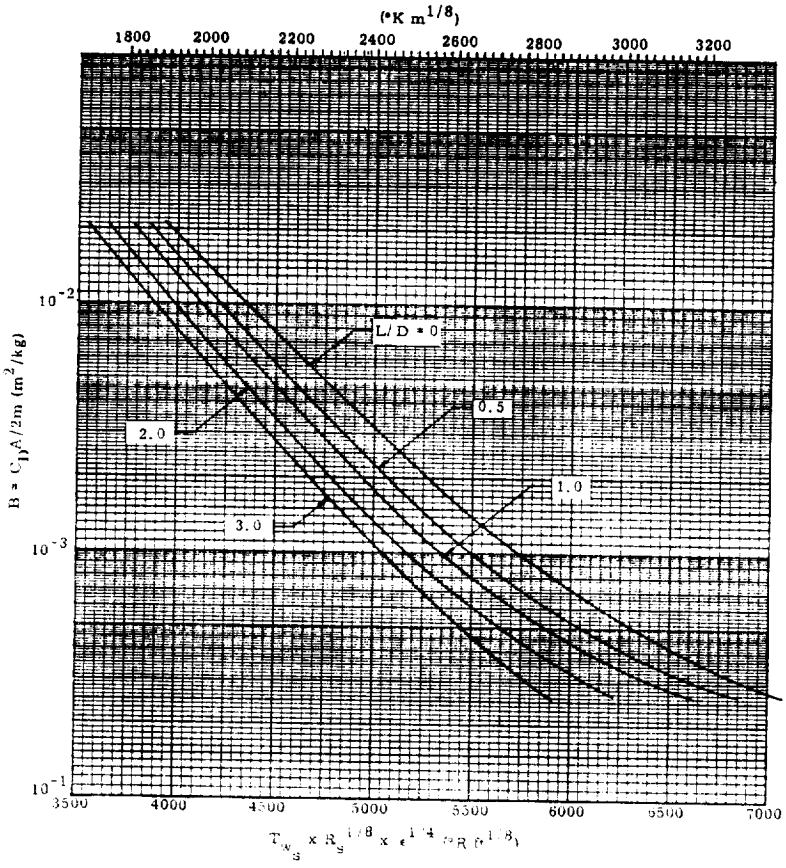

(c) $\gamma_0 = -10°$

Fig. 35. (continued)

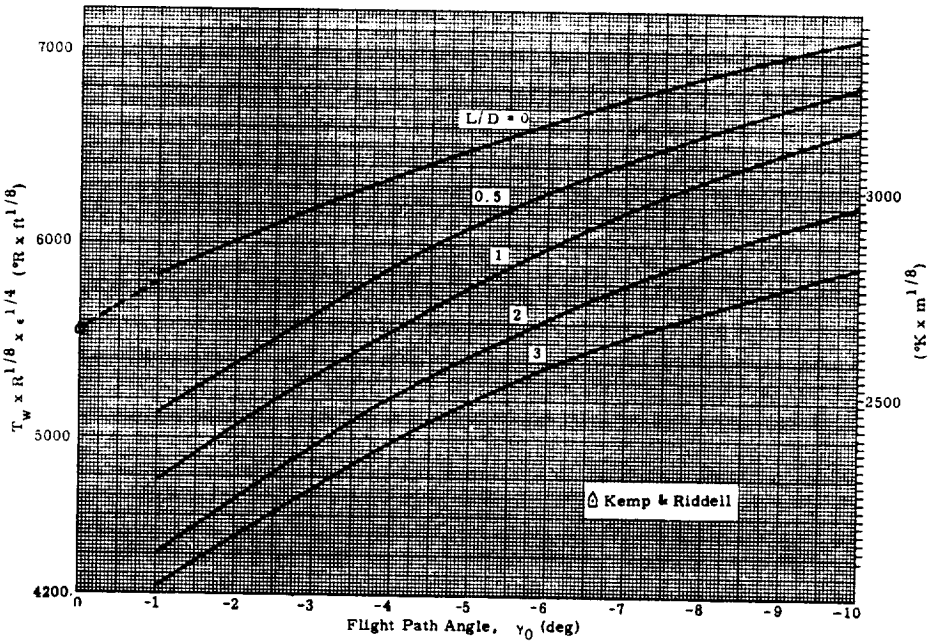

(a) $B = 0.037\ ft^2/slug = 0.234 \times 10^{-3}\ m^2/kg$, $W/C_DA = 438$ psf $= 21000$ newton/m^2

Fig. 36. Maximum Re-Entry Stagnation Point Nose Temperature Versus γ_0
($h_0 = 400{,}000$ ft $= 121{,}920$ m, $v_0 = 25{,}000$ fps $= 7620$ mps)

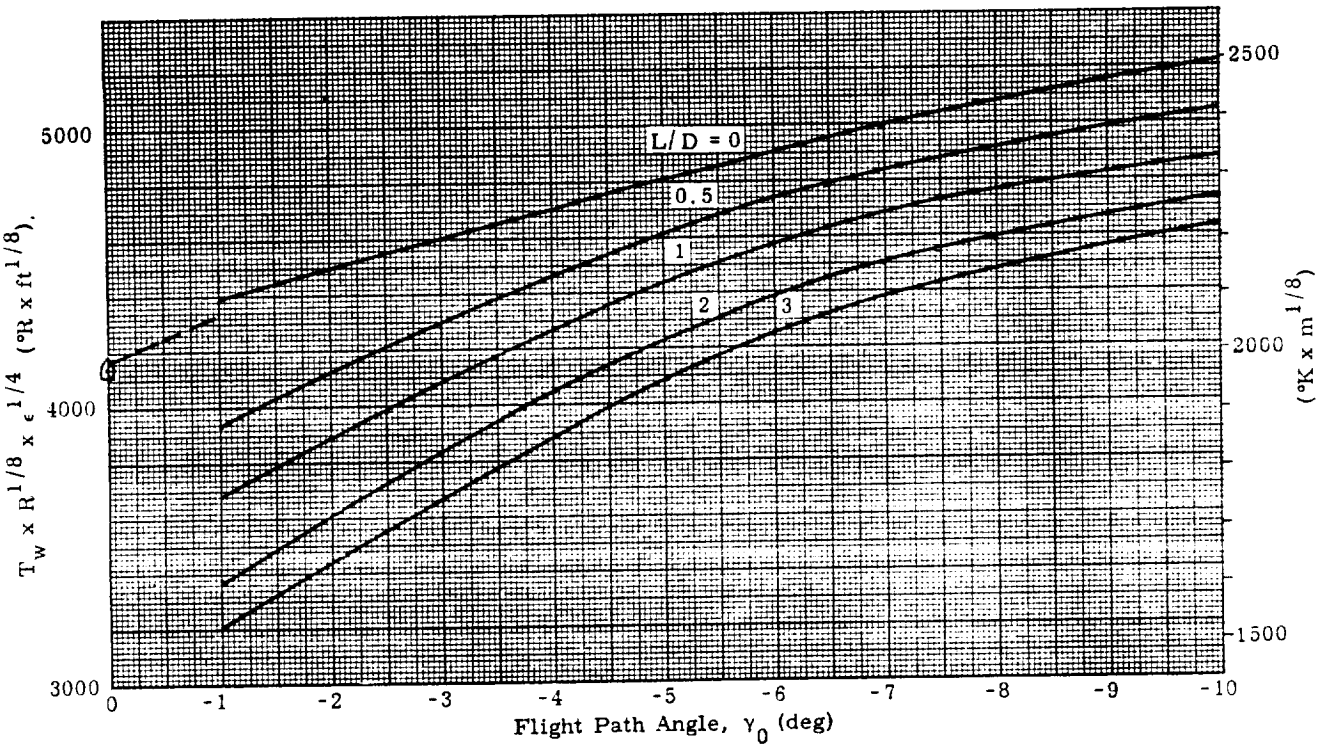

(b) B = 0.322 ft^2/slug = 2.05 x 10^{-3} m^2/kg, W/C_DA = 50 psf = 2390 newton/m^2

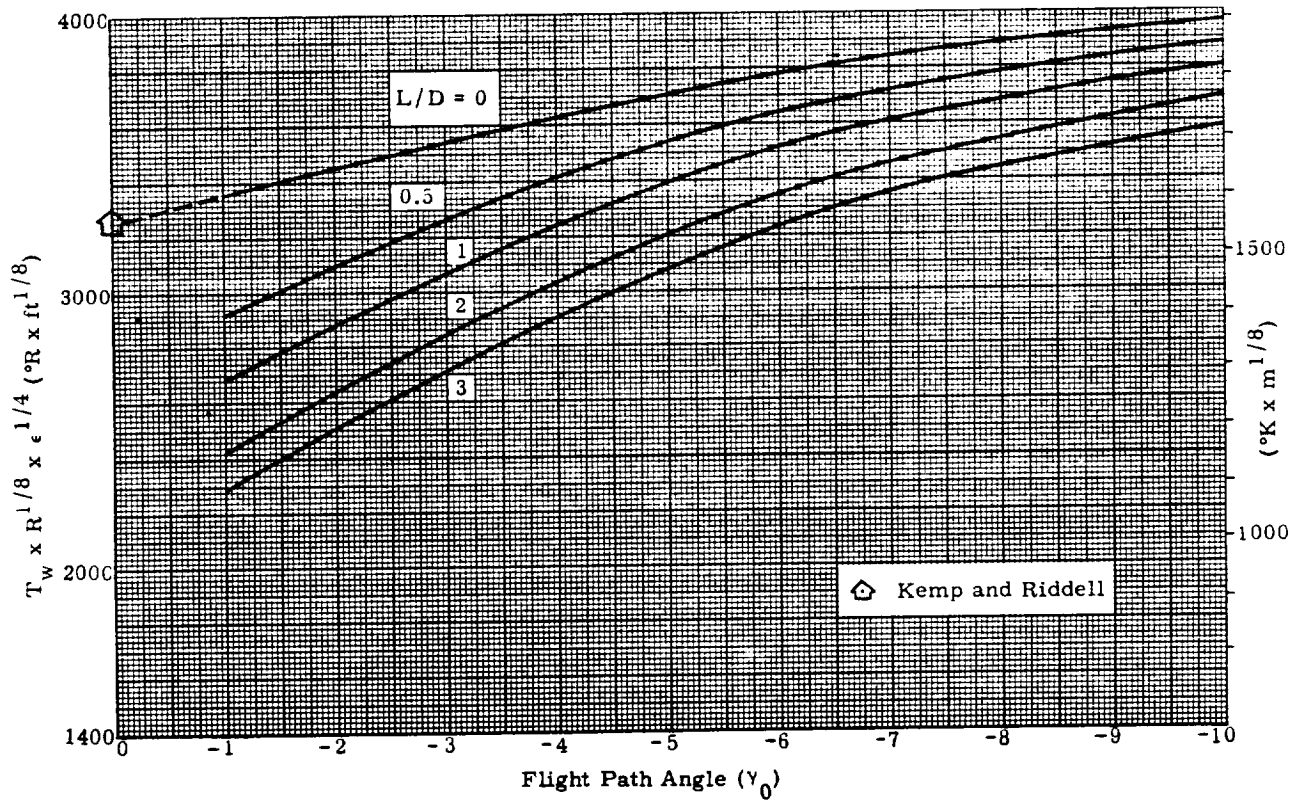

(c) B = 22 ft^2/slug = 0.0205 m^2/kg, W/C_DA = 5 psf = 239 newton/m^2

Fig. 36. (continued)

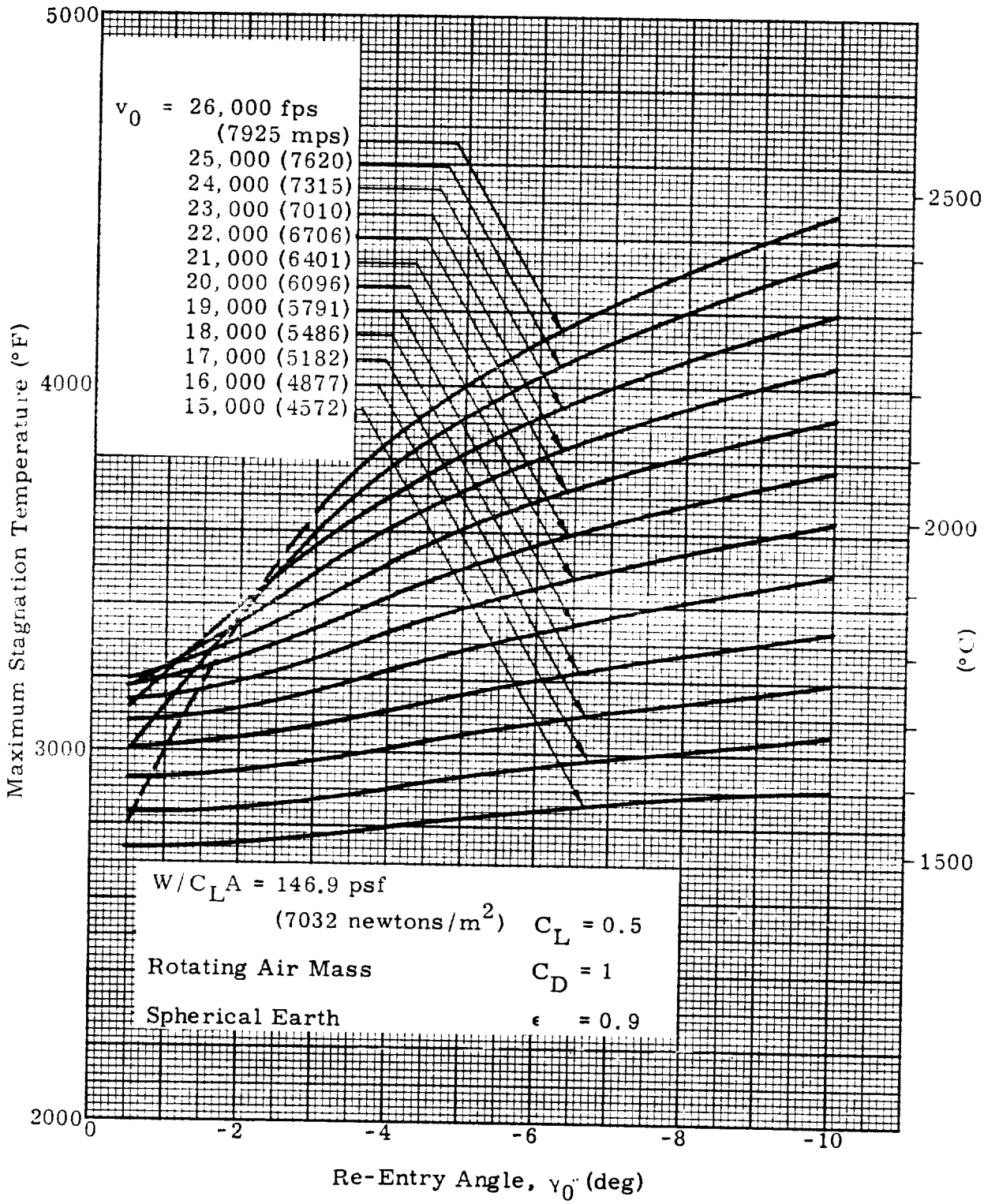

Fig. 37. Effect of Re-Entry Conditions on Maximum Stagnation Point Temperature (L/D = 0.5)

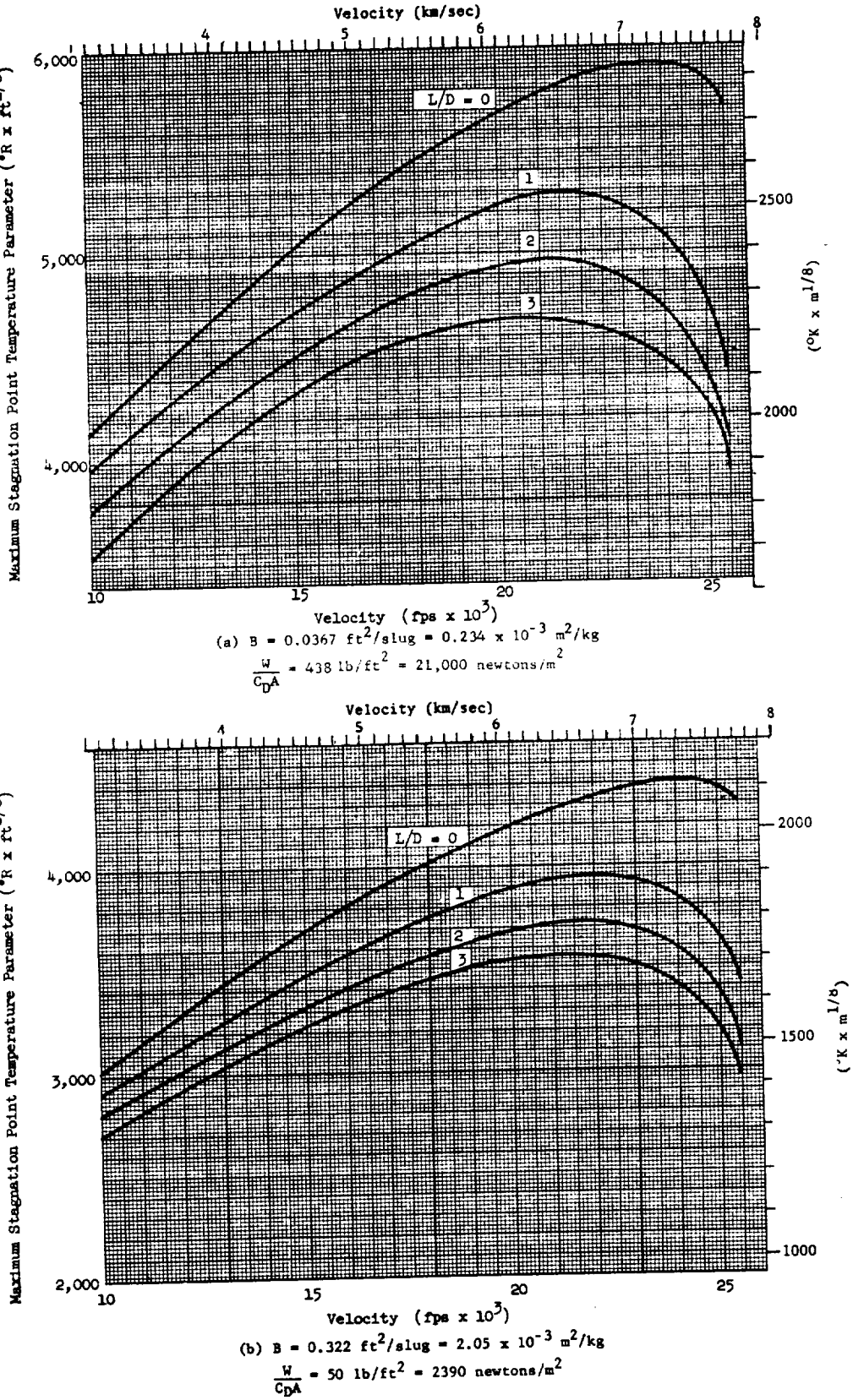

Fig. 38. Maximum Re-Entry Stagnation Point Temperature Parameter Versus Velocity (h_0 = 400,000 ft = 121,920 m; γ_0 = -1°)

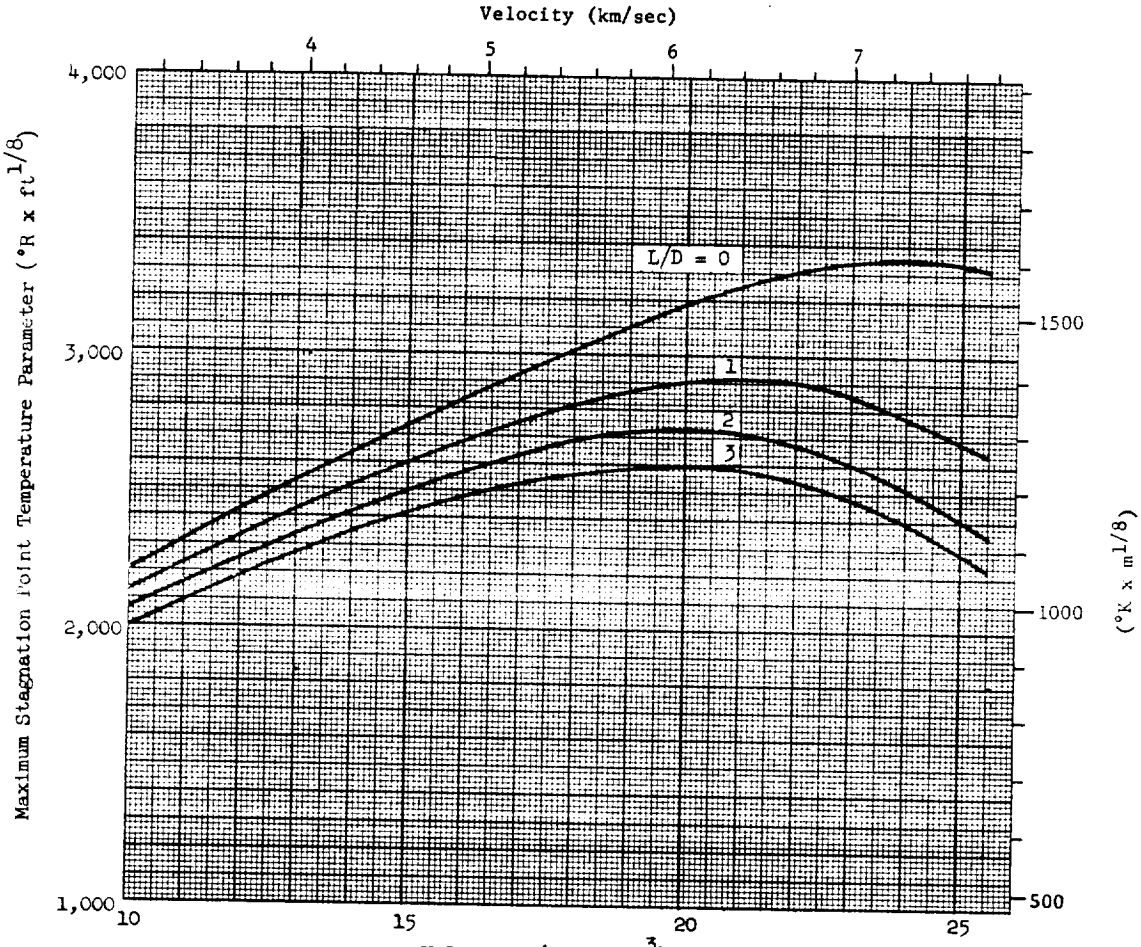

(c) B = 3.22 ft^2/slug = 20.5 x 10^{-3} m^2/kg

$\frac{W}{C_D A}$ = 5 lb/ft^2 = 239 newtons/m^2

Fig. 38. (continued)

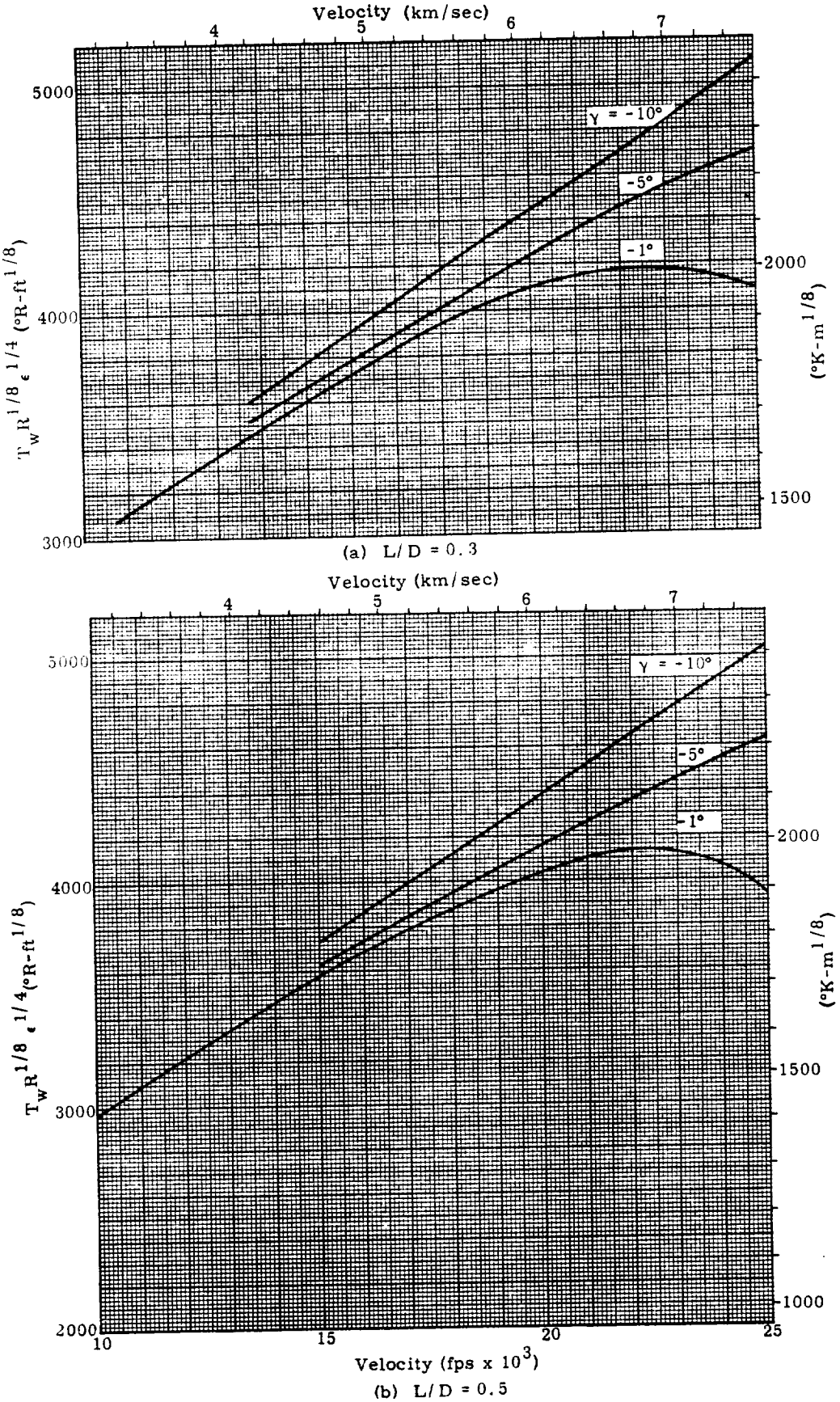

Fig. 39. Maximum $T_w R^{1/8} \epsilon^{1/4}$ Versus Re-Entry Velocity (h_0 = 400,000 ft = 121,920 m, $\frac{W}{C_D A}$ = 50 psf = 2390 newtons/m^2

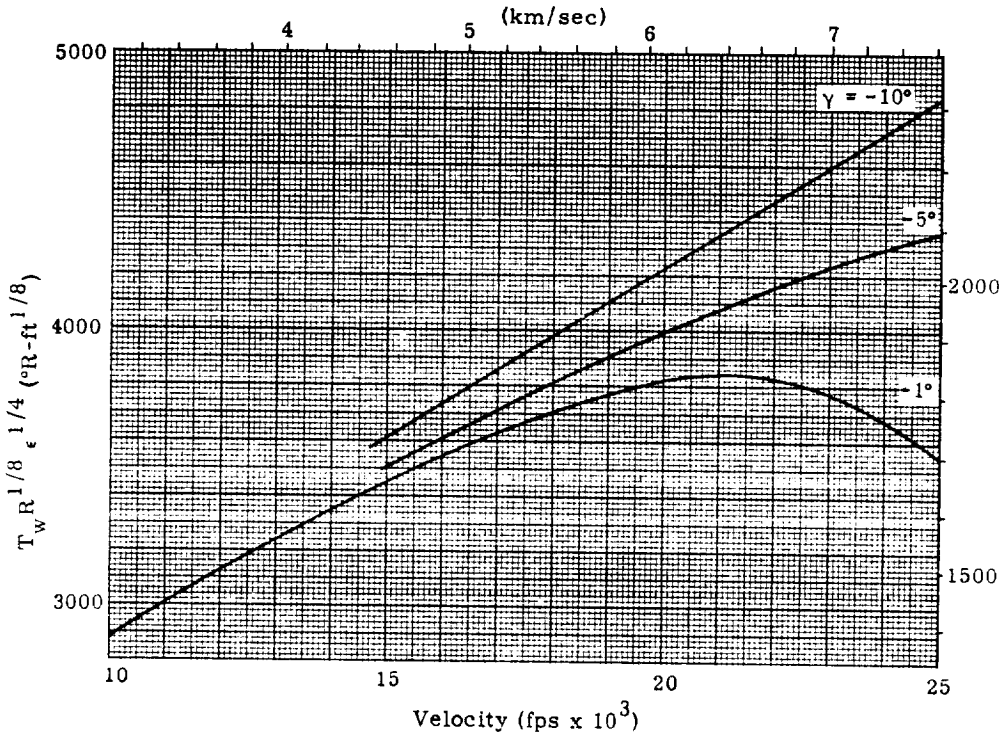

(c) L/D = 1.25

$$\left[\left(TR^{1/8}\,\epsilon^{1/4}\right)_{\frac{W}{C_D A}} = X\right] \simeq \left[\left(TR^{1/8}\,\epsilon^{1/4}\right)_{\frac{W}{C_D A}} = 50\right]\left(\frac{X}{50}\right)^{1/8} \simeq \left[1200\,(q)^{1/4}_{\frac{W}{C_D A}} = X\right] \text{ Btu/ft}^2\text{-sec}$$

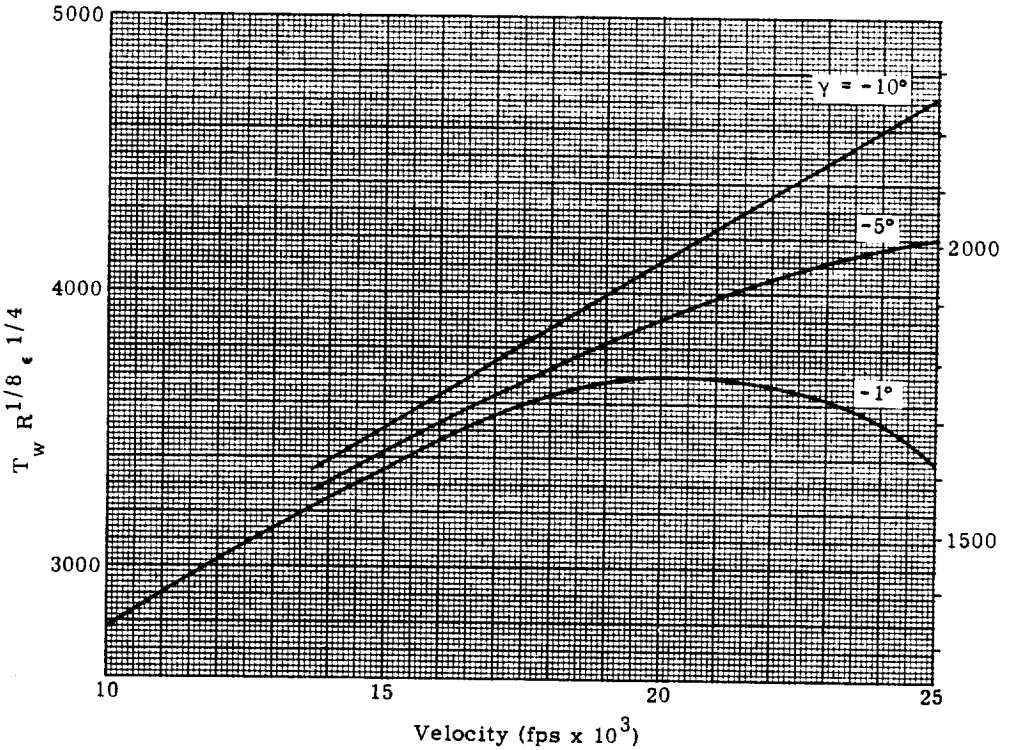

(d) L/D = 2

Fig. 39. (continued)

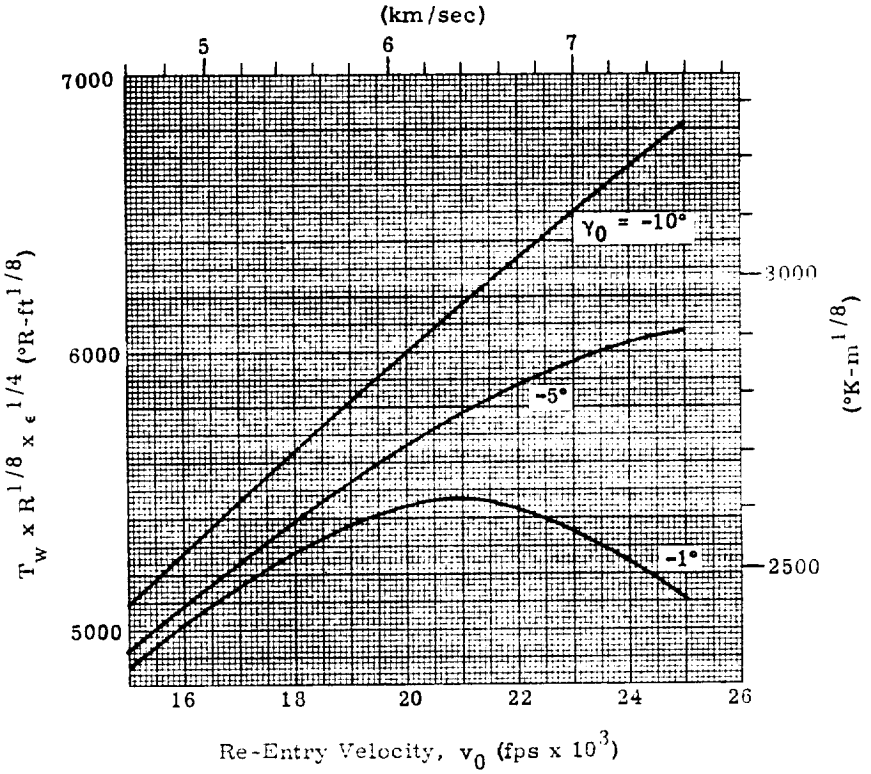

(a) L/D = 0.5

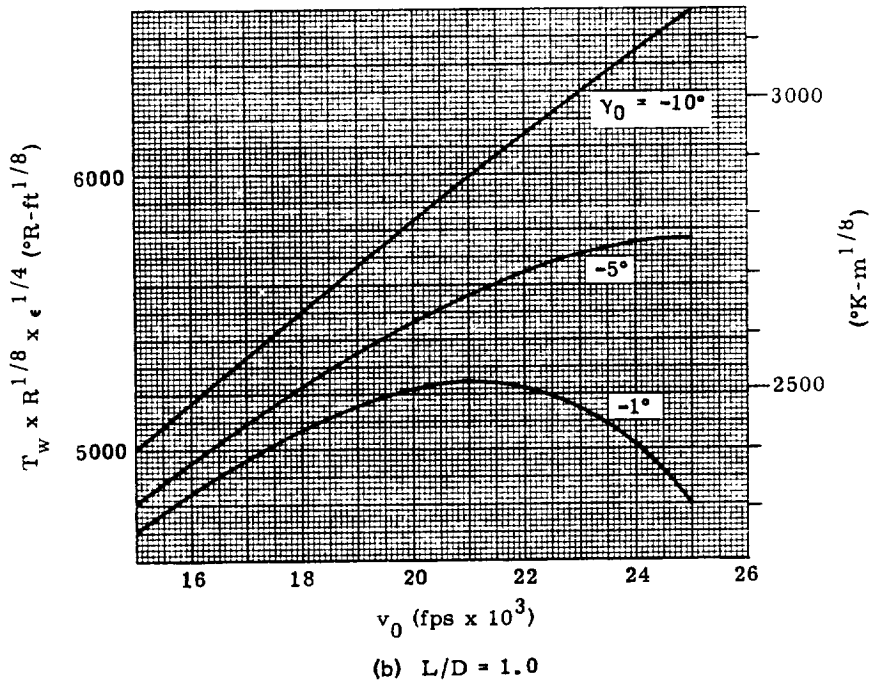

(b) L/D = 1.0

Fig. 40. Maximum Re-Entry Stagnation Point Nose Temperature Versus Velocity (h_0 = 400,000 ft = 121,920 m; W/C_DA = 438 psf = 21,000 newtons/m^2

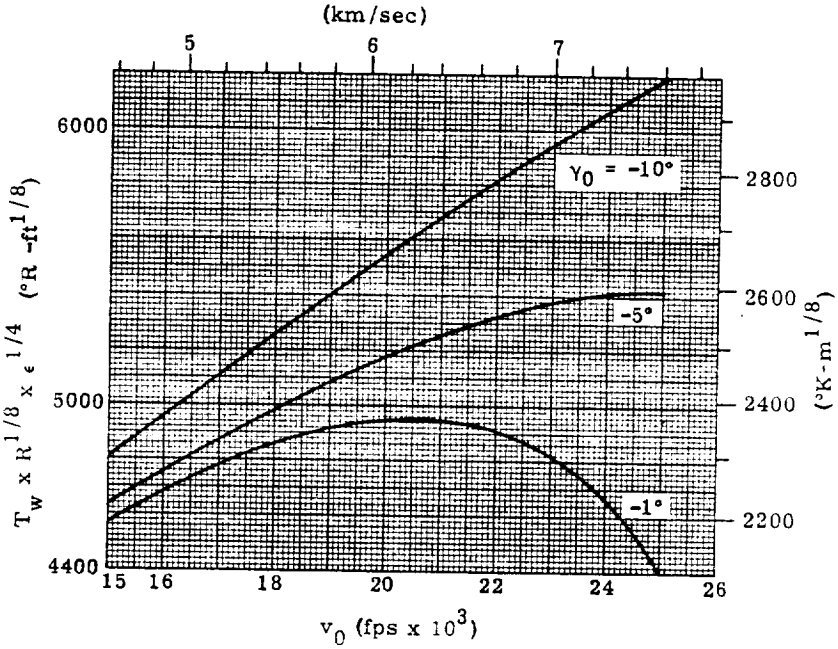

(c) L/D = 2

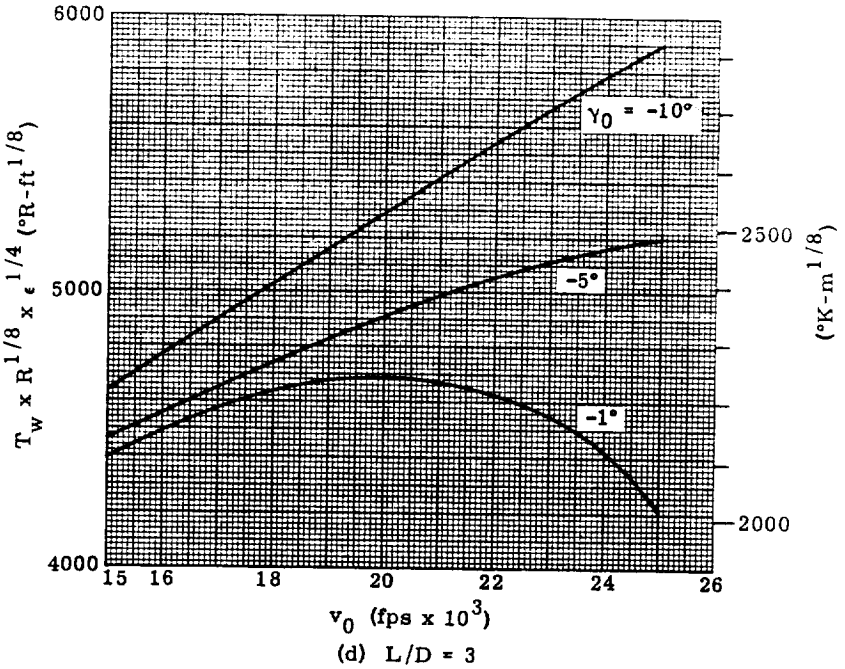

(d) L/D = 3

Fig. 40. (continued)

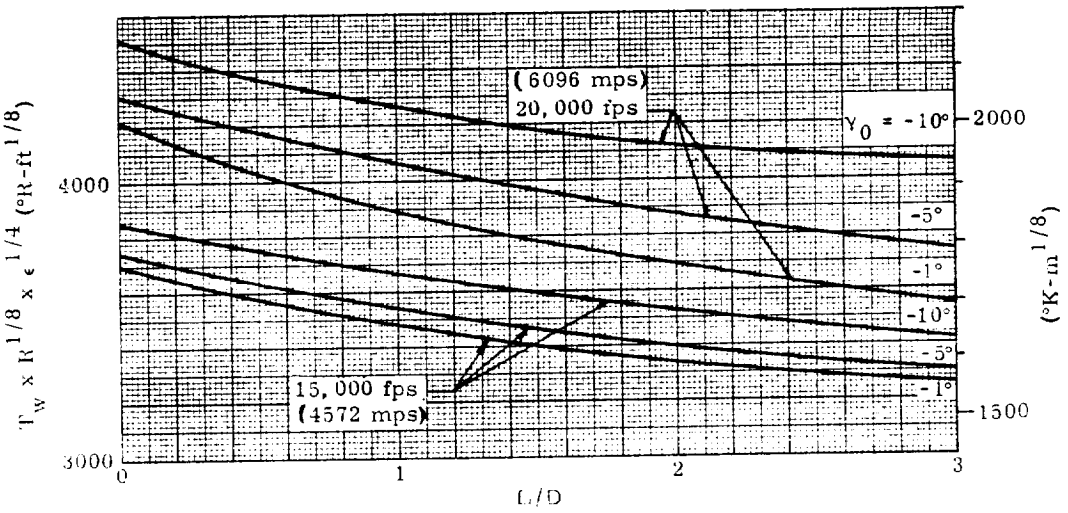

$$\left(T_w R^{1/8} \epsilon^{1/4}\right) W/C_D A = X \simeq \left(T_w R^{1/8} \epsilon^{1/4}\right) W/C_D A = 50 \left(\frac{X}{50}\right)^{1/8} \simeq 1200 (q)^{1/4} \quad W/C_D A = X \text{ Btu/ft}^2\text{-sec}$$

(a) $W/C_D A$ = 50 psf = 2390 newtons/m^2

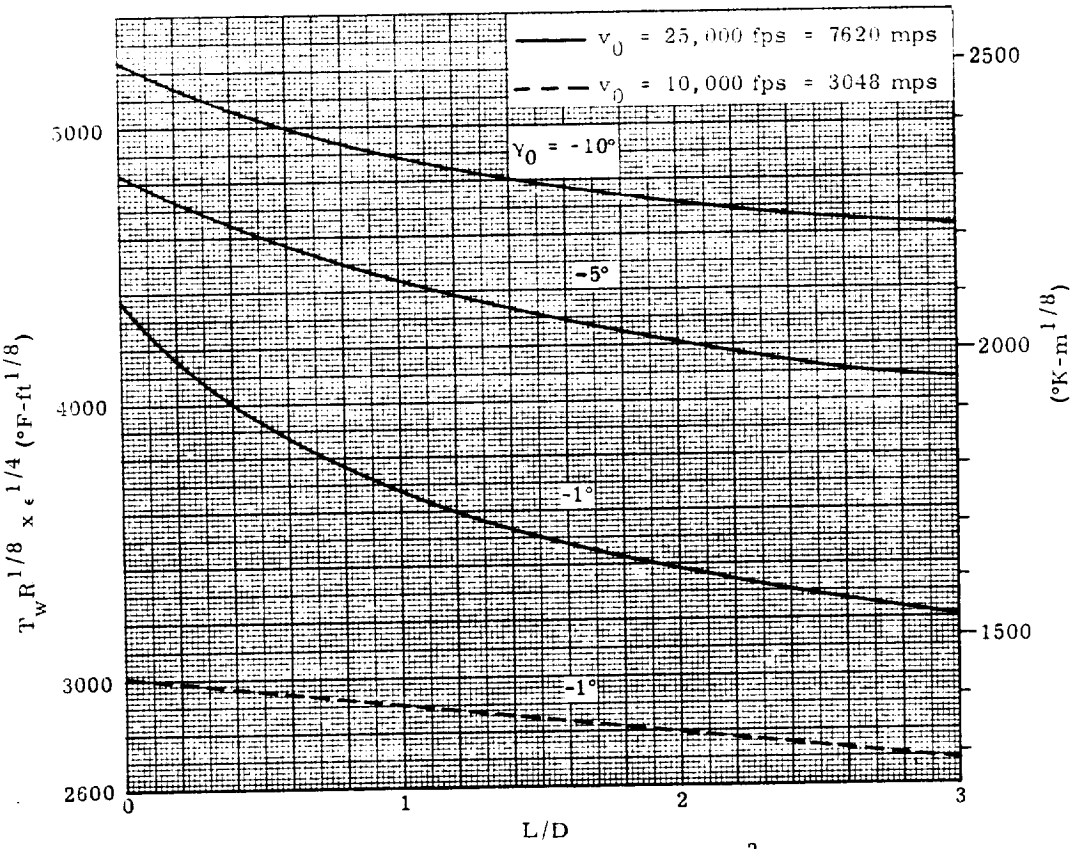

(b) $W/C_D A$ = 50 psf = 2390 newtons/m^2

Fig. 41. $T_w R^{1/8} \epsilon^{1/4}$ Versus Lift-Drag Ratio (h_0 = 400,000 ft = 121,920 m)

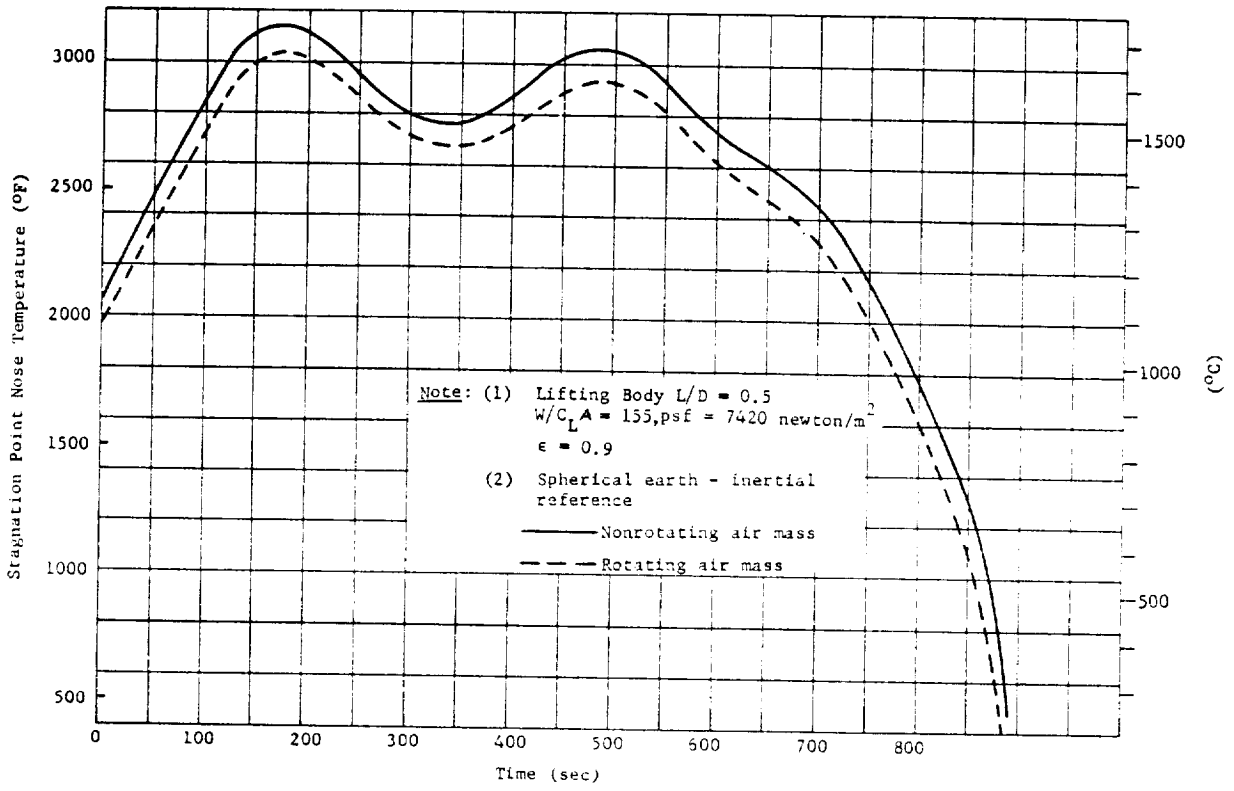

Fig. 42. Equilibrium Temperature History, with and Without Rotating Air Mass

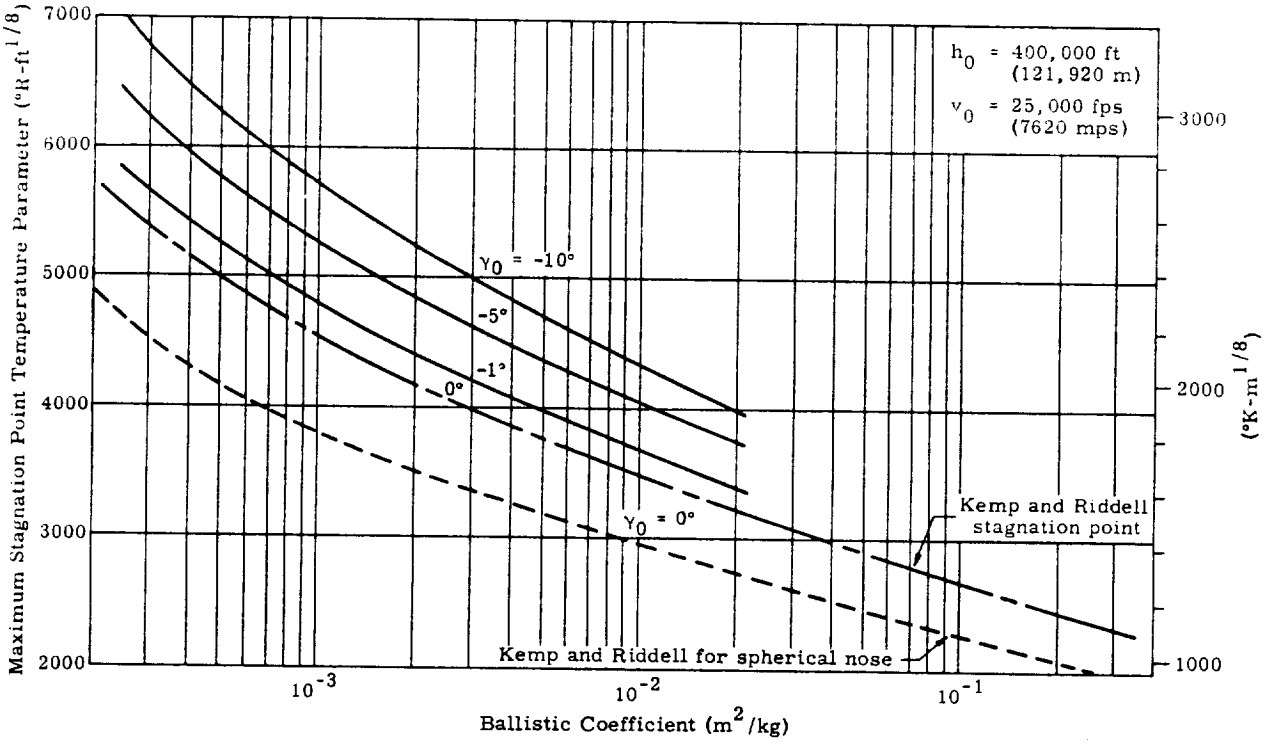

Fig. 43a. Maximum Stagnation Point Temperature Parameter Versus Ballistic Coefficient (ballistic re-entry--L/D = 0)

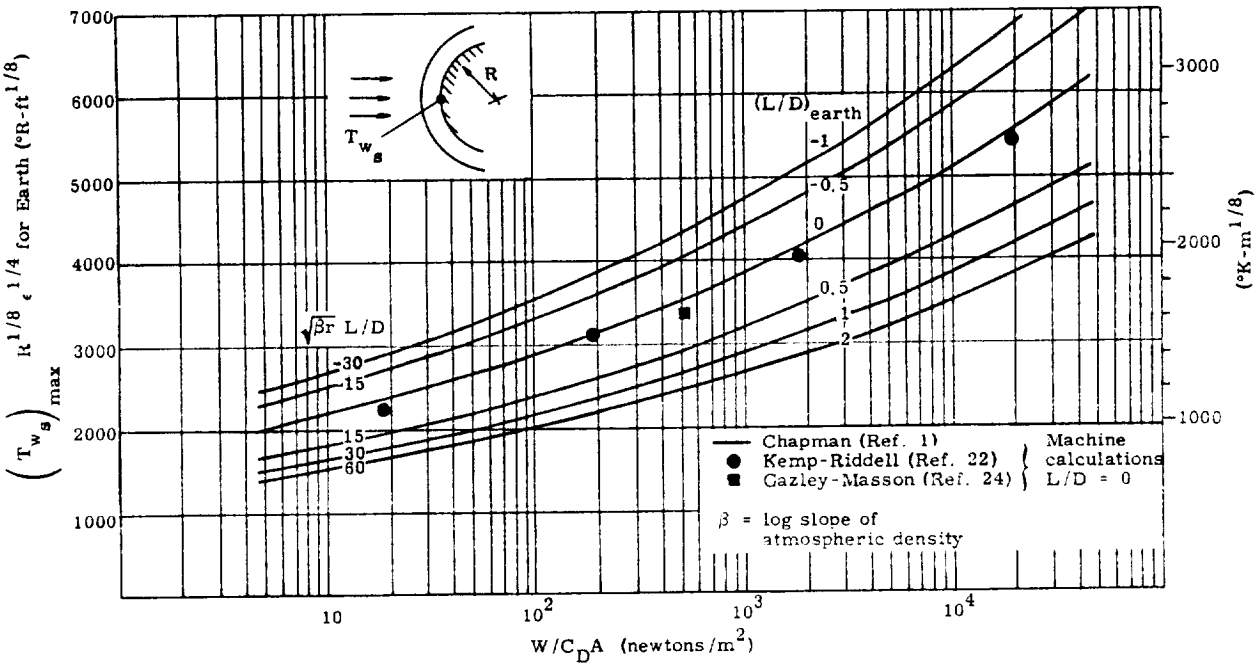

Fig. 43b. Maximum Radiation-Equilibrium Temperature at Laminar Stagnation Point for Entry from Decaying Orbits into Earth Atmosphere (Ref. 1)

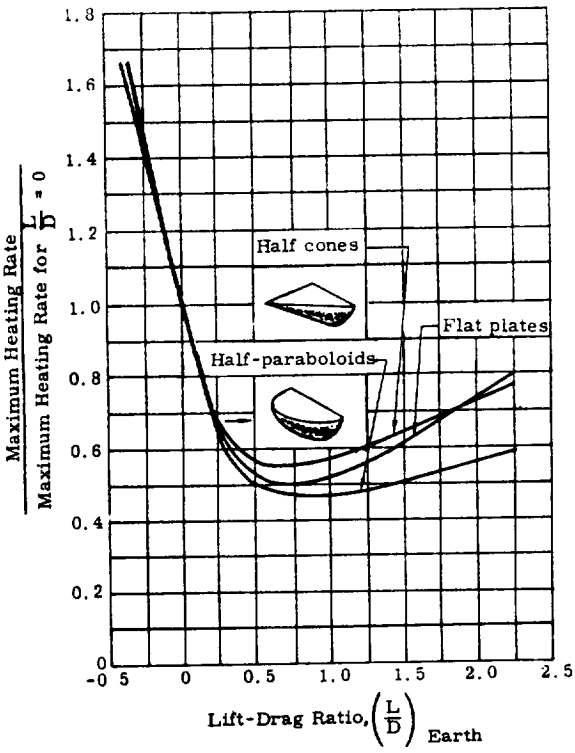

Fig. 44. Effect of Lift-Drag Ratio on Maximum Laminar Heating Rate at Stagnation Point for Entry from Decaying Orbits

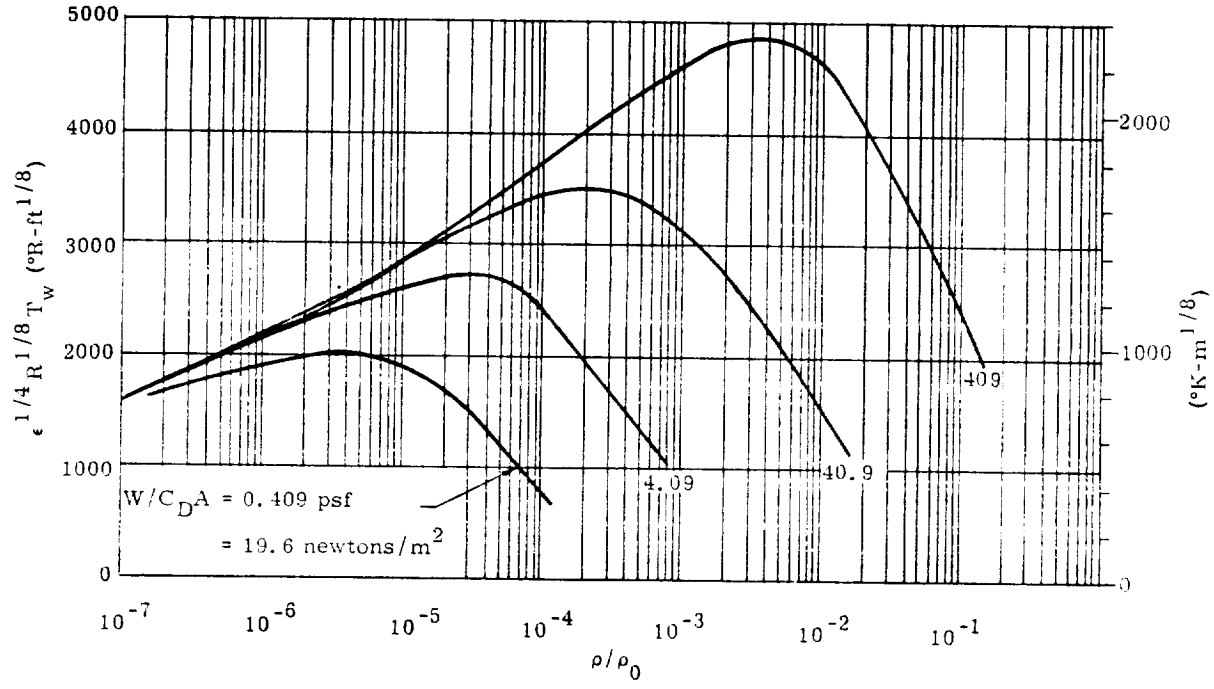

Fig. 45a. Surface Temperature Parameter $\epsilon^{1/4} R^{1/8} T_w$ as a Function of Air Density Ratio ρ/ρ_0. Simple drag bodies (Ref. 22)

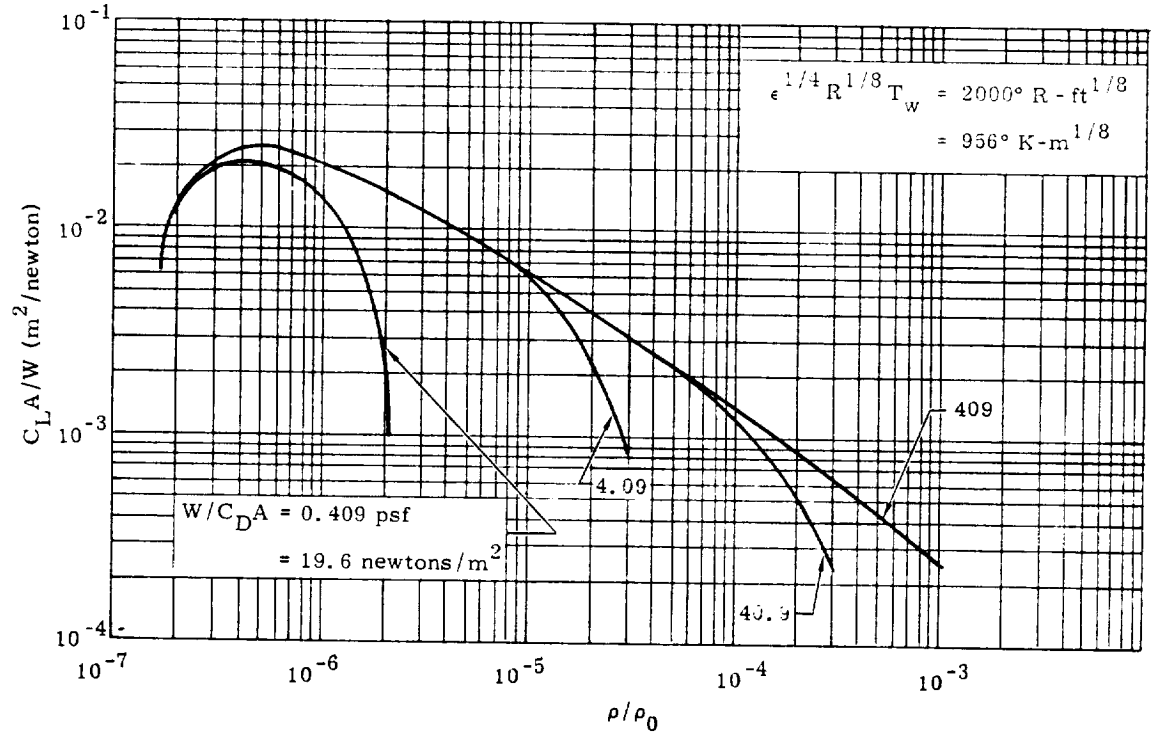

Fig. 45b. Lift Parameter C_LA/W as a Function of Air Density Ratio ρ/ρ_0 for Several Values of the Drag Parameter W/C_DA. Constant Heat Transfer Trajectories (Ref. 22)

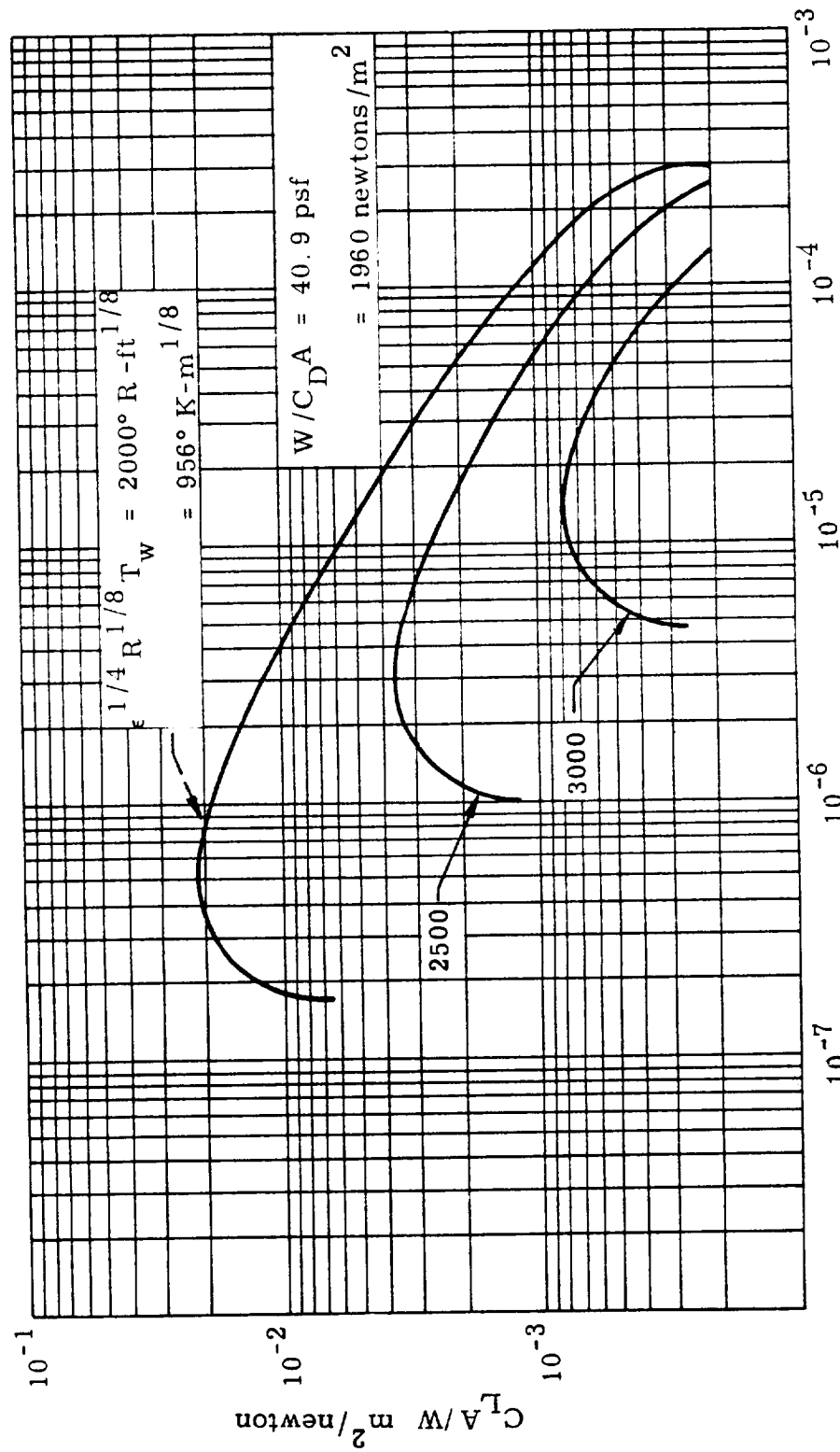

Fig. 45c. Lift Parameter $C_L A/W$ as a Function of Air Density Ratio ρ/ρ_0 for Several Values of the Surface Temperature Parameter $\epsilon^{1/4} R^{1/8} T_w$. (Constant Heat Transfer Trajectories) (Ref. 22)

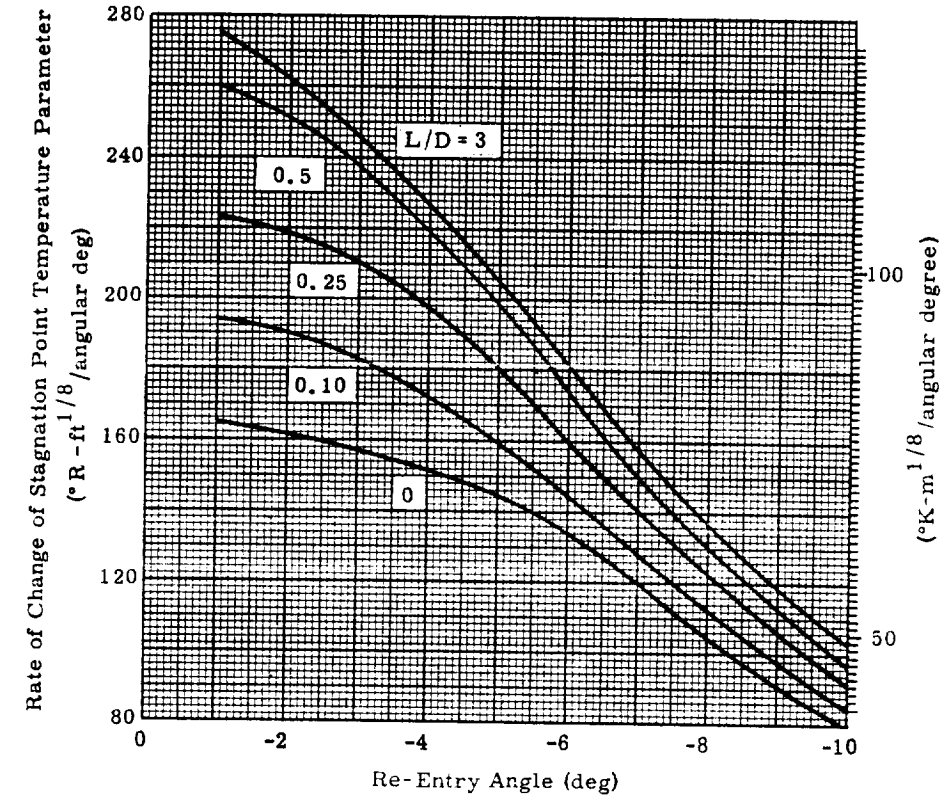

(a) B = 0.0367 ft^2/slug = 0.234 x 10^{-3} m^2/kg

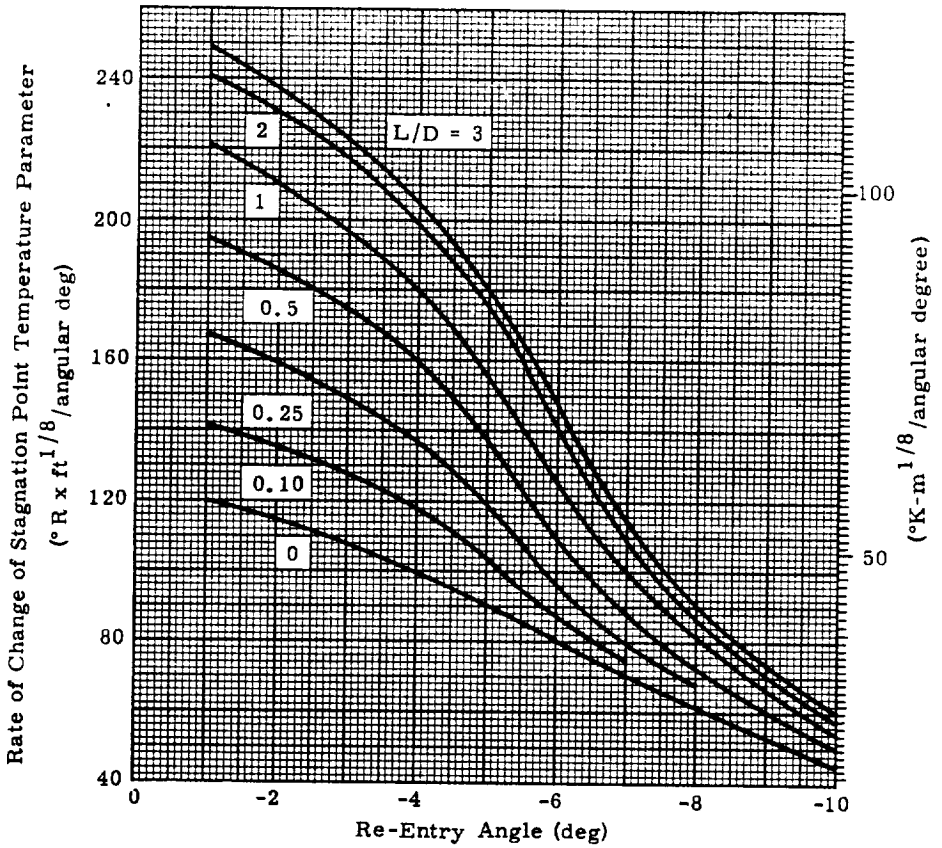

(b) B = 0.322 ft^2/slug = 2.05 x 10^{-3} m^2/kg

Fig. 46. Rate of Change of Stagnation Point Temperature Parameter as a Function of Re-Entry Angle (h_0 = 400,000 ft = 121,920 m, v_0 = 25,000 fps = 7620 mps)

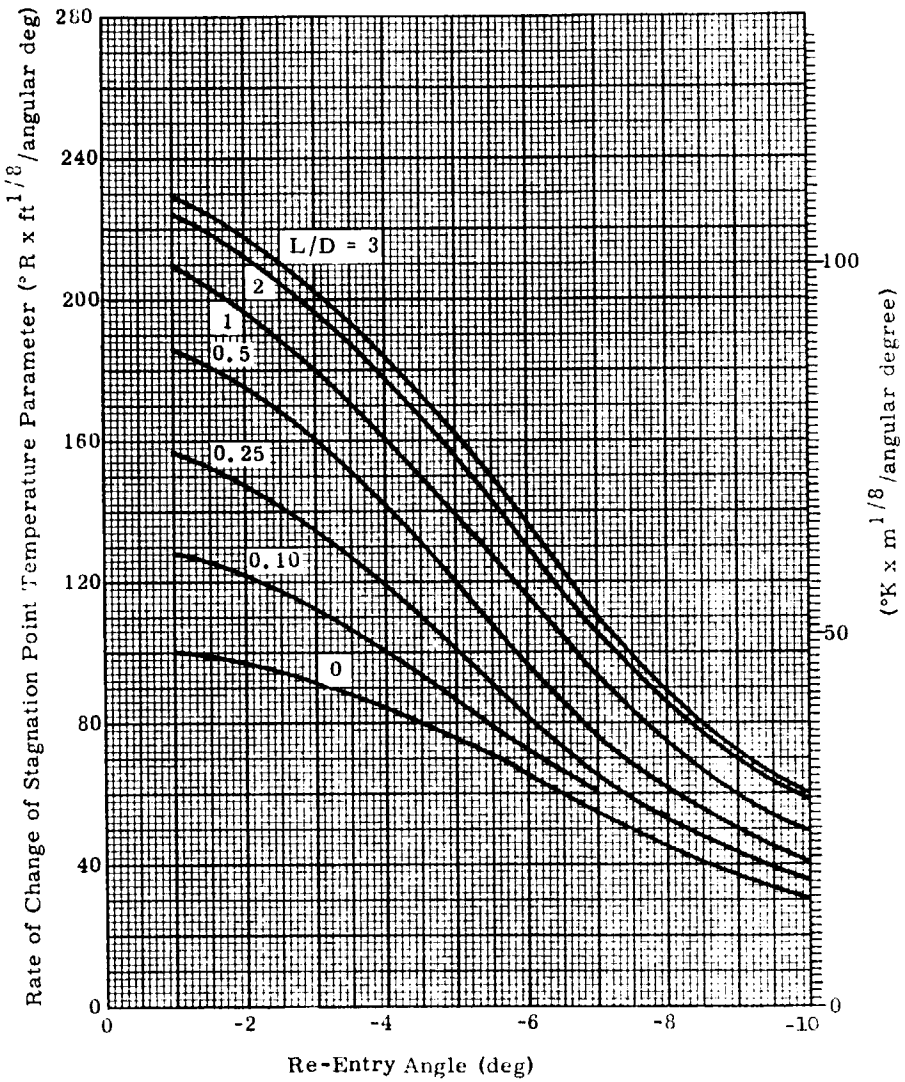

(c) B = 3.22 ft^2/slug = 20.5 x 10^{-3} m^2/kg

Fig. 46. (continued)

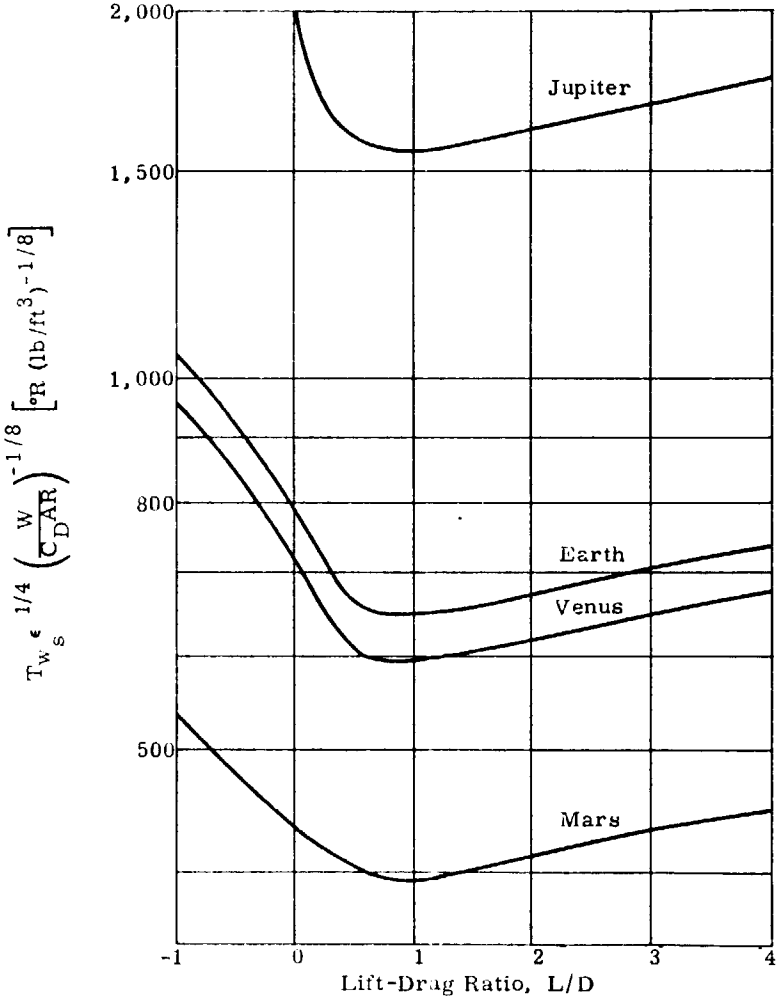

$T_{w_s} \epsilon^{1/4} \left(\frac{W}{C_D AR}\right)^{-1/8}$ [°R (lb/ft^3)$^{-1/8}$]

Fig. 47. Maximum Surface Temperature for Entry into Various Planets from Decaying Orbits

(v_0/v_c = 1, γ_0 = 0°) (Ref 1)

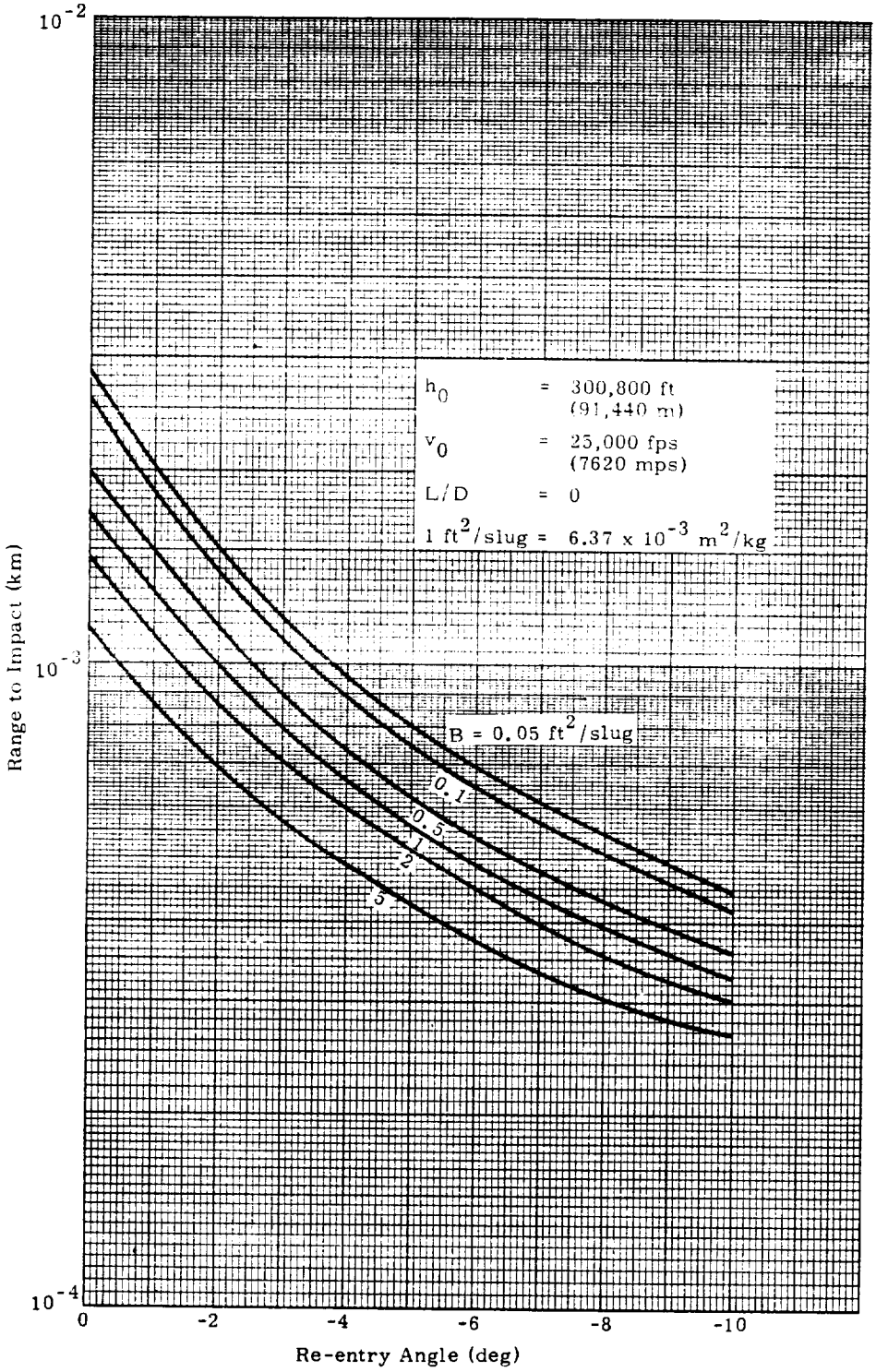

Fig. 48. Range to Impact Versus Re-entry Angle

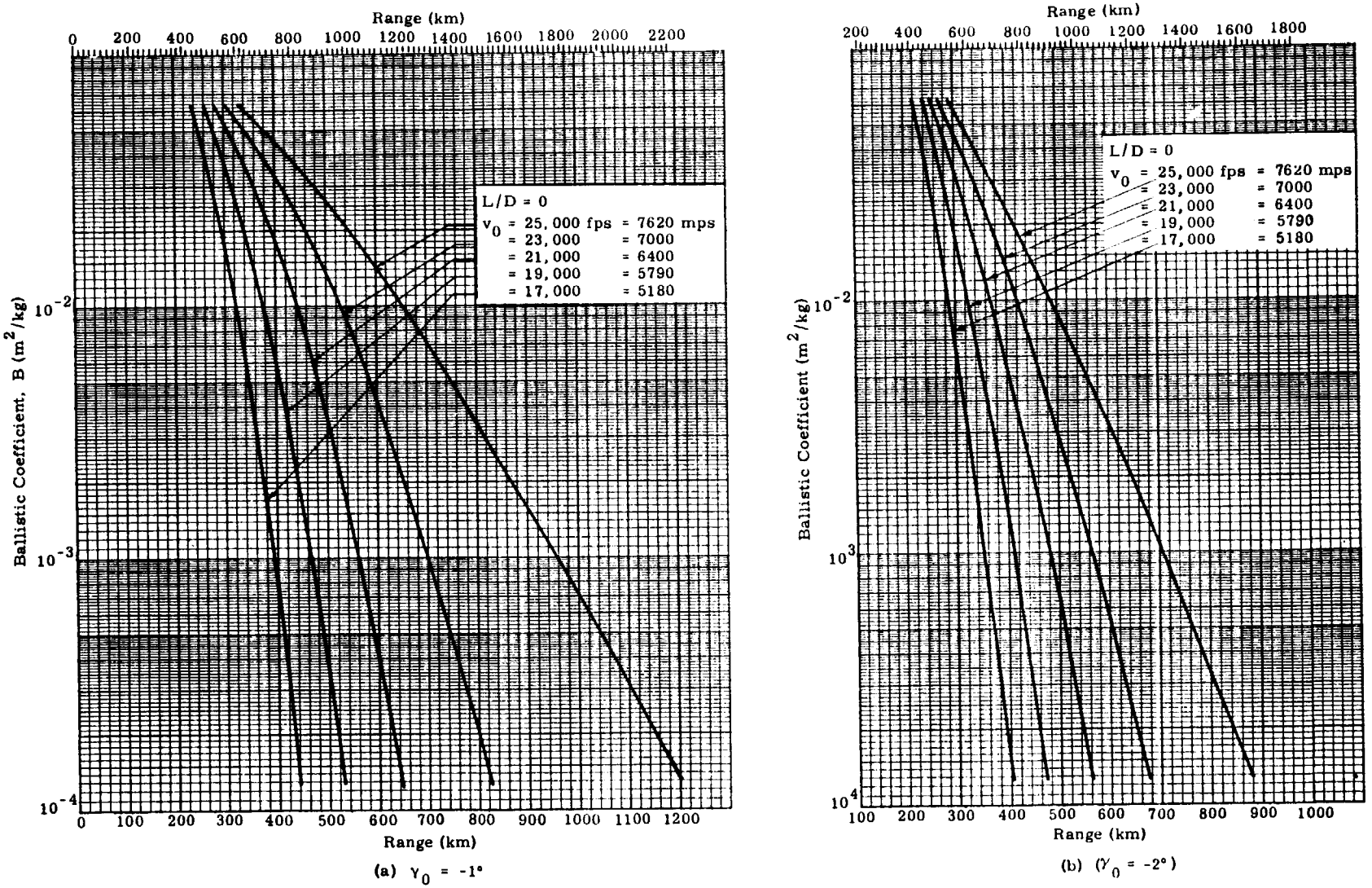

Fig. 49. Range Attained in Descent from 300,000 ft (91,440 m) to Sea Level (L/D = 0)

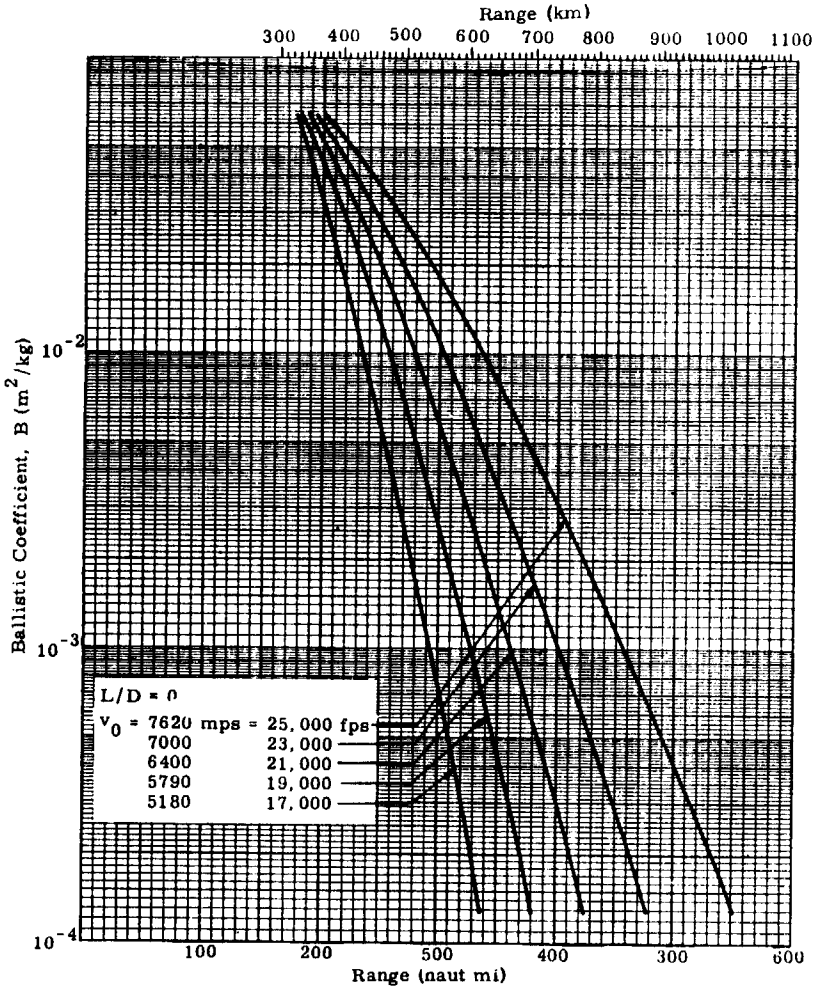

(c) ($\gamma_0 = -4°$)

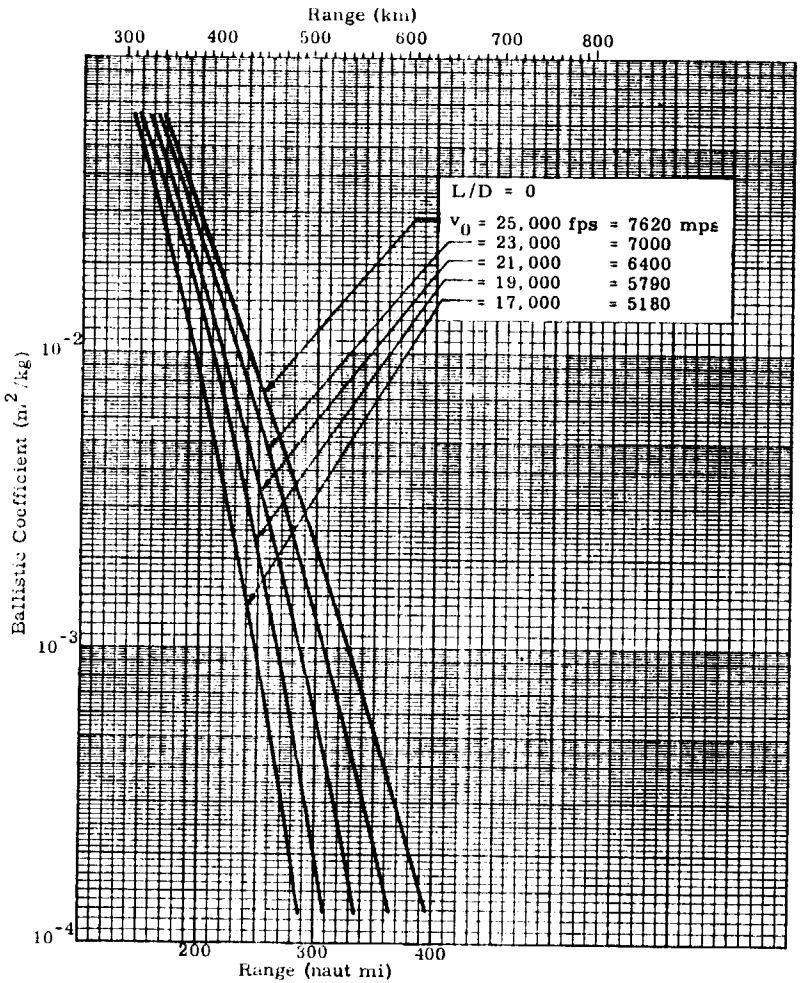

(d) ($\gamma_0 = -6°$)

Fig. 49. (continued)

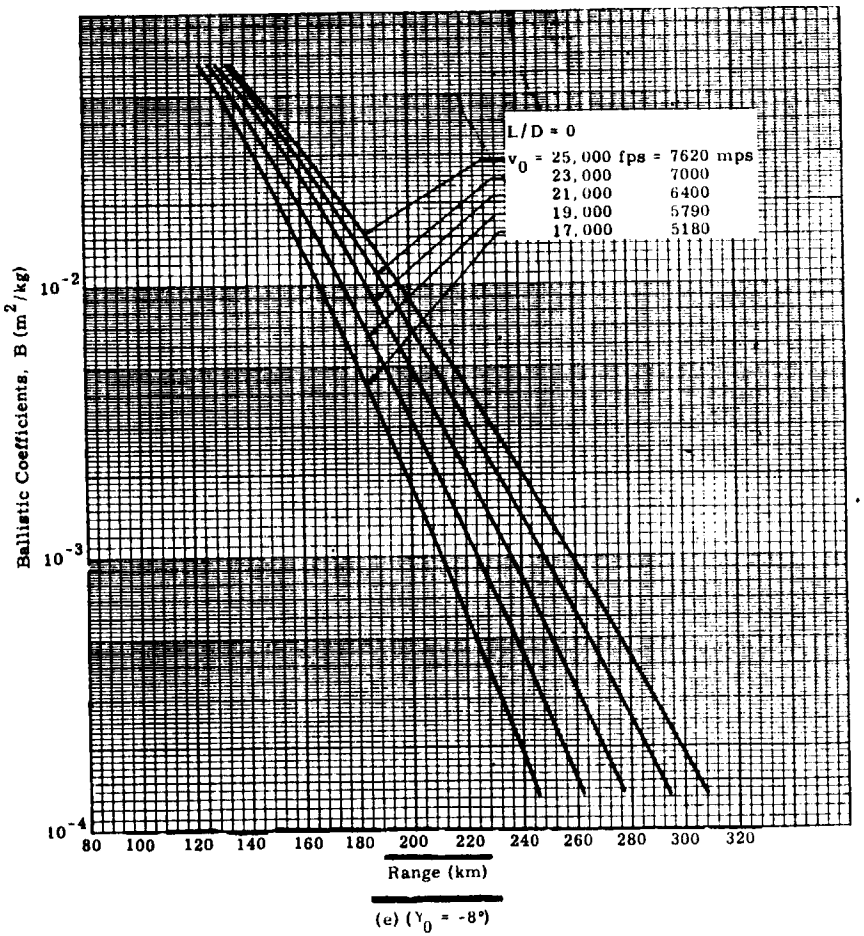

(e) (γ_0 = -8°)

Fig. 49. (continued)

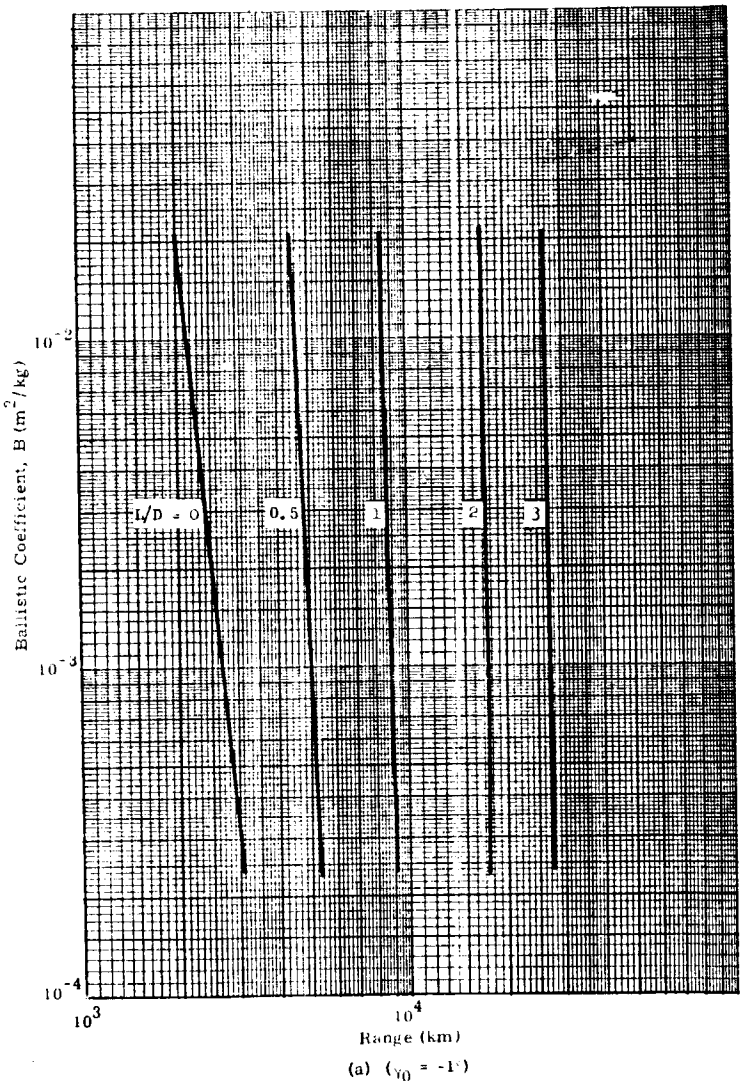

(a) (γ_0 = -1°)

Fig. 50. Range to Impact from 400,000 ft = 121,920 m (v_0 = 25,000 fps = 7620 mps)

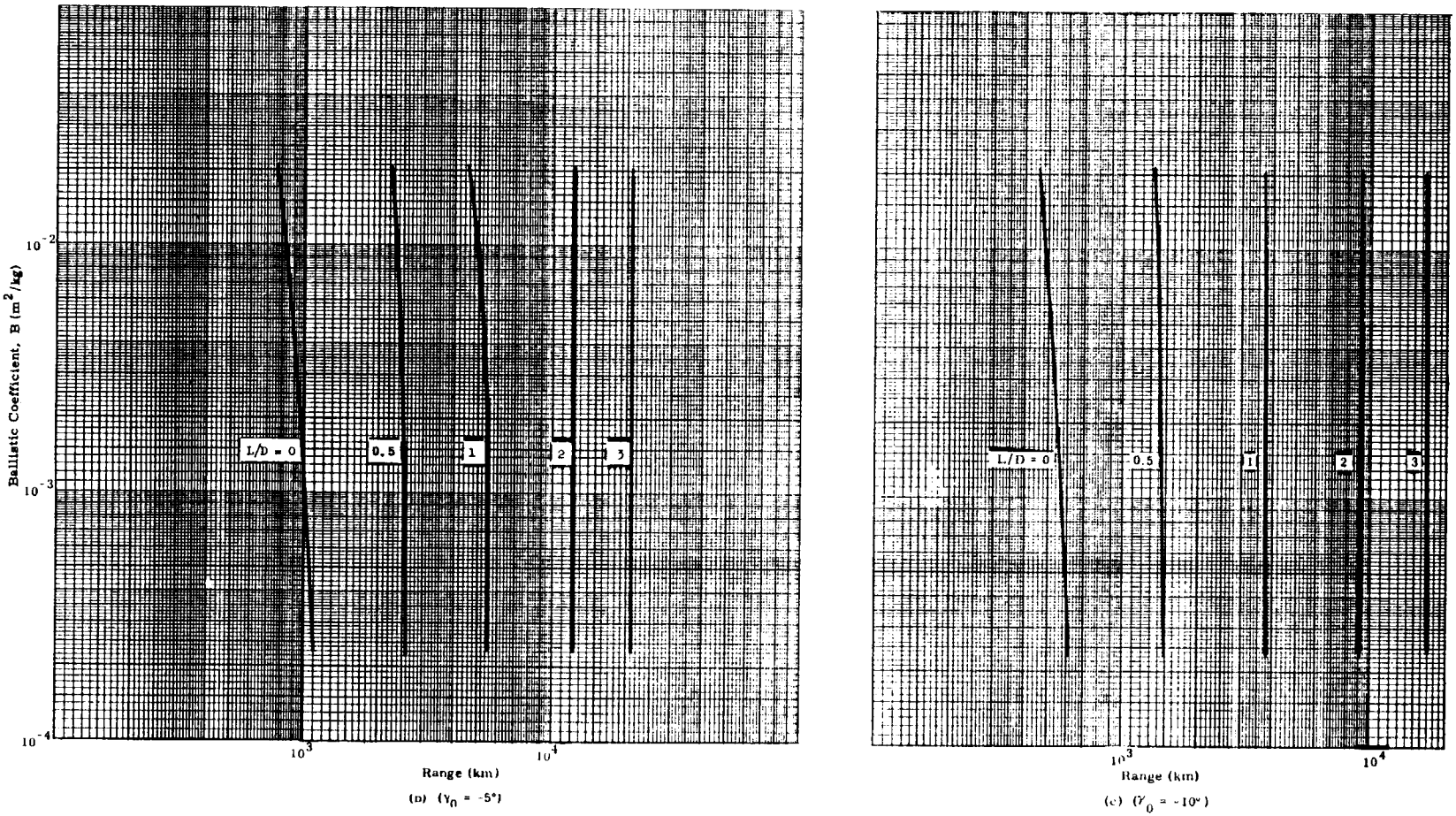

Fig. 50. (continued)

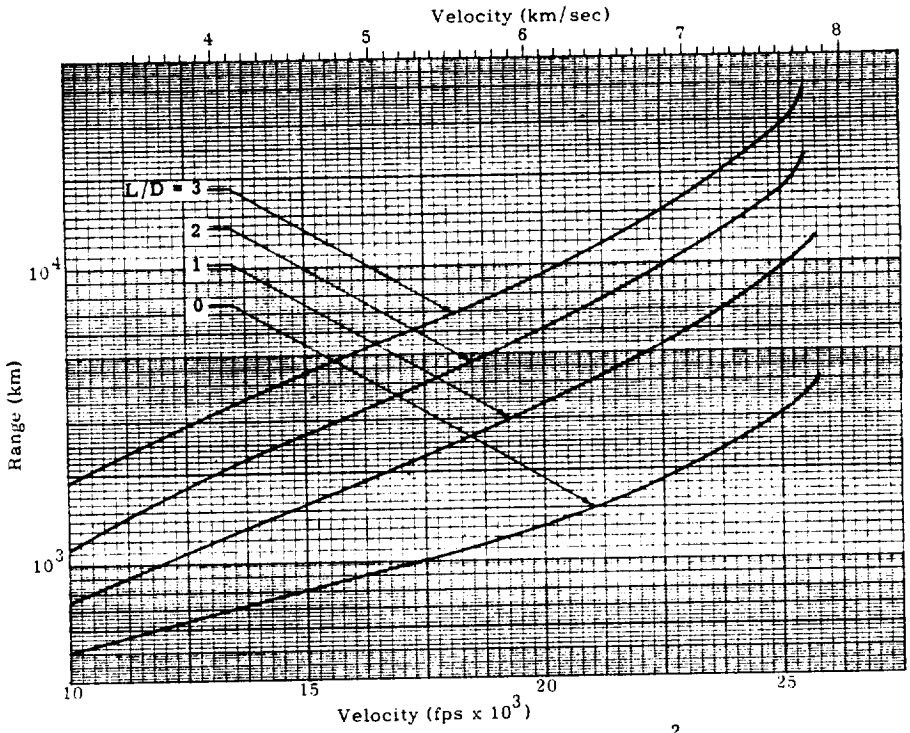

(a) W/C_DA = 438 psf = 21,000 newton/m^2,

B = 0.0367 ft^2/slug = 0.234 x 10^{-3} m^2/kg

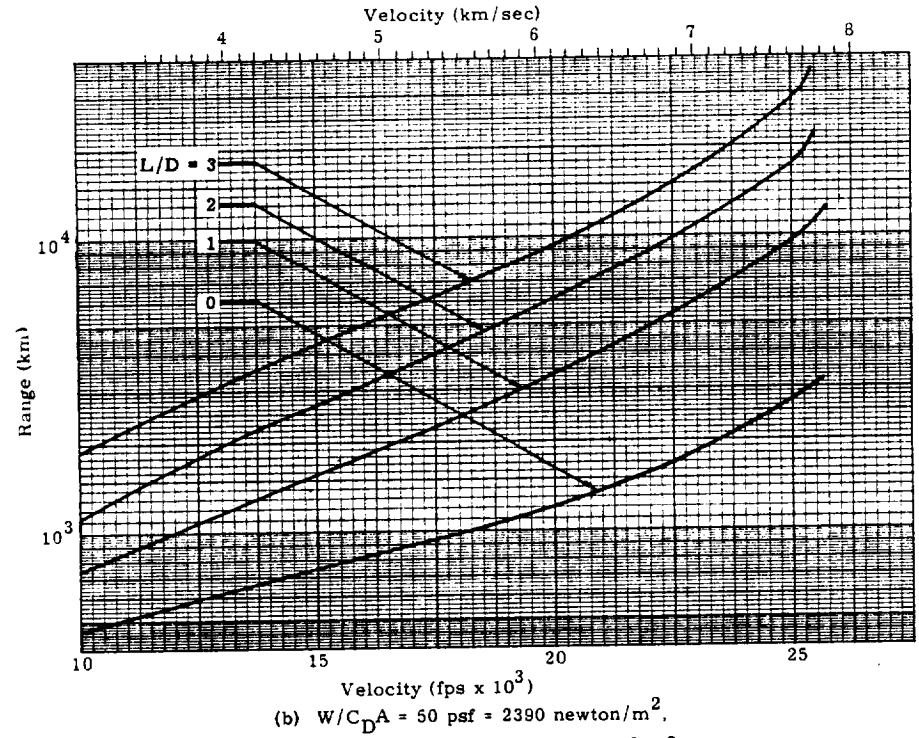

(b) W/C_DA = 50 psf = 2390 newton/m^2,

B = 0.322 ft^2/slug = 2.04 x 10^{-3} m^2/kg

Fig. 51. Range to Impact from 400,000 ft = 121,920 m (γ_0 = -1°)

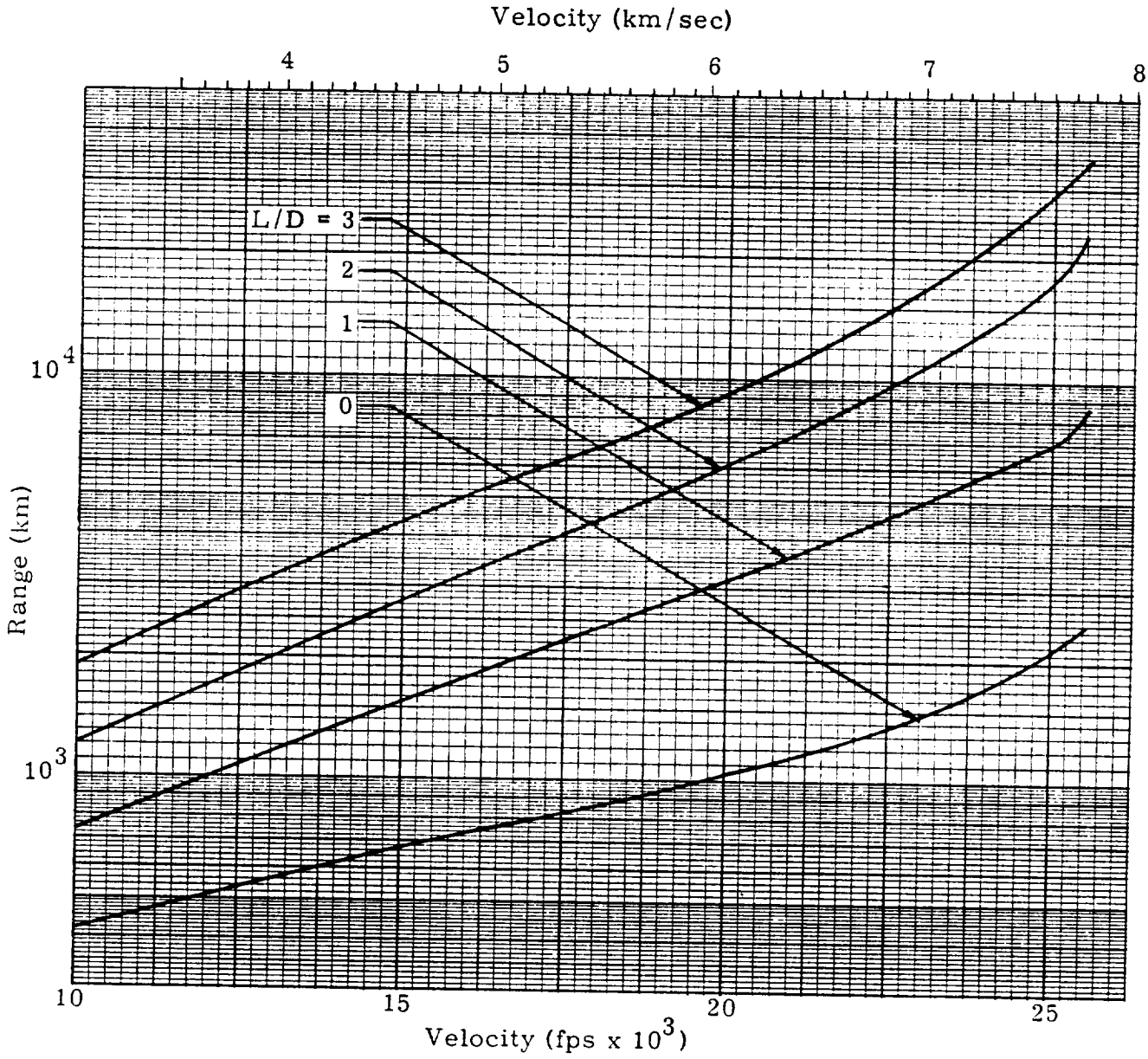

(c) W/C_DA = 5 psf = 239 newton/m^2,

B = 3.22 ft^2/slug = 2.05 x 10^{-2} m^2/kg, γ = -1°

Fig. 51. (continued)

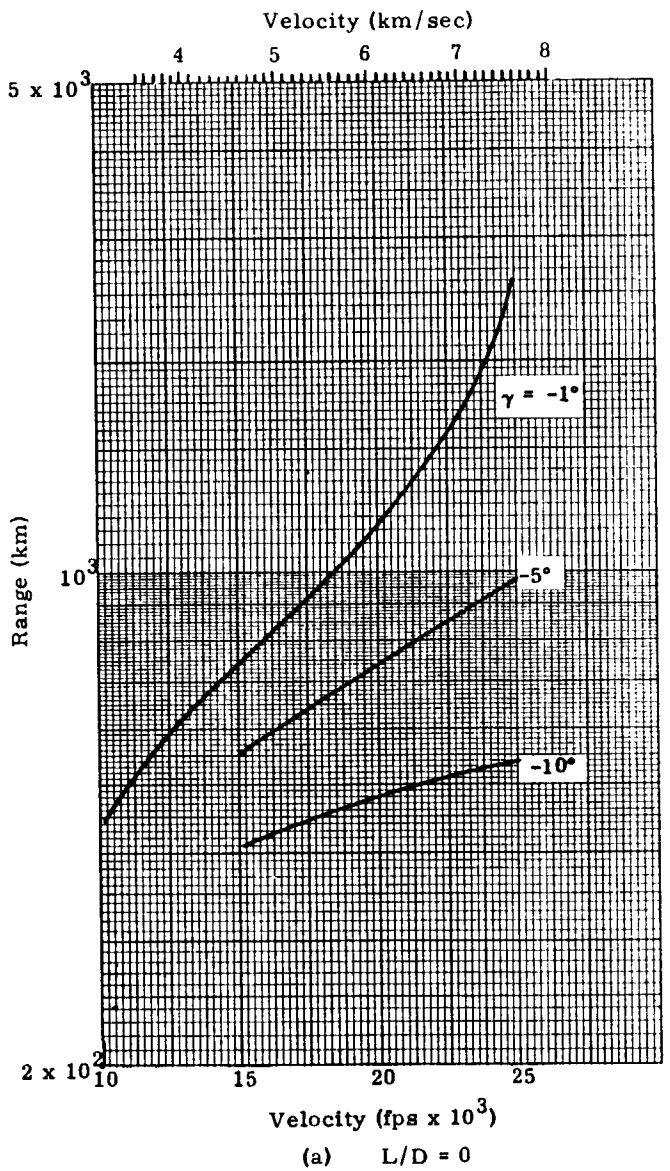

(a) L/D = 0

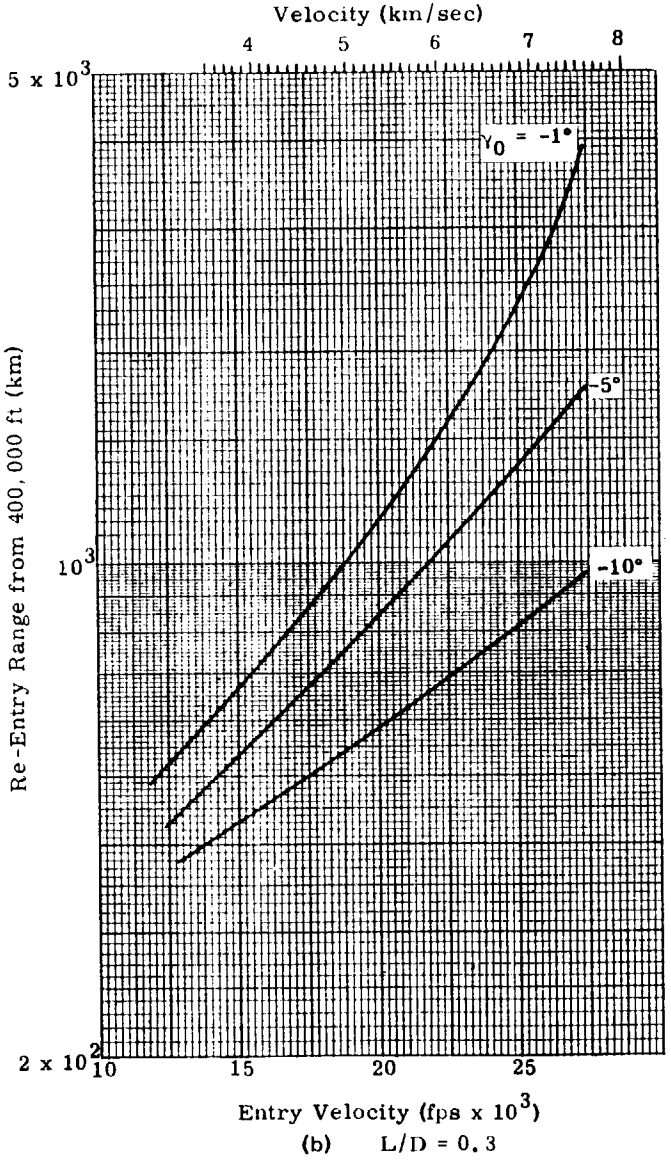

(b) L/D = 0.3

Fig. 52. Impact Range Versus Re-Entry Velocity($\frac{W}{C_D A}$ = 50 psf = 2390 newton/m^2, h_0 = 400,000 ft = 121,920 m)

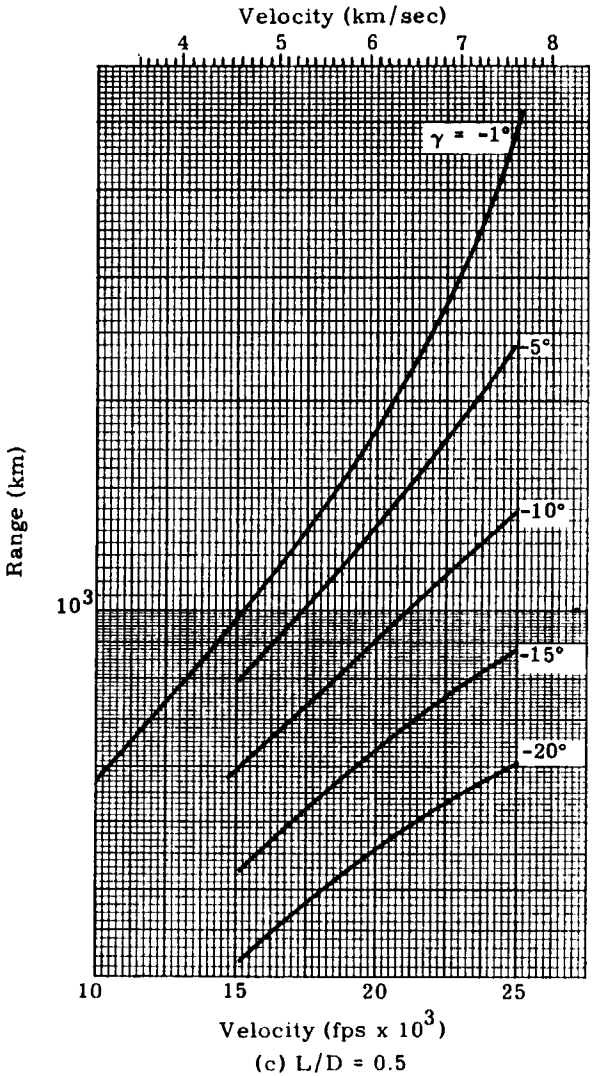

(c) L/D = 0.5

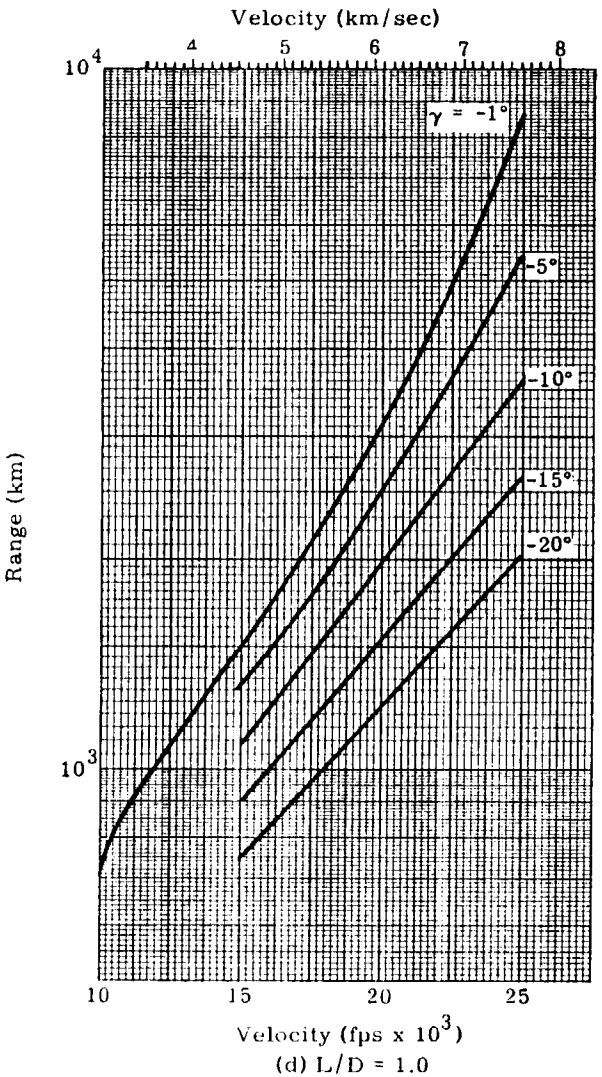

(d) L/D = 1.0

Fig. 52. (continued)

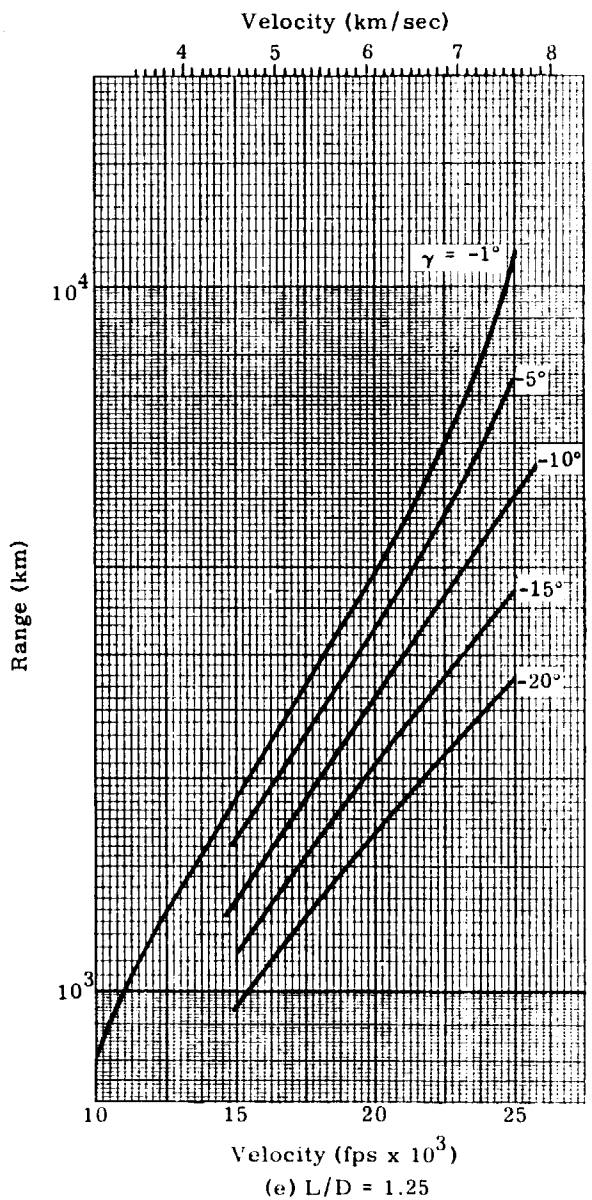

(e) L/D = 1.25

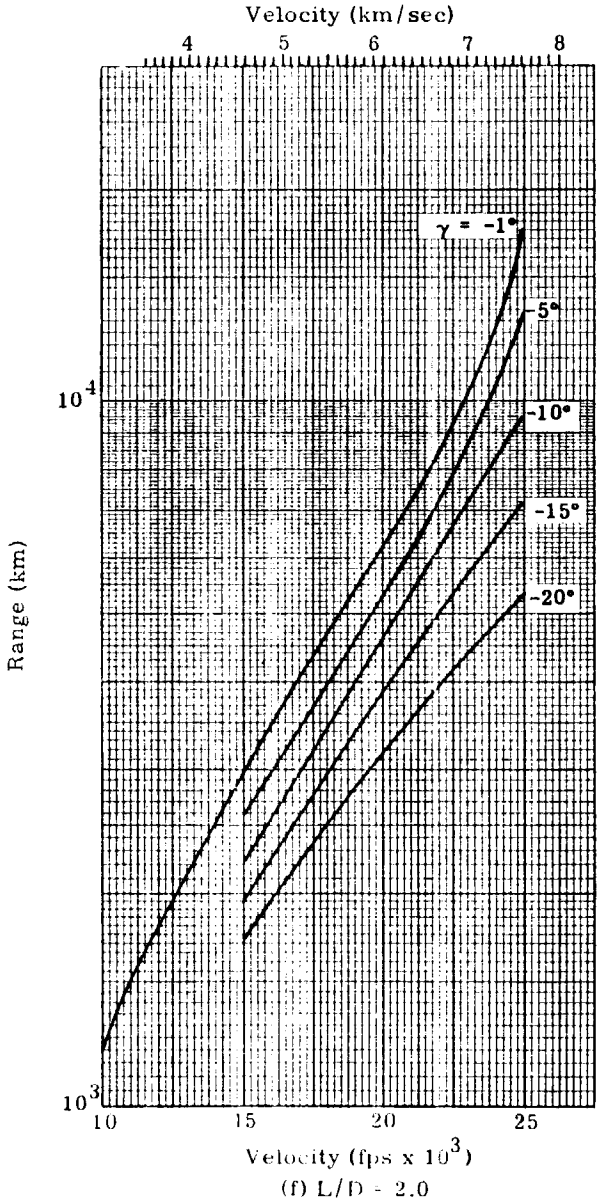

(f) L/D = 2.0

Fig. 52. (continued)

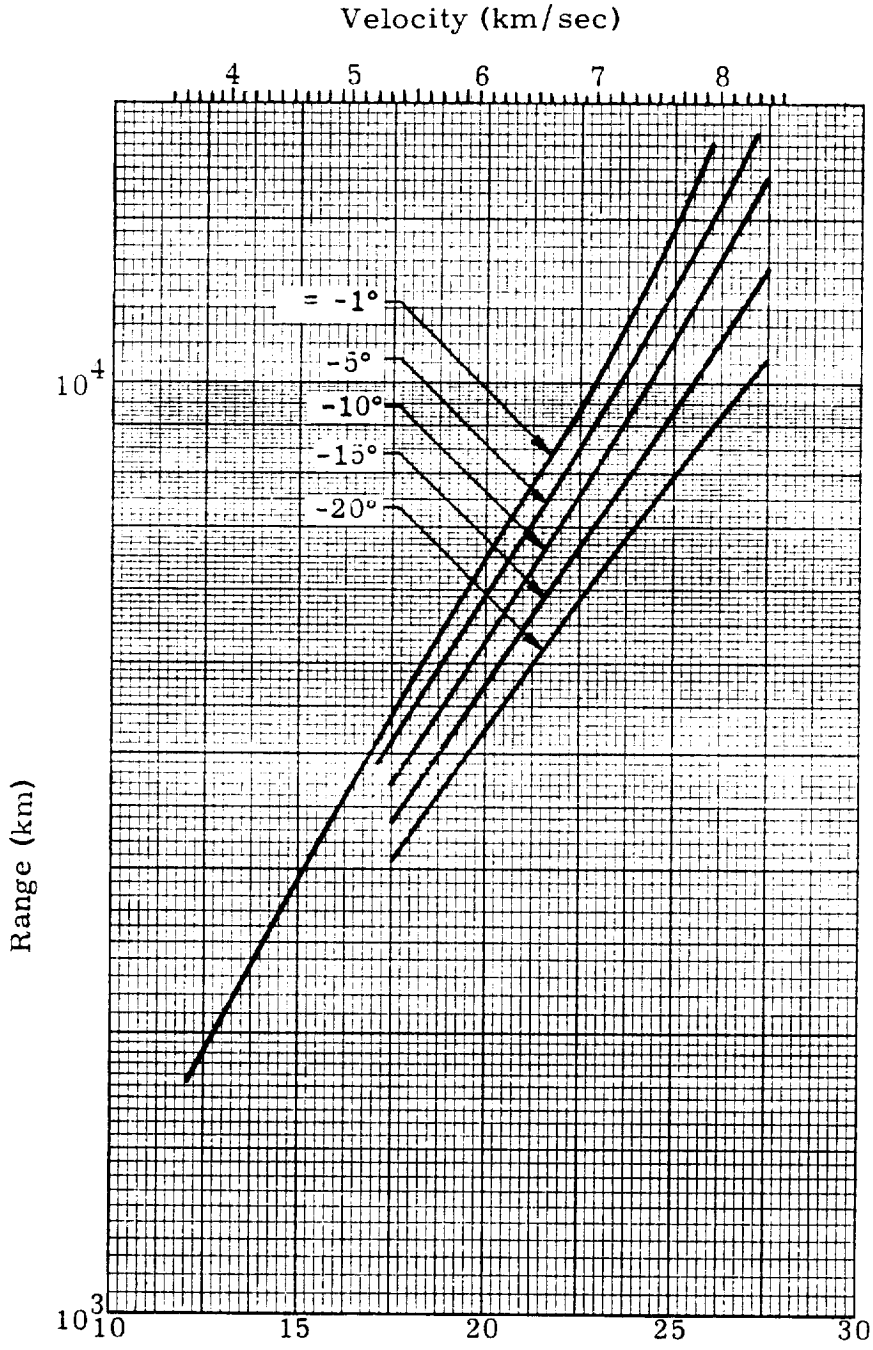

(g) L/D = 3.0

Fig. 52. (continued)

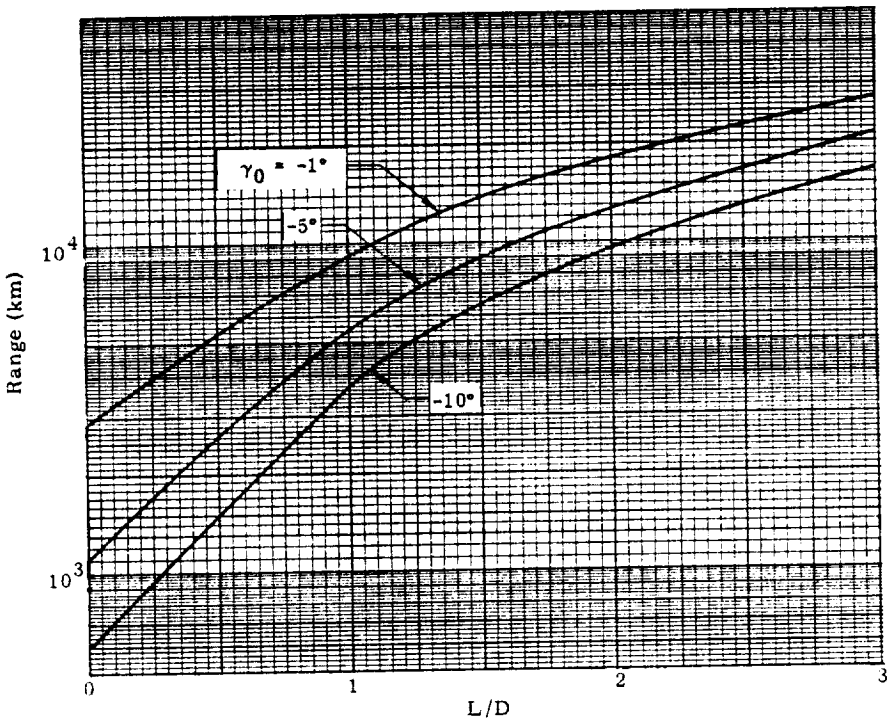

(a) W/C_DA = 438 psf = 21,000 newton/m^2

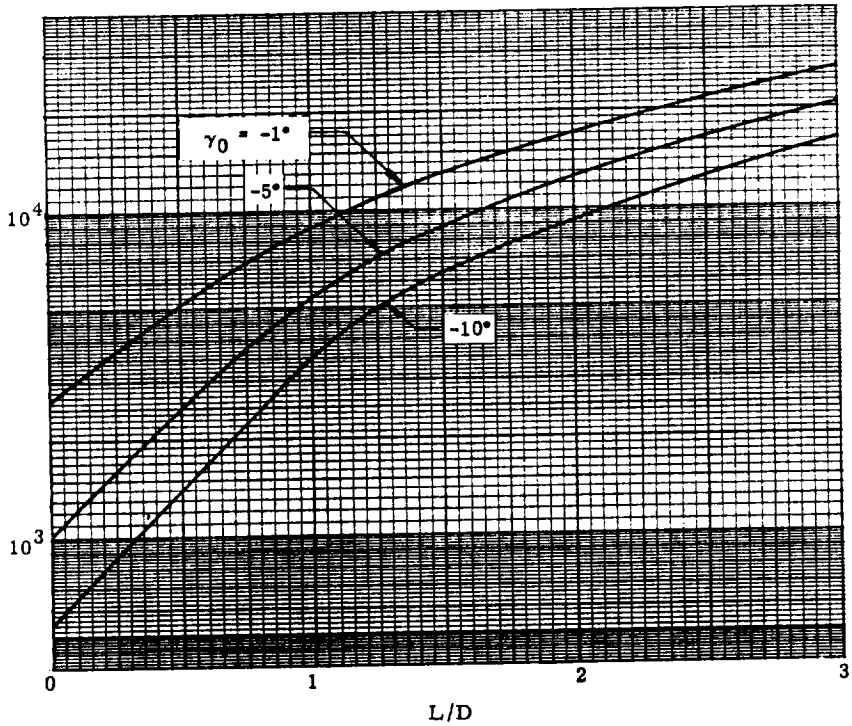

(b) W/C_DA - 50 psf = 2390 newton/m^2

Fig. 53. Range to Impact from 400,000 ft (121,920 m) Versus L/D (v_0 = 25,000 fps = 7620 mps)

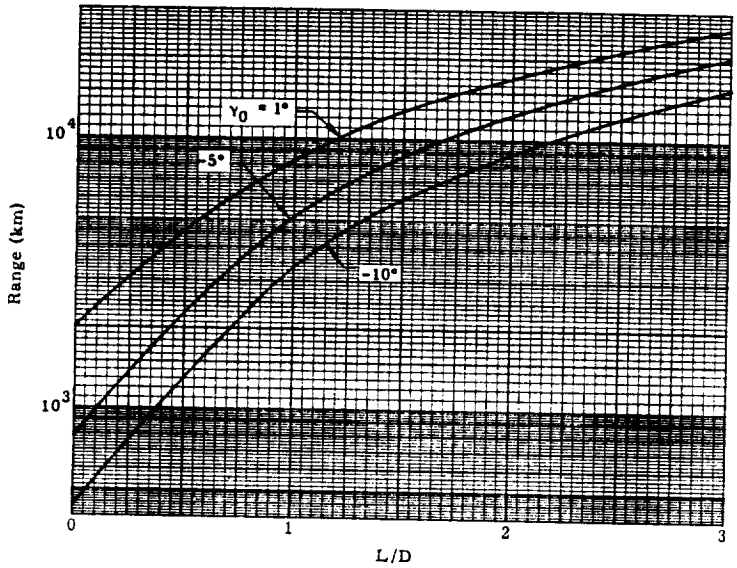

(c) W/C_DA = 5 psf = 239 newton/m^2

Fig. 53. Continued

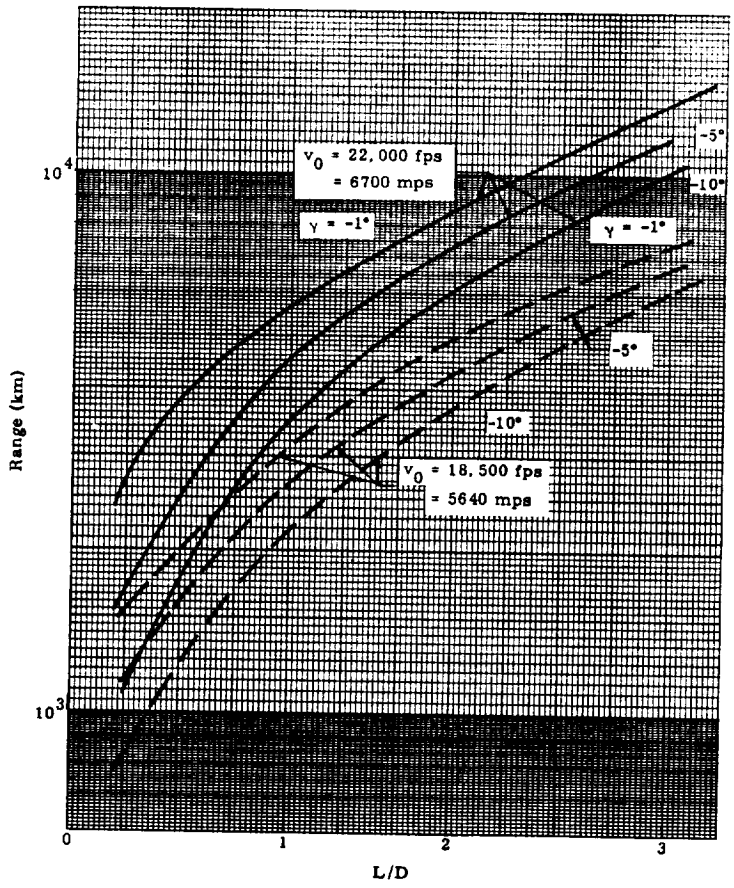

(a) v_0 = 18,500 fps and v_0 = 22,000 fps

Fig. 54. Range Versus Lift-Drag Ratio, $\frac{W}{C_DA}$ = 50 psf (Applies for 5< $\frac{W}{C_DA}$ < 500 psf; h_0 = 400,000 ft)

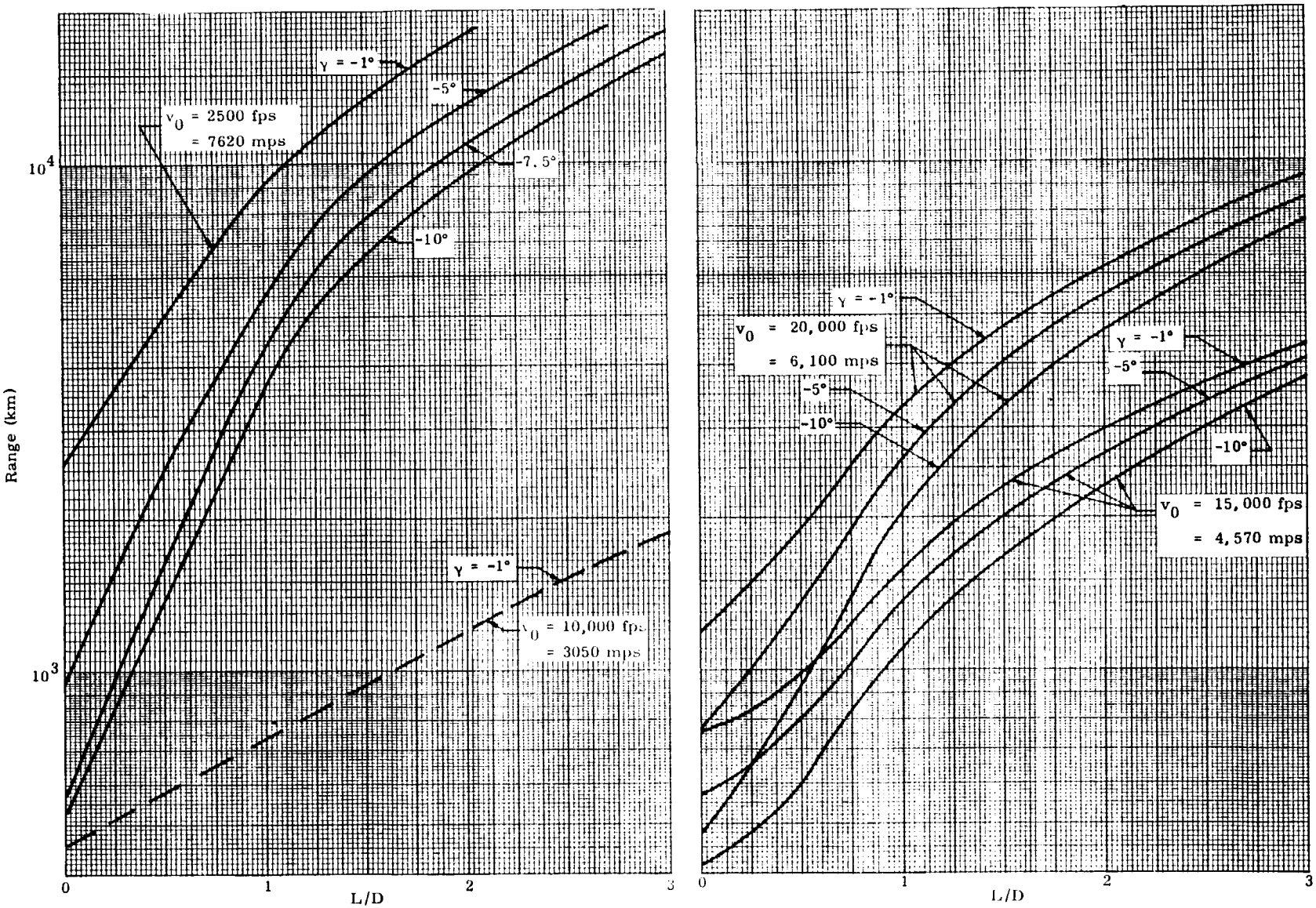

(b) v_0 = 25,000 and 10,000 fps (7620 and 3050 mps)

(c) v_0 = 20,000 and 15,000 fps (6100 and 4570 mps)

Fig. 54. (continued)

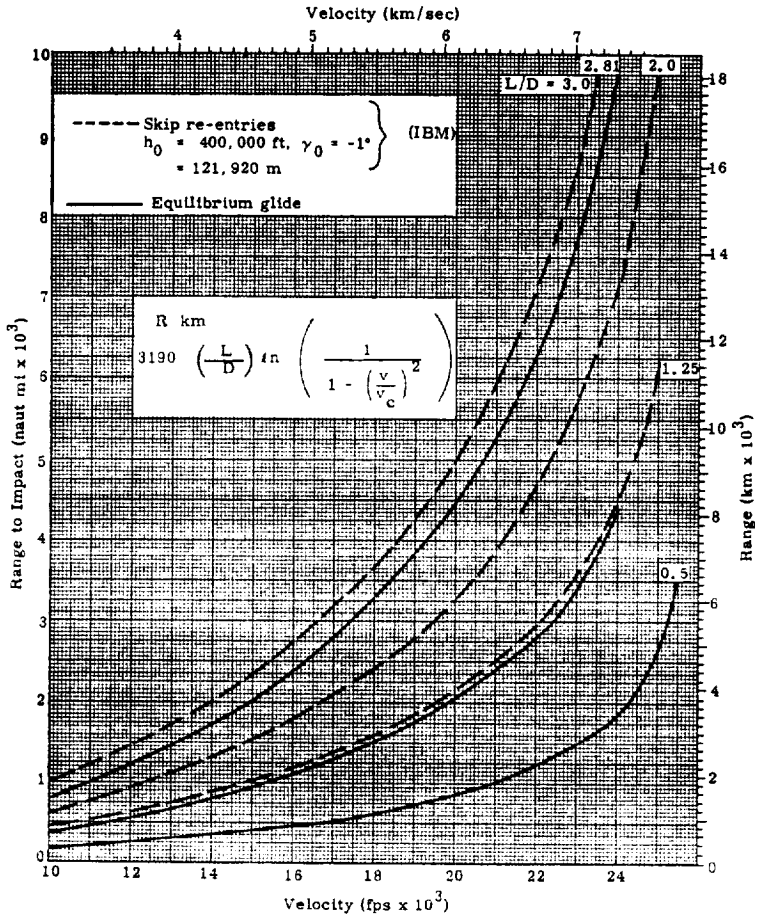

Fig. 55. Equilibrium Glide Range (not dependent on $W/C_L A$)

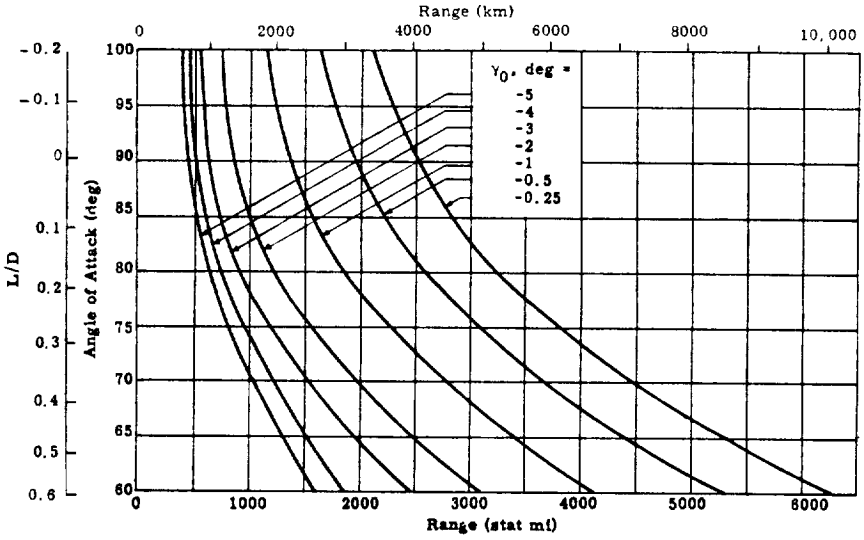

Fig. 56a. Variation in Range as a Function of Angle of Attack and Entry Angle. (Nonrotating Earth; h_0 = 350,000 ft = 106,700 m; v_0 = 25,863 fps = 7870 mps; W/A = 20 lb/ft^2 = 956 newton/m^2) (Ref. 25)

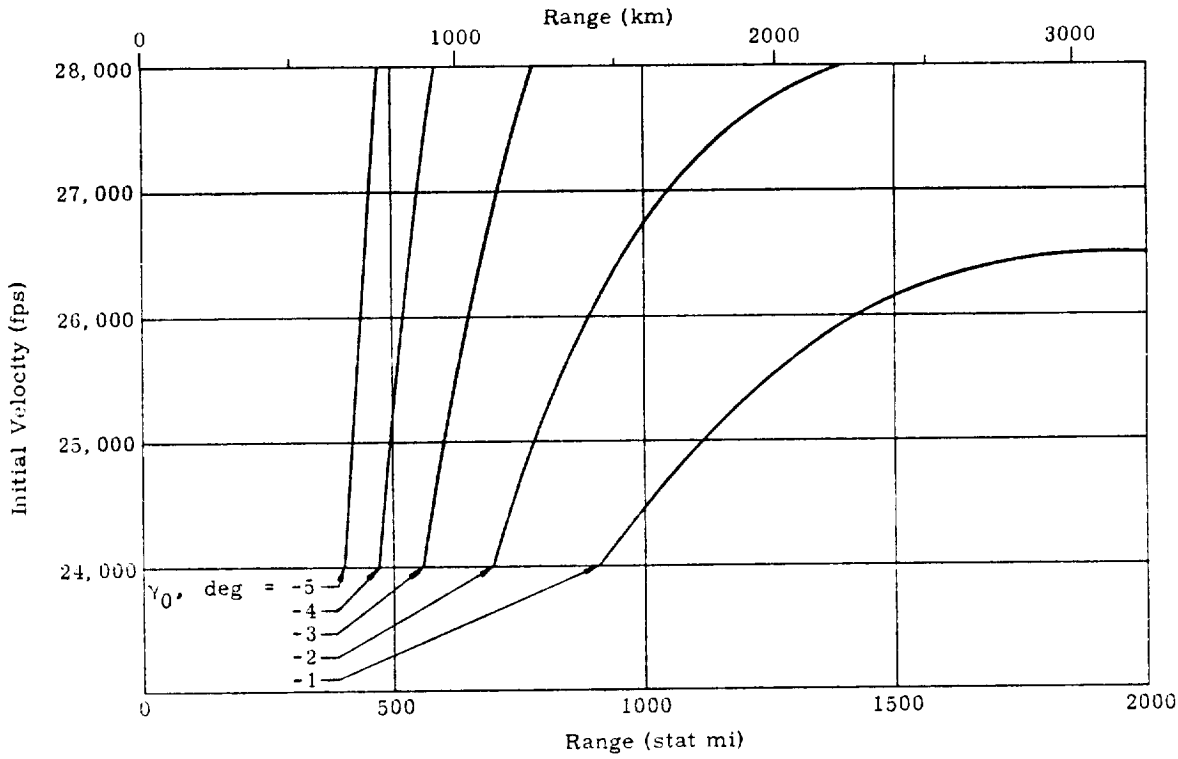

Fig. 56b. Variation in Range as a Function of Initial Velocity and Entry Angle for Ballistic Vehicles (α = 90), (Nonrotating Earth; h_0 = 350,000 ft = 106,800 m; W/A = 20 lb/ft^2 = 955 newtons/m^2] [Ref. 25]

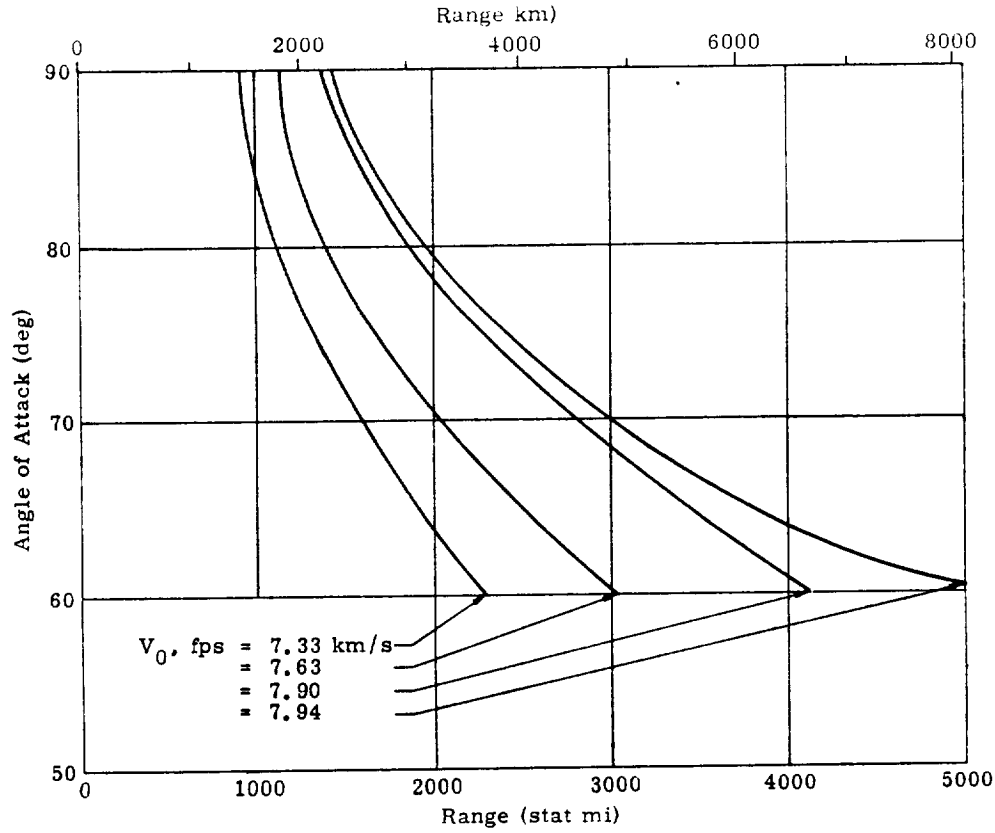

Fig. 56c. Variation in Range as a Function of Angle of Attack and Initial Velocity. (Nonrotating Earth; h_0 = 350,000 ft = 160,800 m; γ_0 = -1°) (Ref 25)

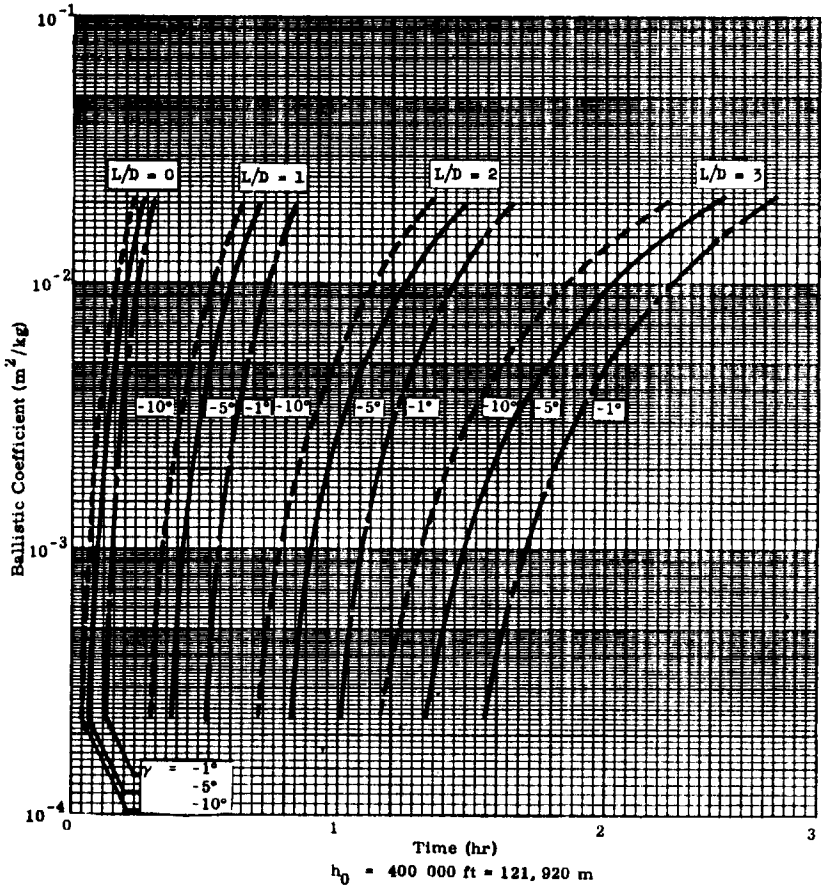

Fig. 57. Time to Impact Versus Ballistic Coefficient (v_0 = 25,000 fps = 7620 mps)

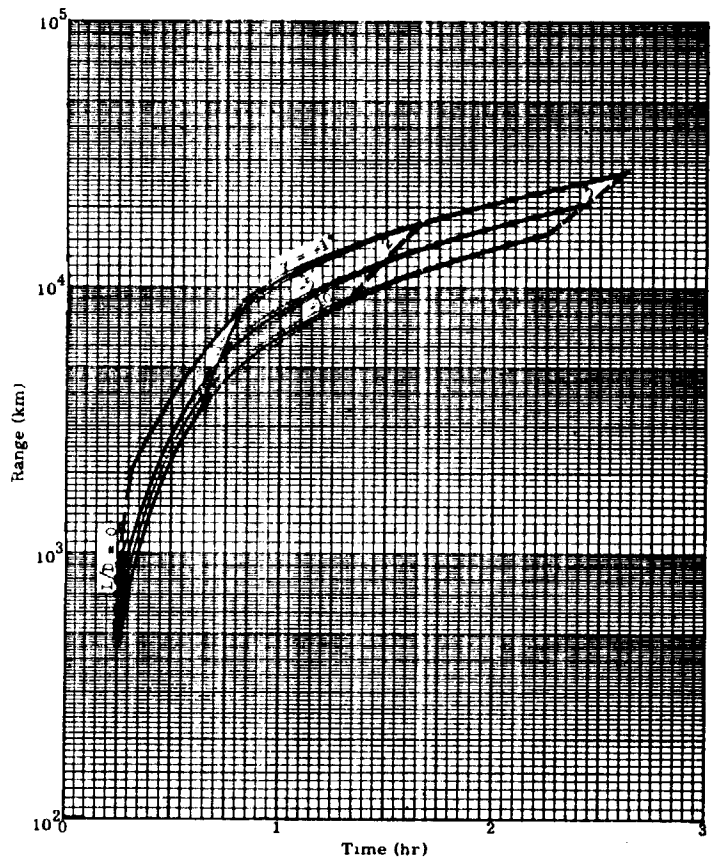

(a) B = 322 ft^2/slug = 2.05 x 10^{-2} m^2/kg

Fig. 58. Time Versus Range to Impact from 400,000 ft = 121,920 m (v_0 = 25,000 fps = 7620 mps)

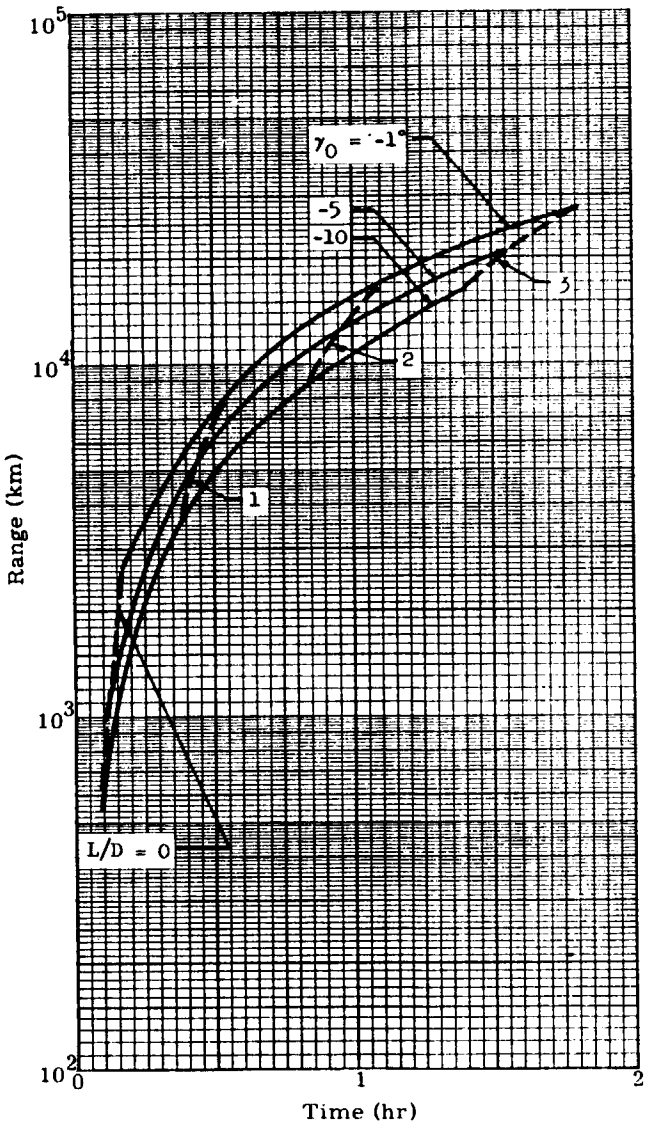

(b) B = 0.322 ft^2/slug = 2.05 x 10^{-3} m^2/kg

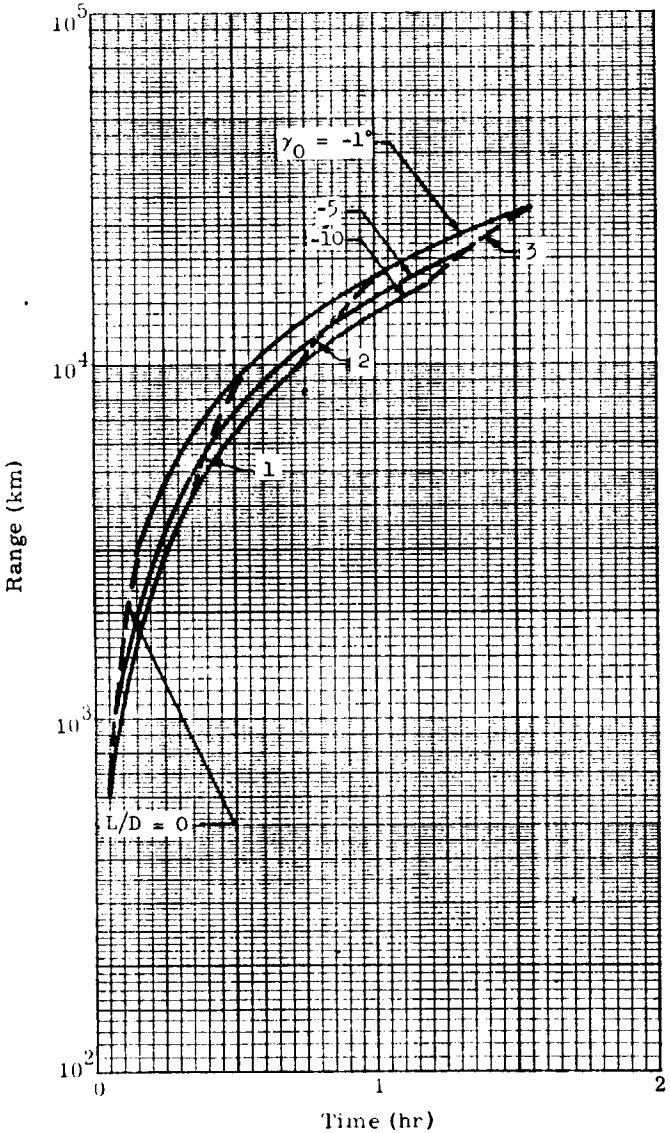

(c) B = 0.0367 ft^2/slug = 0.234 x 10^{-3} m^2/kg

Fig. 58. Continued

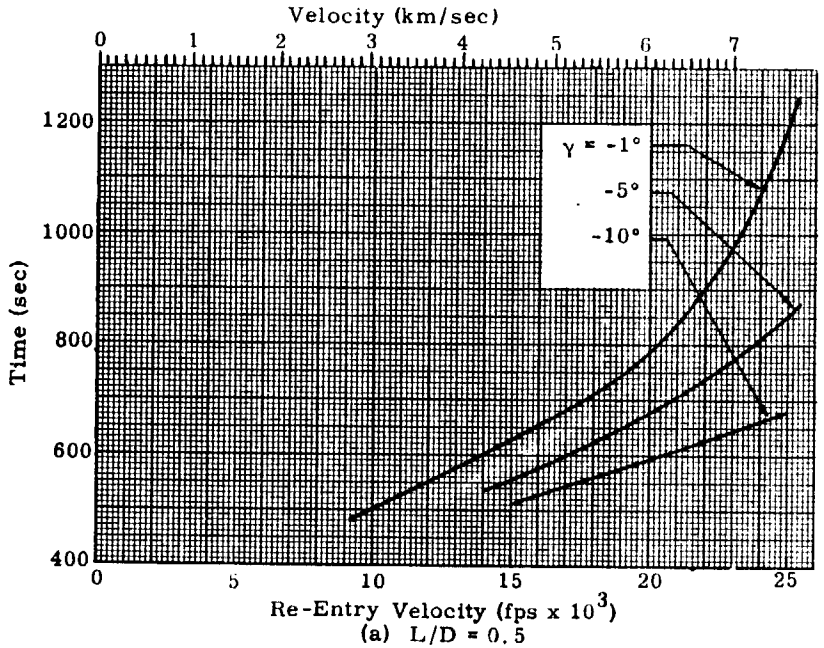

(a) L/D = 0.5

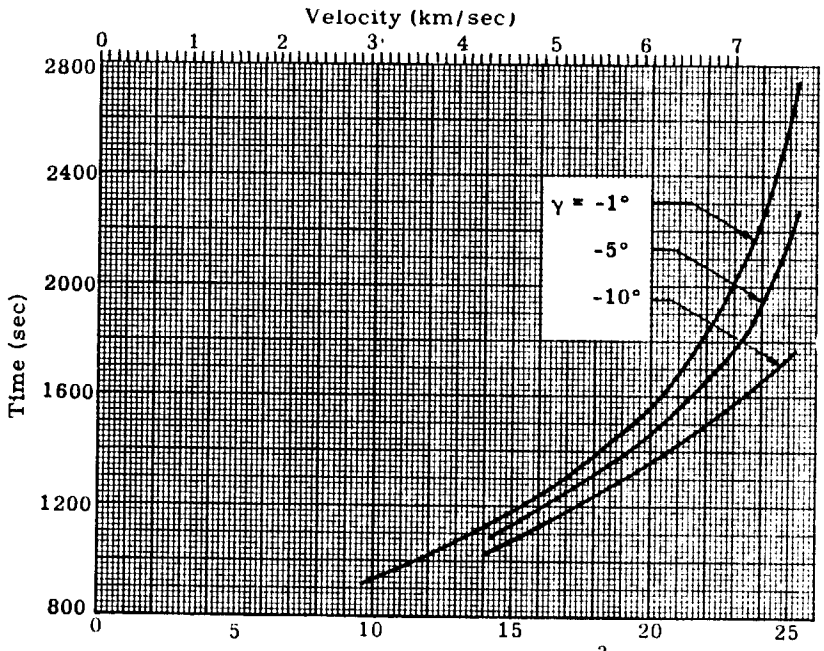

(b) L/D = 1.25

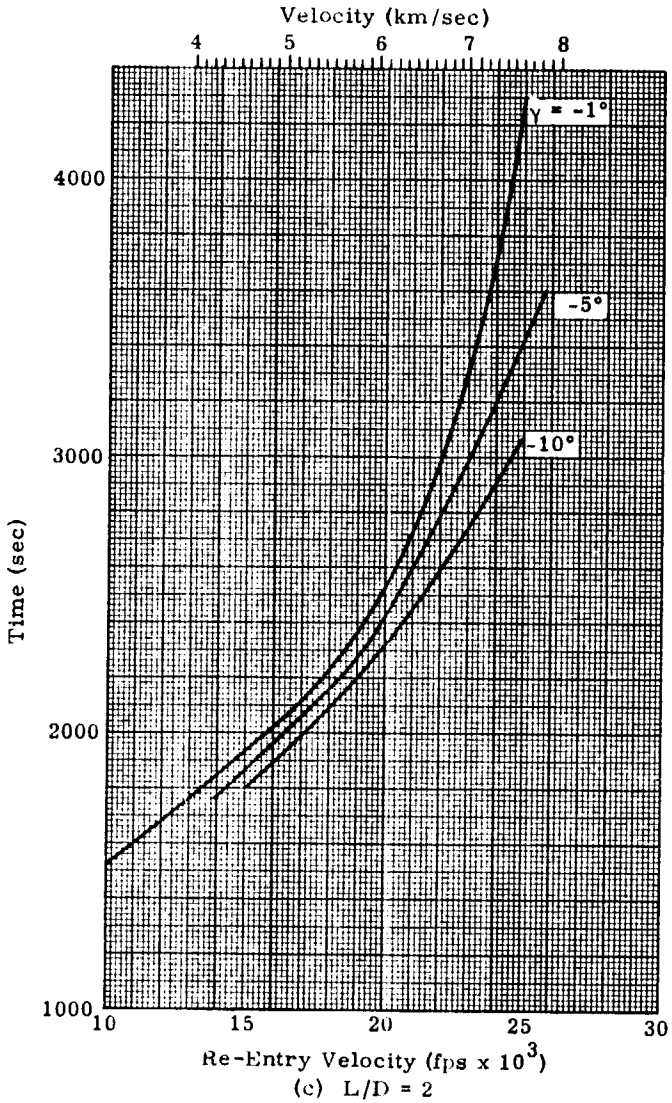

(c) L/D = 2

Fig. 59. Time to Impact Versus Re-Entry Velocity (h_0 = 400,000 ft = 121,920 m, W/C_DA = 50 psf = 2390 newtons/m^2)

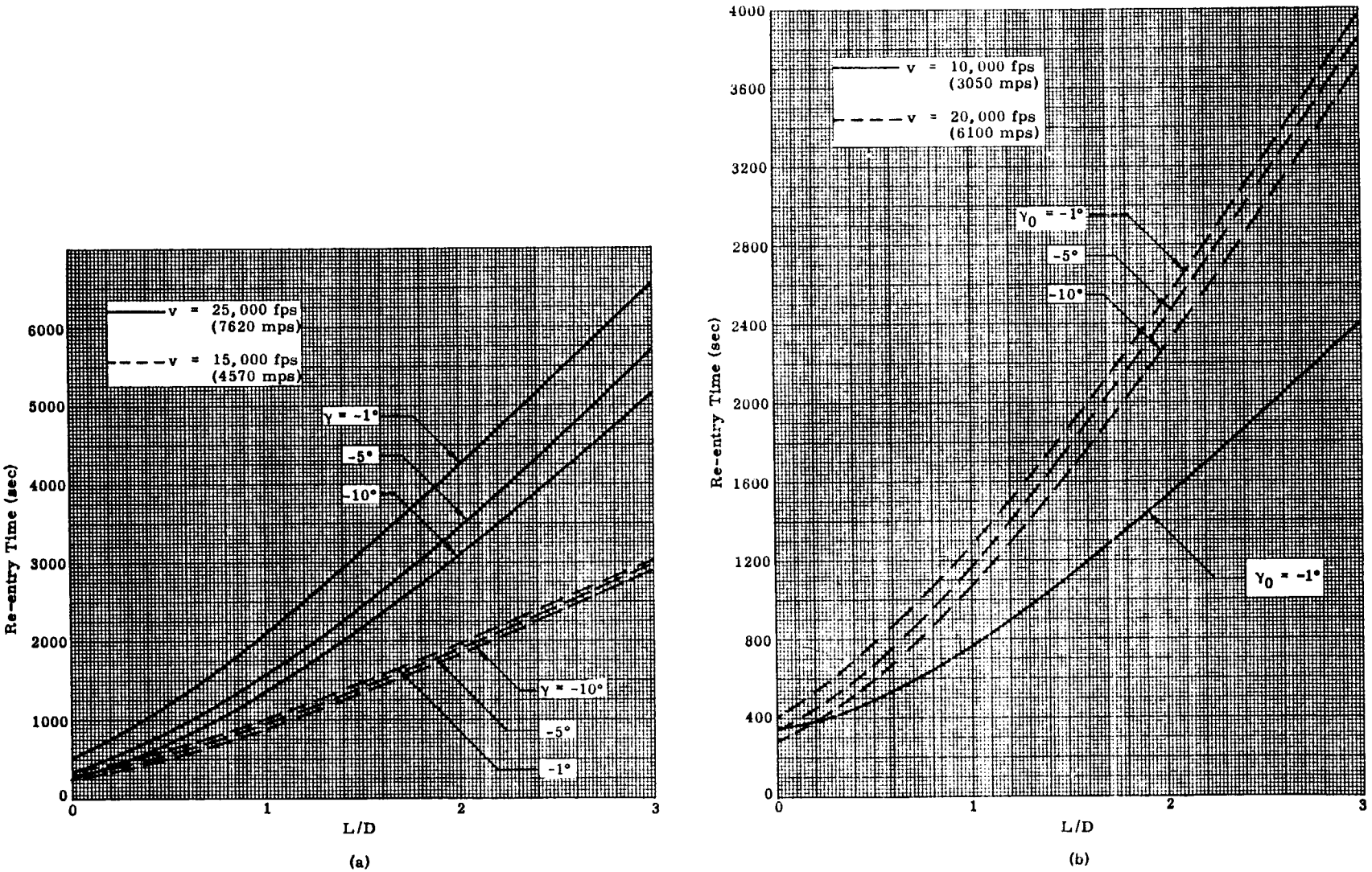

Fig. 60. Re-Entry Time Versus L/D for Various Velocities($\frac{W}{C_D A}$ = 50 psf = 2390 newtons/m^2; h_0 = 400,000 ft = 121,920 m)

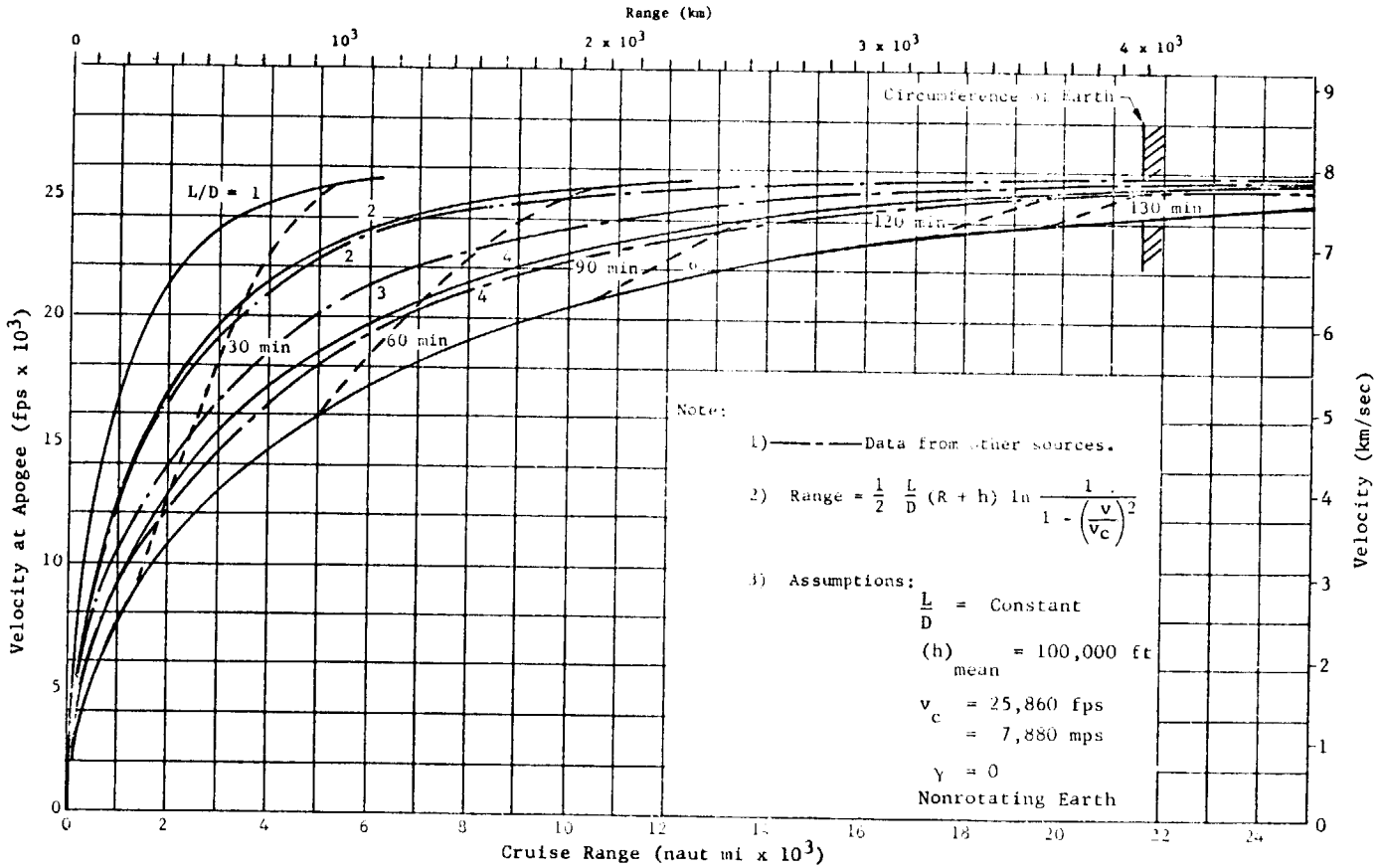

Fig. 61. Velocity at Apogee Versus Range

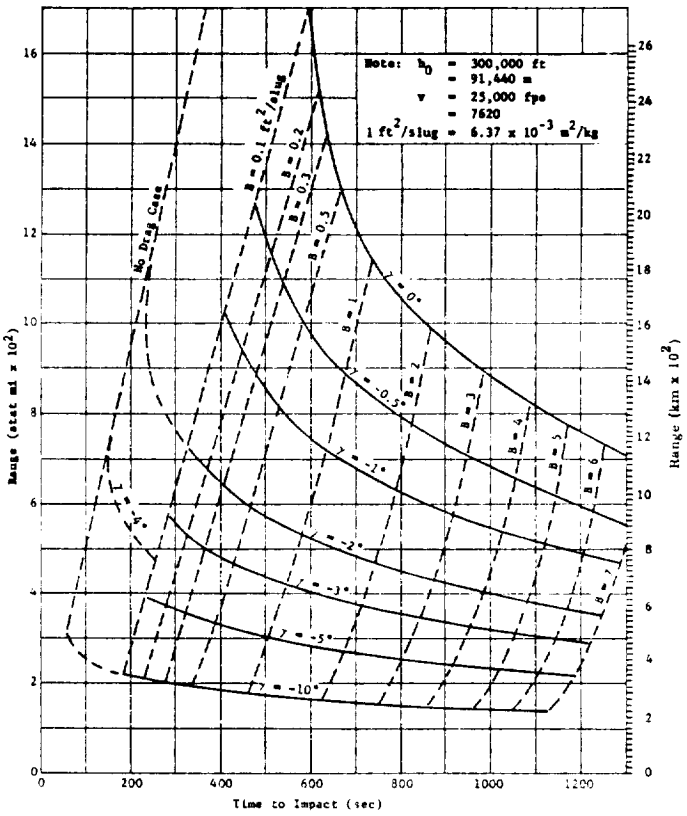

Fig. 62. Range and Time to Impact for Ballistic Entry

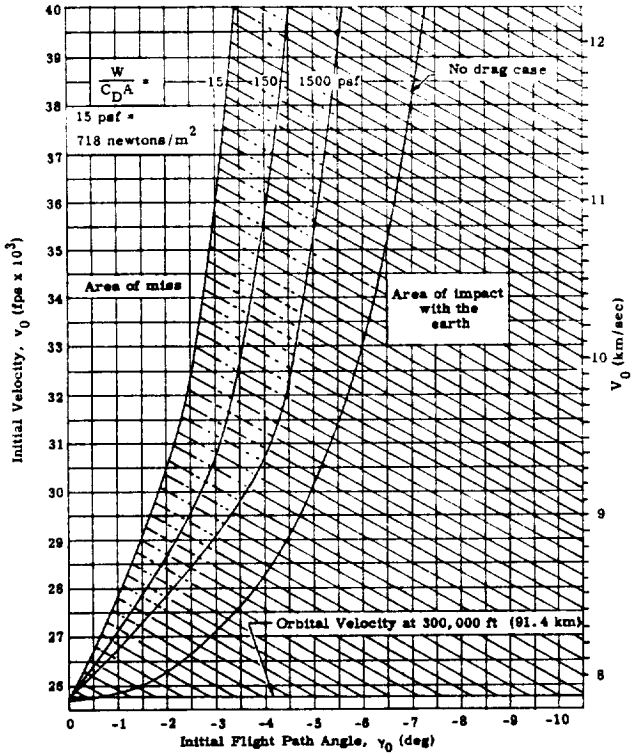

Fig. 63a. Conditions for Impact--Ballistic Case

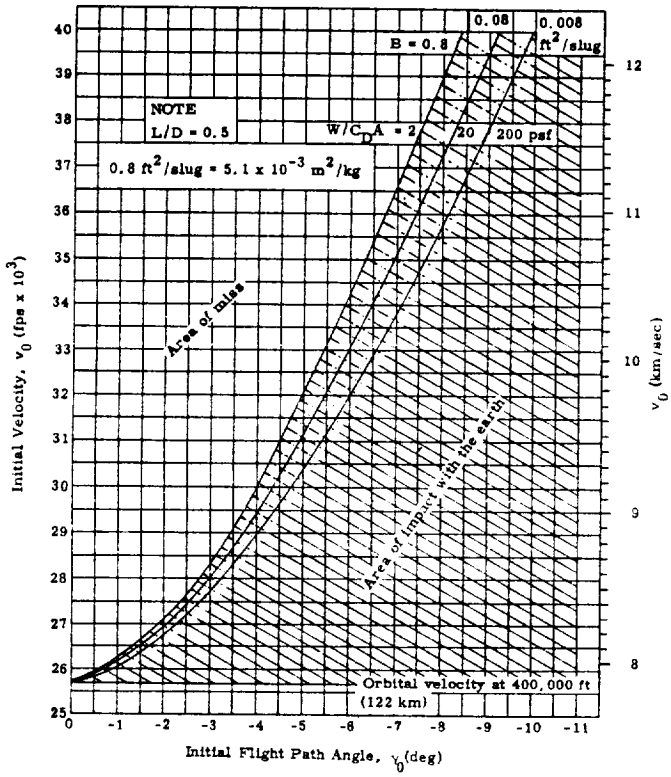

Fig. 63b. Conditions for Impact, Lifting Case

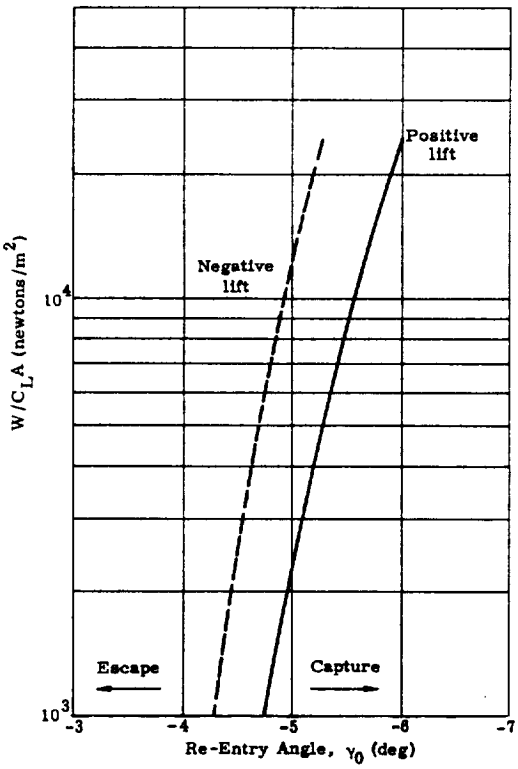

Fig. 63c. Minimum Entry Angle for Capture (at escape velocity) (Ref. 14)

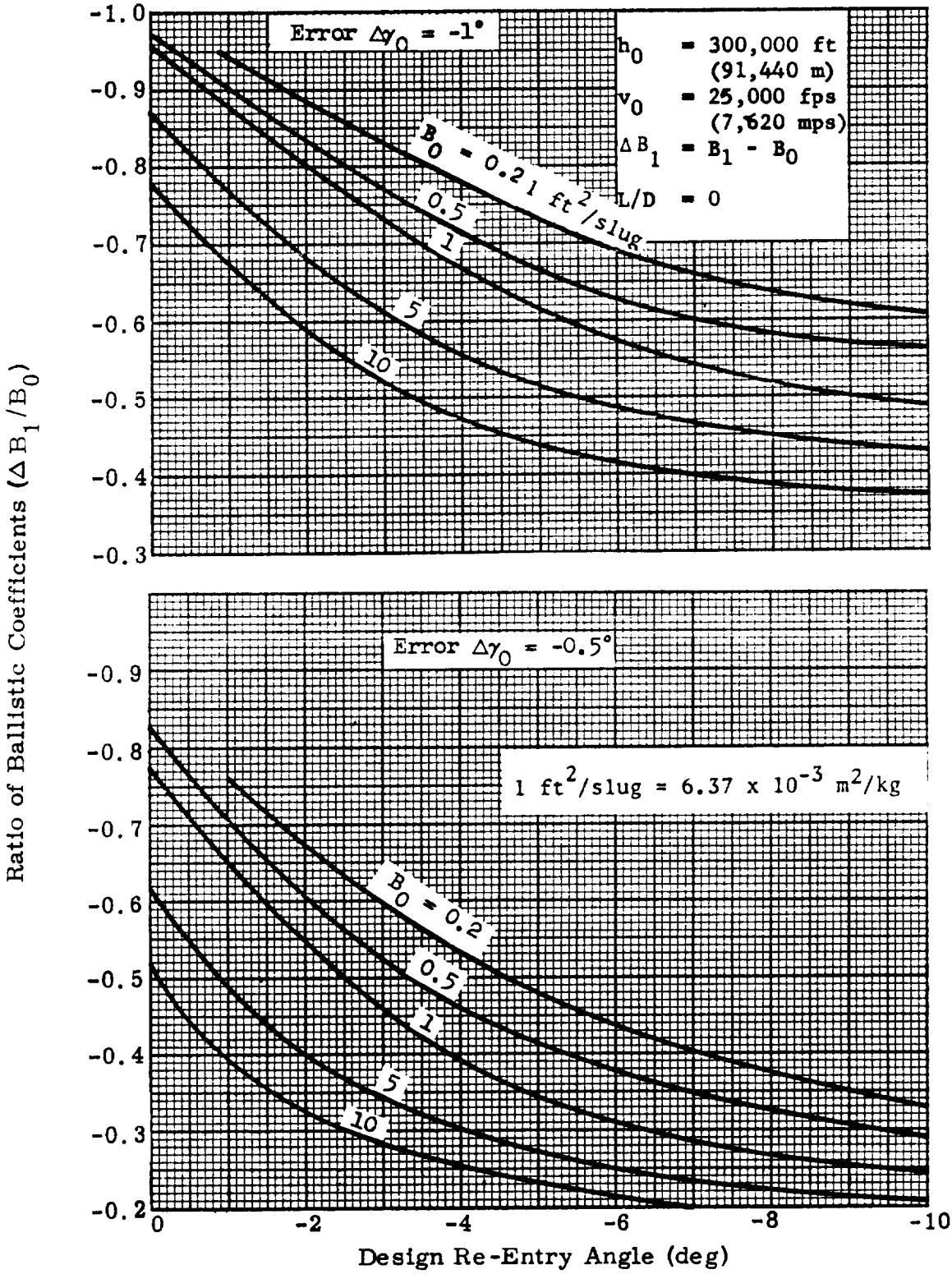

Fig. 64. Range Corrections with Ballistic Coefficient Increments

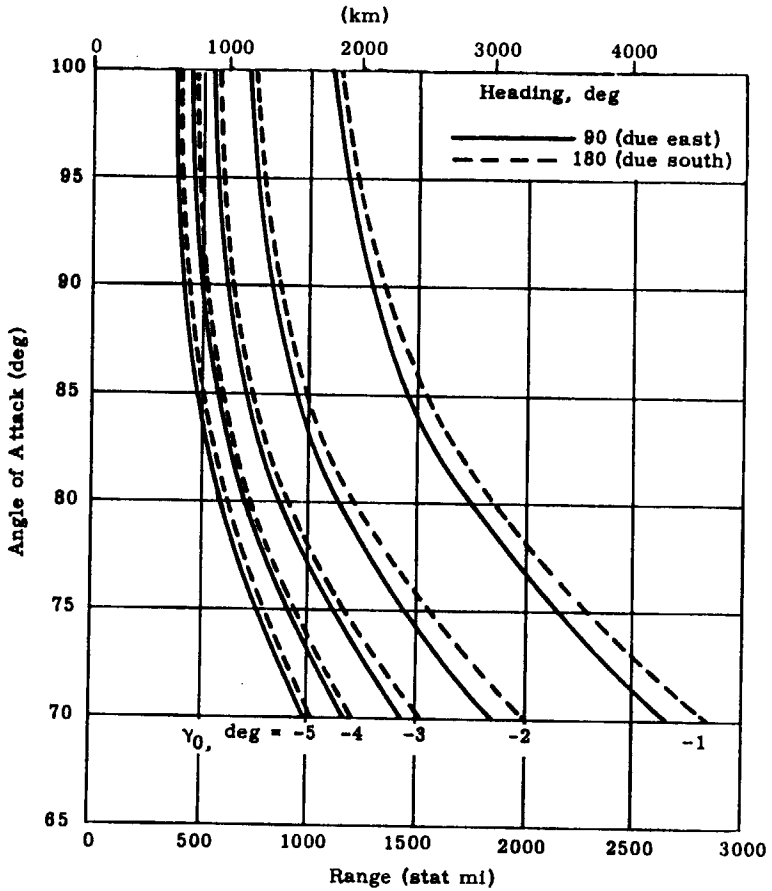

Fig. 65a. Variation in Range as a Function of Angle of Attack and Entry Angle for Headings of 90° and 150° (Rotating Earth; h_0 = 350,000 ft = 106,680 m; v_0 = 25,743 fps = 7846 mps; W/A = 20 lb/ft^2 = 957 newtons/m^2) (Ref. 25)

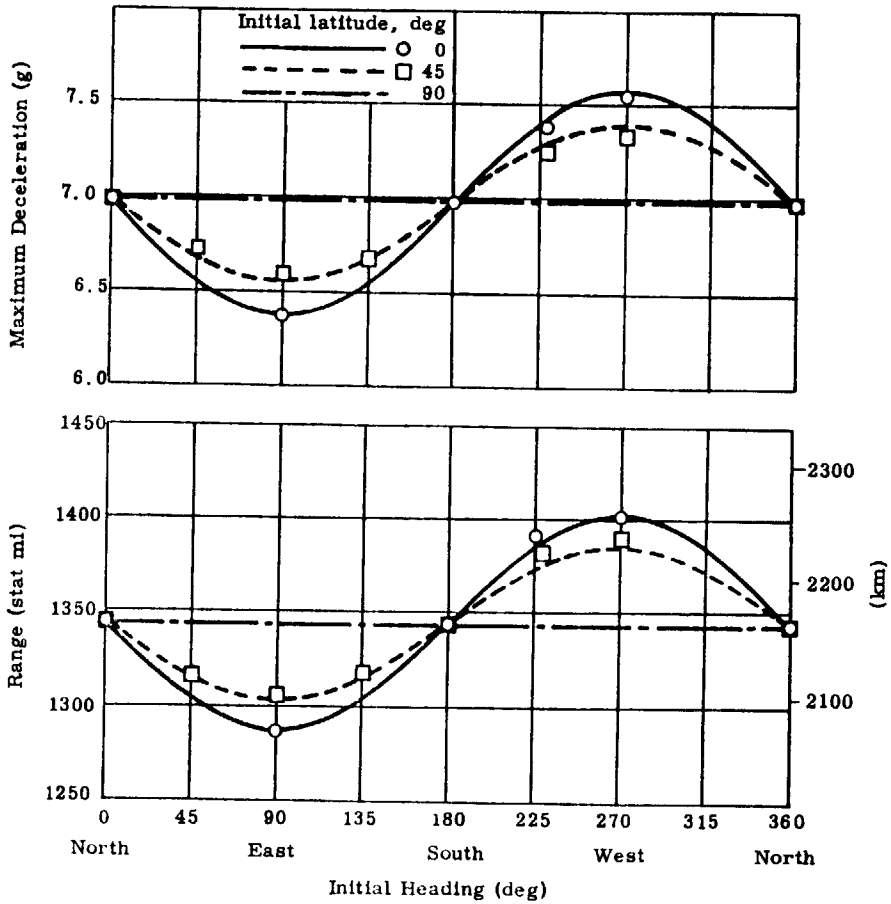

Fig. 65b. Variation in Range and Maximum Deceleration as a Function of Heading and Initial Latitude (Rotating Earth; h_0 = 350,000 ft = 106,650 m; v_0 = 25,743 fps = 7846 mps; W/A = 20 lb/ft^2 = 957 newtons/m^2) (Ref. 25)

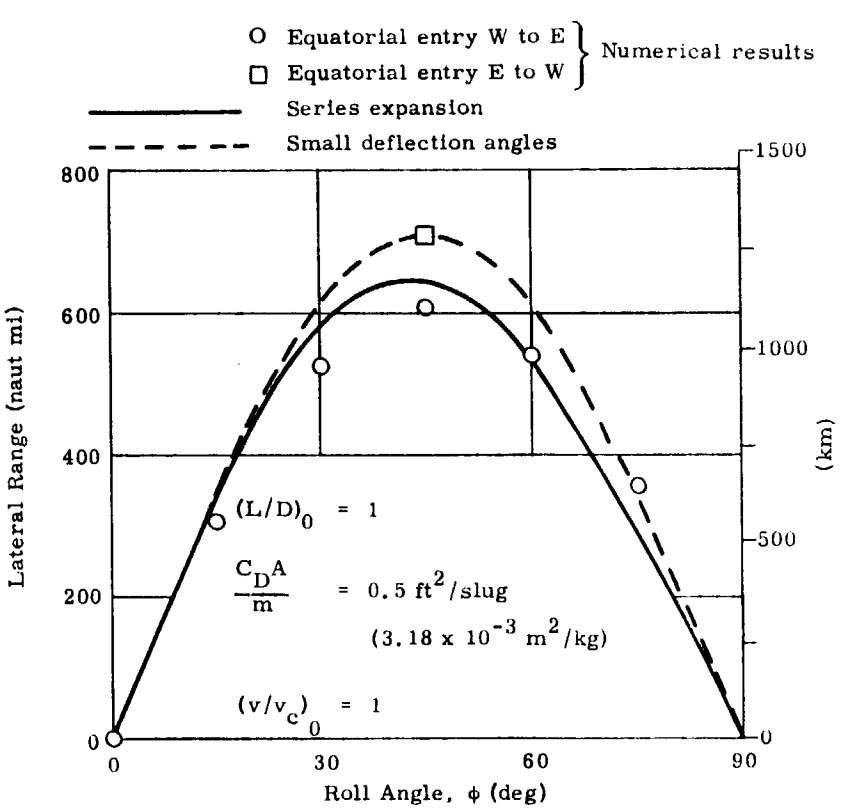

Fig. 66a. Effect of Roll Angle on Lateral Range (Ref. 27)

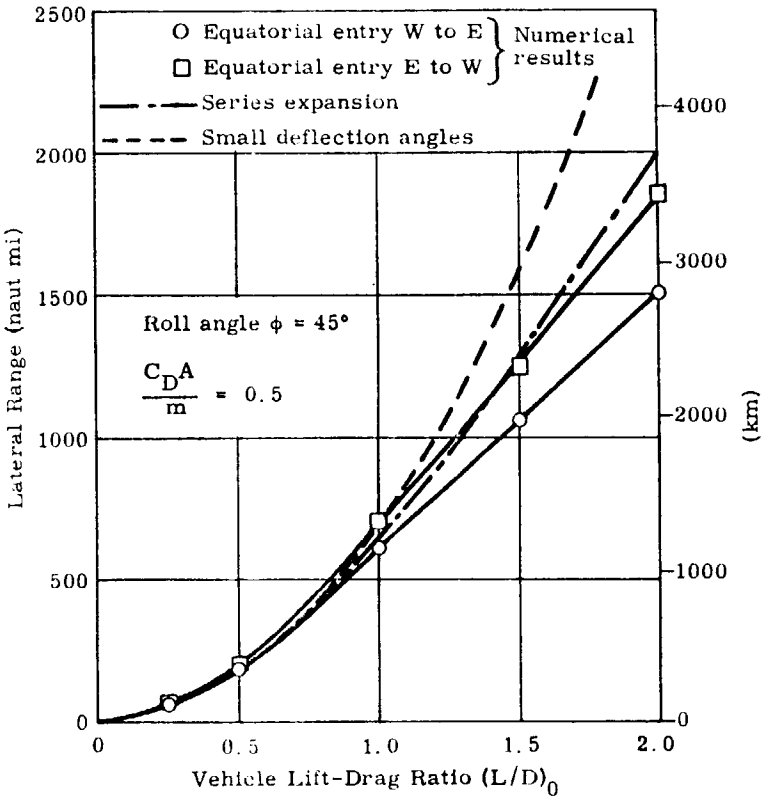

Fig. 66b. Lateral Range Capability ($v_0 = v_c$) (Ref. 27)

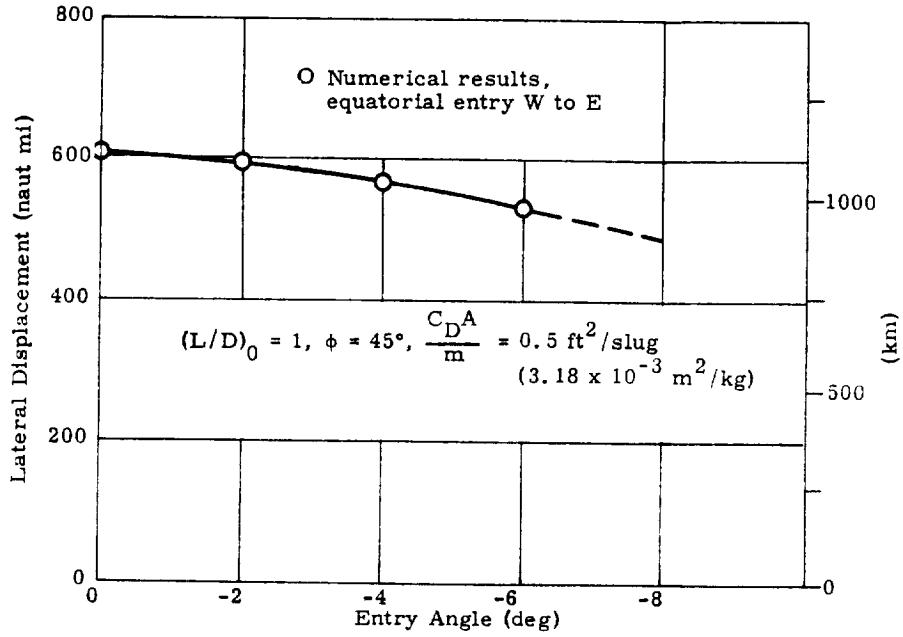

Fig. 66c. Effect of Entry Angle on Lateral Range (Ref 27)

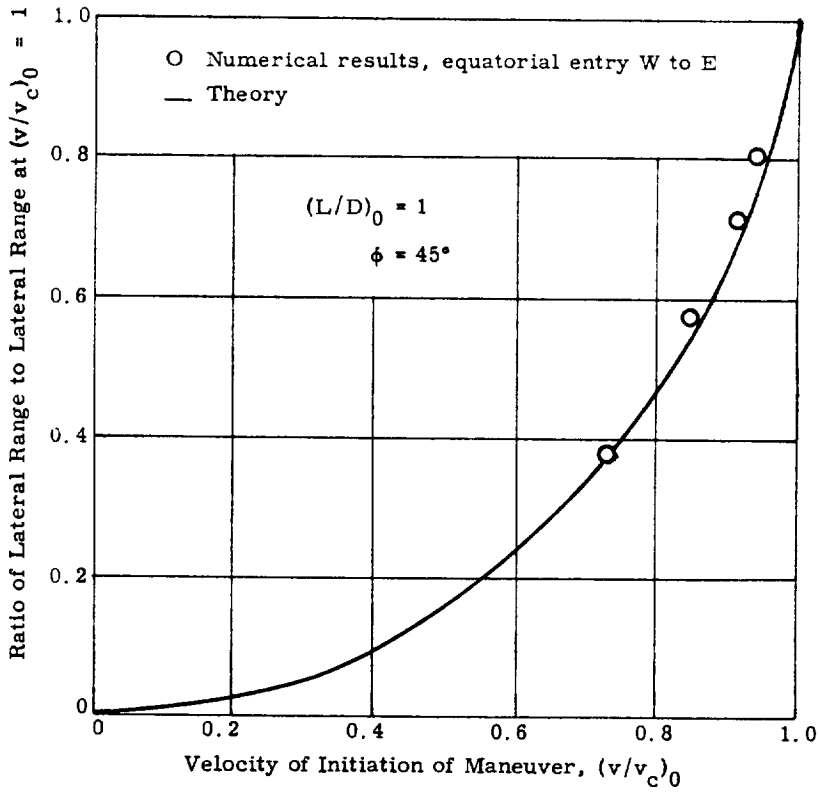

Fig. 66d. Effect of Velocity at Initiation of Maneuver on Lateral Range (Ref 27)

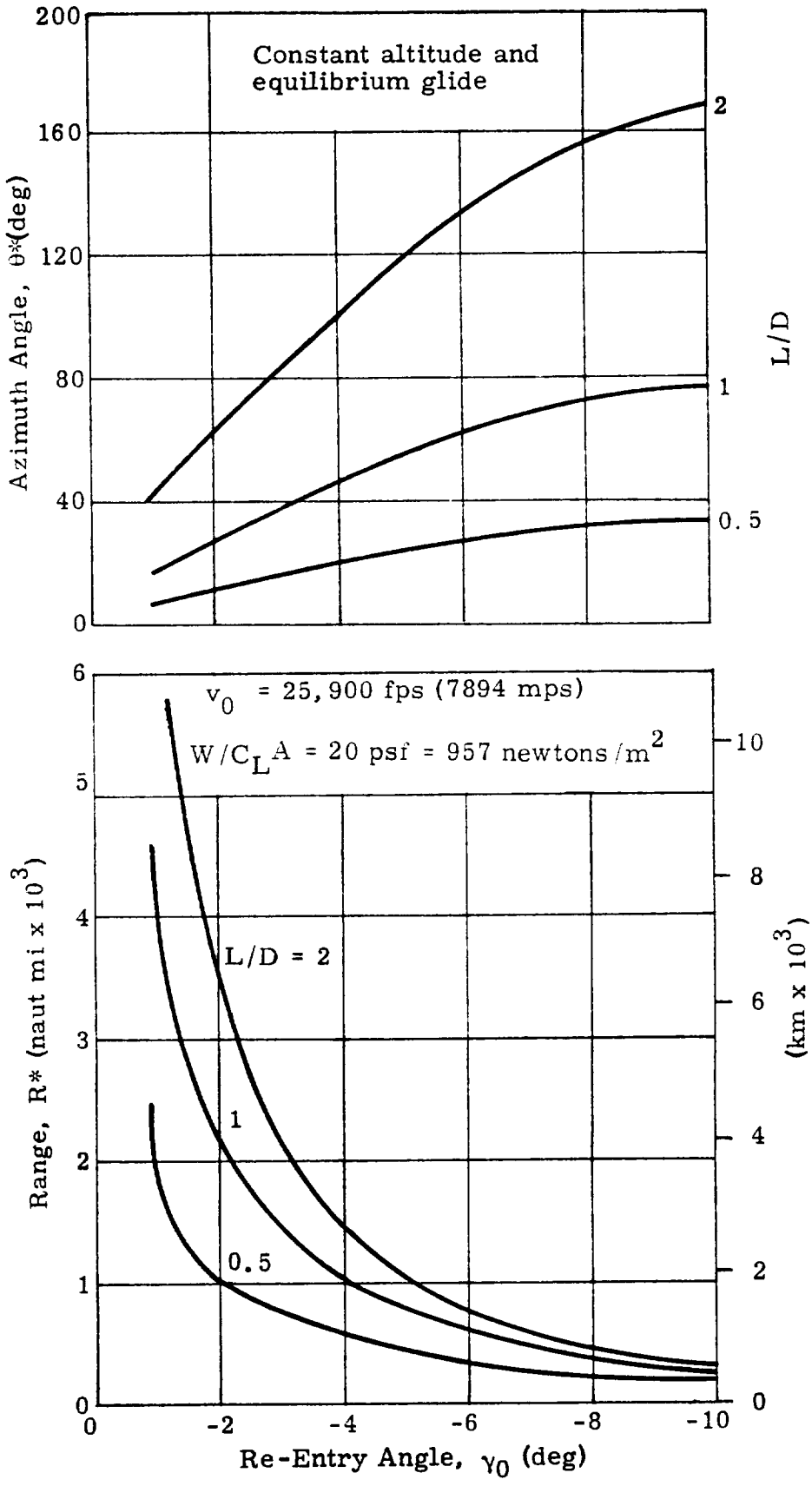

Fig. 67a. Effect of Re-Entry Angle on the Azimuth Angle and Range to Maximum Lateral Deflection Point (Ref 14)

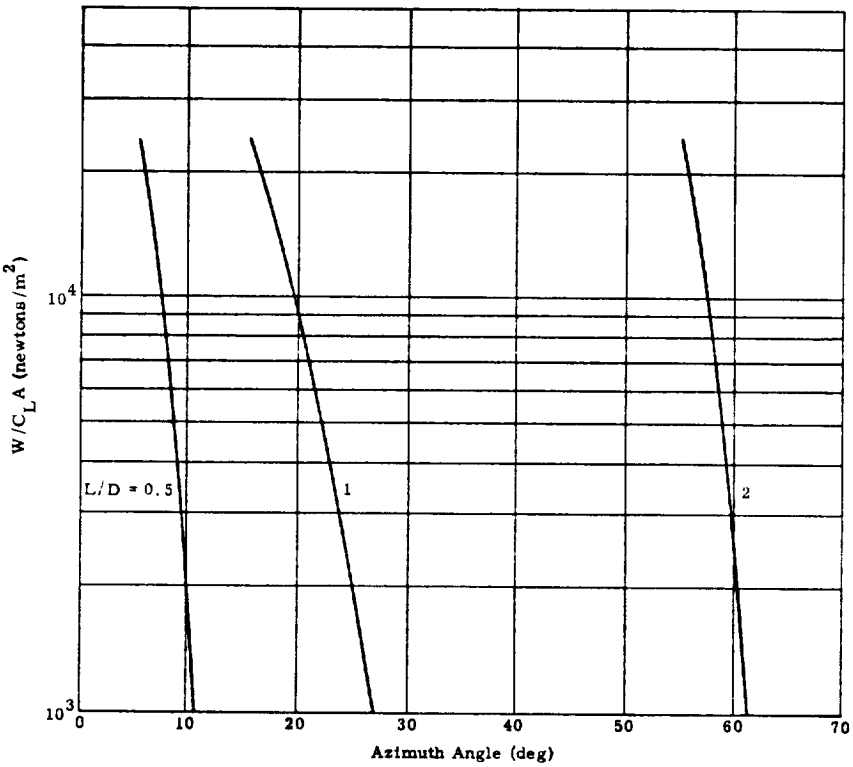

Fig. 67b. Effect of Wing Loading on Azimuth Potential ($\gamma_0 = 2°$; constant altitude and equilibrium glide) (Ref. 14)

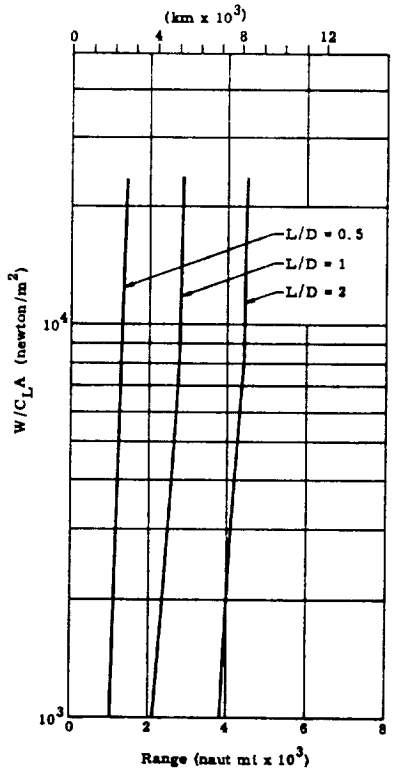

Fig. 67c. Effect of Wing Loading on Range to Maximum Azimuth Potential ($\gamma_0 = -2°$; constant altitude and equilibrium glide) (Ref. 14)

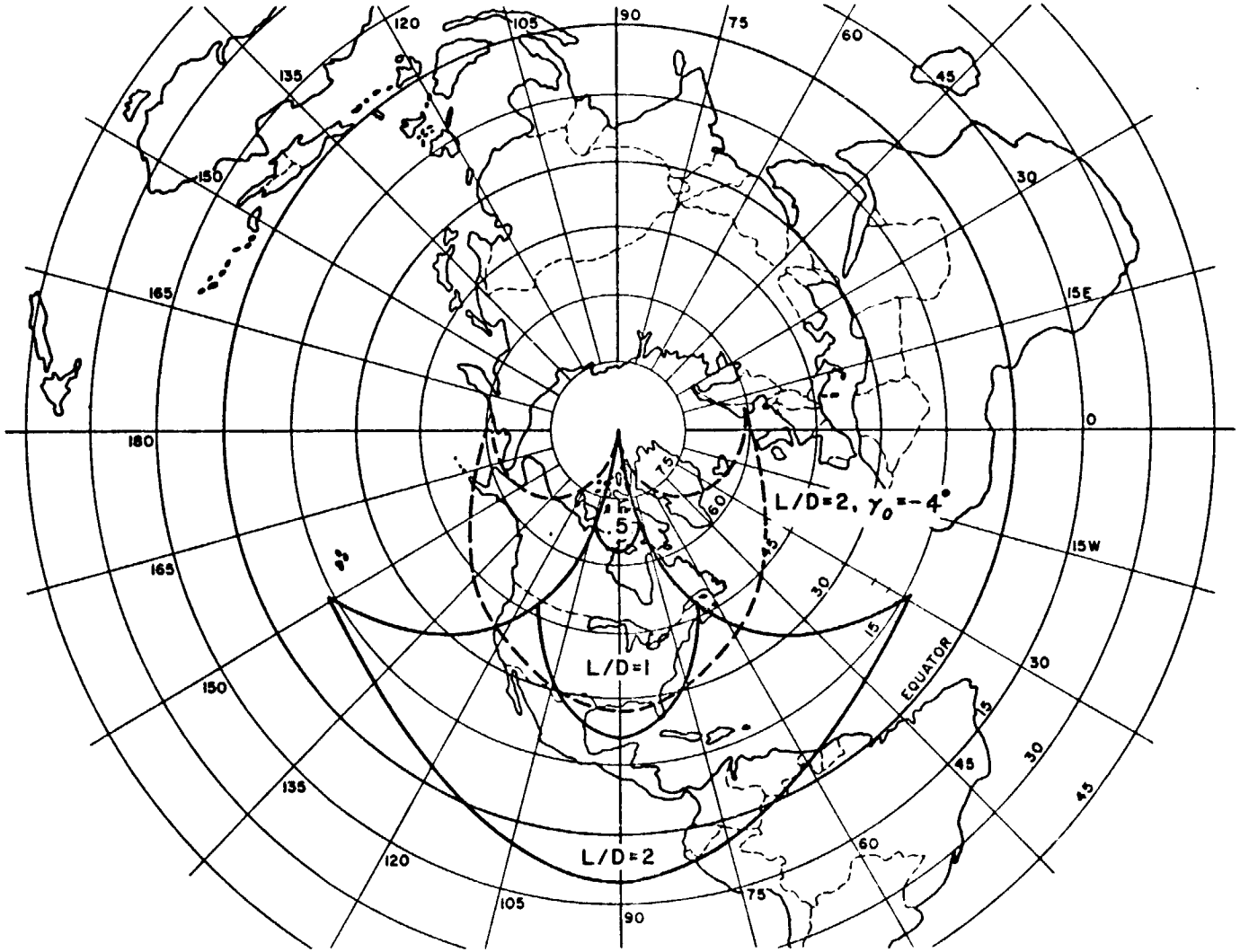

(a) $v_0 = v_c$, $\gamma_0 = -2°$, $W/C_L A$ = 20 psf = 957 newtons/m^2 (Ref. 14)

Fig. 68. Total Maneuverability Envelope

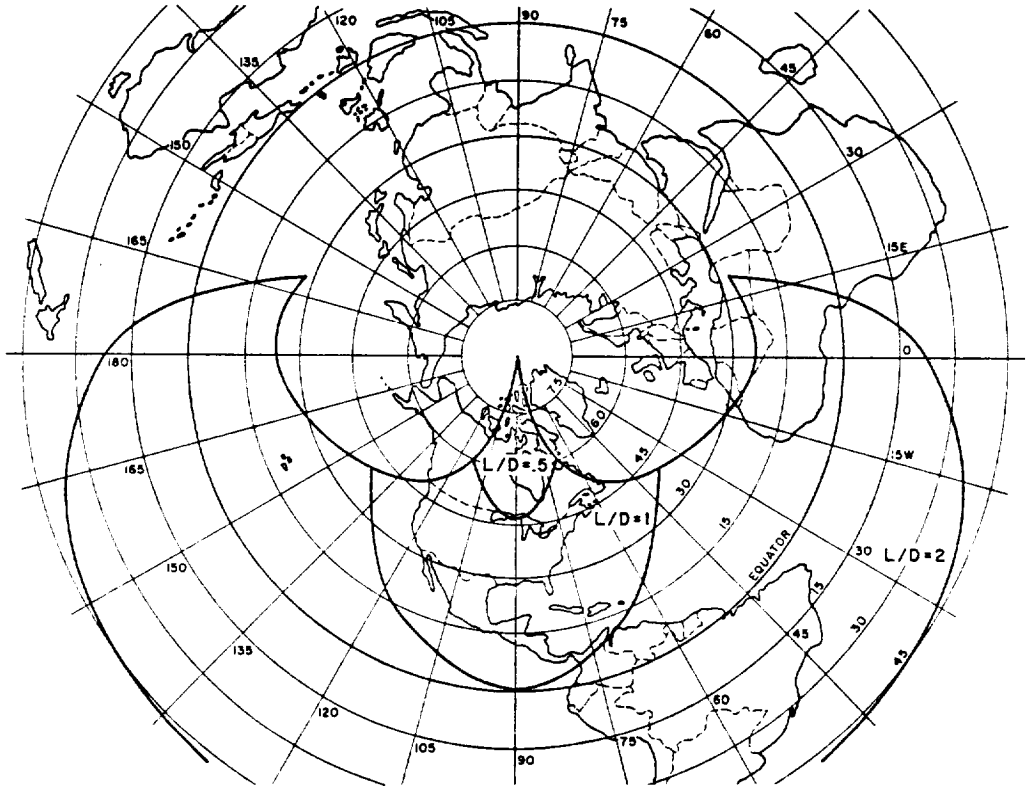

(b) $v_0 = \sqrt{2}\, v_c$, $\gamma_0 = -6°$, $W/C_L A = 100$ psf = 4787 newtons/m^2 (Ref. 14)

Fig. 68. (continued)

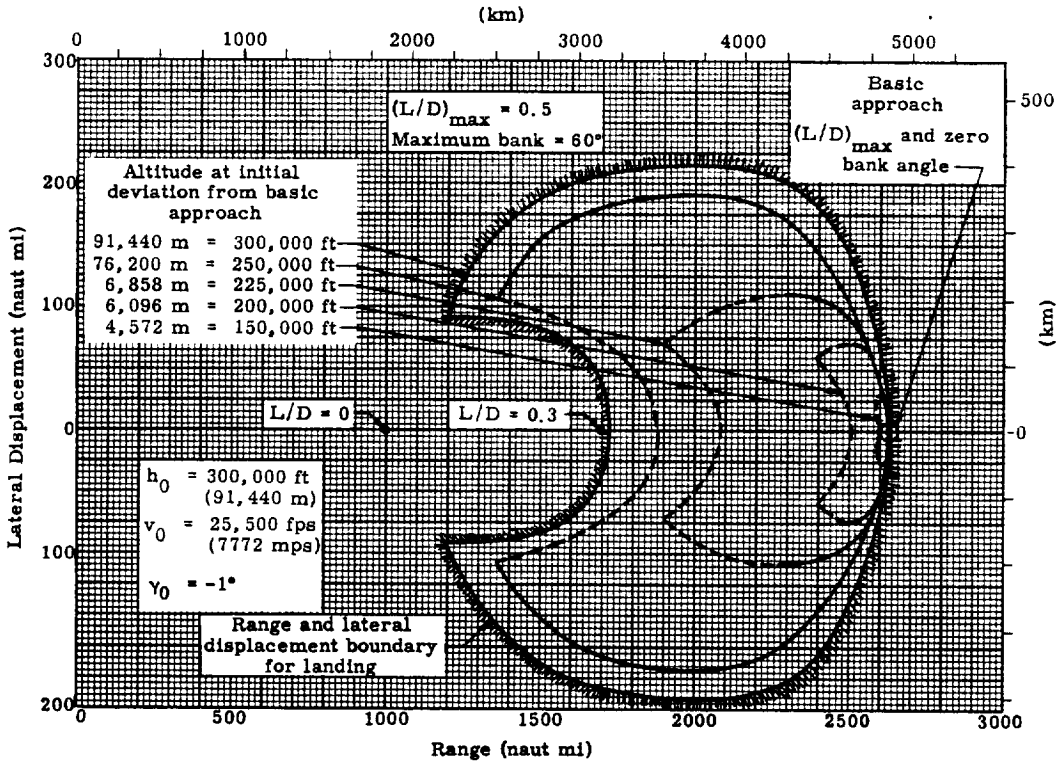

Fig. 69. Range and Lateral Displacement for Lifting Body Re-Entry

CHAPTER X

WAITING ORBIT CRITERIA

		Page
	Symbols	X-1
A.	Introduction	X-2
B.	Payload and Geometrical Restrictions	X-2
C.	Vehicle Temperature Control	X-4
D.	Cryogenic Propellant Storage	X-10
E.	References	X-15
	Illustrations	X-21

LIST OF ILLUSTRATIONS

Figure		Page
1	Equilibrium Temperature of Inert Sphere	X-23
2	Equilibrium Temperature of a Thin Plate Normal to the Sun	X-23
3	Effect of Attitude on Equilibrium Temperature of a Thin Plate Located at One Astronomical Unit from the Sun	X-24
4	Effect of Added Heat Input on Equilibrium Temperature	X-24
5	Vapor Pressure of Cryogenic Fluids	X-25
6	Heat Transfer Rates of Cryogenic Insulations, Thermal Conductivity Versus Vacuum Pressure	X-25
7	Thermal Conductivity at Various Wall Temperatures .	X-26
8	Heat Flux from Sun.	X-26
9	Solar Heating--Temperature of Outer Wall	X-27
10	Heat Transfer to Hydrogen and Oxygen.	X-27
11	No-Loss (Pre-Boiloff) Time--LH_2 Tank.	X-28
12	System Factors (S) Versus Time $S = I_w + \frac{tQ_l T}{v}$ . .	X-28
13	Propellant Boiloff Plus Insulation Weight at Optimum Insulation Thickness for Spherical Tanks on the Lunar Surface	X-29
14	Boiloff Losses for Liquids Contained in Spherical Tanks, General Case	X-30

X. WAITING ORBIT CRITERIA

SYMBOLS

A	Right ascension
A_e, A_i	Reference areas for emitted and incident energy
c_p	Specific heat at constant pressure
G	Solar flux
k	Thermal conductivity
l	Thickness
L	Latitude
p	Pressure
$\vec{P}$	Unit vector to perigee
Q	Transmitted heat flux
$\hat{R}$	Unit vector to the injection point
$\vec{S}$	Unit vector specified by launch time and time of flight to injection point
T	Absolute temperature
W	Weight
α	Absorptivity
γ	Ratio of specific heats
ϵ	Emissivity
θ	True anomaly
Λ	Longitude
ν	Heat of vaporization
ρ	Density
σ	Stefan-Boltzmann constant
τ	Orbital period

A. INTRODUCTION

In the previous chapters of this manual, the concept of waiting orbits or parking orbits was introduced. In some of these discussions the parking orbit was defined completely (i.e., all six elements were obtained) by the mission to be accomplished. The rendezvous discussion utilizing the intermediate orbit is an example of such cases. In other discussions, however, one or more of the orbital elements could be selected based on considerations other than those of the mechanics of the mission. When these degrees of freedom exist, the following factors are among those which become of interest:

		Chapter
(1)	the radiation environment	II
(2)	the meteoroid environment	II
(3)	atmospheric factors, heating, etc.	II, V
(4)	orbital perturbations	IV, V
(5)	satellite lifetimes	V
(6)	maneuver requirements	VI
(7)	recovery considerations	VIII
(8)	trajectory error sensitivities	XII
(9)	guidance and navigation philosophies	XII
(10)	solar elevation and eclipses	XIII
(11)	tracking station, area, and point coverage optimization	XIII
(12)	ground tracks and or synchronous behavior	XIII
(13)	optical resolution, etc.	XIII
(14)	staging considerations, reignition and economics	
(15)	radiation heat loads and cryogenic storage	

Because of the number of constraints which can be imposed, no single set of rules can be constructed which will yield the best orbit in the sense that each constraint is satisfied. Indeed, it is necessary to assign weights to each factor and to select the elements of the intermediate trajectory for each particular mission by a study of the tradeoffs involved. This phase of study will not be attempted here because of the scope of the task and the fact that the 15 previous constraints can be permutated into $\frac{15!}{n!(15-n)!}$ different combinations (taken n at a time) and $\frac{15!}{(15-n)!}$ different permutations.

All of these factors except the last two are discussed within the manual. The next to last item is a practical limitation imposed by the nature of the vehicle used to boost the satellite to orbit and as such was not covered within the present scope of study. Later paragraphs will, however, provide a short qualitative treatment. The final item on the list, though far from completing the possible list of constraints (e.g., human tolerances to radiation), falls into the same general classification of material. However, because of the fact that propellant is required for maneuvers and because radiation heat loads cause problems of storability and boiloff, some of the problems are presented. The level of these discussions, however, will be superficial since the theory of heat transfer is a study in itself and since in any case the specific vehicle must be considered to obtain design data. The presentation of this material, though brief, will begin to tie the purely mechanical analyses of the remainder of the manual to system or operational requirements.

B. PAYLOAD AND GEOMETRICAL RESTRICTIONS

The parking orbit concept was introduced in several chapters (e.g., VII and IX) to assure that some given parameter (usually time) could be factored into the 3-dimensional analysis without requiring drastic maneuvers at launch. Thus, the primary advantage was in the area of timing the mission. However, there are three other distinct advantages:

(1) Flexibility

(2) Energy reductions

(3) Error correction.

Flexibility in planning and executing the mission is afforded because the intermediate orbit, if selected properly, increases the number of times at which transfer to a given position or orbit is possible. Also, since the orbit is to be utilized in any event, the launch can occur at any of the crossings of the orbital plane by the launch site. Thus, the effects of countdown holds can be reduced.

The energy requirement utilizing this technique is generally reduced because of two factors. First, the out-of-plane maneuver can be eliminated (or nearly so if there are small launch time errors) and secondly, the type of transfer trajectories can be energy optimized since the timing problem is handled separately. It is noted, however, that there may be times in which parking orbits will require an increase in energy. These cases are those for which the problem timing was correct for direct launch and ascent via a near optimum trajectory since under such conditions the work expended in transporting propellant to an intermediate orbit for future burning is not recoverable. (If this situation is in fact true, it can, however, be assessed so that in no case should an unnecessarily high energy requirement exist.) This energy loss points up the case for a low altitude parking orbit. The practical limit for this orbit will be mentioned later.

The third advantage is that of affording a convenient interval for either correcting for launch errors or computing changes in the transfer trajectory to compensate for them. Because of this feature, the intermediate orbit approach will result in smaller errors in the position and velocity in space at the time of arrival at the designated transfer point.

The discussions which follow combine the flexibility and energy considerations in a brief summary of some of the material presented elsewhere in the manual (the emphasis here being in the selection of the intermediate orbit). Consider the following sketch and angular definitions:

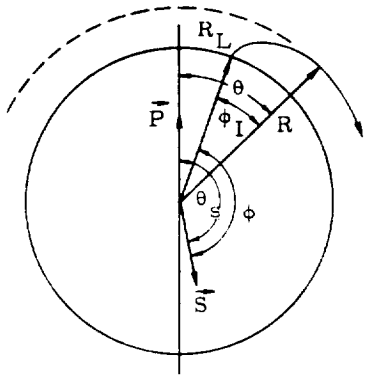

$$\theta = \theta_s - \phi + \phi_I$$

where

θ_s = perigee-outward radial angle

ϕ = launch-outward radial angle

ϕ_I = total burning arc (launch-to-injection)

$\vec{P}$ = unit vector directed toward perigee

$\vec{S}$ = unit vector in outward radial direction (specified by launch date and flight time).

Since θ_s and ϕ_I are relatively invariant (with zero coast capability), it is necessary to vary ϕ by launch azimuth or outward radial declination. (Launch azimuth is restricted by range safety; to change the outward radial declination the mission must be altered). By employing a variable coasting arc ϕ_I may be replaced by $\phi_1 + \phi_c + \phi_2$ where ϕ_1 is the burning arc necessary to get into the parking orbit and ϕ_2 is the burning arc from parking orbit to final injection. Given a launch azimuth (or time) and mission (outward radial declination), the powered flight is matched to the post-injection trajectory by varying launch time (or azimuth) and parking orbit coast time. This is illustrated in the following sketch.

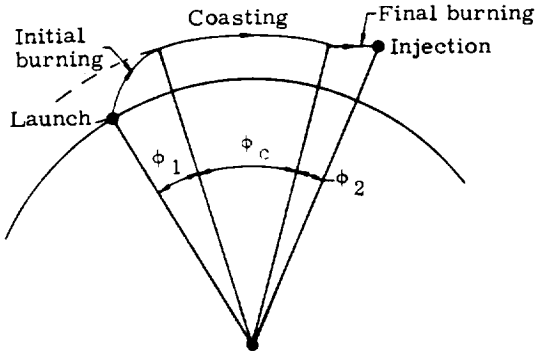

$$\theta = \theta_s - \phi + (\phi_1 + \phi_c + \phi_2)$$

The lowest possible altitude should be selected for the parking orbit from energy considerations. Since the energy requirement is lower, this selection also provides the greatest payload capability. The minimum altitude which can be utilized, however, depends on vehicle engineering constraints such as aerodynamic heating and structural loading, on guidance constraints, such as minimum elevation angle, and on mission constraints requiring specified orbital characteristics (all enumerated in the introduction). However, if the payload capability outweighs the other factors, a parking orbit altitude in the vicinity of 100 to 110 naut mi (i.e., 185 to 204 km) appears to be the best choice.

Thus everything is defined in terms of the parameters of the problem save the vector $\hat{R}$. This unit vector is obtained utilizing the spherical trigonometric relationships in Chapter III for right ascension and declination or latitude and the identity

$$\hat{R} = \cos A \cos L \hat{x} + \sin A \cos L \hat{y} + \sin L \hat{z}$$

where

$\hat{R}$ = unit vector directed from earth's center to injection

A_I = right ascension of injection

L_I = injection latitude

$\hat{x}, \hat{y}, \hat{z}$ = unit vectors, earth centered inertial cartesian system (aligned as x, y, z) with x toward vernal equinox

This location will of course vary considerably with launch time delays since the interval in the intermediate orbit must be adjusted accordingly.

Corresponding to this value of A and L, there is a unique value of longitude for injection. This value may be obtained from the following equation.

$$\Lambda_I = A_I - A_L - \Omega_e t_I + \Lambda_L$$

where

A_L = launcher right ascension

Λ_L = launcher longitude

$t_I = t_1 + t_2 + \phi_c / \dot{\phi}_c$

$\dot{\phi}_c$ = constant parking orbital rate,

$= \frac{2\pi}{\tau} = \sqrt{\frac{\mu}{a^3}}$

This brief review points up some of the factors affecting the selection of a parking orbit and indicates the desirability of restricting the altitude of such an orbit. The discussion has, however, been purely qualitative since more complete discussions are available in Chapters VI and VIII as well as in the literature.

C. VEHICLE TEMPERATURE CONTROL (REF. 1)

The general temperature control problem can be conveniently subdivided into two requirements.

(1) Maintaining the mean temperature of the spacecraft components within limits dictated by tolerances of the components.

(2) Preventing fluctuations about the mean temperature which might impair the general reliability.

Depending on the mission requirements, there are several possible solutions for these problems:

(1) Independent local control of sensitive components.

(2) General control of the mean temperature of the total spacecraft.

(3) General control of the mean temperature of the total spacecraft plus control of the fluctuations about the mean temperature.

(4) Various combinations of the above.

The major factors involved in the temperature control problem will be examined leading to a discussion of various control methods.

1. Heat Balance

The mean temperature of an object in space is determined by the energy balance on that object. Except for the dwell time in a planetary atmosphere, a spacecraft is generally in a vacuum far below that which will support conductive or convective transfer, and since mass transfer is generally negligible, the only significant exchange is by radiation. Consider for simplicity a satellite made of a material of infinite thermal conductivity so that it is at a uniform temperature throughout. If it is not in the vicinity of a planet and has no internal power its energy balance, at equilibrium, is found by equating the absorbed solar energy with the infrared energy emitted from the spacecraft:

$$\alpha G A_i = \epsilon \sigma T^4 A_e$$

$$T^4 = \frac{\alpha}{\epsilon} \frac{G}{\sigma} \frac{A_i}{A_e} \qquad (1)$$

where T is the absolute temperature, α is the absorptance of the surface coating for the zero air mass solar spectrum, ϵ is the emittance of the surface for the black body infrared spectrum corresponding to the temperature of the spacecraft, G is the solar flux at the local radial distance of the spacecraft from the sun, σ is the Stefan-Boltzmann constant, A_i is the cross-sectional area intercepting solar energy, and A_e is the emitting surface area. Kirchhoff's law for opaque materials states that absorptance equals emittance (for bodies at the same temperature) at a given wave length or integrated over the same spectral curve. But since the two bodies of this problem are not at the same temperature and since α is here reserved for the solar wavelengths and ϵ for the infrared wavelengths, α in general does not equal ϵ. The fourth power of the temperature is seen in Eq (1) to be proportional to the ratio of α to ϵ so that the ratio itself becomes a convenient material property of interest (see Fig. 1).

If internal power w is uniformly dissipated throughout the imaginary spacecraft, the energy balance then becomes

$$\alpha G A_i + w = \epsilon \sigma T^4 A_e$$

$$T^4 = \frac{\alpha}{\epsilon} \frac{G}{\sigma} \frac{A_i}{A_e} + \frac{w}{\epsilon \sigma A_e} \qquad (2)$$

The effect of the internal power on the mean temperature depends on the ease with which that energy can reach the surface and be radiated away, which in the case of our infinite conductivity spacecraft is a function of the emittance ϵ only. Thus, the emittance must be considered separately as well as in the ratio of α/ϵ. It has often been the case that the second term on the right of Eq (2), the internal power term, is small relative to the first term, so that the internal power produces a minor effect on the spacecraft mean temperature.

It has been assumed that the spacecraft exterior is a continuous surface of a single material. This is generally not the case. However, under the assumption of infinite conductivity the case of multiple surface materials with no internal power, is expressed by

$$T^4 = \frac{G}{\sigma} \left[\frac{\alpha_1 A_{i1} + \alpha_2 A_{i2} + \dots}{\epsilon_1 A_{e1} + \epsilon_2 A_{e2} + \dots} \right] \qquad (3)$$

where the numerical subscripts represent the n surface materials. If the idealized isothermal spacecraft has moved to the vicinity of a planet, the energy balance including the transient effect becomes:

> [the absorbed solar energy + the absorbed solar energy reflected from the planet + the absorbed planet emitted energy + the internally dissipated power + the stored energy] equated to the infrared energy emitted by the spacecraft.

Symbolically,

$$\Sigma \alpha_j G A_{iSj} + \Sigma \alpha'_j E_R A_{iRj} + \Sigma \epsilon'_j E_E A_{iEj}$$

$$+ w + Wc_p \frac{dT}{dt} = \Sigma \epsilon_j \sigma T_j^4 A_{ej} \qquad (4)$$

where G is the solar flux at local distances of spacecraft from sun, E_R is the flux of solar energy reflected from the planet, E_E is the flux of planet emitted energy at the altitude of the spacecraft, A_{iS} is the area absorbing direct solar energy, A_{iR} is the area absorbing reflected solar energy, A_{iE} is the area absorbing the planet's emitted energy, α' is the absorptance of the solar reflected energy, ϵ' is the absorptance for the planet's emitted energy, w represents the internally dissipated power, Wc_p the thermal capacity of the shell, t is time, and the summation signs indicate that the appropriate terms are summed over the j isothermal surface areas.

Depending on the spacecraft thermal design, and its particular orbit and altitude, the magnitude of the energy exchanges shown in Eq (4) varies, in turn causing changes in the mean temperature of the spacecraft. These factors are discussed qualitatively in the following sections. More detailed analytic discussions are to be found in the bibliography.

a. Solar flux input

The mean value and variations about the mean are most strongly affected by direct solar radiation. Solar flux input is dependent on orientation of the surface, time of exposure, look angles with respect to sun, wavelength of received and emitted radiation. In addition there is the roblem of solar eclipses due to the planets (see Chapter XIII).

One effect of the eclipse of an earth satellite is the transient cooling during the eclipse. The extent of this, in a simplified model, depends on the thermal capacity of the satellite and the external radiation resistance as determined by the surface infrared emittance. In an actual satellite the various components each have different thermal capacities and different thermal couplings to the exterior, and will therefore experience different transient thermal behavior during the eclipse. The other important thermal effect is due to the reduction in the total solar radiation input integrated around the orbit. For example, a satellite in a polar orbit will at one time during the year experience full sun, and at another time of the year, if in a low altitude orbit, the total solar flux averaged around the orbit will be only slightly greater than one-half of the nominal value. The present best estimate of the nominal value of the solar flux at the earth's mean orbital distance from the sun is 442 Btu/hr-ft^2 (1199 kcal/hr-m^2) with an uncertainty of ±2%. The ellipticity of the earth's orbit results in a ±3.7% fluctuation in the solar input throughout the year, so that other factors remaining constant, a satellite will be about 9° R (5° K) hotter in December than in June. The limit cases for the effect of earth orbits in solar radiation input may be divided as:

Ecliptic. A satellite whose orbit lies in the ecliptic plane at same time will be eclipsed by the planet once each orbit throughout the time required for the planet to rotate the orbital plane out of the ecliptic by an amount dependent on the orbital elements.

Equatorial. If the orbit lies in the equatorial plane, and is at a relatively low altitude, the satellite will be eclipsed each orbit. At a sufficiently great altitude, because of the 23-degree tilt of the earth's equatorial plane, the satellite will experience an eclipse once each orbit during two periods of the year and will experience no eclipses for the other two periods. This is the case for a satellite in a circular, equatorial 24-hour orbit about the earth.

Polar. The polar orbit is similar to the high altitude equatorial case in that the satellite is eclipsed once each revolution for two periods during the year and is in full sunlight for the other two periods. Each of the two eclipsing intervals start out with an eclipse of momentary duration, gradually increasing to an eclipse of maximum duration (the time depending on the satellite velocity) and gradually decreasing the shorter eclipse durations.

Special. One special class of orbits [approximately 81° retrograde, depending on the semilatus rectum] has the property that the nodes regress such that the 1° per day shift in the direction to the sun is canceled. In this orbit the satellite will be in full sun continuously throughout the year or, depending on the launch time during the day, eclipsed once each orbit throughout the year. The duration of the eclipse depends on the altitude of the satellite and the ellipticity of the orbit. For example, in a highly elliptical orbit it is possible to have very long eclipses, if they occur at the apogee of the orbit; however, it is possible to delay the occurrence of such an apogee eclipse (resulting from orbital precession) for several years, depending upon the orbit characteristics, by suitable choice of launch time.

b. Planetary emitted flux

For the earth and presumably for any planet with an appreciable atmosphere the infrared energy emitted by the planet is relatively independent of latitude and longitude and varies in a predictable manner with altitude. In the case of the earth at low altitudes the flux is about 68 Btu/hr-ft^2 (184 kcal/hr-m^2). In cases where there is no atmosphere, as for the moon, the emitted flux must be considered to vary with angular position measured from the subsolar point because of the large temperature variations on the surface.

The earth-emitted flux injects two sources of error which must be accounted for in the thermal design of the spacecraft. One is the magnitude of the flux, which is known with much less precision than that of the solar flux. (This lack of knowledge is even more applicable of the moon, and for the other planets there is relatively poor knowledge of the planetary thermal balance conditions and the emitted flux). The second is the lack of adequate knowledge of the emission spectral characteristics. In the case of the earth, for example, it is known that the emitted flux comes primarily from the surrounding gaseous atmosphere which has spectral characteristics differing significantly from the black body spectrum corresponding to the earth's equilibrium temperature. Lack of knowledge of this spectral characteristic results in an uncertainty in the effective absorptance of the spacecraft surface material for the earth emitted energy.

c. Planetary reflected solar energy

The same altitude dependence applies for the solar energy reflected from the earth or nearby planet as for the infrared energy emitted by the planet. In addition the reflected solar energy varies with the orbit plane attitude with respect to the sun and the instantaneous position in the orbit. For example, in a twilight polar orbit the reflected solar flux is approximately constant, whereas in a noon orbit in which the sun

lies in the orbit plane the reflected flux varies from zero to a maximum of about 160 Btu/hr-ft^2 (434 kcal/hr-m^2) at the sub-polar point.

The magnitude of this flux is approximately as uncertain as that of the earth emitted flux and is known to vary with such factors as cloud coverage. The absorptance of the surface materials for the planetary reflected solar energy is not precisely the same as for the direct solar flux because of changes in the spectral characteristics after reflection from the planet and its atmosphere. The magnitude of these changes and the corresponding change in the effective absorptance for this flux is not well known.

d. Spacecraft characteristics affecting heat balance

The internal and surface characteristics of the vehicle itself are important in temperature control since they define the radiation losses to space and to internal heat boundaries (equipment heat dissipation and thermal inertias). A thorough review of thermal balance and uncertainties is given by Comack and Edwards (Ref. 2) and a qualitative discussion is presented below.

Thermal radiation properties. Knowledge of the thermal radiation properties of the spacecraft surfaces can be deficient in two respects. The first has to do with uncertainties in measurement of the properties in the laboratory, and the second is concerned with the changes in those properties due to handling and exposure to the air before launch, to heating during ascent to orbit, and to exposure to the space environment.

Shape and attitude considerations. A spin stabilized spacecraft has the spin axis nominally fixed in inertial space, though various disturbing torques and tip-off errors can decrease the spin rate and gradually shift the spin axis attitude in space. An attitude controlled spacecraft is not affected as much by these uncertainties. Cornog (Ref. 3) shows that if the attitude of the vehicle can be controlled, the same aspect of the vehicle can be presented to the sun at all times. If low vehicle temperatures are desired, the portions of the surface exposed to the sun can be made highly reflective, the unexposed portions can be covered with some material having good radiative properties, and by changing the shape or treating each vehicle quadrant with the desired α/ϵ materials, the effective absorptive area exposed to sunlight can be made quite small.

Internal temperature gradients. The preceding factors all result in either variations or uncertainties in the spacecraft mean temperature. (Mean temperature can be defined as that temperature which the spacecraft would attain assuming zero thermal resistances.) In an actual vehicle, temperature variation can be quite large. For example, temperature differences exceeding 100° F (38° C) were encountered in Explorer VI. Thus a given component in this spacecraft located near one end of the thermal gradient would experience large changes in temperature as the sun orientation changes and during the spacecraft lifetime.

Internal power fluctuations. As various components are turned on and off, or changed in power level, the locally dissipated energy causes local temperature changes, the amount depending on the power dissipated and the particular thermal circuitry of the spacecraft interior. This internal power dissipation may range from a few watts to kilowatts depending on the equipments required for the mission.

2. The Effects of Thermal and Optical Properties on Temperature Control

a. Thermal radiation properties and materials

Coating the surface of the spacecrafts external structure with thin lightweight material may provide the needed thermal radiation properties. These coatings may in some instances be more effective if applied in patterns of several materials (for example the combination of vacuum deposited aluminum and anodized aluminum in adjacent areas). Values of solar absorptance α and infrared emittance ϵ covering the entire range from 0 to 1 are useful for these coatings. In particular, both high and low values of the ratio of α/ϵ are especially useful for certain forms of active temperature control systems. A good material should absorb over the entire thermal spectrum, that is, have high α and high ϵ. (Materials which reflect well over the entire spectrum, that is, have low values of α and ϵ, are also useful, although this combination can sometimes be achieved by insulation.)

A great body of thermal radiation data exists in the literature. While these data are useful as a guide to the kinds of properties obtainable with various types of materials, most of it is useless for space applications. There are a variety of reasons for this fact:

(1) The data is not applicable because of the following reasons: much of it is reported for radiation properties not directly applicable to the spacecraft thermal control problem; in general, the diffuse properties are required, but most data reported is for specular properties; for emittance, hemispherical values are generally required, but most data reported is for normal or near-normal angles; absorptance data is not available as a function of incident angle but most data reported is for a single near-normal angle; much emittance data reported is for a total measurement, which is often made at a relatively high temperature (such data is applicable to a somewhat incorrect spectral curve and to the wrong material temperature); finally the total solar absorptances are often measured directly with the solar energy as it exists at the laboratory (this spectrum is generally markedly different from the solar spectrum in space).

(2) Measurement errors. Only in the past few years have the subtleties of the various types of radiation measurements and techniques been fully appreciated (Refs. 4 and 5). Equipment and techniques to measure directly the appropriate properties are in many cases still lacking. From the standpoint of the designer using the data, such errors represent serious shortcomings and must

be fully recognized. A few of the common sources of errors are: lenses and mirrors which do not have spectrally flat optical characteristics are often present in the instrument optical path; water vapor may be present in detrimental amounts; the reflecting surface in integrating spheres, often MgO, is sensitive to water vapor and may have to be renewed frequently; MgO is partially transparent in the wavelengths for which it is used and must be applied in a relatively heavy coat to avoid erroneous data, a fact not always appreciated by the experimenter; nonuniform wall temperatures with variances in the infrared reflectance yield erroneous data; spectral measurements are difficult to obtain at wavelengths longer than about 50 μ, and much of the available equipment is limited to about 25 μ. This last point is significant in its effect on the property obtained for a low temperature spectrum (for example, 18% of the energy of a 50° F (10° C) black-body spectrum and 36% of a -100° F -73° C spectrum are both beyond 25 μ).

(3) Materials not well defined. Much of the reported data represents materials which are poorly defined. For example, the surface optical properties are usually sensitive to the details of a materials processing technique. Because of incomplete or inadequate description of the material, the materials cannot generally be duplicated, rendering useless a large part of the reported data. In most cases the only solution to this situation is to measure the required properties for each material.

Once the spacecraft has been prepared with materials of the desired properties, there remains a practical problem of making certain that the properties remain unchanged before the spacecraft reaches altitudes above the atmosphere. A certain amount of handling of the exterior surfaces may be unavoidable. Some of the more delicate coatings can be protected by plastic peel-coats until a few days before the scheduled launch, but if any last minute cleaning is necessary to remove fingerprints, grease, dirt, etc., there is always a danger that the cleaning process itself may affect delicate surface properties. During the launch interval the satellite and its materials are presumably protected from aerodynamic heating by a protective fairing, which is jettisoned after leaving the sensible atmosphere. Because of the weight penalty in carrying the fairing along longer than necessary, there is often a tendency to jettison it too soon, thereby heating the satellite surfaces to a level which may affect the optical properties of the surfaces.

b. Optical properties in the space environment

Most of the factors of the space environment represent new and untried conditions for spacecraft materials. Whether these materials and in particular their sensitive surface optical properties remain stable in this environment is a question of importance for all spacecraft with long intended lifetimes. Among the factors of importance are:

(1) The vacuum of space, in which the pressure is such that sublimation and decomposition occur virtually unimpeded.

(2) Ultraviolet radiation, X-rays, and the harder radiation of the radiation belts.

(3) Single particle radiation.

(4) Micrometeorites.

Certain of these factors may present no problems. For example, micrometeorites are generally believed to be of sufficiently low flux that they will have no significant effect in spacecraft thermal control (Ref. 6). Many of the other factors of the space environment are difficult or impossible to reproduce in the laboratory, even singly, let alone in combination. In addition, the designer does not always have the freedom to choose materials which are rugged since certain optical properties are available only in delicate, vacuum deposited forms. Since these surfaces can be delicate, sufficient flexibility must be allowed to provide for some change in materials optical properties due to exposure in the space environment. (Some of the important optical properties of various materials are summarized in Table 1.)

3. Vehicle Temperature Control Systems

a. Passive

A passive thermal control system is defined here to be one employing fixed external coatings in which there is no active element either mechanical or electrical. Since the mission requirements in orbit, the lifetime, the internal component complexity, etc., have generally been sufficiently simple from the thermal environment standpoint to allow a passive system to be used successfully, the great majority of spacecraft flown to date have had passive thermal control systems. Experience demonstrates that a passive design can achieve a spacecraft mean temperature in orbit within about 5 to 10° F (2.8 to 5.6° C) of the designed mean temperature (for example, in the case of Explorer VI).

An interesting application of a passive design was that of Pioneer V, a spacecraft designed to reach the vicinity of the Venus orbit. In the course of its journey, it would experience approximately a doubling of the solar flux from that occurring at the earth's distance from the sun. This spacecraft was spin stabilized, that is, with its spin axis fixed in inertial space. In an approximate manner, the trajectory flown may be considered to be such that the sun moved half-way around the spin axis during the half orbit to Venus. That is, the sun look-angle would increase from zero, looking straight down the spin axis at one end of the spacecraft, to 180°, looking at the opposite end of the spin axis and spacecraft. If the external coating was chosen to be appropriate for the solar flux at the earth's distance from the sun at the start of the flight (sun look-angle equal to zero) and also chosen appropriately on the other half of the spacecraft for the Venus distance from the sun, then in a rough sense the coating would be appropriate at both the earth and at Venus. In actual fact, partly because of three-dimensional effects and partly because of other considerations, the orbit that was flown resulted in a sun look-angle of 35° at the start,

TABLE 1

Optical Properties of Various Materials (Ref. 3)

Material	Degrees Fahrenheit	Degrees Centigrade	Absorption Number α	Emissivity ϵ	Ratio α/ϵ
Silver	100	37.7	0.04	0.02	2.0
Aluminum, polished	100	37.7	0.10	0.05	2.0
	1000	538	-	0.06	
Aluminum, 2024, buffed and polished	100	37.7	0.34 to 0.37	0.03	12.0
Stainless steel, black	100	37.7	-	0.90	-
	1000	538	-	0.90	-
Stainless steel, polished	100	37.7	0.40	0.05	8.0
Fused quartz, bricks, hard rubber, asbestos	100	37.7	0.1 to 0.4	0.90	0.2
	1000	538	-	0.90	-
Lamp black	100	37.7	0.95	0.95	1.0
	1000	538	-	0.95	-
SiO on polished metal	100	37.7	0.1	0.90	0.1
MgO	100	37.7	0.15	0.97	0.15
Titanium, 6A1-4V	100	37.7	0.8	0.18	4.4

decreasing to about 15° at 20 days, back to 35° in about 40 days, and increasing to 135° upon reaching the Venus orbit at approximately 105 days after launch. A pattern was chosen using two materials, one with an α of 0.92 and ϵ of 0.87 and the other with an α of 0.25 and an ϵ of 0.85. A pattern was achieved which maintained a mean temperature within the desired range over the entire trajectory, as well as at the end points of Earth and Venus. During the 3-1/2 months of transmitted data, the measured temperatures followed the predicted curve within about 5° to 10° F. The flight path that was finally selected was not the optimum one from trajectory considerations but rather was chosen to satisfy a thermal control requirement that the sun look-angle increase from approximately 0 to approximately 180°. It would be entirely possible, from trajectory considerations alone, for the sun look-angle to start at 90° at the earth, decrease to zero and increase back to 90° at the Venus orbit. Clearly the coating pattern and therefore the effective α/ϵ of the spinning spacecraft at both the earth and Venus would be the same and would therefore not compensate for the increase in solar flux. The actual sun look-angle history noted above was about the limit of allowable deviation from the ideal 0 to 180° change.

b. Active

A variety of mechanizations of active control may be envisioned:

(1) The spacecraft can be kept relatively cool by means of passive coatings, but still warm enough to satisfy the majority of the components. (Local thermostatically controlled electrical dissipation can be provided to warm those few components requiring a higher temperature.) While this scheme is quite feasible, the types of components which require the heating, (such as liquid fuel tanks and secondary storage batteries) may be so large that the "local" heating may involve a large fraction of the spacecraft power. Unless excess power is available such a design may not be practical from the point of view of the overall system.

(2) With a nonspherical shape, such as a relatively flat disc, the mean temperature can be increased or decreased by orienting the spacecraft so as to increase or decrease the surface area intercepting solar energy (see Figs. 2, 3 and 4). However, normally, this design would not be practical in view of other conflicting requirements for the spacecraft attitude control system.

(3) A number of materials change optical properties as a function of temperature. For example, silicon monoxide and other materials like it have the self-controlling tendency to increase in emittance as temperature increases, thus tending to limit the temperature rise, and vice versa. Various experimenters are currently examining such materials, but the materials unfortunately have a general characteristic that their emissivity is too weak a function of temperature to be advantageously employed.

(4) Some number of materials undergo reversible optical property changes as a result of phase changes, Curie point

transitions, etc. For example, the so-called thermochromic materials reversibly change color, and therefore solar absorptance, as a sharp function of temperature. Unfortunately these materials may be in the form of gels, liquids, etc., generally with low vapor pressures and therefore unsuitable for the exterior surface. They could be encapsulated in materials transparent in solar wave lengths but at the present at least they would not seem to offer enough advantages to overcome their obvious shortcomings for use in a temperature control system.

(5) Mechanical changes of radiation properties and areas are the systems presently given most consideration.

These mechanizations are embodied in two general types of active vehicle temperature control designs, the radiation balance design and the insulated design. Any thermal design is at least partially a combination of the two and there are many designs in which both the external radiation balance and the insulated features are combined in a single application.

Radiation balance type. In a radiation balance design the internally dissipated power is generally a small factor in the overall heat balance and therefore contributes only in a minor way to the mean temperature level, although the dissipated power may have important local effects. The energy relationship is then a balance, in the equilibrium state, between the absorbed incident radiant energy and the emitted radiant energy. Active control of the temperature may be effected by varying the exposed areas of two materials, one with a relatively high α/ϵ ratio and one with a relatively low α/ϵ ratio. This can be accomplished by a venetian blind arrangement, moving vanes, or in a variety of other ways.

The first spacecrafts with such a temperature control system were the Atlas/Able 4 and Able 5 satellites. These were intended to be orbiting satellites of the moon, to be put into lunar orbit by means of monopropellant hydrazine engine aboard the spacecraft to reduce the approach velocity sufficiently to allow lunar capture. Partly because of the hydrazine fuel and fairly severe environmental conditions, such as lunar eclipse durations exceeding two hours, it was necessary to employ an active thermal control system. The spacecraft was spin stabilized, thus an arbitrary sun orientation with respect to the spin axis was possible during the spacecraft lifetime.

Briefly, the thermal design was as follows. Thermal energy exchange took place primarily at 50 circular areas well distributed over the external skin. Each circle consisted of an alternating arrangement of two materials in the eight 45° sectors of the circle, one material with a high α/ϵ ratio and the other a low α/ϵ ratio. The circular areas were covered by a four bladed mask which could completely cover one or the other of the two materials, or some fraction of each at any intermediate position. The mask was driven by a bimetallic spring device at the inner end of the body, arranged so that the bimetallic device sensed a portion of the spacecraft interior. The plastic body of the unit was made of a poor thermal conductor so that the bimetallic spring was better coupled thermally to the spacecraft interior than it was to the skin of the spacecraft. The mask was rotated the 45° of its travel by a 25° F change in temperature of the spring. With the spring at 50° F the mask fully exposed the high α/ϵ material, and at 75° F the low α/ϵ material was fully exposed. The activation thus provided self-powered, closed-loop control of the interior temperature. The remainder of the spacecraft's skin, outside the control circles, was covered with a material of low α and low ϵ so that the contribution to the overall energy balance from the uncontrolled area would be as small as possible. That area was vacuum-deposited aluminum, over a smooth plastic substrate, with an absorptance of 0.10 and an emittance of 0.05. The high α/ϵ material in the control areas was a form of titanium dioxide with an α of 0.65 and an ϵ of 0.13, and the low α/ϵ material was a particular form of anodized aluminum with an α of 0.20 and an ϵ of 0.80. A more complete description of this system is given in Ref. 7.

The system has the capability of compensating for fairly large changes in the external environment, such as an interplanetary mission to Venus, and furthermore it minimizes the decrease in temperature during long eclipses because the masks automatically decrease the effective emittance of the spacecraft during this time.

Insulated type. If a spacecraft is always oriented so that the sun irradiates only certain of its sides but not others, as may be the case in a fully attitude controlled or a spin stabilized spacecraft, it is possible to insulate the solar irradiated sides so that the solar input plays little or no part in the spacecraft energy balance. (A very high order of insulation may be achieved for the spacecraft sides with multiple layer reflective insulation.) If for simplicity the spacecraft is considered to be far removed from a planet, then the energy balance is achieved between the internally dissipated power, the transmitted solar heat load and the spacecraft emitted energy. The unirradiated, uninsulated faces are covered with a surface of high emittance, and the emitted radiation is controlled by a set of louvers (external coverings to the radiation plate). The emitting area is then a function of the louver position, which may be controlled by sensors measuring the radiation plate temperature to which the spacecraft components are mounted. If the louver is irradiated, the system may still be employed if the radiation plate is covered with a material of sufficiently low α and high ϵ, to minimize the solar input. It is required that the internally dissipated power be at least as great as the heat losses from the entire spacecraft when the louvers are fully closed.

The advantages of this design are that the spacecraft is insensitive to eclipses and other changes in the solar flux, such as would occur on an interplanetary journey. The temperatures within the spacecraft are much more uniform than in the radiation balance design since there is no large external input over any part of the surface, and the problem of sensitivity of optical properties

of the space environment is greatly diminished. The primary property of interest is the high emittance on the radiating plate, but this is a property which tends to be stable in space environment (Ref. 8).

D. CRYOGENIC PROPELLANT STORAGE (Ref. 9)

Cryogenics is concerned with the phenomena of low temperatures, normally those below T ≈ - 250° F (-157° C). To be more specific, cryogenic storability involves the prevention of excessive boiloff of cryogenic fluids (e.g., liquid oxygen, liquid fluorine, liquid nitrogen, liquid hydrogen, and liquid helium) over varying periods of time. These stored fluids can be used for any of the following purposes:

(1) Supplying other vehicles or stations (logistic use).

(2) Maintaining state-of-readiness in ballistic missiles or for satellite propulsion (operational use).

(3) Thermal shielding during times of increased flux.

1. Properties of Cryogenic Fluids

Insofar as space vehicles are concerned, there are six important cryogenic fluids: liquid hydrogen, liquid helium, liquid nitrogen, liquid fluorine, liquid oxygen, and liquid ozone. Table 2 gives the basic properties, except vapor pressure, of these fluids and of liquid neon and liquid argon. Figure 5 presents the vapor pressure of these fluids as a function of temperature and pressure. Definition of properties is as follows:

(1) Heat of vaporization (ν). The number of heat units required to vaporize one unit weight of liquid at its normal boiling point.

(2) Boiling point. Absolute temperature, at which liquid boils under one atmosphere of pressure.

(3) Freezing point. Absolute temperature, at which the liquid freezes, under one atmosphere of pressure (except liquid helium).

(4) Critical point. The combination of pressure and temperature of a liquid and its vapor under equilibrium conditions that causes the two phases to be indistinguishable.

(5) Density (ρ). Density of the gas phase in units of force per unit volume.

(6) Specific heat ratio (γ). Ratio of specific heat at constant pressure (c_p) to specific heat at constant volume (c_v).

(7) Vapor pressure (p). The vapor pressure of a liquid is defined as the pressure of saturated vapor over the liquid. It varies with temperature. In the design of cryogenic tankage, the relationship of vapor pressure to other pressures (see below) is of importance in calculating boil-off and "no-loss" times. Figure 5 gives the variation of vapor pressure with temperatures for liquid nitrogen, liquid oxygen, liquid hydrogen, and liquid helium.

2. Properties of Insulations

In the past few years a number of new insulations of extreme value in cryogenic service have been developed. With these much more efficient insulations, the mission analyst is able to plan space flights involving much greater weight of payload and vehicle.

There are six types of insulation now in use for various types of cryogenic service. Some are useless with regard to space vehicles, because of too high a conductivity or density. Others (Fiberglas, SI-4, NRC-2) have great potential in space applications, since the environmental vacuum (either moderate or high) prevents heat leaks into the fluids due to gas conduction and convection. The substance added, whether powder, Fiberglas, aluminum foil, etc., is intended to reduce the radiation heat leak across the vacuum into the fluid.

a. Types of insulation

(1) Cellular. Actually consists of a silica gel with very high absorbing or absolving surface.

(2) Powder. An organic powder, usually perlite, is introduced into a space held at a moderate vacuum (< 100μ Hg).

(3) Opacified powder. Aluminum or bright copper flakes are added to the powder to increase the radiation shielding. The vacuum must be high (< 10μ Hg).

(4) Fiberglas. A very low density inorganic substance placed in a high vacuum (< 1μ Hg).

(5) Organic foams. Usually polystyrene, foamed either with air or freon. These foams have a cell structure which isolates one cell from another. When placed next to a fluid at cryogenic temperatures, the gas condenses within each cell, creating a partial vacuum, which is the insulating agent. Use of such foams with liquid oxygen or liquid fluorine is highly dangerous, due to their organic nature.

(6) Multiple radiation shield. This type has the highest insulating qualities (but also requires high order vacuum for most efficient usage (< 1μ Hg). One type (Linde SI series) consits of alternate layers of aluminum foil and glass fiber paper. Usually 50 to 80 layers are used. NRC-2 uses approximately 100 layers of crinkled mylar which has been aluminized on both sides.

b. Table of properties

Table 3 lists all types of insulations, with some of them reported under different conditions. The properties of Santogel A, given for an ambient operating pressure and under moderate vacuum, show the effect of vacuum on these insulations. The thermal conductivity (k) of Linde SI-4 and the Fiberglas insulations, is measured both in the compressed and uncompressed states. The increase in k value under compression indicates that such insulations must be maintained in an uncompressed state for greatest efficiency, but will also have a reasonable insulating effect when compressed. This fact may be of considerable importance for the insulation of space vehicle stages during flight through the atmosphere. Outer insulation blankets must be compressed to prevent their being lost due to air friction. Once in orbit, or in space flight, the compressing device may be removed, and the high vacuum of space will raise the insulation to its full efficiency.

c. Relationship of thermal conductivity to operating pressure

To obtain the very low thermal conductivity values shown in Table 3, the insulations must be in vacuum. Hence, a double wall is required for most tankage applications--except in space, where the environment is already a vacuum. The thermal conductivity is a function of the degree of vacuum in the interspace. Figure 6 indicates that, in general, the powder and cellular types of insulation are less affected by vacuum changes than the radiation shield and fiber glass types. With the latter, there is a sharp lowering in efficiency when the operating pressure rises above about 10μ of mercury; while with the former, the change in k is more gradual, and pressures of 100 to 1000μ Hg can be tolerated with not too great a degradation of insulating qualities. It may also be seen from Fig. 6 that the multiple radiation shield insulations (at high vacuum) are more efficient than other types by an order of magnitude.

One other criterion for efficient insulation is given in the last column of Table 3 where the thermal conductivity (k) is multiplied by the density of the insulation (ρ). It may be seen that the product k_ρ for the multiple radiation shields is one to three orders of magnitude lower than other types. Hence, for orbital operations, it is concluded that the multiple radiation shield insulations must be used. In the remainder of this section, the insulation used in all calculations will be the Linde SI-4.

d. Relationship of thermal conductivity to wall temperatures

The temperatures of the inner (cold) wall and the outer (warm) wall of the insulation have decided effect on the value of the thermal conductivity factor (Fig. 7). The thermal conductivity varies by about a factor of 30 as the outer wall temperature (T_1) varies by a factor of 10 [100° to 1000° R (56 to 560° K)] for any constant inner wall temperature (T_2). The value of k varies much less with inner wall temperature for constant T_1, and is essentially independent of the value of T_1.

3. Design of Cryogenic Tanks

In order to design cryogenic tankage for space applications, one must determine the heat input into the cryogenic fluid. In order to do this, the temperature of the outer wall must be determined. If the insulation has been selected and the cryogenic fluid specified, all else is known. The ultimate factor to be calculated is the evaporation, or boil-off rate, of the cryogenic fluid.

Space vehicles, or orbiting tankage, receive heat from the sun according to the distance from the sun. Figure 8 shows the relationship of heat flux from the sun (G_s) and the distance from the sun. If the surface of the tankage were either a perfect absorber or a perfect reflector, the problem would be simple. However, since this is not the case, the absorptivity (α) and the emissivity (ϵ) of the surface must be taken into account. Normally, the parameter used is the ratio of these terms, α/ϵ. The higher this ratio, the more heat absorbed, and the higher the temperature T_1. Figure 9 shows the variation of T_1 with $\alpha A_s/\epsilon A_w$ (where A_s = surface area exposed to the sun and A_w = area of the total outer surface of the tank). The greater the proportion of the outer surface exposed to the sun, the greater the heat absorbed.

It is possible to determine the outer wall temperature (T_1) from Fig. 9, once the shape and size of the tankage are known. One first assumes a value of α/ϵ, the practical lower limit of which is approximately 0.25. From the general shape and orientation of the space vehicle or tank, A_s/A_w may be estimated. After obtaining $\alpha A_s/\epsilon A_w$, it is possible to interpolate in Fig. 9 at the expected distance from the sun, reading the temperature. Note that orbits about the earth may be assumed at the same distance as the earth from the sun, with negligible error. Even on the moon at its nearest point to the sun, the temperature of the outer wall will maximize at essentially the same value as if the vehicle were on earth.

Knowing the temperature of the outer wall, it is then possible to determine the heat flux (Q_ℓ) into the cryogenic fluid.

$$Q_\ell = \frac{k}{\ell} (T_1 - T_2)$$

where k/ℓ is the ratio of the thermal conductivity to the thickness of the insulation, and Q_ℓ is the heat flux to the exposed surface. Figure 10 shows the results of calculations for several values of T_1 (thus, for several values of α/ϵ), and for various thicknesses and thermal conductivities.

a. Total heat input

The total heat input per hour into the cryogenic liquid will be $Q_{\ell T} = Q_\ell A_w (A_s/A_w)$ where A_s/A_w = estimated percentage of surface exposed to the sun. From a knowledge of $Q_{\ell T}$, the weight of the cryogenic liquid at the start,

TABLE 2

Properties of Cryogenic Fluids

Element	Mol Weight	Heat of Vaporization (Btu/lb)	Heat of Vaporization (kcal/newton)	Boiling Point (° R at 1 atm)	Freezing Point (° R at 1 atm)	Critical Point Temperature (° R)	Critical Point Pressure (10^6 newtons/m^2)	Density (lb/ft^3)	Density (newton/m^3)	Gas Volume of Liquid (cu ft/gal)	Gas Volume of Liquid (m^3/liter)	Gas Constant (R)	Specific Heat $\gamma = c_p/c_v$	Weight of Liquid (lb/gal)	Weight of Liquid (newton/liter)
Hydrogen	2.02	194.2	11.00	36.54	25	59.87	1.297	0.0052	0.817	114.3	0.735	772	1.4	0.54	0.55
Helium	4.00	10.3	0.583	7.596	0 (25 atm)	9.49	0.230	0.0103	1.62	101.0	0.640	386.3	1.66	1.043	1.053
Neon	20.20	37.5	2.124	48.96	43.0	89.02	2.716	0.0522	8.20	192.0	1.234		1.64	10.0	10.10
Nitrogen	28.02	85.7	4.855	139.32	113.0	227.91	3.395	0.0725	11.39	93.0	0.598	55.1	1.4	6.73	6.80
Oxygen	32.00	91.7	5.20	162.36	99.0	277.85	5.078	0.0828	13.01	115.3	0.741	48.3	1.4	9.53	9.62
Fluorine	38.00	74.1	4.20	153.00	97.0	259.50	557.4	0.0983	15.44	128.5	0.826		1.4	12.6	12.7
Argon	39.91	72.0	4.08	157.14	151.0	271.40	4.865	0.1034	16.24	112.0	0.720	38.7	1.67	11.56	11.67
Ozone	48.00	136.1	7.710	290.34	144.0	469.91	5.573	0.1230	19.32	91.6	0.589		1.4	11.28	11.39

1 Btu/lb = 0.5665 k cal/newton
1 lb/ft^2 = 157.084 newtons/m^3
1 lb/gal = 1.00976 newtons/liter
1 ft^3/gal = 0.006428 m^3/liter
1 lb/$in.^2$ = 144 lb/ft^2 = 6894.4 newtons/m^2

TABLE 3

Properties of Insulations

Insulation	Type	Density (ρ) (lb/ft^3)	Density (ρ) (newtons/m^3)	Vacuum Space Pressure (microns Hg, μ)	Thermal Conductivity (k) A* (Btu/hr-ft-° R)	Thermal Conductivity (k) A* (kcal/sec-m-° K)	Thermal Conductivity (k) B* (Btu/hr-ft-° R)	Thermal Conductivity (k) B* (kcal/sec-m-° K)	kρ (Btu-lb/hr-ft^4-° R) A*	kρ (Btu-lb/hr-ft^4-° R) B*
Santocel A	Cellular	6.0	940	Ambient	1400×10^{-5}	1780×10^{-9}	1400×10^{-5}	1780×10^{-9}	8400×10^{-5}	8400×10^{-5}
Santocel A	Cellular	6.0	940	< 100μ	120×10^{-5}	153×10^{-9}	96×10^{-5}	123×10^{-9}	720×10^{-5}	576×10^{-5}
Polystyrene foam	Freon filled cellular	3.0	470	< 100μ	900×10^{-5}	1150×10^{-9}	700×10^{-5}	890×10^{-9}	2700×10^{-5}	2100×10^{-5}
Polystyrene foam	Air filled cellular	2.4	377	Ambient	--	--	1900×10^{-5}	2400×10^{-9}	--	4500×10^{-5}
Perlite	Powder	8.0	1260	< 100μ	90×10^{-5}	115×10^{-9}	72×10^{-5}	92×10^{-9}	720×10^{-5}	576×10^{-5}
Linde CS-5	Powder w/Cu flakes	11.0	1730	< 10μ	22×10^{-5}	28×10^{-9}	17.6×10^{-5}	22.5×10^{-9}	242×10^{-5}	194×10^{-5}
Linde SI-12	Multiple radiation shields (Al foil + fiber glass)	2.5	390	< 1μ	17×10^{-5}	22×10^{-9}	10×10^{-5}	13×10^{-9}	42.5×10^{-5}	25×10^{-5}
Linde SI-4	Multiple rad shield	4.0	630	< 1μ	2.5×10^{-5}	3.2×10^{-9}	2×10^{-5}	2.6×10^{-9}	12.0×10^{-5}	9.4×10^{-5}
Linde SI-4	Compressed mult rad shield	20.0	3140	< 1μ	80.0×10^{-5}	102×10^{-9}	64.0×10^{-5}	81.6×10^{-9}	1600×10^{-5}	1280×10^{-5}
NRC-2	Multiple rad (aluminated mylar)	3.0	470	< 1μ	3×10^{-5}	3.8×10^{-9}	2.6×10^{-5}	3.3×10^{-9}	9×10^{-5}	7.8×10^{-5}
Fiber glass	Fiber	2.5	390	< 1μ	40.0×10^{-5}	51.0×10^{-9}	32.0×10^{-5}	40.8×10^{-9}	100×10^{-5}	80×10^{-5}
Fiber glass	Compressed fiber	10.0	1570	< 1μ	80×10^{-5}	102×10^{-9}	64×10^{-5}	82×10^{-9}	800×10^{-5}	640×10^{-5}

*A--between 560° R - 162° R (LN_2BP)
*B--between 560° R - 36° R (LH_2BP)

$\frac{1 \text{ Btu-lb}}{\text{hr-ft}^4\text{-° R}} = 2.0042 \times 10^{-2} \frac{\text{kcal-newton}}{\text{sec-m}^4\text{-° K}}$

$\frac{1 \text{ Btu}}{\text{hr-ft-° R}} = 1.27588 \times 10^{-4} \frac{\text{kcal}}{\text{sec-m-° K}}$

and the heat of vaporization of the cryogenic liquid, some knowledge of the evaporation rate can be gained.

b. Relationship of tank pressure, vapor pressure and designed vent pressure

The phenomena occurring in a tank of cryogenic liquid are complex. If the vapor pressure = tank pressure = vent pressure, then the evaporation rate is easily determined. There appear, however, to be three thermodynamic phenomena that occur in distinct phases. When the heat inflow begins, normally the vapor pressure will be below the tank pressure. As heat continues to flow in, the temperature of the liquid increases according to

$$\Delta T = \frac{Q_{\ell T} t}{W c_p}$$

where

t = time in hours

W = weight of cryogenic fluid, and

c_p = specific heat of liquid at constant pressure.

Thus, the pressure is raised, as shown in Fig. 5. During Phase 1, no evaporation can occur because all of the heat used in raising the temperature of the liquid, merely increases its vapor pressure.

Phase 1 ends when the vapor pressure equals the tank pressure. In Phase 2, these two pressures will always be equal, since, if the vapor pressure were greater, evaporation from the liquid into the ullage space would increase the tank pressure. Thus, in Phase 2, the liquid temperature, the vapor pressure and tank pressure all increase, until finally the vent pressure is reached. Although the liquid has evaporated, it has not yet been lost from the tank. It is, however, unusable as a propellant, although it could be used to aid in a pressure transfer of the fluid, if required.

Based on perfect gas laws, the total heat input during Phase 2 can be conveniently divided in the following way

$$t Q_{\ell T} = \Delta T W c_p + M_1 \nu \left[\frac{p_2 T_1}{p_1 T_2} - 1 \right]$$

where

M_1 = mass of gas initially in ullage space

p_1, p_2 = initial and final Phase 2 tank pressures

ν = heat of vaporization of cryogenic liquid, and

ΔT = total temperature change of liquid.

The first term in this equation is the heat input which raises the temperature of the liquid, and the second term is the heat input which vaporizes the liquid. The duration of Phase 2 is given by

$$t = \frac{1}{Q_{\ell T}} \left[\Delta T W c_p + M_1 \nu \left(\frac{p_2 T_1}{p_1 T_2} - 1 \right) \right]$$

if aerodynamic heating is neglected. A term $Q_{aero}/Q_{\ell T}$ must be subtracted from the time to account for this phenomenon.

If the ullage space is small, t can be considered the preboil-off time, because in this case the boil-off time is much less than the liquid heating time. If the ullage is less than 10 to 15% of the total volume,

$$t \approx \frac{\Delta T W c_p}{Q_{\ell T}} \text{ hours,}$$

this is the time during which no boil-off occurs.

Phase 3 is that period during which tank pressure is equivalent to vent pressure. It is during this time that the liquid actually boils off.

$$W_{BO} = \frac{t Q_{\ell T}}{\nu}$$

This equation shows that the boil-off for reasonably well designed systems is moderate even for long times for good quality insulation in moderate thicknesses.

If the tank is filled at the vent pressure then the process will be in Phase 1 until the vapor pressure reaches the vent pressure, at which time the process becomes Phase 3. Thus, preboil-off time and the actual boil-off can be regulated by varying the design vent pressure. Phase 2 is completely eliminated from consideration. Such a system will have the disadvantages of requiring external pressure sources (helium bottles) and a pressure relief system. Thus, by setting a high vent pressure and maintaining a small ullage space, the preboil-off (no loss) time can be extended considerably (see Fig. 11).

c. Insulation performance factor

The weight of the insulation, I_w, represents a performance penalty and since insulation is not perfect, a certain amount of boil-off will be associated with the weight of insulation determined by the $t Q_{\ell T}/\nu$. The penalty exists when

$$I_w + t Q_{\ell T}/\nu > \text{(uninsulated tank boil-off)}.$$

Let

$$S = I_w + \frac{t Q_{\ell T}}{\nu}$$

be called the insulation performance factor. Thus, it is desired to minimize S. Since

$$\ell = \frac{I_w}{\rho A}$$

and

$$Q_{\ell T} = \frac{k \rho A^2 (T_1 - T_2)}{I_w}$$

then

$$S = I_w + \frac{t}{\nu}\left[\frac{k\rho A^2 (T_1 - T_2)}{I_w}\right]$$

and S is a minimum when

$$I_w^2 = \frac{K\rho A^2 (T_2 - T_1)\, t}{\nu}.$$

Thus, the total weight is minimized when the insulation weight is just equal to the weight of the boiled-off liquid. Finally,

$$S_m = 2\sqrt{\frac{K\rho (T_1 - T_2)\, t_A^2}{\nu}}$$

Figure 12 is a plot of the insulation performance factor versus time-in-storage for a 6000-lb (26,700 newton) liquid hydrogen tank under a specific set of conditions and with a surface area of 10^3 ft^2 (93 m^2).

If it is assumed that it is required to have a given amount of LH_2 left (from a 6000-lb [26,700 newton] initial capacity) after a given time and the amount of insulation is to be found, enter Fig. 12 at the time and read S. Subtract the permissible weight of the boiled-off liquid hydrogen, the remainder is left for the weight of the insulation. From Table 3, the density of SI-4 is read. Thus, the volume of SI-4 required to meet the prescribed boil-off can be computed.

Now, since the area of the outer surface of such a tank is known, the thickness of SI-4 wrapped about the tank necessary to provide the proper insulation can be estimated. Before proceeding, it is noted that the insulation for such a tank may actually weigh slightly more than the uninsulated tank.

Once the thickness of insulation is determined, all that remains is to determine the no-loss time (Fig. 11), the boil-off during Phase 3, and the weight of tankage required.

d. Application to other cryogenic fluids

In order to apply the previous discussions to the design of tankage for cryogenic fluids other than liquid hydrogen, the following factors must be taken into account.

(1) The ratio of the weight of the new cryogenic fluid to liquid hydrogen.

(2) Boiling point of the new cryogenic fluid related to LH_2.

(3) The volume occupied by one pound of the new liquid.

It is then possible by means of ratios to use the figures given here to obtain tank designs for all other cryogenic fluids. What must be kept in mind is the high weight of propellants other than hydrogen and helium.

4. Example

The problem is to find the optimum insulation thickness for insulating spherical tanks placed on the illuminated lunar surface (Refs. 10 and 11), that is, to find the minimum combined weight of vaporized propellant and insulation for tanks containing liquid hydrogen, oxygen or fluorine.

For tanks on the lunar surface, an external insulation surface temperature of 607° R (337° K) was assumed (based on an average of the lunar surface temperature and the radiation equilibrium temperature of a surface exposed at normal incidence to solar radiation).

The only need for insulation during the lunar night would be to prevent freezing of the fluorine or oxygen (at 97° to 99° R [54° and 55° K], respectively) and to limit the hydrogen boil-off. However, the average external insulation temperature is estimated to be about 108° R (60° K), so that freezing of fluorine and oxygen will not occur, and the hydrogen vaporization rate will be only about 15% of the day condition. Therefore, the day condition is controlling for insulation thickness if the conservative approach of designing is chosen for propellant tanks to be exposed on either the illuminated or shadowed surface of the moon.

Propellant losses on the lunar surface. The weight shown in Fig. 13 is the sum of insulation weight and boil-off, the two being equal at the optimum. The results are based on conduction through the insulation only. In actual practice the heat leaks through tank support structure are about equal to the heat flow through the insulation. An approximation to the real case would be to increase the value read from the curve by about 70%. The propellant weight loss would then be the total value of the ordinate and the insulation weight would be 70% of that value.

Propellant losses during transfer. To determine losses from the tanks during the earth-moon transfer phase:

(1) Determine optimum insulation thickness based on the lunar day condition and increase by 40%

$$\ell_i = (1.40)\sqrt{\frac{k\Delta T\, t}{\rho_i\, \nu}}$$

(2) Calculate $\Delta T/\nu$ from Table 4.

(3) Enter Fig. 14 to find "β." Vaporized propellant then equals

$$W = \frac{tD^2}{\ell_i}\beta$$

(4) Double the weight found in step (3) to account for heat leaks, and add the insulation weight

$$W_i = A_i \ell_i \rho_i$$

Propellant losses in lunar orbit. Propellant loss from tanks that do not land on the moon but which are a part of the boost, transfer and deboost system are more difficult to define due to their inherently integral fabrication with the flight structure. However, for hydrogen the loss will probably lie between 0.01 to 0.10% per hour of the initial hydrogen weight. The lower value would be a design goal for a thermally well designed flight vehicle with separate tankage. The oxidizer boil-off can be assumed zero for the "well designed" case since the major heat exchange, even with separate tanks, is from the oxidizer to the hydrogen with other modes relatively small so that the oxidizer may actually experience some cooling.

TABLE 4

Propellant Parameters

Propellant	ΔT_a (°R)		ν	
	Lunar Day	Transfer	Btu/lb	kcal/newton
H_2	567	460	190	10.7
O_2	445	338	92	5.2
F_2	454	347	72	4.1

1 Btu/lb = 0.05667 kcal/newton

E. REFERENCES

1. Lipkis, R. P., "Temperature Control of Spacecraft," Space Technology Laboratories, Inc., Memorandum, August 1961.
2. Camack, Walter G., and Edwards, Donald K., "Effect of Surface Thermal Radiation Characteristics on the Temperature Problem in Satellites," Surface Effects on Spacecraft Materials, John Wiley and Sons, 1960.
3. Cornog, R. A., "Temperature Equilibria in Space Vehicles," part of Space Technology Laboratories Engineering Design Manual, 1961.
4. Bevans, J. T., "A Review of Thermal Radiation Properties and Measuring Techniques," Space Technology Laboratories, Inc., TN-60-0000-09096, 24 June 1960.
5. Dunkle, R. V., "Thermal Radiation Characteristics of Surfaces," Invited Paper at the American Society of Mechanical Engineers Annual Meeting, 1960, to be published in the Journal of Heat Transfer, Trans ASME.
6. Beard, David B., "Interplanetary Dust Distribution and Erosion Effects," Surface Effects on Spacecraft Materials, John Wiley and Sons, 1960.
7. Acker, R. M., Lipkis, R. P., and Vehrencamp, J. E., "Temperature Control System for the Atlas Able-4 Lunar Satellite," presented at the Aviation Conference, Dallas, Texas, 5 to 9 June 1960.
8. Fried, E., and Costello, F. A., "The Interface Thermal Contact Resistance Problem in Space Vehicles," Presented at ARS Lifting Re-entry Vehicles Conference, Palm Springs, California, 4 to 6 April 1961.
9. Wolverton, R. W., ed., "Flight Performance Manual for Orbital Operations," Space Technology Laboratories (LA), September 1961 (U).
10. Perkins, D. S., "Cryogenic Propellant Considerations, Lunar Return Vehicle," STL Memo 9862-2-47, 13 July 1961.
11. Fuil, A., "First Approximation to Optimizing Insulation Weight on Propellant Tanks for Long Term Space Storability of Cryogenics," STL Memo 9862-36, 19 July 1961.

F. BIBLIOGRAPHY

1. Bibliography for Staging of Vehicles

(See other chapters for geometrical restrictions and bibliography of pertinent references.)

Amass, W., Bullard, S. A., and Teegarden, W. T., "Collection of Parametric Performance Studies," The Martin Company, Baltimore, Maryland, TM 491/2-02-60, January 1960.

Arens, M., "Staging of Cruising Vehicles," ARS Journal, Vol. 31, No. 6, June 1961, pp 824 to 825.

Ashley, H., and Asher, G. W., "The Virtual Mass of Clustered Boosters," ARS Journal, Vol. 31, No. 6, June 1961, pp 757 to 763.

Builder, C. H., "A General Solution for Optimization of Staging of Multistaged Boost Vehicles," ARS Journal, Vol. 29, No. 7, July 1959, pp 497 to 499.

Byrum, B. L., and Grady, E. R., "General Airframe Dynamics of a Guided Missile," Journal of the Aeronautical Sciences, Vol. 22, No. 8, August 1955.
"Kinematics and Kinetics of Aerospace Vehicles," The Martin Company, Baltimore, Maryland, Engineering Report No. ER 10920, June 1960.

Chase, R. L., "Multistage Rocket Staging Optimization," American Astronautical Society, Preprint No. 60-41, January 1960.

Chin, S. S., "Missile Design Criteria," The Martin Company, Orlando, Florida, Report No. OR-1272, 10 October 1960.

Cobb, E. R., "Optimum Staging Technique to Maximize Payload Total Energy," ARS Journal, Vol. 31, No. 3, March 1961, pp 342 to 344.

Cohen, A. D., and Rhodes, H. H., "Evaluation of Coasting Flight of an Ascending Satellite Vehicle for Circular Orbits," ARS Journal, Vol. 30, No. 8, August 1960, pp 768 to 769.

Cole, D. M., and Epstein, L. I., "Interpretation of Malina-Summerfield Criterion for Optimization of Multistage Rockets," Jet Propulsion, Vol. 26, No. 3, March 1956, p 188.

Cole, D. M., and Marrese, M. A., "Optimization of Rockets for Maximum Payload Energy," American Rocket Society Journal, Vol. 29, No. 1, January 1959, p 71.

Coleman, J. J., "Optimum Stage-Weight Distribution of Multistage Rockets," ARS Journal, Vol. 31, No. 2, February 1961, pp 259 to 260.

Dergarabedian, P., and Ten Dyke, R. P., "Estimating Performance Capabilities of Boost Rockets," Los Angeles, California, Space Technology Laboratories, September 1959, Report No. TR-59-0000-00792.

Dini, D., "Distribution of the Stages of a Missile to Obtain Minimum Takeoff Weight, Minimum Cost, and Maximum Payload Kinetic Energy," L'Aerotecnica, Vol. 41, No. 1, February 1961, pp 3 to 13 (in Italian).

Ehricke, K. A.,
"Powered Flight," Handbook of Astronautical Engineering, New York, McGraw-Hill Book Company, 1961 (Koelle, ed.)
"Ascent of Orbital Vehicles," American Rocket Society, Preprint No. 146-54, 1954.

Fiul, A., and Braham, H., "Optimization of Vehicles and Trajectories for the Twenty-Four Hour Equatorial Satellite Mission," American Rocket Society, Paper No. 1120-60, 1960.

Fried, B. D., "On the Powered Flight Trajectory of an Earth Satellite," Jet Propulsion, Vol. 27, No. 6, June 1957.

Froehlich, J. E., "Capabilities of Multistaged Chemical Rocket Systems," Astronautica Acta, Vol. 6, No. 6, 1960, pp 311 to 321.

Geckler, D., "Ideal Performance of Multistage Rockets," ARS Journal, Vol. 30, No. 6, June 1960, pp 531 to 536.

Goldsmith, M., "On the Optimization of Two Stage Rockets," Jet Propulsion, Vol. 27, April 1957, p 415.

Hall, H. H., and Zambelli, E. D., "On the Optimization of Multistage Rockets," Jet Propulsion, Vol. 28, No. 7, July 1958, pp 463 to 465.

Hughes, J. V., et al., "Trajectories for Continuously Applied Propulsion Thrust," Proceedings of the 4th Symposium on Ballistic Missile and Space Technology (Los Angeles, 1959). New York, Pergamon Press, 1960. (Also, Planetary and Space Science, July 1961, Vol. 7.)

Koelle, H. H., "Optimization Considerations for Orbital Payload Capabilities," American Rocket Society, Preprint No. 491-57, October 1957.

Krause, H. G. L., Koelle, H. H., and Kuebler M. E., "Analytical Method for the Determination of Powered Rocket Trajectory Elements, with a Specific Turning Program and Consideration of Air Drag and Thrust Variation," Stuttgart, Astronautical Research Institute, Report No. 3, Chapter 2, August 1953, pp 18 to 25. (ASTIA Document No. AD-115961.)

MacDonald, J. A., "Probability Approach to Outage Prediction (U)," The Martin Company, Baltimore, Maryland, Engineering Report No. 11712, 1961.

Mackay, J. S., and Weber, R. J., "Performance Charts for Multistage Rocket Boosters," NASA TN D-582, January 1961.

Pollak, R. J., "Rapid Determination of the Interaction Between the Rocket Vehicle and Its Trajectory," Lockheed Aircraft Corporation, Missiles and Space Division, Sunnyvale, California, American Rocket Society, Preprint No. 1476-60, 1960.

Ragsac, R. V., and Patterson, P. L., "Multistage Rocket Optimization," ARS Journal, Vol. 31, No. 3, March 1961, pp 450 to 451.

Schmidt, R., "Preliminary Calculation and Layout Method for Single and Multistage Ballistic and Space Rockets, Huntsville, Alabama, Army Ballistic Missile Agency, Redstone Arsenal, Report No. RA-TR-1-61, 10 February 1961.

Schurmann, E. E. H., "Optimum Staging Technique for Multistaged Rocket Vehicles," Jet Propulsion, Vol. 27, August 1957, p 863.

Subotowicz, M., "The Optimization of the N-Step Rocket with Different Construction Parameters and Propellant Specific Impulses in Each Stage," Jet Propulsion, Vol. 28, No. 7, July 1958, pp 460 to 463.

Ten Dyke, R. P., "Computation of Rocket Step Weights to Minimize Initial Gross Weight," Jet Propulsion, Vol. 28, May 1958, p 338.

Townsend, G., "Ascent to Orbit," Design Guide to Orbital Flight, McGraw-Hill Book Company, New York, Chapter 6, 1962.

Van Pelt, J. M., "Optimum Propellant Distribution for Two-Stage Ballistic Missiles," The Martin Company, Baltimore, Maryland, TM 491/2-66, January 1959.

Vargo, L. G., and Bruce, R. W., "Preliminary Optimization of Clustered Rocket Vehicles," Aeronutronic, Newport Beach, California, November 1959.

Vertregt, M.
"Calculation of Step-Rockets," Journal of the British Interplanetary Society, Vol. 14, January 1955, p 20.
"A Method for Calculating the Mass Ratios of Step-Rockets," Journal of the British Interplanetary Society, Vol. 15, March 1956, p 94.

Wang, C. J., et al., "Thrust Optimization of a Nuclear Rocket of Variable Specific Impulse," ARS Journal, Vol. 29, No. 5, 1959, pp 341 to 344.

Weisbord, L.,
"A Generalized Optimization Procedure for N-Staged Missiles," Jet Propulsion, Vol. 28, July 1958, p 164.
"Optimum Staging Techniques," ARS Journal Vol. 29, June 1959, p 445.

Wilson, M. L., "The Calculation of Fuel Distribution in Step-Rocket," Journal of the British Interplanetary Society, Vol. 16, No. 77, October to December 1957, pp 211 to 215.

2. Bibliography for Thermal Control and Cryogenic Storage

Adelberg, M., "Storage of Cryogenics in Space," STL Report TN-59-0000-00324, 28 September 1959.

Altshuler, T. L., "A Method for Calculating the Thermal Irradiance Upon a Space Vehicle and Determining Its Temperature," General Electric Company, R60SD386, August 1960.

Ballinger, J., et al., "Thermal Environment of Space," Convair Astronautics Division, General Dynamics Corporation, ERR-AN-016, November 1960.

Berenson, P., "Transition Boiling Heat Transfer from a Horizontal Surface," AIChE Paper No. 18, ASME-AIChE Heat Transfer Conference, Buffalo, August 1960.

Bevans, J. T., Grier, J. T., and Dunkle, R. V., "Comparison of Total Emittances with Values Computed from Spectral Measurements," Trans. ASME, Vol. 80, No. 7, October 1958, p 1405.

Birkebak, R. C., and Hartnett, J. P., "Measurements of the Total Absorptivity for Solar Radiation of Several Engineering Materials," ASME Paper 57-SA-27.

Blanchero, J. T., Barker, G. E., and Boll, R. H., "Heat Transfer Characteristics of Boiling Oxygen, Fluorine, and Hydrazine," Eng. Res. Inst., University of Michigan (1951). See also Chem Eng Progr Symposium, Serial No. 17, Vol. 51, 1955, p 21.

Boelter, L. M. K., et al., "A Mechanical Integrator for Determination of Illumination from Diffuse Surface Sources," Transactions of the Illuminating Engineering Society, Vol. 34, No. 9, November 1939, p 1085 to 1092.

Brandt, J. A., Irvine, T. F., and Eckert, E. R. G., "A Method of Measuring Total Hemispherical Emissivities at Low Temperatures--Results for Pure Iron from 300 to 500° R," Proceedings, Heat Transfer and Fluid Mechanics Institute, Stanford University, 1960.

Brock, O. K., "Thermal Radiation Interchange Between Black and Grey Surfaces," Convair, Fort Worth, General Dynamics Corporation, PT-23, 3 June 1960.

Bromley, L. A., "Heat Transfer in Stable Film Boiling," Chem Eng Prog, Vol. 46, 1950, pp 221 to 227.

Brown, A. I., and Marco, S. M., "Introduction to Heat Transfer," McGraw-Hill Book Company, New York, 1942.

Carslaw, H. S., and Jaeger, J. C., "Heat Conduction in Solids," 2nd Edition, Oxford Press, 1959.

Chang, Y. P., and Snyder, N. W., "Heat Transfer in Saturated Boiling," AIChE Preprint No. 104, Third National Heat Transfer Conference, August 1959.

Chelton, D. B., and Mann, D. B., "Cryogenic Data Book," WADC TR 59-8, March 1959.

Class, C. R., DeHaan, J. R., Piccone, M., and Cost, R. B.,
"Pool Boiling Heat Transfer to a Cryogenic Liquid," WADC Tech Rep 58-528, 1958.
"Boiling Heat Transfer to Liquid Hydrogen from Flat Surfaces," Advances in Cryogenic Engineering, Vol. 5, 1960, K. D. Timmerhaus, Editor.

Dean, L. E., and Thompson, L. M., "Heat Transfer Characteristic of Liquid Nitrogen," Bell Aircraft Corporation, Rep No. 56-982-035, 1955. See also ASME Paper 56-SA-4.

Deissler, R. G.,
"Heat Transfer and Fluid Friction for Fully Developed Turbulent Flow of Air and Supercritical Water with Variable Fluid Properties," Trans Am Soc Mech Engrs, 76, pp 73 to 85, 1954.
"Analysis of Turbulent Heat Transfer, Mass Transfer, and Friction in Smooth Tubes at High Prandtl and Schmidt Numbers," NACA Report 1210, 1955.

Drayer, D. E., and Timmerhaus, K. D., "An Experimental Investigation of the Individual Boiling and Condensing Heat Transfer Coefficients for Hydrogen," Paper J-6, Advances in Cryogenic Eng., Vol. 7, 1962, p 401.

Driscoll, D. G., "Cryogenic Tankage for Space Flight Applications," Linde Company, Cryogenics Engineering Conference, 1959.

Dunkle, R. V.,
"Thermal Radiation Characteristics of Surfaces," Lecture presented at Symposium on Theory and Fundamental Research in Heat Transfer, ASME, November 1960; also in Theory and Fundamental Research in Heat Transfer, J. A. Clark, Editor, Pergamon Press, 1962.
"Thermal Radiation Tables and Applications," Trans ASME, Vol. 76, 1954, pp 549 to 552.

Durham, T. F., McClintock, R. M., and Reed, R. P., "Cryogenics Materials Data Handbook," Cryogenics Engineering Laboratory, National Bureau of Standards, U. S. Department of Commerce, Contract AF04(647)-59-3, 8th Quarterly Report, Boulder, Colorado.

Dusinberre, G. M., "Heat Transfer Calculations by Finite Differences," International Textbook Company, 1961.

Eckert, E. R. G., "Introduction to the Transfer of Heat and Mass," McGraw-Hill Book Company, New York, 1950.

Eckert, E. R. G., and Drake, R. M., Jr., "Heat and Mass Transfer," McGraw-Hill Book Company, New York, 1959.

Elrod, H. G., "New Finite-Difference Method for the Solution of the Heat Conduction Equation, Especially near Surfaces with Convective Heat Transfer," Trans. ASME, Vol. 79, No. 7, October 1957, p 1519.

Farkas, A., "Orthohydrogen , Parahydrogen, and Heavy Hydrogen, Cambridge University Press, London, 1935, p 20.

Fenechi, H., "Thermal Conductance of Metallic Surfaces in Contact," SM Thesis, MIT, 1957.

Fenster, S. K., VanWylen, G. J., and Clark, J. A., "Transient Phenomena Associated with the Pressurization of Liquid Nitrogen Boiling at Constant Heat Flux," Advances in Cryogenic Engineering, K. D. Timmerhaus, Editor, Vol. 5, 1960, p 226.

Forster, H. E., and Zuber, N., "Dynamics of Vapor Bubbles and Boiling Heat Transfer," AIChE Journal, Vol. 1, 1955, p 531.

Frainier, R. J., "Experimental Performance and Selection of Rocket Insulation Systems," Linde Company, Cryogenic Engineering Conference (Reprint), 1960.

Frederking, T. H. K.,
"Film Boiling of Helium I and Other Liquefied Gases on Single Wires," AIChE, J. Vol. 5, No. 3, 1959, p 403.
"Remarks on the Heat Transport in Helium II at High Heat Flux Values," University of California, Los Angeles, Report No. 62-5, February 1962.

Frederking, T. H. K., and Clark, J. A., "Natural Convection Film Boiling on a Sphere," Paper submitted to 1962 Cryogenic Engineering Conference Committee, K. D. Timmerhaus, Secretary, May 1962.

Fritz, S., "The Albedo of the Planet Earth and of Clouds," Journal of Meteorology, 1949.

Fulk, M. M., Reynolds, M. M., and Park, O. E., "Thermal Radiation Absorption by Metals," Proceedings, 1954 Cryogenic Engineering Conference, p 151.

Gebhart, B., "Unified Treatment for Thermal Radiation Transfer Processes--Gray Diffuse Radiators and Absorbers," ASME Paper No. 57-A-34. See also, "Heat Transfer," B. Gebhart , McGraw-Hill, 1961.

Giedt, W. H., "Principles of Engineering, Heat Transfer," D. Van Nostrand Company, Princeton, New Jersey, 1958.

Graham, R. W., Hendricks, R. C., Hsu, Y. V., and Friedman, R., "Experimental Heat Transfer and Pressure Drop of Film Boiling Liquid Hydrogen Flowing Through A Heated Tube," Advances in Cryogenic Engineering, K. D. Timmerhaus, Editor, Vol. 6, 1961, p 517.

Hamilton, D. C., and Morgan, W. R., "Radiant-Interchange Configuration Factors," National Advisory Committee for Aeronautics, NACA TN 2836, 1952.

Haselden, G. G., and Prosad, S., "Heat Transfer from Condensing Oxygen and Nitrogen Vapours," Trans Inst Chem Eng (London), Vol. 27, 1949, pp 195 to 200.

Haselden, G. G., and Peters, J. I., "Heat Transfer to Boiling Liquid Oxygen and Liquid Nitrogen," Trans Am Inst Chem Eng (London), Vol. 27, 1949, pp 201 to 208.

Holten, D. C., "A Study of Heat and Mass Transfer to Uninsulated Liquid Oxygen Containers," Advances in Cryogenic Engineering, Vol. 6, K. D. Timmerhaus, Editor, 1961, p 499.

Holter, F. J., "Simplified Matrix Technique for Determining the Average Surface Temperatures of an N-Surface Enclosure Radiation to Space," Personal Communication to J. A. Clark, November 1961.

Hottel, H. C.,
"Some Problems in Radiative Transport," Lecture presented at 1961 International Heat Transfer Conference, Boulder, Colorado, London, England.
"Radiant Heat Transmission," Mechanical Engineering, Vol. 52, No. 7, July 1930, pp 699 to 704.

Hsu, Y. Y., and Smith, J. M., "The Effect of Density Variation on Heat Transfer in the Critical Region," Am Soc Mech Engr, Paper 60-HT-8, 1960.

Irvine, T. F., Hartnett, J. P., and Eckert, E. P. G., "Solar Collector Surfaces with Wave Length Selective Radiation Characteristics," Solar Energy, Vol. II, No. 2-3, July to October 1958. See also addendum: Solar Energy, Vol. III, No. 2, April 1959, p 38.

Ivey, H. J., "Preliminary Results on the Effect of Acceleration on the Critical Heat Flux in Pool Boiling," Reactor Development Division Report AEEW-R99, AEE, Dorchester, Dorset, England, September 1961.

Jakob, M., "Heat Transfer," Vol. I and II, John Wiley and Sons, 1949, 1960.

Kamius, M., and Zabel, E., "Manufacture and Delivery of Liquid Oxygen and Liquid Nitrogen to ICBM Sites," Rand Report, STL 59-3357.

Karagounis, A., "Heat Transfer Coefficient for Liquid Helium," (in French), Bull Inst Intern Froid, Annexe 2. 195-9, 1956.

Keenan, J. H., "Thermodynamics, John Wiley and Sons, Inc., New York, 1941.

King, C. R., "Compilation of Thermodynamic Properties, Transport Properties and Theoretical Rocket Performance of Gaseous Hydrogen," NASA TN D-275, 1960.

Knudsen, J. G., and Katz, D. L., "Fluid Dynamics and Heat Transfer," McGraw-Hill Book Company, Inc., 1958.

Kreith, F.,
"Principles of Heat Transfer," International Textbook Company, 1960.
"Radiation Heat Transfer for Spacecraft and Solar Power Plant Design," International Textbook Company, 1962.

Kreith, F., and Summerfield, M., "Investigation of Heat Transfer at High Heat Flux Densities; Experimental Study with Water of Friction Drop and Forced Convection with and Without Surface Boiling in Tubes," Jet Propulsion Lab Progress Report 4-68, 1948.

Kropschot, R. H., "Insulation Principles," Lecture No. 3, UCLA Symposium, Cryogenic Technology, 1962.

Leonhard, K. E., and McMordie, R. K., "The Nonadiabatic Flow of Evaporating Cryogenic Fluid Through a Horizontal Tube," Advances in Cryogenic Engineering, Vol. 6, K. D. Timmerhaus, Editor, 1961, p 481.

Leuenberger, H., and Person, R. A., "Radiation Shape Factors for Cylindrical Assemblies," American Society of Mechanical Engineers, Paper 56-A-144.

Loper, J. L., and Heatherly, E. R., "Vapor Losses in Cylindrical Containers of Aluminum and Fiberglas Laminate Filled with Liquid Nitrogen and Exposed to Climatic Heating," Tech Note No. G-002, Structures and Mechanics Laboratory, ABMA, Huntsville, Alabama, 4 August 1955.

McAdams, W. H., "Heat Transmission," 3rd Edition, McGraw-Hill, 1954.

McCue, G. A.,
"Program for Determining Temperatures of Orbiting Space Vehicles," Space and Information Systems Division, North American Aviation, Inc., SID 61-105, 20 April 1961.
"Eclipse Characteristics of Close Earth Satellite Orbits," Space and Information Systems Division, North American Avaiation, Inc., SID 61-50, February 1961.

McMordie, R. K., "Steady-State Conduction with Variable Thermal Conductivity," Trans ASME, Heat Transfer Journal, Vol. 84, No. 1, February 1962, p 92.

Merte, H., and Clark, J. A., "Boiling Heat Transfer Data for Liquid Nitrogen at Standard and Near-Zero Gravity," Advances in Cryogenic Engineering, Vol. 7, 1962, K. D. Timmerhaus, Editor.

Moon, P., "The Scientific Basis of Illuminating Engineering," McGraw-Hill Book Company, New York, 1936.

Monroe, A. G., Bristow, A. S., and Newell, J. E., "Heat Transfer to Boiling Liquids at Low Temperatures and Elevated Pressures," J. Appl Chem, Vol. 2, 1952, pp 613 to 624.

Mulford, R. N., Nigon, J. P., Dash, J. G., and Keller, W. E., "Heat Exchange Between a Copper Surface and Liquid Hydrogen and Nitrogen," Ext from Secret Doc, LAMS-1443.

Nordwall, H. L., "Geometrical Configuration Factor Program," Space and Information Systems Division, North American Aviation, Inc., SID 61-90, 30 April 1960.

Obert, E. F., "Elements of Thermodynamics and Heat Transfer," McGraw-Hill Book Company, New York, 1949.

Oppenheim, A. K., "Radiation Analysis by the Network Method," Transaction ASME, Vol. 78, No. 1, May 1956, pp 725 to 735.

Perkins, W. E., and Frainier, R. J., "Practical Storage of Liquid Hydrogen and Helium," Linde Company, 1959 Cryogenic Engineering Conference.

Perry, J. H., "Chemical Engineer's Handbook," McGraw-Hill Book Company, New York, 3rd Edition, 1950, p 205.

Peterson, M., "Radiation Effects," Los Angeles Division, North American Aviation, Inc., NA-56-399, 1956.

Pope, D. H., Killian, W. R., and Corbett, R. J., "Single-Phase Flow Tests with Liquid Hydrogen," Advances in Cryogenic Engineering, Vol. 5, K. D. Timmerhaus, Editor, Plenum Press, 1960, p 449.

Richards, R. J., Robbins, R. F., Jacobs, R. B., and Holten, D. C., "Heat Transfer to Boiling Liquid Nitrogen and Hydrogen Flowing Axially Through Narrow Annular Passages," Adv in Cryogenic Eng., K. D. Timmerhaus, Ed., Plenum Press, Inc., New York, Vol. 3, 1960, p. 375.

Richards, R. J., Steward, W. G., and Jacobs, R. B., "A Survey of the Literature on Heat Transfer from Solid Surfaces to Cryogenic Fluids," NBS TN 122, Boulder Laboratories, October 1961.

Richtmyer, R. D., "Difference Methods for Initial-Value Problems," Interscience Publishers, Inc., New York, 1957.

Riede, P. M., and Wang, D., "Characteristics and Applications of Some Super Insulations," Linde Company, 1959 Cryogenic Engineering Conference (Reprint).

Robsenow, W. M., and Clark, J. A., "Mechanism of Boiling Heat Transfer," Trans ASME, Vol. 73, July 1951.
"Heat Transfer and Pressure Drop Data for High Heat Flux Densities to Water at High Subcritical Pressures," Heat Transfer and Fluid Mechanics Institute, Stanford University, 1951.

Rohsenow, W. M., "Correlating Heat Transfer Data for Surface Boiling Liquids," Trans ASME, Vol. 74, 1952.

Rohsenow, W. M., and Choi, H., "Heat, Mass and Momentum Transfer," Prentice-Hall, 1961.

Ruzicka, J., "Heat Transfer to Boiling Nitrogen," Problems of Low Temperature Physics and Thermodynamics, Pergamon Press, 1959, p 323.

Schneider, P. J., "Conduction Heat Transfer," Addison-Wesley, 1955.

Scott, R. B., "Cryogenic Engineering," D. Van Nostrand Company, 1959.

Smolak, G. R., and Knoll, R. H., "Cryogenics Propellant Storage for Round Trips to Mars and Venus," IAS Paper No. 60-23, presented at the 28th Annual IAS Meeting, New York, 25 to 27 January 1960.

Stevenson, J. A., and Grafton, J. C., "Radiation Heat Transfer Analysis for Space Vehicles," Space and Information Division, North American Aviation, Inc., Downey, California, ASD Technical Report 61-119, Part I, December 1961.

Stock, B. J., "Observations on Transition Boiling Heat Transfer Phenomena," Argonne National Lab, ANL-6175, June 1960.

Sydoriak, S. G., and Roberts, T. R., "A Study of Boiling in Short Narrow Channels and Its Application to Design of Magnets Cooled by Liquid H_2 and N_2," J Appl Phys, Vol. 28, No. 2, 1957, pp 143 to 148.

Thompson, W. R., and Geery, E. L., "Heat Transfer to Cryogenic Hydrogen at Super-Critical Pressure," Advances in Cryogenic Engineering, Vol. 7, K. D. Timmerhaus, Editor, 1962, p 391.

Timmerhaus, K. D., Editor, "Advances in Cryogenic Engineering," Vol. 1 to 7, Plenum Press.

Usiskin, C. M., and Siegel, R., "An Experimental Study of Boiling in Reduced and Zero Gravity Fields," Trans ASME, Journal of Heat Transfer, Vol. 83, No. 3, August 1961.

Van Gundy, D. A., and J. R. Uglum, "Heat Transfer to an Uninsulated Surface at 20° K," Advances in Cryogenic Engineering, Vol. 7, K. D. Timmerhaus, Editor, Paper No. J-3, 1962.

Van Vliet, K. M., "Selective Coatings for Extra-terrestrial Solar Energy Conversion, A Fundamental Analysis," Wright Air Development Division, WADD TR 60-773, 1960.

Von Glahn, U. H., and Lewis, J. P., "Nucleate and Film Boiling Studies with Liquid Hydrogen," Advances in Cryogenic Engineering, Vol. 5, K. D. Timmerhaus, Editor, 1960.

Walters, H. H., "Single Tube Heat Transfer Tests with Liquid Hydrogen," Advances in Cryogenic Engineering, K. D. Timmerhaus, Editor, Vol. 6, 1961, p 509.

Wooley, H. W., Scott, R. B., and Brickwedde, F. G., "Compilation of Thermal Properties of Hydrogen in Its Various Isotopic and Ortho-para Modifications," J. Research National Bureau Standards 41, November 1948, pp 379 to 476.

Wright, C. C., "Design, Construction and Testing of a Helium-To-Hydrogen Heat Exchanger," Advances in Cryogenic Engineering, Vol. 5, K. D. Timmerhaus, Editor, Plenum Press, 1960, p 248.

Zuber, N., and Fried, E., "Two Phase Flow and Boiling Heat Transfer to Cryogenic Liquids," American Rocket Society, Propellants, Combustion and Liquid Rockets Conference, April 1961.

ILLUSTRATIONS

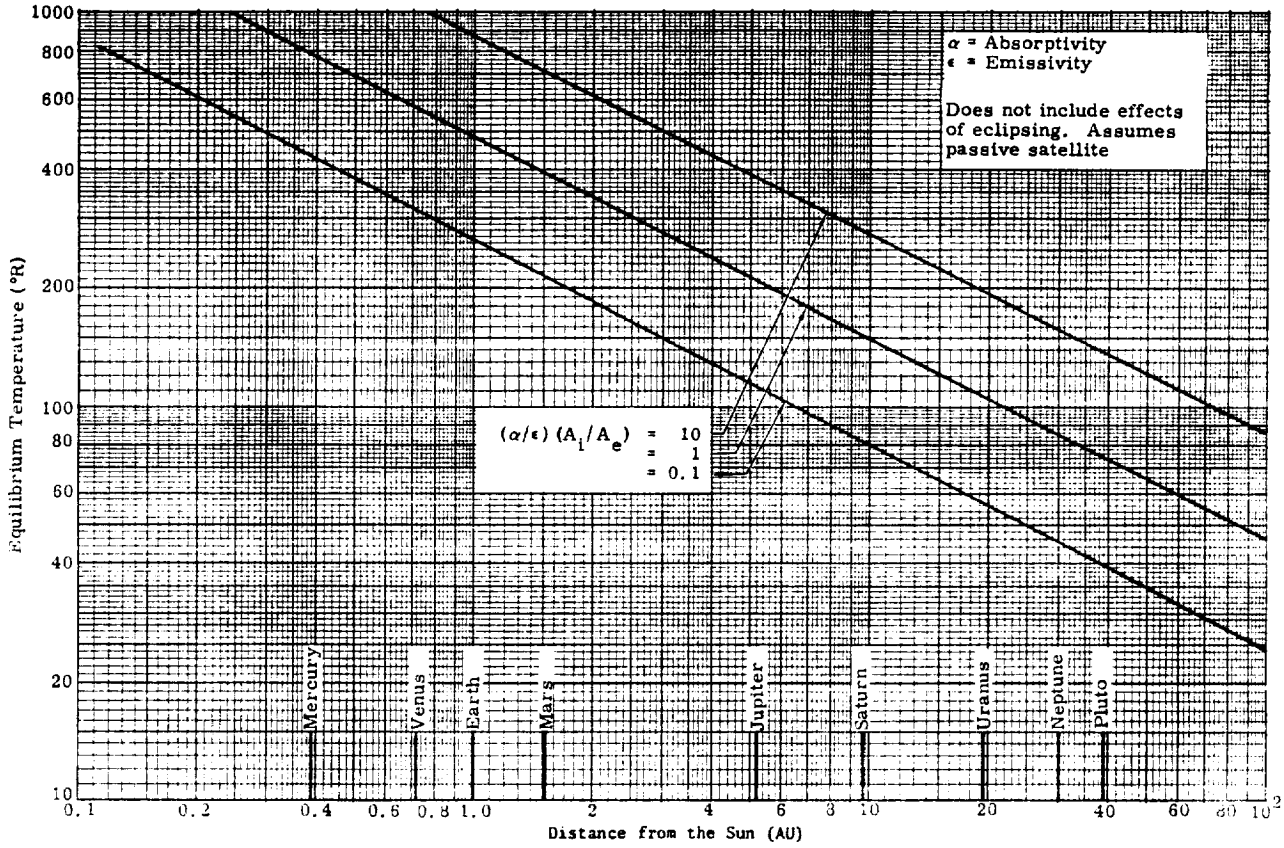

Fig. 1. Equilibrium Temperature of Inert Sphere

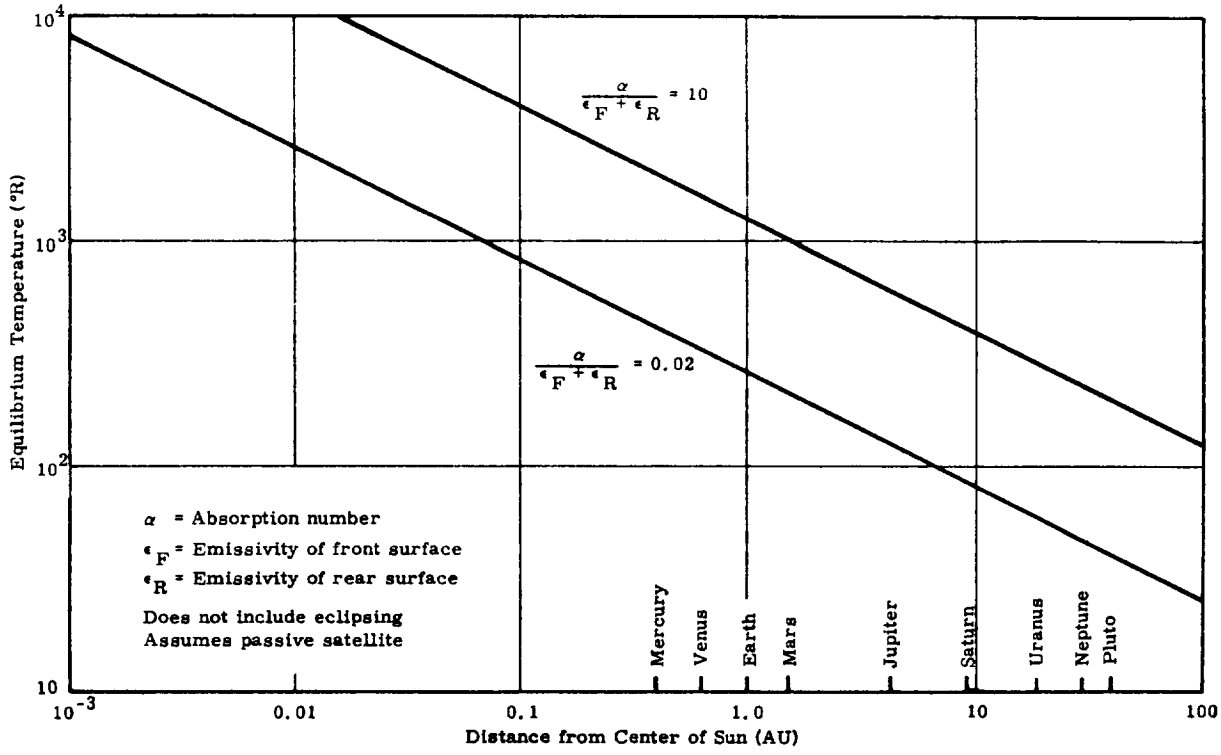

Fig. 2. Equilibrium Temperature of a Thin Plate Normal to the Sun (Ref. 3)

Preceding page blank

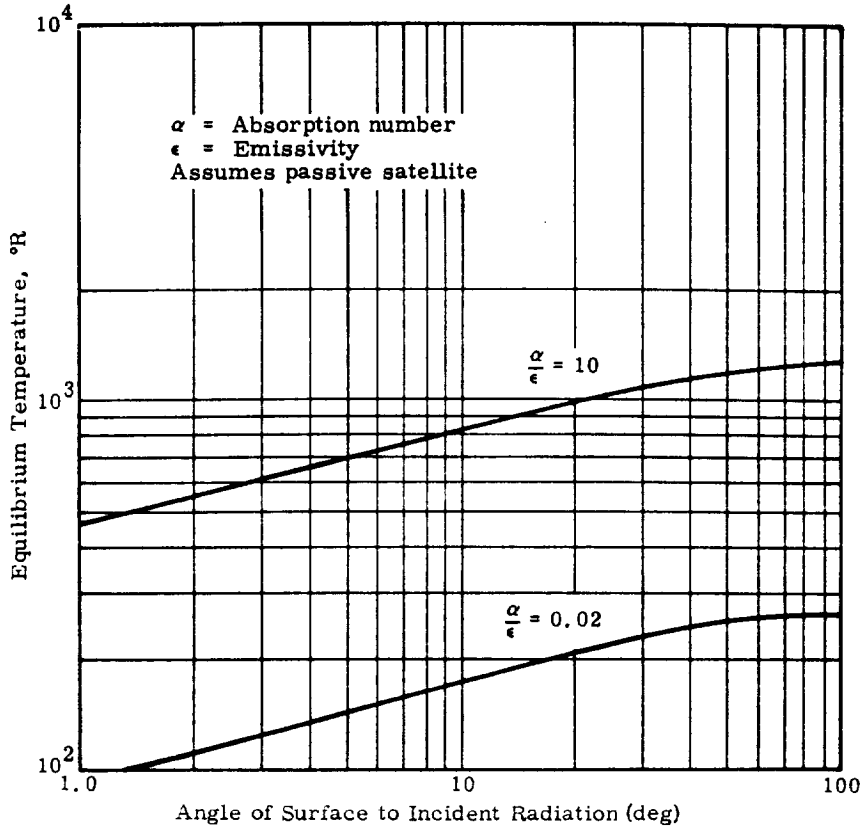

Fig. 3. Effect of Attitude on Equilibrium Temperature of a Thin Plate Located at One Astronomical Unit from the Sun (Ref. 3)

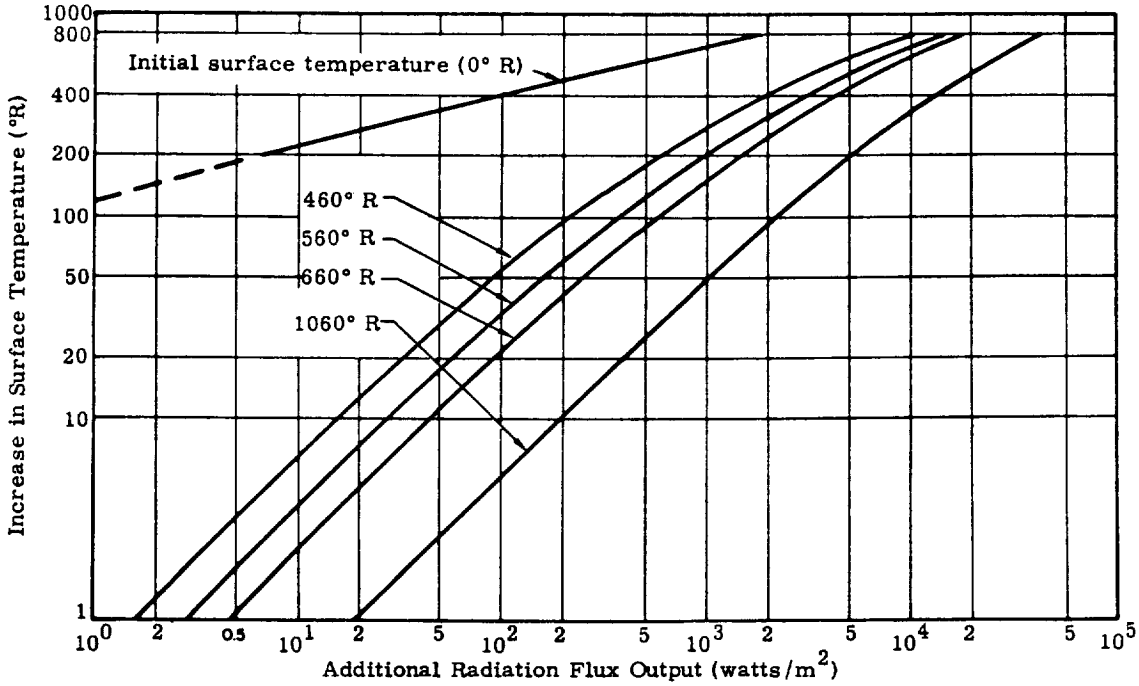

Fig. 4. Effect of Added Heat Input on Equilibrium Temperature (1 w/ft^2 = 10.76 w/m^2) (Ref. 3)

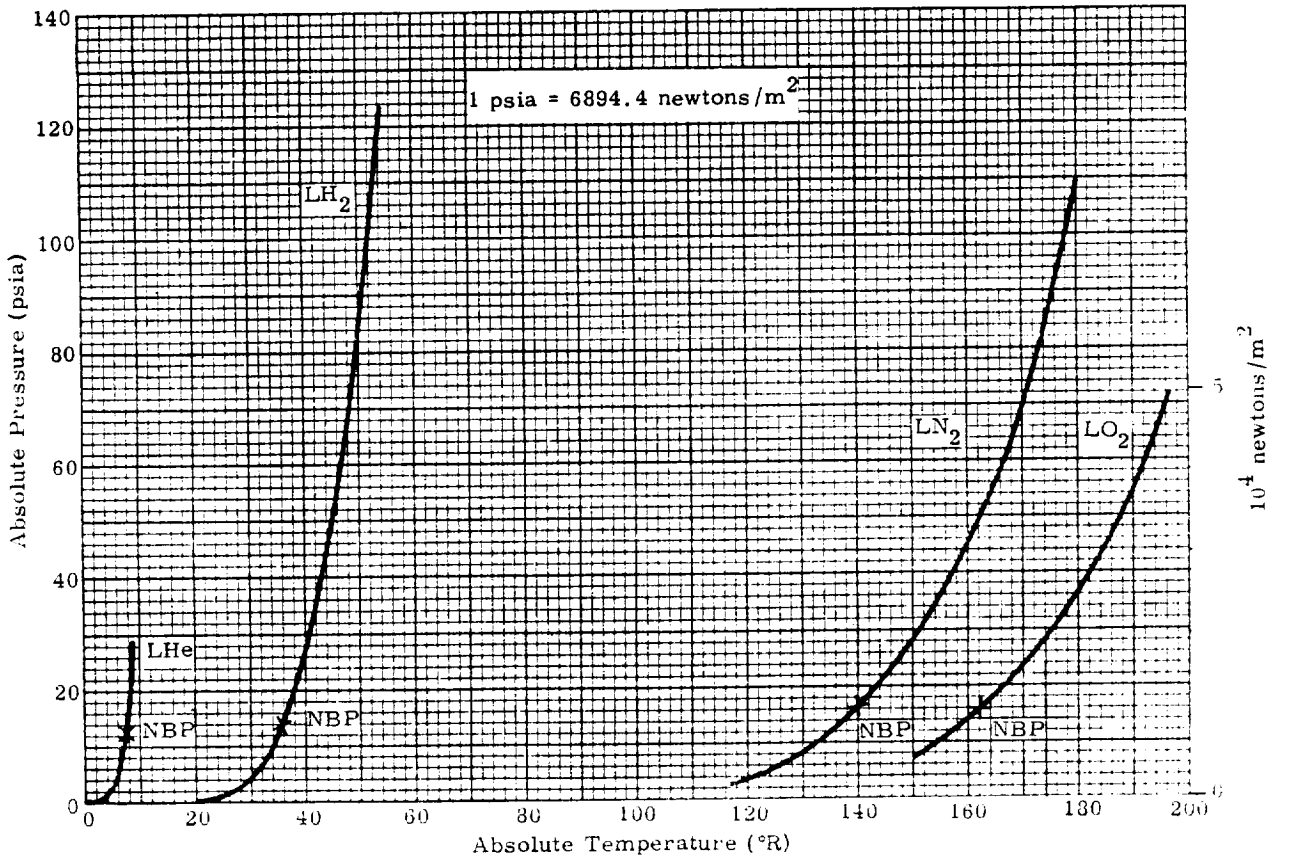

Fig. 5. Vapor Pressure of Cryogenic Fluids

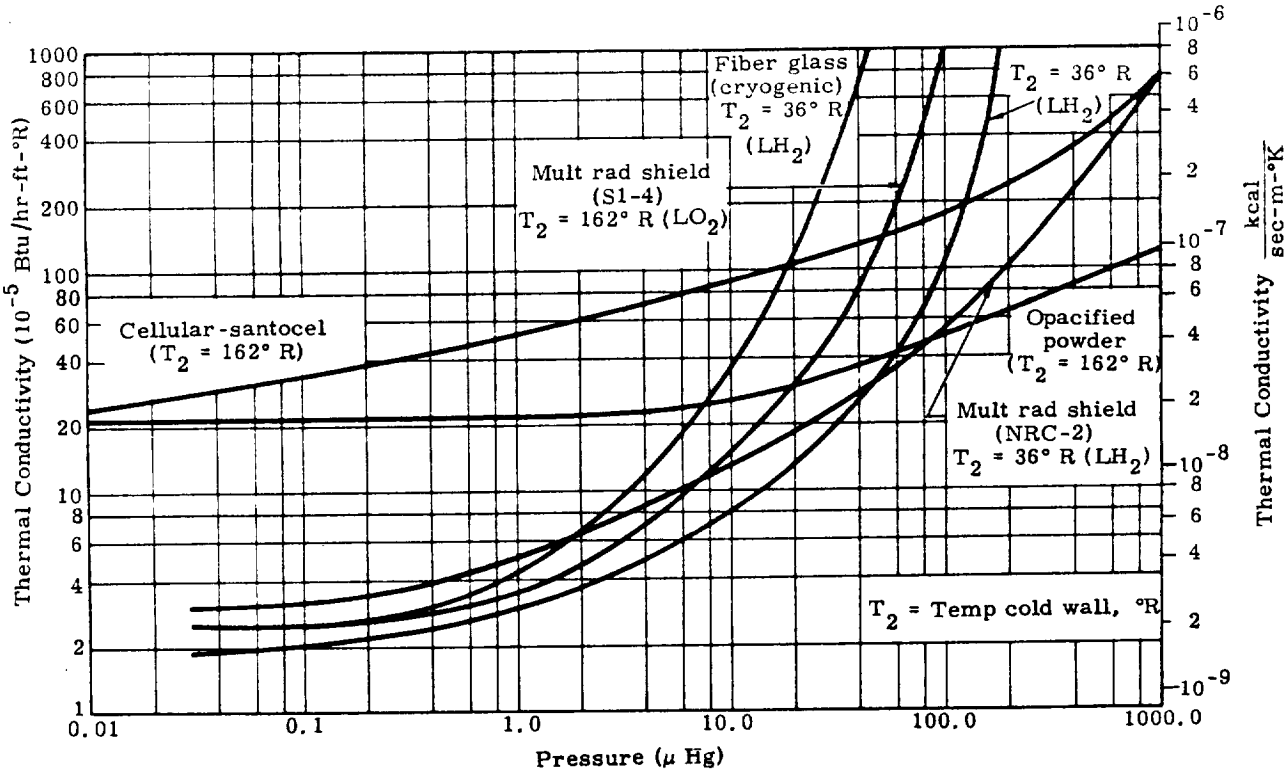

Fig. 6. Heat Transfer Rates of Cryogenic Insulations, Thermal Conductivity Versus Vacuum Pressure (1 Btu/hr-ft-°R = 1.27588 x 10^{-4} kcal/sec-m-°K)

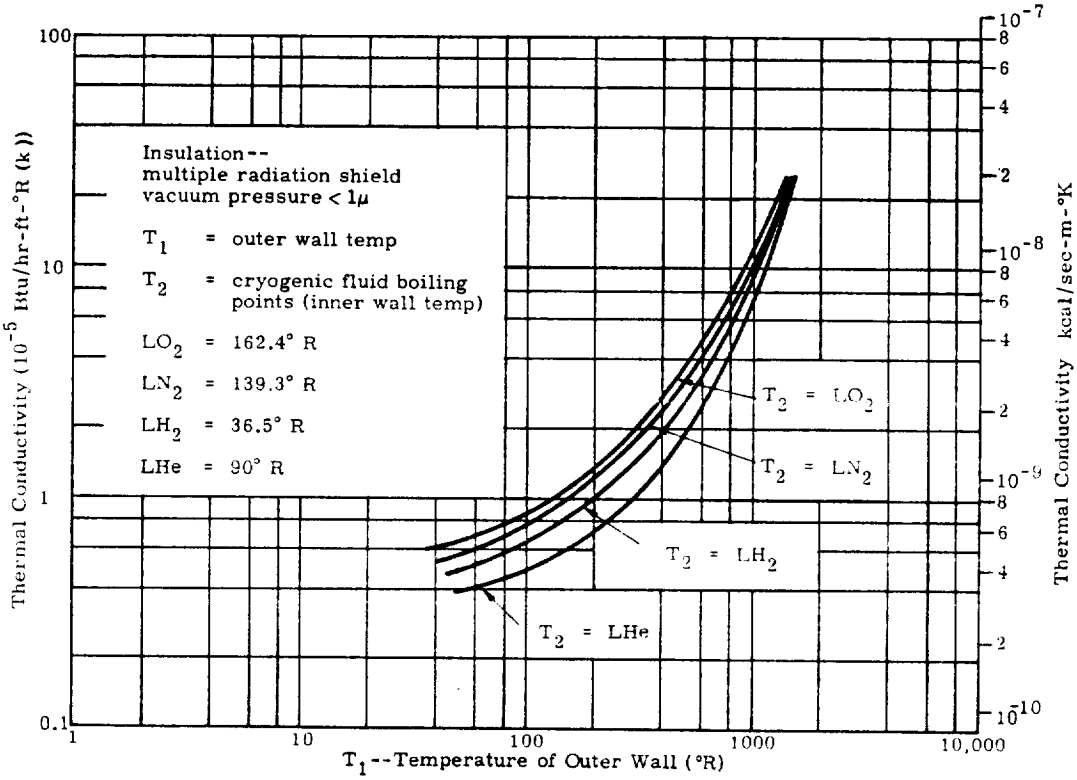

Fig. 7. Thermal Conductivity at Various Wall Temperatures
(1 Btu/hr-ft-°R = 1.27588 x 10^{-4} kcal/sec-m-°K)

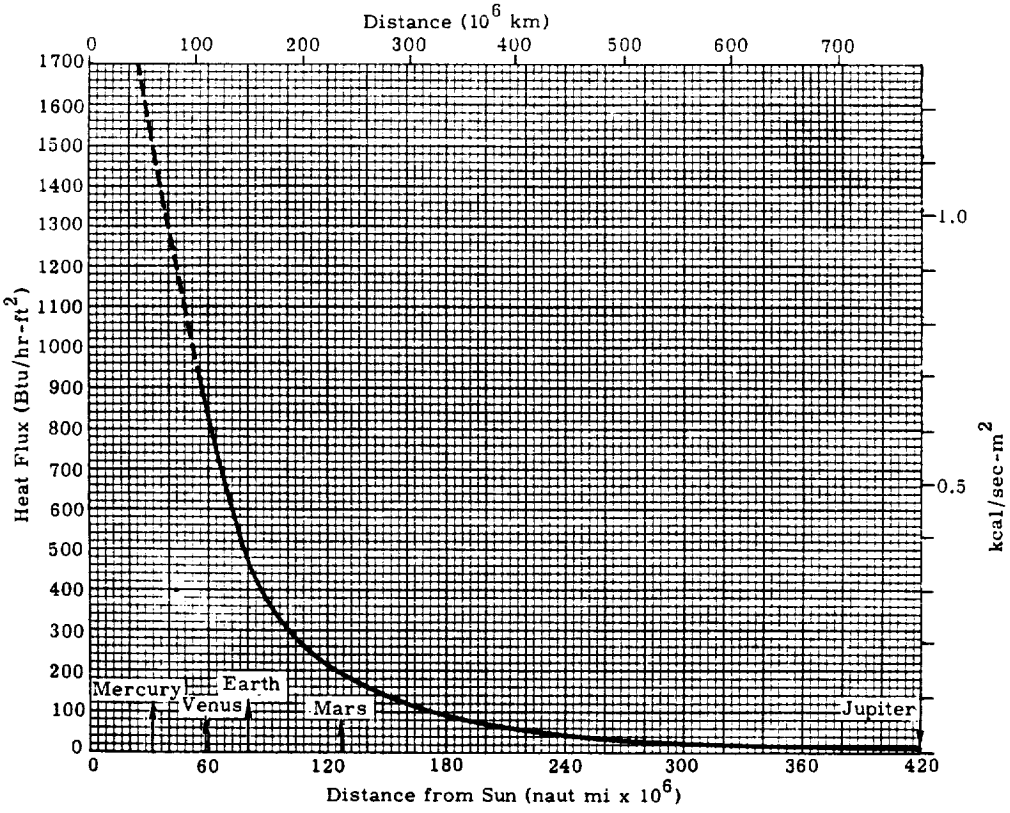

Fig. 8. Heat Flux from Sun (1 Btu/hr-ft^2 = 0.75347 x 10^{-3} kcal/sec-m^2)

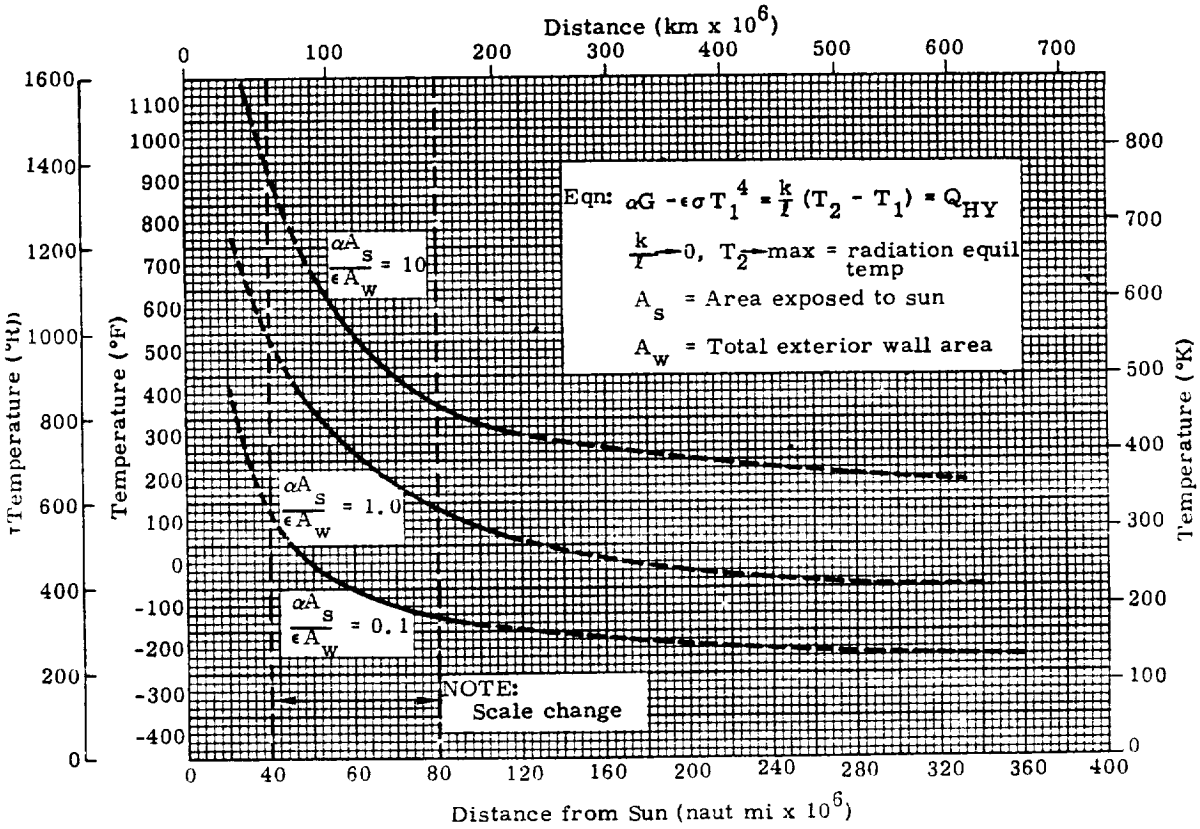

Fig. 9. Solar Heating--Temperature of Outer Wall

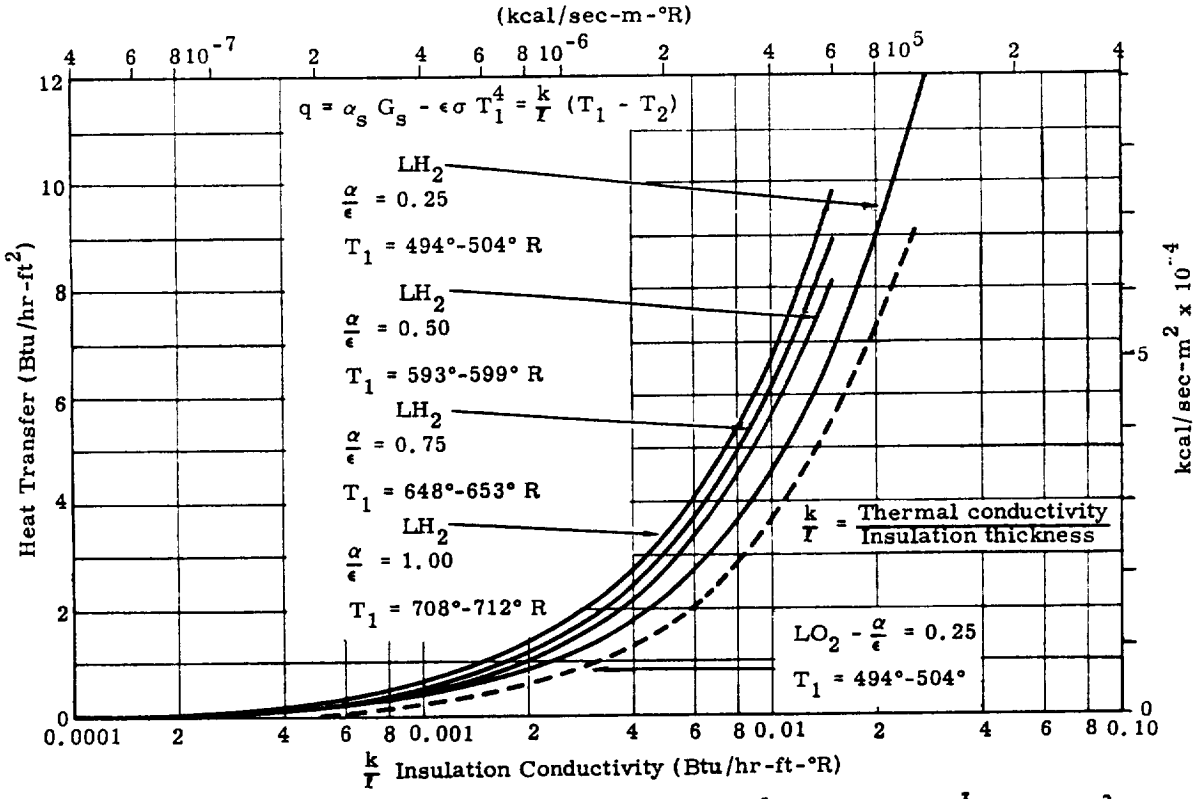

Fig. 10. Heat Transfer to Hydrogen and Oxygen (1 Btu/hr-ft^2 = 0.75347 x 10^{-3} kcal/sec-m^2)

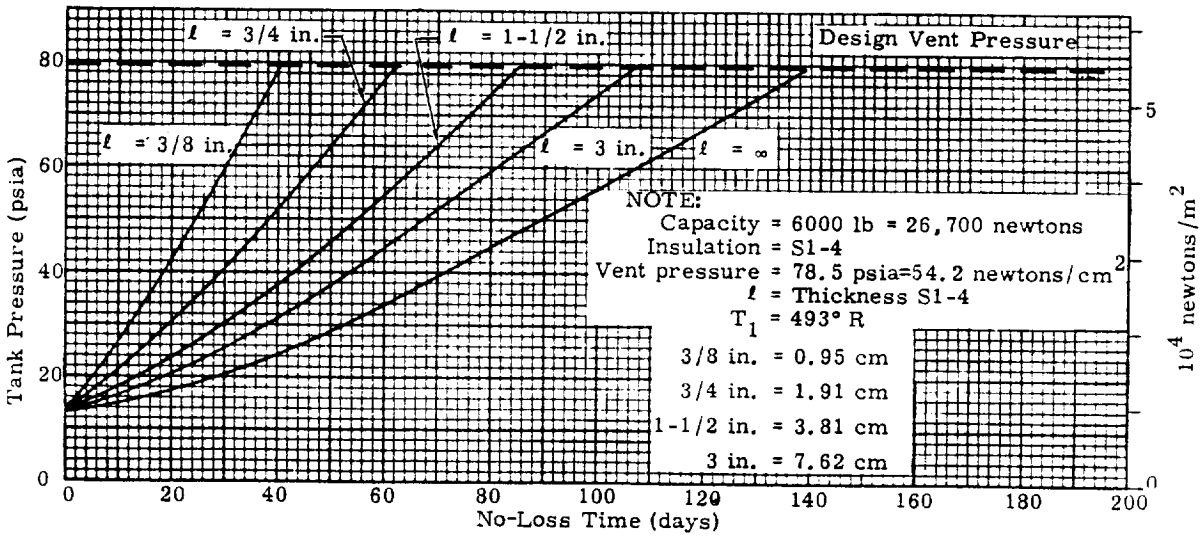

Fig. 11. No-Loss (Pre-Boiloff) Time--LH_2 Tank (1 psia = 6894.4 newtons/m^2)

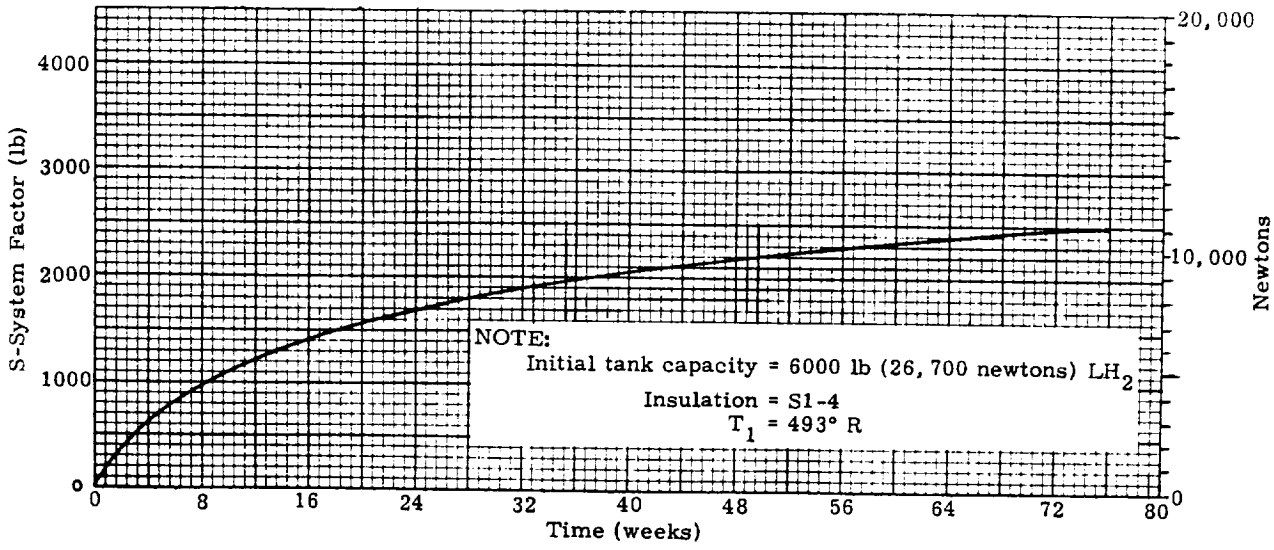

Fig. 12. System Factor (S) Versus Time $S = I_w + \left(\frac{tQ\,T}{\ell\,v}\right)$ **(1 lb = 4.448 newtons)**

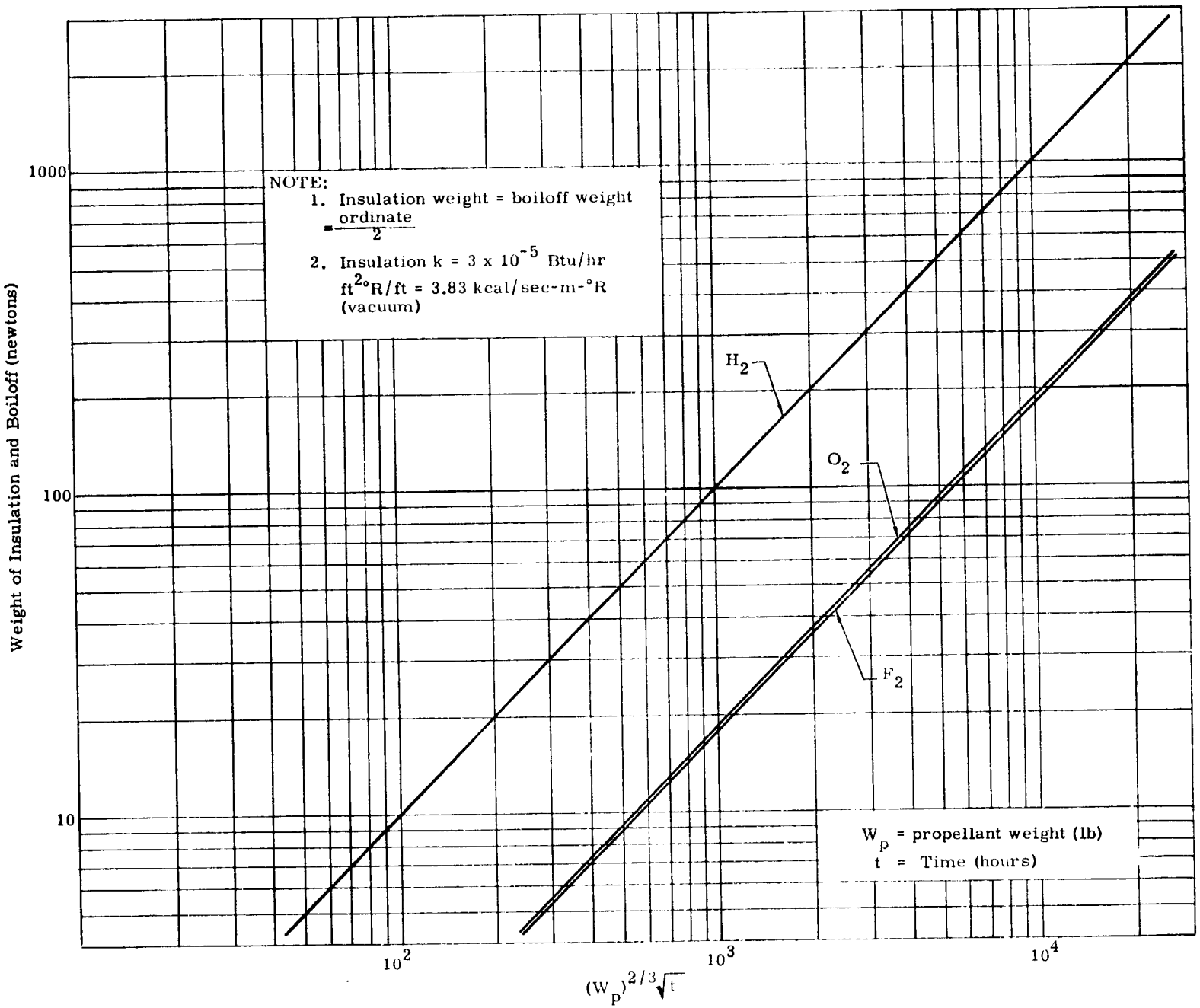

Fig. 13. Propellant Boiloff Plus Insulation Weight at Optimum Insulation Thickness for Spherical Tanks on the Lunar Surface (1 lb = 4.448 newtons)

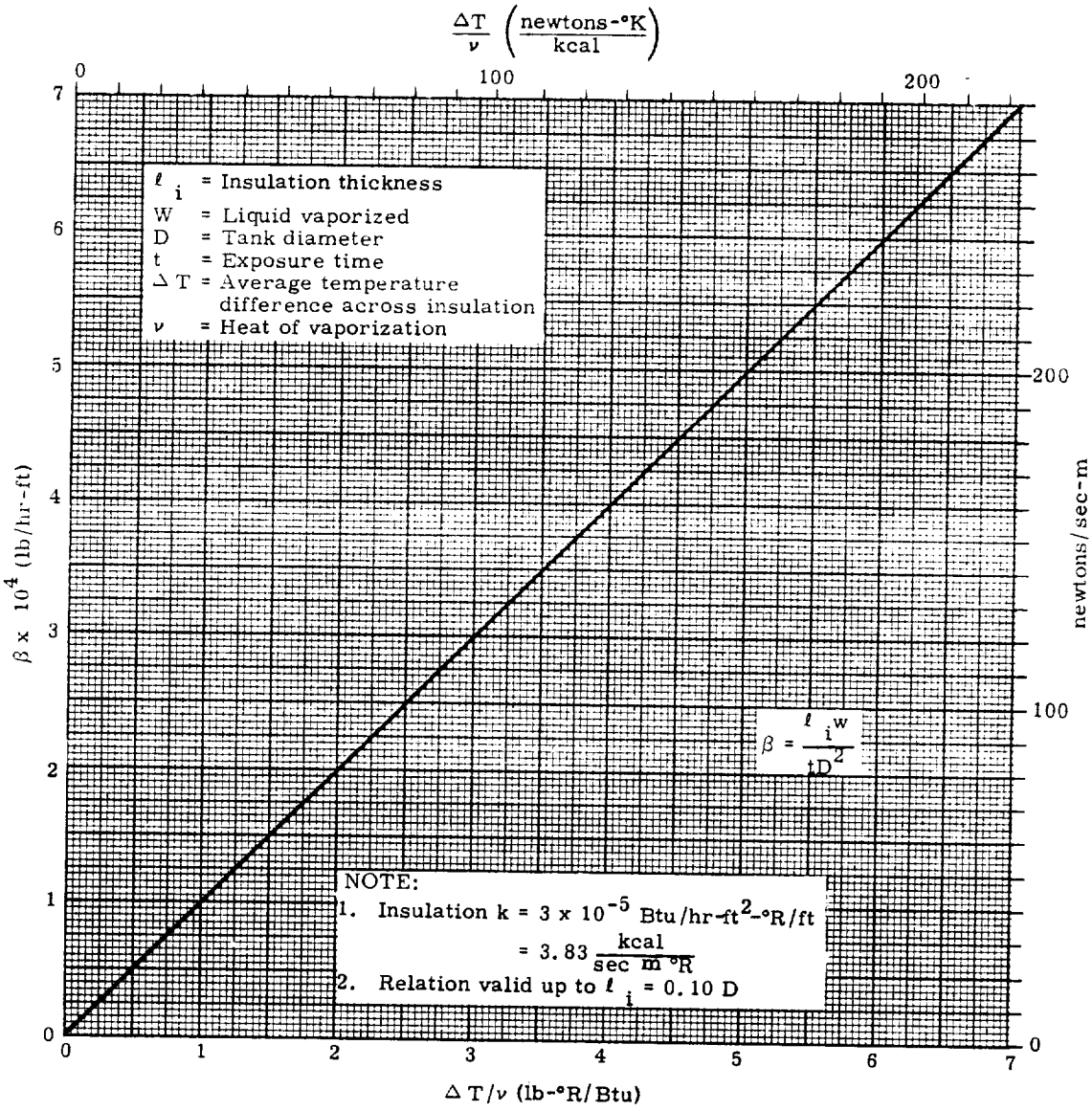

Fig. 14. Boiloff Losses for Liquids Contained in Spherical Tanks, General Case

CHAPTER XI

ORBIT COMPUTATIONS

Prepared by:

J. D. Kraft
Martin Company (Baltimore)
Aerospace Mechanics Department
March 1963

		Page
	Symbols	XI-1
A.	Introduction	XI-2
B.	Coordinate Systems and Transformations	XI-2
C.	Acquisition of Data	XI-14
D.	Determination of Preliminary Orbit Elements	XI-22
E.	Theory of Observation Error	XI-28
F.	Orbit Improvement	XI-37
G.	Accuracy Determinations	XI-43
H.	References	XI-47
I.	Bibliography	XI-47
	Illustrations	XI-51

LIST OF ILLUSTRATIONS

Figure		Page
1	Interferometer System	XI-53
2	Minitrack Modified Interferometer System	XI-53
3	Effect of Spread and Number of Data on Accuracy of Ecentricity Determination	XI-54
4	Effect of Spread and Number of Data on Accuracy of Semilatus Rectum Determination	XI-54
5	Effect of Spread of Data on Accuracy of Inclination and Nodal Longitude Determination	XI-55
6	Effect of a Limited Number of Data on Accuracy of Orbit Determination	XI-56
7	Effect of a Limited Number of Data on Accuracy of Orbit Determination	XI-56
8	Angular Observation Errors, σ_A Versus σ_ϵ ($\sigma_\rho^\bullet$ = 0.3 mps)	XI-57
9	Angular Observation Errors, σ_D Versus σ_ϵ ($\sigma_\rho^\bullet$ = 0.3 mps)	XI-57
10	Angular Observation Errors, σ_ν Versus σ_ϵ ($\sigma_\rho^\bullet$ = 0.3 mps)	XI-58
11	Angular Observation Errors, σ_η Versus σ_ϵ ($\sigma_\rho^\bullet$ = 0.3 mps)	XI-58
12	Angular Observation Errors, σ_r Versus σ_ϵ ($\sigma_\rho^\bullet$ = 0.3 mps)	XI-59
13	Angular Observation Errors, σ_v Versus σ_ϵ ($\sigma_\rho^\bullet$ = 0.3 mps)	XI-59

LIST OF ILLUSTRATIONS (continued)

Figure		Page
14	Angular Observation Errors, σ_a Versus σ_ϵ ($\sigma_\rho^\bullet$ = 0.3 mps)	XI-60
15	Angular Observation Errors, σ_e Versus σ_ϵ ($\sigma_\rho^\bullet$ = 0.3 mps)	XI-60
16	Angular Observation Errors, σ_i Versus σ_ϵ ($\sigma_\rho^\bullet$ = 0.3 mps)	XI-61
17	Angular Observation Errors, σ_Ω Versus σ_ϵ ($\sigma_\rho^\bullet$ = 0.3 mps)	XI-61
18	Angular Observation Errors, σ_ω Versus σ_ϵ ($\sigma_\rho^\bullet$ = 0.3 mps)	XI-62
19	Angular Observation Errors, σ_M Versus σ_ϵ ($\sigma_\rho^\bullet$ = 0.3 mps)	XI-62
20	Angular Observation Errors, σ_A Versus σ_ϵ (σ_ρ = 183 m)	XI-63
21	Angular Observation Errors, σ_D Versus σ_ϵ (σ_ρ = 183 m)	XI-63
22	Angular Observation Errors, σ_ν Versus σ_ϵ (σ_ρ = 183 m)	XI-64
23	Angular Observation Errors, σ_η Versus σ_ϵ (σ_ρ = 183 m)	XI-64
24	Angular Observation Errors, σ_ν Versus σ_ϵ (σ_ρ = 183 m)	XI-65

LIST OF ILLUSTRATIONS (continued)

Figure		Page
25	Angular Observation Errors, σ_r Versus σ_ϵ (σ_ρ = 183 m)	XI-65
26	Angular Observation Errors, σ_a Versus σ_ϵ (σ_ρ = 183 m)	XI-66
27	Angular Observation Errors, σ_e Versus σ_ϵ (σ_ρ = 183 m)	XI-66
28	Angular Observation Errors, σ_i Versus σ_ϵ (σ_ρ = 183 m)	XI-67
29	Angular Observation Errors, σ_Ω Versus σ_ϵ (σ_ρ = 183 m)	XI-67
30	Angular Observation Errors, σ_ω Versus σ_ϵ (σ_ρ = 183 m)	XI-68
31	Angular Observation Errors, σ_M Versus σ_ϵ (σ_ρ = 183 m)	XI-68
32	Range Observation Errors, σ_A Versus σ_ρ (σ_ϵ = 0.05 deg)	XI-69
33	Range Observation Errors, σ_D Versus σ_ρ (σ_ϵ = 0.05 deg)	XI-69
34	Range Observation Errors, σ_ν Versus σ_ρ (σ_ϵ = 0.05 deg)	XI-70
35	Range Observation Errors, σ_η Versus σ_ρ (σ_ϵ = 0.05 deg)	XI-70

LIST OF ILLUSTRATIONS (continued)

Figure		Page
36	Range Observation Errors, σ_v Versus σ_ρ (σ_ϵ = 0.05 deg)	XI-71
37	Range Observation Errors, σ_r Versus σ_ρ (σ_ϵ = 0.05 deg)	XI-71
38	Range Observation Errors, σ_e Versus σ_ρ (σ_ϵ = 0.05 deg)	XI-72
39	Range Observation Errors, σ_a Versus σ_ρ (σ_ϵ = 0.05 deg)	XI-72
40	Range Observation Errors, σ_i Versus σ_ρ (σ_ϵ = 0.05 deg)	XI-73
41	Range Observation Errors, σ_Ω Versus σ_ρ (σ_ϵ = 0.05 deg)	XI-73
42	Range Observation Errors, σ_ω Versus σ_ρ (σ_ϵ = 0.05 deg)	XI-74
43	Range Observation Errors, σ_M Versus σ_ρ (σ_ϵ = 0.05 deg)	XI-74

XI. ORBIT COMPUTATION

SYMBOLS

a	Orbit semimajor axis
A	Right ascension
c	Speed of light; also, variance-covariance matrix
D	Declination
e	Orbit eccentricity
E	Eccentric anomaly
f	Flattening; also, two-way phase coherent Doppler frequency shift
f_{non}	Noncoherent Doppler frequency
h	Altitude above the surface of the earth
H	Hour angle
i	Inclination of the orbit to the equatorial plane
l	Celestial latitude
L	Geocentric latitude
L'	Geodetic latitude
m	Mass
M	Mean anomaly
N	Electron density
p	Semilatus rectum (semiparameter)
r	Radius vector
R	Radius of the earth
R_c	Radius of the earth at the observation site
t	Time
t_p	Time when the vehicle encounters perigee
t_s	Local sidereal time
T	Transformation matrix
v	Velocity; also, diagonal matrix of the inverse variances
x, y, z	Cartesian coordinates. See section A.1 for definitions of the various coordinate systems
α	Azimuth angle
δ	Residual
ϵ	Elevation angle
η	Angle of the velocity vector with north on the local horizontal plane; also, sector-triangle ratio
θ	True anomaly
ι	Obliquity of the ecliptic
λ	Celestial longitude
Λ	Geocentric longitude
μ	Gravitational constant; also, mean value
$\hat{\mu}$	Maximum likelihood estimator for the mean
ν	Angle of the velocity vector to the local geocentric vertical; also, refractive index
ρ	Range, the distance from the observer to a body
$\dot{\rho}$	Range rate
σ	Standard deviation
$\hat{\sigma}^2$	Maximum likelihood estimate of the variance
τ	Orbit period
ω	Argument of perigee
Ω	Right ascension or longitude of the ascending node
Ω_e	Rotation rate of the earth, 0.7292115×10^{-4} rad/sec
Υ	Vernal equinox (Aries)
$\underline{\Omega}$	Autumnal equinox (Libra)

A. INTRODUCTION

The basic problem of orbit computation is the determination, from a set of observations, of six parameters which define an orbit. These parameters may be the Cartesian position and velocity components at some epoch, the classical orbit elements (semimajor axis, eccentricity, inclination, argument of perigee, longitude of ascending node, and mean anomaly at epoch), or any other set of independent quantities which uniquely determine the orbit. The orbit computation problem may involve determination of quantities other than the six orbit parameters, however. For example, improved values of physical constants, drag coefficients, tracking station locations or thrust corrections may also be determined in the orbit computation process.

Whether the goal of a satellite vehicle mission is gathering of accurate geophysical data or safe recovery of a manned capsule, accurate orbit computation is a prime requirement since gravity field or atmospheric density information is only as accurate as the satellite position time-histories from which it is derived. In addition, there is a requirement for continual precise knowledge of the position of manned satellites for the safety of the pilot. The increasing requirement for fast, highly accurate determination of orbits has led to many new developments of theories, techniques and systems as well as modifications of existing astronomical methods. This chapter comprises a general exposition of some methods and system capabilities for locating an earth satellite and predicting its future positions and velocities. Specifically, the areas considered are tracking networks and their capabilities, tracking techniques, data reduction, initial determination of the orbit elements and improvement of the computed orbit.

B. COORDINATE SYSTEMS AND TRANSFORMATIONS

1. Coordinate System Definition

In the determination of orbits a multitude of coordinate systems are frequently used. It is convenient to define these various systems before considering the principal problem of orbit determination, so that the definitions will be available for reference.

Complete specification of a coordinate system involves three geometric quantities, an origin, a principal direction and a fundamental plane. For example, the origin might be an observer on the earth's surface (a topocentric system), the center of the earth (a geocentric system), the center of the moon (selenocentric), the center of the sun (heliocentric), or any other convenient point. The principal direction might be the south point on the horizon, vernal equinox, or any of a number of such directions; and the fundamental plane might be one of the customary planes of reference, i.e., the local horizontal, equatorial or ecliptic planes, or any other convenient plane. In addition, coordinate systems may be time dependent (rotating systems) or fixed in spatial orientation (inertial systems). Table 1 defines the most frequently used systems of coordinates. A list of definitions of the various terms involved in this table and subsequent discussions is presented in Appendix B.

2. Transformation of Coordinates

A rotation ξ about a certain axis is considered positive if counterclockwise as viewed from the positive end of that axis. The general forms for rotations of $+\xi$ about the x, y, and z axes are as follows:

$$\begin{bmatrix} x' \\ y' \\ z' \end{bmatrix} = \begin{bmatrix} 1 & 0 & 0 \\ 0 & \cos\xi & \sin\xi \\ 0 & -\sin\xi & \cos\xi \end{bmatrix} \begin{bmatrix} x \\ y \\ z \end{bmatrix} \qquad (1)$$

$$\equiv T_{x,\,\xi} \left\{x,\ y,\ z\right\}$$

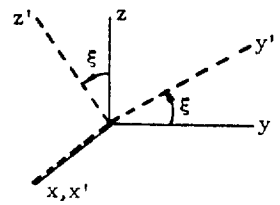

$$\begin{bmatrix} x' \\ y' \\ z' \end{bmatrix} = \begin{bmatrix} \cos\xi & 0 & -\sin\xi \\ 0 & 1 & 0 \\ \sin\xi & 0 & \cos\xi \end{bmatrix} \begin{bmatrix} x \\ y \\ z \end{bmatrix} \qquad (2)$$

$$\equiv T_{y,\,\xi} \left\{x,\ y,\ z\right\}$$

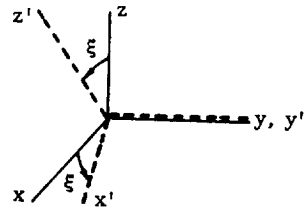

$$\begin{bmatrix} x' \\ y' \\ z' \end{bmatrix} = \begin{bmatrix} \cos\xi & \sin\xi & 0 \\ -\sin\xi & \cos\xi & 0 \\ 0 & 0 & 1 \end{bmatrix} \begin{bmatrix} x \\ y \\ z \end{bmatrix} \qquad (3)$$

$$\equiv T_{z,\,\xi} \left\{x,\ y,\ z\right\}$$

These general rules may be used to derive transformations between the various coordinate systems defined in the preceding subsection.

TABLE 1

Coordinate Systems

Coordinate System	Basis	Origin	Principal Direction	Principal Plane	Poles	Secondary Great Circles	Parallels	Angular Coordinates	Cartesian Coordinates	Transformation References (sections)
Geocentric (geographic) (rotating)	Rotation of earth	Center of earth	Intersection of greenwich meridian with equatorial plane	Equatorial	North and south terrestrial poles (or north and south celestial poles)	Meridians	Parallels of latitude	Geocentric latitude L Geocentric longitude Λ		B. 2. a (geodetic) B. 2. d (topocentric)
Geodetic (rotating)	Reference spheroid, rotation of earth	Intersection of normal to geoid with major axis of earth	Intersection of greenwich meridian with equatorial plane	Equatorial	North and south celestial poles	Meridians	Parallels of latitude	Geodetic latitude L' Geodetic longitude Λ		B. 2. a (geocentric) B. 2. f (general)
Topocentric (horizontal) (rotating)	Direction of gravity	Observer	South point of horizon	True horizon	Zenith and nadir	Vertical circles	Almucantars	Azimuth a Elevation ϵ	x_{oh} y_{oh} z_{oh}	B. 2. b B. 2. c
Equatorial (rotating)	Rotation of earth	Observer or center of earth	Intersection of observer's meridian with equatorial plane	Equator of date	North and south terrestrial poles	Meridians	Parallels of latitude	Declination D or geocentric latitude L Hour angle H or relative longitude $\Delta\Lambda$	x_r y_r z_r	
Earth centered inertial (ECI)	Diurnal motion of celestial sphere	Center of earth	Vernal equinox of date	Equator of date	North and south celestial poles	Hour circles	Parallels of declination	Declination D = L Right ascension A	x_e y_e z_e	B. 2. e (general) B. 2. h (orbit)
General equatorial (inertial)	Diurnal motion of celestial sphere	Any convenient point	Intersection of any convenient secondary circle with the equatorial plane	Equator of date	North and south celestial poles	Meridians	Parallels of declination	Declination D Relative right ascension Δ A	x_i y_i z_i	B. 2. e (ECI) B. 2. f (geodetic) B. 2. g (ecliptic)
Orbit (inertial)	Orbital motion of satellite vehicle	Focus	Orbit major axis in direction of perifocus	Orbit plane	Normal to orbit plane			True anomaly θ	x_ω y_ω z_ω	B. 2. h (ECI)
Ecliptic (inertial)	Orbital motion of earth	Any convenient point	Vernal equinox of date	Ecliptic	Ecliptic poles	Secondaries to the ecliptic	Parallels of latitude	Celestial latitude t Celestial longitude λ	x_ϵ y_ϵ z_ϵ	B. 2. g. (general)
Galactic (inertial)	Geometry of visible universe	Any convenient point	Intersection of galactic circle with celestial equator	Galactic circle	Galactic poles	Secondaries to the galactic	Parallels of latitude	Galactic latitude Galactic longitude		

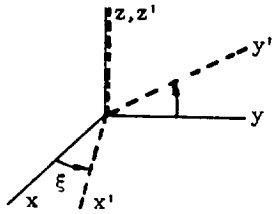

Transformation of geodetic latitude L' to geocentric latitude L

$$L = L' - 695''.6635 \sin 2L' + 1''.1731 \sin 4L' - 0''.0026 \sin 6L' \quad (4)$$

or $\tan L = (1-f)^2 \tan L'$ where

$f = \frac{1}{298.24}$ = flattening

Transformation from topocentric horizontal (x_{oh}, y_{oh}, z_{oh}) axes to topocentric equatorial (x_o, y_o, z_o) rotating axes

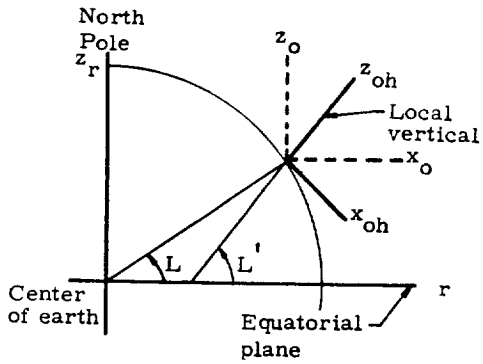

$$\begin{bmatrix} x_o \\ y_o \\ z_o \end{bmatrix} = \begin{bmatrix} \sin L' & 0 & \cos L' \\ 0 & 1 & 0 \\ -\cos L' & 0 & \sin L' \end{bmatrix} \begin{bmatrix} x_{oh} \\ y_{oh} \\ z_{oh} \end{bmatrix} \quad (5)$$

polar coordinates:

$$\left.\begin{aligned} x_{oh} &= \rho \cos \epsilon \cos \alpha \\ y_{oh} &= \rho \cos \epsilon \sin \alpha \\ z_{oh} &= \rho \sin \epsilon \end{aligned}\right\} \quad (6)$$

where ϵ = elevation, α = azimuth

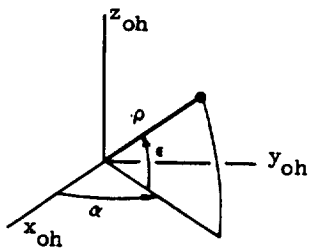

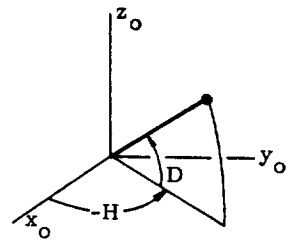

$$\sin D = \sin L' \sin \epsilon - \cos L' \cos \epsilon \cos \alpha$$

$$\sin H = -\frac{\sin \alpha \cos \epsilon}{\cos D} \quad (7)$$

Transformation from topocentric equatorial (x_o, y_o, z_o) rotating axes to topocentric equatorial inertial axes (x_i, y_i, z_i)

$$\begin{bmatrix} x_i \\ y_i \\ z_i \end{bmatrix} = \begin{bmatrix} \cos t_s & -\sin t_s & 0 \\ \sin t_s & \cos t_s & 0 \\ 0 & 0 & 1 \end{bmatrix} \begin{bmatrix} x_o \\ y_o \\ z_o \end{bmatrix} \quad (8)$$

where

t_s = local sidereal time

= hour angle of vernal equinox

= right ascension of local meridian.

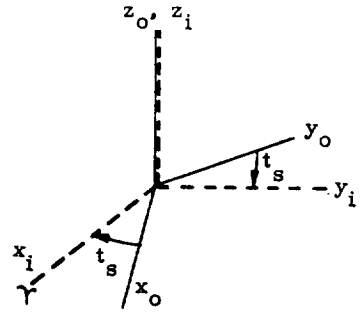

The polar coordinates are related as follows:

$$A = t_s - H \quad (9)$$

D is the same as in subsection b.

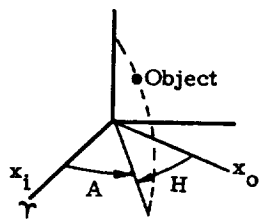

Transformation from topocentric equatorial inertial axes (x_i, y_i, z_i) to geocentric equatorial inertial axes (x_e, y_e, z_e)

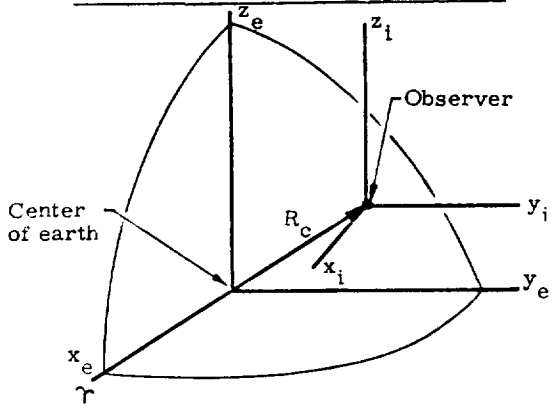

$$x_e = x_i + X_c$$

$$y_e = y_i + Y_c \qquad (10)$$

$$z_e = z_i + Z_c$$

where

$$X_c = (C + h_o) \cos L' \cos t_s$$

$$Y_c = (C + h_o) \cos L' \sin t_s \qquad (11)$$

$$Z_c = (S + h_o) \sin L'$$

are the coordinates of the observer in the equatorial inertial system and

t_s = local sidereal time

L' = geodetic latitude

h_o = observer's height above sea level in units of the equatorial radius of the earth

$$C = \frac{1}{\sqrt{1 - (2f - f^2) \sin^2 L'}}$$

$$S = C(1 - f)^2$$

$$f = \frac{1}{298.24} = \text{flattening of the earth}$$

(C and S, as defined by $\frac{R_c}{R_e} \sin L = S \sin L'$ and $\frac{R_c}{R_e} \cos L = C \cos L'$, are tabulated in the American Ephemeris and Nautical Almanac).

$$R_c = R_e C \sqrt{\cos^2 L' + (1 - f)^4 \sin^2 L'} \qquad (12)$$

$$= \frac{R_e (1 - f)}{\sqrt{1 + f(f - 2) \cos^2 L}} \qquad (13)$$

where

R_e = equatorial radius.

Transformation from general equatorial inertial coordinates (x_i, y_i, z_i) to earth-centered inertial axes (x_e, y_e, z_e)

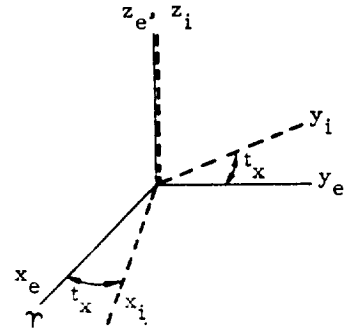

$$\begin{bmatrix} x_e \\ y_e \\ z_e \end{bmatrix} = \begin{bmatrix} \cos t_x & -\sin t_y & 0 \\ \sin t_x & \cos t_x & 0 \\ 0 & 0 & 1 \end{bmatrix} \begin{bmatrix} x_i \\ y_i \\ z_i \end{bmatrix} \qquad (14)$$

where

t_x = right ascension of the x_i-axis meridian

$$A = t_x + \Delta\Lambda \qquad (15)$$

D is the same as in subsection b

$\Delta\Lambda$ = difference in geocentric longitude between the x_i-axis and the object being located.

Transformation from general equatorial inertial coordinates (x_i, y_i, z_i) to geodetic coordinates

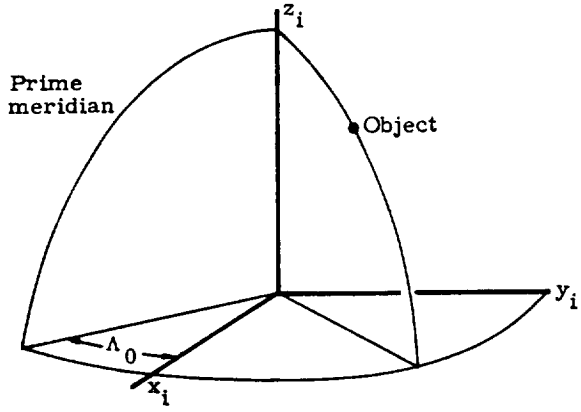

Geodetic or geocentric longitude:

$$\Lambda = \Lambda_0 + \tan^{-1} \frac{y_i}{x_i} - \frac{\Omega_e}{\Delta t} \qquad (16)$$

Geodetic latitude:

$$L' = \tan^{-1}\left[\frac{1}{(1-f)^2}\,\frac{z_i}{\sqrt{x_i^2 + y_i^2}}\right] \qquad (17)$$

where

Λ_0 = geodetic longitude of the prime direction x_i at the time of transformation

Ω_e = rotation rate of the earth, 0.7292115×10^{-4} rad/sec

Δt = time elapsed since the time of transformation

f = flattening = $\frac{1}{298.24}$

Transformation from equatorial inertial coordinates (x_i, y_i, z_i) to ecliptic inertial coordinates $(x_\epsilon, y_\epsilon, z_\epsilon)$

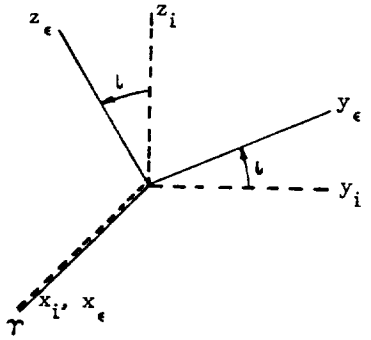

$$\begin{bmatrix} x_\epsilon \\ y_\epsilon \\ z_\epsilon \end{bmatrix} = \begin{bmatrix} 1 & 0 & 0 \\ 0 & \cos\iota & \sin\iota \\ 0 & -\sin\iota & \cos\iota \end{bmatrix} \begin{bmatrix} x_i \\ y_i \\ z_i \end{bmatrix} \qquad (18)$$

or, since

$$x_i = r_i \cos D \cos A$$

$$y_i = r_i \cos D \sin A \qquad (19)$$

$$z_i = r_i \sin D$$

and

$$x_\epsilon = r_\epsilon \cos \ell \cos\lambda$$

$$y_\epsilon = r_\epsilon \cos \ell \sin\lambda \qquad (20)$$

$$z_\epsilon = r_\epsilon \sin \ell$$

$$\cos \ell \cos\lambda = \cos D \cos A$$

$$\cos \ell \sin\lambda = \cos\iota \cos D \sin A + \sin\iota \sin D$$

$$\sin \ell = -\sin\iota \cos D \sin A + \cos\iota \sin D \qquad (21)$$

where

ι = obliquity of the ecliptic

= $23^\circ 27' 08.''26 - 0.''4684\,(t_{years} - 1900)$

$r_i = r_\epsilon$ = radius vector

A = right ascension

D = declination

ℓ = celestial latitude

λ = celestial longitude.

Transformation from orbit system coordinates $(x_\omega, y_\omega, z_\omega)$ to earth-centered inertial coordinates (x_e, y_e, z_e)

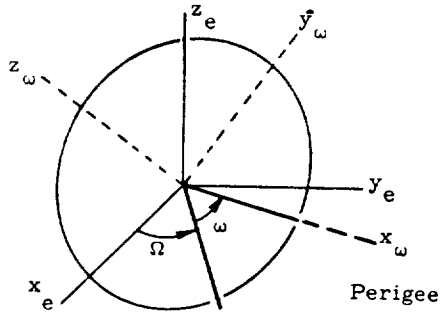

Rotation routine:

(1) Rotation in the orbit plane about the z_ω axis through $-\omega$, $T_{-\omega}$

(2) Rotation about the line of nodes through $-i$, T_{-i}

(3) Rotation in the equatorial plane through $-\Omega$, $T_{-\Omega}$

then

$$\{x_e, y_e, z_e\} = T_{-\Omega}\, T_{-i}\, T_{-\omega}\, \{x_\omega, y_\omega, z_\omega\} \qquad (22)$$

where

$$T_{-\Omega}\, T_{-i}\, T_{-\omega} =$$

$$\left[\begin{array}{c|c|c} \cos\Omega\cos\omega & -\cos\Omega\sin\omega & \\ -\sin\Omega\cos i\sin\omega & -\sin\Omega\cos i\cos\omega & \sin\Omega\sin i \\ \hline \sin\Omega\cos\omega & -\sin\Omega\sin\omega & \\ +\cos\Omega\cos i\sin\omega & +\cos\Omega\cos i\cos\omega & -\cos\Omega\sin i \\ \hline \sin i\sin\omega & \sin i\cos\omega & \cos i \end{array}\right]$$

The elements of this transformation matrix are frequently assigned the following symbols for convenience:

$$T_{-\Omega}\, T_{-i}\, T_{-\omega} = \begin{bmatrix} P_x & Q_x & R_x \\ P_y & Q_y & R_y \\ P_z & Q_z & R_z \end{bmatrix} \qquad (23)$$

3. Data Correction

Various data corrections are usually required to convert apparent coordinates to true coordinates. Depending on the nature of the measurement, corrections may be required to account for aberration, refraction, precession, proper motion, nutation and parallax.

a. Aberration

Since light travels at a finite velocity, the apparent coordinates of any body in space depend upon the motion of the body and the motion of the observer on earth during the time interval required for light from the body to arrive at the observer. This apparent displacement of a body from its actual position due to the finite speed of light and the motions of the observer and the body is called aberration. To elaborate, the observer perceives a ray of light which originated at the body sometime before the instant of observation and which traveled toward a position that the earth would occupy sometime after the ray originated. Therefore, at the time of observation, the moving body is no longer located in the direction from which the light ray is observed. Also, since the earth is moving, the apparent direction of the ray differs from the true direction. Thus the observed direction relative to the stars is neither the actual direction at the time of observation nor the direction to the position of the body at the time the ray was emitted.

Various types of aberration are distinguished. Planetary aberration is the displacement of the observed apparent position from the actual position at the instant of observation. Stellar aberration, a part of the planetary aberration, is the displacement of the observed position from the actual position of the body at the instant when the light ray was emitted. The stellar aberration consists of two parts, diurnal aberration and annual aberration. Diurnal aberration is that part due to the rotation of the earth on its axis. Annual aberration is due to the orbital motion of the earth about the sun.

Obviously, most corrections for aberration are significant only for astronomical determinations on relatively remote bodies. Even for observations of the sun, only stellar aberration need be considered. In the case of a satellite, observed as to its distance and angular position relative to the earth, the stellar aberration may be neglected as being essentially the same for the satellite and the earth. Also, a satellite experiences very nearly the same heliocentric motion as the earth. Therefore, aberration corrections for satellites in practice need include only the effect of motion of the satellite relative to the earth during the time required for light from the satellite to arrive at the observer. (For example, during the time for light to pass from the moon to the earth, the moon moves about 0."7 in geocentric longitude.) Planetary aberration is larger for artificial satellites. In a circular satellite orbit, central angle traversed is proportional to time, i.e.,

$$\frac{\Delta\theta}{2\pi} = \frac{t}{\tau} \quad (\Delta\theta \text{ in radians}).$$

Since the period is

$$\tau = 2\pi r\sqrt{\frac{r}{\mu}}\,,$$

$$\Delta\theta = \frac{t}{r}\sqrt{\frac{\mu}{r}}$$

where r is the satellite orbit radius. The time required for light to travel from an overhead satellite to the earth is

$$t = \frac{r - R}{c}$$

where R is the radius of the earth and c is the speed of light. Therefore, the planetary aberration is

$$\Delta\theta = \frac{r - R}{cr}\sqrt{\frac{\mu}{r}}\,.$$

This quantity has a maximum for r = 3R,

$$\Delta\theta_{max} \approx 2''.1$$

The following sections briefly consider methods used for computing the effect of aberration. A more detailed description is contained in Ref. 1.

(1) Stellar aberration

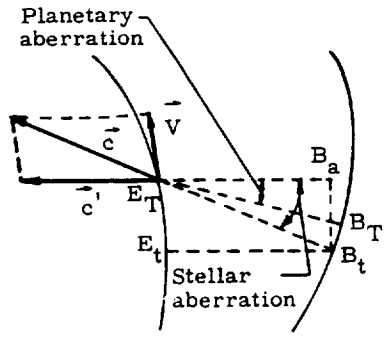

In stellar aberration determinations the following notation is used:

$\vec{v}$ = earth's orbital velocity in inertial, fixed-origin coordinates (x, y, z)

$\vec{c}$ = velocity vector of the actual light ray

$\vec{c}'$ = relative velocity vector of the light ray

T = instant when an observation is made

t = earlier time when the ray observed left the body

E_T, E_t = actual positions of the earth at the times T and t, respectively

B_T, B_t = actual positions of a body at the times T and t, respectively

B_a = apparent position of the body at time T

$\tau = T - t$ = time for light to travel from the body to earth

$\rho = \tau c$ = geometric distance $E_T B_t$

Λ_a, Λ_T = longitudes of the apparent direction $E_T B_a$ and the true light path $E_T B_T$, respectively

L_a, L_T = latitudes corresponding to Λ_a, Λ_T.

Then the direction cosines of $E_T B_a$ are

$$\begin{aligned} \cos L_a \cos \Lambda_a &= \cos L_T \cos \Lambda_T + \frac{v_x}{c} \\ \cos L_a \sin \Lambda_a &= \cos L_T \sin \Lambda_T + \frac{v_y}{c} \\ \sin L_a &= \sin L_T + \frac{v_z}{c} \end{aligned} \tag{24}$$

where V_x, V_y, V_z are the components of v

These direction cosines give

$$\tan (\Lambda_a - \Lambda_T) = \frac{-\sec L_T (v_x \sin \Lambda_T - v_y \cos \Lambda_T)}{c + \sec L_T (v_x \cos \Lambda_T + v_y \sin \Lambda_T)} \tag{25}$$

$$\tan (L_a - L_T) = \frac{v_z \cos L_T - (v_x \cos \Lambda_T + v_y \sin \Lambda_T) \sin L_T}{v_z \sin L_T + (v_x \cos \Lambda_T + v_y \sin \Lambda_T) \cos L_T + c} + O\left(\sin^2 \frac{\Lambda_a - \Lambda_T}{2}\right)$$

where:

$O\left(\sin^2 \frac{\Lambda_a - \Lambda_T}{2}\right)$ denotes terms of the order of the quantity in the brackets.

In rectangular coordinates,

$$X_a - X_t = \frac{v_x \rho_t}{c} = v_x \tau$$

$$Y_a - Y_t = \frac{v_y \rho_t}{c} = v_y \tau$$

$$Z_a - Z_t = \frac{v_z \rho_t}{c} = v_z \tau \tag{26}$$

where

(X_a, Y_a, Z_a) are the apparent coordinates of the body at the instant of observation T

(X_t, Y_t, Z_t) are the true coordinates of the body at the time the light left the body.

(2) Planetary aberration

The planetary aberration is the stellar aberration corrected for the motion of the body from B_t to B_T during the time for light from the body to reach earth (see previous sketch). This correction may be computed from a Taylor series, e.g.,

$$X_T - X_t = \dot{X}_t \tau + \frac{1}{2} \ddot{X}_t \tau^2 + \frac{1}{6} \dddot{X}_t \tau^3 + \ldots$$

Then the rectangular components of the planetary aberration are

$$\begin{aligned} X_a - X_T &= (V_x - \dot{X}_t)\tau - \tfrac{1}{2}\ddot{X}_t \tau^2 - \tfrac{1}{6}\dddot{X}_t \tau^3 \ldots \\ Y_a - Y_T &= (V_y - \dot{Y}_t)\tau - \tfrac{1}{2}\ddot{Y}_t \tau^2 - \tfrac{1}{6}\dddot{Y}_t \tau^3 \ldots \\ Z_a - Z_T &= (V_z - \dot{Z}_t)\tau - \tfrac{1}{2}\ddot{Z}_t \tau^2 - \tfrac{1}{6}\dddot{Z}_t \tau^3 \ldots \end{aligned} \tag{27}$$

where (X_t, Y_t, Z_t) are given in the preceding subsection. The terms of order τ^2 and higher can usually be neglected. In terms of right ascension and declination the planetary aberration can then be expressed as

$$\left.\begin{aligned} \Delta A &= -A \frac{R_T}{c} \\ \Delta D &= -\dot{D} \frac{R_T}{c} \end{aligned}\right\} \tag{28}$$

where $R_T = \sqrt{X_T^2 + Y_T^2 + Z_T^2}$

(3) Diurnal aberration

Because of the earth's rotation, the observer moves toward the east at a rate

$$\zeta = 464 \frac{R_c}{R_e} \cos L \quad \text{meters/sec} \tag{29}$$

where

R_c = radius of the earth at the observer's location

R_e = equatorial radius of the earth

L = geocentric latitude of the observer.

This motion causes a shift in apparent position of remote bodies toward the east given by

$$\frac{\zeta}{c} \sin \xi$$

where ξ is the angular distance from the east point to the body. Then, in terms of right ascension and declination, the diurnal aberration is

$$\left.\begin{aligned} \Delta A &= 0''.319 \frac{R_c}{R_e} \cos L \cos H \sec D \\ \Delta D &= 0''.319 \frac{R_c}{R_e} \cos L \sin H \sin D \end{aligned}\right\} \quad (30)$$

where H = hour angle of the body.

The effect of diurnal aberration may be neglected except where relative positions of widely separated bodies are being measured.

(4) Annual aberration

The annual aberration, due to the earth's orbital motion, in terms of right ascension and declination is

$$\begin{aligned} \Delta A &= C_1 c_1 + C_2 c_2 \\ \Delta D &= C_1 c_1' + C_2 c_2' \end{aligned} \quad (31)$$

where

$$c_1 = \cos A \sec D$$

$$c_2 = \sin A \sec D$$

$$c_1' = \tan \iota \cos D - \sin A \sin D \quad [\iota = \text{obliquity}]$$

$$c_2' = \cos A \sin D$$

and

$$C_1 = -20''.47 \cos \lambda_\odot \cos \iota$$

$[\lambda_\odot$ = true longitude of sun$]$

$$C_2 = -20''.47 \sin \lambda_\odot$$

are tabulated in the American Ephemeris.

b. Precession

Precession is the combination of the slow change of direction of the earth's axis of rotation and the slower change of direction of the axis perpendicular to the ecliptic. The first effect is due to the action of the sun and the moon (luni-solar precession), the second is due to the action of the planets (planetary precession).

As a result of precession the vernal equinox is slowly regressing at a rate of about 50 sec of arc per year; therefore, any coordinate system which has as the principal direction the vernal equinox must specify a date to which it is referred.

To change from one equatorial system, say referred to the mean equinox of date, to another, say to the mean equinox of some other standard date (like 1950.0), the following operations should be performed:

$$\begin{aligned} x_d &= X_x x_{1950} + Y_x y_{1950} + Z_x z_{1950} \\ y_d &= X_y x_{1950} + Y_y y_{1950} + Z_y z_{1950} \\ z_d &= X_z x_{1950} + Y_z y_{1950} + Z_z z_{1950} \end{aligned} \quad (32)$$

or

$$\begin{aligned} x_{1950} &= X_x x_d - Y_x y_d - Z_x z_d \\ y_{1950} &= -X_y x_d + Y_y y_d + Z_y z_d \\ z_{1950} &= -X_z x_d + Y_z y_d + Z_z z_d \end{aligned}$$

where the subindex

d = mean equinox of date

1950 = mean equinox of 1950.0

and

$$X_x = 1.000\,000\,00 - 0.000\,296\,97\,T^2 - 0.000\,000\,13\,T^3$$

$$Y_x = -X_y = -0.022\,349\,88\,T - 0.000\,006\,76\,T^2 + 0.000\,002\,21\,T^3$$

$$Z_x = -X_z = -0.009\,717\,11\,T + 0.000\,002\,07\,T^2 + 0.000\,000\,96\,T^3$$

$$Y_y = 1.000\,000\,00 - 0.000\,249\,76\,T^2 - 0.000\,000\,15\,T^3$$

$$Z_y = Y_z = -0.000\,108\,59\,T^2 - 0.000\,000\,03\,T^3$$

$$Z_z = 1.000\,000\,00 - 0.000\,047\,21\,T^2 + 0.000\,000\,02\,T^3$$

where T is measured in Julian centuries from 1950.0.

The Julian Calendar is discussed and a table presenting Julian Day Numbers presented in Chapter II.

$$T = [\text{Julian date number for epoch} - \text{Julian date number for 1950.0}] / 36525$$

c. Nutation

Due to the solar and lunar attractions on the equatorial protuberance of the earth, the celestial pole travels in a small ellipse around its mean position on the circular precessional path. The correction for nutation is very small and may generally be neglected except in precise astronomica determinations.

Tables for nutation in longitude and in obliquity are tabulated in the American Ephemeris and Nautical Almanac each year. An explanation of how those tables are obtained is given in Astronomical Papers of the American Ephemeris, vol. XV, Part I, p. 153, 1953, and in the joint supplement to the American Ephemeris and Nautical Almanac entitled "Improved Lunar Ephemeris 1952 - 1959," pp. ix-x, 1954.

To obtain rectangular coordinates referred to the mean equinox of date when those referred to the true equinox are available, perform the following computations:

$$\begin{aligned} x &= x_d\, x_y - y_d\, y_z - z_d\, z_z \\ y &= -x_d\, x_y + y_d\, y_z + z_d\, z_z \\ z &= -x_d\, x_z + y_d\, y_z + z_d\, z_z \end{aligned} \qquad (33)$$

where

$$z_z = y_y = x_x = 1$$

$$-y_x = x_y = \Delta\psi \cos\iota \sin 1''$$

$$-z_x = x_z = \Delta\psi \sin\iota \sin 1''$$

$$-z_y = y_z = \Delta\iota \sin 1''$$

ι = obliquity of ecliptic

and

$\Delta\iota$ and $\Delta\psi$ are, respectively, the rates of nutation in obliquity and in longitude (obtained from the tables mentioned above) in units of seconds of arc.

d. Refraction

Refraction is another source of deviation between the apparent and true directions of optical or radio measurements. The curvature of electromagnetic rays due to refraction is greatest for measurements of small elevation above the horizontal plane. From Snell's law, the correction to be added to the observed elevation is

$$\Delta\epsilon = \int_b^o \frac{ds}{\rho_c} = -\int_b^o \frac{\hat{n}\cdot\nabla\nu}{\nu}\, ds \qquad (34)$$

where the integral along the ray path is taken from the body observed, b, to the observer, o, and

ρ_c = radius of curvature of the ray path

ν = refractive index

$\hat{n}$ = unit vector normal to the ray path

s = arc length along the ray path

Specification of the variation in ν along the path may be very difficult. One approach is numerical integration of the integral expressed as

$$\sum_i a_i \tan^{(2i+1)} z_a$$

where the a_i's are empirical coefficients and z_a is the apparent zenith distance. In several studies of radio wave refraction, two components of the refractive index are distinguished:

tropospheric refraction:

$$(\nu - 1)\, 10^6 = \frac{103.49}{K}\,(p_a - p_w) + \left[\frac{86.26}{K} \cdot \left(1 + \frac{5748}{K}\right) p_w\right] \qquad (35)$$

where

p_a = air pressure, mm of mercury

p_w = water pressure, mm of mercury

K = temperature in degrees Kelvin

or

$$\nu - 1 = 105 \times 10^{-6}\, e^{-0.142\,(h - a)}$$

$(\pm 15\%,\ h \geq 9$ km)

ionospheric refraction:

$$\nu = \sqrt{1 - \frac{4\pi N \epsilon^2}{\epsilon_o m \omega^2}} = \sqrt{1 - \frac{3.18 \times 10^9 N}{\omega^2}} \qquad (36)$$

where

N = electron density, electrons /cm^3

ϵ = charge of the electron

m = mass of an electron

ϵ_0 = dielectric constant

ω = frequency in radians per second

Electron density is tabulated in Chapter II. Ref (2) enumerates the phase changes which occur in propagation for the various radio tracking techniques:

Range measurement:

$$\Delta\phi_t = \frac{\omega}{c}\left(\int_{up} \nu ds + \int_{down} \nu ds\right) \qquad (37)$$

Doppler measurement:

$$\Delta\phi = \frac{\omega}{c}\,\frac{d}{dt}\left(\int \nu ds\right) = \frac{\omega}{c}\left(\nu_b\, \hat{t}_b \cdot \frac{\dot{}}{\rho} + \int \frac{\partial\nu}{\partial t}\, ds\right)$$

(assuming isotropic ν) (38)

Interferometer measurement:

$$\Delta\phi_s = \frac{\omega}{c}\left(\int_1 \nu ds - \int_2 \nu ds\right) \tag{39}$$

$$\delta\Delta\phi = \frac{\omega}{c}\ \Delta x \sin\epsilon\ \Delta\epsilon \tag{40}$$

where the integrals are taken over the ray path and

ρ = range

$\Delta\phi_t$ = temporal phase difference

$\Delta\phi_s$ = spatial phase difference

$\Delta\dot{\phi}$ = difference in rate of change of phase

ω = frequency (rad/sec)

c = speed of light

ν = refractive index

b = subscript indicating a value of the body

$\hat{t}$ = unit vector tangent to the ray

Δx = interferometer baseline length

and $\Delta\epsilon$ = is defined in Eq (34)

4. Data conversions

Transformation between topocentric coordinates and direction cosine data

$$l = \cos\epsilon\cos\alpha = \frac{x_{oh}}{\rho}$$

$$m = \cos\epsilon\sin\alpha = \frac{y_{oh}}{\rho}$$

$$n = \sqrt{1 - l^2 - m^2} = \sin\epsilon = \frac{z_{oh}}{\rho} \tag{41}$$

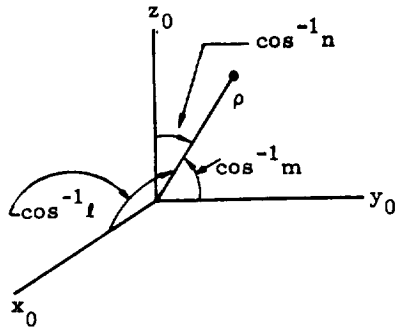

From the differentials of these relations

$$dl = \frac{dx_{oh}}{\rho} - \frac{x_{oh}}{\rho^3}(x_{oh}\,dx_{oh} + y_{oh}\,dy_{oh} + z_{oh}\,dz_{oh})$$

$$dm = \frac{dy_{oh}}{\rho} - \frac{y_{oh}}{\rho^3}(x_{oh}\,dx_{oh} + y_{oh}\,dy_{oh} + z_{oh}\,dz_{oh})$$

$$dn = \frac{dz_{oh}}{\rho} - \frac{z_{oh}}{\rho^3}(x_{oh}\,dx_{oh} + y_{oh}\,dy_{oh} + z_{oh}\,dz_{oh})$$

the correction relationship is

$$\begin{bmatrix} dl \\ dm \\ dn \end{bmatrix} = \begin{bmatrix} 1 - l^2 & -lm & -ln \\ -lm & 1 - m^2 & -mn \\ -ln & -mn & 1 - n^2 \end{bmatrix} \begin{bmatrix} \frac{dx_{oh}}{\rho} \\ \frac{dy_{oh}}{\rho} \\ \frac{dz_{oh}}{\rho} \end{bmatrix} \equiv T_I \left\{ \frac{d\vec{r}_{oh}}{\rho} \right\} \tag{42}$$

Transformation between topocentric coordinates and radar data

$$x_{oh} = \rho\cos\epsilon\cos\alpha$$

$$y_{oh} = \rho\cos\epsilon\sin\alpha \tag{43}$$

$$z_{oh} = \rho\sin\epsilon$$

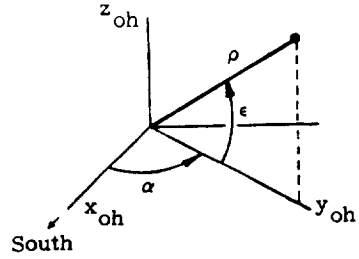

where

ρ = range

α = azimuth

ϵ = elevation

The inverse relationships are

$$\rho = \sqrt{x_{oh}^2 + y_{oh}^2 + z_{oh}^2} \tag{44}$$

$$\sin\epsilon = \frac{z_{oh}}{\rho}$$

$$\tan\alpha = \frac{y_{oh}}{x_{oh}}$$

(continued)

The sensitivities of topocentric coordinates to radar data corrections are obtained from the differentials of the above expressions.

$$d\rho = \frac{1}{\rho}\left(x_{oh}\, dx_{oh} + y_{oh}\, dy_{oh} + z_{oh}\, dz_{oh}\right)$$

$$\cos\epsilon\, d\epsilon = \frac{dz_{oh}}{\rho} - \frac{z_{oh}}{\rho^3}\left(x_{oh}\, dx_{oh} + y_{oh}\, dy_{oh} + z_{oh}\, dz_{oh}\right)$$

$$\sec^2\alpha\, d\alpha = \frac{dy_{oh}}{x_{oh}} - \frac{y_{oh}}{x_{oh}^2}\, dx_{oh}$$

$$\begin{bmatrix} d\rho \\ \cos\epsilon\, d\alpha \\ d\epsilon \end{bmatrix} = \begin{bmatrix} \cos\epsilon\cos\alpha & \cos\epsilon\sin\alpha & \sin\epsilon \\ -\frac{1}{\rho}\sin\alpha & \frac{1}{\rho}\cos\alpha & 0 \\ -\frac{1}{\rho}\sin\epsilon\cos\alpha & -\frac{1}{\rho}\sin\epsilon\sin\alpha & \frac{1}{\rho}\cos\epsilon \end{bmatrix} \begin{bmatrix} dx_{oh} \\ dy_{oh} \\ dz_{oh} \end{bmatrix} \qquad (45)$$

The transformations of the time rates of these variables are as follows:

$$\dot\rho = \frac{1}{\rho}\left(x_{oh}\,\dot x_{oh} + y_{oh}\,\dot y_{oh} + z_{oh}\,\dot z_{oh}\right)$$

$$\dot\alpha = \frac{x_{oh}\,\dot y_{oh} - y_{oh}\,\dot x_{oh}}{x_{oh}^2 + y_{oh}^2} \qquad (46)$$

$$\dot\epsilon = \frac{z_{oh}\left(x_{oh}\,\dot x_{oh} + y_{oh}\,\dot y_{oh}\right) - \dot z_{oh}\left(x_{oh}^2 + y_{oh}^2\right)}{-\rho^2\sqrt{x_{oh}^2 + y_{oh}^2}}$$

C. ACQUISITION OF DATA

1. Tracking Techniques

Orbit data are chiefly acquired by either optical or radio techniques. Optical trackers have the advantage of extremely accurate topocentric angular measurements, and the disadvantage of not being able to measure range directly (range is found by triangulation). Radar trackers, using much longer wave lengths (1 in. to 50 ft), have the advantage of accurate line-of-sight measurements but the disadvantage of relatively poor accuracy in angular measurements. The radar trackers are able to attain their high accuracy in line-of-sight measurements because radio waves can be generated with very narrow bandwidths; hence, the measurements of single frequencies are practical. Since the velocity of electromagnetic wave propagation is known rather accurately, the range (the velocity of light times the transit time) can be measured with good accuracy. The other line-of-sight measurement based on the doppler effect involves a comparison of the transmitter frequency to the received frequency in order to deduce range rate. Since the frequencies of a light transmitter spread out over a wide band and are uncorrelated, great difficulty is encountered in attempting to follow any one frequency and measure its Doppler effect. Only recently has pure light, with a very narrow bandwidth, been generated with high intensity.

Thus optical cameras such as the Baker-Nunn camera are used to measure the topocentric angles of satellites and radars are used for both line-of-sight measurements and angles (even though angles degrade the accuracy).

a. Optical systems

Optical systems which may be used are: Baker-Nunn camera, recording optical tracking instrument (ROTI). Cine theodolite, and ballistic cameras. A complete description of one, the Baker-Nunn camera, follows:

Features:	field of view = 5° x 30° focal length = 20 in. = 50.8 cm accuracies = 2 " (claimed) limiting magnitude: 17.2 (when tracking object on celestial equator).
Description:	Modification basic Schmidt design which has wider field of view than most telescopes or cameras; uses three-element correcting system for aberrations.
Advantages:	Wide field of view, without excessive aberration.
Disadvantages:	Slow processing; no direct range or range rate measurements, sometimes takes a week to process a single photograph, sometimes the star background is too sparse.

b. Radio trackers

Various techniques have been developed to obtain the highest accuracy from radar measurements. Three broad classes of techniques are discussed:

(1) Radar measurements

(2) Interferometer techniques

(3) Special techniques to reduce measurement errors.

Radar measurements can be classified into line-of-sight measurements and angular measurements. Line-of-sight measurements are range and range rate; angular measurements are usually azimuth and elevation. Since the wave lengths of the radio waves used by radars are relatively large compared with the dimensions of the typical radar antenna, the angular measurements are usually less accurate than the line-of-sight measurements. Many systems such as Minitrack and General Electric Mod II use triangulation schemes with only range measurements. By using

at least three stations in a coherent manner, the topocentric angles of the satellite can be computed. Generally, range measurements use monopulse systems.

(1) Range measurements

There are two types of range radars.

Skin track radars depend on the reflection properties of the satellite's skin to reflect the transmitted pulse back to the receiver. Of course, the reflected pulse is greatly reduced in amplitude. Since the reflected pulse is weak, and since it is desirable to send out as many pulses as possible during a pass, complex gates must be built into the receiver and usually high redundancy must be in each pulse to help separate the signal from the noise.

Beacon track radars can either be monopulse or continuous wave-single frequency carrier types. Beacon track radars depend on a transmitter on board the satellite which can be interrogated by a ground transmitter. Since the return pulse is much stronger than that of the skin track radar, beacon track radars are more accurate in range measurements. However, the added weight of the onboard transmitter sometimes precludes using beacon track radars.

(2) Doppler systems

Another radar technique is to measure the change in carrier frequency as the satellite either recedes or approaches the radar station. One of the differences between this technique and the above pulsed systems is that the transmitter and receiver of the tracking station must be phase locked onto the satellite in order to obtain accuracy, which means that phase information of the carrier is retained. The frequency transmitted can be measured by counting its energy maxima or minima; the received frequency is measured the same way. The result is a frequency difference which is proportional to the range rate of the satellite. Range can sometimes be measured by integrating the range rate (provided the constant of integration is known).

(3) Angular measurements

Direct angular measurements (that is, not using triangulation techniques with line-of-sight measurements) can be made as follows: Suppose a radar antenna is highly directional so that when it does not point directly at the satellite (assuming a satellite beacon and neglecting refraction effects), the signal strength falls off. The signal strength is at a maximum when the antenna points directly at the satellite. When the maximum signal strength is indicated the orientation of the antenna can be measured in azimuth and elevation.

(4) Interferometer systems

Interferometer systems measure the difference in times that a radio wave front from a satellite strikes differently located tracking stations (see Fig. 1). By the time that the wave front reaches the tracking stations it is almost planar; and the approximation that

$$b \cos \epsilon = \lambda = c\,(t_2 - t_1)$$

is fairly accurate. The elevation ϵ can be found from the above formula.

Minitrack is an example of a tracking system which uses the above interferometer technique in modified form. The tracking portion (distinguished from the acquisition portion) of each Minitrack "station" consists of five antennas. The central antenna transmits and receives; each of the others only receives. Two of the receivers form a north-south line with central included; the other two receivers form an east-west line with central. The resulting beam width from the length of the baselines is 100° (north-south) by 11° (east-west). See Fig. 2.

Notice that, since the antennas are fixed in direction, the Minitrack station cannot track unless a satellite passes through its fan-shaped radio beam.

(5) Special techniques

Noise reduction techniques may be listed as

(1) Low noise receivers

(2) Choice of frequency

(3) Modulation scheme and redundancy (coding, correlation)

(4) Frequency diversity to avoid multipath errors

(5) Time standards and synchronization

(6) Search or acquisition techniques

(7) Antenna design

(8) Coherent and noncoherent systems

Low noise receivers. These receivers are the masers and reactance amplifiers. Masers (microwave amplification by stimulated emission of radiation) utilize the high Q properties of the natural resonance frequencies of certain materials such as ammonia, cesium vapor and rubidium.

A reactance amplifier increases the signal-to-noise ratio of the receiver by pumping energy into the signal in a manner related to the phase of the incoming signal. In this manner the phase information redundancy of a carrier is not thrown away.

Choice of frequency. The atmosphere is opaque to most radio frequencies; however, there is a "window" to radiation in the region from 300 to 10,000 Mc. Water vapor absorption limits the upper frequencies and thermal excitation limits the lower end of the spectrum.

Modulation schemes and redundancy. One scheme for using the redundancy of the signal has already been mentioned. The common modulation schemes are amplitude modulation, frequency modulation and pulse time.

Frequency diversity. Frequency diversity systems use two or more carrier frequencies to minimize frequency effects in propagation. One of the major sources of error in propagation

is the ionosphere, which acts as a time varying dielectric, thus changing the frequency of a carrier in an unpredictable manner. The ionosphere also refracts radio beams, thus changing the direction of the beam. The following formula shows how the index of refraction is a function of frequency and ion density:

$$\nu = \sqrt{1 - \frac{81N}{f^2}}$$

where

ν = index of refraction

N = ion density in particles/cm^3

f = carrier frequency in kc

Using two frequencies allows the index of refraction to be estimated, thus minimizing the error due to bending of the radio wave.

The change in frequency due to the variable index of refraction has been calculated by Guier and Weiffenbach to be:

$$f - f_0 = \nu_0 \frac{r_c f_0}{c} \left(\cos h \frac{d\psi}{dt} + \frac{1}{r} \frac{dr}{dt} \sqrt{r^2 \frac{\nu}{\nu_0} - \cos^2 h} \right)$$

where

ν_0 = equivalent refractive index at earth's surface

r_c = the geocentric distance of the station

$\psi(t)$ = angle between the station vector and the geocentric distance vector of the satellite

r = geocentric distance

h = height

c = velocity of light $\tilde{=} 3.00 \times 10^{10}$ cm/sec

Time standards and synchronization. Some classes of orbits and some types of orbit computations (determinations) require very tight synchronization, whereas others need considerably less. If three stations are to take simultaneous range measurements, then the simultaneity requirement will generally limit the three stations to smaller baselines, and complicated synchronization techniques are needed. On the other hand, overdetermined orbits do not need such tight synchronization and baselines as wide as the earth are feasible (satellites could also be used for tracking stations resulting in very wide baselines).

One technique for synchronization of precision radars is to use gas filled wave guides in which the temperature are pressure can be controlled to the extent that the velocity of propagation is very precise. Generally, a central station is connected via wave guides to outlying stations; the signals and time are sent to central from the other stations via the wave guides. If line-of-sight radio beams were to be used instead of wave guides, then significant errors, such as multipath errors and variable time delays due to temperature sensitive dielectric constants of the propagation medium, would occur.

Another technique used for synchronization when the time requirements are not quite so stringent, is to use WWV receivers. WWV transmits very accurate radio pulses on frequencies of 2.5, 5, 10, 15, 20, 25 Mc. Through the use of new techniques such as parametric amplifiers, the frequencies are accurate to several parts in 10^{11}. Received frequencies, if by line of sight, can be nearly as accurate as the frequency transmitted by WWV; if the received frequency is received via the ionsphere reflection, then the accuracy varies, sometimes degrading to a few parts in 10^6 during solar storms.

2. Station Properties

Table 2 lists some of the existing satellite tracking stations and their properties. Where the information is incomplete or changes are anticipated, blanks are left so that insertions or modifications can be made. The information presented should allow a good first estimate of whether or not a station might usefully support a given mission.

Additional information on these and other stations is available from Goddard Space Flight Center, Greenbelt, Maryland, attention Code 531.3.

Explanation of Table 2

Station number--An arbitrarily assigned serial number for cross referencing within this handbook.

System--The net of tracking facilities, if any, to which the particular station is assigned.

Cognizant agency--This is the activity responsible for the scheduling and operation of the station; if should be contacted to obtain support from this station. Abbreviations are:

AMR	Atlantic Missile Range Cape Canaveral, Florida
APL	Applied Physics Laboratory Johns Hopkins University Silver Spring, Md.
BRL	Ballistics Research Laboratory Aberdeen Proving Ground Aberdeen, Md.
GE	General Electric Corporation General Engineering Laboratory Schenectady, New York
GSFC	Goddard Space Flight Center Anacostia Naval Station Anacostia, Maryland

JPL	Jet Propulsion Laboratory California Institute of Technology Pasadena, California
MIT	Lincoln Laboratories Massachusetts Institute of Technology Boston, Mass.
NAA	Space and Information Systems Division North American Aviation, Inc. Downey, California
NERA	Radio Receiving Station NERA Nederhorstdenberg, Netherlands
NSSC	National Space Surveillance Center (Spacetrack) Code CRRKI, AFCRC L. G. Hanscom Field Bedford, Mass.
PMR	Pacific Missile Range Pt. Mugu, California
RADC	Rome Air Development Command Griffiss AFB Rome, New York
SRI	Stanford Research Institute Menlo Park, California
STL	Space Technology Laboratories One Space Park Redondo Beach, California
UILL	Electrical Engineering Research Laboratory University of Illinois Champaign, Illinois
USASRDL	US Army Astro Scientific Research and Development Laboratory Deal, New Jersey
VAFB	Vandenberg AFB Lompoc, California
WRE	Weapons Research Establishment Woomera, Australia
WSMR	White Stands Missile Range White Sands, New Mexico

Station name--A designation descriptive of location and/or equipment.

Installation type--Equipment classification (e.g., FPS-16). Several widely distributed radio systems are described in Table 3. Where the installation type is unique or at least not widely used at present, the table gives the particular antenna configuration. In this case, generally only the primary antenna is described, and there may be others for different frequencies or purposes.

Local designation--A code used by the cognizant agency to identify the station within the agency.

N Lat (deg)--The geodetic north latitude of the station, measured in degrees.

E Long. (deg)--The geodetic east longitude of the station, measured in degrees.

Altitude (meters)--The height of the antenna feed at zero degree elevation above mean sea level, measured in meters.

Survey reference--The basic survey to which the station's location is referenced.

Data reported--Advertised and/or known observations from a given station. More may be available.

α	azimuth measurement
ϵ	elevation or astronomical altitude measurement
H	hour angle
D	declination
ρ	range measurement
$\dot{\rho}$	range rate
f_{non}	noncoherent Doppler frequency, the received frequency from the satellite being tracked, including Doppler frequency shifts
f	two-way phase coherent Doppler frequency shift. Range rate can be accurately and directly extracted from f in most cases
Tel	telemetry, analog or digital coded information communicated from the satellite

Units--Basic measurement system in which the data if reported. Data reported and units are on the same respective lines in Table 2.

Coordinate system--Indicates how the station's antenna is mounted and calibrated. Antenna steering data (ephemerides) should be supplied in the system and units specified. The asterisk means that the units desired differ from those reported and are artillery mils for angular measurements.

Accuracy (3σ)--This is statistical 3σ to which a given measurement is accurate.

Data formats--Indicates the data output equipment available. Most manual outputs work into a teletype system. Almost all automatic outputs work into a teletype system. Almost all automatic output systems may be read manually, so only the higher order available output is shown.

Data delay--The estimated nominal time for handling data at the station before it is transmitted to the user. Abbreviations are as follows:

RT Real time, which signifies that the data is transmitted via an on-line process and will be received by the user essentially the same time that the station observes it.

NRT Near real time--less than 1-min delay--essentially the same as real time except for slight delays such as those caused by data going through teletype tape loops, etc.

Maximum range--The range limit on the particular installation when tracking a passive 1-m^2 target.

Antenna gain/frequency--The advertised approximate antenna gain in a particular frequency band.

Table 3 contains descriptions of some of the more widely used radio tracking systems.

3. Data Acquisition

Mission constraints generally dictate the data sources and tracking time available to each source for a given pass. Low altitude earth satellites are usefully visible from a given station for about 5 to 20 min, and, if the satellite's period is on the order of 120 min, three to four stations more or less evenly spaced along the ground track of the satellite can track and produce data so that data processing facilities will not be overloaded. Prelaunch planning must always include the possibility of a nonnominal orbit, and data handling and orbit computation operations must be capable of producing results under this "worst condition." Orbit determination tasks seldom have the problem of an overload of data, and, when it arises, it is easily controlled.

The threat of insufficient data is best met by considered overdesign of the tracking network. Some redundancy in the tracking systems is desirable, so that failure of a single system will not require reliance on optical or skin track radar methods for further data. Optical methods are slow and dependent on such uncontrollable items as weather, and large skin track radars generally have other commitments. One tracking station with high acquisition reliability should be able to track immediately after injection of the satellite into its free flight orbit, since in many cases the data is better at shorter ranges and time-propagating position errors are reduced. Accurate determination of the time of injection (orbit epoch) is possible from telemetry or Doppler data.

The problem of locating tracking stations to provide maximum certainty in orbit determination involves three considerations:

(1) Maximizing basic orbital information.

(2) Maximizing the visibility period, consistent with other requirements.

(3) Measuring with maximum certainty.

Maximizing the basic orbital information depends strongly on what part of the orbit is being observed. For any given coordinate system, there exist orbits and locations on the orbit path which give ambiguous coordinates. For example: (1) it is very difficult to resolve the line of nodes (intersection of orbit plane and equatorial plane) if the orbit is equatorial or near equatorial; (2) it is also extremely difficult to locate perigee when the orbit is nearly circular; (3) if a station is located such that it observes perigee passage, the orbit determination might be very poor because so few observations would be obtained and the noise on the observations would obscure such vital information as time of perigee; (4) in the least-squares fitting of observations in orbit determination (described in Section E. 2) the partial derivatives (of the observation quantities with respect to the orbital elements) can be manipulated to indicate the information content of a pass, orbit, orbits, etc.

Maximizing the visibility period means more observations for a given situation, but careful notice must be taken of the information gained from each observation. This requirement can be approached by attempting to either adjust the network to maximize visibility or to adjust orbits to existing networks. Most system designs are compromises of the above two approaches.

Measuring with maximum certainty means measuring in such a manner that most errors are minimized.

Data rate. To minimize random errors, the highest data rate possible is desirable in order to obtain the maximum number of data per pass. However, the assumptions of independent data become poorer as the data rate is increased.

If the correlation between measurements falls off exponentially with time, then there is a predictable data rate above which greater errors are given in the orbit determination rather than less.

Measurement ambiguities. A simple example of a measurement ambiguity to be avoided follows.

Suppose the tracking station measures range ρ, azimuth α and elevation ϵ, of the satellite with respect to the radar location.

It can be seen that when ϵ equals exactly 90°, the azimuth measurement is ambiguous; and when ϵ only approaches 90°, the azimuth measurements become more uncertain.

Transformation ambiguities. Transformation ambiguities may result in the trigonometric transformations of the topocentric coordinates into orbital elements. An example of this is the transformation of the inertial, geocentric spherical coordinates r, A and D, into the radar quantities ρ, α and ϵ.

One possible transformation equation is

$$\sin (D_s - D) = \frac{\rho}{r} (\cos \epsilon \cos \alpha)$$

TABLE 2

Tracking Systems

No.	System	Cognizant Agency	Station Name	Installation Type	Local Designation	N Lat	E Long.	Altitude (m)	Survey Ref	Data	Units	Coord System	Accuracy 3σ	Data Formats	Data Delay	Max Range (passive 1-sq m target)	Ant Gain / Oper Freq Band	Comments
1	Minitrack	GSFC	Coolidge Field, Antigua Island			17.15	298.217			f_{non}	Cycles							
2			Antofagasta, Chile			-23.6389	289.7278										21 db/UHF	
3			Blossom Point, Md.		B point	38.43045	282.9134	4.9							1 min		30 db/L	
4			Cape Canaveral		{UHF	28.45866	279.43095	6.1		α, ε	Degrees				10 min		12 db/UHF	Minitrack R&D sta. cape has vertical baseline for UHF, provides greater coverage than most Minitrack stations
					{VHF	28.41186	279.40935										VHF	
5			East Grand Forks, Minn.			47.93	262.98						3 cps;					
6			Fairbanks, Alaska			64.73	212.35						[theoretical,					
7			Fort Meyers, Fla.			26.62	278.15						20" of arc			500 n mi		
8			Fort Stewart, Ga.			31.9806	278.5083						(0.006°).			(14 db S/N)		
9			Grand Turk Is.	Radio		21.52	288.90			f_{non}	Cycles	Azimuth elevation	1 millisec	Manual variable				
10			Johannesburg, S. Africa	inter-		-26.1825	28.7356						of time;					
11			Lima, Peru (Ancon)	ferometer		-11.7778	282.8444						experi-					
12			Mayaguana Is.			22.3750	286.9917						mental					
13			Quito, Ecuador (Mt. Cotopaxi)			-0.6278	281.4389						200" of arc (0.06°)]					
14			St Johns, Newfoundland			50.00	304.50											
15			San Diego, Navy Elect. Lab			32.5806	243.0278											
16			Santiago, Chile (Peldehue)			-33.1528	289.3277											
17			South Dakota															
18			Spain															
19			Woomera, Australia			-31.1026	136.7882	160.0									VHF	
20	Atlantic Missile	AMR	Cape Canaveral	Azusa		28.49137	279.44104			ρ, α, ε		Azimuth elevation					33 db/C-band	
21	Range		Cape Canaveral	Azusa MK II		28.41295	279.40752			{ρ, α, dir cos, dir cos rates			{Range 3 ft; 6 pts/million nonambiguous dir cos. 0.75 pts/million ambiguous cos rate				35 db/C-band 36.864 mc or 73.728 mc	
22			Cape Canaveral	Extradop		28.45	279.43											
23			Bassett Cove, GBI	receiver		26.60	280.68											
24			West End, GBI			26.65	281.08											
25			Jupiter, Fla.			26.95	279.93											
26			Cape Canaveral	Mod II	Radar 1.3	28.49245	279.42419	15.7		ρ, α, ε	Ft deg	Azimuth elevation	12 m 1.5 mils				33 db/2650 to 33 db/2950 mc	
27			Grand Bahama Is.		Radar 3.1	26.61645	281.64006	16.3										
28			Eleuthera Is		Radar 4.1	25.26760	283.68677	37.5										
29			San Salvador Is.		Radar 5.1	24.06664	285.46366	14.6										
30			Grand Turk Is.		Radar 7.1	21.43328	288.85452	25.3										
31			Antigua		Radar 9.1	17.17540	292.91181	408.2										
32			Ascension Is.		Radar 12.1	-7.93148	345.59709	275.2										
33			Cape Canaveral	FPS-8		28.4	279.4									220 n mi	35 db/L-band	
34			Grand Bahama Is.			26.61	281.64											
35			Cape Canaveral	FPS-16	116	28.48133	279.52327	13.7	AMS	ρ, α, ε	Ft	Azimuth	50 ft	Auto-	NRT	500 stat mi	44.5 db/C-band	Experimental model XN-1
36			Patrick AFB		216	28.22647	279.40054	8.3	spheroid		deg	elevation	0.012 deg	matic variable				Model XN-2 prototype (5000-mi range capability proposed for all FPS-16's except XN-2)
37			Grand Bahama Is.		316	26.61527	281.65189	14.1										
38			San Salvador		516	24.11837	285.49560	13.1										
39			Ascension Is.		1216	-7.95175	345.58739	94.6										
40			Antigua		916	17.14250	298.20667	45.7										Proposed

TABLE 2 (continued)

No.	System	Cognizant Agency	Station Name	Installation Type	Local Designation	N Lat	E Long.	Altitude (m)	Survey Ref	Data	Units	Coord System	Accuracy 3σ	Data Formats	Data Delay	Max Range (passive 1-sq m target)	Oper Freq Band / Ant. Gain	Comments
41	Atlantic Missile Range	AMR	Tele-2	60-ft parabolic dish	BTM	28.51351	279.22347	20.9		Tel	Deg	Azimuth elevation		Manual variable	5 min		28 db/VHF	Primary telemetry station at Cape Canaveral
42			Tele-3			28.46289	279.41667	20.7		α, ε			0.75 deg				32 db/UHF	
43			AMR mobile	28-ft parabolic dish						Tel Δf, α, ε	Cycles, deg	Azimuth* elevation*	3 cps 1.5 deg	Automatic fixed	NRT		VHF UHF VHF	Has autotrack capability once signal is acquired
44	Pacific Missile Range	PMR	South Arguello	FPS-16	023001	34.58276	239.43944	661.6		ρ, α, ε	Ft, deg	Azimuth elevation	150 ft, 0.03 deg	Automatic variable	RT	200 mi	44.5 db/C-band	Planned 5000-mi range part of Mercury net
45			North Arguello		023002	34.58305	239.43989	661.6								500 mi		Planned 500-mi range
46			South Mugu		003001	34.12144	240.84933	12.8								200 mi		Planned 500-mi range (Mugu has a total of 4 FPS-16's)
47			North Mugu		003002	34.12122	240.84812	12.8								200 mi		500-mi and 5000-mi range capability is planned for one of four FPS-16's on San Nicolas
48			San Nicolas Island		No. 15											200 mi		Kokee has planned 5000-mi range capability
49			Kokee, Kauai, Hawaii		No. 30											500 mi		There are 6 SCR-584/615's at Point Mugu and 4 at San Nicolas
50			Point Mugu	SCR-584/615		34.121	240.848	12.8			Yd, mil		100 yd, 10 mil			440 km	S-band	Two verlorts being acquired
51			San Nicolas															
52			Point Arguello	Verlort		34.58	239.439	661.6					20 yd, 1 mil at 3°/sec			1800 km		
53			Kauai, Hawaii															
54			Point Mugu	Microlock		34.121	239.439	661.6		f							108 mc	
55			South Point, Hawaii			18.94	204.33										70 mc	
56	Transit Program Net	APL	Howard County	20-ft dish	0.01	39.1635	283.1010	145.0	No. Amer Datum	Tel f_{non}	Cycles	Azimuth elevation	0.75 cps	Automatic fixed	NRT		VHF 23db/UHF	Receiver has parametric amplifier uses atomichron time standard
57			Austin		0.02	30.28861	262.26861	179.8					1.5 cps		60 min		VHF	
58			Las Cruces		0.03	32.28157	253.28222	1218.4									VHF	
59			Seattle		0.04	47.56107	237.64471	83.5									VHF	
60			Argentia		0.05	47.31529	306.01029	13.8									VHF	
61			Sao Paulo		0.08									Manual variable			VHF	
62	Deep Space	JPL	Goldstone, Calif.	85-ft parabolic dish	GS	35.3895	243.1518	1054.6		H, D f_{non} Tel	Deg, Cycles	Hour angle declination	0.15 deg 39 cps	Automatic fixed	NRT		UHF	200- to 250-ft dia parabolic antennas are planned for each DSN site, the first for Goldstone in 1965 Goldstone also has Az-El antennas
63			Woomera, Australia		W	-31.382	136.886											
64			Johannesburg, S. Africa		J	-25.891	27.675			H, D	Deg		0.15 deg					
65	Space-track Net	MIT	Millstone Hill	84-ft parabolic dish		42.617	288.509	156.1		ρ, α, ε $\dot{\rho}$	Km, deg	Azimuth elevation	18.3 km 1.2 deg	Automatic variable	NRT		36 db/UHF	High power skin tracking
66		BRL	BRL Lab	Unihelix		39.4744	283.9278	18.3		Δf, α, ε	Cycles, deg		9 cps 12 deg	Manual variable	1 min		1.4 db/UHF	
67		RADC	Rome ADC	28-ft parabolic dish		43.2234	284.5792	164.0		f_{non} α, ε	Cycles		60 cps 15 deg		10 min		28 db/UHF	
68		NSSC	Sagamore Hill Telescope	84-ft parabolic dish		42.6311	289.1846	74.7		H, D f_{non}	Hr, min, sec, deg, min, cycles	Hour angle declination	3 deg 9 cps		15 min		37 db/UHF	

TABLE 2 (continued)

No.	System	Cognizant Agency	Station Name	Installation Type	Local Designation	N Lat	E Long.	Altitude (m)	Survey Ref	Data	Units	Coord System	Accuracy 3σ	Data Formats	Data Delay	Max Range (passive 1 sq m target)	Ant. Gain / Oper Freq Band	Comments
69	Space-track Net	SRI	Stanford Research	61-ft parabolic dish		37.4031	237.8247	150.0		f_{non} α,ϵ	Cycles, deg	Azimuth elevation	4000 cps 5.25 deg	Manual variable			33 db/UHF	
70	White Sands Missile Range	WSMR	White Sands, N. Mex.	FPS-16	R-113	32.35795	253.60737	1234.2		ρ,α,ϵ	Yd deg	Azimuth elevation	15 yd 0.015 deg	Automatic variable	30 min		44.5 db/ C-band	Part of Mercury program net
71			Holloman AFB		R-123	32.91589	253.90139	1264.8										
72			Mid White Sands		R-112	32.35795	253.62977	1234.0										
73			East White Sands		R-114	32.35795	253.63171	1233.6										
74			South Holloman		R-122	32.90222	253.90139	1264.5										
75		WRE/ GSFC	Red Lake			30.81931	136.85847	128.1			Yd art mils		150 ft 0.015 deg	Automatic fixed	60 min	500 mi		Part of Mercury Program net. Data in octal artillery mils
76		WRE	Mirikata			29.87147	135.241	219.1										
77		STL	GGS	Quad helix		28.44853	279.41929	3.5	AMS spheroid	Δf	Cycles		0.18 cps	Manual automatic fixed	15 min		15 db/UHF	
78	Courier Program	USASRDL	Fort Monmouth	50-ft parabolic dish	Decour	40.1833	285.9431	31.7		f_{non} α,ϵ	Cycles, deg	Azimuth Elevation	2 cps 0.5 deg	Manual variable	NHT		33 db/UHF	Receiver has parametric amplifier
79		GE	GE	28-ft parabolic dish		42.84806	285.92917	403.9		f_{non} α,ϵ	Cycles		15 cps 12 deg		5 min		26 db/UHF	
80		GSFC	Huntsville	15-ft parabolic dish		34.6670	273.3564	181.4		f_{non} α,ϵ	Cycles, deg		30 cps 6 deg		60 min		19.5 db/ UHF	
81		U. Ill.	University of Illinois			40.1050	271.7731	240.2					300 cps 6 deg		2 min		28 db/UHF	
82		NERA	NERA Tracking	10-m parabolic dish		52.233	5.083	0.0		Tel f	Cycles		0.3 pts/ million cps		8 hr			
83		RADC	GE-Trinidad	84-ft parabolic dish		10.73923	298.3910	273.3	Clarke spheroid	ρ,α,ϵ	Km, deg		18 km 1.2 deg		5 min		36 db/UHF VHF	High power skin tracking
84		NAA	NAA Tracking	Quad helix		33.92472	241.87268	39.6		f_{non} α,ϵ	Cycles, deg		7.5 cps 15 deg		15 min		22 db/UHF	
85		RCA	Moorestown	FPS-49						$\rho,\dot{\rho},\alpha,\epsilon$							39 db/UHF	Data smoothing interval is 10 sec High power skin tracking
86		GSFC	Cape Canaveral	6-ft parabolic dish	Hangar S	28.48794	279.41378	7.6		f_{non}	Cycles		30 cps		15 min		15 db/UHF	
87		NASA	Cape Canaveral	Microlock		28.41483	279.40583	6.1		α	Deg		1.5 deg				VHF	Uses atomichron time standard
88						28.41436	279.40584	6.1										
89						28.41405	279.40625	6.1										
90		NASA	Cape Canaveral	Microlock		28.41464	279.40516	10.4		α,ϵ Tel	Deg	Azimuth Elevation	15 deg 3 deg	Manual variable			13 db/VHF 33 db/L-band	
91	Discoverer Net	VAFB	Cook Tracking	60-ft parabolic dish		34.82565	239.49507	306.3					α 0.06 deg		5 min		28 db/ VHF UHF	
92	SPANDAR	NASA	Wallops Island	60-ft parabolic dish		37.8546	284.4866	29.0		α,ϵ			ϵ 0.03 deg				S-band	
93	Relay	NASA	Andover, Maine	Cassegrain Antenna		44.6319	289.3017						0.06 deg					
94			Goonhilly, England			50.0494	354.8253						6 min of arc 0.15 deg					
95			Nutley, N. J.			40.816	285.833											
96			Plemeur-Bodou, France			48.7869	356.4758											
97			Rio de Janeiro, Brazil			22.9525	316.6314	9.8										
98			Fucino, Italy			41.9781	13.6014	610.1										

TABLE 3

Tracking Facility Characteristics

Name	Manufacturer	Antenna Type	System Type	Scan Rate	Coverage	Beam Width	Frequency
Minitrack	Navy	Fixed array	CW-bistatic	Stationary	Vertical fan	0.3° x 140°	108 and 135 mc
AN/FPS-16	RCA	12-ft parabolic 44.5-db gain	Monopulse; skin or beacon automatic tracking	Range: 10,000 yd/sec Azimuth: 40°/sec Elevation: 30°/sec	360° az; -10° + 85° el (raster, circular and sector scan)	1.2°	5400 to 5900 mc
Verlort	Reeves	10-ft parabolic	Monopulse; skin or beacon automatic tracking	Range: 10,000 yd/sec Az and El: 900 mils/sec	360° az; -11.25 to 90° el	2.5°	S-band
FPS-49 (BMEWS)	RCA	84-ft parabolic 39-db gain	Pulse-doppler, steerable automatic tracking	3° to 15°/sec	330° az 0 to 90° el	2° x 2° pencil	425 mc
FPS-50 Surveillance (BMEWS)	RCA	165- x 400-ft torus 45-db gain	88 feed horns and 2 dual organ pipe scanners	5°, 6-2/3° and 10°/sec in azimuth	2 fans--3.5° and 7° el angles	1° elev width	425 mc
Millstone FPS-44	Lincoln Labs, MIT	84-ft parabolic 37.3-db gain		2°/sec	360° az 0 to 90° el (conical scan)	2.1°	440 mc
Trinidad FPS-44	GE	84-ft parabolic 37.5-db gain		4.5°/sec (slew)	360° az 0 to 90° el	2.25°	425 and 438 mc
Goldstone	NASA	85-ft HA-DEC parabolic	Deep space	1.0° and 0.03°/sec	360° az 5° to 90° el	1° at 960 mc 0.4° at 2295 mc	890/960 mc 2115/2295 mc (1963)
Stanford Research	SRI	60-ft parabolic	Monostatic pulse	4°/sec (slew)	360° az 0° to 90° el	12°	106.1 mc Calif. 200 to 400 mc Alaska
Doploc	Army BRL-ARPA	Tunable 16-db gain	CW doppler	Stationary	3 fans	8° x 76°	108 mc
Spasur (detection)	NRL-ARPA	50-dipole receiver 400 ft long (1600 ft being installed)	Detection only CW-tristatic fence interferometer	Stationary	Vertical fan	0.4° x 160° (0.3° x 160° proposed)	108 mc (108 and 428 mc proposed)
ESAR	Bendix	90-element linear array			±45° az ±45° el	Transmit 1.5° pencil Receive 1.5° cluster	425 mc 850 mc 1275 mc

where

D = declination of the satellite in inertial coordinates

D_s = declination of the station in inertial coordinates

r = geocentric distance of the satellite.

Examination of this equation shows that D information is lost when the azimuth α measurements approach 90°, that is, when the satellite heads due east from the station. In a like manner, all coordinate transformations have ambiguous answers where the inertial orbital element cannot be determined at that time. One of the ways of resolving ambiguities is to have an overdetermined orbit; another way is to adjust the orbit or the station location such that the ambiguities do not occur.

Errors may be minimized by suitable station calibration techniques and methods.

It is undesirable to attempt an orbit determination from a single station's data on one pass. The station's random errors generally preclude computation or an orbit sufficiently accurate to furnish position predictions which will enable a narrow beam radar to acquire one orbit revolution later. Experience dictates that data from at least one tracking pass from each of two well spaced stations (preferably through apogee, and 90° to 180° from apogee) is required to determine the initial orbit achieved.

Satellites in highly elliptical orbits (perigee high enough to be free from drag effects) and space probes present less stringent requirements on the tracking system, unless midcourse guidance is involved, because more stations have visibility for longer periods of time and data is plentiful. Midcourse guidance requires rapid and accurate orbit determination if satellite fuel requirements are to be kept within reason. As little as an hour may be available to track the satellite, process data, determine the orbit, and calculate the time and duration of the rocket firing for correction of the satellite trajectory.

Under these conditions, prelaunch planning must include limitations on the tracking time and the number of data points, to ensure that adequate computation time is available. Several data handling modes should be available so that last minute equipment failures do not jeopardize the mission.

4. Data Handling

Communications should be established at least one hour prior to the earliest scheduled liftoff to ascertain that complete circuit communication is available. Once liftoff occurs, data should begin to arrive from the tracking stations.

Teleprinter circuits are a favored method for transmitting data because they:

(1) Are readily available as a leased service.

(2) Are the most reliable rapid communication.

(3) Produce punched paper tape and printed, multicopy output.

(4) May be gauged together on a single circuit at little extra cost.

The received information may be:

(1) Supplied as electrical impulses in teletype code to electronic conversion equipment which writes it on a magnetic tape in computer code, or enters it directly into the computer.

(2) Punched onto cards by passing the paper tape through a tape-to-card machine. (These cards are checked for bad points and are then read into the computer.)

(3) Manually transcribed to load sheets, keypunched to cards, and then read into the computer. (This method is used if the data is irregular in some respect and cannot be handled as described in the first two methods.)

The availability of at least two of the above methods is recommended. Experience has shown that flexibility is a prime data handling requirement. Extremely useful observations may be received in an irregular format when previously coordinated sources have failed to acquire the satellite, and the orbit determination agency should be prepared to use them.

Generally, the transmission of information from tracking stations to a central data gathering center is over a narrow bandwidth channel such as a telephone circuit. This means that the information cannot be fed over the lines very rapidly. Error checking slows down the rate even more; to check for all errors would require an extremely long time. The result is that high probability error classes are checked automatically or semi-automatically; low probability errors are not excluded.

5. Data Filtering

Two extreme cases of how the data could be processed are: (1) the raw data could be fed into a central data gathering center and processed there and (2) the data could be processed at each station. If each tracking station completely processes its own data, there is not only a duplication of computing equipment (one for each station) but each station is not taking full advantage of other stations' data. If all data is fed raw from each tracking station to one central computer, then far too much bad data gets into the orbit determination routine. The usual compromise is to have one central computer do the final editing, smoothing and orbit determination, but have each tracking station perform its own local calibrations

and some data smoothing and editing for grossly erroneous data.

When a sufficient number of points have accumulated, the preliminary precision orbit is determined. The differential correction technique using least squared errors is the method usually used; it is described later.

An optimum filtering scheme has two conflicting requirements imposed on it: (1) to use all the information contained in the observation and (2) to reject all misinformation contained in the observations.

Since there are no perfect data, all observations have varying degrees of noise or unknown errors associated with them. Using all the information contained implies accepting all data points. Rejecting all misinformation implies rejecting all data points. Filtering schemes attempt to improve the accuracy of an orbit determination by various compromises with the two above contradictory requirements. One such compromise is to reject all "obviously" bad data. Such data only degrade the curve fits, since they contain so little information. Another compromise is to maximize the probability of the accuracy of the estimates of the orbit parameters. This compromise is effected by determining the maximum likelihood estimates of the orbital parameter. There are two different ways of determining a bad point: (1) by taking more observations, thus increasing the probability of obtaining a more accurate fit, or (2) by a priori knowledge of the true trajectory or a priori knowledge that a given point is bad.

The best filtering of the data, if random errors (only) are present, uses a least square fit (described in Sections E.2 and F) to curves constrained by the known (i.e., well determined) laws of physics. Unfortunately, to use all the points in the curve fitting procedure would degrade the orbit determination so much that the computation would almost always result in an ambiguous answer. (In other words, so many orbits would fit the set of observations that the estimates would not be consistent.) Additionally, if much of the bad data had been rejected previously by quicker methods, fewer computations would be needed to reject the bad data.

An efficient filtering scheme must divide the filtering between the tracking stations and the central computer, such that most of the above problems are minimized. It is instructive to contrast the extremes of too much local filtering at the tracking stations and no local filtering.

Excessive local filtering. If data is rejected on the basis of simple curve fitting, the curve being fit would be in error and there would be a tendency to reject "good" data.

If data is fit to curves representing the known laws of orbital mechanics, then a complex computer is required at each station. However, each station would have the disadvantage of not using data from other stations.

If each station fits all data to curves representing orbital mechanics, then each is really a central station and there is inefficiency in that the same computations are being duplicated in each station.

No filtering at local station. If no filtering occurs at each station, the computation center is swamped with bad data, unknown biases (e.g., biases known to local stations but not to central), increased transmission errors, and less information per unit time being fed to central.

D. DETERMINATION OF PRELIMINARY ORBIT ELEMENTS

Two areas of the problem of orbit determination are generally distinguished:

(1) Preliminary orbit determination--more or less approximate calculation of an orbit which was previously completely unknown.

(2) Orbit improvement--refinement in accuracy of elements already known approximately.

This section considers the problem of preliminary orbit determination; Section F considers orbit improvement. Many methods of determining preliminary orbits are available. The best computation technique to use in a given problem depends on the types of data available. Table 4 shows the appropriate computation schemes to be used for the various combinations of observational data.

Several methods are described briefly below. Reference 4 considers some techniques in greater detail.

1. Method of Laplace

The method of Laplace depends on the solution of the differential equation of motion by Taylor series. That is, a solution of the equation

$$\frac{d^2\vec{r}}{dt^2} = -\mu \frac{\vec{r}}{r^3} \tag{47}$$

will be written in the form

$$\vec{r} = \vec{r}_0 + \frac{d\vec{r}}{dt}\bigg|_0 (t - t_0) + \frac{1}{2}\frac{d^2\vec{r}}{dt^2}\bigg|_0 (t - t_0)^2 + \ldots \tag{48}$$

Evaluation of the derivatives (the series coefficients) of Eq (48) from Eq (47) and collection of terms gives

$$\vec{r}(t) = \left[1 - \mu \frac{(t - t_0)^2}{2r_0^3} + \ldots\right]\vec{r}_0 + \tag{49}$$

(continued)

TABLE 4*

Observation Requirements for Preliminary Orbit Determination

Observational Data	Assumption	Method
Three 3-dimensional fixes	None	Herrick-Gibbs or Gibbs (with or without differential correction to reduce residuals and/or discard bad data)
Overdetermined system with more than three fixes	Random error distribution	Least-square differential correction of initial orbit
Fifteen range measurements	Low eccentricity circular orbit rectilinear parabola	Gibbs
Eight range measurements		Gibbs
Four range measurements		Gibbs
One 1-dimensional fix (can be achieved in several ways: one vector measurement of range and range rate; three range and three range-rate measurements)	None	Laplace, Lagrange
Two 3-dimensional fixes	None	Gauss (and variants)
Azimuth, elevation (α, ϵ)	None	Laplacian
Azimuth, elevation rate ($\dot{\alpha}$, $\dot{\epsilon}$)		
Azimuth, elevation change of rate ($\ddot{\alpha}$, $\ddot{\epsilon}$) all at one time		
Three elevation / Three azimuth } for three times	None	Convert to α, ϵ, $\dot{\alpha}$, $\dot{\epsilon}$, $\ddot{\alpha}$, $\ddot{\epsilon}$ of middle data (Laplacian)
(That is, each $\epsilon_i - \alpha_i$ pair is taken at three separate times)		Retain α, ϵ
		Lagrange with Herrick-Gibbs velocity
		Gauss
		Gibbs expansion method
Three range measurements	None	Differential correction of pseudo-Laplacian
Three range-rate measurements		
Six range measurements	None	Differential correction of pseudo-Laplacian
Six range-rate measurements	None	Probably only differential correction
Other combinations of six observed quantities for three or more times	None	Needs to be developed
Five observed quantities for one or two times	Parabolic or one-condition orbits	Modified Olbers Laplacian or similar method
Four observed quantities: for example, α, ϵ, $\dot{\alpha}$, $\dot{\epsilon}$ for one time; 2α, 2ϵ for two times	Circular or two-condition orbits: for example, two ranges or two r's are assumed	Standard circular orbit methods
Four ranges for four times		
Two ranges, two range rates for two times		
α, ϵ, range, range rate for one time		
Three observed quantities	Three-condition orbit	Needs to be developed
Two observed quantities	Four-condition orbit	Needs to be developed

*Adapted from Ref. 3

$$+ (t - t_0)\left[1 - \mu\frac{(t-t_0)^2}{6r_0^3} + \ldots\right]\left.\frac{d\vec{r}}{dt}\right|_0 \equiv s\,\vec{r}_0 + \sigma\,\dot{\vec{r}}_0 \tag{49}$$

From Eq (49), if the position vector $\vec{r}_0$ and the velocity vector $\dot{\vec{r}}_0$ are known for some time t_0, and if the series s and σ converge, the radius vector at any time, $\vec{r}(t)$, is determined. But the radius vector $\vec{r}$ is related to the observations by

$$\vec{r} = \rho\hat{\rho} + \vec{R} \tag{50}$$

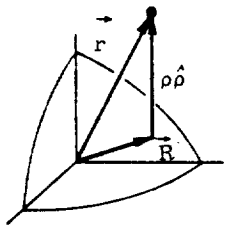

where

$\vec{R}$ = vector position of the observer

ρ = magnitude of the observation vector

$\hat{\rho}$ = unit vector in the direction of observation

Successive differentiation of Eq (50) gives

$$\ddot{\vec{r}} = \ddot{\rho}\hat{\rho} + 2\dot{\rho}\dot{\hat{\rho}} + \rho\ddot{\hat{\rho}} + \ddot{\vec{R}} \tag{51}$$

The acceleration as given by dynamics (Eq (47)) can then be equated to that given by the geometry (Eq (51))

$$\ddot{\rho}\hat{\rho} + 2\dot{\rho}\dot{\hat{\rho}} + \rho\ddot{\hat{\rho}} + \ddot{\vec{R}} = -\frac{\rho\hat{\rho} + \vec{R}}{r^3} \tag{52}$$

The dot product of this equation with $(\hat{\rho} \times \dot{\hat{\rho}})$ gives

$$\rho\,(\hat{\rho} \times \dot{\hat{\rho}} \cdot \ddot{\hat{\rho}}) = -(\hat{\rho} \times \dot{\hat{\rho}} \cdot \ddot{\vec{R}}) - \frac{\hat{\rho} \times \dot{\hat{\rho}} \cdot \vec{R}}{r^3} = (\hat{\rho} \times \dot{\hat{\rho}} \cdot \vec{R})\left(\frac{1}{R^3} - \frac{1}{r^3}\right) \tag{53}$$

Dotting Eq (50) into itself provides the additional relation

$$r^2 = \rho^2 + R^2 + 2\,(\hat{\rho} \cdot \vec{R})\,\rho \tag{54}$$

If only direction data comprise the observations, ρ and r are the only unknowns in Eqs (53) and (54). Each of the vector products can be evaluated from the observations and the known position of the observer. Three observations, each consisting of two angular coordinates and the corresponding time, are sufficient to determine $\hat{\rho}_0$ and $\ddot{\hat{\rho}}_0$ at some time t_0 (generally the middle of the three observations), except when $\hat{\rho} \times \dot{\hat{\rho}} \cdot \ddot{\hat{\rho}} = 0$ at $t = t_0$, or if $\ddot{\beta} = 0$ at $t = t_0$.

A convenient computation method for determination of the preliminary orbit of an earth satellite from three observations of right ascension and declination,

t_a: A_a D_a

t_0: A_0 D_0

t_b: A_b D_b,

proceeds as follows. Four equations in the four unknowns s_a, s_b, σ_a and σ_b are obtained

$$\vec{r}_a = s_a\vec{r}_0 + \sigma_a\dot{\vec{r}}_0 = s_a\,(\rho_0\hat{\rho}_0 + \vec{R}_0) + \sigma_a\dot{\vec{r}}_0 = \rho_a\hat{\rho}_a + \vec{R}_a$$

$$\vec{r}_b = s_b\vec{r}_0 + \sigma_b\dot{\vec{r}}_0 = s_b\,(\rho_0\hat{\rho}_0 + \vec{R}_0) + \sigma_b\dot{\vec{r}}_0 = \rho_b\hat{\rho}_b + \vec{R}_b$$

where

$$\hat{\rho}_i = \cos A_i \cos D_i\hat{i} + \sin A_i \cos D_i\hat{j} + \sin D_i\hat{k}$$

The dot products of these equations with unit vectors $\hat{A}$ and $\hat{D}$,

$\hat{A}$ = $-\sin A\hat{i} + \cos A\hat{j}$ (in the direction of increasing right ascension)

$\hat{D}$ = $-\sin D\cos A\hat{i} - \sin D\sin A\hat{j} + \cos D\hat{k}$ (in the direction of increasing declination)

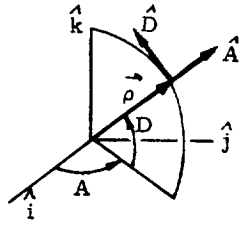

give the following equations to be solved:

$$s_i\,(\hat{\rho}_0 \cdot \hat{A}_i)\,\rho_0 + \sigma_i\hat{A}_i \cdot \dot{\vec{r}}_0 = -s_i\,(\vec{R}_0 \cdot \hat{A}_i) + \vec{R}_i \cdot \hat{A}_i$$

$$s_i\,(\hat{\rho}_0 \cdot \hat{D}_i)\,\rho_0 + \sigma_i\hat{D}_i \cdot \dot{\vec{r}}_0 = -s_i\,(\vec{R}_0 \cdot \hat{D}_i) + \vec{R}_i \cdot \hat{D}_i \tag{55}$$

where

$$i = a, b$$

2. Method of Gauss

If three position vectors, $\vec{r}_1$, $\vec{r}_2$ and $\vec{r}_3$ at times t_1, t_2 and t_3, are coplanar, and if $\vec{r}_1$ is not parallel or anti-parallel to $\vec{r}_3$,

$$\vec{r}_2 = c_1 \vec{r}_1 + c_3 \vec{r}_3 . \tag{56}$$

With the notation of the previous subsection

$$\vec{r}_i = \rho_i \hat{\rho}_i + \vec{R}_i, \quad i = 1, 2, 3.$$

These two equations give,

$$c_1 \vec{\rho}_1 - \vec{\rho}_2 + c_3 \vec{\rho}_3 = - c_1 \vec{R}_1 + \vec{R}_2 - c_3 \vec{R}_3 . \tag{57}$$

Also, from Eq (56),

$$\vec{r}_1 \times \vec{r}_2 = c_3 \vec{r}_1 \times \vec{r}_3$$

$$\vec{r}_2 \times \vec{r}_3 = c_1 \vec{r}_1 \times \vec{r}_3 ,$$

so that

$$c_1 = \frac{\vec{r}_2 \times \vec{r}_3 \cdot \vec{k}}{\vec{r}_1 \times \vec{r}_3 \cdot \vec{k}} = \frac{\text{Area } \triangle OP_2P_3}{\text{Area } \triangle OP_1P_3}$$

$$c_3 = \frac{\vec{r}_1 \times \vec{r}_2 \cdot \vec{k}}{\vec{r}_1 \times \vec{r}_3 \cdot \vec{k}} = \frac{\text{Area } \triangle OP_1P_2}{\text{Area } \triangle OP_1P_3}$$

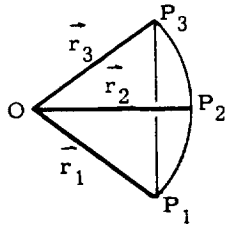

The c's are known as "triangle ratios" "Sector-triangle ratios" can then be defined as

$$\eta_1 = \frac{\text{area of sector } OP_2P_3}{\text{area of triangle } OP_2P_3}$$

$$\eta_2 = \frac{\text{area of sector } OP_1P_3}{\text{area of triangle } OP_1P_3}$$

$$\eta_3 = \frac{\text{area of sector } OP_1P_2}{\text{area of triangle } OP_1P_2}$$

By Kepler's law of areas, the areas of the sectors are proportional to the time. Therefore,

$$c_1 = \frac{t_3 - t_2}{t_3 - t_1} \frac{\eta_2}{\eta_1} \tag{58}$$

$$c_3 = \frac{t_2 - t_1}{t_3 - t_1} \frac{\eta_2}{\eta_3} \tag{59}$$

Additional conditions are imposed by Kepler's equation,

$$\frac{1}{a}\sqrt{\frac{\mu}{a}} (t_j - t_i) = E_j - E_i - e (\sin E_j - \sin E_i)$$

(a dynamic condition) (60)

where

E = eccentric anomaly

e = eccentricity of orbit

a = semimajor axis of orbit

μ = gravitational constant

and

$$r_i + r_j = 2a - ae (\cos E_i + \cos E_j) \tag{61}$$

(a geometric condition).

Defining $2E_{ij} = E_j - E_i$ as the change in eccentric anomaly and $2\theta_{ij} = \theta_j - \theta_i$ as the change in true anomaly, the last equation gives

$$r_i + r_j = 2a \sin^2 E_{ij} + 2\sqrt{r_i r_j} \cos \theta_{ij} \cos E_{ij} \tag{62}$$

and Kepler's equation becomes

$$\frac{1}{a}\sqrt{\frac{\mu}{a}} (t_j - t_i) = 2E_{ij} - \sin 2E_{ij} + \frac{2}{a}\sqrt{r_i r_j} \cos \theta_{ij} \sin E_{ij}. \tag{63}$$

The following definitions will prove convenient.

$$k^2 \equiv 4 r_i r_j \cos^2 \theta_{ij}$$

$$1 + 2\ell \equiv \frac{r_i + r_j}{k}$$

$$m^2 \equiv \frac{\mu}{k^3} (t_j - t_i)^2 \tag{64}$$

$$x \equiv \sin^2 \frac{E_{ij}}{2} .$$

Solution of Eq (62) for a gives

$$2a \sin^2 E_{ij} = \frac{k (r_i + r_j)}{k} - k \cos E_{ij}$$

or

$$a = \frac{k (\ell + x)}{\sin^2 E_{ij}} \tag{65}$$

Substitution of this a, obtained from geometrical constraints, into Kepler's equation, Eq (63), gives

$$\sqrt{\mu} (t_j - t_i) = (2E_{ij} - \sin 2E_{ij}) a^{3/2} + 2\sqrt{r_1 r_3} \cos \theta_{ij} \sin E_{ij} \sqrt{a}$$

or

$$\sqrt{\mu}\,(t_j - t_i) = \frac{2E_{ij} - \sin 2E_{ij}}{\sin^3 E_{ij}} \left[k(\ell + x)\right]^{3/2} + k^{3/2}(\ell + x)^{1/2} = mk^{3/2}$$

With the definitions

$$\ell + x \equiv \frac{m^2}{\eta^2}$$

$$X(x) \equiv \frac{2E_{ij} - \sin 2E_{ij}}{\sin^3 E_{ij}} \qquad (66)$$

this equation reduces to

$$\frac{m^3}{y^3} X(x) + \frac{m}{\eta} = m \qquad (67)$$

or

$$\eta = 1 + \frac{m^2}{\eta^2} X(x)$$

Differentiation of the above definition of X (x) with respect to E_{ij} gives

$$\sin^3 E_{ij} \frac{\partial X}{\partial E_{ij}} = -3 \sin^2 E_{ij} \cos E_{ij} X + 4 \sin^2 E_{ij}$$

Then

$$\frac{dX}{dx} = \frac{dX}{dE_{ij}} \frac{dE_{ij}}{dx} = \frac{4 - 3\cos E_{ij} X}{\sin E_{ij}} \cdot \frac{1}{\frac{1}{2}\sin E_{ij}}.$$

Then expanding X (x) in series gives

$$X(x) = \sum_{i=0}^{\infty} A_i x^i$$

where

$$A_i = \frac{2i+4}{2i+3} A_{(i-1)} \text{ from } \frac{dX}{dx} = \sum i A_i x^{i-1}$$

From Eq (66), $A_0 = \frac{4}{3}$. Therefore,

$$X(x) = \frac{4}{3} + \frac{4}{3}\cdot\frac{6}{5} x + \frac{4}{3}\cdot\frac{6}{5}\cdot\frac{8}{7} x^2 + \cdots \qquad (68)$$

The solution for a preliminary orbit by Gauss' method then proceeds as follows:

(1) Select approximate values for ρ_1, ρ_3, $X \approx \frac{4}{3}$, $\eta_2 \approx \eta_3 \approx 1$, these values to be improved by iteration. Take $c_1 \approx \frac{t_3 - t_2}{t_3 - t_1}$ and $c_3 \approx \frac{t_2 - t_1}{t_3 - t_1}$.

(2) Determine r_1 and r_3 from $\vec{r}_i = \rho_i \hat{\rho}_i + \vec{R}_i$ and determine θ_1, θ_3 and k from Eq (64).

$$\vec{r}_2 = c_1 \vec{r}_1 - c_3 \vec{r}_3$$

$$\vec{\rho}_2 = \vec{r}_2 - \vec{R}_2$$

(3) Determine m from t_1, t_2 and k by Eq (64). Revise $\eta_2 = 1 + \frac{m^2 X_2}{\eta_2^2}$ (iteration loop).

(4) Derive ℓ from r_1, r_2 and k by Eq (64). Derive x from $x = \left(\frac{m}{\eta_2}\right)^2 - \ell$. Revise X from Eq (68) (iteration loop). From x obtain $\theta_j - \theta_i$ and a from Eqs (64) and (65). From E_{ij} and θ_i, θ_j determine ℓ.

(5) Repeat (1) to (4) with ρ_1, ρ_2 to get η_3, X_3.

(6) Repeat (1) to (4) with ρ_2, ρ_3 to get η_1, X_1.

(7) Obtain improved values for c_1 and c_3 from Eqs (58) and (59).

(8) Obtain improved values of ρ_1 and ρ_2 from Eq (57). Note that this is accomplished by dotting in turn by $\hat{\rho}_2 \times \hat{\rho}_3$ and $\hat{\rho}_1 \times \hat{\rho}_2$. The values of $\rho_1 + \rho_2$ are then obtained from the following equations.

$$c_1(\hat{\rho}_1 \cdot \hat{\rho}_2 \times \hat{\rho}_3)\rho_1 = -c_1(\vec{R}_1 \cdot \hat{\rho}_2 \times \hat{\rho}_3) + (\vec{R}_2 \cdot \hat{\rho}_2 \times \hat{\rho}_3) - c_3(\vec{R}_3 \cdot \hat{\rho}_2 \times \hat{\rho}_3)$$

$$c_3(\hat{\rho}_1 \cdot \hat{\rho}_2 \times \hat{\rho}_3)\rho_3 = -c_1(\vec{R}_1 \cdot \hat{\rho}_1 \times \hat{\rho}_2) + (\vec{R}_2 \cdot \hat{\rho}_1 \times \hat{\rho}_2) - c_3(\vec{R}_3 \cdot \hat{\rho}_1 \times \hat{\rho}_2)$$

(9) Repeat (1) through (8) with improved values of ρ_1, ρ_3, until iteration converges.

3. Gibbs' Modification of Gauss' Method

There is an alternative method of solution for c_1 and c_3 in Gauss' Method due to Gibbs. If

$$T_1 = \sqrt{\mu}\ (t_3 - t_2)$$

$$T_2 = \sqrt{\mu}\ (t_3 - t_1)$$

$$T_3 = \sqrt{\mu}\ (t_2 - t_1),$$

$$\vec{r}_1 = \vec{a}_0 - \vec{a}_1 T_3 + \vec{a}_2 T_3^2 - \vec{a}_3 T_3^3 + \vec{a}_4 T_3^4 - \ldots$$

$$\vec{r}_2 = \vec{a}_0$$

$$\vec{r}_3 = \vec{a}_0 + \vec{a}_1 T_1 + \vec{a}_2 T_1^2 + \vec{a}_3 T_1^3 + \vec{a}_4 T_1^4 + \ldots$$

Determination of $\frac{d^2 \vec{r}_i}{dt^2}$ from these series, setting

$$\frac{d^2 r_i}{dt^2} = -\mu \frac{\vec{r}_i}{r_i^3},$$

elimination of the $\vec{a}$ s and substitution in

$$\vec{r}_2 = c_1 \vec{r}_1 + c_3 \vec{r}_3$$

gives

$$\left.\begin{aligned} c_1 &= m\ \frac{1 + B_1/r_1^3}{1 - B_2/r_2^3} \\ c_2 &= n\ \frac{1 + B_3/r_3^2}{1 - B_2/r_2^3} \end{aligned}\right\} \qquad (69)$$

Here

$$B_1 = (mn + n - m)\ \frac{T_2^2}{12}$$

$$B_2 = (mn + 1)\ \frac{T_2^2}{12}$$

$$B_3 = (mn - n + m)\ \frac{T_2^2}{12}$$

where

$$m + n = 1 \text{ and } n = T_3/T_2,\ m = T_1/T_2$$

4. Method of Olbers

The method of Olbers is a technique for determining preliminary parabolic orbits. As in Eq (57),

$$c_1 \vec{\rho}_1 - \vec{\rho}_2 + c_3 \vec{\rho}_3 = -c_1 \vec{R}_1 + \vec{R}_2 - c_3 \vec{R}_3 \equiv \vec{V} \qquad (70)$$

The dot product of this equation and $(\hat{\rho}_2 \times \vec{U})$ where $\vec{U}$ is coplanar with $\vec{V}$ and $\vec{\rho}_2$,

$$\vec{U} = \hat{\rho}_2 \times \vec{V} \times \frac{\hat{\rho}_2}{V}$$

is

$$c_1 \rho_1 (\hat{\rho}_2 \cdot \hat{\rho}_2 \times \vec{U}) + c_3 \rho_3 (\hat{\rho}_3 \cdot \hat{\rho}_2 \times \vec{U}) = 0 \qquad (71)$$

Then

$$\rho_3 = M \rho_1 \qquad (72)$$

where

$$M = -\frac{c_1 (\hat{\rho}_1 \cdot \hat{\rho}_2 \times \vec{U})}{c_3 (\hat{\rho}_3 \cdot \hat{\rho}_2 \times \vec{U})} \qquad (73)$$

The computation then proceeds as follows:

(1) Select initial approximate values for ρ_1 and for c_1 and c_3 such that

$$\frac{c_3}{c_1} = \frac{t_3}{t_1}.$$

Obtain ρ_3 from Eq (72).

(2) Obtain $\vec{r}_1$, c_2 and ρ_2 from ρ_1, ρ_3 and c_3 by Eq (70).

(3) Obtain $\vec{r}_3$ and $S = |\vec{r}_2 - \vec{r}_1|$ from the law of cosines

$$S^2 = r_1^2 + r_2^2 - 2 r_1 r_2 \cos(\theta_2 - \theta_1).$$

(4) Obtain

$$X = \frac{2\sqrt{\mu}\ (t_2 - t_1)}{(r_1 + r_2)^{3/2}}$$

(5) Correct ρ_1 in step (1) by iteration until

$$(r_1 + r_3)\ X\ Y = S \qquad (74)$$

where X Y is the term in Euler's equation,

$$\frac{6\sqrt{\mu}\ (t_j - t_i)}{(r_i + r_j)^{3/2}} = (1 + X\ Y)^{3/2}$$

$$\pm (1 - X\ Y)^{3/2} = 3\ X \qquad (75)$$

(6) Obtain η_1, η_2, η_3 from $\vec{r}_2 = c_1 \vec{r}_1 \mp c_2 \vec{r}_2$ and the sector to triangle area ratios defining the η's.

(7) Determine c_1 and c_3 from Eqs (58) and (59) and iterate until they agree with step (1).

(8) From the corrected values of c_1 and c_2 calculate $\hat{\rho}_2$ and compare with the observed $\hat{\rho}_2$. This checks the assumption of Olbers' method that $e \approx 1$.

E. THEORY OF OBSERVATION ERROR

After a preliminary orbit has been determined as described in Section D, the elements thus determined, together with a theory of motion, may be used to calculate theoretical positions of the orbiting body at any time. If further observations of the body are then made, the observed positions will be found to deviate from the theoretical positions for the corresponding times. The differences in observed and computed positions, or residuals, may be attributed to three causes:

(1) Approximations involved in the theory.

(2) Inaccuracies in the preliminary orbit elements.

(3) Errors in the observations.

In the problem of orbit improvement, to be considered in Section F, these residuals between observed and computed positions are used to improve the accuracy of the preliminary orbit elements. Since the methods of orbit improvement are rather complex in themselves, some benefit may be derived from a review, preparatory to considering these methods in Section F, of those areas of statistics and numerical analysis which are basic to the orbit improvement theories.

1. Data Errors

Data errors are of three types: systematic errors, which affect all measurements alike; mistakes, generally large errors due to careless reading of indicators or incorrect recording, which do not follow any law, and accidental errors, causes of which are unknown and indeterminate, and which are usually relatively small and follow the laws of probability. Systematic errors can be corrected to some extent by calibration of instruments, and large mistakes can be eliminated from data by use of an appropriate data rejection philosophy. The mathematical theory of errors to be discussed applies only to accidental errors, and only these errors will be considered in the analyses.

All kinds of accidental errors may be described by frequency distributions, or probability density functions, curves which give the relative frequency of occurrence of the various values in a set of observations. By far the most useful frequency distribution is the normal or Gaussian distribution,

$$f(x) = \frac{1}{\sqrt{2\pi}\,\sigma} \exp\left[-\frac{1}{2\sigma^2}(x-\mu)^2\right] \qquad (76)$$

which is found to describe most random or accidental data errors. A special usefulness of the normal distribution is also indicated by the mathematical theory as expressed in the central-limit theorem of statistics:

"If a population has a finite variance σ^2 and mean μ, then the distribution of the sample mean approaches the normal distribution with variance $\frac{\sigma^2}{n}$ and mean μ as the sample size n increases."

It is interesting that, regardless of the form of the population distribution function, the sample mean will be approximately normally distributed for large samples.

The parameters of the distribution, as previously indicated, are the variance σ^2 and the mean μ. Sometimes, however, other parameters are employed:

modulus of precision = $h = \frac{\sigma}{\sqrt{2}}$

probable error = 0.6745σ (normal distribution only)

In practice, since the actual parameters σ and μ of the theoretical population distribution are not known, they must be estimated from the available data. Statistical analysis shows that the maximum-likelihood estimates of these parameters for the normal distribution, are

$$\hat{\mu} = \frac{1}{n}\sum_{i=1}^{n} x_i = \bar{x} \qquad (77)$$

$$\hat{\sigma}^2 = \frac{1}{n}\sum_{i=1}^{n} (x_i - \bar{x})^2 \qquad (78)$$

where n is the total number of data, x_i, in a sample.

The significance of the distribution function is further indicated by noting that the area under the function contained between two arbitrary limits, x_1 and x_2, is the probability that a given observation will lie between x_1 and x_2, i.e.,

$$\text{Probability}\left[x_1 \le x \le x_2\right] = \int_{x_1}^{x_2} f(x)\,dx$$

$$= \frac{1}{\sqrt{2\pi}\,\sigma}\int_{x_1}^{x_2} e^{-\frac{1}{2\sigma^2}(x-\mu)^2}\,dx \qquad (79)$$

Viewed from this aspect, the parameters of the normal distribution can be interpreted as follows:

μ = data value corresponding to the maximum value of the frequency distribution

σ = a span of x such that 68.26% of the area under the distribution curve is contained between the limits $\mu-\sigma$ and $\mu+\sigma$.

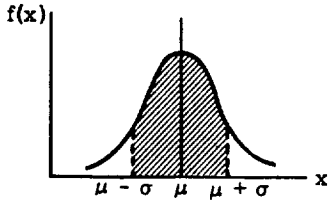

Probability distributions for several variables (multivariate distributions) may be defined in a similar manner, i.e.,

$$\text{Probability}\left[x_1 < x < x_2,\ y_1 < y < y_2\right] = \int_{x_1}^{x_2}\int_{y_1}^{y_2} f(x, y)\, dy\, dx \tag{80}$$

where f (x, y) is called the joint density function for x and y. In particular, the bivariate normal distribution is

$$f(x, y) = \frac{1}{2\pi\sigma_x\sigma_y\sqrt{1-\rho^2}} \exp\left\{-\frac{1}{2(1-\rho^2)}\left[\left(\frac{x-\mu_x}{\sigma_x}\right)^2 - 2\rho\,\frac{x-\mu_x}{\sigma_x}\,\frac{y-\mu_y}{\sigma_y} + \left(\frac{y-\mu_y}{\sigma_y}\right)^2\right]\right\} \tag{81}$$

which represents a bell-shaped surface over the x-y plane. The parameter ρ is called the correlation between x and y. When the correlation is zero, f (x, y) becomes the product of two univariate distributions

$$f(x,y) = g_1(x)\, g_2(y)$$

and the variates are said to be independently distributed. It is sometimes convenient to write Eq (81) in matrix notation:

$$f(x_1, x_2) = \frac{1}{2\pi\sqrt{|\sigma_{ij}|}} \exp\left[-\frac{1}{2}\sum_{i=1}^{2}\sum_{j=1}^{2}\sigma^{ij}(x_i-\mu_i)(x_j-\mu_j)\right] \tag{82}$$

where

$|\sigma_{ij}|$ = determinate of the matrix $\left[\sigma_{ij}\right]$

$$\left[\sigma_{ij}\right] = \begin{bmatrix}\sigma_{11} & \sigma_{12}\\ \sigma_{21} & \sigma_{22}\end{bmatrix} = \text{the variance-covariance matrix}$$

$\sigma_{11} = \sigma_x^2$ and $\sigma_{22} = \sigma_y^2$

$\sigma_{12} = \sigma_{21}$ = covariances

$$\left[\sigma^{ij}\right] = \begin{bmatrix}\dfrac{\sigma_{22}}{|\sigma_{ij}|} & -\dfrac{\sigma_{12}}{|\sigma_{ij}|}\\ -\dfrac{\sigma_{21}}{|\sigma_{ij}|} & \dfrac{\sigma_{11}}{|\sigma_{ij}|}\end{bmatrix} = \text{inverse of } \left[\sigma_{ij}\right]$$

The extension to the general multivariate distribution is obvious:

$$f(x_1, x_2, \ldots x_k) = \left(\frac{1}{2\pi}\right)^{\frac{k}{2}} \frac{1}{\sqrt{|\sigma_{ij}|}} \exp\left[-\frac{1}{2}\sum_{i=1}^{k}\sum_{j=1}^{k}\sigma^{ij}(x_i-\mu_i)(x_j-\mu_j)\right] \tag{83}$$

Error analysis frequently requires consideration not only of random errors in measurements, but of errors in functions of the measurements. That is, the quantity sought is some known function of several measured quantities. Of particular interest is the function consisting of a linear combination of random variables. If $x_1, x_2, \ldots x_k$ are independently and normally distributed random variables with means μ and variances σ_i^2, and if

$$u = \sum_{i=1}^{k} a_i x_i, \tag{84}$$

where the a_i are arbitrary constants, then u is normally distributed with mean

$$\mu_u = \sum_{i=1}^{k} a_i \mu_i \tag{85}$$

and variance

$$\sigma_u^2 = \sum_{i=1}^{k} a_i^2 \sigma_i^2 \tag{86}$$

This case is of special interest because, even if the function of interest, u, is nonlinear, the errors in u, Δu, can usually be accurately approximated by first-order differentials, i.e.,

$$\Delta u = \frac{\partial u}{\partial x_1}\Delta x_1 + \frac{\partial u}{\partial x_2}\Delta x_2 + \ldots + \frac{\partial u}{\partial x_k}\Delta x_k$$

which can then be treated as Eq (84).

2. The Method of Least Squares

The method of least squares is a method of finding the best possible values for a set of m unknowns, $x_1, x_2, \ldots, x_m$, satisfying n linear equations, where $n > m$.

$$a_{11} x_1 + a_{12} x_2 + \ldots + a_{1m} x_m = y_1$$

$$a_{21} x_1 + a_{22} x_2 + \ldots + a_{2m} x_m = y_2$$

$$\ldots$$

$$a_{n1} x_1 + a_{n2} x_2 + \ldots + a_{nm} x_m = y_n$$

Since the number of equations exceeds the number of unknowns, and since the y_i may contain observation errors, the system of equations is not solvable exactly, i.e., there is no set $x_1, x_2, \ldots x_m$ for which each of the n equations is exactly satisfied. Each equation then has a residual of the form

$$\delta_i = y_i - a_{i1} x_1 - a_{i2} x_2 - \ldots - a_{im} x_m.$$

$$(i = 1, 2, n) \qquad (87)$$

The least squares technique attempts to find values for $x_1, x_2, \ldots x_m$ which will make $\sum_{i=1}^{n} \delta_i^2$ as small as possible. This is the criterion for "best" solutions in the least squares method. If such a set of x_i exists, it then satisfies the condition

$$\frac{\partial}{\partial x_1} \sum_{i=1}^{n} \delta_i^2 = 0,$$

$$\frac{\partial}{\partial x_2} \sum_{i=1}^{n} \delta_i^2 = 0,$$

$$\ldots.$$

$$\frac{\partial}{\partial x_n} \sum_{i=1}^{n} \delta_i^2 = 0$$

This differentiation results in the following m equations

$$x_1 \sum_{i=1}^{n} a_{i1} a_{i1} + x_2 \sum_{i=1}^{n} a_{i1} a_{i2} + \ldots + x_m \sum_{i=1}^{n} a_{i1} a_{im} = \sum_{i=1}^{n} a_{i1} y_i$$

$$x_1 \sum_{i=1}^{n} a_{i2} a_{i1} + x_2 \sum_{i=1}^{n} a_{i2} a_{i2} + \ldots + x_m \sum_{i=1}^{n} a_{i2} a_{im} = \sum_{i=1}^{n} a_{i2} y_i \cdots \qquad (88)$$

$$x_1 \sum_{i=1}^{n} a_{im} a_{i1} + x_2 \sum_{i=1}^{n} a_{im} a_{i2} + \ldots + x_m \sum_{i=1}^{n} a_{im} a_{im} = \sum_{i=1}^{n} a_{im} y_i$$

(continued)

These equations comprise a system of m linear equations in the m unknowns $x_1, x_2 \ldots x_m$, which may be solved in a routine manner, e.g., by Cramer's rule. These equations are called the normal equations and are sometimes written in the following shorthand form:

$$[a_1 a_1]\ x_1 + [a_1 a_2]\ x_2 + \ldots + [a_1 a_m]\ x_m = [a_1 y]$$

$$[a_1 a_2]\ x_1 + [a_2 a_2]\ x_2 + \ldots + [a_2 a_m]\ x_m = [a_2 y] \qquad (89)$$

$$\ldots \qquad \ldots$$

$$[a_1 a_m]\ x_1 + [a_2 a_m]\ x_2 + \ldots + [a_m a_m]\ x_m = [a_m y]$$

These equations apply in the case in which the equations of condition, Eq (87), are of equal weight, i.e., all observations are assumed to be made with the same precision. If this is not true, then each of the residuals δ_i must be

assigned an estimated weight p_i, and each equation of condition multiplied by the square root of its weight. Then the normal equations become

$$\sum_{i=1}^{n} \left[p_i a_{i1} (x_1 a_{i1} + x_2 a_{i2} + \cdots + x_m a_{im} - y_i)\right] = 0$$

$$\sum_{i=1}^{n} \left[p_i a_{i2} (x_i a_{i1} + x_2 a_{i2} + \cdots + x_m a_{im} - y_i)\right] = 0 \qquad (90)$$

$$\cdots$$

$$\sum_{i=1}^{n} \left[p_i a_{im} (x_i a_{i1} + x_2 a_{i2} + \cdots + x_m a_{im} - y_i)\right] = 0$$

The weights normally utilized in these equations are inversely proportional to the variances, i.e.,

$$p_i = \frac{\sigma^2}{\sigma_i^2} , \qquad (91)$$

where σ_i^2 is the variance corresponding to weight p_i and σ^2 is the variance corresponding to unity weight.

Use of the least squares method is not strictly limited to sets of linear equations. The method can be applied directly in the case of certain functions of an exponential type, but the usual procedure adopted in dealing with sets of nonlinear equations is to replace the functions by linear Taylor series approximations. Let the n observations α_i be related to n nonlinear functions of the unknowns to be determined, i.e.,

$$f_i (x_1, x_2, \ldots, x_m) = \alpha_i - \delta_i$$

$$i = 1, 2, \ldots, n, \quad n > m$$

where the x_j are the unknowns to be determined and the δ_i are the residuals, or errors in the observations. The desired solutions may be represented by sums of approximate solutions, $(x_1)_0, (x_2)_0, \ldots, (x_m)_0$, and corrections to these approximate solutions,

$$x_j = (x_j)_0 + \Delta x_j .$$

Then expansion of the f_i in Taylor series gives

$$f_i \left[(x_1)_0, (x_2)_0, \ldots, (x_m)_0\right] + \left.\frac{\partial f_i}{\partial x_1}\right|_0 \Delta x_1 + \left.\frac{\partial f_i}{\partial x_2}\right|_0 \Delta x_2 + \ldots + \left.\frac{\partial f_i}{\partial x_m}\right|_0 \Delta x_m$$

$$\approx \alpha_i - \delta_i, \quad \overline{\Sigma x_j}^2 \approx 0 \qquad (92)$$

On setting

$$\alpha_i - f_i \left[(x_j)_0\right] \equiv y_i$$

$$\left.\frac{\partial f_i}{\partial x_j}\right|_0 \equiv a_{ij} ,$$

Eq (92) corresponds to Eq (87), the linear equations of condition, and may therefore be solved for the "best" values of the x_j in the manner outlined previously.

For the present purposes, it is convenient to formulate the weighted least squares estimate in matrix notation. Consider the equations of condition, Eq (87)

$$\delta_i = y_i - \sum_{j=1}^{m} a_{ij} x_j ,$$

the weighted least squares condition is that

$$\sum_{i=1}^{n} \frac{1}{\sigma_i^2} \left[y_i - \sum_{j=1}^{m} a_{ij} x_j\right]^2$$

be minimum. If the σ_i^2 do not vary significantly with x_j, setting the m derivatives

$$\frac{\partial}{\partial x_j} \sum \left(\frac{\delta_i}{\sigma_i}\right)^2 = 0$$

gives the following normal equations,

$$\sum_{i=1}^{n} \frac{1}{\sigma_i^2} \left[y_i - \sum_{j=1}^{m} a_{ij} x_j \right] a_{ik} = 0$$

$$k = 1, 2, \ldots m$$

or

$$\sum_{i=1}^{n} \frac{1}{\sigma_i^2} a_{ik} y_i - \sum_{j=1}^{m} \left[\sum_{i=1}^{n} \frac{1}{\sigma_i^2} a_{ij} a_{ik} \right] x_j = 0$$

In matrix notation, with

$$[v] \equiv \left[\sigma_i^{-2} \delta_{ij} \right] \equiv \begin{bmatrix} \sigma_1^{-2} & 0 & 0 & \ldots & 0 \\ 0 & \sigma_2^{-2} & 0 & \ldots & 0 \\ \cdot & \cdot & \sigma_3^{-2} & & 0 \\ \cdot & \cdot & \cdot & & \\ 0 & 0 & 0 & \ldots & \sigma_n^{-2} \end{bmatrix}$$

the normal equations become

$$\sum_{i=1}^{n} [v\,a]_{ik} y_i - \sum_{j=1}^{m} \left(\sum_{i=1}^{n} [v\,a]_{ik} a_{ij} \right) x_j = 0$$

since

$$[v\,a]_{ik} = \sum_{\ell=1}^{n} v_{i\ell} a_{\ell k} = \sum_{\ell=1}^{n} \sigma_i^{-2} \delta_{i\ell} a_{\ell k}$$

where $\delta_{i\ell}$ is the Kronecker delta and is equal to 1 ($i = \ell$) or 0 ($i \neq \ell$). Thus, $[v\,a]_{ik} = \sigma_i^{-2} a_{ik}$.

But

$$\sum_{i=1}^{n} [v\,a]_{ik} y_i = \sum_{i=1}^{n} [v\,a]^t_{ki} y_i = \left([v\,a]^t y \right)_k$$

and

$$\sum_{j=1}^{m} \left(\sum_{i=1}^{h} [v\,a]_{ik} a_{ij} \right) x_j =$$

$$= \sum_{j=1}^{m} \left(\sum_{i=1}^{n} [v\,a]^t_{ki} a_{ij} \right) x_j$$

(continued)

$$= \sum_{j=1}^{m} \left([v\,a]^t a \right)_{kj} x_j$$

$$= \left\{ [v\,a]^t a\, x \right\}_k .$$

Therefore, the normal equations may be written

$$\left([v\,a]^t y \right)_k - \left\{ \left([v\,a]^t a \right) x \right\}_k = 0$$

$$k = 1, 2, \ldots, m$$

or

$$[v\,a]^t y - \left([v\,a]^t a \right) x = 0$$

Finally, the explicit solution for the m-vector of unknowns is

$$\{x\} = \left[\{v\,a\}^t a \right]^{-1} [v\,a]^t \{y\}$$

or

$$\{x\} = \left[a^t v\, a \right]^{-1} [a]^t [v] \{y\} \qquad (93)$$

where

- a = n x m matrix of the a_{ij}
- v = n x n diagonal matrix of the inverse variances
- y = n-vector of known data

Several examples of the application of the method of least squares are given in the following sections for the cases of equiweighted data.

a. Least squares fit of a straight line

The sum of the squared residuals to be minimized in fitting a straight line by the least squares technique is

$$\sum_{i=1}^{n} \delta_i^2 = \sum_{i=1}^{n} \left[y_i - (m x_i + k) \right]^2$$

$$= \sum_{i=1}^{n} \left(y_i^2 - 2 m x_i y_i - 2 k y_i + 2 k m x_i + m^2 x_i^2 + k^2 \right)$$

which is quadratic in k, i.e.,

$$\sum_{i=1}^{n} \delta_i^2 = n k^2 + 2 k \left(m \sum_{i=1}^{n} x_i - \sum_{i=1}^{n} y_i \right) + C$$

where C contains all terms not involving k.

The minimum occurs for

$$\frac{\partial}{\partial k}\sum_{i=1}^{n}\delta_i^2 = 2nk + 2\left(m\sum_{i=1}^{n}x_i - \sum_{i=1}^{n}y_i\right) = 0$$

or

$$\sum_{i=1}^{n}y_i = m\sum_{i=1}^{n}x_i + nk \qquad (94)$$

Similarly, the quadratic in m gives

$$\sum_{i=1}^{n}x_i y_i = m\sum_{i=1}^{n}x_i^2 + k\sum_{i=1}^{n}x_i \qquad (95)$$

Example: Consider a plot of the inverse of the nondimensional acceleration versus time. Then

$$I_{sp} = -\frac{1}{m},\ x_i = \text{time points},\ y_i = \frac{g}{a_t}$$

From the raw data or specific impulse of an engine in the table, compute x, y, xy and x^2.

Raw Data for Specific Impulse of an Engine

	x	y	xy	x^2
(120 sec)	0	0.1765	0	0
	0.5	0.1748	0.0874	0.25
	1.0	0.1731	0.1731	1.00
	1.5	0.1715	0.25725	2.25
	2.0	0.1697	0.3394	4.00
	2.5	0.1680	0.4200	6.25
	3.0	0.1663	0.4989	9.00
	3.5	0.1645	0.57575	12.25
	4.0	0.1627	0.6508	16.00
	4.5	0.1608	0.7236	20.25
	5.0	0.1590	0.7950	25.00
	5.5	0.1571	0.86405	30.25
	6.0	0.1553	0.9318	36.00
	6.5	0.1537	0.99905	42.25
	7.0	0.1521	1.0647	49.00
	7.5	0.1504	1.1280	56.25
	8.0	0.1484	1.1872	64.00
	8.5	0.1463	1.24355	72.25
	9.0	0.1444	1.2996	81.00
	9.5	0.1426	1.3547	90.25
(130 sec)	10.0	0.1409	1.4090	100.00
	$\Sigma x = 105.0$	$\Sigma y = 3.3381$	$\Sigma xy = 16.00285$	$\Sigma x^2 = 717.50$ (120 to 130 sec)

Then, from

$$\Sigma y = m\,\Sigma x + n\,k$$

$$\Sigma xy = m\,\Sigma x^2 + k\,\Sigma x,$$

$$\begin{cases} 3.3381 = 105\,m + 21\,k \\ 16.00285 = 717.5\,m + 105\,k \end{cases}$$

Simultaneous solution of these equations gives

$$m = -0.003572207$$

$$I_{sp} = 279.938 \text{ sec from 120 to 130 sec.}$$

b. Least squares fit of an ellipse

A determination of the "best" elements of an ellipse from application of the least squares criterion to q sets of data (r, A, L, t),

r = radius vector

A = right ascension

L = declination (geocentric latitude)

t = time

may be based upon q sets of equations of the form

$$\begin{cases} t_k = t_p + a\sqrt{\frac{a}{\mu}}\left[\cos^{-1}\left(\frac{a - r_k}{ea}\right) \pm \sqrt{e^2 - \left(1 - \frac{r_k}{a}\right)^2}\right] & (96) \\ \cos A_k \cos L_k \tan i \sin \Omega - \cos L_k \sin A_k \tan i \cos \Omega + \sin L_k = 0 & (97) \end{cases}$$

where

$$k = 1, 2, \ldots, q, \quad q > 3.$$

Approximate values of the elements are assumed known. These rough values will be designated a_0, e_0, t_{p0}. Then corrections δa_0, δe_0, δt_{p0} must be computed such that

$$a = a_0 + \delta a_0$$

$$e = e_0 + \delta e_0 \qquad (98)$$

$$t_p = t_{p0} + \delta t_{p0}$$

(t_p = time of perigee encounter)

are the elements that best satisfy Eq (96). Equation (96) can be written in residual form as follows:

$$\delta_k = t_{p0} + \delta t_{p0} - t_k + (a_0 + \delta a_0)\left[\frac{1}{\mu}(a_0 + \delta a_0)\right]^{1/2}\left[\cos^{-1}\ (a_0 + \delta a_0 - r_k)(a_0 e_0 + e_0\,\delta a_0 + a_0\,\delta e_0 + \delta a_0\,\delta e_0)^{-1} \pm \sqrt{(e_0 + \delta e_0)^2 - \left(1 - \frac{r_k}{a_0 + \delta a_0}\right)^2}\ \right]$$

This equation may be linearized in terms of the corrections by means of Taylor's expansion,

$$\delta_k = \delta a_0 \frac{\partial t_k}{\partial a} + \delta e \frac{\partial t_k}{\partial e} + \delta t_p \frac{\partial t_k}{\partial t_p} + t_p - t_k + a_0\sqrt{\frac{a_0}{\mu}}\left[\cos^{-1}\left(\frac{a_0 - r_k}{e_0 a_0}\right) \pm \sqrt{e_0^2 - \left(1 - \frac{r_k}{a_0}\right)^2}\ \right], \qquad (99)$$

where terms of order $\{\delta(\ )\}^2$ and higher have been neglected. This approximation of the Taylor series terms involving higher powers of the corrections will not affect the accuracy of the final solutions for which the corrections are very small, provided that further corrections of the form Eq (98) are applied, i.e., that the solution is obtained by a convergent iteration of the form

$$\begin{aligned} a_{n+1} &= a_n + \delta a_n \\ e_{n+1} &= e_n + \delta e_n \qquad (100) \\ t_{p_{n+1}} &= t_{p_n} + \delta t_{p_n} \end{aligned}$$

Then the orbit elements which represent a least squares fit of the (r_k, t_k) data can be determined by stipulating that $\sum_{k=1}^{q} \delta_k^2$ be a minimum. Evaluation of the partial derivatives of Eq (99) and substitution in Eq (100) yields the following final solutions for the planar elements:

$$a_{n+1} = a_n + \frac{1}{d}\begin{vmatrix} -\sum_k \Xi_k \Phi_k & \sum_k \Xi_k \Psi_k & \sum_k \Xi_k \\ -\sum_k \Psi_k \Phi_k & \sum_k \Psi_k^2 & \sum_k \Psi_k \\ -\sum_k \Phi_k & \sum_k \Psi_k & q \end{vmatrix} \qquad (101)$$

$$e_{n+1} = e_n + \frac{1}{d}\begin{vmatrix} \sum_k \Xi_k^2 & -\sum_k \Xi_k \Phi_k & \sum_k \Xi_k \\ \sum_k \Xi_k \Psi_k & -\sum_k \Psi_k \Phi_k & \sum_k \Psi_k \\ \sum_k \Xi_k & -\sum_k \Phi_k & q \end{vmatrix} \qquad (102)$$

$$t_{p_{n+1}} = t_{p_n} + \frac{1}{d}\begin{vmatrix} \sum_k \Xi_k^2 & \sum_k \Xi_k \Psi_k & -\sum_k \Xi_k \Phi_k \\ \sum_k \Xi_k \Psi_k & \sum_k \Psi_k^2 & -\sum_k \Psi_k \Phi_k \\ \sum_k \Xi_k & \sum_k \Psi_k & -\sum_k \Phi_k \end{vmatrix} \qquad (103)$$

where $d = \begin{vmatrix} \sum_k \Xi_k^2 & \sum_k \Xi_k \Psi_k & \sum_k \Xi_k \\ \sum_k \Xi_k \Psi_k & \sum_k \Psi_k^2 & \sum_k \Psi_k \\ \sum_k \Xi_k & \sum_k \Psi_k & q \end{vmatrix}$

$$\Xi_k = \frac{3}{2}\sqrt{\frac{a_n}{\mu}}\,(R_{1k} - R_{2k}) - \frac{1}{R_{2k}}\sqrt{\frac{a_n}{\mu}}\left(\frac{r_k}{a_n}\right)^2$$

$$\Psi_k = \frac{a_n}{R_{2k}}\sqrt{\frac{a_n}{\mu}}\left(\frac{a_n - r_k}{e_n a_n} - e_n\right)$$

$$\Phi_k = t_{pn} - t_k + a_n\sqrt{\frac{a_n}{\mu}}\,(R_{1k} - R_{2k})$$

$$R_{1k} = \cos^{-1}\left(\frac{a_n - r_k}{e_n a_n}\right)$$

$$R_{2k} = e_n \sin R_{1k}$$

In terms of true anomaly instead of time, the solution is much simpler:

$$p_n = p_{n-1} + \frac{1}{D} \begin{vmatrix} \sum_{k=1}^{q} \theta_k r_k - p_{n-1} \sum_{k=1}^{q} \theta_k^2 & -p_{n-1} \sum_{k=1}^{q} \theta_k^3 \cos\theta_k \\ p_{n-1} \sum_{k=1}^{q} \theta_k^3 \cos\theta_k - \sum_{k=1}^{q} \theta_k^2 r_k \cos\theta_k & p_{n-1} \sum_{k=1}^{q} \theta_k^4 \cos^2\theta_k \end{vmatrix} \tag{104}$$

$$e_n = e_{n-1} + \frac{1}{D} \begin{vmatrix} \sum_{k=1}^{q} \theta_k^2 & \sum_{k=1}^{q} \theta_k r_k - p_{n-1} \sum_{k=1}^{q} \theta_k^2 \\ \sum_{k=1}^{q} \theta_k^3 \cos\theta_k & p_{n-1} \sum_{k=1}^{q} \theta_k^3 \cos\theta_k - \sum_{k=1}^{q} \theta_k^2 r_k \cos\theta_k \end{vmatrix} \tag{105}$$

where

p = semilatus rectum of ellipse

$$D = \begin{vmatrix} \sum_{k=1}^{q} \theta_k^2 & -p_{n-1} \sum_{k=1}^{q} \theta_k^3 \cos\theta_k \\ \sum_{k=1}^{q} \theta_k^3 \cos\theta_k & p_{n-1} \sum_{k=1}^{q} \theta_k^4 \cos^2\theta_k \end{vmatrix}$$

$$\theta_k = \frac{1}{1 + e_{n-1} \cos\theta_k}$$

This routine is suitable for computing ellipses, parabolas or hyperbolas. There are no discontinuities since the denominator of θ_k becomes zero only for $\cos\theta_k = \frac{-1}{e}$, i.e., only for infinite orbital radius.

The previous routines are concerned with the computation of the elements which describe satellite position in a plane. There remains the problem of solving for the elements which define the orientation of the orbital plane in space. The equation for the orbital plane in spherical coordinates in Eq (97). Then the q data points can be used to write q residual equations.

$$P_1 \cos L_k \cos A_k - P_2 \cos L_k \sin A_k + \sin L_k = \delta_k$$

The best values of the elements Ω and i are then determined as follows

$$\Omega = \tan^{-1}\left(\frac{P_1}{P_2}\right) \tag{106}$$

$$i = \tan^{-1}\left(\frac{P_1}{\sin\Omega}\right) \tag{107}$$

where

$$P_1 = \frac{\begin{vmatrix} -\sum_k \cos L_k \sin L_k \cos A_k & -\sum_k \cos^2 L_k \cos A_k \sin A_k \\ \sum_k \cos L_k \sin L_k \sin A_k & \sum_k \cos^2 L_k \sin^2 A_k \end{vmatrix}}{\begin{vmatrix} \sum_k \cos^2 L_k \cos^2 A_k & -\sum_k \cos^2 L_k \cos A_k \sin A_k \\ -\sum_k \cos^2 L_k \sin A_k \cos A_k & \sum_k \cos^2 L_k \sin^2 A_k \end{vmatrix}}$$

$$P_2 = \frac{\begin{vmatrix} \sum_k \cos^2 L_k \cos^2 A_k & -\sum_k \cos L_k \sin L_k \cos A_k \\ -\sum_k \cos^2 L_k \sin A_k \cos A_k & \sum_k \cos L_k \sin L_k \sin A_k \end{vmatrix}}{\begin{vmatrix} \sum_k \cos^2 L_k \cos^2 A_k & -\sum_k \cos^2 L_k \cos A_k \sin A_k \\ -\sum_k \cos^2 L_k \sin A_k \cos A_k & \sum_k \cos^2 L_k \sin^2 A_k \end{vmatrix}}$$

Equations (101) through (107) may be used to investigate the effects of number, accuracy and spread of data points on the accuracy of computation.

These equations may be used to show the effects of spread of data over limited arcs of the orbit by letting sets of identical data be associated with various arc lengths. Errors due to limited sample size are to be precluded as far as possible; therefore, each set of data was selected to fit a normal distribution of zero mean and 1000-ft standard deviation in range and 0.005° in azimuth and elevation. The orbit selected for the first series of computations was the circular 6-hr orbit ($r = 5.488164 \times 10^7$ ft). The results of the computations are shown in Figs. 3, 4 and 5. Errors in computed eccentricity, semiparameter, inclination and nodal longitude are plotted against the spread of equally spaced data points for sets of four, nine and twenty-five data. For data spread over arcs of $40° < \text{arc} < 90°$, the iteration converged very slowly and for arcs less than 40° the solutions drifted. These figures provide a qualitative indication of the improvement of results with spread of data over wide arcs.

As indicated in the statement of the central-limit theorem in Section 0.1, the failure of a small sample of data to yield the mean of the true population gives rise to another type of error. The qualitative effect of this error may also be investigated with the previously derived solutions for least squares fit of an ellipse. Limited data samples of 6, 10, 20, 30 and 40 points were selected randomly from a normal population of $\sigma = 1000$ ft. For the case of Fig. 6, the data were taken at equal intervals over two 15° arcs at opposite sides of a 6-hr circular orbit. In Fig. 7

the results with a limited number of data are shown for data taken at equal intervals around two sample orbits, a circular 200-stat mi or 322-km orbit and an ellipse of e = 0.4 and p = 3.07425 x 10^7 ft or 0.937031 x 10^4 km. The errors in computed eccentricity and semilatus rectum are shown as functions of the number of randomly selected data.

3. Other Methods of Parameter Estimation

Although the least squares method is most widely used, it is not the only technique available. Some other approaches are the minimum variance technique, the maximum likelihood estimate and the method of moments.

a. Minimum variance

The minimum variance estimate is that estimate which has a minimum variance-covariance matrix. When the errors are uncorrelated, i.e., when the covariances are zero, the minimum variance and weighted least squares methods are identical. However, when the errors are correlated, the minimum variance approach may be superior because it includes the effects of the correlations. That is, if one data type is highly correlated, the least squares technique may overly weight that data type. However, the least squares technique is generally used because the minimum variance computations are more complicated and require more detailed information about the covariances which is frequently not available. The improvement to be gained by use of the minimum variance technique is not of great significance.

The basic equations of the minimum variance approach may be developed as follows. If x_t is the true value of the unknown parameter x, and x_e is its estimated value,

$$y_i = a_i x_t + \delta_i (x_t)$$

where y_i are the observed data and $\delta_i (x_t)$ are the errors in the true unknowns, and

$$x_e = \sum_{i=1}^{n} b_i y_i.$$

Therefore,

$$x_e = \sum_{i=1}^{n} b_i (a_i x_t + \delta_i)$$

is a random variable since x_e is a function of δ_i. The variance of x_e, from Eq (86), is

$$\sigma_{x_e}^2 = \sum_{i=1}^{n} b_i^2 \sigma_i^2$$

where

σ_i^2 = variance of δ_i

if the δ_i's are uncorrelated. If correlation exists,

$$\sigma_{x_e}^2 = \sum_{i=1}^{n} b_i^2 \sigma_i^2 + \sum_{\substack{i,j=1 \\ i \neq j}}^{n} b_i b_j \rho_{ij} \qquad (108)$$

where

ρ_{ij} = covariance of δ_i and δ_j.

The first summation of Eq (108) comprises the diagonal terms of the variance-covariance matrix, and the second summation represents the off diagonal terms. The minimum variance technique, as the name implies, is based on a minization of $\sigma_{x_e}^2$, subject to the condition that the expected value of x_e is x_t. This minimization results in the following minimum variance estimates.

$$\{x_e\} = \left[a^t c^{-1} a\right]^{-1} a^t c^{-1} \{y\} \qquad (109)$$

where

c = the nxn variance-covariance matrix

This equation is completely analogous to that for the least squares estimate, Eq (93), and the two estimates are obviously identical for the case of zero correlation, $c^{-1} = v$. The variance of the estimates in matrix notation is

$$\sigma_{x_e}^2 = \left[a^t c^{-1} a\right]^{-1}. \qquad (110)$$

b. Maximum likelihood

The maximum likelihood estimate is the estimate which maximizes the probability distribution of the data sample. If the errors are normally distributed, the maximum likelihood estimate reduces to that obtained by the minimum variance technique.

c. Method of moments

As an example of the method of moments, the problem of fitting a straight line, solved in Section D. 2. a by least squares, is presented.

For a set of n values of (x_i, y_i) the rth moment of y is

$$\frac{1}{n} \sum_{1}^{n} x_i^r y_i$$

where

r is zero or a positive integer.

Now obtain two equations in m and k by equating the zeroth and first moments of the observed y's

to the zeroth and first moments, respectively, of the y's computed from an assumed $y = mx + k$ line fit. All moments are taken about the origin of x. These two equations may then be solved for m and k. Let ${}_oy$ be observed y's and ${}_cy$ computed y's. Then for observed y's the first moment is

$$\frac{1}{n}\sum_{1}^{n} x_i\, {}_oy_i$$

and zeroth moment is

$$\frac{1}{n}\sum_{1}^{n} {}_oy_i \,.$$

Obtain computed y's from ${}_cy = mx_i + k$ and get moments

$$\frac{1}{n}\sum_{1}^{n} x_i\,(mx_i + k)$$

and

$$\frac{1}{n}\sum_{1}^{n} mx_i + k.$$

Equating as previously indicated,

$$\frac{1}{n}\sum_{1}^{n} y_i = \frac{1}{n}\sum_{1}^{n} (mx_i + k)$$

$$\frac{1}{n}\sum_{1}^{n} x_i y_i = \frac{1}{n}\sum_{1}^{n} \left[x_i\,(mx_i + k)\right].$$

Simplification of these equations gives

$$\sum_{1}^{n} y_i = m\sum_{1}^{n} x_i + nk \qquad (111)$$

$$\sum_{1}^{n} x_i y_i = m\sum_{1}^{n} x_i^2 + k\sum_{1}^{n} r_i \,. \qquad (112)$$

These equations are the same as Eqs (94) and (95) in the least squares example.

Solve these for m to get

$$m = \frac{\sum_{1}^{n} y \sum_{1}^{n} x - n\sum_{1}^{n} xy}{\left(\sum_{1}^{n} x\right)^2 - n\sum_{1}^{n} x^2}$$

Example.

$$I_{sp} = -\frac{1}{m} \quad \text{when} \begin{cases} x_i = \text{time points} \\ y_i = g/a_T \text{ (corresponding to x points).} \end{cases}$$

Thus

$$I_{sp} = \frac{n\sum_{1}^{n} x_i^2 - \left(\sum_{1}^{n} x_i\right)^2}{\sum_{1}^{n} y_i \sum_{1}^{n} x_i - n\sum_{1}^{n} x_i y_i}.$$

When n goes from 1, 2, ..., n

$$\sum_{1}^{n} x_i = \frac{n\,(n+1)}{2}$$

$$\sum_{1}^{n} x_i^2 = \frac{n\,(n+1)\,(2n+1)}{6} \,.$$

F. ORBIT IMPROVEMENT

It has been noted that the basic problem of orbit determination is solution for the six defining parameters of an orbit from a set of observations. Orbit improvement, as distinguished from preliminary orbit determination, assumes that approximate parameters are already known and that these are to be improved in accuracy. The six parameters may be the classical orbit elements $(a, e, i, \omega, \Omega, t_p)$, or the Cartesian position and velocity components at a specified time, or any set of quantities which uniquely determine the orbit. Other quantities, in addition to the six orbit parameters, could be refined in the orbit improvement process. For example, the accuracy of any geophysical constants which appear in the equations of motion (of which the six orbit parameters are constants of integration) may be improved. Examples of these constants are drag coefficients, the various coefficients of the gravitational potential function harmonics, inaccurately known locations of tracking stations, thrust corrections, etc. The basic method of computing corrections to these constants and orbit parameters is known as the differential correction technique.

1. Differential Correction Technique

The equation of motion can be written, as indicated in Chapter IV, as

$$\frac{d^2\vec{r}}{dt^2} = -\mu\frac{\vec{r}}{r^3} + \sum_i \frac{F_i}{m} \qquad (113)$$

where the F_i are perturbative forces due, for example, to drag, oblateness, thrust, etc. If there were no errors in the observations or inaccuracies

in the physical constants of Eq (113), all data would be exact solutions to this equation. The six constants of integration (the orbit parameters) involved in the solution of this equation could then be evaluated exactly. That is, if there existed an explicit solution for Eq (113),

$$f_i(x_1, x_2, \ldots, x_m) = y_i \qquad i = 1, 2, \ldots, n$$

where

y_i = the observed data

x_j = the unknown orbit parameters and physical constants

f_i = some nonlinear function,

the m values of x_j would be determined if at least m values of data y_i were available. However, no observation will be exactly correct, and so this equation becomes

$$f_i(x_1, x_2, \ldots, x_m) = y_i - \delta_i$$

$$i = 1, \ldots n, \; n > m$$

where δ_i is the error in the ith item of observed information y_i. Although the functional relationship expressed in this equation is very complicated, simple linear approximate functions of the corrections to the unknowns, Δx_i, can be written from Taylor series

$$f_i(x_{01}, x_{02}, \ldots, x_{0m}) + \left.\frac{\partial f_i}{\partial x_1}\right|_0 \Delta x_1 + \left.\frac{\partial f_i}{\partial x_2}\right|_0 \Delta x_2 + \ldots + \left.\frac{\partial f_i}{\partial x_m}\right|_0 \Delta x_m = y_i - \delta_i$$

or

$$\sum_{j=1}^{m} \left.\frac{\partial f_i}{\partial x_j}\right|_0 \Delta x_i = \Delta y_i - \delta_i$$

where $x_{01}, x_{02}, \ldots, x_{0m}$ are known approximate values of x_j Δy_i are the differences in observed and computed or anticipated data and the corrected values of the parameters to be determined are

$$x_j = x_{0j} + \Delta x_j.$$

This procedure is useful in the problem of orbit improvement, where approximate values of the parameters are assumed known from preliminary determinations. Then, if an excess of data is taken, n > m, the "best" values for the corrections can then be determined by the method of least squares as outlined in Section E. 2 for

$$a_{ij} = \left.\frac{\partial f_i}{\partial x_j}\right|_0$$

The normal equations corresponding to Eq (90) are

$$\sum_{i=1}^{n} \frac{1}{\sigma_i^2}\left[\Delta y_i - \sum_{j=1}^{m} \frac{\partial f_i}{\partial x_j} \Delta x_j\right] \frac{\partial f_i}{\partial x_k} = 0$$

$$j, k = 1, 2, \ldots, m \qquad (114)$$

This process of correcting parameters which are known approximately, is referred to as differential correction, and is not strictly limited to orbit improvement. In the case of launch of an artificial satellite, for example, the nominal trajectory parameters can be used as the initial approximate values to be refined. The only restriction is that the approximate values be sufficiently accurate to validate neglecting higher terms in the Taylor series (i.e., assure convergence of the iteration). The results of Section E are applicable to this method of estimation of orbit parameters. In particular, the matrix formulation for the estimated values, from Eq (93), is

$$\{\Delta x\} = \left[a^t v a\right]^{-1}[a]^t[v] \{\Delta y\} \qquad (115)$$

where

$[a]$ = nxm matrix of the partial derivative coefficients

$[v]$ = nxn diagonal matrix of the inverse variances

and the variances of the estimated values are, from Eq (108) or Eq (110)

$$\sigma_{x_e}^2 = \sum_{i=1}^{n} b_i^2 \sigma_i^2 \qquad \text{(no correlation)}$$

or

$$\sigma_{x_e}^2 = \left[a^t v a\right]^{-1} \qquad (116)$$

2. Determination of Partial Derivatives

In the matrix $\left[a^t a\right]$ there are elements of the form

$$\sum_{i=1}^{n} \left(\frac{\partial y_i}{\partial x_j} \; \frac{\partial y_i}{\partial x_k}\right)$$

where x_j and x_k are parameters at initial epoch. It is convenient, in the calculation of partials of the form $\frac{\partial y_i}{\partial x_j}$, to separate the partial into components which may be determined individually with greater ease.

$$\frac{\partial y_i}{\partial x_j} = \frac{\partial y_i}{\partial X}\frac{\partial X}{\partial x_j} + \frac{\partial y_i}{\partial Y}\frac{\partial Y}{\partial x_j} + \frac{\partial y_i}{\partial Z}\frac{\partial Z}{\partial x_j} + \frac{\partial y_i}{\partial \dot{X}}\frac{\partial \dot{X}}{\partial x_j} + \frac{\partial y_i}{\partial \dot{Y}}\frac{\partial \dot{Y}}{\partial x_j} + \frac{\partial y_i}{\partial \dot{Z}}\frac{\partial \dot{Z}}{\partial x_j}$$

where (X, Y, Z) and ($\dot{X}$, $\dot{Y}$, $\dot{Z}$) are the current position and velocity components. The partials of the observed quantities,

$$\frac{\partial y_i}{\partial X}, \quad \frac{\partial y_i}{\partial \dot{X}},$$

etc., are derivable in analytic form from the definitions of the y_i. The derivatives

$$\frac{\partial X}{\partial x_j}, \quad \frac{\partial \dot{X}}{\partial x_j}$$

etc., are obtained by numerical integration. From the equation of motion,

$$\ddot{X} = F,$$

$$\frac{d^2}{dt^2}\left(\frac{\partial X}{\partial x_j}\right) = \frac{\partial F}{\partial X}\frac{\partial X}{\partial x_j} + \frac{\partial F}{\partial Y}\frac{\partial Y}{\partial x_j} + \frac{\partial F}{\partial Z}\frac{\partial Z}{\partial x_j} + \frac{\partial F}{\partial \dot{X}}\frac{\partial \dot{X}}{\partial x_j} + \frac{\partial F}{\partial \dot{Y}}\frac{\partial \dot{Y}}{\partial x_j} + \frac{\partial F}{\partial \dot{Z}}\frac{\partial \dot{Z}}{\partial x_j}$$

Equations of this type are doubly integrated numerically to give

$$\frac{\partial X}{\partial x_j}, \frac{\partial Y}{\partial x_j}, \frac{\partial Z}{\partial x_j}$$

and differentiation of these partials yields

$$\frac{\partial \dot{X}}{\partial x_j}, \frac{\partial \dot{Y}}{\partial x_j}, \frac{\partial \dot{Z}}{\partial x_j}.$$

3. Analytic Solutions for Partial Derivatives

Corrections in a set of orbit elements may be related analytically to corrections in the Cartesian coordinates. One convenient set of orbit element corrections is $d\psi_x$, $d\psi_y$, $d\psi_z$, dM_0, da, de, where the $d\psi$'s are rotations about the Cartesian axes,

$$dx = z\,d\psi_y - y\,d\psi_z$$

$$dy = x\,d\psi_z - z\,d\psi_x$$

$$dz = y\,d\psi_x - x\,d\psi_y \qquad (117)$$

and

dM_0 = correction in mean anomaly

da = correction in semimajor axis

de = correction in eccentricity

The differentials dM_0, da, de are obtained from the equations of Keplerian motion. If $\hat{p}$ and $\hat{q}$ are unit vectors along the x_ω and y_ω axes (the orbit plane coordinates defined in Section B.)

$$\vec{r} = a(\cos E - e)\,\hat{p} + a\sqrt{1-e^2}\sin E\,\hat{q} \qquad (118)$$

$$d\vec{r} = \left[(\cos E - e)\,da + a(-\sin E\,dE - de)\right]\hat{p} + \left[\sqrt{1-e^2}(\sin E\,da + a\cos E\,dE) - a\sin E\frac{e\,de}{\sqrt{1-e^2}}\right]\hat{q} \qquad (119)$$

The nomenclature is that of Chapter III.

But, from Kepler's equation,

$$E - e\sin E = M_0 + \frac{\sqrt{\mu}}{a^{3/2}}(t - t_0), \qquad (120)$$

$$dE = \frac{a}{r}\left[\sin E\,de + dM_0 - \frac{3}{2}\frac{\sqrt{\mu}}{a^{3/2}}(t - t_0)\frac{da}{a}\right]$$

Substitution of this equation in Eq (119) and noting that

$$\sin E = -\frac{\dot{x}_\omega r}{\sqrt{\mu a}}$$

$$\vec{v} = \frac{1}{r}\sqrt{\frac{\mu}{a}}\left[-a\sin E\,\hat{p} + a\sqrt{1-e^2}\cos E\,\hat{q}\right] \qquad (121)$$

gives

$$dx_\omega = \left[x_\omega + m\frac{\dot{x}_\omega}{n}\right]\frac{da}{a} - \left[a - \frac{\dot{x}_\omega}{n}\sin E\right]de + \frac{\dot{x}_\omega}{n}dM_0$$

$$dy_\omega = \left[y_\omega + m\frac{\dot{y}_\omega}{n}\right]\frac{da}{a} - \left[\frac{ey_\omega}{1-e^2} - \frac{\dot{y}_\omega}{n}\sin E\right]de + \frac{\dot{y}_\omega}{n}dM_0 \qquad (122)$$

where

$$n = \frac{\sqrt{\mu}}{a^{3/2}} \qquad (123)$$

$$m = -\frac{3}{2}\frac{\sqrt{\mu}}{a^{3/2}}(t - t_0). \qquad (124)$$

It is desirable to write the eccentricity sensitivities in the form

$$\frac{\partial x}{\partial e} = Hx + K\dot{x}, \quad x \to y, z.$$

Solving the simultaneous equations

$$\begin{cases} \dfrac{\partial x}{\partial e}_{\omega} = Hx_{\omega} + K\dot{x}_{\omega} \\ \dfrac{\partial y}{\partial e}_{\omega} = Hy_{\omega} + K\dot{y}_{\omega} \end{cases}$$

gives

$$H = \frac{\dot{y}_{\omega}\dfrac{\partial x}{\partial e}_{\omega} - \dot{x}_{\omega}\dfrac{\partial y}{\partial e}_{\omega}}{x_{\omega}\dot{y}_{\omega} - y_{\omega}\dot{x}_{\omega}}$$

$$K = \frac{x_{\omega}\dfrac{\partial y}{\partial e}_{\omega} - y_{\omega}\dfrac{\partial x}{\partial e}_{\omega}}{x_{\omega}\dot{y}_{\omega} - y_{\omega}\dot{x}_{\omega}}.$$

Substituting for $\frac{\partial x}{\partial e}_{\omega}$ and $\frac{\partial y}{\partial e}_{\omega}$ from Eq (122) and for x_{ω}, y_{ω}, $\dot{x}_{\omega}$, $\dot{y}_{\omega}$ from Eqs (118) and (121) gives

$$H = -\frac{1}{1-e^2}(\cos E + e) \qquad (125)$$

$$K = \frac{1}{n}\frac{\sin E}{1-e^2}(2 - e^2 - e\cos E). \qquad (126)$$

Then the final form of the differential correction equation is

$$\begin{bmatrix} dx \\ dy \\ dz \end{bmatrix} = \begin{bmatrix} 0 & z & -y & \frac{\dot{x}}{n} & Hx + K\frac{\dot{x}}{n}x + m\frac{\dot{x}}{n} \\ -z & 0 & x & \frac{\dot{y}}{n} & Hy + K\frac{\dot{y}}{n}y + m\frac{\dot{y}}{n} \\ y & -x & 0 & \frac{\dot{z}}{n} & Hz + K\frac{\dot{z}}{n}z + m\frac{\dot{z}}{n} \end{bmatrix} \begin{bmatrix} d\psi_x \\ d\psi_y \\ d\psi_z \\ dM_0 \\ de \\ \frac{da}{a} \end{bmatrix} \qquad (127)$$

where m, n, H and K are given by Eqs (123) through (126). This equation is due to Eckert and Brouwer, Ref (5). In vector notation,

$$d\vec{r} = (d\vec{\psi} \times \vec{r}) + \frac{\vec{v}}{n}dM_0 + (H\vec{r} + K\frac{\vec{v}}{n})de + (\vec{r} + m\frac{\vec{v}}{n})\frac{da}{a}. \qquad (128)$$

Eq (127) can be transformed to the satellite oriented system (X_s, Y_s, Z_s) by

$$dx_s = d\vec{r} \cdot \hat{r}$$
$$dy_s = d\vec{r} \cdot \hat{n}$$
$$dz_s = d\vec{r} \cdot \hat{m}.$$

Evaluation for each term of Eq (128) proceeds as follows.

$$(d\vec{\psi} \times \vec{r}) \cdot \hat{r} = d\vec{\psi} \cdot (\vec{r} \times \hat{r}) = 0$$
$$(d\vec{\psi} \times \vec{r}) \cdot \hat{n} = d\vec{\psi} \cdot (\vec{r} \times \hat{u}) = d\vec{\psi} \cdot r\hat{m} = r d\psi_m$$
$$(d\vec{\psi} \times \vec{r}) \cdot \hat{m} = d\vec{\psi} \cdot (\vec{r} \times \hat{m}) = d\vec{\psi} \cdot (-r\hat{n})$$

If $d\vec{\psi} = d\psi_p \hat{p} + d\psi_q \hat{q} + d\psi_s \hat{s}$,

$$(d\vec{\psi} \times \vec{r}) \cdot \hat{n} = r\, d\psi_s$$
$$(d\vec{\psi} \times \vec{r}) \cdot \hat{m} = -r\, d\psi_p\, p\cdot n - d\psi_q\, r\, \hat{q}\cdot\hat{n}$$
$$= d\psi_p\, b \sin E - d\psi_q\, a(\cos E - e)$$

Also

$$\frac{\vec{v}}{n} \cdot \hat{r} = \frac{V_r}{n} = \frac{a^2}{r} e \sin E$$

$$\frac{\vec{v}}{n} \cdot \hat{n} = \frac{1}{n}\frac{\sqrt{\mu p}}{r} = \frac{a^2}{r}\sqrt{1-e^2}$$

$$\frac{\vec{v}}{n} \cdot \hat{m} = 0$$

$$(H\vec{r} + K\frac{\vec{v}}{n}) \cdot \hat{r} = rH + K\frac{a^2}{r} e \sin E$$
$$(H\vec{r} + K\frac{\vec{v}}{n}) \cdot \hat{n} = K\frac{a^2}{r}\sqrt{1-e^2}$$
$$(H\vec{r} + K\frac{\vec{v}}{n}) \cdot \hat{m} = 0$$

$$(\vec{r} + m\frac{\vec{v}}{n}) \cdot \hat{r} = r + m\frac{a^2}{r} e \sin E$$
$$(\vec{r} + m\frac{\vec{v}}{n}) \cdot \hat{n} = m\frac{a^2}{r}\sqrt{1-e^2}$$
$$(\vec{r} + m\frac{\vec{v}}{n}) \cdot \hat{m} = 0.$$

Then Eq (127) can be written

$$\begin{bmatrix} dx_s \\ dy_s \\ dz_s \end{bmatrix} = \begin{bmatrix} 0 & 0 & 0 & B & rH + KB & r + mB \\ 0 & 0 & r & C & KC & mC \\ b\sin E & -a(\cos E - e) & 0 & 0 & 0 & 0 \end{bmatrix} \begin{bmatrix} d\psi_p \\ d\psi_q \\ d\psi_s \\ dM_0 \\ de \\ \frac{da}{a} \end{bmatrix} \qquad (129)$$

where

$$B = \frac{a^2}{r} e \sin E$$

$$C = \frac{a^2}{r}\sqrt{1-e^2}$$

and H, K, and m are defined by Eqs (124) through (126). The transformations from the rotational element corrections (the $d\psi$'s) to the classical element corrections proceed from a consideration of the accompanying sketch. From a projection of all vectors on the nodal line,

$$di = d\psi_p \cos\omega - d\psi_q \sin\omega . \qquad (130)$$

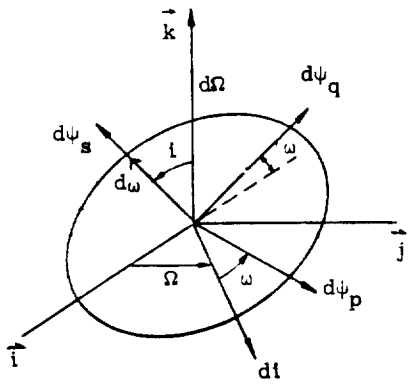

From a projection of all vectors on the line perpendicular to the nodal line in the orbit plane,

$$d\Omega \sin i = d\psi_q \cos\omega + d\psi_p \sin\omega . \qquad (131)$$

From a projection of all vectors on the normal to the orbit plane,

$$d\omega + d\Omega \cos i = d\psi_s . \qquad (132)$$

Eq (129) can be transformed to topocentric coordinates by means of the transformations of Section B.2.

$$\left\{d\vec{r}_0\right\} = T_{-0}\, T_{-\Omega}\, T_{-i}\, T_{-(\omega+\theta)} \left\{d\vec{r}_s\right\} \qquad (133)$$

where T_{-0} symbolizes the transformation from ECI to topocentric coordinates.

The final step in formulating the differential correction equations is the transformation to the differentials in the data. For example, from Eqs (42 or (45),

$$\begin{bmatrix} d\rho' \\ dm \\ dn \end{bmatrix} = T_I \left\{d\vec{r}_0\right\} \qquad (134)$$

or

$$\begin{bmatrix} d\rho \\ \cos\epsilon\, d\alpha \\ d\epsilon \end{bmatrix} = T_r \left\{d\vec{r}_0\right\} \qquad (135)$$

If Doppler data are available, the Eckert Brouwer equations must be modified, as indicated in Ref. (6).

The orbit velocity is

$$\vec{v} = \frac{1}{1 - e\cos E}\sqrt{\frac{\mu}{a}}\,(-\sin E\,\hat{p} + \sqrt{1-e^2}\cos E\,\hat{q}).$$

Since

$$dE = \frac{a}{r}\left[\sin E\, de + dM_0 - \frac{3}{2}\frac{\sqrt{\mu}}{a^{3/2}}(t - t_0)\frac{da}{a}\right],$$

$$\begin{aligned} d\vec{v} = {} & \hat{p}\left[\left(-\frac{\dot{x}_\omega}{2a} - \frac{\sqrt{\mu a}}{r^3}\, m\, x_\omega\right) da \right. \\ & - \frac{\sqrt{\mu}}{r^3}\, a^{3/2}\, x_\omega\, dM_0 \\ & \left. - \frac{\sqrt{\mu}}{r^2}\, a^{3/2} \sin E \left\{\cos E + \frac{a}{r}(\cos E - e)\right\} de\right] \\ & + \hat{q}\left[\left(-\frac{\dot{y}_\omega}{2a} - \frac{\sqrt{\mu a}}{r^3}\, m\, y_\omega\right) da \right. \\ & - \frac{\sqrt{\mu}}{r^3}\, a^{3/2}\, y_\omega\, dM_0 \\ & \left. - \frac{\sqrt{\mu a}}{r}\left(\frac{a^2}{r^2}\sqrt{1-e^2}\sin^2 E - \frac{a}{r}\sqrt{1-e^2}\cos^2 E + \frac{e\cos E}{\sqrt{1-e^2}}\right) de\right] \end{aligned}$$

Then, after a procedure similar to the derivation of $\left\{d\vec{r}_s\right\}$, the result, analogous to Eq (129) is obtained. For example,

$$-\frac{\sqrt{\mu}}{r^3}\, a^{3/2}\, \vec{r}\cdot\hat{r} = -\sqrt{\frac{\mu}{a}}\left(\frac{a}{r}\right)^2$$

$$-\frac{\sqrt{\mu}}{r^3}\, a^{3/2}\, \vec{r}\cdot\hat{n} = 0$$

$$-\frac{\sqrt{\mu}}{r^3}\, a^{3/2}\, \vec{r}\cdot\hat{m} = 0$$

$$\left(-\frac{\vec{v}}{2a} - \frac{\sqrt{\mu a}}{r^3}\, m\, \vec{r}\right)\cdot\hat{r} = -\frac{v_r}{2a} - \frac{\sqrt{\mu a}}{r^2}\, m$$

$$= -\sqrt{\frac{\mu}{a}}\,\frac{a}{r}\left(\frac{e}{2}\sin E + m\,\frac{a}{r}\right)$$

$$\left(-\frac{\vec{v}}{2a} - \sqrt{\frac{\mu a}{r^3}}\, m\vec{r}\right) \cdot \hat{n} = -1/2\, \frac{a}{r}\sqrt{\frac{\mu(1-e^2)}{a}}$$

$$\left(-\frac{\vec{v}}{2a} - \sqrt{\frac{\mu a}{r^3}}\, m\vec{r}\right) \cdot \hat{m} = 0$$

Finally,

$$\left\{d\vec{v}\right\} = \begin{bmatrix} 0 & 0 & \alpha_3 & \alpha_4 & \alpha_5 & \alpha_6 \\ 0 & 0 & \beta_3 & 0 & \beta_5 & \beta_6 \\ \gamma_1 & \gamma_2 & 0 & 0 & 0 & 0 \end{bmatrix} \begin{bmatrix} d\psi_p \\ d\psi_q \\ e\,d\psi_s \\ dM_0 + d\psi_s \\ de \\ \frac{da}{a} \end{bmatrix} \tag{136}$$

where

$$\alpha_3 = \sqrt{\frac{\mu}{a}}\, \frac{a}{r} \left(\frac{a}{r}\cos E + \frac{e}{1+\sqrt{1-e^2}}\right)$$

$$\alpha_4 = \sqrt{\frac{\mu}{a}} \left(\frac{a}{r}\right)^2$$

$$\alpha_5 = \alpha_4 \sin E$$

$$\alpha_6 = \sqrt{\frac{\mu}{a}}\, \frac{a}{r} \left(\frac{e}{2}\sin E + m\frac{a}{r}\right)$$

$$\beta_3 = \sqrt{\frac{\mu}{a}}\, \frac{a}{r} \sin E$$

$$\beta_5 = \frac{a}{r}\cos E \sqrt{\frac{\mu}{p}}$$

$$\beta_6 = -1/2\, \frac{a}{r} \sqrt{\frac{\mu(1-e^2)}{a}}$$

$$\gamma_1 = \sqrt{\frac{\mu a}{r}}\, \sqrt{1-e^2}\cos E$$

$$\gamma_2 = \sqrt{\frac{\mu a}{r}} \sin E$$

The velocity of interest is not the total velocity but the component of relative velocity along the line of sight. If R is the position vector of the observer in geocentric equatorial inertial coordinates (x, y, z) and $\vec{\rho}$ is the position vector of the satellite in topocentric coordinates,

$$\vec{r} = \vec{R} + \vec{\rho}$$

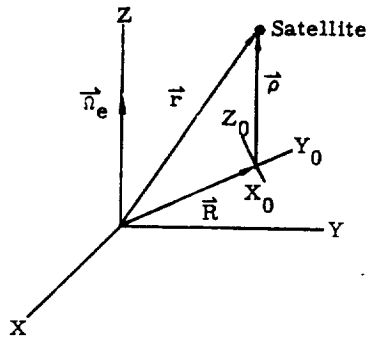

Differentiating,

$$\vec{v} = \frac{d\vec{R}}{dt} + \frac{d\vec{\rho}}{dt} + \vec{\Omega}_e \times \vec{\rho}$$

where $\frac{d\vec{\rho}}{dt}$ is the velocity of the satellite relative to the observer and $\vec{\Omega}_e$ is the angular velocity of the earth's rotation, or

$$\frac{d\vec{\rho}}{dt} = \vec{v} - \vec{\Omega}_e \times \vec{r}$$

The Doppler shift being measured is

$$\frac{d\rho}{dt} = \hat{\rho} \cdot \frac{d\vec{\rho}}{dt} = \hat{\rho} \cdot (\vec{v} - \Omega_e \times \vec{r})$$

where $\hat{\rho}$ is the unit vector along the line of sight. Then, considering variations due to changes in the orbit elements only,

$$\delta\left(\frac{d\rho}{dt}\right) = \hat{\rho} \cdot (\delta\vec{v} - \vec{\Omega}_e \times \delta\vec{r}) + (\vec{v} - \vec{\Omega}_e \times \vec{r}) \cdot \delta\left[\frac{\vec{r} - \vec{R}}{\rho}\right]$$

Since $\delta\vec{R} = 0$ (i.e., the observer's position is not a function of the orbit elements) and $\delta\rho = \delta\vec{r} \cdot \hat{\rho}$,

$$\delta\left(\frac{d\rho}{dt}\right) = \hat{\rho} \cdot \left\{\delta\vec{v}\right\} - \left\{\delta\vec{r}\right\} \cdot \left[\rho \times \vec{\Omega}_e - \frac{d\vec{\rho}}{dt}\frac{1}{\rho} + \left(\frac{d\vec{\rho}}{dt} \cdot \hat{\rho}\right)\frac{\hat{\rho}}{\rho}\right]$$

$$= \hat{\rho} \cdot \left\{\delta\vec{v}\right\} - \left\{\delta\vec{r}\right\} \cdot \left(\hat{\rho} \times \vec{\Omega}_e - \frac{d\hat{\rho}}{dt}\right)$$

where $\delta\vec{v}$ and $\delta\vec{r}$, as previously given, are the differential correction expressions involving the corrections in the elements.

G. ACCURACY OF DETERMINATIONS

1. Sources of Error

The accuracy of an orbit determination depends on not only the precision of the measurements but on knowledge of the errors and how the errors can be eliminated. Errors are broadly divided into two classes: systematic and random. Random errors can be minimized if the statistical properties of the noise spectrum are known; systematic errors, if known, can be removed by various techniques such as calibrations against known standards.

Systematic errors. Systematic errors are errors which occur in the measurements (sensors), the station location (geodetic), and the description of the orbit (simulation). Equipment sensor biases may be due to refraction effects in the measurement of angles, mechanical misalignment of the electrical axis with the geometrical axis of a parabolic reflector antenna (boresighting), drift of d-c reference voltages, surveying errors of true north or of the local horizon plane in the measurement of azimuth and elevation, error in the adopted value for the velocity of light, backlash in the servo gears which move the antenna, and sag in the antenna at different attitudes.

Range measurements, assuming a monopulse radar, can have systematic delays in propagation, false signals due to reflections, timing errors and gating errors. Some of these errors are removed by using a beacon on board the satellite which changes the frequency of the return with a known delay.

Range rate errors, using a doppler technique, can acquire systematic errors due to variable ion densities which change the frequency of the carrier to give spurious doppler effects. If a transponder is used on board, there could be small systematic retransmission errors. If the station location is not well known, there will be systematic errors for example due to errors in the calculated velocity of the station about the earth's axis.

Other geodetic uncertainties, such as in the figure of the earth, gravity anomalies, and representation of the potential function may contribute to significant errors in orbit determination. The degree of completeness of the simulation model, for example the inclusion of nongravitational losses (radiation pressure, atmospheric drag fluctuations, etc.) and perturbations due to, say, other planets or other bodies, will contribute to errors.

Noise. Some of the sources of noise which degrade observational data are atmospheric, cosmic, man-made, and thermal. Atmospheric noise is due mostly to electrical storms and varies widely throughout the year. Cosmic noise comes from the center of the galactic plane, the sun, and from a certain number of "radio" stars such as Cassiopeia.

Man-made noise comes primarily from extraneous electromagnetic radiation generated by electrical devices.

Much of the above noise can be minimized by modulation techniques which translate the information band to carrier frequencies that lie outside the noise bandwidths.

On the other hand, thermal noise covers a very wide bandwidth of frequencies and can be minimized by using specialized techniques such as phase-locked loops and cold-temperature receivers.

One obvious method of minimizing all noise is to increase the signal power. This can be accomplished by putting a transmitter on board the satellite thus eliminating the need for skin tracking.

The best set of carrier frequencies to use to minimize cosmic noise lies in the band between 1000 mc and 10,000 mc. Man-made and atmospheric noise are also extremely low in this band.

Thermal noise power at the receiver of a tracking antenna is caused by thermal agitation of electrons in the resistances in the input network. Thermal noise received power can be expressed by

$$P_N = k \cdot T \cdot \Delta f \cdot NF$$

where

P_N = Available noise power at the receiver (watts)

k = Boltzmann's constant = 1.38×10^{-32} w-sec/° K

T = Effective input temperature (not necessarily the physical ambient temperature) (°K)

Δf = Effective input noise bandwidth (cps)

NF = Noise figure of input circuit (up to the demodulator).

Reducing T, Δf, or NF will reduce the noise power. Temperature T can be reduced by bathing the receiver in a cold environment, using receivers whose effective temperature is low (such as reactive amplifiers and masers), and by "looking" only at cold space. Noise bandwidth can be reduced by using narrowband filtering but this also limits the signal bandwidth.

As long as the signal is above a certain threshold, modulation techniques such as frequency modulation and pulse code modulation can be utilized which very effectively suppress the noise. The improvement of signal to noise ratio is $\sqrt{3}$ by using an f-m system instead of an a-m system with identical input bandwidth (for random noise).

Another method of suppressing noise is to use a phase-locked loop in which a ground transmitter transmits to the satellite transponder which transmits back down to a ground receiver. The ground receiver is kept locked in phase to a multiple of the transmitter frequency by a voltage-controlled-oscillator which beats against the received frequency and whose frequency is controlled by an

error voltage from a phase detector. The voltage controlled oscillator "follows" the received frequency but with just enough lag to allow a very narrow band of frequencies to filter through the loop. This narrow band is used as the information band; and the information can be picked off by filtering. Since the bandwidth is so narrow the noise content is very small.

2. Examples of Probable Errors

Examples of the probable errors of orbit determinations based on measured standard deviations of radar stations versus various parameters follow (see Ref. 7).

Description: The sets of curves are plots of the 1σ errors of the classical elements versus radar errors. Notice that the correlations between orbital parameters have not been plotted.

Altitude	Observations
370 km	Angles and range rate (range rate held fixed)
	Angles and range (range held fixed)
	Angles and range (angles held fixed)
650 km	Same
930 km	Same
3700 km	Same

Briefly, the studies produced outputs which were the standard deviations (1 sigma) of the geocentric spherical coordinates (r, A, D, v, ν, η), orbit elements (a, e, i, Ω, ω, M), and periods (τ) of various orbits of earth satellites.

Key to Symbols:

L_v Λ_v = latitude, longitude respectively of vehicle being tracked

L_s Λ_s = latitude, longitude respectively of station(s) tracking vehicle

A = right ascension of vehicle

D = declination of vehicle

ν = velocity angle with the local geocentric vertical

η = velocity angle with north on the local horizontal plane

r = geocentric distance

v = inertial velocity

a = semimajor axis of ellipse of vehicle orbit

e = eccentricity axis of ellipse of vehicle orbit

i = inclination of orbit plane with the equatorial plane

Ω = location of node of ellipse with respect to vernal equinox Υ

ω = argument of perigee of ellipse

M = mean anomaly

τ = period of orbit

σ_j = standard deviation of any quantity j ($\sigma_\alpha = \sigma_\epsilon$)

N = number of observations

$T_\oplus$ = distance (in degrees) of earth track of vehicle at closest approach to tracking station

h = altitude from surface of $\oplus$

The spherical coordinates, orbital elements and periods were calculated by the computer program and were based on least square fits of observations. The observations were generated from trajectory tapes with noise added.

The inputs to the curve fitting program were observations (range, range rate, azimuth and elevation) of a "satellite" by a tracking station(s) versus time, the station location(s), assumed standard deviations of the observational data, the nominal orbit of the satellite, and the data rate of the station(s).

To obtain the tables and graphs included in this section, many of the input variables were varied to obtain various outputs.

Quantities varied were: observational sigmas, station locations, orbit parameters, number of iterations, earth tracks of satellites and data rates. The earth track (designated $\oplus$ track) of a satellite is the projection of the orbit upon the surface of the earth; the earth track was specified by the number of great circle degrees away from the tracking station at closest approach.

Thus graphs were obtained which were plots of σ_L, σ_ρ, $\sigma_{\dot\rho}$

$\sigma_A, \sigma_D, \sigma_r, \sigma_\nu, \sigma_\eta, \sigma_v$ versus

σ_ϵ, σ_ρ, $\sigma_{\dot\rho}$, $\oplus$ track, h, τ, Λ, L

$\sigma_a, \sigma_e, \sigma_i, \sigma_\Omega, \sigma_\omega, \sigma_M$ versus

σ_ϵ, σ_ρ, $\sigma_{\dot\rho}$, $\oplus$ track, h, τ, Λ, L

σ_τ versus σ_ϵ, σ_ρ, $\sigma_{\dot\rho}$, $\oplus$ track, h, τ, Λ, L

Only graphs showing the spherical and orbital errors versus σ_ϵ and σ_ρ are given in this section; these result in 36 graphs.

Other pertinent points:

(1) All observations were some combination of range, range rate, azimuth and elevation.

(2) All output sigmas are normalized to 16 observations by multiplying by $\sqrt{N/4}$ where N is the number of observations in a given pass of data.

(3) Azimuth and elevation sigmas are always assumed equal and are usually plotted as σ_ϵ. ($\sigma_\alpha = \sigma_\epsilon$)

(4) For comparison, most runs used only one iteration.

(5) Asymptotes are drawn on the graphs as straight lines.

Most of the graphs tend to show diminishing returns in accuracy of orbit determination in attempting to improve the angular accuracy better than 0.5° (if the sigma of range rate is held fixed at 1 fps (0.3 mps) and no range observations are taken).

Using only range and range rate observations, the same accuracies in orbit determination as above i.e., (σ_ϵ = 0.5°, $\sigma_{\dot\rho}$ = 1 fps 0.3 mps) can be obtained if the deviations are 600 ft (183 m) in range and 1 fps in range rate.

Hence a "balanced" tracking system could be defined as one whose measurement standard deviations are as follows:

$\sigma_{\dot\rho}$ = 1 fps 0.3 mps (range rate observation error)

σ_ρ = 600 ft 183 m (range observation error)

σ_ϵ = 0.5° (azimuth and elevation angular observation errors)

The word "balanced" used here is not to be used in the sense of optimum but rather in the sense that improving the accuracy of one (only) type of measurement does not produce a proportionate increase in the orbit determination (assuming a balanced system).

3. Graphical Display of Observation Errors

Three basic sets of information are presented for the mission analyst: (1) angular observation errors for an assumed standard deviation of 1 fps (0.3 mps) in range rate measurement $\sigma_{\dot\rho}$ (2) angular observation errors for an assumed standard deviation of 600 ft (183 m) in range measurement σ_ρ, and (3) range observation errors for an assumed standard deviation of 0.05° in azimuth and elevation angle measurement σ_ϵ. For each set are shown the six spherical coordinates (σ: A, D, r, ν, η, v) and the six orbital elements (σ: a, e, i, Ω, ω, M) for orbits of four different altitudes (approximately 370, 650, 930 and 3700 km).

(1) Figures 8 through 19 (Set 1). These figures show the standard deviations of the six geocentric spherical coordinates and the standard deviations of the six orbital elements as a function of the angular observation error for four altitudes, where $\sigma_{\dot\rho}$ = 1 fps (0.3 mps).

(2) Figures 20 through 31 (Set 2). These figures show the same variables where σ_ρ = 600 ft (180 m).

(3) Figures 32 through 43 (Set 3). These figures show the standard deviations of the six spherical coordinates and the six orbital elements as a function of the range observation error for four altitudes, where σ_ϵ = 0.05°.

The initial conditions for both the angular and range observation error computations are given in Table 5 as a function only of orbital altitude.

The asymptotic values of the standard deviations of the six spherical coordinates and six orbital elements for Sets 1, 2 and 3 are given in Table 6. These are the limiting values in each dependent variable as the independent variable becomes very large. Because the data rate is the same for each orbital altitude, 18 observations are contained in the results for the 365-km orbit, 27 for the 645-km orbit, 33 for the 922-km orbit and 91 for the 3710-km orbit.

TABLE 5

Initial Conditions for Angular and Range Observations
(see Figures 8 to 43)

	Altitude (km)			
	365	645	922	3710
t	0	0	0	0
L_v	0°	0°	0°	0°
L_s	60° N	60° N	60° N	60° N
Λ_v	0°	0°	0°	0°
Λ_s	353° E	353° E	353° E	356° E
A	202.7°	202.7°	202.7°	202.7°
D	0°	0°	0°	0°
ν	90°	90°	90°	90°
η	0°	0°	0°	0°
r	6.745×10^6 m	7.01×10^6 m	7.300×10^6 m	10^7 m
v	7688 m/sec	7534 m/sec	7389 m/sec	6286 m/sec
a	6.742×10^6 m	7.01×10^6 m	7.300×10^6 m	10^7 m
e	0.00069	0.00009	0.0009	0.00012
i	90°	90°	90°	90°
Ω	202.7°	202.7°	202.7°	202.7°
ω	-213.2°	-180°	-180°	-180°
M	4.13	3.14	3.14	3.14
τ	91.86 min	97.6 min	103.4 min	168.07 min
N	18	27	33	91
$T_\oplus$	3.4° E	3° E	3° E	10° W

TABLE 6

Asymptotes of Dependent Variable, Figures 8 to 43

	365 (height in km)	645 (height in km)	922 (height in km)	3710 (height in km)
		Set of 1 as $\sigma_\epsilon \to \infty$ (σ_ρ = 1 fps) (0.3 mps)		
σ_A (deg)	0.033	0.040	0.015	0.040
σ_D (deg)	0.041	0.038	0.017	0.0036
σ_ν (deg)	0.018	0.018	0.008	0.0012
σ_η (deg)	0.018	0.022	0.009	0.023
σ_r (km)	3.688	3.658	1.768	3.048
σ_v (m/sec)	0.43	4.27	2.0	0.30
σ_a (m)	96.0	122	65.8	131
σ_e	0.625×10^{-7}	0.063×10^{-7}	0.030×10^{-7}	0.870×10^{-7}
σ_i (deg)	0.018	0.021	0.009	0.023
σ_Ω (deg)	0.032	0.04	0.015	0.041
σ_ω (deg)	2.6	26.0	12.4	2.1
σ_M (deg)	2.6	26.0	12.4	2.1
		Set 2 as $\sigma_\epsilon \to \infty$ (σ_ρ = 180 m)		
σ_A (deg)	0.040	0.031	0.026	0.019
σ_D (deg)	0.038	0.021	0.016	0.005
σ_ν (deg)	0.018	0.010	0.007	0.0015
σ_η (deg)	0.022	0.016	0.014	0.002
σ_r (km)	3.658	2.377	1.615	4.88
σ_v (m/sec)	4.27	2.0	1.6	0.30
σ_a (m)	122	99.1	94.5	110
σ_e	6.7×10^{-7}	6.3×10^{-7}	7.6×10^{-7}	0.55×10^{-7}
σ_i (deg)	0.021	0.017	0.014	0.019
σ_Ω (deg)	0.037	0.031	0.026	0.019
σ_ω (deg)	25.5	14.0	21.0	2.2
σ_M (deg)	25.6	14.0	21.0	2.2
		Set 3 as $\sigma_\epsilon \to \infty$ (σ_ϵ = 0.05 deg)		
σ_A (deg)	0.015	0.014	0.014	0.013
σ_D (deg)	0.017	0.017	0.018	0.022
σ_ν (deg)	0.0085	0.0083	0.0090	0.0085
σ_η (deg)	0.0087	0.0082	0.0082	0.0077
σ_r (km)	1.768	1.798	1.890	2.012
σ_v (m/sec)	2.01	1.92	1.89	1.83
σ_a (m)	70.4	79.2	88.4	131
σ_e	3.0×10^{-7}	5.3×10^{-7}	9.0×10^{-7}	2.9×10^{-7}
σ_i (deg)	0.009	0.008	0.006	0.008
σ_Ω (deg)	0.015	0.014	0.018	0.013
σ_ω (deg)	12.2	13.0	25.7	12.0
σ_M (deg)	12.2	13.0	25.7	12.0

H. REFERENCES

1. Brouwer, D., and Clemence, G., "Methods of Celestial Mechanics," Academic Press, New York, 1961, pp 187 to 209.

2. Kaula, W., "Celestial Geodesy," NASA TN D-1155, March 1962.

3. Baker, R., Jr., and Makemson, M., "Astrodynamics," Academic Press, 1960, pp 240, 241.

4. Herget, P., "The Computation of Orbits," published privately, 1948.

5. Eckert, W., and Brouwer, D., "The Use of Rectangular Coordinates in the Differential Correction of Orbits," Astronomical Journal, No. 1069, 16 August 1937.

6. Bowden, G., and Flis, J. (editors), "Notes of the Summer Institute in Dynamical Astronomy at Yale University," July 1959.

7. Ireland, R., "Tracking Studies," STL Report 7340.2-172, 30 October 1960.

I. BIBLIOGRAPHY

Baker, R. M. L., Jr.,
"High Precision Orbit Determination," ASI Monthly Progress Report, November 1958. (Also, ASI Monthly Progress Report, December 1958, Appendix B.)
"Orbit Determination from Range and Range-Rate Data," American Rocket Society, 1960, Paper No. 1220-60.

Baker, R. M. L., Jr., et al., "Efficient Precision Orbit Computation Techniques," ARS Journal, Vol. 30, No. 8, August 1960, pp 740 to 747. (Also, Los Angeles, California, University of California, 11 June 1959, Astrodynamical Report No. 3.)

Barr, T. A., and Lundquist, C. A., "Tracking Experiments with Pioneer IV," IRE Transactions on Military Electronics, Vol. MIL-4, Nos. 2-3, April to July 1960, pp 355 to 359.

Batrakov, Yu. V., "Determination of the Preliminary Orbits of Artificial Satellites from Observations with Time Approximately Known," ARS Journal, Russian Supplement, Vol. 30, No. 9, September 1960, pp 859 to 864.

Berger, W. J., and Ricupita, J. R., "Prediction Theory of Missile and Satellite Orbits," ARS Journal, Vol. 29, No. 6, June 1959.

Besag, P. L., and Anderson, J. T., "Determination of the Orbit of an Artificial Satellite," IRE Proceedings, Vol. 48, No. 5, 1960, p 950.

Bode, H. W., and Shannon, C. E., "A Simplified Derivation of Linear Least Squares Smoothing and Prediction Theory," IRE Proceedings, Vol. 38, 1950, pp 417 to 425.

Brown, D. C., "A General Solution to the Problem of the Adjustment of Trajectory Observations," RCA Data Processing, Florida, AFMTC, TM-54, 6 March 1959.

Bryant, R.,
"Interim Definitive Orbits Determined at the NASA Computing Center," California Institute of Technology, Jet Propulsion Laboratory, Pasadena, California, JPL Proceedings of Seminar on Orbit Prediction, February 1960.
"NASA Computing Center Predictions," California Institute of Technology, Jet Propulsion Laboratory, Pasadena, California, JPL Proceedings of Seminar on Orbit Prediction, February 1960.

Cahill, W. F., and Harris, I., "Determination of Satellite Orbits from Radar Data," NASA TN D-489, 1960. (Also, American Rocket Society, Preprint No. 940-59.)

Carr, R., et al., "Tracking and Orbit Determination Program of JPL," California Institute of Technology, Jet Propulsion Laboratory, Pasadena, California, JPL Report No. TR-32-7, February 1960.

Cormier, L. N., Goodwin, N., and Squires, R. K., "Simplified Satellite Prediction from Modified Orbital Elements," Annals of the International Geophysical Year, Vol. XII, Pergamon Press, New York, 1960, pp 83 to 84.

Crawford, R. T., "Determination of Orbits of Comets and Asteroids," New York, McGraw-Hill Book Company, 1930.

Darlington, S., "Linear Least-Squares Smoothing and Prediction with Applications," Bell Systems Technical Journal, Vol. 37, 1958.

Debey, L. G., "Tracking in Space by DOPLOC," IRE Transactions on Military Electronics, Vol. MIL-4, Nos. 2-3, April to July 1960, pp 332 to 335.

Deutch, A., "Orbits for Planetary Satellites from Doppler Data," ARS Journal, Vol. 30, No. 6, June 1960.

Dubyago, A., "The Determination of Orbits," New York, The Macmillan Company, 1961.

Duke, D., "Orbit Determination from Optical Tracking," Journal of the Society of Motion Picture and Television Engineers, Vol. 69, No. 1, 1960, pp 9 to 14.

Eimer, M., et al., "Evaluation of Pioneer 4 Orbit Determination Program," California Institute of Technology, Jet Propulsion Laboratory, Pasadena, California, JPL Technical Release No. 34-26, February 1960.

Friedland, B., "Least Squares Filtering and Prediction of Nonstationary Sampled Data," Information and Control, Vol. 1, 1958, pp 297 to 313.

Glazier, E. V. D. (ed.), et al., "Avionics Research: Satellites and Problems of Long Range Detection and Tracking," London, Pergamon Press, 1960.

Glover, C. C., "Optimum Prediction with a Mean Weighted Square-Error Criterion," Inst. Radio Engrs., Trans. Automatic Control, Vol. AC-6, No. 1, February 1961, pp 43 to 48.

Guier, W. H.,
"Doppler Tracking of Project Transit Satellites," IRE Transactions of the Space Electronics and Telemetry Symposium, September 1960.
"A Satellite Doppler Navigation System," IRE Proceedings, Vol. 48, No. 4, 1960, pp 507 to 516.

Harris, I., and Cahill, W. F., "Determination of Satellite Orbits from Radar Data," IRE Proceedings, Vol. 48, No. 9, September 1960, pp 1657 to 1658.

Herrick, S.,
"Observation Requirements for Precision Orbit Determination," Aeronautics and Astronautics, New York, Pergamon Press, 1960, pp 417 to 434.
"Orbits from Position and Velocity," University of California, Los Angeles, California, Astrodynamical Report No. 8 (AFOSR TN 60-816), July 1960.
"A Comparison of Astronomical and Ballistic Traditions in Orbit Computation," Astrodynamical Report No. 14, University of California Dept. of Astronomy, May 1962.

Kaula, W. M., "Celestial Geodesy," NASA TN D-1155, March 1962.

King-Hele, D. G., and Walker, D. M. C.,
"Methods for Predicting the Orbits of Near Earth-Satellites," Journal of the British Interplanetary Society, Vol. 17, No. 1, 1959, pp 2 to 14.

Kraft, J. D., "Satellite Orbit Computation," Design Guide to Orbital Flight, McGraw-Hill Book Company, New York, 1962, Chapter 11.

Kulikov, D. K., and Batrakov, Yu. V., "Method for Improving Orbits of Artificial Satellites of the Earth Using Observations with Approximate Values of Time," ARS Journal, Russian Supplement, Vol. 30, No. 9, 1960, pp 865 to 874.

Lane, R. E., "Mathematical Processes, Smoothing and Differentiating Experimental Data," University of Texas, Austin, Texas, MPRL-419, 18 June 1958.

Lawden, D. F., "The Calculation of Orbits," Journal of the British Interplanetary Society, Vol. 14, No. 4, July to August 1955.

Magness, T. A., and McGuire, J. B., "Statistics of Orbit Determination-Correlated Observations," STL Report No. 8976-6001-RU-ODO.

Mechau, D. V., "List of Coordinates of Stations Engaged in the Observation of Artificial Earth Satellites," Cambridge, Massachusetts, Smithsonian Astrophysical Observatory, Special Report No. 45, 1960.

Mowlem, A., "The Programming System for Orbit Determination at IBM Space Computing Center," California Institute of Technology, Jet Propulsion Laboratory, Pasadena, California, JPL Technical Release No. 34-26, February 1960.

Muhleman, D., "Satellite Orbit Determination and Prediction Utilizing JPL Goldstone 85-Ft Antenna and JPL Tracking Program," California Institute of Technology, Jet Propulsion Laboratory, Pasadena, California, JPL Technical Release No. 34-27, February 1960.

Munick, H., "Determination of Elements of an Elliptic Orbit from the Orbital Velocity Vector," ARS Journal, Vol. 29, No. 2, February 1959, p 150.

Rechtin, E., "Satellite Tracking," California Institute of Technology, Jet Propulsion Laboratory, Pasadena, California, American Rocket Society Preprint No. 649-58, 1958.

Richards, P. B., "Orbit Determination of a Nontransmitting Satellite Using Doppler Tracking Data," General Electric Company, Missile and Space Vehicle Department, Philadelphia, Pennsylvania, Institute of Aeronautical Sciences, Preprint No. 61-141-1835, June 1961.

Rossoni, J. P., "Technical Aspects of Satellite Tracking on IBM Computers at Smithsonian Astrophysical Observatory in Cambridge," California Institute of Technology, Jet Propulsion Laboratory, Pasadena, California, JPL Technical Release No. 34-26, February 1960.

Shapiro, L., "The Prediction of Ballistic Missile Trajectories from Radar Observations," McGraw-Hill Book Company, New York, 1957.

Silva, R. R., "Millstone Operations Related to the Pioneer V Space Probe," Massachusetts Institute of Technology, Lincoln Laboratories, Cambridge, Massachusetts, Report No. 30-G-0007, 1960.

Siry, J. W., "The Vanguard Orbit Determination Program," Annals of the International Geophysical Year, Vol. XII, Pergamon Press, New York, pp 91 to 104.

Sperling, H. J.,
"On the Computation of Keplerian Ellipses," Huntsville, Alabama, Army Ballistic Missile Agency, ABMA Report No. DA-TM-48-60, 1960.
"Survey of Space Flight Decks Used at ABMA," California Institute of Technology, Jet Propulsion Laboratory, Pasadena, California, JPL Technical Release No. 34-26, February 1960.

Swerling, P., "Computer Program for First Order Error Propagation in Satellite Orbit Prediction," California Institute of Technology, Jet Propulsion Laboratory, Pasadena, California, JPL Proceedings of Orbit Prediction Symposium,

February 1960 (Martin Library No. MR 5982-Z-65).

Szebehely, V. G., "Lunar and Interplanetary Trajectory Determination Activities at General Electric," California Institute of Technology, Jet Propulsion Laboratory, Pasadena, California, JPL Technical Release No. 34-26, February 1960.

Tross, C., "Lunar Vehicle Orbit Determination," California Institute of Technology, Jet Propulsion Laboratory, Pasadena, California, JPL Technical Release No. 34-26, February 1960.

Veis, G., and Moore, C., "Smithsonian Astrophysical Observatory Differential Orbit Improvement Program," California Institute of Technology, Jet Propulsion Laboratory, Pasadena, California, JPL Proceedings of Orbit Prediction Symposium, February 1960 (Martin Library No. MR 5982-Z-65).

Walters, L. G., et al.,
"Differential Correction Experimentation with Low Eccentricity Orbits," American Rocket Society, Preprint No. 960-59, November 1959.
"Differential Orbit Correction Experimentation with Satellites 1958 Alpha 1 and 58 ϵ," California Institute of Technology, Jet Propulsion Laboratory, Pasadena, California, JPL Proceedings of Seminar on Orbit Prediction, February 1960 (Martin Library No. MR 5982-Z-65).

Wasel, A. D., "Orbital Elements, Trajectory Simulation, and Prediction for Earth Satellites," Journal of the British Interplanetary Society, Vol. 17, September to October 1959, pp 130 to 133.

Weirauch, R. F., "On the Accuracy of an Elliptical Orbit Determination," Stockholm, XIth International Astronautical Congress, 1960.

Welborn, E., "Mathematical Processes, Sets of Coefficients for Data Processing Formulas," University of Texas, Austin, Texas, MPRL-475, 5 May 1959.

Westrom, G., and Van Sant, C. T., "Differential Correction of Earth Satellite Orbits Including the Drag Perturbation," Aeronutronic, Division of Ford Motor Company, Newport Beach, California, Institute of Aeronautical Sciences Preprint No. 61-140-1834, 1961.

Williams, K. P., "The Calculation of the Orbits of Asteroids and Comets," Bloomington, Indiana, Principia Press, 1934.

"Contribution to Astrodynamics: Astrodynamic Analysis for the National Space Surveillance Control Center," Volume I and Volume II, Aeronutronic, Newport Beach, California, Publication No. U-880, 1960.

"Curve Fitting and Filtering Theory, Down-Range Antiballistic Measurement Program (DAMP)," RCA, MSRD, Moorestown, New Jersey.

"Seminar Proceedings: Tracking Programs and Orbit Determination," California Institute of Technology, Jet Propulsion Laboratory, Pasadena, California, JPL Technical Release No. 34-26, February 1960 (Martin Library No. MR 5982-Z-65).

ILLUSTRATIONS

Preceding page blank

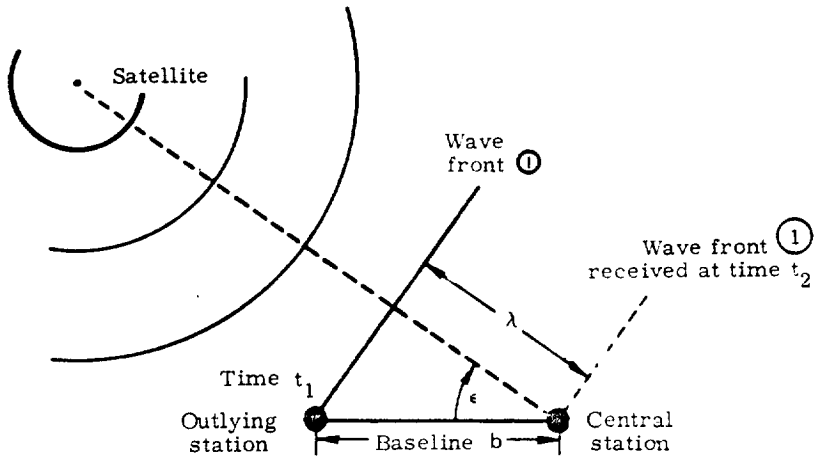

λ is the wavelength of the carrier from the satellite
c is the velocity of propagation
b is the distance between stations

Fig. 1. Interferometer System

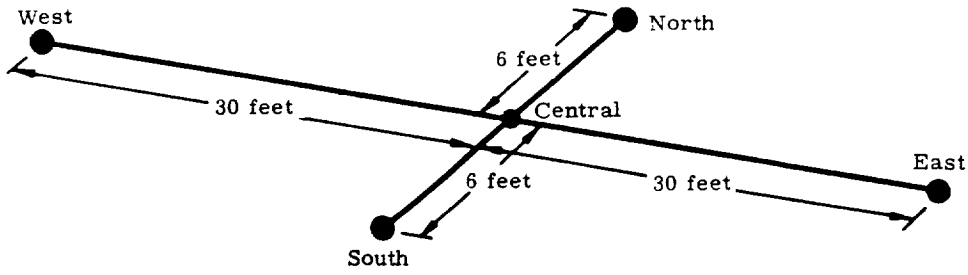

The claimed accuracy in angles: 20" to 40" (0.1 - 0.2 mrad)
in optimum atmosphere conditions
400" in bad weather

Frequency: 108 mc (λ = 9 ft)

Fig. 2. Minitrack Modified Interferometer System

Preceding page blank

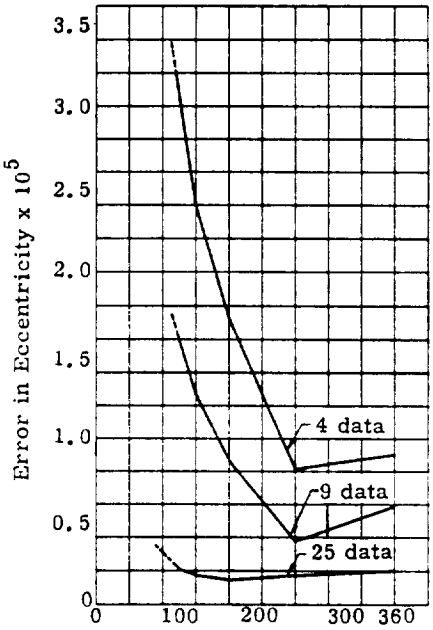

Fig. 3. Effect of Spread and Number of Data on Accuracy of Eccentricity Determination

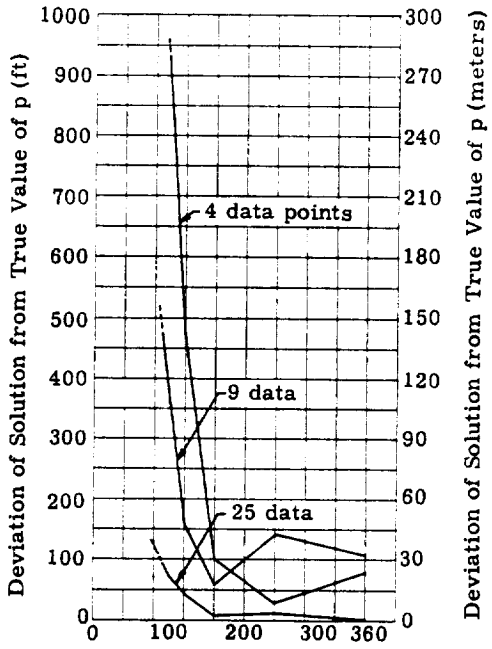

Fig. 4. Effect of Spread and Number of Data on Accuracy of Semilatus Rectum Determination

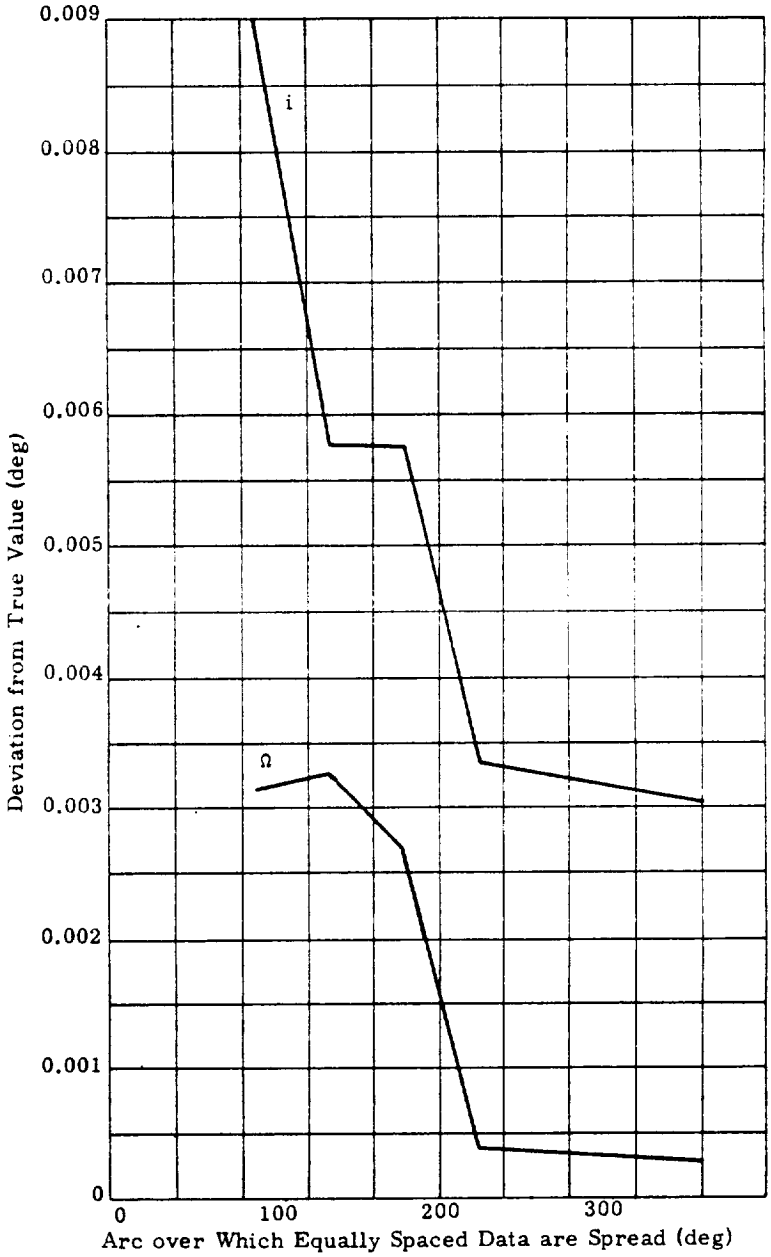

Fig. 5. Effect of Spread of Data on Accuracy of Inclination and Nodal Longitude Determination

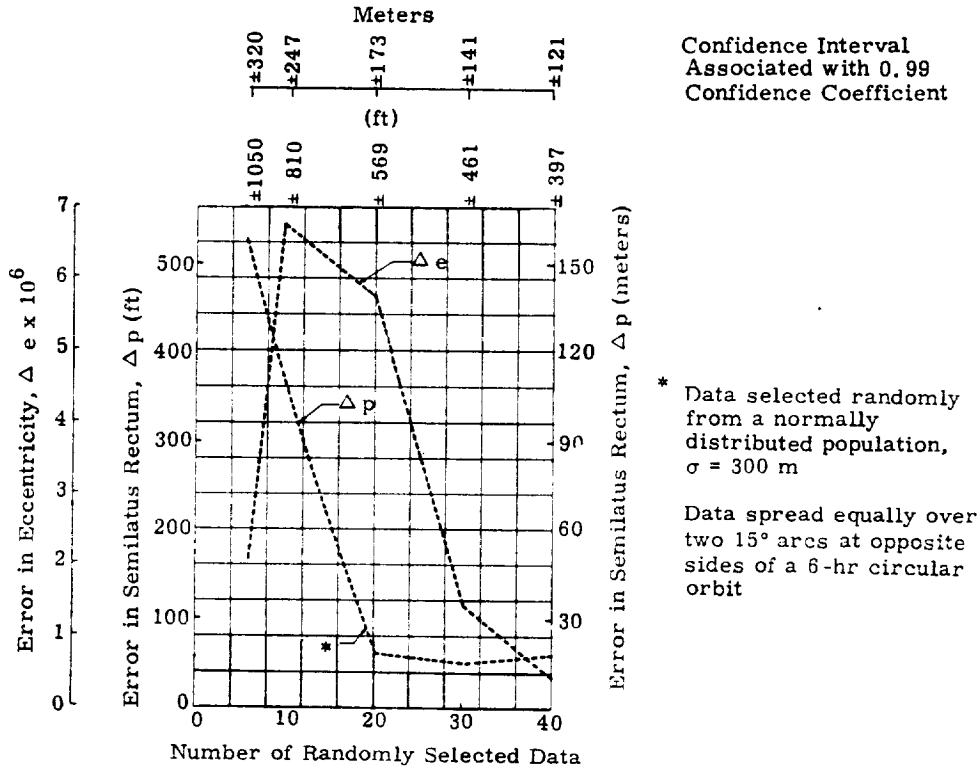

Fig. 6. Effect of a Limited Number of Data on Accuracy of Orbit Determination

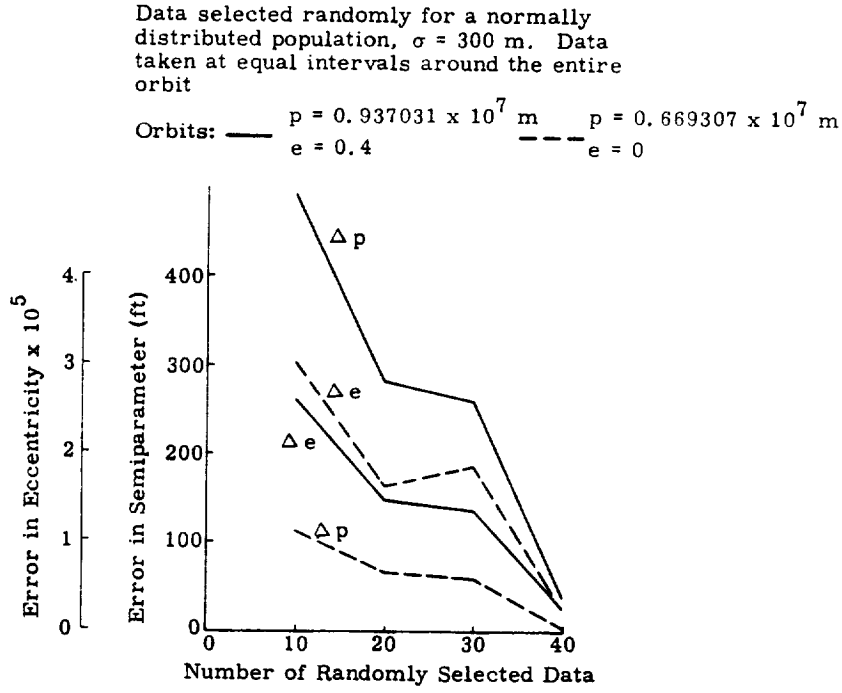

Fig. 7. Effect of a Limited Number of Data on Accuracy of Orbit Determination

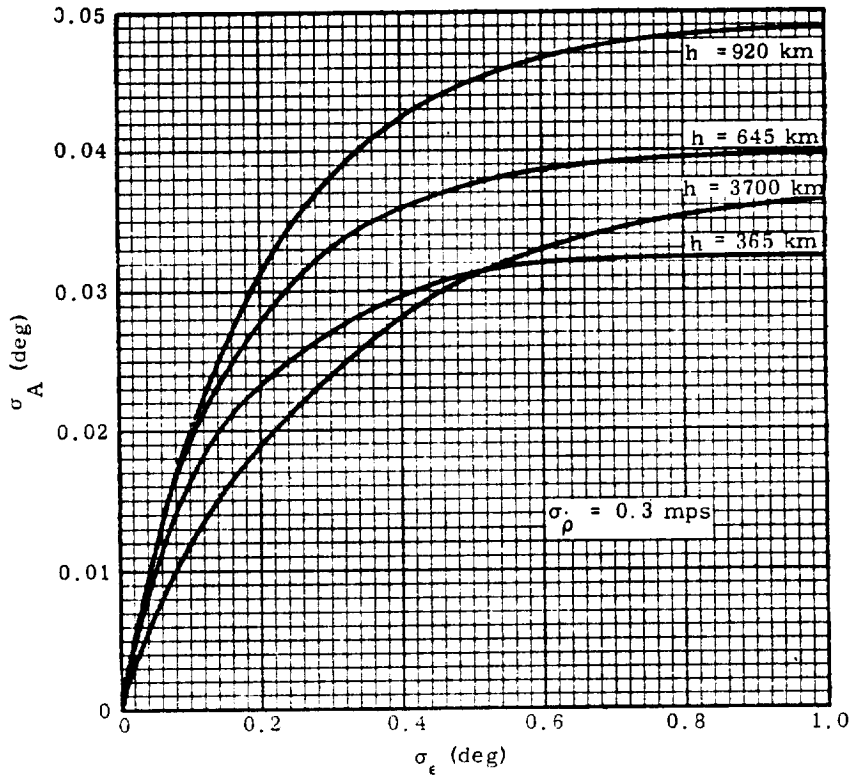

Fig. 8. Angular Observation Errors, σ_A Versus σ_ϵ

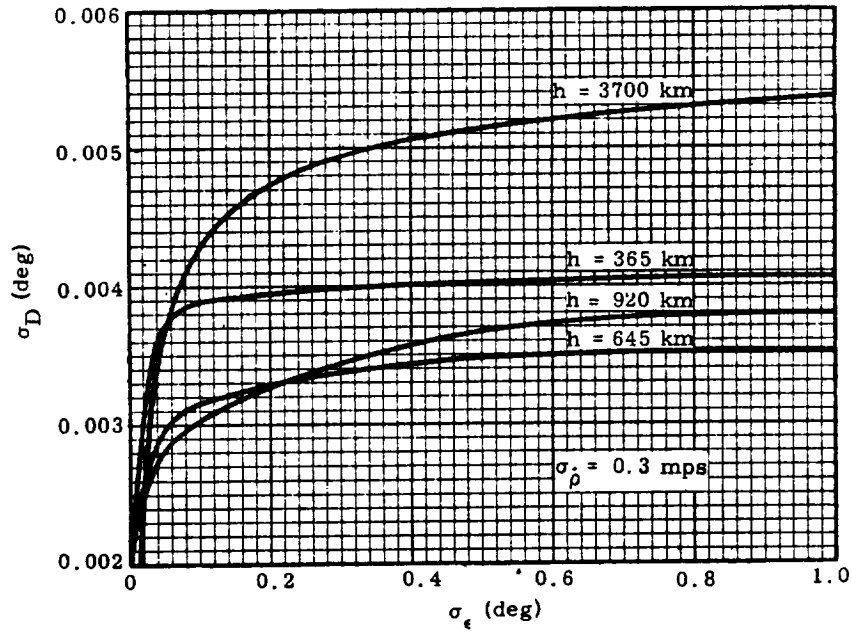

Fig. 9. Angular Observation Errors, σ_D Versus σ_ϵ

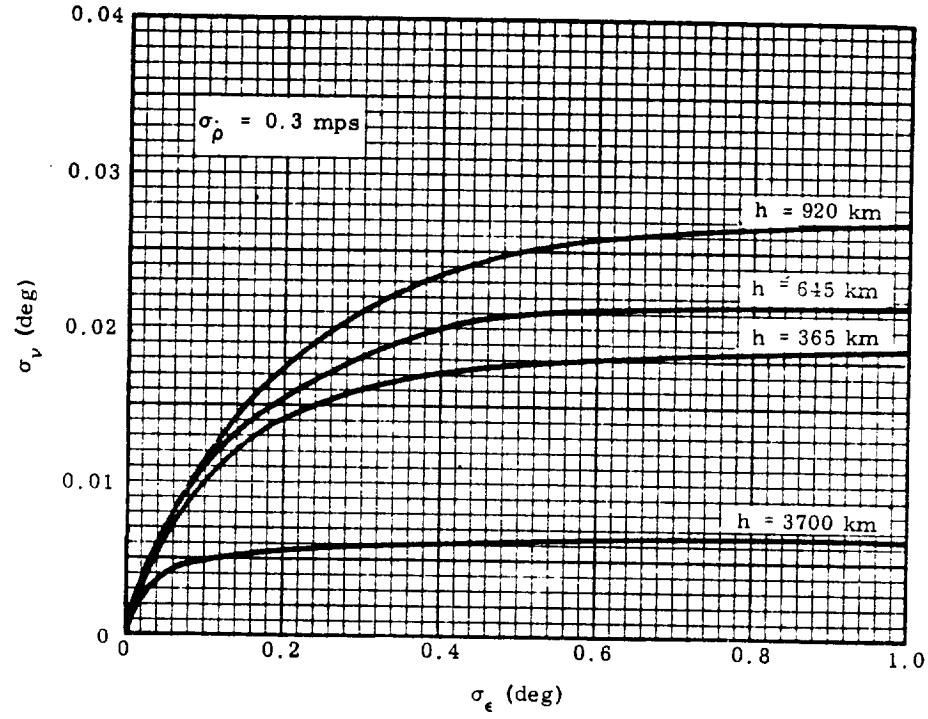

Fig. 10. Angular Observation Errors, σ_ν Versus σ_ϵ

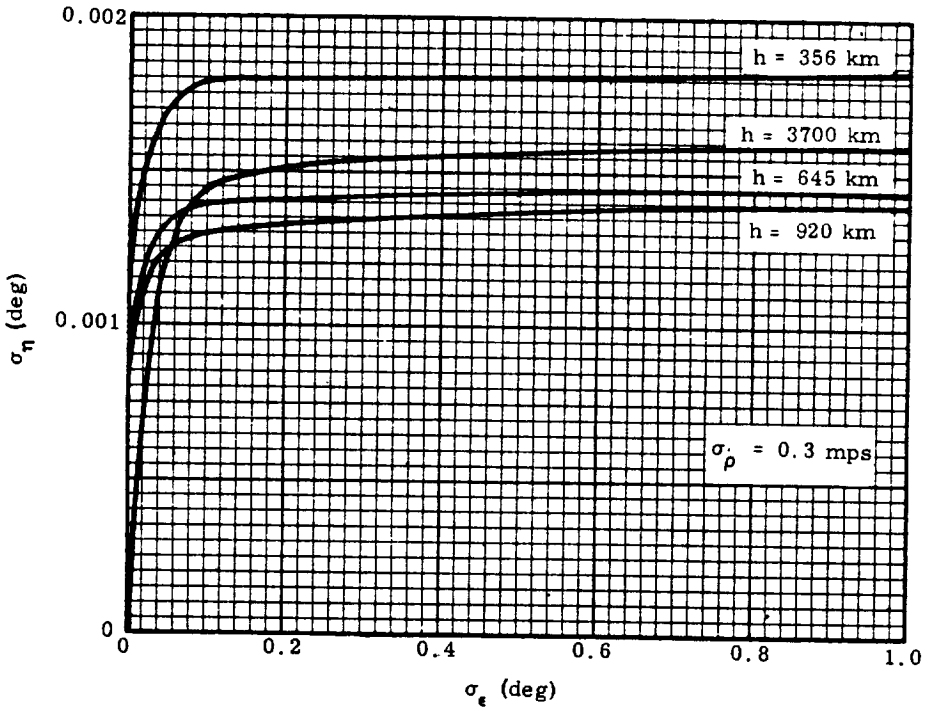

Fig. 11. Angular Observation Errors, σ_η Versus σ_ϵ

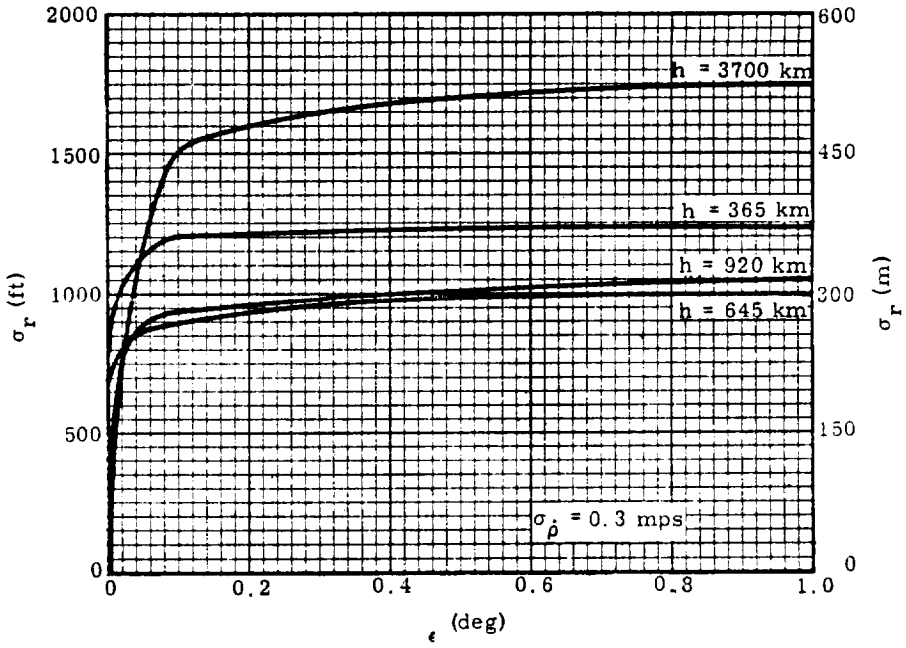

Fig. 12. Angular Observation Errors, σ_r Versus σ_ϵ

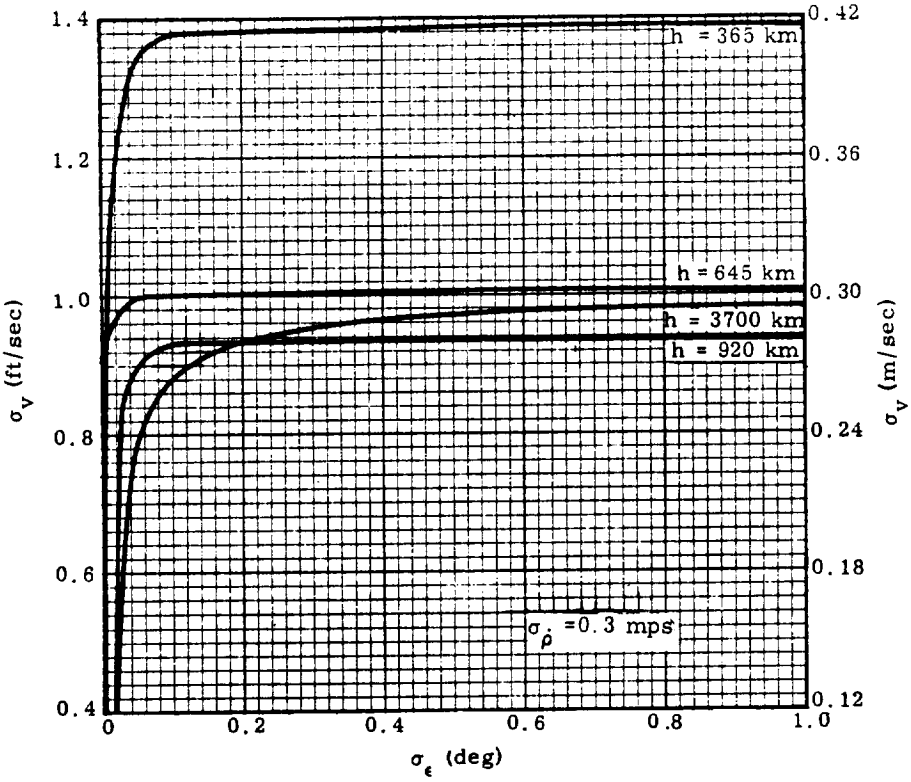

Fig. 13. Angular Observation Errors, σ_V Versus σ_ϵ

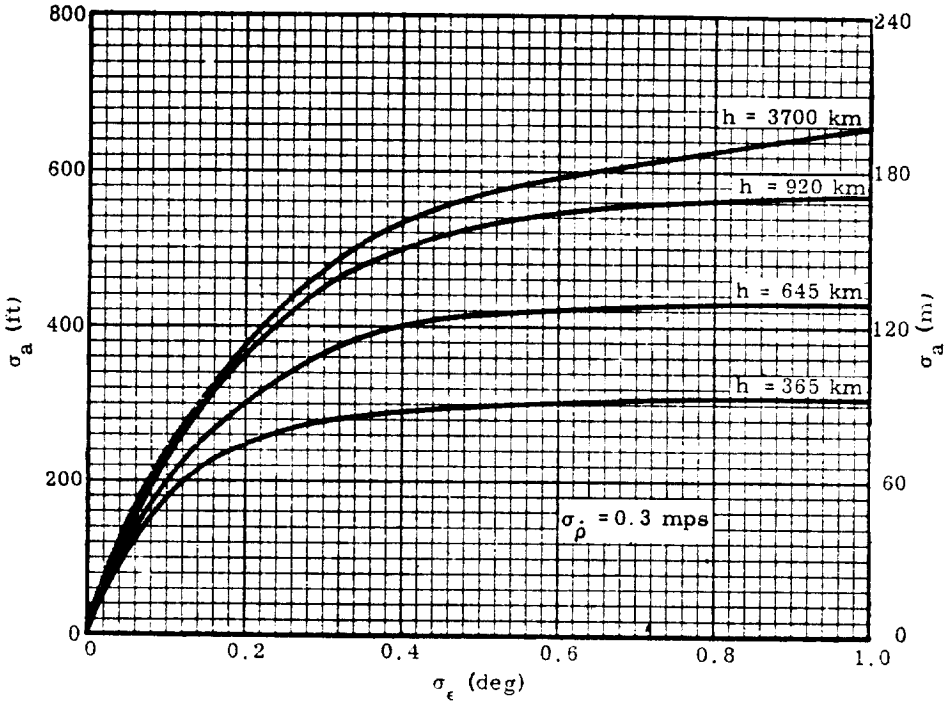

Fig. 14. Angular Observation Errors, σ_a Versus σ_ϵ

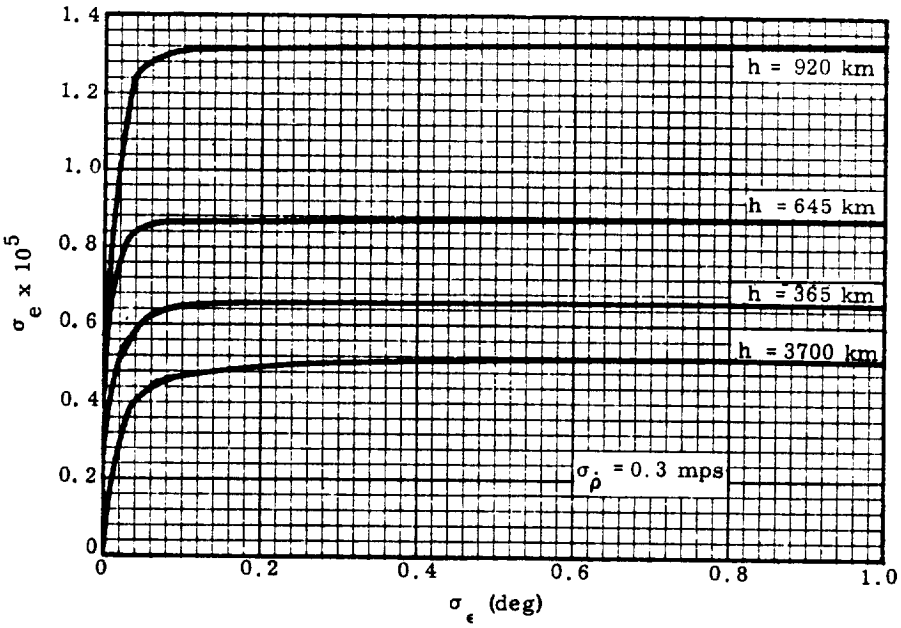

Fig. 15. Angular Observation Errors, σ_e Versus σ_ϵ

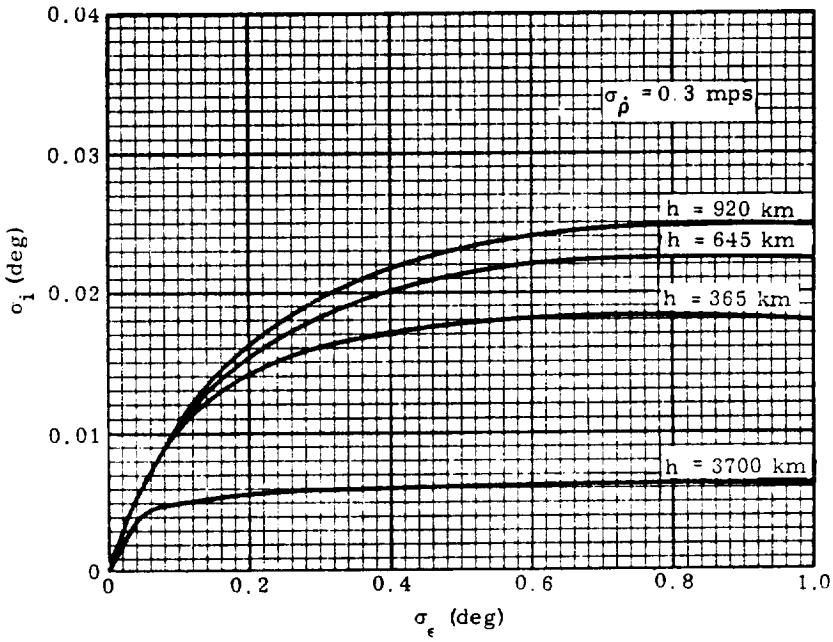

Fig. 16. Angular Observation Errors, σ_i Versus σ_ϵ

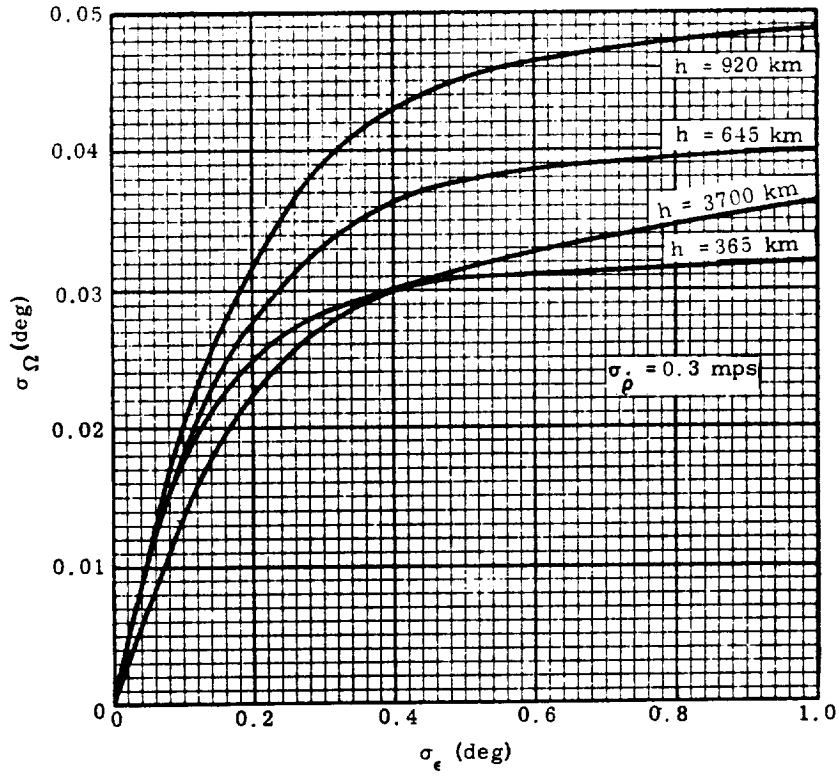

Fig. 17. Angular Observation Errors, σ_Ω Versus σ_ϵ

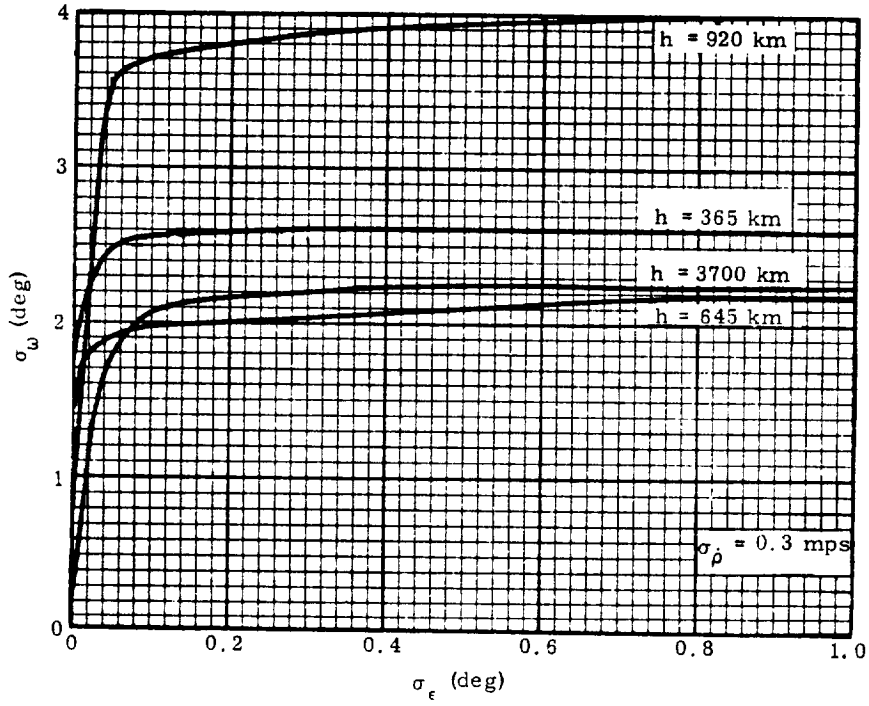

Fig. 18. Angular Observation Errors, σ_ω Versus σ_ϵ

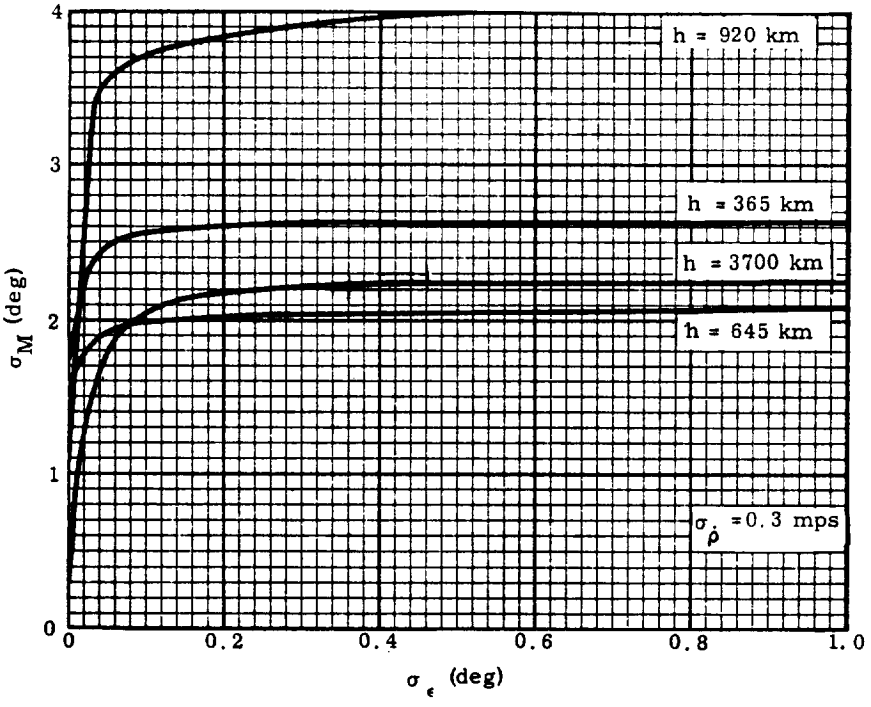

Fig. 19. Angular Observation Errors, σ_M Versus σ_ϵ

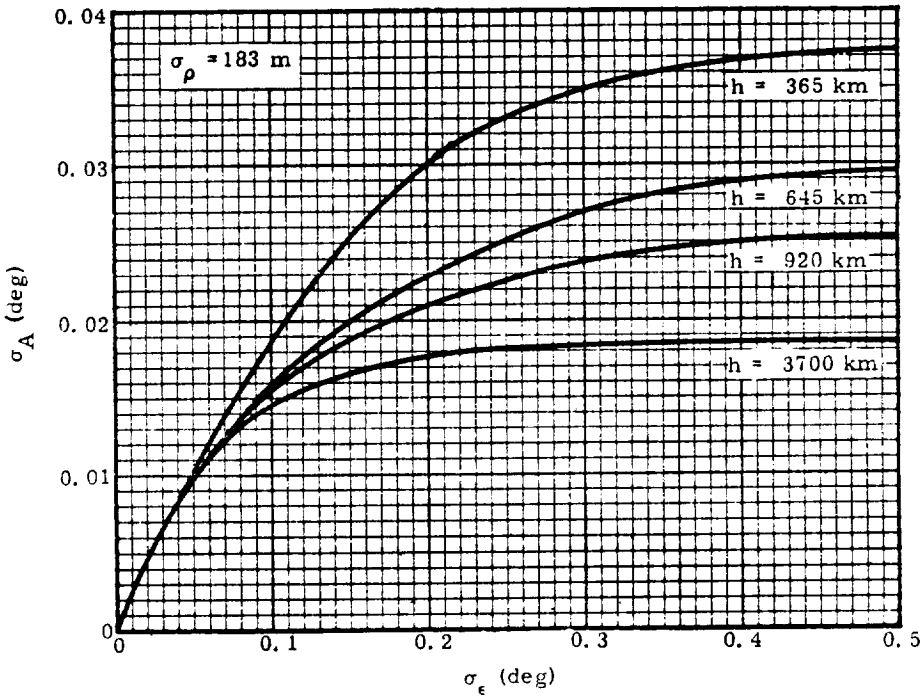

Fig. 20. Angular Observation Errors, σ_A Versus σ_ϵ

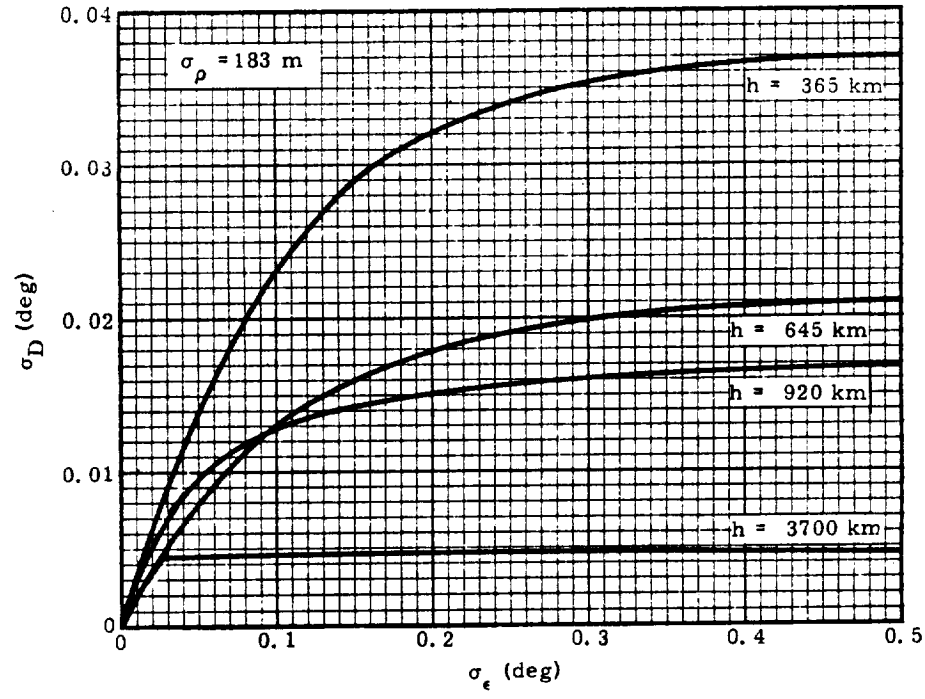

Fig. 21. Angular Observation Errors, σ_D Versus σ_ϵ

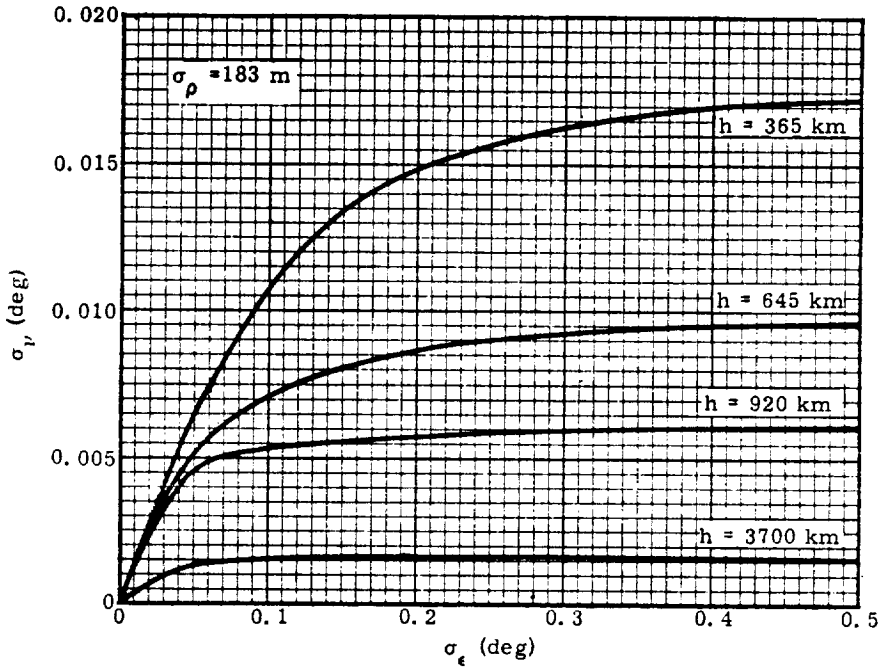

Fig. 22. Angular Observation Errors, σ_ν Versus σ_ϵ

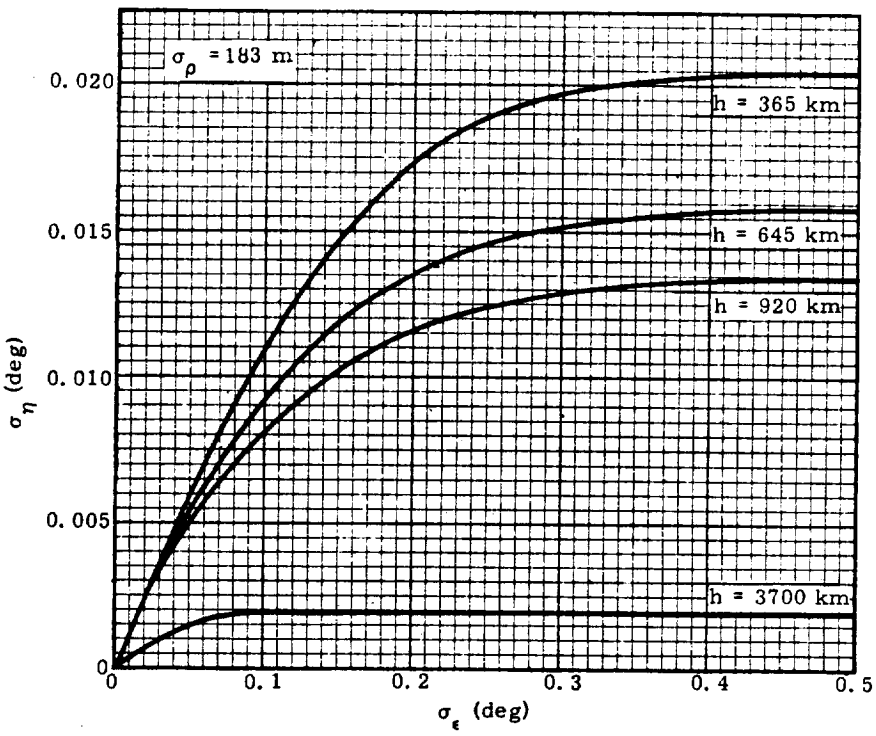

Fig. 23. Angular Observation Errors, σ_η Versus σ_ϵ

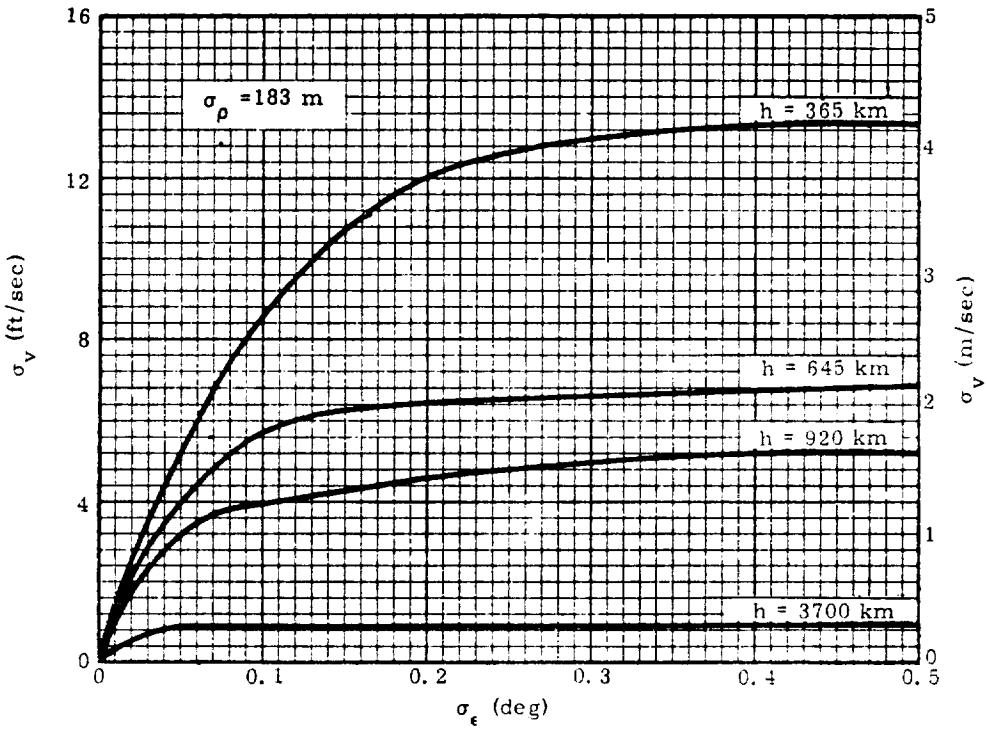

Fig. 24. Angular Observation Errors, σ_v Versus σ_ϵ

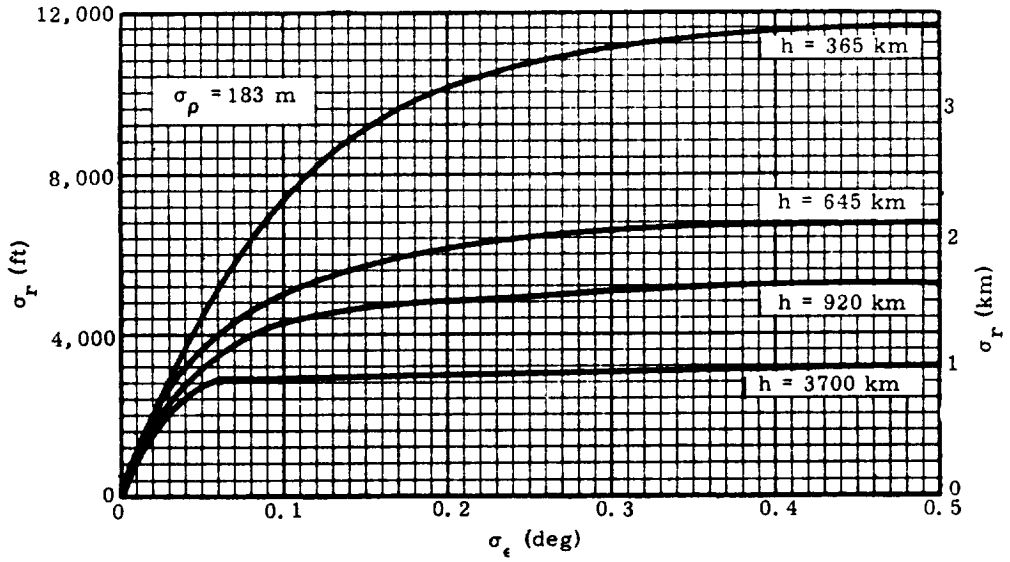

Fig. 25. Angular Observation Errors, σ_r Versus σ_ϵ

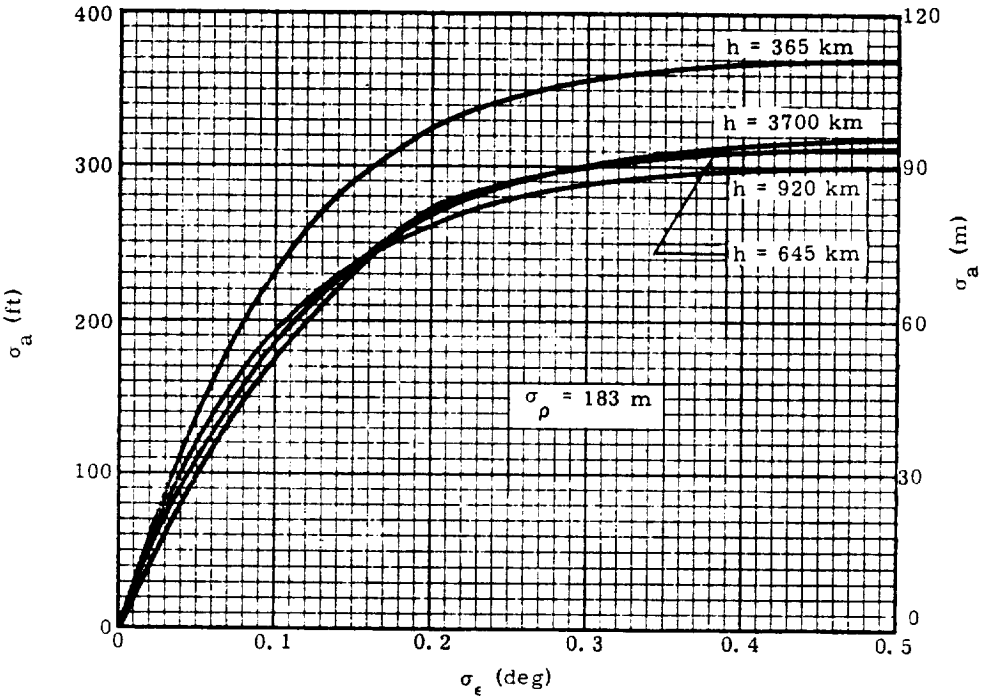

Fig. 26. Angular Observation Errors, σ_a Versus σ_ϵ

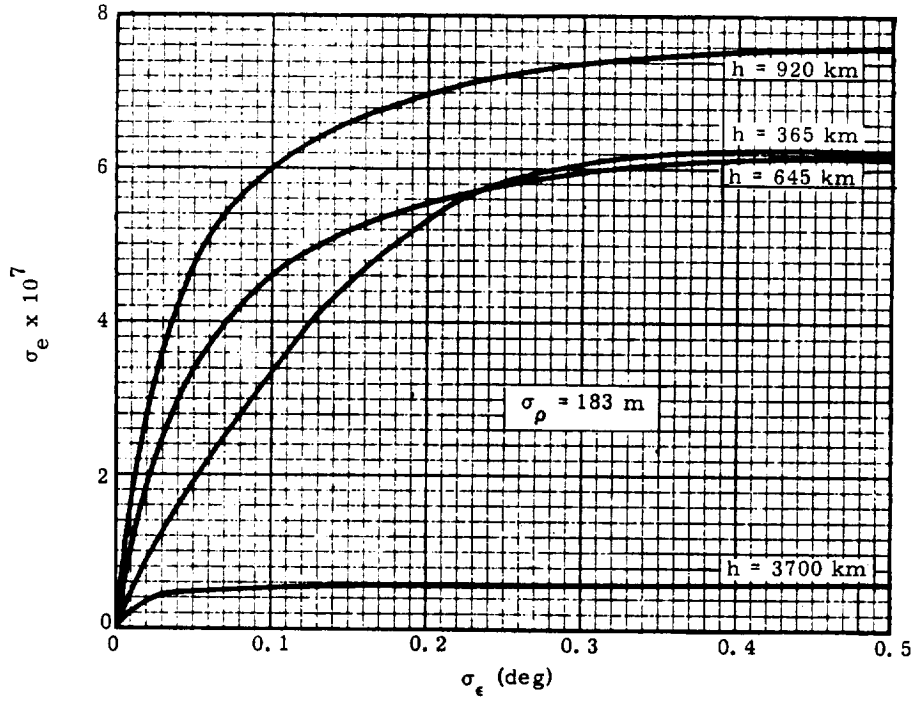

Fig. 27. Angular Observation Errors, σ_e Versus σ_ϵ

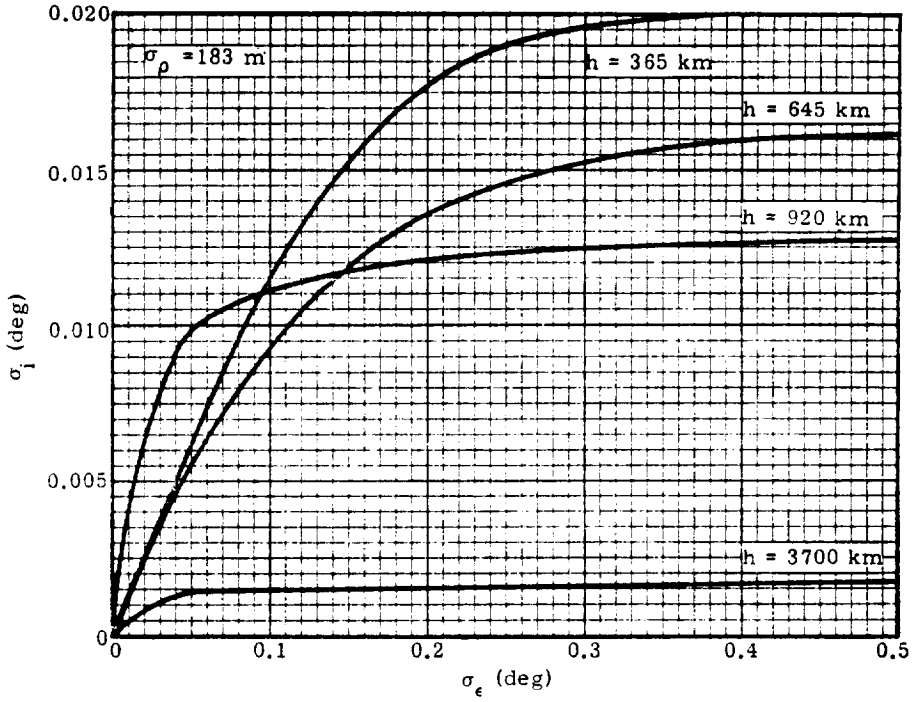

Fig. 28. Angular Observation Errors, σ_i Versus σ_ϵ

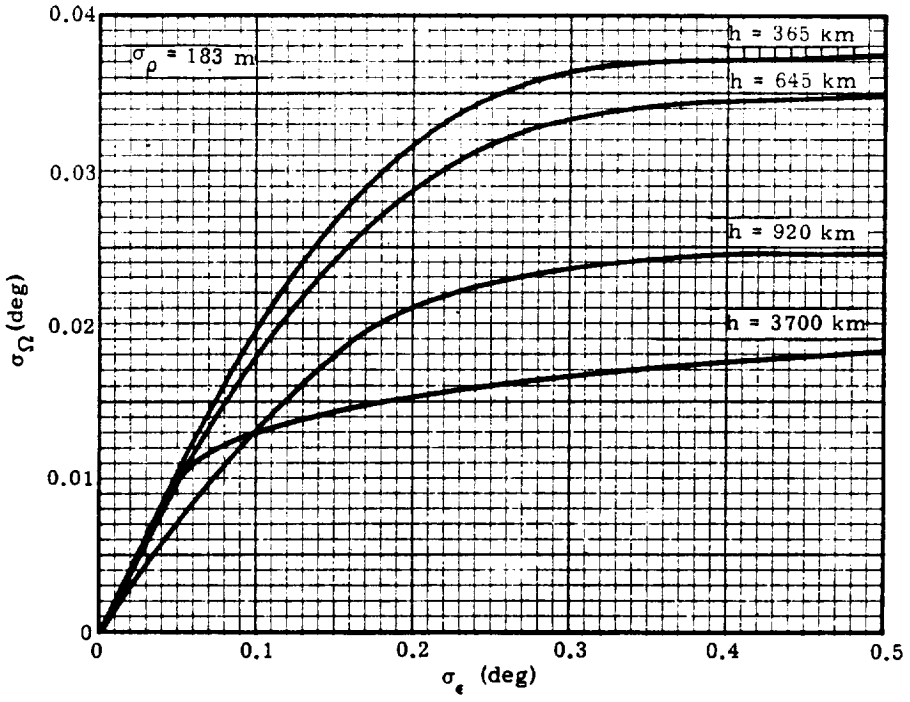

Fig. 29. Angular Observation Errors, σ_Ω Versus σ_ϵ

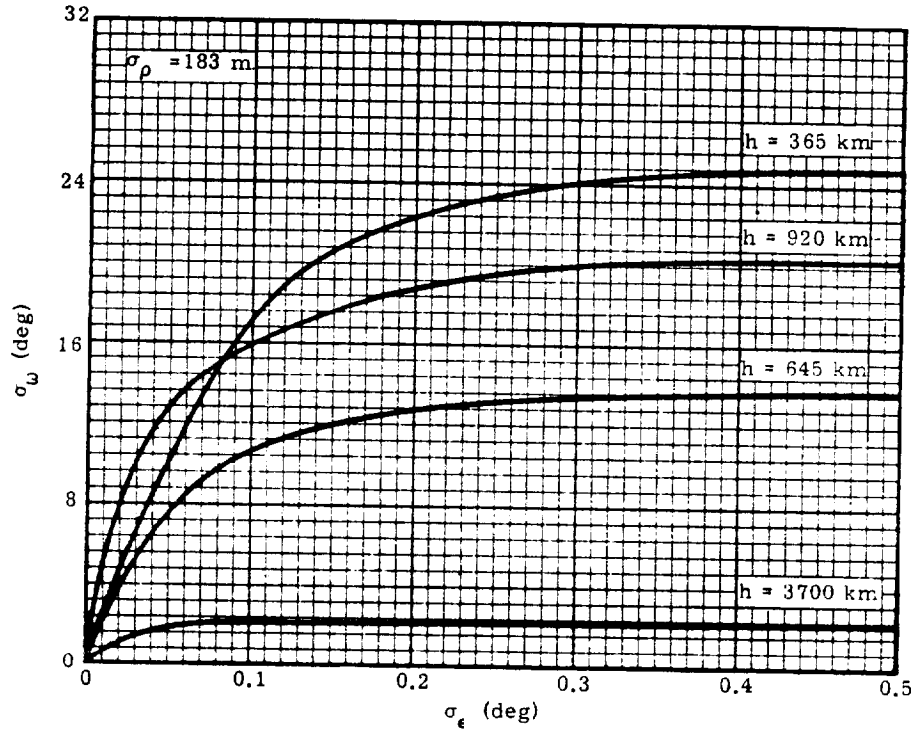

Fig. 30. Angular Observation Errors, σ_ω Versus σ_ϵ

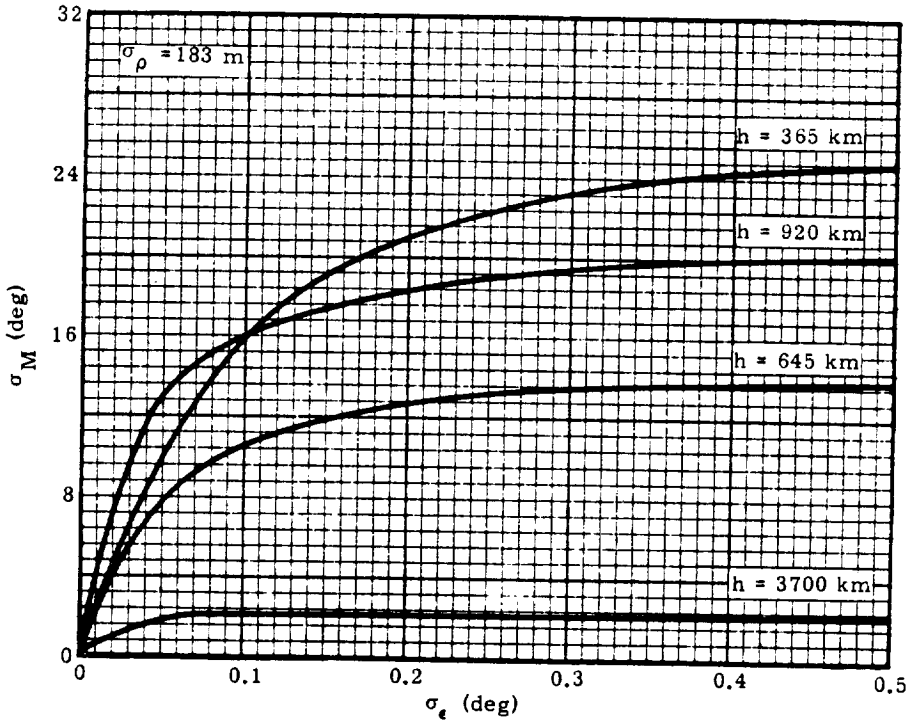

Fig. 31. Angular Observation Errors, σ_M Versus σ_ϵ

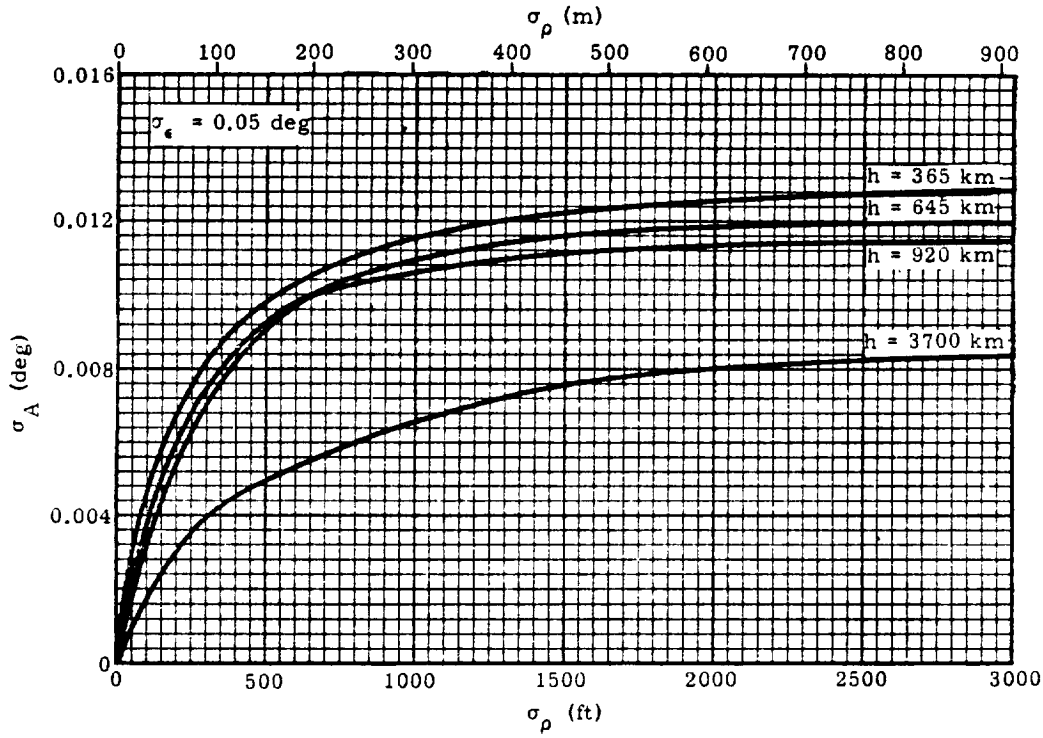

Fig. 32. Range Observation Errors, σ_A Versus σ_ρ

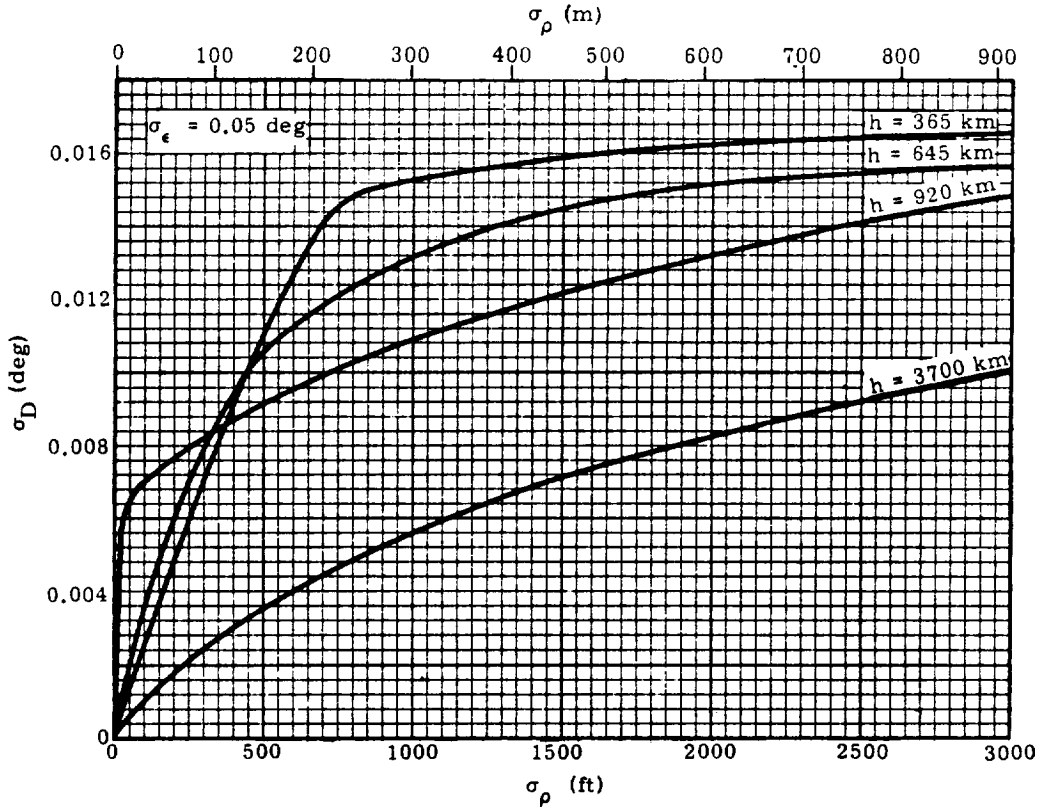

Fig. 33. Range Observation Errors, σ_D Versus σ_ρ

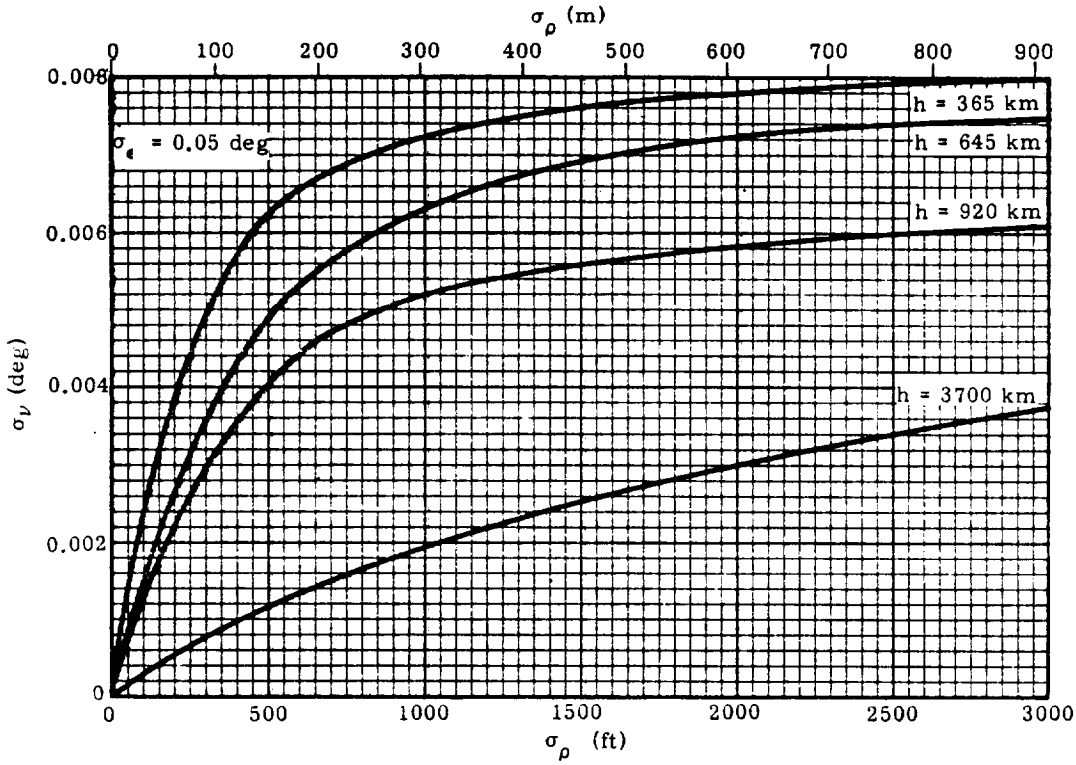

Fig. 34. Range Observation Errors, σ_ν Versus σ_ρ

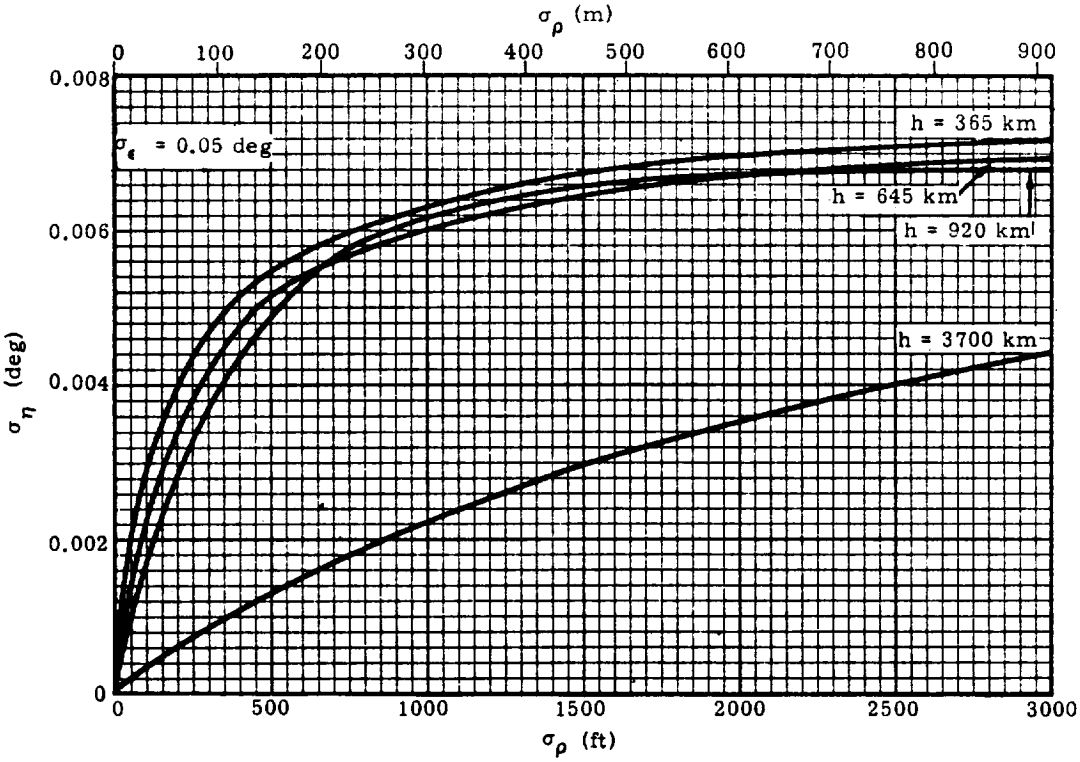

Fig. 35. Range Observation Errors, σ_η Versus σ_ρ

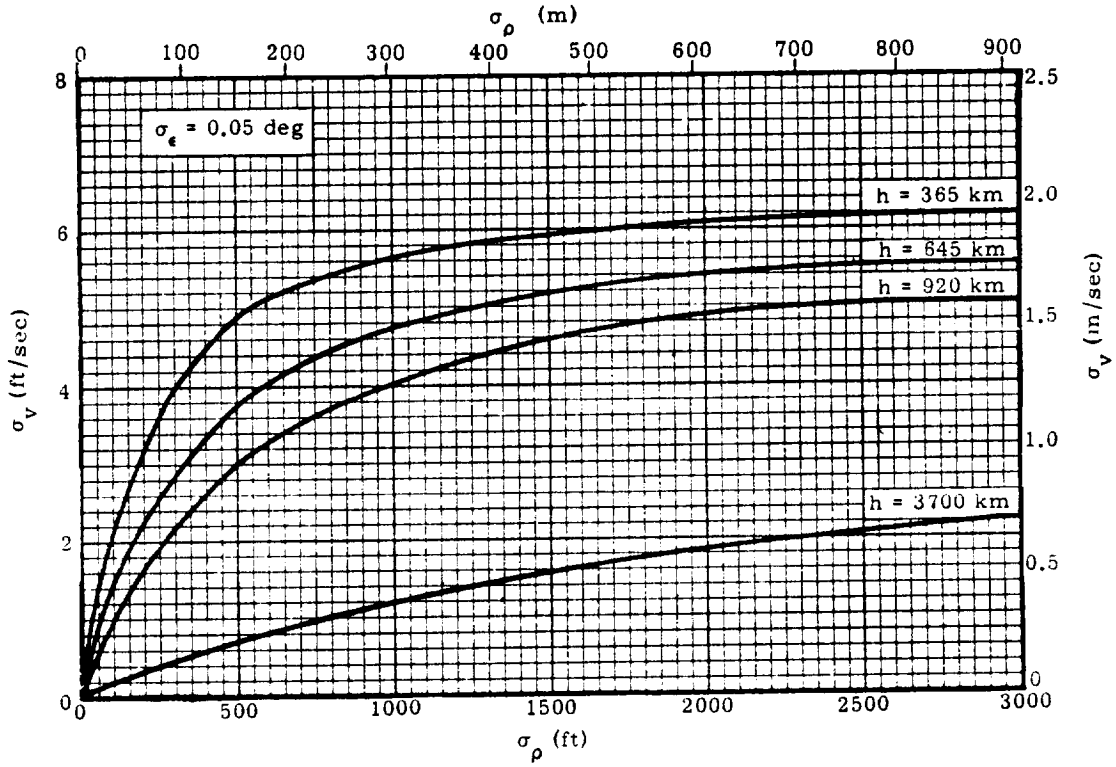

Fig. 36. Range Observation Errors, σ_v Versus σ_ρ

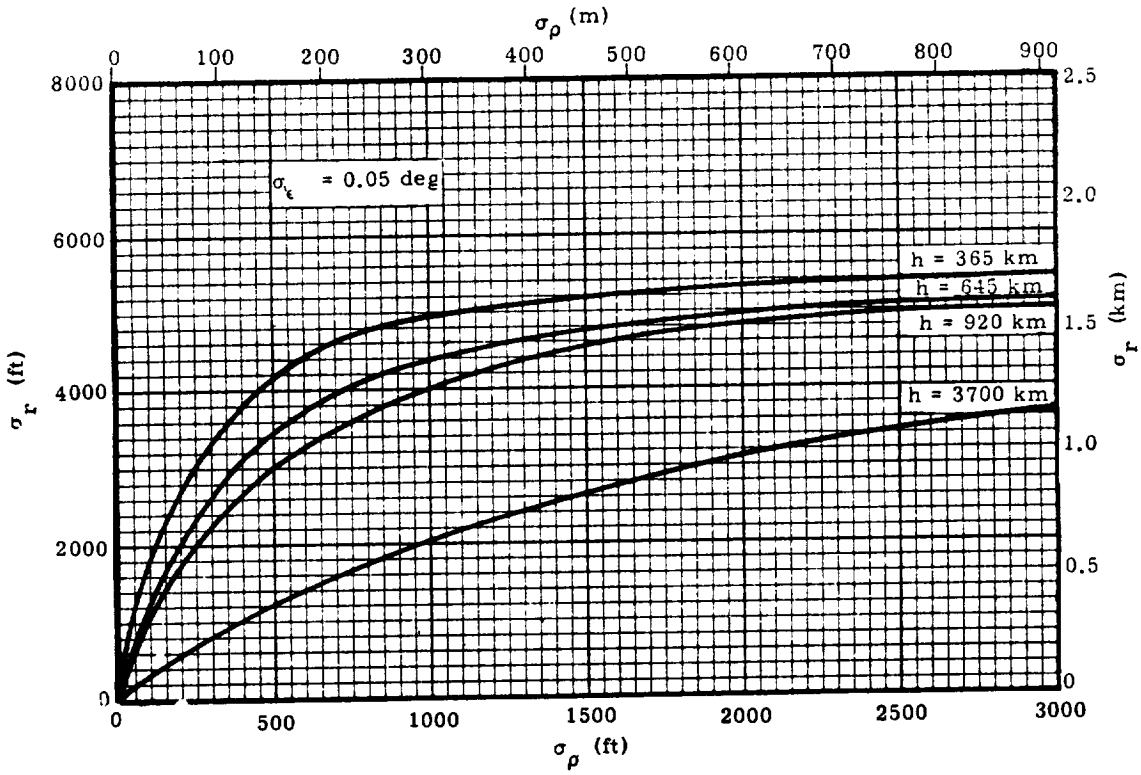

Fig. 37. Range Observation Errors, σ_r Versus σ_ρ

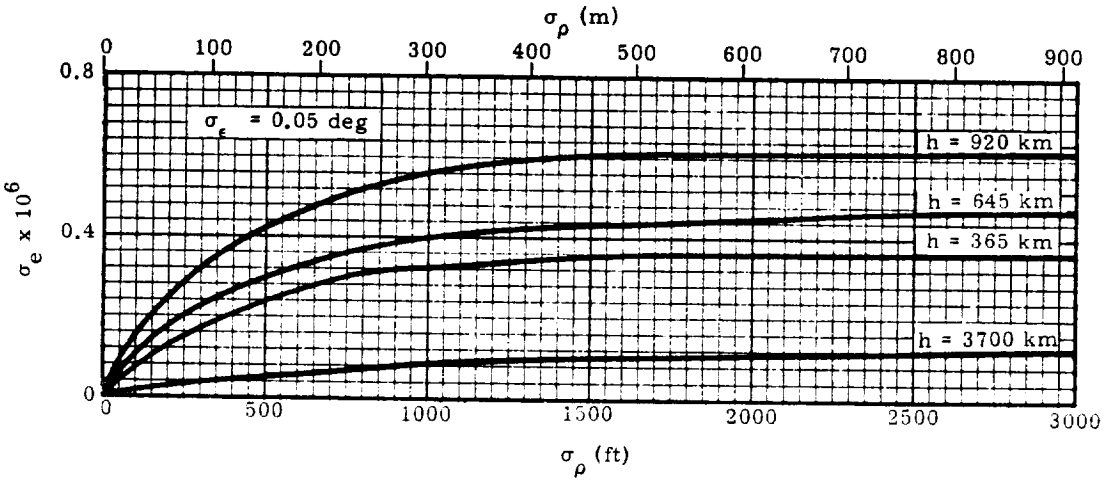

Fig. 38. Range Observation Errors, σ_e Versus σ_ρ

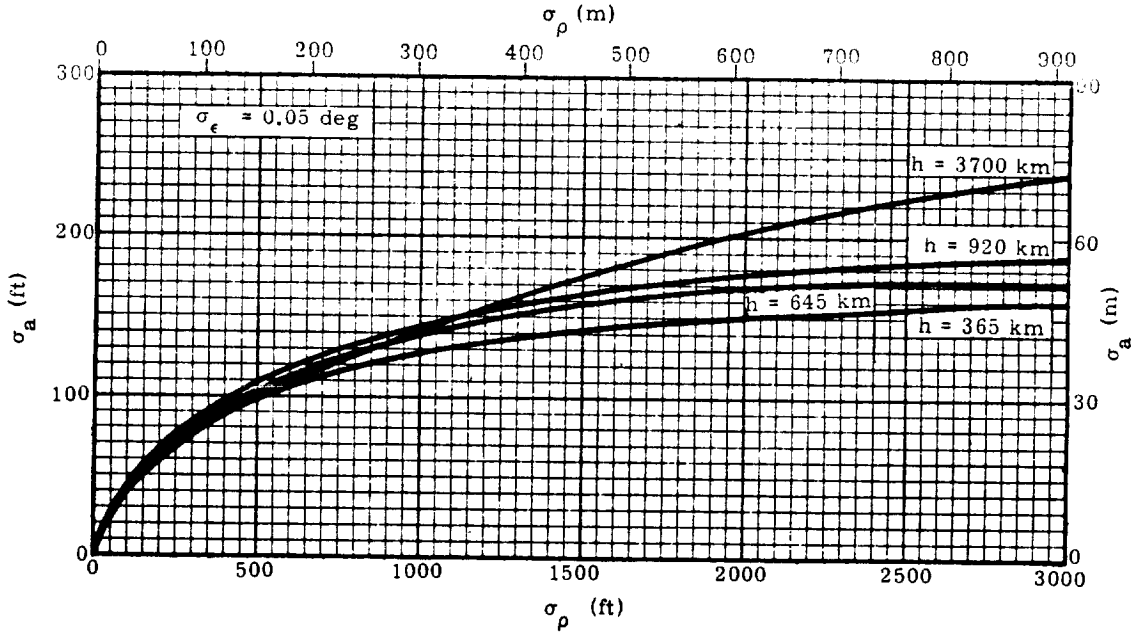

Fig. 39. Range Observation Errors, σ_a Versus σ_ρ

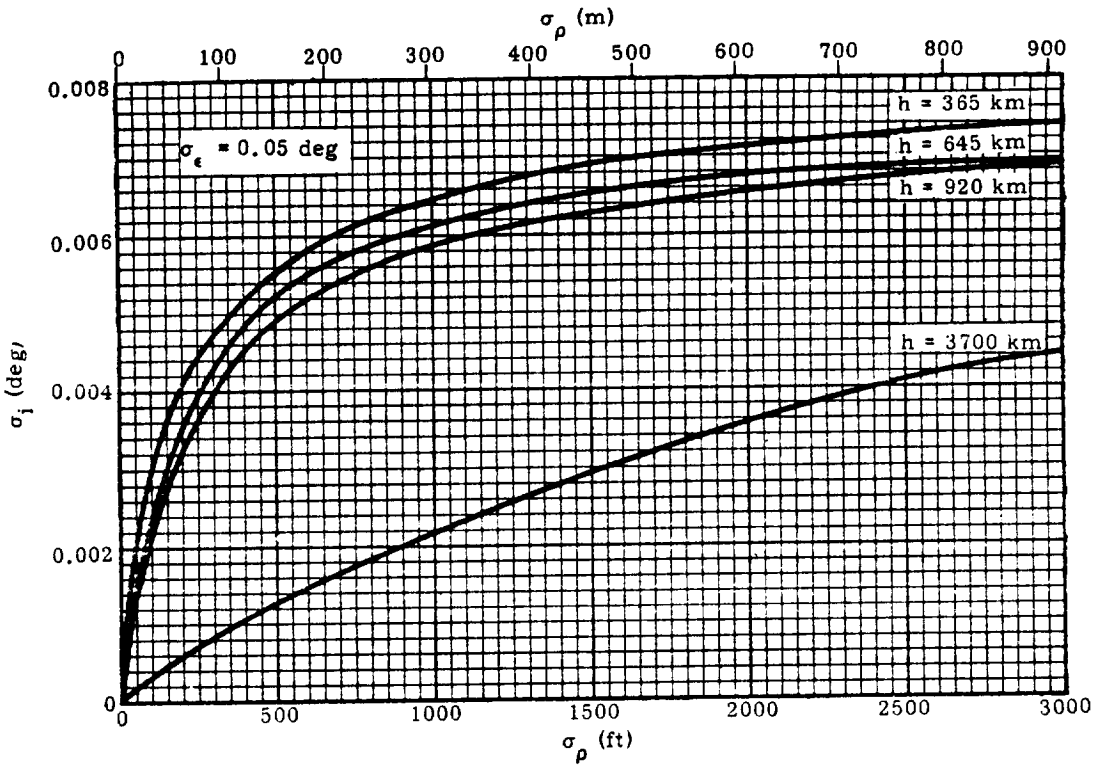

Fig. 40. Range Observation Errors, σ_i Versus σ_ρ

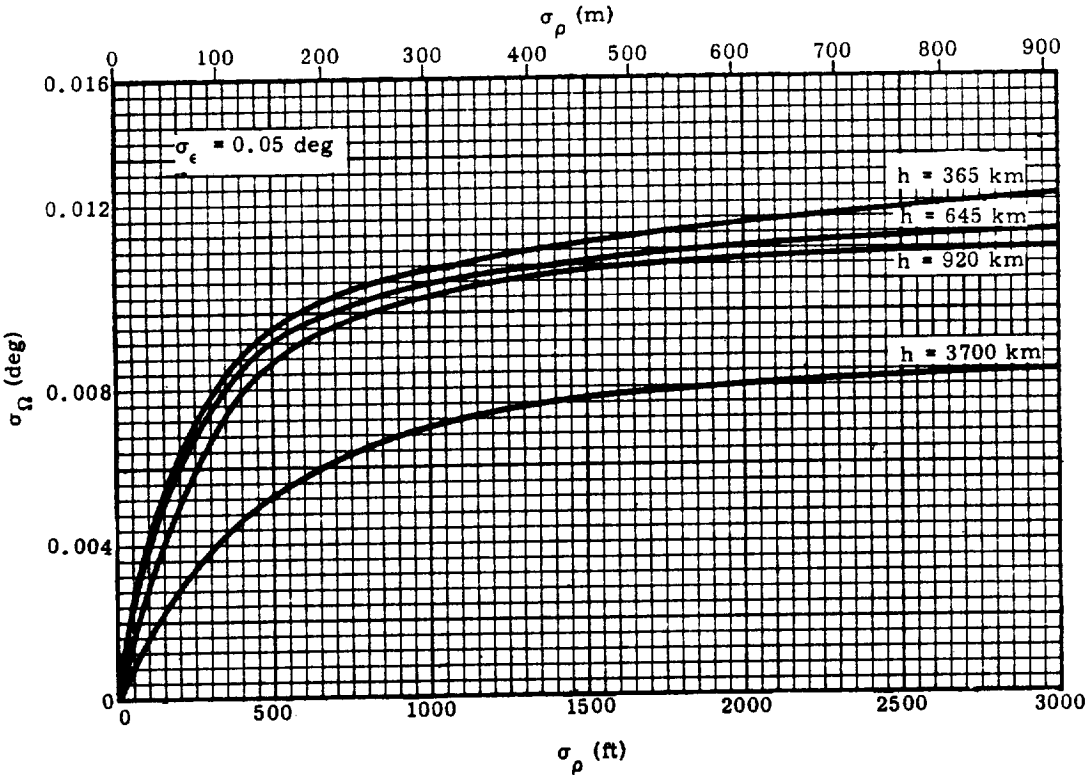

Fig. 41. Range Observation Errors, σ_Ω Versus σ_ρ

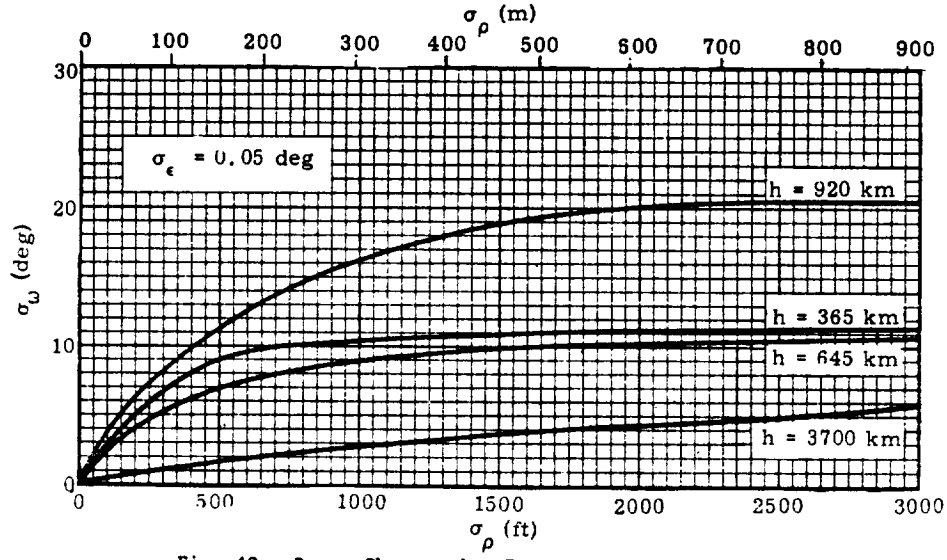

Fig. 42. Range Observation Errors, σ_ω Versus σ_ρ

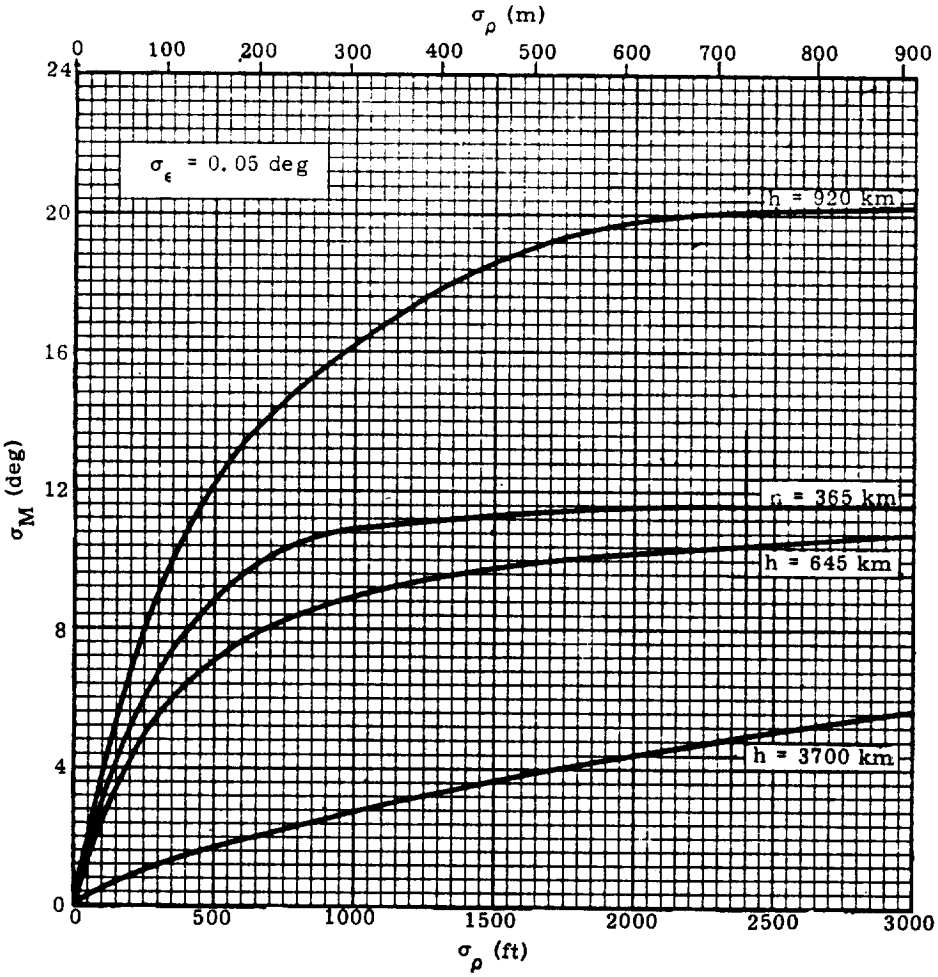

Fig. 43. Range Observation Errors, σ_M Versus σ_ρ

CHAPTER XII

GUIDANCE AND CONTROL

Prepared by:

J. D. Kraft
Martin Company (Baltimore)
Aerospace Mechanics Department
March 1963

		Page
	Symbols	XII-1
A.	Introduction	XII-2
B.	Guidance and Control Requirements	XII-2
C.	Space Vehicle Guidance Techniques	XII-28
D.	Design of Attitude Control Systems for Earth Satellites	XII-31
E.	References	XII-56
F.	Bibliography	XII-56
	Illustrations	XII-63

LIST OF ILLUSTRATIONS

Figure		Page
1	Results of Optimization for Equal σ in Pitch and Yaw Equal to $\sigma_{\Delta_{\epsilon_0}}$	XII-65
2	Normalized Density Function of Δv (Equation 110)	XII-65
3	Vacuum Ballistic Trajectory Error Analysis (velocity and radius, cutoff to apogee, partials)	XII-66
4	Vacuum Ballistic Trajectory Error Analysis (velocity and radius partials, expanded scale)	XII-67
5	Vacuum Ballistic Trajectory Error Analysis (correction for $r_0/r_f = 1.02$)	XII-68
6	Vacuum Ballistic Trajectory Error Analysis (correction for $r_0/r_f = 1.04$)	XII-69
7	Vacuum Ballistic Trajectory Error Analysis (radius partial, apogee to r_f, $r_f = r_0$	XII-70
8	Vacuum Ballistic Trajectory Error Analysis (radius partial, apogee to r_f, $r_f = r_0/1.02$)	XII-71
9	Vacuum Ballistic Trajectory Error Analysis (radius partial, apogee to r_f, $r_f = r_0/1.04$)	XII-72
10	Vacuum Ballistic Trajectory Error Analysis (flight path angle partial, $r_0/r_f = 1.00$)	XII-73
11	Vacuum Ballistic Trajectory Error Analysis (flight path angle partial, extended velocities, $r_0/r_f = 1.00$)	XII-74
12	Vacuum Ballistic Trajectory Error Analysis (flight path angle partial, $r_0/r_f = 1.02$)	XII-75
13	Vacuum Ballistic Trajectory Error Analysis (flight path angle partial, extended, $r_0/r_f = 1.02$) . . .	XII-76
14	Vacuum Ballistic Trajectory Error Analysis (flight path angle partial, $r_0/r_f = 1.04$)	XII-77

LIST OF ILLUSTRATIONS (continued)

Figure		Page
15	Vacuum Ballistic Trajectory Error Analysis (flight path angle partials, extended velocities $r_0/r_f = 1.04$)	XII-78
16	Vacuum Ballistic Trajectory Error Analysis (circular velocity as a function of altitude)	XII-79
17	Vacuum Ballistic Trajectory Error Analysis (r_0/r_f as a function of h_0 and h_f)	XII-80
18	Altitude and Velocity Influence Coefficients Versus Range (for values of elevation angle γ_0)	XII-81
19	Elevation Angle Influence Coefficient Versus Range (for values of elevation angle γ_0)	XII-81
20	Time of Flight Versus Range	XII-82
21	Overall Control System Block Diagram with Radio Guidance Loop	XII-83
22	Functional Block Diagram for a Radio-Inertial System	XII-83
23	Actual Antenna Radiation Pattern Showing Important Trajectory Steering Constraints	XII-84
24	Gravity Computer	XII-84
25	Steering Computer	XII-85
26	Motor Shutoff Computer	XII-85
27	Torque from Solar Radiation as a Function of Area and Lever Arm	XII-86
28a	Field Intensity Versus Altitude for Earth's Magnetic Field	XII-86
28b	Maximum Torque per Ampere-Turn for a 0.3 m Radius Coil Versus Altitude over the Magnetic Equator	XII-86

LIST OF ILLUSTRATIONS (continued)

Figure		Page
29	Flux Density in Inertial Space Versus Position in 400-Naut Mi (741 km) Orbit	XII-87
30	Component of Flux Density Along Earth's Local Vertical in 400-Naut Mi(741 km) Orbit for Several Orbit Inclinations	XII-88
31	Magnitude of Earth's Magnetic Field at 400-Naut Mi (741 km) as a Function of Latitude Assuming the Magnetic Dipole Is Along the Earth's Spin Axes	XII-88
32	Typical Conical Earth Scanning System	XII-89
33	Geometry for Using Edge Tracking to Generate Attitude Information	XII-90
34	A Wide Angle Passive Scanner	XII-90
35	A Possible Yaw and Array Sun Sensor Arrangement	XII-91
36	T Shadow Bar Sun Sensor	XII-91
37	Coordinate System for Computation of Yaw and Solar Array Laws	XII-92
38	Yaw and Solar Array Control Laws	XII-92
39a	Torque in Body Coordinates Due to Solar Radiation Pressure for One Orbit	XII-93
39b	Momentum Change in Inertial Coordinates Due to Solar Radiation Pressure for One Orbit	XII-93
40	Total Stored Momentum During One Orbit Due to Gravity Gradient	XII-93
41	Block Diagram of Simple On-Off Control System . .	XII-94
42	Phase Plane Portrait of a Contractor Control System	XII-94

LIST OF ILLUSTRATIONS (continued)

Figure		Page
43	Block Diagram of Gas Jet Reaction Wheel Dual Mode System	XII-94
44	Typical Phase Portrait Dual Mode System with Constant Disturbance Torque	XII-95
45	Example Attitude Control System Block Diagram for Acquisition Mode	XII-95
46	Phase Portrait of Roll Error and Roll Error Phase of Acquisition	XII-96
47	Angle and Angular Rate at First Switching Line Versus Acceleration for Initial Conditions of 1°/sec and 180° Error	XII-96
48	Angle and Angular Rate Versus Time of Acquisition	XII-97
49	Basic Attitude Control System Block Diagram for Normal Mode	XII-97

XII. GUIDANCE AND CONTROL

SYMBOLS

a	Semimajor axis
e	Orbit eccentricity
E	Eccentric anomaly
g	Acceleration due to gravity
i	Orbit inclination
L	Geocentric latitude
M	Mean anomaly
r	Orbit radius
R	Radius of the earth
t	Time
t_p	Time of perigee passage
v	Magnitude of vehicle velocity
α	Azimuth of velocity vector relative to nominal
β	Azimuth of the orbit path relative to the north point on the horizon
γ	Flight path angle relative to local horizontal
θ	True anomaly
μ	Gravitational constant of the earth; also, mean value in statistical discussions
ν	Angle from the ascending node to the projection of the radius to the vehicle on the equatorial plane
ρ	Range; also, correlation
σ^2	Variance
τ	Orbit period
Φ	Earth central angle in the orbit plane from ascending node to the vehicle position
ψ	Earth central angle normal to the orbit plane
ω	Argument of perigee
Ω	Longitude or right ascension of the ascending node.

Subscripts

a	Apogee value
p	Perigee value

A. INTRODUCTION

The purpose of this chapter is threefold.

(1) Develop the guidance and control requirements as functions of the tolerances imposed on the trajectory.

(2) Introduce the subject of satellite guidance with a discussion of guidance techniques.

(3) Introduce the subject of attitude control.

The first item can generally be discussed by developing an error analysis relating the errors in a specified set of orbit parameters, or, analogously, in position and velocity at a specified time, to errors occurring at injection and then by relating errors at injection to errors in the powered ascent phase. The first analysis is presented in Section B of this chapter (powered ascent trajectories are not covered in this manual) in a general form obtained without sacrifice or assumption. The remaining discussions will be of a more qualitative nature. The difference in emphasis is due to the fact that the field of guidance and control involves studies both of techniques and hardware to implement the desired changes; however, discussions of hardware have been omitted from this text due to its constantly changing nature. These discussions are presented in Sections C and D.

B. GUIDANCE AND CONTROL REQUIREMENTS

Since the goal of a guidance and control system is generally to bring the vehicle to a certain position with a certain velocity, the first step in design of such a system is generally ascertaining the accuracy in this position and velocity required by the mission. The mission requirements are usually expressed in terms of allowable tolerances in orbit elements or required position and velocity accuracies at some terminal point in the trajectory. Therefore, the designer must be able to relate these mission tolerances to tolerances in the final position and velocity of the trajectory phase in which the guidance system is operational. Relations between these tolerances are derived in this section. Errors in elliptic orbits are considered in Subsection 1, and errors in powered flight trajectories are considered in Subsection 2.

1. Error Analysis of Elliptic Orbits

An elliptic orbit can be completely specified by assigning six independent parameters. Of particular interest are the classical elements (semimajor axis (a), eccentricity (e), argument of perigee (ω), time of perigee (t_p), inclination of the orbit plane to the equatorial plane (i) and the celestial longitude or right ascension of the ascending node (Ω) and the polar position and velocity components (radial distance of the vehicle from the center of the earth (r), central angle in the orbit plane from ascending node to vehicle position (ϕ), position angle normal to the orbit plane (ψ = 0 nominally), vehicle velocity magnitude (v), flight path angle in the vertical plane relative to local horizontal (γ) and flight path angle in the horizontal plane (azimuth angle) with respect to north (β). Differentiation of the equations relating these two systems provides a set of error formulas which serves as a basis for specification of guidance system requirements.

a. General differential analysis

Since the equations relating the planar parameters (a, e, ω, t_p and r, ϕ, v, γ) are not coupled with the equations relating the parameters defining planar orientation, the derivation can be conveniently considered in two parts.

(1) Planar parameters

Generation of the four error equations

$$da = f_1 (dr, d\phi, dv, d\gamma)$$

$$de = f_2 (dr, d\phi, dv, d\gamma)$$

$$d\omega = f_3 (dr, d\phi, dv, d\gamma)$$

$$dt_p = f_4 (dr, d\phi, dv, d\gamma)$$

must be based upon four independent relations between the variables (a, e, ω, t_p) and (r, ϕ, v, γ):

$$v^2 = \mu \left(\frac{2}{r} - \frac{1}{a}\right) \tag{1}$$

$$r^2 v^2 \cos^2 \gamma = \mu a (1 - e^2) \tag{2}$$

$$r = \frac{a (1 - e^2)}{1 + e \cos (\phi - \omega)} \tag{3}$$

$$t_p - t = -\sqrt{\frac{a^3}{\mu}} (E - e \sin E)$$

$$= -\sqrt{\frac{a^3}{\mu}} M \tag{4}$$

where

$$E = \cos^{-1} \left(\frac{a - r}{ea}\right)$$

These equations are, respectively, the energy equation, the law of areas (Kepler's second law), the equation of conic form (Kepler's first law) and Kepler's equation. The establishment of these laws is considered in Chapter III. Taking differentials of Eq (1) gives the required linear error formula for the semimajor axis.

$$da = 2 \frac{a^2}{r^2} dr + \frac{2a^2 v}{\mu} dv \tag{5}$$

This equation is most conveniently expressed in normalized form with coefficients written in terms of only one variable, either r or $\theta = \phi - \omega$. From Eqs (1) and (3)

$$da = 2\,\frac{a^2}{r^2}\,dr + 2a^2\sqrt{\frac{1}{\mu}\left(\frac{2}{r}-\frac{1}{a}\right)}\,dv \qquad (6)$$

$$= \frac{2\,(1+e\cos\theta)^2}{(1-e^2)^2}\,dr + 2a\sqrt{\frac{a}{\mu}}\sqrt{\frac{1+2e\cos\theta+e^2}{1-e^2}}\,dv \qquad (7)$$

or

$$\frac{da}{a} = 2\left(\frac{a}{r}\right)\frac{dr}{r} + 2\left(2\,\frac{a}{r}-1\right)\frac{dv}{v} \qquad (8)$$

$$= 2\,\frac{1+e\cos\theta}{1-e^2}\,\frac{dr}{r} + 2\left(2\,\frac{1+e\cos\theta}{1-e^2}-1\right)\frac{dv}{v}. \qquad (9)$$

(Also, since the orbit period $\tau = 2\pi\sqrt{\frac{a^3}{\mu}}$, $\frac{d\tau}{\tau} = \frac{3}{2}\,\frac{da}{a} = 3\,\frac{a}{r}\,\frac{dr}{r} + 3\,(2\frac{a}{r}-1)\,\frac{dv}{v}$.) Differentials of eccentricity may be determined from Eq (2).

$$de = \frac{v^2\cos^2\gamma}{\mu e a}\,(a-r)\,dr + \frac{2rv\cos^2\gamma}{\mu e a}\,(a-r)\,dv + \frac{r^2v^2\sin\gamma\cos\gamma}{\mu e a}\,d\gamma \qquad (10)$$

Substitution of Eqs (1), (2) and (3) and simplification gives

$$de = \frac{1-e^2}{er}\left(\frac{a}{r}-1\right)dr + 2\,\frac{1-e^2}{er}\,(a-r)\,dv \pm \frac{1}{e}\sqrt{(1-e^2)\left[\left(\frac{r}{a}-1\right)^2-e^2\right]}\,d\gamma \qquad (11)$$

$$= \frac{(e+\cos\theta)\,(1+e\cos\theta)}{a\,(1-e^2)}\,dr + 2\,(e+\cos\theta)\left[\frac{a\,(1-e^2)}{\mu\,(1+2e\cos\theta+e^2)}\right]^{1/2}dv + (1-e^2)\,\frac{\sin\theta}{1+e\cos\theta}\,d\gamma \qquad (12)$$

or, in normalized form,

$$de = \frac{1-e^2}{e}\left(\frac{a}{r}-1\right)\frac{dr}{r} + 2\,\frac{1-e^2}{e}\left(\frac{a}{r}-1\right)\frac{dv}{v} \pm \frac{1}{e}\sqrt{(1-e^2)\left[\left(\frac{r}{a}-1\right)^2-e^2\right]}\,d\gamma \qquad (13)$$

$$= (e+\cos\theta)\,\frac{dr}{r} + 2\,(e+\cos\theta)\,\frac{dv}{v} + (1-e^2)\,\frac{\sin\theta}{1+e\cos\theta}\,d\gamma \qquad (14)$$

From Eq (3),

$$\cos(\phi-\omega) = \frac{a\,(1-e^2)-r}{er},$$

differentials of the argument of perigee may be written.

$$-\sin(\phi-\omega)\,(d\phi-d\omega) = \frac{1+e\cos\theta}{e}\,\frac{da}{a} - \left(\frac{\cos\theta}{e}+2\,\frac{1+e\cos\theta}{1-e^2}\right)de - \frac{1+e\cos\theta}{e}\,\frac{dr}{r}$$

Substitution for da and de from Eqs (5) through (14) gives $d\omega$.

$$d\omega = \pm\frac{1}{e}\sqrt{1-\left[\frac{a\,(1-e^2)-r}{er}\right]^2}\,\frac{dr}{r} \pm \frac{2}{e}\sqrt{1-\left[\frac{a\,(1-e^2)-r}{er}\right]^2}\,\frac{dv}{v} - \frac{1}{e^2}\left[1+e^2-\frac{r}{a}\right]d\gamma + d\phi \qquad (15)$$

$$d\omega = \frac{\sin\theta}{e}\,\frac{dr}{r} + 2\,\frac{\sin\theta}{e}\,\frac{dv}{v} - \frac{2e+(1+e^2)\cos\theta}{e\,(1+e\cos\theta)} + d\phi \qquad (16)$$

The linear error relation for the final planar element, t_p, is obtained from Eq (4).

$$\frac{d\,(t_p-t)}{t_p-t} = \frac{3}{2}\,\frac{da}{a} - \frac{\sin E}{E-e\sin E}\,de + \frac{1-e\cos E}{E-e\sin E}\,dE \qquad (17)$$

where

$$dE = -\frac{1}{e \sin E}\left[\frac{r}{a}\frac{da}{a} - \left(1 - \frac{r}{a}\right)\frac{de}{e} - \frac{dr}{a}\right]. \quad (18)$$

Substituting for da and de from Eqs (8) and (13) or (9) and (14), and substituting Eq (18) in Eq (17) gives the required relation

$$\frac{d(t_p - t)}{t_p - t} = \left\{3\frac{a}{r} \pm \frac{1}{M}\left[2\frac{a}{r} - 1 - \left(\frac{a}{r}\right)^2(1 - e^2)\right]^{-1/2}\left[-2 + \frac{r}{a} + \left(\frac{a}{r} - 1\right)\left(\frac{1 - e^2}{e^2}\right)\left(\frac{a}{r}(1 - e^2) - 1\right)\right]\right\}\frac{dr}{r} + \left\{3\left(2\frac{a}{r} - 1\right) \mp \frac{2}{M}\left[e^2 - \left(1 - \frac{r}{a}\right)^2\right]^{1/2}\left[1 + \frac{a}{r}\left(\frac{1 - e^2}{e^2}\right)\right]\right\}\frac{dv}{v} + \frac{1}{M}\frac{(1 - e^2)^{3/2}}{e^2}\left[1 - \frac{r}{a}\left(\frac{1}{1 - e^2}\right)\right]d\gamma \quad (19)$$

$$= \left\{\frac{3(1 + e\cos\theta)}{1 - e^2} + \frac{1}{M}\frac{\sqrt{1 - e^2}}{e\sin\theta}\left[-2 + (e + \cos\theta)\cos\theta + \frac{1 - e^2}{1 + e\cos\theta}\right]\right\}\frac{dr}{r} + \left[3\frac{1 + 2e\cos\theta + e^2}{1 - e^2} - \frac{2}{M}\sqrt{\frac{1 - e^2}{e}}\sin\theta\frac{1 + e\cos\theta + e^2}{1 + e\cos\theta}\right]\frac{dv}{v} + \frac{1}{M}\frac{(1 - e^2)^{3/2}}{e}\frac{\cos\theta}{1 + e\cos\theta}d\gamma \quad (20)$$

where M = mean anomaly = E - e sin E.

(2) Orientation parameters

The out-of-plane coordinates and injection parameters ($d\psi$, the displacement in central angle normal to the orbit plane at injection, and $d\beta$, the error in orbit azimuth or orbit orientation in the horizontal plane) determine the orientation of the orbit plane in space, as defined by the orbit parameters i, the inclination of the orbit plane to the equator, and Ω, the right ascension of the ascending node.

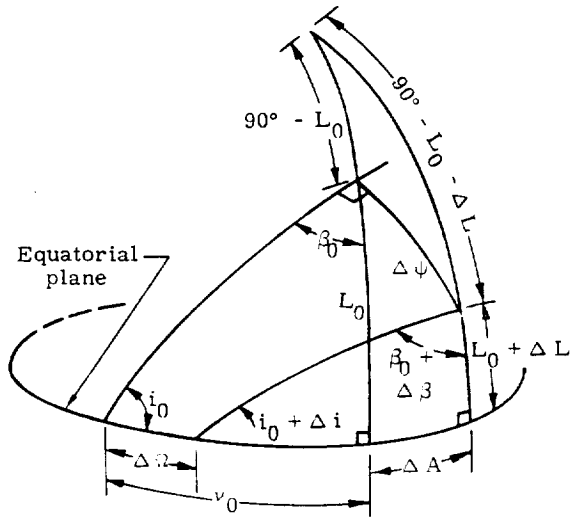

The required error relations

$$di = \frac{\partial i}{\partial \psi}d\psi + \frac{\partial i}{\partial \beta}d\beta$$

$$d\Omega = \frac{d\Omega}{d\psi}d\psi + \frac{\partial \Omega}{\partial \beta}d\beta$$

can be determined from consideration of the accompanying sketch and Table 8 of Chapter III, the table of spherical trigonometry identities.

$$\cos(i_0 + \Delta i) = \cos(L_0 + \Delta L)\sin(\beta_0 + \Delta\beta)$$

Since only a differential approximation to the error is required, the terms of this equation may be expanded in Taylor series, and terms of second order in the errors may be neglected.

$$\cos i_0 - \sin i_0\,\Delta i \approx \cos L_0 \sin\beta_0 + \cos L_0\cos\beta_0\,\Delta\beta - \sin L_0\sin\beta_0\,\Delta L$$

Since $\cos i_0 = \cos L_0 \sin\beta_0$,

$$\Delta i \approx -\frac{\cos L_0\cos\beta_0}{\sin i_0}\Delta\beta + \frac{\sin L_0\sin\beta_0}{\sin i_0}\Delta L. \quad (21)$$

A relation

$$\Delta L = f(\Delta\psi, \Delta\beta)$$

is then required for substitution in Eq (21). Such a relation is obtained from application of the law of cosines to the spherical triangle formed by two meridians and the side $\Delta\psi$ in the sketch.

$$\cos(90° - L_0 - \Delta L) = \cos(90° - L_0)\cos\Delta\psi + \sin(90° - L_0)\sin\Delta\psi\cos(90° + \beta_0)$$

Simplifying and expanding in series gives

$$\Delta L \approx - \sin \beta_0 \, \Delta\psi.$$

Substitution of this equation in Eq (21) gives the error in inclination

$$di = - \frac{\cos L_0 \cos \beta_0}{\sin i_0} \Delta\beta - \frac{\sin L_0 \sin^2 \beta_0}{\sin i_0} \Delta\psi.$$

The error in nodal right ascension may be determined by noting that

$$\cos (\nu_0 + \Delta A - \Delta\Omega) = \frac{\cos (\beta_0 + \Delta\beta)}{\sin (i_0 + \Delta i)}$$

and

$$\frac{\sin \Delta A}{\sin \Delta\psi} = \frac{\sin (90° + \beta_0)}{\sin (90° - L_0 - \Delta L)}$$

These equations on expansion give

$$\tan \nu_0 \, (\Delta A - \Delta\Omega) \approx \tan \beta_0 \, \Delta\beta + \cot i_0 \, \Delta i$$

$$\Delta A \approx \frac{\cos \beta_0}{\cos L_0} \Delta\psi.$$

Then

$$d\Omega = \left[- \frac{\tan \beta_0}{\tan \nu_0} + \frac{\cot i_0 \cos L_0 \cos \beta_0}{\tan \nu_0 \sin i_0} \right] \Delta\beta$$

$$+ \left[\frac{\cos \beta_0}{\cos L_0} + \frac{\cot i_0 \sin L_0 \sin^2 \beta_0}{\tan \nu_0 \sin i_0} \right] \Delta\psi.$$

The di and $d\Omega$ solutions can be written completely in terms of L and i as follows:

$$di = - \frac{\sin L_0 \cos^2 i_0}{\sin i_0 \cos^2 L_0} \, d\psi \mp \sqrt{1 - \frac{\sin^2 L_0}{\sin^2 i_0}} \, d\beta \qquad (22)$$

$$d\Omega = \pm \frac{1}{\cos^2 L_0 \sin i_0} \sqrt{1 - \frac{\sin^2 L_0}{\sin^2 i_0}} \, d\psi$$

$$- \frac{\sin L_0}{\sin^2 i_0} \, d\beta \qquad (23)$$

The orbit plane orientation errors can also be derived in terms of a velocity azimuth error, $d\alpha$ referenced to the local nominal direction of the velocity vector, rather than the orbit azimuth error $d\beta$. That is, from the following sketch, if the orbit orientation is in error due to a $\Delta\psi$ but $\Delta\alpha = 0$, the incorrect orbit (as well as the correct orbit) is normal to the arc $\Delta\psi$. The new orbit azimuth angle, β_1, is not equal to the nominal orbit azimuth angle, β_0, even though the velocity azimuth error is zero. Then, from the spherical trigonometry relations of Chapter III,

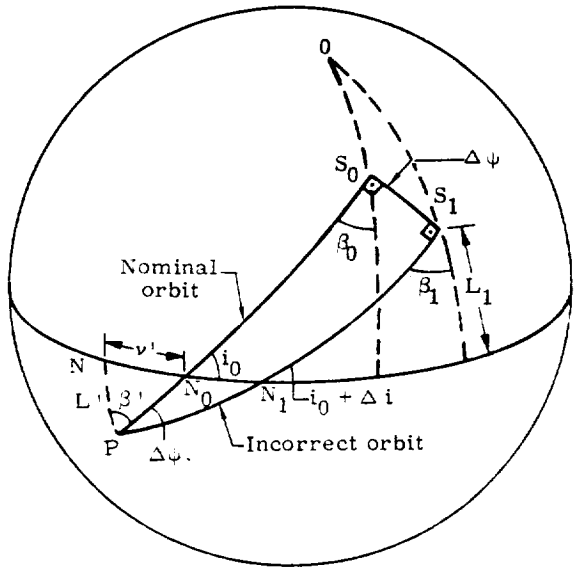

$$\cos (i_0 + \Delta i) = \cos L' \sin (\beta' + \Delta\psi)$$

in ΔNPN_1, where the primed quantities relate to the intersection point of the nominal and incorrect orbit planes. Expansion of this equation in Taylor series and neglecting higher order terms as before gives

$$\Delta i \approx - \frac{\cos L' \cos \beta'}{\sin L_0} \Delta\psi.$$

Since

$$\tan \beta' = \frac{\cot i_0}{\cos (90 - \phi_0)}$$

where

$$\phi_0 = \text{arc } N_0 \, S_0$$

and

$$\sin \beta' = \frac{\cos i_0}{\cos L'}$$

$$\Delta i = - \sin \phi_0 \, \Delta\psi = - \frac{\sin L_0}{\sin i_0} \Delta\psi.$$

Similarly, from

$$\tan (\nu' + \Delta\Omega) = \sin L' \tan (\beta' + \Delta\psi)$$

when

$$\Delta\Omega = \text{arc } N_0 \, N_1$$

$$\Delta\Omega \approx \frac{\sin L' \cos^2 \nu'}{\cos^2 \beta'} \Delta\gamma$$

or

$$\Delta\Omega \approx \frac{\cos \phi}{\sin i_0} \Delta\gamma = \frac{1}{\sin i_0} \sqrt{1 - \frac{\sin^2 L_0}{\sin^2 i_0}} \, \Delta\gamma.$$

Now consider an error due to $\delta\alpha$ superimposed on the previously considered incorrect orbit as shown in the accompanying sketch. The additional errors due to $\delta\alpha$ will be denoted by $\delta(\ )$.

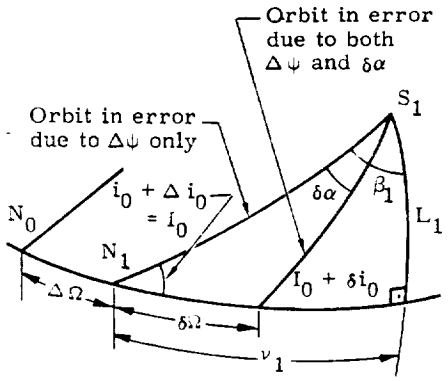

$$\sin(\beta_1 - \delta\alpha) = \frac{\cos(I_0 + \delta i_0)}{\cos L_1}$$

where

$$I_0 = i_0 + \Delta i_0$$

or

$$\delta i_0 \approx \frac{\cos\beta_1 \cos L_1}{\sin I_0}\,\delta\alpha$$

$$\approx \frac{\cos\beta_0 \cos L_0}{\sin i_0}\,\delta\alpha$$

Also, from

$$\cos(\nu_1 - \delta\Omega) = \frac{\cos(\beta_1 - \delta\alpha)}{\sin(I_0 + \delta i)}$$

$$\delta\Omega \approx -\frac{\cos\beta_1}{\sin I_0} - \frac{\cos\beta_1}{\sin I_0}\cot I_0\,\delta i + \frac{\sin\beta_1}{\sin I_0}\,\delta\alpha$$

$$\approx \frac{\sin L_0}{\sin^2 i_0}\,\delta\alpha$$

The the total error formulas, analogous to Eqs (22) and (23), are obtained by adding the contributions due to $\Delta\psi$ and $\delta\alpha$ (that is, forming $\Delta i + \delta i$ and $\Delta\Omega + \delta\Omega$).

$$di = -\frac{\sin L_0}{\sin i_0}\,d\psi + \cos\phi_0\,d\alpha \qquad (24)$$

$$d\Omega = \frac{\cos\phi_0}{\sin i_0}\,d\psi + \frac{\sin L_0}{\sin^2 i_0}\,d\alpha \qquad (25)$$

The differential error expressions derived in this section (Eqs (8), (9), (13) through (16), (19), (20), (24) and (25)) are presented concisely for reference in Table 1.

The inverses of the relations expressed in Table 1 (that is, the errors in polar position and velocity components as functions of errors in the classical elements) are also useful error formulas. These formulas can be generated simply by inverting the matrix of coefficients given in Table 1. If Table 1 is expressed as

$$\{p_i\} = [a_{ij}]\{q_j\}$$

where

$$\{p_i\} = \left\{\frac{da}{a},\ de,\ d\omega,\ \frac{d(t_p - t)}{t_p - t},\ di,\ d\Omega\right\}$$

= the six vector of nondimensional orbit parameter differentials

$$\{q_j\} = \left\{\frac{dr}{r},\ \frac{dv}{v},\ d\gamma,\ d\phi,\ d\psi,\ d\beta\right\}$$

= the six vector of nondimensional polar coordinates

$$[a_{ij}] = \begin{bmatrix} a_{11} & a_{12} & 0 & 0 & 0 & 0 \\ a_{21} & a_{22} & a_{23} & 0 & 0 & 0 \\ a_{31} & a_{32} & a_{33} & 1 & 0 & 0 \\ a_{41} & a_{42} & a_{43} & 0 & 0 & 0 \\ 0 & 0 & 0 & 0 & a_{55} & a_{56} \\ 0 & 0 & 0 & 0 & a_{65} & a_{66} \end{bmatrix}$$

Then the required inverse matrix is

$$[a_{ij}]^{-1} = \frac{[\tilde{a}_{ij}]}{|a_{ij}|}$$

where

$[\tilde{a}_{ij}]$ = adjoint of $[a_{ij}]$ (transpose the cofactor matrix)

$|a_{ij}|$ = determinant with elements a_{ij}.

Inversion is most conveniently accomplished if the 4 x 4 submatrix of planar parameter coefficients and the 2 x 2 submatrix of orientation parameter coefficients are inverted separately. The process is also simplified by noting that

$$\begin{vmatrix} a_{11} & a_{12} & 0 & 0 \\ a_{21} & a_{22} & a_{22} & 0 \\ a_{31} & a_{32} & a_{33} & 1 \\ a_{41} & a_{42} & a_{43} & 0 \end{vmatrix} = -\begin{vmatrix} a_{11} & a_{12} & 0 \\ a_{21} & a_{22} & a_{23} \\ a_{41} & a_{42} & a_{43} \end{vmatrix}$$

$$= -\frac{2}{M}\frac{(1 - e^2)^{3/2}\ (1 + e^2 + 2e\cos\theta)}{e\,(1 + e\cos\theta)^2}$$

The resulting inverse matrix is presented in Table 2.

With the relations of Tables 1 and 2, errors in one phase of an orbit can be determined as functions of errors several phases prior to or subsequent to that phase. For example, errors in position and velocity at orbit injection can be used to solve for errors in the orbit elements, which can in turn be used to determine by the inverse relations, errors in position and velocity at any future time.

b. Errors in orbit extrema

Orbit tolerances are frequently specified in terms of allowable errors in apogee or perigee conditions. For example, in establishment of a low-altitude orbit, a perigee altitude tolerance may be specified in order to assure a long orbit lifetime. Equations for these errors in apogee and perigee conditions can be easily determined as a special case of the previous general analysis (Section B. 1. a.).

From Eqs (1) and (3)

$$r_a = a(1 + e) \tag{26}$$

$$r_p = a(1 - e) \tag{27}$$

$$v_a = \sqrt{\frac{\mu}{a}\,\frac{1 - e}{1 + e}} \tag{28}$$

$$v_p = \sqrt{\frac{\mu}{a}\,\frac{1 + e}{1 - e}} \tag{29}$$

where subscripts a and p denote apogee and perigee conditions, respectively. These equations yield the following differentials.

$$dr_a = (1 + e)\,da + ade \tag{30}$$

$$dr_p = (1 - e)\,da - ade \tag{31}$$

$$dv_a = -\frac{v_a}{2a}\,da - \frac{v_p}{(1 + e)^2}\,de \tag{32}$$

$$dv_p = -\frac{v_p}{2a}\,da + \frac{v_a}{(1 - e)^2}\,de \tag{33}$$

These equations may be expressed in nondimensional form as follows.

$$\frac{dr_a}{r_a} = \frac{da}{a} + \frac{de}{1 + e} \tag{34}$$

$$\frac{dr_p}{r_p} = \frac{da}{a} - \frac{de}{1 - e} \tag{35}$$

$$\frac{dv_a}{v_a} = -\frac{1}{2}\frac{da}{a} - \frac{de}{1 - e^2} \tag{36}$$

$$\frac{dv_p}{vp} = -\frac{1}{2}\frac{da}{a} + \frac{de}{1 - e^2} \tag{37}$$

Then

$$\begin{bmatrix} \frac{dr_a}{r_a} \\ \frac{dr_p}{r_p} \end{bmatrix} = \begin{bmatrix} 1 & \frac{1}{1+e} \\ 1 & \frac{-1}{1-e} \end{bmatrix} \begin{bmatrix} \frac{d_a}{a} \\ de \end{bmatrix}$$

$$= \begin{bmatrix} 1 & \frac{1}{1+e} \\ 1 & \frac{-1}{1-e} \end{bmatrix} \begin{bmatrix} a_{11} & a_{12} & 0 \\ a_{21} & a_{22} & a_{23} \end{bmatrix} \begin{bmatrix} \frac{dr}{r} \\ \frac{dv}{v} \\ d\gamma \end{bmatrix}$$

and

$$\begin{bmatrix} \frac{dv_a}{v_a} \\ \frac{dv_p}{v_p} \end{bmatrix} = \begin{bmatrix} -\frac{1}{2} & \frac{-1}{1-e^2} \\ -\frac{1}{2} & \frac{1}{1-e^2} \end{bmatrix} \begin{bmatrix} \frac{d_a}{a} \\ de \end{bmatrix}$$

$$= \begin{bmatrix} -\frac{1}{2} & \frac{-1}{1-e^2} \\ -\frac{1}{2} & \frac{1}{1-e^2} \end{bmatrix} \begin{bmatrix} a_{11} & a_{12} & 0 \\ a_{21} & a_{22} & a_{23} \end{bmatrix} \begin{bmatrix} \frac{dr}{r} \\ \frac{dv}{v} \\ d\gamma \end{bmatrix}$$

Substitution of the a_{ij} from Table 1 gives the differentials of the apogee and perigee values.

$$\frac{dr_a}{r_a} = \frac{a}{r}\left[2 + \frac{1 - e}{e}\left(1 - \frac{r}{a}\right)\right]\frac{dr}{r} + 2\,\frac{a}{r}\left[1 + \frac{1}{e}\left(1 - \frac{r}{a}\right)\right]\frac{dv}{v} \pm \frac{1 - e}{e}\sqrt{\left(\frac{r}{a}\right)^2\frac{\left(2\frac{a}{r} - 1\right)}{(1 - e^2)} - 1}\;d\gamma \tag{38}$$

$$\frac{dr_p}{r_p} = \frac{a}{r}\left[2 - \frac{(1 + e)}{e}\left(1 - \frac{r}{a}\right)\right]\frac{dr}{r} + 2\,\frac{a}{r}\left[1 - \frac{1}{e}\left(1 - \frac{r}{a}\right)\right]\frac{dv}{v} \mp \frac{1 + e}{e}\sqrt{\left(\frac{r}{a}\right)^2\frac{\left(2\frac{a}{r} - 1\right)}{(1 - e^2)} - 1}\;d\gamma \tag{39}$$

$$\frac{dv_a}{v_a} = \left[-\frac{a}{r} + \frac{1}{e}\left(1 - \frac{a}{r}\right)\right]\frac{dr}{r} + \left[1 - 2\,\frac{a}{r} + \frac{2}{e}\left(1 - \frac{a}{r}\right)\right]\frac{dv}{v} \mp \frac{1}{e}\sqrt{\left(\frac{r}{a}\right)^2\frac{\left(2\frac{a}{r} - 1\right)}{1 - e^2} - 1}\;d\gamma \tag{40}$$

TABLE 1

Error Analysis Equations

$$
\begin{bmatrix} \frac{da}{a} \\ de \\ d\omega \\ \frac{d(t_p - t)}{t_p - t} \\ dt \\ d\Omega \end{bmatrix} =
\begin{bmatrix}
\frac{2(1 + e\cos\theta)}{1 - e^2} & 2\frac{1 + 2e\cos\theta + e^2}{1 - e^2} & 0 & 0 & 0 & 0 \\
e + \cos\theta & 2(e + \cos\theta) & (1 - e^2)\frac{\sin\theta}{1 + e\cos\theta} & 0 & 0 & 0 \\
\frac{\sin\theta}{e} & 2\frac{\sin\theta}{e} & -\frac{2e + (1 + e^2)\cos\theta}{e(1 + e\cos\theta)} & 1 & 0 & 0 \\
\frac{3(1 + e\cos\theta)}{1 - e^2} + \frac{1}{M}\frac{\sqrt{1 - e^2}}{e\sin\theta}\left[-2\right. & 3\frac{1 + 2e\cos\theta + e^2}{1 - e^2} & & 0 & 0 & 0 \\
\left. + (e + \cos\theta)\cos\theta + \frac{1 - e^2}{1 + e\cos\theta}\right] & -\frac{2}{M}\sqrt{\frac{1 - e^2}{e}}\sin\theta\frac{1 + e\cos\theta + e^2}{1 + e\cos\theta} & \frac{1}{M}\frac{(1 - e^2)^{3/2}}{e}\frac{\cos\theta}{1 + e\cos\theta} & & & \\
0 & 0 & 0 & 0 & -\frac{\sin L_0 \sin^2\beta_0}{\sin i_0} & -\frac{\cos L_0 \cos\beta_0}{\sin i_0} \\
0 & 0 & 0 & 0 & \frac{\cos\beta_0}{\cos L_0} + \frac{\cos i_0 \sin\beta_0 \cos\beta_0}{\sin^2 i_0} & \frac{1}{\sin L_0}\left[\cot^2 i_0 \cot^2\beta_0 - 1\right]
\end{bmatrix}
\begin{bmatrix} \frac{dr}{r} \\ \frac{dv}{v} \\ d\gamma \\ d\phi \\ d\psi \\ d\beta \end{bmatrix}
$$

$$
\begin{bmatrix} \frac{da}{a} \\ de \\ d\omega \\ \frac{d(t_p - t)}{t_p - t} \\ dt \\ d\Omega \end{bmatrix} =
\begin{bmatrix}
2\frac{a}{r} & 2\left(2\frac{a}{r} - 1\right) & 0 & 0 & 0 & 0 \\
\frac{1 - e^2}{e}\left(\frac{a}{r} - 1\right) & 2\frac{1 - e^2}{e}\left(\frac{a}{r} - 1\right) & \pm\frac{1}{e}\sqrt{(1 - e^2)\left[\left(\frac{r}{a} - 1\right)^2 - e^2\right]} & 0 & 0 & 0 \\
\pm\frac{1}{e}\sqrt{1 - \left[\frac{a(1 - e^2) - r}{er}\right]^2} & \pm\frac{2}{e}\sqrt{1 - \left[\frac{a(1 - e^2) - r}{er}\right]^2} & -\frac{1}{e^2}\left[1 + e^2 - \frac{r}{a}\right] & 1 & 0 & 0 \\
3\frac{a}{r} \pm \frac{1}{M}\left[3\frac{a}{r} - 1 - \left(\frac{a}{r}\right)^2(1 - e^2)\right]^{-1/2}\left[-2\right. & 3\left(2\frac{a}{r} - 1\right) \mp \frac{2}{M}\left[e^2\right. & \frac{1}{M}\frac{(1 - e^2)^{3/2}}{e^2}\left[1 - \frac{r}{a}\frac{1}{1 - e^2}\right] & 0 & 0 & 0 \\
\left. + \frac{r}{a} + \left(\frac{a}{r} - 1\right)\frac{1 - e^2}{e^2}\left\{\frac{a}{r}(1 - e^2) - 1\right\}\right] & \left. - \left(1 - \frac{r}{a}\right)^2\right]^{1/2}\left[1 + \frac{a}{r}\frac{(1 - e^2)}{e^2}\right] & & & & \\
0 & 0 & 0 & 0 & -\frac{\sin L_0 \cos^2 i_0}{\sin i_0 \cos^2 L_0} & \pm\sqrt{1 - \frac{\sin^2 L_0}{\sin^2 i_0}} \\
0 & 0 & 0 & 0 & \pm\frac{1}{\cos^2 L_0 \sin i_0}\sqrt{1 - \frac{\sin^2 L_0}{\sin^2 i_0}} & -\frac{\sin L_0}{\sin^2 i_0}
\end{bmatrix}
\begin{bmatrix} \frac{dr}{r} \\ \frac{dv}{v} \\ d\gamma \\ d\phi \\ d\psi \\ d\beta \end{bmatrix}
$$

$$\frac{dv_p}{v_p} = \left[-\frac{a}{r} + \frac{1}{e}\left(\frac{a}{r} - 1\right)\right] \frac{dr}{r} + \left[1 - 2\frac{a}{r} + \frac{2}{e}\left(\frac{a}{r} - 1\right)\right] \frac{dv}{v} \pm \frac{1}{e}\sqrt{\left(\frac{r}{a}\right)^2 \frac{\left(2\frac{a}{r} - 1\right)}{1 - e^2} - 1}\, d\gamma \qquad (41)$$

upper sign for + γ, lower sign for - γ

With coefficients expressed in terms of the variable θ, Eqs (38) through (41) become

$$\frac{dr_a}{r_a} = \frac{1}{1-e}(2 - e + \cos\theta)\frac{dr}{r} + \frac{2}{1-e}(1 + \cos\theta)\frac{dv}{v} + (1 - e)\frac{\sin\theta}{1 + e\cos\theta}\, d\gamma \qquad (42)$$

$$\frac{dr_p}{r_p} = \frac{1}{1+e}(2 + e - \cos\theta)\frac{dr}{r} + \frac{2}{1+e}(1 - \cos\theta)\frac{dv}{v} - (1 - e)\frac{\sin\theta}{1 + e\cos\theta}\, d\gamma \qquad (43)$$

$$\frac{dv_a}{v_a} = \frac{-1}{1-e}(1 + \cos\theta)\frac{dr}{r} - \frac{1}{1-e}(1 + e + 2\cos\theta)\frac{dv}{v} - \frac{\sin\theta}{1 + e\cos\theta}\, d\gamma \qquad (44)$$

$$\frac{dv_p}{v_p} = -\frac{1}{1+e}(1 - \cos\theta)\frac{dr}{r} - \frac{1}{1+e}(1 - e - 2\cos\theta)\frac{dv}{v} + \frac{\sin\theta}{1 + e\cos\theta}\, d\gamma \qquad (45)$$

Eqs (38) through (45) are collected in Table 3.

c. Evaluation of critical cases ($e \approx 0$, $i \approx 0°$)

Many of the error formula coefficients involved in transformation from polar coordinate errors to orbit element errors (Table 1) are indeterminate or inaccurate for $e \approx 0$ or $i \approx 0°$. Error formulas for these special cases may be developed by a Taylor series approach, as used in Ref. (1). If $a = a_0 + \Delta a$, $r = r_0 + \Delta r$, $v = v_0 + \Delta v$ are substituted in Eq (1),

$$a_0 + \Delta a = \left[\frac{2}{r_0 + \Delta r} - \frac{(v_0 + \Delta v)^2}{\mu}\right]^{-1}.$$

Since $a_0 = r_0$ and $v_0 = \sqrt{\frac{\mu}{r_0}}$ for nominally circular orbits,

$$1 + \frac{\Delta a}{r_0} = \left[\frac{2}{1 + \frac{\Delta r}{r_0}} - \left(1 + \frac{\Delta v}{v_0}\right)^2\right]^{-1} \qquad (46)$$

Neglecting terms of second order and higher in the Maclaurin series expansion

$$(1+\epsilon)^n = 1 + n\epsilon + \frac{n(n-1)\epsilon^2}{2!} + \frac{n(n-1)(n-2)\epsilon^3}{3!} + \cdots \qquad (47)$$

$(\epsilon^2 << 1)$

of the various terms of Eq (46) gives

$$\frac{\Delta a}{r_0} \approx 2\frac{\Delta r_0}{r_0} + 2\frac{\Delta v_0}{v_0} \quad (1 >> \epsilon^2) \qquad (48)$$

which checks with Eq (8) for nominally circular orbits ($a_0 = r_0$ in the coefficients). However, similar evaluation of Δe from Eq (2) (that is, letting $r = r_0 + \Delta r$, $v = v_0 + \Delta v$, $\gamma = \Delta\gamma$ in

$$e^2 = 1 + \frac{1}{\mu^2} r^2 v^4 \cos^2\gamma - \frac{2}{\mu} r v^2 \cos^2\gamma$$

requires retaining second order terms in approximations by Eq (47) since the first order terms vanish. The resulting solution is

$$e^2 \approx \left(2\frac{\Delta v}{v_0} + \frac{\Delta r}{r_0}\right)^2 + \gamma^2. \qquad (49)$$

$(1 >> e^2)$

TABLE 2

Error Analysis Equations

$$
\begin{bmatrix} \frac{dr}{r} \\ \frac{dv}{v} \\ d\gamma \\ d\phi \\ d\psi \\ d\beta \end{bmatrix} =
\begin{bmatrix}
1 - \frac{3}{2}\frac{e M \sin\theta}{(1-e^2)^{1/2}}(1+e\cos\theta) & -\frac{1}{1-e^2}\cos\theta\,(1+e\cos\theta) & 0 & \frac{M e \sin\theta}{(1-e^2)^{3/2}}(1+e\cos\theta) & 0 & 0 \\
\frac{1}{2}\left[-1+3\frac{e M \sin\theta (1+e\cos\theta)^2}{(1-e^2)^{3/2}(1+e^2+2e\cos\theta)}\right] & \frac{1}{(1-e^2)}\frac{\cos\theta(1+e\cos\theta)^2}{(1+e^2+2e\cos\theta)} & 0 & 2\sin\theta & 0 & 0 \\
-\frac{3 e M (e+\cos\theta)(1+e\cos\theta)^2}{2(1-e^2)^{3/2}(1+e^2+2e\cos\theta)} & \frac{\sin\theta(1+e^2+e\cos\theta)(1+e\cos\theta)}{(1-e^2)(1+e^2+2e\cos\theta)} & 0 & \frac{M e (1+e\cos\theta)^2 (e+\cos\theta)}{(1-e^2)^{3/2}(1+e^2+2e\cos\theta)} & 0 & 0 \\
-\frac{3}{2} M \frac{(1+e\cos\theta)^2}{(1-e^2)^{3/2}} & \frac{1}{1-e^2}\sin\theta\,(2+e\cos\theta) & 1 & \frac{M(1+e\cos\theta)^2}{(1-e^2)^{3/2}} & 0 & 0 \\
0 & 0 & 0 & 0 & \frac{\sin i_0}{\sin L_0}(\cot^2 i_0 \cot^2\beta_0 - 1) & \cos L_0 \cos\beta_0 \\
0 & 0 & 0 & 0 & -\cos\beta_0\left[\frac{\sin i_0}{\cos L_0} + \frac{\cos i_0 \sin\beta_0}{\sin i_0}\right] & -\sin L_0 \sin^2\beta_0
\end{bmatrix}
\begin{bmatrix} \frac{da}{a} \\ de \\ d\omega \\ \frac{d(t_p - t)}{t_p - t} \\ di \\ d\Omega \end{bmatrix}
$$

TABLE 3

Error Analysis Equations

$$
\begin{bmatrix} \frac{dr_a}{r_a} \\ \frac{dr_p}{r_p} \\ \frac{dv_a}{v_a} \\ \frac{dv_p}{v_p} \end{bmatrix} =
\begin{bmatrix}
\frac{1}{1-e}(2-e+\cos\theta) & 2\frac{1}{1-e}(1+\cos\theta) & (1-e)\frac{\sin\theta}{1+e\cos\theta} \\
\frac{1}{1+e}(2+e-\cos\theta) & 2\frac{1}{1+e}(1-\cos\theta) & -(1+e)\frac{\sin\theta}{1+e\cos\theta} \\
-\frac{1}{1-e}(1+\cos\theta) & -\frac{1}{1-e}(1+e+2\cos\theta) & -\frac{\sin\theta}{1+e\cos\theta} \\
-\frac{1}{1+e}(1-\cos\theta) & -\frac{1}{1+e}(1-e-2\cos\theta) & \frac{\sin\theta}{1+e\cos\theta}
\end{bmatrix}
\begin{bmatrix} \frac{dr}{r} \\ \frac{dr}{v} \\ d\gamma \end{bmatrix}
$$

$$
\begin{bmatrix} \frac{dr_a}{r_a} \\ \frac{dr_p}{r_p} \\ \frac{dv_a}{v_a} \\ \frac{dv_p}{v_p} \end{bmatrix} =
\begin{bmatrix}
\frac{a}{r}\left[2+\frac{(1-e)}{e}\left(1-\frac{r}{a}\right)\right] & 2\frac{a}{r}\left[1+\frac{1}{e}\left(1-\frac{r}{a}\right)\right] & \pm\frac{1-e}{e}\left[\left(\frac{r}{a}\right)^2\frac{2\frac{a}{r}-1}{1-e^2}-1\right]^{1/2} \\
\frac{a}{r}\left[2-\frac{1+e}{e}\left(1-\frac{r}{a}\right)\right] & 2\frac{a}{r}\left[1-\frac{1}{e}\left(1-\frac{r}{a}\right)\right] & \mp\frac{1+e}{e}\left[\left(\frac{r}{a}\right)^2\frac{2\frac{a}{r}-1}{1-e^2}-1\right]^{1/2} \\
-\frac{a}{r}+\frac{1}{e}\left(1-\frac{a}{r}\right) & 1-2\frac{a}{r}+\frac{2}{e}\left(1-\frac{a}{r}\right) & \mp\frac{1}{e}\left[\left(\frac{r}{a}\right)^2\frac{2\frac{a}{r}-1}{1-e^2}-1\right]^{1/2} \\
-\frac{a}{r}+\frac{1}{e}\left(\frac{a}{r}-1\right) & 1-2\frac{a}{r}+\frac{2}{e}\left(\frac{a}{r}-1\right) & \pm\frac{1}{e}\left[\left(\frac{r}{a}\right)^2\frac{2\frac{a}{r}-1}{1-e^2}-1\right]^{1/2}
\end{bmatrix}
\begin{bmatrix} \frac{dr}{r} \\ \frac{dv}{v} \\ d\gamma \end{bmatrix}
$$

Similarly the series approximation of Eq (47) gives, from Eqs (26) and (27),

$$\frac{\Delta r_a}{r_0} \approx \frac{\Delta a}{r_0} + e \tag{50}$$

$$\frac{\Delta r_p}{r_0} \approx \frac{\Delta a}{r_0} - e \tag{51}$$

$(1 >> e^2)$

Substitution of Eqs (48) and (49) in Eqs (50) and (51) gives

$$\frac{\Delta r_a}{r_0} \approx 2\frac{\Delta r_0}{r_0} + 2\frac{\Delta v_0}{v_0} + \sqrt{\left(2\frac{\Delta v}{v_0} + \frac{\Delta r}{r_0}\right)^2 + \gamma^2} \tag{52}$$

$$\frac{\Delta r_p}{r_0} \approx 2\frac{\Delta r_0}{r_0} + 2\frac{\Delta v_0}{v_0} - \sqrt{\left(2\frac{\Delta v}{v_0} + \frac{\Delta r}{r_0}\right)^2 + \gamma^2} \tag{53}$$

The elements ω and t_p are not defined in the circular orbit case and, therefore, will not be considered. However, di and $d\Omega$ are indeterminate for i = 0°. For this case, from spherical trigonometry,

$$\cos \Delta i = \cos \Delta\psi \sin (90 + \Delta\beta).$$

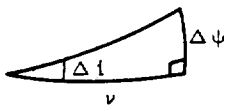

d

The Maclaurin series approximation gives

$$1 - \frac{\Delta i^2}{2} = \left(1 - \frac{\Delta\psi^2}{2}\right)\left(1 - \frac{\Delta\beta^2}{2}\right)$$

or

$$\Delta i^2 = \Delta\psi^2 + \Delta\beta^2 \tag{54}$$

The error in Ω is not defined (since, for the nominally equatorial orbit, the ascending node is not defined). However, the node of the incorrect orbit can be determined from

$$\sin \nu = \frac{\tan \Delta\psi}{\tan \Delta i} \approx \frac{\Delta\psi}{\Delta i} \tag{55}$$

The case of near circular orbits is also considered for the inverse transformation (errors in polar coordinates as functions of orbit element errors) in Ref. (1). For the small eccentricities of this special case, the planar variables can be expressed by the following series expansions, as given in Chapter III.

$$\frac{r}{a} = 1 - e\cos M - \frac{e^2}{2}(\cos 2M - 1) - \frac{e^3}{2!\,2^2}(3\cos 3M - 3M) - \ldots$$

$$\frac{v}{\sqrt{\frac{\mu}{a}}} = 1 + e\cos\theta + \frac{e^2}{4}(3 - \cos 2\theta) + \frac{e^3}{8}(4\cos\theta - \cos 3\theta - 7) + \ldots$$

$$\theta = M + 2e\sin M + \frac{5e^2}{4}\sin 2M + \frac{e^3}{12}(13\sin 3M - 3\sin M)$$

$$\gamma = e\sin\theta - \frac{e^2}{2}\sin 2\theta + \frac{e^3}{3}\sin 3\theta - \ldots$$

$$M = \text{mean anomaly} = \sqrt{\frac{\mu}{a^3}}\,(t - t_p) \tag{56}$$

For $e^2 << 1$, approximate relations can be written.

$$r \approx a\,(1 - e\cos M) \tag{57}$$

$$v \approx \sqrt{\frac{\mu}{a}}\,(1 + e\cos M) \tag{58}$$

$$\theta \approx M + 2e\sin M \tag{59}$$

$$\gamma \approx e\sin M \tag{60}$$

From Eq (56)

$$M = M_0 + \Delta M = \left[\frac{\mu}{r_0^3\left(1 + \frac{\Delta a}{r_1}\right)^3}\right]^{1/2}(t - t_{p0} - \Delta t_p)$$

or

$$\Delta M = -\frac{3}{2}\frac{\Delta a}{r_0}M_0 - \sqrt{\frac{\mu}{r_0^3}}\,\Delta t_p. \tag{61}$$

The errors at any later time Δr_2, Δv_2, $\Delta\gamma_2$ and $\Delta\theta_2$ will be determined as functions of Δr_1, Δv_1, and $\Delta\gamma_1$ by varying one injection parameter at a time and assuming a linear combination of the individual errors.

Case (1) $\left[\Delta r_1 = 0,\ \Delta v_1 = 0,\ \Delta\gamma_1 \neq 0\right]$

If γ_1 is the only launch parameter which is in error, $\Delta r_1 = 0$, $\Delta v_1 = 0$, $\gamma_1 = \Delta\gamma_1$, and from Eq (49), $e \approx |\Delta\gamma_1|$, where $\Delta\gamma_1$ is an error due to a velocity component normal to the desired circular orbit velocity at launch. For the circular orbit, M and t_p are referenced to the perigee direction in the incorrect orbit. Since the semimajor axis a is a function of r and v but not γ, $\Delta a = 0$ for this case. Then, from Eqs (57) through (61),

$$\Delta r_{(1)} \approx -er_0\cos M_0 \approx -r_0\,|\Delta\gamma_1|\cos M_0$$

$$\frac{\Delta v_{(1)}}{v_0} \approx |\Delta\gamma_1|\cos M_0$$

(continued)

$$\Delta\theta_{(1)} \approx -\sqrt{\frac{\mu}{r_0^3}}\,\Delta t_p + 2\left|\Delta\gamma_1\right|\sin M_0$$

$$\Delta r_{(1)} \approx \left|\Delta\gamma_1\right| \sin M_0$$

From the $\Delta r_{(1)}$ equation, $\Delta r = 0$ when $\cos M_0 = 0$. Therefore, for case (1), $M_0 = 90°$ (for γ_1 positive) or $M_0 = 270°$ (for γ_1 negative). The absolute magnitudes in these equations may be removed by defining a mean anomaly M_0, referenced to the initial point. Then $\mathcal{M}_0 = M_0 - 90°$ for positive $\Delta\gamma_1$, and $\mathcal{M}_0 = M_0 + 90°$ for negative $\Delta\gamma_1$. Substitution in the previous equations gives, for either positive or negative $\Delta\gamma_1$,

$$\frac{\Delta r_{(1)}}{r_0} \approx \Delta\gamma_1 \sin \mathcal{M}_0 \qquad (62)$$

$$\frac{\Delta v_{(1)}}{v_0} \approx -\Delta\gamma_1 \sin \mathcal{M}_0 \qquad (63)$$

$$\Delta\theta_{(1)} \approx 2\Delta\gamma_1 (\cos \mathcal{M}_0 - 1) \qquad (64)$$

$$\Delta\gamma_{(1)} \approx \Delta\gamma_1 \cos \mathcal{M}_0 \qquad (65)$$

In derivation of Eq (64) use is made of the fact that $\Delta\theta_{(1)} = 0$ at $\mathcal{M}_0 = 0$ since the correct and incorrect orbits intersect at the initial point.

Case (2) $\left[\Delta\gamma_1 = 0,\ \Delta v_1 = 0,\ \Delta r_1 \neq 0\right]$

For $\Delta\gamma_1 = 0$, $\Delta v_1 = 0$, $\Delta r_1 \neq 0$, Eqs (48) and (49) give

$$\frac{\Delta a_{(2)}}{r_0} \approx 2\,\frac{\Delta r_1}{r_0}$$

$$e_{(2)} \approx \frac{|\Delta r_1|}{r_1}.$$

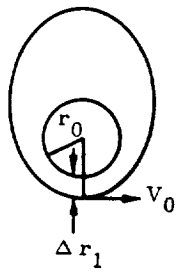

Then, from Eqs (57) through (61)

$$\frac{\Delta r_{(2)}}{r_0} \approx 2\,\frac{\Delta r_1}{r_0} - \frac{|\Delta r_1|}{r_0}\cos M_0$$

$$\frac{\Delta v_{(2)}}{v_0} \approx -\frac{\Delta r_1}{r_0} + \frac{|\Delta r_1|}{r_0}\cos M_0$$

$$\Delta\theta_{(2)} \approx -3\,\frac{\Delta r_1}{r_0} M_0 - \sqrt{\frac{\mu}{r_0^3}}\,\Delta t_p + 2\,\frac{|\Delta r_1|}{r_0}\sin M_0$$

$$\Delta\gamma_{(2)} \approx \frac{|\Delta r_1|}{r_0}\sin M_0$$

But $M_0 = 0°$ for Δr_1 positive, and $M = 180°$ for Δr_1 negative. Then, for $\mathcal{M}_0 = 0°$ at launch,

$$\frac{\Delta r_{(2)}}{r_0} \approx \frac{\Delta r_1}{r_0}(2 - \cos \mathcal{M}_0) \qquad (66)$$

$$\frac{\Delta v_{(2)}}{v_0} \approx \frac{\Delta r_1}{r_0}(\cos \mathcal{M}_0 - 1) \qquad (67)$$

$$\Delta\theta_{(2)} \approx \frac{\Delta r_1}{r_0}(2 \sin \mathcal{M}_0 - 3\,\mathcal{M}_0) \qquad (68)$$

$$\Delta\gamma_{(2)} \approx \frac{\Delta r_1}{r_0}\sin \mathcal{M}_0 \qquad (69)$$

Case (3) $\left[\Delta r_1 = 0,\ \Delta\gamma_1 = 0,\ \Delta v_1 \neq 0\right]$

For the remaining case, where $\Delta r_1 = 0$, $\Delta\gamma_1 = 0$ and $\Delta v_1 \neq 0$, Eqs (48) and (49) gives

$$\frac{\Delta a}{r_0}(3) \approx 2\,\frac{\Delta V_1}{V_0}$$

$$e_{(3)} \approx 2\,\frac{|\Delta V_1|}{V_0}.$$

A procedure similar to that used in cases (1) and (2) gives

$$\frac{\Delta r_{(3)}}{r_0} \approx 2\,\frac{\Delta v_1}{v_0}(1 - \cos \mathcal{M}_0) \qquad (70)$$

$$\frac{\Delta v_{(3)}}{v_0} \approx \frac{\Delta v_1}{v_0}(2 \cos \mathcal{M}_0 - 1) \qquad (71)$$

$$\Delta\theta_{(3)} \approx -3\,\mathcal{M}_0\,\frac{\Delta v_1}{v_0} + 4\,\frac{\Delta v_1}{v_0}\sin \mathcal{M}_0 \qquad (72)$$

$$\Delta\gamma_{(3)} \approx 2\,\frac{\Delta v_1}{v_0}\sin \mathcal{M}_0. \qquad (72)$$

The total error solutions are obtained by combining the effect of all three errors linearly (adding Eqs (62), (66) and (70); Eqs (63), (67) and (71); etc.).

$$\frac{\Delta r}{r_0} \approx \sin \eta_0 \, \Delta \gamma_1 + (2 - \cos \eta_0) \frac{\Delta r_1}{r_0} + 2 (1 - \cos \eta_0) \frac{\Delta v_1}{v_0} \qquad (74)$$

$$\frac{\Delta v}{v_0} \approx - \sin \eta_0 \, \Delta \gamma_1 + (\cos \eta_0 - 1) \frac{\Delta r_1}{r_0} + (2 \cos \eta_0 - 1) \frac{\Delta v_1}{v_0} \qquad (75)$$

$$\Delta \omega \approx \Delta \omega_1 + 2 (\cos \eta_0 - 1) \Delta \gamma_1 + (2 \sin \eta_0 - 3 \eta_0) \frac{\Delta r_1}{r_0} + (4 \sin \eta_0 - 3 \eta_0) \frac{\Delta v_1}{v_0} \qquad (76)$$

$$\Delta \gamma \approx \cos \eta_0 \, \Delta \gamma_1 + \sin \eta_0 \frac{\Delta r_1}{r_0} + 2 \sin \eta_0 \frac{\Delta v_1}{v_0} \qquad (77)$$

$$e^2 << 1$$

d. Statistical analysis

The error formulas developed in previous sections serve to convert a specific set of errors from one system of orbit determining variables to another. However, in preliminary design work, specific sets of errors are frequently not of interest. Rather, the design engineer must determine the probability that a certain error will be less than the tolerable limit. That is, he requires a probabalistic relation rather than an algebraic relation between the errors. This section concerns the determination of the error probabilities from the previously determined error formulas.

(1) Probability of Linear Error Functions

The majority of these error formulas are linear differential approximations of the form.

$$u = \sum_i a_i x_i, \; i = 1, 2, \ldots, k$$

where the a_i are constants. If the x_i (the errors to be transformed) are independently and normally distributed with means μ_i and variances σ_i^2, then the moment generating function $\mu(t)$ for the distribution of the variate u is given as follows:

$$m(t) = \left(\frac{1}{2\pi}\right)^{\frac{k}{2}} \left(\prod_{i=1}^{n} \frac{1}{\sigma_i}\right) \int_{-\infty}^{\infty} \int_{-\infty}^{\infty} \cdots \int_{-\infty}^{\infty} \exp\left[t \sum_i a_i x_i - \frac{1}{2} \sum_i \left(\frac{x_i - \mu_i}{\sigma_i}\right)^2\right] dx_1 \, dx_2 \ldots dx_k$$

Transformation to the standard form is convenient.

Let

$$y_i = \frac{x_i - \mu_i}{\sigma_i}$$

Then

$$m(t) = \left(\frac{1}{2\pi}\right)^{k/2} \prod_i \left(\int_{-\infty}^{\infty} \exp(t a_i \mu_i) \exp(t a_i y_i \sigma_i - \frac{1}{2} y_i^2) \, dy_i \right)$$

$$= \left(\frac{1}{2\pi}\right)^{k/2} \prod_i \left(\exp(t a_i \mu_i) \exp\left(\frac{1}{2} t^2 a_i^2 \sigma_i^2\right) \cdot \int_{-\infty}^{\infty} \exp\left(-\frac{1}{2}\left[y_i^2 - 2 t a_i y_i \sigma_i + t^2 a_i^2 \sigma_i^2\right]\right) dy_i\right)$$

$$= \exp\left[t \sum_i a_i \mu_i + \frac{t^2}{2} \sum_i a_i^2 \sigma_i^2\right] \qquad (78)$$

However, the moment generating function for the normal distribution is

$$m_n(t) = \exp\left(t\mu + \frac{1}{2} t^2 \sigma^2\right)$$

Therefore, Eq (78) is the moment generating function for a normal distribution

$$n(u) = \frac{1}{\sqrt{2\pi}\,\sigma} \exp\left[-\frac{1}{2}\left(\frac{u - \mu}{\sigma}\right)^2\right]$$

with mean and variance given by

$$\mu = \sum_i a_i \mu_i \qquad (79)$$

$$\sigma^2 = \sum_i a_i^2 \sigma_i^2 \qquad (80)$$

Similarly, if the x_i are correlated instead of being independently distributed, u is distributed normally with

$$\mu = \sum_i a_i \mu_i \tag{81}$$

$$\sigma^2 = \sum_i a_i^2 \sigma_i^2 + \sum_{i,j} a_{ij} \sigma_{ij} \tag{82}$$

The covariance, σ_{ij}, is sometimes written $\rho_{ij} \sigma_i \sigma_j$ where ρ_{ij} is the correlation. These results (Eq (79) and (80) or (81) and (82)) then describe the probability distributions of the left-hand column vectors of Tables 1, 2 and 3 if the distributions of the right-hand column vectors are assumed to be normal. For example, from Eq (48), if Δr and Δv are normally distributed with zero means, then Δa is normally distributed with zero mean and variance

$$\frac{\sigma^2_{\Delta a}}{r_0^2} = 4\left[\frac{\sigma^2_{\Delta v}}{v_o^2} + \frac{\sigma^2_{\Delta r}}{r_0^2} + 2\,\frac{\rho_{\Delta v \Delta r}\,\sigma_{\Delta v}\,\sigma_{\Delta r}}{v_0\, r_0}\right].$$

(nominally circular orbits)

Once the distribution of the transformed error is determined, the probability that u will lie between two given values u_1 and u_2 is given by

$$P\left[u_1 < u < u_2\right] = \int_{u_1}^{u_2} n(u)\, du.$$

Since areas under the normal error distribution curve are widely tabulated, the probability that the error u will be less than a specified tolerable limit u*,

$$P\left[|u| < u^*\right] = \int_0^{u^*} n(u)\, du, \tag{83}$$

may be readily evaluated from tables. The solution for error probabilities has thus been obtained in all cases in which the error formula can be approximated by a linear function.

(2) Probability of Nonlinear Error Functions

Although most of the error formulas are linear, certain formulas for nominally circular orbits (for example, Eqs (49), (52), (53) and (54)) involve nonlinear relations of the form

$$u = \sqrt{x_1^2 + x_2^2} \tag{84}$$

Determination of the probability distribution of the function of Eq (84) is not so simple as in the case of the linear error formula, and the resulting distribution is not normal. If x_1 and x_2 are assumed normally and independently distributed, their joint distribution is simply the product of the individual distributions,

$$n(x_1, x_2) = \frac{1}{2\pi\,\sigma_{x_1}\,\sigma_{x_2}} \exp\left\{-\frac{1}{2}\left[\left(\frac{x_1}{\sigma_{x_1}}\right)^2 + \left(\frac{x_2}{\sigma_{x_2}}\right)^2\right]\right\}.$$

The distribution of u may be obtained by eliminating either x_1 or x_2 in terms of u to obtain a density

$$g(u, x_2) = \sum_i n\left[x_1(u, x_2), x_2\right] \left|\frac{\partial x_i}{\partial u}\right|_i$$

where each term in the summation represents one branch of a possibly nonmonotone function $u(x_1)$. The desired distribution, g(u), may then be obtained by integrating over the x_2 in $g(u, x_2)$.

$$g(u) = \int_{-\infty}^{\infty} g(u, x_2)\, dx_2$$

In particular, for $u = \sqrt{x_1^2 + x_2^2}$

$$x_1 = \pm\sqrt{u^2 - x_2^2}$$

$$\left|\frac{\partial x_1}{\partial u}\right| = \frac{u}{\sqrt{u^2 - x_2^2}}$$

$$g(u, x_2) = 2\left\{\frac{1}{2\pi\,\sigma_{x_1}\,\sigma_{x_2}} \exp\left[-\frac{1}{2}\left(\frac{u^2 - x_2^2}{\sigma^2_{x_1}} + \frac{x_2^2}{\sigma^2_{x_2}}\right)\right] \frac{u}{\sqrt{u^2 - x_2^2}}\right\}$$

Thus,

$$g(u) = \frac{u \exp\left[-\frac{1}{2}\,\frac{u^2}{\sigma^2_{x_1}}\right]}{\pi\,\sigma_{x_1}\,\sigma_{x_2}} \int_{-\infty}^{\infty} \frac{1}{\sqrt{u^2 - x_2^2}} \cdot \exp\left\{-\frac{1}{2}\left[x_2^2\left(\frac{1}{\sigma^2_{x_2}} - \frac{1}{\sigma^2_{x_1}}\right)\right]\right\} dx_2$$

$$\left[= \int_{-\infty}^{\infty} g(u, x_2)\, dx_2\right]$$

After the transformation

$$t = x_2^2$$

this expression may be integrated to yield the required distribution

$$g(u) = \frac{u}{\sigma_{x_1}\,\sigma_{x_2}} \exp\left[-\frac{u^2}{4}\left(\frac{1}{\sigma^2_{x_1}} + \frac{1}{\sigma^2_{x_2}}\right)\right] I_0\left[\frac{u^2}{4}\left(\frac{1}{\sigma^2_{x_2}} - \frac{1}{\sigma^2_{x_1}}\right)\right], \quad 0 < x_2^2 < u^2, \tag{85}$$

$$= 0, \quad x_2^2 > u^2$$

This g(u) (and, in particular, the distribution of corrected orbit eccentricity error) is a skewed, single-sided distribution with positive mean and a shape similar to that of the gamma distribution.

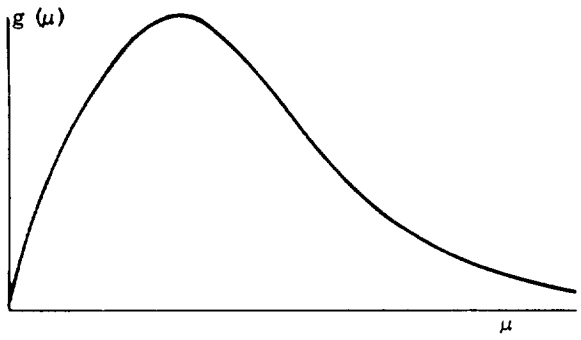

In manipulation of the distribution g(u) the following definitions are convenient.

$$K_1 \equiv \frac{1}{\sigma_{x_1}\sigma_{x_2}}$$

$$K_2 \equiv \frac{1}{4}\left[\frac{1}{\sigma^2_{x_1}} + \frac{1}{\sigma^2_{x_2}}\right]$$

$$K_3 \equiv \frac{1}{4}\left[\frac{1}{\sigma^2_{x_2}} - \frac{1}{\sigma^2_{x_1}}\right]$$

The distribution is then

$$g(u) = K_1 u e^{-K_2 u^2} I_0 (K_3 u^2)$$

Quantities of some significance in describing the properties of the distribution (e.g., central values, spread, skewness, etc.) are the moments of the distribution. The rth moment of g(u) is

$$\bar{\mu}_r = \int_{-\infty}^{\infty} u^r g(u)\, du$$

$$= K_1 \int_{-\infty}^{\infty} u^{r+1} \exp(-K_2 u^2) I_0 (K_3 u^2)\, du$$

After the transformation $t = u^2$, the integral can be evaluated in various forms.

$$\int_0^{\infty} t^n \epsilon^{-K_2 t} I_\nu (K_3 t)\, dt = \Gamma(n + \nu + 1)(K_2^2 - K_3^2)^{-\frac{1}{2}(n+1)} P_n^{-\nu}\left(\frac{K_2}{\sqrt{K_2^2 - K_3^2}}\right)$$

$$K_2 > |K_3|$$

where the generalized Legendre function is given by

$$P_n^m(z) = \frac{1}{\Gamma(1-m)}\left(\frac{z+1}{z-1}\right)^{m/2} {}_2\mathcal{F}_1 (-n, n+1; 1 - m; \tfrac{1}{2} - \tfrac{1}{2} z)$$

and the hypergeometric series is given by

$${}_m\mathcal{F}_n (a_1, \ldots, a_m; \gamma_1, \ldots, \gamma_n; z) = \sum_{i=0}^{\infty} \frac{(a_1)_i \ldots (a_m)_i}{(\gamma_1)_i \ldots (\gamma_n)_i} \frac{z^i}{i!}$$

Then

$$\bar{\mu}_r = \frac{K_1}{2} \frac{\Gamma(\frac{r}{2}+1)}{K_2^{r/2+1}} \mathcal{F}\left[\frac{r+2}{4}, \frac{r+4}{4}, 1; \left(\frac{K_3}{K_2}\right)^2\right]$$

$$= \frac{K_1}{2} \frac{\Gamma(\frac{r}{2}+1)}{K_2^{r/2+1}} \sum_{i=0}^{\infty} \frac{(\frac{r+2}{4}; 1; i)\ (\frac{r+4}{4}; 1; i)}{i!\ (1; 1; i)} \left(\frac{K_3}{K_2}\right)^{2i}$$

In particular, the mean of the distribution g(u) is given by

$$\bar{\mu}_1 = \frac{K_1 \Gamma(\frac{3}{2})}{2K_3^{3/2}} \mathcal{F}\left[\frac{3}{4}, \frac{5}{4}, 1; \left(\frac{K_3}{K_2}\right)^2\right]$$

$$= \frac{K_1 \sqrt{\pi}}{4K_2^{3/2}} \left[1 + \frac{\frac{3}{4}\cdot\frac{5}{4}}{1\cdot 1}\left(\frac{K_3}{K_2}\right)^2 + \frac{\frac{3}{4}\cdot\frac{7}{4}\cdot\frac{5}{4}\cdot\frac{9}{4}}{(2!)^2}\left(\frac{K_3}{K_2}\right)^4 + \frac{\frac{3}{4}\cdot\frac{7}{4}\cdot\frac{11}{4}\cdot\frac{5}{4}\cdot\frac{9}{4}\cdot\frac{13}{4}}{(3!)^2}\left(\frac{K_3}{K_2}\right)^6 + \ldots\right].$$

The second moment is of interest in determination of the variance of g(u).

$$\bar{\mu}_2 = \frac{K_1}{2} \frac{\Gamma(2)}{K_2^2} \mathcal{F}\left[1, \frac{3}{2}, 1; \left(\frac{K_3}{K_2}\right)^2\right]$$

$$= \frac{K_1}{2K_2^2}\left[1 + \frac{3}{2}\left(\frac{K_3}{K_2}\right)^2 + \frac{1}{2!}\frac{3}{2}\cdot\frac{5}{2}\left(\frac{K_3}{K_2}\right)^4 + \frac{1}{3!}\cdot\frac{3}{2}\cdot\frac{5}{2}\cdot\frac{7}{2}\left(\frac{K_3}{K_2}\right)^6 + \ldots\right]$$

Then the variance is

$$\sigma_u^2 = \bar{\mu}_2 - (\bar{\mu}_1)^2$$

Thus, the probability distributions of errors given by nonlinear equations of the form of Eq

(84) are rather complex. Therefore, the probability that the error u will be less than a specified tolerable limit u* must be computed by numerical integration or by the Monte-Carlo technique. The probability could be computed, for the case of Eq (84) by numerical integration.

$$P\left[u < u^*\right] = \int_0^{u^*} g(u)\, du,$$

where g(u) is defined in Eq (85). However, in general, this probability may be more readily computed from

$$P\left[u < u^*\right] = \int\int \cdots \int_{u < u^*} f(x_1, x_2, \ldots x_n)\, dx_1\, dx_2 \ldots dx_n \tag{86}$$

where $f(x_1, x_2 \ldots, x_n)$ is the multivariate distribution of the errors $x_1, x_2 \ldots, x_n$ and the integration limits are defined from the region in which $u < u^*$. If the number of random variables x_i is larger than five, the Monte-Carlo method is a convenient alternate solution for the probability P that a multivariate normal variable lies in a region R. These methods of evaluating the probabilities are considered in the following section.

The determination of the surface defining the region $u < u^*$ (that is, the limits of integration) is generally not difficult. In some cases, however, this surface may be difficult to construct. In this eventuality a more general technique may be employed. Consider for example an error function which is expressible as a sum of a normally distributed error Δp_n and an arbitrary known function $f(\Delta q)$ of a second normally distributed variable, Δq.

$$\Delta p = \Delta p_n + f(\Delta q)$$

For a complicated function $f(\Delta q)$, the determination of constant Δp surfaces in the Δq, Δp_n space become unwieldy. The individual density functions of Δp_n and $f(\Delta q)$ are readily obtainable, the latter by dividing the Gaussian density of Δq by $\frac{df(\Delta q)}{d\Delta q}$. Hence, $f(\Delta p)$, the density function of Δp, can be formulated as a convolution integral of the individual density functions

$$f(\Delta p) = \int_{-\infty}^{\infty} g(\Delta p - \xi)\, z(\xi)\, d\xi \tag{87}$$

where

$g(\Delta p_n)$ = density function of Δp_n

$z\left[f(\Delta q)\right]$ = density function of $f(\Delta q)$

(3) Evaluation of Multivariate Normal Probabilities (Ref. 2)

Error analyses and success probability determination for space missions (as well as other areas) frequently require the integration of a multivariate normal distribution over some appropriate region. In some instances, it is possible to use special computational routines to obtain this integral. In other situations, the Monte-Carlo method may have to be used. A general formulation and an illustration of both methods follow.

Theoretical discussion and special computational routines. The probability P is sought where

$$P = \int_{L'_1}^{U'_1} \int_{L'_2}^{U'_2} \cdots \int_{L'_{n-1}}^{U'_{n-1}} \int_{L'_n}^{U'_n} f(x_1, \ldots, x_n)\, dx_n \ldots dx_1 \tag{88}$$

with $f(x_1, \ldots, x_n)$ the multivariate normal distribution with mean vector $(\mu_1, \ldots, \mu_n)$ and variance-covariance matrix

$$\Sigma = (\sigma_{ij}),\ i, j = 1 \ldots n,\ \sigma_{ij} = \sigma_{ji}.$$

That is,

$$f(x_1, \ldots, x_n) = \frac{1}{(2\pi)^{n/2} \left|\Sigma\right|^{1/2}} \exp\left[- \frac{1}{2} \sum_{j=1}^{n} \sum_{i=1}^{n} \sigma^{ij} (x_i - \mu_i)(x_j - \mu_j) \right] \tag{89}$$

with σ^{ij} the (i, j) element in the matrix Σ^{-1} and $\left|\Sigma\right|$ denoting the determinant of the matrix Σ, and where

$$\begin{aligned} U'_n &= U'_n(x_1, \ldots, x_{n-1}), \quad L'_n = L'_n(x_1, \ldots x_{n-1}) \\ U'_{n-1} &= U'_{n-1}(x_1, \ldots, x_{n-2}), \\ L'_{n-1} &= L'_{n-1}(x_1, \ldots, x_{n-2}) \\ U'_2 &= U'_2(x_1), \quad L'_2 = L'_2(x_1) \\ U'_1 &= \text{constant}, \quad L'_1 = \text{constant} \end{aligned} \tag{90}$$

In order to obtain the number P via the computational routines, a transformation must be made to new variables $z_1, \ldots, z_n$ which have mean vector $(0, \ldots, 0)$ and variance-covariance matrix I_n, the unit matrix of size n. That is, the distribution of $(z_1, \ldots, z_n)$ is

$$\frac{1}{(2\pi)^{n/2}} \exp\left[- \frac{1}{2} \left(z_1^2 + z_2^2 + \ldots + z_n^2 \right) \right] \tag{91}$$

Of course, when a transformation is made to these new variables $(z_1, \ldots, z_n)$, the limits of integration change as well as the integrand. Therefore, among all the possible transformations, one must be chosen which will render the limits in a suitable form for the computational routines. Such a transformation is

$$x_i = \mu_i + \sum_{j=1}^{i} c_{ij} z_j, \quad i = 1, \ldots, n \tag{92}$$

with the coefficients c_{ij} defined recursively by

$$c_{il} = \frac{\sigma_{il}}{\sqrt{\sigma_{11}}}, \quad 1 \leq i \leq n$$

$$c_{il} = \sqrt{\sigma_{ii} - \sum_{k=1}^{i-1} c^2_{ik}}, \quad 1 < i \leq n$$

$$c_{ij} = \frac{\sigma_{ij} - \sum_{k=1}^{j=1} c_{ik} c_{jk}}{c_{jj}}, \quad n \geq i > j > 1 \tag{93}$$

$$c_{ij} = 0, \quad 1 \leq i < j \leq n.$$

Now the integral of Eq (88), giving the probability P, is

$$P = \frac{1}{(2\pi)^{n/2}} \int_{L_1}^{U_1} \int_{L_2}^{U_2} \cdots \int_{L_{n-1}}^{U_{n-1}} \int_{L_n}^{U_n} \exp\left[- \frac{1}{2} \left(z_1^2 + \ldots + z_n^2 \right) \right] dz_n \cdots dz_1 \tag{94}$$

with

$$U_n = U_n (z_1, \ldots, z_{n-1}), \quad L_n = L_n (z_1, \ldots, z_{n-1})$$

$$U_{n-1} = U_{n-1} (z_1, \ldots, z_{n-2}),$$

$$L_{n-1} = L_{n-1} (z_1, \ldots, z_{n-2})$$

$$U_2 = U_2 (z_1), \quad L_2 = L_2 (z_1) \tag{95}$$

$$U_1 = \text{constant}, \quad L_1 = \text{constant}$$

where the limits U_k and L_k are obtained from U'_k and L'_k by substituting into the relations $L'_k \leq x_k \leq U'_k$ expressions (92) for the x's in terms of z's.

The following example may illuminate the preceding generalities. Let the requirement for a successful orbit be

$$-B \leq \delta r_p \leq \delta r_a \leq A \tag{96}$$

for given positive numbers A and B. Equations (52) and (53) can be written more concisely in the following form:

$$\delta r_p = t_3 - \sqrt{t_1^2 + t_2^2} \tag{97}$$

$$\delta r_a = t_3 + \sqrt{t_1^2 + t_2^2} \tag{98}$$

where (t_1, t_2, t_3) has the multivariate normal distribution with mean vector (μ_1, μ_2, μ_3) and variance-covariance matrix

$$\sum = \begin{bmatrix} \sigma_{11} & \sigma_{12} & \sigma_{13} \\ \sigma_{21} & \sigma_{22} & \sigma_{23} \\ \sigma_{31} & \sigma_{32} & \sigma_{33} \end{bmatrix}$$

The numbers A and B are specified in the mission requirements; and μ_1, μ_2, μ_3, σ_{11}, σ_{12}, σ_{13}, σ_{22}, and σ_{33} ($\sigma_{ij} = \sigma_{ji}$) may be computed from the definitions of the t_i (Eqs (52) and (53)), the linear error analysis of Section B.1.d.(1) and given values of $\sigma_{\Delta r}$, $\sigma_{\Delta v}$, σ_γ. To obtain the probability P that Eq (96) holds, Eqs (97) and (98) are substituted into Eq (96) and the condition for success is symmetrized by making the preliminary change of variable $x_1 = t_1$, $x_2 = t_2$, $x_3 = t_3 - 1/2 (A - B)$. Then the criterion for success becomes

$$-1/2 (A + B) \leq x_3 - \sqrt{x_1^2 + x_2^2} \leq x_3 + \sqrt{x_1^2 + x_2^2} \leq 1/2 (A + B) \tag{99}$$

where (x_1, x_2, x_3) has mean vector $\mu_1, \mu_2, \mu_3 - 1/2 (A - B)$ and unchanged variance-covariance matrix $\sum$.

The region in the (x_1, x_2, x_3) space is composed of two conical segments, as shown in the following sketch.

It is desired to integrate the distribution of (x_1, x_2, x_3) over the region determined by Eq (99). The resulting probability, analogous to Eq (88) is the desired result. The upper and lower limits analogous to Eq (90) are

$$U'_3 = 1/2 (A + B) - \sqrt{x_1^2 + x_2^2}$$

$$L'_3 = -1/2 (A + B) + \sqrt{x_1^2 + x_2^2}$$

$$U_2' = \sqrt{1/2\,(A+B)^2 - x_1^2}\,,$$

$$L_2' = -\sqrt{1/2\,(A+B)^2 - x_1^2} \qquad (100)$$

$$U_1' = 1/2\,(A+B),\quad L_1' = -1/2\,(A+B).$$

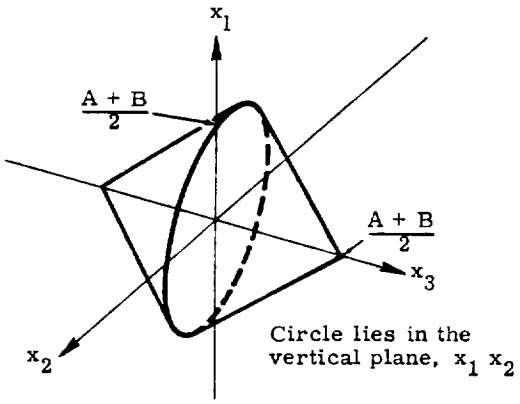

In this instance, the transformation of Eq (92) to the variables (z_1, z_2, z_3) is given by

$$x_1 = \mu_1 + c_{11}\,z_1$$

$$x_2 = \mu_2 + c_{21}\,z_1 + c_{22}\,z_2 \qquad (101)$$

$$x_3 = \mu_3 - 1/2\,(A-B) + c_{31}\,z_1 + c_{32}\,z_2 + c_{33}\,z_3$$

with the coefficients c_{ij} given explicitly by

$$c_{11} = (\sigma_{11})^{1/2},\quad c_{21} = \frac{\sigma_{21}}{(\sigma_{11})^{1/2}},\quad c_{31} = \frac{\sigma_{31}}{(\sigma_{11})^{1/2}}$$

$$c_{22} = \sqrt{\sigma_{22} - c_{21}^2}\,,\quad c_{32} = \frac{\sigma_{32} - c_{31}\,c_{21}}{c_{22}} \qquad (102)$$

$$c_{33} = \sqrt{\sigma_{33} - c_{31}^2 - c_{32}^2}$$

Introducing these c's into Eq (101) and the x's from Eq (101) into the relations $L_k' \le x_k \le U_k'$ (k = 1, 2, 3) yields, analogous to Eq (95),

$$U_3 = \frac{1}{c_{33}}\left[-\mu_3 + A - c_{31}\,z_1 - c_{32}\,z_2 - \sqrt{(\mu_1 + c_{11}\,z_1)^2 + (\mu_2 + c_{21}\,z_1 + c_{22}\,z_2)^2}\right]$$

$$L_3 = \frac{1}{c_{33}}\left[-\mu_3 - B - c_{31}\,z_1 - c_{32}\,z_2 + \sqrt{(\mu_1 + c_{11}\,z_1)^2 + (\mu_2 + c_{21}\,z_1 + c_{22}\,z_2)^2}\right]$$

$$U_2 = \frac{1}{c_{22}}\left\{-\mu_2 - c_{21}\,z_1 + \left[1/4\,(A+B)^2 - (\mu_1 + c_{11}\,z_1)^2\right]^{1/2}\right\}$$

$$L_2 = \frac{1}{c_{22}}\left\{-\mu_2 - c_{21}\,z_1 - \left[1/4\,(A+B)^2 - (\mu_1 + c_{11}\,z_1)^2\right]^{1/2}\right\} \qquad (103)$$

$$U_1 = \frac{1}{c_{11}}\left[-\mu_1 + 1/2\,(A+B)\right]$$

$$L_1 = \frac{1}{c_{11}}\left[-\mu_1 - 1/2\,(A+B)\right].$$

Now the probability

$$P = \frac{1}{(2\pi)^{3/2}}\int_{L_1}^{U_1}\int_{L_2}^{U_2}\int_{L_3}^{U_3}\exp\left[-1/2\,(z_1^2 + z_2^2 + z_2^2)\right]\,dz_3\,dz_2\,dz_1$$

can be obtained from a suitable computational routine.

Monte-Carlo method. Consider again the problem of obtaining the probability P that a multivariate normal variable lies in a region R. The Monte-Carlo method may be used, for example, in situations where the number of components of the random variable is larger than five (the routines previously described are no longer applicable).

The method proceeds as follows. Select a sample of size N of the random variable of interest. Count the number N_0 of these sample values which lie in the region R. The fraction N_0/N is an estimate of P.

The question arises: how to choose the sample size N so as to estimate P with assigned precision. An answer can be given if the problem is formulated this way. Choose N large enough for the probability that $|N_0/N - P| < d$ to equal a for preassigned d and a. Then if a "guess" for P is available, choose

$$N = \frac{P\,(1-P)\,z_a^2}{d^2} \qquad (104)$$

where z_a is defined by

$$\frac{1}{\sqrt{2\pi}}\int_{-z_a}^{z_a}\exp\left(-1/2\,t^2\right)\,dt = a$$

and is obtained from tables of the normal distribution. If no "guess" for P is available, an upper bound on the choice of N is $\frac{z_a^2}{4d^2}$.

Thus, to estimate P within 0.1 with a probability of 0.95, a conservative choice for N is

$$\frac{(1.96)^2}{4\,(0.10)^2} = 96.04$$

To estimate P to within 0.01 with a probability of 0.95, N must be 9,604 at most. To estimate P to within 0.01 with a probability of 0.95, if there is reason to suppose that P is near 0.9, Eq (104) yields

$$N \approx \frac{(0.9)\,(0.1)\,(1.96)^2}{4\,(0.01)^2} = 864.4\,.$$

Thus, a reduction of almost 9000 in the sample size necessary to meet a certain criterion has been achieved by using additional information known to the experimenter.

In conclusion, a remark should be made on the usefulness of the Monte-Carlo method in evaluating probabilities when the random variables of interest are not necessarily normally distributed. The estimate of the sample size required given above does not depend on the normality of the variables under consideration. It is valid no matter what their distribution is. (The fact that z_a in the formulas is obtained from tables of the normal distribution is incidental.)

(4) Probability Analysis of Vehicle Position and Velocity (Ref. 1)

By means of the previously considered statistical theories and the equations of Table 2, the probability distribution of the position and velocity of an orbiting vehicle can be determined at any time. This section deals with a convenient method of analysis for the problem. Let

$$\{p_i\} = \left[a_{ij}\,(\theta)\right]\{q_i\}$$

represent the relation between the position and velocity errors p_i and the orbit injection errors q_j. If the q_j are normally and independently distributed without biases, their multivariate distribution is given by

$$f(q_1, q_2, \ldots q_6) = \prod_{i=1}^{6}\left\{\left(\frac{1}{2\pi\,\sigma_i^2}\right)^{1/2}\exp\left[-\frac{1}{2}\left(\frac{q_i}{\sigma_i}\right)^2\right]\right\} \qquad (105)$$

Then the multivariate distribution of the transformed errors is

$$g(p_1, p_2, \ldots, p_6) = f(q_1, q_2, \ldots, q_6)\left|\frac{\partial(q_1, q_2, \ldots, q_6)}{\partial(p_1, p_2, \ldots, p_6)}\right| \qquad (106)$$

The region $g(p_1, p_2, \ldots, p_6)$ = constant is a six-dimensional ellipsoidal surface of equal probability. This time-varying hypersurface provides a convenient definition of the region of occurrence of the vehicle position and velocity with given probability.

For example, consider the simple case of only two orbit injection errors.

$$p_1 = a_{11}\,q_1 + q_{12}\,q_2$$

$$p_2 = q_{21}\,q_1 + q_{22}\,q_2$$

Then if

$$f(q_1, q_2) = \frac{1}{2\pi\,\sigma_{q1}\,\sigma_{q2}}\exp\left[-\frac{1}{2}\left(\frac{q_1^2}{\sigma_{q1}^2} + \frac{q_2^2}{\sigma_{q2}^2}\right)\right],$$

$$g(p_1, p_2) = \frac{1}{2\pi\,\sigma_{q1}\,\sigma_{q2}\left|a_{11}\,a_{22} - a_{12}\,a_{21}\right|}\,e^{-\frac{1}{2}Q^2} \qquad (107)$$

where the quadratic form is

$$Q^2 = \frac{1}{(a_{11}\,a_{22} - a_{12}\,a_{21})^2}\left[\left(\frac{a_{22}^2}{\sigma_{q1}^2} + \frac{a_{21}^2}{\sigma_{q2}^2}\right)p_1^2 - 2\left(\frac{a_{22}\,a_{12}}{\sigma_{q1}^2} + \frac{a_{11}\,a_{21}}{\sigma_{q2}^2}\right)p_1\,p_2 + \left(\frac{a_{12}^2}{\sigma_{q1}^2} + \frac{a_{22}^2}{\sigma_{q2}^2}\right)p_2^2\right] \qquad (108)$$

Since the coefficients a_{ij} are functions of time, the distribution changes with time. In this two-variable case, g = constant defines an ellipse. Equations (107) and (108) can be written in simplified notation as

$$g(p_1, p_2) = K\exp\left[-\frac{1}{2}\left(Ap_1^2 + 2Bp_1\,p_2 + C\,p_2^2\right)\right]$$

If the axis of the $p_1 - p_2$ coordinate system is rotated through an angle $\frac{1}{2}\tan^{-1}\left(\frac{2B}{A - C}\right)$, the cross product term is eliminated.

$$g(p_1', p_2') = K'\,e^{-\frac{1}{2}\left[p_1'^2 + D^2 p_2'^2\right]} \qquad (109)$$

where p_1' and p_2' are the new coordinates. Also, D can be absorbed by defining new coordinates $p_1'' = p_1'$ and $p_2'' = Dp_2'$.

$$g(p_1'', p_2'') = \frac{K'}{D}\exp\left[-\frac{1}{2}\left(p_1''^2 + p_2''^2\right)\right] \qquad (110)$$

Again, variables can be changed to polar coordinates so that the polar angle can be integrated from 0 to 2π and the radius ($R^2 = p_1''^2 + p_2''^2$) from 0 to R. The probability of a vehicle being within R is then

$$P(R) = 1 - e^{-\frac{R^2}{2}} \qquad (111)$$

because $\frac{2\pi K_1}{D} = 1$ for the normalized distribution.

2. Error Analysis of Powered Trajectories

Typical trajectory sequences consist of alternating powered and free-flight phases. The final mission errors are functions of errors occurring in all such phases. This section considers the contribution of errors in the powered phases just as Section B.1. considered errors in the free-flight phases. If the powered phases are short so that the impulse maneuver theories are reasonably accurate, approximate analytic relations can be developed. However, the increased complexity of motion in powered flight generally requires numerical analysis.

a. Impulse analysis

(1) General case

The equations describing addition of a vector impulse δv are the laws of cosines and sines:

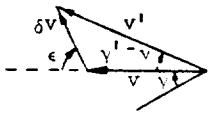

$$f_1 = -\delta v^2 + v^2 + v'^2 - 2vv' \cos(\gamma' - \gamma) = 0 \qquad (112)$$

$$f_2 = \delta v \sin\epsilon + v' \sin(\gamma' - \gamma) = 0 \qquad (113)$$

Symbols are consistent with previous notation and are further defined in the sketch. Errors in v' and γ' are to be determined as functions of errors in v, γ, ϵ and δv. From Eqs (112) and (113) the error relationships, approximated by linear differentials, can be expressed as follows.

$$-\delta v\, d(\delta v) + v'\, dv' + vv' \sin(\gamma' - \gamma)(d\gamma' - d\gamma)$$

$$- \cos(\gamma' - \gamma)(v\, dv' + v'\, dv) + v\, dv = 0$$

and

$$- \sin\epsilon\, d(\delta v) - \delta v \cos\epsilon\, d\epsilon + \sin(\gamma' - \gamma)\, dv'$$

$$+ v' \cos(\gamma' - \gamma)(d\gamma' - d\gamma) = 0$$

Terms may be collected, and the resulting expressions solved by application of Cramer's rule for the errors dv' and $d\gamma'$. In this solution the Jacobian

$$\frac{\partial(f_1, f_2)}{\partial(v', \gamma')} = 2\begin{vmatrix} v' - v\cos(\gamma' - \gamma) & vv' \sin(\gamma' - \gamma) \\ \sin(\gamma' - \gamma) & v' \cos(\gamma' - \gamma) \end{vmatrix}$$

$$= 2v'\left[v' \cos(\gamma' - \gamma) - v\right]$$

is useful. The results are

$$dv' = \left[\frac{\delta v \cos(\gamma' - \gamma) - \frac{vv'}{\delta v}\sin^2(\gamma' - \gamma)}{v' \cos(\gamma' - \gamma) - v}\right] d(\delta v)$$

$$+ \cos(\gamma' - \gamma)\, dv - v \sin(\gamma' - \gamma)\, d\epsilon$$

$$d\gamma' = \frac{\sin(\gamma' - \gamma)\left[\left(v' - v\cos(\gamma' - \gamma)\right)\frac{v'}{\delta v} - \delta v\right]}{v'\left[v' \cos(\gamma' - \gamma) - v\right]} d(\delta v)$$

$$- \frac{\sin(\gamma' - \gamma)}{v'} dv + \left[1 - \frac{v}{v'}\cos(\gamma' - \gamma)\right] d\epsilon + d\gamma$$

In terms of $(\gamma' - \gamma)$ or, in terms of ϵ,

$$dv' = \left[\frac{\delta v}{v'} + \frac{v}{v'}\cos\epsilon\right] d(\delta v) + \left[\frac{\delta v}{v'}\cos\epsilon + \frac{v}{v'}\right] dv$$

$$- v\frac{\delta v}{v'}\sin\epsilon\, d\epsilon \qquad (114)$$

$$d\gamma' = \frac{v}{v'^2}\sin\epsilon\, d(\delta v) - \frac{\delta v}{v'^2}\sin\epsilon\, dv$$

$$+ \frac{\delta v}{v'^2}(\delta v + v\cos\epsilon)\, d\epsilon + d\gamma \qquad (115)$$

(2) Nominally Tangential Impulses ($\epsilon = 0$) (Ref. 2)

In many missions a velocity increment, δv, is added at the apogee of a coast period in a direction nominally parallel to the existing coast velocity, v. An attitude error, $\Delta\epsilon$, during the apogee burning causes a nonlinear speed error in the system, in addition to a speed error representing a linear transformation of the other Gaussian sources. The geometry is shown in the accompanying sketch. The resulting speed error, Δv_1, due to this source is

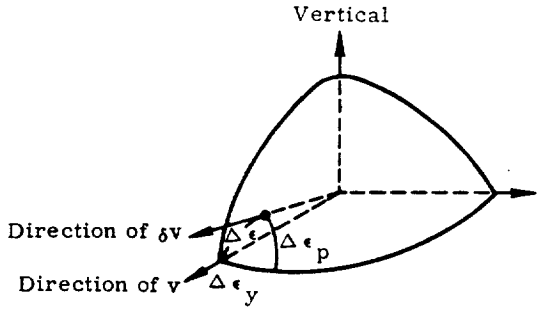

$$\Delta v_1 = v + \delta v - \sqrt{(\delta v)^2 + v^2 + 2\delta v\, v \cos\Delta\epsilon} \qquad (116)$$

For small $\Delta\epsilon$, Eq (116) becomes

$$\Delta v_1 \approx \frac{\delta v}{2\left(1 + \frac{\delta v}{v}\right)}(\Delta\epsilon)^2 \qquad (117)$$

where terms up to second order have been retained.

The $\Delta\epsilon$ in Eq (117) is actually composed of two components in directions normal to v. These are typically a yaw attitude error, $\Delta\epsilon_y$, and a pitch attitude error, $\Delta\epsilon_p$, as shown in the sketch.

Thus Eq (11 7) becomes

$$\Delta v_1 = \frac{\delta v}{2\left(1 + \frac{\delta v}{v}\right)}\left[(\Delta\epsilon_y)^2 + (\Delta\epsilon_p)^2\right] \qquad (118)$$

To this must be added the Gaussian speed error, Δv_n, due to a linear transformation from the other sources (see previous section). The total speed error, Δv, then becomes

$$\Delta v = \frac{\delta v}{2\left(1 + \frac{\delta v}{v}\right)}\left[(\Delta\epsilon_y)^2 + (\Delta\epsilon_p)^2\right] + \Delta v_n \qquad (119)$$

The statistics of Eq (119) are non-Gaussian though $\Delta\epsilon_y$, $\Delta\epsilon_p$, Δv_n are Gaussian. It is again convenient to consider the space of $\Delta\epsilon_y$, $\Delta\epsilon_p$, Δv_n which represents a trivariate normal density. In this space, surfaces of constant Δv are paraboloids of revolution parallel to the axis Δv_n as shown in the sketch. An analogous procedure is described in Section B.1.d(3). Hence integration of the trivariate normal distribution of $\Delta\epsilon_y$, $\Delta\epsilon_p$, Δv_n within the paraboloid (from $\Delta v_n = -\infty$ to Δv) yields the probability that Δv is less than some specified value. Integration for different values of Δv yields the entire statistics of Δv.

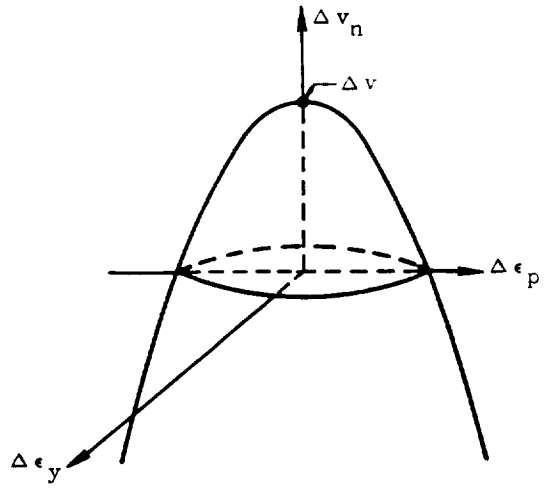

An interesting optimization theory is often applicable, once the complete statistics of Δv are obtained. It may be desirable to modify the nominal value of v in the trajectory such that it is assured to any given probability (say 0.997 or 3σ) that the magnitude of the resulting speed error is less than Δv_0, where it is desirable to minimize Δv_0. This might be the case for example in a satellite which employs orbit corrections after injection, where minimization of the speed error at injection, Δv_0, minimizes the propulsion capability required in the payload. This optimization is carried out as follows.

The cumulative distribution function P (Δv) is obtained as described above. The above optimization requirement can be interpreted as a selection of the minimum continuous span in Δv over which the P (Δv) function changes by 0.997. Designation of the center of that span as the shift in nominal injection speed would then complete the required optimization.

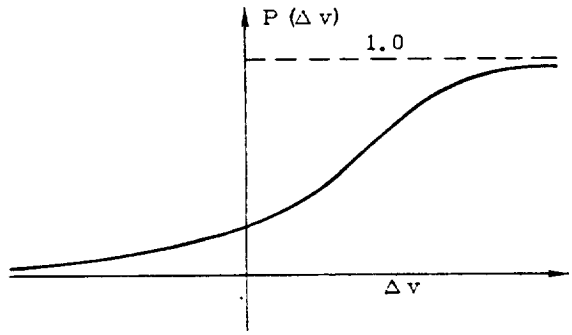

The foregoing is easily carried out by choosing a running variable Δv_0 as a trial smaller extreme of the 0.997 span of Δv, and reading off in the figure the associated span of Δv which contains the necessary 0.997 change in P (Δv). Plotting as a continuous function of Δv_0 the quantities, half the span and the center of the span, permits determination of the optimum operating point as that value of Δv_0 which has the minimum half span. This is shown in the following sketch. The corresponding change in the nominal injection speed and the 0.997 error in speed, Δv_0, are determined from the figure for this optimum Δv_0.

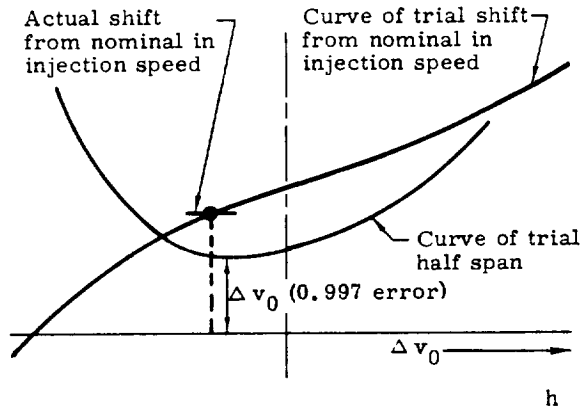

This optimization procedure for nonlinear speed errors has been carried out for equal variances in $\Delta\epsilon_y$ and $\Delta\epsilon_p$, and the results are presented in Fig. 1. The reason that the optimization procedure is useful is the skewed and biased nature of the density function of Δv given by Eq (119), which is shown in Fig. 2. This suggests a shift in nominal operating value of speed as was formally carried out.

The technique Eq (87) could have been employed as an alternative method of solution in Eq (119). Note that $y(\Delta\epsilon)$, the density function of $\Delta\epsilon$ in Eq (119), is a Rayleigh distribution, if the standard deviations of $\Delta\epsilon_y$ and $\Delta\epsilon_p$ are the same, $\Delta\epsilon_0$.

$$y(\Delta\epsilon) = \frac{\Delta\epsilon}{\sigma^2_{\Delta\epsilon_0}} e^{-\frac{(\Delta\epsilon)^2}{2\sigma^2_{\Delta\epsilon_0}}} \qquad 0 < \Delta\epsilon < \infty \quad (120)$$

or

$$z\left[f(\Delta\epsilon)\right] = \frac{1}{k} e^{-\frac{f(\Delta\epsilon)}{k}} \qquad 0 < (\Delta\epsilon) < \infty \quad (121)$$

where

$$k = \frac{\delta v}{1 + \frac{\delta v}{v}} \sigma^2_{\Delta\epsilon_0} \quad (122)$$

and where $f(\Delta\epsilon)$ is the non-Gaussian part of Eq (119). Hence, using Eqs (87) and (121) in (119) yields

$$p(\Delta v) = \int_0^\infty \frac{1}{k} e^{-\frac{\xi}{k}} \frac{e^{-\frac{(\Delta v - \xi)^2}{2\sigma^2_{\Delta v_n}}}}{\sqrt{2\pi\sigma^2_{\Delta v_n}}} d\xi \quad (123)$$

Equation (123) can be expressed in terms of tabulated functions:

$p(\Delta v)$ = density function of Δv

$$= \frac{e^{\left[-\frac{\Delta v}{k} + \frac{1}{2}\left(\frac{\sigma_{\Delta v_n}}{k}\right)^2\right]}}{k}\left[1 - R\left(\frac{\sigma_{\Delta v_n} - \Delta v}{k}\right)\right] \quad (124)$$

where

$$R(u) = \int_{-\infty}^{u} \frac{\exp(-t^2/2)}{\sqrt{2\pi}} dt \quad (125)$$

= a tabulated function

Also the cumulative distribution $P(\Delta v)$ can be found by integrating Eq (124)

$P(\Delta V)$ = cumulative distribution of ΔV

$$= R\frac{\Delta V}{\sigma_{\Delta V_n}} - \left\{\exp\left[\frac{1}{2}\left(\frac{\sigma_{\Delta V_n}}{k}\right)^2 - \frac{\Delta V}{k}\right]\right.$$

$$\left.\cdot\left[1 - R\left(\frac{\sigma_{\Delta V_n}}{k} - \frac{\Delta V}{\sigma_{\Delta V_n}}\right)\right]\right\} \quad (126)$$

b. General guidance error analysis (Ref. 2)

The guidance error analysis procedure to be described is a universal one for satellite missions. It can be applied to any type of trajectory, with guidance provided by an arbitrary type of guidance system, and with an arbitrary criterion employed for error in final orbit.

The type of powered flight trajectory that can be handled is perfectly general, although two or three discrete burns, each followed by a coast period, are the most common. The following sketches show some typical trajectories. Continuous low-thrust burning, characteristic of nuclear stages, can also be accommodated within the error analysis procedure. Also of arbitrary assignment are the nominal orbit parameters at the end of each burning phase.

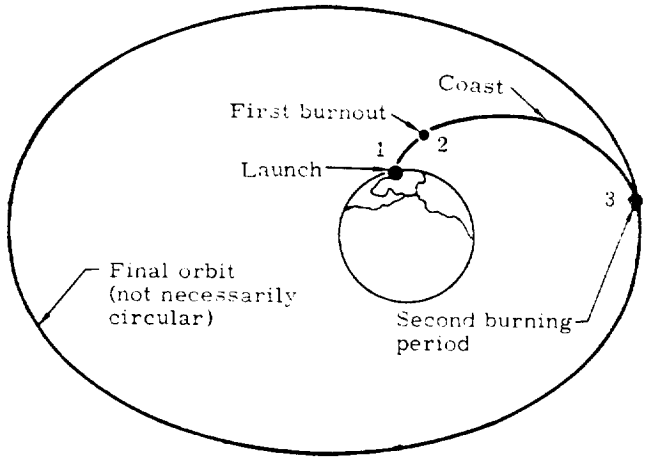

(a) Injection into Arbitrary Orbit Using a Coast Period Between Burns

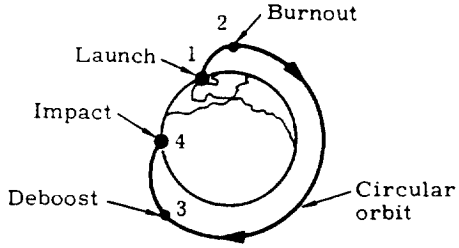

(b) Re-entry from Orbit

The error analysis procedure is capable of treating any type of guidance system, whether it be an inertial platform, a radio guidance system, an open loop autopilot system, or combinations thereof on the different stages.

Finally, the statistical quantities of interest in the final orbit may be the elliptic elements (such as eccentricity, period, etc.) or the band of altitudes within which the orbit should be confined according to some assigned statistical probability; or the impact error associated with a re-entry vehicle; or some other criterion.

Basically, the approach may be considered as consisting of four steps:

(1) Determination of the B matrix which relates the injection error vector X to system error S

$$X = BS$$

(2) Determination of the covariance matrix which contains error-interrelations and is normalized to the one-sigma error values.

(3) Determination of boundaries in Gaussian space along which quantities of interest are constant.

(4) Integration over this boundary (if one variable is of interest) or over the intersections of several boundaries (if several variables are of interest).

(1) Determination of the B matrix

The linearity assumption is made that each of the N statistically independent error sources produces a proportional error in each component of the six-dimensional error vector at end of powered flight, X. Hence, there exists a 6 x N matrix B which relates the N-dimensional vector error source, S, to the six-dimensional vector, X. The element B_{ij} in this matrix is the partial derivative of the ith component of X with respect to the one-sigma value of the jth component of the error source, S (thus each component of S is normalized by its standard deviation for convenience, as defined below). The assumption of linearity is very good in nearly all cases. The notable exceptions and method of treatment have been noted (Section B-1-c).

In the following analysis the basic error sources, S, are assumed statistically independent and unbiased. The above definition is stated explicitly as

$$X = BS \tag{127}$$

where each component S_i is expressed in units of its standard deviation, σ_i. Table 4 shows the error sources that usually are most significant for each type of guidance system.

TABLE 4

Sources of Error for Various Guidance Systems

Guidance System	Inertial Platform Guidance System	Radio Guidance System	Autopilot or Open Loop Guidance System
Internal and external error sources	Platform and component initial alignment errors. Gyro drift. Accelerometer errors: scale factor, bias, cross coupling, etc. Airborne computer errors. Engine shutdown errors.	Errors in measurement of position and velocity coordinates due to basic measurement devices and due to propagation refraction through the medium. Ground based computer errors. Engine shutdown errors.	Initial alignment errors of engine and inertial elements. Gyro drift. Gyro torquing error, due to power supply and gyro itself. Vehicle center of gravity offset. Accelerometer errors. Propulsion system errors: I_{sp} and weight flow. Engine shutdown errors. Timing errors.

The method in determination of the B matrix is to take each independent error source, one at a time, and find the six-dimensional error in X due to this, thereby yielding one column in the 6 x N matrix. This is done most expediently by using the same digital computer program which has previously been used in determination of the complete powered flight trajectory. N + 1 machine runs are made using this program, each one carried out from liftoff through each burning phase and coast phase until the end of the last burning period. On the first of these runs, all input conditions are nominal, and, of course, X is zero. On the second and each subsequent run, one input is perturbed, that being the error source under consideration for that run. As stated above, the amount of the perturbation is taken for convenience as the one-sigma value. The difference from nominal of the resultant output is X, which is the desired column in the B matrix, from Eq (127).

(2) Determination of covariance matrix, Λ

The vector X is a six-dimensional Gaussian density function since each of its components is a linear transformation of Gaussian error sources from Eq (127). The complete statistics of X are therefore given by the covariance matrix, A, defined by

$$\Lambda = E(XX^T)$$

where X^T is the transpose of the column vector and E is the statistical expectation operator defined by

$$E\left[h(x)\right] = \int_{-\infty}^{\infty} h(x)\, f(x)\, dx$$

where h(x) is any function of a variable of distribution f(x). Inserting Eq (127) in the equation for Λ yields

$$\Lambda = E(BSS^TB^T) \qquad (128)$$

$$= BB^T \qquad (129)$$

$$= 6 \times 6 \text{ matrix}$$

In deriving Eq (130), the following fact was used.

$$E(SS^T) = \text{unit matrix} \qquad (130)$$

This follows because of the statistical independence of the error sources in S, and because of the way B was defined in Eq (127).

In unusual circumstances where the assumptions given for Eq (127) are invalid, the same theory applies, but the expressions previously developed have additional terms. Such a situation might physically arise, for example, in a radio guidance system, if uncertainty in refraction causes a correlated (though unbiased) error in several basic measurements such as range, angle and their derivatives. The only change in the equations derived in this section caused by such a correlation between the components of S occurs in Eq (129), which becomes

$$\Lambda = BE(SS^T)B^T \qquad (131)$$

where the matrix $E(SS^T)$ is no longer a unit matrix, but contains the correlation coefficients as off-diagonal terms. Equation (131) then becomes the basic 6 x 6 matrix defining completely the statistics at final burnout, with all other equations remaining the same.

If an error source is biased and the value is known (which is really necessary if it is to be included in the error analysis) then the true system error can be reduced by inserting a compensating offset.

3. Error Analysis of Various Trajectory Sequences (Ref. 2)

As noted in the previous sections, the error analysis procedure generally requires machine computation, although the transformation of errors in free-flight can be expressed analytically. These analytic expressions are useful, especially in cases where the errors at end of first burning can also be obtained analytically (for example, in a radio guidance system). Thus, in these cases, the complete error analysis may be carried out analytically without machine computation.

Table 5 gives the in-plane errors for a fairly general trajectory, which invokes only the usual constraint that second burn occur at apogee of the coast ellipse. These equations become greatly simplified for a Hohmann transfer ellipse, as shown in Table 6. Table 7 is the transformation of errors in a nominally circular orbit. Table 8 gives out-of-plane errors.

The in-plane equations given in Tables 5, 6 and 7 are derived by taking first order perturbations in the two basic equations of motion in a central force field given below. These are:

$$\frac{r_0}{r_f} = \frac{1 - \cos\phi_f}{\lambda_0 \cos^2\gamma_0} + \frac{\cos(\gamma_0 + \phi_f)}{\cos\gamma_0}$$

$$= \frac{1 + e\sin(\phi - \alpha)}{\lambda_0 \cos^2\gamma_0} \qquad (132)$$

$$t = \frac{\lambda_0^2 r_0 \cos^3 \gamma_0}{v_0} \int_0^{\phi_f} \left[1 + e \sin(\phi - \alpha)\right]^{-2} d\phi \qquad (133)$$

where the zero subscript refers to conditions at beginning of coast, and the f subscript refers to quantities at apogee.

TABLE 5

In-Plane Errors at Injection in Terms of Errors Introduced During Each of Two Burns Separated by a Coast Time, t*

Subscript 0 represents beginning of coast
Subscript c represents end of coast
Subscript f represents injection
$\Delta\eta$ represents pitch attitude error in second burn
δv = velocity increment in second burn
μ = gravitational constant times mass of earth
λ = ratio of twice kinetic to potential energy at burnout

1. Altitude Error

$$\Delta r_f = \left(\frac{\partial r}{\partial r_0}\right)_t \Delta r_0 + \left(\frac{\partial r}{\partial v_0}\right)_t \Delta v_0 + \left(\frac{\partial r}{\partial \gamma_0}\right)_t \Delta\gamma_0$$

$$\left(\frac{\partial r}{\partial r_0}\right)_t = \frac{r_f}{r_0}\left[1 + \frac{r_f}{r_0}\frac{(1 - \cos\phi_f)}{\lambda_0 \cos^2\gamma_0}\right]$$

$$\left(\frac{\partial r}{\partial v_0}\right)_t = 2\frac{r_f}{v_0}\frac{r_f}{r_0}\frac{1 - \cos\phi_f}{\lambda_0 \cos^2\gamma_0}$$

$$\left(\frac{\partial r}{\partial \gamma_0}\right)_t = \frac{r_f}{r_0}\frac{r_f}{\cos^2\gamma_0}\left[\frac{2(1 - \cos\phi_f)}{\lambda_0 \tan\beta_0} - \sin\phi_f\right]$$

2. Velocity Error

$$\delta v_f = \left(\frac{\partial v}{\partial r_0}\right)_t \Delta r_0 + \left(\frac{\partial v}{\partial v_0}\right)_t \Delta v_0 + \left(\frac{\partial v}{\partial \gamma_0}\right)_t \Delta\gamma_0$$

$$\left(\frac{\partial v}{\partial r_0}\right)_t = \left[\frac{\mu}{v r_0^2} - \frac{\mu}{v_c r_f^2}\left(\frac{\partial r}{\partial r_0}\right)_t\right]$$

$$\left(\frac{\partial v}{\partial v_0}\right)_t = \left[\frac{v_0}{v_c} - \frac{\mu}{v_c r_f^2}\left(\frac{\partial r}{\partial v_0}\right)_t\right]$$

$$\left(\frac{\partial v}{\partial \gamma_0}\right)_t = -\frac{\mu}{v_c r_f^2}\left(\frac{\partial r}{\partial \gamma_0}\right)_t$$

(continued)

TABLE 5 (continued)

3. Flight Path Angle

$$\delta\gamma_f = \frac{v_c}{v_f}\left[\left(\frac{\partial\gamma}{\partial r_0}\right)_t \Delta r_0 + \left(\frac{\partial\gamma}{\partial v_0}\right)_t \Delta v_0 + \left(\frac{\partial\gamma}{\partial\gamma_0}\right)\Delta\gamma_0 + \left(\frac{\partial\gamma}{\partial t}\right)_t \Delta t\right] + \frac{\Delta v}{v_f}(\Delta\eta - \Delta\phi_f)$$

$$\left(\frac{\partial\gamma}{\partial r_0}\right)_t = -\frac{v_0}{v_c r_0}\frac{\sin\phi_f}{\lambda_0 \cos\gamma_0} - \frac{v_0}{v_c}\left[\frac{\cos\phi_f}{\lambda_0 \cos\gamma_0} - \cos(\gamma_0 + \phi_f)\right]\left(\frac{\partial\phi}{\partial r_0}\right)_t$$

$$\left(\frac{\partial\phi}{\partial r_0}\right)_t = -(1 - e)^2\left[\frac{3}{r_0}k_1 + \frac{4\sin^2\phi_f}{\lambda_0 r_0 \cos^2\gamma_0}k_2 - \frac{2\lambda_0(\lambda_0 - 1)\cos^2\gamma_0}{e r_0}k_3\right]$$

$$\left(\frac{\partial\gamma}{\partial v_0}\right)_t = \frac{2}{v_c}\frac{\sin\phi_f}{\lambda_0 \cos\gamma_0} - \frac{v_0}{v_c}\left[\frac{\cos\varphi_f}{\lambda_0 \cos\gamma_0} - \cos(\gamma_0 + \phi_f)\right]\left(\frac{\partial\phi}{\partial v_0}\right)_t$$

$$\left(\frac{\partial\phi}{\partial v_0}\right)_t = -(1 - e)^2\left[\frac{3}{v_0}k_1 + \frac{8\sin^2\phi_f}{\lambda_0 v_0 \sin 2\gamma_0}k_2 - \frac{4\lambda_0(\lambda_0 - 1)\cos^2\gamma_0}{e v_0}k_3\right]$$

(continued)

* Tables 5 to 8 are analytic expressions for determining B matrix. The only constraint on the trajectory is that the end of coast be apogee of the transfer ellipse. Gyro reference is assumed for apogee burn.

TABLE 5 (continued)

$$\left(\frac{\partial \gamma}{\partial \gamma_0}\right)_t = \frac{v_0}{v_c}\left[\frac{-\sin\phi_f \sin\beta_0}{\lambda_0 \cos^2 {}_0} + \cos(\gamma_0 + \phi_f)\right]$$

$$-\left\{\frac{v_0}{v_c}\left[\frac{\cos\phi_f}{\lambda_0 \cos\gamma_0} - \cos(\gamma_0 + \phi_f)\right]\right.$$

$$\left.\cdot\left(\frac{\partial \phi_f}{\partial \gamma_0}\right)_t\right\}$$

$$\left(\frac{\partial \varphi}{\partial \gamma_0}\right)_t = (1-e)^2\left[3\tan\gamma_0 k_1\right.$$

$$+2\left(-\frac{4\cos 2\gamma_0 \sin^2\phi_f}{\lambda_0 \sin^2 2\gamma_0} + \frac{\sin^2\phi_f}{\sin^2\beta_0}\right)k_2$$

$$\left.-\frac{\lambda_0(2-\lambda_0)\sin 2\gamma_0}{e}k_3\right]$$

$$\alpha = \phi_f + \frac{\pi}{2}$$

$$k_1 = \int_0^{\phi_f} \frac{d\phi}{\left[1 + e\sin(\phi - \alpha)\right]^2}$$

$$= \frac{e}{1-e^2}\,\frac{\sin\phi_f}{1 - e\cos\phi_f} + \frac{1}{1-e^2}k_4$$

$$k_2 = \int_0^{\phi_f} \frac{e\cos(\phi-\alpha)\,d\phi}{\left[1 + e\sin(\phi-\alpha)\right]^3}$$

$$= \frac{1}{2}\left[\frac{1}{(1 - e\cos\phi_f)^2} - \frac{1}{(1-e)^2}\right]$$

$$k_3 = \int_0^{\phi_f} \frac{\sin(\phi-\alpha)\,d\phi}{\left[1 + e\sin(\phi-\alpha)\right]^3}$$

$$= \frac{1}{2}\,\frac{1}{(1-e^2)}\,\frac{\sin\phi_f}{(1 - e\sin\phi_f)^2}$$

$$+\frac{1}{2}\,\frac{2e^2+1}{(1-e^{2)2}}\,\frac{\sin\phi_f}{(1 - e\cos\phi_f)}$$

$$+\frac{\frac{3}{2}e}{(1-e^{2)2}}k_4$$

$$k_4 = \int_0^{\phi_f} \frac{d\phi}{1 + e\,\mathrm{sIn}(\phi_f - \alpha)} = \left\{\frac{2}{\sqrt{1-e^2}}\right.$$

$$\left.\tan^{-1}\left(\sqrt{\frac{1-e}{1+e}}\tan\frac{\phi_f}{2}\right)\right\}$$

TABLE 6

In-Plane Errors at Injection in Terms of Errors Introduced During Each of Two Burns Separated by a Coast Time, t, $\gamma_0 = 0°$ (Hohmann Transfer)

$$\frac{\Delta r_f}{r_f} = \frac{\Delta r_0}{r_0}\left(2 + \frac{r_f}{r_0}\right) + 2\,\frac{\Delta v_0}{v_0}\left(1 + \frac{r_f}{r_0}\right)$$

$$\Delta v_f = -\frac{\Delta r_0}{r_0}\,\frac{2}{\lambda_0}\,v_0 - \Delta v_0\left(2 + \frac{r_0}{r_f}\right) + \Delta(\delta v)$$

$$\Delta\phi_f = \frac{4}{\lambda_0}\,\Delta\gamma_0 - k_5\left(\frac{\Delta r_0}{\lambda_0 r_0} + \frac{\Delta v_0}{v_0}\right) + \Delta t\,\frac{v_c}{r_f}$$

where

$$k_5 = \frac{3\pi}{\lambda_0}\left(\frac{r_f}{r_0}\right)^{1/2}$$

$$\Delta\gamma_f = -\Delta\gamma_0\left[\frac{r_0}{r_f}\,\frac{v_c}{v_f} + \left(\frac{\delta v}{v_f}\,\frac{4}{\lambda_0}\right)^*\right] - \Delta\eta\,\frac{\delta v}{v_f}$$

$$+\left\{\left[\frac{\Delta r_0}{r_0\lambda_0} + \frac{\Delta v_0}{v_0}\right]\right.$$

$$\left.\cdot\left[k_5\,\frac{(\lambda_0 - 1)}{\lambda_0}\,\frac{v_0}{v_f} + \left(\frac{\delta v}{v_f}\kappa_5\right)^*\right]\right\}$$

$$+\delta t\left[\frac{v_0}{v_f}\,\frac{(\lambda_0 - 1)}{\lambda_0} \div \left(\frac{\delta v}{v_f}\right)^*\right]\frac{v_c}{r_f}$$

* The terms encircled are eliminated when a horizon scanner reference is used for apogee.

TABLE 7

Coast Phase Transformation of In-Plane Initial Errors Δr_0, Δv_0, $\Delta\gamma_0$ Into Final Errors δr_f, δv_f, $\delta\beta_f$, $\delta\phi_f$ After Traversing an Angle ϕ_f in a Nominally Circular Orbit

$$\begin{bmatrix} \frac{\Delta r_f}{r_0} \\ \frac{\Delta v_f}{v_0} \\ \Delta\gamma_f \\ \Delta\phi_f \end{bmatrix} = \begin{bmatrix} 2-\cos\phi_f & 2(1-\cos\phi_f) & -\sin\phi_f \\ -(1-\cos\phi_f) & (-1+2\cos\phi_f) & \sin\phi_f \\ -\sin\phi_f & -2\sin\phi_f & \cos\phi_f \\ -3\phi_f+2\sin\phi_f & -3\phi_f+4\sin\phi_f & 2(1-\cos\phi_f) \end{bmatrix} \begin{bmatrix} \frac{\Delta r_0}{r_0} \\ \frac{\Delta v_0}{v_0} \\ \Delta\gamma_0 \end{bmatrix}$$

TABLE 8

Coast Phase Transformation for Out-of-Plane Errors

Out-of-plane error α and ψ in terms of initial errors, α_0, ψ_0 and ϕ_f. ψ and α are defined in Section B.

$$\begin{bmatrix} \delta\alpha \\ \delta\gamma \end{bmatrix} = \begin{bmatrix} \cos\phi_f & -\sin\phi_f \\ \sin\phi_f & \cos\phi_f \end{bmatrix} \begin{bmatrix} \delta\alpha_0 \\ \delta\psi_0 \end{bmatrix}$$

4. Ballistic Trajectory Error Analysis (Ref. 3)

The ground range over a nonrotating earth achieved by a ballistic missile is given by

$$\rho_g = R\tan^{-1}\frac{\sin\gamma_0\cos\gamma_0}{\frac{\mu}{r_0 v_0^2} - \cos^2\gamma_0} + R\tan^{-1}\cos\gamma_0\left[1-\left(\frac{r_0}{r_f}\right)^2\cos^2\gamma_0 + \frac{2\mu}{r_0 v_0^2}\left(\frac{r_0}{r_f}-1\right)\right]\left[\frac{\mu}{r_0 v_0^2} - \frac{r_0}{r_f}\cos^2\gamma_0\right]^{-1} \quad (134)$$

where subscript 0 indicates a cutoff condition, and subscript f indicates a final condition, and R is the radius of the earth, as shown in the accompanying sketch. Differentiation of Eq (134) yields the following error partials.

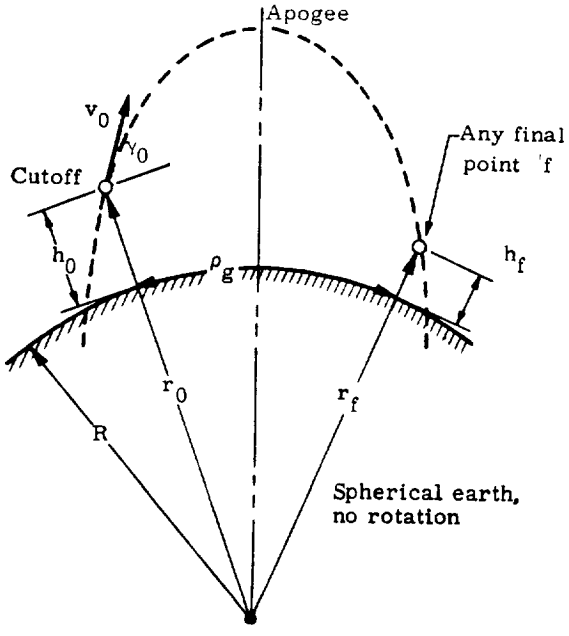

$$v_0\frac{\partial r}{\partial v_0} = 2K_1K_2 \quad (135)$$

$$r_0\frac{\partial r}{\partial r_0} = K_1 + \left\{R\cos\gamma_0\left[\left(\frac{v_c}{v_0}\right)^4\left(2\frac{r_0}{r_f}-1\right) + \left(\frac{v_c}{v_0}\right)^2\left(1-3\frac{r_0}{r_f}\cos^2\gamma_0\right) + \frac{r_0}{r_f}\cos^2\gamma_0\right]\left[\left\{\left[\frac{v_c}{v_0}^2 - \cos^2\gamma_0\right]^2 + \sin^2\gamma_0\cos^2\gamma_0\right\}\sqrt{1-\frac{r_0^2}{r_f^2}\cos^2\gamma_0 + 2\left(\frac{v_c}{v_0}\right)^2\left(\frac{r_0}{r_f}-1\right)}\right]^{-1}\right\} \quad (136)$$

$$K_1 = \left\{R\left(\frac{v_c}{v_0}\right)^2\sin\gamma_0\cos\gamma_0\left\{\left[\frac{v_c}{v_0}^2 - \cos^2\gamma_0\right]^2 + \sin^2\gamma_0\cos^2\gamma_0\right\}^{-1}\right\}$$

$$K_2 = 1 + \left\{1-\frac{r_0}{r_f}\cos^2\gamma_0 + \left(\frac{v_c}{v_0}\right)^2\left(\frac{r_0}{r_f}-1\right)\right\} \cdot \left\{\sin\gamma_0\sqrt{1-\frac{r_0^2}{r_f^2}\cos^2\gamma_0 + 2\left(\frac{v_c}{v_0}\right)^2\left(\frac{r_0}{r_f}-1\right)}\right\}^{-1}$$

$$\frac{\partial r}{\partial\gamma_0} = -\left\{R\left[\left(\frac{v_c}{v_0}\right)^2\left(1-2\cos^2\gamma_0\right) + \cos^2\gamma_0\right]\right\} \cdot \left\{\left[\left(\frac{v_c}{v_0}\right)^2 - \cos^2\gamma_0\right]^2 + \sin^2\gamma_0\cos^2\gamma_0\right\}^{-1} - \left\{R\sin\gamma_0\left[\left(\frac{v_c}{v_0}\right)^2\left(1-2\frac{r_0}{r_f}\cos^2\gamma_0\right) + \frac{r_0}{r_f}\cos^2\gamma_0 + 2\left(\frac{v_c}{v_0}\right)^4\left(\frac{r_0}{r_f}-1\right)\right]\right\} \left[\left\{\left[\left(\frac{v_c}{v_0}\right)^2 - \cos^2\gamma_0\right]^2 + \sin^2\gamma_0\cos^2\gamma_0\right\} \cdot \sqrt{1-\frac{r_0^2}{r_f^2}\cos^2\gamma_0 + 2\left(\frac{v_c}{v_0}\right)^2\left(\frac{r_0}{r_f}-1\right)}\right]^{-1} \quad (137)$$

where

v_c = circular orbit velocity at cutoff altitude.

These error sensitivities are plotted in Figs. 3 through 17. The quantity K_1, which arises from the first term (cutoff to apogee term) of Eq (134), and which appears as the first term of Eq (136) and as a factor of Eq (135), is plotted in Figs. 3 and 4. The multiplying factor K_2 is shown in Figs. 5 and 6. The second term of Eq (136) (that is, the part of the error partial $\frac{\partial \rho_g}{\partial r_0}$ arising during that portion of the trajectory between apogee and the final point) is given by Figs. 7, 8 and 9. The first term of $\frac{\partial \rho_g}{\partial \gamma}$ (cutoff to apogee) is shown in Figs. 10 and 11. The second term is shown in Figs. 10 through 15. Figures 16 and 17 are useful auxiliary graphs in using Figs. 3 through 15. The error sensitivities are also given (Ref. 4) in Figs. 18 and 19 as functions of range and Fig. 20 gives flight time as a function of range.

C. SPACE VEHICLE GUIDANCE TECHNIQUES (Ref. 2)

Once the requirements imposed by the mission on the guidance system have been appraised by the methods of Section B, a guidance philosophy may be selected to meet that requirement. Guidance may be defined as the processes of measurement, data extraction and smoothing, computation and control which are required to assure that a space vehicle reaches a desired destination from a given launch point. For the present purposes, the destination may be a point for injection into an arbitrary parking orbit from a direct ascent trajectory to a point in space, with the proper six-initial conditions to place the vehicle on a coast ellipse (for a transfer maneuver), parabola or hyperbola to establish a lunar or interplanetary trajectory, or some other final-value condition. Thus, it is customary to classify the problem by:

(1) Launch guidance

(2) Midcourse guidance

(3) Terminal guidance

and to further classify the guidance problem by the form of the mechanization and constraints, as:

(1) Radio supervised (maximum radar range, minimum elevation angle, required look-angles for antenna patterns, maximum slewing rates, etc.).

(2) Inertial (platform stability, linearity, threshold levels and dynamic range, integration accuracy, etc.).

(3) Radio-inertial (combination systems where position may be derived from radar with inherent radar constraints, and velocity from inertial measurement with inherent inertial system constraints).

The literature is now becoming extensive on these more specialized problems of theory and mechanization. It is nearly impossible within the span of the handbook to do more than suggest different approaches to the guidance problem insofar as specific mechanizations are concerned. The chief emphasis will be on providing the mission analyst with general methods of guidance analysis applicable to any class of guidance system.

1. Formulation of Guidance Equations

The formulation of the guidance equations for the launch guidance phase may take the form of, (1) explicit guidance, (2) delta guidance, or (3) Q-guidance.

Explicit guidance. The required velocity vector, $\vec{v}_r$, is obtained in closed form as a function of position and time. The velocity-to-be-gained, $\vec{v}_g$, is then obtained as

$$\vec{v}_g = \vec{v}_r - \vec{v} \tag{138}$$

where $\vec{v}$ is the instantaneous velocity of the vehicle. The vehicle is then steered in an efficient manner until $\vec{v}_g = 0$, at which time the engines are shut off.

Delta guidance. In delta guidance, the required velocity vector is approximated by a functional expansion about the nominal expected burnout position and time (x_n, y_n, z_n, t_n) as

$$\vec{v}_r = \vec{v}_{rn} + \vec{A}(x_n - x) + \vec{B}(y_n - y) + \vec{C}(z_n - z) + \vec{D}(t_n - t) + \text{second order terms} \tag{139}$$

where $\vec{v}_{rn}$, $\vec{A}$, $\vec{B}$, $\vec{C}$, $\vec{D}$ are constant vectors and x, y, z denote the platform coordinate system. Several second-order difference terms such as $(x_n - x)(z_n - z)$ may be required to obtain the desired accuracy. The advantage of the above method is that only simple arithmetic operations rather than the square roots and divisions required for explicit guidance need be performed by the airborne digital computer. The disadvantages result from the larger number of constants that must be precalculated and inserted into the onboard digital computer.

Q-guidance. Another method of guidance is referred to as Q-guidance. This method gives the velocity-to-be-gained directly by integration of

$$\dot{v}_g^{\,i} = A_t^{\,i} - \sum_j^3 Q_j^{\,i} v_g^{\,i} \tag{140}$$

where i, j = 1, 2, 3 refer to x, y and z components, A_t^i are the components of thrust-drag acceleration as measured by the accelerometers; and the matrix Q_j^i is defined as

$$Q_j^i = \frac{\partial v_r^i}{\partial x^j}$$

In explicit and delta guidance, it is necessary to perform a gravity computation, which is not required for Q-guidance. The only guidance constants required for Q-guidance are the components of the Q-matrix and three initial values for $\vec{v}_g$. The components of the Q-matrix will contain about 10 trajectory-dependent constants. The disadvantage of Q-guidance is that the computer does not evaluate instantaneous position or velocity. These quantities are useful in orienting the body attitude during the coast period and for resetting the digital computer prior to the later burning periods.

2. Launch Guidance

a. Radio launch guidance

A radio guidance mechanization of a spacecraft steering loop may proceed along the most general lines as shown in the sketch where the guidance complexity is placed in the ground equipment. An entire tracking network may be involved in gathering the tracking data. Depending on the nature of the tracking data (range-only, range-azimuth-elevation, angle-only) and the number of participating stations, an initial and then precision orbit is calculated by, say, an IBM 7990 computer, the actual orbit is compared to the desired orbit, and pitch and yaw steering commands or discrete commands are generated and sent to the control system of the spacecraft for thrust vector control.

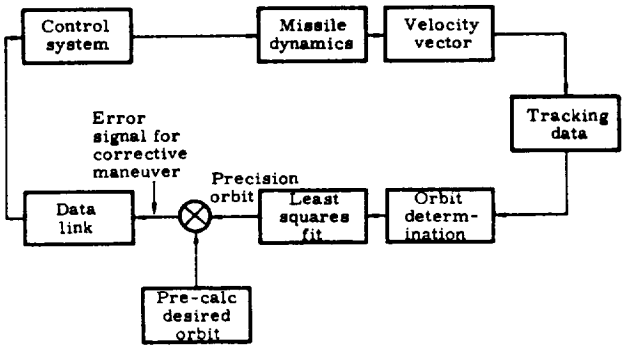

A single semispecial purpose guidance computer located at the launch site may be schematically represented as in Fig. 21.

The missile dynamics for either a symmetric or nonsymmetric shape are given, together with all equations of motion reduced to a form suitable for digital computer calculation. Finally, a functional block diagram is shown in Fig. 22 for a combination CW and pulse radio guidance system. One of the most severe constraints in a radio-inertial system is due to the antenna radiation pattern (see Fig. 23) and signal sensitivities of the spacecraft receivers. One way of overcoming such problems (though introducing other perhaps more flexible constraints) is to consider the usual inertial guidance mechanization.

b. Inertial launch guidance (Ref. 5)

To accomplish inertial navigation in a region containing gravity fields some method must be used for calculating gravity acceleration. If the path of the vehicle can be accurately predicted, the effects of gravity can be precalculated. In this case, guidance during flight would be done in terms of thrust acceleration and its time integrals only. As the path of a specific vehicle becomes difficult to predict (relative to the accuracy requirement), it becomes necessary to make a gravity computation during flight.

The following sketch shows, with an exaggerated scale, the powered flight trajectory of a space vehicle. A rectangular coordinate system with origin in the vicinity of the trajectory and with the y-axis vertical can be used to express the components of gravity relative to a free-fall reference frame at the center of the earth as follows:

$$g_x = -g\frac{x}{r} = \frac{-g_0 r_0^2 x}{\left[x^2 + z^2 + (r_0 + y)^2\right]^{3/2}} \qquad (141)$$

$$g_y = -g\frac{y + r_0}{r} = \frac{-g_0 r_0^2 (y + r_0)}{\left[x^2 + z^2 + (r_0 + y^2\right]^{3/2}} \qquad (142)$$

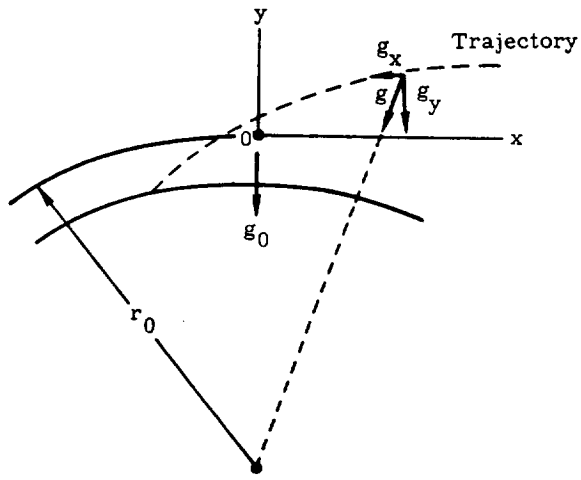

The g_z term is similar to g_x, but for simplicity will be omitted here. x can be taken in the nominal plane of the trajectory and the problem considered in two dimensions. These equations are nonlinear and their mechanization requires considerable computer complexity. Simple linear approximations which are valid near the origin of coordinates are

$$g_x = -\frac{g_0}{r_0} x \tag{143}$$

$$g_y = -g_0\left(1 - \frac{2y}{r_0}\right). \tag{144}$$

The acceleration equations in component form are

$$\ddot{x} = a_{tx} + g_x \tag{145}$$

$$\ddot{y} = a_{ty} + g_y \tag{146}$$

Block diagrams for the solution of these linear equations are shown in Fig. 24. The x channel has negative feedback and two integrations and thus has a sinusoidal response to an input disturbance. The y channel has positive feedback and an input disturbance leads to a diverging value of y.

The effect of the approximation in the gravity computer can, of course, be calculated for a given trajectory. Additional terms to include the nonspherical gravity field of the earth can be included as necessary. If the acceleration free-fall reference frame is located in a satellite, for example, then the gravity components which give the difference in gravity between the location of the accelerometer and the reference frame, would differ from those given in Eqs (141) and (142). Because the satellite moves through the earth's gravity field, the gravity components would vary with time.

The effect of the gravity computation upon position and velocity error buildup caused by accelerometer or initial condition errors is of considerable interest. It can be investigated analytically in terms of perturbation equations of the form

$$\Delta\ddot{x} = \Delta a_{tx} + \Delta g_x = \Delta a_{tx} + \frac{\partial g_x}{\partial x}\Delta x + \frac{\partial g_x}{\partial y}\Delta y \tag{147}$$

$$\Delta\ddot{y} = \Delta a_{ty} + \Delta g_y = \Delta a_{ty} + \frac{\partial g_y}{\partial x}\Delta x + \frac{\partial g_y}{\partial y}\Delta y \tag{148}$$

The differential coefficients are functions of space which can be obtained from Eqs (141) and (142). They should be evaluated along the unperturbed path of the vehicle. However, this leads to differential equations with time varying coefficients which cannot be solved in closed form. For flights in a region of a few hundred miles breadth, the coefficients can be evaluated at one point in the vicinity of the trajectory with adequate accuracy for the purposes here. This gives the following equations for the perturbation in position caused by thrust acceleration perturbation or accelerometer error.

$$\Delta\ddot{x} + \frac{g_0}{r_0}\Delta x = \Delta a_{tx} \tag{149}$$

$$\Delta\ddot{y} - \frac{2g_0}{r_0}\Delta y = \Delta a_{ty}. \tag{150}$$

The physical meaning of these equations is easy to see. For example, a positive error in vertical position leads to a calculated value of gravity acceleration which is too small and thus to a calculated value of true acceleration which is too large. This in turn integrates into an even larger positive position error.

The solution to Eqs (149) and (150) for constant values of thrust acceleration perturbations (accelerometer bias or zero offset) are

$$\Delta x = \frac{\Delta a_{tx}}{g_0/r_0}\left[1 - \cos\sqrt{\frac{g_0}{r_0}}\,t\right] \tag{151}$$

$$\Delta y = \frac{\Delta a_{ty}}{2g_0/r_0}\left[\cosh\sqrt{\frac{2g_0}{r_0}}\,t - 1\right] \tag{152}$$

The terms for initial condition perturbations are similar to these. Near the surface of the earth, the sinusoidal oscillation has a period of about 84 min, that is,

$$2\pi\sqrt{r_0/g_0} \approx 84 \text{ min}.$$

Position errors caused by accelerometer errors other than a constant bias can be calculated by well known methods. An offset in the attitude reference will cause a cross coupling error, thus $\Delta a_{tx} = \beta a_{ty}$, where β is the attitude reference error. A gyro drift rate thus gives an increasing position error.

These perturbations or error equations illustrate a basic limitation of inertial guidance for long times of flight, namely, that errors in the vertical direction increase exponentially with time. However, errors in the horizontal direction caused by accelerometers are oscillatory with a period of 84 min. This makes practical two-dimensional inertial systems for aircraft and ships which can employ altimeters to measure altitudes. For flight times less than about 10 min, Eqs (151) and (152) can be approximated by the simple equations

$$\Delta x = \Delta a_{tx}\frac{t^2}{t}; \qquad \Delta\dot{x} = \Delta a_{tx}\,t \tag{153}$$

$$\Delta y = \Delta a_{ty}\frac{t^2}{t}; \qquad \Delta\dot{y} = \Delta a_{ty}\,t \tag{154}$$

which are those that would be obtained by ignoring the feedback error from the gravity calculation. They would also be those obtained for navigation in a constant gravity field.

Associated with the concept of this guidance is that of the standard or reference trajectory. Such

a trajectory is one which a standard or nominal missile would follow under standard or nominal aerodynamic conditions. The path of any specific missile should follow the standard trajectory quite closely. In general, the specific paths will be statistically distributed about the standard which in some sense will be a mean of the distribution.

A schematic of a steering computer is given in Fig. 25. The angle commanded by the pitch programmer is compared with the gimbal pitch angle to give a pitch steering command to the missile control system. The overall guidance loop is illustrated in Fig. 25 by the feedback from the missile control system through missile dynamics to the inertial measurement unit.

Lateral and pitch steering having been accomplished, the remaining problem is to terminate the missile thrust at the proper time so that the spacecraft will hit the intended aiming point. The proper combination of burnout values can be obtained by considering the effects on target miss of small changes in the horizontal and vertical components of position and velocity. To express this analytically, the range of the missile is expanded as a function of position and velocity components about the standard burnout point.

$$\rho - \rho_s = \frac{\partial \rho}{\partial x}(x - x_s) + \frac{\partial \rho}{\partial y}(y - y_s) + \frac{\partial \rho}{\partial \dot{x}}(\dot{x} - \dot{x}_s) + \frac{\partial \rho}{\partial \dot{y}}(\dot{y} - \dot{y}_s) + \ldots \quad (155)$$

ρ designates range, the subscript s designates standard conditions, and the partial derivative coefficients are evaluated at the standard burnout point, $\partial\rho/\partial x \equiv C_x$, etc. A computer which continuously calculates the downrange miss at the aiming point is shown in Fig. 26. Prior to the start of the flight, values of the standard burnout conditions, x_s, etc., are fed into the computer along with values of the coefficients, C_x, etc., which are calculated for the particular range desired. At some zero time for guidance (which should be within a few seconds of the actual lift-off time of the missile) the accelerometers are connected to the computer and torquing of the gyros at earth rate is stopped. Position and velocity components relative to the launch point then appear in the channels indicated in the figure and the computer calculates the downrange miss, M_r. Early in the flight, the calculated value will be grossly in error because only linear terms are used in the expansion. Near burnout, however, the computation will be quite accurate. The thrust of the missile is terminated when the computed miss becomes zero. This will always occur because the missile is flying toward the impact point with an increasing velocity.

The inertial guidance scheme should be evaluated from several standpoints. For example, the need for the gravity computer should be investigated. If the actual missile flight is sufficiently close to the nominal flight, the effect of gravity can be precalculated with sufficient accuracy and no gravity computer is necessary. On the other hand, and especially for extreme accuracy, additional terms in the gravity expansion might be necessary. If the variation in missile thrust is large, higher order terms might be needed in the expansion of the motor shutoff, Eq (155). Refinements in the guidance scheme would include means of compensation for time of flight variations. The design of the system should include an error analysis of all of the principal components so that a proper balance in design complexity can be obtained. For example, high accuracy in the cutoff expansion in meaningless if the accelerometers are low accuracy devices. A thorough error analysis including the effects of inertial component tolerances is presented in Ref. 6.

3. Midcourse Guidance

Guidance principles applied to launch guidance have been discussed in the earlier sections. The spacecraft may be assumed to travel along a free flight path to its destination without further application of thrust or guidance. This type of guidance is accurate enough in general for establishing earth satellite orbits, and possibly in more refined operations. However, for precise navigation to the moon, to establish satellite orbits about the moon, or for interplanetary orbits midcourse and terminal guidance will be needed. Midcourse corrections for lunar trajectories are considered in detail in the companion work, Lunar Flight Handbook, Ref. 7. Differential corrections are considered in Chapter VI of this manual.

D. DESIGN OF ATTITUDE CONTROL SYSTEMS FOR EARTH SATELLITES (Ref. 2)

The design of a spacecraft attitude control system is a complex problem. The specific stabilization and orientation requirements must be met, and compatibility with other spacecraft subsystems must be ensured. The early spacecraft, which were designed for long term operation, were spin stabilized. More stringent requirements of present experimental, communications, interception or reconnaissance missions have demanded more precise or more complex control. The purpose of this part of the Handbook is to present several important problems which must receive attention in the design of the attitude control system. Tradeoff and systems problems, considerations involved in a particular choice of an attitude control system, and design data which may be helpful for preliminary calculations are presented. The scope of the section is, by and large, limited to consideration of the attitude control of earth-orbiting satellites.

The designer is confronted with the problem of choosing among a number of possible solutions for a particular attitude control system. Since no attitude control system can be broadly classed as optimal for every mission, a range of the possible control system selections must be reviewed in the preliminary design as each relates to both the required control system performance and the design of other subsystems. Often, the number of solutions can be quickly narrowed to one or two

logical choices. The designer must define the flight sequence, particular modes of control, and control laws, evaluate the effects of disturbing forces during operation, and assess the control system reliability to provide an optimum correction technique for fine position and time control.

To aid the designer and mission analyst in this task, the Handbook treats important system considerations of the mission and control specifications; methods of obtaining control orientation; control system sensors and control modes. One typical satellite configuration is shown in the following sketch.

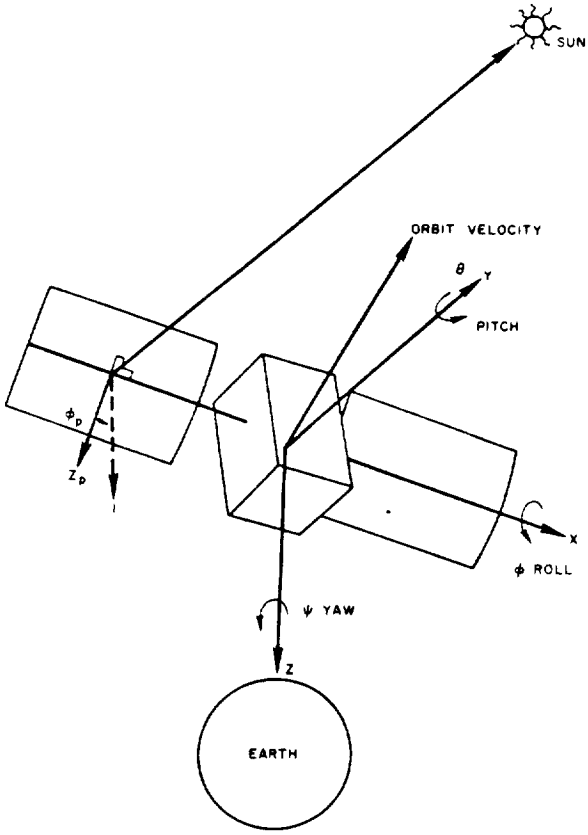

1. Mission and Control Configuration

The purpose of this section is to survey the various types of spacecraft attitude control systems which might be used for various missions. It is important to begin with a general discussion of the broad specifications which are important in the preliminary design. Because control system specifications for the spacecraft often differ depending on the mission, this section treats only broad requirements. Once the mission is determined, the designer can look at various control schemes for the particular payload or range of payloads that can be launched by the available boosters. This means that for some missions, studies involving the tradeoff between booster capability, weight of payload in a particular orbit or set of orbits, costs, reliability, the basic requirements of the mission, and other system interrelations are required. Pointing accuracy, maximum attitude rates, system lifetime, reliability, allowable weight, cost, state of hardware development, orbital requirements, boost environment, etc., are typical inputs to the control system design.

a. Mission

A limited set of possible missions will indicate the range of similarities and differences of probable attitude control system requirements. Broadly, the missions have been categorized into experimental spacecraft, reconnaissance satellites, communication satellites and missions requiring orbital docking.

(1) Experimental spacecraft. The satellites and interplanetary probes launched to date have wide and varied stabilization requirements. Satellites containing equipment for detailed solar or stellar observations may need to stabilize with respect to the sun or star under observation to within a very few seconds of arc with very low rates (Orbiting Astronomical Observatory). To obtain information concerning the earth's magnetic field, cosmic radiation, and the like, a satellite may need stabilization within the limits of only 1° or 2° (Orbiting Geophysical Observatory). Spacecraft for investigating various aspects of the moon, Venus and Mars, may require control during a landing operation as well as stabilization during space transit. The midcourse orientation requirements may be similar to those of a satellite, but as the vehicle approaches the planet, separate terminal control and guidance schemes are generally required. The lifetime of experimental satellites must be considered.

(2) Reconnaissance satellite. Two types of vehicles to perform reconnaissance missions may be distinguished. The first is similar to the earth-pointing experimental satellite in that the mission function is to obtain pictures or data concerning earth topography or activities on the earth. Basically, this system will have control requirements which will be a direct function of the resolution capability of the reconnaissance equipment aboard: good absolute pointing accuracy, and very low pointing error rates are required. A second type of reconnaissance vehicle is one for inspection in orbit of other satellites and space vehicles. Such inspection will probably require accurate orientation with respect to some other object, like the earth or sun.

(3) Communication satellite. Various forms of control systems will be required to meet the needs of varying orbits, synchronism requirements and antenna pointing. An oriented antenna may increase the antenna gain by as much as 10 db. This could simplify the communication system at the expense of additional control system complexity. The number of communication satellites depends on the orbit and coverage requirements. While more low altitude satellites are required for the same coverage as higher altitude satellites, the booster capability will allow more to be launched at lower cost, or alternatively, lower cost may be achieved through the use of simpler, more reliable boosters. The altitude also affects the control system design through

altitude-dependent environmental characteristics such as aerodynamics, gravity gradient, radiation and other phenomena. The number of satellites with synchronized orbits which require the additional complexity of a synchronizing or indexing system must be compared with those required in "random" orbits where such a system is not required. For example, 18 satellites in a 6-hour synchronized circular orbit are required for continuous coverage between New York and Paris, whereas approximately 21 are required in "random" orbits for 99% coverage.

(4) Orbital docking. Studies have indicated that the physical mating of two satellites in orbit is feasible. This system would permit the transfer of fuel to provide additional velocity to one of the vehicles (target vehicle) in orbit, essentially yielding an increase in booster capability. The actual mechanics and dynamics of the docking process and the problems of terminal guidance will require detailed attention by the mission analyst. For search, preterminal and terminal modes, the attitude control may require an earth or sun reference in addition to the target vehicle reference.

b. Control configuration

The limitations on size and shape which arise from the limited booster capabilities immediately constrain the configuration. The shape and particularly the moments of inertia are significant. If, for example, the spacecraft is to be spin stabilized, then for internal energy dissipation to provide stable damping, the moment of inertia about the desired spin axis must be larger than that about the other two axes. If, however, the vehicle is to be a low altitude, fully oriented satellite, the inertia configuration will determine whether or not the spacecraft is stable with respect to the torques generated by the earth's gravity field. In fact, the designer may choose configurations so that there is sufficient control moment to stabilize the vehicle from this effect alone.

If the center of aerodynamic pressure does not coincide with the spacecraft's center of gravity, there may be large aerodynamic overturning moments for the low altitude satellite which can affect the control system design and methods for generating countertorques. Principal axis/control axis alignment, difference in inertias, may be significant in the spacecraft dynamic response. In the design of momentum storage and mass expulsion systems, minimizing the moments of inertia about the axes will help reduce the weight of the momentum storage and mass expulsion device. Unfortunately, the other subsystems, particularly the power supply and temperature control, may have a predominant effect on the configuration.

(1) Power supply system. It is anticipated that power supplies for earth satellites requiring long life will continue to use the sun's energy to provide primary power. Rechargeable batteries will be provided to supply the power during periods of eclipse. The solar array size must meet the electrical power requirements of the system and recharge the batteries during periods of sunlight.

The power supply efficiency is maximum if the control system is capable of orienting the faces containing the solar cells toward the sun throughout the lifetime of the satellite--except, of course, during periods of eclipse (see Chapter XIII). If, however, a spin stabilized satellite is chosen, a maximum of only 25% of this power can be realized for a spherical satellite covered with solar cells in any orbit. Two particular spin axis orientations will provide more efficiency: (1) where the spin axis is continually aligned along the sun line, the efficiency is equivalent to that of the oriented array; and (2) where the spin axis is oriented normal to the sun line, an efficiency of approximately 32% of that of the fully oriented array is achieved.

The cyclic life of the batteries is affected by several things, including temperature, depth of discharge and height of charge. The control system response characteristics during acquisition of the sun can effectively reduce the depth of discharge required for a particular orbit through minimizing the time required for the solar array to reacquire the sun after an eclipse. The longer this takes, the more the batteries will be discharged and the less time there will be for recharge before entering eclipse again. This problem is particularly significant in orbits with eclipse periods which exist for a significant period of time.

During orbits with extremely long periods of sunlight compared to eclipse time, it may be desirable to include in the solar array control laws a provision for charge-control to prevent overcharging the battery. Since both continuous sun and earth orientation are impossible without an extra degree of freedom (except for special orbits and during particular periods in each orbit) systems which do not have a rotatable solar array have a reduced efficiency. However, if the power requirements are not extreme, it may be more reliable to have an unoriented rather than oriented array. This is an important tradeoff study to perform.

The electrical power obtained from rotatable solar arrays must be transmitted from the array to the body. The control system, as will be shown later, can be used to eliminate the need for providing complete rotational freedom which would suggest the need of slip-rings for power transmission. Control laws can be used which limit the required solar array travel to ±90°.

There are a number of other possible array configurations for which specific control laws can be generated. The problems associated with continuous but very slow drives may indicate that stepping the array or providing a set of multiple-fixed positions is an easier and more reliable approach.

(2) Temperature control. A number of active and passive temperature control systems are possible for satellite application. One system which has a great effect on both the control system design and the configuration is one in which the main body is attitude controlled, so that the two surfaces perpendicular to solar array axis

never see the sun. The temperature is controlled by insulating those four surfaces which sometime during the satellite lifetime will see the sun, thus preventing heat absorption. The other two surfaces contain shutters which are actuated to control the emissivity or radiation of internally generated heat into free space. These shutters will not be exposed to direct sunlight for long periods of time if the control system is working properly. If the satellite is earth oriented, sun control about the axis along the local vertical (yaw) will prevent direct sunlight from impinging on these surfaces suggesting four design considerations for the control system. These are:

(1) Quick acquisition must be made to the sun orientation following separation from the boost vehicle to avoid long periods of unoriented attitude.

(2) Special methods of control may be required by the temperature control systems. The time required to acquire the sun when the spacecraft emerges from the eclipse must be controlled. The effect of low control gain during periods of high noon (i.e., a condition obtained when the sun is in or nearly in the orbit plane) must be reviewed to keep from exposing these surfaces to the sun for long periods of time.

(3) Any other modes such as rotation out of the required plane for velocity corrections must take into consideration the possible exposure of these surfaces.

(4) The sun-pointing accuracy during periods of normal control must satisfy the temperature requirements.

(3) Orbit control system. For many earth oriented satellites, a system to provide change in the satellite's velocity during its time in orbit will be necessary. The indexing into a synchronous orbit of a communication satellite, the terminal guidance of a docking satellite, or the deboost of a vehicle for re-entry, are examples of systems which will utilize a propulsion system to change the spacecraft velocity while in orbit. The control system must be capable of properly reorienting the vehicle in space so the nozzle or rocket thrust will have the correct spatial attitude when the rocket is fired. Furthermore, since the thrust of this rocket will probably not pass exactly through the spacecraft center of gravity, an overturning moment will occur. Sufficient control authority must be available to correct for these moments. In addition, most orbit control systems will have a fine or precise vernier correction and/or a station-keeping mode that could easily use the control system nozzles and obtain energy from the attitude control system. Some simplification in hardware design will be obtained through integration of these systems.

(4) Data link. Earth satellites will be required to communicate with earth based stations. For many systems specific antenna pointing is required. Antenna gain and beamwidth, communication security, ground receiver flexibility and coverage are areas which affect the system design. For earth satellites, pointing accuracy of a few degrees is sufficient to retain most of the power in the transmitted signal. With proper orientation of antennas for interplanetary probes, increased data transmission rate may be possible.

The data link, or communication system, can also be used to command special modes of control. For example, through analysis of telemetry data it may be learned that a component has failed. The communications system may then send a command to switch in a redundant component.

(5) Control configuration environment and reliability. The environment in which the attitude control system will be required to operate is of extreme importance. Control and disturbance torque generation and sensing requirements are discussed later. The principal considerations which affect the control system reliability and equipment design may be itemized as follows:

Boost environment. The control system in the satellite must meet the requirement that it be operable after boost into orbit. During the first seconds of boost, the high accelerations (say 10 g), vibration, and heat environment impose severe restrictions on all components.

Vacuum. The pressure at 100 naut mi or 185 km is approximately 10^{-5} mm Hg, decreasing rapidly to 10^{-10} mm at 1000 naut mi (1850 km) and to 10^{-13} mm at 100,000 naut mi (18,500 km). In vacuum, there is no resistance to sublimation and evaporation of molecules of surface materials. There is a tendency for systems to "out-gas," creating additional control system torques and reducing the supply required for control torque generation. Substances with a low vapor pressure should be used to reduce the evaporation. The positive elimination or proper sealing of rubbing surfaces can reduce the problem to negligible proportions. As an example, slip rings for transferring power from the solar array to the main body can be eliminated by employing special yaw and solar array control laws (described later) which limit the solar array travel to ±90°. If motor-driven sensors, inertial wheels, and servos are used, they must be sealed to prevent the evaporation of lubricants from reducing the lifetime of the bearings.

Micrometeoroids. The average control system torque caused by this effect is small and can generally be ignored in comparison with other torques experienced in space. Chapter II considers the quantity and energy distribution of micrometeoroids in space. Two additional considerations are the possible puncture of the gas tank by a large micrometeoroid, and the general effect of bombardment on control system sensors and other components which are directly exposed.

Particle radiation. Shielding is necessary to protect such components or surfaces as are exposed to the bombardment of high energy protons and neutrons. Radiation damage can occur to sun sensors using solar cells, horizon scanners utilizing susceptible optical and detector materials, solid-state electronics, etc. Radiation damage depends on orbit altitude and inclination and must be evaluated.

Other considerations. Other environmental considerations include ultraviolet rays which serve only to increase the rate of sublimation; X-rays and gamma rays which are only significant during solar storms and can be essentially eliminated by the same mechanisms that protect against high energy protons and neutrons; and cosmic flux which appears to be of insignificant consequence in ionization.

Reliability. The degradation of system reliability due to space environment is difficult to predict. The use of failure rate data to assess the reliability of the control system is an important design tool and warrants further consideration. The number of components in the preliminary control configuration can usually be estimated. These estimates then form the basis for a reliability study.

Assume that the failure of a single component will cause the entire system to fail and that the extrapolation from a laboratory environment to an operating space environment can be performed realistically. Even in the event of errors in extrapolation, the relative reliability of different design approaches can still be evaluated.

The failure rate data for some commonly used components are given in Table 9. These data refer to a laboratory environment with an ambient temperature of 30° C and applied electrical stresses of approximately 25% of the rated. In the period between "infant mortality" and "wear out," most components experience a constant percentage random failure rate, λ_c. The probability of a system operating successfully for time, t_1, is defined by

$$P_s = e^{-\lambda t_1} \tag{156}$$

where

λ = composite system failure rate in space environment

t_1 = length of operating time.

TABLE 9

Some Commonly Used Failure Rates

Component	Inherent Laboratory Failure Rate Per 10^9 Hours
Silicon transistors	153
Silicon diodes	51
Resistors (film)	8
Pots (composition)	38
Capacitors (paper)	3
Capacitors (solid tantalum)	40
Transformer/winding (low voltage)	10
Relays (DPDT)	296
Motors and tachometers (ac)	200
Magnetic amplifiers	30
Control windings	10

The failure rate data is often expressed in units of frits which are defined as the number of failures in 10^9 hr. If there is a requirement for a 1-year operation and the system in space environment is assumed to be degraded over the laboratory environment by a factor of 3, the probability of one year's successful operation is then

$$P_{1\ \text{year}} = \frac{\sum \text{frits} \times 3 \times 8760\ \text{hours}}{10^9} \tag{157}$$

2. Control Orientation Methods

This and the succeeding sections define some of the methods, techniques, and problems associated with the design of the attitude control orientation and stabilization system. A most important choice in the early design is the method of obtaining attitude control torques. This section provides brief discussions of the important methods for providing control orientation.

Each method is specifically concerned with the effects of space environment and other changes of momentum the spacecraft may experience. It is important to remember the fundamental differences between torques which are constant in inertial space, always resulting in additional momentum to the system, and torques which are constant with respect to body coordinates and are in many cases cyclic in inertial space. Such cyclic torques do not necessarily require the removal of momentum from the system.

The following items and combinations of them are briefly discussed: (1) methods such as inertial orientation (spin stabilization); (2) the manipulation of the natural forces of space, such as gravity gradient, solar pressure, earth magnetic field, and aerodynamics; (3) the merits of internal rotating momentum storage and mass expulsion. A choice from among the several possible approaches is generally necessary quite early in the design. Special modes, such as separation rate control, acquisition, eclipse, indexing, terminal guidance, etc., may dictate special control requirements. These modes are discussed separately in a later section.

a. Inertial orientation

The simplest means of obtaining control is to spin the vehicle about a known axis. If this axis is either the minimum or maximum principal axis of inertia, the momentum imparted by the spin rate will cause (without the influence of external disturbances) the spin axis to remain fixed in inertial space. If there is no need to orient a particular axis or antenna on the vehicle to the earth and if sufficient energy can be obtained from the sun for electrical power, this method is the simplest. Pioneer V, Explorer VI, Courier, and others have been stabilized in such a manner. The final orientation of the spin axis in space will be the inertial orientation which exists at the time the spacecraft is spun. If there is initial momentum not along the spin axis, the system is stable only if the spin axis is also the axis of maximum inertia. Mercury ring

dampers are sometimes utilized to remove the wobble which occurs due to separation rates and dynamic unbalance effects.

There are several possible control orientations that might be required. Some of the more usual ones are sun orientation and stellar orientation:

(1) Sun orientation. It is possible to orient the spin axis toward the sun. This orientation gives the same power efficiency as an oriented solar array but it could complicate a communication system because of the time-dependent orientation of a body-fixed antenna with respect to the earth. To maintain the spin axis orientation to the sun will require precession of the spin axis at the rate of one revolution per year plus that required to compensate for the regression of the orbit line of nodes. A very simple attitude system can be used to obtain this orientation, if the pointing requirements are not too stringent.

(2) Orbit plane orientation. A spin stabilized satellite with its spin axis normal to the orbit plane can be used for a number of applications, for example, satellites required to photograph or otherwise survey the earth's surface and communication satellites where the antenna provides a toroidal pattern about the spin axis. If the earth-sun line remains normal to the orbit plane, then a high efficiency solar array can be mounted normal to the spin axis. If the inclination of the orbital plane to the ecliptic plane is small, solar cells mounted on a cylindrical surface about the spin axis will operate for the satellite lifetime but provide a maximum power per cell of only $1/\pi$ x the power per cell that would be achieved with cells in a comparable fully oriented array. If the orbit is unrestricted, then on the average each solar cell on the spinning vehicle will provide only 1/4 the power per cell of cells in the comparable fully oriented array.

(3) Other orientations. Spin stabilized satellites can conceivably be employed to maintain other orientations than those discussed above. Such tasks as pointing telescopes at fixed stars can easily be performed; however, such requirements are often associated with scientific missions where data transmission considerations require earth oriented antennas for communication, and an oriented solar array for power. These auxiliary tasks cannot easily be performed with a spin stabilized satellite.

Spin stabilization does not appear to be a satisfactory control scheme for earth orientation of an axis of an earth orbiting satellite. Either large torques (large energy expenditure) are required to maintain this spin axis rotation, or internal moving parts such as reaction wheels are required. Torque impulse, if applied properly, will require an energy expenditure of $H\omega$ per revolution where H is the total momentum of the satellite and ω is the average satellite orbital rate. If wheels are used, they must be capable of storing momentum at least equal to the spin momentum; for this reason they introduce significant stability problems and require complex implementation. Other problems, such as achieving the proper initial orientation and devices for damping the nutation must be considered. The spacecraft design yielding maximum flexibility will not, for most cases, rely on spin momentum for stabilization and orientation.

A symmetric body spinning at an angular velocity, p_0, about either maximum or minimum principal axes of inertia will, in the absence of any external moments, maintain its initial orientation constant in inertial space. If the body total angular momentum vector initially coincides with the spin axis, and if an impulse angular momentum is now added normal to the spin axis, the body spin axis will precess about the new system total angular momentum vector. The rigid body axes are defined in the sketch. The body is considered to be symmetrical about the spin axis.

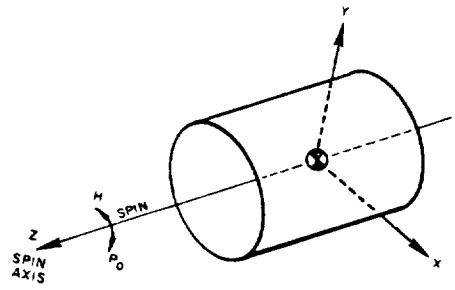

The motion of the satellite spinning at a constant spin rate in the absence of any external torques will generally be periodic about the spin axis. To simplify the solution of the equations of motion, a complex angular velocity, ω_n, is defined as

$$\omega_n = \omega_x + i\omega_y . \qquad (158)$$

Substituting this equation into Euler's equations of motion for a rigid body, the solution which defines the frequency of angular nutation is obtained in body coordinates. This means if the total body angular momentum, H_t, is about some other axis than the spin axis, the spin axis will experience nutation (free precession) about the total momentum vector. The following sketch shows the trace of the tip of the body spin axis under such an influence.

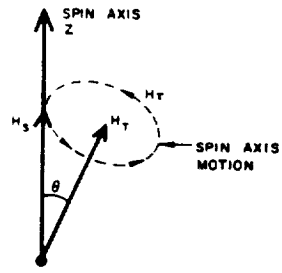

A point on the nutating body rotates at a frequency, given by

$$\Omega = \left(\frac{I_z}{I_x} - 1\right) p_0 \qquad (159)$$

where I_z is the moment of inertia about the spin axis and I_x is the moment of inertia about a transverse axis. For an inertial observer watching a fixed point on the body, this frequency is simply

$$\Omega_i = \frac{I_z p_0}{I_x} \text{ for small } \theta. \tag{160}$$

The half angle cone, θ, for the motion of z is given by

$$\tan \theta = \frac{I_z p_0}{I_x \omega_n} . \tag{161}$$

Passive dampers dissipate energy to remove the nutation (but do not change the system angular momentum) causing the z-axis to be aligned with H_t. Precession of the vehicle angular momentum vector is obtained by application of a moment impulse applied normal to the momentum vector. Any nutation that results from momentum vector reorientation can be damped passively by several schemes and it can also be prevented by proper application of another impulse also normal to the z-axis.

If an impulse is applied normal to the spin axis to cause a precession, then the application of another moment impulse (equal to the first and also normal to the spin axis), after the body has rotated through an angle φ given by

$$\varphi = \frac{I_x}{I_z} \pi \quad \text{radians} \tag{162}$$

will eliminate the nutation and will have caused the z-axis to precess through an angle of 2θ. Energy considerations will show that, for passive damping schemes, the moment of inertia about the spin axis must be greater than that about a transverse axis.

The advantages and disadvantages of spin stabilization as contrasted with control of non-spin configurations are presented below.

Advantages. (1) Fixed inertial orientation with limited accuracy can be achieved with a completely passive system; (2) accurate orientation with respect to a fixed star or slowly rotating line of sight can generally be achieved with a fairly simple, lightweight system; and (3) most disturbances including torques from velocity correction jet misalignments have only a small effect on the accuracy of a spin stabilized body.

Disadvantages. (1) Only one axis can be controlled; (2) a complex control system is required to point the spin axis along a rapidly rotating line of desired orientation; and (3) spin speed control may be required on systems where disturbance torques may cause large changes in the spin momentum of the system.

b. Use of natural forces of space environment

This section discusses the major sources of torques which will be experienced by the vehicle during its lifetime in orbit. These torques may be harnessed for control purposes or treated simply as disturbing influences for which control moments from other sources must be provided. Four major sources of torque which might be used for control are solar radiation pressure, gravity gradient, earth's magnetic field and aerodynamics. Gravity gradient, aerodynamics and earth's magnetic field have their greatest effect at low altitudes; solar radiation pressure is largely independent of altitude, and depends on the spacecraft surface area facing the sun.

(1) Solar radiation torque. The torque due to solar radiation pressure forces acting on a satellite vehicle is significant and must be evaluated. The combined equations necessary to express these torques in the general equations of motion of the vehicle are highly nonlinear. The purpose here will be to discuss briefly the cause of solar radiation torque and its effect on spin stabilized spacecraft and satellites with active attitude control orientation in an earth-sun reference.

Every satellite vehicle is composed of a number of distinct surfaces, each with particular surface reflective properties and characteristics. The bombardment of these surfaces by photons emanating from the sun will create forces on the spacecraft. The magnitude and direction of these forces are determined by the reflective properties of the surface. If the center of radiation pressure through which these forces act is not coincident with the vehicle center of mass, then a torque acting on the vehicle will be developed. This torque may be of sufficient magnitude to affect the control system design.

The radiation power in the vicinity of the earth is 1.94 cal/cm^2-min corresponding to a pressure of 9.4×10^{-8} psf (4.48×10^{-6} n/m^2) for complete absorption. In preliminary design it is necessary to calculate an upper bound on the radiation torque in order to determine the spacecraft momentum storage requirements for control system design.

The effect of the solar radiation torque on a spin stabilized satellite depends on the orientation of the spin axis with respect to the earth-sun line and the vehicle projected area facing the sun. The force parallel to the spin axis during one spin cycle will have no net effect on the vehicle. That force perpendicular to the spin axis can create precession of the spacecraft if it does not pass through the center of mass. The nature of the momentum change will depend on the orbit. For example, in a polar orbit (where there is no orbit plane regression) the net momentum caused by this torque will average to zero in one year.

For a fully oriented satellite with sun-earth orientation the torques will depend on the control laws and the inclination of the orbit with respect to the sun. Where the sun lies in the plane of the orbit, the torques in two axes will be cyclic in inertial space except for any rectification because of the constraint of earth orientation. Consider the example where the solar radiation torques are due solely to a solar array, as shown in the following sketch.

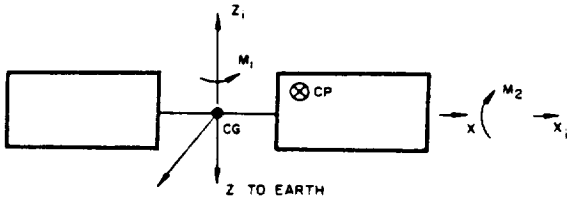

The radiation force acts through the center of pressure (CP) and creates constant moments about the z- and x-body axes, M_1 and M_2 respectively. If the z-axis is continuously oriented toward the earth and the sun is perpendicular to the orbit plane, the torques are cyclic in inertial space. For the sun in the orbit plane the moment is constant in inertial space. A plot of these torques in inertial space for orbits possessing inclination with respect to the sun of 90° and 0° is shown in the following sketches.

The solar radiation torque may also be used to provide useful control system torques. It has been proposed to equip the spacecraft with a large weather-vane type of reflective sail and control the vehicle by actuating this sail to create control torques. Such a scheme is difficult to implement and requires special control during eclipse and some form of momentum storage during periods when control torques about required axes cannot be obtained. Figure 27 presents the torque from solar radiation as a function of area and radiation pressure lever arm for total absorption.

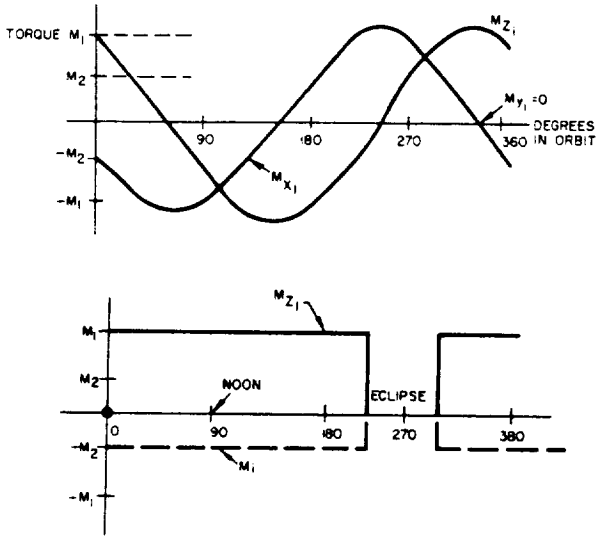

(2) Gravity gradient. The earth's gravitational potential varies with altitude. For this reason the center of gravity and the center of mass of a satellite are not exactly coincident. Unless the force of gravity, applied at the center of gravity, acts along a line passing through the center of mass, a torque tending to rotate the satellite will result. This torque can be employed to stabilize a satellite with respect to the earth's gravitational field. The gravitational torque may represent a disturbing input which must be overcome by the satellite control system.

The force due to gravity on a unit mass can be expressed in terms of the negative gradient of the gravitational potential as

$$\vec{F} = -\nabla\left(\frac{-\mu}{r}\right) \tag{163}$$

where

r = the magnitude of $\vec{r}$, a radius vector from the earth's center to the unit mass

μ = the product of the universal gravitational constant and the mass of the earth

$-\mu/r$ = the gravitational potential, a representation sufficientiy accurate for the purpose here.

The torque $\vec{M}_g$ tending to rotate the satellite about its center of mass is then

$$\vec{M}_g = -\int \vec{\rho} \times \nabla\left(\frac{-\mu}{r}\right) dm \tag{164}$$

where $\vec{\rho}$ is a radius vector from the satellite center of mass to the differential mass dm and the integration includes all mass of the satellite. For conditions where ρ is very small with respect to r, a condition always satisfied for earth satellites, the preceding integral expression for torque can be evaluated to yield

$$M_{g_x} = \frac{3\mu}{r_0^3}(\vec{u}_r \cdot \vec{j})(\vec{u}_r \cdot \vec{k})(I_{yy} - I_{zz}) \tag{165}$$

$$M_{g_y} = \frac{3\mu}{r_0^3}(\vec{u}_r \cdot \vec{i})(\vec{u}_r \cdot \vec{k})(I_{zz} - I_{xx}) \tag{166}$$

$$M_{g_z} = \frac{3\mu}{r_0^3}(\vec{u}_r \cdot \vec{i})(\vec{u}_r \cdot \vec{j})(I_{xx} - I_{yy}) \tag{167}$$

where

$$M_g = M_{g_x}\vec{i} + M_{g_y}\vec{j} + M_{g_z}\vec{k} \tag{168}$$

and

$\vec{i}, \vec{j}, \vec{k}$ = unit vectors along satellite principal axes of inertia

$\vec{u}_r$, r_0 = unit vector for and magnitude of radius vector from the center of the earth to the satellite center of mass, respectively

I_{xx}, I_{yy}, I_{zz} = moments of inertia about i, j, k respectively

Examination of these torque equations shows that all three torque components will be zero when $\vec{u}_r$ is aligned with a principal axis of inertia. However, a stable torque-free orientation will exist only when the principal axis with minimum

moment of inertia is aligned with $\vec{u}_r$. Complete stable orientation is possible only for the above condition when, in addition, the axis of maximum moment of inertia is aligned perpendicular to the satellite orbit plane. Gravity gradient torques provide the vertical orientation of the axis of minimum moment of inertia and result in a satellite rotation of the orbit rate. Gyroscopic action tends to orient the axis of maximum moment of inertia perpendicular to the orbit plane and thus along the angular rotation vector.

To establish more clearly the effects of gravity gradient on a satellite it is convenient to consider the satellite in a circular orbit shown in the following sketch. If all error angles are small, then the torque components due to gravity gradient are

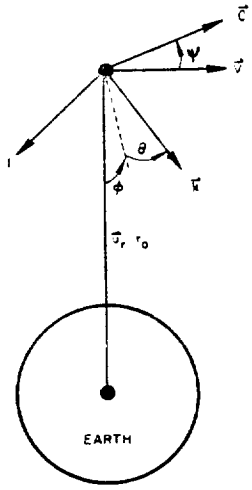

$$M_{g_x} = -3\omega_0^2 (I_{yy} - I_{zz})\,\phi \qquad (169)$$

$$M_{g_y} = -3\omega_0^2 (I_{xx} - I_{zz})\,\theta \qquad (170)$$

$$M_{g_z} = 0 \qquad (171)$$

where ω_0 is the orbit rate. The time rate of change of angular momentum of the system is equal to the applied torque and for small error angles, the angular velocity vector $\vec{\Omega}$, is given by

$$\vec{\Omega} = \vec{i}\,(\dot{\phi} - \omega_0\psi) + \vec{j}\,(\dot{\theta} - \omega_0) + \vec{k}\,(\dot{\psi} + \omega_0\phi) \qquad (172)$$

The linearized equations of motion for the system become

$$I_{xx}\ddot{\phi} + 4\omega_0^2 (I_{yy} - I_{zz})\,\phi = 0 \qquad (173)$$

$$I_{yy}\ddot{\theta} + 3\omega_0^2 (I_{xx} - I_{zz})\,\theta = 0 \qquad (174)$$

$$I_{zz}\ddot{\psi} + \omega_0^2 (I_{yy} - I_{xx})\,\psi = 0 \qquad (175)$$

where cross-coupling terms have been neglected.

An undamped motion will occur about the orientation where all three error angles are zero if $I_{yy} > I_{xx} > I_{zz}$. In order to stabilize a satellite by use of gravity gradient torque some auxiliary damping system is required. Such damping can be provided by reaction wheels driven from sensors within the satellite.

A more attractive scheme is to provide the necessary damping by passive means such as body flexure, liquid dampers, or passive interactions with the earth's magnetic field. Unfortunately, such passive techniques are not yet completely understood, and at present their design is difficult unless very small damping factors can be tolerated.

The limitations of the usefulness of gravity gradient torque for stablizing a satellite with respect to local vertical and the orbit plane are:

(1) Gravity gradient torques decrease with altitude while some disturbance torques (notably solar radiation pressure torques) are invariant with altitude, thus it is difficult to design high altitude satellites to operate primarily with gravity gradient stabilization.

(2) Orbit eccentricity introduces disturbances in the gravity gradient control which preclude the use of this type of control for highly eccentric orbits.

(3) At low altitudes aerodynamic torques are encountered which greatly complicate the design of a gravity gradient controlled satellite.

(4) Satellite requirements such as solar arrays to collect solar energy, communication antenna placement, booms for experiments, and restrictions on configuration for compatibility with the boost vehicle may so constrain the satellite configuration that gravity gradient stabilization cannot be achieved.

(5) Highly accurate orientation is difficult to achieve since attitude errors must be developed to provide gravity gradient torques to counter disturbance torques.

Gravity gradient torques become disturbance torques when other than local vertical orientation is desired, or when control is accomplished primarily with other techniques such as gas expulsion systems operated from a horizon scanner. In the latter case, gravity gradient torques will generally constitute system disturbances even when the desired orientation is apparently the stable gravity gradient orientation. The active control system will always attempt to align with respect to the control axes, which will coincide with the principal axes of inertia only in the case

of perfect alignment. Furthermore, if a solar array that rotates with respect to the satellite proper is used to generate electrical energy, the principal axis of inertia will rotate with respect to the control axes and an additional system disturbance will result.

(3) Earth's magnetic field. The magnetic field of the earth can be used in conjunction with magnetic rods or current carrying coils to provide control torques. The earth's magnetic field has already been used with magnetic rod arrays to provide "despin systems" on Transit 1B and 2A satellites. It is now evident that a complete control system is feasible based on obtaining control moments from the energizing of satellite-fixed, current-carrying coils. For lower altitudes, the torque obtained from the coils can offset the effects of disturbance torques without large expenditures of power or extremely weighty coils. For designs utilizing other torquing schemes it is imperative that care be taken to reduce the magnetic moment of the spacecraft so that magnetically induced disturbance torques are not significant.

All the factors contributing to the earth's magnetic field are not well understood, but it is clear that for satellites greater than 100 mi above the surface of the earth, circulating currents in the atmosphere and surface field irregularities do not significantly affect the approximation of a field which will be produced by assuming a simple magnetic dipole at the center of the earth.

The axis of this dipole, which best represents the magnetic field, is skewed at an angle of approximately 18° with respect to the earth's spin axis. The North Magnetic Pole is at approximately 70° N Latitude, 97° W Longitude. The South Magnetic Pole is at approximately 73.5° S Latitude and 155° E Longitude. This means that the axis of the dipole, and hence the field, precesses around the earth's spin axis. This precession is significant and means that only in orbits which are synchronous with respect to the earth's spin will the effects of the magnetic field be the same during successive orbits or sets of orbits (depending on the synchronous period). Only in a 24-hour orbit which contains the dipole is it impossible to generate torques for complete three-axis control. In general, the field will vary constantly with respect to system axes. In any one day (due to the field's precession about the earth's spin axis) it appears possible to generate control torques about all of the required control axes. These torques may not be available at the instant they are required, suggesting the requirement for momentum storage. Further, the magnitude of the field is different on each successive orbit, depending on the altitude, inclination, eccentricity, time of launch, point of injection, control axis orientation (control laws) etc. Knowledge of the field magnitude and direction is essential to the proper energizing of coils and must be supplied either by computation or measurement. The data essential to the preliminary designer is the magnitude of the field as a function of altitude and variations typical of those which will be experienced in the particular orbit. Figure 28 shows the total magnetic field as a function of altitude for the dipole representation.

A current carrying coil in the magnetic field tends to assume a position that will result in the largest possible flux through it in a positive sense. That is, the force F on an element of wire in a flux field, B, is given by

$$\vec{F} = i\, \vec{dl} \times \vec{B} \qquad (176)$$

or a coil whose center is along the spacecraft z-axis would cause the spacecraft to experience a torque, $\vec{M}_m$ in dyne-centimeters of

$$\vec{M}_m = \frac{\pi r_c^2}{10} n (\vec{u}_x B_y + \vec{u}_y B_x) \qquad (177)$$

where

$\vec{u}_x$ and $\vec{u}_y$ = unit vectors along x and y spacecraft axes respectively

r_c = the radius of the coil in centimeters

i = the current in amperes

B = the flux density in gauss

n = the number of turns.

It is interesting to note that 0.1 gauss acting normal to a 10-turn coil of No. 14 (standard household wiring) copper wire 1 ft in (0.3 m) radius (weight less than 1 lb (4.4 newtons) without supports) when energized with 1 w will produce a torque approximately 5.8×10^{-5} ft-lb. (7.9×10^{-5} m-newtons) This is potentially an extremely attractive torque for control. This torque is about an order of magnitude above that anticipated for either solar radiation or gravity gradient with reasonable design practices. The magnitude of the control torque obtainable for a coil with a 1-ft (0.3 m) radius over the magnetic equator is plotted in Fig. 28 as a function of altitude.

There are some interesting tradeoff studies between weight, power, wire size, and the use of materials that can be considered. For example, for a circular coil the torque in a constant field is equivalent to

$$\text{Torque} = k_1 P^{1/2} W^{1/2} R \rho^{-1/2} \qquad (178)$$

k_i = constant of proportionality (i = 1, 2, 3)

P = applied power

W = weight of the coil

R = radius of the coil

ρ = relative resistivity of the material.

The most significant increase in torque is obtained with larger radius coils. Larger coils of the same size wire with the same power show

$$W = k_2 R$$

$$T = k_3 R^{3/2}.$$

A knowledge of the variations of the earth's magnetic field along the orbit is important. The combination of nodal regression, dipole axis precession, and orbit period means that the flux will vary each revolution and is different from time to time, except for those that have a period which is a multiple of the earth's spin rate. The variations of the flux density in an inertial coordinate system are plotted as a function of time for orbit inclinations of 0°, 30°, 60° and 90° for two consecutive orbits of 400 naut mi (741 km) in Fig. 29. The inertial coordinate system for these plots has the x-axis along the earth-sun line at the vernal equinox, the z-axis essentially along the positive earth spin vector, and the y-axis to form the right-handed set. To see the effectiveness of control, the component of flux density along the earth's local vertical is plotted as a function of time for the 400-naut mi orbit in Fig. 30.

For the purposes of calculation, the earth's field can be simply expressed in terms of the axial and normal component from the earth's magnetic dipole. The equations are

$$H_{axial} = 0.308 \frac{(1 - 3\cos^2 \delta)}{(r/R)^3} \qquad (179)$$

$$H_{normal} = 0.461 \frac{\sin 2\delta}{(r/R)^3} \qquad (180)$$

where

H_{axial} and H_{normal} = the components of field intensity in oersteds

δ = the angle between the earth's magnetic dipole axis and the radius vector to the satellite

r = the radius vector to the satellite from the center of the earth in centimeters

R = the radius of the earth (6.371×10^8 cm)

If the dipole is aligned along the earth's spin axis (a reasonable assumption for preliminary calculations), then the latitude, L, is equal to $(90 - \delta)°$. Figure 31 shows the total magnetic field $(H_{axial}^2 + H_{normal}^2)^{1/2}$ as a function of latitude for this assumption.

Some of the limitations and considerations on the usefulness of earth's magnetic field for stabilizing a satellite are:

(1) Since the torque generated is always about an axis perpendicular to the earth's field, only two axes can be controlled at once. It is necessary to add devices such as inertia flywheels or gyros to store the momentum along the axis which cannot be controlled until the spacecraft reaches an orbit position where the momentum may be magnetically transferred from that axis.

(2) The magnitude of the control torque must be greater than the sum of the internal and external disturbance torques. It is not difficult to achieve fairly significant control torques at altitudes up to 10,000 mi. (16,000 km)

(3) The earth's field in body coordinates is continually changing. In-flight computation based on this field must be performed or the direction of the field must be sensed in order to determine proper current patterns required by the coils. This might be done using magnetometers as magnetic field sensors and primary orientation signals obtained from earth local vertical sensors, sun sensors, or star trackers and others.

(4) The stability of a system using body-fixed coils in the earth's magnetic field is questionable because of the difficulty imposed by the inherent cross-coupling torques due to the action of the magnetic field on the coil. Current carrying rods or sheets may provide one solution. Another possible solution would be to use the magnetic field to induce momentum in a controlled way by providing eddy current damping to the momentum wheels. Unfortunately the amount of momentum imparted to the body by this method is, for practical purposes, quite low.

(4) Aerodynamic torques. The earth satellite in a low altitude orbit, or with a low altitude perigee, will experience aerodynamic forces during its lifetime. The nature of these forces, depending on the orientation of the vehicle and its altitude, may be of consequence and may require an expenditure of a significant amount of control system momentum. In fact, for some extremely low altitude satellites, certain proposals have been made to use the aerodynamic torques through a large rudder or actuating trailing drag device to obtain control torques. Since somewhat higher altitude satellites are being considered here, the aerodynamic torque will be treated as a disturbance torque with simplified methods for computing its effects.

Knowledge of the density of the upper atmosphere is constantly improving. The ARDC 1959 Atmosphere, which is frequently used, represents the average density when perigee is in twilight near the time of a sunspot maximum. The density can vary considerably from the ARDC 1959 model.

"Hyperthermal free molecule" flow theory is generally used to obtain the shearing and normal stresses on the various flat surfaces of a space vehicle. Although this theory has been adequately described, two important criteria associated with it are worthy of note.

(1) The mean free path of the air molecules must be many times greater than the size of the body moving through the air. In the vicinity of the body, the frequency of collisions between air molecules is negligible relative to the frequency of collisions between the molecules and the body surface. The above condition

is realized for most spacecraft since at an altitude of 150 mi (280 km), the mean free path of free stream molecules is approximately 1000 ft (300 m) whereas the largest body dimension is usually less than 15 ft. (5 m)

(2) The term "hyperthermal" implies a vehicle speed much greater than the mean free stream molecular speed. The orbital speed of spacecraft at 150 mi (280 km) is roughly an order of magnitude greater than the mean molecular speed, and hence, the hyperthermal condition is deemed acceptable.

The equations which describe the pressure, P, and the shearing stress, S, are

$$P = 2(2 - \sigma') q \sin^2 \beta \qquad (181)$$

$$S = 2\sigma q \sin \beta \cos \beta \qquad (182)$$

where the pressure, P, acts normal to the surface and the shearing stress, S, tangent to the surface in the direction of the normal projection of the velocity vector on the surface. The angle of attack, β, may be expressed in terms of the yawing angle, ψ, for the body surface. Hence, $\beta = \psi$ and $\beta = 90° - \psi$ for surfaces whose normals are along the y- and x-body-axes, respectively (see sketch Section D.1.). It can be shown for the solar array that $\sin \beta = \sin \psi \cos \phi_p$. The previous angle relations are valid only when the velocity vector lies in the x_b, y_b plane. Computation of force on the body and array surfaces as a function of β or ψ and ϕ_p is a straightforward process provided the surface area is known. The question of surface area arises when it is realized that at most yaw angles the leading paddle partially shades the body and portions of the body partially shade the trailing paddle from possible molecular collisions. As a result, shading factors must be calculated. Since for this type of flow the center of pressure is essentially at the center of the exposed surfaces, it is necessary to calculate the latter in conjunction with the shading factors.

The two quantities, σ and σ', respectively, defined as the surface reflection coefficients for tangential and normal momentum exchange, have a significant influence on the magnitude of the pressure and shearing stress. The nature of the molecular re-emission, and hence the value of σ and σ', are functions of the type of surface material, the velocity angle of incidence, and the wall temperature. The value of σ and σ' can vary between 0 and 1. The few measurements made on typical engineering surfaces indicate values of σ between 0.8 and 1.0. For low angles of attack it appears that the characteristic of re-emission may be altered sufficiently to cause considerable deviations of σ' from these values. The quantity, σ', had not yet been measured experimentally; however, the values of σ and σ' should not differ greatly. The surface interaction experiments which have been conducted imply that most molecules do not rebound in billiard-ball fashion, i.e., with the angles of incidence and reflection equal, but that they are diffusely scattered due to (1) physical roughness of the surface, and (2) temporary trapping on the surface. The effect of changes of these coefficients on the maximum disturbing moments must also be considered in the design until better data are available.

For preliminary design, an approximate maximum moment due to aerodynamics for a spacecraft similar to that shown in the sketch of Section D.1. can be computed quickly. Compute the offset of the center of area from the center of mass and the exposed area for the β or b's which appear critical. The torque due to drag is simply

$$M_D = C_D L_D A q \qquad (183)$$

where

C_D = the drag coefficient or $2(2 - \sigma')$

L_D = the assumed center of area offset from the center of gravity

A = the total area bombarded by molecules

q = dynamic pressure at the spacecraft altitude equal to $1/2\ \rho\ v^2$.

If aerodynamic torques are a problem, the length, L_D, which is determined by the center of area normal to the airstream, must be closely controlled.

If the yaw angle is such that the spacecraft does not shade impinging molecules from one paddle, then no net equivalent lift torque is experienced. However, there will be a torque if the yaw angle is such that one of the paddles is shaded. The moment which tends to rotate the body about the axis is given approximately by

$$M_L = C_L (1 - f) L_L A_p q \sin^2 \psi \cos^2 \phi_p \sin \phi_p \qquad (184)$$

where

C_L = lift coefficient or $2(2 - \sigma' - \sigma)$

L_L = the distance of center of solar paddle area from center of vehicle mass

f = the shading factor on one paddle

A_p = the area of one solar paddle

ψ = the angle with respect to the velocity vector (yaw angle)

ϕ_p = the solar array angle.

This expression is not evaluated since the shading factor is also a function of ψ and possibly ϕ_p. The equations presented for these torques are approximate and are presented only to allow a rough determination. Different equations, of course, must be derived for other configurations and, in any event, a more refined analysis of these torques should be performed if a problem area is suspected.

c. Use of momentum storage devices

The use of rotating devices to provide momentum storage in a spacecraft has been described extensively in the literature. Such devices are generally used to continuously absorb the effect of disturbance torques, to store momentum due to orbital rate, and to perform special control maneuvers. Constant speed rotating inertial devices may be used to change the gyroscopic coupling torques about a particular axis or axes. In designing a system for momentum storage, it must be remembered that the momentum storage requirements are determined by inertial torques as they appear in body axes. A constant external torque with respect to inertial space will change the total momentum of the system, and hence the storage requirements will increase with time. However, disturbance torques which are fixed in the body may require momentum storage that is cyclic in inertial space, dependent on the orientation of the body axes with respect to inertial space. Understanding the relationship of the inertial and body reference frames is a fundamental point in determining how stored momentum must be handled. For example, assume a spacecraft is to rotate uniformly in such a way as to point to the earth as it progresses in orbit; to do so requires a rotation of 360° per orbit. In the absence of any applied torques, the stored momentum of the system will remain constant with respect to inertial space. In general, at any point in orbit, the momentum can be considered to be stored in three-body-fixed wheels whose axes may not coincide with the inertial frame. In such an instance the wheels will change speed continuously in order to transfer momentum from one body axis to another (although the momenta are fixed in inertial space) in order that at every instant the sum of the individual momenta will equal the total constant momentum.

The effectiveness of reaction wheels is based on the law that the time rate of change of wheel momentum is equal to the torque. The attitude error signal is used with filtering to control the wheel speed, meaning that for nonzero constant momentum storage there must be an angular pointing error. Integral control can be used to alleviate this problem in the steady state. Since most momentum storage devices are limited in their storage capability, momentum storage may be used in conjunction with momentum expulsion devices to allow operation beyond the capability of the storage device for removing the momentum. Such systems then combine the most useful function of the momentum storage (to absorb continuously without extreme energy expenditure the momentum imparted by disturbance torques and orbital maneuvers) and that of the mass expulsion system (to remove momentum from the system only when it saturates the storage device).

The momentum storage system adds complexity to the system. If the problem of coupling between axes is significant, careful design will be required. Methods proposed for obtaining momentum storage include rotating inertia (a motor-driven inertial flywheel, gyro stabilizer gimballed gyroscopes) and the control of the motion of a fluid moving in an enclosed circuit. In an attempt to reduce the cross-coupling terms, a free sphere has been proposed. The present satellite designs generally use the single-axis, motor-driven flywheels.

d. Use of mass expulsion devices

The attitude control of a spacecraft with initial rates in the presence of an external torque field can be simply achieved through the use of a variety of mass expulsion devices. The actuation of such devices will be controlled by the output of a sensor and used to change the angular rate of the spacecraft to keep it within some attitude error limit or to precess the spin axis of a spin stabilized spacecraft. The mass expulsion system may either produce a torque proportional to the error signal or produce quantized torque levels for controlled periods of time to maintain the vehicle angular momentum below some prescribed limit.

The governing problem in design is the tradeoff between weight and reliability. The simplest system is the single level thrust, on-off system used to maintain the spacecraft attitude error and error rate within certain limits. The impulse required for such systems is a direct function of the limit cycle rate, the lowest value of which is determined by such parameters as rate gain, position gain, filtering, sensor noise, valve actuation hysteresis, valve time delay, thrust build-up and decay characteristics, design thrust level, etc.

The use of cold gas such as dry nitrogen with nozzles and regulators designed to produce thrusts of the order of 0.1 to 0.001 lb (.4 to .004 newtons) is acceptable for most present spacecraft weights and lifetimes. Of course, larger thrusts will be required to provide control moments for large satellites or during periods when the booster stage is attached to the spacecraft or when misalignments of the thrust used for midcourse corrections require a larger control authority to overcome overturning moments. Hot gas systems will have a specific impulse considerably greater than that of the cold gas; however, problems associated with multiple starts, obtaining the low-thrust level, and thrust characteristics may not make such a system attractive except where larger thrust levels are required.

The on-off system, when used as the only means of obtaining control torques, requires a significant amount of impulse for long-term operation. If thrust is made proportional to the attitude error (such as is possible with proportional jets) it will react to disturbance torques continuously except when operation is within the low signal nonlinearities of the valve. The continuous operation in response to cyclic disturbance torques will also require a large expenditure of impulse over a significant lifetime. A more suitable design for long lifetime missions will be to expend electrical power (which can be replenished easily using solar cells) to control body-fixed reaction wheels in response to the angular momentum changes. The mass expulsion system would only be used to remove the effects of secular torques.

The development of more efficient, higher impulse systems such as plasma, ion and vapor propulsion is necessary for propulsive systems

in satellites which must achieve the longer lifetimes of several years--probably a requirement of the near future. With these systems, a significant weight advantage will be obtained if their reliability is acceptable.

Proportional and simple on-off controls have been mentioned as possible means of obtaining control torques without any additional torque-producing requirements. Other schemes have been proposed. One reduces the gas required by a simple on-off single level thruster by using the flexibility of a two-level thrusting system. Such a system, if properly designed, does not require rate information for stable operation. Another method with some advantages is modulation of the pulse duration applied by a single level jet as a function of the error signal. This system is also stable without rate information.

e. Combination systems

Momentum expulsion and momentum storage devices can be designed to complement one another. The storage device will control or store momentum due to cyclical torques on the spacecraft without gas expulsion and the jets will overcome long-term constant disturbance torques by periodically desaturating the storage device by expelling mass from the spacecraft. The jets will be needed also to counter initial body attitude rates, when the vehicle is separated from its booster, and perhaps torques produced by rocket thrust misalignment during guidance maneuvers.

The desirability of such combined systems will be determined on the basis of the factors of weight (including power consumption) and reliability for a given lifetime.

3. Methods of Attitude Sensing

The purpose of this section is to examine important methods which could be used for sensing the attitude of spacecraft from which attitude error signals can be generated. Basically, the methods will include earth, sun and stellar sighting, the use of inertial instruments, and the use of ambient fields.

a. Earth horizon sensors

The achievement of many earth orbiting missions will require the spacecraft to point one axis along or at some preset fixed angle with respect to the earth's instantaneous local vertical. There are a number of earth sensing devices, generally referred to as horizon scanners, which may be employed for this purpose. Horizon scanner operation depends on the detection of the difference in radiation emitted or reflected by the earth and the earth's atmosphere, and the radiation emitted by free space. The radiation emitted by the earth and the earth's atmosphere approximates black body radiation at a temperature which varies from 220° K to 280° K. In addition to the emitted radiation, the earth reflects solar radiation dependent on the relative earth and sun positions. This discussion will be confined to devices which utilize only earth and earth's atmosphere emitted radiation and thus capable of both night and day operation. operation.

A horizon scanner consists of four basic parts: an optical system; a scanning system; a radiation detector; and an information processing system. The optical system's principal function is to concentrate the energy in the optical field of view onto a suitable detector system. The scanning system moves the optical field of view in some precise manner relative to the spacecraft. The radiation detector may be a single element or system of elements which are sensitive to the radiation to be measured. The information processing system contains the logic circuitry necessary to provide proper error signals to the control system.

There are basic limitations to the accuracy of horizon scanners which are dependent on the altitude of the spacecraft relative to the earth. The limitations involve the shape of the earth, and the variations in the earth-space radiation difference. By proper selection of the radiation spectra used by the detector and canning mechanism used to locate the earth, these inaccuracies may be minimized.

The most widely accepted detector for application in horizon scanners is the thermistor balometer. This device has substantially a flat spectral response from ultraviolet to the far infrared and, for uncooled detectors, exhibits the best detection in the infrared spectral range. The precise spectral range for detector operation is determined by the selection of elements in the optical system.

The method used for scanning depends upon the orbital parameters of the spacecraft mission, overall system accuracy, and the requirements for earth acquisition.

There are three principal types of scanning techniques: a fixed field of view continuously scanning in a cone; an edge tracker system which locates and tracks the horizon in a fixed plane; and a passive scanner which utilizes a wide field of view imaged on a detector array. There are other scanning systems which will not be discussed, such as a rosette scan pattern or the possible use of image tube techniques for electronic image plane scanning.

(1) Conical scanning. Figure 32 depicts a typical conical scanner system (two scanners) in normal operation. The optics for each scanner consists of a prism and lens system which causes the field of view, focused on the detector, to scan in a circle in some fixed half-angle cone by continuous rotation of the prism.

A schematic of the scanner optics is shown in Fig. 32b. The detector output signal for each revolution of the prism is shown in Fig. 32c. Each scanner controls one of the vehicle axes. The control signal is generated by sensing the width of the balometer output pulse on either side of a reference signal, which is aligned with the vehicle control axis. Referring to Fig. 32d, the vehicle is aligned in roll when A-C is equal to C-B. Control relative to two axes may also be obtained with the same type of scanners in alternate scan orientation. Referring to Fig. 32e, the vehicle is aligned in roll when A-C is equal to C-B, and aligned in pitch when A-B is equal to A'-B'. This

type of scan technique is best applied to spacecraft missions which have nearly circular orbits. Since the scanner is generally best designed for operation over a limited range of altitudes, the large variation in the ratio of earth-to-space return signals obtained in highly eccentric orbits will create a special design problem if accuracy is required.

The conical scanner can be designed also to operate with a half-angle cone equal to 90°. Two such scanners would control a spacecraft in two axes in the same manner as the scanner described above, where the axes of rotation of the prisms are normal to each other. The scan pattern would appear similar to Fig. 33 except the scans would intersect along the vehicle yaw axis, coincident with the local vertical when no spacecraft pitch or roll attitude error exists.

(2) Edge Tracking. The sketch shows a schematic of a single edge tracking horizon scanner. This scanner uses the detector output to drive a mirror. The field of view of the mirror is continuously oscillated through some small angle in a plane independent of the mirror drive. The mirror drive is nulled when the detector output is a square wave, which indicates that the mean position of the small oscillation of the field of view, and hence the mirror, coincides with the earth horizon.

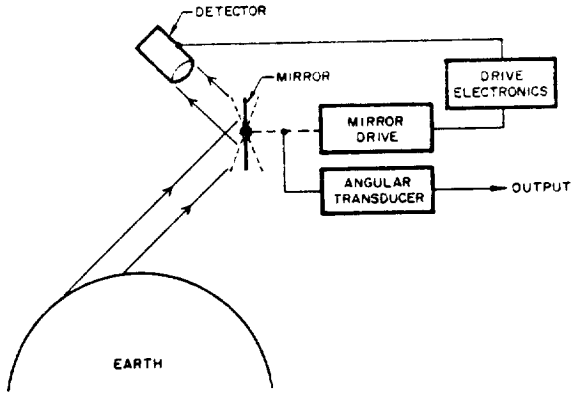

The field of view of the mirror may be oscillated by many techniques--for example, by oscillating the mirror as shown in the figure, or by interrupting the incoming radiation with a shaped reticle. Figure 33 indicates how three-edge tracking scanners may be used to generate spacecraft pitch and roll control signals. The angle of each mirror is measured relative to a vehicle reference axis. The field of view of each scanner searches in a fixed plane relative to the spacecraft. The pitch and roll attitude error signal may be generated by processing the difference in the angles measured by trackers A and D, and the angles measured by trackers A and B. A fourth tracker, C, may be used to provide the redundant error signals.

(3) Passive scanner. A simple example of a passive scanner is shown in Fig. 34. A wide-angle lens system images the earth's radiation on a detector array. The control error signals are obtained by differencing the detector outputs. This system is only workable for spacecraft missions with near circular orbits, since the detector array must be sized for a near constant size earth image. Other passive scanners might include electronic imaging tubes and simple shadow bar techniques for operation at extreme disturbances.

The scanners also suffer from the problem of sun interference. The presence of the sun with its high energy in the balometer field of view for extended periods will cause erroneous signals to be generated and may possibly damage the detector. Means of determining the sun's presence and eliminating its effect on the control signal must be provided. The passive scanner with its large field of view will contain the sun more during orbital life than the other scanners. During this time the scanner must not only be made inoperative but, in order to protect the detector system from damage due to solar radiation, some positive filtering of the sun's energy must be accomplished.

b. V/H technique

The V/H technique, as applied to attitude control, is described in Ref. (8). The V/H technique is also a potentially accurate navigation system for close orbits of a planet. From correlation of stored strip pictures of the expected track of the vehicle and real-time pictures taken from the satellite, deviations from the desired orbital position could be determined. Velocity information could be obtained by correlating two successive pictures taken with a fixed time delay.

Basically, the method consists of measuring the ratio of satellite velocity (V) to altitude (H) by the use of the following equation:

$$\frac{V}{H} = \frac{\dot{\alpha}}{\cos^2 \alpha} \quad \frac{\dot{H}}{H} \tan \alpha$$

where α is the angle between some object on the ground and the vertical. This is mechanized by correlation of video signals from successive frames of a vidicon. Image velocity V' is directly proportional to V/H.

$$V' = H' \cdot \frac{V}{H}$$

where H' is the focal length of the instrument.

A mechanization diagram of the optical correlator for the V/H orbital guidance system is shown in the following sketch.

The reference map is formed electronically by exciting an optically thin CdS (cadmium sulfide) film by a long persistence blue phosphor light, thus creating a pattern of absorption. The blue phosphor light renders transparent object areas upon illumination. The CdS film must be of sufficient thickness to provide a volume absorption which would prevent obtaining false results. False results would be obtained if the film were not thick enough, and some unmatched part of the scene would have greater transmitted brightness than the correlation peak. The optimum film thickness should be obtained by experimentation. The green emission is eliminated by the green filter, and the transmitted light will have the characteristic of two patterns multiplied together. When this distribution is integrated, the correlation function is formed except that some background level will be transmitted. However, the peak will exist and can be detected.

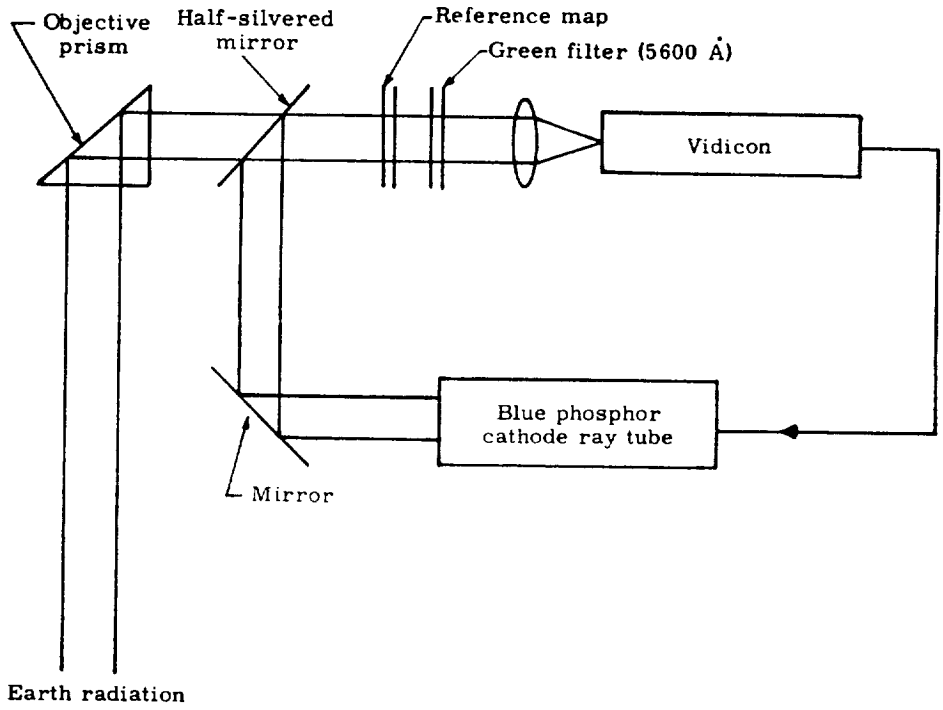

c. Sun sensors

The sun is an excellent reference for many satellites in that fairly simple sensors can be used to attain both a measure of yaw orientation and, if a rotatable solar array is used, solar array orientation. Spacecraft for solar experiments will use such devices for orienting along the sun-line. The principal problem with sun sensors occurs when the vehicle is in eclipse and such sensors can no longer be used. As will be indicated later in the discussion of modes of attitude control, several steps may be taken to minimize effects of such a problem.

The simplest form of sun sensor employs photovoltaic solar cells. These cells can be used in a variety of ways to provide angular error information. For most applications the linear range is limited to ±20 to 40° with a saturated output over the rest of the 360°. The following sketch illustrates such a characteristic.

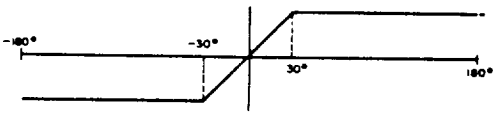

If relatively high accuracy is required, a device similar to that indicated as yaw scanner in Fig. 35 will, by measuring dwell amplitude on the scanning mirror, give about 0.05° for linear ranges up to 10°. (A reduction in accuracy will be imposed if greater linear ranges are required.) If accuracies no better than about 0.5° to 1° are of interest, then the extremely simple shadowing array such as the array orientation sensor, one-half of which is shown in Fig. 35, or the T-bar arrangement shown in Fig. 36 may be employed. It should be noted that such devices are subject to null shifts and gain variation, due to the difference in thermal properties of the cells.

A relatively new method of sun sensing is the use of a spot position transducer. This device is a solid-state transducer whose output is sensitive to the position of a light spot on its surface. This transducer converts the light-spot x and y displacement into a pair of voltages V_x and V_y proportional to the displacement. The displacements are referred to the cell center where x, y, V_x and V_y are all zero. By using a simple lens, the sun may be imaged on the transducer. A function of the angular position of the sun is then obtained in the two axes normal to the position of optical axis of the system. The linearity and accuracy which may be obtained with this device are determined by the sophistication employed in the optics and the desired field of view.

Many systems are available for measuring deviations from the sun. The three presented here represent only a very small sample.

d. Gyro mechanisms

Error signals for control to an inertial reference can be provided by gyro mechanisms. Both single-degree-of-freedom and two-degree-of-freedom gyros could be used for this application. For long term operation, gyro drift will cause major attitude reference errors unless means for resetting the gyro and/or in-flight calibration to eliminate drift are incorporated. This might be done with information derived in the vehicle with relationship to stars, sun, etc., or on ground-command based on ephemeris or telemetry data.

One means of determining spacecraft error from the orbit plane is to operate a gyro whose input axis is to be aligned in the orbit plane in a rate mode. Such a gyro, if not oriented in the orbit plane, will sense some fraction of the orbital rate of the earth-oriented vehicle as it proceeds in its orbit around the earth. The use of this rate essentially provides a gyrocompass

scheme for determining orbit plane reference above very low altitude orbits where the orbital rate is high. Such a system has practical difficulties. Compensation will be required for the spacecraft rates in roll (or pitch) which will also appear in the output of the gyro. The drift characteristics and basic accuracy of the gyro limit the ultimate accuracy of the system. For a small input axis alignment error, e_z, the gyro output, $\dot{e}_g$, will be the component of pitch and roll rate, $\dot{e}_h$, along the axis plus the component of orbital rate, $\omega_0 e_z$.

$$\dot{e}_g = \dot{e}_h + \omega_0 e_z \qquad (185)$$

By properly introducing the component of error due to input other than orbital rate, e_h, (see sketch) the output of a rate integrating gyro in a rate mode can be approximately that of the component of orbital rate. For convenience, the roll axis is to be aligned in the orbit plane. Thus e_h becomes e_x. Note that the noise introduced from the sensed motions about the roll axis may be significant, and if the orbital rate is too low (reduced as a function of altitude) the system is impractical.

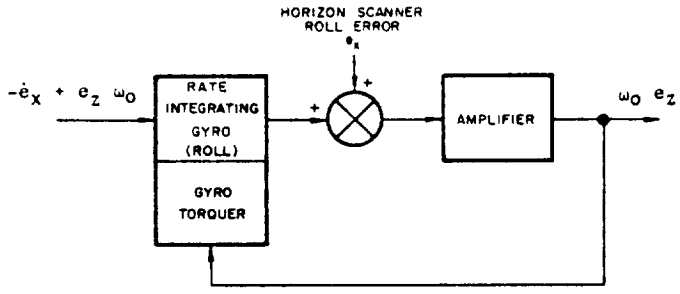

The use of the gyrocompass technique as standard practice requires additional power for temperature control, and is subject to the long term reliability problems generally associated with most gyros.

Other schemes for orienting the body with respect to the orbit plane should be studied. It is possible to use ephemeris data, from which sun/orbit plane orientation with respect to one another can be predicted. This, combined with the control laws, will provide knowledge of the satellite yaw attitude with respect to the orbit plane. Sun sensors can be used to determine when the spacecraft is in the noon, or near-noon, condition (that is, when the solar array goes through 0°). At this time the vehicle yaw angle is known and can be used. A gyro will maintain inertial orientation about the yaw axis and additional commands are necessary only to remove the errors due to gyro drift and to the regression of nodes.

e. Celestial observations

The star field may be used in two ways for the orientation of the satellite. First, a particular star might be used as the sun or the earth are used to maintain a fixed orientation with respect to that star. (In the case of complete star orientation perhaps two or more stars may be chosen for such an orientation.) Secondly, the star field of motion as observed in the vehicle can be used to measure the rate of change of the vehicle.

(1) Attitude. Sighting on distant stars may be used with an inertially established frame of reference to achieve initial alignment of the references or to prevent long term drift, if necessary. It is possible to use optical sightings, such as a telescope, or even the radio frequency noise sensed by a radio-telescope. The two severe problems encountered in the use of celestial sensing are the acquisition of the star, and the amount of computation required to transform the star reference set of axes into the appropriate vehicle control error signals. One excellent way in which a star may be used to obtain continuous or intermittent information without complicated computation is in orbits where a pole star is available. A very good application of this method is in an earth equatorial orbit. Actually, any inclined orbit about a spherical body with a pole star would be acceptable, but, because of the regression of the line of nodes due to the earth's obiateness, computation is required for most earth-orbiting vehicles. The tracking of stars with high precision telescopes and very accurate telescopic drives is necessary to obtain exceptional accuracy. Of particular interest is the Orbiting Astronomical Observatory which is under development by NASA, in which absolute sensor accuracies on the order of seconds of arc are required.

(2) Attitude rate. Considerable interest has been expressed in what are often called "celestial driftometers." A telescope or some other optical means is fixed relative to the axes of the satellite and drift velocities of the stars across the field are measured. From this, one can obtain a component of the angular velocity of the star field relative to the vehicle which is then a component of the angular velocity in inertial space. The main purpose for this device is to provide rate measurements for precise control with respect to the orbital rate vector.

f. Other ambient field sensors

It is possible to obtain certain information about the vehicle's orientation in space through the use of ambient fields other than those previously discussed. Fields which can be used appear to be the gravity field, the magnetic field, and, for extremely low altitude orbits, the atmosphere. It has been suggested that if cosmic rays are directional in space, the gradient in its intensity may be used as a sensor.

(1) Gravity gradient. A vehicle will tend to align its axis of minimum inertia along the local vertical to the earth, and its axis of maximum inertia normal to the orbit plane, due to the effect of the gravitational field. This effect acts as a torque which provides control, and also as a sensor of direction of the gravitational potential. In other words, the restoring torque appears in the equations of motion as if it had been introduced by an independent control system operating on

external information. It is also impossible to imagine instruments constructed such that they would operate independently on the gravity field to determine the direction of the local vertical. Such instruments have been mentioned as possibilities, but none have been given serious consideration. The two possible types are the pendulum type, utilizing two pendulums forming a dumbbell free to turn about one axis, and the other involving the use of accelerometers operating differently to provide a direct measure of the gravity gradient.

(2) Magnetic fields. The earth's magnetic field could conveniently be used as an orientation reference for satellites in near-earth orbits. This is reported to have been done in Sputnik III. Moreover, it seems that the magnetometers could be put to good advantage measuring the magnitude of the earth's magnetic field. The primary difficulty is not so much one of the inherent measuring capability of the instrument itself, but of measuring the precise direction of the magnetic field with respect to the vehicle in its orbit because of heterogeneities in the earth's field, ionospheric currents, geomagnetic storms, and fields present in the spacecraft itself. However, if magnetice torques are to be used to advantage, some measure of at least the direction of the magnetic field must be obtained.

(3) Atmosphere. In any low altitude orbit it may be possible to use such devices as are employed in airplanes, missiles, etc., which are most sensitive to the very nearly negligible atmosphere. For example, a weather vane might provide information about the relative winds for one set of axes. Using an extremely sensitive pressure device would allow the nulling of such pressures to achieve appropriate orientation. However, the pressure at the altitudes above 100 mi suggests that, at present, this is an impractical approach.

(4) Other ambient fields. Natural radiation such as cosmic rays, micrometeoroids and ion streams could be exploited for the use of attitude control system sensors. Most of these devices, however, appear to present no advantage over those being used and are not receiving a great deal of consideration. For example, the direction of the spacecraft velocity can be determined by the relative bombardment of charged particles with respect to the body axis. Ion "traps" flown on Explorer VIII have indicated that sufficient current can be obtained to orient the vehicle relative to the velocity vector. The accuracy of a system using ion traps will probably be below that of optical systems, but it may find application when other sensors are inoperative due to occulting of the sensed body.

Another potential method would include the use of radio techniques wherein the difference between the received signals of two antennas would be a measure of the attitude error in a plane containing the two antennas. This differencing could be obtained electrically in the spacecraft or through the use of interference techniques. An additional method might be the use of return signals from a body which is receiving the output of a satellite-contained radar. Such schemes have been proposed for the landing of spacecraft on distant planets, as well as for achieving some measure of stabilization information at low altitudes.

4. Modes of Attitude Control

This section will discuss some primary modes of operation that are generally necessary in order that the spacecraft mission can be performed.

In general, the spacecraft will be separated from its booster with potentially sizable errors with respect to the final orientation requirements in both attitude and attitude rate. An initial mode of operation will be to control the initial rates and provide the proper attitude orientation. The process which describes the acquisition from separation to the final orientation is often called "acquisition" and generally consists of at least three separate modes--initial rate adjustment, search, and final acquisition. The actual switching and sequencing for achieving acquisition will vary between spacecraft systems, depending on the orientation requirements, sensor limitations, methods of obtaining control orientation, etc.

The second major control mode will be the mode of operation required to maintain the proper attitude orientation and stabilization. This mode is often referred to as the "normal" operating mode. Special operating provisions may be required when the normal control system operation is not possible; this occurs, for example, when the sun or star sensors are occulted by the earth, or when the spacecraft axis about which sun sensor information is used lies along the sun lines. Each orientation requirement defines a set of operating requirements, for example, control laws associated with solar array orientation, orbit plane orientation, and the like must be implemented. Other modes of control might include providing proper orientation of the spacecraft during velocity corrections required for orbit control, terminal maneuvering for docking, and deboost preparatory to re-entry.

a. Acquisition

During the separation of the spacecraft from its booster, angular impulses will be imparted to the spacecraft, resulting in initial rates which cannot be ignored. The first step after the control system has been electrically activated will be to control or null these rates with respect to some reference axes. For a spacecraft which uses a solar array, it is often desirable to null the rates in two axes about the earth-sun line by immediately orienting the solar array (held fixed with respect to the spacecraft during acquisition) to the sun. In the case of systems using the manipulation of the forces of space such as gravity gradient, earth's magnetic field, etc., momentum storage and/or mass expulsion devices are generally needed to reduce initial body rates to an acceptable level. Body-fixed rate measuring instruments providing attitude rate signals to momentum transfer devices can be used to reduce these rates before orientation of the body axes is achieved.

Once the body rates are reduced to small magnitudes, a search mode of operation will generally

be required. During this mode the sensors are caused to perform a search for those objects which they will sense to provide attitude error signals. There are many alternative approaches to the search mode. The selection of the approach is often dependent on a tradeoff between the dynamic range of the sensor, orbit conditions for acquisition, operational launch time requirements, etc. Depending on the sensor and the control system, either the entire spacecraft is rotated or it may be desirable to perform the search by articulating the sensor (like a radar dish, star tracker, etc.) with respect to the body.

Acquisition of proper orientation when the control torques are generated by essentially passive means is generally simpler than acquisition with active control systems. In the case of spinning satellites, lateral impulses at separation of satellite and booster will produce a free precession or nutation of the vehicle. An inertially fixed orientation is established by this satellite as soon as the nutation of the vehicle about its momentum vector has been damped. Such damping, as indicated previously, may be provided by a simple device like an annular ring of mercury located about the spin axis. A new inertial orientation of the spinning body is achieved by a controlled precession of the spin axis in a plane containing the initial momentum vector and the final desired orientation of the spin axis.

With the use of gravity gradient, once the initial rates have been stopped and sufficient damping has been added, the system will automatically acquire the earth's local vertical with the principal axis of minimum inertia and have the principal axis of maximum inertia normal to orbit plane. The angular error associated with the acquisition will depend on the relative magnitude of the disturbance and control torques and the misalignment of the control axis with the local vertical. The time required for acquisition depends on the capability of the damping devices and the initial conditions.

In the design of the acquisition mode, any requirements which severely limit the time to "acquire" must be carefully reviewed. Such limitations are significant in the determination of the amount of gas used, size of the pneumatic jets, torque requirements of the reaction wheel, etc. For example, the gas jet control moment may have been determined to provide a certain factor of desaturation to a set of reaction wheels operating in dual mode operation. However, the jet control moment that is determined for desaturation is usually not the best size to meet the rate nulling requirements. If this is true, a compromise solution will be necessary. The sensors used for acquisition may significantly affect the gas consumption. It may be desirable, for example, to add an auxiliary rate gyro and/or provide a sensor with a wider dynamic range. Neither of these requirements is necessary for normal operation. Additional electronics are required to perform the switching and logic functions required in this mode.

Final operational steps of acquisition, consisting of separate and successively more accurate modes of control, each operating over the dynamic range consistent with the devices which are used for control sensing and orientation may be necessary. To obtain extremely precise accuracies, several of these modes of operation, each successively more accurate than the previous one, could be used.

b. Normal control

The orientation requirements of the spacecraft are mission-dependent. Those satellites oriented with a particular axis to be aligned along the earth's local vertical will have simple control in pitch and roll, generally nulling the outputs of earth horizon scanners. The control about the axis aligned along the local vertical (yaw axis) may depend on the orientation requirements with respect to the sun or other bodies. The yaw control may involve: orientation of the roll axis in the orbit plane; orientation of the solar array about the roll axis when the yaw axis points to the earth; special star orientation; or be simply unspecified.

The essential modes of control within the normal control for a nonspin earth-oriented satellite follow.

(1) Pitch/roll control. For purposes of discussion, the yaw axis is to be pointed along the earth's local vertical. Angular deviations from the local vertical can be determined by horizon scanners, processed and used directly for attitude control error signals.

(2) Yaw control. The yaw control problem is significant and depends on the spacecraft control requirements. The three most interesting cases are yaw orientation with respect to the orbit plane, yaw orientation to provide maximum solar energy on rotatable or nonrotatable solar cells, and no yaw requirements.

(a) Orbit plane orientation. Orientation with respect to the orbit plane is often a difficult control problem. The difficulty is primarily one of sensing rather than the need for any unique control laws. Gyrocompassing provided by the orbit rate coupling either through the use of gravity gradient or by mulling to the output of an orbital rate sensor are excellent schemes if there is sufficient orbital rate.

(b) Solar array/yaw orientation. Since the orbit plane can have any inclination with respect to the earth-sun line, it is necessary to provide two degrees of freedom to maintain a flat plate oriented normal to the sun line. In addition to solar array rotation, yaw orientation must be performed for maximum efficiency. If the solar array is not oriented, then yaw control with respect to the sun will in general improve efficiency over control with respect to the orbit plane or no control.

If the coordinate system shown in Fig. 37 is used, the following control laws indicate the yaw motion of the spacecraft (zero yaw angle occurs when the roll axis is in the orbit plane, and zero array angle when the sun is perpendicular to the earth satellite line). From the figure it follows that

$$\vec{u}_r = \vec{i}(\sin\alpha) + \vec{j}(\cos\alpha) \quad (186)$$

$$\vec{u}_s = \vec{j}(\cos\xi) + \vec{k}(\sin\xi) \quad (187)$$

$$\vec{u}_r \times \vec{u}_s = \vec{u}_p \sin\left(\frac{\pi}{2} - \phi_p\right) \quad (188)$$

$$\sin\psi = \vec{u}_p \cdot \vec{k} \quad (189)$$

$$\sin\phi_p = \vec{u}_r \cdot \vec{u}_s \quad (190)$$

combining Eqs (186), (187) and (190), the ideal array angle is given by

$$\sin\phi_p = \cos\alpha \cdot \cos\xi \quad (191)$$

combining Eqs (186), (187), (188) and (189)

$$\sin\psi = \frac{\sin\alpha\cos\xi}{\cos\phi_p} \quad (192)$$

and

$$\cos\psi = \frac{\sin\xi}{\cos\phi_p} \quad (193)$$

combining Eqs (192) and (193), the ideal yaw angle is given by

$$\tan\psi = \frac{\sin\alpha}{\tan\xi} \quad (194)$$

In order to eliminate the need for slip rings, the array angle and hence the yaw angle may be restricted to ±90°. Figure 38 shows variation of array angle and yaw angle, respectively, with satellite location in orbit.

(c) Unspecified yaw orientation. For some missions there may be no specific requirements for orientation about the yaw axis. However, a requirement to maintain low yaw rates may exist due to requirements of on-board equipment or experiments. Even when such is not the case, it will generally be necessary to reduce yaw rates to within limits tolerable to the other axes controls before acquisition is complete.

(3) Eclipse. On systems where the sun information is used to determine yaw attitude error, the mode of operation during eclipse of the sun must be carefully reviewed. Often, yaw control is not required during eclipse. In such instances reacquisition of the sun when the spacecraft emerges from eclipse is necessary. If yaw control is required during occulting, then a special sensor or sensors must be provided in order to obtain appropriate attitude error signals. Yaw orientation might be maintained inertially with a programmed angle with respect to the orbit plane in order to have proper orientation at the time of emerging. A simpler scheme would be to maintain the spacecraft rate about the yaw axis below a known low value. In this case, reacquisition of the sun is still required upon emergence from eclipse, but may not require expenditure of as much impulse as the uncontrolled method.

It is interesting to note that, unless special provisions are incorporated, when the eclipse region is entered, the momentum stored in the yaw inertia wheel will be dumped into the vehicle, creating an uncontrolled rotation. This occurs because the yaw loop is essentially opened, resulting in a zero wheel speed command. It may be desirable in some systems to damp the initial yaw wheel speed during eclipse to avoid the momentum transfer. For a sun-oriented, spin-stabilized spacecraft the problem of eclipse is not serious since the sun is essentially fixed in inertial space during the time of eclipse.

(4) Noon control. An additional control problem arises when the axis for which control information is being obtained is aligned along the line of sight of the sensed object providing that information. A sun-oriented spacecraft requires special control system operating provisions to maintain proper attitude orientation during periods in some orbits where the angle of the control axis with respect to the line of sight is not sufficient to obtain useful attitude angle information. For an earth-oriented satellite with a solar array, this condition occurs when the sun is in the orbit plane ($\xi = 0$) and the satellite yaw axis lies along the earth-sun line. This situation is often referred to as "high noon." If a sun sensor is used, the gain in the yaw axis will go to zero at this point again causing the momentum in the yaw wheel to be dumped into the body. For the control laws shown in Fig. 38, a 180° yaw rotation of the spacecraft is required at this time ($\alpha = 0$). This is often referred to as the "yaw-turn" and can be performed in a variety of ways. If there is a gyro present in the yaw axis, it can be used to provide stabilization during the maneuver. In many cases, the turn can be adequately performed by programming yaw reaction wheel speed in a manner which will cause the vehicle to rotate. In any case, precautions must be taken to minimize expenditure of impulse for eclipse and noon control.

c. Orbit control

Frequently velocity changes are required for orbit control or midcourse correction. The control system must have sufficient control authority to offset the disturbing torques caused by thrust misalignments from the propulsive devices used to correct the velocity. For system design simplicity it is usually desirable to have only one thrust nozzle on the vehicle. The control system is then required to orient the vehicle to allow the nozzle thrust to be applied in the correct direction. This will require a special orientation mode and perhaps a special sensor, depending on the orientation accuracy required. Large propulsive devices will be used for coarse orbit corrections. If precise corrections are required, it is likely that low thrust (probably cold gas) devices will be used to perform vernier indexing and long term station keeping. The required design of the vernier system in terms of the nozzles, gas supply, etc., should be integrated with the pneumatic system used for attitude control.

d. Other modes

The flight sequence must be determined early in the preliminary design. Such a sequence, if properly conceived, will define the operational requirements for the control system and, hence, the

major modes of control. This, coupled with a failure analysis, will be used to completely determine the primary and various alternate or backup modes of operation. A major number of modes of control beyond those described above are possible. Most of these modes are purely mission-dependent and must be considered for each particular mission.

The terminal mode of operation involved in the orbital docking maneuver of two satellites in orbit will be based on the particular design of the terminal sensors and the terminal guidance equipment that is used. A large number of possible modes exist with manned spacecraft wherein the primary motive is to recover the pilot (or crew) and allow him to participate in the navigation and control of the spacecraft. Clearly, modes of control covering such flight phenomenon as abort, re-entry, orbit maneuvering, etc., each using a combination of ground-based, on-board and manual sensing and torquing, may be required to achieve a well-integrated guidance and control design. In addition, special modes of unmanned vehicles such as a picture-taking mode, a mode for obtaining a star fix, etc., are conceivable.

5. Design of Spacecraft Control Systems

An example is provided to show specific design procedures for attitude control systems. From a given vehicle configuration and for a 400-naut mi (740 km) orbit, a reaction wheel/gas jet dual mode system is to be designed. Consider the following problem.

Example

a. Problem statement

Given the following control and spacecraft configuration specifications, design a dual mode reaction wheel/gas jet attitude control system.

	Specifications
Orbit	400-naut mi, (740 km) circular
Lifetime	One year
Orientation requirements	Yaw axis pointed to earth local vertical to ±1°, solar array face perpendicular to sun line within ±5°
No slip rings	
Acquisition	Thirty min after separation from booster, maximum initial body rate 1°/sec in all axes.

Vehicle Configuration

The vehicle configuration will be the same as shown in the sketch of Section D-1, with the following specific properties. Vehicle inertias for two solar array angles

	I_{xx}	I_{yy}	I_{zz}
For $\phi_p = 0°$	100	160	115
For $\phi_p = 90°$	100	150	125
Solar array area	50 ft^2 or (5 x 5 ft each paddle) 4.65 m^2		
Gas jet lever arms	2.5 ft all axes (7.63 m)		
Vehicle dimension	4 x 4 x 5 ft (1.2 x 1.2 x 1.5 m)		

b. Control laws

The requirement for elimination of slip-rings on the solar array means that the laws derived in Section C-4 are applicable. These laws are shown in Fig. 38.

c. Disturbance torques and momentum storage requirements

The calculation of disturbance torques for this example is limited to those due to solar radiation and gravity gradient. Other torques are considered negligible in comparison. In practice, all torques must be estimated.

(1) Solar radiation torque. We will assume a 0.5-ft (0.5 m) offset between the center of gravity, and a 50% reflectivity yielding an effective radiation pressure 1.5 times that for total absorption. The projected areas are 50 sq ft (4.65 m^2) for solar array, 20 sq ft (1.86 m^2) as seen along the pitch or roll axis, and 16 sq ft (1.49 m^2) as seen along the yaw axis.

In the case where the sun lies in the plane of the orbit the torques will be cyclic except for rectification which occurs because of eclipse and yaw control law (see Fig. 39a). In the case where the sun is perpendicular to the plane of the orbit where no eclipses occur, the torque will be periodic in inertial space. Then, the net momentum change per cycle will be zero. The component of momentum in inertial space is shown for sun inclination of 0° in Fig. 39b.

(2) Gravity gradient torques. The torques due to the gravity potential have been treated in Section D-2. By applying the vehicle parameters to the equations for determining gravity gradient torques, the total momentum change per orbit can be determined and is plotted in Fig. 40. Since the rotation of the solar array changes the spacecraft inertia, the momentum change is a function of the inclination of the sun with respect to the orbit plane. The stored momentum is plotted for three sun inclinations. As expected, the spacecraft is unstable with respect to gravity torques since the z-axis is not the axis of principal inertia.

(3) Total momentum requirement. The cyclical value of momentum shown in Figs. 39a and 39b will be used to provide information for the sizing of the inertia wheel. A conservative value of cyclical momentum would be 0.02 ft-lb/sec (0.27 $\frac{\text{m-newtons}}{\text{sec}}$) gravity gradient (height in Fig. 40) and

0.006 ft-lb/sec (0.008 $\frac{\text{m-newtons}}{\text{sec}}$) for solar radiation (height in Fig. 39). These are crude estimates for the preliminary design, but fortunately, as will be seen, turn out to be of secondary importance to the total storage requirements.

Over each orbit the momentum added to the system will be that which is not cyclical. Gravity gradient for $\xi = 45°$ will add about 0.052 ft-lb/sec (0.071 m-n/s) and solar radiation for $\xi = 0$ will add 0.008 ft-lb/(0.011 m-n/s) sec per orbit. The inclination of $\xi = 0$ is the worst case for solar radiation since the maximum eclipse time occurs at this inclination. The gravity gradient dictates the most stringent requirement. Integrating 0.06 ft-lb/sec (0.08 m-n/s) over the 5250 orbits in one year, an impulse of approximately 125 lb-sec (557 n-s) is obtained.

(4) Design of a torque-producing system. The torque-producing system must provide sufficient impulse to overcome the secular effects of disturbance torques and must be designed to provide the minimum system weight while not appreciably reducing system reliability. Only two of these several approaches will be compared. These are the simple on-off (or contractor) mass expulsion control system using gas jets, and the dual mode system utilizing thrust devices (gas jets) and momentum storage (motor driven inertial flywheels).

The simple on-off or contractor control system will be acceptable if the resultant body rates are not too high and if the gas consumption over the required lifetime does not appreciably exceed the equivalent weight required for the momentum storage system. A block diagram of such a system is shown in Fig. 41; the system produces a limit cycle in attitude error with error rates as shown in the phase portrait of Fig. 42.

The design of these systems is well-known. The choice of acceleration (torque-to-inertia ratio) depends on the initial acquisition conditions and the characteristics of the sensor. A total thrust per axis of 0.02 lb (0.09 n) adequately satisfies the acquisition requirement. A jet lever arm of 2.5 ft (0.61 m) an attitude error dead zone of 0.5°, hysteresis of 1%, rate-to-position gain of 10, and negligible time delay were chosen for sample calculation. The resulting limit cycle period was 800 sec with a limit cycle rate of approximately 0.0025°/sec. For three channels of operation the total impulse requirements for one year will be approximately 3000 lb-sec (13,400 n-s), or for a cold gas pneumatic system like nitrogen or argon, approximately 120 lb (535 n) are required for the gas and tankage weight. This weight represents a large fraction of the total satellite weight and should be reduced, if possible. For low body rates such as this system produces, the most significant term is hysteresis. Since this example uses 1% hysteresis, considered a present state-of-the-art limit, and ignores time delay, which is also significant, a practical design would probably result in increased gas consumption for the on-off system.

(5) Design of dual mode system. The block diagram shown in Fig. (43) is that of a dual mode system and represents the addition to the gas jet system of motor-driven flywheels, which provides the capability of storing the cyclical momentum. Since the gas jets are not used to force the system into a hard limit cycle, the only gas required is that to remove stored momentum due to secular torques and that necessary for initial sun-earth acquisition and special modes requiring the use of gas jets. Figure 44 shows the typical error angle-angular rate plot for the system under the effect of a constant disturbance torque.

(a) Momentum storage system. The first job to be treated in the design of the system will be to size the inertia wheels and determine the torque requirements on the drive motor. The requirements for pitch and roll reaction wheels are determined separately from those for the yaw wheel.

Pitch/roll wheel sizing. The pitch and roll wheels will be required to store the momentum due to torques which are cyclical in inertial space and to store the momentum which must be transferred from another axis to that body axis as the vehicle rotates in inertial space. In the disturbance torque calculations a peak cyclical momentum storage requirement of 0.026 ft-lb/sec (0.035 m-n/s) was determined, including the effects of both gravity gradient and solar radiation. In general, the wheels must also be capable of storing the body momentum required for the spacecraft orbital rate which is 1.05×10^{-3} rad/sec of 0.17 ft-lb/sec (0.23 m-n/s) if it occurs in the pitch axis or 0.105 ft-lb/sec (0.143 m-n/s) in the roll axis. Combining this with the disturbance torque requirements, momentum storage of 0.250 ft-lb/sec (0.341 m-n/s) will be chosen. If we choose the maximum allowable speed of the motor to be 500 rad/sec, the flywheel inertia then must be 0.5×10^{-3} slug-ft^2 (0.68×10^{-3} kg-m^2). Since the orbital momentum in any one axis can be transferred to any other axis, during orbital maneuvers, a wheel of this size will be used in both the pitch and roll axes. This represents a solid steel wheel approximately 4 in. (10.2 cm) in diameter, 1/2-in. (1.2 cm) thick and weighing approximately 2 lb (8.9 n).

It is well to review the pitch and roll momentum storage capability from the standpoint of acquisition. Generally wheels will not have sufficient momentum storage capability to continue the initial rates. During acquisition the body rates must be reduced to a sufficiently low magnitude so that the wheel is able to store the residual momentum in the body. In many cases this will correspond to the contractor servo limit cycle rates. For the acquisition system design, which is discussed later, a torque-to-inertia ratio of approximately 3.5×10^{-4} rad/sec^2 will be determined to meet the acquisition system requirements. If an equivalent hysteresis of 5% is used for the design, a limit cycle rate of approximately 0.05°/sec will exist. This rate dictates wheel momentum storage capability of at least 0.05 ft-lb/sec (0.08 n-m/s), well within our previously determined wheel storage capability. Further, it might be required that under normal operation the momentum storage capability be such as to maximize the time between gas jet firings. Note from Fig. 44 that, after gas is fired, it appears that the most desirable attitude would be at zero error signal or that represented by complete wheel desaturation (a). If the wheel mementum is not completely removed or if too much is added by the gas system, the final attitude

will occur at (b) or (c), respectively. With a torque-to-inertia ratio of 3.5×10^{-4} rad/sec^2, a rate-to-position gain of 11.25 and a hysteresis of 5%, a gas jet firing will remove approximately 30% of the wheel's saturation momentum.

If the jet firing is required to completely desaturate the wheel, a spacecraft angular rate at the time the jet is turned off, approximately 0.0015 rad/sec is necessary. For a system with the same gain ratio and hysteresis, a torque-to-inertia ratio of 3.8×10^{-3} rad/sec is required to completely desaturate the wheel. The presently chosen 3.5×10^{-4} rad/sec^2 will remove only 30% of the stored momentum.

Yaw wheel size and motor torque. The yaw wheel must not only be able to store the same momentum as the pitch and roll wheel but it must help to perform the yaw turn required at high noon. If it is assumed that the yaw turn is to be performed within 15° of high noon (solar array angle equal to 75°) and if it is assumed that the turn is to be performed strictly on wheels (i.e., no gas is to be fired), it is possible to determine the yaw wheel and motor torque requirements. The time for the satellite to move 15° in its orbit is 250 sec. Then for a maximum effort turn (constant torque) as shown in the following sketch, the motor torque required is 1.25 in.-oz (0.0089 m-z). At the maximum spacecraft rate, the momentum which must be stored is approximately 1.56 ft-lb/sec (2.13 n-m/s). Since in a practical motor it is not possible to attain full torque as the speed increases, a 2-in.-oz (0.014 m-n) motor is chosen. The momentum to be stored is 1.56 ft-lb/sec (2.13 m-n/s) for the turn, plus the 0.25 ft-lb/sec (0.34 m-n/s) (storage requirement capability necessary for momentum transfer from pitch and/or roll wheels). The yaw wheel inertia will be 3.2×10^{-3} slug-ft^2 (4.3×10^{-3} kg-m^2) for the 500 rad/sec top motor speed. About a 6-in. diameter by 1-in. (2.5 cm) thick solid steel wheel weighing approximately 7 lb (31 n) is necessary.

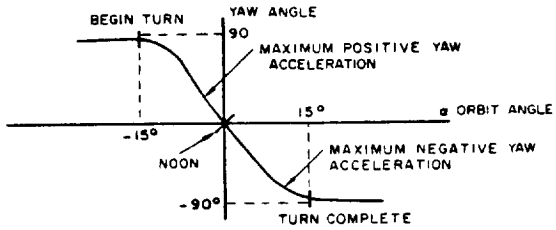

Yaw Angle During Noon Turn

Pitch and roll motor torque requirements. The torque requirement for the pitch and roll motors may be based either on the "high noon" turn requirement or on the cancellation of spacecraft momentum before the phase plane trajectory reaches the opposite switching line (trajectory d in Fig. 44 is such an example) thus causing unnecessary gas to be fired. Each time a jet fires, about 0.5 in.-oz (0.0036 m-n) of torque is required to provide a trajectory to keep the other gas jet from firing. For this example, it has been assumed that the yaw turn maneuver must occur within ± 15° of the noon condition. This means that the pitch and roll wheels must be capable of transferring the maximum momentum stored by each to the other in 250 sec. For the maximum effort turn as shown in the previous sketch, the torque required to accomplish the transfer of the maximum momentum (0.250 ft-lb/sec) (0.34 m-n/s) is 0.71 in.-oz (0.0051/m-n) in pitch and 0.82 in.-oz (0.0058 m-n) in roll. Commercially available 1 in.-oz (0.00711 m-n) motors are chosen for the pitch and roll motors.

(b) Mass expulsion system. The mass expulsion system is designed on the basis of three requirements: first, the torque level is determined in concert with the sun sensor linear range and to obtain acquisition within the required time with minimum gas consumption; second, the total impulse requirements are equal to the sum of separate impulses required for acquisition, removal of secular disturbance torques, reacquisition, redundancy and contingency and; third, the design parameters are determined on the basis of practical values of equivalent hysteresis, dead zone, valve dynamics, etc. For a 1° limitation in local vertical, if the maximum orientation pitch occurs at the same instant that the roll error is maximum, then the errors in individual axes must be no greater than the 0.707° to meet the 1° requirement. The maximum dead zone in pitch and roll axes, for this example, will be designed to approximately 0.5° to allow for sensor errors, noise and misalignment.

As will be shown in the acquisition design, the thrust level per axis (usually two nozzles) will be about 0.02 lb (0.08 n). An impulse of 210 lb-sec (938 n-s) for 1 yr of operation will be required from the following sources.

	(Lb-Sec)	(n-s)
Disturbance torques for 1 yr	120	536
Initial acquisition	36	161
Three reacquisitions	3*	13.4
20% contingency	32	143
Required because of pressure regulator limitations 10%	19	85
	210	938.4

*Assuming that the maximum momentum of all the wheels is dumped into the body, the reacquisition requirement is still less than 1 lb-sec (1.4 n-s).

The pneumatic gas system including the tankage will weigh approximately 9 lb (40 n), assuming nitrogen with about 60 lb-sec of impulse (80 n-s) per pound (4.4 n) of weight, plus a nominal 140% allotment for tankage factor. The comparison of the two systems in weight for a year's operation finds the on-off system weighing a minimum of 120 lb (536 n) compared to the dual mode system weighing approximately 39 lb (173 n) including 20 lb (89 n) for the reaction wheels, motors, and circuitry plus 9 lb (40 n) for pneumatic system, plus the additional power supply required to drive the motors (estimated to be less than 10 lb).

(c) Acquisition sequence. For power supply requirements and temperature control it is necessary to cause either the yaw or pitch axes to lie along the sun line within 30 min of the time of separation from the booster vehicle. The spacecraft initial rates and initial attitude orientation will be assumed the most adverse, namely: 1°/sec and 180° from desired orientation.

When separated from the booster, the spacecraft is misoriented and possesses booster separation-imparted body rates. The process of achieving normal control requires that the rates be nulled and that the sun and earth be acquired while the vehicle is in the sunlight. Of the several possible sequences the one chosen is as follows.

The rate null mode. During this mode the solar array is fixed at +90° and the yaw axis of the spacecraft is pointed at the sun, and rates about this axis are nulled. Information is provided by sun sensors and a yaw rate gyro. The array sun sensor provides roll signals and the yaw sun sensor provides pitch signals. By pointing the body at the sun initially, the power supply is immediately oriented for maximum charging and the orientation is proper for temperature control. In addition, the need for rate gyros in the pitch and roll axes is eliminated.

The orientation mode. During this mode the spacecraft is slowly rotated about the yaw axis to obtain horizon scanner returns from the earth. The solar array meanwhile maintains itself normal to the sun line. This method requires simple logic, little gas consumption, and ensures earth acquisition regardless of the position in orbit provided that the spacecraft is not in eclipse and that the scan angle coverage of the horizon scanner is sufficient.

The vehicle is now in its normal operating mode, the horizon scanners and sun sensors provide the information in pitch/roll and yaw to stabilize the spacecraft in the presence of disturbance torques, and the solar array is oriented so that the solar cells are facing the sun. If earth reference is lost, the vehicle will automatically return to the orientation of the rate null mode and reacquire the earth by repeating the above sequence. The block diagram of the acquisition mode is shown in Fig. 45.

(d) Design for acquisition. The following design is based on single axis computations which are considered adequate for preliminary design. All details of switching and choice of parameters must ultimately be determined by a three-axis study. The filter in the gas jet system is to be designed for rapid convergence from high rates to low limit cycle rates. The larger the rate gain, for a single axis at least, the lower the time and the less the gas that will be required to converge. For passive networks, practical upper limit for K_R is approximately 15. A filter F(s) is assumed where

$$F(s) = \frac{12.5\,s + 1}{1.25\,s + 1} \tag{195}$$

The equivalent rate-to-position gain for the switching line is assumed to be 11.25.* Clearly one of the principal design parameters to be chosen will be angular acceleration (torque-to-inertia ratio). A decrease in torque will increase the gas consumption and the time required for sun acquisition. An increase in thrust will suggest an increase in sun sensor linear range in order to keep the gas consumption down.

Assume that the thrust is essentially the same for all axes and that yaw rates and error signal coupling between pitch and roll can be neglected. A conservative estimate of the total time for acquisition can be obtained by assuming consecutive pitch and roll system operation. The phase plane of Fig. 46 shows the operation in one axis, assuming the worst initial conditions. Figure 47 shows the maximum angular rate that the spacecraft will encounter versus torque-to-inertia ratio, assuming the initial condition of 1°/sec and 180° attitude error. This curve is for the switching lines for the filter that is used. With a dead zone of about 1° about the yaw axes the rate at switching, if the sun sensor linear range is ± 30°, will be 2.6°/sec and a torque-to-inertia ratio of 3.5×10^{-4} rad/sec^2 will be required. It is next necessary to compute the time to acquire and the gas consumption. These can be determined approximately from the phase plot or from the rate diagram. An approximate closed form solution for the convergence in a single axis has been developed and is given by

$$t_{acq} = \frac{(\pi/180)^2\,\omega_0^2}{2K_R F^2 r^2}\left[I_{xx}^2 + I_{yy}^2{}_{(\phi_\rho = -90°)}\right] \tag{196}$$

where

ω_0 = initial crossover rate in degrees per second which is approximately 2.6°/sec

F = thrust per axis

R = thrust level arm

and since torque-to-inertia, λ, is given by

$$\lambda = \frac{Fr}{I} \tag{197}$$

$$t_{acq} = \frac{1.53 \times 10^{-4}}{11.25}\left(\frac{2.6}{3.5 \times 10^{-4}}\right)^2 \times 2 = 1720 \text{ sec} \tag{198}$$

which is slightly less than the specified 30 min. Here the torque-to-inertia ratio is assumed the

*In practice, the effect of acceleration and higher terms in the expansion $F(s) = 1 + 11.25\,s - 14.2\,s^2 + \ldots$ must be considered. These terms may alter the limit cycle switching line, and hence gas consumption, significantly.

same in both axes. Figure 48 shows a few cycles of the settling transient for a similar system.

Because of the differences in inertia, and if $\lambda = 3.5 \times 10^{-4}$, the total thrust should be 0.014 lb (0.062 n) in the roll axis and 0.22 lb (0.98 n) in the pitch axis. We will use a thrust of 0.02 lb (0.089 n) per axis or nozzles acting in pairs with a thrust of 0.01 lb (0.044 n). (Some of the foregoing calculations could now be refined using the correct λ's rather than the same λ for both axes.) A crude estimate of gas consumption for acquisition would be (assuming the jets are on at all times)

$$\text{Pitch and roll} \quad (1720)(0.02) \approx 35 \text{ lb-sec} \approx 156 \text{ n-s}$$

$$\text{Yaw} = \frac{I}{r}\omega \quad \frac{115}{2.5}(1/57.3) \approx 1 \text{ lb-sec} \approx 4.4 \text{ n-s}$$

$$\text{Total} = 36 \text{ lb-sec} = 160 \text{ n-s} \quad (199)$$

If, instead of ± 30°, a linear range of ± 15° is chosen for the sun sensor, the necessary λ to keep the solution in the linear range of the sensor would decrease by a factor of about 7 and the acquisition time would be increased by a factor of about 10. The resultant gas consumption would be up by only 40%. For the λ of 3.8×10^{-3}, which provides for perfect wheel desaturation (see Fig. 44), the sensor linear range should be at least 65°.

(6) Sensor design

(a) Sun sensor. The sun sensors located on the array for array error angles and on the body (or array) for yaw error angles will have a linear range of ± 30. The operation around the null and the absolute linearity are not critical since accuracy to no better than ± 2° is all that is required for the 5° pointing requirement, indicating that simple shadowing techniques can be used. Although the calculations of acquisition are based on a ± 1° dead zone for yaw, they are crude and will not be seriously altered with the 2° dead zone.

(b) Horizon scanner. The scan angle, λ, (see sketch) for this system must be determined. Two requirements aid in the selection of this angle.

In order to ensure acquisition, the edge of the scan pattern must scan the earth for any spacecraft position. At 400 naut mi (740 km) the earth subtends approximately 135° at the satellite, indicating that a half angle cone of at least 24° is required to ensure acquisition. This, however, since it is at the very edge of the earth, will provide a very noisy signal.

From the linearity consideration of a change in pulse width per change in angle, a scan angle which normally crosses at 45° of the portion of the earth that is seen by the satellite is reasonable (see the following sketch).

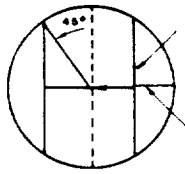

Scan chord

Equivalent earth's radius seen at 400 nautical miles (740 km) is approximately 1520 nautical miles (2815 km)

The scan angle for this configuration then should be approximately 50°. The uncertainty due to ionospheric noise considered to be about 7 mi (13 km) indicates that a scanner error of about 0.27° in roll and pitch is possible. Other errors due typically to optical irregularities, mounting misalignment, thermistor balometer characteristics, etc., must also be considered. The proper scan rate would be determined on the basis of the tradeoff between inherent scanner signal-to-noise ratio and system bandwidth. This is not a significant problem for a 400-naut mi (740 km) orbit. Typical system bandwidth in excess of 3 cps is easily attained with a nominal scanner rate of 30 rps.

(7) System description. The system block diagram is shown in Fig. 49. The reaction wheel size has been selected and the torque requirements of the motor obtained, the gas jet has been determined and the impulse requirements per year established. The sun sensor and horizon scanner requirements have been briefly examined. To complete the study, a reliability analysis is necessary but has been excluded for this example. The acquisition noon-turn logic and solar array drive must, of course, be included. No special eclipse requirements are assumed. Reacquisition of sun must be studied and if only a small amount

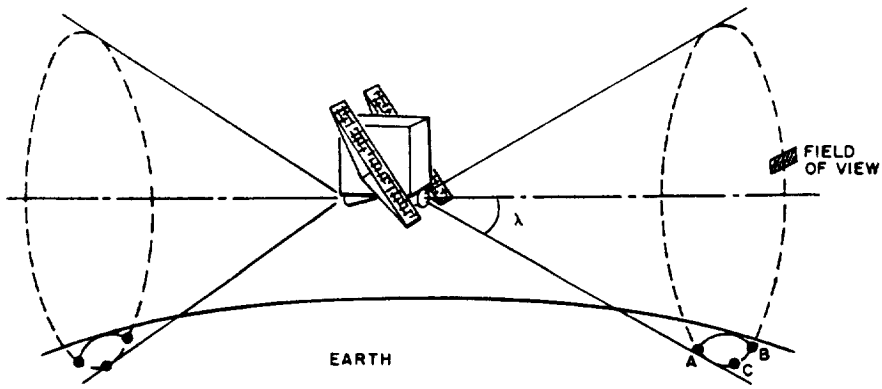

of gas is required, it can probably be performed upon emergence from each eclipse. A simplified block diagram of the normal mode is shown in Fig. 49.

E. REFERENCES

1. Leach, R. and Townsend, G., "Guidance and Control Requirements," (Chapter XII of "Orbital Flight Manual") McGraw-Hill Book Company, Inc., 1962.

2. Wolverton, R. W. (editor), "Flight Performance Handbook for Orbital Operations," Space Technology Laboratories, Inc., September 1961.

3. Sparrow, W., and Bursey, C., "Vacuum Ballistic Trajectory Range Errors," Martin-Marietta Internal Report.

4. Air Force Technical Document USAFA/1-582.

5. Russell, W. T., "Inertial Guidance for Ballistic Vehicles," "Space Technology," edited by Seifert, H. S., John Wiley and Sons, New York, 1959.

6. Moore, R. A. and Meronek, D. F., "Generalized Inertial Guidance System Error Equations," Proceedings of the Third National Conference on Military Electronics, Washington, D. C., 29 June 1959.

7. Lunar Flight Handbook, Martin Company, ER 12685, Apr 1963.

8. Button, P. A., et al., "V/H Satellite Attitude Control," Radiation, Inc., Research Division.

F. BIBLIOGRAPHY

Battin, R. H., "A Statistical Optimizing Navigation Procedure for Space Flight," ARS Journal, Vol. 32, No. 11, November 1962, p 1681.

Bedford, L. H., "Guidance and Control," Journal of the Royal Aeronautical Society, May 1958, Vol. 62, pp 348 to 354.

Bellman, R., Dreyfus, S. and Kalaba, R., "Applications of Dynamic Programming to Space Guidance, Satellites and Trajectories," The Rand Corporation, Santa Monica, California, August 1959.

Blazek, H. F., "Performance of Inertial Components on an Unstabilized Base," American Rocket Society, May 1959, Preprint No. 775-59.

Buglia, James J., Young, George R., Timmons, Jesse D. and Brinkworth, Helen S., "Analytical Method of Approximating the Motion of a Spinning Vehicle with Variable Mass and Inertia Properties Acted Upon by Several Disturbing Parameters," National Aeronautics and Space Administration, Report R-110, 1961.

Button, P. A., "Study of Satellite Guidance Sensors, Compendium of Technical Analysis," Radiation, Inc., Orlando, Florida, Final Report No. IR-1761-VI, 30 January 1961.

Cannon, R. H. Jr., "Some Basic Response Relations for Reaction-Wheel Attitude Control of Space Vehicles."

Cashmore, D. J. and Gordon, G. N., "Manned Navigation and Guidance in the Solar System," Journal of the British Interplanetary Society, March to April 1959, Vol. 17, No. 2.

Collins, O. C., "Determination of the Velocity Vector of a Space Vehicle from Apparent Changes in the Angular Separation of Stars," American Astronautical Society, Tenth Meeting, December 1960.

Crowley, J. C., Kolodkin, S. S. and Schneider, A. M., "Some Properties of the Gravitational Field and Their Possible Application to Space Navigation," Proceedings on the East Coast Conference on Aeronautical and Navigational Electronics, IRE, 1958.

Doolittle, J. H. and Pearson, J. R., "Study of Satellite Vehicle Orbital Guidance," Radiation, Inc., Orlando, Florida, Report No. RR 1188-59-01, February 1959.

Dow, P. C., Jr., "Re-entry Guidance at Escape Velocity," American Rocket Society, Preprint No. 2296-61, October 1961.

Draper, C. S., "Performance Requirements of Guidance Systems for Ballistic Missiles, Satellites and Space Vehicles," Cambridge, Massachusetts, Massachusetts Institute of Technology, MIT Instrumentation Laboratory, Report No. R-172, March 1958.

Drake, D. E. and Keown, E. R., "Programming of Digital Computers for Determination of Stability and Control Characteristics," WADC TR 59-290, July 1959.

Duncan, D. B., "Inertial Guidance and Space Navigation," Journal of the Institute of Navigation, Vol. 6, No. 1, p 30; "Analysis of an Inertial Guidance System," Jet Propulsion, Vol. 28, No. 2, pp 111 to 116, February 1958.

Dworetzky, L. H. and Edwards, A., "Principles of Doppler Inertial Guidance," ARS Journal, December 1959, Vol. 29, No. 12.

Ehricke, K. A., "Error Analysis of Keplerian Flights Involving a Single Central Force Field and Transfer Between Two Central Force Fields," Navigation Spring 1958, pp 5 to 23.

Fried, W. R., "Doppler Radars for Guidance, Design Techniques and Performance," ARS Journal, December 1959, Vol. 29, No. 12.

Frye, W. E., "Fundamentals of Inertial Guidance and Navigation," American Astronautical Society, Fourth Annual Meeting, January 1958.

Garber, T., "Ascent Guidance for Satellite Rendezvous," Aerospace Engineering, Vol. 19, May 1960.

Goetze, D., "Accuracy and Range of Infrared Horizon Sensors as Limited by Detector Noise," ARS Journal, Vol. 32, No. 7, July 1962, p 1039.

Gretz, R. W., "Error Sensitivities in Satellite Ascent and Orbital Transfer," ARS Journal, Vol. 32, No. 12, December 1962, p 1860.

Grube, R. H., "Optical Tracking for Terminal Guidance," Automatic Control, August 1960, Vol. 13, No. 2, pp 20 to 22.

Gurley, J. G., "On the Propagation of Errors in a Schuler-Type Inertial Navigation System," American Rocket Society, May 1960, Preprint No. 1173-60.

Harry, D. P. and Friedlander, A. L., "Exploratory Statistical Analysis of Planet Approach Phase Guidance Schemes," NASA TN D-268, March 1960.

Haeussermann, W., "Considerations About a Guidance and Control System for a 24-Hour Communication Satellite Launched with the Saturn Vehicle," American Rocket Society, December 1960, Preprint No. 1479-60.

Hayes, J. E. and Vander Velde, W. E., "Satellite Landing Control System Using Drag Modulation," ARS Journal, Vol. 32, No. 5, May 1962, p 722.

Hutchinson, R. C., "Geometrical and Astronomical Aspects of Employing a Star Tracker to Correct the Attitude of a Stable Platform," Massachusetts Institute of Technology, Instrumentation Laboratory, February 1961.

Ives, N. E., "Principles of Attitude Control of Artificial Satellites," Farnborough, Great Britain, Royal Aircraft Establishment, 1959, Report No. TN GW 534.

Jarmolow, K., "Dynamics of Spinning Rocket with Varying Inertial and Applied Moment," Journal of Applied Physics, March 1957, Vol. 28, No. 3, pp 208 to 213.

Juelich, O. C., "Passive Aerodynamic Attitude Stabilization of Near Earth Satellites," Vol. 3, Mathematical Techniques and Computer Program, North American Aviation, Inc., WADD TR 61-133, Aeronautical Systems Division, Flight Dynamics Laboratory, Columbus, Ohio, July 1961.

Karrenberg, H. K. and Roberson, R. E., "Guidance and Control of 24-Hour Communication Satellites," Stockholm, XIth International Astronautical Congress, 1960.
"Celestial Rate Sensing," ARS Journal, Vol. 31, No. 3, March 1961, pp 440 and 441.

Keeler, R. J., et al., "Injection Guidance," Astronautics, Vol. 6, No. 11, November 1961.

Ketchum, H. B.
"Navigational Calculations in Space Flight; Part I--Planetary Orbital Distances," Journal of Space Flight, April 1953, Vol. 5.
"Navigational Calculations in Space Flight; Part II--Planetary Orbital Velocities and Gravitational Fields," Journal of Space Flight, September 1953, Vol. 5.
"Navigational Calculations in Space Flight; Part III--Satellite Gravitational Field, Orbital Velocities and Elements of Orbits," Journal of Space Flight, December 1953, Vol. 5.

"Navigational Calculations in Space Flight; Part IV--The Effects of Atmospheric Friction," Journal of Space Flight, June 1954, Vol. 6.

Kooy, J. M. J., "On the Orbital Computations and the Guidance Problem of a Deep Space Rocket," Amsterdam, Ninth International Astronautical Congress, 1958.

Laning, J. H., Jr and Battin, R. H., "Theoretical Principle for a Class of Inertial Guidance Computers for Ballistic Missiles (U)," Massachusetts Institute of Technology, Instrumentation Laboratory, Cambridge, Massachusetts, Report No. R-125, June 21 and 22, 1956.

Lapaz, L., "On the Magnetic Damping of Rotation of Artificial Satellites of the Earth," Journal of Geophysical Research, Vol. 65, No. 7, July 1960, pp 2201 and 2202.

Larmore, L., "Celestial Observations for Space Navigation," Aerospace Engineering, January 1959, pp 37 to 42.

Lee, D. E., "Trajectory Control Development," Los Angeles, Fourth Symposium on Ballistic Missiles and Space Technology, August 1959.

Legalley, D. P., "Guidance, Navigation, Tracking and Space Physics," Ballistic Missile and Space Technology, New York, Academic Press, 1960, Vol. 3.

Longchamp, W. F., "Guidance Equipment Survey," Los Angeles, Convair Astronautics, Report No. AZP-095, April 1959.

Lorell, J., "Velocity Increments Required to Reduce Target Miss on Coasting Trajectories," Advances in the Astronautical Sciences, Vol. 6, The Macmillan Company, New York, 1960.

MacDonald, R. B. and Johnson, G. W., "Inertial Guidance for Hypersonic and Orbital Vehicles," Institute of Aeronautical Sciences, January 1957, Paper No. 59-33.

Mathews, K. C., "Orientation Errors in Command Guidance Systems," ARS Journal, January 1960, Vol. 30.

Miner, W. E. and Schmieder, D. H., "The Path-Adaptive Mode for Guiding Space Flight Vehicles," American Rocket Society, George Marshall Space Flight Center, for presentation at the ARS Guidance, Control and Navigation Conference, August 7 to 9, 1961, Stanford University.

Mueller, R. R., "Investigation of Possible Satellite Position-Sensing Methods," American Rocket Society, November 1959, Reprint No. 913-59.

Myers, G., "Guidance of Tiros 1," ARS Journal, Vol. 31, No. 5, 1961.

Newman, T. V., "Inertial Navigation and Space Flight," American Astronautical Society, New York, 4th Annual Meeting, January 1958.

Novak, D., "Inertial Guidance for Ascent and Injection into a Precise Orbit on a Predetermined Schedule," the Martin Company, Baltimore, Maryland, Engineering Report No. ER 11518, October 6, 1960.

Nyland, F., "Digital Computers for Control in Missiles and Space Vehicles," the Martin Company, Denver, Colorado, Report No. R-60-19, August 1960.

O'Mara, H. R. and Gabler, R. T., "The Propagation of Errors in Keplerian Orbits," The Rand Corporation, Santa Monica, California, Report No. P-1481, August 1958.

Palmer, R. R., et al., "Multiple Inertial System Operation in Long-Term Navigation," North American Aviation, Inc., for presentation at the ARS Guidance, Control and Navigation Conference, Stanford University, August 7 to 9, 1961.

Perret, E. E. and Corbin, J. L., "Effects of Small Changes in Position and Velocity at Burnout on the Orbit of a Ballistic Missile," WADC TN 59-336, October 1959.

Pearson, J. R., "Technique Development of Orbital Guidance Equipment for Satellite Vehicles," Radiation, Inc., Orlando, Florida, Technical Note No. 1188-59-01, 17 April 1959.

Pfeiffer, C. G.
"Simple Guidance of Deep Space Booster Vehicles," Astronautics, Vol. 6, No. 11, November 1961.
"Rudimentary Launch Guidance Methods for Space Missions," American Rocket Society, Preprint No. 1172-60, 1960.

Reis, R. J., "Passive Detection of Lunar Features for Terminal Guidance," ITT Laboratories, Fort Wayne, Indiana, April 1959.

Reiss, M. H., "Systems Approach to Space Vehicle Guidance," WADC Report, September 1958.

Roberson, R. E.
"General Guidance and Control Concepts for Satellites and Space Vehicles," Amsterdam, 9th Congress of the International Astronautical Federation, August 1958.
"On Guidance and Control Requirements in Astronautics," Journal of the Franklin Institute, Vol. 269, pp 196 to 220, March 1960.
"Astronavigation Guidance and Control in Space," Journal of the Astronautical Sciences, Vol. 7, No. 4, pp 87 to 95, Winter 1960.

Rosen, B. M., "Lunar Mission Guidance Requirements," Sperry Engineering Review, Vol. 12, June 1959.

Rosenstock, H. B., "The Effect of the Earth's Magnetic Field on the Spin of the Satellite," Astronautica Acta, Vol. 3, pp 215 to 221, 1957.

Russell, W. T., "Inertial Guidance for Rocket-Propelled Missiles," Jet Propulsion, Vol. 28, pp 17 to 24, January 1958.

Satyendra, K. N. and Bradford, R. E., "Self-Contained Navigational System for Determination of Orbital Elements of a Satellite," ARS Journal, Vol. 31, No. 7, pp 949 to 956, July 1961.

Savet, P. H., "Attitude Control of Orbiting Satellites at High Eccentricity," ARS Journal, Vol. 32, No. 10, p 1577, October 1962.

Savet, P. H. and Carroll, J., "Space Navigation and Exploration by Gravity Gradient Detection," Institute of Aeronautical Sciences, Los Angeles, National Summer Meeting, June 1959.

Schlitt, H., "Advanced Instrumentation Concepts in the Field of Inertial Navigation," Institute of Aeronautical Sciences, St. Louis, Midwestern Meeting on Guided Missiles, May 1958.

Schmaedeke, W. and Swanlund, G., "Optimalizing Techniques for Injection Guidance, Minneapolis-Honeywell Regulator Company, presented at ARS Guidance, Control and Navigation Conference, Stanford University, August 7 to 9, 1961.

Scull, J. R., "Space Guidance," American Rocket Society, Preprint No. 2113-61, October 1961.

Seward, H. H., "Sunfinder for an Interplanetary Vehicle (U)," Massachusetts Institute of Technology, Instrumentation Laboratory, Cambridge, Massachusetts, December 1960.

Shepler, H. C., "Visual Tracking of Space Vehicles," American Astronautical Society, Preprint No. 60-51, 1960.

Shklovskii, I. S., "Optical Methods for Tracking Earth Satellites," Planetary and Space Sciences, Vol. 5, No. 3, pp 233 to 237, July 1961.

Sirri, N., "Space-Vehicle Attitude Control," California Institute of Technology, Jet Propulsion Laboratory, Pasadena, California, JPL Report No. TR 34-121, 1960.

Stubbs, H. E., "Investigation of Physical Phenomena for Space Navigation (U)," Geophysics Corporation of America, Bedford, Massachusetts, Report No. ASD TR 61-286, August 1961.

Swanlund, G. and Ito, W., "Analysis Techniques to Determine the Guidance Computer Requirements for Space Vehicles," American Rocket Society, Preprint No. 2292-61, October 1961.

Thompson, J. W., "Lunar Parralax Method of Astro Navigation," The Rand Corporation, Santa Monica, California, Report No. P-181, December 1950.

Townsend, G. and Leach, R., "Guidance and Control Requirements," Design Guide to Orbital Flight, McGraw-Hill Book Company, New York, Chapter 12, 1962.

Townsend, G., Kork, J. and Kraft, D. "Guidance Requirements for a 24-hr Satellite," the Martin Company, Baltimore, Maryland, Engineering Report No. ER 10718-6, October 1959.
"Orbital Guidance Systems Study," The Martin Company, Baltimore, Maryland, Engineering Report No. ER 11439-3, November 1960.

Tripp, C. N. and Boardman, W. P, "Attitude Control Rocket Requirements for Space Vehicles," Marquardt Corporation, presented at the National IAS-ARS Joint Meeting, Los Angeles, Calif., June 13 to 16, 1961.

Vertregt, M., "Orientation in Space," Journal of the British Interplanetary Society, Vol. 15, No. 6, pp 324 to 338, November and December 1956.

Wheelon, A. D., "Midcourse and Terminal Guidance," University of California, Engineering Extension, Berkeley, California, April 1958, Eng X461-AEC, Space Technology Lecture 12B. (Also, Space Technology, John Wiley & Sons, New York, 1959 (Siefert, H., ed.))

White, J. A.
"A Study of the Guidance of Space Vehicles Returning to a Braking Ellipse About the Earth," NASA TN D-191, January 1960.
"A Study of the Effect of Errors in Measurement of Velocity and Flight-Path Angle on the Guidance of a Space Vehicle Approaching the Earth," NASA TN D-957, October 1961.

Wing, W. G., "State of the Art: Inertial Guidance," Space/Aeronautics, Vol. 31, p 24, January 1959.

West, C. T. and Goodstein, R., "On the Simplification of the Attitude Equations of a Satellite," American Astronautical Society, Preprint No. 60-13, 1960.

Widrow, B., "Rate of Adaptation in Control Systems," ARS Journal, Vol. 32, No. 9, p 1378, September 1962.

Windeknecht, T. G., "A Simple System of Sun Orientation for a Spinning Satellite," Institute of Aerospace Sciences, Preprint No. 61-204-1898, June 1961.

Williams, O. S. and Wiseman, J. R., "Low-Thrust Bipropellant Pulse-Rockets for Satellite Attitude Control," American Rocket Society, Preprint No. 1503-60, 1960.

Williams, O. S., "Performance and Reliability of Rocket Attitude Control Systems," Thiokol Astronaut, Vol. 2, No. 1, pp 3 to 6, 1960.

Wilson, R. H., Jr., "Magnetic Field Effects on Artificial Satellites," Sky and Telescope, Vol. 20, No. 2, pp 77 to 79, August 1960.

Wisneski, M. L., "Error Matrix for a Flight on a Circular Orbit," ARS Journal, Vol. 32, No. 9, p 1416, September 1962.

Wolaver, L. E., "Derivation and Burnout Errors," "A Study of the Satellite Equations of Motion," WADC Aeronautical Research Laboratory, WCLJY Internal Memo 58-0, Part I, March 1958.

Zajac, E. E., "Damping of a Gravitationally Oriented Two-Body Satellite," ARS Journal, Vol. 32, No. 12, p 1871, December 1962.

"Analytical Investigation to Determine the Dynamic Requirements of Missile Flight Control Systems," Systems Technology, Inc., Report No. TN-3, 6 January 1959.

"Detection and Analysis of Missile Guidance Systems," ITT Laboratories, Fort Wayne, Indiana, August 1958 to February 1961.

1st Quarterly Report, August 1958.
2nd Quarterly Report 72001, March 1959.
3rd Quarterly Report 72027, October 1959.
4th Quarterly Report 72037, November 1959.
5th Quarterly Report 72042, November 1959.
6th Quarterly Report 72050, December 1959.
7th Quarterly Report 72082, May 1960.
8th Quarterly Report 72095, July 1960.
9th Quarterly Report 72143, January 1961.
10th Quarterly Report 72155, February 1961.

"Developmental Star Tracker Final Report," Santa Barbara Research Department, Santa Barbara, California, Report No. 1030-F, July 1956.

"Doppler Velocity for Space Navigation," General Precision Laboratory, New York, Interim Engineering Reports Nos. A18-3 and A18-4.

"First Quarterly Engineering Report on the Study of Electromagnetic Phenomena for Space Navigation," The Franklin Institute, Philadelphia, Pennsylvania, Report No. Q-A2183-1, 1 July to 30 September 1958.

"First Quarterly Technical Note on Study of Automatic Position Fixing," General Precision Laboratory, New York, Report No. A20-1, 1 December 1958.

"Guidance and Control; Trajectories; Radio Propagation," Transactions of Second Technical Symposium on Ballistic Missiles, Ramo-Wooldridge, AFBMD, ARDC, Vol. II, 12 to 14 June 1957.

"Proceedings of the National Specialists Meetings on Guidance of Aerospace Vehicles," Institute of the Aeronautical Sciences, New York, 1960.
Antes, L. L.
"Command and Data Link for an Astronomical Satellite."
Spradlin, L. W.
"The Long-Time Satellite Rendezvous Trajectory."
Lowry, J. H., Jr. and Buehrle, C. D.
"Guidance and Control of Point Return Vehicles,"

Haywood, W. J., Jr.
"Application of Optical Techniques to Interplanetary Navigation."
Ormsby, R. D.
"A Free Reaction Sphere Satellite Attitude Control System."
Useller, J. W. and Algranti, J. S.
"Pilot Control of Space Vehicle Tumbling."
Alonso, R. L. and Laning, J. H., Jr.
"Design Principles for a Control Computer for Space Guidance."
Grube, R. H.
"Terminal Guidance for Lunar and Planetary Probes."

"Study of Satellite Guidance Sensors," Radiation, Inc., Final Technical Report No. IR-1761-VI, Orlando, Florida, 2 Vols., January 1961.

"Technique Development of Orbital Guidance Equipment for Satellite Vehicles," Radiation, Inc., Orlando, Florida, April 1959 to July 1960.
Quarterly Technical Note 1188-59-01, April 1959.
Quarterly Technical Note 1188-59-02, July 1959.
Quarterly Technical Note 1188-59-03, October 1959.
Quarterly Technical Note 1188-59-04, January 1960.
Quarterly Technical Note 1188-60-01, April 1960.
Quarterly Technical Note 1188-60-02, July 1960.

Techniques of Indication and Control for Inertial Guidance of Ballistic Missiles," Massachusetts Institute of Technology, Cambridge, Massachusetts, Instrumentation Laboratory, February 1959.

"Radio and Inertial Guidance," Transactions of the First Technical Symposium on Ballistic Missiles, Ramo-Wooldridge, Report No. GM 01.1-266, Vols. 1 and 2, 21 and 22 June 1956.

"Radio and Inertial Guidance," Transactions of the Second Technical Symposium on Ballistic Missiles. Ramo-Wooldridge, Report No. GM TR 202, Vols. 1 and 2, 12 to 14 June 1957.

"Radio and Inertial Guidance," Transactions of the Third Technical Symposium on Ballistic Missiles, Ramo-Wooldridge, Vols. 1 and 2, 14 to 15 July 1958.

"USAF Symposium on Guidance of Ballistic Missiles and Space Vehicles," WADC TR 58-270, March 1958.

Adams, J. J. and Chilton, R. E.
"A Weight Comparison of Several Attitude Control Systems for Satellites," NASA Memorandum 12-30-586, February 1959

Arck, M. H. and Merlen, M. M.
"Horizon Sensors for Vertical Stabilization of Satellites and Space Vehicles," IAS Symposium, Boston, May 1960.

Barnes, J. L., "Precision Position and Attitude Control for Synchronous Satellites," Stockholm, XIth International Astronautical Congress, Astrodynamics Colloquium, 1960.

Chatkoff, M. and Lynch, G., "Attitude Control of a Space Vehicle by a Gyroscopic Reference Unit," Aero/Space Engineering, Vol. 19, May 1960.

Davis, W. R., "Determination of a Unique Attitude for an Earth Satellite," American Astronautical Society, 4th Annual Meeting, New York, January 1958.

DeLisle, J. E., et al., "Attitude Control of Spacecraft," Astronautics, Vol. 6, No. 11, November 1961.

Freed, L. E., "Attitude Control System for a Spinning Body," Institute of Aerospace Sciences, Preprint No. 61-207-1901, June 1961.

Gates, C. R., "Attitude Control of Space Vehicles," California Institute of Technology, Pasadena, California, Jet Propulsion Laboratory, JPL Report No. EP 795, February 5, 1960. (Presented at the National Automatic Control Conference, Dallas, Texas, November 4 to 6, 1959.)

Gillespie, W., Jr., "Some Notes on Attitude Control on Earth Satellite Vehicles," NASA TN D-40, December 1959.

Grasshoff, L., "Method for Controlling the Attitude of a Spin-Stabilized Satellite," ARS Journal, Vol. 31, No. 5, 1961.

Haeussermann, W. E., "Recent Advances in Attitude Control of Space Vehicles," ARS Journal Vol. 32, No. 2, p 188, February 1962.

Kalman, R. E. and Bertrom, J. E., "Control System Analyses and Design via the Second Method of Liapunov," RIAS, Inc., Baltimore, Maryland, Monograph 59-13. (Also, ASME Paper No. 59-NAC-2, 1959.)

Levin, S. M. and Manusevich, L. G., "A Vector Method for Calculating One Class of Control Systems," Automation and Remote Control, Vol. 21, No. 10, pp 962 to 970, October 1960.

Lillestrand, R. L., "Use of a Stellar Aberrascope in Space Systems," XIth International Astronautical Congress, Astrodynamics Colloquium, Stockholm, 1960.

Litovchenko, I. A., "On a Problem of Optimum Control," Automation and Remote Control, Vol. 21, No. 8, pp 791 to 798, August 1960.

Mueller, H., "An Attitude Control System for Extremely Small Control Forces," XIth International Astronautical Congress, Astrodynamics Colloquium, Stockholm, 1960.

Ormsby, R., "Capabilities and Limitations of Reaction Spheres for Attitude Control," ARS Journal, Vol. 31, No. 6, 1961.

Ormsby, R. and Smith, M. C., "A Reaction Spheres Attitude Control System," American Rocket Society, Preprint No. 1500-60, 1960.

Pistiner, J. S., "On-Off Control System for Attitude Stabilization of a Space Vehicle," ARS Journal, Vol. 29, No. 4, pp 283 to 289, April 1959.

Potter, N. S., "Orientation Sensing in Inertial Space by Celestial Pattern Recognition Techniques," American Rocket Society, Preprint No. 1482-60, 1960.

Ritchie, M. L., Hanes, L. F. and Hainsworth, T. C., "Some Display-Control Aspects of Manual Attitude Control in Space," American Astronautical Society, Preprint No. 60-14, January 1960.

Roberson, R. E.
"Optical Determination of Orientation and Position near a Planet," American Rocket Society, Preprint No. 643-58, 1958.
"Principle of Inertial Control of Satellite Attitude," 9th International Astronautical Congress, 1958.
"Gyroscopic Sensing of Satellite Yaw," International Congress on Automatic Control, Moscow, June 1960.
"Attitude Sensing and Control for a Satellite Vehicle," The Rand Corporation, Santa Monica, California, Research Memo No. RM-1050, January 1953.
"Gravitational Torque on a Satellite Vehicle," Journal of the Franklin Institute, Vol. 265, No. 1, January 1958.
"Control of Satellites," WADD TR 60-643, 31 July 1960.
"Methods of Attitude Sensing," Proceedings of the Manned Space Station Symposium, Los Angeles, April 1960.
"Gravity Gradient Determination of the Vertical," American Rocket Society, Preprint No. 1496-60, December 1960.

Roman, N. G., "Attitude Control and Stabilization Required for Satellite Telescopes," Proceedings of the Manned Space Station Symposium, Los Angeles, April 1960.

Sohn, R. L., "Attitude Stabilization by Means of Solar Radiation Pressure," ARS Journal, Vol. 29, No. 5, pp 371 to 373, May 1959.

Stalony-Dobrzanski, J. and Imai, O., "Attitude and Flight Path Control System for a Space Station Supply Vehicle," Aero/Space Engineering, Vol. 19, May 1960.

Thomson, W. T. and Reiter, G. S., "Attitude Drift of Space Vehicles," Journal of the Astronautical Sciences, Vol. 7, No. 2, pp 29 to 34, 1960.

Tripp, C. N., "Attitude Control Rocket Requirements for Space Vehicles," Institute of the Aerospace Sciences, Preprint No. 61-205-1899, 1961.

Von Pahlen, F., "An Accurate Determination of Attitude by Optical Means," IAS Symposium, Boston, May 1960.

ILLUSTRATIONS

Preceding page blank

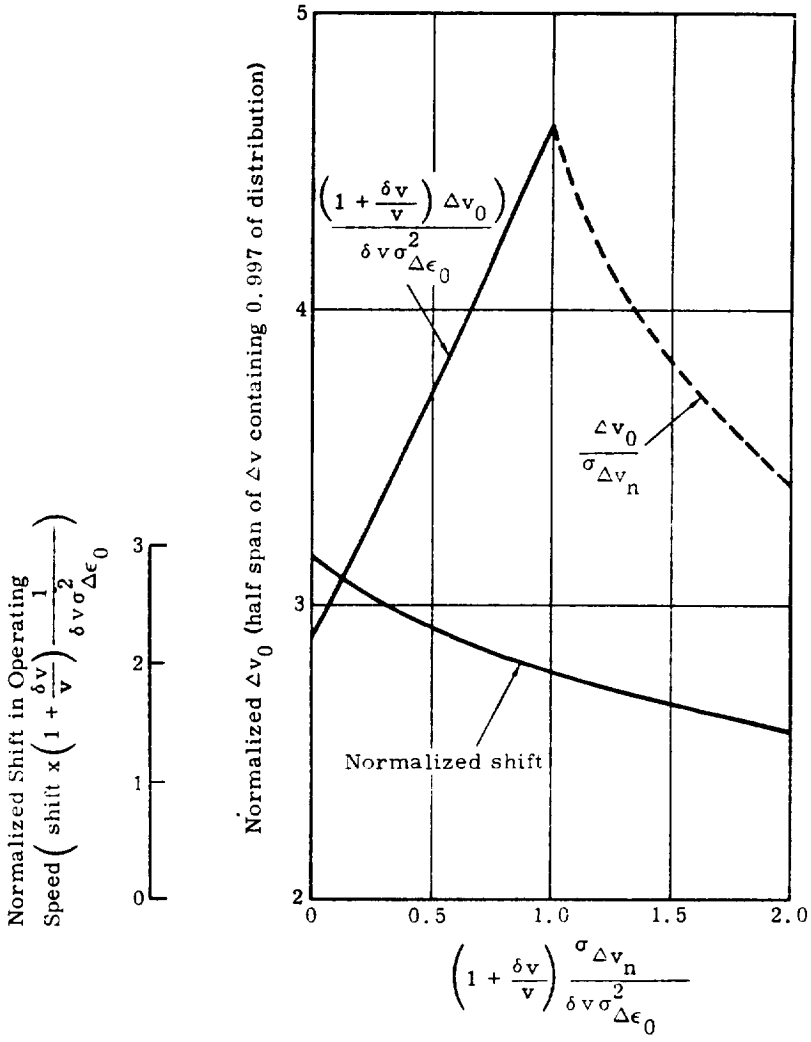

Fig. 1. Results of Optimization for Equal σ in Pitch and Yaw Equal to $\sigma_{\Delta\epsilon_0}$

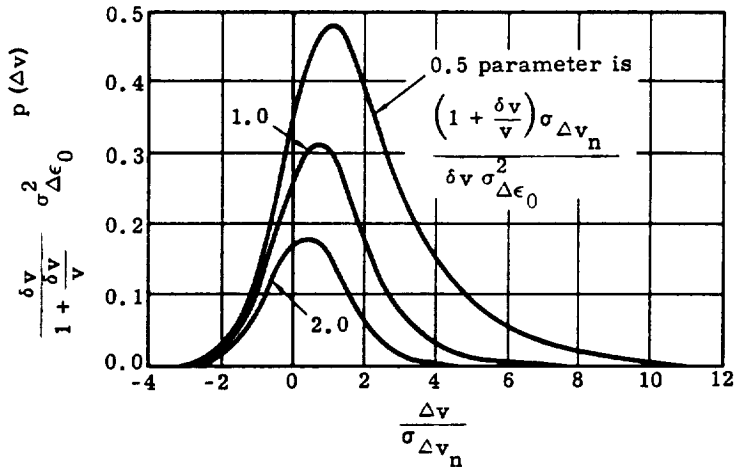

Fig. 2. Normalized Density Function of Δv (Equation 119)

Preceding page blank

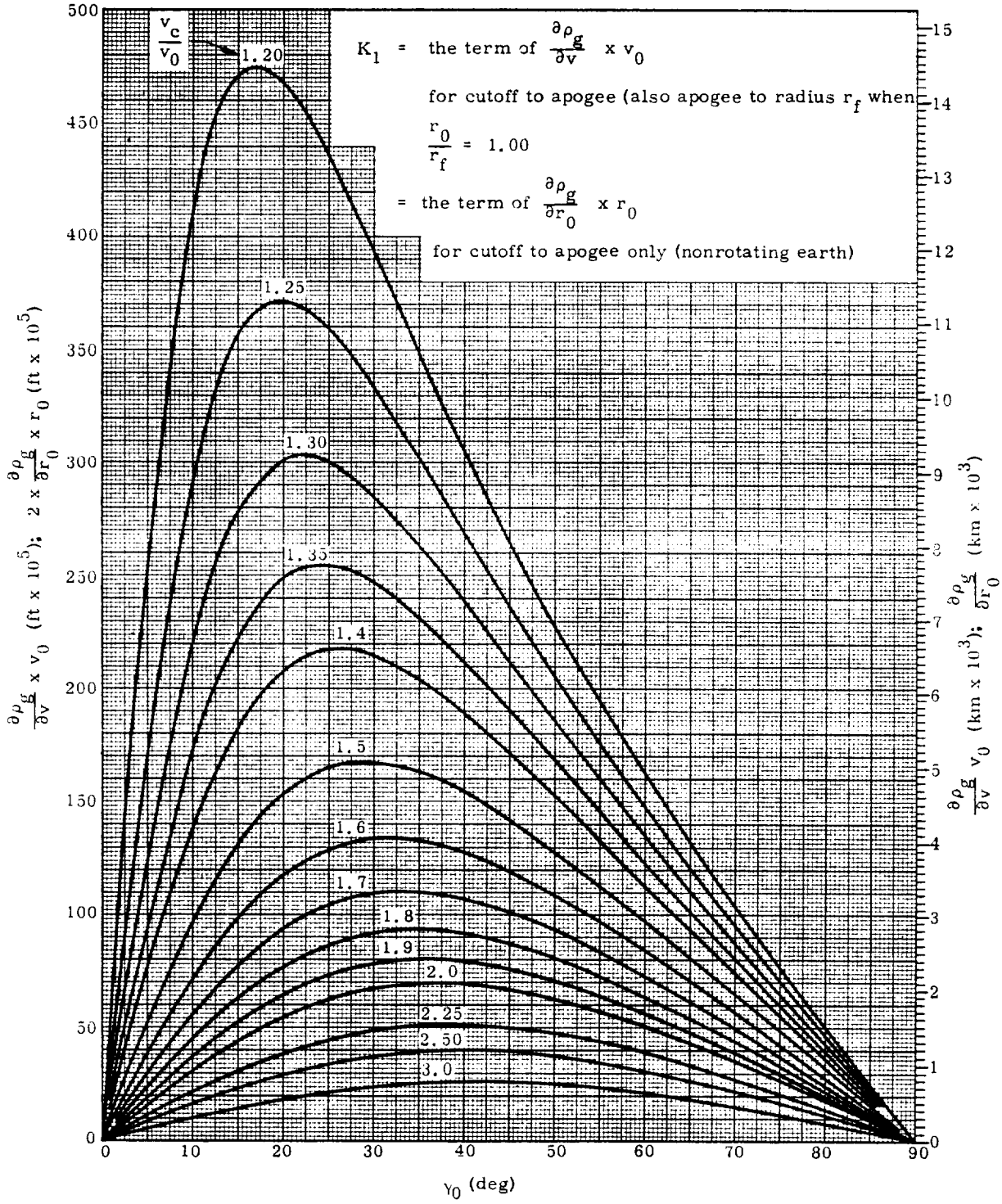

Fig. 3. Vacuum Ballistic Trajectory Error Analysis
(velocity and radius, cutoff to apogee, partials)

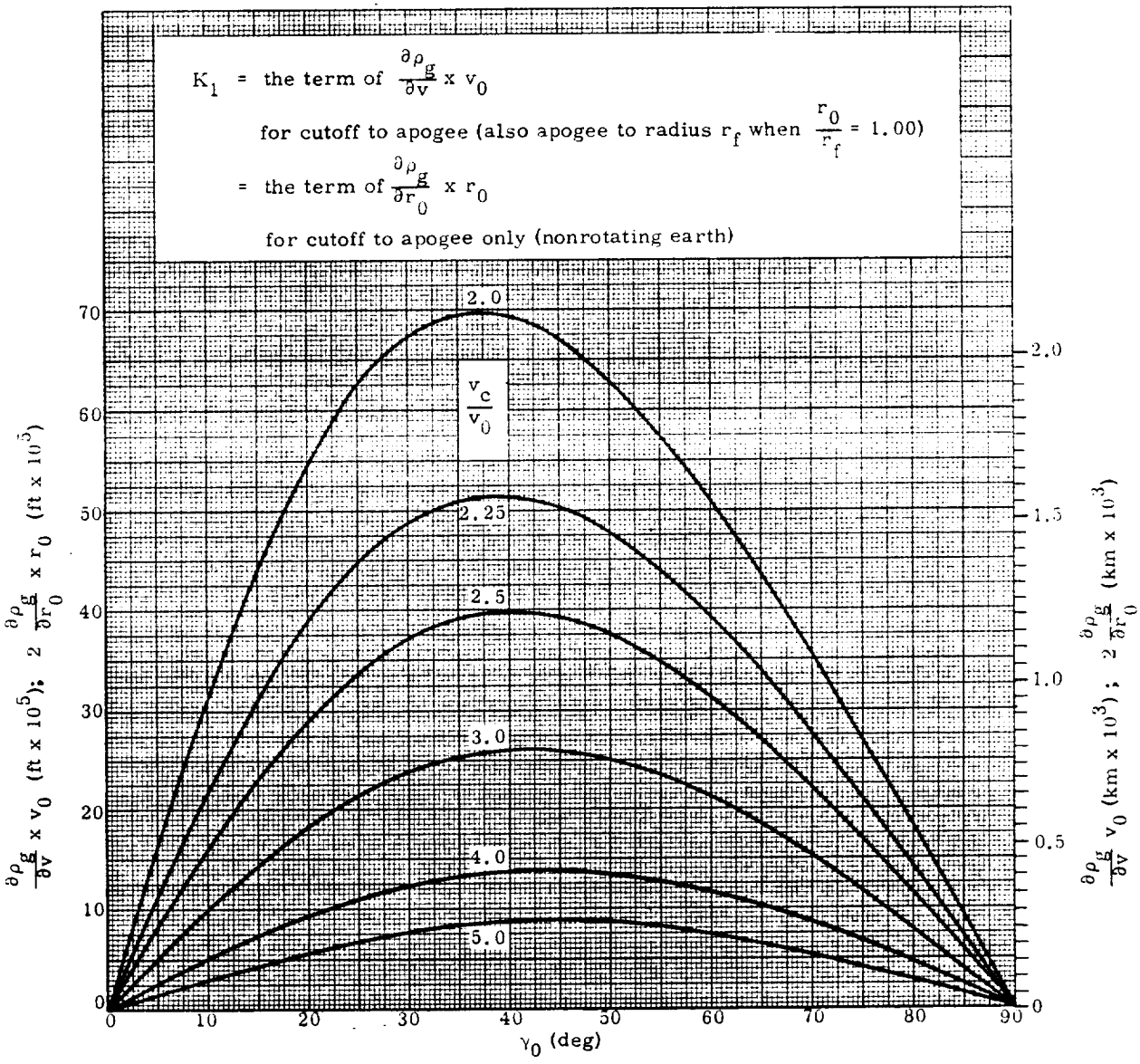

Fig. 4. Vacuum Ballistic Trajectory Error Analysis (velocity and radius partials, expanded scale)

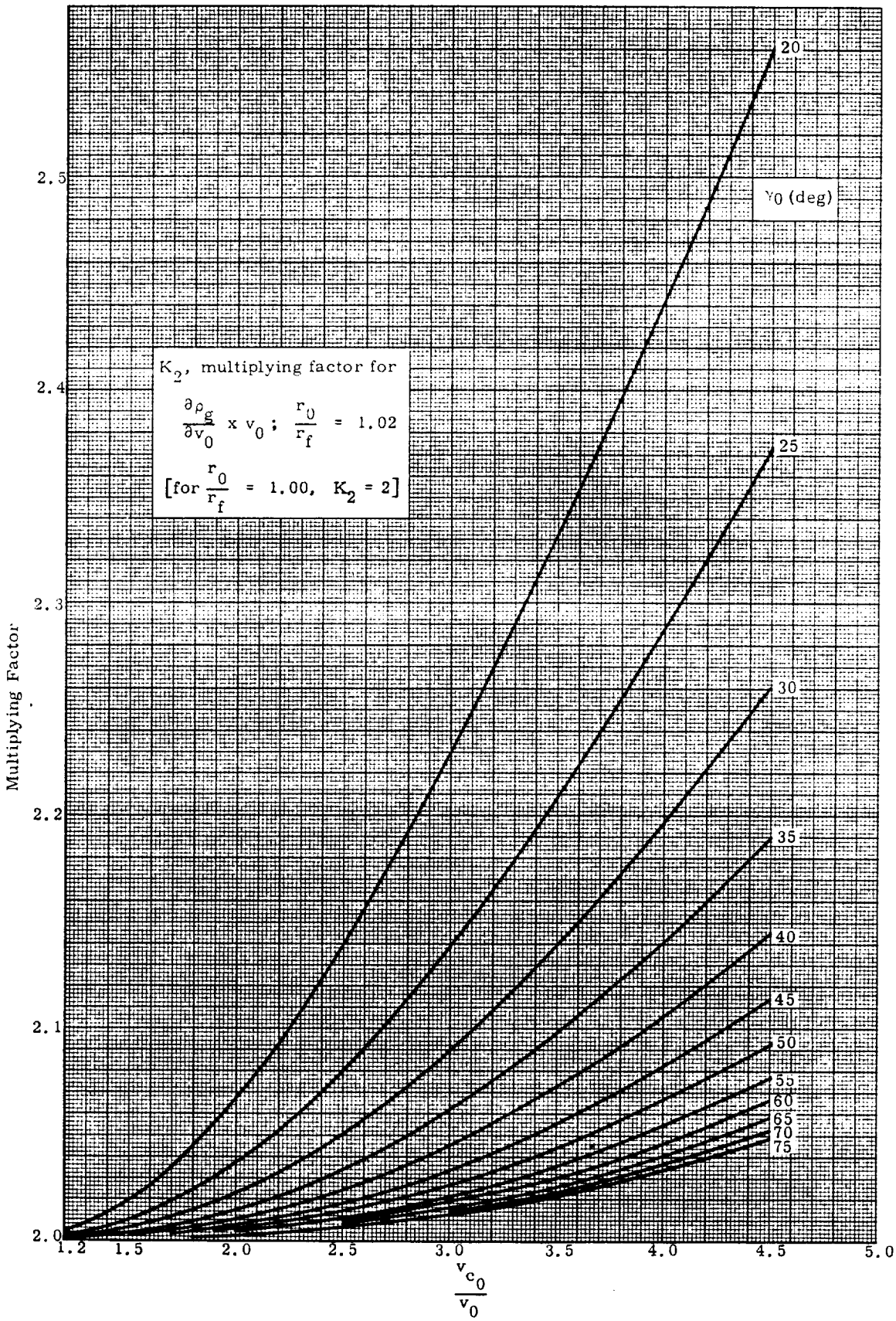

Fig. 5. Vacuum Ballistic Trajectory Error Analysis (correction for $r_0/r_f = 1.02$)

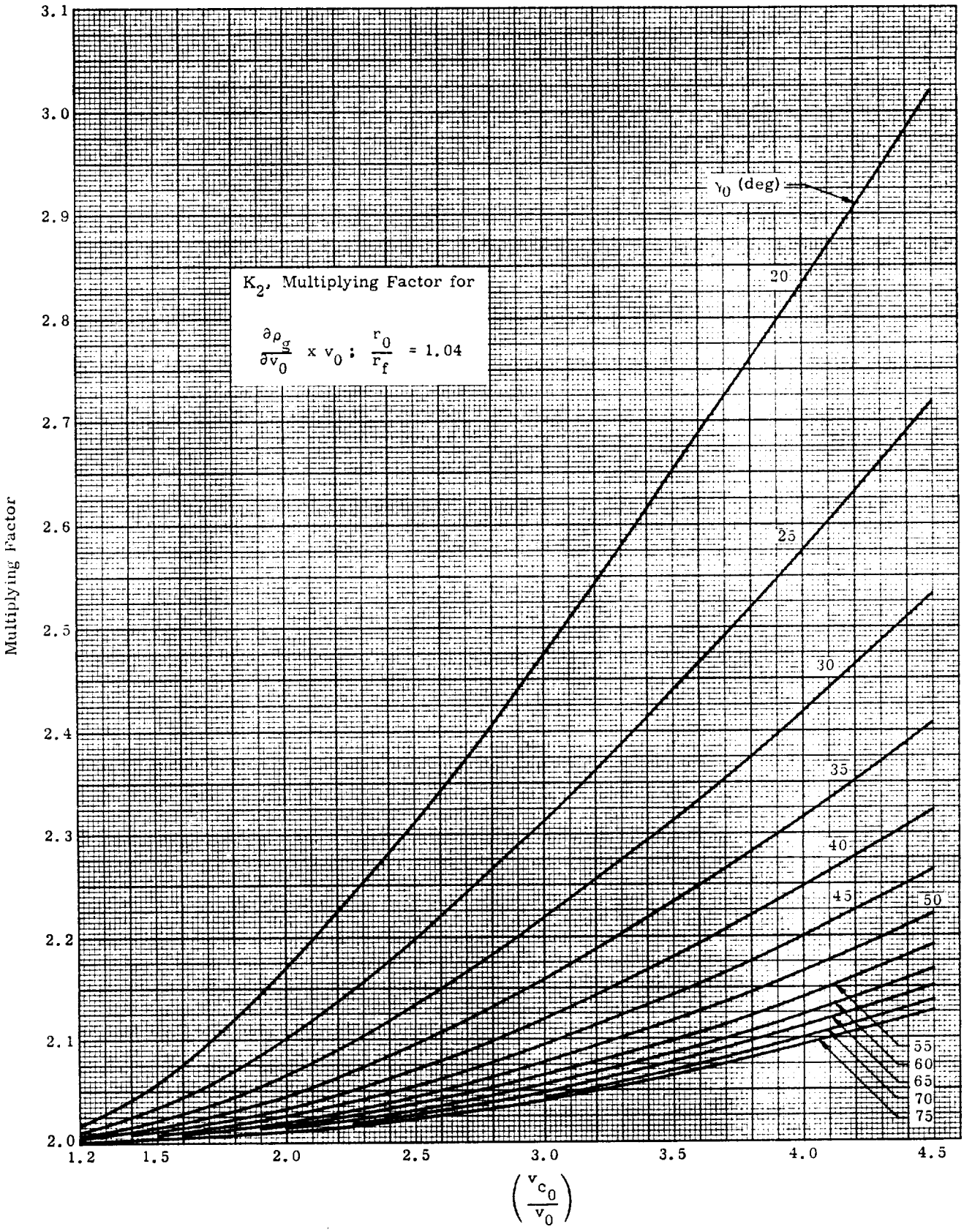

Fig. 6. Vacuum Ballistic Trajectory Error Analysis (correction for $r_0/r_f = 1.04$)

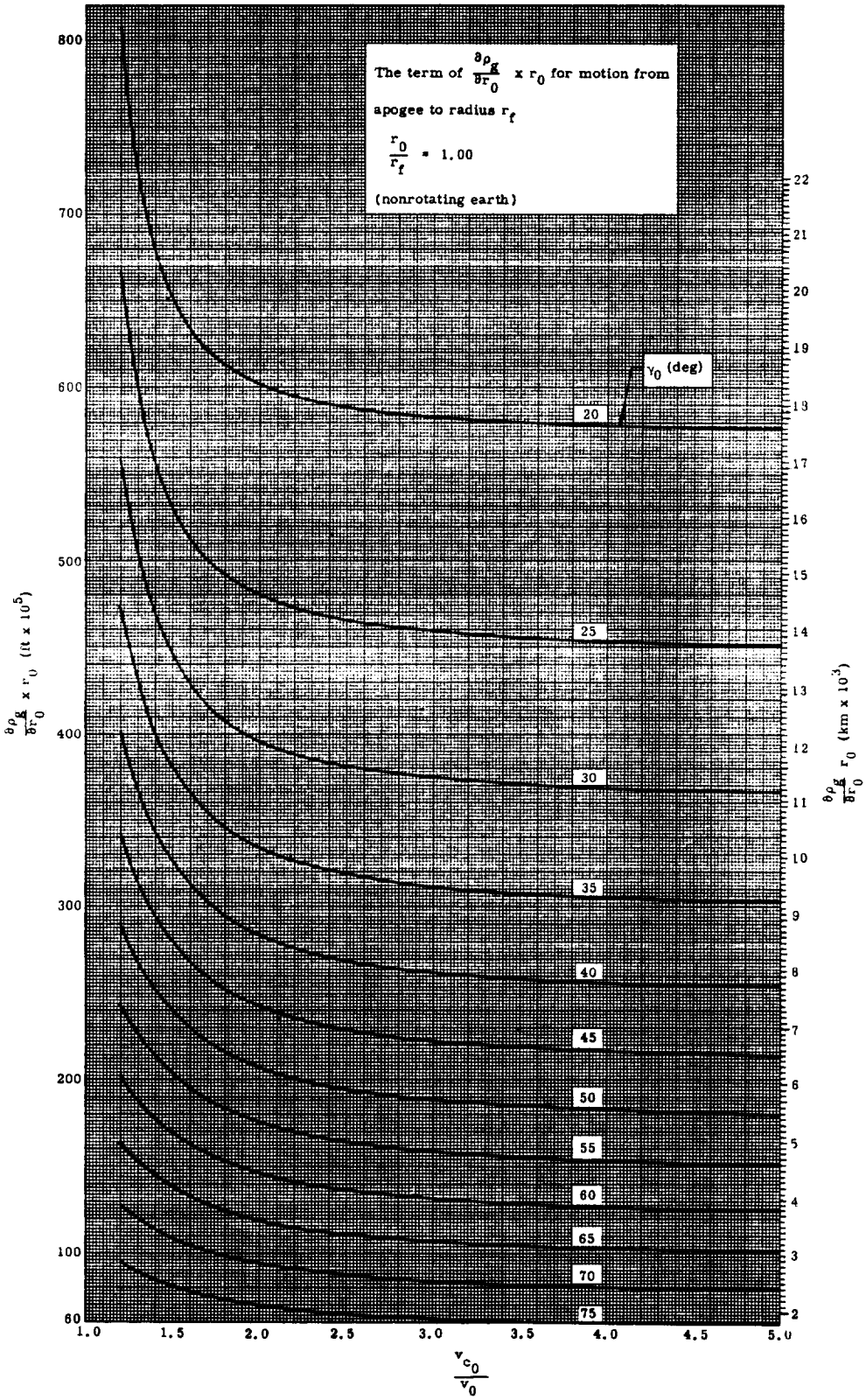

Fig. 7. Vacuum Ballistic Trajectory Error Analysis (radius partial, apogee to r_f, $r_f = r_0$)

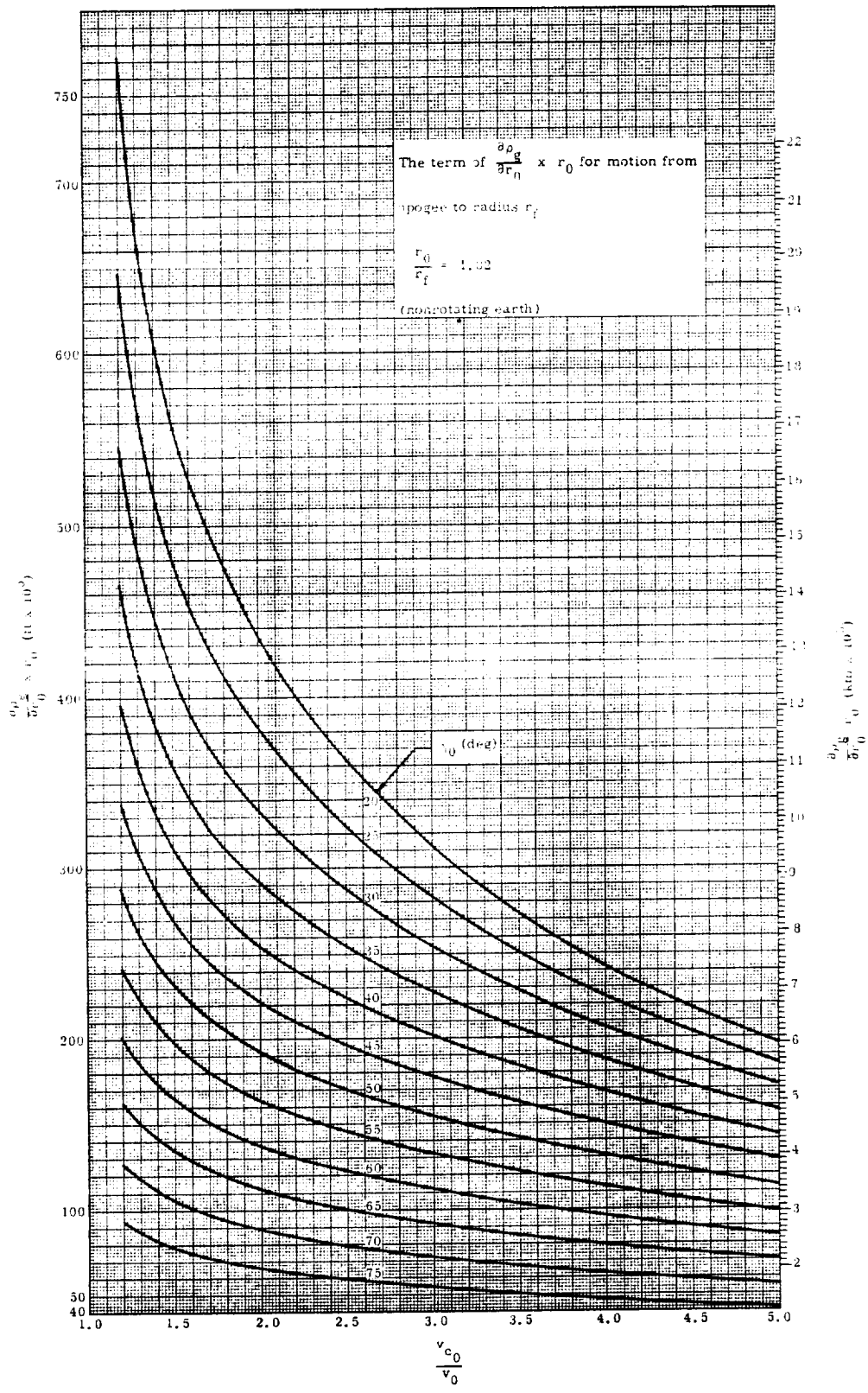

Fig. 8. Vacuum Ballistic Trajectory Error Analysis (radius partial, apogee to r_f, $r_f = r_0/1.02$)

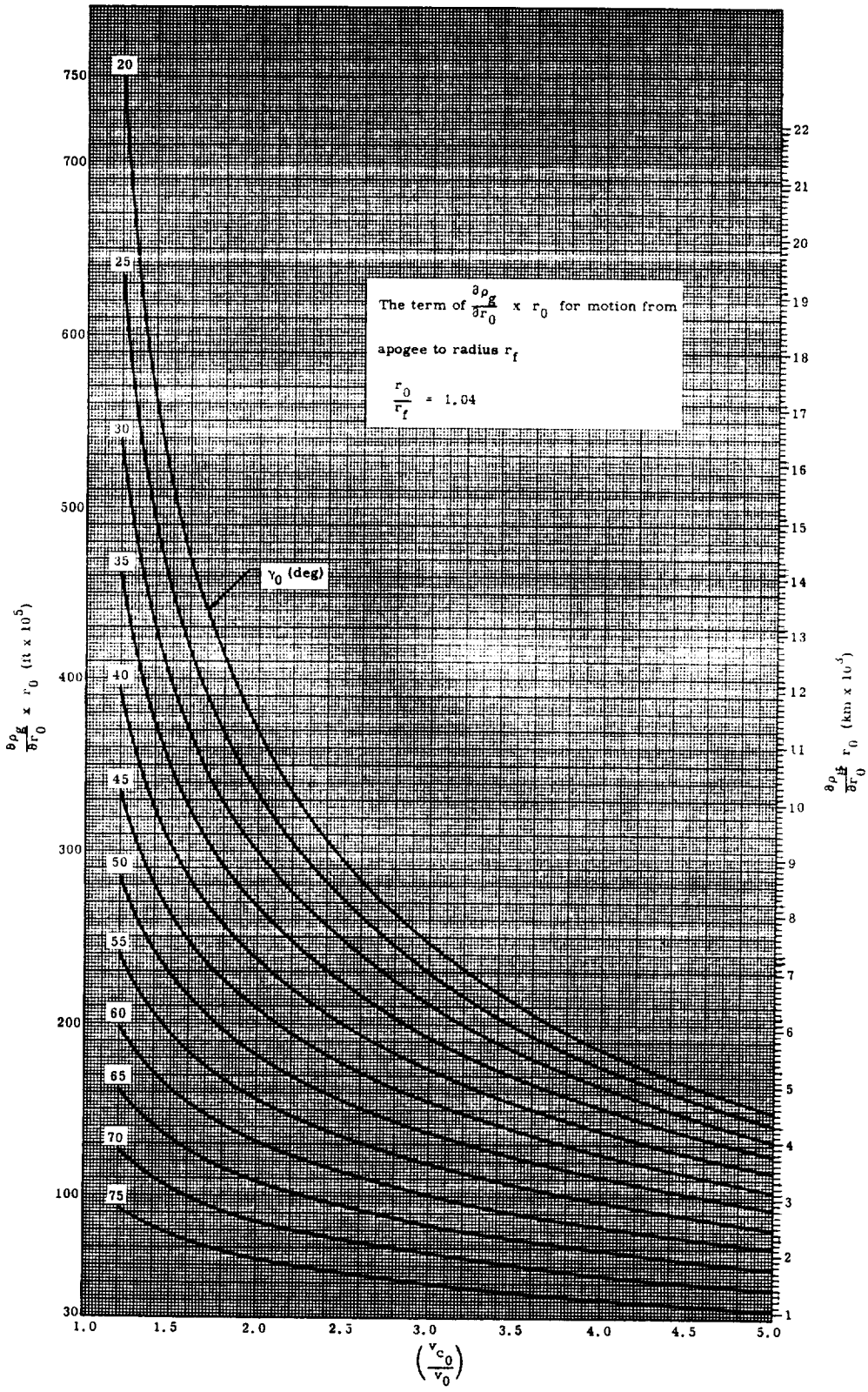

Fig. 9. Vacuum Ballistic Trajectory Error Analysis (radius partial, apogee to r_f, $r_f = r_0/1.04$)

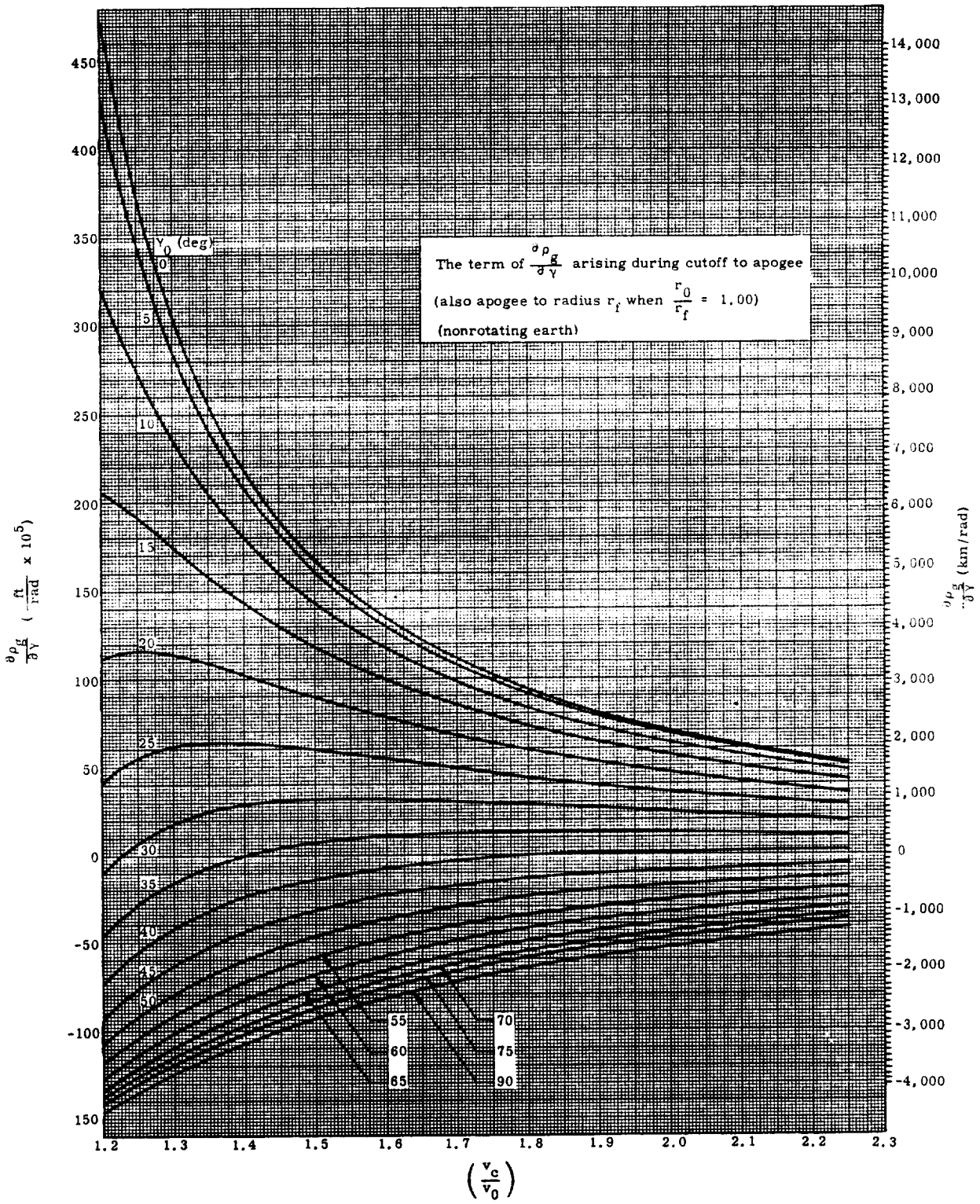

Fig. 10. Vacuum Ballistic Trajectory Error Analysis (flight path angle partial, $r_0/r_f = 1.00$)

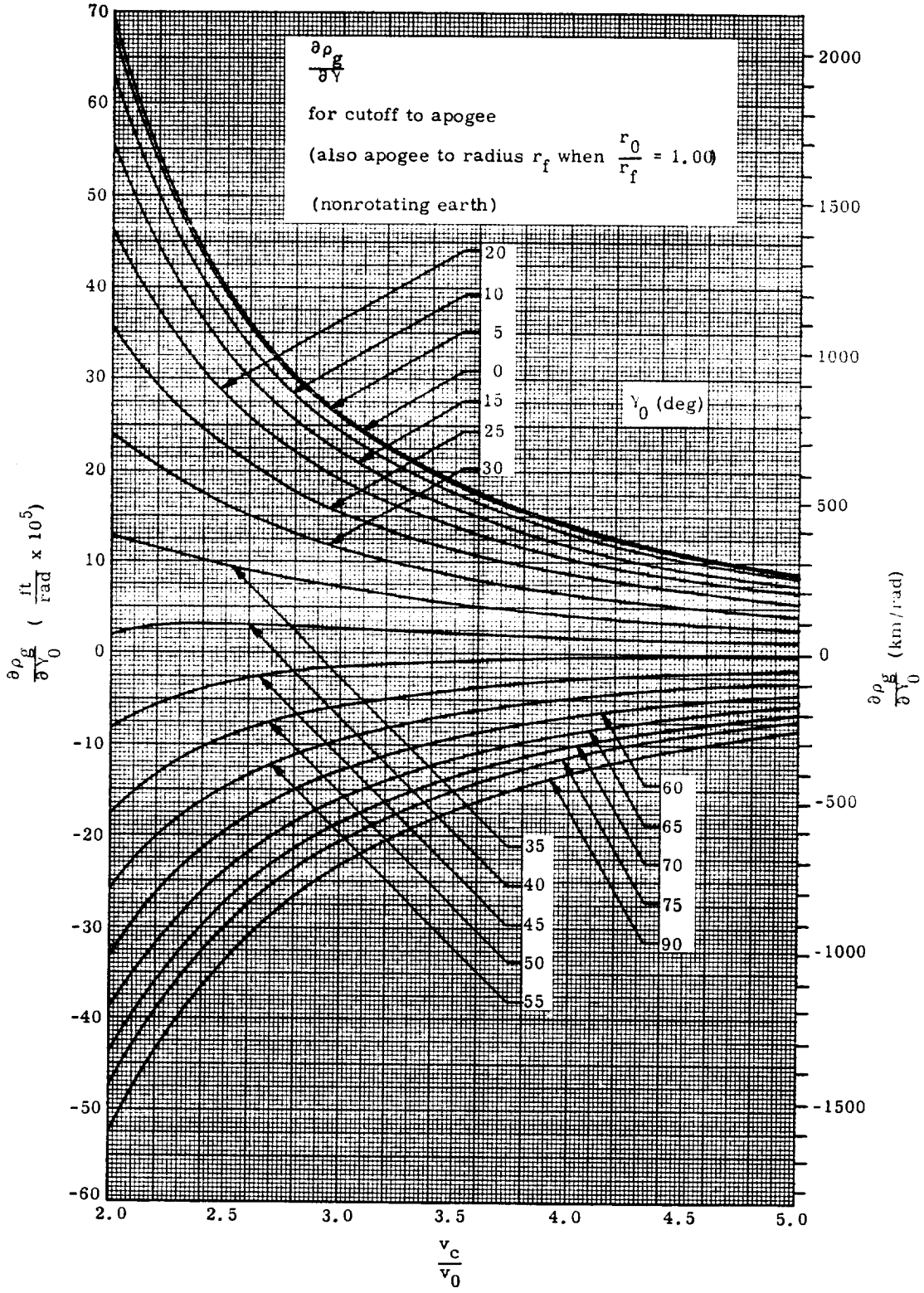

Fig. 11. Vacuum Ballistic Trajectory Error Analysis (flight path angle partial, extended velocities, $r_0/r_f = 1.00$)

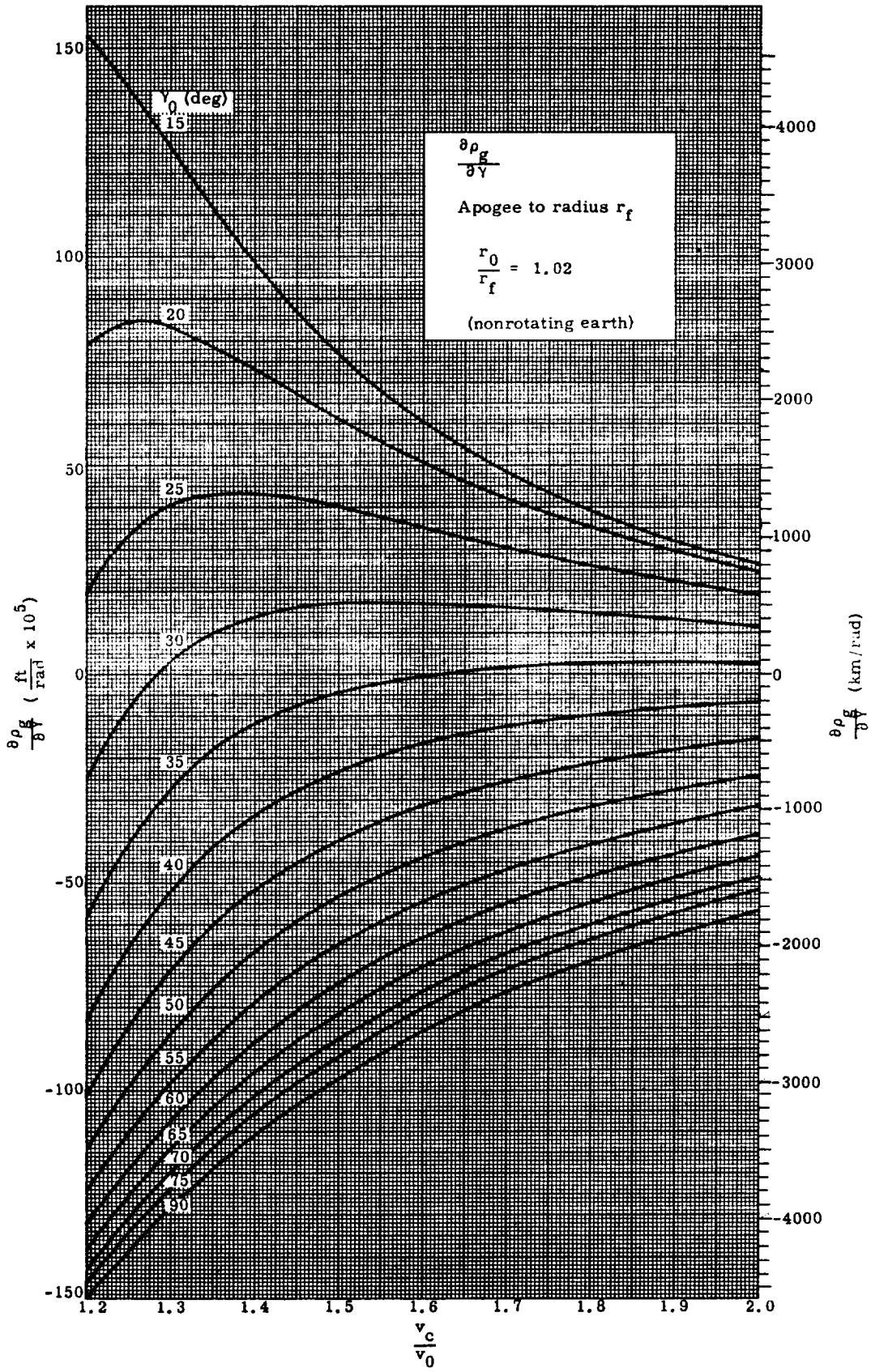

Fig. 12. Vacuum Ballistic Trajectory Error Analysis (flight path angle partial, $r_0/r_f = 1.02$)

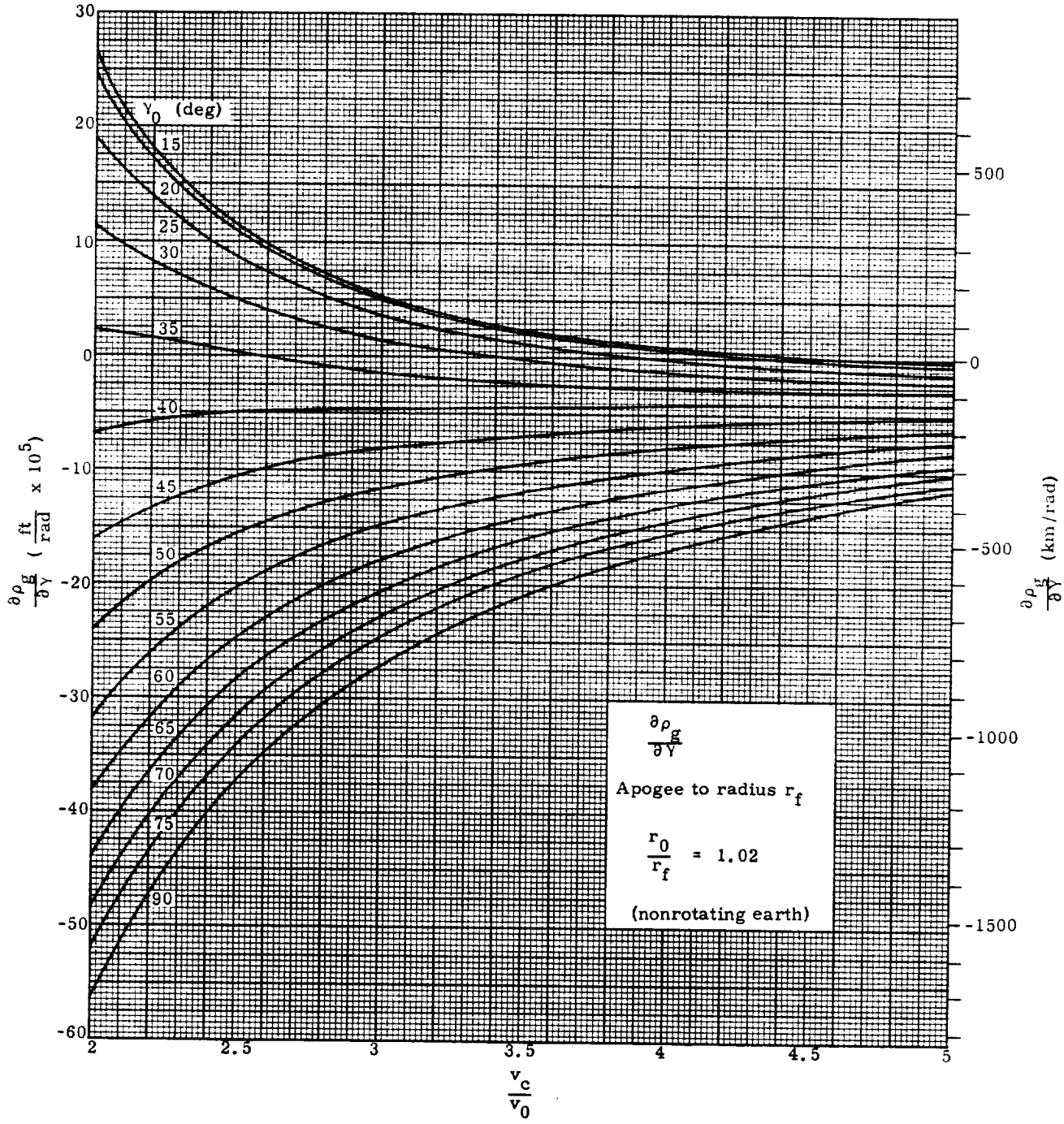

Fig. 13. Vacuum Ballistic Trajectory Error Analysis
(flight path angle partial, extended, r_0/r_f = 1.02)

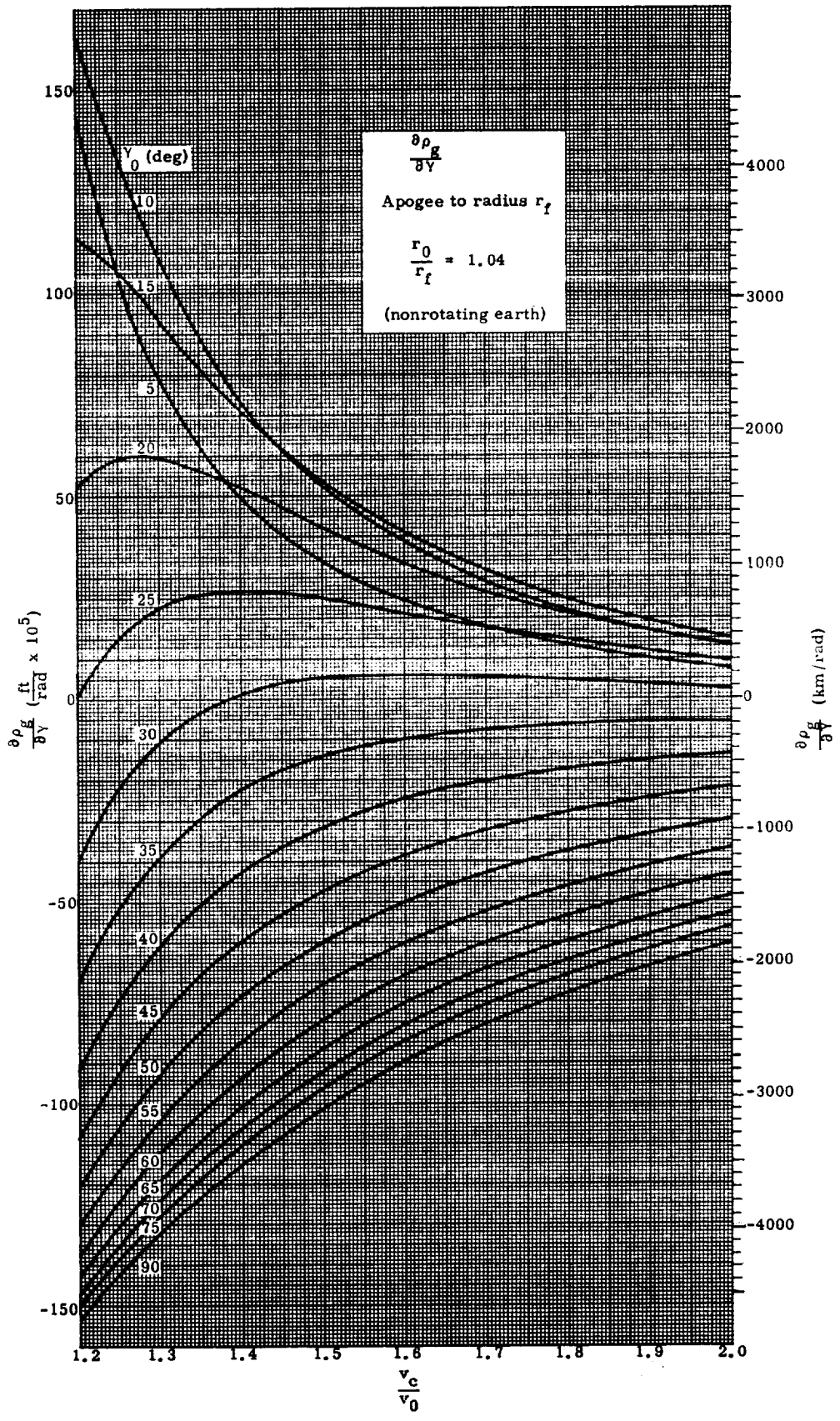

Fig. 14. Vacuum Ballistic Trajectory Error Analysis (flight path angle partial r_0/r_f = 1.04)

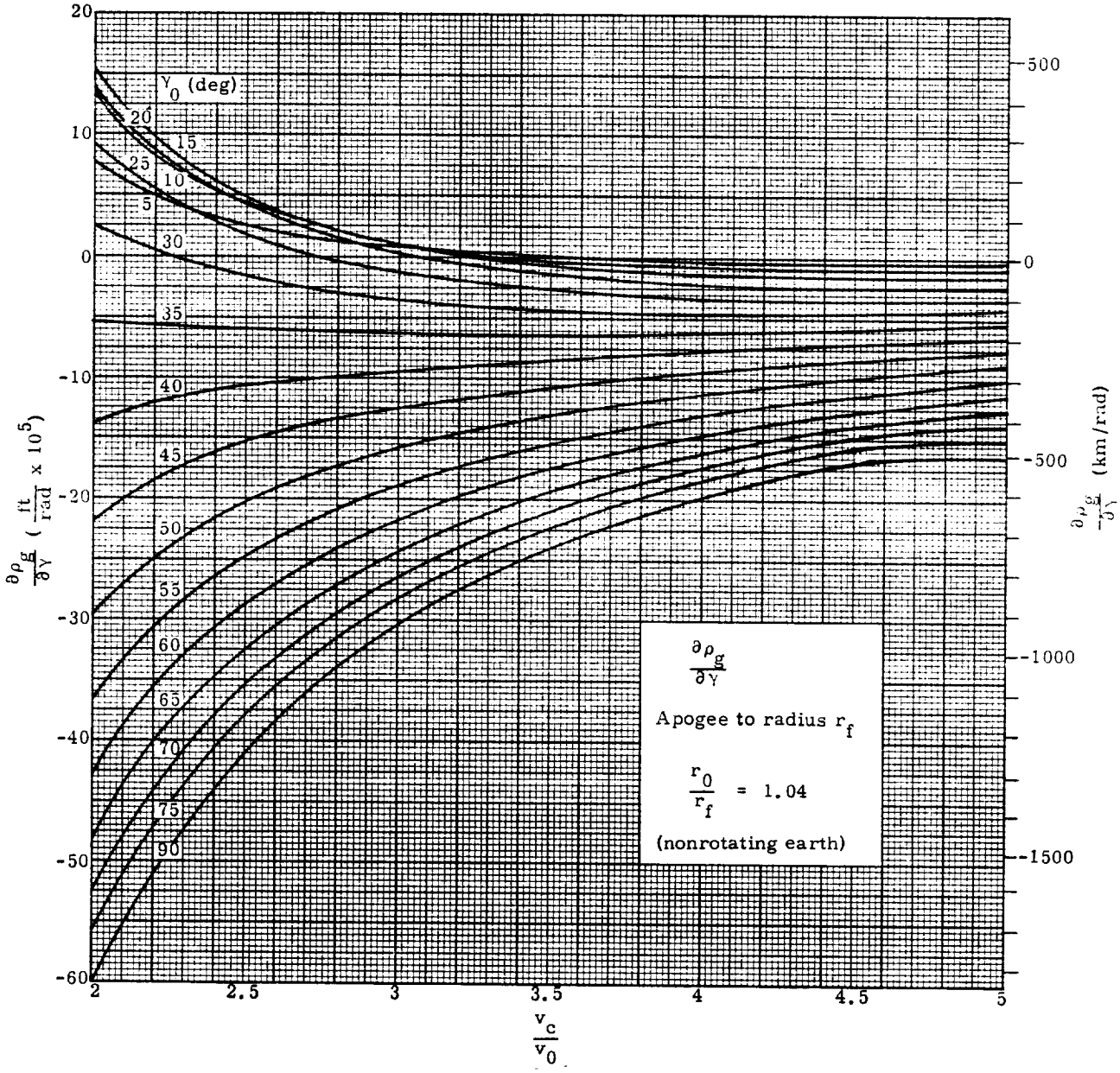

Fig. 15. Vacuum Ballistic Trajectory Error Analysis (flight path angle partials, extended velocities, r_0/r_f = 1.04)

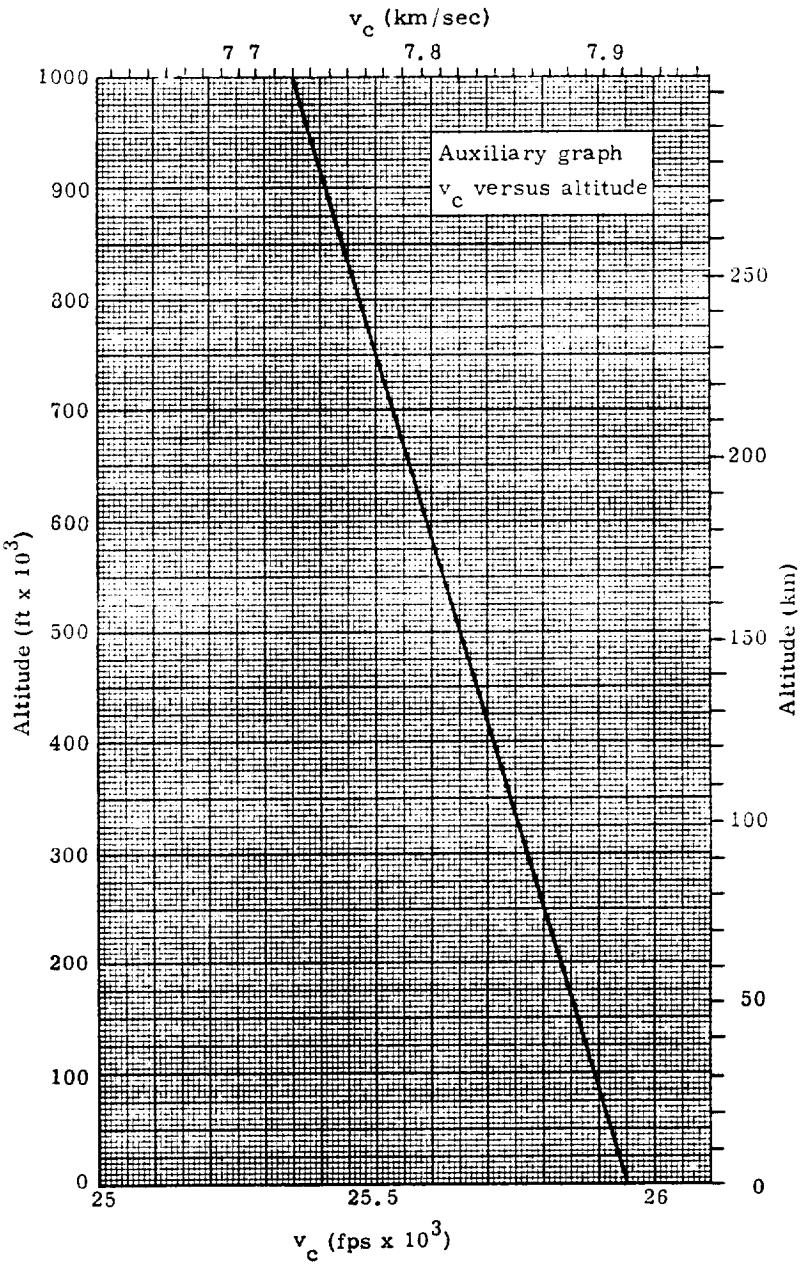

Fig. 16. Vacuum Ballistic Trajectory Error Analysis
(circular velocity as a function of altitude)

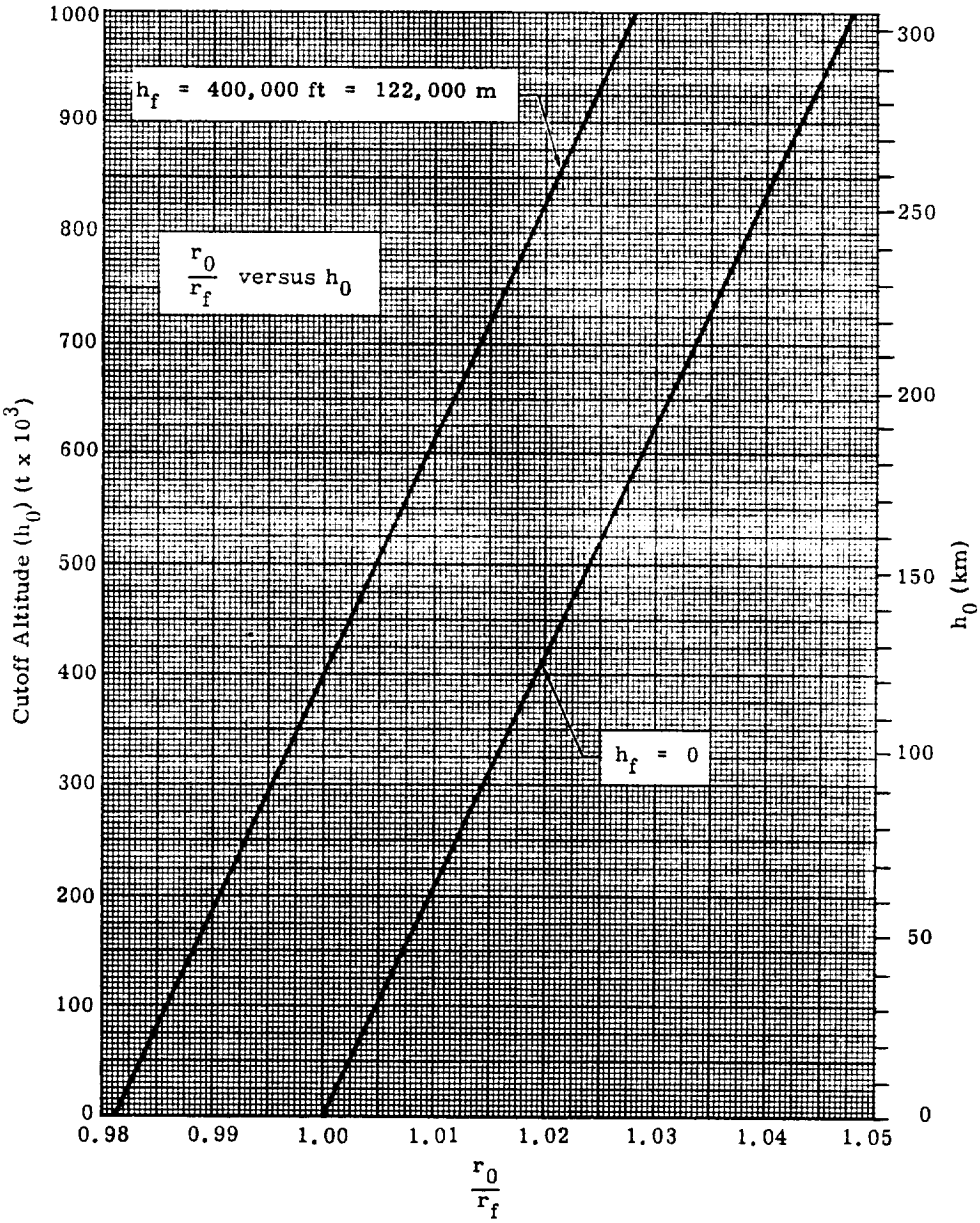

Fig. 17. Vacuum Ballistic Trajectory Error Analysis (r_0/r_f as a function of h_0 and h_f)

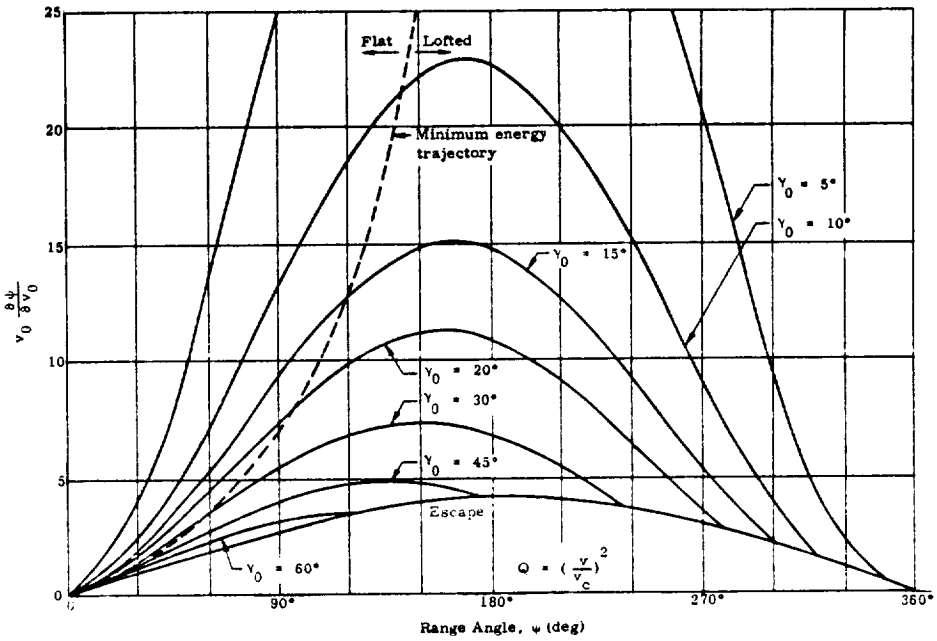

Fig. 18. Altitude and Velocity Influence Coefficients Versus Range (for values of elevation angle γ_0)

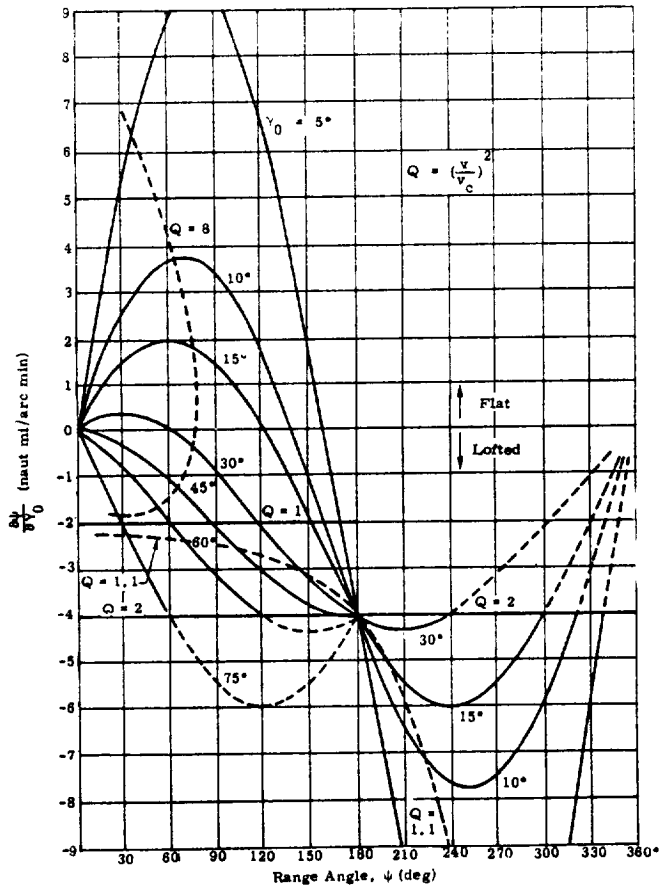

Fig. 19. Elevation Angle Influence Coefficient Versus Range (for values of elevation angle γ_0)

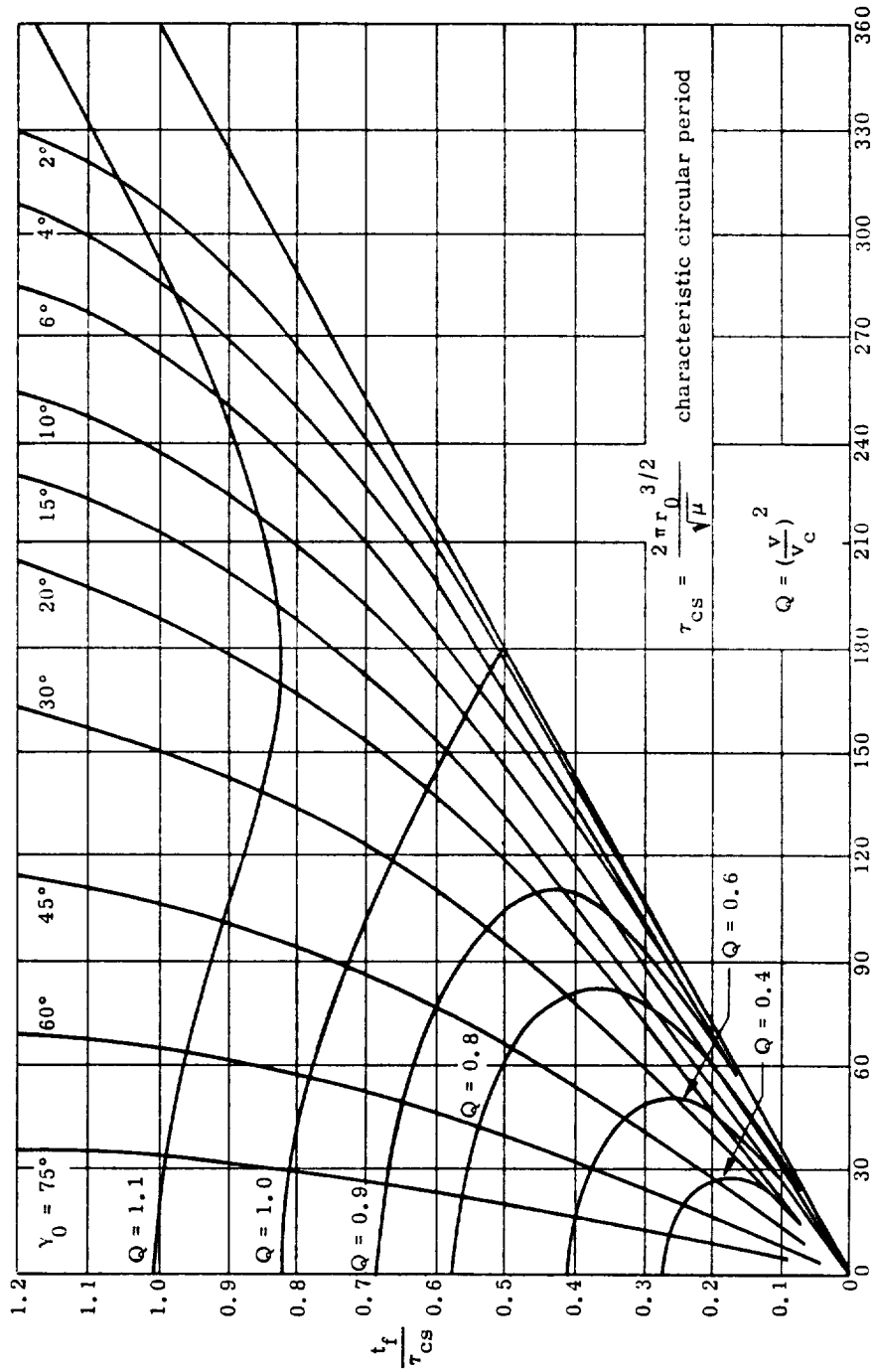

Fig. 20. Time of Flight Versus Range

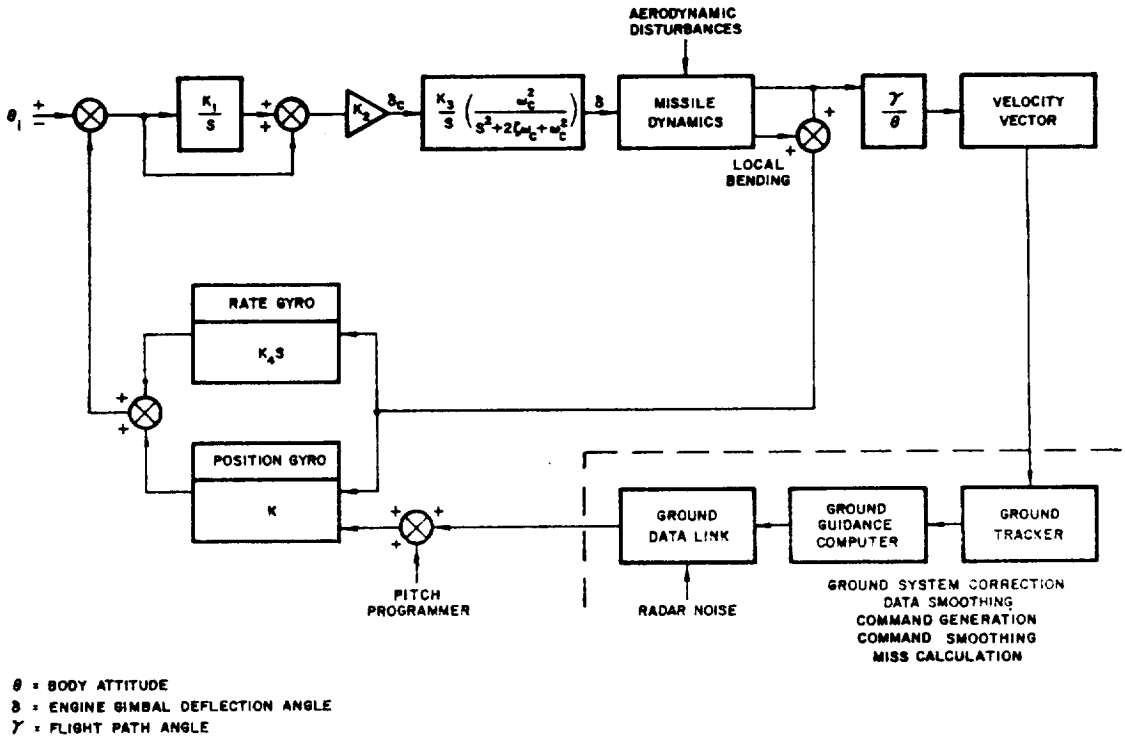

θ = BODY ATTITUDE
δ = ENGINE GIMBAL DEFLECTION ANGLE
γ = FLIGHT PATH ANGLE

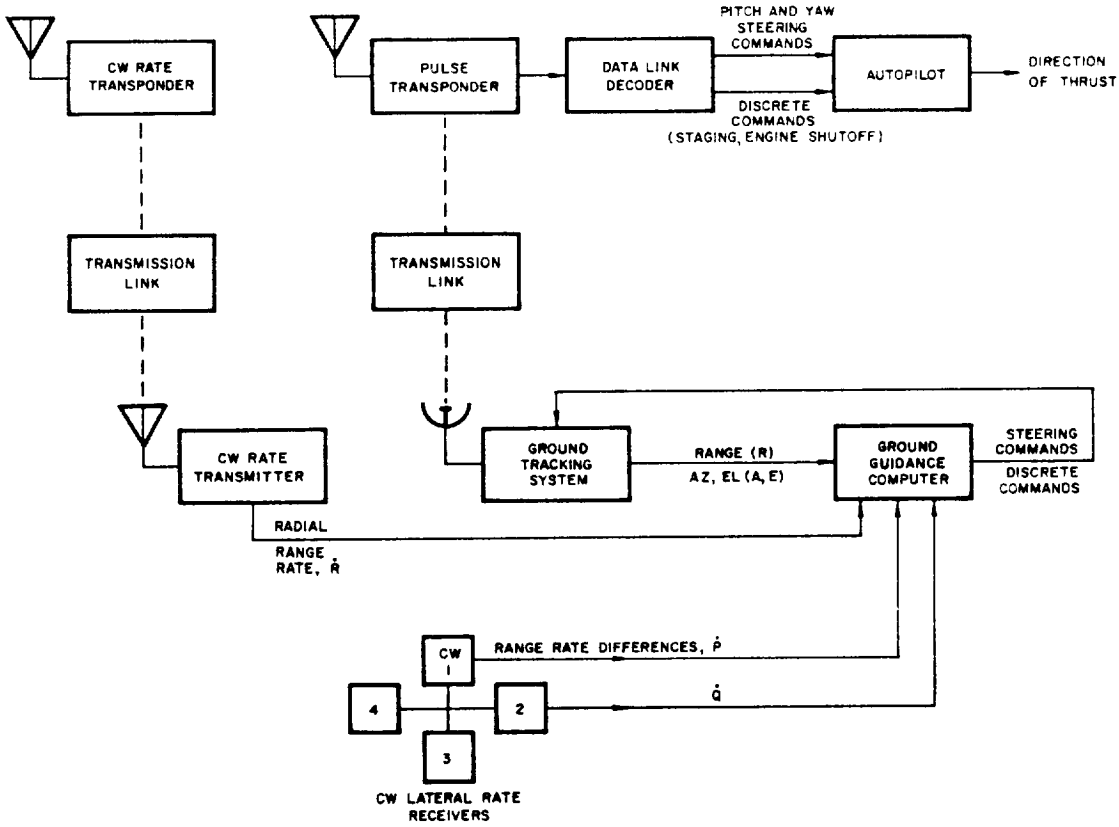

Fig. 22. Functional Block Diagram for a Radio-Inertial System

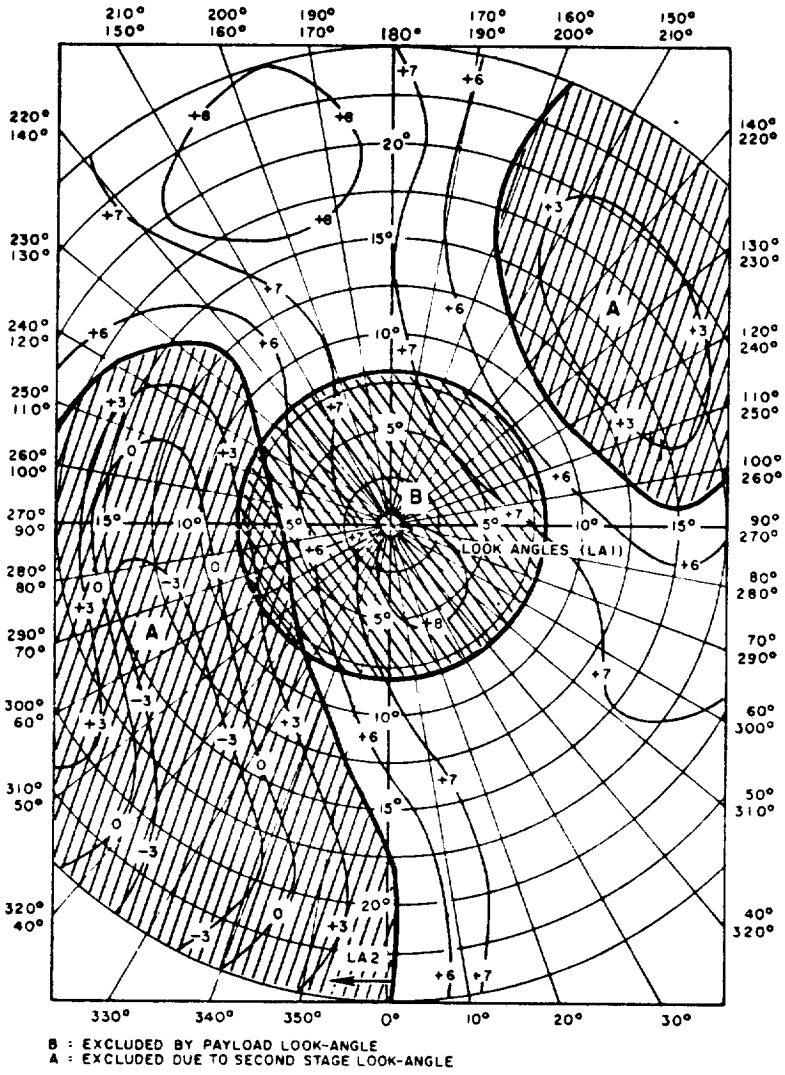

Fig. 23. Actual Antenna Radiation Pattern Showing Important Trajectory Steering Constraints

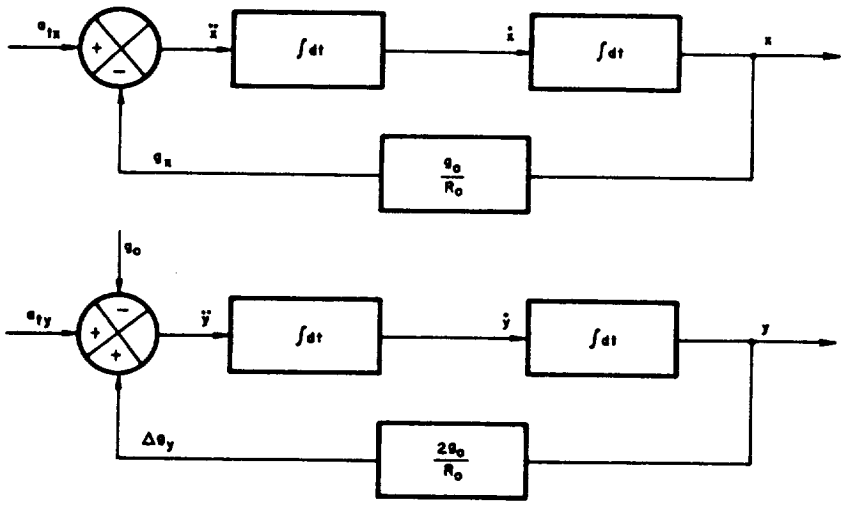

Fig. 24. Gravity Computer

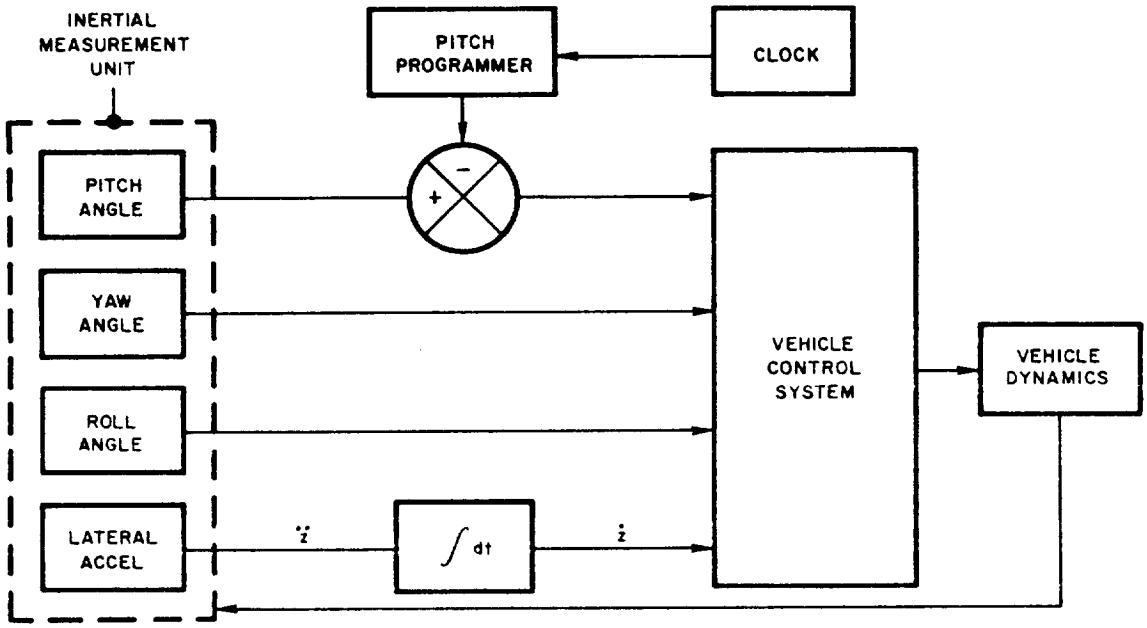

Fig. 25. Steering Computer

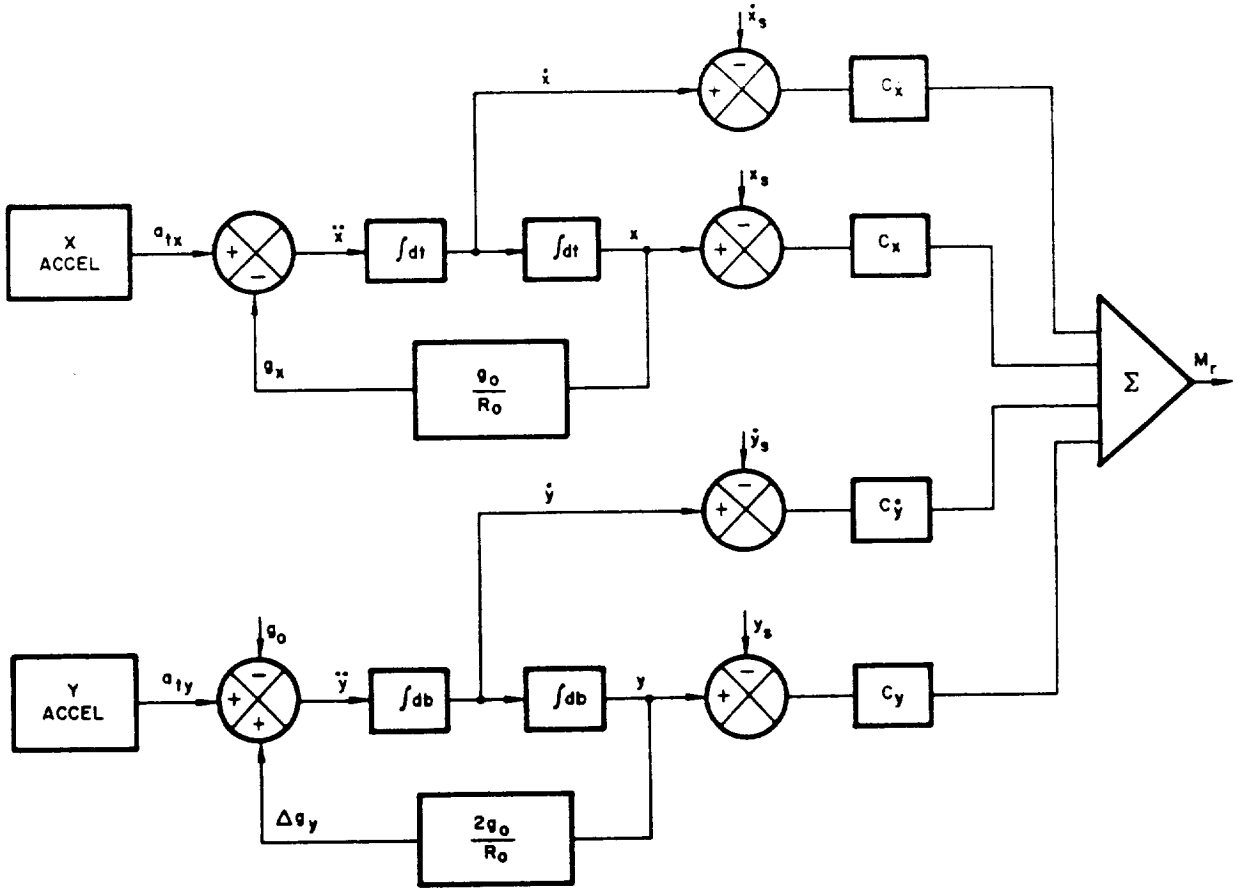

Fig. 26. Motor Shutoff Computer

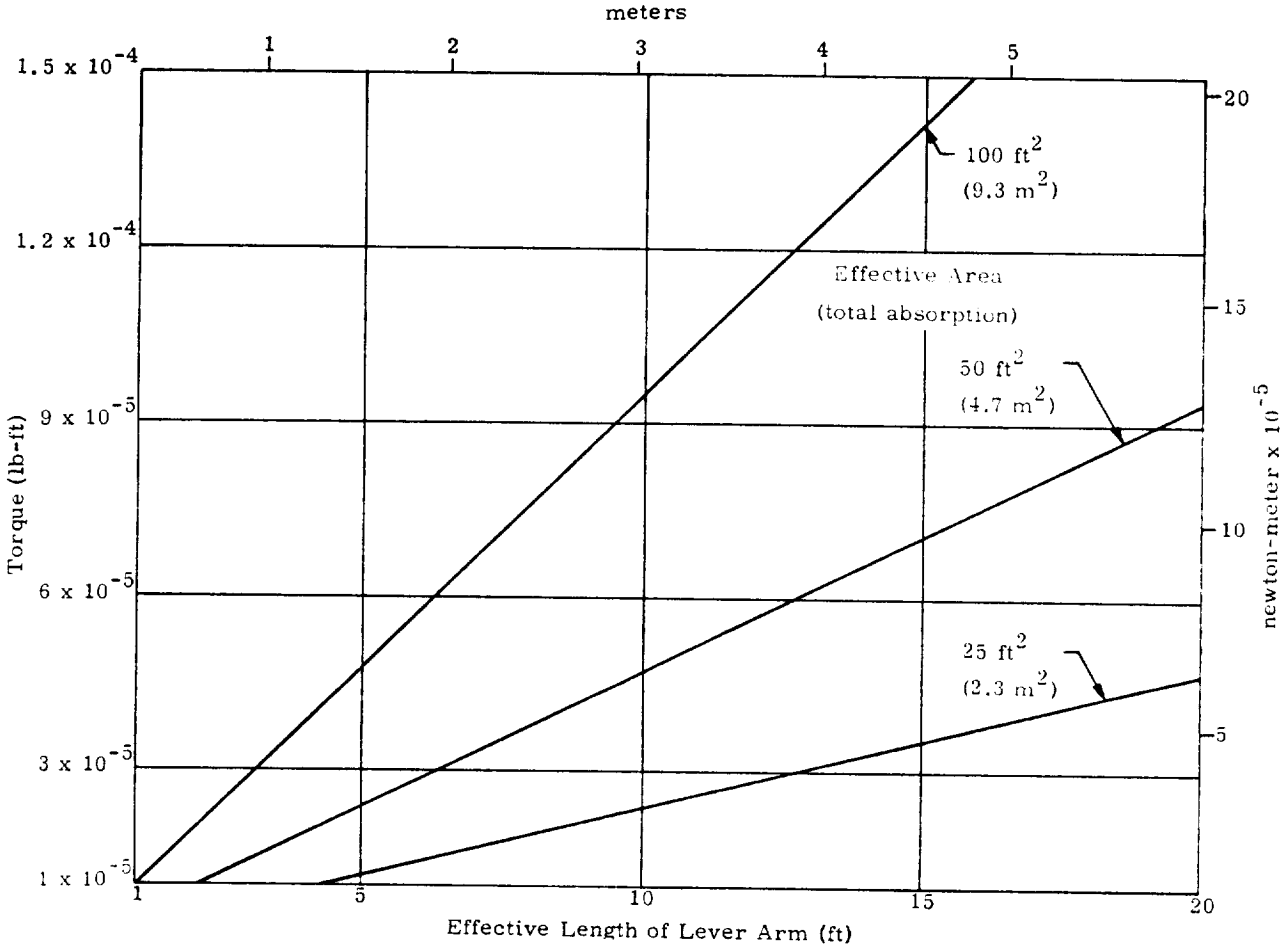

Fig. 27. Torque from Solar Radiation as a Function of Area and Lever Arm

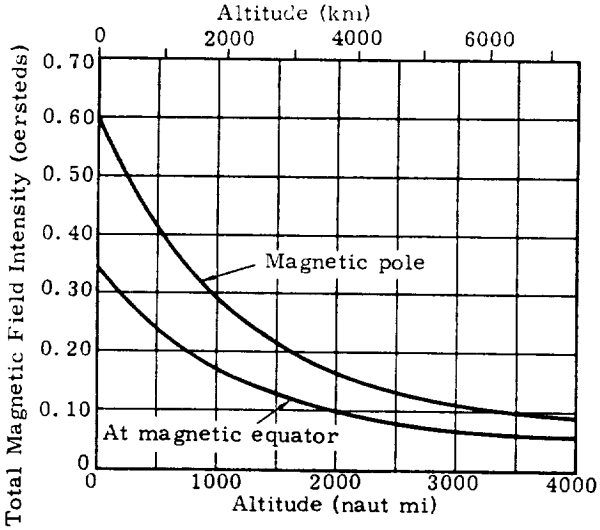

Fig. 28a. Field Intensity Versus Altitude for Earth's Magnetic Field

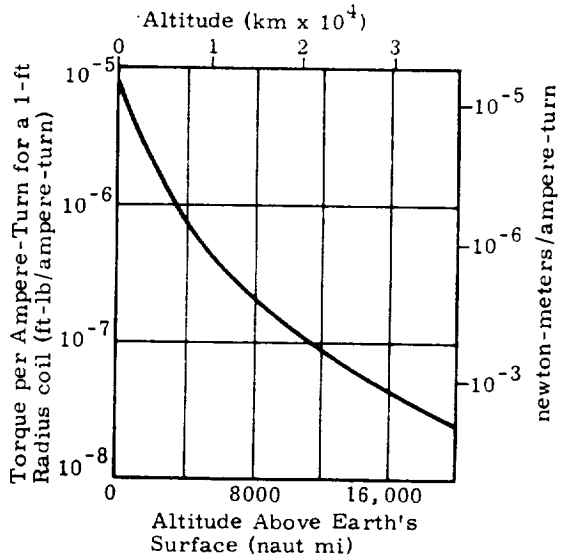

Fig. 28b. Maximum Torque per Ampere-Turn for a 1-ft Radius Coil Versus Altitude over the Magnetic Equator

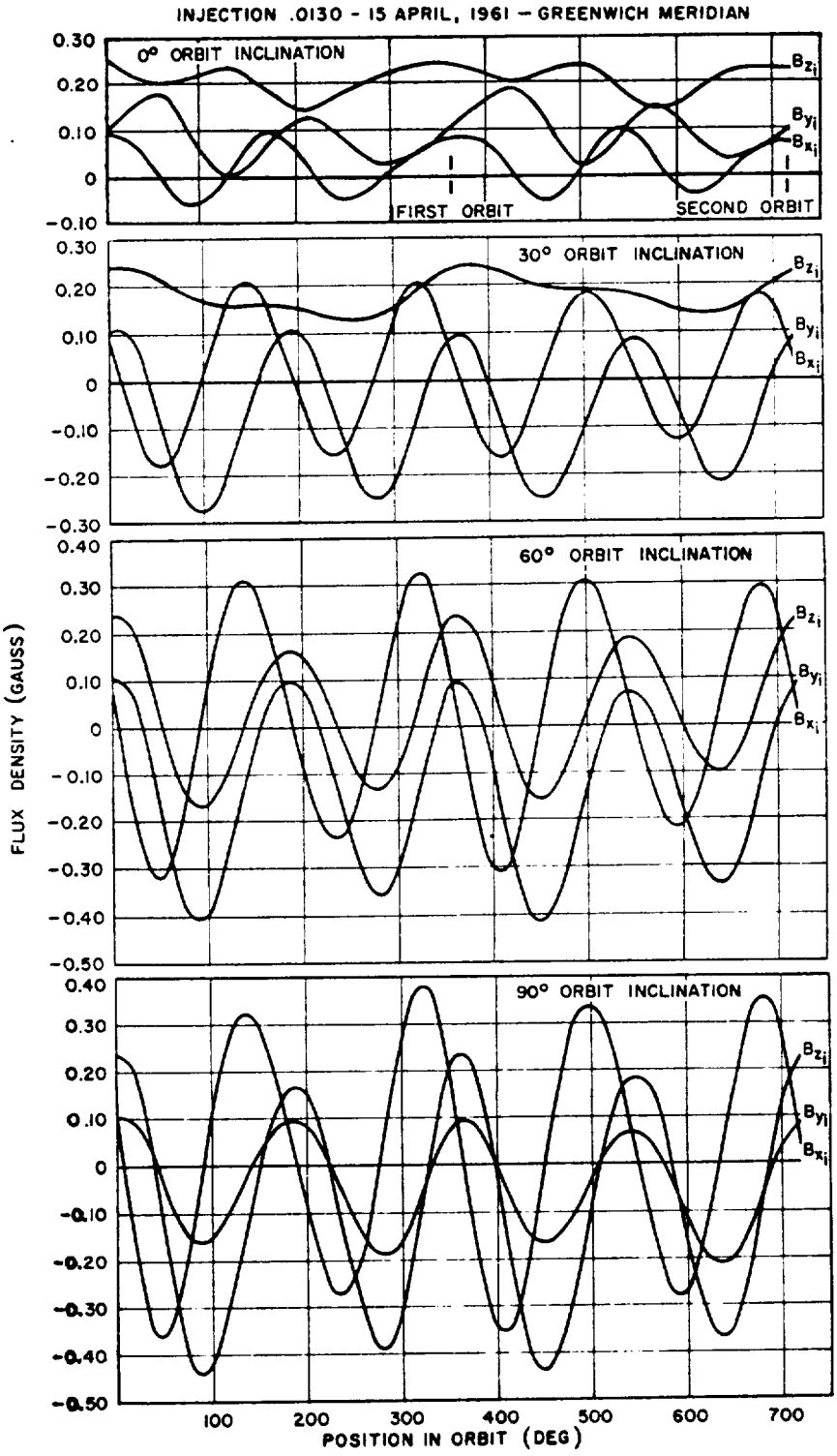

Fig. 29. Flux Density in Inertial Space Versus Position in 400-naut mi (741 km) Orbit

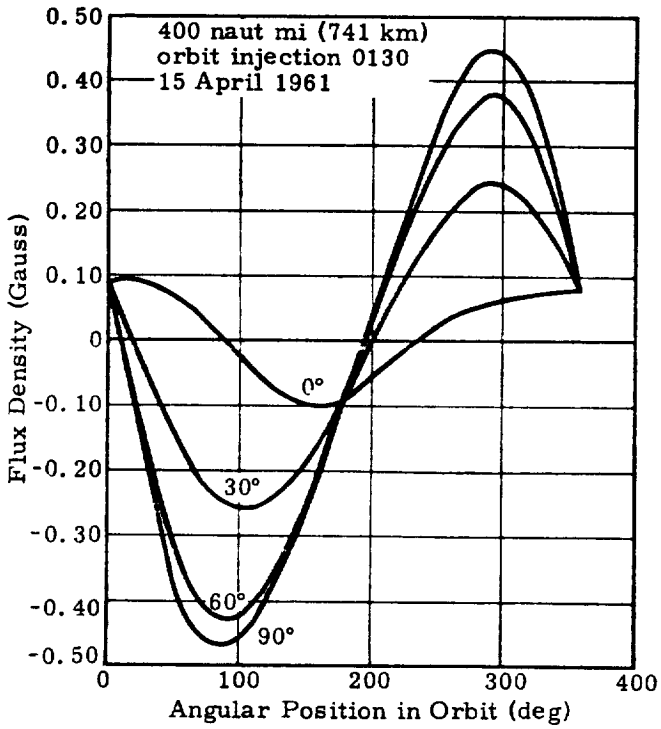

Fig. 30. Component of Flux Density Along Earth's Local Vertical in 400-naut mi Orbit for Several Orbit Inclinations (741 km)

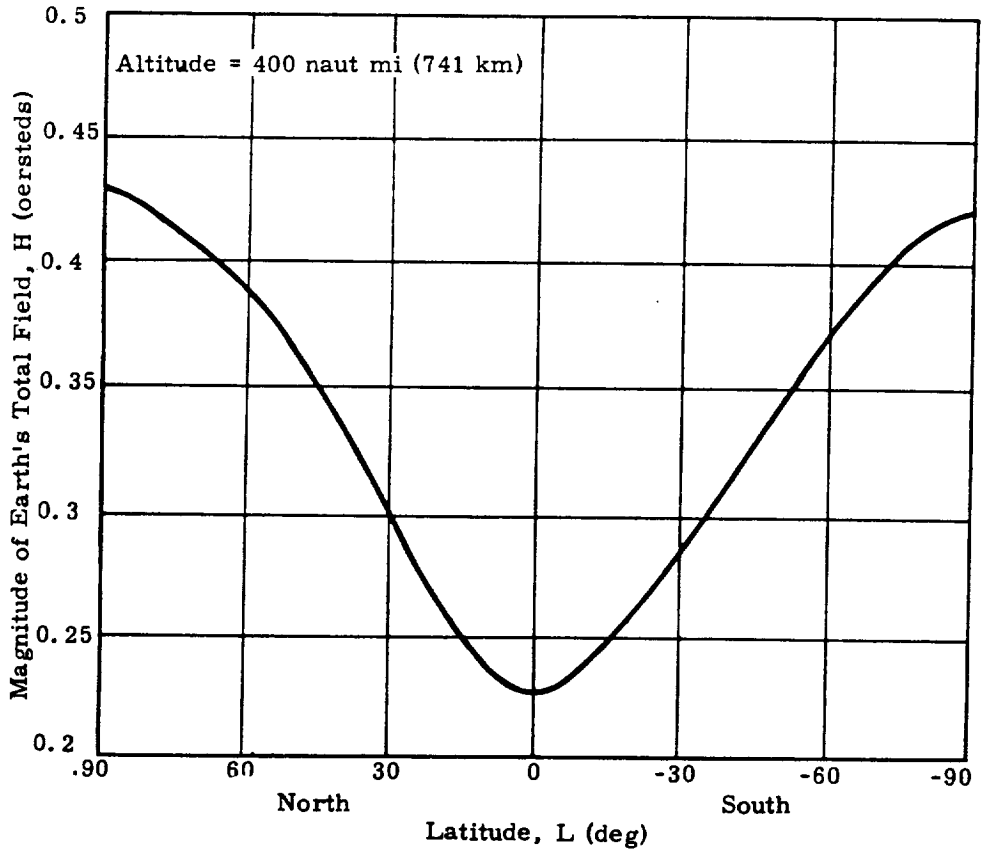

Fig. 31. Magnitude of Earth's Magnetic Field at 400 naut mi (741 km) as a Function of Latitude Assuming the Magnetic Dipole is Along the Earth's Spin Axis

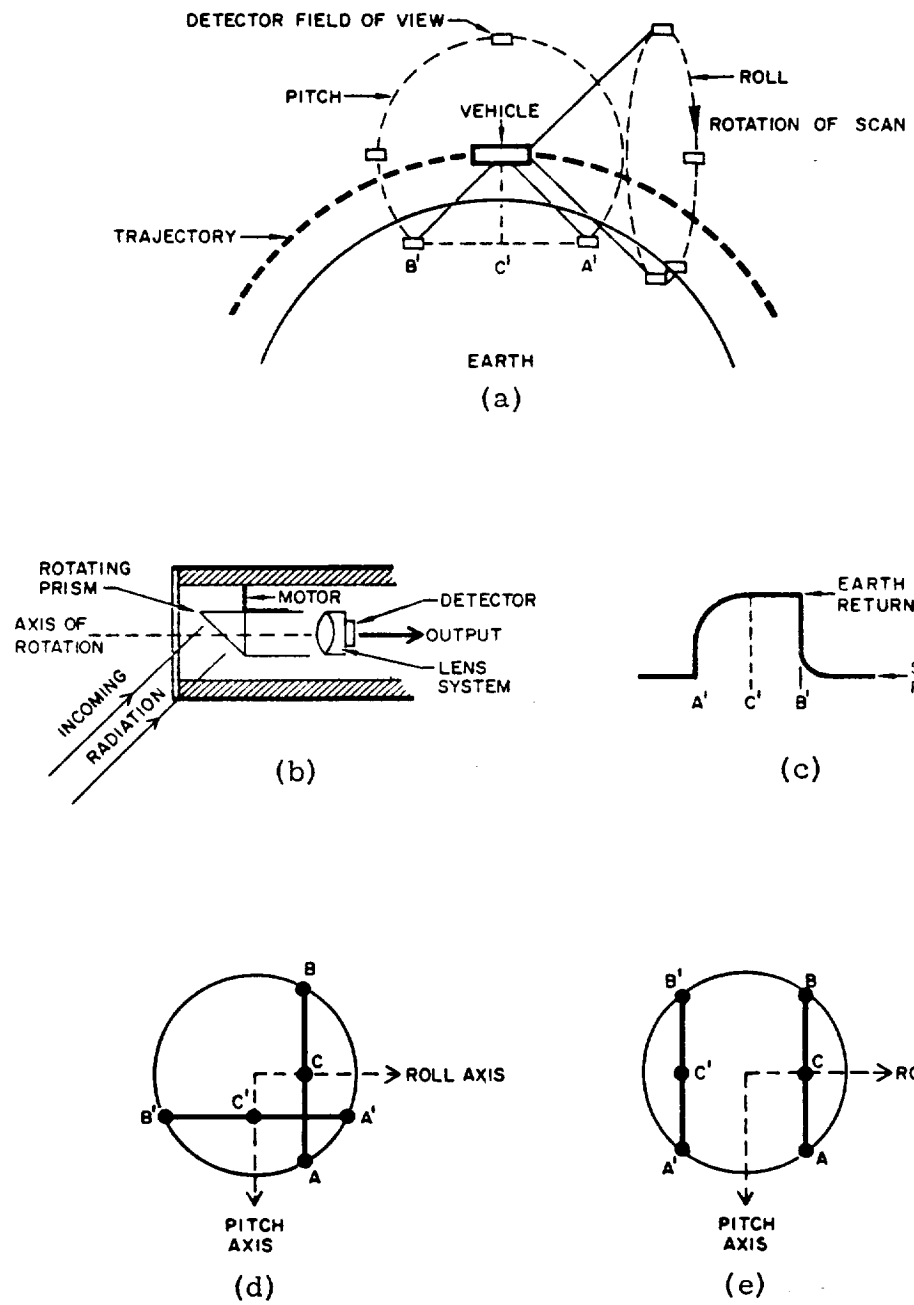

Fig. 32. Typical Conical Earth Scanning System

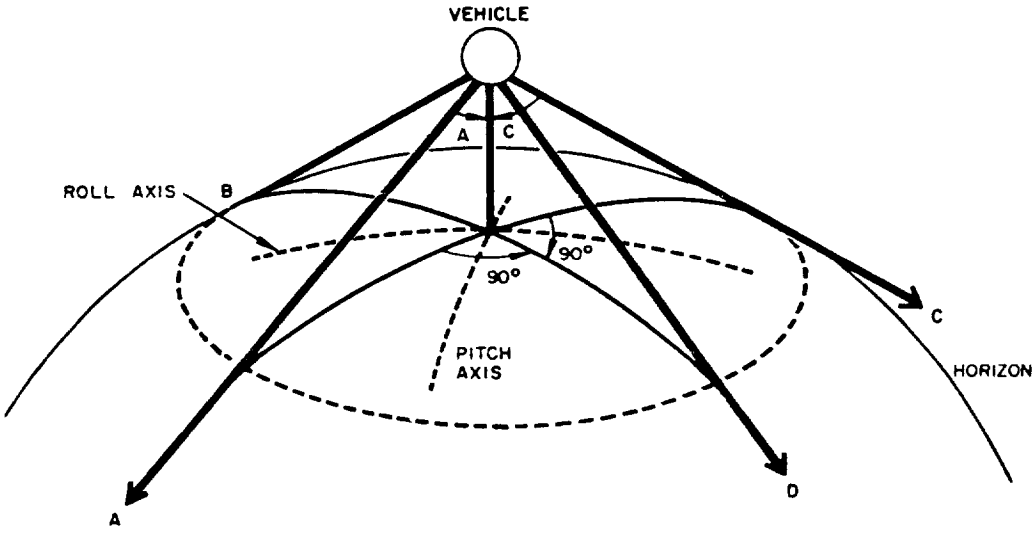

Fig. 33. Geometry for Using Edge Tracking to Generate Attitude Information

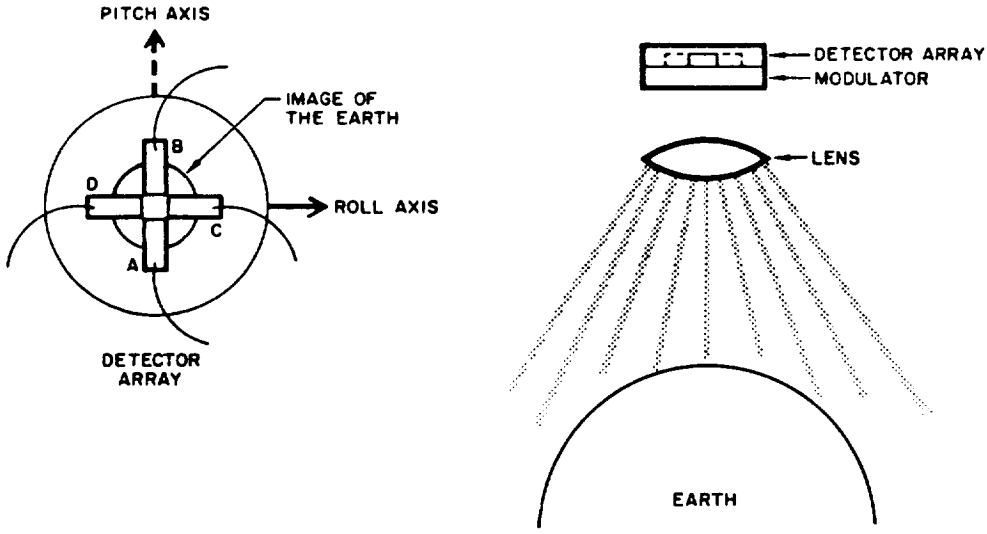

Fig. 34. A Wide Angle Passive Scanner

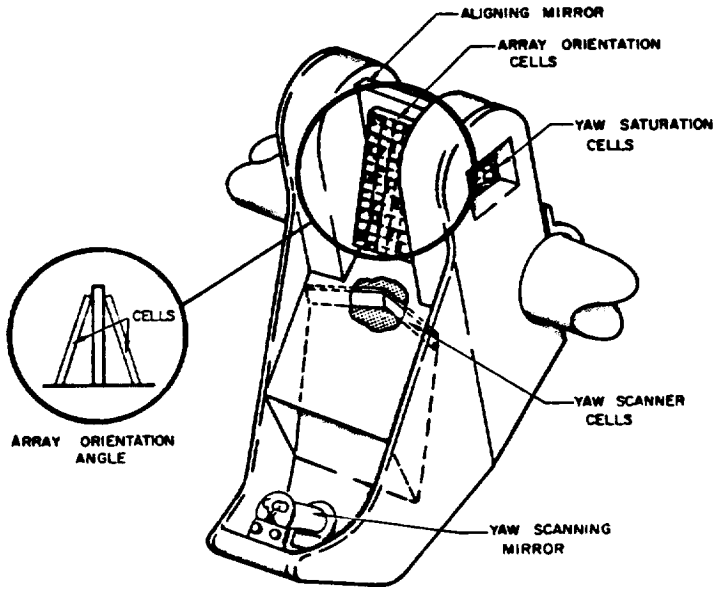

Fig. 35. A Possible Yaw and Array Sun Sensor Arrangement

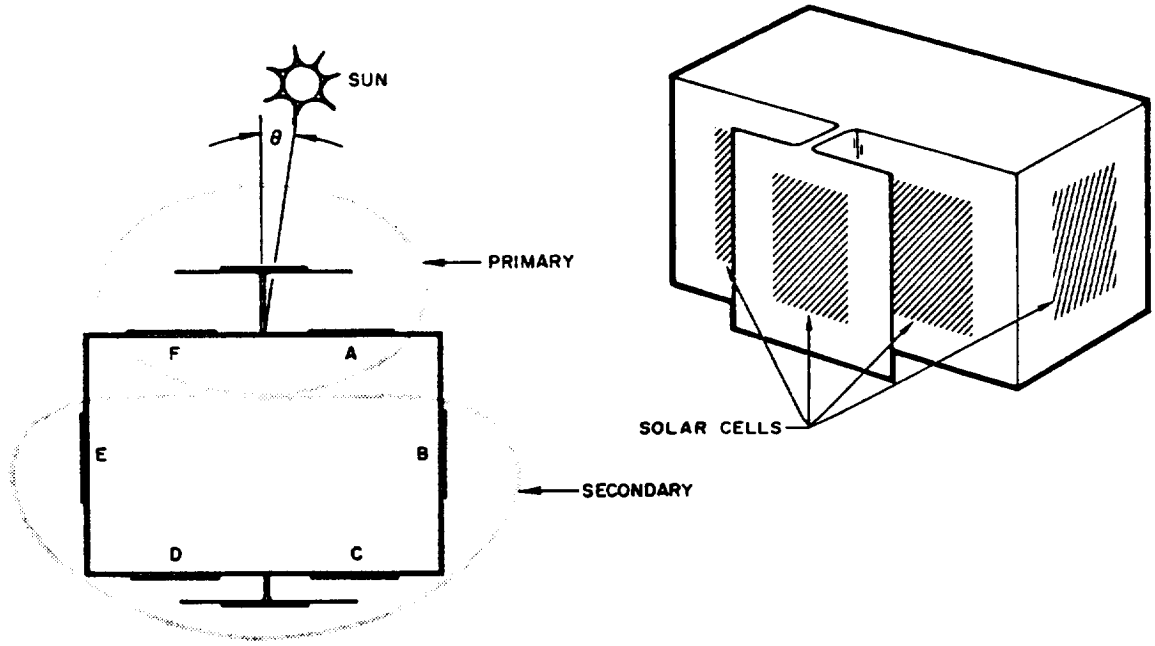

Fig. 36. T Shadow Bar Sun Sensor

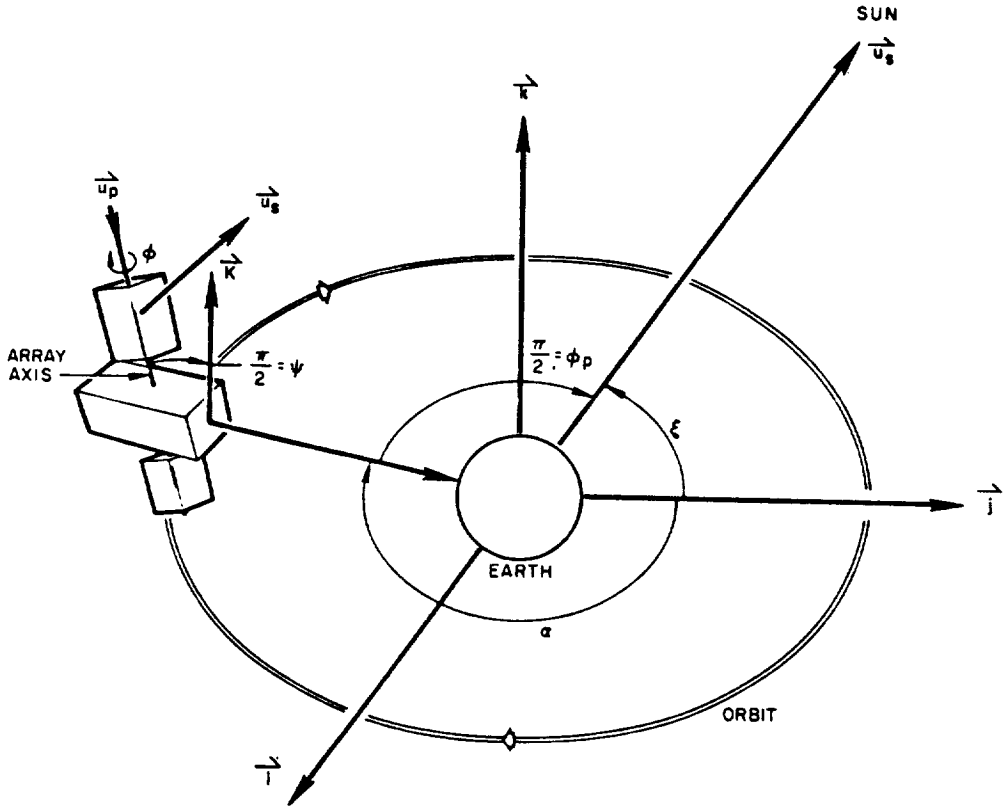

Fig. 37. Coordinate System for Computation of Yaw and Solar Array Laws

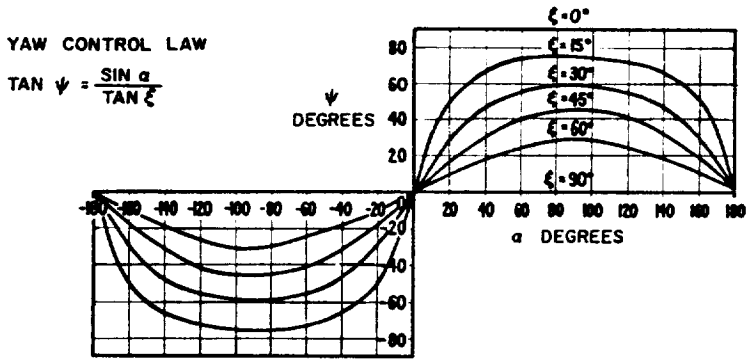

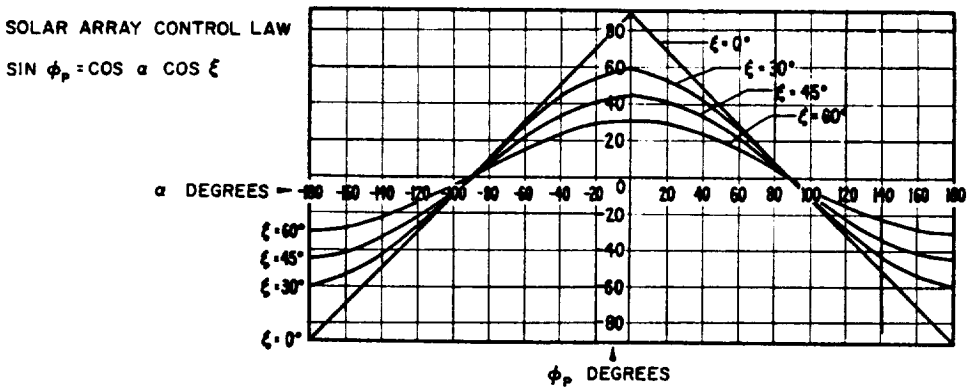

Fig. 38. Yaw and Solar Array Control Laws

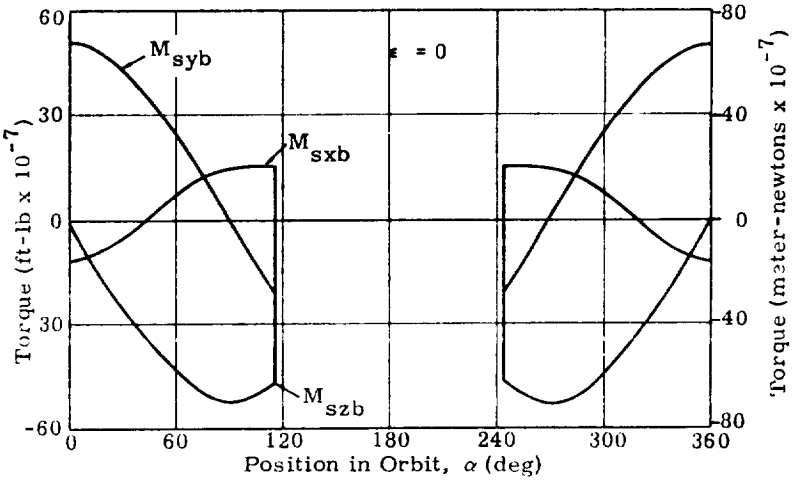

Fig. 39a. Torque in Body Coordinates Due to Solar Radiation Pressure for One Orbit

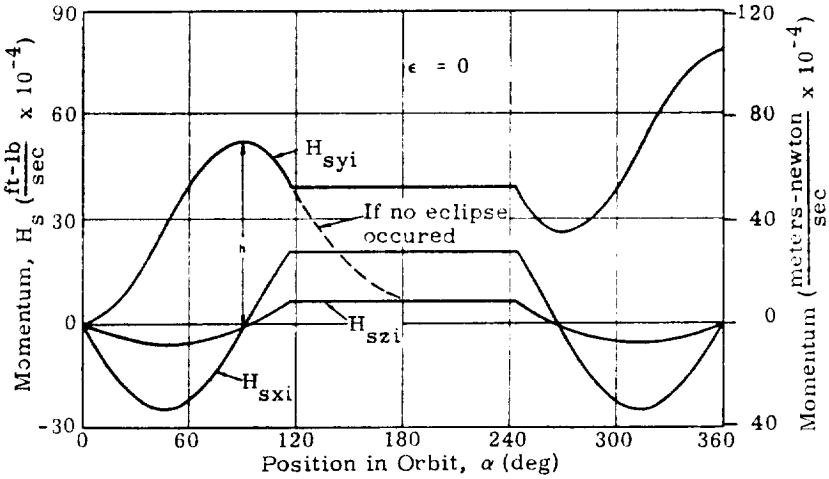

Fig. 39b. Momentum Change in Inertial Coordinates Due to Solar Radiation Pressure for One Orbit

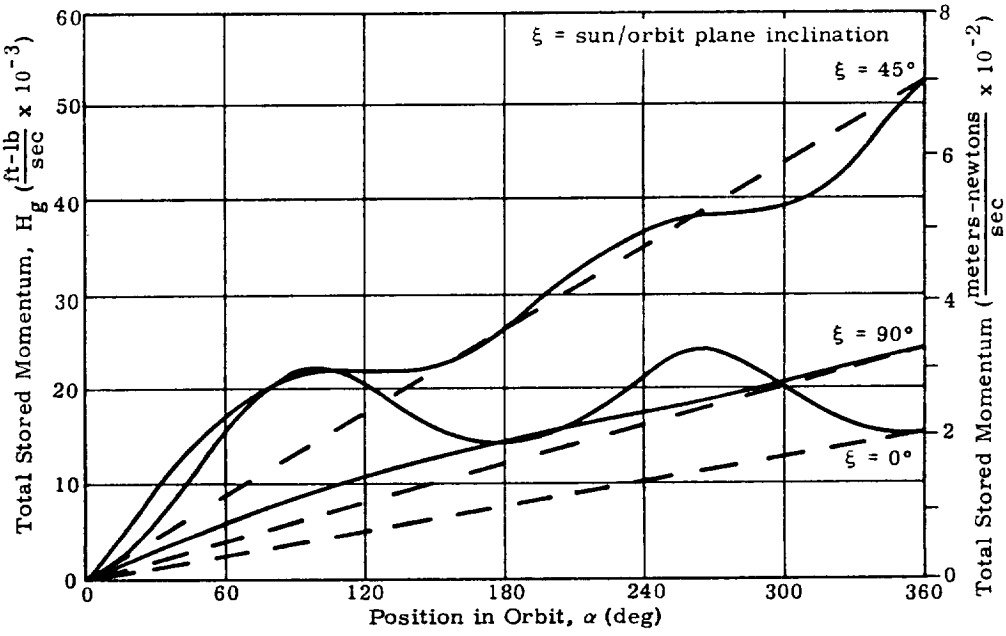

Fig. 40. Total Stored Momentum During One Orbit Due to Gravity Gradient

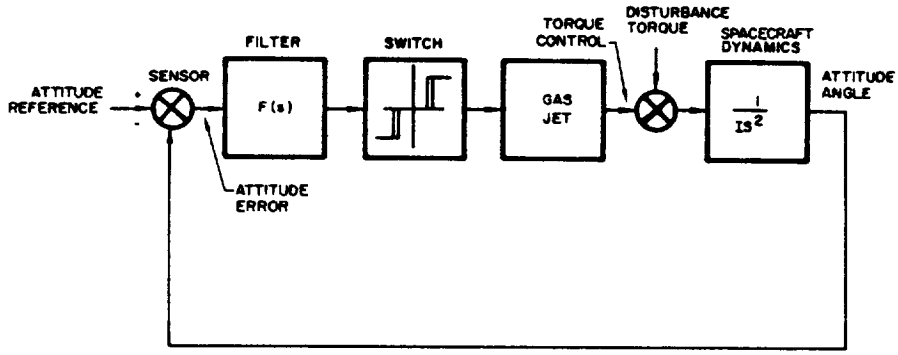

Fig. 41. Block Diagram of Simple On-Off Control System

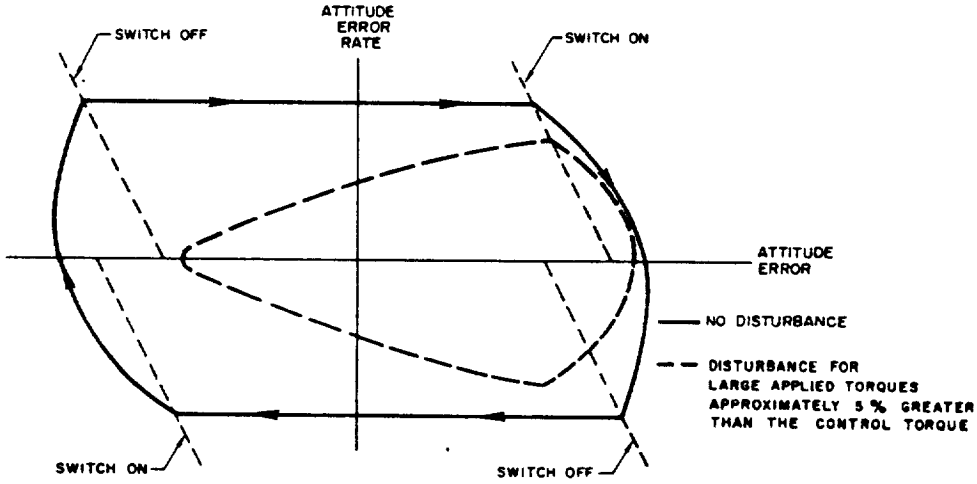

Fig. 42. Phase Plane Portrait of a Contractor Control System

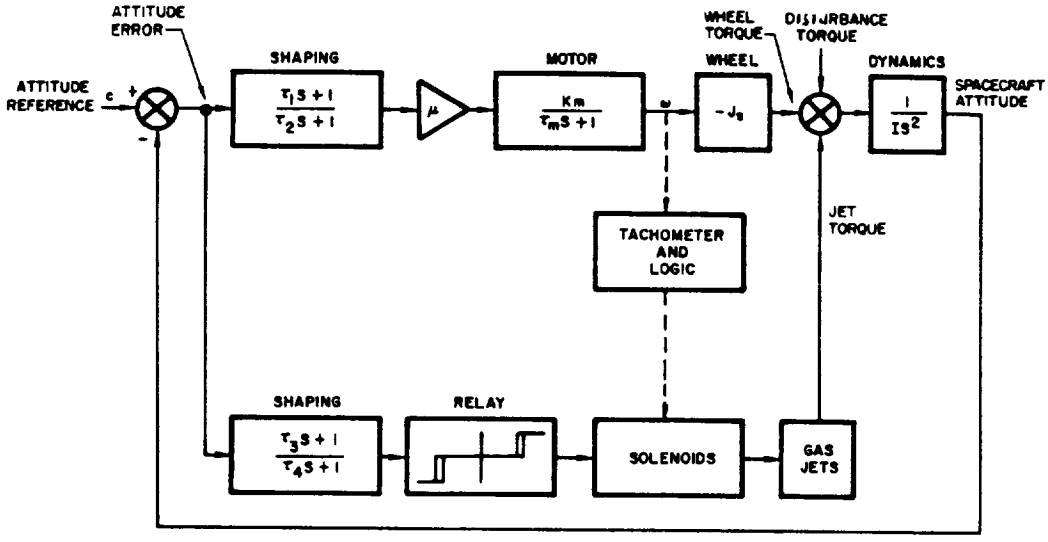

Fig. 43. Block Diagram of Gas Jet Reaction Wheel Dual Mode System

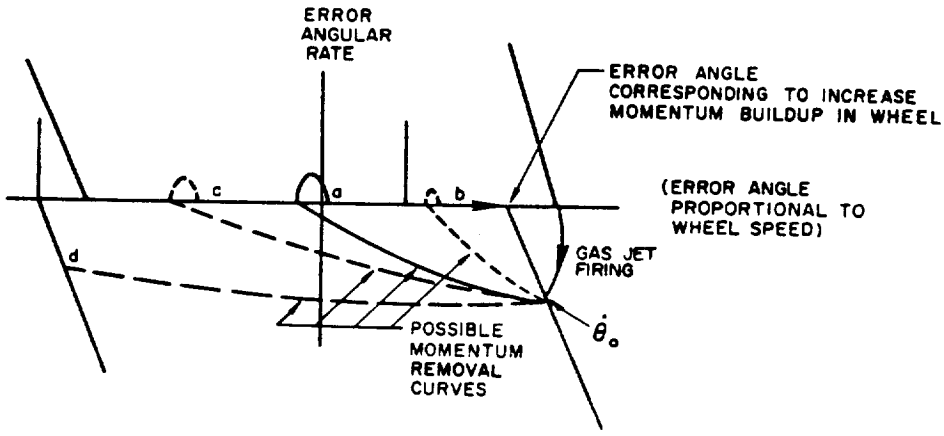

Fig. 44. Typical Phase Portrait Dual Mode System with Constant Disturbance Torque

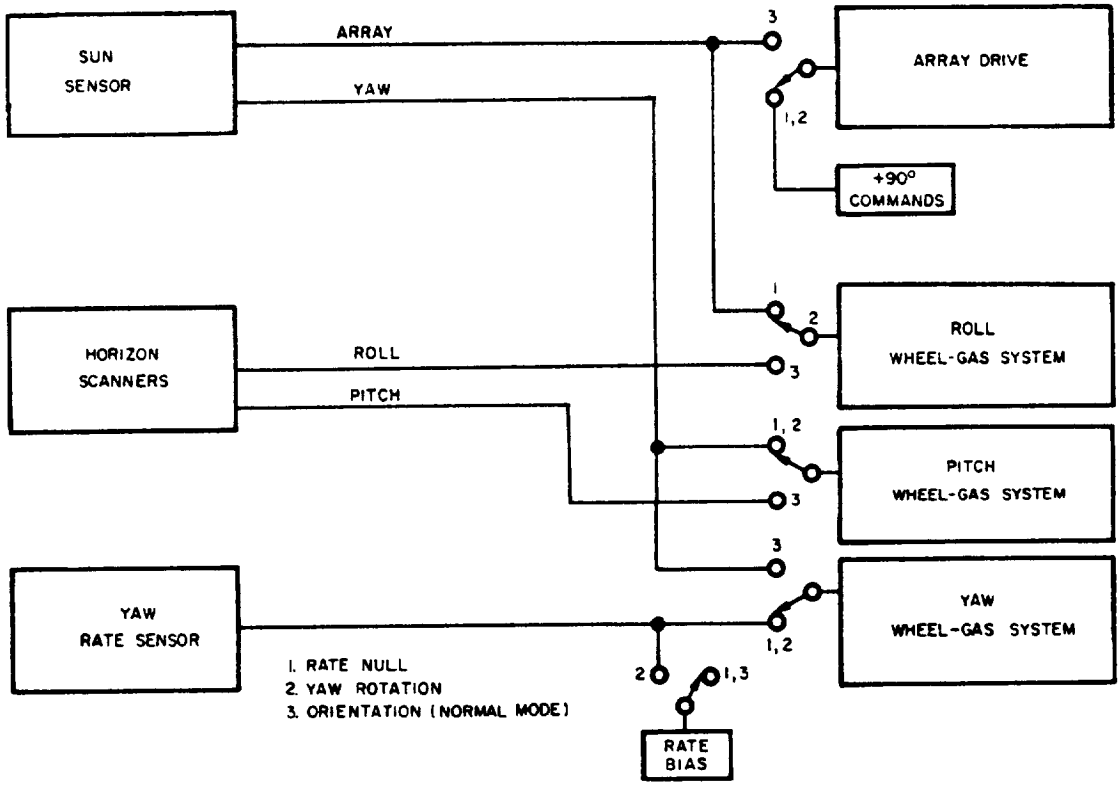

Fig. 45. Example Attitude Control System Block Diagram for Acquisition Mode

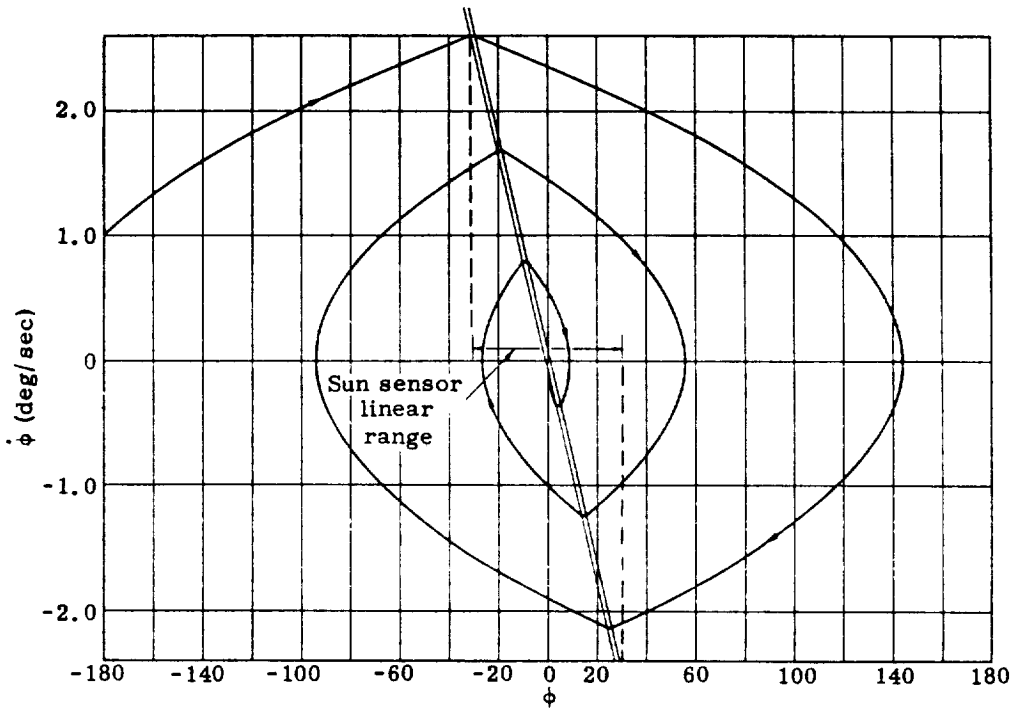

Fig. 46. Phase Portrait of Roll Error and Roll Error Phase of Acquisition

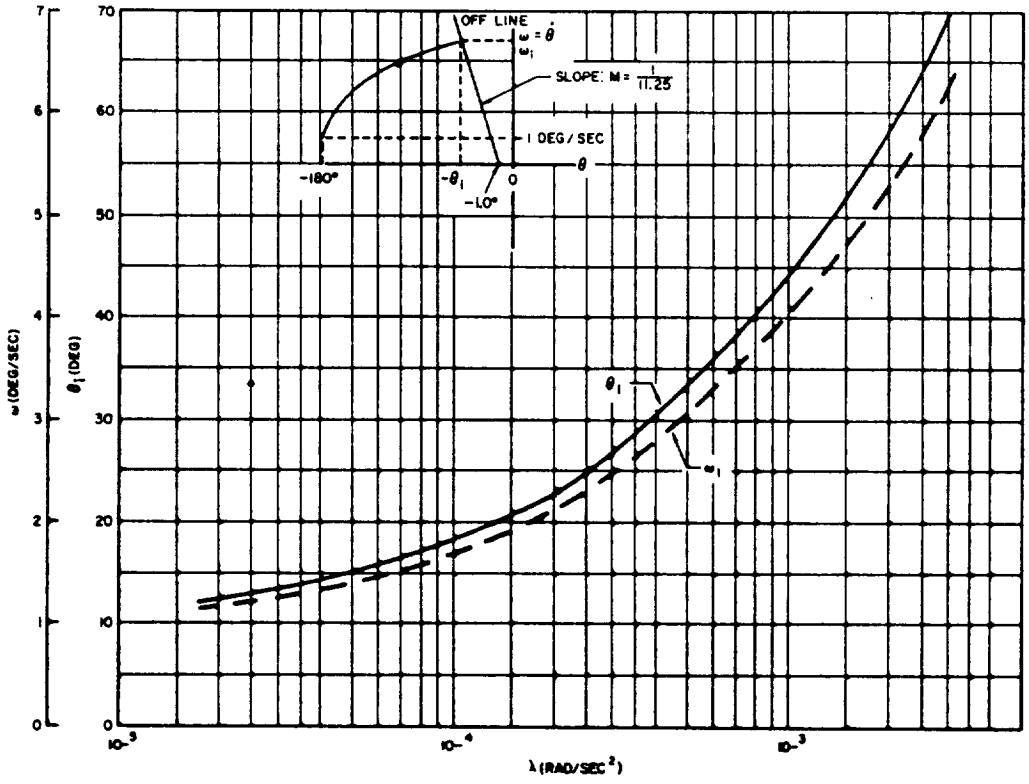

Fig. 47. Angle and Angular Rate at First Switching Line Versus Acceleration for Initial Conditions of 1°/sec and 180° Error

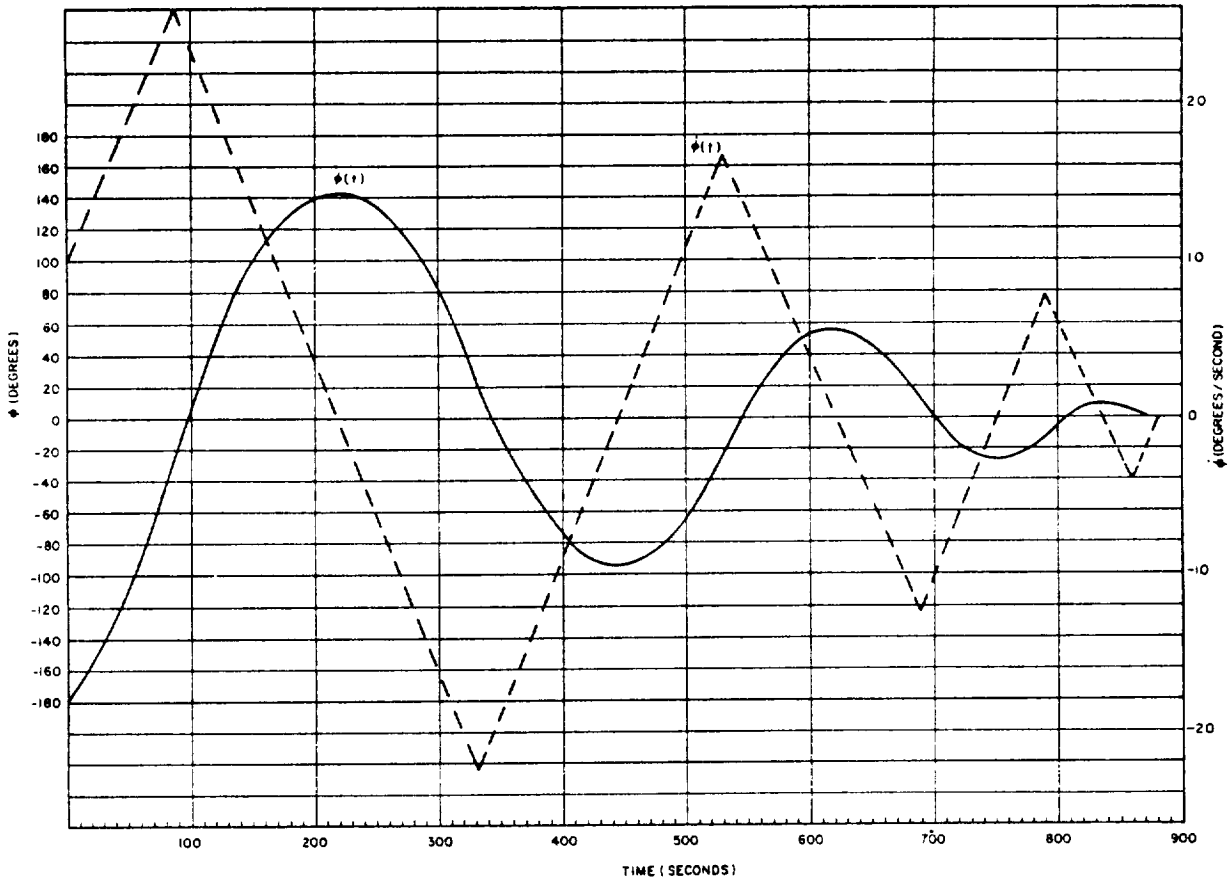

Fig. 48. Angle and Angular Rate Versus Time of Acquisition

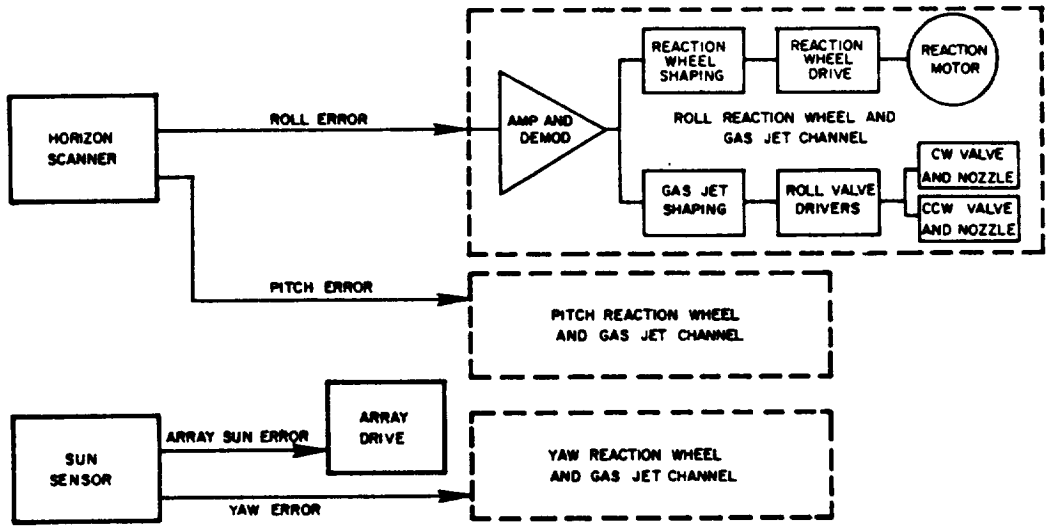

Fig. 49. Basic Attitude Control System Block Diagram for Normal Mode

CHAPTER XIII

MISSION REQUIREMENTS

Prepared by:

J. D. Kraft
Martin Company (Baltimore)
Aerospace Mechanics Department
March 1963

		Page
	Symbols	XIII-1
A.	Introduction	XIII-2
B.	Mission Considerations	XIII-2
C.	Solar Problems	XIII-6
D.	Ground Tracks	XIII-14
E.	Satellite Coverage	XIII-17
F.	Sensor Limitations on Orbit Selection	XIII-26
G.	References	XIII-32
H.	Bibliography	XIII-32
	Illustrations	XIII-35

LIST OF ILLUSTRATIONS

Figure		Page
1	Sine of the Angle Between the Normal to the Orbit Plane and the Earth-Sun Line, i = 90°	XIII-37
2	Cosine of the Angle Between the Normal to the Orbit Plane and the Earth-Sun Line, i = 90°	XIII-38
3	Cross Section of Orbit Through Shadow Cone	XIII-39
4	Orbit Going Through Shadow When Shadow Is at the Node	XIII-39
5	Orbit Going Through Shadow When Shadow Is Not at the Node	XIII-39
6	Cross Section of Orbit Through Penumbra Cone	XIII-40
7	Orbit Going Through Penumbra When It Is at the Node	XIII-40
8	Vector Analysis of Eclipse Time	XIII-41
9	Geometry of Eclipse Season	XIII-41
10	Maximum Time in Umbra and Penumbra Versus Semimajor Axis	XIII-42
11	Maximum Time in Umbra and Penumbra Versus Semimajor Axis	XIII-43
12	Maximum Time in Penumbra (No Umbra Eclipse) Versus Semimajor Axis	XIII-44
13	Maximum Time in Penumbra (No Umbra Eclipse) Versus Semimajor Axis	XIII-44
14	Eclipse Season (Umbra Only) Versus Semimajor Axis	XIII-45
15	Eclipse Season (Umbra and Penumbra) Versus Semimajor Axis	XIII-46

LIST OF ILLUSTRATIONS (continued)

Figure		Page
16	Geometry of the Simplified Eclipse Problem	XIII-47
17	Time in Sunlight Versus Cosine of Angle Between Earth-Sun Line and Normal to Orbit	XIII-47
18	Percent Time in Shadow for Circular Unperturbed Orbits	XIII-48
19	Eclipse Durations and Eclipse Seasons for Unperturbed Circular Orbits	XIII-49
20	Eclipse Durations and Eclipse Seasons for Unperturbed Circular Orbits	XIII-50
21	Eclipse Durations and Eclipse Seasons for Unperturbed Circular Orbits, i = 90°, h = 926 km	XIII-51
22	Eclipse Durations and Eclipse Seasons for an Unperturbed Circular Orbit, i = 60°, h = 926 km . . .	XIII-52
23	Eclipse Durations and Eclipse Seasons for Unperturbed Circular Orbits, i = 32°, h = 926 km	XIII-53
24	Inclination with Respect to the Ecliptic (i_ϵ) Versus Longitude of the Node with Respect to the Equator (Ω) for Different Inclinations with Respect to the Equator (i)	XIII-54
25	Angular Radius of Shadow Versus Distance from Center of Earth	XIII-55
26	Angular Radius of Shadow Versus Distance from Center of Earth	XIII-56
27	Flow Chart of a Simple Eclipse Program	XIII-57
28	Example of Eclipse Patterns When Launching a Vehicle on Different Dates in 1963 at the Same Time of Day	XIII-58
29	Example of Eclipse Patterns When Launching a Vehicle at Different Times on the Same Date	XIII-59

LIST OF ILLUSTRATIONS (continued)

Figure		Page
30	Example of Eclipse Patterns for One Satellite Taking into Account Different Perturbations	XIII-60
31	Geometry of the Ground Track Problem	XIII-60
32	Ground Tracks of Circular 24-Hr Orbits	XIII-61
33	Ground Track of Elliptical 24-Hr Orbits	XIII-61
34	Ground Track of an Elliptical 24-Hr Orbit	XIII-61
35	Satellite Coverage	XIII-62
36	Satellite Coverage	XIII-63
37	Longitudinal Ground Track Shift	XIII-64
38	Nodal Orbit Period	XIII-65
39	Diurnal Longitudinal Shift of the Ground Track ..	XIII-66
40	Number and Distribution of Satellites in a Polar Network Providing Complete Global Coverage (σ = 0 deg)	XIII-67
41	Theoretical and Practical Optimum Satellite Utilization in a Polar Network Providing Complete Global Coverage	XIII-67
42	Comparison of Polar Satellite Networks Providing Coverage from the Poles to Minimum Latitude, L_{min} (σ = 0 deg)	XIII-68
43	Comparison of Inclined and Polar Satellite Networks Providing Coverage from the Equator to Maximum Latitude, L_{max} (σ = 0 deg)	XIII-68
44	Eccentricity Effects on the Spacing of Six Satellites (placed at equal time intervals)	XIII-69
45	Ground Track for One Satellite During a Day ...	XIII-70

LIST OF ILLUSTRATIONS (continued)

Figure		Page
46	Ground Tracks for 16 Satellites During Half a Revolution	XIII-71
47	Three-Dimensional Orbit Pattern	XIII-72
48	Areas Not Covered by Ground Swaths at Time Zero	XIII-73
49	Maximum Longitudinal Increment of Area Not Covered by Ground Swath as a Function of the Orbital Inclination	XIII-74
50	The Coordinate System for Satellite Tracking	XIII-75
51	Satellite Depression Angle Relative to Local Vertical	XIII-75
52	Cosine ψ Versus Nodal Reference Angle	XIII-76
53	Cosine ψ Versus Nodal Reference Angle (detailed view)	XIII-77
54	Diagram for Finding the Distance at Subsatellite Point and Line-of-Sight Range	XIII-78
55	Chart for Determining Elevation and Slant Range of Satellite (0 to 185,000 km)	XIII-79
56	Chart for Determining Elevation and Slant Range of Satellite (0 to 8340 km)	XIII-80
57	Visibility Time for Circular Orbits (nonrotating earth)	XIII-81
58	Effect of Earth Rotation on Visibility Time (circular orbits)	XIII-82
59	Maximum Orbit Altitude as a Function of Ground Resolution Desired, Focal Length and System Resolution	XIII-83

LIST OF ILLUSTRATIONS (continued)

Figure		Page
60	Transfer Function (scene-lens combination)	XIII-84
61	Transfer Function of Scene Contrast	XIII-84
62	Diffraction Limited Lens	XIII-85
63	Transfer Function of Diffraction Limited Lens . . .	XIII-85
64	Transfer Function of Diffraction Limited Lens . . .	XIII-86
65	Transfer Function for Linear Motion	XIII-86
66	Typical Photographic Film Transfer Function	XIII-87
67	Illustrative Example	XIII-87

SYMBOLS

a = orbit semimajor axis

b = orbit semiminor axis

d = ground range

e = orbit eccentricity

E = eccentric anomaly

h = orbit altitude

i = inclination of the orbit plane to the equatorial plane

i_ϵ = inclination of the orbit plane to the ecliptic plane

$i_\odot$ = obliquity of the ecliptic

J_2 = coefficient of the gravitational potential function, 1.0823×10^{-3}

ℓ = Celestial latitude (referenced to ecliptic)

L = geocentric latitude (referenced to equator)

M = mean anomaly

n = mean motion $= \sqrt{\frac{\mu}{a^3}}$

n_1 = number of orbit planes in a pattern

n_2 = number of satellites in an orbit

p = orbit semilatus rectum

r = radial distance from the center of the earth

R = radius of a sphere of volume equivalent to that of the earth

R_e = equatorial radius of the earth

s = angular radius of shadow

t = time

t_v = visibility time

v = velocity magnitude

x, y, z = Cartesian position coordinates

α = central angle between the subsatellite point and the edge of the area visible from the satellite

β = azimuth angle relative to north

γ = flight path angle with respect to local horizontal

γ_n = angle between the earth-sun line and the normal to the orbit plane

$\cos\alpha, \cos\beta, \cos\gamma$ = direction cosines

ϵ = elevation angle with respect to the horizontal plane

θ = true anomaly

ϑ = central angle in the ecliptic plane from vernal equinox to the sun

λ = celestial longitude (referenced to ecliptic)

Λ = geocentric longitude (referenced to equator)

μ = gravitational constant of the earth ($398,601.5\ km^3/sec^2$)

ρ = line-of-sight range

σ = viewing angle with respect to the horizontal plane

τ = Keplerian orbit period

τ_{nodal} = nodal orbit period, the interval between two successive transits through the ascending node

$\tau_{sidereal}$ = sidereal orbit period, the interval between two successive crossings of the same hour circle on the celestial sphere

τ_e = period of the earth's rotation

ϕ = central angle in the orbit plane from the ascending node to the satellite

ω = argument of perigee

Ω = right ascension or longitude of the ascending node

Ω_e = rate of rotation of the earth

Υ = vernal equinox

SUBSCRIPTS

o observer

$\odot$ sun

$\oplus$ earth

ϵ ecliptic

0 initial value

A. INTRODUCTION

Once a satellite mission has been conceived to accomplish a given function (e.g., reconnaissance, communications, meteorological determinations, etc.), the question arises as to what orbit or orbits would best be suited to accomplishing the specified mission. Selection of the best orbit depends upon a multitude of factors such as periodicity, area coverage capability, target coverage capability, satellite and subsatellite point illumination and vehicle tracking considerations. These factors will be investigated in order to provide a basis for orbit selection in a given mission plan. Section B considers the general nature of the various types of missions and indicates how the above factors are involved in orbit design for each mission. Detailed quantitative analyses of the various factors are contained in Sections C, D and E.

B. MISSION CONSIDERATIONS

Although each mission has its individual requirements, most satellites may be categorized for general study as follows:

(1) Reconnaissance satellites.

(2) Communications satellites.

(3) Navigation satellites.

(4) Meteorological satellites.

(5) Scientific satellites.

In general, orbit design for each of the missions will require consideration of ground tracks, coverage and sensor limitations. In addition, whenever photographic determinations are made, or solar power supplies are used, various solar problems (e.g., heating, time in sunlight, relative orientation of the vehicle-sun-line, etc.) must be considered. Table 1 lists most of the factors involved in selection of each orbit element. The following subsections qualitatively relate these factors to the above mission types.

1. Reconnaissance Satellites

One function in which satellite systems are well suited is that of scientific or military reconnaissance. Observations made by a satellite system can provide valuable information on the nature of this surface of the earth, and of the number, locations and state of development of installations. In making these observations, a satellite system has the advantage of covering large areas rapidly and periodically with no risk to the observer.

From a general point of view, selection of an optimum reconnaissance satellite orbit, involving specification of six orbit elements, is based upon the following philosophy:

(1) In most missions, orbits of low eccentricity should be selected to allow uniform sensor performance throughout the orbit. Thus, for the limiting case of $e = 0$, two additional elements ω and T_p (the argument of perigee and the time of perigee passage) may be selected arbitrarily because they have no real meaning.

(2) In general, choice of orbit altitude depends on a tradeoff between sensor power and resolution requirements for low altitude on one hand and coverage and orbit lifetime requirements for high altitude on the other. Decay of the orbit altitude due to atmospheric drag is prohibitive for altitudes less than 150 km, and orbits of altitude less than about 225 km will require periodic corrections even for useful lifetimes of a few weeks. The added complexity of orbit correction systems and the added fuel requirement, as determined in Chapter VI, are certainly factors in the selection of an orbit altitude for extended missions. The effect of low altitude in decreasing area coverage is discussed in some detail in Section E. This factor is especially significant for missions requiring continuous photographic coverage for extended periods, where the film bulk can be quite large. The sensor requirement for low altitudes is discussed in Section F.

(3) For fairly low altitude satellites, the inclination of the orbit to the equatorial plane must be at least as large as the latitude of geographical areas to be observed. Thus, as an example, if there is a requirement for complete coverage with low altitudes, polar orbits are required (Section E).

(4) The right ascension of the ascending node, as determined by the launch time, could be selected arbitrarily for missions of extended duration or missions aimed at more or less total coverage. However, for short-term missions requiring photographic inspection of a specific geographic area, the node should be selected so that the satellite passes over the area of interest during the local daytime.

2. Communications Satellites

Satellites can be used as component stations of a communication system relaying signals from one point on the earth's surface to another. Their advantage in this application is primarily one of coverage. Range limitations of conventional radio transmission can be overcome and reliable intercontinental radio telephone links established.

Communications satellites may function actively or passively. That is, an active satellite contains receiving and transmitting equipment so that it can receive a signal from earth, amplify it and retransmit the same signal signal back to earth. A passive satellite, which may take the form of a large, metallic skin balloon, merely reflects incident radiation from the earth so that a portion of this radition is scattered back in the direction of the earth. Examples of the two types are the ECHO balloon satellites and the TELSTAR active satellites. Passive systems would require ground

TABLE 1

Factors Involved in Orbit Selection

Altitude	Factor	Eccentricity	Factor	Inclination	Factor	Node	Factor
High	(1) Maximum coverage	Low ($e \approx 0$)	(1) Uniform coverage over large areas	Low	(1) Elimination of earth relative motion in the case of the 24-hr orbit	Special value	(1) Selection of daytime over a reconnaissance or coverage area
High	(2) Minimum drag perturbations	Low ($e \approx 0$)	(2) Uniform sensor resolution and power requirements	High	(2) Complete global coverage	Special value	(2) Selection of an optimum or uniform coverage pattern
High	(3) Minimum oblateness perturbations	Low ($e \approx 0$)	(3) Elimination of earth relative motion in the case of the 24-hr orbit	Specific values	(3) Optimum or uniform coverage	Special value	(3) Maximization of time in sunlight for solar power
Low	(4) Sensor resolution and power limitations	Low ($e \approx 0$)	(4) Ease of position prediction and uniform ground track	Specific values	(4) Tracking station utilization		
Low	(5) Minimum solar and lunar perturbations	Low ($e \approx 0$)	(5) Secular perturbations can be largely compensated for in achieving synchronous orbits	Specific values	(5) Reconnaissance or coverage of a particular area		
Low	(6) Propellant expenditure in launch	High	(6) Increased coverage over limited areas for fixed launch propellant expenditure	Specific values	(6) Regression rate set to 0.986°/day for a given altitude (allows orbit plane to follow the sun)		
Specific altitudes (24-hr, 6-hr, etc., see Section D.2.)	(7) Achieving synchronous performance (orbit period a rational fraction of a day)						
See Chapter II	(8) Avoiding Van Allen belts						

station transmitters of much higher power than would active satellites. On the other hand, the complexity of vehicle-borne equipment leads to limitations on reliability and mission duration for active systems.

Mission requirements for a complete communications system would probably aim for continuous 24-hr coverage between virtually every pair of points on the earth's surface. One orbit design which has been frequently mentioned in connection with this requirement employs the 24-hr satellite orbit. Because this orbit has a period of one day, satellite motion is synchronized with the rotation of the earth. In the case of the 24-hr equatorial circular orbit, the satellite would appear to hang motionless in the sky above an observer on the earth. Elliptic or nonequatorial 24-hr satellites perform diurnal excursions relative to the observer. The 24-hr orbit is described in greater detail in Section D. The advantages of the 24-hr orbit in communications systems lie in the stationary nature of the satellite and the wide coverage of each satellite (the 24-hr circular orbit altitude is 35,777 km). At the 24-hr orbit altitude, each satellite can view very nearly half of the earth's surface. Thus, three satellites could provide very adequate coverage which could only be achieved by hundreds of satellites in low altitude orbits. Also, ground antennas could be fixed, and tracking would be extremely simple. A disadvantage of the 24-hr orbit system is the relatively high power required to transmit to this high altitude.

Whatever altitude is chosen, it should be such that an integral number of periods are contained in a day. Then the ground track, the trace of the subsatellite point on the surface of the rotating earth, will repeat daily. This condition is obviously desirable from the standpoints of ease of prediction of satellite position and utilization of the system. That is, the user would know what satellite service is available at a given time without referring to a complicated ephemeris because a satellite is at the same place at the same time each day. Synchronous orbits, which exhibit a daily repeating ground track, are those of 24, 12, 8, 6, 4, 3 and 2 sidereal hour periods. The altitudes corresponding to these periods are tabulated in Section D.

For communications systems which aim for literally world-wide service, circular orbits offer the advantage of uniformity in coverage. However, if the system is to provide coverage primarily in one hemisphere or primarily during the daytime, high eccentricity orbits could be chosen. These orbits can be achieved more economically than could circular orbits of their apogee altitude (apogee altitude is the criteria here in order to provide a large communication range). The elliptical orbits would, of course, be launched so that apogee conditions occur over the daylight side of the earth or over the hemisphere of interest.

3. Navigation Satellites

Artificial satellites can be used as references for all-weather navigation systems determining position and velocity of a surface vehicle, aircraft or space vehicle. The conventional navigation methods, e.g., dead-reckoning, star and sun sighting during clear weather and storage of reference information by inertial guidance instruments, provide navigation information of adequate accuracy. However, such information must be periodically corrected to maintain accuracy, and the replacement of star and sun sighting with satellite sighting would permit this updating to be performed at any time, regardless of weather conditions.

a. Satellite navigation methods

Various methods of satellite navigation may be considered, depending on the nature of available equipment, data available from sources other than the satellites and the nature of the position or velocity information to be obtained.

(1) Sphereographical navigation

The position of an observer on the earth's surface can be determined from a pair of observations of the angle between the local vertical and the line of sight to a celestial body. Of course, in order to make these observations, the local vertical must be obtained by means of a pendulum, plumb bob or some other device. Any celestial body, e.g., the sun, a star or a satellite, could be observed as long as its angular position is accurately known. Determinations based on satellite positions will obviously be complicated by the high relative velocity of the observer and the satellite. However, the fundamental technique is the same. The observer, equipped with a vertical reference and an electronic sextant, measures the direction angles of a radio signal continuously emitted from the navigation satellite.

(2) Doppler navigation

The sphereographical technique employs the classical angular measurements of celestial navigation. Satellite systems employing radio techniques are not limited to these methods. One radio technique is based on the Doppler effect. Radio signals received from a moving vehicle appear higher in frequency as the vehicle approaches the observer and lower in frequency as the vehicle recedes from the observer. The difference between the observed frequency and the known transmitter frequency, the "Doppler shift," is a measure of relative motion (or relative position when these shifts are integrated) of the vehicle and observer and, therefore, can serve as input to a navigation system. Knowledge of local vertical is not required. The TRANSIT satellite program employs a purely Doppler system.

(3) Complete geometric determination

Systems for navigation on the surface of the earth can implicitly make use of the knowledge that the observer is a known distance from the center of the earth, the origin of the coordinate system in which the satellite positions are known. A more general problem may be hypothesized as follows: the position and velocity of a vehicle in space is to be determined solely from data consisting of range and range rate relative to the navigation satellites. The observer is assumed to have no knowledge of his orientation, position or velocity

from other sources such as plumb bobs, altimeters, etc. If a complete determination is to be made from a set of observations made at any given time, the observer must simultaneously note the range and range rate of three navigation satellites, the positions and velocities of which are known. Then his position is determined as the intersection of three spheres.

$$(x_o - x_i)^2 + (y_o - y_i)^2 + (z_o - z_i)^2 = \rho_{io}^2 \qquad (1)$$

$$i = 1, 2, 3$$

where

x_o, y_o, z_o = Cartesian position coordinates of observer

x_i, y_i, z_i = known Cartesian position coordinates of the three navigation satellites

ρ_{io} = ranges from the three navigation satellites to the observer.

The observer's velocity is determined from

$$\dot{\rho}_{io} = \frac{(\vec{V}_o - \vec{V}_i) \cdot \vec{\rho}_{io}}{\rho_{io}} \qquad (2)$$

where

$$\vec{V}_o - \vec{V}_i = (\dot{x}_o - \dot{x}_i)\,\vec{i} + (\dot{y}_o - \dot{y}_i)\,\vec{j} + (\dot{z}_o - \dot{z}_i)\,\vec{k}$$

$\dot{x}_o, \dot{y}_o, \dot{z}_o$ = Cartesian velocity coordinates of observer

$\dot{x}_i, \dot{y}_i, \dot{z}_i$ = Cartesian velocity components of the three navigation satellites

$\dot{\rho}_{io}$ = the range rate data

and $\vec{\rho}_{io}$ is given from Eq (1).

Differentiation of Eqs (1) and (2) gives the following error formulas.

$$\begin{pmatrix} dx_o \\ dy_o \\ dz_o \end{pmatrix} = \frac{1}{K} \begin{bmatrix} C_{11} & C_{12} & C_{13} \\ C_{21} & C_{22} & C_{23} \\ C_{31} & C_{32} & C_{33} \end{bmatrix} \begin{pmatrix} \Delta_1 \\ \Delta_2 \\ \Delta_3 \end{pmatrix} \qquad (3)$$

where

$$\Delta_i = (x_o - x_i)\,dx_i + (y_o - y_i)\,dy_i + (z_o - z_i)\,dz_i + \rho_{io}\,d\rho_{io} \quad i = 1, 2, 3$$

$$K = |K_{v_{ij}}| = \begin{vmatrix} (x_s - x_1) & (y_s - y_1) & (z_s - z_1) \\ (x_s - x_2) & (y_s - y_2) & (z_s - z_2) \\ (x_s - x_3) & (y_s - y_3) & (z_s - z_3) \end{vmatrix}$$

and C_{ij} is the cofactor of the $(ij)^{th}$ element of K^T.

$$\begin{pmatrix} d\dot{x}_o \\ d\dot{y}_o \\ d\dot{z}_o \end{pmatrix} = \frac{1}{K} \begin{bmatrix} C_{11} & C_{12} & C_{13} \\ C_{21} & C_{22} & C_{23} \\ C_{31} & C_{32} & C_{33} \end{bmatrix} \begin{pmatrix} \delta_1 + \frac{\dot{\rho}_{10}}{\rho_{10}}\,\delta'_1 + \delta_1'' \\ \delta_2 + \frac{\dot{\rho}_{20}}{\rho_{20}}\,\delta'_2 + \delta_2'' \\ \delta_3 + \frac{\dot{\rho}_{30}}{\rho_{30}}\,\delta'_3 + \delta_3'' \end{pmatrix} \qquad (4)$$

where

$$\delta_i \equiv (\dot{x}_o - \dot{x}_i)(dx_i - dx_o) + (\dot{y}_o - \dot{y}_i)(dy_i - dy_o) + (\dot{z}_o - \dot{z}_i)(dz_i - dz_o)$$

$$\delta'_i \equiv (x_o - x_i)(dx_o - dx_i) + (y_o - y_i)(dy_o - dy_i) + (z_o - z_i)(dz_o - dz_i)$$

$$\delta_i'' \equiv (x_s - x_i)\,\Delta\dot{x}_i + (y_s - y_i)\,\Delta\dot{y}_i + (z_s - z_i)\,\Delta\dot{z}_i + \rho_{is}\,\Delta\dot{\rho}_{is}$$

and K and C_{ij} are those defined in Eq (3).

b. Selection of navigation satellite orbits

The navigation satellite system is similar in most functional requirement aspects to the communications satellite system, with perhaps more emphasis on precise orbit determination and minimum sensor power requirements in the navigation system case. Here again, the requirements of wide, uniform coverage with the fewest satellites, low transmitter power and synchronous motion are important considerations in specifying optimum orbits. Since navigation requires satellite tracking by each observer as opposed to tracking by a few high-powered transmitters in the communications system, an increased emphasis on lower altitudes is required in navigation system orbit design. Also, since each observer must locate the satellites by means of an accurate ephemeris, the ephemeris should be as simple and easily updated as possible. This requirement makes selection of one of the synchronous orbits attractive. From a general standpoint, the requirements taken as a whole seem to indicate choice of circular 4- or 6-hr orbits for use in navigation system orbit patterns. For specific missions, Sections C, D, E and F offer data upon which a quantitative tradeoff may be based.

4. Meteorological Satellites

Satellite systems offer several advantages in meteorological determinations. The area over which observations can be made is, of course, much larger for a satellite system than for a ground station. By means of this greater coverage, a complete storm structure, as evinced by component cloud formations, may be observed from the satellite. During daylight conditions the satellite determinations can be photographic. The photographs could provide information on the size, structure and location of a storm, and series of photographs would reveal the nature and time history of the storm development and its motion. When the satellite is above the night side of the earth, observations can be made by an infrared scanning system operating at wavelengths which are emitted from the earth and on a spectral band which is reflected or absorbed by clouds.

In addition to storm observations, satellite determinations could include atmospheric moisture content from radar and infrared measurements of water vapor absorption bands, atmospheric density, and radio noise, which indicates the location of thunderstorms, line squalls and fronts where the atmosphere is unstable.

The TIROS satellites, a series of experimental television-equipped meteorological satellites launched in a NASA program, have proved very successful. In addition to known cloud and weather phenomena, processes which apparently had not been previously investigated were observed.

From the standpoint of orbit design the requirements of the meteorological satellite mission primarily involve achieving proper altitude and coverage. The orbit should be high enough to permit adequate area coverage (Section E) of high altitude cloud formations and yet be low enough to provide good resolution with available sensors (Section F). Eccentricity should generally be low to provide uniform coverage and resolution. The TIROS I orbit altitude was approximately 750 km. Required orbit inclination is determined from the latitude range to be covered, as considered in Section E.

C. SOLAR PROBLEMS

For many satellite missions the following considerations involving the relative positions of the sun and the vehicle are important from a mission design standpoint:

(1) Times of satellite eclipse, i.e., times when a vehicle enters and leaves the shadow of the earth.

(2) The duration of an eclipse, or the percentage of time spent in shadow.

(3) The time history of the relative positions of the vehicle, the sun and the earth.

These factors are useful in analysis of the following mission requirements:

(1) Compensation for radiant heat absorbed through the vehicle skin.

(2) Provision for adequate power supply by solar cells.

(3) Provision for tracking the sun.

(4) Assurance of optimum illumination of the subsatellite point for photographing certain geographical phenomena.

These various problems related to solar effects and their effects on mission performance therefore merit some consideration.

1. Relative Geometry of the Vehicle, Earth and Sun Positions

Since analyses of these solar problems depend on knowledge of the positions of the vehicle, earth and sun relative to each other, it is convenient to first derive equations for the instantaneous relative positions. These equations will provide a basis for the individual analyses.

a. Position of the satellite in an earth centered inertial (ECI) coordinate system

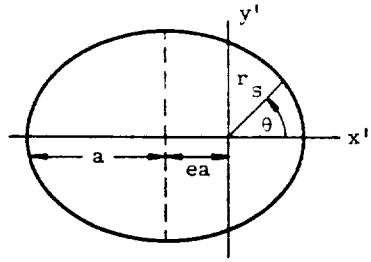

The equation of an ellipse in polar coordinates is

$$r_s = \frac{a\,(1 - e^2)}{1 + e \cos \theta} \qquad (5)$$

or in rectangular coordinates

$$\frac{(x' - ea)^2}{a^2} + \frac{y'^2}{a^2\,(1 - e^2)} = 1$$

for coordinates in the orbit plane, x' toward perigee. These coordinates may be transformed to ECI by the following rotations as outlined in Chapter XI.

$$\begin{pmatrix} x \\ y \\ z \end{pmatrix} = \begin{bmatrix} \cos \Omega & -\sin \Omega & 0 \\ \sin \Omega & \cos \Omega & 0 \\ 0 & 0 & 1 \end{bmatrix} \begin{bmatrix} 1 & 0 & 0 \\ 0 & \cos i & -\sin i \\ 0 & \sin i & \cos i \end{bmatrix}$$

$$\begin{bmatrix} \cos \omega & -\sin \omega & 0 \\ \sin \omega & \cos \omega & 0 \\ 0 & 0 & 1 \end{bmatrix} \begin{pmatrix} x' \\ y' \\ z' \end{pmatrix} \qquad (6)$$

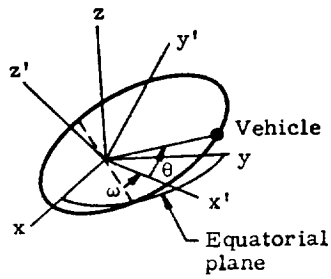

The direction cosines of the position of the vehicle in ECI are obtained by substitution of Eq (5) in Eq (6):

$$\frac{x_s}{r_s} = \cos(\theta + \omega)\cos\Omega - \cos i \sin(\theta + \omega)\sin\Omega$$

$$\frac{y_s}{r_s} = \cos(\theta + \omega)\sin\Omega + \cos i \sin(\theta + \omega)\cos\Omega$$

$$\frac{z_s}{r_s} = \sin(\theta + \omega)\sin i \qquad (7)$$

The rectangular coordinates (x_s, y_s, z_s) are obtained in terms of the parameter θ by substitution of Eq (5) in Eq (7).

b. Position of the sun in an ECI coordinate system

The definition of solar position in the ECI system is simplified by choice of vernal equinox, Υ, the direction of the intersection line of the ecliptic and equatorial planes, as one of the system axes. Many astronomical tables provide solar position in terms of right ascension, A, and declination, D, as functions of time.

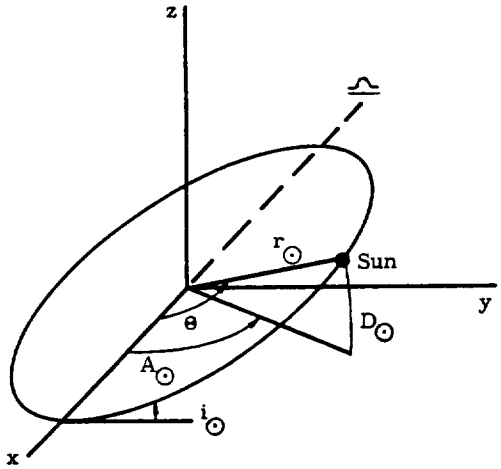

$$x_\odot = r_\odot \cos D_\odot \cos A_\odot$$
$$y_\odot = r_\odot \cos D_\odot \sin A_\odot$$
$$z_\odot = r_\odot \sin D_\odot \qquad (8)$$

However, a more convenient system for study purposes is one employing obliquity, $i_\odot$, and ecliptic angle from equinox, Θ. The obliquity

$$i_\odot = 23^\circ\ 27'\ 08.26'' - 0.4684''\ (t - 1900)$$

(where t is the calendar year) is practically constant, and the solar position can then be specified by only two variables, $r_\odot$ and Θ. The angle Θ can be found by the inverse solution of Kepler's equation for the eccentric anomaly as a function of time. Then, the Θ can be found as a function of E. However, since the orbit of the earth is nearly circular,

$$e_\oplus = 0.0167272,$$

$r_\odot$ is nearly constant (0.983273 au $\leq r_\odot \leq$ 1.016727 au) and Θ can be approximated as

$$\Theta = 0.98563\ d_\Upsilon$$

where d_Υ is the number of days past vernal equinox ($\approx$ March 21).

In either case, the solar position in terms of $i_\odot$ and Θ is given as follows:

$$x_\odot = r_\odot \cos\Theta$$
$$y_\odot = r_\odot \cos i_\odot \sin\Theta \qquad (9)$$
$$z_\odot = r_\odot \sin i_\odot \sin\Theta$$

c. Position of the sun in a vehicle-centered inertial coordinate system (VCI)

The position of the sun in the VCI system is obtained by subtracting corresponding ECI components of the vehicle and the sun.

$$X = x_\odot - x_s$$
$$Y = y_\odot - y_s \qquad (10)$$
$$Z = z_\odot - z_s$$

where $(x_\odot, y_\odot, z_\odot)$ and (x_s, y_s, z_s) are given by Eqs (7) and (8) or (9). The distance from the vehicle to the sun is

$$r_{s\odot} = \sqrt{(x_\odot - x_s)^2 + (y_\odot - y_s)^2 + (z_\odot - z_s)^2} \qquad (11)$$

and so Eq (10) may be expressed in direction cosine form as follows:

$$\cos\alpha_X = \frac{x_\odot - x_s}{r_{s\odot}}$$

$$\cos\beta_Y = \frac{y_\odot - y_s}{r_{s\odot}} \qquad (12)$$

$$\cos\gamma_Z = \frac{z_\odot - z_s}{r_{s\odot}}$$

d. Position of the sun in a vehicle-centered local horizontal coordinate system (VCL)

ECI coordinates may be transformed to VCL by successive counterclockwise rotations about z through Ω, about x through i and about z through $(\theta + \omega)$.

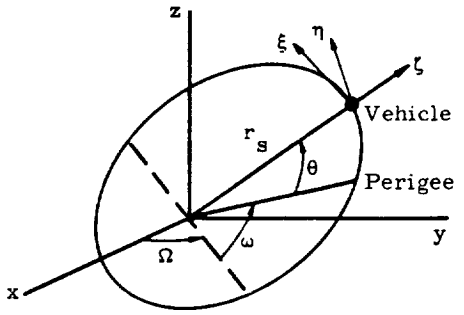

$$\begin{bmatrix}\zeta\\ \eta\\ \xi\end{bmatrix} = \begin{bmatrix}\cos(\theta+\omega) & \sin(\theta+\omega) & 0\\ -\sin(\theta+\omega) & \cos(\theta+\omega) & 0\\ 0 & 0 & 1\end{bmatrix}$$

$$\begin{bmatrix}1 & 0 & 0\\ 0 & \cos i & \sin i\\ 0 & -\sin i & \cos i\end{bmatrix}\begin{bmatrix}\cos\Omega & \sin\Omega & 0\\ -\sin\Omega & \cos\Omega & 0\\ 0 & 0 & 1\end{bmatrix}\begin{bmatrix}x\\ y\\ z\end{bmatrix}$$

$$\begin{bmatrix}\cos\Omega\cos(\theta+\omega) - \sin\Omega\cos i\sin(\theta+\omega) & \sin\Omega\cos(\theta+\omega) + \cos\Omega\cos i\sin(\theta+\omega) & \sin i\sin(\theta+\omega)\\ -\cos\Omega\sin(\theta+\omega) - \sin\Omega\cos i\cos(\theta+\omega) & -\sin\Omega\sin(\theta+\omega) + \cos\Omega\cos i\cos(\theta+\omega) & \sin i\cos(\theta+\omega)\\ \sin\Omega\sin i & -\cos\Omega\sin i & \cos i\end{bmatrix}\begin{bmatrix}x\\ y\\ z\end{bmatrix} \qquad (13)$$

Substitution of Eq (9) in Eq (13), followed by translation of the vehicle radius r_s in the ζ direction, gives the direction cosines of the solar position in VCL coordinates:

$$\cos\alpha_\zeta = \frac{\zeta_\odot}{r_{s\odot}} = \frac{r_\odot}{r_{s\odot}}\Big\{\cos\theta\Big[\cos\Omega\cos(\theta+\omega) - \sin\Omega\cos i\sin(\theta+\omega)\Big] + \sin\theta\cos i_\odot\Big[\sin\Omega\cos(\theta+\omega) + \cos\Omega\cos i\sin(\theta+\omega)\Big] + \sin\theta\sin i_\odot\Big[\sin i\sin(\theta+\omega)\Big]\Big\} - \frac{r_s}{r_{s\odot}}$$

$$\cos\beta_\eta = \frac{\eta_\odot}{r_{s\odot}} = \frac{r_\odot}{r_{s\odot}}\Big\{\cos\theta\Big[-\cos\Omega\sin(\theta+\omega) - \sin\Omega\cos i\cos(\theta+\omega)\Big] + \sin\theta\cos i_\odot\Big[-\sin\Omega\sin(\theta+\omega) + \cos\Omega\cos i\cos(\theta+\omega)\Big] + \sin\theta\sin i_\odot\sin i\cos(\theta+\omega)\Big\} \qquad (14)$$

$$\cos\gamma_\xi = \frac{\xi_\odot}{r_{s\odot}} = \frac{r_\odot}{r_{s\odot}}\Big[\cos\theta\sin\Omega\sin i - \sin\theta\cos i_\odot\cos\Omega\sin i + \sin\theta\sin i_\odot\cos i\Big]$$

The last equation of Eq (14) is especially interesting since the true anomaly θ is not involved, i.e., $\cos\gamma_\xi$ is a function only of the time of year (Θ) and the orbit orientation (Ω and i). In fact, for low altitude orbits $r_\odot \approx r_{s\odot}$ and γ_ξ approaches the angle between the earth-sun line and the normal to the orbit plane.

$$\cos\gamma_n = \cos\Theta\sin\Omega\sin i - \sin\Theta\cos i_\odot\cos\Omega\sin i + \sin\Theta\sin i_\odot\cos i \qquad (15)$$

This is a useful parameter in determining time in sunlight (Section E). The $\sin\gamma_n$ and $\cos\gamma_n$ are plotted in Figs. 1 and 2 (Ref. 1) for a particular orbit to show the form.

2. Eclipses of Earth Satellites

There are several important areas to be considered in the study of eclipsing of earth satellites by the earth's shadow. The areas discussed in this section include the following.

(1) General geometry of eclipses by the shadow.

(2) Equations leading to the prediction of eclipses by the shadow.

(3) General geometry of eclipses by the penumbra.

(4) Equations leading to the prediction of eclipses by the penumbra.

(5) Eclipse information obtained by analytical means.

(6) Complications involved in the problem.

(7) Chart and equations for a computer program.

In the material to be presented, all angular orbital elements are referred to the plane of the ecliptic. Since these angles are referred to the plane of the equator for earth satellites, the reader should see Chapter XI for the appropriate coordinate transformation.

a. General geometry of eclipses by the shadow (Ref. 2)

For simplicity, Figs. 3 through 5 show the orbit of the satellite through the center of the shadow. Figure 5 shows a case where the shadow is not at the node. In all three figures, P_1 is the point where the satellite enters the shadow and P_2 the point where it leaves the shadow. P_3 is some point outside the shadow (that is, in sunlight). Let s be the size (angular radius) of the shadow and θ_s the angular distance from the center of the shadow to any point in the orbit. When $\theta_s > s$ the satellite is in sunlight; when $\theta_s < s$ the satellite is in shadow.

b. Equations involved in prediction of eclipses by the shadow (Ref. 2)

The angular size of the earth's shadow is computed from

$$s = \frac{102}{100}\left[\sin^{-1}\left(\frac{R}{r}\right) - 16'\right] \qquad (16)$$

where R is the earth's radius

and

$$r = \frac{a(1-e)^2}{1+e\cos\theta}$$

a = semimajor axis
e = eccentricity
θ = true anomaly

and the factor 102/100 is due to the refraction of the atmosphere. Now, using the following sketch

$$\cos\theta_s = \cos\Delta\lambda\cos\Delta\theta + \sin\Delta\lambda\sin\Delta\theta\cos i_\epsilon \qquad (17)$$

where

$$\Delta\lambda = \Omega - \lambda\,(\text{shadow})$$

$$\Delta\theta = \theta - \theta\,(\Omega)$$

and

λ (shadow) = longitude of the shadow
= longitude of the sun + 180°

$\theta\,(\Omega)$ = true anomaly at the node
$= -\omega$

i_ϵ = inclination of orbit plane to ecliptic plane

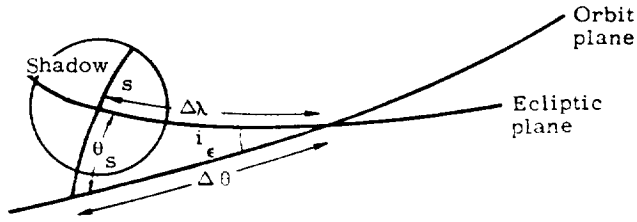

The solution of the equations for $s = \theta_s$ will give values θ_1 and θ_2, the true anomaly at the point of entering the shadow (P_1) and at the point of leaving the shadow (P_2) respectively. For each of those conditions

$$\cos E = \frac{\cos\theta + e}{1 + e\cos\theta} \qquad (18)$$

$$M = E - e\sin E \qquad (19)$$

If	$0 \le \theta \le 180$ or	If	$180 \le \theta \le 360$
then	$0 \le E \le 180$	then	$180 \le E \le 360$
and	$0 \le M \le 180$	and	$180 \le M \le 360$

$$\text{and } t = \frac{M}{n},\quad n = \frac{\sqrt{\mu}}{a^{3/2}} \qquad (20)$$

where

e = eccentricity

E = eccentric anomaly

M = mean anomaly

t = time from perigee passage (t_p)

n = mean motion

μ = GM, the product of the universal gravity constant and the mass of the earth
= 1.407648×10^{16} ft^3/sec^2 (adopted value)
= 398,601.5 km^3/sec^2

then

$$\text{Time in umbra} = t_{2u} - t_{1u} \qquad (21)$$

If Eq (21) is negative, add the orbital period to the answer.

To determine eclipse duration on any later revolution, it is necessary to update the past values of the orbital elements which have been changed as a result of various perturbations (see Chapter IV), and the position of the shadow (approximately 0.9856 deg/day). The equations for s and θ_s are again solved for the points where $s = \theta_s$.

c. General geometry of eclipses by the penumbra (Ref. 2)

To find time in penumbra, an approach is followed similar to the study for the time in umbra or shadow. In this case, however, the penumbra is a ring around the umbra as shown in Figs. 6 and 7.

From Fig. 6, it can be seen that, if the satellite orbit is circular (i.e., $r_1 = r_2$),

$$\Delta T_1 OP_1 \approx \Delta T_2 OP_2$$

$$\therefore \angle T_1 OP_1 = \angle T_2 OP_2$$

But

$$\begin{aligned} \angle T_1 OT_2 &= 180° - \angle O_1 OT_1 - \angle T_2 O O_2 \\ &= 180° - (90° - \alpha) - (90° - \beta) \\ &= \alpha + \beta \end{aligned}$$

and

$$\begin{aligned} \psi &= \angle T_1 OT_2 + \angle T_2 OP_2 - \angle T_1 OP_1 \\ &= \angle T_1 OT_2 = \alpha + \beta. \end{aligned}$$

Thus the angle ψ is very nearly constant regardless of the size of the circular orbit and is approximately equal to 0.54°.

d. Equations involved in prediction of eclipses by the penumbra (Ref. 2)

Whether a satellite enters the penumbra or not (in a particular revolution about the earth) is a similar problem to that of finding out whether it enters the umbra (shadow) or not. We simply increase s by ψ and then compare θ_s with $s + \psi$. The satellite enters and leaves the penumbra cone at the points $\theta_s = s + \psi$. For these points use Eqs (18), (19) and (20) obtaining t_{1p} and t_{2p}, relative time of entering penumbra and time out of penumbra. If there is not an umbra eclipse in that revolution, then

$$\text{Time in penumbra} = t_{2p} - t_{1p} \qquad (22)$$

If there is an umbra eclipse in that revolution, then there will be two times in penumbra (first going from point P_1 to point P_2 and then going from point P_3 to point P_4 as shown in Fig. 7, namely,

$$\text{Time in penumbra (1)} = t_{1u} - t_{1p} \qquad (23)$$

$$\text{Time in penumbra (2)} = t_{2p} - t_{2u} \qquad (24)$$

If any of Eqs (22), (23) and (24) is negative, add the orbital period to the answer.

e. Alternative solution for eclipse times

An alternative solution for eclipse times may be formulated from consideration of Fig. 9. Let $(\hat{x}, \hat{y}, \hat{z})$ be unit vectors in an ecliptic coordinate system $(x_\epsilon, y_\epsilon, z_\epsilon)$.

$R_\odot$ = radius of the sun

$R_\oplus$ = radius of the earth

$\vec{r}$ = geocentric radius vector to the satellite (unit vector $\hat{r}$)

$r_\oplus$ = distance between the centers of earth and sun

$\hat{s}$ = unit vector along the direction of the earth-sun line

λ = geocentric celestial longitude of the vehicle (ecliptic)

ℓ = geocentric celestial latitude of the vehicle (ecliptic)

$\lambda_\oplus$ = heliocentric celestial longitude of the earth (ecliptic)

ϕ = angle between $\hat{r}$ and $\hat{s}$

Then

$$\hat{r} = \cos \ell \cos \lambda \, \hat{x} + \cos \ell \sin \lambda \, \hat{y} + \sin \ell \, \hat{z}$$

$$\hat{s} = -\cos \lambda_\oplus \, \hat{x} - \sin \lambda_\oplus \, \hat{y}$$

and

$$\cos \phi = \hat{r} \cdot \hat{s}$$

The condition for entering or leaving the penumbra is that $\epsilon = 0$ (ϵ defined in Fig. 8). This condition can be determined from

$$\epsilon = \alpha - \beta + \pi - \phi - \sin^{-1} \frac{R_\oplus}{r}$$

where

$$\begin{aligned} \alpha &= \sin^{-1} \frac{R_\odot}{\sqrt{r_\oplus^2 + r^2 - 2 r_\oplus r \cos}} \\ &\approx \frac{R_\odot}{r_\oplus} \left[1 + \frac{1}{6} \left(\frac{R_\odot}{r_\oplus} \right)^2 - \frac{1}{2} \left(\frac{r}{r_\oplus} \right)^2 + \frac{r}{r_\oplus} \cos \phi \right. \\ &\quad \left. + \frac{3}{2} \left(\frac{r}{r_\oplus} \right)^2 \cos^2 \phi \right] \end{aligned}$$

$$\left[1 >> \left(\frac{R_\odot}{r_\oplus} \right)^2 ; \; 1 >> \left(\frac{r}{r_\oplus} \right)^2 \right],$$

and

$$\beta = \sin^{-1} \frac{r \sin\phi}{\sqrt{r_\oplus^2 + r^2 - 2 r_\oplus\, r \cos\phi}}$$

$$\approx \frac{r}{r_\oplus} \sin\phi \left[1 - \frac{1}{2}\left(\frac{r}{r_\oplus}\right)^2 + \frac{1}{6}\left(\frac{r}{r_\oplus}\right)^2 \sin^2\phi + \frac{r}{r_\oplus}\cos\phi + \frac{3}{2}\left(\frac{r}{r_\oplus}\right)^2 \cos\phi\right]$$

$$\left[1 >> \left(\frac{R_\odot}{r_\oplus}\right)^2 ;\ 1 >> \left(\frac{r}{r_\oplus}\right)^2\right]$$

The solutions for penumbra entrance and exit thus satisfy

$$\epsilon \approx \frac{R_\odot}{r_\oplus}\left[1 + \frac{r}{r_\oplus}\cos\phi - \frac{r}{R_\odot}\sin\phi\right] + \pi - \phi - \sin^{-1}\frac{R_\oplus}{r} = 0$$

$$\left[1 >> \left(\frac{R_\odot}{r_\oplus}\right)^2 ;\ 1 >> \left(\frac{r}{r_\oplus}\right)^2\right]$$

The umbra entrance and exit conditions can be written by taking

$$\epsilon = \pi - \phi - (\alpha - \beta) - \sin^{-1}\frac{R_\oplus}{r}$$

where

$$\alpha + \beta \approx \frac{R_\odot}{r_\oplus}\left(1 + \frac{r}{r_\oplus}\cos\phi + \frac{r}{r_\odot}\sin\phi\right)$$

(as indicated by Fig. 8) and where α is taken in the opposite direction to that for the penumbra solution, i.e., α is the angle between the vehicle-sun line and the lower tangent to the solar surface.

No correction for refraction of the light waves has been made in this material. However, it is noted that the apparent effect at the vehicle will be to make the sun appear larger. Thus, an accurate correction can be made by utilizing the apparent rather than the true radius of the sun.

f. Eclipse information obtained by analytical means (Refs. 1, 2 and 3)

An exact closed-form analysis of general satellite eclipses is impracticable; however, some useful information can be obtained by this type of analysis. Very little can be done with an eccentric orbit, as may be inferred from the previous sections, but with unperturbed circular orbits several important eclipse properties may be determined.

(1) Eclipse season

If it is desired to find the days on which an eclipse occurs, or so-called eclipse season, one may do so with the aid of Fig. 9

$$\sin\lambda_u = \frac{\sin s}{\sin i_\epsilon} \tag{25}$$

where s would be the maximum size of the shadow for an eccentric orbit.

Then

$$\text{eclipse season} \begin{pmatrix}\text{umbra}\\ \text{only}\end{pmatrix} \approx 2\,\frac{\lambda_u}{0.986}\ \text{days} \tag{26}$$

where 0.986 is the mean velocity of the sun in degrees per day.

The exact eclipse season is difficult to compute analytically: (1) due to the regression of the nodes the inclination with respect to the ecliptic varies and it is difficult to predict the inclination when the earth's shadow is near the node; (2) if the orbit is very eccentric the size of the shadow at perigee would be much larger than that at apogee, and again it would be necessary to predict the position of perigee at the time the shadow is approaching the node. For many applications, however, the simple method presented above is adequate.

To determine the eclipse season including the penumbra, the above equations may be used but s must be increased by ψ ($\psi = 0°.54$), as shown in the following sketch.

$$\text{eclipse season} \begin{pmatrix}\text{umbra and}\\ \text{penumbra}\end{pmatrix} \approx 2\,\frac{\lambda_{up}}{0.98563} = 2\,\frac{\sin^{-1}\left[\frac{\sin(s+\psi)}{\sin i_\epsilon}\right]}{0.98563} \tag{27}$$

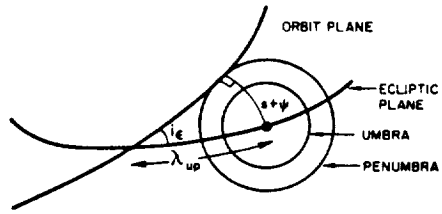

Obviously, if the inclination with respect to the ecliptic is smaller than the angular radius of the shadow ($i_\epsilon < s$), there will be an eclipse at every revolution.

Also it must be remembered that due to oblateness (and also luni-solar perturbations in certain cases) the nodes regress, and a more realistic expression for Eq (26) would be

$$\text{eclipse season} = 2\,\frac{\lambda_u}{0.98563 + \frac{d\Omega}{dt}} \tag{28}$$

where $d\Omega/dt$ = rate of regression of the nodes with respect to the ecliptic. It should be noted that, with proper selection of orbit inclination and altitude, the regression rate can be made

equal to the earth revolution rate, $\frac{d\Omega}{dt} = 0.986°/$ day (i.e., the orbit would follow the sun). In particular, if the initial orbit were chosen to have this regression rate and, furthermore, to be continuously in sunlight with

$$i_\epsilon > \cos^{-1}\sqrt{1 - \left(\frac{R}{r}\right)^2},$$

the satellite would be in sunlight for its entire lifetime. The orbit condition for $\frac{d\Omega}{dt} = 1°/\text{day}$ is

$$\cos i \approx -0.1\left(\frac{r}{R}\right)^{7/2}$$

i. e., $90 < i < 180°$.

No straightforward analytical expression exists to give the rate of regression of the nodes with respect to the ecliptic similar to the expression (to first order) which gives the rate of regression of the nodes with respect to the equator. The reason for this fact is shown in the following sketch.

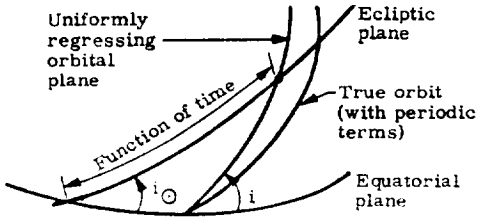

Thus, the equatorial nodal position and the periodic perturbutions of the node must both be considered in the definition of nodal position relative to the ecliptic. A graphic study shows, however, that the regression of the nodes with respect to the ecliptic is negligible in most cases. In cases for which it is not; $i_\epsilon < s$ and, therefore, is of no consequence in the computation of the eclipse season, since for $i_\epsilon < s$ there is an eclipse in every revolution.

(2) Maximum time in umbra (eccentric orbits)

To get an idea of the maximum time in the umbra the following method may be used.

Let the size of the shadow at apogee be s_a and the angular velocity at apogee, w_a

where

$$w_a = \frac{v_a}{r_a} = \sqrt{\frac{\mu}{a^3 (1+e)^3 (1-e)}}$$

$$v_a = \sqrt{\mu\left(\frac{2}{r_a} - \frac{1}{a}\right)}$$

$$r_a = a(1+e)$$

then

$$\text{maximum duration of eclipse} = 2\left(\frac{s_a}{w_a}\right)$$

where s_a is given by Eq (16).

(3) Curves of maximum eclipse duration and eclipse season (circular orbits)

In the case of unperturbed circular orbits a simplified approach is possible. A set of general curves is included for circular orbits; clearly, the results obtained from these curves cannot be extended to eccentric orbits. A simple method of computing and presenting maximum eclipse durations and eclipse seasons is given in the following material.

Figure 10 shows maximum time in umbra versus semimajor axis, which is obtained from

$$\text{maximum time in umbra} = 2\frac{s}{n} \qquad (29)$$

where n is the mean motion

$$n = \frac{\sqrt{\mu}}{a^{3/2}} \qquad (30)$$

Maximum time in umbra and penumbra versus semimajor axis is obtained simply from

$$\text{maximum time in umbra and penumbra} = 2\frac{s+\psi}{n}. \qquad (31)$$

Figure 11 shows the same information as Fig. 10, but with expanded scale.

Maximum time in penumbra where there is no umbra eclipse is computed from

$$\cos \delta\theta = \frac{\cos(s+\psi)}{\cos s} \qquad (32)$$

which is obtained from the following sketch.

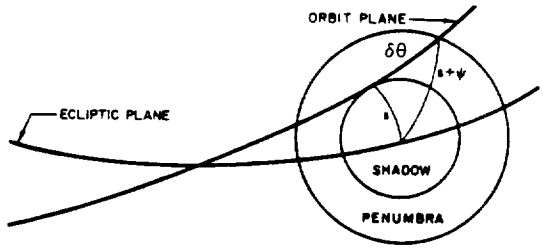

Then, maximum time in penumbra $= 2\frac{\delta\theta}{n}$.

Figure 12 shows maximum time in penumbra versus semimajor axis. Figure 13 shows the same information as Fig. 12, but with expanded scale.

Figure 14 shows eclipse season (umbra only) versus semimajor axis and inclination, which is obtained as illustrated in Fig. 9. Figure 15 shows eclipse season (umbra and penumbra) versus semimajor axis and inclination obtained as illustrated in Fig. 9.

Figure 10 showed that, for fairly low altitude orbits (less than one earth radius), the times in umbra and penumbra differ by a fraction of a minute or less than 1% of the orbit period. In this region the earth shadow can be accurately approximated by a cylinder. With this assumption the eclipse duration solution for unperturbed circular orbits can be further simplified. The simplified problem has been considered in various references, e.g., Refs. 1, 3 and 4.

If the shadow made by the earth is approximated by a cylinder, this cylinder will intersect the orbit plane in an ellipse with semimajor axis of $\frac{R}{\cos \gamma_n}$ and semiminor axis of R, as shown in Fig. 16, where cos γn is given in Eq (15) and plotted in Fig. 2. The per cent time in sunlight is then the same as the per cent of the orbit arc not contained in the shadow ellipse, as shown in Fig. 16. The problem then reduces to the simple determination of the angle ϕ from the intersection of the orbit and the projected shadow ellipse:

$$\begin{cases} x^2 + y^2 = r_s^2 \text{ (orbit)} \\ \dfrac{x^2}{\left(\dfrac{R}{\cos \gamma_n}\right)^2} + \dfrac{y^2}{R^2} = 1 \text{ (shadow ellipse)} \end{cases}$$

Substitution of y from the first equation in the second equation gives

$$x^2 \cos^2 \gamma_n + r^2 - x^2 = R^2$$

or

$$x = \frac{\sqrt{r_s^2 - R^2}}{\sin \gamma_n}$$

Then

$$\cos \phi = \frac{x}{r_s} = \frac{\sqrt{1 - \left(\frac{R}{r_s}\right)^2}}{\sin \gamma_n}, \quad 0° < \phi < 90°$$

The per cent time in sunlight is

$$t_s = \frac{180 - \phi}{180} \times 100\% \text{ for } \sin \gamma_n > \sqrt{1 - \left(\frac{R}{r_s}\right)^2}$$

$$= 100\% \text{ for } \sin \gamma_n \leq 1 - \sqrt{\left(\frac{R}{r_s}\right)^2}$$

Substitution for ϕ in this equation gives

$$\sin \gamma_n = \pm \frac{\sqrt{1 - \left(\frac{R}{r_s}\right)^2}}{\cos (1.8\, t_s)} \qquad (33)$$

This equation determines the orbit orientation γ_n required for any desired per cent sunlight time t_s. Equation (15) in turn provides the combinations of time of year, orbit ascending node and orbit inclination possible for a given t_s.

As examples, circular orbits of various altitudes and inclinations were considered. The value of cos γ_n for various orbit altitudes as a function of per cent sunlight time is plotted in Fig. 17. Another presentation of the same relationship is given in Fig. 18. These values are obtained from Eq (33). Then horizontal lines across Fig. 1 or Fig. 2 at each t_s level determine the (θ, Ω) loci for the given per cent time in sunlight. These loci have been replotted in different form in Figs. 19 through 23. These figures show very clearly the required longitude of ascending node, Ω, required to provide a given sunlight time t_s at any given time of the year. For example, for 125-naut mi (232 km) orbits, 100% sunlight may be achieved only in alternate quarters of the year, the quarters near autumnal and vernal equinoxes. During quarters centered about the summer and winter solstices, the maximum time in sunlight is 80%. For 500-naut mi (930 km) orbits, 100% sunlight may be obtained at any time in the year.

Other curves which may prove to be useful are:

(1) Inclination with respect to the ecliptic (i_ϵ) versus longitude of the node with respect to equator (Ω) for different inclinations with respect to equator (i) (Fig. 24), computed from

$$\cos i_\epsilon = \cos 23.4 \cos i + \sin 23.4 \sin i \cos \Omega \qquad (34)$$

which is obtained from the following sketch.

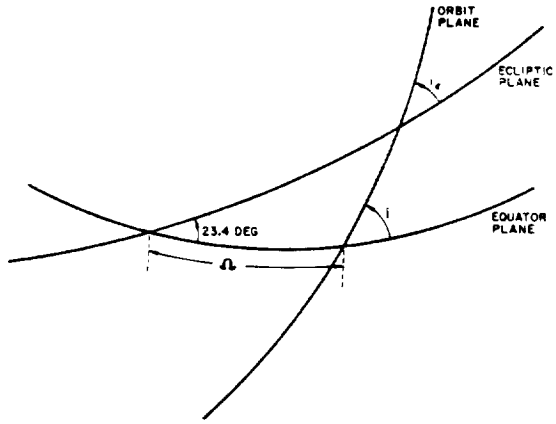

(2) Angular radius of shadow versus distance from center of earth, Fig. 25 [see Fig. 3 and Eq (16)]. Figure 26 shows the same information as Fig. 25, but with expanded scale.

g. Chart and equations for a computer program

The following reasons indicate why a closed-form analytical solution is not easily obtained:

(1) Time of launch--the longitude of the node at burnout will vary with the time of launch.

(2) Date of launch--the initial position of the sun will be different for different dates of launch.

(3) Eccentricity of orbit--the shadow is not a circle, but has an egg-shaped contour.

(4) Regression of the nodes--the longitude of the node will vary constantly due to oblateness.

(5) Advance of perigee--the argument of perigee will vary constantly due to oblateness; the size of the shadow at the nodes will vary from maximum if perigee is at the node to minimum if apogee is at the node.

(6) Drag--the size of the semimajor axis of the orbit will decrease due to atmospheric drag.

(7) Luni-solar perturbations--all of the orbital elements will vary to some extent due to luni-solar perturbations.

A method for obtaining a more precise solution to the general problem of earth's satellite eclipses is given in this section.

The most efficient method of calculating eclipses is by means of a computer program, a simple example of which is represented in Fig. 27, from Ref. 2.

It must be noted at this point that this program, as well as any of the analytical methods described, will produce only times in umbra and times in penumbra at a given revolution, but not the time of day at which these phenomena happen. This can be roughly determined by knowing the time from perigee passage at which the phenomena occur, the period, and the time of perigee passage for some date. If the time of perigee passage for date D_1 is T_1 and the period is τ, then the approximate time of perigee passage for some other date D_2, ΔD days from D_1, is

$$T_2 = T_1 + N\tau \qquad (35)$$

where N is the integral number of periods in ΔD. If the motion of perigee due to perturbations is large, the anomalistic period (time from perigee to perigee) should be used in Eq (35).

The results of machine computations are shown in Figs. 28 through 30. The luni-solar perturbations were added by first running another program which computes changes in equatorial elements due to various perturbations (a complicated program in itself), and then using the output as the input to the eclipse program. Also included in the above set of curves is one showing the eclipse pattern when launching the same vehicle at different times of day on the same date and at the same time of day on different dates.

D. GROUND TRACKS (REF. 3)

The equations for the ground track of a satellite orbit may be written, from an application of spherical trigonometry to Fig. 31, as follows:

Geocentric latitude:

$$L = \sin^{-1} (\sin i \sin \phi) \qquad (36)$$

Geocentric longitude:

$$\Lambda = \tan^{-1} (\cos i \tan \phi) + \Lambda_{n0} - \Omega_e \Delta t - \frac{3}{2} Kn J_2 \Delta t \left(\frac{R_e}{a}\right)^2 \frac{\cos i}{(1 - e^2)^2} \qquad (37)$$

where

i = inclination of the orbit plane to the ecliptic plane, $0 \leq i < 180°$, measured + from east at ascending node

ϕ = orbit central angle between the satellite and the ascending node

Λ_{n0} = initial geocentric longitude of the ascending node, $0 \leq \Lambda_{n0} \leq 360°$, measured + toward the east

Ω_e = rotation rate of the earth, 4.178074×10^{-3} deg/sec

Λ_{n0} = initial geocentric longitude of the ascending node

Δt = time measured from the initial condition

K = 57.2958 deg/rad

n = mean motion = $\sqrt{\frac{\mu}{a^3}}$

J_2 = 1.0823×10^{-3}

R_e = equatorial radius of the earth

a = orbit semimajor axis

e = orbit eccentricity.

Equations (36) and (37), presenting satellite position with respect to a rotating oblate earth, neglect second order oblateness perturbations.

These equations may be used to generate the ground track as a series of points (L, Λ) as a function of the parameter ϕ. This determination is simple in the case of circular orbits, but somewhat complicated for elliptical orbits due to the nonlinear behavior of the angular rate.

1. Elliptical Orbit Ground Tracks

The difficulties of ground track predictions for elliptical orbits arise from the fact that the angle in orbit plane (from ascending node to satellite) is a nonlinear function of time. For large eccentricities, Chapter III expresses this angle in the form of a Fourier-Bessel infinite series. For small eccentricities, the angle can be expressed as a simple sine series where the constants are determined by the corresponding eccentricities.

Satellite latitude and longitude are first established with respect to a nonrotating earth, as a function of time. Rotation of the earth, regression of the nodes and precession of the perigee are then used as corrections for longitude and latitude on a rotating earth. Six input parameters are needed (e.g., h_0, v_0, γ_0, L_0, Λ_0 and β_0). From these data all the necessary information is obtained by the equations of spherical trigonometry and planetary motion along the Keplerian ellipses.

The geometrical representation of the problem, indicating the most important quantities used in the calculation procedure, is given in Fig. 31. It should be noted that the longitude of the ascending node (Ω), as well as the angle of perigee (ω) and the angle of the satellite (ϕ) from the node are all functions of time.

The properties of the Keplerian ellipse are as follows:

Semimajor axis:

$$a = \frac{r_0}{2 - r_0 v_0^2/\mu} \tag{38}$$

Eccentricity:

$$e = \sqrt{1 - \frac{r_0^2 v_0^2 \cos^2 \gamma_0}{a\mu}} \tag{39}$$

Period:

$$\tau = 2\pi \sqrt{a^3/\mu} \tag{40}$$

Next the central angle from perigee is derived. First, the local flight path angle is seen from the following geometry to be

$$\tan \gamma = \frac{\dot{r}}{r\dot{\theta}} = \frac{1}{r}\frac{dr}{d\theta}$$

$$r = \frac{p}{1 + e \cos \theta}$$

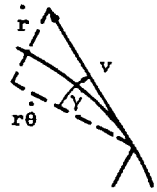

Therefore,

$$\frac{dr}{d\theta} = \frac{p e \sin \theta}{(1 + e \cos \theta)^2} \quad \text{and} \quad \tan \gamma = \frac{e \sin \theta}{1 + e \cos \theta}$$

This is expressed as

$$\tan \gamma = \frac{e\sqrt{1 - \cos^2 \theta}}{1 + e \cos \theta}$$

and the following is derived.

$$e \cos \theta = \sin^2 \gamma \pm \cos \gamma \sqrt{e^2 - \sin^2 \gamma}$$

From this, the initial central angle from perigee is obtained.

$$\theta_0 = \pm \cos^{-1} \left[\frac{\sin^2 \gamma_0 \pm \cos \gamma_0 \sqrt{e^2 - \sin^2 \gamma_0}}{e} \right] \tag{41}$$

Equation (41) gives four possible answers and the correct one should be selected as follows:

Flight Path Angle	Radius	θ_0 (from perigee)
$\gamma_0 > 0$	$r_0 < a$	$0° < \theta_0 < \theta^*$
$\gamma_0 > 0$	$r_0 > a$	$\theta^* < \theta_0 < 180°$
$\gamma_0 < 0$	$r_0 > a$	$180° < \theta_0 < 360° - \theta^*$
$\gamma_0 < 0$	$r_0 < a$	$360° - \theta^* < \theta_0 < 360°$

where $\theta^* \equiv 180° - \cos^{-1} e$ (see Fig. 31) (42)

Now the inclination of the orbit is obtained by spherical trigonometry.

$$i = \cos^{-1} (\cos L_0 \sin \beta_{0I}), \tag{43}$$

where β_{0I} is obtained as follows.

$$\beta_{0I} = \beta_0 + \frac{R_e \Omega_e}{v_0 \cos \gamma_0} \cos L_0 \cos \beta_0$$

The component of velocity parallel to the earth's surface is found by $v' = v_0 \cos \gamma_0$. The component due to the earth's rotation is simply

$$v_e = R\, \Omega_e \cos L_0.$$

From trigonometry,

$$\frac{v_e}{\sin \Delta\beta} = \frac{v'}{\sin (90° + \beta_0)} = \frac{v'}{\cos \beta_0}.$$

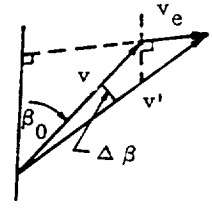

Because $\Delta\beta$ is a small angle, $\sin \Delta\beta \approx \Delta\beta$ is a good approximation. Finally, since

$$\Delta\beta = \frac{v_e}{v'} \cos \beta_0 = \frac{R\, \Omega_e}{v_0 \cos \gamma_0} \cos L_0 \cos \beta_0. \tag{44}$$

Now

$$\beta_{0I} = \beta_0 + \Delta\beta. \tag{45}$$

The initial angle from the ascending node is

$$\phi_0 = \sin^{-1} \left[\frac{\sin L_0}{\sin i} \right] \tag{46}$$

and the initial perigee angle from the node (Eqs (41) and (46)) is

$$\omega_0 = \phi_0 - \theta_0. \tag{47}$$

Denoting the time from the initial point (L_0, Λ_0, h_0) by Δt. Then,

$$t = t_0 + \Delta t. \tag{48}$$

where t_0 is the time from perigee found from Kepler's equation

$$t_0 = \frac{\tau}{2\pi}\left\{\frac{-e\sqrt{1 - e^2 \sin\theta_0}}{1 + e\cos\theta_0} + 2\tan^{-1}\left[\frac{\sqrt{1 - e^2}\tan(\theta_0/2)}{1 + e}\right]\right\}. \tag{49}$$

For a nonrotating earth, the following equations are derived from spherical trigonometry.

$$\text{Latitude:}\quad L_I = \sin^{-1}(\sin i \sin\phi) \tag{50}$$

$$\text{Longitude:}\quad \Lambda_I = \tan^{-1}(\cos i \tan\phi) + \Lambda_h \tag{51}$$

Next, consider a rotating earth with oblateness effects. Due to the precession of the apsides, the perigee of the orbit is a function of time, and the angle of perigee from the ascending node is given by

$$\omega = \omega_0 + K\dot{\omega}\frac{\Delta t}{\tau} = \omega_0 + \frac{3}{2}Kn J_2 \Delta t \left(\frac{R_e}{a}\right)^2 \frac{\left(2 - \frac{5}{2}\sin^2 i\right)}{(1 - e^2)^2} \tag{52}$$

where

$$n \equiv \frac{2\pi}{\tau} = \sqrt{\frac{\mu}{a^3}} \tag{53}$$

For an easterly launch, the node is given for a rotating oblate earth as

$$\Omega = \Omega_0 - \Omega_e \Delta t - K\dot{\Omega}\frac{\Delta t}{\tau} = \Omega_0 - \Omega_e \Delta t - KnJ \Delta t \left(\frac{R_e}{a}\right)^2 \frac{\cos i}{(1 - e^2)^2} \tag{54}$$

where $\Omega_0 = \Lambda_{n0}$ + Greenwich Sidereal Time

$$= \Lambda_0 - \cos^{-1}\left(\frac{\cos\phi_0}{\cos L_0}\right) + \text{GST} \tag{55}$$

(Longitudinal shift of the ground track is plotted in Fig. 30.) Now, the angle from node can be found from a Fourier-Bessel series expansion as a function of time.

$$\phi = \omega + nt + 2e \sin nt + \frac{5}{4}e^2 \sin 2nt + \ldots. \tag{56}$$

Expressing Eq (56) in terms of t_0 and using Eq (52),

$$\phi = \phi_0 + n\Delta t\left[1 + \frac{3}{2}KJ_2\left(\frac{R_e}{a}\right)^2 \frac{(2 - \frac{5}{2}\sin^2 i)}{(1 - e^2)^2}\right] + 2e(\sin nt - \sin nt_0) + \frac{5}{4}e^2(\sin 2nt - \sin 2nt_0) + \ldots. \tag{57}$$

For a few revolutions, Eq (57) can be approximated by

$$\phi = \phi_0 + n\Delta t + 2e(\sin nt - \sin nt_0). \tag{58}$$

Finally, the desired relations for satellite position with respect to a rotating oblate earth are given by Eqs (36) and (37). Also, the orbit radius can be expressed in series form as

$$r = a\left[1 - e\cos nt - \frac{e^2}{2}(\cos 2nt - 1) - \ldots\right]. \tag{59}$$

If extreme accuracies are needed, it should be remembered that $\dot{\Omega}$ and $\dot{\omega}$ in Eqs (52) and (54) can be considered as simple constants only for integral numbers of revolutions. For some fraction of a revolution, the rates of regression of the nodes and precession of the apsides are actually periodic functions, which contain sines or cosines of the geocentric latitude. These functions result in an oscillation about the mean values given by $\dot{\Omega}$ and $\dot{\omega}$ utilized here. The more accurate perturbation models are described in greater detail in Chapter IV.

2. Synchronous Orbits

As noted previously, because synchronous orbits yield ground tracks which repeat daily, they have special advantages for certain missions, e.g., navigation and communication, and, therefore, merit special consideration. The periods and altitudes of the synchronous orbits are given in Table 2. This table is based on the following equation.

$$\tau_{\text{sidereal}} \approx 2\pi a\sqrt{\frac{a}{\mu}}\left[1 - 3J_2\left(\frac{R_e}{a}\right)^2\right]$$

Of particular interest, because of limited ground track excursion, is the 24-hr satellite. The circular equatorial 24-hr satellite does not move relative to the rotating earth, and so its ground track is simply a point on the equator. Circular 24-hr orbits of nonzero inclination exhibit limited excursions. The ground tracks for these orbits, shown for i = 40°, 50° and 60° in Fig. 32, have the shape of a figure eight. Elliptical inclined 24-hr orbits have ground tracks resembling skewed figure eights. Examples of these are shown in Figs. 33 and 34.

TABLE 2

Synchronous Orbits

$\tau_{sidereal}$ (sid hr)	$\tau_{sideral}$ (sol sec)	Semimajor Axis a (ft x 10^8)	Semimajor Axis a (km)	Circular Orbit Altitude (R_e = 6378.15 km) h (km)
24	86,164.09	1.383408	42,166.28	35,788.13
12	43,082.05	0.871558	26,565.08	20,186.93
8	28,721.36	0.665182	20,274.76	13,896.61
6	21,541.02	0.549151	16,738.13	10,359.98
4	14,360.68	0.419175	12,776.46	6,398.31
3	10,770.51	0.346109	10,549.40	4,171.25
2	7,180.34	0.264281	8,055.28	1,677.13

E. SATELLITE COVERAGE

Coverage concerns the ability of a satellite-borne observer or sensor to view a point or area on the surface of the earth or, from the opposite standpoint, the ability of a satellite to be viewed from a point or area on the earth. As noted in Section B, most types of satellite missions, including reconnaissance, communications and navigation missions, impose certain coverage requirements. This section considers the degree of coverage available with a given orbit or pattern of orbits. Because of the basic differences in area coverage and point coverage, these topics will be considered separately.

1. Area Coverage

Area coverage, as distinguished from point coverage, will be taken to imply interest in a wide area, e.g., the entire globe, a certain range of latitudes, a continent, etc. Point coverage involves coverage of specific areas of limited extent, such as specified landing sites, tracking stations, small reconnaissance targets, etc.

a. Coverage by a single satellite

The total area on the earth's surface theoretically visible from a satellite at a given instant is given by the following expression:

$$d = R\alpha = R \cos^{-1}\left(\frac{R}{R+h}\right) \qquad (60)$$

where

R = earths's radius (6371.02 km)

α = central angle between the subsatellite point and the outer edge of area visible from the satellite

h = altitude of the satellite (in km)

If the angle of incidence is restricted to be larger than a given minimum viewing angle σ, then the coverage arc length can be expressed by the following equation (see sketch).

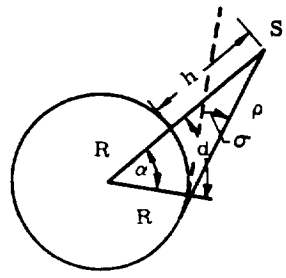

$$d = R\alpha = R\left[\cos^{-1}\left(\frac{R\cos\sigma}{R+h}\right) - \sigma\right] \qquad (61)$$

This equation is plotted in Figs. 35 and 36. The coverage angle, α, in degrees can be found from the corresponding arc length by the conversion

$$\alpha = 0.0089929\, d \text{ (deg)}$$

where d is in kilometers. This conversion is based on the radius of a sphere of volume equivalent to that of the earth. The percent of earth's surface area visible from the satellite can be found immediately from the coverage angle, α, by comparing the area of the visible segment with the total area of the globe.

Area of segment

$$A_s = 2\pi R^2 (1 - \cos\alpha)$$

Total area

$$A_t = 4\pi R^2$$

Percent area visible

$$A\% = \frac{A_s}{A_t} \times 100\% = \left[\frac{1 - \cos\alpha}{2}\right] \times 100\%$$

If range, in addition to viewing angle, is a sensor limitation, the dashed lines on Fig. 35 (the loci of maximum range) together with the maximum viewing angle loci determine permissible regions of coverage half-angle and altitude.

$$\rho = \frac{R \sin\alpha}{\cos(\alpha + \sigma)} \qquad (62)$$

It is frequently necessary to relate the coverage information of Eq (61) and Figs. 35 and 36 to geocentric longitude and latitude on the earth's surface. If at a certain time the subsatellite point is located at geocentric longitude Λ_0 and geocentric latitude L_0, the circular perimeter of the spherical segment of half-angle α (the area in view of the satellite) may be determined as follows. In the following sketch, let (L, Λ) denote a point of the perimeter to be determined. If

$$\Delta\Lambda \equiv \Lambda - \Lambda_0$$

and $\Delta\Lambda^*$ is measured on a great circle, the law of sines of spherical trigonometry gives

$$\sin \Delta\Lambda^* = \sin \Delta\Lambda \sin (90° - L)$$

or

$$\sin \Delta\Lambda = \frac{\sin \Delta\Lambda^*}{\cos L} \qquad (63)$$

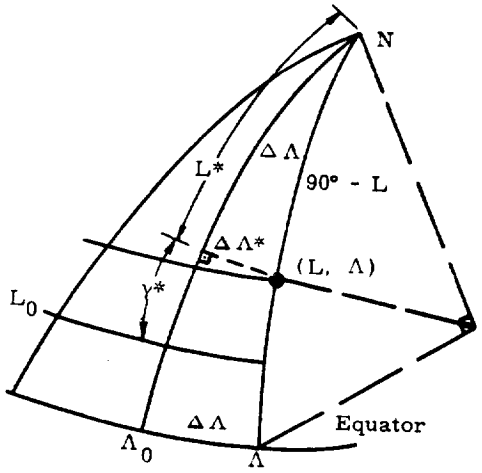

From the following sketch, also by the law of sines,

$$\sin \Delta\Lambda^* = \sin \beta \sin \alpha \qquad (64)$$

where β is an arbitrary azimuth angle (the parameter of the perimeter solution) and α is the coverage half-angle defined in Eq (60). Equations (63) and (64) give

$$\sin \Delta\Lambda = \frac{\sin \alpha \sin \beta}{\cos L} \qquad (65)$$

Also from spherical trigonometry

$$\cos \gamma^* = \frac{\cos \alpha}{\cos \Delta\Lambda^*}$$

Since

$$\gamma^* = 90° - L_0 - L^*,$$

$$90° - L^* = L_0 + \cos^{-1} \left(\frac{\cos \alpha}{\cos \Delta\Lambda^*} \right) . \qquad (66)$$

But, from the preceding sketch

$$\cos L^* = \frac{\cos (90° - L)}{\cos \Delta\Lambda^*}$$

or

$$\sin (90° - L^*) = \frac{\sin L}{\cos \Delta\Lambda^*} \qquad (67)$$

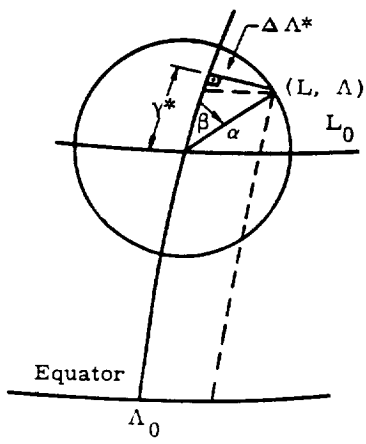

Eqs (66) and (67) give

$$\sin L = \cos \Delta\Lambda^* \sin \left[L_0 + \cos^{-1} \left(\frac{\cos \alpha}{\cos \Delta\Lambda^*} \right) \right]$$

which, after substitution into Eq (64) and simplification, yields

$$\sin L = \sin L_0 \cos \alpha + \cos L_0 \sin \alpha \cos \beta \qquad (68)$$

Equations (65) and (68) then comprise a solution for the perimeter of the instantaneous coverage area in terms of the parameter β, the coverage half-angle α, and the geocentric longitude and latitude of the subsatellite point (λ_0, L_0).

Equations (65) and (68) may also be used to define the areas on earth which are not visible from a given ring by making the following substitutions:

$$L_0 = \pm (\pi/2 - i)$$

$$\alpha = \pm (\pi/2 - \alpha).$$

Now, differentiating Eq (65) with respect to β and equating the result to zero yields the maximum longitudinal increment of an area which is uncovered by a particular ground swath. This derivative is

$$\cos \Delta\Lambda \frac{d(\Delta\Lambda)}{d\beta} = \frac{1}{\cos^2 L} \left[\cos \beta \sin \alpha \cos L - \sin \beta \sin \alpha \frac{d}{d\beta} (\cos L) \right] \qquad (69)$$

Using Eq (68) and the trigonometric identity

$$\cos^2 L = 1 - \sin^2 L$$

it follows that

$$2 \cos L \frac{d}{d\beta} (\cos L) = 2 \sin L (\cos L_0 \sin \alpha \sin \beta)$$

or

$$\frac{d}{d\beta} (\cos L) = \tan L \cos L_0 \sin \alpha \sin \beta \qquad (70)$$

From Eqs (69) and (70),

$$\frac{d(\Delta\Lambda)}{d\beta} = \frac{\cos\beta \sin\alpha \cos L - \sin^2\beta \sin^2\alpha \cos L_0 \tan L}{\cos\Delta\Lambda \cos^2 L} \tag{71}$$

If

$$\frac{d(\Delta\Lambda)}{d\beta} = 0,$$

it is implied that

$$\cos\beta \sin\alpha \cos L - \sin^2\beta \sin^2\alpha \cos L_0 \tan L = 0 \tag{72}$$

Squaring Eq (68) and substituting into Eq (72) yields

$$(\sin L_0 \cos L_0 \sin\alpha \cos\alpha) \cos^2\beta - (1 - \sin^2 L_0 \cos^2\alpha - \sin^2\alpha \cos^2 L_0) \cos\beta + \sin L_0 \cos L_0 \sin\alpha \cos\alpha = 0 \tag{73}$$

Equation (73) can be simplified, yielding

$$\cos^2\beta - 2\left[\frac{\cot\alpha}{\sin 2L_0} - \frac{\tan L_0}{\tan 2\alpha}\right] \cos\beta + 1 = 0 \tag{74}$$

Defining

$$K = \frac{\cot\alpha}{\sin 2L_0} - \frac{\tan L_0}{\tan 2\alpha} \tag{75}$$

the azimuth for maximum longitude deviation, $\Delta\Lambda_{max}$ is given by

$$\cos\beta_{\Delta\Lambda_{max}} = K - \sqrt{K^2 - 1} \tag{76}$$

Taking the limit in Eq (75) as $L_0 \to 0$, $K \to \infty$ and $\lim_{L_0 \to 0} (\cos\beta_{\Delta\Lambda_{max}}) = 0$. Thus, the time that the azimuth angle $\beta_{\Delta\Lambda_{max}}$ (which locates the maximum value of $\Delta\Lambda$) equals 90° corresponds to the center of the area uncovered by the ground swath on the equator. The angle $\beta_{\Delta\Lambda_{max}}$ is less than 90° for northern latitudes and greater than 90° for southern latitudes.

The previous analyses concern the instantaneous coverage available from a satellite. Since the satellite is moving relative to the earth's surface, the spherical segment of covered area also moves along the surface, thus generating a track (the "ground swath") of area covered at some time during the lifetime of the satellite.

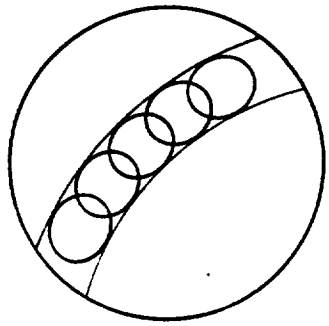

The edges of the ground swath of a single satellite may be determined from the area coverage perimeter solutions previously obtained and the ground track equations developed in Section D. The problem is illustrated in the following sketch.

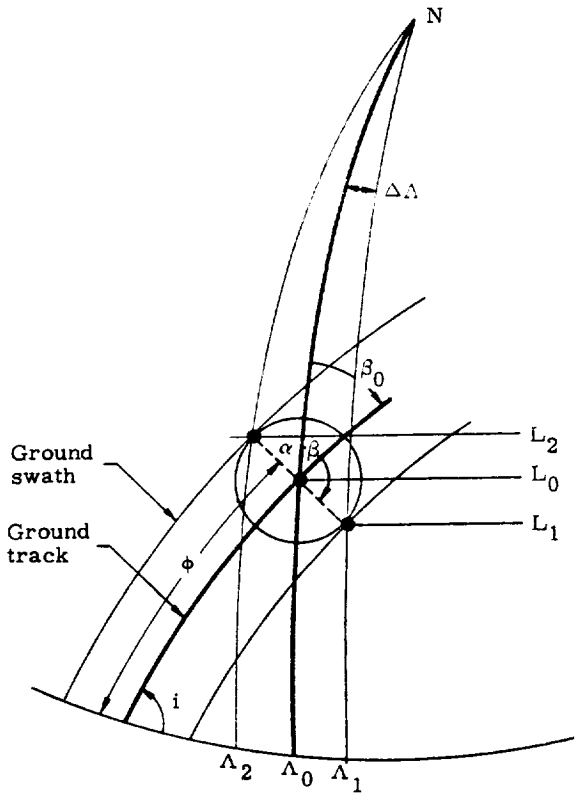

Again, let the position of the subsatellite point in geocentric coordinates at a certain time be (L_0, Λ_0). The locus of points on the perimeter of the area covered when the satellite is located at this position is given by Eqs (65) and (68). Two

of these points will also be points on the ground swath edges to be determined. Namely, the two points are those at the intersections of the circular perimeter and the major circle through (L_0, Λ_0) and perpendicular to the ground track. Thus, the two intersection points may be determined by solving Eqs (65) and (68) for two particular values of β,

$$\beta = \beta_0 \pm 90°$$

where β_0 is the orbit azimuth angle relative to the rotating earth defined in the previous ground track analysis, Section D, Eqs (44) and (45). That is, the solution of

$$\sin L = \sin L_0 \cos \alpha \mp \cos L_0 \sin \alpha \sin \beta_0 \tag{77}$$

$$\sin \Delta\Lambda = \pm \frac{\sin \alpha \cos \beta_0}{\cos L} \tag{78}$$

provides two points on the ground swath edges. Then the complete ground swath outline may be generated by solution of Eqs (77) and (78) for sets of values (L_0, Λ_0, β_0) generated from the ground track solutions, Eqs (36), (37), (44) and (45). For low altitude orbits, ground swath outlines can usually be calculated to adequate accuracies without correcting the orbit azimuth angle in inertial space, β_{0I}, for rotation of the earth. Of course, rotation must be included in the ground track equations used to generate the set of base points (Λ_0, L_0).

In determination of the long term coverage available from a given satellite, the longitudinal shift of the ground swath, as computed from Eqs (77) and (78), is of interest. At each latitude, the longitude of the ground track (and hence the longitudes of the ground swath outlines) shifts an amount

$$\Delta\Lambda_\tau = \Omega_e \tau_{nodal} \tag{79}$$

where

Ω_e = rotation rate of the earth
= 4.178074×10^{-3} deg/sec

τ_{nodal} = nodal period of the satellite orbit.

For circular orbits,

$$\tau_{nodal} \approx \tau\left[1 - \frac{3}{2} J_2 \left(\frac{R_e}{r_o}\right)^2 \frac{7\cos^2 i - 1}{4}\right], \quad 1 >> J_3 \tag{80}$$

where

τ = Keplerian orbit period = $2\pi r_0 \sqrt{\frac{r_0}{\mu}}$

r_0 = circular orbit radius

Equation (79) is plotted for the case of circular orbits in Fig. 37. The longitudinal shift may be obtained to five place accuracy by multiplying $\frac{\tau_{nodal}}{\tau}$ from Fig. 38 by τ from Table 1 of Chapter III and multiplying this result by Ω_e.

The previous analyses, and those of Section D, are concerned with the determination of the ground track and ground swath for a given set of orbit elements and sensor limitations. From the opposite point of view, the equations of these sections can be used to select orbit elements and sensor requirements to achieve total or optimum coverage in a certain area. The typical pattern of area covered by two consecutive ground swaths is shown in the following sketch. During any given day every point in the latitude region of total coverage is in view of the satellite at some time. This region can be determined from the previously derived ground track and ground swath equations by solving for the intersection points of two consecutive swath outlines. However, if mission requirements permit coverage of each point in a latitude band once in several days, the total coverage area may be increased. That is, if the orbit altitude and inclination are selected so that the longitudinal shift

$$\Delta\Lambda = m\,\Delta\Lambda_\tau\,(h, i) \tag{81}$$

(where m = number of orbit periods in one day, $\Delta\Lambda_\tau$ is given by Eq (79)) experienced in one day is of such a magnitude that the orbits of the second day are out of phase with those of the first day, then the lune-shaped uncovered areas below the total coverage region will be partially or totally covered by the swaths of the second day. The diurnal longitudinal shift of the ground track is

$$\Delta\Lambda_d = n\,\Delta\Lambda_\tau - 360° \tag{82}$$

where

n = the integral number closest to $\frac{d}{\tau_{nodal}}$, or that for which $\Delta\Lambda_d$ is minimum

d = one sidereal day, 86,164 mean solar seconds.

Equation 82, plotted in Fig. 39, is then a quantity of interest in determining coverage available over several days. Of course, for missions of long duration, total coverage is available in the latitude range $L = \pm i + \alpha$, provided that the ground track does not repeat diurnally. When mission length is limited to a few days or weeks, and total coverage of a specified latitude range is required, optimum coverage is achieved by selection of orbit altitude and inclination such that

$$\Delta\Lambda_d = \pm \frac{k}{m}\,\Delta\Lambda_\tau\,(h, i) \tag{83}$$

where

k = an integer

m = mission length in days.

An orbit chosen on this basis would obviously provide the most uniform coverage with minimum overlapping of ground swaths.

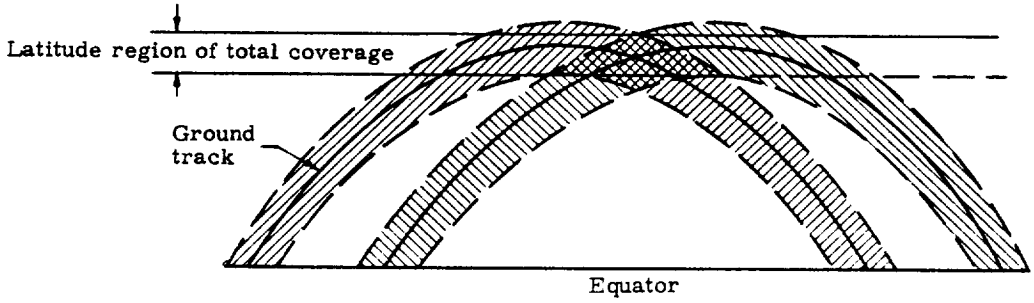

b. Pattern coverage (Ref. 3)

If mission requirements specify continuous total coverage of a large area by at least one satellite or frequent coverage from low altitudes, more than one satellite will be required. Optimization of coverage available from a pattern of several satellite orbits requires a somewhat different approach then that for the single satellite case.

(1) General approach

It is obvious that infinitely many possible arrangements of orbital planes and satellites in orbit could be considered for a satellite pattern covering either some well-defined region or the total surface area of the earth. To simplify the problem and provide for constant angular separations between the orbital planes, consider that the orbit planes are equally inclined to the equator. Second, the uniform coverage requirements can be best met by arranging the nodes of orbital planes at equal distances along the equator, by distributing satellites in equal numbers among all the orbital planes and by placing satellites in circular orbits of common altitude (so that the distances between all the satellites in one ring will be as uniform as possible).

In Ref. 5 the following set of equations is presented for optimization of satellite networks for zonal coverage of a latitude belt in both hemispheres (see the accompanying sketch), considering N the total number of satellites, n_1 the number of orbit planes and n_2 the number of satellites in each orbit plane:

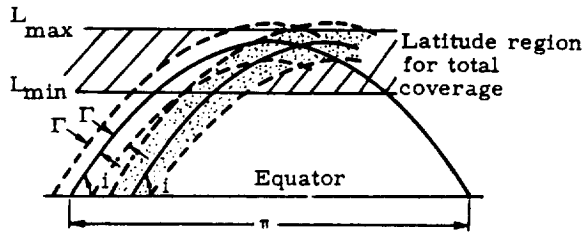

$$h = R\left(\cos\sigma/\cos\left\{\cos^{-1}\left[\cos\left(\frac{\pi n_1}{N}\right)\cos\Gamma\right] + \sigma\right\} - 1\right) \qquad (84)$$

$$L_{min} = \tan^{-1}\left\{\tan i \cos\left[\left(\frac{k+1}{n_1}\right)\pi\right]\right\} - \sin^{-1}\left\{\frac{\sin\Gamma}{\sqrt{1-\sin^2 i \sin^2\left[\left(\frac{k+1}{n_1}\right)\pi\right]}}\right\} \qquad (85)$$

where Γ is the ground swath angular half-width, given by

$$\Gamma = \sin^{-1}\left[\sin L_{max}\cos i - \cos\frac{\pi}{n_1}\cos L_{max}\sin i\right] \qquad (86)$$

Note: $0 < \Gamma < 90°$ is required, also

$$\Gamma \leq \cos^{-1}\sqrt{1 - \sin^2 i \sin^2\frac{\pi}{n_1}} \qquad (87)$$

k = the least integer such that

$$k \geq \frac{n_1}{2} - 2 - \frac{n_1}{\pi}\tan^{-1}\left[\frac{\cos i}{\sin\Gamma}\sqrt{\frac{\cos^2\Gamma}{1-\sin^2 i\sin^2\frac{\pi}{n_1}} - 1}\right] \qquad (88)$$

σ = minimum incidence angle for the sensor.

The relationship between the ground swath angular half-width, Γ, and the ground coverage angle, α, is given by

$$\cos\alpha = \cos\Gamma\cos\frac{\pi}{n_2}, \qquad (89)$$

as shown in the accompanying sketch, in which consecutive satellites in the same orbit are located at A and B.

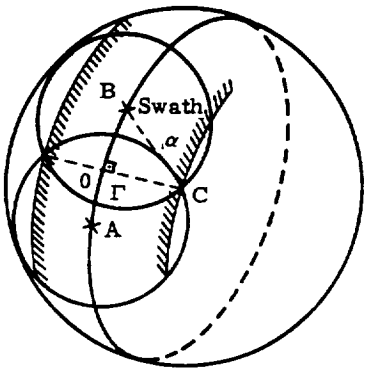

In Ref. 5 the above equations are solved for various polar and inclined orbit planes, as shown in Figs. 40 through 43.

Figure 40 gives the total number of satellites, N, required for polar orbits consisting of from 2 to 6 orbit planes. As a numerical example, a reconnaissance system of 36 satellites providing complete global coverage is considered. The results are shown in the following table:

Orbit Planes n_1	Satellites/ Plane n_2	Required Altitude h (km)
2	18	2780
3	12	1245
4	9	968
6	6	1245
9	4	2780

Considering sensor limitations, the 4-orbit plane system is obviously optimum for the case considered.

Figure 41 gives the comparison between the theoretical optimum curve and the practical optimum curve for polar orbits with minimum incidence angle $\sigma = 0°$. The effects of increasing minimum incidence angles are also shown.

Figure 42 gives the comparison of polar satellite networks providing coverage from the poles to a fixed minimum latitude L_{min}, considering $\sigma = 0°$ and $L_{min} = 60°$, 30° and 0° (note that $L_{min} = 0°$ gives the complete global coverage given by the step-function on Fig. 41).

Finally, Fig. 43 shows the comparison of inclined satellite patterns to the polar pattern for complete coverage. It can be seen that polar orbits are preferable, at least under 3500-km altitudes.

As a more particular example, following slightly different lines of approach, the optimization of a specific orbit pattern is analyzed more fully in the next subsection.

(2) Specific example: 6-hour orbit pattern

Although the equations and data presented in the preceding subsection provide a general basis for orbit pattern selection, a specific mission may present special problems. As an interesting example, consider the selection of a navigation satellite orbit pattern which must fulfill the requirement that at least three satellites be visible from any point on the earth's surface (and, therefore, from any point in space near the earth) at any given time. Definition of the required pattern entails specification of each of the following parameters:

(1) Orbital period (i.e., altitude).

(2) Number of satellites in each ring.

(3) Orbital nodal positions (number of rings).

(4) Orbital inclination.

(5) Orbital eccentricity.

The synchronized pattern obtained from these considerations must also be subjected to a pattern proof, including the effects of small changes in inclination. The earth's oblateness effects are included in the determination of the exact orbital altitude.

The altitude of the navigation satellites depends on a large number of factors as noted in Section A. Some of the most important are:

(1) Resolution limitations.

(2) Perturbations.

(3) Repeatable daily ground track.

(4) Number of satellites employed.

(5) Van Allen radiation belts.

For the best resolution at sea level, the satellite orbits should be as low as possible. On the other hand, oblateness perturbations are largest for low altitude orbits; for higher orbits the perturbations caused by the sun and the moon increase in relative importance. A repeatable daily ground track will simplify the preparation of the required ephemeris which makes navigation possible; therefore, it is desirable to have an integral number of revolutions per day. The number of satellites in a given ring will further define the necessary altitude and period for the desired ground coverage. To keep the molecular breakdown of the solar cells and similar electronic apparatus to a minimum, the Van Allen radiation belts should be avoided as much as possible.

From all the above considerations, the 6-hr orbit was considered as the most promising for the present application.

The 6-hr orbit retraces its ground track on a daily basis and that ground track results from four orbital revolutions. For an ideal spherical earth, the period of this orbit would be exactly one-fourth of a sidereal day. Since the earth is actually oblate, the orbit plane regresses slowly; and in order to repeat the desired ground track (i.e., to achieve a sidereal period of 21,541.02 mean solar seconds), the semimajor axis required is 16738.13 km. (A complete set of synchronous orbit semimajor axes is included in Section D.2.) The circular orbit altitude corresponding to this value of semimajor axis is about 10,360 km.

At this altitude, the ground coverage is 135.26°, as can be seen in the following sketch:

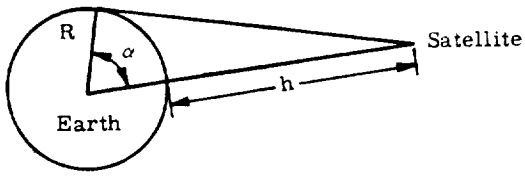

$$2\alpha = 2\cos^{-1}\left(\frac{R}{R+h}\right) = 135.26°$$

Thus, three or more satellites will be required to provide continuous coverage of a band on the earth (the width of this band being a function of the number of satellites). Because the overlap of the covered areas is small with only three satellites per ring, four satellites will be placed in each ring at 90° intervals. In general, only one satellite is seen on the earth's surface from a given satellite ring. Furthermore, there are two areas around the axis perpendicular to the orbital place of a given satellite ring where no satellites from this ring are visible. To ensure that in these regions at least three satellites are visible, three more satellite rings are required, placed so as to make at least one satellite visible from each additional ring at all times. Since uniform ground coverage is desirable, the nodes for the four satellite rings must be displaced from each other by 90° on the equator. This brings the total number of satellites employed in the navigation pattern to 16.

To equalize oblateness perturbations for the four orbital planes, the inclinations must be equal. From this condition, it can be seen that the most symmetrical distribution of orbital planes in inertial space results if each set of two planes intersects at a latitude of 45° (that is, halfway between the poles and the equator). The orbital inclination which satisfies these conditions was found from spherical trigonometry as:

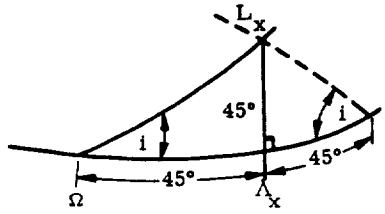

$$i = \tan^{-1}\left[\frac{\tan L_x}{\sin(\Lambda_x - \Omega)}\right] = 54.736°$$

Orbital eccentricity produces periodic relative motion of the satellites in each ring (Fig. 44) which, in turn, produces irregular ground coverage. While this in itself does not eliminate eccentric orbits from consideration, it does make the resulting analysis and pattern utilization more difficult, because the solution for position as a function of time becomes transcendental. For these reasons, the orbits considered are circular (i.e., zero eccentricity).

To avoid crowding a considerable number of satellites over the same region of the globe, one satellite was placed at the node for Planes I and II (which are consecutive), while the positions in Planes III and IV were displaced by 45°. The initial latitudes, longitudes and central angles of all 16 satellites are given in Table 3.

TABLE 3

Initial Positions of 16 Satellites

Orbit Plane and Satellite Numbers	Latitude (L_0) (deg)	Longitude (Λ_0) (deg)	Initial Central Angle (θ_0) (deg)
I-1	0	180 W	0
I-2	54.7 N	90 W	90
I-3	0	0	180
I-4	54.7 S	90 E	270
II-1	0	90 W	0
II-2	54.7 N	0	90
II-3	0	90 E	180
II-4	54.7 S	180 E	270
III-1	35.3 N	30 E	45
III-2	35.3 N	150 E	135
III-3	35.3 S	150 W	225
III-4	35.3 S	30 W	315
IV-1	35.3 N	120 E	45
IV-2	35.3 N	120 W	135
IV-3	35.3 S	60 W	225
IV-4	35.3 S	60 E	315

The ground track of a satellite, as noted in Section C, is given by the equations:

$$L = \sin^{-1}\left[\sin i \sin(\theta_0 + \theta)\right] \qquad (90)$$

$$\Lambda = \tan^{-1}\left[\cos i \tan(\theta_0 + \theta)\right] + \Omega_o - \Omega_e t \qquad (91)$$

where flight time is given for a circular orbit by the equation

$$t = \left(\frac{\tau}{2\pi}\right)\theta. \qquad (92)$$

A complete ground track during one day was computed for the first satellite in the first orbit plane by Eqs (90) and (91). The result was plotted in Fig. 45. It should be noted that the same pattern of four revolutions is identically repeated during each day. This is due to the fact that the sidereal period is exactly one-fourth of a sidereal day.

Initial positions and ground tracks for one-half of a revolution are given in Fig. 46. It is obvious from this figure that the distribution of satellites is not completely uniform over the earth's surface at all times. However, there are no serious crowding problems and thus, this pattern is satisfactory.

The placement of the four orbit planes in three-dimensional space is indicated in Fig. 47. The first of the two drawings shows the intersections of the orbital planes in inertial space (the earth should be visualized as rotating within this fixed framework). The second drawing shows the initial positions of the 16 satellites as given in Table 3 and Fig. 46 (except the ones hidden by the earth).

The proof of satellite pattern. It must now be shown that the pattern specified actually satisfies the requirement that at least three of the vehicles are always visible at any point on earth's surface. Secondly, small changes in the orbit inclination must be investigated in order to justify the optimum inclination selected (i = 54.736°).

In order to rigorously prove the satellite pattern, the concept of ground swath was used. Swath in the case of this problem is defined as the region on a nonrotating earth where at least one of the four satellites in the ring is always visible.

From Eq (89), it can be seen that the width of the ground swath (to either side of the ground track) is given by:

$$\Gamma = \cos^{-1}\left(\frac{\cos\alpha}{\cos\frac{180°}{n_2}}\right) = 57.421°$$

$$\frac{180°}{n_2} = \frac{180°}{4} = 45°$$

Outlines of ground swaths were obtained as indicated in Section E.1.a. Areas not included by the swath generated by the satellites in four orbit planes are shown in Fig. 48. No satellite from the ring indicated by the Roman numeral is visible inside either cross-hatched area of the same number. Because no cross-hatched areas intersect, the figure proves that at least three satellites are visible at all times at every point on the earth's surface. On a rotating earth the eight cross-hatched areas must be visualized as moving with a 24-hour period but maintaining the given topological pattern. The horizontal and vertical distances between any two adjacent cross-hatched areas are essentially equal (5.4° on a great circle).

The effects of small changes in orbit inclination on the pattern of circular areas shown in Fig. 48 may be investigated by means of the equations of Section E.1.a, with swath width denoted by Γ instead of α.

The results of the foregoing analysis are presented in Fig. 49 which shows that the requirements placed upon the pattern can only be met in the range of orbital inclinations between 49.6° and 57.4°. The selection of the optimum inclination with this range must be based on visibility criteria because there are definite limits which must be imposed on the minimum elevation angle between the satellites of the pattern and the horizon to make navigation practical. This optimum inclination angle is 54.736° because only this inclination ensures that all of the visible satellites will be at least 5° above the horizon. This analysis also proves that the minimum altitude for a pattern of 16 satellites, which will ensure a minimum elevation angle above the horizon of 5° for at least three of the satellites at all times, is that of the 6-hr orbit.

2. Point Coverage

In many satellite missions, area coverage as discussed in the previous section is not a firm requirement; rather, it is desired to maximize the time spent over a specific set of points on the earth. These locations may be tracking stations, ground data links, landing sites, or points under surveillance. Various problems connected with point coverage are considered in this section.

a. Determination of the zenith angle of a satellite

A problem of interest to satellite tracking and communication is that of determining the conditions under which the satellite is visible, or above the horizon, when viewed from a point on the earth. To solve this problem assume that a satellite S is in an orbit inclined at angle i to the earth's equator, and assume a point of observation P on the earth at a latitude L. Consider a coordinate system, its origin at the point of observation, with the Z-axis vertical, the X-axis due east (i.e., in the direction of motion of the point of observation) and the Y-axis due north. Let the distance from the center of earth to the point of observation be R_e and the distance from the center of the earth to the satellite be r.

The satellite's position is determined by a central angle ϕ_s measured in the orbital plane from the ascending node, and the position of the point of

observation is determined by an angle ϕ_e measured from the longitude of the ascending node (Fig. 50). In terms of the usual variables, the angles ϕ_s and ϕ_e are given as

$$\phi_s = \omega + \theta \qquad \text{where } \Lambda_p = \text{longitude of observation point}$$
$$\phi_e = \Lambda_p - \Lambda_n \qquad \Lambda_n = \text{longitude of nodal point}$$

The coordinates of the satellite in the X, Y, Z system are as follows:

$$x = r\,(\cos i \sin \phi_S \cos \phi_e - \cos \phi_S \sin \phi_e)$$

$$y = r\left[\cos L \sin i \sin \phi_S - \sin L\,(\cos \phi_S \cos \phi_e + \cos i \sin \phi_S \sin \phi_e)\right]$$

$$z = r\left[\sin L \sin i \sin \phi_S + \cos L\,(\cos \phi_S \cos \phi_e + \cos i \sin \phi_S \sin \phi_e)\right] - R$$

The distance between the point of observation and the satellite is

$$\rho = \sqrt{r^2 + R - 2\,r\,R \cos \psi}$$

where

$$\cos \psi = \sin L_p \sin i \sin \phi_S + \cos L_p\,(\cos \phi_e \cos \phi_S + \cos i \sin \phi_e \sin \phi_S)$$

and ψ is the angle between the radius vectors from the earth's center to the point of observation and to the satellite (see Fig. 50).

The direction cosine, ℓ_z, (i.e., the cosine of the angle δ between the Z-axis and the radius vector from P to S) is

$$\ell_z = \frac{z}{\rho} = \frac{r \cos \psi - R}{\sqrt{r^2 + R - 2r\,R \cos \psi}} = \frac{\frac{r}{R} \cos \psi - 1}{\sqrt{1 + \left(\frac{r}{R}\right)^2 - \frac{2r}{R} \cos \psi}}$$

The satellite is above the horizon as viewed from the point of observation if $\ell_z > 0$ and, since ℓ_z is the cosine of the satellite's zenith angle, any value of the satellite elevation angle can be specified and the corresponding ℓ_z determined. Any ℓ_z above this value corresponds to a satellite passage at an elevation angle equal to, or higher than, the specified value.

For the point of observation $\phi_e = (\Omega_e + \dot{\Omega})\,t + \phi_1$, where

$\dot{\Omega}$ = the rate of regression of the nodes of the satellite (rad/sec)

$$\phi_1 = \Lambda_{p0} - \Lambda_{n0}$$

For the satellite $\phi_S = \phi_S(t) + \phi_0$, where $\phi_S(t)$ is the equation relating the central angle to time in the general elliptical case, and ϕ_0 is the initial angle of the satellite with respect to the ascending node. For a circular orbit $\phi_S(t) = \omega_S t$, where ω_S is the angular velocity of the satellite. The use of these equations is illustrated by the following example.

Assume an orbital inclination angle of 30° and a point of observation at a latitude of 30°. Assume further that the satellite is in a circular orbit at an altitude such that it makes 15 revolutions relative to the ascending node in the time it takes the earth to make one revolution relative to this node. The regression period is then about 50 days and the period of the satellite about 1.59 hr, rather than the 1.6-hr period if the regression were neglected. For this example this small difference is neglected and a satellite altitude of 357 stat mi and $r/R_e = 1.0902$ is assumed. To find when the satellite is above the horizon for a point originally along the meridian through the node at the time the satellite was at the node (i.e., $\phi_1 = \phi_0 = 0$, $\phi_e = \Omega_e t$ and $\phi_S = 15\,\Omega_e t$), the procedure is first to plot

$$\ell_z = \cos \delta = \frac{1.0902 \cos \psi - 1}{\sqrt{1 + (1.0902)^2 - 2\,(1.0902 \cos \psi)}}$$

as a function of cos ψ (Fig. 51). Note that $\ell_z > 0$ for $0.9173 \cos \psi < 1$. Next plot cos ψ as a function of $\phi_e = \Omega_e t$ (Figs. 52 and 53). The values of ϕ_e for which $0.9173 \leq \cos \psi$ (indicated on the figure by a solid line) then represent the values of $t = \phi_e/\Omega_e$, for which the satellite is above the horizon. If it is required that the satellite be 30° above the horizon, then $0.5 < \ell_z$ and $0.9916 \leq \cos \psi$. This line is indicated on the figure by a dotted line. The angle δ, defined by $\cos \delta = \ell_z$, is actually the zenith distance of the satellite and the angle ϕ_e can be considered the "hour angle" of P with respect to satellite node.

Finally, Fig. 54 presents in English units a solution for the line-of-sight range to the satellite and the distance of the subsatellite point from the observation point on the earth's surface. This information is presented in different form in Figs. 55 and 56, also in English units. It should be noted that Figs. 35 and 36 present the same information in metric units when the coverage

half-angle, α, is interpreted as ground range, d, and the minimum viewing angle, σ, is interpreted as elevation, ϵ.

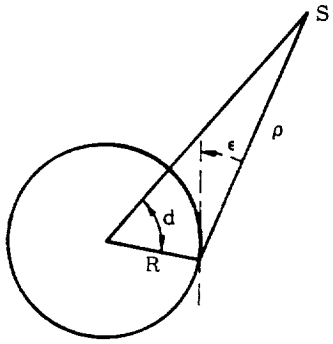

b. Visibility time durations

Visibility times for satellites in elliptical orbits must be computed from Kepler's equation, tabulated in Chapter 3. However, in the case of circular orbits, the equations for visibility time are sufficiently simple to warrant presenting parametric results. Visibility time from a point on a nonrotating earth is then

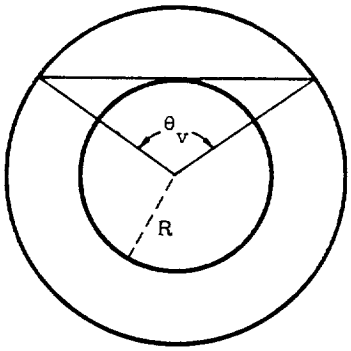

$$t_v = \frac{\cos^{-1}\frac{R}{r}}{180^\circ}\left(2\pi r\sqrt{\frac{r}{\mu}}\right) \qquad (93)$$

where r = circular orbit radius. The visibility time of a satellite moving in a circular orbit exactly in the direction of the earth's rotation is

$$t_{v+} = t_v \frac{\tau_e}{\tau_e - \tau} \qquad (94)$$

where

τ_e = period of earth rotation, 86,164 sec

τ = orbit period = $2\pi r\sqrt{\frac{r}{\mu}}$

For satellites moving directly opposite to the direction of the earth's rotation, the visibility time is

$$t_v - t_v \frac{\tau_e}{\tau_e + \tau}. \qquad (95)$$

Equations (93), (94) and (95) are plotted in Figs. 57 and 58.

c. Visibility and call-down time computation

The computation of call-down time (the time interval during which a vehicle may initiate a landing sequence terminating at a specified landing site) or visibility time proceeds by solution for the intersections of the ground track, as given by the equations of Section D, and the perimeter of a test region. In the case of visibility time, the test region is simply the spherical segment determined by the maximum ground range of the tracking station. The perimeter of the test region is then given by Eqs (65) and (63) where (L_0, Λ_0) is interpreted as the location of the tracking station and α is the maximum ground range. In the case of call-down time the shape of the test region is a function of the maneuverability of the landing vehicle. This particular subject is treated in some length in Chapter VIII.

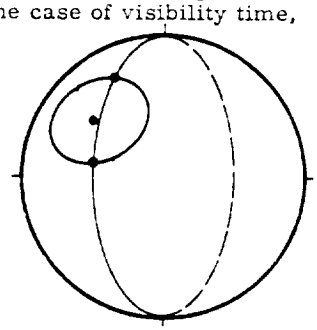

F. SENSOR LIMITATIONS ON ORBIT SELECTION

The selection of orbit elements to best fulfill given mission requirements must obviously be subject to any sensor limitations. Although sensors may take a wide variety of forms, consideration will be limited to the two largest classes, optical and radio systems. The primary limitations of these systems are power and resolution requirements.

1. Radio Systems

An important limitation of radio systems and the primary limitation for communication applications is the restriction on range imposed by transmission power limits. The range equation may be written in several forms:

$$\frac{P_r}{P_t} = \frac{G_t A_r}{4\pi \rho^3} = \frac{G_r A_t}{4\pi \rho^2} = \frac{G_t G_r \lambda^2}{(4\pi\rho)^2} = \frac{A_t A_r}{(\lambda \rho)^2} \qquad (96)$$

for simple one-way transmission.

Where

P_r = received signal power

P_t = transmitted power

A_r = effective area of the receiving antenna

A_t = effective area of the transmitting antenna

G_r = receiving antenna gain

G_t = transmitting antenna gain

λ = wavelength

ρ = range from the transmitter to the receiver.

In skin tracking, the transmitted radio beam is reflected by the object tracked, and a portion of the reflected energy is then received at the transmitter station. For skin tracking, then,

$$\frac{P_r}{P_t} = \frac{A_o A_r G_t}{(4\pi \rho^2)^2} = \frac{G_t G_r \lambda^2 A_o}{4\pi (4\pi \rho^2)^2} \qquad (97)$$

where

A_o = scattering cross-section area.

Typical gains and effective areas for use in the above equations are contained in Table 4 from Ref. 6.

TABLE 4

Antenna	Gain	Effective Area
Isotropic	1	$\frac{\lambda^2}{4\pi}$
Infinitesimal dipole	1.5	$\frac{1.5\lambda^2}{4\pi}$
Half-wave dipole	1.64	$\frac{1.65\lambda^2}{4\pi}$
Optimum horn	$\frac{10.0 A}{\lambda^2}$	0.81 A
Parabola or lens	$\frac{(6.3 \text{ to } 7.5) A}{\lambda^2}$	(0.5 to 0.6) A
Broadside array	$\frac{4\pi A}{\lambda^2}$ (maximum)	A (maximum)

The minimum detectable signal is not determined by the ability to amplify the signal, but by the noise which obscures the signal. That is, if no interference were present, any signal transmitted over any distance could be detected by providing sufficient amplification in the receiver. Noise limiting the usable range may enter the radio system at the transmitter, at the receiver or in the space link. The noise power produced in a bandwidth Δf is given by

$$P_n = kT \Delta f \qquad (98)$$

where

k = Boltzmann's constant = 1.38×10^{-23}, w-sec/° K

T = absolute temperature of the circuitry, ° K

Δf = bandwidth, cps

The temperature T is the weighted sum of the various component source temperatures, the weights being high (unity) for noise sources internal to or surrounding the receiver or low if the noise enters through a fraction of the receiver surroundings. Typical equivalent temperatures of internal receiver noise are 2000° K for conventional receivers, 100° K for parametric amplifier receivers and 10° K for masers. Equivalent temperatures of external noise are dependent on frequency and, in the case of atmospheric noise, on elevation angle. External noise is shown in the following sketches from Ref. 6. The blackbody radiation of the earth also comprises a noise source which increases for low elevation angles. Thus, low altitude satellites, which spend relatively long times near the horizon of an observer on earth, entail greater noise problems. Other sources of noise are the sun, the moon and the planets.

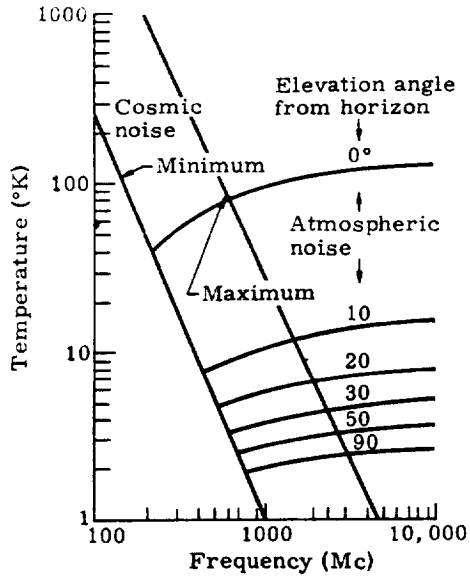

The ratio of received power, P_r, to interference power in the bandwidth Δf determines the range at which communication is feasible. A ratio of unity is defined as threshold reception. The threshold reception range for space-to-earth communication is

$$\rho' = \sqrt{\frac{P_t A_t G_r}{4\pi k T \Delta f}} \qquad (99)$$

Usable ranges may be about one-third of this value.

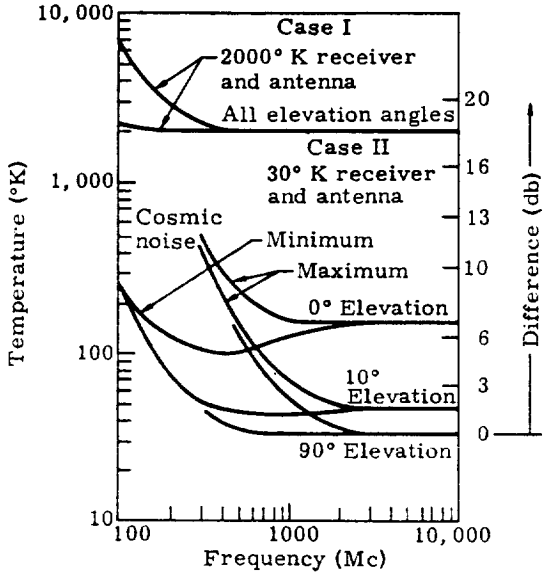

In addition to range limitations, missions employing radar systems may encounter resolution problems. The angular resolution of a radar is determined by the narrowness of the antenna beam. The apparent angular extent of an object detected is increased by the width of the antenna beam, and objects separated by less than the beamwidth are interpreted as a single object. Consequently, for a given system bandwidth, the minimum resolution distance increases with increased altitude. Range resolution depends mainly on the pulse duration of the transmitted signal.

Just as noise determines the minimum detectable signal for range limitations, the obscuring of echoes by ground clutter and sea return is closely related to resolution capability. For example, in detection of a ship by means of an overhead airborne radar, difficulty is experienced in distinguishing the ship from the sea because the ranges differ by less than the pulse duration. The problem of relating radar resolution in the presence of clutter to orbit altitude is too complex to consider here except by generally noting the importance of low altitudes in achieving high resolution and minimizing power consumption.

2. Satellite Photography Systems

Resolution attainable in satellite photography is related to orbit altitude, and so the photographic system limitations are factors in choice of orbit elements. Investigation of this relationship, in order to be meaningful, must consider the entire photographic system performance in some detail.

Among the factors which determine the degree of detail that can be detected or identified by a visual or photographic system are the object distance and the focal length of the viewing lens. The ratio of object distance, d, to focal length, f, is referred to as the scale number, S.

$$S = \frac{d}{f} \qquad (100)$$

Then one cm on a photograph corresponds to S cms on the ground. Thus larger scale numbers mean greater difficulty in discerning fine detail.

A second parameter useful in defining optical system capability is resolution, the ability to distinguish parts of an image. In photography, resolution is the ability of a film-lens system to distinguish a standard pattern of black and white lines. Thus a film-lens system may be described as providing resolution of r_f lines per millimeter. Ground resolution is the distance on the ground equivalent to one barely resolvable line. Thus, if a film-lens system provides a system resolution of r_f lines per mm, and the scale number is S, the ground resolution, r_g, is

$$r_g = \frac{S}{r_f} \qquad (102)$$

In terms of commonly used units,

$$r_g \text{ (meters)} = \frac{S}{1000\, r_f \text{ (lines per millimeter)}}.$$

Although ground resolution is a ratio, the effects of graininess influence a selection of lower values of S and r_f to attain a given r_g. From Eqs (101) and (102), the maximum orbit altitude can be determined as a function of system resolution, focal length and ground resolution.

$$h = 1000\, f r_f r_g \qquad (103)$$

where

h = orbit altitude in meters

f = focal length in meters

r_g = ground resolution in meters

r_f = system resolution in lines per mm.

Equation (103) is plotted in Fig. 59. However, in order to use this data or Eq (103) it is necessary to describe the quantity r_f (or system resolution). This resolution is a function of many separate factors and will be discussed in the following paragraphs.

The overall performance of a photographic system depends on the contribution of each element of the system. The elements of a photographic system are:

(1) The scene, with its contrasts.

(2) The atmosphere, which modifies the light from the scene before it enters the optical system.

(3) The optical system, which images the scene on the film.

(4) The camera system, through which uncompensated motion and vibration enter the system.

(5) The film, which records the final image.

Each of the elements which follows the scene alters the contrast in a different manner. It is desirable to have a method of analysis which permits the examination of each of these elements in the same terms so that the individual elements can be compared on a common basis, and which presents the result in the same terms.

Such a method is the sine wave response analysis which describes the effects of each element in terms of its modulation transfer function, T (K). The method is analogous to the transfer function analysis of servomechanisms in which the modulation transfer function describes the response of the element as a function of the spatial frequency. The overall system performance is then the product of the modulation transfer functions of the individual elements.

a. Modulation transfer function

Consider a scene in which the intensity varies according to the following relation

$$I = I_A + I_V \sin\left(\frac{2\pi K}{K_0}\right).$$

This is a series of lines spaced K_0 units apart (see following sketch). The maximum intensity is $I_A + I_V$ and the minimum intensity is $I_A - I_V$, with the intensity varying sinusoidally between these limits. Since all of the lines are the same distance apart, they represent a constant spatial frequency, K_0. The modulation transfer function can be defined as the ratio of I_V to I_A. Therefore for this scene the modulation transfer function T (K_0) is given by I_V/I_A.

Now consider the image which is produced when light from a scene (see following sketch) which has a modulation transfer function of unity but

increasing spatial frequency is passed through a diffraction limited lens. At some spatial frequency the diffraction patterns of the individual lines begin to overlap and the contrast in the image is reduced. As the lines become closer together the contrast becomes further reduced until at some frequency the lens gives essentially no response to the modulation in the scene. The modulation of the scene-lens combination might appear as shown in the following sketch. The corresponding transfer function is given in Fig. 60. Since the scene has a modulation transfer function of unity, Fig. 60 is the transfer function of the lens alone.

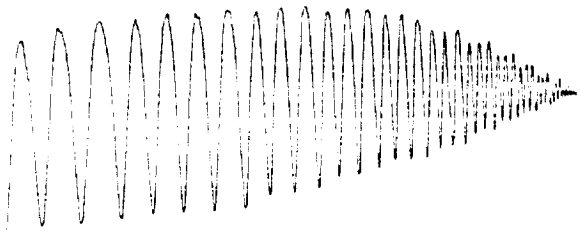

By determining the modulation transfer function of each element of the system, the modulation transfer function of the final image as recorded on film can be determined, thereby determining the

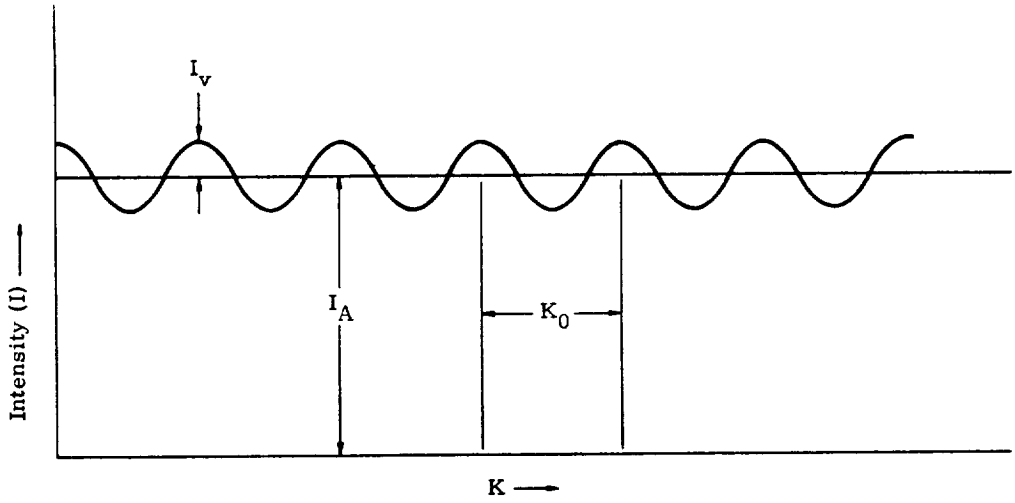

performance of the system. The modulation transfer function of each of the elements of the system is discussed in the following paragraphs.

b. The scene

The scene to be photographed is usually a complex mixture of contrasts and spacings, and its transfer function, although theoretically obtainable, is too complex to be of practical value. Fortunately, we are rarely interested in the performance of the system against a particular scene; we are usually interested in the ability of the system to resolve detail. This can be done by evaluating the system performance against an artificial scene which lends itself to analysis, such as the scene represented in the foregoing sketch.

Such artificial "target" scenes are characterized by a constant contrast, and therefore a constant transfer function, for all spatial frequencies. The transfer function varies with the contrast in the following manner:

$$T_C = \frac{C - 1}{C + 1} \qquad (104)$$

where C is the brightness ratio of the peaks to the valleys of the sine wave.

Equation (104) is plotted in Fig. 61. The scene contrast is seen to act as a "gain" factor which multiplies the system sine wave response, and, therefore, to compare systems on a common basis, it is necessary to use a common value of scene contrast. For satellite photography a brightness ratio of 8.1 is usually assumed.

c. The atmosphere

In addition to the obvious effect of clouds, the atmosphere affects the system in two ways. The first of these, scattering, causes some light from the sun to be scattered directly into the system and some image forming light from the scene is scattered out of the system. From a satellite, looking through the entire thickness of the atmosphere, the scattering causes the target contrast to be reduced by a factor of four, so that the effective contrast seen by the system is 2:1, giving a transfer function of 0.33 from Eq (104).

The second effect is due to turbulence, and it affects only very high acquity systems. The turbulence causes a random angular displacement of the rays making up the image, and its value for satellite photography has not yet been adequately determined. It is felt that it will limit the ultimate system performance to the order of one foot.

d. The lens

The transfer function of the lens depends on its diffraction pattern and aberations, and for a particular lens this can be measured after the lens is manufactured. For system design, which must be performed before the lens is manufactured, it can be assumed that the lens has no aberations and is diffraction limited. For a well designed lens, this will be very nearly true on axis, but at the edges of the field the performance will be considerably reduced.

The modulation transfer function for a diffraction limited circular aperture, when viewing a line image, is given by Ref. 7

$$T(K) = \frac{2}{\pi}\left[\cos^{-1}(AK) - AK\sqrt{1 - (AK)^2}\right] \qquad (105)$$

where

$A = N\lambda$

λ = wavelength of light

N = focal ratio (f-number) of the lens

K = spatial frequency

The transfer function of an f/4 lens for light of 6000 A was given in Fig. 60. Equation (102) is plotted in Fig. 62 and the transfer function for f/1 to f/12 lenses is given in Figs. 63 and 64.

e. Image motion

The camera introduces two types of image motion into the system, vibration and linear motion. Although it is generally impossible to determine the expected vibration environment at the time of system design, the transfer function for vibration is useful in that it can be used to determine an allowable vibration level which will not seriously degrade the system. By finding that transfer function which degrades the system performance by the allowable amount, the vibration level which produces the transfer function is determined.

The transfer function for vibration is given by

$$T(K) = J_0(\pi AK) \quad \text{(Ref. 7)} \qquad (106)$$

where

J_0 = zero order Bessel function

A = amplitude of the vibration

K = spatial frequency

Linear motion between the film and the image during the exposure time can arise from several sources. These include:

(1) Uncompensated vehicle rotation rates.

(2) V/H measurement errors.

(3) Camera pointing errors.

(4) Film drive speed errors.

The magnitude of the motion from these sources can usually be predicted at the system design stage and the effects of the motion can be calculated.

The transfer function for linear motion is given by Ref. 7.

$$T(K) = \frac{\sin \pi AK}{\pi AK} \qquad (107)$$

where

A = distance of the motion (in the focal plane)

K = spatial frequency

Equation (107) is plotted in Fig. 65.

f. The film

The modulation transfer function of the photographic film is determined experimentally and can be obtained from the film manufacturer. An example of the transfer function that might be obtained from satellite photography films is shown in Fig. 66.

g. Interpretation

The overall system transfer function represents the response of the system to lines of width which vary from very broad, to lines which are finer than the system can resolve, and therefore is a good description of the system performance. However, it is often desirable to describe the system performance in terms of a single number, the resolution. It has been found that the minimum detectable resolution occurs at a response of 0.04, and the spatial frequency at which 4% response occurs is becoming accepted as the system resolution.

h. Illustrative example

To illustrate the use of modulation transfer functions in analyzing systems, the following example is presented. Assume the following system characteristics:

Aperture--18 in. or 0.492 m

Focal ratio--f/4

Orbital altitude--125 naut mi or 232 km

Image motion--equivalent to 2.5×10^{-6} rad

Target contrast 8:1, reduced to 2:1 by the atmosphere.

These values lead to the following transfer functions:

The lens, being f/4, is described in Fig. 60.

The image motion is determined as follows:

$A = 2.5 \times 10^{-6}$ rad x 72 in. (focal length) x 25.4 millimeters/in. $= 4.57 \times 10^{-3}$ mm.

This yields the transfer function shown in Fig. 67 for image motion. The film will be represented by the transfer function of Fig. 66. Table 5 gives the values of the transfer function for the example, and they are plotted in Fig. 67.

The 4% response point is seen to occur at 140 lines per millimeter. The corresponding resolution in the scene is determined by multiplying the distance in the image (1/140 mm), by the scale number, as in Eq (103)* or utilizing Fig. 59.

TABLE 5

Transfer Functions for Illustrative Example

Spatial Frequency (lines/mm)	The Scene + Atmosphere	Lens	Image Motion	Film	Overall System
10	0.33	0.96	0.99	0.96	0.30
20		0.93	0.98	0.90	0.27
30		0.90	0.96	0.85	0.24
40		0.87	0.94	0.80	0.22
50		0.84	0.91	0.74	0.19
60		0.81	0.88	0.70	0.16
70		0.78	0.84	0.66	0.14
80		0.75	0.79	0.63	0.12
90		0.72	0.74	0.60	0.11
100		0.69	0.68	0.58	0.09
110		0.66	0.63	0.55	0.08
120		0.63	0.57	0.53	0.06
130		0.60	0.51	0.51	0.05
140		0.57	0.45	0.50	0.04
150		0.54	0.39	0.48	0.03
160		0.51	0.33	0.47	0.026
170		0.48	0.27	0.45	0.019
180		0.45	0.21	0.44	0.013
190		0.43	0.16	0.43	0.010
200		0.40	0.10	0.41	0.005

$$r_f = \frac{1}{140}\ \text{mm} \times \frac{125\ \text{miles}}{72\ \text{in.}} \times \frac{1\ \text{in.}}{25.4\ \text{mm}}$$

$$\times\ 6076\ \frac{\text{ft}}{\text{mi}} = 2.97\ \text{ft}$$

$$= 0.974\ \text{m}$$

i. Tabulation of transfer function values

Reference 7 also presents the following table of values for the transfer functions.

TABLE 6

Values of T(K)

AK	$J_0(\pi AK)$	$\sin \pi AK / \pi AK$	$\frac{2}{\pi}\left[\cos^{-1}(AK) - AK\sqrt{1-(AK^2)}\right]$
0.05	0.994	0.996	0.963
0.10	0.975	0.983	0.873
0.15	0.945	0.963	0.810
0.20	0.904	0.935	0.747
0.25	0.854	0.900	0.685
0.30	0.790	0.858	0.623
0.40	0.646	0.756	0.506
0.45	0.560	0.699	0.442

(continued)

TABLE 6 (continued)

AK	$J_0(\pi AK)$	$\sin \pi AK / \pi AK$	$\frac{2}{\pi}\left[\cos^{-1}(AK) - AK\sqrt{1-(AK^2)}\right]$
0.50	0.473	0.636	0.389
0.60	0.293	0.525	0.285
0.70	0.110	0.368	0.188
0.75	0.025	0.300	0.138
0.80		0.234	0.104
0.90		0.109	0.038
0.95		0.052	0.015
1.00		0	0

G. REFERENCES

1. Kraft, D., "Position of the Sun with Respect to an Earth Satellite," Martin Company, ER 12507, April 1962.

2. Wolverton, R. (editor), "Flight Performance Handbook for Orbital Operations," STL, September 1961.

3. Jensen, J., Townsend, G., Kork, J. and Kraft, D., "Design Guide to Orbital Flight," McGraw-Hill, 1962.

4. Patterson, G., "Graphical Method for Prediction of Time in Sunlight for a Circular Orbit," ARS Journal, Vol. 31, No. 3, p 441.

5. Lüders, R. D., "Satellite Networks for Continuous Zonal Coverage," ARS Journal, Vol. 31, No. 2, February 1961, p 179.

6. Rechtin, E., "Deep Space Communications," Astronautics, Vol. 6, No. 4, April 1961, p 37.

7. Scott, R. M., "Contrast Rendition as a Design Tool," Photographic Science and Engineering, Vol. 3, No. 5, September to October 1959.

H. BIBLIOGRAPHY

Vargo, L. G., Pasquall, J., and Gersten, R. H., "Observation Satellite Orbits," ARS Journal, Vol. 32, pp 105 to 106, 1962.

Kaula, W. M., "Analysis of Gravitational and Geometric Aspects of Geodetic Utilization of Satellites," National Aeronautics and Space Administration, (NASA Technical Note D-572), March 1961.

Levin, E., "The Reflected Radiation Received by an Earth Satellite," Aerospace Corporation, El Segundo, California (Report No. TDR-594 (1560-01) TN-3), 8 May 1961, 21 p incl illus.

Greenwood, S. W., "Reconnaissance Orbits Normal to the Ecliptic Plane," Royal Aeron Soc, J, Vol. 65, No. 606, June 1961, pp 437 to 438.

Cunningham, F. G., "Calculation of the Eclipse Factor for Elliptical Satellite Orbits," National Aeronautics and Space Administration (NASA) Technical Note D-1347), June 1962.

Katz, A. H., "Observation Satellites," Astronautics:

Part I, Vol. 5, No. 5, May 1960.
Part II, Vol. 5, No. 6, June 1960, p 26.
Part III, Vol. 5, No. 7, July 1960, p 28.
Part IV, Vol. 5, No. 8, August 1960, p 30.
Part V, Vol. 5, No. 9, September 1960, p 32.
Part VI, Vol. 5, No. 10, October 1960, p 36.

Rechtin, E., "Deep Space Communications," Astronautics:

Part I, Vol. 6, No. 4, April 1961, p 37.
Part II, Vol. 6, No. 5, May 1961, p 26.

Mueller, G. E., Hebenstreit, W. B., and Spangler, E. R., "Communication Satellites--How High?," Astronautics, Vol. 6, No. 7, July 1961, p 42.

Tepper, M., "Tiros Program Results," Astronautics, Vol. 6, No. 5, May 1961, p 28.

Kershner, R. B., "Transit Program Results," Astronautics, Vol. 6, No. 5, May 1961, p 30.

Jaffe, L., "Project Echo Results," Astronautics, Vol. 6, No. 5, May 1961, p 32.

Pierce, J. R., "Practical Problems of Satellite Communication, Astronautics, Vol. 6, No. 5, May 1961, p 34.

Ziemer, R. R., "Orbiting Astronomical Observatories," Astronautics, Vol. 6, No. 5, May 1961, p 36.

Freitag, R. F., "Project Transit: A Navigation Satellite," Navigation, Summer-Autumn 1960, Vol. 7, Nos. 2 and 3.

Holahan, J., "Transit: Navy Claims World's First Operational Satellite," Space Aeronautics, June 1960, Vol. 33, No. 6, p 154.

Kershner, R. B., "The Transit Program," Astronautics, June 1960, Vol. 5, No. 6, p 30.

Graves, C. D., "Radio Propagation Measurements Using the Explorer Six Satellite," Journal of Geophysical Research, September 1960, Vol. 65, No. 9, p 2585.

Heller, G., "Thermal Control of the Explorer Satellites," ARS Journal, April 1960, Vol. 30, No. 4.

Keigler, J. E., and Krawitz, L., "Weather Radar Observation from an Earth Satellite," Journal of Geophysical Research, September 1960, Vol. 65, No. 9, p 2793.

"First Navigation Satellite," Missiles and Rockets, 18 April 1960, Vol. 6, No. 16, p 15.

"Navy Tests Transit Navigational Potential," Aviation Week, 18 April 1960, Vol. 72, No. 16, pp 29 to 30.

"Refraction Error No Problem in Transit," Missiles and Rockets, 14 November 1960, Vol. 7, No. 20, p 19.

Mueller, G. E., "Telebit--An Integrated Space Navigation and Communication System," Astronautics, May 1960, Vol. 5, No. 5, p 26.

"Explorer Eight Mapping Ionosphere," Aviation Week, 7 November 1960, Vol. 73, No. 19, p 31.

"Explorer Eight Probes Ionosphere," Missiles and Rockets, 14 November 1960, Vol. 7, No. 20, p 42.

"Explorer Eight Relays Ionospheric Data," Aviation Week, 21 November 1960, Vol. 73, No. 21, p 71.

Basler, R. P., Dewitt, R. N., and Reid, G. C., "Radiation Information from 1958 Delta 2," Journal of Geophysical Research, April 1960, Vol. 65, No. 4, p 1135.

Davies, M. E.,
"Are the Lunik III Photos Fake?," Astronautics, June 1960, Vol. 5, No. 6, p 46.
"How Good Is the Lunik III Photography?," Astronautics, May 1960, Vol. 5, No. 5, p 28.

Krasovskii, V. I., "Results of Scientific Investigations Made by Soviet Sputniks and Cosmic Rockets," ARS Journal, January 1960, Vol. 30, No. 1, p 27.

Clarke, E., "Tiros Exceeds Weather Bureau Hopes," Aviation Week, 2 May 1960, Vol. 72, No. 18, p 30.

Goldberg, E. A., and Landon, V. D., "Key Equipment for Tiros I," Astronautics, June 1960, Vol. 5, No. 6, p 36.

Holmes, J., "Tiros II Maps Hurt by Poor TV Photos," Missiles and Rockets, 5 December 1960, Vol. 7, No. 23, p 15.

Keigler, J. E. and Krawitz, L., "Weather Radar Observations from an Earth Satellite," Journal of Geophysical Research, September 1960, Vol. 65, No. 9, p 2793.

Keigler, J. E., and Oakley, C. B., "The Tiros System on the Ground," Astronautics, June 1960, Vol. 5, No. 6, p 44.

Lewis, C., "NASA Tiros I Demonstrates Potential Satellite Reconnaissance Utility," Aviation Week, 11 April 1960, Vol. 72, No. 15, p 28.

Means, P., "Tiros Presages Long-Range Forecasts," Missiles and Rockets, 11 April 1960, Vol. 6, No. 14, p 21.

Osgood, C. C., "Structural Design of Tiros I," Astronautics, June 1960, Vol. 5, No. 6, p 42.

Perkel, H., "Tiros I Spin Stabilization," Astronautics, June 1960, Vol. 5, No. 6, p 38.

Ritter, M., "Thermal Design for Tiros," Astronautics, June 1960, Vol. 5, No. 6, p 40.

Sternberg, S., and Stroud, W. G., "Tiros I--Meteorological Satellite," Astronautics, June 1960, Vol. 5, No. 6, p 32.

Wexler, H., and Fritz, S., "Tiros Reveals Cloud Formation," Science, 10 June 1960, Vol. 131, No. 3415, p 1708.

"Aerospace Engineering Intelligence--Tiros Satellite is Powered by 9200 Solar Cells," Space Aeronautics, May 1960, Vol. 33, No. 5, p 31.

"The Satellite Echo One," Nature, 27 August 1960, Vol. 187, No. 4739, p 741.

"The Echo Communications Satellite," IGY Bulletin, September 1960, No. 39, p 14.

"Tiros II Transmits Cloud, Infrared Data," Aviation Week, 28 November 1960, Vol. 73, No. 22, p 32.

"NASA Tiros I Demonstrates Potential Satellite Reconnaissance Utility," Space Technology, July 1960, Vol. 3, No. 3, p 24.

"Sputnik III Results," Missiles and Rockets, 11 January 1960, Vol. 6, No. 2, p 38.

"Sputnik IV," Spaceflight, October 1960, Vol. 11, No. 8, p 230.

"The Other Side of the Moon," Spaceflight, January 1960, Vol. 11, No. 5, p 130.

"Triumph of Sputnik V," Spaceflight, October 1960, Vol. 11, No. 8, p 225.

Heppner, J. P., Stolarik, J. D., Shapiro, I. R., and Cain, J. C., "Project Vanguard Magnetic-Field Instrumentation and Measurements," NASA TN D-486, September 1960. (Also, Nice, France, First International and Space Symposium, January 1960.)

Mansir, D., "Magnetic Measurements in Space," Electronics, 5 August 1960, Vol. 33, No. 32, p 47.

O'Keefe, J. A., Eckels, A., and, Squires, R. K., "Vanguard Measurements Give Pear-Shaped Component of Earth's Figure," Science, 27 February 1959, Vol. 129, No. 3348, pp 565 to 566.

Siry, J. W., "The Vanguard IGY Earth Satellite Program," Moscow, 5th General Assembly of CSAGI, 30 July to 10 August.

ILLUSTRATIONS

Preceding page blank

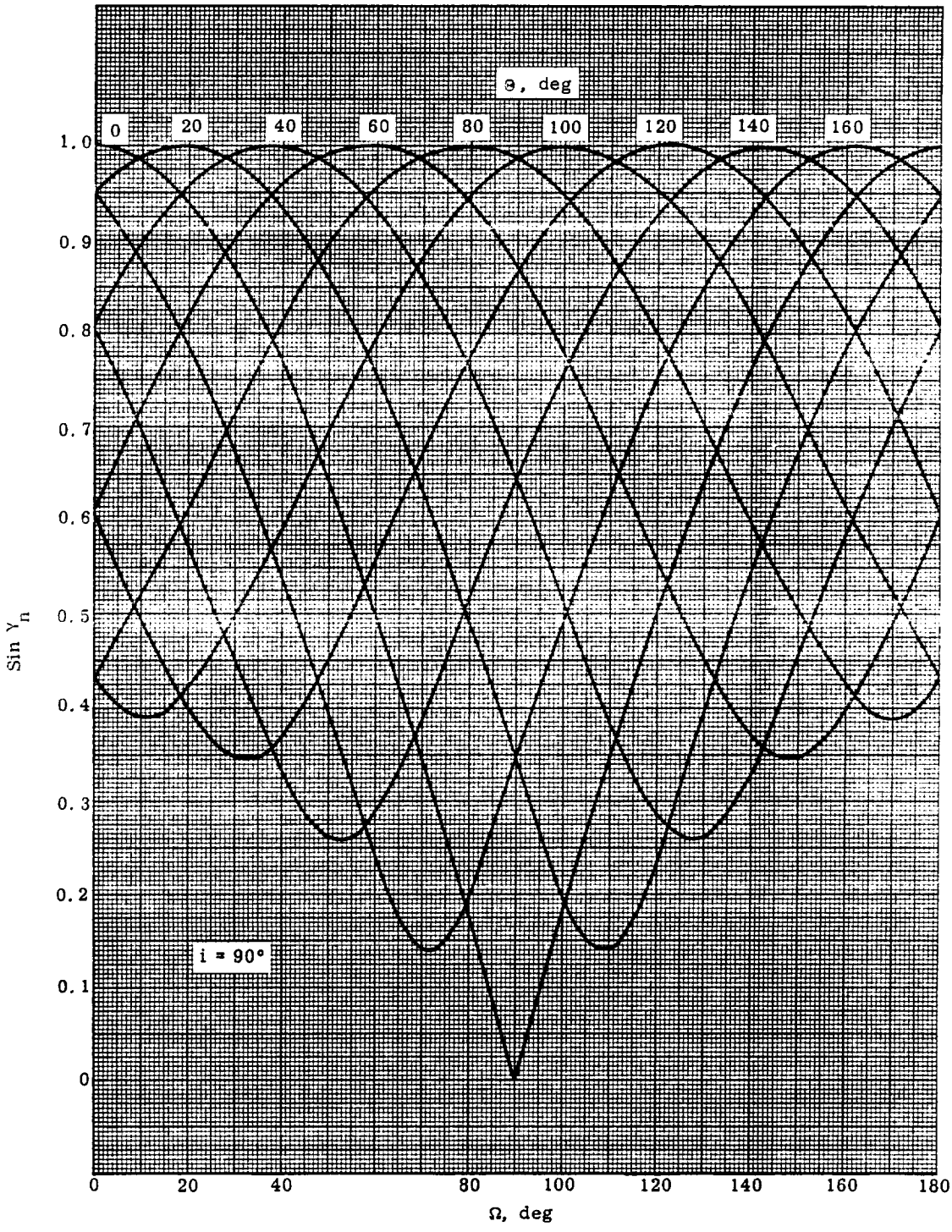

Fig. 1. Sine of the Angle Between the Normal to the Orbit Plane and the Earth-Sun Line, i = 90°

Preceding page blank

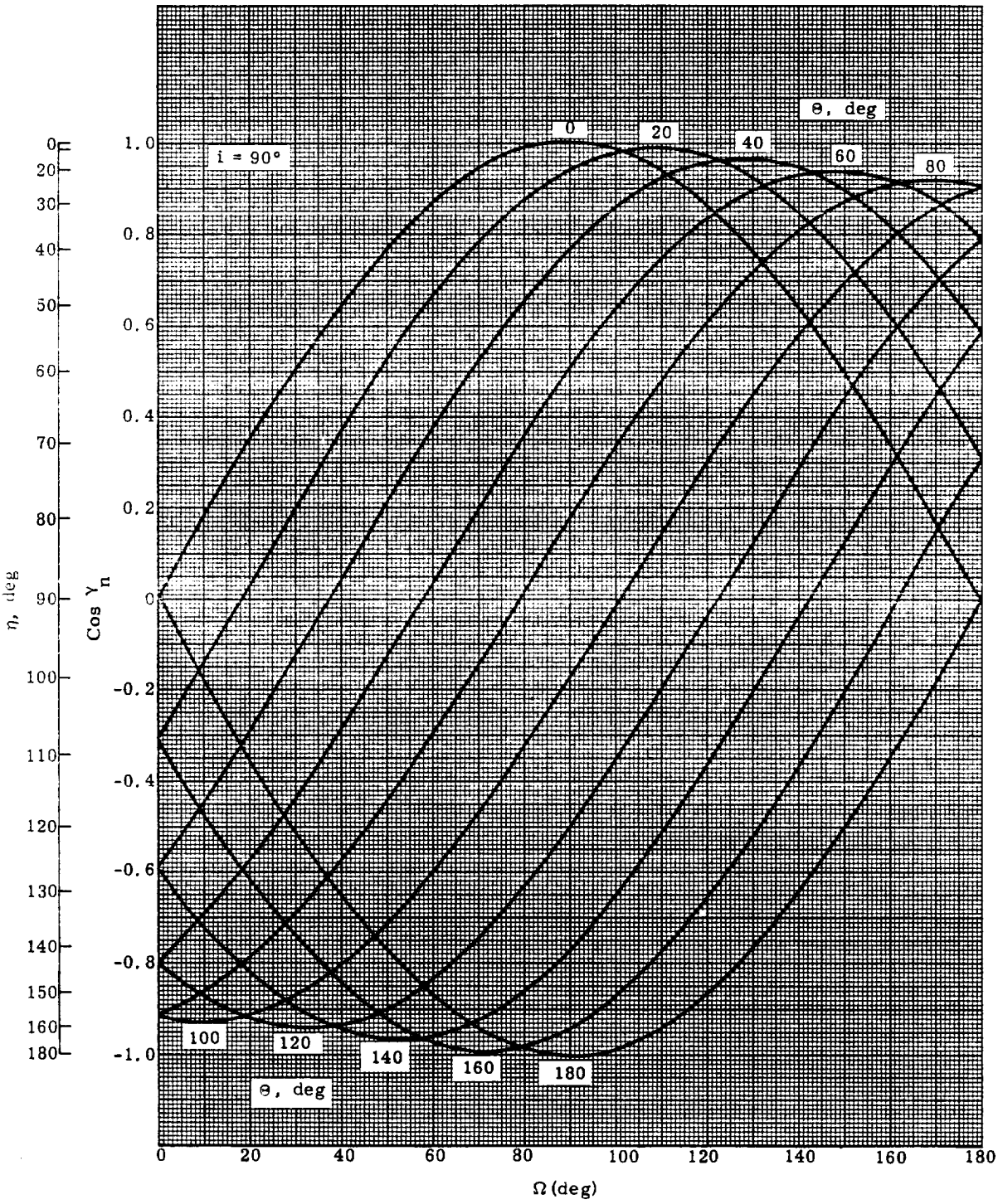

Fig. 2. Cosine of the Angle Between the Normal to the Orbit Plane and the Earth-Sun Line, i = 90°

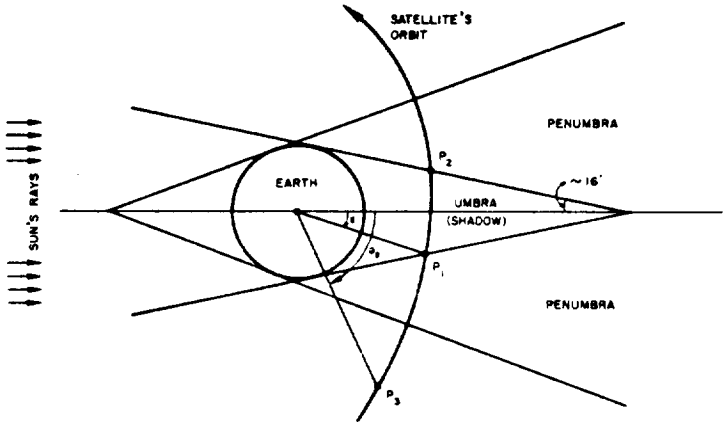

Fig. 3. Cross Section of Orbit Through Shadow Cone

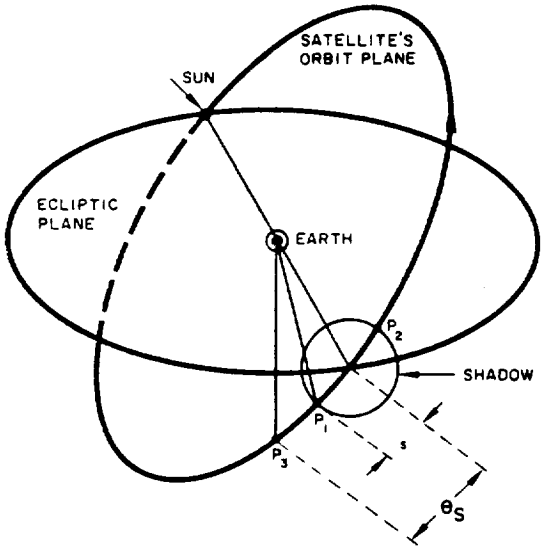

Fig. 4. Orbit Going Through Shadow When Shadow Is at the Node

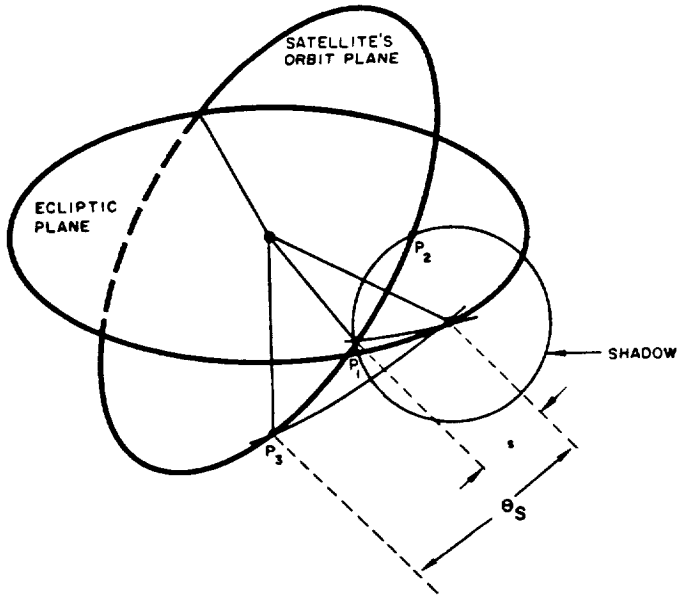

Fig. 5. Orbit Going Through Shadow When Shadow Is Not at the Node

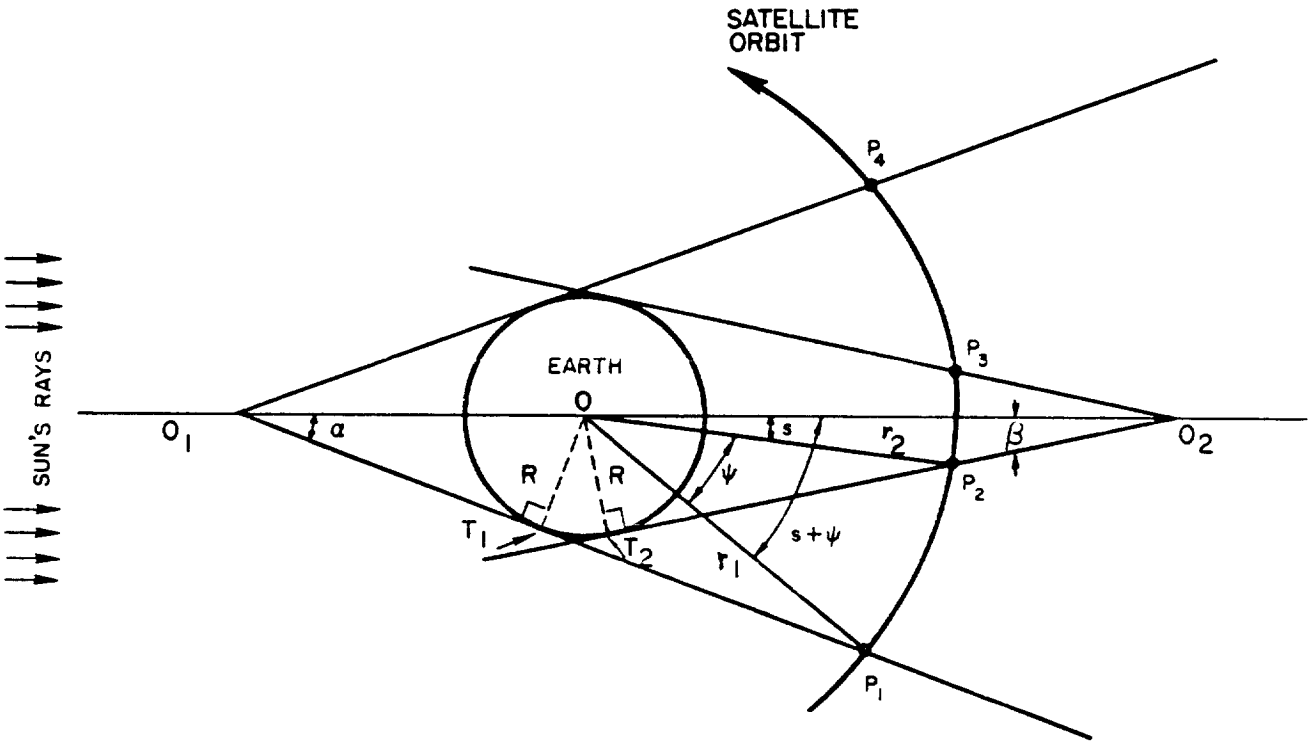

Fig. 6. Cross Section of Orbit Through Penumbra Cone

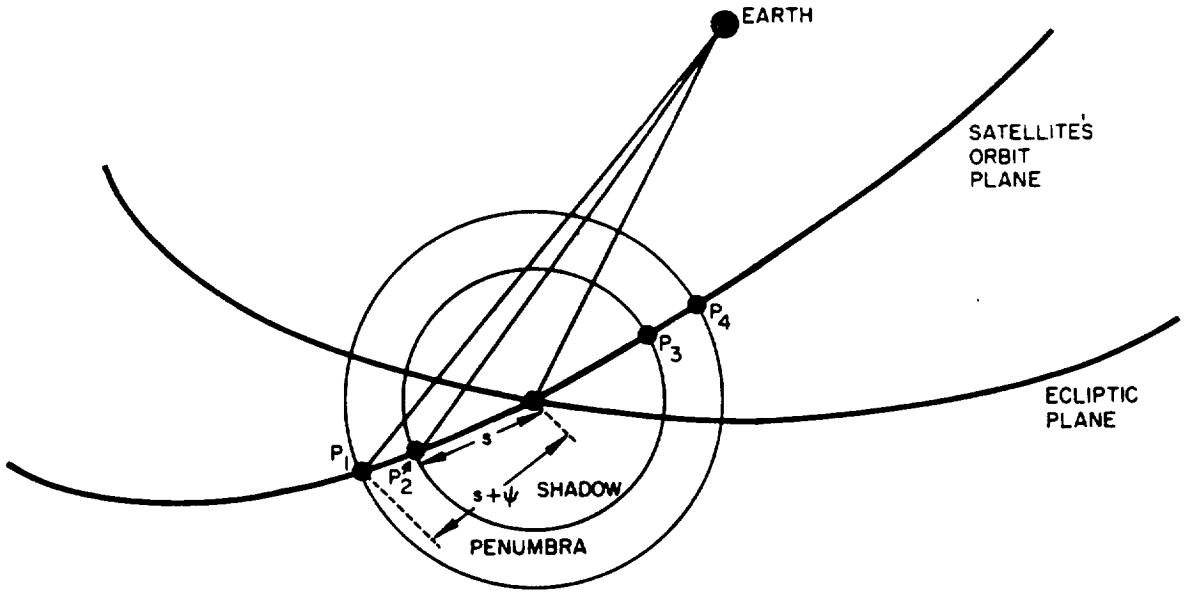

Fig. 7. Orbit Going Through Penumbra When It Is at the Node

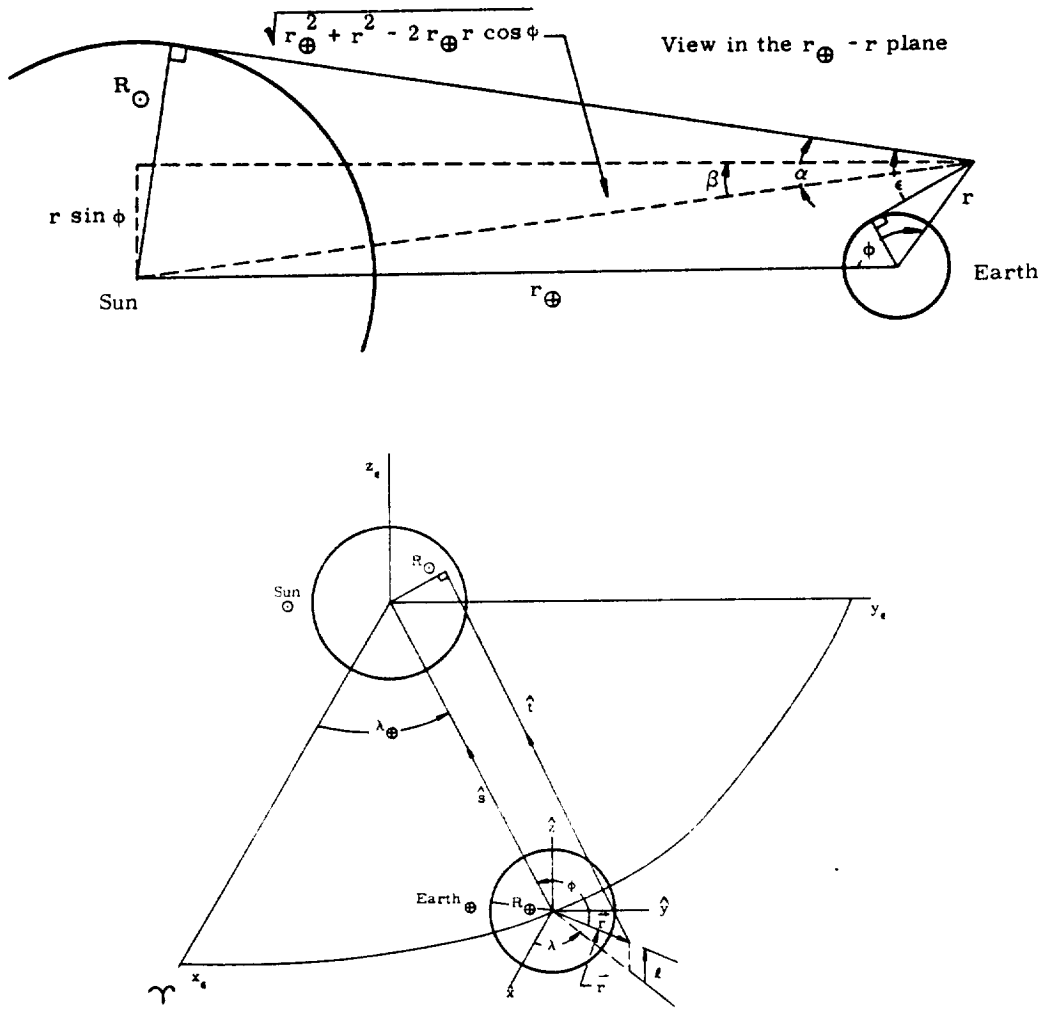

Fig. 8. Vector Analysis of Eclipse Time

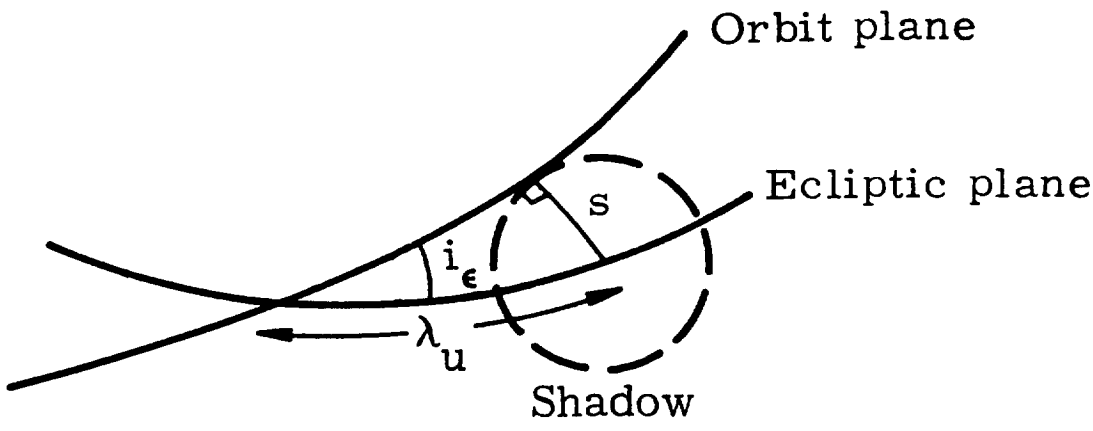

Fig. 9. Geometry of Eclipse Season

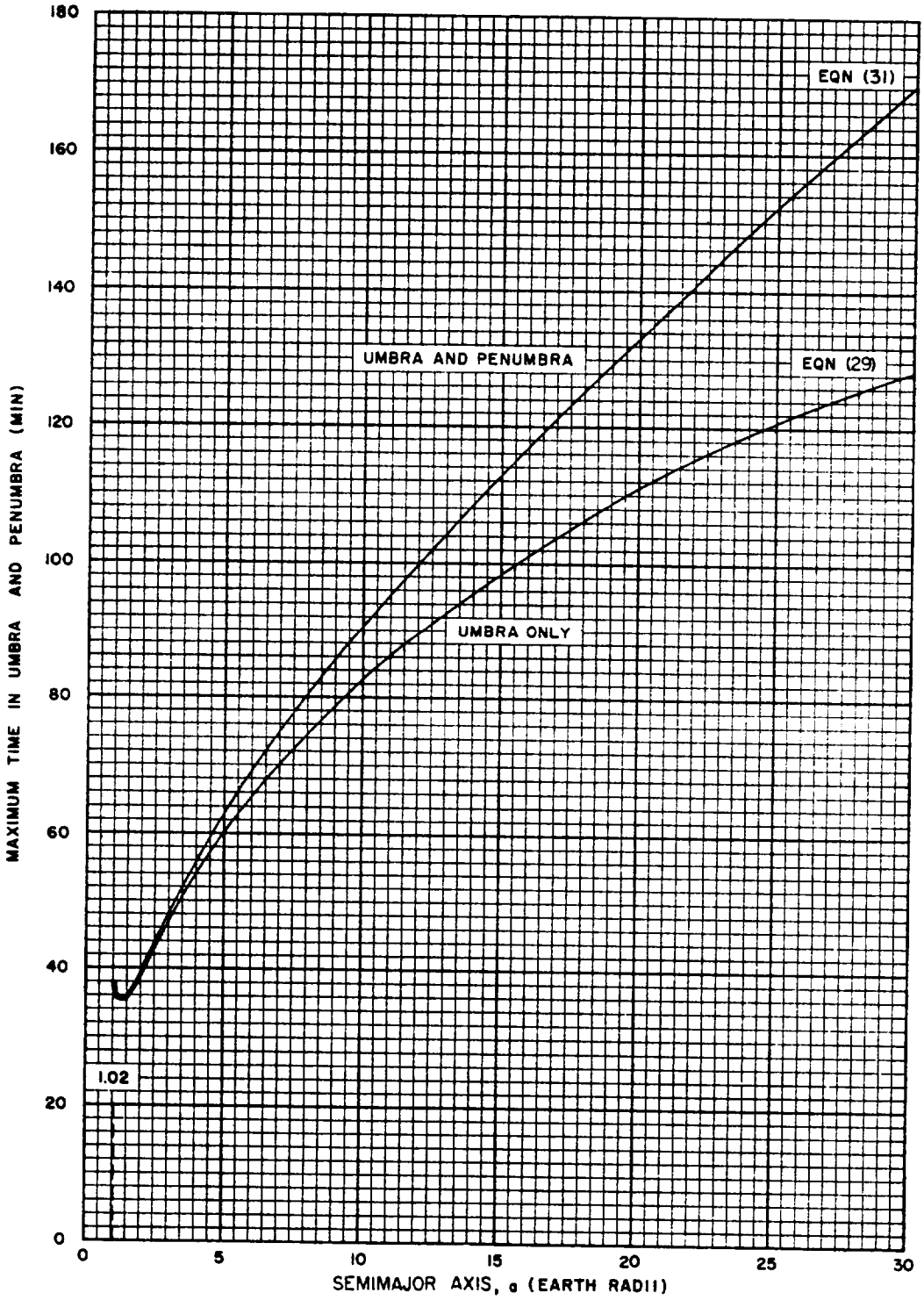

Fig. 10. Maximum Time in Umbra and Penumbra Versus Semimajor Axis

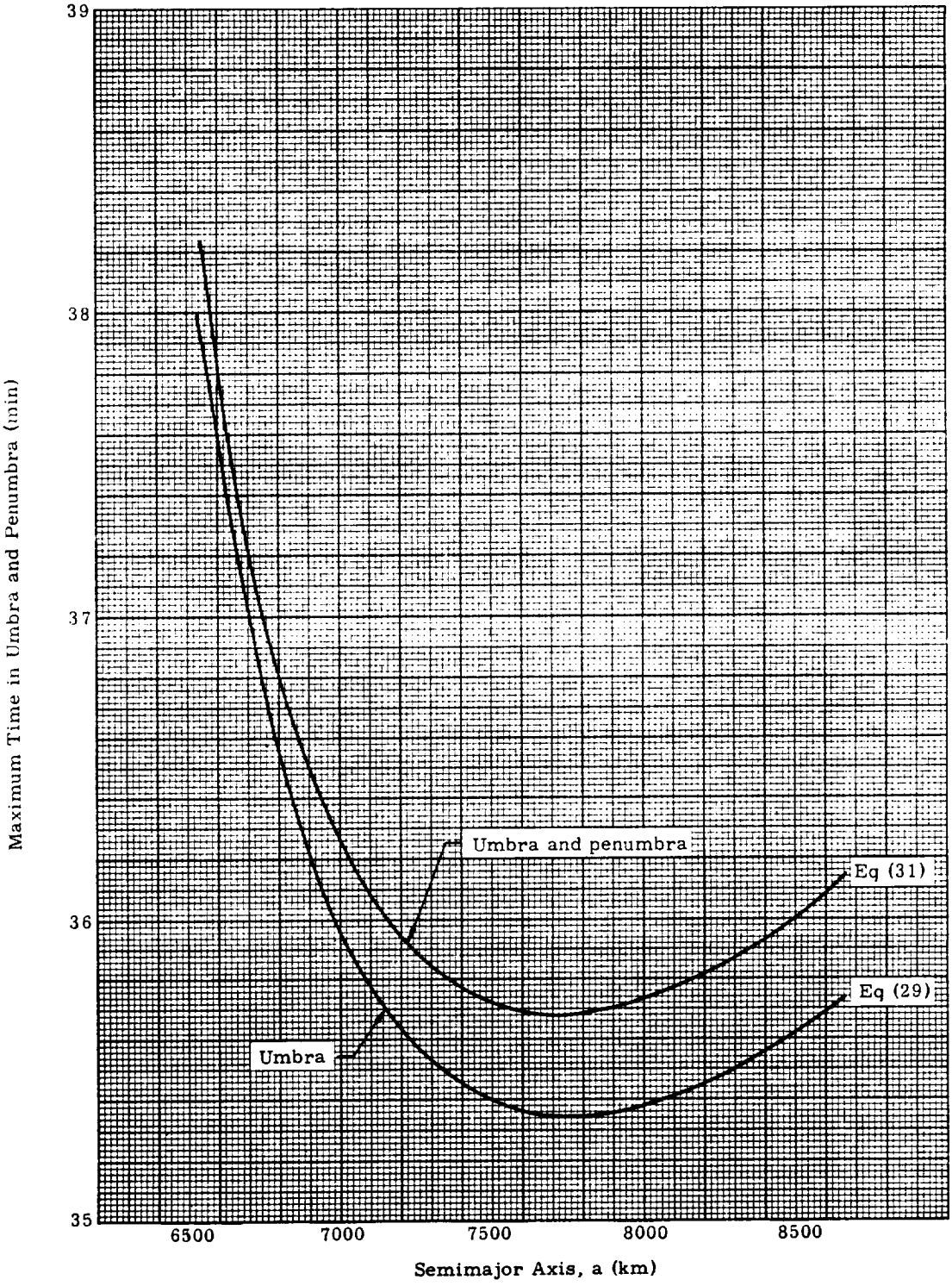

Fig. 11. Maximum Time in Umbra and Penumbra Versus Semimajor Axis

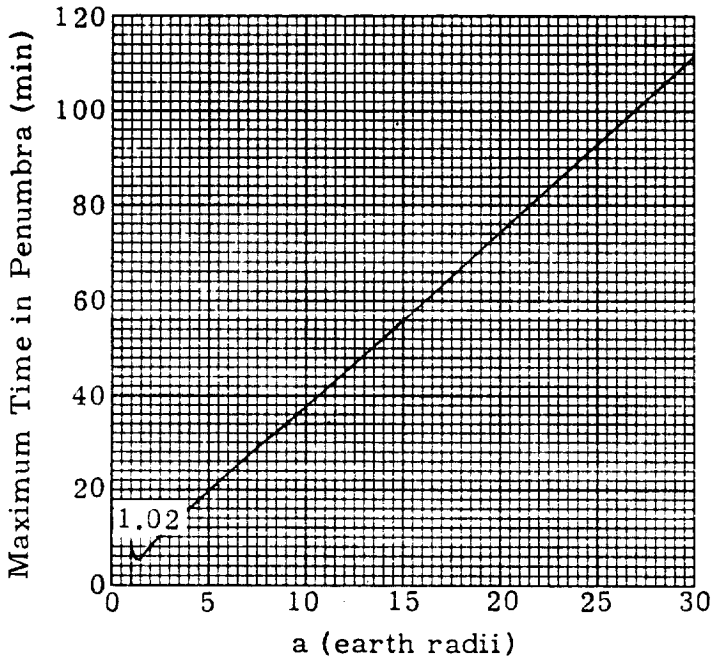

Fig. 12. Maximum Time in Penumbra (No Umbra Eclipse) Versus Semimajor Axis

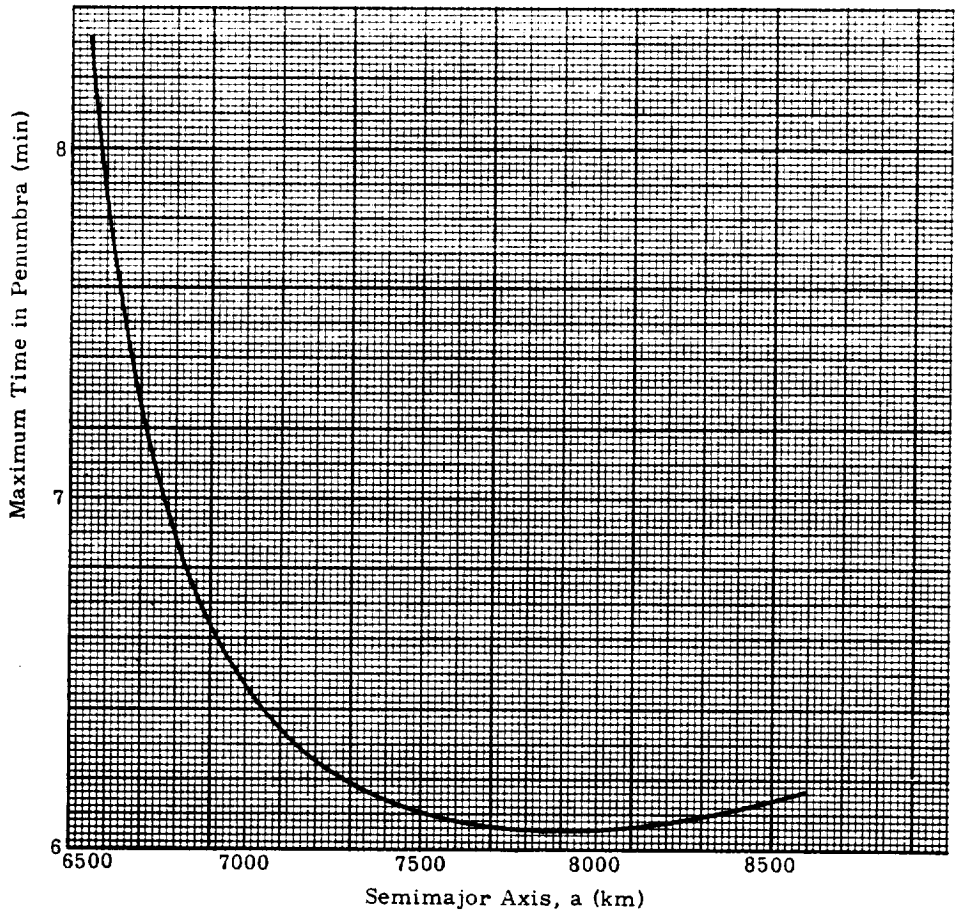

Fig. 13. Maximum Time in Penumbra (No Umbra Eclipse) Versus Semimajor Axis

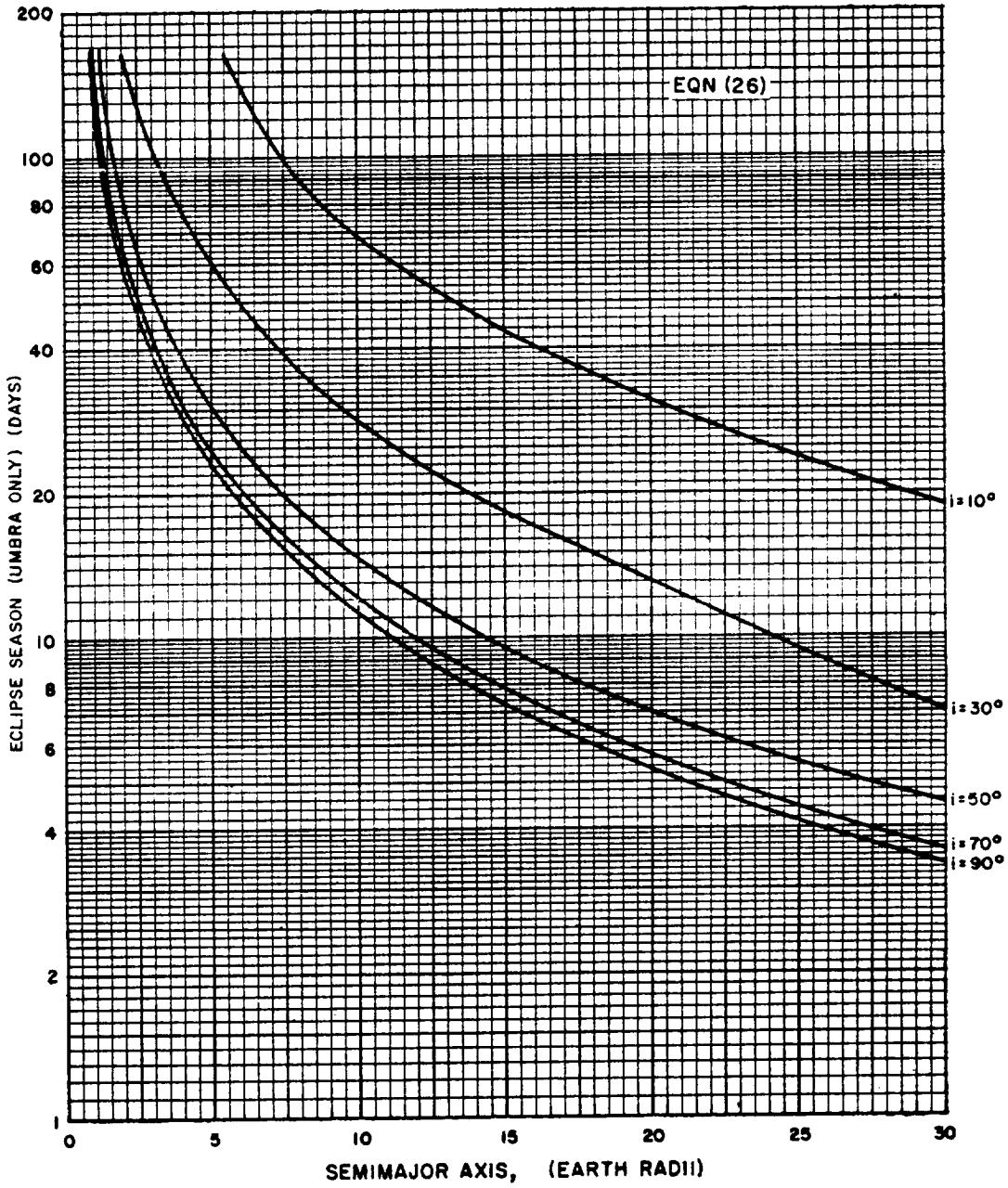

Fig. 14. Eclipse Season (Umbra Only) Versus Semimajor Axis

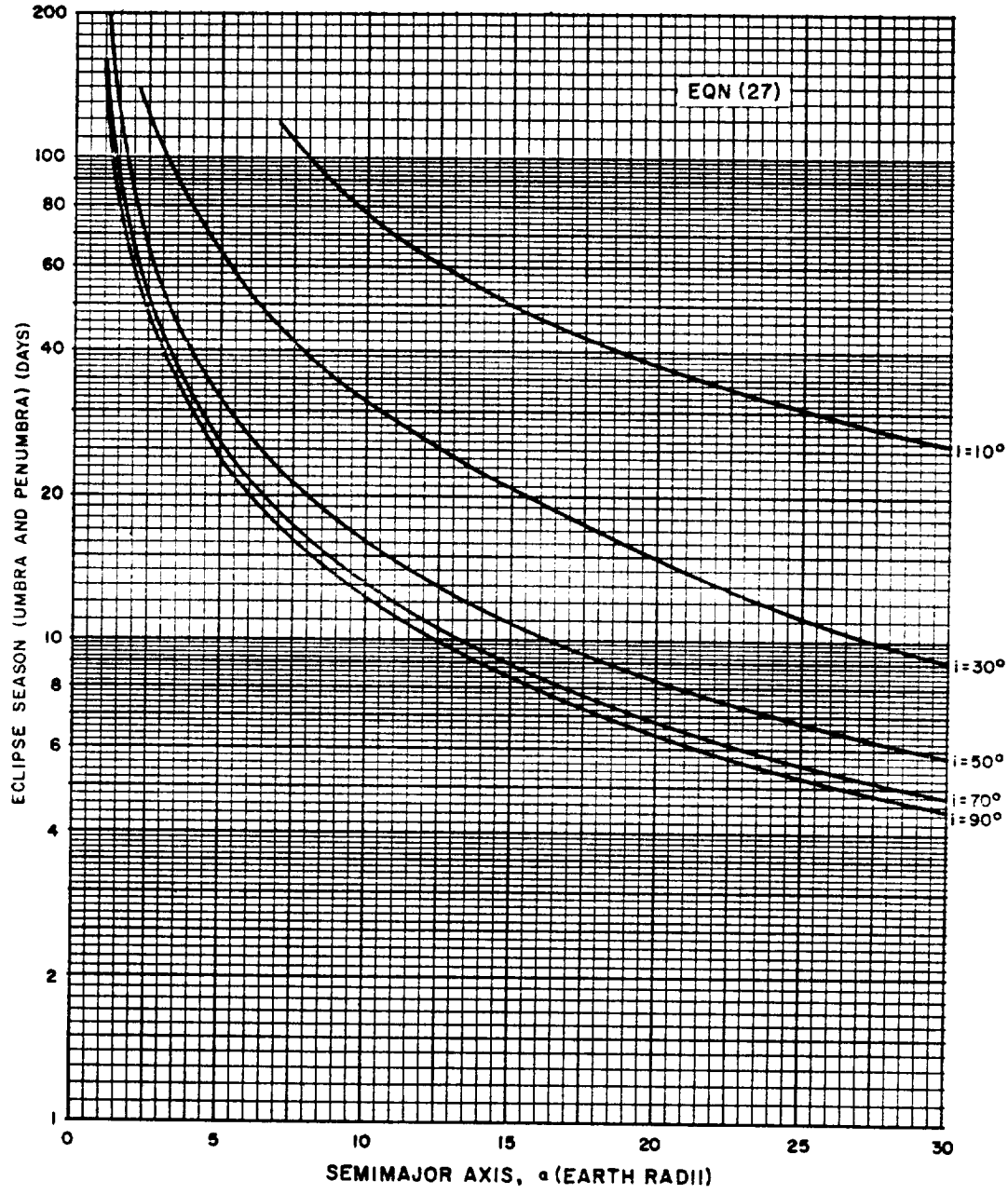

Fig. 15. Eclipse Season (Umbra and Penumbra) Versus Semimajor Axis

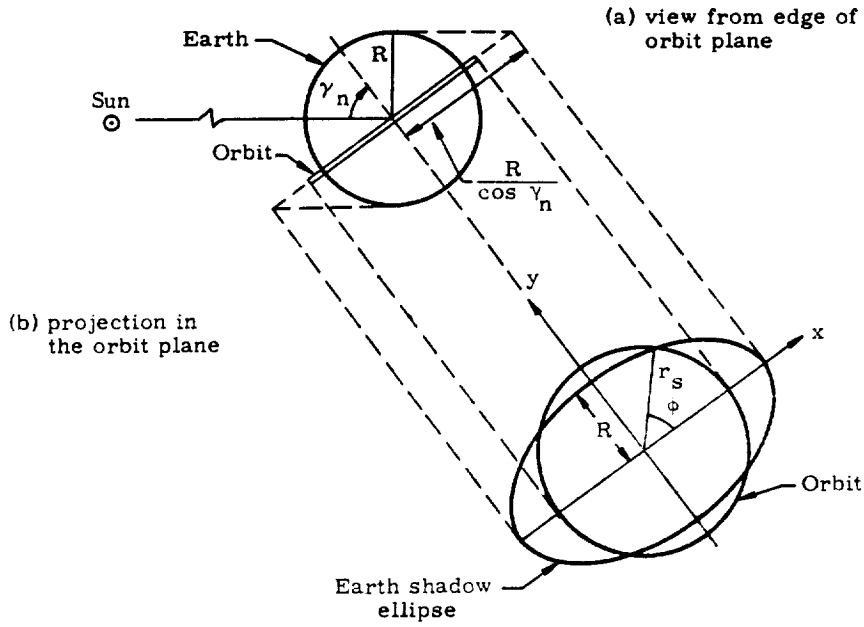

Fig. 16. Geometry of the Simplified Eclipse Problem

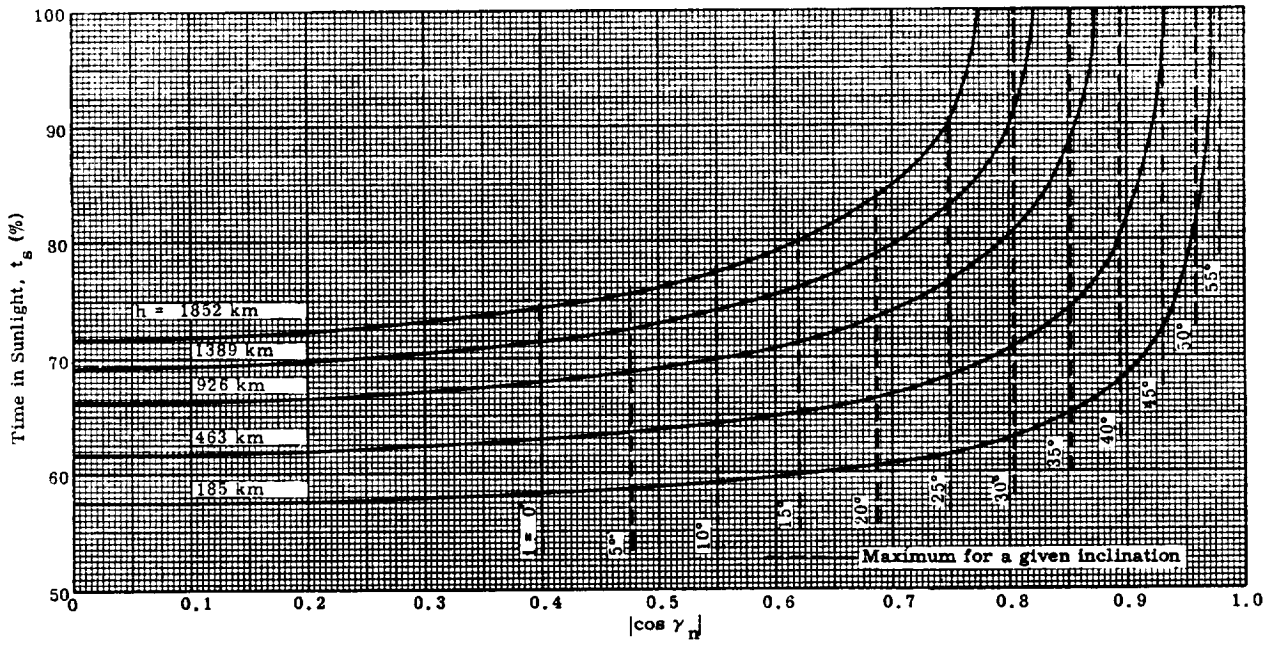

Fig. 17. Time in Sunlight Versus Cosine of Angle Between Earth-Sun Line and Normal to Orbit

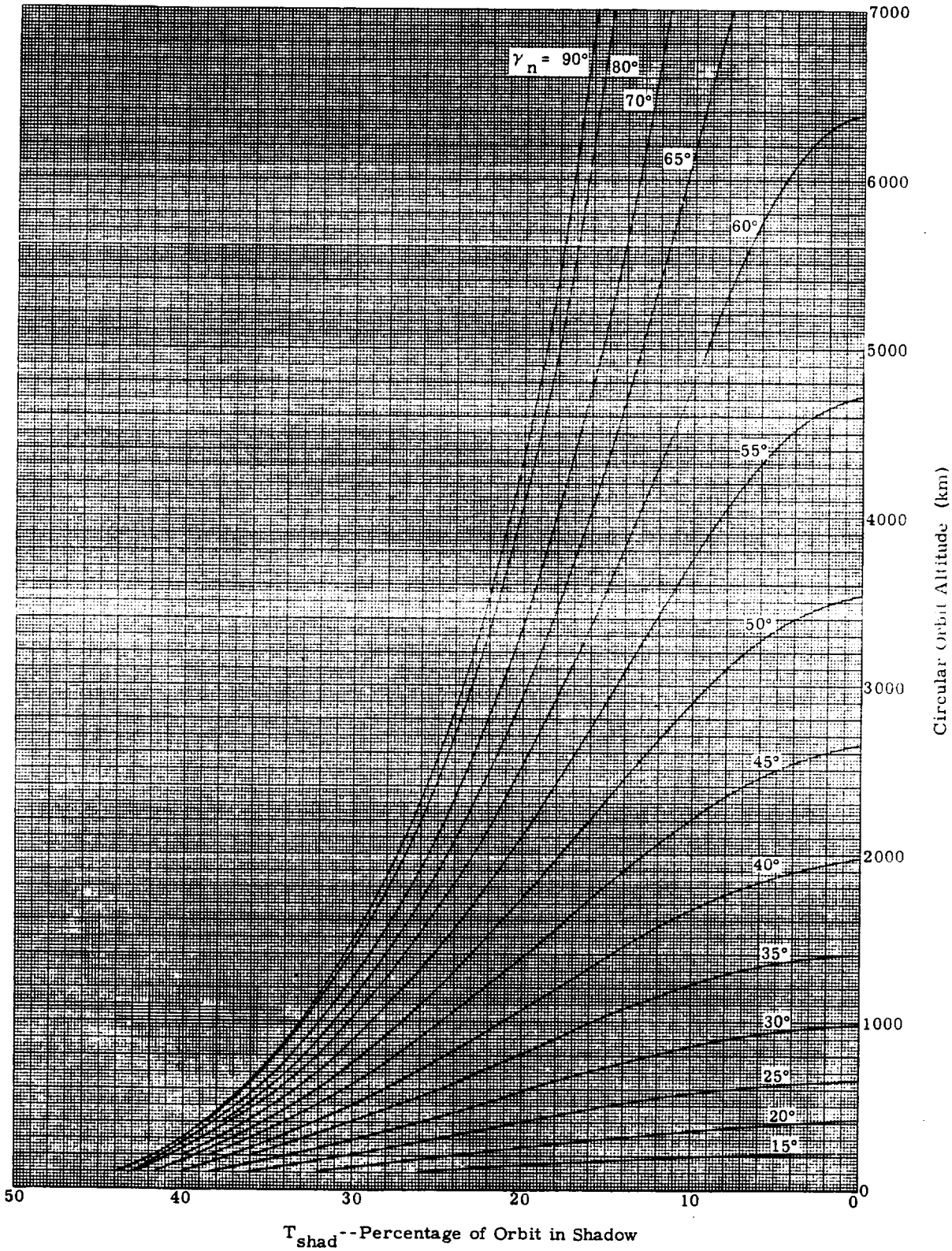

Fig. 18. Percent Time in Shadow for Circular Unperturbed Orbits

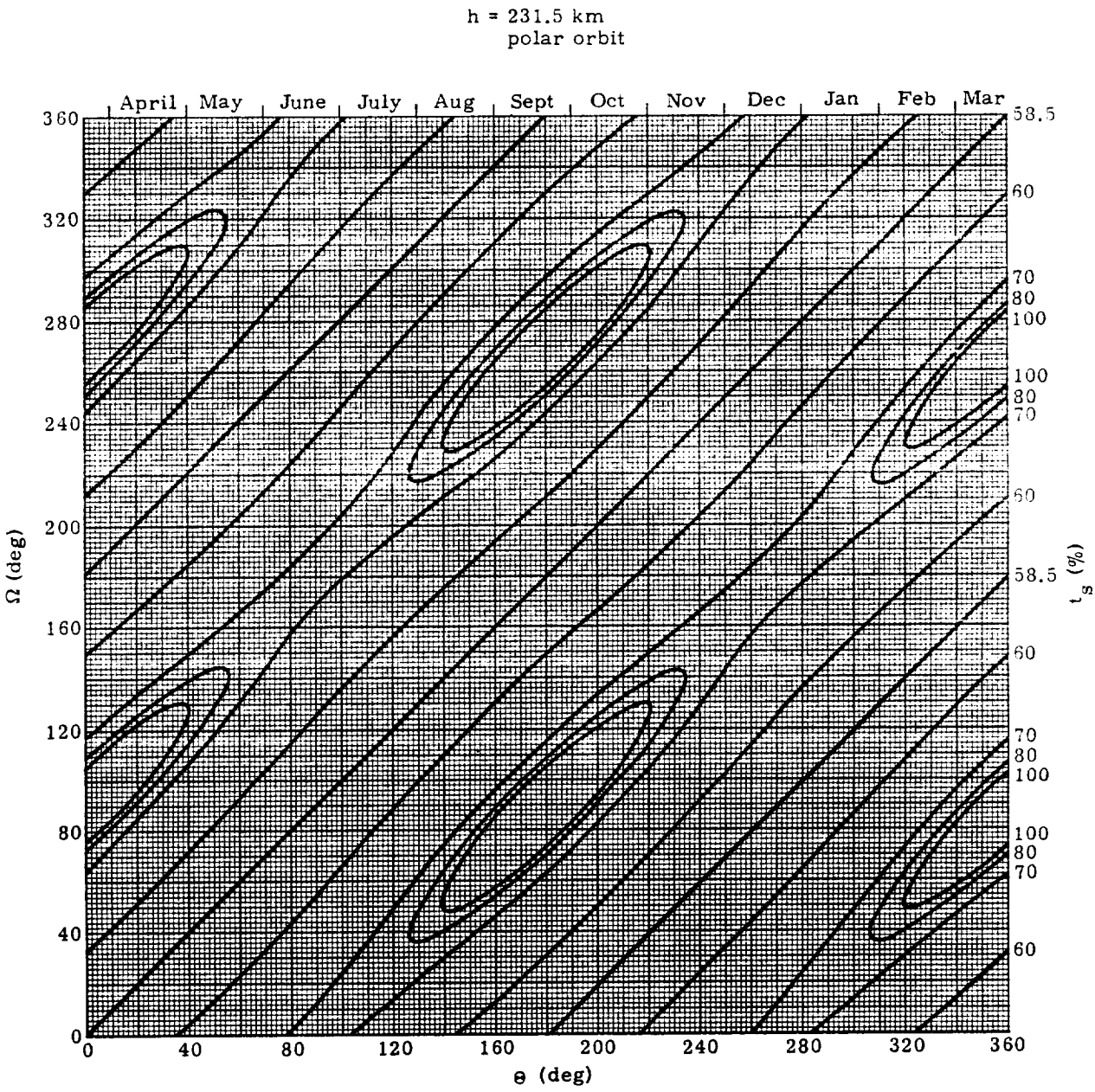

Fig. 19. Eclipse Durations and Eclipse Seasons for Unperturbed Circular Orbits

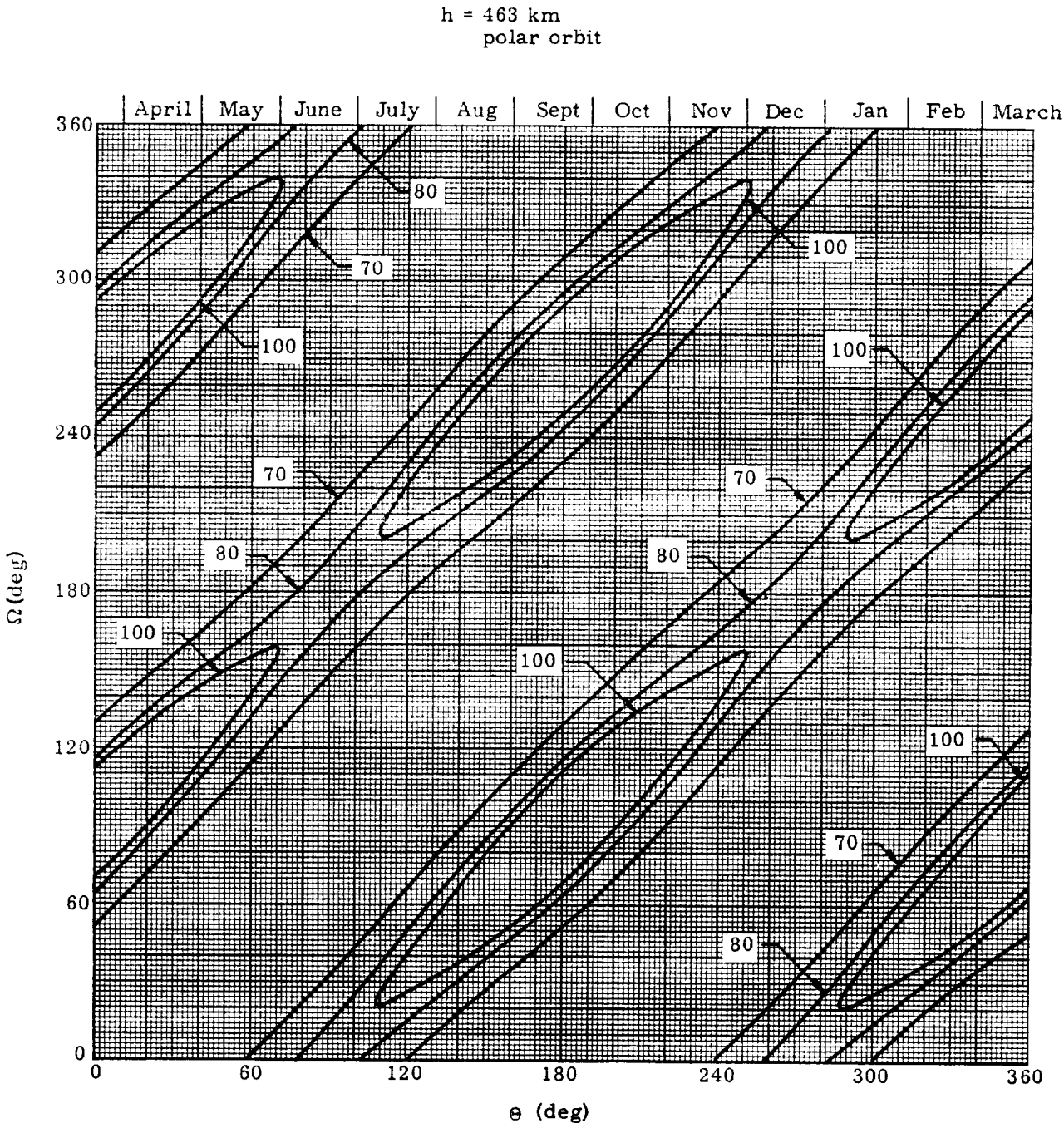

Fig. 20. Eclipse Durations and Eclipse Seasons for Unperturbed Circular Orbits

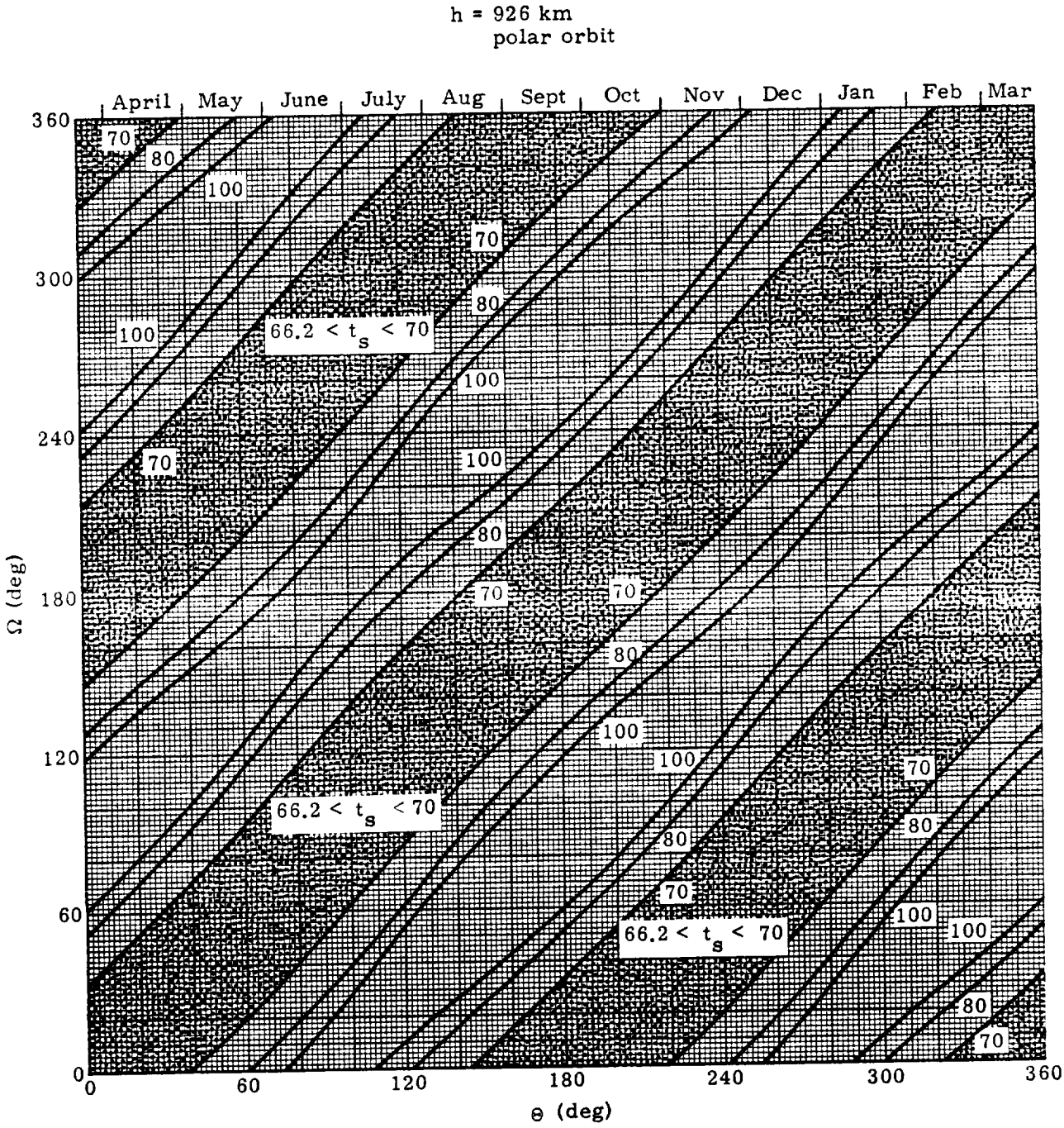

Fig. 21. Eclipse Durations and Eclipse Seasons for Unperturbed Circular Orbits, i = 90°, h = 926 km

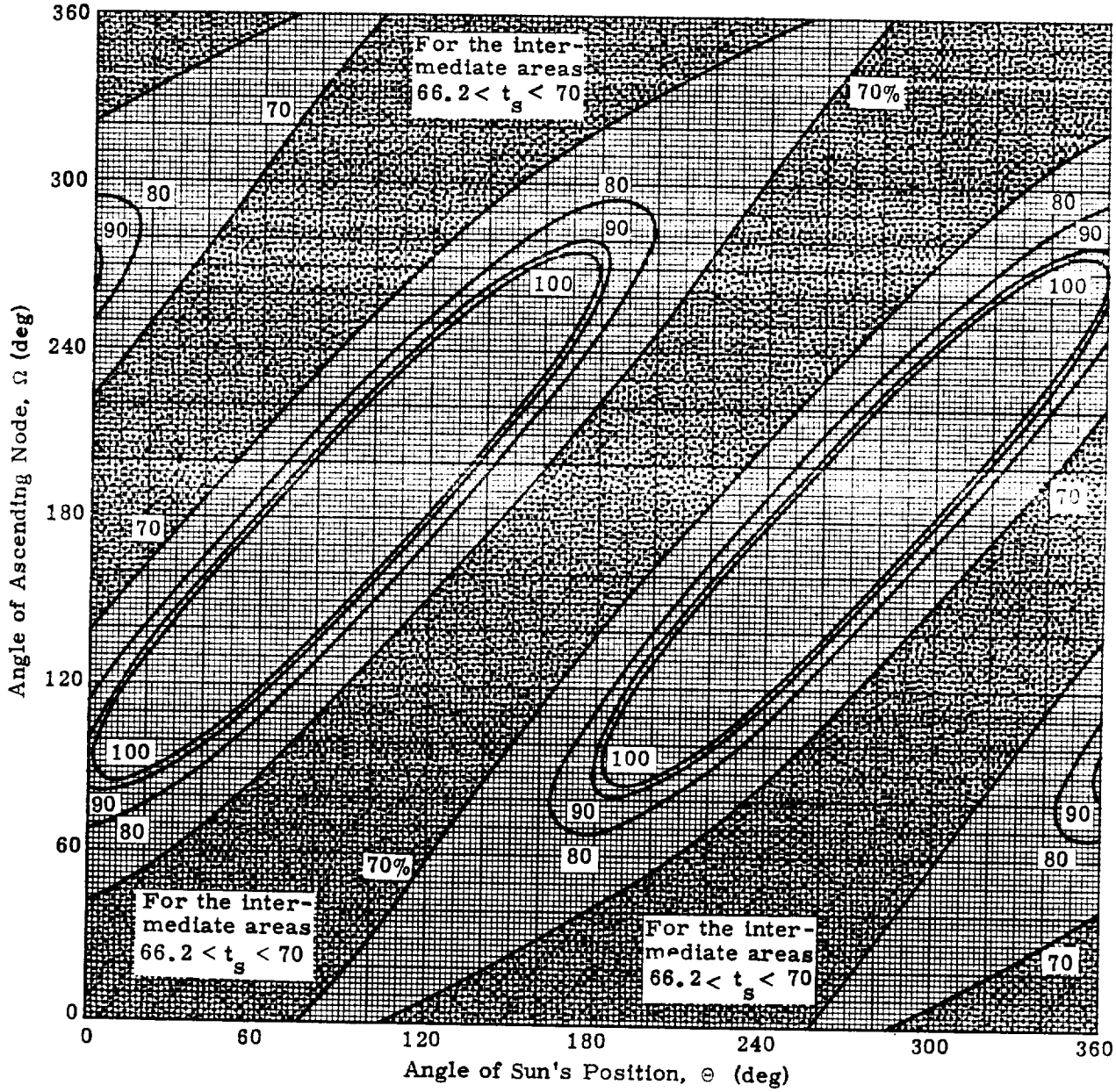

Fig. 22. Eclipse Durations and Eclipse Seasons for an Unperturbed Circular Orbit, i = 60°, h = 926 km

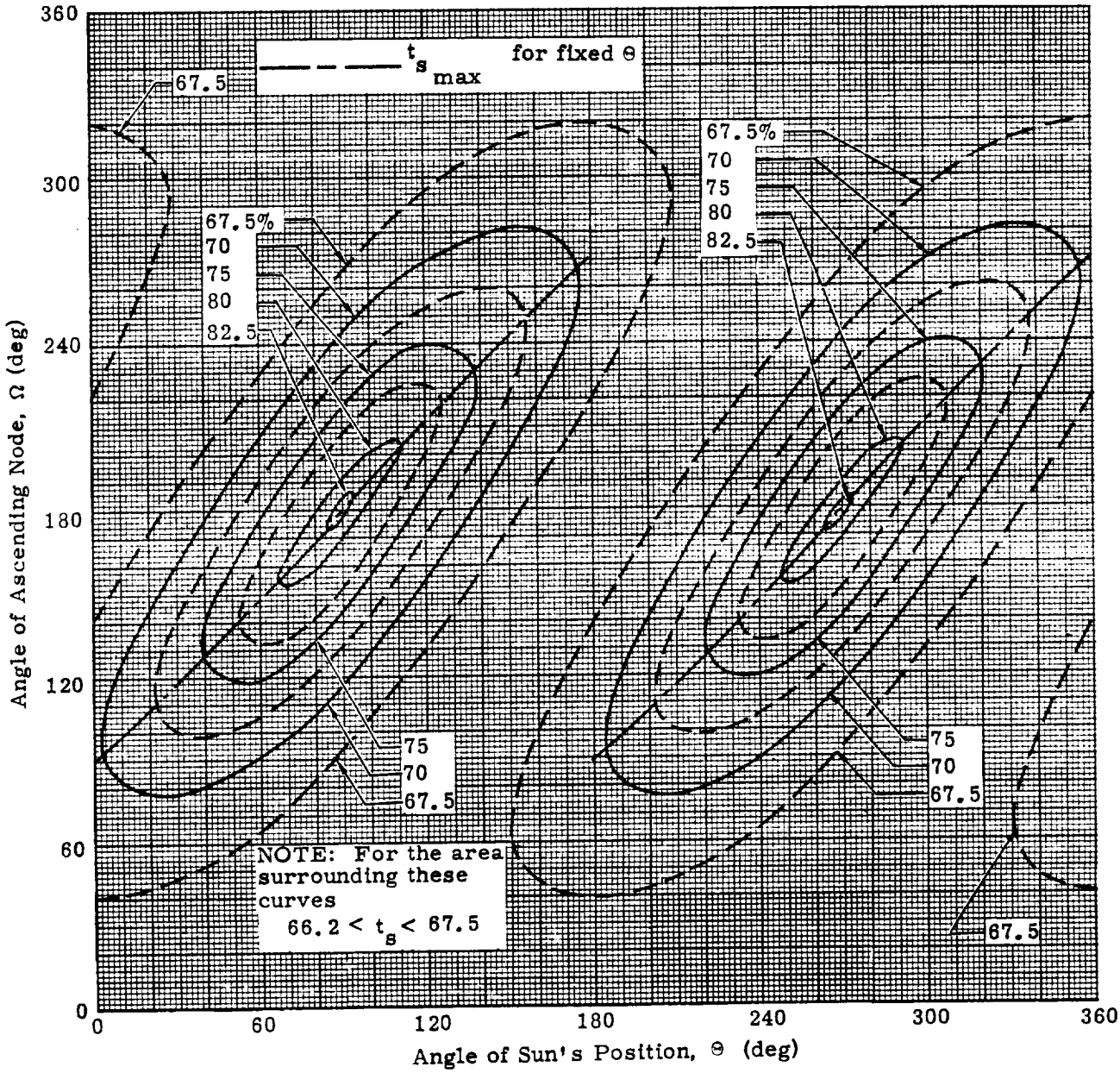

Fig. 23. Eclipse Durations and Eclipse Seasons for Unperturbed Circular Orbits, i = 32°, h = 926 km

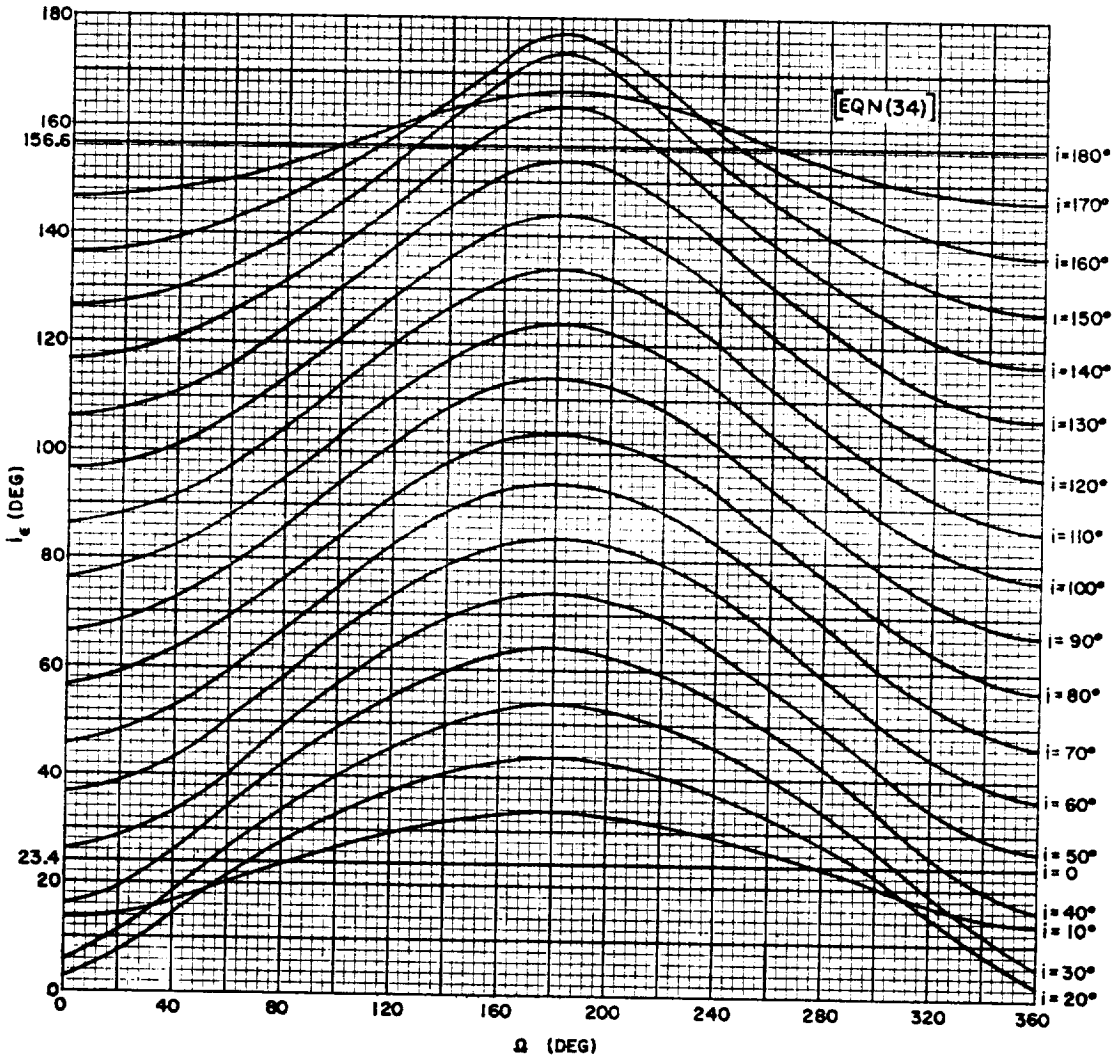

Fig. 24. Inclination with Respect to the Ecliptic (i_ϵ) Versus Longitude of the Node with Respect to the Equator (Ω) for Different Inclinations with Respect to the Equator (i)

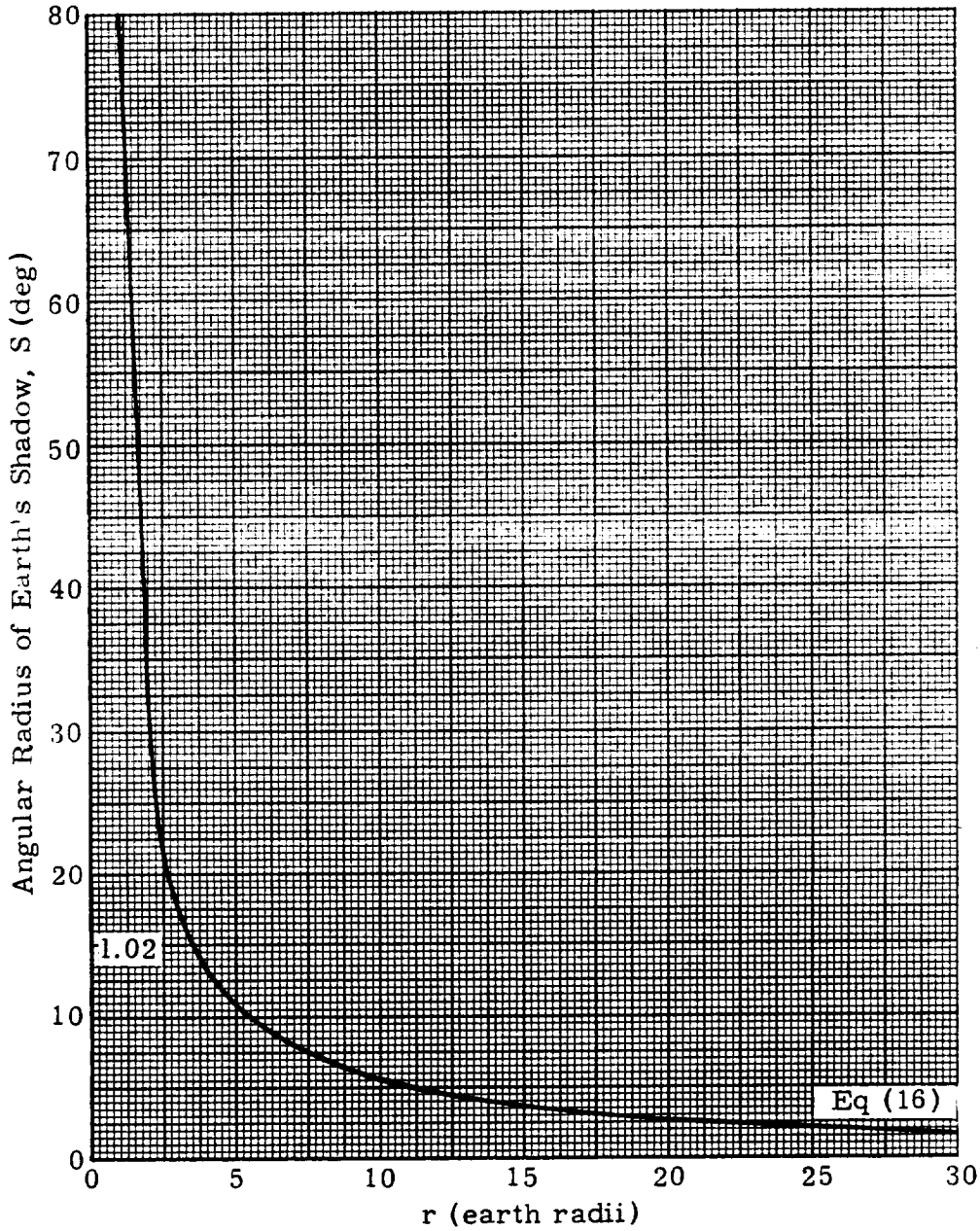

Fig. 25. Angular Radius of Shadow Versus Distance from Center of Earth

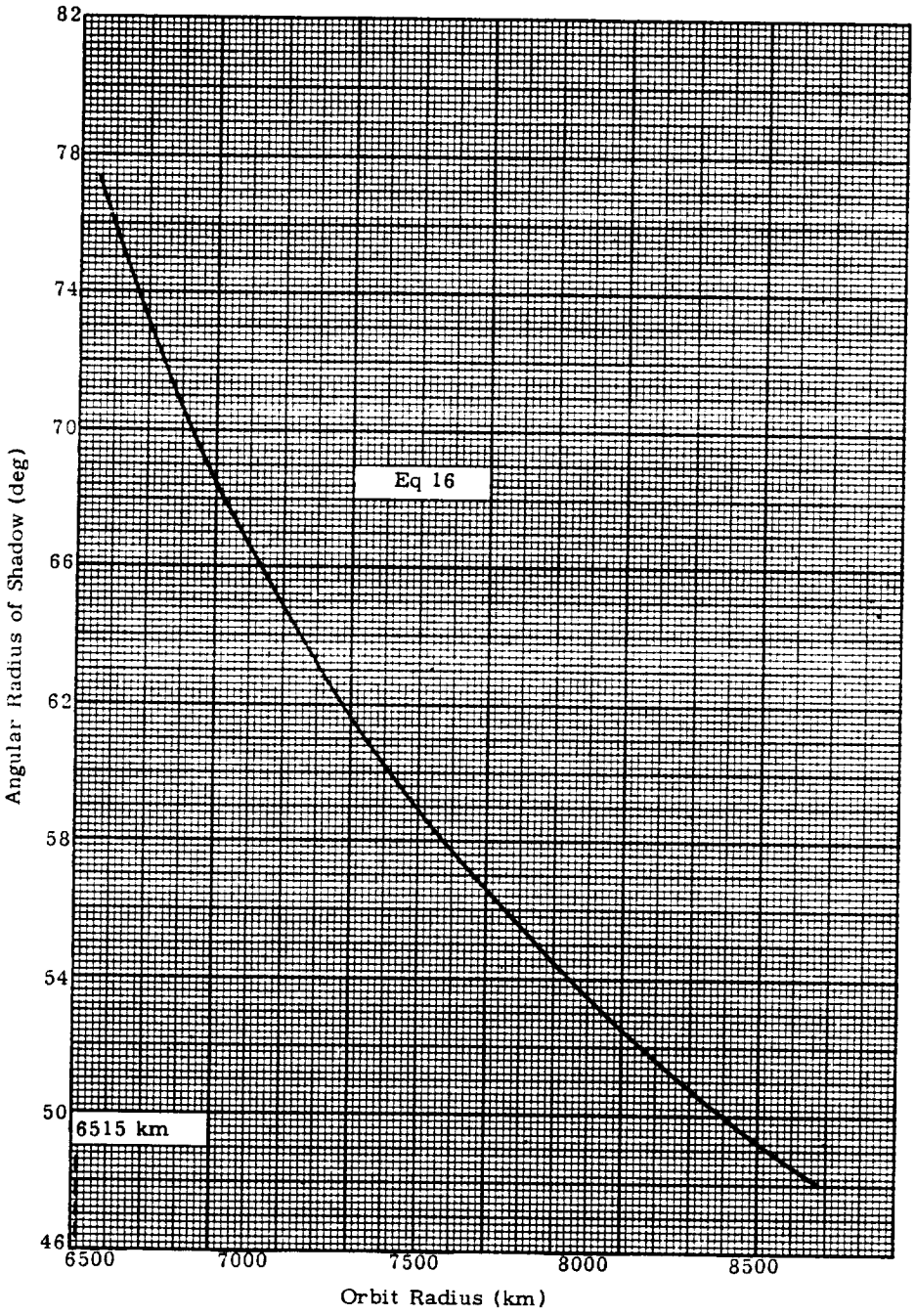

Fig. 26. Angular Radius of Shadow Versus Distance from Center of Earth

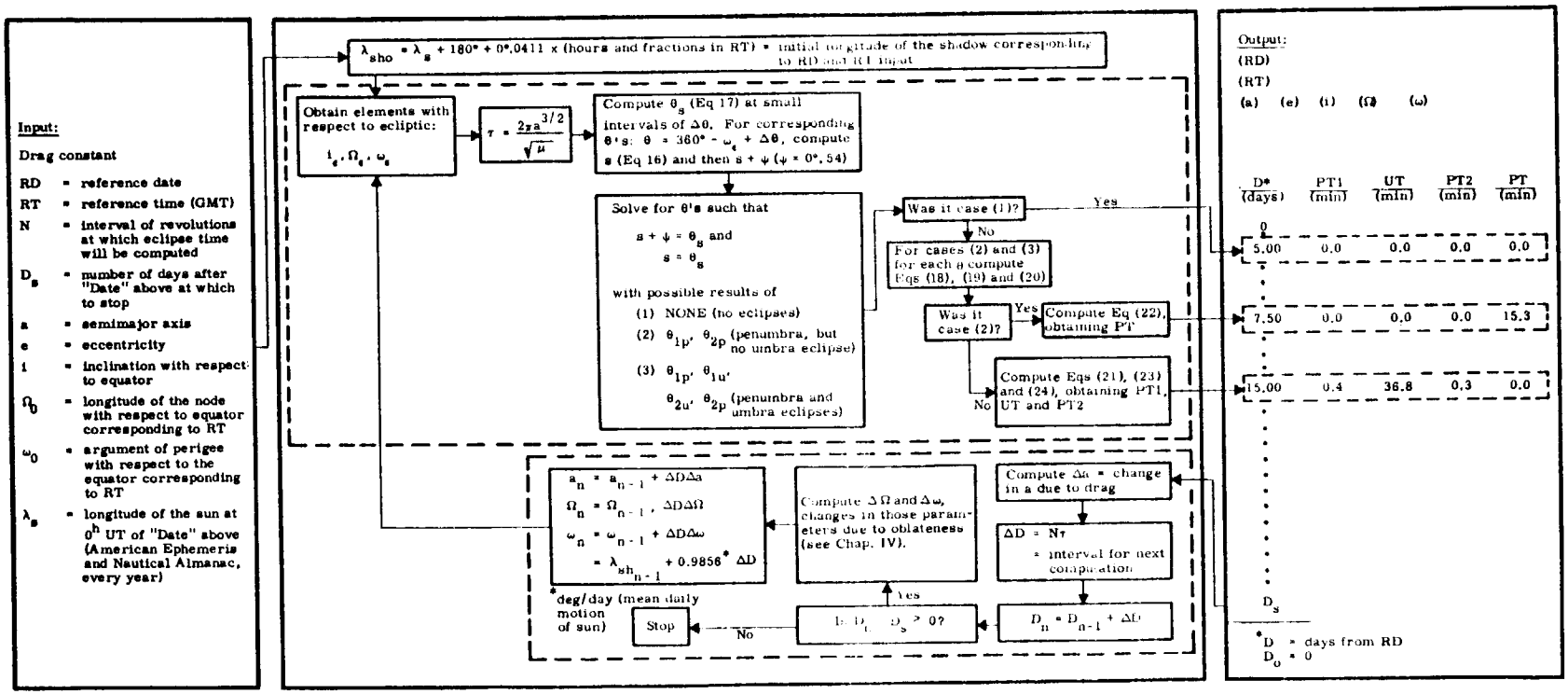

Fig. 27. Flow Chart of a Simple Eclipse Program

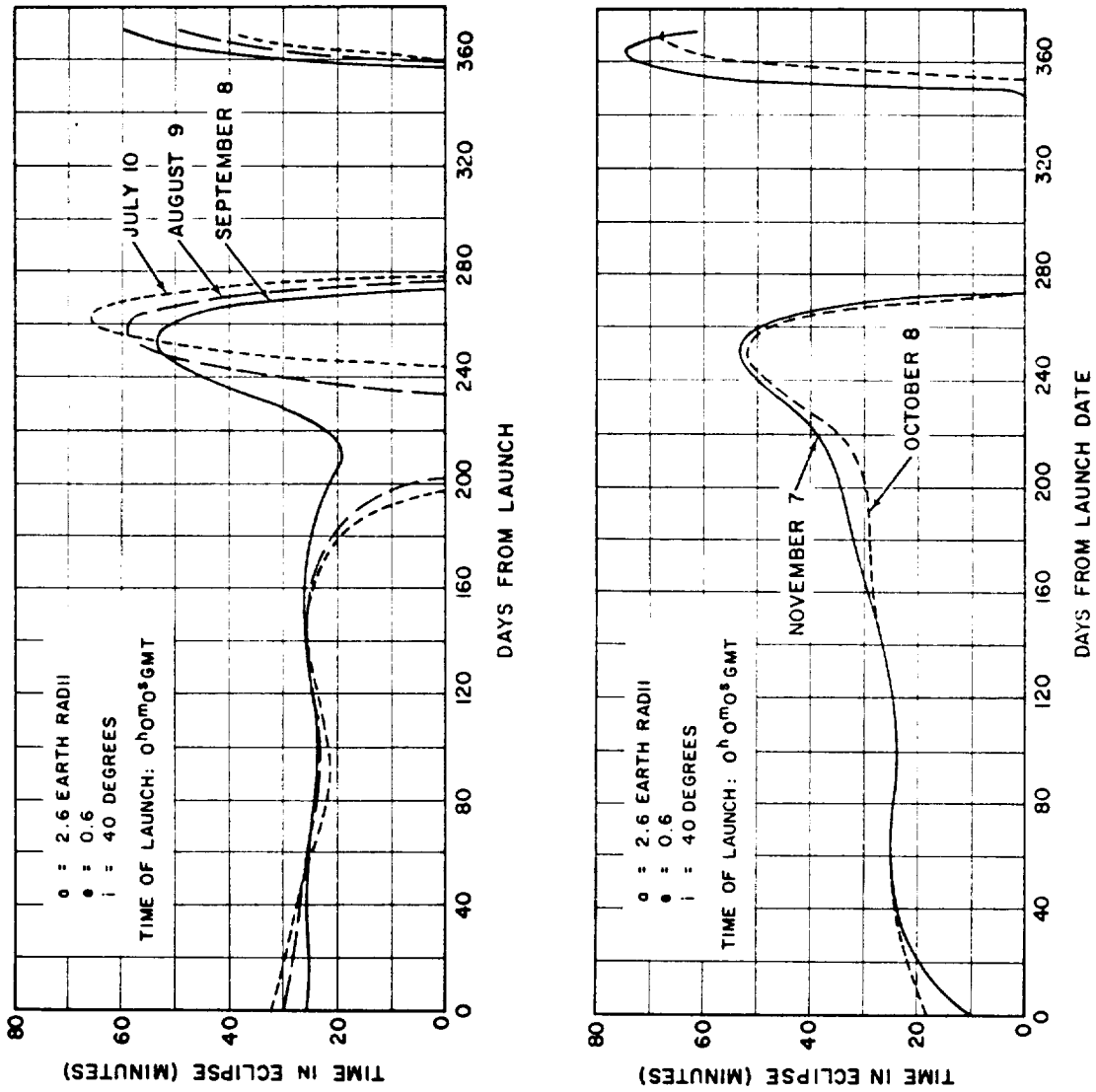

Fig. 28. Example of Eclipse Patterns When Launching a Vehicle on Different Dates in 1963 at the Same Time of Day

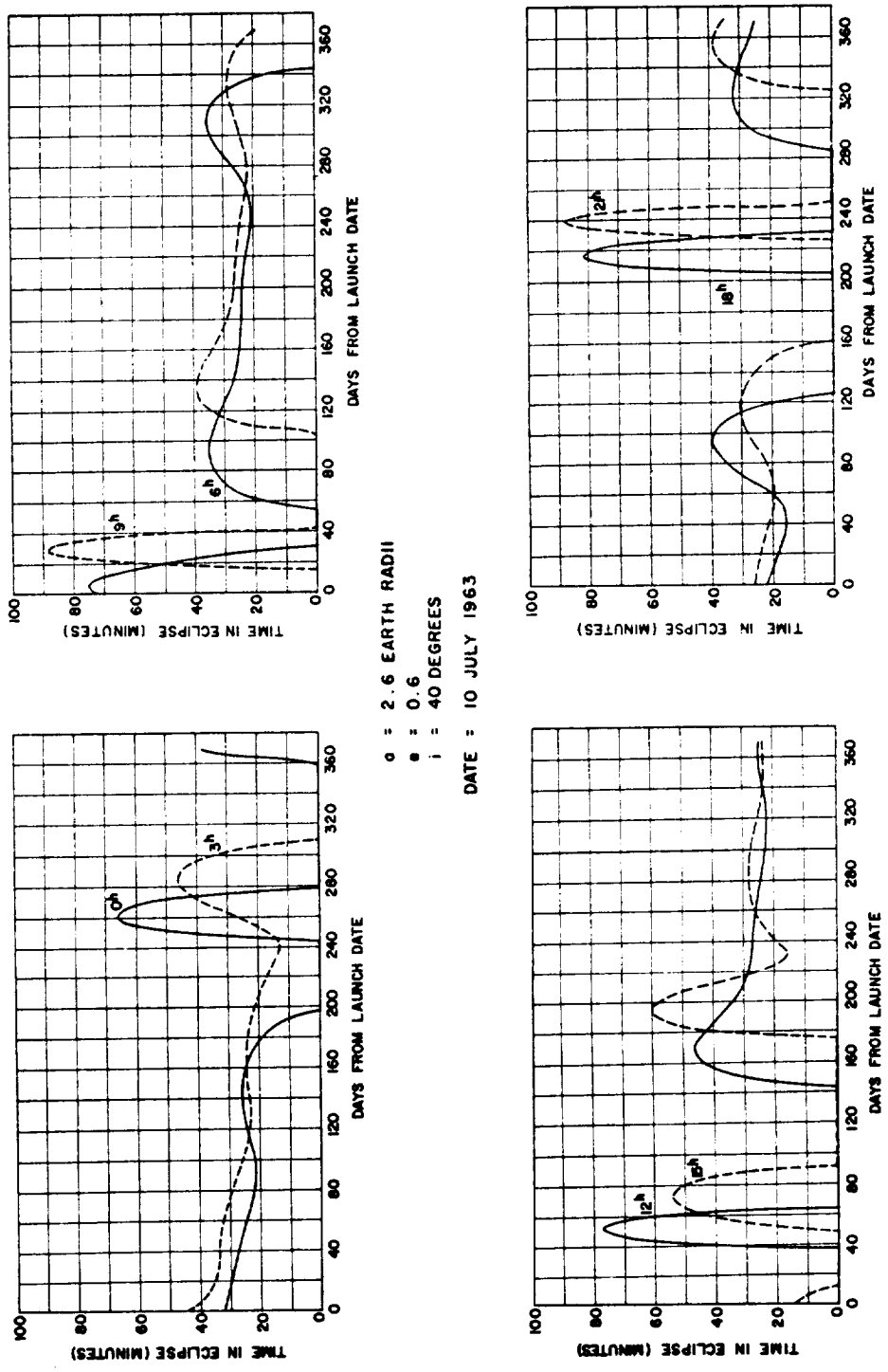

Fig. 29. Example of Eclipse Patterns When Launching a Vehicle at Different Times on the Same Date

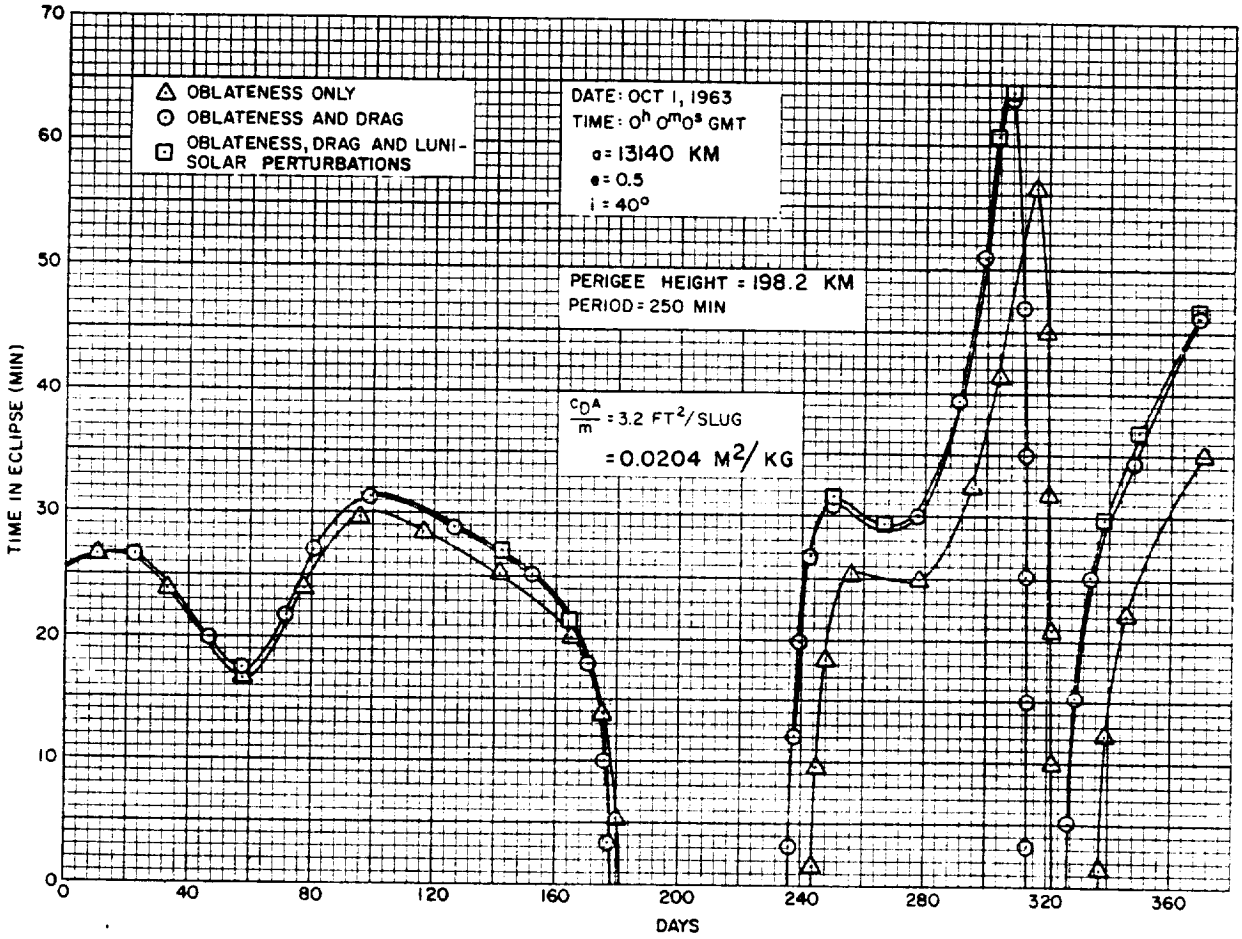

Fig. 30. Example of Eclipse Patterns for One Satellite Taking into Account Different Perturbations (the luni-solar effects are small for this orbit; however, in some orbits these predominate)

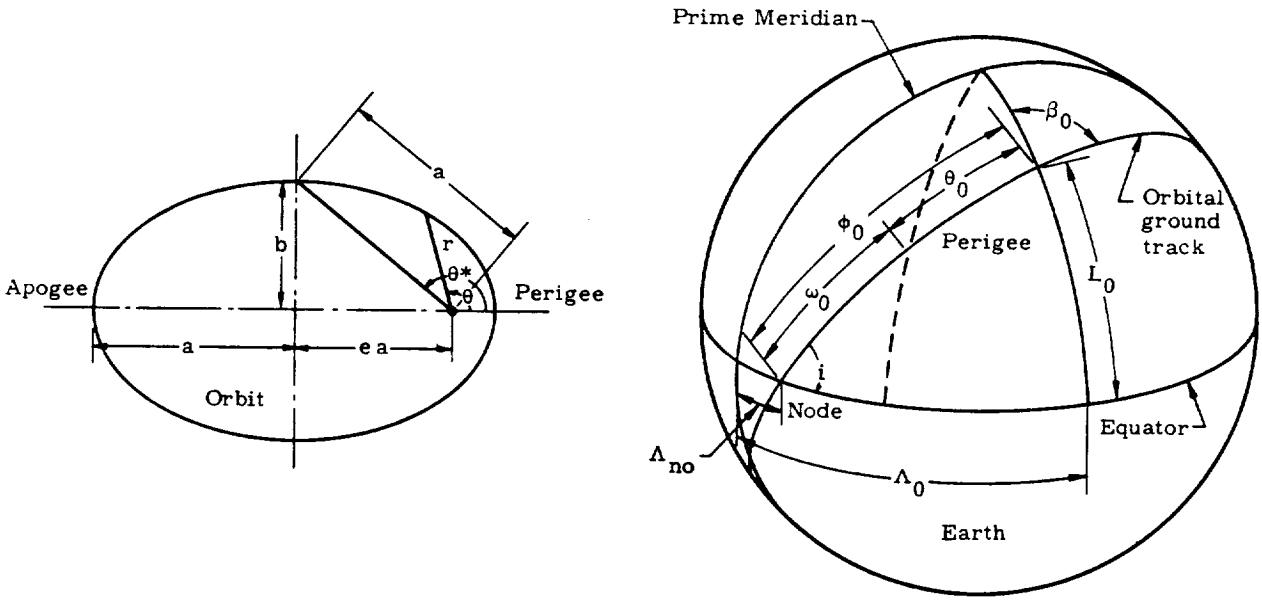

Fig. 31. Geometry of the Ground Track Problem

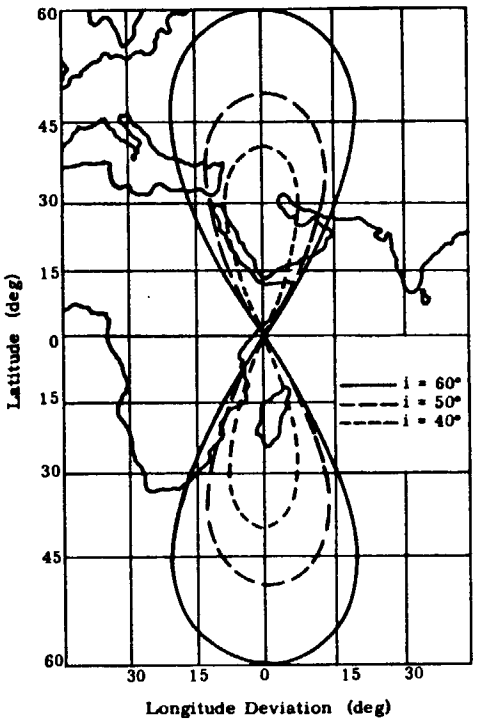

Fig. 32. Ground Tracks of Circular 24-hr Orbits

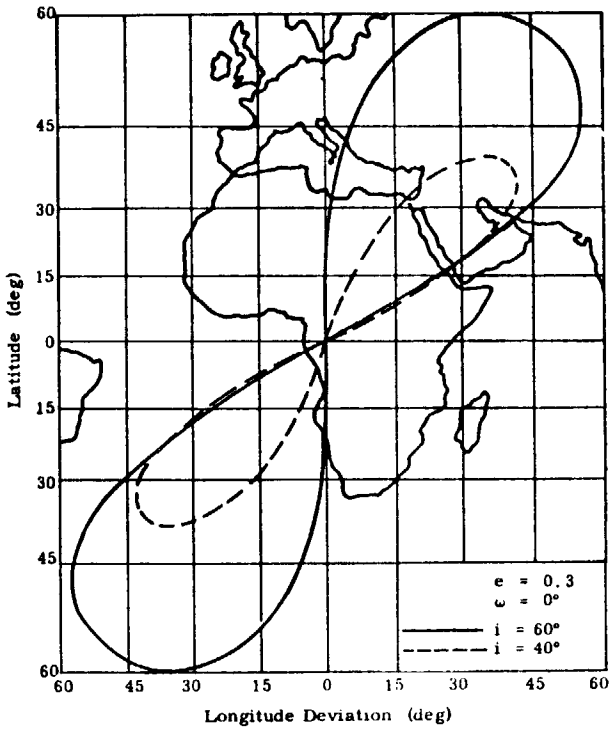

Fig. 33. Ground Tracks of Elliptical 24-hr Orbits

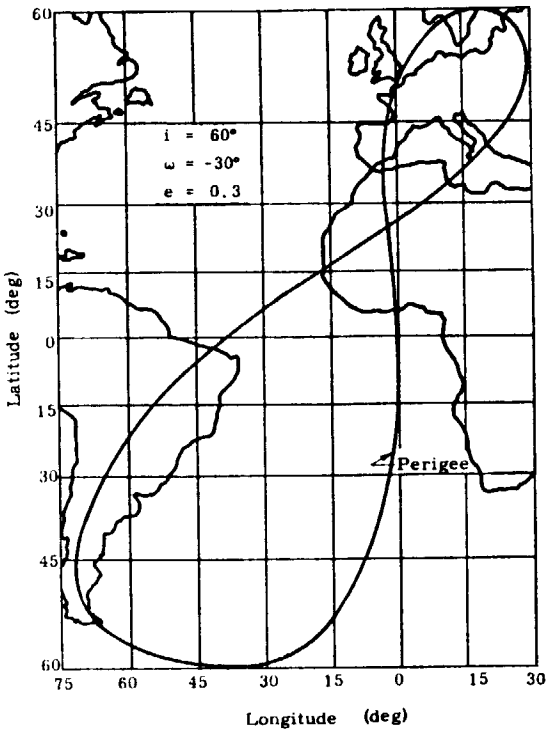

Fig. 34. Ground Track of an Elliptical 24-hr Orbit

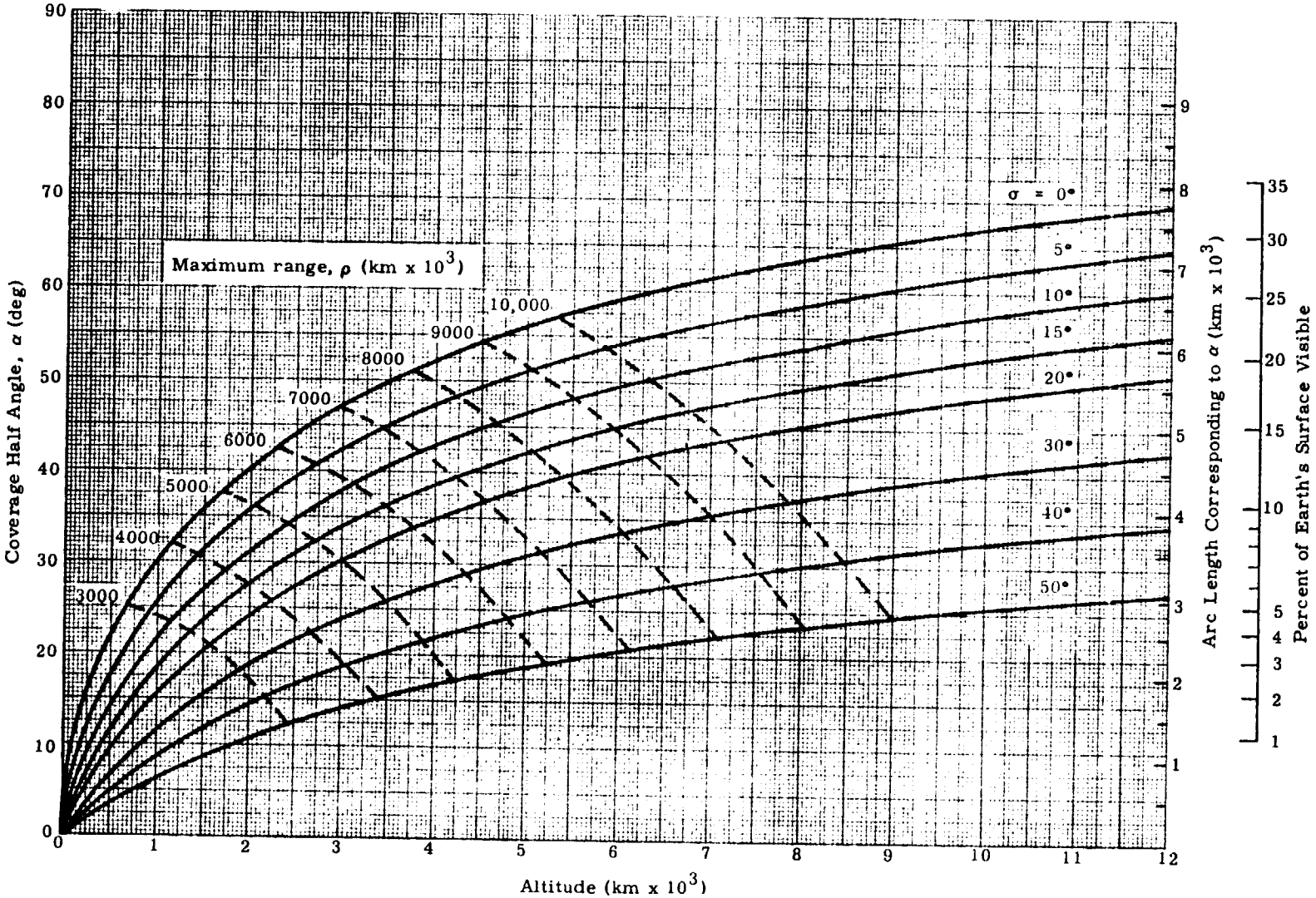

Fig. 35. Satellite Coverage

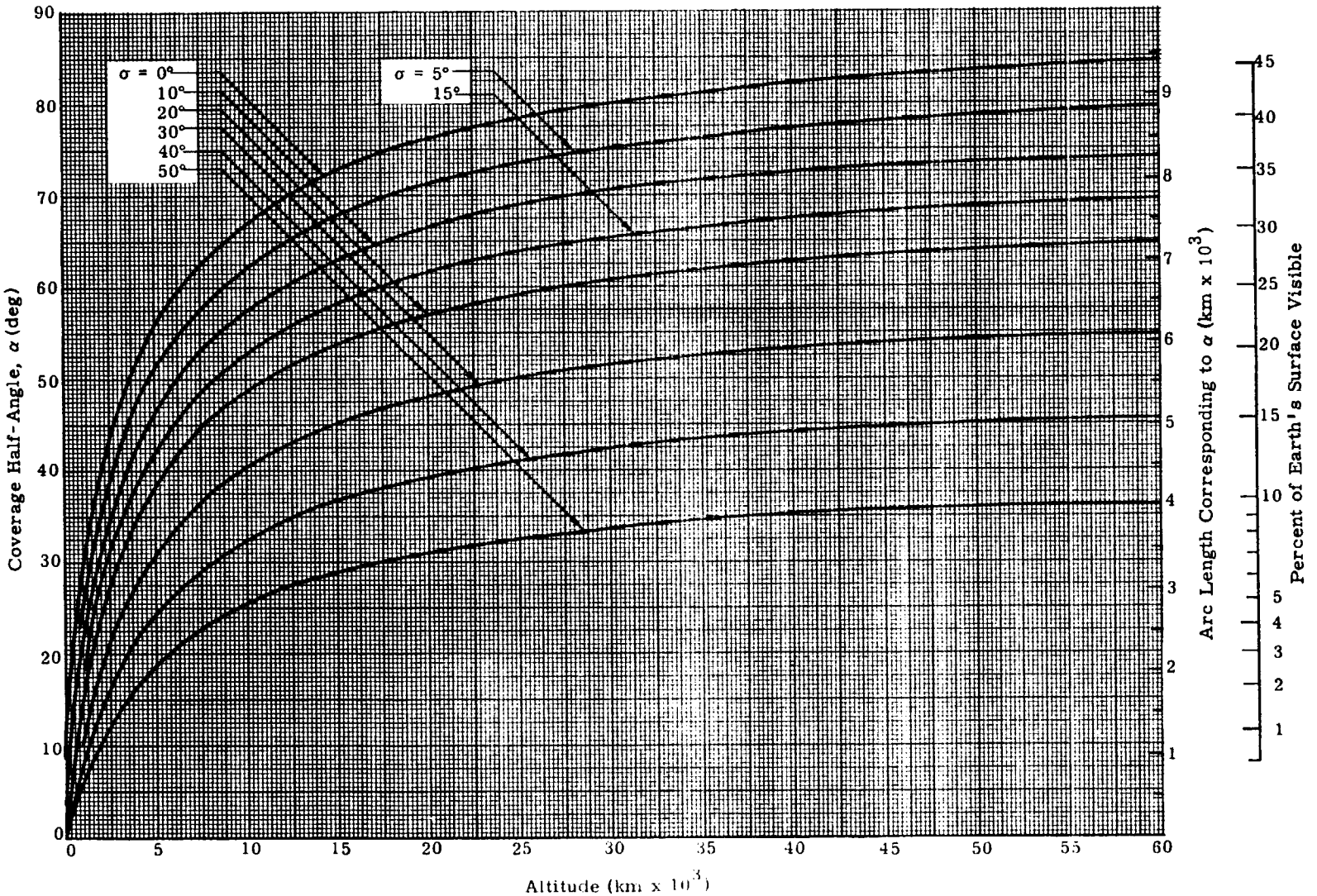

Fig. 36. Satellite Coverage

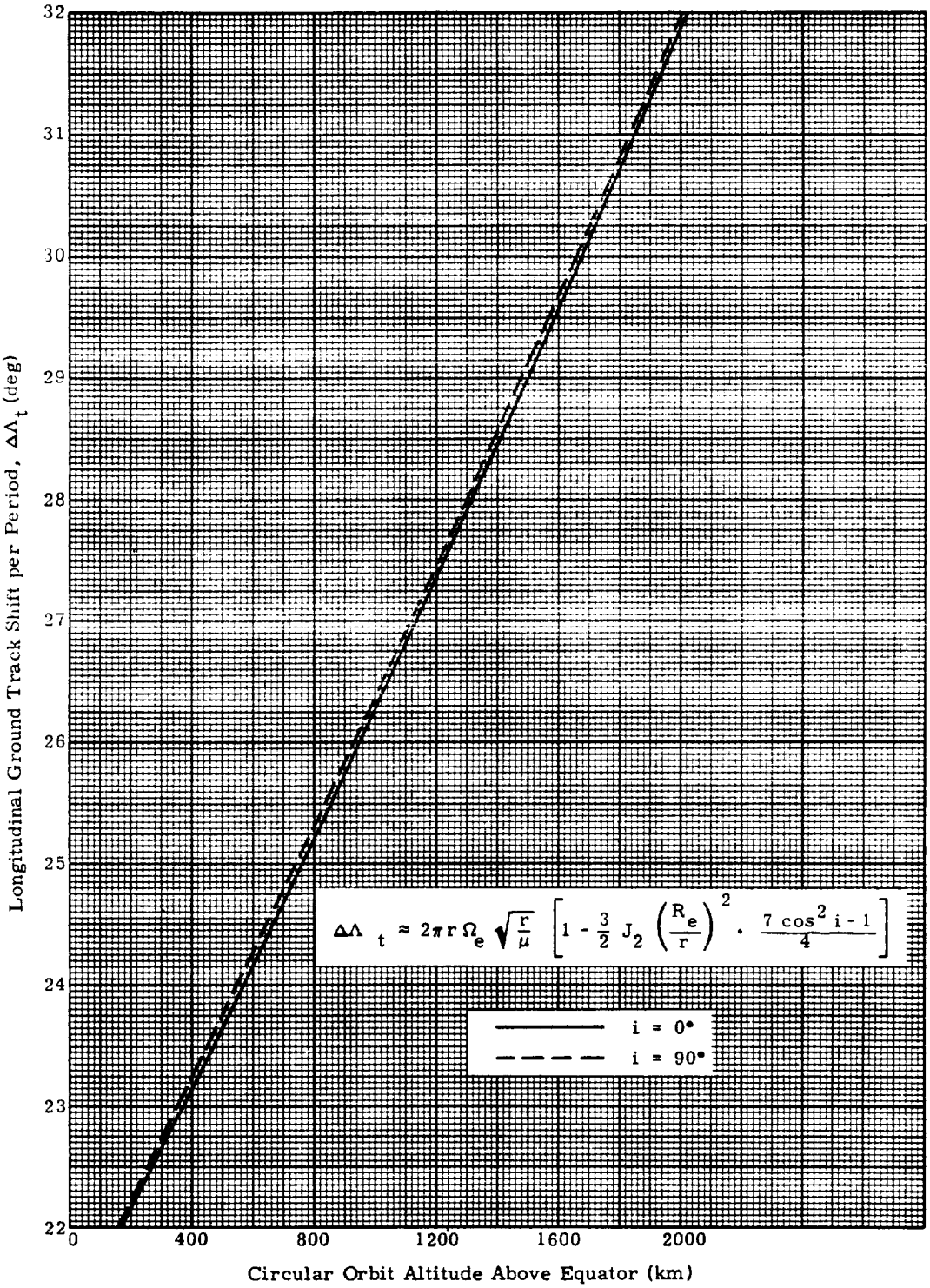

Fig. 37. Longitudinal Ground Track Shift

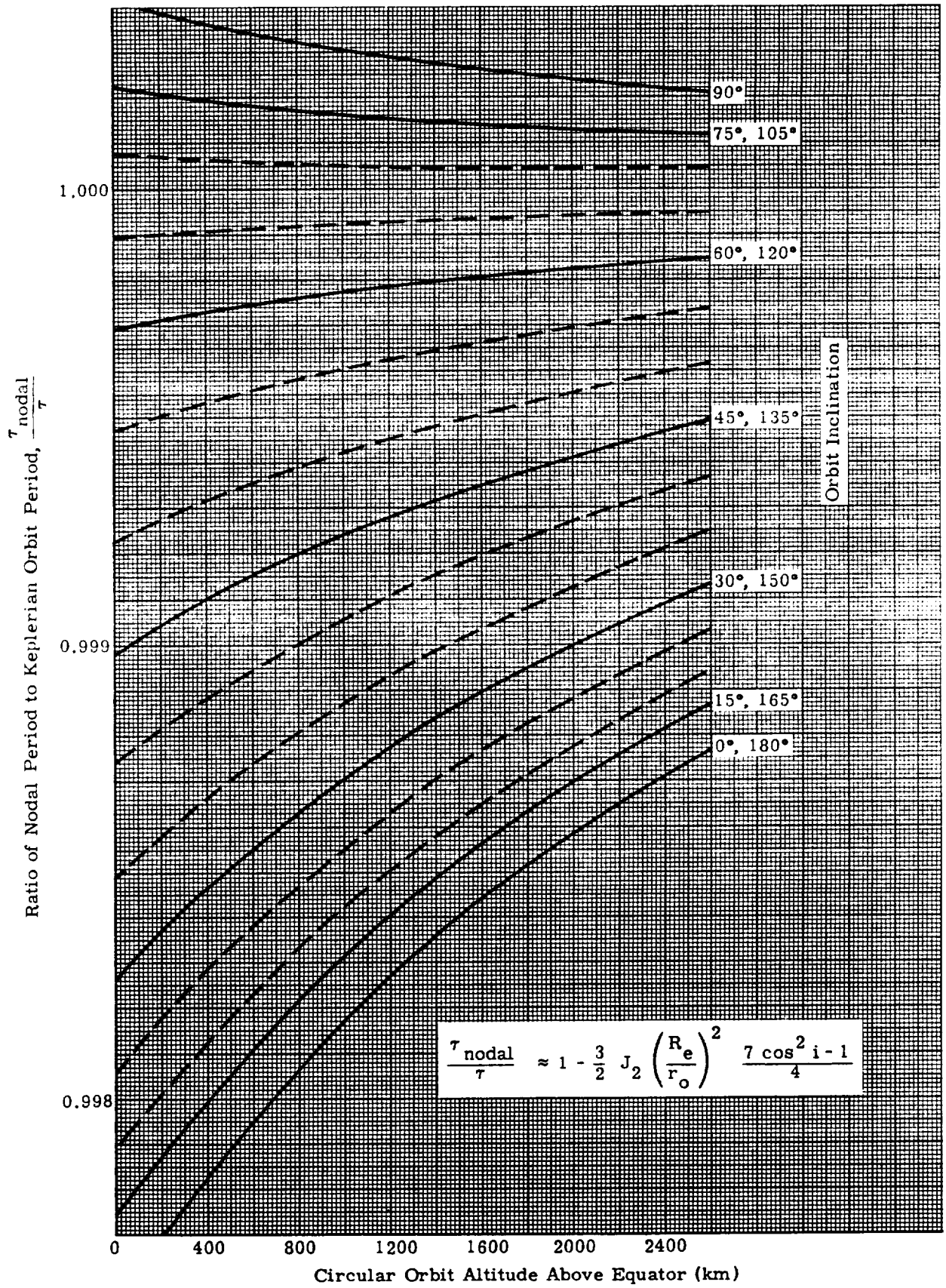

Fig. 38. Nodal Orbit Period

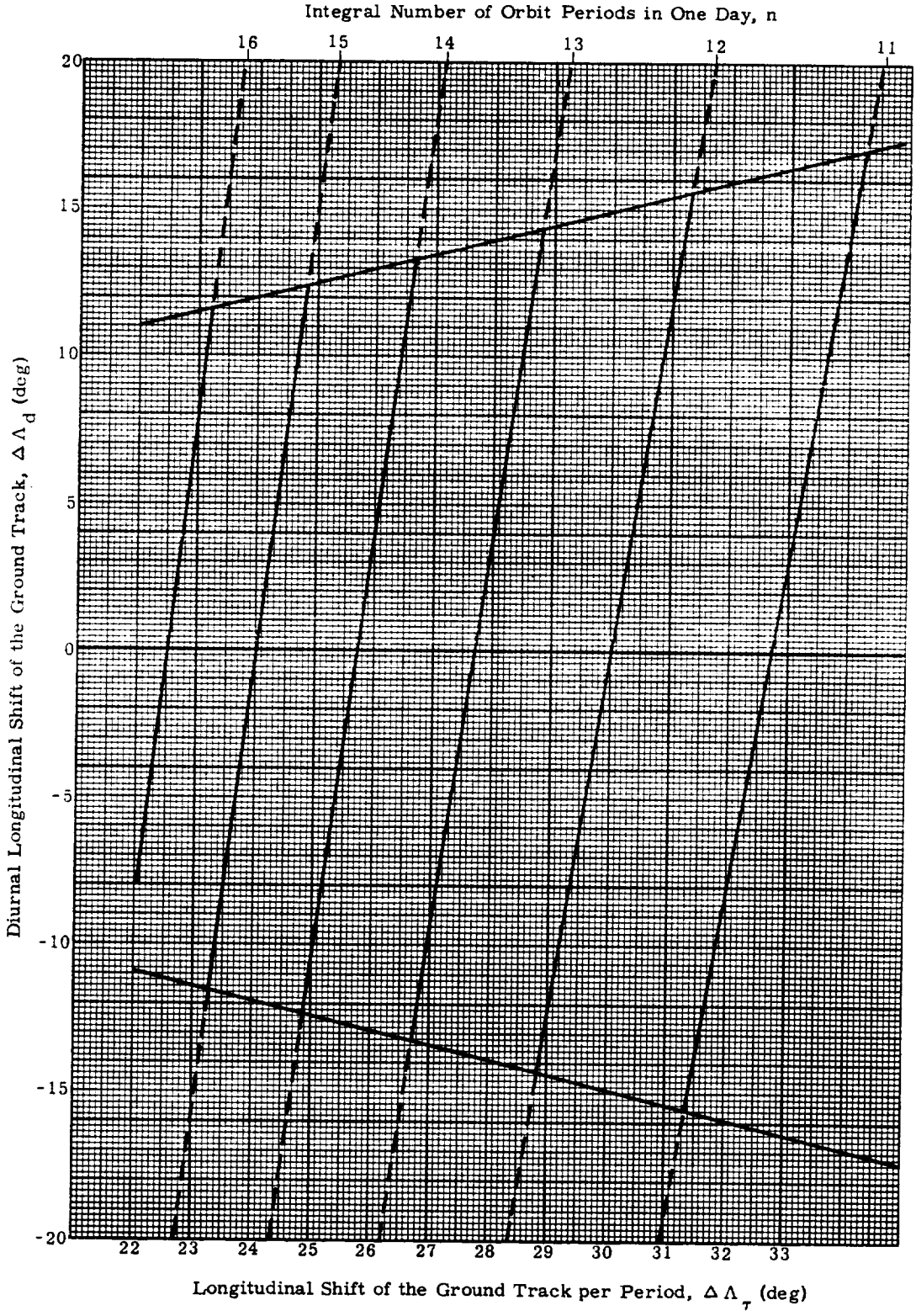

Fig. 39. Diurnal Longitudinal Shift of the Ground Track

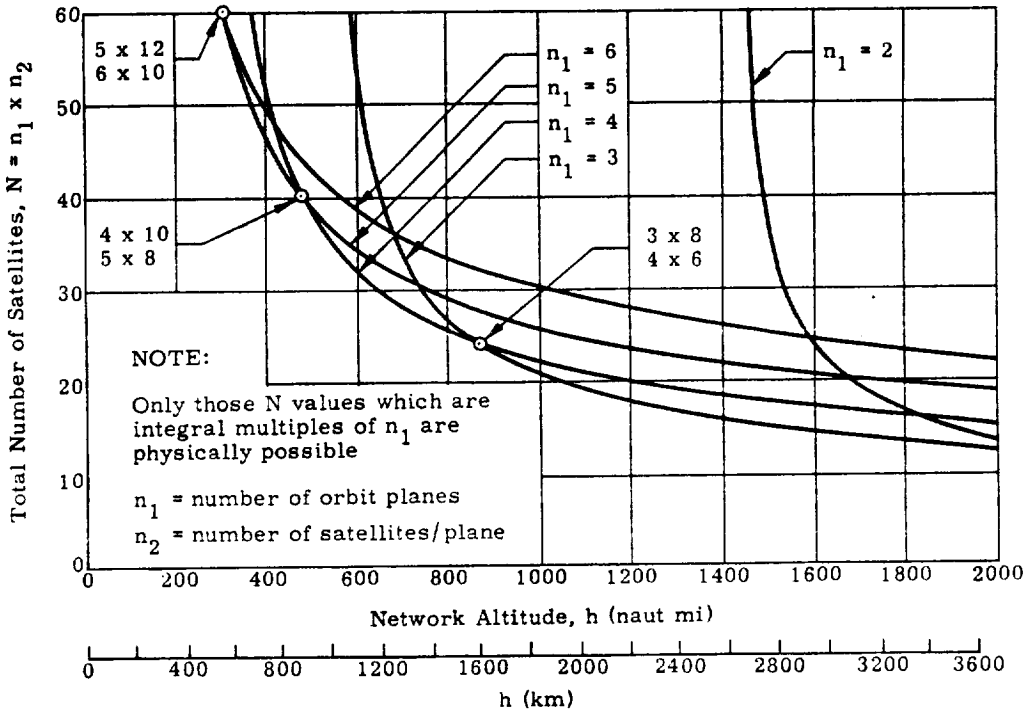

Fig. 40. Number and Distribution of Satellites in a Polar Network Providing Complete Global Coverage (σ = 0 deg)

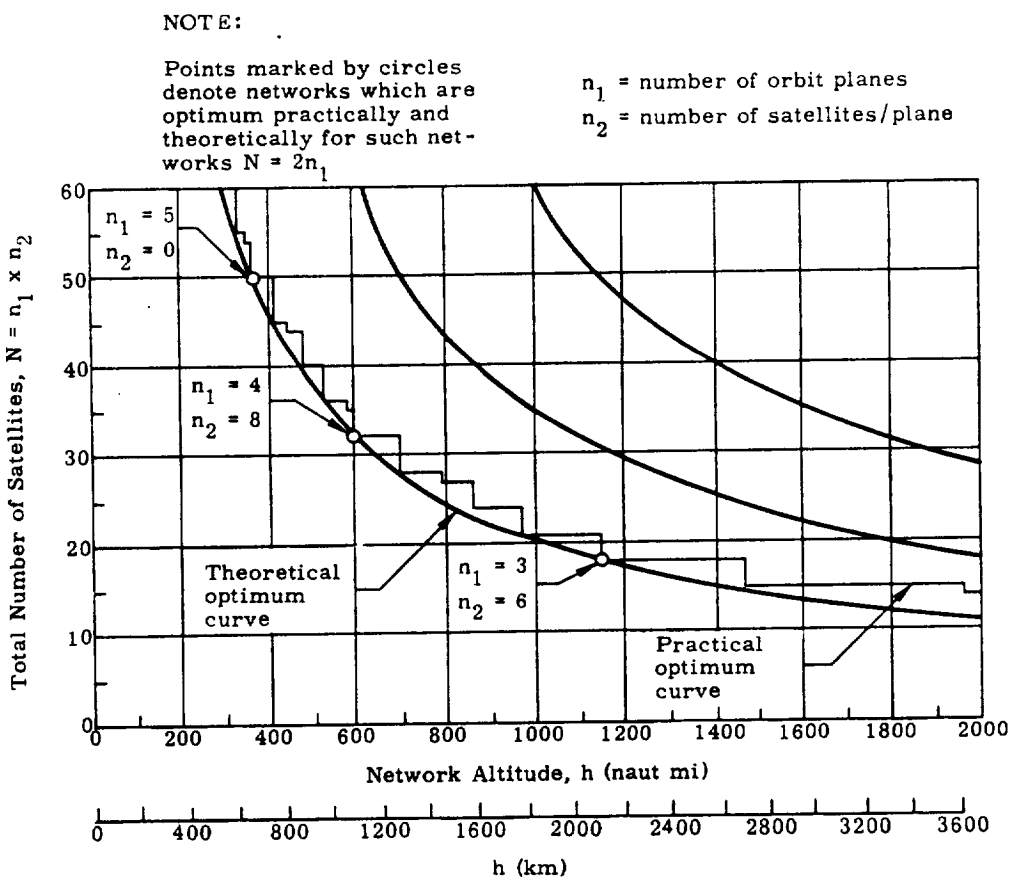

Fig. 41. Theoretical and Practical Optimum Satellite Utilization in a Polar Network Providing Complete Global Coverage

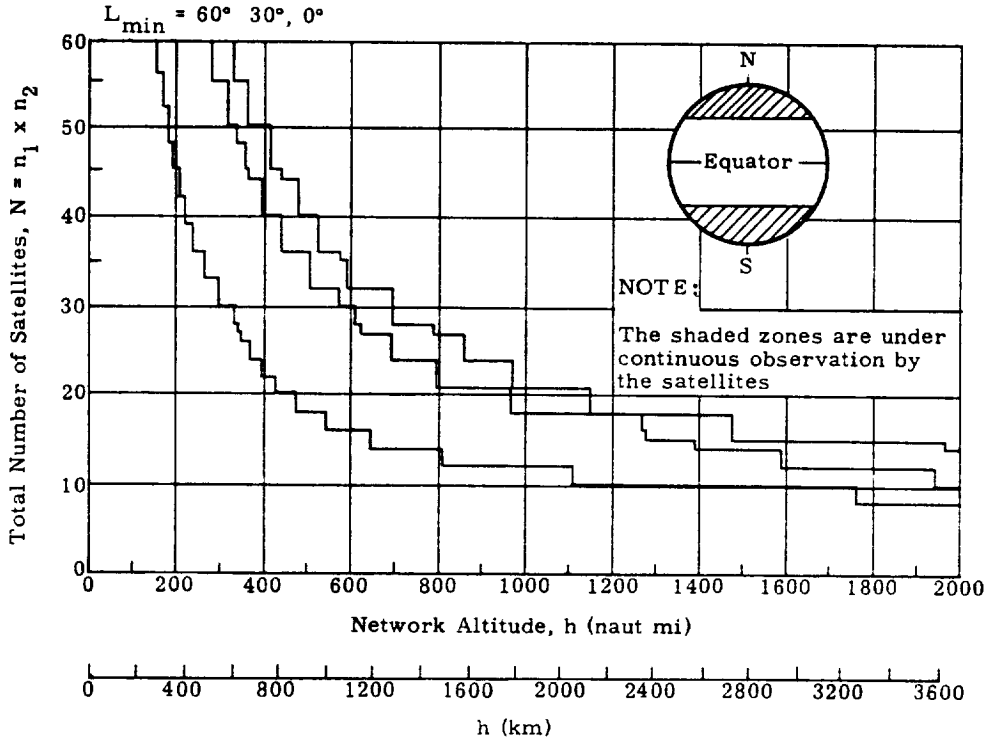

Fig. 42. Comparison of Polar Satellite Networks Providing Coverage from the Poles to Minimum Latitude, L_{min} (σ = 0 deg)

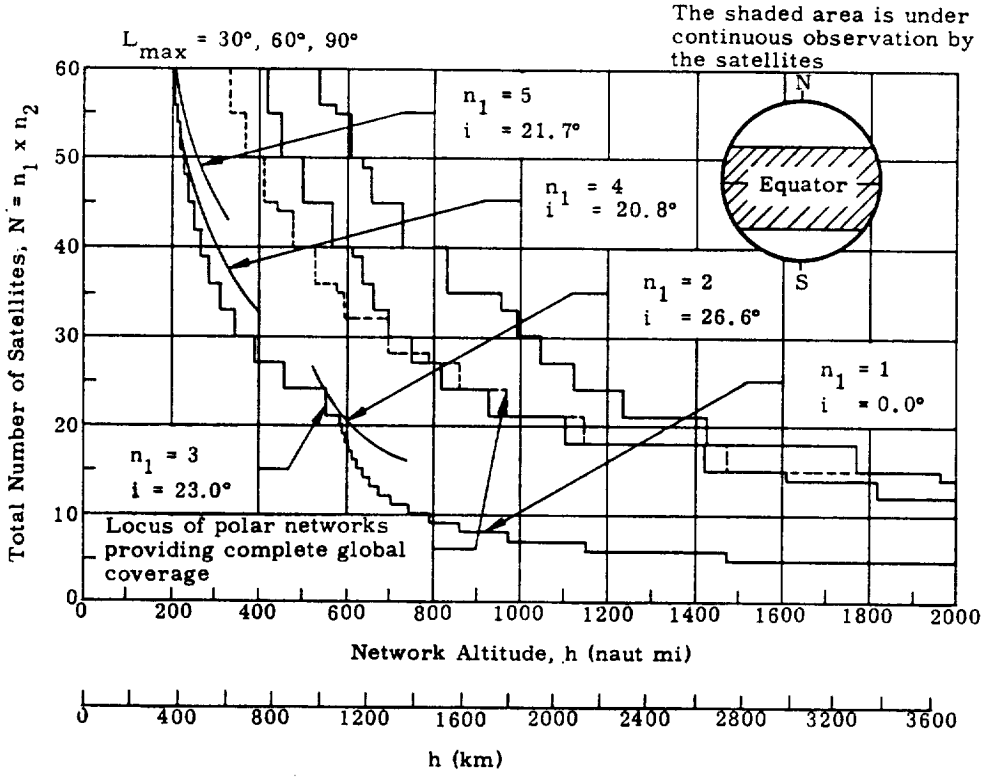

Fig. 43. Comparison of Inclined and Polar Satellite Networks Providing Coverage from the Equator to Maximum Latitude, L_{max} (σ = 0 deg)

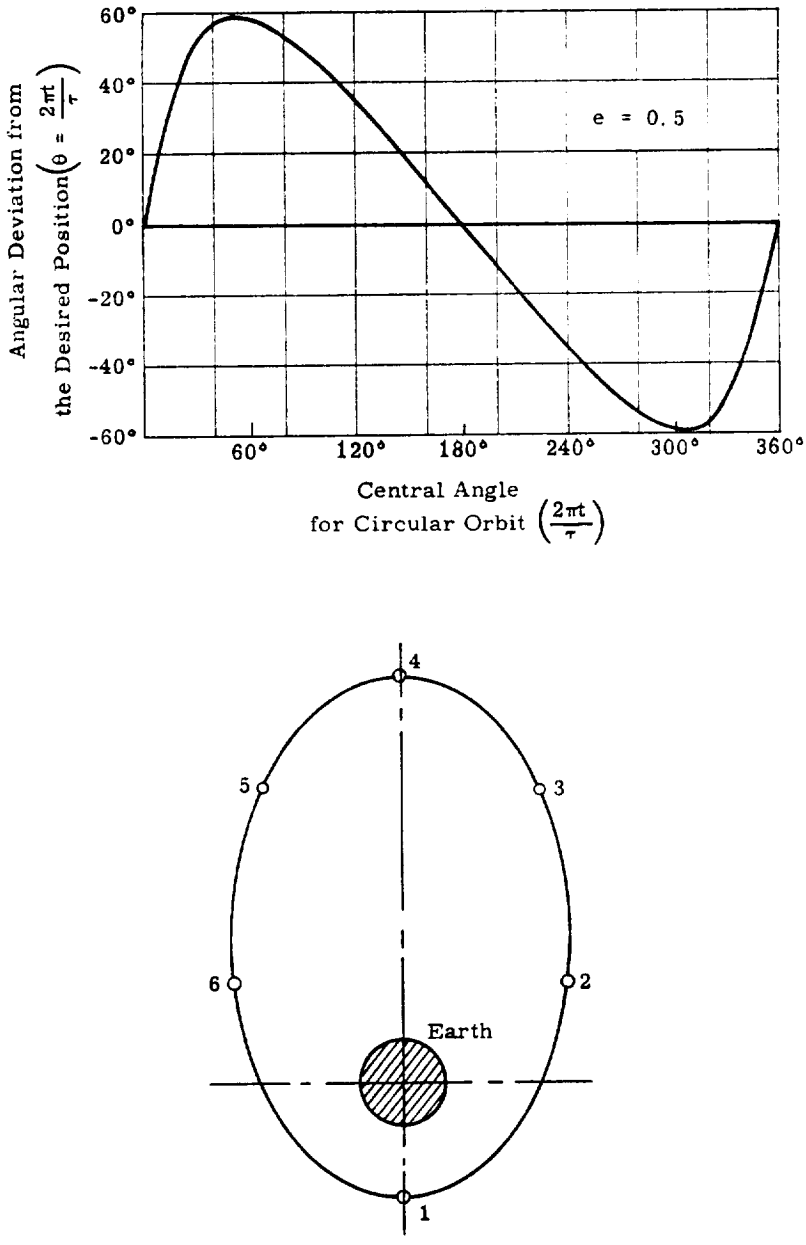

Fig. 44. Eccentricity Effects on the Spacing of Six Satellites (placed at equal time intervals)

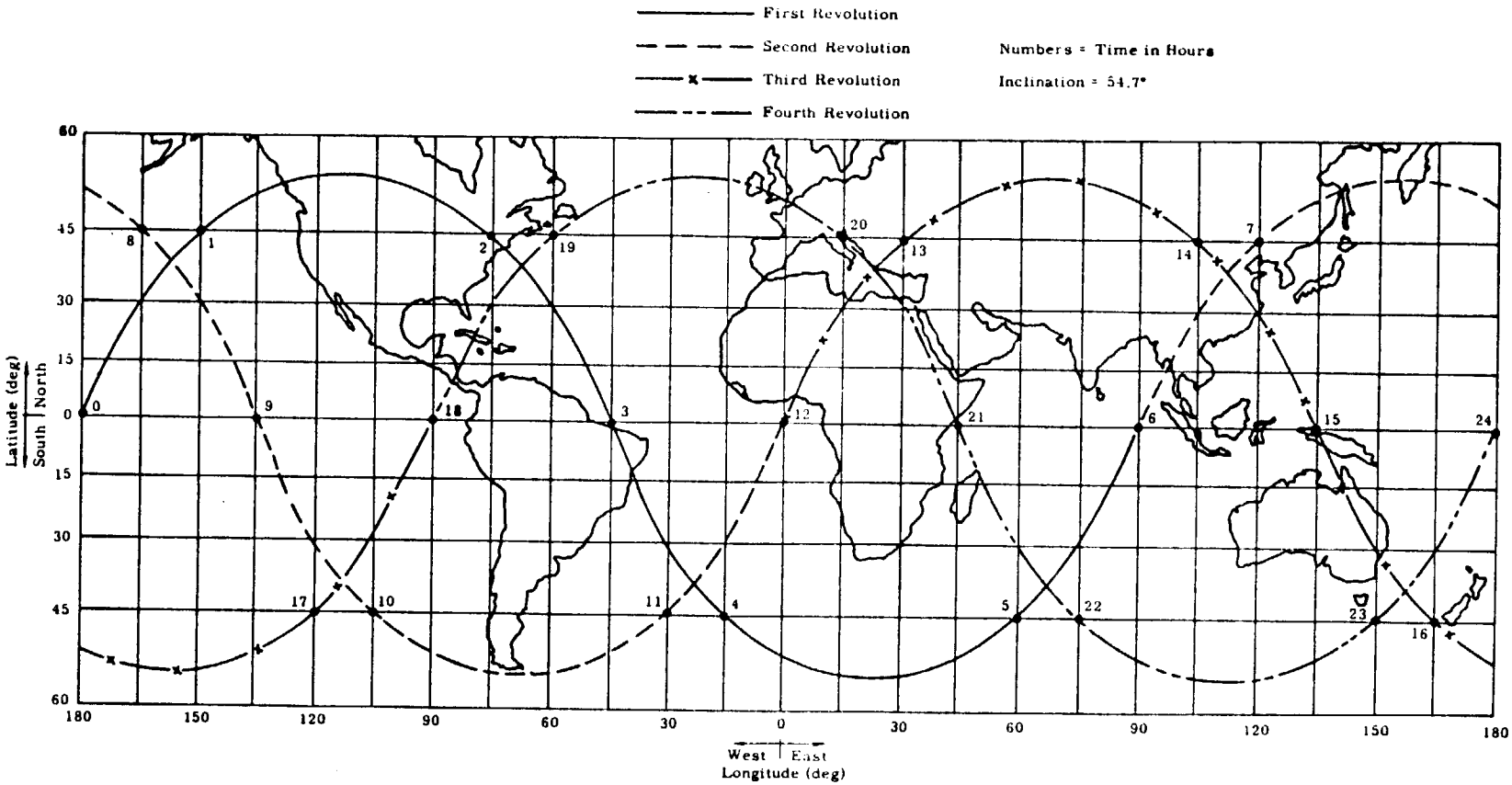

Fig. 45. Ground Track for One Satellite During a Day

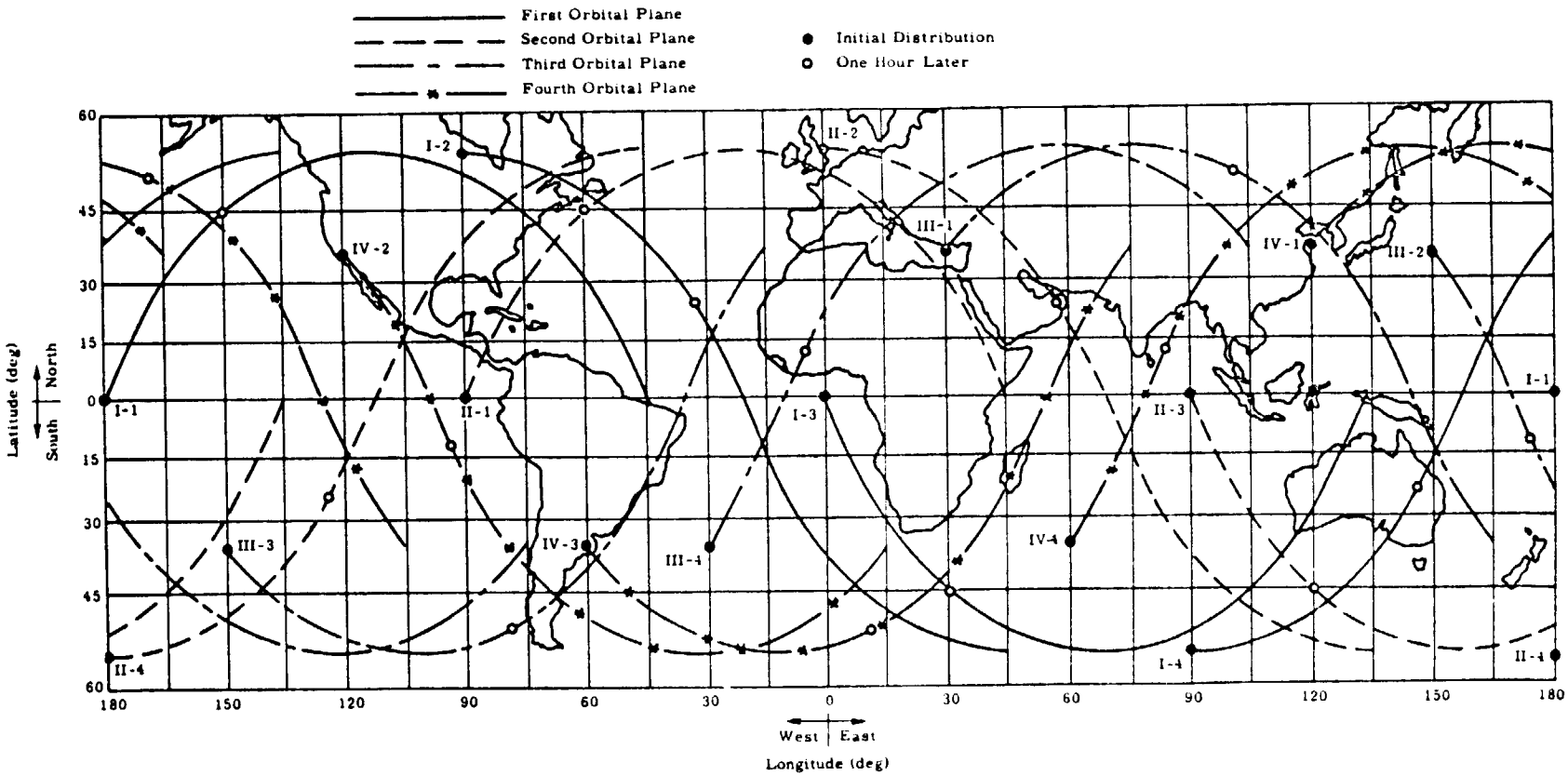

Fig. 46. Ground Tracks for 16 Satellites During Half a Revolution

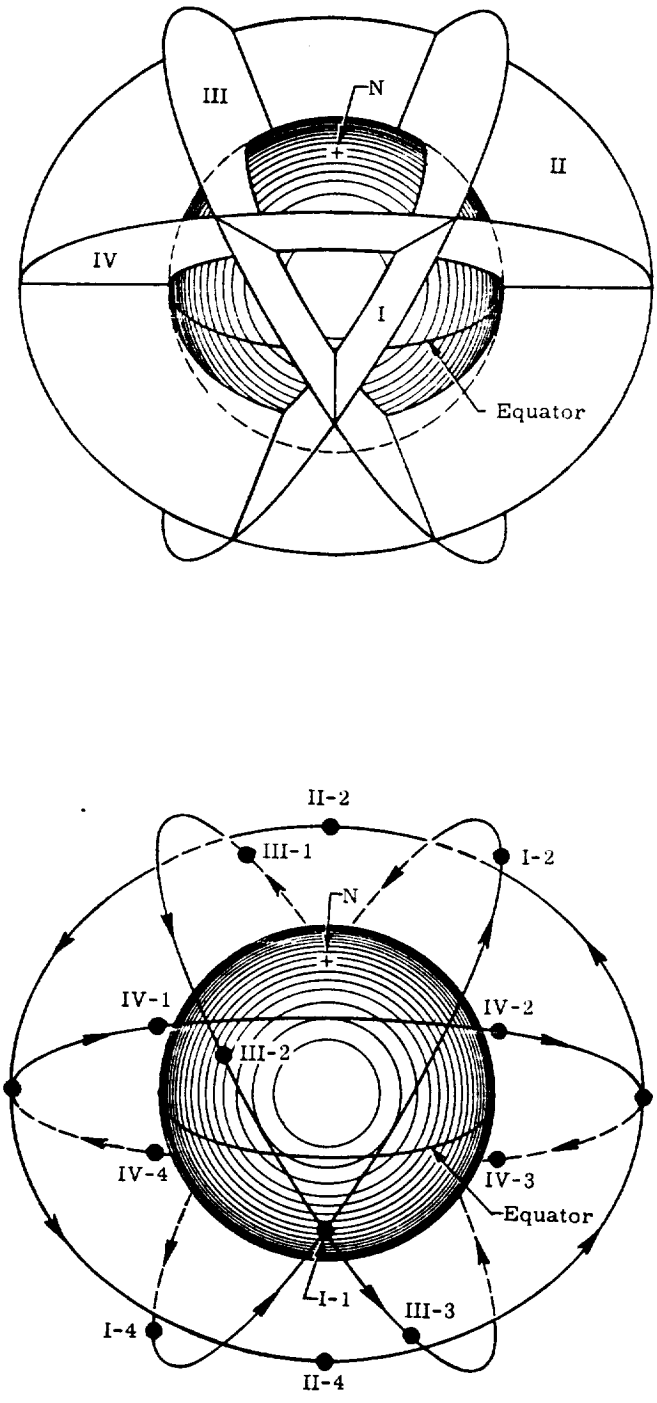

Fig. 47. Three-Dimensional Orbit Pattern

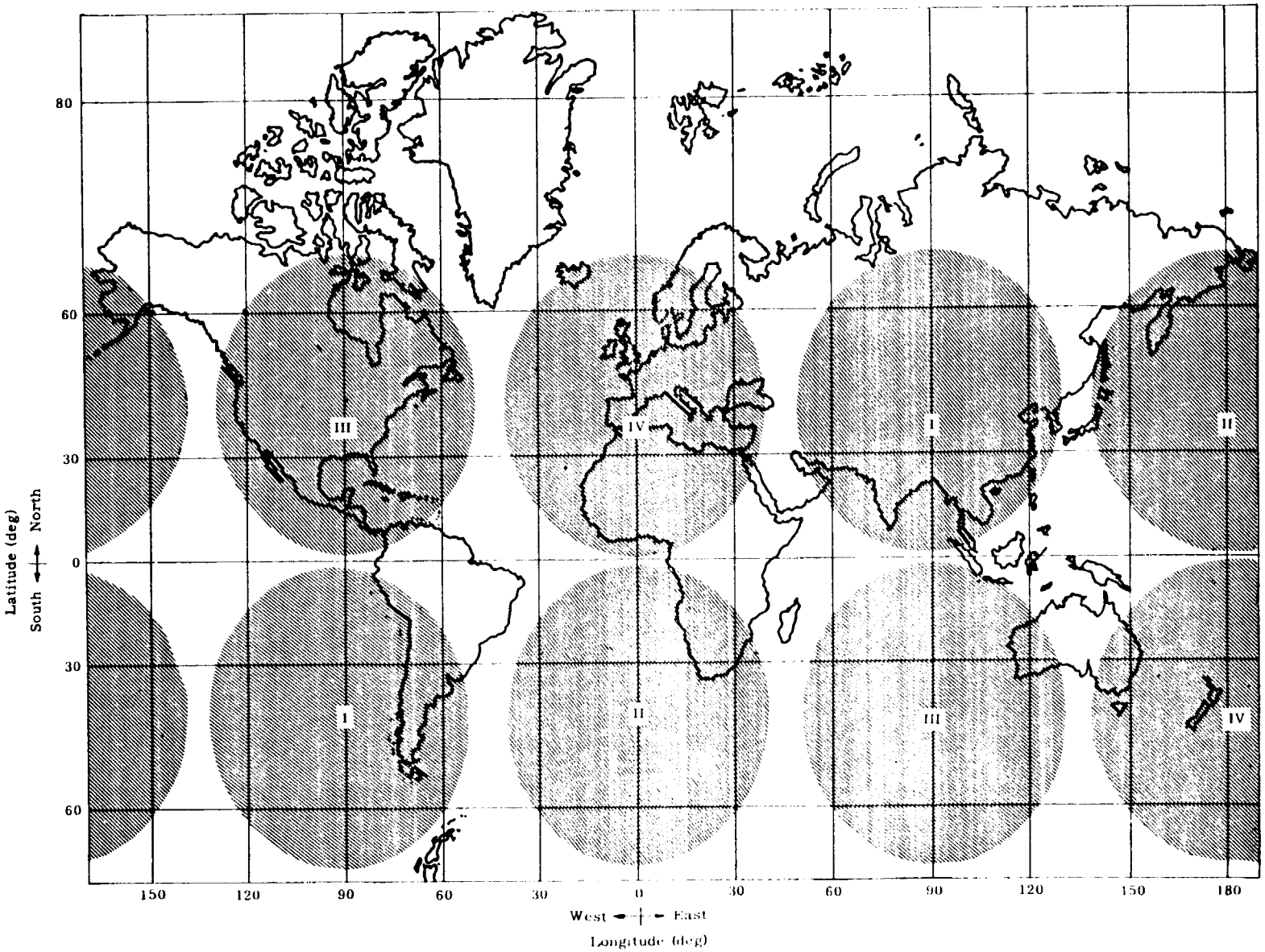

Fig. 48. Areas Not Covered by Ground Swaths at Time Zero

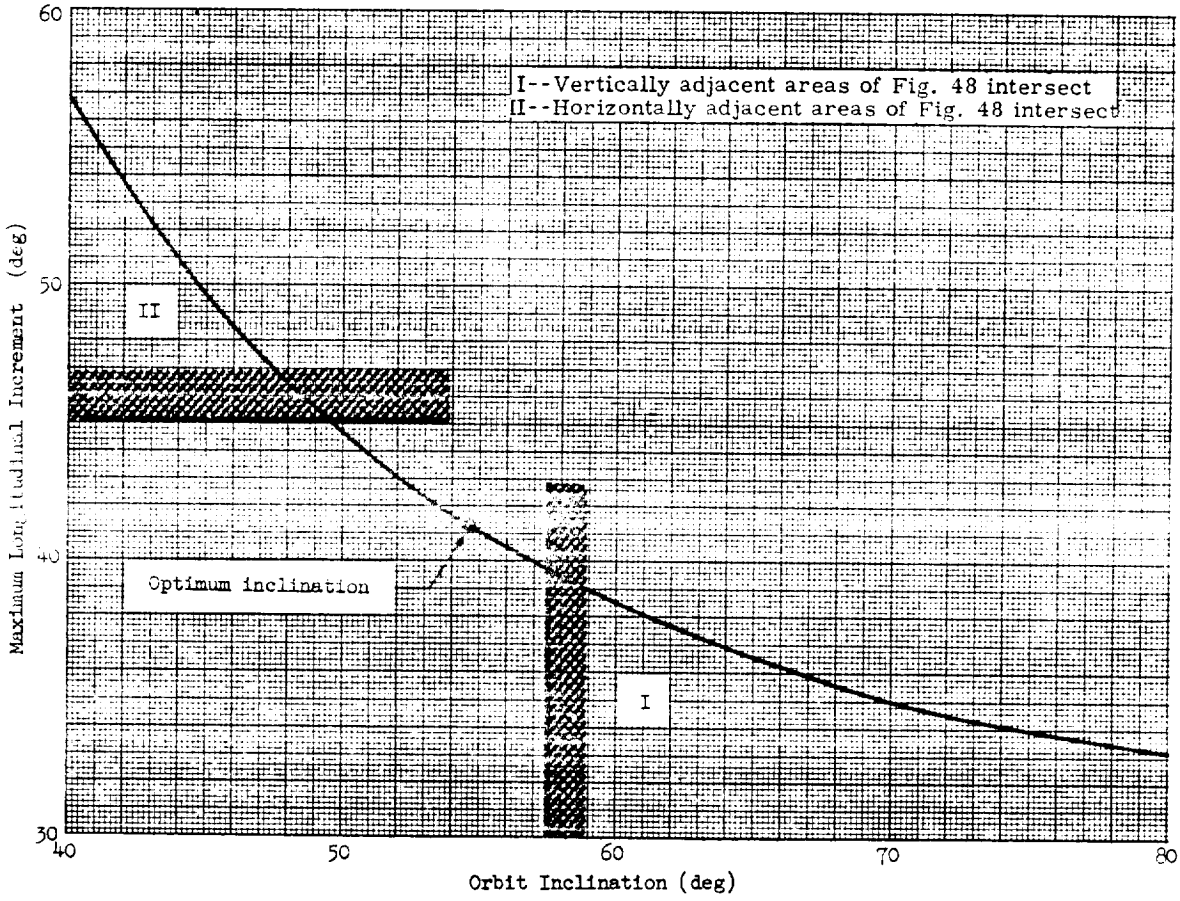

Fig. 49. Maximum Longitudinal Increment of Area Not Covered by Ground Swath as a Function of the Orbital Inclination

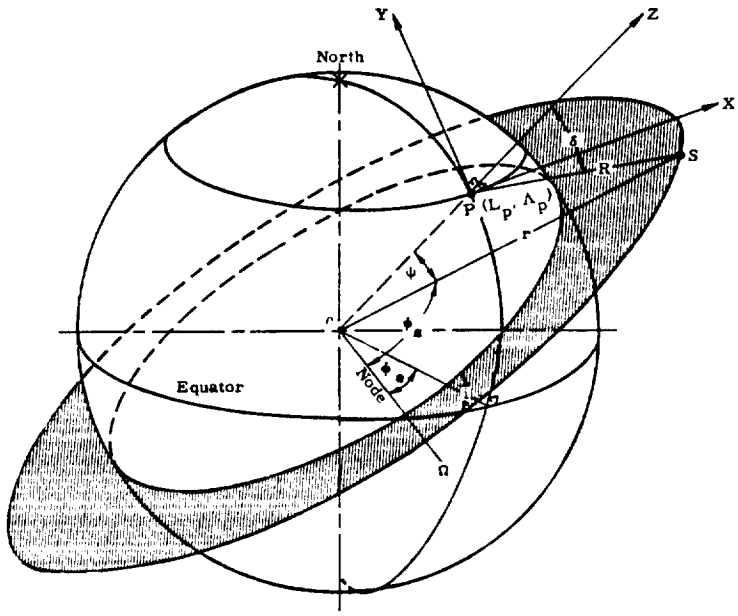

Fig. 50. The Coordinate System for Satellite Tracking

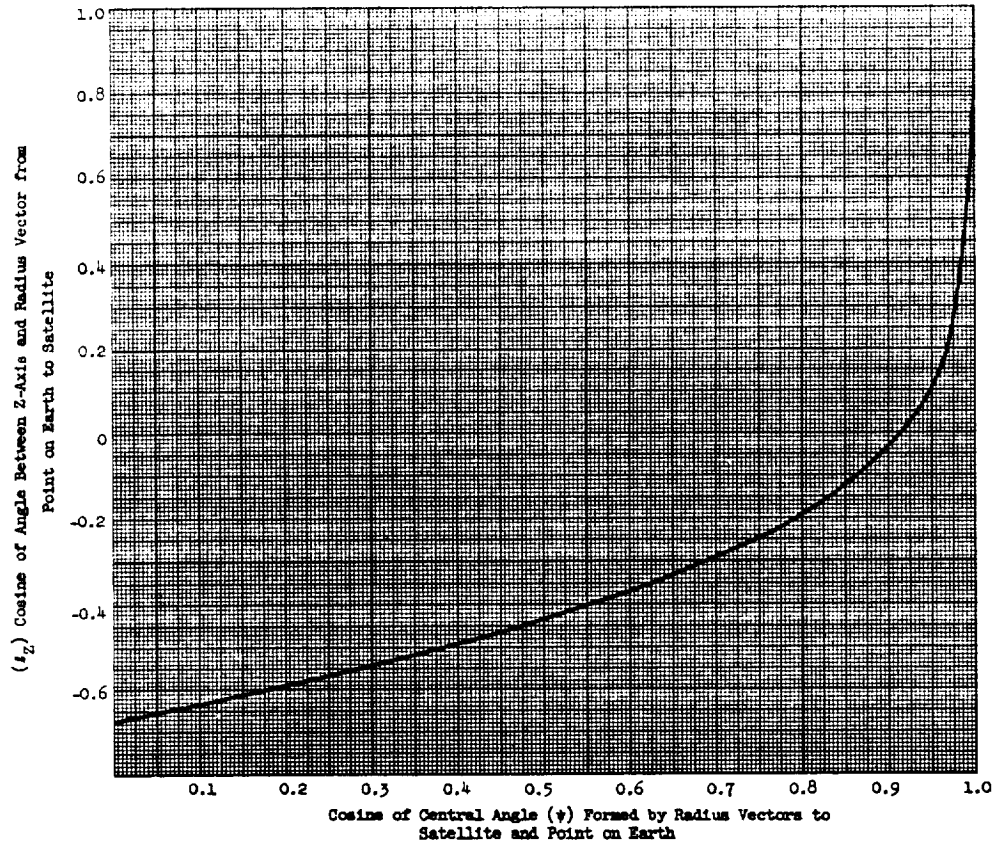

Fig. 51. Satellite Depression Angle Relative to Local Vertical

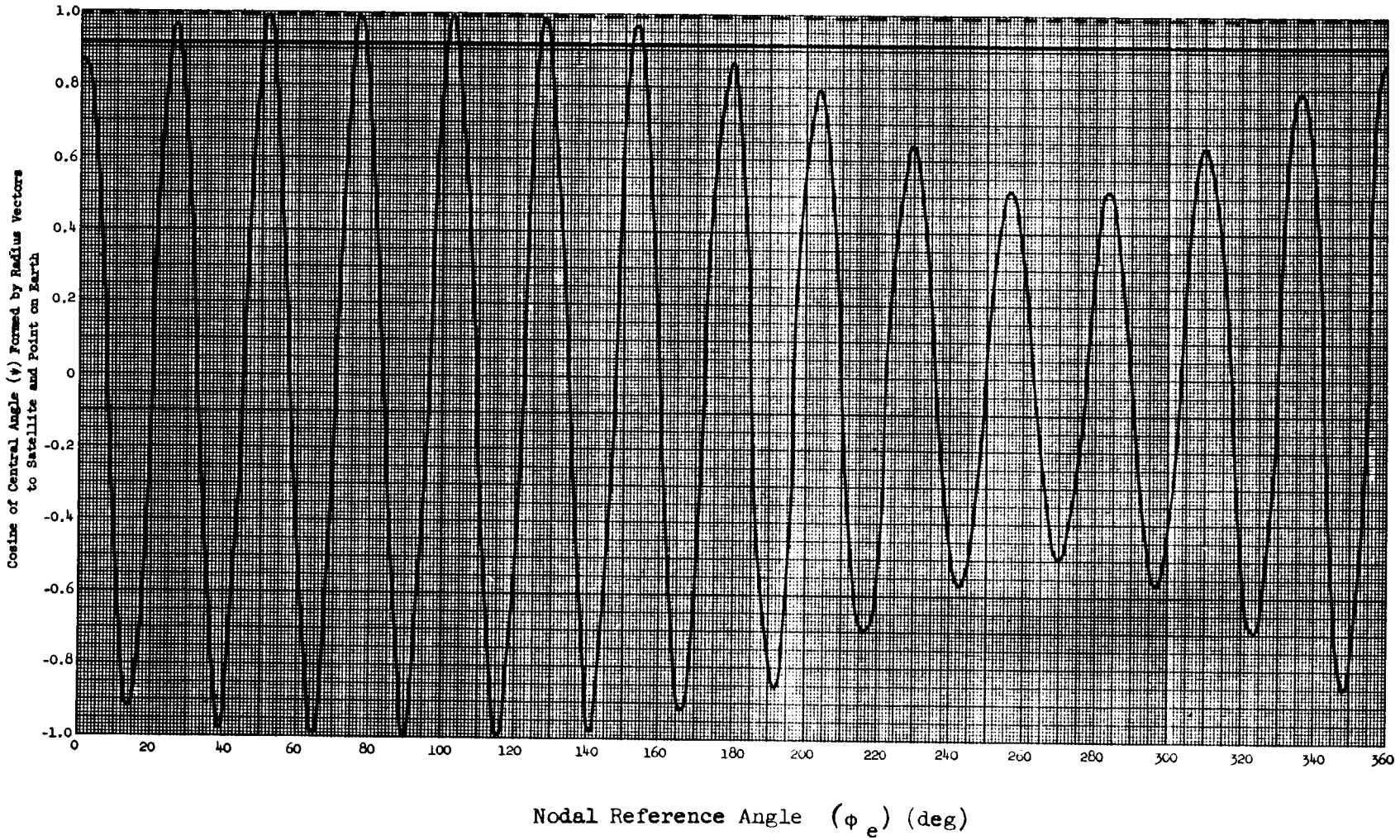

Fig. 52. Cosine ψ Versus Nodal Reference Angle

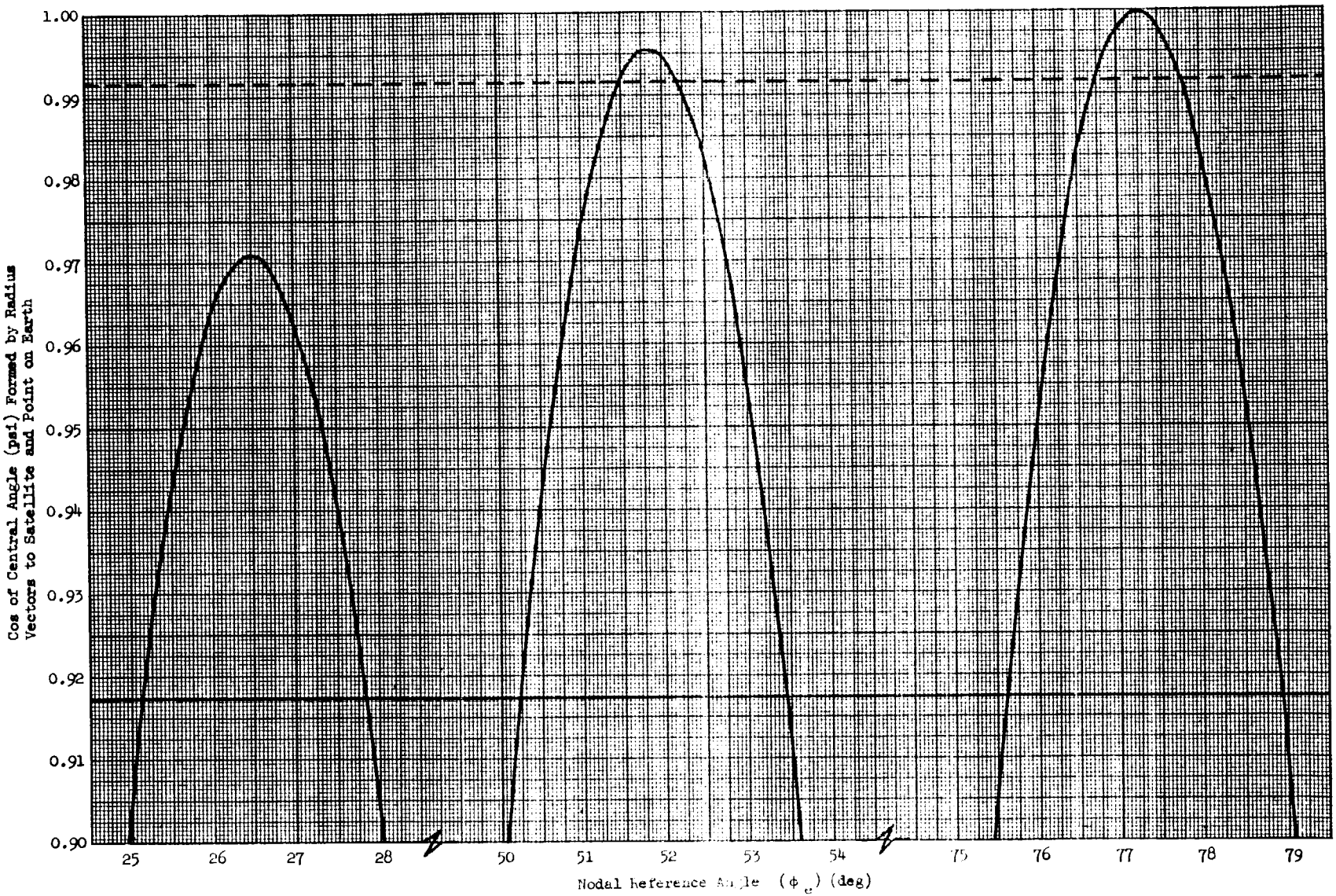

Fig. 53. Cosine ψ Versus Nodal Reference Angle (detailed view)

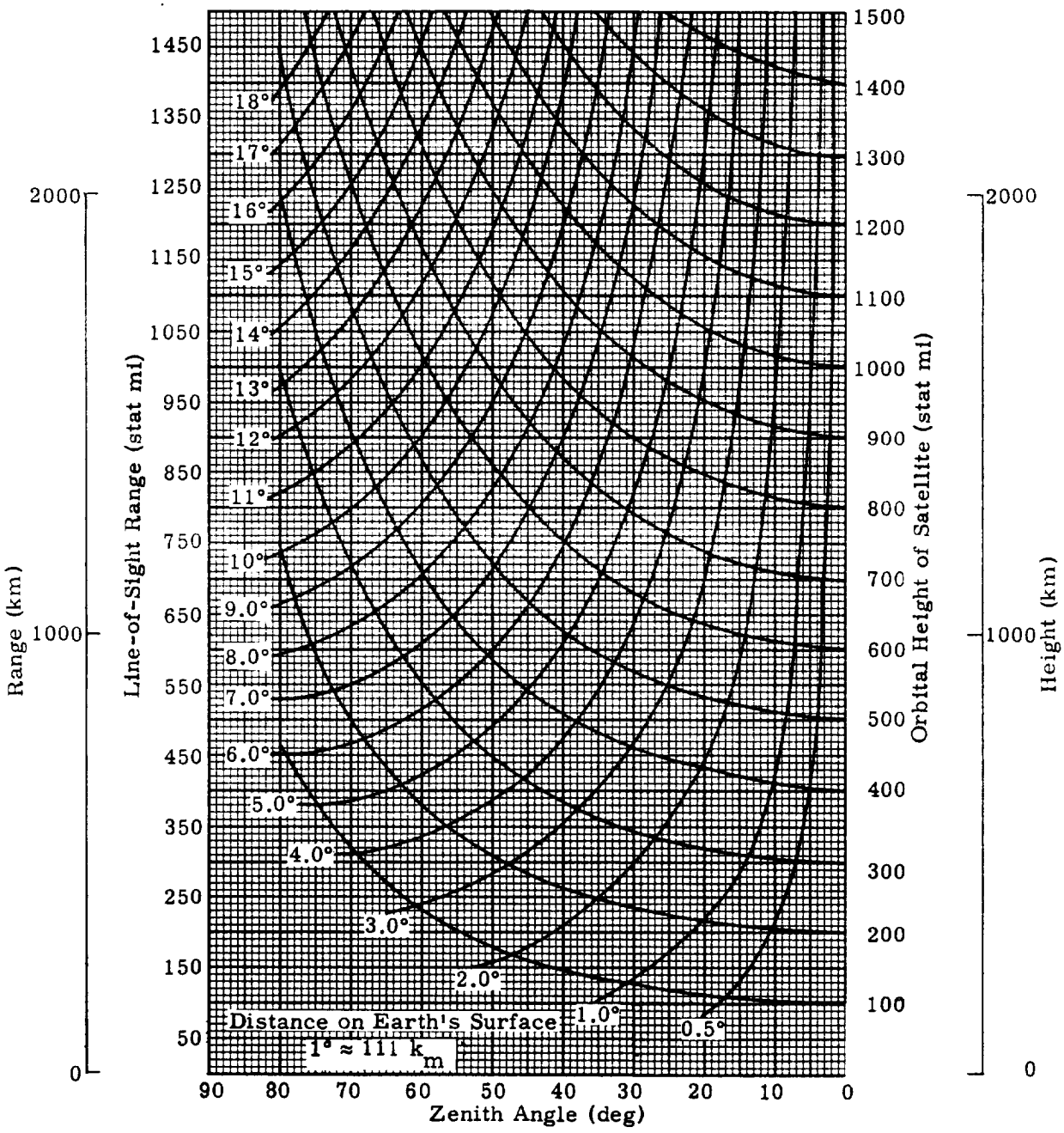

Fig. 54. Diagram for Finding the Distance at Subsatellite Point and Line-of-Sight Range

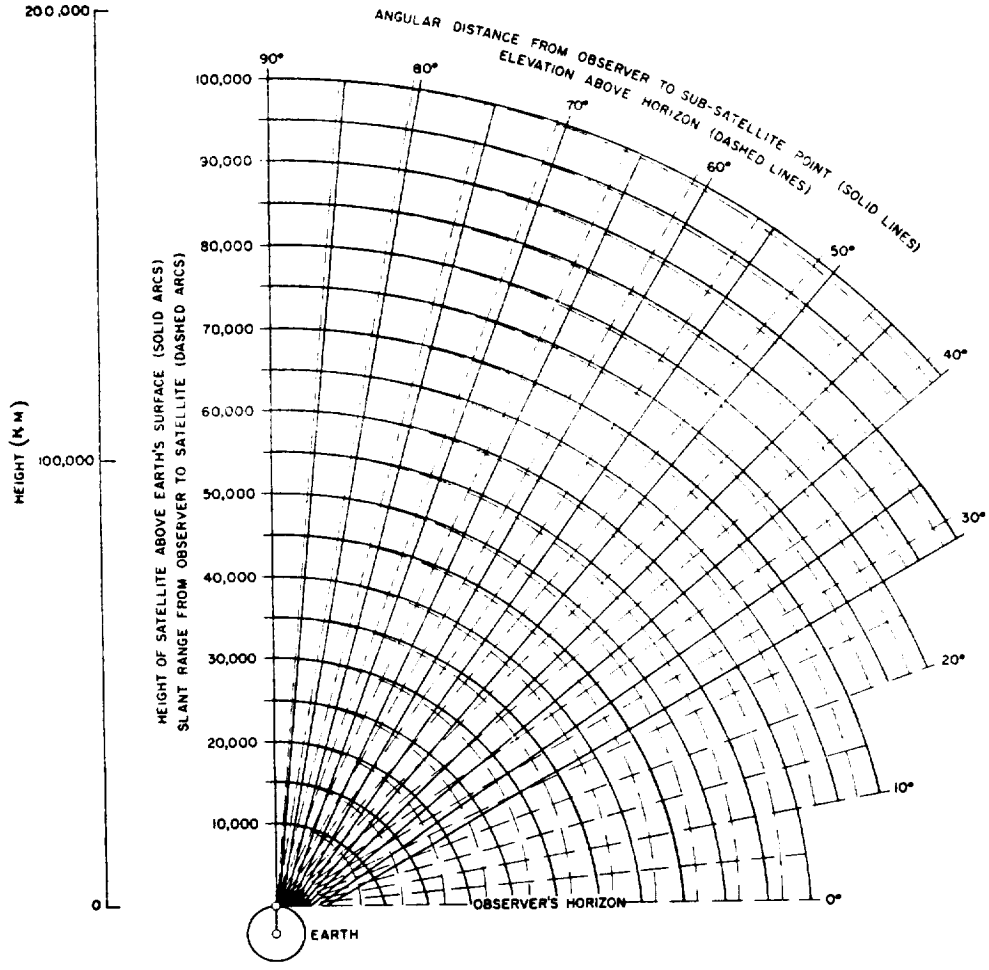

Fig. 55. Chart for Determining Elevation and Slant Range of Satellite (0 to 100,000 naut mi, 185,000 km)

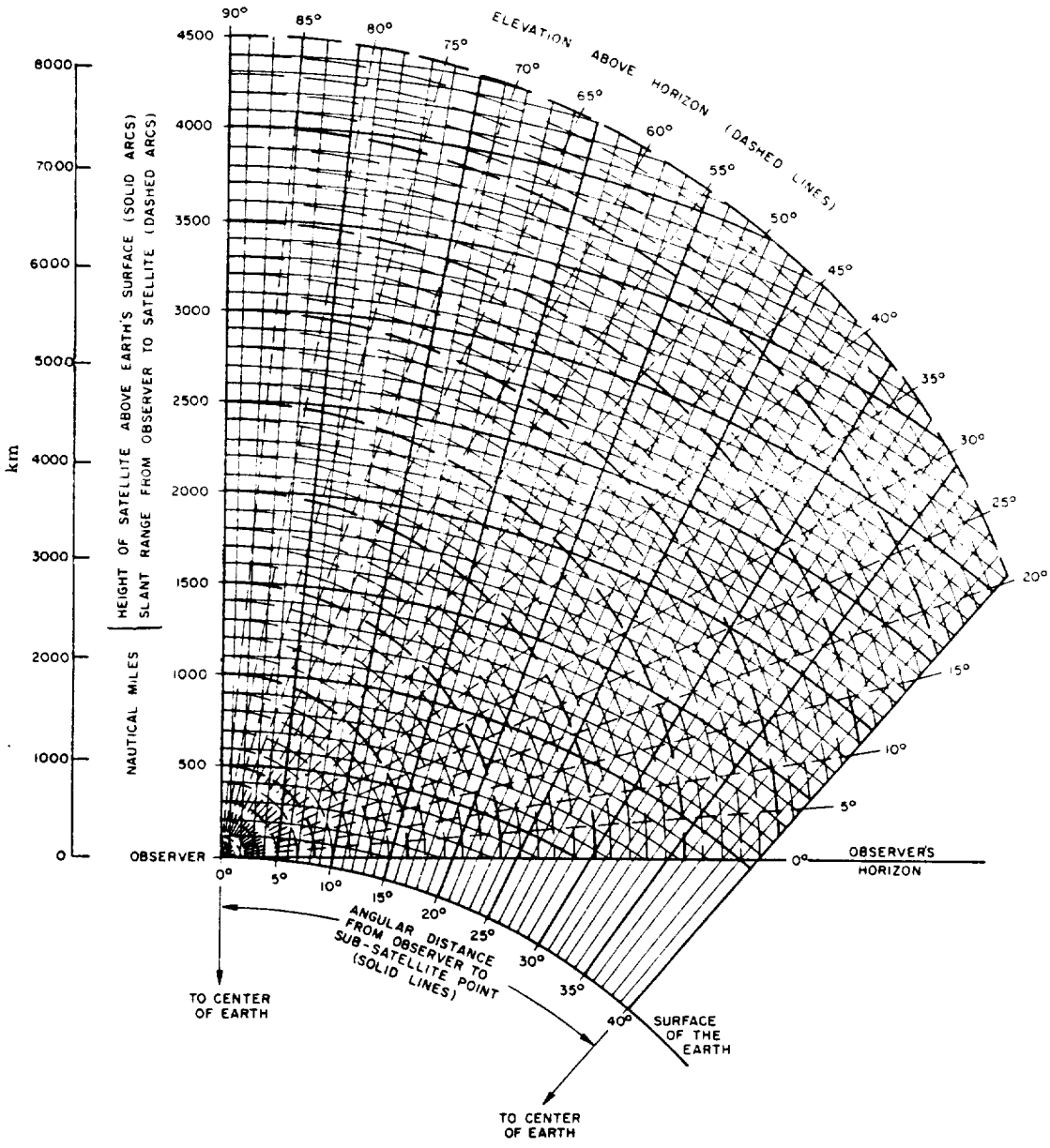

Fig. 56. Chart for Determining Elevation and Slant Range of Satellite (0 to 4500 naut mi, 8150 km)

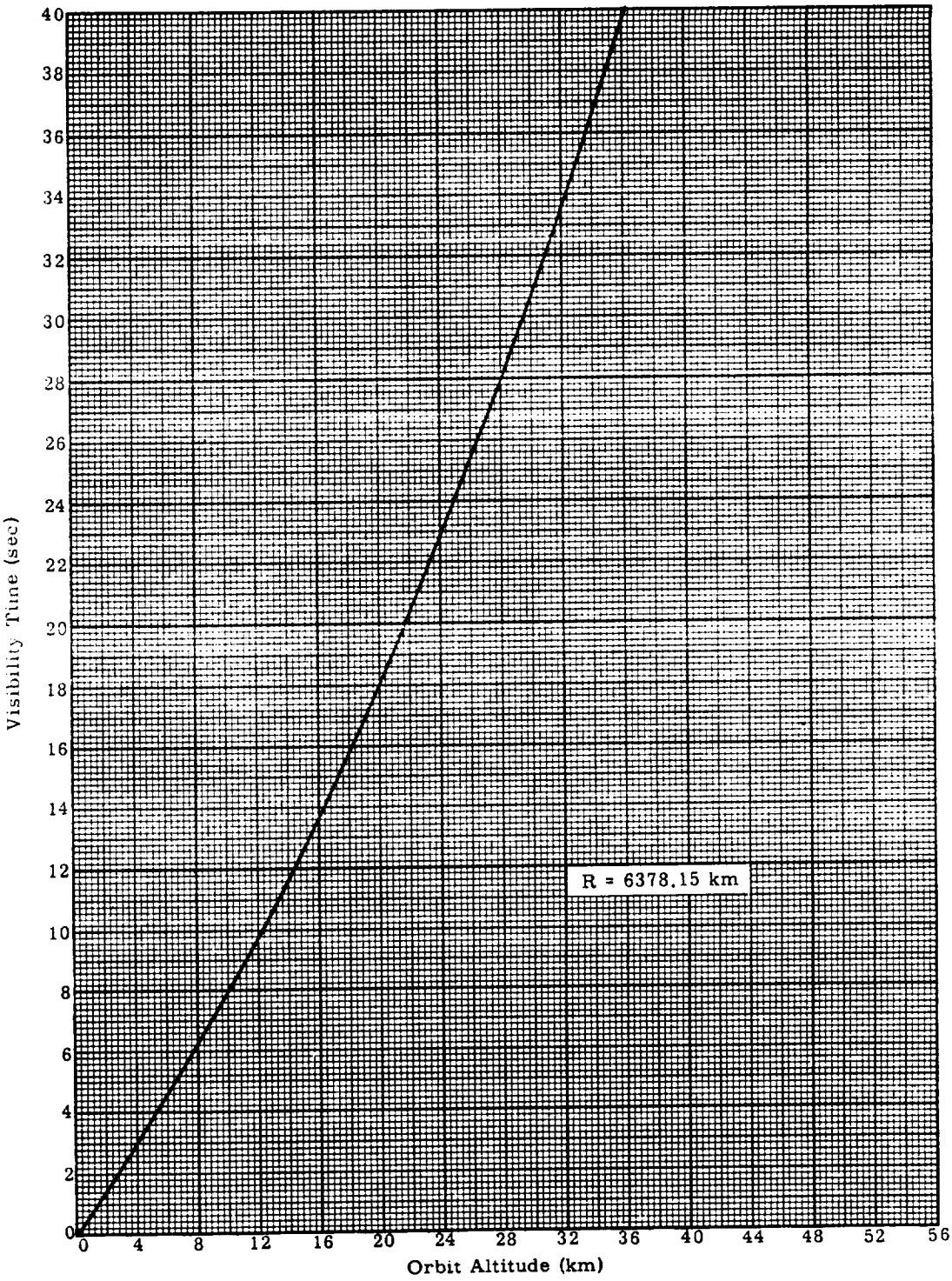

Fig. 57. Visibility Time for Circular Orbits (nonrotating earth)

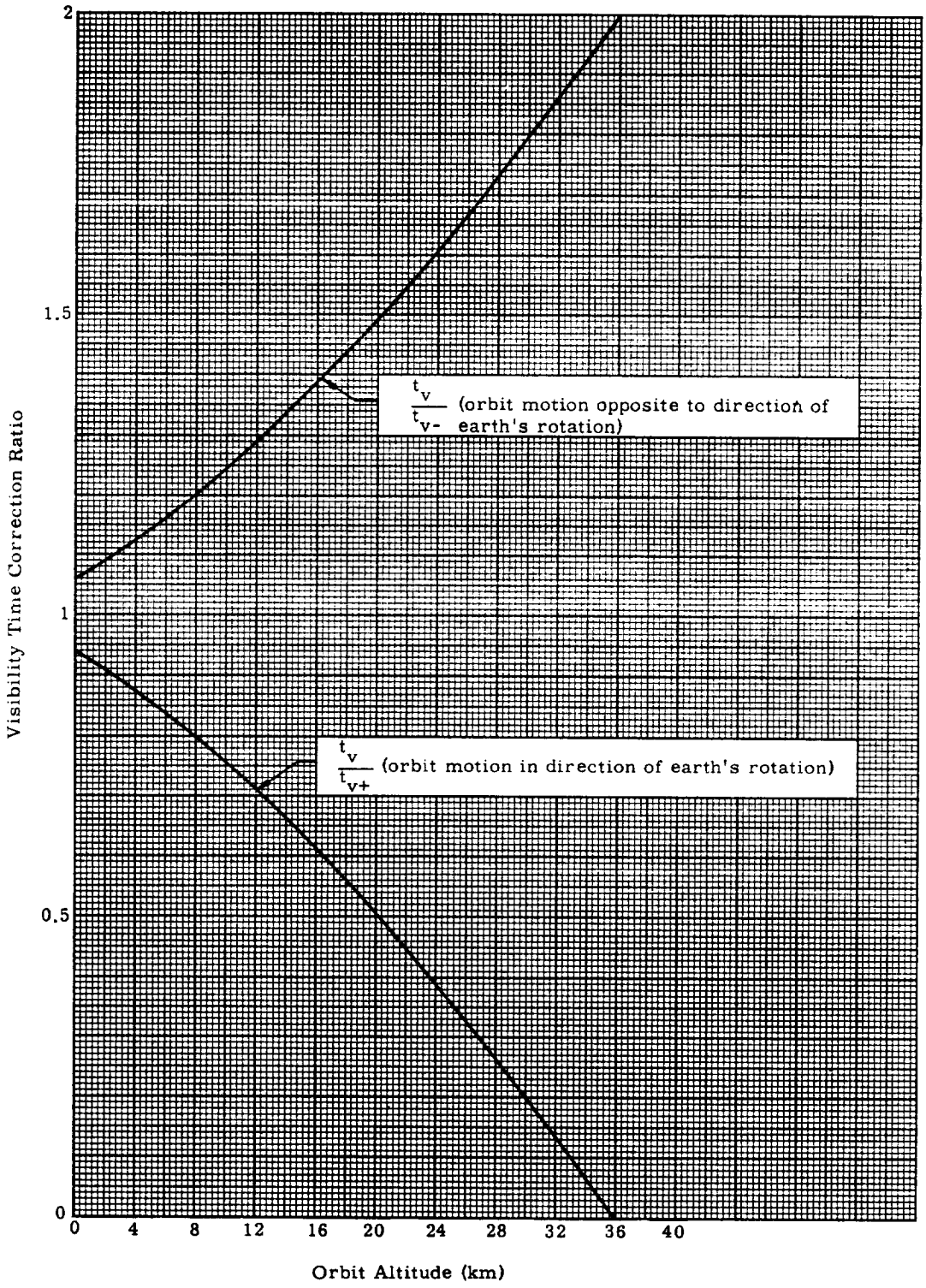

Fig. 58. Effect of Earth Rotation of Visibility Time (circular orbits)

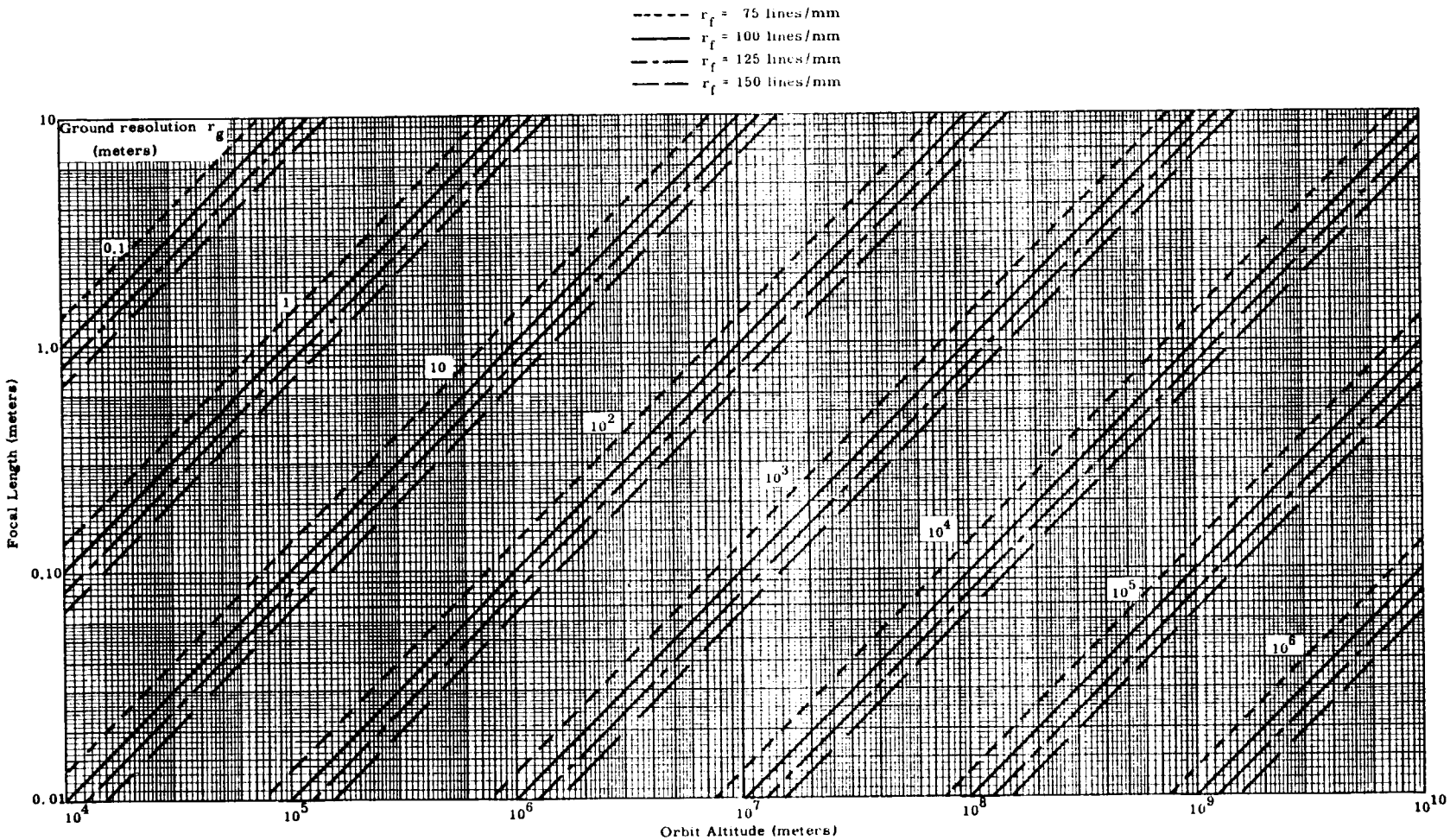

Fig. 59. Maximum Orbit Altitude as a Function of Ground Resolution Desired, Focal Length and System Resolution

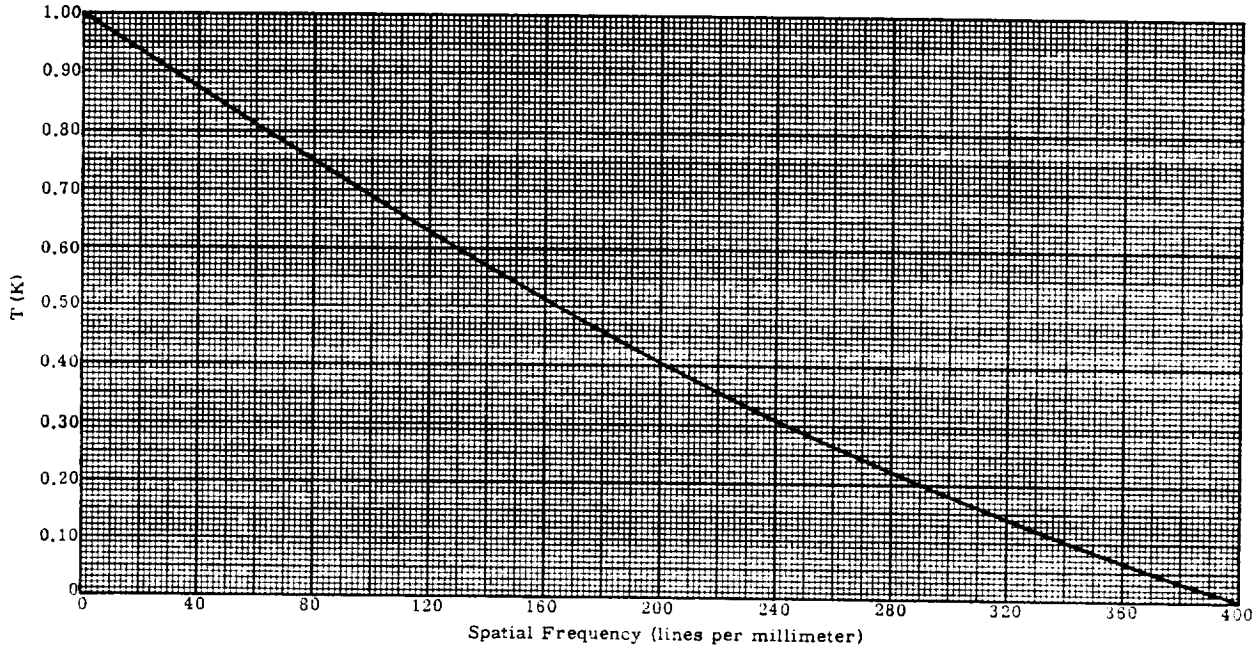

Fig. 60. Transfer Function (scene-lens combination)

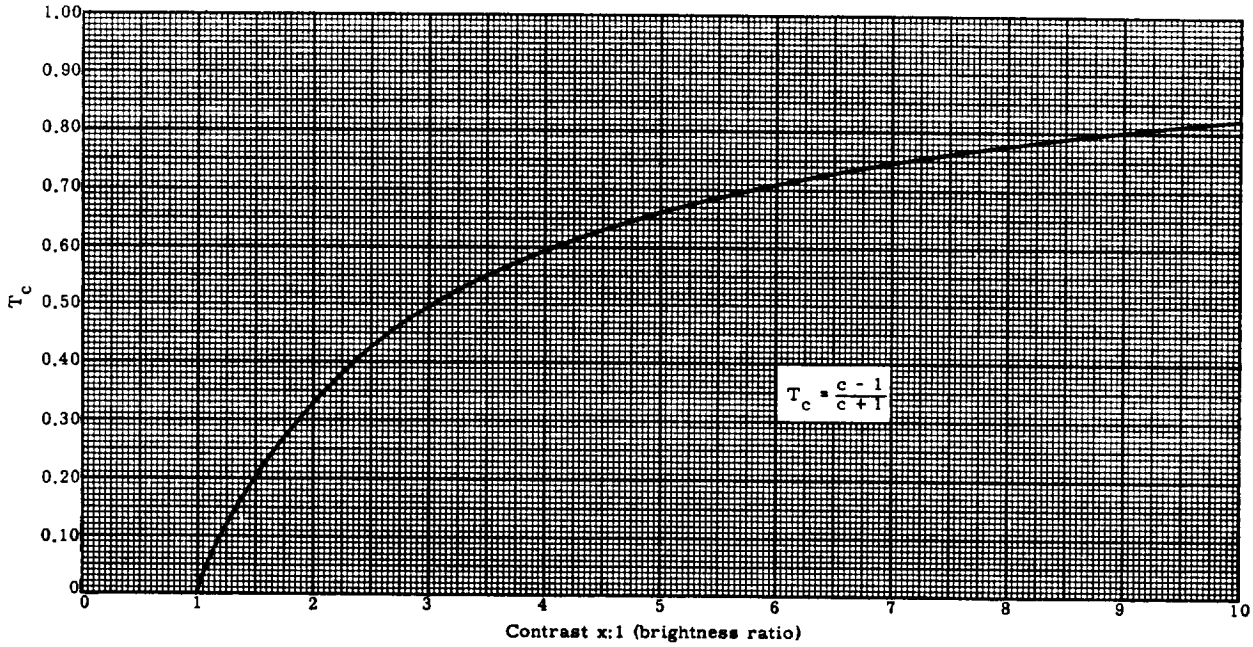

Fig. 61. Transfer Function of Scene Contrast

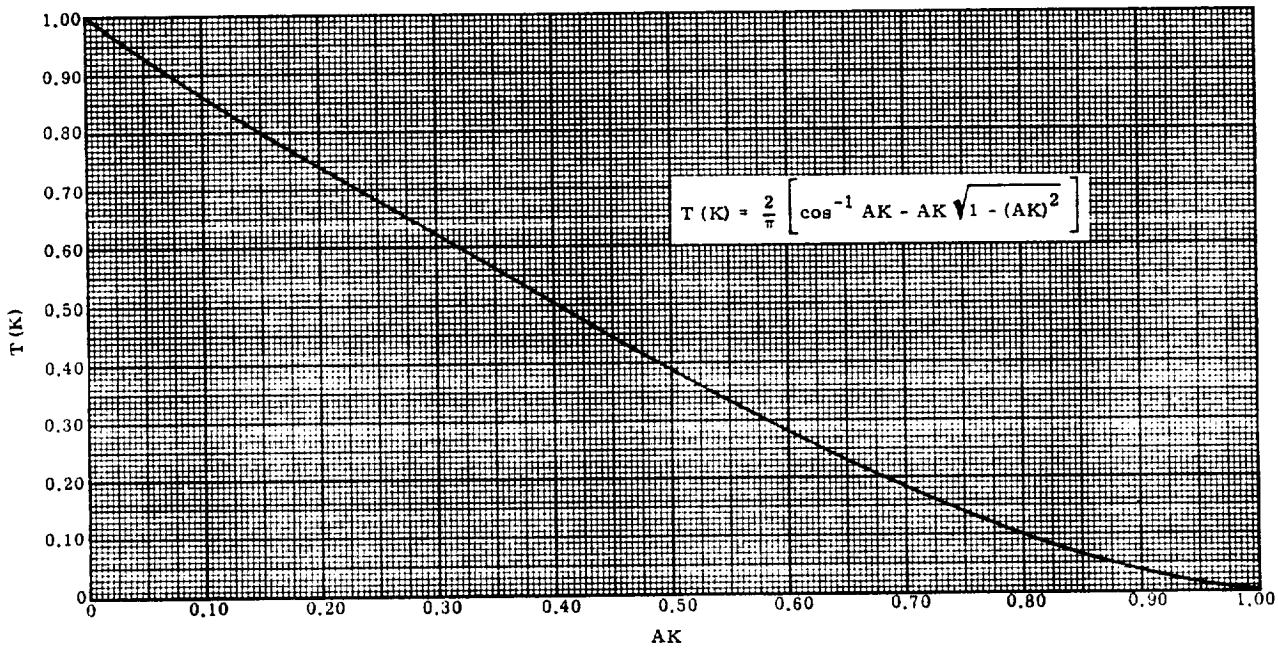

Fig. 62. Diffraction Limited Lens

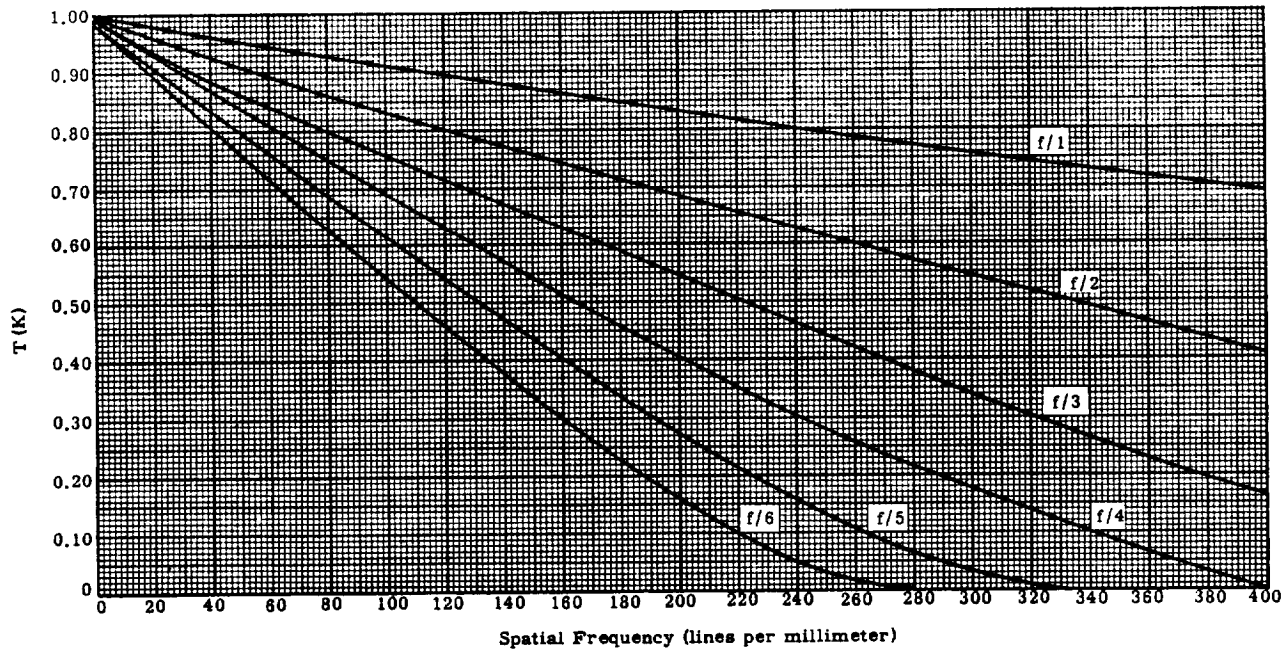

Fig. 63. Transfer Function of Diffraction Limited Lens

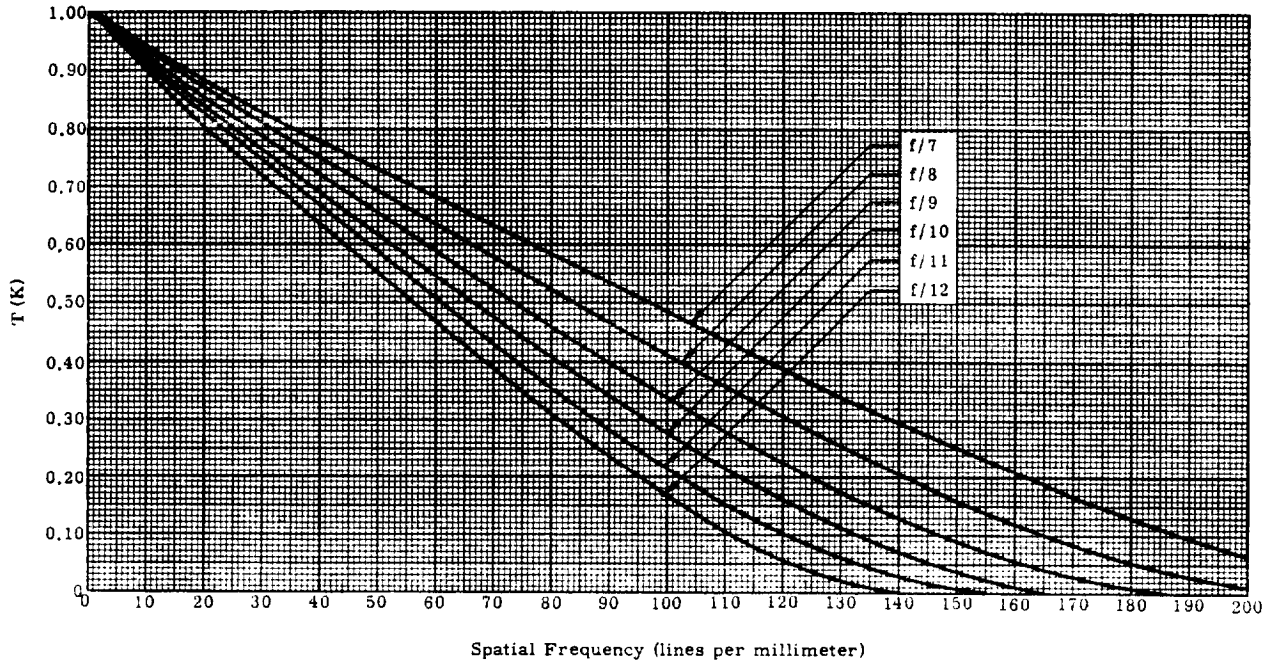

Fig. 64. Transfer Function of Diffraction Limited Lens

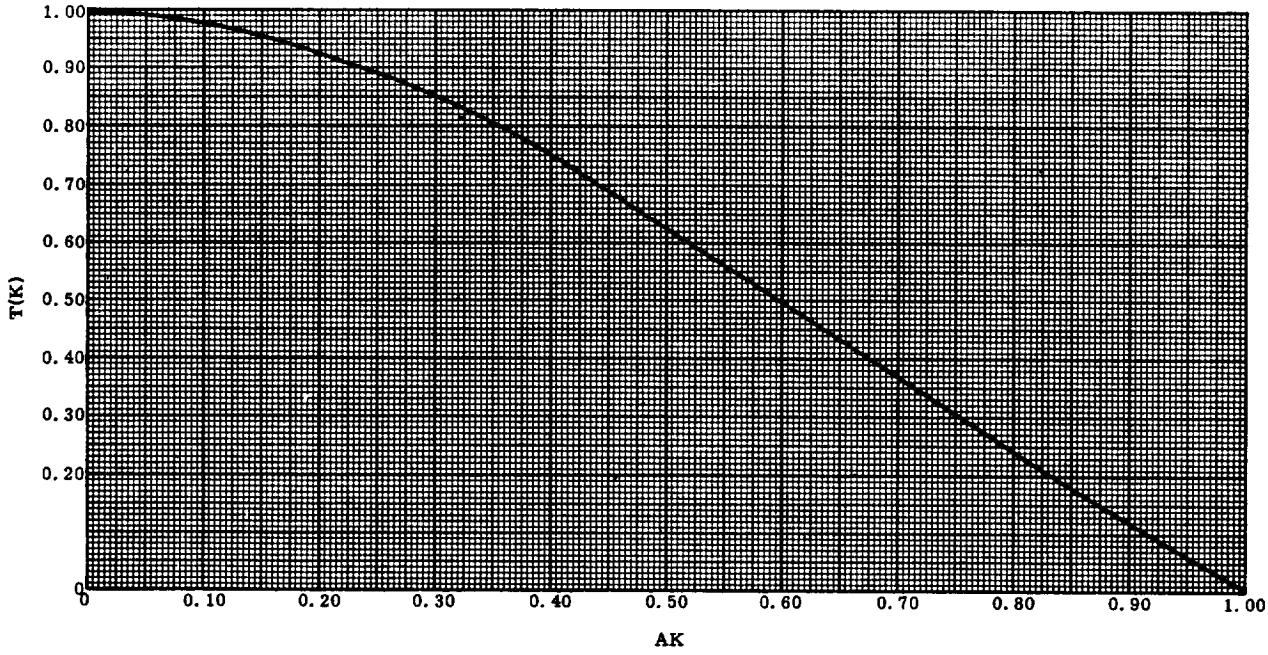

Fig. 65. Transfer Function for Linear Motion

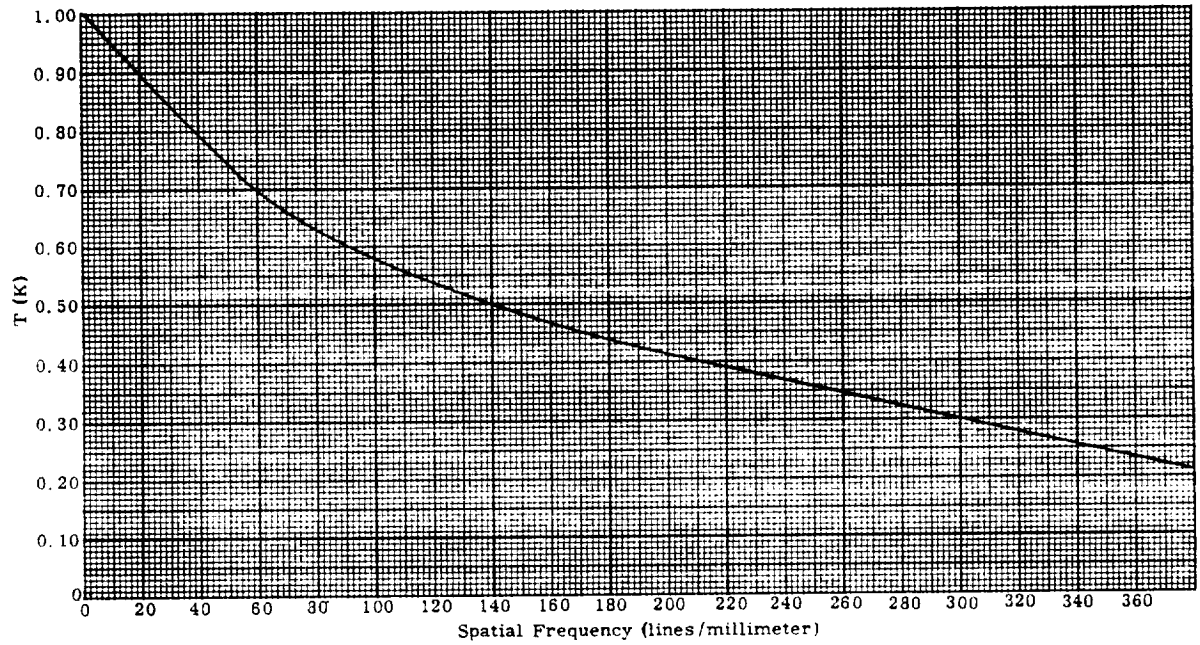

Fig. 66. Typical Photographic Film Transfer Function

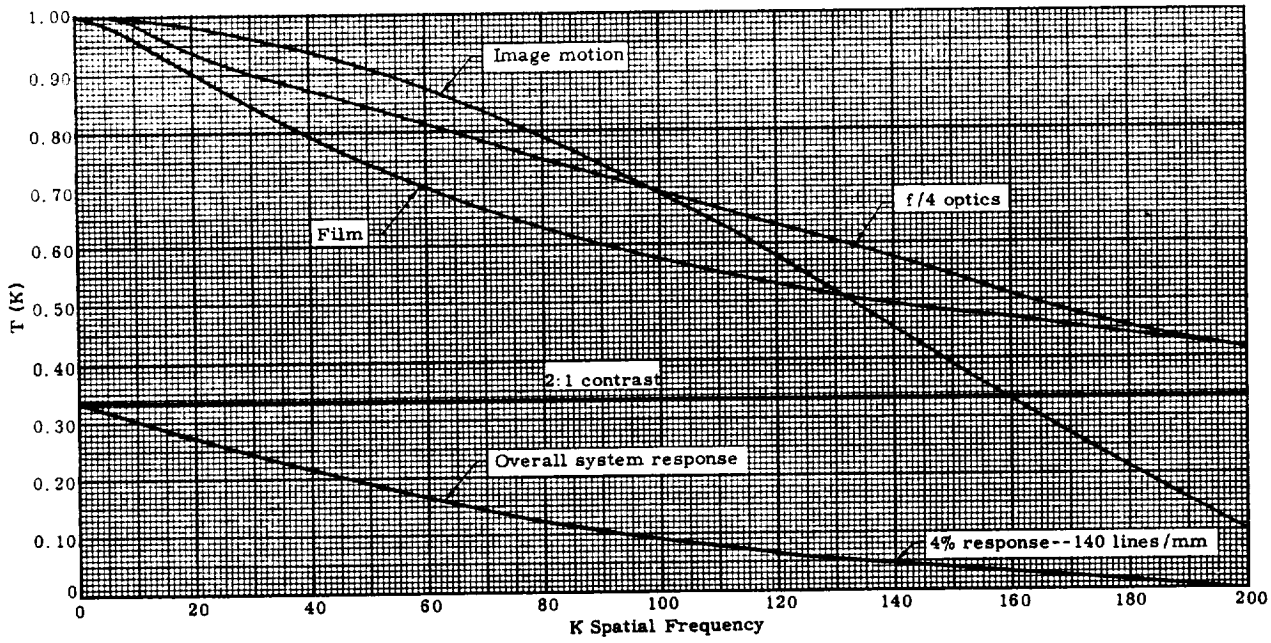

Fig. 67. Illustrative Example

APPENDIX A

GLOSSARY (REF. 1)

A

Aberration: apparent displacement of a body from its actual position due to the observer's motion, the object's motion and the finite speed of light.

Aberration, planetary: aberration including effects of the object's motion as well as the observer's motion during the time light travels from the object to the observer.

Aberration, stellar: aberration including only the effect of the earth's motion around the sun, mean value 29.9 km/sec.

Ablation: the gradual removal or erosion of an exposed surface of an object resulting from its high speed passage through a resistive medium.

Abort: the termination of a space mission after an emergency forces return to earth.

Albedo: fraction of total incident light reflected by a body.

Albedo, average geometric: ratio between the average brightness of the object to the brightness of a white screen of the same size normal to the incident light (lunar albedo 0.105).

Albedo, spherical: ratio of the light scattered in all directions by the object to the total incident light (lunar albedo = 0.073).

Almucantar: a parallel to the horizon.

Altitude (also elevation): a topocentric coordinate in the horizon system; the angular distance of an object above the horizon, measured on a vertical circle. Also synonymous with the height of an object above some surface.

Analytical integration: the specification of an explicit closed algebraic or series relation to represent the integral of a given function.

Angular momentum: the quantity $m\vec{r} \times \dot{\vec{r}}$ ($= r^2 \dot{\theta}$ in polar coordinates) constant for conic motion.

Anomaly: or angle; see true anomaly, mean anomaly, and eccentric anomaly.

Aphelion: the point on a heliocentric ellipse farthest from the sun.

Apocynthion (also aposelene or apolune): the point on a selenocentric elliptic orbit farthest from the moon's center.

Apofocus: the apsis on an elliptic orbit farthest from the principal focus or center of force.

Apogee: the point on a geocentric elliptical orbit farthest from the earth's center.

Apsis (plural, apsides): the point on a conic where the radius vector is a maximum or minimum. The line of apsides is the major axis extended indefinitely.

Argument of latitude: the angle in the orbit from the ascending node to the object in the direction of motion; the sum of the argument of perifocus and the true anomaly.

Argument of perifocus: the angular distance measured in the orbit plane in the direction of motion from the lines of nodes to line of apsides.

Aries: an astronomical constellation; a portion of the celestial sphere which contained the vernal equinox.

Aries, first line of: the direction of the vernal equinox (the name is a carryover from a time that the vernal equinox was in the constellation Aries).

Aspect: angular position of a body relative to its line of advance in orbit.

Astrodynamics: the engineering or practical application of celestial mechanics and other allied fields such as high altitude aerodynamics; geophysics; attitude dynamics; and electromagnetic, optimization, observation, navigation, and propulsion theory, to the contemporary problems of space vehicles. Astrodynamics is sometimes also meant to include the study of natural objects such as comets, meteorites and planets.

Astronomical unit (AU): the mean distance or semimajor axis of the orbit of a fictitious unperturbed planet having the mass (0.000,002,819 solar masses) and sidereal period (365.256,383,5 mean solar days) that Gauss adopted for the earth in his original determination of the gravitational constant K_s (= 0.017,202,089,95). Approximately equal to 92,914,000 statute miles or 149,530,000 km.

Azimuth: a topocentric coordinate measured in the plane of the horizon from the north (or south) point on the horizon clockwise to the object.

B

Ballistic trajectory (also coast trajectory or free-flight trajectory): motion of the space vehicle without rocket burning or thrust forces.

Barker's equation: an equation that relates position to time for an object traveling in a parabolic orbit.

Barycenter: center of mass of a system of masses.

Base altitudes: reference altitudes or levels of the atmosphere between which the atmospheric temperature gradient is assumed to be a constant.

Boltzmann's constant: the ratio of the mean total energy of a molecule to its absolute temperature. Its value is 1.380×10^{-23} joule/°K.

Braking: the deceleration of a space vehicle by rocket thrust or by atmospheric drag.

Braking ellipses: a series of ellipses whose semi-major axes decrease due to the atmosphere of a planet when a vehicle attempts a landing on that planet.

Burnout: end of rocket burning for a particular rocket engine in a given stage of the rocket.

C

Call-down frequency: the frequency with which a vehicle can be recalled from orbit and landed at a specific site.

Cartesian coordinate system: a set of (usually three) mutually orthogonal straight coordinate axes which form a right-handed coordinate system.

Celestial equator: the great circle in which the plane of the terrestrial equator intersects the celestial sphere. The north celestial pole is the point of intersection of the earth's spin vector with the celestial sphere.

Celestial sphere: a hypothetical sphere of infinite dimensions, centered at the observer (or center of the earth or sun, etc.), on the inner surface of which the celestial bodies are projected and appear to move. This sphere is fixed in space, and thus, because of the earth's rotation, appears to rotate from east to west.

Centrifugal force: a fictitious position-dependent force that apparently arises when the motion of an object is observed with respect to a rotating coordinate system. The relationship yielding this "force" is $-m\vec{\omega} \times (\vec{\omega} \times \vec{r})$, where m is the mass of the object and $\vec{\omega}$ is the angular velocity vector of the rotating coordinate system.

Characteristic velocity: the sum of all absolute velocity changes required of a vehicle for a particular space flight (a measure of the total energy requirement for a flight).

Circle, galactic: fundamental plane of the galactic reference system (north pole at $12^h\ 44^m$ right ascension and +27° declination), inclined 62° to the celestial equator.

Circle, hour: secondary circles of the equatorial coordinate system, i.e., planes normal to the celestial equator.

Circle, secondary: great circles (or planes through the origin) which pass through the poles of a given coordinate system.

Circle, vertical: intersections of the celestial sphere by vertical planes in a horizontal coordinate system.

Circumlunar trajectory: a trajectory from the vicinity of the earth which passes behind the moon and returns ballistically to the vicinity of the earth.

Cislunar space: the region of space around the earth and moon, usually taken as being synonymous with the sphere of influence of the earth-moon system.

Collision parameter: the offset distance between the extension of a velocity vector of an object at a great distance from a center of attraction or repulsion and this center.

Colure, equinoctial: the plane, secondary to the equator, which passes through both the celestial poles and the equinoxes.

Colure, solstitial: the plane, secondary to the equator, which passes through both the celestial poles and the solstices.

Conjunction: a point in the orbit of a planet (or moon) where its celestial longitude equals that of the sun. If the alignment is sun-planet-earth, the planet is said to be in "inferior conjunction." This configuration is possible only with inferior planets; if it is planet-sun-earth, the planet is in "superior conjunction." Similarly, when the moon (or a superior planet) is between the earth and the sun, i.e., "new," it is said to be at conjunction.

Coordinate systems: one of a number of sets of celestial coordinate systems used in astronautics (Chapter XI).

(1) Ecliptic System uses the plane of the earth's orbit (ecliptic) as the reference. The axis of the poles of the ecliptic is at right angles to this plane. This system is most useful for intrasolar system work since all the planets move in or near the plane of the ecliptic.

(2) Equatorial System uses the celestial equator as the reference plane. The celestial equator and celestial poles coincide with extensions of the earth's equator and poles on the celestial sphere. This system is the one most commonly used in astronomy.

(3) Horizon System uses the observed horizon as the reference plane and is the common system of celestial navigation.

Coriolis force: a fictitious velocity dependent force that apparently arises when the motion of an object is reckoned with respect to a rotating coordinate system. The relationship yielding this "force" is $-2m\vec{\omega} \times \dot{\vec{r}}_r$, where m is the mass of the object, $\vec{\omega}$ is the angular velocity vector of the rotating coordinate system, and $\dot{\vec{r}}_r$ is the velocity of the object reckoned with respect to the rotating system.

Cosmic dust: fine dust particles (micrometeorites) that are concentrated in the solar system in the plane of the ecliptic (e.g., giving rise to the phenomenon of "zodiacal light") and also dispersed in a more rarefied manner in interstellar space, being more concentrated in the galactic spiral arms; also a component of comets.

Cosmic rays (direct): high-energy charged particles (e.g., with energies in excess of 100 Mev) such as protons, alpha particles and heavy nuclei which have apparently been ejected by stars and accelerated by vast magnetic fields in interstellar space.

Cosmoparticle: discrete material entities of submeteoritic mass, either in or from space. They may be "free" or individual molecules or atoms, or molecular or atomic constituents of any kind, e.g., ions, atomic nuclei, protons, neutrons, electrons, positrons, etc.

Cross product: or vector product (denoted by $\vec{A} \times \vec{B}$) of two typical vector quantities $\vec{A}$ and $\vec{B}$ can be defined either as a vector mutually perpendicular to both $\vec{A}$ and $\vec{B}$ with magnitude A B sin (A, B) or equivalently as

$$(A_yB_z - A_zB_y)\,I + (A_zB_x - A_xB_z)\,J + (A_xB_y - A_yB_x)\,K$$

where the subscripts denote the components of the vectors on the three orthogonal axes denoted by the unit vectors I, J, K.

Culmination: The time at which a heavenly body reaches the meridian of an observer. Upper culmination occurs near zenith, lower culmination near nadir.

D

Day, sidereal: the period of one rotation of the earth relative to inertial space (the stars), $23^h\ 56^m\ 04^s.090$ mean solar time.

Day, solar: the time between two successive upper (or lower) culminations of the sun, $24^h\ 03^m\ 56^s.556$ sidereal time.

Declination: the arc of an hour circle (great circles passing through the poles) intercepted between the celestial equator and the object; angular distance north or south of the celestial equator.

Definitive orbit: an orbit that is defined in a highly precise manner with due regard taken for accurate constants and observational data, and precision computational techniques including perturbations.

Differential correction: a method for finding from the observed minus computed (O - C) residuals small corrections which, when applied to the elements or constants, will reduce the deviations from the observed motion to a minimum.

Dip: the angular distance between the true horizontal and the observed horizon for an observer above ground level.

Direct motion: the term applied to eastward or counterclockwise motion of a planet or other object as seen from the North Pole (i.e., in the direction of increasing right ascension). Thus, it is motion on an orbit in which $i \leq 90$ degrees.

Diurnal: daily.

Diurnal motion: the apparent revolution of the heavenly bodies around the earth.

Dot product: or scalar product (denoted by $\vec{A} \cdot \vec{B}$) of two typical vector quantities $\vec{A}$ and $\vec{B}$ can be defined as AB cos (A, B) or equivalently as $A_xB_x + A_yB_y + A_zB_z$ where the subscripts denote the components of the vectors on three orthogonal axes.

Drag: the force occasioned by the passage of an object through a resistive medium acting in a direction opposite to that of the object's motion relative to the medium.

Drag coefficient: the total drag force acting on an object divided by one-half the local atmospheric density, the projected frontal area of the object, and the square of the magnitude of the velocity of the object relative to the resistive medium.

Drift, anomalistic: the variation or drift of a frequency source (e.g., a crystal oscillator) such that the frequency changes due to a variety of causes (e.g., temperature variation, component aging, etc.), none of which can be predicted in advance or completely controlled.

E

Eccentric anomaly: an angle at the center of an ellipse between the line of apsides and the radius of the auxiliary circle (which has radius equal to semimajor axis of ellipse and center at center of ellipse) through a point that has the same x-coordinate as a given point on the ellipse.

Eccentricity: the ratio of the radius vector through a point on a conic to the distance from the point to the directrix.

Eclipse: a name applied to cases where a nonluminous body passes into the shadow of another; eclipse of the sun means the interposition of the moon's disc between the observer and the sun.

Ecliptic: the great circle formed by the intersection of the orbital plane of the earth (the ecliptic plane) and the celestial sphere.

Ecliptic coordinate system: axes with the ecliptic as the fundamental plane and with spherical coordinates: celestial longitude and latitude.

Elements of orbit: any six independent constants defining the orbit, e.g., (1) orientation elements: Ω longitude of ascending node; i inclination of orbit plane; ω argument of perifocus; (2) dimensional elements: e eccentricity; a semimajor axis; (3) time element: T time of perifocus passage.

Elevation, angle of: the angle between the inertial velocity vector $\vec{r}$ and the local horizontal, i.e., the plane normal to $\vec{r}$ passing through the vehicle.

Eliminant: a determinant that is formed when n - 1 linear unknowns are eliminated from a set of n equations. The elimination of x and y, for example, from

$$a_1x + b_1y = c_1$$

$$a_2x + b_2y = c_2$$

$$a_3x + b_3y = c_3$$

yields the eliminant:

$$\begin{vmatrix} a_1 & b_1 & c_1 \\ a_2 & b_2 & c_2 \\ a_3 & b_3 & c_3 \end{vmatrix} = 0$$

Elongation, angle of: the angle between the direction to an object and to the center of the coordinate system reckoned at the observer.

Energy integral: one of the integrals of two-body motion expressing conservation of energy.

Entry angle: the angle between the velocity vector of a space vehicle relative to a resistive medium and the local horizontal.

Ephemeris (plural, ephemerdies): a table of calculated coordinates of an orbject with equidistant dates as arguments.

Ephemeris time (ET): uniform or Newtonian time, defined by mean frequency of rotation of the earth around the sun for the year 1900.

Epoch: arbitrary instant of time for which the elements of an orbit are valid (e.g., initial, injection, or correction time).

Equator, celestial: the great circle in which the plane of the terrestrial equator intersects the celestial sphere.

Equator, terrestrial: the circle in which the plane through the earth's center normal to its axis of rotation (the equatorial plane) intersects the earth's surface.

Equatorial bulge: the excess of the earth's equatorial diameter over the polar diameter (i.e., about 27 miles, 43 km); oblateness.

Equatorial satellite: a satellite whose orbit plane coincides with the earth's equatorial plane.

Equatorial system: rectangular axes referred to the equator as the fundamental plane and having spherical coordinates, right ascension and declination.

Equilateral triangle solutions: a particular solution of the three-body problem in which an object situated at one vertex of an equilateral triangle formed with the sun and a planet has a stable orbit. It was predicted by Lagrange (1772) and amply confirmed in the case of Jupiter. See Trojan asteroids.

Equinox, nutation of: arises from nutation of equator.

Equinox of date: position of equinox at epoch being used in discussion.

Equinox, precession of: arises from precession of equator.

Equinox, true: equals equinox or vernal equinox, q.v., "true" being used to emphasize distinction from mean equinox.

Equinoxes: intersections of the equator and ecliptic, the vernal equinox being the point where the sun crosses the equator going from south to north (descending node of earth's orbit).

Euler's equation: a relation in a parabolic orbit involving two radii vectors, their chord, and the time interval between them; discovered by Euler (1744).

Evection: a large perturbative term in the moon's longitude discovered by Hipparchus, amounting to 1° 15' at maximum.

F

Feasibility orbit: an orbit that can be rapidly and inexpensively computed on the basis of simplifying assumptions (e.g., two-body motion, circular orbit, three-body motion approximated by 2 two-body orbits, etc.) and yields an indication of the general feasibility of a system based upon the orbit without having to carry out a definitive orbit computation.

Free-molecule flow (or free-molecular flow): flow regime in aerodynamics in which molecules emitted from an object, as it passes through a resistive medium, do not affect the flow of oncoming molecules by scattering interactions, i.e., the mean free path of the

emitted molecules is much longer than a characteristic linear dimension of an object.

G

Galactic system: a system based on the center-line of the milky way.

Gaussian gravitational constant, K_s: factor of proportionality in Kepler's third law; the numerical value depending on the units employed. See astronautical unit.

Geocentric: referred to the center of the earth as origin.

Geocentric parallax: see parallax.

Geocentric subvehicle point: the point where the radius vector from the geocenter to a space vehicle intersects the spheroid.

Geodetic subvehicle point: the point where a line through a space vehicle normal to the spheroid intersects the spheroid.

Geoid: the mean sea-level figure of the earth.

Geoidal surface: the mean sea-level surface of the earth; surface of gravitational equipotential.

Geometric meter: the standard meter.

Geopotential meter: a unit of length employed in reckoning geopotential altitude.

Gravitational potential: at a point, the work required to remove unit mass from that point to infinity.

Greenwich meridian: the zero meridian from which geographical longitude is measured (passes through the Greenwich Observatory, England).

Ground trace: a succession of subvehicle points on earth or on any other celestial body.

Ground swath: a region around the ground trace, the boundaries of which are specified by the lateral distance from the ground trace.

Guidance and control system: a system that actively counteracts or overcomes the effects of deviations (from nominal conditions) in order to accomplish the given mission with the desired degree of exactness. Navigational inputs allow the guidance and control system to sense these deviations.

Guidance law: the equations which are mechanized in the guidance and control system.

Guidance law, explicit: the guidance computer in the vehicle predicts and the vehicle is steered along a trajectory which brings it to the desired end conditions.

Guidance law, implicit: the vehicle follows a nominal trajectory while the guidance system is active.

H

Harmonics of the earth's gravitational field: a series representing the gravitational potential of the earth whose terms form a harmonic progression, i.e., include powers of the reciprocal of distance.

Heliocentric: referred to the center of the sun as origin.

Hohmann orbit: an elliptic heliocentric trajectory for interplanetary flight, having tangency to the earth at one apsis and to another planetary orbit (e.g., that of Venus or Mars) at the opposite apsis. More generally stands for any such doubly tangent transfer ellipse.

Horizon, apparent: the horizon formed by the horizontal plane through the position of the observer.

Horizon, rational: the horizon formed by the plane through the center of the earth parallel to the observer's horizon.

Horizon coordinate system: a system of topocentric coordinates either spherical (azimuth and altitude) or rectangular, having as reference plane the celestial horizon, which is perpendicular to the direction of gravity at the observer.

Horizon scanner: an optical device that senses the radiation discontinuity between a planet or lunar surface and the stellar background of space. It can be utilized to establish a "vertical" reference based upon a "visual" horizon (which differs from both the astronomical and geodetic horizon).

Horizontal plane: that plane perpendicular to the direction of gravity at any place.

Hour angle (LHA): angle between the observer's meridian and the hour circle passing through the object, a coordinate in the rotating equator system, positive toward west, 0 to 24 hr.

Hour circle: any one of the great circles that pass through the celestial poles and, therefore, are at right angles to the equator.

I

Inclination i: angle between orbit plane and reference plane (e.g., the equator is the reference plane for geocentric orbits and the ecliptic for heliocentric orbits).

Inertial axes: axes that are not in accelerated or rotational motion.

Injection: the addition of an "instantaneous" incremental velocity vector to the satellite velocity vector at a prescribed time and place to establish a new orbit.

Injection conditions: position and velocity of rocket at the instant when the thrusting of rocket motor ends and the ballistic portion of the trajectory begins.

Intermediate orbit: an orbit tangent to the actual (or disturbed) orbit, having the same coordinates but not velocity at point of tangency.

Inversion: in this context is meant to be synonymous with the numerical solution of a set of linear algebraic equations.

Ionosphere: the ionized portion of the atmosphere above about 60 km.

Isostatic equilibrium: a situation in which the pressure under the earth's surface is the same regardless of whether it is measured under a mountain, valley or ocean, i.e., lower density strata underlie mountains while higher density strata underlie oceans.

J

Jacobi's integral: an integral of the equations of motion in a rotating coordinate system which relates the square of the velocity and the coordinates of an infinitesimal body referred to the rotating coordinate system. The constant of integration associated with Jacobi's integral is known as Jacobi's constant.

Julian date: the number of mean solar days that have elapsed since midnight, January 1, 4713 BC; e.g., the Julian date of January 1, 1960 is 2,436,934, and of February 1, 1965 is 2,438,792, etc.

K

Kepler's planetary laws: (1) every planet moves in an ellipse about the sun with the sun at one focus; (2) every planet moves in such a way that its radius vector sweeps over equal areas in equal intervals of time; (3) the squares of the periods of revolution of two planets are to each other as the cubes of their mean distances from the sun.

K_e^{-1} min: the characteristic time for geocentric orbits, i.e., the time required by hypothetical satellites to move 1 radian in a circular orbit of radius a_e (equatorial earth's radius); equal to 13,447,052 min.

K_s^{-1} day: the characteristic time for heliocentric orbits, i.e., the time required for a planet at 1 astronomical unit to move 1 radian (or 1 a.u.) along its orbit; equal to 58.132,440,87 days.

L

Lagrangian solutions: particular solutions of the three-body problem in which an infinitesimal object moves under the attraction of two finite bodies (e.g., the sun and Jupiter) which revolve in circles around their center of mass and in which the distances from the infinitesimal object to the finite bodies remain constant. See also equilateral triangle solutions and synodic satellites, i.e., the so-called straight line solutions.

Lambert's equation: an equation of the 8th degree expressing the curvature of the apparent path of a body moving around the sun, as seen from the earth: discovered by Lambert (1771).

Latitude, astronomical: the angle between the direction of gravity through a point and the equatorial plane.

Latitude, celestial: the angular distance of an object north (+) or south (-) of the ecliptic plane; a coordinate in the ecliptic system.

Latitude, geocentric: the angle between the equatorial plane and a straight line from the observer to the center of the earth. It differs from astronomical and geodetic latitudes because of the oblateness of the earth, 0° to 90° north or south.

Latitude, geodetic (or geographic latitude): the angle between the plane of the equator and a normal to a reference spheroid. Geodetic and astronomical latitudes differ only because of local deviations in the direction of gravity, 0° to 90° north or south.

Least squares inversion: a solution of a set of overdetermined linear equations such that the sum of the squares of the residuals is a minimum.

Legendre polynomials: the coefficients $P_n(c)$ in the expansion $(1 - 2ch + h^2)^{-1/2} = \sum_{n=0}^{\infty} P_x(c)\, h^n$ where $P_0(c) = 1$, $P_1(c) = 1/2\,(3c^2 - 1)$, $P_3(c) = 1/2\,(5c^3 - 3c)$, or, in general, $(n + 1)\, P_{n+1}(c) - (2n + 1)\, cP_n(c) + nP_{n-1}(c) = 0$.

Libration: (1) apparent or optical and physical tilting and side-to-side movements of the moon that render 18 percent of its surface alternately visible and invisible, (2) long-period orbital motions of the Trojan asteroids around the equilateral triangle points of the three-body Lagrangian solutions, (3) periodic perturbative oscillations in orbital elements.

Lift: the force arising from the passage of a vehicle through a resistive medium when the vehicle presents an asymmetrical form or orientation; which force acts in a direction normal to the object's motion relative to the medium.

Limb: the edge of the visible disk of the sun, moon, planet, etc.

Line of apsides: a line connecting the near to the far apsis, i.e., defines the major or transverse axis.

Line of nodes: the intersection of a reference plane and the orbit plane.

Line-of-sight: the apparent or observed direction of an object.

Longitude, celestial: the angular distance measured along the ecliptic from the vernal equinox eastward to the great circle passing through the object and normal to the ecliptic.

Longitude, ephemeris: analogous to ordinary geographic longitude, but referred to the ephemeris meridian, rather than to the Meridian of Greenwich.

Longitude, geocentric: the angular distance from the foot of the Greenwich meridian, measured along the equator, east or west, to the foot of the meridian through the place.

Longitude of ascending node: the angular distance from the vernal equinox measured eastward in the fundamental plane (ecliptic or equator) to the point of intersection with the orbit plane at the point that the object crosses from south to north.

Longitude of perifocus: sum of the angle in the fundamental plane between the vernal equinox and the line of nodes and the angle in the orbit plane between the line of nodes and the line of apsides, measured in the direction of motion.

Lunar equation: a factor required for reducing observations to the barycenter of the earth/moon system.

Lunar theory: the analytical theory of the motion of the moon. The lunar theories of Delavnay, Hansen, and Hill-Brown are used most frequently today.

Lunar unit (LU): the mean distance from the center of the earth to the center of a fictitious unperturbed moon having the mass and sidereal period of the moon. One lunar unit is approximately equal to 384,747 km or 239,122 statute miles.

Lunicentric: referred to the moon's center as origin; selenocentric.

M

Mach number: the ratio of the speed of a vehicle to the local speed of sound.

Macrometeorites: meteorites that are sufficiently massive to become fallen meteorites (and whose origin appears to be related to that of minor planets).

Magnetic storms: extensive disturbances in the earth's magnetic field.

Magnitude, stellar: a measure of the brightness of a star. A difference of five magnitudes represents a factor of 100 in brightness.

Mean anomaly: the angle through which an object would move at the uniform average angular speed n, measured from perifocus; $M = t\sqrt{\frac{\mu}{a^3}}$.

Mean center of moon (MCP): the point on the lunar surface intersected by the lunar radius that is directed toward the earth's center when the moon is at the mean ascending node and when the node coincides with the mean perigee or the mean apogee. The MCP is a specified distance from the crater Mösting A in the Sinus Medii.

Mean distance: the semimajor axis (it can be considered as an historical term).

Mean equinox of date: a fictitious equinox whose position is that of the vernal equinox at a particular date with the effect of nutation removed.

Mean free path: the path of a molecule when molecules are assumed to be smooth, rigid spheres with no external field of force acting on them; each molecule travels freely on a straight line between impacts with other molecules. The distance traversed between two successive impacts is called the free path and the average value of this distance the mean free path.

Mean solar day: the elapsed time between successive passage of the mean fictitious sun across the observer's meridian, 86,400 mean solar sec, the mean fictitious sun being a fictitious sun that moves along the celestial equator with the mean speed with which the true sun apparently moves along the ecliptic throughout the year.

Meridian: (1) Terrestrial meridians: great circles passing through North and South Poles, e.g., the observer's local meridian passes through his local zenith and the North and South Poles. (2) Celestial meridian: a great circle on the celestial sphere in the plane of the observer's terrestrial meridian.

Meridian, ephemeris: the geographical meridian which lies east of Greenwich by the amount 1.002738 times the difference (ET-UT).

Meridian passage: also called "transit" or "culmination" of a celestial object is marked by its crossing an observer's meridian.

Mesometeorites: intermediate meteorites having characteristic dimension of the order of a fraction of an inch that are stopped by the atmosphere, consumed, and are seen as common "meteors." The origin of these bodies appears to be related to that of comets

Meteor swarms: a large collection of mesometeorites (probably the remains of an "old" comet) that enters the earth's atmosphere and is seen as a swarm of meteors. The term is often applied to the actual collection of mesometeorites on heliocentric orbits in space.

Micrometeorites: very small meteorites (having a characteristic dimension of a few microns) that are stopped by the atmosphere without being consumed in flight or without producing luminous phenomena visible at the earth's surface.

Minor planets (or asteroids): small planets revolving about the sun, estimated to number more than 30,000, with diameters of more than 1 mile. The largest, Ceres, has a diameter of 488 miles.

Molecular scale temperature: the actual temperature of the atmosphere at any given height multiplied by the ratio of the mean molecular weight of the atmosphere at sea level to the mean molecular weight of the atmosphere at the given height.

Month, nodal: the time for one revolution of the moon with respect to either node.

Month, sidereal: the time between two successive arrivals of the moon at a given apparent place on the celestial sphere as indicated by the stars.

Month, synodic: the time for one revolution of the moon with respect to the apparent place of the sun, e.g., the time between conjunctions.

Moon's celestial equator: a great circle on the celestial sphere in the plane of the moon's equator, i.e., in a plane perpendicular to the moon's axis of rotation.

Moon's orbital plane (MOP): the instantaneous orbital plane of the moon around the earth, defined by the moon's geocentric radius and velocity vectors.

N

Nadir: the downward plumb-bob direction, or the point where the downward extension of the direction of a plumb-bob intersects the celestial sphere.

Navigation: the process of determining the position and velocity of a submarine, ship, airplane, or space vehicle by making observations from the vehicle of objects in the environment of the vehicle.

n-body problem: concerned with the gravitational interactions of masses m_i, m_j, i, j = 1, 2,..., n which are assumed homogeneous in spherical layers, under the Newtonian law. If n = 2, one has a two-body problem, while n = 3 is known as the three-body problem.

Newton's laws: Law of gravitation: Every particle of matter in the universe attracts every other particle with a force varying directly as the product of their masses and inversely as the square of the distance between them. Laws of motion: (1) Every particle continues in its state of rest, or of uniform motion in a straight line, unless it is compelled to change that state by a force impressed upon it. (2) The rate of change of momentum is proportional to the force impressed, and takes place in the direction of the straight line in which the force acts. (3) To every action there is an equal and opposite reaction; or the mutual actions of two bodies are always equal and oppositely directed.

Nodal passage, time of: the time T_Ω when an object passes through the node from the southern hemisphere to the northern hemisphere.

Node: the points of intersection of the great circle on the celestial sphere cut by the orbit plane and a reference plane (e.g., the ecliptic or equator reference plane).

Node, ascending: the node in the reference plane through which the body passes from South to North.

Node, descending: the node in the reference plane through which the body passes from North to South.

Node, longitude of ascending: see longitude of ascending node.

Nominal orbit: the true or ideal orbit in which space vehicle is expected to travel.

Normal places: curve formed, when several observations are available very close together in time, by smoothing observed coordinates.

Numerical differentiation: a process that allows for the numerical evaluation of the derivative of quantity, given tabular values of the quantity.

Numerical integration: a process that allows for the numerical evaluation of a definite integral.

Nutation: short period terms in the precession arising from the obliquity, the eccentricity, and the inclination of the moon's orbit and the regression of its nodes (approximately a 19-year period).

O

Obliquity of the ecliptic: the inclination of the ecliptic to the celestial equator; the angle of approximately 23° 27' between the earth's orbital plane and its equator.

Occultation: the interruption of the light from one celestial body by the intervention of another.

Opposition: the position of an object when its celestial longitude is 180° from sun, i.e., opposite to sun. (Configuration possible only with moon and superior planets.)

Orientation angles: the classical orientation elements, i.e., the inclination, longitude of the ascending node, and longitude of perifocus.

Osculating orbit: an orbit tangent to the actual or disturbed trajectory, having the same coordinates and velocity at that instant.

P

Parallactic angle: the angle between the hour circle of and the vertical circle through a body.

Parallactic inequality: a secondary effect on the solar perturbations in the moon's longitude due to the ellipticity of the earth's orbit.

Parallax: (1) Geocentric parallax: the angle at the object subtended by the earth's equatorial radius; applied to objects in the solar system. (2) Heliocentric parallax: the angle at a star, etc., subtended by the radius of the earth's orbit; applied to objects outside the solar system.

Pericynthion: the point on a selenocentric orbit nearest the moon's center.

Perifocus: the point on an orbit nearest the central force.

Perigee: the point on a geocentric orbit nearest the earth's center.

Perihelion: the point on a heliocentric orbit nearest the sun.

Period: the time required for one complete circuit of the orbit.

Period, anomalistic: interval of time from one perifocus passage to the next.

Period, nodal (also draconic): interval of time from one nodal crossing to the next.

Period, sidereal: the time required for the projection of a planet or other body to make a complete circuit of the celestial sphere. This is the true period.

Period, synodic: the time between successive oppositions of a superior planet or successive inferior conjunctions of an inferior planet.

Perturbations: deviations from exact reference motion caused by the gravitational attractions of other bodies or other forces.

General perturbations: A method of calculating the perturbative effects by expanding and integrating in series.

Special perturbations: methods of deriving the disturbed orbit by numerically integrating the rectangular coordinates or the elements.

Piecewise continuous: a function that can be divided into a finite number of pieces such that the function is continuous on the interior of each piece and such that the function approaches a finite limit at the point of connection of one piece with another. In the context of the temperature profile discussion the term is used in a more restricted sense to imply a function that is divided into a finite number or series of connected linear pieces (straight line segments).

Planetocentric: referred to the center of a planet as dynamical center or origin of coordinates.

Planets: bodies in the solar system which move in essentially elliptical paths around the sun (see Kepler's laws).

Inferior planets:	Inner, or terrestrial, planets:
Mercury	Mercury
Venus	Venus
Superior planets:	Earth
Mars	Mars
Asteroids	Asteroids, or minor planets.
Jupiter	
Saturn	
Uranus	Outer, or major, planets:
Neptune	
Pluto	Jupiter
	Saturn
	Uranus
	Neptune
	Pluto

Plasma: a collection of positive and negative ions that has no overall or gross charge.

Polar satellite: a satellite that passes over the north and south poles of the earth, i.e., that has an inclination of 90° with respect to the earth's equator.

Polar distance, ecliptic: complement of the celestial latitude.

Polar distance, north: complement of the declination.

Poles, celestial: the points in which the axis of rotation intersects the celestial sphere.

Poles, ecliptic: the points in which the normal to the ecliptic through the origin intersects the celestial sphere.

Poles, galactic: the points in which the fundamental galactic axis intersects the celestial sphere. The north galactic pole is at $12^h\ 44^m$ right ascension and +27° declination.

Position, apparent: coordinates of a celestial body as seen by an observer at the center of the earth referred to a coordinate system defined by the instantaneous equator, ecliptic, and equinox. The tabulated positions of the sun, moon, and planets in the American Ephemeris and Nautical Almanac are usually apparent positions.

Position, mean: coordinates of a celestial body referred to a coordinate system defined by the mean equator, ecliptic and equinox of date. This means that the periodic effects of nutation have been neglected.

Position, true: coordinates of a celestial body if corrections for planetary aberration are applied to the apparent position. A sequence of true positions as a function of time is known as a geometric ephemeris.

Potential function: see gravitational potential.

Poynting-Robertson effect: the gradual decrease in the orbital semimajor axis and eccentricity of a micrometeorite caused by the re-emission of radiant energy from the micrometeorite. The theory was first announced by Poynting and later improved and brought into conformity with the theory of relativity by Robertson.

Precession of the equinoxes: the slow, 26,000-year period westward motion of the equinoxes (and equator) along the ecliptic, arising from solar and lunar perturbations on the earth's equatorial bulge, which cause the earth's axis to precess.

Predicting a satellite's position: the six elements are the same in number as the three coordinates of position and the three components of velocity required to specify the launching conditions completely.

Primary: the body having the strongest gravitational field (most ponderous mass) in a system of bodies revolving about their common center of gravity. (Sun is the solar system's primary, earth is earth-moon system primary, etc.)

Prime meridian: the meridian defining 0° and 180° E or 180° W longitude. On earth the Greenwich meridian is the prime meridian.

R

Radiation pressure: the pressure acting on a surface exposed to incident electromagnetic radiation caused by the momentum transferred to the surface by the absorption and reflection of the radiation.

Ratios of the triangles: in the orbit determination methods of Gauss, Olbers, et al., the ratios of the triangles formed by the radii and the chords are assumed in a first approximation to be ratios of the sectors, which are the ratios of the corresponding time intervals by Kepler's second law.

Rectilinear orbit: a trajectory for which perifocus distance is zero and eccentricity is one.

Red shift, gravitational: an effect predicted by the General Theory of Relativity in which the frequency of light emitted by atoms in stellar atmospheres is decreased by a factor proportional to the (mass/radius) quotient of the star: confirmed observationally by the spectra of white dwarfs.

Re-entry: portion of a trajectory in the atmosphere of a planet; in the case of the earth it is usually taken as the portion below 400,000 ft or 122 km.

Re-entry corridor: all possible re-entry trajectories which do not produce excessive aerodynamic heating or deceleration.

Reduction to orbit: quantity added to celestial heliocentric longitude to give true longitude, q.v.

Reference ellipsoid (or spheroid): oblate spheroid closely approximating the geoid.

Reference orbit: an orbit, usually but not exclusively the best two-body orbit available, on the basis of which the perturbations are computed.

Refractive index (of a medium): the ratio of the speed of light in a vacuum to that in the medium, hence it is a measure of how greatly electromagnetic radiation rays are bent during their transit through a medium such as the earth's atmosphere.

Regression of the moon's nodes: the movement of the nodes of the moon's orbit westward along the ecliptic, due to solar perturbations, with period $\simeq$ 19 years.

Relativity effects: effects on a space vehicle trajectory and on time measurement arising by use of Einstein's special theory of relativity or of Einstein's general theory of relativity instead of the customary Newtonian mechanics for determining the trajectory. The fundamentals of these theories of relativity are discussed in Chapter IV of the Lunar Flight Handbook. Relativity effects are small in the weak gravitational field of the solar system if the space vehicle velocity is small compared to the speed of light. There are many such effects, the most prominent of which are: the time dilation predicted from the Lorentz transformation of special relativity; the time dilation, secular advance of perigee, and red-shift of spectral lines predicted by general relativity.

Rendezvous: the approach and contact of two vehicles in space.

Representation: the computation of the position of a space vehicle given the orbital elements and the time.

Residuals (O - C): differences between the observed and computed coordinates in the sense observed minus computed.

Residuals (O - 1): differences between the precomputed ideal observational data and the actual observed data on, for example, an interplanetary voyage.

Restricted n-body problem: the motion of n masses under their mutual gravitational attraction, but with one of the n masses having negligible mass and hence not influencing the motion of the other (n - 1) masses. This term is usually applied to n = 3 (see also n-body problem).

Retrograde motion: westward or clockwise motion as seen from the North Pole, i.e., motion in an orbit in which i > 90 degrees (opposite earth's rotation).

Retrorocket: a rocket attached to a space vehicle whose thrust is directed in a general direction against the inertial velocity of the space vehicle.

Reynolds number: the ratio of inertial forces to viscous forces--it is proportional to the Mach number, vehicle diameter, and the density, or, in equivalent terms, proportional to the diameter of the space vehicle in mean free paths and the vehicle speed measured in terms of the average thermal speeds of gas molecules that constitute the oncoming flow.

Right ascension: angular position of an object (e.g., star) measured eastward along the celestial equator from the vernal equinox to the great circle passing through the north celestial pole and the star (hour circle). Right ascension is often expressed in hours, minutes, and seconds ($1^h = 15°$).

S

Scale height: the distance in which an isothermal atmosphere decreases in density from 1 to 1/e.

Secular terms: expressions for perturbations that are proportional to the time.

Selenocentric: referred to the center of the moon; lunicentric.

Selenocentric equatorial coordinates: a right-handed coordinate system centered at the moon with its three axes defined by the vernal equinox, north celestial pole (of the earth), and a direction perpendicular to these two, i.e., an equatorial coordinate system translated to the moon.

Selenographic coordinates: coordinates that are rigidly attached to the moon (as geographic coordinates are attached to the earth) defined by the moon's equator and prime meridian. See mean center of moon.

Semimajor axis: the distance from the center of an ellipse to an apsis; one-half the longest diameter; one of the orbital elements.

Semiminor axis: one-half the shortest diameter of an ellipse.

Semiparameter: semilatus rectum; the perpendicular distance from the conic to the semimajor axis through either focus (not to be confused with the generic term "parameters").

Setting circles: a graduated scale that can be read visually and indicates the direction (e.g., altitude and azimuth or right ascension and declination) in which a telescope is pointed. Ordinarily they are employed to set or point a conventional astronomical telescope in the proper direction to make a given observation.

Sidereal period of a planet: see period, sidereal.

Sidereal time: the hour angle of the vernal equinox. (See Chapter II for conversion of sidereal time to mean solar time).

Sidereal year: time required by the earth to complete one revolution of its orbit; equal to 365.25636 mean solar days.

Slip flow: a flow regime in aerodynamics in which there is some departure from continuum flow and the layer of compressible fluid immediately adjacent to the surface of an object is no longer at rest but has a finite tangential "slipping" velocity.

Solar flares: short-lived areas of brilliance (covering areas of 10 million square miles or so) on the sun's chromosphere that are associated with other solar activity. Often accompanied by bursts of emitted charged corpuscles and electromagnetic radiation. They reach several times normal brightness within one or two minutes and then subside slowly over 15 to 30 minutes.

Solar parallax: the ratio of the earth's equatorial radius to its mean distance from the sun.

Solar time, mean: hour angle of fictitious mean sun increased by 12 hours. (The fictitious mean sun is a fictitious sun moving on the celestial equator with a mean motion of the real sun.) See pages 474 to 476, American Ephemeris and Nautical Almanac for conversion of mean solar time to sidereal time.

Solar wind: those low energy particles, i.e., corpuscular radiation (electrons and protons) emanating from the sun. Typical flux rates are 10^8 to 10^{10} particles per cm^2 per second, and typical energies are 1000 to 100,000 electron volts for the protons and a few electron volts for the electrons.

Solstices: the two times a year when the sun's declination is greatest north or south (about June 22 and December 22).

Space range system: a system or network of observation stations, together with their associated communication links and computational facilities, that are utilized to observe and track space vehicles, e.g., the Pacific Missile Range, the National Space Surveillance System, etc.

Specular reflection: characterized by the relation that the angle of incidence equals the angle of reflection, in contrast to diffuse reflection.

Sphere, celestial: an imaginary reference sphere; generally considered to be of infinite radius, and having its visible representation in the sky.

Spheroid: an oblate ellipsoid which closely approximates the mean sea-level figure of the earth or geoid.

Stability of a point or orbit: a point or orbit is stable if the space vehicle will remain near the point or orbit if given a small displacement and velocity. The point or orbit is unstable if the space vehicle will depart from it rapidly.

Standard atmosphere: a table of atmospheric density as a function of altitude which is accepted as a standard and used as a model to portray a typical average atmospheric density variation.

Standard deviation: the square root of the arithmetic mean of the squares of the deviations from the mean; also called root mean square error and sigma deviation.

Stationary points: points in the apparent path of a planet, etc., against the star background where the object appears to stand still because relative to the observer it is moving only in the line of sight. Such a point occurs when a planet changes its apparent motion from direct to retrograde and vice-versa.

Station error: small, usually negligible, differences between the astronomical and geodetic latitudes, due to certain anomalies (such as a mountain) in the local gravitational field.

Stratosphere: a region in which the temperature remains constant from about 18 km up to a height of 30 to 35 km.

Surface-circular satellite: a hypothetical satellite on a circular orbit about the earth having a semimajor axis equal to the earth's equatorial radius. Hence, such a satellite would "skim the surface of the earth" as it revolved on its orbit.

Synodic satellite: a hypothetical satellite, situated 0.84 of the distance to the moon on a line joining the centers of the earth and moon and having the same period of revolution as the moon, according to the Lagrangian "straight line solution" of the three-body problem.

T

Terminator: the boundary between the illuminated and dark sides of a planet or satellite. Usually one distinguishes between a morning and an evening terminator.

Three-body problem: the problem of integrating the equations of motion of three bodies (e.g., sun-moon-earth) moving under their mutual gravitational attractions: directly soluble only in particular cases. See Lagrangian solutions.

Thrust: the force exerted on a vehicle, by the discharge of a gas or propellant, in accordance with the conservation of linear momentum.

Time, ephemeris: time reckoning based upon "constant" frequency rather than frequency of earth's rotation. The current difference between ephemeris and universal time is about 35 seconds.

Time dilation: the apparent slowing-down of moving clocks. This effect arises from the special and general theory of relativity.

Time of perifocal passage: the time when a space vehicle traveling upon an orbit passes by the nearer apsis or perifocal point.

Topocentric: referred to the position of the observer on the surface of the earth, as origin.

Topocentric parallax: the difference between the geocentric and topocentric positions of a satellite.

Topocentric equatorial coordinates: a right-handed coordinate system centered at the observer with its three axes defined by the vernal equinox, north celestial pole, and a direction perpendicular to these two, i.e., an equatorial coordinate system translated to the topos.

Tracking: the process of determining the position and velocity of a celestial body by making observations from earth by optical or electromagnetic means.

Trajectory sensitivities: the partial derivatives of dependent trajectory variables with respect to independent trajectory variables.

Transitional flow: a flow regime in aerodynamics between the free-molecule flow and slip-flow regimes in which the molecules emitted from the surface of an object affect the flow of oncoming molecules, i.e., in which the mean free path of the emitted molecules becomes comparable to a characteristic linear dimension of an object.

Transearth trajectory: trajectory from the vicinity of the moon to the vicinity of the earth.

Translunar trajectory: trajectory from the vicinity of the earth to the vicinity of the moon.

Transverse axis: the distance between the apsides --identical to the semimajor axis for elliptical orbits.

Triaxial ellipsoid: a solid aspherical figure which when cut or sectioned in three (orthogonal, normal or mutually perpendicular) directions exhibits three elliptical cross sections of differing semimajor axes and eccentricities.

Tropopause: the height (varying from about 9 km over the poles to 18 km over the equator) where the gradual decrease in temperature with elevation above sea level ceases.

True anomaly: the angle about the focus between the perifocus and the radius vector in the direction of the motion.

True equinox of date: the actual position of the equinox including both precession and nutation.

Twenty-four-hour satellite: a satellite whose orbital period is approximately 24 hr. If such a satellite is on circular equatorial orbit, then it will theoretically remain fixed or "stationary" relative to the rotating earth.

Two-body orbit: the motion of a body of negligible mass around a center of attraction.

U

Umbra: the dark central portion of the shadow of a large body such as the earth or moon (used in connection with eclipses). The outer, less dark shadow is known as the penumbra.

Unit vector: a vector whose magnitude or length is unity--utilized to define directions in space.

Universal time (UT): mean solar time referred to the meridian of Greenwich, slightly nonuniform owing to the irregular rotation of the earth.

V

Van Allen radiation belt: two toroidal-shaped zones or belts of charged particles roughly situated in the plane of earth's equator. The inner belt commences at about one-fifth on an earth's radius above the equator and extends out to a little less than one earth's radius. The outer belt is located at about two-and one-half earth radii from the earth at the equator and is about one-earth radius thick. Actually the outer belt has a cross section that is shaped somewhat like a banana and extends north and south of the equatorial plane two earth radii. The northern and southern extremes of the belt's cross section (at about 45 degrees latitude) approach the earth one-half of an earth radius closer than at the equator.

Variant orbits: computed orbits in which one of the initial conditions (or parameters) is varied slightly from those of the nominal trajectory--such orbits are utilized to compute numerical partial derivatives or to determine the effects of errors in launch conditions.

Variation of latitude: small periodic changes in the position of the earth's poles due to a "wobbling" of the axis of rotation about the geometrical axis (the shortest diameter) of the earth.

Vector component: the projection of a vector on a given axis in space, e.g., if it is the X-axis then the component of the vector A on this axis is denoted by A_x.

Vector equation: an equation, whose terms include vectors, that can be resolved into component equations; e.g., $\ddot{\vec{r}} = \frac{-\mu \vec{r}}{r^3}$ actually represents the three component equations:

$$\ddot{x} = -\mu x/r^3$$

$$\ddot{y} = -\mu y/r^3$$

$$\ddot{z} = -\mu z/r^3$$

where $\underline{\ddot{r}}$ has been replaced by its three components $\ddot{x}$, $\ddot{y}$, and $\ddot{z}$ and $\underline{r}$ by its three components x, y, and z.

Velocity, circular: the magnitude of the velocity required of a body at a given point in a gravitational field which will result in the body following a circular orbital path about the center of the field.

Velocity, escape (also parabolic velocity): the minimum magnitude of the velocity required of a body at a given point in a gravitational field which will permit the body to escape from the field.

Velocity, orbital: with respect to the planets, usually the mean magnitude of the velocity in orbit--computed as the total distance traveled in one circuit divided by the period.

Vernal equinox: that point of intersection of the ecliptic and celestial equator where the sun crosses the equator from south to north in its apparent annual motion along the ecliptic.

Vis viva integral: see energy integral.

Voice trajectory program (Volume of Influence Calculated Envelopes): a patched conic lunar mission trajectory program. It uses the analytical solutions of the two-body trajectories to construct a complete trajectory from the vicinity of the earth to the moon and back.

Y

Year: the orbital period of the earth. When unqualified, it refers to the equatorial or to the calendar year, depending on its use.

Year, anomalistic: the time interval between successive passes through perihelion = 365.259,641,34 + 0.000,003,04 T days (T denotes centuries since 1900).

Year, Besselian: a time reckoning in terms of actual rather than calendar years.

Year, calendar: a variable year containing either 365 or 366 days.

Year, equatorial (also tropical or ordinary year, not calendar year): interval between transits of the sun through the moon equator 365.242, 198,79 - 0.000,006,14 T days.

Year, Julian: the year of the Julian calendar = 365.25 days.

Year, sidereal: the period of the earth relative to the stars = 365.256,360,42 + 0.000,000,11 T days.

Z

Zedir technique: the use of two cameras on a satellite whose optical axes are parallel, one of which photographs the sky (zenith) while the other simultaneously photographs the ground (nadir). Upon development and measurement, the photographs can be utilized to find the attitude of the camera's optical axis at the time of photograph.

Zenith: the point where the upward extension of the plumb-bob direction intersects the celestial sphere.

REFERENCE

1. "Flight Performance Handbook for Orbital Operations," Appendix A, Space Technology Laboratories, Inc. (Redondo Beach, California), September 1961.

APPENDIX B

ACKNOWLEDGEMENT

The Martin Company expresses its grateful appreciation to Dr. Helmut G. L. Krause of NASA for his permission to reproduce his study, "On a Consistent System of Astrodynamic Constants." It was formerly published by the George C. Marshall Space Flight Center, Propulsion and Vehicle Engineering Division, Huntsville, Alabama.

1. THE ASTRONOMICAL UNIT AND THE SOLAR PARALLAX

The astronomical unit (A.U.), or the Earth's mean distance from the Sun, is connected with the solar parallax ($\pi_\odot$) by the following relation (with $R_e = 6378.170 \pm 0.020$ km the equatorial radius of the Earth):

$$1 \text{ A.U.} = \frac{R_e}{\sin \pi_\odot} = \frac{R_e}{\pi_\odot'' \sin 1''} = \frac{206264.''806247}{\pi_\odot''} R_e = \frac{1\,315\,592\,000 \pm 4000}{\pi_\odot''} \quad (1)$$

Modern determinations of the solar parallax usually are included between the two values $\pi_\odot = 8.''790 \pm 0.''001$ (H. Spencer Jones, 1941) and $\pi_\odot = 8.''79835 \pm 0.''00039$ (E. Rabe, 1949). The mean value of both determinations, $\pi_\odot = 8.''794 \pm 0.''002$, has been accepted by C. W. Allen (Ref. 1, p. 131) in his book on "Astrophysical Quantities" (1955). Exactly in the middle of these two values are also the recently obtained data of radar echoes from Venus, which have a considerably higher accuracy than previous determinations. Furthermore, agreement of the different radio observatories is also very good, as shown in the following table:

Radio Observatory	Author (Year)	Ref.	Radar Frequency (MC/sec)	Astronomical Unit (km)	Solar Parallax ($R_e = 6378.170$ km)
Millstone (Lincoln Lab., M.I.T.)	Pettengill, Price et. al. (1961)	2	440	149 597 850 ± 400	$8.''79419_1$
Goldstone (J.P.L.)	Victor, Stevens and Muhlemann (1961)	3	2388	149 598 845 ± 250	$8.''79413_2$
Jodrell Bank (U. of Manchester)	Thomson et. al. (1961)		408	149 601 000 ± 5000	$8.''79400_5$
Moorestown (R.C.A.)	Maron et. al. (1961)		---	149 596 000	$8.''79429_9$
U. S. S. R.	Kotelnikov (1961)		700	149 599 500 ± 800	$8.''79409_4$
					$8.''79414_4$

According to Newcomb and de Sitter the semimajor axis of the Earth's orbit around the Sun is given by $a_\oplus = 1.000\,000\,236 \pm 0.000\,000\,004$ A.U. (or approximately 35 km more than 1 A.U.). For practical purposes both distances will be assumed equal to

$$a_\oplus = 149\,598\,700 \pm 400 = 149\,598\,700\ (1 \pm 2.7 \times 10^{-6}) \text{ km} \quad (2)$$

The corresponding solar parallax will be

$$\pi_\odot = \frac{R_e}{a_\oplus \sin 1''} = 206\,264.''806\,247\ \frac{6378.170 \pm 0.020}{149\,598\,700 \pm 400} = 8.''79414 \pm 0.''00005 \quad (3)$$

Taking as best value for the light velocity the value determined by Froome (Ref. 4) in 1958:

$$c = 299\,792.5 \pm 0.1 = 299\,792.5\ (1 \pm 3.3 \times 10^{-7}) \text{ km/sec} \quad (4)$$

the light-time for unit distance (1 A.U.) is therefore

$$\tau = \frac{a_\oplus}{c} = 499.007_5 \pm 0.018 = 499.007_5\ (1 \pm 3.6 \times 10^{-5})\ \text{sec} \qquad (5)$$

2. DEFINITION OF TIME UNITS, MEAN ORBITAL MOTIONS, AND ROTATIONAL ANGULAR VELOCITIES OF EARTH AND MOON

There are three different times which are in use, namely, the Greenwich mean solar time or universal time (U.T.), the Greenwich mean siderial time (G.M.S.T.) and the ephemeris time (E.T.) or Newtonian time. Due to the variable rotation of the Earth, the mean solar time and the mean siderial time do not have a constant rate. The observations are therefore functions of a variable time, while the gravitational theories for the Sun and the planets use a uniform time. The ephemeris time, having a constant rate is defined by the orbital motion of the Earth as given by Newcomb's Tables of the Sun. It is therefore necessary to apply corrections to our practical determinations of time. In addition to the fluctuations and the tidal slowing down of the Earth's rotation, the Moon also shows a real diminution in the angular mean motion which is not given by Brown's lunar theory.

The correction to Newcomb's tabulated tropical mean longitude of the Sun (Ref. 5)

$$L_\odot = 279^\circ\ 41'\ 48.''04 + 129\,602\,768.''13\ T_E + 1.''089\ T_E^2 \qquad (6)$$

is, according to H. Spencer Jones (Ref. 6),

$$\Delta L_\odot = +1.''00 + 2.''97\ T + 1.''23\ T^2 + 0.0748\ B \qquad (7)$$

when the observation times are in U.T. The time T is in Julian centuries of 36525^d counted from 1900 Jan. 0, 12^h U.T. (Greenwich mean noon) and B is the irregular fluctuation in the Moon's mean longitude in arc seconds (time of observation again expressed in U.T.). The Sun's tropical mean longitude, $L_\odot$, increases at the rate of $1''$ in $86400/(0.985\,647\,3354 \times 3600) = 24.349\,48$ sec, so that the correction to universal time, required to obtain ephemeris time is, according to H. Clemence (Ref. 7),

$$\Delta t \equiv t_E - t_U = 24.349\,48\ \Delta L_\odot = +24^s.349 + 72^s.318\ T + 29^s.950\ T^2 + 1.82134\ B \qquad (8)$$

H. Spencer Jones gives for the irregular fluctuation (Ref. 6)

$$B = (L_{\mathfrak{C},\,\text{obs.}} - L_{\mathfrak{C},\,\text{tabular}}) + 10.''71 \sin(140.^\circ0\ T + 240.^\circ7) - 4.''65 - 12.''96\ T - 5.''22\ T^2 \qquad (9)$$

The periodic term is Brown's empirical term in his lunar theory. Therefore the correction to the Moon's mean longitude, as given by Brown's Tables of the Motion of the Moon (Ref. 8), is

$$\Delta L_{\mathfrak{C}} \equiv L_{\mathfrak{C},\,\text{obs.}} - L_{\mathfrak{C},\,\text{tabular}} = +4.''65 + 12.''96\ T + 5.''22\ T^2 + B - 10.''71 \sin(140.^\circ0\ T + 240.^\circ7) \qquad (10)$$

in order to obtain the actual mean longitude determined by observations in U.T. In the time

interval $\Delta t = t_E - t_U$ the Moon's mean longitude increases by (n = 13.176 396 5268 × 3600/86400 = = 0.549 016 522″/sec)

$$\Delta L_t = 0.549\ \Delta t = 13.368\ \Delta L_\odot = +13.''37 + 39.''70\ T + 16.''44\ T^2 + B \tag{11}$$

Therefore the correction to Brown's Tables is

$$\Delta L_\iota - \Delta L_t = -8.''72 - 26.''74\ T - 11.''22\ T^2 - 10.''71 \sin (140°.0\ T + 240°.7) \tag{12}$$

when the observations are in ephemeris time. Brown's theory is now reduced to a gravitational theory with the same measure of time as defined by Newcomb's Tables of the Sun. Clemence's corrected value for the Moon's mean longitude (Ref. 7)

$$L_\iota = 270°\ 26'\ 2.''99 + 1\,732\,564\,379.''31\ T_E - 4.''08\ T_E^2 + 0.''0068\ T_E^3 \tag{13}$$

is used in the American Ephemeris and Nautical Almanac.

By means of equation (6) the tropical year, from mean equinox to mean equinox, thus has the length

$$P_{\text{trop}} = \frac{2\pi}{L'_\odot} = \frac{1\,296\,000'' \times 36\,525^{dE}}{129\,602\,768.''13 + 2.''178\ T} = 365.^{dE}242\,198\,78 - 0.^{dE}000\,006\,138\ T$$

$$= 365^{dE}05^{hE}\,48^{mE}\,45.^{sE}\,9747 - 0.^{sE}\,5303\ T = 31\,556\,925.^{sE}\,9747 - 0.^{sE}\,5303\ T \tag{14}$$

In 1957 the ephemeris second has been adopted as the fundamental invariable unit of time, and it is the fraction 1/31 556 925.9747 of the tropical year for 1900 Jan. 0, 12^h E.T. (Ref. 9)

The basis for all civil time-keeping is the universal time which is non-uniform. In practical life, however, the difference between mean solar time and ephemeris time can be neglected because there is $1^d \approx (1 \pm 10^{-8})^{dE}$. To define universal time Newcomb introduced a fictitious mean Sun which moves with the same constant siderial rate, in the equator, as the mean siderial motion is for the true Sun, affected by aberration (20.″50) in the ecliptic. According to Newcomb, the right ascension of the fictitious mean Sun is (neglecting nutation in right ascension)

$$R_E = 279°\,41'\,27.''54 + 129\,602\,768.''13\ T_E + 1.''394\ T_E^2$$

$$= 18^h\,38^m\,45.^s836 + 8\,640\,184.^s542\ T_E + 0.^s0929\ T_E^2 \tag{15}$$

Defining a point on the equator whose right ascension, measured from the mean equinox of date, is

$$R_U = 18^h\,38^m\,45.^s\,836 + 8\,640\,184.^s\,542\ T_U + 0.^s\,0929\ T_U^2\ , \tag{16}$$

and where R_E differs from R_U by 0.002738 Δt (see equation 8), the Greenwich hour angle

$\tau_{Gr\,(R_U)}$ of the point whose right ascension is R_U [equal to universal time (U.T.) $\pm 12^h$], increased by the right ascension R_U, is the Greenwich hour angle, $\tau_{Gr(\Upsilon)}$, of the mean vernal equinox of date which is Greenwich mean siderial time, Θ_{Gr} . That is,

$$\text{U.T.} \pm 12^h + R_U = \tau_{Gr(R_U)} + R_U = \tau_{Gr\,(\Upsilon)} \equiv \Theta_{Gr} \tag{17}$$

Adding the East longitude to both sides gives the local mean time on the left side of the equation and the local mean siderial time on the right side, because

$$\Theta = \Theta_{Gr} + \lambda_{east.}$$

The time rate of the right ascension, given by differientation of equation (16), is

$$\begin{aligned}
\dot{R}_U &= 8\,640\,184.542 + 0.1858\ T_U \ [\text{sec/Jul. century}] \\
&= 129\,602\,768.13 + 2.788\ T_U \ [''/\text{Jul.century}] \\
&= 3548.330\,4074 + 0.000\,076\,33\ T_U \ [''/\text{d}] \\
&= 0.985\,647\,3354 + 2.1203 \times 10^{-8}\ T_U \ [°/\text{d}],
\end{aligned} \tag{18}$$

Adding to this the time rate of the hour angle, $\dot{\tau} = 360\ °/\text{d} = 1296\,000\ ''/\text{d}$, the time rate of the mean siderial time is then

$$\begin{aligned}
\dot{\Theta}_m &= 1\,299\,548.330\,4074 + 0.000\,076\,33\ T \ [''/\text{d}] \\
&= 360.985\,647\,3354 + 2.1203 \times 10^{-8}\ T \ [°/\text{d}] \\
&= 15.041\,068\,638\,97 + 8.835 \times 10^{-10}\ T \ [''/\text{s or } °/\text{h}] \\
&= 1.002\,737\,909\,265 + 0.5890 \times 10^{-10}\ T \ [\text{d}_*/\text{d or } \text{s}_*/\text{s}] \\
&= 7.292\,115\,854\,58 \times 10^{-5} + 4.283 \times 10^{-15}\ T \ [\text{rad/s}]
\end{aligned} \tag{19}$$

This motion is the result of the spin of the Earth and the motion of the vernal equinox (precession). Because the latter motion takes place in the ecliptic the equatorial component or the general precession in right ascension, m, must be used here. The mean angular velocity of the Earth's rotation is, therefore,

$$\Omega_m = \dot{\Theta}_m - m \tag{20}$$

It is very probable that Newcomb's value for the general precession in longitude, p, must be increased by $\Delta p = +\ 0.''80$ per tropical century (see Part 9), thus

$$\begin{aligned}
p &= 5026.441 + 2.2229\ T + 0.00026\ T^2 \ [''/\text{trop. century}] \\
&= 0.137\,619\,4 + 0.000\,060\,861\ T + 0.712 \times 10^{-8}\ T^2 \ [''/\text{d}] \\
&= 0.000\,038\,227\,61 + 0.000\,000\,016\,906\ T + 1.98 \times 10^{-12}\ T^2 \ [°/\text{d}]
\end{aligned} \tag{21}$$

Neglecting the correction in planetary precession ($\Delta\lambda = 0$) the correction for the general precession in right ascension would be $\Delta m = \Delta p \cdot \cos\epsilon = 0.''80 \times 0.917 = +0.''73$. Thus,

$$m = 4609.236 + 2.7945\ T + 0.000\,12\ T^2\ [''/\text{trop. century}]$$

$$= 0.126\,1967 + 0.000\,076\,511\ T + 0.33 \times 10^{-8}\ T^2\ [''/\text{d}]$$

$$= 0.000\,035\,054\,64 + 0.000\,000\,021\,253\ T + 0.92 \times 10^{-12} T^2\ [^\circ/\text{d}] \qquad (22)$$

The angular velocity of the Earth's rotation is, therefore,

$$\Omega_m = 1\,299\,548.204\,2107 - 0.000\,000\,18\ T\ [''/\text{d}]$$

$$= 360.985\,612\,2808 - 0.0050 \times 10^{-8}\ T\ [^\circ/\text{d}]$$

$$= 15.041\,067\,178\,37 - 0.021 \times 10^{-10}\ T\ [''/\text{s or } ^\circ/\text{h}]$$

$$= 1.002\,737\,811\,891 - 0.0014 \times 10^{-10} T\ [\text{rot/d}]$$

$$= 7.292\,115\,146\,46 \times 10^{-5} - 0.010 \times 10^{-15}\ T\ [\text{rad/s}] \qquad (23)$$

Using equations (19) and (23) the following periods are obtained:

1. Mean solar day (culmination period of the mean Sun)

$$1^d = 1.^d\!\bullet\ 002\,737\,909\,265 + 0.^d\!\bullet\ 589 \times 10^{-10}\ T$$

$$= 86\,636.^s\!\bullet\ 555\,360\,50 + 0.^s\!\bullet 050\,889\,6 \times 10^{-4}\ T$$

$$= 24^h\!\bullet 03^m\!\bullet 56.^s\!\bullet\ 555\,360\,50 + 0.^s\!\bullet\ 050\,889\,6 \times 10^{-4}\ T$$

$$= 1.^{\text{rot}}\ 002\,737\,811\,891 - 0.^{\text{rot}}\ 001\,4 \times 10^{-10}\ T$$

$$= (1 + 10^{-8})^{dE} \qquad (24)$$

2. Mean siderial day or mean equinoctial day (culmination period of the vernal equinox)

$$1^{d}\!\bullet = 1^d - 0.^d 002\,730\,433\,586 - 0.^d 587 \times 10^{-10}\ T$$

$$= 0.^d\ 997\,269\,566\,414 - 0.^d\ 587 \times 10^{-10} T$$

$$= 86164.^s\ 090\,538\,17 - 0.^s\ 050\,716\,8 \times 10^{-4} T$$

$$= 23^h 56^m 04.^s\ 090\,538\,17 - 0.^s\ 050\,716\,8 \times 10^{-4}\ T$$

$$= \frac{\Omega}{\dot{\Theta}} = 1 - \frac{m}{\dot{\Theta}} = (1 - 0.000\,000\,097\,108)^{\text{rot}} - 0.^{\text{rot}}\ 589 \times 10^{-10}\ T$$

$$= 0.^{\text{rot}}\ 999\,999\,902\,892 - 0.^{\text{rot}}\ 589 \times 10^{-10}\ T \qquad (25)$$

3. Period of the Earth's rotation (culmination period of an equatorial star without proper motion)

$$1^{rot} = \frac{\dot{\Theta}}{\Omega} = 1 + \frac{m}{\Omega} = 1^d.000\,000\,097\,108 + 0^d.589 \times 10^{-10}\ T$$

$$= 86400^s.008\,390\,13 + 0^s.050\,889\,6 \times 10^{-4}\ T$$

$$= 1^d - 0^d.002\,730\,336\,743 + 0^d.001\,4 \times 10^{-10}\ T$$

$$= 1^d - 235^s.901\,094\,60 + 0^s.000\,120\,96 \times 10^{-4}\ T$$

$$= 0^d.997\,269\,663\,257 + 0^d.001\,4 \times 10^{-10}\ T$$

$$= 86\,164^s.098\,905\,40 + 0^s.001\,209\,6 \times 10^{-5}\ T \qquad (26)$$

Because

$$1^d - 1^d. = 236^s.555\,360\,50 + 0^s.050\,889\,6 \times 10^{-4}\ T$$

$$= 235^s.909\,461\,83 + 0^s.050\,7168 \times 10^{-4}\ T$$

or

$$1^h - 1^h. = 9^s.856\,473 = 9^s.829\,561$$

the change of mean siderial time against mean solar time is $9^s.856\,47$ in a mean solar hour and $9^s.829\,56$ in a mean siderial hour.

In order to apply Kepler's third law, the siderial mean angular motions of the Earth about the Sun and the Moon about the Earth will be needed. Differentiation of equation (6) gives the tropical mean motion of the Earth:

$$n_\odot\,(\text{trop.}) = \dot{L}_\odot = 129\,602\,768.13 + 2.178\ T\ [''/\text{Jul. century}]$$

$$= 3548.330\,407\,4 + 0.000\,059\,63\ T\ [''/d]$$

$$= 0.985\,647\,335\,4 + 1.6564 \times 10^{-8}\ T\ [°/d] \qquad (27)$$

Subtracting from this the general precession in longitude (equation 21) yields the siderial mean motion of the Earth:

$$n_\odot\,(\text{sid.}) = \dot{L}_\odot - p = 3548.192\,788\,0 - 0.000\,001\,23\ T\ [''/d]$$

$$= 0.985\,609\,1078 - 0.0342 \times 10^{-8}\ T\ [°/d]$$

$$= 0.041\,067\,046\,16 - 0.1424 \times 10^{-10} T\ [''/s]$$

$$= 1.990\,986\,582\,0 \times 10^{-7} - 0.690\,374\,68 \times 10^{-16}\ T\ [\text{rad/s}] \qquad (28)$$

Differentiating equation (13) provides the tropical mean motion of the Moon:

$$n_\mathbb{C}\ (\text{trop}) = \dot{L}_\mathbb{C} = 1\,732\,564\,379.31 - 8.16\,T + 0.0204\,T^2\ [''/\text{Jul. century}]$$

$$= 47\,435.027\,496\,5 - 2.234 \times 10^{-4}\ T + 0.559 \times 10^{-6} T^2\ [''/\text{d}]$$

$$= 13.176\,396\,5268 - 6.206 \times 10^{-8}\ T + 1.55 \times 10^{-10} T^2\ [^\circ/\text{d}]$$

$$= 0.549\,016\,521\,950 - 2.586 \times 10^{-9}\ T + 6.46 \times 10^{-12} T^2\ [''/\text{s}] \qquad (29)$$

and subtraction of the general precession in longitude, p, gives the siderial mean motion of the Moon:

$$n_\mathbb{C}\ (\text{sid.}) = \dot{L}_\mathbb{C} - p = 47\,434.889\,8771 - 2.843 \times 10^{-4}\ T + 0.552 \times 10^{-6} T^2\ [''/\text{d}]$$

$$= 13.176\,358\,2992 - 7.897 \times 10^{-8}\ T + 1.53 \times 10^{-10} T^2\ [^\circ/\text{d}]$$

$$= 0.549\,014\,929\,133 - 3.290 \times 10^{-8}\ T + 6.38 \times 10^{-12} T^2\ [''/\text{s}]$$

$$= 2.661\,699\,487\,73 \times 10^{-6} - 1.595 \times 10^{-13} T + 3.09 \times 10^{-17} T^2\ [\text{rad/s}] \qquad (30)$$

Because the distance of the Earth to the Sun is now known more accurately than before, it is possible to give the mean orbital velocity of the Earth about the Sun with high accuracy, namely

$$v_\oplus = a_\oplus\ n_\oplus = 29784.90 \pm 0.08\ [\text{m/s}] \qquad (31)$$

There are two constants connected with this velocity. Taking $e = 0.01675$ for the orbital eccentricity of the Earth the value for the constant of aberration will be

$$K = \frac{v_\oplus/c}{\sqrt{1-e^2}\ \sin 1''} = \frac{r\,n_\oplus}{\sqrt{1-e^2}\ \sin 1''} = 20.''4956 \pm 0.''0007, \qquad (32)$$

and using the formula of de Sitter (Ref. 10) the geodetic precession, due to the special theory of relativity, is

$$p_g = \frac{3}{2}\,(v_\oplus/c)^2\ n_\oplus = \frac{3}{2}\,(K \sin 1''\sqrt{1-e^2})^2 n_\oplus = 1.''9188 \pm 0.''0002 \qquad (33)$$

3. THE LUNAR DISTANCE AND THE LUNAR PARALLAX

The mean observed distance, $\overline{r}_\mathbb{C}$, of the Moon from the Earth is connected with the mean perturbed lunar parallax, $\pi_\mathbb{C}$, and the constant $\pi_\mathbb{C}'$ of the sine of the perturbed lunar parallax by the following relation:

$$\frac{\overline{r}_\mathbb{C}}{R_\oplus} = \frac{1}{\sin \pi_\mathbb{C}} = \frac{1}{\pi_\mathbb{C}'\ \sin 1''} \qquad (34)$$

Dividing both sides of the series development

$$\pi_\mathbb{C} = \sin \pi_\mathbb{C} + \frac{1}{6}\ \sin^3 \pi_\mathbb{C} + \cdots$$

by sin 1″ yields (because $\pi_\ell' = \sin \pi_\ell / \sin 1''$)

$$\pi_\ell'' = \pi_\ell' + \frac{1}{6}(\pi_\ell')^3 (\sin 1'')^2 + \cdots = \pi_\ell' \left[1 + \frac{1}{6}\left(\frac{R_\oplus}{\bar{r}_\ell}\right)^2 + \cdots \right]$$

$$= \pi_\ell' \times 1.000045885 = \pi_\ell' + 0.''157 \tag{35}$$

Newer determinations are

$\pi_\ell' = 3422.''54$	$\pi_\ell = 3422.70$	(E.W. Brown, Ref. 8)
3422.526 ± 0.009	3422.683 ± 0.009	(W. deSitter, Ref. 10)
3422.419 ± 0.024	3422.576 ± 0.024	(H. Jeffreys, Ref. 11, p. 193)
3422.493	3422.650	(Herrick, Baker, Ref. 12)

Recent determinations of the mean lunar distance, $\bar{r}_\ell$, by means of radar echoes to the Moon are in very close agreement (see Reference 13). This value is given by

$$\bar{r}_\ell = 384\,402.0 + 1.0 = 384\,402.0\,(1 \pm 2.6 \times 10^{-6})\ \text{km} \tag{36}$$

thus

$$\frac{\bar{r}_\ell}{R_\oplus} = \frac{384\,402.0\,(1 \pm 2.6 \times 10^{-6})}{6378.170\,(1 \pm 3.2 \times 10^{-6})} = 60.26838\,(1 \pm 5.8 \times 10^{-6}) = 60.26838 \pm 0.00035 \tag{37}$$

and

$$\pi_\ell' = \frac{\sin \pi_\ell}{\sin 1''} = \frac{206\,264.''806\,247}{(\bar{r}_\ell / R_\oplus)} = 3422.''438 \pm 0.''020 \tag{38}$$

$$\pi_\ell = 3422.''595 + 0.''020 \tag{39}$$

To obtain the semi-major axis, a_ℓ, it is necessary to add to the mean lunar distance the constant part of the solar perturbations according to Brown's lunar theory. There is now

$$a_\ell = 1.000\,907\,681\ \bar{r}_\ell = 384\,750.9 \pm 1.0\ \text{km} \tag{40}$$

and the mean orbital velocity of the Moon about the Earth is

$$v_\ell = a_\ell\, n_\ell = 1024.091 \pm 0.003\ \text{m/s} \tag{41}$$

4. MASS RATIOS OF THE SUN AND THE EARTH-MOON SYSTEM

Taking the already given values for $a_\oplus$, $n_\oplus$ (sid.), and a_ℓ, n_ℓ (sid.) then Kepler's third law gives

$$n_\oplus^2\, a_\oplus^3 = G\,(M_\odot + M_\oplus + M_\ell) = G\,M_\oplus\,(\nu + 1)(1 + \kappa) \tag{42}$$

$$n_\ell^2\, a_\ell^3 = G\,(M_\oplus + M_\ell) = G\,M_\oplus\,(1 + \kappa) \tag{43}$$

with

$$\nu = \frac{M_\odot}{M_\oplus + M_\leftmoon} \gg 1 \qquad ; \qquad \kappa = \frac{M_\leftmoon}{M_\oplus} \ll 1 \tag{44}$$

Dividing the two equations yields

$$\nu \equiv \frac{M_\odot}{M_\oplus + M_\leftmoon} = \left(\frac{n_\oplus}{n_\leftmoon}\right)^2 \left(\frac{a_\oplus}{a_\leftmoon}\right)^3 - 1 = \left(\frac{v_\oplus}{v_\leftmoon}\right)^2 \left(\frac{a_\oplus}{a_\leftmoon}\right) - 1$$

$$= 328\,898.6 \ (1 \pm 1.6 \times 10^{-5}) = 328\,898.6 \pm 5.2 \tag{45}$$

This value is approximately in the middle between the value 329 390 obtained by S. Newcomb (Ref. 14), adopted by Am. Ephemeris, and the value 328 446 ± 43 determined by E. Rabe (Ref. 15).

The second equation gives

$$\mu_\oplus (1 + \kappa) = n_\leftmoon^2 \ a_\leftmoon^3 = v_\leftmoon^2 \ a_\leftmoon = 403\,512.3 \pm 3.2 \ \mathrm{km^3/s^2} \tag{46}$$

which connects the gravitational parameter $\mu_\oplus = GM_\oplus$ for the Earth with κ, the ratio of the Moon's mass to the Earth's mass.

5. THE CONSTANT OF LUNAR INEQUALITY AND THE PARALLACTIC INEQUALITY IN MOON'S ECLIPTIC LONGITUDE

The Parallactic Inequality in the Moon's ecliptic longitude is given by E. W. Brown's lunar theory as follows

$$P_* = (49853.''2 \pm 1.''2) \ \frac{1-\kappa}{1+\kappa} \ \frac{\pi_\odot}{\pi_\leftmoon'} = (49853.''2 \pm 1.''2) \ \frac{1/\kappa - 1}{1/\kappa + 1} \ \frac{\bar{r}_\leftmoon}{a_\odot} \tag{47}$$

or with the newest data for the lunar distance and the astronomical unit

$$P_* = (128.''1005 \pm 0.''0037) \ \frac{1/\kappa - 1}{1/\kappa + 1} \tag{48}$$

Newer determinations are:

$P_* = 124.''86 \pm 0.''15$	(J. Bauschinger, Ref. 16)
$= 125.154$	(E. W. Brown, Ref. 8)
$= 124.93$	(H. Battermann, Ref. 17)
$= 124.969 \pm 0.042$	(D. Brouwer and O. B. Watts, Ref. 18)

On the other hand, the constant of Lunar Inequality is defined by W. deSitter (Ref. 10) as

$$L = \frac{\kappa}{1+\kappa} \ \frac{\pi_\odot}{\sin \pi_\leftmoon} = \frac{206\,264.''806\,247}{1/\kappa + 1} \ \frac{\pi_\odot}{\pi_\leftmoon'} = \frac{530.''0089 \pm 0.''0028}{1/\kappa + 1} \tag{49}$$

Newcomb used the lunar inequality in the Sun's longitude which is, according to deSitter, $L_\odot = 1.00450\,L$. The ratio of P_* and L, depending only on κ, is

$$P_*/L = \frac{49\,853.''2 \pm 1.''2}{206\,264.''806\,247}\ (1/\kappa - 1) = (0.241\,695 \pm 0.000\,006)\,(1/\kappa - 1) \qquad (50)$$

The mass ratio is therefore

$$1/\kappa = (4.13744_4 \pm 0.00010)\,\frac{P_*}{L} + 1 = \frac{530.''0089 \pm 0.''0028}{L} - 1 = \frac{128.''1005 + P_*}{128.''1005 - P_*} \qquad (51)$$

Observed values for the constant of Lunar Inequality are:

$L = 6.''456 \pm 0.''012$	(Newcomb, Ref. 14)	From observations of	Sun
6.414 ± 0.009	(D. Gill, Ref. 19)	"	Victoria
6.4305 ± 0.0031	(A.R. Hinks, Ref. 20)	"	Eros (opp. of 1901)
6.4390 ± 0.0015	(H. Spencer Jones, Ref.21)	"	Eros (opp. of 1931)
6.450 ± 0.010	(Morgan and Scott, Ref. 22)	"	Sun
6.4378 ± 0.0015	(H. Jeffreys, Ref. 23)	"	Eros (opp. of 1931)
6.4356 ± 0.0028	(E. Rabe, Ref. 15)	"	Eros (opp. of 1931)
6.4428 ± 0.0014) 6.4430 ± 0.0017)	(E. Delano, Ref. 24)	"	Eros (opp. of 1931)

The latest reevaluation of all Eros observations during the opposition of 1930/31 by E. Delano (Ref. 24) gave

$L = 6.''4428 \pm 0.''0014$ (from right ascensions of Eros)
$L = 6.4430 \pm 0.0017$ (from declinations of Eros)

Delano used the old value $\pi_\odot = 8.''790$ for the solar parallax and obtained therefore $1/\kappa = 81.222 \pm 0.027$ and 81.219 ± 0.030, respectively. With the newest values for $\pi_\odot$ and π_ℓ' there is now

$$1/\kappa = 81.263_7 \quad \text{and} \quad 1/\kappa = 81.261_2$$

respectively.

6. ANOTHER METHOD FOR THE DETERMINATION OF THE RATIO OF THE MASSES OF EARTH AND MOON

The mass of the Earth is given by

$$M_\oplus = \frac{4}{3}\,\pi\,R_\oplus^3\,(1-f)\,\rho_\oplus \qquad (52)$$

where f is the flattening (oblateness) and $\rho_\oplus$ is the mean density of the Earth. On the other hand the mass of the triaxial figure of the Moon is given by

$$M_\ell = \frac{4}{3}\,\pi\,a\,b\,c\,\rho_\ell = \frac{4}{3}\,\pi\,a^3\left(\frac{b}{a}\right)\left(\frac{c}{a}\right)\rho_\ell \qquad (53)$$

Because the longest axis is always directed to the Earth (neglecting the small librations) and can never be seen, the lunar radius of the visible disk is

$$R_\ell = \frac{b+c}{2} \quad ; \quad \frac{R_\ell}{a} = \frac{1}{2}\left(\frac{b}{a} + \frac{c}{a}\right) = \sigma \tag{54}$$

That yields for the mass of the moon

$$M_\ell = \frac{4}{3}\,\pi\, R_\ell^3 \quad \frac{(b/a)(c/a)}{\sigma^3}\,\rho_\ell \tag{55}$$

The mass ratio is therefore

$$1/\kappa \equiv M_\oplus/M_\ell = \left(\frac{R_\oplus}{R_\ell}\right)^3 \frac{(1-f)\,\sigma^3}{(b/a)(c/a)}\left(\frac{\rho_\oplus}{\rho_\ell}\right) \quad \frac{(1-f)\,\sigma^3}{(b/a)(c/a)} \quad \frac{\rho_\oplus/\rho_\ell}{k^3} \tag{56}$$

where

$$k = \frac{R_\ell}{R_\oplus} = \frac{\sin s_\ell}{\sin \pi_\ell} = \frac{s_\ell'}{\pi_\ell'} = \frac{s_\ell - 0.''003}{\pi_\ell - 0.''157} \tag{57}$$

is given by the lunar parallax, π_ℓ, and the apparent semi-diameter of the Moon, s_ℓ .

A reevaluation of Sir Harold Jeffrey's best data on the Moon's figure by the author gave (see section 12)

$$\frac{b}{a} = 0.9998116 \quad ; \quad \frac{c}{a} = 0.9993720 \quad ; \quad \sigma = 0.9995918$$

From the secular perturbations of artificial Earth satellites there follows as best value for the Earth oblateness

$$1/f = 298.30 \quad ; \quad 1 - f = 0.9966\,4767$$

so that

$$1/\kappa = 0.9962409 \quad \frac{\rho_\oplus/\rho_\ell}{k^3} \tag{58}$$

Taking for the mean densities the well-known and frequently used values

$$\rho_\oplus = 5.517 \pm 0.004 \ \text{g/cm}^3 \ \text{(Heyl)} \ ; \ \rho_\ell = 3.342 \pm 0.005 \ \text{g/cm}^3 \ \text{(Jeffreys)}$$

the density ratio, independent from the assumed value of the gravitational constant, G, becomes $\rho_\oplus/\rho_\ell = 1.6508$. Therefore

$$1/\kappa = 1.6446/k^3 \tag{59}$$

With $\pi_\mathbb{C}' = 3422.''438$ and various values for $s_\mathbb{C}$ the following table is obtained

$s_\mathbb{C}$	k	$1/\kappa$
932.''58 (Newcomb, Ref. 25)	0.2724891	81.286
932.63 (American Ephem., Ref. 26)	0.2725037	81.272
932.80 + 0.07 (Hirose & Manabe, Ref. 27)	0.2725534	81.228

The American Ephemeris is using $k = 0.2724953$, based on Brown's lunar parallax. The values for $1/\kappa$ obtained in the previous paragraph are between the two latter values in this table. The arithmetic mean of these two latter values will be taken as the presently best value, namely

$$1/\kappa \equiv \frac{M_\oplus}{M_\mathbb{C}} = 81.250\,(1 \pm 3 \times 10^{-4}) = 81.250 \pm 0.024 \tag{60}$$

and therefore

$$k \equiv \frac{R_\mathbb{C}}{R_\oplus} = 0.2725289 \pm 0.0000273 \tag{61}$$

The last equation of paragraph 4 now gives

$$\mu_\oplus \equiv GM_\oplus = \frac{403512.3}{1.0123077} = 398606.4 \pm 4.9 \ \text{km}^3/\text{sec}^2 \tag{62}$$

for the Earth, while, for the Moon,

$$\mu_\mathbb{C} \equiv GM_\mathbb{C} = \kappa \mu_\oplus = 4905.92 \pm 1.52 \ \text{km}^3/\text{sec}^2 \tag{63}$$

7. GEODYNAMIC (TERRESTRIAL) RELATIONS

The surface of the Earth (geoid) can be approximated as the surface of an spheroid assumed as an equipotential surface. The equation for the Earth's radius, as function of the latitude, is then given by

$$R = R_\oplus \left[1 - f \sin^2 \varphi + \left(\frac{5}{8} f^2 - \kappa\right) \sin^2 2\varphi\right] = R_\oplus \left[1 - f \sin^2 \phi - \left(\frac{3}{8} f^2 + \kappa\right) \sin^2 2\phi\right] \tag{64}$$

where φ is the geodetic (geographic) latitude and ϕ the geocentric latitude. They are related by

$$\tan \phi = (1 - f)^2 \tan \varphi = (1 - e^2) \tan \varphi \tag{65}$$

where $e = \sqrt{f\,(2 - f)}$ is the eccentricity of the meridian ellipse of the Earth. The equation of the Earth-ellipsoid is obtained by setting $\kappa = 0$. The maximum depression, $-\kappa R_\oplus$, of the spheroid from the ellipsoid is reached at the latitude 45°. It will never be more than 5.17 m. For the spheroid as equipotential surface there is

$$U = \frac{GM}{R}\left[1 - \frac{2}{3} J \left(\frac{R}{R_\oplus}\right)^2 P_2 (\sin \phi) + \frac{4}{15} K \left(\frac{R}{R_\oplus}\right)^4 P_4 (\sin \phi) + \cdots\right] + \frac{1}{2} \Omega^2 R^2 \cos^2 \phi$$

$$= \frac{GM}{R}\left[1 - \sum_{n=2}^{\infty} J_n \left(\frac{R}{R_\oplus}\right)^n P_n (\sin \phi)\right] + \frac{1}{2} \Omega^2 R^2 \cos^2 \phi = \text{const.} \tag{66}$$

and the acceleration of gravity at this surface is

$$g = |\operatorname{grad} U| = g_e [1 + \beta \sin^2 \varphi + \gamma \sin^2 2\varphi] = g_e [1 + \beta \sin^2 \phi + (\gamma + \beta f) \sin^2 2\phi] \qquad (67)$$

where Ω is the angular velocity of the Earth's rotation, β and γ are constant gravity coefficients and J_n or J and K are constant oblateness coefficients. These coefficients depend only on f, κ, and a parameter containing Ω^2 (centrifugal force parameter). This latter parameter is a little different in the various second-order theories which have been developed. Taking

$$\Omega = 7.292\,115\,146 \times 10^{-5} \text{ rad/sec}$$

$$1/f = 298.30 \quad ; \quad 1 - f = 0.996\,647\,670$$

$$G = 6.670 \times 10^{-8} \text{cm}^3/(\text{g}\cdot\text{sec}^2) \quad ; \quad \rho_m = 5.517 \text{ g/cm}^3 \quad ; \quad G\rho_m = 3.679\,839 \times 10^{-7} \qquad (68)$$

then the following parameters could be used

$$\varpi = \frac{\Omega^2 R_e^3}{GM} = \frac{\Omega^2}{4/3\,\pi\, G \rho_m (1 - f)} = 0.003\,461\,369 \text{ [Herrick, (Ref.12]} \qquad (69)$$

$$\varpi' = \frac{\Omega^2 R_v^3}{GM} = \frac{\Omega^2}{4/3\,\pi G \rho_m} = \varpi (1 - f) = 0.003\,449\,766 \text{ [Jeffreys, Ref.11]} \qquad (70)$$

$$\varpi_1 = \frac{\Omega^2 R_1^3}{GM} = \varpi \left(1 - f + 2f^2 - \frac{8}{3}\kappa\right) = \varpi'(1 + 2f^2 - \frac{8}{3}\kappa) = 0.003\,449\,843 \text{ [deSitter, Ref.10]} \qquad (71)$$

$$m = \frac{\Omega^2 R_e}{g_e} = \frac{\varpi}{1 - A - \frac{3}{2}\varpi + f + f^2 - \frac{3}{7} f\varpi + \frac{16}{7}\kappa} = \frac{\varpi}{1 - A - \varpi + J + 1/2\,K}$$

$$= 0.003\,467\,730 \text{ [Darwin, Ref.28; Helmert, Ref.29]} \qquad (72)$$

where $R_v = R_e (1 - f)^{1/3}$ is the radius for a sphere of same volume as the Earth and $R_1 = R_e (1 - 1/3\, f + 5/9\, f^2 - 8/9\kappa)$ is the mean radius for which $P_2 (\sin \varphi) = 0$ or $\varphi = \sin^{-1}\sqrt{1/3} = 35°15'51.''8$. $A = 0.88 \times 10^{-6}$ is the mass of the Earth's atmosphere (expressed in mass of the Earth) which does not contribute to the surface gravity of the Earth. Different assumptions have been made for κ. Bullard (Ref.30) found $10^6 \kappa = 0.68$. This value was accepted later by Herrick, Baker, and Hilton (Ref.12) On the other hand, deSitter found values of only $10^6 \kappa = 0.47$ to 0.52 and used the round mean value $10^6 \kappa = 0.50$. The theoretical limits are according to deSitter (Ref. 31)

$$0 \leqslant \kappa \leqslant \frac{5}{16} f\varpi - \frac{1}{4} f^2 = (3.62 - 2.81) \times 10^{-6} = 0.81 \times 10^{-6} \qquad (73)$$

The different formula systems now yield

$$J = f - \frac{1}{2}\varpi - \frac{1}{2}f^2 + \frac{9}{14}f\tilde{\omega} + \frac{4}{7}\kappa$$

$$= f - \frac{1}{2}\varpi' - \frac{1}{2}f^2 + \frac{1}{7}f\tilde{\omega}' + \frac{4}{7}\kappa$$

$$= f - \frac{1}{2}\tilde{\omega}_1 - \frac{1}{2}f^2 + \frac{1}{7}f\tilde{\omega}_1 + \frac{4}{7}\kappa$$

$$= f - \frac{1}{2}m - \frac{1}{2}f^2 + \frac{1}{7}fm + \frac{3}{4}m^2 + \frac{4}{7}\kappa \qquad (74)$$

$$K = \frac{6}{7}D = 3f^2 - \frac{15}{7}f\tilde{\omega} + \frac{24}{7}\kappa$$

$$= 3f^2 - \frac{15}{7}f\tilde{\omega}' + \frac{24}{7}\kappa$$

$$= 3f^2 - \frac{15}{7}f\tilde{\omega}_1 + \frac{24}{7}\kappa$$

$$= 3f^2 - \frac{15}{7}fm + \frac{24}{7}\kappa \qquad (75)$$

$$\beta = \frac{5}{2}\tilde{\omega} - f - \frac{26}{7}f\tilde{\omega} + \frac{15}{4}\varpi^2 + \frac{8}{7}\kappa$$

$$= \frac{5}{2}\tilde{\omega}' - f - \frac{17}{14}f\tilde{\omega}' + \frac{15}{4}\tilde{\omega}'^2 + \frac{8}{7}\kappa$$

$$= \frac{5}{2}\tilde{\omega}_1 - f - \frac{17}{14}f\varpi_1 + \frac{15}{4}\varpi_1^2 + \frac{8}{7}\kappa$$

$$= \frac{5}{2}m - f - \frac{17}{14}fm + \frac{8}{7}\kappa \qquad (76)$$

$$\gamma = \frac{1}{8}f^2 - \frac{5}{8}f\varpi - 3\kappa$$

$$= \frac{1}{8}f^2 - \frac{5}{8}f\varpi' - 3\kappa$$

$$= \frac{1}{8}f^2 - \frac{5}{8}f\tilde{\omega}_1 - 3\kappa$$

$$= \frac{1}{8}f^2 - \frac{5}{8}fm - 3\kappa \qquad (77)$$

$$\chi \equiv g_e/(GM/R_e^2) = 1 - A - \varpi + J + \frac{1}{2} K$$

$$= 1 - A - \frac{3}{2} \varpi + f + f^2 - \frac{3}{7} f\varpi + \frac{16}{7} \kappa$$

$$= 1 - A - \frac{3}{2} \varpi' + f + f^2 - \frac{27}{14} f\varpi' + \frac{16}{7} \kappa$$

$$= 1 - A - \frac{3}{2} \varpi_1 + f + f^2 - \frac{27}{14} f\varpi_1 + \frac{16}{7} \kappa$$

$$= 1 - A - \frac{3}{2} m + f + f^2 - \frac{27}{14} fm + \frac{9}{4} m^2 + \frac{16}{7} \kappa \qquad (78)$$

Using these equations and the above-given constants for the Earth then the following table is obtained with $J_2 = (C - A)/(M R_e^2) = \frac{2}{3} J$ and $J_4 = -\frac{4}{15} K = -\frac{8}{35} D$:

Coefficient	$\kappa = 0$	$\kappa = 0.50 \times 10^{-6}$	$\kappa = 0.68 \times 10^{-6}$
$10^6 J$	1623.48	1623.77	1623.87
$10^6 K$	8.85	10.56	11.18
$10^6 J_2$	1082.32	1082.51	1082.58
$10^6 J_4$	- 2.36	- 2.82	- 2.98
$10^6 \beta$	5302.92	5303.49	5303.70
$10^6 \gamma$	- 5.85	- 7.35	- 7.89
χ	0.9981 6566	0.9981 6680	0.9981 6721

The numerical values for $|J_4|$ are a little higher than the values derived from the observed secular perturbations of artificial satellites. Thus the data for $\kappa = 0$ will be used here.

The gravitational parameter of the Earth is now given by

$$\mu_\oplus \equiv GM_\oplus = \frac{4}{3} \pi G\rho_\oplus R_e^3 (1 - f) = \frac{g_e R_e^2}{\chi} = 398\,606.4 \pm 4.9 \text{ km}^3/\text{sec}^2 \qquad (79)$$

which corresponds to $1/\kappa = 81.250$. Taking, furthermore, $\frac{4}{3} \pi = 4.188\,790\,204$; $1 - f = 0.996\,647\,670$; $\chi = 0.998\,165\,66$ that yields

$$g_e R_e^2 = \chi \mu_\oplus = 397\,875.2 \pm 4.9 \text{ km}^3/\text{sec}^2 = 3.978\,752 \times 10^{14} \text{ m}^3/\text{sec}^2 \qquad (80)$$

and

$$\frac{g_e}{R_e} = \frac{4}{3} \pi (1 - f) \chi G \rho_\oplus = 4.167\,090\,090\, G\rho_\oplus \qquad (81)$$

or with $G = 6.670 \times 10^{-8}\ \mathrm{cm^3/g \cdot sec^2}$

$$\rho_\oplus = \frac{(g_e/R_e)\times 10^7}{2.779\,45} \quad [\mathrm{g/cm^3}] \tag{82}$$

8. EXPERIMENTAL VALUES OF THE GRAVITATIONAL ACCELERATION OF THE EARTH

The observed gravitational acceleration at the surface of the rotating Earth can be represented by the formula

$$g = g_e [1 + \beta \sin^2 \varphi + \gamma \sin^2 2\varphi + \delta \cos^2 \varphi \cos 2(\lambda - \lambda_0)] \tag{83}$$

where λ is the geographic longitude measured eastwards of Greenwich meridian. The first term corresponds to a sphere. The next two terms give the contribution due to the oblateness of the Earth spheroid, while the longitude term is due to the non-ellipticity of the equator when the Earth is assumed as a triaxial figure. The longitude, λ_0, gives the direction of the longest semi-axis of the equator. δ is connected with the difference $B - A$ of the equatorial moments of inertia or with the flattening, f_e, of the equator by the relation

$$\delta = \frac{9}{4}\,\frac{B-A}{M_\oplus R_e^2} = \frac{9}{4}\,\Lambda f_e(2 - f_e) \approx \frac{3}{8}\,f_e \tag{84}$$

because the inhomogenity factor of the Earth is given by

$$\Lambda = \frac{C}{M_\oplus(a^2 + b^2)} \approx \frac{C}{2M_\oplus R_e^2} \approx \frac{1}{6} \tag{85}$$

The most important determinations from gravity measurements since 1915 have been compiled in a table on the following page.

All these gravity measurements are still based on the standard gravity value of Potsdam ($\varphi = 52^\circ\,22.'86$; $\lambda = +\,13^\circ\,4.'06$; $h = 87$ m)

$$g = 981.2740 \text{ gal}$$

obtained by F. Kuhnen and Ph. Furtwangler (Ref. 43). It is necessary to revise the Potsdam system. For the correction of the Potsdam value, the following data are given (Refs. 44 and 45):

P. R. Heyl and G. S. Cook (Wash. D.C.)	: − 20	milligal	according to absolute gravity measurements
Bullard (Teddington, G. Brit.)	: − 15	"	
J. S. Clarke (Teddington, Gt. Brit.)	: − 13	"	
Ivanoff (Leningrad, U.S.S.R.)	: − 4	"	
P. R. Heyl	: − 15	"	according to recalculations
Bullard and Browne	: − 16	"	
Morelli (1954)	: − 16	"	
H. Jeffreys	: − 13.4	"	
Wollard	: − 14 to − 18	"	
A. Berroth	: − 12.5	"	
Morelli (1959)	: − 12.9	"	

Author	Year	Ref.	g_0 (gal)	$10^6\beta$	$10^6\gamma$	$10^6\delta$	λ_0	ΔR_0 (m)	$1:f_1$	$1:f_2$	$1:f_m$	$1:f_0$
F. R. Helmert	1915	32	978.052 ± 3	5285 ± 5		18 ± 3	− 17° ± 4	230 ± 51			296.7 ± 0.4	28 000
A. Berroth	1916	33	978.046	5296		11.6 ± 4	− 10	150 ± 58	296.7	298.8	297.8 ± 0.7	42 000
W. Heiskanen	1924	34	978.048 ± 3	5293 ± 6		---	---	---	---	---	297.4 ± 0.5	---
"	1924	34	978.052 ± 3	5285 ± 6	− 7	27 ± 3	+ 18 ± 5	345 ± 38	294.3 ± 0.6	299.0 ± 0.6	296.7 ± 0.5	18 700
"	1928	35	978.049 ± 1	5289		---	---	---	---	---	297.06	---
"	1928	35	978.049 ± 1	5293		19 ± 3	0 ± 5	242	295.7	299.0	297.3	26 703
"	1938	36	978.0451	5302.7		---	---	---	---	---	298.25 ± 0.3	---
"	1938	36	978.0524	5297.0		27.6	− 25	352 ± 30	295.3 + 0.4	300.2 + 0.4	297.8 ± 0.4	18 314
N. F. Shuravlev	1940	37	978.0484	5303		---	---	---	---	---	298.3	---
E. Niskanen	1945	38	978.0468	5297.8	−5.9	23.0	− 3.9	293	295.7 ± 0.2	299.8 ± 0.2	297.8 ± 0.2	21 550
H. Jeffreys	1948	39	978.0513	5285.9		---	---	---	---	---	296.85 ± 0.66	---
H. Schütte	1950	40	978.0520 ± 33	5282.7 ± 6.0		---	---	---	---	---	296.3	---
U. A. Uotila	1957	41	978.0516	5291.0		10.6	− 6	---	---	---	297.2	47 600
Heiskanen & Uotila	1957	42	978.0496	5293.4		---	---	---	---	---	297.4	---
Mean Value			978.049_5	$5292._4$							297.3	

Taking for g_e the latest determination of Heiskanen and Uotila (Ref. 42) which is nearly in agreement with the average value of all determinations, and using the correction due to H.Jeffreys (Ref.39) the following value is obtained

$$g_e = 978.0496 - 0.0134 = 978.0362 \text{ gal} = 9.780362 \text{ m/sec}^2 \tag{86}$$

9. THE DYNAMIC OBLATENESS AND THE CONSTANTS OF PRECESSION AND NUTATION

The dynamic flattening $H = (C - A)/C$ is connected with Newcomb's constant of precession, P, by the relation

$$\frac{P}{H} = 530977.''04 + \frac{94419319''}{1/\kappa + 1} = 1678932.''29 \quad \text{for } 1/\kappa = 81.250 \tag{87}$$

while the constant of nutation, N, is given by

$$\frac{N}{H} = \frac{252871''}{1/\kappa + 1} \cos\epsilon = \frac{231982''}{1/\kappa + 1} = 2820.''45 \quad \text{for } 1/\kappa = 81.250 \tag{88}$$

where $\cos\epsilon = 0.9173917$ (for 1900.0) has been used for the cosine of the obliquity, ϵ, of the ecliptic. The constants in the equations are obtained from Brown's theory of the motion of the Moon and are well known. Both equations yield

$$\frac{P}{N} = 2.288872\,(1/\kappa + 1) + 407.01140 = 595.271 \quad \text{for } 1/\kappa = 81.250$$

while observed modern values of P and N lead to

$$\frac{P}{N} = \frac{5493.''62}{9.''208} = 596.614 \quad \text{and thus} \quad 1/\kappa = \frac{P/N}{2.288872} - 178.8218 = 81.84$$

This value for $1/\kappa$ is by far too large. H. Jeffreys (Ref. 39) has shown that in the equation for the constant of nutation, N, another constant H' for the dynamic flattening must be used due to the deviation of the Earth's interior from the isostatic equilibrium ($H' < H$). Therefore H can be determined only from P and $1/\kappa$. With $p_0 = p_\odot + p_\ell$, the lunisolar precession, $p_\ell = \frac{3}{2}\frac{\nu_\oplus^2}{c^2} n_\oplus$, the geodetic precession (a relativistic term due to W. deSitter), p, the general precession in longitude, and λ, the planetary precession in right ascension, Newcomb's precessional constant is

$$P = \frac{p_0}{\cos\epsilon} = \frac{p + p_\ell}{\cos\epsilon} + \lambda \tag{89}$$

Values for 1900.0 derived from observations are (for a tropical century)

$P = 5490.''66$	$p = 5025.''641$	$\lambda = 12.''473$	$p_\ell = 0$	(Newcomb & Andoyer, Ref.46)
5493.156 ± 0.175	5026.000	12.493	1.915	(deSitter & Brouwer, Ref.10)
5493.847	$5026.''650$	12.469	1.921	(Clemence, Ref.7)

According to newer investigations, Newcomb's value of the general precession in longitude

must be corrected by $\Delta p = +\ 0.''75$ (H. R. Morgan, Ref. 47), $\Delta p = +\ 0.''71$ (J. H. Oort, Ref. 48), $\Delta p = +\ 0.''86$ (Dirk Brouwer, Ref. 48), $\Delta p = +\ 0.''84$ (Poulkovo Obs., Ref. 48). The average value for the correction may be $\Delta p = +\ 0.''80$. All these investigators take $\Delta\lambda = 0$. In another paper, J. H. Oort (1943, Ref. 49) takes $\Delta\lambda = +\ 0.''02$, a correction also used by deSitter. The correction for P is therefore

$$\Delta P = \frac{\Delta p + \Delta p_{\mathcal{S}}}{\cos \epsilon} + \Delta\lambda = \frac{0.''80 + 1.92}{0.917\,3917} + 0.00 = 2.''96 \tag{90}$$

The value

$$P = 5490.''66 + 2.''96 = 5493.''62 \tag{91}$$

will be accepted here. The dynamic flattening is now

$$H \equiv \frac{C - A}{C} = \frac{5493.''62}{1\,678\,932.''29} = 0.003\,272\,091 = \frac{1}{305.615 \pm 0.05} \tag{92}$$

and thus

$$q \equiv \frac{3}{2}\,\frac{C}{M_{\oplus} R_{\bullet}^2} = \frac{J}{H} = 0.49616_0 \pm 0.00017 \tag{93}$$

and

$$\frac{C}{m_{\oplus} R_{\bullet}^2} = \frac{J_2}{H} = 0.33077_3 \pm 0.00011 \tag{94}$$

The quantity q may be calculated in another way. Clairant's theory for the Earth in hydrostatic equilibrium has been developed to the second order by Radau (Ref. 50), Callandreau (Ref. 51), and Darwin (Ref. 28). deSitter (Ref. 31) gives

$$q \equiv \frac{3}{2}\,\frac{C}{M R_{\bullet}^2} = 1 - \frac{1}{3}\,\varpi_1 - \frac{2}{5}\left(1 - \frac{2}{3}\,f\right)\frac{\sqrt{1 + \eta_1}}{1 + \lambda_1} \tag{95}$$

where

$$\eta_1 = \frac{\frac{5}{2}\,\varpi_1 + \frac{10}{21}\,\varpi_1^2 + \frac{4}{7}\,f^2 - \frac{6}{7}\,f\varpi_1}{f - \frac{5}{42}\,f^2 + \frac{4}{7}\,\kappa} - 2 \tag{96}$$

and $1 + \lambda_1$ is an average value of Radau's function, $f(\eta)$, depending on the internal density distribution of the Earth. The most reliable value, $1 + \lambda_1 = 1.00016$, was derived by Bullard (Ref. 30). With the above data for f and ϖ_1 the above-mentioned equations give, for $\kappa = 0$,

$$\eta_1 = 0.57440 \quad ; \quad q = 0.49815$$

$$\frac{C}{M R_{\bullet}^2} = \frac{2}{3}\,q = 0.33210$$

These data are not compatible with the previously derived data (eqs. 93 and 94), showing that the hypothesis of hydrostatic equilibrium is not fulfilled for the Earth.

10. DENSITY DISTRIBUTION WITHIN THE MOON

It is very difficult to derive a consistent system of lunar constants. Most reports on this subject are based on the work of Sir Harold Jeffreys. However, not even this source is free of inconsistencies. The reason is that many lunar constants are coupled with each other by relations. Therefore a systematic investigation of these relations will be necessary.

It is assumed that the density ρ within the Moon is constant over concentric ellipsoidal shells

$$\frac{\xi^2}{a^2} + \frac{\eta^2}{b^2} + \frac{\zeta^2}{c^2} = \mu^2 \tag{97}$$

where μ varies from 0 at the center to 1 at the surface, and where

$$\begin{aligned} \xi/a &= \mu \cos\phi \cos\theta \\ \eta/b &= \mu \cos\phi \sin\theta \\ \zeta/c &= \mu \sin\phi \end{aligned} \tag{98}$$

are the relative coordinates of the mass element

$$dm = \rho(\mu)\, d\xi\, d\eta\, d\zeta = \rho(\mu)\, a\, b\, c\, \mu^2 \cos\phi\, d\mu\, d\phi\, d\theta \tag{99}$$

The angle ϕ is the lunicentric latitude and θ the longitude. a is the longest semi-axis of the surface ellipsoid pointing toward the Earth, b the smallest semi-axis in the lunar equator, and c the rotational or polar semi-axis.

Using equations (98) and (99) after observing that

$$\int_0^{2\pi} \sin^2\theta\, d\theta = \int_0^{2\pi} \cos^2\theta\, d\theta = \pi\,; \quad \int_{-\pi/2}^{\pi/2} \cos^3\phi\, d\phi = \frac{4}{3}\,; \quad \int_{-\pi/2}^{\pi/2} \sin^2\phi \cos\phi\, d\phi = \frac{2}{3}$$

the moments of inertia around the a, b, c axes, respectively, become

$$\begin{aligned} A &= \int_0^M (\eta^2 + \zeta^2)\, dm = \lambda M (b^2 + c^2) \\ B &= \int_0^M (\zeta^2 + \xi^2)\, dm = \lambda M (c^2 + a^2) \\ C &= \int_0^M (\xi^2 + \eta^2)\, dm = \lambda M (a^2 + b^2) \end{aligned} \tag{100}$$

where the integrations are taken from 0 to 2π with respect to θ, from $-\pi/2$ to $\pi/2$ with respect to ϕ and from 0 to 1 with respect to μ. In the last equation $M = 4/3\, \pi\, a\, b\, c\, \rho_m$ is the total mass (ρ_m is the mean density) and the inhomogenity factor, λ, is given by

$$\lambda = \frac{\int_0^1 \rho \mu^4 d\mu}{\rho_m} = \frac{\int_0^1 \rho \mu^4\, d\mu}{3\int_0^1 \rho \mu^2\, d\mu} \tag{101}$$

Because $a > b > c$, there is $A < B < C$. A constant density model gives $\lambda = 1/5 = 0.2$. For Jeffreys compressional model with constant bulk modulus (Ref. 52) Roche's density law [with $\rho_m = 3.342\ g/cm^3$ (mean density), $\rho_0 = 3.290\ g/cm^3$ (surface density) and $\rho_c = 3.420\ g/cm^3$ (central density)] becomes

$$\rho = \rho_c - (\rho_c - \rho_0)\,\mu^2 = 3.420 - 0.130\,\mu^2 \quad [g/cm^3] \tag{102}$$

The inhomogenity factor is, therefore,

$$\lambda = \frac{1}{5}\,\frac{\rho_c - \frac{5}{7}(\rho_c - \rho_0)}{\rho_m} = \frac{1}{5}\,\frac{\rho_c - \frac{5}{7}(\rho_c - \rho_0)}{\rho_c - \frac{3}{5}(\rho_c - \rho_0)} = \frac{0.9955}{5} =$$

$$= 0.1991 \pm 0.0001 \tag{103}$$

11. CONSTANTS OF THE PHYSICAL LIBRATION OF THE MOON

The values of $f \equiv \frac{C - B}{C - A}$ and the inclination of the Moon's equator to the ecliptic can be determined from observations of the physical libration of the Moon. Due to the difficulty of observations near the irregular limb of varied illumination the values for f scatter widely, as can be seen from the following table (Refs. 11 and 13):

Author	Year	$f \equiv \frac{C - B}{C - A}$
F. Hayn	1907	0.75 ± 0.04
F. Hayn		0.85 ± 0.07
J. Stratton	1909	0.50 ± 0.03
I. V. Belkovich	1936	0.84 ± 0.08
I. V. Belkovich	1949	0.67 ± 0.03
K. Koziel	1949	0.71 ± 0.051
K. Koziel	1949	0.60 ± 0.055
A.A. Nefedjev	1950	0.65 ± 0.045
A.A. Yakovkin	1950	0.85 ± 0.03
T. Weimer	1954	0.60
Mean Value		0.70_2

Sir Harold Jeffreys used $f = 0.84$ in his book *The Earth* (Ref. 11). Later he recommended $f = 0.67$ (Ref. 53) and used $f = 0.639 \pm 0.014$ in his latest paper (Ref.54).

The secular motions of the perigee and node of the lunar orbit are also influenced by the Moon's oblateness coefficients (L and K). From Jeffreys equation for the perigee motion follows (Ref. 11):

$$380\,L - 1192\,K = 6.420 - 3896\,J_\bullet \gtrsim 0$$

and thus

$$f = 1 - \frac{K}{L} \geqslant 1 - \frac{380}{1192} = \frac{812}{1192} = 0.6812$$

The mean value of the table is consistent with this lower limit for f and therefore

$$f = 0.70 \pm 0.02 \tag{104}$$

will be adopted in this paper.

A new investigation of the libration of the Moon's axis by H. Jeffreys (Ref. 54) leads to

$$\beta \equiv \frac{C - A}{C} = 0.0006279 \pm 0.0000010 \tag{105}$$

taking into account a solar effect not evaluated by Hayn.

The three quantities λ, f, and β are sufficient to calculate all other quantities, provided the mass and the mean radius of the Moon are known.

12. RELATIONS AND NUMERICAL VALUES FOR THE DIMENSIONLESS MOMENT OF INERTIA PARAMETERS

The same symbols for moment of inertia parameters will be used as they have been introduced mainly by H. Jeffreys (Ref. 11). The numerical values are based on the above-given parameters λ, f, and β; namely

$$\lambda = \frac{A}{M(b^2 + c^2)} = \frac{B}{M(c^2 + a^2)} = \frac{C}{M(a^2 + b^2)}$$

$$= \frac{C - B}{M(b^2 - c^2)} = \frac{C - A}{M(a^2 - c^2)} = \frac{C - B}{M(b^2 - c^2)} = 0.1991 \pm 0.0001 \tag{106}$$

$$f = \frac{\alpha}{\beta} = \frac{C - B}{C - A} = \frac{2J - K}{2J + K} = \frac{J - 1/2\ K}{L} = \frac{b^2 - c^2}{a^2 - c^2} = 0.70 \pm 0.02 \tag{107}$$

$$\beta = \frac{C - A}{C} = \frac{J + 1/2\ K}{g} = \frac{L}{g} = \frac{a^2 - c^2}{a^2 + b^2} = 0.0006279 \pm 0.0000010 \tag{108}$$

The other parameters can be derived from these as follows:

$$1 - f = \frac{\gamma}{\beta} = \frac{B - A}{C - A} = \frac{K}{J + 1/2\ K} = \frac{K}{L} = \frac{a^2 - b^2}{a^2 - c^2} = \frac{3\lambda - g}{L} = \frac{3\lambda/g - 1}{\beta} =$$

$$= 0.30 \pm 0.02 \tag{109}$$

$$\alpha = \frac{C - B}{C} = f\beta = \frac{J - 1/2\ K}{g} = \frac{L - K}{g} = \frac{b^2 - c^2}{a^2 + b^2} = 0.000\,4395 \pm 0.000\,0133 \tag{110}$$

$$\gamma = \frac{B - A}{C} = \beta - \alpha = \frac{K}{g} = (1 - f)\beta = \frac{a^2 - b^2}{a^2 + b^2} = 0.000\,1884 \pm 0.000\,0129 \tag{111}$$

$$g = \frac{3}{2}\ \frac{C}{Ma^2} = \frac{3\lambda}{1 + \gamma} = \frac{3}{2}\ \lambda\ \frac{a^2 + b^2}{a^2} = 0.5972 \pm 0.0003 \tag{112}$$

$$L = \frac{3}{2}\ \frac{C - A}{Ma^2} = J + \frac{1}{2}\ K = g\beta = \frac{3}{2}\ \lambda\ \frac{a^2 - c^2}{a^2} = 0.000\,3750 \pm 0.000\,0008 \tag{113}$$

$$J = \frac{3}{2}\ \frac{C - \frac{A + B}{2}}{Ma^2} = L - \frac{1}{2}\ K = \frac{1 + f}{2}\ L = \frac{1}{2}\ \frac{1 + f}{1 - f}\ K = \frac{3}{2}\lambda\ \frac{\frac{a^2 + b^2}{2} - c^2}{a^2}$$

$$= g\left(\beta - \frac{1}{2}\ \gamma\right) = g\ \frac{\alpha + \beta}{2} = g\left(\alpha + \frac{1}{2}\ \gamma\right) = 0.000\,3187_5 \pm 0.000\,0044 \tag{114}$$

$$K = \frac{3}{2}\ \frac{B - A}{Ma^2} = (1 - f)\ L = g\gamma = \frac{3}{2}\ \lambda\ \frac{a^2 - b^2}{a^2} = 0.000\,1125 \pm 0.000\,0077 \tag{115}$$

The dimensionless moments of inertia and their differences are obtained from the above-mentioned data as:

$$\frac{C - A}{Ma^2} = \frac{2}{3}\ L = \frac{2J + K}{3} = \lambda\ \frac{a^2 - c^2}{a^2} = 0.000\,2500 \pm 0.000\,0005 \tag{116}$$

$$\frac{C - B}{Ma^2} = \frac{2}{3}\ fL = \frac{2J - K}{3} = \lambda\ \frac{b^2 - c^2}{a^2} = 0.000\,1750 \pm 0.000\,0054 \tag{117}$$

$$\frac{B - A}{Ma^2} = \frac{2}{3}\ (1 - f)\ L = \frac{2}{3}\ K = \lambda\ \frac{a^2 - b^2}{a^2} = 0.000\,0750 \pm 0.000\,0051 \tag{118}$$

$$\frac{A}{Ma^2} = \frac{2}{3}\ g\ (1 - \beta) = \frac{2}{3}\ (g - L) = \lambda\ \frac{b^2 + c^2}{a^2} = 0.3978_{77} \pm 0.0002 \tag{119}$$

$$\frac{B}{Ma^2} = \frac{2}{3}\ g\,(1 - \alpha) = \frac{2}{3}\ (g - fL) = \lambda\ \frac{c^2 + a^2}{a^2} = 0.3979_{52} \pm 0.0002 \tag{120}$$

$$\frac{C}{Ma^2} = \frac{2}{3}\, g = \frac{2\lambda}{1+\gamma} = \lambda\, \frac{a^2 + b^2}{a^2} = 0.3981_{27} \pm 0.0002 \qquad (121)$$

The ratios of the semi-axes now become

$$\frac{b}{a} = \sqrt{\frac{1-\gamma}{1+\gamma}} = \sqrt{1 - \frac{2\gamma}{1+\gamma}} = 0.9998116 \pm 0.0000129 \qquad (122)$$

$$\frac{c}{\bar{a}} = \sqrt{1 - \frac{2\beta}{1+\gamma}} = \sqrt{1 - \frac{2\gamma}{(1-f)(1+\gamma)}} = 0.9993720 \pm 0.0000010 \qquad (123)$$

These data seem, at present, to be the most reasonable. H. Jeffreys' value

$$g \equiv \frac{3}{2}\, \frac{C}{Ma^2} = 0.5956 \pm 0.0010$$

is slightly low, and affords a higher density concentration towards the center as has been assumed by Jeffreys.

13. THE FINAL DETERMINATION OF THE DIMENSIONS, MASSES AND MOMENTS OF INERTIA FOR THE EARTH AND THE MOON

Using the obtained value of the gravitational acceleration, g_e, at the equator (eq. 86) in the relations (eq. 80) and (eq. 82) at the end of Section 7 there follows at once $R_e = \sqrt{\chi \mu_\oplus / g_e} = 6378169.835$ m and $\rho_\oplus = 5.516964$ g/cm^3. The final values, adopted for the Earth, will be taken as

$$R_e = 6378170\ (1 \pm 3.2 \times 10^{-6})\ \text{m} = 6378170 \pm 20\ \text{m} \qquad (124)$$

and

$$\rho_\oplus = 5.5170\ (1 \pm 7.3 \times 10^{-4})\ \text{g/cm}^3 = 5.5170 \pm 0.0040\ \text{g/cm}^3 \qquad (125)$$

The volume of the Earth is

$$V_\oplus = \frac{4}{3}\, \pi\, R_e^3\, (1-f) = 1.083225 \times 10^{27}\ (1 \pm 1.02 \times 10^{-5})\ \text{cm}^3$$

$$= (1.083225 \pm 0.000011) \times 10^{27}\ \text{cm}^3 \qquad (126)$$

while the mass is given by

$$M_\oplus = \frac{\mu_\oplus}{G} = V_\oplus\, \rho_\oplus = 5.9761 \times 10^{27}\ (1 \pm 7.2 \times 10^{-4})\ \text{g} = (5.9761 \pm 0.0043) \times 10^{27}\ \text{g} \qquad (127)$$

and the polar radius now becomes

$$R_p = R_e\, (1-f) = 6356788\ (1 \pm 3.7 \times 10^{-6})\ \text{m} = 6356788 \pm 24\ \text{m} \qquad (128)$$

The unit for the moments of inertia is

$$M_\oplus R_e^2 = 2.4311_4 \times 10^{45} (1 \pm 7.3 \times 10^{-4}) g\ cm^2 = (2.4311_4 \pm 0.0018) \times 10^{45} g\ cm^2 \quad (129)$$

and therefore

$$C - A = J_2 \times M_\oplus R_e^2 = 2.6313 \times 10^{42} (1 \pm 9.1 \times 10^{-4}) g\ cm^2 = (2.6313 \pm 0.0024) \times 10^{42} g\ cm^2 \quad (130)$$

$$C = \frac{2}{3} q \times M_\oplus R_e^2 = 8.0415 \times 10^{44} (1 \pm 1.07 \times 10^{-3}) g\ cm^2 = (8.0415 \pm 0.0086) \times 10^{44} g\ cm^2 \quad (131)$$

It is now possible to give corresponding data for the Moon. The mass is given by

$$M_\leftmoon = \kappa M_\oplus = 7.3552 \times 10^{25} (1 \pm 1.02 \times 10^{-3})\ g = (7.3552 \pm 0.0075) \times 10^{25}\ g \quad (132)$$

while the mean visible radius is

$$R_\leftmoon = k R_e = 1\,738\,236\ (1 \pm 1.0 \times 10^{-4}) = 1\,738\,236 \pm 174\ m \quad (133)$$

and therefore the semi-axes of the three-axial Moon are

$$a = \frac{R_\leftmoon}{\sigma} = 1\,738\,946 \pm 186\ m \quad (134)$$

$$b = a \left(\frac{b}{a}\right) = 1\,738\,618 \pm 209\ m \quad (135)$$

$$c = a \left(\frac{c}{a}\right) = 1\,737\,854 \pm 188\ m \quad (136)$$

The unit for the Moon's moments of inertia is

$$M_\leftmoon a^2 = 2.2241_6 \times 10^{42} (1 \pm 1.23 \times 10^{-3})\ g\ cm^2 = (2.2241_6 \pm 0.0027) \times 10^{42} g\ cm^2 \quad (137)$$

and thus the moments of inertia are

$$A = 0.8849_{42} \times 10^{42} (1 \pm 1.73 \times 10^{-3})\ g\ cm^2 = (0.8849_{42} \pm 0.0015_3) \times 10^{42} g\ cm^2 \quad (138)$$

$$B = 0.8851_{09} \times 10^{42} (1 \pm 1.73 \times 10^{-3})\ g\ cm^2 = (0.8851_{09} \pm 0.0015_3) \times 10^{42} g\ cm^2 \quad (139)$$

$$C = 0.8854_{98} \times 10^{42} (1 \pm 1.73 \times 10^{-3})\ g\ cm^2 = (0.8854_{98} \pm 0.0015_3) \times 10^{42} g\ cm^2 \quad (140)$$

$$C - \frac{A + B}{2} = (0.000\,473 \pm 0.000\,007) \times 10^{42}\ g\ cm^2 \quad (141)$$

$$B - A = (0.000\,167 \pm 0.000\,012) \times 10^{42}\ g\ cm^2 \quad (142)$$

The oblateness coefficients of the potential function of the Moon are

$$J_2 = \frac{C - (A + B)/2}{M_\leftmoon a^2} = \frac{2}{3} J = 0.000\,2125 \pm 0.000\,0029 \quad (143)$$

$$J_2^{(2)} = \frac{B-A}{4\,M_\leftmoon\,a^2} = \frac{1}{6}\,K = 0.000\,0188 \pm 0.000\,0013 \qquad (144)$$

The derived value for the equatorial radius of the Earth (eq. 124) is in good agreement with the following values:

Author	Year	Ref.	$R_\oplus$
W. M. Kaula	1961	55	6 378 163 ± 21 m
V. C. Clarke, Jr.	1962	56	6 378 165 ± 25
I. Fischer	1962	57	6 378 166
Present Report	1962		6 378 170 ± 20

I. Fisher's value for $1/\kappa = M_\oplus / M_\leftmoon = 81.268$ is also in good agreement with the value in this report. The presented system of constants is not only a consistent one, but the most serious discrepancy has been removed in determining the gravitational parameter $\mu_\oplus$ from terrestrial data and, on the other hand, from the lunar mean motion in combination with radar measurements of the Moon's distance.

Finally, the present data for the Moon's moments of inertia are compared with the values of other authors in the following table:

Author	Ref.	A 10^{35} kg·m^2	B 10^{35} kg·m^2	C 10^{35} kg·m^2	$C-(A+B)/2$ 10^{35} kg·m^2	$B-A$ 10^{35} kg·m^2
B. E. Kalensher	58	0.87976	0.87985	0.88032	0.00051	0.00009
Makemson, Baker, Westrom	13	0.88837	0.88856	0.88893	0.00047	0.00019
V. C. Clarke, Jr.	56	0.88746	0.88764	0.88801	0.00046	0.00018
Present Report	---	0.88494	0.88511	0.88550	0.00047	0.00017

The values of V. C. Clarke, Jr. are used for the Ranger Program.

14. THE EARTH ELLIPSOID

The equation of the rotational ellipsoid or spheroid is

$$\frac{x^2+y^2}{R_\oplus^2} + \frac{z^2}{R_p^2} = 1 \qquad (145)$$

where

$$x = R\cos\phi\cos\lambda = R_\oplus\cos\psi\cos\lambda = \rho_n\cos\varphi\cos\lambda \qquad (146)$$

$$y = R\cos\phi\sin\lambda = R_\oplus\cos\psi\sin\lambda = \rho_n\cos\varphi\sin\lambda \qquad (147)$$

$$z = R\sin\phi = R_p\sin\psi = \rho_n(1-e^2)\sin\varphi \qquad (148)$$

and R_e is the equatorial Earth radius, R_p the polar Earth radius, R the local Earth radius, ρ_n the normal radius of curvature, λ the geographic longitude (positive eastward of Greenwich), ϕ the geocentric latitude, ψ the reduced latitude, φ the geodetic or geographic ($\approx$ astronomical) latitude, and e the first eccentricity of the meridian ellipse. Introducing the second eccentricity, ϵ, and the flattening (oblateness, ellipticity), f, the following relations hold

$$f = \frac{R_e - R_p}{R_e} = 1 - \sqrt{1 - e^2} = 1 - \frac{1}{\sqrt{1 + \epsilon^2}} \approx \frac{1}{2} e^2 + \frac{1}{8} e^4 + \cdots + \frac{1 \cdot 1 \cdot 3 \cdot 5 \cdots (2\kappa - 3)}{2 \cdot 4 \cdot 6 \cdot 8 \cdots (2\kappa)} e^{2\kappa} + \cdots \tag{149}$$

$$e^2 = \frac{R_e^2 - R_p^2}{R_e^2} = \frac{\epsilon^2}{1 + \epsilon^2} = f(2 - f) = 2f - f^2 \tag{150}$$

$$\epsilon^2 = \frac{R_e^2 - R_p^2}{R_p^2} = \frac{e^2}{1 - e^2} = \frac{f(2 - f)}{(1 - f)^2} = 2f + 3f^2 + \cdots + (\kappa + 1) f^\kappa + \cdots \tag{151}$$

thus

$$\frac{R_p}{R_e} = 1 - f = \sqrt{1 - e^2} = \frac{1}{\sqrt{1 + \epsilon^2}} \tag{152}$$

The different latitude angles are related by

$$\tan \phi = \sqrt{1 - e^2} \tan \psi = (1 - e^2) \tan \varphi \tag{153}$$

$$\tan \phi = (1 - f) \tan \psi = (1 - f)^2 \tan \varphi \tag{154}$$

By differentiation the relation

$$\frac{R^2}{R_p} d\phi = R_e \, d\psi = \rho \, d\varphi \tag{155}$$

follows.

Thus the line element is

$$ds^2 = dx^2 + dy^2 + dz^2 = dr^2 + r^2 d\phi^2 + r^2 \cos^2 \phi \, d\lambda^2 = R_e^2 (1 - e^2 \cos^2 \psi) \, d\psi^2 + R_e^2 \cos^2 \psi \, d\lambda^2 \tag{156}$$

The parameter ρ is the mean radius of curvature, and is correlated with the normal radius of curvature

$$\rho_n = \frac{R_e}{(1 - e^2 \sin^2 \varphi)^{1/2}} = \frac{R_e^2 / R_p}{(1 + \epsilon^2 \cos^2 \varphi)^{1/2}} = R \frac{\cos \phi}{\cos \varphi} = \tag{157}$$

$$= R_e \left[1 + \frac{1}{2} e^2 \sin^2 \varphi + \frac{3}{8} e^4 \sin^4 \varphi + \frac{5}{16} e^6 \sin^6 \varphi + \cdots \right]$$

and to the meridional radius of curvature

$$\rho_m = \frac{R_e(1-e^2)}{(1-e^2\sin^2\varphi)^{3/2}} = \frac{R_p^2/R_e}{(1-e^2\sin^2\varphi)^{3/2}} = \frac{R_e^2/R_p}{(1+\epsilon^2\cos^2\varphi)^{3/2}}$$

$$= R_e(1-e^2)\left[1+\frac{3}{2}e^2\sin^2\varphi+\frac{15}{8}e^4\sin^4\varphi+\frac{35}{16}e^6\sin^6\varphi+\cdots\right] \tag{158}$$

by the relation

$$\rho = \sqrt{\rho_m\rho_n} = \frac{R_p}{1-e^2\sin^2\varphi} = \frac{R_e^2/R_p}{1+\epsilon^2\cos^2\varphi} = R_p\left[1+e^2\sin^2\varphi+e^4\sin^4\varphi+e^6\sin^6\varphi+\cdots\right] \tag{159}$$

The radius of a parallel of latitude is $\rho_n\cos\varphi = R_e\cos\psi = R\cos\phi$. Because f or e^2 are small quantities the latitudes ϕ, ψ, and φ will not differ very much from each other. Therefore it is very useful to have rapidly converging series developments available for the differences $\phi-\varphi$ and $\psi-\varphi$. With

$$m = \frac{R_e^2-R_p^2}{R_e^2+R_p^2} = \frac{1-(1-e^2)}{1+(1-e^2)} = \frac{e^2}{2-e^2} = f+\frac{1}{2}f^2-\frac{1}{4}f^4+\cdots \tag{160}$$

there is

$$\phi = \varphi - m\sin 2\varphi+\frac{m^2}{2}\sin 4\varphi-\frac{m^3}{3}\sin 6\varphi\pm\cdots \tag{161}$$

$$\varphi = \phi + m\sin 2\phi+\frac{m^2}{2}\sin 4\phi+\frac{m^3}{3}\sin 6\phi+\cdots \tag{162}$$

and with

$$n = \frac{R_e-R_p}{R_e+R_p} = \frac{1-(1-f)}{1+(1-f)} = \frac{f}{2-f} = \frac{1}{2}f+\frac{1}{4}f^2+\cdots \tag{163}$$

there is

$$\psi = \varphi - n\sin 2\varphi+\frac{n^2}{2}\sin 4\varphi-\frac{n^3}{3}\sin 6\varphi\pm\cdots \tag{164}$$

$$\varphi = \psi + n\sin 2\psi+\frac{n^2}{2}\sin 4\psi+\frac{n^3}{3}\sin 6\psi+\cdots \tag{165}$$

An accurate formula for the difference $\varphi-\phi$ is given by

$$\tan(\varphi-\phi) = \frac{e^2\tan\varphi}{1+(1-e^2)\tan^2\varphi} = \frac{e^2\sin\varphi\cos\varphi}{1-e^2\sin^2\varphi} \tag{166}$$

The local Earth radius (radius vector) can be accurately calculated from the relations

$$R = \sqrt{x^2+y^2+z^2} = \frac{R_p}{\sqrt{1-e^2\cos^2\phi}} = R_e\sqrt{1-e^2\sin^2\psi} = R_e\sqrt{\frac{1-e^2(2-e^2)\sin^2\varphi}{1-e^2\sin^2\varphi}}$$

$$= R_e\sqrt{\frac{1-4m(1+m)^{-2}\sin^2\varphi}{1-4n(1+n)^{-2}\sin^2\varphi}} = \frac{1+n}{1+m}R_e\sqrt{\frac{1+m^2+2m\cos 2\varphi}{1+n^2+2n\cos 2\varphi}} \tag{167}$$

By taking the logarithm of the last relation there follows

$$\ln \frac{R}{R_e} = \ln \frac{1+n}{1+m} + \frac{1}{2} \ln (1 + m^2 + 2m \cos 2\varphi) - \frac{1}{2} \ln (1 + n^2 + 2n \cos 2\varphi)$$

or, using a known series development,

$$\log \frac{R}{R_e} = \log \frac{1+n}{1+m} + M \left[(m-n) \cos 2\varphi - \frac{m^2 - n^2}{2} \cos 4\varphi + \frac{m^3 - n^3}{3} \cos 6\varphi \mp \cdots \right] \quad (168)$$

where M is the module ($M = 0.43\,429\,44819$). This series is due to Encke.

Conventional power series for R/R_e can be obtained as follows:

$$\frac{R}{R_e} = (1 + \epsilon^2 \sin^2 \phi)^{-1/2} = 1 - \frac{1}{2} \epsilon^2 \sin^2 \phi + \frac{3}{8} \epsilon^4 \sin^4 \phi - \frac{5}{16} \epsilon^6 \sin^6 \phi \pm \cdots \quad (169)$$

The above-mentioned power series for the local Earth radius can also be written

$$\frac{R}{R_e} = 1 - \left(\frac{1}{2} \epsilon^2 - \frac{3}{8} \epsilon^4 + \frac{5}{16} \epsilon^6 \right) \sin^2 \phi - \left(\frac{3}{32} \epsilon^4 - \frac{5}{64} \epsilon^6 \right) \sin^2 2\phi + \frac{5}{64} \epsilon^6 \sin^2 \phi \sin^2 2\phi + \cdots \quad (170)$$

or

$$\frac{R}{R_e} = 1 - f \sin^2 \phi - \left(\frac{3}{8} f^2 + \frac{1}{2} f^3 \right) \sin^2 2\phi + \frac{5}{8} f^3 \sin^2 \phi \sin^2 2\phi + \cdots \quad (171)$$

using eq. (151).

In order to obtain power series for the local Earth radius as a function of the geodetic latitude, φ, it is useful to set

$$k = \frac{4m}{(1+m)^2} = e^2 (2 - e^2) \; ; \; k' = \frac{4n}{(1+n)^2} = f (2 - f) = e^2 \; ; \; k/k' = 2 - e^2 \quad (172)$$

the non-dimensional local Earth radius is now

$$\frac{R}{R_e} = 1 - \frac{1}{2} (k - k') \sin^2 \varphi - \frac{1}{8} (k^2 + 2kk' - 3k'^2) \sin^4 \varphi - \frac{1}{16} (k^3 + k^2 k' + 3kk'^2 - 5k'^3) \sin^6 \varphi - \cdots \quad (173)$$

or

$$\frac{R}{R_e} = 1 - \frac{1}{2} e^2 [(2 - e^2) - 1] \sin^2 \varphi - \frac{1}{8} e^4 [(2 - e^2)^2 + 2 (2 - e^2) - 3] \sin^4 \varphi$$

$$- \frac{1}{16} e^6 [(2 - e^2)^3 + (2 - e^2)^2 + 3 (2 - e^2) - 5] \sin^6 \varphi - \cdots \quad (174)$$

Because

$$e^2 = 2f - f^2 \; ; \quad 2 - e^2 = 2 - 2f + f^2$$

there is, also,

$$\frac{R}{R_e} = 1 - \left(f - \frac{5}{2}f^2 + 2f^3\right)\sin^2\varphi - \left(\frac{5}{2}f^2 - \frac{17}{2}f^3\right)\sin^4\varphi - \frac{13}{2}f^3\sin^6\varphi - \cdots$$

$$= 1 - f\sin^2\varphi + \left(\frac{5}{8}f^2 - \frac{1}{2}f^3\right)\sin^2 2\varphi + \frac{13}{8}f^3\sin^2\varphi\,\sin^2 2\varphi + \cdots$$

$$= 1 - \frac{1}{2}f + \frac{5}{16}f^2 + \frac{5}{32}f^3 + \left(\frac{1}{2}f - \frac{13}{64}f^3\right)\cos 2\varphi - \left(\frac{5}{16}f^2 + \frac{5}{32}f^3\right)\cos 4\varphi + \frac{13}{64}f^3\cos 6\varphi + \cdots \tag{175}$$

It is also important to know the arc corresponding to 1° in longitude, namely

$$\nu = \frac{\pi}{180}\rho_n\cos\varphi = \frac{\pi}{180}\frac{R_e\cos\varphi}{(1 - e^2\sin^2\varphi)^{1/2}}$$

$$= \frac{\pi}{180}R_e\cos\varphi\left(1 + \frac{1}{2}e^2\sin^2\varphi + \frac{3}{8}e^4\sin^4\varphi + \cdots\right)$$

$$= \frac{\pi}{180}R_e\left(1 + \frac{1}{8}e^2 + \frac{3}{64}e^4\right)\cos\varphi - \left(\frac{e^2}{8} + \frac{9}{128}e^4\right)\cos 3\varphi + \frac{3}{128}e^4\cos 5\varphi \mp \cdots \tag{176}$$

and the arc corresponding to 1° in latitude, namely

$$\mu = \frac{\pi}{180}\rho_m = \frac{\pi}{180}\frac{R_e(1 - e^2)}{(1 - e^2\sin^2\varphi)^{3/2}} = \frac{\pi}{180}R_e(1 - e^2)\left[1 + \frac{3}{2}e^2\sin^2\varphi + \frac{15}{8}e^4\sin^4\varphi + \cdots\right]$$

$$= \frac{\pi}{180}\frac{R_p^2}{R_e}\left[1 + \frac{3}{4}e^2 + \frac{45}{64}e^4 - \left(\frac{3}{4}e^2 + \frac{15}{16}e^4\right)\cos 2\varphi + \frac{15}{64}e^4\cos 4\varphi \mp \cdots\right] \tag{177}$$

The length of a meridian quadrant is given by

$$Q_m = \frac{\pi}{2}\overline{\rho}_m = \int_0^{\pi/2}\frac{R_e(1 - e^2)}{(1 - e^2\sin^2\varphi)^{3/2}}\,d\varphi = R_e(1 - e^2)\int_0^1\frac{dz}{(1 - e^2z^2)\sqrt{(1 - z^2)(1 - e^2z^2)}}$$

$$= R_e(1 - e^2)\prod\left(\frac{\pi}{2}, -e^2, e\right) = R_e(1 - e^2)\int_0^{\pi/2}\left[1 + \frac{3}{2}e^2\sin^2\varphi + \frac{15}{8}e^4\sin^4\varphi + \frac{35}{16}e^6\sin^6\varphi + \cdots\right]d\varphi$$

$$= \frac{\pi}{2}R_e(1 - e^2)\left[1 + \frac{3}{4}e^2 + \frac{45}{64}e^4 + \frac{175}{256}e^6 + \cdots\right]$$

$$= \frac{\pi}{2}R_e\left(1 - \frac{1}{4}e^2 - \frac{3}{64}e^4 - \frac{5}{256}e^6 - \cdots\right)$$

$$= \frac{\pi}{2}R_e\left(1 - \frac{1}{2}f + \frac{1}{16}f^2 + \frac{1}{32}f^3 + \cdots\right) \tag{178}$$

The volume of the Earth spheroid is simply given by

$$V = \frac{4}{3}\pi R_e^2 R_p = \frac{4}{3}\pi R_e^3 (1-f) \tag{179}$$

while the surface area follows from

$$S = 4\pi R_e R_p \int_0^1 \sqrt{1+\epsilon^2 z^2}\, dz = 2\pi R_e R_p \left[\sqrt{1+\epsilon^2} + \frac{1}{\epsilon}\sinh^{-1}\epsilon\right]$$

$$= 2\pi R_e^2 \left[1 + \frac{\sinh^{-1}\epsilon}{\epsilon\sqrt{1+\epsilon^2}}\right] = 2\pi R_e^2 \left[1 + \frac{\ln(\epsilon+\sqrt{1+\epsilon^2})}{\epsilon\sqrt{1+\epsilon^2}}\right]$$

$$= 2\pi R_e^2 \left[1 + \left(1 - \frac{1}{6}\epsilon^2 + \frac{3}{40}\epsilon^4 - \frac{5}{112}\epsilon^6 \pm\cdots\right)\left(1 - \frac{1}{2}\epsilon^2 + \frac{3}{8}\epsilon^4 - \frac{5}{16}\epsilon^6 \pm\cdots\right)\right]$$

$$= 4\pi R_e^2 \left(1 - \frac{1}{3}\epsilon^2 + \frac{4}{15}\epsilon^4 - \frac{8}{35}\epsilon^6 - \cdots\right) = 4\pi R_e^2 \left(1 - \frac{2}{3}f + \frac{1}{15}f^2 + \frac{4}{105}f^3 + \cdots\right) \tag{180}$$

These formulas will now be used to derive the Earth's dimensions and other Earth parameters. Taking $R_e = 6378170 \pm 20$ m and $1/f = 298.30 \pm 0.05$ yields

$$e^2 = 0.006\,693\,422 \quad , \quad e = 0.081\,813\,334$$

$$\epsilon^2 = 0.006\,738\,525 \quad , \quad \epsilon = 0.082\,088\,522$$

$$m = 0.003\,357\,949 = 692.''627$$

$$n = 0.001\,678\,979 = 346.''314$$

The mean radius is

$$\bar{R} = \frac{2R_e + R_p}{3} = 6\,371\,043 \pm 21 \text{ m} \tag{181}$$

The radius for the geodetic latitude $\varphi = \sin^{-1}\sqrt{1/3} = 35°\,15'\,51.''8$ ($\phi = 35°\,4'\,59.''5$) is

$$R_1 = R_e \sqrt{1 - \frac{e^2(1-e^2)}{3-e^2}} = R_e \left[1 - \frac{1}{3}f + \frac{5}{9}f^2 + \frac{1}{3}f^2 + \cdots\right] = 6.371\,083 \pm 21 \text{ m} \tag{182}$$

The radius for the geocentric latitude $\phi = \sin^{-1}\sqrt{1/3} = 35°\,15'\,51.''8$ ($\varphi = 35°\,26'\,45.''5$) is

$$R_2 = R_e \sqrt{1 - \frac{e^2}{3-2e^2}} = R_e \left[1 - \frac{1}{3}f - \frac{1}{3}f^2 - \frac{7}{27}f^3 - \cdots\right] = 6\,371\,019 \pm 21 \text{ m} \tag{183}$$

The radius for a sphere of equal area is

$$R_S = (S/4\pi)^{1/2} = R_e \left(1 - \frac{1}{3}f^2 - \frac{1}{45}f^3 + \frac{11}{945}f + \cdots\right) = 6\,371\,041 \pm 21 \text{ m} \tag{184}$$

while the radius for a sphere of equal volume is

$$R_V = (3V/4\pi)^{1/3} = R_e (1-f)^{1/3} = R_e \left(1 - \frac{1}{3}f - \frac{1}{9}f^2 - \frac{5}{81}f^3 - \cdots\right) = 6\,371\,035 \pm 21 \text{ m} \tag{185}$$

The surface area is

$$S = 4\pi R_e^2 \left(1 - \frac{2}{3} f + \frac{1}{15} f^2 + \frac{4}{105} f^3 + \cdots\right) = (5.100\,711 \pm 0.000\,034) \times 10^{14}\ \mathrm{m}^2 \quad (186)$$

while the volume is given by

$$V = \frac{4}{3}\pi R_e^3 (1 - f) = (1.083\,225 \pm 0.000\,011) \times 10^{21}\ \mathrm{m}^3 \quad (187)$$

The radius of curvature at the pole is

$$\rho_p = R_e^2 / R_p = R_e / (1 - f) = 6\,399\,624 \pm 24\ \mathrm{m} \quad (188)$$

while the meridional radius of curvature at the equator is given by

$$\rho_{m_e} = R_p^2 / R_e = R_e (1 - f)^2 = R_e (1 - e^2) = 6\,335\,478 \pm 27\ \mathrm{m} \quad (189)$$

The length of an equatorial quadrant is

$$Q_e = \frac{\pi}{2} R_e = 10\,018\,806 \pm 31\ \mathrm{m} \quad (190)$$

while the length of a meridional quadrant is

$$Q_m = \frac{\pi}{2} R_e \left(1 - \frac{1}{2} f + \frac{1}{16} f^2 + \frac{1}{32} f^3 + \cdots\right) = 10\,002\,020 \pm 34\ \mathrm{m} \quad (191)$$

Therefore the arc corresponding to 1° in longitude is at the equator

$$\nu_e = Q_e / 90 = \frac{\pi}{180} R_e = 111\,320.07 \pm 0.35\ \mathrm{m} \quad (192)$$

while the arc corresponding to 1° in latitude is at the equator

$$\mu_e = \frac{\pi}{180} \rho_{m_e} = \frac{\pi}{180} R_e (1 - f)^2 = 110\,574.95 \pm 0.47\ \mathrm{m} \quad (193)$$

at the pole

$$\mu_p = \frac{\pi}{180} \rho_p = \frac{\pi}{180} R_e / (1 - f) = 111\,694.51 \pm 0.41\ \mathrm{m} \quad (194)$$

and in the average

$$\bar{\mu} = Q_m / 90 = \frac{\pi}{180} R_e \left(1 - \frac{1}{2} f + \frac{1}{16} f^2 + \frac{1}{32} f^3 + \cdots\right) = 111\,133.56 \pm 0.38\ \mathrm{m} \quad (195)$$

Finally, a few series developments are given for the Earth radius, for the various definitions of latitude, and for the radii of curvature:

$$\phi = \varphi - 692.''627 \sin 2\varphi + 1.''163 \sin 4\varphi \mp \cdots$$

$$\varphi = \phi + 692.''627 \sin 2\phi + 1.''163 \sin 4\phi + \cdots \quad (196)$$

and

$$\psi = \varphi - 346.''314 \sin 2\varphi + 0.''291 \sin 4\varphi \mp \cdots$$

$$\varphi = \psi + 346.''314 \sin 2\psi + 0.''291 \sin 4\psi + \cdots \quad (197)$$

furthermore

$$\log \frac{R}{R_e} = 9.9992\,7266 + 0.0007\,2917 \cos 2\varphi - 0.0000\,0184 \cos 4\varphi + \cdots \quad (198)$$

and

$$\frac{R}{R_e} = 1 - 0.00336\,9263 \sin^2\phi + 0.00001\,7028 \sin^4\phi - 0.00000\,0096 \sin^6\phi \pm \cdots$$

$$= 1 - 0.00335\,2330 \sin^2\phi - 0.00000\,4233 \sin^2 2\phi + 0.00000\,0024 \sin^2\phi \sin^2 2\phi + \cdots$$

$$= 0.99832\,1724 + 0.00167\,6162 \cos 2\phi + 0.00000\,2111 \cos 4\phi + 0.00000\,0003 \cos 6\phi + \cdots \quad (199)$$

or

$$R = 6378\,170.0 - 21489.7 \sin^2\phi + 108.6 \sin^4\phi - 0.6 \sin^6\phi \pm \cdots$$

$$= 6378\,170.0 - 21381.7 \sin^2\phi - 27.0 \sin^2 2\phi + 0.2 \sin^2\phi \sin^2 2\phi + \cdots$$

$$= 6367\,465.7 + 10690.8 \cos 2\varphi + 13.5 \cos 4\varphi + 0.0_2 \cos 6\varphi + \cdots \quad (200)$$

and

$$\frac{R}{R_e} = 1 - 0.00332\,4310 \sin^2\varphi - 0.00002\,7777 \sin^4\varphi - 0.00000\,0241 \sin^6\varphi - \cdots$$

$$= 1 - 0.00335\,2330 \sin^2\varphi - 0.00000\,7004 \sin^2 2\phi + 0.00000\,0060 \sin^2\phi \sin^2 2\phi + \cdots$$

$$= 0.99832\,0349 + 0.00167\,6156 \cos 2\varphi + 0.00000\,3487 \cos 4\varphi + 0.00000\,0008 \cos 6\varphi + \cdots \quad (201)$$

or

$$R = 6378\,170.0 - 21203.0 \sin^2\varphi - 177.2 \sin^4\varphi - 1.5 \sin^6\varphi - \cdots$$

$$= 6378\,170.0 - 21381.7 \sin^2\varphi - 44.7 \sin^2 2\varphi + 0.4 \sin^2\varphi \sin^2 2\varphi + \cdots$$

$$= 6367\,456.9 + 10690.8 \cos 2\varphi + 22.2 \cos 4\varphi + 0.0_5 \cos 6\varphi + \cdots \quad (202)$$

and

$$\frac{\mu}{\mu_e} = \frac{\rho_m}{\rho_{m_e}} = 1 + 0.01004\,0132 \sin^2 \varphi + 0.00008\,4004 \sin^4 \varphi$$

$$= 1.00505\,1568 - 0.00506\,2068 \cos 2\varphi + 0.00001\,0500 \cos 4\varphi \mp \cdots \quad (203)$$

or

$$\mu = 110\,574.95 + 1110.19 \sin^2 \varphi + 9.29 \sin^4 \varphi + \cdots$$

$$= 111\,133.53 - 559.74 \cos 2\varphi + 1.16 \cos 4\varphi \mp \cdots \quad (204)$$

$$\frac{\nu}{\nu_e} = \frac{\rho_n}{R_e} \cos \varphi = 1.00083\,8785 \cos \varphi - 0.00083\,9841 \cos 3\varphi + 0.00000\,1059 \cos 5\varphi + \cdots \quad (205)$$

or

$$\nu = 111\,413.44 \cos \varphi - 93.49 \cos 3\varphi + 0.12 \cos 5\varphi \quad (206)$$

and

$$\frac{\rho_n}{R_e} = 1 + 0.00334\,6711 \sin^2 \varphi + 0.00001\,6801 \sin^4 \varphi + 0.00000\,0094 \sin^6 \varphi + \cdots$$

$$= 1 + 0.00336\,3605 \sin^2 \varphi - 0.00000\,4224 \sin^2 2\varphi - 0.00000\,0023 \sin^2 \varphi \sin^2 2\varphi$$

$$= 1.00167\,9685 - 0.00168\,1800 \cos 2\varphi + 0.00000\,2118 \cos 4\varphi - 0.00000\,0003 \cos 6\varphi \quad (207)$$

or

$$\rho_n = 6378\,170.0 + 21345.9 \sin^2 \varphi + 107.2 \sin^4 \varphi + 0.6 \sin^6 \varphi + \cdots$$

$$= 6378\,170.0 + 21453.6 \sin^2 \varphi - 26.9 \sin^2 2\varphi - 0.1_5 \sin^2 \varphi \sin^2 2\varphi + \cdots$$

$$= 6388\,883.\dot{3} - 10726.8 \cos 2\varphi + 13.5 \cos 4\varphi - \cdots \quad (208)$$

REFERENCES

1. C. W. Allen: *Astrophysical Quantities.* 263pp., The Athlone Press, University of London, 1955.

2. G. W. Pettengill, H. W. Briscoe, J. V. Evans, E. Gehrels, G. M. Hyde, L. G. Kraft, R. Price, and W. B. Smith: *A Radar Investigation of Venus.* The Astronomical Journal, vol. 67, no. 4, pp. 181-190, May 1962.

3. D. O. Muhleman, D. B. Holdridge, and N. Block: *The Astronomical Unit Determined by Radar Reflections from Venus.* The Astronomical Journal, vol. 67, no. 4, pp. 191 - 203, May 1962.

4. K. D. Froome: *Precision Determination of the Velocity of Electromagnetic Waves.* Nature, vol. 181, no. 4604, p. 258, 25 Jan. 1958.

5. Simon Newcomb: *Tables of the Motion of the Earth on Its Axis and Around the Sun.* Astronomical Papers prepared for the use of the American Ephemeris and Nautical Almanac, vol. vi, part 1, 1895.

6. H. Spencer Jones: *The Rotation of the Earth, and the Secular Accelerations of the Sun, Moon and Planets.* Monthly Notices, Royal Astron. Soc., vol. 99, no. 7, pp. 541- 558, 1939.

7. G. M. Clemence: *On the System of Astronomical Constants.* The Astronomical Journal, vol. 53, no. 6, pp. 169-179, May 1948.

8. E. W. Brown: *Tables of the Motion of the Moon.* Yale University Press, New Haven, 1919.

9. *Procès Verbaux des Séances du Comité International des Poids et Mesures*, deuxième Série, tôme 25, p. 77, 1957.

10. W. deSitter and Dirk Brouwer: *On the System of Astronomical Constants.* Bulletin of the Astronomical Institutes of the Netherlands, vol. VIII, no. 307, pp. 213-231, 8 July 1938.

11. Harold Jeffreys: *The Earth. Its Origins, History and Physical Constitution.* Cambridge University Press, Fourth Edition, 1959.

12. S. Herrick, R.M.L. Baker, Jr. and C. G. Hilton: *Gravitational and Related Constants for Accurate Space Navigation.* American Rocket Society Paper 497-57, October 1957.

13. M. W. Makemson, R.M.L. Baker, Jr. and G. B. Westrom: *Analysis and Standardization of Astrodynamic Constants.* Univ. of California, Los Angeles. Astrodynamical Report no. 12, February 1961. Journal of the Astronautical Sciences, vol. VIII, no. 1, Spring 1961; AAS Preprint 61-27, January 1961.

14. Simon Newcomb: *The Elements of the Four Inner Planets and the Fundamental Constants of Astronomy.* Washington, D.C., 1895 (Supplement to The American Ephemeris and Nautical Almanac for 1897).

REFERENCES (Continued)

15. Eugene Rabe: *Derivation of Fundamental Astronomical Constants from Observations of Eros During 1926-1945.* The Astronomical Journal, vol. 55, no. 1184, pp. 112-126, 1950. *Additional Note on the Solar Parallax from Eros.* The Astronomical Journal, vol. 59, pp. 409-411, 1954.

16. Julius Bauschinger: Enzykl. d. Math. Wiss. 6 II, no. 17, 1919. (The value is given in Ref. 45, p. 51).

17. H. Battermann: Veröffentl. d. Sternw. Koenigsberg/Pr. (The value is given in Ref. 45, p. 51)

18. Dirk Brouwer and O. B. Watts: Unpublished. (The value is given in Ref. 45, p. 52).

19. David Gill: *Determination of the Solar Parallax and the Mass of the Moon from Heliometer Observations of Iris, Victoria and Sappho Made in the Years 1888 and 1890.* Ann. Cape Observatory, vol. 6, 1896, and vol. 7, 1897.

20. A. R. Hinks: *Solar Parallax.* Monthly notices, Royal Astronomical Soc., vol. 70, no. 9, p. 588, 1909.

21. H. Spencer Jones: *The Solar Parallax and the Mass of the Moon from Observations of Eros at the Opposition of 1931.* Mem. Royal Astr. Soc., vol. 66, pt. 2, 56pp., London, 1941.

22. H. R. Morgan and F. P. Scott: *Observations of the Sun 1900-1937 Compared with Newcomb's Tables.* The Astronomical Journal, vol. 47, p. 193, 1939.

23. Harold Jeffreys: *On the Lunar Equation.* Monthly Notices of the Royal Astronomical Soc. (London), vol. 102, no. 4, pp. 194-204, 1942.

24. Erwin Delano: *The Lunar Equation from Observations of Eros 1930-31.* The Astronomical Journal, vol. 55, pp. 129-132, 1950.

25. Simon Newcomb: *Researches on the Motion of the Moon, Part II.* Astr. Paper. Amer. Eph., vol. IX, p. 39, 1912.

26. The American Ephemeris and Nautical Almanac for the Year 1962, U.S. Government Printing Office, Washington, D.C., 1960. Explanatory Supplement to the Astronomical Ephemeris and the American Ephemeris and Nautical Almanac, London, 1961.

27. H. Hirose and R. Manabe: *Motion and Figure of the Moon.* Transactions I.A.U., vol. 9, p. 265, 1955.

28. George H. Darwin: *The Theory of the Figure of the Earth, Carried to the Second Order of Small Quantities.* Monthly Notices Roy. Astron. Soc., vol. 60, pp. 82-124, 1899.

29. F. R. Helmert: *Die mathematischen und physikalischen Theorien der Höheren Geodäsie.* I. *Die mathematischen Theorien.* Leipzig, 1880. II. *Die physikalischen Theorien.* Leipzig, 1884.

REFERENCES (Continued)

30. E. C. Bullard: *The Figure of the Earth.* Monthly Notices Roy. Astron. Soc., Geophys. Suppl., vol. 5, no. 6, 1948.

31. W. deSitter: *On the Flattening and the Constitution of the Earth.* Bulletin of the Astronomical Institutes of the Netherlands, vol. II, no. 55, pp. 97-108, 14 May 1924.

32. F. R. Helmert: *Neue Formeln für den Verlauf der Schwerkraft im Meeresniveau beim Festland.* Sitz-Ber. d. Kgl. Preuss. Akad. d. Wiss, vol. 41, pp. 676-68, Berlin 1915.

33. A. Berroth: *Die Erdgestalt und die Hauptträgheitsmomente A und B im Äquator aus Messungen der Schwerkraft.* Gerl. Beitr. Geophys., vol. 14, pp. 215-257, Leipzig, 1915-1918.

34. W. A. Heiskanen: *Untersuchungen über Schwerkraft und Isostasie.* Publ. Finn. Geod. Inst., no. 4, Helsinki, 1924.

35. W. A. Heiskanen: *Ist die Erde ein dreiachsiges Ellipsoid?* Gerlands Beitr. Geophys., vol. 19, pp. 356-377, Leipzig, 1928, Astr. Nachr., vol. 234, no. 5562, Kiel, 1928.

36. W. A. Heiskanen: *Investigations on the Gravity Formula.* Ann. Acad. Scient. Fennicae, series A, vol. 51, no. 8, Helsinki, 1938.

37. N. F. Shuravlev: *Die Bestimmung der Abplattung des Erdellipsoides aus gravimetrischen Messungen* (in Russian with English Abstract) Publ. Astro. Inst. Sternberg, vol. 14, pt. 2, Moscow, 1940.

38. Erkki Niskanen: *Gravity Formulas Derived by the Aid of the Level Land Stations.* Publ. Isos. Inst. IAG (Helsinki), no. 16, 1945; Ann. Acad. Scient. Fennicae, series A, no. III, 10, pp. 1-16, Helsinki, 1945.

39. Harold Jeffreys: *The Figures of the Earth and Moon* (Third Paper). Monthly Notices of the Roy. Astr. Soc., Geophys. Suppl, vol. 5, no. 7, pp. 219-247, July 1948.

40. H. Schütte: *Die Bestimmung der Abplattung der Erde aus der Schwereverteilung nach denn Schwereverzeichnis von N. F. Shuravlev.* Gerl. Beitr. Geophys., vol. 62, pp. 9-26, Leipsig, 1950.

41. U. A. Uotila: *Determination of the Shape of the Geoid.* Symposium: Size and Shape of the Earth, held at the Ohio State University, Columbus, Ohio, Nov. 13-15, 1956. Publ. no. 7, Inst. of Geodesy, Photogrammetry and Cartography, 1957.

42. W. A. Heiskanen; *Achievements of the World-wide Gravity Program of the Mapping and Charting Research Laboratory of the Ohio State University.* Report to the Toronto General Assembly of the IUGG in 1957.

43. F. Kühnen und Ph. Furtwängler: *Bestimmung der absoluten Grösse der Schwerkraft zu* Potsdam mit Reversionspendeln. Veröff. d. Preuss. Geod. Inst. N.F. 27, 1906.

44. W. A. Heiskanen and F. A. Vening Meinesz: *The Earth and Its Gravity Field.* x + 470 pp., McGraw-Hill Book Co., New York, 1958 (p. 75).

REFERENCES (Continued)

45. Landolt-Börnstein: *Zahlenwerte und Funktionen aus Physik, Chemie, Astronomie, Geophysik und Technik.* Vol. III, pp. 43-52 (A. Kopff: Astrometrische Konstanten) and pp. 256-270 (K. Jung: Schwerkraft und Erdfigur), Springer-Verlag, Berlin, 1952.

46. H. Andoyer: *Les formules de la précession après S. Newcomb.* Bulletin Astronomique (Paris), vol. 28, p. 67-76, 1911.

47. H. R. Morgan: *Systematic Corrections to the Albany General Catalogue.* The Astron. Jour., vol. 54, no. 1, pp. 1-9, Sept. 1948; Corrections to the Fundamental Catalogs. The Astron. Jour., vol. 54, no. 6, pp. 145-150, June 1949

48. Landolt-Börnstein: *Zahlenwerte und Funktionen.* (Ref. 45, p. 52.)

49. J. H. Oort: *The Constants of Precession of Galactic Rotation.* Bulletin of the Astron. Institutes of the Netherlands, vol. 9, p. 424 - 427, 1943.

50. R. R. Radau: *Sur la loi des densitées à l'intérieur de la Terre.* Comptes Rendus Acad. Sci. (Paris), vol. 100, pp. 972-974, 1885; Bulletin Astronomique 2, p. 157, 1885.

51. O. Callandreau: *Sur le développement en série du potential.* J. Polytech., 1889; Ann.de l'Observ. de Paris 19 E, 1889.

52. Harold Jeffreys: *On the Figures of the Earth and Moon.* Monthly Notices of the Roy. Astr. Soc., vol. 97, no. 1, pp. 3-15, Nov. 1936 or Geophys. Suppl., vol. 4, no. 1, pp. 1-13, Jan. 1937.

53. Harold Jeffreys: *The Moon's Libration in Longitude.* Monthly Notices of the Roy. Astr. Soc., vol. 117, no. 5, pp. 475-477, 1957.

54. Harold Jeffreys: *On the Figure of the Moon.* Monthly Notices Roy. Astr. Soc., vol. 122, pp. 421-432, 1961.

55. W. M. Kaula: *A Geoid and World Geodetic System Based on a Combination of Gravimetric, Astrogeodetic, and Satellite Data.* Jour. Geophys. Res., vol. 66, no. 6, pp. 1799-1811, June 1961.

56. Victor C. Clarke Jr.: *Constants and Related Data Used in Trajectory Calculations at the Jet Propulsion Laboratory.* Jet Propulsion Laboratory, Technical Report No. 32-273, 14 pp., 1 May 1962.

57. Irene Fischer: *Parallax of the Moon in Terms of a World Geodetic System.* The Astronomical Jour., vol. 67, no. 6, pp. 373-378, Aug. 1962.

58. B. E. Kalensher: *Selenographic Coordinates.* Jet Propulsion Laboratory, Technical Report No. 32-41, 31 pp., 24 February 1961.

SUMMARY

An internally consistent system of astrodynamic constants is derived based upon theoretical coupling relationships and the most recent available experimental data. A previously existing discrepancy in the value of the gravitational parameter of the earth (as derived by different methods) has been eliminated. Likewise, several inconsistencies in the previously available system of lunar constants have been removed.

A new method of determining the ratio of the masses of the Earth and Moon has been derived and the results are in agreement with other determinations.

An error study of each constant is presented; both relative and absolute probable errors are listed.

The results of this study can be summarized in the following list of astrodynamic constants:

1. GENERAL CONSTANTS

1. Newton's gravitation constant:

$$G = 6.670\ (1 \pm 0.0007) \times 10^{-8} = (6.670 \pm 0.005) \times 10^{-8}\ \mathrm{cm^3\ g^{-1}\ s^{-2}}(\mathrm{dyn\ cm^2\ g^{-2}})$$

2. Velocity of light:

$$c = 299\,792.5\ (1 \pm 3.3 \times 10^{-7}) = 299\,792.5 \pm 0.1\ \ \mathrm{km/s}$$

3. Solar parallax (Sun's equatorial horizontal parallax):

$$\pi_\odot = 8.''794\,14\ (1 \pm 5.8 \times 10^{-6}) = 8.''794\,14 \pm 0.''000\,05$$

4. Astronomical unit (mean Earth-Sun distance = $R_\oplus / \pi_\odot \sin 1''$):

$$\text{a. u.} = 149\,598\,700\ (1 \pm 2.7 \times 10^{-6}) = 149\,598\,700 \pm 400\ \ \mathrm{km}$$

5. Light year (distance which light travels in a year = $P_\oplus\ c$):

$$\text{l. y.} = 31\,556\,925.9747\ \ c = (9.460\,530 \pm 0.000\,003) \times 10^{12}\ \mathrm{km} = 63\,239.39 \pm 0.15\ \text{a. u.}$$

6. Parsec (distance in which 1 a. u. appears as $1'' = 1$ a. u./sin $1''$):

$$\mathrm{pc} = 206\,264.806\,247\ \text{a. u.} = (3.085\,695 \pm 0.000\,008) \times 10^{13}\,\mathrm{km} = 3.261\,651 \pm 0.000\,008\ \ \text{l. y.}$$

7. Light time for 1 a. u. :

$$\tau = \text{a.u.}/c = 499.008\ (1 \pm 3.6 \times 10^{-5}) = 499.008 \pm 0.018\ \ \mathrm{s}$$

8. Constant of aberration:

$$K = 20.''4956\ (1 \pm 3.5 \times 10^{-5}) = 20.''4956 \pm 0.''0007$$

9. Obliquity of ecliptic

$$\epsilon = 23°27'8.''26\ -\ 46.''844\ \mathrm{T} - 0.''0060\ \mathrm{T}^2 + 0.''00183\ \mathrm{T}^3$$

$$\cos\epsilon = 0.917\,3917\ ;\ \sin\epsilon = 0.397\,985\,5\ (1900.0)$$

10. Newcomb's constant of precession (per tropical century):

$$P = \frac{p_0}{\cos\epsilon} = 5493.''62 - 0.''003\,64\ \mathrm{T} = (N + 2.''96)^*$$

11. Luni-solar precession in longitude:

$$p_0 = p_\odot + p_\zeta = 5039.''804 + 0.''4930\ \mathrm{T} - 0.''000\,04\ \mathrm{T}^2 = (N + 2.''72)$$

---

* N refers to Newcomb's precessional data

12. Geodetic precession in longitude:

$$p_g = \frac{3}{2} (v_\oplus / c)^2 \, n_\oplus = 1.''9188 \pm 0.''0002 = (N + 1.''92)$$

13. Observed luni-solar precession in longitude:

$$p_1 = p_0 - p_g = 5037.''885 + 0.''4930 \, T - 0.''00004 \, T^2 = (N + 0.''80)$$

14. Planetary precession in right ascension:

$$\lambda = -m + n \cot \epsilon = 12.''473 - 1.''8870 \, T - 0.''00014 \, T^2 = (N + 0.''00)$$

15. General precession in longitude:

$$p = p_1 - \lambda \cos \epsilon = m \cos \epsilon + n \sin \epsilon = 5026.''441 + 2.''2229 \, T + 0.''00026 \, T^2 = (N + 0.''80)$$

16. General precession in right ascension:

$$m = p_1 \cos \epsilon - \lambda = 4609.''236 + 2.''7945 \, T + 0.''00012 \, T^2 = (N + 0.''73)$$

$$= 307.^s 2824 + 0.^s 18630 + 0.^s 000008 \, T^2 = (N + 0.^s 0487)$$

17. General precession in declination:

$$n = p_1 \sin \epsilon = 2005.''005 - 0.''8533 \, T - 0.''00037 \, T^2 = (N + 0.''32)$$

$$= 133.^s 6670 - 0.^s 05689 \, T - 0.^s 000025 \, T^2 = (N + 0.^s 0213)$$

18. Mean siderial time rate (for 1950.0):

$$\dot{\Theta}_m = 7.292\,115\,854\,79 \times 10^{-5} \text{ rad/s} = 1.002\,737\,909\,294 \; d_*/d \; (s_*/s)$$

$$= 15.041\,068\,639\,41 \; ''/s \; (°/h) = 360.985\,647\,346\,0 \; °/d$$

2. EARTH CONSTANTS

19. Semi-major axis of the Earth's orbit:

$$a_\oplus = 149\,598\,700 \, (1 \pm 2.7 \times 10^{-6}) = 149\,598\,700 \pm 400 \text{ km}$$

20. Siderial mean orbital motion (for 1950.0):

$$n_\oplus = 0.985\,609\,108\,0 \; °/d = 0.041\,067\,046\,15 \; ''/s \; (°/h)$$

$$= 1.990\,986\,581\,7 \times 10^{-7} \text{ rad/s}$$

21. Mean orbital velocity:

$$v_\oplus = a_\oplus n_\oplus = 29\,784.90\ (1 \pm 2.7 \times 10^{-6}) = 29\,784.90 \pm 0.08 \quad \text{m/s}$$

22. Mass ratio of the Sun to the Earth-Moon system:

$$\nu = \frac{M_\odot}{M_\oplus + M_4} = 328\,898.6\ (1 \pm 1.6 \times 10^{-5}) = 328\,898.6 \pm 5.2$$

23. Mass ratio of the Sun to the Earth:

$$\nu\ (1 + \kappa) = \frac{M_\odot}{M_\oplus} = 332\,947.6\ (1 \pm 2.0 \times 10^{-5}) = 332\,947.6 \pm 6.7$$

24. Gravitational parameter of the Earth:

$$\mu_\oplus = GM_\oplus = 398\,606.4\ (1 \pm 1.23 \times 10^{-5}) = 398\,606.4 \pm 4.9\ \text{km}^3/\text{s}^2$$

25. Mass:

$$M_\oplus = 5.9761 \times 10^{27} (1 \pm 7.2 \times 10^{-4}) = (5.9761 \pm 0.0043) \times 10^{27}\ \text{g}$$

26. Equatorial radius:

$$R_e = 6\,378\,170\ (1 \pm 3.14 \times 10^{-6}) = 6\,378\,170 \pm 20\ \text{m}$$

27. Polar radius:

$$R_p = 6\,356\,788\ (1 \pm 3.70 \times 10^{-6}) = 6\,356\,788 \pm 24\ \text{m}$$

28. Flattening (oblateness, ellipticity):

$$f = \frac{R_e - R_p}{R_e} = 0.003\,352\,33\ (1 \pm 1.7 \times 10^{-4}) = 0.003\,352\,33 \pm 0.000\,000\,56 = 1{:}\ (298.30 \pm 0.05)$$

$$1 - f = (1 - e^2)^{1/2} = (1 + \epsilon^2)^{-1/2} = R_p / R_e = 0.996\,647\,67\ (1 \pm 5.6 \times 10^{-7})$$

29. First eccentricity of the meridian ellipse:

$$e = 0.081\,813\,33 + 0.000\,006\,80$$

$$e^2 = f\,(2 - f) = 0.006\,693\,42 + 0.000\,001\,11$$

30. Second eccentricity of the meridian ellipse:

$$\epsilon = 0.082\,088\,52 \pm 0.000\,006\,87$$

$$\epsilon^2 = \frac{e^2}{1 - e^2} = 0.006\,738\,53 \pm 0.000\,001\,13$$

31. Mean radius:

$$\bar{R} = (2\ R_e + R_p)\ /\ 3 = 6\,371\,043\ (1 \pm 3.3 \times 10^{-6}) = 6\,371\,043 \pm 21\ \text{m}$$

32. Radius for geodetic latitude $\varphi = \sin^{-1}\sqrt{1/3} = 35°15'51.''8$

$$R_1 = 6\,371\,083\,(1 \pm 3.3 \times 10^{-6}) = 6\,371\,083 \pm 21 \text{ m}$$

33. Radius for geocentric latitude $\phi = \sin^{-1}\sqrt{1/3} = 35°15'51.''8$

$$R_2 = 6\,371\,019\,(1 \pm 3.3 \times 10^{-6}) = 6\,371\,019 \pm 21 \text{ m}$$

34. Radius for sphere of same surface area:

$$R_S = 6\,371\,041\,(1 \pm 3.3 \times 10^{-6}) = 6\,371\,041 \pm 21 \text{ m}$$

35. Radius for sphere of same volume:

$$R_V = 6\,371\,035\,(1 \pm 3.3 \times 10^{-6}) = 6\,371\,035 \pm 21 \text{ m}$$

36. Surface area:

$$S_\oplus = 5.100\,711 \times 10^{14}\,(1 \pm 6.6 \times 10^{-6}) = (5.100\,711 \pm 0.000\,034) \times 10^{14} \text{ m}^2$$

37. Volume:

$$V_\oplus = 1.083\,225 \times 10^{21}(1 \pm 1.0 \times 10^{-5}) = (1.083\,225 \pm 0.000\,011) \times 10^{21}\text{m}^3$$

38. Mean density:

$$\bar{\rho}_\oplus = 5.5170\,(1 \pm 7.3 \times 10^{-4}) = 5.5170 \pm 0.0040 \text{ g/cm}^3$$

39. Angular velocity of the Earth's rotation:

$$\Omega_m = 7.292\,115\,146\,46 \times 10^{-5} \text{rad/s} = 1.002\,737\,811\,891 \text{ rot/d}$$

$$= 15.041\,067\,178\,37 \text{ ''/s } (°/\text{h}) = 360.985\,612\,280\,8 \text{ °/d}$$

40. Rotational velocity at the equator:

$$\Omega_m R_e = 465.1035\,(1 \pm 3.2 \times 10^{-6}) = 465.1035 \pm 0.0015 \text{ m/s}$$

41. Centrifugal acceleration at the equator:

$$\Omega_m^2 R_e = 0.033\,915\,88\,(1 \pm 3.2 \times 10^{-6}) = 0.033\,915\,88 \pm 0.000\,000\,11 \text{ m/s}^2$$

42. Centrifugal acceleration factor:

$$\varpi_\oplus = \frac{\Omega^2 R_e^3}{G M_\oplus} = 3461.369 \times 10^{-6}(1 \pm 2.2 \times 10^{-5}) = (3461.369 \pm 0.076) \times 10^{-6}$$

43. Oblateness coefficients of the Earth's potential:

$$J = 1623.48 \times 10^{-6}(1 \pm 1.8 \times 10^{-4}) = (1623.48 \pm 0.29) \times 10^{-6}$$

$$K = \frac{6}{7} D = 8.85 \times 10^{-6}$$

$$J_2 = \frac{2}{3} J = 1082.32 \times 10^{-6}(1 \pm 1.8 \times 10^{-4}) = (1082.32 \pm 0.19) \times 10^{-6}$$

$$J_4 = -\frac{4}{15} K = -\frac{8}{35} D = -2.36 \times 10^{-6}$$

44. Coefficients of the Earth's gravity formula:

$$\beta = 5302.92 \times 10^{-6}; \quad \gamma = -5.85 \times 10^{-6}$$

45. Mass of the Earth's atmosphere:

$$M_{atm} = \frac{p_0}{g} \cdot S_\oplus = (10\,332.275 \text{ kg/m}^2) \cdot S_\oplus$$

$$= 5.270\,195 \times 10^{18}(1 \pm 6.6 \times 10^{-6}) = (5.270\,195 \pm 0.000\,035) \times 10^{18} \text{ kg}$$

46. Relative mass of the Earth's atmosphere:

$$A = M_{atm}/M_\oplus = 0.881\,88 \times 10^{-6}(1 \pm 7.3 \times 10^{-4}) = (0.881\,88 \pm 0.000\,64) \times 10^{-6}$$

47. Gravity acceleration correction factor:

$$\chi = g_e/(GM_\oplus/R_e^2) = 0.998\,165\,66\,(1 \pm 4.0 \times 10^{-7}) = 0.998\,165\,66 \pm 0.000\,000\,40$$

$$1 - \chi = A + \bar{\omega} - J - \frac{1}{2} K = 1834.34 \times 10^{-6}(1 \pm 2.2 \times 10^{-4}) = (1834.34 \pm 0.40) \times 10^{-6}$$

48. Gravity acceleration at the Earth's equator:

$$g_e = 9.780\,362\,(1 \pm 3.3 \times 10^{-6}) = 9.780\,362 \pm 0.000\,032 \text{ m/s}^2$$

49. Dynamic oblateness:

$$H = \frac{C - A}{C} = 3272.09 \times 10^{-6}(1 \pm 1.6 \times 10^{-4}) = (3272.09 \pm 0.54) \times 10^{-6} = 1/305.615 \pm 0.05$$

50. Moment of inertia parameter:

$$q = \frac{3}{2} \frac{C}{M_\oplus R_e^2} = \frac{J}{H} = 0.496\,16\,(1 \pm 3.4 \times 10^{-4}) = 0.496\,16 \pm 0.000\,17$$

51. Dimensionless moments of inertia:

$$\frac{A}{M_\oplus R_e^2} = J_2\left(\frac{1}{H} - 1\right) = 0.329\,69 \pm 0.000\,11$$

$$\frac{C}{M_\oplus R_e^2} = J_2/H = 0.330\,77 \pm 0.000\,11$$

52. Unit for the Earth's moments of inertia:

$$M_\oplus R_e^2 = 2.4311_4 \times 10^{38} (1 \pm 7.3 \times 10^{-4}) = (2.4311_4 \pm 0.0018) \times 10^{38} \text{ kg m}^2$$

53. Earth's moments of inertia:

$$A = 0.801\,52 \times 10^{38} (1 \pm 1.07 \times 10^{-3}) = (0.801\,52 \pm 0.000\,86) \times 10^{38} \text{ kg m}^2$$

$$C = 0.804\,15 \times 10^{38} (1 \pm 1.07 \times 10^{-3}) = (0.804\,15 \pm 0.00086) \times 10^{38} \text{ kg m}^2$$

$$C - A = 2.6313 \times 10^{35} (1 \pm 9.1 \times 10^{-4}) = (2.6313 \pm 0.0024) \times 10^{35} \text{ kg m}^2$$

54. Angular momentum:

$$C\,\Omega = 5.8640 \times 10^{33} (1 \pm 1.07 \times 10^{-3}) = (5.8640 \pm 0.0063) \times 10^{33} \text{ kg m}^2/\text{s}$$

55. Rotational energy:

$$\frac{1}{2} C\Omega^2 = 2.1380 \times 10^{29} (1 \pm 1.07 \times 10^{-3}) = 2.1380 \pm 0.0023) \times 10^{29} \text{ kg m}^2/\text{s}^2 \text{(joule)}$$

56. Circular velocity at the Earth's equator:

$$v_{cir} = \sqrt{\mu_\oplus / R_e} = 7905.404\ (1 \pm 7.7 \times 10^{-6}) = 7905.404 \pm 0.061 \text{ m/s}$$

3. LUNAR CONSTANTS

57. Mean observed distance from the Earth:

$$\bar{r}_\mathbb{C} = 384\,402.0\ (1 \pm 2.6 \times 10^{-6}) = 384\,402.0 \pm 1.0 \text{ km}$$

58. Relative mean lunar distance:

$$\bar{r}_\mathbb{C} / R_e = 1/\sin \pi_\mathbb{C} = 60.268\,38\ (1 \pm 5.8 \times 10^{-6}) = 60.268\,38 \pm 0.000\,35$$

59. Constant part of the sine of the perturbed lunar parallax:

$$\pi_\mathbb{C}' = \frac{\sin \pi_\mathbb{C}}{\sin 1''} = 3422.''438\ (1 \pm 5.8 \times 10^{-6}) = 3422.''438 \pm 0.''020$$

60. Mean perturbed equatorial horizontal parallax:

$$\pi_\mathbb{C} = 3422.''595\ (1 \pm 5.8 \times 10^{-6}) = 3422.''595 \pm 0.''020$$

61. Semi-major axis of the Moon's orbit:

$$a_\mathbb{C} = 1.000\,907\,681\ \bar{r}_\mathbb{C} = 384\,750.9\ (1 \pm 2.6 \times 10^{-6}) = 384\,750.9 \pm 1.0 \text{ km}$$

62. Siderial mean orbital motion (for 1950.0):

$$n_\mathbb{C} = 13.176\,358\,259\,8\ ^\circ/\text{d} = 0.549\,014\,912\,685\ ''/\text{s}\ (^\circ/\text{h})$$

$$= 2.661\,699\,407\,99 \times 10^{-6} \text{ rad/s}$$

63. Mean orbital velocity:

$$v_{\leftmoon} = a_{\leftmoon}\, n_{\leftmoon} = 1024.091\ (1 \pm 2.9 \times 10^{-6}) = 1024.091 \pm 0.003\ \text{m/s}$$

64. Lunar inequality in the Moon's ecliptic longitude:

$$L = 6.''4439\ (1 \pm 3.0 \times 10^{-4}) = 6.''4439 \pm 0.''0019$$

65. Parallactic inequality in the Moon's ecliptic longitude:

$$P_{\leftmoon} = 124.''986\ (1 \pm 3.3 \times 10^{-5}) = 124.''986 \pm 0.''004$$

66. Mass ratio of the Earth to the Moon:

$$1/\kappa = M_{\oplus}/M_{\leftmoon} = 81.250\ (1 \pm 3.0 \times 10^{-4}) = 81.250 \pm 0.024$$

67. Mass ratio of the Earth-Moon system to the Earth:

$$1 + \kappa = (M_{\oplus} + M_{\leftmoon})/M_{\oplus} = 1.012\,307\,7\ (1 \pm 3.7 \times 10^{-6}) = 1.012\,307\,7 \pm 0.000\,0037$$

68. Gravitational parameter of the Moon:

$$\mu_{\leftmoon} = GM_{\leftmoon} = 4905.92\ (1 \pm 3.1 \times 10^{-4}) = 4905.92 \pm 1.52\ \text{km}^3/\text{s}^2$$

69. Mass:

$$M_{\leftmoon} = 7.3552 \times 10^{25}\ (1 \pm 1.02 \times 10^{-3}) = (7.3552 \pm 0.0075) \times 10^{25}\ \text{g}$$

70. Moon's semi-diameter at mean distance:

$$s_{\leftmoon} = 932.''72\ (1 \pm 1.0 \times 10^{-4}) = 932.''72 \pm 0.''09$$

71. Relative radius of the visible disk of the Moon:

$$k = R_{\leftmoon}/R_{\odot} = 0.2725\,289\ (1 \pm 1.0 \times 10^{-4}) = 0.2725\,289 \pm 0.0000\,273$$

72. Radius of the visible disk of the Moon:

$$R_{\leftmoon} = \frac{b + c}{2} = 1738\ 236\ (1 \pm 1.0 \times 10^{-4}) = 1738\ 236 \pm 174\ \text{m}$$

73. Longest semi-axis directed to the Earth:

$$a = R_{\leftmoon}/0.9995\,918 = 1738\,946\ (1 \pm 1.07 \times 10^{-4}) = 1738\,946 \pm 186\ \text{m}$$

74. Medium semi-axis in orbital direction:

$$b = 0.9998\,116\ a = 1738\,618\ (1 \pm 1.20 \times 10^{-4}) = 1\,738\,618 \pm 209\ \text{m}$$

75. Shortest semi-axis (rotational or polar radius):

$$c = 0.9993\,720\ a = 1\,737\,854\ (1 \pm 1.08 \times 10^{-4}) = 1\,737\,854 \pm 188\ \text{m}$$

76. **Volume:**

$$V_\ell = \frac{4}{3}\ \pi\ abc\ = 2.200\,86 \times 10^{25}\,(1 \pm 3.35 \times 10^{-4}) = (2.200\,86 \pm 0.000\,74) \times 10^{25}\,\mathrm{cm}^3$$

77. Mean density:

$$\bar{\rho}_\ell = 3.3420\ (1 \pm 1.5 \times 10^{-3}) = 3.3420 \pm 0.0050\ \ \mathrm{g/cm}^3$$

78. Surface density:

$$\rho_0 = 3.290\ \ \mathrm{g/cm}^3$$

79. Central density:

$$\rho_c = 3.420\ \ \mathrm{g/cm}^3$$

80. Inhomogenity factor of the Moon:

$$\lambda = 0.1991\ (1 \pm 5.0 \times 10^{-4}) = 0.1991 \pm 0.0001$$

81. Dimensionless moment of inertia parameters:

$$f = \frac{C - B}{C - A}\ = 0.70\ (1 \pm 2.86 \times 10^{-2}) = 0.70 \pm 0.02$$

$$\alpha = \frac{C - B}{C} = 0.000\,4395\ (1 \pm 3.03 \times 10^{-2}) = 0.000\,4395 \pm 0.000\,0133$$

$$\beta = \frac{C - A}{C}\ = 0.000\,6279\ \ (1 \pm 1.6 \times 10^{-4}) = 0.000\,6279 \pm 0.000\,0001$$

$$\gamma = \frac{B - A}{C}\ = 0.000\,1884\ (1 \pm 6.85 \times 10^{-2}) = 0.000\,1884 \pm 0.000\,0129$$

$$g = \frac{3}{2}\ \frac{C}{M_\ell\ a^2} = 0.5972\ (\ 1 \pm 5.0 \times 10^{-4}) = 0.5972 \pm 0.0003$$

$$J = \frac{3}{2}\ \frac{C - 1/2\ \ (A + B)}{M_\ell\ a^2}\ = 0.000\,3187\ (1 \pm 1.38 \times 10^{-2}) = 0.000\,3187 \pm 0.000\,0044$$

$$K = \frac{3}{2}\ \frac{B - A}{M_\ell\ a^2}\ = 0.000\,1125\ (1 \pm 6.84 \times 10^{-2}) = 0.000\,1125 \pm 0.000\,0077$$

$$L = \frac{3}{2}\ \frac{C - A}{M_\ell\ a^2}\ = 0.000\,3750\ (1 \pm 2.1 \times 10^{-3})\ = 0.000\,3750 \pm 0.000\,0008$$

82. **Dimensionless moment of inertia differences:**

$$\frac{C - A}{M_\ell\ a^2}\ = 0.000\,2500\ \ (1 \pm 2.1 \times 10^{-3}) = 0.000\,2500 \pm 0.000\,0005$$

$$\frac{C - B}{M_\ell\ a^2}\ = 0.000\,1750\ (1 \pm\ 3.09 \times 10^{-2}) = 0.000\,1750 \pm 0.000\,0054$$

82. Dimensionless moment of inertia differences (Continued):

$$\frac{B-A}{M_\ell a^2} = 0.000\,0750\,(1 \pm 6.84 \times 10^{-2}) = 0.000\,0750 \pm 0.000\,0051$$

83. Dimensionless moments of inertia:

$$\frac{A}{M_\ell a^2} = 0.397\,87_7\,(1 \pm 5.0 \times 10^{-4}) = 0.397\,87_7 \pm 0.00020$$

$$\frac{B}{M_\ell a^2} = 0.397\,95_2\,(1 \pm 5.0 \times 10^{-4}) = 0.397\,95_2 \pm 0.000\,20$$

$$\frac{C}{M_\ell a^2} = 0.398\,12_7\,(1 \pm 5.0 \times 10^{-4}) = 0.398\,12_7 \pm 0.000\,20$$

84. Axial ratios of the Moon:

$$\frac{b}{a} = \sqrt{1 - \frac{2\gamma}{1+\gamma}} = 0.9998\,116\,(1 \pm 1.3 \times 10^{-5}) = 0.9998\,116 \pm 0.0000\,129$$

$$\frac{c}{a} = \sqrt{1 - \frac{2\beta}{1+\gamma}} = 0.9993\,720\,(1 \pm 1.0 \times 10^{-6}) = 0.9993\,720 \pm 0.0000\,010$$

$$\sigma = R_\ell / a = \frac{1}{2}\left(\frac{b}{a} + \frac{c}{a}\right) = 0.9995\,918\,(1 \pm 7.0 \times 10^{-6}) = 0.9995\,918 \pm 0.0000\,070$$

85. Oblateness coefficients of the potential function of the Moon:

$$J_2 = \frac{C - 1/2\,(A+B)}{M_\ell a^2} = \frac{2}{3}\,J = 0.000\,2125 \pm 0.000\,0029$$

$$J_2^{(2)} = \frac{B-A}{4\,M_\ell a^2} = \frac{1}{6}\,K = 0.000\,0188 \pm 0.000\,0013$$

86. Unit for the Moon's moments of inertia:

$$M_\ell a^2 = 2.224\,1_6 \times 10^{35}(1 \pm 1.2 \times 10^{-3}) = (2.224\,1_6 \pm 0.0027) \times 10^{35}\ \text{kg m}^2$$

87. Moment of inertia differences:

$$C - \frac{1}{2}\,(A+B) = 0.000\,473 \times 10^{35}\,(1 \pm 1.50 \times 10^{-2}) = (0.000\,473 \pm 0.000\,007) \times 10^{35}\,\text{kg m}^2$$

$$B - A = 0.000\,167 \times 10^{35}(1 \pm 6.96 \times 10^{-2}) = (0.000\,167 \pm 0.000\,012) \times 10^{35}\ \text{kg m}^2$$

88. Moon's moments of inertia:

$$A = 0.884\,94 \times 10^{35}\,(1 \pm 1.73 \times 10^{-3}) = (0.884\,94 \pm 0.001\,53) \times 10^{35}\,\text{kg m}^2$$

$$B = 0.885\,11 \times 10^{35}\,(1 \pm 1.73 \times 10^{-3}) = (0.885\,11 \pm 0.001\,53) \times 10^{35}\,\text{kg m}^2$$

$$C = 0.885\,50 \times 10^{35}\,(1 \pm 1.73 \times 10^{-3}) = (0.885\,50 \pm 0.001\,53) \times 10^{35}\,\text{kg m}^2$$

INDEX

(A)

	Page
Acceleration, gravitational,	II-9-14
Accuracy, tracking,	XI-12-20
Adams-Bashforth method,	IV-9-10
Aerodynamic heating,	IX-14-17
Air drag, perturbation of satellite orbits by,	V-1-55, IV-3
Angular momentum smoothing,	VII-44-46
Angular orbital elements,	III-4-37
Anomaly, eccentric, equations for,	III-21
series expansions,	III-26
mean, equations for,	III-25
figures,	III-76-87
series in,	III-26-34
true, equations for,	III-23
series for,	III-27
Apogee radius, equations for,	III-19
Apogee velocity, equations for,	III-20
Area coverage,	XIII-17-26
Areas, law of,	III-2
Argument of perigee, equations for,	III-24
Ascending node, equations for,	III-24
Astronomical unit,	II-2-15
Astronautical constants,	II-4
Atmospheric density, U.S. Standard 1962,	II-21-31
variability,	II-31-38
Attitude control, modes of,	XII-31-55
Attitude sensing, methods of,	XII-44-48
Axis, semimajor, equations for,	III-17
semiminor, equations for,	III-17
Azimuth, equations for,	III-37

Page

(B)

Ballistic coefficient, ... V-4-6
effective, ... V-20
tumbling, ... V-6-8
Bessel functions, ... V-16
asymptotic series, ... V-17
integrals, ... V-16
modified, ... V-17
reduction formulas, ... V-17
Bibliographies (see references)

(C)

Central force field, ... III-2
Change in orbital velocity due to
impulsive burning of an injection rocket, ... VI-2, 6
in satellite in-orbit position, ... VI-6-8, 11
Closure (rendezvous), (see final closure)
Coefficient of drag, ... V-3-6
effective, ... V-20
Coefficients of potential, function, ... II-9-14
Compatible orbits rendezvous, ... VII-9-12
Computation of orbits, ... IX-25-30
Conic motion, ... III-1-7
Constants, astronautical, ... II-2
conversion, ... II-50-56
geocentric, ... II-9-14
heliocentric, ... II-4-5
planetocentric, ... II-5-8
selenocentric, ... II-14-15
Control requirements, ... XII-47-55
Conversion factors, table of, ... II-50-56

Page

Coordinate systems, geometrical properties of, ... IX-2
Coordinate systems, important, summary, ... IX-3
Coordinates and transformations, ... IX-2-6
Cosmic radiation, ... II-41-45
Cryogenic fluids, properties of, ... X-10
Cryogenic tanks, design of, ... X-11
Coverage, area, ... XIII-17-24
  effects of sensor limitations, ... XIII-26-31
Cowell's method, ... IV-4

(D)

Decay histories, ... IX-2-18
  circular orbits, ... V-9-10
  effects on coverage, ... VIII-25-26
  elliptic orbits, ... V-13-21
Decay rates, circular orbits, ... V-18
  elliptic orbits, ... V-19
  expansions for small parameter, ... V-11
Deceleration, re-entry, ... IX-12-14
Declination, equations, ... III-37
Definitions, ... Appendix A
Density, atmospheric (see atmospheric density)
Departure, orbital (see Orbital Departure)
Direct launch (rendezvous), ... VII-12-13
Docking, orbital (see Rendezvous)
Drag, atmospheric, ... V-3-8
  in circular orbits, ... V-9-10
  coefficient, ... V-4-8
  effect on the orbit (perturbations), ... V-8-55
  for tumbling bodies, ... V-6-8
Differential corrections, maneuvers, ... VI-33-39
  orbit improvement, ... XI-37-43

Page

(E)

Eccentricity, equations for, ... III-18
series expansions in, ... III-26-34
Eckert-Brouwer differential corrections, ... XI-37-42
Eclipses of earth satellites, ... XIII-6-14
Ecliptic coordinates, ... XI-2-6
Elements, elliptic, equations for, ... III-16-34
hyperbolic, equations for, ... III-34-38
Elliptic orbits, computation of, ... XI-22-47
correction of, ... VI-2-52
discussion of, ... III-2-13
Encke's method, ... IV-4-5
Energy, equation, ... III-5
kinetic, ... II-5
loss due to drag, ... V-9
minimization of, ... VI-43-50
potential, ... II-5
total, ... II-5
Error analysis, of elliptic orbits, ... XII-2-28
of orbital departure, ... VIII-5-6, 22-23
of maneuvers, ... VI-39-42
Errors in numerical integration, ... IV-7-14
Extraction of information (see Orbit Computation) XI-12-22

(F)

Final closure (rendezvous), ... VII-15-54
analytic solutions, ... VII-50-54
techniques, ... VII-26-54
energy and time requirements, ... VII-40-44
terminal smoothing, ... VII-44-50
Finite burning times--effects on departure, ... VIII-19-22
effects on maneuvers, ... VI-50-53

Page

Flight path angle, equations for, ... III-22
Flight time, equations for, ... III-6
figures, ... III-45, 76-87
lifetimes, ... V-2-30
re-entry, ... IX-2-12
rendezvous, ... VII-40-44
return from orbit, ... VIII-19-22
Flow regimes, ... V-2-3
Force, central, ... III-2
Formulations for elliptic orbits, ... III-16-34
Fourier-Bessel expansions, ... III-30-34
Frequency-departure, ... VIII-24-30

(G)

Gauss-Jackson method, ... IV-11
General maneuver, ... VI-23-26
General perturbations, ... IV-14-50
Geocentric constants, ... II-9-14
coefficients of the potential function, ... II-12
flattening and equatorial radius, ... II-12-14
gravitational constant, ... II-11
Geodetic latitude, ... XI-4
Geometry, of ellipse, ... III-46
of hyperbola, ... III-47
of orbit in 3-D, ... III-46
of parabola, ... III-47
Geophysical data, ... II-15-50
Glossary, ... Appendix A
Ground resolution, ... XIII-26-32
Ground swath, ... XIII-17-26
Guidance and control requirements, ... XII-2-28

Page

(H)

Heat balance, ... X-4
Heat input, ... X-5
Heat transfer, ... X-11
Heliocentric constants, ... II-4-5
  planetary geometry, ... II-5-8
  planetary masses, ... II-5
  planetary orbits, ... II-8-9
  solar gravitation constant, ... II-4
  solar parallax, ... II-4
Hyperbolic orbits, element relations, ... III-35-36
  time variant relations, ... III-36-37

(I)

Illumination of satellites, ... XIII-6-14
Improvement of orbit, ... XI-37-43
Impulsive maneuvers, ... VI-2-38
Inclination, equations for, ... III-24
Integration, numerical, errors in, ... IV-12-14
Intermediate orbits, rendezvous, ... VII-5-9

(J)

J_i (coefficients of the gravitational potential), ... II-9-14

(K)

Keplerian orbits, ... III-1-14
Kepler's equation, ... III-6
  solution by Newton's method, ... III-6
Krylov-Bogoliuboff averaging method, ... V-15

(L)

Lagrange's planetary equations, ... IV-20-21
Lambert's theorem, ... III-7-9

Page

Lifetimes, ... V-1-29
drag coefficients, ... V-4-6
drag force, ... V-3-4
drag on tumbling bodies, ... V-6-8
effect of density variability, ... V-25-30
flow regimes, ... V-2-3
three dimensional perturbation, ... V-21-25
change in elements, ... V-22-25
perturbing force, ... V-21-22
two-dimensional perturbation, ... V-8-21
elliptic orbits, ... V-10-12
near circular orbits, ... V-9-10, 18-19
variation of elements, ... V-12-18
Low altitude orbits, departure from, ... VIII-17-23
Low level thrust maneuvers, ... VI-56-64
Lunar perturbations, ... IV-36-40

(M)

Maneuverability, ... IX-18-21
envelopes, ... IX-21
lifting bodies, ... IX-21
re-entry, ... IX-18-21
Maneuvers, ... VI-1-64
differential corrections, ... VI-33-39
distribution of the resulting orbit, ... VI-39-43
effects of finite burning time, ... VI-50-53
general, ... VI-23-26
impulsive corrections, ... VI-2-3
in orbit propulsion system, ... VI-53-56
independent adjustment of elements, ... VI-3-15
microthrust study, ... VI-56-64
optimization, ... VI-43-50

Page

propulsion for canceling drag and
oblateness, ... VI-26-33
small maneuvers in nearly circular orbits, ... VI-15-23
Mean anomaly (see Anomaly, mean)
Meteoroid, data, ... II-46-50
hazard and shielding, ... II-50
penetration, ... II-49
Method of least squares, ... XI-30-36
Microthrust, normal to the plane, ... VI-60
circumferential, ... VI-58
general, ... VI-60-64
radial, ... VI-57-58
tangential, ... VI-58
Minimum energy transfers, ... VI-43-50
Mission requirements, ... XIII-1-32
area coverage, ... XIII-17-21
communication satellites, ... XIII-2-4
eclipses, ... XIII-8-14
ground tracks, ... XIII-14-17
meteorological satellites, ... XIII-6
mission considerations, ... XIII-2-6
navigation satellites, ... XIII-4-6
pattern coverage, ... XIII-21-24
point coverage, ... XIII-24-26
reconnaissance satellites, ... XIII-2
relative geometry vehicle, earth, sun, ... XIII-6-8
satellite coverage, ... XIII-17-26
sensor limitations, ... XIII-26-32
solar problems, ... XIII-6-14
synchronous orbits, ... XIII-16-17
Model atmospheres, ... II-15-38

Page

Molecular speed ratio, ... V-4
Motion, equations of, ... III-2

(N)

Node, ascending, equations for, ... III-24
Nomography, ... III-14-15
Nongravitational forces, ... IV-3-4
Numerical integration, ... IV-7-14

(O)

Orbit computation, ... XI-1-47
accuracy determination, ... XI-43-47
acquisition of data, ... XI-14-22
coordinate systems and transformations, ... XI-2-14
data correction, ... XI-2-11
Gibbs' modification, ... XI-26-27
maximum likelihood, ... XI-36
method of Laplace, ... XI-22-25
method of least squares, ... XI-30-37
method of Gauss, ... XI-25-26
method of moments, ... XI-36-37
minimum variance, ... XI-36
observational error, ... XI-28-37
orbit improvement, ... XI-37-43
preliminary orbits, ... XI-22-28
station properties, ... XI-14-16
tracking techniques, ... XI-12-14
Orbital departure, ... VIII-3-30
analysis of departure frequencies, ... VIII-24-30
generalized return problem, ... VIII-3-17
planar analysis of deorbit from low altitude circular orbits, ... VIII-17-23
three-dimensional impulse analyses, ... VIII-23-24

Page

Orbit mechanics, ... III-1-39
graphical data, ... III-39-87
Lagrangian equations, ... III-3
Lambert's theorem, ... III-7-9
motions in central force field, ... III-2-3
motion in 3-D, ... III-4
N-body problem, ... III-9-12
nomograms, ... III-14-15
orbital elements, ... III-3
properties of elliptic motion, ... III-4-7
series expansion for elliptic orbits, ... III-12-14
tables of equations for elliptic motion, ... III-15-38
Oblate earth, ... II-9-14
Oblateness, comparison of theories, ... IV-31-36
perturbations, ... IV-21-31
long period, ... IV-24
secular, ... IV-23-24
short period, ... IV-24-25
Observational theory and trajectory prediction, ... XI-28-37
Optimization, of area coverage, ... XIII-17-26
of maneuvers, ... VI-43-50
of satellite patterns, ... XIII-21-26
Orbit determination, ... XI-22-28
Orbit improvement, ... XI-37-42
Orbital parameters, equations for, ... III-17-38
Orbital perturbations, equations for, ... IV-23-40
Orientation, satellite, ... XIII-6-14
Osculating orbital elements, ... IV-15-21

(P)

Parallax, lunar, ... II-14
solar, ... II-4

Page

Parameters, variation of, ... IV-15-21
Parking orbits, utilization of, ... VII-5-9
Penetration, meteorite, ... VIII-3-17
Perigee advance, due to drag, ... V-13
due to oblateness, ... IV-23-24
Perigee radius, equations for, ... III-19
Perigee velocity, equations for, ... III-20
Period, anomalistic, ... IV-22
changes due to drag, ... VIII-25-27
changes due to oblateness, ... IV-21-22
nodal, ... IV-22
sidereal, ... IV-22
Perkins' method for decay rates, ... V-18-19
Perturbation theories, analytic comparison of, ... IV-31-36
Cowell's method, ... IV-4-5
drag perturbations, ... IV-40-45
Encke's method, ... IV-5-6
first order secular, ... IV-21-23
general, ... IV-15-40
higher order, ... IV-23-31
numerical integration, ... IV-7-14
oblateness, ... IV-21-31
precession of apsides, ... IV-24
regression of nodes, ... IV-24
solar-lunar, ... IV-36-40
special, ... IV-2-7
stability, ... IV-47-50
variation of parameters, ... IV-6-7-15-21
Physical data, ... II-2-56
astronomical constants, ... II-2-15

	Page
astrophysical data,	II-15-50
conversion data,	II-50-56
Planets, geometry of,	II-5-9
masses of,	II-5
elements of orbits,	II-8
Potential function,	II-9
Precession of apsides,	IV-24
Primary cosmic radiation,	II-43-45
Propellant storage in orbit,	X-10-15
Propulsion requirements to cancel effects of oblateness,	VI-26-33
Propulsion system,	VI-53-56
chamber sizing,	VI-55
nozzle sizing,	VI-54
propellant flow rates,	VI-56
requirements,	VI-53
thrust level,	VI-54

(R)

Radar data,	XI-12-22
Radial acceleration, equations for,	III-22
Radial velocity, equations for,	II-21, 22
Radiation, damage thresholds,	II-45
penetrating electromagnetic,	II-45
primary cosmic,	II-41-45
solar flare radiations,	II-39, 40
Van Allen belts,	II-40, 41
Radius, earth's equatorial,	II-12-14
equivalent,	II-19
polar,	II-12-14
orbital, equations for,	III-21
series,	III-27, 28

Page

Range, descent from orbit to re-entry, ... VIII-17-23
ballistic vehicles re-entry to impact, ... IX-17, 18
equilibrium glide re-entry to impact, ... IX-19
lateral re-entry to impact, ... IX-18-21
lifting vehicles re-entry to impact, ... IX-17-21
Re-entry, aerodynamic heating, ... IX-14-17
deceleration and loads, ... IX-12-14
range and maneuverability, ... IX-17-21
theory, ... IX-2-22
trajectories, ... IX-2-12
References and bibliography, guidance and control, . XII-56-63
lifetime, ... V-30-35
maneuvers, ... VI-64-75
mission requirements, ... XIII-32-35
orbit computation, ... XI-47-49
orbit mechanics, ... III-39-41
orbital departure, ... VIII-30
perturbations, ... IV-50-59
physical data, ... II-56-63
re-entry, ... IX-21-29
rendezvous, ... VII-54-57
waiting orbit criteria, ... X-15-21
Regression of the nodes, ... IV-24
Rendezvous, ... VII-1-53
compatible orbits, ... VII-9-12
direct launch, ... VII-12-13
energy and time requirements, ... VII-40-44
final closure techniques, ... VII-26-40
gross maneuvers, ... VII-3-13
homing phase errors, ... VII-53-59
intermediate orbits, ... VII-2-9
long time closures, ... VII-50-53

Page

relative motion, ... VII-13-26
terminal guidance smoothing, ... VII-44-50
terminal manuever, ... VII-13-54
Return from orbit (see Re-entry and Orbit Departure)
Runge-Kutta method, ... IV-7-8

(S)

Satellite, energy, ... III-5
ground tracks, ... XIII-14-17
illumination, ... XIII-6-14
orbital data, ... III-15-39
orientation with respect to the sun, ... XIII-6-14
recovery, ... VIII, IX
Selenocentric constants, ... II-14-15
Simulatus rectum (see Semiparameter)
Semimajor axis, equations for, ... III-17
Semiparameter, equations for, ... III-18
Sensitivities, trajectories, ... XII-2-28
Series expansions of orbital parameters, ... III-26-34
Smoothing techniques, general, ... XI-28-42
rendezvous, ... VII-44-50
Solar, gravitational constant, ... II-5
parallax, ... II-4
perturbations, ... IV-36-40
radiation, ... II-39-40
Special perturbations, ... IV-2-14
Spherical trigonometric relations, ... III-37, 38
Statistical error analysis (maneuvers), ... IV-39-43
Storability, cryogenic, ... X-10-15
Swath, ... XIII-17-26

(T)

Temperatures, histories for re-entry, ... IX-14-17
parameters, ... IX-14-17
radiation equilibrium, ... IX-16
skin, ... IX-14-17
stagnation point, ... IX-14-17
Terminal guidance for rendezvous, ... VII-13-54
Theory of errors in orbital prediction, ... XII-2-2
Three dimensional elliptic relations, ... III-4
Time dependent variables for elliptic orbits, ... III-21-23
Time standards and conversions, ... II-50-56
Tracking facilities, ... XI-12-22
Trajectories, re-entry, ... IX-2-12
Transfer maneuvers, ... VI-2-33
Transformation of coordinates, ... XI-2-12
True anomaly, equations for, ... III-23
series expansions, ... III-27

(U)

Umbra, time in, ... XIII-6-14
Upper atmosphere, models of, ... II-15-38
Universal gravitation, low of, ... II-2

(V)

Van Allen radiation, ... II-40, 41
Variation of parameters, ... IV-15-21
Vis Viva integral, ... III-5
Visibility times, ... XIII-17-26

(W)

Waiting orbit criteria, ... X-2-15
cryogenic propellant storage, ... X-10-15

Page

payload and geometrical restrictions X-2-4
vehicle temperature control, ... X-4-10
Weights and volume conversions, ... II-50-56

(Z)

Z function for re-entry, ... IX-2-12
Zenith angle of a satellite, ... XIII-24-25